EANM'21

Annual Congress of the
European Association of Nuclear Medicine
October 20-23, 2021
Virtual

Abstracts

European Journal of Nuclear Medicine and
Molecular Imaging (2021) 48 (Suppl 1): S1–S648

This supplement was not sponsored by outside commercial interests. It was funded entirely by the association's own resources.

Dear Colleagues, dear Friends,

On behalf of the European Association of Nuclear Medicine, it is my honour to invite you to the 34th Annual EANM Congress. The event will run virtually from 20 to 23 October 2021.

Despite the difficult time we are experiencing due to the pandemic, nuclear medicine continues to grow both in diagnostic imaging and therapy. New radiopharmaceuticals which facilitate the study and treatment of new targets are being introduced, more and more protocols which cover unmet clinical needs and new applications are running, and the use of nuclear medicine procedures is increasingly being incorporated into clinical practice and guidelines. This success remains related to that very peculiar characteristic of our specialty, namely, its functional approach to medicine. This is mainly true with respect to imaging, but also for therapy.

In recent years we have proudly celebrated the status of the EANM Congress as the world's leading meeting for nuclear medicine. In 2019, for example, we reached almost 7000 participants, a truly memorable record. As we all know, the pandemic of 2020 forced all events to move to a virtual format and we did our best to prepare a great event. We succeeded in keeping all of our scientific programmes running with 11 parallel channels and received excellent feedback from participants. As mentioned, we are unable to return to the live format we are used to and would have all hoped for in 2021. Therefore, we have planned a great event with a full scientific programme once more, but have arranged some significant improvements after the lessons learnt last year. In 2021, pre-congress symposia will run a couple of weeks before the congress, which, as a result, has been shortened by one day. Furthermore, most of the several parallel tracks will not run according to the traditional time sequence but will always be available on demand to facilitate access and productivity for attendees.

In summary, we are working on providing you a congress with superb and comprehensive scientific content as well as a lot of other features to make your participation enjoyable whatever you are looking to achieve.

Stefano Fanti

EANM Congress Chair 2020-2022

PRE-CONGRESS SYMPOSIA OCTOBER 4-6, 2021

Time (CEST)	Channel 1 Monday, Oct 4, 2021	Channel 1 Tuesday, Oct 5, 2021	Channel 1 Wednesday, Oct 6, 2021	Time (CEST)
09:00 - 12:00	**Pre-Congress Symposium 1** Dosimetry + Translational Molecular Imaging & Therapy Committee **Pre-Clinical Dosimetry and Extrapolations from Animal Models to Humans**	**Pre-Congress Symposium 3** Bone & Joint + Oncology & Theranostics + Paediatrics Committee **Radiosynoviorthesis - Master Class in Science and Practice**	**Pre-Congress Symposium 5** Neuroimaging + Radiopharmacy + Drug Development Committee **Imaging of Protein Misfolding in Parkinson's Disease and Related Disorders - Where are we and What do we need?**	09:00 - 12:00
14:00 - 17:00	**Pre-Congress Symposium 2** Cardiovascular + Physics Committee **Signal Quantification in Cardiac SPECT – Dream or Reality?**	**Pre-Congress Symposium 4** Oncology & Theranostics Committee **Structured Reporting of Oncology PET-CT – Are we Ready for Template-Based Reporting?**	**Pre-Congress Symposium 6** Oncology & Theranostics Committee / ESTRO **Oligocare Concept in Radiation Oncology**	14:00 - 17:00

PRE-CONGRESS SYMPOSIA OCTOBER 11-13, 2021

Time (CEST)	Channel 1 Monday, Oct 11, 2021	Channel 1 Tuesday, Oct 12, 2021	Channel 1 Wednesday, Oct 13, 2021	Time (CEST)
09:00 - 12:00	**Pre-Congress Symposium 7** Radiation Protection + Dosimetry Committee **Biokinetic Modelling in Cancer Therapy and Clinical Impact**	**Pre-Congress Symposium 9** Oncology & Theranostics + Thyroid Committee / ESES **Nuclear Endocrinology in the Era of Precision Medicine**	**Pre-Congress Symposium 11** Inflammation & Infection Committee **Light in the Dark - Hybrid Imaging in Patients with Sepsis/Bacteremia**	09:00 - 12:00
14:00 - 17:00	**Pre-Congress Symposium 8** Radiopharmacy + Oncology & Theranostics + Drug Development Committee **Novel Radionuclides for Theranostics on the Horizon**	**Pre-Congress Symposium 10** Physics + Dosimetry Committee **Total Body PET**	**Pre-Congress Symposium 12** Technologists Committee **PET/MR - The Cross Path of Morphology and Functionality**	14:00 - 17:00

WEDNESDAY OCTOBER 20, 2021

Time (CEST)	Channel 1	Channel 2	Channel 3
08:45 - 09:10	**Opening Ceremony**		
09:10 - 10:00	101 **Plenary 1** **Highlights Lecture**		
10:15 - 11:00	201 CME **CME 1** Oncology & Theranostics Committee **Prostate Cancer - Greatest Hits**	202-1 **Special Track** Interview with the Expert 1 **Therapy** (10:15 - 10:40)	203 **Industry Channel** Satellite Symposium by GE Healthcare
11:00 - 11:45		202-2 **Special Track** Interview with the Expert 2 **Imaging Myeloma** (11:00 - 11:20)	
12:00 - 12:45	301 CME **CME 2** Physics Committee **AI in Radiomics**	302-1 **Special Track** Interview with the Expert 3 **Nuclear Endocrinology** (12:00 - 12:25)	303 **Industry Channel** Satellite Symposium by Advanced Accelerator Applications, A Novartis Company
12:45 - 13:30		302-2 **Special Track** Interview with the Expert 4 **Neuroimaging**	
13:30 - 13:50	**Awards Ceremony**		
13:50 - 14:20	**Lunch Break**		403 **Industry Channel** Satellite Symposium by Hermes Medical Solutions (13:50-14:15)
14:20 - 14:40	**Plenary Quiz**		
14:40 - 16:00	401 **Plenary 2** **incl. Marie Curie Lecture Theranostics Applications and Challenges**		
16:15 - 17:45	501 CME **CME 3** Inflammation & Infection Committee **The Battle Continues - WBC Scan vs FDG PET/CT**	502 **Special Track** **The Top 3 Trials Sessions 1 Prostate**	503 **Industry Channel** Satellite Symposium by Advanced Accelerator Applications, A Novartis Company
18:00 - 19:30	601 CME **CME 4** Neuroimaging Committee **Imaging Neuroinflammation - Everything You Always Wanted to Know, But Were Afraid to Ask**	602 **Special Track** **Case Report Session What's the Case? Report it Now!**	603 **Industry Channel** Satellite Symposium by Telix Pharmaceuticals

THURSDAY OCTOBER 21, 2021

Time (CEST)	Channel 1	Channel 2	Channel 3
09:00 - 09:45	801 CME **CME 5** Cardiovascular + Inflammation & Infection Committee **Infiltration, Infection and Infiltrative Nuclear Cardiovascular Diseases - Think Nuclear!**	802-1 **Special Track** Interview with the Expert 5 **Creating Tracers** (09:00 - 09:35)	803-1 **Industry Channel** Satellite Symposium by GE Healthcare
09:45- 10:30		802-2 **Special Track** Interview with the Expert 6 **Paediatric NM Today**	803-2 **Industry Channel** Satellite Symposium by GE Healthcare
10:45 - 12:15	901 CME **CME 6** Oncology & Theranostics Committee **Quo vadis PET/MRI?**	902 **Industry Channel** Satellite Symposium by Siemens Healthineers	903 **Industry Channel** Satellite Symposium by GE Healthcare
12:15 - 13:10	**Lunch Break**		
13:10 - 13:30	**Plenary Quiz**		
13:30 - 14:50	1001 **Plenary 3** **Conventional Nuclear Medicine - Oldies but Goldies**		
15:05 - 16:35	1101 CME **CME 7** Physics + Dosimetry Committee **Developments and Challenges in Theranostics**	1102 **Special Track** **The Top 3 Trials Sessions 2 Rest of the Science**	1103 **Industry Channel** Satellite Symposium by Terumo Interventional Systems
16:50 - 17:35	1201 CME **CME 8** Radiation Protection + Dosimetry Committee **Pregnancy and Breastfeeding in the Context of Nuclear Medicine**	1202-1 **Special Track** Interview with the Expert 7 **The Theranostic Unit** (16:50 - 17:10)	1203 **Industry Channel** Satellite Symposium by Bayer AG
17:35 - 18:20			

Plenary Sessions | CME Sessions | Joint Symposia | Technologists' Track | M2M Track | Cutting Edge Science Track | Pitfalls & Artefacts / Teaching Sessions | Clinical Oncology Track | Further TROP/Featured Sessions | e-Poster Presentation Sessions | Special Track | Satellite Symposia

FRIDAY OCTOBER 22, 2021

Time (CEST)	Channel 1	Channel 2	Channel 3
09:00 - 09:45	1301 CME 9 Radiopharmacy + Drug Development Committee **Back to the Future - New Kit-Based Approaches for Labelling Radiopharmaceuticals (^{68}Ga, Al[^{18}F]F,...)**	1302-1 Special Track Interview with the Expert 8 **Vision Trial** (09:00 - 09:30)	1303-1 Industry Channel Satellite Symposium by GE Healthcare
09:45 - 10:30		1302-2 Special Track Interview with the Expert 9 **The Best Young NM**	1303-2 Industry Channel Satellite Symposium by GE Healthcare
10:45 - 11:30	1401 CME 10 Thyroid + Oncology & Theranostics Committee **Radionuclide Therapies - Management of Side Effects and Complications**	1402-1 Special Track Interview with the Expert 10 **Running a Preclinical Lab in New York City** (10:45 - 11:20)	1403 Industry Channel Satellite Symposium by Sirtex Medical Europe GmbH
11:30 - 12:15		1402-2 Special Track Interview with the Expert 11 **New PET Tracers in Oncology**	
12:15 - 13:10	**Lunch Break**		
13:10 - 13:30	**Plenary Quiz**		
13:30 - 14:50	1501 Plenary 4 **Isotopes' Past and Future**		
15:05 - 16:35	1601 CME 11 Bone & Joint Committee **New Concepts for Imaging and Therapy of Bone Metastases**	1602 Special Track **The Top 3 Trials Sessions 3 New Tracers**	1603 Industry Channel Satellite Symposium by Boston Scientific
16:50 - 17:35	1701 CME 12 Paediatrics Committee **Nuclear Medicine in the Evaluation of Child Abuse**	1702-1 Special Track Interview with the Expert 12 **Radiopharmacy Running** (16:50 - 17:25)	1703 Industry Channel Satellite Symposium by Spectrum Dynamics Medical Ltd.
17:35 - 18:20			

SATURDAY OCTOBER 23, 2021

Time (CEST)	Channel 1	Channel 2	Channel 3
09:00 - 09:45	1801 CME 13 Translational Molecular Imaging & Therapy + Oncology & Theranostics Committee **Immunotheranostics**	1802-1 Special Track Interview with the Expert 13 **A Life in NM**	
09:45 - 10:30		1802-2 Special Track Interview with the Expert 14 **Prostate Cancer Imaging**	
10:45 - 11:30	1901 CME 14 Drug Development + Translational Molecular Imaging & Therapy Committee **Probing Tumour Metabolism - An Update**	1902-1 Special Track Special Talk by Declan Murphy **Prostate Cancer along the Yellow Brick Road**	
11:30 - 12:15		1902-2 Special Track Interview with the Expert 15 **Reflections on the Development of PET and Theranostics Downunder - A 25-Year Journey into the Light**	
12:25 - 12:45	**Closing Session**		

Plenary Sessions | CME Sessions | Joint Symposia | Technologists' Track | M2M Track | Cutting Edge Science Track | Pitfalls & Artefacts / Teaching Sessions | Clinical Oncology Track | Further TROP/Featured Sessions | e-Poster Presentation Sessions | Special Track | Satellite Symposia

ON-DEMAND CONTENT
AVAILABLE FROM OCTOBER 20, 2021 | 09:00

204 **Technologists' Track CTE 1** Technologists Committee / SNMMI **Tech Guide Launch**	205 **Joint Symposium 1** Bone & Joint + Inflammation & Infection + Paediatrics Committee / ESSR **PET/MRI in MSK - Be Hybrid!**	206 **Joint Symposium 2** Cardiovascular Committee / ASNC **PET-MPI vs. SPECT-MPI - Is it Worth the Price?**	207 **Pitfalls & Artefacts 1** Cardiovascular + Physics + Technologists Committee **Pitfalls in Cardiovascular Imaging**	208 **M2M Track TROP Session** Drug Development + Radiopharmacy + Translational Molecular Imaging & Therapy Committee **Prostate Cancer Imaging - The Various Angles of Attack**	209 **Cutting Edge Science Track TROP Session** Dosimetry Committee **Radiobiology Meets Dosimetry**	210 **Clinical Oncology Track TROP Session** Oncology & Theranostics Committee **Head and Neck / Colorectal**	211 **Featured Session** Cardiovascular Committee **Quantification in MPI - A Must!**	212 **e-Poster Presentation Session 1** Cardiovascular Committee **The Nuclear Cardiovascular World at its Best**
304 **Technologists' Track CTE 2** Technologists + Paediatrics Committee **Managing the Paediatric Patient in Nuclear Medicine Departments**	305 **Joint Symposium 3** Cardiovascular Committee / EACVI **MPI after the ISCHEMIA Trial - Still Alive?**	306 **Joint Symposium 4** Dosimetry Committee / CIRSE **Biokinetics and Dosimetry in Intraarterial Therapy**	307 **Pitfalls & Artefacts 2** Neuroimaging + Oncology Committee **Pseudoprogression and Pseudoresponse in Brain Tumours**	308 **M2M Track TROP Session** Drug Development + Radiopharmacy + Translational Molecular Imaging & Therapy Committee **It's the Alpha, not the Beta**	309 **Cutting Edge Science Track TROP Session** Dosimetry Committee **Dosimetry Methods**	310 **Clinical Oncology Track TROP Session** Oncology & Theranostics Committee **Breast**	311 **Featured Session** Cardiovascular Committee **Show me your Heart!**	312 **e-Poster Presentation Session 2** Dosimetry Committee **Dosimetry**
404 **Technologists' Track CTE 3** Technologists Committee / ESTRO **PET/CT for RT Planning**	405 **Joint Symposium 5** Drug Development + Radiopharmacy + Oncology & Theranostics Committee / SRS **Targeting Cancer with Peptides, Fragments or Antibodies**	406 **Joint Symposium 6** Drug Development + Radiopharmacy + Translational Molecular Imaging & Therapy Committee / SRS **Modifying Radiopharmaceuticals to Alter Pharmacokinetics**	407 **Pitfalls & Artefacts 3** Neuroimaging Committee **Challenging Cases in Nuclear Neurology**	408 **M2M Track TROP Session** Drug Development + Radiopharmacy + Translational Molecular Imaging & Therapy Committee **Theranostics - Various Targets**	409 **Cutting Edge Science Track TROP Session** Dosimetry Committee **Lu-177 Dosimetry**	410 **Clinical Oncology Track TROP Session** Oncology & Theranostics Committee **Lung**	411 **Featured Session** Cardiovascular Committee **New Kids on the Cardiovascular Block!**	412 **e-Poster Presentation Session 3** Inflammation & Infection Committee **More on Infection & Inflammation Imaging and NM in COVID-19**
504 **Technologists' Track CTE 4** Technologists Committee **Cardiac PET/CT**	505 **Joint Symposium 7** Inflammation & Infection Committee / EASD **My Foot is on Fire - Find the Hot Spot**	506 **Joint Symposium 8** Inflammation & Infection + Bone & Joint Committee / EULAR **PET/CT and PET/MRI in Patients with Autoimmune Disorders**	507 **Pitfalls & Artefacts 4** Oncology & Theranostics + Translational Molecular Imaging & Therapy Committee **Sentinel Lymph Node in Head & Neck, Penile and Gynaecological Cancers**	508 **M2M Track Featured Session** Drug Development + Radiopharmacy + Translational Molecular Imaging & Therapy Committee **Mapping Brain Structures**	509 **Cutting Edge Science Track TROP Session** Dosimetry Committee **Clinical Dosimetry and Radioembolisation**	510 **Clinical Oncology Track TROP Session** Oncology & Theranostics Committee **Gastro-Intestinal**	511 **TROP Session** Inflammation & Infection Committee **Top of Cardiovascular and Soft Tissue Infection/Inflammation Imaging**	512 **e-Poster Presentation Session 4** Drug Development + Radiopharmacy + Translational Molecular Imaging & Therapy Committee **Radiochemistry**
604 **Technologists' Track CTE 5** Technologists + Inflammation & Infection Committee **Update in Inflammation Imaging**	605 **Joint Symposium 9** Neuroimaging Committee / EAN **The New ATN Diagnostic Concept in Alzheimer's Disease**	606 **Joint Symposium 10** Neuroimaging Committee / ILAE **PET/MRI in Epilepsy**	607 **Pitfalls & Artefacts 5** Paediatrics Committee **Pitfalls & Pearls in Paediatric Musculoskeletal**	608 **M2M Track Featured Session** Drug Development + Radiopharmacy + Translational Molecular Imaging & Therapy Committee **Functional Brain Imaging**	609 **Cutting Edge Science Track TROP Session** Dosimetry Committee **Diagnostic Dosimetry**	610 **Clinical Oncology Track TROP Session** Oncology & Theranostics Committee **Neuroendocrine**	611 **TROP Session** Inflammation & Infection Committee **Top of Nuclear Medicine in COVID-19**	612 **e-Poster Presentation Session 5** Drug Development + Radiopharmacy + Translational Molecular Imaging & Therapy Committee **Theranostics**
904 **Technologists' Track CTE 6** Technologists Committee **Radionuclide Therapy Management**	905 **Joint Symposium 11** Neuroimaging + Oncology & Theranostics Committee / EANO **Advancements in Neuro-Oncology**	906 **Joint Symposium 12** Oncology & Theranostics Committee / EORTC **Nuclear Medicine in Precision Oncology**	907 **Pitfalls & Artefacts 6** Thyroid Committee **Pitfalls & Artefacts in Endocrine Imaging**	908 **M2M Track TROP Session** Drug Development + Radiopharmacy + Translational Molecular Imaging & Therapy Committee **Tumour Microenvironment and Immunotherapy**	909 **Cutting Edge Science Track Featured Session** Radiation Protection Committee **From Safety Culture to Fieldwork in Radiation Protection**	910 **Clinical Oncology Track Featured Session** Oncology & Theranostics Committee **Radioguided Surgery and Sentinel Lymph Nodes**	911 **Featured Session** Neuroimaging Committee **Molecular Imaging of Alzheimer's Disease**	912 **e-Poster Presentation Session 6** Neuroimaging Committee **Molecular Brain Imaging**
					1009 **Cutting Edge Science Track TROP Session** Physics Committee **New Imaging Equipment and Techniques**			1012 **e-Poster Presentation Session 7** Thyroid Committee **An Overview on Endocrine Disease**
1104 **Technologists' Track CTE 7** Technologists Committee **Research - Technologist's Involvement**	1105 **Joint Symposium 13** Oncology & Theranostics Committee / EHA **Biomarkers in Lymphoma**	1106 **Joint Symposium 14** Oncology & Theranostics Committee / EHA **New Therapies in Lymphoma - Is Deauville Still Good Enough?**	1107 **Teaching Session 1** Bone & Joint + Inflammation & Infection Committee / AGA **Imaging of Prosthetic Knee Joint Loosening - Spotlight on Quantitative and Multidisciplinary Algorithms**	1108 **M2M Track TROP Session** Drug Development + Radiopharmacy + Translational Molecular Imaging & Therapy Committee **Peptides Only!**	1109 **Cutting Edge Science Track Featured Session** Physics Committee **Software Developments in Total Body PET**	1110 **Clinical Oncology Track TROP Session** Oncology & Theranostics Committee **Prostate Staging**	1111 **Featured Session** Neuroimaging Committee **Molecular Imaging of Movement Disorders**	1112 **e-Poster Presentation Session 8** Oncology & Theranostics Committee **Imaging in Recurrent Prostate Cancer**
1204 **Technologists' Track Technologists' Oral Presentations 1** Technologists Committee **TROP - Sharing Technologist's Experience 1**	1205 **Joint Symposium 15** Oncology & Theranostics Committee / EHA **Imaging Challenges in Multiple Myeloma - Quo Vadis 2021?**	1206 **Joint Symposium 16** Oncology & Theranostics Committee / ESMO **Combination Treatments - What can Radioligand Therapy be Combined with?**	1207 **Teaching Session 2** Cardiovascular Committee **All About Cardiac SPECT**	1208 **M2M Track TROP Session** Drug Development + Radiopharmacy + Translational Molecular Imaging & Therapy Committee **Radiochemistry - Cook it or Leave it**	1209 **Cutting Edge Science Track TROP Session** Physics Committee **Imaging of Non-Standard Radionuclides**	1210 **Clinical Oncology Track TROP Session** Oncology & Theranostics Committee **Prostate Varia and Others**	1211 **Featured Session** Neuroimaging Committee **Amino Acid Imaging of Gliomas**	1212 **e-Poster Presentation Session 9** Oncology & Theranostics Committee **Imaging in Primary Prostate Cancer**
1304 **Technologists' Track Technologists' Oral Presentations 2** Technologists Committee **TROP - Sharing Technologist's Experience 2**	1305 **Joint Symposium 17** Oncology & Theranostics Committee / EAU **What to Do and Not Do in Prostate Imaging**	1306 **Joint Symposium 18** Oncology & Theranostics Committee / EAU **Urological Challenges for Imaging Beyond Prostate**	1307 **Teaching Session 3** Dosimetry + Translational Molecular Imaging & Therapy + Radiation Protection Committee **Radiobiology as a Missing Link in Improving and Understanding Nuclear Medicine**	1308 **M2M Track TROP Session** Drug Development + Radiopharmacy + Translational Molecular Imaging & Therapy Committee **Out of the Box Innovations**	1309 **Cutting Edge Science Track Featured Session** Physics Committee **Harmonisation and Standardisation**	1310 **Clinical Oncology Track TROP Session** Oncology & Theranostics Committee **Prostate BC Recurrence**	1311 **Featured Session** Neuroimaging Committee **Brain Tumor Imaging - More than Amino Acids in Gliomas**	1312 **e-Poster Presentation Session 10** Oncology & Theranostics Committee **Lymphoma and Other Hematological Diseases**
1404 **Technologists' Track Technologists' Oral Presentations 3** Technologists Committee **TROP - Sharing Technologist's Experience 3**	1405 **Joint Symposium 19** Physics Committee / EFOMP **Harmonisation and Standardisation**	1406 **Joint Symposium 20** Physics Committee / AAPM **Artificial Intelligence for Image Processing and Quantification**	1407 **Teaching Session 4** Oncology & Theranostics Committee **Immunotherapy - Assessing Organs and Events on ^{18}F]FDG PET/CT**		1409 **Cutting Edge Science Track TROP Session** Physics Committee **Data Analysis**	1410 **Clinical Oncology Track TROP Session** Oncology & Theranostics Committee **Local Radionuclide Therapy and Other Oncological Treatments**	1411 **Featured Session** Neuroimaging Committee **Novel Molecular Brain Imaging Applications**	1412 **e-Poster Presentation Session 11** Oncology & Theranostics Committee **Neuroendocrine and Lymphoma**
1504 **Technologists' Track Mini Course 1 (60 minutes)** Technologists Committee **Safety in PET/MRI**	1505 **Joint Symposium 21** Physics Committee / AAPM **Numerical and Computer Phantoms**	1506 **Joint Symposium 22** Radiation Protection + Thyroid + Dosimetry Committee / EURAMED **The MEDIRAD Project - Impact on Nuclear Medicine Practice**	1507 **Teaching Session 5** Radiation Protection + Physics Committee **Radiation Detection and Measurement**		1509 **Cutting Edge Science Track Featured Session** Physics Committee **PET Reconstructions and Corrections**	1510 **Clinical Oncology Track Featured Session** Oncology & Theranostics Committee **Prostate Cancer Therapy**	1511 **TROP Session** Paediatrics Committee **Paediatric Nuclear Medicine**	1512 **e-Poster Presentation Session 12** Oncology & Theranostics Committee **Head Neck / Breast / Lung**
1704 **Technologists' Track Mini Course 2 (60 minutes)** Technologists Committee **Case Studies (PET/CT & PET/MRI)**	1705 **Joint Symposium 23** Radiation Protection + Technologists Committee / EURADOS **Extremity Dosimetry - It's in Your Hands!**	1706 **Joint Symposium 24** Thyroid + Oncology & Theranostics Committee / ESMO **Theranostics in Thyroid Cancer Beyond Radioactive Iodine**	1707 **Teaching Session 6** Translational Molecular Imaging & Therapy + Drug Development + Radiopharmacy + Technologists Committee **Animal Models - Technical Considerations and Recommendations**		1709 **Cutting Edge Science Track TROP Session** Physics Committee **Data/Image Processing Based on Deep Learning**	1710 **Clinical Oncology Track Featured Session** Oncology & Theranostics Committee **Neuroendocrine Therapy**	1711 **TROP Session** Paediatrics Committee **General Nuclear Medicine**	1712 **e-Poster Presentation Session 13** Physics Committee **Image Acquisition / Reconstruction / Processing 1**
1804 **Technologists' Track Mini Course 3 (60 minutes)** Technologists Committee **Case Studies (Conventional Nuclear Medicine)**	1805 **Joint Symposium 25** Thyroid Committee / ESES / ESSO **Global Cost-Effectiveness of Different DTC Management Strategies**	1806 **Joint Symposium 26** Translational Molecular Imaging & Therapy Committee / ESMI / WMIS **Imaging Mitochondria and Mitochondrial Dysfunction**			1809 **Cutting Edge Science Track TROP Session** Physics Committee **Artificial Intelligence - Clinical Applications**	1810 **Clinical Oncology Track TROP Session** Oncology & Theranostics Committee **Lymphoma and Other Hematological Tumours**	1811 **TROP Session** Thyroid Committee **Nuclear Thyroidologist and Thyroid Cancer Management - Current Update and Future Perspectives**	1812 **e-Poster Presentation Session 14** Physics Committee **Image Acquisition / Reconstruction / Processing 2**
1904 **Technologists' Track Technologists' e-Poster Presentations** Technologists Committee **Technologist e-Poster Presentations - Sharing Technologist's Experience**	1905 **Joint Symposium 27** Neuroimaging Committee / JSNM **Advances in Molecular Imaging of Neurodegenerative Disorders**	1906 **Joint Symposium 28** EANM / IAEA **Lancet Oncology Commission on Medical Imaging and Nuclear Medicine**			1909 **Cutting Edge Science Track TROP Session** Physics Committee **Radiomics - Methodology and Clinical Applications**	1910 **Clinical Oncology Track TROP Session** Oncology & Theranostics Committee **Gynaecological and Melanoma**	1911 **TROP Session** Thyroid Committee **Nuclear Medicine Imaging and Therapy in Thyroid and Parathyroid Disorders**	1912 **e-Poster Presentation Session 15** Physics Committee **AI and Radiomics**

Plenary Sessions | CME Sessions | Joint Symposia | Technologists' Track | M2M Track | Cutting Edge Science Track | Pitfalls & Artefacts / Teaching Sessions | Clinical Oncology Track | Further TROP/Featured Sessions | e-Poster Presentation Sessions | Special Track | Satellite Symposia

PCS1

Monday, October 4, 2021, 09:00 - 12:00

Channel 1

Pre-Congress-Symposium 1: Pre-Clinical Dosimetry and Extrapolations from Animal Models to Humans

PCS-001

Introduction - Preclinical Dosimetry, Challenges and Prospects

F. Cicone; Università degli Studi "Magna Graecia" di Catanzaro, Catanzaro, ITALY.

PCS-002

Comparative Anatomy and Physiology - It's Not Just Size That Matters

J. Ruberte; Universitat Autonoma de Barcelona, Barcelona, SPAIN.

PCS-003

"Clinical" Challenges, Animal Handling and Reproducibility

R. Beck; Technische Universität München, Munich, GERMANY.

PCS-005

Building Bridges Between Humans and Animals - Technological Developments

C. Pettinato; Policlinico di Milano, Milan, ITALY.

PCS-006

Methodological Aspects of Dose Extrapolations

S. Gnesin; Institut universitaire de radiophysique appliquée (IRA) - CHUV, Lausanne, SWITZERLAND.

PCS-007

In Vivo Radiobiology and Dose/Response Effects

N. Chouin; LUNAM Université, Oniris, «AMaROC», Nantes, FRANCE.

PCS2

Monday, October 4, 2021, 14:00 - 17:00

Channel 1

Pre-Congress-Symposium 2: Signal Quantification in Cardiac SPECT - Dream or Reality?

PCS-009

Clinical Needs for Quantification in Cardiac SPECT

H. Verberne; Academic Medical Center, Department of Nuclear Medicine, Amsterdam, NETHERLANDS.

PCS-010

Myocardial Blood Flow

I. Armstrong; Manchester University NHS Foundation Trust, Nuclear Medicine, Manchester, UNITED KINGDOM.

PCS-011

MIBG for Cardiac Innervation

K. Prigent; CHU Côte de Nacre, Service de Médecine Nucléaire, Caen, FRANCE.

PCS-013

Bone Tracers in Amyloidosis

M. Burniston; Burnington, Barts Health NHS Trust, Nuclear Medicine, London, UNITED KINGDOM.

PCS-014

Is Whole-Body CZT the Future?

L. Imbert; CHRU Nancy, Nuclear Medicine, Nancy, FRANCE.

PCS3

Tuesday, October 5, 2021, 09:00 - 12:00

Channel 1

Pre-Congress-Symposium 3: Radiosynoviorthesis - Master Class in Science and Practice

PCS-016

Changing Paradigms in (Osteo)Arthritis Management

L. Terslev; Rigshospitalet Glostrup, Copenhagen Center for Arthritis Research Copenhagen University Hospital, Copenhagen, DENMARK.

PCS-017

Challenges in the Management of Haemophilia

T. T. Yee; Royal Free Hospital - University College London, Hematology, London, UNITED KINGDOM.

PCS-018

Tackling the Target Joint - Radiosynoviorthesis Versus Surgery

Y. Jabbar; Great Ormond Street Hospital, Paediatric orthopaedic surgery, London, UNITED KINGDOM.

PCS-020

EANM Guideline - Patient Selection, Isotopes, Multidisciplinary Collaboration

F. M. van der Zant; Noordwest Ziekenhuisgroep, Nucleaire geneeskunde, Alkmaar, NETHERLANDS.

PCS-021
EANM Guideline - Procedural Aspects, Arthrocentesis and Radiation Protection
W. U. Kampen; Radiologische Allianz Hamburg - Nuklearmedizin Spitalerhof, Hamburg, GERMANY.

PCS4

Tuesday, October 5, 2021, 14:00 - 17:00

Channel 1

Pre-Congress-Symposium 4: Structured Reporting of Oncology PET-CT - Are we Ready for Template-Based Reporting?

PCS-023
Essential Elements of PET-CT Reporting - An Overview
G. Gnanasegaran; Royal Free London NHS Foundation Trust, Department of Nuclear Medicine, London, UNITED KINGDOM.

PCS-024
How to Report PET-CT in Lymphoma
C. Kobe; University of Cologne, Department of Nuclear Medicine, Cologne, GERMANY.

PCS-025
How to Report PET-CT in Lung Cancer
E. Lopci; Nuclear Medicine Unit, IRCCS – Humanitas Research Hospital, Milan, ITALY.

PCS-026
How to Report PET-CT in GI and HPB Cancer
S. Carrilho Vaz; Champalimaud Foundation Centre for the Unkown, Nuclear Medicine, Radiopharmacology, Lisbon, PORTUGAL.

PCS-028
How to Report PET-CT in Prostate Cancer
K. Rahbar; University Hospital Muenster, Department of Nuclear Medicine, Münster, GERMANY.

PCS-029
How to Report PET-CT in Melanoma and Myeloma
C. Nanni; Azienda Ospedaliero-Universitaria di Bologna Policlinico S.Orsola, Nuclear Medicine, Bologna, ITALY.

PCS-030
How to Report PET-CT in Gynaecological Cancers
S. Balogová; Comenius University of Bratislava, St.Elisabeth Oncology Institute, Nuclear medicine, Bratislava, SLOVAKIA.

PCS-031
How to Report PET-CT in Neuroendocrine Tumour
V. Ambrosini; University of Bologna, Policlinico S.Orsola Malpighi Bologna, DIMES, Nuclear Medicine, Bologna, ITALY.

PCS5

Wednesday, October 6, 2021, 09:00 - 12:00

Channel 1

Pre-Congress-Symposium 5: Imaging of Protein Misfolding in Parkinson's Disease and Related Disorders - Where are we and What do we need?

PCS-034
Molecular Neuroimaging of PD and Related Disorders - Current State
S. Morbelli; San Martino Hospital, University of Genoa, Nuclear Medicine, Genoa, ITALY.

PCS-035
Amyloid and Tau Pathology in PD, DLB, PSP/CBD and MSA
G. Kovacs; University of Toronto, Department of Laboratory Medicine and Pathobiology, Toronto, CANADA.

PCS-036
Relevance of Amyloid Imaging in Parkinson's Disease and Related Disorders
N. Bohnen; University of Michigan, Department of Radiology, Michigan, UNITED STATES OF AMERICA.

PCS-038
Tau Imaging in PSP/CBD - Ready for Clinical Trials?
H. Barthel; University of Leipzig, Department of Nuclear Medicine, Leipzig, GERMANY.

PCS-039
Alpha-Syn Pathology in PD, DLB, PSP/CBD and MSA
L. Walker; Newcastle University, Institute of Neuroscience, Newcastle, UNITED KINGDOM.

PCS-040
Alpha-Syn Imaging in PD, MSA and DLB - Will We Ever Get There?
J. Seibyl; Institute for Neurodegenerative Disorders, New Haven, UNITED STATES OF AMERICA.

PCS6

Wednesday, October 6, 2021, 14:00 - 17:00

Channel 1

Pre-Congress-Symposium 6 (EANM/ESTRO): Oligocare Concept in Radiation Oncology

PCS-042
Oligocare for Tailored Medicine
M. Guckenberger; Department of Radiation Oncology, University Hospital Zurich (USZ), Zürich, SWITZERLAND

PCS-043
Radiation Oncologist's Point of View
M. Scorsetti; Radiotherapy and Radiosurgery Unit, Humanitas University, Pieve Emanuele, ITALY.

PCS-044
Targeted Imaging and Therapy in Oligomets
E. Lopci; Nuclear Medicine Unit, IRCCS – Humanitas Research Hospital, Milan, ITALY.

PCS-046
The Future of Imaging in Radiotherapy
P. Ost; Department of Radiation Oncology, Iridium Network, Antwerp, BELGIUM.

PCS-047
Ongoing Projects and Initiatives
Y. Lievens; Radiation Oncology Department, Ghent University Hospital and Ghent University, Ghent, BELGIUM.

PCS7

Monday, October 11, 2021, 09:00 - 12:00

Channel 1

Pre-Congress-Symposium 7: Biokinetic Modelling in Cancer Therapy and Clinical Impact

PCS-049
Introduction and Overview
C. Stokke; Oslo University Hospital, Division of Radiology and Nuclear Medicine, Oslo , NORWAY.

PCS-050
Biokinetic Modelling and its Clinical Impact for ^{131}I Therapy of Thyroid Disease
F. Verburg; Erasmus MC, Nuclear Medicine, Rotterdam, NETHERLANDS.

PCS-051
Modelling of ^{177}Lu-PRRT Biokinetics and Impact on Clinical Dosimetry
M. Cremonesi; European Institute of Oncology, Radiation Research Unit, Milan, ITALY.

PCS-053
Dosimetry and Treatment Planning for ^{177}Lu-PSMA Using PBPK Modelling
G. Glatting; Universität Ulm, Abteilung Nuklearmedizin, Medizinische Strahlenphysik, Ulm, GERMANY.

PCS-054
Modelling of ^{223}Ra Biokinetics and its Application for Clinical Dosimetry
J. Taprogge; St. George's University Hospital NHS FT / Royal Marsden Hospital NHS FT, Medical Physics, London, UNITED KINGDOM.

PCS-055
Biokinetics of the ^{212}Pb in vivo Alpha Particle Generator and its Radioactive Daughters
N. Zaid; Ulm University, Ulm, GERMANY.

PCS-056
Biokinetic Modelling and Dosimetry for Optimizing Treatment using ^{211}At-Labelled Antibodies
S. Palm; University of Gothenburg, Radiation Physics, Gothenburg, SWEDEN.

PCS8

Monday, October 11, 2021, 14:00 - 17:00

Channel 1

Pre-Congress-Symposium 8: Novel Radionuclides for Theranostics on the Horizon

PCS-059
Novel Radionuclides for Theranostics - What for?
C. Deroose; University Hospitals Leuven, Nuclear Medicine, Leuven, BELGIUM.

PCS-060
PRISMAP - The European Medical Isotope Programme Providing Novel Radionuclides
T. Stora; CERN Geneva, Geneva, SWITZERLAND.

PCS-061
Mass Separation Techniques - The Way to High Quality?
M. Manzolaro; Istituto Nazionale di Fisica Nucleare, Rome, ITALY.

PCS-062
The Technical Challenges to Provide Novel Radionuclides
R. Mikolajczak; National Centre for Nuclear research-POLATOM, Otwock, POLAND.

PCS-064
Novel Radionuclides - Preclinical Proof of Concept
C. Müller; Paul Scherrer Institute, Center for Radiopharmaceutical Sciences, Zürich, SWITZERLAND.

PCS-065
Novel Radionuclides - But in Right Quality and for the Right Target
D. Niculae; Horia Hulubei National Institute for R&D in Physics and Nuclear Engineering, Bucharest, ROMANIA.

PCS-066
Novel Radionuclides - What Do We Already Know in Clinical Applications?
I. Rauscher; Department of Nuclear Medicine, Klinikum rechts der Isar, Technical University Munich, Munich, GERMANY.

PCS-067
Novel Radionuclides - Don't Forget the Regulatory Side
O. Neels; Institute of Radiopharmaceutical Cancer Research Helmholtz-Zentrum Dresden - Rossendorf (HZDR), Dresden, GERMANY.

PCS9

Tuesday, October 12, 2021, 09:00 - 12:00

Channel 1

Pre-Congress-Symposium 9 (EANM/ESES): Nuclear Endocrinology in the Era of Precision Medicine

PCS-070
Precision Medicine in Endocrinology. The Radiopharmacist's View
M. Fani; University Hospital Basel, Dept. of Nuclear Medicine, Basel, SWITZERLAND.

PCS-071
Functional and Molecular Thyroid Imaging
L. Giovanella; Imaging Institute of Southern Switzerland, Clinic for Nuclear Medicine, Bellinzona, SWITZERLAND.

PCS-072
Molecular imaging of endocrine neoplasms: a practical approach for well-tailored imaging protocols
D. Taïeb; Centre Hospitalo-Universitaire Timone, Médecine Nucléaire, Marseille, FRANCE.

PCS-074
Impact of Imaging on Personalized Parathyroidectomy in Primary and Renal Hyperparathyroidism
P. Petranović Ovčariček; University Hospital Center Sestre milosrdnice, Oncology and nuclear medicine, Zagreb, CROATIA.

PCS-075
Integration of Molecular Imaging in the Personalized Approach to Patients with Adrenal Masses
M. Raffaelli; Fondazione Policlinico Universitario Agostino Gemelli IRCCS, Università Cattolica del Sacro Cuore, Division of Endocrine and Metabolic Surgery, Department of Medical and Surgical Sciences, Rome, ITALY.

PCS-076
Imaging of MEN1, MEN2 and VHL - The Endocrine Surgeon's View
F. Sebag; Alc-Marseille university, APHM, Department of Endocrine Surgery, Marseille, FRANCE.

PCS10

Tuesday, October 12, 2021, 14:00 - 17:00

Channel 1

Pre-Congress-Symposium 10: Total Body PET

PCS-079
Translation of the Technical Innovations of Total Body PET in Clinic
L. Nardo; University of California at Davis, Division of Nuclear Medicine, Davis, UNITED STATES OF AMERICA.

PCS-080
Clinical Applications of Total Body PET - Bern Experience
A. Rominger; University of Bern, Department of Nuclear Medicine, Bern, SWITZERLAND.

PCS-081
Clinical Applications of Total Body PET - Shanghai Experience
H. Shi; Zhongshan Hospital of Fudan University, Department of Nuclear Medicine, Shanghai, CHINA.

PCS-082
Clinical and Research Benefits of a Long Axial Field-of-View System
M. Daube-Witherspoon; University of Pennsylvania, Department of Radiology, Philadelphia, UNITED STATES OF AMERICA.

PCS-084
Development of Detector for Total Body PET
S. Ziegler; University of Munich, Department of Nuclear Medicine, Munich, GERMANY.

PCS-085
Instrumentation of Total Body PET
S. Vandenberghe; Ghent University, Department of Electronics and Information Systems, Ghent, BELGIUM.

PCS-086
Image Reconstruction for Total Body PET
D. Visvikis; National Institute of Health and Medical Research (INSERM), Medical Image Processing Lab in Brest, Brest, FRANCE.

PCS11

Wednesday, October 13, 2021, 09:00 - 12:00

Channel 1

Pre-Congress-Symposium 11: Light in the Dark - Hybrid Imaging in Patients with Sepsis/ Bacteremia

PCS-088
Game Intro - Sepsis/Bacteremia and the Questions from Clinicians to NM Physicians
A. L. Goodman; Centre for Clinical Infection and Diagnostics Research, King's College London, Guy's and St Thomas' NHS Foundation Trust, London, UNITED KINGDOM.

PCS-089
Level 1 - Diagnostic Yield of FDG PET/CT in Patients with Sepsis/Bacteremia
A. W. J. M. Glaudemans; University Medical Center Groningen, Medical Imaging Center, Groningen, NETHERLANDS.

PCS-090
Level 2 - Clinical Impact and Outcome Using FDG PET/CT in Patients with Sepsis/Bacteremia
S. Hess; Department of Radiology and Nuclear Medicine, Hospital Southwest Jutland, Esbjerg, DENMARK.

PCS-092
Level 3 - Cost-Effectiveness and Proposed Optimal Use of FDG PET/CT in Patients with Sepsis/Bacteremia
I. J. Kouijzer; Department of Internal Medicine and Radboud Center for Infectious Diseases, Radboudumc, Nijmegen, NETHERLANDS.

PCS-093
Bonus Level - Other Tracers Beyond FDG
A. Roivainen; Turku PET Centre, University of Turku and Turku University Hospital, Turku, FINLAND.

PCS-094
Next Level - Possible Role of FDG PET/MRI
P. Veit-Haibach; University Health Network, Joint Dept. Medical Imaging, Toronto, CANADA.

PCS12

Wednesday, October 13, 2021, 14:00 - 17:00

Channel 1

Pre-Congress-Symposium 12: PET/MR - The Cross Path of Morphology and Functionality

PCS-096
Intro
R. Strand Olsen; Bispebjerg and Frederiksberg Hospital, Clinical Physiology; Nuclear Medicine, Copenhagen, DENMARK.

PCS-097
The PET/MR
T. Lund Andersen; Rigshospitalet, Dept. of Clinical Physiology, Nuclear Medicine and PET, Copenhagen, DENMARK.

PCS-098
Performing PET/MR
L. Grønnemark; Aarhus University Hospital, Department of Nuclear medicine and PET, Aarhus, DENMARK.

PCS-099
Onsite Experience with PET/MR
S. Stienaers; University hospitals Leuven, Nuclear Medicine department, Leuven, BELGIUM.

PCS-101
PET/MR Motion Correction
M. Ganz-Benjaminsen; Rigshospitalet, Copenhagen University Hospital, Neurobiology Research Unit, Copenhagen, DENMARK.

PCS-102
Interpretation of PET/MR
A. Beer; Ulm University Hospital, Department of Nuclear Medicine, Ulm , GERMANY.

100

Wednesday, October 20, 2021, 08:45 - 09:10

Channel 1

Opening Ceremony

OP-0001
Opening Ceremony

S. Fanti; EANM Congress Chair, Bologna, ITALY.

101

Wednesday, October 20, 2021, 09:10 - 10:00

Channel 1

Plenary 1: Highlights Lecture

OP-0002
Highlight Lecture

I. Burger; Kantonsspital Baden, Nuclear Medicine, Baden, SWITZERLAND.
& N. Albert; LMU, Munich, GERMANY.

201

Wednesday, October 20, 2021, 10:15 - 11:45

Channel 1

CME 1: Prostate Cancer - Greatest Hits

OP-0004
Immunohistochemistry and PET Targeting ProstateSpecific Membrane Antigen - Now You See Me?

D. Ferraro; University Hospital Zurich, Department of Nuclear Medicine, Zurich, SWITZERLAND.

OP-0005
PSMA PET in Primary Staging - Ready for Prime Time? The Urologist's Perspective

O. Ettala; Turku University Hospital, Department of Urology, Turku, FINLAND.

OP-0006
PSMA PET After Primary Treatment - Anything New?

D. Oprea-Lager; Amsterdam University Medical Centers, Department of Radiology & Nuclear Medicine, Amsterdam, NETHERLANDS.

OP-0007
PSMA PET for Castration-Resistant Prostate Cancer - How Far Have We Come?

W. Fendler; University Hospital Essen, Department of Nuclear Medicine, Essen, GERMANY.

202-1

Wednesday, October 20, 2021, 10:15 - 10:40

Channel 2

Interview with the Expert 1 - Therapy

OP-0009
Interview - Therapy

S. Fanti; University of Bologna, Radiological Sciences - Nuclear Medicine, Bologna, ITALY.

OP-0010
Interview - Therapy

I. Virgolini; Medizinischen Universität Innsbruck, Innsbruck, AUSTRIA.

202-2

Wednesday, October 20, 2021, 11:00 - 11:20

Channel 2

Interview with the Expert 2 - Imaging Myeloma

OP-0011
Interview - Imaging Myeloma

C. Nanni; Azienda Ospedaliero-Universitaria di Bologna Policlinico S.Orsola, Nuclear Medicine, Bologna, ITALY.

OP-0012
Interview - Imaging Myeloma

P. Castellucci; IRCCS Azienda Ospedaliero-Universitaria di Bologna, Nuclear Medicine Unit, Bologna, ITALY.

204

Wednesday, October 20 - Saturday, October 23, 2021

on-demand pool, release on Wednesday, October 20 at 09:00

CTE 1 (EANM/SNMMI): Tech Guide Launch

OP-0013
PET/CT Artefacts and Pitfalls

J. T. Middlebrooks; Radiation Safety and Health Physics Consultant, Board Certified in Radiation Safety Medical Imaging Consultants, Benton, UNITED STATES OF AMERICA.

OP-0014
New Solutions in Oncology
A. Doma; Institute of Oncology Ljubljana, Nuclear Medicine Dep., Ljubljana, SLOVENIA.

OP-0015
Advancements in Neuroimaging
D. van Weehaeghe; Division of Nuclear Medicine and Molecular Imaging, University Hospitals of Leuven and KU Leuven, Leuven, BELGIUM.

205

Wednesday, October 20 - Saturday, October 23, 2021

on-demand pool, release on Wednesday, October 20 at 09:00

Joint Symposium 1 (EANM/ESSR): PET/MRI in MSK - Be Hybrid!

OP-0017
MR Protocols for Hybrid PET/MRI in MSK
L. Sconfienza; I.R.C.C.S. Istituto Ortopedico Galeazzi, Unit of Diagnostic and Interventional Radiology, Milan, ITALY.

OP-0018
PET/MRI in MSK Malignant Diseases
L. Garcia Canamaque; HM Hospitales, Madrid, SPAIN.

OP-0019
PET/MRI in MSK Benign Conditions
S. Wan; University College London , London, UNITED KINGDOM.

OP-0020
PET/MRI in MSK - Be Hybrid!
S. Annunziata; Fondazione Policlinico Gemelli , Rome , ITALY.

206

Wednesday, October 20 - Saturday, October 23, 2021

on-demand pool, release on Wednesday, October 20 at 09:00

Joint Symposium 2 (EANM/ASNC): PET-MPI vs. SPECT-MPI - Is it Worth the Price?

OP-0022
On Stable Chest Pain?
P. Arumugam; Department of Nuclear Medicine, Central Manchester Foundation Trust, Manchester, UNITED KINGDOM.

OP-0023
For Detecting Microvessel Disease
C. Nappi; Federico II University of Naples, Department of Advanced Biomedical Sciences, Naples, ITALY.

OP-0024
For Guiding Coronary Revascularisation
R. C. Thompson; University of Missouri - Kansas City, St. Luke's Mid America Heart Institute, Kansas City, UNITED STATES OF AMERICA.

OP-0025
In Inflammatory and Infiltrative Diseases
S. Dorbala; Brigham and Women's Hospital, Harvard Medical School, Boston, UNITED STATES OF AMERICA.

207

Wednesday, October 20 - Saturday, October 23, 2021

on-demand pool, release on Wednesday, October 20 at 09:00

Pitfalls & Artefacts 1: Pitfalls in Cardiovascular Imaging

OP-0027
Clinical Cases
J. Diekmann; Hannover Medical School (MHH), Department of Nuclear Medicine, Hanover, GERMANY.

OP-0028
Technologist Cases
L. Camoni; University of Brescia, Nuclear Medicine and Molecular Imaging Department, Brescia, ITALY.

OP-0029
Physics Cases
S. G. Nekolla; Technical University of Munich, Klinikum rechts der Isar, Department of Nuclear Medicine, Munich, GERMANY.

208

Wednesday, October 20 - Saturday, October 23, 2021

on-demand pool, release on Wednesday, October 20 at 09:00

M2M Track - TROP Session: Prostate Cancer Imaging - The Various Angles of Attack

OP-0031

^{61}Cu-PSMA: a new radiotracer for PET imaging of prostate cancer

T. Basaco Bernabeu[1], R. Mansi[1], L. Del Pozzo[1], S. Zanger[1], M. Blagoev[2], R. H. Gaonkar[1], L. McDougall[1], J. Anass[2], L. Jaafar-Thiel[3], M. Fani[1];

[1]Division of Radiopharmaceutical Chemistry, University Hospital Basel, Basel, SWITZERLAND, [2]Department of Nuclear Medicine, University Hospital of Zurich, Zurich, SWITZERLAND, [3]Swiss Nuclides AG, Aarau, SWITZERLAND.

Aim/Introduction: In the last few years, radiotracers targeting prostate-specific membrane antigen (PSMA) have influenced imaging and management of prostate cancer. ^{68}Ga-labeled urea-based PSMA inhibitors are the most commonly used radiotracers in this disease entity. ^{18}F-labeled derivatives have become an alternative mainly for meeting the increasing demand for PSMA-targeted PET imaging. This comes, however, at the cost of the facile chelator-based kit radiolabeling and the possibility of a therapeutic companion (theranostics); options possible with radiometals. As an alternative, we propose the cyclotron produced Copper-61 ($E_{\beta+_{mean}}$ =500 keV, $E_{\beta+_{max}}$ =1216 keV, $t_{1/2}$ =3.34 h) that combines the attractive logistics of ^{18}F, chelator-based radiochemistry, and further therapeutic options (^{67}Cu). We report - to the best of our knowledge - first preclinical data on ^{61}Cu-PSMA radiotracers. **Materials and Methods:** [^{61}Cu]$CuCl_2$ was produced from an irradiated Ni-target at the University Hospital Zurich cyclotron followed by cassette-based automated separation as described previously (1). DOTAGA-(l-y)fk(Sub-KuE) (PSMA-I&T, herein DOTAGA-PSMA-I&T) (2) and NODAGA-(l-y)fk(Sub-KuE) (NODAGA-PSMA-I&T) were labeled with [^{61}Cu]$CuCl_2$ in ammonium acetate buffer, pH 8 at 95°C. Both ^{61}Cu-PSMA radiotracers were evaluated head-to-head in vitro using LNCaP cells and by dynamic PET/CT imaging in LNCaP-xenografted nude mice. Results: [^{61}Cu]Cu-NODAGA-PSMA-I&T and [^{61}Cu]Cu-DOTAGA-PSMA-I&T were prepared at an apparent molar activity of 24 MBq/nmol, without the need of post-purification. [^{61}Cu]Cu-NODAGA-PSMA-I&T was more hydrophilic than [^{61}Cu]Cu-DOTAGA-PSMA-I&T (logD = -2.95±0.08 and -2.69±0.44, respectively). In vitro, both radiotracers showed similar PSMA-mediated cellular uptake (approx. 35% after 2h at 37°C), with 50-60% being internalized. PET/CT images of [^{61}Cu]Cu-NODAGA-PSMA-I&T vs [^{61}Cu]Cu-DOTAGA-PSMA-I&T indicated clear differences. [^{61}Cu]Cu-NODAGA-PSMA-I&T accumulated in the tumor, increasing from 15 up to 60 min p.i., and in the kidneys. Kidney uptake could be reduced by modulating the injected mass. [^{61}Cu]Cu-DOTAGA-PSMA-I&T showed lower tumor, but also lower kidney uptake, than [^{61}Cu]Cu-NODAGA-PSMA-I&T, and high activity in the liver. The accumulation in the liver may be due to in vivo instability of the ^{61}Cu-DOTAGA complex. Comprehensive biodistribution studies of both radiotracers in LNCaP xenografts are in progress and will be presented. **Conclusion:** The NODAGA chelator is confirmed to be a perfect match for ^{61}Cu-based radiotracers compared with the DOTAGA chelator. [^{61}Cu]Cu-NODAGA-PSMA-I&T showed better characteristics, including but not limited to higher tumor uptake and lower background activity than [^{61}Cu]Cu-DOTAGA-PSMA-I&T, potentially attributed to its higher in vivo stability. [^{61}Cu]Cu-NODAGA-PSMA-I&T is, therefore, the potential candidate for clinical translation of ^{61}Cu-based PSMA-targeted PET imaging. **References:** 1.J. Svedjehed et al., EJNMMI Radiopharmacy and Chemistry 2020;5:21 2.M. Weineisen et al., J Nucl Med 2015;56:1169-1176

OP-0032

Use of the fibroblast activation protein inhibitor [^{64}Cu]Cu-$DOTHA_2$-FAPI-04 to overcome heterogeneity in prostate cancer

O. Bélissant[1], V. Dumulon-Perreault[2], M. Milot[3], I. Ben-Salem[1], E. Croteau[2], S. Ait-Mohand[2], E. Turcotte[1], B. Guérin[1,2], E. Rousseau[1];

[1]Département de médecine nucléaire et radiobiologie, Université de Sherbrooke, Sherbrooke, QC, CANADA, [2]Centre d'imagerie moléculaire de Sherbrooke (CIMS) du CRCHUS, Sherbrooke, QC, CANADA, [3]Université de Sherbrooke, Sherbrooke, QC, CANADA.

Aim/Introduction: Prostate Specific Membrane Antigen (PSMA) ligands are used for diagnosis of recurrent or metastatic prostate cancer (PCa) but are less sensitive for neuroendocrine differentiated lesions [1] which are however relevant in these indications. Multiple PET imaging is sometimes needed for heterogeneous disease. With development of fibroblast activation protein inhibitor (FAPI), this need for multiple PET could be overcome [2]. The aim of this study is to assess the tumoral uptakes of [^{64}Cu]Cu-$DOTHA_2$-FAPI-04, [^{18}F]FDG, [^{68}Ga]Ga-DOTA-TATE and [^{68}Ga]Ga-PSMA-617 in cell lines reflecting PCa heterogeneity. **Materials and Methods:** Mice bearing xenografts of prostate adenocarcinoma (LNCaP, PC-3), small cells neuroendocrine prostate cancer (NCI-H660), and pancreatic cancer (BxPC-3, known to express FAP, positive controls) were imaged within a week by static PET, 60 minutes post-injection of [^{68}Ga]Ga-PSMA-617, [^{18}F]FDG, [^{68}Ga]Ga-DOTA-TATE and [^{64}Cu]Cu-$DOTHA_2$-FAPI-04. Washout times between imagings were at least 18 half-lives of the injected radiotracers. Visual analysis and percentages of injected activity per cubic centimeter (%IA/cc) in tumors were determined. After the last imaging session, mice were euthanized, and biodistribution of [^{64}Cu]Cu-$DOTHA_2$-FAPI-04 (%IA/g) in tumor and organs

determined. Results: [^{64}Cu]Cu-DOTHA$_2$-FAPI-04 labelling yield was >95%, with 100% purity according to ITLC and UPLC, and effective molar activity (EMA) 85-100MBq/nmol. EMA for [^{68}Ga]Ga-PSMA-617 and [^{68}Ga]Ga-DOTA-TATE (mainly labelled with cyclotron produced gallium-68) were 364 and 419 MBq/nmol respectively. Three LNCaP (5 tumors), six PC-3, three NCI-H660 and six BxPC-3 (7 tumors) tumor bearing mice have completed their series of imaging at this time. [^{64}Cu]Cu-DOTHA$_2$-FAPI-04 mean uptakes were respectively 2.81±0.61, 2.23±0.36, 2.02±0.19 and 2.45±0.61 %IA/cc in these tumors on PET. [^{64}Cu]Cu-DOTHA$_2$-FAPI-04 allowed good visualization of all tumors, and its uptake was higher or similar to the other tracers for all cell lines, except for [^{18}F]FDG in PC-3. Volume did not significantly affect tumor uptake in this series. Biodistribution results showed 3.94±0.29, 2.26±0.005, 3.24±0.003 and 3.03±1.05 %IA/g of [^{64}Cu]Cu-DOTHA$_2$-FAPI-04 respectively in the same tumors. **Conclusion:** [^{64}Cu]Cu-DOTHA$_2$-FAPI-04 allows good visualization of three types of PCa tumors in xenografts bearing mice, including castrate sensitive and resistant adenocarcinomas and neuroendocrine prostate cancer. There is thus a strong potential for imaging heterogeneous disease with [^{64}Cu]Cu-DOTHA$_2$-FAPI-04 PET/CT. **References:** 1. Sheikhbahaei S, Afshar-Oromieh A, Eiber M, et al. Pearls and pitfalls in clinical interpretation of prostate-specific membrane antigen (PSMA)-targeted PET imaging. Eur J Nucl Med Mol Imaging. 2017;44(12):2117-36.2. Khreish F, Rosar F, Kratochwil C, et al. Positive FAPI-PET/CT in a metastatic castration-resistant prostate cancer patient with PSMA-negative/FDG-positive disease. Eur J Nucl Med Mol Imaging. 2020 Jul;47(8):2040-2041.

OP-0033

Click chemistry-based PSMA ligands for multimodal intraoperative tumor detection of prostate cancer

Y. Derks[1], M. Rijpkema[1], H. Amatdjais-Groenen[2], A. Kip[1], P. Laverman[1], S. Lütje[3], S. Heskamp[1], D. Löwik[2];
[1]Radboud university medical center, Nijmegen, NETHERLANDS, [2]Radboud University, Nijmegen, NETHERLANDS, [3]University Hospital Bonn, Bonn, GERMANY.

Aim/Introduction: Incomplete resection of prostate cancer (PCa) leads to disease recurrence and consequently poor patient outcome. To achieve complete resection, prostate specific membrane antigen (PSMA) targeting ligands containing both a radiolabel and a fluorophore can be used for multimodal intraoperative tumor detection and delineation. The aim of our study was to develop ligands, either conjugated with IRDye800CW using click- or NHS-based chemistry, for intraoperative detection of PSMA-positive tumor lesions. **Materials and Methods:** Four PSMA ligands were developed. Ligands were conjugated with IRDye800CW via strain promoted click- or NHS-based chemistry and with either DOTA (for ^{111}In labeling) or MAG3 (for ^{99m}Tc labeling). PSMA-mediated binding and internalization were determined using PSMA-expressing LS174T-PSMA and control LS174T wildtype (WT) cells. IC_{50} values of the ligands were determined in LS174T-PSMA competitive binding assays. Moreover, LogD values and stability in human serum (0.8 µg/ml, 2h, 37°C) were determined. Tumor targeting properties were evaluated in BALB/c nude mice with subcutaneous LS174T-PSMA and LS174T WT tumors using µSPECT/CT, fluorescence imaging, and biodistribution studies (2h p.i., 0.3 nmol ligand and 10 MBq/mouse). Results: In vitro, NHS-conjugated variants showed a significantly higher ligand binding and internalization (23.7% ± 0.6% for ^{99m}Tc and 20.3% ± 0.4% for ^{111}In) compared with click-conjugated variants (4.0% ± 0.6% for ^{99m}Tc and 9.1 % ± 0.4% for ^{111}In, $p < 0.001$). All ligands were stable in serum and IC_{50} values ranged from 312 to 474 nM. Click chemistry and use of MAG3 as a chelator increased lipophilicity of the ligands. In vivo, tumors were clearly visualized using both µSPECT/CT and fluorescence imaging. The four ligands showed rapid blood clearance and specific accumulation in LS174T-PSMA tumors. For the ^{99m}Tc labeled ligands, tumor uptake of the click variant was 11.9 ± 1.4 %ID/g compared with 17.7 ± 3.9 %ID/g for NHS ($p < 0.05$). For the ^{111}In labeled ligands, click and NHS showed a tumor uptake of 21.2 ± 1.2 %ID/g and 25.3 ± 2.0 %ID/g ($p > 0.05$), respectively. Overall, the click variants showed a higher liver accumulation compared with the NHS variants. **Conclusion:** Here we demonstrate efficient PSMA-specific tumor targeting of newly developed PSMA ligands. Use of NHS-chemistry resulted in the highest tumor uptake. Nonetheless, click-chemistry based PSMA ligand development offers the potential of more versatile conjugation of multiple imaging moieties and/or drugs. In the future, these ligands can potentially be used for intraoperative image-guided prostate cancer treatment. **References:** None

OP-0034

Clinical translation of the GRPR antagonist [^{99m}Tc]Tc-maSSS-PEG$_2$-RM26 for targeting prostate tumors

A. Abouzayed[1], S. S. Rinne[1], N. Lushnikova[2], A. Rybina[2], E. Usynin[2], J. Sörensen[1], V. Tolmachev[1], V. Chernov[2], A. Orlova[1];
[1]Uppsala University, Uppsala, SWEDEN, [2]Tomsk National Research Medical Center of the Russian Academy of Sciences, Tomsk, RUSSIAN FEDERATION.

Aim/Introduction: Treatment output for prostate cancer depends on diagnostic accuracy. Gastrin-releasing peptide receptor (GRPR) is an important target for imaging of early prostate cancer. The GRPR antagonist [^{99m}Tc]Tc-maSSS-PEG$_2$-RM26 (^{99m}Tc-RM26) with high affinity (61 pM) and specificity for GRPR was presented previously. The aim of this study was to develop a single-step labeling procedure for clinical translation, to evaluate the radiotracer in vivo to assess its utility for SPECT imaging, and to test its safety in first-in-human study. **Materials and Methods:** Sterile lyophilized kit containing maSSS-PEG$_2$-RM26 for the single-step labeling

was developed. ^{99m}Tc-RM26 was injected in mice bearing PC-3 tumors. Biodistribution of ^{99m}Tc-RM26 was studied 3 and 6 hours post-injection. Targeting specificity was studied by co-injection of excess unlabeled RM26. microSPECT/CT imaging was performed to confirm in vivo data. Two patients with localized prostate cancer were examined. ^{99m}Tc-RM26 was injected as an intravenous bolus in dose of 40 µg/300 MBq. Patients were imaged using Siemens Symbia Intevo Bold scanner equipped with a high-resolution low-energy collimator. Whole-body imaging (2, 4, 6, 24 h) and SPECT/CT scans (2, 4, 6 h) were performed. Results: The single-step radiolabeling procedure using kit containing maSSS-PEG$_2$-RM26 (40 µg), gluconic acid (5 mg), EDTA (100 µg), and stannous chloride (75 µg) and freshly eluted pertechnetate (400-650 MBq) resulted in high radiochemical yields (>98%) and low reduced-hydrolyzed technetium-99m (<0.5%) determined by ITLC and RP-HPLC. Addition of unlabeled RM26 to injected ^{99m}Tc-RM26 resulted in significant decrease of activity uptake in GRPR positive xenografts (7.5 ± 2.3%ID/g vs 1.2 ± 0.9%ID/g) and pancreas (6.1 ± 0.9%ID/g vs 1.3 ± 0.2%ID/g), demonstrating agent specificity. Radiolabeled peptide demonstrated appreciable hepatobiliary excretion. The microSPECT/CT images were in good agreement with the biodistribution data, GRPR-expressing xenografts were clearly visualized. The dosimetry estimated based on in vivo data showed the highest absorbed dose in the small intestine ($1.65 \cdot 10^{-3}$ mGy/MBq), and the effective dose was $3.49 \cdot 10^{-3}$ mSv/MBq. No side effects were observed after the administration of the ^{99m}Tc-RM26 in patients. Liver, gallbladder, small and large intestines, kidneys and bladder were the organs with the highest activity uptake. In both patients, the tumor was visualized as a focus of increased ^{99m}Tc-RM26 accumulation, not extending beyond the prostate. **Conclusion:** [^{99m}Tc]Tc-maSSS-PEG2-RM26 demonstrated specific GRPR targeting in vivo, and along with the simple method for labeling, clinical translation of the GRPR-targeting radiotracer is underway, with early results showing high safety and effectiveness in detecting primary prostate tumors. **References:** none

OP-0035

^{68}Ga- versus ^{18}F-PSMA for Cerenkov Luminescence and autoradiography in a prostate cancer mouse model

P. Fragoso Costa[1,2], L. Püllen[3,2], J. M. Klose[1,2], J. Iking[1,2], P. Sandach[1,2], M. Staniszewska[1,2], K. Herrmann[1,2], J. P. Radtke[3,2], S. Tschirdewahn[3,2], B. Hadaschik[3,2], W. P. Fendler[1,2], C. Darr[3,2];
[1]Clinic for Nuclear Medicine, Essen, GERMANY, [2]German Cancer Consortium (DKTK)-University Hospital Essen, Essen, GERMANY, [3]Department of Urology, Essen, GERMANY.

Aim/Introduction: Cerenkov luminescence imaging (CLI) is a novel imaging modality for the assessment of resection margins. ^{18}F-PSMA and ^{68}Ga-PSMA are available tracers for CLI based assessment of resection margins. Due to its decay characteristics, ^{68}Ga outperforms ^{18}F in terms of Cerenkov light yield. However, the short half-live of ^{68}Ga causes logistic challenges. The aim of this study is to investigate the detection limits of both tracers in terms of CLI and evaluate the added benefit of a flexible scintillation foil, enabling autoradiography imaging (ARI), using mouse models for prostate cancer. **Materials and Methods:** A total of 10 mice bearing subcutaneous PSMA-avid RM1-PGLS tumors were examined. After PET/CT imaging, mice were sacrificed and immediately subjected to whole body CLI, positioned to focus on tumor and kidney visualisation for 300 seconds. Median time from tracer injection to whole body CLI was 4.74 (2.43; 5.20) h. After organ removal, ex-vivo CLI of kidneys and tumor tissue was performed. A flexible scintillator foil was applied when CLI signal was not conspicuous. CLI signal was correlated with PET data, decay corrected to the time of CLI and ARI. Contrast-to-noise ratios were calculated for PET, CLI and ARI. Results: PET/CT was performed 2-4 hours after intraperitoneal administration of (median; IQR) 4.67 (4.34 - 6.57) MBq ^{68}Ga-PSMA and 2.61 (2.27 - 2.93) MBq ^{18}F-PSMA in five mice each. Tumors and kidneys were visible in PET images (CNR > 4). At time of extracted ex-vivo organ CLI, the median activity concentration (AC) of ^{68}Ga-PSMA was 1.54 (0.96; 3.93) kB/mL in lesions and 11.63 (9.69; 32.03) kBq/mL in kidneys; and ^{18}F-PSMA median AC was 9.02 (8.17; 10.22) kBq/mL in lesions and 106.68 (95; 121.75) kBq/mL in kidneys. ^{68}Ga and ^{18}F average PET tracer AC showed a significant Pearson correlation for contrast-to-noise ratio in both whole body and ex-vivo organ/lesion CLI (whole body ^{68}Ga: r=0.63 p<0.05 and ^{18}F: r=0.93, p<0.01; ex-vivo organ CLI ^{68}Ga: r=0.96, p<0.01 and ^{18}F: r=0.96, p<0.01). In CLI the minimum detected AC for ^{68}Ga was 0.84 kBq/mL and for ^{18}F 30.66 kBq/mL. Regarding ^{18}F, ARI significantly improved the representation of low activities (p<0.001), lowering the minimal detectable AC to 7.25 kBq/mL. **Conclusion:** Detection limits for CLI using ^{18}F and ^{68}Ga in biological tissue were identified and validated by an independent measurement (PET), showing higher sensitivity for ^{68}Ga-based-CLI. Using ARI, it is possible to detect low signals of ^{18}F that are otherwise not detectable by CLI. **References:** none

OP-0036

Impact of the specific activity of ^{18}F-PSMA-11 on tumor uptake in a preclinical prostate cancer model

***S. Piron[1]**, J. Verhoeven[1], B. Descamps[1], K. Kersemans[2], C. Vanhove[1], F. De Vos[1];*
[1]Ghent University, Ghent, BELGIUM, [2]Ghent University Hospital, Ghent, BELGIUM.

Aim/Introduction: When using radioligands that target a saturable receptor, the amount of unlabeled compound may affect the tumor uptake because of competitive binding at the target site. This preclinical study aims to determine the potential impact of changes in the specific activity (SA) of the PSMA-targeting radioligand ^{18}F-PSMA-11 on tumor

uptake and visualization in mice. **Materials and Methods:** Six male NOD/SCID mice bearing C4-2 xenograft tumors each underwent three PET/CT scans within a period of two weeks. Each mouse was administered 9.29 ± 0.37 MBq ^{18}F-PSMA-11 with either a high SA (196.8 ± 32.4 MBq/µg), medium SA (19.10 ± 1.69 MBq/µg) and low SA (1.944 ± 0.274 MBq/µg). One hour after injection, static PET/CT scans were performed for 15 minutes. All tumors and a background region contralateral to the tumor were delineated and standardized uptake values (SUV_{mean} and SUV_{max}) as well as tumor-to-background ratios (TBR_{mean} and TBR_{max}) were determined. The statistical analysis was performed using multiple pairwise comparison with Holm correction. Results: SUV_{mean} values were significantly lower for the low vs medium SA (0.60 ± 0.12 vs 1.44 ± 0.48, p=0.012) and low vs high SA (0.60 ± 0.12 vs 2.28 ± 0.69, p=0.012), but did not differ significantly for the medium vs high SA (1.44 ± 0.48 vs 2.28 ± 0.69, p=0.055). SUV_{max} showed a similar trend when comparing low vs medium SA (1.19 ± 0.24 vs 3.20 ± 1.02, p=0.012), low vs high SA (1.19 ± 0.24 vs 5.04 ± 2.14, p=0.012) and medium vs high SA (3.20 ± 1.02 vs 5.04 ± 2.14, p=0.13). TBR_{mean} and TBR_{max} demonstrated the highest values for the medium SA (18.71 ± 2.64 and 41.58 ± 4.88, respectively), followed by the high SA (13.89 ± 2.30 and 29.80 ± 5.85, respectively) and low SA (9.48 ± 0.91 and 19.07 ± 3.33, respectively). All were significantly different from each other (p<0.05). The higher TBR values for medium vs high SA suggest improved tumor contrast when administering a higher amount of PSMA-11 (0.495 ± 0.062 µg vs 0.048 ± 0.007 µg), which resulted in decreasing activity in the background region while tumor uptake (SUV_{mean} and SUV_{max}) was not significantly different. **Conclusion:** These results indicate a significant impact of the specific activity on both SUV values and tumor-to-background ratios, as administration of a high SA resulted in increased tumor uptake while surprisingly a medium SA lead to higher tumor-to-background ratios. **References:** none

OP-0037

Evaluation of the HET-CAM model for biodistribution studies of ^{18}F-siPSMA-14

J. Loeffler[1,2], C. Hamp[2], A. B. Koch[2], C. Solbach[2], L. Hao[1], G. Glatting[3], V. Rasche[1,4], A. J. Beer[2], G. Winter[2];
[1]Center for Translational Imaging, Core Facility Small Animal Imaging, Ulm University, Ulm, GERMANY, [2]Department of Nuclear Medicine, Ulm University Medical Faculty, Ulm, GERMANY, [3]Department of Nuclear Medicine, Medical Radiation Physics, Ulm University Medical Faculty, Ulm, GERMANY, [4]Department of Internal Medicine, Ulm University Medical Faculty, Ulm, GERMANY.

Aim/Introduction: The assessment of the biodistribution of newly developed radiopharmaceuticals always requires animal testing, usually done in rodents. Over the past years there has been a steadily increasing demand for alternative methods that comply with the 3Rs principles of animal welfare. The HET-CAM (hen's egg test-chorioallantoic membrane) model is a promising alternative to meet these demands. Preceding studies in chicken eggs could help reducing the number of necessary animal experiments. Our aim was to evaluate the model, particularly in regards to quantifiability and reproducibility of data using the PSMA-specific tracer ^{18}F-siPSMA-14. **Materials and Methods:** Tumor xenografts of a PSMA-positive (LNCaP C4-2) and a PSMA-negative cell line (PC-3) were established. MRI and PET measurements were performed between embryo development days 12 and 16. MRI (BioSpec 117/16, Bruker) included an overview scan (Flash3D) of the whole egg and a high-resolution scan (RARE) of the tumor region. After i.v. application of ^{18}F-siPSMA-14 a 60min dynamic PET (Focus 120, Siemens Medical Solutions, Inc.) was performed. PET data were evaluated using Pmod ver. 4.105 (PMOD Technologies Ltd.). Subsequently, tumor xenografts were excised and the corresponding radioactivity was determined using a γ-counter (Cobra II, PerkinElmer). To detect the PSMA protein, tumors were lysed, and Western blots (WB) were generated. In addition, immunohistochemistry (IHC) was performed to detect the PSMA protein. Based on MRI data VOIs were placed to calculate TACs of the tumors and organs of interest. Results: In the WB and IHC analysis PSMA was detected only in the LNCaP C4-2 cells. Tumor volumes were determined based on MRI data revealing a volume of (29.2+/-9.3) mm^3 for LNCaP C4-2 and (23.4+/-11.3) mm^3 for PC-3 (n=8). A high accumulated activity was detected in the LNCaP C4-2 tumor xenografts after superposition of PET and MRI data: LNCaP C4-2 (2.6+/-1.1) %IA/mL; PC-3 (1.5+/-1.0) %IA/mL, resulting in a ratio of C4-2/PC-3 = 2.5+/-1.3 γ-counter measurements indicate similar results: LNCaP C4-2 (13.0+/-6.9) %IA/mL; PC-3 (7.5+/-3.0) %IA/mL; C4-2/PC-3 = 1.7+/-0.8. **Conclusion:** For both quantification methods, PET and γ-counter, a high specific accumulation of ^{18}F-siPSMA-14 in PSMA-positive tumors was observed using the HET-CAM model. Thus, the presented platform provides the opportunity to determine tumor volume and to quantify the target specific accumulation, allowing a pre-selection of newly developed radiopharmaceuticals. Therefore, the HET-CAM model has great potential as an alternative model to reduce the number of animal experiments. **References:** none

OP-0038

Investigation of the Molecular Design of PSMA-targeting Radioligands for Imaging of Prostate Cancer

F. Lundmark, G. Olanders, S. S. Rinne, A. Abouzayed, A. Orlova, U. Rosenström;
Department of Medicinal Chemistry at Uppsala University, Uppsala, SWEDEN.

Aim/Introduction: Prostate-specific membrane antigen (PSMA) is a promising target for imaging prostate cancer since it is frequently overexpressed in both poorly differentiated tumours and metastatic lesions. For PSMA-inhibitors, urea-

based ligands are preferable as they provide favourable interactions with the active site leading to high affinity. For labelling with radiometals, a need for a linker between the urea-moiety and the bulky metal chelator has been emphasized. The introduction of a linker also enables additional interactions with the entrance tunnel of the active site, leading to more potent inhibitors. This ongoing project aims to investigate how structural modifications in the linker of PSMA-binding radioligands would affect the binding to PSMA. **Materials and Methods:** Computational modelling was used to design different linkers based on the ability to interact with Tyr549, Tyr552, Tyr700 (subpocket 1) and Arg463, Phe546, Trp541 (subpocket 2) in the entrance tunnel of PSMA. In total, 11 novel urea-based PSMA-targeting analogues were synthesized using solid-phase peptide synthesis. Structural modifications were made by incorporation of naphthyl, phenylalanine, 4-bromo-phenylalanine, tyrosine, cyclohexane, or alanine in different positions in the linker. NOTA chelator was coupled to all analogues for labelling with indium-111. Specific binding and affinity to PSMA were evaluated in vitro using PC3-pip cells. Results: All analogues were labelled with indium-111 in high radio-chemical yields (>98%) and demonstrated stable radionuclide/chelator complexes as well as specific binding to PSMA in vitro. When comparing their binding properties, a 10-fold difference in affinity was observed with K_D values ranging from 4-40 nM. Analogues with a naphthyl group targeting subpocket 1 and an alanine, phenylalanine, or tyrosine sidechain positioned to interact with subpocket 2 demonstrated higher affinities compared to those with other substituents. Results were in good agreement with the observed size and structure of the two subpockets investigated using the crystal structure of PSMA, where subpocket 2 seems to be stricter in size compared to the more spacious subpocket 1. **Conclusion:** Herein, 11 novel PSMA-binding radioligands for imaging of prostate cancer are presented. By structural modifications of the linker placed between the urea-moiety and the metal chelator, a 10-fold higher affinity could be obtained. Ultimately, it was emphasized that interactions between subpocket 1 and a bulky hydrophobic moiety, and subpocket 2 and a less bulky moiety, led to the highest affinity for PSMA. **References:** none

OP-0039

Selection of Optimal Radiolabel Position and Composition in DARPin Ec1 for High-Contrast Imaging of EpCAM Expression in Prostate Cancer

A. Vorobyeva[1,2], T. Xu[1], A. Schulga[3,2], E. Konovalova[3], Y. Liu[1], J. Garousi[1], S. S. Rinne[1], M. Larkina[2], H. Ding[4], T. Gräslund[4], A. Orlova[1,2], S. M. Deyev[3,2], V. Tolmachev[1,2];

[1]Uppsala University, Uppsala, SWEDEN, [2]National Research Tomsk Polytechnic University, Tomsk, RUSSIAN FEDERATION, [3]Shemyakin & Ovchinnikov Institute of Bioorganic Chemistry, Moscow, RUSSIAN FEDERATION, [4]KTH Royal Institute of Technology, Stockholm, SWEDEN.

Aim/Introduction: Up to a quarter of patients with oligometastatic prostate cancer (PC) are not eligible for prostate-specific membrane antigen-targeted therapy and require a complementary targeted treatment. Epithelial cell adhesion molecule (EpCAM) has intense overexpression in 40-60% of PC cases and is associated with metastasis, chemo- and radioresistance and increased risk of recurrence, which makes it a promising therapeutic target. To select patients for EpCAM-targeted treatment, radionuclide molecular imaging of EpCAM expression could be performed. Designed ankyrin repeat protein (DARPin) Ec1 has high affinity to EpCAM (68 pM), small size (18 kDa) and might be used as a diagnostic counterpart for therapy. The aim of the study was to investigate the influence of radiolabel position (N- and C-terminal) and composition (radiometal and radiohalogen) in DARPin Ec1 targeting EpCAM on imaging contrast in PC. **Materials and Methods:** Two DARPins Ec1 variants having N- or C-terminal cysteine were produced, site-specifically conjugated to DOTA chelator and labeled with cobalt-57, gallium-68 and indium-111. Radioiodination of ((4-hydroxyphenyl)ethyl)maleimide (HPEM) provided non-residualizing [^{125}I]I-HPEM label, which was site-specifically conjugated to the DARPins. EpCAM-expressing PC-3 and DU145 PC cells were used to evaluate binding specificity in vitro. Affinity and internalization were studied in DU145 cells. Biodistribution of eight radiolabeled conjugates was measured in Balb/c nu/nu mice bearing DU145 and Ramos (negative control) xenografts 3 and 24 h post-injection (p.i.). MicroSPECT/CT and microPET/CT imaging was used to confirm the biodistribution data. Results: Radiolabeling and purification provided conjugates in over 97% radiochemical purity. Binding of all conjugates to PC cells was specific with picomolar affinity. Slow internalization in vitro suggested the suitability of non-residualizing label for in vivo imaging. C-terminal label position in DARPin Ec1 provided lower uptake in normal organs than N-terminal for all label types. [^{125}I]I-HPEM label provided the lowest retention of activity in normal organs, however, resulted in high hepatobiliary excretion (21±2%ID/g). Three hours p.i. C-terminal [^{125}I]I-HPEM label provided the highest ratios of tumor-to-blood (20 ± 6), tumor-to-muscle (83 ± 40) and tumor-to-bone (11±2). Tumor targeting was highly specific. Imaging confirmed the biodistribution results. **Conclusion:** Label position and composition are important for DARPin Ec1. Non-residualizing [^{125}I]I-HPEM label at C-terminus provided the highest tumor-to-muscle and tumor-to-bone ratios 3 h p.i. and is more suitable for imaging of EpCAM in early stage PC. Among radiometals, indium-111 at C-terminus provided as high tumor-to-blood ratio as [^{125}I]I-HPEM, the highest tumor-to-lung and tumor-to-liver ratios and could be used at late stage PC. **References:** None

OP-0040

HER3 targeting ^{68}Ga-labeled affibody provides superior PET imaging contrast compared with ^{89}Zr-labeled antibody and antibody-fragment based tracers

S. Rinne[1], A. Abouzayed[1], C. Dahlsson Leitao[2], A. Vorobyeva[1], V. Tolmachev[1], S. Ståhl[2], J. Löfblom[2], A. Orlova[1];
[1]Uppsala University, Uppsala, SWEDEN, [2]KTH - Royal Institute of Technology, Stockholm, SWEDEN.

Aim/Introduction: PET-imaging of HER3 expression in oncology could improve patient care. Because of the low overexpression in tumors and substantial expression in normal tissue achieving sufficient HER3 image contrast is challenging. The choice of the targeting molecule can appreciably influence the PET-image contrast. The aim of this study was to perform a preclinical head-to-head comparison of radiotracers based on different types targeting proteins for PET-imaging of HER3 expression: the anti-HER3 antibody [^{89}Zr]Zr-DFO-MM121, a newly synthesized MM121-derived fragment [^{89}Zr]Zr-DFO-MM121-F(ab')$_2$, and the previously developed affibody-based tracer [^{68}Ga]Ga-(HE)$_3$-Z$_{HER3}$-NODAGA. **Materials and Methods:** MM121 and MM121-F(ab')$_2$ were coupled with a DFO chelator and labeled with ^{89}Zr. The stability of the radioconjugates was tested in PBS and human serum. Binding specificity and internalization assays were performed using HER3-expressing BxPC-3 (pancreatic carcinoma) and DU145 (prostate carcinoma) cells. The biodistribution of [^{89}Zr]Zr-DFO-MM121 (48h and 96h pi) and [^{89}Zr]Zr-DFO-MM121-F(ab')$_2$ (3h, 24h, 48h pi) was studied in BxPC-3 xenografted mice. Mice with RAMOS xenografts were used as a HER3-negative control. Biodistribution of [^{68}Ga]Ga-(HE)$_3$-Z$_{HER3}$-NODAGA was performed 3h pi for reference. nanoPET/CT was performed for all conjugates at the respective time points. Results: DFO-MM121 and DFO-MM121-F(ab')$_2$ were successfully labeled with ^{89}Zr (purity>97%). Stability test showed high stability in PBS, but up to 25% release of activity in human serum within 24h. Binding to cells was HER3 specific; in both cells lines 31-35% of added activity was internalized for both ^{89}Zr-labeled tracers after 24h of continuous incubation. In vivo, the ^{89}Zr-conjugates bound specifically to HER3-expressing BxPC-3 xenografts. The highest tumor uptake among all tracers was achieved with [^{89}Zr]Zr-DFO-MM121-F(ab')$_2$ 3h pi (7±2 %ID/g), but it decreased with time and at 48h pi it was comparable to the tumor uptake of [^{89}Zr]Zr-DFO-MM121 (4-5.6 %ID/g, 48h and 96h pi). [^{89}Zr]Zr-DFO-MM121 and [^{89}Zr]Zr-DFO-MM121-F(ab')$_2$ cleared significantly slower from blood than [^{68}Ga]Ga-(HE)$_3$-Z$_{HER3}$-NODAGA. Both ^{89}Zr-labeled radioconjugates showed significantly higher uptake in liver, spleen, and bone compared with [^{68}Ga]Ga-(HE)$_3$-Z$_{HER3}$-NODAGA. The highest tumor-to-organ ratios and image contrast with [^{89}Zr]Zr-DFO-MM121 and [^{89}Zr]Zr-DFO-MM121-F(ab')$_2$ were observed 96h and 48h pi, respectively. The tumor-to-blood ratio of [^{89}Zr]Zr-DFO-MM121-F(ab')$_2$ 48h pi (15±4) was 2.3-fold higher than with [^{89}Zr]Zr-DFO-MM121 96h pi. Despite lower tumor uptake, [^{68}Ga]Ga-(HE)$_3$-Z$_{HER3}$-NODAGA provided higher tumor-to-non-tumor ratios than both ^{89}Zr-labeled tracers at their respective optimal imaging time points. nanoPET/CT confirmed the biodistribution results. **Conclusion:** [^{68}Ga]Ga-(HE)$_3$-Z$_{HER3}$-NODAGA provided significantly better HER3 imaging contrast than [^{89}Zr]Zr-DFO-MM121 and [^{89}Zr]Zr-DFO-MM121-F(ab')$_2$, suggesting that affibody-based tracers could be considered superior to monoclonal antibodies and F(ab')$_2$-fragments for PET-imaging of HER3 expression. **References:** None.

OP-0041

^{61}Cu-PSMA versus ^{68}Ga-PSMA for PET imaging of prostate cancer

T. Basaco Bernabeu[1], R. Mansi[1], L. Del Pozzo[1], R. H. Gaonkar[1], L. McDougall[1], S. Zanger[1], L. Jaafar-Thiel[2], M. Fani[1];
[1]Division of Radiopharmaceutical Chemistry, University Hospital Basel, Basel, SWITZERLAND,
[2]Swiss Nuclides AG, Aarau, SWITZERLAND.

Aim/Introduction: Prostate-specific membrane antigen (PSMA)-targeting is highly relevant in prostate cancer for detection and therapy (theranostics). A number of low-molecular-weight PSMA inhibitors have been developed for this purpose, with ^{68}Ga-PSMA-11 being recently approved. Others, like ^{68}Ga-PSMA-617 and ^{68}Ga-PSMA-I&T, offer additionally the possibility of theranostics when labeled with ^{177}Lu. In view of the increasing clinical demand, the production capacity of the generator produced ^{68}Ga-tracers (2-3 patient doses) raises certain concerns. A valuable alternative is Copper-61 ($E_{\beta+_{mean}}$=500 keV, $E_{\beta+_{max}}$=1216 keV, $t_{1/2}$=3.34 h). ^{61}Cu can be produced in cyclotrons in large scale, while its lower energy and longer half-life (enabling delayed imaging), compared to ^{68}Ga, may result to refined imaging quality. In addition, ^{61}Cu has the therapeutic companion ^{67}Cu. We report herein the comparison of ^{61}Cu-PSMA versus ^{68}Ga-PSMA, based on PSMA-I&T. **Materials and Methods:** The chelator DOTAGA on PSMA-I&T (herein referred as DOTAGA-PSMA-I&T) was replaced with NODAGA for labeling with ^{61}Cu, due to the stable Cu-NODAGA complex in vivo, compared to Cu-DOTAGA. [^{61}Cu]CuCl$_2$ was produced from irradiated Ni-target at the University Hospital Zurich cyclotron followed by cassette-based automated separation, as described previously (1). [^{61}Cu]Cu-NODAGA-PSMA-I&T was evaluated head-to-head with [^{68}Ga]Ga-DOTAGA-PSMA-I&T in terms of lipophilicity, in vitro cellular uptake in LNCaP cells and PET/CT imaging in LNCaP-xenografted nude mice. Biodistribution studies are on-going. Results: The two radiotracers were prepared at apparent molar activities of 24-30 MBq/nmol. [^{61}Cu]Cu-NODAGA-PSMA-I&T, compared with [^{68}Ga]Ga-DOTAGA-PSMA-I&T, showed higher hydrophilicity (logD= -2.95±0.08 and -2.79±0.41, respectively) and higher cellular uptake in vitro (26.6±0.9% after 1 h at 37°C, with 12±1.9%

being internalized versus 20.6±2.3% cellular uptake and 9.8±1.3% internalized fraction, respectively). PET/CT images 1 h p.i. revealed the same biodistribution pattern for both radiotracers, which was characterized by accumulation mainly in the tumor - with [^{61}Cu]Cu-NODAGA-PSMA-I&T showing higher uptake - and in the kidneys. The biodistribution pattern of [^{61}Cu]Cu-NODAGA-PSMA-I&T was the same on PET/CT images at 4 h p.i.. The kidney uptake of [^{61}Cu]Cu-NODAGA-PSMA-I&T could be reduced significantly, from 96% to 72% to 34% IA/g at 1h p.i. by increasing the injected amount, from 200 to 400 to 1000 pmol, respectively. Quantitative biodistribution studies in LNCaP xenografts are in progress and will be presented. **Conclusion:** [^{61}Cu]Cu-NODAGA-PSMA-I&T compared well with [^{68}Ga]Ga-DOTAGA-PSMA-I&T on PET/CT images in terms of total body distribution, while showing higher tumor uptake and offering the possibility of delayed images. [^{61}Cu]Cu-NODAGA-PSMA-I&T is considered for clinical evaluation versus established ^{68}Ga-PSMA tracers. **References:** 1.J. Svedjehed et al., EJNMMI Radiopharmacy and Chemistry 2020;5:21

OP-0042

Synthesis, radiolabelling and in vitro characterisation of a bimodal BODIPY-labelled PSMA-targeting bioconjugate for dual imaging of prostate cancer

T. Stemler[1], I. Hierlmeier[1], S. Maus[1], F. Rosar[1], F. Khreish[1], S. Ezziddin[1], E. Krause[2], C. Hoffmann[3], G. Jung[3], M. Bartholomä[1];
[1]Department of Nuclear Medicine, Saarland University – Medical Center, Homburg/Saar, GERMANY, [2]Department of Cellular Neurophysiology, Saarland University, Center for Integrative Physiology and Molecular Medicine, Homburg/Saar, GERMANY, [3]Department of Biophysical Chemistry, Saarland University, Saarbrücken, GERMANY.

Aim/Introduction: BODIPY dyes represent a promising class of fluorophores with excellent fluorescence properties. These dyes also offer the possibility to introduce the positron-emitter fluorine-18, allowing the development of hybrid nuclear and fluorescent imaging probes.[1,2] The aim of the study was to demonstrate the use of [^{18}F]F-labelled BODIPY dyes for dual imaging of prostate cancer. Therefore, a BODIPY peptidomimetic targeting the prostate specific membrane antigen (PSMA) was synthesised, radiolabelled and tested in terms of its biological applicability. **Materials and Methods:** For the preparation of the bimodal PSMA-targeting conjugate Glu-CO-Lys-Ahx-BODIPY 1, both the synthesis of the PSMA-binding motif Glu-CO-Lys and the coupling of the Ahx spacer were performed on solid support using standard Fmoc-chemistry. Conjugation of BODIPY was carried out in solution to obtain the final bioconjugate. Fluorescence properties were measured by fluorescence spectroscopy. The bioconjugate was radiolabelled by Lewis-acid catalysed isotopic ^{18}F/^{19}F exchange for 15 min at room temperature. Binding affinities of the conjugates were determined by competitive cell binding experiments in the human prostate cancer cell line LNCaP. Specific internalisation of the ^{18}F-labelled compound was demonstrated along with blocking experiments using 2-PMPA. Cellular localisation of the BODIPY-PSMA conjugate was studied by fluorescence microscopy. Results: The bioconjugate was obtained in 38 % yield after purification by semi-preparative RP-HPLC. Absorption and emission maxima of 1 were detected at wavelengths of 490 nm and 510 nm, with high fluorescent quantum yields and fluorescence lifetimes in the nanosecond range. Bioconjugate 1 showed a high PSMA affinity comparable to PSMA-11. Radiolabelling was achieved in molar activities of ~ 1 MBq nmol^{-1} with radiochemical purities of >99 % after C_{18} Sep-Pak purification. After 1 h, 0.4 % of compound [^{18}F]F-1 were bound to PSMA on the cell surface of LNCaP cells and 3.4 % were specifically internalised. PSMA-mediated uptake of compound 1 into LNCaP cells was confirmed by fluorescence microscopy showing gradual internalisation over time. **Conclusion:** Compound 1 was readily prepared and radiolabelled under mild conditions in moderate molar activities and high radiochemical purities, without altering the fluorescent properties of the BODIPY dye. In cell experiments, 1 showed a high PSMA-affinity and might be a suitable candidate for the development of PSMA-specific dual-imaging agents. **References:** 1. Kowada, T., Maeda, H. & Kikuchi, K. Chem. Soc. Rev. 44, 4953-4972 (2015). 2. Paulus, A. et al. EJNMMI Res 5, 120 (2015).

209

Wednesday, October 20 - Saturday, October 23, 2021

on-demand pool, release on Wednesday, October 20 at 09:00

Cutting Edge Science Track - TROP Session: Radiobiology Meets Dosimetry

OP-0044

Quantitative Ex Vivo Imaging of ^{225}Ac with the iQID Alpha Camera

C. Miller[1,2], J. Rousseau[3], J. Crawford[4], B. Miller[5,6], F. Bénard[7,3,8], A. Rahmim[1,2,8], C. Uribe[7,8];
[1]Department of Physics and Astronomy, University of British Columbia, Vancouver, BC, CANADA, [2]Department of Integrative Oncology, BC Cancer Research Institute, Vancouver, BC, CANADA, [3]Department of Molecular Oncology, BC Cancer Research Institute, Vancouver, BC, CANADA, [4]Department of Physics and Physical Oceanography, Memorial University of Newfoundland, St. John's, NL, CANADA, [5]Department of Radiation Oncology, University of Colorado School of Medicine, Aurora, CO, UNITED STATES OF AMERICA, [6]College of Optical Sciences, University of Arizona, Tucson, AZ, UNITED STATES OF AMERICA, [7]PET Functional Imaging, BC Cancer, Vancouver, BC, CANADA, [8]Department of Radiology, University of British Columbia, Vancouver, BC, CANADA.

Aim/Introduction: Quantitative measures such as the intratumoural activity distribution of a radiopharmaceutical and the corresponding absorbed dose distribution are useful information for radiopharmaceutical therapy (RPT) and radiopharmaceutical development. The ionizing-radiation Quantum Imaging Detector (iQID) is a scintillation-based detector able to image alpha particles, such as those emitted from tissue sections of mice injected with an alpha-emitting radiopharmaceutical. Quantitative imaging enables the determination of dose rates and time integrated activities within tumour sections. The aim of this work is to generate quantitative images of the activity distribution and dose rates within tumour sections of mice who were injected with an ^{225}Ac labelled antibody. **Materials and Methods:** Small drops of a solution containing ^{225}Ac with activities ranging from 0.8 Bq to 95 Bq were pipetted onto a silver-doped Zinc Sulfide (ZnS:Ag) scintillator and imaged with the iQID detector. The images were segmented and a calibration factor was calculated by generating a calibration curve and performing a linear fit. Four tumour bearing mice were injected with 18.4 kBq ± 2 kBq of an ^{225}Ac labelled antibody. Three days post injection, the tumours were collected, frozen, and sliced into 14 um slices for autoradiography with the iQID detector. The calibration factor was used to convert the iQID images into units of activity (Bq). A dose kernel for ^{225}Ac was created using GATE version 9.0 assuming water as the medium. The kernel was convolved with the iQID image to generate dose rate maps of each tumour slice. The tumour slices were segmented and the total dose rate within each slice was calculated. Results: The measured calibration factor for the ^{225}Ac isotope in the iQID camera was 0.33 cps/Bq. Using this factor, activity maps in units of Bq and dose rate maps in units of Gy/s were generated. Total activities within the slices range from 1.1 Bq to 2.7 Bq and total dose rates ranged from 0.6 to 1.5 Gy/s. Visually, activity distributions were heterogeneous. **Conclusion:** We present a method to generate ^{225}Ac quantitative images of the activity distribution and dose rates within mouse tissue sections using the iQID detector. This work has the potential to find correlations between dose, dose rates, and the degree of tumour heterogeneity with the therapeutic efficacy and other biological variables. Moreover, it will allow us to understand the distributions of different radiopharmaceuticals within tissue and correlate it with therapeutic outcomes. **References:** None

OP-0045

The Impact of Cell Shape on the Doses Delivered to the Nucleus from ^{177}Lu-labelled Radiotracers

C. Miller[1,2], G. Chaussé[3], J. Brosch-Lenz[2,4], F. Bénard[3,5,6], A. Rahmim[1,2,6], C. Uribe[3,6];
[1]Department of Physics and Astronomy, University of British Columbia, Vancouver, BC, CANADA, [2]Department of Integrative Oncology, BC Cancer Research Institute, Vancouver, BC, CANADA, [3]PET Functional Imaging, BC Cancer, Vancouver, BC, CANADA, [4]Department of Nuclear Medicine, University Hospital, LMU Munich, Munich, GERMANY, [5]Department of Molecular Oncology, BC Cancer Research Institute, Vancouver, BC, CANADA, [6]Department of Radiology, University of British Columbia, Vancouver, BC, CANADA.

Aim/Introduction: Targeted radiopharmaceutical therapy (RPT) is a promising treatment option for various tumour types and metastases. While most dosimetry estimates in RPT are done on a macroscopic level, e.g. with PET or SPECT imaging, dosimetry on a cellular level is key to enhance our understanding of the mechanisms of RPT and to increase the chances of treatment success. Cellular dosimetry is often based on Monte Carlo (MC) simulations, however the choice of cell shape and distribution of the radiopharmaceutical within the cell may impact the calculated dose and therefore the accuracy of these methods. This work aims to compare S-values to the nucleus from ^{177}Lu in two in vitro models of LNCaP (human prostate cancer cell line) cells: a spherical model and an 'egg-white' shaped model representing an adherent cell. **Materials and Methods:** A spherical and an 'egg-white' shaped cancer cell were modelled using GATE version 9.0 Monte Carlo software. Both models include a nucleus, nuclear membrane, cytoplasm, and cellular membrane. All cell regions were assumed to have the density of water (1g/cm^3). The total areas of both models were identical and were based on dimensions of LNCaP cells. The spherical cell was 13.5µm in diameter and the maximum dimensions of the egg-white cell was 39µm x 7µm x 14µm. ^{177}Lu activity was homogeneously distributed either throughout the cytoplasm or at the cell membrane of each model to represent levels of internalization of the radioisotope. Absorbed dose was scored on a voxel level (0.04µm)^3 with GATE's dose actor. S-values to the nucleus were calculated for each of the source regions and models. Results: The S-values to the nucleus of the 'egg-white' cell were 1.4x10^{-4} Gy/Bqs and 1.5x10^{-4} Gy/Bqs from the cytoplasm and membrane respectively. These values were 2.1 and 1.2 times lower than those from the spherical cell respectively. **Conclusion:** The S-values to the nucleus of the spherical cell were larger than those from the 'egg-white' cell, likely due to the symmetrical distribution of activity. This indicates that the shape of the cell model influences the S-value and therefore the total dose to the nucleus of the cell. Consequently, absorbed dose simulations at a microscopic level must take

into account the cell size and shape and care should be taken to ensure the use of an accurate cell model referring to human cell lines. Future steps will include the comparison of different radionuclides on a cellular level. **References:** None

OP-0046

A physiologically-based pharmacokinetic model of ^{212}Pb-labelled pharmaceuticals targeting neuroendocrine tumors in mice

N. Zaid, P. Kletting, G. Winter, A. Beer, G. Glatting;
Ulm University, Ulm, GERMANY.

Aim/Introduction: ^{212}Pb-labelled pharmaceuticals are promising in vivo sources of alpha particles through the short-lived ^{212}Pb-daughter ^{212}Bi. Cytotoxic alpha particles have a great potential in the treatment of aggressive neuroendocrine tumours that are resistant to beta radiation. Quantitative analysis of the distributed free radioactive products is challenging in targeted alpha particle therapy (TAT). Mathematical modelling allows for describing separately and simultaneously the pharmacokinetics of each of the decay products of alpha generators. Therefore, a first physiologically-based pharmacokinetic (PBPK) model was developed to describe the pharmacokinetics of [^{212}Pb]Pb-DOTAMTATE targeting somatostatin receptor type2 (SSTR2) in mice. **Materials and Methods:** A whole-body ^{212}Pb-PBPK model for mice was developed and implemented in both modelling software SAAM II (version 2.3) and Simbiology/MATLAB (MATLAB R2020a). All relevant physiological mechanisms are described in the ^{212}Pb-PBPK model with parameter values from the literature. Another PBPK model for free ^{212}Bi was developed, evaluated and integrated into the ^{212}Pb-PBPK model. The pharmacokinetic parameters in the ^{212}Pb-PBPK model were estimated using [^{212}Pb]Pb-DOTAMTATE biokinetic data in AR42J-bearing mice after intravenous administration of 0.0013 nmol (0.185 MBq) of [^{212}Pb]Pb-DOTAMTATE [1]. Absorbed dose coefficients (ADC) due to bound and unbound conjugated and released radionuclides were calculated. Results: The developed model successfully describes the experimental data. The fitted curves were good by visual inspection. The tumour plasma flow rate was (0.33±0.45) ml/min/g. SSTR2 densities in tumour, kidneys, liver, pancreas, spleen and lung were (5.94±1.04), (3.04±0.31), (0.13±0.03), (4.05±1.48), (0.57±0.04) and (1.39±0.05) nmol/l. The calculated ADC in tumour, kidneys, liver, spleen, lung, and pancreas were 0.23, 0.14, 0.01, 0.03, 0.07 and 0.10 Gy/kBq, respectively. In kidneys, the contributions of alpha radiation to total ADC due to conjugated ^{212}Bi, conjugated ^{212}Po, free ^{212}Bi and free ^{212}Po were 17.3 %, 44.6 %, 3.6 % and 8.6 %, respectively. The contributions of beta radiation due to conjugated ^{212}Pb, conjugated ^{212}Bi, free ^{212}Bi and free ^{208}Tl were 5.8 %, 11.5 %, 2.2% and 6.5%, respectively. **Conclusion:** The developed ^{212}Pb-PBPK model describes the pharmacokinetics of a ^{212}Pb-labelled pharmaceutical and the decay products in mice. The ^{212}Pb-PBPK model can be used to determine the contribution of distributed free radionuclides to the absorbed dose in non-target tissues. Hence, the efficacy and safety of using ^{212}Pb-labelled pharmaceuticals can be evaluated, reducing the time required for translation from bench to bedside. **References:** [1] Stallons, T. A. R., et al. (2019). Molecular Cancer Therapeutics 18(5): 1012-1021.

OP-0047

Therapeutic efficacy of heterogeneously distributed radiolabelled peptides: influence of radionuclide choice

G. Tamborino[1,2], J. Nonnekens[2,3,4], M. De Saint-Hubert[1], L. Struelens[1], M. De Jong[2], M. Konijnenberg[2];
[1]Research in Dosimetric Application, Belgian Nuclear Research Centre (SCK CEN), Mol, BELGIUM, [2]Department of Radiology & Nuclear Medicine, Erasmus MC, Rotterdam, NETHERLANDS, [3]Department of Molecular Genetics, Erasmus MC, Rotterdam, NETHERLANDS, [4]Oncode Institute, Erasmus MC, Rotterdam, NETHERLANDS.

Aim/Introduction: To model dose-response relationships for in vivo experiments with radiolabelled peptides enabling therapeutic efficacy comparison. **Materials and Methods:** Distribution of somatostatin receptor type-2 ($SSTR_2$) expression was imaged in NCI-H69 xenografts on mice, at 0,2,5,11 days after injection with ^{177}Lu-DOTATATE. Realistic 3D heterogeneous activity distributions (5.7x5.7x10µm voxels) were reconstructed in tissue geometries of cancer and heathy cells. The resulting spatial absorbed dose rate distributions at each time-point were calculated using GATE and compared to homogenous dose rate distribution. Calculations were performed for the most commonly used radionuclides (^{90}Y, ^{161}Tb,^{177}Lu, ^{213}Bi), assuming comparable biodistributions. The added activity was in all cases 30 MBq, except for ^{213}Bi with 10 MBq. The averaged absorbed dose on the mm-scale tissue sections delivered over the whole treatment (complete decay) was correlated to the modelled in vivo survival. Radiobiological parameters were derived from experimental data on ^{177}Lu-DOTATATE: DNA-damage repair half-life (T_{μ}) by fitting the in vitro DSBs over time and linear quadratic (LQ) model radiosensitivity parameters (α,β) by comparison with cell death assay and volume response over time. The tumor doubling time T_D was obtained by fitting the tumor volume data over time. An RBE of 3.4 was used for the calculations with ^{213}Bi. The absorbed dose (0-2days) on µm-scale sections was correlated with DSBs induction, measured by γH2AX-foci for ^{177}Lu-DOTATATE. Results: The average S-values for the initial heterogeneous dose-distributions (S_{Lu}=3.36±0.32 µGyBq^{-1}h^{-1}, S_{Tb}=4.84±0.48 µGyBq^{-1}h^{-1},S_{Y}=6.35±0.47 µGyBq^{-1}h^{-1},S_{Bi}=218±0.22 µGyBq^{-1}h^{-1}) are not significantly different from the homogeneous ones, irrespectively of the radionuclide choice. The reduction of $SSTR_2$ expression over time, accounted for ^{177}Lu-DOTATATE, causes an increase in this S-value difference up to +58% at day 11. No significant difference between the heterogeneous and homogeneous in vivo survival is observed, unless the $SSTR_2$ reduction over time is significant and taken into account in the calculations. Within the LQ-model, the best matching in vivo survival

correlation for ^{177}Lu-DOTATATE corresponds to α=0.14 Gy^{-1},α/β=100Gy,T_μ=60h,T_D=14.5d, indicating an RBE of 0.4. The lowest in vivo survival corresponds to ^{213}Bi (11%) followed by ^{161}Tb (39%), ^{90}Y (37%) and ^{177}Lu (58%). The minimal effective dose rate for cell kill is 13.24-13.66 mGy/h for beta-emitters and 131.29 mGy/h for ^{213}Bi, below these values proliferation takes over. A linear correlation (slope=0.0223DSBs/cell mGy^{-1},R^2 =0.7) between the absorbed dose delivered by ^{177}Lu and the number of DSBs/cell was found. **Conclusion:** Heterogeneity in receptor expression leads to differences between cellular and average doses to tumors which might impact clinical tumor dosimetry. **References:** none

OP-0048

Modeling early radiation DNA damage occurring during [^{177}Lu]Lu-DOTA-[Tyr^3]octreotate radionuclide therapy

G. Tamborino[1,2], Y. Perrot[3], M. De Saint-Hubert[1], L. Struelens[1], J. Nonnekens[2,4], M. De Jong[2], M. Konijnenberg[2], C. Villagrasa[3];
[1]Research in Dosimetric Application, Belgian Nuclear Research Centre (SCK CEN), Mol, BELGIUM, [2]Department of Radiology & Nuclear Medicine, Erasmus MC, Rotterdam, NETHERLANDS, [3]IRSN, Institut de Radioprotection et de Sûreté Nucléaire, Fontenay aux Roses, FRANCE, [4]Department of Molecular Genetics, Erasmus MC, Rotterdam, NETHERLANDS.

Aim/Introduction: The aim of this study is to build a simulation framework to evaluate the number of DNA double strand breaks (DSBs) induced by in vitro targeted radionuclide therapy (TRT) by adapting a simulation chain, including direct and indirect damage, that has been benchmarked against external beam radiotherapy. This work represents the first step towards modeling DSBs during TRT with the ultimate goal of exploring underlying biological mechanisms and influence of physical/chemical parameters to enable a better response prediction in patients. We used this tool to characterize early DSB induction by [^{177}Lu]Lu-DOTA-[Tyr^3]octreotate (^{177}Lu-DOTATATE), a commonly used TRT for neuroendocrine tumors. **Materials and Methods:** A multiscale approach is implemented to simulate the number of DSBs produced by the cumulated decays over 4 hours of the beta and IC-electrons components of ^{177}Lu-DOTATATE. The approach involves 2 sequential simulations performed with Geant4/Geant4-DNA. First, the radioactive source is sampled according to previous uptake experiments on the distribution of activities within medium and cells (U2OS+$SSTR_2$), assuming instant and permanent internalization, and a phase space (PHSP) is scored around the nucleus (ellipsoid or elliptic cylinder) of the central cell. The cell population is rendered by polygonal mesh models. Then, the PHSP is used to generate particles entering the nucleus containing a multi-scale description of the DNA (6Gbp) in order to score the number of DSBs/particle source. The final DSB computations are compared to experimental data, measured by immunofluorescent detection of 53BP1 foci. Results: Our results reveal that accurate cellular morphology modelling and activity localization sampling influence significantly the probability of electrons reaching the nucleus and their energy deposition pattern within the nucleus, causing a spread in the induction of DSBs. A significant difference was found in the DSB yields induced by bound and unbound fractions of activity, explained by the specific energy (z) distributions within the nuclear geometries. The average number of simulated DSBs is 14 DSBs/cell (range 7-24 DSBs/cell) compared to 13 DSBs/cell experimentally determined (2-30 DSBs/cell). We found a linear correlation between the mean absorbed dose to the nucleus and the number of DSBs/cell with a slope of either 0.0144 DSBs/cell mGy^{-1} or 0.017 DSBs/cell mGy^{-1} (internalization in Golgi apparatus or cytoplasm, respectively). **Conclusion:** Our results demonstrate that integrating realistic cellular and organelle geometries and their uptake with a simulation chain characterizing biological damage is crucial to model DNA damage and hence, to find more reliable dose-effect correlations for DSBs with TRT. **References:** none

OP-0049

In silico study on the heterogeneity of the dose distribution and radiobiological efficacy of Ac-225 and Lu-177 for PSMA-guided radiotherapy

G. Birindelli[1], M. Drobnjakovic[1], V. Morath[2], K. Steiger[3], C. D'Alessandria[2], E. Gourni[1], A. Afshar-Oromieh[1], W. Weber[2], A. Rominger[1], M. Eiber[2], K. Shi[1];
[1]Inselspital, University of Bern, Bern, SWITZERLAND, [2]Klinikum rechts der Isar, Technical University of Munich, München, GERMANY, [3]Technical University of Munich, München, GERMANY.

Aim/Introduction: Lutetium-177 (^{177}Lu) radioligand therapy (RLT) targeting prostate specific-membrane antigen (PSMA) is an effective treatment for metastatic castration-resistant prostate cancer (mCRPC). The use of radionuclides emitting α-particles such as Actinium-225 (^{225}Ac) is under investigation in order to improve the treatment efficacy in patients with a suboptimal outcome. Indeed, large hypoxic regions in the tumor microenvironment can strongly influence the dose distribution. Although microdosimetry is critical for RLT treatment outcome, it is difficult to clinically establish the quantitative relation. Based on mice histology images, we propose a histology-driven in silico model to quantitatively investigate the microdosimetry and its influence on the treatment outcome for PSMA-directed RLT with ^{177}Lu and ^{225}Ac. **Materials and Methods:** Three immunohistochemistry (IHC) for CD31 (vessel endothelium) slices were used to simulate the tumor microenvironment. Ten regions of interest with varying hypoxia severity have been analyzed. The dynamic distribution of ^{177}Lu and ^{225}Ac-PSMA-ligands was simulated by establishing a PBPK-based convection-reaction-diffusion model. A validated PBPK model for RLT studies has been adopted to calculate the arterial input function (AIF).

The amount of radiopharmaceutical was chosen to obtain a mean deposited dose in the prostate tumor model of 10 Gy after 20 days post-injection. A kernel-based method was developed for dose calculation and a dose to tissue histogram (DTH) metric was established to study the dose distribution for each region of the tumor microenvironment (physioxia, physiological hypoxia, pathological hypoxia and radiobiological hypoxia). The probability of cell survival was calculated in relation to the linear-quadratic model. Results: The statistical analysis from all the ROIs shows a higher standard deviation in the dose distributions obtained with ^{225}Ac compared to ^{177}Lu. The more homogenous dose distribution is due to the larger range covered by the β-particles emitted by ^{177}Lu. The DTH metric shows that in poorly vascularized ROIs only the 10% of radiobiological hypoxic tissue receives the target dose using ^{177}Lu-PSMA-ligands treatment. This percentage drops down to 5% using ^{225}Ac. In highly vascularized ROIs the percentage of hypoxic tissue receiving the target dose increases to more than 85% and 65% for the ^{177}Lu and ^{225}Ac-PSMA-ligands respectively. Nevertheless, for the same mean irradiation dose 20 days p.i., the ^{225}Ac-PSMA-ligand has a significantly higher cell-killing potency. **Conclusion:** The proposed hybrid model shows that ^{177}Lu-PSMA-ligands treatment assures a more homogeneously distributed dose and a lower dependency of treatment efficacy on the domain vascularization. Nevertheless, the ^{225}Ac-PSMA-ligands demonstrate higher cytotoxicity even in a hypoxic environment. **References:** none

OP-0050

Time and dose dependent DNA double strand damage induction and repair in peripheral blood mononuclear cells after internal ex vivo irradiation with [^{223}Ra]$RaCl_2$

L. Göring[1], H. Scherthan[2], J. Müller[2], S. Schumann[1], A. K. Buck[1], M. Port[2], M. Lassmann[1], U. Eberlein[1];
[1]Department of Nuclear Medicine, University Hospital Würzburg, Würzburg, GERMANY, [2]Bundeswehr Institute of Radiobiology affiliated to the University of Ulm, Munich, GERMANY.

Aim/Introduction: This study's aim was to investigate the time and dose dependence of DNA double strand damage induction and repair in peripheral blood mononuclear cells (PBMCs) after internal ex vivo irradiation with [^{223}Ra]$RaCl_2$ **Materials and Methods:** 25 blood samples of five healthy volunteers were collected, with one non-irradiated sample of each volunteer serving as baseline reference. The remaining blood samples were incubated for 1h with different [^{223}Ra]$RaCl_2$ activities to achieve nominal absorbed doses to the blood of 3, 25, 50 and 100mGy. Following internal exposure in a rolling test tube at 37°C, the PBMCs were isolated from the radioactive blood samples. To study the time course of DNA repair, the PBMCs of each sample were divided in three subsamples and fixed with ethanol either directly or after culture in RPMI for 4h or 24h. DNA damage tracks along alpha-particle trajectories (alpha-tracks) in PBMCs were revealed by immunofluorescent staining of DNA double-strand break markers γ-H2AX and 53BP1. The alpha-tracks were counted in 500 nuclei per sample manually in a microscope by an experienced operator (HS). Results: The mean absorbed doses to the blood were (2.9±0.0)mGy, (24.5±0.5)mGy, (48.5±0.6) mGy and (98.0±1.8)mGy. Directly after internal [^{223}Ra]$RaCl_2$ irradiation the alpha-track counts (unit: alpha-tracks per 100 cells) were: 0.71±0.28 (3mGy), 3.83±0.97 (25mGy), 7.24±1.87 (50mGy), 14.24±2.44 (100mGy), non-irradiated baseline 0.04±0.08. After 4h and 24h the alpha-track numbers per 100 cells decreased significantly ($p<0.05$) to 1.40±0.49 and 0.32±0.20 (25mGy), 3.95±0.91 and 0.92±0.30 (50mGy), 8.20±1.31 and 1.48±0.43 (100mGy), while the decrease for 3mGy was not significant due to the high uncertainty of the low alpha-track numbers per 500 cells. The counts in the non-irradiated baselines for 4h and 24h were 0.04±0.08 and 0.00. The resulting decay rates of the mean alpha-track reduction, approximated by mono-exponential fits, were (0.25±0.06)h^{-1} at 25mGy, (0.09±0.02)h^{-1} at 50mGy, (0.10±0.01)h^{-1} at 100mGy. Repair kinetics for 50 and 100mGy show similar time dependence in contrast to 25mGy samples. **Conclusion:** Our analysis revealed a significant radiation-induced increase of alpha-track frequency for absorbed doses of 3, 25, 50, 100mGy after internal irradiation with [^{223}Ra]$RaCl_2$ relative to the non-irradiated baseline. The significant decrease of alpha-tracks for 25, 50 and 100mGy after 4h and 24h in culture indicates the repair of most alpha-induced DNA double strand break damage. Further data collection in this ongoing study shall provide for more statistical power to reveal better insights and to differentiate between faithful repair and residual damage after internal high-LET irradiation. **References:** none

OP-0051

DSB repair in peripheral blood mononuclear cells after internal ex vivo irradiation of blood with [^{131}I]NaI in patients before radioiodine therapy

*S. Schumann[1], H. Scherthan[2], K. Pfestroff[3], S. Schoof[2], A. Pfestroff[3], P. Hartrampf[1], N. Hasenauer[1], A. K. Buck[1], M. Luster[3], M. Port[2], M. Lassmann[1], **U. Eberlein**[1];*
[1]Department of Nuclear Medicine, University of Würzburg, Würzburg, GERMANY, [2]Bundeswehr Institute of Radiobiology affiliated to the University of Ulm, Munich, GERMANY, [3]Department of Nuclear Medicine, Philips University Marburg, Marburg, GERMANY.

Aim/Introduction: The aim of the sub-study of the MEDIRAD project was to analyse ex vivo the DNA double strand break (DSB) induction and repair in isolated peripheral blood mononuclear cells (PBMCs) after an internal ex vivo irradiation of whole blood with [^{131}I]NaI with a nominal absorbed dose of 50 mGy. The co-localizing biomarkers γ-H2AX and 53BP1 were used to quantify the induced DSB. **Materials**

and Methods: Blood samples of 33 patients (Würzburg: 20, Marburg: 13) were obtained immediately before radioiodine therapy of differentiated thyroid cancer (DTC). 1 ml of [^{131}I] NaI solution was added to 7 ml of blood and incubated for 1 h. The remaining non-irradiated blood served as baseline sample. To investigate the ex vivo repair, isolated PBMCs were either directly ethanol-fixed, or fixed after 4 h and 24 h short-time culture in RPMI followed by storage at -20°C. An immunofluorescence staining was performed with γ-H2AX and 53BP1 antibodies. An experienced observer (H.S.) performed manual microscopic focus analysis of DSB-indicating co-localizing γ-H2AX and 53BP1 foci in 100 cells per sample. Results: 32 out of 33 blood samples could be analysed. The mean absorbed dose of 32 samples irradiated ex vivo was (50.1±2.3) mGy. For all time points (0 h, 4 h, 24 h), the baseline average number of foci per cell were statistically similar and the average number of radiation-induced foci per cell (RIF) was significantly different ($p<0.05$) compared to baseline and the respective other time points for all time points. The average number of RIF after irradiation was 0.72±0.16 at t =0 h, 0.26±0.09 at t = 4 h, and 0.04±0.09 at t = 24 h. A monoexponential fit of the mean values at the three time points provided a decay rate of (0.25±0.05) h^{-1}, which is in good agreement with data obtained from studies with external irradiation. **Conclusion:** Our study is the first to investigate ex vivo DNA damage repair in internally irradiated isolated PBMCs of patients before radionuclide therapy. Our findings with 50 mGy absorbed dose to the blood show, in a large patient sample, that internal irradiation with [^{131}I] NaI induces efficient DSB repair and that the repair rate triggered by internal beta and gamma irradiation of PBMCs is comparable to the repair rate observed after external irradiation with gamma- or x-rays. The MEDIRAD project has received funding from the Euratom research and training programme 2014-2018 under grant agreement No 75552. **References:** none

210

Wednesday, October 20 - Saturday, October 23, 2021

on-demand pool, release on Wednesday, October 20 at 09:00

Clinical Oncology Track - TROP Session: Head and Neck / Colorectal

OP-0053

Do we know what we're looking at? Increasing our understanding of ^{18}F-FDG distribution in oncology by direct coregistration of histopathology and autoradiography in malignancies of the head and neck

J. Debacker[1,2,3], D. Creytens[4,5], Y. D'Asseler[5,6], K. De Man[6], B. Descamps[7,8], V. Keereman[8,9], S. Libbrecht[4], V. Schelfhout[5,6], K. Van de Vijver[4,5], C. Vanhove[7,8], W. Huvenne[1,2];

[1]Department of Head and Skin, Ghent University, Ghent, BELGIUM, [2]Department of Head and Neck Surgery, Ghent University Hospital, Ghent, BELGIUM, [3]Department of Nuclear Medicine, University Hospital Brussels, Brussels, BELGIUM, [4]Department of Pathology, Ghent University Hospital, Ghent, BELGIUM, [5]Department of Diagnostic Sciences, Ghent University, Ghent, BELGIUM, [6]Department of Medical Imaging, Nuclear Medicine, Ghent University Hospital, Ghent, BELGIUM, [7]INFINITY Lab, Ghent University, Ghent, BELGIUM, [8]Department of Electronics and Information Systems, Ghent University, Ghent, BELGIUM, [9]XEOS Medical, Ghent, BELGIUM.

Aim/Introduction: Over the last decades, the use of ^{18}F-FDG has taken a pivotal role in oncological diagnosis, staging and follow-up. While endless research has shown the clinical importance of ^{18}F-FDG, we remain unaware how ^{18}F-FDG behaves in and around human malignancies on a submillimetric scale. Unfortunately, as glucose metabolism is an active process, pathological assessment of relevant protein markers was found to be inadequate in correctly predicting ^{18}F-FDG-uptake. Technological improvements are resulting in increasing spatial resolution for PET-scanners, therefore an urgent understanding of ^{18}F-FDG-distribution on these higher resolutions is required. **Materials and Methods:** In the current study, we developed a methodology that enabled direct coregistration of the radioactivity-distribution in a surgically resected specimen with histopathological assessment. Patients were injected with 4 MBq/kg of ^{18}F-FDG prior to the initiation of standard of care surgical oncological resection. After resection of the malignancy, the surgical specimen was imaged using preclinical micro-PET and -CT devices with a spatial resolution of 800µm and 50µm, respectively. After imaging, the specimen was freshly sliced into thin slices of approximately 2mm by a pathologist. One slice was snap-frozen and frozen sections were imaged using an autoradiographic film overnight. Following the imaging, frozen sections were stained with standard hematoxylin and eosin staining. Pathological results were overlayed with the

results of ^{18}F-FDG PET/CT and autoradiography to coregister the histopathological and imaging results. Results: We performed this methodology on a total of four patients with cutaneous squamous cell carcinoma (n=2), angiosarcoma (n=1) and thyroid medullary carcinoma (n=1). While the mean time between injection and autoradiography was 3h49, we were able to image sufficient radioactivity to directly coregister the results with the clinical pathological frozen sections. All regions with identified malignant tissue displayed increased ^{18}F-FDG-uptake. However, uptake was not limited to these regions, as a similar increased uptake was identified in adjacent benign sebaceous glands. Interestingly, we also identified a heterogeneous ^{18}F-FDG-uptake in separate clusters of malignant tissue, which could partly be explained by the cluster's amount of peritumoral inflammatory cells. **Conclusion:** To the best of our knowledge, these results are the first to describe direct coregistration of ^{18}F-FDG with the gold standard of histopathology in any human malignancy. These heterogeneous results display an important diversity in metabolic activity between different tumor and peritumoral tissues. The use of this methodology could increase our understanding of radiotracer distribution in human diseases on a previously unprecedented scale in clinical nuclear medicine. **References:** none

OP-0054

Correlation of FAPI-PET and contrast enhanced T1w / T2w MRI in 12 adenoid cystic carcinomas

D. Liew[1], M. Röhrich[1], L. Loi[2], S. Adeberg[1], M. Syed[1], U. Haberkorn[1], D. Paech[2];
[1]University Hospital, Heidelberg, GERMANY, [2]German Cancer Research Centre, Heidelberg, GERMANY.

Aim/Introduction: Fibroblast Activation Protein (FAP) is a new target for Positron emission tomography and computed tomography (PET/CT) imaging of epithelial tumours embedded in a fibrous stroma. Adenoid cystic carcinomas (ACC) showed elevated FAP-specific tracer uptake in a pilot study [1] and display intertumoral heterogeneity on contrast enhanced (ce) T1w and T2w MRI scans [2]. In this study, we correlated FAP-specific signaling with T1w and T2w MRI signals to further characterize the significance of FAP uptake in ACCs. **Materials and Methods:** Clinical PET/CT scans of 12 ACC patients were performed at 10, 60 and 180 minutes post i.v. administration of ^{68}Ga-labelled-FAP-specific tracer molecules. PET- and corresponding MRI-scans were co-registered and 3D volumetric segmentations were performed on ce T1w and T2w lesions of co-registered MRI slides. Signal intensity values of FAP-specific PET signalling and ce T1w/T2w MRI scans were analysed for their pixel-wise correlation in each patient. Pooled estimates of the correlation coefficients were calculated using the Fisher z-transformation. Results: FAP-specific PET signals showed a slight positive correlation with ce T1w values (pooled correlation 0.114, 0.147, 0.162 at 10, 60 and 180 minutes) and a slight negative correlation with T2w values (pooled correlation -0.149, -0.121, -0.225 at 10, 60 and 180 minutes). Individual r-values at 60 minutes ranged from -0.080 to 0.434 in ce T1w and from -0.466 to 0.637 in T2w. **Conclusion:** There are only slight correlations between the intensity of FAP-specific signals and tumour appearance in ce T1w or T2w MRI scans, which underlines that FAP-specific signalling is not only a surrogate marker of MRI sequences, but an independent signal. Due to the heterogeneity of the patient population (treatment naïve, post-treatment and recurrent ACC), as well as probable differences in histological subtypes, further investigation with a larger, stratified sample is needed. **References:** [1] Kratochwil C, Flechsig P, Lindner T, et al. 68Ga-FAPI PET/CT: Tracer Uptake in 28 Different Kinds of Cancer. J Nucl Med. 2019;60(6):801-805. doi:10.2967/jnumed.119.227967 [2] Li Y, Hao D, Song X, Zhang C. Computed tomography and magnetic resonance imaging of adenoid cystic carcinoma in the maxillary sinus: a retrospective study with radiologic-histopathologic correlations. Oral Surg Oral Med Oral Pathol Oral Radiol. 2021;131(1):111-121. doi:10.1016/j.oooo.2020.06.019

OP-0055

Non-invasive Grading of Oropharyngeal Squamous Carcinomas with FDG PET/CT Textural Parameters

M. Novikov;
LISOD Hospital, Pliuty village, Obuhovskiy district, UKRAINE.

Aim/Introduction: FDG PET/CT is frequently performed for routine staging purposes in patients with head and neck carcinomas. Metabolic images contain data beyond qualitative or semantic features utilized to detect malignant disease. Heterogeneity of FDG distribution assessed by textural analysis may provide insights into connection of biologic or morphologic tumor features with imaging features. In current study we aim to calculate metabolic textural parameters of FDG PET/CT images and investigate their ability to predict tumor differentiation grade, as one of the prognostic factors for squamous oropharyngeal carcinomas. **Materials and Methods:** We retrospectively analyzed data from pretreatment FDG PET/CT scans of 64 patients (median age 62.4 years, 65.7% males, 34.3% females) with histologically proven squamous oropharyngeal carcinomas, 20 (31.2%) patients with low-grade tumors, 23 (35.9%) with moderately differentiated tumors and 21 (32.9%) with high-grade carcinomas. All PET/CT exams were performed in concordance with EANM guidelines for FDG imaging of solid tumors [1]. Metabolic volumes of primary tumors were identified with semiautomatic technique utilizing 3D active contour segmentation (ITK SNAP) [2]. Consequently, textural features were extracted from resulting volumes with LIFEx software, and six indices (homogeneity and entropy from GLCM, short and long run emphasis from GLRLM, low and high gray-level zone emphasis from GLZLM), from different

matrices were selected for further analysis, to test an ability to non-invasively discriminate tumor grade. Statistical analysis of extracted data was performed with SPSS Statistics 21.0 software (IBM, NY, USA). Results: Non of the parameters were able to distinguish low-grade tumors. When separating moderately differentiated tumors and high-grade tumors, high gray-level zone emphasis from GLZLM was the relatively most successful parameter. It demonstrated AUC of 0.684 for discrimination of moderately differentiated tumors with threshold of ≤372.7 (sensitivity 97.1%, specificity 38.1), and AUC of 0.717 for discrimination of high-grade tumors with threshold of >386.7 (sensitivity 42.3%, specificity 96.2%). **Conclusion:** Textural parameters from metabolic PET/CT images of squamous oropharyngeal carcinomas showed moderate accuracy in non-invasive differentiation of tumor grade: none of the indices were able to reliably discriminate low-grade tumors, but showed overall increase of FDG uptake heterogeneity, moderately-differentiated and high-grade tumors. **References:** 1. Boellaard R, Delgado-Bolton R, Oyen WJG et al (2014) FDG PET/CT: EANM procedure guidelines for tumour imaging: version 2.0. Eur J Nucl Med Mol Imaging 42:328-354. doi: 10.1007/s00259-014-2961-x 2. Yushkevich PA, Piven J, Hazlett HC et al (2006) User-guided 3D active contour segmentation of anatomical structures: Significantly improved efficiency and reliability. NeuroImage 31:1116-1128. doi: 10.1016/j.neuroimage.2006.01.015

OP-0056

Pretreatment metabolic and molecular profiling of locally advanced head and neck cancer

H. Minn[1,2], A. Silvoniemi[3], L. Nissi[1], J. Hirvonen[4], M. Seppänen[5], J. Laine[6];

[1]University of Turku, Turku, FINLAND, [2]Department of Oncology, Turku University Hospital, Turku, FINLAND, [3]Department of Otorhinolaryngology - Head and Neck Surgery. Turku University Hospital and University of Turku, Turku, FINLAND, [4]Department of Radiology. Turku University Hospital and University of Turku, Turku, FINLAND, [5]Department of Clinical Physiology, Nuclear Medicine and Turku PET Centre.University of Turku, Turku, FINLAND, [6]Department of Pathology. Turku University Hospital and University of Turku, Turku, FINLAND.

Aim/Introduction: We aimed to study the relationship between mutational landscape and molecular imaging findings in patients with head and neck squamous cell carcinoma (HNSCC). **Materials and Methods:** Fourteen patients (median age 67 years, male/female-ratio 11/3) with diagnosis of HNSCC underwent FDG PET/CT, multiparametric MRI and liquid biopsy before onset of chemoradiotherapy (CRT) and/or surgery. All patients signed informed consent form approved by local Ethical Board. Biopsy-confirmed primary tumour location was supraglottic larynx in 1, oropharynx in 9, and hypopharynx in 4 patients, respectively. Ten patients presented with lymph node metastases in neck. Metabolic tumour volume (MTV) and total lesion glycolysis (TLG) were calculated from PET/CT and apparent diffusion coefficient (ADC) from diffusion-weighted (DWI) MRI and compared with tumour mutational burden (TMB), number of tumour-based DNA changes in primary tumour and simultaneously obtained cell-free liquid biopsy. p16 was used as a surrogate biomarker for human papilloma virus (HPV) infection. Results: Median primary tumour maximum diameter was 40 (range, 20-80) mm, ADC 1173 (range, 840-2021), MTV 12 (range, 3-72) cm^3, and TLG 153 (range, 17-615). Median MTV for both primary and metastatic lymph nodes (MTV total) was 20 (range, 10-79) cm^3, and TLG total 268 (range, 45-660). Five patients had p16 +ve HNSCC and 10 had mutation(s) in tumour suppression protein p53. Ten patients showed cell-free tumour DNA in their liquid biopsy. ADC, MTV, and TLG (both primary and total) were comparable between p16/p53+ve and p16/p53-ve patients. A borderline significance was found for correlation between TMB and MTV total (p=0.1429) and TLG total (p=0.1561). Similarly an inverse relationship between ADC and MTV total was found (p=0.146). We expect the statistical power of these findings to improve while we hope to finish enrollment in this ongoing study to our predetermined target of 30 patients within the next 3 months. **Conclusion:** Metabolic activity as determined by MTV/TLG and DWI may reflect mutational landscape in HNSCC. Molecular imaging combined to gene expression profiling may thus help predict HNSCC recurrence or metastatic potential and assist in planning of novel therapeutic approaches such as modulation of tumour and host immune activity. **References:** None.

OP-0057

Monitoring the Response of Radiation Therapy in Head and Neck Squamous Cell Carcinoma (HNSCC) Patients with "Full Digital" ^{18}F-FDG-PET/CT

M. Mihaylova[1], E. Piperkova[1], L. Chavdarova[1], K. Nikolova[1], S. Petrov[1], I. Mihaylova[2];

[1]University Specialized Hospital for Active Treatment in Oncology, Clinic of Nuclear Medicine, Sofia, BULGARIA, [2]University Specialized Hospital for Active Treatment in Oncology, Department of Radiation Therapy, Sofia, BULGARIA.

Aim/Introduction: ^{18}F-FDG PET/CT imaging plays an increasing role in radio-chemo therapy (RCT/RT) planning and response evaluation in patients with squamous cell carcinoma (HNSCC). The aim of our prospective study was to assess the new generation ultra-high resolution (UHR) "full digital" PET/CT input for the RCT/RT response evaluation and to precise the time-point for patients' follow-up. **Materials and Methods:** The study included 94 PET/CT studies in 83 RCT/RT-treated patients with HNSCC (70 male and 13 female, mean age 63y), for a 10 months period since the initiation

of last generation UHR "full-digital" PET/CT-scanner. 43 pts underwent definitive RCT (total dose of 70-72 Gy) for the site of the primary tumor and regional lymph nodes and in 40 - RT followed the surgery. RCT/RT response was evaluated with PET/CT qualitative interpretation and quantitative indices: standardized uptake value (SUVmax), tumor lesion glycolysis (TLG) and metabolic tumor volume (MTV), classified as PET negative (-) - complete response (CR), PET unclear (+/-) - partial response (PR) and PET positive with non-response (NR) to RCT/RT. Results: All 83 patients received at least one (PET-1) scan 3 months after RCT/RT. In 44 PET-1 scan was evaluated as negative (-) with CR to RCT/RT, in 10 - PET-1 (+/-) with PR and in 29 - PET-1 was positive with avid tumor and significantly high SUVmax and TLG value (Score 4-5). PET-2 was done in all 10 pts with PET-1 (+/-). In 5 of them (5/10) PET-2 turned negative with CR and other 5 remained unclear (+/-) with residual increased 18F-FDG uptake areas in the tumor bed and secondary irradiated surrounding soft tissue inflammation and inflammatory lymph nodes. Only one PET-2 positive patient received a third PET-3, evaluated as negative with late CR. The most common site of involvement was oral cavity (28pts), followed by larynx (26pts), nasal cavity and paranasal sinuses (15pts), hypopharynx (8pts) and tonsils (6pts). PET1-3 resulted in 50 patients with CR (44 after PET-1, 5 after PET-2 and 1 on PET-3), 4 - with PR and 29 - with NR directed to further treatment. **Conclusion:** ^{18}FDG - PET/CT is a promising hybrid imaging modality for RCT/RT response assessment in HNSCC patients, able to identify smaller viable residual tumor and characterize secondary irradiated surrounding soft tissue inflammation and inflammatory lymph nodes. Additional data and further investigations will be needed to precise the right time-point of individual RT-response assessment with UHR "full digital" PET/CT. **References:** None

OP-0058

Molecular Imaging parameters with 18F-FDG PET/CT comparison with MRI in the evaluation of recurrence of nasopharyngeal cancer a Mexican population

S. Medina-Ornelas[1], K. Luna-Ortiz[1], J. Lopez-Gomez[2], J. Altamirano-Garcia[1], J. Alegria-Baños[1], O. Martinez-Juarez[3]; [1]Instituto Nacional de Cancerologia, Mexico City, MEXICO, [2]Hospital Angeles Pedregal, Mexico City, MEXICO, [3]Hospital Angeles Lindavista, Mexico City, MEXICO.

Aim/Introduction: Determine the value of ^{18}F-FDG PET/CT compared to MRI using the variables standardized uptake values (SUV), total lesion glycolysis (TLG), and molecular tumor volume (MTV) in the assessment of recurrence. **Materials and Methods:** 33 patients were studied. The gold standard was histopathology or clinical/ imaging follow-up. ^{18}F-FDG PET/CT and MRI results were classified as true positive (TP), true negative (TN), false positive (FP) or false negative (FN). The McNemar chi-square test was used to evaluate the efficacy of each imaging method and compare the percentage of the false imaging findings between the two imaging modalities. ^{18}F-FDG-PET/CT, the correlation between 18F-FDG-uptake parameters (SUVmax, MTV, TLG) were analyzed by a simple regression analysis Results: Based on the reference standard, 23 patients were positive and 10 patients were negative for tumor recurrence The median follow-up time was 23.4 months (range 6.9-36.7 months). Overall sensitivity, specificity, positive predicted value (PPV), and negative predicted value (NPV) of 18F-FDG PET/CT, before using the cut-off points of the SUVmax, MTV, and TLG variables obtained using the ROC curve, were 86%, 63%, 82% y 70%, respectively. While for MRI were 90%, 90%, 95% y 80%, respectively. The cut-off values with statistical p values were SUVmax =12.5 (p =0.048), MTV =55 cm^3 (p =0.0039) and TLG =310 g (p =0.0209) were significantly effective in differentiating recurrence. After using these cutoff points, there was a significant improvement in the recurrence detection rate, obtaining a sensitivity, specificity, PPV and NPV de 100%, 90%, 95% y 100%, respectively **Conclusion:** A higher TLG may be a more accurate predictor of recurrence than MTV or SUVmax; with better diagnostic accuracy compared with MRI, we also determined that application of a cut-off of molecular imaging parameters SUVmax, MTV, and TLG maybe it can help in the interpretation of the images and be more concluding. **References:**

OP-0059

Disease free and Progression free survivals in metabolic responders and non-responder on follow up FDG PET/CT after chemoradiation in nasopharynx cancer patients

***N. Fatima[1]**, M. U. Zaman[1], S. Zaman[2], A. Zaman[3], U. U. Zaman[4]; [1]Aga Khan University, Karachi, PAKISTAN, [2]Dow Medical College, Dow University of Health Sciences (DUHS), Karachi, PAKISTAN, [3]Dr Ruth Pfau (CHK), Karachi, PAKISTAN, [4]Sunny Downstate Medical Center, NY, New York, NY, UNITED STATES OF AMERICA.*

Aim/Introduction: To determine disease free survival (DFS) and progression free survival (PFS) in patients with nasopharyngeal cancer (NPC) having achieved complete and partial metabolic response on post-chemoradiation (CRT) FDG PET/CT using standardized imaging and reporting protocols. **Materials and Methods:** This retrospective study was conducted at PET/CT Section of a JCIA accredited healthcare facility of Pakistan and accrued 46 NPC patients who had baseline and post-CRT FDG PET/CT from April-2016 till April-2019 and followed-up till April-2021. Based on complete metabolic response (CMR) on post-CRT FDG PET/CT, 29 patients were categorized as responders and 17 were labeled as non-responder based on partial metabolic response (PMR) respectively. Both groups were followed for a median period of 14 months (range = 4 - 60 months). Kaplan Meier's survival curves were analyzed to measure DFS in responders and PFS in non-responders respectively. Results: On follow-up, mean DFS in responders was 41.14 ± 6.87 month and recurrence was found in 06 (21%) patients. Baseline SUVmax >7.4 of primary tumor, body mass index

>24.609 and female gender were found significant predictors of recurrence in responder group using receiver operating characteristics curve analysis (p <0.05). In non-responders group, the mean PFS was 4.17 ± 1.37 months. Higher primary tumor SUVmax and more stage IV disease on baseline FDG PET/CT were found significant predictors of shorter PFS in non-responders on multiple regression analysis (p <0.05). **Conclusion:** Female gender, higher BMI and primary tumor SUVmax (>7.4) on baseline FDG PET/CT predict shorter DFS in patients who achieved complete metabolic response after CRT. In patients with partial metabolic response on post-CRT FDG PET/CT, higher primary tumor SUVmax and stage IV disease on baseline FDG PET/CT were found significant predictors of shorter PFS. **References:** -

OP-0060

Comparison of ^{68}Ga-FAPI-04 and ^{18}F-FDG PET/CT for the Diagnosis of Lesions in Patients with Colorectal Cancer

***X. Lin**, H. Zhu, W. Zhao, Y. Zhang, A. Wu, Z. Yang, X. Wang;*
Peking University Cancer Hospital & Institute, Beijing, CHINA.

Aim/Introduction: Colorectal cancer is a common gastrointestinal cancer with higher mortality and morbidity, and its treatment decision-making relies on accurate clinical staging. The conventional fluorine 18 (^{18}F) fluorodeoxyglucose (FDG) PET/CT has some limitations. Targeting fibroblast-activation protein (FAP) overexpressed in colorectal cancer with a prominent stroma including cancer-associated fibroblasts (CAFs), is a novel tracer, gallium 68 (^{68}Ga)-labeled fibroblast-activation protein inhibitors (FAPIs). The aim of this study is to assess the diagnostic performance of ^{68}Ga-FAPI PET/CT in primary and metastatic lesions of colorectal cancer by comparing with that of ^{18}F-FDG PET/CT. **Materials and Methods:** The images of all enrolled patients sequentially received ^{18}F-FDG and ^{68}Ga-FAPI-04 PET/CT examinations between December 2019 through May 2020 were retrospectively analyzed. The uptake and diagnostic performance were compared respectively using the Wilcoxon signed-rank and McNemar test between the two techniques. Results: Of all 37 patients enrolled, 18 newly diagnosed patients were examined by PET/CT for tumor staging and the others for tumor restaging or efficacy assessment. Compare to ^{18}F-FDG PET/CT, ^{68}Ga-FAPI-04 PET/CT led to upstaging of the clinical TNM stages in 4 patients (22%). In primary lesions of colorectal cancer, the uptake of ^{68}Ga-FAPI-04 were not significant different (median, 13.1 VS 12.7, p = 0.384) and detection rates were both 100% (18 of 18). In lymph node metastases, the uptake of ^{68}Ga-FAPI-04 in abdominal and pelvic lymph nodes was both higher than that of ^{18}F-FDG (median, 3.5 VS 6.6, p = 0.000; median, 1.85 VS 3.95, p = 0.000), and the sensitivity of ^{68}Ga-FAPI-04 PET/CT was superior to that of ^{18}F-FDG PET/CT (80% VS 43%, p = 0.01). However, the specificity of ^{68}Ga-FAPI-04 PET/CT was not higher than that of 18F-FDG PET/CT (75% vs 85%, p = 0.695). In peritoneal metastases, the SUVmax value of ^{68}Ga-FAPI-04 PET/CT was higher than that of ^{18}F-FDG PET/CT (3.7 VS 2.6, p = 0.016). In liver Metastases, the target-to-background ratio (TBR) of 68Ga-FAPI was significantly higher than that of ^{18}F-FDG PET/CT (p = 0.012). All of the 8 positive liver lesions detected by ^{68}Ga-FAPI-04 PET/CT were confirmed to be metastases (operation or biopsy), only 5 of them were detected by ^{18}F-FDG PET/CT (62.5%, 5 of 8). **Conclusion:** As a novel tracer for PET/CT scan, ^{68}Ga-FAPI-04 PET/CT presented its advantages in detection of lymph node and distant metastases by comparing to that of ^{18}F-FDG PET/CT. The clinical value of ^{68}Ga-FAPI-04 PET/CT should be further investigated. **References:** none

OP-0061

Combined ^{18}F-FDG PET/CT-based metabolically active tumor volume and dissemination parameter improve outcome prediction in metastatic colorectal cancer

***E. Woff**, G. Critchi, T. Guiot, L. Ameye, A. Hendlisz, P. Flamen;*
Institut Jules Bordet, Brussels, BELGIUM.

Aim/Introduction: Stratification of metastatic colorectal cancer (mCRC) patients is mostly based on clinical and biological characteristics. Baseline whole-body metabolically active tumor volume (WB-MATV) reflecting the active tumor load and measured by ^{18}F-FDG PET/CT, has recently been demonstrated to be a strong prognostic biomarker in mCRC (1). The dissemination parameter (Dmax), reflecting the tumor load dissemination and also measured by ^{18}F-FDG PET/CT, has recently been shown to predict outcome in high grade lymphoma (2). The aim of this study is to evaluate the added prognostic value of this new parameter on WB-MATV in large exploratory and validation cohorts of mCRC patients. **Materials and Methods:** Three prospective multicenter studies and one monocenter study enrolled mCRC patients in first and last-line treatment settings. Baseline WB-MATV was defined as the sum of metabolically active volumes of all target lesions identified on the baseline ^{18}F-FDG PET/CT according to the PERCIST methodology. Distance between target lesions was measured and the largest distance between two lesions (Dmax) was calculated for each patient. Optimal Dmax cutoff for survival prediction was determined in the development set by the Contal and O'Quigley method. Kaplan-Meier analyses of overall survival (OS) were performed. Results: Baseline WB-MATV and Dmax were evaluable in 201/239 (1^{rst} development set), 94/125 (2nd development set) and 44/47 (validation set) patients. Among the patients with a high WB-MATV (≥100 cm^3), Dmax was significantly associated with OS (hazard ratio (HR) of Dmax ≥ vs < 32.5 cm: 1.47 (1.01-2.16), P < 0.05 in the 1^{rst} development set; 3.48 (1.76-6.90), P < 0.001 in the 2nd development set; and 4.38 (1.85-10.36), P < 0.001 in the validation set). By contrast, Dmax was not significantly associated with OS among the patients with a low WB-MATV (<100 cm3). **Conclusion:** This

study demonstrates that both baseline WB-MATV and Dmax independently predict OS in mCRC, regardless of treatment received. Among the mCRC patients with high WB-MATV, Dmax further improves risk stratification by the identification of a high-risk group of early death. **References:** 1. Woff E, Hendlisz A, Ameye L, et al. Validation of Metabolically Active Tumor Volume and Total Lesion Glycolysis as ^{18}F-FDG PET/CT-derived Prognostic Biomarkers in Chemorefractory Metastatic Colorectal Cancer. J Nucl Med. 2019;60:178-184.2. Cottereau A-S, Nioche C, Dirand A-S, et al. ^{18}F-FDG PET Dissemination Features in Diffuse Large B-Cell Lymphoma Are Predictive of Outcome. J Nucl Med. 2020;61:40-45.

OP-0062

Preliminary evaluation of ^{64}Cu-ATSM as a tracer of predictive assessment of neoadjuvant treatment response in locally advanced rectal cancer

M. Colombié[1], L. Ferrer[1,2], M. Lacombe[3], V. Fleury[1], M. Le Thiec[1], A. Morel[1], B. Maucherat[1], D. Rusu[1], N. Varmenot[1,4], P. Tremolieres[3], N. Allam[1], E. Rio[1], V. Guimas[1], I. Masson[1], H. Senellart[1], S. Hiret[1], P. Salaun[5,6], L. Campion[1], A. Vidal[4], F. Haddad[4,7], A. Rauscher[1], F. Kraeber-Bodéré[8,2], M. Bourgeois[8,2,4], C. Rousseau[1,2];
[1]ICO René Gauducheau, Saint-Herblain, FRANCE, [2]Université de Nantes, CNRS, Inserm, CRCINA, Nantes, FRANCE, [3]ICO Paul Papin, Angers, FRANCE, [4]Arronax, Saint-Herblain, FRANCE, [5]University Hospital, Brest, FRANCE, [6]EA GETBO 3878, University Western Brittany, Brest, FRANCE, [7]SUBATECH, IMT Atlantique, CNRS/IN2P3, Université de Nantes, Nantes, FRANCE, [8]University Hospital, Nantes, FRANCE.

Aim/Introduction: In locally advanced rectal cancers, neoadjuvant treatment is a standard. Recent studies highlight the ability of ^{64}Cu-ATSM to illustrate redox status at the tumor scale, a factor of aggressiveness, invasion, pejorative prognosis. Our hypothesis is to use ^{64}Cu-ATSM PET/CT to evaluate redox status in primary tumor to predict tumor regression and neoadjuvant therapy efficacy. The aim is as well to evaluate the application of semi-quantitative analysis of PET/CT to identify features predictive of response to neoadjuvant treatment. **Materials and Methods:** Seventy patients with a newly diagnosed rectal carcinoma will be include in a prospective multicenter study. Before neoadjuvant treatment ^{18}FDG and ^{64}Cu-ATSM PET/CT scans are performed. ^{64}Cu-ATSM acquisitions are performed 1h and 24h after injection of 3MBq/kg from the liver to the pelvis. After surgery, histological data are collected to obtain residual tumor grading and IHC oxidative stress marks. Standard and advanced quantitative imaging features are extracted using slicer3D [1] as delineating and visualizing tool. Rectal tumor and gluteal muscle VOIs are respectively delineated by a threshold varying on patient basis and manually. In this work, we focused our analysis on tumor/muscle ratio (T/M), percentage of injected activity per tumor mass and tumor volume as descriptors. Results: So far, 9/70 patients were enrolled (3 women, 6 men; mean age 66.1). No adverse events occurred. 7/9 patients were N+. Median CEA pre-treatment was 3 µg/L (range 0.9 - 28.7). ^{64}Cu-ATSM visual assessment showed a primary tumor good uptake with a visual pattern heterogeneity in inter-patients. The late ^{64}Cu-ATSM acquisitions showed a visual increase of digestive uptake. On quantitative analysis, median ^{18}FDG T/M was 11.39 [7.7-21.8]. For all patients, ^{64}Cu-ATSM T/M increased between 1h and 24h after injection. Median 1h and 24h ^{64}Cu-ATSM T/M were 2.95 [2.3-5.1] and 6.3 [4.4-11.9] respectively. Regarding 1h and 24h ^{64}Cu-ATSM examinations, median % activity/g were 30.9 [21.5 - 36/7] and 15.7 [8.6-26.4] respectively. Median MTV was 34.4 cm3 [13.4-49.9]. Five patients had already surgery results showing a residual tumor after neoadjuvant therapy for all of them with 2/5 patients pN+. **Conclusion:** These preliminary analyses in locally advanced rectal cancers suggest that ^{64}Cu-ATSM might have the potential to individualize tumor characteristics with different uptake patterns. Benefit of late acquisition could be discuss due to digestive elimination of this tracer. The study is ongoing and supplementary data will be presented at the congress. **References:** [1] Fedorov A et al. Magn Reson Imaging. 2012;Nov;30(9):1323-41

OP-0063

Predictive value of ^{18}FDG-PET / CT tumor SUVmax value in terms of overall survival after neoadjuvant therapy in rectal cancer

F. Demir, G. G. Avcı;
Tokat Gaziosmanpasa University, Tokat, TURKEY.

Aim/Introduction: ^{18}FDG-PET / CT is particularly useful in staging colorectal cancers and determining occult metastatic disease and causes substantial changes in the treatment plan in patients. Also, it has been shown that ^{18}FDG-PET / CT contributes significantly to other diagnostic methods in determining the response to treatment after neoadjuvant CRT. Aim of this study was to investigate whether tumor SUVmax value in ^{18}FDG-PET / CT after neoadjuvant treatment is a predictor of overall survival in rectal cancer. **Materials and Methods:** Sixty-four rectal cancer patients who underwent ^{18}FDG-PET / CT imaging to evaluate staging and neoadjuvant CRT response were included in the study. In ^{18}FDG-PET / CT axial images, the volume-of-interest (VOI) was drawn semi-automatically including the tumor tissue in the rectum area, and the pre-treatment SUVmax1 and post-treatment SUVmax2 values were calculated. To determine the predictive value of ^{18}FDG-PET / CT SUVmax parameters in terms of the death, the area under the curve (AUC), and cut-off values were calculated using Receiver Operator Characteristic ROC analysis. Kaplan Meier analysis was used to evaluate the effect of cut of SUVmax value on overall survival. Results: 25 (39%) were female and 39 (61%) were male of the 64 patients included in the study. The average age was 65.67 ± 9.27. The median follow-up period was 37.5 months

(3-69). During the follow-up period, death was observed in 25 (39%) patients, while 39 (61%) patients were alive. 52 (81%) of the patients were operated on. All of the patients received neoadjuvant radiotherapy and 59 (91%) of them had received chemotherapy concurrently. When the ^{18}FDG-PET / CT parameters of the rectum tumor are examined; The mean SUVmax1 was 20.1 ± 9.5, and SUVmax2 7.6 ± 4.8. When we investigated the predictive value of ^{18}FDG-PET / CT parameters before and after treatment in terms of death; the SUVmax2 value was a significant predictive parameter. When the cut-off value for SUVmax2 value was taken as 8.6, the sensitivity and specificity were 70% (p = 0.037). In addition, when the cut-off value of 8.6 was used for the SUVmax2 value, there was a significant difference in terms of overall survival (p = 0.006). While the median survival was 66 months in those with Suvmax2 value below 8.6, it was 46 months in those above 8.6. **Conclusion:** ^{18}FDG-PET / CT tumor SUVmax value after neoadjuvant therapy has a significant predictive value in terms of overall survival in rectal cancer.

OP-0064

Postradiation pelvic fractures on FDG PET - types, incidence and lack of recognition

P. Bochev, G. Mateva, N. Novoselska;
Acibadem Cityclinic UMBAL Mladost hospital, Sofia, BULGARIA.

Aim/Introduction: To asses the incidence, types, specific imaging features and degree of recognition of postradition pelvic /sacral fractures. **Materials and Methods:** Screening: Patient database of Acibadem Citiclinic Mladost, Sofia was retrospectively reviewed for the period 01/2020 to 04/2021 for patients that underwent previous external beam radio(chemo)therapy of the pelvic region. Inclusion criteria: Reported or suspected sacral/pelvic fractures on FDG PET CT scans or reported "postradiation changes", "mixed or sclerotic changes". Validation of the reports was based on the presence of obvious fracture lines; presence of clear sclerotic consolidation lines; linear FDG PET activity within sacrum and pelvic ring, concomitant with fracture lines or consecutive linear sclerotic transformation at the site of activity or confirmed by other imaging . Exclusion criteria: Bone metastases of any location, brachytherapy alone, major pelvic trauma. Positive findings were further classified based on Dennis zones for sacral fractures as well as anterior and posterior arch involvement. Reports were assessed for conclusive declaration of pelvic fracture or lack of such. Results: A total of 294 patients were screened, distributed by diagnosis as follows: 68 endometrial cancer, 151 cervical, 57 rectal, 11 bladder cancer, 7 vaginal cancers. 20 patients met the inclusion criteria. The total incidence of recognized postradiation insufficiency fractures was 4,46%, being the lowest in endometrial cancer (2,9%) and highest in rectal cancer (12,3%). 19/20 patients had posterior arc sacral fractures, 18/19 being in Denis I zone. One patient had a consecutive iliac bone fracture after having a sacral fracture and one patients - complex pelvic fracture. Six patients had anterior arc fractures but only in one it was isolated. 11/20 patients were reported as having insufficiency fractures. The rest were either not recognized or described inconclusively, which led to further imaging. **Conclusion:** Postradiation pelvic fractures are, in fact, a common complication after radiotherapy (especially in rectal cancer) with posterior arc/sacrum being the most common fracture point. They remain unrecognized or misinterpreted on routine FDG PET CT in almost half of the cases, which leads to further unnecessary imaging. **References:** none

211

Wednesday, October 20 - Saturday, October 23, 2021

on-demand pool, release on Wednesday, October 20 at 09:00

Featured Session: Quantification in MPI - A Must!

OP-0066

Quantification in MPI - Let's do it?

H. Verberne; Academic Medical Center, Department of Nuclear Medicine, Amsterdam, NETHERLANDS.

OP-0067

Left Ventricular Hypertrophy in CZT SPECT Imaging: comparison with Cardiac Magnetic Resonance

E. Cerudelli[1,2], M. Gazzilli[1], L. Camoni[1], F. Dondi[1], A. Mazzoletti[1], P. Bellini[1], D. Albano[1,2], R. Giubbini[1,2];
[1]Azienda Socio Sanitaria Territoriale degli Spedali Civili di Brescia, Brescia, ITALY, [2]Università degli Studi di Brescia, Brescia, ITALY.

Aim/Introduction: It is widely known the increasing importance of the identification of left ventricular hypertrophy (LVH) due to its correlation with occurrence of myocardial infarction and cardiac death. The goal of the study is to validate the diagnostic accuracy of Cadmium-Zinc-Telluride (CZT) myocardial perfusion imaging (MPI) in correctly quantifying LV mass (LVM) and unmasking the presence of LVH, using cardiac magnetic resonance (CMR) as reference. **Materials and Methods:** Seventy-one patients (mean age 64±10; 79% male) underwent 99mTc-tetrofosmin stress/rest CZT MPI and 1,5T CMR within maximum 120 days (50±37 days). Only rest images were selected for LVM determination. Corridor 4DM (4DM) and Emory Cardiac Toolbox (ECTb) were used for MPI analyses. LVM MPI data were compared to those obtained with CMR, considered as gold standard. The presence of LVH in MPI was defined based on validated CMR cut-offs (>74 g/m^2 in men and >63 g/m^2 in women). Results: Mean LVM values obtained were respectively 156 g ± 39 by CMR, 164 g ± 42 by 4DM (p=NS vs CMR) and 155 g ± 37,6 by ECTb (p=NS vs CMR).

The correlation between LVM estimated with CZT SPECT and CMR was good, but better with 4DM than ECTb (R = 0,85, p<0,001 for 4DM vs. 0,78, p<0,001 for ECTb). On Bland-Altman plots the limits of agreement relative to CMR LVM were quite narrow (-21,5 to +12,6 % for 4DM and -20,1 to +22,3% for ECTb). Applying CMR standardized cut-offs and using CMR as reference, between 55 subjects classified as hypertrophic by 4DM, 52 were similarly categorized as pathologic by CMR but no false negative case was registered. On the contrary, using ECTb 48 patients were classified as hypertrophic, of which 45 were equally categorized as pathological by CMR, but 7 patients were wrongly defined as not hypertrophic by the MPI software. These findings result in the same specificity for the two MPI software packages (84,2%), but 4DM showed a higher sensitivity and accuracy than ECTb (100 vs. 86,5% for sensitivity; 95,8 vs. 85,9% for accuracy). **Conclusion:** Our results suggest the high accuracy of CZT SPECT, especially using 4DM software, in the evaluation of LV mass and in identification of LVH, opening new opportunities for new applications of MPI in clinical routine. **References:** Okwuosa TM, Hampole CV, Ali J et al. Left ventricular mass from gated SPECT myocardial perfusion imaging: comparison with cardiac computed tomography, J Nucl Cardiol 2009;16:775-83

OP-0068

Prognostic value of myocardial perfusion imaging using cardio-dedicated CZT-camera

T. Mannarino[1], A. D'Antonio[1], R. Bologna[1], E. Criscuolo[1], P. Buongiorno[1], E. Caiazzo[1], R. Assante[1], E. Zampella[1], V. Gaudieri[1], R. Green[1], V. Cantoni[1], M. Petretta[2], W. Acampa[1], A. Cuocolo[1];
[1]Department of Advanced Biomedical Sciences, University of Naples Federico II, Naples, ITALY, [2]IRCCS SDN, Diagnostic Imaging, Naples, ITALY.

Aim/Introduction: Myocardial perfusion imaging (MPI) using novel cardio-dedicated camera with cadmium-zinc-telluride (CZT) detectors has an important role in diagnosis and risk-stratification of patients with suspected or known coronary artery disease (CAD). Aim of our study was to evaluate the prognostic value of CZT-MPI in a large cohort of patients with suspected or known CAD using a low-dose CZT protocol. **Materials and Methods:** We evaluated 2063 patients (1429 men, 634 women, mean age 64±11 years) with suspected or known CAD. All patients underwent single-day stress/rest CZT-MPI after the injection of 185 MBq and 555 MBq of ^{99m}Tc-sestamibi, respectively. Summed stress score (SSS), summed difference score (SDS), left ventricle (LV) post-stress volumes and ejection fraction were automatically calculated using a commercially available software. Patients were categorized into three groups according to SDS values (no ischemia: SDS=0, mild ischemia: SDS <7, severe ischemia: SDS ≥7). The outcome end points were cardiac death, myocardial infarction or unstable angina requiring late (6 months) coronary revascularization. Results: During a mean follow-up of 26±9 months, 79 events occurred (3.8% cumulative event rate). Patients with events showed higher prevalence of male gender, diabetes (both p<0.05) and known CAD (p<0.001) as compared to patients without. SSS was significantly higher in patients with events as compared to those without (7.7±9.4 vs. 3.7±7.0), as well as SDS (4.4±4.5 vs. 2.3±2.7), LV post-stress end-diastolic and end-systolic volumes (115±65 mL vs. 91±42 mL and 65±56 mL vs. 43.9±35.2 mL) (all p<0.001). Moreover, patients with events had reduced post-stress LV ejection fraction as compared to patients without events (49±14% vs. 56±13%, p<0.001). At univariable Cox regression analysis, male gender, diabetes, known CAD, SSS, SDS, LV post-stress end-diastolic and end-systolic volumes and LV ejection fraction were significant predictors of event (all p<0.001). At multivariable analysis, only SDS resulted as independent predictor of events (p<0.001). Kaplan-Meier survival curves showed that patients with severe ischemia had lower event-free survival compared to patients with no ischemia or mild ischemia (log-rank p<0.001). **Conclusion:** Low-dose MPI obtained by CZT camera is a powerful tool in risk stratification of patients with suspected or known CAD. In particular, patients with no ischemia and those with mild ischemia showed similar event- free survival. Differently, severe ischemia was associated with a high risk of major adverse cardiac events at a mid-term follow-up. **References:** None.

OP-0069

Dynamic SPECT myocardial perfusion imaging in coronary disease ; correlation with angiographic findings

J. Pinaquy, E. Riahi, F. Debordeaux, H. Douard, T. Couffinhal, P. Coste, L. Bordenave;
University Hospital of Bordeaux, Bordeaux, FRANCE.

Aim/Introduction: To assess the association between stress (sMBF), rest (rMBF) myocardial blood flow, coronary reserve (CFR) and lesions objectified by coronary angiography.The secondary objectives were to assess the performance of the visual analysis and to determine the thresholds for the best performing flows. **Materials and Methods:** 64 patients who underwent dynamic myocardial perfusion imaging on a CZT camera and coronary angiography within 4 months without an intercurrent event were included. The sMBF, rMBF and MFR were measured (Corridor 4DM). Visual analysis was considered positive in the presence of ischemia of more than one segment. Coronary angiography involvement was considered positive if there was a stenosis greater than 70% or if the FFR was <0.8. Necrotic territories in scintigraphy were excluded. Results: 147 territories could be analyzed. 31 presented with a significant abnormality on coronary angiography. The visual scintigraphy analysis by territory has a sensitivity of 67% and a specificity of 97%. The best quantitative parameter was sMBF. The area under the ROC curve is 0.9. For a threshold of 1.75 ml · g-1 · min-1, the

sensitivity and specificity were 84% and 90%, respectively. **Conclusion:** The sMBF measured on CZT gamma cameras can be used to determine coronary artery status by territory and significantly increases the specificity of the examination without altering its specificity. The presence of an underlying necrosis is however an obstacle to the analysis of the territory concerned. **References:** None

OP-0070

Coronary Vascular Function Assessed by Low Dose Dynamic CZT-SPECT MPI in Patients with Diabetes Mellitus

A. D'Antonio[1], T. Mannarino[1], E. Criscuolo[1], R. Bologna[1], P. Buongiorno[1], R. Assante[1], E. Zampella[1], V. Gaudieri[1], C. Nappi[1], R. Green[1], V. Cantoni[1], M. Petretta[2], W. Acampa[1], A. Cuocolo[1];
[1]Department of Advanced Biomedical Sciences, University of Naples "Federico II", Naples, ITALY, [2]IRCCS SDN, Diagnostic Imaging, Naples, ITALY.

Aim/Introduction: Diabetes mellitus (DM) is a major risk factor for cardiovascular disease, related to both obstructive coronary artery disease (CAD) and coronary vascular dysfunction. It is also well known that diabetic patients present a reduced myocardial perfusion reserve (MPR). The recent introduction of cadmium-zinc-telluride (CZT) single-photon emission computed tomography (SPECT) may allow the quantification of myocardial blood flow (MBF) and MPR in addition to standard myocardial perfusion imaging (MPI) and functional parameters. The aim of the study was to assess coronary vascular function by dynamic CZT-SPECT in diabetic and non-diabetic patients with suspected or known CAD. **Materials and Methods:** We evaluated 230 consecutive patients (147 non-diabetic and 83 diabetic patients) with suspected or known CAD, referred to MPI for clinical evaluation. All patients underwent dynamic rest/stress CZT-SPECT after the injection of 185 MBq and 555 MBq of ^{99m}Tc-sestamibi, respectively. Standard rest and stress perfusion images were acquired at the end of each dynamic scan. Summed stress score (SSS) >3 was considered as abnormal. Perfusion defects were also quantitated as % of LV myocardium and expressed as total perfusion defect (TPD). MBF was computed from the dynamic rest and stress imaging. MPR was defined as the ratio of hyperemic to baseline MBF and it was considered reduced when <2.1. Results: Diabetic patients were older and had a higher prevalence of hypertension compared to non-diabetic patients (both p<0.05). All the other clinical characteristics and imaging findings were comparable between the two groups. No significant difference was found in the prevalence of abnormal MPI in diabetic and non-diabetic patients (p=0.22). In particular, SSS (5.7±8.8 vs. 3.9±7.3, p=0.10) and TPD (8.5±13.1% vs. 5.5 ± 10.3%, p=0.06) were comparable between the two groups. However, diabetic patients showed lower values of MPR compared to non-diabetic patients (2.13±0.5 vs. 2.38 ± 0.6, p<0.01). MPR was reduced in 45 (54%) diabetic patients and in 54 (24%) non-diabetic patients (p<0.01). At multivariable logistic regression analysis, male gender and diabetes were associated with reduced MPR (both p<0.01). **Conclusion:** Diabetic patients with suspected or known CAD have a higher prevalence of reduced MPR compared to non-diabetic patients. Measurement of MBF and MPR by low dose dynamic CZT-SPECT represents a powerful tool in evaluation of coronary vascular function. The assessment of MPR by dynamic CZT-SPECT could provide incremental risk stratification beyond clinical and perfusion variables in patients with diabetes. **References:** None

OP-0071

Exercise Ischemia is an Efficient Predictor of Significant Coronary Artery Disease in Routine Reports of a Large-Scale Clinical Cohort using Very Low-Dose Myocardial Perfusion SPECT

M. B. Chawki[1], T. Gonçalves[1], C. Boursier[1], M. Bordonné[1], A. Verger[2], L. Imbert[2], M. Perrin[1], M. Claudin[1], V. Roch[1], K. Djaballah[3], B. Popovic[4], E. Camenzind[4], P. Marie[5];
[1]Université de Lorraine, CHRU-Nancy, Department of Nuclear Medicine and Nancyclotep Imaging Platform, Nancy, FRANCE, [2]Université de Lorraine, CHRU-Nancy, Department of Nuclear Medicine and Nancyclotep Imaging Platform, INSERM U1254, IADI, Nancy, FRANCE, [3]Université de Lorraine, CHRU-Nancy, Department of Cardiology, Nancy, FRANCE, [4]Université de Lorraine, CHRU-Nancy, Department of Cardiology, INSERM, UMR-1116 DCAC, Nancy, FRANCE, [5]Université de Lorraine, CHRU-Nancy, Department of Nuclear Medicine and Nancyclotep Imaging Platform, INSERM, UMR-1116 DCAC, Nancy, FRANCE.

Aim/Introduction: This study assesses results from large-scale and real-life routine interpretations by multiple observers of very low-dose exercise-myocardial perfusion SPECT imaging (MPI) and the correlation of MPI ischemia with subsequent routine reports of coronary stenosis by angiography. **Materials and Methods:** Data from 13,126 routine exercise-MPI reports, from 11,952 patients (31% women), using very low doses of Sestamibi and a high-sensitivity cardiac CZT-camera, were extracted to assess the reporting of significant MPI-ischemia (≥ 10% of the left ventricle), to determine the normalcy rate for MPI in a group with < 5% pretest likelihood of coronary artery disease (CAD) (n=378), and to assess the ability of MPI to predict a > 50% coronary stenosis in patients with available coronary angiography reports within the next three months of MPI (n=713). Results: The median of patients' effective dose was 2.51 [interquartile range: 1.00-4.71], the normalcy rate was 97%, and the overall rate of reporting MPI-ischemia was 12%. The MPI-ischemia rate was independently related to a previous CAD history, the male gender, obesity, and a < 50% resting LV ejection fraction, ranging from 31% with all these risk factors represented, to 2% when there were no risk factors. A > 50% coronary stenosis was reported in 58% of the angiography group and it was significantly predicted by MPI-ischemia, although this prediction was less significant for mild (odd-ratio [95% confidence interval]: 1.61 [1.11-2.32]) than for moderate-to-severe MPI-ischemia (3.91 [2.24-6.84]) and was also impacted by other independent

risk factors, notably a history of CAD (2.31 [1.56-3.44]), a sub-maximal exercise test (1.61 [1.11-2.34]) and age ≥ 65 years (1.41 [1.00-1.97]). The rates of the subsequent reporting of a > 50% coronary stenosis ranged from 48% for mild MPI-ischemia with no additional risk factor, to 88%, for moderate-to-severe MPI-ischemia combined with all other risk factors. **Conclusion:** Exercise ischemia is an efficient predictor of significant CAD in routine reports of a large-scale clinical cohort and using a very low-dose MPI protocol, although this prediction is significantly enhanced by other variables. This weakly irradiating investigation could likely be repeated at shorter time intervals, especially in targeted patient groups with high risk of ischemia. **References:** none

OP-0072

Prognostic value of heart rate reserve in patients with suspected coronary artery disease undergoing stress myocardial perfusion imaging

F. Reina[1], C. Nappi[1], M. Petretta[2], R. Assante[1], E. Zampella[1], V. Gaudieri[1], V. Cantoni[1], R. Green[1], L. Piscopo[1], F. Volpe[1], C. Mainolfi[1], E. Nicolai[2], W. Acampa[1], A. Cuocolo[1];
[1]Department of Advanced Biomedical Sciences, University Federico II, Naples, ITALY, [2]IRCCS-SDN, Naples, ITALY.

Aim/Introduction: The prognostic value of myocardial perfusion single-photon emission computed tomography (MPS) has been demonstrated. Also, chronotropic incompetence, evaluated by heart rate reserve (HRR), is associated with increased risk of adverse events. Yet, the incremental prognostic value of HRR over stress MPS data has not been fully investigated. We assessed the prognostic value of HRR in patients with suspected coronary artery disease (CAD) undergoing stress MPS. **Materials and Methods:** We studied 866 patients with suspected CAD undergoing exercise-stress MPS between May 2002 and January 2014 as part of their diagnostic program. The primary study endpoint was all-cause mortality. All patients were followed for ≥60 months. HRR was calculated as the difference between peak exercise and resting HR, divided by the difference of age-predicted maximal and resting HR and expressed as percent. Patients with a summed difference score (SDS) ≥5% were considered to have an ischemic response. The occurrence of all-cause of deaths was noted and considered as event. Follow-up was censored at 84 months. Results: During follow-up, 61 deaths occurred (7% cumulative event rate). Patients experiencing death were older, with higher prevalence of male gender and diabetes, lower HRR and higher prevalence of ischemia. The best trade-off between sensitivity and specificity for identifying chronotropic incompetence was a HRR <67% with an area under the receiver operating characteristic curve of 0.62. Event free survival was lower in patients with HRR <67% compared to those with HRR ≥67%. Event-free survival analysis was also performed categorizing the patients in four groups according to HHR and SDS cut-offs (group 1: HRR ≥67% and SDS <5%; group 2: HRR <67% and SDS<5%; group 3: HRR ≥67% and SDS ≥5%; group 4: HRR <67% and SDS ≥5%). There was a trend in survival function across the four categories (chi-square 29.6, P<0.0001), the worst outcome being detectable in patients of group 4. Accordingly, the annualized event rate was 0.006 in patients with HRR <67% and 0.014 in those with HRR ≥67% (P<0.001). Univariable predictors of events were age, gender, diabetes, HRR and ischemia, while age, gender, HRR and ischemia were independent predictors of all-cause mortality. HRR improved the prognostic power of a model including clinical data and MPS findings for predicting all-cause mortality, increasing the global chi-square from 76 to 82 (P<0.005). **Conclusion:** Chronotropic incompetence has independent and incremental prognostic value in predicting all cause of death in patients with suspected CAD undergoing exercise-stress MPS. **References:** None

OP-0073

Negative Determinant Value of Myocardial Perfusion Scintigraphy on Solid State Gamma Cameras

N. Talay, E. Sahin Kutuk, T. Bahceci, E. Ozdemir;
Ankara City Hospital Nuclear Medicine Department, Ankara, TURKEY.

Aim/Introduction: Myocardial Perfusion Scintigraphy (MPS) is a non-invasive imaging method that has been widely used for many years in the diagnosis of coronary artery disease (CAD). High resolution images can be obtained in a shorter time with lower doses of radiopharmaceuticals with Cadmium-Zinc-Telluride (CZT) cameras specific to cardiac imaging, which have been used in recent years. We aimed to determine the negative predictive value for CAD of MPS monitored by solid state cardiac cameras within normal limits. **Materials and Methods:** The records of 6432 patients who were referred to our clinic with suspected CAD were retrospectively elaborated. These patients underwent MPS imaging using the Cardiac Spect NM 530 GE device were retrospectively evaluated and 1554 patients who were reported in normal limits were detected. 4 patients with non-cardiac death during follow-up were excluded from the study (2 cases Covid-19 infection, 2 cases malignancy). The clinical follow-up of 1550 patients (mean age: 59, female/male:943/607) were in the study with an average of 17.94 ± 3.7 (12-24) months time period. During the follow-up, the rates of death, myocardial infarction or revascularization (PTCA and/or CABG) events were evaluated in line with the MACE criteria (major adverse cardiac event). Results: The CAD risk factors of the patients are summarized in Table 1. Treadmill stress (n: 1246) was applied in 80% of the patients. Pharmacological stress with adenosine (n: 304) was applied in 20% of the patients. During the follow-up, coronary angiography (n: 41) was performed in 3% of the patients and it was found that 0.3% received PTCA (n: 4), 0.1% CABG

(n: 2) and 24% (n: 371) was suitable for medical treatment. (Table 2).). 1 of the patients who underwent CABG was later dead as a result of postoperative mediastinitis complications (0.1%). It was observed that all patients with a major cardiac event previously had a known CAD. The negative predictive value of MPS was calculated as 99.6% with follow-up data. **Conclusion:** Negative predictive value (NPV) of MPS for CAD with conventional gamma cameras has been reported in the literature at values varying between 82-97%. In our study, very high NPV of 99.6% was detected for CAD with solid state cardiac cameras. With this finding, we recommend using cardiac solid state gamma cameras and MPS as the initial test in order to identify low-risk patients for CAD and to prevent unnecessary additional examination and invasive procedures. **References:** none

OP-0074

Added value of Myocardial Flow Reserve measurement in cardiac SPECT for coronary artery disease screening

M. Bailly[1], F. Thibault[1], G. Metrard[1], M. Courtehoux[2], D. Angoulvant[2], M. Ribeiro[2];
[1]CHR Orléans, Orleans, FRANCE, [2]CHRU Tours, Tours, FRANCE.

Aim/Introduction: Myocardial blood flow (MBF) and flow reserve (MFR) measurement have been shown to improve diagnostic performances of coronary artery disease (CAD) in cardiac PET. Dedicated CZT cardiac cameras provide accurate evaluation of MBF and MFR during dynamic Myocardial Perfusion Imaging (MPI) in SPECT, but its correlation with patient's risk of CAD remains to be investigated. In this study, we evaluated the results of SPECT MFR measurement in patients referred for CAD screening. **Materials and Methods:** 137 patients (61 male, 76 female) referred for CAD screening MPI between November 2018 and March 2020 were included in a prospective trial (CFR-OR). 10 years risk of cardiovascular death according to the European Society of Cardiology (SCORE) was calculated. SPECT data were acquired on a CZT-cardiac camera using a stress/rest one-day Tc-99m-tetrofosmin protocol. Low dose thoracic CT was used for coronary calcium score (CCS) evaluation. Invasive Coronary Angiography (ICA) was performed upon decision of the referring cardiologist. Results: Mean SCORE was 4 ± 3.1 %. Mean global MFR was 2.50 ± 0.74. There was a significant inverse correlation between MFR and SCORE (p=0.006), gender (p=0.019), and number of cardiovascular risk factors (p=0.01). MFR was significantly reduced in patients with CCS above 1 (p=0.01). 23 patients underwent ICA. 18 showed coronary plaques qualifying for high-risk patients; among them, 16 patients had impaired MFR (the 2 other patients had moderate stenosis, <50%, with negative FFR), whereas only 4 had abnormal visual MPI. Based on global MFR, and with a threshold of 2, sensitivity and specificity were respectively 83.3% and 100%, and Area Under Curve (AUC) was 0.94. **Conclusion:** Global MFR measured during MPI SPECT for CAD screening may contribute to high-risk patient identification. It significantly enhances SPECT diagnostic performances and could help physician decision to perform ICA. **References:** None

OP-0075

Prone Myocardial Perfusion SPECT Imaging in attenuation artefacts may obviate the need for a Rest Study: Our Experience

C. Fragkaki, A. T. Archontaki;
Chania General Hospital "St. George", Chania, GREECE.

Aim/Introduction: In myocardial perfusion SPECT studies, inferior wall artefact caused by diaphragmatic attenuation and anterior wall artefact, due usually to breast attenuation, is a common finding.[1,2,3] Our aim was to assess the value of prone imaging in both attenuation artefacts and to evaluate how often a subsequent rest study was avoided in our Nuclear Medicine department.[4,5] **Materials and Methods:** In a two-year period, a total of 1678 patients underwent myocardial perfusion imaging with a dual-detector SPECT γ-camera, with either ^{99m}Tc-MIBI or ^{99m}Tc-Tetrofosmin. From those, 874 studies with both supine and prone acquisitions were reviewed. Prone imaging acquisition was performed when there was what seemed to be reduced perfusion in the anterior wall (181), in the inferior wall (482) or both (211). Rest imaging acquisition was not performed when stress prone images showed normal myocardial perfusion. Results: From 874 prone studies, improvement was shown in 180/392 anterior wall defects (45.9%) and in 427/693 inferior wall defects (61.6%) proving attenuation artefacts. From those, 71/211 patients showed improvement in both defects (33.6%) simultaneously. Rest imaging acquisition was safely omitted in 399/874 patients (45.6%) with normal prone stress studies, avoiding patient's unnecessary radiation exposure. **Conclusion:** We concluded that prone imaging helps diagnose soft tissue attenuation artefacts not only to inferior wall defects but to anterior wall defects, known as "breast attenuation artefact" as well. With prone imaging, patients can often avoid unnecessary radiation exposure since rest myocardial perfusion studies with ^{99m}Tc agents, need a second radiopharmaceutical injection. **References:** 1.Taasan V et al. Comparative accuracy of supine-only and combined supine-prone myocardial perfusion imaging in men. J Nucl Cardiol. 2016 Dec;23(6):1470-1476. 2.Arsanjani R et al. Two-position supine/prone myocardial perfusion SPECT (MPS) imaging improves visual inter-observer correlation and agreement. J Nucl Cardiol. 2014 Aug;21(4):703-11. 3.Stathaki M et al. The Benefits of Prone SPECT Myocardial Perfusion Imaging in Reducing Both Artifact Defects and Patient Radiation Exposure. Arq Bras Cardiol. 2015 Oct;105(4):345-52. 4.Cantoni V et al. A. Prone-only SPECT myocardial perfusion imaging: An alternative standard in clinical practice?. J. Nucl. Cardiol. (2020). 5.Ceylan Gunay E et al. Prone imaging

allows efficient radiopharmaceutical usage by obviating the necessity of a rest study in Tc-99m-methoxyisobutylisonitrile myocardial perfusion scintigraphy. Nucl Med Commun. 2011 Apr;32(4):284-8.

OP-0076

Correlation between myocardial flow, coronary reserve and Framingham and ESC-SCORE cardiovascular risk scores

J. Pinaquy, P. Ferenczi, F. Debordeaux, H. Douard, Y. Pucheu, T. Couffinhal, L. Bordenave;
University Hospital of Bordeaux, Bordeaux, FRANCE.

Aim/Introduction: To find an association between the level of cardiovascular risk and myocardial stress flows (sMBF), resting (rMBF) and myocardial flow reserves (MFR) in a population of patients having undergone a myocardial evaluation by CZT gamma camera. **Materials and Methods:** Retrospective analysis including 75 non-coronary patients randomly selected from all the patients referred to the Bordeaux University Hospital (Haut Lévêque hospital) from December 2018 to June 2020 for a myocardial scintigraphy with quantitative analysis of flows and reserves.The inclusion criteria were the negativity of the scintigraphy in visual analysis, clinical data attesting to the absence of anterior myocardial heart disease and complete and reconciled data from the examination concerning their cardiovascular risk factors. For each patient were calculated two cardiovascular risk scores. The Framingham score, with adaptation to European and French populations, and the European cardio vascular risk score (ESC-SCORE). The values used to classify the level of risk were: for Framingham 2008, <10% for a low risk,> 10% for an intermediate to high risk. For ESC-SCORE, <5% for low risk,> 5% for intermediate to high risk. Results: No linear correlation was found between the cardiovascular risk values according to Framigham or ESC-SCORE and the sMBf, rMBF or MFR.sMBF were significantly lower in patients with intermediate and high cardiovascular risk according to Framingham (> 10%) compared with low risk patients (mean values of 1.89ml.min-1.g-1 versus 2.32 ml.min-1 .g-1 respectively (p =0.028)). The MFR was not significantly different.Significantly lower values of sMBF are also found in patients with high risk compared with low risk patients according to ESC-SCORE (> 10%) (mean values of 1.73 ml.min-1.g-1 versus 2.17 ml.min-1 .g-1 respectively (p = 0.005)). The MFR was also not significantly different. **Conclusion:** This study confirmed that sMBFs measured with CZT is correlated with risk factor scores and should be of cardiovascular events in non-coronary patients.No differences were found for MFR. **References:** None

301

Wednesday, October 20, 2021, 12:00 - 13:30

Channel 1

CME 2: AI in Radiomics

OP-0079

Challenges in Multi-Center Trials Using Radiomics Models - The Role of AI Based Harmonisation

V. Jaouen; Institut Mines Telecom Atlantique, Plouzane, FRANCE.

OP-0080

AI and Radiomics for Oncology Applications

M. Sollini; Humanitas University, Nuclear Medicine Division, Milan, ITALY.

OP-0081

Potential Role of AI and Radiomics in Cardiac Imaging

C. Rischpler; Hospital/Institute, Department of Nuclear Medicine, University Hospital Essen, Essen, GERMANY.

OP-0082

What May AI and Radiomics Bring in Neuroimaging?

R. Buchert; University Medical Center Hamburg-Eppendorf, Department of Nuclear Medicine, Hamburg, GERMANY.

302-1

Wednesday, October 20, 2021, 12:00 - 12:45

Channel 2

Interview with the Expert 3 - Nuclear Endocrinology

OP-0084

Interview - Nuclear Endocrinology

G. Treglia; Ente Ospedaliero Cantonale, Nuclear Medicine and PET/CT Center, Bellinzona, SWITZERLAND.

OP-0085

Interview - Nuclear Endocrinology

L. Giovanella; Imaging Institute of Southern Switzerland, Clinic for Nuclear Medicine, Bellinzona, SWITZERLAND.

302-2

Wednesday, October 20, 2021, 12:45 - 13:30

Channel 2

Interview with the Expert 4 - Neuroimaging

OP-0086
Interview - Neuroimaging

A. Lammertsma; *Amsterdam University Medical Centers, Department of Nuclear Medicine and PET Research, Amsterdam, NETHERLANDS.*

OP-0087
Interview - Neuroimaging

E. van de Giessen; *Academic University Medical Centers, Dept. of Nuclear Medicine, Amsterdam, NETHERLANDS.*

304

Wednesday, October 20 - Saturday, October 23, 2021

on-demand pool, release on Wednesday, October 20 at 09:00

CTE 2: Managing the Paediatric Patient in Nuclear Medicine Departments

OP-0088
Paediatric Patient Care - Technologist's Practice Improvement

A. Santos; *Hospital CUF Descobertas, Medicina Nuclear Department, Lisbon, PORTUGAL.*

OP-0089
Paediatric Patient Care - Clinician's Perspective

Z. Bar-Sever; *Schneider Children's Hospital, Department of Nuclear Medicine, Petach Tikva, ISRAEL.*

OP-0090
Paediatric Patient Care - Communication Improvement

A. Grilo; *Escola Superior de Tecnologia da Saúde, Instituto Politécnico de Lisboa, Lisbon, PORTUGAL.*

305

Wednesday, October 20 - Saturday, October 23, 2021

on-demand pool, release on Wednesday, October 20 at 09:00

Joint Symposium 3 (EANM/EACVI): MPI after the ISCHEMIA Trial - Still Alive?

OP-0092
The ISCHEMIA Trial - Design and Results

R. Liga; *Universita di Pisa, Cardiac-Thoracic-Vascular Department, Pisa, ITALY.*

OP-0093
Role of Anatomical Imaging after the ISCHEMIA Trial

M. R. Dweck; *University of Edinburgh, Department of Cardiology, Edinburgh, UNITED KINGDOM.*

OP-0094
Role of Functional Imaging after the ISCHEMIA Trial

A. Saraste; *Turku University Hospital, Heart Center, Turku, FINLAND.*

OP-0095
The ISCHEMIA Trial - Clear Answers, Open Questions

E. Reyes-Torres; *St Thomas' Hospital, The PET Imaging Centre, London, UNITED KINGDOM.*

306

Wednesday, October 20 - Saturday, October 23, 2021

on-demand pool, release on Wednesday, October 20 at 09:00

Joint Symposium 4 (EANM/CIRSE): Biokinetics and Dosimetry in Intraarterial Therapy

OP-0097
Radio-Embolization and HCC – Where Are We in the Guidelines and Why?

A. Denys; *CHUV centre hospitalier universitaire vaudois, Radiodiagnostic et radiologie interventionnelle, Lausanne, SWITZERLAND.*

OP-0098
Dosimetry and Radio-Embolization - Dose Specific Issues and New Solutions

N. Schaeffer; *Centre Hospitalier Universitaire Vaudois (CHUV), Department of Nuclear Medicine and Molecular Imaging, Lausanne, SWITZERLAND.*

OP-0099

Dose-Effect Guided 90Y Microspheres Treatment Planning

L. Strigari; University of Bologna, Medical Physics department, Bologna, ITALY.

OP-0100

Yttrium-90 Radioembolization as a Possible New Treatment for Brain Cancer

A. Pasciak; The Johns Hopkins University School of Medicine, Baltimore, UNITED STATES OF AMERICA.

307

Wednesday, October 20 - Saturday, October 23, 2021

on-demand pool, release on Wednesday, October 20 at 09:00

Pitfalls & Artefacts 2: Pseudoprogression and Pseudoresponse in Brain Tumours

OP-0102

Neurooncologist - The Neurooncologist's Perspective

M. Glas; University of Essen, Department of Clinical Neuro-oncology at the Essen University Hospital, Essen, GERMANY.

OP-0103

Neuroradiologist - An MRI Overview

P. C. M. Sundgren; Lund University, Department of Diagnostic Radiology, Lund, SWEDEN.

OP-0104

Nuclear Medicine Physician - ...And What About PET?

I. Law; Copenhagen University Hospital, Dep. of Clinical Physiology, Copenhagen, DENMARK.

308

Wednesday, October 20 - Saturday, October 23, 2021

on-demand pool, release on Wednesday, October 20 at 09:00

"M2M Track - TROP Session: It's the Alpha, not the Beta"

OP-0106

Preclinical study of Targeted Alpha Therapy using ^{211}At-labeled phenylalaline derivative in a syngeneic Multiple Myeloma model

J. Gaschet[1], R. Echeynne[1], N. Chouin[2], S. Gazzola[1], F. Guérard[1], S. Gouard[1], S. Marionnaud-Lambot[3], A. Maubert[1], C. Alliot[1,4], P. O. Hofgaard[5], B. Bogen[5], E. Yan[6], F. Haddad[4,7], F. Kraeber-Bodéré[8], M. Wheatcroft[6], J. Gestin[1], M. Chérel[9,4];
[1]Université de Nantes, CNRS, INSERM, CRCINA, Nantes, FRANCE, [2]Université de Nantes, CNRS, INSERM, CRCINA, Oniris, Nantes, FRANCE, [3]Université de Nantes, CNRS, INSERM, CRCINA, CHU of Nantes, Nantes, FRANCE, [4]GIP Arronax, Saint-Herblain, FRANCE, [5]Department of Immunology, Centre for Immune Regulation, Institute of Clinical Medicine, University of Oslo, Oslo, NORWAY, [6]Telix Pharmaceuticals Ltd, Melbourne, AUSTRALIA, [7]Université de Nantes, IMT Atlantique, CNRS, Subatech, Nantes, FRANCE, [8]Université de Nantes, CNRS, INSERM, CRCINA, CHU of Nantes, ICO Gauducheau, Nantes, FRANCE, [9]Université de Nantes, CNRS, INSERM, CRCINA, ICO Gauducheau, Nantes, FRANCE.

Aim/Introduction: Multiple myeloma (MM) is a malignant gammopathy characterized by an uncontrolled proliferation of monoclonal plasma cells within the bone marrow. New therapeutic regimens including combination of drugs have significantly improved the overall survival rate for patients in the past decade. However, MM remains an incurable disease, notably because of treatment resistance. L-type amino acid transporter-1 (LAT1) mediates the influx of neutral amino acids into the cells and the overexpression of this transporter correlates with malignancy in MM. LAT1 is also the target of the standard MM treatment melphalan. Given the high radiation sensitivity of plasma cells and the short path length of alpha particles, potentially allowing minimal bone marrow toxicity, ^{211}At-labeled phenylalanine derivative (^{211}At-APA) appeared a promising candidate for molecular targeting in MM and was assessed in a preclinical model of MM. **Materials and Methods:** The first part of the study aimed at evaluating in vitro uptake of radiolabeled-phenylalanine derivative in different MM cell lines and establishing dose-response curve to ^{211}At-APA. Then dose escalation, biodistribution and dosimetry studies were done as preamble to efficacy evaluation. Finally anti-tumor activity of ^{211}At-APA in vivo following i.v. injection was assessed in an orthotopic syngeneic MM mouse model. Results: In vitro studies showed excellent cell uptake of radiolabeled-phenylalanine derivative and radiosensitivity to ^{211}At-APA as well as stability of the radiopharmaceutical.

Maximum tolerated activity was defined at 4MBq ^{211}At-APA by a dose escalation study. No major durable toxicity was observed, however biodistribution and dosimetry studies underlined that the limiting organ with ^{211}At-APA treatment in that preclinical model would be the stomach. Efficacy study demonstrated a significant improvement in animal survival with a median survival of 43 days for treatment at 4MBq ^{211}At-APA versus 26 days in control group (p=0.0005). **Conclusion:** This study provides the first proof-of-concept of the efficacy of ^{211}At-labeled phenylalanine derivative in MM. **References:** none

OP-0107

FGFR3 Targeted Alpha Therapeutic [^{225}Ac]-FPI-1966 induces regression in preclinical bladder xenograft model

Y. Storozhuk, N. Grinshtein, N. Robinson, D. Rodriguez, I. Duffy, R. Simms, E. Burak, J. Valliant;
Fusion Pharmaceuticals, Hamiton, ON, CANADA.

Aim/Introduction: Fibroblast growth factor receptor 3 (FGFR3) is a receptor tyrosine kinase that regulates cell proliferation, survival, and migration. FGFR3 is frequently dysregulated and overexpressed in multiple solid tumors, specifically in bladder and head and neck cancers. Targeted alpha therapeutics (TATs) represent an ideal strategy to exploit FGFR3 as a therapeutic target due inherent potency of TAT approach. Herewith we describe the preclinical biodistribution and efficacy of FGFR3-targeted therapeutic, [^{225}Ac]-FPI-1966, in a preclinical bladder xenograft model. **Materials and Methods:** Phage-derived human FGFR3-targeted monoclonal antibody vofatamab was conjugated using a bifunctional chelate and radiolabeled with lutetium-177 or actinium-225: [^{177}Lu]-FPI-1965 was used to evaluate tissue biodistribution and [^{225}Ac]-FPI-1966 to determine therapeutic efficacy. For biodistribution studies, Balb/c nude mice with established RT112 bladder xenografts were injected intravenously with [^{177}Lu]-FPI-1965 (0.1 mg/kg) in the presence of 10 mg/kg cold vofatamab, followed by dissection of selected organs at different time points for 4-168 hours and radioactivity measurements using the gamma counter. For efficacy studies, single doses of [^{225}Ac]-FPI-1966 (92.5-740 kBq/kg) or weekly/bi-weekly fractionated doses (4 x 92.5, 4 x 185, or 2 x 370 kBq/kg) were co-administered with 10 mg/kg cold vofatamab to RT112-bearing animals. Tumor growth was monitored for 54 days and study endpoints included tumor volume measurement and/or impact on animal health status. Results: The biodistribution profile of [^{177}Lu]-FPI-1965 when co-dosed with 10 mg/kg of cold vofatamab was characterized by sustained blood concentrations (31.06 ± 0.13 %ID/g at 4h and 7.56 ± 1.99 % at 168h), minimal tissue uptake (below 10 %ID/g) and high tumour uptake peaking at 168 hours (46.67 ± 19.67 %ID/g). To evaluate the radiotherapeutic efficacy of [^{225}Ac]-FPI-1966 in RT112 bladder xenograft model, a head-to-head comparison study was undertaken with single doses as compared to multiple doses. Tumor regression was detected in mice treated with a single dose of [^{225}Ac]-FPI-1966 (either 370 or 740 kBq/kg). In addition to that, four weekly doses of 185 kBq/kg were sufficient to induce complete RT112 regression in all the mice. Two bi-weekly doses of 370 kBq/kg were similarly effective as a single dose of 370 kBq/kg but led to a more durable regression. **Conclusion:** Favorable biodistribution profile of [^{177}Lu]-FPI-1965 was observed when co-dosed with 10 mg/kg cold vofatamab, resulting in prolonged blood concentrations, minimal normal tissue uptake and high tumor uptake. Therapeutic efficacy was obtained with both single and multiple doses of [^{225}Ac]-FPI-1966 in a preclinical bladder xenograft model. **References:** none

OP-0108

Synergy of ^{224}Ra-labeled microparticles and chemotherapy in a murine ovarian cancer model

R. Wouters[1,2], S. Westrøm[2], I. Vergote[3,4], T. B. Bønsdorff[2], A. Coosemans[1];
[1]Laboratory of Tumor Immunology and Immunotherapy, Department of Oncology, Leuven Cancer Institute, KU Leuven, Leuven, BELGIUM, [2]Oncoinvent AS, Oslo, NORWAY, [3]Department of Obstetrics and Gynecology, University Hospitals Leuven, Leuven Cancer Institute, Leuven, BELGIUM, [4]Department of Oncology, Gynecological Oncology, KU Leuven, Leuven, BELGIUM.

Aim/Introduction: A novel alpha-therapy consisting of radium-224-labeled calcium carbonate microparticles (^{224}Ra-$CaCO_3$-MP) has been designed to treat micrometastatic disease in the peritoneal cavity via intraperitoneal (IP) administration. This preclinical study aimed to evaluate the effects of combining ^{224}Ra-$CaCO_3$-MP with either first line chemotherapy for ovarian cancer, carboplatin-paclitaxel, or second line chemotherapy, carboplatin-pegylated liposomal doxorubicin (PLD), in an immune competent murine ovarian cancer model. **Materials and Methods:** Mice with ID8-fLuc ovarian cancer were treated with ^{224}Ra-$CaCO_3$-MP (5 mg, 14-22 kBq/animal) one day after IP tumor cell inoculation. Additionally, ^{224}Ra-$CaCO_3$-MP treatment was combined with either carboplatin (100 mg/kg)-paclitaxel (10 mg/kg) on day 14, 21 or 28 post tumor cell inoculation, or carboplatin (80 mg/kg)-PLD (1.6 mg/kg) on day 14 post tumor cell inoculation. All treatments were given IP. Readouts included survival and time to ascites development. Results: Our results showed that, as a single treatment, ^{224}Ra-$CaCO_3$-MP was able to delay the onset of malignant ascites development compared to vehicle control (median onset of ascites 62.5 and 53.5 days, respectively, p_{adj}=0.0002), but was not able to prolong survival significantly (median survival 78 and 71 days, respectively). However, when ^{224}Ra-$CaCO_3$-MP treatment was administered in combination with carboplatin-PLD, survival was significantly prolonged compared to mice that received

carboplatin-PLD alone (median survival 113 and 94 days, respectively, p_{adj}=0.0102). At the time of submission, the study combining ^{224}Ra-$CaCO_3$-MP treatment with carboplatin-paclitaxel was still ongoing. **Conclusion:** This research demonstrated that ^{224}Ra-$CaCO_3$-MP as a single treatment was able to delay ascites formation but not to provide a survival benefit in this immune competent murine ovarian cancer model. However, a biological synergistic effect was achieved with ^{224}Ra-$CaCO_3$-MP treatment in combination with second line chemotherapy treatment. It is of further interest to identify combinations of ^{224}Ra-$CaCO_3$-MP treatment with the right type of chemotherapy regimen so that an additional survival benefit can be obtained compared to chemotherapy alone. **References:** None.

OP-0109

NTSR1 Targeted Alpha Therapeutic [^{225}Ac]-FPI-2059 induces regression in preclinical colorectal xenograft model

S. Mahammad[1], I. Duffy[1], R. Simms[1], J. Forbes[1], C. Smerling[2], N. Grinshtein[1], E. Burak[1];
[1]Fusion Pharmaceuticals Inc., Hamilton, ON, CANADA,
[2]3B Pharmaceuticals GmbH, Berlin, GERMANY.

Aim/Introduction: Neurotensin receptor 1 (NTSR1) is a validated cancer target known to be upregulated in multiple solid tumor types including colorectal and pancreatic cancers with limited treatment options and unmet medical need. Fusion utilizes targeted alpha therapy (TAT) which enables delivery of high energy alpha particle emitting isotopes (actinium 225) to the targeted tumor cells. Herewith we describe the preclinical therapeutic efficacy studies of NTSR1-targeted therapeutic [^{225}Ac]-FPI-2059 and provide a direct comparison to [^{177}Lu]-IPN-1087 ([^{177}Lu]-3BP-227) when tested in preclinical colorectal xenograft model. **Materials and Methods:** IPN-1087, a small molecule antagonist targeting NTSR1, was radiolabeled with either lutetium-177 or actinium-225. For therapeutic efficacy studies, single doses of 3,885-8,325 MBq/kg of [^{177}Lu]-IPN-1087 (2,100-4,500 µCi) or 1.85-5.55 MBq/kg of [^{225}Ac]-FPI-2059 (1-3 µCi) were administered to animals bearing HT29 xenografts (average tumor volume = 212 ± 46 mm^3), and tumor growth was monitored for 77 days. Mice in the control group were administered vehicle alone (10% ethanol in PBS). Study endpoints included tumor volume measurement and/or impact on animal health status. Results: Therapeutic efficacy study results indicated a significant and durable tumor growth inhibition in animals treated with 8,325 MBq/kg of [^{177}Lu]-IPN-1087 as compared to the control group. In contrast to that, mice administered 3,885 MBq/kg of [^{177}Lu]-IPN-1087 showed no discernable tumor growth inhibition. Importantly, therapeutic efficacy with [^{225}Ac]-FPI-2059 was far superior to that obtained with [^{177}Lu]-IPN-1087 since durable tumor regression was observed with both low and high treatment doses of [^{225}Ac]-FPI-2059 (1.85 and 5.55 MBq/kg, respectively). There were no treatment-related toxicities observed in any of the studies. **Conclusion:** Head-to-head comparison of therapeutic efficacy obtained with IPN-1087 radiolabelled with either actinium-225 or lutetium-177 highlighted that treatment with [^{225}Ac]-FPI-2059 results in superior efficacy in mice as compared to [^{177}Lu]-IPN-1087 in a xenograft model of colorectal cancer. **References:** None

OP-0110

Estimated absorbed dose in human after intravenous administration of [^{211}At]NaAt for the FIH clinical trial of targeted alpha therapy

T. Watabe[1,2], T. Sato[3], K. Kaneda[2], K. Ooe[1], Y. Liu[1], K. Kurimoto[1], A. Toyoshima[2], A. Shinohara[2], Y. Shirakami[2];
[1]Osaka University Graduate School of Medicine, Suita, JAPAN, [2]Institute for Radiation Sciences, Osaka University, Suita, JAPAN, [3]Nuclear Science and Engineering Center, Japan Atomic Energy Agency, Tokai, JAPAN.

Aim/Introduction: Sodium astatide ([^{211}At]NaAt) can be used for a promising targeted alpha therapy of differentiated thyroid cancer (DTC). Preparations are in progress for the first-in-human (FIH) clinical trial in DTC patients refractory to ^{131}I treatment. The purpose of this study was to evaluate the estimated absorbed dose in human after intravenous administration of [^{211}At]NaAt to identify the risk organs for the clinical trial. **Materials and Methods:** [^{211}At]NaAt solution (approximately 0.1MBq) was injected into the normal ICR mice (6 weeks old, male (n = 25) and female (n = 25)). Mice were dissected after euthanasia at 10 min, 1, 3, 6, and 24 hours after administration, and the radioactivity and weight of each organ were measured. The residence time (hr) was calculated from the area under the curve of the time radioactivity curve interpolated by the exponential function which decayed with the physical half-life. Assuming that the distribution in the human body is the same as that of the mouse, the weight of each organ of the mouse is converted into the reference organ weight of ICRP (Pub 110). The absorbed dose (mGy/MBq) of each organ was calculated from the residence time using dosimetry software IDAC-Dose 2.1. The results were also compared with the extended single-dose toxicity study of [^{211}At]NaAt in mice (Watabe T, et al. Ann Nucl Med. 2021). Results: Reflecting the whole-body distribution, the estimated absorbed doses in the thyroid gland were the largest in both adult males and females, at 6.39 and 6.11 mGy/MBq, respectively. This is followed by the stomach (0.830, 0.854 mGy/MBq) and salivary glands (0.553, 0.404 mGy/MBq), and the others are myocardium, spleen, and bladder (0.2-0.3 mGy/MBq), testis, uterus, and ovary (0.1-0.15 mGy/MBq), kidney, pancreas, small intestine, and colon (0.07-0.12 mGy/MBq), liver (0.049, 0.062 mGy/MBq), and brain, lung, and red bone marrow (0.01-0.03 mGy/MBq), respectively. In comparison with the histology results of the toxicity study, stomach and salivary gland showed no significant change, whereas testis showed pathological change with a considerable weight

decrease. **Conclusion:** The absorbed dose in human was estimated from the results of while-body distribution after a single intravenous administration of [^{211}At]NaAt in ICR mice. Stomach and salivary gland showed relatively high absorbed doses, but associated with no significant pathological change. On the other hand, attentions should be paid in the testis as a radiosensitive organ in the FIH clinical trial of [^{211}At]NaAt. **References:** Watabe T, et al. Ann Nucl Med. 2021

OP-0111

Dose response of ^{212}Pb-labeled calcium carbonate microparticles in mice with intraperitoneal ovarian cancer

R. G. Li[1,2,3], T. B. Bønsdorff[3], K. Lindland[3], M. M. Malenge[3], R. H. Larsen[3];
[1]University of Oslo, Oslo, NORWAY, [2]Oslo university hospital, Oslo, NORWAY, [3]Oncoinvent AS, Oslo, NORWAY.

Aim/Introduction: Calcium carbonate ($CaCO_3$) microparticles functioning as carriers of alpha emitting radionuclides provide containment of the radiation at the target site. We have previously employed this concept for treating cavitary micrometastases with microparticles labeled with ^{224}Ra, which are currently in clinical trials. Lead-212, a daughter of ^{224}Ra, has high affinity for $CaCO_3$ and serves as an in vivo generator of alpha particles. The possibility for on-site single-step-labeling of $CaCO_3$ microparticles makes ^{212}Pb an interesting candidate radionuclide for treatment of cavitary cancers. The aim of this study was to evaluate the intraperitoneal (i.p.) retention of ^{212}Pb-$CaCO_3$ microparticles in a biodistribution study, and their therapeutic potential in mice with i.p. ovarian cancer. **Materials and Methods:** The $CaCO_3$ microparticles were produced by spontaneous precipitation, suspended in saline, added the recrystallization inhibitor pamidronate, and autoclaved for sterilization. A sterile solution of ^{212}Pb was injected directly into the sealed vial with microparticles and the contents were mixed for 3 min by orbital shaking. In the biodistribution study, tumor-free nude athymic mice received a single i.p. injection of either ^{212}Pb-$CaCO_3$ microparticles, or free $^{212}Pb^{2+}$ in 0.9% NaCl, and were sacrificed after 2 hours for radioactivity measurements of selected tissues. In the therapeutic efficacy study, the survival of nude athymic mice inoculated i.p. with ES-2 ovarian cancer cells was monitored, after treating the mice with 2-5 mg ^{212}Pb-$CaCO_3$ microparticles with doses ranging from 57-390 kBq. Results: The labeling procedure resulted in high yields (≥99%) of ^{212}Pb precipitated on the microparticles. Microparticle-bound ^{212}Pb resulted in substantial retention of ^{212}Pb within the peritoneal cavity compared to free $^{212}Pb^{2+}$; a significant reduction of released ^{212}Pb was reflected by the percentage injected dose per gram of tissue found in the blood, kidneys, femur and skull of mice ($p < 0.015$). The survival of mice with tumors that were treated with ^{212}Pb-$CaCO_3$ was dose-dependent and significant for all of the tested doses; the median survival increased from 19 days in the control, to 26, 32, and 39 days for mice treated with 57, 147, and 390 kBq, respectively. **Conclusion:** Lead-212-labeled $CaCO_3$ microparticles can be prepared in a fast and efficient process, and represent a promising therapeutic option against cavitary cancers. **References:** None.

OP-0112

Large-scale production experiment for Ac-225 using an electron linear accelerator

M. Maeda[1], T. Tadokoro[1], Y. Ueno[1], K. Nishida[1], Y. Kani[1], M. Itoh[2], T. Sasaki[2], T. Watanabe[2], H. Kikunaga[3], S. Kashiwagi[3], K. Shirasaki[4], S. Sekimoto[5], T. Ohtsuki[5], M. Inagaki[5];
[1]Hitachi, Ltd., Research & Development Group, Hitachi, JAPAN, [2]Hitachi, Ltd., Healthcare Buisiness Unit, Tokyo, JAPAN, [3]Research Center for Electron Photon Science, Tohoku University, Sendai, JAPAN, [4]Institute for Materials Research, Tohoku University, Sendai, JAPAN, [5]Institute for Integrated Radiation and Nuclear Science, Kyoto University, Kumatori-Cho, JAPAN.

Aim/Introduction: Ac-225 has nuclear properties that make it well suited for use in targeted alpha therapy. Clinical trials have demonstrated the applicability of radiopharmaceuticals containing Ac-225 to treat various cancers. Despite these promising results, Ac-225-radiopharmaceutical development has been prevented by insufficient supplies of Ac-225. Production of Ac-225 using an electron linear accelerator has the advantages of producing no additional Ac isotopes, a relatively small accelerator size, and an easily achievable high beam current. Previously, we made a basic study of Ac-225 production, and now we report on a large-scale production experiment. **Materials and Methods:** We used the electron linear accelerator in the Tohoku University Research Center for Electron Photon Science. The target nuclide was Ra-226 (50 MBq, 1000 times the amount we used in our basic study), in the form of Ra-226•Cl_2 and provided by the Institute for Materials Research, Tohoku University. The electron beam energy was 44.5 MeV and the beam current was 149.5 uA. Irradiation time was 6 h. We used DGA and Sr resins to isolate Ac-225 from Ra-225/Ra-226 and its daughter nuclides. Ac-225 is in radiation equilibrium with Bi-213, hence we evaluated Ac-225 production amount using gamma-spectroscopy of Bi-213 with a HP-Ge detector. We also carried out an Ac-225 production calculation using the Monte Carlo radiation transport calculation code PHITS [1]. We determined the production rate of Ra-225 using the experimentally derived bremsstrahlung radiation distribution and theoretical reaction cross section data [2]. Ac-225 production amount was derived by calculation of radiation balance with Ra-225. Results: The produced amount of Ac-225 was 365.6 kBq, which was 1.46 times larger than the calculated value. We confirmed that the production amounts of Ac-225 were about 1000 times that of the basic study. **Conclusion:**

365.6 kBq of Ac-225 was produced using an electron linear accelerator from Ra-226•Cl_2 (Ra-226, 50 MBq) target. The isolation process was successfully done and high purity Ac-225 was obtained. It was confirmed that the production amount of Ac-225 increased almost in proportional to the amount of Ra-226 under almost the same beam conditions and Ra-226 installation conditions. **References:** [1] T. Sato et al. Features of Particle and Heavy Ion Transport code System (PHITS) version 3.02, J. Nucl. Sci. Technol. 55. 684-690 (2018). [2] TENDLE-2017 Nuclear data library Gamma sub-library for Ra(Z=88) and A=226, https://tendle.web.psi.ch/tendle_2017/gamma_html/Ra/GammaRa226xs.html (accessed on August 20, 2019)

OP-0113

Comparison of PSMA-TO-1 and PSMA-617 labelled with ^{68}Ga, ^{177}Lu and ^{225}Ac: a first in-human translational study

C. Meyer[1], V. Prasad[2], A. Stuparu[1], G. Glatting[2], P. Kletting[2], J. Miksch[2], C. Solbach[2], K. Lueckerath[1], L. Nyiranshuti[1], S. Zhu[1], J. Czernin[1], M. Dahlbom[1], J. Calais[1], A. Beer[2], R. Slavik[1];
[1]UCLA, Los Angeles, CA, UNITED STATES OF AMERICA, [2]Department of Nuclear Medicine University Hospital Ulm, Ulm, GERMANY.

Aim/Introduction: PSMA-TO-1 ("Tumor-Optimized-1") is a novel PSMA ligand with longer circulation time than PSMA-617. In this translational study, we first compared tumor uptake of ^{68}Ga-PSMA-TO-1/-617/-11 and the biodistribution of ^{177}Lu-PSMA-TO-1/-617 in murine models. We then assessed survival after treatment with ^{225}Ac-PSMA-TO-1/-617 in a murine model of disseminated prostate cancer. We also report first-in-human dosimetry data of PSMA-TO1/-617 labelled with lutetium-177 in prostate cancer patients. **Materials and Methods:** PET images were acquired 60 minutes after administration of ^{68}Ga-PSMA-TO-1/-617/-11 on consecutive days in mice bearing subcutaneous C4-2 xenografts. For biodistribution studies, 50 mice were treated with either 30 MBq of ^{177}Lu-PSMA-617 or ^{177}Lu-PSMA-TO-1 and sacrificed at 1, 4, 24, 48, and 168 hours for ex-vivo gamma counting. Then, mice with disseminated prostate cancer lesions were treated with either 40 kBq of ^{225}Ac-PSMA-617 (n=10), ^{225}Ac-PSMA-TO-1 (n=10) or remained untreated (n=5) and followed for survival. For human dosimetry studies, 3 metastatic castration-resistant prostate cancer patients received 500 MBq of ^{177}Lu-PSMA-TO-1. A dual imaging approach was used: planar images were acquired at 1-2, 3-4, 18-22, 48, 90-94, and +/- 162-164 hours with an additional SPECT/CT acquisition at 18-24 hours. Results: Tumor uptake one hour after administration of ^{68}Ga-labeled agents was highest using PSMA-617, followed by PSMA-TO-1 and PSMA-11. Nevertheless, ^{177}Lu-PSMA tumor uptake at subsequent time points was greater for PSMA-TO-1 up to one week following treatment. This was however accompanied by increased kidney uptake of PSMA-TO-1 compared with PSMA-617 (24 and 0.5 %IA/g, respectively, 24 hours after administration; p=0.0001). Mice treated with a single cycle ^{225}Ac-PSMA-TO-1 survived longer than those treated with ^{225}Ac-PSMA-617 or remained untreated (17.8, 14.5 and 7.7 weeks respectively; p<0.0001). Kidney, salivary gland, bone marrow, and mean ± SD tumor doses (Gy/GBq) for ^{177}Lu-PSMA-TO-1 in patient #01/#02/#03 were 2.5/2.4/3.0, 1.0/2.5/2.3, 0.14/0.11/0.10 and 0.42±0.03/4.45±0.07/1.8±0.57, respectively. **Conclusion:** In this translational study, PSMA-TO-1 tumor uptake tended to be greater than that of PSMA-617 in both clinical and preclinical settings. However, PSMA-TO-1 resulted in higher radiation doses to kidneys, salivary glands, and bone marrow. Nevertheless, ^{225}Ac-PSMA-TO-1 resulted in significant preclinical survival benefits over ^{225}Ac-PSMA-617 suggesting that further clinical evaluations in prospective phase 0/1 trials would be warranted. **References:** None.

309

Wednesday, October 20 - Saturday, October 23, 2021

on-demand pool, release on Wednesday, October 20 at 09:00

Cutting Edge Science Track - TROP Session: Dosimetry Methods

OP-0115

An organ specific compartment TIAC fitting tool for IDAC-Dose

M. Andersson[1,2], S. Mattsson[2];
[1]Department of Radiation Physics, Institute of Clinical Sciences, Sahlgrenska Cancer Center, Sahlgrenska Academy, University of Gothenburg, Gothenburg, SWEDEN, [2]Medical Radiation Physics, Department of Translational Medicine Lund University, Malmö, SWEDEN.

Aim/Introduction: The main objective of biokinetic modelling in nuclear medicine is to create a model, which describes the spatial distribution of all decays of an administered radiopharmaceutical and estimate source organ specific time-integrated activity coefficients (TIAC). All organs and tissues as well as other relevant structures which have an increased activity concentration compared to the general background uptake should have a specific TIAC. The increased organ uptake depends on different mechanism. The uptake phase is both radiopharmaceutical specific and organ dependent and often followed by a longer retention phase. If enough time-activity data is gathered, an organ specific compartment model describing the transport of the radiopharmaceutical can be created. Compartment modelling is a mathematical representation to describe physiological and pharmacological kinetic characteristics. The transfer rate describe the probability of a radiopharmaceutical

to be transferred from one compartment to another per unit time. A compartment model parameter fitting tool has been developed to facilitate organ specific TIAC calculations from measured data in blood or urine samples, or from SPECT/CT or PET/CT quantitative imaging. **Materials and Methods:** The fitting tool is a graphical interface and an integrated module to the online version of IDAC-Dose2.1 (1). It is developed in MatLab and each organ specific TIAC can be fitted using four different compartmental configurations, from 1 uptake phase and no retention phase to 3 uptake phases and 2 retention phases. The fitting of model parameters to data points is based on a numerical integration with a least squares criterion. The fitting tool is strictly a mathematical representation using the predefined compartmental configuration. Results: The fitting tool has been tested on several different data sets and compared with SAAMII. The user need to validate that the fitting tool do not reach a local minimum and that the selected compartmental configuration is realistic to represented the patient data. The organ retention fitting tool was also applied on a biokinetic model for metastatic castration resistant prostate cancer patients treated with ^{223}Ra-dichloride **Conclusion:** The new software provides a possibility to create organ specific TIACs. As the fitting tool also will be part of the internal dosimetry software IDAC-Dose2.1, it will facilitate absorbed dose and effective dose calculations directly from measured data. Further information: Both the organ compartment fitting tool and IDAC-Dose2.1 are free research software and are available online from the idac-dose.org webpage. **References:** 1. Andersson M. et al. EJNMMI Res 2017;7(1):88

OP-0116

Evaluation of a new dual-energy quantitative computed tomography (DEQCT) method against 2-point Dixon MRI to quantify the yellow marrow and red marrow volume fraction for bone marrow dosimetry in molecular radiotherapy

M. Salas Ramirez[1], J. Tran-Gia[1], P. Hartrampf[1], A. Heidemeier[2], M. Lassmann[1];
[1]Department of Nuclear Medicine, University of Würzburg, GERMANY, [2]Department of Diagnostic and Interventional Radiology, University of Würzburg, GERMANY.

Aim/Introduction: This study validates a phantom-independent dual-energy quantitative computed tomography (PI-DEQCT) method against 2-point Dixon MRI to quantify the volume fraction of yellow marrow (YMVF) and red marrow (RMVF) to apply patient-specific radionuclide S values for bone marrow dosimetry. **Materials and Methods:** First, a new PI-DEQCT method based on calculated Hounsfield units obtained from a parametrization function of the photon cross-sections of the elements that make up human tissues in the range of diagnostic x-ray energies was implemented for a dual-source computed tomography (DSCT) system (Somatom Force, Siemens Healthineers). Second, the Hounsfield units for adipose tissue (yellow marrow surrogate), red marrow, and mineral bone for 90kVp and 150kVp images were calculated. The elemental composition and density of adipose tissue and red marrow were obtained from the International Commission on Radiation Units Report 44. The mineral bone composition was based on the hydroxyapatite chemical formula [$Ca_{10}(OH)_2(PO_4)_6$] with a density of 3 g/cm^3. Lastly, an empirical function that corrects for beam hardening was estimated using an electron density phantom. The quantification of the YMVF, RMVF, and bone mineral volume fraction (BMVF) using the PI-DEQCT method was performed in the spongiosa region of the five lumbar vertebrae of a 52-year-old patient suffering from multiple myeloma. The patient was treated with multiple cycles of monoclonal antibodies and two high-dose chemotherapies followed by autologous stem cell rescue. After treatment and as part of the diagnostic protocol, whole-body images of the patient using dual-energy CT (DECT) with the DSCT system and 2-point Dixon MRI using a 1.5T system (Magnetom Avanto, Siemens Healthineers) were acquired on the same day. In analogy to previous work [1], YMVF and RMVF were quantified using the 2-point Dixon MRI data. These values were re-scaled to the volume not occupied by BMVF based on the PI-DEQCT method and compared with the PI-DEQCT-based YMVF and RMVF. Results: The mean [YMVF, RMVF] across the five lumbar vertebrae for the 2-point Dixon MRI and the PI-DEQCT method were [0.69±0.03, 0.27±0.03] and [0.68±0.06, 0.27±0.06], respectively. The maximum relative errors between both methods in the five lumbar vertebrae were 7% (YMVF) and 20%. **Conclusion:** The good agreement between the DEQCT-PI method and the 2-point Dixon MRI shows that YMVF and RMVF quantification are possible using our newly developed PI-DEQCT method. This is an essential step for applying patient-specific radionuclide S values for bone marrow dosimetry. **References:** [1] M. Salas-Ramirez et al. Phys.Med.Biol. 63 025029 (2018).

OP-0117

Physiologically-based pharmacokinetic modelling for radiopharmaceuticals using a multilevel object-oriented modelling methodology

R. Bouwman[1], S. Herrero[2], G. de With[1];
[1]NRG, Arnhem, NETHERLANDS, [2]Empresarios Agrupados Internacional, Madrid, SPAIN.

Aim/Introduction: Novel therapeutic radiopharmaceuticals (RPs) are focusing on the use of alpha-emitting nuclides. Comparing the dosimetric impact of the different RPs requires more accurate simulations of the uptake and distribution of the RP within the body up to cellular level. Physiology based pharmacokinetic (PBPK) models are currently explored to model this uptake and distribution. These models are compartment based

and include individual details of the patient specific and pharmacokinetic parameters of the RP. Standard approaches for modelling the uptake and distribution of the RP focusses on the transport of activity including the important transport mechanisms in a sequence of first-order differential equations. To advance these models, requires incorporation of a multilevel mathematical description of the physiological processes from organisms up to tissue and cellular level. In this study we therefore implemented a previously proposed PBPK model of SST2 targeting ligands in a novel software tool that focusses on the physiological functionality of an organ at different levels resulting in the transport of the activity and compared the results with the standard approach. **Materials and Methods:** The starting point for this study is the PBPK model developed by Kletting et al for the treatment of neuroendocrine tumours which has been slightly modified. The full chain of events following intravenous administration, including extravasation, binding, internalization and release of the RP are included. The model is implemented in SAAM II (standard approach), and in PhysPK (novel approach). Prior to therapy a pre-therapeutic scan provides information about the patient specific uptake of the RP in healthy and tumorous tissue. Based on this scan decisions are made for subsequent therapy. To benchmark the developed models pre-therapeutic data from the original publication (^{111}In-DOTATATE) was used to compare both implementations. Results: A comparison of both models was carried out using identical model parameterisation. Differences in time integrated activity between the two approaches were less than 10% for the kidney, spleen, red-bone-marrow and liver and less than 20% for the tumours. The differences were mostly a result of computational inconveniencies in the standard approach. Trends in time activity curves were however comparable and therefor it was concluded that despite the differences in approach both models are equivalent. **Conclusion:** The multi-level PBPK model demonstrated to be useful for further development as part of dosimetry procedures of therapeutic RPs. The next step would be to validate the newly developed model in a clinical setting. **References:** Kletting, P. et al (2016).

OP-0118

Manual versus artificial intelligence-based segmentations as a pre-processing step in whole-body dosimetry calculations

J. van Sluis, W. Noordzij, E. G. De Vries, I. C. Kok, D. A. De Groot, M. Jalving, M. N. Lub-de Hooge, A. H. Brouwers, R. Boellaard; University Medical Center Groningen, Groningen, NETHERLANDS.

Aim/Introduction: Over the last decades, labelling of monoclonal antibodies (MAbs) with zirconium-89 (^{89}Zr) allowed whole body assessment of MAb distribution and tumour targeting over time with molecular imaging. The main advantage of ^{89}Zr is the long half-life of 78.4h, matching the pharmacokinetic behaviour of antibodies, making it suitable for labelling of MAbs. The long physical half-life of ^{89}Zr and the long biological half-life of MAbs may cause high radiation burden and limit the amount of activity that can be administered, limiting image quality. Especially with emerging MAb fragments and nanobodies associated with different size and affinity kinetics, it is important to obtain reliable radiation dose estimates to optimize the amount of activity that can be administered while keeping radiation burden within acceptable limits. Organ segmentation is required for whole-body dosimetry but is a very time-consuming task. Therefore, we explored using an AI-based automated segmentation tool as a pre-processing step for calculating the organ and whole-body effective doses. **Materials and Methods:** Retrospective PET/CT data of six patients undergoing treatment with ^{89}Zr-labelled pembrolizumab were included in this study. Manual organ segmentations were performed using in-house developed software, and biodistribution information was obtained. Using the activity biodistribution information, residence times were calculated. The obtained residence times served as input for OLINDA/EXM version 1.0 (Vanderbilt University, 2003) to calculate the effective dose per organ and the whole-body effective dose (mSv/MBq) according to ICRP publication 103. Subsequently, organ segmentations were also performed using Recomia (available at: https://www.recomia.org/), a cloud-based AI platform for nuclear medicine and radiology research [1]. The workflow for calculating residence times and whole-body effective doses, as described above, was repeated. Results: Patient data were obtained at three different time-points, day 2, 4, and 7 post-injection, resulting in 18 PET/CT scans. Overall analysis time per scan was approximately 3h for manual segmentations compared to ≤30min using Recomia. Whole-body effective doses differed minimally for the six patients with a median difference in received mSv/MBq of 0.52% (range 0.15-1.95%) according to ICRP publication 103. **Conclusion:** These first results suggest that whole-body dosimetry calculations can benefit from fast automated AI-based whole-organ segmentations using Recomia. As several newly developed MAbs (e.g., MAb fragments and nanobodies) are emerging in anti-cancer therapy, whole-body effective doses for these different therapeutic agents can be assessed rapidly and efficiently. **References:** 1. Trägårdh E et al. RECOMIA - a cloud-based platform for artificial intelligence research in nuclear medicine and radiology. EJNMMI Physics; 2020;7.

OP-0119

A thyroid iodide uptake and volume determination tool for the online version of IDAC-Iodide

M. Andersson[1,2], S. Mattsson[2];
[1]Department of Radiation Physics, Institute of Clinical Sciences, Sahlgrenska Cancer Center, Sahlgrenska Academy, University of Gothenburg, Gothenburg, SWEDEN, [2]Medical Radiation Physics, Department of Translational Medicine Lund University, Malmö, SWEDEN.

Aim/Introduction: Radioactive iodide is commonly used for the treatment of different thyroid conditions since the 1940s. The new software IDAC-Iodide (1) combines the detailed biokinetic model for iodide given by the ICRP for diagnostic nuclear medicine and combines it with the EANM pre-therapeutic procedure to estimate patient specific thyroid uptake. The software gives both an improved patient specific dosimetry for the thyroid and an estimation of the absorbed dose to non-target organs and tissues. However, the activity needed to produce the prescribed absorbed dose to the thyroid starts with quantifying the pre-therapeutic thyroid uptake of iodide from patient images. **Materials and Methods:** A graphical software tool was developed in MatLab. The code reads and display planar thyroid images. The tool allows the possibility to draw regions of interest around the left and right thyroid lobes, respectively, in all pre-therapeutic images to determine the count rate within the lobes. By including a count rate to activity conversion factor and the administered iodide activity can the fractional I-131 uptake in the thyroid at time t, RIU(t), be determined for each measurement. The time period t, from administration to the specific measurement and the RIU(t) will then be the initial data in the patient specific biokinetic and dosimetric estimations for the IDAC-Iodide calculation. The software tool also provides the possibility to estimate the thyroid volume. The volume determination is based on assuming a prolate spheroid volume of both the left and right thyroid lobes. The mass of the thyroid is calculated assuming the tissue density of 1.04 g/cm^3 for thyroid (2). Results: The DICOM reader was tested on different planar images. The measurement tool to determine the distances of the prolate spheroid was validated with ImageJ. The segmentation tool for region of interest was also validated with ImageJ. The results of the thyroid iodide uptake and volume determination tool was in agreement with the results generated with ImageJ. **Conclusion:** The inclusion of provides the possibility to determine patient specific time-integrated activity coefficient and the absorbed dose coefficients for the thyroid and also for other relevant organs directly form the pre-therapeutic images. Further information: Both the thyroid iodide uptake and volume determination tool and IDAC-Iodide are free research software and are available online from the idac-dose.org webpage. **References:** 1)Andersson M, Mattsson S. Front Endocrinol 2021;12:634955. 2)ICRP. Ann ICRP (2016) 45:1-74.

OP-0120

Investigation of the effect of small but frequently occurring patient movements onto 3D activity quantitation in Siemens xSPECT Quant reconstruction with integrated motion correction

A. Gosewisch[1], M. Reymann[2], H. Ilhan[1], L. Beyer[1], G. Platsch[2], P. Bartenstein[1], A. H. Vija[3], G. Böning[1];
[1]Department of Nuclear Medicine, University Hospital, LMU Munich, Muenchen, GERMANY, [2]Siemens Healthcare GmbH, Molecular Imaging, Forchheim, GERMANY, [3]Siemens Medical Solutions USA, Inc., Molecular Imaging, Hoffman Estates, IL, UNITED STATES OF AMERICA.

Aim/Introduction: In radionuclide, therapy post-therapeutic estimation of the delivered radiation dose to tumors and organs-at-risk is important for the evaluation of therapy effects and for further therapy planning. The accuracy of dose estimation techniques highly depends on the accuracy of the underlying sequential quantitative SPECT/CT measurements. In clinical routine patients often suffer from pain and consequently perform small pain-induced movements during SPECT acquisition. We have therefore established a workflow to generate simulated SPECT projection data being affected by small patient movements and assessed the resulting quantitation errors. **Materials and Methods:** Projection data of a NEMA sphere phantom (total phantom activity: 781 MBq Lu-177; foreground-to-background ratio: 8-1) were simulated with SIMIND in 128 steps over 360 degree, in 128x128 matrices (4.7952mm/4.7952mm) and in baseline position as well as in +/-1cm horizontal offset positions. Final projection data sets containing object motion were generated by randomly sampling (i) the time between motions from a normal distribution with a mean of 60 seconds, and (ii) the motion direction. The following combinations of motion duration (MD, in sec) and acquisition step time (ST, in sec) were investigated: MD=15 with ST=15, MD=5 and ST=15, and MD=5 and ST=5, yielding three projection data sets with motion. Poisson noise was applied and projection data were reconstructed with Siemens xSPECT Quant with and without making use of the integrated reprojection-based motion correction algorithm. The reconstructed signal in the spheres was analyzed in comparison to the baseline without motion. Results: Mean motion-induced quantitation errors in the three largest spheres (diameter: 37mm, 28mm, 22mm) were 7.7% (MD=15, ST=15), 8.2% (MD=5, ST=15), and 6.4% (MD=5, ST=5), and were reduced to 5.1%, 5.5%, and 5.9% by motion correction. **Conclusion:** This preliminary investigation demonstrates that even small and very rarely occurring movements can alter the estimated activity in quantitative SPECT. Integrated motion compensation algorithms may have the potential to reduce these effects and improve the robustness of subsequent image-based dosimetry. We observed a dependency of quantitation error from motion frequency and duration, and of acquisition

step duration. This ongoing work will further aim for gaining insight into these relationships to optimize clinical dosimetry by focusing on analyzing a large collection of projection data sets with randomly sampled motion. Furthermore, a human CT template will be filled with realistic organ and tumor activities and processed accordingly. **References:** None

OP-0121

Bone marrow dosimetry for terbium-161 reveals higher dependence on source distribution within the bone marrow cavities compared to lutetium-177

J. Hemmingsson[1], J. Svensson[2], N. P. van der Meulen[3,4], C. Müller[3], P. Bernhardt[1];
[1]Department of Medical Radiation Sciences, the Sahlgrenska Academy, University of Gothenburg, Gothenburg, SWEDEN, [2]Department of Oncology, Sahlgrenska University Hospital, Gothenburg, SWEDEN, [3]Center for Radiopharmaceutical Sciences ETH-PSI-USZ, Paul Scherrer Institute, Villigen, SWITZERLAND, [4]Laboratory of Radiochemistry, Paul Scherrer Institute, Villigen, SWITZERLAND.

Aim/Introduction: Through encouraging preclinical results, terbium-161 is now considered an alternative to lutetium-177 for use in radionuclide therapies. While chemically similar, terbium-161 emits more low-energy electrons per decay than lutetium-177, a favorable feature when treating disseminated disease but potentially hazardous to the radiosensitive bone marrow. In the development of skeletal dosimetry models, the active marrow is identified as the target region to evaluate radiation-induced bone marrow toxicities. The purpose of this study was to evaluate the source distribution dependence of terbium-161 and lutetium-177 in bone marrow cavities and its dosimetric impact on active bone marrow. **Materials and Methods:** The male and female image-based bone marrow dosimetry models of Hough et al. (1) and O'Reilly et al. (2) were used to produce S values for terbium-161 and lutetium-177, respectively. Specific absorbed fractions for 13 bone sites were combined with decay data from ICRP 107 to calculate active marrow S values, both bone site-specific and skeletal averaged, for the source distributions: active marrow (AM), inactive marrow (IM), trabecular bone surface (TBS) and trabecular bone volume (TBV). Results: Male/Female skeletal-averaged S values (mGy/MBq) for lutetium-177 were: S(AM ← AM): 1.29e-5/1.40e-5, S(AM ← IM): 2.92e-6/4.30e-6, S(AM ← TBS): 3.89e-6/5.03e-6 and S(AM ← TBV): 2.34e-6/2.27e-6. Similarly for terbium-161: S(AM ← AM): 1.92e-5/2.10e-5 , S(AM ← IM): 3.37e-6/5.01e-6, S(AM ← TBS): 5.28e-6/6.78e-6 and S(AM ← TBV): 2.77e-6/2.70e-6. Increased S values was seen for terbium-161 for all source/target combinations corresponding to 48.9/50.4, 15.3/16.5, 35.9/34.6 and 18.4/18.7 percent, respectively. These higher values are attributed to the 36% higher electron energy emission from terbium-161 compared to lutetium-177. **Conclusion:** The high emission of low-energy electrons emitted from terbium-161 make it highly dependent on its distribution within the bone marrow cavity. If uniformly distributed within the active marrow the absorbed dose, compared to lutetium-177, will be increased, while for other distributions the absorbed dose to the active marrow will be decreased. Consequently, the bone marrow toxicity profile of ^{161}Tb- compared to ^{177}Lu-labeled pharmaceuticals will be more dependent on the source distribution. **References:** 1.Hough M, Johnson P, Rajon D, Jokisch D, Lee C, Bolch W. An image-based skeletal dosimetry model for the ICRP reference adult male—internal electron sources. Physics in Medicine & Biology. 2011;56:2309. 2.O'Reilly SE, DeWeese LS, Maynard MR, et al. An image-based skeletal dosimetry model for the ICRP reference adult female—internal electron sources. Physics in Medicine & Biology. 2016;61:8794.

OP-0122

The feasibility of dose estimation to thyroid remnants and salivary glands and avid following therapeutic ^{131}I administration

M. Abuqbeitah;
Istanbul University, Istanbul, TURKEY.

Aim/Introduction: the main purpose was to validate a dosimetry method for estimating absorbed dose to salivary glands and lesions after radioiodine therapy, that help to evaluate salivary glands induced dysfunctions and dose-effect relationship. **Materials and Methods:** IEC body phantom was filled with 1983.2 MBq and 20 SPECT/CT scans were acquired using 128 projections/2π, 25 seconds/projection, 15%±7 photo-peak window, OSEM reconstruction with 8 subsets and 10- 40 iterations. A set of functions were derived to correct for scatter, dead time, and partial volume effect. The salivary glands were delineated over CT images and thyroid residuesover SPECT images with 30% iso-contour. In the patients study, 31 patients underwent subsequent single bed SPECT/CT scans 4-6, 20-25, and 168 h after orally administered 5062±1913 MBq ^{131}I. Results: mean volume of right parotid glands via CT was 29.4±13.3 cm^3, left parotid 28.7±11.9 cm^3. Right and left submandibular volumes were 12.6±3.9 cm^3 and 12.6±3.8 cm^3, respectively. The absorbed dose to parotids was 0.47±0.46 Gy/GBq, and to submandibular glands was 0.16±10 Gy/GBq, while whole salivary glands dose (n=26) was 0.51±0.25 (0.21-1.11) Gy/GBq. The absorbed dose to thyroid remnants and distal metastases was 0.5-400 Gy/GBq an 0.8-15 Gy/GBq, respectively. Consequently, only 41% of thyroid residues had dose > 80 Gy, 18 % received 70-80 Gy, 18 % showed 40-70 Gy, while 23 % had dose ≤ 40 Gy. In metastases, 18 % of lesions had dose ≥ 80 Gy, while the dose 9% was 40-60 Gy, and to the remaining 73% was ≤ 40 Gy. **Conclusion:** No improvement was observed on the recovery coefficients of the lesions with ≥ 35 iterations. The conformity between salivary glands dose estimates after RIT via SPECT/CT and ^{124}I PET/CT approves the reliability of the presented method. A wide dose range was emphasized that necessitates establishing dose-effect relationship based on actual post-therapeutic dose estimates. **References:** none

310

Wednesday, October 20 - Saturday, October 23, 2021

on-demand pool, release on Wednesday, October 20 at 09:00

Clinical Oncology Track - TROP Session: Breast

OP-0124

First Results of Simultaneous FAPi-PET/MRI Targeting the Fibroblast Activation Protein in Primary Breast Cancer

P. Backhaus[1,2], M. C. Burg[3], W. Roll[1], F. Büther[1,2], H. Breyholz[1], S. B. Weigel[3], W. Heindel[3], M. Pixberg[1], P. J. Barth[4], J. Tio[5], M. Schäfers[1,2]; [1]Department of Nuclear Medicine, University Hospital Münster, Münster, GERMANY, [2]European Institute for Molecular Imaging, University of Münster, Münster, GERMANY, [3]Clinic for Radiology, University Hospital Münster, Münster, GERMANY, [4]Gerhard-Domagk Institute for Pathology, University Hospital Münster, Münster, GERMANY, [5]Department of Gynecology & Obstetrics, University Hospital Münster, Münster, GERMANY.

Aim/Introduction: ^{18}F-FDG Is the most established PET radiotracer in breast cancer is and it has proven value especially in unraveling inconclusive conventional staging results and in therapy monitoring of advanced disease. Considering the clinical role of MRI and the difficult co-registration of the highly plastic organ, breast PET/MRI is a particular promising modality that offers to uniquely overlay accurate morphological and functional imaging with molecular biomarkers. However, uptake of ^{18}F-FDG in primary breast lesions is not reliable across different breast cancer subtypes and its accuracy is limited. The fibroblast activation protein (FAP) is abundantly expressed in invasive breast cancer and FAP-directed PET tracers have recently become available. The aim of this study was to initially evaluate the potential of FAP-directed breast PET/MRI and consecutive whole-body scanning using the ligand ^{68}Ga-FAPi-46 for staging of local disease extent, lymph node and distant staging in clinical use. **Materials and Methods:** In 19 female patients with breast cancer, we retrospectively analyzed ^{68}Ga-FAPi-PET/MRI and PET/CT scans; 18 to complement initial staging and 1 for re-staging after therapy for distant metastases. 30 min after injection of 149 ± 48 MBq (mean ± SD) ^{68}Ga-FAPi-46 patients underwent a 25-min prone breast PET/MRI and subsequently either received supine whole-body PET/MRI or PET/CT. Results: Strong tracer accumulation was observed in every untreated primary breast malignancy (mean Standardized Uptake Values, SUV_{max}: 13.9, range: 7.9 - 29.9, median lesion diameter 26 mm, 9 - 155 mm) resulting in clear tumor delineation in every case independent of tumor grading, hormone receptor and histological type. Even sub-centimeter lesions demonstrated reliable tracer accumulation. All preoperatively verified lymph node metastases in 13 patients demonstrated strong tracer accumulation (mean SUV_{max} 12.2, 3.3 - 22.4, mean diameter 21 mm, 14 - 35 mm). Tracer uptake established or supported extra-axillary lymph node involvement in 7 patients and impacted therapy decisions in 3 patients. In cases with distant metastases, FAPi-PET uncovered additional lesions. **Conclusion:** Combining ^{68}Ga-FAPi-46 in simultaneous breast PET/MRI demonstrated highly favorable imaging characteristics. Subsequent whole-body scanning added incremental diagnostic information for detection of lymph node and distant metastases. Further studies are needed to quantify the diagnostic accuracy of FAPi-PET/MRI and to evaluate its impact in clinically relevant scenarios. **References:** none

OP-0125

Correlation between tumoral infiltrating lymphocytes, ^{99m}Tc HYNIC-iFAP SPECT/CT and ^{18}FDG PET/CT: a potential imaging biomarker of tumoral microenvironment aggressiveness in breast cancer

O. Garcia-Perez[1], P. Vallejo-Armenta[1], L. Torres-Agredo[2], P. Casanova[1], F. Porras-Reyes[1], J. Vargas-Ahumada[1], I. Soldevilla-Gallardo[1], Q. Pitalua-Cortes[1], E. Bargallo[1], G. Ferro-Flores[3], C. Santos-Cuevas[3], B. Ocampo-García[1], E. Estrada-Lobato[4], P. Cabrera-Galeana[5]; [1]Instituto Nacional de Cancerologia, Mexico city, MEXICO, [2]Universidad Autonoma de Bucaramanga, Bucaramanga, COLOMBIA, [3]Instituto Nacional de Investigaciones Nucleares, Mexico city, MEXICO, [4]International Atomic Energy Agency, Wien, AUSTRIA, [5]Instituto Nacional de Cancerología, Mexico City, MEXICO.

Aim/Introduction: Stromal cells have a particularly important role in the mechanisms of action of cancer hallmarks. The interactions between cancer-associated fibroblasts(CAF) and tumor infiltrating lymphocytes (TILs) have been studied due to their potential role in cancer progression; immunohistochemical studies have shown a negative regulation between both cell populations of the microenvironment and a potential predictive role in therapy response in breast cancer. This together with the development of new inhibitors that evaluate the expression of the fibroblastactivation protein (FAP) of CAF´s allow the integration of histological-imaginginformation to stratify patients with tumor microenvironments prone to bad prognosis. Aim of this investigation was to correlate the uptake of 99mTc HYNIC-iFAP and 18FDG with the expression in percentage of TILs. **Materials and Methods:** Thirteen female patients (mean age 49 y/o +/- 14.4) with histopathological confirmed primary breast cancer were included (3 Luminal A, 4 Luminal B, 2 HER2 enriched and 4 basal-like). Both studies, 18FDG PET/CT and 99mTc-HYNIC-iFAP SPECT/CT were performed the same week. Maximum target-to-background ratio (TBR) and SUVmax values were correlated with percentage of TIL, histologic tumor grade (Scarff Bloom Richardson or SBR) and Ki67 index. Results: There was a negative correlation between the TBR of 99mTc-

HYNIC-iFAP and TILs (r=0.455, p=0.059) for 18FDG and TILs was positive (r=0.458, p=0.058). No significant differences were encountered between TBR and all immunophenotypes, although it was markedly decreased for Luminal A (5.91+/-2.14) compared to the rest of the groups (Luminal B 13.57 +/-5.67, HER2 enriched 11.60+/-5.84 and Basal-like 6.31 +/- 4.57). Pearson coefficient between TBR 99mTc-HYNIC-iFAP and Ki67 (r=0.184) or SBR (r=0.333) was not significant and between FDG and Ki67 or the SBR did show a significant correlation (r 0.669 and r=0.747, p=0.002). **Conclusion:** This work found a negative correlation between the TBRs with 99mTc-HYNIC-FAPI and TILs, similar to those described between CAFs and TILs,suggesting that this image biomarker is correlated with the presence of CAFs in the tumoral microenvironment, which has potential role in the prediction of highly immunogenic tumors and prone to develop epitelial-mesenchymal transition. We also noticed that 18FDG shows high correlation with known predictive markers like Ki67 and SBR and could be considered as a complementary predictor marker. The low variability between the values of 99mTc-HYNIC-iFAP and the molecular subtypes gives it the ability to offer a potential theragnostic use to any tumor variant. **References:** none

OP-0126

Comparison [68Ga]GaFAPİ-46 PET/CT and [18F]FDG PET/CT in Breast carcinoma staging: Preliminary results of randomised prospective clinical trial from Azerbaijan

F. Novruzov[1], E. Mehdi[1], N. Orucova[1], Q. Abdullayev[1], N. Talibova[2], M. Moore[3], F. Valla[3], S. Rahimzade[4], J. Aliyev[5];
[1]Azerbaijan National Centre Of Oncology, Department of Nuclear Medicine, Baku, AZERBAIJAN, [2]Azerbaijan National Centre Of Oncology, Department of Medical Oncology, Baku, AZERBAIJAN, [3]SOFIE, TOTOWA, NJ, UNITED STATES OF AMERICA, [4]Azerbaijan National Centre Of Oncology, Department of Woman Health, Baku, AZERBAIJAN, [5]Azerbaijan National Centre Of Oncology, Department of General Surgery, Baku, AZERBAIJAN.

Aim/Introduction: Accurate clinical staging is important for treatment management of breast cancer, but [18F]FDG PET/CT has some limitations. Labelling fibroblast-activation protein with PET radiotracers is a newer diagnostic approach for the visualization of tumor stroma. The aim of his study is to compare the diagnostic performance of [68Ga]FAPI-46 PET/CT and [18F]FDG PET/CT in primary and metastatic lesions of breast cancer and to reveal the best diagnostic imaging time of [68Ga]FAPI-46 PET/CT. **Materials and Methods:** We have included 24 patients (with median age 53 years) consecutive naive breast carcinoma patients. The pathology confirmed by lesion tru-cut biopsy. [18F]FDG and [68Ga]FAPI-46 PET/CT exam performed to all patients within 2 days. All patients have been scanned 10 minute, 30 minute and 1 hour after [68Ga]FAPI-46 injected. To find out the highest tumor-to background ratio we choose SUVmean values from aorta blood pool and liver parenchyma as a background. To standardise the ratio values, the new variable was defined as percentage of the 10th, 30th and 60th minute scan time. Results: Tracer uptake was higher with [68Ga]FAPI-46 PET/CT than with [18F]FDG PET/CT in primary lesions (SUVmax: 15.9 vs 11.5, respectively, P=0.004). There was a significant increase in [68Ga]FAPI-46 SUVmax values when the lesion size increased. But, in lesions smaller than 3 cm in size [68Ga]FAPI-46 SUVmax values showed slightly better correlation than [18F]FDG (rs(20)=0.552, p=0.012 vs rs(20)=0.494, p=0.027). The tumor-to background ratio values increased over the 10th, 30th and 60th minute scan time (F(2, 40)=10.95, p=0.002). The 30th minute tumor-to-background ratio was significantly higher from 10th minute scan values (63.3%, p=0.001), but not from 60th minute scan ones (-7.1%, p=1.000) when aorta SUVmean values taken into account as background. In five patients [68Ga]FAPI-46 PET/CT revealed extra lesions which had not been found with FDG. In nine of 24 patients had mild to high FAPI-46 uptake in benign inflammatory and degenerative changes. **Conclusion:** [68Ga]FAPI-46 PET/CT is a new alternative diagnostic method in breast cancer staging. In contrast to 18F-FDG, no diet or fasting in preparation is necessary, and image acquisition can be started even 30 minute after tracer injection. FAPI-46 showed better tumor-to-background ratio rather than FDG. This may indicate potential for targeted radionuclide treatment with beta and alpha emitters in the near future. **References:**
Clemens Kratochwil, Paul Flechsig, Thomas Lindner ett. all. ^{68}Ga-FAPI PET/CT: Tracer Uptake in 28 Different Kinds of Cancer. Journal of Nuclear Medicine, 2019

OP-0127

PET/CT radiomics in breast cancer: promising tool for prediction of the Ki67 expression

C. Shen[1], X. Duan[1], Q. Nie[2], C. Ding[2];
[1]Xi'an Jiaotong University, Xi'an, CHINA,
[2]Philips Healthcare, Shanghai, CHINA.

Aim/Introduction: The aim of this study was to validate the value of radiomics parameters of fluorine-18 fluorodeoxyglucose (18F-FDG) PET/computed tomography (CT) imaging in breast cancer patients in the prediction of ki-67 expression. **Materials and Methods:** A total of 115 patients who were diagnosed with breast cancer and then examined by 18F-FDG PET/CT for staging were included in this study. Ki-67 proliferation index was determined. Standardized uptake value (SUV)-based and radiomics findings were obtained from 18F-FDG PET/CT images. Independent t-test, and least absolute shrinkage selection operator (LASSO) were used to select the most discriminative radiomics features. Radiomics score incorporated with all the selected features and the clinical features were used to construct the binary logistic regression and nomogram classifier. A receiver operating characteristic curve (ROC) analysis was used to predict the accuracy. Decision curve analysis (DCA) was performed to assess clinical utility of

the prediction model. Results: 944 features were reduced to 14 potential predictors.The RRS were significantly different between two groups (ki67+ vs ki67-, 0.440±0.473 vs 1.039 ± 0.430, t = -6.663, p < 0.001). Of all clinical parameters, the N stage (OR [95% CI], 5.752 [2.032, 16.286], p<0.001) and RRS (OR [95% CI], 20.540 [5.521, 76.423], p<0.001) were identified as independent factors in predicting Ki67 expression.AUC was 0.866 (0.790, 0.922), p < 0.001, with the sensitivity, specificity, Youden index and cutoff value of 82.50%, 80.00%, 0.6250, 0.66718, respectively. The DCA indicated that the use of the clinical-radiomic nomogram added more benefit than either the clinical or radiomic features alone. **Conclusion:** Radiomics-derived evaluation score combined with the N stage could effectively predict of Ki67 expression in breast cancer base on PET/CT images, which can provide the therapeutic selections for these patients. **References:** 1. Siegel RL, Miller KD, Jemal A. Cancer statistics, 2020. CA: a cancer journal for clinicians. 2020;70(1):7-30. 2. Perou CM, Sorlie T, Eisen MB, et al. Molecular portraits of human breast tumours. Nature. 2000;406(6797):747-752. 3. Baker E, Whiteoak N, Hall L, France J, Wilson D, Bhaskar P. Mammaglobin-A, VEGFR3, and Ki67 in Human Breast Cancer Pathology and Five Year Survival. Breast cancer : basic and clinical research. 2019;13:1178223419858957. 4. Gallardo A, Garcia-Valdecasas B, Murata P, et al. Inverse relationship between Ki67 and survival in early luminal breast cancer: confirmation in a multivariate analysis. Breast cancer research and treatment. 2018;167(1):31-37.

OP-0128

First-in-human study of ^{99m}Tc-labelled HER2-binding DARPin G3

O. Bragina[1,2], *V. Chernov*[1,2], *A. Schulga*[2,3], *E. Konovalova*[3], *A. Vorobyeva*[4,2], *A. Orlova*[4,2], *J. Sörensen*[5], *R. Zelchan*[1,2], *A. Medvedeva*[1], *S. M. Deyev*[2,3], *V. Tolmachev*[2,6];
[1]*Cancer Research Institute, Tomsk National Research Medical Center, Tomsk, RUSSIAN FEDERATION,* [2]*Research Centrum for Oncotheranostics, Research School of Chemistry and Applied Biomedical Sciences, Tomsk Polytechnic University, Tomsk, RUSSIAN FEDERATION,* [3]*Shemyakin-Ovchinnikov Institute of Bioorganic Chemistry of the Russian Academy of Sciences, Moscow, RUSSIAN FEDERATION,* [4]*Department of Medicinal Chemistry, Uppsala University, Uppsala, SWEDEN,* [5]*Radiology and Nuclear Medicine, Department of Surgical Sciences, Uppsala University, Uppsala, SWEDEN,* [6]*Department of Immunology, Genetics and Pathology, Uppsala University, Uppsala, SWEDEN.*

Aim/Introduction: Human epidermal growth factor receptor type 2 (HER2) is druggable target in breast and gastroesophageal cancer. Overexpression of HER2 is a predictive biomarker for response to HER2-targeted therapeutics. Radionuclide molecular imaging of HER2 might be instrumental in stratification for HER2-targeted treatments. Designed ankyrin repeat protein (DARPin) G3 binds to HER2 with affinity of 90 pM (1). Preclinical studies demonstrated that positioning of $(HE)_3$ tag at C-terminus of G3 provides stable labelling using [^{99m}Tc]Tc$(CO)_3$ and favourable distribution of the labelled DARPin (2). The aim of this Phase I clinical study was to evaluate safety, tolerability, biodistribution and dosimetry of [^{99m}Tc]Tc-$(HE)_3$-G3. **Materials and Methods:** The study has been approved by the Board of Medical Ethics and Scientific Council of Cancer Research Institute, Tomsk National Research Medical Center of the Russian Academy of Sciences and all subjects signed a written informed consent. Patients with primary breast cancer were enrolled. At least 5 patients per cohort had HER2-postive and at least 4 had HER2-negative tumours. [^{99m}Tc]Tc-$(HE)_3$-G3 was injected with a protein dose of 1000 µg (9 patients), 2000 µg (10 patients) and 3000 µg (9 patients). The injected activity was 287±170 MBq. Patients were observed up to 7 days after injection to detect possible side effects. At 2, 4, 6, and 24 h after injection, a planar scintigraphy and SPECT imaging were performed. Dosimetry was calculated as described by Bragina and co-workers (3). Results: No side effects were observed after injection of [^{99m}Tc]Tc-$(HE)_3$-G3. The highest uptake was found in kidney, liver, small intestines content, lung and breast. Increase of injected protein dose to 3000 µg reduced the hepatic uptake two-fold compared to injected dose of 1000 µg. An average effective dose was 0.011± 0.004 mSv/MBq (no significant difference between cohorts). Visualization of tumours was clear already 2 h after injection. Tumour-to-contralateral site ratio for clinically HER2-positive tumours was significantly higher (p < 0.05, Mann-Whitney test) that the ratio for HER2-negative tumours. In one patient (cohort 3000 µg), liver and bone metastases were found and confirmed by CT imaging. **Conclusion:** Injections of [^{99m}Tc]Tc-$(HE)_3$-G3 are safe, well-tolerated and associated with low absorbed doses. Imaging using [^{99m}Tc]Tc-$(HE)_3$-G3 enables discrimination between clinically HER2-positive and negative tumours. Further clinical development of [^{99m}Tc]Tc-$(HE)_3$-G3 might result in a useful molecular imaging probe. **References:** 1.Zahnd C et al.,. Cancer Res. 2010;70:1595-605. 2.Vorobyeva A et al.. Sci Rep. 2019;9:9405. 3.Bragina O et al, J Nucl Med. 2021;62:493-499.

OP-0129

Impact of hybrid whole-body ^{18}F-FDG PET/MRI for breast cancer patients staging according to accepted guidelines: prognostic bioimaging markers associated with tumour aggressiveness

E. Valls, *A. Compte, J. Garcia, S. Ortiz, M. Cozar, P. Bassa, C. Galan, S. Mourelo, M. Soler, M. Buxeda, A. Blanch, E. Riera;*
CETIR-ASCIRES, Barcelona, SPAIN.

Aim/Introduction: To assess the clinical value of hybrid ^{18}F-FDG PET/MRI in staging breast cancer patients and to establish prognostic value of derived pre-treatment PET/MRI imaging biomarkers. **Materials and Methods:** Fifteen patients (54.6±15.8-year-old) stage IIB-III of invasive ductal breast cancer, HER2-positive, underwent ^{18}F-FDG PET/

MRI study before treatment decision for staging purposes. The synchronic PET/MRI (Signa-3T,GE) acquisition protocol included dedicated-breast-prone PET (1.bed)/MRI (3D-T2, T2-Fat, T1, DWE, CDE) and whole-body PET (5.beds)/MRI (LAVA-Flex, MRAC, DWI, T2-SSFSE). Dual-phase PET/MRI studies were jointly reviewed by a Nuclear and a Radiologist. A consensus was reached over T-staging, as well as for nodal disease and distant metastases. Patients were categorized in two groups: 1)TxN0M0 or TxN1M0; 2)Tx N>1 and/or M1. Results correlated with histopathological study and/or other diagnostic procedures. A region of interest was automatically drawn of the entire primary tumour on each patient's dedicated-breast-prone PET/MRI. The following biomarkers were recorded for each lesion: SUVmax, SUVpeak, MTV (in ^{18}F-FDG), ADC (in DWI) and Gd-peak enhancement (in DCE). T-student test was used to investigate the association between N>1 and/or M1 on whole-body ^{18}F-FDG PET imaging with these biomarkers in dedicated-breast-prone ^{18}F-FDG PET/MRI. Results: Dedicated-breast-prone ^{18}F-FDG PET/MRI correctly identified 100% of primary tumours. For T-stage assessment, added value of ^{18}F-FDG findings as compared to MRI showed: agreement (n:8), better boundary (n:5), hypermetabolic uptake not depicted on MRI (n:2). Whole-body ^{18}F-FDG PET/MRI detected axillary, extra-axillar lymph-nodes and distant metastases in 8 out of 15 patients (53.3%). Patient categorization was: 7 patients N0 or N1 M0: T1cN0M0 (n:2); T2N0M0, T2N1M0 (n:3); T3N1M0. 8 patients N>1 and/or M1: T2N3aM0, T2N3bM0, T3N3bM0, T4dN3aM0 (n: 2); T3N1M1, T3N3cM1, T4d3cM1. Site of M1 lesions were: mediastinal lymph-nodes (n:2); lung (n:1); bone (n:2); corresponding to 3 patients. Mean±SD values in both groups for each biomarker were: SUVmax (7.88±4.03 vs. 19.38±14.68); SUVpeak (4.77±2.24 vs. 13.89±10.12); MTV (2.93±2.10 vs. 5.12±4.78); ADC (0.82±0.32 vs. 0.88±0.26); DCEpeak (247.6±127.0 vs. 465.67±265.04), with significant differences in both groups for each biomarker, except for ADC. Significant correlation was found only with SUVpeak and DCEpeak, with both biomarkers being prognostic factors to present with N>1 and/or M1. **Conclusion:** Hybrid ^{18}F-FDG PET/MRI provided advantages for both local tumour staging and axillar lymph-nodes detection (in dedicated-breast-prone imaging), improving also extra-axillar lymph-nodes and distant metastases detection (in whole-body imaging). SUVpeak and peak enhancement DCE obtained in ^{18}F-FDG PET/MRI were predictive of extra-axillar lymph-nodes and distant metastases. Further evaluation is warranted to confirm these preliminary results. **References:** None

OP-0130

Impact on the long-term prognosis of FDG PET/CT in luminal breast cancer

M. Caracciolo[1], L. Urso[1], L. Evangelista[2], S. Panareo[1], N. Quartuccio[3], N. Ortolan[1], I. Zamberlan[1], A. Schirone[4], A. Frassoldati[4], C. Cittanti[1], G. Arnone[3], M. Bartolomei[1];

[1]Nuclear Medicine Unit, Oncological Medical and Specialists Department, University Hospital of Ferrara, Ferrara, ITALY, [2]Nuclear Medicine Unit, Department of Nuclear Medicine DIMED, University of Padua, Padova, ITALY, [3]Nuclear Medicine Unit, ARNAS Ospedali Civico, Di Cristina e Benfratelli, Palermo, ITALY, [4]Clinical Oncology, Oncological Medical and Specialists Department, University Hospital of Ferrara, Ferrara, ITALY.

Aim/Introduction: In the perspective of precision medicine, molecular classification of breast cancer apperars of paramount importance. According to the current International guidelines, FDG PET/CT is suggested as an optional examination during follow-up only in case of inconclusive conventional imaging. The aim of the present study study was to explore the possible prognostic role of FDG PET/CT, measured in terms of survival, in breast cancer in the recurrent setting, also in accordance with different molecular subtypes. **Materials and Methods:** From two institutional databases, we retrospectively retrieved data about breast cancer patients undergoing FDG PET/CT between 2011 and 2018 for the assessment of recurrency. Molecular subtypes of breast cancer were defined based on the expression of estrogen, progesterone, HER2-b receptors and proliferation index. FDG PET/CT images were revised without knowledge of the molecular subtypes in order to detect local recurrence or lymph node and distant metastases. Overall survival (OS, intended as the time from PET/CT and time of death) was registered for each patient, by checking the medical charts. Parametric and survival analysis were computed. Results: 250 patients were retrieved. FDG PET/CT resulted suggestive for disease recurrence in 159 (63.2%) patients (4 patients with only local breast recurrence, 36 with lymph node recurrence without distant metastases, and 119 with distant metastic lesions). The median time from FDG PET/CT to the last clinical follow-up visit was 54 months (1-192 months). In the whole study group, patients with PET evidence of disease recurrence at any site showed a significantly shorter OS compared to patients with no evidence of recurrence at PET scan ($p<0.001$). Based on molecular classification, 64 patients were classified as Luminal A, 92 as Luminal B, and 29 as Luminal B/HER2-b. Subjects affected by B and B/He molecular type were merged in a single group (B+B/HER2-b). In luminal A patients and B+B/He, a positive PET scan was related to a worse outcome ($p=0.004$, $p=0.001$, respectively). Moreover, PET evidence of distant metastases resulted a

significant discriminator between long and short survivors, either in the A or B+/B-He patient subgroup (p=0.015, p<0.0001). **Conclusion:** These preliminary data suggest that FDG PET/CT may ben an attractive prognostic tool in recurrent breast cancer evlauation. In particular our study supports its prognostic role both in Luminal A and B-type molecular subtypes. **References:** Gradishar, et al. J Natl Compr Can Netw. 2020; 18:452-478Piva R, et al. Breast Cancer (Dove Med Press). 2017; 9:461-471

OP-0131

The Relationship Between Tumor/ Lymph Node Suv Ratio And Immunohistochemical Features With Distant Metastases In Initial Staging F18-PET/CT In Breast Cancer

H. Tosun, B. B. Demirel, G. Uçmak;
Dr. Abdurrahman Yurtaslan Ankara Oncology Training and Research Hospital, Ankara, TURKEY.

Aim/Introduction: We aimed to investigate the relationship between immunohistochemical features, tumor and lymph node PET parameters with the presence of distant metastases at initial staging of breast cancer. **Materials and Methods:** Eighty-five women who were referred to our clinic for PET/CT for staging purposes with diagnosis of breast cancer were included in the study. Age and immunohistochemical (IHC) features of the patients [hormone receptor (HR), her2 status, ki67 index and subtypes] were recorded. Primary tumor SUVmax (Tmax), lymph node SUVmax (Nmax) and tumor / lymph node SUVmax ratios (T/N) were calculated in PET/CT. Patients were divided into two groups as metastatic and non-metastatic according to PET/CT findings. The differences between groups in terms of age, IHC and SUV values were statistically analyzed using t-test. Results: The mean age of the patients was 52±13.8 (range 25-79 years). They were observed in 4 subtypes as, 69% HR +, her2- (n=58), 12% HR +, her2 + (n=10), 10% isolated her2 + (n=9), 9% triple negative (n=8). According to PET/CT findings, the patients were divided in two groups, 45% metastatic (n = 39) and 55% non-metastatic (n = 46). While no statistically significant difference was observed between the two groups in terms of age, HR, Her2 status, ki67 index, subtypes, Tmax and Nmax averages, only a statistically significant difference was found between T/N ratios (p <0.01, Table 1). The mean T/N ratios in metastatic and non-metastatic groups were 2.1 and 4.9, respectively. **Conclusion:** Accurate staging is important in terms of treatment plan and prediction of disease prognosis in breast cancer. In our study, it was thought that the difference in T/N ratio, independent of Tmax and Nmax values, could be a determinant in terms of the overlooked and possible micrometastatic disease indicator in the patient group without known distant metastasis. **References:** 1) Prognostic Significance of MetabolicTumor Volume Measured by (18)F-FDG PET/CT in Operable Primary Breast Cancer DOI: 10.1007/s13139-012-0161-9 2) Predictive and prognosticpotential of volume-based metabolic variables obtained by a baseline18 F-FDG PET/CT in breast cancer with neoadjuvant chemotherapy indication DOI: 10.1016/j.remn.2017.09.002 3) Axillary Lymph Node-to-Primary Tumor Standard Uptake Value Ratio on Preoperative (18)F-FDG PET/CT: A Prognostic Factor for Invasive Ductal Breast Cancer DOI: 10.4048/jbc.2015.18.2.173

OP-0132

Ga-68 PSMA and F-18 FDG PET/CT Imaging in Patients with Triple Negative Breast Cancer and PSMA and Claudin 1, Claudin 4 and Claudin 7 Receptors in Primary Tumor Tissues

E. Arslan[1], N. Ergül[1], E. Beyhan[1], Ö. Erol[1], M. Cin[2], S. Battal Havare[2], F. D. Can Trabulus[3], Ö. Mermut[4], S. Akbaş[5], T. F. Çermik[1];
[1]Istanbul Training and Research Hospital, Clinic of Nuclear Medicine, Istanbul, TURKEY, [2]Istanbul Training and Research Hospital, Department of Pathology, Istanbul, TURKEY, [3]Istanbul Training and Research Hospital, Clinic of Surgery, Istanbul, TURKEY, [4]Istanbul Training and Research Hospital, Department of Radiation Oncology, Istanbul, TURKEY, [5]Koç University Hospital, Department of Medical Oncology, Istanbul, TURKEY.

Aim/Introduction: In this study, we aimed to investigate the diagnostic and prognostic role of PSMA expression in primary and metastatic lesions in 68Ga-PSMA-PET/CT imaging in patient with triple negative breast cancer (TNBC), and also the presence and level of PSMA, Claudin1, Claudin 4 and Claudin 7 receptors in the primary tumoral tissue with immunohistochemically. **Materials and Methods:** 42 women with TNBC (mean age 49.8 ± 10.3 (range: 26-72) underwent Ga-68 PSMA and F-18 FDG PET/CT imaging. The presence of PSMA and Claudin1, 4 and 7 receptors in 29 of the 42 cases was scored immunohistochemically in primary tumor. Results: In Ga-68 PSMA PET/CT, 34/36 (94%) primary lesions were PSMA(+), while 2/36 (6%) were PSMA(-). While 24/42 axillary lymph node metastases were positive in F-18 FDG PET/CT, 22 (92%) cases were PSMA(+) and 2 (8%) cases were PSMA(-) in Ga-68 PSMA PET/CT. Distant metastasis was observed in 24 cases in Ga-68 PSMA PET/CT. Ga-68 PSMA PET/CT showed multiorgan metastasis in 3 cases, 10 liver metastasis [6 PSMA(+), 4 PSMA(-)], 6 bone metastasis [5 PSMA (+), 1 PSMA (-)], 4 lung metastasis [2 PSMA (+), 2PSMA (-)], and 3 brain metastasis [3 PSMA(+) detected lesions were not be detected with F-18 FDG PET/CT], 1 distant nodal metastasis [1 PSMA(+)] was present. 25/29 tissues (86%) were stained with claudin 1, 25/29 (86%) with claudin 4, 13/29 (45%) with

claudin 7, 14/29 (48%) with PSMA. A high positive correlation was found between Ga-68 PSMA SUVmax results and PSMA receptor scoring (Table 2). **Conclusion:** The Ga-68 PSMA PET/CT results were satisfactory in detecting the primary tumors. Ga-68 PSMA PET/CT was observed to be superior to F-18 FDG PET/CT in detecting brain metastasis in TNBC. F-18 FDG uptake and diagnostic sensitivity are higher in metastatic regions other than brain. We suggest that Ga-68 PSMA may have a potential role for radionuclide therapy in the presence of high tumoral uptake in metastatic cases with TNBC due to the theragnostic value. **References:** No

OP-0133

FDG-PET/CT versus CE-CT for response monitoring in metastatic breast cancer - a prospective comparative study

M. Vogsen[1,2,3], F. Harbo[4], N. Jakobsen[1], H. Nissen[1], S. E. Dahlsgaard-Wallenius[1], O. Gerke[1,2], J. Jensen[3], J. Asmussen[4], A. Jylling[5,2], P. Braad[1], W. Vach[6], M. Ewertz[2], M. Hildebrandt[1,2,7];
[1]Odense University Hospital, Department of Nuclear Medicine, Odense, DENMARK, [2]University of Southern Denmark, Department of Clinical Research, Odense, DENMARK, [3]Odense University Hospital, Department of Oncology, Odense, DENMARK, [4]Odense University Hospital, Department of Radiology, Odense, DENMARK, [5]Odense University Hospital, Department of Pathology, Odense, DENMARK, [6]Basel Academy for Quality and Research in Medicine, Basel, SWITZERLAND, [7]Centre for Innovative Medical Technology, Odense University Hospital, Odense, DENMARK.

Aim/Introduction: This study aimed to compare contrast-enhanced CT (CE-CT) and FDG-PET/CT for response monitoring in metastatic breast cancer (MBC) using the standardized response evaluation criteria RECIST 1.1 and PERCIST. The objective was to analyze if FDG-PET/CT detected progressive disease earlier than CE-CT. **Materials and Methods:** Women with MBC were enrolled prospectively and monitored using a combined CE-CT and FDG-PET/CT scan every 9-12 weeks to evaluate response to first-line treatment. CE-CT scans and RECIST 1.1 were used for clinical decision-making without access to the FDG-PET/CT scans. At completion, FDG-PET/CT scans were unblinded and assessed according to PERCIST. Visual assessment was used if response criteria could not be applied. Paired comparative analyses for CE-CT vs. FDG-PET/CT were applied. The primary endpoint was the first detection of progression, and the secondary endpoints were time to detection of progression and the number of scans with measurable disease. Results: A total of 87 women were enrolled in the study with a median of six (range 1-11) follow-up scans. Their distribution according to progression is seen in Table 1. Progression was detected first by FDG-PET/CT in 43/87 patients (49.4%) while CE-CT detected progression first in 1/87 patients (1.11%) ($p < 0.0001$). Excluding patients without progression (n=32), progression was seen first by FDG-PET/CT in 78% (43/55). On average, progression was seen in two follow-up scans (range 1-4) earlier on FDG-PET/CT than on CE-CT. Of 87 patients, 76 (87.4%) had measurable disease according to PERCIST and 51 (58.6%) according to RECIST 1.1. **Conclusion:** In most patients, FDG-PET/CT detected progression earlier than CE-CT, FDG-PET-CT being later only in one. Using FDG-PET/CT offers the opportunity to optimize treatment planning allowing earlier termination of ineffective toxic treatments for MBC. The question about the magnitude of the final benefit for patients is a perspective for future research. **References:** ClinicalTrials.gov registration: NCT03358589

OP-0134

Evaluation of Cardiac Toxicity in Patients Undergoing Breast Cancer Treatment with HER2-inhibitors

A. Lazar[1], M. Mutuleanu[1], M. Gherghe[1,2], I. Irimescu[2];
[1]Carol Davila University of Medicine and Pharmacy, Bucharest, ROMANIA, [2]Oncology Institute "Professor Doctor Alexandru Trestioreanu", Bucharest, ROMANIA.

Aim/Introduction: The human epidermal growth factor receptor 2 (HER2) is overexpressed in up to 25% of the breast cancers diagnosed. The main HER2-inhibitors used in HER2-positive metastatic breast cancer treatment are the monoclonal antibodies Trastuzumab and Pertuzumab, usually associated with other types of chemotherapy, such as anthracyclines, taxanes or hormonal therapy. The clinical benefits of HER2-inhibitors are well documented, however the important cardiac adverse reactions must be taken into consideration. In this study we evaluate the cardiac function of patients undergoing combined therapy with HER2-inhibitors, by comparing results obtained through equilibrium radionuclide angiogram and cardiac ultrasound, with the aims of assessing early cardiac toxicity of the treatment and the necessity of further treatment adjustment. **Materials and Methods:** Participants were requested to provide results from the most recent echocardiographic exam. Multigated acquisition (MUGA) scans were performed in 48 female patients aged 31-69 years old, diagnosed with HER2-positive breast cancer, stages IIB - IV, undergoing treatment with both Trastuzumab and Pertuzumab. Erythrocytes were radiolabeled "in vivo" using a technique in which a solution of pyrophosphate is injected intravenously and, after 20 minutes, a dose of 20 mCi of ^{99m}Tc-pertechnetate is administered. Planar (LAO45 on detector 1) and SPECT/CT acquisitions were performed on a gamma camera (Discovery 670 DR, GE Healthcare) after 10 minutes from the last injection, using EKG-gated parameters of 16 frames/cycle for both studies. Results: Most left ventricular ejection fractions (LVEF) obtained through the MUGA scans were lower than the ones estimated on echocardiography (p=0.004), but still in the normal range, with only 6 patients exhibiting higher EFs on both planar radionuclide ventriculography (RNV) and cardiac SPECT. The incidence of decreased LVEF on the equilibrium radionuclide angiogram was 3% (ranging from 22-49%, with an average decrease of 18%), with one patient

(0.5%) fulfilling the ESC criteria for cardiac toxicity, presenting an LVEF=22%. It is notable that none of the subjects who presented echocardiographic LVEF lower than 60% had an abnormal ejection fraction on MUGA scans. **Conclusion:** The majority of patients undergoing therapy with Pertuzumab and Trastuzumab for breast cancer exhibited low normal LVEF, probably corelated with cardiotoxicity given by previous treatment with taxanes and anthracyclines, which most of the patients underwent as preoperative care. As an ongoing study, assessment of LVEF at both at the beginning and the ending of the treatment is necessary to evaluate the toxic potential of this treatment combination. **References:** None.

OP-0135

The significance of the intramammarian sentinel lymph nodes in the lymphatic mapping

Z. Koc, P. P. Özcan, F. Daloğlu, M. Berkeşoğlu, Z. S. Sağlam; Mersin University, Mersin, TURKEY.

Aim/Introduction: The limited number of series in the literature about the intramammarian sentinel lymph nodes point out clinical significance of this entity. The aim of this study was to evaluate the pathologic status of the intramammarian sentinel lymph nodes as well as compare these results with sentinel node imaging and F-18 FDG PET/CT findings. **Materials and Methods:** 30 women (36-72; 52,mean: 73±11,19 years old) with diagnosis of breast cancer who underwent sentinel lymph node evaluation were the subject of this study. The patients' pathology results pointed out the intramammarian sentinel lymph nodes and there were 15 patients with sentinel lymph node scintigraphy and 23 patients with F-18 FDG PET/CT results. The detection rates of the imaging studies were analyzed and compared with pathology results. Results: Four of the patients included in the study were operated previously (mastectomy) and the others primary tumor was 20,94±11,19 mm mean in size and the mean uptake value was 11,08±6,88 (SUVmax). The axillary lymph nodes that were observed in the F-18 FDG PET/CT were mean 13±8,66 mm in diameter and the mean SUVmax value of these lymph nodes was 5,3±5,4. The detection rate of the intramammarian lymph nodes in the F-18 FDG PET/CT was 7/23 (30,43%) and 5/15 (33,3%) in the sentinel lymph node imaging. Among the 29 sentinal intramammarian lymph nodes 16 were positive and intramammarian sentinel lymph nodes were only metastatic lymph node in 7 patients. Additionally in 5 of the patients with sentinel lymph node scintigraphy the sentinel node was not detected. **Conclusion:** The intramammarian lymph nodes changed patients management in 7/30 patients in this study. The detection rates of nor the sentinel lymph node scintigraphy neither F-18 FDG PET/CT was sufficient. **References:** 1. Koc ZP, Özcan Kara P, Dağ A, Tuncel Daloğlu F.In-transit sentinel lymph nodes predicted by F-18 Fluorodeoxyglucose Positron Emission Tomography/Computed Tomography.Nucl Med Rev Cent East Eur. 2019;22(1):37-39.

311

Wednesday, October 20 - Saturday, October 23, 2021

on-demand pool, release on Wednesday, October 20 at 09:00

Featured Session: Show me your Heart!

OP-0137

Cardiac Sarcoid and Amyloid Imaging Are Here to Stay

O. Lairez; University. hospital of Toulouse, Department of Nuclear Medicine and Cardiac Imaging Center, Toulouse, FRANCE.

OP-0138

Volumetric Evaluation of ^{99m}Tc-pyrophosphate SPECT/CT in Patients with Transthyretin Cardiac Amyloidosis: Correlation with Cardiac Functional Parameters

S. Watanabe, K. Nakajima, H. Wakabayashi, H. Yoneyama, S. Yoshida, J. Komatsu, A. Inaki, T. Konishi, S. Kinuya; Kanazawa University Hospital, Kanazawa, JAPAN.

Aim/Introduction: Volumetric evaluation of ^{99m}Technetium-pyrophosphate (^{99m}Tc-PYP) SPECT/CT is an objective and useful method for diagnosing transthyretin cardiac amyloidosis (ATTR-CA) [1, 2]. The aim of this study was to assess its relationship to cardiac functional parameters and SUVmax. **Materials and Methods:** We retrospectively evaluated 22 patients with ATTR-CA, and who underwent ^{99m}Tc-PYP SPECT/CT at our hospital between October 2018 and January 2021 (76.5±11.6 years old). All patients underwent endomyocardial biopsy and/or TTR gene test; 12 patients were diagnosed with wild type and 10 patients were diagnosed with hereditary type. Patients were imaged at 1 hour (n = 8) or 3 hours (n = 14) after ^{99m}Tc-PYP injection. First, we evaluated an aortic blood pool ^{99m}Tc-PYP activity (ABPmax) using SUVmax in the ascending aorta at the level of the pulmonary artery bifurcation [3]. Next, we objectively evaluated the total volume of the region where ^{99m}Tc-PYP uptake > 1.2 times ABPmax in the left and right ventricular myocardium and defined it as cardiac metabolic volume (CMV). SUV and CMV were calculated using xSPECT Quant. We assessed the correlation of CMV with cardiac functional parameters of echocardiography (LVEF, left ventricular posterior wall thickness at end-diastole: LVPWTd, and E to early diastolic mitral annular tissue velocity ratio: E/e'), electrocardiography (QRS duration), and blood examination (BNP and troponin T: TnT). As a conventional uptake parameter, myocardial SUVmax was also calculated. Results: CMV (mean±SD = 170.4±169.1cm^3) negatively correlated with LVEF (59.0±15.9%; r = -0.59, p = 0.004) and correlated with LVPWTd (14.5±4.1mm; r = 0.62, p = 0.002), E/e' (18.6±5.4; r = 0.47, p = 0.03), QRS(113.3±28.3ms; r = 0.47, p = 0.03), BNP (346.0±401.0pg/mL; r = 0.64, p = 0.001; n = 17), and TnT(0.071±0.032ng/mL; r = 0.61, p = 0.047; n = 11). Myocardial SUVmax cannot be objectively assessed in 2 biopsy-proven ATTR-CA patients because ^{99m}Tc-PYP uptakes

in the myocardium were diffusely low (CMV < 0.2cm^3) and the adjacent blood pool uptakes were high. In the other 20 patients, SUVmax (4.1±1.6) negatively correlated with LVEF, while did not significantly correlate with other parameters (CMV, LVPWTd, E/e', QRS, BNP, and TnT). **Conclusion:** Volumetric evaluation of ^{99m}Tc-PYP SPECT/CT may be superior to SUVmax in assessing the disease burden of ATTR-CA, which could be a useful non-invasive marker to precisely stratify and follow the amyloid burden. **References:** 1) Miller RJH et al. JNC. 2021; online ahead of print. 2) Watanabe S et al. EJNMMI. 2020; 47(S1): S524.

OP-0139

Diagnostic value of bone scintigraphy in cardiac amyloidosis after domino liver transplantation

E. Piekarski[1], L. Eliahou[2,3], R. Chequer[1], F. Scalbert[1], D. Adams[3,4], D. Le Guludec[1], M. S. Slama[3,5], D. Samuel[3,6], I. Kounis[6], F. Rouzet[1], V. Algalarrondo[2,3];

[1]Nuclear Medicine Department, Bichat-Claude Bernard Hospital, Assistance Publique Hôpitaux de Paris (AP-HP), DHU APOLLO, Inserm UMR 1148, Université de Paris, Paris, FRANCE, [2]Cardiology Department, Bichat-Claude Bernard Hospital, AP-HP, Inserm UMR-S 1180, Université de Paris, Paris, FRANCE, [3]French Referent Center for Rare Diseases for FAP (Familial Amyloid Polyneuropathy) (CRMR-NNERF), Bicêtre, FRANCE, [4]Neurology Department, AP-HP, Université Paris-Saclay, INSERM 1195, Bicêtre, FRANCE, [5]Cardiology Department, Bichat-Claude Bernard Hospital, AP-HP, Université de Paris, Paris, FRANCE, [6]Centre Hépato Biliaire, AP-HP, Université Paris-Saclay, Hopital Paul Brousse, Villejuif, FRANCE.

Aim/Introduction: Domino liver transplantation (DLT) consists in reimplanting liver from transplanted patients suffering from transthyretin amyloidosis (TTR) in recipients (DLR) with end stage liver disease. Secondary amyloidosis has been reported within 10 years in DLR. The aim of the study was to evaluate bone scintigraphy (DPD) for the diagnosis of cardiac amyloidosis (CA) in DLR. **Materials and Methods:** We retrospectively included consecutive DLR undergoing assessment of CA in the French Reference Center for Amyloidosis (CRMR-NNERF) from 2012 to 2020 who had undergone at least one DPD. All patients underwent clinical evaluation of their cardiac and neurological condition, ECG, echocardiography, cMRI, BNP and Troponin T serum levels, and target organ biopsy. The diagnosis of CA was made by expert consensus. Results: A total of 48 patients were included. DPD was performed 10 [3 to 19] years after DLT. The mean age was 71 y, 85%, were male and 77% were symptomatic with a predominance of neurologic symptoms. Patients with final diagnosis of CA (N=16) were older than patients without CA (75 vs 69, p=0.007), had higher troponin levels (0.08 vs 0.04, p=0.037), increased myocardial thickness (IVS 13.8 vs 10.6mm, p<0.001), uptake on DPD (7 patients vs none, p<0.001), LGE on MRI (12 vs 2, p<0.001). Of the 16 patients with CA, only 7 presented positive DPD; 2 patients with negative DPD had positive myocardial biopsy.Therefore, DPD for the diagnosis of CA in DLR had a sensitivity of 44%, with negative predictive value of 78%. However, specificity was 100%. Patients with CA and positive DPD were older than patients with CA and negative DPD (78 [70-86] vs 70 [50-83], p=0.006). In the 7 patients with positive DPD, Perugini grade was 1 in 1 patient, 2 in 2 patients and 3 in 4 patients. All showed diffuse cardiac uptake (with apical sparring in 3 patients) except for 2 (no uptake in a necrotic wall from previous myocardial infarction). Out of 16 patients who underwent repeated DPD, 3 with initially negative DPD presented cardiac uptake onset during follow-up. **Conclusion:** CA can develop during follow up in DLR, thus patients should be monitored closely with multimodal evaluation. DPD shows high specificity but in contrast with published data in wild-type or hereditary TTR CA, the present study shows that in the DLR population, the diagnostic performance of DPD is lower with limited sensitivity so that a negative DPD does not rule out CA. **References:** None

OP-0140

Bone scintigraphy in hereditary ATTR patients: characteristics and prognostic impact of the different clinical phenotypes

F. Mattana[1], M. Sguazzotti[2], P. Massa[2], A. Ponziani[2], A. G. Caponetti[2], G. Saturi[2], R. Bonfiglioli[1], S. Longhi[2], C. Gagliardi[2], E. Biagini[2], P. Cortelli[3], N. Gallie[2], S. Fanti[1];

[1]IRCCS Azienda Ospedaliero-Universitaria di Bologna, Metropolitan Nuclear Medicine, Bologna, ITALY, [2]IRCCS Azienda Ospedaliero-Universitaria di Bologna, Cardiology Unit, Bologna, ITALY, [3]IRCCS Institute of Neurological Sciences of Bologna, Bellaria Hospital, Bologna, ITALY.

Aim/Introduction: Hereditary transthyretin-related amyloidosis (h-ATTR) is a rare autosomal-dominant infiltrative disease, caused by a single amino acid mutation on the transthyretin (TTR) gene. TTR mutations lead to formation of amyloid fibrils, which are consecutively deposited extracellularly in multiple organs, including heart and peripheral nervous system. We aimed to characterize and compare clinical, instrumental, and prognostic features of patients affected by h-ATTR by dividing the population into the disease's main phenotypes (unaffected carriers-UC, cardiac-CP, neurological-NP or mixed phenotype-MP). We tried to correlate the phenotypes with technetium-99m 3,3-diphosphono-1,2-propanodicarboxylic acid (99mTc-DPD) bone scintigraphy (BS) and the correlation with the visual analysis using Perugini score (PS). **Materials and Methods:** 285 patients (pts) of a single-centre cohort with a recognized pathogenic mutation on TTR gene were retrospectively included in the analysis. Phenotypes of disease were defined at baseline. NP was defined according to sensorimotor and/or autonomic dysfunction, while CP was defined in the presence of unexplained maximum wall thickness >12 mm

and other typical echocardiographic findings. UC and MP presented none or both of the above-mentioned features, respectively. 99mTc-DPD BS was performed according to EANM guidelines with standard procedures. PS is considered positive when is ≥2, as well established. Results: Out of 285 pts, 210 pts showed clinical signs of the disease, 37 (13%) with CP, 65 (23%) with NP and 108 (38%) with MP, while 75 subjects (26%) were UC. 162 pts underwent (99mTc-DPD) BS at baseline: among CP pts, 20 showed PS=2, 9 PS=3; in NP pts, 20 showed score 0, 2 PS=1, 6 had PS=2, 1 had PS=3; in MP pts 1 had PS=1, 31 had PS=2, 23 showed PS=3. After a mean follow-up of 59 months, 98 (34%) patients died. On a Kaplan-Meier survival analysis, mean survival times were 208, 150, 123 and 95 months for UC, NP, CP, and MP, respectively, with a statistically significant difference in affected patients between NP and MP (p=0.012). NYHA class, ECG findings, left ventricular wall thickness and ejection fraction did not significantly differ between CP and MP. **Conclusion:** These results suggest that primary phenotypes strongly influence the natural history of the h-ATTR; prognosis could range from excellent in unaffected carriers to inauspicious in MP. PS positive at BS were mostly frequent observed in MP and CP pts when compared to NP pts, in which PS are negative or low grade, resulting in a better outcome. **References:** none

OP-0141

Does semiquantification using the H/CL ratio on 3h planar [^{99m}Tc]Tc-DPD imaging have additional prognostic value in cardiac amyloidosis?

L. Lemos[1], P. Soeiro[1], R. Ferreira[1,2], M. J. Cunha[1], G. Costa[1,3], J. Pedroso de Lima[1,2,3];
[1]Centro Hospitalar e Universitário de Coimbra, Coimbra, PORTUGAL, [2]Instituto de Ciências Nucleares Aplicadas à Saúde (ICNAS), Faculdade de Medicina, Universidade de Coimbra, Coimbra, PORTUGAL, [3]Faculdade de Medicina, Universidade de Coimbra, Coimbra, PORTUGAL.

Aim/Introduction: Cardiac scintigraphy with bone-seeking agents has high sensitivity and specificity for the diagnosis of ATTR amyloidosis. Images are evaluated using a visual grading scale, but the prognostic value of each category is unclear. Planar imaging semiquantification techniques, using metrics such as the heart-to-contralateral (H/CL) ratio, are easy to perform and have been proposed as possible prognostic markers. The objective of this study is to assess whether H/CL ratio on 3h planar [^{99m}Tc]Tc-DPD imaging correlates with mortality or any analytical or imaging parameters with prognostic value. **Materials and Methods:** We reviewed the clinical charts of 107 patients (65 male, 42 female; average age 78.9±9.9 years) with suspected cardiac amyloidosis who underwent [^{99m}Tc]Tc-DPD scintigraphy, between October/2018-March/2021. Each patient performed whole-body anterior and posterior images and left anterior oblique images of the thorax, 3h after injection. Myocardial uptake was graded from 0-3 by visual comparison with rib uptake, according to the ASNC/EANM Cardiac Amyloidosis Practice Points. H/CL ratio was also calculated, using the mean counts within ROI placed over the heart and mirrored over the contralateral chest. A study displaying grade 2-3 myocardial uptake or a H/CL ratio>1.3 was considered positive. Relevant demographic data were also collected, as well as analytical (ntproBNP, immunofixation), echocardiographical (LVEF; interventricular septum thickness); MRI (LVEF, LV volume, estimated mass, late gadolinium enhancement) and AngioCT parameters (coronary and aortic calcium scores), as well as biopsy results, when available. Results: The average H/CL ratio at 3 hours of our sample was 1.29±0.52, with 31 patients (29%) considered to have positive studies. 69 patients were classified as having grade 0 myocardial uptake (64.5%), 7 as grade 1 (6.5%), 1 as grade 2 (0.9%) and 30 as grade 3 (28%). H/CL ratio was significantly different between all the visual grading categories (Kruskal-Wallis, p<0.01). The visual grading scales and semi-quantification also showed very high agreement (Cohen's kappa 0.955; p<0.01) in classifying studies as positive or negative. When analytical and imagiological parameters were analyzed, weak statistically significant correlations were found between H/CL ratio and ntproBNP (Spearman's rho 0.312; p<0.01) and the interventricular septum thickness (rho 0.339; p<0.01) and LVEF values determined by echocardiography (rho -0.289; p=0.015). There was no association between the H/CL ratio and survival (Cox regression, HR 0.973; CI95% 0.439-2.160; p=0.947). **Conclusion:** In our population, H/CL ratio calculation on 3h planar [^{99m}Tc]Tc-DPD imaging did not show any significant additional prognostic value compared to visual grading. **References:** none

OP-0142

Multiparametricassessment Of The Mechanical Function Of The Left Ventricleby CZT MPI: Comparison With Cardiac Magnetic Resonance

E. Cerudelli[1,2], M. Gazzilli[1], L. Camoni[1], F. Dondi[2], A. Mazzoletti[2], P. Bellini[2], D. Albano[1,2], F. Bertagna[1,2], R. Giubbini[1,2];
[1]Azienda Socio Sanitaria Territoriale degli Spedali Civili di Brescia, Brescia, ITALY, [2]Università degli Studi di Brescia, Brescia, ITALY.

Aim/Introduction: We aimed to verify the accuracy of Cadmium-Zinc-Telluride (CZT) myocardial perfusion imaging (MPI) in assessing left ventricle (LV) mechanical parameters using two commonly employed softwares, comparing results with cardiac magnetic resonance (CMR), considered as reference. **Materials and Methods:** Within maximum 120 days (50±37 days), seventy-one patients (mean age 64±10; 21% female) underwent 99mTc tetrofosmin stress/rest CZT MPI and 1,5 T CMR. Corridor 4DM (4DM) and Emory Cardiac Toolbox (ECTb) were selected for MPI analyses. End diastolic volume (EDV), end systolic volume (ESV), ejection fraction (EF) and LV mass (LVM) were quantified. Results: Considering mean values,

only EF values obtained with ECTb were significantly different than the CMR ones (p<0,01). Correlation between results of CZT SPECT and CMR was high for both the software packages analysed, but superior using 4DM than ECTb (EDV: R = 0,981 vs. 0,947; ESV: R = 0,978 vs. 0,942; EF 4DM: R = 0,859; Mass: R = 0,849 vs. 0,781). Bland-Altman analysis showed systematic error only in EDV computation, with a trend of overestimation of the lower and progressive underestimation of the higher values by CMR with quite narrow limits of agreement for both SPECT softwares (4DM -14,3% to 8,8%; ECT - 12,4% to 25,7%). Considering separately patients with and without previous myocardial infarction (MI) the strengths of correlation were the greatest for the second group, with always higher values for 4DM than ECTb for all the parameters analysed (with previous MI, EDV: R = 0,977 vs. 0,943; ESV: R = 0,971 vs. 0,936; EF 4DM: R = 0,825; Mass: R = 0,799 vs. 0,756; without MI, EDV: R = 0,985 vs. 0,948; ESV: R = 0,987 vs. 0,961; EF 4DM: R = 0,887; Mass: R = 0,949 vs. 0,838). **Conclusion:** The evaluation of the mechanical function of LV with CZT MPI is feasible, with high levels of agreement, especially using 4DM software. These results support the growing emphasis to systematically include the LV mechanical parameters in all MPI reports. **References:** Schaefer WM, Lipke CSA, Standke D, et al. Quantification of left ventricle volumes and ejection fraction from Gated 99mTC-MIBI SPECT: MRI validation and comparison of the Emory Cardiac Tool Box with QGS and 4D-MSPECT. J Nucl Med, 2005;46:1256-1263

OP-0143

Qualitative and quantitative cardiac 18F-FDG-PET findings in patients with suspected inflammatory cardiomyopathy: a pilot study

A. Franchini[1], *A. Scarale*[2], *F. Baldassi*[1], *G. Cabrini*[2], *E. Gay*[2], *M. Milella*[2], *C. Rossetti*[2], *S. Capitanio*[2];
[1]*University of Milano-Bicocca, Milano, ITALY,* [2]*ASST Grande Ospedale Metropolitano Niguarda, Milano, ITALY.*

Aim/Introduction: Inflammatory cardiomyopathies refer to a broad group of disorders characterized by myocardial inflammation as a primary cause of cardiac dysfunction with heterogeneous substrates (postinfectious, autoimmune, toxic and infiltrative). The aim of this pilot study was to evaluate the incidence of myocardial inflammation detected by 18F-FDG PET/CT imaging in a group of patients with non-sarcoidotic and non-ischemic cardiomyopathy (NICM) with the support of a semiquantitative analysis. **Materials and Methods:** We retrospectively evaluated all cardiac PET examinations performed in Niguarda Hospital from January 2018 to December 2020. We selected from this population 14 unexplained non-sarcoidotic NICM patients (mean age = 57; average left ventricular ejection fraction 35 ± 10%) that underwent 18F-FDG PET/CT studies after 12 hour fasting and under high-fat, low-carbohydrate diet for at least 24 hours before the scan, in order to identify a possible underlying inflammatory etiology of cardiomyopathy. At visual analysis, cardiac PET images were considered positive if there was any area of myocardial FDG uptake having greater activity than the left ventricular blood pool. Myocardial FDG uptake was reported as either none, focal, diffuse, or focal on diffuse uptake. A dedicated software was used to estimate global and regional cardiac uptake of FDG through 17 segment polar maps. Results: 9/14 patients showed myocardial pathological FDG uptake at PET/CT scan. In particular, 2, 4, and 3 individuals exhibited diffuse, focal, and focal on diffuse patterns, respectively. The quantitative analysis of FDG distribution in myocardium confirmed the qualitative interpretation, showing average SUV values significantly higher in positive patients than in those visually considered negative (p<0.01). In PET positive subjects, FDG uptake was heterogeneously distributed throughout the left ventricle with a variation coefficient of 34±14%. No significant difference in SUV max values was found among three vascular territories (LAD, RCA and CX). However, the difference between CX and LAD variation coefficient approached statistical significance. Positive patients with a prevalence of myocardial segments with SUV greater than 1.5 tended to have a more pronounced increase in ejection fraction after PET scan compared to baseline value, even if still under statistical significance. **Conclusion:** This pilot study underlines the utility of 18F-FDG-PET in the identification of myocardial inflammatory burden in patients with unexplained cardiomyopathy. In particular, if confirmed by further studies, the complementary use of qualitative image assessment and quantitative PET analysis could have a potential capability to obtain prognostic information with a consequent impact on patient management. **References:** none

OP-0144

Are stress-induced dyssynchrony parameters obtained from different nuclear modalities comparable in terms of identifying high-risk patients after surgical treatment of ischemic cardiomyopathy?

V. Shipulin*, A. Pryakhin, S. Andreev, V. M. Shipulin, K. Zavadovsky; Cardiology Research Institute, Tomsk National Research Medical Centre, Russian Academy of Sciences, Tomsk, RUSSIAN FEDERATION.*

Aim/Introduction: Stress tests can be used to unmask mechanical dyssynchrony (MD). However, stress-induced changes in left ventricle (LV) MD by data of nuclear imaging modalities are not well-understood, especially predictive value [1]. The ai of our study was to assess the role of stress-induced changes of LV MD obtained by nuclear modalities in evaluating high-risk patients after surgical treatment of ischemic cardiomyopathy (ICM). **Materials and Methods:** 69 patients with ICM were enrolled. Before surgical treatment, all patients underwent gated myocardial perfusion imaging (gMPI) (Tc^{99m}-MIBI; 2 days stress-rest protocol, adenosine 140mkg/kg/min) and gated blood pool SPECT (gBPS) (rest - stress, dobutamine doses of 5/10/15 μg/kg/min). After surgical treatment, patients were divided into 2 groups: with (death,

IABP, extra inotropic support) (n=21) and without (n=48) complications in early postoperative period. The following parameters were estimated: perfusion (SSS, SRS, SDS); phase, standard deviation (PSD) and histogram bandwidth (HBW); phase entropy (only by gBPS). Stress-induced changes (Δ) were calculated for MPI indices as [stress value-rest value], for gBPS indices as [value on each dobutamine dose-rest value]. For gBPS the maximum changes of MD were calculated as well. Results: Rest gBPS MD correlated with SRS better than rest gMPI (gMPI: PSD r=0.31, p=0.005; HBW r=0.28, p=0.008; gBPS: PSD r=0.47, p<0.001; HBW r=0.36, p=0.006; entropy r=0.39, p=0.003). Stress gBPS MD correlated better with post stress gMPI MD at the dobutamine dose of 5μg/kg/min. The following increase of the dobutamine dose led to a decrease in the r-value, but it remained significant for all indices. Stress-induced MD changes didn't correlate between gMPI and gBPS. Mann-Whitney test showed significant differences in SDS (p=0.02) between the groups. Both methods didn't show any differences at rest study. Stress-induced changes of MD showed differences between groups in only ΔEntropy rest-10μg/kg/min (p=0.02) and maximum ΔEntropy (p=0.01) by gBPS, as well as Δphase mean (p=0.03) by gMPI. Logistic regression analysis showed that only maximum ΔEntropy has prognostic value in prediction of the course of early postoperative period (OR 1.2 95%CI 1.04; 1.37). ROC-analysis showed sensitivity of 80% and specificity of 55% with AUC of 0.7 for cut-off value >0 **Conclusion:** Only maximum ΔEntropy obtained from dobutamine gBPS was associated with the adverse course of early postoperative period in patients with ICM. **References:** 1. Saushkin V.V., Mishkina A.I., Shipilin V.V., Zavadovsky K.V. The value of radionuclide assessment of mechanical dyssynchrony in patients with cardiac diseases. REJR 2019; 9(1):186-202. DOI:10.21569/2222-7415-2019-9-1-186-202 2.

OP-0145

Clinical differences between patients with Perugini's grade 2 and grade 3 cardiac ATTR amyloidosis confirmed by ^{99m}Tc-DPD scan

F. Sebastián Palacid, N. Álvarez Mena, B. Pérez López, C. Gamazo Laherrán, P. Turbay Eljach, M. Alonso Rodriguez, A. Sáinz Esteban, C. F. García García, M. Ruiz Gómez, M. J. González Soto, R. Ruano Pérez;
Hospital Clínico Universitario Valladolid, Valladolid, SPAIN.

Aim/Introduction: To describe the clinical differences between patients with scintigraphy-confirmed ATTR cardiac amyloidosis, based on Perugini's uptake degree in which they have been classified (grade 2 vs. grade 3). **Materials and Methods:** Retrospective study between February 2017 and April 2021. 80 patients were included (72 men and 8 women). 71 patients were classified as Perugini's uptake grade 3 by scintigraphy. We have assessed 22 clinical variables, such as sex, age, distribution pattern of the radiopharnaceutical in the myocardium, cardiovascular risk factors, echocardiogram or proteinogram abnormalities, etc. Results: The differences have been found between both groups show that patients with ATTR grade 2 cardiac amyloidosis were more likely to develop moderate or severe concentric left ventricular hypertrophy (p=0.0000), to have a preserved LVEF (LVEF >50%) (p=0.0047) and to present proteinogram abnormalities (p=0.0206). On the other hand, patients with Perugini's grade 3 ATTR cardiac amyloidosis were more likely to develop interventricular septal hypertrophy (p=0.0001), to have a LVEF restriction (LVEF <50%) (p=0.0047) and to suffer severe chronic kidney disease (p=0.0027). We have not found other differences with statistical significance between the rest of the clinical variables. **Conclusion:** Although the sample of patients with grade 2 ATTR cardiac amyloidosis was small, we can infere that there are clinical differences between both groups of patients. Therefore, Perugini's scintigraphic grading would allow us to estimate the clinical impact of the disease on patients and allow us to know what are the implicit clinical characteristics based on the uptake of the radiopharmaceutical in the myocardium. **References:** None

OP-0146

Possibility of scintigraphic indexes of left ventricle mechanical dyssynchrony for predicting benefit from cardiac resynchronization therapy with comparing different response criteria

A. Mishkina, V. Saushkin, T. Atabekov, K. Zavadovsky;
Cardiology Research Institute, Tomsk National Research Medical Centre, Russian Academy of Sciences, Tomsk, RUSSIAN FEDERATION.

Aim/Introduction: The assessment of left ventricular mechanical dyssynchrony is essential in identifying patients who may benefit from cardiac resynchronization therapy (CRT). Numerous criteria are used in the literature to define a positive response to CRT. Recently, echocardiographic indexes more often used to determine the response to CRT [1]. The aim of this study was to assess the prognostic significance of LV mechanical dyssynchrony indexes, assessed by myocardial perfusion imaging (MPI), to predict benefit from CRT, using different criteria of response. **Materials and Methods:** This study included 40 HF patients, referred for CRT. Before CRT all patients underwent rest gated MPI. Based on the phase analysis, the following indexes were estimated: phase standard deviation (SD) and phase histogram bandwidth (HBW). One year after CRT response was defined as each of the following criteria: left ventricle end-systolic volume (LV_ESV) decreased by ≥15%, left ventricle ejection fraction (LV EF) increase by ≥5%, and 10% and their combination. Results: SD and HBW were significantly different between responder and non-responders when using various response criteria, except LV_ESV decrease ≥15%. According to ROC-analysis, SD and HBW were statistically significant predictors of response to CRT, with the listed response criteria, except LV_ESV. Then the response was defined as LV_EF increase ≥5% following

ROC-characteristics were received: for SD cut-off point was ≤132ms, sensitivity (Se)=63%, specificity (Sp)=87%, area under the curve (AUC)=0.696; for HBW cut-off point was ≤401ms, Se=63%, Sp=87%, AUC=0.696; p<0.05. The following ROC-characteristics were found for LV_EF increase ≥10% response: for SD cut-off point was ≤132ms, Se=76%, Sp=81%, AUC=0.75; for HBW cut-off point was ≤440ms, Se=76%, Sp=72%, AUC=0.74; p<0.05. Then the response was defined as LV_ESV decrease ≥15% following ROC-characteristics were received: for SD cut-off point was ≤130ms, Se=53%, Sp=75%, AUC=0.57, p=0.28; for HBW cut-off point was ≤491ms, Se=66%, Sp=60%, AUC=0.578, p=0.27. Then the response was defined as a combination of LV_ESV decrease ≥15% and LV_EF increase ≥5% following ROC-characteristics were received: for SD cut-off point was ≤164ms, Se=91%, Sp=54%, AUC=0.726; for HBW cut-off point was ≤541ms, Se=83%, Sp=54%, AUC=0.667; p<0.05. **Conclusion:** The LV mechanical dyssynchrony indexes, assessed by MPI, are matters for predicting benefit from CRT when improvement of LV_EF was used as response criteria. Thus, MPI may be used as a tool to optimize patient selection to CRT. **References:** 1. Saushkin V.V., Mishkina A.I., Shipilin V.V., Zavadovsky K.V. The value of radionuclide assessment of mechanical dyssynchrony in patients with cardiac diseases. REJR 2019; 9(1):186-202. DOI:10.21569/2222-7415-2019-9-1-186-202

OP-0147

Impact of hybrid ^{18}F-FDG PET/CMR on cardiac sarcoidosis diagnosis and disease stage differentiation

J. Garcia, R. Olivero, P. Bassa, M. Lopez, J. Monmeneu, E. Riera, L. Higueras, M. Garcia, A. Maceira;
CETIR ASCIRES Grupo biomédico, Barcelona, SPAIN.

Aim/Introduction: To evaluate diagnostic impact of hybrid ^{18}F-FDG PET/CMR in patients with cardiac sarcoidosis (CS) and to discern their disease stages. **Materials and Methods:** Twelve patients (56±9-year-old; 8 male) suspected for CS were prospectively included. Seven presented with known extracardiac involvement, and 5 with clinical,, ECG and cardiac-US suspicious for CS. Exclusion criteria were pregnancy/breast-feeding, pacemaker/other metallic implants, kidney failure. Patients were submitted to dietary for 5 days, with a high-protein and fat diet, carbohydrates restriction, and intravenous heparin administration (50 IU/Kg) 15 min before injection of 0.125 mCi/kg ^{18}F-FDG, with the aim to supress glucose miocadial uptake (except for 2 patients on anticoagulant treatment). Synchronous PET/CMR study (Signa-3T,GE) included: 1)Whole-body PET/MRI 1h after ^{18}F-FDG injection: 5 beds; 4 min/bed. MRI: DIXON, T1, T2 and diffusion sequences. 2) Cardiac PET/MR: PET: 1 bed/10 min with cardiac and respiratory gating. CMR: anatomical sequences; cine; phase contrast; STIR; rest first-pass perfusion with Gd, late Gd enhancement (LGE). Cardiac volumes, mass, biventricular ejection fraction (EF) and segmental systolic function were all measured on the CMR. Hypoperfusion was assessed on the rest first-pass, and LGE pattern was also sought. Whole-body PET images were reviewed for detection of extracardiac uptake sites, and myocardium ^{18}F-FDG uptake in cardiac PET images, with activity pattern and uptake intensity (SUVmax) assessment. Results: Procedure was successfully completed in all patients, with no artifacts due to synchronous PET/MRI acquisition. There were no technical incidences and adequate myocardial suppression was always achieved. The averaged time for each study was 60 min: 20 min (whole-body) and 40 min (cardiac). LVEF was significantly reduced in 5 patients, and RVEF in 1 patient. LGE+ consistent with CS was detected in 9 patients (75%), with transmural injury (n:3); intramyocardial (n:2); subendocardial (n:2) and subepicardial (n:2). Abnormal focal segmental cardiac ^{18}F-FDG uptake was detected in 5 patients. Mean SUVmax was 3.2 (2.9-4.9). In 4 out of 5 patients, 18F-FDG uptake corresponded with LGE+. Combined findings allowed patient categorization into 3 groups: 1)Active CS (PET+MRI+) in 5 patients; 2)Inactive CS (PET-RM+) in 4 patients; and 3) No imaging criteria for CS (PET-RM-) in 3 patients. Moreover, active focal extracardiac ^{18}F-FDG uptake was detected in 7 patients: mediastinum (n:5), and mediastinum and lung (n:2). **Conclusion:** Synchronous ^{18}F-FDG PET/MRI acquisition allowed reliable cardiac and extracardiac assessment of sarcoidosis and stage disease categorization all in one-step procedure, thus providing valuable information about sarcoidosis impact on heart function and extracardiac involvement. **References:** None

313

Wednesday, October 20, 2021, 13:30 - 13:50

Channel 1

EANM Awards Ceremony

OP-0150

EANM Awards Ceremony

W. Wadsak; *EANM Secretary/Treasurer, Vienna, AUSTRIA.*

314

Wednesday, October 20, 2021, 14:20 - 14:40

Channel 1

Plenary Quiz (for Plenary 2)

OP-0151

Plenary Quiz

V. Garibotto; *University Hospital of Geneva, Nuclear Medicine and Molecular Imaging Division, Geneva, SWITZERLAND.*

401

Wednesday, October 20, 2021, 14:40 - 16:00

Channel 1

Plenary 2: Theranostics Applications and Challenges (incl. Marie Curie Lecture)

OP-0152
We are Theranostics

B. Guillet; *Radiopharmacy department, University Hospital Marseille, Marseille, FRANCE.*

OP-0153
PSMA Theranostics in 2021

D. Oprea-Lager; *Amsterdam University Medical Centers, Department of Radiology & Nuclear Medicine, Amsterdam, NETHERLANDS.*

OP-0154
Marie Curie Lecture: Other New Theranostics

R. Hicks; *The Sir Peter MacCallum Cancer Center, Department of Oncology, Molecular Imaging and Therapeutic Nuclear Medicine, Melbourne, AUSTRALIA.*

OP-0155
Handling Challenges

L. Evangelista; *University of Padova, Department of Medicine (DIMED), Padua, ITALY.*

OP-0156
Risk Analysis in Radionuclide Therapy

R. Dierckx; *UMCG - University Medical Center Groningen, Department of Nuclear Medicine & Molecular Imaging, Groningen, NETHERLANDS.*

OP-0157
Tech Challenges

A. Santos; *Hospital CUF Descobertas, Medicina Nuclear Department, Lisbon, PORTUGAL.*

OP-0158
Reimbursement Challenges

J. Kunikowska; *Medical University of Warsaw, Nuclear Medicine Department, Warsaw, POLAND.*

501

Wednesday, October 20, 2021, 16:15 - 17:45

Channel 1

CME 3: The Battle Continues - WBC Scan vs FDG PET/CT

OP-0161
Radiolabelled WBC Scintigraphy for Musculoskeletal Infections - Pros and Cons

E. Noriega-Álvarez; *Hospital General Universitario de Ciudad Real, Department of Nuclear Medicine, Ciudad Real, SPAIN.*

OP-0162
FDG-PET for Musculoskeletal Infections - Pros and Cons

Z. Keidar; *Rambam Health Care Campus, Director, Department of Nuclear Medicine, Haifa, ISRAEL.*

OP-0163
Radiolabelled WBC Scintigraphy for Cardiovascular Infections - Pros and Cons

F. Rouzet; *GH Bichat-Claude Bernard, Department of Nuclear Medicine, Paris, FRANCE.*

OP-0164
FDG-PET for Cardiovascular Infections - Pros and Cons

L. Leccisotti; *Fondazione Policlinico Universitario Agostino Gemelli IRCCS, Nuclear Medicine Unit, Rome, ITALY.*

502

Wednesday, October 20, 2021, 16:15 - 17:45

Channel 2

The Top 3 Trials Sessions - 1- Prostate

OP-0166

External Validation and Addition of PSMA-PET to the Most Frequently Used Nomograms for the Prediction of Pelvic Lymph-node Metastases: an International Multicenter Study

D. Meijer[1], P. J. van Leeuwen[2], M. J. Roberts[3], A. R. Siriwardana[3], A. Morton[3], J. W. Yaxley[3], H. Samaratunga[4], L. Emmett[5], P. M. van de Ven[1], H. G. van der Poel[2], M. L. Donswijk[2], T. N. Boellaard[2], I. G. Schoots[2], D. E. Oprea-Lager[1], G. D. Coughlin[6], A. N. Vis[1];
[1]Amsterdam UMC, Amsterdam, NETHERLANDS, [2]Netherlands Cancer Institute, Amsterdam, NETHERLANDS, [3]Royal Brisbane and Women's Hospital, Brisbane, AUSTRALIA, [4]Aquesta Uropathology, Brisbane, AUSTRALIA, [5]St. Vincent's Hospital, Darlinghurst, AUSTRALIA, [6]Wesley Hospital, Brisbane, AUSTRALIA.

Aim/Introduction: Different nomograms exist for the preoperative prediction of pelvic lymph-node metastatic disease in individual patients with prostate cancer (PCa). These nomograms do not incorporate modern staging imaging techniques such as prostate-specific membrane antigen (PSMA)-positron emission tomography (PET). The aim of this study, was to determine the predictive performance of the Briganti 2017, the Memorial Sloan Kettering Cancer Center (MSKCC), and the Briganti 2019-nomograms with the addition of PSMA-PET in an international, multicenter present-day cohort of patients undergoing robot-assisted radical prostatectomy (RARP) and extended pelvic lymph-node dissection (ePLND) for localized PCa. **Materials and Methods:** All 1156 eligible patients who underwent RARP and ePLND in three reference centers for PCa surgery between January 2016 and November 2020 were included. Performance of the three nomograms was assessed using the receiver operating characteristic (ROC) curve derived area under the curve (AUC), calibration plots and decision curve analyses. Subsequently, recalibration and addition of PSMA-PET to the nomograms were performed. Results: Overall, 273/1156 patients (24%) had pelvic lymph-node metastatic (pN1) disease on histopathological examination. AUCs of the Briganti 2017, the MSKCC, and the Briganti 2019-nomograms were 0.70 (95%Confidence Interval (95%CI): 0.64-0.76), 0.71 (95%CI: 0.65-0.77) and 0.77 (95%CI: 0.70-0.82), respectively. PSMA-PET findings showed a significant association with pN1-disease when added to the nomograms (p<0.001). Addition of PSMA-PET substantially improved the discriminative ability of the models yielding cross-validated AUCs of 0.76 (95%CI: 0.70-0.82), 0.78 (95%CI: 0.70-0.82) and 0.82 (95%CI: 0.75-0.86), respectively. In decision curve analyses, the addition of PSMA-PET to the three existing nomograms resulted in increased net-benefits. **Conclusion:** The addition of PSMA-PET to the previously developed nomograms showed a substantially improved predictive performance, which suggests that PSMA PET is a likely future candidate for a modern predictive nomogram. **References:** None.

OP-0167

Quantitative ^{68}Ga-PSMA-11 PET/CT Parameters of Intraprostatic Malignancy in Men with Prostate Adenocarcinoma in the proPSMA Study: Comparison to ISUP Grade Group

J. P. Buteau[1], F. de Galiza Barbosa[2], R. Alipour[1], S. Koschel[1], E. Link[1], O. Alghazo[1,3], C. Mitchell[1], S. F. Oon[1], N. Lawrentschuk[1,4], R. J. Francis[5], S. Williams[1], D. G. Murphy[1], M. S. Hofman[1];
[1]Peter MacCallum Cancer Centre, Melbourne, AUSTRALIA, [2]Hospital Sirio-Libanes, Sao Paulo, BRAZIL, [3]Urology Division, Clinical Sciences Department, Yarmouk University, Irbid, JORDAN, [4]Royal Melbourne Hospital, Melbourne, AUSTRALIA, [5]Sir Charles Gairdner Hospital, Perth, AUSTRALIA.

Aim/Introduction: The proPSMA multicentre, randomised, phase 3 study demonstrated superior accuracy for detection of nodal or distant metastatic disease with ^{68}Ga-PSMA-11 PET/CT compared to conventional imaging (92% vs 65%)[1]. We conducted a post-hoc analysis of the proPSMA cohort for quantitative parameters of intraprostatic malignancy. The primary objective was to define the association between SUVmax and ISUP grade group (GG) of the index lesion. Secondary objectives included determining the associations between quantitative PSMA PET parameters with baseline PSA and risk of nodal and/or distant metastases, as well as percentage of PSMA-negative cancers by GG. **Materials and Methods:** Men with histopathologically-confirmed prostate cancer with high-risk features were recruited from 10 Australian centres. Sites of PSMA uptake within the prostate were segmented using an absolute threshold of SUVmax ≥4 (excluding physiological urine). Quantitative parameters analysed were SUVmax, SUVmean, molecular imaging tumour volume (MiTV) and total lesion activity (TLA) defined as SUVmean x MiTV. PSMA negative studies were defined as intraprostatic SUVmax<4. Histopathology was from transperineal biopsy performed prior to imaging. The association between SUVmax and GG was assessed with a Kruskal-Wallis test. The association between quantitative PSMA parameters and baseline PSA was assessed with linear regression, while the association with risk of metastases was with logistic regression. Results: 293 of 302 men recruited had an available staging PSMA PET/CT. 283/293 (97%) had PSMA-positive intraprostatic malignancy, with SUVmax 19.1 (mean), SUVmean 7.4, MiTV 14.1 mL and TLA 129.6. PSMA-negative studies were GG3 (5 patients) and GG5 (5 patients), with highest SUVmax 3.15. In PSMA-positive patients, there was a significant difference in mean SUVmax of 16.4, 20.3 and 22.0 for

GG3, GG4 and GG5, respectively (Kruskal-Wallis test p=0.0037). There were associations of all quantitative PSMA parameters and PSA, most significant between MiTV and baseline PSA (1 unit higher MiTV 0.87 (standard error 0.08) higher PSA p<0.0001)). There were associations with presence of nodal and/or distant metastases, most significant for MiTV (odds ratio 1.03 [95% confidence interval 1.01-1.04] p=0.001). **Conclusion:** In men with prostate cancer with high-risk features, 97% had PSMA-positive intraprostatic malignancy. SUVmax differed significantly between GG3 and GG5, increasing with grade, although with significant overlap. The volume of PSMA-avid intraprostatic malignancy (MiTV) had the strongest association with higher baseline PSA and risk of nodal and/or distant metastases. **References:** 1.Hofman,M.S. et al.(2020) 'Prostate-specific membrane antigen PET/CT in patients with high-risk prostate cancer before curative-intent surgery or radiotherapy (proPSMA): a prospective, randomised, multicentre study',The Lancet, 395(10231),pp.1208-1216.

OP-0168

Comparing the clinical performance and cost efficacy of [^{68}Ga]Ga-PSMA-11 and [^{18}F]PSMA-1007 in the diagnosis of recurrent prostate cancer: a Markov-chain decision analysis

I. Alberts, *C. Mingels, A. Rominger, A. Afshar-Oromieh; Institut für Nuklearmedizin, Bern, SWITZERLAND.*

Aim/Introduction: Amongst others, [^{68}Ga]Ga-PSMA-11 and [^{18}F]PSMA-1007 are available for the detection of recurrent prostate cancer (rPC). While PET/CT with PSMA-radioligands is known to influence clinical decision-making, the relative performance of these two radiotracers with respect to clinical outcomes or cost efficacy is less well understood. The objective of this study was to compare and contrast the performance of these tworadiotracers in rPC using Markov-chain decision analysis model informed by real-world clinical data. **Materials and Methods:** 244 patients undergoing PSMA PET/CT for rPC were included in this study (122 with [^{18}F]PSMA-1007 and 122 with [^{68}Ga]Ga-PSMA-11) to generate real-world data with regard to rates of PET positivity, negativity, unclear findings and rates of clinical follow up. We generate a Markov-chain decision process to model clinical decision-making processes and cost efficacy using the generated real-world data and literature-derived values. Results: The detection rate was minimally and non-significantly higher for [^{18}F]PSMA-1007 compared to [^{68}Ga]Ga-PSMA-11 (91.8% vs. 86.9%, p=0.68). A significantly higher rate of uncertain findings was found for [^{18}F]PSMA-1007 (17.2% vs. 8.25%, p=0.02). The likelihood of a true positive findings was higher for [68 Ga]Ga-PSMA-11 compared to [^{18}F]PSMA-1007 (0.903 ± 0.033 vs. 0.803 ± 0.041) with a higher PPV for[^{68}Ga]Ga-PSMA-11 (0.990 ± 0.034 vs. 0.854 ± 0.125). The overall cost-per patient is slightly lower for [^{18}F]PSMA-1007 (3193 vs 3337 CHF; $3557 vs. $3717 USD). However, the incremental cost effective ratio (ICER) favours [^{68}Ga]Ga-PSMA-11, where the cost per outcome (a true positive scan) is lower (3697 vs 3975 CHF; $4118 vs. $4429). A intervention efficacy analysis (numbers needed to treat and harm) favours [^{68}Ga]Ga-PSMA-11, where the number needed to image (to yield one extra patient-level TP) is 10.1 and to harm is -7.8(number needed to image to yield one extra patient-level FP). **Conclusion:** The study confirms the higher detection rate for [^{18}F]PSMA-1007, but finds greater rates of uncertain findings and false positives when compared to [^{68}Ga]Ga-PSMA-11. A higher rate of negative scans for [^{68}Ga]Ga-PSMA-11 resulted in higher average costs per patient, but a cost-efficacy analysis favours [68 Ga]Ga-PSMA-11 where the diagnostic yield(probability of a patient receiving a true positive result) is higher. These data point toward [^{68}Ga]Ga-PSMA-11 as a cost-effective radiotracer in recurrent PC. **References:** None

OP-0169

PSMA PET validates higher rates of metastatic disease for European Association of Urology Biochemical Recurrence Risk Groups: an international multicentre study

W. Fendler[1], *J. Ferdinandus*[1], *A. Farolfi*[1], *W. Samuel*[2], *M. Osama*[3], *P. Scott*[4], *M. Rodnick*[4], *M. Pampaloni*[5], *B. Viglianti*[4], *M. Eiber*[6], *K. Herrmann*[1], *J. Czernin*[7], *W. Armstrong*[8], *J. Calais*[8], *T. Hope*[5], *M. Piert*[4]; [1]*Department of Nuclear Medicine, Essen, GERMANY,* [2]*Department of Urology, University of California San Francisco, CA, UNITED STATES OF AMERICA,* [3]*Department of Radiation Oncology, University of California San Francisco, CA, UNITED STATES OF AMERICA,* [4]*Department of Radiology, University of Michigan, Ann Arbor, Michigan, IL, UNITED STATES OF AMERICA,* [5]*Department of Radiology and Biomedical Imaging, University of California San Francisco, CA, UNITED STATES OF AMERICA,* [6]*Department of Nuclear Medicine, Klinikum rechts der Isar Munich, GERMANY,* [7]*Ahmanson Translational Imaging Division, Department of Molecular and Medical Pharmacology, University of California Los Angeles, Los Angele, CA, UNITED STATES OF AMERICA,* [8]*Ahmanson Translational Imaging Division, Department of Molecular and Medical Pharmacology, University of California Los Angeles, Los Angeles, CA, UNITED STATES OF AMERICA.*

Aim/Introduction: The European Association of Urology (EAU) Prostate Cancer Guidelines Panel recommends risk groups for biochemically recurrent prostate cancer (BCR) to identify men at high risk of progression or metastatic disease. Recent United States Food and Drug Administration approval for ^{68}Ga-PSMA-11 and growing global availability of PSMA-directed PET imaging (PSMA PET) will impact disease localization in majority of men with BCR. We determined the rates of local and metastatic disease in recurrent and persistent prostate cancer stratified by EAU BCR risk groups and biochemical persistence (BCP). **Materials and Methods:** A total of 1960 patients from three prospective trials and one institutional database were included. Results: Post-RP EAU BCR low risk, EAU BCR high risk, and BCP groups yield distant metastatic (M1) detection in 43/176 (24%), 342/931 (37%),

and 154/386 (40%) of patients. For post-RT EAU BCR low risk and EAU BCR high risk groups, M1 detection rate was 113/309 (37%) and 110/158 (70%), respectively. BCP, high risk BCR and higher levels of serum PSA were significantly associated with PSMA PET M1 disease in multivariate regression analysis. PSMA-PET revealed no disease in 25% and locoregional only disease in 33% of patients with post-RP or post-RT EAU BCR high risk. **Conclusion:** By showing that the novel EAU BCR high-risk groups have higher rates of metastatic disease on PSMA PET than the low-risk groups, our findings further support the new EAU classification. Additionally, PSMA PET identified relevant patient subgroups with undetectable or locoregional only disease in all EAU risk groups, which might refine risk assessment. **References:** none

OP-0170

Phase 3 Study of ^{177}Lu-PSMA-617 in Patients with Metastatic Castration-Resistant Prostate Cancer (VISION)

B. Krause[1], J. de Bono[2], K. N. Chi[3], K. Fizazi[4], K. Herrmann[5], K. Rahbar[6], S. T. Tagawa[7], L. T. Nordquist[8], N. Vaishampayan[9], G. El-Haddad[10], C. H. Park[11], T. M. Beer[12], W. J. Pérez-Contreras[13], M. DeSilvio[13], E. Kpamegan[13], G. Gericke[14], R. A. Messmann[13], M. J. Morris[15], O. Sartor[16];

[1]Rostock University Medical Centre, Rostock, GERMANY, [2]The Institute of Cancer Research and Royal Marsden Hospital, London, UNITED KINGDOM, [3]British Columbia Cancer Agency, Vancouver, BC, CANADA, [4]Gustave Roussy Institute, Paris-Saclay University, Villejuif, FRANCE, [5]University Hospital Essen, Essen, GERMANY, [6]University Hospital Münster, Münster, GERMANY, [7]Weill Cornell Medicine, New York, NY, UNITED STATES OF AMERICA, [8]Urology Cancer Center, Omaha, NE, UNITED STATES OF AMERICA, [9]School of Medicine, Wayne State University, Detroit, MI, UNITED STATES OF AMERICA, [10]Moffitt Cancer Center and Research Institute, Tampa, FL, UNITED STATES OF AMERICA, [11]Norton Cancer Institute, Louisville, KY, UNITED STATES OF AMERICA, [12]Knight Cancer Institute, Oregon Health & Science University, Portland, OR, UNITED STATES OF AMERICA, [13]Novartis Pharmaceuticals Corporation, East Hanover, NJ, UNITED STATES OF AMERICA, [14]Novartis Pharma AG, Basel, SWITZERLAND, [15]Memorial Sloan Kettering Cancer Center, New York, NY, UNITED STATES OF AMERICA, [16]Tulane University School of Medicine, New Orleans, LA, UNITED STATES OF AMERICA.

Aim/Introduction: Metastatic castration-resistant prostate cancer (mCRPC) remains fatal despite recent therapeutic advances. Prostate-specific membrane antigen (PSMA) is highly expressed in mCRPC lesions. [^{177}Lu]Lu-PSMA-617 (^{177}Lu-PSMA-617) is a targeted radioligand therapy that delivers β-particle radiation to PSMA-expressing cells and surrounding microenvironment. **Materials and Methods:** VISION was an international, randomized, open-label phase 3 study evaluating ^{177}Lu-PSMA-617 in adults with PSMA-positive mCRPC previously treated with ≥1 modern androgen axis inhibitor and 1-2 taxane regimens. PSMA positivity was determined by independent central review of ^{68}Ga-PSMA-11 PET/CT scans (uptake greater than liver). Patients were randomized 2:1 to ^{177}Lu-PSMA-617 (7.4 GBq every 6 weeks, ≤6 cycles) plus investigator-determined standard of care (SOC) or to SOC alone. Protocol-permitted SOC excluded chemotherapy and ^{223}Ra. The alternate primary endpoints were radiographic progression-free survival (rPFS) using PCWG3 criteria by independent central review and overall survival (OS), powered for hazard ratios (HR) of 0.67 and 0.7306, respectively. Key secondary endpoints were independently centrally reviewed RECIST v1.1 objective response rate (ORR) and disease control rate (DCR), and time to first symptomatic skeletal event (SSE). Results: From 4 June 2018 to 23 October 2019, 831 of 1179 screened patients were randomized to receive ^{177}Lu-PSMA-617 + SOC (n = 551) or SOC alone (n = 280). Median study follow-up was 20.9 months at the data cut-off (27 January 2021). Demographics and baseline characteristics were balanced between treatment arms. ^{177}Lu-PSMA-617 plus SOC significantly improved rPFS versus SOC alone (HR, 0.40 [99.2% confidence interval [CI]: 0.29–0.57]; p < 0.001, one-sided; median, 8.7 vs 3.4 months). ^{177}Lu-PSMA-617 plus SOC also significantly improved OS versus SOC alone (HR, 0.62 [95% CI: 0.52–0.74]; p < 0.001, one-sided; median, 15.3 vs 11.3 months). All key secondary endpoints were statistically significant between the treatment arms in favor of ^{177}Lu-PSMA-617 + SOC, including ORR (29.8% vs 1.7%), DCR (89.0% vs 66.7%) and time to first SSE (HR, 0.50; median, 11.5 vs 6.8 months). While a higher rate of treatment-emergent adverse events of grade 3 or higher was observed with ^{177}Lu-PSMA-617 (52.7% vs 38.0%), therapy was well tolerated. **Conclusion:** Radioligand therapy with ^{177}Lu-PSMA-617 is well tolerated, improves rPFS and prolongs survival when added to safely combinable SOC in patients with advanced PSMA-positive mCRPC. These findings warrant adoption of ^{177}Lu-PSMA-617 as a new treatment option in patients with mCRPC. NCT03511664. Funded by Endocyte, Inc., a Novartis company. **References:** None

OP-0171

Nomograms to predict outcome after LuPSMA radionuclide therapy in men with metastatic castration-resistant prostate cancer: an international multicenter retrospective study

A. Gafita[1], J. Calais[1], T. R. Grogan[1], B. Hadaschik[2], H. Wang[3], M. Weber[4], S. Sandhu[5], C. Kratochwil[6], R. Esfandiari[7], R. Tauber[3], A. Zeldin[8], H. Rathke[6], W. R. Armstrong[1], A. Robertson[3], P. Thin[1], C. D'Alessandria[3], M. B. Rettig[1], E. S. Delpassand[7], U. Haberkorn[6], D. Elashoff[1], K. Herrmann[4], J. Czernin[1], M. S. Hofman[5], W. P. Fendler[4], M. Eiber[3];

[1]UCLA, Los Angeles, CA, UNITED STATES OF AMERICA, [2]University of Duisburg-Essen, Essen, CA, UNITED STATES OF AMERICA, [3]Technical University Munich, Munich, GERMANY, [4]University of Duisburg-Essen, Essen, GERMANY, [5]Peter MacCallum Cancer Center, Melbourne, AUSTRALIA, [6]University of Heidelberg, Heidelberg, GERMANY, [7]Excel Diagnostics, Houston, TX, UNITED STATES OF AMERICA, [8]Silicon Albion Ltd, London, UNITED KINGDOM.

Aim/Introduction: Lutetium-177-prostate-specific membrane antigen (LuPSMA) is a novel targeted treatment for patients with metastatic castration-resistant prostate cancer (mCRPC). Predictors of outcome after LuPSMA to enhance its clinical implementation are yet to be identified. **Materials and Methods:** To develop predictive nomograms for treatment outcome, patients who underwent LuPSMA between December 10, 2014 and July 19, 2019 under phase II trials (NCT03042312, ACTRN12615000912583) or compassionate access programs at six institutions across Europe, USA, and Australia were retrospectively screened. Eligible patients had available baseline [^{68}Ga]Ga-PSMA-11 PET/CT, clinical data, and survival outcomes. Putative predictors included 18 pretherapeutic clinicopathologic and ^{68}Ga-PSMA-11 PET/CT variables. Primary outcome for the nomograms were overall survival (OS) and prostate-specific antigen progression-free survival (PSA-PFS). Nomograms for each outcome were computed from Cox regression models with lasso penalty for variable selection. Models performance was measured by examining discrimination (Harrell's C-index), calibration (calibration plots), and utility (patient stratification into low vs. high-risk group). Models were validated internally using bootstrapping and externally by calculating their performance on a validation cohort. Results: Data were centrally collected from April 23, 2019 to January 13, 2020. 270 (65%) of 414 screened patients were eligible and divided into development (n=196) and validation cohort (n=74). The median follow-up was 21·5 (IQR 13·3-30·7) months. Predictors included in the nomograms were time since initial diagnosis, chemotherapy status, hemoglobin levels, and ^{68}Ga-PSMA-11 PET/CT parameters (miTNM classification and tumor burden). The C-indices of the OS and PSA-PFS models were 0·72 (95%CI 0·68-0·76) and 0·71 (95%CI 0·68-0·74), respectively. Both models were adequately calibrated and their predictions correlated with the observed outcome. Low- vs. high-risk patients had significantly different OS (24·9 vs. 7·4 months; p<0·0001) and PSA-PFS (6·6 vs. 2·5 months; p=0·022). **Conclusion:** These externally validated nomograms predictive for outcome after LuPSMA in patients with mCRPC can help in clinical trial design and individual clinical decision making, particularly at institutions where LuPSMA is introduced as a novel therapeutic option. An online risk calculator is available at www.uclahealth.org/nuc/nomograms. **References:** none

504

Wednesday, October 20 - Saturday, October 23, 2021

on-demand pool, release on Wednesday, October 20 at 09:00

CTE 3: PET/CT for RT Planning

OP-0173

20 years of Positron Emission Tomography in Radiation Therapy - Clinical Perspective

R. Durmo; Arcispedale Santa Maria Nuova, Nuclear medicine, Reggio Emilia, ITALY.

OP-0174

Recent Advances in Radiotherapy

B. Bak; Greater Poland Cancer Centre, Radiotherapy Department II, Poznan, POLAND.

OP-0175

Recent Updates of PET Imaging in Radiotherapy Planning

R. Allie; University College London Hospital, Institute of Nuclear Medicine, London, UNITED KINGDOM.
& J. Heywood; University College London Hospital, Radiotherapy, London, UNITED KINGDOM.

505

Wednesday, October 20 - Saturday, October 23, 2021

on-demand pool, release on Wednesday, October 20 at 09:00

Joint Symposium 5 (EANM/SRS): Targeting Cancer with Peptides, Fragments or Antibodies

OP-0178

In Peptides, We Trust!

S. Dalm; Erasmus Medical Center, Department of Radiology and Nuclear Medicine, Rotterdam, NETHERLANDS.

OP-0179

Antibody Fragments, Fast Kinetics are Essential!

N. Devoogdt; Vrije Universiteit Brussel, Department of Medical Imaging, Brussels, BELGIUM.

OP-0180

Antibodies as Radiopharmaceutical Vectors - Do the Benefits Outweigh the Costs?

B. M. Zeglis; Hunter College, Department of Chemistry, New York, UNITED STATES OF AMERICA.

506

Wednesday, October 20 - Saturday, October 23, 2021

on-demand pool, release on Wednesday, October 20 at 09:00

Joint Symposium 6 (EANM/SRS): Modifying Radiopharmaceuticals to Alter Pharmacokinetics

OP-0182

How to "Fix" Tracer Pharmacokinetics - The Chemist's Toolbox

M. Schottelius; Centre Hospitalier Universitaire Vaudois (CHUV), Dept. of Nuclear Medicine, University of Lausanne (UNIL) and Ludwig Institute of Cancer Research (LICR), Dept. of Oncology, Lausanne, SWITZERLAND.

OP-0183

Linker Modification Strategies to Alter the Pharmacokinetic Profile of Low Molecular Weight Radiopharmaceuticals

A.-C. Eder; University Medical Center, Department of Nuclear Medicine, Division of Radiopharmaceutical Development, Freiburg, GERMANY.

OP-0184

Incorporation of an Albumin Binder to Optimize Tumour Delivery of PSMA-Targeting Radiotherapeutic Agents

K.-S. Lin; University of British Columbia, Department of Radiology, Vancouver, CANADA.

OP-0185

Blood-Brain Barrier Permeation of Brain-Targeted Radioligands

T. Billard; Université Claude Bernard - Lyon, ICBMS - Institut de Chimie et Biochimie Moléculaires et Supramoléculaires, Lyon, FRANCE.

507

Wednesday, October 20 - Saturday, October 23, 2021

on-demand pool, release on Wednesday, October 20 at 09:00

Pitfalls & Artefacts 3: Challenging Cases in Nuclear Neurology

OP-0187

Challenging Cases in Neurodegenerative Dementia

A. Chiaravalloti; University Tor Vergata, Department of Biomedicine and Prevention, Rome, ITALY.

OP-0188

Challenging Cases in Movement Disorders

M. Brendel; Department of Nuclear Medicine, University Hospital of Munich; Munich Cluster for Systems Neurology (SyNergy), Munich, GERMANY.

OP-0189

Challenging Cases in Neuroncology

T. Traub-Weidinger; Department of Biomedical Imaging and Image-Guided Therapy, Medical University of Vienna, Vienna, AUSTRIA.

508

Wednesday, October 20 - Saturday, October 23, 2021

on-demand pool, release on Wednesday, October 20 at 09:00

M2M Track - TROP Session: Theranostics - Various Targets

OP-0191

Enhanced Therapeutic Effect of the Albumin-Binding [^{177}Lu]Lu-Ibu-DAB-PSMA as Compared to [^{177}Lu]Lu-PSMA-617 - A Preclinical Therapy Study

V. Tschan[1], F. Borgna[1], R. Schibli[1,2], C. Müller[1,2]; [1]Paul Scherrer Institute, 5232 Villigen-PSI, SWITZERLAND, [2]ETH Zurich, 8093 Zurich, SWITZERLAND.

Aim/Introduction: Among a new class of PSMA-targeting radioligands comprising ibuprofen as an albumin-binding entity, [^{177}Lu]Lu-Ibu-DAB-PSMA was identified as the most promising candidate due to its high tumour accumulation (1). In this preclinical study, the in vivo therapeutic efficacy of [^{177}Lu]Lu-Ibu-DAB-PSMA was investigated and compared to [^{177}Lu]Lu-PSMA-617. **Materials and Methods:** Preclinical therapy studies were conducted with athymic nude mice bearing PSMA-expressing PC-3 PIP tumour xenografts. Seven groups of mice (n = 6-12) were injected with [^{177}Lu]Lu-Ibu-DAB-PSMA or [^{177}Lu]Lu-PSMA-617 at an activity of 2 MBq, 5 MBq or 10 MBq per mouse or only saline. The tumour sizes and body weights were monitored every second day over 3 months. Potential early side effects were assessed in a separate experiment in mice without tumours, 10 days or 28 days after the injection of 10 MBq [^{177}Lu]Lu-Ibu-DAB-PSMA or [^{177}Lu]Lu-PSMA-617. Several biochemical blood plasma parameters, indicative for hepatic and renal function, were compared with those obtained from untreated control mice. Tissue sections of paraffin-embedded kidneys, bone marrow and spleen were (patho)histologically investigated. Results: At all investigated activity levels, [^{177}Lu]Lu-Ibu-DAB-PSMA was more effective to treat tumours than [^{177}Lu]Lu-PSMA-617. The median survival time of mice treated with 2 MBq [^{177}Lu]Lu-Ibu-DAB-PSMA or [^{177}Lu]Lu-PSMA-617 was 34 days and 19 days,

respectively. The majority of mice (8/12 and 5/6, respectively) treated with 5 MBq or 10 MBq [^{177}Lu]Lu-Ibu-DAB-PSMA were still alive at study end (Day 84). In contrast, mice treated with 5 MBq or 10 MBq [^{177}Lu]Lu-PSMA-617 had a median survival time of 32 days and 51 days, respectively. Even the highest activity (10 MBq/mouse) of either radioligand did not affect blood plasma parameters investigated 10 days or 28 days after treatment. No histological abnormalities were observed in radiosensitive tissue (kidneys, bone marrow and spleen) of treated mice relative to untreated controls. **Conclusion:** Our data revealed a significantly increased therapeutic efficacy of [^{177}Lu]Lu-Ibu-DAB-PSMA compared to [^{177}Lu]Lu-PSMA-617 when applied at the same activity while early side effects were not observed. These exciting results open new perspectives for the treatment of prostate cancer patients with this novel radioligand. **References:** (1) Deberle & Benešová et al. Theranostics 2020:10(4):1678.

OP-0192

Therapeutic response of CCKBR-positive tumors to combinatory treatment with RAD001 and radiolabeled minigastrin analogue [^{177}Lu]Lu-PP-F11N

M. Grzmil[1], S. Imobersteg[1], A. Blanc[1], R. Schibli[1,2], M. Behe[1];
[1]Paul Scherrer Institute, Villigen PSI, SWITZERLAND, [2]Department of Chemistry and Applied Biosciences, ETH Zürich, SWITZERLAND.

Aim/Introduction: High expression of cholecystokinin B receptor (CCKBR) was reported in a variety of human cancers including medullary thyroid cancer (MTC). The small peptide hormone minigastrin binds to CCKBR with high affinity and the previous studies developed radiolabeled gastrin analogues with favorable pharmacokinetics for theranostics applications. Recently we have shown clinically feasible way for augmented tumor-specific uptake of radiolabeled minigastrin analogue [^{177}Lu]Lu-PP-F11N by pharmacological interference with activity of mammalian target of rapamycin complex 1 (mTORC1). Inhibition of mTORC1 by RAD001 led to increased CCKBR protein level in cancer cells, and consequently higher uptake of radiolabeled minigastrin in CCKBR-positive tumor bearing nude mice [1]. In the present study we investigated efficacy of combinatory treatment with RAD001 and [^{177}Lu]Lu-PP-F11N. **Materials and Methods:** Radiolabeling efficiency of N-terminal DOTA-conjugated gastrin analogue PP-F11N (DOTA-$(DGlu)_6$-Ala-Tyr-Gly-Trp-Nle-Asp-Phe) was analyzed by HPLC. To evaluate the therapeutic effects of the combinatory treatment in vivo, human A431 cells, which overexpress CCKBR, were used in xenograft nude mouse model. Tumor growth and the mean survival time were investigated after administration of 5 or 10 doses of RAD001 alone or in combination with [^{177}Lu]Lu-PP-F11N and dissected tumors were used for histological analysis. Results: Both RAD001 and [^{177}Lu]Lu-PP-F11N single treatments as well as their combination inhibited tumor growth. The average tumor size in concomitant treated mice with RAD001 and [^{177}Lu]Lu-PP-F11N was significantly reduced as compared to monotherapies. Kaplan-Meier curves showed increased life-span in all treated groups. The median survival time in the control group was 19.5 days, whereas the median survival in the mice treated with 5 and 10 doses of RAD001 in combination with [^{177}Lu]Lu-PP-F11N was extended as compared to monotherapies and reached 36 and 43 days, respectively. During therapy, there was a constant increase in the body weight of the mice without severe adverse effects. **Conclusion:** Taken together, our study data demonstrates potential of mTORC1 inhibition to substantially improve therapeutic efficacy of radiolabeled minigastrin analogues in CCKBR-positive cancers. **References:** 1. Grzmil M, Qin Y, Schleuniger C, Frank S, Imobersteg S, Blanc A, Spillmann M, Berger P, Schibli R, Behe M. Pharmacological inhibition of mTORC1 increases CCKBR-specific tumor uptake of radiolabeled minigastrin analogue [^{177}Lu]Lu-PP-F11N. Theranostics. 2020 Aug 29;10(24):10861-10873.

OP-0193

A new class of radiopharmaceuticals for CXCR4-expressing malignancies based on the endogenous antagonist EPI-X4

R. Gaonkar[1], Y. Schmidt[1], R. Mansi[1], M. Harms[2], A. Seidel[2], J. Münch[2], M. Fani[1];
[1]Division of Radiopharmaceutical Chemistry, University Hospital Basel, Basel, SWITZERLAND, [2]Institute of Molecular Virology, Ulm University Medical Center, Ulm, GERMANY.

Aim/Introduction: The pathologic overexpression of the C-X-C motif chemokine receptor (CXCR4) in more than 20 types of cancer designates it as an interesting target for theranostic interventions in oncology. Among all CXCR4-targeting radiotracers, the cyclic pentapeptides ^{177}Lu-Pentixather/^{68}Ga-Pentixafor are the most advanced theranostic pair. Recently, Münch et al (1) identified the first endogenous peptide antagonist of CXCR4, termed EPI-X4, a human serum albumin fragment generated by pH-regulated proteases. We aim to develop a new class of theranostics based on EPI-X4 analogs, shown to be stable in blood plasma and robust to chemical modifications. The new radiotracers are compared head-to-head with ^{177}Lu-Pentixather. **Materials and Methods:** Seven DOTA-conjugated peptide analogs of EPI-X4 were synthesized, JMF-01 to JMF-07. The affinity of their complexes with natural Lu - and with Ga for selective analogs - was tested against the human CXCR4 expressed in GHOST cells (GHOST-CXCR4+), using the CXCR4-specific 12G5 antibody. The ^{177}Lu-labeled conjugates were evaluated in terms of lipophilicity and in-vitro cellular uptake in GHOST-CXCR4+ cells. PET/CT and SPECT/CT imaging were performed in healthy Balb/c mice

1h and 4h after injection of ^{68}Ga-/^{177}Lu-JMF-04, respectively. In all studies, ^{nat}Lu/^{177}Lu-Pentixather was used as reference. Results: The IC_{50} of the ^{nat}Lu-complexes were in the range of 6.2 nM (^{nat}Lu-JMF-07) to 1012 nM (^{nat}Lu-JMF-01) vs 70 nM for ^{nat}Lu-Pentixather. No significant difference in affinity was observed between ^{nat}Lu- and ^{nat}Ga-complexes of the same analog. The radiotracers had variable lipophilicity, with ^{177}Lu-JMF-01 and -05 being similar to ^{177}Lu-Pentixather (logD=-1.49 and -1.91 vs -1.53, respectively), ^{177}Lu-JMF-02, -04 and -06 having improved hydrophilicity (logD=-2.7 to -3.2) and ^{177}Lu-JMF-03 and -07 being lipophilic (logD=-0.58 and 0.29, respectively). In-vitro, ^{177}Lu-JMF-02, -05 and -06 showed similar CXCR4-mediated cellular uptake as ^{177}Lu-Pentixather (0.9-1.2% vs 1.2%, respectively, at 1h/37°C), while ^{177}Lu-JMF-02 and -04 had significantly higher uptake (2.0 and 8.4%, respectively). So far, ^{177}Lu-JMF-04 showed the best characteristics, similarly to its ^{68}Ga-counterpart (logD=-2.75 and cellular uptake of 10.4%). PET/CT and SPECT/CT images indicated that the biodistribution pattern of ^{68}Ga-/^{177}Lu-JMF-04 is characterized by low background activity and accumulation in the kidneys, compared with ^{68}Ga-/^{177}Lu-Pentixather which displayed higher background activity and high liver uptake. **Conclusion:** Our data support the idea of developing CXCR4-targeting theranostics based on EPI-X4. The new radiotracers compare fairly with ^{177}Lu-Pentixather, in terms of hydrophilicity and affinity, while they may display improved biodistribution profile. A thorough in-vivo assessment in CXCR4-expressing xenografts is in progress. **References:** 1. Zirafi O et al., Cell Reports 11, 737-747, 2015.

OP-0194

In Vitro Metabolic Activity and Internalisation Investigation of Copper-64 Radiopharmaceuticals As Theranostic Agents for Hypoxic Tumours

T. Liu[1,2], M. Dahle[1], M. Karlsen[2], K. Redalen[1];
[1]Department of Physics, Norwegian University of Science and Technology, Trondheim, NORWAY, [2]Department of Radiology and Nuclear Medicine, St. Olavs Hospital, Trondheim University Hospital, Trondheim, NORWAY.

Aim/Introduction: Tumour hypoxia (oxygen deficiency) is an adverse factor of the tumour microenvironment associated with malignant progression and therapy resistance. Positron emission tomography (PET) may image tumour hypoxia using a tracer accumulating in hypoxic regions, such as [copper-64][copper-diacetyl-bis(N(4)-methylthiosemicarbazone)] ([^{64}Cu][Cu(ATSM)]). Hypoxia signalling- and copper transport pathways have shown to be interrelated, and ^{64}Cu radiopharmaceuticals may also elicit a dual role as therapeutic agent under hypoxia due to emission of high linear energy transfer (LET) Auger electrons, delivering radiation to surrounding cells upon internalisation. Recognising that the underlying mechanisms behind the therapeutic effect are not fully understood, our aim was to investigate in vitro effects of [^{64}Cu]$CuCl_2$ and [^{64}Cu][Cu(ATSM)] on metabolic activity and internalisation in experimental prostate cancer. **Materials and Methods:** Cu-64 was produced in a 12 MeV cyclotron following ^{64}Ni(p,n)^{64}Cu reaction. End-of-production [^{64}Cu]$CuCl_2$ and [^{64}Cu][Cu(ATSM)] were analysed using high performance liquid chromatography (HPLC). Using the 22Rv1 prostate cancer cell line, metabolic activity was determined using the XTT cell proliferation assay on natural copper (^{nat}Cu) and four different ^{64}Cu doses. Hypoxia was created using an anaerobic gas-generating sachet in a polycarbonate container maintaining pO_2<1%, pCO_2=8% for 6 hours. Cellular uptake of ^{64}Cu was determined by quantifying the activity in medium and cells following treatment with 4 Bq/cell. Cell lysates (whole protein and cytoplasmic/nuclear fractions) were prepared. Activities in cytoplasmic and nuclear fraction lysates were measured to determine the intracellular uptake of ^{64}Cu. Western blot immunostaining of lysates evaluated expression of the hypoxia-inducible factor-1α (HIF-1α) and copper transporter-1 (CTR-1). Results: Metabolic activity assessed by XTT showed a dose-dependent decrease for both [^{64}Cu]$CuCl_2$ and [^{64}Cu][Cu(ATSM)]. The results from [^{nat}Cu] evaluated with HPLC confirmed that the decrease in metabolic activity was due to radiation and not chemical toxicity. Quantification of cellular uptake activities showed significantly higher hypoxic-to-normoxic (H/N) uptake ratio in [^{64}Cu][Cu(ATSM)] (H/N=5.37) compared to in [^{64}Cu]$CuCl_2$ (H/N=1.54) (P=0.0068). Under hypoxia, internalisation of [^{64}Cu][Cu(ATSM)] and [^{64}Cu]$CuCl_2$ into the nucleus was increased compared to in normoxia. Western blot confirmed HIF-1α expression in hypoxic but not normoxic cells. For hypoxic cells, expression of both HIF-1α and CTR-1 was higher in the nucleus. **Conclusion:** [^{64}Cu]$CuCl_2$ and [^{64}Cu][Cu(ATSM)] reduced the metabolic activity of experimental prostate cancer in a dose-dependent manner. Internalisation of ^{64}Cu increased under hypoxia, although the uptake of [^{64}Cu][Cu(ATSM)] was higher than of [^{64}Cu]$CuCl_2$, suggesting different uptake mechanisms. Investigations of key cellular uptake mechanisms and in vivo PET are ongoing and will be presented. **References:** None

OP-0195

Alternating PSMA Expression Levels by Ionizing Radiation Exposure as an Additional Feature in PSMA-Targeting Prostate Cancer Treatment: First In Vitro Evaluation

D. Arbuznikova[1,2,3], M. Boll[1,2,4], A. Grosu[3,5], P. T. Meyer[1,5], M. Eder[1,2,4], C. Zamboglou[3,5], A. Eder[1,2,4];
[1]Department of Nuclear Medicine, University Medical Centre Freiburg, Freiburg, GERMANY, [2]Division of Radiopharmaceutical Development, German Cancer Consortium (DKTK), Partner Site Freiburg, Freiburg, GERMANY, [3]Department of Radiation Oncology, University Medical Centre Freiburg, Freiburg, GERMANY, [4]German Cancer Research Centre (DKFZ), Heidelberg, GERMANY, [5]German Cancer Consortium (DKTK), Partner Site Freiburg, Freiburg, GERMANY.

Aim/Introduction: The prostate-specific membrane antigen (PSMA) is a cell surface protein with glutamate carboxypeptidase activity that is upregulated in prostate cancer and the expression of which rises with higher progression of disease. To date, metastatic castration-refractory prostate cancer remains incurable. However, treatment with PSMA-targeting radiopharmaceuticals appears to be an effective therapy option currently investigated in clinical phase III studies. Enhancing PSMA expression by ionizing radiation (e.g. percutaneous radiotherapy) might improve the specific delivery of radioactivity to the cancer cells and, ultimately, result in better therapy success. In this study, the impact of exposure to external ionizing radiation on PSMA expression levels was investigated. **Materials and Methods:** Human PSMA overexpressing LNCaP cells received various doses of ionizing radiation (0.5-8 Gy). 1-24 h post-irradiation, expression of PSMA was examined by cell surface staining of viable cells with an Alexa-488-labelled anti-PSMA antibody and flow cytometry. Additionally, PSMA levels were determined 4-48 h following irradiation by western blotting using a primary anti-PSMA antibody and a secondary infrared fluorescent dye-coupled antibody. Results: Irradiation of LNCaP cells resulted in distinct effects on the PSMA expression level measured by flow cytometry. While no effect was detected at 1 h post-irradiation, the PSMA expression increased by around 20 %, as compared to non-irradiated control cells, at 4 h post-irradiation for all applied irradiation doses. Afterwards, PSMA expression levels decreased until 24 h post-irradiation in a dose-dependent manner by -11 to -18 % for the high doses. However, these preliminary effects have to be further validated in additional sensitive in vitro assays, as the effect was not within the detection limit of the corresponding western blotting experiments. **Conclusion:** Our first in vitro data suggest a short-term influence of ionizing radiation on PSMA expression levels with an upregulation of PSMA on the cell surface at 4 h post-irradiation. Further studies are planned to validate these findings and particularly assess the time course of expression levels. Finally, we aim at understanding the underlying molecular mechanisms behind the observed effects and their implication for clinical practice. **References:** none

OP-0196

Long-term radiotoxicity study with [^{177}Lu]Lu-NeoB

M. Verhoeven[1], E. A. Ruigrok[1], M. W. Konijnenberg[1], E. de Blois[1], C. M. de Ridder[1], D. C. Stuurman[1], M. J. Klomp[1], L. W. de Kreij-de Bruin[1], L. Bertarione[2], K. Rolfo[2], R. Manno[3], M. de Jong[1], S. U. Dalm[1];
[1]Erasmus MC, Rotterdam, NETHERLANDS, [2]Advanced Accelerator Applications, a Novartis Company, Colleretto Giacosa, ITALY, [3]European Research Biology Center, Pomezia, ITALY.

Aim/Introduction: The gastrin releasing peptide receptor (GRPR)-targeting antagonist NeoB is a promising tracer for imaging and therapy of GRPR-expressing malignancies, e.g. prostate and breast cancer. Prior studies showed that NeoB has good in vivo stability, high tumor uptake and retention. However, it has a relatively high uptake in GRPR-expressing pancreas and in kidneys, the latter as a consequence of renal excretion. We performed extensive biodistribution/dosimetry studies and investigated long term radiotoxicity of [^{177}Lu]Lu-NeoB in Balb/c AnNRj healthy mice. **Materials and Methods:** In the biodistribution study, mice were injected with 40 MBq/400 pmol, 80 MBq/800 pmol or 120 MBq/1200 pmol [^{177}Lu]Lu-NeoB. Blood and organs were collected (1, 2, 24, 48 and 96 h p.i.) from 3 animals/group, for biodistribution/dosimetry assessment. To determine radiotoxicity, mice were administered the same doses, 1x week, for 3 consecutive weeks. Two control groups received vehicle or non-radioactive [^{175}Lu]Lu-NeoB with the same experimental design. Laboratory investigations (-1, 5, 11, 19, 30, and 43 weeks p.i.), gross pathology (5, 19 and 43 weeks p.i.) and histopathology were performed. Binary logistics regression analysis was performed to determine dose-effect relations. Results: The biodistribution study showed the highest absorbed radiation doses in kidneys, liver and pancreas for both genders. In the radiotoxicity study no clinical signs or changes in body weight and food consumption were observed. Slight to moderate increase in urea levels and decrease in red blood cells indices were observed in females of mid and high dose groups compared to control groups. Histopathological evaluation indicated kidney hydronephrosis and nephropathy in high and mid dose groups, and with minor incidence, in the low dose group, at weeks 19 and 43. Sometimes these signs were associated with urothelial cell degeneration in the urinary bladder. Only bilateral hydronephrosis at 43 weeks showed a clear dose-effect relation ($P<0.0001$) with ED_{50} at 20 Gy

(95%CI: 16-30 Gy). Ovarian atrophy was observed in treated females at week 43 only. Relevance hereof remains to be investigated as this was not observed at earlier timepoints. No histopathological findings were observed in pancreas, liver and bone marrow. **Conclusion:** This study revealed the kidneys as dose limiting organs for toxicity in mice, observed at histopathology. This is not surprising as the kidneys are the main excretion organs for [^{177}Lu]Lu-NeoB, thus this organ is exposed to relatively high radiation doses. Interestingly, no signs of toxicity were found in liver and pancreas, despite the relatively high absorbed radiation doses. **References:** None

OP-0197

Imaging-guided co-targeting of HER2 and EpCAM using trastuzumab and DARPin-toxin fusion protein for theranostics of ovarian cancer

T. Xu[1], A. Schulga[2,3], O. Vorontsova[1], H. Ding[4], T. Gräslund[4], A. Orlova[1,3], V. Tolmachev[1,3], S. Deyev[2,3,5], A. Vorobyeva[1,3]; [1]Uppsala University, Uppsala, SWEDEN, [2]Russian Academy of Sciences, Moscow, RUSSIAN FEDERATION, [3]National Research Tomsk Polytechnic University, Tomsk, RUSSIAN FEDERATION, [4]KTH Royal Institute of Technology, Stockholm, SWEDEN, [5]National Research Nuclear University 'MEPhI', Moscow, RUSSIAN FEDERATION.

Aim/Introduction: Human epidermal growth factor receptor 2 (HER2) and epithelial cell adhesion molecule (EpCAM) are expressed in ca. 30% and ca. 70% of ovarian cancers, respectively. Their co-expression allows for co-targeted treatment of ovarian cancer. Designed ankyrin repeat protein (DARPin) Ec1 is a small engineered scaffold protein (18 kDa) that binds to EpCAM with high affinity. It was fused to the catalytic subunit of Pseudomonas exotoxin A with reduced immunogenicity and toxicity (LoPE toxin, 25 kDa). Ec1-LoPE was studied in vitro, and its therapeutic efficacy was evaluated alone and in combination with trastuzumab in EpCAM- and HER2- co-expressing SKOV-3 xenografts in vivo. **Materials and Methods:** Ec1-LoPE was labeled with technetium-99m and iodine-125 and studied for affinity, binding specificity, cellular processing and cytotoxicity in SKOV-3 and OVCAR-3 cells. The cross-blockability by trastuzumab was investigated. Biodistribution of [^{125}I]I-PIB-Ec1-LoPE was performed in Balb/c nu/nu mice bearing SKOV-3 xenografts 4 h, 24 h and 48 h post-injection. In vivo specificity was studied using EpCAM-negative Ramos xenografts. Therapy using Ec1-LoPE and trastuzumab was performed in Balb/c nu/nu mice bearing SKOV-3 xenografts. Imaging of HER2 expression was performed using [^{99m}Tc]Tc-ZV2 affibody molecule. Imaging of EpCAM expression was performed using [^{125}I]I-PIB-Ec1. Results: Radiolabeled Ec1-LoPE demonstrated EpCAM-specific binding and subnanomolar affinity to SKOV-3 and OVCAR-3 cells. No cross-blocking between the binding of Ec1-LoPE to EpCAM and trastuzumab to HER2 was observed. Cellular processing showed rapid binding of Ec1-LoPE and internalization of ca. 30% by 6 h in both cell lines. Ec1-LoPE provided dose-dependent cytotoxic effect with IC_{50} value 0.53 μM on SKOV-3 cells and 83 pM on OVCAR-3 cells. Biodistribution of Ec1-LoPE was characterized by fast renal excretion. A significantly ($p<0.05$) lower accumulation of Ec1-LoPE was observed in Ramos xenografts compared to SKOV-3 xenografts. Eight cycles of treatment using Ec1-LoPE were well tolerated by mice and reduced the growth of SKOV-3 xenografts compared to the control group. The co-treatment using Ec1-LoPE and trastuzumab prolonged median survival of mice compared with the control and mono-treatment groups. No pathological changes in liver and kidneys were observed during histology examination. SPECT/CT imaging enabled clear visualization of SKOV-3 tumors expressing EpCAM and HER2 and correlated well with the measurements of tumor size. **Conclusion:** The addition of Ec1-LoPE improved survival of trastuzumab-treated mice bearing EpCAM- and HER2-expressing xenografts. Radionuclide imaging permits identification of tumors with co-expression of both targets. Ec1-LoPE and trastuzumab co-treatment is a promising therapeutic strategy in ovarian cancers. **References:** none

OP-0198

Novel Radiolabelled CCK_2R Antagonists Show Promise for In Vivo Theranostic Use

D. Novak[1,2], M. Anderluh[2], R. Mansi[3], M. Krošelj[1], P. Kolenc[1,2]; [1]Department of Nuclear Medicine, University Medical Centre Ljubljana, Ljubljana, SLOVENIA, [2]Faculty of Pharmacy, University of Ljubljana, Ljubljana, SLOVENIA, [3]Division of Radiopharmaceutical Chemistry, University Hospital Basel, Basel, SWITZERLAND.

Aim/Introduction: With the use of radiolabelled cholecystokinin-2/gastrin receptor (CCK_2R) antagonists (CCK_2R-ANTs) possible adverse effects of current state-of-the-art radiolabelled CCK_2R agonists may be avoided. Therefore, we designed, synthesized and evaluated novel radiolabelled CCK_2R-ANTs based on CRL1 or CRL3[1] bearing acyclic N3S-BFC (bifunctional chelator) suitable for ^{99m}Tc-radiolabelling. By introducing different hydrophilic spacer, such as PEG_n[2], and/or BFC suitable for theranostics, we aimed to obtain CCK_2R-ANTs with improved in vitro and in vivo tumour targeting properties compared to the selected radiolabelled agonist CP04 (DOTA-(D-Glu)$_6$-Ala-Tyr-Gly-Trp-Met-Asp-Phe-NH_2). **Materials and Methods:** Two sets of CRL1 and CRL3 analogues conjugated to DOTA (DN12 and DN13) and DOTAGA (DN14 and DN15) were synthesized manually on solid phase and in combination with synthesis in solution. After purification by RP-HPLC, the compounds were characterized by ESIMS and analytical RP-HPLC. The IP1-based functional cell assay (IPOne®) was used to confirm antagonistic properties of the newly synthesized compound. The novel CCK_2R-ANTs were radiolabelled with gallium-68. For radiolabelled compounds, $logD_{7.4}$, stability in PBS, metabolic stability and binding to serum proteins were assessed. Cell association fraction and

saturation binding assays to determine binding properties were carried out in human-CCK_2R transfected A431 (A431-CCK_2R) and mock cells (A431-mock). For comparison, agonist [^{68}Ga]Ga-CP04 as well as [^{99m}Tc]Tc-CRL1/CRL3 were used in all experiments. Results: All radiolabelled compounds exhibited high stability, with >95% intact compounds at h h 4h in PBS and human serum. A gradual increase in hydrophilicity was achieved for DOTA-/DOTAGA-analogues ($logD_{7.4}$<-2.5 for all vs. -1.63±0.07 for [^{99m}Tc]Tc-CRL1 vs. -3.84±0.43 for [^{68}Ga]GaCP04). These results are in accordance with protein bound fraction for [^{68}Ga]Ga-CCK_2R-ANTs being as low as 3.4±1.1% ([^{68}Ga]Ga-DN14) compared to 25.3±7.6 % for [^{99m}Tc]Tc-CRL1 and 7.7±0.7 for [^{68}Ga]GaCP04. The specific cell associated fractions for [^{68}Ga]Ga-CCK_2R-ANTs ranged from 26.8±4.2% for [^{68}Ga]Ga-DN12 to 30.5±6.6% for [^{68}Ga]Ga-DN15 compared to 25.30±7.60 for [^{99m}Tc]Tc-CRL1 and 14.1±0.5% for [^{68}Ga]Ga-CP04, attributing the higher percentage to antagonistic mode of action. Apart from the agonism/antagonism, the most distinct difference between CCK_2R-ANTs and [^{68}Ga]GaCP04 was observed in maximal specific binding (B_{max}), since B_{max} value for each CCK_2R-ANTs was at least 5-times higher compared to [^{68}Ga]GaCP04. The dissociation constants (K_d) showed no dependence neither on BFC selection nor agonism/antagonism. **Conclusion:** We successfully synthesized, characterized and evaluated novel CCK_2R-ANTs, with promising in vitro properties. Animal studies are planned to further investigate theranostic potential of CCK_2R-ANTs in in vivo setting. **References:** [1] Wayua C, Low PS. J Nucl Med. 2015;56(1):113-119. [2] Novak D, et al. ChemMedChem. 2021;16:155 -163.

OP-0199

In vivo theranostic evaluation of a ^{64}Cu-radiolabelled antibody in a murine model of multiple myeloma

C. Métivier[1], P. Remaud-Le-Saec[1], S. Marionneau-Lambot[1], F. Davodeau[1], C. Chauvet[1], C. Saï-Maurel[1], P. Hofgaard[2,3], B. Bogen[2,3], R. Tripier[4], F. Haddad[5], J. Gaschet[1], M. Chérel[1], N. Chouin[1], A. Faivre-Chauvet[1], L. Rbah-Vidal[1];

[1]Université de Nantes, CHU Nantes, CNRS, Inserm, CRCINA, F-44000 Nantes, FRANCE, [2]Department of Immunology, Centre for Immune Regulation, Institute of Clinical Medicine, University of Oslo, Oslo, NORWAY, [3]KG Jebsen Centre for Influenza Vaccine Research, Institute of Clinical Medicine, University of Oslo, Oslo, NORWAY, [4]UMR CNRS 6521 CEMCA, University of Brest, Brest, FRANCE, [5]GIP Arronax, Saint-Herblain, FRANCE.

Aim/Introduction: Nuclear medicine offers a unique advantage for a theranostic approach to cancer in a context of personalized medicine by combining imaging and targeted radionuclide therapy (TRT). Copper-64, due to its radiological properties (β^+ 17.4%, β^- 39,0%) appears to be an attractive radionuclide combining diagnostic and therapeutic capabilities into a single agent. However, in recent years, some ^{64}Cu-radiolabelled vectors have been tested for cancer preclinical radiotherapy, with divergent results[1]. This project aimed to explore the theranostic potential of an anti-CD138 radiolabelled antibody ([^{64}Cu]Cu-HTE1PA-9E7.4) in the syngeneic murine MOPC315.BM multiple myeloma (MM) model. **Materials and Methods:** PET imaging and ex vivo biodistribution studies using [^{64}Cu]Cu-HTE1PA-9E7.4 were carried out at several times after tracer injection. The pharmacokinetic profile and parameters were evaluated, and absorbed doses to tissues were estimated based on biodistribution. Then, single and repeated-dose regimens of TRT were tested using different activities (22, 35, 55 and 65 MBq) in our preclinical model of MM. Antitumoral efficiency was monitored by survival of treated mice compared to control ones (saline or mAb alone). All mice were assessed daily throughout the TRT study for outward signs of toxicity as lethargy and body weight loss, and weekly for hematological and renal parameters. Results: PET imaging and ex vivo biodistribution results demonstrated a favourable profile of [^{64}Cu]Cu-HTE1PA-9E7.4 with a high and long lasting uptake CD138 positive cells (> 50% IA/g at 24 h and 48 h p.i). TRT using 22 MBq single dose shows no significant effect on survival whereas 35 and 65 MBq increased the median survival by 5 and 7 days respectively compared to the control mice (4 weeks post-inoculation of MOPC315.BM). Interestingly, repeated-dose regimens were significantly more effective with increasing median survival by 3 weeks (2X 55 MBq) compared to control groups, and 50% of mice treated with two injections of 35 MBq still alive more than 10 weeks after cell injection. A moderate and transient hematotoxicity was observed and its grade correlates with the injected activities. **Conclusion:** As expected, copper-64 properties allow to use it as a theranostic agent. These promising results show that repeated injections of ^{64}Cu-radiolabelled antibody are safe and effective in this syngeneic preclinical model of MM, and pave the way to further theranostic evaluation of ^{64}Cu-based therapies. **References:** 1. Gutfilen, B., Souza, S. A. & Valentini, G. Copper-64: a real theranostic agent. Drug Des Devel Ther 12, 3235-3245 (2018).

OP-0200

Novel Synthetic Strategies Enable the Efficient Development of Folate Conjugates for Radiotheragnostic Application

L. Deberle[1], M. Benešová[1,2], A. E. Becker[1], P. Guzik[1], R. Schibli[1,2], C. Müller[1,2];

[1]Paul Scherrer Institute, Villigen, SWITZERLAND, [2]ETH Zurich, Zurich, SWITZERLAND.

Aim/Introduction: The folate receptor (FR) is a promising target for radiotheragnostics due to its overexpression in numerous tumor types. It is, thus, of interest to develop novel folate radioconjugates for theragnostic application. This study aimed to establish a synthetic approach to overcome the challenges in folate chemistry and facilitate a convenient

preparation of a broad spectrum of folate radioconjugates. **Materials and Methods:** Two solid support-based synthesis pathways were established using orthogonal Fmoc-protection strategies for a modular build-up of an albumin-binding DOTA-folate conjugate (OxFol-1) which served as our model compound.[1] In Approach 1, the folate entity (folic acid) was connected to a resin-immobilized lysine-based linker followed by the DOTA chelator and a p-iodophenyl entity as albumin binder. In Approach 2, the DOTA chelator was first conjugated to the resin-bound linker, followed by the albumin binder and, in the last step, the folate entity was attached. The latter approach also enabled to introduce 6R- or 6S-5-methyltetrahydrofolate (5-MTHF) as folate entity (6R-RedFol-1 and 6S-RedFol-1). The synthesized conjugates were labeled with lutetium-177 and preclinically investigated. Results: Both solid phase-based synthesis approaches enabled the preparation of OxFol-1 within one week and yielded a highly pure (>98%) product in moderate yields (7-8%) without the need to purify intermediate products. Approach 2 appeared advantageous for the synthesis of 6R- and 6S-5-MTHF-based conjugates. All three conjugates, containing either 6R-5-MTHF, 6S-5-MTHF or folic acid as targeting entity and a p-iodophenyl-based albumin binder[2], were obtained in 8–12 steps with high chemical purity (>98%). FR affinity (1.0-3.6 nM) of the ^{177}Lu-labeled conjugates (50 MBq/nmol; >98% radiochemical purity) was in the nanomolar range and in vitro binding to human plasma proteins was high (>94%). Biodistribution and SPECT/CT imaging studies in KB tumor-bearing mice showed the most promising results for 6R-RedFol-1 with a high tumor uptake (47 ± 4% IA/g, 24 h p.i.) and tumor-to-kidney ratio (2.0 ± 0.4, 24 h p.i.).[3] **Conclusion:** The established synthesis approach enabled a straightforward preparation of folic acid- or 5-MTHF-based FR-targeting agents. The results demonstrated a favorable effect of using 5-MTHF instead of folic acid as targeting agent and opened new perspectives for radiotheragnostic application of this novel class of radiofolates. **References:** [1] Müller et al. Journal of nuclear medicine : official publication, Society of Nuclear Medicine 2014, 55, (10), 1658-64. [2] Dumelin et al. Angew Chem 2008, 17, 3240-3245. [3] Guzik et al. Eur J Nucl Med Mol Imaging 2021, 48, 972-983.

OP-0201

Production and in vitro evaluation of no-carrier-added radio-cisplatin emitting Auger electrons

H. Obata[1], *A. B. Tsuji*[1], *K. Nagatsu*[1], *M. Ogawa*[2], *M. R. Zhang*[1]; *[1]National Institutes for Quantum and Radiological Science and Technology, Chiba, JAPAN, [2]Hokkaido University, Hokkaido, JAPAN.*

Aim/Introduction: Auger electrons (Auger e^-) have the potential for therapeutic applications by inducing nano-scale physiochemical damage to biomolecules due to their short-range (2-500 nm). Although DNA is the primary target of Auger e^-, it remains challenging to maximize the interaction between Auger e^- and DNA. To assess the DNA-damaging effect of Auger e^- released as close as possible to DNA, we focused on a platinum(Pt)-based antineoplastic drug, cisplatin, because it can form direct DNA adducts between Pt and nucleobases. Here, to evaluate the effect of Auger e^- without chemical factors we radio-synthesized no-carrier-added (n.c.a.) [$^{189, 191}$Pt]cisplatin (radio-cisplatin), and investigated its in vitro properties and DNA-damaging effect in cultured cells. **Materials and Methods:** N.c.a. radio-cisplatin was radio-synthesized by treating n.c.a. radio-$PtCl_4^{2-}$ with excess NH_3 and heating the reaction mixture, and the product was isolated by preparative HPLC. As in vitro evaluation of radio-cisplatin, cellular uptake, intracellular distribution, and DNA binding were investigated, and DNA double-strand breaks (DSBs) were evaluated by immunofluorescence staining of γH2AX. Results: Our production method provided n.c.a. radio-cisplatin with a radiochemical purity of 99% at the end of synthesis. Although uptake of radio-cisplatin was low (0.6% incubated dose after 25-h incubation), approximately 20% of intracellular radio-Pt was in a nucleus, and 2% of intra-nucleus radio-Pt bound to DNA. Due to the low accumulation of radio-Pt, the frequency of cells with γH2AX foci was low (1%) in the γH2AX assays. Nevertheless, strong signals in nuclei of tumor cells treated with radio-cisplatin were found more often than with saline or nonradioactive cisplatin, suggesting Auger e^- released very close to DNA cause more DSB. **Conclusion:** N.c.a. radio-cisplatin was successfully prepared at high radiochemical purities as an effective tool to evaluate DNA damage induced by Auger e^- without chemical factors. Radio-cisplatin binding to DNA caused severe DSBs by the release of Auger e^- very close to DNA without chemical damage by carriers. **References:** Obata, et al. Int. J. Mol. Sci. 2021, 22, 4622. Obata, et al. Sci Rep 2021, 11, 8140.

OP-0202

Preparation and preclinical assessment of ^{188}Re-Rituximab for Radioimmunotherapy

B. Alirezapour[1], *H. Yousefnia*[1], *A. Bahrami-Samani*[1], *F. Shakeri*[2], *M. Alizadeh*[2], *M. Hashemizadeh*[3], *M. Fathi*[2], *B. Azizkalantari*[3]; *[1]Nuclear Science and Technology Research Institute (NSTRI), Tehran, IRAN, ISLAMIC REPUBLIC OF, [2]Zanjan University of Medical Sciences, Zanjan, IRAN, ISLAMIC REPUBLIC OF, [3]Pars Isotope Company, Tehran, IRAN, ISLAMIC REPUBLIC OF.*

Aim/Introduction: Radiolabeled monoclonal antibodies have shown great promise for cancer diagnosis and therapy. Rituximab is a chimeric monoclonal antibody against the protein CD20, which is primarily found on the surface of immune system B cells. Has been attempted to label Rituximab with ^{188}Re ($T_{1/2}$ = 16.9 h, E_β- max= 2.12 Mev, Eγ= 155 KeV (15%)) through using (HYNIC & MDP) BFCs in order to shows that Rituximab and radiation treatment combined will increase

therapeutic efficacy. In this regard, cell based assays as well as biodistribution studies in CD20+ cell lines and tumor bearing mice have been performed, respectively. **Materials and Methods:** The high radionuclide and radiochemical purity of the ^{188}Re-perrhenate solution was eluted from ^{188}W/^{188}Re generator which was manufactured by Pars Isotope Company. Rituximab was conjugated with HYNIC & MDP. HYNIC-Rituximab & MDP-Rituximab were labeled with ^{188}Re then Radiochemical purity as well as immunoreactivity, Cell Cytotoxicity and internalization studies by Raji cell line (CD20+ cell line) and serum stability of ^{188}Re-Rituximab were determined. The biodistribution studies and radioimmunoscintigraphy were performed in tumor bearing mice (^{188}Re-Rituximab i.v., 100 µl, 25±5 µg mAb, 12, 24 and 48 h). Results: ^{188}Re-HYNIC-Rituximab & ^{188}Re-MDP-Rituximab were prepared (RCP >95% ± 0.9, Specific activity 4.8 ± 1.2 µCi/µg- RCP >98% ± 0.7, Specific activity 5.2 ± 1.1 µCi/µg). Immunoreaction of ^{188}Re-HYNIC-Rituximab and ^{188}Re-MDP-Rituximab complex towards CD20 were determined by RIA and the complexes showed high immunoreactivity towards CD20. In vitro and in vivo stability of radioimmunoconjugates were investigated respectively in PBS and blood serum by RTLC method. In vitro stability for ^{188}Re-HYNIC-Rituximab was more than 84% ± 2.1 in PBS and 67% ± 3.1 in serum and for ^{188}Re-MDP-Rituximab was more than 91% ± 1.1 in PBS and 77% ± 3.8 in serum over 24 h . The Immunoreactivity of the radiolabeled Rituximab towards Raji cell line was found to be around 0.76 for both by using Lindmo assay protocol. Cell Cytotoxicity study by MTT assay showed increased effects of ^{188}Re-Rituximab on cell death of CD20-overexpressing cell line in camparison to unlabeled Rituximab. The biodistribution of ^{188}Re-Rituximab complexes in the tumor bearing mice at 12, 24 and 48 h after intravenous administration, expressed as %ID/g. The accumulation of the radiolabeled antibody in Tumor and other tissues demonstrates a similar pattern to the other radiolabeled anti-CD20 immunoconjugates. **Conclusion:** ^{188}Re-Rituximab is a potential compound for Radioimmunotherapy of CD20 expression in oncology. **References:** None

509

Wednesday, October 20 - Saturday, October 23, 2021

on-demand pool, release on Wednesday, October 20 at 09:00

Cutting Edge Science Track - TROP Session: Lu-177 Dosimetry

OP-0204

Impact of dead-time correction method on ^{177}Lu quantitative SPECT and dosimetry in personalized PRRT

A. Desy[1,2], G. F. Bouvet[1,2], J. M. Beauregard[1,2];
[1]Department of Medical Imaging, and Research Center (Oncology Axis), CHU de Québec – Université Laval, Québec City, QC, CANADA, [2]Department of Radiology and Nuclear Medicine, and Cancer Research Center, Université Laval, Québec City, QC, CANADA.

Aim/Introduction: Personalized ^{177}Lu-octreotate peptide receptor radionuclide therapy (PRRT) relies on quantitative SPECT (QSPECT)/CT dosimetry. Dead-time correction is required in this setting. To date, we have applied an average dead-time correction factor (DTCF) to the reconstructed QSPECT. However, the count rate and the corresponding dead time vary from one projection to another. Here we investigated to which extent correcting dead time per projection impacts quantification and dosimetry. **Materials and Methods:** Data from 12 patients (one cycle each) enrolled in our personalized PRRT trial (NCT02754297) was selected to obtain a wide range of DTCF (1.004-1.297). QSPECT/CT was performed at 23.2±1.3 and 70.4±1.0 h (Siemens Symbia T6). DTCF is based on the wide-spectrum count rate and retrieved from a lookup table. Firstly, following our current method[1], the average DTCF based on the average acquisition count rate was applied to the voxel data after reconstruction (4i8s-ACSCRR-OSEM; MIM Software). Secondly, the per-projection DTCFs were obtained and lost counts were injected into each projection before reconstruction. 2-cm spherical volumes of interest (VOIs) were placed over the kidneys (n=24), L4 & L5 bone marrow (n=24) and up to five tumours (n=57). Dosimetry was computed from the monoexponential time-activity curve (kidneys and bone marrow averaged, n=12)[2]. Counts and absorbed doses were compared between the per-projection vs. average methods and per dead-time groups: low (DTCF<1.10; n=13 QSPECTs) and high (DTCF≥1.10; n=11). Results: The median deviations (range) of VOI counts at low dead time were -0.2% (-2.7-3.8%), -0.2% (-6.9-3.9%) and 0.7% (-2.7%-16.2%) for the kidneys, tumours and bone-marrow, respectively. At high dead time, these were 0.5% (-2.2%-3.1%), 0.4% (-1.8%-3.3%) and 1.8% (-10.9%-9.8%), respectively. Regardless of the magnitude of dead time, kidney and tumour absorbed doses showed small differences between methods: 0.3% (-1.8%-2.1%) and -0.2% (-3.9%-5.7%) deviations, respectively, with only 3/57 tumours exceeding

±3%. Whereas, for bone marrow absorbed dose, slightly larger deviations were observed: 1.9% (-1.4%-9.0%), with 3/12 cases exceeding ±3%. A possible factor contributing to the bone marrow results is its very low activity, with consequent noisy signal. **Conclusion:** ^{177}Lu-QSPECT and dosimetry are minimally influenced by the choice of dead-time correction method, in particular for target tissues such as the kidneys and tumours. The use of an average acquisition DTCF appears suitable in personalized PRRT based on renal dosimetry. **References:** 1. Frezza A et al., EJNMMI Phys., 2020;7:10; 2. Del Prete M et al., EJNMMI Phys., 2018;5:25

OP-0205

Optimisation of the Radiation Dosimetry Protocol in ^{177}Lu-PSMA Therapy

M. Mink[1,2], S. M. Peters[1], B. M. Privé[1], M. de Bakker[1], C. H. Muselaers[3], N. Mehra[4], J. A. Witjes[3], M. Gotthardt[1], C. W. Timmermans[2,5], J. Nagarajah[1], M. W. Konijnenberg[1,6];
[1]Department of Medical Imaging, Radboud university medical center, Nijmegen, NETHERLANDS, [2]Radboud University, Nijmegen, NETHERLANDS, [3]Department of Urology, Radboud university medical center, Nijmegen, NETHERLANDS, [4]Department of Medical Oncology, Radboud university medical center, Nijmegen, NETHERLANDS, [5]Nikhef, Amsterdam, NETHERLANDS, [6]Department of Radiology and Nuclear Medicine, Erasmus Medical Center, Rotterdam, NETHERLANDS.

Aim/Introduction: Dosimetry in ^{177}Lu-PSMA therapy is a valuable tool to assess treatment efficacy and toxicity. For dosimetry, accurate sampling of the radiotracer uptake time-activity-curve using post-treatment imaging is important. It is of interest to minimise the number of scans without compromising the accuracy of dose calculations, since these scans put a burden on both patients and hospital resources. This study aims to develop an optimal protocol to determine the patient-specific absorbed dose in organs and lesions efficiently and accurately. **Materials and Methods:** Ten patients with metastatic hormone-sensitive prostate cancer received two cycles of ^{177}Lu-PSMA-617 treatment (NCT03828838). Post-treatment imaging was performed at 1h, 24h, 48h, 72h and 168h, including three bed positions SPECT/CT and a whole-body planar scan. Five-time-point SPECT dosimetry was performed for lesions and organs with physiological uptake (kidneys, liver and salivary glands), and used as reference standard. Absorbed dose values for various compositions of time-points were compared to the reference standard to determine the optimal simplified dosimetry protocol. The optimal combinations were selected by considering Lin's concordance correlation coefficient ρ_C, the uncertainty in the absorbed dose u(D) (acceptable limit u(D)<25%) and the normalised error E_n (pass for E_n<1). Results: The reference median absorbed dose for lesions was 2.07 Gy/GBq [range: 0.30-16.40] with a mean uncertainty of 13.6±3.1%. It was possible to obtain satisfactory lesion absorbed dose results from one-time-point imaging at 168h (ρ_C=0.98, $E_{n,mean}$=0.59±0.45 and $u(D)_{mean}$=20.1±1.3%). The best two-time-point combination was 24h+168h (ρ_C=0.99, $E_{n,mean}$=0.44±0.35 and $u(D)_{mean}$=12.9±2.3%). The organ reference median absorbed doses were 0.52 Gy/GBq [range: 0.21-0.88] with $u(D)_{mean}$=15.1±2.8% for kidneys, 0.08 Gy/GBq [range: 0.06-0.14] with $u(D)_{mean}$=21.7±4.8% for liver and 0.50 Gy/GBq [range: 0.15-1.28] with $u(D)_{mean}$=13.4±1.8% for salivary glands. Simplification of organ dosimetry based on SPECT or planar scans is still being investigated. **Conclusion:** Lesion dosimetry based on one-time-point SPECT imaging at 168h provides a good representation for the absorbed dose, though with an increase in uncertainty. By including the 24h time-point, a more accurate dose estimation is obtained. Simplification of the organ dosimetry protocol is still being analysed. This study shows that accurate lesion dosimetry in ^{177}Lu-PSMA therapy can be performed with minimal imaging time-points, making dosimetry assessments more adaptable for routine clinical implementation. **References:** none

OP-0206

Validation of a simplified single time point image-based dosimetry approach for ^{177}Lu-PSMA therapy

J. Brosch-Lenz[1,2], A. Gosewisch[1], F. Völter[1], L. Kaiser[1], P. Bartenstein[1], S. Ziegler[1], A. Rahmim[2,3,4], C. Uribe[5,3], G. Böning[1];
[1]Department of Nuclear Medicine, University Hospital, LMU Munich, Munich, GERMANY, [2]Department of Integrative Oncology, BC Cancer Research Institute, Vancouver, BC, CANADA, [3]Department of Radiology, University of British Columbia, Vancouver, BC, CANADA, [4]Department of Physics, University of British Columbia, Vancouver, BC, UNITED STATES OF AMERICA, [5]Functional Imaging, BC Cancer, Vancouver, BC, CANADA.

Aim/Introduction: Quantitative imaging is required for absorbed dose estimation in organs/tumors. Currently, most protocols require scans at multiple time points (MTP) following the radiopharmaceutical injection. However, this is not always feasible and puts a high burden on patients. Single time point (STP) image-based dosimetry has gained increasing interest as it can simplify the procedure and optimize resources. Large variations in effective half-lives ($effT_{1/2}$) between patients have been observed, especially in tumors, therefore patient-individual dosimetry is emphasized. This work aimed to validate a simplified dosimetry approach for ^{177}Lu-PSMA therapy using patient-individual measurements of organ/tumor $effT_{1/2}$ from MTP imaging from the 1st therapy cycle to estimate doses to organs/tumors with a STP in subsequent cycles. **Materials and Methods:** The 1st and 2nd therapy cycles of 10 patients, each with multi-bed quantitative ^{177}Lu-SPECT/CT at 24h, 48h and 72h post-injection, were analyzed. SPECT/CT images were registered to the 24h scan of each cycle. Volumes of interest (VOIs) for kidneys and bone lesions were segmented on the 24h SPECT images of 1st and 2nd cycle using thresholds and k-means clustering. $EffT_{1/2}$ for

kidneys, whole-bone tumor burden and up to 4 individual lesions per patient (apparent in both cycles) were obtained using mono-exponential fits. The absorbed doses were calculated using VOI-wise time-integrated activities and mass-scaled organ/tumor S-values according to the MIRD formalism. The eff$T_{1/2}$ from the 1st cycle were used to perform STP dosimetry for the 2nd cycle with the 24h, 48h, and 72h scan separately. Percentage differences (PD) of doses were calculated for all VOIs for the STP approaches against the reference of MTP dosimetry for the 2nd cycle. Results: STP against MTP PDs for kidney doses were -4.2±5.0%, 0.1±4.9%, and 14.8±26.6% for the 24h, 48h, and 72h scans, respectively. Whole-bone tumor burden PDs were 7.1±22.9%, 4.4±14.3%, and 7.3±12.5% for the 24h, 48h, and 72h scans, respectively. Lastly, for the individual lesions PDs of 3.8±23.3%, 3.4±10.6%, and 8.0±25.1% were observed for the 24h, 48h, and 72 scans, respectively. **Conclusion:** We evaluated the feasibility of a simplified dosimetry approach that uses the eff$T_{1/2}$ of organs/tumors measured from MTP scans performed during 1st cycle of ^{177}Lu-PSMA therapy and applies it to a STP scan on the 2nd cycle. Our results suggest that this is a valid approach with smallest errors with a STP performed at 48h. Future steps will include expanding the analysis for more organs and testing it on a larger cohort of patients. **References:** none

OP-0207

A simplified method for kidney dosimetry in ^{177}Lu therapies based on single SPECT-CT and multiple external probe measurements

D. Pistone[1,2], T. Ligonnet[3], L. Auditore[4], A. Italiano[2,1], E. Amato[4,2], A. Campenni[4,5], N. Schaefer[6], S. Boughdad[6], S. Baldari[4,5], S. Gnesin[3]; [1]MIFT Department, University of Messina, Messina, ITALY, [2]INFN Section of Catania, Catania, ITALY, [3]Institute of Radiation Physics, Lausanne University Hospital and University of Lausanne, Lausanne, SWITZERLAND, [4]BIOMORF Department, University of Messina, Messina, ITALY, [5]Nuclear Medicine Unit, University Hospital "G. Martino", Messina, ITALY, [6]Department of Nuclear Medicine and Molecular Imaging, Lausanne University Hospital and University of Lausanne, Lausanne, SWITZERLAND.

Aim/Introduction: Image-based patient-specific kidney dosimetry provides a significant contribution to the optimization of activity administration in ^{177}Lu peptide receptor radionuclide therapy (PRRT) of neuroendocrine tumors and metastatic prostate cancer. However, the need of multiple SPECT-CT acquisitions and the subsequent dosimetric workflow can imply a remarkable resource effort. The aim of this proof-of-concept study is to propose a simplified personalized kidney dosimetry procedure in ^{177}Lu therapies, relying on a single quantitative SPECT-CT acquisition and multiple radiometric measurements executed with a collimated external probe, properly directed on kidneys. **Materials and Methods:** Firstly, a phantom study was conducted, performing sequential external count-rate measurements in an abdominal phantom setup including kidneys, liver and bowel compartments filled with activity concentrations of ^{99m}Tc reproducing relevant organ effective half-lives occurring in ^{177}Lu-PRRT: 55, 79 and 85 hrs in kidneys, liver and bowel, respectively. Effective half-life in kidneys was evaluated via mono-exponential fit of count-rates measured directing the collimated probe towards left kidney and in an intermediate position between the two kidneys (for background subtraction), and was compared with the expected value known from the experimental construction. Secondly, GATE Monte Carlo (MC) simulations reproducing the experiment were performed, using ^{99m}Tc and ^{177}Lu as sources. Finally the proposed method was tested via MC simulation on a clinical case of ^{177}Lu-DOTATATE PRRT with SPECT-CT images at three time points (2, 20 and 70 hrs), simulating external probe measurements analogous to the ones of phantom study. A simplified kidney dosimetry workflow, employing a single SPECT-CT and an effective half-life derived from probe measurements at three time points, was compared to a complete direct MC dosimetry workflow. Results: The estimated kidney half-life obtained from collimated count-rate measurements with background subtraction performed on the phantom was consistent within 3% of the expected value. Phantom study MC simulations with both ^{99m}Tc and ^{177}Lu confirmed a similar level of accuracy. The simplified dosimetric workflow, tested on the examined clinical case, led to kidney dose estimations compatible within 6%, 12% and 2% with the complete MC workflow, using respectively the SPECT-CT at 2, 20 and 70 hours. **Conclusion:** The proposed simplified procedure to perform kidney dosimetry in ^{177}Lu therapies, taking advantage of external probe measurements for the estimation of patient-specific renal effective half-life, provides satisfactory accuracy and would reduce to a unique quantitative SPECT-CT the imaging required to derive the kidney absorbed dose, with consequent benefits in terms of clinic workflows and patient comfort. **References:** none

OP-0208

Evaluation of 2D/3D hybrid dosimetry in PSMA-targeted radioligand therapy

F. Rosar, N. Schön, H. Bohnenberger, M. Bartholomä, T. Stemler, S. Maus, F. Khreish, S. Ezziddin, A. Schaefer-Schuler; Department of Nuclear Medicine, Saarland University - Medical Center, Homburg, GERMANY.

Aim/Introduction: Dosimetry is needed to optimize individualized PSMA-targeted radioligand therapy. However, there is no international consensus on the optimal dosimetry method. Our aim was to evaluate the feasibility of 2D/3D hybrid dosimetry in [^{177}Lu]Lu-PSMA-617 radioligand therapy

as this method may offer the possibility of being more accurate than 2D dosimetry and less time consuming than 3D dosimetry. **Materials and Methods:** Whole-body planar images and SPECT/CT images were acquired from n=24 patients with 65 cycles at three time points (24h, 48h and ≥96h) after administration of [^{177}Lu]Lu-PSMA-617. 2D/3D hybrid dosimetry was performed based on one SPECT/CT and three whole-body planar images. Absorbed doses were calculated for the kidneys, the liver, the salivary glands and bone metastases. Results were compared to 3D dosimetry based on three SPECT/CT images. Results: Mean absorbed doses estimated by 2D/3D hybrid dosimetry were 0.52 ± 0.27 Gy/GBq for the kidneys, 0.10 ± 0.05 Gy/GBq for the liver, 0.81 ± 0.34 Gy/GBq for the parotid gland, 0.73 ± 0.39 Gy/GBq for the submandibular gland and 1.55 ± 1.28 Gy/GBq for bone metastases. Compared to 3D dosimetry estimated absorbed doses by 2D/3D hybrid dosimetry showed non-significant differences for normal organs (median difference up to 4%). In contrast, significantly different absorbed doses to bone metastases were observed (median difference 7%, p<0.001). In addition, Bland-Altman analysis revealed high agreement between 2D/3D hybrid dosimetry and 3D dosimetry. **Conclusion:** 2D/3D hybrid dosimetry is feasible for use in individualized PSMA-RLT providing high accuracy in absorbed dose estimation. **References:** none

OP-0209

Comparison of Voxel S-values and Monte Carlo Simulation in [^{177}Lu]Lu-DOTA-TATE Quantification for Patient-Specific Dosimetry

C. Rodrigues[1,2,3], P. Ferreira[1], F. P. M. Oliveira[1], Â. Silva[1], L. Peralta[2,3], D. C. Costa[1];
[1]Champalimaud Centre for the Unknown, Champalimaud Foundation, Lisbon, PORTUGAL, [2]Faculdade de Ciências da Universidade de Lisboa, Lisbon, PORTUGAL, [3]Laboratório de Instrumentação e Física Experimental de Partículas, Lisbon, PORTUGAL.

Aim/Introduction: Peptide receptor radionuclide therapy (PRRT) with [^{177}Lu]Lu-DOTA-TATE is remarkably effective in the treatment of neuroendocrine tumours (NETs) over-expressing somatostatin receptors. Apart from potential renal and/or haematological toxicity, the significant absorbed dose variability among patients requires individual treatment optimisation. Several methods have been used to quantify tissue exposure. This study compares the dosimetry calculated by two computational methods on a retrospective analysis of [^{177}Lu]Lu-DOTA-TATE PRRT clinical cases. **Materials and Methods:** Twenty-four treatments from 6 patients with histologically confirmed inoperable and/or metastatic neuroendocrine neoplasia over-expressing somatostatin receptors were retrospectively analysed (4 cycles/patient). A mean activity of 7.2 ± 0.5 GBq/cycle of [^{177}Lu]Lu-DOTA-TATE was administered. For 5 patients, two abdominal SPECT and CT acquisitions (24h and 120h post administration) were performed. For the other patient only one acquisition was performed (24h post administration). These acquisitions were used for absorbed dose quantification based on two methods. Voxel-based dosimetry with pre-calculated voxel S-values (VSV) was performed with an in-house program. Monte Carlo (MC) based dosimetry, with 100 million events, was performed with TOPAS (Geant4) tool. Organ 3D absorbed dose maps were qualitatively compared using dose-volume histograms (DVHs) and mean absorbed doses were quantitatively compared using the intraclass correlation coefficient (ICC) and relative difference (RD), with respect to MC. Results: MC based dosimetry entailed a simulation time of around 40 hours/simulation while the VSV method took less than 1 minute/computation, in the same workstation. Very good agreement (ICC > 0.90) was found for organ absorbed dose maps obtained with the two methods, with similar dose distribution given by the DVHs. Mean absorbed dose in the liver, right kidney, left kidney, spleen, bone marrow and NETs showed an ICC of 1.000, 0.992, 0.998, 0.999, 0.999 and 0.999, respectively. The greatest median RD of -3.6% (min = -25.6, max = 3.8) was seen for the bone marrow. Liver, right kidney, left kidney, spleen and NETs presented median RD of -1.0% (-5.5, 0.7), -2.9% (-11.1, 2.6), -1.9% (-15.4, 1.7), 0.2% (-4.3, 4.1) and 0.4% (-10.3, 8.2), respectively. These differences are most likely due to patient morphology considerations in MC simulations. **Conclusion:** This preliminary study reveals similar 3D absorbed dose maps for both VSV and MC methods, with slightly lower VSV than MC dose values. Therefore, the VSV-based method appears to be a reasonable choice for clinical dosimetry calculations in [^{177}Lu]Lu-DOTA-TATE PRRT patients, considering the significantly short computation time and dosimetry accuracy. **References:** none

OP-0210

Impact of SPECT Segmentation on Accuracy of Lu-177 Activity Quantification for Dosimetry in Radionuclide Therapy

J. Pfeil[1], Z. Zsebe[2], I. Apostolova[2], R. Buchert[2], S. Klutmann[2], W. Lehnert[2];
[1]Humboldt Universität zu Berlin, Berlin, GERMANY, [2]University Medical Center, Hamburg, GERMANY.

Aim/Introduction: Accurate quantification of activity in organs and tumours is essential for dosimetry in Lu-177 radionuclide therapy. In this context the method of segmentation plays an important role, especially for small structures affected by partial volume effects. The aim of this study was to analyse different segmentation methods with respect to their quantitative accuracy in dependence on object volume, object-to-background-ratio (OBR) and image noise. **Materials and Methods:** Lu-177 phantom SPECT/CT-scans were performed in List-Mode using a Mediso AnyScan SPECT/CT triple head camera (MLEGP-

collimators), processed into projections with 40 to 5 s per projection and then reconstructed using the iterative Tera-Tomo 3D SPECT/CT OSEM-algorithm (110 effective iterations, attenuation and scatter correction, resolution recovery). The IEC-NEMA body phantom was used with different spherical and cylindrical inserts with volumes between 350 and 0.5 ml, filled with activity concentrations relevant for patient scans and OBRs between 20:1 and 3:1. Activity segmentation was performed using the dosimetry software QDOSE. The following segmentation methods were investigated: anatomic segmentation (AS), convolution of the anatomical VOI with a Gaussian (CS), fixed SPECT thresholds (FS), SPECT segmentation with background subtraction (BS) and multiplication of the mean activity concentration of a 50 %-threshold VOI with the object volume (MS). Activity recovery for all objects was considered for quantitative analysis. Results: In general, AS and MS underestimated the activity, with increasing inaccuracies for small volumes. Results of FS had a strong volume and OBR dependence for all thresholds. CS with a full width at half maximum (FWHM) of 5 mm was most robust against partial volume effects and noise with mean deviations of 6% for OBR ≥ 15/ volume ≥ 2,6 ml/ ≥ 5 s per projection (-13% to 17%) and OBR ≥ 5/ volume ≥ 50 ml/ ≥ 15 s per projection (-11% to 5%). BS provided similar results for OBR ≥ 15 with a mean deviation of 9 %. **Conclusion:** The choice of segmentation method is crucial, in particular for small organs and tumours. Amongst the investigated methods CS (FWHM 5 mm) produced the most accurate quantification. In view of the dosimetry imaging after therapy, a higher inaccuracy of the activity for smaller volumes for SPECT imaging shortly after therapy (with low contrast, but also lower noise) may only have a small effect on the overall absorbed dose calculation due to the relatively small expected contribution of this first time point to the cumulated activity. **References:** none

OP-0211

Ga-68-PSMA-11 PET Imaging as a Predictor for Absorbed Doses in Organs at Risk and Small Lesions in Lu-177-PSMA-617 Treatment

S. Peters[1], *R. Hofferber*[2], *B. Privé*[1], *M. De Bakker*[1], *M. Gotthardt*[1], *F. De Lange*[1], *C. Muselaers*[1], *N. Mehra*[1], *A. Witjes*[1], *P. Costa*[2], *J. Nagarajah*[1], *M. Konijnenberg*[1], *W. Jentzen*[2];
[1]*Radboudumc, Nijmegen, NETHERLANDS,* [2]*Essen University Hospital, Essen, GERMANY.*

Aim/Introduction: Patient eligibility for ^{177}Lu-PSMA therapy is usually checked by evaluating the lesion uptake (SUV) on ^{68}Ga-PSMA-PET/CT. Yet, this pre-therapeutic PSMA-PET scan may also be used to predict the absorbed dose of ^{177}Lu-PSMA therapy. This could improve patient selection and further individualize the treatment by elucidating the ideal dose for the target lesions while adhering to the threshold absorbed doses for the organs at risk (kidneys, salivary glands, and liver). This study aims to predict the absorbed doses of ^{177}Lu-PSMA therapy in the organs at risk and target lesions using pre-therapeutic single time point ^{68}Ga-PSMA-PET/CT and compares the outcomes to the actual delivered absorbed doses after therapy. **Materials and Methods:** In this study (NCT03828838), 10 patients with low volume hormone-sensitive prostate cancer were evaluated. Each patient received a pre-therapeutic ^{68}Ga-PSMA-11 PET/CT, followed by therapy with 3 GBq ^{177}Lu-PSMA-617. Post-therapy, 3 bed positions SPECT/CT were acquired at 1, 24, 48, 72 and 168 h. Absorbed dose in organs and lesions (n = 22) was determined according to the MIRD scheme, using CT or PET derived volumes. Tracer uptake of ^{68}Ga-PSMA-PET/CT at 1 h post injection was used to predict the absorbed dose for ^{177}Lu-PSMA using the mean effective half-life of the 10 patients on SPECT. Predicted PET/actual SPECT absorbed dose ratios were determined for each target volume. Results: Tissue specific tracer kinetics for organs could be established with low variability (SD 6% - 21%). PET/SPECT absorbed dose ratio was 2.21 ± 0.46, 1.10 ± 0.15, 1.20 ± 0.34, 1.11 ± 0.29 for kidneys, liver, submandibular and parotid glands, respectively. For kidneys a mean scaling factor of 2.21 was applied, resulting in PET/SPECT absorbed dose ratio of 1.01 ± 0.21. A large inter-patient variation of 54% was observed in the lesion kinetics resulting in PET/SPECT absorbed dose ratio: 1.3 ± 0.7 (range: 0.4 - 2.7). This means the absorbed dose estimation in a single lesion is at maximum a factor 3 off. **Conclusion:** This study showed that a single time-point ^{68}Ga-PSMA-PET/CT scan can be used to predict absorbed doses in the organs at risk. The dose prediction of the target lesions is limited by extensive variance, which could be the result of tumor heterogeneity or biochemical behavior of the tracer. However, even a lesion absorbed dose indication that is at maximum a factor of 3 off can provide the treating physician with valuable information before start of treatment. **References:** -

OP-0212

Comparison of Red Marrow Dosimetry Methodologies for Lu-177-PSMA Radionuclide Therapy

W. Lehnert, *I. Apostolova, R. Buchert, S. Klutmann; University Medical Center, Hamburg, GERMANY.*

Aim/Introduction: Haematological toxicity is a potential confounding factor for Lu-177-PSMA radionuclide therapy. Hence red marrow (RM) is considered an organ at risk. The aim of this study was to investigate RM dosimetry by (1) comparing the blood-based (BB) approach with an imaging-based (IB) approach and (2) evaluating the influence of dose calculation software on RM absorbed dose (AD). **Materials and Methods:** This study included 8 patients (cycle 1 or 2 of ^{177}Lu-PSMA-617), 4 with a high skeletal tumour load (TL) and 4 with a low skeletal TL. They underwent whole body SPECT imaging and blood sampling at 2h, 24h, 48h and 72h. RM time-integrated activity coefficients were calculated based on the

activity concentration in blood and for the IB approach using the activity in the lumbar vertebrae segmented in the SPECT images scaled to total RM mass. RM AD was calculated using OLINDA/EXM 1.1, IDAC-Dose 1.0 and IDAC-Dose 2.1 with RM, major organs and remainder body (RB) (including tumours) as source organs. Results: For the BB approach the mean RM AD was 46.4 mGy/GBq for IDAC-Dose 2.1 across all patients and 56.0 mGy/GBq and 36.1 mGy/GBq for patients with high TL and low TL, respectively. The AD with OLINDA/EXM 1.1 was 53%, 65% and 43% higher. Independent of patient group the AD was also 22% higher for IDAC-Dose 1.0 compared to IDAC-Dose 2.1. The contribution of RM self-dose to total AD was lower for OLINDA 1.1 with 40% than for IDAC-Dose 1.0 and 2.1 with 48% due to different assumptions regarding the RB contribution to RM AD. When RM was excluded as source organ, IDAC-Dose 2.1 and 1.0 overestimated the RM AD by 88% and 46% for high TL patients and underestimated it by -3.5% and -25% for low TL patients, respectively, compared to the RM BB approach. OLINDA 1.1 underestimated the AD for high TL patients by -21% and for low TL patients by -53%. The IB approach could only be applied to patients without extensive skeletal metastases, but showed much slower kinetics and hence higher RM AD compared to the BB approach with increases between 139% and 166%. **Conclusion:** The choice of RM dosimetry approach and dosimetry calculation software severely impacts the calculated AD, which poses difficulties for applying the 2Gy RM dose limit and predicting haematotoxicity using clinical routine dosimetry. It is therefore essential to monitor haematotoxicity in particular for patients with high skeletal TL. **References:** None

OP-0213

Simplified dosimetry for peptide-receptor radionuclide therapy using physiologically-based pharmacokinetic and nonlinear mixed effect modelling

D. Hardiansyah[1], A. Riana[1], P. Kletting[2], A. J. Beer[2], G. Glatting[2];
[1]Universitas Indonesia, Depok, INDONESIA,
[2]Ulm University, Ulm, GERMANY.

Aim/Introduction: Estimation of accurate time-integrated activity coefficients (TIACs) is important for treatment planning in peptide-receptor radionuclide therapy (PRRT). The aim of this study was to investigate the accuracy of a simplified dosimetry using a physiologically-based pharmacokinetic (PBPK) model, a nonlinear mixed effect (NLME) model and a single planar measurement to calculate the TIACs of ^{111}In-DOTATATE in various organs used for dosimetry in PRRT. **Materials and Methods:** Biokinetic data of ^{111}In-DOTATATE in tumours, kidneys, liver, spleen and whole body were obtained from eight patients using planar imaging at 2, 4, 24, 48 and 72 h post injection. Serum activity was measured at 5 and 15 min; 0.5, 1, 2, and 4 h; and 1, 2, and 3 d p.i.. A published PBPK model for PRRT, NLME and a single biokinetic datum at different time points, i.e. T1=(2.9±0.6) h, T2=(4.6±0.4) h, T3=(22.8±1.6) h, T4=(46.7±1.7) h and T5=(70.9±1.0) h, were used to calculate TIACs in tumours, kidneys, liver, spleen, whole body and serum. Relative deviations (RDs) (median [min, max]) between the calculated TIACs from a single biokinetic datum were compared to the TIACs calculated from all-time points fit. Results: Using PBPK and NLME modelling together with a single biokinetic datum resulted in a good fit based on visual inspection of the fitted curves and the coefficient of variation CV of the fitted parameters (<50%). T4 was identified being the time point with the lowest RDs for kidneys TIACs with RD_{tumor}=2% [-16, 21]%, $RD_{kidneys}$=5% [0, 18]%, RD_{liver}=0% [-13, 11]%, RD_{spleen} =9% [-11, 16]%, RD_{WB}=2% [-3, 7]% and RD_{serum} =4% [-23, 25]%. Furthermore, using T5 also resulted in low RD of the TIACs, i.e. RD_{tumor}=3% [-27, 34]%, $RD_{kidneys}$=-1% [-12, 28]%, RD_{liver}=-7% [-18, 18]%, RD_{spleen} =9% [-17, 24]%, RD_{WB}=-1% [-7, 4]% and RD_{serum} =4%[-21, 24]%. The RDs of the calculated kidneys TIACs in this study were similar to the RDs of the calculated kidneys TIACS reported by Devasia et al. [1] using a NLME model, exponential functions and a single biokinetic datum at 96 h from SPECT/CT, i.e. $RD_{kidneys}$=-3% [-16, 4]%. **Conclusion:** In this study, we introduced for the first time a simplified calculation of TIACs using a PBPK model, a NLME model and a single biokinetic datum from planar imaging. Our results suggest a single measurement with planar imaging might be used to calculate TIACs in the OAR and tumours during PRRT. **References:** 1. Devasia, T., et al., J Nucl Med, 2020: p. jnumed.120.256255.

OP-0214

Optimization of three imaging time points for most reliable renal dosimetry in Peptide Receptor Radionuclide Therapy

A. Konuparamban[1,2], A. Nautiyal[1,2], A. K. Jha[1,2], S. Mithun[1,2], V. Rangarajan[1,2];
[1]Tata Memorial Hospital, Mumbai, INDIA, [2]Homi Bhabha National Institute(HBNI), Deemed University, Mumbai, INDIA.

Aim/Introduction: The use of peptide receptor radionuclide therapy (PRRT) with [^{177}Lu]Lu-DOTATATE has gained wide acceptance for treatment of metastatic neuroendocrine tumour. Individualized dosimetry based dose estimation of tumour and critical organs is one of the necessary steps to ensure the efficacy of the treatment in radionuclide therapy. Renal dosimetry is an important step in PRRT as the kidney is a critical organ. Renal dosimetry in PRRT is usually performed by acquiring 3 to 5 whole-body planar scans to extrapolate the tracer kinetics. However, it is a time consuming and cumbersome procedure for patients and professionals. Aim of our study is to optimize three most appropriate imaging time-points for reliable renal dosimetry in PRRT. **Materials and Methods:** This study was approved by the institutional ethics committee of our institution. Twenty patients'(age=49.34±14.79yrs;

height=162.48±11.67cm and weight=60.16±16.11kg) dosimetry data who underwent PRRT between 2019 to 2020 were utilized. Whole-body planar scans were acquired at five time-points (0.5, 4, 24, 72 and 160h) using Discovery 670-Pro-SPECT/CT system post administration of [^{177}Lu]Lu-DOTATATE(average activity 6494.185±1932.03MBq). Renal volume was calculated using Q.Metrix software installed on Xeleris 4.1 workstation. Normalized cumulated activity(NCA) and absorbed dose were estimated for kidneys by using Dosimetry Toolkit and OLINDA-EXM 2.0 for following time subsets i.e. for all five time points, and for three time points in seven combinations[T1=(0.5,4,24h); T2= (4,24,72h); T3= (0.5,4,160); T4=(4,24,160h); T5=(24,72,160h); T6=(4,72,160h); T7=(0.5,4,72h)]. NCA and absorbed dose calculated with five imaging time points subset was considered as the gold standard. The NCA and absorbed dose calculated for the rest of the subsets were compared with that of the gold standard by performing Pearson correlation using SPSS software. Results: For standard set, mean NCA and absorbed dose in kidneys were 3.13±1.49h and 0.86±0.39mGy/MBq respectively. Mean NCA and absorbed dose in each subset were 2.57±1.48, 0.65±0.44(T1); 5.51±2.09, 1.52±0.57(T2); 2.97±0.92, 0.82±0.24(T3); 5.54±2.10, 1.76±0.94(T4); 11.46±4.99, 3.19±1.45(T5); 5.49±2.19, 1.52±0.602(T6); 3.02±1.31h, 0.84±0.35mGy/MBq (T7), respectively. Among all the subsets, T7 showed the best correlation for NCA and absorbed dose with gold standard i.e. r=0.98 and 0.97 respectively and T1, worst correlation i.e. r= -0.13 and -0.19 respectively. Table 1 shows the correlation of NCA and absorbed dose for all the subsets. **Conclusion:** With our study, we were able to demonstrate that the renal dosimetry study can be completed within 72 hours with three time point imaging i.e. 0.5, 4, 72 hours with most reliable accuracy in comparison to that of five time point imaging. **References:** None

OP-0215

Estimation of kidney absorbed doses from ^{177}Lu-DOTATATE using single time point SPECT/CT

S. Ballout[1], D. Gillett[1], E. Varzakis[1], I. Harper[1], D. Pitfield[2], A. Powell[1], R. T. Casey[3,2], S. Heard[1], L. Aloj[4,1];

[1]Department of Nuclear Medicine, Cambridge University Hospitals NHSFT, Cambridge, UNITED KINGDOM, [2]Department of Endocrinology, Cambridge University Hospitals NHSFT, Cambridge, UNITED KINGDOM, [3]Department of Genetics, University of Cambridge, Cambridge, UNITED KINGDOM, Cambridge, UNITED KINGDOM, [4]Department of Radiology, University of Cambridge, Cambridge, UNITED KINGDOM, Cambridge, UNITED KINGDOM.

Aim/Introduction: Lutetium-177 (^{177}Lu)-DOTATATE therapy is used to treat metastatic neuroendocrine tumours. Patients receive up to 4 cycles at 8 week intervals. Currently, patients are imaged on days 0, 1, 4, and 7 post-therapy after each treatment to enable dosimetry to be carried out. These repeated visits to the hospital can be challenging for patients and also require hours of time on the gamma cameras. To address these challenges we have investigated whether it is possible to estimate kidney absorbed doses in subsequent treatments by using a single treatment-specific SPECT/CT and effective half-lives calculated from cycle 1. **Materials and Methods:** Kidney time-activity curves (TAC) were generated from planar images acquired 0, 1, 4 and 7 days post treatment. In addition a single SPECT/CT was carried out at a single time-point after each treatment (usually day 4) and used to scale the TAC to activity concentration. From these TACs the effective half-lives and the kidney absorbed doses were calculated. The subsequent treatment kidney absorbed doses were also estimated by using the TACs from treatment 1 and scaled using the single SPECT/CT. These estimates were compared to the doses calculated using the full datasets from each treatment. Results: From a total of 16 patients treated and imaged using this method two were excluded due to the kidney uptake being obscured by tumour lesion uptake on the planar images. Using the full datasets of the remaining 14 patients (49 treatment cycles) the average absorbed doses for the right and left kidneys was calculated to be 3.3 + 0.2 Gy and 3.2 + 0.1 Gy respectively. The estimated doses for subsequent treatments based on the effective half-lives from treatment 1 and a treatment-specific SPECT/CT resulted in mean differences of 1.2% (IQR = 25%) and -3.0% (IQR = 28%) for the right and left kidneys respectively. The maximum differences observed were 44% and -43% for the right and left kidneys respectively. In all patients the calculated total treatment doses and estimated doses were within the commonly used 23 Gy kidney dose threshold. **Conclusion:** Our work has shown that in 87.5% of patients the absorbed kidney doses can be estimated using a single time point SPECT/CT for subsequent treatments, providing a full set of data for at least one treatment has been acquired. Use of this simplified acquisition protocol will allow more flexibility to perform dosimetry in more treatments, reduce camera time and hospital visits. **References:** None

510

Wednesday, October 20 - Saturday, October 23, 2021

on-demand pool, release on Wednesday, October 20 at 09:00

Clinical Oncology Track - TROP Session: Lung

OP-0217

Frequency and prognostic value of immune-related adverse effects assessed on18F-FDGPET/CT in NSCLC treated with immune checkpoint inhibitors

O. Humbert[1], M. Bauckneht[2], J. Gal[1], D. Rener[1], M. Paquet[1], A. Schiazza[1], D. Chardin[1], C. Genova[3], R. Schiappa[1], G. Rossi[4], L. Zullo[3], J. Darcourt[1], S. Morbelli[3], J. Otto[1];
[1]Antoine Lacassagne Cancer Center, Nice, FRANCE, [2]Nuclear Medicine Unit, IRCCS Ospedale Policlinico San Martino, Genova, ITALY, [3]IRCCS Ospedale Policlinico San Martino, Genova, ITALY, [4]Ospedale Pare Antero Micone, Genova, ITALY.

Aim/Introduction: Beyond tumor response monitoring, ^{18}FDG PET can assess organ-related inflammation triggered by systemic therapies. We aimed to evaluate, in patients with non-small cell lung cancer (NSCLC) treated with immune checkpoint inhibitors (ICPI), the prognostic value of immune-related adverse events (iRAEs) observed on interim ^{18}FDG PET. **Materials and Methods:** We used data from two independent prospective cohorts. 1) Exploratory cohort (Nice, France): 92 consecutive patients with metastatic NSCLC were prospectively included before initiation of ICPI (pembrolizumab or nivolumab) in first or later line (MR 2610080620). ^{18}FDG PET scans were performed before treatment, after 7 weeks ($PET_{Interim}1$) and 3 months ($PET_{Interim}2$) of treatment. 2) Validation cohort (Genova, Italy): 45 consecutive patients with stage metastatic NSCLC were prospectively included before initiation of Nivolumab in second or later line (NCT02475382 trial). ^{18}FDG PET scans were performed before treatment, after 8 weeks of treatment ($PET_{Interim}1$) and after either 2 or 4 additional cycles ($PET_{Interim}2$). The iPERCIST criteria were used. Abnormal homogenous organ ^{18}FDG uptakes, deemed to be due to a therapy-related immune activation, were collected as imaging iRAEs. Overall survival (OS) and durable clinical benefit (DCB), defined as treatment continuation over a 6-month period, were the primary and secondary endpoints of the study. Results: 1) Exploratory cohort : The median OS was 21 months. According to iPERCIST criteria, 29.3% (27/92) of patients had a metabolic complete/partial response; 6.6% (6/92) had a stable metabolic disease; 64.1% (59/92) had a metabolic progressive disease. $PET_{interim}1$ and $PET_{interim}2$ revealed at least one iRAE site in 72.8% of patients (67/92) in various organs: midgut/hindgut inflammation (33.7% of patients), gastritis (21.7%), thyroiditis (18.5%), pneumonitis (17.4%), and other organ inflammations (9.8%). PD-L1 tumor expression and iPERCIST tumor response were the only variables significantly associated with a higher probability to reach a DCB (p= 0.01 and < 0.001, respectively). iPERCIST tumor response and immuno-induced gastritis occurrence on interim PET were the only variables significantly associated with improved OS (p< 0.001 and p=0.026, respectively). Patients with gastritis on PET had a 2-fold improved 2-year OS compared to patients without (75% vs 37%, respectively). 2) Validation cohort: Patients' median overall survival was 10 months. Immuno-induced gastritis was observed in 19.6% (9/46) of patients and was significantly associated with better OS (p=0.04). **Conclusion:** Immuno-induced gastritis, revealed by interim ^{18}FDG PET in around 20% of patients treated with ICPI monotherapy, is an imaging biomarker of improved overall survival. **References:** None

OP-0218

Using a semi-supervised clustering method to determine whether a radiomic phenotype can distinguish primary lung tumors from lung metastases

V. Cuplov, N. Captier, I. Buvat, F. Orlhac;
Laboratory of Translational Imaging in Oncology, U1288 Inserm, Institut Curie, Univ. Paris Saclay, Orsay, FRANCE.

Aim/Introduction: To investigate a semi-supervised clustering method for identifying tumors with similar radiomic phenotypes and derive a tumor classification approach including an uncertainty estimate. **Materials and Methods:** A cohort of 371 patients with lung primary tumor or lung metastases were retrospectively studied [1]. Each patient underwent a baseline 18F-FDG PET/CT scan and the lung lesion was segmented (threshold=0.4 SUVmax). Using LIFEx [2], 84 radiomic features were extracted from both PET and CT images. Patients were grouped into communities using the unsupervised PhenoGraph clustering method [3]. This method represents the data as a network, connecting phenotypically similar profiles, and then extracts communities by optimizing the network modularity. The data input to PhenoGraph was either composed of all features or of a sub-group of features selected using importance scores of an optimized random forest classifier trained to predict the tumor type (primary or metastases). This method was applied on PET or CT-based features and on the combination of both. The clustering purity (P) was obtained from clusters and tumor types. Using the configuration maximizing the purity, the ability to distinguish lung primary tumors from lung metastases based on the cluster assignment was determined. Results: The cohort was composed of 266 patients with lung primary tumor and 105 with lung metastases. The purity showed that the clustering using PET features (0.616<P<0.763, depending on the selected features) was more discriminant than using

CT features (0.629<P<0.635) or the combination of both (0.626<P<0.731). The maximal purity (P=0.763±0.012) was obtained with PET and a sub-group of 10 features. This configuration corresponded to 8 clusters among which 4 contained only primary lesions (165 out of 266 primary). The other clusters contained 70%, 61%, 18% and 33% of primary lesions. Based on the clustering assignment, 44% of the lesions could be identified with 100% certainty, 35% could be classified with an accuracy higher than 70%, while the other 21% could not be identified trustfully (accuracy lower than 70%). **Conclusion:** The semi-supervised method proposed showed that the most relevant radiomic information to distinguish primary lung tumors from lung metastases is contained in a PET radiomic phenotype composed of 10 features. This method allows one to classify about 80% of the tumors with an acceptable uncertainty, where the lesion classification uncertainty depends on the cluster it belongs to. **References:** [1] Kirienko et al. EJNMMI 2018. [2] Nioche et al. Cancer Res 2018. [3] Levine et al. Cell 2015.

OP-0219

The immune metabolic prognostic index discloses the presence of radiological progression in patients with non-small cell lung cancer (NSCLC) treated with Nivolumab

F. Lanfranchi[1,2], M. Bauckneht[1,2], C. Genova[1,3], G. Rossi[1,3], E. Rijavec[4], M. G. Dal Bello[1], G. Ferrarazzo[1,2], M. Tagliamento[1,3], C. Delucchi[1,2], M. I. Donegani[1,2], F. Biello[5], S. Chiola[6,7], L. Zullo[1,3], S. Raffa[1,2], G. Cittadini[1], C. Marini[1,8], G. Sambuceti[1,2], F. Grossi[4], S. Morbelli[1,2];
[1]IRCCS Ospedale Policlinico San Martino, Largo Rosanna Benzi 10, 16132, Genoa, ITALY, [2]Department of Health Sciences (DISSAL), University of Genoa, Via Antonio Pastore 1, 16132, Genoa, ITALY, [3]Department of Internal Medicine (DIMI), University of Genoa, Viale Benedetto XV 6, 16132, Genoa, ITALY, [4]Medical Oncology Unit, Fondazione IRCCS Ca' Granda Ospedale Maggiore Policlinico, Via Francesco Sforza 28, 20122, Milan, ITALY, [5]Department of Transitional Medicine, University of Eastern Piedmont, Via Solaroli 17, 28100, Novara, ITALY, [6]Humanitas Clinical and Research Center–IRCCS, Via Manzoni 56, Rozzano, 20089, Milan, ITALY, [7]Department of Biomedical Sciences, Humanitas University, Via Rita Levi Montalcini 4, Pieve Emanuele, 20090, Milan, ITALY, [8]Institute of Molecular Bioimaging and Physiology (IBFM), National Research Council (CNR), Via Fratelli Cervi 93, 20090, Segrate, Milan, ITALY.

Aim/Introduction: Identifying reliable biomarkers for the response assessment during immunotherapy represents an urgent clinical need in non-small cell lung cancer (NSCLC). In fact, 3-7% of patients with clinical benefit from immune checkpoint inhibitors show atypical response patterns at computed tomography (CT), including the stabilization or objective response following an initial radiological progression. We thus combined peripheral-blood systemic inflammation indexes and 18F-fluorodeoxyglucose positron emission tomography (FDG-PET)/CT volumetric parameters in disclosing the radiological progression occurring in NSCLC patients treated with Nivolumab. **Materials and Methods:** Thirty-six patients with advanced pre-treated NSCLC treated with Nivolumab and classified as progressive disease (PD) according to response evaluation criteria in solid tumours 1.1 (RECIST) were considered eligible. We assessed the prognostic value of FDG-PET/CT parameters (maximum standardized uptake value, SUVmax; metabolic tumour volume, MTV; total lesion glycolysis, TLG), and systemic inflammation indexes (neutrophil-to-lymphocyte ratio, NLR; derived-NLR, dNLR; lymphocyte-to-monocyte ratio, LMR; platelets-to-lymphocyte ratio, PLR; systemic inflammation index, SII), and their combination. Classes of response based on FDG-PET criteria (PERCIST), immune-related criteria (irRC), and immunotherapy-adapted RECIST criteria (iRECIST) at the time of PD were recorded. Analyses were repeated twice either considering all PD (including PD occurring in the same patients at different time-points) or considering only first PD in the thirty-six patients. Results: The multivariate analysis indicated dNLR and MTV at the time of PD as independent prognosticators. MTV and dNLR combination allowed to calculate the Immune-Metabolic Prognostic Index (IMPI), which identified three groups associated with significantly different Overall Survival (OS, median duration expressed in months; p<0.001): low-IMPI (neither MTV≥179.08 nor dNLR≥2.67; n=17; OS=27.2, 95%CI=19.9-35), intermediate-IMPI (MTV≥179.08 or dNLR≥2.67; n=27; OS=12.6, 95%CI=10.9-18) and high-IMPI (MTV≥179.08 and dNLR≥2.67; n=10; OS=4.2, 95%CI=3.4-8.1). Also dNLR and TLG variations from baseline (delta-dNLR and delta-TLG, respectively) resulted in independent prognosticators and were combined in the IMPI Response (IMPIR). Low-IMPIR (neither delta-dNLR≥-15% nor deltaTLG≥80%; n=14; OS=33.6, 95%CI=25.8-36), intermediate-IMPIR (delta-dNLR≥-15% or deltaTLG≥80%; n=22; OS=12.2, 95%CI=9.5-20), and high-IMPIR (delta-dNLR≥-15% and deltaTLG≥80%; n=18; OS=10; 95%CI=4.5-15.5) showed significantly different OS (p<0.001), even after adjusting for PERCIST, irRC, and iRECIST classes. IMPI and IMPIR resulted in independent prognosticators. **Conclusion:** The degree of systemic inflammation, the quantification of the metabolically active tumour burden, their combination, and their variation compared to baseline could be used for the prognostic assessment of NSCLC patients showing radiological progression after Nivolumab. Further studies in a larger group of patients are needed to confirm this preliminary evidence. **References:** None

OP-0220

Machine Learning Radiomics for Prediction of Survival in Non Small Cell Lung Cancer Patients Studied with PET/CT and FDG

E. Giovannini[1], *L. Florimonte*[2], *E. Bonatto*[3], *C. Bareggi*[4], *L. Dellavedova*[5], *A. Milano*[6], *G. Giovacchini*[1], *V. Duce*[1], *C. Aschele*[6], *M. Castellani*[2], *A. Ciarmiello*[1];
[1]*Nuclear Medicine O.U. - Sant'Andrea Hospital, La Spezia, ITALY,* [2]*Nuclear Medicine Department Fondazione IRCCS Ca' Granda Ospedale Maggiore Policlinico, Milano, ITALY,* [3]*University of Milan, Milano, ITALY,* [4]*Medical Oncology Unit Fondazione IRCCS Ca' Granda Ospedale Maggiore Policlinico, Milano, ITALY,* [5]*Nuclear Medicine Department Ovest Milanese, Legnano, Milano, ITALY,* [6]*Oncology Dip. S. Andrea Hospital, La Spezia, ITALY.*

Aim/Introduction: Machine-learning radiomics is a promising approach to improve the clinical management of non-small cell lung cancer (NSCLC). We aimed to assess the prognostic role of radiomics in NSCLC patients. **Materials and Methods:** 321 NSCLC patients that underwent PET/CT with FDG were divided into an early stage group (n=79) and advanced stage (n=242). A total of 42 radiomics features and standardized uptake values (SUVmax) were extracted from PET studies. Feature selection occurred with a 3-step process consisting of: 1) Spearman's rank correlation versus clinical stage; 2) least absolute shrinkage and selection operator (LASSO) regression model; 3) evaluation of model predictive performance with bootstrap resampling and area under the curve (AUC). Results: The variable combination that best distinguished the two groups of patients included 8 textural features and SUVmax. All considered statistical features (specificity, sensitivity, Chi-Square, relative risk and 95% confidence interval, 95% CI) indicate a higher statistical significance of the combined model vs SUVmax. This combined 9-parameter model predicted progression-free survival (P=0.0006 and P=0.01) and overall survival better than SUVmax alone (P=0.0003 vs P=0.08). **Conclusion:** These data indicate that machine learning radiomic analysis can aid in the distinction between early stage and advanced stage NSCLC patients and can be used to predict survival in NSCLC with greater statistical power than SUVmax alone. **References:** none

OP-0221

Therapeutic response assessment using [18F]-FDG-PET/CT in NSCLC patients treated with immune checkpoint inhibitors

I. Duran Derijckere[1], *N. Gohimont*[2], *I. Karfis*[1], *G. Critchi*[1], *T. Berghmans*[3], *P. Flamen*[1];
[1]*Nuclear medicine department, Institut Jules Bordet, Université Libre de Bruxelles (ULB), Brussels, BELGIUM,* [2]*Nuclear medicine department, CHU Saint Pierre, Université Libre de Bruxelles (ULB), Brussels, BELGIUM,* [3]*Thoracic oncology clinic, Institut Jules Bordet, Université Libre de Bruxelles (ULB), Brussels, BELGIUM.*

Aim/Introduction: Immunotherapy using anti-PD-1 immune checkpoint inhibitors (ICIs) are well-established treatments of various cancers, including advanced non-small cell lung carcinoma (NSCLC). However, there are still difficulties in predicting and assessing response to treatment using conventional anatomical and metabolic criteria. For this purpose, specific criteria such as dual-time-point iPERCIST and PERCIMT have been developed. Our study aimed to evaluate iPERCIST and PERCIMT response criteria and metabolic predictive biomarkers in patients treated with anti-PD-1 ICIs for an advanced NSCLC. **Materials and Methods:** From 01/01/2015 and 31/05/2019 we retrospectively identified patients who were treated with anti-PD-1 ICIs (nivolumab or pembrolizumab) for an advanced NSCLC and underwent an 18FDG PET/CT at baseline no more than 6 weeks before the start of treatment. Metabolic predictive biomarkers were assessed at baseline including SUV_{spleen}, MTV and TLG. Response assessment was evaluated using iPERCIST and PERCIMT criteria on a follow-up FDG PET/CT (FU1) performed within 100 days after the start of treatment. If unconfirmed progressive metabolic disease (UPMD) was observed at FU1, a second follow-up FDG PET/CT (FU2) was evaluated if available. OS was determined as end-point and defined as the time elapsed from the start of ICIs to death from any cause. The minimal time of exposure to immunotherapy was 1 cycle. All PET/CT examinations were performed in respect to EARL specifications. Results: A total of 43 patients were analyzed of whom 9 had a baseline FDG PET/CT only, and 34 had both baseline and FU1. Response assessment using iPERCIST criteria revealed 2 CMR, 10 PMR, 5 SMD and 17 UPMD. Further follow-up of patients with UPMD at FU2 showed SMD in 3/17 (18%) and confirmed PMD in 4/17 (23%); 10/17 (59%) patients didn't perform a FU2. Median OS was significantly shorter in patients with PMD/UPMD compared to patients with CMR/PMR/SMD (8.2 months vs mOS not-reached respectively, HR= 6.32 [IC95%: 1.79-22.31], p<0.0001). Response assessment using PERCIMT criteria showed 2 CR, 17 PR, 7 SD and 8 PD. Median OS was also significantly shorter in patients with PD compared to patients with CR/PR/SD (5.3 months vs mOS not-reached respectively, HR= 6.31 [IC95%: 0.92-43.09], p<0.0001). No significant difference was observed in median OS for baseline SUV_{spleen}, MTV and TLG using medians as cut-offs. **Conclusion:** Both iPERCIST and PERCIMT criteria correctly detected disease progression in patients with advanced NSCLC treated with anti-PD-1 ICIs. However, neither SUV_{spleen}, MTV nor TLG measured at baseline were related to treatment outcome. **References:** none

OP-0222

The role of 18F-FDG PET/CT for evaluating immunotherapy response in patients with NSCLC: a systematic review and meta-analysis

M. Huang;
The Department of Nuclear Medicine, West China Hospital, Sichuan University, Chengdu, Sichuan, China, Chengdu, CHINA.

Aim/Introduction: Our study aimed to investigate the ability of 18F-FDG PET/CT to assess the immunotherapy response of patients with non-small-cell lung cancer(NSCLC). **Materials and Methods:** MEDLINE, PubMed, Cochrane, Scopus, Embase, and Web of Science databases were searched until April 25, 2021. The keywords "immune checkpoint inhibitor OR immunotherapy", "nivolumab OR pembrolizumab OR atezolizumab OR ipilimumab", AND "non-small-cell lung cancer OR NSCLC", were used in combination with "^{18}F-FDG" OR "fluorodeoxyglucose" OR "positron emission tomography" AND "response" OR "prognostic" OR "survival". We also screened the references of the included articles to identify any other relevant studies. Outcome measures were assessed by hazard ratios of SUVmax, SUVmean, MTV, and TLG for overall survival (OS) and progression-free survival (PFS). Inclusion criteria were studies of patients with NSCLC treated with immunotherapy and had response assessed by FDG-PET. Of the 337 articles identified, 16 studies including 838 patients were included in the analysis. Detailed data were extracted and categorized. Comprehensive meta-analysis software was used for analysis. Results: Sixteen articles were eligible and included in our study. Based on the baseline 18F-FDG PET/CT imaging, the pooled hazard ratios of SUVmax, SUVmean, MTV, and TLG for overall survival (OS) were 0.753 (95%CI:0.486-1.167, p = 0.204), 0.456 (95%CI: 0.224-0.927, p = 0.03), 2.009 (95%CI: 1.247-3.237, p = 0.004), and 1.663 (95%CI:1.027-2.693 p = 0.038), respectively. Meanwhile, the pooled hazard ratios of SUVmax, SUVmean, MTV, and TLG for progression-free survival (PFS) were 0.685 (95%CI:0.497-0.979, p = 0.038), 0.475 (95%CI: 0.277-0.815, p = 0.03), 1.002 (95%CI: 0.908-1.106, p = 0.965), and 0.967 (95%CI:0.887-1.067 p = 0.503), respectively. Among the above parameters, only MTV could distinguish the difference between responders and non-responders (P=0.003). We reviewed several studies to compare different response criteria, and found that immunotherapy-modified response assessment criteria were correlated with patient survival outcomes, with OS and PFS significantly longer in responders than in non-responders. **Conclusion:** The baseline 18F-FDG PET/CT parameters SUVmax, SUVmean, MTV, and TLG were effective in predicting the final response to immunotherapy in NSCLC patients. Among them, MTV seems to be more correlated with tumor response. Modified response assessment criteria for immunotherapy are likely to be an appropriate method for monitoring immunotherapy. **References:** none

OP-0223

The role of ^{18}F-FDG PET/CT in Predicting Response to PD-1 Blocking Immunotherapy and the prognostic significance of immune organs activation

C. Ferrari[1], G. Santo[1], N. C. Merenda[1], M. C. Bellomo[1], G. Ranieri[2], C. D. Gadaleta[2], G. Rubini[1];
[1]Section of Nuclear Medicine, DIM, University "Aldo Moro", Bari, ITALY, [2]Interventional Oncology Unit with Integrated Section of Translational Medical Oncology, National Cancer Research Centre, Istituto Tumori "Giovanni Paolo II", Bari, ITALY.

Aim/Introduction: The advent of immunotherapy with checkpoint inhibitors (ICI), targeted programmed cell death protein 1 (PD-1), revolutioned the management of solid tumors in clinical practice, providing new therapeutic opportunities for cancer patients. In this new scenario, an adequate imaging tool for predicting therapies response is essential in order to avoid overtreatment. This study aims to evaluate the predictive role of ^{18}F-FDG PET/CT-derived semi-quantitative parameters as well as immune-related adverse events (irAEs) and lymphoid cell-rich organs in treatment response evaluation. **Materials and Methods:** Forty cancer patients who underwent ^{18}F-FDG PET/CT scans before and at first restating after the beginning of immunotherapy were retrospectively enrolled (malignant melanoma, n=15; non-small cell lung cancer, n=25). PET-based semi-quantitative parameters extracted from both scans were respectively: SUVmax and SUVpeak of the target lesion (preSUVmax$_{TL}$, postSUVmax$_{TL}$, preSUVpeak$_{TL}$, postSUVpeak$_{TL}$), whole-body metabolic tumor volume (preMTV$_{WB}$ and postMTV$_{WB}$) and whole-body total lesion glycolysis (preTLG$_{WB}$ and postTLG$_{WB}$), as well as interval changes of SUVmax (ΔSUVmax$_{TL}$), MTV (ΔMTV$_{WB}$), TLG (ΔTLG$_{WB}$). All these PET-derived parameters were correlated to treatment response assessed by Response Evaluation Criteria in Solid Tumors (RECIST1.1) at first restaging. IrAEs, if present, were also described. Moreover, SUVmax of the spleen (pre-/post-SUVmax$_{Sp}$), bone marrow (pre-/post-SUVmax$_{Bm}$) and thyroid (pre/postSUVmax$_{Th}$) at baseline and restaging scans as well as the correspondent ΔSUVmax were also correlated to the clinical benefit (CB) at follow up. The continuous variables were compared using the Student's t test for normal distributions and the Mann-Whitney U test for non-normal distributions ($p<0.05$). Results: Twenty/40 (50%) eligible patients, experienced progressive disease (PD) at first restaging (median: 4.5 months, range: 2-11). PostSUVmax$_{TL}$ ($p<0.001$) and ΔSUVmax$_{TL}$ ($p=0.002$), as well as postTLG$_{WB}$ ($p=0.003$) and ΔTLG$_{WB}$ ($p<0.001$) were significantly associated with PD vs. non-PD. Twelve/40 patients (30%) developed an irAEs: 3/12 (25%) thyroiditis, 1/12 (8.2%) pneumonia, 2/12 (16.7%) arthritis, 2/12 (16.7%) myositis, 1/12 lymphadenopathy (8.2%), 1/12 esophagitis (8.2%), 1 enterocolitis and 1 colitis (2/12, 16.7%). Among these

patients, 5/12 (41.7%) had no-CB, while 7/12 (58.3%) had CB even though no statistically significant difference between groups was found. PostSUVmax$_{Bm}$ was significantly correlated to CB (p=0.005) at follow-up (median 10 months, range, 3-53). **Conclusion:** Our preliminary results suggest that ^{18}F-FDG PET/CT could represent a reliable tool in immunotherapy treatment response evaluation. Several PET-derived semi-quantitative parameters correlate with different therapy response. Moreover, bone marrow SUVmax at first restaging scan could be associated with clinical benefit and potentially representing an indicator of the efficacy of immune system activation. **References:** None

OP-0224

Digital and respiratory-gated FDG PET/CT for characterization of lung lesions

T. Bartel, W. P. Fendler, K. Pabst, F. Barbato, C. Rischpler, K. Herrmann, H. Hautzel;
Nuklearmedizin Universitätsklinikum Essen, Essen, GERMANY.

Aim/Introduction: Identification and differentiation between benign and malignant lung lesions by molecular means is one of the core indications of FDG PET/CT imaging. However, due to motion artefacts especially small lesions and those close to the diaphragm are prone to metabolic underestimation. To overcome this respiratory gating of FDG data was introduced. With the development of digital PET/CT's count sensitivity and spatial resolution further improved. Here, we addressed the question if respiratory motion correction still implies an additional benefit on pulmonary lesion identification and tumor characterisation as compared to standard reconstruction techniques not adjusting for motion-related data blurring. **Materials and Methods:** 104 patients were included who underwent FDG-PET/CT (digital Siemens Vision 600 scanner) for either differentiation of a pulmonary lesion in terms of malignancy or for staging / restaging. Histology revealed adenocarcinoma (48%), squamous cell carcinoma (21%), SCLC (11%), a benign lesion (14%) or another malignant entity (6%). The data were reconstructed with (1) an iterative algorithm, (2) a point spread function algorithm (PSF), (3) according the EARL certification protocol and (4) a commercially available reconstruction tool correcting for respiratory motion (Onco freeze, Siemens Healthineers, Germany). SUVmax, SUVpeak, SUVmax lesion-to-background ratio, SUVpeak lesion-to-background ratio, lesion diameter in z-axis and the distance from lesion to diaphragm as a measure of breathing-related motion were calculated. For statistical comparisons multiple regression analyses regarding histology, z-axis diameter and lesion to diaphragm distance as independent variables were performed (Statistica V.11) ($p < 0.05$ regarded as significant). Results: With respect to SUVmax all reconstruction protocols could differentiate between benign and malignant lesions but the lesion-to-background correction did not improve this. However, the averaged lesion-to-background ratio was at least 18% higher for the motion corrected data as compared to the motion-uncorrected reconstructions. Neither SUVmax nor SUVpeak could further subdivide the various malignant tumor entities. A positive correlation between z-axis diameter and both SUVmax and SUVpeak was found for all reconstructions but the orthogonal distance between lesion and diaphragm had no impact on the SUV measures of any of the reconstruction types. **Conclusion:** When using a digital PET/CT with standard reconstruction iterative, PSF or EARL demonstrate a similar performance as compared to respiratory motion corrected reconstruction. Respiratory motion corrected reconstruction demonstrated highest lesion-to-background ratio, but all four reconstructions allowed for differentiation between benign and malignant pulmonary lesions. **References:** none

OP-0225

Prognostic value of ^{18}F-FDG PET/CT quantitative metrics in non-small cell lung cancer

S. Fontão de Castro, I. Próspero, L. S. Violante, G. Ferreira, J. Teixeiro, H. Duarte;
Instituto Português de Oncologia do Porto Francisco Gentil, EPE, Porto, PORTUGAL.

Aim/Introduction: Tumor-node-metastasis system is the most important tool to estimate prognosis and guide therapy in lung cancer patients. However, quantitative measurement of glycolytic metabolism as a derivative of biologic aggressiveness, using ^{18}F-FDG-PET/CT, may add additional value in estimating the risk of recurrence. The aim of this study is to explore if maximum standardized uptake (SUV$_{max}$), total metabolic tumor volume (MTV), total lesion glycolysis (TLG) and SUV$_{peak}$ corrected to lean body mass (SUL$_{peak}$) values can predict recurrence in non-small cell lung cancer. **Materials and Methods:** Retrospective study of 166 consecutive patients who performed ^{18}F-FDG-PET/CT scan for lung disease staging in an Oncology Institute, between 01/11/2017 and 01/11/2019, before surgery treatment (curative intent). A total of 105 patients were included [mean age 65.8±9.1 years; 62.9% male (N=66); 72.4% adenocarcinoma (N=76), 20.0% squamous cells (N=21) and 7.6% other histological types (N=8); 52.4% treated only with surgery (N=54); 48.6% stage IA/IB (N=51), 21.9% stage IIA/IIB (N=23), 24.8% stage IIIA/IIIB (N=26) and 4.8% stage IVA (N=5)]. SUV$_{max}$, MTV, TLG and SUL$_{peak}$ tumor values were determined using a semi-automatic quantification tool (Syngo.via software, Siemens®), through boundaries of voxels presenting with SUV≥2.5. Patients were followed until last observation or death and progression free survival (PFS) was evaluated based on radiologic findings. Univariable and multivariable Cox regression analysis was used to determine factors associating with PFS. The best cut-off value for each variable was defined using ROC analysis. Results: The 105

patients treated with curative intent were followed for 0.5 to 3.5 years (mean 2.3±0.6), during which time 29.5% relapsed (N=31) and 14.3% died (N=15). Median PFS was 2.1 years [95% CI:0.18-3.45]. Overall survival was not reached. Cox regression model showed association between relapse and MTV [HR:1.008 (95% CI:1.005-1.011); p<0.001], TLG [HR:1.001 (95% CI:1.001-1.002); p<0.001], SUL_{peak} [HR:1.989 (95% CI:1.007-1.177); p<0.032] and disease stage [HR:1.704 (95% CI:1.213-2.394); p=0.002]. ROC curves analysis showed an optimal cut-off point of 7.88cm^3 for MTV (sensibility: 67.7%; specificity: 66.2%), 28.96 for TLG (sensibility 74.2%; specificity 66.2%) and 5.375 for SUL_{peak} (sensibility 61.3%; specificity 70.3%). Cox regression analysis did not demonstrate a statistically significant association between relapse and SUV_{max} (p=0.082). Multivariable analysis proved that both MTV and TLG were predictors of PFS independently of disease stage (HR:1.007, p=0.013; HR:1.001 p<0.001, respectively). **Conclusion:** This work suggests that regardless disease stage, MTV and TLG values may provide additional value in predicting relapse for non-small cell lung cancer patients treated with surgical curative intent. **References:** None.

OP-0226

Tc99m MAA tumor distribution as a predictive risk factor of occult nodal metastasis in clinically N0 non small cell lung cancer patient

***V. Murad**, M. Suh, H. Choi, G. J. Cheon, K. J. Na, Y. T. Kim;*
Seoul National University Hospital, Seoul, KOREA, REPUBLIC OF.

Aim/Introduction: Lung perfusion SPECT/CT with labeled ^{99m}Tc macro aggregated albumin (MAA) is currently used in the preoperative setting of patients with non-small cell lung cancer (NSCLC) to determine the best surgical approach. ^{99m}Tc MAA particles distribute according to the blood flow and get trapped in the arteriolar-capillary bed. As the tumor progresses, the arteriolar-capillary bed is modified into highly permeable vessels, increasing the risk of tumor spread. We hypothesized that the ^{99m}Tc MAA accumulation in the tumor may represent the arteriolar-capillary bed architecture and functional status, which may serve as an independent risk factor for occult nodal metastasis. **Materials and Methods:** A total of 239 NSCLC patients with clinical N0 status who underwent preoperative lung perfusion SPECT/CT were retrospectively evaluated. According to the visual grading of ^{99m}Tc MAA accumulation in the tumor, patients were classified into uptake and no-uptake groups. Logistic regression and survival analysis were performed. Results: Of the 239 patients, 89 (37.2%) were allocated in the uptake group and 150 (62.8%) in the no-uptake group. In the univariate analysis, no-uptake group (p=0.0001), large tumor size (>3cm) (p=0.0002), and histologic type non-adenocarcinoma (p<0.0001) were statistically significant factors predicting occult nodal metastasis. Multivariate analysis revealed that, tumor with no ^{99m}Tc MAA uptake remained as an independent risk factor for occult nodal metastasis (OR, 3.8; p=0.0052, 95% IC). In addition, prognostic significance of ^{99m}Tc MAA tumor distribution was evaluated. Compared to the uptake group (21.3%), no-uptake group (45.4%) showed significantly higher lymphovascular invasion (p=0.0002). With a median follow-up of 31.5 months, the recurrence free survival (RFS) was significantly shorter in stage III-IV (p<0.0001), no-uptake group (p=0.0044), and non-adenocarcinoma patients (p=0.0058) at univariate analysis. At multivariate analysis, stage (p<0.0001) was the only remaining independent predictor for RFS. **Conclusion:** The absence of ^{99m}Tc MAA tumor uptake in preoperative lung perfusion SPECT/CT represents an independent risk factor for occult nodal metastasis. Furthermore, the absence of uptake was associated with higher chance of lymphovascular invasion and shorter RFS. ^{99m}Tc MAA tumor distribution may serve as an imaging biomarker for determining the extent of surgery and adjuvant treatment strategy. **References:** None.

OP-0227

Discriminative capacity of the ^{18}F-FDG PET/CT quantitative parameters in the solitary pulmonary nodule

***M. Rashki**[1], E. Triviño-Ibáñez[1], D. Rivas-Navas[1], A. González-Jiménez[2], A. Rodríguez-Fernández[1];*
[1]Nuclear Medicine department, University Virgen de las Nieves Hospital, Granada, SPAIN, [2]Nuclear Medicine department, Jaén Hospital, Jaén, SPAIN.

Aim/Introduction: To evaluate the discriminative capacity of the new quantification parameters of ^{18}F-FDG-PET/CT by semi-automatic independent operator processing in the differentiation of malignant and benign solitary pulmonary nodules (SPNs). **Materials and Methods:** An observational and retrospective study in patients with incidental SPN, without inflammatory-infectious pulmonary disease or oncological pathology, who underwent ^{18}F-FDG PET/CT between January and December of 2015 with a follow up of more than 5 years. Visual and quantitative analysis was performed by semi-automatic segmentation of the lesion, calculating maximum, peak, and minimum standard uptake value (SUV); normalized according to body weight (SUVbw); body surface area (SUVbsa) and lean body mass (SUL), as well as MTV (Metabolic tumor volume) and TLG (Total lesion glycolysis). Volume, RECIST diameters, maximum orthogonal diameter, WHO area, max, mean, and min Hounsfield Units (HU) were analyzed in CT images. The benign/malignant nature of the SPN was determined according to the histological analysis and/or clinical-radiological follow up > 5 years. The efficiency of PET/CT, PET, and CT in the diagnosis of benign and malignant SPNs was calculated. We studied the association of the different parameters with the malignancy risk through binary logistic regression analysis and the malignancy discriminative capacity through ROC analysis. Results: 77 patients (mean age: 62.86±12.03; 74.7% men

and mean follow-up: 53.14 months). 53.2% of the SPN were benign. Parameters statistically significantly associated with a higher risk of malignancy were: ever smoking (OR: 10.35; p=0.0.31), mean value of the $SUVbw_{max}$ (OR: 3.60; p<0.001); $SUVbw_{peak}$ (OR: 5.30, p<0.001); $SUVbw_{min}$ (OR: 19.36, p=0.001); $SUVbs_{max}$ (OR: 54.15, p<0.001); $SUVbs_{peak}$ (OR: 574.61, p<0.001); SUL_{max} (OR: 5.39, p<0.001); SUL_{peak} (OR: 4.17, p<0.001); SUL_{min} (OR: 53.39, p=0.001) and TLG (OR:1.23, p=0.002). None of the CT parameters were significantly associated with malignancy. The ROC analysis for each of these parameters showed that SUL_{max} presents a higher diagnostic yield, with an area under the curve of 0.853 (standard error: 0.05, p<0.001; 95% CI: 0.754 to 0.952), being the optimal threshold 1.17. **Conclusion:** The new quantitative parameters of ^{18}F-FDG PET/CT, and more specifically SUL_{max}, present an optimal diagnosis capacity to differentiate the benign or malignant nature of SPN. **References:** None

OP-0228

Clinical validation of a fully automated lung segmentation method in patients with pulmonary nodules: preliminary results

Z. Mikó[1,2], E. Szabó[2], J. Csirik[2], S. Urbán[1], Z. Besenyi[1], L. Pávics[1]; [1]Department of Nuclear Medicine, University of Szeged, Szeged, HUNGARY, [2]Institute of Informatics, University of Szeged, Szeged, HUNGARY.

Aim/Introduction: The lung is a common site of primary malignancies and metastases. The exact localisation of pulmonary nodules is important in therapy planning and follow-up. There is a need for a fully automated method analyzing imaging data in a reproducible way to localise soliter or multiple pulmonar lesions. The aim of the current study is to evaluate the efficacy of our newly developed automated algorithm in localisation of pulmonary abnormalities. **Materials and Methods:** 48 pulmonary nodules of 28 patients were evaluated in the study. The patients underwent a whole body low-dose FDG-PET/CT during shallow breathing (group A). In all cases an additional native, low-dose chest CT was performed in breath-hold (group B). The localisation of each pulmonary nodules were determined by two experienced nuclear medicine specialists according to Boyden's nomenclature. In case of disagreement a consensus of opinion was formed. The findings were analyzed on lobar and also on segmental level in both groups. A comparison was made between the results of the visual assessment and the automated method. For comparison a three-point scale was used. 1: full agreement, 2: partial agreement -the algorithm localised the lesion in the proper area, a merged segment, but not in the visually identified single segment-, 3: no agreement. Results: On the level of lung lobes our results showed full agreement in both groups. In group A most of the segmental findings (38/48) showed good agreement (score 1-2). In group B this rate was 36/48. In group A the algorithm was accurate (score 1) in 13/38 cases and in group B in 24/36 cases. Poor agreement (score 3) was shown 10 times in group A and 12 times in group B. In these cases the lesions were mostly localized in the nearby segments. **Conclusion:** There is a good correlation between the visual and the automated findings. Our newly developed method is a promosing tool to improve lung nodule detection accuracy which can be useful in daily clinical practice. **References:** None

511

Wednesday, October 20 - Saturday, October 23, 2021

on-demand pool, release on Wednesday, October 20 at 09:00

Featured Session: New Kids on the Cardiovascular Block!

OP-0230

Diamonds in the Rough - New Opportunities in Cardiovascular Imaging

F. Hyafil; *Assistance Publique - Hopitaux de Paris, European Hospital Georges Pompidou, Nuclear Medicine, Paris, FRANCE.*

OP-0231

Glycoprotein IIb/IIIa receptor targeted PET/CT imaging for detecting prosthetic valve thrombosis: a proof-of-concept study

***V. Hugenberg[1]**, R. Zabel[1], R. Preuss[1], K. Friedrichs[2], T. Rudolph[2], V. Rudolph[2], S. Bleiziffer[3], H. Milting[4], A. Stephens[5], N. Koglin[5], J. Gummert[3], W. Burchert[1], M. Deutsch[3];*
[1]Institute of Radiology, Nuclear Medicine and Molecular Imaging, Heart and Diabetes Center North Rhine-Westphalia, University Hospital Ruhr-University Bochum, Bad Oeynhausen, GERMANY, [2]Department of General und Interventional Cardiology/Angiology, Heart and Diabetes Center North Rhine-Westphalia, University Hospital Ruhr-University Bochum, Bad Oeynhausen, GERMANY, [3]Department of Thoracic and Cardiovascular Surgery, Heart and Diabetes Center North Rhine-Westphalia, University Hospital Ruhr-University Bochum, Bad Oeynhausen, GERMANY, [4]Erich and Hanna Klessmann Institute for Cardiovascular Research & Development (EHKI), Heart and Diabetes Center North Rhine-Westphalia, University Hospital Ruhr-University Bochum, Bad Oeynhausen, GERMANY, [5]Life Molecular Imaging GmbH, Berlin, GERMANY.

Aim/Introduction: Prosthetic valve thrombosis (PVT) is a well-documented phenomenon in mechanical heart valves. Although dynamic 4-dimensional multidetector computed tomography (4D-MDCT) has greatly improved the diagnosis of bioprosthetic valve thrombosis (BPVT), more sensitive imaging tools are lacking. Furthermore, 4D-MDCT is not applicable for the detection of thrombi in mechanical valve

replacement. The novel glycoprotein IIb/IIIa receptor targeted PET tracer [^{18}F]GP1 has been investigated for visualizing acute venous and arterial thrombi as well as thrombi inside LVADs. We hypothesized that [^{18}F]GP1 PET/CT imaging is suitable to detect PVT. **Materials and Methods:** Our proof-of-concept case study was conducted under compassionate use regulations and in accordance with the Declaration of Helsinki. [^{18}F]GP1 PET/CT was performed in two patients with symptomatic, severe hemodynamic bioprosthetic valve dysfunction. In both patients contrast-enhanced 4D-MDCT had previously shown hypoattenuating opacities at the base of the valve leaflets suggestive of a thrombotic mass. Another patient with a non-dysfunctional mechanical valve prosthesis underwent [^{18}F]GP1 PET/CT for suspected PVT due to recurrent cerebrovascular events. After a 12-16-week course of therapeutic oral anticoagulation [^{18}F]GP1 PET/CT imaging was repeated in all patients to monitor therapeutic effects on thrombus resolution. Results: Focal [^{18}F]GP1 uptake on valve leaflets was observed in all patients with suspected PVT. [^{18}F]GP1 PET/CT of the two patients with obstructive BPVT clearly distinguished between blood pool activity and thrombotic foci. Clot-to-blood ratios at baseline were 8.2 and 4.5, respectively. Follow-up 4D-MDCT corroborated thrombus resolution and reversal of hypoattenuated leaflet thickening after a 12-week course of therapeutic oral anticoagulation. Correspondingly, [^{18}F]GP1 PET/CT imaging demonstrated decreased tracer uptake in both patients. Clot-to-blood ratio at follow-up visit decreased to 1.2 and 2.9, respectively. While absent tracer uptake was seen in patient #1, residual tracer uptake was observed in patient #2 suggestive of ongoing platelet aggregation. [^{18}F]GP1 imaging of the patient with the mechanical aortic valve revealed activity accumulation mainly on the valve rims at baseline. A slight decrease in tracer uptake was observed after a 16-week course of anticoagulation. **Conclusion:** [^{18}F]GP1 PET/CT is a novel useful imaging technique in patients with suspected PVT. [^{18}F]GP1 PET/CT may serve as a novel, highly sensitive tool to overcome some limitations of current diagnostic imaging modalities for detecting PVT and may prove useful for the monitoring and guidance of therapeutic interventions. **References:** Chae, EJNMMI Research (2019) 9:3. Kim, J Nucl Med (2019) 60:224. Hugenberg, EJNMMI (2019) 46:SI98.

OP-0232

^{18}F-FDG in patients with embolic stroke of undetermined source (ESUS): A pilot study to identify and evaluate atherosclerotic plaques

L. Romero Robles, M. Garrastachu Zumaran, F. Julian Villaverde, X. Boulvard Chollet, M. Mangas Losada, I. Garcia Megias, A. Cabrera Villegas, R. Ramirez Lasanta, R. Delgado Bolton;
Hospital San Pedro, Logroño (La Rioja), SPAIN.

Aim/Introduction: Ischemic strokes are caused by embolism (26%, most frequent cause atrial fibrillation, AF), atherosclerosis (20%, defined as plaque >50% diameter), small-vessel-disease (21%), unknown or ESUS (26%), and multifactorial (7%). ^{18}F-FDG PET/CT is a reliable technique to evaluate the degree of inflammation and vulnerability in atherosclerotic plaques [1]. The aim of this study was to assess the degree of glucose hypermetabolism (based of the ^{18}F-FDG uptake) and, therefore, the degree of inflammation in nonstenosing (<50% diameter) carotid artery plaques in ESUS. **Materials and Methods:** The inclusion criteria of this observational pilot study were: (1) patients with acute ischemic strokes; (2) restricted to a single carotid artery territory with a nonstenosing plaque <50% diameter evaluated in CT angiography; (3) classified as ESUS; (4) in whom a post-ictal ^{18}F-FDG PET/CT (Siemens Biograph, Erlangen, Germany) was performed to evaluate the degree of inflammation. Exclusion criteria were: history of cancer, corticoid therapy, fever of unknown origin, infection, and vasculitis. Thirteen patients met all these criteria. PET-image analysis (visual and semi-quantitative) of the carotid plaque ipsilateral to the stroke included SUVmax and target-to-background-ratio (TBR). Plaques were categorized as positive or vulnerable if TBR ≥1.6 and negative or non-vulnerable otherwise [1]. Results: Thirteen patients were included (7 male; median-age 70 years-old, range 47-82). All patients had cardiovascular risk factors and dyslipidemia was the most frequent condition (92%). ^{18}F-FDG PET/CT was performed after ESUS with a range of 1-40 months. ^{18}F-FDG PET/CT was positive in 11 cases (85%) and negative in 2 (15%). SUVmax and TBR were 2.1 and 1.8 in the positive cases, and 1.2 and 1.2 in the negative ones, respectively. One negative patient had a PET-visual diagnosis of large vessels vasculitis (previously unknown and therefore not excluded), a potential cause of stroke, currently under investigation. One positive patient presented AF 9 months after the stroke and 2 months after PET/CT. **Conclusion:** ^{18}F-FDG PET/CT showed that most of our patients with ESUS presented increased glucose metabolism in their nonstenosing carotid plaques. Based on the literature, de degree of hypermetabolism demonstrated in our patients' plaques could allow the categorization as inflammatory and vulnerable plaques. Therefore, this pilot study concludes that ^{18}F-FDG PET/CT may help evaluating the etiology of ESUS and guiding further diagnostic procedures, although further studies are warranted. **References:** 1. Bucerius et al. EANM position paper on PET imaging of atherosclerosis. EJNMMI.2016;43:780-92.

OP-0233

Detection of acute myocarditis with ^{68}GA-DOTATOC digital-PET as compared with cardiac MRI : preliminary results

C. Boursier, E. Chevalier, J. Varlot, L. Filippetti, O. Huttin, V. Roch, L. Imbert, E. Albuisson, M. Claudin, D. Mandry, P. Marie;
CHRU Nancy, Vandoeuvre-les Nancy, FRANCE.

Aim/Introduction: Cardiac MRI is the reference imaging technique for the diagnosis of myocarditis at the acute phase. The study aim was to determine whether the digital-PET imaging of ^{68}Ga-DOTATOC, an analog of somatostatin receptors, (i) constitutes an alternative to MRI for identifying myocarditis at the acute phase and (ii) whether it could be more sensitive than MRI for identifying myocarditis at later stages. **Materials and Methods:** Thirty patients hospitalized for acute myocarditis (chest pain, rise in blood cardiac enzymes) confirmed by cardiac MRI (abnormal T1 and T2 maps, according to modified lake Louise criteria), are planned to be recruited in this study (ClinicalTrials.gov identifier: NCT03347760). Cardiac recordings of 15min, obtained by a digital-PET at one hour after the injection of 2 MBq/kg of ^{68}Ga-DOTATOC, are analyzed at the acute phase and 4-months later, on the day of a control cardiac MRI. The cardiac uptake of ^{68}Ga-DOTATOC is quantified with a cardiac/blood SUVmax ratio with volumes of interest placed over the left ventricle, at a > 1 cm distance from liver, and within the right atrium. A non-myocarditis group is retrospectively built from patients with no history of cardiac disease and having undergone a ^{68}Ga-DOTATOC digital-PET for a known or suspected neuroendocrine tumor. Results: Up to now, we included nine male patients who underwent the first PET exam at 6±3 days after peak troponin and 2.3±1.0 days after MRI, and 6 of them had the second PET and MRI exams 4.3±0.3 months later. The non-myocarditis group includes 16 patients with a comparable age (24±5 years) than that of the myocarditis group (24±5 years). The SUVmax cardiac/blood ratio is significantly higher on the 1st PET than on the 2nd PET of myocarditis patients (3.02±0.53 vs. 2.17±0.39, p< 0.001), and this ratio is further lower in the non-myocarditis group (1.11±0.36, p<0.001 vs. 1st or 2nd myocarditis PET). A SUVmax ratio > 2 was observed on (i) all the 1st PET of myocarditis patients (100%), (ii) none of the PET from non-myocarditis patients (0%), and (iii) in 3 among the six 2nd PET of myocarditis patients (50%), whereas none had any persistence of inflammation signs on the control MRI obtained on the same day. **Conclusion:** This ongoing study provides encouraging preliminary results on the potential of ^{68}Ga-DOTATOC digital-PET for detecting acute myocarditis with an ability to identify myocarditis comparable to that of MRI at an early stage but higher at later stages. **References:** None

OP-0234

Early detection of anthracycline cardiotoxicity by^{18}F-FDG PET/MRI in oncology patients

T. Yuan, M. Wei, X. Chen, X. Wang;
Department of Nuclear Medicine, Peking University Cancer Hospital & Institute,, Beijing, CHINA.

Aim/Introduction: The purpose of this study was to identify the availability of ^{18}F-FDG PET/MRI in early detection of anthracycline cardiotoxicity in oncology patients and to evaluate the diagnostic efficacy of different multiparametric values. **Materials and Methods:** Cancer patients after anthracyclinechemotherapy and controls without chemotherapywere prospectively recruited. All patients fasted for at least 12 hours and had their blood glucose level measured prior to injection of ^{18}F-FDG. Cardiac magnetic resonance examinations including LVEF, mass, T1 and T2mapping was explored. Myocardial uptake of ^{18}F-FDG were analyzed by semi-quantitative (maximum standardized uptake value, SUV_{max}) methods. $SUV_{max\text{-}heart}/SUV_{max\text{-}mediastinum}$, $SUV_{max\text{-}heart}/SUV_{max\text{-}liver}$, $SUV_{max\text{-}heart}/SUV_{max\text{-}background\ (scapularmuscles)}$, $SUV_{max\text{-}heart}/SUV_{max\text{-}erector\ spinae}$ratios were calculated.Receiver operator characteristics (ROC) curve analysis was performed to determine optimal cut-off values of those PET/MRI imaging criteria for evaluating early anthracycline cardiotoxicity, taking ECG-positive as the end point. Results: 28 patients (mean age 47±14 years) and 17 controls (mean age 28±7 years) were recruited. There was no significant difference between both groups in terms of LVEF(p=0.880), mass(p=0.163) and T2mapping (septal p=0.415, lateral wallp=0.170). Native T1 of patients were significantly higher than controls (lateral wall: 1168.17.12±48.52 vs 1136.14±51.15; t=-2.104, p=0.041). There were significant differences in myocardial uptake between ECG-positive group(n=8) and ECG-negative group (n=11) (SUV_{max}:12.75±2.92 vs 7.10±4.04; t=-3.356, p=0.004). ROC curves showed optimal thresholds of T1 value (lateral wall) and $SUV_{max\text{-}heart}/SUV_{max\text{-}mediastinum}$, $SUV_{max\text{-}heart}/SUV_{max\text{-}liver}$, $SUV_{max\text{-}heart}/SUV_{max\text{-}capularmuscles}$, $SUV_{max\text{-}heart}/SUV_{max\text{-}erector\ spinae}$ratios were 1182, 9.9, 4.5, 10.2, 9.7 respectively.The corresponding areas under the curves (AUC) were 0.558, 0.761, 0.795, 0.886, 0.818 respectively. The sensitivity, specificity, positive predictive value, negative predictive value and accuracy of T1 value (lateral wall) and $SUV_{max\text{-}heart}/SUV_{max\text{-}mediastinum}$, $SUV_{max\text{-}heart}/SUV_{max\text{-}liver}$, $SUV_{max\text{-}heart}/SUV_{max\text{-}scapularmuscles}$,$SUV_{max\text{-}heart}/SUV_{max\text{-}erector\ spinae}$ratios were 57.14% (4/7), 66.67% (14/21), 36.36% (4/11), 82.35% (14/17), 64.29% (18/28); 100.00%(8/8), 54.50%(6/11), 61.54%(8/13), 100.00%(6/6), 73.68%(14/19); 100.00%(8/8), 54.50%(6/11), 61.54%(8/13), 100.00%(6/6), 73.68%(14/19); 100.00%(8/8), 72.73%(8/11), 72.73%(8/11), 100.00%(8/8), 84.21%(16/19); 100.00%(8/8), 63.64%(7/11), 66.67%(8/12), 100.00%(7/7), 78.95%(15/19). When MRI and PET parameters were combined and positive was classified by both T1 value

greater than 1182ms and $SUV_{max\text{-}heart}$/$SUV_{max\text{-}scapularmuscles}$ratio greater than 10.2, the specificity and accuracy were 77.78% (7/9) and 85.71%(12/14), respectively. **Conclusion:** ^{18}F-FDG PET/CT could early identify anthracycline cardiotoxicity in oncology patients, and if using 10.2 as the threshold of after treatment $SUV_{max\text{-}heart}$/$SUV_{max\text{-}scapularmuscles}$ratio, the negative predictive efficacy and accuracy of^{18}F-FDG PET/CT for early TACT prediction are up to 80%, the specificity and positive predictive efficacy can up to 70%. It may improve diagnostic accuracy of anthracycline cardiotoxicity when combined with T1 value. **References:** None

OP-0235

Gated tomographic radionuclide angiography using 3D-ring CZT Starguide SPECT/CT : head-to-head comparison with a cardiac-dedicated CZT camera

T. Carsuzaa, F. Thibault, M. Bailly;
CHR Orleans, Orleans, FRANCE.

Aim/Introduction: The StarGuide 3D-ring CZT camera (GE Healthcare, Haifa, Israel) is equipped with 12 swiveling high-resolution CZT detectors and a CT in a hybrid system. Gated tomographic radionuclide angiography is a gold standard for the assessment and monitoring of left cardiac function in patients under treatment at risk of cardiotoxicity (oncology). In this preliminary work, we compared the evaluation of left ventricle ejection fraction (LVEF) between the new CZT SPECT/CT StarGuide system and a cardiac-dedicated CZT camera. **Materials and Methods:** We conducted a prospective single-center comparative study (with intra-patient comparisons). Patients underwent a 7-minutes acquisition on a cardiac-dedicated CZT camera (Discovery NM 530c, GE Healthcare, Haifa, Israel) and a 9-minutes acquisition on the new StarGuide CZT system, after mean injection of 321.4 +/- 55.9 MBq ^{99m}Tc-labeled human serum albumin. The primary outcome was the comparison of LVEF between both cameras. Secondary outcomes included the measurement of right ventricle ejection fraction (RVEF) and left ventricular volumes. All data were analyzed using BPGs software. Results: Between December 2020 and April 2021, 26 patients were included (22 women; 4 men; mean age 56.9 Y; mean BMI 29.5 kg/m^2 (range (17-42)). Mean LVEF was 69.7% +/- 11.6% (range (46% - 94%). There was no-significant difference between the two acquisition methods ($p<0.02$) with a Pearson correlation coefficient of 0.75. The only abnormal patient (LVEF < 50%) was correctly classified as abnormal on both systems (LVEF were 46% and 48% respectively for cardiac dedicated and 3D-ring CZT systems). Left ventricular volumes were also not significantly different between the two systems ($p<0.05$). Overall image quality seemed visually similar. RVEF seemed lower using StarGuide (mean RVEF 47.4 % +/- 9.4% and 46.2% +/- 10.4% respectively for cardiac-dedicated and 3D-ring CZT systems; $p=0.61$), that might be explained by the difficult contouring due to the RV shape. **Conclusion:** Our preliminary results seem to indicate that the use of StarGuide system for the measurements of LVEF and ventricular volumes measurement gives similar results to those of a cardiac-dedicated CZT camera. These results should be confirmed on a larger scale. **References:** none

OP-0236

Incremental Value of ^{18}F-FDG Cardiac PET Imaging Over Dobutamine Stress Echocardiography in Predicting Myocardial Ischemia in Patients with Suspected Coronary Artery Disease

E. Zampella[1], R. Assante[1], A. D'Antonio[1], T. Mannarino[1], E. Criscuolo[1], R. Bologna[1], P. Buongiorno[1], V. Gaudieri[1], C. Nappi[1], R. Green[1], V. Cantoni[1], M. Petretta[2], W. Acampa[1], A. Cuocolo[1];
[1]Department of Advanced Biomedical Sciences, University Federico II, Naples, ITALY, [2]IRCCS SDN, Diagnostic Imaging, Naples, ITALY.

Aim/Introduction: Metabolic imaging using radiolabeled glucose analogues ^{18}F-fluorodeoxyglucose (^{18}FDG) has been proposed for direct imaging of myocardial ischemia by PET imaging. We evaluated the incremental value of ^{18}F-FDG PET imaging over dobutamine stress echocardiography (DSE) in predicting myocardial ischemia at ^{82}Rubidium (^{82}Rb) imaging in patients with suspected coronary artery disease (CAD). **Materials and Methods:** Forty-one patients with suspected CAD underwent within seven days apart cardiac PET with ^{82}Rb and DSE followed by cardiac ^{18}F-FDG PET imaging. For ^{82}Rb PET, total perfusion defect (TPD) was calculated and considered abnormal if ≥5%. Ischemic TPD was calculated as stress TPD - rest TPD and considered abnormal when ≥5%. ^{18}F -FDG images were scored on a 0 to 2 scale and ischemia was defined as an uptake score 2 of at least a myocardial segment. For DSE, regional wall motion was evaluated on a 4-point scoring system (1, normal; 2, hypokinetic; 3, akinetic; 4, dyskinetic) and classified as biphasic response, worsening, sustained improvement or no change. Patients with biphasic or worsening response patterns in ≥1 segment were considered to have ischemia. Logistic regression analysis was performed to identify predictors of ischemia at ^{82}Rb-PET. The incremental value of ^{18}F-FDG PET over DSE was assessed by the likelihood ratio chi-square. Results: Stress-induced myocardial ischemia was detected in 20 (49%) patients at ^{82}Rb-PET, in 21 (51%) at ^{18}F-FDG PET and in 22 (54%) at DSE. Among ischemic patients at ^{82}Rb-PET, 15 (75%) showed ischemia at both ^{18}F-FDG PET and DSE. Three (15%) patients resulted false negative at DSE; of those, 2 (67%) were reclassified as ischemic at ^{18}F-FDG PET. Among 21 patients without ischemia at ^{82}Rb-PET, 15 (71%) were negative at both 18F-FDG PET and DSE. Five (24%) patients were false positive at DSE and 2 (40%) of these resulted as negative at ^{18}F-FDG PET. At univariate analysis, both ^{18}F-FDG PET and DSE results were significant predictors of ischemia at ^{82}Rb-PET ($P<0.001$), while ^{18}F-FDG PET resulted the only independent predictor of ischemia ($P<0.05$). At incremental analysis, the addition

of ^{18}F-FDG PET to DSE significantly increased the global chi-square of the model for predicting ischemia at ^{82}Rb-PET from 17 to 33 (P<0.05). **Conclusion:** ^{18}F-FDG PET performed after dobutamine stress test may provide an incremental value as compared to DSE in the evaluation of myocardial ischemia. Stress-induced myocardial ischemia can be imaged directly by using ^{18}F-FDG PET after dobutamine stress test. **References:** none

OP-0237

Comparison of early imaging of ^{123}I-BMIPP and myocardial washout rate for diagnosis of triglyceride deposit cardiomyovasculopathy

R. Ono[1], H. Miyauchi[1], K. Hoshi[2,3], T. Iimori[4], M. Oyama[5], K. Hirano[6], Y. Kobayashi[1];
[1]Department of Cardiovascular Medicine, Chiba University Graduate School of Medicine, Chiba, JAPAN, [2]Faculty of Medicine, Chiba University School of Medicine, Chiba, JAPAN, [3]Internal Medicine, National Hospital Organization Disaster Medicine Center, Tachikawa City, JAPAN, [4]Department of Radiology, Chiba University Hospital, Chiba, JAPAN, [5]Division of Laboratory Medicine, Chiba University Hospital, Chiba, JAPAN, [6]Laboratory of Cardiovascular Disease, Novel, Non-invasive, and Nutritional Therapeutics and Triglyceride Research Center, Graduate School of Medicine, Osaka University, Osaka, JAPAN.

Aim/Introduction: Triglyceride deposit cardiomyovasculopathy (TGCV) is a novel cardiovascular disorder discovered in Japanese patients waiting for heart transplant (ORPHA code: 565612). TGCV is characterized by the excessive accumulation of triglycerides in the myocardium and coronary artery caused by intracellularly impaired fatty acid metabolism. However, diagnosing TGCV is often difficult because the patients are generally treated only for coronary artery disease, heart failure, or cardiomyopathy. In addition, the serum triglyceride level is not directly associated with TGCV. The diagnostic criteria for TGCV include decreased myocardial washout rate (WR) of iodine-123-beta-methyl iodophenyl-pentadecanoic acid (^{123}I-BMIPP), diffuse narrowing coronary arteries, impaired left ventricular systolic function, and Jordan's anomaly. Therefore, the WR of ^{123}I-BMIPP plays an important role for the diagnosis of TGCV. However, executing the early and delayed imaging is burdensome because of its procedure time. The aim of this study was to evaluate the early imaging of ^{123}I-BMIPP to detect the impaired fatty acid metabolism in patients with TGCV. **Materials and Methods:** We performed ^{123}I-BMIPP and 201Thallium (^{201}Tl) scintigraphy in 212 patients with cardiac disease to measure the total counts of ^{201}Tl and ^{123}I-BMIPP in the early and delayed phase. All patients were applied to diagnostic criteria for TGCV. To assess the fatty acid metabolism, we calculated early ^{123}I-BMIPP indices including the heart to mediastinum ratio (H/M) of ^{123}I-BMIPP and the relative accumulation of ^{123}I-BMIPP to ^{201}Tl (BMIPP/Tl) in the early phase. The diagnostic values of the early indices and the WRs of ^{123}I-BMIPP were evaluated by ROC analysis. Results: Among 212 patients, 84 received the definitive diagnosis of TGCV. The diagnostic values of the ^{123}I-BMIPP indices were evaluated by ROC analysis. Area under the curve (AUC) of H/M, BMIPP/Tl and WR of ^{123}I-BMIPP were 0.516 (95% CI: 0.418-0.613), 0.744 (95%CI: 0.667-0.821) and 0.873 (95%CI: 0.820-0.927), respectively. In early indices, the AUC of BMIPP/Tl is significantly larger than that of H/M ($p < 0.05$). **Conclusion:** For the diagnosis of TGCV, reduced WR of ^{123}I-BMIPP is a crucial index. Although H/M does not replace the WR, BMIPP/Tl uptake ratio in early imaging would be useful to detect the impaired fatty acid metabolism in patients with TGCV. **References:** 1. Hirano, et al. Triglyceride deposit cardiomyovasculopathy. N Engl J Med. 2008;359(22):2396-8. 2. Li M, et al. Triglyceride deposit cardiomyovasculopathy: a rare cardiovascular disorder. Orphanet J Rare Dis. 2019;14:134. 3. Kobayashi, et al. The Diagnostic Criteria 2020 for Triglyceride Deposit Cardiomyovasculopathy. Ann of Nucl Cardiol. 2020;6:99-104.

OP-0238

The impact of lung perfusion scintigraphy in the work-up of Acute Pulmonary Embolism diagnosis: healthcare and economic aspects

G. Rubini[1], P. Mammucci[1], C. Ferrari[1], C. G. Leo[2], P. Mincarone[3];
[1]Section of Nuclear Medicine, DIM, University "Aldo Moro", Bari, ITALY, [2]National Research Council, Institute of Clinical Physiology, Branch of Lecce c/o Campus Ecotekne via Monteroni, Lecce, ITALY, [3]National Research Council, Institute for Research on Population and Social Policies, Research Unit of Brindisi, Brindisi, ITALY.

Aim/Introduction: Acute pulmonary embolism (APE) is a cardiovascular emergency, representing the main cause of mortality, morbidity and hospitalization in Europe. Early diagnosis is critical for reducing mortality. Lung Perfusion Scintigraphy (LPS) is a simple, easy-to-perform and inexpensive nuclear medicine method with no contraindications or side effects, showing high performance in the diagnosis of APE in patients with high clinical suspicion but with inconclusive computed tomography pulmonary angiography (CTPA) imaging.This study aims to evaluate the economic and healthcare impact of LPS in patients with suspected APE and a non-conclusive or contraindicated CTPA. **Materials and Methods:** We retrospectively evaluated 1,846 patients who underwent LPS at our Nuclear Medicine Unit, over a 4-year-period. We interpreted LPS according to PISAPED criteria and performed a risk assessment according to the Simplified Pulmonary Embolism Severity Index (sPESI). Two alternative healthcare strategies for the diagnosis and treatment of APE in the acute phase, either with or without LPS, were modelled and represented with the Unified Modeling LanguageTM. Direct healthcare costs from the National Health Service perspective were considered and the economic model was fed either with retrospective data

or national and regional official fares. Results: LPS resulted positive in 309/1,846 (16.7%) patients and negative in 1,537/1,846 (83.3%). Out of LPS positive patients, 9 had a low severity and were discharged while 300 were hospitalized. Among patients requiring hospitalization, 204/300 (68%) needed intensive care, whereas 96/300 (32%) required only ordinary hospitalization. The average per-patient costs for diagnosis and treatment of the acute phase of PE in low-risk patients with a non-conclusive/contraindicated CTPA, with or without LPS, were 2,145.25€ and 4,912.45€ respectively. Considering our patient flow, the overall annual reduction of hospital direct costs could be estimated as varying from 691,800€ to 2,075,400€. **Conclusion:** Our analysis suggests that the strategy with LPS, excluding the APE suspicion in an emergency scenario, offers a huge advantage in terms of healthcare cost and resources. Furthermore, this diagnostic tool is reliable for a better patient risk stratification and for the management optimization of those who do not require admission to intensive care or ordinary hospitalization. **References:** None.

OP-0239

Left-ventricular volumes and ejection fraction from cardiac ECG-gated ^{15}O-water positron emission tomography compared to cardiac magnetic resonance imaging using simultaneous hybrid PET/MR

J. Nordström, S. Kvernby, T. Kero, J. Sörensen, H. Harms, M. Lubberink;
PET Center Uppsala Akademiska sjukhuset, Uppsala, SWEDEN.

Aim/Introduction: ^{15}O-water PET is the gold standard for non-invasive quantification of myocardial blood flow. In addition to evaluation of ischemia, assessment of cardiac function and remodeling is important in all cardiac diseases. However, since ^{15}O-water is freely diffusible and standard uptake images show little contrast between the myocardium and blood pool, assessment of left-ventricular (LV) volumes and ejection fraction (EF) is challenging. Therefore, the aim of the present study was to investigate the feasibility of LV volumes and EF calculations from first pass analysis of ^{15}O-water PET by comparison with cardiac magnetic resonance imaging (CMR) using a hybrid PET/MR scanner. **Materials and Methods:** Twenty-four patients with known or suspected CAD underwent a simultaneous ECG-gated cardiac PET/MR scan. ^{15}O-water first-pass (FP) images (0-50 s) were analyzed in aQuant software and CMR images were analyzed in the software Segment, for LV volumes and EF calculations. LV volumes and EF were compared using correlation and Bland-Altman analysis. In addition, inter- and intra-observer variability of LV volumes and EF were assessed for both modalities. Results: Correlation between PET and CMR was strong for volumes (r>0.84) and moderate for EF (r=0.52), with the moderate correlation for EF at least in part due to the small range of EF values. Agreement was high for all parameters with a slight overestimation of PET values for end-diastolic volume but with no significant mean bias for other parameters. Inter- and intra-observer agreement of volumes was high and comparable between PET and CMR. For EF, inter-observer agreement was higher for PET and intra-observer agreement was higher for CMR. **Conclusion:** LV volumes and EF can be calculated by first pass analysis of a ^{15}O-water PET scan with high accuracy and comparable precision as with CMR. **References:** None

OP-0240

Incomplete Anatomical Revascularization in Multivessel Coronary Artery Disease: a Quantitative Myocardial Perfusion PET Study

A. Guarneri[1], L. Leccisotti[2,1], M. Grandinetti[3], G. Locorotondo[4], M. Iafrancesco[3], P. Bruno[3], F. Crea[4], M. Massetti[3], A. Giordano[1,5];
[1]Section of Nuclear Medicine, University Department of Radiological Sciences and Haematology, Università Cattolica del Sacro Cuore, Rome, ITALY, [2]Unit of Nuclear Medicine, Department of Diagnostic Imaging, Radiation Oncology and Haematology, Fondazione Policlinico Universitario Agostino Gemelli IRCCS, Rome, ITALY, [3]Unit of Cardiac Surgery, Department of Cardiovascular Sciences, Fondazione Policlinico Universitario Agostino Gemelli IRCCS, Rome, ITALY, [4]Unit of Cardiology, Department of Cardiovascular Sciences, Fondazione Policlinico Universitario Agostino Gemelli IRCCS, Rome, ITALY, [5]Unit of Nuclear Medicine, Department of Diagnostic Imaging, Radiation Oncology and Hematology, Fondazione Policlinico Universitario Agostino Gemelli IRCCS, Rome, ITALY.

Aim/Introduction: complete coronary revascularization by coronary artery bypass grafting (CABG) is the gold standard treatment in multivessel coronary artery disease (CAD). However, an "incomplete anatomical revascularization" strategy could be the preferred therapeutic approach for selected patient categories. So far, the effects of an incomplete coronary revascularization on myocardial blood flow (MBF) and coronary flow reserve (CFR) are unknown, especially in non-revascularized segments. The aim of this study is to prospectively evaluate regional and global changes of MBF and CFR in patients undergoing incomplete versus complete anatomical coronary revascularization by CABG using myocardial perfusion PET. **Materials and Methods:** inclusion criteria were age≥18years and multivessel CAD (stenosis diameter≥70% in at least 2 epicardial coronary arteries). Myocardial perfusion PET with ^{13}N-ammonia (370+370 MBq) was performed at rest and during adenosine stress before and 4-6 months after CABG. Resting MBF (mL/min/g) was corrected for rate pressure product and CFR was calculated as the ratio of stress MBF (mL/min/g) to corrected resting MBF. All data were calculated for the whole left ventricle, for each coronary territory and for each of 17 myocardial segments according to the individual anatomy of coronary tree and CABG surgery data. Results: seven male patients were prospectively enrolled

(mean age 61 years, range 51-77). Three patients underwent complete anatomical revascularization and 4 patients incomplete anatomical revascularization. A total of 101/119 (85%) myocardial segments were completely revascularized, including 51 from patients completely revascularized and 50 from patients non completely revascularized. Eighteen (15%) myocardial segments were not revascularized. CFR significantly increased after CABG in revascularized and not revascularized segments, with a greater increase in revascularized segments: from 1.21±0.45 to 1.82±0.53 in revascularized segments vs. 1.25±0.49 to 1.44±0.33 in not revascularized segments ($p<0.001$ within each group, $p=0.013$ between groups). Stress MBF increased from 1.23±0.44 to 1.64±0.42 in revascularized segments vs. 1.20±0.53 to 1.41±0.44 in not revascularized segments ($p\leq0.004$ within each group, $p=0.037$ between groups). Per coronary territory and per patient analysis showed that CFR and stress MBF significantly increased after CABG in both revascularized and not revascularized groups, with a greater increase in the revascularized group. **Conclusion:** this pilot study shows that the "incomplete anatomical revascularization" strategy could have beneficial effects even in myocardial segments not directly revascularized, through a significant increase of CFR and stress MBF values. Large-scale studies are needed to confirm these results and to obtain information on the clinical effect of this strategy on selected categories of patients. **References:** none

601

Wednesday, October 20, 2021, 18:00 - 19:30

Channel 1

CME 4: Imaging Neuroinflammation – Everything You Always Wanted to Know, But Were Afraid to Ask

OP-0243

Background of TSPO and Non-TSPO Targets and Their Radiotracers

M. Brendel; *Department of Nuclear Medicine, University Hospital of Munich; Munich Cluster for Systems Neurology (SyNergy), Munich, GERMANY.*

OP-0244

Imaging Neuroinflammation with TSPO Ligands - A Critical Reappraisal

B. van Berckel; *VU University Medical Center, Department of Radiology and Nuclear Medicine, Amsterdam, NETHERLANDS.*

OP-0245

Imaging Neuroinflammation - Beyond TSPO Receptors

D. van Weehaeghe; *Division of Nuclear Medicine and Molecular Imaging, University Hospitals of Leuven and KU Leuven, Leuven, BELGIUM.*

602

Wednesday, October 20, 2021, 18:00 - 19:30

Channel 2

Case Report Session: What's the Case? Report it Now!

OP-0396

PET/MRI Advantages in Primary Inferior Vena Cava Leiomyosarcoma

B. Ronchi, G. Peña, C. Sacchi; FUESMEN, Mendoza, ARGENTINA.

Aim/Introduction: To present three rare cases of leiomyosarcoma of the inferior vena cava (IVC) in which 18-F fluorodeoxyglucose (18-F FDG) nuclear magnetic resonance (MRI) in Hybrid Resonator, PET/MRI General Electric SIGNA of 3 Tesla, given its low incidence in order to know its anatomo-metabolic behavior, forms of presentation, dissemination and the benefits of this technique at the time of diagnosis. **Materials and Methods:** We present three cases with history of abdominal pain and abdominal distension. Complementary studies were performed that failed to determine the etiology of the injury, so these patients were evaluated with PET/MRI with 18-F Fluorodeoxyglucose (FDG) in a full-body PET 3D TOF acquisition scan in Hybrid Resonator, PET/MRI General Electric SIGNA 3 Tesla. Results: 18-F FDG PET/MRI showed the presence of wide retroperitoneal hypermetabolic mass in vena cava in all patients. It was possible to determine its probable etiology, location, extension, distant metastasis and metabolic degree. The Mingoli classification was also applied to determine the VC compromise area. High-grade vena cava leiomyosarcoma was confirmed by microscopic evaluation and immunohistochemical analysis. The three-dimensional capability of MR imaging allows to delimit the vascular and neural structures with more accuracy, under zero exposure to radiation. PET imaging is appropiate to identify metabolic activity and the presence of distant metastases. **Conclusion:** This hybrid methodology combines the two best complementary techniques, in a single exam, which provides a more certain diagnostic approach. **References:** Coindre JM. Grading of soft tissue sarcomas: review and update. Arch Pathol Lab Med 2006;130(10):1448-1453. V. N. Reddy- PET imaging features of Leiomyosarcomas in various anatomic locations. A case series.- ECR 2020 / C-14798.

OP-0397

Giant Pelvic Plasmacytoma Detected by F-18 FDG PET/CT in a Patient with Multiple Myeloma

S. Kesim, T. Ones, N. Filizoglu, C. O. Sahin, T. N. Kissa, Z. C. Balaban Genc, K. Niftaliyeva, K. Oksuzoglu, S. Ozguven, F. Sen, S. Inanir, H. T. Turoglu, T. Y. Erdil;
Marmara University Istanbul Pendik Training and Research Hospital, Istanbul, TURKEY.

Aim/Introduction: Plasmacytomas are defined as solid lesions of multiple myeloma. Extramedullary plasmacytoma is seen in less than 5% of all plasma cell neoplasms and although it is usually observed in the head and neck region, plasmacytomas of the mesentery are extremely rare. Herein, we present F-18 FDG PET/CT images of a patient with aggressive multiple myeloma and paramedullary/extramedullary involvement. **Materials and Methods:** A 47-year-old man with suspected multiple myeloma was referred to F-18 FDG PET/CT for staging. Results: F-18 FDG PET/CT scan revealed multiple lytic lesions with increased FDG uptake in the entire skeleton. Interestingly, increased FDG uptake was noted in the 185x228 mm measured multilobulated expansile lesion with punctate calcifications, involving the sacrum, left and right iliac bone and L5 vertebra. Besides, multiple soft tissue lesions with punctate calcification foci presenting increased FDG uptake, were evaluated in favor of independent plasmacytomas within the mesenteric fatty planes. The patient was diagnosed with plasma cell neoplasia due to bone marrow biopsy performed after F-18 FDG PET/CT examination. **Conclusion:** F-18 FDG PET/CT is used as a reference imaging tool in detecting bone lesions at the initial diagnosis, evaluating the response to treatment and showing the presence of extramedullary disease in patients with multiple myeloma. Dystrophic calcifications can be seen in the plasmacytomas of multiple myeloma. Although this appearance can be associated with intratumoral necrosis as in other neoplasms, it can also be secondary to amyloid deposition. This characteristic pattern should be kept in mind while evaluating the FDG PET/CT images in patients with multiple myeloma. **References:** none

OP-0398

Mosaic Pattern of Skin Granuloma Annulare on[18F] FDG PET/CT

G. Abdullayev, E. Mehdi, F. Novruzov;
Azerbaijan National Centre of Oncology, Department of Nuclear Medicine, Baku, AZERBAIJAN.

Aim/Introduction: Granuloma annulare is a relatively common, often self-limited disorder that can affect both children and adults. The generalized form of granuloma annulare typically presents with numerous erythematous papules and plaques on the trunk and extremities. The connective tissue disease, rheumatoid arthritis, lymphoma, solid organ malignancies including breast, endometrial, lung, esophageal cancer may be associated with granulomatous dermatitis. [18F]FDG PET/CT has been shown to be useful in assessing many tumors because of its high sensitivity and specificity. Here we described [18F]FDG PET/CT findings of the rare form of the granulomatous diseases like granuloma annulare. **Materials and Methods:** A 70-year-old man presented with progressive annulare skin lesions on the surface of the whole body, especially in the back and lumbar region. Patient underwent [18F]FDG PET/CT scan for revealing the suspected malignancy. The tru-cut biopsy was performed from newly appeared skin lesions. Granuloma annulare is confirmed by clinical manifestation and immunohistochemistry. Results: PET/CT scan showed increased mosaic [18F]FDG uptake on all skin lesions. Skin biopsy demonstrated noncaseating epithelioid granulomas, mainly made up of giant cells, histiocytes and neutrophil leukocytes. There are no FDG avid characteristic pathologic findings revealed on bilateral mediastinal and thoracic images. **Conclusion:** In our case we found the mosaic and ring-shaped intense FDG uptake on progressive annulare skin lesions on the surface of the whole body, which is why we prefer to call this sign - mosaic pattern for guiding clinicians to recognize the characteristic patterns. The granuloma annulare can have high 18F-FDG uptake, without any other FDG avid lesions in whole body, which help clinicians to differentiate other common granulomatous diseases like cutaneous sarcoidosis and langerhans cell histiocytosis. **References:** Kesim S, Ozguven S. Granuloma annulare show diffuse 18F-fluorodeoxyglucose uptake on PET/CT. Report of a case. Rev Esp Med Nucl Imagen Mol. 2020 Dec 17:S2253-654X(20)30078-0. English, Spanish. doi: 10.1016/j.remn.2020.04.007.

OP-0399

A Case of Lumbar Osteomyelitis Imitating a Malignant Tumor

C. Sahin, K. Oksuzoglu, S. Kesim, N. Filizoglu, T. N. Kıssa, K. Niftaliyeva, Z. C. Balaban, S. Ozguven, F. Sen, T. Ones, H. T. Turoglu, S. Inanir, T. Y. Erdil;
Marmara University Pendik Training and Research Hospital, Department of Nuclear Medicine, Istanbul, TURKEY.

Aim/Introduction: Vertebral osteomyelitis is an infectious disease of the vertebral corpus. It is called spondylodiscitis when avascular intervertebral disc involvement is observed. Vertebral osteomyelitis is seen in 3-5% of all osteomyelitis cases. Herein, we presented a male patient who was operated on due to a mass in the lumbar region that mimics malignant tumor infiltration, which was diagnosed as methicillin-susceptible Staf. aureus osteomyelitis on postoperative pathology. **Materials and Methods:** A 63-year-old male patient who was operated for a mass extending to the surrounding soft tissues at the level of the L4-L5

vertebrae, was referred for FDG PET/CT to find the primary focus of malignancy. Results: In FDG PET / CT examination; a dense hypermetabolic lesion which was extended to the surrounding muscle planes and spinal canal, destroying the L4-L5 vertebral bodies was observed, . In addition, mild hypermetabolic lymph nodes were observed in the distal paraaortacaval area and bilateral main iliac loci. Although the findings suggest infectious changes in the foreground, malignancy could not be ruled out. After PET scan, histopathological examination was demonstrated that active inflammation. On tissue culture, methicillin-susceptible Staf. aureus was isolated. Following antibiotherapy, the patient's complaints and symptoms regressed. **Conclusion:** The incidence of vertebral osteomyelitis (VO) is 2.4 / 100,000 (years) and increased with age. Pyogenic infections are among vertebral OM etiologies. DM is one of the most important risk factors that predispose to pyogenic infections. Staph aureus is the most common pyogenic agent (39.3%). Its rarity, symptoms being similar to other diseases (lymphoma, disc herniation ..) and the absence of fever causing delays in the diagnosis. Inflammatory cells (neutrophils and macrophages) are activated with cytokines released in case of infection and inflammation. Expression of glucose transporters (GLUT) increases in activated inflammatory cells and FDG entry into the intracellular space increases. FDG PET / CT imaging was found to be more successful in the diagnosis of primary osteomyelitis than MRI and conventional imaging. For this reason, OM should be kept in mind in the differential diagnosis in cases where FDG PET / CT examination was performed to investigate malignancy, and a primary focus that could represent malignancy could not be detected on imaging but had vertebral involvement. **References:** None

OP-0400

Whole Body Lymphoscintigraphy and WB DWIBS-MRI in two cases of thoracic lymphangiomatosis

C. Olianti[1], A. Arena[2], A. Perrone[3], A. Tondo[3];
[1]University Hospital of Florence, Florence, ITALY, [2]Hospital of Prato, Prato, ITALY, [3]University Hospital Meyer, Florence, ITALY.

Aim/Introduction: Thoracic lymphangiomatosis is a rare systemic disorder affecting children (1-2). Due to its rarity and wide spectrum of clinical, histological and imaging features, diagnostic pathway can be challenging. We report the case of a young adult and an adolescent submitted to whole body lymphoscintigraphy (WB-LYM) and whole body MRI to the aim of surgical planning. **Materials and Methods:** A 16year old male and a 30y old female underwent a WB-LYM at 10 min, 1.5, 3, 8 and 24 hours, vertex-feet 8cm/min scan. ^{99m}TC-labelled nanocolloid (7,4 mBq for each limb) was administered simultaneously in 2nd interdigital space for superficial lymphatic circulation. MRI was performed using a 3T scanner and an imaging protocol consistent of coronal T2W-STIR and DWIBS sequences under free breathing. Also chest-CT was performed before surgery. Results: WB-LYM showed in the boy asymmetric lymphatic flux between upper (left-delay) and lower limbs (right-delay) with abnormal visualization of left scapular, retro-clavicular, inferior cervical, paraspinal lymphatic sites and important bilateral chest disease (more on the left), pleural chylous effusion and thoracic duct enlargement. A bilateral lower limbs delay was seen for the female with collateral enlarged circulation, left delay with lymphatic stasis in left axillary, sub-clavicular sites and right mean-superior pulmonary field. MRI allowed acquisition of anatomical details with a superimposable pattern of WB-LYM results, but not the localization and quantification of lymphatic peripheral delays. **Conclusion:** Lymphangiomatosis is a rare disorder with a broad range of clinicopathological and imaging features. MRI allows a WB evaluation of disease extent, CT allows a good evaluation for surgical planning, WB-LYM allows the WB lymphatic circulation, showing also the sites of delays and collateral enlarged circulation. **References:** 1) Alvarez OA, Kjellin I, Zuppan CW. Thoracic lymphangiomatosis in a child. J Pediatr Hematol Oncol. 2004 Feb;26(2):136-41. doi: 10.1097/00043426-200402000-00018. PMID: 14767208. 2) Faul JL, Berry GJ, Colby TV, Ruoss SJ, Walter MB, Rosen GD, Raffin TA. Thoracic lymphangiomas, lymphangiectasis, lymphangiomatosis, and lymphatic dysplasia syndrome. Am J Respir Crit Care Med. 2000 Mar;161(3 Pt 1):1037-46. doi: 10.1164/ajrccm.161.3.9904056. PMID: 10712360.

OP-0401

PET/CT as a key role imaging tool in infectious endocarditis (IE) complications: two cases of splenic abscesses, in patients with prosthetic valve endocarditis (PVE)

Z. Dancheva, M. Dyankova, T. Stoeva, S. Chausheva, T. Yordanova, B. Chaushev, A. Klisarova;
St Marina University Hospital, Varna, BULGARIA.

Aim/Introduction: Infective endocarditis (IE) carries a high risk of morbidity and mortality. In the latest update of the European Society of Cardiology guidelines for the management of IE, 18FDG PET/CT was included as one of the diagnostic tools in the diagnostic flow chart of IE. The role of PET/CT is not only confined in IE recognition, but also in IE complications finding, as they might spread all over the body. Splenic assess is a rare IE complication, while the splenic infarction is more common. It is estimated, that 5% of patients with splenic infarction, will eventually develop splenic abscess. Aim. We present two consecutive patients in which PET/CT had successfully recognized the prosthetic aortic valve IE, but also had a crucial role in septic emboli recognition, comprising splenic abscesses, which lead to their prompt treatment. **Materials and Methods:** We report two cases of patients with had a clinical history of aortic valve replacement, recent fever and infectious syndrome, positive

blood cultures, and suspected artificial valve structures on cardioechography and transoesophageal echography studies. The patients were resistant to antibiotic therapy, chosen according to the blood cultures. Both patients were referred for a PET/CT as a non-invasive tool for IE diagnosis confirmation and also excluding of other infectious emboli spread. We used the widely accepted patient preparation protocols including diet lacking carbohydrates for 12-24 h prior to the scan. Also strenuous exercise was avoided for at least 12 h. A non-gated cardiac protocol and a whole body PET/CT imaging were performed. Before image interpretation, good image quality was verified. Results: In both of our patients, high metabolic activity was registered in the prosthetic valve region with an SUV max value of 4.2 and 5.3, respectively. Both patients had enlarged spleen, measuring 143mm and 150mm, with a cystic lesion, engaging almost the whole spleen with a periphery with high metabolic activity. After the diagnosis, the patients were consulted with a surgeon and abscesses were drained. They were successfully treated and discharged when permanently afebrile with an appointment for an urgent aortic valve reoperation. **Conclusion:** On those patients, PET/CT acted as a key imaging method, which was able to recognize the PVE life threatening complication - splenic abscess, in two of our patients. This case report underlines the need for a whole body imaging and directed search of IE infectious complications in therapy resistant cases of IE. **References:** None

OP-0402

Extensive dermatomyositis mimicking insulin-induced skeletal muscle uptake in 18F-FDG PET/CT

J. Zhang-Yin[1], N. Weynants[2], G. Piret-Gerard[3], P. Pierre[2], B. Tang[1];
[1]CSL hospital, Vivalia, Arlon, BELGIUM, [2]Oncology, CSL hospital, Vivalia, Arlon, BELGIUM, [3]Radiology, CSL hospital, Vivalia, Arlon, BELGIUM.

Aim/Introduction: Dermatomyositis is a rare type of the idiopathic inflammatory myopathies and considered as an autoimmune disease. It could be a paraneoplastic manifestation for which ^{18}F-FDG PET/CT is useful. **Materials and Methods:** We reported a case of 67 years-old female patient which was admitted for skin rash, thigh pain and weakness. The laboratory test revealed an uncommonly high blood creatine kinase level (9000 U/L). For this severe dermatomyositis, a workshop by thigh MRI, ^{18}F-FDG PET/CT and muscle biopsy were performed. As the patient also suffered from type 2 diabetes requiring insulin injections, were carefully given instructions before perfoming the ^{18}F-FDG PET/CT which aimed to seek malignancy. Results: The PET/CT's MIP image (Fig 1) showed an extensive and moderate muscle uptake, similar to diffuse skeletal muscle uptake encoutered in patients in postprandial state or having insulin injections less than 4 hours. After investigation, the patient has respected strictly the instructions for diet and insulin injection delay. Moreover, a careful reading of the examen revealed some unusually patterns of muscle uptake. Indeed, there were no uptake in latissimus dorsi, leg muscles and medial or posterior compartments of thigh (Fig 2). These findings were highly consistent with those by MRI showing an extensively involvement of anterior compartments of thigh (Fig 3), corresponding exactly the uptake territories. The PET/CT is negative for malignancy search. This result was supported by findings from the muscle biopsy in the right quadriceps: the positivity for anti-Mi2 antibody suggesting an idiopathic origin of dermatomyositis. The patient then were treated by association of corticosteroid and methotrexate, allowing symptoms disappear and the creatine kinase level down to 900 U/L within several days. **Conclusion:** Plasma insulin can increase the muscle glucose uptake by inducing the translocation of GLUT4 from intracellular vesicles to the plasma membrane. Before PET/CT, instructions should be performed in order to prevent this situation. This case illustrated an extensive dermatomyositis which mimick insulin-induced skeletal muscle uptake. The distinction has been made thanks to some special patterns of muscle uptake and MRI findings. **References:** 1. Okiyama N. Clinical Features and Cutaneous Manifestations of Juvenile and Adult Patients of Dermatomyositis Associated with Myositis-Specific Autoantibodies. J Clin Med. 2021 Apr 16;10(8):1725. 2. Parida GK, Roy SG, Kumar R. FDG-PET/CT in Skeletal Muscle: Pitfalls and Pathologies. Semin Nucl Med. 2017 Jul;47(4):362-372.

OP-0403

The usefulness of ^{67}Gallium-citrate scintigraphy in renal transplant infection

A. Marques, F. Abreu, S. Pintão;
Centro Hospitalar de Lisboa Ocidental, Lisbon, PORTUGAL.

Aim/Introduction: Patients who have received a renal transplant are more susceptible to urinary tract infections due to immunosuppression and a shorter ureter. ^{67}Gallium (^{67}Ga) citrate scintigraphy has been used to identify and localize suspected infection in these patients. The authors present a clinical case illustrating the usefulness of ^{67}Gallium - citrate scintigraphy in the diagnosis of renal infection. **Materials and Methods:** A 55-year-old woman who had end-stage renal failure and undergone renal transplantation five months ago, presented with fever, abdominal distention, leukocytosis and normal urine analysis.The patient had a personal history of three recent hospitalizations for renal graft infection. Graft ecodoppler showed diffuse urethral thickening, with no other relevant changes.Given the clinical context, a ^{67}Ga citrate scintigraphy was performed to diagnose and localize any focus of infection. 10 mCi of ^{67}Ga citrate were administered and images were taken at 24, 48 and 72 hours as well as SPECT / CT of the abdomen at

24 and 48 hours. Results: ^{67}Ga citrate scintigraphy showed a persistent focal area of increased uptake in the superior region of the renal graft, compatible with infectious focus. Antibiotherapy was instituted and the patient showed significant clinical and analytical improvement. **Conclusion:** ^{67}Ga citrate scintigraphy is an useful method for diagnosing and eventual therapy monitoring in patients with renal graft infections. **References:** None.

OP-0404

The role of F18 FDG PET/CT imaging in the incidental diagnosis of cancer patients with asymptomatic COVID-19 infection

M. Keskin;
Mersin City Training and Research Hospital, Mersin, TURKEY.

Aim/Introduction: The aim of this study was to present the findings of COVID-19 patients who had no complaints due to infection in known cancer patients, but were found incidentally during F18-FDG PET/CT scan. **Materials and Methods:** Three patients with high probability viral pneumonia among 334 patients who is a known cancer underwent F18-FDG PET/CT scans between January and February 2021 were analyzed. None of the patients included in the study had symptoms of acute respiratory disease, and the diagnosis of viral pneumonia due to COVID-19 was confirmed by PCR test. Results: The rate of cancer patients with asymptomatic COVID-19 lung involvement detected incidentally in F18-FDG-PET/CT was 0.89%. Although patients had no respiratory distress, viral pneumonia with FDG uptake was observed in the lungs. **Conclusion:** Lung infection due to COVID-19 can be seen rarely in asymptomatic cancer patients. Proper management of this process will contribute to the survival of patients. **References:** None

OP-0405

Utility of ^{18}Ffluorodeoxyglucose PET- CT in a Rare case of Granulomatosis with Polyangiitis (GPA) with Multi-organ involvement without raised serum Proteinase 3 antineutrophil cytoplasmic antibodies (c-ANCA)

A. Dixit;
MPCT cancer hospital, Navi Mumbai, INDIA.

Aim/Introduction: Granulomatosis with polyangiitis (GPA, formerly Wegener's) is a rare autoimmune disorder involving classical triad of kidneys, respiratory tract and blood vessels but can also present as limited or widespread which cannot be categorised with only clinical and lab investigations. **Materials and Methods:** We report an interesting case of (GPA) with rare multi-organ involvement in a young 35 year old male who presented with complaints of burning micturition, swelling over face, multiple violet reddish skin ulcerative lesions over nose, face, scalp, chest and significant weight loss (~13 kg) since last 6 months. Urine examination revealed hematuria and abnormal urinary albumin and micro-albumin. USG abdomen suggested bilateral small renal simple cortical cysts. Microscopic examination from the skin lesions of scalp suggested hyperplasia and hyperkeratosis with areas of surface ulceration over epidermis and necrobiotic collagen with infiltrate of histiocytes between collagen bundles of deposition of mucinous material consistent with granuloma annulare (interstitial pattern) of unknown etiology. Granulomatous infiltrations have been reported with malignant blood disease in literature. Laboratory tests revealed a normal complete blood count (CBC), antistreptolysin O (ASO), erythrocyte sedimentation rate (ESR), rheumatoid factor (RF), blood glucose level (BGL) but weakly positive ANA (anti-nuclear antibody)with speckled pattern. Fluorine-18- fluorodeoxyglucose (^{18}F FDG) positron emission tomography (PET)-CT scan was advised to rule out paraneoplastic etiology. There are multiple hypermetabolic cutaneous subcutaneous lesions over face, nose, scalp, chest with multiple cavitatory pulmonary nodules, bilateral cystic hypermetabolic kidney lesions with multiple intramuscular lesions along thigh muscle (R > L), paravertebral muscles of back, bilateral thyroid gland and pancreas. The scan findings raised suspicion for autoimmune disease etiology. C-reactive proteins (CRP) were raised without elevated c -ANCA titres. Microscopic examination of right thigh metabolically active lesion confirmed granulomatous inflammation with giant cell and tissue necrosis suggesting necrotizing vasculitis. Results: Based on the clinical, laboratory, ^{18}F FDG PET-CT scan and histopathological findings, diagnosis of c-ANCA negative GPA was made. Patient improved on immunosuppressive therapy (Rituximab) and steroids on clinical follow up. **Conclusion:** ^{18}F FDG PET-CT scan helps in diagnosis, extent of disease involvement, guiding appropriate accessible biopsy site in suspected cases of GPA and can be further used for response assessment to treatment. **References:** 1. Ogan N, et al. Positron emission tomography in the management of five cases with granulomatosis with polyangiitis. Turk J Clin Lab 2017;8:8076.2. 2. Soussan M, et al. FDGPET/CT in patients with ANCAassociated vasculitis: Caseseries and literature review. Autoimmun Rev 2014;13:12531.

OP-0406

18-FDG-PET/CT in thoracic sarcoidosis, mimicking a chondrosarcoma progression - a case report

***Z. Dancheva*[1]**, *A. Konsoulova[2], M. Dyankova[1], T. Yordanova[1], B. Chaushev[1], T. Stoeva[1], S. Chausheva[1], A. Klisarova[1];*
[1]St Marina University Hospital, Varna, BULGARIA, [2]Department of Oncology, Complex Oncological Centre, Burgas, BULGARIA.

Aim/Introduction: As a non-tumor-specific agent, 18F-FDG accumulates not only in tumor, but also in inflammatory cells - activated macrophages and leucocytes. Sarcoidosis is a disease, involving abnormal collection of inflammatory cells, forming granulomas, that may present as nodules in

multiple organs, most often in lungs. It may mimic nodular parenchymal involvement or mediastinal lymphadenopathy of substantial dimensions. Aim. We present case of a patient with chondrosarcoma with regular follow-up computer tomography (CT), interpreted as disease progression. The patient was thus referred to ^{18}F-FDG PET/CT which showed a constellation, suggestive for sarcoidosis which was further on histologically confirmed. **Materials and Methods:** A 38-year-old male patient with partial resection of the left scapula for a low-grade chondrosarcoma, pT1cN0cM0G1, had a follow-up thorax CT three years after initial surgery. The CT suggested progression in lungs with appearance of parenchymal and subpleural nodules, and gross mediastinal and hilar lymphadenopathy. The patient was in excellent performance status with no signs of progressive malignant disease and was referred to PET/CT for further assessment. Results: 18F-FDG -PET/CT demonstrated enlarged metabolically active cervical left supraclavicular and infraclavicular lymph nodes (LNs). The MIP images demonstrated symmetrical bilateral clusters of large and grouped mediastinal and hilar LNs, reminding the Lambda sign on Gallium - 67 scan. Bilateral pulmonary parenchymal and subpleural nodules were also apparent in the metabolic images. Some metabolically active abdominal and pelvic LNs <12mm were also found. The differential diagnosis included stage II sarcoidosis, lymphoma as a metachronous disease or, less likely, sarcoma progression. The constellation of thoracic, cervical and left supra- and subclavicular LNs was highly suspicious of sarcoidosis. Another sign, suggesting potential multisystem inflammatory disease, was the excellent condition of the patient with no symptom of a progressive malignancy or lymphoma. The patient was referred to mediastinoscopy, confirming histologically the diagnosis of sarcoidosis. **Conclusion:** Metabolically active mediastinal lymph nodes raise wide differential diagnosis that should not only discuss the 18F-FDG -PET/CT images, but also consider the past history, tumor clinical behavior and histology, as well as relevant risk factors. This case report broadens the library of every nuclear medicine physician and oncologist, reminding that sarcoidosis might behave as a systemic disease, involving parenchymal organs and lymph nodes. **References:** None

OP-0407

Molecular Neuroimage and Parkinsonism after SARS-CoV2 Infection

A. Silva Mascarenhas, F. Menegatti Marino;
Imagens Médicas de Brasília - IMEB, Brasília, BRAZIL.

Aim/Introduction: Parkinsonism is described as a clinical presentation after some infections by viruses and in the current world scenario we face a new infectious pathology that teaches us something new every day, such as post-infectious neurological sequels. There are several reports in the literature of neurological symptoms after SARS-CoV2 infection, suggesting the potential for neurotropism of the virus. In the current work, we present a description of the findings of molecular neuroimaging exams in two cases of patients with clinical manifestations of parkinsonism after SARS-CoV2 infection. **Materials and Methods:** Presentation description of the findings in molecular neuroimaging exams of SPECT TRODAT and cardiac scintigraphy with MIBG in two different cases of patients with a clinical picture of parkinsonian syndrome after SARS-CoV2 infection. Results: Two cases of young female patients, diagnosed with SARS-CoV2 infection, who started to present with parkinsonism after recovery of the initial clinical picture of respiratory symptoms were evaluated. In both cases, we found an asymmetric uptake pattern of the TRODAT tracer in striatum, with a reduction in uptake in the projection of the middle third of the striatum contralateral to motor symptoms, in addition to this finding, we performed a cardiac scintigraphy with MIBG that showed signs of preservation of density and functional tone in post-ganglionic sympathetic nerve endings - ruling out the hypothesis of Parkinson's Disease. **Conclusion:** We found a peculiar image pattern in the SPECT TRODAT exam of these patients, with an involvement in the middle third of the striatum, different from other findings in the literature, which makes us think that this finding may be a form of initial presentation of the condition, however a larger volume of data is require for a more accurate assessment. We need more studies for a better understanding of the neurological sequels after a SARS-CoV2 infection, and in this still uncertain context it is particularly important to have the availability of non-invasive imaging tests that can help to better understand the behavior and evolution of this new pathology which is already part of the daily routine. **References:** COHEN, M.E., et. al. A case of probable Parkinson's disease after SARS-CoV-2 infection. The Lancet, 2020; MENDEZ-GUERRERO, A., et. al. Acute hypokinetic-rigid syndrome following SARS-CoV-2 infection. Academy of Neurology, 2020; FABER, I., et. al. Covid-19 and Parkinsonism: A non-post-encephalitic case. Mov Disord, 2020; BEAUCHAMP, L.C., et. al. Parkinsonism as a Third Wave of the COVID-19 Pandemic? Journal of Parkinson's Disease, 2020.

OP-0408

Covid Incidental infection finding in 18 FPSMA1007 PET CT in asymptomatic patient

M. Agolti, L. Solari;
Centro de Medicina Nuclear Clinica Modelo, Parana, ARGENTINA.

Aim/Introduction: In Argentina we are having COVID Infection second wave with more than 1650000 infected patients, since the COVID pandemic started. Due to the geographical situation of our Nuclear Medicine department, more than 500km from cyclotron , and due to the expensive cost of Ga 68 PSMA generator we evaluate our Prostate high risk/ biochemical recurrence prostate cancer patients with 18 FPSMA 100 PET CT, with excellent results mostly regarding local

relapse and lymph nodes relapse. **Materials and Methods:** Asymptomatic patient with Prostate Adenocarcinoma Gleason 6 who underwent radical prostatectomy in 2011, with biochemical recurrence diagnosed through PSA : 10,24 ng/ml. We performed 18 FPSMA 1007 in a Phillips Gemini TF PET/CT with an integrated 16-slice CT, the dose was 7 mCI according to Body Mass Index BMI, and the images were acquired 100 min after injection. Results: We found a local relapse in prostate bed, and right seminal vesicle (SUV Max 8,4) and we also found peripheral ground grass opacities in both lungs with mild radiopharmaceutical uptake (SUV Max 2,8) and a pseudonodular image in lower inferior right lobe (SUV Max 3,4) image. This CT pattern is described as typical appearance in RSNA consensus regarding COVID -19 . We contacted referent physician , who indicated PCR COVID -19 test which was positive. **Conclusion:** There is no publication on 18FPSMA uptake in COVID, however we know there are other causes of increased uptake in inflammatory process like tuberculosis, we believe from other publications on GA 68 PSMA, this mild uptake could be related to inflammatory changes. This was a low risk of metastasis patient, due to low Gleason, and lung metastasis are not very common in Prostate adenocarcinoma. Although extraordinary measures of cleaning and personal protection are taken during COVID pandemic, it is very important to be aware of infected patients in order to apply home isolation, symptom surveillance, and treatment. There are highly suggestive findings of Covid-19 including pulmonary round-glass opacities and consolidations, in more than two segments, mainly bilateral; the opacities can present as circumscribed areas of involving a whole segment/lobe. Nodal uptake can also be visualized.Nuclear medicine physicians should be alert to the risk of COVID 19 pulmonary infection patterns, even in asymptomatic patient in order to adopt safety measures for other patients and hospital staff, in order to block the spread of infection, and to improve patients treatment and surveillance. **References:** None

OP-0409

^{18}F-FDG brain PET in a patient with neurological involvement after severe SARS-CoV-2 infection: a rather fast recovery of brain metabolic function

A. Martini[1,2], G. Carli[3], I. Laghai[1], L. Kiferle[4], P. Piersanti[4], D. Perani[3], S. Sestini[1];

[1]Hospital Santo Stefano Nuclear Medicine Unit, Prato, ITALY, [2]University of Florence, AUOC Careggi, Department of Nuclear Medicine, Florence, ITALY, [3]University Vita Salute San Raffaele, Nuclear Medicine Unit Division of Neuroscieces, Milan, ITALY, [4]Hospital Santo Stefano Neurology Unit, Prato, ITALY.

Aim/Introduction: Along primary respiratory target, ther's evidence that many patients with SARS-CoV-2 infection develop neurological signs and symptoms.Herein, we describe case of patient with newly originated neurological symptoms due to SARS-CoV-2 which underwent fluorine-18-fluoro-deoxy-glucose positron emission tomography (^{18}F-FDG-PET) two times, first one during onset of neurological symptoms and second one after significative remission of clinical symptoms. Aim of study was highlight strategical role of ^{18}F-FDG-PET to detect brain functional impairment and provide understanding of physiopathology underlying central nervous system involvement due to SARS-CoV-2. **Materials and Methods:** A 60-y old patient developed SARS-CoV-2 infection in november 2020. During acute phase of disease (1 month), presented anosmia and severe respiratory symptomatology which required admission to intensive care unit and prolonged mechanical respiratory treatment. Thereafter, he was tested negative SARS-CoV-2 and was moved to home care in rather good clinical conditions. After two months from november 2020 started to present significative cognitive impairment and focal neurological signs including motor deficit and ideomotor slow-down. The Mini-Mental State Evaluation was 21.2/30 with significant impairment of recent memory, attention, and calculation. He also presented insomnia episodes and hyperkinetic delirium. No abnormalities were present in cerebro spinal fluid including presence SARS-CoV-2 RT-PCR and on brain MRI. After five months from november 2020, we observed significant clinical improvement with almost total disappearance of neurological symptoms. We performed two ^{18}F -FDG-PET scans at two (during neurological symptoms) and five (during clinical remission) months after acute phase of infection. Brain metabolism was analysed using optimised and validated voxel-based SPM method at the single-subject based on comparisons with large and well-selected dataset of healthy control level ($p = 0.01$). Results: visual reading and SPM analysis at the single-subject level of PET scan performed two months' time-point showed functional pattern characterised by significant severe and extended hypometabolism affecting almost all brain cortices, particularly frontal regions. On contrary, second PET scan five months' time-point revealed rather slight cortical hypometabolism in orbito-frontal and medial-frontal cortices. **Conclusion:** ^{18}F-FDG PET neuroimaging studies results provide evidence that along clinical symptoms remission, functional impairment of cortical grey matter areas observed in this patients is likely to be transient and reversible. According emerging neuropathological findings, neuronal functional impairment could be likely attributed to synergistic effects of systemic virus-mediated inflammation sustained by systemic cytokine release and transient hypoxia inducing local microglial activation rather than to direct viral invasion of brain parenchyma or vasculitis. **References:** none

OP-0410

The role of ^{18}F-FDG PET/CT in diagnosis and evaluation of an unsuspected secondary cutaneous lesion in a patient with tumor of unknown origin (TUO) in times of COVID-19 pandemic - a case report

T. Stoeva, T. Yordanova, M. Dyankova, S. Chausheva, Z. Dancheva, B. Chaushev, A. Klisarova;
UMHAT "Sveta Marina" EAD- Varna, Varna, BULGARIA.

Aim/Introduction: Herein, we aimed to report the advantages of ^{18}F-FDG PET/CT for finding a proper biopsy place and accurate staging of a tumor of unknown origin (TUO). Moreover, PET/CT was able to reveal an unsuspected secondary skin lesion, not reported in clinical exam, due to the necessity of wearing face masks owing to coronavirus 2019 disease (COVID-19). **Materials and Methods:** We present a case of a 75-years-old female patient with TUO. Due to complaints in the upper gastrointestinal tract, the patient was admitted into a hospital. The abdominal magnetic resonance imaging (MRI) showed hypervascular liver lesions, retroperitoneal lymphadenopathy and pathological bone-marrow involvement from TUO. It was suggested that the possible primary site was lymphoma or secondary lesions from breast, ovarian cancer or carcinoid. We performed a^{18}F-FDG PET/CT for the detection of primary tumor. Results: Baseline ^{18}F-FDG PET/CT was positive for metabolically active retroperitoneal lymph nodes and liver lesions. Also, we found a^{18}FDG-avid skin lesion in the right nasolabial fold, which no one had noticed on the clinical exams, probably because of the face mask that the patient was constantly wearing for protection against SARS-CoV-2 virus. Suspicious lesions in the right breast were found as well. The mammography findings were negative. Liver, skin and bone marrow biopsy were performed. Histology and immunohistochemistry of liver lesions and bone marrow showed mixed, small cleaved and large cell non-Hodgkin lymphoma. Biopsy of the skin lesion showed cutaneous Non Hodgkin involvement. The patient started a chemotherapy regimen, including six cycles of Obinutuzumab and Bendamustine. **Conclusion:** ^{18}F-FDG PET/CT is an irreplaceable imaging modality for evaluating patients with TUO. In this case, we showed the important role of ^{18}F- FGD PET/CT for finding a proper biopsy place, accurate staging and evaluating of an unnoticed prior the exam, non-Hodgkin lymphoma skin involvement. **References:** None.

OP-0411

^{18}F-FDG PET/CT diagnostic challenges in differentiating between post-COVID-19 vaccination lymphadenopathy and acral lentiginous melanoma metastasis: A Case Report

I. Almasan, G. Rusu, L. Hitu, G. Kermoison, H. Haba, I. Alexiev, D. Piciu;
Institute of Oncology „Prof Dr. Ion Chiricuta",
Cluj-Napoca, ROMANIA.

Aim/Introduction: Acral lentiginous melanoma (ALM) is a rare subtype of cutaneous malignancy accounting for only 2-3% of all melanomas. ALM is characterized by a delay in diagnosis, leading primarily to advanced disease at presentation, which determines a very poor prognosis. In this case report, we discuss the ^{18}F-FDG PET/CT findings in a patient with acral lentiginous melanoma associated with vaccination-induced lymphadenopathy which mimics metastatic disease. **Materials and Methods:** We report a case of a 72-year-old male with a history of acral lentiginous melanoma on the right palm, referred to ^{18}F-FDG PET/CT for follow-up, 19 days after the second dose of mRNA COVID-19 vaccine to the right deltoid muscle. Results: Compared to the previous exam, 3-month follow-up ^{18}F-FDG PET/CT scan revealed stationary FDG uptake to the mediastinal lymph nodes (right paratracheal, subaortic, bilateral hilar) with SUVlbm max 4.6 and newly enlarged metabolically active right axillary lymph nodes with SUVlbm max 5.87, measuring between 9.7-17.5 mm on CT, concerning for malignancy. An FDG avid lesion to the right deltoid muscle with SUVlbm max 2.24 was also detected. In this scenario, the observed lymphadenopathy ipsilateral to the injection site couldn't undoubtedly be attributed to the vaccination, as the melanoma was located on the same right side. These findings were discussed with the patient and he opted for ultrasound-guided fine-needle aspiration cytology of the axillary lymph nodes. Cytological examination demonstrated reactive patterns without evidence of malignancy. **Conclusion:** As immunization rates increase, cases of patients with unilateral vaccination-induced adenopathy are being observed in clinical practice. This phenomenon is especially relevant for oncology patients undergoing imaging, as it can contribute to diagnostic errors. Systematically collecting vaccination data (time of last administered dose, injection site, type of vaccine used) before imaging along with administering the vaccine contralateral to the cancer side are crucial steps in avoiding misdiagnosis and further invasive procedures. **References:** None

OP-0412

Inguinal Bladder Hernia on FDG PET/CT

N. Filizoglu, S. Kesim, C. O. Sahin, T. N. Kissa, K. Niftaliyeva, Z. C. Balaban Genc, K. Oksuzoglu, S. Ozguven, F. Sen, S. Inanır, T. Ones, H. T. Turoglu, T. Y. Erdil;
Marmara University Pendik Training and
Research Hospital, Istanbul, TURKEY.

Aim/Introduction: Herniation of the bladder into the inguinal canal is rare and is usually detected incidentally in asymptomatic patients. However, symptoms such as dysuria, frequent urination, nocturia, and hematuria are also common. It is difficult to evaluate the bladder in nuclear medicine examinations due to many radioactive materials are excreted through the urinary tract. Bladder activity can easily

be confused with an abnormal uptake in the bowel, rectum, or scrotum, leading to misinterpretation of pelvic images in many nuclear medicine studies. Herein, we presented an inguinal bladder hernia that was incidentally detected during ^{18}F-fluorodeoxyglucose (FDG) positron emission tomography (PET)/computed tomography (CT) in a patient who was followed up with a diagnosis of gastric cancer. **Materials and Methods:** FDG PET/CT imaging was performed on an 80-year-old male patient who had a diagnosis of gastric cancer to evaluate the response to treatment. Results: FDG PET/CT showed mild hypermetabolic metastatic lymph nodes in the aortocaval area. Intense FDG uptake was observed in the right inguinal area on MIP images. Transaxial CT and PET images were evaluated together and it was understood that this intense FDG uptake was caused by the intense urinary activity of the bladder herniated into the inguinal canal. **Conclusion:** Inguinal bladder hernia represents 0.5% -3% of all lower abdominal hernias and 1-3% of all inguinal hernias. It usually presents in obese men aged 50-70 years. As seen in our case, most of these herniations are direct inguinal hernias and occurs on the right side. Bladder neck obstruction due to prostatic hypertrophy, decreased bladder tone, weak pelvic muscles, and obesity are among the possible causes. Most of them are asymptomatic and are detected incidentally on radiological imaging. Intense FDG uptake is seen in kidneys, ureters, and bladders due to normal urine excretion. Patients are routinely asked to micturate before nuclear imaging, in particular, if the pathology is in the pelvis. The presence of abnormally increased FDG activity may lead to misdiagnosis and problems in cancer staging. We describe an interesting case of incidentally detected inguinal bladder hernia and emphasize the importance of hybrid imaging in distinguishing benign findings that will cause FDG uptake in the inguinal canal from malignant causes such as metastasis. **References:** none.

OP-0413

Demonstration of Peritoneal-Scrotal Communication by^{99m}Tc-MAA Scintigraphy

***A. Marques**, F. Abreu, S. Pintão;*
Centro Hospitalar de Lisboa Ocidental, Lisbon, PORTUGAL.

Aim/Introduction: Continuous Ambulatory Peritoneal Dialysis (CAPD) is an effective renal function replacement technique in patients with end stage renal disease (ESRD). However, several complications can occur, including inguinal hernias and dialysate leaks, mainly due to increased intra-abdominal pressure from the dialysate fluid in the peritoneal cavity. Peritoneal scintigraphy with technetium-99m macroaggregated human albumin (^{99m}Tc-MAA) helps to establish the diagnosis of these complications. **Materials and Methods:** A 61-year old male patient in ESRD undergoing CAPD treatment for three years, developed a sudden onset of bilateral scrotal swelling, more marked on the left side. To confirm and demonstrate the dialysate fluid leak into the scrotum, a peritoneal scintigraphy was performed. A dose of 185 MBq (5 mCi) of 99mTc-MAA was injected into the dialysate bag and instilled into the peritoneal cavity through the indwelling Tenckhoff catheter.Planar and SPECT/CT images of the abdominopelvic region were acquired 5 hours after radiotracer administration. Results: The images demonstrated tracer-labeled dialysate fluid in the left scrotal sac, consistent with a peritoneo-scrotal communication, as well as increased linear activity in the right inguinal canal, but not in the right scrotum. Low dose CT images showed presence of a right inguinal hernia. Patient underwent surgical correction of the left side dialysate leakage and the right inguinal hernia. **Conclusion:** Peritoneal scintigraphy is a simple, safe and effective method for the identification of dialysate leaks and hernial sites in patients undergoing CAPD. **References:** None.

OP-0414

Pulmonary Embolism on Azygos Lobe Detected by Ventilation/Perfusion SPECT/CT

***S. Kesim**, N. Filizoglu, C. O. Sahin, Z. C. Balaban Genc, K. Niftaliyeva, T. N. Kissa, K. Oksuzoglu, S. Ozguven, F. Sen, T. Ones, S. Inanir, H. T. Turoglu, T. Y. Erdil;*
Marmara University Istanbul Pendik Training and Research Hospital, Istanbul, TURKEY.

Aim/Introduction: Azygos lobe is a rare, anatomically separated segment of the upper lobe of the right lung that does not have a unique bronchus or blood supply. Although tumors, pneumothorax or extralobar pulmonary sequestrations have previously been reported to occur in this lobe, there are limited reports of thromboembolism on azygos lobe detected by lung scintigraphy. Herein, we present a case of 64-year-old woman with pulmonary embolism on azygos lobe detected by ventilation/perfusion single-photon emission computed tomography/computed tomography. **Materials and Methods:** An immobilized 64-year-old woman with clinical suspicion of pulmonary embolism, who underwent surgery for glioblastoma multiforme, was referred to ventilation/perfusion scintigraphy. Results: Perfusion lung scintigraphy (A) with Tc-99m-labelled macroaggregated human albumin (99mTc-MAA) and ventilation lung scintigraphy (B), which was performed after inhalation of Tc-99m-labelled Technegas, revealed subsegmental mismatch perfusion defects including azygos lobe of right lung. **Conclusion:** Clinical importance of azygos lobe is that it may simulate bulla, enlarged thymus, a substernal goiter, localised pneumothorax, abscess or nodule and a consolidated azygos lobe may mimic neoplasm. Although prior studies indicate that there may be a relative hypoperfusion and hypoventilation of azygos lobe, here is a lack of literature showing perfusion defects due to pulmonary embolism. Since it is an anatomically separated variant, perfusion only planar SPECT images may be inadequate for an embolism

on azygos lobe, as in our case. Hybrid imaging combining single-photon emission computed tomography (SPECT) with a low-dose CT have proved to improve diagnostic accuracy. **References:** none

OP-0415

Use of 2- [^{18}F] FDG PET / CT in unusual pediatric tumors

M. Acuña Hernandez[1], R. Palma Rosillo[2], R. Mora Ramírez[2]; [1]Universidad Autónoma de Bucaramanga, Bucaramanga, COLOMBIA, [2]Instituto Nacional de Pediatría, Ciudad de México, MEXICO.

Aim/Introduction: Lymphoblastic lymphoma comprises approximately 20% of pediatrics non-Hodgkin lymphoma and the 2-[^{18}F] FDG PET/CT can be util in the initial staging of newly diagnosed, assessment of response after induction chemotherapy. Extrarenal malignant rhabdoid tumor, is a rare malignancy in childhood and has a poor prognosis. The 2-[^{18}F] FDG PET/CT was helpful in the initial staging, assessing response to treatment, and in clinical decisions at various stages of management. **Materials and Methods:** A case series of two pediatrics patients with lymphoblastic lymphoma preB from histopathological diagnosis by renal biopsy and extrarenal malignant rabdoid tumor with histopathological diagnosis on biopsy of left frontal lesion. Results: Case 1 is a 4-year-old male consulted for febrile syndrome associated with polyarticular and abdominal pain, night sweats and lower limb edema, abdominal ultrasonography documenting bilateral nephromegaly, in blood bicytopenia and renal disfuntion. Histopathological renal biopsy diagnosis of pre-B lymphoblastic lymphoma. 2-[^{18}F] FDG PET/CT for initial staging, finding an abnormal increase in metabolism in the kidneys, bone marrow, bone, and abdominal adenopathies. Management was started with chemotherapy, but the patient died before completing the treatment. Case 2 is a 5-year-old male presented trauma due to a foreign object in the left eye, requiring surgical intervention to remove. , Two weeks later recite ocular pain, decreased visual acuity, ipsilateral headache and emesis in two occasions. Orbital MR evidence in the left orbital cavity towards the intraconal space, a solid space-occupying lesion, measuring 34 x 18.5 cm, which displaces extraocular muscles, proptosis, and optic nerve. Histopathological biopsy report extrarenal malignant rhabdoid tumor. 2-[^{18}F] FDG PET/CT fused with MR for initial staging, finding an abnormal increase in metabolism in the tumor described in the left orbit. with extension to the left cavernous sinus, meninges, and left temporal lobe. Surgical management was carried out with subsequent adjuvant chemotherapy. **Conclusion:** 2-[^{18}F]FDG PET/CT is a useful for staging infrequent pediatric tumors. **References:** 1. Society of Nuclear Medicine and Molecular Imaging. Procedure Standard/EANM Practice Guideline on Pediatric 18 F-FDG PET/CT for Oncology 1.0. J Nucl Med. 2021 Jan; 62(1):99-110. DOI: 10.2967/jnumed.120.254110. 2. Elhussein, A. Fawzy, M. Rahman, HA. Omar, W. Hussein. EM. Productivity of 18 F-FDG-PET/CT Diagnostic Tool in the Management of Pediatric Lymphoblastic Lymphoma. Nuclear Medicine Review. 2019; 22 (1): 23-28. DOI: 10.5603/NMR.2019.0004 3. Giles, RH. McCowage, G. Kellie, S. Graf, N. Extrarenal Malignant Rhabdoid Tumor in Childhood Application of 18 F-FDG PET/CT. J Pediatr Hematol Oncol. 2012; 34: 17-21. DOI: 10.1097/MPH.0b013e31822541a6.

OP-0416

Comparison [68Ga]FAPİ-46 PET/CT and [131I] SPECT/CT findings after ablation therapy with high-activity 131-I therapy of metastatic papillary thyroid cancer patients: Two case reports

F. Novruzov[1], A. Aliyev[2], S. Novruzova[1], N. Orucova[1], I. Aliyeva[3], M. Moore[4], F. Valla[4], F. Giammarile[5,1], E. Mehdi[1]; [1]Azerbaijan National Centre of Oncology, Department of Nuclear Medicine, Baku, AZERBAIJAN, [2]Azerbaijan National Centre of Oncology, Department of Head and Neck Surgery, Baku, AZERBAIJAN, [3]Azerbaijan Medical University, Department of Internal Medicine, Baku, AZERBAIJAN, [4]SOFIE, Totowa, NJ, UNITED STATES OF AMERICA, [5]International Atomic Energy Agency, Vienna, AUSTRIA.

Aim/Introduction: The aim of our study is to define the biodistribution of [68Ga]FAPI-46 in high-risk metastatic thyroid cancer patients who are treated with high activities of 131-I and the make a correlation of [68Ga]FAPI-46 findings with post-therapy 131-I SPECT/CT. **Materials and Methods:** A 19-year old female and a 43-year old male patient were diagnosed with papillary thyroid cancer. Both patients had undergone total thyroidectomy with neck dissection surgery. High thyroglobulin levels (310 ng/ml and 475 ng/ml, respectively) were detected after surgery. The patients were diagnosed with the classical variant of papillary thyroid carcinoma with lymph node metastasis. There were no perineural and muscle invasions. Both patients were deemed "high-risk" and underwent high-activity 131-I therapy (5.55 and 7.4 GBq respectively). 131-I SPECT/CT was performed according to our protocol for dosimetry analysis and [68Ga]FAPI-46 PET/CT for tumor re-staging. The male patient also performed bone scan with [18F]NaF. Results: Both patients demonstrated high uptake of 131-I and [68Ga]FAPI-46 in the thyroid bed and cervical lymph nodes. In the female patient, CT showed multiple subcentimeter lung nodules with high 131-I and [68Ga]FAPI-46 uptake[68Ga]FAPI-46 PET/CT showed better spatial resolution especially in localising smaller lymph nodes and lesions. Although radioiodine is the gold standard for thyroid cancer imaging, the intense physiological uptake of 131-I in the gastrointestinal system and salivary glands is another limitation of image interpretation, which was not observed in [68Ga]FAPI-46 PET/CT. There was focal and moderate uptake of [18F]NaF in the left parietal bone of male patient, without evident uptake in 131-I and [68Ga]FAPI-46

PET/CT scan, thus considered as non metastatic. **Conclusion:** [68Ga]FAPI-46 PET/CT is a new diagnostic method in imaging cancer patients. No diet or fasting in preparation for the examination is necessary, and image acquisition can potentially be started a few minutes after tracer injection. Locally aggressive or metastatic thyroid cancer showed high tumor to background [68Ga]FAPI-46 uptake. Thus, [68Ga] FAPI-46 is an alternative imaging method for thyroid cancer with better image quality than 131I SPECT. Furthermore, in the near future, [68Ga]FAPI-46 may indicate potential for targeted radionuclide therapy with alpha emitters in the theranostic approach of disseminated small lesions, such as lung metastases of thyroid cancer. **References:** Clemens Kratochwil, Paul Flechsig, Thomas Lindner ett. all. ^{68}Ga-FAPI PET/CT: Tracer Uptake in 28 Different Kinds of Cancer. Journal of Nuclear Medicine, 2019

OP-0417

Peptide Receptor Radionuclide Therapy (PRRT) in Radioiodine-Refractory Thyroid Cancer. A Case Report of Significant Response to 177Lu-Dotatate Treatment

S. Ataei, K. Aryiana, S. Mostafavi, M. Esmati nia, H. Mohammad Zadeh Kosari, A. Aghaei;
Mashhad university of medical science, Mashhad, IRAN, ISLAMIC REPUBLIC OF.

Aim/Introduction: In the cases of radioiodine-refractory differentiated thyroid cancer (RrDTC), iodine-therapy is not effective due to the fact that tumor cells lose their iodine uptake ability. RrDTCs can, in some cases, express somatostatin receptors (SSRT). For these patients 68Ga/177Lu-DOTATATE could be used for both diagnosis and treatment, providing novel treatment option. In order to evaluate PRRT on RrDTCs, we present a 59-year-old woman with follicular thyroid carcinoma, who underwent total thyroidectomy followed by receiving 30 mCi 131I for ablation. On the follow-up, there was a marked increase in thyroglobulin (Tg) level up to >500 ng/ml with suppressed TSH (first Tg: 0.01 ng/ml). Cervical ultrasonography and diagnostic I131 scan were negative. An empirical dose of 200 mCi I131 was administered. However, post-treatment scan was negative. Rising serum Tg levels (>30000 ng/ml), in absence of Tg-Ab, bindicated a metastatic disease. Also, the patient reported severe sternal region pain. **Materials and Methods:** This patient, as a case of RrDTC, underwent FDG PET/CT that showed pulmonary nodules and sternal manubrium lytic lesion with FDG uptake. Then Ga-68 DOTATE PET/CT was performed, confirming the lesions detected by FDG PET/CT. Therefore, the patient as an expressing somatostatin receptors (SSRT) case, received 200 mci of Lu-177 DOTATATE. Response to therapy was assessed by Tg, post-treatment Lu-177 DOTATATE SPECT/CT and patient's clinical symptoms. Results: Post-treatment Lu-177 DOTATATE SPECT/CT showed good uptake in pulmonary nodules and sternal lesion. Blood analysis 3 months after the first treatment showed diminished Tg level to 1760 ng/ml, being 982 ng/ml after completing the second treatment. Additionally, patient declared significant improvement of clinical symptoms. **Conclusion:** About 25-50% of patients with locally advanced or metastatic DTC become refractory to RAI [1]. Treatment options are limited, one of which is recently proposed in PRRT [2]. However, Lu-177 DOTATATE had a significant effect in reducing Tg levels and improving our patient's clinical manifestations. **References:** 1. Schlumberger M, Brose M, Elisei R, Leboulleux S, Luster M, Pitoia F, et al. Definition and management of radioactive iodine-refractory differentiated thyroid cancer. Lancet Diabetes Endocrinol 2014; 2: 356-8. doi: https://doi.org/10.1016/S2213- 8587(13)70215-8 2. Budiawan H, Salavati A, Kulkarni HR, et al. Peptide receptor radionuclide therapy of treatment-refractory metastatic thyroid cancer using (90)Yttrium and (177) Lutetium labeled somatostatin analogs: toxicity, response and survival analysis. Am J Nucl Med Mol Imaging 2013;4:39-52.

OP-0418

Subacute Thyroiditis and Cardiovascular Events - a Report of Two Clinical Cases

K. Bajuk Studen[1,2], K. Zaletel[1,2], E. Pirnat[1,2], S. Gaberscek[1,2];
[1]University Medical Centre Ljubljana, Ljubljana, SLOVENIA, [2]Faculty of Medicine, University of Ljubljana, Ljubljana, SLOVENIA.

Aim/Introduction: The combination of long-lasting inflammation and hyperthyroidism could increase the risk for cardiovascular (CV) events in the clinical course of subacute thyroiditis (ST). We report two clinical cases of patients diagnosed with ST and treated with methylprednisolone (a starting dose of 24 mg/day with decreasing the dose for 4 mg every 5 days). **Materials and Methods:** None. Results: Patient 1 was a 53-year old male smoker who presented with pain in the neck located in the thyroid and fever for a couple of weeks. During the clinical examination for ST he complained of chest pain. Electrocardiogram (ECG) did not show signs of acute ischemia, nevertheless he was admitted because of slighlty elevated troponin I 0.16 μg/L (normal level <0.1 μg/L). He was hyperthyrotic with TSH 0.01 mIU/L (ref. range 0.59-4.23), free T_4 52.0 pmol/L (ref. range 11.5-22.7) and free T_3 16.44 pmol/L (ref. range 3.5-6.5). He had sedimentation rate (SR) 105 mm/h. Treatment with methylprednisolone was initiated. After 2 days of observation, further elevation of troponin I to 0.898 μg/L and dynamic ECG changes were observed. Percutaneous coronary intervention in two coronary arteries was performed. In addition to methylprednisolone, aspirin, ticagrelor, perindopril, rosuvastatin and bisoprolol were prescribed. The patient recovered fully with a mild transient hypothyroidism. Patient 2 was a 60-year old male with arterial hypertension, hyperlipidemia, type 2 diabetes, and he was an ex-smoker. He complained of malaise and growing tender mass in the right thyroid lobe for four months. In this

period, he was evaluated twice at emergency department - first because of temporary loss of vision in the right half of the visual field that lasted several hours and 2 months later because of transient paresis in the left hand. Both times, he was diagnosed with transitory ischemic attack. Clopidogrel was added to aspirin for 3 weeks, along with treatment of pre-existing diseases. Due to suspicion of having thyroid tumor, fine-needle biopsy was performed and confirmed the diagnosis of ST. He was also found to be hyperthyrotic with TSH 0.01 mIU/L, free T_4 32.8 pmol/L and free T_3 6.9 pmol/L. He had SR 42 mm/h. Treatment with methylprednisolone led to quick clinical and laboratory improvement of ST. **Conclusion:** Although the course of ST is usually mild, we must not overlook the associated pathology that could lead to life-threatening complications. Further research should focus on the combined effect of inflammation and hyperthyroidism on cardiovascular events. **References:** None

OP-0419

Imaging pituitary microadenoma by using ^{18}F-FDOPA, ^{68}Ga-DOTA-NOC and ^{18}F-FDG PET/CT

S. Li, T. Wollenweber, A. Göllner, T. Traub-Weidinger, J. Furtner-Sajer, G. Karanikas, A. Haug, M. Hacker;
Medical University of Vienna, Vienna, AUSTRIA.

Aim/Introduction: The visualization of pituitary microadenoma, especially in Cushing´s syndrome, is a major challenge. The purpose of this case report was to compare the diagnostic value of [^{18}F]-FDOPA, [^{68}Ga]-DOTA-NOC and [^{18}F]-FDG PET/CT in a patient with pituitary Cushing´s syndrome. **Materials and Methods:** We report a 56-year-old woman presented with pituitary Cushing´s syndrome and central hypothyroidism due to pituitary microadenoma. The patient received dynamic magnetic resonance imaging (MRI), [^{18}F]-FDOPA, [^{68}Ga]-DOTA-NOC and [^{18}F]-FDG PET/CT scans for staging and evaluation before surgery. Transsphenoidal surgery was then performed and histological results were obtained. Results: MRI detected a 5 mm mass lesion in the left pituitary gland. [^{18}F]-FDOPA PET/CT revealed clearly focal and remarkable FDOPA uptake, consistent with the localization of tumour lesion detected by MRI. Whereas [^{68}Ga]-NOTA-NOC PET/CT visualized a homogenous physiological uptake in the pituitary gland. In comparison to [^{18}F]-FDOPA PET/CT, [^{18}F]-FDG PET/CT showed an absence of uptake in the lesion. The histological analysis confirmed an aggressive pituitary corticotroph microadenoma. **Conclusion:** This case report showed the first within-patient comparison results that [^{18}F]-FDOPA PET/CT has higher sensitivity as compared with [^{18}F]-FDG or [^{68}Ga]-DOTA-NOC PET/CT in the detection of pituitary corticotroph microadenoma. We speculated that [^{18}F]-FDOPA PET/CT might be more useful for precise diagnosis of hormone active pituitary microadenomas. **References:** none

OP-0420

A Benign Adrenal Mass with Changing Metabolism Mimicking Metastasis During Follow-up in a GIST Patient

Ü. Yararbas, F. Tamer;
Ege University Medical Faculty, Izmir, TURKEY.

Aim/Introduction: Gastrointestinal stromal tumor (GIST) are mesenchymal tumors that usually spreads to the liver and the peritoneum. Metastatic spread to the adrenal gland is very rare. Adrenal adenomas are common benign lesions and the vast majority of them are non-functional and asymptomatic. Non-functional adrenal adenomas have usually low metabolic activity with some exceptions. In this case report, we present a gastric GIST patient with liver and multiple gross peritoneal metastases and a co-existing adrenal mass. **Materials and Methods:** Forty year-old male was diagnosed as gastric GIST with peritoneum and liver metastases 14 months ago and Imatinib treatment was started. During the period of diagnosis and follow-up, four consecutive FDG PET/CT imaging were obtained. For the differential diagnosis of left adrenal mass, tru-cut biopsy was performed. Results: Staging PET/CT scan revealed a left adrenal mass having a diameter of 4.2x4 cm with moderately increased FDG uptake besides gastric GIST lesion and its metastatic spreads in the peritoneum and liver. While a metabolic and morphologic regression was observed in the first follow up FDG PET/CT scan in primary and metastatic lesions, progressive findings were noted in the two subsequent scans. Starting from the first (staging) FDG PET/CT study, left adrenal mass was stable morphologically but the metabolic activity of the lesion has been changed dramatically during the follow up examinations. The change in metabolic activity of the adrenal mass was not in accordance with other GIST lesions; in the first follow-up, while all lesions demonstrated regression in size and metabolic activity, adrenal lesion showed prominent metabolic progression (SUVmax: 12.6). In the light of the suspicious finding, tru-cut sampling was performed from the left adrenal lesion and the lesion was reported as adrenal cortical adenoma. In the following two PET/CT scans, metabolic activity of the adrenal mass declined first (SUVmax: 5.4) and then increased (SUVmax: 8.9). **Conclusion:** Although the main reason for the finding described is not clearly defined, considering the circadian secretion pattern of functional tumoral lesions, the intermittent hyperfunction in adrenal adenoma may explain the alterations in FDG uptake (3). The relatively rare occurrence of adrenal metastasis in cases of GIST and discordant findings in the patient's follow-up created the need for histopathological confirmation in this case. Care should be taken in primary tumors metastasizing frequently to adrenal glands to prevent false positive reportings. **References:** none

OP-0421

^{99m}Tc-MIBI Retention in Graves' Disease

B. Seven[1], M. Aslan[1], M. Çapraz[2];
[1]Department of Nuclear Medicine, Sabuncuoglu Serefeddin Training and Research Hospital, Amasya, TURKEY, [2]Department of Internal Medicine, School of Medicine, University of Amasya, Amasya, TURKEY.

Aim/Introduction: Parathyroid scintigraphy using ^{99m}Tc-MIBI in the diagnosis of functional parathyroid adenoma is the most effective image to detect the lesion. Differences in MIBI kinetics in the thyroid and parathyroid glands have led to the development of a dual-phase imaging technique performed after a single injection of the radiotracer. False-positive results may occur in patients with thyroid nodules, but the addition of ^{99m}Tc-pertechnetate scintigraphy to the protocol helps distinguish between the two. Concomitant cases of primary hyperparathyroidism and Graves' disease are well documented, but little is known about handling MIBI in the second condition. **Materials and Methods:** A 62-year-old woman with a history of Graves' disease and hyperparathyroidism was referred to our department for a ^{99m}Tc-MIBI parathyroid scintigraphy to preoperative localization of an abnormal parathyroid gland. Early and delayed images showed diffuse delay in radiotracer washout in both lobes of the thyroid. A ^{99m}Tc-pertechnetate scintigraphy performed 2 days later showed uniformly increased uptake consistent with Graves' disease. Results: This case shows a finding of ^{99m}Tc-MIBI retention in Graves' disease. **Conclusion:** Mitochondrial content and p glycoprotein expression may be responsible factors for this finding, as in thyroid and parathyroid nodules. **References:** None.

604

Wednesday, October 20 - Saturday, October 23, 2021

on-demand pool, release on Wednesday, October 20 at 09:00

CTE 4: Cardiac PET/CT

OP-0251

Session Introduction

M.C. Attard; PRA Health Sciences, Isala, Nuclear Medicine, Zwolle , NETHERLANDS.

OP-0252

Clinical Examples of Rubidium PET/CT

M. Mouden; Isala Hospital, Zwolle , NETHERLANDS.

OP-0253

Research Tracers Used in Cardiac PET/CT

A. Saraste; Turku University Hospital, Heart Center, Truku, FINLAND.

605

Wednesday, October 20 - Saturday, October 23, 2021

on-demand pool, release on Wednesday, October 20 at 09:00

Joint Symposium 7 (EANM/EASD): My Foot is on Fire - Find the Hot Spot

OP-0255

Diabetic Foot Infections - Clinical Challenges for Diabetologists

F. Game; University Hospitals of Derby and Burton NHS Foundation Trust, Department of Diabetes and Endocrinology, Derby, UNITED KINGDOM.

OP-0256

Diabetic Foot Infections - Clinical Challenges for Radiologists

T. Kwee; University Medical Center Groeningen, Department of Radiology, Groningen, NETHERLANDS.

OP-0257

Diabetic Foot Infections - Clinical Challenges for Nuclear Medicine Physicians

C. Lauri; Sant'Andrea Hospital, Nuclear Medicine Unit, Department of Medical-Surgical Sciences and of Translational Medicine of "Sapienza" University, Rome, ITALY.

606

Wednesday, October 20 - Saturday, October 23, 2021

on-demand pool, release on Wednesday, October 20 at 09:00

Joint Symposium 8 (EANM/EULAR): PET/CT and PET/MRI in Patients with Autoimmune Disorders

OP-0259

Autoimmune Rheumatic Disorders - The Rheumatologist's Questions

R. Seror; Rheumatology Department, Université Paris Sud, Hôpitaux Universitaires Paris-Sud, Paris, FRANCE.

OP-0260

Autoimmune Paraneoplastic Syndromes - The Clinician's Point of View

Z. Szekanecz; Department of Rheumatology, University of Debrecen, Debrecen, HUNGARY.

OP-0261

The Current Role of FDG Imaging in Autoimmune Disorders

L. Leccisotti; Fondazione Policlinico Universitario Agostino Gemelli IRCCS, Nuclear Medicine Unit, Rome, ITALY.

OP-0262

The Role of Novel Radiotracers - FAPI Imaging in Systemic Sclerosis and IgG4-Related Disease

C. Schmidkonz; University Hospital Erlangen, Department of Nuclear Medicine, Erlangen, GERMANY.

607

Wednesday, October 20 - Saturday, October 23, 2021

on-demand pool, release on Wednesday, October 20 at 09:00

Pitfalls & Artefacts 4: Sentinel Lymph Node in Head & Neck, Penile and Gynaecological Cancers

OP-0264

Sentinel Lymph Node in Malignant Skin Melanoma

S. Balogová; Comenius University of Bratislava, St.Elisabeth Oncology Institute, Nuclear medicine, Bratislava, SLOVAKIA.

OP-0265

Sentinel Lymph Node in Head and Neck Cancers

R. A. Valdés Olmos; Leiden University Medical Centre, Radiology, Section of Nuclear Medicine & Interventional Molecular Imaging Laboratory, Leiden, NETHERLANDS.

OP-0266

Sentinel Lymph Node in Penile Carcinoma

O. Brouwer; Netherlands Cancer Institute, Department of Surgical Oncology (Urology), Amsterdam, NETHERLANDS.

OP-0267

Sentinel Lymph Node in Gynaecological Cancers

S. Vidal Sicart; Hospital Clínic Barcelona, Nuclear Medicine Dpt., Barcelona, SPAIN.

608

Wednesday, October 20 - Saturday, October 23, 2021

on-demand pool, release on Wednesday, October 20 at 09:00

M2M Track - Featured Session: Mapping Brain Structures

OP-0269

Evolution of Brain Mapping - From Bedside to Bench…

F. Mottaghy; Universitätsklinikum Aachen, Klinik für Nuklearmedizin, Aachen, GERMANY.

OP-0270

Preclinical Evaluation, Kinetic Modelling, And Assessment Of Test-Retest Reproducibility Of [^{18}F] Synvest-1 For PET Imaging Of Synaptic Vesicle Glycoprotein 2A

D. Bertoglio[1], J. Verhaeghe[1], F. Zajicek[1], S. De Lombaerde[1,2], A. Miranda[1], S. Stroobants[1,2], V. Khetarpal[3], M. Skinbjerg[3], C. Dominguez[3], Y. Wang[3], I. Munoz-Sanjuan[3], J. Bard[3], L. Liu[3], S. Staelens[1];

[1]University of Antwerp, Wilrijk, BELGIUM, [2]Antwerp University Hospital, Edegem, BELGIUM, [3]CHDI Management/CHDI Foundation, Los Angeles, CA, UNITED STATES OF AMERICA.

Aim/Introduction: The synaptic vesicle glycoprotein 2A (SV2A) is an essential vesicle transmembrane protein ubiquitously expressed in all synapses. Since synaptic pathology is associated with several neuropsychiatric and neurodegenerative disorders, PET imaging of SV2A[1,2] may provide a unique tool to assist in drug discovery and assessment of therapeutic response. This study aims to validate and characterize the novel clinically available radioligand [^{18}F]SynVesT-1[3] for preclinical application. **Materials and Methods:** Dynamic microPET/CT imaging was performed in adult (10-moth-old) male wild-type (wt) C57Bl/6J mice (n = 29). We performed a blocking study using the SV2A drug levetiracetam (50 or 200 mg/kg, i.p.) and estimated the receptor occupancy using Lassen plots. The use of an image-derived input function (IDIF) for noninvasive assessment of V_T, $V_{T\,(IDIF)}$, was validated against an arterial input function measured with an invasive arteriovenous (AV) shunt and using a population-based curve for radiometabolite correction. We further investigated the pharmacokinetic modelling, stability of the $V_{T\,(IDIF)}$ estimate, and the test-retest reproducibility of [^{18}F]SynVesT-1 in the mouse brain. Results: In vivo plasma availability of [^{18}F]SynVesT-1 decreased rapidly (22.4 ± 3.6% of the unchanged parent at 10 min p.i.). The two-tissue compartmental model (2TCM) was the best-fitted model and the Logan plot showed optimal agreement with 2TCM (r^2 = 0.99, $p<0.0001$). The noninvasive $V_{T\,(IDIF)}$ showed excellent agreement with the V_T based on the measured metabolite-corrected plasma input function (r^2 = 0.95, $p<0.0001$). Shortening the scan from 120-min down to 60-min did not affect the $V_{T\,(IDIF)}$ estimation (r^2 = 0.98, $p<0.0001$). Levetiracetam pretreatment (50 and 200 mg/kg i.p.) resulted in a complete blockade (97.4 ± 3.2% and 100.3 ± 1.3%, respectively, according to Lassen plots) of [^{18}F]SynVesT-1, confirming target engagement in a dose-dependent manner and extremely low non-displaceable binding (V_{ND}). No suitable reference region was observed in the mouse brain. Evaluation of test-retest reproducibility is currently ongoing. **Conclusion:** [^{18}F]SynVesT-1 selectively binds to SV2A with no suitable reference region in the mouse brain. By applying 2TCM or Logan plot with metabolite-corrected image-derived input function, SV2A density could be reliably estimated

noninvasively. [^{18}F]SynVesT-1 PET imaging offers a readily applicable high-throughput tool to assist in drug discovery and assessment of therapeutic response in neuropsychiatric and neurodegenerative disorders. **References:** 1 Finnema et al., Sci Transl Med, 2016; https://doi.org/10.1126/scitranslmed.aaf6667;2 Bertoglio et al., J Cereb Blood Flow Metab, 2020; https://doi.org/10.1177/0271678X19864081;3 Li et al., ACS Chem Neurosci, 2019; https://doi.org/10.1021/acschemneuro.8b00526.

OP-0271

Head-to-Head Comparison of beta-Amyloid-PET Quantification in PET, PET/CT and PET/MRI: Towards Small Animal Multicenter Studies

M. Koehler[1], K. Wind[1], C. Klaus[2], A. Zatcepin[1,2], L. Sebastian Monasor[2,3], J. Gnörich[1,2], L. Beyer[1], F. Eckenweber[1], M. Scheifele[1], F. Gildehaus[1], B. von Ungern-Sternberg[1], M. Patt[4], C. Haass[2,5,6], P. Bartenstein[1,6], J. Herms[2,6,7], S. Tahirovic[2], S. Ziegler[1], M. Brendel[1,2,6]; [1]Department of Nuclear Medicine, University Hospital of Munich, LMU Munich, Munich, GERMANY, [2]German Center for Neurodegenerative Diseases (DZNE) Munich, Munich, GERMANY, [3]Graduate School of Systemic Neuroscience, Ludwig-Maximilians-University Munich, Munich, GERMANY, [4]Department of Nuclear Medicine, University of Leipzig, Leipzig, GERMANY, [5]Chair of Metabolic Biochemistry, Biomedical Center (BMC), Faculty of Medicine, LMU Munich, Munich, GERMANY, [6]Munich Cluster for Systems Neurology (SyNergy), Munich, GERMANY, [7]Center of Neuropathology and Prion Research, University of Munich, Munich, GERMANY.

Aim/Introduction: β-amyloid (Aβ) small animal PET facilitates robust quantification of fibrillar amyloidosis in Alzheimer's disease (AD) mouse models. Thus, the methodology receives growing interest as a monitoring tool in preclinical drug trials. In this regard, harmonization of different scanners at multiple sites would allow establishing of joint normal cohorts and may facilitate efficacy comparison of different treatments. Therefore, we objected to determine the level of agreement of Aβ-PET quantification by a head-to-head comparison of three different state of the art μPET scanners, which could help pave the way for future multicenter studies. **Materials and Methods:** Within a timeframe of 5±2 weeks, transgenic APPPS1 (n=9) and wild-type (n=8) mice (age range: 13-16mo) were examined three times by Aβ-PET ([^{18}F]-florbetaben) using a Siemens Inveon DPET, a Mediso nanoScan PET/MR, and a Mediso nanoScan PET/CT with harmonized reconstruction protocols. Cortex-to-white-matter standardized uptake value ratios ($SUVR_{CTX/WM}$) were consistently calculated to compare percentage difference, effect sizes (Cohen's d) and z-score values relative to WT mice. Correlation coefficients (Pearson's r) were calculated for the agreement of individual SUVR between different scanners. Voxelwise analysis was used to determine the agreement of spatial pathology patterns. Results: All three μPET scanners yielded comparable group differences between TG and WT mice ($\%_{PETmean}$ = 20.4, $\%_{PET/MRmean}$ = 18.4, $\%_{PET/CTmean}$ = 18.1). Voxelwise analysis confirmed a high degree of congruency of the spatial pattern (Dice coefficient$_{PETvs.PET/MR}$ = 83.0%, $DC_{PETvs.PET/CT}$ = 69.3%, $DC_{PET/MRvs.PET/CT}$ = 81.9%). Noticeable differences in the group level variance of the three scanners resulted in divergent z-scores and effect sizes (d_{PET} = 8.47, $d_{PET/MR}$ = 4.57, $d_{PET/CT}$ = 4.14). However, correlations at the individual mouse level were still strong between scanners ($r_{PETvs.PET/MR}$ = 0.961, $r_{PETvs.PET/CT}$ = 0.912, $r_{PET/MRvs.PET/CT}$ = 0.867; all $p \leq 0.0001$). **Conclusion:** Our comparison of standardized small animal Aβ-PET acquired by three different scanners substantiates the possibility of moving towards a multicentric approach in preclinical AD research. The alignment of image acquisition and analysis methods achieved good overall comparability between data sets. Nevertheless, differences in variance of different scanners may limit data interpretation at the individual mouse level and deserves methodological optimization. **References:** none

OP-0272

Development and Translational Study of Novel Alpha-Synuclein PET Tracers

B. Uzuegbunam[1], W. Paslawski[2], H. Ågren[3], C. Halldin[2], D. Librizzi[4], W. Weber[1], M. Luster[4], T. Arzberger[5], B. H. Yousefi[4]; [1]Technical University of Munich, Munich, GERMANY, [2]Karolinska Institute, Stockholm, SWEDEN, [3]University of Uppsala, Uppsala, SWEDEN, [4]Philipps-University of Marburg, Marburg, GERMANY, [5]Ludwig-Maximilians-University of Munich, Munich, GERMANY.

Aim/Introduction: α-Synuclein aggregates (a-syn) imaging in the living brain would enable to diagnose and track the degree and location of α-synucleinopathies over time. We identified highly promising a-syn PET tracers based on 4,4'-diaryl-2,2'-bithiazole compounds (DABTA), showing very high binding affinity to α-syn fibrils (Ki as low as 0.5 nM) and high (> 100-fold) selectivity to a-syn versus Aβ and tau. Here, we report the results of studies including clinical translation research. **Materials and Methods:** Several DABTAs show high binding affinity for a-syn and high selectivity were ^{18}F-labeled. A combination of molecular dynamics and quantum/molecular mechanics approaches were applied to calculate the binding. Machine learning methods (MLM) were used to model the physiochemical properties and pharmacokinetics of the ligands. The ligands were further screened via experimental logD, binding assays, plasma stability, biodistribution, and brain metabolite analyses. Imaging with E46K a-syn mutation and controls using dynamic PET coregistered to a 7T-MRI and NHP PET were carried out. The in vivo stability and autoradiography using animal tissues were performed. Results: The rational design was based on binding sites revealed by in silico which helped characterize and evaluate the binding of the candidates. The DABTAs showed promising affinity based on these

calculations. The most promising second generation tracers [^{18}F]7 and [^{18}F]8 (log D 2.88 and 2.65 respectively) showed in biodistribution experiments in healthy mice initial brain uptakes of up to 7.3 %ID/g and 6.1 %ID/g. The latter showed a relatively faster brain washout 0.39% ID/g at 120 min p.i., with an affinity of 0.5 nM to our target, ~400-fold selectivity over Aβ and 870-fold selective over tau. The DABTAs showed almost no presence of brain radiometabolites at 20 min p.i., together with 72% plasma stability at the same time point in healthy mice. **Conclusion:** The optimization results hold promise and encourage us to further investigate the tracers towards imaging in humans. Furthermore, the revealed binding features from in silico modeling will facilitate the rational design of the tracers with desired properties. **References:** None

OP-0273

[^{18}F]MC225 PET for the dose-response assessment of tariquidar inhibition of blood-brain barrier P-glycoprotein function in vivo

L. Garcia-Varela[1,2], P. Mossel[1], P. Aguiar[2], D. A. Vazquez-Matias[1], A. van Waarde[1], A. T. Willemsen[1], A. L. Bartels[3], R. A. Dierckx[1], P. H. Elsinga[1], G. Luurtsema[1];
[1]University Medical Center of Groningen, Groningen, NETHERLANDS, [2]Department of Nuclear Medicine and Molecular Imaging Group, Clinical University Hospital, IDIS Health Research Institute, Santiago de Compostela, SPAIN, [3]Department of Neurology, University Medical Center Groningen, Groningen, NETHERLANDS.

Aim/Introduction: At the blood-brain barrier (BBB), P-glycoprotein (P-gp) is an efflux transporter that maintains homeostasis by protecting the brain from neurotoxic substances. BBB P-gp function may not be completely blocked but partially due to the effect of different Central-Nervous-System drugs or in patients with neurodegenerative diseases [1]. [^{18}F]MC225 is a weak P-gp substrate tracer that may show higher sensitivity to detect small changes in the P-gp function than previously developed P-gp tracers [2,3]. This study aims to explore the sensitivity of [^{18}F]MC225 to measure the effect of different doses of tariquidar (a P-gp inhibitor) and find the most appropriate fit to the dose-response curve. **Materials and Methods:** Twenty-three rats were divided into seven groups (n=3-4) and injected with different doses of tariquidar (0 (control), 0.75, 1.5, 3, 6, 8, and 12mg/kg). Tariquidar was administered intravenously 30 min before the PET acquisition with arterial sampling. Tissue and blood data were fitted to a 1-Tissue-Compartment-Model to obtain the kinetic parameters K_1 and V_T, which allow the estimation of the P-gp function [2]. Dose-response curve was fitted to different models using GraphPad Prism v6. ANOVA and post-hoc analyses were performed to explore the differences in K_1 and V_T among groups. Results: The best fit was obtained using the four-parameters sigmoidal curve. The IC_{50} was 2.18±0.27 mg/kg, the minimum K_1 value was 0.25 (0.15-0.36 95%CI) and the maximum K_1 value was 0.99 (0.90-1.08 95%CI), which was reached with a dose of 6mg/kg. K_1 values increased from 0.25±0.03 (control) to 0.39±0.14 in the 1.5mg/kg group, however, significant differences compared to controls were only found from a dose of 3 mg/kg on (K_1=0.82±0.16; p=0.001). Similar results were obtained using the V_T to estimate the P-gp function. **Conclusion:** The dose-response curve using either K_1 or V_T provided similar results. A tariquidar dose of 6mg/kg completely inhibited the P-gp function. A significant increase of K_1 values was detected at 3mg/kg dose and a trend to increase was already seen after 1.5mg/kg. This study shows that [^{18}F]MC225 seems an adequate tracer to measure small changes in the P-gp function in vivo and thus may be useful in Alzheimer and drug resistance studies where P-gp function can be partially altered. **References:** 1. Wanek T, et al. Mol Pharm. 2015;12:3214-252. Savolainen H, et al. J Cereb Blood Flow Metab. 2017;37:1286-983. Bauer M, et al. Clin Pharmacol Ther. 2019;105:1061-4

OP-0274

Longitudinal follow-up of APJ receptor expression by microPET/CT in a rodent model of cerebral ischemia-reperfusion

***O. Nachar**, N. Hugues, B. Louis, L. Balasse, V. Nail, A. Moyon, A. Bouhlel, G. Hache, F. Dignat-George, J. Laurin, P. Garrigue, B. Guillet; Aix-Marseille University, Marseille, FRANCE.*

Aim/Introduction: The Apelin/APJ system is a target of interest for angiogenesis-based monitoring and therapies in oncologic and cardiovascular diseases. During ischemic stroke, Apelin/APJ promotes neuroprotection and angiogenesis (1). The administration of apelin-13 during the hyper-acute phase of cerebral ischemia provides very early benefits in terms of neuronal survival and infarct size (2). An experimental PET radiotracer of APJ receptor expression, [^{68}Ga]Ga-AP747, was recently developed by our team and exhibited an early prognostic value and superiority over [^{68}Ga]Ga-RGD2 in a hindlimb ischemia mouse model. As the literature lacked data about APJ expression later than 1 day after cerebral ischemia, this study aimed at evaluating APJ expression using [^{68}Ga]Ga-AP747 microPET/CT up to 16 days after cerebral ischemia/reperfusion in middle-aged rats. **Materials and Methods:** A 1h-transient middle cerebral artery occlusion (MCAO) was induced in 350-400g female Sprague-Dawley rats (n=6) under 3% sevoflurane anesthesia. Neurological function was graded using the modified neurological severity score (mNSS) (3) and adhesive removal test (ART) on days 1, 7 and 14 post-MCAO. Animals were intravenously injected with 13.5±1.9 MBq/200µL of [^{68}Ga]Ga-AP747 on days 2,3,5,6,7,13 and 16 after MCAO (radiochemical purity: 98.54±0.71%). Blocking was performed using a 100-fold excess of APJ ligand (n=4). [^{68}Ga]Ga-RGD_2 microPET/CT

was performed on days 6,8,12,15 (n=3). MicroPET/CT images were acquired 120min after injection on a Mediso Nanoscan PET/CT under 2% isoflurane anesthesia. Quantitative region-of-interest (ROI) analysis of the PET images was performed using VivoQuant software and a rat brain atlas (4). [^{68}Ga]Ga-AP747 activity inside each ROI was quantified in cortex and caudate putamen and expressed as ipsilateral-to-contralateral (i/c) ratios. Results: Scoring with mNSS and ART confirmed the intensity of cerebral ischemia repercussion on neuromotor function ($mNSS_{day1}$=11.4±4.2; $mNSS_{day7}$=6.8±2.2; $mNSS_{day14}$=6.8±2.2; $ART_{i,Day1}$=5.8±2.2s, $ART_{c,Day1}$=51±46s). [^{68}Ga]Ga-AP747 microPET/CT highlighted the overexpression of APJ in the region of the infarct no later than 2 days after ischemia and sustained for at least 16 days. [^{68}Ga]Ga-AP747 i/c (166.25±24.95) significantly decreased after blocking in the same animal (107.25±8.46; **p=0.0021, n=4). [^{68}Ga]Ga-RGD_2 microPET/CT showed less i/c activity than [^{68}Ga]Ga-AP747 (*p=0,0458). **Conclusion:** To date, the literature suggested an overexpression of APJ limited to the short time-frame of hypercritic ischemia ending with reperfusion, and no study evaluated APJ expression later than 1 day after cerebral ischemia. This study provides interesting data at later time points underlying new treatment windows for Apelin that will need to be investigated in further experiments. **References:** (1) https://doi.org/10.3389/fneur.2020.00075 ; (2) https://doi.org/10.1016/j.jchemneu.2020.101886 ; (3) https://doi.org/10.1161/hs1101.098367 ; (4) https://bit.ly/3tdFGwR ;

OP-0275

Preclinical evaluation of [^{11}C]HSP990 for in vivo visualization of heat shock protein 90 (Hsp90) in brain with positron emission tomography (PET)

R. Cools[1], K. Vermeulen[2], C. Cawthorne[3], G. Bormans[1];
[1]Laboratory for Radiopharmaceutical Research, Department of Pharmacy and Pharmacological Sciences, KU Leuven, Leuven, BELGIUM, [2]SCK CEN Belgian Nuclear Research Centre, Mol, BELGIUM, [3]Nuclear Medicine & Molecular Imaging & MoSAIC, Department of Imaging & Pathology KU Leuven, Leuven, BELGIUM.

Aim/Introduction: The molecular chaperone, heat shock protein 90kDa, is a key player in the protein quality control system to maintain homeostasis upon stress conditions. An aberrant role of Hsp90 has been attributed to several neurodegenerative disorders, including Alzheimer's and Parkinson's disease. The development of a suitable Hsp90 PET probe can provide in vivo quantification of the expression levels of Hsp90 as a biomarker for diagnosis and follow-up of CNS disease progression. In this respect, the radiosynthesis of [^{11}C]HSP990 was developed and the tracer was evaluated as an Hsp90 PET probe. **Materials and Methods:** In vitro binding of [^{11}C]HSP990 to rodent brain tissue slices was evaluated using autoradiography. Binding specificity was assessed by co-incubation with HSP990, Onalespib, PU-H71 and SNX-0723. Ex vivo biodistribution and metabolization of [^{11}C]HSP990 was evaluated in healthy rodents at baseline conditions and after pre-treatment with Onalespib (30mg/kg), HSP990 (5mg/kg) and SNX-0723 (5mg/kg). In vivo brain uptake was assessed by dynamic µPET studies in rodents after combined pre-treatment with Onalespib (30mg/kg) and HSP990 (5mg/kg) or SNX-0723 (5mg/kg). Dynamic µPET brain scans with arterial blood sampling was performed in a rhesus monkey at baseline and blocking (HSP990, 1mg/kg) conditions. Results: In vitro [^{11}C]HSP990 binding was deemed Hsp90 specific by competition studies with Hsp90 inhibitors. Ex vivo biodistribution studies indicated saturable Hsp90 binding in brain, bone marrow, blood and blood rich organs in healthy rodents. Hsp90-specific binding was observed in the blood cell fraction. In combined pre-treatment and displacement µPET studies, reversible and Hsp90-specific binding of [^{11}C]HSP990 was observed in rat brain. Dynamic µPET brain scans in a rhesus monkey demonstrated high and sustained [^{11}C]HSP990 uptake in cortical brain regions. Arterial blood sampling confirmed the presence of a saturable Hsp90 binding pool in the blood cell fraction of a rhesus monkey. This saturable binding pool functions as a reservoir for Hsp90 inhibitors, which may substantially influence the pharmacokinetics and dynamics of Hsp90 inhibitors. The fraction of radio-metabolites accounted for only 10% of total plasma activity at 60 min post tracer injection. **Conclusion:** This study shows that despite the ubiquitous expression of Hsp90, saturable pools of Hsp90 inhibitor binding are present in blood, bone marrow and brain in healthy animals. PET with [^{11}C]HSP990 may allow to evaluate whether the amount of saturable Hsp90 in brain is different in patients with neurodegenerative disorders compared to age-matched controls to confirm the putative role of Hsp90 in these disorders. **References:** None

OP-0276

Upregulation of Sigma-1 receptor expression depends on the severity of ischemia: Based on the imaging study with the sigma-1 receptor imaging agent, I-125-OI5V

J. Taki[1], H. wakabayashi[1], H. Mori[1], T. Hiromasa[1], N. Akatani[1], K. Shiba[2], K. Ogawa[3], S. Kinuya[1];
[1]Kanazawa University Hospital, Kanazawa, JAPAN, [2]Kanazawa University, Advanced Science Research Center, Kanazawa, JAPAN, [3]Kanazawa University, Institute for Frontier Science Initiative, Kanazawa, JAPAN.

Aim/Introduction: Sigma receptor was first recognized as an opioid receptor subtype in the 1970s. One of the subtypes, sigma-1 receptor (Sig-1R) was first reported in the central nervous system and has been shown to relate many neurodegenerative diseases. The Sig-1R primarily resides at the endoplasmic reticulum (ER) membrane associated with mitochondria (MAM) as a molecular chaperon and functions based on interaction with various proteins and is also translocated to the plasma membrane when living system

is under abnormal state. We previously reported that serial expression of Sig-1R after myocardial ischemia using I-125-iodophenyl-piperidino-cyclopenntanon (OI5V); the uptake in area at risk peaked at day 3 after ischemia followed by gradual decline over 1 month. We aimed to explore how myocardial severity of ischemia affect spatiotemporal myocardial Sig-1R expression using I-125-OI5V. **Materials and Methods:** The left coronary artery (LCA) was occluded for 30, 20, 10-min and reperfusion was achieved. At 3 and 7 days after reperfusion, I-125- OI5V (1.5MBq), was injected at 30 min before sacrifice. Just before sacrifice, LCA was reoccluded and Tc-MIBI (150-180MBq) was injected to verify the area at risk. Then, the dual-tracer autoradiography of the left ventricular short axis slices was performed. The I-125-OI5V uptake ratios were calculated by dividing the count density in the area at risk by those of normally perfused area. Results: At day 3, intense uptake was observed in area at risk in 30 min LCA occlusion (1.89 ± 0.20) and the uptake reduced to 1.52 ± 0.17 at day 7. In 20 min ischemia, the uptakes at day 3 and 7 declined to 1.60 ± 0.15 and 1.30 ± 0.09, respectively. In 10 min ischemia, the uptakes further reduced to 1.34 ± 0.21 and 1.18± 0.16, respectively. **Conclusion:** Significant I-125 labeled OI5V uptake was observed in area at risk at day 3 and 7 by depending on the duration of the LCA occlusion. These results indicate that I-125 labeled OI5V is a promising tool for visualizing cardiac Sig-1R expression by depending on the severity of ischemic burden. **References:** none

OP-0277

Pharmacological characterization of [^{18}F]-FNM and evaluation of NMDA receptors activation in rat brain injury model

M. Beaurain[1], F. Talmont[2], D. Pierre[3], S. Boucher[1], P. Payoux[1], A. Salabert[1];
[1]Toulouse Neuroimaging Center (ToNIC, Inserm UMR1214), Toulouse, FRANCE, [2]Institut de Pharmacologie et de Biologie Structurale (IPBS, CNRS), Toulouse, FRANCE, [3]CHU de Toulouse, Toulouse, FRANCE.

Aim/Introduction: NMDA receptors (NMDARs) dysfunction seems to play a central role in physiopathology of psychiatric and neurodegenerative disorders, but this role is still poorly understood. The development of a PET tracer able to selectively bind the NMDARs intra-channel PCP site may make it possible to visualize NMDARs in an open and active state. In this study, we describe in vitro pharmacological characterization (affinity and selectivity) of [^{18}F]-fluoroethylnormemantine ([^{18}F]-FNM), and evaluate its ability to localize activated NMDA receptors in a rat preclinical model. **Materials and Methods:** The affinity of the non-radioactive analog, [^{19}F]-FNM, for the intra-channel PCP site was determined in a radioligand competition assay using [^{3}H]-TCP (N-(1-[2-thienyl]-cyclohexyl)-3,4-[3H] piperidine) on mice and rats brain homogenates. Selectivity was also investigated by the same method with specific radioligands targeting NMDARs glycine site, AMPA, opioid, and dopaminergic receptors. We performed, in vivo, brain lesions using stereotaxic quinolinic acid injections in the left motor area (M1) of seven Sprague Dawley rats. Each rat was imaged on a microPET/CT camera 40 minutes after receiving a dose of 30 MBq +/-20 of [^{18}F]-FNM, 24 and 72 hours after injury. Nine non-injured rats (control rats) were also imaged using the same protocol. A descriptive voxel-wise analysis with SPM software was performed in order to determine a Z-score map between injured rats and controls. Results: In rats, using the [^{3}H]-TCP binding assay, FNM displayed Ki values of 35,38 ± 4,58 µM and 55,13 ± 10,04 µM in hippocampus and frontal cortex homogenates, respectively. FNM also showed significant bindings on NMDARs glycine site, and opioid receptors, but no interaction with AMPA and dopaminergic receptors were detected. The average of [^{18}F]-FNM uptake in motor cortex of control rats and in controlateral cortex of injured rats was homogeneous. 24 hours after injury, -1.5 Z-score into the lesion, and 6 in the peri-lesioned area were determined. 72 hours after injury, we observed Z-scores 3 into the lesion, and 0 into the peri-lesioned area. **Conclusion:** In vitro pharmacological characterization is an essential step into the development of molecular imaging probes. These assays considerably improved the interpretation of preclinical in vivo images especially in the case of a multispecific probe as [^{18}F]-FNM. In this study, they support the ability of this tracer to track the variation of NMDARs activation chronologically and topographically. **References:** Evaluation of [18F]FNM biodistribution and dosimetry based on whole-body PET imaging of rats. Salabert et al. Nucl Med Biol. 2017 Dec 21;59:1-8.

OP-0278

Measuring histamine H3 receptor occupancy of the experimental anti-Parkinson drug AG0029, using [^{11}C] GSK-189254 and PET

N. Ghazanfari[1], A. van Waarde[1], J. Sijbesma[1], J. Doorduin[1], D. Vallez-Garcia[1], M. Kominia[1], M. Koelewijn[2], K. Attia[1], T. J. Visser[2], A. Heeres[2], A. T. Willemsen[1], E. F. de Vries[1], R. A. Dierckx[1], P. H. Elsinga[1];
[1]UMCG, Groningen, NETHERLANDS, [2]Symeres, Groningen, NETHERLANDS.

Aim/Introduction: Inadequacies of currently designed drugs in treating neurodegenerative disorders have promoted efforts to develop novel drugs interacting with multiple targets. As part of a collaborative drug discovery program, AG-0029 was developed. This compound has agonist affinity to dopamine (0.08 nM) and antagonist affinity (111 nM) to histamine H3 receptors and may enhance both the motor and cognitive symptoms of Parkinson's disease. Previously, we reported on the occupancy of dopamine D2/D3 receptors in the rodent brain by AG0029 [1]. In the present study, we aimed to quantitatively assess the engagement of AG-0029

with cerebral histamine H3 receptors, using PET. **Materials and Methods:** Two dynamic PET scans of 60 min with arterial blood sampling were made in 12 healthy male Wistar rats (body weight 373±32 g), at a one-week interval, using 49±8 MBq of the histamine H3 receptor ligand [^{11}C]GSK-189254. The animals were first scanned at baseline and subsequently after administration of either 1 or 10 mg/kg of AG-0029 in saline (i.v., 5 min before tracer injection, n=6 for each drug dose). Results: In baseline scans, the regional distribution of the tracer corresponded to the known distribution of histamine H3 receptors in the rodent brain. Considerable uptake was noticed in frontal-cortex and olfactory-bulb, and low uptake in occipital-cortex and cerebellum. A region-of-interest was manually drawn around the frontal areas with high uptake and a standard elliptical ROI was placed in the cerebellum. Tracer uptake in the cerebellum was not significantly affected by drug pretreatment, in contrast to uptake in the frontal target regions. Frontal-to-cerebellum ratios of radioactivity minus one were plotted as a function of time. The maximum of this curve is an estimation of tracer binding potential (BP). BP values were not reduced after pretreatment with 1 mg/kg AG-0029 (from 2.03±0.24 to 1.97±0.20) but were significantly reduced by 10 mg/kg of the test drug (to 1.33±0.22). Calculated H3 receptor occupancies were 3±10 and 34±11%, respectively. The tracer was slowly metabolized and tracer metabolism was not significantly affected by drug pretreatment. At 62±9 min after injection, 50% of the plasma radioactivity still represented parent compound. Preliminary data analysis using a simplified reference tissue model fit showed the same trends as the ratio method. **Conclusion:** Our PET data indicated negligible histamine H3 receptor occupancy after administration of 1 mg/kg, but considerable (34%) occupancy after administration of 10 mg/kg AG-0029. **References:** A. van Waarde, EJNMM, vol. 47, no. Suppl. 1, p. S114, 2020.

OP-0279

Early detection of Amyloid-β pathology via ^{89}Zr-DFO*-Immuno-PET with a novel bispecific monoclonal antibody

N. Stergiou[1], T. Wünsche[1], M. Schreurs[1], I. Mes[1], M. Verlaan[1], E. Kooijman[1], A. Windhorst[1], G. van Dongen[1], L. Helboe[2], S. Vergo[2], S. Christensen[2], A. Asuni[2], A. Jensen[2], B. Bang-Andersen[2], D. Vugts[1], W. Beaino[1];

[1]Amsterdam UMC, Vrije Universiteit Amsterdam, Radiology & Nuclear Medicine, Amsterdam, NETHERLANDS, [2]H. Lundbeck A/S, Nykøbing Sjælland, DENMARK.

Aim/Introduction: New developments in the treatment of Alzheimer Disease (AD) focus on antibodies targeting amyloid-β; (Aβ). To increase the brain uptake of antibodies, the transferrin receptor 1 (TfR1) shuttling mechanism has been used. Immuno-PET with ^{89}Zr-labelled antibodies poses the opportunity to be a powerful tool to quantify brain uptake. We have labelled an aducanumab-based bispecific antibody, Abeta-mAb-scFab8D3 targeting Aβ as well as TfR1, with ^{89}Zr for immuno-PET imaging. The aim was to study the brain uptake of [^{89}Zr]Zr-DFO*-NCS-Abeta-mAb-scFab8D3 in a preclinical model of AD to assess TfR1 saturation and the potential of detecting different Aβ plaque load as function of age. **Materials and Methods:** Abeta-mAb-scFab8D3, monospecific Abeta-mAb and nonspecific control B12-mAb-scFab8D3 were modified with DFO*-NCS and subsequently labelled with ^{89}Zr. Ten months old APP/PS1 transgenic mice were intravenously (i.v.) injected with different antibody doses (30, 100, 200, and 400 micrograms; 5 MBq/mouse). Blood kinetics were determined up to 7 days post-injection (p.i.). In order to correlate the brain uptake of [^{89}Zr]Zr-DFO*-NCS-Abeta-mAb-scFab8D3 with different Aβ plaque loads, we compared the uptake in 3-, 7- and 10-months old APP/PS1 transgenic mice and age matched wild type (WT) littermates (i.v., 30 micrograms; 5 MBq/mouse). For both studies PET imaging was acquired at day 7 p.i. and followed by ex vivo biodistribution, ex vivo autoradiography and immunofluorescence staining to confirm antibody accumulation and target engagement in the brain. Results: [^{89}Zr]Zr-DFO*-NCS-Abeta-mAb-scFab8D3 showed high brain uptake (1.8 % ID/g) in 10- months old APP/PS1 transgenic mice, while the monospecific control [^{89}Zr]Zr-DFO*-NCS-Abeta-mAb (0.4% ID/g) and the bispecific isotype control [^{89}Zr]Zr-DFO*-NCS-B12-mAb-scFab8D3 (0.6% ID/g) showed low brain uptake, which was at the same low level of brain uptake as [^{89}Zr]Zr-DFO*-NCS-Abeta-mAb-scFab8D3 in WT littermates (0.7% ID/g). Saturation of the TfR1 binding with increased antibody doses resulted in gradually lower brain uptake until 0.6% ID/g for the highest dose of 400 micrograms which was as low as for the isotype control. Already in 3- months old APP/PS1 mice with low Aβ plaque load, higher uptake of [^{89}Zr]Zr-DFO*-NCS-Abeta-mAb-scFab8D3 was clearly detectable (1.7% ID/g) in comparison to WT littermates (1.2% ID/g). The ratio of specific uptake in APP/PS1 mice to nonspecific uptake in WT littermates increased with older age/higher plaque load respectively. **Conclusion:** [^{89}Zr]Zr-DFO*-NCS-Abeta-mAb-scFab8D3 revealed high and specific uptake in the APP/PS1 mice brain and can be used for the detection of Aβ plaque pathology. Moreover, brain shuttling via the TfR1 represents a viable option to deliver antibodies into the brain. **References:** none

609

Wednesday, October 20 - Saturday, October 23, 2021

on-demand pool, release on Wednesday, October 20 at 09:00

Cutting Edge Science Track - TROP Session: Clinical Dosimetry and Radioembolisation

OP-0281

Preliminary results of INSPIRE clinical dosimetry study

C. Abreu[1], L. Carnegie-Peake[1], J. Taprogge[1], P. Gape[1], D. Rushforth[1], C. Barker[1], A. Divoli[1], J. Gear[1], L. McAreavey[1], I. Murray[1], B. Pratt[1], B. Rojas[1], L. Vavrova[1], K. Wong[2], K. Newbold[2], G. Flux[1];
[1]Joint Department of Physics, Royal Marsden NHS Foundation Trust and Institute of Cancer Research, London, UNITED KINGDOM, [2]Head and Neck Oncology Unit, Royal Marsden NHS Foundation Trust, London, UNITED KINGDOM.

Aim/Introduction: Investigating National Solutions for Personalised Iodine-131 Radiation Exposure (INSPIRE, ClinicalTrials.gov Identifier: NCT04391244) forms part of a concurrent series of multi-centre clinical trials within Work Package 3 of MEDIRAD. The aim of INSPIRE and Work Package 3 is to determine a threshold absorbed dose required to ensure a successful outcome for radioiodine therapy following thyroidectomy. Furthermore, the range of radiation doses delivered to organs-at-risk and other healthy organs will be established to better inform risk estimates from radioiodine therapy. **Materials and Methods:** Patients that are recruited to the study will undergo a series of SPECT/CT, SPECT-only and whole-body scans to quantify the radioiodine activity retained in thyroid remnant and normal tissues at a single or multiple time points following the administration of Iodine-131. Radiation dosimetry of thyroid remnant is performed using maximum voxel dosimetry following the MIRD formalism. Maximum voxel dosimetry is used to avoid issues owing to volume delineation. Normal tissues dosimetry is performed using an in-house developed 3D voxel dosimetry package, DoDose, which uses a dose-point kernel for electrons only. For single scan patients, time integrated activities were obtained assuming population half-lives. Results: Dosimetry results for twenty-one patients participating in the INSPIRE trial from single time and multiple time point scans showed a range of maximum absorbed doses to the thyroid remnants from 0.2 to 27.5 Gy. Whole-body, lung and bone absorbed doses were < 0.1 Gy for all patients. **Conclusion:** INSPIRE clinical dosimetry study aims to recruit a total of 50 patients at the Royal Marsden NHS Foundation Trust. Preliminary results from the study suggest a broad range of absorbed doses to the thyroid remnant. Additionally, the relationship between absorbed doses delivered and treatment success will be investigated. **References:** none

OP-0282

Therapy with ^{177}Lu-DOTATATE: correlation between relative platelets reduction and image based bone marrow low absorbed dose

S. Mazzaglia, G. Argiroffi, V. Fuoco, M. Maccauro, E. Seregni, A. Lorenzoni, G. Aliberti, M. Kirienko, C. Chiesa;
IRCCS Istituto Nazionale Tumori, Milan, ITALY.

Aim/Introduction: During the sequence of administrations with ^{177}Lu-DOTATATE, in rare cases the limiting organ is the bone marrow (BM). This work aims to study the still unclear correlation between the blood count reduction and the BM absorbed dose (BMAD) after the first administration. **Materials and Methods:** We studied the hemochrome after the first administration of 25 patients treated according to the radiopharmaceutical indication. The relative reduction and absolute clinical toxicity according to CTCAE of platelets (PLT) and white blood cells (WBC) were considered. Two risk factors were considered, in addition to BMAD: chemotherapy before PRRT and different glomerular filtration rate (GFR) reduction after the first therapeutic administration. Two SPECT/CT scans were taken at 20±1 and 147±37 hours p.i. BM dosimetry was based on a VOI drawn on the body of lumbar vertebrae L2-L3-L4. OLINDA1.1 calculation considered all the source organs. The total BM residence time was obtained considering a fraction of 6.7 % in the VOI. Individual BM mass was calculated with a linear scaling of the VOI with respect to standard 70 mL. The count reduction at nadir was considered at 20% and 30% for PLT, while 30% and 40% for WBC. Dose-reduction correlation was studied. Patients were grouped in two classes, according to reduction above/below the threshold. Mann-Whitney test and AUC-ROC analysis were performed. The best BM dose cut-off corresponding to maximum sum of sensitivity plus specificity was determined. The association between BMAD and PLT reduction was studied. Results: PLT/WBC nadir occurred 5.6±2/6.9±2 weeks p.i. respectively. Dose-reduction correlation was statistically significant for PLT with r=0.43, p=0.03. The difference between median BM doses of the group with PLT reduction <30% (21 patients) and reduction >30% (4 patients) was statistically significant at Mann-Whitney test (0.10 Gy vs 0.25 Gy, p=0.02). AUC was 0.88±0.08 (p=0.02). The BM dose optimal cut-off to predict reduction >30% for PLT was 0.13 Gy, with sensitivity=100%, specificity=71%. Using this value, PLT reduction >30% was associated with BM dose (p=0.016). No statistical significance was obtained considering absolute clinical toxicity for PLT (9/25 patient with G1). No association of PLT relative reduction with previous chemo or GRF reduction was observed. For WBC, no significance was obtained. No association between blood count reduction and previous chemotherapy nor GFR reduction was found. **Conclusion:** BMAD>0.13 Gy was associated with PLT relative reduction at nadir >30% after the first PRRT administration. Absolute toxicity should not be considered in similar studies. **References:** none

OP-0283

Global Tumour Absorbed Dose Heterogeneity for Patients Treated with 177-Lilotomab Satetraxetan

J. Blakkisrud[1,2], A. Løndalen[1,3], J. Dahle[4], A. Kolstad[5], C. Stokke[1,2]; [1]Division of Radiology and Nuclear Medicine, Oslo University Hospital, Oslo, NORWAY, [2]Department of Physics, University of Oslo, Oslo, NORWAY, [3]Faculty of Medicine, University of Oslo, Oslo, NORWAY, [4]Nordic Nanovector ASA, Oslo, NORWAY, [5]Department of Oncology, Oslo University Hospital, Oslo, NORWAY.

Aim/Introduction: 177-Lu-lilotomab satetraxetan is a radioimmunoconjugate currently undergoing clinical trials to treat patients with indolent non-Hodgkin B-cell lymphoma. Cumulative dose voxel histograms (cDVH) can be used to assess the distribution of absorbed dose. In the current work we aimed to investigate the relationship between cDVH parameters for tumour tissue and clinical response. **Materials and Methods:** Fourteen patients with indolent non-Hodgkin lymphoma from the phase 1/2a LYMRIT37-01 trial injected with 177-Lu-lilotomab satetraxetan (median 1362, range 756-2189 MBq) and subjected to post-therapy SPECT/CT imaging were included. Manual masking of physiological uptake and a global threshold previously found for this patient group was used to segment tumour regions. Absorbed dose rate maps were derived from SPECT/CT-images acquired 96 hours post injection. A patient-averaged effective half-life calculated from the total activity in the tumours 96 and 168 hours post injection was used to form dose maps. The D98 and D02, the minimum absorbed dose covering 98 and 2 percent of the patient total tumour tissue respectively was calculated. A heterogeneity index (HI) defined as (D02-D98)/D50 was also found. An analysis performed on individual tumour volumes, defined as connected regions in the tumour mask, where the relative difference between minimum and maximum D50-absorbed dose, to measure intra-patient variation. Patients were grouped into complete and partial responders (CR+PR), and stable disease and progressive disease (SD+PD). Spearman rank was used to test correlation between D98, D02 and D50-values and the Mann-Whitney-U-test was used to test differences between groups. Results: Patient global D98-absorbed doses ranged from 0.26 to 2.60 Gy. The patient global D02-values ranged from 0.85 to 8.41 Gy. There was a higher patient global D98-absorbed dose for the CR+PR-group (median 0.87, range 0.26-2.62 Gy) compared to the SD+PD-group (median 0.55, range 0.32-1.37 Gy) but this difference was not significant ($p = 0.25$). There were strong correlations between the DVH-parameters (rho 0.95-0.97, $p<10\text{-}7$). The HI did not differ between the two groups, median HI (ranges) were 1.50 (1.10-1.60) and 1.40 (1.04-1.76) for the CR+PR and SD+PD-group respectively. The number of tumour regions in the patients varied from a single region to 23 regions. Intra-patient relative difference in D50-values ranged from 30 to 140 %. **Conclusion:** Estimated cDVH-parameters calculated from global threshold segmented tumour regions from post therapy SPECT/CT-images proved insufficient to explain differences between clinical response for patients treated with 177-Lu-lilotomab satetraxetan. Possible future directions encompass incorporation of baseline FDG-PET/CT-information to define tumour anatomy. **References:** None

OP-0284

Clinical dosimetry study of kidney absorbed radiation doses for [^{177}Lu]Lu-PSMA-617 and [^{177}Lu]Lu-PSMA-I&T

***M. Uijen**, B. Privé, C. van Herpen, M. Gotthardt, M. Konijnenberg, S. Peters, J. Nagarajah;*
Radboudumc, Nijmegen, NETHERLANDS.

Aim/Introduction: Prostate specific membrane antigen (PSMA) targeted radionuclide therapy is a promising treatment modality in prostate cancer. [177Lu]Lu-PSMA-617 and [177Lu]Lu-PSMA-I&T are the most often used compounds in clinical trials or compassionate use programs. Results from preclinical studies revealed around 30 times higher kidney absorbed dose for [177Lu]Lu-PSMA-I&T compared to [177Lu]Lu-PSMA-617, which may lead to an increased risk of kidney toxicity in patients treated with [177Lu]Lu-PSMA-I&T. We performed dosimetry in patients from two different prospective clinical trials treated with [177Lu]Lu-PSMA-617 or [177Lu]Lu-PSMA-I&T, using exactly the same dosimetry protocol in a single center. **Materials and Methods:** Ten low volume hormone-sensitive metastatic prostate cancer patients (mHSPC) were treated with a total activity of 9 GBq [177Lu]Lu-PSMA-617 in two cycles (NCT03828838). Six recurrent or metastatic salivary gland cancer (R/M SGC) patients, four female and two male, were treated with 2-4 cycles of 7.4 GBq [177Lu]Lu-PSMA-I&T (NCT04291300). Whole-body scans and SPECT/CT imaging of the kidneys were performed at 5 time points (1h, 24h, 48h, 72h, and 168h post injection) for both studies with identical scanning parameters. In mHSPC patients SPECT/CT imaging was performed after both cycles and in SGC patients only after the first cycle. Kidney absorbed dose (Gy/GBq) was calculated by organ-based dosimetry using commercial software (Olinda 2.1, Hermes). A Wilcoxon-Mann-Whitney test was used to test for difference in kidney absorbed dose between [177Lu]Lu-PSMA-617 and [177Lu]Lu-PSMA-I&T. Results: All sixteen patients had an adequate kidney function (creatinine clearance ≥50 mL/min). Median kidney absorbed dose was 0.49 Gy/GBq (range: 0.34-0.66) in mHSPC patients treated with [177Lu]Lu-PSMA-617. Median kidney absorbed dose was 0.73 Gy/GBq (range: 0.42-0.89) in R/M SGC patients treated with [177Lu]Lu-PSMA-I&T. The difference in absorbed dose between [177Lu]Lu-PSMA-617 and [177Lu]Lu-PSMA-I&T showed to be statistically significant ($p=0.023$). **Conclusion:** This study reveals a statistically significant difference in kidney absorbed dose between [177Lu]Lu-PSMA-617 and

[177Lu]Lu-PSMA-I&T. The median kidney absorbed dose for [177Lu]Lu-PSMA-I&T was approximately 1.5 times higher than for [177Lu]Lu-PSMA-617. The individual variation of the kidney absorbed dose was for both ligands 65%. These results should be interpreted with caution, as this is based on different patient populations and tumor loads. Yet, other relevant dosimetry factors (e.g. imaging time points, SPECT scanner, dosimetry software) were the same for both groups. Overall, the difference of kidney radiation doses in the clinical setting is considerably lower than published preclinical results suggest. **References:** none

OP-0285

Dose volume histogram comparison between pre-treatment ^{99m}Tc-MAA SPECT/CT and post treatment ^{90}Y PET/CT voxel-based dosimetry with rigid and deformable contour registration algorithms in radioembolization with resin ^{90}Y microspheres

G. Della Gala[1], M. Santoro[1], G. Paolani[1], S. Strolin[1], E. Lodi Rizzini[2], A. Cappelli[3], C. Mosconi[3], L. Calderoni[4], A. Morganti[2], S. Fanti[4], R. Golfieri[3], L. Strigari[1];

[1]Medical Physics Department IRCCS Azienda Ospedaliera Universitaria di Bologna, Bologna, ITALY, [2]Radiation Oncology Center, Department of Experimental, Diagnostic and Specialty Medicine, IRCCS Azienda Ospedaliera Universitaria di Bologna, Bologna, ITALY, [3]Radiology Unit, Department of Experimental, Diagnostic, and Specialty Medicine, IRCCS Azienda Ospedaliera Universitaria di Bologna, Bologna, ITALY, [4]Department of Nuclear Medicine, IRCCS Azienda Ospedaliera Universitaria di Bologna, Bologna, ITALY.

Aim/Introduction: Transarterial radioembolization with ^{90}Y-loaded resin microspheres is used to treat hepatic lesions where surgery is considered not feasible. Prior to the treatment, ^{99m}Tc macroaggregated albumin (99mTc-MAA) are injected to simulate the treatment using the SPECT/CT. In this study, voxel-based dosimetry is performed on both ^{99m}Tc-MAA SPECT/CT and ^{90}Y-PET/CT with Bayesian penalized likelihood (BPL) reconstruction to evaluate the agreement between the predicted and the administered dose distributions in terms of mean dose and dose volume histograms (DVHs), comparing two (i.e. rigid and deformable) image fusion methods. **Materials and Methods:** 79 patients consecutively underwent dosimetric planning and therapy up to March 2021. All patients underwent SPECT/CT imaging within 2 hours after the administration of 370 MBq of ^{99m}Tc-MAA in the arteries supplying blood to the tumor. Within 2 weeks they underwent radioembolization and, the day after, ^{90}Y PET/CT imaging. Liver, tumor and non-tumoral liver (NTL) were delineated by a multidisciplinary team on multiphasic CT and SPECT/CT images. The pre-therapy dosimetry was performed using the local deposition method (LDM). The post-treatment dose distribution was calculated on the BPL-reconstructed PET/CT images using LDM and two workflows employing either rigid or deformable registration to transfer on the PET/CT images the delineated contours. The Wilcoxon test was used to compare pre-therapy and post-therapy DVH at several dose-points and overall mean doses to tumor and NTL. Correlation was tested with Pearson's coefficient. Results: Overall, mean doses to NTL and tumor in pre- and post-therapy dosimetry with rigid contour registration were comparable (14.9 vs 13.8 Gy and 116.4 vs 101.9 Gy, respectively), as well as V_{50Gy} (75.8% vs 76.1%) and V_{100Gy} (47.1% vs 43.3%) in tumor and V_{20Gy} (17.6% vs 19.3%) and V_{40Gy} (10.1% vs 9.9%) in NTL (all $p>0.05$). All dosimetric data showed significant correlation (e.g., tumor mean dose 0.74, $p<0.01$; NTL mean dose 0.83, $p<0.01$). Deformable registration showed poorer performance, resulting in a lower post-therapy tumor mean dose ($p<0.05$), probably due to the increase of transferred volumes (about 14%) using the deformable approach. **Conclusion:** Pre-therapy dosimetry showed predictive capability towards post-therapy dose distribution. Rigid contour registration approach was more robust in terms of tumor mean dose. **References:** none

OP-0286

Dosimetric comparison between planning SPECT and monitoring PET for ^{90}Y-radioembolisation

J. Labour, T. Baudier, S. Parisse-Di Martino, F. Khayi, D. Sarrut, J. Badel;

Centre Léon Bérard, Université de Lyon; CREATIS; CNRS UMR5220; Inserm U1044; INSA-Lyon; Université Lyon 1, Lyon, FRANCE.

Aim/Introduction: This study analysed different workflows to compare dosimetry computed from SPECT ^{99m}Tc-MAA images and PET treatment monitoring images following ^{90}Y-radioembolisation. **Materials and Methods:** A cohort of 20 patients is currently being studied. For each patient, ^{99m}Tc-MAA SPECT/CT images were acquired, reconstructed with attenuation- and diffusion-corrections, and calibrated in MBq.mL^{-1}. Treatment monitoring was performed with a digital PET/CT using reconstruction parameters [1] optimised with dose-volume histograms (DVHs). The whole liver (WL) and total tumour (T_{total}) were contoured on the CT acquired during the workup session and propagated to the SPECT images. The perfused liver volume (PLV) was defined using a 5% threshold on the SPECT. Contours were propagated to PET images with four registration methods, $rigid_{global}$, $deformable_{global}$, $rigid_{local}$ and $rigid_{local,functional}$. The two firsts consider CT (SPECT) to CT (PET) rigid/deformable (BSpline) transformations. The third uses a rigid transformation between the two CTs, centred on the liver only. The last one considers rigid local registration between SPECT and PET images with a rigid local transformation centred on the liver. Absorbed dose distributions were calculated using Voxel S-values convolution. The predictive and treatment follow-up DVHs were compared using the mean absorbed dose (D_{mean}) and absorbed dose at 2% volume ($D_{2\%}$). Results: For

the first patients, D_{mean} were within 5.4% and 6.4% and D2% were within 2.0% and 2.1% for the WL and PLV whatever the registration method, respectively. However, for T_{total}, the range was larger. For example, for patient #3, the SPECT-predicted D_{mean} was 125.4 Gy while it was 39.07, 43.6, 30.7 and 168.3 Gy from the PET images for all methods, respectively. In that case, only locally rigid registration between functional images (SPECT and PET) instead of CT images provided comparable DVHs. This might be due to inaccurate location of the lesions due to respiratory motion and internal organ movements between workup and treatment sessions. Even if liver CT contours were well registered, the activity measured from SPECT and PET, integrated over a longer acquisition duration than CT (12.5 min/bed for SPECT, 10 min/bed for PET) mismatched. **Conclusion:** $rigid_{local,functional}$ method is recommended in addition to other CT registration methods to propagate contours from SPECT/CT to PET/CT. The analysis on the entire cohort will be presented at the conference. **References:** [1] Labour, J. et al. "Yttrium-90 Quantitative Phantom Study Using Digital Photon Counting PET." EJNMMI Physics, in revision, (2021).

OP-0287

The Impact of an Optimised Methodology of Lung Shunt Fraction Estimation in Planar ^{99m}Tc-MAA Imaging on Prescribed Activity and Estimated Doses to Liver and Lungs for ^{90}Y SIRT Treatments

N. McArdle[1], S. Cournane[1,2], J. McCavana[1], J. Lucey[1], L. León Vintró[2]; [1]St Vincent's University Hospital, Dublin, IRELAND, [2]University College Dublin, Dublin, IRELAND.

Aim/Introduction: ^{90}Y Selective internal radiation therapy (SIRT) is planned using ^{99m}Tc-macroaggregated albumin (^{99m}Tc-MAA) imaging. Extra-hepatic uptake is assessed and the lung shunt fraction (LSF) is quantified. The LSF is utilised in the calculation of the therapeutic activity. While it is recommended that the LSF is estimated using the geometric mean of counts from liver and lung planar images, this methodology employs a simplified inherent attenuation correction and neglects contribution from scattered radiation. The objective of this study was to correct for these limitations, assessing the impact this would have on the prescribed ^{90}Y activity and estimated doses to liver and lungs. **Materials and Methods:** An anthropomorphic thorax phantom with fillable and removable organs was used to simulate a number of known LSFs. Planar scintigraphy images were acquired using a number of scatter windows, allowing for spectral analysis. Attenuation of the overlying tissue was determined through CT measurements. Subsequently, the liver and lung phantom organs were imaged with and without the overlying attenuation material. Scatter ratios between lung and liver counts for the known LSFs were used to determine the effect of scatter contributions from each organ. The uncertainties associated with scatter, as well as the attenuation and scatter contributions from the liver were evaluated for each case and corrected for in the LSF calculation. This optimised calculation was then applied to patient data. Results: The percentage overestimation of the geometric mean method when compared to the known LSF values (0 - 25%) was up to 45%. Using scatter correction, the accuracy of the LSF in the clinically-relevant range (3-15%) improved, although the mean overestimation was 20%. To further improve the LSF accuracy, an optimum scatter window selection and more robust attenuation correction will be further investigated and presented. **Conclusion:** This work presents a simple process, applicable in any imaging centre, employing CT and planar imaging data to more accurately estimate the LSF. In patient and phantom studies, we observed a percentage overestimation in LSF estimation greater than 150%. By implementing our optimised methodology, the lung dose was estimated to be a third of that estimated by standard empirical methods, with the prescribed activity reduced by up to 4%. Although there are minimal changes in the prescribed activity, dose to the lungs is greatly overestimated. This revised methodology facilitates improved accuracy in the dosimetry estimation and a more optimised prescribed patient therapy dose. **References:** None

OP-0288

Comparison of Two ^{90}Y-charged Glass Microspheres Liver Radioembolisation Dosimetry Methods: Voxel S-values and Monte Carlo - GATE

M. Ribeiro[1,2], P. Ferreira[1], F. P. Oliveira[1], J. Cruz[2], D. C. Costa[1]; [1]Champalimaud Centre for the Unknown, Champalimaud Foundation, Lisboa, PORTUGAL, [2]NOVA School of Science and Technology, Almada, PORTUGAL.

Aim/Introduction: Personalized dosimetry is paramount in treatment planning and verification of ^{90}Y-glass microspheres ([^{90}Y]-GMS) liver radioembolisation. The voxel S-values (VSV) method accomplishes clinical dosimetry but neglects tissue heterogeneities. GATE is a Monte Carlo (MC) code capable to perform dosimetry calculations based on medical images, addressing patient-specific tissue heterogeneities. This study aims to compare 3D absorbed dose maps obtained from the VSV method and MC-GATE simulations. **Materials and Methods:** In this preliminary study, non-hybrid [^{99m}Tc]-MAA SPECT and CT planning images, and hybrid [^{90}Y]-GMS PET/CT treatment verification images from three patients were retrospectively selected. A clinical expert segmented the total liver, the planning tumour volume (PTV), and the normal liver volume (NLV) for each patient based on the CT. Yttrium-90 3D absorbed dose maps were estimated using the VSV method and MC-GATE simulation, assuming a distribution pattern identical to the SPECT and PET acquired images. The total administered activity was used to scale the absorbed dose maps in the field of view. Within each PTV and NLV regions of interest (ROI), the mean, median, maximum, and standard deviation absorbed dose maps were compared using the

intraclass correlation coefficient (ICC) and relative difference (RD). Dose maps were also compared using dose-volume histograms (DVH). The MC was considered as the reference method. Results: To obtain a statistical uncertainty below 1% within the PTV, the simulation time for MC-GATE dosimetry was 32 ± 5 hours on a personal computer. Differently, VSV dosimetry took only a few seconds. Excellent agreement (ICC > 0.98) was reached for all measures within each ROI, resulting in similar DVH, although slightly higher values were found using the VSV. In the PTV, the mean, median, maximum, and standard deviation of the absorbed doses showed a median RD of 1.9% [min = 1.3, max = 2.6], 2.0% [-0.2, 2.4], 0.8% [-2.1, 1.7] and 1.7% [1.6, 2.7]. In the NLV, the same measures showed an RD of 1.7% [0.0, 5.4], 1.2% [-2.0, 4.8], 0.6% [-3.4, 3.3] and 1.9% [0.7, 5.4]. **Conclusion:** The time needed for MC dosimetry is acceptable in clinical practice. All features used to compare the absorbed dose distributions within each ROI showed excellent agreement. However, VSV dosimetry consistently produced slightly higher mean absorbed doses than MC simulations. This is most likely due to the latter truly considering the heterogeneities of the liver and surrounding tissues. We demonstrated both methods to be feasible in clinical practice for personalised dosimetry. **References:** None

OP-0289

Post-treatment three-dimensional voxel-based dosimetry after Yttrium-90 resin microsphere radioembolization in HCC

E. Veenstra, S. J. Ruiter, R. P. Bokkers, K. P. de Jong, W. Noordzij; University Medical Center Groningen, Groningen, NETHERLANDS.

Aim/Introduction: Selective internal radiation therapy (SIRT) with yttrium-90 (^{90}Y) has been established as treatment of non-operable and locally advanced hepatocellular carcinoma (HCC) patients. Current pre-treatment dosimetry with technetium-99m SPECT/CT can be a poor predictor of subsequent absorbed ^{90}Y dose. Instead, post-therapy ^{90}Y-PET/CT voxel-based dosimetry enables true quantification of absorbed dose. The aim of this study was to compare ^{90}Y PET/CT dosimetry to tumour response characteristics and overall survival (OS) in HCC patients treated with ^{90}Y resin microspheres. **Materials and Methods:** Thirty patients (26 male, 4 female) with unresectable HCC underwent thirty-six ^{90}Y-SIRT resin microspheres treatments and subsequent post-therapy ^{90}Y-PET/CT scanning in our institution, between May 2018 and November 2020. OS was determined after a minimal follow-up of 6 months. Dose delivered to lesions and unaffected liver tissue was calculated using MIM SurePlan™ Liver Y90 software. Lesions were divided to a <120 Gy or >120 Gy group. Response rate was determined using mRECIST criteria on follow-up MRI. Disease control was defined as a lesion showing complete response, partial response, or stable disease. Objective response was defined as complete or partial response. Results: A total of 43 treated lesions were included, with 15 lesions in the <120 Gy group (median, interquartile range [IQR]: 62,6 Gy, 48,5 - 97,2 Gy) and 28 in >120 Gy (207 Gy, IQR: 154 - 311 Gy). Median OS was longer for patients in >120 Gy group (33 months [95% CI: 31 - 34 months]), versus 17 months [95% CI: 13 - 27 months], p<.001). Lesion size was significantly reduced only in the >120 Gy group (p=.025), with larger effect at final follow-up (p=.010, median 240 days, IQR: 210 - 280 days). Tumour dose was moderately correlated with reduction in lesion size (df = 41, r=.28, p=.031). Although non-significant, tumour dose and mRECIST-score were moderately correlated (r=.243, p=.483). For all lesions, disease control and objective response rates were 93% and 77%. Complications were rare, with one patient suffering from radiation induced duodenal ulceration. **Conclusion:** As computed by post-therapy PET/CT dosimetry, patients that received higher tumour radiation-absorbed dose of ^{90}Y-SIRT showed both larger reductions in tumour size and better overall survival. **References:** None.

610

Wednesday, October 20 - Saturday, October 23, 2021

on-demand pool, release on Wednesday, October 20 at 09:00

Clinical Oncology Track - TROP Session: Gastro-Intestinal

OP-0291

Head-to-head Comparison of [^{68}Ga]Ga-Fapi-04 and [^{18}F]-FDG PET/CT in Evaluating the Extent of Disease in Gastric Adenocarcinoma

***J. Kuten*[1,2], *C. Levine*[1,2], *O. Shamni*[3], *S. Pelles*[4,2], *I. Wolf*[4,2], *G. Lahat*[5,2], *E. Mishani*[3], *E. Even-Sapir*[1,2];**

[1]Department of Nuclear Medicine, Tel Aviv Sourasky Medical Center, Tel Aviv, ISRAEL, [2]Sackler School of Medicine, Tel Aviv University, Tel Aviv, ISRAEL, [3]Cyclotron Radiochemistry Unit, Hadassah Medical Organization and Faculty of Medicine, Jerusalem, ISRAEL, [4]Division of Oncology, Tel Aviv Sourasky Medical Center, Tel Aviv, ISRAEL, [5]Department of Surgery, Tel Aviv Sourasky Medical Center, Tel Aviv, ISRAEL.

Aim/Introduction: [^{18}F]-Fluorodeoxyglucose (FDG) positron emission tomography-computed tomography (PET/CT) may sometimes be suboptimal for imaging gastric adenocarcinoma. The recently introduced [^{68}Ga]Ga-FAPI-04 (FAPI) PET/CT targets tumor stroma and has shown considerable potential in evaluating the extent of disease in a variety of tumors. **Materials and Methods:** We performed a head-to-head prospective comparison of FAPI and FDG PET/CT in the same group of 13 patients with gastric adenocarcinoma who presented for either initial staging (n = 10) or restaging (n = 3) of disease. Lesion detection and maximum standardized uptake value (SUV_{max}) were compared between the two types of radiotracers. Results:

All ten primary gastric tumors were FAPI-positive (100% detection rate), whereas only five were also FDG-positive (50%). SUV_{max} was not significantly different, but the tumor-to-background ratio was higher for FAPI (mean, median, and range of 4.5, 3.2, and 0.8-9.7 for FDG and 12.9, 11.9, and 2.2-23.9 for FAPI, P = 0.007). The level of detection of regional lymph node involvement was comparable. FAPI showed a superior detection rate for peritoneal carcinomatosis (100% vs. none). Two patients with widespread peritoneal carcinomatosis underwent a follow-up FAPI scan after chemotherapy: one showed partial remission and the other showed progressive disease. **Conclusion:** The findings of this study suggest that FAPI PET/CT outperforms FDG PET/CT in detecting both primary gastric adenocarcinoma and peritoneal carcinomatosis from gastric cancer. FAPI PET/CT also shows promise for monitoring response to treatment in patients with peritoneal carcinomatosis from gastric cancer, however, larger trials are needed to validate these findings. **References:** 1. Zhao L, Pang Y, Luo Z, et al. Role of [68Ga] Ga-DOTA-FAPI-04 PET/CT in the evaluation of peritoneal carcinomatosis and comparison with [18F]-FDG PET/CT. Eur J Nucl Med Mol Imaging. 2021; 2. Lindner T, Loktev A, Altmann A, et al. Development of quinoline-based theranostic ligands for the targeting of fibroblast activation protein. J Nucl Med. 2018;59(9):1415-22. 3. Lindner T, Loktev A, Giesel F, et al. Targeting of activated fibroblasts for imaging and therapy. EJNMMI Radiopharm Chem. 2019;4(1):1-15. 4. Kratochwil C, Flechsig P, Lindner T, et al. 68Ga-FAPI PET/CT: Tracer uptake in 28 different kinds of cancer. J Nucl Med. 2019;60(6):801-5. 5. Pang Y, Zhao L, Luo Z, et al. Comparison of 68 Ga-FAPI and 18 F-FDG Uptake in Gastric, Duodenal, and Colorectal Cancers . Radiology. 2021;298(2):393-402.

OP-0292

Respiratory-gated FDG PET/MRI in Evaluation of Primary Gastric Lesions and Gastric Lymph Nodes in Patients with Gastric Cancer

S. Gulbahar Ates[1], U. Aydos[2], U. O. Akdemir[2], O. Yuksel[3], A. Uner[4], A. Dursun[5], L. O. Atay[2];

[1]Department of Nuclear Medicine, Dr. Abdurrahman Yurtaslan Ankara Oncology Training and Research Hospital, Ankara, TURKEY, [2]Department of Nuclear Medicine, Faculty of Medicine, Gazi University, Ankara, TURKEY, [3]Department of General Surgery, Faculty of Medicine, Gazi University, Ankara, TURKEY, [4]Department of Internal Medicine, Division of Medical Oncology, Faculty of Medicine, Gazi University, Ankara, TURKEY, [5]Department of Pathology, Faculty of Medicine, Gazi University, Ankara, TURKEY.

Aim/Introduction: To evaluate the added value of respiratory-gated ^{18}F FDG PET/MRI in the visual and the semiquantitative assessment of primary gastric lesions and peri-gastric lymph nodes (LN) in the patients with gastric cancer. **Materials and Methods:** 102 upper abdominal respiratory-gated and whole-body (WB) ^{18}F FDG PET/MRI of 88 patients with gastric cancer were evaluated visually and semi-quantitatively. For 41 patients who underwent surgery, histopathological and PET findings were compared. Three PET images were obtained from upper abdominal PET data, non-Q static(non-QS) PET from all counts, respiratory-gated Q static (QS) PET from counts in end-expiration phase of breathing, shortened 4-minute PET that reconstructed to obtain similar counts to QS PET. The semi-quantitative parameters of primary lesions were recorded for each PET image. The percentage changes of all quantitative values in respiratory-gated QS PET images compared to the other PET images were calculated. The sizes of primary lesions and patients' body mass indexes (BMI) were also recorded. According to LN stations, the presence and the numbers of positive LNs for each PET image were recorded. LNs were scored visually according to a 4-point-scale: no uptake as 1, background < uptake < liver as 2, slightly higher than liver as 3 and markedly higher than liver as 4. Results: The patients whose primary lesion sizes were ≤ 30mm had significantly higher SUV percentage changes than the patients who had > 60mm lesions in QS PET compared to non-QS PET. The patients whose BMIs were >30 had higher percentage changes than the patients with BMI ≤30 in QS PET compared to the other PET images ($p<0.05$, Table). In the comparison of histopathological LN status and PET findings (as positive or negative), sensitivity, specificity, positive predictive value (PPV), negative predictive value (NPV), and accuracy was 78.57%, 61.54%, 81.48%, 57.14%, and %73.17, respectively. 3rd (lesser curvature), 4th (greater curvature) and 6th (infrapyloric) LN stations had significantly higher visual score in the QS PET than in the other PET images. 4th LN station had significantly higher number of FDG-positive RLN in the QS PET than in the non-QS and the WB PET images. In the 4th station, sensitivity, PPV, NPV and accuracy increased in the QS PET compared to the other PET images. **Conclusion:** Respiratory-gated PET/MRI was found significantly superior in the evaluation of especially 4th LN station, smaller gastric lesions, and in the patients with higher BMİ compared to the non-respiratory gated PET images. **References:** Nope

OP-0293

Static and dynamic FAPI-PET for the differentiation of low grade and high grade intraductal papillary mucinous neoplasms

A. Spektor[1], M. Lang[2], E. Gutjahr[3], U. Heger[2], C. Tjaden[2], H. Rathke[1], U. Haberkorn[1], M. Röhrich[1];

[1]Department of Nuclear Medicine, University Hospital Heidelberg, Heidelberg, GERMANY, [2]Department of Surgery, University Hospital Heidelberg, Heidelberg, GERMANY, [3]Department of Pathology, University Hospital Heidelberg, Heidelberg, GERMANY.

Aim/Introduction: Fibroblast Activation Protein (FAP) is a novel target for Positron emission tomography (PET) imaging of various tumours. In previous studies, pancreatic ductal adenocarcinomas (PDAC) have shown high FAPI-uptake.

Intraductal papillary mucinous neoplasm (IPMN) are divided into low-grade (LG) and high-grade (HG) subtypes, of which HG IPMN may develop into PDAC. Conventional imaging modalities (ultrasound, computed tomography, magnetic resonance imaging) cannot differentiate LG and HG IPMN satisfactorily, which frequently leads to the surgical resection of LG IPMN. In this study, we applied static and dynamic FAPI-PET in 12 patients with suspected IPMN. All patients have undergone biopsy or resection after PET-imaging. Imaging properties of LG and HG IPMN were analyzed retrospectively. **Materials and Methods:** Dynamic PET-scans were acquired over 60 minutes after the i.v. administration of 68Ga-labelled-FAPI-tracer (FAPI-74) followed by static imaging 60 minutes p.i.. SUVmax and SUVmean values of IPMN lesions and healthy organs were measured using spheric volumes of interest and target to background ratios (TBR) were calculated. Time-activity curves (TACs) derived from dynamic imaging were analyzed and kinetic modeling parameters were gained using a 2 compartment model. Results: HG IPMN showed significantly higher FAPI-uptake than LG IPMN (average SUVmax 6,78 +/- 2,67 versus 3,40 +/- 0,64, SUVmean 5,60 +/- 2,84 versus 2,57 +/- 0,30, TBRmax 2,85 +/- 1,27 versus 1,43 +/- 0,31, TBRmean 2,36 +/- 1,35 versus 1,08 +/- 0,14). TAC analysis revealed a delayed avaraged time to peak in HG IPMN (1.937,61 +/- 1516,04s) compared to LG IPMN (90s) and pancreatic background tissue (248,56 +/- 229,13s). Kinetic modelling showed differential average in K2 values of HG IPMN (0,39 +/- 0,31), LG IPMN (0,91 +/- 0,04). **Conclusion:** FAPI-PET imaging is a new, extremely promising imaging modality for the differentiation of LG and HG IPMN, which is clinically highly relevant in order to avoid resection of LG IPMN. **References:** none

OP-0294

The Role of ^{99m}Tc-HFAPi SPECT/CT for Patients with Malignancies of the Digestive Tract

X. Jia[1], Y. Wang[1], Y. Liu[1], Y. Yang[1], G. Qiu[1], S. Chen[2], F. Wang[3], J. Zhang[1], A. Yang[1], R. Gao[1];
[1]The first affiliated hospital of Xi'an jiaotong university, Xi'an, CHINA, [2]Foshan Atomical Medical Equipment Ltd, Foshan, CHINA, [3]Chinese Academy of Sciences;;Medical Isotopes Research Center, Peking, CHINA.

Aim/Introduction: Recently, molecular PET/CT imaging with radiolabeled FAP inhibitor (FAPi) has been evaluated in different diseases. Promising results have been demonstrated in its clinical application in malignancies within the digestive tract. Since SPECT is a lower cost and more widely available alternative to PET, ^{99m}Tc-labeled FAPis represent attractive tracers for imaging applicable in a larger number of patients. The current study aimed to evaluate the role of ^{99m}Tc-labeled FAPi (^{99m}Tc-HFAPi) in clinical analysis for digestive tract tumors. **Materials and Methods:** A total of 33 patients with digestive tract tumors, including 4 patient with suspected local relapse and 29 treatment-naive patients, underwent ^{99m}Tc-HFAPi SPECT/CT. SPECT/CT scans were taken 60-90 min after administration of ^{99m}Tc-HFAPi and physiologic biodistribution and tumor uptake were semiquantitatively evaluated. Uptake of ^{99m}Tc-HFAPi was compared with standard imaging, changes in tumor stage and in oncologic management were recorded. Results: Physiological uptake of ^{99m}Tc-HFAPi was observed in the liver, gallbladder, kidneys, pancreas, intestine, and to a lesser extent in the salivary glands and thyroid glands. The highest contrast was achieved in colorectal cancer, liver metastasis and head and neck metastasis, with an T/B ratio more than 6. Because of low background activity in normal tissue, there was a high tumor-to-background ratio of more than 3 in most lesions. In treatment-naive patients, TNM was changed in 20.69%, whereas in patients with metastases, new findings occurred in 40%. **Conclusion:** ^{99m}Tc-HFAPi represents a powerful tracer for diagnostic scintigraphy in DT tumors, especially in cases where PET imaging is not available. **References:** None

OP-0295

Measure of future liver remnant function (FLR-F) in patients candidate to major liver resection with a new imaging tracer of hepatobiliary system: a pilot study

T. Graziani[1], G. Baldari[1], G. Serreli[2], C. Cidda[1], M. Scarlattei[1], S. Migliari[1], A. Sammartano[1], L. Ruffini[1];
[1]Nuclear Medicine Division, Azienda Ospedaliero-Universitaria of Parma, Parma, ITALY, [2]Medical Physic, Azienda Ospedaliero-Universitaria of Parma, Parma, ITALY.

Aim/Introduction: Estimation of future liver remnant function (FLR-F) is used in our center, associated with CT-volumetry (FLR-V), for the pre-operative assessment of patients candidate to major liver resection. In the past the radiotracer used was 99mTc-mebrofenin (HIDA), actually not available on the market. The suggested HIDA cut-off value of mebrofenin uptake to predict postoperative liver failure (LF) is 2.69%/min/mq (De Graaf 2010). Since August 2020 we use 99mTc-MBrIDA. Our aim was to demonstrate efficacy of the new tracer in measuring FLR-F and to assess the use of HIDA cut-off value for 99mTc-MBrIDA. Additionally, we evaluated the predictive value of FLR-F/FRL-V in our population. **Materials and Methods:** From January 2016 to April 2021 patients scheduled for major liver surgery were submitted to FLR-F measure with 99mTc-mebrofenin (HIDA-group) or 99mTc-MBrIDA (MbrIDA-group). To determine total and regional liver function we used the formulas from Ekman 1996 and the recomended guidelines (Rassam 2019). All patients performed CT volumetry. MBrIDA acquisition consisted of early dynamic, fast SPECT-CT, late dynamic scan for tracer excretion. Results: We assessed FLR-F in 16 patients candidate to liver surgery for colorectal liver metastasis (5 patients), hepatocellular carcinoma (4), cholangiocarcinoma (5), gallbladder cancer (1), Klatskin cancer (1). In the HIDA-group (4 pts) FLR-F resulted >2%/min/mq in 3 patients (2.42, 3.01,

2.94) and 2.02%min/mq in one patient, that was submitted to portal vein embolization (PVE) increasing FLR-F to 3.95%/min/mq. No patient had post-surgery complications or LF. In the MbrIDA-group (12 pts), seven patients with FLR-F 2.81%/min/mq (FLR-V 34%), 4.27 (38%), 2.47 (38%), 2.37 (39%), 2.99 (32%), 2.61 (33%) and 1.49 (32%) went straight to surgery; 3 patients with FLR-F 1.12%min/mq (FLR-V 32.6), 1.81 (29%) and 1.27 (27%) underwent ALPPS. The FLR-F was re-assessed at least 2 weeks after ALPPS resulting increased to 2.65 (FLR-V 36.7%), 2.24 (33%) and 2.39 (43%), respectively. Two patients underwent FLR-F measure only after ALPPS resulting 2.39 (FLR-V 43%) and 1.47 (40%). In the MBrIDA-group 1 patient developed liver failure (basal FLR-F 1.49) and 2 pts showed reversible signs of liver impairment (one with post ALPPS FLR-F 1.47). Patients with FLR-F<2 developed complications even if FLR-V was >30%. **Conclusion:** In the preoperative work-up of major liver surgery, FLR-F estimation led to a "function oriented" use of PVE or/and ALPPS. HIDA cut-off value for FLR-F may be used with the new tracer 99mTc-MBrIDA. Volumetric index is not sufficient alone to assess patients candidate to major liver surgery. **References:** none

OP-0296

18F-FDG PET/MRI in intraductal papillary mucinous neoplasms (IPMNs) of pancreas: a preliminary monocentric experience

M. Frigo, P. Bartoletti, V. Bodanza, R. Simeone, P. Zucchetta, D. Cecchin, L. Evangelista;
University of Padua, Padova, ITALY.

Aim/Introduction: IPMNs of pancreas are a heterogeneous group of tumors that can anticipate the development of a ductal adenocarcinoma. Their incidence is difficult to assess although they show an increasingly rate. An early differential diagnosis between malignant and benign lesions is crucial to establish the best patient management. Surgery offers an opportunity to prevent pancreatic adenocarcinoma, but it may represent an overtreatment, with a considerable morbidity and mortality. International guidelines set the risk stratification and the therapeutic approach based on patient's clinical, biochemical, and morphological characteristics. However, although metabolic features are not stated, 18-FDG hybrid PET/CT has shown a possible role for the management of IPMNs. The aim of this study was to evaluate the role of 18F-FDG hybrid PET/MRI for the identification of malignant lesion in patients with a confirmed IPMN. **Materials and Methods:** Between 2015 to 2021, 29 patients with a confirmed IPMN underwent 18F-FDG PET/MRI (Siemens, mMR Biograph) at Nuclear Medicine Unit of the University of Padova, Italy. Inclusion criteria were: 1) the same MRI sequences for the PET/MRI examination, and 2) the availability of morphological IPMN characteristics at contrast enhanced CT imaging. For each patient, the worrisome features (cysts ≥3 cm in size, or enhancing mural nodules <5 mm, or thickened and enhanced cyst walls, or a main pancreatic duct-MPD 5-9 mm in size, or abrupt changes in MPD caliber with distal pancreatic atrophy, lymphadenopathy, or high serum levels of CA19.9, or a rapid rate of cyst growth) were recovered. Results: Seventeen patients met the inclusion criteria. MRI sequences included T1-VIBE opp-in, T1 VIBE-fs, T1-VIBE, T2-TSE, T2-SPACE, three-phase enhanced T1-VIBE and Diffusion Weighted Imaging (DWI). Worrisome features were present in 11/17 (64.7%) patients. CA19.9 and CEA levels were increased in 7/17 (41.2%) and 3/17 (17.6%), respectively. PET showed a focal FDG uptake in 4/17 (23.5%) subjects, while MRI was positive for pancreatic lesions in all patients. Follow-up data were available in 8/17 (47%) patients. Three out of these 8 (37.5%) patients developed a pancreatic adenocarcinoma. All 3 subjects had worrisome features at morphological imaging. 18F-FDG PET/MRI resulted true positive in all 3 cases (sensitivity: 100%), with a semiquantitative standardized uptake value ranged between 3.4-5.9. **Conclusion:** 18F-FDG PET/MRI can be useful in patients with IPMN and worrisome features at morphological imaging, being able to early identify those who will develop an aggressive tumor. **References:** 1. Yamashita YI. Anticancer Res. 2019;39:2493-99. 2. Huo L. Clin Nucl Med. 2016;41:989-90.

OP-0297

Accuracy of [^{18}F]FDG PET-CT in the evaluation of the post-neoadjuvant local response in esophageal cancer by using cualitative and PERCIST criteria

S. Martin Aguilar[1], C. Ponce Herrera[1], C. Montiel Casado[1], F. Moreno Ruiz[1], M. Florez Rial[1], M. Requena Santos[1], A. Gutierrez Cardo[1], V. Marín Parrilla[1], M. Nicolás Aguado[1], N. Álvarez Mena[2], L. Lumbreras Vega[1], D. Ramirez Ocaña[1], M. Puentes Zarzuela[1];
[1]Hospital Regional de Málaga, Málaga, SPAIN, [2]Hospital Clínico Universitario de Valladolid, Valladolid, SPAIN.

Aim/Introduction: Evaluate the suitability of [^{18}F]FDG PET-CT as a method of evaluating the post-neoadjuvant response of the primary lesion in locally advanced esophageal cancer. **Materials and Methods:** A total of 34 consecutive patients diagnosed with locally advanced esophageal cancer between 12/2016-09/2020, who underwent neoadjuvant therapy followed by surgical resection (performed 48,47± 22,36 days after treatment), were selected. All tissue specimens were assessed as per the tumor regression grade (TRG) system by Ryan (0-complete response, 1-almost complete response, 2-moderate response or 3-poor response). Basal and post-neoadjuvant [^{18}F]FDG PET-CT were performed. Post-neoadjuvant response was evaluated qualitatively and quantitatively by PERCIST (Δ%SUL peak>30). Studies were classified qualitatively as complete, indeterminate, partial or minimal response, and by PERCIST as complete or partial response or stable disease. The PET-TC results were also compared with the pathological findings of the surgical specimen. Results: 47,05% patient had adenocarcinoma (ADC) (n=16), 20.58% squamous cell carcinoma (n=7) and 1 TNE, all of them undergoing chemoradiotherapy, and

29,49% patient had ADC undergoing chemotherapy (n=10), were selected. [^{18}F]FDG PET-CT detected post-neoadyuvant cualitative complete response in 10% ADC-chemotherapy and 6,25% ADC-chemoradiotherapy; partial response in 80% ADC-chemotherapy, 56,25% ADC-chemoradiotherapy, 57.14% squamous carcinoma and in the TNE; and minimal response in 18,75% ADC-chemoradiotherapy. 20,58% patients had indeterminate results. PERCIST detected post-neoadyuvant complete response in 10% ADC-chemotherapy and 6,25% ADC-chemoradiotherapy; partial response in 80% ADC-chemotherapy, 50% ADC-chemoradiotherapy, 100% squamous carcinoma and in the TNE; and stable disease in 10% ADC-chemotherapy and 43,75% ADC-chemoradiotherapy. Histological analysis showed TRG 0 in 25% ADC-chemoradiotherapy and 42,85% squamous carcinoma; grade 1 in 40% ADC-chemotherapy, 31,25% ADC-chemoradiotherapy and 1 squamous carcinoma; grade 2 in 20% ADC-chemotherapy, 25% ADC-chemoradiotherapy and 28,57% squamous carcinoma; and poor regression in 40% ADC-chemotherapy, 18,75% ADC-chemoradiotherapy, 14,28% squamous carcinoma and in the TNE. [^{18}F]FDG PET-CT was able to identify through qualitative criteria 64% of patients with response (83% ADC-chemotherapy, 61.53% ADC-chemoradiotherapy and 50% squamous carcinoma) and 76% by PERCIST (better in squamous carcinoma), but only 11% (qualitative criteria) and 22% (PERCIST) patients without response were identified. The agreement in the degree of response between histology and PET-TC was 32.35% by qualitative analysis (40% ADC-chemotherapy, 31.25% ADC-chemoradiotherapy and 28.57% squamous carcinoma) and 41.17% by PERCIST (50% ADC-chemotherapy, 37.5% ADC-chemoradiotherapy, and 42.85% squamous cell carcinoma). **Conclusion:** [^{18}F]FDG PET-CT appears to have good sensitivity to identify patients with post-neoadjuvant response, but with low specificity. In addition, it showed lacks of precision to differentiate the degree of response. **References:** None

OP-0298

Reliability and Prognostic value of qualitative and semiquantitative 18F-FDG PET/CT analysis in patients with gastrointestinal stromal tumours undergoing imatinib adjuvant treatment after surgery

C. Altini, C. D'Alò, N. C. Merenda, A. Di Palo, A. R. Pisani, G. Rubini; Section of Nuclear Medicine, DIM, University "Aldo Moro", Bari, ITALY.

Aim/Introduction: Gastrointestinal stromal tumours (GISTs) are the most common mesenchymal tumours of the gastrointestinal tract, mostly located in the stomach and small intestine. Adjuvant therapy with imatinib is the standard treatment option for recurrent or metastatic GIST after surgery. The role of ^{18}F-FDG-PET/CT in this setting of patients is not clearly established and its prognostic value is not well investigated.This study aims to investigate the reliability and the prognostic role of ^{18}F-FDG-PET/CT qualitative and semi-quantitative analysis in post-operative GIST patients treated with adjuvant imatinib. **Materials and Methods:** we retrospectively evaluated 17 patients (mean age 65y) with histologically confirmed GIST who underwent ^{18}F-FDG-PET/CT before and after imatinib treatment. PET/CT images were analyzed both qualitatively and semi-quantitatively. PET-based semi-quantitative parameters extracted from both scans respectively were: whole body SUVmax corrected for body weight (pre/post-$SUVbw_{WB}$), metabolic tumor volume ($preMTV_{WB}$ and $postMTV_{WB}$) and total lesion glycolysis ($preTLG_{WB}$ and $postTLG_{WB}$), as well as percentage interval changes ($\%\Delta SUVmax_{WB}$, $\%\Delta MTV_{WB}$, $\%\Delta TLG_{WB}$). According to PET Evaluations Response Criteria for solid tumors (PERCIST), patients were classified in complete metabolic responders (CMR), partial metabolic responders (PMR), stable metabolic disease (SMD) and progressive metabolic disease (PMD) and then grouped in metabolic responders (MR=CMR+PMR+SMD) and no-metabolic responders (nMR=PMD) respectively. Both clinical and instrumental follow-up was used to evaluate time to progression (TTP) disease. The continuous variables were compared into R/NR groups using the Student's t-test with 95%CI. TTP was estimated by the Kaplan-Meier method and results between MR/nMR groups were compared using long-rank test. A $p<0.05$ was considered statistically significant. Results: according to PERCIST, CMR was found in 1/17 (5,9%) patients, PMR in 5/17 (29,4%), SMD in 5/17 (29,4%), PMD in 6/17 (35,4%). Among semi-quantitative PET-based parameters, statistical analysis demonstrated a significant difference into MR/nMR groups for both $\%\Delta TLG_{WB}$ ($p= 0.03$) and $\%\Delta MTV_{WB}$ ($p= 0.008$). TTP for the whole cohort resulted of 27.7 ± 4.8 months. MR showed a significantly longer TTP (24.6 ± 2.1 months) than nMR (14.7 ± 6.3 months) (p=0.006). **Conclusion:** Our preliminary results suggest that ^{18}F-FDG PET/CT could represents a reliable imaging tool to assess disease response in patients with GIST treated with adjuvant imatinib, relying both on the qualitative and semiquantitative analysis, particularly on MTV and TLG volume-based parameters. Further studies are mandatory to assess the accuracy of these results in larger populations and to standardize these parameters. **References:** none

OP-0299

Comparison of 18F-DOPA and 68Ga-DOTA-TOC as a PET imaging tracer before peptide receptor radionuclide therapy

E. Veenstra[1], A. H. Brouwers[1], D. A. de Groot[1], J. Hofland[2], A. M. Walenkamp[1], T. Brabander[2], Z. T. Wouter[1], W. Noordzij[1]; [1]University Medical Center Groningen, Groningen, NETHERLANDS, [2]Erasmus University Medical Center, Rotterdam, NETHERLANDS.

Aim/Introduction: In treatment of neuroendocrine neoplasms (NENs), confirmation of somatostatin receptor expression with ^{68}Ga-DOTA somatostatin analogues is mandatory to determine eligibility for peptide receptor

radionuclide therapy (PRRT). ^{18}F-DOPA is also used in the diagnostic imaging of NENs, sometimes detecting additional lesions compared to ^{68}Ga-DOTA-TOC. The aim of this study was to explore differences in tumour detection of both tracers and their relevance for selecting patients for PRRT with ^{177}Lu-DOTA-TATE. **Materials and Methods:** We retrospectively studied eight patients with NENs who underwent both ^{68}Ga-DOTA-TOC and carbidopa-enhanced ^{18}F-DOPA PET/CT, before first-time PRRT with ^{177}Lu-DOTA-TATE. No routine scanning of either one tracer was preferred above the other. Tracer order was influenced due to stock availability or to detect suspected metastases with a second tracer. On CT, treatment response was classified according to RECIST 1.1 as partial response (PR), stable (SD), progressive disease (PD), or undetermined (UD). Results: Seven patients with in total 89 lesions completed four infusions of 7.4 GBq ^{177}Lu-DOTA-TATE, one patient received only two cycles. Before treatment, ^{18}F-DOPA PET/CT detected significantly more lesions than ^{68}Ga-DOTA-TOC PET/CT (79 vs. 62, p<.001). After treatment, the number of lesions with disease control were not considered significantly different between ^{18}F-DOPA-only (5/27) and ^{68}Ga-DOTA-TOC-only lesions (4/10, p=.25). ^{18}F-DOPA detected more liver metastases (24/27) compared to ^{68}Ga-DOTA-TOC (7/10, p=.006). Seven out of eight patients displayed a mismatch pattern by having at least one lesion not detected by both tracers, while other lesions did. Six patients showed in-patient heterogeneity in treatment response between ^{18}F-DOPA-only and ^{68}Ga-DOTA-TOC-only lesions. **Conclusion:** Response to PRRT with ^{177}Lu-DOTA-TATE was comparable for both ^{68}Ga-DOTA-TOC- and ^{18}F-DOPA-only NEN lesions. ^{18}F-DOPA may be equally capable of predicting response to PRRT, if ^{68}Ga-DOTA-TOC is unavailable. **References:** None

OP-0300

[^{18}F] FDG PET-CT: Prognostic capacity of baseline SUVmax and %ΔSUL peak in locally advanced esophageal cancer undergoing neoadjuvant therapy followed by curative surgery: a single-center study

S. Martin Aguilar, C. Ponce Herrera, C. Montiel Casado, F. J. Moreno Ruiz, M. Florez Rial, M. Requena Santos, E. Muñoz Espinosa, A. L. Gutierrez Cardo, M. Nicolás Aguado, D. Ramirez Ocaña, L. Lumbreras Vega, M. Puentes Zarzuela;
Hospital Regional de Málaga, Málaga, SPAIN.

Aim/Introduction: Evaluate the prognostic capacity of [^{18}F] FDG PET-CT in locally advanced esophageal cancer undergoing neoadjuvant therapy based on cuantitative values. **Materials and Methods:** Retrospective observational study with n=34 patients diagnosed with locally advanced esophageal cancer between 12/2016-09/2020, submitted to neoadjuvant therapy followed by surgical resection. Surgical resection was subsequently performed in a mean interval of 48,47± 22,36 days after treatment. Patients were followed with clinical evaluations, peripheral blood analysis, CT scans, and endoscopies. All patients were staged with endoscopy and 18F-FDG PET-CT, 33 underwent CT scans and 27 underwent endoscopic ultrasound. Post-neoadyuvant 18F-FDG PET-CT was perform between 31,41± 25,62 days after treatment. The results of baseline and post-neoadyuvant PET-CT were also compared with the evolution of the patients after surgery, assessing postoperative complications, recurrence/progression, overall survival and progression-free time. Results: 47,05% patient had adenocarcinoma (ADC) (n=16) and 20.58% squamous cell carcinoma (n=7), both of them undergoing chemoradiotherapy CROSS; 29,49% patient had ADC undergoing chemotherapy FLOT (n=10), and 1 TNE undergoing chemoradiotherapy CDDP + VP-16, with a mean follow-up of 10.79±12,12 months; overall survival (OS) 12.9±12,45 / progression-free time 9.7±9,42 months in ADC-chemotherapy, OS 10.43±11,67 / progression-free time 8.09±10,84 months in ADC-chemoradiotherapy, OS and progression-free time 4.71± 6,68 month in squamous carcinoma, and OS and progression-free time of 41 months in NET.55.88% patients presented postoperative complications; 3 ADC-chemotherapy (28.81±5,03 baseline SUVmax and 57.5±42 %ΔSUL peak vs 14.09±4,37 baseline SUVmax and 43.14±12,7 %ΔSUL peak of patients without complications), 10 ADC-chemoradiotherapy (4.32±6,35 baseline SUVmax and 43.8±28,86 %ΔSUL peak vs. 9.88±3,5 baseline SUVmax and 37.66±21,69 %ΔSUL peak of the patients without complications), and 6 squamous carcinoma (17.58±8,91 baseline SUVmax and 69.83±15,53 %ΔSUL peak vs. 26,69±14,31 baseline SUVmax and 75,5±4,95 %ΔSUL peak of patients without complications).17.64% patients presented recurrence / progression; 3 ADC-chemotherapy (with 14.94±5,78 baseline SUVmax and 60.66±6,51 %ΔSUL peak vs. 9.81±3,07 baseline SUVmax and 42.66±28,79 %ΔSUL peak of the patients without progression) and 3 ADC-chemoradiotherapy (with 10.75±2,04 baseline SUVmax and 43±23,64 %ΔSUL peak vs. 12.27±6,3 baseline SUVmax and 53.5±27,17 %ΔSUL peak of the patients without progression). **Conclusion:** A high baseline SUVmax seems to be related to greater postoperative complications in ADC with chemotherapy or chemoradiotherapy, and with a higher risk of recurrence / progression in ADC-chemotherapy, while a lower %ΔSUVmax and %ΔSUL peak seems to be related to greater postoperative complications in carcinoma squamous cell and increased risk of recurrence / progression in ADC-chemoradiotherapy. **References:** none

OP-0301

Accuracy of [18F] FDG PET-CT to identify the location and extent of local residual disease in esophageal cancer

S. Martin Aguilar, C. Ponce Herrera, C. Montiel Casado, F. Moreno Ruiz, M. Requena Santos, M. Florez Rial, V. Marín Parrilla, E. López Rodriguez, M. Nicolás Aguado, L. Lumbreras Vega, D. Ramirez Ocaña, M. Puentes Zarzuela;
Hospital Regional de Málaga, Málaga, SPAIN.

Aim/Introduction: Assess the capacity of 18F-FDG PET-CT to define the location and size of local residual disease in esophageal cancer after neoadjuvant. **Materials and Methods:** A total of 34 consecutive patients diagnosed with locally advanced esophageal cancer between 12/2016-09/2020, submitted to neoadjuvant therapy followed by surgical resection, were selected. Surgical resection was subsequently performed, obtaining an esophagogastrectomy specimen in 88.23% of cases, 3 only stomach and 1 only esophagus. All tissue specimens were assessed macro and microscopically. All of them underwent basal and post-neoadjuvant [18F] FDG PET-CT. Localization of region with residual disease was performed by identifying the hypermetabolic area and its measurement in the craniocaudal direction. The lesions were divided into the middle or distal third of the esophagus, esophagus-gastric junction (EGJ), stomach, or a combination of the above. The post-neoadjuvant PET-CT results also were compared with the pathological findings of the surgical specimen. Results: 47,05% patient with adenocarcinoma (ADC) (n=16), 20.58% squamous cell carcinoma (n=7) and 1 TNE, all of them undergoing chemoradiotherapy, and 29,49% patient had ADC undergoing chemotherapy (n=10), were selected. [18F] FDG PET-CT detected 5,82% stomach residual disease, 5,82% stomach-EGJ, 11,76% EGJ, 20,58% distal esophagus-EGJ, 29,41% distal esophagus, 8,82% mid-distal esophagus, and 8,82% mid esophagus. Histological analysis showed 44,11% EGJ residual disease, 20,58% distal esophagus-EGJ, 8,82% distal esophagus, and 5,88% mid esophagus. 20,58% showed no tumor remainder. 58.82% patients evidenced coincident localization (60% ADC-chemotherapy, 50% ADCchemoradiotherapy and 85.71% squamous carcinoma), 17.64% approximate localization (20% ADC-chemotherapy, 18.75% ADC-chemoradiotherapy and in NET) and 23.52% different localization (20% ADC-chemotherapy, 31.25% ADC-chemoradiotherapy, and 14.28% squamous carcinoma). A similar size was observed in 25% cases with coincident location (30% ADC-chemotherapy and 12.5% ADC-chemoradiotherapy); smaller histological size was observed in 60% cases with coincident location (37.5% ADC-chemoradiotherapy and 85.71% squamous carcinoma) and in 83.33% with approximate localization (10% ADC-chemotherapy, 18.75% ADC-chemoradiotherapy and NET); and greater histological size was observed in 15% cases with coincident location (30 % ADC-chemotherapy) and in 16.66% with approximate localization (10% ADC-chemotherapy). **Conclusion:** [18F] FDG PET-CT was able to correctly identify the location of the tumor remainders / fibrotic region in squamous carcinoma, and less precisely in ADC. The measurement of tumor extension was less precise, although in most cases the histological lesion / fibrosis showed smaller or equal size than the hypermetabolic region. **References:** None.

OP-0302

Se-75-SehCAT in the diagnostic procedure of chronic diarrhoe

C. Körber, N. Körber-Hafner;
Nuclearmedicine, Fulda, GERMANY.

Aim/Introduction: A chronic diarrhoe is a frequent disease in adult patients with a prevalence of 4 to 5% in a western population 1. A subgroup of primarily chologenic diarrhoe is present in up to 1 % of the population (Walters et al./2010). The gold standard in the differentiation of the specificity of the diarrhoe is the test using 75 Se taurocholic acid. (SehCAT) that is performed since 1982. **Materials and Methods:** We used the following protocol for SehCAT testing on a GE NM 670 gamma camera. On the day 0 of the administration of 370 kBq Se-75-SehCAT a planar scintigraphy was obtained 3 to 6 hours after swallowing the capsule. On day 7 the following protocol was repeated: planar scintigraphy of the abdomen, 5 min scanning time, enery window 280 keV +/- 20%, maximal distance between patient and collimator, equal positioning on both days on the gamma camera. The measurement of the Se-75 retention rate was performed using a GEHC standardized formula that we obtained from GE. Results: Since May 2020 28 patients received SehCAT testing. 11 patients (39%) showed a retention rate between 0 and 5 % after 7 days, 7 patients (25%) between 6 and 10 % and 10 patients (36%) had a retention greater than 15%. **Conclusion:** We can show that the correct SehCAT testing can lead to an ensured differentiation of chologenic diarrhoe and give hints to the severity of bile acid malabsorption. The reliable diagnose can ensure a consistent therapy with bile acid sequestrants. Furthermore we found more patients with a severe bile acid malabsoprtion than expected from literature (64%). **References:** 1Arasaradnam, R. P. et al.Guidelines for the investigation of chronic diarrhoea in adults: British Society of Gastroenterology, 3rd edition. Gut 67, 1380-1399 (2018)2Walters JR. Defining primary bile acid diarrhea: making the diagnosis and recognizing the disorder. Expert Rev Gastroenterol Hepatol 2010; 4: 561-567.

611

Wednesday, October 20 - Saturday, October 23, 2021

on-demand pool, release on Wednesday, October 20 at 09:00

TROP Session: Top of Cardiovascular and Soft Tissue Infection/Inflammation Imaging

OP-0304

Investigation of Pediatric Cardiac-Related Infections with ^{18}F-FDG PET/CT: Optimization and Performance

G. April, R. Lambert, S. Turpin;
CHU Ste-Justine, Montreal, QC, CANADA.

Aim/Introduction: The use of ^{18}F-FDG PET/CT is frequent for the detection of cardiac infection or inflammation in adults, however literature remains scarce for pediatric applications. The purpose of our study was to review our experience as a tertiary pediatric center, including the feasibility of myocardial suppression protocol in children. **Materials and Methods:** One hundred and five cardiac ^{18}F-FDG PET/CT scans performed in 67 children age 3 weeks to 17-year-old were reviewed. ^{18}F-FDG PET/CT was performed without (Group A, 72 studies) or with (Group B, 33 studies) myocardial suppression protocol. Standard protocol included minimal 4 hours fasting, with cessation of D5% perfusion for a least 2 hours. Age-permitting suppression protocol, implemented since 2015, included 24 hours low-carbohydrate diet, minimal 12 hours fasting, with/without IV heparin administration. Cardiac suppression was classified as absent, partial or complete. Infection was classified as intracardiac, extra-cardiac cardiovascular, remote septic emboli and miscellaneous. Infection foci were individually analyzed. Final diagnosis was obtained by combining other modalities findings, microbiological sampling and clinical response to antibiotics.Comparison between groups A and B was made using student t-test for age and Chi-Square analysis for imaging protocolization and infection compatibilization. Results: Patients in A were younger than in B (2.63 ± 5.8 vs 10.74 ± 4.24 years, $p < 0.0001$). Myocardial suppression failed in 57% of A and 9% of B; complete suppression was achieved in 24% of A and 85% of B; and partial suppression in 19% of A and 6 % of B ($p < 0.0001$). In 29 studies (patients 2-years-old and younger), complete or partial suppression was found in 9. Sensitivity for global detection of infection was 89.1% for A, 96% for B ($p = 0.379$), and was 86.7% for children 2-years and younger. Intracardiac infection identification was superior in B ($p= 0.003$). Fifty-four studies identified cardiac-related infection, including 15 RV-AP conduits, 7 pacemakers, 3 sternal osteomyelitis, 5 superficial wound infections, 7 pneumonias and 8 miscellaneous infections. Only one native valve endocarditis was identified. Septic emboli were demonstrated in 15 studies, including 2 where they were the only manifestation of underlying endocarditis. **Conclusion:** Sensitivity for infection detection was high in our population, even in infants/babies where myocardial suppression is not feasible. However, best detection of intra-cardiac foci was achieved with suppression protocol. Identification of septic emboli also seemed valuable for indirect detection and suspicion of endocarditis. **References:** None

OP-0305

Diagnostic performance of digital PET with a dedicated head and neck protocol for the assessment of inflammation of cranial arteries in Giant Cell Arteritis

B. Durand-Bailloud[1], T. Thibault[2], A. Bertaut[3], C. Drouet[1], R. popoff[1], F. Godard[1], G. Nodari[1], B. Bonnotte[2,4], M. Samson[2,4], A. Cochet[1,5,6], J. Alberini[1,5,6];
[1]Department of Nuclear Medicine, Georges-François Leclerc Cancer Center, Dijon, FRANCE, [2]Department of Internal Medicine and Clinical Immunology, François Mitterrand University Hospital, Dijon, FRANCE, [3]Department of Methodology and Biostatistics, Georges-Francois Leclerc Research Cancer Center, Dijon, FRANCE, [4]INSERM, UMR 1098, University of Bourgogne Franche-Comté, Dijon, FRANCE, [5]Department of NMR spectroscopy and Nuclear Medicine, François Mitterrand University Hospital, Dijon, FRANCE, [6]ImViA EA 7535, University of Burgundy, Dijon, FRANCE.

Aim/Introduction: Diagnosis of Giant cell arteritis (GCA) may be difficult, but is an emergency. Recently FDG-PET/CT imaging was not recommended for the assessment of wall inflammation of cranial arteries by the European League Against Rheumatism (EULAR). The aim of this prospective study was to evaluate the diagnostic performance of digital PET with a dedicated acquisition protocol for the assessment of wall inflammation of cranial arteries and to evaluate the inter-observer variability. **Materials and Methods:** FDG-PET/CT scans were performed between November 2018 and July 2020 with 5-min PET images acquisition time on the head and neck. Images were acquired 60 min after injection of 3 MBq/kg of FDG. Patients over 50 years newly suspected of having GCA before or within 3 days of glucocorticoid treatment were referred by the internal medicine department. The Total Vascular Score established on 7 arterial segments according to the EANM recommendations (TVS corresponding to a visual analysis comprising 4 levels) was compared with a score including 20 segments due to the inclusion of right and left sides segments and cranial segments (vertebral, temporal, maxillary and occipital) as well as a score including only cranial segments. These scores were assessed by 2 nuclear medicine physicians and, in case of disagreement between the 2 observers in any segment, a final score was resolved by a consensus obtained by a reading of a 3rd nuclear medicine physician. All observers were blinded to the clinical context and the final diagnosis. Inter-observer variability was assessed. The final GCA diagnosis was established by the internists in charge of patients. Results: The GCA diagnosis was established for 15 among 52 patients (mean age ± SD = 73.4y ± 10.8). From the Receiving Operating Characteristic curve analysis based on the clinical diagnosis,

sensitivity and specificity were 80% and 97% respectively for the 20-segments-score and for the cranial score, higher than those of TVS (sensitivity and specificity of 73% and 89%, respectively). 13 patients were positive on PET/CT with the 20-segments score or cranial score, versus 11 with the TVS. The inter-observer variability was substantial (weighted kappa = 0.68), and higher in the cranial segments (kappa > 0.75 in temporal, maxillary and occipital segments) than aorta and primary branches. **Conclusion:** This prospective study showed high performance of FDG-PET/CT imaging in the detection of inflammation of cranial segments in patients newly suspected of having GCA and a better inter-observer variability for cranial segments. **References:** none

OP-0306

New Possible Interpretation Criteria In 18F-FDG PET/CT SCAN For The Diagnosis Of Infective Endocarditis

M. Gazzilli[1], D. Albano[1], S. Lucchini[1], A. Peli[1], E. Cerudelli[1], F. Dondi[2], A. Mazzoletti[2], P. Bellini[2], F. Bertagna[2], R. Giubbini[2];
[1]Azienda Socio Sanitaria Territoriale degli Spedali Civili di Brescia, Brescia, ITALY, [2]University of Brescia, Brescia, ITALY.

Aim/Introduction: We proposed two interpretative criteria in FDG-PET/CT scan for the diagnosis of infective endocarditis (IE), qualitative and semi-quantitative criteria. The aim of our study was to evaluate the value of this PET/CT-based interpretation system to assess the diagnosis of IE. **Materials and Methods:** We retrospectively included 108 patients who underwent 18F-FDG-PET/CT for suspected IE. PET/CT scans were interpreted according to a 4-point score (0=no uptake; 1=cardiac uptake <blood-pool activity; 2= blood-pool <uptake< liver activity; 3= uptake>liver). For semi-quantitative criterion: SUVmax and SUVmean of the suspected valve lesion, liver, spleen and of the bone marrow (BM) were calculated. BM and spleen SUVmean were normalized to those of the liver, and hypermetabolism (HSBM) was defined as a BM or spleen-to-liver ratio>1. Results: Comparing the score criteria results with the clinical final diagnosis the sensitivity, specificity, positive predictive value, negative predictive value and accuracy of qualitative criteria were 92.8%, 80.7%, 83.8%, 91.3% and 87%, respectively. There was a high agreement between the two readers applying these criteria (k=0,902). A definite IE was documented in 83% of patients showing HSBM and abnormal cardiac uptake, 44% with abnormal cardiac uptake, 28% with HSBM and 10% with neither one. Comparing the two proposed methods for the analysis of 18F-FDG PET/CT images with Spearman test, we obtained a rho=0.473 with a p<0.0001 (95% CI 0.304-0.613). **Conclusion:** We demonstrated that the association of both PET/CT criteria perfectly IE responds to the need of standardization of the PET/CT images interpretation in IE and they could be useful for evaluating treatment response. **References:** 1. Gazzilli M, Albano D, Durmo R, et al. Improvement of diagnostic accuracy of 18fluorine-fluorodeoxyglucose PET/computed tomography in detection of infective endocarditis using a 72-h low carbs protocol. Nucl Med Comm. 2020; 41:753-758.1. Albano D, Dondi F, Gazzilli M, et al. Meta-analysis of the Diagnostic Performance of 18F FDG-PET/CT in Native Valve Endocarditis. JACC: Cardiovascular Imaging 2020 doi:10.1016/j.jcmg.2020.09.021.

OP-0307

Clinical Management in Patients with suspected Mycotic Aneurysms: Impact of FDG-PET/CT

L. Husmann[1], M. W. Huellner[1], H. Gruenig[1], N. Eberhard[2], C. A. Mestres[3], Z. Rancic[4], B. Hasse[5];
[1]Department of Nuclear Medicine, University Hospital of Zurich / University of Zurich, Zurich, SWITZERLAND, [2]Division of Infectious Diseases and Hospital Epidemiology, University Hospital of Zurich / University of Zurich, Zurich, SWITZERLAND, [3]Clinic for Cardiac Surgery, University Hospital of Zurich / University of Zurich, Zurich, SWITZERLAND, [4]Clinic for Vascular Surgery, University Hospital of Zurich/ University of Zurich, Zurich, SWITZERLAND, [5]Division of Infectious Diseases and Hospital Epidemiology, University Hospital of Zurich, Zurich, SWITZERLAND.

Aim/Introduction: The aim of the present study was to determine the impact of positron emission tomography/computed tomography with ^{18}F-fluorodeoxyglucose (PET/CT) on clinical management in patients with suspected mycotic aortic aneurysms (MAA). **Materials and Methods:** One hundred and one PET/CT were acquired in 50 patients, thereof 50 for the initial diagnosis/baseline scan, 51 for follow-up. Impact on patient management was defined in three categories: "confirmed" (PET/CT resultsconfirmed by clinical follow-up), "suspected" (conclusive PET/CT results, not confirmed by clinical follow-up), or "misleading" (results of PET/CT proven wrong by follow-up). For clinical follow-up patient data were recorded at the time of imaging, and at the latest recorded clinical visit. It included patient demographics, clinical information, laboratory data, results of microbiology, results from other diagnostic procedures, information about treatment, and patient's general health condition. Results: In four patients (8%) no clinical follow-up was feasible, the other 46 patients were clinically followed for a median of 898 days (IQR 320-4105). The combined evaluation of all 101 PET/CT demonstrated an impact on patient management in 78,5% of cases (48,5% confirmed, 30% suspected). Results of 21,5% of the PET/CT examinations were misleading. Respective values at baseline and at follow-up were: impact on patient management in 82% and 74,5% (70% and 27.5% confirmed, and 12% and 47% suspected), misleading cases in 18% and 25.5%. **Conclusion:** In MAA, PET/CT has a high impact on patient management, which is more pronounced with baseline than with follow-up examinations. However, PET/CT results may be misleading in a smaller proportion of cases. **References:** none

OP-0308

[^{18}F]FDG hypermetabolisms of the spleen and/or bone marrow: indirect signs of bacteremia

R. Zanca[1], *F. Bartoli*[1], *E. Esposito*[1], *E. Lazzeri*[1], *M. Sollini*[2,3], *R. Slart*[4,5], *P. Erba*[1,4];
[1]*Regional Center of Nuclear Medicine, Department of Translational Research and New Technology in Medicine, University of Pisa and AOUP, Pisa, ITALY,* [2]*Nuclear Medicine, Humanitas Clinical and Research Center - IRCCS, Rozzano (Milan), ITALY,* [3]*Department of Biomedical Sciences, Humanitas University, Pieve Emanuele (Milan), ITALY,* [4]*Department of Nuclear Medicine and Molecular Imaging, University of Groningen, University Medical Center Groningen, Groningen, NETHERLANDS,* [5]*Department of Biomedical Photonic Imaging, University of Twente, Enschede, NETHERLANDS.*

Aim/Introduction: Recently hypermetabolisms of the spleen and/or bone marrow has been proposed as an indirect sign of infective endocarditis (IE), useful to reinforce the suspicion of IE in the absence of any other infectious, inflammatory, or malignant disease. However, in our experience this is a common findings also in patients with other type of infections rather IE. Therefore, with the present work we aim to determine whether hypermetabolisms of the spleen and/or bone marrow represent an indirect signs of bacteremia rather than of IE. **Materials and Methods:** We retrospectively evaluated a series 300 patients who performed between January 2015 to December 2020 [^{18}F]FDG PET/CT (Discovery 710 GE) for suspected infection. In particular, 100 pts had infections from different origin and a positive blood culture (PBC), 100 pts presented localized infection, but negative blood culture (IDBCN) and 100 pts were classified as definite IE (IED) according to the 2015 ESCcriteria. [^{18}F]FDG SUVmax SUVmean in bone marrow, spleen and liver were measured drawind a 14 cm^3 regions of interest (ROIs) positioned close to the centers of the spleen and of the right liver lobe, but excluding abscess and/or ischemic lesions., as previously described (Caroline Boursier et al. ; Jordy P.Pijl et al.). BM SUVmax and SUVmean was obtained from ROIs placed on the bodies of each of the five lumbar vertebrae, excluding any damaged vertebra. BM to liver SUV ratios (BLR) and spleen to liver SUV ratios (SLR) were calculated. Kruskal-Wallis tests and the Dunn's test procedure for multiple comparison were performed using JMP Statistical Discovery^{tm} Results: We didn't find any significant difference among the three groups in SUVmax/mean or in SLR. Nevertheless, by grouping patients for the presence of positive (169 pts) or negative blood culture (131 pts), irrespectively from the final diagnosis we were able to demonstrate a significant difference in SLR between the two groups (p=0.0055). No significant associations were found with BLR. **Conclusion:** Our data support the concept that increased uptake in the spleen can be considered an indirect signs of bacteremia, rather than a specific type of infection such as IE. **References:** NONE

OP-0309

Blood Ketone Measurements Can Be Used to Predict Myocardial FDG Uptake

P. Francis, *C. Eland;*
Royal Children's Hospital, Melbourne, AUSTRALIA.

Aim/Introduction: Infection imaging is an important utilization of Fluorodeoxyglucose(FDG) Positron Emission Tomography (PET) scanning. When there is concern regarding cardiac infection eg endocarditis, suppression of normal physiological uptake improves sensitivity and specificity of the study. Prolonged fasting, low carbohydrate diets and pre-treatment with heparin may minimise myocardial uptake but these rely on adequate preparation or anticoagulation that may be of risk in some patients. It is not always practical to prepare patients with urgent clinical indications with a prolonged fast. Blood Ketone levels rise as a physiological consequence of fasting and relative carbohydrate deficiency. We aimed to assess whether the point of care measurement of blood ketones prior to FDG PET scan predicts myocardial FDG uptake. **Materials and Methods:** 75 patients were included in the study with ages ranging from 7 months to 18 years. Patient preparation included a minimum fasting time of 6 hours and 12 hours for patients with a clinical indication of infection. Ketone measurements were taken at the time of blood glucose measurement, just prior to FDG administration. Maximum Standard Unit Value (SUVmax) values were collected using Siemens' syngo.via software system. Three different regions of the myocardium were analysed including the true lateral wall, the apical wall and the cavity of the left ventricle. Results: Graphs were created comparing the SUVmax value and the ketone measurement of each patient. The graph demonstrates that. A ketone measurement of >0.5 correlated with myocardial SUV <2. **Conclusion:** Our results demonstrate that as ketone measurements increase, SUV values decrease. A ketone measurement of >0.5 provides a SUVmax value of <2 in all cases. This information can be used to predict suppressed myocardial FDG PET uptake, in infection imaging, thereby limiting the need to use other pre-treatments and interventions. **References:** none

OP-0310

The diagnostic value of [^{18}F]FDG-PET/CT in detecting septic thrombosis in patients with venous catheter-related Staphylococcus aureus bacteremia

R. Tuinte[1], M. Gompelman[1], E. Aarntzen[1], I. Kouijzer[1], E. van Leerdam[1], M. Berrevoets[2], J. ten Oever[1], C. Bleeker-Rovers[1], G. Wanten[1];
[1]Radboud University Medical Center, Nijmegen, NETHERLANDS, [2]Elisabeth-TweeSteden Ziekenhuis, Tilburg, NETHERLANDS.

Aim/Introduction: Catheter-related septic thrombosis often complicates Staphylococcus aureus bacteremia (SAB) in patients with a central venous catheter. Diagnosis and management of septic thrombosis remains difficult and currently there is no reference standard for diagnosis. We describe the diagnostic value of [^{18}F]FDG-PET/CT imaging in a patient cohort and the potential contribution of quantitative measurements in detecting septic thrombosis. **Materials and Methods:** We selected patients with catheter-related SAB from our institutional database (period 2013-2020). The contribution of [^{18}F]FDG-PET/CT imaging on decision of final clinical diagnosis was evaluated. Additionally, Standardized Uptake Values (SUV) were measured and compared with a composite reference standard (clinical signs, initial result of the [^{18}F]FDG-PET/CT, and outcome of the Multidisciplinary Team (MDT) meeting) to identify a potential cut-off value for detection of septic thrombosis. Results: We identified 93 patients with a catheter-related SAB. Quantitative measurements were possible for 43 of the 56 patients in whom a [^{18}F]FDG-PET/CT scan was performed. A septic thrombosis was clinically diagnosed in 30% (13/43) of the cases. In 85% of these cases, significant [^{18}F]FDG-PET/CT uptake at the site of the thrombus was the deciding factor for diagnosis of septic thrombosis during the MDT Meeting. All mean SUV values of thrombotic lesions were significantly higher in patients with clinically proven septic thrombosis compared to patients in whom this diagnosis was rejected ($p<0.001$). A SUV_{peak} thrombus/SUV_{mean} blood ratio of 1.6 as cut-off to differentiate between septic thrombosis and non-septic thrombosis had a sensitivity of 92% (95% CI 64-100) and specificity of 89% (95% CI 65-99). A decision rule-based algorithm was designed to guide diagnosis of septic thrombosis. **Conclusion:** Quantitative [^{18}F]FDG-PET/CT derived parameters can be helpful to differentiate between septic and non-septic thrombosis in patients with catheter-related SAB. **References:** None

OP-0311

Inflammatory-Directed Whole-Body PET Can Alter Diagnosis in Treatment-Naïve Patients with Suspected Rheumatic Disease

R. Werner[1], K. V. Guggenberger[2], S. Serfling[1], T. Higuchi[3], M. G. Pomper[4], S. P. Rowe[4], M. Schmalzing[5], A. K. Buck[1], T. Bley[2], M. Fröhlich[5];
[1]Department of Nuclear Medicine, University Hospital Würzburg, Würzburg, GERMANY, [2]Department of Diagnostic and Interventional Radiology, University Hospital Würzburg, Würzburg, GERMANY, [3]Graduate School of Medicine, Dentistry and Pharmaceutical Sciences, Okayama University, Osaka, JAPAN, [4]The Russell H Morgan Department of Radiology and Radiological Science, Division of Nuclear Medicine, Baltimore, MD, UNITED STATES OF AMERICA, [5]Department of Internal Medicine II, Rheumatology/Clinical Immunology, University Hospital Würzburg, Würzburg, GERMANY.

Aim/Introduction: [^{18}F]FDG PET/CT has been widely utilized to assess the inflammatory burden in vasculature and joints of patients with suspected diagnosis of rheumatic disease. We aimed to elucidate the impact of [^{18}F]FDG on change in initially established diagnosis in treatment-naïve patients at time of scan. **Materials and Methods:** 60 patients, which were referred from our Department of Rheumatology for an [^{18}F]FDG PET/CT to assist in diagnosis, were analyzed. We compared the initially suspected diagnosis prior to PET to the final diagnosis, which was established by board-certified rheumatologists after the scan. In addition, vessel wall-to-liver (VLR) and joint-to-liver ratio (JLR) were assessed in 11 vessel segments and 10 joints, respectively and the derived semiquantitative uptake levels were also compared. Results: 37/60 (61.7%) of patients were treatment-naïve at time of scan (defined as no or only low-dose prednisone prior to imaging). After PET, the established diagnosis was large vessel vasculitis (LVV) in 21/37 (56.8%); polymyalgia rheumatica (PMR) in 6/37 (16.2%) and combined PMR+LVV in the remaining 10/37 (27%). PET altered suspected diagnosis in 28/37 (75.7%) of the patients (LVV, 15/21 [71.4%]; PMR, 4/6 [66.7%]; LVV+PMR, 9/10 [90%]). In patients with final diagnosis of LVV or PMR alone, the vast majority of patients had an unclear diagnosis prior to PET (LVV, 14/15 [93.3%]; PMR, 4/6 [66.7%]). However, if the final diagnosis was PMR+LVV, PMR had been suspected in 5/10 (50%), followed by an unclear diagnosis prior to the scan (3/10 [30%]). VLR of patients finally diagnosed with LVV tended to be significantly higher when compared to VLR in PMR (1.02±0.08 [95%CI, 0.96-1.1] vs. 0.92±0.1 [95%CI, 0.85-0.99], P=0.07), but not when compared to PMR+LVV (1.02±0.13 [95%CI, 0.93-1.1], P=1). JLR of individuals finally diagnosed with PMR (0.92±0.16, [95%CI, 0.8-1.03]), however, was significantly increased relative to JLR in LVV (0.56±0.04 [95%CI, 0.53-0.59]) and PMR+LVV (0.63±0.09 [95%CI, 0.56-0.69], P<0.001, respectively). **Conclusion:** In treatment-naïve individuals with suspected diagnosis of rheumatic disease, an

inflammatory-directed PET can alter diagnosis in >75% of the cases. Semiquantitative assessment assists in establishing final diagnosis, supporting the notion that a quantitative whole-body read-out of the entire vasculature and joints should be performed, independent of initially suspected diagnosis. **References:** none

OP-0312

Evaluation of F-18-FDG-PET/MRI in patients with echinococcosis

N. Eberhardt[1], J. P. Steinacker[1], L. Peters[2], S. Kapp-Schwoerer[2], P. Korf[3], M. Beer[4], C. Solbach[1], T. Kull[1], B. Grüner[2], A. J. Beer[1];
[1]Ulm University Medical Center, Department of Nuclear Medicine, Ulm, GERMANY, [2]Ulm University Medical Center, Department of Internal Medicine III – Section for Infectious Diseases, Ulm, GERMANY, [3]Siemens Healthcare GmbH, Erlangen, GERMANY, [4]Ulm University Medical Center, Department of Diagnostic and Interventional Radiology, Ulm, GERMANY.

Aim/Introduction: For evaluation of the inflammatory activity of infections with Echinococcus-multilocularis (EM), F-18-FDG-PET/CT is used both in primary diagnosis as well as for therapy monitoring. In this respect PET/MRI is a promising method by combining the advantages of the high sensitivity of molecular imaging with PET with the superior soft tissue contrast of MRI with a reduction of radiation exposure compared to PET/CT as well. Furthermore, the combination of morphological, functional and biological data from PET, MRI and DW-MRI in simultaneous PET/MRI has the potential of showing valuable additional biological information compared to PET/CT. **Materials and Methods:** Retrospectively 52 PET/MRI scans (Siemens Biograph mMR, 3 T) of patients with EM-infections were evaluated both under ongoing anthelminthic treatment as well as after operation (30F, 22M, median age 49yrs). One hour before the scans F-18-FDG was administered i.v. (approx. 350 MBq) and they were performed from mid-thorax to groin (native + contrast enhanced (CE) with Gadovist, 0.1 ml/kgBW) for approx. 30-40min (MRI sequences: axial T1-Flash CAIPI, T2-Haste STIR, T1-Flash CAIPI CE & liver: T2-Haste, DWI, dynamic CE T1-Flash; coronal: T2-Haste, T1-Flash fat sat CE). We assessed the visual identification and qualitative evaluation of potential EM-lesions and evaluated SUVs and ADC values semi-quantitatively using a region-of-interest (ROI) approach in representative solid non-cystic areas of EM-lesions with high FDG-uptake. Additionally, we performed voxel-based analysis of SUVs and ADC values. Results were analysed by Pearson's pairwise correlation analysis. Results: After resection all 13 patients had no residual EM-lesions or EM-recurrence during follow-up. For the 38 patients without prior resection, EM-lesions could be successfully identified, for 23/38 with elevated FDG uptake (SUVmean 2.8+/-1.6, ADCavg 1233+/-374mm^2/s). No significant correlation was found for SUV and ADC (R=0.004, p=0.973). In 14/52 further unclear liver lesions without notable FDG-uptake, MRI substantially facilitated differential diagnosis of an EM-lesion versus other entities. In comparison to equivalent PET/CT protocols, PET/MRI is associated with a ca. 70% reduction in radiation exposure. **Conclusion:** F-18-FDG-PET/MRI is a promising method in echinococcosis for detection of EM-lesions and evaluation of their inflammatory activity in both primary staging as well as for therapy monitoring. Compared to PET/CT a significant reduction of radiation exposure is possible. Moreover, differential diagnosis in non-FDG-avid unclear liver lesions is substantially facilitated. The missing correlation of the imaging biomarkers SUV and ADC suggests that they provide complementary information on the biology of EM-lesions, which warrants further evaluation in future studies. **References:** None

OP-0313

Disentangling inflammatory from fibrotic disease activity by fibroblast activation protein imaging

C. Schmidkonz[1], S. Rauber[2], A. Atzinger[1], T. Götz[1], A. Soare[2], M. Cordes[1], O. Prante[1], P. Ritt[1], T. Bäuerle[1], M. Köhner[1], U. Haberkorn[3], T. Kuwert[1], G. Schett[1], A. Ramming[2];
[1]University Hospital Erlangen, Department of Nuclear Medicine, Erlangen, GERMANY, [2]University Hospital Erlangen, Department of Rheumatology, Erlangen, GERMANY, [3]University Hospital Heidelberg, Department of Nuclear Medicine, Heidelberg, GERMANY.

Aim/Introduction: To date, there is no valuable tool to assess fibrotic disease activity in humans in vivo in a non-invasive way. This study aims to uncouple inflammatory from fibrotic disease activity in fibroinflammatory diseases such as IgG4-related disease. **Materials and Methods:** In this cross-sectional clinical study, 27 patients with inflammatory, fibrotic and overlapping manifestations of IgG4-related disease underwent positron emission tomography (PET) scanning with tracers specific for fibroblast activation protein (FAP; 68Ga-FAP inhibitor (FAPI)-04), 18F-fluorodeoxyglucose (FDG), magnetic resonance imaging (MRI) and histopathological assessment. In a longitudinal approach, 18F-FDG and 68Ga-FAPI-04 PET/CT data were evaluated before and after immunosuppressive treatment and correlated to clinical and MRI data. Results: Using combination of 68Ga-FAPI-04 and 18F-FDG-PET, we demonstrate that non-invasive functional tracking of IgG4-related disease evolution from inflammatory towards a fibrotic outcome becomes feasible. 18F-FDG-PET positive lesions showed dense lymphoplasmacytic infiltration of IgG4 + cells in histology, while 68Ga-FAPI-04

PET positive lesions showed abundant activated fibroblasts expressing FAP according to results from RNA-sequencing of activated fibroblasts. The responsiveness of fibrotic lesions to anti-inflammatory treatment was far less pronounced than that of inflammatory lesions. **Conclusion:** FAP-specific PET/CT permits the discrimination between inflammatory and fibrotic activity in IgG4-related disease. This finding may profoundly change the management of certain forms of immune-mediated disease, such as IgG4-related disease, as subtypes dominated by fibrosis may require different approaches to control disease progression, for example, specific antifibrotic agents rather than broad spectrum anti-inflammatory treatments such as glucocorticoids. **References:** none

OP-0314

[68Ga]Ga-Deferoxamine for Imaging of Bacterial Infections- Preliminary Results of a Phase I/II Study

B. Nilica[1], M. Petrik[2], C. Rangger[1], C. Uprimny[1], J. Pfister[1], M. Hajduch[3], G. Weiss[4], I. Virgolini[1], C. Decristoforo[1];
[1]Department of Nuclear Medicine, Medical University Innsbruck, Innsbruck, AUSTRIA, [2]Institute of Molecular and Translational Medicine, Faculty of Medicine and Dentistry, Palacky University, Innsbruck, CZECH REPUBLIC, [3]Institute of Molecular and Translational Medicine, Faculty of Medicine and Dentistry, Palacky University, Olomouc, CZECH REPUBLIC, [4]Department of Internal Medicine II, Innsbruck Medical University, Innsbruck, AUSTRIA.

Aim/Introduction: Timely and accurate diagnosis of bacterial infections is crucial for effective patient care. Molecular imaging has the potential for specific and sensitive detection of infections, replacing current methods based on biopsy or anatomical imaging. One of few microbe specific targets is the Siderophore system, not existing in mammalian cells. In recent studies we could show that the siderophore deferoxamine, established for treating iron overload diseases (as Desferal®), can be radiolabelled with ^{68}Ga and used for imaging of bacterial infections by PET (1). In preclinical studies excellent targeting of various clinically relevant bacteria such as Pseudomonas, Staphylococcus and Streptococcus ssp. finally resulting in high contrast imaging in Micro-PET/CT studies was shown, whereas microorganisms lacking Deferoxamine transporters (e.g. E.coli) provided no signal, indicating the specificity of this approach. We here report preliminary results of a Phase I/IIa study (EuEudraCT Nr: 2020-002868-31) on safety, tolerability, pharmacokinetics, radiation dosimetry and preliminary diagnostic performance in patients with bacterial infections using ^{68}Ga-deferoxamin. **Materials and Methods:** The clinical trial is designed in 2 Phases. In the initial Phase A with 4 patients sequential PET imaging is performed after injection of ^{68}Ga-deferoxamine for assessment of initial safety, tolerability and , pharmacokinetics and to calculate radiation absorbed doses. Phase B will include 11 patients to additionally assess initial diagnostic sensitivity for bacterial infections. Patients with a variety of clinically relevant infections are eligible for recruitment. ^{68}Ga-deferoxamine is prepared using an automated module and released based on defined quality criteria. Inclusion criteria include a proven bacterial muscoskeletal or pulmonary infections. Pharmacokinetics are assessed by sequential imaging, measuring activity in blood and urine and HPLC-analysis of blood and urine metabolites. Results: 68Ga-deferoxamine production resulted in high radiochemical yields and purity. So far one patient was included with a proven hip-joint infection. No sign of metabolic degradation was seen in blood samples, with a moderate rate of blood elimination, in urine 30-50% metabolites were detected. Serial PET imaging revealed rapid and stable accumulation in the infected area from 30-180min, corresponding with previous positivity in ^{18}F-FDG scan. Recruitment of further patients is currently ongoing and its outcome will be reported. **Conclusion:** This clinical study will, for the first time provide human data of a novel diagnostic PET radiopharmaceutical for direct imaging of infection. Initial results are promising and will be further complemented. **References:** (1) Petrik M, et al. ^{68}Ga-labelled desferrioxamine-B for bacterial infection imaging. Eur J Nucl Med Mol Imaging. 2021 Feb;48(2):372-382.

OP-0315

PET-CT Imaging of Pulmonary Inflammation with [68Ga]Ga-DOTATATE

E. Puuvuori[1,2], F. Liggieri[3], E. Chiodaroli[3], I. Velikyan[1], J. Sigfridsson[3], H. Romelin[3], S. Ingvast[4], O. Korsgren[4], O. Eriksson[1], G. Perchiazzi[3];
[1]Science for Life Laboratory, Uppsala University, Uppsala, SWEDEN, [2]Department of Medicinal Chemistry, Uppsala, SWEDEN, [3]Department of Surgical Sciences, Uppsala University, Uppsala, SWEDEN, [4]Department of IGP, Uppsala University, Uppsala, SWEDEN.

Aim/Introduction: In the characterization of various lung diseases, including nCOVID-19, detection of inflammatory cells would provide a tremendous benefit. For instance, macrophages participate to several stages of pulmonary inflammation by activating the inflammatory process and coordinating the repair cascade. Most importantly, they contribute to regulating the resolution and termination of the inflammation, which makes them a suitable target for measuring the severity and progress of lung diseases. [^{68}Ga]Ga-DOTATATE is extensively used in clinical imaging of neuroendocrine tumours overexpressing somatostatin receptor subtype 2 (SSTR-2). Since activated macrophages also overexpress SSTR-2, in this study we wanted to examine

if [^{68}Ga]Ga-DOTATATE could be utilized as a positron emission tomography (PET) marker for visualization of M1 macrophages in pulmonary inflammation. **Materials and Methods:** In order to induce inflammation in the lungs, lavage by warm saline was conducted to remove the alveolar surfactant and expose the lungs to ventilator inducted injury in farm pigs (n=7). Healthy pigs (n=3) were used as control. A 60 minutes dynamic PET scan over the lungs was performed after [^{68}Ga]Ga-DOTATATE injection. The tracer uptake and Hounsfield units (HU) in distinct segments of the lungs were assessed as mean standard uptake values (SUV) 30-60 minutes post injection. The lungs were independently visualized by contrast enhanced computed tomography (CECT) to assist segmentation of PET images and locate inflammation. Samples of basal and apical segments were harvested for histology staining. For binding specificity, SPRD rats were treated with lipopolysaccharides (LPS) by oropharyngeal aspiration. Organ biodistribution and ex vivo autoradiography (ARG) data were conducted on LPS treated, somatostatin induced blocking and control animals. Results: The accumulation of [^{68}Ga]Ga-DOTATATE on pigs was pronounced in the more severely damaged dorsal segments of the lungs (SUV_{mean}= 1.00 ± 0.54), compared with ventral segments (SUV_{mean}= 0.23 ± 0.05). On healthy pigs the uptake in the dorsal segment was SUV_{mean}= 0.31 ± 0.19, $p < 0.05$. Regional uptake of the tracer corresponded to the expected areas of injury as assessed by CT and were in line with HU analysis and histology. The uptake in rat lungs treated with LPS could be blocked and it was significantly higher compared with control group. **Conclusion:** [^{68}Ga]Ga-DOTATATE demonstrated significantly increased uptake in the severely injured parts of the porcine lungs and in rat LPS model the uptake could be blocked. According to these results, [^{68}Ga]Ga-DOTATATE is a potential candidate for future diagnostic clinical studies in the fight against severe lung diseases. **References:** none

801

Thursday, October 21, 2021, 09:00 - 10:30

Channel 1

CME 5: Infiltration, Infection and Infiltrative Nuclear Cardiovascular Diseases - Think Nuclear!

OP-0318
Cardiac Sarcoidosis

O. Gheysens; *Cliniques Universitaires Saint-Luc, Leuven, BELGIUM.*

OP-0319
Cardiac Amyloidosis

T. Kero; *Uppsala University, Department of Surgical Sciences/Nuclear Medicine & PET, Uppsala, SWEDEN.*

OP-0320
Enodcarditis

A. Scholtens; *Meander Medical Center, Department of Nuclear Medicine, Amersfoort, NETHERLANDS.*

OP-0321
Vasculitis

L. Gormsen; *Aarhus University Hospital, Department of Nuclear Medicine and PET Center, Aarhus, DENMARK.*

802-1

Thursday, October 21, 2021, 09:00 - 09:35

Channel 2

Interview with the Expert 5 - Creating Tracers

OP-0323
Interview - Creating Tracers

S. Fanti; *University of Bologna, Radiological Sciences - Nuclear Medicine, Bologna, ITALY.*

OP-0324
Interview - Creating Tracers

U. Haberkorn; *University Hospital Heidelberg, Department of Nuclear Medicine, Heidelberg, GERMANY.*

802-2

Thursday, October 21, 2021, 09:45 - 10:30

Channel 2

Interview with the Expert 6 - Paediatric NM today

OP-0325
Interview - Paediatric NM today

L. Biassoni; *Great Ormond Street Hospital for Children, Radiology, London, UNITED KINGDOM.*

OP-0326
Interview - Paediatric NM today

T. D. Barwick; *Imperial College, London, UNITED KINGDOM.*

804

Wednesday, October 20 - Saturday, October 23, 2021

on-demand pool, release on Wednesday, October 20 at 09:00

CTE 5: Update in Inflammation Imaging

OP-0327

Overview of Nuclear Medicine Techniques and Radiopharmaceuticals for Infectious and Inflammatory Diseases

C. Lund Denholt; Bispebjerg and Frederiksberg Hospital, Clinical department of physiology and nuclear medicine, PET & Cyclotron, Copenhagen, DENMARK.

OP-0328

Radiolabeled WBC Scan for Infectious Diseases

E. Noriega-Álvarez; Hospital General Universitario de Ciudad Real, Department of Nuclear Medicine, Ciudad Real, SPAIN.

OP-0329

PET/CT for Infectious and Inflammatory Diseases

A. W. J. M. Glaudemans; University Medical Center Groningen, Medical Imaging Center, Groningen, NETHERLANDS.

805

Wednesday, October 20 - Saturday, October 23, 2021

on-demand pool, release on Wednesday, October 20 at 09:00

Joint Symposium 9 (EANM/EAN): The New ATN Diagnostic Concept in Alzheimer's Disease

OP-0331

Introduction into the ATN Concept

B. Dubois; Salpétrière University Hospital, Behavioural Neurology Department and Dementia Research Center, Paris, FRANCE.

OP-0332

PET Tracers to Establish the ATN Profile

V. Villemagne; University of Pittsburgh, Department of Psychiatry, Pittsburgh, UNITED STATES OF AMERICA.

OP-0333

A Critical Clinician's Perspective on the ATN Concept

G. Frisoni; Geneva University Hospital, Memory Clinic, Geneva, SWITZERLAND.

OP-0334

PET Data Supporting/Opposing the ATN Concept

G. Chételat; Université de Caen Basse-Normandie, Multimodal Neuroimaging in Brain diseases Lab, Caen, FRANCE.

806

Wednesday, October 20 - Saturday, October 23, 2021

on-demand pool, release on Wednesday, October 20 at 09:00

Joint Symposium 10 (EANM/ILAE): PET/MRI in Epilepsy

OP-0336

Introduction

P. Federico; Hotchkiss Brain Institute, Cumming School of Medicine, University of Calgary, Calgary, CANADA.

OP-0337

Epilepsy - The Role of MRI in Patients with Focal Epilepsy

A. E. Vaudano; OCB Hospital, Neurological Unit, AOU Modena, Modena, ITALY.

OP-0338

Epilepsy - The Role of FDG-PET and FDG-PET/MR in Patients with Focal Epilepsy

E. Guedj; APHM, Service Central de Biophysique et Medecine Nucleaire, Marseille, FRANCE.

OP-0339

Is FDG the Only PET Tracer Useful for Patients with Epilepsy?

A. Hammers; PET Imaging Centre, King's College London, London, UNITED KINGDOM.

807

Wednesday, October 20 - Saturday, October 23, 2021

on-demand pool, release on Wednesday, October 20 at 09:00

Pitfalls & Artefacts 5: Pitfalls & Pearls in Paediatric Musculoskeletal

OP-0341

Physiological, Variants & Benign Tumours

D. de Palma; A.O. Ospedale di Circolo e Fondazione Macchi, Department of Nuclear Medicine, Varese, ITALY.

OP-0342

Non-Tumoural and Paraneoplastics Pitfalls

I. Roca; University Hospital Vall d'Hebron, Department of Nuclear Medicine, Barcelona, SPAIN.

OP-0343

Challenging Cases

M. Terroir Cassou; Oncopole, Department of Nuclear Medicine, Toulouse, FRANCE.

808

Wednesday, October 20 - Saturday, October 23, 2021

on-demand pool, release on Wednesday, October 20 at 09:00

M2M Track - Featured Session: Functional Brain Imaging

OP-0345

Introduction Talk

P. Payoux; *CHU Purpan, Nuclear Medicine Department, Toulouse, FRANCE.*

OP-0346

Longitudinal Evaluation Of The First Mutant Huntingtin PET Radioligand As A Marker For mHTT Lowering Therapies For Huntington's Disease

D. Bertoglio[1], J. Verhaeghe[1], S. De Lombaerde[1,2], F. Zajicek[1], T. Vasilkovska[1], A. Miranda[3], A. Gaertner[4], B. Huscher[4], A. Kakoulidou[4], I. Cardaun[4], A. Cornelius[4], T. Schwagarus[4], A. Van der Linden[1], S. Stroobants[1,2], Y. Wang[5], M. Skinbjerg[5], C. Dominguez[5], V. Khetarpal[5], L. Liu[5], I. Munoz-Sanjuan[5], J. Bard[5], S. Staelens[1];
[1]University of Antwerp, Wilrijk, BELGIUM, [2]Antwerp University Hospital, Edegem, BELGIUM, [3]University of Antwerp, Antwerpen, BELGIUM, [4]Evotec SE, Hamburg, GERMANY, [5]CHDI Management/ CHDI Foundation, Los Angeles, CA, UNITED STATES OF AMERICA.

Aim/Introduction: Huntington's Disease (HD) is a progressive autosomal dominant neurodegenerative disorder caused by mutant huntingtin (mHTT) protein; therefore, lowering mHtt expression is a key therapeutic strategy. The use of an allele-selective engineered transcription repressor (mHTT-ZFP) offers one mHTT-lowering approach[1]. Here, we assess the time-dependent therapeutic effects of this mHTT-ZFP in the Q175DN mouse model of HD at different ages using non-invasive in vivo PET imaging for mHtt aggregates as well as different phenotypic biomarkers (PDE10a, D_1R, and $D_{2/3}R$[2-4]). **Materials and Methods:** Intra-striatal injection of mHTT-ZFP using AAV-mediated gene transfer was performed in heterozygous (Het) zQ175DN mice either early (n=21; 2 month-old: mHTT-ZFP2M; no detectable mHTT aggregates) or late (n=23; 5 month-old: mHTT-ZFP5M; significantly detectable mHTT aggregates) in disease progression. As controls, het (n=22/study) and wt (n=20/study) mice were injected with DNA-binding domain mutant, mHTT-deltaDBD/ZFP (i.e. fails to lower mHTT) in the contralateral striatum. Dynamic PET imaging at 3 (only mHTT-ZFP2M paradigm), 6, and 10 months of age was performed with the radioligands: [^{11}C]CHDI-180R (mHTT aggregates), [^{18}F]MNI-659 (PDE10a), [^{11}C]SCH23390 (D_1 Receptor), and [^{11}C]Raclopride ($D_{2/3}$ Receptors) and were followed by post-mortem autoradiography and immunostaining analyses to confirm in vivo findings. Results: At 10M, all investigated biomarkers showed a significant therapeutic response following mHTT-ZFP treatment at 2M and 5M. A significant decrease in mHTT aggregate levels was measurable by [^{11}C]CHDI-180R in both the mHTT-ZFP2M (-41.5%, p<0.0001) and mHTT-ZFP5M (-25.5%, p<0.0001) paradigms. PDE10a was the most responsive phenotypic biomarker for both the mHTT-ZFP2M (+98.1%, p<0.0001) and mHTT-ZFP5M (+43.6%, p<0.0001) paradigms, followed by D_1R (mHTT-ZFP2M = +28.5%, p<0.0001), and $D_{2/3}R$ (mHTT-ZFP2M = +17.0%, p<0.01). Post-mortem analyses supported the in vivo PET quantification demonstrating significant reduction in mHTT levels as measured by in vitro [^{3}H]CHDI-180 autoradiography for both the mHTT-ZFP2M (-53.6%, p<0.0001) and mHTT-ZFP5M (-42.1%, p<0.0001) paradigms. Immunostaining confirmed the reduction in mHtt aggregates and lack of GFAP and Iba1 immunoreactivity as result of AAV delivery. **Conclusion:** Using PET imaging, we could quantify the time-dependent suppression of mHTT levels in response to therapeutic intervention as well as the functional restorative effects on different striatal markers. This study demonstrates mHTT lowering can be measured in the living brain, therefore enabling, for the first time, a translational path to assess a functional impact of mHTT lowering therapeutics. **References:** 1. Zeitler et al., Nat Med, 2019; https://doi.org/10.1038/s41591-019-0478-3;2. Bertoglio et al., PONE, 2018; https://dopi/org/10.1371/journal.pone.0206613;3. Häggkvist et al., J Nucl Med, 2017; https://doi.org/10.2967/jnumed.116.180497;4. Bertoglio et al., Mol Imaging Biol, 2021; https://doi.org/10.1007/s11307-020-01561-1.

OP-0347

Microglia Phenotypes Impact Metabolic Connectivity in Mouse Models of Neurodegenerative Diseases

J. Gnörich[1,2], A. Reifschneider[3], K. Wind[1,2], A. Zatcepin[1,2], T. Wiedemann[3], M. Grosch[4], X. Xiang[3,5], M. Khojasteh-Fard[3], F. Ruch-Rubinstein[1], M. Koehler[1], T. Blume[2,6], Y. Shi[2], G. Biechele[1], L. Beyer[1], F. Eckenweber[1], M. Scheifele[1], P. Bartenstein[1,7], J. Herms[2,6,7], S. Tahirovic[2], A. Capell[2,3], C. Haass[2,3,7], S. Ziegler[1,7], M. Brendel[1,2,7];
[1]Department of Nuclear Medicine, University Hospital of Munich, Munich, GERMANY, [2]German Center for Neurodegenerative Diseases (DZNE), Munich, GERMANY, [3]Biomedical Center (BMC), Division of Metabolic Biochemistry, Faculty of Medicine, Ludwig-Maximilians-Universität München, Munich, GERMANY, [4]German Center for Vertigo and Balance Disorders, University Hospital of Munich, LMU Munich, Munich, GERMANY, [5]CAS Key Laboratory of Brain Connectome and Manipulation, the Brain Cognition and Brain Disease Institute, Shenzhen Institutes of Advanced Technology, Chinese Academy of Sciences; Shenzhen-Hong Kong Institute of Brain Science-Shenzhen Fundamental Research, Shenzhen, CHINA, [6]Center for Neuropathology and Prion Research, Ludwig-Maximilians-University München, Munich, GERMANY, [7]Munich Cluster for Systems Neurology (SyNergy), Munich, GERMANY.

Aim/Introduction: Assessment of metabolic connectivity by brain FDG-PET has recently gained growing interest in approaching complex cerebral metabolic networks in neurodegenerative diseases. In this preclinical study, we

aimed to investigate metabolic connectivity during ageing and in presence of distinct microglia phenotypes. **Materials and Methods:** We analyzed metabolic networks measured by interregional correlation coefficients (ICCs) of FDG-PET scans in wild-type and transgenic mice with progranulin (Grn) knock-out (KO, = severe disease associated microglia), Trem2-KO mice (= microglia locked in homeostasis) and the double mutant Grn-KO x Trem2-KO. The impact of microglia on metabolic networks was determined by microglia depletion via a CSF1R inhibitor in wild-type mice at two different ages. FDG-PET images were acquired 30-60 min post injection by Siemens Inveon DPET and a 3T PET-MRI Mediso nanoScan with harmonized protocols. Intensity normalization of individual FDG-PET images was performed by scaling to the global mean after spatial normalization to a predefined FDG-PET template. Within maps of relative regional FDG uptake, 24 different pre-evaluated volumes of interest were applied and assigned to either cortical or subcortical networks. ICCs of 24 x 24 regional pairs were calculated and z-transformed prior to group comparisons. Results: Metabolic connectivity in cortical regions decreased as a logarithmic function of age in wild-type mice ($R^2 = 0.95$). Contrary, subcortical ICCs peaked as a quadratic function at 6 months of age ($R^2 = 0.83$). Microglia depletion by CSF1R inhibition resulted in a strong decrease of metabolic connectivity in wild-type mice at both ages studied (6-7m; $p < 0.002$, 9-10m; $p < 0.002$), when compared to untreated age-matched wild-type mice. In transgenic models we observed a dramatic increase of ICC's in Grn-KO mice when compared to wild-type mice in cortical ($p < 0.0001$) and hippocampal ($p < 0.0002$) networks. Trem2-KO mice did not show significant alterations in metabolic connectivity when compared to wild-type and the altered metabolic connectivity of Grn-KO mice was completely rescued in Grn-KO x Trem2-KO mice. **Conclusion:** Metabolic connectivity of cortical networks in mice decreases with ageing despite the known increased glucose uptake in older mice. We demonstrate that the presence of microglia has a strong impact on metabolic connectivity and that metabolic connectivity is linked to the microglia phenotype. Thus, metabolic connectivity comprises an important complementary read-out of FDG-PET when microglia activation states change. **References:** none

OP-0348

TREM2 Deficiency Desynchronises Microglial Activity in the Mouse Brain

A. Zatcepin[1,2], X. Xiang[3,4], S. Parhizkar[5], J. Gnörich[1,2], M. Grosch[6], K. Wind[1,2], Y. Shi[2], L. Beyer[1], G. Biechele[1], F. Eckenweber[1], T. Wiedemann[1], S. Lindner[1], A. Rominger[1,7], P. Bartenstein[1,8], M. Willem[3], S. Tahirovic[2], J. Herms[2,8,9], C. Haass[2,3,8], S. I. Ziegler[1,8], M. Brendel[1,2,8];

[1]Department of Nuclear Medicine, University Hospital of Munich, LMU Munich, Munich, GERMANY, [2]German Center for Neurodegenerative Diseases (DZNE) Munich, Munich, GERMANY, [3]Biomedical Center (BMC), Division of Metabolic Biochemistry, Faculty of Medicine, LMU Munich, Munich, GERMANY, [4]CAS Key Laboratory of Brain Connectome and Manipulation, the Brain Cognition and Brain Disease Institute, Shenzhen Institutes of Advanced Technology, Chinese Academy of Sciences; Shenzhen-Hong Kong Institute of Brain Science, Shenzhen, CHINA, [5]Department of Neurology, Washington University in St. Louis, St. Louis, MO, UNITED STATES OF AMERICA, [6]German Center for Vertigo and Balance Disorders, University Hospital of Munich, LMU Munich, Munich, GERMANY, [7]Department of Nuclear Medicine, University of Bern, Inselspital, Bern, SWITZERLAND, [8]Munich Cluster for Systems Neurology (SyNergy), Munich, GERMANY, [9]Center for Neuropathology and Prion Research, LMU Munich, Munich, GERMANY.

Aim/Introduction: Microglial activation is a hallmark of Alzheimer disease (AD) neuropathology, and the triggering receptor expressed on myeloid cells 2 (TREM2) is known to be a key component required for disease-associated microglia. However, the regional interplay of microglia cells in the brain has not been investigated yet. We tested if we could find evidence for a microglia connectome and if TREM2 deficiency has an impact on microglial synchronisation. **Materials and Methods:** In this work, we analysed interregional correlation coefficients (ICCs) of TSPO-PET scans deriving from APPPS1 and wild-type mice with and without additional TREM2 loss-of-function ($TREM2^{-/-}$). 60-90 min post injection ^{18}F-GE-180 PET scans were acquired for all mice using Siemens Inveon DPET. All images were manually registered to a T1 MR template in Ma-Benveniste-Mirrione atlas space. The individual images were elastically matched to corresponding PET templates in the atlas space to account for minor differences in individual brain anatomy. Myocardial correction was applied to normalize ^{18}F-GE-180 binding (Deussing et al. 2017). Regional values were extracted from a set of 21 volumes of interest (VOIs, 10 cortical and 11 subcortical), analogous to metabolic connectivity studies. First, we performed microglia depletion by CSF1R inhibition in wild-type mice to test if ICCs of TSPO-PET change when microglia are cleared from the brain. Second, we compared TSPO-PET ICC matrices between 18 wild-type/$TREM2^{+/+}$, 15 wild-type/$TREM2^{-/-}$, 11 APPPS1/$TREM2^{+/+}$, and 12 APPPS1/$TREM2^{-/-}$ mice. Results: Microglia-depleted mice showed the

most dramatic reduction of ICCs in all the compartments of the brain. Furthermore, we observed a significant decrease of ICCs in wild-type/TREM2$^{-/-}$ mice when compared to wild-type/TREM2$^{+/+}$mice in most of the VOI pairs, including both cortical and subcortical VOIs. In contrast, APPPS1/TREM2$^{-/-}$ mice indicated a reduction of ICCs only in subcortical regions including the cerebellum and the brainstem, when compared to APPPS1/TREM2$^{+/+}$ mice. **Conclusion:** Our ICC analysis of TSPO-PET scans in mice with depleted microglia provides the first evidence of a microglia connectome in the mouse brain and that molecular connectivity methods can potentially be applied to TSPO tracers. Microglia activity desynchronises upon TREM2 deficiency and in dependency of regional amyloid accumulation. **References:** Deussing, M., Blume, T., Vomacka, L., Mahler, C., Focke, C., Todica, A., ... & Brendel, M. (2018). Coupling between physiological TSPO expression in brain and myocardium allows stabilization of late-phase cerebral [18F] GE180 PET quantification. Neuroimage, 165, 83-91.

OP-0349

Exploring The Neuroprotective Effects Of Montelukast Treatment In A Rat Model Of Quinolinic Acid-Induced Neurotoxicity

M. Tassan Mazzocco[1,2], V. Murtaj[1,2], S. Belloli[2,3], L. Presotto[2], G. Mennuni[2,3], T. Canu[4], A. Coliva[2], E. Toninelli[2], R. M. Moresco[2,3,5];
[1]PhD Program in Neuroscience, Medicine and Surgery Department, University of Milano-Bicocca, Milan, ITALY, [2]Nuclear Medicine Department, San Raffaele Scientific Institute (IRCCS), Milan, ITALY, [3]Institute of Molecular Bioimaging and Physiology (IBFM), CNR, Milan, ITALY, [4]Department of Radiology, Experimental Imaging Center, San Raffaele Scientific Institute (IRCCS), Milan, ITALY, [5]Medicine and Surgery Department, University of Milano-Bicocca, Milan, ITALY.

Aim/Introduction: One intrastriatal administration of quinolinic acid (QA) in rats is sufficient to induce a lesion with features observed in Huntington's disease (HD) such as neurodegeneration and neuroinflammation. Our aim was to evaluate the effects of the leukotriene receptor antagonist Montelukast (MLK), which exhibited neuroprotection in different preclinical models, on QA-induced neurotoxicity using in vivo neuroimaging. Moreover, we tested whether and how functional interaction between brain areas was affected by QA lesion and MLK treatment by applying a connectomics analysis method. **Materials and Methods:** Healthy Sprague Dawley rats underwent Positron Emission Tomography (PET) with 2-Deoxy-2-[^{18}F]fluoroglucose ([^{18}F]-FDG) to assess basal brain glucose metabolism in regions of interest (ROIs). The right and left striatum of all animals were injected with QA and vehicle (VEH), respectively. Starting from the day before QA injection, animals were treated with MLK or VEH for 14 days. At 14- and 30-days post-lesion, animals were monitored with Magnetic Resonance Imaging (MRI) and PET using [^{18}F]-VC701, a translocator protein-specific radiotracer. At 4 months post-lesion, [^{18}F]-FDG PET was repeated. Pearson's correlation coefficient and Fisher-transformed z score were calculated between pairs of ROIs to compare metabolic connectivity between groups. Results: [^{18}F]-FDG uptake was higher in the lesioned hemisphere of MLK compared to VEH rats. This difference was significant ($p<0.05$) in the orbitofrontal cortex (OFC), motor cortex, somatosensory cortex and striatum. Including pre-lesion animals, QA significantly reduced [^{18}F]-FDG in the lesioned hemisphere of VEH compared to healthy rats. This difference was not found in MLK rats in most cortical areas. In the right OFC of MLK rats [^{18}F]-FDG uptake was significantly higher compared to VEH rats ($p<0.05$). No effect of MLK on neuroinflammation was detected by [^{18}F]-VC701, while a trend toward a reduction in MRI lesion volume was found in MLK compared to VEH rats. VEH rats exhibited stronger connectivity than healthy rats and several inversions in correlation, mainly involving prefrontal cortex (PFC) and striatum. MLK reverted several correlations involving PFC, while establishing new patterns related to the striatum and connections between left midbrain and right cortical regions. **Conclusion:** Chronic MLK treatment partially recovered metabolic activity after QA lesion in the striatum and several cortical regions. Connectomics data highlighted how brain circuits rearrange to compensate the lesion and showed that MLK was able to reverse some of the connections to the healthy condition pattern. Overall, these findings emphasize a potential clinical application of MLK in the management of HD-like symptoms. **References:** None

OP-0350

New Brain Atlas tool for Parkinson's Disease Images Analysis

S. Belloli[1,2], L. Presotto[3], D. Mercatelli[4], G. Mennuni[1,2], M. Tassan Mazzocco[2,5], A. Coliva[2], E. Toninelli[2], T. Canu[6], V. Bettinardi[2], M. Morari[4], R. M. Moresco[1,2,7];
[1]IBFM-CNR, Segrate, ITALY, [2]Nuclear Medicine Department, IRCCS San Raffaele, Milan, ITALY, [3]Nuclear Medicine Department, IRCCS San Raffaele, Segrate, ITALY, [4]Department of Neuroscience and Rehabilitation, University of the Study of Ferrara, Ferrara, ITALY, [5]PhD Program in Neuroscience, Medicine and Surgery Department, University of Milano-Bicocca, Milan, ITALY, [6]Department of Radiology, Experimental Imaging Center, IRCCS San Raffaele, Milan, ITALY, [7]Medicine and Surgery Department, University of Milano - Bicocca, Milan, ITALY.

Aim/Introduction: Parkinson's disease (PD) is characterized by the loss of dopaminergic (DA) neurons and the appearance of α-synuclein aggregates in the substantia nigra pars compacta (SNc) which are associated with chronic neuroinflammation. Several PD mouse models have been studied using Positron Emission Tomography (PET) with different radiotracers to shed light on disease features and progression. Images analysis standardization and correlation

of PET findings with different information as "omics" data are one of the biggest challenges in studying neurodegeneration models. The aim of this study is to develop a brain atlas tool with the common coordinate framework (CCFv3) of the Allen Mouse Brain Atlas[1] for the application in brain disorders. **Materials and Methods:** Twenty C57BL/6 male mice of three months of age were acquired with ^{18}F-FDG PET/CT (Molecubes, Gent, BE). Twelve of them underwent also 3D-T2 high resolution MR scans (isotropic voxel size 0.11 mm). All the images were elastically registered to the reference Allen Brain Atlas and then averaged to build a reference template on which 27 brain regions of volume of interest (VOI) were defined. To validate the toolbox, we applied the template to the study of mice subacutely injected with the parkinsonian drug 1-methyl-4-phenyl-1,2,3,6-tetrahydro-piridine (MPTP; 30 mg/kg/day for 7 days) subjected to a test re-test study (n=6) with the translocator protein (TSPO) radioligand ^{18}F-VC701. Analysis was performed in comparison to the PMOD software VOI template[2,3] to identify microglia/macrophages regions of activation in the PD model. Results: The toolbox application allowed the identification of 11 brain areas of significant ^{18}F-VC701 uptake increase, including left and right dorsal basal ganglia ($p<0.05$), left and right thalamus ($p<0.05$), and somatomotor and somatosensory cortex ($p<0.001$). The PMOD template, instead, identified significant radiotracer increase in basal ganglia and thalamus ($p<0.001$) but not in cortical regions, due to its broader areas partition. **Conclusion:** We developed a brain atlas tool for mouse that conforms to the CCFv3 providing regions that are optimized for in vivo imaging analysis and defined within its ontology. This tool allows to recognize more precisely the regions involved in microglia/macrophages activation in a PD mouse model compared to PMOD template and could potentially be applied to other models and processes. **References:** 1. https://mouse.brain-map.org/static/atlas 2. Ma Y et al. Neuroscience. 2005;135(4):1203-15. DOI 3. Mirrione MM et al. Neuroimage. 2007;38(1):34-42. DOI; Acknowledgement: - PRIN 2017-LYTE9M funded by Italian Ministry of Education, University and Research (MIUR); - ESFRI RoadMap: EuroBioimaging (Facility N. 45).

OP-0351

Dynamic behavior of brain and muscle glucose uptake during insulin challenges

C.-H. Malbert[1], *C. Marathe*[2], *A. Chauvin*[3], *M. Genissel*[3], *J. Georges*[3], *M. Horowitz*[4], *K. Jones*[5];
[1]*INRAE - Aniscan, Saint-Gilles, FRANCE,* [2]*University of Adelaide, Endocrine and metabolic unit, Adelaide, AUSTRALIA,* [3]*INRAE - UE3P, Saint-Gilles, FRANCE,* [4]*University of Adelaide, Adelaide Medical school, Adelaide, AUSTRALIA,* [5]*University of Adelaide, Endocrine and Metabolic unit, Adelaide, AUSTRALIA.*

Aim/Introduction: Recent animal and human data emphasized that brain glucose uptake (CMRglu) was increased in insulin-resistant obese during hyperinsulinemic-euglycemic clamp. This was reversed in the skeletal muscle, for which glucose uptake (MMRglu) decreased in identical conditions. While the clamp procedure was a proxy for postprandial insulin secretion, it did not reproduce the physiological pulsatility of insulin secretion, especially since peaks amplitudes were tripled in obese compared to lean. Our study aimed to quantify CMRglu vs. MMRglu, using dynamic PET and fPET, during a pulsatile insulin infusion clamp compared with fasted and steady insulin infusion clamp. **Materials and Methods:** CMRglu and MMRglu were quantified in twenty-four adult miniature pigs, half of them being insulin-resistant obese (81.6 ± 4.37 Kg) using a 4 months high-fat high-carbohydrate diet while the remaining being qualified as lean group (35.9 ± 1.08 Kg). CMRglu and MMRglu were obtained using dynamic PET ^{18}FDG scanning and direct measurement of arterial input function using an external arterio-veinous shunt. Three imaging sessions were performed per animal during either fasting, pulsatile insulin euglycemic clamp, and steady insulin euglycemic clamp. fPET was also achieved during pulsatile insulin clamp using continuous ^{18}FDG infusion (0.02 MBq/kg/min) to investigate the instantaneous relationship between glucose uptake and pulsatile insulin infusion. Pmod VOI-based and SPM statistical parameter mapping analyses were performed. Results: Whole-brain CMRglu was significantly ($p > 0.01$) increased during pulsatile insulin clamp compared to fasted condition both in lean (13.8 ± 0.28 vs. 8.3 ± 0.35 µmol/min/100g) and obese groups (12.8 ± 0.27 vs. 9.2 ± 0.23 µmol/min/100g). On the contrary, it was increased only in the obese group (16.2 ± 0.27 vs. 9.2 ± 0.40 µmol/min/100g obese vs lean) during steady insulin clamp while not significantly different the fasted condition. Kinetics analyses showed that plasma to tissue transfert was not entirely responsible for these modifications. MMRglu did not exhibit identical changes with a steady increase from fasting, pulsatile and steady insulin clamp observed in the lean group. No significant changes in MMRglu were observed during pulsatile or steady insulin infusion compared to fasting in the obese group. **Conclusion:** We demonstrated that pulsatile insulin infusion mimicking the postprandial condition was equally effective in lean and obese to increase CMRglu. In contrast, an equal amount of insulin steadily infused increased CMRglu in obese only. MMRglu increased in the lean only during insulin infusion irrespective of its delivery schedule. **References:** Rebelos et al, J clin Med, 2021

OP-0352

Neuroinflammation PET imaging for in vivo evaluation of aging process in a Down syndrome animal model

L. Estessi de Souza, M. Penido da Silva, C. Cristiano Real, D. De Paula Faria;
Universidade de São Paulo, São Paulo, BRAZIL.

Aim/Introduction: Down Syndrome (DS) is the most common genetic cause of intellectual disability in the world. Positron Emission Tomography (PET) using ^{11}C-PK11195 is a tool for evaluating innate immune cells activation in the central nervous system. The aim of this study was to evaluate neuroinflammation appearance during the aging process of an animal model of Down syndrome. **Materials and Methods:** DS transgenic mice (TS65Dn, n=6) and its littermate wild type (WT n=6), were evaluated with ^{11}C-PK11195 PET imaging. Tracer (±15 MBq) was injected intravenously and 30 min after, a static image was acquired for 20 min in a PET scanner for small animals. Images were quantified by PMOD™ software and the data was expressed in percentage of tracer increase compared to the 2-month time point. Data was analyzed by general linear model repeated measures (significant when $p \leq 0.05$). Iba-1 imunohistochemistry was performed to confirm neuroinflammation in the post-mortem tissue (microglia activation). Results: ^{11}C-PK11195 uptake was increased in the age of 5 months for the Ts65Dn and WT animals when compared to its respective 2-month-old time point, where the increases were: striatum, WT 93% (p=0.005), Ts65Dn 48% (p=0.033); cortex, WT 123% (p=0.002), Ts65Dn 60% (p=0.016); hippocampus, WT 63% (p=0.017), Ts65Dn 62% (p=0.010); thalamus, WT 57% (p=0.021), Ts65Dn 42% (p=0.032); cerebellum, WT 80% (p=0.016); brainstem, WT 59% (p=0.001), Ts65Dn 64% (p=0.022); midbrain, Ts65Dn 43% (p=0.046). Comparing the age of 14 months to 2 months-old, the increase of tracer uptake was even more expressive, striatum: WT 172% (p=0.0001), Ts65Dn 100% (p=0.001); cortex WT 205% (p=0.0001), Ts65Dn 109% (p=0.0001); hippocampus WT 143% (p=0.0001), Ts65Dn 95% (p=0.0001); thalamus WT 140% (p=0.0001), Ts65Dn 208% (p=0.0001); cerebellum WT 187% (p=0.0001), Ts65Dn 97% (p=0.001); brainstem, Ts65Dn 87% (p=0.015) and midbrain WT 133% (p=0.001), Ts65Dn 71% (p=0.006). All statistical differences were related to uptake increase within ages and there were no differences between Ts65Dn and WT animals at any time point, and this data agrees with Iba-1 immunohistochemistry. **Conclusion:** ^{11}C-PK11195 PET imaging was able to detect neuroinflammation during aging of a transgenic model of Down syndrome and its littermate wild-type. These data suggest that the neuroinflammation is related to the aging process per se and there is no influence by the presence of the 21 trisomy. **References:** none

OP-0353

Evaluation of [^{18}F]F-DPA PET for detecting microglial activation in the spinal cord of a rat model of neuropathic pain

S. Shimochi[1,2], T. Keller[1], J. Rajander[3], E. Löyttyniemi[4], O. Solin[1], P. Nuutila[1], S. Kanaya[2], E. Yatkin[5], T. J. Grönroos[1], H. Iida[1];
[1]Turku PET Centre, University of Turku, Turku, FINLAND, [2]Nara Institute of Science and Technology, Ikoma City, JAPAN, [3]Accelerator Laboratory, Turku PET Centre, Åbo Akademi University, Turku, FINLAND, [4]Department of Biostatistics, University of Turku, Turku, FINLAND, [5]Central Animal Laboratory, University of Turku, Turku, FINLAND.

Aim/Introduction: Recent studies have linked activated spinal glia to neuropathic pain. Here, using a positron emission tomography (PET) scanner with high spatial resolution and sensitivity, we evaluated the feasibility and sensitivity of N,N-diethyl-2-(2-(4-([^{18}F]fluoro)phenyl)-5,7-dimethylpyrazolo[1,5-a] pyrimidin-3-yl)acetamide ([^{18}F] F-DPA) PET imaging technique for detecting spinal cord microglial activation after partial sciatic nerve ligation (PSNL) in rats. **Materials and Methods:** Neuropathic pain was induced in rats (n = 14) by PSNL, and pain sensation tests were conducted before surgery and 3 and 7 days post-injury. On day 7, in vivo PET imaging and ex vivo autoradiography were performed using [^{18}F]F-DPA or [^{11}C]PK11195. Biodistribution and ex vivo PET imaging of the removed spinal cord was carried out with [^{18}F]F-DPA. Results: Mechanical allodynia was confirmed in the PSNL rats from day 3 through day 7. Ex vivo autoradiography showed a higher lesion-to-background uptake with [^{18}F]F-DPA compared with [^{11}C]PK11195. Ex vivo PET imaging of the removed spinal cord showed clear [^{18}F] F-DPA accumulation in the inflammation site. However, the standardized uptake value (SUV) of in vivo [^{18}F]F-DPA PET was not significantly increased in the lesion compared with the reference region. The likely explanation was that lesion SUVs were much higher with in vivo PET (1.00 ± 0.10) compared with ex vivo PET (0.20 ± 0.02) and biodistribution (0.35 ± 0.10), which disturbed observation of tracer accumulation. The same pattern applied for in vivo [^{11}C]PK11195 PET. **Conclusion:** Novel [^{18}F]F-DPA aided visualization of the spinal cord inflammation site in PSNL rats on ex vivo autoradiography and was superior to [^{11}C]PK11195. However, in vivo [^{18}F]F-DPA PET did not allow for visualization of tracer accumulation. The main reasons for this result were the small lesion size and insufficient SUVs relative to intrinsic background noise in the restricted spinal cord region, which is surrounded by organs with high radioactivity, and associated with several potential physical factors. **References:** none

OP-0354

Validation of 2-Deoxy-2-[^{18}F]fluorosorbitol (^{18}F-FDS) repurposed as a PET imaging biomarker of Blood Brain Barrier integrity in vivo

G. Hugon, S. Goutal, A. Dauba, A. Winkeler, A. Novell, N. Tournier; Université Paris-Saclay, CEA, CNRS, Inserm, BioMaps, Service Hospitalier Frédéric Joliot, Orsay, FRANCE.

Aim/Introduction: Non-transported low molecular weight sugars or polyols such as sucrose or mannitol are widely used for quantitative determination of paracellular (between-cell) transport across membranes in vitro. They provide sensitive and quantitative markers of biological membrane integrity. Sorbitol is an isomer of mannitol. 2-Deoxy-2-[^{18}F]fluorosorbitol (^{18}F-FDS) is a non-transported and non-metabolized sorbitol derivative, easily obtained from the reduction of ^{18}F-FDG. Biodistribution ^{18}F-FDS shows negligible baseline brain uptake. We hypothesized that ^{18}F-FDS may provide a quantitative PET imaging biomarker of blood-brain barrier (BBB) integrity in vivo. **Materials and Methods:** A protocol using Focused Ultrasound technology with microbubbles (FUS) was performed to generate a transient and hemispheric opening of the BBB in the right brain hemisphere in 6 Balb/c nude mice, compared with 3 control mice (no FUS). Five min after FUS, ^{18}F-FDS (4.2±0.7 MBq) was injected i.v followed by 60 min microPET acquisition. Animals were then sacrificed and brain removed to visually check Evan's blue extravasation as a post-mortem marker of BBB disruption. Time-activity curves (TACs) were measured in the right and left hemisphere. An image-derived input function was obtained from radioactivity the aorta. A 1-tissue compartment model was used to estimate the influx (K_1) and efflux (k_2) transfer constants as well as the total volume of distribution ($V_T = K_1/k_2$). Results: In FUS mice, higher uptake of ^{18}F-FDS was observed in opened hemisphere. Area Under the TACs (0-60 min) was significantly higher in the hemisphere with disrupted BBB compared to contralateral hemisphere (1.81±0.9-fold increase, $p<0.01$); or any hemisphere of control mice ($p<0.01$). Significant increase in K_1 (1.4±0.69-fold, $p<0.05$), V_T (2.43±0.8-fold, $p<0.001$) and decrease in k_2 (1.72±0.37-fold, $p<0.01$) was observed in the sonicated compared with the contralateral hemisphere in the FUS group but not in the control group, consistent with ex vivo Evan's blue extravasation. **Conclusion:** Our results show that ^{18}F-FDS PET signal is increased with suitable sensitivity when BBB integrity is compromised. Compared with other imaging techniques such as contrast (gadolinium)-enhanced MRI, quantitative PET allows for kinetic modelling. This revealed that BBB disruption had consequences on both the influx and the efflux transport of solutes across the BBB.^{18}F-FDS was initially developed for imaging of bacterial infection or renal function. Our preclinical data suggest that ^{18}F-FDS PET may be repurposed as a biomarker of BBB integrity for non-invasive and quantitative investigation of BBB integrity in the living brain in several pathophysiological situation. **References:** none

OP-0355

The (-)[^{18}F]FBVM to in vivo vizualise the VAChT by PET

J. Vercouillie[1], F. Buron[2], P. Emond[1], G. Chicheri[1], S. Serrière[1], J. Busson[1], Z. Gulhan[3], S. Bodard[1], A. Oury[1], L. Galineau[1], H. Marzag[2], D. Guilloteau[1], S. Routier[2], S. Chalon[1];
[1]UMR 1253, iBrain, Université de Tours, Inserm, Tours, FRANCE,
[2]ICOA, UMR 7311, Univesrity of Orléans, Orleans, FRANCE,
[3]INSERM 1253, CERRP, Tours Hospital, Tours, FRANCE.

Aim/Introduction: The vesicular acetylcholine transporter (VAChT) is a relevant biomarker to assess cholinergic dysfunction in neurodegenerative diseases[1-2] or to measure cholinergic cardiac parasympathetic activity[3]. Many efforts have been made to develop suitable imaging agents (PET or SPECT) to in vivo vizualise the VAChT. We report here the first radiosynthesis of [^{18}F]FBVM and the enantiomeric purification. (+/-), (+) and (-)[^{18}F]FBVM were evaluated in rodents as well as (-)[^{18}F]FEOBV for comparison. **Materials and Methods:** (+/-)[^{18}F]FBVM was synthetized from its corresponding (+/-) pinacol borane precursor in one step. The enantiomeric purification of (+) and (-)[^{18}F]FBVM were performed using the Chiralcel OD column. (-)[^{18}F]FEOBV was obtained in a one step process using the commercial enantiomerically pure precursor according to standard procedure[4]. The brain accumulation of radiotracers was measured ex vivo by biodistribution study at 2 hours after i.v. injection, and in vivo using the microPET-CT SuperArgus system (Sedecal, Madrid, Spain) in adult Wistar rats. Competition studies to evaluate non specific binding were performed using the VAChT antagonist (-)vesamicol (1mg/kg). Results: (+/-)[^{18}F] FBVM was obtained in 62 ± 2 min in 20 to 43 %RCY. The isolation of both enantiomers was initially obtained after two HPLC purifications (C18 and chiral columns), then optimized with only the chiral purification. (+) and (-)[^{18}F]FBVM were respectively obtained in 66 and 71 min with RCY up to 29 %. Molar activities of the four radiotracers were between 100 and 200 GBq/µmole. The brain uptake of all tracers was significantly higher in the striatum and significantly lower in the cerebellum than in other regions. The striatum/cerebellum uptake ratio was significantly higher for (-)[^{18}F]-FBVM (5.84), than for (+/-)[^{18}F]-FBVM (3.91), (-)[^{18}F]-FEOBV (3.59) and (+)[^{18}F]-FBVM (1.52). The pre-injection of vesamicol induced a reduction of the 4 tracers uptake in all brain regions although it was more significant for (-)[^{18}F]-FBVM than for (-)[^{18}F]-FEOBV (e.g., -46% and -30% in the striatum, respectively). PET images confirmed a higher signal/noise ratio for (-)[^{18}F]-FBVM than for the 3 other tracers. **Conclusion:** We were able to radiolabel and isolate the (-)[^{18}F]FBVM in good yield and high ee purity and we demonstrated that it has a better sensitivity for the VAChT PET imaging than (+)[^{18}F]FBVM and (-)[^{18}F]FEOBV. **References:** (1) Van der Zee et al. Movement Disorders. 2021. 36(3):642-650. (2) Aghourian et al. Mol Psychiatry. 2017. 22(11):1531-1538. (3) Saint-Georges et al. Journal of Nuclear Cardiology. 2021. 28, 1;50-4. (4) Mulholland et al. Synapse. 1998. 30:263-274

809

Wednesday, October 20 - Saturday, October 23, 2021

on-demand pool, release on Wednesday, October 20 at 09:00

Cutting Edge Science Track - TROP Session: Diagnostic Dosimetry

OP-0357

[^{123}I]IMAZA: Biodistribution and Radiation Dosimetry in Patients with Adrenal Tumors

S. Beykan[1], H. Hänscheid[1], S. Andreas[1], S. Hahner[2], A. K. Buck[1], M. Lassmann[1];

[1]Department of Nuclear Medicine, University of Würzburg, Würzburg, GERMANY, [2]Division of Endocrinology and Diabetes, Department of Medicine I, University Hospital of Würzburg, University of Würzburg, Würzburg, GERMANY.

Aim/Introduction: The newly developed compound IMAZA labelled with I-123 is a promising diagnostic tracer for the differential diagnosis of adrenal incidentalomas. We provide first results on the biodistribution and dosimetry of [^{123}I]IMAZA. **Materials and Methods:** 21 patients' sequential whole-body planar scans at nominally 0.17, 0.75, 2, 5, and 24 h, several blood samples between 0.02 h and 24 h and a single SPECT/CT scan at 5 h after the administration of 131-189 MBq [^{123}I]IMAZA were analyzed. The specific uptake values as a function of time were measured for the whole-body, kidneys, liver and the blood. Whole-body retention was derived by normalizing the geometric mean of the net count rates in the planar scans to the first scan. The SPECT/CT scan was used to normalize the planar count rates in the kidneys, bladder and the liver to the absolute activity concentrations. The blood samples were measured in a calibrated well counter. The time-integrated activity coefficients (TIACs) including uncertainties were calculated with NUKFIT (1). The kidney-bladder model with 3.5 h voiding interval was used to estimate the urinary bladder TIAC. The absorbed dose (AD) and effective dose (ED) coefficients were calculated with IDAC-Dose2.1 (2) using ICRP 110 adult computational voxel phantoms. Results: While [^{123}I]IMAZA showed high specific accumulation in adrenocortical tumors in many of the patients, healthy adrenal glands were scintigraphically not visible. Increased activity concentrations were evident in the liver and weakly detectable in the kidneys. Activity excretion was almost exclusively renal; a minor hepatobiliary component was dosimetrically irrelevant. The mean TIACs were: whole body: 5.47±1.28 h, liver: 1.41±0.08 h, kidneys: 0.09±0.04 h, urinary bladder: 1.43±0.16 h and red bone marrow: 0.41±0.08h. The highest AD coefficient was calculated for the urinary bladder wall (0.06±0.01 mGy/MBq). The calculated EDs were in the range of 0.6-2.4 mSv (Mean ED coefficient: 0.009±0.003 mSv/MBq). **Conclusion:** Observed low background activity associated with the rapid clearance of [^{123}I]IMAZA improves the diagnostic evaluation at similar or lower doses to organs as compared to [^{18}F]FDG and other ^{123}I- and ^{68}Ga-labeled agents. The bladder TIAC and thus the voiding interval largely determine the individual radiation exposure. **References:** (1)Kletting P, et al. Med Phys 2013. (2) Andersson M, et al. EJNMMI research, 2017.

OP-0358

Pre-therapy ^{123}I-NaI dosimetry for predicting salivary gland absorbed doses from ^{131}I-NaI therapy

L. Vávrová[1], J. Gear[1], J. Taprogge[1], I. Murray[1], S. Brown[2], J. Swain[2], J. Wadsley[3], G. Flux[1];

[1]The Royal Marsden NHS Foundation Trust and Institute of Cancer Research, Sutton, UNITED KINGDOM, [2]CTRU, University of Leeds, Leeds, UNITED KINGDOM, [3]Weston Park Hospital, Sheffield, UNITED KINGDOM.

Aim/Introduction: Salivary gland hypofunction or xerostomia has been reported as a common side effect following ^{131}I-NaI therapy for differentiated thyroid cancer patients (DTC) after thyroidectomy. The aim of this study was to assess the absorbed doses per administered activity delivered to the salivary glands during ^{131}I-NaI therapy and investigate the correlation between absorbed doses predicted based on ^{123}I-NaI pre-therapeutic scans and ^{131}I-NaI therapy absorbed doses. **Materials and Methods:** For a subset of patients in the UK-based multi-centre clinical trial SELIMETRY (EudraCT No 2015-002269-47), pre- and post-therapeutic dosimetry was performed. This involved up to five SPECT/CT scans at 5, 24, 30, 48 and 72 hours after administration of 370 MBq of ^{123}I-NaI under rhTSH stimulation. Four post-therapy dosimetry scans were performed at 24, 48, 72 and 144 hours following radioiodine therapy with 5.5 GBq of ^{131}I-NaI under rhTSH stimulation. The SPECT scans were quantified using system calibration factors [1]. Volumes of left and right parotid and submandibular glands were determined from CT scans. Activity retention was determined from SPECT scans using volumes of interest defined by a threshold matching the CT-derived volumes. The time activity curves were fitted with a double exponential function to obtain cumulated activity. The correlation between predicted and actual absorbed doses was approximated with a linear function and assessed using R^2 and F-test for regression analysis. Results: Based on preliminary results, the median absorbed doses per administered activity of parotid and submandibular glands were 0.16 mGy/MBq (range 0.00-0.60) and 0.30 mGy/MBq (range 0.07-0.51) for ^{123}I-NaI prediction and ^{131}I-NaI post-therapy imaging, respectively. For the linear regression of ^{131}I-NaI absorbed doses on ^{123}I-NaI predicted absorbed doses to the salivary glands, R^2 was 0.89 and p-value < 0.001 (F-test for regression). **Conclusion:** Estimated absorbed doses per administered activity are in a good agreement with values published in literature. A strong and significant correlation was observed between absorbed doses predicted from pre-

therapeutic scans and those estimated from post-therapeutic imaging. These results suggest that absorbed dose to salivary glands can be predicted using pre-therapy ^{123}I-NaI dosimetry and considered while planning the therapeutic activity in order to prevent adverse effects. **References:** [1] Gregory RA et al. Phys Med Biol. 2019;64(24):24501

OP-0359

First Evaluation of PET-Based Human Biodistribution and Radiation Dosimetry of ^{64}Cu-iPSMA

B. Góngora-Servín[1], B. Rivera-Bravo[1], A. R. Jalilian[2], M. Avila-Rodriguez[1];
[1]Universidad Nacional Autónoma de México, Ciudad de Mexico, MEXICO, [2]International Atomic Energy Agency, Vienna, AUSTRIA.

Aim/Introduction: Following the successful preparation and preclinical evaluation of [^{64}Cu]Cu-NOTA-HYNIC-iPSMA (^{64}Cu-iPSMA) as a potential radiopharmaceutical for therasnostic applications in prostate cancer [1], the aim of this research was to determine the human biodistribution and estimate the radiation dosimetry of ^{64}Cu-iPSMA, using whole-body (WB) PET scans in healthy volunteers. **Materials and Methods:** Three healthy volunteers were included in this study (male, 44.3±14.4 y.o., mean weight 71.6±1.5 kg). After I.V. injection of the tracer (4.0 MBq/kg), 3 consecutive WB emission scans were acquired at 5, 30, and 60 min after injection. Additional scans were acquired at 5, 9 and 24 h p.i. Low-dose CT scans without contrast were used for anatomic localization and attenuation correction. OLINDA/EXM software was used to calculate human radiation doses using the reference male adult model. Sphere model was used to calculate the doses to prostate, salivary and lacrimal glands, while for bladder and bowel well stablished dynamic urinary bladder model (MIRD Pamphlet No. 14) and gastrointestinal model (ICRU 30) were used. Results: The injection of 287±6 MBq of ^{64}Cu-iPSMA produced no observable adverse events or clinically detectable pharmacologic effects in any of the 3 subjects. Renal excretion of the tracer was observed at early times p.i., while biliary/gastrointestinal excretion was apparent at late times. The highest uptake ratio was observed in the liver, kidneys, and bowel. As expected, images also revealed uptake of ^{64}Cu-iPSMA in the salivary and lacrimal glands. Calculated mean absorbed doses per administered activity for large intestine, small intestine, urinary bladder wall, kidneys and liver were 335±35, 111±20, 82±1, 79±54 and 74±3 (μGy/MBq), respectively. Calculated doses using the sphere model were 9.2±0.6, 156±32, 178±81, 116±77, and 897±43 (μGy/MBq) for the prostate, parotid, submandibular, sublingual, and lacrimal glands, respectively. Finally, the calculated mean effective dose per administered activity was 73.2±10.1 μSv/MBq. **Conclusion:** To our knowledge, dosimetry estimates for a PSMA-based radiopharmaceutical labeled with ^{64}Cu have not previously been reported for humans. Effective dose calculated for ^{64}Cu-iPSMA is somewhat higher than the reported for ^{18}F and ^{68}Ga labeled PSMA ligands, however, still safe and more suitable for imaging purposes in theranostic applications. Research supported by International Atomic Energy Agency CRP code F22067-RC 20569. **References:** [1] G. Ferro-Flores, B. Ocampo-García, M. Luna-Gutierrez, C.L. Santos-Cuevas, Synthesis and preclinical evaluation of ^{64}Cu-NOTA-HYNIC-iPSMA, International Symposium on Trends in Radiopharmaceuticals (ISTR-2019), IAEA Conference Proceedings.

OP-0360

^{64}Cu-ATSM as a therapeutic agent in solid tumor? preliminary results of a whole body human dosimetry study

N. Varmenot[1,2,3], M. Colombié[1], C. Rousseau[1,2,4], F. Haddad[5,3,4], L. Ferrer[1];
[1]ICO René Gauducheau, F-44800 Saint-Herblain, FRANCE, [2]CRCINA UMR 1232 INSERM, F-44000 Nantes, FRANCE, [3]GIP ARRONAX, F-44800 Saint-Herblain, FRANCE, [4]Université de Nantes, F-44000 Nantes, FRANCE, [5]SUBATECH, IMT Atlantique, CNRS/IN2P3, F-44000 Nantes, FRANCE.

Aim/Introduction: Preclinical and clinical studies demonstrated the interest of ^{64}Cu-ATSM as an hypoxia imaging agent, illustrating redox at the tumor scale as a pejorative prognosis factor [1]. Due to its beta minus (0.574 MeV, 40%) and electron capture (42.6%) decay emission components, ^{64}Cu-ATSM has also been considered as a potential therapeutic agent, able to target hypoxic tumors directly [2, 3]. In the frame of a clinical study involving ^{64}Cu-ATSM evaluation in locally advanced rectal cancer (NCT03951337), an ancillary dosimetry study is conducted to evaluate the potential interest of this tracer as therapeutic agent. We report here dosimetric results of the first patient over the tenth to be enrolled. **Materials and Methods:** Whole body PET/CT acquisitions were performed with a Biograph Vision 450 (Siemens Medical Solution, USA) at 1.5h, 4h, 24h, 28h and 48h after intravenous injection of ^{64}Cu-ATSM (3MBq/kg). Absorbed doses were evaluated for the tumor and organs presenting major uptake assessed by a physician visual review. Organ and tumor delineation and absorbed doses calculation were performed with OpenDose3D a freely available module of 3DSlicer [4]. Monoexponential fit was used to determine cumulated activities in organs and tumor. Results: After intravenous injection of 320 MBq of ^{64}Cu-ATSM, main uptakes were observed in liver and colon with 24.2±9.2 mGy and 19.7±9.9 mGy as respective absorbed doses and standard deviations. Rectal tumor revealed an heterogeneous uptake related to its hypoxic status and the respective absorbed dose and standard deviation were 2.6±3.0 mGy. **Conclusion:** These first dosimetric results based on a diagnostic evaluation of ^{64}Cu-ATSM in one rectal cancer patient showed a relative high uptake in liver and colon as compared to tumor uptake. With such a differential uptake

ratio, therapeutic activity required for controlling the tumor would led to complication for the organs at risk. The potential inter-patient variability in tumor uptake should be confirmed with the other patients to be enrolled in this study. We expect supplementary data to be presented at the congress. **References:** 1. Laforest R et al. Dosimetry of $^{60/61/62/64}$Cu-ATSM: a hypoxia imaging agent for PET. Eur J Nucl Med Mol Imaging. 2005. 2. Gutfilen B et al. Copper-64: a real theranostic agent. DDDT. 2018. 3. Obata A et al. Basic characterization of ^{64}Cu-ATSM as a radiotherapy agent. Nuclear Medicine and Biology. 2005. 4. Fedorov A et al. 3D Slicer as an Image Computing Platform for the Quantitative Imaging Network. Magn Reson Imaging. 2012.

OP-0361

Biokinetics and radiation dosimetry of [^{18}F]-PSMA-1007

E. Hvittfeldt[1], M. Björsdorff[1], J. Oddstig[2], S. Leide Svegborn[3], G. Brolin[2], D. Minarik[3], E. Trägårdh[1,4];
[1]Clinical Physiology and Nuclear Medicine, Skåne University Hospital and Lund University, Malmö, SWEDEN, [2]Radiation Physics, Skåne University Hospital and Lund University, Lund, SWEDEN, [3]Radiation Physics, Skåne University Hospital and Lund University, Malmö, SWEDEN, [4]Wallenberg Centre for Molecular Medicine, Lund, SWEDEN.

Aim/Introduction: PET-CT using prostate-specific membrane antigen (PSMA) ligands is a recent method for imaging of prostate cancer. The most commonly used tracer is [^{68}Ga]Ga-PSMA-11. A more recent tracer, [^{18}F]-PSMA-1007, offers possible advantages concerning production and biokinetics. Radiation dosimetry data for this ligand is limited to a material of three healthy volunteers[1]. The purpose of this study was to study the biokinetics and dosimetry of [^{18}F]-PSMA-1007 in patients with prostate cancer. **Materials and Methods:** Twelve patients with prostate cancer referred for [^{18}F]-PSMA-1007 PET-CT were injected with 4.0 MBq/kg [^{18}F]-PSMA-1007. Eight PET-CT scans with concomitant blood sampling was performed, the first four scans within 30 minutes of injection and the eighth after 330 minutes. Urine was collected until the following morning. With the support of a previously developed AI[2], volumes of interest for radiation sensitive organs and organs with high uptake of [^{18}F]-PSMA-1007 were created in the PET images. A biokinetic compartment model was developed using activity data from PET images and blood and urine samples. Time-activity curves and normalized cumulated activity for all delineated organs were calculated. The software IDAC 2.1 was used to calculate the effective dose and absorbed dose to various organs. Results: High concentrations of activity is seen in the liver, kidneys, parts of the small intestine, spleen, salivary glands and lacrimal glands with seemingly irreversible uptake. Approximately 8% of injected activity is eliminated through urine in 20 hours. The hepatobiliary elimination was approximated to 6% after 5.5 hrs. The highest absorbed doses are in the lacrimal glands, kidneys, salivary glands, liver and spleen (0.11 - 0.066 mGy/MBq). The effective dose is 0.025 mSv/MBq. **Conclusion:** Biokinetics and radiation dosimetry of [^{18}F]-PSMA-1007 was studied in twelve patients with prostate cancer. [^{18}F]-PSMA-1007 is taken up preferentially in the liver, kidneys, parts of the small intestine, spleen, salivary glands and lacrimal glands. Binding to organs seems largely irreversible but there is some excretion through bile and urine. The highest absorbed doses are in the lacrimal glands, kidneys, salivary glands, liver and spleen. The effective dose is 0.025 mSv/MBq (8.0 mSv to a man weighing 80 kg using our clinical protocol). **References:** [1] F-18 labelled PSMA-1007: biodistribution, radiation dosimetry and histopathological validation of tumor lesions in prostate cancer patients. Giesel et al EJNMMI . (2017) 44:678-688[2] RECOMIA-a cloud-based platform for artificial intelligence research in nuclear medicine and radiology. Trägårdh et al EJNMMI Phys. (2020) 7:51

OP-0362

A revised compartmental model for biokinetics and dosimetry of ^{18}F-FDG

M. Andersson[1,2], A. Kamp[3], D. Noßke[4], S. Mattsson[2], A. Giussani[3];
[1]Department of Radiation Physics, Institute of Clinical Sciences, Sahlgrenska Cancer Center, Sahlgrenska Academy, University of Gothenburg, Gothenburg, SWEDEN, [2]Medical Radiation Physics, Department of Translational Medicine Lund University, Malmö, SWEDEN, [3]Department of Medical and Occupational Radiation Protection, Federal Office for Radiation Protection (BfS), Neuherberg, GERMANY, [4]Department of Medical and Occupational Radiation Protection, Federal Office for Radiation Protection (BfS), (retired), Neuherberg, GERMANY.

Aim/Introduction: The objective of this study was to review available biokinetic data and propose an updated compartmental model for ^{18}F-FDG in the frame of the work of ICRP Task Group 36 "Radiation dose to patients in diagnostic nuclear medicine". **Materials and Methods:** The compartmental model was developed based on biokinetic data from Hays et al. [1-2], Deloar et al. [3], Meija et al. [4] and the time-resolved activity of ^{18}F-FDG in blood obtained within the study by Brix et al. [5]. The biokinetic model of ICRP Publication 128 [6] was improved by explicitly including blood as the central exchange compartment and by allowing more complex model structures. Analogously to Hays and Segall [1], blood was modelled by two sub-compartments - plasma and red blood cells. The urinary excretion of ^{18}F-FDG was described by a transfer from plasma to kidneys compartment and a subsequent flux from kidneys to urinary bladder. Any arbitrary voiding interval can be set in the model. Similar to other reported biokinetic models for ^{18}F-FDG [1,6], brain, heart wall, lungs and liver were considered to be source regions and corresponding tissue compartments exchanging with plasma were included in the model. To account for ^{18}F-FDG transported by plasma to

body tissues besides the explicitly modelled source regions two sub-compartments "Other" defining a short- and a long-term retention of ^{18}F-FDG were added. The biokinetic model parameters and the corresponding model predictions were derived using independently a commercial software and a modified software version of IDAC-Iodide [7]. Results: The model predictions showed a good agreement with experimental data for blood, brain, liver, lungs and heart wall. Due to substantial variations in urine activity data published by different authors, further validation of urinary excretion is planned. Updated time-integrated activity coefficients and corresponding dose coefficients were calculated with the proposed model. **Conclusion:** Based on the published data including recently measured activity in blood, the biokinetic model of ^{18}F-FDG was revised and updated. The proposed compartmental model can be used for improved clinical dosimetry for patients administered with ^{18}F-FDG. **References:** 1. Hays M.T., Segall G.M. J Nucl Med 1999;40:1358-1366.2. Hays M.T. et al. J Nucl Med 2002;43(2):210-214.3. Deloar H.M. et al. Eur J Nucl Med 1998;25:565-574.4. Meija A.A. et al. J Nucl Med 1991;32:699-706.5. Brix G. et al. EJNMMI Res. 2020;10(1):43.6. ICRP, 2015. ICRP Publication 128. Ann. ICRP 44(2S).7. Andersson M., Mattsson S. Front Endocrinol 2021;12:634955.

OP-0363

Radiation dosimetry of ^{18}F-CETO, a PET tracer for adrenocortical imaging

M. Lubberink[1], *I. Silins*[1], *A. Moreno*[1], *F. Aigbirhio*[2], *M. Gurnell*[2], *M. Brown*[3], *S. Roslin*[1], *G. Antoni*[1], *P. Hellman*[1], *A. Sundin*[1]; *[1]Uppsala University, Uppsala, SWEDEN, [2]University of Cambridge, Cambridge, UNITED KINGDOM, [3]Queen Mary University of London, London, UNITED KINGDOM.*

Aim/Introduction: Para-chloro-2-^{18}F-fluoroethyl etomidate (^{18}F-CETO) is a novel fluorine-18 labelled analogue of ^{11}C-metomidate, a tracer mainly used for lateralization of primary aldosteronism and detection, staging and surveillance in adrenocortical carcinoma. Due to the short half-life of carbon-11 and the high liver uptake, the clinical use of ^{11}C-metomidate is still sparse. The longer half-life of ^{18}F-CETO and its lower liver uptake make it a promising alternative to ^{11}C-metomidate[1]. The aim of this study was to perform pre-clinical and human radiation dosimetry of ^{18}F-CETO. **Materials and Methods:** Pre-clinical dosimetry was based on an ex-vivo biodistribution study in rats (n=30) and a 90 min dynamic PET scan in cynomolgus (n=1). Dosimetry in humans was based on 90 min dynamic PET scans over the abdomen followed by whole-body scans at 2, 3 and 5 h p.i. of ^{18}F-CETO in patients with adrenal pathology (n=9). Uptake in animals was translated to humans assuming equal standardized uptake values. Volumes of interest were drawn over representative subsamples of organs with visually observable uptake. Residence times were calculated by trapezoidal integration, and residence time in the urinary bladder was based on sampling. Olinda/EXM 1.1 was used to calculate absorbed doses. Results: Effective dose was similar independent of species: 18.4 µSv/MBq based on rat data, 16.1 µSv/MBq based on cynomolgus data and 16.2 ± 0.7 µSv/MBq based on human data. Of all organs with clearly observable uptake, residence time was highest in liver (0.16 ± 0.07 h in humans). Regardless of species used for input data, adrenal glands received the highest absorbed dose of 0.09 ± 0.03 mGy/MBq based on human data, followed by urinary bladder wall (0.05 ± 0.01 mGy/MBq), osteogenic cells (0.026 ± 0.002 mGy/MBq) and liver (0.025 ± 0.008 mGy/MBq). **Conclusion:** The adrenal glands were found to be the dose-limiting organ for ^{18}F-CETO. A typical clinical scan using 200 MBq ^{18}F-CETO will result in an effective dose of 3.2 ± 0.6 mSv. **References:** [1]Silins et al, Int J Med Sci 2021

810

Wednesday, October 20 - Saturday, October 23, 2021

on-demand pool, release on Wednesday, October 20 at 09:00

Clinical Oncology Track - TROP Session: Neuroendocrine

OP-0365

[^{18}F]AlF-NOTA-octreotide vs. [^{68}Ga]Ga-DOTA-somatostatin analogue imaging in neuroendocrine tumour patients: results of planned interim analysis of a prospective registration trial

E. Pauwels[1], *F. Cleeren*[2], *T. Tshibangu*[2], *M. Koole*[1], *K. Serdons*[1], *L. Boeckxstaens*[1], *J. Dekervel*[3], *E. Van Cutsem*[3], *C. Verslype*[3], *S. Stroobants*[4], *T. Vandamme*[5,6], *W. Lybaert*[6], *K. Geboes*[7], *G. Bormans*[2], *C. M. Deroose*[1]; *[1]Nuclear Medicine, University Hospitals Leuven; Nuclear Medicine and Molecular Imaging, Department of Imaging and Pathology, KU Leuven, Leuven, BELGIUM, [2]Radiopharmaceutical Research, Department of Pharmacy and Pharmacology, KU Leuven, Leuven, BELGIUM, [3]Digestive Oncology, University Hospitals Leuven, Leuven, BELGIUM, [4]Nuclear Medicine, Antwerp University Hospital; Molecular Imaging and radiology, Faculty of Medicine and Health Sciences, University of Antwerp, Wilrijk, BELGIUM, [5]Center for Oncological Research (CORE), Integrated Personalized and Precision Oncology Network (IPPON), University of Antwerp, Antwerp, BELGIUM, [6]Oncology, NETwerk Antwerpen-Waasland CoE, Antwerp, BELGIUM, [7]Digestive Oncology, Department of Gastroenterology, Ghent University Hospital, Ghent, BELGIUM.*

Aim/Introduction: To meet the increasing demand for somatostatin receptor PET imaging in neuroendocrine tumour (NET) patients, fluorine-18-labelled somatostatin analogue (SSA) tracers could represent a key alternative to the current gold standard gallium-68-labelled SSAs given

their beneficial manufacturing properties and increased cost-effectiveness. [^{18}F]AlF-NOTA-octreotide ([^{18}F]AlF-OC) has shown to be a promising candidate [1,2], but further validation and comparison with [^{68}Ga]Ga-DOTA-SSA in large patient groups is lacking. Our ongoing prospective, multicentre, registration trial (clinicaltrials.gov:NCT04552847) aims to demonstrate non-inferiority of [^{18}F]AlF-OC compared with [^{68}Ga]Ga-DOTA-SSA PET in NET patients. We report the results of a planned interim analysis after 20 patients scanned with PET/CT. **Materials and Methods:** Patients with histologically confirmed NET and a routine clinical [^{68}Ga]Ga-DOTA-SSA PET scheduled within 3 months prior to or after the study scan, were eligible. An interim analysis was performed for the first 20 patients (16M/4F; age 39-84y). Patients received an IV bolus of 4 MBq/kg [^{18}F]AlF-OC. Two hours post-injection, a whole-body PET with low-dose CT was acquired. The median time between [^{18}F]AlF-OC PET and clinical [^{68}Ga]Ga-DOTATATE (n=10) or [^{68}Ga]Ga-DOTANOC (n=10) PET performed according to the EANM guidelines [3], was 8 days (range: minus 12 to plus 27 days). Tumour lesions were counted in consensus by two experienced readers who were blinded for patient data and the radiopharmaceutical that was used. To this purpose, routine and study scans were randomized. Since uptake in the salivary glands is significantly lower for [^{18}F]AlF-OC compared with [^{68}Ga]-DOTATATE [2], datasets were trimmed by another operator to remove the head region. Following blinded readout, the detection ratio (DR) was determined for each scan, i.e. the fraction of lesions detected using the union of lesions detected by both modalities ([^{18}F]AlF-OC and [^{68}Ga]Ga-DOTATATE/NOC) in a patient as the reference. Finally, the differential detection ratio (DDR; difference in DR between [^{18}F]AlF-OC and [^{68}Ga]Ga-DOTATATE/NOC) was calculated. Results: In total, 1245 different tumour lesions were detected, of which 1218 with [^{18}F]AlF-OC and 865 with [^{68}Ga]Ga-DOTATATE/NOC. In 15 patients, [^{18}F]AlF-OC detected more lesions, while only in 3 patients less lesions were detected on [^{18}F]AlF-OC compared to [^{68}Ga]Ga-DOTATATE/NOC. The DR was significantly higher for [^{18}F]AlF-OC than for [^{68}Ga]Ga-DOTATATE/NOC (mean DR 96.9% vs. 75.3%; p=0.001). The mean DDR was 21.6% (95% confidence interval: 11.9%-31.3%). **Conclusion:** The interim analysis indicates that the diagnostic performance of [^{18}F]AlF-OC is non-inferior, and even superior, to that of [^{68}Ga]Ga-DOTA-SSA PET in NET patients. Further patients will be included to validate these preliminary results. **References:** [1] Long.Clin.Nucl.Med.2019;44:452-8 [2]Pauwels.Eur.J.Nucl.Med.Mol.Imaging.2020;47:3033-46[3]Bozkurt Eur.J.Nucl.Med.Mol.Imaging.2017;44:1588-1601

OP-0366

Prognostic value of whole-body PET volumetric parameters extracted from ^{68}Ga-DOTATOC-PET/CT in well-differentiated neuroendocrine tumors

P. Thuillier[1,2], V. Liberini[1], S. Grimaldi[1], O. Rampado[3], E. Gallio[3], B. De Santi[4], E. Arvat[5], A. Piovesan[5], R. Filippi[6], F. Molinari[4], D. Deandreis[1]; [1]Nuclear Medicine Unit, Department of Medical Sciences, University of Turin, Turin, ITALY, [2]Department of Endocrinology, University Hospital of Brest, Brest, FRANCE, [3]Medical Physics Unit, AOU Città della Salute e della Scienza, Turin, ITALY, [4]Biolab, Department of Electronics and Telecomunications, Politecnico di Torino, Turin, ITALY, [5]Oncological Endocrinology Unit, Department of Medical Sciences, University of Turin, Turin, ITALY, [6]Department of Oncology Department of Medical Sciences, University of Turin, Turin, ITALY.

Aim/Introduction: The objective of this study was to evaluate the prognostic value of somatostatin receptor tumor burden (SRTB) extracted from ^{68}Ga-DOTATOC PET/CT in patients presenting WD-NETs. **Materials and Methods:** We retrospectively analyzed PET/CT of 84 patients with histologically confirmed WD-NETs (51 G1, 30 G2 and 3 G3). Primary sites were as follows: gastroenteropancreatic (n=72), lung (n=9) and unknown (n=3) NETs. For each PET/CT, all DOTATOC-avid lesions were segmented by 2 operators using a customized threshold based on the healthy liver maximum standardize uptake value (SUVmax) to calculate the somatostatin receptor expressing tumor volume (SRETV) and total lesion somatostatin receptor expression (TLSRE=SRETV*SUVmean), using LIFEx 5.1. The sum of all lesions SRETV (SRETVwb) and TLSRE (TLSREwb) were calculated for each patient. Time to progression (TTP), defined as the time between PET imaging to the first event, and overall survival (OS) were studied using Kaplan-Meier analysis. Cox regression model was used to evaluate predictors of progression. Results: Progression was confirmed in 35 patients(41.7%) and 14 patients died (median follow-up 23 months). For SRTB parameters, optimal cut-offs for predicting progression were defined using the receiver operating characteristic (ROC) curve which revealed AUC of 0.83 and 0.79 for SRETVwb and TLSREwb, respectively. Higher SRETVwb (≥39.1ml) and TLSREwb (>306.8g) were correlated with significantly shorter median TTP (TTP=12months vs not reached for both; p<0.001) and shorter median OS (OS not reached for both; p<0.001). SUVmax was not associated with TTP and OS (p=0.08 and p=0.09, respectively). TNM stage at PET time, Ki67% level, and treatment history were also significantly associated with a shorter TTP and OS (p<0.05), while age, gender and secretory syndrome were not associated with TTP and OS (p>0.05). In multivariate analysis using the Cox proportional regression model including only SRETVwb as SRTB parameter, SRETVwb (>39.1ml) was the only independent predictor of TTP (HR = 4.76 [1.56; 14.53]; p=0.006), regardless of TNM stage, Ki67% level and treatment

history (p=0.58, 0.85 and 0.39, respectively). **Conclusion:** In our cohort, whole-body volumetric ^{68}Ga-DOTATOC PET/CT parameters (SRETVwb and TLSREwb) were associated with TTP and OS. SRTB could has an additional value in comparison to conventional prognosis parameters (especially Ki67% level and TNM staging) and other PET parameters (e.g. SUVmax) to predict patient prognosis, thus supporting the implementation of these parameters in clinical practice in patients with WD-NETs. However, our findings need to be further confirmed in more homogeneous cohorts of patients and larger prospective studies are needed. **References:** None

OP-0367

Role of volumetric parameters on ^{68}Ga-DOTATOC PET/CT in NET patients treated with PRRT

L. Urso[1], M. Caracciolo[1], N. Ortolan[1], I. Zamberlan[1], A. Castello[1], E. Tonini[2], S. Panareo[1], A. Nieri[1], C. Cittanti[1], L. Uccelli[1], L. Lodi[1], S. Bertelli[1], S. Romani[1], S. Zaccaria[1], A. Turra[2], M. Bartolomei[1];
[1]Nuclear Medicine Unit, Oncological Medical and Specialists Department, University Hospital of Ferrara, Ferrara, ITALY,
[2]Sant'Anna Hospital, Medical Physics Unit, Ferrara, ITALY.

Aim/Introduction: to assess the role of volumetric parameters, evaluated by ^{68}Ga-DOTATOC PET/CT, in relation to clinical outcomes in NET patients treated with Peptide Receptor Radionuclide Therapy (PRRT). **Materials and Methods:** we retrospectively evaluated 39 patients (21 male, 18 female, mean age 60.7y) affected by NET who underwent PRRT with ^{177}Lu-DOTATOC alone or combined with ^{90}Y-DOTATOC within FENET-2016 phase II clinical trial (CTiD:NCT04790708). ^{68}Ga-DOTATOC PET/CT was performed 3 months before and after PRRT. For each PET/CT, we calculated SUVmax, SUVmean, somatostatin receptor expressing tumour volume (SRETV) and total lesion somatostatin receptor expression (TLSRE), as well as their percentage of changes (Δ) for liver tumor burden and for total tumor burden, referred to the five most relevant lesions according to RECIST 1.1 criteria. SRETV was estimated by a semiautomatic tumor-contouring software with a predefined threshold of 40% of SUVmax, while TLSRE was obtained multiplying SRETV and SUVmean. Early clinical response was evaluated according to RECIST 1.1 criteria and NET board. Results: we treated NET from pancreas (n=19), midgut (n=7), bronchial (n=6), cerebral (n=1), paraganglioma (n=1) and unknown origin (n=5). Grading was G1, G2, and G3 for 4, 31, and 3 patients respectively, while for 1 was unknown. Median Ki67 was 8%. Early clinical response documented 9 partial response (PR), 25 stable disease (SD), and 5 progressive disease (PD). Post-treatment SRETV and ΔSRETV for total tumor burden were progressively increased among response groups (median post-SRETV was 11.3 for PR, 37.4 for SD and 139.2 for PD, p=0.02; median ΔSRETV was -37.4% for PR, +14.5% for SD and +24.8% for PD, p=0.03). Likewise, median post-SRETV for liver burden was significantly higher in PD patients (10.1 for PR, 63.8 for SD and 468.4 for PD, p=0.03). Contrarily, SUVmax and TLSRE were not associated with early clinical response, both for total and liver tumor burden. Furthermore, no correlation was found between volumetric parameters and Ki67. **Conclusion:** our results suggest that liver and total tumor burden SRETV might be a valid parameter to assess tumor response after PRRT. In particular, SRETV seems more consistent than SUVmax, which only express single hot pixel within a tumor mass and does not necessarily represent the whole tumor status. Moreover, SRETV appears more accurate than TLSRE being not related to SUVmean, which is less reliable in widespread heterogeneous tumors as in our cohort. Further prospective investigations are necessary to confirm our preliminary results. **References:** Toriihara et al. Eur_J_Nucl_Med_Mol_Imaging. 2019 Oct;46(11):2244-2251.

OP-0368

Prediction of transient bone marrow suppression after [^{177}Lu]Lu-DOTA-TATE treatment using [^{68}Ga]Ga-DOTA-TOC PET/CT and clinical parameters in patients with gastroenteropancreatic neuroendocrine tumors

H. Ryoo, H. Choi, J. Paeng, K. Kang, G. Cheon;
Department of Nuclear Medicine, Seoul National University Hospital, Seoul, KOREA, REPUBLIC OF.

Aim/Introduction: Bone marrow (BM) suppression is a dose-limiting complication commonly observed in peptide receptor radionuclide therapy (PRRT) with [^{177}Lu]Lu-DOTA-TATE. [^{68}Ga]Ga-DOTA-TOC positron emission tomography (PET) is routinely performed for the selection of candidates for PRRT. Here, we performed analyses on the utility of pretreatment [^{68}Ga]Ga-DOTA-TOC PET/CT and clinical parameters for the prediction of transient BM suppression after PRRT. **Materials and Methods:** Seventy-eight patients with gastroenteropancreatic neuroendocrine tumors underwent the first cycle of [^{177}Lu]Lu-DOTA-TATE PRRT, and hemoglobin (Hb), white blood cell (WBC), platelet (PLT) counts were monitored. Pretreatment [^{68}Ga]Ga-DOTA-TOC PET/CT (n=59) and baseline clinical parameters (n=78) were retrospective collected. Quantitative and qualitative measurements of BM, spleen, and bone metastasis were performed on [^{68}Ga]Ga-DOTA-TOC PET/CT. Hematologic toxicity was assessed according to Common Terminology Criteria for Adverse Events (CTCAE v5.0). Worsening of CTCAE grade, and the relative percent decline of blood counts at nadir per time after PPRT were used as indicators of transient BM suppression. Clinical and PET variables were analyzed using the Mann-Whitney test, Fischer's exact test, and Spearman's ρ correlation analysis to assess predictive values of transient BM suppression. Results: Transient BM suppression occurred in 17.9% (14/78), 28.2% (22/78), and 10.3% (8/78) in Hb, WBC, and PLT of 78 patients. Baseline clinical parameters that were significantly associated with transient BM suppression were: low Hb (11.8 ± 2.0 vs 12.9 ± 1.8, p=0.017) and WBC (5.60 ± 1.37 vs 6.80 ± 2.31, p=0.017) counts at baseline for toxicity in WBC; low PLT counts at baseline (178 ± 44 vs 253 ± 106, p=0.013) and previous radiotherapy to bone (p=0.05) for toxicity in PLT. BM and bone metastasis parameters on [^{68}Ga]Ga-DOTA-TOC PET/CT showed correlation with relative percent decline

per time in WBC, but not in Hb and PLT: burden of bone metastasis uptake (i.e. product of bone metastasis extent and Krenning score; ρ = 0.316, p = 0.015) and BM to liver uptake ratio (ρ = 0.248, p = 0.059). None of the clinical and PET parameters were associated with toxicity in Hb. **Conclusion:** [^{68}Ga]Ga-DOTA-TOC PET/CT does provide information for the prediction of transient BM suppression in terms of WBC, but not in Hb and PLT. Low baseline blood counts and previous radiotherapy are potential prognostic factors for the toxicity in WBC and PLT. The combination of [^{68}Ga]Ga-DOTA-TOC PET/CT and baseline clinical parameters may predict transient BM suppression after PRRT and can be used for treatment personalization. **References:** none

OP-0369

18fluoro-Dopa positon emission tomography computed tomography and whole body magnetic resonance imaging are efficient and complementary imaging modalities for evaluation of extension in well-differentiated neuroendocrine tumor of small intestine patients

M. Terroir Cassou Mounat, C. Caramella, M. Attard, M. Faron, H. Tissot, L. Lamartina, J. Hadoux, T. Henry, M. Schlumberger, S. Leboulleux, E. Baudin;
Institut Gustave Roussy, Villejuif, FRANCE.

Aim/Introduction: In neuroendocrine tumor of small intestine (SI NET), the best imaging for work up is not yet well known. The aim of the study was to compare 18fluoro-dopa (F-18-Dopa) positon emission tomography/computed tomography (PET/CT) and whole body magnetic resonance imaging (WB MRI) in patients under watch and see policy or under somatostatin analogs. **Materials and Methods:** Consecutive patients were prospectively recorded with the following criteria (i) well differentiated SI NET grade 1 or 2, (ii) absence of previous treatment except surgery of the primitive lesion and somatostatin analogs (iii) F-18-Dopa PET/CT and WB MRI performed at our center within 5 months. One expert nuclear physician and one expert radiologist read each imaging modality unaware of other results. We performed per patient, per organ and per lesion analysis. The reference assessment for structural disease was concordance between two imaging modalities and/or confirmation during follow-up. Results: Forty-three patients were included. On the per patient analysis, the sensitivity of F-18-Dopa PET/CT and WB MRI was respectively 100% and 91.7% (p=0.18) and the specificity was respectively 57.1% and 85.7% (p=0.8). The positive predictive value of F-18-Dopa PET/CT and WB MRI was respectively 92% and 97% (p=0.33). The negative predictive value of F-18-Dopa PET/CT and WB MRI was respectively 100% and 66.7% (p=0.1). On the per organ/lesion analysis, the gold standard showed an amount of 583 lesions. The sensitivity of F-18-Dopa PET/CT was significantly different from WB MRI in upper diaphragmatic lymph nodes (100% and 33% respectively; p=0.0001) and in peritoneum (85% and 45% respectively; p=0.0001). The sensitivity and specificity in all others location were not significantly different between the two modalities. The accuracy of F-18-Dopa PET/CT and WB MRI was 94% and 88% for liver, 95% and 100% for under diaphragmatic lymph nodes, 80% and 50% for peritoneum, 77% and 50% for upper diaphragmatic lymph nodes, 100% and 0% for lung, 36% and 50% for pleura, 100% and 58% for bone. **Conclusion:** F-18-Dopa PET/CT and WB MRI are two efficient and complementary imaging modalities in SI NET. F-18-Dopa PET/CT is more sensitive for peritoneum and upper lymph node involving which could change the support of SI NET patients. **References:** none

OP-0370

Two Birds with One Stone: Can [68Ga]Ga-DOTANOC PET/CT Image Quality Be Improved through BMI-Adjusted Injected Activity in Neuroendocrine Tumour Patients?

E. Fortunati[1], G. Argalia[1], L. Zanoni[2], D. Calabrò[1], C. Malizia[2], V. Allegri[2], S. Civollani[2], S. Fanti[1,2], V. Ambrosini[1,2];
[1]Nuclear Medicine, Department of Experimental, Diagnostic and Specialty Medicine, University of Bologna, Bologna, ITALY, [2]Nuclear Medicine, IRCCS, Azienda Ospedaliero-Universitaria di Bologna, Bologna, ITALY.

Aim/Introduction: The aim of this study was to assess how patients (pts)' dependent parameters may affect [68Ga]Ga-DOTANOC PET/CT image quality and to propose a theoretical body mass index (BMI)-adjusted injected activity (IA) scheme, to improve imaging of high weight pts. **Materials and Methods:** Among pts prospectively enrolled in an Institutional Ethics Committee-approved (131/2017/O/Oss) electronic archive between June-2019 and May-2020, we included only those followed at Our Center with a gastro-entero-pancreatic or lung primary tumour excluding those presenting even minimal radiopharmaceutical extravasation, movement artifacts or renal insufficiency. If more than one scan of the same pt was present, we included only the first [68Ga]Ga-DOTANOC PET/CT. All [68Ga]Ga-DOTANOC PET/CT images were acquired following EANM (European Association of Nuclear Medicine) guidelines and rated for visual quality (1= non-diagnostic, 2= poor, 3= moderate, 4=good). Collected data included pt's body weight, height, BMI, age, IA, IA per Kg, IA per BMI, liver SUVmean, liver SUVmax standard deviation, liver signal-to-noise ratio (LSNR), normalized_LSNR (LSNR_norm) and contrast-to-noise ratio (CNR) for positive scans and were compared to image rating (poor vs moderate/good). Results: Overall, 77 pts were included. Rating concordance was high (agreement= 81.8%, Fleiss k score= 0.806). All pts' dependent parameters resulted significantly different between poor-rated and moderate/good scans (IA: p=0.006, IAkg: p=0.0001, body weight: p<0.0001, BMI: p<0.0001, IABMI: p<0.0001). Factors significantly associated with moderate/good rating were BMI (p<0.0001), body weight (p=0.0001), IABMI (p=0.0004), IAkg

(p=0.001), IA (p=0.003), LSNR_norm (p=0.01). The BMI-based model presented the best predictive efficiency (81.82%). IABMI performance to differentiate moderate/good from poor rating resulted statistically significant (IAUC=0.78; 95%CI: 0.68-0.89; cut-off value of 4.17MBq*m^2/kg, sensitivity=81.1%, specificity=66.7%). If BMI-adjusted IA (=4.17*BMI) would have been applied in this population, the median IA would have slightly inferior (-4.8%), despite a different IA in each patient. **Conclusion:** BMI resulted the best predictor of image quality. The proposed theoretical BMI- adjusted IA scheme (4.17*BMI) should yield images of better quality (especially in high-BMI pts) maintaining practical scanning times (3minutes/bed). Further validation is warranted. **References:** None.

OP-0371

[68Ga]Ga-DOTANOC PET/CT Derived Radiomic Features Can Discriminate Pancreatic Neuroendocrine Tumours from Accessory Spleens: Preliminary Results

G. Argalia[1], S. Malavasi[2,3], E. Fortunati[1], D. Calabrò[1], D. Campana[4,5], R. Casadei[6,5], C. Ricci[6,5], A. Bevilacqua[2,7], S. Fanti[1,8], V. Ambrosini[1,8];
[1]Nuclear Medicine, Department of Experimental, Diagnostic and Specialty Medicine, University of Bologna, Bologna, ITALY, [2]Advanced Research Center for Electronic Systems (ARCES), University of Bologna, Bologna, ITALY, [3]Research Institute on Global Challenges and Climate Change (Alma Climate), University of Bologna, Bologna, ITALY, [4]Oncology, IRCCS, Azienda Ospedaliero-Universitaria di Bologna, Bologna, ITALY, [5]DIMEC, IRCCS, Azienda Ospedaliero-Universitaria di Bologna, Bologna, ITALY, [6]Surgery, IRCCS, Azienda Ospedaliero-Universitaria di Bologna, Bologna, ITALY, [7]Department of Computer Science and Engineering (DISI), University of Bologna, Bologna, ITALY, [8]Nuclear Medicine, IRCCS, Azienda Ospedaliero-Universitaria di Bologna, Bologna, ITALY.

Aim/Introduction: Accessory spleens (AS) may represent a pitfall in [68Ga]Ga-DOTANOC PET/CT image interpretation, especially when intra-pancreatic. Aim of the study was to evaluate whether [68Ga]Ga-DOTANOC PET/CT derived radiomic features can be used to discriminate pancreatic neuroendocrine tumours (pNET) from AS. **Materials and Methods:** 41 patients with AS (3/41 intra-pancreatic) and 55 pts with primary pNET and a positive [68Ga]Ga-DOTANOC PET/CT were selected from a CE-approved electronic archive. [68Ga]Ga-DOTANOC PET/CT was performed and interpreted following standard EANM procedure. Nuclear medicine physician manually performed segmentation of the whole volume of both the pNET lesion and the AS on the fused [68Ga]Ga-DOTANOC PET/CT images. Within these regions of interest, four symmetric grey-level co-occurrence matrices (GLCMs) were generated over SUV maps, considering four distances d, averaged over four angles. 14 first-order and 22 second-order radiomic features were then computed on SUV maps and GLCMs, respectively. All radiomic features were normalized and considered in couples. Highly linearly correlated radiomic features were excluded and linear discriminant analysis was performed on the remaining 566 couples to build as many radiomic models. Wilcoxon rank-sum test was applied and Area Under the Curve (AUC) of the receiver operating characteristic (ROC), together with sensitivity, specificity and accuracy, were used to assess model performance. The couple showing the lowest p-values and the highest AUC was finally selected. Results: The radiomic model made of first-order kurtosis and second-order joint entropy (d=2) showed the highest significant performance (p-value=2.11E-14) with sensitivity=91%, specificity=88%, accuracy=90%, AUC=96%, true negative=36, false positive=5, false negative=5, true positive=50. In particular, it is worth noticing that 2/3 intra-pancreatic AS were correctly discriminated by the radiomic model. **Conclusion:** Our preliminary results showed that the identified [68Ga]Ga-DOTANOC PET/CT derived radiomic features may be used to discriminate pNET from AS. From a clinical perspective, if confirmed on larger samples, these data may be relevant for discriminating pNET from intra-pancreatic AS. **References:** None.

OP-0372

Pancreatic uptake of radiolabeled exendin as a measure of beta cell mass in remission of type 2 diabetes in patients having metabolic surgery

L. Deden[1], M. Boss[2], H. de Boer[3], E. Aarts[1], M. Brom[2], E. Hazebroek[1], F. Berends[1], M. Gotthardt[2];
[1]Vitalys, Rijnstate Hospital, Arnhem, NETHERLANDS, [2]Radboud University Medical Center, Nijmegen, NETHERLANDS, [3]Rijnstate Hospital, Arnhem, NETHERLANDS.

Aim/Introduction: The role of beta cells in the onset, course and remission type 2 diabetes mellitus (T2DM) is not clear. Beta cell mass (BCM) and function (BCF) might be related to T2DM remission after metabolic bypass surgery (RYGB). An approach for in vivo beta cell imaging is targeting the glucagon-like peptide-1 (GLP-1) receptor. The aim of this study is examining BCF and pancreatic uptake of ^{68}Ga-exendin-4 (EX) before and after RYGB in patients with T2DM by radiolabeled exendin-4. **Materials and Methods:** Arginine stimulation test (AST), oral glucose tolerance test (OGTT) and EX PET/CT were performed pre- and one year post-RYGB. Total pancreatic uptake of EX (kBq) was measured quantitatively on PET/CT as marker for BCM. Results: Thirteen patients were included: ten female, mean age of 52 years and mean duration of T2DM of 10 years. One patient was withdrawn at one year follow-up. Preoperatively, seven patients were on insulin therapy (99±47 IU/day) and six on metformin (1-2g/day). Postoperatively, average BMI and HbA1c decreased from 39±4.0 to 28±3.4 kg/m2 and from 63±11 to 43±15 mmol/mol, respectively. Preoperatively, pancreatic uptake of EX tends tob e lower in the insulin than the metformin group: 221±107 vs 324±101 kBq (p=0.104). In addition, the c-peptide response during OGTT tends to be smaller in the insulin as compared to the

metformin group (1.3 vs 2.6 nmol/l, p=0.081). Postoperatively, in the insulin group, two patients had complete remission (i.e. no antidiabetics and normal HbA1c), two patients had little improvement (insulin or sulfonylurea treatment and unchanged HbA1c) and three patients had improvements in between. Mean pancreatic uptake increased to 321±67 kBq (p=0.025) in the insulin group. This seems to be related to the degree of improvement. In the metformin group all patients had complete remission. Average pancreatic uptake remained stable, with relative changes ranges from -11% to +22%. **Conclusion:** Patients with insulin-dependent T2DM might have lower beta cell mass and function as compared to patients with noninsulin-dependent T2DM. In the metformin group, average pancreatic EX uptake remained stable and c-peptide response decreased after RYGB, probably reflecting normalistion of BCF. Decreased uptake in few patients may also reflect normalisation of BCM. In insulin-dependent patients, largest increase in pancreatic uptake was observed after partial or complete T2DM. This may indicate towards recovered beta cells and has not been observed in patients so far. Mechanisms behind changes in pancreatic EX uptake and possibly recovering of BCM need further investigation. **References:** none

OP-0373

Ga-68 DOTATATE PET / Lu-177 DOTATATE SPECT Theranostics: Discordance in Neuroendocrine Tumor and Organ Distributions

***K. Wong**, K. A. Frey, J. Niedbala, R. K. Kaza, F. P. Worden, Y. K. Dewaraja;*
Michigan Medicine, Ann Arbor, MI, UNITED STATES OF AMERICA.

Aim/Introduction: Peptide radionuclide receptor therapy (PRRT) requires molecular targeting of neuroendocrine tumor (NET) metastases that have overexpression of somatostatin receptor type 2 (SSTR2). Our aim is to evaluate Ga-68 DOTATATE PET/CT activity within tumors, non-tumoral liver, kidneys and spleen, compared to that of Lu-177 DOTATATE on post-therapy SPECT/CT. **Materials and Methods:** PET and SPECT images were available for patients who underwent standard (7.4 GBq per cycle x 4 cycles) Lu-177 DOTATATE PRRT followed by multi-time point Lu-177 SPECT/CT. Ga-68 DOTATATE PET/CT was performed with mean interval of 6.2 months (range 1- 16) before Cycle#1 PRRT. Lu-177 DOTATATE SPECT/CT imaging was performed at 4 hours (T1), 24 h (T2), Day4-5 (T3) and Day7-9 (T4) post-Cycle#1. SPECT/CT was reconstructed using commercial software, xSPECT Quant with images displayed in SUV units. Manual contouring of up to 5 index lesions performed by a radiologist on baseline CT or MRI were applied to co-registered SPECT/CT and PET/CT followed by deep learning-based CT auto-segmentation of the normal organs to extract SUVpeak, SUVmean and SUV tumor:organ ratios. A hot-sphere phantom study was also performed to compare SUV on Ga-68 PET to Lu-177 SPECT. Results: 73 lesions in 18 patients with progressive metastatic NET were analyzed. PET-derived tumor SUVpeak were predictive of SPECT SUVpeak at all 4 time-points with moderate correlation (R2= 0.43, 0.36, 0.35, 0.24 , T1, T2, T3, T4; regression p<0.001). For organs, the correlation was worse, and the PET SUVmean was significantly higher compared to SPECT including at the 4h time point (for T1 average SUV across patients: liver 6.0 vs. 1.5, kidneys 9.2 vs. 4.8, spleen 13.1 vs. 4.5; p < 0.001). Tumor SUVpeak-to-organ-SUVmean ratios were significantly higher on the SPECT at all time points compared to pre-treatment PET, (T1 average SUV ratio: tumor:liver 18.1 vs 5.9, tumor:kidneys 5.0 vs 3.3 and tumor:spleen 5.2 vs 2.3; p< 0.001). The ratios increased further at subsequent SPECT time points. Phantom results demonstrated that these findings are not attributed to differences in imaging modality alone. **Conclusion:** We found quantitative evidence for discordance in relative tumor vs. normal organ biodistribution between the theranostic pairs, with significant higher ratios shown in Lu-177 SPECT compared with Ga-68 PET. We postulate this phenomenon is due to temporal differences in DOTATATE uptake and internalization in tumors as compared to normal organs. These observations have implications for selection of patients for PRRT using PET and over-reliance on tumor:organ ratios. **References:** none

OP-0374

[68Ga]Ga-DOTA-TOC PET/MRI validation compared to PET/CT, in patients with paraganglioma and pheochromocytoma. Initial results

***S. Prado Wohlwend**, M. Ballesta Moratalla, P. Bello Arques, M. del Olmo García, I. Torres Espallardo, J. Merino Torres;*
Universitary and Polytechnic Hospital La Fe, Valencia, SPAIN.

Aim/Introduction: To validate the usefulness and diagnostic performance of [68Ga]Ga-DOTA-TOC PET/MRI compared with the current standard of care, PET/CT, in patients with paraganglioma and pheoctomocytoma. **Materials and Methods:** Prospective study in patients with locally advanced or metastatic pheochromocytoma(PHEO) or paraganglioma(PGL), it was performed with local ethics committee approval 2020-432-1. After administration of [68Ga]Ga-DOTA-TOC, we acquired first a whole body PET/CT scan, followed immediately by PET/MRI obtaining T1 in and out of phase, T2, T2FS, STIR and diffusion sequences. Intermodality agreement between radiotracer uptake, anatomical images confirmation (true positive), no tumor viability verification in the absence of uptake (true negative), Krenning scale, highest SUVmax and target-to-liver-ratio (TLR) were calculated. Results: 6 patients completed the protocol, 3 women, mean age 50.33(38-71) years. Primary tumor location was: 1 PHEO, 4 cervical PGL and 1 retroperitoneal PG. Genetic syndromes were 1 SDHD, 2 SDHB, 2 sporadic cases and 1 unknown. The average of [68Ga]Ga-DOTA-TOC activity administered was 188.33Mbq. PET/CT

was performed at a mean of 54min(67-45) post-injection, and PET/MRI at 96.83min(81-134). A total of 34 lesions were detected with a complete radiotracer uptake intermodality agreement between PET/CT anf PET/MRI (K coefficient:1). PET/CT confirmed 32 true positive lesions and PET/MRI other 32 (K coefficient 0.6). A PGL in the carotid glomus treated with RT showed radiopharmaceutical uptake but was not characterizable by PET/CT or PET/MRI. Furthermore, PET/CT did not characterized a millimetric sacral bone lesion, and PET/MRI did not define the uptake on a tympanic PGL with bone involvement at the base of the skull. The semiquantitive analysis for PET/CT and PET/MRI SUVmax and TLR were 61.1/97.1g/mL and 12.11/18.21g/mL respectively. Krenning score was 2/2pat, 3/1pat and 4/3pat in PET/CT scan. In PET/MRI only a sacral bone microscopic lesion changed from 2 to 4 score. (probably due to an improved time of fligt and the point spread function). The PET/MRI confirmed a true negative on a necrotic splenic lesion, supporting the later radionuclide therapy. The change of Krenning score in a lesion, did not modify the therapeutic attitude, but confirmed a higher somatostatin expression. **Conclusion:** [68Ga]Ga-DOTA-TOC PET/MRI provides an accurate detection of radiotracer uptake, with adecuate anatomical correlation in PHEO and PGL. It is especially useful in small lesions, providing better delimitation and quantification of the uptake intensity than PET/CT. Larger series are necessary to clarify in which anatomical regions or clinical context PET/MRI may be more useful or be more limited. **References:** None

OP-0375

Prevalence and Significance of 68Ga-DOTA-conjugated Somatostatin Receptor-Targeting Peptide PET/CT Incidental Findings - A Systematic Review

M. Bentestuen, F. Gossili, C. E. Almasi, H. D. Zacho;
Department of Nuclear Medicine, Aalborg University Hospital, Aalborg, DENMARK.

Aim/Introduction: We aimed to evaluate the prevalence of 68Ga-DOTA-conjugated somatostatin receptor (SSTR)-targeting peptide PET/CT incidentalomas and risk of malignancy in incidental findings. **Materials and Methods:** Studies reporting incidentalomas on 68Ga-DOTA-conjugated SSTR-targeting peptide PET/CT were systematically searched in Pubmed, Cochrane, Embase and Web of Science published prior to 1st of May 2020. Studies were filtered by two independent readers for eligibility based on title and abstract, and subsequently on full text. The main exclusion criteria were: 1) Pathological findings that matched scan indication, 2) known organ specific disease and/or incidental findings confirmed on other scan modality prior to 68GaDOTA PET/CT, 3) lack of diagnosis/follow-up and/or insufficient information regarding reported cases, and 4) results published in annual meetings, conferences etc.. Results: Twenty-one studies met the preset criteria, comprising a total of 2906 subjects. The majority of study subjects were from retrospective cohort studies on incidentalomas in a specific organ (n=2888). However, most included studies were case reports (n=14, 67%). A total of 133 subjects had incidentalomas on PET/CT. In decreasing order, incidentalomas were reported in the thyroid gland (n=65), spine (n=30), brain (n=26), breast (n=6) and other locations (n=6). Overall, a total of 17 out of 114 (15%) incidentalomas were identified as malignant on final diagnosis. Incidentalomas in the thyroid gland was associated with goiter and Hashimotos disease in benign cases. Five patients (8%) with thyroid incidentalomas were diagnosed with malignancy, all presenting as focal uptake on PET/CT. Incidentaloma in the breast was associated with high risk of malignancy (67%). Benign causes of incidental uptake in the breast were gynecomastia and breast fibroadenoma. Five patients (19%) with intracranial incidentalomas were diagnosed with malignancy in the form of metastatic paragangliomas (n=4) and medulloblastoma (n=1). Among benign findings meningeomas were the most prevalent. Incidentalomas in the spine had a low risk of malignancy (3%) and benign cases were interpreted as vertebral hemangiomas on CT. Incidentalomas in other locations were individual cases and were most likely benign. **Conclusion:** To the authors knowledge, this is the first review that aim to assess incidental 68Ga-DOTA-conjugated SSTR-targeting peptide PET/CT findings. Most incidentalomas were found in the thyroid gland, spine and brain. The risk of malignancy was greatest in the breast, brain and thyroid gland. **References:** none

OP-0376

Higher diagnostic accuracy of FDG PET/CT than contrast enhance CT in initial staging of pancreatic cancers; Hybrid is better than Solo

M. Zaman[1], N. Fatima[1], S. Zaman[2], A. Zaman[3], U. U. Zaman[4];
[1]AKUH, Karachi, PAKISTAN, [2]Dow Medical College, Dow University of Health Sciences (DUHS), Karachi, PAKISTAN, [3]Dr Ruth Pfau (CHK), Karachi, PAKISTAN, [4]Sunny Downstate Medical Center, NY, New York, NY, UNITED STATES OF AMERICA.

Aim/Introduction: Pancreatic adenocarcinomas (PCs) are very aggressive tumor and about 80% are surgically un-resectable with a 5 -year survival of 2%. Contrast enhanced CT (CECT) is the mainstay diagnostic and staging tool while role of FGD PET/CT is currently not clear. Aim of this study is to observe the clinical impact of FDG PET/CT in PC in initial staging and compare it with CECT. **Materials and Methods:** This retrospective study was conducted at PET/CT Imaging facility of JCIA healthcare facility of Pakistan from (March 2017 till December 2020). Total 67 patients with biopsy proven pancreatic cancers were included who had contrast CECT and FDG PET/CT for primary staging. All patients have had FDG PET/CT study as per institutional imaging and reporting protocol which is based on EANM 2015 recommendations.

FDG PET/CT based staging was compared with CECT to see the impact on treatment strategy. Results: Total 67 patients with mean age of 59 years (30 - 81 years) and male preponderance (63% male and 37% female) were accrued. Histopathology revealed adenocarcinoma in 63/67 (94%) and mucinous cancer in 04/67 (6%) patients. Mean primary tumor size was 42 mm (10-113 mm) with a mean SUVmax 7.4 (1-24). Metabolically active perilesional nodes were seen in 25/67 (37%) patients. FDG PET/CT findings categorized 29/67 (43%) patients with stage IV disease. Compared with CECT, FDG PET/CT has upstaged disease in 26/67 (39%) and had a concordance in remaining 41/67 (61%) patients. FDG PET/CT was not found to downstage the disease in this study population. **Conclusion:** In newly diagnosed PCs, FDG PET/CT in comparison to CECT has upstaged the disease in 39% and had concordance in 61% cases. Based on these findings, FDG PET/CT must be included in initial staging protocol of pancreatic cancer to avoid futile surgical procedures. **References:** None

811

Wednesday, October 20 - Saturday, October 23, 2021

on-demand pool, release on Wednesday, October 20 at 09:00

TROP Session: Top of Nuclear Medicine in COVID-19

OP-0378

Long Covid hallmarks on [18F]FDG-PET/CT: a case-control study

F. Gelardi[1], M. Sollini[1], S. Morbelli[2], M. Ciccarelli[3], M. Cecconi[1], A. Aghemo[1], P. Morelli[3], S. Chiola[1], A. Chiti[1];
[1]Humanitas University, Pieve Emanuele, ITALY, [2]University of Genoa, Genoa, ITALY, [3]Humanitas Research Hospital, Rozzano, ITALY.

Aim/Introduction: After SARS-CoV-2 outbreak, an increasing number of patients complain a wide range of symptoms after infection recovery, defined as Long Covid. We recognized [18F]FDG PET/CT as the optimal imaging technique to elucidate the underlying pathophysiology of Long Covid, being extensively used in assessment of infectious and inflammatory diseases. **Materials and Methods:** Thirteen adult patients presenting at least one persisting symptom and the onset of limitation in daily activities after 30 days from Covid-19 recovery were prospectively enrolled. All patients underwent a whole-body [18F]FDG PET/CT. A control group of twenty-six negative whole-body [18F]FDG PET/CT of melanoma patients matched for sex and age were selected. Control patients were only surgically treated and negative for neurological disorders. Whole-body PET/CT images were visually and semi-quantitatively analysed. Voxel-based analysis to compare brain metabolism in cases/controls were performed using SPM. Subgroup of patients were established according to prevalent clinical symptoms and [18F]FDG PET/CT findings. Results: CT images showed bilateral lung abnormalities with mild [18F]FDG uptake in four Covid-19 patients, corresponding to who requested oxygen support. Alongside target organs, different healthy organs showed increased [18F]FDG uptake and target-to-background ratio, including healthy lung parenchyma, muscles, skin, and gastrointestinal system. Despite an increased [18F]FDG uptake on vessels (61%) and bone marrow (46%) was observed in Long Covid, prevalence does not differ from melanoma patients (73% and 46%, respectively). Long Covid showed areas of brain hypo-metabolism in the right para-hippocampal gyrus and right thalamus. Clusters of hypo-metabolism were observed in para-hippocampal gyrus and orbitofrontal cortex in patients complaining anosmia/ageusia. Similarly, para-hippocampal gyrus, brainstem (substantia nigra), and thalamus exhibit hypo-metabolism in patients with persistent fatigue. **Conclusion:** Our results support the view of Long Covid as a multiorgan inflammatory syndrome, suggesting a change in Covid-19 patients long-term management. A prolonged post-infection inflammatory reaction might affect both typical organs involved in the acute disease and non-target tissues. Brain hypo-metabolism patterns matched with prevalent symptoms reflect a transitory synaptic dysfunction which may result in long-term sequelae. **References:** None.

OP-0379

[^{68}Ga]Ga-DOTA-(RGD)$_2$ PET/CT imaging of endothelial activation in COVID-19 patients

E. Aarntzen, E. van Genugten, J. van Steenis, W. Hoefsloot, F. van de Veerdonk, M. Netea, M. Prokop;
Radboud University Nijmegen Medical Centre, Nijmegen, NETHERLANDS.

Aim/Introduction: Endothelial cells are regulators of inflammatory processes [1] and interact with their environment via integrin signaling [2]. During SARS-CoV2 infection, endothelial cells play a central role [3,4], their expression of ACE2 allows viral entry in distant organs. Loss of ACE2 function might result in angioedema [4, 5] at early stages. In response to circulating inflammatory mediators, activated endothelial cells facilitate extravasation of immune cells [6] during systemic phases. At recovery, endothelial cells initiate tissue regeneration [3]. Inadequate endothelial responses however, associate with vascular complications [7] and multi-organ failure [8]. Positron emission tomography (PET) imaging with [^{68}Ga]Ga-DOTA-(RGD)$_2$ targets avb3 integrin expression. We hypothesized that PET imaging provides insight in localization and magnitude of endothelial activation in lung parenchyma of COVID-19 patients, complementary to anatomical imaging or laboratory biomarkers, and in relation to changes in lung perfusion. **Materials and Methods:** We

performed a prospective observational study in n=10 patients with proven SARS-CoV2 infection admitted with respiratory insufficiency (NCT04596943). Patients underwent a [^{68}Ga]Ga-DOTA-(RGD)$_2$ PET scan followed by CT-subtraction. Routine clinical parameters were recorded. PET imaging findings were correlated to CT-severity score and local perfusion differences in the lung parenchyma (analysis ongoing). PET data from a previous study [9] served as reference. Results: [^{68}Ga]Ga-DOTA-(RGD)$_2$ uptake in total lung parenchyma was increased as compared to controls (p=0.0049), independent of lung lobe. Uptake in affected lung parenchyma, as determined by ground glass opacities or consolidations on CT, was significantly increased in all patients (p<0.0001) and as such highly correlated with CT-severity score (R^2 = 0.6433). Also in non-affected lung parenchyma, [^{68}Ga]Ga-DOTA-(RGD)$_2$ uptake was significantly increased in 8/10, group difference p=0.0058. Preliminary analyses of CT-subtraction showed local variations in lung perfusion, partly correlated with [^{68}Ga]Ga-DOTA-(RGD)$_2$ uptake. **Conclusion:** [^{68}Ga]Ga-DOTA-(RGD) PET imaging enables in vivo quantification of endothelial cell activation in lung parenchyma in COVID-19 patients with respiratory insufficiency. Our results suggest involvement endothelial cells in both local complications in the lung parenchyma, as well as at sites distant from infection, reflecting systemic endothial cell responses. **References:** [1] Pober et al. Nat Rev Immunol 2007[2] Cooper et al. Cancer Cell 2019[3] Ackermann et al. New Engl J Med 2020[4] Jin et al. Signal Transduct Target Ther 2020[5] Van de Veerdonk et al. JAMA Netw Open 2020[6] Doerschuk et al. Microcirculation 2001[7] Klok et al. Thromb Res 2020[8] Bikdeli et al. J Am Coll Cardiol 2020[9] Lobeek et al. Eur J Nucl Med Mol Imaging 2020

OP-0380

From early limbic inflammation to long COVID sequelae: targetting the transition from brain PET hypermetabolism to hypometabolism

E. Guedj[1], S. Morbelli[2], E. Kaphan[3], J. Y. Campion[1], P. Dudouet[1], M. Ceccaldi[1], S. Cammilleri[1], F. Nobili[1], C. Eldin[1];
[1]Aix Marseille Univ, Marseille, FRANCE, [2]Genoa University, Genoa, ITALY, [3]APHM, Marseille, FRANCE.

Aim/Introduction: COVID longitudinal PET studies are required to specify the relationship between brain metabolic abnormalities and temporal sequence of functional complaints, and especially early ^{18}F-FDG PET examinations to investigate the hypothesis of brain hypometabolic dysfunction secondary to earlier brain hypermetabolic inflammation as described in encephalitis. **Materials and Methods:** We studied spatial covariance metabolic PET pattern using SSMPCA toolbox in 35 patients with long COVID, 73 patients with autoimmune encephalitis (AE) and 6 patients with subacute COVID-19, in comparison to 44 age-matched healthy subjects. Results: The second PC comparing 35 patients with long COVID and 44 healthy subjects accounted for 8.4% of the variance with a difference between groups (p<0.001) and correlated with the clinical severity (r=0.371, p=0.028). This spatial covariance pattern included negative weights within the limbic system, brainstem and cerebellum, and positive weights within neocortical areas. The first PC comparing 73 patients with AE and 44 healthy subjects accounted for 18.9%, with a difference between groups (p<0.001). This spatial covariance pattern was inversed of those found in long COVID (r=- 0.93; p<0.001), demonstrating same regions involvement with opposite bottom/up weights from hypermetabolism to hypometabolism. The first PC comparing 6 patients with subacute COVID and 44 healthy subjects accounted for 16.3%, with a difference between groups (p<0.001), and a similar pattern of those found in AE (r=0.49; p=0.001), inversed to those found in long COVID (r=-0.37; p=0.013). **Conclusion:** The confirmation of brain hypermetabolism as feature of subacute COVID-19, with an encephalitis-like pattern in the same regions showing hypometabolism at later stages of COVID-19, reinforces the hypothesis of network disruption through early diffusion of inflammation/infection followed by hypometabolic sequelae in long COVID, with therapeutic implications for early intervention. **References:** (18)F-FDG brain PET hypometabolism in patients with long COVID. Guedj E, Campion JY, Dudouet P, Kaphan E, Bregeon F, Tissot-Dupont H, Guis S, Barthelemy F, Habert P, Ceccaldi M, Million M, Raoult D, Cammilleri S, Eldin C. Eur J Nucl Med Mol Imaging. 2021 Jan 26:1-11.

OP-0381

Metabolic network underlying persistent hyposmia after mild or moderate Coronavirus disease 2019 (COVID-19)

M. Donegani[1], S. Chiola[2,3], M. Pardini[4], F. Lanfranchi[1], F. D'Amico[1], S. Raffa[1], A. A. Miceli[1], C. Mantarro[5], C. Delucchi[6], M. Bauckneht[6], F. Massa[4], D. Arnaldi[6], L. Benedetti[4], F. Nobili[4], S. Morbelli[1];
[1]Department of Health Sciences (DISSAL), University of Genoa, Genova, ITALY, [2]Humanitas Clinical and Research Center–IRCCS, Rozzano (Mi), ITALY, [3]Humanitas University, Department of Biomedical Sciences, Milan, ITALY, [4]Department of Neuroscience (DINOGMI), University of Genoa, Genova, ITALY, [5]Department of Biomedical and Dental Sciences and Morphological and Functional Images, University of Messina, Messina, ITALY, [6]IRCCS Ospedale Policlinico San Martino, Genova, ITALY.

Aim/Introduction: COVID-19 due to SARS-CoV-2 infection has been associated with a number of neurological complications, including persistent hyposmia (frequently reported also in mild disease). Despite its relative frequency, to date the neural bases of hyposmia post-SARS-CoV-2 infection are poorly understood. We aimed to evaluate brain metabolic correlate of persistent isolated olfactory dysfunction after SARS-CoV-2 infection. **Materials and Methods:** Sixty-five patients underwent whole-body [18F]-FDG PET/CT, including a dedicated brain acquisition at our institution between May

2020 and March 2021 at least four weeks after their recovery after SARS-CoV-2 infection. Olfactory test (16 items smell diskettes olfaction test) was available in forty-five of them (27 males and 18 females; mean age 60 ± 13.1 years, range 35-86) and was scored as abnormal in twenty-two patients. Brain regions of relative hypometabolism in patients with or without hyposmia with respect to controls were assessed means of voxel-based analysis (SPM8). Patients' subgroups were also compared. Multiple regression analysis was used to identify correlation between anosmia test results and brain metabolism in both patients' subgroups. Age, gender and time from positive swab were included as nuisances. $p<0.001$ was accepted as significant. Results: Mean time interval between the first positive swab and PET acquisition was 12 weeks (range 4-28) for patients with hyposmia and 18 weeks (range 4-40) for patients with normal olfactory function. Eight patients with hyposmia were able to correctly identify between 7 and 9/16 smells; nine patients recognized between 4 and 6 smells, while five patients recognized ≤ 3 smells. Relative hypometabolism was demonstrated in bilateral parahippocampal and fusiform gyri and in left insula in hyposmic patients with respect to controls while no regions of significant hypometabolism were highlighted in non-hyposmic group. Furthermore, patients with hyposmia exhibited significant hypometabolism with respect to non-hyposmic patients in bilateral orbitofrontal cortex and gyrus rectus. Finally, only in patients with hyposmia, olfactory test scores were directly correlated with metabolism within a wide cluster encompassing corpus callosum, orbitofrontal, temporo-lateral cortex, amigdala, parahippocampal gyrus on both hemispheres. No correlations were highlighted between time from the first positive swab and brain metabolism. **Conclusion:** Hyposmia after SARS-CoV-2 infection without a history of severe respiratory distress is associated with significant metabolic alterations in regions beyond those involved in primary olfactory processing. If the present results will be confirmed on an individual basis, [18F]-FDG PET may play a role in the identification of presence (and resolution) of brain functional sequelae of COVID-19. **References:** none

OP-0382

Lung scintigraphy for pulmonary embolism diagnosis in COVID-19 patients: a multicenter observational study

P. Le Roux[1], P. Bonnefoy[2], A. Bahloul[3], B. Denizot[4], B. Barres[5], C. Moreau-Triby[6], A. Girma[7], A. Pallardy[8], Q. Ceyrat[9], L. Sarda-Mantel[10], M. Razzouk-Cadet[11], R. Zsigmond[12], F. Cachin[5], G. Karcher[3], P. Salaun[1];

[1]CHRU Brest, Brest, FRANCE, [2]CHU Saint-Etienne, Saint-Etienne, FRANCE, [3]CHU Nancy, Nancy, FRANCE, [4]CH Alpes Léman, Contamine-sur-Arve, FRANCE, [5]Jean Perrin Comprehensive Cancer Center, Clermont-Ferrand, FRANCE, [6]Hospices Civils de Lyon, Lyon, FRANCE, [7]Hôpital Foch, Suresnes, FRANCE, [8]CHU Nantes, Nantes, FRANCE, [9]Centre d'imagerie fonctionnelle, Bordeaux, FRANCE, [10]Assistance Publique-Hôpitaux de Paris, Hôpital Saint-Louis, Paris, FRANCE, [11]CHU Nice, Nice, FRANCE, [12]Centre d'Imagerie Nucléaire d'Annecy, Annecy, FRANCE.

Aim/Introduction: Pulmonary embolism (PE) has been described as a frequent complication of COVID-19 disease. Lung ventilation/perfusion (V/P) scintigraphy is a well-established test for PE diagnosis. However, in COVID-19 patients, there has been an ongoing debate within the nuclear medicine community as to whether and when the ventilation study should be performed. Indeed, the ventilation procedure potentially increases the risk of contamination to the healthcare workers. On the other hand, omitting the ventilation has been described to decrease the diagnostic accuracy of the test. As a consequence, it has been proposed either to omit the ventilation, to only perform the ventilation in a second time when the P SPECT/CT was inconclusive, or to systematically perform ventilation imaging. The aim was to describe practices and to assess the role of ventilation imaging when performing lung scintigraphy for suspected PE in COVID-19 patients. **Materials and Methods:** A national registry was created in collaboration with the French Society of Nuclear Medicine to collect lung scans performed in COVID-19 patients for suspected PE. Practices of departments were assessed regarding imaging protocols and aerosol precautions. A retrospective review of V/P SPECT/CT scans was then conducted. Two physicians blinded to clinical information reviewed each case by sequentially using P SPECT, P SPECT/CT and V/P SPECT/CT images. Scans were classified in one of the four following categories: patients for whom PE could reasonably be excluded based on 1) perfusion SPECT only, 2) P SPECT/CT, 3) V/P SPECT/CT; or 4) patients with mismatched defects suggestive of PE according to the EANM criteria. Results: Data from 188 COVID-19 patients who underwent lung scintigraphy for suspected PE between 03/2020 and 04/2021 in 12 French nuclear medicine departments were collected. Personal protective equipment and dedicated cleaning procedures were used in all departments. Of the 188 patients, 175(93%) had a ventilation scan. 24(13%) only had a planar scan and 162(86%) had SPECT/CT imaging. Out of the 150 V/Q SPECT/CT included in the central review, PE could be excluded using only P SPECT, P SPECT/CT and V/P SPECT/CT in 27(18%), 57(38%) and 48(32%) patients, respectively. V/P SPECT/CT was positive for PE in 18(12%) patients, including 12(67%) with a low burden of PE (≤10%). **Conclusion:** In this population of COVID-19 patients assessed with lung scintigraphy, the prevalence of PE was low(12%). Only 18% of patients had a normal perfusion scan. Ventilation imaging was required to confidently rule out PE in 32% of patients. **References:** None

OP-0383

Functional alterations due to COVID-19 lung lesions - Lessons from a multicenter V/Q scan-based registry

P. Bonnefoy[1], A. Bahloul[2], B. Denizot[3], B. Barres[4], C. Moreau-Triby[5], A. Girma[6], A. Pallardy[7], Q. Ceyrat[8], L. Sarda-Mantel[9], M. Razzouk-Cadet[10], R. Zsigmond[11], F. Cachin[4], G. Karcher[2], P. Salaun[12], P. Le Roux[12];

[1]CHU Saint-Etienne, Saint Etienne, FRANCE, [2]CHU Nancy, Nancy, FRANCE, [3]CH Alpes Léman, Contamine-sur-Arve, FRANCE, [4]Jean Perrin Comprehensive Cancer Center, Clermont-Ferrand, FRANCE, [5]Hospices Civils de Lyon, Lyon, FRANCE, [6]Hôpital Foch, Suresnes, FRANCE, [7]CHU Nantes, Nantes, FRANCE, [8]Centre d'imagerie fonctionnelle, Bordeaux, FRANCE, [9]Assistance Publique-Hôpitaux de Paris, Hôpital Saint-Louis, Paris, FRANCE, [10]CHU Nice, Nice, FRANCE, [11]Centre d'Imagerie Nucléaire d'Annecy, Annecy, FRANCE, [12]CHRU Brest, Brest, FRANCE.

Aim/Introduction: Clinical manifestations of COVID-19 are variable and range from incidental finding in asymptomatic patient to acute respiratory injury. The lung lesions observed also seem to be variable. The impact of these lesions on ventilation (V) and pulmonary perfusion (Q) functions has only been reported in a limited number of patients. The main objective of this work is to describe V/Q injury by type of COVID-19 lesions visible on CT. **Materials and Methods:** For this purpose, we explored the registry powered by the French Society of Nuclear Medicine (SFMN) which included patients who underwent V/Q scan for PE suspicion during a proven acute COVID-19 infection. This study analyzed patients explored with V/Q SPECT/CT scans between 03/2020 and 04/2021. A centrally blinded review of all V/Q SPECT/CT scans was performed. CT lesions consistent with COVID-19 infection were recorded and a qualitative evaluation of perfusion and ventilation was performed using a 5-points score (0=Normal function,1=mild impairment, 2=moderate impairment, 3=severe impairment, 4=Absent function). Results: V/Q SPECT/CT was performed in 150 patients with confirmed COVID-19 infection recruited in 12 nuclear medicine departments. Parenchymal lesions were visible in 131 patients (87%). Lesions were most often bilateral (110 patients) with subpleural (65%), peribronchovascular (9%) or mixed topography (25%). The lesions were extended to 0%, 1-10%, 11-25%, 26-50%, 51-75%, >75% of lung parenchyma in 19, 42, 51, 30, 7 and 1 patients, respectively. Analysis by lesion revealed the presence of frosted glass lesions in 33 patients, crazy-paving in 47 patients and alveolar condensations in 91 patients. Frosted glass lesions were responsible for minimal perfusion impairment (Perfusion score [mean+/-] 0.85+/-0.6) and moderate ventilation impairment (Ventilation score 1.67+/-1); Crazy-paving for moderate perfusion impairment (Perfusion score 2.06+/-1.1) and moderate-to-severe ventilation impairment (Ventilation score 2.45+/-1.1); Alveolar condensations for moderate perfusion impairment (Perfusion score 2.07+/-1) and severe ventilation impairment (Ventilation score 2.98+/-0.9). **Conclusion:** In this population of COVID-19 patients assessed with V/Q SPECT/CT scans for suspected acute PE, a large proportion of patients had COVID-19 parenchymal lesions on CT images. COVID-19 related pulmonary lesions were, in order of frequency and functional impairment, alveolar condensations, crazy-paving and frosted glass lesions with V/Q impairment predominating in ventilation. **References:** none

OP-0384

Quantification of Loss of Hypoxic Pulmonary Vasoconstriction Using Lung Perfusion SPECT/CT and FDG-PET/CT in Patients with Covid-19

C. Ramos, A. Fernandes, M. Takahashi, S. Souza, M. Fujiwara, N. Tobar, S. Dertkigil, J. Rodrigues, E. Gonçales, P. Trabasso, D. Zantut-Wittmann;

University of Campinas, Campinas, BRAZIL.

Aim/Introduction: Loss of hypoxic pulmonary vasoconstriction leading to functional right-to-left intrapulmonary shunt has been related to severe hypoxemia in some patients with Covid-19 (1-3). This results in arterial pulmonary perfusion occurring in inflamed non-aerated lung areas. The aim of this study was to quantify the percent of total pulmonary perfusion that occurs in inflamed areas in patients with acute Covid-19 pneumopathy. **Materials and Methods:** Twenty-four patients (14 women, median age 54.5 [28-78] years) admitted to hospital with respiratory failure and nasopharyngeal swab test (RT-PCR) positive for Covid-19 were studied. In order to assess simultaneously pulmonary perfusion and inflammation, Lung Perfusion SPECT/CT (5 minutes after the intravenous injection of 2.4 MBq/kg ^{99m}Tc-MAA) and PET/CT (1h after injection of 4.4 MBq/kg of ^{18}F-FDG) were performed sequentially. Lung metabolic volume (MV) was defined as that above the mediastinal uptake on ^{18}F-FDG PET images. A MV-mask, representing total lung inflammation, was then registered to the Lung Perfusion SPECT volume. The counts within the MV-mask were divided by the total counts of the SPECT image. This resulted in the percentage of lung perfusion occurring in inflamed lung tissue, assigned as functional right-to-left shunt (Shunt%). Flow rate of supplemental oxygen (O_2flow) and clinical parameters were noted for each patient. Spearman's correlation coefficient was used to evaluate the strength of relationship between paired data. Results: PET/CT images demonstrated increased glycolytic metabolism in consolidation and ground-glass opacities areas of the lungs, with different degrees of ^{18}F-FDG uptake. Ten/24 patients presented normal or increased perfusion in areas with ^{18}F-FDG uptake. The other 14/24 patients presented the expected reduced lung perfusion in these affected areas. Wedge-shaped perfusion defects consistent with thromboembolism were detected in 3/24 patients. The mean±SD of the O_2flow, MV, and Shunt% were respectively 2.7±1.5 L/min, 558±453 mL, and 22.5%±18.7%. Shunt% presented positive correlation with O_2flow (r=0.70229, p=0.0001). **Conclusion:** Simultaneous evaluation

of Lung Perfusion SPECT/CT and FDG PET/CT allows the non-invasive identification and quantification of loss of hypoxic pulmonary vasoconstriction in patients with acute Covid-19 pneumopathy. Shunt% presented a strong relationship with O_2flow. Other aspects of Covid-19 pulmonary disease can be assessed by the combination of both techniques such as inflammatory burden and pulmonary thromboembolism (3). **References:** (1) Gattinoni L, et al. Am J Respir Crit Care Med. 2020; 201:1299-1300. (2) Patel BV, et al. Am J Respir Crit Care Med. 2020; 202(5):690-699. (3) Ramos CD, et al. Am J Respir Crit Care Med. 2021; 203(9):1186-1187.

OP-0385

Myocardial Perfusion SPECT Findings In Postcovid Period

M. Araz, G. Sutcu, B. Demir, E. Ozkan, C. Soydal;
Ankara University, Ankara, TURKEY.

Aim/Introduction: It has been reported that risk of cardiac events has increased after Covid-19 infection, which is soon related with late thrombotic and microcirculatory complications induced by inflammatory cascade. Myocardial perfusion scan (MPS) is fundamental imaging method in evaluation of ischemia and coronary risk assessment. In this study, we investigated if MPS can be used in the assessment of patients with history of Covid-19 and cardiac symptoms **Materials and Methods:** Patients who were referred to Nuclear Medicine Department between August 2020-April 2021 with a history of active symptomatic Covid-19 infection (confirmed by PCR positivity) in the last 6 months were involved in the study group. Age-and gender matched control group was composed of randomly chosen patients who attended for MPS between January 2019 - September 2019, before pandemic. Age, gender, risk factors for coronary artery disease (hypertension, diabetes mellitus, hyperlipidemia, family history for coronary artery disease, obesity) as well as the active symptoms were noted in both groups. The history of percutaneous coronary investigations or by-pass grefting were also recorded from the hospital registry. Myocardial perfusion SPECT results were categorized in the groups as either normal, ischemia or infarct Chi-square test was performed for comparison of frequency of reported ischemia on MPS. P value<0.05 was considered significant Results: A total of 179 patients (84F, 95M, mean age 58.28±9.28) were involved retrospectively. 85 patients were included in the study group and 94 in the control group. The study and control groups were matched in terms of age and sex. No significant differences were found in the frequency of risk factors and previous coronary interventions or operations for coronary artery disease between two groups. Ischemia was reported more frequently among patients with a history of Covid-19 infection (p<0.001). Among 39 patients with ischemia on MPS in the study group, 11 patients were taken under follow up without coronary angiography, 5 patients refused coronary angiography and 23 patients were evaluated with coronary angiography. Stent implantation was performed in 2/23 patients, CABG in 1 patient and in 20/23 patients medical therapy was preferred due to noncritical stenosis in the coronaries **Conclusion:** There exists a significant increase in the frequency of ischemia on MPS in patients with a history of Covid-19 infection in the last 6 months. MPS is a reliable method to investigate ischemia in patients with Covid-19 history **References:** None

OP-0386

Prior COVID-19 History Increases The Risk of Ischemia in Myocardial Perfusion CZT Detectors Scintigraphy

E. Sahin Kutuk, N. B. Talay, T. Bahceci, E. Ozdemir;
Ankara City Hospital, Ankara, TURKEY.

Aim/Introduction: The aim of this study is to evaluate the rate of ischemia on myocardial perfusion imaging (MPI) at our department during the pandemic compared to prior to the pandemic. **Materials and Methods:** This is a single centre retrospective assessment of the rate of patients with ischemia on myocardial perfusion SPECT imaging (MPI) during the COVID-19 pandemic (August - November 2020, cohort of 896 patients) in comparison to that of the same period before the pandemic (cohort of 1415 patients). Results: The number of SPECT-MPIs in 2020 cohort was lower than 2019 (p <0.01). However the rate of ischemic MPI in the 2020 cohort was higher than prior to the pandemic (42.2% vs. 31.0%, p <0.01). When the group of the pandemic period was examined independently, ischemia rate was higher in patients with prior COVID-19 history compared to those without (52.4% vs 41.1%) (p = 0.049). The prior COVID-19 history increased the possibility of ischemia in MPI approximately 1.5 times (OR: 1.57, 95% CI, 1.003-2.470) (p = 0.048). **Conclusion:** We found that the rate of ischemia in SPECT-MPI was statistically higher than the period before the pandemic. In addition, when the group in the pandemic period was examined, a higher rate of ischemia was observed in those with a history of COVID-19 compared to those without. According to our study, COVID-19 causes an increased risk of ischemia in myocardial perfusion CZT detectors scintigraphy **References:** None.

OP-0387

Evaluation of the findings in [^{18}F]-FDG PET/CT studies of patients with incidental diagnosis of lung tumors in radiological imaging, which are performed due to the clinical suspicion of SARS-CoV-2 pneumonia

G. Guzmán Prudencio, S. Alvarez Ruiz, L. Del Barco Diez Canseco, N. Canchumanya Huatuco, M. Calderón Calvente, L. De la Cueva Barrao, M. Falgás Lacueva, P. Navarro Beltrán, M. Sangrós Sahún, D. Abós Olivares;
Hospital Universitario Miguel Servet, Zaragoza, SPAIN.

Aim/Introduction: To analyze the added diagnostic value of chest imaging techniques in the incidental diagnosis of lung cancer, in patients with clinical suspicion of SARS-CoV-2 pneumonia. **Materials and Methods:** We reviewed the findings in [^{18}F]-FDG PET/CT studies performed between February 2020 and March 2021, whose reason for request was the evaluation of a radiological finding on CT (solitary pulmonary nodule, lung mass with or without hilar and / or mediastinal lymphadenopathy), in patients initially studied for suspected SARS-CoV-2 pneumonia.Based on the findings of the PET-CT study, using the current TNM classification, and the pathological correlation for small cell lung cancer (SCLC) and non-small cell lung cancer (NSCLC), we classified the patients in six different groups. Group 1: Stage I and II (NSCLC), Group 2: Stage III (NSCLC), Group 3: Stage I-IIIB (limited stage-SCLC), Group 4: Stage IV (NSCLC and extensive stage-SCLC), Group 5: metastasis of non-lung carcinoma, and Group 6: benign findings. Results: In total, 36 [18F]-FDG PET-CT studies were obtained, of 13 women and 23 men, in the age range of 30 to 81 years. The correlation between imaging and pathological anatomy studies confirms lung carcinoma in 21(58%) cases (14 NSCLC and 7 SCLC), in 2(5%) cases of non-lung carcinoma metastasis (Group 5) and in 13 (36%) cases benign and / or inflammatory lesions (Group 6).From the 21 patients diagnosed of lung carcinoma, 3 cases (Group 1) were in early stages of the disease, which were candidates for complete surgical resection, and 3 cases (Group 2) were subsidiary for possible surgery after systemic treatment. The remaining patients were in an advanced stage of the disease 2 cases (Group 3) and 13 cases (Group 4), that were candidates to systemic treatment. **Conclusion:** 1.- The imaging studies in patients with suspected SARS CoV-2 pneumonia have had a beneficial side effect in a significant number of patients in whom unsuspected lung carcinoma have been diagnosed at a presumably earlier stage than following their natural history. 2.- Although, in most of the cases of lung cancer the diagnosis was made in advanced stages of the disease, we also found patients that were in early stages, candidates of potentially curative surgical treatment and probable greater long-term survival. 3.- Likewise, they have been useful in the extension study of distant metastasis of non-pulmonary tumors and they also made possible to rule out malignancy in patients with benign lung lesions. **References:** None.

OP-0388

Ipsilateral nodal uptake post COVID-19 vaccination and the impact on interpretation of 18F-FDG PET/CT scans

M. Arora, A. Gomes Moura, M. Carmody, Z. Win, N. H. Patel, C. Bowen, S. R. Khan, T. Barwick;
Imperial College Healthcare Trust, London, UNITED KINGDOM.

Aim/Introduction: Implementation of mass vaccination amidst the COVID-19 pandemic has posed new interpretative challenges in Nuclear Medicine.18F-FDG avid nodes have been reported ipsilateral to the side of mRNA vaccination on PET/CT(1),increasing the potential for false-positive diagnoses. Our aims were to assess the incidence of ipsilateral nodal uptake on PET/CT post COVID-19 vaccination(mRNA and vector-based),imaging characteristics of nodal uptake and impact on image interpretation. **Materials and Methods:** Local Institutional approval was obtained.18F-FDG PET/CT studies of 134 patients who had received COVID-19 vaccination and a routine patient questionnaire (brand,laterality and date of vaccination) were retrospectively evaluated. Two experienced observers documented the presence of ipsilateral avid nodes visible above background, including SUVmax and size of the most avid node. Cases impacting interpretation/management were noted. The incidence of nodal uptake was calculated and differences within age, gender, vaccine brand assessed(Fisher's exact test). Results: The overall incidence of ipsilateral post-vaccine nodal uptake on 18F-FDG PET/CT was 13.4%(18 patients). This was significantly higher amongst females(23% vs 4% males;p=0.002). Our data suggests there is a trend of higher incidence in younger age groups, which will be explored further with larger patient numbers. A higher incidence was also observed in patients vaccinated<40 days(18%; n=13/72) compared to>40 days(8%; n=4/51), 11/134 patients recorded their vaccination dates too vaguely to be included. No significant difference was demonstrated between nodal uptake and vaccine type (p=0.598).All avid nodes involved the axilla only. Multiple avid nodes were seen in 14 cases(78%) and a single avid node in 4 cases(22%). The SUV max range was 1.5-6.8 (SUVmax=3.3±0.3) and short-axis nodal size range was 3-12mm (size= 8±0.6mm). Interpretation was confounded in 7/18 cases, 4 of which were breast cancer cases and 3 of these had been vaccinated ipsilateral to the side of malignancy. **Conclusion:** The incidence of 18F-FDG nodal uptake ipsilateral to side of COVID-19 vaccination (mRNA and vector-based vaccinations) is 13.4% in our series, with an increased frequency amongst females and younger age groups. This impacted image interpretation, particularly in breast cancer cases. Interpretation can be aided by documenting vaccination details and vaccinating contralateral to the side of known pathology.In addition,deferring imaging to after 40 days of vaccination may allow vaccine-related nodal activity to resolve.This concurs with other imaging recommendations(2) to delay scanning by 4-6 weeks following vaccination where possible. **References:** (1)Doss

et al.Clin Nucl Med 2021 May;46(5):439-441; (2)Grimm et al.SBI Recommendations for the Management of Axillary Adenopathy in Patients with Recent COVID-19 Vaccination Mar 2021.

OP-0389

Global Impact of COVID-19 on Nuclear Medicine Departments; an International Follow-up Survey

F. Giammarile, D. Paez, E. Estrada-Lobato, M. Mikhail, O. Pellet; Division of Human Health, Department of Nuclear Sciences and Applications International Atomic Energy Agency, Vienna, AUSTRIA.

Aim/Introduction: As a follow-up to the international survey conducted in April 2020, this survey aims to provide a situational snapshot of the COVID-19 impact on nuclear medicine services worldwide, one year later. The survey was designed to determine the impact of the pandemic at two specific time-points: June and October 2020 and compare them to the previously collected data. **Materials and Methods:** A web-based questionnaire, in the same format as the April 2020 survey was disseminated to nuclear medicine facilities worldwide. Survey data was collected using a secure software platform hosted by the International Atomic Energy Agency (IAEA); it was made available for 6 weeks, from November 23 to December 31, 2020. Results: From 505 replies from 96 countries, data was extracted from 355 questionnaires (of which 338 were fully completed). The responses came from centres evenly distributed in different regions of the world and with different income status. Regional differences and challenges across the world were identified and analysed. Globally, the volume of nuclear medicine procedures decreased by 73.3% in June 2020 and 56.9% in October 2020. Among the nuclear medicine procedures, oncological PET studies showed less of a decline in utilization compared to conventional nuclear medicine and particularly nuclear cardiology. The impact was also significantly less in high-income countries. A trend towards a return to the pre-COVID-19 situation of the supply chains of radioisotopes, generators, and other essential materials was evident. **Conclusion:** The impact of the COVID-19 pandemic was associated with a significant reduction in nuclear medicine diagnostic and therapeutic procedures throughout 2020. In June, the global decline recorded in the survey was greater than in October when there was a slight improvement. However, the total number of procedures continued below that recorded in April 2020, and less than half of the volumes normally carried out before the pandemic **References:** Freudenberg LS, Paez D, Giammarile F, Cerci J, Modiselle M, Pascual TNB, et al. Global Impact of COVID-19 on Nuclear Medicine Departments: An International Survey in April 2020. J Nucl Med. 2020;61(9):1278-83.

901

Thursday, October 21, 2021, 10:45 - 12:15

Channel 1

CME 6: Quo vadis PET/MRI?

OP-0392

Methodological Developments

H. Quick; *University Hospital Essen, Hybrid and High-Field MR Imaging, Essen, GERMANY.*

OP-0393

Oncological Applications

I. Burger; *Kantonsspital Baden, Nuclear Medicine, Baden, SWITZERLAND.*

OP-0394

Beyond Oncological Applications

A. Hammers; *King's College London & Guy's and St Thomas' PET Centre, School of Biomedical Engineering and Imaging Sciences, Faculty of Life Sciences and Medicine, London, UNITED KINGDOM.*

904

Wednesday, October 20 - Saturday, October 23, 2021

on-demand pool, release on Wednesday, October 20 at 09:00

CTE 6: Radionuclide Therapy Management

OP-0423

Informed Consent in Radionuclide Therapy Management

C. Deroose; *University Hospitals Leuven, Nuclear Medicine, Leuven, BELGIUM.*

OP-0424

Patient Care during Radionuclide Therapy Treatment

L. Pereira; *Maidstone and Tunbridge Wells NHS Trust, Nuclear Medicine, Royal Turnbridge Wells, UNITED KINGDOM.*

OP-0425

Radionuclide Therapy Waste Management

P. Fragoso Costa; *Clinic for Nuclear Medicine, University Hospital Essen, Essen, GERMANY.*

905

Wednesday, October 20 - Saturday, October 23, 2021

on-demand pool, release on Wednesday, October 20 at 09:00

Joint Symposium 11 (EANM/EANO): Advancements in Neuro-Oncology

OP-0427

Artificial Intelligence in Glioma Imaging

L. Papp; Medical University Vienna, Center for Medical Physics and Biomedical Engineering, Vienna, AUSTRIA.

OP-0428

New PET Tracers for Brain Tumour Imaging

N. Albert; LMU, Munich, GERMANY.

OP-0429

The 2020 EANO Guidelines on Diagnosis and Management of Gliomas - Take-Home Messages for the Clinician

J.-C. Tonn; University Hospital Munich (LMU), Department of Neurosurgery, Munich, GERMANY.

906

Wednesday, October 20 - Saturday, October 23, 2021

on-demand pool, release on Wednesday, October 20 at 09:00

Joint Symposium 12 (EANM/EORTC): Nuclear Medicine in Precision Oncology

OP-0431

Molecular Imaging of the Immune System

A. Wu; Department of Immunology & Theranostics, Beckman Research Institute of the City of Hope, Duarte, UNITED STATES OF AMERICA.

OP-0432

Targeted Alpha Therapy

M. Koole; KU Leuven, Department of Nuclear Medicine and Molecular Imaging, Leuven, BELGIUM.

OP-0433

Managing Radioiodine Refractory Thyroid Cancer

D. Vriens; Leiden University Medical Center, Department of Radiology, Leiden, NETHERLANDS.

907

Wednesday, October 20 - Saturday, October 23, 2021

on-demand pool, release on Wednesday, October 20 at 09:00

Pitfalls & Artefacts 6: Pitfalls & Artefacts in Endocrine Imaging

OP-0435

FDG-PET/CT - Endocrine Incidentalomas and Beyond

D. Deandreis; Director of Nuclear Medicine Division, Department of Medical Sciences, University of Turin, AOU Città della Salute e della Scienza, Turin, ITALY.

OP-0436

Somatostatin Receptor Targeted PET - Often Obvious, But Not Always

A. Haug; AKH Vienna, Division of Nuclear Medicine, Vienna, AUSTRIA.

OP-0437

Non-FDG Thyroid Incidentalomas

L. Heijmen; Radboud University Medical Centre, Division of Nuclear Medicine, Nijmegen, NETHERLANDS.

908

Wednesday, October 20 - Saturday, October 23, 2021

on-demand pool, release on Wednesday, October 20 at 09:00

M2M Track - TROP Session: Tumour Microenvironment and Immunotherapy

OP-0439

Fluorescent FAPI, does it stain FAP or something else?

T. Buckle, R. van Leeuwerden, D. van Willigen, F. van Leeuwen; LUMC, Leiden, NETHERLANDS.

Aim/Introduction: In recent years imaging of the fibroblast activate protein has emerged as a high potential extension of the tracer arsenal within nuclear medicine. Based on the success stories of FAPI-PET one may argue that the same target may also help advance the field of image-guided surgery. Using a known FAP targeting vector Gly-Pro (GP; (1)) and its variant ERGTGP a family of GP-fluorescent FAPI-tracers was created. Validation of in vitro performance was focused on their sub-cellular accumulation. **Materials and Methods:** Four different GP-fluorescent FAPI tracers were synthesized by functionalizing GP or ERGTGP with QAmine(SO3)Cy5, resulting in QAmine-(SO3)Cy5-GP, QAmine-(SO3)Cy5-ERGETGP, and QAmine-(SO3)Cy5-CPGTEGRE. MCF7 (known FAP positive human breast cancer cells; (1)) cells and three control cell lines (MDAMB231 (human breast carcinoma),

RT4D12 (rat schwannoma), GeB3 (dog epithelial)) were incubated with 1uM of tracer, either alone or in competition with the FAP inhibitor Ac-Gly-BoroPro. Incubation with non-functionalized dye variants and blocking with a mitochondrial tracer (1nM) were performed as control. Fluorescence confocal microscopy was used to assess the cellular distribution of the tracer signal (Cy5). Nuclear, lysosomal and mitochondrial counter stains were used as reference for intracellular localization. Immunohistochemical staining with an anti-FAP antibody was applied to confirm the presence of FAP within the different cell cultures. Results: QAmine-(SO3)Cy5-GP, QAmine-(SO3)Cy5-ERGETGP and QAmine-(SO3)Cy5-CPGTEGRE showed intracellular tracer uptake in all cell lines, with a staining pattern similar to literature reports (1). Non-functionalized dyes did not show cellular uptake. Neither incubation time (1 or 4 hours) nor temperature (4 or 37 degrees) influenced the staining of QAmine-(SO3) Cy5-GP, QAmine-(SO3)Cy5-ERGETGP or QAmine-(SO3)Cy5-CPGTEGRE. Interestingly, blocking experiments with the FAP inhibitor Ac-Gly-BoroPro (1000-fold excess) revealed a 62% decrease in fluorescence in RT4D12 cells, while uptake in MCF-7 and Geb3 cells was unaffected. Blocking with a mitochondrial stain affected uptake of the FAPI tracers in MCF-7 (60% signal decrease) but not Geb3 cells while lysosomal and mitochondrial counterstains were completely diminished. In contradiction to fluorescence imaging, FAP-specific immunohistochemistry showed intracellular presence of FAP in MCF-7, but not in RT4D12, MDAMB231 and GEB3 cells. **Conclusion:** The fluorescent FAPI-tracers were able to stain a wide range of cells, but the observed staining patterns did not seem to correlate with FAP IHC. At this point this discrepancy is unexplained, but the bulky nature of the fluorescent dyes could play a role. **References:** 1) Brennen et al, JNCI, 2012

OP-0440

Optimization of immune cell labeling efficiency using [^{111}In]In-PLGA-NH$_2$ nanoparticles modified with TAT cell penetrating peptides

R. Raavé[1], B. Manandhar[1], M. Krekorian[1,2], M. Srinivas[2], J. de Vries[2], S. Heskamp[1], E. Aarntzen[1];
[1]Department of Medical Imaging, Radboud Institute for Molecular Life Sciences, Radboud university medical center, Nijmegen, NETHERLANDS, [2]Department of Tumor Immunology, Radboud Institute for Molecular Life Sciences, Radboud university medical center, Nijmegen, NETHERLANDS.

Aim/Introduction: Nanoparticles (NPs) have been widely used for the purpose of multimodal imaging. Recently, we have developed a NP platform of poly (lactic-co-glycolic acid) (PLGA)-NH$_2$ for radiolabeling of monocytes using [^{111}In]InCl$_3$ as opposed to conventional [^{111}In]In-oxine, which is limited by its low cellular retention and cytotoxicity. However, these NPs show limited cell labeling efficiency. Hence, to improve the labeling, we modified the NPs with cell penetrating peptides to increase cellular uptake while maintaining cellular retention and cell viability. In this study, we conjugated PLGA-NH$_2$ NPs with TAT cell penetrating peptides (Ac-C-Ahx-YGRKKRRQRRR-NH$_2$, TAT-PLGA-NH$_2$). These [^{111}In]In-TAT-PLGA-NH$_2$ NPs were used to radiolabel human monocytes (THP-1 cell line). **Materials and Methods:** PLGA-NH$_2$ and TAT-PLGA-NH$_2$ were radiolabeled with [^{111}In]InCl$_3$ by incubation at 37°C at 550 rpm for 30 minutes and washed three times to determine the labeling efficiency. THP-1 cells were labeled using [^{111}In]In-PLGA-NH$_2$ NPs with or without TAT ([^{111}In]In-THP-1 cells) by incubating at 37°C for 2 hours. [^{111}In]In-THP-1 cells were washed three times and subsequently the labeling efficiency was determined. The cell viability was assessed through trypan blue exclusion. The ^{111}In-retention and cell viability was determined after incubation in RPMI-1640 media (supplemented with 10% fetal calf serum) at 37°C for 1, 2, 4, 6, 24 and 48 hours. Results: TAT conjugated and nonconjugated NPs had a similar labeling efficiency of 29.15 ± 11.22% and 31.47 ± 14.24%, respectively. When radiolabeling THP-1 cells, the TAT-PLGA-NH$_2$ NPs significantly improved the cellular uptake to 17.02 ± 7.05% compared to 4.32 ± 2.52 % for nonconjugated NPs; corresponding with cell-specific activity of 33.5 ± 11.5 and 21.9 ± 18.5 kBq/10^6 cells, respectively. The retention of radioactivity in ^{111}In-THP-1 cells over 48 hours was comparable with 84.95 ± 4.63 % for TAT-PLGA-NH$_2$ and 81.99 ± 9.49 % for PLGA-NH$_2$ NP. Similarly, viability was 75.92 ± 18.46 % and 76.95 ± 15.90 % for TAT-PLGA-NH$_2$ and PLGA-NH$_2$ labeled cells at 48 hours, respectively. **Conclusion:** PLGA-NH$_2$ NPs modified with TAT cell penetrating peptide resulted in improved labeling efficiency while maintaining the cellular retention and viability over 48 hours. This approach allows in vivo tracking of ex vivo labeled cells with enhanced sensitivity. **References:** None.

OP-0441

Evaluation of novel anti-CAIX antibodies by PET imaging and biodistribution studies in a colorectal adenocarcinoma model

H. Law[1], J. Rousseau[1], P. C. McDonald[2], A. E. Lenferink[3], N. Colpo[1], J. Zeisler[1], R. Tan[1], S. Dedhar[2], K. Lin[1], F. Bénard[1];
[1]Molecular Oncology, BC Cancer Research Institute, Vancouver, BC, CANADA, [2]Integrative Oncology, BC Cancer Research Institute, Vancouver, BC, CANADA, [3]National Research Council, Biotechnology Research Institute, Montreal, QC, CANADA.

Aim/Introduction: Hypoxia creates a microenvironment that drives tumour cells towards aggressive phenotypes, in addition to inducing radiation and chemotherapy resistance. Metabolic rates increase, creating an acidic environment within each cell. To maintain an optimal intracellular pH for survival and proliferation, cancer cells overexpress a surface protein called carbonic anhydrase IX (CAIX). CAIX is a component of the hypoxia-induced signalling cascade

that can be targeted for imaging and therapy. CAIX is overexpressed in many solid cancers while expressed at low levels in normal tissues. The aim of this study is to assess if novel anti-CAIX monoclonal antibodies (mAbs) are suitable for radioimmunotherapy (RIT) of CAIX-positive cancers by positron emission tomography (PET) in a colorectal adenocarcinoma model. **Materials and Methods:** High affinity chimeric mouse/human (c11H9 and c2C7) and murine (m4A2) mAbs targeting CAIX were produced; c11H9 binds the proteoglycan-like domain, while c2C7 and m4A2 bind the catalytic domain. All mAbs were conjugated to the chelator DFO*-pPhe-NCS (DFO*) at a chelator:mAb ratio of 5:1, and radiolabelled with ^{89}Zr. Radiochemical purity and specific activities were determined by iTLC-SG chromatography and size exclusion chromatography using HPLC. The radiolabelled mAbs (20.2 ± 0.3 µg, 1.4 ± 0.1 MBq) were injected intravenously into athymic nude mice bearing subcutaneous HT-29 colorectal adenocarcinoma xenografts. PET/CT imaging was performed at days 1, 3, and 6 post-injection (p.i.), and biodistribution studies were carried out at days 3 and 6 p.i. (n=5 per group). Results: All mAbs were efficiently conjugated with DFO* and radiolabelled with ^{89}Zr. Radiochemical purities of ^{89}Zr-labelled immunoconjugates were >97% and specific activities were 0.2-0.4 MBq/µg. PET-CT imaging with all mAbs showed robust tumour uptake and high tumour-to-background ratios across days 1, 3, and 6 p.i. Biodistribution at day 6 p.i. confirmed the high tumour uptake with 15.88±1.08, 20.22±1.5, and 10.3±4.0 %ID/g for c11H9, c2C7, and m4A2 respectively. High tumour-to-muscle ratios (>26 for c11H9, >21 for c2C7, and >36 for m4A2) were also observed at day 6 p.i. **Conclusion:** The three novel anti-CAIX mAbs showed clear tumour uptake in a CAIX-expressing colorectal adenocarcinoma model. The high tumour uptake and tumour-to-background ratios achieved by immunoPET imaging warrant further investigation to evaluate the potential of these mAbs for diagnostic and radioimmunotherapy applications. **References:** none

OP-0442

Development of ^{89}Zr and ^{68}Ga-anti-CD103 Fab fragment-based PET imaging for non-invasive assessment of cancer reactive T cell infiltration

M. Wazynska, X. Fan, A. Kol, M. de Bruyn, P. H. Elsinga, H. W. Nijman; University Medical Center Groningen, Groningen, NETHERLANDS.

Aim/Introduction: CD103, an integrin specifically expressed on the surface of cancer-reactive T cells, shows significantly increased expression during successful immunotherapy across human malignancies. Previously, it has also been linked with better disease-specific survival in patients with ovarian, cervical, and endometrial cancer. Therefore, CD103 is an attractive biomarker for non-invasive immune PET imaging of T cell infiltration. **Materials and Methods:** Previously, we developed a monoclonal antibody (mAb) that specifically targets human CD103-positive cells. Here, we used this mAb to generate a Fab derivative radiolabeled it with 89Zr and 68Ga. We examined in vitro stability in phosphate buffer saline, serum and by implementing EDTA challenge, as well as in vitro binding using CD103 expressing CHO or CHO wild-type cell lines. For in vivo studies, nude mice (BALB/cOlaHsd-Foxn1nu) with established CD103 expressing CHO or CHO wild-type xenografts were injected with ^{89}Zr and ^{68}Ga-anti-human CD103 Fabs and underwent serial PET imaging, followed by ex vivo biodistribution. Results: We developed ^{89}Zr- and ^{68}Ga-radiolabeled Fab fragment (Fab) clones that specifically recognize human CD103 in vitro and in vivo. Tracers were synthesized with radiochemical purity greater than 95% and molar activity 13.4 ± 0.8, 58.3 ± 0.5 GBq/µmol (^{89}Zr- and ^{68}Ga-radiolabeled molecule respectively). In vivo, both ^{89}Zr- and ^{68}Ga-anti-human CD103 tracers showed high target-to-background ratios, high target site selectivity and a high sensitivity in human CD103 positive xenografts. **Conclusion:** We developed two novel human CD103 immuno-PET tracers for future non-invasive assessment of cancer reactive T cell infiltration. Consequently, both ^{89}Zr and ^{68}Ga-anti-CD103 Fab fragment-based PET tracer could be successfully used in clinical settings for stratification patients who could benefit from immune checkpoint inhibition therapy. **References:** [1] Sharma P, Allison JP. The future of immune checkpoint therapy. Science. 2015;348(6230):56-61. [2] Topalian SL, Drake CG, Pardoll DM. Immune checkpoint blockade: a common denominator approach to cancer therapy. Cancer Cell. 2015 Apr 13;27(4):450-61.[3] Mahoney KM, Rennert PD, Freeman GJ. Combination cancer immunotherapy and new immunomodulatory targets. Nat Rev Drug Discov. 2015 Aug;14(8):561-84. [4] Workel HH, Komdeur FL, Wouters MCA, Plat A, Klip HG, Eggink FA, et al. CD103 defines intraepithelial CD8+ PD1+ tumour-infiltrating lymphocytes of prognostic significance in endometrial adenocarcinoma. Eur J Cancer. 2016;60:1-11.[5] Edwards J, Wilmott JS, Madore J, Gide TN, Quek C, Tasker A, et al. CD103+tumor-resident CD8+T cells are associated with improved survival in immunotherapy-naïve melanoma patients and expand significantly during anti-PD-1 treatment. Clin Cancer Res. 2018;24(13):3036-45.

OP-0443

Anti-tumor efficacy of a combination therapy with PD-L1 targeted alpha therapy and adoptive cell transfer of PD-1 deficient melanoma-specific human lymphocytes

L. Marotte[1,2], M. Capitao[1,2], C. Deleine[1,2], T. Beauvais[3,2], G. Cadiou[1,2], J. Perrin[1,2], M. Chérel[4,5,6], Y. Guilloux[1,2], E. Scotet[1,2], F. Bruchertseifer[7], A. Morgenstern[7], A. Jarry[1,2], N. Labarrière[1,2], **J. Gaschet***[1,2]; *[1]University of Nantes, CNRS, INSERM, CRCINA, Nantes, FRANCE, [2]LabEx IGO "Immunotherapy, Graft, Oncology", Nantes, FRANCE, [3]University of Nantes, CNRS, INSERM, CRCINA, CHU of Nantes, Nantes, FRANCE, [4]University of Nantes, CNRS, INSERM, CRCINA, ICO Gauducheau, Nantes, FRANCE, [5]LabEx IRON "Innovative Radiopharmaceuticals in Oncology and Neurology", Nantes, FRANCE, [6]GIP Arronax, Saint-Herblain, FRANCE, [7]European Commission, Joint Research Centre, Karlsruhe, GERMANY. (*shared last authors)*

Aim/Introduction: The optimization of adoptive transfer approaches of anti-tumor T cells requires both the functional improvement of the injected T cells and the modulation of the tumor microenvironment, favoring the recruitment of these T cells and their activation. We have recently shown the therapeutic benefit of two approaches tested individually in a melanoma model: the adoptive transfer of specific T cells invalidated for the expression of the inhibitory receptor PD-1, and PD-L1 targeted alpha therapy (TAT). In this study, we sought to investigate the efficacy of these two therapies combined, compared to each monotherapy, in order to evaluate the synergy between these two approaches, in the same melanoma model. **Materials and Methods:** Here we used melanoma-specific T-cell clones, previously validated for the edition of PDCD1 gene and their wild-type counterparts, and already tested in vivo for adoptive transfer in NSG mice engrafted with PD-L1 expressing human melanoma tumors. We also used a previously validated TAT approach, using a ^{213}Bi-anti-human-PD-L1 mAb, alone or in combination with adoptive cell transfer, in the same mouse model. Results: Here we confirmed previous results obtained with each monotherapy (1,2) and documented the superior ability of a combination between the adoptive transfer of PD-1 deficient T cells and TAT targeting PD-L1 to control the growth of melanoma tumors in NSG mice. **Conclusion:** This study provides the first proof-of-concept of the efficacy of a combination therapy using TAT, adoptive cell transfer and genomic editing of IC-encoding genes. **References:** (1) Marotte L, Simon S, Vignard V, Dupre E, Gantier M, Cruard J, Alberge JB, Hussong M, Deleine C, Heslan JM, Shaffer J, Beauvais T, Gaschet J, Scotet E, Fradin D, Jarry A, Nguyen T, Labarriere N. Increased antitumor efficacy of PD-1-deficient melanoma-specific human lymphocytes. J Immunother Cancer. 2020 Jan;8(1):e000311. doi: 10.1136/jitc-2019-000311. (2) Capitao M, Perrin J, Simon S, Gouard S, Chouin N, Bruchertseifer F, Morgenstern A, Rbah-Vidal L, Chérel M, Scotet E, Labarrière N, Guilloux Y, Gaschet J. Anti-Tumor Efficacy of PD-L1 Targeted Alpha-Particle Therapy in a Human Melanoma Xenograft Model. Cancers (Basel). 2021 Mar 12;13(6):1256. doi: 10.3390/cancers13061256.

OP-0444

Development of ^{89}Zr-anti-CD103 PET imaging for non-invasive assessment of cancer reactive T cell infiltration

X. Fan*, A. Kol, M. Wazynska, M. de Bruyn, P. H. Elsinga, H. W. Nijman; University Medical Center Groningen, Groningen, NETHERLANDS.*

Aim/Introduction: CD103, an integrin specifically expressed on the surface of cancer-reactive T cells, is significantly increased during successful immunotherapy across human malignancies. In this study, we describe zirconium-89 (^{89}Zr) radiolabeling of monoclonal antibody (mAb) clones that specifically recognize human CD103 for non-invasive immune PET imaging of T cell infiltration as potential biomarker for effective anti-cancer immune responses. **Materials and Methods:** Firstly, we developed an ^{89}Zr-anti-murine CD103 PET tracer for feasibility of CD103 PET. Healthy, non-tumor bearing C57BL/6 mice underwent serial PET imaging after intravenous injection, followed by ex vivo biodistribution. Tracer specificity and macroscopic tissue distribution were studied using autoradiography combined with CD103 immunohistochemistry (IHC). Next, we generated CD103 antibodies that specifically target human CD103 positive cells. Nude mice (BALB/cOlaHsd-Foxn1nu) with established CD103 expressing CHO or CHO wild-type xenografts were injected with ^{89}Zr-anti-human CD103 antibodies and underwent serial PET imaging, followed by ex vivo biodistribution. Results: We developed ^{89}Zr antibody-based tracers targeting both murine and human CD103 molecule with high radiochemical purity (RCP>95%). ^{89}Zr-anti-murine CD103 PET imaging identified CD103-positive tissues at clinically relevant target densities. In vitro, anti-human CD103 PET traces revealed strong binding to the CD103+ CD8+ T cell subpopulation in ovarian cancer tumor digests. In vivo, ^{89}Zr-anti-human CD103 tracers showed high target-to-background ratios, high target site selectivity and a high sensitivity in human CD103 positive xenografts. **Conclusion:** We developed novel human CD103 immuno-PET tracers for future non-invasive assessment of cancer reactive T cell infiltration. **References:** [1] Sharma P, Allison JP. The future of immune checkpoint therapy. Science. 2015;348(6230):56-61. [2] Topalian SL, Drake CG, Pardoll DM. Immune checkpoint blockade: a common denominator approach to cancer therapy. Cancer Cell. 2015 Apr 13;27(4):450-61.[3] Mahoney KM, Rennert PD, Freeman GJ. Combination cancer immunotherapy and new immunomodulatory targets. Nat Rev Drug Discov. 2015 Aug;14(8):561-84. [4] Workel HH, Komdeur FL, Wouters MCA, Plat A, Klip HG, Eggink FA, et al. CD103 defines intraepithelial CD8+ PD1+ tumour-infiltrating lymphocytes of prognostic significance in endometrial adenocarcinoma. Eur J Cancer. 2016;60:1-11.[5] Edwards J, Wilmott JS, Madore J, Gide TN, Quek C, Tasker A, et al. CD103+tumor-resident CD8+T cells are associated with improved survival in immunotherapy-naïve melanoma patients and expand significantly during anti-PD-1 treatment. Clin Cancer Res. 2018;24(13):3036-45.

OP-0445

Preclinical pharmacokinetic and dosimetry of a 89 Zr labelled anti-PDL1 in an orthotopic lung cancer model

A. Krache[1,2], C. Fontan[3], C. Pestouri[4], M. Bardies[5,6], P. Payoux[7,8], E. Chatelut[1], M. White-koning[1], A. Salabert[2,8];
[1]INSERM UMR1037 - CRCT (centre de recherche en cancérologie de toulouse), team 14 DIAD, Toulouse, FRANCE, [2]INSERM UMR1214 - TONIC (Toulouse neuroimaging center), team DEVIN, Toulouse, FRANCE, [3]Zionexa, Toulouse, FRANCE, [4]US006/CREFRE - équipes de zootechnie expérimentale et d'exploration non invasive, Toulouse, FRANCE, [5]INSERM UMR1194 - IRCM (Institut de recherche en cancérologie de Montpellier), Toulouse, FRANCE, [6]INSERM UMR1194 - IRCM (Institut en cancérologie de Montpellier), Toulouse, FRANCE, [7]INSERM UMR1214 - TONIC (Toulouse neuroimaging center), Toulouse, FRANCE, [8]CHU Toulouse, Toulouse, FRANCE.

Aim/Introduction: 10F.9G2 is an murine immunoglobulin monoclonal antibody targeting programmed death cell ligand (PDL1) and preventing its ligation to programmed death protein (PD1) to restore antitumoral immune response of infiltrated T-cells. Before anti-PDL1 therapy, PDL1 expression is conducted on tumoral tissue and depending on biopsy extraction site, PDL1 expression could be very heterogeneous. Non-invasive PET imaging could be used for a whole-body mapping on PDL1 site. **Materials and Methods:** We assessed in vitro binding and immunoreactivity of a murine anti-PDL1 radiolabelled with zirconium 89 on PDL1 expressing cells. We also evaluated the pharmacokinetic, biodistribution and dosimetry [89Zr]DFO-anti-PDL1 in both healthy mice and in immunocompetent lung cancer mice model. PET imaging was used to analyse [89Zr]DFO-anti-PDL1 distribution in whole-body and in the induced lung tumour. We used pharmacokinetic modelling to describe major pharmacokinetics' key parameters and to assess AUC computation for dosimetry evaluation in both mice and human. Results: We estimated PK parameter using non-compartmental method and compartmental method. We found in average a distribution volume of 4.3 mL and half-life of 29h in blood. We were able to target the tumour within 24h after [89Zr]DFO-Anti-PDL1 injection and best time imaging was at 48h. AUC simulated in organs by 1-CMT model was used to predict absorbed dose radiation in healthy mice and extrapolated to human. All tumours were successfully target by [89Zr]Anti-PDL1 and estimated dosimetry was about 50 µSv/MBq in human. **Conclusion:** Radiolabelled antibodies could allow personalized medicine and provide a new monitoring method for clinician before and during PD-1/PD-L1 treatment to evaluate PD1 expression and predict treatment response. Thus, 89Z radiolabelled antibody had low organ absorbed dose and effective dose that makes it suitable for potential human use. **References:** none

OP-0446

68Ga DOTA FAPI 46 and 18F FDG PET/CT for the diagnosis of primary and metastatic lesions in patients with various types of cancer

***P. U N**, A. R. Bharathi, S. M. Desai, B. Srinath, H. Mohan;*
Sri Shankara cancer hospital and Research center, Bangalore, INDIA.

Aim/Introduction: As 70 to 90 % of the tumor mass constitute cancer-associated fibroblasts (CAFs) which has become an attractive target for diagnostic imaging and as well as therapy. One unique biomarker that is abundant on CAFs but absent from quiescent fibroblasts is Fibroblast Activation Protein alpha (FAP) (1). FAP is a transmembrane serine protease that facilitates remodeling of the extracellular matrix, promoting cell invasion, cell motility, cell adhesion, and angiogenesis (2) which are critical to tumor progression. FAP is virtually absent from healthy cells, (3) and seen in several tumour entities. Therefore, FAP-specific inhibitors (FAPI) were advanced into tumour-targeting radiopharmaceuticals. Recently, it has been identified that FAPI-46 is a promising agent. Aim is to assess the potential usefulness of 68Ga-DOTA-FAPI-46 positron emission tomography/computed tomography (PET/CT) for the diagnosis of primary and metastatic lesions in various types of cancer, compared with 18F FDG PET/CT **Materials and Methods:** 22 patients with different cancers underwent serial 68Ga-DOTA-FAPI-46 PET/CT and 18F FDG PET/CT at 60 minutes with an interval of 1 to 2 days. Standardized uptake values (SUV) and TBR were generated Results: A total of 22 patients with 13 different tumor entities were included. All patients tolerated the examination well and no adverse side effects were observed. It was observed that the highest SUVmax was found in lung, breast, ovary, stomach, RCC, prostate and HCC. The 68Ga-DOTA-FAPI-46 tracer uptake was comparable with 18F-FDG tracer uptake at respective 60 mins post injection. It was also observed that there is no preparations for normalised blood sugar levels in 68Ga FAPI PET/CT scan. In case of Ca-Prostate, the 68Ga-DOTA-FAPI-46 PET/CT was compared with 68Ga-PSMA-11 PET/CT and the tracer uptake was comparable with the same **Conclusion:** The 68Ga-DOTA-FAPI-46 is safe to use in humans beings. The 68Ga-DOTA-FAPI-46 PET/CT scan results are comparable with the 18F FDG PET/CT in various types of cancer; however there is no significant advantages were demonstrated. The theranostic application is an emerging advantage in future **References:** 1. Zi F, He J, He D, Li Y, Yang L, Cai Z. Fibroblast activation protein alpha in tumor microenvironment: recent progression and implications (review) Mol Med Rep. 2015;11:3203-11. 2. Liu R, Li H, Liu L, Yu J, Ren X. Fibroblast activation protein: a potential therapeutic target in cancer. Cancer Biol Ther. 2012;13:123-9. 3. Brennen WN, Isaacs JT, Denmeade SR. Rationale behind targeting fibroblast activation protein-expressing carcinoma-associated fibroblasts as a novel chemotherapeutic strategy. Mol Cancer Ther. 2012;11:257-66.

OP-0447

Synthesis and preclinical evaluation of [^{18}F]AlF-NODA-C6-CTHRSSVVC as a PET tracer for tumor-associated CD163^{+} macrophages

B. Fernandes[1,2], I. F. Antunes[1], D. A. Vazquez-Matias[1], K. Prasad[1], E. De Mattos[3], W. Szymanski[4], C. M. Jeckel[2], E. F. de Vries[1], P. H. Elsinga[1]; [1]Dept. of Nuclear Medicine and Molecular Imaging, University Medical Center Groningen, University of Groningen, Groningen, NETHERLANDS, [2]Graduate Program in Biomedical Gerontology, School of Medicine, Pontifical Catholic University of Rio Grande do Sul (PUCRS), Porto Alegre, BRAZIL, [3]Dept. of Biomedical Sciences of Cells & Systems, Section Molecular Cell Biology, University Medical Center Groningen, University of Groningen, Groningen, NETHERLANDS, [4]Dept. of of Radiology, University Medical Center Groningen, Stratingh Institute for Chemistry, University of Groningen, Groningen, NETHERLANDS.

Aim/Introduction: M1 and M2-type macrophages play an important role in the tumor microenvironment[1]. There is increasing evidence demonstrating that M2 signature is linked to worse prognosis of cancer, whereas M1 infiltration has been correlated to a better prognosis[2]. Therefore, assessing the phenotype signature might improve the assessment of tumor-associated macrophages (TAM) infiltration, tumor progression, and treatment response. This study aimed to develop a new radiotracer for positron emission tomography (PET) based on the peptide CTHRSSVVC[3] targeting the CD163 receptor, which is specifically expressed on M2-TAM. **Materials and Methods:** [^{18}F]AlF-NODA-C6-CTHRSSVVC was synthesized using the aluminum [^{18}F]fluoride technology. In vivo studies were carried out to monitor the modulation of CD163 expression by chemotherapy in tumor-bearing mice. The animals were divided into three treatment groups: High cyclophosphamide dose group to promote immunosuppression and infiltration of M2 macrophage phenotype; low cyclophosphamide dose to avoid immunosuppression, leading to recruitment of M1 macrophage phenotype; and high cyclophosphamide dose combined with zoledronic acid drug to promote the reduction of M2 phenotype infiltration and repolarization from M1 to M2. After 7 days of treatment, animals were injected with [^{18}F]AlF-NODA-C6-CTHRSSVVC and scanned for 60 minutes, followed by ex vivo biodistribution. Western blot was performed to confirm CD163 expression. Results: [^{18}F]AlF-NODA-C6-CTHRSSVVC was synthesized with a radiochemical yield, radiochemical purity, and a molar activity of 23 ± 6%, 92 ± 2%, 1059 ± 978 GBq.µmol^{-1}, respectively. Tracer uptake in the tumor was expressed as tumor-to-muscle ratio (TMR) to compensate for the variability due to differences in tracer delivery. Macrophages in tumor microenvironment were well visualized with PET and a positive correlation was found between CD163 expression and the TMR obtained from the PET images (r_s=0.737, p⊠0.001). Despite a significant difference in CD163 expression was detected by Western blot, no significant difference in the tumor tracer uptake between treatment groups was found. **Conclusion:** [^{18}F]AlF-NODA-C6-CTHRSSVVC was successfully developed. [^{18}F]AlF-NODA-C6-CTHRSSVVC PET was able to visualize M2-type macrophages in tumors. Tracer uptake correlated well with CD163 expression, but treatment-associated differences in macrophage infiltration could not be detected by PET. **References:** 1. Malyshev, I. & Malyshev, Y. Current Concept and Update of the Macrophage Plasticity Concept: Intracellular Mechanisms of Reprogramming and M3 Macrophage (Switch) Phenotype. (2015) 2. DeNardo, D. G. & Ruffell, B. Macrophages as regulators of tumour immunity and immunotherapy. Nature Reviews Immunology 1 (2019) 3. Silva, R. A. et al. CTHRSSVVC Peptide as a Possible Early Molecular Imaging Target for Atherosclerosis. (2016)

OP-0448

Expression of fibroblast activation protein by three prostate cancer cell lines

O. Bélissant[1], S. Geha[2], M. I. Messihad[3], A. Rioux-Chevalier[3], J. V. Leyton[1], E. Rousseau[1];
[1]Département de médecine nucléaire et radiobiologie, Université de Sherbrooke, Sherbrooke, QC, CANADA, [2]Département de Pathologie, Université de Sherbrooke, Sherbrooke, QC, CANADA, [3]Université de Sherbrooke, Sherbrooke, QC, CANADA.

Aim/Introduction: The radiolabeled fibroblast activation protein inhibitors (FAPI) allow PET imaging for numerous cancer types, and therapeutic radioligands are under development. Even if predominantly expressed in tumor stroma, FAP expression was also shown in pancreatic [1] and gastric cancer cells [2], and in circulating tumor cells from metastatic castration-resistant prostate cancer [3]. As FAPI could be used for imaging of prostate cancer regardless of its differentiation, the aim of this study is to assess the expression of FAP in three cell lines reflecting heterogeneity of prostate cancer lesions. **Materials and Methods:** All cell lines were acquired cultivated following provided instructions. Two were prostate adenocarcinomas (LNCaP and PC-3), and one was a small cell prostate neuroendocrine line (NCI-H660). Pancreatic cancer cell line BxPC3 was used as a positive control. Cells were subcutaneously injected into the flank of NSG mice. When tumors reached 10mm, mice were euthanized and tumors were removed, fixed, and embedded in paraffin for section. Immunohistochemical staining was performed to confirm FAP expression in tumor xenografts using a commercial polyclonal anti FAP-1 antibody. Immunostained sections were evaluated by an experienced pathologist, and expression of FAP scored from 0 to 3+. Results: Immunohistochemical staining revealed FAP staining in all prostate cancer cells' cytoplasm, and not in stroma fibroblasts, with a score 2+. This was stronger than in positive control cells. In BxPC3 cells staining was as strong in fibroblast as well as in cancer cells. A western blot analysis

confirmed FAP expression in the cultured cell line PC-3, with a higher visual score than BxPC3. **Conclusion:** We found FAP was expressed in three prostatic cancer cell lines, by cancer lines themselves rather than by activated fibroblasts. This highly interesting finding warrants further study to assess if it is also the case in humans, since this would guide the choice of isotope for radioligand therapy based on necessity or not for crossfire effect for cancer-cell irradiation. **References:** 1. Shi M, Yu DH, Chen Y, et al. Expression of fibroblast activation protein in human pancreatic adenocarcinoma and its clinicopathological significance. World J Gastroenterol. 2012 Feb 28;18(8):840-6. 2. Mori Y, Kono K, Matsumoto Y, et al. The expression of a type II transmembrane serine protease (Seprase) in human gastric carcinoma. Oncology. 2004;67(5-6):411-9. 3. Friedlander TW, Ngo VT, Dong H, et al. (2014), Detection and characterization of invasive circulating tumor cells derived from men with metastatic castration-resistant prostate cancer. Int. J. Cancer, 134: 2284-2293.

OP-0449

Combined treatment of mice bearing HER2-expressing xenografts by trastuzumab and Affibody-mediated PNA-based pretargeting improves their survival

M. Oroujeni[1], H. Tano[2], A. Vorobyeva[1,3], Y. Liu[1], O. Vorontsova[1], T. Xu[1], K. Westerlund[2], A. Orlova[1,3], V. Tolmachev[1,3], A. Eriksson Karlström[2];

[1]Uppsala University, Uppsala, SWEDEN, [2]KTH Royal Institute of Technology, Stockholm, SWEDEN, [3]Tomsk Polytechnic University, Tomsk, RUSSIAN FEDERATION.

Aim/Introduction: Therapy of patients with HER2-expressing tumours using monoclonal antibody trastuzumab enhanced their survival. Our previous study has demonstrated that affibody-mediated peptide nucleic acid (PNA)-based pretargeting extended significantly survival of mice bearing HER2-expressing SKOV-3 xenografts. Since affibody molecules and trastuzumab bind to different epitopes on HER2, we aimed to test the hypothesis that a combination of PNA-mediated pretargeted therapy with trastuzumab could extend mice survival compared to monotherapies (trastuzumab or pretargeting alone). **Materials and Methods:** To confirm that affibody molecules and trastuzumab bind to different epitopes on HER2, mutual interference of primary pretargeting probe ZHER2:342-SR-HP1 and trastuzumab in binding to HER2-expressing cell-lines, was investigated in vitro. Experimental therapy was designed to evaluate the survival of mice bearing HER2-expressing SKOV-3 xenografts (4 groups) treated with: vehicle (group A); trastuzumab (group B) by subcutaneous injection of 4 mg/kg mouse for two weeks followed by 2 mg/kg weekly; pretargeting (group C) using affibody-PNA chimera ZHER2:342-SR-HP1 and complementary probe [^{177}Lu]Lu-HP2, by intravenous injection of 100 µg of ZHER2:342-SR-HP1 and 16 h later by 3.5 µg /16 MBq of [^{177}Lu]Lu-HP2 in a solution containing 2 mg of Gelofusine once a week; and combination of trastuzumab and pretargeting (group D). Treatment regimens for trastuzumab and pretargeting in group D were same as groups B and C, respectively. Animals' weight and tumours' size were monitored twice per week. After the study termination (by 90 days based on ethical permit), samples of liver and kidneys were evaluated for toxicity signs. Results: A large molar excess of trastuzumab had no influence on affinity of ZHER2:342-SR-HP1 to HER2-expressing cells in vitro. Affinity of trastuzumab was not affected by the presence of a large excess of ZHER2:342-SR-HP1 in vitro. Median survival of mice treated with trastuzumab (75.5 d) was significantly longer than the survival of mice treated with a vehicle (59.5 d). Median survival of mice treated with pretargeting was not reached by day 90. Six mice of this group survived and two had complete remission. All mice in the combined treatment group survived by day 90. Tumours in seven mice in this group disappeared at the treatment termination. There was no significant difference between animal weights in different treatment groups. No significant evidence of renal toxicity was observed in all treated mice **Conclusion:** Combination of trastuzumab and affibody-mediated PNA-based radionuclide pretargeting for treatment of mice bearing SKOV-3 xenografts significantly increased the mice survival compared to monotherapies. **References:** none

OP-0450

^{68}Ga-FAPI-04 PET/CT for molecular assessment of fibroblast activation and risk evaluation in systemic sclerosis-related interstitial lung disease

C. Schmidkonz[1], J. Distler[2], C. Treutlein[3], A. Atzinger[1], O. Prante[1], P. Ritt[1], T. Götz[1], T. Bäuerle[1], M. Cordes[1], M. Köhner[1], T. Kuwert[1], A. Ramming[2], G. Schett[2], C. Bergmann[2];

[1]University Hospital Erlangen, Department of Nuclear Medicine, Erlangen, GERMANY, [2]University Hospital Erlangen, Department of Rheumatology, Erlangen, GERMANY, [3]University Hospital Erlangen, Department of Radiology, Erlangen, GERMANY.

Aim/Introduction: Interstitial lung disease (ILD) is the most common cause of death in systemic sclerosis (SSc). To date, the progression of SSc-ILD is judged by the accrual of lung damage on computed tomography (CT) and lung function testing. However, diagnostic tools to assess current activity are lacking. Here, we tested the hypothesis that quantification of fibroblast activation by FAPI PET/CT may correlate with ILD activity and disease progression in SSc-ILD. **Materials and Methods:** 21 patients with SSc-ILD confirmed by HRCT and 21 controls without ILD were consecutively enrolled. All participants underwent FAPI PET/CT imaging and standard-of-care procedures including HRCT and lung function testing (PFT) at baseline. Patients with SSc-ILD patients were followed-up for 6 months with HRCT and PFT. We compared baseline FAPI PET/CT uptake to standard diagnostic tools and currently used predictors of ILD progression. Follow-

up FAPI PET/CT scans were obtained in a subset of patients treated with nintedanib to assess change over time. Results: FAPI accumulated in fibrotic areas of the lungs in SSc-ILD compared to controls with a median wlSUVmean of 0.8 (0.6 to 2.1) in the SSc-ILD group and 0.5 (0.4 to 0.5) in the control group (p<0.0001) and a median whole lung maximal standardized uptake value (wlSUVmax) of 4.4 (3.05 to 5.2) in the SSc-ILD group compared to 0.7 (0.65 to 0.7) in the control group (p<0.0001). FAPI uptake was higher in patients with extensive disease, with previous ILD progression or high EUSTAR activity scores. Increased FAPI uptake at baseline was associated with progression of ILD independently of extent of involvement on HRCT scan and the forced vital capacity at baseline. In consecutive FAPI PET/CTs, changes in tracer uptake was concordant with the observed response to the fibroblast-targeting antifibrotic agent nintedanib. **Conclusion:** Our study presents first in human evidence that fibroblast activation correlates with fibrotic activity and disease progression in the lungs of SSc-ILD patients and that FAPI PET/CT may be of potential to improve risk assessment of SSc-ILD. **References:** none

909

Wednesday, October 20 - Saturday, October 23, 2021

on-demand pool, release on Wednesday, October 20 at 09:00

Cutting Edge Science Track - Featured Session: From Safety Culture to Fieldwork in Radiation Protection

OP-0452

Radiation Protection in Nuclear Medicine - Opportunities and Challenges from Many Different Perspectives

S. L. Svegborn; Dept of radiation physics, Skåne university hospital, Malmö, SWEDEN.

OP-0453

A novel method to determine radiation protection advice following radioisotope therapy by modelling public exposure

B. Rojas, J. Gear, D. Rushforth, I. Murray, J. Robinson, J. Patel, G. Flux; Royal Marsden NHS Foundation Trust, Sutton, UNITED KINGDOM.

Aim/Introduction: Contact restrictions are often necessary to reduce exposure to members of the public from patients receiving radioisotope therapy. Methods of dose estimation generally assume the recipient receives zero dose whilst the patient is following restriction advice. In practice, this is often untrue, especially for persons in the same household. We aimed to create a system for generating behavioural restrictions based on direct patient measurements and models of contact that account for exposure during the restriction period. **Materials and Methods:** Dose rate as a function of distance, and activity retention over time were measured for 40 patients receiving $Na^{131}I$ for thyroid cancer. Models of patient contact were divided into three phases: (1) A period of total isolation from others, for example whilst in hospital. (2) A period of restricted contact with others after leaving hospital. (3) A normal contact pattern. Models of contact were developed for a range of persons likely to be exposed to the patient. Normal contact models were derived from the literature. Restricted contact models were based on advice given to patients at our institute. The dose to a recipient was estimated by integrating the time varying dose rate data at different distances and summing across all distances in the contact model. Minimum periods for hospital isolation and restricted contact after discharge were determined iteratively to meet the required dose constraint. Results: Estimated doses during restriction periods are non-zero, and in some cases contribute a significant proportion of a person's total exposure. Average doses received from our patients during and after restrictions were 345 and 402 µSv respectively. The effect of considering the dose to others during the period of restricted contact was to increase the period of time for which restrictions must be followed. In a few cases the length of time the patient had to stay in hospital isolation also increased. For the case of doses to a patient's partner, hospital isolation increased by an average of 0.1 days (max 3) and restrictions increased by an average of 2.6 days (max 14). **Conclusion:** Doses to the public during periods of restricting behaviour should be accounted for. A method has been developed to generate isolation and behavioural restriction advice by modelling all public exposure after therapy. The parameters of this model can be personalised. **References:** none

OP-0454

Communicating Radiation Issues with Patients: Can We Do Better?

L. Cunha[1], A. R. Roda[1,2], P. Ratão[1,3], M. Capoulas[1,4], H. C. Vasconcelos[5,6], M. Sousa[7], A. S. Moreira[1], L. F. Metello[1,8]; [1]IsoPor-Azores, Azores, PORTUGAL, [2]Medical Physics Department, IPOFG, Coimbra, PORTUGAL, [3]Nuclear Medicine Department, IPOFG, Lisboa, PORTUGAL, [4]Pharmacy Department, HBA, Loures, PORTUGAL, [5]Sc. Techn. Fac., Univ. Azores, Azores, PORTUGAL, [6]CEFITEC, Physics Dept, Universidade Nova de Lisboa, Lisbon, PORTUGAL, [7]Interdisciplinary Studies Research Center, ISEP.IPP, Porto, PORTUGAL, [8]ESS-IPP, Porto, PORTUGAL.

Aim/Introduction: Communicating with patients is part of the daily job of any health professional and in the Internet era, this has become a more challenging task. Often patients present opinions based on information collected from random sources. Therefore, health professionals should be well prepared before engaging in conversations with patients, particularly when the subject is sensitive or complex, such as radiation exposure. **Materials and Methods:** We realized that

at our department, when discussing radiation issues with patients not all of us have the same speech, and sometimes, personal views were conveyed instead of facts and current scientific knowledge. This is undesirable as may hinder patient and community trust not only in health professionals but in the organization as a whole. Recognizing it as a potential problem, we started a reflection on how could we improve the communication with patients regarding the benefits/risks of radiation: who should discuss it, when, which information is relevant, and in which format. We started by collecting and analyzing the written information usually provided to patients. Additionally, the dialogs between patients and staff members regarding radiation issues were examined. Patients were asked to rank the level of awareness they got, after reading our documents, about the risks and benefits of the prescribed procedure and how they think we might improve. We compared our written information with some examples from other departments and the literature. Results: Most patients considered the written messages were not clear enough regarding the benefits nor the risks of procedures. We found out when talking to patients, some staff members tend to focus on the risks, increasing the level of patient anxiety while others would just say "the procedure is 100% safe" and that also was not satisfactory to the patient, leading to some mistrust. Interestingly, we noticed that patients with renal xenografts were usually more worried about the chemical toxicity of the injected products rather than the radiation risk. Based on these findings, we prepared two additional leaflets: one focused on the benefits vs. risks of NM procedures, emphasizing the benefits, and another one directed to xenografted patients. Furthermore, we arrived at a consensus on how to effectively talk to patients. Staff was trained to present clear and concise messages confidently. **Conclusion:** Effective communication might be challenging, but it worth putting effort into as it adds value to the value chain in NM and improves the patient level of confidence. **References:** None

OP-0455

A Systematic National Review: Safety Assessment as a Tool for Development of Safety Culture in Nuclear Medicine Facilities in Finland

J. Liukkonen, S. Kaijaluoto;
Radiation and Nuclear Safety Authority (STUK), Helsinki, FINLAND.

Aim/Introduction: The aim of the study was to determine how safety assessment processes were conducted in Finland and how safety assessments affected safety culture. Finnish Radiation Act 859/2018 was introduced based on EU directive 2013/59/Euratom. The legislation contains a detailed requirement for safety assessment in nuclear medical facilities. National Radiation and Nuclear Safety Authority (STUK) confirms the safety assessment when the requirements are met. The research questions were 1) What were the most common deficiencies in safety assessments and how they were revised? 2) What were the benefits and demerits in the national safety assessment process. 3) Can safety assessments be used as a supervisory tool? **Materials and Methods:** A detailed list of requirements containing 334 items was made for evaluation of safety assessment. Based on the list all safety assessments (N=27) were evaluated. The revised safety assessments were re-evaluated with the same method. In addition, an internet survey was executed for all licensees. The safety assessments were used to profile relevant radiation safety considerations for on-site inspections. Quantitative and qualitative data were collected during the process. Statistical methods were used in the quantitative part and action research approach in the qualitative part. Results: All safety assessments were drafted in time. The preliminary results show that none of the original safety assessments were confirmed. The main deficiencies were lack of dose constraints, misclassifications, and absence of coverage. The majority of reviewed safety assessments were confirmed on time. Statistical analysis of all distributions is in progress. The survey is upcoming. **Conclusion:** Safety assessments provide an insight to risk management on a practical level in nuclear medicine. The safety assessment process can reveal deficiencies in daily practice and the operational environment. The preliminary data enables risk-based profiling of nuclear medicine activities and facilities. Safety assessments can be used to improve and evaluate safety culture. This justifies the legislative requirement for up-to-date safety assessments in nuclear medicine. Finally, safety assessment should cover technical aspects e.g. radiation protection, and human factors e.g. operational instructions. The survey will enable the evaluation of resource efficiency locally and nationwide. **References:** Radiation Act 859/2018, EU directive 2013/59/Euratom

OP-0456

A single center analysis of cumulative effective dose arising from multiple PET/CT scans over 11 years

M. Abuqbeitah[1], M. Rehani[2];
[1]Istanbul University-Cerrahpasa/Cerrahpasa medical school, Istanbul, TURKEY, [2]Oxford university/Massachusetts General Hospital, Boston, MA, UNITED STATES OF AMERICA.

Aim/Introduction: To estimate number of patients undergoing multiple FDG-PET/CT imaging exams, the frequency of exams, broad clinical indications for scanning, cumulative effective dose (CED) in one year and over the last decade. **Materials and Methods:** Records of 18F-FDG PET/CT scans were retrospectively analyzed at Instanbul University-Cerrahpaşa/Cerrahpaşa medical school, for 11 years from 04 Jan 2010 to 04 Nov 2020. Patient's name, ID, indications, administered activity, date and time of administration were derived from the dedicated documents. The effective dose E from 18F-FDG PET/CT scans for each patient was computed by: Total E = [n × A (MBq) ×0.019 (mGy/MBq)] + [n × CF× DLP]. E: effective dose, n: number of scans, A: administered 18F-FDG

activity, CF: conversion factor, DLP: dose linear product (mGy. cm2). Results: A total of 55424 patients (60%: F, 40%: M) underwent PET/CT using 421± 101 MBq 18F-FDG over 11 years. The medical indications were: 82% malignant diseases, 5% inflammatory diseases, 4% cardiac and neural conditions, while the remaining 9% for tumor survey and other conditions. Around 10 % of the patients underwent 18F-FDG PET/CT exam twice in a year, 4 % scanned 3 times in a year, while 1 % and 0.1 % were imaged 4 and 5 times in a year, respectively. The CED to patients were 54, 81, 108, and 135 mSv/year after 2,3,4 and 5 18F-FDG scans respectively. An estimated 1 % of the patients exceeded 100 mSv in a year. Furthermore, 17 % of the whole population underwent 2-23 ^{18}F-FDG PET/CT scans over11 years with CED ranging from 54-621 mSv; among them, 30 % (2756 patients) with CED dose above 100 mSv and the rest 70% were below 100 mSv. **Conclusion:** Sizeable number of patients are undergoing multiple FDG-PET/CT exams during one year and 4.3% patients exceeded 100 mSv in one year. Nearly 18 % of scanned patients were with non-malignant conditions. **References:** none

OP-0457

Adaptation of ICRP 128 Iodine Population Bio-kinetic Model to Thyroid Cancer Patients After Thyroidectomy

L. Peake[1,2], J. Taprogge[1,2], I. Murray[1,2], J. Gear[1,2], G. Flux[1,2]; [1]Joint Department of Physics, Royal Marsden Hospital NHSFT, London, UNITED KINGDOM, [2]The Institute of Cancer Research, London, UNITED KINGDOM.

Aim/Introduction: The bio-kinetics of iodine in thyroid cancer patients who only have a thyroid remnant following thyroidectomy may differ from healthy populations. Iodine bio-kinetic models published in ICRP Report 128 [1] consider four scenarios in healthy reference populations. The aim of this work was to adapt the population model presented in ICRP 128 to thyroid cancer patients after thyroidectomy. **Materials and Methods:** Population modelling was performed using Monolix software. Activity retention data for 23 thyroid cancer patients, including: whole-body, thyroid, blood and protein-bound iodine data were used. Rate constants were adjusted and compared to the four models presented in ICRP 128 (low, medium, high and blocked thyroid uptakes). Results: Compared to the medium thyroid uptake population model, four rate constants differed for this patient population. Flow from the iodide in blood compartment into the iodide in thyroid compartment was determined to be 0.14 day^{-1} . Flow from the organic iodine in thyroid compartment to the organic iodine in blood was 0.35 day^{-1}. The rate constant from the iodide in blood compartment to the kidneys 3 compartment was determined to be 6.96 day^{-1} and the rate constant from urinary bladder content compartment to the urine compartment was 25.49 day^{-1}. Using these rate constants, the population model and activity retention data in this thyroid cancer patient population showed good agreement. **Conclusion:** To apply population bio-kinetic models in a clinical setting, the changes in bio-kinetics caused by the disease must be considered. Model development should be performed with data from the specific patient population. The rate constants proposed for use with the published ICRP 128 model provide increased accuracy in describing the biokinetics of radioiodine in the thyroid cancer patient population. **References:** [1] Mattsson, S et al. (2015). ICRP Publication 128, Annals of the ICRP, 44(2_ suppl), 7-321. Acknowledgements: The MEDIRAD project has received funding from the Euratom research and training programme 2014-2018 under grant agreement No 755523.

OP-0458

Models of Internal Liver Vasculature within the Mesh-Type ICRP Adult Reference Phantom to Support Internal Dosimetry in Radiopharmaceutical Therapy

C. Correa Alfonso[1], S. Domal[1], J. Withrow[1], M. Abdulla[1], C. Grassberger[2,3], S. Xing[2,3], J. Shin[2,3], H. Paganetti[2,3], W. Bolch[1]; [1]University of Florida, Gainesville, FL, UNITED STATES OF AMERICA, [2]Massachusetts General Hospital, Boston, MA, UNITED STATES OF AMERICA, [3]Harvard Medical School, Boston, MA, UNITED STATES OF AMERICA.

Aim/Introduction: Organ dose in radiopharmaceutical dosimetry under the MIRD schema is computed as the product of the time-integrated activity (TIA), assessed via quantitative imaging, and the radionuclide S-value. For the former, the TIA is typically assessed as the cumulative number of nuclear decays irrespective of whether they occur in source organ parenchyma or in its blood. Similarly, S values are typically computed using anatomic patient models in which organs are modeled as single-region volumes within which organ parenchyma and blood are homogenously mixed. In this study, we sought to explicitly model the blood vasculature within the ICRP adult male (AM) and adult female (AF) liver to produce dual-region organ models allowing a differentiation of parenchyma and blood decay sites. **Materials and Methods:** Virtual models of arterial (HA), portal (HPV) and hepatic vein (HV) trees were generated inside the segments of the ICRP AF/AM livers via Constrained-Constructive-Optimization (CCO). The CCO algorithm was used to generate independent vascular trees for all inflows (HA and HPV) and outflows (HV). Hemodynamic and geometric parameters of the main vessels were used as inputs. Within the algorithm, pressure, blood flow, and radius of vessels in each tree were updated as each new vessel was created and connected to the optimal bifurcation site. The vascular networks created inside the AF/AM livers were tetrahedralized using TETGEN software to perform radiation transport using PHITS. Specific Absorbed Fractions (SAF) were computed for monoenergetic electrons, photons, and alpha particles in which blood decays were modeled in two stages: (1) sites within explicitly modeled hepatic vessels, and

(2) sites within the hepatic blood pool outside these vessels - capillaries and blood sinuses. Results: Vascular models of ~6000 non-intersecting cylinders representing the HA, HPV and HV vascular networks were created independently for the AF/AM livers. Computed SAFs as a function of particle energy were obtained after which radionuclide S-values were generated. As hypothesized, the dual-region liver model allowed for explicit accounting for a sizeable fraction of alpha and low-energy electron blood self-absorption across energy ranges of interest to radiopharmaceutical therapy. **Conclusion:** Computational models of human liver vasculature have been developed by implementing a vessel generation algorithm that creates binary trees inside AF/AM reference livers. Although the present model does not include the precapillary and capillary vasculature, or blood sinusoids, the incorporation of the vasculature inside the ICRP reference adult livers allows for more accurate dose assessments in radiopharmaceutical therapy. **References:** None

OP-0459

Relevance of Internal Bremsstrahlung for estimating the exposure to pure beta emitters

L. Auditore[1], F. Juget[2], A. Italiano[3], D. Pistone[4], Y. Nedjadi[2], S. Gnesin[2], E. Amato[5];
[1]Section of Radiological Sciences, Department of Biomedical and Dental Sciences and Morphofunctional Imaging, University of Messina, Messina, ITALY, [2]Institute of Radiation Physics, Lausanne University Hospital and University of Lausanne, Lausanne, SWITZERLAND, [3]INFN, National Institute for Nuclear Physics, Section of Catania & MIFT Department, University of Messina, Messina, ITALY, [4]MIFT Department, University of Messina & INFN, National Institute for Nuclear Physics, Section of Catania, Messina, ITALY, [5]Section of Radiological Sciences, Department of Biomedical and Dental Sciences and Morphofunctional Imaging, University of Messina & INFN, National Institute for Nuclear Physics, Section of Catania, Messina, ITALY.

Aim/Introduction: β-decay is accompanied by Internal Bremsstrahlung (IB) consisting of the emission of photons showing a continuous energy spectrum. Although theoretical approaches have been developed and several measurements have been carried out for modelling the IB spectral distribution, this process is disregarded in most estimates of exposure to pure β-emitters. In our recent work [1], we demonstrated that the contribution of IB to the exposure to a ^{90}Y source can ben worth of consideration. We set up two models for the IB spectral distribution and implemented them in Monte Carlo (MC) simulations to evaluate the absorbed dose in case of external irradiation from liquid sources in vials, both without and with the emission of IB photons. We found that, depending on the chosen model, IB photons can contribute to the total absorbed dose up to 30-60%.The aim of this study was to compare our MC simulations with radiometric measurements for a ^{90}Y source and to extend the analysis also to other high-energy beta emitters such as ^{32}P. **Materials and Methods:** We compared radiometric measurements in a well ionization chamber with Monte Carlo simulations for ^{32}P and ^{90}Y. MC setup was preliminarily validated by comparing measurements and simulations for ^{57}Co, ^{133}Ba, ^{137}Cs and ^{60}Co γ-emitters. Measurements were carried out using a commercial radionuclide calibrator and, for each isotope, a vial was filled with a standardized solution. MC simulations were performed using GAMOS. Concerning ^{32}P and ^{90}Y, a first set of MC estimates was obtained by neglecting IB photons; then, IB spectral distribution was properly modelled for each beta emitter and a second set of simulations was run including IB photons. Results: We found that MC estimates deviate up to about -15% from measurements when IB process is disregarded in simulations, while the inclusion of IB photons allows achieving a reasonable agreement thus also giving indications on the appropriate modelling of the IB spectral distribution. The obtained results outline the need to include IB among the interaction processes to be considered when high-energy pure β-emitters are simulated. **Conclusion:** IB process is usually neglected when estimating the exposure to pure beta emitters. However, we demonstrated that for high-energy beta emitters such as ^{90}Y and ^{32}P, Internal Bremsstrahlung can play a relevant role for enhancing the absorbed dose values. For some β-emitters, the inclusion of IB in MC simulations deserves, in our opinion, consideration. **References:** [1] Italiano A., et al. Physica Medica 2020;76:159-65.

OP-0460

How To Assess the Real Extremities Dosimetry Based On the Results of a Dosimeter Ring ?

M. Armando[1], A. Huet[2], F. Vial[1], M. Rannou[1], R. Valette[2], H. Hida[3];
[1]Radiopharmacy unit, Pharmacy, Valence Hospital Center, Valence, FRANCE, [2]Radiation Protection, Valence Hospital Center, Valence, FRANCE, [3]Pharmacy, Valence Hospital Center, Valence, FRANCE.

Aim/Introduction: In Nuclear Medicine, monitoring workers' exposure to ionizing radiation is essential. Working Group 4 of the ORAMED project was concerned with the optimization of the extremities dosimetry in nuclear medicine departments. They concluded that correction factors should be applied to the dosimeter ring results to evaluate maximal hand dosimetry. To verify the applicability of these factors in our department, we conducted a dosimetry study in which we evaluated dose equivalents ratio between the index pulp (where the dose is most of the time the highest) and the index base (where the dose is routinely measured) of the non-dominant hand (1). **Materials and Methods:** Skin dose equivalents (Hp 0,07) were measured on 17 operators during multiple preparation and administration procedures with four most commonly used radionuclides (^{99m}Tc, ^{123}I, ^{18}F and ^{90}Y). For ^{18}F administration, two procedures were evaluated (syringe + shield or cartridge

+ shield). Operators wore a thermoluminescent dosimeter (TLD) ring at the base of the index of the non-dominant hand and a TLD pellet on the pulp of each index. Dose equivalents ratio between the pulp and the base of the index of the non-dominant hand (Ratio A) was calculated for each procedure and radionuclide. Ratio between index pulp from non-dominant hand and dominant-hand was also calculated (Ratio B). Results: For preparation, ratio A was 2.5, 6, 5.3 and 3.4 for ^{99m}Tc, ^{123}I, ^{18}F and ^{90}Y respectively. Ratio B was 1.2, 2.3, 2.2 and 2.4 respectively. For administration, ratio A was 5.4, 3, 3.3 and 3.75 respectively for ^{99m}Tc, ^{123}I, ^{18}F syringe and ^{18}F cartridge (^{90}Y wasn't evaluated). Ratios B was 5.1, 2.7, 1.2 and 2.7 respectively. In every situation, the most exposed index was on the non-dominant hand. **Conclusion:** Results are very heterogeneous depending on the radionuclide and the gesture (preparation or administration) evaluated. However, ratio A was a minimum of 2.5 (for preparation with ^{99m}Tc) and a maximum of 6 (for preparation with^{123}I), which confirm that the raw dosimeter ring results are not representative as they stand for the extremities dosimetry. A mean correction factor must be applied to assess the real dose at the extremities, associated with a risk of over or underestimation depending on the situation. Ideally, dosimetry studies should be conducted to best adapt the correction factor to the operators activities and the radionuclides handled. **References:** (1) ORAMED (Work Package 4): Practical guidelines to reduce hand exposure for standard nuclear medicine procedures.

OP-0461

Calibration for ^{41}Ar of radiation detectors for air exhaust systems

F. Zagni[1], *S. Vichi*[2], *G. Pantalone*[3], *V. Cabitza*[4], *N. Sabba*[5], *E. Moretti*[5], *M. D'Arienzo*[6], *S. Fanti*[7], *L. Strigari*[1];
[1]*Medical Physics Department, IRCCS Azienda Ospedaliero-Universitaria di Bologna, Bologna, ITALY,* [2]*Clinical engeneering department, IRCCS Azienda Ospedaliero-Universitaria di Bologna, Bologna, ITALY,* [3]*Department of Industrial Engineering, University of Bologna, Bologna, ITALY,* [4]*PET Radiopharmacy Unit, IRCCS Azienda Ospedaliero-Universitaria di Bologna, Bologna, ITALY,* [5]*Picomed srl, Mirnadola (MO), Italy, Mirandola (MO), ITALY,* [6]*ENEA, National Institute of Ionizing Radiation Metrology, Rome, ITALY,* [7]*Nuclear Medicine Department, IRCCS Azienda Ospedaliero-Universitaria di Bologna, Bologna, ITALY.*

Aim/Introduction: Air exhaust systems in cyclotron vaults involve the use of radiation detectors in order to monitor the release of contaminated air. The calibration of these devices, once mounted along the chimney/fume hood, is not straightforward; in this work, we propose a method for the evaluation of the calibration factor of a NaI detector specifically for ^{41}Ar. The work includes both experimental measurements and Monte Carlo (MC) simulations. **Materials and Methods:** We compared MC results with experimental measurements performed using the NaI detector and a known activity of ^{41}Ar. To this aim, a Marinelli beaker was filled with ^{40}Ar and exposed to the neutron flux inside the biomedical cyclotron bunker installed at our institution. The sample was measured with a HPGe-spectrometry system, independently calibrated with multipeak reference source.Using the obtained reference activity, the efficiency of the NaI detector was evaluated after proper spectrum acquisition of the same beaker. The NaI detector and the beaker were modeled with MC simulations and the efficiency was compared to the experimental value. The ratio simulated/experimental was used as a scaling factor for the subsequent calibration factor evaluated through simulations, in order to take into account the different count-rate between real and modeled probe, due to the intrinsic efficiency of the scintillation material, light and charge collection by the PMT. The final geometrical configuration (the NaI detector mounted inside the chimney) was modeled with MC simulations. The duct was modeled considering a uniform activity concentration in air and a total length of 4 meters. Minimum detectable activity (MDA) was also estimaned (Currie method) considering 10-minutes acquisitions.The experimental measurements were repeated three times, while MC simulations (performed with both Geant4 and FLUKA toolkits) were run to reach a statistical uncertainty of about 1%. Results: The obtained simulated/experimental efficiency ratio of the NaI detector for the beaker geometry was 0.80+/-0.07. Calibration factor for ^{41}Ar was 182+/-16 cps/(Bq/cm3). Estimated MDA: 0.7 Bq/g **Conclusion:** This method provides a feasible and accurate approach for calibration of ^{41}Ar which does not rely solely on MC simulations but is supported by inter-comparison using the same radionuclide that is being calibrated (in fact often only a single ^{137}Cs-point-source is used for experimental validation of simulations). This work also confirms that both the MC toolkits used are able to properly support the calibration procedure of detectors dedicated to the monitoring of air exhaust systems. **References:** None

OP-0462

Ambient Dose Measured at a Nuclear Medicine Department

V. de Sousa, *G. Cardoso*, *A. I. Santos*;
Hospital Garcia de Orta, E.P.E., Almada, PORTUGAL.

Aim/Introduction: Given the complexity of Nuclear Medicine Departments (NMD), demonstration of safety is of the utmost importance. Ambient dosimetry allows control of dose rates in locations where there is exposure to ionizing radiation, both for occupationally exposed workers and patients, as well as for the public in general. This study was conducted with the aim of evaluating ambient radiation dose rate levels in the different areas of a NMD and compared them against the limits legally established for controlled areas. **Materials and Methods:** A monitoring system (40 keV - 1.3 MeV) with 12 probes fixed at the ceiling registers continuously the dose rates in several locations: nursing areas, imaging rooms, waiting rooms, radiopharmacy, waste storage room and decay tanks. Data from 2018 to 2020 were analysed and

annual median values during clinical activity periods were estimated for each room, considering the period between 7 A.M and 8 P.M.. Dose values were then compared against legally established limits for controlled areas, defined as areas where effective dose can be greater than 6 mSv/year or an equivalent dose greater than 3/10 of one of the dose limits established for occupational workers, assuming different time occupations for each area. Background values were estimated for each room by analysing values registered between 3 and 4 A.M. Results: Background values ranged from 0.070 to 0.479 µSv/h, being highest in waste storage room. The median values, for each area were: nursing room A 0.090 [P25: 0.070; P75: 0.280] µSv/h; nursing room B 0.209 [P25: 0.100; P75: 0.540] µSv/h; nursing room C 0.239 [P25: 0.108; P75: 1.250] µSv/h; nursing room D 1.570 [P25: 0.100; P75: 4.289] µSv/h; SPECT/CT 0.409 [P25: 0.158; P75: 0.709] µSv/h; PET/CT 0.360 [P25: 0.170; P75: 0.569] µSv/h; adult patients waiting room 1.330 [P25: 0.500; P75: 2.539] µSv/h; children waiting room 0.170 [P25: 0.079; P75: 0.680] µSv/h; bedridden patients waiting room 0.230 [P25: 0.090; P75: 0.810] µSv/h; radiopharmacy 0.189 [P25: 0.129; P75: 0.389] µSv/h; waste storage room 0.490 [P25: 0.200; P75: 0.790] µSv/h; and decay tanks 0.100 [P25: 0.070; P75: 0.150] µSv/h. **Conclusion:** The room with higher dose rates was nursing room D, which is mainly used for the uptake phase of PET/CT studies, and the lowest dose rate values were registered in nursing room A. Although all the evaluated rooms were classified as controlled zones, even the highest estimated annual dose values are below the occupational dose limit for controlled areas. **References:** None

910

Wednesday, October 20 - Saturday, October 23, 2021

on-demand pool, release on Wednesday, October 20 at 09:00

Clinical Oncology Track - Featured Session: Radioguided Surgery and Sentinel Lymph Nodes

OP-0464

Radioguided Surgery in Prostate Cancer - Facilitating Cure?

T. Maurer; *University of Hamburg-Eppendorf (UKE), Hamburg, GERMANY.*

OP-0465

Hot needles can confirm accurate lesion sampling intraoperatively using [^{18}F]PSMA-1007 PET guided biopsy in patients with suspected prostate cancer

R. Laudicella[1,2], D. A. Ferraro[1,3], K. G. Zeimpekis[1], I. Mebert[1,4], J. Müller[1], O. Donati[5], M. T. Sapienza[3], J. H. Rüschoff[6], N. Rupp[6], D. Eberli[4], I. A. Burger[1,7];

[1]Department of Nuclear Medicine, University Hospital Zurich, University of Zurich, Zurich, SWITZERLAND, [2]Nuclear Medicine Unit, Department of Biomedical and Dental Sciences and Morpho-Functional Imaging, University of Messina, Messina, ITALY, [3]Department of Radiology and Oncology, Faculdade de Medicina FMUSP, Universidade de Sao Paulo, Sao Paulo, BRAZIL, [4]Department of Urology, University Hospital Zürich, University of Zurich, Zurich, SWITZERLAND, [5]Interventional and Diagnostic Radiology, University Hospital Zurich, University of Zurich, Zurich, SWITZERLAND, [6]Department of Pathology and Molecular Pathology, University Hospital Zurich, University of Zurich, Zurich, SWITZERLAND, [7]Department of Nuclear Medicine, Kantonsspital Baden, Baden, SWITZERLAND.

Aim/Introduction: The increasing use of prostate-specific membrane antigen (PSMA) targeted PET for staging prostate cancer (PCa) improved the confidence in this modality to detect significant PCa. Attempts to use PSMA PET/MRI guided fusion biopsy showed promising results but also the persisting limitation of sampling error due to impaired image fusion. Therefore, we aimed to assess the possibility of intraoperative quantification of PSMA tracer uptake in core biopsies as an instant confirmation for accurate lesion sampling. **Materials and Methods:** In this IRB approved, prospective, proof of concept study, we included five patients with suspected PCa by elevation of PSA level and a suspicious lesion on multiparametric MRI (mpMRI). All patients underwent [^{18}F]PSMA-1007 PET/CT scans followed by immediate PET/CT-guided and saturation template biopsy, a mean of 3.1h ± 0.3 (range 2.5-3.5) after the PET scan between 01.06.2020 and 30.11.2020. The activity in biopsy cores was measured as counts per minute (cpm) in a gamma spectrometer. Counts were correlated with histopathology in terms of WHO/ISUP grade, tumor length, and membranous PSMA expression on immunohistochemistry (IHC). Results: In 43 out of 113 needles, PCa was present (defined as any ISUP 1 or higher). The median and mean cpm was overall significantly higher in needles with PCa (97cpm; mean 260cpm ± 397) compared to needles without PCa (64cpm; mean 73cpm ± 44, $p < 0.001$). In one patient with diffuse moderate tracer uptake on PSMA PET (SUV_{max} 9.6), 13 out of 24 needles had moderate cpm ranging between 100-200, but only signs of acute inflammation; among them, in 11/13 IHC could confirm mild to strong PSMA expression. Excluding this case, ROC analysis resulted in an AUC of 0.789, with an optimal cut-off to confirm PCa at 75cpm, with a sensitivity and specificity of 63% and 87%, respectively. In all 4 patients with significant cancer, the first or second PSMA PET-guided needle correlated with the highest ISUP grade of PSMA positive tumor with high cpm ranging from 224-2079cpm. **Conclusion:** [^{18}F]PSMA-1007 uptake in PCa can be used to confirm accurate lesion sampling of the dominant tumor intraoperatively. This technique could improve confidence in imaging-based biopsy guidance and reduce the need for saturation biopsy. **References:** none

OP-0466

The value of SSTR2 receptor-targeted PET/CT in proton irradiation of grade I meningioma

M. Pelak, B. Flechl, R. Galalae, S. Tubin, M. Mumot, E. Hug, C. Lütgendorf-Caucig;
MedAustron Ion Therapy Center, Wiener Neustadt, AUSTRIA.

Aim/Introduction: Meningioma is the most common intracranial tumour in adults. Surgery is a well-established primary therapy of choice and radiation therapy has significantly improved local control for incompletely resected or inoperable tumours. Due to excellent long-term outcomes for WHO Grade I meningiomas, proper delineation is critical to avoid both marginal failures and unnecessary late toxicity. In the present study we investigate the value of SSTR2 (somatostatin receptor type 2) -specific PET/CT as means to support this process. **Materials and Methods:** Thirty cases of intracranial meningiomas were independently presented to 4 radiation oncologists of various experience and expertise from our department. All patients had WHO Grad I disease with macroscopic tumour and all had received at least one surgery. The cases were anonymized and the previous contours were erased. In the first phase of the study all radiation oncologists had to independently define the macroscopic tumour volume based on fused images of planning CT with multiparametric preoperative and planning MRIs. Subsequently, the contours were locked, DOTA-conjugate PET-CTs were added to the cases and the participants had to adapt copies of their previous volumes, now considering additional information from PET/CT. Conformity indices between MRI-only and PET/CT-aided series defined as intersection to union ratio were evaluated, both collectively and between all possible combinations of observer pairs. Results: In 7 out of 30 cases (23.3%) PET/CT revealed additional lesions corresponding to meningiomas distinct from primary diagnosis: four lesions in the falx which were a coincidental finding as well as two intraosseous and one intraorbital extensions which would significantly alter the target volumes and resulting treatment fields done using MRI only. Overall there was a trend towards a slight increase of the contoured tumour volume compared to MRI-only delineation (median volume change +6.9%, range: -25.7 to +73.6%). The conformity indices of PET/CT-aided contours were statistically significantly higher than of ones done based on MRI only in 23 (76.7%) out of 30 case pairs (median = +0.1, range: -0.23 to + 0.32, $p = 0.0028$ for all contours collectively and median = +0.084, range: -0.212 to +0.26, $p = 0.0034$ between all possible observer pairs). **Conclusion:** SSTR2 receptor-targeted PET/CT is a valuable tool in meningioma which should be routinely used for planning of particle therapy of incompletely resected meningioma. It serves both as a workup procedure and an aid for delineation process that reduces the likelihood of marginal misses or unnecessary toxicity. **References:** none

OP-0467

Preliminary evaluation of the hybrid tracer Indocyanine Green (ICG)-^{99m}Tc-nanocolloid for sentinel lymph node biopsy in bladder cancer

D. Rietbergen[1], E. van Gennep[1], G. KleinJan[1], M. Donswijk[2], B. van Rijn[2], R. Valdes Olmos[1], H. van der Poel[2], F. van Leeuwen[1];
[1]Leids Universitair Medisch Centrum (LUMC), Leiden, NETHERLANDS, [2]Netherlands Cancer Institute, Amsterdam, NETHERLANDS.

Aim/Introduction: Radical cystectomy combined with extended pelvic lymph node dissection (ePLND) is considered routine care for non-metastatic muscle-invasive bladder cancer (MIBC). Hereby, lymph node invasion has proven to be an independent predictor of disease recurrence and cancer-specific survival. The purpose of this trial is to evaluate the feasibility of targeting the SN in bladder cancer patients for sentinel node (SN) biopsy, using the hybrid tracer Indocyanine Green (ICG)-^{99m}Tc-nanocolloid. **Materials and Methods:** Twenty patients (mean age: 63,3 y, range: 30-82 y) with histologically confirmed cN0M0 MIBC, scheduled for radical cystectomy with SN biopsy and ePLND, were prospectively included. Twelve patients were operated following neoadjuvant chemotherapy, 7 patients did not receive prior therapy. After 4 transurethral injections of ICG-^{99m}Tc-nanocolloid (mean 208 MBq) around the tumor in the detrusor muscle, early and delayed lymphoscintigraphy as well as SPECT-CT. Using the guidance of the nuclear images, the patients were operated on day two using a combination of radio and fluorescence guidance. Surgical samples were examined at pathology. Results: One patient was operated in another hospital and had to be excluded from analysis, resulting in a group of 19 patients analyzed. Using preoperative imaging, SNs were observed in 10 patients (52,6%), meaning 9 patients (47,4%) yielded non-visualizations. The number of identified SNs was statistical higher for NAC than noNAC patients (7 vs 3 SNs); non visualization was not statistical different for both NAC and noNAC patients (5 vs 4 patients). Histopathology confirmed tumor positive SNs in 4/19 patients; 21% of the total population. Of the patients with preoperative SN visualization, in 2/10 SNs turned out to be tumor positive (one in the NAC group, one in the noNAC group) while the ePLND specimens were tumor negative. In the other 8 patients, the SNs and ePLND specimens were tumor negative. In the preoperative nonvisualization group, two of the NAC stage III patients were false negative where a tumor positive node was seen in the ePLND specimens. No additional (micro)metastatic disease was seen in tumor stage below III nor in the noNAC group. **Conclusion:** While SN identification was only effective in about half of the patients, the preoperative imaging data indicated a proper staging for patients with MIBC. Furthermore, preoperative imaging did indicate that the tumor drainage pathways can deviate from routine ePLND templates which did not contain tumor. In case of nonvisualization in advanced tumor stages, ePLND could be needed. **References:** none

OP-0468

How signal intensity influences utility of a robotic DROP-IN gamma probe during surgery - a clinical comparison between sentinel lymph node and PSMA-receptor targeted tracers

M. van Oosterom[1], P. Dell'Oglio[1], H. de Barros[2], P. Meershoek[1], T. Maurer[3], E. M. Wit[2], P. Stricker[4], H. G. van der Poel[2], P. J. van Leeuwen[2], F. W. van Leeuwen[1];
[1]Leiden University Medical Center, Leiden, NETHERLANDS, [2]Netherlands Cancer Institute - Antoni van Leeuwenhoek Hospital, Amsterdam, NETHERLANDS, [3]Martini-Clinic, University Medical Center Hamburg-Eppendorf, Hamburg, GERMANY, [4]St. Vincent's Prostate Cancer Centre, Darlinghurst, AUSTRALIA.

Aim/Introduction: Among the rapidly growing field of minimal-invasive surgery, urology has been one of the first disciplines to embrace robotic surgery; the management of prostate cancer being a prime indication. While robotic systems deliver many advantages for the minimal-invasive setting, they also give rise to specific challenges. When applying radioguided surgery for example, the restricted access and the detachment of the robotic surgeon from the surgical bed impairs the utility of traditional laparoscopic gamma probes. To improve maneuverability and regain control for the surgeon, we designed and translated a tethered DROP-IN gamma probe. By applying the technology during both sentinel lymph node (SLN) and PSMA-targeted radioguided surgery procedures, we are able to evaluate how the differences in signal intensity and signal to background ratios in these two indications impact on the utility of the DROP-IN gamma probe. **Materials and Methods:** The DROP-IN gamma probe was applied in 50 patients with (recurrent) prostate cancer (period 2018-2021). In the primary tumor setting, SLN resections were guided by ICG-^{99m}Tc-nanocolloid (intraprostatic injection of ~200MBq). PSMA-targeted salvage resections were guided by ^{99m}Tc-PSMA I&S (intravenous injection ~550MBq). Imaging-based preoperative roadmaps were acquired with SPECT/CT-scans and/or PET/CT in the case of PSMA targeting. Performance of the DROP-IN was evaluated based on sensitivity, specificity and background activity of relevant tissues. Results: In SLN procedures, the SPECT/CT images only revealed background signal in the prostate and liver. In the PSMA-targeted procedures, the SPECT/CT images indicated background signals in, among others, bladder, urine and intestines. During the PSMA-targeted procedures, nodal count rates were about 5-times lower than for the SLN procedures (on average 160 versus 850 counts/s, respectively). On top of that, more interference was observed from background tissues (i.e., bladder, bowel, urine, blood), resulting in a lower signal-to-background ratio for the PSMA-targeted procedures. Therefore, in vivo lesion identification took more time in the PSMA-targeted procedure with respect to the SLN procedure. Ex vivo evaluation of the specimens excised, helped to confirm a successful lesion retrieval in all cases. **Conclusion:** The DROP-IN technology has proven its potential for robotic radioguided SLN and PSMA-targeted surgery. Differences in tracer accumulation and tracer pharmacokinetics, however, need to be accounted for, rendering in vivo lesion localization different in a PSMA-targeted procedure as opposed to a SLN procedure. **References:** none

OP-0469

Promising results of I125 Radioguided seed localization (RSL) surgery of papillary thyroid cancer recurrence

O. Ajuria Illarramendi, P. Azpeitia Hernandez, A. Martinez-Lorca, M. Gutierrez Guerrero, P. Paredes Rodriguez, J. Bonilla Plaza, T. Navarro Martinez, M. Rioja Martin, M. Orduña Diez;
Hospital universitario ramon y cajal, Madrid, SPAIN.

Aim/Introduction: Recurrence of papillary thyroid cancer (PTC) has been reported on 5 - 30% of patients. Central compartment lymph nodes and thyroidectomy bed are the most common sites of recurrence and surgery is considered an accepted therapeutic option. This lesions need to be localized accurately for their optimal excision. We describe our experience with 125I radioguided seed localization (RSL) surgery of nonpalpable recurrent papillary thyroid cancer. **Materials and Methods:** Retrospective review of patients who underwent radioguided surgery with 125I seed between August 2018 and April 2021 in our center. 8 patients were considered for the study, five women and three men, with a mean age of 53.7 years. All of them had previous thyroidectomy. 10 seeds were placed in 10 lesions in 8 patients. One patient had 3 seeds placed. All seeds were placed under ultrasound guidance (3/10 the same day, 4/10 prior day and 2/10 two days before). 4/10 lesions were biopsy proven nonpalpable PTC on the surgical bed and the other 6/10 lesions were pathologic lymph nodes detected on ultrasound. Results: 10 seeds were placed in 8 patients. 10/10 were correctly placed. There was no seed migration. The target was successfully localized in 100% of cases. No complications were reported during the placement of the seed, neither during nor after surgery (recurrent laryngeal nerve injury, hipoparathyroidism or haematoma). In 4/8 patients local recurrence was confirmed, 1/8 had no disease and 5/8 had lymph node metastasis (the patient with 3 seed showed both local and lymphatic disease). To date, all patients remain disease free. **Conclusion:** RSL surgery with I125 seeds accomplished the excision of 100% of the lesions, without complications. Due to its simplicity and high accuracy, it has become the elected technique in our hospital for the excision of nonpalpable recurrent papillary thyroid cancer. **References:** None

OP-0470

Incidence and risk factoranalysis ofcomplications after sentinel node biopsy for penile cancer: a call for more precise identification of the true sentinel node only?

L. Wever[1], H. M. de Vries[1,2], B. W. van Rhijn[1], H. G. van der Poel[1], N. M. Graafland[1], M. L. Donswijk[1], K. Sikorska[1], S. Horenblas[1], F. W. van Leeuwen[1,2], O. R. Brouwer[1,2];
[1]Netherlands Cancer Institute-Antoni van Leeuwenhoek Hospital, Amsterdam, NETHERLANDS, [2]Leiden University Medical Center, Leiden, NETHERLANDS.

Aim/Introduction: Surgical staging is recommended in intermediate to high risk and clinically node negative (cN0) penile cancer (PeCa). However, (modified) inguinal lymph node dissection (ILND) is associated with high morbidity. Therefore, dynamic sentinel node biopsy (DSNB) was introduced as an alternative with the aim to reduce morbidity while maintaining diagnostic accuracy. The objective of this study is to determine the incidence and types of complications after DSNB and identify risk factors for the occurrence of postoperative complications. **Materials and Methods:** We evaluated 644 PeCa patients (1,284 DSNB procedures/groins) who underwent hybrid radio- and fluorescence guided DSNB DSNB between 2011 and 2020 at a single high-volume centre. After injection with ICG-^{99m}-Tc-nanocolloid, SNs were preoperatively identified using lymphoscintigraphy and SPECT/CT. Intraoperative SN detection was performed using a combination of gamma-tracing and fluorescence imaging. 30-day postoperative complications were assessed using the modified Clavien-Dindo classification system. Univariable and multivariable generalized linear mixed models were used to identify risk factors for the occurrence of complications per groin. Results: 768 SNs were identified on early planar lymphoscintigraphy (10mins) and 1806 SNs on late lymphoscintigraphy. 114 additional SNs were identified on SPECT/CT. During surgery a median of 2 LNs per groin (range 0 - 10) were removed. Histopathology showed a median of 2 LNs per groin (range 0 - 10) were found. A 30-day postoperative complication occurred in 20% of the groins (n=263). 95% of those complications were mild to moderate (grade I-II). Wound infection and lymphocele formation were the most common,compromising 47% and 34% of all complications, respectively. The number of removed lymph nodes (LNs) per groin was the main predictor for developing any grade of 30-day complication (OR 1.44; p<0.001), grade ≥ complications (OR 1.34; p<0.001), and early postoperative infections (OR 1.36; p<0.001). **Conclusion:** DSNB is still associated with a considerable risk of mild to moderate (grade I-II) postoperative complications. A higher number of removed LNs is the main risk factor for developing postoperative complications. This implies that further multidisciplinary procedural refinement aimed at more precise definition and identification of only the true SN(s) may help further reduce the morbidity of surgical staging in PeCa. **References:** none

OP-0471

Utility Of The 99MTC-Tilmanocept In Sentinel Lymph Node Biopsy Of Endometrial Cancer

A. Laverde Mächler, J. Suárez Fernández, C. Vigil Díaz, D. Lisei Coscia, J. Maraña González, L. Rodríguez Díaz, M. Domínguez Grande, N. Martín Fernández, F. González García;
HUCA, Oviedo, SPAIN.

Aim/Introduction: To present our preliminary results about the performance of ^{99m}Tc -Tilmanocept as an alternative radiotracer for sentinel lymph node biopsy (SLNB) in endometrial cancer. **Materials and Methods:** We conducted a prospective study including 17 patients from 47-74 years (median: 58 years) with the diagnosis of endometrial cancer who had provisional FIGO stages IA (n = 10), IB (n = 6) or II (n = 10).The day before surgery, 3mCi of ^{99m}Tc -Tilmanocept was injected in 4 doses into the stroma of the uterine cervix mucosa. Planar scintigraphy and SPECT/CT images were acquired 30 and 120 minutes after injection. Dye was injected in the operating room before surgery, with the same technique as ^{99m}Tc -Tilmanocept (15 patients with methylene blue patients and 2 with indocyanine green). For ethical reasons, pelvic lymphadenectomy was only performed in provisional stages IB or II (n = 7) or in those with high suspicion of metastatic lymphadenopathies (n = 1). Results: Scintigraphic images obtained had very good quality, showing bilateral lymphatic drainage in 12 patients (71%) and unilateral in 5 (29%). All patients had drainage to at least one external iliac chain (100% sensitivity), with also drainage to a common iliac (n=7), internal iliac (n=3), or both (n=2). At least one sentinel lymph node (SLN) was detected intraoperatively in 15 patients (detection rate 93%). The ^{99m}Tc -Tilmanocept / dye correlation was exact in 9 patients, partial in 5 and absent in 3. Pelvic lymphadenectomy was performed in 5 patients with negative SLN, without false negative results. Three patients presented positive lymph nodes for isolated tumor cells, with negative lymphadenectomy. The definitive FIGO stages were IA (n = 13), IB (n = 2), II (n = 1), and IIIC1 (n = 1). **Conclusion:** ^{99m}Tc -Tilmanocept is an alternative radiopharmaceutical suitable for use in SLNB of endometrial cancer, offering high-quality scintigraphic images and preliminary results non-inferior to those obtained with the current radiopharmaceuticals or dyes. **References:** Vidal-Sicart S, Vera DR, Valdés Olmos RA. Next generation of radiotracers for sentinel lymph node biopsy: What is still necessary to establish new imaging paradigms? Rev Esp Med Nucl Imagen Mol. 2018 Nov-Dec;37(6):373-379. English, Spanish. doi: 10.1016/j.remn.2018.09.001. Epub 2018 Nov 5. PMID: 30409688.

OP-0472

The impact of drainage pathways on the detection of nodal metastases in prostate cancer: a phase II randomized comparison of intratumoral vs. intraprostatic tracer injection for sentinel node detection

E. Wit;
NKI-AvL, Amsterdam, NETHERLANDS.

Aim/Introduction: Surgical management of local regional micrometastates in pelvic lymph nodes (LN) of prostate cancer (PCa) provides a substantial challenges. Focus sentinel node (SN) resections have been explored to complemented, or even replace, extended pelvic lymph node resections (ePLND). Previous studies, however, indicated that the location and the amount of detected sentinel nodes (SNs) in PCa is substantially influenced by the way a SN-tracer is deposited within the prostate. To validate whether intratumoral (IT) tracer injection helps to increase the identification of tumor positive LNs better than intraprostatic (IP) tracer injection, a prospective randomized phase II trial was performed **Materials and Methods:** PCa patients with a >5% risk of lymphatic involvement were randomized between ultrasound guided transrectal injection of indocyanine green-^{99m}Tc-nanocolloid in 2 depots of 1 mL in the tumor (n=55, IT-group) or in 4 depots of 0.5 mL in the peripheral zone of the prostate (n=58, IP-group). Preoperative lymphoscintigraphy and SPECT/CT were used to define the location of the SNs. SNs were dissected using a combination of radio- and fluorescence-guidance, followed by an extended pelvic LN dissection and robot-assisted radical prostatectomy. Outcome measurements were number of tumor-bearing SNs, tumor-bearing LNs, removed nodes, number of patients with nodal metastases and metastasis-free survival (MFS) of 4-7 year follow up data Results: IT-injection did not result in significant difference of removed SNs (5.0 vs 6.0, p=0.317) and histologically positive SNs (28 vs 22, p=0.571). However, in IT-group the SN positive nodes were 73.7% of total positive nodes compared to 37.3% in IP-group (p=0.015). Moreover, significantly more node-positive patients were found in IT-group (42% vs 24%, p=0.045), which did not result in a worse MFS. In two patients (1.8%) from whom the IT-tracer injection only partly covered intraprostatic tumor spread, nodal metastases in ePLND without tumor positive SNs were yielded **Conclusion:** The percentage positive SNs found after IT-injection was significantly higher compared to IP-injection. Significantly more node-positive patients were found using IT-injection. IT-injection failed to detect nodal metastases from non-index satellite lesions. Therefore we suggest to combine IT- and IP-tracer injections in men with visible tumor on imaging **References:** none

OP-0473

Is the hottest sentinel lymph node (SLN) the true SLN in breast cancer or do we need to resect more to find it correctly?

A. Bronte, A. Echaide, J. J. Rosales, J. F. Bastidas, V. Betech, F. Pareja, B. Olartecoechea, N. Rodríguez-Spiteri, F. Martínez-Regueira, M. J. García-Velloso, M. Rodríguez-Fraile;
University Clinic of Navarra, Pamplona, SPAIN.

Aim/Introduction: The aim of this study was to determine if the SLN with the highest counts seen in the lymphoscintigraphy and detected with gamma probe during SLN dissection corresponds to the true SLN (the one that provides accurate information on lymph node tumour involvement). Additionally, to determine if there are tumoral or technical factors which have an effect on the highest uptake node to not be the true SLN. **Materials and Methods:** 194 patients with unilateral breast cancer were retrospectively studied. The uptake each excised SLN was correlated with: patient (age and sex), tumour (laterality, location, size, histology, molecular type, clinical stage, neoadjuvant chemotherapy) and technical characteristics (surgical location, ex vivo counts per second, and methylene blue uptake), the latest prospectively collected. For the diagnostic study hypothesis (the node with the highest activity is the true SLN) the false negative ratio (FNRh) and the accuracy (Ah) were determined. To verify the veracity of the true negatives SLNs, the false negative rate was determined through the clinical follow-up for each patient. Results: Based upon a 10% rule, mean number of SLN removed per patient was 1.8. In 40/194 (21%) patients there was lymph node tumour involvement. During follow-up period (median 19[3-120] months) 2/173 (1.2%) patients presented axillary lymph node recurrence and were included as false negative SLN. For our series, the resection of the hottest node would have resulted in an Ah of 94.8% (FNRh=23,1%), of 2 SLNs an Ah of 98.1% (FNRh=15.4%), of 3 SLNs an Ah of 100% (FNRh=0%). Resecting 4 or more SLNs did not increased the Ah. Neoadjuvant chemotherapy ($p<0.048$) and clinical stage IIA ($p<0.001$) had a significantly effect on the highest uptake node to not be the true SLN. **Conclusion:** The hottest SLN was the true SLN in 94.8% of the patients. However, the resection of the 3 hottest SLNs detected the true SLN in 100% of patients. Neoadjuvant chemotherapy and clinical stage IIA can negatively influence the lymph node with the highest uptake being the true sentinel. Therefore, in this patient group, it is advisable to resect at least 3 SLNs to ensure 100% accuracy. **References:** None.

OP-0474

Long Term Results of Sentinel Lymph Node Biopsy Using Combined Method: A Single Institution Experience

B. Zengel[1], *U. Yararbas*[2], *I. C. Tercan*[3], *R. I. Durusoy*[4];
[1]*University of Health Sciences Turkey, İzmir Bozyaka Health Practice and Research Center, Department of General Surgery, Izmir, TURKEY,* [2]*Ege University Medical Faculty, Department of Nuclear Medicine, Izmir, TURKEY,* [3]*University of Health Sciences Turkey, Izmir Bozyaka Health Practice and Research Center, Department of General Surgery, Izmir, TURKEY,* [4]*Ege University, Faculty of Medicine, Department of Public Health, Izmir, TURKEY.*

Aim/Introduction: Sentinel lymph node biopsy (SLNB) is currently a standard approach in the management of axilla in early breast cancer. Although there are some minor differences in SLN detection rate using different injection modalities or radiocolloid types, as mentioned in major guidelines, satisfactory SLN detection rates have been reported for all approaches. Since it is easily performed, periareolar radiocolloid injection in combination with blue dye is preferred in our practice. While gradually a more conservative approach to axillary staging such as inclusion of patients with neoadjuvant chemotherapy (NACT) and omitting axillary dissection in the presence of micrometastatic or oligometastatic SLNs has been accepted in recent years, we aimed to review long term results of our practice. **Materials and Methods:** Study group consisted of 661patients who underwent SLNB between 2007-2020. A total of 688 SLNB was performed in these 661 patients since 27 cases had bilateral lesions. Mean age was 54,9±13,0. SLN detection rates, number of SLNs, locoregional recurrence rates were evaluated in two subgroups including patients that SLNB performed before any therapeutic intervention (582 patients; group A) and following neoadjuvant chemotherapy (NACT) (106 patients; group B). Additionally locoregional recurrence ratio was also evaluated in patient with micrometastasic SLN. Results: Overall SLN detection rate was %96,2. There was a significant difference in group A (97.9%) and B (%86.8) ($p<0.001$) in terms of SLN detection rates. Mean number of SLN detected was 3.9 in group A and 4.8 in group B (p: 0.47). Mean follow-up time was 5.7±4.4 years in group A and 2.6±2.2 years in group B. Locoregional recurrence occurred in 4 of 582 patients (0.68%) in group A, in none of the group B patients (106). In patients with micrometastasic SLNs, no locoregional recurrence was detected whether a complementary dissection was performed (11 patients) or not (34 patients). **Conclusion:** Successful SLN detection rate is significantly lower in patients with NACT. In succesful SLNBs, the difference between number of SLN harvested was not statistically significant in group A and B. Although there is a difference in mean follow-up times, in both groups locoregional recurrence rates were low. Complementary dissection in patients with micrometastic SLN did not provide additional benefit. **References:** None

OP-0475

Sentinel lymph node biopsy in muscle-invasive bladder cancer: single-center experience

R. Sadeghi, *L. Zarifmahmoudi*, *H. Ghorbani*, *K. Sadri*;
Mashhad University of Medical Sciences, Mashhad, IRAN, ISLAMIC REPUBLIC OF.

Aim/Introduction: In this study, the validity of sentinel node biopsy procedure as our index test was assessed and compared with bilateral pelvic lymphadenectomy for staging and detecting the regional lymph nodes metastasis in patients with muscle-invasive bladder cancer (MIBC). **Materials and Methods:** Consecutive series of cases with T1-T4 urothelial MIBC were included. Following the injection of radiotracer, sentinel nodes were sought using a handheld gamma probe and all hot nodes were harvested. Bilateral pelvic lymphadenectomy was done for all patients following sentinel node biopsy. The tumor specimen, sentinel nodes, and excised lymph nodes were evaluated histopathologically. Same as the other midline tumors, detection rate and false negative rates were calculated using patient basis and side basis methods. Results: By evaluating each patient as a unit of analysis, sentinel nodes were detected in 35 of 41 patients (85%), 13/16 (81%) of the neoadjuvant chemotherapy (NAC) and 22/25 (88%) of the no-neoadjuvant chemotherapy (No-NAC) participants. The false negative rate was 3/7 (42%): 1/3 (33%) for NAC, and 2/4 (50%) for No-NAC patients. By evaluating each hemipelvis as a unit of analysis, sentinel nodes were detected in 53 of 82 hemipelves (65%), 19/32 (66%) of the NAC, and 34/50 (68%) of the No-NAC hemipelves. No false-negative result was found by assessing each hemipelvis as a unit of analysis. **Conclusion:** Sentinel node biopsy is a feasible method for lymph node staging in MIBC, including patients with a history of NAC. To optimize the sensitivity, the decision regarding the lymphadenectomy is best to be based on the pathological status of sentinel node harvested from each hemipelvis separately as the unilateral finding of a sentinel node, does not rule out the possibility of metastatic involvement of contralateral pelvic lymph nodes. **References:** None

OP-0476

The impact of the COVID-19 outbreak on breast cancer with indication of surgical treatment and SLNB

E. López Llobet, *D. Monachello Araujo*, *C. Escabias Del Pozo*, *D. Travaglio Morales*, *Y. Abadi Sedraoui*, *J. Cordero García*, *L. Dominguez Gadea*;
Hospital Universitario La Paz, Madrid, SPAIN.

Aim/Introduction: The health emergency caused by COVID19 and the Lockdown that began in Spain on March 14, 2020, wreaked significant havoc on the organization and health care in all its fields. The objective of this study is to analyze the impact caused in patients with diagnose of breast cancer, mainly related to the reduction in the number of procedures

performed and treatment modifications, as well as the indirect impact on the results of the sentinel lymph node biopsy (SLNB). **Materials and Methods:** Patients who underwent sentinel node detection by lymphoscintigraphy in the Nuclear Medicine department of the Hospital Universitario La Paz in March, April and May 2020, during COVID19 first wave, were retrospectively reviewed and compared with a control group of patients submitted to the same procedure in those months of the previous year. The variables of: number of procedures performed, tumor characteristics, neoadjuvant treatment administration, SLNB results, axillary lymph node dissection (ALND) and type of surgery were analyzed. Results: Medical records of a total of 78 patients were reviewed, 25 were operated in 2020 and 43 in 2019, objectifying a reduction of 26% in 2020 compared to the previous year. No significant differences were observed in the mean age of the patients (p=0,08), tumor grade (p=0,31) neither histology (p=0,31), however, a significant difference in tumor size was observed (p0,005). Regarding patient's management, 52% received neoadjuvant treatment in 2020 and 23% in 2019. Positive results for SLNB were obtained in 24% of patients in 2020 compared to 9% in 2019, 12% of patients underwent ALND in 2020 and 6% in 2019. We observed a percentage of 68% of conservative surgeries in 2020 and 77% in 2019, and 24% of immediate breast reconstruction in 2020 up from 30% in 2019. **Conclusion:** During the COVID19 health crisis, fewer surgeries were performed, patients with worse prognosis and those who had received neoadjuvant treatment were priorized, and immediate reconstructive surgeries were reduced in order to minimize surgical time. We observed an increase in tumor size and in lymp node involvement, and also in lymphadenectomies performed, probably related to diagnosis delay. **References:** Fancellu, A., et al. 2020. The COVID-19 Outbreak May Be Associated to a Reduced Level of Care for Breast Cancer. A Comparative Study with the Pre-COVID Era in an Italian Breast Unit. Healthcare, 8(4), p.474Vanni, G. et al. 2020. Delay in Breast Cancer Treatments During the First COVID-19 Lockdown. Anticancer Research, 40(12), pp.7119-7125.

911

Wednesday, October 20 - Saturday, October 23, 2021

on-demand pool, release on Wednesday, October 20 at 09:00

Featured Session: Molecular Imaging of Alzheimer's Disease

OP-0478

Brain Imaging for a Biological Definition of Alzheimer's Disease

A. Drzezga; Cologne University, Nuclear Medicine, Cologne, GERMANY.

OP-0479

Visual assessment and Centiloid quantification across diagnostic groups: the AMYPAD project

L. Collij[1], C. Buckley[2], A. Palombit[3], K. Gray[3], M. Shekari[4], G. Salvadó[4], M. Battle[2], D. Altomare[5], R. Gismondi[6], A. Stephens[7], V. Garibotto[8], B. N. van Berckel[1], C. Ritchie[9], P. Payoux[10], B. Vellas[10], O. Grau[4], M. Boada[11], A. Drzezga[12], P. Scheltens[1], Z. Walker[13], J. Démonet[14], A. Nordberg[15], P. Visser[1], G. Frisoni[16], G. Farrar[2], F. Barkhof[1], J. Gispert[4], On behalf of the AMYPAD consortium;
[1]Amsterdam UMC, location VUmc, Amsterdam, NETHERLANDS, [2]GE Healthcare, Hammersham, UNITED KINGDOM, [3]IXICO, London, UNITED KINGDOM, [4]BarcelonaBeta Brain Research Center, Barcelona, SPAIN, [5]University Hospital Geneva, Geneva, SWITZERLAND, [6]Life Molecular Imaging, Geneva, SWITZERLAND, [7]Life Molecular Imaging, Berlin, GERMANY, [8]University Hospital Geneva, Geneva, SWITZERLAND, [9]University of Edinburgh, Edinburgh, UNITED KINGDOM, [10]University Hospital of Toulouse, Toulouse, FRANCE, [11]Ace Alzheimer Center Barcelona, Barcelona, SPAIN, [12]University College Cologne, Cologne, GERMANY, [13]University College London, London, UNITED KINGDOM, [14]Le Centre hospitalier universitaire vaudois, Laussane, FRANCE, [15]Karolinska Institutet, Solna, SWEDEN, [16]University Hospital of Geneva, Geneva, SWITZERLAND.

Aim/Introduction: To assess the distribution in Centiloid (CL) units across the two Amyloid Imaging to Prevent Alzheimer's Disease (AMYPAD) studies, within diagnostic groups (i.e. cognitively unimpaired participants, subjective cognitive decline plus (SCD+), mild cognitive impairment (MCI), and dementia) and to derive the optimal cut-off against visual reads (VR). **Materials and Methods:** As per April 2021, 541 participants (SCD+: N=161 [29.8%)], MCI: N=228 [42.1%], Dementia: N=152 [28.1%]) of the Diagnostic and Patient Management Study (DPMS) and 243 participants (CDR=0: N=210 [86.4%]), CDR=0.5: N=33 [13.6%]) of the Prognostic and Natural History Study (PNHS) had valid CL quantification and VR amyloid PET ([^{18}F]flutemetamol or [^{18}F]florbetaben) information. For DPMS, CL quantification was performed using the Cortex-ID PET-only pipeline, while CL quantification for the PNHS was performed using the MR-based LEAP pipeline. For both studies, whole cerebellum was the reference region. VR was performed by local readers (from 10 sites) trained for the specific radiotracer according to product guidelines. For this work, the final VR classification (i.e. negative/positive) was used. The optimal CL cut-off compared to visual assessment was determined using a ROC analysis and maximized Youden index. The AUC, sensitivity and specificity are provided. Results: Across the DPMS population, the mean CL burden was 44.6 (SD=49.9, range=-52.4-221.9) and 275 (50.8%) patients were assessed as VR+. Against VR, the optimal CL cut-off was 21.2 (AUC=.966, 95% CI =.950-.982, sensitivity=95.6%, specificity=89.1%). Across diagnostic groups, there was a stepwise increase in mean CL burden (F=30.75, p<.001; SCD: M=22.65, SD=38.97; MCI: M=47.04, SD=48.91; Dementia:

M=64.28, SD=52.73) (Figure 1). In the PNHS, the mean CL value was 20.72 (SD=29.27, range=-30.29-113.72) and 57 (23.46%) participants were assessed as VR+. Against VR, the optimal CL cut-off was 20.71 (AUC=.872, 95%CI=.816-.929, sensitivity= 84.2%, specificity=81.2%). Individuals classified as CDR=0.5 showed a higher CL value compared to CDR=0 participants (t=2.587, p=0.014; CDR=0: M=18.25, SD=26.73; CDR=0.5: M=36.44, SD=38.98) (Figure 2). **Conclusion:** The optimal CL cut-off against amyloid-PET visual assessment was remarkably concordant (CL~21) across the two AMYPAD trials, irrespective of the notable differences in their respective recruited populations, quantification approaches, and distribution of CL values. This accordance was achieved by the assessments of local readers using the approved product guidelines and without any kind of consensus reads. Therefore, our results support the construct validity of VR for detection of early amyloid deposition. They also support the validity of pooling CL units, acquired with different radiotracers and using different quantification pipelines. **References:** none

OP-0480

Calibration and Evaluation of the Centiloid Scale for Amyloid Quantitation with Multiple Fluorine-18 Radiotracers

W. Balhorn, K. Krawiec, N. Cole, A. S. Nelson;
MIM Software, Beachwood, OH, UNITED STATES OF AMERICA.

Aim/Introduction: Consistency of amyloid imaging has vastly improved, but there is still variability in reported quantitative values. The Centiloid scale was designed to standardize amyloid PET quantitation for various amyloid PET radiotracers and analysis methods. Using commercial software, we calibrated the quantitative output of a PET-based amyloid processing method to the Centiloid scale for florbetapir, florbetaben, and flutemetamol tracers. Centiloid values were collected for independent datasets with each tracer and results using a single Centiloid cutoff were compared to expert visual reads. **Materials and Methods:** Centiloid conversion equations were generated by following Klunk et al. [1]. A global cortical SUVr value was calculated by averaging six VOIs (medial orbital frontal, lateral temporal, parietal, anterior cingulate, posterior cingulate, and precuneus) in reference to the whole cerebellum. 100 florbetapir, 109 florbetaben, and 72 flutemetamol PET scans were selected for analysis. These were collected at 50-70, 90-110, and 90 minutes post-injection, respectively. Florbetapir, florbetaben, and flutemetamol exams were obtained, respectively, from the Alzheimer's Disease Neuroimaging Initiative (ADNI), a clinical trial [2], and the Australian Imaging, Biomarker & Lifestyle Flagship Study of Ageing (AIBL). Florbetapir and florbetaben scans were classified as visually positive or negative by three readers with the majority classification taken. Flutemetamol scans were classified as patients with Alzheimer's disease or amyloid negative by a single expert reader. Commercial software for image analysis was used to calculate Centiloid values and the exams were classified using a cutoff of 24 as determined by La Joie R et al. [3]. Accuracy was evaluated as the percentage of correctly classified exams. Results: Centiloid conversion equations for each fluorine-18 radiotracer passed all requirements [1] and correlation coefficients (R^2) between the commercial software and published Centiloid values were: florbetapir (0.97), florbetaben (0.98), and flutemetamol (0.96). Given a Centiloid cutoff of 24, the accuracy for all, amyloid negative, and amyloid positive subjects for each tracer was: florbetapir (92%, 91%, 93%), florbetaben (94%, 90%, 96%), and flutemetamol (97%, 100%, 89%). **Conclusion:** The imaging software was successfully calibrated to the Centiloid scale for multiple fluorine-18 radiotracers. Using a common cutoff, classification accuracy for amyloid negative and positive scans with florbetapir, florbetaben, and flutemetamol was acceptable and consistent. These results show promise in creating a universal cutoff and common quantitative scale across amyloid tracers. **References:** [1] Klunk W et al. Alzheimer's & Dementia (2015) [2]Barthel H et al. Lancet Neurol (2011) [3]La Joie R et al. Alzheimer's & Dementia (2019)

OP-0481

Concordance between molecular imaging, CSF and plasma biomarkers of Alzheimer's disease: evidence from the memory clinic

S. Stampacchia[1], D. Altomare[1], B. Melnic[1], F. Ribaldi[1], S. E. Tomczyk[1], M. Martins[1], M. Marizzoni[1], N. Ashton[2], H. Zetterberg[2], K. Blennow[2], I. Kern[3], G. B. Frisoni[4], V. Garibotto[4];
[1]University of Geneva, Geneva, SWITZERLAND, [2]University of Gothenburg, Gothenburg, SWEDEN, [3]Geneva University Hospital, Geneva, SWITZERLAND, [4]University of Geneva and Geneva University Hospital, Geneva, SWITZERLAND.

Aim/Introduction: The biological definition of Alzheimer's disease (AD) requires, in addition to amyloid (A), in vivo detection of abnormal tau deposits (T), while neurodegeneration (N) is considered AD-unspecific. The concentration of both T and A is currently determined using positron emission tomography (PET) and/or within cerebrospinal fluid (CSF), which are costly and invasive procedures. Most recently, the availability of new techniques allowing to determine ATN biomarkers in plasma, has opened the new and exciting perspective of large-scale screening of AD. Nevertheless, research is still needed to validate their clinical use. This study aims to provide new evidence on the concordance between PET, CSF and plasma AT(N) biomarkers in a memory clinic setting. **Materials and Methods:** We analysed participants from our cohort having at least one of the following couple of measures within a maximum gap of 12 months: CSF + amyloid-PET (N=75), CSF + tau-PET (N=36), plasma + tau-PET (N=73), plasma + amyloid-PET

(N=70), CSF + plasma (N=21). The following fluid biomarkers were analysed: Aß42, t-tau and p-tau181 in CSF; p-tau181 and NFL in plasma. Plasma analyses were performed using Single molecule array (Simoa) technology. CSF values were binarized using validated thresholds, while thresholds for plasma were derived from an independent study using the same assays. PET images acquired using different tracers (florbetapir or flutemetamol for Aß, and flortaucipir for tau) were binarized by means of visual assessment performed by an expert nuclear medicine specialist and SUVR validated positivity thresholds. Levels of plasma Aß40 e Aß42, t-tau, p-tau181, p-tau231, NFL, GFAP are currently under analyses for an enlarged sample. Results will be presented during the conference. Results: Amyloid-PET visual assessment and CSF Aß42 were concordant in 82% of the cases. Tau-PET visual assessment was concordant with CSF t-tau in 72% of individuals, CSF p-tau181 in 67% and plasma p-tau181 in 72%. In line with existing literature, there was a positive correlation between plasma p-tau181 and plasma NFL [r =0.36, p = .003], tau-PET global SUVR [r = 0.34, p = .006], Amyloid-PET Centiloid [r = 0.47, p = .001], CSF t-tau [r = 0.54, p = .015], CSF p-tau [r = 0.55, p = .012] and a negative trend with CSF Aß [r = -0.45, p = .051]. **Conclusion:** Fluids and brain imaging biomarkers of A and T pathology were concordant in most cases. A deeper understanding of the causes of discordance is a clinical priority. **References:** none

OP-0482

A PET only ^{18}F-flortaucipir quantification: comparison with an MRI-based method

R. Fahmi;
Siemens Healthineers, Molecular Imaging, Knoxville, TN, UNITED STATES OF AMERICA.

Aim/Introduction: Tau-PET enables in-vivo quantification of regional tau pathology. Most published tau-PET quantification methods use MRI for processing. This abstract describes the development/evaluation of an MR-free tau-PET quantification prototype, and its use in calculating SUVRs on Braak regions using flortaucipir (FTP) images from the ADNI database. The computed SUVRs are compared against those derived using an MR-based tau-PET quantification method. **Materials and Methods:** We extended our amyloid PET-based deformable registration method[1] to register tau-PET images to MNI space. This method is based on a deformable database-feature-matching (DFM) algorithm which matches points-of-interest (POIs) in the patient's brain against a template of POIs in the MNI geometry generated as follows. We obtained pairs of ^{18}F -flortaucipir and ^{18}F-florbetapir images, corresponding to 40 ADNI subjects representing different diagnostic groups. For each subject, the amyloid image was registered to MNI space using the amyloid-based DFM and the resulting transformation was applied to the corresponding FTP image followed by the generation of a set of POIs and their local feature descriptors. We quantified tau in N=717 FTP images from ADNI. Each image was registered to MNI-space using the new DFM algorithm, followed by SUVR computation on predefined Braak regions, normalized to the inferior-cerebellar-cortex. The Braak regions [2] were defined using the AAL-atlas. Calculated SUVRs were compared to publicly available SUVRs computed using an MR-based quantification method of FTP[2]. Results: Most scans were successfully registered to MNI space and required no manual adjustments. Moderate to good correlations were found between size-weighted composite SUVRs calculated with the two methods (Braak1-2: R^2=0.86; Braak3-4: R^2=0.945; Braak5-6: R^2=0.948; and meta-temporal [2]: R^2=0.952). The corresponding regression fits (MR-based SUVRs vs. MR-free SUVRs) were: y=1.067x+0.05; y= 1.107x - 0.014; y= y=1.002x + 0.074; and y=1.078x + 0.019, respectively. Note that there is no AAL region for the entorhinal cortex so a manually delineated mask was used, which might not be optimal and could explain the lower correlation-coefficient for Braak1-2. **Conclusion:** Automatic PET-only flortaucipir quantification using a novel PET-to-PET deformable registration algorithm yielded cortex-to-inferior cerebellar grey SUVRs in Braak regions which are well correlated with ADNI values calculated using an MRI-based approach. This suggests that ^{18}F-flortaucipir SUVRs are in good agreement, whether calculated with or without the use of MRI for processing (e.g., for segmentation and for spatial normalization). **References:** [1] Ludovic Sibille et al., 'Deformable registration for 18F-florbetapir PET quantification', EANM'2015. [2] Susan Landau et al., 'UC-Berkeley-Flortaucipir (AV-1451) processing methods', https://ida.loni.usc.edu/.

OP-0483

In vivo Braak staging of tau pathology in Alzheimer's disease: A multicenter [18F]PI-2620 PET study

M. Rullmann[1], *M. Brendel*[2], *M. L. Schroeter*[3], *D. Saur*[4], *J. Levin*[5], *R. Perneczky*[6], *S. Tiepolt*[1], *M. Patt*[1], *A. Mueller*[7], *V. Villemagne*[8], *J. Classen*[4], *A. W. Stephens*[7], *O. Sabri*[1], *H. Barthel*[1];
[1]*Department of Nuclear Medicine, University of Leipzig, Leipzig, GERMANY,* [2]*Department of Nuclear Medicine, University Hospital of Munich, LMU Munich, Munich, GERMANY,* [3]*Clinic for Cognitive Neurology, University of Leipzig, Leipzig, GERMANY,* [4]*Department of Neurology, University of Leipzig, Leipzig, GERMANY,* [5]*Department of Neurology, University Hospital of Munich, LMU Munich, Munich, GERMANY,* [6]*Department of Psychiatry and Psychotherapy, University Hospital, LMU Munich, Munich, GERMANY,* [7]*Life Molecular Imaging GmbH, Berlin, GERMANY,* [8]*Department of Molecular Imaging & Therapy, Austin Health, Heidelberg, AUSTRALIA.*

Aim/Introduction: Tau aggregates accumulate in the Alzheimer's disease (AD) brain according to the established Braak staging scheme and spread from transentorhinal over limbic regions to the neocortex. To impact the management

of AD patients, an in vivo tool for tau Braak staging is needed. First-generation tau tracers have limited performance in detecting early stages of tau. Therefore, we tested the corresponding capability of the next-generation tau tracer, [18F]PI-2620. **Materials and Methods:** We analyzed [18F]PI-2620 PET data from 37 beta-amyloid-positive AD dementia patients (69 ± 9 years, 20 females, MMSE scores: 20 ± 6) and those from 19 healthy controls (63 ± 10 years, 10 women, MMSE scores: 29 ± 1). Data were collected in four different centers (Leipzig, Germany; Melbourne, Australia; Munich, Germany; New Haven, USA). We applied kinetic modeling of the 0-60min p.i. PET data using MRTM2 with the lower cerebellum as the reference region. We used the Tau-Braak staging atlas of Schwarz et al. 2016 to extract corresponding DVRs. Controls were used to define stage-dependent PET positivity (>mv+2.5sd). In addition, we condensed the six-stage model data into an established three-class model (I+II, III+IV, and V+VI). Results: Stage-dependent PET positivity largely followed the Braak scheme (except Braak stage III). The frequency of PET positivity decreased from Braak I (43 %), II (35 %), III (59 %), IV (30 %), V (24 %) to VI (19 %). A hierarchical model (defining a stage>I as positive only if the lower stage(s) is positive) was met by 54 % of AD dementia cases for the six-stage model, whereas this was the case for 78 % of cases for the three-class Braak staging model. Six cases (16 %) showed a "hippocampal sparing" tauopathy pattern. **Conclusion:** [18F] PI-2620 PET appears to be able to perform Braak tau staging of AD in vivo. The results should benefit from further analysis such as correction for partial volume effect. **References:** Adam J Schwarz, Peng Yu, Bradley B Miller, Sergey Shcherbinin, James Dickson, Michael Navitsky, Abhinay D Joshi, Michael D Devous Sr, Mark S Mintun. Regional profiles of the candidate tau PET ligand 18F-AV-1451 recapitulate key features of Braak histopathological stages. Brain. 2016 May;139(Pt 5):1539-50. doi: 10.1093/brain/aww023

OP-0484

Multi-parametric [^{18}F]PI-2620 tau PET/MRI in Alzheimer's disease variants: A proof-of-concept study

J. Melasch[1], M. Rullmann[1], C. Scherlach[2], D. Saur[3], M. L. Schroeter[4], S. Tiepolt[1], A. Stephens[5], N. Koglin[5], S. Hesse[1], M. Strauss[6], M. Brendel[7], G. Aghakhanyan[8], A. Schildan[1], O. Mishchenko[1], M. Patt[1], J. Claßen[3], K. Hoffmann[2], O. Sabri[1], H. Barthel[1];
[1]Department of Nuclear Medicine, University Hospital, Leipzig, GERMANY, [2]Department of Neuroradiology, University Hospital, Leipzig, GERMANY, [3]Department of Neurology, University Hospital, Leipzig, GERMANY, [4]Clinic for Cognitive Neurology, University Hospital, Leipzig, GERMANY, [5]Life Molecular Imaging, Berlin, GERMANY, [6]Department of Psychiatry and Psychotherapy, University Hospital, Leipzig, GERMANY, [7]Department of Nuclear Medicine, University Hospital, Munich, GERMANY, [8]Department of Translational Research and of New Surgical and Medical Technology, University of Pisa, Pisa, ITALY.

Aim/Introduction: In the last years, hybrid PET/MRI has become a promising tool to image multiple aspects of Alzheimer's disease (AD). In this study, we used the new-generation tau radiotracer [^{18}F]PI-2620 to evaluate tau pathology together with structural and functional brain parameters in different AD phenotype variants. **Materials and Methods:** 15 patients (8 female, 70±14 years old, MMSE score=20±8) with different AD dementia phenotypes and with positive amyloid biomarker constellation were so far included into this study. These were 9 patients with classical AD, 3 patients with visual-variant (posterior cortical atrophy, PCA), 2 patients with language-variant (logopenic aphasia, LPA), and 1 patient with genetic variant (autosomal-dominant AD, ADAD) of AD. The patients underwent 0-60min p.i. [^{18}F]PI-2620 tau PET/MRI (Siemens Biograph mMR). The AD data were compared with those of respective healthy control groups (n=10). Kinetic modeling (MRTM2, reference region=lower cerebellum) of the dynamic PET data resulted in [^{18}F]PI-2620 DVR (tau load) and R_1(blood flow) maps, while voxel-based MR morphometry yielded atrophy, resting-state functional MRI (default mode network, seed=posterior cingulate cortex) yielded functional connectivity readouts, and diffusion-tensor imaging yielded fractional anisotropy values as structural connectivity readouts. The data were analyzed VOI-based (PMOD) and voxel-based (SPM). Results: In classical AD, [^{18}F]PI-2620 DVRs were increased in the typical Braak histopathology regions, while [^{18}F]PI-2620 R1s were mainly decreased in temporoparietal and posterior cingulate/precuneus regions. Atrophy was most-pronounced in mesial temporal and temporoparietal areas. Functional connectivity of the DMN was globally reduced, while this was the case for structural connectivity in posterior thalamic radiation, superior longitudinal fasciculus and parts of corpus callosum. Different to classical AD, the PCA cases showed additional [^{18}F]PI-2620 DVR increases in occipital areas, with concomitant atrophy/[^{18}F]PI-2620 R1 reduction and reduced DMN activity as well as disturbed structural connectivity mainly in the posterior thalamic radiations. The LPA cases revealed left-hemispherical predominance of DVR, R1 and functional connectivity together with partial co-involvement of frontal areas, but no further structural connectivity deficits. The ADAD case showed a multi-parameter constellation similar to that of the classical AD cases. **Conclusion:** The PET patterns observed in the different AD subtypes are consistent with recently published larger studies for other tau tracers. These preliminary data point to multi-parametric [^{18}F]PI-2620 PET/MRI being able to provide a range of different brain state readouts which show characteristic patterns for different AD phenotype variants. Larger studies are thus justified to investigate the potential of this approach for AD subtype differential diagnosis. **References:** none

OP-0485

Total P-Tau Brain Load (TTBL) quantification using F18-MK6240 PET: new approach and correlations with CSF phospho-tau and visual Braak staging

T. Gérard, V. Malotaux, V. Van Pesch, A. Ivanoiu, B. Hanseeuw, R. Lhommel;
Université Catholique de Louvain, Bruxelles, BELGIUM.

Aim/Introduction: F18-MK6240 is a promising second-generation PET radiopharmaceutical for evaluation of cerebral tauopathy in MCI/AD. To date, association between F18-MK6240 PET and cerebrospinal fluid (CSF) P-tau protein remains poorly documented. **Materials and Methods:** Twenty-four patients attending the Memory Clinic underwent both a F18-MK6240 tau-PET (dynamic-6x5min ; 90 min_pi), a 3D-T1-MRI and a lumbar punction. Average and partial volume correction were applied on PET using constructor software. Imaging data were then processed using PMOD_Neuro(v4.1) tools. Neocortical region were defined by 3DT1-MRI segmentation (Hammers Atlas), PET images were normalized by cerebellar grey-matter SUV and voxels units converted to SUV-ratio (SUVr). Only voxels showing SUVr values >cut-offs were considered for TTBL. Eleven cut-offs were tested (increment 0.1, from SUVr [1.0-2.0]). Regional/global(=TTBL) percentages of Tau_cortical involvement were calculated as follow: =[(number of voxels>cut-off)/(total number of regional/global voxels)].The different TTBL (one value for each cut-off) were correlated with P-tau CSF values (lab cut-off for positivity: 61 pg/ml) by linear regression. Independently, a visual reading of the scans was performed and used as reference to assess the Braak classification for each patient. Results: Percentages of tauopathy significantly correlate with CSF P-tau, for every tested cut-off.Best correlation was found with cut-off 1.1 SUVr (R^2:0.309; p=0.005). This filter was thus kept for further analysis. A good separation of individual visual read groups Braak [0-1-2], Braak [3-4] and Braak [5-6] corresponds to respective percentages ranges of taupathy (TTBL): [9-21]%, [20-57]% and [63-88]%.The linear correlation of TTBL with CSF p-TAU values depicted discrepancies for 5/24 patients (21%): 4/24 patients (17%) have a positive PET but a negative CSF P-tau and 1/24 (4%) have a negative PET but a positive CSF P-tau level. All other patients have consistent results between PET and P-Tau CSF (+/+or-/-). **Conclusion:** We propose a new approach for F18-MK6240 tau-PET quantification using a percentage of tauopathy calculated on the whole neocortex. The cut-off (1.1 SUVr) for TTBL was defined to obtain the best correlation with CSF P-tau. TTBL significantly correlated with CSF P-tau levels but individual discrepancies appear in near 1/5 patient. Conversely, a very good correlation of the percentage of tauopathy compared to PET-visual-Braak-staging. Further investigations are ongoing to affine regional SUVr cut-offs based on the visual-reading -reference and to clarify the clinical situation of the discordant cases. **References:** none

OP-0486

Association between tau and synaptic density in amnestic mild cognitive impairment: a longitudinal follow-up study

G. Vanderlinden[1], T. Vande Casteele[2,3], J. Ceccarini[1], L. Michiels[4,5], R. Lemmens[4,5], E. Triau[6], K. Serdons[7], M. Koole[1], M. Vandenbulcke[2,3,8], K. Van Laere[1,7];
[1]Nuclear Medicine and Molecular Imaging, Imaging Pathology, KU Leuven, Leuven, BELGIUM, [2]Research Group Psychiatry, KU Leuven, Leuven, BELGIUM, [3]Leuven Brain Institute, Leuven, BELGIUM, [4]Department of Neurology, University Hospitals UZ Leuven, Leuven, BELGIUM, [5]VIB, Center for Brain & Disease Research, Laboratory of Neurobiology, Leuven, BELGIUM, [6]Private Practice Neurology, Leuven, BELGIUM, [7]Department of Nuclear Medicine, University Hospitals UZ Leuven, Leuven, BELGIUM, [8]Department of Old-Age Psychiatry, University Hospitals UZ Leuven, Leuven, BELGIUM.

Aim/Introduction: Longitudinal rates of tau accumulation and their association with synaptic density and cognition remain to be fully elucidated in the progress of amnestic mild cognitive impairment (aMCI) to AD. The aim of this study was to investigate how increased tau accumulation and its spreading pattern is related to regional changes in synaptic density and progressive cognitive dysfunction in patients with aMCI. **Materials and Methods:** Nineteen aMCI patients (70.0±7.3 yrs, 8M/11F, MMSE 21-30) and 26 healthy controls (HC) (68.9±9.1 yrs, 14M/12F, MMSE 28-30) underwent [^{18}F]MK-6240 and [^{11}C]UCB-J PET scans (GE Signa 3T PET-MR), and neuropsychological examination at baseline (ongoing extension of Vanhaute et al (2020)[1]). So far, 8 aMCI patients underwent a 2-year follow-up investigation. Associations between [^{11}C]UCB-J SUVR, [^{18}F]MK-6240 SUVR and cognitive performance were investigated cross-sectionally both by a volume-of-interest (Hammers N30R83 atlas PMODv4.1) and a voxel-wise (SPM12) approach, with partial volume correction (PVC). Voxel-based morphometry was performed to determine grey matter (GM) atrophy. Results: Compared to HC, aMCI patients showed GM atrophy in the medial temporal lobe bilaterally (15-24%), increased [^{18}F]MK-6240 binding in the temporal lobe bilaterally (70%, p<0.001, k_{ext}=174356 voxels), and decreased [^{11}C]UCB-J binding in the right temporal lobe (14%, p=0.013, k_{ext}=1545 voxels) at baseline. Hippocampal [^{18}F]MK-6240 SUVR was inversely correlated with MMSE, RAVLT and AVF scores (r_s=-0.71, r_s=-0.62 and r_s=-0.65 respectively, all p<0.0001). A positive association between hippocampal [^{11}C]UCB-J SUVR and MMSE, RAVLT and AVF scores was found (r_s=0.52, r_p=0.49 and r_p=0.41 respectively, p=0.0002-0.005). In aMCI patients, [^{11}C]UCB-J and [^{18}F]MK-6240 SUVR were inversely correlated in the left medial temporal lobe (r_p=-0.63, p=0.0042). Furthermore, 4 out of 8 aMCI patients showed a progressive cognitive decline based on MMSE and RAVLT scores. At 2-year follow-up, a significant average increase in tau accumulation in the parietal, occipital and temporal cortex (34-43%, p=0,02-0,04), alongside a significant decrease in [^{11}C]UCB-J

binding in the hippocampus and medial temporal, frontal, parietal and cingulate cortex (7.5-10.3%, p=0,008-0,04) was observed across all subjects. **Conclusion:** In this extended study, previous baseline findings between tau, synaptic density and cognitive performance were corroborated in aMCI patients. Furthermore, pilot longitudinal results show a significant increase in tau load over time, accompanied by a more restricted decrease in synaptic density. Spatially, the increase in tau load extended wider compared to the decrease in synaptic density, in line with the hypothesis that tau deposition is a primary driver to synaptic loss and cognitive decline. **References:** 1. Vanhaute,H.et al;Neurology;95(5),e545-e553(2020)

OP-0487

In-vivo MRI imaging of locus coeruleus degeneration is coupled to brain glucose metabolism in Alzheimer's disease pathology

G. Aghakhanyan[1], A. Galgani[2], F. Lombardo[3], N. Martini[4], H. Hlavata[3], A. Leo[1], F. Guidoccio[1], G. Tognoni[2], P. A. Erba[1], N. Pavese[5], F. S. Giorgi[2], D. Volterrani[1];

[1]Nuclear Medicine Unit, Department of Translational Research and of New Surgical and Medical Technologies, University of Pisa, Pisa, ITALY, [2]Neurology Unit, Department of Translational Research and of New Surgical and Medical Technologies, University of Pisa, Pisa, ITALY, [3]Cardiovascular and Neuroradiological Multimodal Imaging Unit, Fondazione "G. Monasterio"- National Research Council/Tuscany Region, Pisa, ITALY, [4]Deep Health Unit, Fondazione "G. Monasterio"- National Research Council/Tuscany Region, Pisa, ITALY, [5]Clinical Ageing Research Unit, Newcastle University, Newcastle upon Tyne NE4 5PL, UNITED KINGDOM.

Aim/Introduction: The loss of noradrenergic neurons and reduction of brain noradrenaline (NA) levels are associated with Alzheimer's disease (AD). The majority of NA neurons are located in the locus coeruleus (LC), a small, bilateral structure in the brainstem. Novel MRI approaches provide an opportunity to quantify structural features of the LC. We aim to investigate brain glucose metabolism related to MRI-derived LC parameters in AD. **Materials and Methods:** Our cohort consisted of forty-four (n=44) subjects including fourteen (n=14) patients with the diagnosis of probable AD and thirty (n=30) patients with mild cognitive impairment (MCI). All patients underwent brain MRI (3.0T) and 20 minutes brain [18F]FDG PET studies. LC segmentation was performed using a dedicated LC-template developed from a larger group of healthy controls. LC scans were warped into the template and three quantitative parameters were extracted for left and right LC: the number of voxels (Nvox), the maximum (Rmax) and mean (Rmean) contrast-ratios. [18F]FDG PET preprocessing was performed by SPM12. Voxel-wise regression analysis was applied using GLM to identify brain regions that display significant relationship between local metabolic demand and MRI-derived LC-parameters accounting for age as a nuisance covariate. A voxel-wise P < .001 significance threshold with minimum cluster extent kE > 50 voxels was set to t-maps. Results: Voxel-wise regression analysis depicted a significant association between Rmax of the left LC and [18F]FDG PET uptake in the frontal regions, more prominent in the left hemisphere, and in the bilateral para-central regions (p<0.001,kE>50 voxels). The Rmax of the right LC was associated with [18F]FDG PET uptake, but with minor number of significant clusters, mapping out the parietal, right middle and left superior frontal regions. The volume of the left LC was positively related with [18F]FDG PET uptake (p<0.001,kE>50 voxels) in the left superior and middle frontal gyrus, extending to the paracentral lobule and supplementary motor cortex, and in the bilateral cerebellum, while the volume of the right LC was coupled with [18F]FDG PET uptake (p<0.001,kE>50 voxels) in the frontal-parietal-occipital regions with explicit left hemispheric predominance. **Conclusion:** These findings may allow understanding the interplay between LC-degeneration coupled with the loss of efferent projections, and brain metabolism in AD-pathology. Longitudinal research is warranted, given that the LC-degeneration is gradual and compensatory mechanisms might occur to maintain homeostasis at the early stages of the disease. Founded by Italian Ministry of Health [RicercaFinalizzata2013,#PE2013-02359574 "In-vivo-assessment-of-the-role-of-Locus-Coeruleus-in-the-development-of-Alzheimer's-Disease-and-other-types-of Dementia" (P.I.:F.S.G.)] **References:** None

OP-0488

Accuracy of FDG-PET at the individual level in MCI-LB versus MCI-AD: a stepwise approach from visual to semi-quantitative analysis

S. Raffa[1], F. Massa[2], A. Chincarini[3], M. Bauckneht[1,4], E. Peira[2,3], D. Arnaldi[2,4], M. Pardini[2,4], M. Pagani[5,6], B. Orso[2], M. Donegani[1], A. Brugnolo[2,4], E. Biassoni[2], P. Mattioli[2], N. Girtler[2,4], U. Guerra[7], S. Morbelli[1,4], F. Nobili[2,4];

[1]Department of Health Science (DISSAL), University of Genoa, Genoa, ITALY, [2]Department of Neuroscience, Rehabilitation, Ophthalmology, Genetics, Maternal and Child Health (DINOGMI), University of Genoa, Genoa, ITALY, [3]National Institute of Nuclear Physics (INFN), Genoa section, Genoa, ITALY, [4]IRCCS Ospedale Policlinico San Martino, Genoa, ITALY, [5]Institute of Cognitive Sciences and Technologies, Consiglio Nazionale delle Ricerche (CNR), Rome, ITALY, [6]Department of Medical Radiation Physics and Nuclear Medicine, Karolinska Hospital, Stockholm, SWEDEN, [7]formerly at Nuclear Medicine Unit, Fondazione Poliambulanza, Brescia, ITALY.

Aim/Introduction: FDG-PET is considered a supportive biomarker dementia with Lewy bodies (DLB). Its diagnostic accuracy is still unknown in prodromal stages (MCI-LB) in which the typical DLB metabolic pattern may be difficultly recognized at the individual level. Semiquantitative analysis of scans is thought to enhance accuracy especially in less skilled readers, but their added role with respect to visual

assessment at this DLB stage is still unknown. **Materials and Methods:** Two groups of patients (40 with prodromal MCI-AD and 39 MCI-LB) retrospectively selected from our database. Subjects were matched for age, education, gender and cognitive status. Patients' diagnosis was confirmed by in vivo biomarkers of either amyloidosis or nigrostriatal impairment though dopamine transporter (DAT)-SPECT, respectively. PET scans were evaluated by six expert readers aware of sex, age, education and MMSE score but blinded regarding the diagnosis of patients. In the first round of the assessment readers were required to visually evaluate the PET scans of each patient (and to choose between three diagnostic outcomes (MCI-AD, MCI-LB and uncertain). In the second round readers received T-maps obtained by the univariate single-subject voxel-based analysis (VBA) with respect to a control group of 40 age- and sex-matched healthy subjects. In the third round the readers were asked to visually re-evaluate the scans and the VBA T-maps and in addition they received an individual odds-ratio (OR) plots obtained by the volumetric regions of interest (VROI) semiquantitative analysis of the two main hypometabolic clusters deriving from the comparison of MCI-AD and MCI-LB patients in the two directions, respectively. Results: Mean diagnostic accuracy of visual assessment was 76.8±5.0% (range 68.4-83.5%) and did not significantly benefit from adding the univariate VBA T-map reading (77.4±8.3%, range 63.3-87.3%), whereas VROI-derived OR plot reading significantly increased both accuracy (89.7±2.3%, range 87.3-92.4%) and inter-rater reliability (ICC 0.97[0.96-0.98]), regardless of the readers' expertise. **Conclusion:** We highlighted a high diagnostic accuracy of 18-FDG PET to distinguish MCI-AD and MCI-LB patients which seems valuable considering the still limited evidence of accuracy of even for indicative biomarkers in prodromal DLB. Conventional visual reading is moderately accurate, is not improved by univariate statistical map reading but by a VROI analysis built on macro-regions, and this independently of reader skills. **References:** none

913

Thursday, October 21, 2021, 13:10 - 13:30

Channel 1

Plenary Quiz (for Plenary 3)

OP-0491

Plenary Quiz

T. Van den Wyngaert; Antwerp University Hospital, Nuclear Medicine, Antwerp, BELGIUM.

1001

Thursday, October 21, 2021, 13:30 - 14:50

Channel 1

Plenary 3: Conventional Nuclear Medicine - Oldies but Goldies

OP-0492

Why some Scans are Evergreen?

O. Israel; Rappaport School of Medicine, Technion - Israel Institute of Technology, Haifa, ISRAEL.

OP-0493

Bone Scan

G. Gnanasegaran; Royal Free London NHS Foundation Trust, Department of Nuclear Medicine, London, UNITED KINGDOM.

OP-0494

Thyroid Scan

E. G. Karamanou; Aristotle University of Thessaloniki, University General Hospital AHEPA, Second Academic Nuclear Medicine Dpt., Thessaloniki, GREECE.

OP-0495

Renal Scan

M. Kalnina; Pauls Stradins Clinical University Hospital, Riga, LATVIA.

OP-0496

V/Q Scan

P. Pilkington; University Hospital 12 de Octubre, Servicio de Medicina Nuclear, Madrid, SPAIN.

OP-0497

Parathyroid Imaging

P. Petranović Ovčariček; University Hospital Center Sestre milosrdnice, Oncology and nuclear medicine, Zagreb, CROATIA.

OP-0498

Lessons from the Past

F. Verzijlbergen; Radboudumc, Erasmus MC Centreal Location, Nijmegen, NETHERLANDS.

1009

Wednesday, October 20 - Saturday, October 23, 2021

on-demand pool, release on Wednesday, October 20 at 09:00

Cutting Edge Science Track - TROP Session: New Imaging Equipment and Techniques

OP-0501

Performance Testing of a Novel, Fully 3D, Gamma Camera

S. Cade, R. Leigh, M. Evans;
Royal United Hospitals Bath NHS Foundation Trust, Bath, UNITED KINGDOM.

Aim/Introduction: Guidelines for performance testing of gamma camera systems (1-5) have been developed assuming flat plate detector geometry and many of the tests recommended are not applicable to the latest generation of fully 3D gamma cameras with multiple small detectors. Following the installation of a novel multi-detector CZT gamma camera we have reviewed the current testing recommendations and how they can be adapted to novel system design. **Materials and Methods:** For a traditional gamma camera, measurements of uniformity are routinely performed for each detector using a cobalt-57 flood source and/or a technetium-99m flood or point source. This setup cannot be used for multi-detector systems. Instead, a cobalt rod source is positioned along the centre of the field of view. A dedicated QC procedure directs each line of detectors towards the source for a consistent amount of time. The uniformity is assessed for each detector bank to give measures of regional and global homogeneity, energy resolution and sensitivity. The same data are used to assess the registration of the heads. There currently isn't an option for users to perform similar tests using other isotopes. Planar tests of resolution and sensitivity cannot be performed for the fully 3D system and so tomographic alternatives must be used. Resolution without scatter was measured using three point sources (5). Total system performance was assessed using the Jaszczack and NEMA image quality phantoms demonstrating improvements in qualitative and quantitative performance compared to traditional systems. A uniform technetium-99m cylinder was used to assess system volume sensitivity (SVS), tomographic uniformity and quantification accuracy. Results: Reconstructed resolution was 5.99mm at the centre and 4.50mm at the periphery. When reconstruction was performed with point spread corrections, resolution of between 2.56mm and 2.78mm was achieved. The quantification was accurate to within 1.6% for the uniform phantom with SVS of 510(kcnts/s)/(MBq/ml) compared to 340(kcnts/s)/(MBq/ml) for a conventional system. **Conclusion:** Assessments were developed for testing performance of a novel fully 3D gamma camera system. **References:** 1. IPEM report 111. Quality Control of Gamma Cameras and Nuclear Medicine Computer Systems. 2015 2. Report of the AAPM Task Group 117. Acceptance Testing and Annual Physics Survey Recommendations for Gamma Camera, SPECT and SPECT/CT Systems. 2019 3. EANM Physics Committee. Routine quality control recommendations of nuclear medicine instrumentation. 2010 4. IAEA human Health Series No.36. SPECT/CT Atlas of Quality Control and Image Artefacts. 2019 5. NEMA NU 1-2018. Standard for Performance Measurements of Gamma Cameras. 2018

OP-0502

First NEMA performance measurements of a new multi-detector CZT-Based SPECT/CT system

G. Le Rouzic[1], R. Zananiri[2], M. Bailly[1];
[1]Centre Hospitalier Régional d'Orléans, Orléans, FRANCE, [2]General Electric, Haïfa, ISRAEL.

Aim/Introduction: StarGuide is a new multi-detector CZT-Based SPECT/CT system. The NM system, associated to a conventional CT, is composed of 12 detectors each of which comprising 7 modules of 16x16 2.46mm-collimated pixels and a registered Tungsten collimator. The aim of this study is to evaluate physical performance of the system for ^{99m}Tc. **Materials and Methods:** In planar mode, sensitivity, spatial resolution and energy resolution were measured following NEMA NU1-2018 [1]. Due to the system geometric configuration, spatial resolution and sensitivity could not be performed with the recommended 10 cm source-collimator distance. Sensitivity was then measured at 15 cm. 10 cm spatial resolution was extrapolated from a linear regression of spatial resolution variation with source-collimator distance (from 15 cm to 27.5 cm). Average ± Standard deviation (over the twelve detectors simultaneous measurements) is reported. In tomographic mode, system volume sensitivity (SVS), SPECT resolution with scatter and tomographic contrast were also evaluated following NEMA NU1-2018 [1]. SVS measurements included data recording and camera motion times. Tomographic contrast was obtained with the imaging phantom described in NEMA NU2-2018 [2]. Results: Detector Planar Sensitivity, is (96.9 ± 1.9) counts/(MBq.s). Detector spatial resolution at 10 cm is (8.4 ± 0.4) mm. Energy resolution is (5.5 ± 0.4) %. System volume sensitivity is 539.8 kcount.s^{-1}/(MBq.ml^{-1}) and system volume sensitivity per axial centimetre is 29.02 kcount.s^{-1}/(MBq.ml^{-2}). Central, radial and tangential resolution are (4.25 ± 0.61) mm, (3.29 ± 0.36) mm and (3.7 ± 0.83) mm, respectively. Contrast recovery and background variability range from 52.5% to 2.2% and 5.6% to 7.8%, respectively. Lung contrast insert is evaluated at (0.30 ± 0.02) %. **Conclusion:** StarGuide shows good and consistent detection performances for ^{99m}Tc-labelled exams. Those performances should be compared with those of conventional NaI(Tl) gamma-cameras. **References:** [1] « NEMA NU 1-2018 Standard for Performance Measurements of Gamma Cameras ». [2] « NEMA NU 2-2018 Performance Measurements of Positron Emission Tomographs ».

OP-0503

Dopamine transporter imaging using 3D-ring CZT StarGuide SPECT/CT: head-to-head comparison with a conventional system

M. Bailly, G. Le Rouzic, G. Metrard;
CHR Orléans, Orleans, FRANCE.

Aim/Introduction: The StarGuide 3D-ring CZT-camera (GE Healthcare, Haifa, Israel) is equipped with 12 swiveling high-resolution CZT detectors and a CT in a hybrid system enabling acquisition closer to the patient and also focused scanning modes. Dopamine transporter imaging with 123I-DaTSCAN is widely used in parkinsonism. In this preliminary work, we compared this new 3D general purpose CZT SPECT/CT system to a conventional camera in both phantom and patients referred for DaTSCAN imaging. **Materials and Methods:** An anthropomorphic striatal phantom filled with 123I solution at a normal striatum-to-background radioactivity ratio (8:1) was acquired on a conventional camera (Discovery 670, GE Healthcare, Haifa, Israel) and on the new StarGuide CZT system without focus and with skull and striata focus. Focus scan consisted of detectors collecting 80% of data in a reduced field-of-view, defined before the acquisition. Resolution profile of the striata were established. 8 patients (4 men and 4 women, age range 27 - 87 years, mean 65.7 years) were double scanned, on the conventional and the new CZT system with focus on striata, 3 hours after mean injection of 123.8 +/- 5.7MBq of 123I-DaTSCAN. Acquisition lasted for 30min on conventional system and 24min on StarGuide. Data were visually analyzed by 3 board-certified Nuclear Medicine Physicians to score final diagnosis, image quality and resolution using a 5-point Likert scale. Striatal Binding Ratios (SBR) were calculated using DaTQUANT (GE Healthcare, Haifa, Israel) for each putamen and caudate (right and left), and each striatum. Results: In both phantom experiments and patients, image quality and resolution scores were visually assessed as superior to conventional technology for the 3 raters. Striata profile showed a significantly better spatial resolution on the new system. This improvement in image quality and resolution was confirmed on patients. SBR were significantly higher using StarGuide SPECT: considering each region as a separate SBR, mean SBR were 2.8 +/-0.94 and 2.9+/-1.1 respectively for conventional and 3D-ring CZT systems (p=0.02). SBR calculated from normal phantom was 4.51 and 4.81 for conventional and new SPECT systems. Final diagnosis for patients remained unchanged in patients independently of the system (2 pathological and 5 normal). **Conclusion:** The use of StarGuide for DaTSCAN acquisitions improved visual image quality and resolution without impairing final diagnosis. SBR tends to be a little higher on this small sample. These results should be confirmed on a larger scale considering normal and pathological patients. **References:** None

OP-0504

Digital SPECT: Improved Imaging using the Continuous Scan Mode on a General Purpose Whole-body Solid-State CZT Camera

J. Kennedy, Z. Keidar;
Rambam - Health Care Campus, Haifa, ISRAEL.

Aim/Introduction: Image quality obtained using the continuous scan mode on a general purpose dual-head whole body solid-state CZT (cadmium zinc telluride) camera (CS-CZTC) was compared to the traditional step-and-shoot mode on both the CZT camera (CZTC), and a standard sodium iodide based device (NaIC). **Materials and Methods:** Image quality was assessed for SPECT scans of a deluxe Jaszczak phantom containing 600 MBq ^{99m}Tc solution (120 projections, 128×128 matrix, 2.2 mm pixel size), at times per stop of 1 s, 2 s, 4 s, 8 s, 16 s, 32 s, and 64 s. Counts acquired during motion between stops were binned to supplement the CS-CZTC projections. Unsupplemented projections provided the CZTC data. Separate step-and-shoot trials provided NaIC data from an Anger camera. Images were reconstructed with filtered back projection, Chang attenuation correction, and no regularization. The contrast-to-noise ratios (CNR) of the 6 cold spheres and 6 cold rod arrays of the phantom were measured using in-house software that was fully automated to preclude user bias. CNR of resolved features and total counts were compared. Results: The 3 smaller spheres and 3 smaller rod arrays were typically unresolved (CNR<<1) for scans with ≤16 s/stop using filtered back projection reconstructions. Scans with ≤2 s/stop displayed no resolvable cold features. Total counts for CS-CZTC were higher than CZTC by 48 % for the 4 s/stop scans and by 3 % for 64 s/stop. These increases were 68 % and 15 % respectively compared to NaIC. The summed time for rotation between scans was 2 minutes for the CZT camera, regardless of stop time, providing proportionately more counts for shorter acquisition times using CS-CZTC. CNR for the largest 3 spheres was 1.11 (range ±0.07) for CS-CZTC, 1.06±0.06 for CZTC, and 0.88±0.06 for NaIC, averaged over the range 4 s to 64 s per stop. Similarly, the CNR for the largest 3 rod arrays was 1.38±0.09 for CS-CZTC, 1.33±0.09 for CZTC, and 1.03±0.08 for NaIC. **Conclusion:** Overall, image quality obtained using the digital whole-body solid-state CZT SPECT/CT camera was improved by acquiring data during motion between stops and was superior to that of a standard Anger camera. The continuous scan mode has the potential for improving clinical image quality of short acquisitions such as found in dynamic imaging protocols. **References:** none

OP-0505

New multi-focal collimator designed for quantitative SPECT imaging in nuclear neurology applications

F. Massanes[1], A. H. Vija[1], X. Ding[1], D. Spence[1], G. Platsch[2], A. Yahil[1], R. Malmin[1];
[1]Siemens Medical Solutions USA, Inc., Hoffman Estates, IL, UNITED STATES OF AMERICA, [2]Siemens Healthcare Gmb, Erlangen, GERMANY.

Aim/Introduction: We designed a new multifocal "SMARTZoom" class collimator [1, 2] with a suitable High Resolution and eXtended magnification imaging volume for applications of brain and heart at nominal radius of rotation of 28cm ("SZHRX"). The SZHRX collimator is a new design with smaller holes, and higher order polynomial design equation. For I-123 isotope, the septal penetration is comparable to that of an MELP collimator. The radius of 28cm in a circular orbit, brain centered, is set to clear most shoulder width's while improving patient comfort by reducing anxiety during the scan. The target resolution is set to achieve at 28cm similar resolution as the LEHR at close orbit. The sensitivity improvement at that distance and for the larger volume is expected to be >1.8x in comparison to LEHR. In this abstract, we seek to demonstrate on phantoms that the design goals are achieved and show quantitative results. **Materials and Methods:** We use the Hoffman Brain phantom as test object and compare the images from LEHR acquired, close orbit scan, to SZHRX at nominal distance. The reconstruction is absolute quantitative for all multi-channel collimators using the xSPECT Quant approach for Tc-99m. The comparison is based on visual assessment and standard quantitative assessment of regions-of-interest. The imaging time is set to LEHR at the same noise level for Tc-99m. Results: The structure of the Hoffman Brain with the SZHRX at nominal distance is not worse than the LEHR acquisition at NCO orbit and at least as good as the LEHR acquisition at 28 cm. A calibrated scan at 26cm is used for quantitative validation, done by choosing 12 volumes of interest of approximately 1ml in volume. The values of the ROIs are, in average, within 6% between LEHR and SZHRX. The largest difference, in percentage, is seen in cold areas were the SZHRX recovers less uptake than the LEHR. The sensitivity is evaluated by decay-correcting the tomographic data and identifying that the SZHRX detects 53% more counts at 26cm than LEHR at NCO orbit. **Conclusion:** The new multifocal collimator "SZHRX" achieves the design goal for use in quantitative SPECT application of nuclear neurology. **References:** 1. Zeintl, J., et al., Performance Characteristics of the SMARTZOOM® Collimator. IEEE Medical Imaging Conference Record, 2011. 2. Rajaram, R., et al., Tomographic Performance Characteristics of the IQ•SPECT System. IEEE Medical Imaging Conference Record, 2011.

OP-0506

Evaluation Of New Features Of A Triple Head SPECT-PET-CT System

L. Torres Aroche[1], Y. Reyes González[2], K. Batista García-Ramo[2], C. Calderón Marín[3], Y. Sánchez González[2];
[1]CENTIS, Havana, CUBA, [2]Centis, Havana, CUBA, [3]Inor, Havana, CUBA.

Aim/Introduction: Multi modality imaging systems has become an important tool for the diagnosis, follow up and treatment of many diseases. The objective of this work was to evaluate and describe the performance of the new features of the triple head SPECT-CT-PET system Mediso AnyScan® SCP TRIO. **Materials and Methods:** To evaluate the performance parameters of the SPECT-PET-CT system the manufacturer recommendations based on the NEMA standards were followed, combined with methods suggested by the IAEA and AAPM publications. To check other new features of the imaging system a set of physical and clinical phantoms were used, combining commercial and home-made phantoms. The evaluated set of new features included the multi-pinhole collimators for brain studies, the list mode functionality, whole body SPECT-CT performance and the potential use of SPECT-CT and PET-CT sequential studies. The performance of basic parameters from the SPECT detectors fitted with new LEHRHS collimators was evaluated and compared with conventional configurations. The available tools for data acquisition and processing, such as the Nucline protocols and the MEDISO Interview and Fusion software were used for data processing and analysis. Results: The general performance of the TRIO system was evaluated with satisfactory results. Some intrinsic parameters such as energy resolution (≤8.98%), intrinsic spatial resolution (≤2.8mm) and maximum count rate (>700Kc/sec) showed very appropriate results. The extrinsic spatial resolution and sensitivity for multi-pinhole collimators for brain studies were measured and evaluated using a point source located at different axial and radial positions of the FOV. It was identified the highest sensitivity close to the center of rotation, decreasing up to 50 percent of the maximum in the borders. No significant changes were found on spatial resolution in the radial direction (mean value about 3mm). It suggests an optimal use of MPH SPECT studies to image central organs such as basal ganglia. The list mode functionality was evaluated for static, SPECT, whole-body-SPECT and dynamic acquisitions; it was checked its practical usefulness to implement optimization strategies for NM examinations. On the other hand, the whole-Body SPECT-CT functionally was also evaluated and verified with satisfactory results. New features such as the system benefits for cardiac studies using MPH collimators or 360 degrees image acquisition are being evaluated. **Conclusion:** The new features of the evaluated SPECT-PET-CT system showed excellent performance; main advantages were identified for the SPECT-CT component. Potential clinical applications and advantages of the triple image modality are currently under evaluation. **References:** none

OP-0507

The First Clinical Trial of the Ultra-Compact Fully Integrated Brain PET System BPET

E. Mikhaylova[1], A. Buck[1], V. Dao[2], M. Hofbauer[3], M. Hüllner[3], P. Kaufmann[3], K. Thielemans[4], C. Tsoumpas[2], V. Treyer[3], M. Ahnen[1], J. Fischer[1];
[1]Positrigo AG, Zurich, SWITZERLAND, [2]University of Leeds, West Yorkshire, UNITED KINGDOM, [3]University Hospital Zurich, Zurich, SWITZERLAND, [4]Algorithms and Software Consulting Ltd, London, UNITED KINGDOM.

Aim/Introduction: We report the results of the first feasibility study using the exploratory prototype of an ultra-compact brain positron emission tomography system (PET) BPET, as well as on the scanning procedure feedback recorded for both patients and medical technologists (MT). **Materials and Methods:** BPET is a LYSO-based scanner with the diameter of 24.2 cm and axial length of 12.8 cm. BPET data of 10 patients injected with [^{18}F]-FDG or [^{18}F]-FET were acquired immediately after a clinical PET/CT scan on a 5-ring LYSO-based commercial reference PET (rPET) scanner on a voluntary basis. BPET scan duration was 15 minutes. The images were reconstructed using open-source tomographic reconstruction software STIR and include normalization, random, scatter and attenuation corrections. Due to the exploratory nature of the study, no statistical methods were employed on images. The tracer uptake was compared qualitatively to rPET by co-registering the BPET images with the images of the rPET scan and comparing them side-by-side. After the scan, each patient and involved MT was interviewed about their experience with the scanning procedure. Results: A qualitative comparison of the images showed that the new system is capable of acquiring brain PET images. For five patients, the top part of brain images was truncated owing to limited axial field-of-view of BPET. A statistical analysis of the received feedback showed: Two-sided heteroscedastic t-test on patient comfort during BPET scan vs the rPET scan measured by Visual Analog Scale (VAS) gave p-value=0.5. Therefore, no difference in patient comfort was detected. Patient comfort measured by question showed that out of 10 patients a) 3 found BPET more comfortable; b) 3 found BPET less comfortable than rPET; c) 4 felt no difference. Therefore no difference in patient comfort was detected. An equivalent test on MT comfort during BPET scan vs the rPET scan measured by VAS gave p-value=0.001 with BPET comfort being lower. Therefore, significant difference in MT comfort detected. A total of 9 out of 10 patients liked sitting during BPET scan. A total of 8 out of 10 patients liked being able to look out during BPET scan. **Conclusion:** The ultra-compact BPET scanner showed feasibility for human brain in-vivo imaging. We received overall promising usability feedback from the patients and MTs and identified areas of improvement for the next prototype generation. **References:** none

OP-0508

Dedicated PET/MRI insert for Breast Cancer

V. Schulz[1,2,3], B. Weissler[1,2], V. Nadig[1], D. Schug[1,2], F. Mueller[1], H. Radermacher[1], N. Gross-Weege[1], T. Nolte[1], m. Borgo[4], M. d. Koning[4], M. Mathlener[5], J. Koelemann[4], S. Aussenhofer[6], T. Celik[6], A. Salomon[7], D. Schaart[8], D. Kuznetsov[8], P. Bakker[8], K. Langen[9], C. Kuhl[10];
[1]Physics of Molecular Imaging Systems / University RWTH Aachen, Aachen, GERMANY, [2]Hyperion Hybrid Imaging Systems GmbH, Aachen, GERMANY, [3]Physics Institute III B, RWTH Aachen University, Aachen, GERMANY, [4]5Futura Composites b.v., Heerhugowaard, NETHERLANDS, [5]Futura Composites b.v., Heerhugowaard, NETHERLANDS, [6]NORAS MRI Products GmbH, Hoechberg, GERMANY, [7]Philips Research, Eindhoven, NETHERLANDS, [8]Delft University of Technology, Delft, NETHERLANDS, [9]Forschungszentrum Juelich, Juelich, GERMANY, [10]Department of Diagnostic and Interventional Radiology, University Hospital Aachen, Aachen, GERMANY.

Aim/Introduction: Improving the spatial resolution and system sensitivity of PET has always been a driver for innovation. Recently developed total-body PET/CT systems introduce an at least 4-fold sensitivity increase to single-organ imaging. However, they are unfortunately subject to the same physical limitations w.r.t. spatial resolution of ~3-4 mm, which is insufficient to reliably diagnose small/early-stage tumors e.g. in breast cancer. The EU H2020 project HYPMED will address the above needs by developing a PET insert for a clinical 1.5T MRI for breast cancer imaging. **Materials and Methods:** The Hypmed insert consists of a combination of 2x2-channel local receive coils and two local PET rings allowing simultaneous imaging of the female breast at 1.5-Tesla. The PET detector rings are positioned at an out-of-plane angle of +/- 20° to better follow the thoracic contour. Each ring consists of 2x14 detectors that have two individual FOVs of 10 cm in height. A 3-layer DOI-capable crystal array design with 1.33 mm pitch was chosen to support high and homogeneous resolution. The MR-compatible detector is based on the Hyperion III platform and features a sensor tile with 12x12 individual channels of DPC-3200 (Philips) forming a sensitive area of ~48×48 mm^2 [1,2]. Results: All system components are completed. MR-compatibility studies of the Hyperion III detector are presented using previous protocols [3]. The PET electronics has been tested for gradient interference and show a B0 disturbance <1 ppm within FOV. At the highest slew rates and duty cycles of the MRI, a slight temperature effect on the detector stacks was observed, but no data rate loss was noticed. Flood maps of the 3-layer detector stack were measured and show excellent ability to identify all 3,425 crystals. **Conclusion:** Local PET detectors in combination with a stand-alone clinical 1.5T MRI are a promising approach for high-resolution PET/MRI of single organs, e.g., the female breast. With its higher sensitivity and improved spatial resolution, it offers an attractive alternative

to commercial integrated PET/MRI systems. **References:** [1] Weissler et al. IEEE TMI, 34.11 (2015): 2258-2270. [2] ADDIN Mendeley Bibliography CSL_BIBLIOGRAPHY Weissler, Bjoern, et al. "A digital preclinical PET/MRI insert and initial results." IEEE transactions on medical imaging 34.11 (2015): 2258-2270. [3] Wehner, J., Weissler, B., Dueppenbecker, P.M., Gebhardt, P., Goldschmidt, B., Schug, D., Kiessling, F. and Schulz, V., 2015. MR-compatibility assessment of the first preclinical PET-MRI insert equipped with digital silicon photomultipliers. Physics in Medicine & Biology, 60(6), p.2231.

OP-0509

Monte Carlo simulation of a last generation PET scanner: preliminary results according to the NEMA NU2-2018 standard

A. Merlet[1], *B. Presles*[1], *A. Cochet*[1,2], *J. M. Vrigneaud*[1,2];
[1]*ImViA EA 7535, University of Burgundy, Dijon, FRANCE,* [2]*Department of Nuclear Medicine, Georges-François Leclerc Cancer Center, Dijon, FRANCE.*

Aim/Introduction: A realistic PET model may offer wide opportunities to study the impact of different imaging parameters or techniques to improve image quality. The aim of this study was to build a Monte Carlo model of a recent digital PET scanner using the GATE software toolkit. We present the first results of the validation of the model according to the NEMA NU2-2018 standard tests. **Materials and Methods:** Experimental and simulated data were obtained on a Discovery MI scanner. The geometry (including the gantry cover and the patient bed) was modeled using data provided by the manufacturer. Simulated count rates were optimised using the scatter fraction and count losses test: 24 acquisitions were used to span the whole range of activities of the scanner, between 20 and 800 MBq. A dedicated iterative process was followed to determine some specific parameters such as background noise and dead time values and adjust the system in both low- and high- activity regions. Energy, time resolutions and coincidence time window were set according to the scanner specifications. The sensitivity test was simulated according to the NEMA specifications and the resulting 3D sinograms were single-slice rebinned using an in-house Python program. Total system sensitivity and axial sensitivity profiles were reported and compared with experimental results. Results: Single and prompt count rates were found to be within 2.4% and 7.0% of the respective experimental ones. Simulated system sensitivities were 12.98 cps/kBq at the center of the scanner and 12.57 cps/kBq at the 10-cm radial offset position. Respective experimental measurements were 12.81 cps/kBq and 12.83 cps/kBq, showing good agreement between simulations and experiments. Simulated and experimental axial sensitivity profiles were undistinguishable. **Conclusion:** This present study showed that a proper GATE modeling of the DMI count rates and sensitivities is feasible. The model elaboration is still ongoing and needs to be validated against the remaining NEMA tests.The first author was supported by General Electric Healthcare. There was no conflict of interest. **References:** None

OP-0510

Snapshot of Global Nuclear Medicine Resources, Country by Country: the IAEA IMAGINE database

M. Mikhail*, D. Paez, Y. Pynda, T. Okolielova, F. Giammarile, E. Estrada-Lobato, O. Pellet;*
International Atomic Energy Agency, Vienna, AUSTRIA.

Aim/Introduction: Presented here is a novel snapshot, statistical modelling, and nuanced discussion of current global gaps and trends in the provision of nuclear medicine. IMAGINE, the IAEA Medical Imaging and Nuclear Medicine Global Resources Database, is a dynamic comprehensive compilation of medical imaging and nuclear medicine resources. **Materials and Methods:** Metrics are detailed worldwide for equipment and human resources, with information on infrastructure from over 170 countries and territories. Datapoints are sought through research and are provided voluntarily from myriad sources such as IAEA fact-finding missions, professional organizations, societies, extensive literature review, and individual experts. The database is updated continuously. Results: New 2021 data for nuclear medicine are presented here, accompanied by a discussion of trends since the database launch in 2019. Our data depict how over 100 countries worldwide have functional PET scanners. Approximately 48% of these are high-income countries, 32% upper-middle income, 19% lower-middle income, and <1% low-income. Over 140 countries have SPECT . Approximately 40% of these are high-income countries, 29% upper-middle income, 24% lower-middle income, and 7% low-income. In an unprecedented fashion, these data are further stratified by evidence-based, epidemiologic indications for nuclear medicine and by UN regional maps. Further, these facts on equipment are subdivided and contrasted with the current availability of nuclear medicine physicians, obtained through global surveys for which IMAGINE serves as a repository, and compared longitudinally. **Conclusion:** Overcoming a paucity of country-specific data on nuclear medicine enabled a comprehensive bird's eye view of global nuclear medicine landscape, presented herein, updated for 2021. Health systems endowed with the right tools deliver better outcomes for patients as a whole. Though most of humanity still lacks access to nuclear medicine, long-term goals for the establishment or improvement of nuclear medicine are discussed. **References:** Hricak H, Abdel-Wahab M, Atun R, Lette MM, Paez D, Brink JA, Donoso-Bach L, Frija G, Hierath M, Holmberg O, Khong PL, Lewis JS, McGinty G, Oyen WJG, Shulman LN, Ward ZJ, Scott AM. Medical imaging

and nuclear medicine: a Lancet Oncology Commission. Lancet Oncol. 2021 Apr;22(4):e136-e172. doi: 10.1016/S1470-2045(20)30751-8. Epub 2021 Mar 4. PMID: 33676609. Gallach M, Mikhail Lette M, Abdel-Wahab M, Giammarile F, Pellet O, Paez D. Addressing Global Inequities in Positron Emission Tomography-Computed Tomography (PET-CT) for Cancer Management: A Statistical Model to Guide Strategic Planning. Med Sci Monit. 2020 Aug 27;26:e926544. doi: 10.12659/MSM.926544. PMID: 32848125; PMCID: PMC7476356. IAEA IMAGINE: the IAEA Medical Imaging and Nuclear Medicine Global Resources Databasehttps://humanhealth.iaea.org/HHW/DBStatistics/IMAGINE.html

OP-0511

Compton 3D Imaging with Sparse Number of Views: Progress on Image Quality @ 511 keV

M. Hmissi[1], G. Lebonvallet[1], A. Iltis[1], B. Mehadji[2], C. Morel[2]; [1]Damavan Imaging, 2 Rue Gustave Eiffel, 10430 Rosières-prés-Troyes, FRANCE, [2]Aix-Marseille University, CNRS/IN2P3, CPPM, Marseille, FRANCE.

Aim/Introduction: Compton imaging has been proposed as a promising nuclear medicine modality for imaging isotopes emitting radiations poorly imaged by SPECT or PET such as for α or β radiotherapy isotopes (^{90}Y, ^{211}At, etc.). But in order to qualify the imaging performances of a Compton camera, 511 keV radiation imaged in single photon mode is the best suitable comparison standard. Our goal is to propose a 3D Compton image reconstruction using only a limited number of views in order to keep equipment lightweight and affordable. **Materials and Methods:** Compton imaging of 511 keV gamma rays has been demonstrated but its image quality is far from typical positron emission tomography (PET) images. Therefore, the aim of this study is to evaluate the potential of the Temporal Compton camera technology to visualize the 3D distribution of 511 keV gamma ray source. We have developed a hand-held Compton camera based on Temporal imaging with $CeBr_3$ monolithic scintillator plates read out by digital-Si-PM arrays, which is using time distributions of the light pulses to improve events characterization. This camera has an angular resolution of 7° FWHM in 2D mode. We have developed an image reconstruction method based on a List-Mode Maximum Likelihood Expectation Maximization (LM-MLEM) algorithm incorporating the detector response function. To make better reconstruction of the Compton events as LM-MLEM tends to bend the reconstructed volumes, we have tested the usage of a total variation denoising algorithm as for regularization. This step allows us to sharpen the edges of the volume while removing unwanted artifacts from the reconstruction. Results: With this Compton camera, we have imaged a homogeneous cylinder 1.5 MBq ^{22}Na source with a length of 11 cm and a diameter of 7.5 cm and a mini-DELUXE phantom where rods were filled with a ^{18}F solution of 33 MBq. We have obtained 2D images from a single view and tomographic 3D image by using at least 3 views. For the cylinder, the 3D images show a volume with correct length and width, whose shape looks like a cylinder. On the other hand, although we have succeeded to reconstruct clearly the sectors of the phantom in 2D, we cannot resolve its rods yet and this work is ongoing. **Conclusion:** In conclusion, we have made progress in the quality of the reconstructed Compton image. We now have the clues to resolve complex objects and are looking forward to perform preclinical tests. **References:** None

OP-0512

The addition of PET-CT in CT-guided bone biopsies

D. Rietbergen, M. Droste, I. Boekestijn, M. Oosterom, M. Burgmans, F. van Velden, F. van Leeuwen, D. Rietbergen; Leids Universitair Medisch Centrum (LUMC), Leiden, NETHERLANDS.

Aim/Introduction: CT-guided percutaneous core biopsies are currently the golden standard for bone lesions of unknown kind. These biopsy can, however, be challenging, especially for small, heterogeneous lesions or lesions without radiographic substrate. The rationale of this retrospective study was to investigate if addition of molecular imaging in the form of PET-CT could help improve the accuracy of biopsies. **Materials and Methods:** 112 patients (median age: 63 y, range: 25-74y) with histologically confirmed CT-guided biopsy of either a vertebral or peripheral bone were retrospectively included. 6 Patients were excluded due to absence of histopathology. Patients were divided in those that received PET-CT imaging within 75 days prior to CT-guided bone biopsy (n=36; PET group) and those that did not (n=70; noPET group). PET images were evaluated by two experienced nuclear medicine physicians with respect to FDG uptake, tumor size and heterogeneity an CT-guided bone lesions. All biopsies were classified by the pathologist and categorized by histopathologic findings in 5 subgroups (benign, malignant disease, normal healthy tissue, infection (osteomyelitis) and inconclusive biopsy). Results: Of the 36 biopsies in the PET group, 33 biopsies (91.7%) showed to be conclusive and only 3 of them (8.3%) were inconclusive. In the noPET group only 53 (75.7%) were conclusive and 17 (24.3%) showed inconclusive results. When subdividing the results in histopathologic categories, 25 lesions were found malignant in both the groups (69.4% PET group and 35.7% noPET group). In the benign category 8.3% in the PET group and 25.7% in the noPET group were seen. **Conclusion:** In the PET group, the number of conclusive biopsies were significant higher compared to the noPET group ($P<0.05$). Based on these findings one can argue that PET/CT prior to a biopsy of a bone lesions can provide a benefit in the diagnosis of a bone lesion to a significantly increased amount of first try biopsy success with less inconclusive biopsies.

Further prospective research is needed to assess the precise improvement in biopsies with this relative new imaging modality. **References:** none

1101

Thursday, October 21, 2021, 15:05 - 16:35

Channel 1

CME 7: Developments and Challenges in Theranostics

OP-0515

Where Are We with Theranostic Imaging Today?

L.-F. de Geus-Oei; Department of Radiology, University Medical Center (LUMC), Leiden, NETHERLANDS.

OP-0516

Terbium Radioisotopes for Theranostics, What to Expect?

C. Müller; Paul Scherrer Institute, Center for Radiopharmaceutical Sciences, Villingen, SWITZERLAND.

OP-0517

Quantitative Theranostic Imaging - Challenges and Opportunities

M. Konijnenberg; Radiologie & Nucleaire Geneeskunde, Klinische Fysica, Erasmus Medical Center, Rotterdam, NETHERLANDS.

1102

Thursday, October 21, 2021, 15:05 – 16:35

Channel 2

The Top 3 Trials Sessions - 2 - Rest of the Science

OP-0519

A pilot study comparing ^{18}F-FDG PET/CT and ^{68}Ga-FAPI PET/CT for initial staging of early operable and locally advanced breast cancers

P. Chandra, K. Senthil, M. Sridev, G. Chandran, J. Kumar, M. Merlin, P. Priya, J. Sangeetha, S. Nath;
MIOT international, Chennai, INDIA.

Aim/Introduction: Fluoro-deoxyglucose (FDG) PET/CT continues to be the standard molecular imaging for staging breast cancers. However it has limited clinical utility in hormone receptor (HR) positive tumours. Recent studies show strong fibroblast activation protein (FAP) expression in stroma of most breast cancer cells which can be imaged in-vivo using the Ga-68 labelled FAP-inhibitors (FAPI). **Materials and Methods:** Prospective observational study in patients with treatment naïve breast cancers who underwent pre-operative 18F-FDG and 68Ga-FAPI PET/CT scans. Both the PET scans were done 24 hours apart. Histopatological correlation and/or follow up were standard of reference. Study was approved by institutional ethics committee. Results: 25 female patients, mean age 57.44 years (Range 43-83) were included. Mean primary tumour size was 3.8 cm (range:1.1-9.8) and mean axillary node size 2.14cm (Range:1.1-6). Except 2 patients with lobular carcinoma, all patients had infiltrating ductal carcinoma. 76% (n=19) patients were HR+ and 24% (n=6) patients HR-. 56% (n=14) patients had low grade (I/II) and 44% (n=11) patients had high grade (III) tumours. 52% (n=13) patients has node positive and 48% (n=12) had node negative disease on FNAC/histopathology. Mean SUVmax of HR+ primary tumours was significantly higher on FAPI PET compared to FDG PET (11.35 vs. 7.27, p- 0.0098). Mean SUVmax of HR+ axillary nodes was higher on FAPI PET compared to FDG PET, although not significant (10.44 vs. 6.59, p-0.078). For HR- tumours, no significant difference was noted between mean SUVmax values of either primary lesions (13.74 vs. 13.59, p-0.485) or enlarged axillary nodes (10.39 vs. 9.17, p- 0.420). Using SUVmax cut-off of 2.5, FAPI PET shows better sensitivity and specificity for axillary nodal staging (91.6% and 100% respectively) compared to FDG PET (66% and 100% respectively). 16% (n=4) patients had distant metastases (3 bone and 1 liver limited) with equal number of lesions identified on both PET/CT's. However, both liver and bone metastases had higher mean SUVmax values on FAPI PET compared to FDG (mean SUVmax-liver was 8.39 vs. 4.5 and mean SUVmax of bone lesions 12.46 vs. 7.02) **Conclusion:** Our initial observation in small cohort of breast cancer patients suggests FAPI PET to be more sensitive than FDG PET in staging HR+ and low grade tumours by displaying a significantly better tumour to background uptake ratio in primary, nodal and metastatic lesions. Other obvious advantage of FAPI PET is absence of patient preparation, faster scans and lower effective dose compared to FDG PET. **References:** None

OP-0520

Safety analysis of a large European cohort on transarterial radioembolization using the adverse event burden score

G. Maleux[1], T. Albrecht[2], D. Arnold[3], I. Bargellini[4], N. De Jong[5], T. Helmberger[6], N. Schaefer[7];
[1]University Hospitals Leuven, Leuven, BELGIUM, [2]Vivantes Klinikum Neukölln, Berlin, GERMANY, [3]Asklepios Tumorzentrum Hamburg, Hamburg, GERMANY, [4]University of Pisa, Pisa, ITALY, [5]Cardiovascular and Interventional Radiological Society of Europe, Vienna, AUSTRIA, [6]Klinikum Bogenhausen, München, GERMANY, [7]Inselspital Hospital Lausanne, Lausanne, SWITZERLAND.

Aim/Introduction: Transarterial radioembolization (TARE) is considered a treatment option for patients with primary and metastatic liver tumours due to its low toxicity. Using the data from the CIRSE Registry for SIR-Spheres Therapy (CIRT, NCT02305459), we evaluated the impact of TARE on the adverse event (AE) burden of the patient and its influence on quality-of-life (QOL). **Materials and Methods:** CIRT is a European-wide prospective multi-centre observational study, which enrolled patients between Jan 2015 and Dec 2017. Eligible patients were adults treated with TARE with Y90 resin microspheres for primary and metastatic malignant liver tumours. Patient and treatment characteristics were collected, as well as effectiveness and toxicity data, including AE and QOL data (by EORTC QLQ-C30) every 3 months up to 24-month follow-up. Relationships between AEs and TARE treatments were investigator-assessed. AEs that occurred after another treatment were censored. AEs were transformed according to the Adverse Event Burden Score (AEBS) and used to analyse prognostic factors for AEs and associations of AEs with Global Health Status (GHS). For the QOL scores, a decrease in 10 item points was defined as deterioration. Results: 1027 patients from 27 sites in 8 countries were included in the analysis. During the follow-up period, 39.6% (n=407) of the patients experienced 992 AEs. 305 (26.7%) AEs were considered treatment-related, 424 (41.3%) unrelated; 263 (25.6%) were censored. Serious adverse events (SAEs, grade 3-5) accounted for 11.4% (n=113) of the AEs; in total 2.4% (n=24) were related to the treatment. The mean AEBS of all patients that experienced AEs was 1.4 (SD 3.8): 0.4 (SD 1.4) for treatment-related AEs, compared to 0.7 (SD 2.7) for the non-treatment related AEs. Mean AEBS for the SAEs was 0.2 (SD 1.2). For the overall population, predictors for treatment-related AEs are single liver tumours (p=0.002), unilateral treatment applications (p<0.0001), and delivered dose of 1.1-1.5 GBq and >1.82 GBq (p=0.0086). Deterioration in QOL was associated with an increase in AEBS (p<0.0001). For patients that experienced deterioration in GHS, treatment-related AEs had an AEBS of 0.9 (SD 1.8), while unrelated AEs had an AEBS of 2.2 (SD 4.7). Updated analysis will include additional prognostic factors and comparisons between related and unrelated AEs for QOL dimensions besides GHS. **Conclusion:** Our data suggests that after TARE, treatment related AEBS, including deterioration of QOL, were less important than non-treatment related AEBS. This underlines the low toxicity of TARE and the beneficial QOL after this treatment. **References:** None

OP-0521

Added Value of F18-FDG PET/MR Imaging for Detecting Liver Metastases in Patients with Colorectal Cancer

P. Gündüz[1], E. Özkan[1], D. Kuru Öz[2], M. Araz[1], Ç. Soydal[1], Ö. Küçük[1], G. Erden[2], K. Kır[1];

[1]Ankara University Faculty of Medicine Nuclear Medicine Department, Ankara, TURKEY, [2]Ankara University Faculty of Medicine Radiology Department, Ankara, TURKEY.

Aim/Introduction: The presence of liver metastases in colorectal cancer is an important factor that affects the prognosis. Early diagnosis and correct staging of liver metastasis affects the clinical approach. The aim of this study was to evaluate the added value of liver PET/MR imaging compared with whole-body FDG PET/CT for detecting liver metastases in patients with colorectal cancer. **Materials and Methods:** A total of 78 patients (29 F, 49 M) with colorectal cancer who underwent F18-FDG PET/CT for staging or restaging were enrolled in this prospective study. Liver PET/MR imaging was performed in all patients after whole body FDG PET/CT. Diagnostic accuracy of liver PET/MR and PET/CT imaging findings were determined based on at least 3 months of clinical follow-up and/or histopathology results. Results: Whole-body F18-FDG PET/CT followed by liver PET/MR imagings were performed for staging in 24 patients and restaging in 54 patients. 24 patients had elevated tumor markers and 30 patients had suspicious radiological findings who underwent FDG PET/CT for restaging. In 68 patients, liver PET/MRI and PET/CT findings were compatible, while the remaining 10 patients were incompatible. Among the compatible patients, more liver lesions were detected in PET/MR than PET/CT in 14 patients. 8 patients had liver lesions that could only be detected by PET/MR and 2 patients had elevated FDG uptake on liver in PET/CT but no liver lesions or activity uptake were seen in PET/MRI. In the lesion-based analysis Se, Sp, PPV, NPV, accuracy of PET/CT and PET/MR were %62, %76, %97, %10, %63 and %98, %100, %100, %76, %98, respectively. In the patients-based analysis Se, Sp, PPV, NPV, accuracy of PET/CT and PET/MR were %77, %94, %88, %80, %85 and %97, %100, %100, %97, %98, respectively. The additional information from PET/MRI led to a change in treatment strategy for 11 of 78 (%14) patients. **Conclusion:** PET/MR provides higher diagnostic accuracy than PET/CT for detecting liver metastases. Liver PET/MR images in addition to whole-body PET/CT in patients with colorectal cancer have the potential to change the clinical approach. **References:** Nishino M, Howard SA, Krajewski KM, Jagannathan JP, et al. Update on the role of imaging in management of metastatic colorectal cancer. Radiographics. 2014;34(7):1908-28.Hong SB, Choi SH, Kim KW, Park SH, Kim SY, Lee SJ, et al. Diagnostic performance of [18F]FDG-PET/MRI for liver metastasis in patients with primary malignancy: a systematic review and meta-analysis. Eur Radiol. 2019;29(7):3553-63.

OP-0522

Efficacy of [18F]FDG-PET/CT in Evaluation of Cytologically Indeterminate Thyroid Nodules Prior to Surgery (EfFECTS): a Randomised-Controlled Multicentre Trial

E. de Koster[1], L. de Geus-Oei[2,1,3], A. Brouwers[4], E. van Dam[5], L. Dijkhorst-Oei[6], I. van Engen-van Grunsven[1], T. Klooker[7,8], R. Netea-Maier[1], M. Snel[2], W. Oyen[1,9,10], D. Vriens[2];
[1]Radboud University Medical Center, Nijmegen, NETHERLANDS, [2]Leiden University Medical Center, Leiden, NETHERLANDS, [3]University of Twente, Enschede, NETHERLANDS, [4]University of Groningen, University Medical Center Groningen, Groningen, NETHERLANDS, [5]Amsterdam University Medical Center, VU University Medical Center, Amsterdam, NETHERLANDS, [6]Meander Medical Centre, Amersfoort, NETHERLANDS, [7]Amsterdam University Medical Center, University of Amsterdam, Amsterdam, NETHERLANDS, [8]Flevo Hospital, Almere, NETHERLANDS, [9]Rijnstate Hospital, Arnhem, NETHERLANDS, [10]Humanitas University, Milan, ITALY.

Aim/Introduction: Approximately 75% of thyroid nodules with indeterminate cytology (atypia of undetermined significance or follicular lesions of undetermined significance (Bethesda III, AUS/FLUS) and (suspicious for a) follicular neoplasm (Bethesda IV, FN/SFN) or Hürthle cell neoplasm (Bethesda IV, HCN/SHCN) are benign. Avoiding unbeneficial diagnostic hemithyroidectomies for these nodules is crucial. [18F]FDG-PET/CT has shown promise as an additional diagnostic to improve preoperative differentiation. **Materials and Methods:** In this triple-blinded, multicentre, randomised-controlled trial in the Netherlands (NCT02208544), 132 patients with an indeterminate thyroid nodule underwent one [18F]FDG-PET/CT of the neck and were randomised to the [18F]FDG-PET/CT-driven or standard management group in a 2:1 ratio. In the [18F]FDG-PET/CT-driven group, patient management was based on the undisclosed [18F]FDG-PET/CT result: in case of a visually [18F]FDG-positive nodule, diagnostic surgery was advised; if the nodule was [18F]FDG-negative, watchful waiting was recommended with a confirmatory ultrasound after one year. In the standard management group, diagnostic hemithyroidectomy was advised to all patients. The primary outcome was the accurate reduction in unbeneficial management, i.e., diagnostic surgery for benign nodules or watchful waiting for malignant/borderline nodules. Intention to treat analysis was performed. Results: In the [18F]FDG-PET/CT-driven group, the rate of unbeneficial patient management was 42% (38/91) as compared to 83% (34/41) in the standard management group (p<0.001). [18F]FDG-PET/CT-driven management resulted in a 40% (25/63) reduction in unbeneficial diagnostic surgeries for benign thyroid nodules. In the standard management group, 2.9% (1/35) of benign nodules did not undergo surgery (p<0.001). There were no cases of unbeneficial watchful waiting for malignant/borderline nodules. Overall sensitivity, specificity, NPV and PPV (95% confidence interval) of [18F]FDG-PET/CT were 94.1% (80.3%-99.3%), 39.8% (30.0%-50.2%), 95.1% (83.5%-99.4%) and 35.2% (25.4%-45.9%), respectively. The benign call rate was 31.1%. In the 101 non-oncocytic nodules (60 AUS/FLUS and 40 FN/SFN), the reduction in unbeneficial surgeries for benign nodules was 48% (23/48) in the [18F]FDG-PET/CT-driven group, compared to 0% (0/28) in the standard management group (p<0.001). Sensitivity, specificity, NPV, PPV and benign call rate were 92.0% (74.0%-99.0%), 50.0% (38.3%-61.7%), 95.0% (83.1%-99.4%), 37.7% (25.6%-51.0%) and 39.6%, The benign call rate in HCN/SHCN nodules was only 3% (1/31) and no reduction in unbeneficial management was seen. **Conclusion:** Implementation of [18F]FDG-PET/CT-driven management in the preoperative workup of indeterminate thyroid nodules accurately reduces the rate of unbeneficial diagnostic surgeries for benign nodules. As nearly all HCN/SHCN nodules are [18F]FDG-positive, application of [18F]FDG-PET/CT should be limited to non-oncocytic nodules to optimise diagnostic yield and use of resources. **References:** none

OP-0523

Lung Dose Assessment on PET/CTs Acquired After Yttrium-90 Radioembolization Showed Occurrence of Radiation Pneumonitis at Lung Dose Lower than 30 Gy

M. Stella, R. van Rooij, M. Lam, H. de Jong, A. Braat;
University Medical Center, Utrecht, NETHERLANDS.

Aim/Introduction: Radiation pneumonitis is a rare but often fatal side effect of Yttrium-90 (^{90}Y) radioembolization, which may occur 1 to 6 months after therapy. In current clinical practice, a predicted value of lung dose >30 Gy during the planning phase is considered a criterion to exclude patients from treatment. However, this value is adapted from external beam radiation therapy[1]. In this study, lung dose computed on post-treatment ^{90}Y-PET/CT and its relation to development of radiation pneumonitis is investigated. **Materials and Methods:** 317 ^{90}Y post liver radioembolization PET/CTs performed during an 8-years period (Feb. 2012- Sep. 2020) were retrospectively analyzed. For the lung dose computation it was chosen to use the left lung dose (LD_{left}) as representative volume to compensate for scatter from the liver and breathing issue, assuming a homogenous distribution of microspheres in the lungs in case of shunting[2]. Results: 272 patients underwent ^{90}Y procedures (mean number of sessions and PET/CTs per patient=1.17, range 1-5). Of these patients 38% had metastatic colorectal carcinoma, 25% hepatocellular carcinoma, 16% neuroendocrine tumor, 8% intrahepatic cholangiocarcinoma, while the remaining were diagnosed with different types of tumor with liver metastases. Out of the total 317 procedures, 63% were performed with glass spheres and 37% with resin spheres. Median injected activity was 1974 MBq (range:242-9538). Mean left lung volume

within the PET FoV was 795 cc (range:80-3792). Median LD_{left} was 1 Gy (range:0-22.1). No patients had a LD_{left} >30 Gy. Of the four patients with a LD_{left} >10 Gy, two patients (LD_{left} = 22.1 Gy and 17.7 Gy respectively) developed radiation pneumonitis and consequently died. A patient with a LD_{left} equal to 18.4 Gy died 2 months after treatment, before evaluation scan, due to progressive disease, while a patient with LD_{left} of 11.7 Gy did not report any lung-dose related side effects. **Conclusion:** Radiation pneumonitis following ^{90}Y radioembolization is rare. In this study, 2 out of 272 patients developed radiation pneumonitis. With 22 and 18 Gy, both these patients had lung doses amongst the highest three encountered in this study. Based on this quantitative estimation of the lung dose on post-treatment data, a lower lung dose threshold for patient exclusion seems more appropriate than the currently used 30 Gy, when calculated using SPECT/CT in the pre-treatment phase. **References:** 1. Bastiaannet, R. et al. EJNMMI Phys. 5, 22 (2018). 2. Salem, R. et al. Am. J. Clin. Oncol. Cancer Clin. Trials 31, 431-438 (2008).

OP-0524

The surgical benefits of using bimodal tracers for image-guided surgery; multicenter experience in >1900 patients

T. Buckle[1], P. Dell'Oglio[1], E. Mazzone[1], D. Rietbergen[1], H. de Vries[1], S. Vidal-Sicart[2], B. Karakullukcu[3], M. Klop[3], O. Brouwer[3], E. Wit[3], P. van Leeuwen[4], H. van der Poel[3], F. van Leeuwen[1];
[1]LUMC, Leiden, NETHERLANDS, [2]University Hospital Clinic Barcelona, Barcelona, SPAIN, [3]Netherlands Cancer Institute - Antoni van Leeuwenhoek Hospital, Amsterdam, NETHERLANDS, [4]Netherlands Cancer Institute - Antoni van Leeuwenhoek Hospital, Leiden, NETHERLANDS.

Aim/Introduction: Hybrid image-guided surgery concepts using combined radio- and fluorescence-image guidance are increasingly gaining traction. Most of these efforts, however, are preclinical or small first-in-human trials. The bimodal tracer ICG-^{99m}Tc-nanocolloid has already been extensively applied at multiple clinical sites and therefore can be used to evaluate if and how hybrid approaches can help realize improvements beyond the current state-of-the-art radioguided approaches. **Materials and Methods:** 1910 patients that underwent sentinel node procedures guided by ICG-^{99m}Tc-nanocolloid (500 Prostate, 700 penis, 60 vulva, 20 breast, 20 cervical, and 590 head and neck cancer (melanoma and oral cavity) cancer patients) were retrospectively included. Preoperative SNs were identified based on lymphoscintigraphy and single-photon emission computed tomography combined with computed tomography (SPECT/CT). Intraoperatively, SNs were detected via gamma tracing and fluorescence imaging. The use of hybrid guidance could be compared to conventional radioguidance methods within the same patient. Outcome was based on reported surgical complications, overall survival, LN recurrence free survival (5yr follow up), and false negative rates (FNR). Results: Interim analysis of all combined results showed that between 98 and 100% of preoperatively identified SNs could be intraoperatively detected with a combination of radio- and fluorescence guidance for respectively prostate, penile, vulva, breast and head and neck cancer. The synergistic approach yielded enhanced intraoperative find rates (radioguidance: rough indication, fluorescence: visual validation of localization and accurate resection). Furthermore, aberrant drainage patterns outside the standard dissection template were revealed (in 29.4% of patients, containing metastases in 22.2% of cases), allowing adaptation of the resection template during surgery. The inability to detect a radioactive signal in SN's (2%) was linked to low tracer uptake and radioactive decay. Overall, the preoperative SPECT/CT roadmap was shown to be indispensable for accurate guidance towards the SNs. Use of ICG-^{99m}Tc-nanocolloid was not associated with increased risk of postoperative complications (Clavidien-Dindo >- II, p>0.041) and no tracer-related (allergic) reactions were reported. No significant difference FNR or overall operation time was seen, compared to the routine radioguided approach. At 5 yr follow up the hybrid approach revealed lower rates of biochemical recurrence (0.79, 95%CI 0.63-0.98) and clinical recurrence (HR 0.76, p=0.035). **Conclusion:** Large scale implementation of the bimodal SN tracer ICG-^{99m}Tc-nanocolloid, indicates that intraoperative fluorescence imaging complements preoperative lymphoscintigraphy/SPECT/CT as well as intraoperative gamma tracing. This helps make detailed nodal identification more intuitive for the operating surgeon. **References:** None

OP-0525

In vivo imaging of tau pathology across PET-based stages of amyloid deposition

A. Moscoso Rial[1], M. J. Grothe[2,1], M. Schöll[1];
[1]Wallenberg Centre for Molecular and Translational Medicine and the Department of Psychiatry and Neurochemistry, Institute of Neuroscience and Physiology, University of Gothenburg, Gothenburg, SWEDEN, [2]Movement Disorders Group, Institute of Biomedicine of Seville-IBiS, Seville, SPAIN.

Aim/Introduction: Previous research has consistently reported widespread tau aggregation in the presence of global amyloid-β (Aβ) pathology, but the association of Aβ pathology severity with tau accumulation remains unclear. Here, we studied cross-sectional and longitudinal tau aggregation in relation to progressive stages of regional Aβ deposition as determined by a recently established Aβ PET-based staging approach. **Materials and Methods:** We examined 244 cognitively unimpaired (CU) and 180 impaired (CI) subjects from the Alzheimer's Disease Neuroimaging Initiative with concurrent T1 MRI, ^{18}F-Florbetapir-PET (FBP), and ^{18}F-Flortaucipir-PET (FTP) scans. A subset of 153

individuals had at least one follow-up FTP scan. An Aβ PET-based staging method for FBP was used to stratify participants into four progressive stages of Aβ deposition. Linear regressions adjusted for age and sex were used to assess regional FTP uptake across Aβ stages in CU and CI individuals (additionally controlled for clinical diagnosis - MCI/AD). Longitudinal tau accumulation was assessed in the pooled CU and CI sample, using linear mixed effects models adjusted for age, sex, and clinical diagnosis. Finally, we assessed cross-sectional tau-related markers (p-tau181 and p-tau181/$A\beta_{1-42}$) in cerebrospinal fluid (CSF) across Aβ stages in another subset of participants (n=227), as well as analyzed associations between neuropathologically defined Braak stages and in vivo Aβ stages in a subset of individuals who have been followed up to autopsy (n=29). Results: Cross-sectionally, FTP uptake in Braak I/II regions increased gradually from Aβ stages 1 through 4, though only Aβ stage 4 in CU and stages 3 and 4 in CI resulted in widespread neocortical tau deposition compared to stage 0. In longitudinal analyses, faster longitudinal FTP increases in Braak I/II regions were observed across Aβ stage 2 onwards, but only Aβ stages 3 and 4 showed faster tau accumulation in regions exceeding Braak I/II. Confirming the PET findings, cross-sectional levels of p-tau181 and p-tau181/$A\beta_{1-42}$ in CSF showed gradual increases across Aβ stages 2-4; neuropathological Braak stages were also strongly correlated with in vivo Aβ stages (rho=0.73, p<0.001). **Conclusion:** Early stages of Aβ pathology seem to associate with medial temporal lobe tau deposition, but more severe and widespread tau pathology does not occur before more advanced stages of Aβ deposition. Since these subjects only cover a subpopulation of Aβ-positive individuals as conventionally defined, recruiting individuals at advanced Aβ stages might represent an effective strategy for clinical trials in which longitudinal tau PET is used as an end point. **References:** None.

OP-0526

Cognitive change in frail individuals with intermediate amyloid load: insight from the MAPT interventional study

L. Saint-Aubert[1], I. Carrié[2], A. Hitzel[3], A. Salabert[3], P. Payoux[1]; [1]INSERM laboratory ToNIC, Toulouse, FRANCE, [2]Gérontopôle - CHU de Toulouse, Toulouse, FRANCE, [3]Service de médecine nucléaire, CHU de Toulouse, Toulouse, FRANCE.

Aim/Introduction: In the past decade, in vivo cerebral amyloid load in the spectrum of cognitive impairment has been extensively explored using positron emission tomography (PET), and is now a key part of screening visits for most therapeutic studies. However, to date, little if no distinction is made between patients with low to medium amyloid load versus patients with high amyloid load, in terms of both the risk of developing AD and the progression of cognitive change. Here we investigated the cognitive changes in frail participants to a multidomain interventional study [1] , according to the degree of cerebral amyloid load : absent/low, medium, high. **Materials and Methods:** Two hundred and forty five participants to the MAPT study were selected. All of them underwent a full cognitive assessment, and were follow-up for up to five years. They all underwent a cerebral amyloid PET scan using [^{18}F]florbetapir. All of them had been randomized at the beginning of the trial into one of four intervention groups: 1/ multidomain intervention and daily omega-3 intake; 2/ multidomain intervention and placebo; 3/ omega-3 uptake alone; 4/ the placebo alone. Cortical amyloid load was quantified from PET imaging as the mean standard uptake value ratio in all regions of the brain (parcelated according to the AAL atlas; cerebellar grey matter as reference). Patients were categorized into "low", "medium", or "high" cerebral amyloid using k-clustering. Cognitive functions were measured as a composite score combining four tests. Using a linear regression model, we investigated how cognition progressed over time according to amyloid status and the intervention group. Results: Our findings were two-fold: patients in the "high amyloid" group showed cognitive decline over time, while patients in the "medium amyloid" group exhibited a cognitive profile stable and similar to the patients with "low amyloid" load (p<0.001). In addition, in the "medium amyloid" group only, we observed an improvement of cognitive performance over time for patients of all intervention group, except for patients in the placebo group (i.e without intervention at all), who showed stable cognitive performance (p<0.05). **Conclusion:** Our findings suggest that having a moderate or high amyloid load is not equivalent in terms of impact on cognitive progression in the short-term (5 years), and that patients with moderate rather than high amyloid load may be a better suited target for drug studies. **References:** [1] Andrieu S et al. Lancet Neurol. 2017. PMID: 28359749

OP-0527

The Phase 3 NETTER-1 Study of [^{177}Lu]Lu-DOTA-TATE in Patients with Midgut Neuroendocrine Tumours: Final Overall Survival and Long-Term Renal Safety

P. Kunz[1], M. E. Caplin[2], P. B. Ruszniewski[3], L. Bodei[4], A. Hendifar[5], E. Mittra[6], E. M. Wolin[7], J. C. Yao[8], M. E. Pavel[9], E. Grande[10], E. Van Cutsem[11], E. Seregni[12], H. Duarte[13], A. Demange[14], S. Mutevelic[14], J. R. Strosberg[15], E. P. Krenning[16];

[1]Yale School of Medicine, New Haven, CT, UNITED STATES OF AMERICA, [2]Royal Free Hospital, London, UNITED KINGDOM, [3]Université de Paris et Hôpital Beaujon, AP-HP, Clichy, FRANCE, [4]Memorial Sloan Kettering Cancer Center, New York, NY, UNITED STATES OF AMERICA, [5]Cedars-Sinai Medical Center, Los Angeles, CA, UNITED STATES OF AMERICA, [6]Oregon Health & Science University, Portland, OR, UNITED STATES OF AMERICA, [7]Icahn School of Medicine at Mount Sinai, New York, NY, UNITED STATES OF AMERICA, [8]University of Texas MD Anderson Cancer Center, Houston, TX, UNITED STATES OF AMERICA, [9]Friedrich-Alexander University of Erlangen-Nürnberg, Erlangen, GERMANY, [10]MD Anderson Cancer Center Madrid, Madrid, SPAIN, [11]University of Leuven, University Hospital Gasthuisberg, Leuven, BELGIUM, [12]Fondazione IRCCS Istituto Nazionale dei Tumori, Milan, ITALY, [13]Instituto Português de Oncologia, Porto, PORTUGAL, [14]Novartis Pharma AG, Basel, SWITZERLAND, [15]Moffitt Cancer Center, Tampa, FL, UNITED STATES OF AMERICA, [16]Erasmus Medical Centre, Rotterdam, NETHERLANDS.

Aim/Introduction: In the primary analysis of the phase 3 NETTER-1 trial, [^{177}Lu]Lu-DOTA-TATE (^{177}Lu-DOTATATE) significantly prolonged progression-free survival versus high-dose long-acting octreotide (HR, 0.18 [95% CI: 0.11, 0.29]; $p < 0.0001$) in patients with advanced, progressive, well-differentiated, somatostatin receptor-positive midgut neuroendocrine tumours (NETs). Here we report final overall survival (OS) and renal safety in NETTER-1. **Materials and Methods:** In this international open-label trial, 231 patients were randomized 1:1 to receive four cycles of ^{177}Lu-DOTATATE 7.4 GBq (200 mCi) every 8 weeks plus long-acting octreotide 30 mg (^{177}Lu-DOTATATE arm), or high-dose long-acting octreotide 60 mg every 4 weeks (control arm), both on top of best supportive care. Patients received treatment until disease progression or completion of an 18-month treatment period, after which they entered long-term follow-up. OS was a key secondary endpoint. Primary intention-to-treat (ITT) analysis of OS was prespecified to occur after 158 deaths or 5 years after the last patient was randomized, whichever occurred first, using Cox proportional-hazards regression and unstratified log-rank test. Long-term renal function was evaluated in both arms using calculated creatinine clearance (Cockcroft-Gault method). Results: Most ^{177}Lu-DOTATATE treated patients (84/111 [76%]) received all four cycles. Final analysis occurred 5 years after the last patient was randomized, following 142 deaths, with a median follow-up of more than 6.3 years in each arm. During long-term follow-up, 41/114 (36%) patients in the control arm received subsequent radioligand therapy ('cross-over'), 26/114 (22.8%) within 24 months after randomization. Median OS was 48.0 months (95% CI: 37.4, 55.2) in the ^{177}Lu-DOTATATE arm and 36.3 months (95% CI: 25.9, 51.7) in the control arm (HR, 0.84 [95% CI: 0.60, 1.17]; p=0.30, two-sided). During the study, most nephrotoxicity in ^{177}Lu-DOTATATE treated patients was mild or moderate (grade 1-2 in 45/111 [40.5%] patients; ≥grade 3 in 6/111 [5.4%] patients). Mean change from baseline in creatinine clearance over time was similar between treatment arms (at 5 years follow-up [evaluable n=26]: -21.6 [SD, 11.7] mL/min and -24.7 [22.1] mL/min in the ^{177}Lu-DOTATATE arm and control arm, respectively). No new cases of myelodysplastic syndrome or acute leukaemia were reported during long-term follow-up. **Conclusion:** Final analysis of OS did not reach statistical significance, potentially impacted by the high rate of cross-over to radioligand therapy in the control arm (36%). Nevertheless, treatment with ^{177}Lu-DOTATATE led to a clinically meaningful improvement in median OS of 11.7 months. No new safety signals emerged during long-term follow-up, with no long-term nephrotoxicity. **References:** None.

1104

Wednesday, October 20 - Saturday, October 23, 2021

on-demand pool, release on Wednesday, October 20 at 09:00

CTE 7: Research - Technologist's Involvement

OP-0529

Conducting the Research

S. Rep; *University Medical Centre, Department of Nuclera Medicine, Ljubljana, SLOVENIA.*

OP-0530

Database Analysis - The Opportunity for Technologists

I. Melo e Costa; *Department of Biomedical Engineering & Imaging Sciences, King's College London, London, UNITED KINGDOM.*

OP-0531

Team Science - Theory and Practice

D. Albano; *University of Brescia and ASST Spedali Civili of Brescia, Department of Nuclear Medicine, Brescia, ITALY.*

1105

Wednesday, October 20 - Saturday, October 23, 2021

on-demand pool, release on Wednesday, October 20 at 09:00

Joint Symposium 13 (EANM/EHA): Biomarkers in Lymphoma

OP-0533

Non-PET Biomarkers in Lymphoma

F. Broussais-Guillaumot; Hematology Department, LYSARC CHU Lyon Pierre Bénite, Caen, FRANCE.

OP-0534

PET for Prognosis and Response Prediction

S. Barrington; King's College London and Guy's and St Thomas' PET Centre, School of Biomedical Engineering and Imaging Sciences, London, UNITED KINGDOM.

OP-0535

How to Combine PET and Non-PET Biomarkers

A.-S. Cottereau; Cochin, Nuclear Medicine, Paris, FRANCE.

1106

Wednesday, October 20 - Saturday, October 23, 2021

on-demand pool, release on Wednesday, October 20 at 09:00

Joint Symposium 14 (EANM/EHA): New Therapies in Lymphoma - Is Deauville Still Good Enough?

OP-0537

From Checkpoint Inhibitors to Cell Therapy - New Standards in Malignant Lymphoma

P. Bröckelmann; Faculty of Medicine and University Hospital of Cologne, Department I of Internal Medicine, Center for Integrated Oncology Aachen Bonn Cologne Düsseldorf, University of Cologne, Cologne, GERMANY.

OP-0538

Evolution of Response Criteria in Lymphoma

J. J. Eertink; Amsterdam UMC, VUmc, Hematology, Amsterdam, NETHERLANDS.

OP-0539

Is Deauville Score Still the Solution?

L. Dercle; University of Toulouse, Physics and signal processing, Toulouse, FRANCE.

1107

Wednesday, October 20 - Saturday, October 23, 2021

on-demand pool, release on Wednesday, October 20 at 09:00

Teaching Session 1 (EANM/AGA): Imaging of Prosthetic Knee Joint Loosening - Spotlight on Quantitative and Multidisciplinary Algorithms

OP-0541

Clinical Point of View for Selecting Imaging Modalities for the Assessment of Knee Endoprosthesis

D. Mathis; Kantonsspital Baselland Bruderholz, Department of Orthopedics, Basel, SWITZERLAND.

OP-0542

Anatomical Imaging in the Management of Prosthetic Loosening

L. M. Sconfienza; I.R.C.C.S. Istituto Ortopedico Galeazzi, Unit of Diagnostic and Interventional Radiology, Milan, ITALY.

OP-0543

Nuclear Medicine Modalities and Quantitative Approaches in the Management of Knee Prosthetic Loosening

C. Lauri; Sant'Andrea Hospital, Nuclear Medicine Unit, Department of Medical-Surgical Sciences and of Translational Medicine of "Sapienza" University, Rome, ITALY.

OP-0544

Summary Suggestion - A Consensus Document in the Diagnosis of Knee Prosthetic Joint Loosening

F. Paycha; Assistance Publique-Hôpitaux de Paris, Université de Paris, Department of Nuclear Medicine, Paris, FRANCE.

1108

Wednesday, October 20 - Saturday, October 23, 2021

on-demand pool, release on Wednesday, October 20 at 09:00

M2M Track - TROP Session: Peptides Only!

OP-0546

[^{18}F]AlF-NOTA-DV1-k-(DV3) for translational CXCR4-targeted molecular imaging

K. Luyten[1], T. Van Loy[2], C. Cawthorne[3], C. Deroose[3], D. Schols[2], G. Bormans[1], F. Cleeren[1];

[1]Laboratory for Radiopharmaceutical Research, Department of Pharmaceutical and Pharmacological Sciences, KU Leuven, Leuven, BELGIUM, [2]Laboratory of Virology and Chemotherapy, Department of Microbiology, Immunology and Transplantation, KU Leuven, Leuven, BELGIUM, [3]Nuclear Medicine and Molecular Imaging, Department of Imaging and Pathology, KU Leuven, Leuven, BELGIUM.

Aim/Introduction: CXCR4-PET imaging with [^{68}Ga]PentixaFor has intrinsic diagnostic value and is used to select patients for personalized CXCR4-targeted radionuclide therapy.[1] However, a CXCR4 targeting radiopharmaceutical labelled with fluorine-18 is still of high value due to its favourable characteristics over gallium-68. Therefore, this study aims to develop an alternative CXCR4-targeting scaffold (DV1-k-DV3, vMIP-II-derived CXCR4 antagonist composed entirely of D-amino acids)[2] that conserves high CXCR4 binding affinity after Al^{18}F-labelling. **Materials and Methods:** Binding affinity of AlF-NOTA-DV1-k-(DV3) towards human CXCR4 (hCXCR4) and mouse CXCR4 (mCXCR4) was determined in a competitive binding assay with fluorescently labelled CXCL12. [^{18}F]AlF-NOTA-DV1-k-(DV3) was synthesized in an automated AllInOne® synthesis module (Trasis, Belgium). In vitro and in vivo stability of [^{18}F]AlF-NOTA-DV1-k-(DV3) was evaluated. Finally, in vivo specific binding of [^{18}F]AlF-NOTA-DV1-k-(DV3) was determined in an U87.hCXCR4 tumour xenograft mouse model using µPET/CT with or without co-injection of 5 mg/kg of the CXCR4 antagonist AMD3100, followed by ex vivo biodistribution at 75min. Data was compared with those obtained with [^{68}Ga]PentixaFor. Results: AlF-NOTA-DV1-k-(DV3) showed slightly higher in vitro binding affinity to hCXCR4 than [^{nat}Ga]PentixaFor (IC_{50}: 5nM and 9nM, respectively). AlF-NOTA-DV1-k-(DV3) also binds to mCXCR4 with high affinity (IC_{50}: 33nM), while [^{nat}Ga]PentixaFor is selective for hCXCR4 (IC_{50}>1000nM for mCXCR4). [^{18}F]AlF-NOTA-DV1-k-(DV3) was successfully produced in high yield (45%) and demonstrated high in vitro (>97% in human serum after 2h) and in vivo stability (>87% in plasma 15min p.i.). Further, [^{18}F]AlF-NOTA-DV1-k-(DV3) shows CXCR4-specific uptake in mCXCR4-expressing organs e.g. liver (SUV_{mean} 8.2), spleen (SUV_{mean} 2.5), and bone (SUV_{mean} 0.4, femur harbouring bone marrow). Tumour uptake of [^{18}F]AlF-NOTA-DV1-k-(DV3) was significantly lower (SUV_{mean} 0.6) compared to [^{68}Ga]PentixaFor (SUV_{mean} 3.0) however, this might be explained by the high affinity of [^{18}F]AlF-NOTA-DV1-k-(DV3) towards both mCXCR4 and hCXCR4. High CXCR4 expression in the liver combined with the high cardiac output to this organ (±25%) may result in a large fraction of [^{18}F]AlF-NOTA-DV1-k-(DV3) binding to mCXCR4 in the liver before it reaches the tumour site. This results in lower tumour accumulation compared to [^{68}Ga]PentixaFor, despite higher in vitro affinity. Therefore, these findings do not preclude human trials to determine the biodistribution and tumour targeting of this tracer. **Conclusion:** The CXCR4-targeting scaffold DV1-k-(DV3) shows high affinity to both mCXCR4 and hCXCR4. [^{18}F]AlF-NOTA-DV1-k-(DV3) can be used for translational research in which CXCR4 upregulation is involved, including cardiologic application and infection/inflammation. **References:** 1. Maurer, S., et al., J Nucl Med. 2019; 60:1399-1405 2. Mao, Y., et al. Cell Transplantation. 2018; 27:1249-1255

OP-0547

Functionalising a PET nanoradiotracer towards integrins enables better tumour targeting in a mouse orthotopic glioblastoma model

L. Sakiroff, B. Louis, J. Ou, L. Balasse, V. Nail, O. Nachar, A. Moyon, A. Bouhlel, T. Roussel, F. Dignat-George, L. Peng, P. Garrigue, B. Guillet; Aix-Marseille University, Marseille, FRANCE.

Aim/Introduction: Nanometric size promotes penetration of chemicals into solid tumours via the enhanced permeability and retention effect (EPR effect), a characteristic of tumours but not constantly found from a tumour to another. Hence, we designed highly flexible, supramolecular, radiolabellable dendrimers self-assembling into "dendrimersomes" enabling PET imaging of the EPR effect heterogeneity (1,2,3). To improve targeting efficiency and specificity, functionalisation of the dendrimers with tumour-cell-specific binding molecules was considered. αvβ3 integrin being widely overexpressed in many tumours including glioblastoma, a specific RGD moiety was designed to be integrated by self-assembling into the dendrimer. This study aimed at evaluating the impact of the functionalization on the in vitro binding specificity of dendrimersomes, and on their in vivo biodistribution and tumour targeting. **Materials and Methods:** The dendrimers were radiolabelled with [^{68}Ga]GaCl3. The radiochemical purity was checked for 4 hours in human serum and NaCl 0.9% at room temperature and 37°C (n=3) by iTLC method. Different ratios of radiolabelled dendrimers / RGD dendrimer (6:1, 3:1, 1:0, 1:3, 1:6, 1:9) were evaluated by cell-based receptor binding assay on U87 human glioblastoma cells (n=3). Small-animal microPET/CT studies were performed in athymic nude mice (n=4) bearing orthotopic U87 glioblastoma xenografts with the best functionalised dendrimersome identified in vitro, compared to the non-functionalised dendrimersome. Results were expressed as percentage of incubated dose (%ID) for in vitro tests and as a brain-to-cerebellum activity ratio for in vivo. Statistical significances were assessed using Kruskal-Wallis test with Dunn's post hoc test for in vitro and paired t-test for in vivo studies. Results: The radiochemical purities were ≥97% and stable for 4h in every studied conditions. The 6:1, 3:1, and 1:3 ratios showed a significant improvement of the dendrimersome binding on U87 cells compared to the 1:0 control ratio (Table 1). The 1:3 ratio was selected for in vivo studies. A significant increase of microPET/CT quantifications in tumours was observed with the 1:3 ratio functionalised dendrimersome compared with the non-functionalised dendrimersome (respectively 1.80± 0.65 and 1.47±0.62; *P = 0.0382). **Conclusion:** Functionalisation of radiolabelled dendrimersomes provides a new perspective for adding molecular targeting to passive EPR targeting, illustrating the high versatility of this type of nanosystem for molecular imaging and offering novel outlooks for theranostics applications. **References:** (1) https://doi.org/10.1073/pnas.1812938115 ;(2) https://doi.org/10.1039/C9CC07750B ;(3) https://doi.org/10.1002/smll.202003290 ;

OP-0548

Synthesis and biological evaluation of the first ^{68}Ga/^{111}In-radiolabelled peptide targeting the neuropeptide-Y receptor 5 (Y_5) in cancers

S. Bodin[1,2], D. J. Worm[3], E. Jestin[4], D. Vimont[1], I. Ait-Arsa[4], E. Hindié[1,2], A. G. Beck-Sickinger[3], C. Morgat[1,2];
[1]Univ. Bordeaux, CNRS, INCIA, UMR5287, F-33000 Bordeaux, FRANCE, [2]University Hospital of Bordeaux, Nuclear Medicine Department, F-33000 Bordeaux, FRANCE, [3]Institute of Biochemistry, Leipzig University, Brüderstrasse 34, 04103 Leipzig, GERMANY, [4]CYclotron Réunion Océan Indien CYROI, 2 rue Maxime Rivière, F-97490 Sainte-Clotilde, FRANCE.

Aim/Introduction: The neuropeptide-Y (NPY) family is composed of four G protein- coupled receptor subtypes (Y_1, Y_2, Y_4 and Y_5). Over-expression of the Y_5 has been reported in some breast cancer cell lines. This work describes the expression of Y_5 in a panel of 11 human cancer cell lines and the radiopharmaceutical characterization of a Y_5-targeting peptide radiolabelled with gallium-68 (^{68}Ga) and indium-111 (^{111}In). **Materials and Methods:** Y_5 expression was assessed using western blot and immunochemistry on breast cancer cell lines (MCF-7, MDA-MB-453, MDA-MB-468, SKBR3, T47D, ZR75.1), prostate cancer cells (LNCaP, DU-145, PC3), colon cancer cells HT-29 and ovary cancer cells SKOV3. Xenografts from MCF-7, PC-3 and HT-29 cells were also tested. Proliferation tests (MTT, sulforhodamine B) were carried out on MCF-7 cells using specific Y_5-agonists and -antagonists. Next, DOTA-[cPP(1-7),NPY(19-32),Ala^{31},Aib^{32},Gln^{34}]-hPP (abbreviated tg3) was prepared by using solid-phase synthesis, purified and then radiolabelled with ^{68}Ga and ^{111}In. In vitro characterization (hydrophilicity, saturation studies, internalization, plasma protein binding) was performed on the human breast cancer cell line MCF-7 (expressing also Y_1). Tissular micro-imaging was also performed on 9 primary prostate cancer samples using [^{111}In]In-tg3. Biodistribution of [^{68}Ga]Ga-tg3 in mice is under analysis. Results: All human cancer cell lines and xenografts express high level of Y_5 except LNCaP cells. [^{68}Ga]Ga-tg3 and [^{111}In]In-tg3 were obtained at high apparent molar activity (14.1 ± 1.3 GBq/µmol and 4.3 ± 3.4 GBq/µmol, respectively). [^{68}Ga]Ga-tg3 and [^{111}In]In-tg3 exhibited hydrophilic properties ($logD_{7.4}$ = -2.58 ± 0.25 and -2.63 ± 0.17), suggesting renal clearance and low brain uptake. Saturation binding experiments demonstrated very good affinity for Y_5 (Kd_{high} (two sites) = 13.2 ± 10.9 nM) and good selectivity (Kd Y_5R / Kd Y_1R > 1000). The Y_5-mediated internalized fraction was low (< 5 % at 60 min) consistent with the known weak β-arrestin coupling of Y_5. Consequently, the membrane-bound fraction reached 6.6% ± 3.9 % for[^{68}Ga]Ga-tg3 and 9.9 ± 4.5 % for [^{111}In]In-tg3. Also, plasma protein binding of [^{68}Ga]Ga-tg3 was low (<1%IA/mg) up to 45 min after incubation. Unlabelled tg3 behaves like a full agonist based on proliferation tests performed on MCF-7 cells. Preliminary tissular micro-imaging study showed Y_5-specific binding of [^{111}In]In-tg3 on intermediate (3/4 samples) and high (2/3 samples) risk prostate tumors while none of the low risk samples bind [^{111}In]In-tg3 (0/2). **Conclusion:** This is the first report of a radiolabelled NPY-analogue designed for Y_5 targeting, which may allow specific imaging of Y_5-overexpressing tumors and potentially theranostic purposes. **References:** None.

OP-0549

Double targeting of NTS_1 and GRPR receptors using ^{68}Ga-labelled heterodimers

S. Bodin[1,2], S. Previti[3], E. Jestin[4], D. Vimont[1], F. Lamare[1,2], I. Ait-Arsa[4], E. Hindié[1,2], F. Cavelier[3], C. Morgat[1,2];
[1]Univ. Bordeaux, CNRS, INCIA, UMR5287, F-33000 Bordeaux, FRANCE, [2]University Hospital of Bordeaux, Nuclear Medicine Department, F-33000 Bordeaux, FRANCE, [3]Univ. Montpellier, CNRS, Institut des Biomolécules Max Mousseron, IBMM, UMR-5247, F-34000 Montpellier, FRANCE, [4]CYclotron Réunion Océan Indien CYROI, 2 rue Maxime Rivière, F-97490 Sainte-Clotilde, FRANCE.

Aim/Introduction: Neurotensin receptor-1 (NTS_1) and gastrin-releasing peptide receptor GRPR (bombesin receptor-2, BB2) are interesting targets for nuclear oncology applications. In some tumors, these receptors exhibit complementary expression profiles considering the stage or the aggressiveness of tumors, such as in breast cancer, colorectal cancer or prostate carcinomas. Targeting both receptors in the same time with a single molecule could enhance the potential for imaging and therapy of such tumors. In this work we describe the in vitro and in vivo properties of [^{68}Ga]Ga-JMV7110, [^{68}Ga]Ga-JMV7253 and [^{68}Ga]Ga-JMV7266, the first heterodimers designed to target both NTS_1 and GRPR. **Materials and Methods:** JMV7110 (DOTA-βAla-βAla-(D)Phe-Gln-Trp-Ala-Val-Gly-His-(3S,4S) Sta-Leu-βAla-βAla-Lys-Lys-Pro-Phe-Ile-Leu-OH), JMV7253 (DOTA-βAla-βAla-(D)Phe-Gln-Trp-Ala-Val-Gly-His-(3S,4S) Sta-Leu-βAla-βAla-Lys-Lys-Pro-Phe-Ile-TMSAla-OH) and JMV7266 (DOTA-βAla-Glu(βAla-βAla-(D)Phe-Gln-Trp-Ala-Val-Gly-His-(3S,4S)Sta-Leu-NH_2)-βAla-Lys-Lys-Pro-Tyr-Ile-Leu-OH, branched compound) were prepared using solid-phase synthesis, purified and then radiolabelled with gallium-68. In vitro characterization was performed on human colorectal adenocarcinoma HT29 cell lines, expressing high levels of NTS_1 and GRPR. Corresponding ^{68}Ga-monomers were used as controls. In vivo pharmacology was complemented by dynamic microPET/CT imaging on HT29-xenografted nude mice. Results: Radiolabelling heterodimers with ^{68}Ga was achieved with moderate yield (44.4 ± 6.3 %) and high apparent molar activity (> 15 GBq/µmol). The three compounds exhibited hydrophilic properties, suggesting renal clearance and low brain uptake, although hydrophilicity was somewhat reduced for [^{68}Ga]GaJMV7253 due to the adjunction of the non-natural amino acid trimethylsilylalanine (TMSAla). Saturation studies demonstrated moderate affinities for

NTS_1 and GRPR (Kd values 100-500 nM), which remain lower than the corresponding ^{68}Ga-monomers. JMV7266 branched structure correlated with better affinity compared with the two linear compounds. High levels of internalization were observed at 60 min, mediated by NTS_1 (> 40 %) and GRPR (> 15 %) with very low membrane bindings (< 11 % via NTS1 and < 5% via GRPR). An early intense efflux was observed for [^{68}Ga]Ga-JMV7110 (> 80% at 5 min) and [^{68}Ga]Ga-JMV7253 but efflux was < 40% with [^{68}Ga]Ga-JMV7266. In vivo biodistribution studies on HT29-grafted mice showed moderate tumor uptake (0.44 ± 0.21% ID/g for [^{68}Ga]Ga-JMV7266 and 0.33 ± 0.11% ID/g for [^{68}Ga]Ga-JMV7110) 90 min post-injection. Kidneys showed the highest uptake at 90min (18.3 ± 9.6% ID/g and 19.4 ± 7.4% ID/g). Dynamic PET/CT data are under analysies. **Conclusion:** To our knowledge, the compounds presented in this work are the first radiolabelled heterodimers targeting both NTS_1 and GRPR. Despite moderate affinities, [^{68}Ga]Ga-JMV7110 and [^{68}Ga]Ga-JMV7266 exhibited promising tumor uptake. **References:** None.

OP-0550

Pyridyl-Ala substitution in the third position of somatostatin receptor antagonists: regioisomerisation modulates their biodistribution

R. Mansi, N. Bertarelli, L. Del Pozzo, S. Zanger, H. Maecke, M. Fani; Div. Radiopharmaceutical Chemistry. University Hospital Basel, Basel, SWITZERLAND.

Aim/Introduction: Radiolabeled somatostatin receptor subtype 2 (SST2) antagonists are under clinical evaluation for imaging and treatment of neuroendocrine tumors. A number of promising SST2 antagonists are based on octapeptide format (octreotide), having Tyr in position 3. The crucial role of this position was reported for SST agonists[1]. In the case of SST antagonists, 3-Pyridylalanine (3Pal) in this position was reported to enhance antagonistic potency and to improve hydrophilicity2. We investigated whether replacement of Tyr^3 on the SST2 antagonist DOTA-LM3 (DOTA-pClPhe-c(DCys-Tyr-DAph(Cbm)-Lys-Thr-Cys)-DTyr-NH_2) by 3Pal^3 has any significant influence, and whether the regioisomers 2Pal and 4Pal impact differently. DOTA-[2Pal^3]-LM3, DOTA-[3Pal^3]-LM3 and DOTA-[4Pal^3]-LM3 were studied comparatively to DOTA-LM3, shown to be very promising for therapy labeled with Lu-177[3]. **Materials and Methods:** All conjugates were synthesized on solid phase and labeled with Lu-177. Their hydrophilicity and their in vitro cellular uptake on HEK cells stably transfected with the human SST2 (HEK-SST2) were determined. Saturation binding studies were performed on cell membranes at 37°C using increased concentrations, ranging from 0.075 to 10 nM. Head-to-head SPECT/CT images were acquired in HEK-SST2 xenografts at 4h p.i. for all four ^{177}Lu-conjugates. Results: The hydrophilicity of [^{177}Lu]Lu-DOTA-[xPal^3]-LM3 increased in the order of 2Pal<3Pal<4Pal (logD=-2.3±0.1 -2.5±0.1 and -2.6±0.1, respectively), being similar or significantly higher than [^{177}Lu]Lu-DOTA-LM3 (logD=-2.3±0.1). All three Pal-radiotracers showed higher cellular uptake than [^{177}Lu]Lu-DOTA-LM3 (77-83% vs 67%, respectively after 4h at 37°C). Saturation binding studies indicated a trend of affinity improvement by 2Pal<3Pal<4Pal (K_D= 0.18±0.02, 0.15±0.01 and 0.11±0.01 nM, respectively), being at the end similar to [^{177}Lu]Lu-DOTA-LM3 (K_D= 0.09±0.02 nM). Surprisingly, despite similar accumulation in the SST2-positive tumors seen in SPECT/CT images, differences were observed in the body distribution. [^{177}Lu]Lu-DOTA-[2Pal^3]-LM3 displayed the best tumor-to-background and tumor-to-kidney ratios, being comparable to [^{177}Lu]Lu-DOTA-LM3. [^{177}Lu]Lu-DOTA-[3Pal^3]-LM3 accumulated mainly in the kidney, while [^{177}Lu]Lu-DOTA-[4Pal^3]-LM3 is additionally accumulated in the abdomen, possibly due to SST2-positive organs. **Conclusion:** Replacement of Tyr^3 by Pal^3 isomers on DOTA-LM3 leads to radiolabeled somatostatin antagonists that compare well with [^{177}Lu]Lu-DOTA-LM3 in terms of affinity and SST2-mediated in vitro uptake. Interestingly, this small structural modification seems to impact on their total body distribution. Further in vivo investigations are in progress to assess which Pal-analog presents the best pharmacokinetic properties in terms of tumor uptake and retention for potential clinical translation. **References:** 1.Ginj M et al. Chemistry & Biology. 2006;13:10812.Hocart SJ et al. J Med Chem. 1998;41:11463.Baum R et al. J Nucl Med. 2021 [ahead of print]

OP-0551

Biodistribution and pharmacokinetics of Zr^{89}-antiVEGF mAbs using PET in glioblastoma rat models

D. Rey Bretal[1], L. García Varela[1], X. García Otero[2,3], N. Gómez Lado[1], A. Moscoso[2], M. Piñeiro Fiel[1,2], C. Mondelo García[3,4], A. Costoya Sánchez[1], A. Fernández Ferreiro[3,4], J. Silva Rodríguez[2], Á. Ruibal[1,2], P. Aguiar[1,2];

[1]Molecular Imaging Group, Department of Radiology, Faculty of Medicine, University of Santiago de Compostela (USC), IDIS, Campus Vida, 15782, Santiago de Compostela, SPAIN, [2]Nuclear Medicine Department and Molecular Imaging Group, IDIS and University Hospital Santiago de Compostela (CHUS), Travesía da Choupana s/n, 15706, Santiago de Compostela, SPAIN, [3]Pharmacy Department, University Clinical Hospital of Santiago de Compostela (SERGAS), 15706, Santiago de Compostela, SPAIN, [4]Pharmacology Group, Health Research Institute of Santiago de Compostela (FIDIS), 15706, Santiago de Compostela, SPAIN.

Aim/Introduction: Bevacizumab and Aflibercept are monoclonal antibodies (mAbs)-based therapies used in clinical oncology since they bind to the vascular endothelial growth factor (VEGF), which is related to the angiogenesis processes implicated in brain tumor proliferation. Although these antiVEGF-based therapies have shown to be advantageous for patients with glioblastoma [1,2], their systemic distribution and pharmacokinetic has been

poorly studied. Our study aims to evaluate the in vivo biodistribution and pharmacokinetics of Zr^{89}-Bevacizumab and Zr^{89}-Aflibercept using PET in a rat model of glioblastoma. **Materials and Methods:** Rat models of glioblastoma were inducted in 6 male Sprague-Dawley rats by injecting 100.000 F98 cells in the frontal cortex of the brain. The animals were then injected with either Zr^{89}-Bevacizumab (n=3) or Zr^{89}-Aflibercept (n=3) and multiple follow-up PET scans were performed on 7, 11, 14, 18 and 21 days post tumor induction. PET images were analyzed using predefined VOIs of the W. Schiffer Rat Brain atlas and a specific VOI covering the tumor and other organs such as the liver. The uptake of the tracer inside the tumor was reported as a tumor-to-brain ratio obtained from SUV(Tumor)/SUV(Cerebellum) and the uptake in other organs was reported as SUV values. The elimination rate of the tracers was calculated by dividing the total radioactivity concentration of a whole-body VOI and volume by the injected dose. Results: Zr^{89}-Bevacizumab showed a tumor-to-brain ratio of 1,32±0,19 at day 7 which increased up to 2,74±0,49 at day 11; 2,72±0,62 at day 14; 3,14±0,65 at day 18 until a value of 3,02±0,33 at day 21. However, Zr^{89}-Aflibercept did not cross the blood-brain barrier (BBB), thus it did not show any uptake inside the tumor [tumor-to-brain ratio of 0,63±0,03 not exceeding 8,7% increase]. At systemic level, elimination rate of the two antiVEGF were similar [0,24 for Zr^{89}-Bevacizumab and 0,20 for Zr^{89}-Aflibercept]. Zr^{89}-Aflibercept showed higher SUV in the liver at day 7 [SUV= 2,14±0,38] than Zr^{89}-Bevacizumab [SUV= 1,03±0,27]. At day 21, Zr^{89}-Aflibercept maintained a greater accumulation in the liver [SUV= 0,68±0,12 vs SUV= 0,49±0,09]. **Conclusion:** Our results suggest that Bevacizumab remains in blood circulation for longer time-period and is able to cross the BBB at early stages of tumor development, being, therefore, a more adequate antiVEGF therapy to treat glioblastomas than Aflibercept. **References:** 1. Jansen MHA, Lagerweij T, et al. Mol Cancer Ther. 2016;15(9):2166-742. 2. de Groot JF, Lamborn KR, et al. J Clin Oncol. 2011;29(19):2689-95

OP-0552

Proof-of-concept of a pretargeting strategy mediated by sstr2 antagonist for the therapy of neuroendocrine tumours

***S. Koustoulidou**, M. Handula, J. Nonnekens, M. Hendriks-de Jong, Y. Seimbille;*
Erasmus MC, Rotterdam, NETHERLANDS.

Aim/Introduction: Peptide receptor radionuclide therapy with somatostatin (sst) analogues has been largely used for the treatment of patients with neuroendocrine tumours (NETs). Somatostatin receptor subtype 2 (sstr2) is the most commonly expressed subtype and hence, several targeting peptides (mostly agonists) have been developed. More recently, a number of reports have shown that radiolabelled sstr2 antagonists demonstrate a better tumour targeting in both pre-clinical and clinical setting. However, accumulation of such peptides in healthy organs could be a dose-limiting factor. In contrast to direct targeting, the pretargeting approach, based on the bioorthogonal inverse electron-demand Diels-Alder (IEDDA) reaction between tetrazine (Tz) and trans-cyclooctene (TCO), has shown a lot of promise as an alternative strategy since it allows safer administration and potentially more effective therapy. Taken together, the aim of this study was to investigate whether the pretargeting approach could work with such peptides in various sstr2-positive in vitro models. **Materials and Methods:** The sstr2 antagonist JR11 was covalently modified with a TCO group and a small molecule containing a DOTA chelator. The Tz molecule was labelled with $^{111}InCl_3$. Binding affinity of JR11-TCO and the reference JR11 were analysed using purified membrane expressing sstr2. The pretargeting approach was validated in the same purified membrane using a filtration-based assay, as well as in U20S +sstr2 cells and in cryosections (H69 xenograft tumours). Results: The binding affinity of JR11-TCO was lower than the reference peptide JR11 (IC_{50}: 10^{-6} M vs 10^{-8} M, respectively). The in vitro assays proved the ability of JR11-TCO and the labelled tetrazine to click in all three experimental setups. More specifically, in purified membrane the percentage (%) added dose of ^{111}In-labelled Tz that reacted with the TCO-modified peptide JR11 was significantly higher than the refence peptide JR11 (4.9 ± 0.2 vs 2.32 ± 0.09 %, respectively). Same significant ratio was observed in H69 tumour sections. In U2OS +sstr2 cells, the overall uptake values were lower but still significantly different between JR11-TCO and JR11 (0.036 ± 0.003 vs 0.018 ± 0.003), probably due to the higher expression of sstr2 in purified membrane. **Conclusion:** To our knowledge, this is the first report of IEDDA-based pretargeting concept in vitro using small molecules, such as the sstr2 antagonist JR11. Such strategy might pave the way for a more effective therapy of NETs in the future. **References:** none

OP-0553

Physiologically Based Pharmacokinetic Models to Predict Organ and Tumor Distribution and Assess the Tumor Sink Effect of ^{68}Ga-DOTATATE and ^{68}Ga-HA-DOTATATE in Patients with Gastroenteropancreatic Neuroendocrine Tumors

***H. Siebinga**[1,2], B. de Wit-van der Veen[2], T. P. Dorlo[1], A. D. Huitema[1,3,4], J. J. Hendrikx[1,2];*
[1]Department of Pharmacy & Pharmacology, Netherlands Cancer Institute, Amsterdam, NETHERLANDS, [2]Department of Nuclear Medicine, Netherlands Cancer Institute, Amsterdam, NETHERLANDS, [3]Department of Clinical Pharmacy, University Medical Center Utrecht, Utrecht, NETHERLANDS, [4]Department of Pharmacology, Princess Máxima Center for Pediatric Oncology, Utrecht, NETHERLANDS.

Aim/Introduction: Uptake differences and similarities of ^{68}Ga-labeled somatostatin analogues have been described previously. However, more insights into the underlying biological and chemical causes for these (dis)similarities are of interest to increase tumor uptake while limiting organ uptake for both diagnosis and therapy. In addition, the effect of total tumor volume on organ uptake is still unclear. Envisaging these potentials, the aim of this research was to develop physiologically based pharmacokinetic (PBPK) models to describe and compare organ and tumor distribution of ^{68}Ga-DOTATATE and ^{68}Ga-HA-DOTATATE and to demonstrate and predict the relevance of a potential tumor sink effect in patients with neuroendocrine tumors (NETs). **Materials and Methods:** Two PBPK models were developed for ^{68}Ga-DOTATATE and ^{68}Ga-HA-DOTATATE separately using PK-Sim and MoBi® open software tools. Three tumor compartments were added, representing primary tumor, liver metastases and other metastases. Furthermore, reactions describing somatostatin receptor (SSTR) binding, internalization and recycling, renal clearance and intracellular degradation were added to the model. Patients with gastroenteropancreatic (GEP) NET who received whole-body ^{68}Ga-DOTATATE or ^{68}Ga-HA-DOTATATE PET/CT on clinical indication were included for validation of PBPK model predictions. Scans were performed at 45 minutes after injection of ~100 MBq ^{68}Ga-(HA)-DOTATATE. Image-based tumor, organ (spleen, liver, thyroid) and blood activity levels were derived (MBq/mL) and corresponding peptide concentrations (µg/mL) were calculated. Results: Data of 39 and 59 GEP-NET patients receiving ^{68}Ga-DOTATATE or ^{68}Ga-HA-DOTATATE, respectively, were included. Mean±SD total peptide amounts and administered radioactivity were 13.1±2.18 µg and 85.8±16.0 MBq for ^{68}Ga-DOTATATE and 6.06±2.26 µg, and 85.7±14.1 MBq for ^{68}Ga-HA-DOTATATE. Minimum and maximum ranges were applied to administered peptide amounts, SSTR organ amounts, tumor blood flow and tumor blood volumes, resulting in model predictions representative for the population. Validations showed that these models adequately described image-based patient data. Sensitivity analysis indicated that input parameters tumor blood flow and tumor blood volume had high impact on tumor distribution. Tumor sink predictions showed decreasing maximum accumulation in spleen with increasing total tumor volume, independent of the tracer (decrease of 25.8% with 1500 mL total tumor volume). However, at clinically relevant tumor volumes (<500mL) only a slight decrease in spleen uptake was predicted (10.5%), indicating an almost neglectable tumor sink effect for most patients. **Conclusion:** The developed PBPK models adequately predicted tumor and organ uptake for this GEP-NET population. Furthermore, predictions with increasing tumor volume showed that for the majority of patients a tumor sink effect on organ uptake is not expected. **References:** None.

OP-0554

Automated preparation and preclinical evaluation of ^{68}Ga-labelled DOTA-MGS5 for PET/CT imaging of CCK2R expressing tumours

A. Hörmann, M. Klingler, C. Rangger, C. Mair, C. Decristoforo, C. Uprimny, I. Virgolini, E. von Guggenberg;
Medical University of Innsbruck, Innsbruck, AUSTRIA.

Aim/Introduction: The novel minigastrin (MG) analogue DOTA-DGlu-Ala-Tyr-Gly-Trp-(N-Me)Nle-Asp-1-Nal-NH_2 (DOTA-MGS5) with enhanced tumour targeting and improved tumour-to-kidney ratio is a promising new candidate for targeting cholecystokinin-2 receptor (CCK2R)-expressing tumours. This receptor is expressed at high incidence in medullary thyroid carcinoma (>90%), small cell lung cancer (>50%) and other tumours. Aiming towards the clinical translation of ^{68}Ga-labelled DOTA-MGS5 (^{68}Ga-DOTA-MGS5) for PET/CT imaging an automated synthesis process was validated and specific preclinical studies were performed. **Materials and Methods:** The validation of the radiolabelling process was carried out using a cassette-based automated synthesis module, DOTA-MGS5 in GMP quality and a pharmaceutical ^{68}Ge/^{68}Ga-generator. Product specifications and analytical procedures were defined according to European Pharmacopoeia monographs available for other ^{68}Ga-labelled radiopharmaceuticals. The receptor specific cell uptake of ^{68}Ga-DOTA-MGS5 was studied using AR42J and A431-CCK2R cells, including blocking experiments and evaluation of the interaction with other receptors. Pharmacokinetic biodistribution studies up to 90 min after injection were carried out in BALB/c mice. An extended single-dose toxicity study was conducted in Wistar rats in a GLP-compliant laboratory. Results: The automated preparation of ^{68}Ga-DOTA-MGS5 was accomplished within 35 min and the final product fulfilled the defined acceptance criteria with a radiochemical purity of >91% up to 3 h post preparation. A high cell uptake of 52% in A431 cells stably transfected with human CCK2R and 33% in AR42J cells expressing rat CCK2R was observed at 2 h after incubation. Efficient blocking of the cell uptake was achieved by co-incubation with pentagastrin and proglumide, whereas no blockage with octreotide or bombesin was observed. ^{68}Ga-DOTA-MGS5 showed a favourable biodistribution profile in mice with rapid blood clearance and renal excretion. An effective dose of ~0.01 mSv/MBq comparable to other ^{68}Ga-labelled ligands was extrapolated to humans. From the toxicity study in rats, the safe administration of a dose of 50 µg DOTA-MGS5 was established for the clinical use. **Conclusion:** ^{68}Ga-DOTA-MGS5 was produced at high quality using an automated synthesis module allowing the clinical use. Preclinical testing revealed a low risk connected with the intravenous administration of ^{68}Ga-DOTA-MGS5. The potential of this promising new PET imaging agent is currently investigated in patients with advanced CCK2R-expressing tumours. **References:** Klingler M et al., J Nucl Med 2019; 60:1010-1016; Uprimny C et al., EJNMMI 2021; 48:935-936

OP-0555

Development and Pre-clinical evaluation of a novel hybrid peptide analog based on Mucin1 ^{68}Ga-NODAGA-MUC1 and ^{68}Ga-NODAGA-MUC1-FA hybrid peptide conjugates and Folic acid: Potential breast/ovarian cancers PET imaging agent

I. Aljammaz[1], S. Alhabardi[2], B. Alotaibi[1], S. Okarvi[1];
[1]King Faisal Specialist Hospital and Research centre, Riyadh, SAUDI ARABIA, [2]King Saud University, Riyadh, SAUDI ARABIA.

Aim/Introduction: Epithelial mucin1 (MUC1) and folic acid (FA) are overexpressed by most epithelial cancers hence attracting increasing interest as potential targets for imaging and therapy. The high expression of MUC1 and FA on breast and ovarian cancers and low expression on normal tissues makes them potential targets for diagnosis and therapy of cancers. To develop an efficient ^{68}Ga-labeled radiopharmaceutical with enhanced breast/ovarian cancer targeting capacity we have designed and synthesized a novel MUC1-derived peptide and also conjugated MUC1 to FA in order to formulate MUC1-FA hybrid peptide conjugate for targeting MUC1/FA receptors. **Materials and Methods:** MUC1 and hybrid MUC1-FA were prepared by solid-phase synthesis following Fmoc/HBTU method. FA was attached to MUC1 via terminal Lys by manual conjugation. The key precursors NODAGA-MUC1 and NODAGA-MUC1-FA hybrid peptide (20 µg each) were reacted with solutions of $^{68}GaCl_3$ (37-300 MBq) in acetate buffer (pH ~4.5) at 90°C and different time range. In vitro receptor binding studies were performed on KB cell lines and biological evaluation was done in normal Balb-c and nude mice bearing KB cells xenografts. Results: Work up of these conjugates gave ^{68}Ga-NODAGA-MUC1 and ^{68}Ga-NODAGA-MUC1-FA hybrid peptide conjugates in almost quantitative radiochemical yield and purity as assessed by TLC and HPLC in less than 20 min. In vitro tests have shown that a significant amount of the ^{68}Ga-NODAGA-MUC1 and ^{68}Ga-NODAGA-MUC1-FA hybrid peptide conjugates are associated with cancer cell fractions. In vivo characterization in normal mice revealed rapid blood clearance of both conjugates with excretion predominantly by urinary pathway. Biodistribution of ^{68}Ga-NODAGA-MUC1 and ^{68}Ga-NODAGA-MUC1-FA hybrid peptide conjugates in nude mice bearing KB xenografts demonstrated significant tumor uptakes (2.8% and 13% ID/g, respectively). These uptakes were blocked by excess co-injection of FA and MUC1, suggesting a receptor-mediated process. In vivo imaging using animal PET/CT is in progress and will be reported. **Conclusion:** These results demonstrate that ^{68}Ga-NODAGA-MUC1 and ^{68}Ga-NODAGA-MUC1-FA hybrid peptide conjugates may be useful as molecular probes for detecting and staging ovarian and breast cancers and their metastasis as well as monitoring tumor response to treatment and deserves further evaluation. **References:** None

OP-0556

Al^{18}F-3p-C-NETA-TATE: Combining a versatile and highly effective chelator with an established somatostatin analogue

S. Ahenkorah[1], E. Murce[2], Y. Seimbille[2], T. Cardinaels[3], C. M. Deroose[4], G. Bormans[1], M. Ooms[3], F. Cleeren[1];
[1]KU Leuven, Leuven, BELGIUM, [2]Erasmus MC, Rotherdam, NETHERLANDS, [3]SCK CEN, Mol, BELGIUM, [4]UZ Leuven, Leuven, BELGIUM.

Aim/Introduction: Somatostatin-based radiopharmaceuticals (e.g. [^{68}Ga]Ga-DOTATATE and [^{177}Lu]Lu-DOTATATE) have been used to diagnose, monitor, and treat neuroendocrine tumour patients with great success. [^{18}F]AlF-NOTA-octreotide, a promising ^{18}F-labeled somatostatin analogue and potential alternative for ^{68}Ga-DOTA-peptides, is under clinical evaluation.[1] Ideally, the same precursor (combination of chelator-linker-vector) can be used for production of both diagnostic and therapeutic radiopharmaceuticals with very similar (e.g. Al^{18}F/^{213}Bi/^{177}Lu) or identical (e.g. complementary Tb-radionuclides) pharmacokinetic properties, allowing accurate, personalised dosimetry estimation and radionuclide therapy of NET patients.[2] In this study we evaluate the versatile and highly effective chelator 3p-C-NETA[3] and present first results of radiosynthesis and stability of Al[^{18}F]F-3p-C-NETA-TATE. **Materials and Methods:** 3p-C-NETA was radiolabelled with diagnostic (^{68}Ga, Al^{18}F) or therapeutic (^{177}Lu, ^{161}Tb,^{213}Bi) radionuclides at different temperatures. The in vitro stability of the corresponding radiocomplexes was determined in PBS and human serum at 37 °C. 3p-C-NETA-TATE was synthesised using standard solid-phase peptide synthesis and purified using HPLC. Al[^{18}F]F-3p-C-NETA-TATE was synthesised in an automated AllInOne module and analysed using radio-HPLC. Finally, the in vitro stability of Al[^{18}F]F-3p-C-NETA-TATE was evaluated in formulation buffer, PBS and human serum at 37 °C. Results: 3p-C-NETA was efficiently labelled with ^{177}Lu and ^{213}Bi (RCY>95%) at room temperature and with ^{161}Tb (>95%) and ^{68}Ga (>90%) at 55 °C. Al^{18}F-labeling required a higher temperature of 95 °C to achieve good yields (>85%). The ^{177}Lu- and ^{161}Tb-3p-C-NETA-complex showed excellent in vitro stability in both PBS and human serum over a period of eight days (97% intact). We also observed high in vitro stability up to 2 h for Al[^{18}F]F-3p-C-NETA-TATE (>93% intact in PBS and human serum). In contrast, [^{68}Ga]Ga-3p-C-NETA was stable in PBS (>90% intact), but not in human serum (only 60% intact after 2h). Al[^{18}F]F-3p-C-NETA-TATE was obtained in good RCY (56%) and radiochemical purity (98%). Al[^{18}F]F-3p-C-NETA-TATE displayed excellent in vitro stability with >95% intact tracer after 4 hours in all tested conditions. **Conclusion:** 3p-C-NETA is an excellent chelator that can be used for both targeted radionuclide therapy (^{177}Lu, ^{213}Bi and ^{161}Tb) and diagnostic applications (Al^{18}F) and has the potential to replace DOTA analogues in current clinical use. Al[^{18}F]F-3p-C-

NETA-TATE will be further evaluated using μPET/MRI imaging in healthy rats and SSTR2 positive tumour mice, in a head-to-head comparison with Al^{18}F-NOTA-octreotide. **References:** 1. Pauwels E, et al. Eur J Nucl Med Mol Imaging 2020, 47, 3033-46. 2. Ahenkorah S, et al. Pharmaceutics 2021, 13, 599. 3. Chong HS, et al. Bioorg Med Chem Lett. 2008, 18, 3436-9.

OP-0557

99mTc-HYNIC-LHRH analog as novel breast cancer imaging agent

L. Alfaya[1], X. Camacho[1], F. García[1], M. Cabrera[1], M. Tassano[1], M. Fernández[1], T. Freire[2], E. Osinaga[3], J. Gambini[4], P. Cabral[1];
[1]Centro de Investigaciones Nucleares, Facultad de Ciencias, Universidad de la República, Montevideo, URUGUAY, [2]Facultad de Medicina, Universidad de la República, Montevideo, URUGUAY, [3]Instituto Pasteur de Montevideo; Facultad de Medicina, Universidad de la República, Montevideo, URUGUAY, [4]Hospital de Clínicas, Facultad de Medicina, Universidad de la República, Montevideo, URUGUAY.

Aim/Introduction: Breast cancer is the most common and the leading cause of death-related cancer in women in the developed world . It has been proved that luteinizing hormone-releasing hormone (LHRH or GnRH) receptors are overexpressed in this pathology, and different agonists and antagonists of LHRH have been used for its treatment . We therefor aimed to developed a radiolabeled LHRH analog (HYNIC-GSG-(DLys6-LHRH) with 99mTc using different co-ligands; comparing radiochemical purity, hydrophobicity and stability over time. In vitro studies with different breast cancer cell lines were performed to evaluate the ability of 99mTc-GSG-HYNIC-(DLys6)LHRH to detect breast cancers overexpressing the LHRH receptor. **Materials and Methods:** HYNIC-GSG-LHRH (D-Lys)(C72H100N24O18) was acquired from Siquimia Srl. (Uruguay). 99mTc labeling was achieved at 50ºC, in the presence of different co-ligands (Tricine, Tricine/Nicotinic Acid (AN); ethylenediaminediacetic acid (EDDA) and Tricine/EDDA). Radiolabeling conditions were optimized to achieve the highest radiochemical purity (≥98%), evaluated by HPLC and ITLC. Log P and stability in serum and L-Cysteine were evaluated up to 4 h. In vitro cell binding studies were done in different human breast cancer cell lines (MDA-MB-231, MDA-MB-435, MCF-7, BT-474) as well as in normal murine fibroblasts (NIH-3T3) as negative control and murine breast cancer cell lines (4T1), up to 60 min. Biodistiribution studies were developed in normal and in 4T1 tumor-bearing Balb/c mice, up to 24 h p.i., using a high purity germanium detector (HPGe) (Canberra) with 20% counting efficiency (at 1332 keV). Spectra were analyzed off-line using Genie 2000 v 3.2. Results: 99mTc-HYNIC-GSG-(DLys6-LHRH)/Tricine/AN complex proved to be easy to label (radiochemical purity of 99.83 ± 0.29 % by HPLC and 99.50 ± 0.17 % by ITLC, 20 min at 50 ºC), with good hydrophilicity (Log P= -2.82 ± 0.04) and stable in vitro (radiochemical purity of >95% in PBS, >90% in BSA and >90% in L-Cysteine over 4 h. at 37ºC). The affinity and specificity of the binding in different breast cancer cell lines (MCF-7, MDA-MB-231, MDA-MB-435, BT-474 and 4T1) was evaluated, yielding good membrane-bound results in all of them, and high specificity, with little internalization for all cell lines. Biodistribution in normal Balb/c and 4T1 tumor-bearing mice revealed high kidney and relevant tumor uptake. **Conclusion:** Our data suggest that the use of the 99mTc-HYNIC-GSG(D-Lys6-LHRH)/Tricin/NA complex represents a potential molecular imaging agent for the diagnosis of LHRH receptor-expressing breast cancers, which would lead to selective targeting. Key words: LHRH, GnRH, Breast Cancer, Molecular Imaging, 99mTechnectium. **References:** None

1109

Wednesday, October 20 - Saturday, October 23, 2021

on-demand pool, release on Wednesday, October 20 at 09:00

Cutting Edge Science Track - Featured Session: Software Developments in Total Body PET

OP-0559

Software Developments in Total Body PET

K. Shi; Inselspital, University of Bern, Bern, SWITZERLAND.

OP-0560

176Lu detection for daily PET quality control: initial clinical experiences

S. McQuaid, J. C. Dickson;
Institute of Nuclear Medicine, UCLH, London, UNITED KINGDOM.

Aim/Introduction: The emissions from the ^{176}Lu present in LSO PET crystals can be utilised for monitoring PET performance and stability, without the need for an external source [1]. This feature is implemented in our PET-CT system (Siemens Vision 600) and has been used for daily PET QC in our department for 18 months. The purpose of this work was to establish the reliability of this PET QC approach and to compare its output with the conventional ^{68}Ge cylinder based QC. **Materials and Methods:** The ^{176}Lu QC acquisition was performed before every day of clinical use, except when ^{68}Ge QC was required for periodic tuning. Results from both QC methods were extracted and and assessed for concordance in overall outcomes and trend pattern agreement. The approaches produce different outputs, preventing individual parameter comparison, but trends in parameter outputs were assessed individually to indicate overall system performance and determine whether the approaches gave comparable findings. Results: The outputs of 436 ^{176}Lu and 76 ^{68}Ge QC results acquired over 18 months were analysed. In this period the ^{176}Lu QC produced a fail outcome on 4 occasions. Each ^{176}Lu QC failure was immediately followed by ^{68}Ge QC, which

also produced a fail outcome on these occasions. All were confirmed to be true PET-related issues (2 were PET blocks not producing an output, and 2 were communication issues, preventing the PET system acquiring correctly. All required corrective action before recommencing clinical scanning). The concordance in outcomes indicates there were no false positives in the ^{176}Lu QC failures. Similarly, no false negatives (i.e. image quality issues arising not being identified through QC procedures) were found. No impact of ^{68}Ge tuning on quantitative ^{176}Lu output parameters was detected, although notably, the ^{176}Lu QC output parameters were stable over this duration and hence not expected to be affected by tuning. The system sensitivity (monitored via ^{68}Ge QC, since the ^{176}Lu QC does not measure this directly) was also stable; further monitoring would therefore be required to ascertain the impact of any sensitivity changes on ^{176}Lu QC outputs. **Conclusion:** QC outcomes using intrinsic ^{176}Lu measurements agreed with conventional ^{68}Ge external source QC, with all failures in PET performance being correctly identified. The reliability of this approach means it is a practical alternative to conventional PET QC methods, with ^{68}Ge acquisitions required only periodically for tuning and sensitivity measurement purposes. **References:** [1] Conti et al Phys. Med. Biol, 2017

OP-0561

Development and evaluation of a CT-less reconstruction framework for long-axial FOV PET scanners using LSO background radiation

H. Sari[1,2], M. Teimoorisichani[3], C. Mingels[2], I. Alberts[2], V. Panin[3], D. Bharkhada[3], K. Shi[2], A. Rominger[2], M. Conti[3];
[1]Siemens Healthineers A.G., Lausanne, SWITZERLAND, [2]Department of Nuclear Medicine, Inselspital, Bern, SWITZERLAND, [3]Siemens Medical Solutions USA Inc., Knoxville, TN, UNITED STATES OF AMERICA.

Aim/Introduction: Lutetium-based scintillators are widely used in the present generation of PET scanners. Radioisotope ^{176}Lu, present in natural occurring Lu, emits γ photons at 307 and 202 keV. The high sensitivity of long-axial FOV PET scanners can be utilized to detect the background LSO radiation (LSO-TX). In this work, we use LSO-TX together with a deep-learning and maximum-likelihood activity and attenuation correction factors estimation (MLACF) based method to generate attenuation maps (μ-maps) with no CT information. **Materials and Methods:** Biograph Vision Quadra (Siemens Healthineers) PET/CT scanner was used to acquire 5-min of LSO-TX at 202 and 307 keV from 9 patients using a special acquisition protocol. Following the LSO-TX acquisition, patients had an intravenous administration of ^{18}F-FDG and PET data were acquired for 65 minutes. Only the 55-65 mins p.i. portion of PET data was used in this work. A second 5-minute LSO-TX acquisition was performed at the end of the PET acquisition. We refer to LSO-TX data acquired before and after the PET scans as cold LSO-TX and hot LSO-TX data respectively. CT images were also obtained at each study. Using the recorded LSO-TX events, μ-maps were generated using maximum likelihood for transmission tomography (MLTR) algorithm. These μ-maps were then denoised using a U-Net convolutional neural network, where the data were split to 7 training and 2 testing data. Two separate networks were trained using the cold and hot LSO-TX datasets. The denoised μ-maps were fed into a MLACF method to generate ACFs and PET images. The ACF sinograms were then used to reconstruct final patient μ-maps at 511 keV. For comparison purposes, PET images were also reconstructed using PSF-TOF method with CT-based μ-maps. PET images were normalized to average uptake in the liver for a quantitative analysis. Results: No significant difference was observed between μ-maps derived from cold and hot LSO-TX data. A good agreement between average ACFs in different organs was observed between LSO-TX derived μ-maps and CT derived μ-maps. Similarly, average normalized UVs in different organs agreed well with less than 5% error in lung, kidney, aorta, heart, and spleen. PET images reconstructed using LSO-TX based μ-maps underestimated mean whole brain UV by 19%. **Conclusion:** We presented a method which utilizes LSO-TX data and a deep-learning based approach to generate CT-free attenuation maps in long-axial FOV PET scanners. Work in progress includes fine tuning and further assessment of the method with more datasets. **References:** None

OP-0562

Development of a deep learning method for CT-free correction for an ultra-long axial field of view PET scanner

S. Xue[1], K. Bohn[1], R. Guo[2], H. Sari[3], M. Viscione[1], A. Rominger[1], B. Li[2], K. Shi[1];
[1]University of Bern, Bern, SWITZERLAND, [2]Shanghai Jiaotong University, Shanghai, CHINA, [3]Siemens Healthcare AG, Lausanne, SWITZERLAND.

Aim/Introduction: The possibility of reduced ionization dose of ultra-high-sensitivity total-body PET makes computed tomography (CT) a critical radiation burden in clinical applications. Artificial intelligence has shown the potential to generate PET images from non-corrected PET images. Our aim in this work is to develop a CT-free correction for an ultra-long field of view (FOV) PET scanner. **Materials and Methods:** Whole body PET images of 165 patients scanned with a digital regular FOV PET scanner (Siemens Biograph Vision in Shanghai and Bern) was included for the development and testing of the deep learning methods. Furthermore, the developed algorithm was tested on data of 7 patients scanned with an ultra-long axial FOV scanner (Siemens Biograph Vision Quadra in Bern). A 2D generative adversarial network (GAN) was developed featuring a residual dense block, which enables the model to fully exploit hierarchical

features from all network layers. The normalized root mean squared error (NRMSE) and peak signal-to-noise ratio (PSNR), were calculated to evaluate the results generated by deep learning. Results: The preliminary results showed that, the developed deep learning method achieved an average NRMSE of 0.4±0.3% and PSNR of 51.4±6.4 for the test on Biograph Vision, and an average NRMSE of 0.5±0.4% and PSNR of 47.9±9.4 for the validation on Biograph Vision Quadra, after applied transfer learning. **Conclusion:** The developed deep learning method to shows the potential for CT-free correction for an ultra-long FOV PET scanner. Work in progress includes clinical assessment of PET images by independent nuclear medicine physicians. Training and fine-tuning with more datasets will be performed to further consolidate the development. **References:** None

OP-0563

Dynamic total-body ^{18}F-FDG parametric imaging on a long-axial FOV PET/CT scanner

H. Sari[1,2], J. Hu[3], C. Mingels[2], I. Alberts[2], J. Hong[2], V. Panin[3], L. Eriksson[3], M. Conti[3], K. Shi[2], P. Cumming[2,4], A. Rominger[2];
[1]Siemens Healthineers AG, Bern, SWITZERLAND, [2]Department of Nuclear Medicine, Inselspital, Bern, SWITZERLAND, [3]Siemens Medical Solutions USA, Inc., Knoxville, TN, UNITED STATES OF AMERICA, [4]School of Psychology and Counselling, Queensland University of Technology, Brisbane, AUSTRALIA.

Aim/Introduction: The introduction of long-axial FOV scanners with SiPM-based PET technology has enabled high temporal and spatial resolution imaging with increased sensitivity, thus opening new frontiers in dynamic total-body PET imaging. In this work, we explore the feasibility of direct and indirect parametric image generation on ^{18}F-FDG datasets acquired using a long-axial FOV PET/CT system, and present an initial comparison of parametric images and routine SUV images. **Materials and Methods:** Twelve oncological patients underwent a 65-minute PET acquisition on a Biograph Vision Quadra PET/CT scanner (Siemens Healthineers), initiated upon intravenous bolus injection of ^{18}F-FDG. Images were reconstructed using PSF-TOF with 4 iterations and 5 subsets and a 2 mm Gaussian filter was applied. Image-derived input functions (IDIFs) were extracted from the descending aorta using a 10 mm diameter cylinder placed in the center of the structure. Influx (K_i) and distribution volume (DV) images were generated using (i) direct Patlak reconstruction method (40-65 min post injection), based on the nested EM algorithm[1], (ii) indirect Patlak method (40-65 min post injection) and (iii) two-tissue compartmental (2TC) model (0-65 min), whereas $K_i=(K_1*k_3)/(k_2+k_3)$. Conventional SUV images (55-65 min post injection) were also reconstructed for purposes of comparison. Contrast-to-noise (CNR) and target-to-background ratio (TBR) metrics were used to perform a quantitative comparison of K_i maps and SUV images. Results: Visual comparison of parametric and SUV images showed reduced background in the direct K_i images compared against SUV, indirect K_i, and 2TC derived K_i images. K_i images generated using all three methods showed higher TBR in detected lesions (n=4) compared to SUV images. Direct K_i images had the highest CNR in these tumor lesions, showing a 54% increase compared to SUV images. Average CNR computed between brain grey and white matters was highest in the SUV images, followed by direct K_i, 2-TC K_i, and indirect K_i. However, these CNR differences in the brain were not significant (One-way ANOVA, p=0.35). **Conclusion:** The present preliminary results show that ^{18}F-FDG parametric imaging in total-body PET can provide improved visualization of target regions with relatively lower background signal, and thus furnishing better tumor quantitation in oncological PET imaging. Direct Patlak reconstruction has superior noise properties. Future work includes analysis of more tumor types, as well as examining the information present in the microparameter (K_1, k_2, k_3 and k_4) maps. **References:** 1. G. Wang and J. Qi, Phys. Med. Biol., vol. 55, 1505-1517, 2010.

OP-0564

Clinical validation of a population-based input function for dynamic whole-body 18F-FDG multiparametric PET imaging using a standard injector

A. H. Dias[1], D. Pigg[2], A. M. Smith[2], V. Shah[2], L. C. Gormsen[1], O. L. Munk[1];
[1]Aarhus University Hospital, Aarhus, DENMARK, [2]Siemens Medical Solutions USA, Inc., Knoxville, TN, UNITED STATES OF AMERICA.

Aim/Introduction: Recently, an automated dynamic whole-body (D-WB) FDG PET/CT scan protocol has been developed for imaging the metabolic rate of ^{18}FDG (MR_{FDG}) based on the Patlak model, which requires the late (e.g. 50-70 min) D-WB data combined with the full (0-70 min) image-derived input function (IDIF). Our aim was to validate the use of a population-based input function (PBIF) to replace the early part of the IDIF, which will allow for a shorter 20-min multiparametric scan protocol. **Materials and Methods:** Twenty patients were scanned for 70 min using the multiparametric PET scan protocol on a Siemens Biograph Vision 600 (Siemens Healthineers) PET/CT scanner. A Medrad Intego PET infusion system (Bayer) was used for standardized injections of ^{18}FDG. A reference arterial input function (AIF) was measured using invasive arterial blood sampling. An IDIF was automatically extracted from the central part of the descending aorta (from bottom-of-descending-aortic-arch to the liver-centre) using prototype deep-learning organ-segmentation and ALPHA technology (Siemens Healthineers). A PBIF was generated by averaging the 20 fits of time-shifted and normalized AIFs using a multi-exponential model, describing tracer behaviour in the circulation, convolved by the shape of the tracer infusion. For each patient, the PBIF was scaled to the late IDIF values from 50-70 min to obtain an individually scaled PBIF (sPBIF). Results: In all cases visual inspection of

the measurements showed good agreement between IDIF and AIF including around the early peak. Comparing the IDIF to the AIF, Pearsons r and relative difference (rd, mean ± SD, N=20) for the area under the curve (AUC) from 0-60 min was r=0.90, rd=3%±6%; and for the difference between average value of late samples from 50-70 min was r=0.91, rd=3%±8%. For Patlak imaging, the AUC is particularly important because any bias directly affects the MR_{FDG} estimates. Comparing the sPBIF to the IDIF, the correlation was r=0.92, and the relative difference was rd=0.3%±6.6% for the AUC from 0-60 min. **Conclusion:** The high spatial resolution of the Siemens Biograph Vision allows the extraction of an IDIF that closely match an invasively measured AIF. A PBIF scaled the late IDIF can be used as input function for Patlak modelling, which suggest that a short 20-min scan protocol is feasible to appropriately scale the PBIF, which can be used to derive parametric images. **References:** None

OP-0565

Normative tissue FDG uptake values from 112 patients undergoing whole-body dynamic 18F-FDG PET/CT - Validation of automated software tools and a normal value database

A. H. Dias, O. L. Munk, L. C. Gormsen;
Aarhus University Hospital, Aarhus, DENMARK.

Aim/Introduction: Advances in software and PET/CT systems now allows for automated dynamic whole-body (D-WB) PET/CT scans with parametric imaging of rate of tracer uptake (K_i) or metabolic rate of FDG (MR_{FDG}=K_i x blood glucose) based on Patlak linearization. The parametric images reflect metabolic activity more accurately than semiquantitative SUV imaging but the altered image appearance and lesion-to-background patterns necessitate updated reporting practices. The aim of this study was to validate the accuracy of parametric images versus manually calculated Patlak parameters, and to report normal vales for organs, tissues and a select group of pathologies. **Materials and Methods:** The study was a retrospective analysis of prospectively recruited patients (12 diabetic and 100 non-diabetic) spanning a range of malignant and inflammatory diseases. Participants were scanned using a 70-min multiparametric PET acquisition protocol on a Siemens Biograph Vision 600 PET/CT scanner. An image derived input function (IDIF) was automatically extracted from the descending aorta. Parametric images (MR_{FDG}) were reconstructed using data from 50-70min and the IDIF. A standard-of-care static PET image was reconstructed using data from 60-70min. SUV values of healthy tissues were compared with K_i and MR_{FDG}. Volumes of interests (VOIs) were defined on healthy tissues and pathologies, and MR_{FDG} values were extracted from the parametric image and time-activity curves (TACs) from the D-WB series. The TAC and IDIF were used to manually calculate K_i and MR_{FDG}, using PMOD4.0. Results: Normative values of SUV, MR_{FDG} and DV were obtained for the blood, bone, brain grey and white matter, colon, heart, kidney, liver, lung, skeletal muscle, pancreas, spleen and stomach, and a few select pathologies. All values extracted from the parametric images correlated well with manual calculations performed in PMOD ($p<0.0001$) as well as with estimates from the literature. As expected, no correlations were observed between glucose levels and MR_{FDG} in tissues known not to be substrate driven (brain and heart), while tissues with substrate driven glucose uptake had significantly correlated glucose levels and MR_{FDG} values (skeletal muscle, liver and pancreas). By contrast, SUV values were mostly not correlated with glucose levels, with the notable exception of the brain. Also of interest, brain MR_{FDG} was inversely correlated with age confirming previous observations. **Conclusion:** The automated multiparametric ^{18}FDG scan protocol provide images and MR_{FDG} values in agreement with manual calculations and literature values. The technique therefore facilitates both accurate clinical reports and simpler acquisition of precise estimates of whole-body tissue glucose metabolism. **References:** None

OP-0566

Non-invasive method for quantitative measurement of the cerebral glucose metabolic rate

A. Cuculiza Henriksen[1], M. Lonsdale[1], V. Nersesjan[2], D. Kondziella[2], L. Marner[1];
[1]Department of Clinical Physiology and Nuclear Medicine, Copenhagen University Hospital Bispebjerg, Copenhagen, DENMARK, [2]Department of Neurology, Rigshospitalet, Copenhagen University Hospital, Copenhagen, DENMARK.

Aim/Introduction: In dementia, regional cerebral hypometabolism may be diagnosed using a short static [18F] FDG scan with the use of a non-affected reference region. However, global changes seen in systemic illness, traumatic brain damage, or in relation to changes in medication or diet require quantitative measurements as no robust reference region exist. We aimed to develop a non-invasive method to measure the cerebral glucose metabolic rate (CMRglu) with a Gjedde-Patlak plot obtaining an image derived input function (IDIF) from the aorta before and after the cerebral scan in comparison to an arterial input function (AIF). **Materials and Methods:** Six healthy subjects (3 men, age 30-68) were injected with a bolus of 200 MBq [18F] FDG simultaneous with initiation of a three-part dynamic PET consisting of a 15-min-recording of the heart, 40-min-recording of the brain and 2-min-recording of the heart. Concurrently, the AIF was measured in the radial or brachial artery using an on-line automated sampler (Allogg ABSS) for continuous measurement the first 15 min and arterial plasma and whole blood samples the remaining 50 min. Plasma glucose was measured. Regions were drawn in aorta (for IDIF), grey matter, hippocampus and cerebellum and time-activity curves extracted. A triexponential model was used

for fitting the input functions after the peak, and the IDIF was weighted due to frame-length. CMRglu was calculated from a Gjedde-Patlak plot using respectively the IDIF and AIF using Pmod software with lumped constant set to 0.61. Results from the two methods were compared by Wilcoxins signed-rank test, and agreement between the methods was analyzed by a Bland-Altman plot. Results: No significant differences were found between CMRglu using AIF and IDIF as input function (grey matter: 36.5±3.7 vs. 36.2±3.3 µmol/100g/min, p=0.44; Hippocampus: 23.6±2.6 vs. 23.4±2.7 µmol/100 g/min, p=0.84; cerebellum 27.9±3.5 vs. 27.4±3.1 µmol/100 g/min, p=0.22). Further, agreement was excellent with low bias (µmol/100 g/min [95% confidence intervals]) and narrow upper and lower limits of agreement (LoA)(grey matter: Bias:0.33 [-0.45;1.13], LoA_{upper} 1.81 [0.37;3.26], LoA_{lower} -1.15 [-2.59;0.29], hippocampus: Bias:0.20 [-0.38;0.78], LoA_{upper} 1.28 [0.22;2.33], LoA_{lower} -0.89 [-1.94;0.17], cerebellum: Bias:0.48 [-0.27;1.23], LoA_{upper} 1.88 [0.51;3.24], LoA_{lower} -0.92 [-2.28;0.44]. **Conclusion:** A non-invasive three-part dynamic [18F]FDG PET recording allow for reliably measuring CMRglu with an IDIF from aorta. The method allows for quantitative measures in patients with presumed global changes in brain glucose consumption. **References:** none

OP-0567

Population-based input function and image-derived input function for whole-body dynamic 68Ga-DOTATOC-PET/CT acquisition: methodology and clinical validation

P. Thuillier[1,2], D. Bourhis[3,2], J. Metges[4], R. Le Pennec[3,2], U. Schick[5], F. Blanc-Beguin[3,2], S. Hennebicq[3,2], P. Salaun[3,2], V. Kerlan[1,2], N. Karakatsanis[6], R. Abgral[3,2];

[1]Department of Endocrinology, University Hospital of Brest, Brest, FRANCE, [2]EA GETBO 3878, University Hospital of Brest, Brest, FRANCE, [3]Department of Nuclear Medicine, University Hospital of Brest, Brest, FRANCE, [4]Department of Oncology, University Hospital of Brest, Brest, FRANCE, [5]Department of Radiotherapy, University Hospital of Brest, Brest, FRANCE, [6]Department of Radiology, Weil Cornell Medical College of Cornell University, New York, NY, UNITED STATES OF AMERICA.

Aim/Introduction: Whole-body dynamic (WBdyn) acquisition methods in positron-emission tomography (PET) have been proposed to assess the spatio-temporal distribution of radiotracers across the human body. It allows to estimate kinetic parameters of clinical relevance, such as the tracer uptake rate constant Ki (slope), on a voxel-by-voxel basis using Patlak graphical analysis. The resulting Ki images have been reported to assist in lesion detectability and characterization of oncologic diseases, including well-differentiated neuroendocrine tumors (WD-NETs), compared to the standard-of-care SUV-metric alone. However, the challenge of reducing the long acquisition times associated with such methods remains. The purpose of this study is the validation of a population-based input function (PBIF) model allowing to accurately estimate Ki from fewer WB-passes in WBdyn-68GaDOTATOC-PET. **Materials and Methods:** Thirty-seven patients with a suspected or known WD-NETs were included (GAPETNET trial:NTC03576040). All WBdyn 68GaDOTATOC-PET acquisitions were performed on a Biograph Vision 600 system, including a 6min cardiac step followed by 9 WB-passes. Image-derived input functions (IDIFs) were obtained using a region-of-interest automatically defined in the heart left ventricle. Datasets of 20 patients were used to model the PBIF from their IDIF. All IDIF peaks were aligned to the median time-to-peak, normalized to patient weight and administrated activity, and then fitted to an exponential model function using labfit software. The final PBIF was then applied to 17 independent patients studies by scaling it to match the respective IDIF at 3 post-injection time windows: 3rd-7th, 5th-7th and 5th-9th pass ($PBIF_{3-7}$, $PBIF_{5-7}$ and $PBIF_{5-9}$, respectively). The Area Under the Curves (AUCs) of individual IDIF and scaled PBIF were compared one-by-one. Patlak Ki imaging was also performed using IDIF and PBIF, and Ki_{IDIF} and Ki_{PBIF} values were extracted on homogeneous areas of physiological uptake (liver, spleen). Data comparisons were performed using a Bland-Altmann test. Results: The highest IDIF vs. PBIF AUC correlation was found with $PBIF_{3-7}$ [R^2= 0.96(slope=1.00)]. Results using $PBIF_{5-7}$ and $PBIF_{7-9}$ were slightly lower [R^2=0.94(slope=1.01) and R^2=0.93(slope=0.99)]. The mean bias between $PBIF_{3-7}$ and IDIF was -1.5±6.5%[95%CI:-4.9;1.8]. In Ki_{IDIF} vs. Ki_{PBIF} comparisons, R^2 using $PBIF_{3-7}$ method was 0.98 and 0.99 for Ki-liver and Ki-spleen, respectively. The mean bias between Ki-$liver_{IDIF}$ and Ki-$liver_{PBIF}$ was -3.4±5.4%[95%CI:-6.1;-0.6]. The mean bias between spleen-Ki_{IDIF} and spleen-Ki_{PBIF} was -1.1±4.8%[95%CI:-3.6;1.2]. **Conclusion:** Our study shows the feasibility of using a PBIF to reduce significantly WBdyn acquisition time, thereby facilitating its use in routine clinical practice. Further evaluation with a larger dataset is needed to confirm this promising results. **References:** none

OP-0568

Motion correction using multi-resolution scheme (MOTIONLESS) for 18F-FDG Total-body PET/CT systems

L. Shiyam Sundar[1], Y. Wang[2], B. A. Spencer[2], G. Wang[2], E. Li[2], S. R. Cherry[2], T. Beyer[1], R. D. Badawi[2];

[1]Medical university of Vienna, Vienna, AUSTRIA, [2]University of California, Davis, CA, UNITED STATES OF AMERICA.

Aim/Introduction: Extended axial field-of-view PET systems hold great potential for parametric imaging. However, estimation of total-body (TB), parametric maps may be limited by subject motion. We translate the Large deformation diffeomorphic metric mapping (LDDMM) approach from neuroinformatics to TBPET by proposing a fast, multi-resolution scheme-based motion correction (MOTIONLESS) for performing motion compensation

of TBPET data. **Materials and Methods:** Fifteen healthy volunteers (26-78 years, weight 53-112 kg) underwent TB PET examinations in the uEXPLORER PET/CT system after giving informed consent. Subjects were asked to limit voluntary movement throughout the entire scan duration. A 60-min PET list-mode acquisition was initiated with the intravenous injection of [18F]FDG ((372 ± 17) MBq). PET list-mode data were rebinned into a dynamic frame sequence (30x2s, 12x10s, 6x30s, 12x120s, 6x300s). The frames were reconstructed into a 150 x 150 x 486 matrices using 3D TOF OSEM with all corrections applied. Frames that did not contain enough structural information (< 60s post-injection (p.i)) were omitted from motion correction. To evaluate the impact of our methodology in a clinical setting, we assessed the tracer kinetic values of a tumour in a genitourinary cancer subject. The dataset was reconstructed using the same parameters as the healthy controls. Results: As expected, the deformations were high around abdominal regions (deformable organs) and low in the cranial areas (rigid organs). Ki maps derived from motion compensated images showed increased tumor Ki values in comparison to the non-motion compensated counterpart. The quantitative assessment of the tumor Ki values was also in agreement with the parametric Ki maps. The Ki values of the motion-compensated tumour were high (0.0675 min^{-1}) in comparison to manually motion-compensated tumour (0.0436 min^{-1}) and non-motion compensated tumour (0.0362 min^{-1}), which warrants further investigation. **Conclusion:** In this work, we propose a fast, diffeomorphic motion compensation approach, to perform total-body PET motion correction. Visual assessment of the tumour indicates improved sharpness and contrast following motion correction. Quantitative assessment of the tumour uptake curve after motion correction agreed well with the manually motion-corrected images. Our data indicates that the proposed MOTIONLESS technique shows potential in performing total-body motion correction with the aid of 3D dense deformation fields **References:** None.

OP-0569

ENHANCE-PET: Exploring the Human Functional Connectome Using Total-Body [18F]FDG-PET

L. Shiyam Sundar[1], R. D. Badawi[2], B. A. Spencer[2], E. Li[2], S. R. Cherry[2], Y. G. Abdelhafez[2], M. Hacker[1], T. Jones[2], T. Beyer[1];
[1]Medical university of Vienna, Vienna, AUSTRIA, [2]University of California, Davis, CA, UNITED STATES OF AMERICA.

Aim/Introduction: Recently, total-body PET (TB-PET) systems with up to 194 cm axial coverage were introduced that offer synchronous kinetic imaging of multiple distant organs at a higher volume sensitivity. Using TBPET kinetic imaging of [18F]FDG, we propose to use assessments of glucose metabolism in multiple organs to automatically build inter-organ pathways that can be used to explore metabolic homeostasis of the human body and disease associated perturbations. **Materials and Methods:** Fifteen healthy volunteers (26-78 years, weight 53-112 kg, 6M/9F) underwent total-body PET examinations on the uEXPLORER PET/CT system. PET list-mode data was initiated with an intravenous injection of [18F] FDG ((372 ± 17) MBq) and was re-binned into a dynamic frame sequence (30x2s, 12x10s, 6x30s, 12x120s, 6x300s) with all corrections applied. As a preliminary step, we have established an automated software suite as a tool to identify functional connectivity between different organs using the 18F-FDG PET/CT datasets from the uEXPLORER TB-PET/CT system. Our software has three components: i) a 3D-unet based multi-organ segmentation tool to segment 13 different organs (brain, thyroid, aorta, lung, inferior vena cava, heart, liver, pancreas, spleen, kidneys, adrenal glands, bones and bladder) from low-dose CT, ii) a diffeomorphic registration algorithm to perform motion correction and iii) a normative functional connectivity module to identify group connectivity of like metabolic rates based upon measuring temporal correlations between time-activity curves of different organs. From the data derived in this processing, a - group-averaged normative correlation network was created for male and female cohort by using Fisher's Z-transformation. Results: In a network plot, the nodes indicate the organs, and the thickness of the curves indicate the strength of the correlation. The node length of an organ depicts its 'connectedness' to other organs. From the data, we saw differences in nodal sizes of brain, heart, liver, bone, and lung between the male and female cohort, hence suggesting connectivity differences between male and female healthy population. **Conclusion:** The results show the possibility of using TB-PET to produce high quality, kinetically derived data to investigate the inter-organ functional connectome of the human body. However, the demonstrated metabolic connectivity poses the challenge to implement paradigms to interrogate the degrees of 'effective connectivity' rather than 'assimilated functional connectivity' within the derived data. **References:** None.

1110

Wednesday, October 20 - Saturday, October 23, 2021

on-demand pool, release on Wednesday, October 20 at 09:00

Clinical Oncology Track - TROP Session: Prostate Staging

OP-0571

Predicting Early Biochemical Progression in Prostate Cancer Patients staged with PSMA PET and multiparametric Magnetic Resonance Imaging

D. Meijer[1], P. J. van Leeuwen[2], M. L. Donswijk[2], T. N. Boellaard[2], I. G. Schoots[2], H. G. van der Poel[2], N. H. Hendrikse[1], D. E. Oprea-Lager[1], A. N. Vis[1];

[1]Amsterdam UMC, Amsterdam, NETHERLANDS, [2]Netherlands Cancer Institute, Amsterdam, NETHERLANDS.

Aim/Introduction: The aim of this study was to point out predictors for early oncological outcome in patients who opt for robot-assisted laparoscopic radical prostatectomy (RARP) for localized prostate cancer (PCa) including conventional prognostic variables as well as multiparametric magnetic resonance imaging (mpMRI) and prostate-specific membrane antigen (PSMA) positron emission tomography (PET) imaging. **Materials and Methods:** This observational study included 500 patients who underwent RARP and extended pelvic lymph node dissection (ePLND). Outcome measurement was biochemical progression of disease, defined as any post-operative PSA ≥0.2 ng/mL. A Cox-regression analysis was performed to assess predictors for biochemical progression, including initial prostate-specific antigen (PSA)-value, biopsy Grade Group (GG), T-stage on mpMRI, and lymph node status on PSMA PET imaging (miN0 vs. miN1). Results: The median total follow-up of all included patients was 12.8 months (IQR 6.6-22.3). When assessing biochemical progression after surgery, initial PSA-value (per doubling; OR 1.24 (95%CI 1.08-1.43), p=0.003), biopsy GG ≥4 vs. GG 1-2 (OR 2.33 (95%CI 1.47-3.69), p<0.001), T-stage on mpMRI (rT3a vs. rT2: OR 2.04 (95%CI 1.30-3.20), p=0.002; ≥rT3b vs. rT2: OR 4.87 (95%CI 3.24-7.32), p<0.001) and miN1 on PSMA PET imaging (OR 2.16 (95%CI 1.46-3.20), p<0.001) were independent predictors of biochemical progression of disease. Moreover, the number of pelvic lymph node metastases on PSMA PET was significantly associated with biochemical progression: one pelvic lymph node metastasis vs. no metastatic disease resulted in an OR 2.60 (95%CI 1.57-4.31), p<0.001; two pelvic lymph node metastases or more on PSMA PET vs. no metastatic disease resulted in an OR 4.61 (95%CI 2.84-7.48), p<0.001. **Conclusion:** Initial PSA-value, biopsy GG ≥4, ≥rT3 disease on mpMRI and miN1 disease on PSMA PET were predictors for early biochemical progression after RARP. Furthermore, the number of pelvic lymph node metastases on staging PSMA PET was associated with biochemical progression. Identifying patients with an increased risk of biochemical progression after surgery may have implications for patient counseling in radical treatment decisions and on patient selection for modern (neo-)adjuvant and systematic treatments. **References:** None

OP-0572

Multiparametric MRI and [^{18}F]PSMA-1007 PET to detect local prostate cancer; a prospective comparative study with correlation to histopathology

B. Privé, B. Israel, M. J. Janssen, M. M. van der Leest, C. H. Muselaers, M. G. Schilham, P. Zamecnik, J. G. Bomers, G. De Lauw, A. J. Smits-van de Camp, J. Sedelaar, W. A. van Gemert, M. Gotthardt, J. O. Barentsz, I. M. van Oort, J. Nagarajah;

Radboudumc, Nijmegen, NETHERLANDS.

Aim/Introduction: Multi-parametric MRI (mpMRI) of the prostate is an effective tool to discriminate between healthy and malignant prostate tissue. Nonetheless, prostate mpMRI has room for improvement with a sensitivity and specificity to detect clinically significant (Gleason score ≥7) prostate cancer (PCa) of 91% and 37%, respectively (1). Potentially, this could be improved by prostate-specific membrane antigen (PSMA) PET imaging. In this setting, [^{18}F]PSMA-1007 is of particular interest as it offers lower renal excretion compared to other available PSMA tracers. The present study aimed to evaluate if [^{18}F]PSMA-1007 PET following the mpMRI improves the detection of local PCa, with biopsy histopathology as reference standard. **Materials and Methods:** In this prospective study (NCT04487847), 75 men with elevated PSA levels and referred for prostate mpMRI will receive additional [^{18}F]PSMA-1007 PET imaging (25 patients with PIRADS I-II, 25 patients with PIRADS III, and 25 patients with PIRADS IV-V). All patients will undergo [^{18}F]PSMA-1007 PET with diagnostic CT within 30 days of the mpMRI and prior to biopsy. MR-directed biopsies will be performed of lesions that are PIRADS ≥III on mpMRI and/or level of suspicion (LOS) ≥III on PSMA-PET. PIRADS ≤II and LOS ≤II are considered non-suspicious and will not undergo biopsy. Those patients will be clinically monitored during follow-up. Results: To date, 25 patients with PIRADS I-II, six patients with PIRADS III, and 17 patients with PIRADS IV-V (total n=48) completed the study protocol. The median (range) age and PSA at baseline was 67 (52-77) years and 7 (2.5-24) µg/l. In these 48 patients, 68 lesions were identified of which 39 were PIRADS ≥III and/or LOS ≥III and underwent target-biopsy. The mpMRI and PSMA-PET showed comparable efficacy to detect PCa lesions with a sensitivity of 93% and 93% and specificity of 70% and 69%, respectively. Four of 68 lesions were classified as tumor suspicious by both mpMRI and PSMA-PET but were negative on pathology. In total, 12 patients had PCa. One patient had a Gleason 3+4 tumor detected by PSMA-PET imaging that was not visible on mpMRI (PIRADS II). Four of six PIRADS III cases were correctly up- or downscaled by PSMA-PET

imaging. **Conclusion:** Screening diagnostics of the prostate may improve by adding [^{18}F]PSMA-1007 PET imaging to the mpMRI. In this regard, PSMA-PET could further improve the negative predictive value and/or help stratifying equivocal mpMRI (PIRADS III) results. The final results of this ongoing study are awaited. **References:** (1) Drost et al. 2019

OP-0573

The Prognostic Value of Histopathological Nodal Features and PSMA-PET findings in Patients with Pelvic Lymph Node Metastases of Prostate Cancer after Extended Pelvic Lymph Node Dissection

D. Meijer[1], R. H. Ettema[1], P. J. van Leeuwen[2], H. G. van der Poel[2], N. H. Hendrikse[1], D. E. Oprea-Lager[1], E. M. Bekers[2], A. N. Vis[1];
[1]Amsterdam UMC, Amsterdam, NETHERLANDS, [2]Netherlands Cancer Institute, Amsterdam, NETHERLANDS.

Aim/Introduction: The aim of this study was to investigate the prognostic value of different morphologic characteristics of pelvic lymph node metastases on the oncological outcome. Moreover, it was assessed whether patients with signs of pelvic lymph node metastases on staging prostate specific-membrane antigen (PSMA) PET/CT (miN1) had a different oncological outcome compared to patients in which the PSMA PET/CT did not reveal any pelvic lymph node metastases (miN0). **Materials and Methods:** All patients who underwent a PSMA PET/CT prior to robot-assisted laparoscopic radical prostatectomy (RARP) and extended pelvic lymph node dissection (ePLND) with histopathological evidence of pelvic lymph node metastatic disease (pN1) were included. To assess lymph-node specific predictors for biochemical progression after RARP, a multivariable Cox regression analysis was performed, including extra-nodal extension (ENE), the diameter of the largest nodal metastasis and the lymph node density (LND; number of tumor positive lymph nodes divided by the total number of resected lymph nodes). Biochemical progression was defined as a PSA-level ≥0.2 ng/mL during follow-up, or the start of adjuvant treatment. Results: In total, 129 patients were studied with a median follow-up of 15 months (interquartile range (IQR) 8-22). The median biochemical progression-free survival for patients with miN0 on PSMA PET/CT was 8.8 months, compared to 4.1 months in patients with miN1 on PSMA PET/CT (hazard ratio (HR) 1.56, 95% confidence interval (CI) 1.01-2.42; p=0.046). Both the diameter of the largest nodal metastasis (HR 1.42, 95%CI 1.02-1.96; p=0.037) and LND (HR 1.03, 95%CI 1.01-1.05; p=0.004) were significant predictors for developing biochemical progression, whereas the presence of ENE (HR 1.27, 95%CI 0.75-2.15; p=0.37) was not a significant predictor for developing biochemical progression. **Conclusion:** Patients with pN1 prostate cancer have a poor prognosis, especially patients with PSMA-avid pelvic lymph node metastases on preoperative PET/CT. A higher lymph node density and a larger diameter of the largest nodal metastasis were significantly associated with biochemical progression after surgery, while the presence of extra-nodal extension was not. **References:** None

OP-0574

Standardized Uptake Values as Determined on Prostate-specific Membrane Antigen Positron Emission Tomography/Computer Tomography are associated with Gleason Grade and Biochemical Recurrence of Disease in Patients with Prostate Cancer

Y. Bodar[1], H. Veerman[2], K. De Bie[1], D. Meijer[1], H. N. Hendrikse[1], P. J. van Leeuwen[2], B. A. Windhorst[1], M. Donswijk[2], R. Boellaard[1], A. N. Vis[1], D. E. Oprea-Lager[1];
[1]Amsterdam UMC, location VUmc, Amsterdam, NETHERLANDS, [2]Netherlands Cancer Institute, Amsterdam, NETHERLANDS.

Aim/Introduction: Prostate cancer (PCa) staging has been improved by prostate-specific membrane antigen (PSMA) positron emission tomography/computed tomography (PSMA-PET/CT). Intraprostatic PSMA uptake, as semi-quantitatively measured by standardized uptake values (SUV), might predict clinically relevant oncological outcomes for PCa. This study aims to investigate the correlation between SUV in patients with PCa, prior to radical prostatectomy (RP) and diverse pathology outcomes, including Gleason score (GS), pN1 status and biochemical progression-free survival (PFS). **Materials and Methods:** A total of 318 patients with biopsy-proven PCa scheduled for RP with a pelvic lymph node dissection in 84.5%, (269/318 patients) were retrospectively analysed (median PSA: 10.5 ng/ml). Prior to RP, patients received a PET/CT with either ^{68}Ga-PSMA-11 (189/318=59% patients) or ^{18}F-DCFPyL (129/318 =41% patients). PET/CT images were analysed visually and semi-quantitatively by measuring the maximum SUV (i.e., SUV_{max}) of the most intense suspect lesions in the prostate. The SUV_{max} of the primary tumour was assessed in relation to GS, pN1 status and PFS. Results: SUV_{max} was associated with clinical and biopsy pre-operative variables, as well as to ISUP grade in the prostate and with pathological tumour stage. Patients with pISUP≤2 showed significantly lower SUV_{max} compared to patients with pISUP>2 for both tracers (SUV_{max} ^{18}F: 5.1 versus 9.6; p=0.002, SUV_{max} ^{68}Ga: 6.63 versus 8.63; p=0.0003, respectively). Moreover, patients with proven lymph node metastatic PCa (pN1) exhibited significantly higher median SUV_{max} than those without or with uncertain lymph node metastases (pN0/pNx) for both tracers (SUV_{max} ^{18}F: 7.9 versus 12.3; p=0.04, SUV_{max} ^{68}Ga: 7.6 versus 12.0 p<0.001). When analysing pre-operative parameters, independent predictors for pN1 on multivariable analysis included ^{68}Ga-PSMA-11 PET/CT intraprostatic SUV_{max} (per doubling: odds ratio (OR) 1.96 (95% Confidence Interval(CI) 1.27-3.01), p<0.001), and ^{18}F-DCFPyL PET/CT intraprostatic SUV_{max} (per doubling: OR 1.79 (95%CI 1.06-3.03). Of the total cohort, 77.6% (247/318) of patients were free from progression at a median follow-up

of 11.6 months (Range 1.4-32.8 months). The pooled lower quartiles of SUV_{max} for both tracers showed a favourable PFS versus the upper 2 quartiles (p<0.001). **Conclusion:** Intraprostatic PSMA-PET/CT uptake, as semi-quantitatively measured by SUV_{max} is prognostic and may represent a valuable new biomarker in localised PCa. The GS, pN1 status and PFS correlated with the intensity of the tracer expression in the primary prostate tumours on PSMA PET/CT with both the ^{68}Ga-PSMA-11 and ^{18}F-DCFPyL tracers. **References:** None

OP-0575

A Pilot Study of ^{68}Ga-PSMA11 and ^{68}Ga-RM2 PET/MRI for Biopsy Guidance in Patients with Suspected Prostate Cancer

***H. Duan**, V. Ferri, P. Ghanouni, B. Daniel, N. Hatami, G. A. Davidzon, C. Mari Aparici, A. Thong, G. A. Sonn, A. Iagaru;*
Stanford University, Stanford, CA, UNITED STATES OF AMERICA.

Aim/Introduction: Targeting of lesions seen on prostate multiparametric MRI (mpMRI) improves prostate cancer (PC) detection at biopsy. However, 20-65% of highly suspicious lesions on MRI (PIRADS 4 or 5) prove to be false positives (FP) at biopsy. Here, we evaluated the potential utility of ^{68}Ga-PSMA11 and ^{68}Ga-RM2 PET/MRI for biopsy guidance in patients with suspected PC and prior negative biopsy or equivocal MRI. **Materials and Methods:** Nine men, aged 59.8±4.6 years, with suspected PC were prospectively enrolled to undergo ^{68}Ga-PSMA11 and ^{68}Ga-RM2 PET/MRI, including mpMRI. The prostate was divided into 12 segments (apex lateral, apex medial, base lateral, base medial, mid lateral, mid medial, left and right, respectively) using PET/MRI data and MIM software. Maximum standardized uptake values (SUV_{max}) of suspected PC lesions and background for each segment were collected. Biopsies after PET/MRI included 1 core through each of the 12 segments and targeted sampling of any lesions seen on PET. PET/MRI results were then compared to the gold standard biopsy. Results: PSA and PSA density were 11.07±6.57 ng/mL and 0.20±0.12 ng/mL^2, respectively. Prostate biopsy prior to imaging was available in 7/9 patients of which 4 were negative and 3 showed Gleason score (GS) 7. mpMRI was negative in 4 patients, 4 showed PIRADS 4 and 1 patient PIRADS 5. ^{68}Ga-PSMA11 and ^{68}Ga-RM2 PET/MRI each identified 18 lesions, however 6 lesions in 3 patients were incongruent. PET/MRI guided biopsy led to the additional finding of 3 clinically significant tumors with GS 7 in 3 patients as well as 2 with GS 6 in 2 patients. Suspected lesions concordant between mpMRI and both radiotracers were seen in 2 patients: PET/MRI guided biopsy confirmed GS 7 in one patient and GS 6 for the other patient, whereas 1 GS 7 lesion was missed by all modalities. All other biopsy verified GS 7 and GS 6 lesions were identified by both radiotracers. Mean SUV_{max} for true positives (TP) was slightly higher than FP, however not statistically significant (Mean SUV_{max} for TP (GS 7) vs. FP lesions: 10.64±8.07 vs. 6.44±4.64 [P=0.38] for ^{68}Ga-PSMA11, and 19.24±17.8 vs. 12.5±13 [P=0.47] for ^{68}Ga-RM2). **Conclusion:** Our preliminary results show that both ^{68}Ga-PSMA11 and ^{68}Ga-RM2 PET/MRI are not only feasible for biopsy guidance in suspected PC, but also identified additional cancers not seen on mpMRI. However, larger studies are needed to shed light on the different expression patterns of PSMA and gastrin releasing peptide receptor in PC. **References:** None

OP-0576

Prospective Pilot Trial On ^{68}Ga-PSMA And ^{68}Ga-DOTA-RM2 PET/MRI In High-Risk Prostate Cancer Staging

***S. Ghezzo**[1], P. Mapelli[1,2], E. Preza[2], G. Brembilla[1], V. Cucchiara[1], A. Samanes Gajate[2], C. Bezzi[1], L. Presotto[2], V. Bettinardi[2], A. Savi[2], P. Magnani[2], R. Menichini[2], A. Coliva[2], I. Neri[2], E. Di Gaeta[3], L. Gianolli[2], A. Briganti[1,4], F. De Cobelli[1,3], P. Scifo[2], M. Picchio[1,2];*
[1]Vita-Salute San Raffaele University, Milan, ITALY, [2]Nuclear Medicine Department, IRCCS San Raffaele Scientific Institute, Milan, ITALY, [3]Department of Radiology, IRCCS San Raffaele Scientific Institute, Milan, ITALY, [4]Department of Urology, IRCCS San Raffaele Scientific Institute, Milan, ITALY.

Aim/Introduction: Hybrid PET/MRI allows the simultaneous acquisition of metabolic, structural, and functional imaging information regarding prostate cancer (PCa) status in a total-body (TB) single session examination. While ^{68}Ga-PSMA PET and multi-parametric MRI (mpMRI) are widely used for PCa characterization, little evidence is available in support of the role of ^{68}Ga-DOTA-RM2 PET. The aim of the present study was to investigate the synergic role of ^{68}Ga-PSMA PET/MRI and ^{68}Ga-DOTA-RM2 PET/MRI in prostate cancer staging. **Materials and Methods:** 15 patients with biopsy-proven PCa underwent both ^{68}Ga-PSMA and ^{68}Ga-DOTA-RM2 PET/MRI within one month. A qualitative analysis of TNM classification was performed and semi-quantitative PET, quantitative MRI and clinical data were collected for each patient. Specifically, maximum standardized uptake value (SUV), mean SUV at different thresholds (40%, 50%, 60% of the maximum - SUVmean40, SUVmean50, SUVmean60); minimum apparent diffusion coefficient (ADC), mean ADC, Ktrans were calculated; Gleason score, prostate-specific antigen (PSA) and ISUP grade were gathered. Spearman correlation between multi-tracer PET, MRI and clinical data was performed. Pvalues < 0.05 were considered statistically significant. DICE score between regions of interest manually segmented on the primary tumor on ^{68}Ga-PSMA, ^{68}Ga-DOTA-RM2 PET and T2 MRI was computed. Results: All imaging modalities detected the primary PCa in 15 patients, with slight differences regarding the multifocality of intra-prostatic findings. One patient presented seminal vesicles involvement detected by both ^{68}Ga-PSMA and MRI, while no uptake was present on ^{68}Ga-DOTA-RM2 images. In one patient multi-tracer PET showed an increased focal uptake in the left side of the prostate, while MRI detected a lesion in the right peripheral zone. TB

^{68}Ga-PSMA, TB ^{68}Ga-DOTA-RM2 PET and MRI were positive in 6, 2 and 4 patients at lymph-nodal level, respectively; positivity at bone-level was also detected by TB ^{68}Ga-PSMA in two patients, and by MRI in one patient. ^{68}Ga-DOTA-RM2 SUVmax, SUVmean50 and SUVmean60 correlated with PSA level at diagnosis (ρ=-0.55, -0.53, -0.53 and p-value=0.04, 0.04, 0.04 respectively). Mean DICE between ^{68}Ga-PSMA and T2= 0.52, ^{68}Ga-PSMA and ^{68}Ga-DOTA-RM2= 0,43, ^{68}Ga-DOTA-RM2 and T2= 0,39. **Conclusion:** The different findings detected by ^{68}Ga-PSMA and ^{68}Ga-DOTA-RM2 potentially reflect the complementary role of these radiotracers in PCa staging. A synergic role of ^{68}Ga-PSMA, ^{68}Ga-DOTA-RM2 PET and mpMRI in PCa characterization during the staging phase is also enlightened. Further studies on larger cohorts are needed to validate these findings and to ultimately assess the utility of hybrid ^{68}Ga-PSMA PET/MRI and ^{68}Ga-DOTA-RM2 PET/MRI in the clinical management of PCa. **References:** none

OP-0577

Prospective analysis of Prostate Cancer Local Staging with ^{18}F-DCFPyL PET/MRI combined with multiparametric MRI - a comparison to histopathology in the radical prostatectomy specimen

Y. Bodar, G. J. Zwezerijnen, J. P. van der Voorn, B. Jansen, R. Smit, S. Kol, D. Meijer, K. De Bie, A. Windhorst, N. Hendrikse, A. Vis, D. Oprea-Lager;
Amsterdam UMC, location VUmc, Amsterdam, NETHERLANDS.

Aim/Introduction: In primary prostate cancer (PCa), the staging of patients and risk stratification are crucial to guide treatment decisions. ^{68}Ga- or ^{18}F-labeled PSMA PET has been successfully introduced for (re)staging of PCa. The use of ^{18}F-DCFPyL PET/MRI might be of additional value to localise primary PCa. The aim of this study was to assess the diagnostic performance of ^{18}F-DCFPyL PET/MRI imaging to localize primary PCa, and to investigate if ^{18}F-DCFPyL PET/MRI imaging may facilitate PSMA-guided targeted prostate biopsy, similarly to mpMRI imaging. **Materials and Methods:** Twentyfive patients with intermediate to high-risk PCa were prospectively enrolled, prior to radical prostatecomy. Before surgery, all patients underwent ^{18}F-DCFPyL PET/MRI and mpMRI, sequentially, on the same day. Two experienced nuclear medicine physicians and two experienced radiologists assessed the tumour localisation on PET/MRI and mpMRI respectively, using a 12-segment model of the prostate. Similar images using a 12-segment prostate model were obtained by the uro-pathologist for the radical prostatectomy specimen. Based on imaging, an index lesion biopsy advice (2 segments) was given per patient. Clinically significant PCa (csPCa) was defined as any PCa with Gleason score ≥ 3 + 4 = 7. The biopsy advice based on PET/MRI and mpMRI was correlated to final histology in the radical prostatectomy specimen. Sensitivity, specificity, positive predictive value (PPV) and negative predictive value (NPV) for csPCa were assessed. Results: In 25 evaluated patients, local PSMA uptake in the prostate gland was observed in all patients. Overall, 142 of 350 segments (40.6%) contained csPCa at final pathologic examination. Sensitivity, specificity, NPV and PPV for csPCa per segment using ^{18}F-DCFPyL -PET/MRI were 51.2%, 89.5%, 72.0% and 77.7%, respectively. Sensitivity, specificity, NPV and PPV for csPCa per segment using mpMRI were 58.7%, 93.0%, 81.6% and 81.0%, respectively. The segments recommended for targeted biopsy contained the highest Gleason score PCa segment in 23/25 patients (91%) both for PSMA-PET/MRI and mpMRI. **Conclusion:** An accurate detection (91%) of csPCa was found when correlating ^{18}F-DCFPyL PET/MRI with the RALP specimen. ^{18}F-DCFPyL PET/MRI adequately localised csPCa, similar to mpMRI, potentially allowing accurate PSMA-targeted biopsy. **References:** None

OP-0578

A Pilot Study of ^{68}Ga-PSMA11 and ^{68}Ga-RM2 PET/MRI for Evaluation of Prostate Cancer Response to High Intensity Focused Ultrasound (HIFU) Therapy

H. Duan, P. Ghanouni, N. Hatami, G. A. Davidzon, C. Mari Aparici, A. Thong, G. A. Sonn, A. Iagaru;
Stanford University, Stanford, CA, UNITED STATES OF AMERICA.

Aim/Introduction: Prostate specific membrane antigen (PSMA) and gastrin-releasing peptide receptors (GRPR) are both overexpressed in prostate cancer (PC). The degree of their expression at various stages of PC is not yet well understood. In this study, we evaluated a novel approach combining both ^{68}Ga-RM2 and ^{68}Ga-PSMA11 PET/MRI within each PC patient before and after treatment with high intensity focused ultrasound (HIFU) to assess accuracy of localization and response to treatment. **Materials and Methods:** Nine men, aged 63.7±8.8 years, with newly diagnosed PC were prospectively enrolled. Pre HIFU, patients underwent prostate biopsy, prostate multiparametric MRI (mpMRI), ^{68}Ga-PSMA11 and ^{68}Ga-RM2 PET/MRI. Response to HIFU treatment was assessed with ^{68}Ga-PSMA11 and ^{68}Ga-RM2 PET/MRI. For localization, the prostate was contoured and divided into 12 segments (apex lateral, apex medial, base lateral, base medial, mid lateral, mid medial, left and right, respectively) using PET/MRI data and MIM software (MIM Software Inc, Cleveland, OH, USA). Maximum standardized uptake values (SUV_{max}) of PC lesions, as well as of background uptake in each segment were collected. Results: Pre HIFU biopsy revealed 16 lesions of which of 12 were clinically significant with a Gleason score (GS) ≥7 and mpMRI showed 10 lesions with 9 being ≥PIRADS 4. ^{68}Ga-PSMA11 and ^{68}Ga-RM2 PET/MRI demonstrated 20 and 19 positive lesions respectively with 17 congruent in 9 patients and 6 incongruent lesions in 4 patients. HIFU treated 21 zones whereas 20 were identified with both radiotracers and one was negative in ^{68}Ga-RM2, but positive in ^{68}Ga-PSMA11. In this patient, pre HIFU biopsy showed a GS 4+3 and mpMRI PIRADS 4. For treatment evaluation, ^{68}Ga-

PSMA11 and ^{68}Ga-RM2 PET/MRI were performed 8.59±4.23 and 9.21±2.45 months, respectively, after HIFU. In all patients PET/MRI were negative for the respective treated area. Pre-treatment PSA prostate specific antigen (PSA) and PSA density were 9.04±3.59 ng/mL and 0.21±0.09 ng/ml^2, respectively, and decreased significantly after HIFU to 3.93±2.62 ng/mL (P=0.00) and 0.10±0.07 ng/ml^2 (P=0.02), respectively. Concordantly, pre-treatment SUV_{max} decreased significantly for ^{68}Ga-PSMA11 and ^{68}Ga-RM2 (^{68}Ga-PSMA11: 13.80±10.72 vs 3.45±3.58 [P=0.03] and ^{68}Ga-RM2 12.09±9.95 vs 3.70±4.10 [P=0.02] before and after HIFU, respectively). **Conclusion:** Our results show that ^{68}Ga-PSMA11 and ^{68}Ga-RM2 PET/MRI identified the dominant lesion for HIFU in 100% and 88.9%, respectively. Both radiotracers accurately verified response to treatment in all patients. The 6 incongruent lesions suggest different expression patterns of PSMA and GRPR in PC. Larger studies are needed to shed light on that. **References:** None

OP-0579

Quantitative imaging parameters to predict local staging of prostate cancer in intermediate- to high-risk patients

R. Laudicella[1,2], S. Skawran[1], D. A. Ferraro[1,3], U. Mühlematter[1], A. Maurer[1], H. Grünig[1], O. Donati[4], D. Eberli[5], I. A. Burger[1,6];
[1]Department of Nuclear Medicine, University Hospital Zurich, University of Zurich, Zurich, SWITZERLAND, [2]Department of Biomedical and Dental Sciences and Morpho-Functional Imaging, Nuclear Medicine Unit, University of Messina, Messina, ITALY, [3]Department of Radiology and Oncology, Faculdade de Medicina, FMUSP, Universidade de Sao Paulo, Sao Paulo, BRAZIL, [4]Interventional and Diagnostic Radiology, University Hospital Zurich, University of Zurich, Zurich, SWITZERLAND, [5]Department of Urology, University Hospital Zürich, University of Zurich, Zurich, SWITZERLAND, [6]Department of Nuclear Medicine, Kantonsspital Baden, Baden, SWITZERLAND.

Aim/Introduction: An increasing number of patients undergo PSMA PET for staging of intermediate or high-risk prostate cancer (PCa). Previous studies showed that PSMA PET/MRI might increase the sensitivity for extracapsular extension (ECE) or seminal vesicle infiltration (SVI). However, the interreader variability for extraprostatic disease (EPD) is still high for multiparametric MRI (mpMRI) and PSMA PET/MRI. This study aimed to assess whether mpMRI and PET/MRI quantitative imaging parameters could yield a more robust prediction of EPD (ECE and/or SVI). **Materials and Methods:** We retrospectively evaluated PCa patients who underwent staging mpMRI and [^{68}Ga]PSMA PET/MRI or PET/CT, followed by radical prostatectomy at our institution between 01.02.2016 and 31.07.2019. This study was approved by the institutional review board. ECE and SVI were determined on histopathology and compared with quantitative PSMA and mpMRI parameters. On mpMRI, ADC values (min and mean mm^2/1000s), longest capsular contact (LCC, mm), and tumor volume (cm^3) were assessed. PSMA-uptake was quantified using a fixed threshold at SUV > 4 to delineate total PSMA uptake ($PSMA_{tot}$, g/ml), and the PSMA volume ($PSMA_{vol}$, cm^3). The t-test was used to compare means, Pearson's test for the categorical correlation, and receiver operating characteristics (ROC) curve to determine the best cut-off. Results: 73 patients were included (mean age 64.5 ± 6.0; mean PSA 14.4 ± 17.1) and among them 31 showed EPD (42.5%). From mpMRI only LCC reached significance (p=0.043), whilst from PSMA PET, both $PSMA_{tot}$ and $PSMA_{vol}$ were significantly associated with a EPD (p = 0.002 and p < 0.001, respectively). On ROC analysis, LCC, $PSMA_{tot}$, and $PSMA_{vol}$ reached an AUC of 0.695 (p = 0.005), 0.709 (p = 0.002), 0.718 (p = 0.002), respectively. **Conclusion:** Quantitative PSMA parameters have a similar potential as mpMRI LCC to predict EPD of PCa. **References:** none

OP-0580

Heterogeneous PSMA expression in prostate cancer: reason for negative ^{68}Ga-PSMA PET/CT scan? Immunohistochemical validation of 40 surgical specimens

W. Cytawa[1], S. Kircher[2], A. K. Seitz[2], S. Weber[2], P. Hartrampf[2], T. Bandurski[1], P. Lass[1], W. Polom[1], C. Lapa[3], A. K. Buck[2];
[1]Medical University of Gdansk, Gdansk, POLAND,
[2]University Hospital Würzburg, Würzburg, GERMANY,
[3]University of Augsburg, Augsburg, GERMANY.

Aim/Introduction: The aim of this study was to immunohistochemically validate the primary tumor PSMA expression in prostate cancer (PCa) patients imaged with ^{68}Ga-PSMA PET/CT prior to surgery, with special consideration to PET negative cases. **Materials and Methods:** The study included 40 men with newly diagnosed, treatment-naïve PCa who were imaged with ^{68}Ga-PSMA I&T PET/CT before radical prostatectomy. All the primary tumors were routinely stained with H&E for diagnosis, with immunohistochemical validation of PSMA expression of the specimens, expressed as immunoreactive score (IRS) classification. Imaging findings were correlated with histopathologic data. Results: 83% (33/40) of patients presented focal uptake of ^{68}Ga-PSMA I&T in the primary tumor in at least one prostate lobe. Among PSMA PET positive patients one third had lymph node metastases (LNMs) detected in post-operative histopathology, while in PET negative patients only 1 out of 7 suffered from regional LN involvement; PSMA-avid distant lesions, predominantly in bones, were observed in 15% and 0% of patients, respectively. The median IRS classification of PSMA expression in tumor tissue was 2 (range 1-3) both in PSMA positive and negative prostate lobes, with significantly different interquartile range: 2-3 vs. 2-2, respectively (p=0.03). The median volume of PSMA-PET positive tumors was 6.0 ml (0.2-32.9) as compared to 1.6 ml (0.3-24.4) of PET negative tumors (p<0.001). **Conclusion:** Heterogeneity of PSMA expression justifies the presence or absence of focal uptake in PSMA PET imaging only to a

certain extent, other factors, including tumor volume, also influence this. Focal accumulation in the primary tumor may correlate positively with aggressiveness of PCa, harboring higher risk of regional lymph node involvement and distant metastatic spread. **References:** None

OP-0581

Pre-Therapeutic n.c.a. ^{177}Lu-PSMA I&T ("LuteScan") as a SPECT compatible radioligand for Imaging of Metastatic Prostate Cancer Patients

G. Limouris[1], M. B. Dolgushin[2], V. Krylov[3], A. G. Zafeirakis[4]; [1]Nuclear Medicine, Medical School, National and Kapodistrian University of Athens, Athens, GREECE, [2]N.N. Blokhin Russian Oncological Research Center, Moscow, RUSSIAN FEDERATION, [3]Nucl Med Dept, Anatoly Tsyb Research Center, Obninsk, RUSSIAN FEDERATION, [4]Nucl Med Dept, Army Share Fund Hospital of Athens, Athens, GREECE.

Aim/Introduction: Intense PSMA activity on ^{68}Ga-PSMA functional imaging is one of the inclusion criteria for implementing ^{177}Lu PSMA radioligand therapy, ensuring adequate PSMA expression on the tumoral lesions. By the present, we introduce n.c.a. ^{177} Lu-PSMA I&T as a diagnostic whole-body scan ("LuteScan") before the initialization of the radioligand therapy as an alternative to the prerequisite ^{68}Ga-PSMA staging PET/CT scan, principally where the latter is not available; aiming to assess the intensity of PSMA activity not only with regard to the prostate metastatic extent but particularly to lacrimal, parotid, sub-mandibular, sublingual glands and kidneys, being the dose-limiting organs. **Materials and Methods:** After institutional review board approval and informed consent, in 9 patients with metastatic castration-resistant prostate cancer (mCRPC), candidates for radiopeptide therapy (median age 76 years) 444 MBq of n.c.a. ^{177} Lu-PSMA I&T ("LuteScan") was pre-therapeutically, i.v. infused. For dosimetry reasons, whole-body acquisitions followed immediately, 24 and 48 hrs p.i. as well as 24 and 48 hr tomo-scintigraphy over (a) the lower part of the head, including the lacrimal and all salivary glands, and (b) the upper abdomen/lumbar region, including kidneys. Results: Pre-therapeutic n.c.a. ^{177} Lu-PSMA I&T SPECT scan ("LuteScan") in mCRPC patients demonstrates them to be PSMA-avid. The absorbed dose for the lacrimal and parotid glands was 2.6 ± 1.4 and 2.1 ± 1.2 Gy/GBq respectively, for kidneys 0.81 ± 0.28 Gy/GBq and for bone marrow 0.038 ± 0.009 Gy/GBq. **Conclusion:** The pre-therapeutic n.c.a. ^{177} Lu-PSMA I&T avid-scan ("LuteScan") in mCRPC patients (a) refer them for further ^{177}Lu PSMA therapy and (b) might represent a clinical alternative to ^{68}Ga-PSMA, where the latter is not available. Dosimetry of lacrimal, salivary glands and kidneys exhibiting high physiological uptake of radiolabeled PSMA-ligands, considered as dose-limiting organs is a sine qua non procedure. **References:** none

OP-0582

Infiltrative growth-pattern on histopathology is associated with lower diffusion restriction: a potential reason for false-negative mpMRI in prostate cancer

R. Laudicella[1,2], J. H. Rüschoff[3], D. A. Ferraro[1,4], D. Hausmann[5,6], I. Mebert[1], A. Maurer[1], T. Hermanns[7], D. Eberli[7], N. Rupp[3], I. A. Burger[1,8]; [1]Department of Nuclear Medicine, University Hospital Zurich, University of Zurich, Zurich, SWITZERLAND, [2]Department of Biomedical and Dental Sciences and Morpho-Functional Imaging, Nuclear Medicine Unit, University of Messina, Messina, ITALY, [3]Department of Pathology and Molecular Pathology, University Hospital Zurich, University of Zurich, Zurich, SWITZERLAND, [4]Department of Radiology and Oncology, Faculdade de Medicina, FMUSP, Universidade de Sao Paulo, Sao Paulo, BRAZIL, [5]Department of Radiology, Kantonsspital Baden, Baden, SWITZERLAND, [6]Department of Clinical Radiology and Nuclear Medicine, University Medical Center Mannheim, Medical Faculty Mannheim, Heidelberg University, Mannheim, GERMANY, [7]Department of Urology, University Hospital Zurich, University of Zurich, Zurich, SWITZERLAND, [8]Department of Nuclear Medicine, Kantonsspital Baden, Baden, SWITZERLAND.

Aim/Introduction: Recently a significant association between a novel growth-pattern on histopathology of prostate cancer (PCa) and prostate-specific membrane antigen (PSMA) uptake on [^{68}Ga]PSMA-PET was shown. This study aims to evaluate an association between this growth-pattern and apparent diffusion coefficient (ADC, mm^2/1000s) values, in direct comparison to [^{68}Ga]PSMA uptake on PET/MRI. **Materials and Methods:** We retrospectively evaluated patients who underwent [^{68}Ga]PSMA PET/MRI for staging or biopsy-guidance, followed by radical prostatectomy at our institution between 01.07.2016 and 31.01.2020. This study was approved by the institutional review board. The dominant lesion per patient was selected, comparing its corresponding histopathology slide to PET/MRI in a multidisciplinary meeting. Namely, the PSMA-uptake was quantified with the maximum standard uptake value (SUV_{max}) and ADC_{mean}. PCa growth-pattern was classified as expansive (EXP) or infiltrative (INF) according to its properties of forming a tumoral mass or infiltrating diffusely between benign glands. Furthermore, the corresponding WHO2016 Gleason score prognostic grade group (ISUP) was evaluated. The t-test was used to compare means, Pearson's test for the categorical correlation, and receiver operating characteristics (ROC) curve to determine the best cut-off. Results: 62 patients were included (mean age 64.2 ± 6.2; mean PSA 11.7 ± 12.5). 25 lesions had an EXP-growth with an ADC_{mean} of 0.777 ± 0.109, whilst 37 showed an INF-growth with a significantly higher ADC_{mean} of 1.079 ± 0.262 ($p<0.001$). We also observed a significant difference in terms of PSMA SUV_{max} for the EXP (19.2 ± 10.9) versus the INF-growth (9.4 ± 6.2, $p<0.001$). Overall, both ADC_{mean} and SUV_{max} correlated with ISUP groups with $r = -0.221$ and $r = 0.453$, respectively ($p=0.084$ and $p<0.001$). Interestingly,

within the lesions encompassing the EXP or the INF-growth no significant correlation between ISUP groups and ADC_{mean} could be observed (p=0.844 and p=0.986). **Conclusion:** PCa with INF-growth showed overall significantly higher ADC_{mean} values compared to PCa with EXP-growth, independent from ISUP grading. **References:** none

1111

Wednesday, October 20 - Saturday, October 23, 2021

on-demand pool, release on Wednesday, October 20 at 09:00

Featured Session: Molecular Imaging of Movement Disorders

OP-0584

What Lies Behind Cognitive Deficits in Parkinsonisms?

F. Nobili; University of Genoa and Polyclinic San Martino Hospital, Department of Neuroscience (DINOGMI), Genoa, ITALY.

OP-0585

Prospective paired comparison of ^{123}I-FP-CIT SPECT images obtained with a 360°-CZT and a conventional cameras

Y. Piatkova[1], P. Payoux[2,3], C. Boursier[1], M. Bordonne[1], V. Roch[1], P. Y. Marie[1,4], L. Imbert[1,5], A. Verger[1,5];
[1]Université de Lorraine, Department of Nuclear Medicine and Nancyclotep Imaging Platform, CHRU Nancy, Nancy, FRANCE, [2]Department of Nuclear Medicine, Toulouse CHU, Purpan University Hospital, Toulouse, FRANCE, [3]Toulouse NeuroImaging Center, University of Toulouse, INSERM, UPS, Toulouse, FRANCE, [4]Université de Lorraine, INSERM, DCAC, Nancy, FRANCE, [5]Université de Lorraine, IADI, INSERM U1254, Nancy, FRANCE.

Aim/Introduction: This study aims to compare ^{123}I-FP-CIT SPECT imaging obtained from a 360°-CZT camera allowing different focus configurations and a conventional Anger camera. **Materials and Methods:** This prospective study (NCT03980418) included patients referred to ^{123}I-FP-CIT SPECT imaging who underwent consecutively a 30 minutes-acquisition on a conventional camera immediately followed by two 15 minutes-acquisitions on the 360°-CZT camera with respectively striatum and brain focus, the reconstruction parameters reaching equivalent contrast ratios albeit higher spatial resolution for the CZT camera. Tomographic count sensitivities were calculated. The images were analyzed through visual, according to 5 independent physicians, and automatic semi-quantitative analyses. Results: Ninety-two patients were included in this study. The CZT camera tomographic count sensitivities showed +25% and +18% of increase for striatum and brain focus respectively as well as a significant higher quality scores (p≤0.04) in comparison to the conventional camera. Kappa scores of consensual visual analysis were at 0.80 and 0.85, and correlation coefficients of semi-quantitative analysis for striatum uptakes were at 0.75 and 0.76 for the comparisons of images obtained with the two cameras, with respectively CZT striatum and brain focus. Advanced age was the single predictor of discordant cases (10/92, 11%) showing systematically abnormal scans with the conventional camera, the latter potentially suffering from partial volume effect. **Conclusion:** Whatever its focus mode, this high-sensitivity 360°-CZT camera provides concordant ^{123}I-FP-CIT SPECT results with a conventional one, but with shorter acquisition time, higher image quality, and a few discordant cases possibly explained by its higher spatial resolution. **References:** None

OP-0586

Imaging With [^{18}F]FE-PE2I Suggests a Non-Linear Relationship Between Dopamine Transporter Availability and Motor Symptom Severity in Patients With Non-Advanced Parkinson´s Disease

***V. Kerstens**, P. Fazio, M. Sundgren, C. Halldin, P. Svenningsson, A. Varrone;*
Karolinska Institute, Stockholm, SWEDEN.

Aim/Introduction: Motor symptom severity in patients with Parkinson's disease (PD) is considered to be related to the neurodegeneration of nigro-striatal dopaminergic projections. However, dopamine transporter (DAT) imaging studies have shown that DAT availability and clinical motor symptom scores are not strongly correlated. The lack of correlations in earlier studies might be related to suboptimal resolution of the imaging technique, choice of striatal regions of interest (ROI), and whether motor scores assessed only bradykinesia and rigidity or also tremor. The aim of this study was to examine the correlations between DAT availability in motor-specific striatal regions and clinical outcome measures, using high-resolution [^{18}F]FE-PE2I PET imaging. Motor symptom severity was evaluated using the MDS-UPDRS-III score with and without tremor. **Materials and Methods:** Twenty-one patients with idiopathic PD (age: 65.9±9.3 years; Hoehn & Yahr (H&Y) stage 1—3, median 1; symptom duration 1—14 years, median 3 yrs) underwent MDS-UPDRS-III assessment and [^{18}F]FE-PE2I PET on the same day, in practically defined OFF state. DAT availability (BP_{ND}) was measured in caudate (CAU), putamen (PUT), sensorimotor striatum (SMS), and substantia nigra (SN). Correlations with clinical outcome measures were examined with linear and non-linear regression. The study analysis plan was pre-registered (https://aspredicted.org/f3rq6.pdf). Results: Significant correlation was found between symptom duration and DAT availability in the SMS only (Spearman σ=-0.45, p=0.038); between H&Y stage and DAT CAU (σ=-0.43, p=0.0491), PUT (σ=-0.70, p=0.0004), SMS (σ=-0.69, p=0.0006), and SN (σ=-0.46, p=0.0365). No correlation was found between symptom duration and DAT availability in CAU, PUT, and SN, nor between MDS-UPDRS-III score and DAT availability in PUT and

SMS. When the correlation between DAT availability and MDS-UPDRS-III data was examined with exponential fitting instead, significant correlations were found between DAT availability in PUT and SMS with total MDS-UPDRS-III score ($p<0.04$) and with MDS-UPDRS-III score with the tremor score omitted ($p<0.03$). Correlations were stronger when looking at the less affected ROI instead of the bilateral or more affected ROI side, except for SN. **Conclusion:** The findings of this study showed that H&Y stage is the clinical outcome measure best correlated with nigrostriatal DAT. A non-linear relationship between motor scores and DAT availability was found, suggesting that DAT deficit is highly variable when motor symptoms develop and approaches a plateau when the disease has progressed. Correlations were stronger in the regions of the less affected hemisphere, which displays a larger dynamic range of DAT availability. **References:** None

OP-0587

18F-FDOPA PET for the diagnosis of cortico-basal syndromes

J. Darcourt[1], A. Schiazza[1], D. Chardin[1], A. El Ouartassi[2], N. Sapin[1], P. Koulibaly[1], O. Humbert[1], C. Giordana[2];
[1]Centre Antoine Lacassagne - UCA, Nice, FRANCE, [2]CHU - UCA, Nice, FRANCE.

Aim/Introduction: Corticobasal degeneration (CBD) is a neurodegenerative disease affecting the nigro-striatal pathway. Patients with lifetime diagnosis of CBD are found after autopsy to have CBD pathology but also other tauopathies like progressive supranuclear palsy (PSP), Alzheimer's disease (AD) or frontotemporal dementia (DFT). Therefore, the term of corticobasal syndrome (CBS) is preferred. Its diagnostic criteria (Armstrong et al.) are purely clinical. We investigated the potential role of 18F-FDOPA PET. **Materials and Methods:** 66 patients were included retrospectively: 27 CBS, 27 matched Parkinson disease (PD) and 12 PSP patients. All underwent brain 18F-FDOPA PET and were compared to 53 normal controls (NC). Visual analysis was performed by considering the following patterns: (i) normal (NP); (ii) faint unilateral striatal uptake (SU) reduction involving homogeneously caudate and putamen (SP); (iii) unilateral or bilateral putaminal uptake (PU) reduction with posterior-anterior gradient (PP). Two observers reviewed the images. A semi-quantitative analysis was performed using the Scenium® striatal analysis software (Siemens) providing automatic VOI over the striatum and the occipital area and computing SORs. 24 CBS patients also underwent 18F-FDG brain PET analyzed by Scenium® brain analysis for FDG which provides z-score expression of FDG uptake compared to NC and automated anatomical VOIs: pre and post-central gyri were studied as most frequently involved in CBD, frontal and temporal as in FTD and parieto-temporal as in AD. Results: DOPA visual profiles were 18 NP, 5 SP and 4 PP for CBS, PP for all PD and 1 NP, 2 SP and 9 PP for PSP patients. Quantitative FDOPA PET analysis compared to NC showed: lower SU on the contralateral side to the symptoms ($p<0.05$) in CBS; more severe PU reduction on both sides in PD ($p<0.0001$), PU reduction equal to PD in PSP. Interestingly, among the 18 N CBS visual patterns, 8 (44%) had a significant (>2SD) asymmetry on quantitative analysis. CBS FDG uptake of the pre and post central gyri were asymmetrical ($p<0.006$). FDG patterns were: 13 CBD, 5 FTD, 2 AD and 4 others. Within each pattern, asymmetry was significant in CBD ($p<0.0005$) and AD ($p<0.04$). **Conclusion:** This study shows that (i) 66% of CBS patients have visually normal 18F-FDOPA SU; (ii) quantitative analysis reduces this number to 37%; (iii) diffuse unilateral SU reduction including caudate is relatively specific of CBS (83%); (iv) the combination of FDG asymmetrical pre and post-central uptake increases the sensitivity of CBS diagnosis from 63 to 88%. **References:** none

OP-0588

Dopaminergic Activity and Functional Connectivity After Intranasal Insulin. A ^{11}C-raclopride PET/MRI Study

D. Blum[1], S. Kullmann[2], B. A. Jaghutriz[2], C. Gassenmaier[3], B. Bender[4], H. Häring[2], G. Reischl[5], H. Preissl[2], C. la Fougère[1], A. Fritsche[2], M. Reimold[1], M. Heni[2];
[1]Nuclear Medicine and Molecular Imaging, Tübingen, GERMANY, [2]Institute for Diabetes Research and Metabolic Diseases of the Helmholtz Center Munich, Tübingen, GERMANY, [3]Department of Internal Medicine, Division of Hematology, Oncology, Clinical Immunology and Rheumatology, Tübingen, GERMANY, [4]Department of Diagnostic and Interventional Neuroradiology, Tübingen, GERMANY, [5]Werner Siemens Imaging Center, Department of Preclinical Imaging and Radiopharmacy, Tübingen, GERMANY.

Aim/Introduction: Animal studies provided evidence that effects from insulin on food intake are in part mediated by central dopaminergic activity. To improve understanding of insulin-dopamine interactions and their role in whole-body metabolism regulation, we performed a ^{11}C-raclopride PET/MRI study and reported higher binding potentials (BPnd) in the ventral striatum after intranasal insulin administration (compared to placebo), which correlated with increased functional connectivity (FC) between the ventral striatum and VTA. Here, we present further analyses of striatal BPnd and FC with other extra-striatal regions, including the WHO well-being index (WHO-5) as covariate. **Materials and Methods:** 10 healthy normal weight men (age 27±3 years, BMI 23.6±2.3 kg/m^2) underwent two ^{11}C-raclopride-PET/MRI (376±79 MBq) including resting-state fMRI after intranasal application of insulin or placebo (randomized). BPnd was estimated in the ventral striatum using the multilinear reference tissue model MRTM2 (t^*=10 min, cerebellum as reference region). FC was calculated 45 minutes after spray application between regions from the mesocorticolimbic circuitry: bilateral ventral tegmental area, dorsal and ventral striatum, lateral hypothalamus and medial prefrontal cortex.

ΔBPnd=BPnd^{insulin} - BPnd^{placebo} was correlated with ΔFC = FC^{insulin} - FC^{placebo} between the ten possible connections (primary analyses: ventral striatum vs. 3 extra-striatal regions). WHO-5 was assessed on each measurement day. We calculated ΔWHO-5 = WHO-5^{insulin} - WHO-5^{placebo} to test if differences in WHO-5 may confound estimates of dopamine release and compared ΔBPnd with average WHO5. Results: In agreement with the literature[1], ΔBPnd correlated positively with ΔWHO-5 (p=0.004), accordingly, correcting each BPnd for WHO-5, the effect size (Cohen's D) increased from 0.7 to 1.0 for insulin induced ΔBPnd, presumably reflecting reduced dopamine release due to inhibited excitatory synaptic transmission in the VTA. ΔBPnd correlated significantly with average WHO-5 (p=0.027). We identified significant correlations between ΔBPnd of the ventral striatum and ΔFC of the connections: ventral striatum-VTA (Pearson's r=0.72, p=0.01), ventral striatum-hypothalamus (r=0.67, p=0.01) and PFC-VTA (r=0.81, p=0.002). **Conclusion:** When estimating changes in synaptic dopamine from repeated D2-PET on separate days, self-rated well-being may be an important covariate to improve the effect size. Measuring PET & fMRI simultaneously allowed us to detect associations, modulated by insulin, between striatal dopaminergic tone and functional connectivity within and beyond the mesocorticolimbic network. In further studies, we will evaluate these associations in persons with obesity and diabetes and deepen our understanding of its contribution to the proper control of reward, eating and metabolism. **References:** [1]doi: 10.1001/archpsyc.63.9.999

OP-0589

18F-PI-2620 binding in dopaminergic pathways is associated with decreased dopamine transporter availability in four-repeat tauopathies

C. Ferschmann[1], M. Scheifele[1], H. Barthel[2], K. Marek[3,4], C. Palleis[5,6], S. Katzdobler[5], U. Fietzek[5], A. Finze[1], G. Biechele[1], L. Beyer[1], F. Eckenweber[1], S. Wall[1], D. Saur[7], M. Schroeter[7,8,9], J. Rumpf[7], M. Rullmann[2], A. Schildan[2], M. Patt[2], A. Stephens[10], J. Classen[7], P. Bartenstein[1,11], J. Seibyl[3,4], J. Levin[5,6,11], G. Höglinger[6,11,12], O. Sabri[2], M. Brendel[1];

[1]Department of Nuclear Medicine, University Hospital of Munich, LMU Munich, Munich, GERMANY, [2]Department of Nuclear Medicine, University Hospital Leipzig, Leipzig, GERMANY, [3]InviCRO, LLC, Boston, MA, UNITED STATES OF AMERICA, [4]Molecular Neuroimaging, A Division of inviCRO, New Haven, CT, UNITED STATES OF AMERICA, [5]Department of Neurology, University Hospital of Munich, LMU Munich, Munich, GERMANY, [6]German Center for Neurodegenerative Diseases (DZNE), Bonn, GERMANY, [7]Department of Neurology, University Hospital Leipzig, Leipzig, GERMANY, [8]Clinic for Cognitive Neurology, University Hospital Leipzig, Leipzig, GERMANY, [9]LIFE - Leipzig Research Center for Civilization Diseases, University of Leipzig, Leipzig, GERMANY, [10]Life Molecular Imaging GmbH, Berlin, GERMANY, [11]Munich Cluster for Systems Neurology (SyNergy), Munich, GERMANY, [12]Department of Neurology, Medizinische Hochschule Hannover, Hannover, GERMANY.

Aim/Introduction: In this study, we hypothesized that high levels of tau burden in the midbrain and the basal ganglia are correlated to more severe striatal dopaminergic loss in 4-repeat-tauopathies. To address this research question, we correlated tau-PET imaging with the 2nd generation tracer 18F-PI-2620 and 123I-Ioflupane single-photon-emission-computed tomography (SPECT) for dopamine transporter (DAT) availability. **Materials and Methods:** In this cross-sectional study, 32 patients with 4-repeat tauopathies and 13 assumed tau-negative disease controls (Parkinson's disease, multiple system atrophy, Psychiatric disorders), who underwent dual imaging with a time gap of 3±5 months (maximum allowed time gap 2yrs) were evaluated. 18F-PI-2620 PET scans were performed in a dynamic setting 0-60 minutes post injection (p. i.) and 18F-PI-2620 binding was quantified in a static 20-40 min time frame in 4-repeat tauopathy target regions (basal ganglia, midbrain, dentate nucleus; reference region: inferior cerebellar grey). DAT-SPECT binding was quantified in the bilateral basal ganglia (reference region: occipital lobe). Z-scores were calculated against age matched control cohorts. Associations between 18F-PI-2620 and DAT-SPECT Z-scores were analyzed using linear regression analyses, controlling for age and sex. Results: In patients with 4-repeat tauopathies (19 male; 69±8 years) we found a significant negative association between 18F-PI-2620 binding in the internal part of the globus pallidus with dopaminergic loss in the putamen ($r = -0.40$, $p = 0.019$). Similar results were obtained for 18F-PI-2620 binding in other midbrain/ basal ganglia regions and dopaminergic loss in the putamen. Contrary, 18F-PI-2620 binding in the dentate nucleus showed no correlation with dopaminergic loss in the putamen ($r = -0.06$, $p = 0.740$). In 13 tau-negative disease controls (7 male; 66±10 years), no negative regional associations between 18F-PI-2620-binding and dopaminergic loss were detected (all $r > -0.10$, all $p > 0.250$). **Conclusion:** Higher levels of tau pathology in midbrain and basal ganglia regions involved in dopaminergic pathways are associated with more severe dopaminergic loss in primary tauopathies. Lacking associations between 18F-PI-2620-binding and dopaminergic loss in assumed tau-negative controls and for the dentate nucleus of 4-repeat tauopathy patients underpin the validity of the observed biomarker linkage. **References:** none

OP-0590

Interplay of tau and functional network connectivity in progressive supranuclear palsy: A [18F]PI-2620 PET/MRI study

G. Aghakhanyan[1,2], M. Rullmann[1], J. Rumpf[3], M. L. Schroeter[4], C. Scherlach[5], M. Patt[1], M. Brendel[6], J. Classen[3], K. T. Hoffmann[7], O. Sabri[1], H. Barthel[1];

[1]Department of Nuclear Medicine, University of Leipzig, Leipzig, GERMANY, [2]Regional Center of Nuclear Medicine, University Hospital of Pisa and Department of Translational Research on New Technologies in Medicine and Surgery, University of Pisa, Pisa, ITALY, [3]Department of Neurology, University of Leipzig, Leipzig, GERMANY, [4]Max Planck Institute for Human Cognitive and Brain Sciences, Leipzig, GERMANY, [5]Department of Neuroradiology, University of Leipzig, Leipzig, GERMANY, [6]Department of Nuclear Medicine, University Hospital of Munich, LMU Munich, Munich, GERMANY, [7]Department of Neuroradiolgy, University of Leipzig, Leipzig, GERMANY.

Aim/Introduction: Progressive supranuclear palsy (PSP) is the most common primary 4R tauopathy. The success of tau-PET imaging opens perspectives to look at the consequence of tau accumulation to the functional neural networks. Our goal was to assess the potential link between regional tau burden and functional network connectivity in PSP using the next-generation tau PET tracer [^{18}F]PI-2620 on a hybrid PET/MRI system. **Materials and Methods:** Twenty-five probable PSP patients (age 70.7 ± 6.8 years, 13 female), including 14 Richardson syndrome (RS) and 11 non-RS phenotypes, underwent 60 minutes dynamic [^{18}F]PI-2620 PET imaging on a 3T PET/MRI system. The tracer binding potential (BP_{ND}) was estimated using non-invasive pharmacokinetic modeling (MRTM2, reference region=lower cerebellum). For functional connectomics analysis (CONN toolbox), the resting-state fMRI was acquired in PSP patients and thirteen older healthy controls (age 64 ± 9.4 years, 4 female). Network-Based Statistic was used to control false discovery rate when performing mass univariate testing to search for differences of either between-group connectivity or in association with subcortical tau burden. Results: In total, 9870 functional connections among 141 ROIs were analyzed. The PSP patients, compared to the healthy controls, expressed altered functional network connectivity with large network mass value (network mass = 4714, p-FDR < 0.05). Basal ganglia appeared to have lower connectivity with the cerebellum, right hippocampus, inferior temporal, inferior frontal and postcentral regions. The cerebellum showed lower connectivity with the striatum, brainstem, and limbic cortex; and intense hyper-connectivity with temporal, supplementary motor, auditory and primary visual cortices. [^{18}F]PI-2620 BP_{ND}in the bilateral external globus pallidum (GPe) was associated with hyper-connectivity of low-scale intra-opercular circuits (Mass 455 and 778, p-FDR < 0.05), while that in the left dentate nucleus (DN) was associated with intra-cerebellar hyper-connectivity and cortico-cerebellar hypo-connectivity (Mass 938.89, p-FDR < 0.01). **Conclusion:** PSP patients have altered functional connectivity operating at the level of large and short-scale neuronal networks. Networks incorporating deep gray matter structures demonstrated hypo-connectivity, while cortico-cortical connections show variable changes. Subcortical tau load in the bilateral GPe and left cerebellar DN modulate functional networks by strengthening low-scale cortico-cortical and intra-cerebellar networks and weakening large-scale cortico-cerebellar networks. These results support the network degradation/reorganization concept in response to tau pathology and motivate future longitudinal investigations to assess the potential of this multi-modality approach for improved disease progression monitoring. **References:** None

OP-0591

[18F]FDG PET/CT assessed by supervised machine learning classify Parkinson's and Atypical Parkinsonian Disorders

G. Aghakhanyan[1], G. Puccini[2], D. Frosini[3], M. Allocca[4], E. Esposito[1], A. Leo[1], D. Genovesi[5], P. A. Erba[1], A. Giorgetti[5], R. Ceravolo[3], V. Berti[4], D. Volterrani[1], AIMN Neurology Study Group;

[1]Nuclear Medicine Unit, Department of Translational Research and of New Surgical and Medical Technologies, University of Pisa, Pisa, ITALY, [2]Department of Nuclear Medicine, Hospital of Prato, Prato, ITALY, [3]Unit of Neurology, Department of Clinical and Experimental Medicine, University of Pisa, Pisa, ITALY, [4]Nuclear Medicine Unit, Department of Experimental and Clinical Biomedical Sciences "Mario Serio", University of Florence, Florence, ITALY, [5]Division of Nuclear Medicine, Fondazione CNR/Regione Toscana, Pisa, ITALY.

Aim/Introduction: Artificial intelligence has made it possible to analyze large data with great potential to classify patients without making a priori selection of characteristics or regions of interest. Idiopathic Parkinson's Disease (iPD) patients and atypical parkinsonian syndromes share many phenotypic manifestations, especially in the early stages of the disease, creating clinical challenges, and herein, the patterns of regional glucose metabolism play a relevant role. We aimed to create [18F]FDG PET/CT predictive model using Random Forest (RF) classifier to distinguish: a) parkinsonian patients from healthy controls and b) iPD and atypical parkinsonian patients. **Materials and Methods:** A retrospective study was conducted on a multi-center cohort consisted of 150 patients (mean age 70±7; 80 female) including 29 iPD and other atypical parkinsonian syndromes, such as Multiple System Atrophy (MSA, n=37), Progressive Supranuclear Palsy (PSP, n=43), Corticobasal Degeneration (CBD, n=29) and Lewy Body Dementia (LBD, n=12). A healthy control dataset of n=153 subjects (mean age 60±14; 66 female) provided by the AIMN Neurology-Study-Group was included. All scans were proceeded using SPM12. An atlas-based cortical/subcortical regional standardized uptake ratio (SUVr) was

generated using MarsBaRthe toolbox including white-matter as a reference region. A supervised learning model, based on RF algorithm was developed to train the disease classifier (Tidymodels-RStudio). The dataset was split into training (80%) and testing (20%) particles. RF stabilization with 500 trees and five-fold cross-validation was carried out. The prediction model was applied to classify, first, the diseased patients and controls, and second, the iPD and atypical PD patients. The prediction performance of a model was validated while considering the overall accuracy, area under curve (AUC), sensitivity and specificity. Results: The RF model, incorporating basal ganglia and thalamus, showed excellent classification efficiency distinguishing the diseased patients and control group, with an accuracy of 92%, AUC of 0.94, sensitivity of 91% and specificity of 92% for test-dataset. The accuracy of diagnosis was not improved adding to the model the cortical regions. The classification accuracy of iPD from other atypical parkinsonian syndromes was achieved to 76%, and AUC 0.89 in the test dataset with the model embedding both subcortical and cortical regions. The caudate, putamen and globus pallidus showed significantly higher weight of diagnostic importance than cortical regions. The accuracy of diagnosis was not improved with and without thalamus. **Conclusion:** The [18F]FDG PET/CT based RF prediction model shows excellent diagnostic performance classifying diseased patients from controls and iPD patients from other parkinsonian syndromes. **References:** None

OP-0592

Different metabolism characteristics of 18F-FDG PET/CT imaging associated with non-motor symptoms in Parkinson's disease

M. Xin, X. Yu, C. Zhang, C. Wang, J. Liu;
Renji hospital, School of medicine, Shanghai Jiao Tong university, Shanghai, CHINA.

Aim/Introduction: Clinical diagnosis of Parkinson's disease is primarily based on motor symptoms characterized, while patient's history including non-motor symptoms (NMSs) are sometimes subtle and neglected. These NMSs can appear as prodromal features and continue to develop throughout the disease duration that repeatedly make disturbance on patients' daily life. A better understanding of brain glucose metabolism of NMSs will contribute to PD individual diagnosis and precise treatment. **Materials and Methods:** Seventy-six patients diagnosed with PD (62.5±9.9 yrs; Male:Female=40:36) were recruited for this study. All subjects underwent neuropsychological assessment by trained neurologists, and whole brain 18F-FDG PET/CT scans. The specific cerebral glucose metabolism characters in all regions were analyzed quantitatively with average pixel value by NeuroQ software. Results: Most of the enrolled patients (55/76, 72.4%) complained about different autonomic dysfunction NMSs, eg. constipation (42.1%), sialorrhoea (39.5%), hidrosis/night sweat (21.0%) and orthostatic hypotension (13.1%). 49/76 (64.5%) patients suffered from sleep disturbance, including night-time sleep disorders (52.6%) and daytime somnolence (34.2%). Nearly half of the patients (33/76, 43.4%) displayed various psychiatric dysfunctions, such as anxiety (18.4%), depression (27.6%), apathy (23.7%), and hallucination (6.6%). About one-third of the patients (23/76, 30.3%) presented cognitive impairments, including memory loss (27.6%), cognitive decline/dementia (5.3%). In addition, 27.6% (21/76) of the subjects displayed sensory symptoms, like hyposmia (25.0%) and visual disturbance (3.9%). Quantitative findings compared to patients without the specific NMSs presented different regional cerebral glucose metabolic distributions. For patients with autonomic dysfunctions of orthostatic hypotension, hypermetabolism was found in the left thalamus, midbrain, pons and right cerebellum, and hypometabolism in the right parietotemporal and lateral temporal cortices (all $p<0.05$). In patients with psychiatric dysfunction of anxiety, there was hypermetabolism in the pons and bilateral cerebella ($p<0.01$), and hypometabolism in the bilateral Broca's regions, inferior frontal and inferior parietal cortices ($p<0.05$). PD patients with memory loss displayed a decrease glucose uptake in the right medial frontal, and posterior cingulate cortices, and bilateral superior lateral temporal cortices, while an increase glucose uptake in the pons and bilateral cerebella (all $p<0.05$). **Conclusion:** This study demonstrated diverse regional glucose uptake features in PD patients with various NMSs. The brain metabolic changes may benefit to the definition of a pre-motor prodrome in early PD diagnosis, as well as the treatment options for concomitant symptoms in later disease stages. **References:** 1. Schapira AHV, et al. Non-motor features of Parkinson disease. Nat Rev Neurosci. 2017;18(7):435-450.

OP-0593

Cerebral[^{18}F]FDG PET in the diagnosis of Atypical Parkinson Disease - a retrospective study

N. Houssein[1,2], L. Marner[1], A. Hejl[3];
[1]Department of Clinical Physiology and Nuclear Medicine, Copenhagen University Hospital Bispebjerg, Copenhagen, DENMARK, [2]Faculty of Health and Medical Sciences, University of Copenhagen, Copenhagen, DENMARK, [3]Department of Neurology, Copenhagen University Hospital Bispebjerg, Copenhagen, DENMARK.

Aim/Introduction: Atypical parkinsonian disease (APD) often present with Parkinson symptoms but have a much poorer long-term prognosis. The diagnosis is presently based on clinical features but a cerebral PET scan with [^{18}F] fluoro-2-deoxy-2-D-glucose ([^{18}F]FDG) may assist in the diagnosis of APD such as multiple system atrophy (MSA), progressive supranuclear palsy (PSP), corticobasal disease (CBD) and Lewy body dementia (DLB)[1]. Only few studies

have evaluated the sensitivity and specificity of [18F]FDG PET in a mixed patient population, which we aim to measure in a retrospective material. **Materials and Methods:** We identified 355 patients referred for a cerebral [18F]FDG PET from Department of Neurology during 2017-2019. 197 patients were excluded due to suspicion of malignancy, dementia, primary progressive aphasia and cerebellar ataxia. The remaining 158 were suspicious of APD and of these 132 has so far been examined. The clinic has specialist function for movement disorders covering Eastern Denmark and about 2 mio of the Danish population. Scans were generally performed at first admission to the clinic.The [18F]FDG PET was analysed using SyngoVia by a nuclear medicine specialist blinded to clinical information. The accuracy of the image-based classification was assessed by comparison with the follow-up clinical diagnosis (median follow-up: 31 months). Results: The 132 patients examined so far (MSA: 18 , PSP: 40 , CBD: 18 , DLB: 14 , PD: 18 and other: 24) were assessed and the overall accuracy was 68%. The accuracy for APD was 74%. Imagine-based classification for APD had 77% sensitivity, 69% specificity, 84% positive predictive value (PPV) and 58% negative predictive value (NPV). For the subtypes, we found that MSA had 100% sensitivity, 90% specificity, 61% PPV and 100% NPV. For DLB, we found 71% sensitivity, 94% specificity, 59% PPV and 97% NPV. For CBD/PSP, we found 57% sensitivity, 96% specificity, 92% PPV and 74% NPV. **Conclusion:** This is among the largest diagnostic accuracy studies to date in a mixed population of patients with symptoms of atypical parkinsonism. The use of [18F]FDG PET for the clinical diagnosis of APD show high sensitivity and specificity even when blinded to clinical information. The findings are in line with previous reports supporting the use of [18F]FDG PET for diagnosis of APD. Early and reliable diagnosis is important for prognosis and supportive treatment of the patients and useful for future clinical treatment trials. **References:** [1]Nobili et al.Eur.J.Neurol.2018.25:1201-17

OP-0594

Widespread loss of presynaptic terminal marker SV2A in early Huntington's disease

A. Delva[1,2], L. Michiels[1,2], M. Koole[2], K. Van Laere[1,2], W. Vandenberghe[1,2];
[1]UZ Leuven, Leuven, BELGIUM, [2]KU Leuven, Leuven, BELGIUM.

Aim/Introduction: Synaptic damage has long been suspected to play a major role in the pathophysiology of HD, but in vivo evidence in humans is limited. To assess synaptic damage in early stages of Huntington's disease (HD) in vivo. **Materials and Methods:** Eighteen HD mutation carriers (51.4 ± 11.6 years; 6F/12M; 7 premanifest, 11 early manifest [7 Shoulson-Fahn stage 1, 4 stage 2]; CAG repeat 41.9 ± 1.7; disease burden 317 ± 50) and 15 age- and gender-matched healthy controls (52.3 ± 3.5 years; 4F/11M) participated in a PET/MR study with ^{11}C-UCB-J, a radioligand for the ubiquitous presynaptic terminal marker SV2A. We also performed ^{18}F-FDG PET in all subjects, as regional cerebral glucose consumption is thought to largely reflect synaptic activity. All subjects were clinically assessed for motor and non-motor manifestations of HD. Volumes of interest were delineated based on individual 3D T1 MRI. SUVR-1 images were calculated for ^{11}C-UCB-J with the centrum semiovale as reference region. ^{18}F-FDG PET images were normalized to the pons. PET images were corrected for partial volume effects. Results: ^{11}C-UCB-J PET showed loss of SV2A binding in the HD group in putamen (-28%, p<0.001), caudate (-25%, p<0.001), pallidum (-24%, p<0.001), frontal (-8%, p=0.004) and parietal cortex (-9%, p=0.002) and cerebellum (-11%,p=0.002). By contrast, ^{18}F-FDG PET only showed significantly lower uptake in caudate and putamen (both -31%, p<0.001). In the premanifest subgroup, ^{11}C-UCB-J PET and ^{18}F-FDG PET showed significant reductions in putamen and caudate only. In the HD group, ^{11}C-UCB-J binding in caudate correlated with UHDRS motor score (r_p= -0.70, p=0.001), SDMT (r_p=0.67, p=0.002) and AVLT sum (r_p=0.69, p=0.002), and ^{11}C-UCB-J binding in putamen correlated with UHDRS motor score (r_p= -0.82, p<0.001) and SDMT (r_p=0.69, p=0.001). **Conclusion:** ^{11}C-UCB-J PET revealed extensive loss of SV2A in early HD, suggesting widespread synaptic disconnection. SV2A loss in the striatum correlated with motor and cognitive functioning. ^{11}C-UCB-J PET is more sensitive than ^{18}F-FDG PET for detection of extrastriatal changes in early HD. **References:** 1. DiProspero NA et al. (2004) 'Early changes in Huntington's disease patient brains involve alterations in cytoskeletal and synaptic elements', J Neurocytol 33:517-533. 2. Niccolini F et al. (2017) 'Striatal molecular alterations in HD gene carriers: a systematic review and meta-analysis of PET studie', J Neurol Neurosurg Psychiatry, 89(2), 185-196. 3. Finnema SJ et al. (2016) 'Imaging synaptic density in the living human brain', Sci Transl Med, 8, 348ra96.

1201

Thursday, October 21, 2021, 16:50 - 18:20

Channel 1

CME 8: Pregnancy and Breastfeeding in the Context of Nuclear Medicine

OP-0597

Status of Guidelines on Breastfeeding

S. Leide-Svegborn; *Radiation Physics, Skåne University Hospital Malmö and Medical Radiation Physics Malmö, Lund University, Malmö, SWEDEN.*

OP-0598

The Pregnant Patient - Risks for the Foetus

F. Jamar; Cliniques universitaires St-Luc, Nuclear Medicine, Brussels, BELGIUM.

OP-0599

How to Estimate the Radiation Doses?

M. Cremonesi; European Institute of Oncology, Radiation Research Unit, Milan, ITALY.

1202-1

Thursday, October 21, 2021, 16:50 - 17:35

Channel 2

Interview with the Expert 7 - The Theranostic Unit

OP-0601

Interview - The Theranostic Unit

A. Iagaru; Stanford University, Stanford Hospital and Clinics, Radiology / Nuclear Medicine and Molecular Imaging, Stanford, UNITED STATES OF AMERICA.

OP-0602

Interview - The Theranostic Unit

C. Mari Aparici; Stanford University, Nuclear Medicine and Molecular Imaging, Stanford, UNITED STATES OF AMERICA.

1204

Wednesday, October 20 - Saturday, October 23, 2021

on-demand pool, release on Wednesday, October 20 at 09:00

Technologists - TROP Session: Sharing Technologist's Experience 1

OP-0603

Feasibility of dose reduction in [^{18}F]-FE-PE2I PET in DAT imaging

T. Lehnskov, D. Riisberg, L. Marner, M. Lonsdale; Bispebjerg/Frederiksberg Hospitall, Copenhagen, DENMARK.

Aim/Introduction: The recommended dose range in dopamine transporter (DAT) imaging of patients with [^{18}F]-FE-PE2I PET/CT is 100-250MBq (typically 200MBq) according to EANM guidelines. The ALARA principle obliges us to find the right balance between radiation dose and a satisfying image quality. In addition, the production of [^{18}F]-FE-PE2I is challenging with a limited and varying yield. Thus, dose reduction of [^{18}F]-FE-PE2I will allow for both an increased number of patients examined per production and contribute to ALARA. The Aim was to find the optimal [^{18}F]-FE-PE2I dose level at our department. **Materials and Methods:** 65 patients referred for [^{18}F]-FE-PE2I PET/CT were included prospectively after written informed consent. Patients were injected with >150MBq as part of our clinical routine and scanned on a GE Discovery 710 or GE Discovery MI, for 10 minutes, 30 minutes post injection. To simulate reduced dose, we used the Varian Real-time Position Management (RPM) system, which is normally used to track the patient tidal volume during the PET scan, to correct for lung movements. In this study we used it for a simulated breathing curve to select a subset of the PET data. The acquired data was reduced to imitate injected doses of 100MBq, 75MBq and 50MBq. Regions of interest (ROI) (putamen and nucleus caudatus) were created by using artificial intelligence (AI) algorithm and the putamen/caudatus ratios calculated (EANM2019 OP-388). The resulting ratios of the three reconstruction with dose reduction were compared to those of the full dose reconstruction. Student´s T-tests were used to assess bias. Agreement between the methods was analysed by a Bland-Altman plot with calculation of limits of agreement (LoA). Results: No-significant biases were found between putamen/caudatus ratios of the full dose and the reduced dose reconstructions: 100MBq: Bias: 0.0006, P=0.838, LoA_{upper} 0.025, LoA_{lower} -0,024 and 75MBq: Bias: -0.0001, P=0.289, LoA_{upper} 0.035, LoA_{lower} -0.038 and 50MBq: Bias: 0.0014, P=0.175, LoA_{upper} 0.058, LoA_{lower} -0.051 Visual inspection revealed that the AI quality in placement of ROI's, decreasing whit reduced dose. Simulated dose of 75MBq and 50MBq resulted in an increased risk of false positive, i.e. abnormal putamen/caudatus ratio, while 100MBq did not show false positive results. **Conclusion:** Dose reduction to 100MBq is feasible and can be used to increase the number of scans per production, simultaneously with a lower radiation exposure for each patient. **References:** None

OP-0604

Development of a brain perfusion SPECT attenuation correction method using synthetic CT images generated by MR images with a deep convolutional neural network

Y. Morisawa[1], Y. Uchiyama[2], A. Takaki[3], S. Ito[2]; [1]Graduate School of Health Sciences, Kumamoto University, Kumamoto, JAPAN, [2]Faculty of Life Sciences, Kumamoto University, Kumamoto, JAPAN, [3]Department of Radiological Technology, Faculty of Fukuoka Medical Technology, Teikyo University, Fukuoka, JAPAN.

Aim/Introduction: An attenuation correction (AC) method for brain perfusion single-photon emission computed tomography (SPECT) is necessary to analyse and quantify cerebral blood flow (CBF). The CT-based attenuation correction (CTAC) method, which is a nonuniform AC method, has been used for brain perfusion SPECT. However, the use of CT scans increase radiation exposure to patients.

Moreover, the CTAC method requires a SPECT/CT system, which is substantially more expensive than the SPECT-only system. Therefore, a nonuniform AC method without radiation exposure and a CT scan are both required for clinical studies. Currently, most patients undergo MRI scans for head imaging because it provides superior soft tissue contrast and does not require radiation exposure of the patient. If synthetic CT (SCT) images based on MR images are directly obtained using a deep convolutional neural network, the CTAC method can be applied to SPECT-only systems without radiation exposure. The purpose of this study is to develop a brain perfusion SPECT attenuation correction method, using SCT images generated by MR images with a deep convolutional neural network (DCNN). **Materials and Methods:** Image data from 73 patients who underwent head MRI and CT scans were used for training and testing of the DCNN. A U-net architecture was used to generate the SCT and was trained to predict SCT images from MR images. Images of 53 of the 73 patients were used as training images, and those of the remaining 20 patients were used as the examination set for accuracy evaluation of the SCT generated from the U-net. The accuracy of the attenuation correction map (μ-map) obtained by the SCT was compared with that obtained by the original CT. Results: The normalised mean absolute error (NMSE) between the SCT and original CT images was 0.59±0.21, and the NMSE of the μ-map calculated from each image was 0.06±0.02 in 20 test subjects. The μ-map of the SCT was approximately equal to that of the original CT. Further study is necessary to confirm the feasibility of this method in SPECT images corrected by the μ-map obtained by the SCT. **Conclusion:** A brain perfusion SPECT attenuation correction method using the SCT with the U-net architecture was developed. This method can contribute to accurate attenuation correction without radiation exposure. **References:** none

OP-0605

Comparative study of Dopamine transporter Imaging between a conventional camera and an innovative 3D-ring hybrid gamma-camera: technologist's point of view

J. Dessoubrais, P. Oudot, F. Clouse, M. Bailly;
Regional Hospital Center of Orleans, Orléans, FRANCE.

Aim/Introduction: We compared the acquisition workflow of Dopamine transporter Imaging on a new 3D-ring CZT-camera to a conventional hybrid camera. We aimed to evaluate the patient workflow using this new device. **Materials and Methods:** The new 3D-ring camera is equipped with 12 swiveling wide energy high resolution and sensitivity CZT (Cadmium Zinc Telluride) detectors and a CT in a hybrid system. This device enables acquisition closer to the patient thanks to its detectors architecture and to a "body contour" mechanism. It also allows focused scanning modes. A panel of 39 patients had their ^{123}I-Ioflupane acquisition on the 3D-ring CZT SPECT-CT system. 8 of them had both acquisitions on the new and the conventional NaI hybrid camera with low energy high resolution and sensitivity collimators. On these 8 patients, we compared image quality, duration of the acquisitions, ease of positioning and patient's experience. The 31 others exams allowed us to confirm our observations on patient's installation and about their feeling in the 3D-ring system. Results: During scan setup, the body contour sensors detect the head of the patient (positioned in a dedicated head support), and the 12 detectors are automatically positioned as close as possible. As a result, positioning is simpler and faster with the new system : 3 min time reduction approximately per patient. This can lead to a reduction of technologist exposure to patient radiation. Exam duration was reduced : 24 minutes on the new 3D-ring CZT system and 30 minutes on the conventional NaI. Total counts were similar for both acquisitions, but image quality was improved on the nuclear medicine physician point of view, because of the spatial resolution improvement. Despite the fact that the 12 detectors come very close to the patient's head, none of them refused their exam, asked for an interruption during the acquisition or felt oppressed. All those findings were confirmed on the other patients that were only explored using this new device. **Conclusion:** The 3D-ring CZT SPECT-CT simplify the positioning of patients for Dopamine transporter Imaging SPECT. It also enhances patient's comfort with a 20%-time reduction, while improving image quality and especially resolution, in those often difficult patients. **References:** None

OP-0606

Bayesian penalized-likelihood reconstruction algorithm in the advanced digital PET/CT system for 18F DOPA PET/CT in patients with Parkinson's disease and Glioblastoma Multiforme

***R. Alhemaidani**, M. AL-Daas, A. Esmail, F. Marafi;*
Jaber Alahmad Center for Molecular Imaging, Kuwait, KUWAIT.

Aim/Introduction: Flourodopa F18 (F-Dopa) is a radioactive tracer that can be used to image dopaminergic neuron nerve endings in order to diagnose Parkinson's disease (PD) and other parkinsonian disorders using positron emission tomography (PET). As a result , we need tools to improve image quality and signal to noise ratio. Q.Clear is a Bayesian penalized-likelihood reconstruction algorithm for PET that was recently implemented by GE Healthcare to improve clinical image quality and quantification on their PET scanners. Our aim is to determine the optimum penalization factor (beta) for clinical use of Q.Clear using an advanced PET/CT system and compare it with the standard PET reconstruction **Materials and Methods:** A total of 20 patients (11 females, 9 male) were referred for 18F-Dopa PET/CT scan, 10 patients indicated with Parkinson disease (PD) and 10

with glioblastoma Multiforme (GBM). All patients (BMI 45.8 ± 18.8) were injected with 8.21mCi ± 3.66 using automatic injector. Images were obtained 60min post injection using GE Health care Digital system (MI). Scout and CT images were first obtained on the brain. Then PET images were acquired using protocol (table 1) then were reconstructed using two different reconstruction tools Measured attenuation correction (MAC) and Bayesian penalized likelihood (BPL) algorithm (Q. Clear, with 3 different Beta (B) value 200,400,600). All images were analyzed by drawing region of interest on the right and left basal ganglia for PD and on the tumor for patients with GBM. SUV mean and standard deviation (std) of the signal were obtained along with SUV mean of the Background (BKG) to calculate signal to noise ratio (SNR_{MAX}). Images were reviewed by two experienced nuclear medicine consultants to access image quality blindly. Results: All 20 patients had interpretable 18F-DOPA studies using conventional reconstruction. Both consultants had consensus opinion on the quality of the images obtained with the different beta values of reconstruction using Q.Clear reconstruction. All the Q.Clear reconstructions with various beta values had image quality comparable with conventional reconstructions. Reconstructions with beta values of MAC and 600 gave smother images. On the other hand, 400 gave more structure than 600. The SNR values progressively increased with increase in beta value. Q.Clear reconstructions with beta value of 200 gave the best image quality as it shows more details . **Conclusion:** Q.Clear reconstructions with beta value of 200 gave best image quality as it add up noise to the image so the boundaries visualized clearly. **References:** None

OP-0607

Development of the ascending aorta region of interest setting program using deep neural networks for ^{99m}Tc-ECD regional cerebral blood flow quantification

T. Sakata[1], Y. Uchiyama[2], A. Takaki[3], S. Ito[2];
[1]Graduate School of Health Sciences, Kumamoto University, Kumamoto, JAPAN, [2]Faculty of Life Science, Kumamoto University, Kumamoto, JAPAN, [3]Department of Radiological Technology, Faculty of Fukuoka Medical Technology, Teikyou University, Fukuoka, JAPAN.

Aim/Introduction: The improved brain uptake ratio (IBUR) method for ^{99m}Tc-ECD single-photon emission computed tomography (SPECT), which is an automatic non-invasive quantitative measurement method of regional cerebral blood flow (rCBF), was developed by reconstructing the determination process of the input function and the regression equation based on measurement of the rCBF by $H_2{}^{15}O$ PET as conducted in a previous study. The input function of this method was determined using the administered dose, which was obtained by analysing the count-time activity curve of the ascending aorta (AAo) in dynamic chest images. The automatic region of interest (ROI) setting program for the AAo was developed by mathematically and statistically analysing a chest RI angiogram (mathematical method). The coincidence ratio between the location of the AAo-ROI obtained using the mathematical method and that obtained using manual methods was approximately 90%. However, to use this program practically, further improvements of 10% are required. If the AAo region can be determined using deep neural networks for segmentation, the accuracy of the AAo-ROI setting program can be improved in terms of simple analytical operation, repeatability, and reproducibility. The purpose of this study was to develop a new AAo-ROI setting program using deep neural networks. **Materials and Methods:** A U-Net architecture based on convolutional neural networks was used to determine the AAo candidate region. Images of 83 patients who underwent chest RI angiography were used as the training images. An ROI with a radius of 4 pixels (8.76 mm) was set on the candidate AAo region, and the highest mean pixel value on the ROI was identified. To confirm the usefulness of this program, 16 patients were examined using the AAo-ROI setting program, and the results were compared with those obtained using the manual method. Results: The coincidence ratios between the location of the AAo-ROI obtained using the mathematical method and this program and that using manual methods was 91% and 98%, respectively. The dice coefficient between the training and segmented AAo regions was 76.5%. A strong correlation was observed between the AAo-ROI and manual setting methods. **Conclusion:** We developed a fully automated AAo-ROI setting program using deep neural networks for ^{99m}Tc-ECD regional cerebral blood flow quantification. This program improves the reproducibility, repeatability, and accuracy of the ROI setting. **References:** none

OP-0608

Eating should be avoided during the administration and early biodistribution of PSMA-directed radioligand therapy

N. Bruin, V. Mohan, J. van de Kamer, J. Sonke, W. Vogel;
The Netherlands Cancer Institute, Amsterdam, NETHERLANDS.

Aim/Introduction: Radionuclide therapy with prostate-specific membrane antigen (PSMA) ligands suffers from unwanted uptake in salivary glands, potentially resulting in dose-limiting xerostomia (dry mouth syndrome) with a severe negative effect on quality of life. Factors that can enhance this toxicity need to be identified and avoided. Oral intake is known to stimulate salivation and salivary gland perfusion, especially in the parotid glands, and therefore eating may increase uptake of PSMA-ligands in salivary glands and aggravate toxicity. The purpose of this study was to determine if eating during the intravenous administration of PSMA-ligands would induce a significant increase in the uptake of PSMA-ligands. **Materials and Methods:** 10

patients with prostate cancer who had already received a whole-body ^{18}F-DCFPyL PET/CT scan on clinical indication, underwent a repeat (intervention) PET/CT scan within a month of the first (baseline) scan without changes in treatment between the two scans. For the intervention scan, patients chose from an assortment of sweet/fatty/acidic foods, which they continuously chewed and swallowed for a period of 10 minutes, beginning one minute prior to the tracer administration. Data from both scans was analyzed by measuring differences in SUL_{mean} and SUL_{max} in VOIs encompassing the parotid and submandibular salivary glands, which were each segmented using a 20% SUL_{max} threshold. Results: A slight increase in average uptake of ^{18}F-DCFPyL in the parotid glands was observed on the intervention scan when compared to the baseline scan (+7.1% SUL_{mean} and +9.2% SUL_{max}, $p<0.05$). No significant difference in uptake was seen in the submandibular glands. **Conclusion:** Eating during the early biodistribution phase slightly increases uptake of PSMA-ligands in the parotid glands. It is currently unknown if this small increase represents a clinically relevant difference in the setting of PSMA-directed radioligand therapy, but any unnecessary additional risk on dose-limiting toxicity should be avoided. We recommend refraining from oral intake during the administration and early biodistribution phase of radiolabeled PSMA-ligands in therapeutic doses, to avoid unnecessary loss in quality of life. **References:** none

OP-0609

Validation process of a new radiolabeled tracers preparation : ^{177}Lu-PSMA-1

P. Orhon[1], M. Piquemal[1], P. Bedouch[2], J. Vuillez[3], L. Djaileb[3], M. Desruet[1], J. Leenhardt[1];
[1]Radiopharmacy, Grenoble Alpes University Hospital, Grenoble, FRANCE, [2]Pharmacy department, Grenoble Alpes University Hospital, Grenoble, FRANCE, [3]Nuclear Medicine, Grenoble Alpes University Hospital, Grenoble, FRANCE.

Aim/Introduction: ^{177}Lu-PSMA-1 radioligand therapy is indicated for the treatment of metastasized castration-resistant prostate cancer. This new therapy using PSMA-1 ligand labeled with ^{177}Lutetium is prepared in the radiopharmacy laboratory. In order to validate the process, three validation batches and several quality controls are required. **Materials and Methods:** 3 production batches were carried out using a miniAIO synthesis device. The various quality controls performed on each ^{177}Lu-PSMA-1 radiolabeling were as follows: Appearance of the solution with visual examination; pH of final product; Radiochemical purity through high-performance liquid chromatography (HPLC) and Thin Layer Chromatography (TLC) methods; Radionucleidic identification by gamma spectroscopy and half-life calculation; Sterility test with direct inoculation in Trypcase Soy Broth (TSB) and Thioglycollate broth with resazurin (THIO-ST) Bacterial endotoxins test (BET) performed with Endosafe® equipment. Furthermore, in order to comply with good preparation practices regarding the aseptic process of the synthesis of 177Lu-PSMA-1, several tests were completed: Media Fill Test (MFT): used to validate an aseptic process by using a sterile microbiological growth medium instead of the drug solution. The final product obtained was incubated for 7 days under ambient conditions and then for 7 days at 30-35°C in the oven; Applicability of sterility tests: European Pharmacopoeia recommends to perform an applicability test of the method in order to confirm the non-antimicrobial effect of the radiopharmaceutical; Determination of the bioburden before sterilizing filtration by an external laboratory. Results: All quality controls performed on the production batches were within specifications: final solution was colourless, with no visible particles; pH of the solution was between 4 and 8; half-life was 6.65 days and the two main gamma photons had energies of 112 and 208 keV; impurities were less than 5% and 3% respectively for TLC and HPLC. Regarding the evaluation of the aseptic process, after 5 days the applicability test was compliant. MFT and sterility tubes were read at day 0, 2, 7 and 14. For all these incubated tubes, none showed any growth of microorganisms. Finally, endotoxin test and bioburden were compliant as the measurements for each production batch were below the expected limits. **Conclusion:** All these controls validated the process of our automated preparation of ^{177}Lu-PSMA-1. For this new radiopharmaceutical drug synthesis, we submitted an investigational medicinal product dossier for authorization by the French National Agency for the Safety of Medicines (ANSM). **References:** EANM guideline on the validation of analytical methods for radiopharmaceuticals

OP-0610

Image quality assessment in two different SPECT scanners: study with a phantom

L. Vieira[1,2], E. Pereira[3], A. Geão[4], L. Freire[5];
[1]Health & Technology Research Center, ESTeSL - Escola Superior de Tecnologia da Saúde de Lisboa, Lisbon, PORTUGAL, [2]Centro de Investigação em Modelação e Optimização de Sistemas Multifuncionais, Escola Superior de Tecnologia da Saúde, Instituto Politécnico de Lisboa, Lisbon, PORTUGAL, [3]NuclearMed, Hospital Particular de Almada, Almada, PORTUGAL, [4]Serviço de Medicina Nuclear, Hospital CUF Descobertas, Lisbon, PORTUGAL, [5]Escola Superior de Tecnologia da Saúde de Lisboa, Instituto Politécnico de Lisboa, Lisbon, PORTUGAL.

Aim/Introduction: Image quality assessment between different NM scanners remains an important issue, due to the need for standardization and harmonization of image acquisition, reconstruction and processing protocols. The aim of this study is to evaluate the quality of two SPECT scanners using a Jaszczak phantom. **Materials and**

Methods: Two GE-Healthcare Gamma Camera (GC), models Infinia-2 and NM/CT-850 were studied using a phantom, model ECAT/DLX/P [1] (7155ml of water; 740MBq; ^{99m}Tc). The same acquisition and processing protocols were used in both GC, namely detectors positioned at 180º with LEHR collimators, 360° acquisition, step-and-shoot circular orbit, 120-projections (60/detector, 15sec/projection), 64×64 matrix, 140keV±10%, FBP reconstruction, Butterworth-filter, cutoff frequency: 0.5 and power:10, and Chang's attenuation correction. Image quality was assessed considering 3 parameters: noise, sensitivity and contrast. For each GC, 3 images were acquired. For noise and sensitivity quantification, 4-ROI's were defined in each image according to [1]; for contrast, 4-ROI-pairs were drawn between the phantom's "cold" spheres (Ø 31.8, 25.4, 19.1, 15.9mm) and close vicinity "hot" background. Statistical analysis was conducted using the Microsoft-Excel program. Results: Noise) The 12-ROI's yielded mean count values of 11346±665 and 10173±471 (mean±sd) for the Infinia-2 and NM/CT scanners; Shapiro-Wilk (S-W) tests indicated that these followed gaussian distributions (p-values=0.171 and 1.000). An unpaired t-test revealed that mean values' difference is statistically significant (p-value=3.56×10^{-5}). Sensitivity) The second set of 12-ROI's yielded mean count values of 10276±708 and 9881±631 for the two GC's. The S-W test indicated that, for the first scanner, ROI values were not gaussian distributed (p-value=0.012). An unpaired Mann-Whitney test indicated that differences between the two scanners were not statistically different (p-value=0.153, one-tailed). Contrast) Assuming the 12-sphere-background ROI-pairs as independent, the S-W test indicated that these followed a gaussian distribution for both GC's (p-values=0.297 and 0.966). An unpaired t-test indicated that differences between the two scanners were not statistically different (p-value=0.251, one-tailed); repeating the t-test for each set of 3 sphere-background pairs in the two GC's, one observed that for spheres 1, 3 and 4 the differences were not statistically significant (p-values=0.092, 0.383 and 0.252), whereas for sphere 2, the p-value=0,0487 (<0.05). **Conclusion:** The characteristics of both scanners may differ regarding noise but, probably not on sensitivity and contrast. However, the reduced sample calls for the need to re-assessment, already ongoing, on these and other equipment, using a more robust protocol, enabling strengthening the conclusions. **References:** [1]-Greer KS. SPECT phantom user's manual. Data Spectrum, 2001

OP-0611

Basic study on imaging acquisition conditions for somatostatin receptor scintigraphy with phantom

M. Nishio[1], N. Fujita[2], H. Ikeda[1], Y. Ochi[1], S. Abe[2], K. Kato[1];
[1]Nagoya University, Nagoya, JAPAN, [2]Nagoya University Hospital, Nagoya, JAPAN.

Aim/Introduction: Somatostatin receptor scintigraphy using ^{111}In-pentetreotide is effective for the detection of neuroendocrine tumors expressing somatostatin receptors. However, somatostatin receptor scintigraphy involves less accumulation of the tracer in tumors and may have less accumulation difference from the physiological accumulation. Additionally, it is associated with lower drug doses and higher statistical noise of collected counts. In addition, ^{111}In-pentetreotide has two energy peaks. Thus, the scattering component mixed in the energy window increases. These effects are considered to differ depending on the setting of imaging conditions such as the energy window width and pixel size. Therefore, in this study, we simulated a neuroendocrine tumor, evaluated the spherical phantom images, and examined the optimal imaging conditions for somatostatin receptor scintigraphy. **Materials and Methods:** A spherical phantom simulating a neuroendocrine tumor was used. The imaging conditions were based on the ones of the Nagoya University Hospital including the main window width of (± 7.5%, ± 10%), sub-window width of (± 3%, ± 5%), and pixel size of (3.3 mm, 4.8 mm) with or without scattering/attenuation correction (total six ways). For the image evaluation, five indices of scattering component ratio, fluctuation coefficient, recovery coefficient, contrast, and contrast noise ratio were used. In addition, a visual evaluation was performed by a nuclear medicine physician. Results: Best results were obtained with the main window width of ± 7.5%, sub-window width of ± 5%, and pixel size of 3.3 mm, with scattering/attenuation correction, being reference conditions for the ratio of scattered components, fluctuation coefficient, and recovery coefficient. For contrast and contrast noise ratio the main window width of ± 7.5%, the sub-window width ± 5%, and the pixel size of 3.3 mm, yielded the most optimum results without scattering/attenuation correction. For visual evaluation, the main window width of ± 10%, the sub-window width of ± 5%, and pixel size of 4.8 mm with scattering/attenuation correction condition gave the most recognizable results for the sphere. **Conclusion:** As the imaging conditions for somatostatin receptor scintigraphy, a main window width of± 7.5%, sub-window width of ± 5%, and pixel size of 3.3 mm are considered to be appropriate. **References:** None

OP-0612

Gallium-68 cyclotron production from liquid target: Experiences and challenges in the integration into routine production of ^{68}Ga-labelled radiotracers

A. Uhlending, J. Wegener, T. Ortgies, G. Höger, H. März, W. Burchert, V. Hugenberg;
Institut für Nuklearmedizin, Radiologie und Molekulare Bildgebung, Bad Oeynhausen, GERMANY.

Aim/Introduction: The nuclide gallium-68 is becoming increasingly important in PET. The cyclotron production of gallium-68 from liquid target via ^{68}Zn(p,n)^{68}Ga nuclear reaction is an elegant solution for the routine production of ^{68}Ga-labelled radiotracers. Here we report on our experiences during the development of a routine-suitable method, starting from the target installation up to routine production. **Materials and Methods:** The 18MeV cyclotron is equipped with a niobium conical target degraded to 16MeV, metal-free loading valve and effective helium cooling. Irradiation parameters for highly enriched zinc-68 nitrate-solution (33 and 66mg/ml) were 60min at 45µA. Post-processing of the irradiated solution and peptide labelling with the post-processed [^{68}Ga]$GaCl_3$ was performed on cassette based automated synthesis modules. Quality control of the [^{68}Ga]$GaCl_3$-solution and the ^{68}Ga-labelled peptides were performed according to Ph. Eur.. Results: After target installation, optimization of irradiation parameters and target seal material, irradiation of enriched zinc-68-solution provided routine-suitable quantities of gallium-68. Post-processing of the irradiated solution consisting of short-lived nuclides and high amounts of zinc turned out to be the major challenge. Attempts of using the predefined methods and cartridges resulted in [^{68}Ga]$GaCl_3$-solutions not applicable for peptide labelling due to high zinc concentrations >2mg/l, leading to low radiochemical yields and purities of the desired peptide radiotracers. The post-processing steps mainly consist of two solid-phase extraction steps (cation and anion exchange cartridges). Substitution of the given cartridges to cartridges with higher capacity and introduction of a rinsing step of the anion change cartridge prior to the elution of the gallium-68 with water finally resulted in reduced and reproduceable low zinc concentrations values of >0.2mg/l. Furthermore, due to the high volume in combination with the higher acid concentration of the [^{68}Ga]$GaCl_3$-solution, a concentration and an elution step of gallium-68 on and from the cation exchange cartridge are required. However, elution of the cartridge with the same predefined volume of eluent resulted in different amounts of buffer addition to reach the required pH-values for the reaction. An additional rinsing step of the cartridge with water prior to elution led to reproduceable amounts of buffer addition. **Conclusion:** Implementing the described changes of the predefined processes enabled the integration of the production of gallium-68 via cyclotron using a liquid target into the routine procedure for the production of ^{68}Ga-labelled radiotracers. [^{68}Ga]Ga-PSMA-11 and [^{68}Ga]Ga-DOTA-TOC were successfully synthesized with radiochemical yields of >70% and quality control specifications were fulfilled. **References:** Alves, Instruments (2018) 2:17.Alves, J. Label Compd Rad (2017) 60:Sl611

1205

Wednesday, October 20 - Saturday, October 23, 2021

on-demand pool, release on Wednesday, October 20 at 09:00

Joint Symposium 15 (EANM/EHA): Imaging Challenges in Multiple Myeloma - Quo Vadis 2021?

OP-0614

Therapy Assessment with FDG

F. Kraeber-Bodéré; University Hospital of Nantes, Nuclear Medicine Department, Nantes, FRANCE.

OP-0615

WB-MRI - My Favourite!

F. Lecouvet; Clinique Universitaires Saint-Luc UCL Brussels, Department of Radiology, Louvain, BELGIUM.

OP-0616

Update in Non FDG

C. Lapa; University Hospital Augsburg Department of Nuclear Medicine, Augsburg, GERMANY.

1206

Wednesday, October 20 - Saturday, October 23, 2021

on-demand pool, release on Wednesday, October 20 at 09:00

Joint Symposium 16 (EANM/ESMO): Combination Treatments - What can Radioligand Therapy be Combined with?

OP-0618

Combination Treatment in Prostate Cancer

U. Vogl; Oncology Institute of Southern Switzerland, Ospedale Regionale die Bellinzona e Valli, Bellinzona, SWITZERLAND.

OP-0619

Combination Treatment in NETs

M. Pavel; Universitätsklinikum Erlangen, Department of Internal Medicine 1, Erlangen, GERMANY.

OP-0620

Preclinical Considerations for Combination Treatment

J. Czernin; University of California Los Angeles, Molecular and Medical Pharmacology, Los Angeles, UNITED STATES OF AMERICA.

1207

Wednesday, October 20 - Saturday, October 23, 2021

on-demand pool, release on Wednesday, October 20 at 09:00

Teaching Session 2: All About Cardiac SPECT

OP-0622

SPECT-MPI

F. Caobelli; Universitätsspital Basel, Klinik für Nuklearmedizin, Basel, SWITZERLAND.

OP-0623

Cardiac Bone Scans

O. Lairez; University. hospital of Toulouse, Department of Nuclear Medicine and Cardiac Imaging Center, Toulouse, FRANCE.

OP-0624

WBC-SPECT

K. Benali; APHP, Department of Nuclear Medicine, Paris, FRANCE.

OP-0625

ERNA

S. Massalha; Rambam HealthCare Campus, Haifa, ISRAEL.

1208

Wednesday, October 20 - Saturday, October 23, 2021

on-demand pool, release on Wednesday, October 20 at 09:00

M2M Track - TROP Session: Radiochemistry - Cook it or Leave it

OP-0627

Toward a reproductive radiolabeling with $\{Al^{18}F\}^{2+}$ complex?

S. Schmitt, E. Moreau;
UMR INSER/UCA 1240 IMOST, Clermont-Ferrand, FRANCE.

Aim/Introduction: Fluoride-18 is the most widely used radionuclide for PET imaging but radiolabeling generally requires drastic conditions (high temperature or basic medium) and time-consuming purification by HPLC. Attractiveness of radiometallation (fast complexation and purification generally performed by SPE) have led to develop, in 2009, a radiolabeling strategy using $\{Al^{18}F\}^{2+}$ complex to mimic a radiometal. Since then, many groups described various radiolabeling conditions, but radiochemical yields are disparate, and some parameters seem unclear. That is why we propose a comprehensive comparison of the radiolabeling parameters in order to have an optimal and reproductive methodology for future clinical developments. **Materials and Methods:** With the aim to obtain probes usable for pretargeting strategies or coupling with peptides, we selected NOTA-PEG_n-X (X = N_3 or Tz and n = 0, 4, 11) and NOTA-maleimide precursors as model compounds for optimization studies. Manually radiolabeling of NOTA precursors with $\{Al^{18}F\}^{2+}$ complex were focused on the following key points: (i) conditioning, and elution of the QMA cartridge (0.9 % NaCl and/or 0.4 M $KHCO_3$, 100-200 µL) for the purification of the fluoride-18; (ii) amount of NOTA-precursors compared to Al^{3+} (1-10 molar equivalents); (iii) use of NaOAc buffer (pH 4) alone or with organic co-solvent (ACN or EtOH, 200-700 µL) at 50-90 °C for 5-20 min for radiolabeling step; (iv) geometry of the reaction vessel and (v) cartridge (C18, tC18, HLB or alumina) for purification step. Radiosyntheses were then automated on SynChrom R&D EVOI module. Complexation efficiency, identity of the radiolabeled probes and radiochemical purities were determined by radio-TLC and radio-HPLC. Results: [^{18}F]AlF-NOTA-PEG_n-X and [^{18}F] AlF-NOTA-maleimide were obtained in 50-63 % decay-corrected (dc) radiochemical yield (RCY) after incubation heating of the appropriated precursors, 2 mM $AlCl_3.6H_20$ and purified $^{18}F^-$ in 0.9 % NaCl/EtOH mixture at 90 °C for 15 min, followed by SPE purification with Oasis HLB cartridge. The overall procedure time was only 30 min. According to automated method, RCY are ranging from 30 % to 35 % in 40-45 min. In each case, radiolabeled probes were obtained with excellent radiochemical purities (> 99%). **Conclusion:** Among all the conditions described in the literature, we were able to determine optimal parameters for radiolabeling with $\{Al^{18}F\}^{2+}$ complex. We have also demonstrated that, despite the optimization of each parameter, similar results cannot be obtained with automated radiosynthesis, which could be a limitation for this methodology **References:** McBride, J. Nucl. Med. 2009, 50, 991. Fersing, Molecules 2019, 24, 2866

OP-0628

Fully Automated Radiosynthesis of [^{89}Zr]Zr-DFOSq-Durvalumab for Clinical PET Imaging of PD-L1

C. Wichmann[1,2,3], S. Poniger[3], N. Guo[1], P. Roselt[4], S. Rudd[5], P. S. Donnelly[5], F. Hegi-Johnson[4], M. MacManus[4], A. M. Scott[1,2,3]; [1]Olivia Newton-John Cancer Research Institute, Heidelberg, AUSTRALIA, [2]La Trobe University, Bundoora, AUSTRALIA, [3]Austin Health, Heidelberg, AUSTRALIA, [4]Peter MacCallum Cancer Centre, Melbourne, AUSTRALIA, [5]The University of Melbourne, Parkville, AUSTRALIA.

Aim/Introduction: Targeting immune checkpoint proteins such as PD-1/PD-L1 is changing the landscape of cancer therapy. However, changes in PD-L1 expression over the course of chemoradiotherapy treatment have not been well characterised. The ImmunoPET study aims to examine

the dynamics of PD-L1 expression via ^{89}Zr-Durvalumab PET imaging before, during and after chemoradiotherapy. To support the large number of clinical productions required for this study, we have developed a fully automated protocol for the radiosynthesis of [^{89}Zr]Zr-DFOSq-Durvalumab. **Materials and Methods:** Automated radiolabelling of DFOSq-Durvalumab with zirconium-89 and subsequent formulation was optimized using a disposable cassette-based synthesis module. Activity losses were minimized by optimizing fluid transfers, reaction buffer, antibody formulation additives and pH. Quality control was performed on the formulated product to satisfy clinical release criteria. Results: DFOSq-Durvalumab with an average chelator-to-antibody ratio of 3.69 was used for radiolabelling experiments. Reaction kinetics in sodium succinate pH 6 were significantly faster compared to HEPES pH 7.2 with 90% conversion observed in 15 and 60 minutes, respectively. This buffer and pH change also reduced the amount of residual radioactivity in the Zr-89 isotope vial from 24% to 0.4% ± 0.2% (n=7). Further radioactivity losses in the form of [^{89}Zr]Zr-DFOSq-Durvalumab were seen in the reactor vial which could be reduced by addition of 0.02% Tween 80 to the reaction buffer decreasing losses from 36% ± 6% (n=4) to 0.8% ± 0.8% (n=4). Interactive peak collection via the PD-10 column radiation profile allowed reproducible collection of the product fraction with low amounts of radioactivity remaining on the PD-10 column (2.9% ± 1.0%, n=5). Residual on the sterile filter was 5.0% ± 2.7% (n=4) and the remaining kit components accounted for 4.3% ± 1.4% (n=3) of radioactivity losses. Overall, the process yield was improved from 13% to 73% ± 7% (n=4) and the process time was 45 minutes. Typically, 164 MBq of product was formulated in a volume of 2.1 mL with a specific activity of 182 MBq/mg. Radiochemical purity and immunoreactive fraction were always >99% and >93% at end-of-synthesis, respectively, and dropped to 90% and 74% after incubation in human serum for 7 days at 37°C. SE-HPLC analysis of formulated [^{89}Zr]Zr-DFOSq-Durvalumab showed very good antibody integrity with levels of aggregation at 3.8% ± 0.7% (n=4). **Conclusion:** Fully automated production of [^{89}Zr]Zr-DFOSq-Durvalumab for clinical use was achieved with minimal exposure to the operator. **References:** none

OP-0629

Optimization and automation of radiolabeling FAPI-74 using [^{18}F]AlF chemistry

M. Laube, J. Pietzsch, T. Kniess, K. Kopka, O. Neels;
Helmholtz-Zentrum Dresden-Rossendorf, Dresden, GERMANY.

Aim/Introduction: In recent years quinoline-based small molecules targeting the fibroblast activation protein alpha (FAP) have gained interest for imaging a variety of tumor entities (1). A number of radiotracers for SPECT and PET have been developed, but so far only three FAP inhibitor (FAPI) radioligands have been reported to be radiolabeled with fluorine-18 (2,3,4). This study shows the optimization and automation of the radiofluorination of FAPI-74. **Materials and Methods:** (S)-(4-Carboxymethyl-7-{2-[4-(3-{4-[2-(2-cyano-pyrrolidin-1-yl)-2-oxoethylcarbamoyl]-quinolin-6-yloxy}-propyl)-piperazin-1-yl]-2-oxo-ethyl}-[1,4,7]triazonan-1-yl)-acetic acid, commonly referred to as FAPI-74, was radiolabeled using the [^{18}F]AlF chelation method. Starting from [^{18}F]fluoride, the reaction with $AlCl_3$, chelate formation and subsequent purification was initially optimized by manual syntheses. Optimization included the examination of different anion exchangers (QMA light, $PSHCO_3$) and elution solutions (NaOAc buffer pH4, 0.9% NaCl) as well as careful adjustment of the reaction parameters time (0-20 min), temperature (r.t. to 100°C), amount of $AlCl_3$ and NaOAc buffer pH4, solvents (DMSO, EtOH), and precursor concentration (1-350 µM). Radiochemical conversion (RCC) was determined by radio-UPLC of the crude reaction mixtures. Selected reaction mixtures were analyzed after decay using UPLC-MS to identify non-radioactive byproducts. The optimized radiosynthetic procedure was transferred to a fully automated radiosynthesizer (TRACERlab FX_{FN}) and the final product was purified and formulated using semi-preparative HPLC and SPE. Results: Under optimized conditions, RCC of [^{18}F]AlF-FAPI-74 of > 99% was still observed at precursor concentrations as low as 12 µM FAPI-74 after reaction in a 1:1 molar ratio with $AlCl_3$ in DMSO/sodium acetate buffer at pH 4 at 80°C for 15 minutes. Transfer of optimized conditions and upscaling was successfully achieved and delivered radiochemical pure [^{18}F]AlF-FAPI-74 formulated in EtOH suitable for further preclinical experiments. Work on a more rapid SPE-purification and full characterization according to GMP guidelines is in progress. **Conclusion:** The radiosynthesis of [^{18}F]AlF-FAPI-74 was optimized and automated, which in the future will allow the production of large quantities and the distribution of this promising radiotracer to other (clinical) centers. **References:**
(1) Altmann A et al. The latest developments in imaging fibroblast activation protein (FAP). J. Nucl. Med. 2021, 62(2) 160-167. (2) Giesel FL et al. FAPI-74 PET/CT Using Either ^{18}F-AlF or Cold-Kit ^{68}Ga Labeling: Biodistribution, Radiation Dosimetry, and Tumor Delineation in Lung Cancer Patients. J. Nucl. Med. 2021, 62(2) 201-207. (3) Jiang X et al. FAPI-04 PET/CT using [^{18}F]AlF Labeling Strategy: Automatic Synthesis, Quality Control, and in vivo Assessment in Patient. Front. Oncol. 2021, 11:649148.

OP-0630

An efficient route to obtain (radio)fluorinated or (radio) iodinated 1,2,3,4-tetrahydro-7-hydroxyisoquinoline-3-carboxylic acid (TIC(OH)) analogues as potential radiotracers for imaging of solid tumours

A. Maisonial Besset[1], M. Chao[1], A. Serre[1], E. Debiton[1], D. Canitrot[1], T. Witkowski[1], F. Degoul[1], S. Tarrit[1], B. Wenzel[2], E. Miot-Noirault[1], J. M. Chezal[1];
[1]UMR1240 IMoST INSERM Clermont Auvergne University, Clermont-Ferrand, FRANCE, [2]Helmholtz-Zentrum Dresden-Rossendorf, Institute of Radiopharmaceutical Cancer Research, Research Site Leipzig, Leipzig, GERMANY.

Aim/Introduction: The use of radiolabelled amino acids (AAs) can provide high contrast SPECT/PET imaging of solid tumours. Among them, radiohalogenated tyrosine analogues ([^{123}I]IMT, [^{18}F]FDOPA, [^{123}I]8-iodo-L-TIC(OH), etc) were developed mainly for imaging of neuroendocrine, prostatic and brain tumours. While radioiodinated derivatives are easily available via electrophilic aromatic substitutions with radioactive I^+, radiofluorinated tyrosine analogues are difficult to obtain. Indeed, direct radiofluorination of electron-rich aromatic structures from [^{18}F]F^- remains a challenge as evidenced by the number of emerging methods recently published. The progresses reported for the radiosynthesis of the [^{18}F]FDOPA illustrate the new opportunities to produce radiofluorinated arenes that could not be routinely accessed even a few years ago. Surprisingly, the [^{123}I]8-iodo-L-TIC(OH), a promising radiotracer for SPECT imaging of prostatic tumours, did not benefit from these methodological advances and no corresponding radiofluorinated derivatives, which could allow the use of the TIC(OH) scaffold for PET imaging, were reported so far. **Materials and Methods:** A convergent synthetic route was developed to produce radioiodinated [^{125}I]iodo-L-TIC(OH), and radiofluorinated [^{18}F]fluoro-L-TIC(OH) tracers from common organotin intermediates, synthesized from iodinated analogues via palladium catalyzed I/$SnMe_3$ exchange. The [^{125}I]iodo-L-TIC(OH) radiotracers were obtained by electrophilic radioiododestannylation with [^{125}I]I^+, while the radiofluorinated analogues [^{18}F]fluoro-L-TIC(OH) were produced from the organotin precursors by copper-mediated aromatic radiofluorination using nucleophilic [^{18}F]F^-. For control of the purity, molar activity and enantiomeric excess, corresponding iodinated and fluorinated derivatives from the L and D series were synthesized. Results: Organotin compounds were radiolabelled using no-carrier-added [^{125}I]NaI in the presence of Chloramine-T as mild oxidative agent at room temperature for 5 minutes with excellent labelling efficiencies (> 95%). After a two-step deprotection sequence and semipreparative RP-HPLC purification, [^{125}I]iodo-L-TIC(OH) compounds were isolated with good radiochemical yields (RCY, 51-78%), high radiochemical purities (RCP, > 98%), molar activities (> 1.5-2.9 GBq/µmol) and enantiomeric excess (e.e., > 99%). [^{18}F]fluoro-L-TIC(OH) derivatives were obtained by radiofluorination of organotin compounds in presence of tetrakis(pyridine)copper(II) triflate catalyst and nucleophilic [^{18}F]F^- at 110 °C for 10 minutes with high labelling efficiencies (54-92%). After purification by C18 solid phase extraction, deprotection under acidic conditions and semipreparative RP-HPLC purification, [^{18}F]fluoro-L-TIC(OH) radiotracers were produced with good RCY (23-37% d.c.), high RCP (> 99%), molar activities (19,7-107 GBq/µmol) and e.e. (> 99%). **Conclusion:** A short and efficient synthetic pathway was developed to produce [^{125}I]iodo-L-TIC(OH) and [^{18}F]fluoro-L-TIC(OH) compounds from common organotin intermediates. In vitro studies on human cancer cell lines are ongoing to evaluate the potential of these radioligands to target AAs transporters. **References:** none

OP-0631

Synthesis and characterisation of the corresponding Cu, In and Lu complexes of a cyclen based chelator with four methylimidazole arms

***I. Hierlmeier**, P. Pfeiffer, T. Stemler, S. Maus, S. Ezziddin, M. Bartholomä;*
Saarland University Medical Centre, Homburg, GERMANY.

Aim/Introduction: We recently introduced a chelating platform based on the macrocycle tacn (1,4,7-triazacyclononane) with additional azaheterocyclic arms.[1] As this chelator enabled the synthesis of trimeric tracers proving to be more potent than monomeric tracers, we aimed to prepare the novel chelator DOTI-Me with four methylimidazole substituents based on the macrocycle cyclen (1,4,7,10-tetraazacyclododecane).[2] The study included the determination of the complex formation and radiolabelling properties with the clinically relevant metal ions $^{64}Cu^{2+}$, $^{111}In^{3+}$ and $^{177}Lu^{3+}$. **Materials and Methods:** DOTI-Me was synthesised in analogy to the methods described for NOTI-Me by reductive amination.[1] Radiolabelling with $^{64}Cu^{2+}$, $^{111}In^{3+}$ and $^{177}Lu^{3+}$ was tested in 0.1 M NaOAc pH 4.0, 4.5, 5.5, 0.1 M MES pH 5.5, 0.1 M HEPES pH 7.4, 8.2, 0.1 M NH_4OAc pH 8.2 for 15 min at 95°C for $^{111}In^{3+}$ and $^{177}Lu^{3+}$, and at RT for $^{64}Cu^{2+}$. Radiochemical yield (RCY) was determined by TLC and HPLC. Radiocomplex stability was assessed by serum stability and DTPA challenge experiments. DOTI-Me and corresponding non-radioactive metal-complexes were characterised by NMR spectroscopy and single crystal X-ray diffraction. Results: DOTI-Me was prepared in nearly quantitative yield (90%). RCYs for ^{64}Cu were >95% for all conditions except 0.1 M HEPES 7.4 and >95% for ^{111}In for all conditions. For ^{177}Lu, only in media with pH >5.5, RCYs ~80% could be achieved. The ^{177}Lu, ^{111}In and ^{64}Cu DOTI-Me complexes were of high stability with >80%, >95% and >91% intact radiocomplex after 21 h for ^{64}Cu/^{111}In and 44 h for ^{177}Lu in both serum stability and DTPA challenge experiments, respectively. The

Cu(DOTI-Me) complex revealed either a 5- or 6-coordinate geometry in the solid state. X-ray analysis of the In(DOTI-Me) complex showed a 8-coordinate complex, in which the In^{3+} cation is bound to four amino groups of cyclen and four imidazole N donors. NMR studies suggest a 9-coordinate complex in solution with an additionally coordinated water molecule. In solution, the Lu(DOTI-Me) complex exhibited an 8-fold coordination similar to the In-complex. **Conclusion:** DOTI-Me exhibited excellent radiolabelling properties for ^{64}Cu, ^{111}In and ^{177}Lu and corresponding complexes were of high stability in vitro. Results suggest that DOTI-Me might be a suitable candidate for the development of ^{64}Cu-, ^{111}In- and ^{177}Lu-labeled radiopharmaceuticals. **References:** [1] RSC Adv., 2016, 6, 119-131[2] Mol Imaging Biol, 2021, 23, 95-108

OP-0632

Preclinical proof of concept study towards modifiable ^{225}Ac-chelators for mild condition labeling and PSMA-targeting

F. Reissig[1], D. Bauer[1], K. Zarschler[1], Z. Novy[2], K. Bendova[2], M. Ludik[1], K. Kopka[1], H. Pietzsch[1], M. Petrik[2], C. Mamat[1];
[1]Helmholtz-Zentrum Dresden-Rossendorf, Institute of Radiopharmaceutical Cancer Research, Dresden, GERMANY, [2]Palacky University Olomouc, Faculty of Medicine and Dentistry, Institute of Molecular and Translational Medicine, Olomouc, CZECH REPUBLIC.

Aim/Introduction: Targeted alpha therapy is intensively investigated in radiopharmaceutical sciences and cancer management in nuclear medicine. Especially, the alpha emitter ^{225}Ac provides excellent physical and chemical properties ($t_{1/2}$ = 10 d). Thus, it is gaining an increasing interest for the radioligand therapy of various tumor entities. The aim of this study was to synthesize macropa-based chelators that allow room temperature labeling and offer functionalization properties for a straightforward coupling of temperature-sensitive biomolecules. As a proof of concept study, the chelators were coupled to known PSMA-targeting vector molecules and were evaluated in vitro and in vivo. **Materials and Methods:** We report on the chemical synthesis and radiolabeling of two PSMA-targeting ligands. Radiolabeling was performed using [^{225}Ac]Ac^{3+} and 0.2 M ammonium acetate at room temperature. Complex formation and stability were verified by HPLC and TLC analyses. Long-term complex stability was investigated over 10 days in 0.2 M ammonium acetate as well as with and without 0.1 M ascorbic acid or 0.1 M 2,5-dihydroxybenzoic acid, respectively. Binding affinity studies and cell survival were performed on human PSMA-positive prostate adenocarcinoma (LNCaP) cells and biodistribution studies were performed in healthy and LNCaP tumor-bearing mice. Results: Two PSMA-targeting molecules (one vs. two binding motifs) were synthesized and the radiolabeling procedure was established. Complex formation was successfully tested for both conjugates applying ligand concentrations ≥10^{-6} M (RCY >99%). Stability up to 10 d was increased by adding of 0.1 M 2,5-dihydroxybenzoic acid to the reaction mixture. Affinity studies on LNCaP cells revealed higher binding affinity for the PSMA conjugate with two binding motifs compared to the counterpart with only one (9.9±0.6 nM vs. 38±8 nM). These differences were verified by cell survival evaluation and biodistribution studies, both showing higher efficiency for the same radioactivity amount on a cellular level, a higher tumor uptake (6.8±0.5%ID/g vs. 12.2±4.3%ID/g) and a rapid whole body clearance within 24 hours p.i.. **Conclusion:** The developed chelators represent potent alternatives for ^{225}Ac complexation compared to the often-used DOTA as they outcompete that ligand regarding complex stability and labeling conditions. Moreover, the broad modification possibilities expand the application of these macrocyclic chelators, especially in combination with sensitive biomolecules. Thereby, every established tumor surface target can be addressed by the presented respective ^{225}Ac-macropa labeling approach to be adapted on the respective binding vector by using the right conjugate chemistry. Thus giving us the promise on bright prospects for the future targeted alpha therapy options. **References:** none

OP-0633

Radiosynthesis of [^{11}C]Flumazenil and [^{11}C]Deprenyl using a fully automated iMiDEV microfluidic radiosynthesizer

H. Mallapura Chandrashekara[1], L. Tanguy[2], B. Långström[3], L. Le Meunier[2], C. Halldin[1], S. Nag[1];
[1]Karolinska Institutet, Stockholm, SWEDEN, [2]PMB Alcen, Peynier, FRANCE, [3]Uppsala University, Uppsala, SWEDEN.

Aim/Introduction: Positron emission tomography (PET) is a molecular imaging technique for diagnosis of various clinical applications and drug discovery. Many PET ligands labelled with different radionuclides such as ^{11}C, ^{18}F are already available. There still is a need to develop platforms to facilitate easy production of those radioligands or to be developed. Microfluidic technology can increase the speed of the labelling and improve efficiency of the labelling process. We have recently introduced a fully automated microfluidic platform (iMiDEV) with a microfluidic-based cassette for a single dose or on-demand dose production of Na^{18}F.[1] [^{11}C]flumazenil and [^{11}C]deprenyl are two radioligands for benzodiazepine receptors and monoamine oxidase-B (MAO-B) respectively. In this study, we aimed to explore methods for the routine syntheses of [^{11}C]flumazenil and [^{11}C]deprenyl using the automated iMiDEV radiosynthesizer. **Materials and Methods:** [^{11}C]CH_3I or [^{11}C]CH_3OTf synthesized from [^{11}C] methane, produced from a GEMS PET-trace Cyclotron using 16.4 MeV protons was transferred to the connected iMiDEV microfluidic synthesizer using a dedicated microfluidic-based cassette. A semi-preparative HPLC system was used for the purification. Appropriate precursors were loaded with a

base on the micro-scale reactor filled with C-18 beads. [^{11}C]CH_3I or [^{11}C]CH_3OTf in a carrier-gas was passed through the reactor at room temperature. After the reaction, the crude reaction mixture was injected into the HPLC for further purification followed by the isolation on C-18 beads as well as the formulation of the products with phosphate-buffered saline containing 10% ethanol. All steps except the HPLC purification were performed automatically in the microfluidic cassette by the synthesizer. The radiochemical purity and identity of the products were determined by analytical HPLC. Results: Different parameters, such as precursor quantity (150-600 µg), starting volume of the precursor solution (100-200 µL), an initial amount of radioactivity of [^{11}C]CH_3I/[^{11}C]CH_3OTf (1,5-5 GBq) were explored to assess their influence on the final yields. After optimizing suitable conditions for both radioligands [volume: 150 µL and precursor: 300 µg], we successfully synthesized [^{11}C]flumazenil (n=14, Y=30±13%) and [^{11}C]deprenyl (n=8, Y=33±7%). Radiochemical purity was >99% and total synthesis time was about 30 min for both. **Conclusion:** Synthesis of [^{11}C]flumazenil and [^{11}C]deprenyl using microfluidic cassette on an automated iMiDEV microfluidic synthesizer were explored. **References:** 1. O. Ovdiichuk, H. Mallapura, F. Pineda, V. Hourtané, B. Långström, C. Halldin, S. Nag, F. Maskali, G. Karcher and C. Collet, Implementation of iMiDEV™, a new fully automated microfluidic platform for radiopharmaceutical production, Lab Chip 2021, In press.

OP-0634

Development of in-House Synthesis and Quality Control of [^{99m}Tc]Tc-PSMA-I&S

E. Plhak[1,2], C. Pichler[2], E. Gößnitzer[2], R. M. Aigner[1], H. Kvaternik[1];
[1]Medical University of Graz, Department of Radiology, Division of Nuclear Medicine, Graz, AUSTRIA, [2]University of Graz, Institute of Pharmaceutical Sciences, Department of Pharmaceutical Chemistry, Graz, AUSTRIA.

Aim/Introduction: [^{99m}Tc]Tc-PSMA-I&S is not only intended to use in the diagnosis, but also can be a therapeutic option for prostate cancer patients by radio guided surgery (1). Since there is no approved kit available [^{99m}Tc]Tc-PSMA-I&S has to be prepared in the radiopharmacy.(2) Therefore, our aim was to establish a validated preparation of [^{99m}Tc]Tc-PSMA-I&S in our laboratory. **Materials and Methods:** A Scintomics GRP 4V module with the SCC software package for programming sequences was used. Disposable cassettes for the labelling of ^{68}Ga-peptides were modified. The precursor (40 µg of PSMA-I&S in 4 mg mannitol) was dissolved in HEPES buffer and transferred into the reaction vessel. An acidic solution of $SnCl_2$ and ascorbic acid was added as well as NaOH. [^{99m}Tc]TcO_4^- was purged into the reaction vessel with N_2. After labelling at 105 °C for 20 min the reaction solution was purified on the Sep-Pak C18 light cartridge. Subsequently it was sterile filtered and formulated by addition of PBS. A HPLC method was validated for the determination of radiochemical and chemical purity using an ACE®3 C18 column (150 x 3.0 mm) eluted by gradient elution with acetonitrile/water + 0.1 % TFA (v/v). ITLC SG plates and the standard solvent for the quality control of ^{68}Ga-labelled peptides MAM (methanol: ammonium acetate 1 M, 1:1.) were used for determination of reduced hydrolysed [^{99m}Tc]TcO_2. Results: An automatic sequence for the synthesis of [^{99m}Tc]Tc-PSMA-I&S was created. A concentration of 0.3 µmol/ml NaOH (pH 8.5) in the reaction mixture resulted in maximum radiochemical yields of 59.2 ± 2.8 % (n=3). The addition of ascorbic acid was essential to prevent radiolysis of the peptide. The radiochemical purity of the product was 93.6 ± 0.4 %. The amount of free [^{99m}Tc]TcO_4^- and reduced hydrolysed [^{99m}Tc]TcO_2 was <2 %. HEPES amount per patient dose was <200 µg. All preparations were free of endotoxins and sterile. **Conclusion:** We developed an automated process for the preparation of [^{99m}Tc]Tc-PSMA-I&S with respect to good manufacturing practice (GMP). The addition of NaOH and ascorbic acid to the reaction solution had a positive impact on the radiochemical yield. The presented procedure for the automatic preparation and quality control is reliable and well applicable in the clinical setting. **References:** (1)Robu S, et al. J Nucl Med. 2017; 58:235-242. (2)Aalbersberg EA, et al. EJNMMI Radiopharmacy and Chemistry. 2020; 5:10

OP-0635

Patient Dose Formulation of ^{90}Y-CHX-A″-DTPA-Rituximab Using Indigenously sourced ^{90}Y-Acetate sourced from Nuclear Reprocessing Waste

A. Mitra[1], A. Chakraborty[2,3], S. Sahu[2], M. Tawate[2], S. Lad[2], S. Gaikwad[2,3], T. Upadhye[2], S. Menon[3,4], M. Ray[2], A. Damle[2], S. Kulkarni[2,3], S. Banerjee[3,5];
[1]MCF, RMC, BRIT, Parel, Mumbai, INDIA, [2]RMC, BARC, Parel, Mumbai, INDIA, [3]HBNI, Mumbai, INDIA, [4]HPD, BARC, Trombay, Mumbai, INDIA, [5]ACTREC, TMC, Navi Mumbai, INDIA.

Aim/Introduction: Zevalin® (^{90}Y-DTPA-Rituximab) predominantly used in treatment of low-grade non-Hodgkin's lymphoma (NHL). Constituents for cold kits of methyl-DTPA-Rituximab were murine rituximab and methyl-DTPA (MX-DTPA). The inherent shortfall of this rituximab lies in the fact that the murine MAb induces Human Anti-Mouse Antibody (HAMA) responses. While the BFC, MX-DTPA is susceptible to higher chances of dissociation of ^{90}Y from DTPA due to radiolytic damage. To obviate these problems, standardization of ^{90}Y-labeled-Rituximab, using p-SCN-Bn-CHX-A″-DTPA and humanized Rituximab was envisaged. The present study describes the preparation of a single patient dose of ^{90}Y-CHX-A″-DTPA-Rituximab, using rituximab (γ-DNA origin), p-SCN-Bn-CHX-A″-DTPA and indigenously sourced ^{90}Y-Acetate. Towards this, the single patient dose preparation has been optimized. The QC parameters and in-vitro stability were validated and compared with commercial product. Pre-

clinical evaluation involving immunoreactivity, cell-binding, internalization, cell-surface absorption was carried out in Daudi cell lines whereas in-vivo biodistribution were carried out in tumors bearing SCID mice expressing circulating CD20 receptor. **Materials and Methods:** Clinical grade, indigenously sourced ^{90}Y-Acetate were used. Rituximab (10mg/mL) pre-concentrated to 100µL using ultra-centrifugal filters at 3000g (17min). Coupling of rituximab [5mg (95µL, 34.75nM)] with p-SCN-Bn-CHX-A"-DTPA [244.64µg (24.46µL, 347.5nM)] carried out at 1:10 molar ratio(pH~8) incubating at 24°C(2h) followed by 4°C(18h). The crude CHX-A"-DTPA-Rituximab purified and eluted from PD-10 using 0.2M CH_3COONa buffer(pH~5.5). pH of ^{90}Y-Acetate [100mCi(100µL)] was adjusted to 6.0 using 0.5M CH_3COONa buffer(pH~7). ^{90}Y-Acetate incubated with purified CHX-A"-DTPA-Rituximab at 37°C(60min). The crude ^{90}Y-CHX-A"-DTPA-Rituximab purified using PD-10. In-vitro stability was ascertained by evaluating RCP using radio-TLC and radio-HPLC. Human B-Cell Burkitt's lymphoma Daudi expressing CD20, used for in-vitro evaluation. In-vivo biodistribution carried out in SCID mice bearing tumor xenograft induced by Daudi cell-lines. Results: Using ^{90}Y-Acetate, pharmaceutical grade ^{90}Y-CHX-A"-DTPA-Rituximab (60mCi, n=7) were formulated with ~55% RCY ^{90}Y-CHX-A"-DTPA-Rituximab was clear, colorless, pH~4.5, RAC~10mCi/mL, RCP (TLC, R_f:0.00-0.10) and (HPLC, R_t:12.0-14.0min) was >98%. EL was <6EU/mL. Product was sterile, also stable upto 24h, on storage at -20°C. ^{90}Y-CHX-A"-DTPA-Rituximab showed rapid binding (18%) reaching plateau at 120min. The immunoreactive-fraction was 67%. Post-injection(3h), uptake in blood and kidney were 22% and 9.8% ID/gm respectively. At 24h p.i, uptake reduced to 12%(blood) and 5%(kidney) ID/gm indicating clearance. **Conclusion:** The ^{90}Y isolated from high level liquid waste, has been approved as clinical grade radiochemical. This has been utilized in the formulation of patient doses of ^{90}Y-CHX-A"-DTPA-Rituximab. This development offers an affordable treatment option to NHL patients. Further studies towards clinical translation of this promising radiopharmaceutical in patients are underway. **References:** None

OP-0636

Crown, a macrocyclic chelator for Lu-177, Bi-213, and Ac-225

H. Yang[1], L. Wharton[2], C. Zhang[3], F. Bénard[3], V. Radchenko[1], P. Schaffer[1];
[1]TRIUMF, Vancouver, BC, CANADA, [2]University of British Columbia, Vancouver, BC, CANADA, [3]BC Cancer Research Centre, Vancouver, BC, CANADA.

Aim/Introduction: Targeted radionuclide therapy (TRT) relies on three components: a targeting vector, a therapeutic isotope, and a chelator that can strongly bind with the isotope. When using DOTA (2,2',2'',2'''-(1,4,7,10-Tetraazacyclododecane-1,4,7,10-tetrayl)tetraacetic acid) to label radiometals, extensive heating is required, which may compromise the targeting vector. Furthermore, for certain isotopes such as Ac, a high precursor concentration is needed, which may cause low molar activity. New chelators that can bind with the therapeutic isotopes efficiently and stably are required to advance TRT development. **Materials and Methods:** We have developed a new macrocyclic chelator, crown (2,2',2'',2'''-(1,10-dioxa-4,7,13,16-tetraazacyclooctadecane-4,7,13,16-tetrayl)tetraacetic acid) (1). We studied its complexation with Lu-177, Bi-213, and Ac-225. We then synthesized crown-αMSH peptide and studied its radiolabeling and serum stabilities with the isotopes. Furthermore, we also studied the biodistribution of Ac-225-crown-αMSH in B16F10 tumor-bearing mice at 2 hours post-injection. Results: Crown can label Lu-177, Bi-213, and Ac-225 at ambient temperature and low concentrations efficiently. In the case of Ac-225 and Lu-177, crown can quantitatively label at a concentration 100 times lower than DOTA. The crown-αMSH peptide can coordinate with these radioisotopes under similar conditions, and the resulting complexes are stable in human serum for up to 7 days. Biodistribution of Ac-225-crown-αMSH in B16F10 tumor-bearing mice demonstrated high tumor uptake and low uptake in other tissues or organs, including the liver, indicating good in vivo stability. **Conclusion:** Crown is a useful chelator for radioisotopes such as Lu-177, Bi-213, and Ac-225. Future studies include the therapy studies and its radiolabeling with other isotopes, especially imaging isotopes. **References:**
1. Yang, Hua, Chengcheng Zhang, Zheliang Yuan, Cristina Rodriguez-Rodriguez, Andrew Robertson, Valery Radchenko, Randy Perron, Denise Gendron, Patrick Causey, Feng Gao, François Bénard, and Paul Schaffer. 2020. "Synthesis and Evaluation of a New Macrocyclic Actinium-225 Chelator, Quality Control and in Vivo Evaluation of 225Ac-crown-αMSH Peptide." Chemistry - A European Journal 26(50):11435-40.

OP-0637

Impact of DOTA position on biodistribution of ^{177}Lu-labelled ABD-fused affibody molecules

Y. Liu[1], A. Vorobyeva[1,2], T. Xu[1], A. Orlova[1,2], A. Loftenius[3], J. Feldwisch[3], P. Jonasson[3], F. Frejd[3,1], V. Tolmachev[1,2];
[1]Uppsala University, Uppsala, SWEDEN, [2]National Research Tomsk Polytechnic University, Tomsk, RUSSIAN FEDERATION, [3]Affibody AB, Solna, SWEDEN.

Aim/Introduction: Human epidermal growth factor receptor 2 (HER2) is overexpressed in many cancers. Affibody molecules, small (7 kDa) scaffold proteins, demonstrated excellent targeting of HER2 in vivo, but their renal uptake is too high for radionuclide therapy. We have previously demonstrated that lutetium-177 labelled fusion of anti-HER2 Affibody molecule with albumin binding domain (ABD) had significantly reduced renal uptake. In this study we aimed to evaluate if the position of DOTA

chelator influences biodistribution and targeting properties of ABD-fused Affibody molecules. **Materials and Methods:** The targeting agents contained an affibody molecule ZHER2:2981 and ABD fused to the C-terminus of the Affibody molecules. For site-specific labelling, unique cysteines were introduced either at C-terminus (construct designated ABY-027) or at position 76 of ABD, opposite to albumin binding site (construct designated ABY-271). A maleimido derivative of DOTA chelator was conjugated to these cysteines, and conjugates were labelled with ^{177}Lu. In vitro evaluation was performed using HER2-expressing SKOV-3 and BT-474 cell lines. The biodistribution of ^{177}Lu-labeled conjugates was measured in Balb/c nu/nu mice bearing HER2-positive SKOV-3 and HER2-negative Ramos xenografts. Results: The labelling of ABY-271 and ABY-027 with ^{177}Lu provided radiochemical yield of over 95%. The labelled compounds were stable in the presence of large excess of EDTA. The binding of radiolabelled conjugates to SKOV-3 and BT-474 cells was specific. The affinity of binding to SKOV-3 cells was 321±66 pM (^{177}Lu-ABY-271) and 674±29 pM (^{177}Lu-ABY-027) in the presence of human serum albumin. Biodistribution of both variants demonstrated a slow blood clearance and low renal uptake. The in vivo targeting of HER2-expressing xenografts was specific. The tumour uptake of ^{177}Lu-ABY-027 (36±14 and 12±2 %ID/g at 48 and 168 h, respectively) did not differ significantly ($p<0.05$) from the tumour uptake of ^{177}Lu-ABY-271 (21±2 and 13±2 %ID/g at 48 and 168 h, respectively). However, the renal uptake of ^{177}Lu-ABY-271 (12±1 and 5.4±2 %ID/g at 48 and 168 h, respectively) was significantly higher that the uptake of ^{177}Lu-ABY-027 (6.0±0.5 and 2.4±0.5 %ID/g at 48 and 168 h, respectively). The biodistribution data were confirmed by microSPECT/CT imaging. **Conclusion:** Positioning of a ^{177}Lu-DOTA label at C-terminus of ZHER2:2891-ABD provides noticeable better biodistribution. Even a small modification, such as the position of DOTA on ABD domain makes an appreciable impact on the biodistribution properties of radiometal-labelled Affibody molecules. Systematic studies of such impact might help to select a therapeutic conjugated with the best targeting properties. **References:** None

1209

Wednesday, October 20 - Saturday, October 23, 2021

on-demand pool, release on Wednesday, October 20 at 09:00

Cutting Edge Science Track - TROP Session: Imaging of Non-Standard Radionuclides

OP-0640

The Impact of Different ^{99m}Tc Activities on Dual Isotope Imaging for ^{166}Holmium Scout Radioembolization Procedure

M. Stella, A. Braat, M. Lam, H. de Jong, R. van Rooij;
University Medical Center, Utrecht, NETHERLANDS.

Aim/Introduction: Partition modelling allows a personalized activity calculation for holmium-166 (^{166}Ho) radioembolization. However, it requires the definition of tumor and non-tumorous liver, typically by segmentation and registration of a separately acquired contrast enhanced CT, which is time-consuming and prone to error. A dual-isotope protocol including ^{166}Ho-scout, for treatment simulation, and technetium-99m (^{99m}Tc) stannous phytate (accumulating in the healthy liver) for automated, robust healthy liver delineation was proposed[1,2]. This phantom study investigates the effect of different ^{99m}Tc activities on the ^{166}Ho-scout images and on the usability of the ^{99m}Tc images for liver segmentation. **Materials and Methods:** The liver compartment, including two tumors, of an anthropomorphic phantom was filled with 250 MBq of ^{166}Ho-chloride, with a tumor to non-tumorous activity concentration ratio of 10:1. Multiple SPECT/CT scans were acquired, ranging up to 125 MBq of ^{99m}Tc activities in the non-tumorous liver. Images were reconstructed using a commercially available protocol incorporating partial volume correction, attenuation and window-based scatter correction by applying a single combined k-factor previously estimated[3,4]. The resulting contrast recovery coefficient (CRC) of hot and cold spheres for ^{166}Ho and ^{99m}Tc respectively was measured in the tumors. Automatic segmentation of the healthy liver and the tumor volumes using ^{99m}Tc images was evaluated by recovered volume and Sørensen-Dice Index. ***Results:*** ^{166}Ho scout scatter-corrected image quality was not hampered by the different ^{99m}Tc. CRC for partial volume corrected cold spheres were approximately 100% independently of the ^{99m}Tc activity. The applied ^{99m}Tc activities were all suitable for automatic healthy liver segmentation using phantom data. **Conclusion:** It is possible to inject ^{99m}Tc activities up to at least 125 MBq without compromising the ^{166}Ho image quality, provided that a proper scatter correction is applied. ^{99m}Tc images acquired in the activity range from 25 MBq up to 125 MBq all performed equally well for the purpose of segmentation of the healthy liver. **References:** 1. Lam, M. G. E. H. et al. Eur. J. Nucl. Med. Mol. Imaging 42, 1192-1201 (2015). 2. Braat, A. J. A. T. et al. J. Nucl. Med. 57, 1423-1423 (2016). 3. van Nierop, B. J. et al. Med. Phys. 45, 3871-3879 (2018). 4. Stella, M. et al. EJNMMI Phys. 8, (2021).

OP-0641

Dicentric trial with iodine-124 PET dosimetry to optimize therapy of metastatic thyroid cancer: PET scanner's SUV verification used to check accuracy of activimeters

C. Chiesa[1], F. Severi[2], W. Jentzen[3], S. Mazzaglia[1], S. Ferretti[2], G. Gorgoni[4], E. Cazzola[4], A. Alessi[1], M. Salgarello[5], E. Seregni[1], M. Maccauro[1];

[1]Nuclear Medicine, Foundation IRCCS Istituto Nazionale Tumori, Milan, ITALY, [2]Medical Physics, Hospital IRCCS Sacro Cuore Don Calabria, Negrar, ITALY, [3]Nuclear Medicine, University Hospital, Essen, GERMANY, [4]Radiopharmacy & Cyclotron, Hospital IRCCS Sacro Cuore Don Calabria, Negrar, ITALY, [5]Nuclear Medine, Hospital IRCCS Sacro Cuore Don Calabria, Negrar, ITALY.

Aim/Introduction: The National Tumour Institute of Milan (INT) and the Sacro Cuore hospital of Negrar (Verona) recently started an AIRC funded dicentric trial based on optimization of iodine-131 therapy of metastatic differentiated thyroid cancer using iodine-124 PET dosimetry. Iodine-124 activity determination with activimeters is prone to inaccuracy in particular caused by a large amount of low energy X-rays. High accuracy in activity measurement is important in pre-treatment dosimetry. The present work aimed at the cross-calibration of activimeters and PET scanners between the two centres. **Materials and Methods:** A 15-mL vial consisting of heavy borosilicate glass (19.5 g) was used and filled with iodine-124 solution. This kind of vial will be used for oral administration. Activimeter accuracy were routinely checked with certified sources. Iodine-124 was produced in Negrar. A sealed vial was measured in Negrar with activimeter Capintec CR-25 PET, shipped with authorized vector to INT, where it was measured with the activimeter ISOMED-2010, and finally to the Italian metrology institute ENEA-INRMI close to Rome, to obtain the reference value. In INT the default setting for iodine-124 was used, while in Negrar an ad-hoc calibration factor had been previously determined. Other independent iodine-124 solutions were measured with the same instruments and settings and used to fill two NEMA94 cylindrical phantoms. PET acquisitions for SUV body weight verification were performed in Negrar with PET scanners Siemens Biograph mCT (2010) and Siemens Biograph mCT-flow (2015), while in INT with Philips Gemini 64 TF (2011) and General Electric Discovery 710 (2016). PET scanners were calibrated with fluorine-18 using the above activimeters. SUV=1.00 was verified with fluorine-18. The PET manufacturers' settings for iodine-124 and prompt gamma correction were applied. Results: The ENEA-INRMI reference value of the sealed vial was provided with an uncertainty of 2.6% (1 standard deviation). After decay correction, inaccuracy of activimeters were -15% and -5% for Negrar and INT activimeters respectively. SUV inaccuracy was +15% and +9% with mCT and mCT-Flow in Negrar, while zero percentage deviations with the two PET scanners in INT. **Conclusion:** SUV is inversely proportional to activity. Three PET scanners except the oldest seem to indicate a -9% (Negrar), 0% (INT) inaccuracy of the corresponding activimeters, as if the ENEA reference value was overestimated of 5%. This overestimation will be further investigated. If confirmed, SUV verification with the three PET scanners except the oldest could be used in reversed way to check activimeter accuracy with iodine-124. **References:** none

OP-0642

Imaging Properties and Quantification Accuracy of ^{68}Ga and ^{124}I in a New Generation Preclinical PET/CT System: A Phantom Study

A. Moraitis[1], W. Jentzen[1], P. Mollet[2], S. L. Kazek[1], J. M. Klose[1], W. P. Fendler[1], P. Fragoso Costa[1];

[1]Department of Nuclear Medicine, University Hospital Essen, Essen, GERMANY, [2]MOLECUBES NV, Ghent, BELGIUM.

Aim/Introduction: ^{68}Ga and ^{124}I are radionuclides of high interest for PET imaging and have been used both clinically and pre-clinically in the context of drug development and dosimetry. However, reliable PET requires adequate image quality and accurate quantification, which in turn is affected by the radionuclides' non-ideal physical properties (e.g., prompt gamma emission, long positron range). In this phantom study, imaging properties were assessed experimentally in the β-cube preclinical PET/CT system (MOLECUBES, Gent, Belgium), and quantification accuracy was evaluated to support image data interpretation when using Ga-68 and I-124 in the preclinical setting. **Materials and Methods:** All activities measured in this study were traceable to national standards. Four phantoms were used, namely a self-made line-source phantom, the Derenzo phantom, a point-source phantom and the NEMA NU-4 2008 image quality phantom. Data were acquired within the 511 keV ± 15% energy window and were reconstructed using OSEM3D reconstruction. Corrections for dead-time, attenuation, random and scattered coincidences were applied. Spatial resolution was assessed in terms of FWHM by fitting a Gaussian function to the line profiles. Image contrast was estimated in each of the triangular sections in the Derenzo phantom. Sensitivity was determined along the axial FOV by means of prompt coincidence rate per unit activity. Recovery coefficients (RC) and spill-over ratios (SOR) were obtained according to the NEMA NU-4 2008 standard. All experiments were also conducted with ^{18}F, serving as reference. Results: Overall spatial resolution was 0.86, 1.87 and 1.98 mm for ^{18}F, ^{68}Ga and ^{124}I, respectively. The maximum value of the section-based image contrast was similar for ^{68}Ga (0.39) and ^{124}I (0.42), while about twice smaller compared to ^{18}F (0.74). Sensitivity was highest for ^{18}F with 34 cps/kBq and lowest for ^{124}I with 10 cps/kBq (30 cps/kBq for ^{68}Ga); however, differences were almost compensated after correcting for branching ratio. SORs were 13 % (^{68}Ga) and 16 % (^{124}I) in water

and 7 % in air (8 % and 6 % for ^{18}F). RCs exceeded 0.8 for ^{18}F for rods larger than 3 mm in diameter, whereas maximum RCs of 0.62 and 0.66 were obtained with ^{68}Ga and ^{124}I in the 5-mm rods, respectively. **Conclusion:** With the selected reconstruction parameters, ^{68}Ga and ^{124}I performed similarly and limitations compared to ^{18}F were primarily caused by the long positron range. Consideration of the specific limitations may help in the interpretation of image data when using these radionuclides in a preclinical setting. **References:** none

OP-0643

^{90}Y quantification using PMT- and SiPM-based PET systems: A phantom study

P. Fragoso Costa[1], W. Jentzen[1], D. Jeromin[1], W. P. Fendler[1], C. Rischpler[1], K. Herrmann[1], M. Conti[2], M. Manuel[1], D. Kersting[1];
[1]Clinic for Nuclear Medicine, Essen, GERMANY, [2]2Siemens Medical Solutions, Knoxville, TN, UNITED STATES OF AMERICA.

Aim/Introduction: Internal radiopharmaceutical dosimetry relies on accurate in-vivo quantification. Y-90 is widely used in radioembolisation, but also has applications in systemic therapies. The development of novel Y-90 based therapies such as Y-90-FAPI-46, needs accurate dosimetry. As a consequence of the low beta-plus branching ratio, Y-90 PET images are noisy. Silicon based detectors (SiPM) improve sensitivity and timing resolution. SiPM equipped PET scanners are expected to outperform the former photomultiplier tube (PMT)-based PET scanners for Y-90 imaging. We compare the size-dependent minimal quantifiable activity of Y-90 PET/CT data in SiPM- and PMT-based scanners, using a body phantom with spherical inserts, to improve dosimetry by choosing the most appropriate scanner. **Materials and Methods:** Radionuclide preparation was performed using a dose calibrator calibrated with traceable standards. The six spheres (9.7, 12.6, 17.4, 22.2, 28.0 and 37.0 mm in diameter) of a NEMA body phantom and the phantom cavity were filled with radioactive solution (signal-to-background ratio of 40). Two PET scanners were used, Biograph mCT and Biograph Vision 600, PMT and SiPM-based scanners, accordingly. A single-bed PET/CT scan with a duration of 15 min was performed. Seven scans were conducted on both scanners consecutively with an interval between each scans equivalent to one Y-90 physical half-life, resulting in a sphere activity concentration (AC) range of 3.3 MBq/mL to 120 kBq/mL. PET data were reconstructed in analogy to the QUEST study using TOF and PSF modelling. The percentage deviations between the imaged AC at different time points and the expected actual AC were calculated. A percentage deviation range of ±20% was considered acceptable. Results: Using the mCT, only spheres with diameters from 17 to 37.0 mm could be visualised. For the largest sphere, acceptable quantification was achieved for ≥700 and ≥1200 kBq/mL for PSF+TOF and TOF, respectively. For the spheres from 17 to 28 mm, the minimum quantifiable AC was ≥1200 and ≥2000 kBq/mL for PSF+TOF and TOF, respectively. Regarding the Vision, all spheres were detected. The largest sphere quantification was acceptable from ≥120 kBq/mL for both PSF+TOF and TOF. For the spheres from 17 to 28 mm, the minimum quantifiable AC was ≥700 kBq/mL for both PSF+TOF and TOF. For the two smallest spheres, acceptable quantification was achieved for ≥1200 kBq/mL. **Conclusion:** The results of this study demonstrate that Y-90 PET quantification on a SiPM-based scanner is improved compared to a PTM-based scanner, suggesting new applications for systemic targeted radionuclide therapy dosimetry. **References:** none

OP-0644

Phantom study of the effect of varying acquisition duration on optimisation of Bayesian penalized likelihood reconstruction for Zirconium-89 PET/CT

L. Bonney[1], M. D. Walker[1], D. R. McGowan[1,2];
[1]Oxford University Hospitals NHS Foundation Trust, Oxford, UNITED KINGDOM, [2]Oxford University, Oxford, UNITED KINGDOM.

Aim/Introduction: This investigation aims to optimise the weighting factor (beta) in Bayesian penalized likelihood (BPL) reconstruction (Q.Clear) for Zr-89 PET and investigate the effect of varying acquisition duration on the optimal beta value for quantification, beta-Q, and image quality, beta-I. The results have implications for the quantitative use of Zr-89 PET studies, such as in dosimetry and for tumour response to radionuclide therapy. In addition investigating short frame duration (high noise) Zr-89 PET images allows for an assessment of the use of gated acquisitions. **Materials and Methods:** The NEMA IEC image quality phantom was filled with 9.61 MBq Zr-89. The ratio of activity concentration in the six spheres to the background was approximately 10:1. A 60-minute acquisition was acquired on a time-of-flight (TOF) PET/CT scanner (GE Discovery 710). The data was retrospectively re-binned into acquisitions of length 3, 4, 5, 10, 15, 20 and 60 minutes. Reconstruction was performed using BPL (varying beta from 500-9000) and ordered subset expectation maximisation (OSEM). OSEM reconstruction parameters were as used by Kirchner et al. (2 iterations, 16 subsets 6.4-mm, heavy z-axis filtering and point-spread-function modelling)[1]. Mean Activity Recovery (RC), Contrast Recovery (CR) and Background Variability (BV) were measured as per the NEMA-2018 protocol. The contrast-to-noise ratio (CNR=CR/BV) was then calculated for each sphere. Beta-I was defined as the beta value that gave the maximum CNR, while beta-Q was defined as that giving the maximum RC. Beta-I and beta-Q were then compared as a function of acquisition duration. Results: For the 37-mm sphere the optimal beta-I were determined to be 6000, 6000, 6000, 3500, 3000, 2500, 1500 (±500) for 3, 4, 5, 10, 15, 20 and 60 minute acquisitions respectively. All had a greater CNR than the corresponding OSEM reconstruction. The optimal beta-Q values were determined to be 1500,

1000, 1000 for 3, 4, and 5 minute acquisitions. For longer acquisitions, the best quantification was achieved with the minimum beta investigated (500). All had a greater RC than the corresponding OSEM reconstruction. **Conclusion:** The preliminary results indicate that both beta-I and beta-Q vary with acquisition duration. Both optimised beta values are higher for shorter durations, due to the increased noise in the images. The difference between beta-I and beta-Q is greater for shorter acquisitions, due to a significant increase in beta-I to counteract the increased noise in short frames, which otherwise degrades the CNR. **References:** 1. Kirchner,J., et al. EJNMMI Phys 8, 6(2021).

OP-0645

Use of [^{89}Zr]Zr-Df-IAB22M2C CD8 PET for Directing Solid Tumor Biopsies to Assess the Immune Status Within the Tumor Microenviroment (TME)

D. Hays[1], E. St. Amour[1], C. Randall[1], I. Wilson[2], W. Le[2], R. Korn[3];
[1]CARTI Cancer Center, Little Rock, AR, UNITED STATES OF AMERICA, [2]ImaginAb, Inc., Inglewood, CA, UNITED STATES OF AMERICA, [3]Imaging Endpoints, Scottsdale, AZ, UNITED STATES OF AMERICA.

Aim/Introduction: The presence of CD8 T cells in the tumor microenviorment (TME) is predictive of treatment response to immunotherapy (IOT). Currently, only invasive procedures are available to determine CD8 T cell density which may not capture the true picture of the immune state of a lesion or patient. [^{89}Zr]Zr-Df-IAB22M2C (CD8 PET) is a novel 80 kDa minibody imaging agent that binds tightly to the CD8+ cell receptor and can be used to non-invasively track CD8 cells in the TME. An ongoing mulitcenter, phase II clinical trial is being conducted to assess the diagnostic performance of this agent compared to CD8+ cell densities by IHC. Successful outcomes of this trial requires careful percutaneous biopsy strategies to target the appropriate regions of CD8 PET activity. Our institutional approach for percutaneous biopsies for successful tissue sampling will be presented. **Materials and Methods:** Adult subjects (>18 y.o.) with metastatic solid tumors recruited into a prospective Phase II clinical trial NCT#03802123 underwent percutaneous biopsy of RECIST1.1-measurable lesions prior to and 4-6 weeks after the start of IOT. All subjects had a whole body CD8 PET. The percutaneous biopsy planning required selecting lesions that were >1.0 cm and in an anatomic location that would be safe for the passage of 18 core biopsy needles into the targeted lesion. Up to 5 core tissue samples were obtained from a single lesion either by CT or US guided approaches. The CD8 PET scan was available for review to help direct biopsy needle placement in the regions of highest CD8 PET uptake in several subjects. CD8 cell density by IHC and CD8 PET uptake with SUV-based measurements were performed through central review. Results: Of the 29 biopsy samples analyzed, a high percentage (75.9%) were considered acceptable for CD8+ cell density determination by IHC and low complication rates. Rejected samples included lack of viable tissue (10.4%) and IHC staining failures in bone lesions (13.7%). At present, the CD8 PET scans are being reviewed prior to the percutaneous biopsy session to better assist in targeting relevant regions within the tumor based on CD8 PET uptake for better tissue sampling results. **Conclusion:** Successful percutaneous biopsy planning of tumor lesions for CD8 IHC determination is critical for assessing the immune TME which in turn may be supplemented with CD8 PET scan information. **References:** None

OP-0646

Modelling Aspects for Quantitative Monte Carlo-based SPECT Reconstruction of Radium-223

J. Gustafsson[1], P. Mínguez[2,3];
[1]Department of Medical Radiation Physics, Clinical Sciences Lund, Lund University, Lund, SWEDEN, [2]Department of Medical Physics and Radiation Protection, Gurutzeta/ Cruces University Hospital/Biocruces Health Research Institute, Barakaldo, SPAIN, [3]Faculty of Engineering, Department of Applied Physics, UPV/EHU, Bilbao, SPAIN.

Aim/Introduction: The use of Monte Carlo (MC) based SPECT reconstruction for ^{223}Ra is studied using the SIMREC program [1], which in turn is based on the SIMIND MC program. Two models for the collimator and the effect of including the background count-rate in the reconstruction are investigated. **Materials and Methods:** Three spheres filled with ^{223}Ra (sphere 1: 5.5 mL, sphere 2: 11.5 mL, sphere 3: 26.4 mL) were studied. Measurements were made for 4.5 kBq/mL (cold background) and for 3.4 kBq/mL, 2.5 kBq/mL, and 1.6 kBq/mL (sphere-to-background ratio 20:1) using a SPECT/CT with a high-energy collimator, 60 projections, 55 s per projection, 4.42×4.42 cm^2 pixels, and 20% energy window at 82 keV. Images were reconstructed with SIMREC (OS-EM 40 iterations, 6 subsets). The background count-rate, i.e., the detector count-rate without any source, was measured and included as an additive term in the reconstruction. To increase speed, a collimator model based on the angular-response function (ARF) was implemented. The ARF is based on a pre-simulation where the photon detection-probability is scored as function of direction and energy. Reconstructed images using ARF were compared with the full collimator model for 20 iterations. The relative sphere activity-concentration errors were calculated. For 4.5 kBq/mL, dilated VOIs (7×7×7 dilation) were constructed, and the activity estimated for each sphere. The total activity in the phantom was studied when excluding the background count-rate in the reconstruction using whole-phantom VOIs. Results: The relative errors in sphere 3 (ARF 20 iterations) were -21%, 1%, -32%, and -35% for 4.5 kBq/mL, 3.4 kBq/mL, 2.5 kBq/mL, and 1.6 kBq/mL, and approximately the same for 40 iterations. For the full collimator model (20 iterations), the errors were -15%, -14%, -29%, and -30%. For the dilated VOIs at 4.5 kBq/mL, the relative activity errors at 20 iterations were -24%, -9%, and -3% for sphere 1, 2, and 3 for the ARF model and -13%, -4%, and 1% for the full model. For ARF 40 iterations, the total activity in the phantom was overestimated by 4% to 68%,

but the errors increased to 25% to 160% when excluding the background count-rate. The sphere activity-concentrations changed approximately 1 percentage point. **Conclusion:** The ARF collimator model allows for considerably faster reconstructions, but the activity-concentration estimates are slightly worse. Including the background count-rate in the reconstruction has small effect in high-activity regions but reduces background signal. **References:** [1] Gustafsson et al. 2018 Phys Med Biol 63 245012

OP-0647

I-131 Quantitative SUV-SPECT/CT Standardisation and Validation

T. Alkahtani[1,2,3], V. Lewington[1,2], L. Livieratos[1,2];
[1]King's College London, London, UNITED KINGDOM, [2]Guy's & St Thomas' Hospitals NHS Foundation Trust, London, UNITED KINGDOM, [3]Princess Nourah bint Abdulrahman University, Riyadh, SAUDI ARABIA.

Aim/Introduction: In addition to qualitative image assessment, quantitative SPECT/CT imaging has potential applications for I-131 molecular radiotherapy (MRT) treatment planning and response assessment in patients with benign and malignant thyroid disease. Quantitative SPECT/CT can estimate the standardised uptake value (SUV) in areas of interest. We investigated the accuracy of absolute SUV quantification of I-131 SPECT images, mainly for MRT planning purposes and potential dosimetry applications. **Materials and Methods:** Standardisation and validation were undertaken using phantom data. We used a cylindrical homogeneous phantom filled with I-131 55MBq (6.2kBq/ml) to assess the scintillation camera calibration factor (CF) (cps/MBq). The CF values for two Intevo Bold (Siemens Healthineers, Germany) systems were used to estimate SUVs. A NEMA IEC Body Phantom comprising a body/thorax-size compartment and six spherical inserts of various sizes (from 10mm to 37mm in diameter) was used to validate the accuracy of SUV quantification. The sphere-to-background ratio was 10:1(sphere concentration 0.3MBq/ml). Concentration recovery coefficients (cRC) and SUVmax were calculated for objects of different sizes. OSEM image reconstruction was performed for both phantom studies using 8 subsets over a range of iterations. Attenuation, scatter, and collimator-detector resolution, were compensated. Results: Total activity convergence reached 90% at 48 updates (iteration*subsets). Both Intevo Bold scanners presented a calibration factor of 41 cps/MBq. Maximum coefficient-of-variation (CoV) of 6% was reached at 240 updates and the lowest of 3.3% at 40 updates. However, the relative error (RE) was constantly decreasing from 4.1% after 32 updates. OSEM iterations for optimised activity concentration values, good precision was observed at 48 updates as coefficient-of-variation became 3.4% and RE 4%. Spheres cRC and SUVmax of the largest sphere reached the optimum cRC of 1 and SUVmax of 10 at 48 updates. Spheres with 28 and 22mm diameter reached 0.6 and 0.5 cRC, respectively. Eighty updates showed 1.2 cRC and 11 SUVmax followed by 0.8 and 0.6 cRC for the 28and 22mm. **Conclusion:** Reproducible, quantitative SUV estimates can be derived from I-131 SPECT/CT images using appropriate reconstruction and compensation methods. Accuracy relies upon optimising calibration factors and OSEM updates for accurate recovery (cRC, CoV, and RE). This method will now be applied prospectively to measure normal and abnormal tissue SUVs in patients undergoing SPECT/CT following I-131 MRT. **References:** none

OP-0648

Sequential vs simultaneous acquisition of 81mKr-99mTc V/Q SPECT - Influence in pulmonary embolism quantification

H. Fernando[1,2], C. Sibley- Allen[2], L. Livieratos[1,2], C. Fowler[1,2];
[1]King's College London, London, UNITED KINGDOM, [2]Guy's & St Thomas' Hospitals NHS Foundation Trust, London, UNITED KINGDOM.

Aim/Introduction: In 81mKr-99mTc V/Q SPECT for pulmonary embolism it is possible to optimise acquisition and processing parameters to manage the effects of 81mKr downscatter to produce simultaneous V/Q acquisition images with good visual diagnostic accuracy as sequential acquisition images. This results in benefits such as reduction of imaging time and reduction of misregistration, motion artefacts. In quantitative V/Q SPECT for PE the %PE is dependent on the the difference of total lung volume to perfusion volume. The effect of simultaneous 81mK - 99mTc V/Q SPECT acquisition in the perfusion volume is yet to be determined. In this study, we aim to analyse the influence of sequential and simultaneous V/Q SPECT acquisition in perfusion volume quantification. **Materials and Methods:** 17 retrospective 81mKr - 99mTc V/Q SPECT clinical studies demonstrating a good sequential/simultaneous correlation via visual reporting, with both PE positive and negative cases were selected for this study. All studies contained images from both sequential and simultaneous acquisition protocols reconstructed as per departmental standard clinical protocol with an estimation of 81mKr downscatter. Images were analysed using a SPECT volumetric quantification platform. For perfusion quantification a 30% voxel intensity threshold for sequential and 33% for simultaneous images were selected as per results of a V/Q SPECT volumetrically assessable photophenic phantom study utilizing the same protocol by our group previously. 10% higher and lower voxel intensity thresholds were also assessed for both sequential and simultaneous images for accountability of any discrepancies between the phantom and clinical studies. Results: VOIs created by the 30% and 33% thresholds for sequential and simultaneous images respectively showed the most compatibility with the visual assessment of images and the corresponding

visual reports. The quantification results of these thresholds demonstrated that 13 perfusion images displayed a >5% volume increase in simultaneous acquisition as compared to the sequential acquisition, with a range from 5% -28%. The average 81mKr percentage downscatter and the average 81mKr total counts of the >5% increased volume group were statistically significantly higher with p=0.009, p= 0.412 respectively. **Conclusion:** The mode of data acquisition (sequential/ simultaneous) may influence perfusion volume quantification in V/Q SPECT thus analysis protocols may require acquisition mode specific optimisation. **References:** None

OP-0649

Influence of V/Q SPECT reconstruction parameters on pulmonary embolism quantification

H. Fernando[1,2], S. Allen[1,2], C. Fowler[1,2], L. Livieratos[1,2];
[1]King's College London, London, UNITED KINGDOM,
[2]Guy's & St Thomas' Hospitals NHS Foundation Trust, London, UNITED KINGDOM.

Aim/Introduction: V/Q SPECT is one of the most sensitive methods for investigation of Pulmonary embolism (PE) in both acute and chronic settings that forms the basis of the 2019 EANM guidelines for PE evaluation. While current guidelines result in binary present/absent outcomes via visual assessment, additional quantification of the extent of PE may allow prognostication of patient outcomes to assist in stratification of treatment and follow up strategies. The aim of this study was to develop a phantom with a volumetrically assessable photophenic defect for optimisation of V/Q SPECT reconstruction parameters in PE quantification. **Materials and Methods:** Specially sourced sponge which allows krypton ventilation after loading with Tc99m-MAA activity was used to construct a lung compartment of 270ml containing a conical shaped defect of 70ml, the size of an average lung segment. The sponge was drenched in 200MBq Tc99mMAA then drip-dried before being introduced into the lung cavity of an anthropometric torso phantom. The lung compartment was supplied with 81mKr gas through a tube connecting to a generator. Imaging was performed using a sequential acquisition protocol. Images were reconstructed using OSEM with sub-iterations 2,4,8,16,32,64,128,256, 512 and 1024 and varying levels of Gaussian filter. The resulting 30 datasets were analysed using a SPECT viewing platform with volumetric quantification using different threshold levels. The quantified volumes were compared to the physical sponge and mismatched defect volumes. Results: The choice of voxel value thresholds for VOI quantification was affected by the reconstruction parameters used. In both ventilation and perfusion images for all reconstruction parameter variants tested, a % count intensity threshold was obtainable with a corresponding volume of <5% relative error. A count intensity threshold of 31% applied on iterations 8/ subsets 16 for ventilation images and a count intensity threshold of 24% applied on iterations 16/ subsets 16 for perfusion images with no post reconstruction filtering were determined as optimum parameters. The V/Q quotient image with a ratio threshold of 2 resulting from the above reconstruction parameters resulted in the optimum quotient image with a 0.3% relative error of the physical defect volume. **Conclusion:** From this pilot phantom assessment, volume quantification in V/Q SPECT appears feasible; the accuracy of quantification is influenced by the choice of reconstruction parameters and intensity thresholds. **References:** None

OP-0650

Ex vivo tissue analysis for translation of targeted image-guided surgery solutions

T. Buckle[1], H. de Vries[2], M. van Oosterom[1], D. van Willigen[1], M. van Alphen[2], P. van Leeuwen[2], O. Brouwer[2], B. Karakullukcu[2], H. van der Poel[2], F. van Leeuwen[1];
[1]LUMC, Leiden, NETHERLANDS, [2]Netherlands Cancer Institute - Antoni van Leeuwenhoek Hospital, Amsterdam, NETHERLANDS.

Aim/Introduction: Intraoperative tumour identification (extension/margins/metastases) via receptor specific targeting is one of the ultimate promises of fluorescence-guided surgery. The translation of receptor-specific fluorescent tracers into clinical trials forms a critical component in maturing this treatment concept. To close the gap between preclinical studies and first-in-human trials we have studied the potential of using topical applications on surgical specimens to assess both tracer and camera performance. **Materials and Methods:** Ex vivo tracer performance was assessed via incubation of freshly excised penile squamous cell carcinoma (pSCC; N=10) and oral squamous cell carcinoma (OSCC; N=10) specimens in a solution containing the c-Met targeting tracer EMI-137 (500 nM; (1)). Three prostate specimens were incubated with the PSMA-targeting tracer EuK-(SO_3)Cy5-mas3 (500 nM; (2)). Both tracers contained Cy5 as fluorescent label. All specimens were analysed using a Cy5-compatible prototype clinical grade laparoscopic camera system. In-house developed image processing software allowed video-rate/real-time tumour identification and assessment of the tumour-to-background ratio (TBR). Fluorescence imaging results were related to standard pathological tumour evaluation and immunohistochemistry. The in vivo potential of c-MET targeting, and intraoperative tumour visualization was confirmed following intravenous administration of EMI-137 in five pSCC patients using the same camera system as used for ex vivo measurements. Results: After incubation with EMI-137 or EuK-(SO_3)Cy5-mas3 91.3% of tumours could be fluorescently illuminated and detected (9/10 OSCC, 10/10 pSCC and 2/3 prostate tumours). Immunohistochemistry

revealed overlap between the fluorescence staining and c-Met or PSMA receptor expression in all illuminated specimens. Non-visualization (2/23, 8.7%) could be linked to lesions that resided deeper below the resection surface (OSCC) or highly diffuse, low grade tumour with very low density of PSMA positive cells. Tumour margin assessment was improved using video-rate representation of the TBR (median TBR: 2.5 +/- 0.2; range 1.9-4.2). This visualization technique also allowed recognition of heterogeneity in receptor expression within the lesion. With regard to EMI-137, studies on surgical specimens successfully translated to in vivo fluorescence-guided surgery, confirming the potential of the topical evaluation steps. **Conclusion:** Ex vivo evaluation on fresh tumour specimens helps 1) evaluate the ability of fluorescent tracers to target tumour specific receptors in human tissue and 2) highlights the possible limitations for in vivo use (e.g., tissue penetration, low/diffuse receptor expression). Initial data obtained with EMI-137 indicate that successful ex vivo staining could be predictive for successful in vivo use. **References:** 1) Burggraaf et al, Nat Med 2015 2) Hensbergen et al, JNM 2020

1210

Wednesday, October 20 - Saturday, October 23, 2021

on-demand pool, release on Wednesday, October 20 at 09:00

Clinical Oncology Track - TROP Session: Prostate Varia and Others

OP-0652

Combining Diffusion Weighted MRI and ^{68}Ga-PSMA PET/CT and using SUVmax/ADC ratio as a biomarker for diagnosis of biopsy naïve prostate cancer

P. Chandra[1], S. Chinnappan[2], A. Sharma[1], G. Chandran[1], J. Kumar[1], S. Nath[1];
[1]MIOT international, Chennai, INDIA, [2]Dept. of Radiodiagnosis, SRIHER, Chennai, INDIA.

Aim/Introduction: ^{68}Ga-Prostate specific membrane antigen (PSMA) PET/CT has very high accuracy in prostate cancer (PCa) detection and can potentially improve the diagnostic accuracy overcoming the low specificity noted with diffusion weighted magnetic resonance imaging (DW-MRI), especially in instances of prostate inflammation. In this study we aimed to compare these two techniques in the pre-biopsy setting as well as develop a hybrid-quantifiable parameter for PCa diagnosis. **Materials and Methods:** Prospective observation study comparing and analyzing the diagnostic accuracy of pre-biopsy DW-MRI and ^{68}Ga-Prostate specific membrane antigen (PSMA) PET/CT's done in patients with suspected PCa (raised PSA and/or positive digital rectal examination). Standard of reference was systemic 12 core trans-rectal ultrasound (TRUS) guided biopsies. Results: 67 patients were included in the study, mean age: 70 years (Range 49-84), mean PSA: 23.2ng/ml (Range 2.97-45.6). Biopsy was positive for PCa in 56% (n=38) and negative in 43% (n=29). Of the benign results, benign hyperplasia was noted in 75% (n=22) and prostatitis in 25% (n=7). Of the PCa, 55% (n=21) of were high (international society of urological pathology) ISUP grade (4-5) and 45% (n=17) low/intermediate ISUP grade (1-3). Mean apparent diffusion co-efficient (mean ADC) value of benign lesions and PCa was 1.135 x 10^{-3}mm^2/sec and 0.723 x 10^{-3}mm^2/sec respectively (p-0.00001). Mean standardized uptake maximum (SUVmax) and ADC of benign and PCa lesions was 4.01 and 16.4 (p=0.000246). Mean SUVmax/ADC ratio of benign and malignant lesions was 3.8 vs. 25.21 (p <0.000026). Inverse correlation was noted between ADC and SUVmax values (R= -0.609), inverse correlation noted between ADC and Gleason's score (R= -0.198) and positive correlation of SUVmax and SUVmax/ADC with Gleason's score (R- 0.438 and R-0.448). ROC curve analysis revealed a SUVmax cut-off 6.03 (Sensitivity/Specificity- 76%/90%, AUC-0.935, Youden index-YI- 0.66), ADC cut-off of 0.817 (Sensitivity/Specificity- 79%/86%, AUC-0.890, YI-0.65) and SUVmax/ADC ratio cut-off of 7.43 (Sensitivity/Specificity- 87%/98%, AUC-0.966, YI-0.85) for PCa diagnosis. **Conclusion:** Combination of DW-MRI and PSMA PET/CT appears to have better diagnostic accuracy than either used alone for PCa detection. SUVmax/ADC ratio is a highly accurate and promising metric and should be further validated in larger clinical trials as molecular imaging biomarker for Pca diagnosis. **References:** None

OP-0653

^{68}Ga-PSMA-11 PET/CT volumetric parameters as prognostic biomarkers in metastatic castration-resistant prostate cancer patients treated with cabazitaxel

***Q. A. Shagera**, C. Artigas, T. Gil, P. Flamen;*
Institut Jules Bordet, Université Libre de Bruxelles, Brussels, BELGIUM.

Aim/Introduction: Recent emerging data suggests ^{177}Lu-PSMA-617 is a more effective therapy than cabazitaxel in metastatic castration-resistant prostate cancer (mCRPC). Therefore, there is a need to identify patients who might not benefit from cabazitaxel therapy. We aimed to evaluate whether quantitative baseline parameters on ^{68}Ga-PSMA-11 PET/CT (PSMA-PET) can predict outcomes in mCRPC patients receiving 2nd line chemotherapy with cabazitaxel. **Materials and Methods:** We retrospectively analyzed all consecutive PSMA-PET performed in our institution between November 2014 and February 2021. Patients were included if they had been previously treated with docetaxel and novel anti-androgen therapies; underwent a PSMA-PET within eight weeks before treatment initiation; and received at least 2 cycles of cabazitaxel. PET parameters, including maximum standardized uptake value (SUVmax), mean SUV (SUVmean),

peak SUV (SUVpeak), total lesion PSMA uptake (TL-PSMA) and PSMA molecular tumor volume (PSMA-MTV) using the SUV=3 threshold, were measured. Progression-free survival (PFS) and overall survival (OS) were estimated as per PCWG3 criteria. A log-rank cut-off finder was used to define high vs. low values of the statistically significant parameters associated with PFS and OS on Cox regression. Kaplan-Meier curves and log-rank test analyses were performed. Results: Thirty-two mCRPC patients were evaluated. Median baseline PSA was 40ng/mL (interquartile, IQ 17-160). Patients received a median of 6 cycles of cabazitaxel (range 2-10). After a median follow-up of 12 months (range 2-29), 29/32 patients progressed and 18/32 died. The median (IQ) of SUVmax, SUVmean, SUVpeak, PSMA-MTV and TL-PSMA were: 19 (13-48), 5 (4-10), 15 (10-38), 165mL (87-709) and 1,164mL (458-4,977), respectively. Only PSMA-MTV was significantly associated with PFS (p=0.035). Association with OS was present for PSMA-MTV (p=0.002) and TL-PSMA (p=0.006). Optimal cut-offs of PSMA-MTV were 515mL for PFS and 473mL for OS, and TL-PSMA optimal cut-off was 2,093mL for OS. Patients with low PSMA-MTV had longer PFS and OS compared to high PSMA-MTV: median PFS 21 vs 12 weeks (HR 0.32, 95%CI: 0.13-0.82, p=0.017) and median OS 24 vs 8.5 months (HR 0.21, 95%CI: 0.08-0.57, p=0.002). Also, patients with low TL-PSMA had longer OS than those with high TL-PSMA: median OS 24 vs 9.3 months (HR 0.29, 95%CI: 0.11-0.81, p=0.018). **Conclusion:** This analysis shows that baseline PSMA-MTV and TL-PSMA are potential prognosticators of outcome in mCRPC patients receiving 2nd line chemotherapy with cabazitaxel. Between both, PSMA-MTV seems to be a stronger prognostic factor. Whether PSMA-MTV might be used to select the optimal therapeutic strategy needs further prospective validation. **References:** None

OP-0654

Japanese multicenter cohort study in patients with prostate cancer with bone metastasis using bone scan index: hormonal therapy and chemotherapy

K. Nakajima[1], A. Mizokami[1], H. Matsuyama[2], T. Ichikawa[3], G. Kaneko[4], S. Takahashi[5], H. Shiina[6], H. Horikoshi[7], K. Hashine[8], Y. Sugiyama[9], T. Miyao[10], M. Kamiyama[11], K. Harada[12], A. Ito[13], PROSTAT-BSI Investigators;

[1]Kanazawa University, Kanazawa, JAPAN, [2]Yamaguchi University, Ube, JAPAN, [3]Chiba University, Chiba, JAPAN, [4]Saitama Medical University International Medical Center, Saitama, JAPAN, [5]Nihon University School of Medicine, Tokyo, JAPAN, [6]Shimane University Faculty of Medicine, Shimane, JAPAN, [7]Gunma Prefectural Cancer Center, Ota, JAPAN, [8]National Hospital Organization Shikoku Cancer Center, Matsuyama, JAPAN, [9]Kumamoto University, Kumamoto, JAPAN, [10]Gunma University Graduate School of Medicine, Maebashi, JAPAN, [11]University of Yamanashi, Yamanashi, JAPAN, [12]Kobe University Graduate School of Medicine, Kobe, JAPAN, [13]Iwate Medical University, Yahaba, JAPAN.

Aim/Introduction: The amount of bone metastasis calculated by bone scan index (BSI) is a potential prognostic factor among patients with prostate cancer and bone metastasis. This multicenter PROSTAT-BSI study aimed to determine prognostic factors in patients under standard hormonal therapy and chemotherapy. **Materials and Methods:** A total of 247 patients (age 71 ± 8 years) with metastatic hormone-sensitive prostate cancer (mHSPC; n=148) under hormone therapy and metastatic castration-resistant prostate cancer (mCRPC; n=99) under chemotherapy were enrolled from 30 hospitals in Japan. The patients were assessed by bone scintigraphy using ^{99m}Tc-methylenediphosphonate before, and every 3-months for 12 months, then 2 and 3 years after treatment. Predictors of all-cause death including BSI, prostate-specific antigen (PSA) and bone metabolic markers were determined using proportional hazard analysis and survival analysis. Initial response rate to therapy was judged at 6 months, and compared with all-cause death. Results: During a mean follow-up of 716 ± 404 days, 81 (33%) of the patients died, and 3-year mortality rates were 20% and 52% in the mHSPC and mCRPC groups, respectively. When the patients were equally classified into tertiles based on BSI, the cutoff values were 0.9% and 3.5% for the mHSPC group, and 1% and 4% for the mCRPC group. Survival analysis showed that BSI >3.5% was a significant determinant of death in the mHSPC group. In contrast, mortality tended to higher among patients with mCRPC and high BSI (>4.0%) but not significant (p=0.073). PSA >55 ng/mL before chemotherapy, however, was a determinant of prognosis in the mCRPC group. Multiple factors such as bone alkaline phosphatase, cross-linked telopeptide parts of type I collagen, c-reactive protein, hemoglobin, BSI, and number of hot spots were significantly associated with death. When contribution of PSA and the BSI to all-cause death was compared by multivariable proportional hazard analysis, BSI was more significant (p=0.011) than PSA (p=ns) in the mHSPC group but neither was significant in the mCRPC group. A BSI >3.5% was also associated with a high incidence of PSA progression in the mHSPC group. Patients with mHSPC and a better BSI response during 6-month period (>45%) to treatment had lower mortality rates than those without such response. **Conclusion:** The amount of BSI determined before and after treatments were significant determinants of 3-year mortality, and combining BSI with PSA should contribute to management of patients with bone metastasis. **References:** none

OP-0655

PSMA PET and radiomics for the evaluation of liver metastases in castration-resistant prostate cancer patients: a multicenter retrospective study

S. Mattoni[1], F. Formaggio[1], G. Bruno[2], P. Caroli[3], J. Cerci[4], M. Eiber[5], W. Fendler[6], R. Golfieri[7], K. Herrmann[6], F. Matteucci[3], C. Mosconi[7], G. Paolani[8], M. Santoro[8], L. Strigari[8], C. Nanni[1], P. Castellucci[1], S. Fanti[1], A. Farolfi[1];

[1]Division of Nuclear Medicine, IRCCS Azienda Ospedaliero-Universitaria di Bologna, Bologna, ITALY, [2]Fundación Centro Diagnóstico Nuclear (FCDN), Buenos Aires, ARGENTINA, [3]Department of Nuclear Medicine, Istituto Scientifico Romagnolo per lo Studio e la Cura dei Tumori "Dino Amadori" (IRST), Meldola, ITALY, [4]Department of Nuclear Medicine, Quanta Diagnóstico e Terapia, Curitiba, BRAZIL, [5]Department of Nuclear Medicine, Klinikum rechts der Isar, Technical University Munich (TUM), Munich, GERMANY, [6]Department of Nuclear Medicine, University of Duisburg-Essen and German Cancer Consortium (DKTK)-University Hospital Essen, Essen, GERMANY, [7]Department of Radiology, IRCCS Azienda Ospedaliero-Universitaria of Bologna, Bologna, ITALY, [8]Department of Medical Physics, IRCCS Azienda Ospedaliero-Universitaria di Bologna, Bologna, ITALY.

Aim/Introduction: Liver metastases in prostate cancer (PC) have unfavorable prognosis. Prostate-specific membrane antigen (PSMA)-ligand positron-emission-tomography (PSMA-PET) for screening of liver lesions has not an established role, due to the high physiological background in the liver parenchyma and potential loss of PSMA-expression due to tumor dedifferentiation. We evaluated the diagnostic performance of PSMA-PET in the detection of liver metastases in castration-resistant PC (CRPC) patients, compared to conventional imaging, i.e. mupti-phase contrast enhanced CT (ceCT) or MRI, or liver biopsy. We also evaluated the ability of radiomics employed in PSMA PET/CT to predict the presence of liver metastases. **Materials and Methods:** Multicenter retrospective study enrolling patients with (a) CRPC, (b) PSMA-PET within 6 months of conventional imaging or liver biopsy, (c) no therapy changes between PSMA-PET and conventional imaging/liver biopsy. PSMA PET/CT scans were independently evaluated by three blinded readers. PSMA-PET sensitivity, specificity, positive predictive value (PPV), negative predictive value (NPV) and accuracy for liver metastases were calculated. A prediction model for presence of liver metastases was built after extraction of radiomic features. Results: Sixty CRPC patients were included among 6 recruitment centers. The median serum PSA level at the time of PSMA-PET was 6.3 ng/mL (IQR 1.6-45.3 ng/mL). Within 6 months before or after PSMA-PET, conventional imaging included CT in 32/60 (53%) patients and MRI in 19/60 (32%), whereas liver biopsy in 9/60 (15%). Overall, conventional imaging and liver biopsy identified 24/60 (40%) patients with liver metastases. PSMA-PET sensitivity, specificity, PPV, NPV, and accuracy for liver metastases were 0.58, 0.92, 0.82, 0.77, and 0.78, respectively. Inter-reader agreement for liver metastases was substantial with a Fleiss kappa of 0.762 (95% CI 0.757 - 0.767). The number of liver metastases and the maximum lesion diameter were significantly associated with the presence of a positive PSMA-PET ($p < 0.05$). Three CT-derived and four PET-derived features were significantly associated with the presence of liver metastases at conventional imaging or liver biopsy. On multivariate regression analysis, the model combining sphericity, and the moment of inverse difference (Idm), had an AUC of 0.807 (95% CI 0.686-0.920) and achieved a sensitivity and sensitivity of 0,75 and 0,87 respectively. **Conclusion:** [68Ga]Ga-PSMA-11-PET demonstrated moderate sensitivity while high specificity, positive predictive value and inter-reader agreement in the assessment of liver metastases in CRPC patients compared to conventional imaging and liver biopsy. The radiomic feature-based model may support Nuclear Physicians in correctly identifying liver metastases. **References:** None

OP-0656

Sarcopenia represents an independent adverse event in metastatic castration-resistant prostate cancer (mCRPC) patients candidates to Radium-223 therapy

F. D'Amico[1,2], R. Lai[3], M. Donegani[1,2], A. Miceli[1,2], S. Raffa[1,2], C. Campi[3], C. Delucchi[1,2], D. Schenone[3], S. Rebuzzi[4,5], G. Fornarini[4], M. Piana[3], C. Marini[1,6], S. Morbelli[1,2], G. Sambuceti[1,2], M. Bauckneht[1,2];

[1]IRCCS Ospedale Policlinico San Martino, Genova, ITALY, [2]Nuclear Medicine Unit, Department of Health Sciences, University of Genoa, Genova, ITALY, [3]Department of Mathematics (DIMA), University of Genoa, Genova, ITALY, [4]Medical Oncology Unit 1, IRCCS Ospedale Policlinico San Martino, Genova, ITALY, [5]Department of Internal Medicine and Medical Specialities (Di.M.I.), University of Genova, Genova, ITALY, [6]CNR Institute of Molecular Bioimaging and Physiology (IBFM), Segrate, ITALY.

Aim/Introduction: Androgens are known to activate anabolic pathways, which result in the gain of lean skeletal muscle (SM) mass. Androgen deprivation therapy, the standard approach for patients with metastatic prostate cancer, alters the patients' body composition promoting a significant loss in SM mass. In the present study, we aimed to assess whether SM composition parameters are associated with unfavorable overall survival (OS) in a cohort of metastatic castration-resistant prostate cancer (mCRPC) patients undergoing Radium-223 administration. **Materials and Methods:** We retrospectively evaluated 45 consecutive mCRPC patients who underwent 18F-Fluorodeoxyglucose (FDG) PET/CT before Radium-223 administration between 2015 and 2021. A computational operator-independent 3D-approach was used to extract whole psoas muscle's volumes (SM-Vol), the percentage of psoas muscle fat content (SM-%fat), and its average standardized uptake value (SM-SUVmean) from FDG PET/CT scans. Baseline established prognosticator including International Society of Urological

Pathology (ISUP) grade at diagnosis, serum Prostate-Specific Antigen (PSA), the number of metastases at bone scan, the number of previous lines of systemic treatment, the prior chemotherapy, as well as the Metabolic Tumour Volume (MTV), and Total Lesion Glycolysis (TGL) calculated from PET/CT images, were also analyzed. Results: Patients were clinically followed up for a median interval of 18.3 months. Overall, 35 (77%) patients died during this period. At the univariate analysis, along with established prognosticator such as PSA value (HR 1.001, 95% CI 1.00-1.01, p=0.02), MTV (HR 1.001, 95% CI 1.00-1.02, p=0.002), and TLG (HR 1.01, 95% CI 1.00-1.02, p=0.001), we observed that lower SM-vol (HR 0.98, 95% CI 0.97-0.99, p=0.02), higher SM-%fat (HR 534.7, 95% CI 21.9-13011.6, p=0.0001), and higher SM-SUVmean (HR 20.17, 95% CI 1.85-219.73, p=0.01) were associated with shorter OS. At the multivariate analysis, TLG and SM-%fat resulted in independent prognosticator (p=0.001 both), while SM-vol showed a tendency for OS prediction (p=0.09). **Conclusion:** The occurrence of sarcopenia (represented by the increase in SM-fat content and the reduction in SM-volume) represents an independent adverse event in mCRPC patients candidates to receive Radium-223 therapy. The mechanisms responsible for this association have not been elucidated. However, based on the increased SM-SUVmean, we presume that this phenomenon might at least partially involve the occurrence of SM inflammation. The present data suggest that assessing individual patients' sarcopenia through FDG PET/CT data may potentially guide customized strategies and support tailored treatment decision-making in mCRPC patients candidates to Radium-223. **References:** none

OP-0657

Clinical Utility of Molecular Imaging in Neuroendocrine Prostate Cancer: Comparison of ^{18}F-FDG, DOTATOC and PSMA PET/CT

J. Vargas Ahumada, O. Garcia Pérez, S. Medina Ornelas, Q. Pitalúa Cortés, E. Gomez Argumosa, E. Ignacio Álvarez, I. Soldevilla Gallardo, A. Scabuzzo, M. Jimenez Rios, L. Vargas Ahumada; Instituto Nacional de Cancerologia, Mexico city, MEXICO.

Aim/Introduction: Neuroendocrine differentiation of prostate cancer (NEDPC) includes de novo presentation or secondary to epigenetic changes (therapy induced t-NEPC). Molecular imaging with PSMA and DOTATOC PET/CT in NEDPC has not been yet validated. ^{18}F-FDG PET/CT has numerous limitations in prostate cancer (PCa) and the utility in NEDPC has only been reported in few series of cases. The objective is to compare the detection rate and SUVmax value of PSMA, DOTATOC and FDG PET/CT. **Materials and Methods:** A total of 9 histologically proven NEDPC patients; Seven t-NEPC with median age of 71 (Range, 53-87), median time from the diagnosis of adenocarcinoma (Gleason score range 8-9) to the confirmed diagnosis of NEDPC was 50 months (range, 15-120), they were all treated with androgen deprivation therapy. Five out of the seven patients had received chemotherapy, a novel androgen receptor pathway inhibitor, or both. Mean prostate-specific antigen (PSA) at the time of NEDPC diagnosis was 31.4 ng/ml (Range, 0.003-137.3 ng/ml); underwent PSMA, DOTATOC and FDG PET/CT within 2 months.Two de novo presentation patients; mean age 72, histologically report in both cases were acinar adenocarcinoma mixed with neuroendocrine cells (Synaptophysin +, Chromogranin + and PSA +) and mean PSA 29.9 ng/ml at diagnosis underwent PSMA and DOTATOC PET/CT within 2 months.We evaluated all metastatic lesions in each one of them (bone, lymph node and visceral, total of 617). Seven patients (t-NEPC) underwent 3 radiotracers and 2 patients with de novo presentation only with two radiotracers (PSMA and DOTATOC). Results: In t-NEPC patients a total of 426 lesions were identified, ^{18}F-FDG PET/CT detected 200 (Visceral n=117, Bone n=73, Lymph node n=10); PSMA-PET/CT detected 179 (Visceral n=17, Bone n=140, Lymph node n=22) and DOTATOC detected 59 lesions (Visceral n=18, Bone n=35, Lymph node n=6).In NEDPC de novo patients a total of 191 lesions were evaluated, PSMA PET/CT detected 105 lesions (Bone n=101 and Lymph node n=4) DOTATOC PET/CT 86 lesions (Bone n=81 and Lymph node n=5) and no visceral lesions were identified. In t-NEDPC the differences between ^{18}F-FDG, DOTATOC and PSMA SUVmax was statistically significance (p<0.005) **Conclusion:** NEDPC demonstrated wide inter and intra patient molecular imaging heterogeneity by PSMA, DOTATOC and ^{18}F-FDG PET/CT. ^{18}F-FDG detected most lesions in t-NEPC among all radiotracers, especially in visceral sites, even though PSMA detected more bone lesions. In de novo patients PSMA detected more lesions. DOTATOC showed no superiority in none of the scenarios. **References:** https://doi.org/10.1016/j.clgc.2021.01.008.2. doi:10.3389/fonc.2020.571308.

OP-0658

The Impact of PSMA Peptide Amount and Tumor Volume on Tumor Uptake on ^{68}Ga-PSMA PET/CT in Primary Prostate Cancer Patients

H. Siebinga[1,2], J. olde Heuvel[1], E. J. Rijkhorst[3], J. J. Hendrikx[1,2], B. J. de Wit-van der Veen[1];

[1]Department of Nuclear Medicine, Netherlands Cancer Institute, Amsterdam, NETHERLANDS, [2]Department of Pharmacy & Pharmacology, Netherlands Cancer Institute, Amsterdam, NETHERLANDS, [3]Department of Medical Physics and Technology, Netherlands Cancer Institute, Amsterdam, NETHERLANDS.

Aim/Introduction: Labelling of Gallium-68 (^{68}Ga) to PSMA-directed ligands involves conjugation of a usually fixed amount of peptide to the generator-eluate. As the radioactivity levels in the ^{68}Ge/^{68}Ga-generator eluate decrease over time, also the specific activity of the tracer will fluctuate. In most clinics the administered radioactive dose is standardized but the injected amount of peptide will vary per patient, which might influence tracer distribution and tumor accumulation. Therefore, our aim was to investigate

the relationship between administered peptide amount and PSMA uptake. Additionally, the impact of total tumor burden on tumor and organ uptake will be assessed. **Materials and Methods:** Data of 358 men with primary prostate cancer who underwent ^{68}Ga-PSMA PET/CT prior to treatment between January 2016 and May 2020 were retrospectively included. ^{68}Ga-PSMA-11 was produced according to local protocol combining 10 µg PSMA-11 to the eluate, resulting in specific activity levels between 22.6-79.1 MBq/µg. PET scans were acquired approximately 45 minutes after injection of ~100 MBq ^{68}Ga-PSMA-11. Quantification was performed by placing spherical volumes-of-interests (at least Ø 2cm) in parotid, aortic arch, liver, kidney cortex, and gluteus muscle. Primary prostatic lesions were segmented using two methods; using a threshold (20% SUV_{max}) and manual contouring at fixed window level (SUVmin-max: 0-5). Both segmentations were performed independently by two observers in 50 patients, and Dice Similarity Coefficients (DSC) were calculated. Thereafter, the most suitable approach was chosen for further segmenting. Patients were divided in three groups based on lesion volume. Correlation and multivariate regression analyses were performed to assess the impact of peptide amount and tumor volume on tumor uptake. Results: Interim analysis showed best agreement between observers for the manual segmentation approach (mean DSC=0.73). Median tumor volume was 6.72 mL (range 0.064-174 mL). Groups were based on quartiles of prostatic lesion volume: ≤4.10 mL, 4.10-20.3 mL and ≥20.3 mL. No significant differences in patient characteristics between the groups were observed. No correlation was found between administered peptide amount and SUV_{peak} or SUV_{mean} for all groups, except for a slightly significant correlation for SUV_{mean} in the first group (≤4.10 mL; R=0.27, p<0.001). Group 3 (≥20.3 mL) showed significant increased uptake in liver (SUV_{peak} and SUV_{mean}) and blood pool (SUV_{mean}). **Conclusion:** Overall, no clear relationship was observed between administered peptide amount and PSMA-11 uptake in tumor lesions or organs. The findings imply that no receptor saturation occurs in men with primary prostate cancer at peptide levels of ~2.5 µg PSMA-11. **References:** None.

OP-0659

Contribution of Ga-68 DOTA-FAPI-4 PET / CT to Tumor Imaging; First Results in 20 Different Types of Cancer

N. Ergul[1], *B. Yılmaz*[1], *G. Olguner Mercanoğlu*[2], *T. F. Çermik*[1];
[1]*Istanbul Training and Research Hospital, Department of Nuclear Medicine, Istanbul, TURKEY,* [2]*University of Health Sciences, Faculty of Pharmacy, Istanbul, TURKEY.*

Aim/Introduction: Cancer-associated fibroblasts, which are densely found in tumor tissue, express high levels of fibroblast activation protein (FAP), and FAP inhibitors (FAPI) labelled with radionuclides can be used in the diagnosis and treatment of cancer. In this study, the role of Ga-68 FAPI-4 PET / CT in imaging of primary, metastatic and recurrent cancers was investigated. **Materials and Methods:** A total of 45 patients [14 females, 31 males, mean age 58.5 (31-84)] with 20 different types of malignant diseases were included in the study. Ga-68 DOTA-FAPI-4 PET / CT imaging was performed 1-7 days after F-18 FDG PET / CT or Ga-68 PSMA PET / CT. Whole body imaging was performed approximately 60 minutes after the 7-10 mCi Ga-68 DOTA-FAPI-4 intravenous injection. Regions with more intense uptake than background activity in areas other than physiological uptake sites were considered pathological. PET findings were evaluated by comparing them with histopathological, radiological and clinical follow-up results. Results: Of the 45 patients in the study group, 37 patients were included for staging, 7 for restaging, and 1 for response to treatment. Ga-68 DOTA-FAPI-04 PET/CT showed intense uptake in 90.6% of primary tumoral lesions. It was observed that Ga-68 DOTA-FAPI-04 PET / CT detected bone, liver and peritoneum metastases with 100% sensitivity and accuracy rates were higher than F-18 FDG PET / CT for all metastases. In all 5 prostate adenocarcinoma cases with low Ga-68 PSMA uptake, increased uptake was observed in Ga-68 FAPI PET / CT in regions defined by mpMRI and malignity detected in histopathological examination. On the other hand, a very low level of Ga-68 FAPI uptake was observed in primary tumors and metastases in 2 patients with intense uptake in Ga-68 PSMA PET / CT. **Conclusion:** The findings of this study showed that Ga-68 FAPI can contribute to the diagnostic process in solid tumors. Especially in malignancies with mild uptake on F-18 FDG PET / CT, it stands out in diagnosis, staging and restaging. It can be useful in the diagnosis and treatment management of prostate cancer, especially in cases with weak uptake on Ga-68 PSMA PET / CT. It is also predicted that FAPI molecules can be used for radionuclide therapy in patients with metastatic disease and unresponsive to other treatments having intense uptake on Ga-68 FAPI PET / CT. **References:** None.

OP-0660

Utility Of ^{18}F-FDG PET / CT In The Staging And Restaging Of Thymic Epithelial Tumors

A. Laverde Mächler, *M. Domínguez Grande, H. Torres, D. Lisei, B. Fernández Llana, C. Vigil Díaz, J. Suárez Fernández, J. Maraña González, A. Álvarez, L. Rodríguez Díaz, N. Martín Fernández, F. González García;*
HUCA, Oviedo, SPAIN.

Aim/Introduction: To contribute our experience in the usefulness of ^{18}F-FDG PET/CT in the staging and restaging of Thymic Epithelial Tumors (TET) **Materials and Methods:** We retrospective analyzed a cohort of 30 patients diagnosed of TET who underwent staging and/or restaging ^{18}F-FDG PET/CT due to suspected disease relapse or analysis of metabolic response to treatment, between January 2015 and April 2021In the staging studies (12 patients), semiquantitative analysis of metabolic parameters of primary lesions was performed: maximum standardized uptake value (SUVmax), metabolic

tumor Volume (MTV) and total lesion glycolysis(TLG), investigating the relationship with their clinicopathologic stages based on the World Health Organization classification (low-risk [A-AB- B1] and high risk [B2-B3-C]) as well as and Ki67 proliferative index (<30% and> 30%). The restaging ^{18}F-FDG PET/CT findings (18 patients/46 PET/CT) were confirmed by histopathologic examination and/or follow-up and compared with those of recent contrast-enhanced CT (28 studies), if available. Results: In the staging studies, TETs had a median SUVmax/MTV/TLG of 4.79/25.11cm3/80.85g respectively. The median SUVmax/MTV/TLG of high-grade tumors (n=4) were higher (8.64/34.84cm3/285.21g, respectively) than those with low-grade (4.2/18.62cm3/58.13g, respectively), being also higher those with Ki67>30% (n=6) (7.8/39.52cm3/153.5g, respectively) compared to Ki67 <30% (n=6) (4.5/10.82cm3/25.4g). Only 2 patients had pleural metastases at diagnosis, 1 of them with a previous negative CT scan. Restaging ^{18}F-FDG PET/CT diagnosed: 4 patients with local recurrences (6 PET / CT), 7 patients with pleural metastases (16 PET / CT), 4 patients with lymphatic metastases (5 PET/CT) and 2 patients with hematogenous metastases (3 PET/CT). In patients with previous CT, false positives were detected in 4 studies and unsuspected lesions in 7, implying a change in Masaoka tumour stage in 45.4% of patients. **Conclusion:** In our experience, in the 18F-FDG PET / CT staging, the metabolic parameters of the TETs had a positive correlation with the degree of histological malignancy. The results of restaging ^{18}F-FDG PET/CT were superior to those of the contrast enhanced CT. **References:** Zhao J, Wang H, Li Q. Value of 18F-FDG PET/computed tomography in predicting the simplified WHO grade of malignancy in thymic epithelial tumors. Nucl Med Commun. 2020 Apr;41(4):405-410. doi: 10.1097/MNM.0000000000001158. PMID: 32032191. Sung YM, Lee KS, Kim BT, Choi JY, Shim YM, Yi CA. 18F-FDG PET/CT of thymic epithelial tumors: usefulness for distinguishing and staging tumor subgroups. J Nucl Med. 2006 Oct;47(10):1628-34. PMID: 17015898.

OP-0661

Usefulness of ^{18}F-FDG PET/CT in patients affected by locally advanced cutaneous squamous-cell carcinoma submitted to anti PD-1 immunotherapy with cemiplimab

L. Filippi[1], I. Proietti[2], R. Pirisino[1], C. Potenza[2], O. Bagni[1]; [1]Department of Nuclear Medicine, Santa Maria Goretti Hospital, Latina, ITALY, [2]Department of Medical-Surgical Sciences and Biotechnologies, Dermatology Unit "Daniele Innocenzi", Sapienza University of Rome, Rome, ITALY.

Aim/Introduction: Our aim was to assess the value of positron emission tomography (PET/CT) with ^{18}F-fluorodeoxyglucose (18F-FDG) in patients affected by cutaneous squamous-cell carcinoma (cSCC) submitted to the recently approved immune-checkpoint blocker cemiplimab, directed against the programmed cell death protein-1 (PD-1). **Materials and Methods:** All the subjects were submitted to PET/CT with ^{18}F-FDG before starting cemiplimab (PET-1) and after 3 months (PET-2). The following quantitative parameters were extracted from PET-1: maximum and mean standardized uptake value (SUVmax and SUVmean), metabolic tumor volume (MTV), total lesion glycolysis (TLG). Response to therapy was assessed by immune PET Response Criteria in Solid Tumors (iPERCIST), entailing a dual-time evaluation of "unconfirmed progressive metabolic disease" (UPMD) status at PET-2. Subjects with UPMD at PET-2 were re-evaluated after 4 weeks (PET-3) to confirm PMD. Patients with complete/partial metabolic response (CMR or PMR) or stable metabolic disease (SMD) at PET-2 or -3 were considered responders, while those with UPMD confirmed at PET-3 were considered non-responders and submitted to histological/cytological examination before cemiplimab discontinuation. Results: Ten patients with histologically proven cSCC and 1 with orbital cutaneous baso-squamous cell carcinoma were included. PET-1 showed tracer incorporation in sCC primary sites while five subjects (45.4%) also presented 18F-FDG uptake within regional lymph nodes. At PET-1, the average SUVmax value was 8.9, average SUVmean was 4.7, average MTV was 6.1 cc and average TLG was 27.5 g. According to iPERCIST criteria, seven subjects (63.3%) were responders (6 PMR and 1 CMR) at PET-2. Four patients presented UPMD at PET-2 and were therefore re-evaluated after 4 weeks: in all cases PET-3 confirmed PMD. In these subjects with UPMD confirmed at PET-3, progression was confirmed by histology (n =3) or cytology (n =1). Histology was also performed in the patient with baso-squamous cell carcinoma, classified as responder (PMR) at PET-2: in such a case microscopic examination showed complete regression of the squamous-cell component and persistence only of basal cell carcinoma. **Conclusion:** Our results show that 18F-FDG PET/CT, performed according to iPERCIST approach, represents a useful tool for monitoring cSCC treated with cemiplimab. **References:** None

OP-0662

Prognostic Value of Volumetric-Metabolic Parameters Obtained in F18-FDG PET/CT Imaging for the Short-term Follow-up of Patients with Advanced Bladder Cancer

T. Bahceci, E. Şahin Kütük, N. Talay, E. Özdemir; Ankara City Hospital, Ankara, TURKEY.

Aim/Introduction: In this study, it was aimed to investigate the prognostic value of volumetric-metabolic parameters and clinical parameters, which were obtained from F18-FDG PET/CT imaging, in the short-term follow-up of patients with advanced bladder cancer and to determine their impacts on overall survival (OS) and progression-free survival (PFS). **Materials and Methods:** Fifty (47 male, 3 female) patients

with advanced-stage bladder cancer who had been referred to our clinic for F-18 FDG PET/CT imaging were included in the study. Univariate and multivariate analyzes were conducted to assess the impact of TLG, MTV, SUVmax, SUVmean parameters, which were obtained from PET images, and the age, gender, histopathology, and presence of lymph node metastasis (LN) and distant organ metastasis on OS and PFS. The predictive impact of these parameters was assessed via Kaplan-Meier curves and ROC curves. Results: It was determined in the univariate analysis, which was conducted in terms of PFS, that MTV and TLG values had a significant impact on progression-free survival ($p<0.05$). It was found that those with higher MTV levels had 2,690 times more progression (95% CI 1,405-5,148). Besides, it was observed in the multivariate analysis that the presence of LN impacted PFS significantly ($p<0.05$). It was determined in the univariate analysis, which was performed in terms of OS, that the presence of LN and liver metastasis, as well as MTV and TLG variables, had a significant impact on overall survival ($p<0.05$). In the multivariate analysis, it was detected that the presence of liver and lymph node metastasis affected OS ($p<0.05$). When the patients who died and survived throughout the follow-up period were compared, it was found that MTV was higher among the patient group who died. No significant difference was determined in terms of other parameters. Accordingly, based on the ROC analysis, the cut-off value for MTV was measured to be 49.4. **Conclusion:** When clinical and metabolic parameters were assessed, it was found out that MTV was the strongest predict for OS and PFS. We suggest that in patients with advanced bladder cancer the metabolic tumor volume should be definitely evaluated in PET/CT imaging. **References:** "none"

OP-0663

Comparison 2- [18F] FDG and [68Ga] Ga-DOTA-NOC PET / CT in re-staging of patients with Esthesioneuroblastoma

L. Torres[1], F. O. García Perez[2], E. Ignacio Álvarez[2], F. A. Sinisterra Solís[2], D. A. Arguelles Pérez[2];
[1]Autonomous University of Bucaramanga, Bucaramanga, Santander, COLOMBIA, [2]The National Cancer Institute (INCan), Mexico City, MEXICO.

Aim/Introduction: Objective: To compare the PET / CT techniques using 2- [18F] FDG and PET / CT [68Ga] Ga-DOTA-NOC in esthesioneuroblastoma re-staging. **Materials and Methods:** A retrospective review of patients diagnosed with esthesioneuroblastoma who underwent PET / CT with 2- [18F] FDG and [68Ga] Ga-DOTA-NOC was conducted. The data obtained were analyzed using the STATA 14.0 statistical software. The univariate analysis performed included sociodemographic and clinical characterization of patients; A bivariate analysis was also conducted to evaluate the capacity to differentiate the PET / CT findings based on the calculation of the area under the ROC curve. Predictive values, sensitivity, specificity, and likelihood ratios evaluated the validity of the criteria used. Results: 7 patients underwent PET / CT imaging with 2- [18F] FDG while 4 patients were performed a conjoint exam with PET / CT [68Ga] Ga-DOTA-NOC. 71.43% of patients (n = 5) were men with an medin age value of 50 years old; 57.14% (n = 4) showed a modified - D Kadish classification; 28.5% (n = 2) showed progression and 57.14% (n = 4) presented relapse of the disease.20 lesions located at various areas were analyzed and the SUVmax, MTV and TLG median values of both radiotracers were evaluated, as follows. The SUVmax 2- [18F] FDG value was 4.15 (0- 8.9) while for [68Ga] Ga-DOTA-NOC was 9.6 (2.54-22.3). The MTV value of 2- [18F] FDG was 10 (5.75-42.6) while for [68Ga] Ga-DOTA-NOC was 7 (1.5-26.3); the TLG value for the 2- [18F] FDG was 21.9 (0-30.45) while for [68Ga] Ga-DOTANOC was 25.9 (7.31-114.5). A correlation analysis was conducted between the SUVmax of 2- [18F] FDG and [68Ga] Ga-DOTA-NOC to yield a weak positive result of 0.54, p = 0.02. For the volume (MTV) cm3, it was a null value of 0.57 with a p = 0.01 and for the TLG SUV-BwXcm3 it was a moderate value of 0.76 with a p = 0.001. The Cut-off points with 2- [18F] FDG were SUVmax value of 3, 9 with 60% sensitivity, 87.5% specificity, 85.6% VPP and 63.6% VPN. The cut-off points fvor 68Ga] Ga-DOTA-NOC was 4.4 with 95% sensitivity, 68.7% specificity, 79% VPP and 91% VPN **Conclusion:** We recommend the conduction of a dual study for the re-staging of patients with esthesioneuroblastoma. **References:** 1.10.1097/RLU.0000000000026442.10.1055/s-0035-15640533.10.1097/RLU.0000000000003133

1211

Wednesday, October 20 - Saturday, October 23, 2021

on-demand pool, release on Wednesday, October 20 at 09:00

Featured Session: Amino Acid Imaging of Gliomas

OP-0665

Impact of Point-Spread Function Reconstruction on Dynamic and Static FDOPA PET/CT Quantitative Parameters in Glioma

A. Girard[1], F. Madani[2], N. Chaboub[2], P. Le Reste[3], A. Devillers[1], H. Saint-Jalmes[4], F. Le Jeune[1], X. Palard-Novello[1];
[1]Centre Eugène Marquis, Rennes, FRANCE, [2]Université Rennes 1, Rennes, FRANCE, [3]University Hospital of Rennes, Rennes, FRANCE, [4]LTSI - Rennes 1 University, Rennes, FRANCE.

Aim/Introduction: Quantification of dynamic and static parameters extracted from FDOPA PET/CT plays a critical role for glioma assessment. The objective of the present study was to investigate the impact of point-spread function (PSF) reconstruction on these quantitative parameters. **Materials**

and Methods: Fourteen patients with untreated gliomas and investigated with FDOPA PET/CT were included. A 20-min dynamic images (8x15sec, 2x30sec, 2x60sec, and 3x300sec post-injection) and a 20-min static image were reconstructed with and without PSF. Volume-of-interests (VOI) were generated on the 20-min static image without PSF and projected onto the other series. Static parameters (SUVmax and SUVmean) of the tumoral and the background VOI and kinetic parameters (K1 and k2) of the tumoral VOI extracted from using full kinetic analysis and were provided. PSF and non-PSF quantitative parameters values were compared. Results: Thirty-three tumoral VOI and fourteen background VOI were analysed. PSF showed significantly higher tumor SUVmax (mean relative difference, + 7.0 %; p< 0.001), SUVmean (mean relative difference, +1.5 %; p= 0.004), K1 (mean relative difference, -20.5 %; p< 0.001), and k2 (mean relative difference -16.0 %; p< 0.001) than non-PSF parameters. Background SUVmax and SUVmean were unaffected (mean relative difference +1.2 %; p = 0.346 for background SUVmax and mean relative difference +0.9 %; p = 0.371 for background SUVmean). **Conclusion:** The present study confirms that PSF significantly increases tumor activity concentrations measured on PET images. However, the use of PSF algorithms for quantitative PET data should be performed with caution, especially for kinetic parameters. **References:** None

OP-0666

Dynamic ^{18}F-FDopa PET imaging for gliomas: is a semi-quantitative model sufficient?

T. Zaragori[1,2], M. Doyen[1,2], F. Rech[3,4], M. Blonski[5,4], L. Taillandier[5,4], L. Imbert[1,2], A. Verger[1,2];
[1]Université de Lorraine, IADI, INSERM, UMR 1254, Vandoeuvre-lès-Nancy, FRANCE, [2]CHRU-Nancy, Université de Lorraine, Department of Nuclear Medicine & Nancyclotep Imaging platform, Nancy, FRANCE, [3]CHRU-Nancy, Université de Lorraine, Department of Neurosurgery, Vandoeuvre-lès-Nancy, FRANCE, [4]Université de Lorraine, Centre de Recherche en Automatique de Nancy CRAN, CNRS UMR 7039, Nancy, FRANCE, [5]CHRU-Nancy, Université de Lorraine, Department of Neuro-oncology, Nancy, FRANCE.

Aim/Introduction: Dynamic analysis of ^{18}F-FDOPA PET very efficiently and non-invasively predicts isocitrate dehydrogenase (IDH) mutations in newly diagnosed gliomas [1]. However, the underlying kinetic model of ^{18}F-FDOPA is complex, raising the question of the rightness of using such analysis in comparison to more sophisticated graphical and compartmental models. **Materials and Methods:** Thirty-seven tumour time-activity curves from ^{18}F-FDOPA PET dynamic acquisitions of newly-diagnosed gliomas were analysed using a semi quantitative model with (Ref SQ) or without reference region (SQ), a graphical Logan model with input function (Logan) or reference region (Ref Logan), and a two-tissue compartmental model validated for ^{18}F-FDOPA PET imaging in gliomas (2TCM) [2]. The overall predictive performance of each model was assessed, by an area under the curve (AUC) comparison of multivariate analyses of all parameters included in the model. Results: The SQ model with an AUC of 0.733 showed comparable performances to other models with AUCs of 0.814, 0.693, 0.786, 0.863, respectively corresponding to Ref SQ, Logan, Ref Logan and 2 TCM (p≥0.11 for the pairwise comparisons with the other models). The SQ time-to-peak parameter had the best diagnostic performance relative to all individual parameters with an accuracy of 75.7%. **Conclusion:** The SQ model circumvents the complexities of the ^{18}F-FDOPA kinetic model and yields similar performances compared to other models most notably the compartmental model. This validates the application of the SQ model for the dynamic analysis of ^{18}F-FDOPA PET images in routine clinical practice. **References:** [1] Ginet et al. Integration of dynamic parameters in the analysis of 18F-FDopa PET imaging improves the prediction of molecular features of gliomas. Eur J Nucl Med Mol Imaging. 2020[2] Wardak et al. 18F-FLT and 18F-FDOPA PET kinetics in recurrent brain tumors. Eur J Nucl Med Mol Imaging. 2014

OP-0667

^{11}C-methionine PET for the preoperative assessment of molecular subtype and prognosis in patients with grade II/III gliomas: a retrospective study

G. Ninatti[1], M. Sollini[1], B. Bono[1], N. Gozzi[2], D. Fedorov[1], L. Antunovic[2], F. Gelardi[1], F. Pessina[1], A. Chiti[1];
[1]Humanitas University, Pieve Emanuele (MI), ITALY,
[2]Humanitas Research Hospital, Rozzano (MI), ITALY.

Aim/Introduction: PET with radiolabelled amino acids is used in the management of glial neoplasms. Guidelines recommend its implementation for the preoperative evaluation of tumour extent, biology, and prognosis, which is a crucial step in neurosurgical planning. This work aimed to study the role of [^{11}C]Methionine (MET) PET in differentiating molecular subtypes and predicting prognosis in newly-diagnosed grade II/III gliomas surgically treated. **Materials and Methods:** In this single-center, retrospective study we included patients with a new diagnosis of grade II/III glioma who underwent surgery at our institution between July 2011 and January 2021 and were imaged preoperatively (<100 days) using [^{11}C]MET-PET/CT. For all patients, we collected clinical, imaging, treatment, and outcome data. [11C]MET-PET images were qualitatively and semiquantitatively analyzed using tumour-to-background ratio (TBR). Negative exams at qualitative analysis were further classified as isometabolic or hypometabolic. We delineated the metabolically active tumour volume with LIFEx software using a TBRmax threshold >1.3. Disease recurrence or progression after treatment were defined according to the Response Assessment in Neuro-Oncology criteria. Progression-free survival (PFS) was calculated from the time of surgery. PFS rates were estimated using the Kaplan-Meier method and survival curves were compared using the log-rank test. Results: 201 histologically-

confirmed cases of grade II/III glioma met the inclusion criteria. Overall, 150 lesions (75%) showed increased [^{11}C]MET uptake. Forty (20%) and eleven (5%) were isometabolic and hypometabolic at [^{11}C]MET-PET, respectively. [^{11}C]MET uptake was more common in oligodendrogliomas and grade III IDH-wildtype astrocytomas compared to IDH-mutant and grade II IDH-wildtype astrocytomas (87% and 93% vs. 48% and 63% of cases, respectively). In [^{11}C]MET-positive gliomas, median TBRmax was highest in grade III IDH-wildtype astrocytomas and grade III oligodendrogliomas (4.65 and 3.22, respectively) and lowest in grade II IDH-wildtype and grade II IDH-mutant astrocytomas (2.34 and 2.14, respectively). Median PFS was 53.5, 38.4, and 16.6 months in oligodendrogliomas, IDH-mutant astrocytomas, and IDH-wildtype astrocytomas, respectively. Overall, 1-, 2-, and 3-year PFS rates were higher in PET-negative patients than in PET-positive ones (97.7%, 82.4%, 64.3% vs. 84.8%, 57.4%, 38.2%, respectively; p=0.022, p=0.009, p=0.015). The difference in 3-year PFS rate was greatest for IDH-mutant astrocytomas (62.5% for PET-negative and 25% for PET-positive tumours, respectively; p = 0.033). **Conclusion:** This work highlights the role of preoperative [^{11}C]MET-PET in estimating the molecular subtype of grade II/III gliomas and predicting their biological behaviour and prognosis. Our findings support the implementation of [^{11}C]MET-PET in routine clinical practice for the better management of these neoplasms. **References:** none

OP-0668

^{18}F-FET PET diagnostic and prognostic value in pre-treated glioma patients presenting with equivocal MRI findings for glioma recurrence

M. Celli, *P. Caroli, L. Fantini, V. Rossetti, I. Marini, G. Paganelli, F. Matteucci;*
Istituto Romagnolo per lo Studio dei Tumori "Dino Amadori" - IRST IRCCS, Meldola, ITALY.

Aim/Introduction: MRI-based differentiation of glioma recurrence from treatment-induced changes remains elusive in up to 30% of treated glioma patients. The aim of this study was to determine ^{18}F-FET PET diagnostic performance in this clinical scenario, its outcome dependency on established prognostic factors, optimal ^{18}F-FET semi-quantitative thresholds and whether ^{18}F-FET parameters may predict progression free survival (PFS) and overall survival (OS). **Materials and Methods:** forty-five treated glioma patients with equivocal MRI findings underwent ^{18}F-FET PET. ^{18}F-FET PET outcome relied on maximum lesion-to-brain ratio (LBRmax), time-to-peak (TTP) and time-activity curve pattern (TAC). Metabolic lesion volume (MLV) and total lesion metabolism (TLM) were calculated. Standard of reference was MRI and clinical follow-up or histology. Nonparametric statistics tested ^{18}F-FET-based parameters for dependency on prognostic markers. ROC curve analysis determined optimal ^{18}F-FET semi-quantitative cut-off values. ^{18}F-FET parameters and prognostic factors were evaluated for PFS and OS by Kaplan-Meier, univariate and multivariate analysis. Results: ^{18}F-FET PET sensitivity, specificity, positive predictive value, negative predictive value were 93.1%, 81.3%, 90%, and 86.7%. ^{18}F-FET PET outcome only differed according to performance status (KPS). ^{18}F-FET cut-off values for GR were LBRmax ≥ 2.1, SUVmax ≥ 3.5 and TTP ≤ 29 minutes. PFS differed on ^{18}F-FET outcome and related metrics and on KPS; different OS was observed according to KPS only. On multivariate analysis, ^{18}F-FET PET outcome was the only significant PFS factor; KPS and age were the only significant OS predictive factors. **Conclusion:** ^{18}F-FET PET demonstrated good diagnostic performance. ^{18}F-FET outcome and metrics were significantly predictive for PFS but not for OS. **References:** None

OP-0669

Voxel-wise Correlation of Amino Acid and TSPO PET with Relative Contrast Enhancement in T1-Weighted MRI in Gliomas

L. Kaiser[1], *A. Holzgreve*[1], *M. Unterrainer*[1,2], *F. Vettermann*[1], *J. Brosch-Lenz*[1], *A. Gosewisch*[1], *G. Böning*[1], *R. Rupprecht*[3], *J. C. Tonn*[4], *P. Bartenstein*[1], *S. Ziegler*[1], *N. L. Albert*[1];
[1]*Department of Nuclear Medicine, University Hospital, LMU Munich, Munich, GERMANY,* [2]*Department of Radiology, University Hospital, LMU Munich, Munich, GERMANY,* [3]*Department of Psychiatry and Psychotherapy, University of Regensburg, Regensburg, GERMANY,* [4]*Department of Neurosurgery, University Hospital, LMU Munich, Munich, GERMANY.*

Aim/Introduction: To enable individualized treatment and prognosis of glioma patients, a detailed spatial characterization of the tumor and its microenvironment is of high importance. In this study, voxel-wise signal from amino acid ([^{18}F]FET) and TSPO PET ([^{18}F]GE180) images was correlated with relative contrast enhancement in T1-weighted MRI data. Thus, a potential correlation between PET tracer uptake and blood-brain barrier (BBB) disruption visualized by MRI was evaluated. **Materials and Methods:** To analyze the spatial correlation between the different modalities, PET images from 28 glioma patients were normalized to healthy background (tumor-to-background ratio, TBR), and contrast enhanced (CE) MRI images were normalized voxel-wise with the respective native T1-weighted MRI images (relative CE, rCE). Dice coefficients (D) were used to quantify the spatial concordance and discordance of volume fractions. For this purpose, the total tumor volumes (D_{tot}) were segmented with a TBR or rCE threshold of 1.6. The corresponding hotspots (D_{hot}) were defined as the volumes containing the 80 hottest voxels around the voxel with maximum intensity. Additionally, voxel-wise correlation plots were used to assess the associations between TBR_{FET}, TBR_{GE180}, and rCE. Results: Only a moderate overlap of the tumor volumes from CE-MRI and PET was found (D_{tot} for rCE vs. TBR_{FET} on average 30%, rCE vs. TBR_{GE180} 28%). The overlap of the corresponding hotspots

was very small, with a mean D_{hot} of 7% and 9%, respectively. For TBR_{GE180} vs. TBR_{FET} D_{tot} was on average 54% and D_{hot} 24%. In particular, in the sub-volumes without significant contrast enhancement, a BBB-independent high uptake could be observed for both tracers. For the sub-volumes with contrast enhancement, there was a positive voxel-wise correlation of rCE with TBR_{FET} and TBR_{GE180}, but with very large variance. **Conclusion:** The discordant hotspots and high signal in volumes without contrast enhancement indicate that a potential influence of BBB-permeability on the PET signal might be small and emphasize the specificity of the PET signal. **References:** none

OP-0670

Prognostic parameters of post-therapeutic positron emission tomography using amino acids (AA PET) in malignant brain tumours

M. Schürer[1], S. Striepe[1,2], K. Jähne[3], S. Klagges[4], C. Scherlach[5], P. Kuzman[6], M. Patt[1], C. Seidel[2], O. Sabri[1], S. Hesse[1];
[1]Department of Nuclear Medicine, University of Leipzig Medical Centre, Leipzig, GERMANY, [2]Department of Radiotherapy and Radiooncology, University of Leipzig Medical Centre, Leipzig, GERMANY, [3]Department of Neurosurgery, University of Leipzig Medical Centre, Leipzig, GERMANY, [4]Clinical Cancer Registry, University of Leipzig Medical Centre, Leipzig, GERMANY, [5]Department of Neuroradiology, University of Leipzig Medical Centre, Leipzig, GERMANY, [6]Department of Neuropathology, University of Leipzig Medical Centre, Leipzig, GERMANY.

Aim/Introduction: AA PET is increasingly used in malignant brain tumours(primary, as well as metastases)after initial therapy for the differentiation of tumour progression and therapy-induced changes(e.g. radionecrosis). Besides this diagnostic value, there is also an ongoing debate about prognostic qualities of AA PET with regard to overall survival(OS). **Materials and Methods:** In order to further evaluate the prognostic significance of post-therapeutic AA-PET, we screened the database of the University of Leipzig Medical Centres Department of Nuclear Medicine for patients that received an PET with either [^{11}C]methionine or [^{18}F] fluoroethyltyrosine with simultaneous PET-MRT following initial therapy of a malignant brain tumour between October 2013 and July 2020. Clinical data and the course of the disease were extracted from clinical records and the local cancer registry. Mean and maximum standardized uptake values(SUV_{mean}/SUV_{max}), as well as mean and maximum tumor-to-backround ratios(TBR_{mean}/TBR_{max})were determined by two experienced readers. OS after PET-MRI was compared using Kaplan-Meier estimator and log-rank test after grouping patients by low/high SUV_{mean}, SUV_{max}, TBR_{mean}, TBR_{max} with the median as the cut-off. Additionally, we examined the association of those parameters with dynamic PET data, using time-activity curves(TACs), with type I(low-grade)and type II/III(intermediate to high-grade)TACs[1,2]. Results: Sixty-four patients(42 with malignant glioma, 22 with metastases; 18 female; age 54.7±14.0 years)were included. The median OS after PET was 320 days for malignant glioma and 308 days for metastases. In malignant glioma, medians were for SUV_{mean} 1.98, SUV_{max} 3.63, TBR_{mean} 1.76, TBR_{max} 3.12. Patients with values above these medians showed significantly shorter OS(SUV_{mean} p=0.034, SUV_{max} p=0.139, TBR_{mean} p=0.017, TBR_{max} p=0.039). In patients with metastases, these observations were only significant for median SUVs(SUV_{mean} 1.55(p=0.034), SUV_{max} 2.73(p=0.011), but not for median TBRs(TBR_{mean} 1.34(p=0.376), TBR_{max} 2.25(p=0.756). Brain metastases with shorter OS showed a significantly higher ratio of type II and III to type I TACs, than those with longer OS(4.0 and 0.82). In this study, the same relation between OS and TACs was not found in primary tumours(5.25 and 2.45). **Conclusion:** Post-therapeutically acquired AA PET parameters have a prognostic significance regarding OS and could gain further clinical importance in evaluating the course of the disease in malignant brain tumours. However, it appears that the distinct PET-derived parameters have specific prognostic value in either primary brain tumour or metastases but this needs further investigations in combination with MR-derived and neuro-pathological factors. **References:** 1-Law I. et al. PMID: 305198672-Galldiks N. et al PMID: 30519867 2-Galldiks N. et al. PMID: 22872742

OP-0671

Sensitivity of 18F-fluoroethyltyrosine PET in the diagnosis of recurrent high grade glioma

T. Schlürmann, S. Kleiner, W. Weber, I. Yakushev;
Technical University of Munich, School of Medicine, Klinikum rechts der Isar, Department of Nuclear Medicine, Munich, GERMANY.

Aim/Introduction: The joint EANM/EANO/RANO practice guidelines/SNMMI procedure standards for imaging of gliomas using PET with radiolabelled amino acids (Law et al., 2019) represent an important step toward standardisation of this diagnostic tool. To differentiate treatment-related changes from recurrent disease by means of 18F-fluoroethyltyrosine (FET) PET, the guidelines recommend a mean tumour-to-background ratio (TBR) of 2.0 or 1.9. In this study, we evaluated sensitivity of this cut-off in a natural cohort of patients with high grade gliomas. **Materials and Methods:** We searched our clinical data base (years 2010 to 2019) for consecutive cases with WHO III and IV gliomas, who had been referred to our department for FET-PET for the differential diagnosis of tumour recurrence and who were operated within 4 weeks (median 1.4 weeks) following imaging. Due to uncertainty in measuring the size of a purely ring-shape contrast enhancement (CE), only cases with a nodular aspect of CE were selected for further analyses (n=117). The maximum size of CE lesions was measured on T1 images by an experienced radiologist. Results: On a histopathological examination glioma recurrence was diagnosed in 113 patients. Among them a TBR ≥ 2.0 was measured in 76 patients, resulting in a cut-off sensitivity of 67 %. This subgroup showed significantly

larger CE lesions (median 23 mm) relative to the remaining 27 subjects (median 11 mm, p<0.001). TBR significantly correlated with the lesion size (Spearman r=0.50, p<0.001). There was no association with the tumour grade. When the analyses were restricted to subjects with a lesion size of > 10 mm (permutation test), cut-off sensitivity increased to 90 %. **Conclusion:** The recommended cut-off provides a rather low sensitivity in detecting high grade glioma recurrence, likely due to partial volume effects in smaller lesions. A lower cut-off may be appropriate for nodular lesions with a size of 10 mm and smaller, i.e. below a double spatial resolution (FWHM) of a conventional PET scanner. To address the issue of specificity, ongoing analyses engage cases with imaging and clinical follow-up. **References:** None

OP-0672

The Utility of Dual Time-Point FET-PET/CT in Recurrence Assessment of Glioma Patients

A. Spataro[1], R. Laudicella[1], A. Vento[1], D. Romeo[1], S. Russo[1], D. Cardile[1], G. Giacoppo[1], F. La Torre[1], B. Pagano[1], S. Bisdas[2,3], F. Minutoli[1], S. Baldari[1];
[1]Nuclear Medicine Unit, Department of Biomedical and Dental Sciences and Morpho-Functional Imaging, University of Messina, Messina, ITALY, [2]Department of Neuroradiology, University College London Hospitals NHS Trust, London, UNITED KINGDOM, [3]Department of Brain Repair and Rehabilitation, University College London, London, UNITED KINGDOM.

Aim/Introduction: [18F]FET PET is a well-established functional imaging technique for the differential diagnosis and evaluation of glioma patients. Generating time-activity curves (TAC) on dynamic [18F]FET PET acquisitions allows obtaining information about gliomas grading: in particular, a continuously increasing uptake is characteristic of low-grade-glioma (LGG), while an early peak followed by a plateau or a decreasing TACs usually characterizes high-grade glioma (HGG). Also to support the patient's comfort, it is possible to perform early and late acquisitions (dual time-point). This preliminary study aims to evaluate the potential clinical advantages of dual time-point [18F]FET-PET/CT in the management of glioma, also in comparison with MRI. **Materials and Methods:** We retrospectively analyzed data of 31 patients (24 male and 7 female, mean age 49±13,5 years old, range 29-75) affected by glioma (11 G2, 5 G3, and 15 G4 according to WHO classification) who underwent surveillance MRI and [18F]FET-PET/CT static acquisition 10 and 50min after the administration of a mean dose of 282,5±47,8 MBq. We correlated PET findings with clinical, radiological (MRI) and follow-up data for a mean period of 3 months after the [18F]FET-PET/CT scan. Results: 22/31 patients resulted positive for recurrence at [18F]FET-PET/CT: among them, the dual time-point acquisition showed the usual TAC trend in 18/22 patients (81%) well correlating with histopathology. In particular, we observed an increasing uptake in 6/6 LGG (100%), and an early peak followed by a decreasing uptake in 12/16 HGG (75%). In 25/31 patients, FET-PET findings were in accordance with MRI. Therefore, in 6/31 patients MRI and FET-PET findings were discordant; among them, 5/6 patients were HGG (83%) and resulted negative/doubtful at MRI whilst positive for recurrence at FET-PET. Accordingly, their therapeutic strategy was changed, with a dramatic impact on management. **Conclusion:** In our preliminary experience, dual time-point [18F]FET PET/CT resulted as a useful tool in the evaluation of LGG and HGG glioma, able to identify tumour progression in case of doubtful MRI results, thus influencing the clinical and therapeutic management. **References:** None.

OP-0673

Diagnostic utility of amino acid PET in the differential diagnosis of recurrent brain metastases and pseudoprogression: a meta-analysis

T. Schlürmann[1], B. Waschulzik[2], W. Weber[1], I. Yakushev[1];
[1]Technical University of Munich, School of Medicine, Klinikum rechts der Isar, Department of Nuclear Medicine, Munich, GERMANY, [2]Technical University of Munich, School of Medicine, Institute of Medical Informatics, Statistics and Epidemiology, Munich, GERMANY.

Aim/Introduction: Vast majority of patients with brain metastases receive radiotherapy. At a follow-up, a substantial proportion of them develop new or progressive contrast enhancement on MRI that may represent both tumor recurrence and treatment related changes termed pseudoprogression. Amino acid PET is an established method to assist differential diagnosis of therapy related changes vs. recurrence in gliomas. However, its diagnostic value in brain metastases is yet to be determined. The aim is to summarize evidence on diagnostic utility of amino acid PET in brain metastases in terms of a meta-analysis. **Materials and Methods:** Medical databases MEDLINE (via PubMed), EMBASE and the Cochrane Library of the Cochrane Collaboration (CENTRAL)) were screened for appropriate studies using combinations of key words "amino acid", "positron emission tomography", "PET", "brain metastases", "cerebral metastases", "radiation necrosis", "radionecrosis", "pseudoprogression". Considered were studies in English with at least 10 patients, who had undergone first-line treatment including radiotherapy and in whom a final diagnosis had been determined by histological examination and/or imaging and clinical follow-up, with the feasibility to extract 2x2 tables. Pooled estimates with 95% confidence intervals were calculated. Heterogeneity was assessed using I2- statistic. Results: Following the above criteria, 14 studies with the tracers methyl-[11C]-methionine (n = 6), O-(2-[18F] fluoroethyl)-L-tyrosine (n = 6), and O-3-(2-[18F]fluoroethyl)-LDopamine (n = 2), with a total of 681 lesions in 481 patients were included. Pooled sensitivity and specificity were 81%

(95%-CI 76-85) and 85% (95%-CI 81-89). Positive, negative likelihood ratios and diagnostic odds ratio were 3.93 (95%-CI 3.2-4.9) ,0.27 (95%-CI 0.22-0.33), and 17.65 (95%-CI 11.9-26.2). Heterogeneity was overall low. **Conclusion:** The present meta-analysis provides IIa class evidence on diagnostic utility of amino acid PET in the differential diagnosis of recurrent brain metastases. These results suggest a good accuracy of this diagnostic tool. In particular, a specificity of 85% indicates that amino acid PET may help to reduce the number of invasive procedures and overtreatment in patients with pseudoprogression. Future studies should identify tumor entities that are more (and less) suitable for the PET diagnostics. **References:** None

OP-0674

A prospective, multi-centre trial of FET PET inGlioblastoma patients - the TROG 18.06 FIG Study

A. Scott[1,2,3], R. Francis[4,5], M. Ebert[4,5], H. Gan[1,2,3], S. Lee[1,3], E. Lau[2,3], A. Moore[6], A. Grose[6], E. Barnes[7], B. Moffat[3], F. Scott[1], L. Adda[1], F. Foroudi[2,1], R. De Abreu Lourenco[8], A. Nowak[5,4], D. Bailey[9], E. Koh[10,11,12];

[1]Olivia Newton-John Cancer Research Institute and La Trobe University, Melbourne, AUSTRALIA, [2]Austin Health, Melbourne, AUSTRALIA, [3]University of Melbourne, Melbourne, AUSTRALIA, [4]Sir Charles Gairdner Hospital, Perth, AUSTRALIA, [5]University of Western Australia, Perth, AUSTRALIA, [6]Trans Tasman Radiation Oncology Group (TROG), Newcastle, AUSTRALIA, [7]NHMRC Clinical Trials Centre, University of Sydney, Sydney, AUSTRALIA, [8]Centre for Health Economics Research and Evaluation, University of Technology Sydney, Sydney, AUSTRALIA, [9]Royal North Shore Hospital and University of Sydney, Sydney, AUSTRALIA, [10]Liverpool and Macarthur Cancer Therapy Centres, Liverpool, Sydney, AUSTRALIA, [11]University of New South Wales, Sydney, AUSTRALIA, [12]Collaboration for Cancer Outcomes, Research and Evaluation, Ingham Institute for Applied Medical Research, Liverpool,Sydney, AUSTRALIA.

Aim/Introduction: [18F] fluoroethyl-L-tyrosine positron emission tomography (FET-PET) has a proposed role in grading of brain lesions, surgical and radiation therapy (RT) planning in Glioblastoma (GBM) and differentiating progressive disease from post-treatment changes, however multi-centre studies are lacking. The FIG study is a prospective non-randomised cohort study which will recruit up to 210 participants with newly diagnosed GBM across ten Australian sites. Study outcomes will address FET-PETs role in RT planning, treatment response evaluation versus standard/advanced MRI and prognostication. We describe here the methodology for site credentialing for the FET-PET In GBM (FIG) study. **Materials and Methods:** Eligible participants with GBM undergo FET-PET imaging at three time-points: FET1 post-operative pre-chemo-RT, FET2 one month post-chemo-RT, with FET3 (+/-FDG-PET) triggered when clinical and/or MRI progression is suspected. Dynamic and static FET-PET images are analysed qualitatively and quantitatively. The RT delivered is as per standard care with the treating Radiation Oncologist (RO) blinded to FET-PET1. Site nuclear medicine (NM) physicians are required to delineate a biological target volume based on FET-PET1 with hybrid RT volumes derived post-hoc. Pre-trial NM quality assurance comprised certification from the Australasian Radiopharmaceutical Trials Network (ARTnet) encompassing FET radiochemistry QC and PET camera calibration. Site and central workflows for documentation and analysis of FET-PET and MRI imaging and credentialing have also been established via TROG. Results: An integrated workflow using MiM v7.0 has been developed incorporating multi-modality image registration, target volume/region of interest contouring and analysis. For benchmarking exercises, each site NM physician involved in FET-PET image interpretation is required to delineate biological target volumes using FET-PET imaging in 3 cases, with a further 3 cases addressing interpretation of response criteria, scoring and assessment of disease status, all accompanied by detailed worksheets. Response criteria for FET-PET vs MRI and FDG-PET have been harmonized. Similarly, the site RO is required to complete 3 cases involving derivation of standard and then hybrid target volume delineation based on pre-derived FET-PET biological volumes. All NM and RO cases undergo detailed appraisal by a central reviewer. To date, three sites have completed all credentialing components. **Conclusion:** The FIG study will be a pivotal prospective trial in establishing the role of FET-PET in GBM management and represents a significant collaborative effort across oncology, imaging, and translational science disciplines. The NM credentialing program has served to build substantial capacity and expertise in FET-PET production, acquisition and imaging interpretation across Australian sites. Trial recruitment is ongoing. **References:** none

1301

Friday, October 22, 2021, 09:00 - 10:30

Channel 1

CME 9: Back to the Future - New Kit-Based Approaches for Labelling Radiopharmaceuticals (^{68}Ga, Al[^{18}F]F,...)

OP-0677

Labelling Cold Kit With ^{68}Ga - The Future is Bright

C. Morgat; *Centre Hospitalier Universitaire de Bordeaux, Service de Médecine Nucléaire, Groupe Hospitalier Pellegrin, Bordeaux, FRANCE.*

OP-0678

Al[^{18}F]F - From Modules Toward a Kit-Based Radiofluorination?

C. Da Pieve; Institute of Cancer Research, Division of Radiotherapy and Imaging, London, UNITED KINGDOM.

OP-0679

Regulatory Aspects of Cold Kit-Based Radiopharmaceuticals in the EU

O. Neels; Institute of Radiopharmaceutical Cancer Research Helmholtz-Zentrum Dresden - Rossendorf (HZDR), Dresden, GERMANY.

1302-1

Friday, October 22, 2021, 09:00 - 09:30

Channel 2

Interview with the Expert 8 - Vision Trial

OP-0681

Interview - Vision Trial

S. Fanti; University of Bologna, Radiological Sciences - Nuclear Medicine, Bologna, ITALY.

OP-0682

Interview - Vision Trial

B. Krause; University Medical Center Rostock, Rostock, GERMANY.

1302-2

Friday, October 22, 2021, 09:45 - 10:30

Channel 2

Interview with the Expert 9 - The Best Young NM

OP-0683

Interview - The Best Young NM

S. Fanti; University of Bologna, Radiological Sciences - Nuclear Medicine, Bologna, ITALY.

OP-0684

Interview - The Best Young NM

K. Herrmann; Universitätsklinikum Essen, Nuclear Medicine, Essen, GERMANY.

1304

Wednesday, October 20 - Saturday, October 23, 2021

on-demand pool, release on Wednesday, October 20 at 09:00

Technologists - TROP Session: Sharing Technologist's Experience 2

OP-0685

Reduction of effective dose using single-CT for attenuation correction in myocardial perfusion imaging

C. Bruneby[1], C. Hasselbring[1], M. Simonsson[1], M. Toth Cervin[1], R. Madru[2];
[1]Centralsjukhuset Kristianstad, Kristianstad, SWEDEN,
[2]Skane University Hospital, Lund, SWEDEN.

Aim/Introduction: Myocardial perfusion imaging (MPI) with digital SPECT-CT is often performed as a two-day protocol with acquisition of two separate CT-examinations for attenuation correction (AC) of stress and rest images. According to EANM guidelines, the CT images entails an additional effective dose of 0,7 -1 mSv to the effective dose from the injected activity (2,32 + 3,2 mSv). The aim of the study is to evaluate the feasibility of MPI images using a single-CT for AC to keep the radiation dose as low as reasonably achievable (ALARA) and to shorten the examination time. **Materials and Methods:** The study was conducted in two groups: 1) 20 consecutively examined patients of both genders and 2) 10 female patients with BMI 27-40 (> 85 kg), who benefit the most from AC, underwent both stress/rest imaging according to standard protocol. Stress and rest images were post processed with respective CT and compared with stress and rest using CT from the stress scanning only. During post processing, SPECT and CT images are manually adjusted in x, y, z-directions. A third-party software 17-segment method was used to determine the summed rest score (SRS), summed stress score (SSS), and the difference, SDS. The statistical evaluation was performed through a Pearson correlation coefficent with SPSS. The images were reviewed by two experienced physicians independently in a blind test. Results: We found good correlation in SRS between two-CT and single-CT attenuated images ($r = 0.80$ for the first group and $r = 0.97$ for the female patients, $p < 0.01$). The SSS was found to be 0.95 for the first group and 0.98 for the second group. The correlation for SDS was found to be 0.93 respective 0.92 for the two groups. In single-CT (AC) images, a slightly larger adjustments may be necessary in y-direction, average of 49 mm, but less significant difference in x and z directions (mean 9 mm respectively 4 mm). The visual review by the experienced physicians did not show a clinically relevant difference between two-CT and single-CT images. **Conclusion:** The preliminary results show that single-CT images could be applied for SPECT-CT MPI. Using single-

CT, we could reduce the effective dose with 0.3-0.5 mSv and 2 min in examination time at our department. **References:** Verberne, H.J., Acampa, W., Anagnostopoulos, C. et al. EANM procedural guidelines for radionuclide myocardial perfusion imaging with SPECT and SPECT/CT: 2015 revision. Eur J Nucl Med Mol Imaging 42, 1929-1940 (2015).

OP-0686

Cardiac scintigraphy examination for high BMI patients using 3D-ring CZT SPECT/CT

P. Oudot, J. Dessoubrais, F. Clouse, M. Bailly;
Centre Hospitalier Regional d'Orléans, Orleans, FRANCE.

Aim/Introduction: A new type of 3D-ring CZT-camera is equipped with 12 swiveling high-resolution CZT detectors and a CT in a hybrid system. This system enables acquisition closer to the patient and also focused scanning modes. For this study, we compared this new 360-ring CZT SPECT/CT system to a cardiac-dedicated CZT camera in Myocardial Perfusion Imaging (MPI) for patients with very high Body Mass Index (BMI). **Materials and Methods:** A panel of 22 patients with high BMI (over 30) had their Stress and/or Rest acquisition on both 3D-ring CZT-camera and the cardiac-dedicated CZT camera. Mean BMI was 39.8 (30 to 55, that covers Obesity class I to IV). Cardiac-dedicated SPECT MPI scans were acquired on prone or supine position, lasting for 10 minutes. 3D-ring CZT SPECT MPI scans were acquired using a Focus mode (which allow to spend 90% of the acquisition on the ROI determined by the technologist) lasting for 12 minutes + low-dose CT acquisition (mean DLP of 39.8 mGy.cm). Mean stress injected activity was 384 MBq +/- 257. All acquisitions were ECG-gated and patients were positioned on the back, arms above the head or along the body. Attenuation correction (AC) was applied to 3D-ring CZT SPECT MPI data. Results: Positioning on the cardiac-dedicated CZT camera can be challenging in high BMI patients, time-consuming and difficult. Image quality was considered at least equal or superior for 14 patients (64%) using 3D-ring CZT SPECT MPI by the NM physicians, especially when applying Attenuation Correction (AC). AC MPI allow us to avoid multiples acquisitions currently done on the dedicated-CZT system (switching position and/or after a meal) because of digestive uptakes and/or centering artifacts. In 6 patients with BMI>45, 3D-ring CZT SPECT stress MPI was strictly normal and could avoid rest acquisition, whereas it wasn't the case if only considering dedicated cardiac CZT MPI. Image improvement was mostly in the inferior and septal wall. The simplicity of positioning and centering and image quality in these patients with this new system make it a first-choice exam both on technologist and a physician point of view. **Conclusion:** The 3D-ring CZT-camera enables us to change and simplify the management of high BMI patients, with less acquisitions and an improvement in terms of image quality and patient comfort. This helped to reduce the number of rest examinations to be scheduled and improved the nuclear cardiology workflow for patients in our department. **References:** None

OP-0687

Intra- and interobserver variability in LVEF measurements by Multi-Gated Nuclear Ventriculography using semi-automatic and manual postprocessing

L. Plet[1], T. Q. Christensen[2], S. Hess[1,3], M. W. Kusk[1];
[1]Department of Radiology and Nuclear Medicine. Hospital South West Jutland, Esbjerg, DENMARK, [2]Department of Clinical Engineering, Region of Southern Denmark, Esbjerg, DENMARK, [3]Department of Regional Health Research, Faculty of Health Sciences, University of Southern Denmark, Odense, DENMARK.

Aim/Introduction: Multi-gated radionuclide ventriculography (MUGA) is a well-established, non-invasive modality for the evaluation of left ventricular ejection fraction (LVEF), e.g. sequentially in patients treated with potentially cardiotoxic chemotherapy or cardiac patients with equivocal LVEF from other examinations and accurate, reproducible LVEF measurements is pivotal. To relieve physician workload technologists with dedicated software often carry out LVEF measurements, but most studies do not include differences between physicians and technologists or difference between manual and semi-automatic postprocessing techniques. Thus, we set out to evaluate inter-reader and intra-reader variations using manual and semi-automatic post-processing techniques and to evaluate differences between physicians and technologists. **Materials and Methods:** Thirty consecutive anonymized datasets from routine examinations (17 oncology patients and 13 cardiology patients) were included retrospectively. Eight observers (Two nuclear medicine physicians and six nuclear medicine technologists calculated LVEF using manual and semi-automated methods on a Xeleris 3.0 workstation (GE Healthcare). Datasets were re-anonymized and after 2-4 weeks all observers repeated the process, blinded to the results of the previous round. Bland-Altman analysis was used for comparison between timepoints and techniques. Inter-observer agreement was analysed with intra-class-corellation coefficient. Overall mean LVEF was calculated for each case and deviations were calculated. Results: For technologists reproducibility and inter- and intra-reader agreement were larger between sessions when using semiautomated ROI. For physicians, no clear pattern could be discerned. Significantly more patients were classified with reduced LVEF using semi-automatic technique. Limits of agreement were larger than +/- 5% for comparison between timepoints regardless of technique and for the same timepoints with different techniques

Conclusion: Results indicate a need for structured training, rigorous protocols for post processing, agreement on choice of technique, and quality control for physicians and technologists. Postproccessing procedures needs to be standardised to increase inter-reader reproducibility. To minimize variability, semiautomatic technique should be preferred. **References:** none

OP-0688

Could the quality and the quantitative amount of ^{99m}Tc-albumin colloidal particles injected could affect the lymph node detection failure in breast cancer patients?

M. Marazzini, C. Cidda, T. Graziani, S. Migliari, A. Sammartano, C. Lazzara, L. Ruffini;
Nuclear Medicine Division, Azienda Ospedaliero-Universitaria of Parma, Parma, ITALY.

Aim/Introduction: The standard method for axillary lymph node staging in early breast cancer is sentinel lymph node (SLN) detection and localization using ^{99m}Tc-albumin colloidal particles , as recommended by the existing Guidelines (Eusoma, EANM, AIOM). However, in some patients the SLN can not be localized during scintigraphy or surgery. Aim of the study was to verify if the quality of preparation and the quantitative amount of ^{99m}Tc-albumin colloidal particles injected could affect the lymph node detection rate in breast cancer patients. **Materials and Methods:** We have assessed 305 radiopharmaceutical productions of ^{99m}Tc-albumin colloidal particles (153 of year 2020 and 152 of year 2018) for radiochemical purity (RCP%), activity concentration (Mbq/mL), injected doses (MBq) and content of albumin colloidal particles (µg/dose). In 2020 the injected dose was increased of 5 MBq Tc-99m and 2.77 µg nanocolloid to obtain a better detection rate of SLN. In addition, we have collected data of 566 patients with early stage breast cancer injected with the prepared radiopharmaceuticals (275 for 2020 and 291 for 2018). The evaluated parameters were time elapsed between injection and visualization, scintigraphic lymph node site and intraoperatively gammaprobe outcomes. Results: The ready-labelling-kits were reconstituted with a mean concentration of 414,71 MBq/mL for 2020 and 396,50MBq/mL for 2018 (minimum activity concentration 100 MBq/mL). Analysis of 2020 samples showed mean RCP% 98.12% and 28.98 µg nanocolloids in a mean injected dose of 30.21 MBq; in 2018 mean RCP% was 98.44% and nanocolloids 26.21µg in a mean injected dose of 24.16 MBq. SLN was succesfully located within 1h from injection in 239 pts (86.9%) in 2020 and 255 (87.6%) in 2018; SLN was detected belatedly, but within 5h from injection, in 34 patients (12%) of 2020 and 27 pts (9%) of 2018. Global detection rate was 99.8% in 2020 and 96.9% in 2018. Both pre-operative lymphoscintigraphy and intraoperative probe did not reveal SLN in 2/275 patients of 2020 (0.7%). The following nodal sampling resulted negative at pathology. In 2018 lymphoscintigraphy did not locate SLN in 9/291 patients (3%) and in 2/9 nor the intraoperative probe did it. Nodal sampling showed metastatic disease in 1 case. **Conclusion:** This study shows that an increased amount of colloidal particles as well as the increased injected dose of the tracer together with high radiochemical purity have an impact on sentinel lymph node detection in breast cancer patients increasing the detection rate and reducing the technique failure. **References:** none

OP-0689

Glomerular filtration rate in terms of Tc-99m-DTPA clearance: Injection and blood sampling by port

C. Holm Led[1], L. J. Jeppesen[1], J. A. Simonsen[1], T. L. Andersen[1,2], L. B. Petersen[1], S. Hvidsten[1];
[1]Department of Nuclear Medicine, Odense, DENMARK,
[2]Department of Clinical Physiology, Nuclear Medicine and PET, Copenhagen, DENMARK.

Aim/Introduction: Glomerular filtration rate (GFR) is frequently determined, especially in cancer patients, whose treatment depends on their renal function. To avoid recurrent venous puncture in these patients, who often have fragile vessels, a port can be installed beneath the skin connecting the port through a catheter to a vein. The port has a silicone membrane through which drugs can be injected and blood samples can be drawn. When calculating the GFR in terms of Tc-99m-DTPA clearance, the precise amount of injected tracer is important to ensure the validity of the results. Injection through membranes is inadvisable because of the risk that they will retain part of the tracer biasing calculations and hence GFR. Furthermore, the port has a reservoir compartment in which the tracer may accumulate and eventually be withdrawn by blood sampling. We set out to investigate the feasibility of injection and blood sampling by port. **Materials and Methods:** In a laboratory model we simulated a single-sample GFR examination with a port, a catheter ending in a cup, and a needle—a so-called gripper—inserted into the port membrane. We injected 8 MBq of Tc-99m-DTPA through a three-way stopcock and flushed with isotonic saline as in a clinical setting. After flushing the injection system, the residual activity of the port, gripper, and catheter was measured using a thyroid counter (AtomLab) or a properly shielded gamma camera. Ten series of 6 ml volume of saline were subsequently withdrawn from a new saline filled cup through the system to simulate blood sampling. 2 ml of each sample were counted in a well counter along with a prepared standard and a background sample. All measurements were compared to the injected activity. Results: The initial activity in the port with catheter and the early sample activity varied quite a lot; from 1.6-33 ppm of the injected activity. In general, the simulated blood sample activity fell drastically from the first to the second sample, reaching a stable level of 0-0.06 ppm of the injected activity in each 2-ml sample. The final activity in the system

was generally low and comparable to the background. **Conclusion:** GFR determination by injection and blood sampling through the port system seems feasible, as the residual activity from the injection system and contamination of the blood samples are insignificant compared to the injected activity. **References:** None

OP-0690

Comparison of low pulmonary perfusion index using ^{99m}Tc-MAA SPECT images and hemodynamic indices in chronic thromboembolic pulmonary hypertension

Y. Ochi, Y. Tsutsumi, N. Fujita, H. Ikeda, M. Nishio, Y. Asano, S. Abe, K. Kato;
Aichi, Nagoya, JAPAN.

Aim/Introduction: Right-sided heart catheterization (RHC) and pulmonary ventilation/perfusion scintigraphy are routinely performed to diagnose chronic thromboembolic pulmonary hypertension (CTEPH). The severity of this disease is evaluated based on hemodynamic indices (mean pulmonary artery pressure, mPAP; pulmonary vascular resistance, PVR; cardiac index, CI) obtained with RHC. However, this is an invasive approach. Therefore, a new index based on SPECT images of pulmonary perfusion could be beneficial as the procedure is non-invasive and used for evaluating disease severity. Hence in this study, we calculated the low pulmonary perfusion (LPP) index using SPECT images. The correlations between this quantitative index and the RHC-based hemodynamic indices were evaluated. **Materials and Methods:** Forty-four patients with a confirmed diagnosis of CTEPH were selected. Using the homebrew application, a histogram was created from the ^{99m}Tc-MAA SPECT images. The regions between 1%-5% or lower than the maximum count and the remaining 99%-95% represented the background (BG) and the total lung region respectively. Based on count values, the latter was divided into four regions: 0%-25%, 25%-50%, 50%-75%, and 75%-100%. The 0%-25% and 0%-50% regions were considered as low perfusion regions, and the LPP index was calculated by dividing the volume of the low perfusion region by the volume of the total lung region. Thereafter, the correlations between the two types of LPP indices and hemodynamic indices were analyzed. Results: BG was same for all patients. With BG 1%, a weak positive correlation was found between the LPP index (0-25%) and mPAP ($r = 0.313$, $P < 0.05$). Though there were weak positive correlations between the LPP index (0-25%) and PVR at all BG thresholds, the best correlation was found at BG 1% ($r = 0.364$, $P < 0.05$). Similarly, there were weak positive correlations between the LPP index (0-50%) and PVR at all BG thresholds, with the best correlation being observed at BG 1% ($r = 0.361$, $P < 0.05$). However, there were no correlations between the two types of the LPP indices and CI. **Conclusion:** The LPP index calculated using ^{99m}Tc-MAA SPECT images weakly correlates with the hemodynamic indices (mPAP and PVR) obtained with RHC. BG thresholds from SPECT images need to be considered and in future studies it may be necessary to determine BG for each patient individually. **References:** none

OP-0691

Comparison Between Different Acquisition Times And Different Reference Tissues In The Interpretation Of The Scintigraphy With 99MTC-HMPAO-Leucocytes In Muscle-Skeleton Infections

R. Rinaldi, D. Albano, F. Dondi;
Nuclear Medicine dpt - ASST Spedali Civili, Brescia, ITALY.

Aim/Introduction: Scintigraphy with labeled autologous leukocytes is considered the gold standard exam for the study and diagnosis of musculoskeletal infections. The aim of our study was to evaluate the reproducibility and image quality both in the visual and in the semi-quantitative analysis using different reconstruction times, in order to identify the correct compromise of acquisition times. The second objective of the study was to compare the interobserver reproducibility to evaluate the semi-quantitative analysis using two different tissues (contralateral region and ipsilateral bone marrow) as the background to calculate the ration with the lesion/region of interest. **Materials and Methods:** Scintigraphic images of 50 patients were acquired according to the standard protocol and evaluated at different times, as defined by the EANM guidelines (300, 200, 150 and 100 seconds). The scintigraphic images were evaluated visually (using scores 1:poor or 2:good to describe the image quality) and semi-quantitative (using appropriate ROIs in all reconstructed images) by two different operators. Intraclass correlation (ICC) , concordance between operators and correlation between acquisition times and semiquantitative ratio were assessed. Results: Interobserver reproducibility of the semiquantitative analysis was found excellent (ICC > 0.9) using the contralateral tissue, regardless of acquisition times, and it was good (ICC 0.775-0.918) when ipsilateral bone marrow was used as background. The ICC between semiquantitative analysis ratios and acquisition time was excellent (> 0.9), regardless of reduced acquisition times. Due to the high concordance between the readers, the readers have scored the imaging time acquisition in order to obtain a qualitative analysis consensus. The qualitative analysis of the images, using a starter acquisition time of 300, 200, 150 and 100 seconds, considering the score 2, were respectively: 0.96, 0.94, 0.90 and 0.72 for delayed at 3-4 hour, and 0.96, 0.86, 0.62 and 0.38 for late imaging at 20-22 hour. **Conclusion:** The semi-quantitative analysis was more reproducible using the contralateral tissue as a background in comparison to the ipsilateral. The starter acquisition time of 300 and 200 second provide a similar image quality in delayed and late imaging. The 200 second acquisition time should be preferred when a late imaging (20-22 hour) is required, in order to optimize the timing and the patient comfort. **References:** Signore A, Jamar F, Israel O, Buscombe J, Martin-Comin J, Lazzeri E. Clinical

indications, image acquisition and data interpretation for white blood cells and anti-granulocyte monoclonal antibody scintigraphy: an EANM procedural guideline. Eur J Nucl Med Mol Imaging. 2018;45:1816-1831.

OP-0692

A Phantom Study on Compton Scatter Correction Methods in ^{99m}Tc Imaging

M. Can[1], *Ö. Karadeniz*[2,1], *T. Ertay*[3,1], *G. Çapa Kaya*[3,1]; *[1]Department of Medical Physics, Institute of Health Sciences, Dokuz Eylül University, Izmir, TURKEY, [2]Department of Physics, Faculty of Sciences, Dokuz Eylül University, Izmir, TURKEY, [3]Department of Nuclear Medicine, Faculty of Medicine, Dokuz Eylül University, Izmir, TURKEY.*

Aim/Introduction: Technetium-99m (^{99m}Tc), emits a 140 keV photon, is the most widely used radionuclide in Nuclear Medicine. In imaging with gamma emitter radioisotopes, photons generated within the human body are scattered, which affects their direction and energy. These scattered photons contribute to the counts in the main energy window at 140 keV. This situation distorts the image in both planar and tomographic imaging. Accordingly, several techniques have been proposed for this distortion caused by scattered photons. In the presented study, the effect of DEW (Dual Energy Window) and TEW (Triple Energy Window) Compton Scatter Correction Method on ^{99m}Tc imaging was investigated. **Materials and Methods:** A cardiac insert phantom, sphere and rods were inserted into a Jaszczak SPECT phantom and all phantoms were filled with ^{99m}Tc water solutions. Planar and single-photon emission computed tomography (SPECT) images were acquired on General Electric (GE) Healthcare system, including the use of low energy high resolution (LEHR) collimator. The scatter correction methods were applied on images with the various main window and scatter window widths. To compare the scatter correction methods, the contrast and full-width half maximum (FWHM) are calculated with and without scatter correction images. Results: Both in planar and SPECT images acquisition with the phantoms, after scattering correction an increase in the image contrasts was observed, while there was a decrease in FWHM values. The results of this study shows that as the ^{99m}Tc source activity increased, the effect of scatter correction methods increased. **Conclusion:** In ^{99m}Tc imaging, the DEW scatter correction method was found to be more successful than the TEW method. We recommend the use of DEW scatter correction for ^{99m}Tc acquisition. **References:** none

OP-0693

First clinical experiences with a new long axial field-of-view PET/CT: the technologist's point-of-view

R. Schepers, *I. Alberts, A. Afshar-Oromieh, M. Viscione, A. Rominger; Inselspital, Bern, SWITZERLAND.*

Aim/Introduction: A new long axial field-of-view (LAFOV) PET/CT system (Biograph Vision Quadra) was installed at our department in October 2020. The aim of this study was to investigate and summarize the first experiences of technologists when working with a new LAFOV system, and in doing so to identify the challenges and new opportunities encountered with this novel system. **Materials and Methods:** Once the LAFOV PET/CT had been in routine clinical use for six months, the initial experiences of technologists were gathered by means of a structured SWOT-based questionnaire. All six technologists working on both the LAFOV scanner and a standard FOV (SAFOV) digital PET/CT system were asked to report the: strengths, weaknesses, opportunities and threats of the new LAFOV scanner compared to the SAFOV system. Results: Recurring positive answers were: shorter acquisition times and the reduction in motion artifacts this induces. Additionally, lower injection doses were highlighted as an advantage of the LAFOV system. These are made possible by the system's high spatial and TOF resolution in combination with an axial FOV of 106cm. These factors can allow for substantial reductions in the acquisition time, making it possible to scan more patients within the same time window and can positively impact upon scan waiting times. Implementing a new LAFOV PET/CT also brought some challenges. The physical bore of the scanner has a length of 235cm, which can be challenging for severely claustrophobic patients and can make it hard for technologists to get close to a patient; e.g. to inject radiopharmaceuticals for dynamic acquisitions or to connect contrast media infusions. As a potential solution, we find the use of lighting can make the bore appear shorter and can improve patient comfort. Other challenges identified where logistics regarding personnel and availability of patient uptake rooms, which can place limits on the number of patients who can actually be examined per day. The high effective sensitivity results in large data sets, and data-storage and transfer needs were highlighted as areas which require consideration when using a LAFOV system. **Conclusion:** Following six months routine clinical experience with a novel LAFOV PET/CT, we identify a number of possibilities and challenges. One of the biggest advantages identified by our survey was the possibility to reduce of injected activity, which lowers radiation exposure for patients and technologists. Although some challenges were highlighted, e.g. claustrophobia, we found that these can be surmounted by qualified technologists. **References:** none

OP-0694

Learning from our mistakes: a teaching tool to improve the quality of Nuclear Medicine Technologist's practices

E. Lemos Pereira, A. Garcia, A. Malaia, M. Fateixa; NuclearMed - Hospital Particular Almada, Almada, PORTUGAL.

Aim/Introduction: Learning is a dynamic and continuous process. Even for experienced professionals, continuing education should be a priority; on one hand, inaccurate work habits are eventually installed and on the other hand, best practices are to be constantly updated. Our NM department runs with four NM Technologists, whose experience range from 3 to 17 years.The aim of this study was to: 1) understand the type of inaccurate procedures; 2) design and implement a teaching tool for practices quality improvement; 3) evaluate the impact of the project. **Materials and Methods:** Study was conducted on three phases: 1) on the first 3 months, observation and proof collecting; 2) a weekly moment for discussion; 3) re-evaluation. On this project, we decided to focus on three error sources: a) radiopharmacy practices, b) radiopharmaceuticals administration and c) records keeping regarding technical aspects of the procedure, material or equipment. On Radiopharmacy, main failures founded were related to the hot cell organization, hygiene or doors handling; On Radiopharmaceuticals administration, most frequent errors were related to the organization of the work table, the sanitation procedures and the residues separation; Finally, regarding records keeping, most errors were related do the lack of technical aspects of the exam registered, quality control and equipment failures records. Results: The initial survey founded that radiopharmacy related errors were frequent (up to 3 events, weekly), and both radiopharmaceuticals administration and record keeping failures were very frequent (more than 3 events per week). After re-evaluation at 1 month, both radiopharmacy and radiopharmaceuticals administration failures become rare (up to 1 event per week), and record keeping errors are now frequent (up to 3 events, weekly). **Conclusion:** Despite initially only the senior technologist was involved on data collection, younger technologists started gradually to get involved, both on data collection but also as discussion promoters. We implemented a weekly "Learning from each other" session, and on each session, one of the technologists should present at least two procedure errors, collected by him on that week. Discussion was then promoted, with the aim of understanding the procedure and the reason that lead to the error. One of the most significant outcomes was the possibility to deconstruct some preconceived incorrect ideas. Re-evaluation revealed significant decrease on the frequency of all events. Re-evaluation at 6M and at 1Y is to be considered. A monthly gathering for discussion of procedures should be a common practice for Nuclear Medicine Technologists. **References:** None

1305

Wednesday, October 20 - Saturday, October 23, 2021

on-demand pool, release on Wednesday, October 20 at 09:00

Joint Symposium 17 (EANM/EAU): What to Do and Not Do in Prostate Imaging

OP-0696

What does Urology want to know from NM?

T. Maurer ; University of Hamburg-Eppendorf (UKE), Hamburg, GERMANY.

OP-0697

9 years of PSMA - Where do we have Evidence for Being Helpful?

H. Zacho; University Hospital, Department of Nuclear Medicine, Aalborg, DENMARK.

OP-0698

9 years of PSMA - Where do we have Evidence for not Being Helpful (yet)?

A. Afshar-Oromieh; University Hospital Insel-Spital, Department of Nuclear Medicine, Bern, SWITZERLAND.

OP-0699

Prostate Cancer Imaging - Others than PSMA Ligands

L. Evangelista; University of Padova, Department of Medicine (DIMED), Padua, ITALY.

1306

Wednesday, October 20 - Saturday, October 23, 2021

on-demand pool, release on Wednesday, October 20 at 09:00

Joint Symposium 18 (EANM/EAU): Urological Challenges for Imaging Beyond Prostate

OP-0701

The Needs of Urologists and Oncologists in Urological Disease Beyond Prostate Cancer

J. Walz; Department of Urology, Institut Paoli-Calmettes Cancer Centre, Marseille, FRANCE.

OP-0702

The Role of PET Imaging in Bladder Cancer

A. Capozza; ASST Santi Paolo e Carlo, Department of Nuclear Medicine, Milan, ITALY.

OP-0703

PET Imaging with Diverse Radiopharmaceuticals in Renal Cancer

L. Evangelista; University of Padova, Department of Medicine (DIMED), Padua, ITALY.

OP-0704

The Role of PET Imaging in the Management of Testicular Cancer

Y. Loriot; Gustave Roussy Institute, Oncology Department, Villejuif, FRANCE.

1307

Wednesday, October 20 - Saturday, October 23, 2021

on-demand pool, release on Wednesday, October 20 at 09:00

Teaching Session 3: Radiobiology as a Missing Link in Improving and Understanding Nuclear Medicine

OP-0706

Radiobiology in Nuclear Medicine

S. Terry; King's College London, School of Biomedical Engineering & Imaging Sciences, London, UNITED KINGDOM.

OP-0707

Why We Cannot Rely on EBRT Radiobiology

M. Konijnenberg; Radiologie & Nucleaire Geneeskunde, Klinische Fysica, Erasmus Medical Center, Rotterdam, NETHERLANDS.

OP-0708

Need for Radiobiology in Preclinical Research

K. Lückerath; University Hospital Essen, Clinic for Nuclear Medicine, Essen, GERMANY.

OP-0709

Need for Radiobiology in the Clinic

R. Hustinx; Centre hospitalier Universitaire de Liège, Liege, BELGIUM.

1308

Wednesday, October 20 - Saturday, October 23, 2021

on-demand pool, release on Wednesday, October 20 at 09:00

M2M Track - TROP Session: Out of the Box Innovations

OP-0711

The Imageable Genome

P. Jané[1], V. Taelman[2], E. Jané[3], O. Bejuy[2], M. Gómez Martínez[4], R. A. Dumont[5], M. A. Walter[1];
[1]Hôpitaux Universitaires de Genève, Geneva, SWITZERLAND, [2]Centre d'imagerie biomédicale (CIBM), Geneva, SWITZERLAND, [3]Universidad Politécnica de Madrid, Madrid, SPAIN, [4]Hospital Universitario Ramón y Cajal, Madrid, SPAIN, [5]Université de Genève, Geneva, SWITZERLAND.

Aim/Introduction: The fraction of the human genome whose expression can be assessed with molecular imaging is unknown. We aimed to define the part of the human genome targetable with molecular imaging through the development of an artificial intelligence-based search pipeline. **Materials and Methods:** We bulk-downloaded and parsed the entire MEDLINE/PubMed Baseline dataset into a local SQL database. We trained a convolutional neural network (spaCy 2.3, Python 3.8) with over 11'000 examples to identify entries related to molecular imaging. We updated a pre-trained natural language processing (NLP) model for biomedical text (ScispaCy) to identify radiopharmaceuticals, and reveal associations with their target proteins. We then searched the UniProt and SwissProt databases to obtain the genes associated to the target proteins. Finally, we analyzed the identified gene set via pathway enrichment and network analyses. Results: We bulk-downloaded and screened over 29 million entries from MEDLINE/PubMed. The convolutional neural network was trained to achieve an overall accuracy (F-score) of 97%, and within the entire MEDLINE/PubMed database it identified 632'000 abstracts related to molecular imaging. Within these abstracts, we identified 2117 unique radiotracers, 512 target proteins and 561 respective genes. These genes were homogeneously distributed over all chromosomes, with the exception of the y chromosome. Pathway analyses revealed an enrichment in heterotrimeric G-protein signaling, and inflammation mediated by chemokine and cytokine signaling. Network analysis revealed that the immune system and signal transduction were amongst the most frequent and interconnected groups within the "Imageable Genome". **Conclusion:** Here we describe the "Imageable Genome", the part of the human genome whose gene products can be targeted with molecular imaging, which will serve as a vital tool for future radiopharmaceutical development with the intent to bridge molecular imaging with genomics and proteomics. **References:** PUBMED/MEDLINE Baseline Database: "Courtesy of the U.S. National Library of Medicine"

OP-0712

Optimizing a PET nanoradiotracer to overcome tumor heterogeneity

B. Louis, L. Balasse, L. Sakiroff, J. Ou, V. Nail, O. Nachar, A. Moyon, A. Bouhlel, T. Roussel, F. Dignat-George, L. Peng, P. Garrigue, B. Guillet; Aix-Marseille Université, Marseille, FRANCE.

Aim/Introduction: Nanometric size promotes penetration of chemicals into solid tumors via the enhanced permeability and retention effect (EPR effect) that is not constantly found. Hence, we designed flexible, supramolecular, radiolabelable dendrimers self-assembling into a dendrimersome to assess EPR effect heterogeneity (1,2,3). Aiming at lowering healthy organs exposure, dendrimers underwent chemical modifications including chain length modulation and

halogenation. This study aimed at evaluating the impact of these chemical modifications on dendrimer biodistribution and tumor targeting. **Materials and Methods:** Five different dendrimer formulations (A,B,C,D,E) were radiolabeled with gallium-68. Healthy Swiss mice (n=6 per formulation) were injected intravenously and dynamically imaged using microPositron Emission Tomography (microPET/CT). Acitivities were quantified at 5, 10, 15, 20, 30, 45, 60, 75, 90 and 120 min post-injection in the organs of interest: brain, heart, liver, lungs, kidneys, bladder, muscle. To assess blood pharmacokinetics, 6 mice /formulation were injected intravenously with gallium-68 dendrimersome, 20µL blood samples were withdrawn at PET time points, and quantified using a calibrated gamma counter. Both imaged and sampled mice were euthanized at 120 min and organs (pancreas, spleen, kidneys, liver, intestines, heart, lungs, muscle, brain and bone) were harvested and counted using gamma-counter. Comparison of the best formulation with the reference (A) was done on SOJ6 adenocarcinoma pancreatic orthotopic mice model (n=6) with static images using microPET/CT 2h and 4h p.i. Quantifications were expressed as % of injected dose per gram of tissue (%ID/g) or as a tumor-to-liver ratio. Statistical significance was analyzed using Tukey's multiple comparisons test. Results: Radiochemical purity was superior than 95% and remained stable at least up to 4h in 37°C serum. Amongst the 5 formulations, microPET results with formulation E showed significantly lower retention in the liver and increased urinary elimination compared to the others with a significantly higher activity in the bladder at 2h (Table 1). These results were confirmed by gamma-counting: formulation E was significantly less retained in the liver than the other formulations (P<0,001, Table 2). In orthotopic pancreatic adenocarcinoma mice model, tumor-to-liver ratios were significantly higher for formulation E 2h (P=0.0489) and 4h p.i. (P=0.0230). **Conclusion:** Late diagnosis and variability of drug penetration in tumors are both regularly associated with poor prognosis. To these concerns, nanotechnology and molecular imaging can provide innovative answers. Formulation E appears as the optimal dendrimer with an optimized biodistribution profile and an enhanced tumor-to-liver in an orthotopic pancreatic adenocarcinoma model.

References: (1) https://doi.org/10.1073/pnas.1812938115 (2) https://doi.org/10.1039/C9CC07750B (3) https://doi.org/10.1002/smll.202003290

OP-0713

Pharmacokinetic studies and modeling to efficiently predict nanoradiotracer PET biodistribution

J. Ou, B. Louis, L. Sakiroff, V. Nail, L. Balasse, A. Bouhlel, O. Nachar, A. Moyon, T. Roussel, F. Dignat-George, L. Peng, B. Guillet, P. Garrigue, F. Gattacceca;

Aix-Marseille University, Marseille, FRANCE.

Aim/Introduction: Nanometric size promotes the penetration of chemicals into solid tumors via the enhanced permeability and retention (EPR) effect, which varies depending on the tumor type. Hence, we designed a flexible, supramolecular, radiolabeled self-assembling dendrimersome to assess EPR effect heterogeneity (1,2,3). Dendrimersome biodistribution was then optimized via chemical modifications, in order to lower exposure to healthy organs. Each structural modification impacts biodistribution and requires new animal experiments. To spare time, costs, and animal lives, pharmacokinetic (PK) modeling was considered to predict nanoparticle biodistribution. **Materials and Methods:** Two-hour-long microPET/CT and gamma-counting biodistribution data of 5 optimized [^{68}Ga]Ga-radiolabeled dendrimersome formulations (A,B,C,D,E) were collected from Swiss mice (n=6). Non-compartmental analysis (NCA) and compartmental analysis (CA) were achieved with PKanalix and Monolix softwares respectively. NCA was used to determine exposure (area under concentration versus time curve, AUC) and PK parameters (clearance, volume of distribution, terminal half-life) in blood and organs for each dendrimer. CA enabled a semi-mechanistic compartmental model and the estimation of transfer rate constants between compartments using differential equations. PK metrics were compared using one-/two-way ANOVA and Tukey post-hoc test. A physiologically-based pharmacokinetic (PBPK) model tailored to dendrimersomes was developed using physiological parameters, dendrimers characteristics (size and charge), and PK data with Simbiology/Matlab. Results: Dendrimersome E displayed the lowest systemic exposure with an AUC of 0.038 %ID/mm3.h, and consistently the highest clearance (2.656 mL/h) and a short blood terminal half-life (2.21 h), which could be ascribed to a more efficient renal elimination as suggested by bladder data (Table 1). The volume of distribution was higher than for other dendrimers (8.002mL versus 4.031-5.954mL), suggesting a wider distribution in the organism, in line with the higher concentrations observed at the first time points in the main organs. AUCs in the main organs were contrarily lower for dendrimersome E, due to a short half-life. The semi-mechanistic model confirmed other dendrimersomes were retained longer in the liver, with lower transfer rates from the liver to blood. The PBPK model allowed simulating the kinetics of dendrimersomes in the main organs. **Conclusion:** NCA enabled the selection of the best-optimized dendrimer with the lowest hepatic retention and the fastest clearance.

CA allowed understanding behaviors of dendrimers in organs. The PBPK model will be enriched with several other parameters such as the choice of bifunctional chelator and radionuclide to become a predictive tool to guide further dendrimers development and optimization. **References:** (1) https://doi.org/10.1073/pnas.1812938115 (2) https://doi.org/10.1039/C9CC07750B (3) https://doi.org/10.1002/smll.202003290

OP-0714

The evaluation of [^{18}F]FDG and [^{18}F]FLT radiotracers as potential biomarkers of early treatment outcome in triple negative breast cancer (TNBC)

P. Rainone[1,2], S. Valtorta[1,3,2], S. Todde[1,3], D. Salvatore[1,2], R. Moresco[1,3,2];
[1]Department of Medicine and Surgery and Tecnomed Foundation, University of Milano – Bicocca, Monza, ITALY, [2]Nuclear Medicine Department, IRCCS San Raffaele Scientific Institute, Milan, ITALY, [3]Institute of Molecular Bioimaging and Physiology, National Research Council (IBFM-CNR), Segrate, ITALY.

Aim/Introduction: Breast cancer is the most common cancer among women and patients who do not achieve a pathologic complete response demonstrate a high relapse rate. A typical feature of BC cells is the metabolic shift towards increased glycolysis, which in recent years has become an interesting therapeutic target for drugs with metabolic action such as metformin. Metformin impact on cancer treatment are corroborated by in vitro and in vivo studies, in which inhibits the growth of tumor cells on a wide variety of tumor phenotypes such as breast cancer.[1-3] Despite these generally favorable pictures, there is a persistent background of studies where metformin administration alone shows little to no effect in cancer[4,5] in comparison with other antidiabetics.[6,7] Recently, was confirmed that the administration of the antihypertensive syrosingopine, in combination with metformin provide a synergistic lethal effect toward a variety of cancer cell types with substantially drop of the toxic threshold for either compound alone, whereas was not reported activity against non-transformed cells, suggesting a novel option in cancer therapy.[8] A fundamental need remain the development of in vivo biomarkers predicting clinical response, for avoid administering ineffective therapies and to characterize tumor heterogeneity. Molecular functional imaging, including Positron Emission Tomography (PET), offers an important non-invasive approach to characterize heterogeneity and predict response to treatment.[9] **Materials and Methods:** Balb/c female mice were inoculated subcutaneously with murine TNBC cells (4T1), when the tumor was palpable, the animals were divided into six treatment groups: vehicle, cisplatin, metformin, syrosingopine or cis-platinum plus metformin and metformin plus syrosingopine. The response to treatment was monitored by caliper measuring for tumor volume (bi-weekly) and by PET/CT studies performed before and after seven days of treatment. Results: Results revealed a significant tumor growth inhibition (%TGI) exclusively after metformin plus syrosingopine administration, confirming a synergist effect after ten days of treatment. PET studies showed a significant reduction of [^{18}F]FLT tumor uptake in cis-platinum plus metformin (*p<0.05) and metformin plus syrosingopine (*p<0.001) treated groups, whereas [^{18}F]FDG uptake increased in all groups. Molecular evaluations of the outcomes identified by PET imaging are ongoing, on each treatment group by immunohistochemistry analysis. **Conclusion:** Preliminary results, promote the use of [^{18}F]FLT as a potential biomarker for the early response to treatment of TNBC. **References:** 1. Junttila M. R. et al., Nature, 2013; 501:346-354. 2. Shipitsin M. et al., Cancer Cell, 2007; 1:259-273. 3. Lee J. O. et al., Breast Cancer Research, 2019; 21:115. 4. Stevens R. J. et al., Diabetologia, 2012; 55,2593-2603. 5. Nayan M. et al., Clin.Genitourin. Cancer, 2016; S1558-7673(16)30159-8. 6. Home P. D. et al., Diabetologia, 2010; 53, 1838-1845. 7. Tsilidis K. K. et al., Diabetes Care, 2014; 37,2522-2532. 8. Benjamin D. et al., Cell Reports, 2018; 25:3047-3058. 9. Cottone L. et al., The Journal of Nuclear Medicine, 2011; 52:1770-1777.

OP-0715

Copper-64 as a translational tool for evaluating pharmacodynamics and efficacy of a new gene therapy treatment in a preclinical mouse model of Wilson's disease

M. Collantes[1,2], M. Ecay[3], G. Quincoces[4,2], D. Moreno[5], O. Murillo[5], V. Ferrer[6], B. Bénichou[6], G. González-Aseguinolaza[7], I. Peñuelas[1,3,4];
[1]Nuclear Medicine Department, Clínica Universidad de Navarra, Pamplona, SPAIN, [2]Navarra Institute for Health Research (IdisNA), Pamplona, SPAIN, [3]Translational Molecular Imaging Unit (UNIMTRA), University of Navarra, Pamplona, SPAIN, [4]Radiopharmacy Unit, Clínica Universidad de Navarra, Pamplona, SPAIN, [5]Gene Therapy and Regulation of Gene Expression, CIMA, Pamplona, SPAIN, [6]Vivet Therapeutics SAS, Paris, FRANCE, [7]Vivet Therapeutics SL, Pamplona, SPAIN.

Aim/Introduction: Wilson's disease (WD) is an autosomal recessive metabolic defect of hepatocyte copper excretion into the bile, caused by absent or reduced ATP7B copper transporter function. We have evaluated the biodistribution of copper-64 in WD mice treated with a variant of VTX-801*, a gene therapy product. **Materials and Methods:** 6 weeks-old male WD mice were intravenously injected with a capsid variant of VTX-801, in which a mouse liver tropic AAV capsid carries a short version of the ATP7B gene (AAV-miniATP7B). Three months later, copper-64 (T1/2 =12.7 h, β+ 17%) was injected intravenously in treated mice as well as in control mice of the same age (Atp7b$^{+/+}$, WT and Atp7b$^{-/-}$, WD) (n = 3). In vivo PET studies were performed at 1.5, 24 and 48 hours post copper-64 injection and quantified by drawing volumes of interest (VOIs) in the liver. Additionally, total

feces were collected in metabolic cages over a period of 72h post copper-64 injection, at which time animals were sacrificed for liver dissection. The radioactive signal from each biological sample was measured with a gamma counter to calculate % of injected dose excreted. Results: All techniques detected statistically significant differences ($p<0.0001$) in the distribution of copper-64 between healthy and WD animals, with PET analysis demonstrating an intense retention of copper-64 in liver of WD mice over time, unlike in healthy animals. WD mice treated with AAV-miniATP7B exhibited restoration of copper-64 excretion in feces and a reduction of copper-64 retention in the liver. **Conclusion:** Copper-64 is an excellent tracer to assess the efficacy of transformative treatments as VTX-801 in a simple, non-invasive and sensitive manner. Copper-64 excretion evaluated by PET imaging and/or the measurement in feces represents a very promising biomarker to evaluate the therapeutic efficacy of ATP7B gene supplementation in WD patients and could serve as a powerful diagnostic tool.* Property of Vivet Therapeutics **References:** None

OP-0716

Defining a clinical imaging protocol for platinum-195m SPECT/CT

J. R. Hendriksen*, D. M. Huizing, B. J. de Wit-van der Veen, W. V. Vogel, E. A. Aalbersberg;*
Department of Nuclear Medicine, Netherlands Cancer Institute, Amsterdam, NETHERLANDS.

Aim/Introduction: Cisplatin is widely used chemotherapy for multiple solid malignancies, but nephrotoxicity and resistance are common limiting factors for treatment continuation. Efficacy and nephrotoxicity may potentially be predicted using pre-therapy [^{195m}Pt]cisplatin imaging. However, optimal parameters for quantitative SPECT/CT imaging of platinum-195m in humans are currently not known. Therefore, a clinical SPECT/CT protocol was developed and evaluated in this study. **Materials and Methods:** The NEMA 2012/IEC phantom was filled with 75 MBq [^{195m}Pt]cisplatin in the background and a sphere-to-background ratio of 1:3 due to the expected high background noise clinically. Acquisition parameters were optimized for the acceptable acquisition time for clinical application of 20 minutes per bed position with administration of 100 MBq [^{195m}Pt]cisplatin. Energy windows of 20% were positioned around the 99 keV, and 25% around 71 keV photopeak (containing both the 67 and 75 photopeaks). A down scatter window of 15% was applied for 71 keV. Imaging was performed on a Siemens Symbia T system with 64 views, 20 seconds per view in continuous mode, noncircular orbit and 128x128 matrix, equipped with a Low Energy High Resolution (LEHR) collimator. Iterative reconstruction was performed with multiple parameters: with/without scatter correction (SC), with/without 5mm Gaussian filter, 71 keV peak alone or with both 71 and 99 keV peaks and different iterations (i) and subsets (s) (3i4s, 4i4s, 6i8s, 4i8s). CT-based attenuation correction was applied on all reconstructions. Quantification and quality was assessed based on the recovery coefficients (RC), line profiles, image noise and visual assessment. Results: The RC mean of the reconstructions with 3i4s, 4i4s were substantially lower compared to 6i8s, and 4i8s (drop of 25%). This also applied for the reconstructions without SC compared to SC. There was a negligible difference in RC in reconstructions with/without Gaussian filter and reconstructions with 71 keV alone or with both peaks. Line profiles showed best image contrast in 6i8s and 4i8s reconstructions, whereas image noise was slightly higher in those reconstructions compared to 3i4s and 4i4s. Quantitatively 4i8s and 6i8s with 5mm Gaussian filter, SC and both 71 keV and 99 keV peaks were comparable, visually however 4i8s was most optimal for clinical usage. **Conclusion:** The best image quality and signal quantification for clinical ^{195m}Pt-SPECT/CT is obtained with 4i8s, 5mm Gaussian filter, SC and the use of both photopeaks (71 and 99 keV). These parameters will be applied and verified in upcoming clinical research with [^{195m}Pt]cisplatin. **References:** None

OP-0717

Solid Targets Made Simple: Making >25 GBq of [^{68}Ga]Ga-PSMA-11 in 60 Minutes Including Beam Time

K. Gagnon*, J. Svedjehed, M. Pärnaste;*
GEMS PET Systems, Uppsala, SWEDEN.

Aim/Introduction: With the ever-growing interest in ^{68}Ga, our goal was to simplify solid-target-based production efforts, whereby a single cassette-based synthesis platform could be used to automatically control all chemical aspects of column conditioning, dissolution, nuclide purification, labelling chemistry, and tracer purification within a single time-list/sequence. To test this concept, the data herein focuses on three sequential [^{68}Ga]Ga-PSMA-11 productions for which the total time from start-of-bombardment (SOB) to end-of-synthesis (EOS) was ≤60 minutes. **Materials and Methods:** Enriched ^{68}Zn was electroplated (~1cm dia.) on silver backings, and targets were irradiated on a PETtrace cyclotron using a fully automated (i.e. no tongs/telepliers) capsule handling station and a prototype in-house developed solid target. Irradiations were sequentially 10, 15, and 20 minutes at a nominal 13.0MeV and 80μA. Chemical processing was controlled by a single FASTlab, for which the sequence was optimized between productions. Automated dissolution of ^{68}Zn (60°C; 5.5min; 4mL 6M HCl+200μL H_2O_2) and column conditioning occurred in parallel. The Ga purification method of [1] was adapted to the solid target process by loading and rinsing in a high HCl/NaCl environment (121mmol total HCl per production). Labelling was performed at 50°C for 5min in acetate buffer with 8μg precursor and ~5mg ascorbic acid, followed by C18 purification and formulation in saline (12mL; <10% EtOH). Results: Respectively, for the irradiations at 10,

15, and 20 minutes, with ^{68}Zn masses of 147, 111, and 150 mg and SOB-to-EOS times of 56, 56, and 60 minutes, we produced 15.8, 17.8, and 28.2 GBq of [^{68}Ga]Ga-PSMA-11 at EOS. Based on residual activity distribution, an average RCY of 57.0±6.6% was assessed. Product QC revealed a pH of 5.5-6.0, RCP >98% (via radioTLC), and RNP ≥99.94% at EOS (≥98%@6hrs post-EOS). **Conclusion:** Simple and automated solid target production of up to 28GBq [^{68}Ga]Ga-PSMA-11 within 60 minutes from SOB-to-EOS was successfully demonstrated. All production chemistry was implemented on a single platform with a single time-list, with manual operations limited to a few mouse-clicks. Moreover, efforts have led to >15-fold [^{68}Ga]Ga-PSMA-11 yields vs. that demonstrated using liquid targets [2] assuming similar ^{68}Zn- and PSMA precursor masses (i.e. up to 150mg and 10µg, respectively). With the goal of producing >100GBq of [^{68}Ga]Ga-PSMA-11, preliminary efforts have commenced, however optimization is required. Nevertheless, preliminary (non-optimized) tests have resulted in 62-75GBq (n=6) to date (RCY=40.3±6.3%) with consistent RCP >98% noted, even when testing to 10 hours (n=1) post-EOS. **References:** [1]Sci.Rep, 2021, 11:3631. [2]EJNMMI Radiopharm. Chem., 2020, 5:25.

OP-0718

[^{68}Ga]Ga-THP-Pam: A PET Radiotracer for Imaging Vascular Calcification

G. Keeling[1], F. Baark[1], O. L. Katsamenis[2], A. J. Reader[1], G. E. Smith[3], S. Y. Terry[1], P. J. Blower[1], R. T. M. de Rosales[1];
[1]King's College London, London, UNITED KINGDOM, [2]University of Southampton, Southampton, UNITED KINGDOM, [3]Theragnostics Ltd, Bracknell, UNITED KINGDOM.

Aim/Introduction: [^{68}Ga]Ga-THP-Pam was previously demonstrated to have high affinity towards a number of calcium salts while [^{18}F]NaF, the most used PET radiotracer for bone imaging has high affinity only for hydroxyapatite (the main component of bone mineral).[1] We hypothesised that the broad calcium mineral affinity of [^{68}Ga]Ga-THP-Pam may be advantageous in detection of vascular calcification (VC), where the composition of solid calcium mineral may be more varied than the composition of bone.[2] We report a direct comparison of [^{68}Ga]Ga-THP-Pam and [^{18}F]NaF in a rat model of VC. **Materials and Methods:** We used a model of VC in which rats were fed a diet containing warfarin and vitamin K_1 along with subcutaneous administration of vitamin D_3 to induce severe VC.[3] Anaesthetised rats were injected with [^{68}Ga]Ga-THP-Pam and scanned using preclinical PET/CT 60-120 min post-injection. The rats were imaged using [^{18}F]NaF the following day. As a control study, animals fed a healthy diet were imaged using the same procedure. Results: Imaging showed high uptake of [^{68}Ga]Ga-THP-Pam and [^{18}F]NaF (3.44 ± 0.69 and 0.91 ± 0.24 %ID respectively, p = 0.002) in a region of tissue around the stomach, with severe calcification as identified by CT. Additionally, [^{68}Ga]Ga-THP-Pam demonstrated increased uptake in the VC group vs. the healthy group across several major organs, most notably in the kidneys (2.21 ± 0.76 vs. 0.25 ± 0.13 %ID, p = 0.002). Ex vivo biodistribution data confirmed the increased uptake of [^{68}Ga]Ga-THP-Pam seen in the imaging data. The presence of calcification in the kidneys, stomach and other organs of interest was confirmed by microCT-based 3D X-ray histology and conventional histology. To visualise small areas of interest such as the aorta, we present preliminary results highlighting the potential utility of a post-reconstruction method to improve the spatial resolution of preclinical PET with gallium-68. Analysis of the mineral composition of the calcifications is ongoing. **Conclusion:** These results demonstrate that [^{68}Ga]Ga-THP-Pam may offer improved detection of VC in comparison to [^{18}F]NaF, including microcalcifications undetectable by preclinical CT. **References:** 1. G. P. Keeling, B. Sherin, J. Kim, B. San Juan, T. Grus, T. R. Eykyn, F. Rösch, G. E. Smith, P. J. Blower, S. Y. A. Terry and R. T. M. de Rosales, Bioconjugate Chem., 2020. 2. E. Tsolaki and S. Bertazzo, Materials, 2019, 12, 3126. 3. J. Bordoloi, PhD Thesis, King's College London, 2015.

OP-0719

Preclinical evaluation of ^{68}Ga-labelled artificial siderophores of the Ferrioxamine type

I. Hubmann[1], A. Mular[2], E. Gumienna-Kontecka[3], M. Misslinger[4], J. Pfister[1], H. Haas[5], M. Petrik[6], C. Decristoforo[1];
[1]Department of Nuclear Medicine, Medical University Innsbruck, Innsbruck, AUSTRIA, [2]Faculty of Chemistry, University of Wroclaw, Wroclaw, POLAND, [3]Faculty of Chemistry, University of Wroclaw, Wrozlaw, POLAND, [4]Division of Molecular Biology, Medical University Innsbruck, Innsbruck, AUSTRIA, [5]Division of Molecular Biology, Medizinische Universität Innsbruck, Innsbruck, AUSTRIA, [6]IMTM, Faculty of Medicine and Dentistry, Palacky University, Innsbruck, AUSTRIA.

Aim/Introduction: Iron is an essential nutrient for growth and virulence of pathogenic microorganisms. Siderophores are low molecular weight organic molecules, biosynthesized and secreted by microorganisms to take up environmental iron. Cyclic Ferrioxamines (FOX), produced by Streptomycetes, can be utilized by a variety of bacteria and fungi. These siderophores are difficult to synthetize and modify, e.g. with fluorescent dyes or antifungal drugs, due to a lack of residual moieties. Therefore, artificial cyclic FOX analogs with different ring sizes were synthesized. We aimed to label these siderophores with radioactive gallium-68 to investigate in vitro and in vivo properties of these novel compounds for molecular imaging of infections using Positron Emission Tomography (PET). **Materials and Methods:** Artificial FOX E derivatives were characterised by HPLC and MALDI-TOF-MS. The compounds were labelled with gallium-68 to perform in vitro (LogD, protein binding) and in vivo tests (biodistribution, PET/CT imaging). Uptake assays using iron sufficient and

depleted microbial cultures (Staph.aureus, Psedomonas aeruginosa, Aspergillus fumigatus) were performed, as well as blocking studies with iron labelled FOX E and NaN_3. Furthermore, biodistribution studies in normal BALBc mice after 45 and 90 min were performed and microPET-CT imaging in a pulmonary Aspergillosis model in rats. Results: Radiolabelling of artificial FOX E siderophores was achieved after 10 min at room temperature with moderate yields and high specific activities of gallium-68. Lipophilicities expressed in logD ranged from -0,5 to -2,5, depending on the structural size of the siderophore. Large cyclic compounds showed a higher lipophilicity in contrast to smaller and open-chain compounds. Protein binding resulted in values <10% for FOX E derivatives. In vitro uptake assays using showed a specific uptake for artificial siderophores with variable uptake specificity in microorganisms dependent on ring size. Biodistribution assays for selected siderophores complemented these findings, PET/CT imaging of one siderophore confirmed in vivo targeting with ^{68}Ga-artificial siderophores in a pulmonary aspergillosis rat-model, further characterisation is ongoing. **Conclusion:** Overall our work gives a first insight into the pharmacological properties of artificial FOX E derivatives to use them as potential lead compounds for modifications for molecular imaging and theranostic applications. **References:** None

OP-0720

New opportunity for imaging in oncology: targeting the neurotensin receptor-2 with JMV7488, a new peptide analogue radiolabelled with gallium-68

S. Bodin[1,2], *S. Previti*[3], *E. Jestin*[4], *D. Vimont*[1], *F. Lamare*[1,2], *I. Ait-Arsa*[4], *S. S. Bertrand*[1], *E. Hindié*[1,2], *F. Cavelier*[3], *C. Morgat*[1,2];
[1]*Univ. Bordeaux, CNRS, INCIA, UMR5287, F-33000 Bordeaux, FRANCE,* [2]*University Hospital of Bordeaux, Nuclear Medicine Department, F-33000 Bordeaux, FRANCE,* [3]*Univ. Montpellier, CNRS, Institut des Biomolécules Max Mousseron, IBMM, UMR-5247, F-34000 Montpellier, FRANCE,* [4]*CYclotron Réunion Océan Indien CYROI, 2 rue Maxime Rivière, F-97490 Sainte-Clotilde, FRANCE.*

Aim/Introduction: Neurotensin receptor 2 (NTS_2) is a well-known mediator of central opioid-independent analgesia. NTS_2 is also overexpressed in a variety of tumor types including prostate, pancreas and breast carcinoma (1,2). In this work, we describe the radiopharmaceutical characterization of [^{68}Ga]Ga-JMV7488, a new silylated peptide radiolabelled with gallium 68 (^{68}Ga) targeting NTS_2. **Materials and Methods:** JMV7488 (DOTA-βAla-βAla-Lys-Lys-Pro-(D)Trp-Ile-TMSAla-OH) was prepared using solid-phase synthesis, purified and then radiolabelled with gallium-68. In vitro characterization was carried out on the human colorectal adenocarcinoma HT29 cell line. In vivo pharmacology was assessed by µPET/CT and animals sacrifice on HT29-xenografted nude mice. Results: [^{68}Ga]Ga-JMV7488 radiolabelling was achieved with moderate yield (53.9 ± 8.34 %) and high apparent molar activity (8.77 ± 1.23 GBq/µmol). It exhibited hydrophilic properties (octanol/PBS partition coefficient = -3.11 ± 0.24), suggesting renal clearance and low brain uptake. Saturation studies showed good affinity for NTS_2 (Kd = 37.10 ± 18.47 nM) and moderate selectivity (Kd NTS_2 / Kd NTS_1 = 15.90). The NTS_2-mediated internalized fraction reached 20.53 ± 6.50% at 10 min and remains stable until 60 min (23.98 ± 4.79 %), with very low membrane binding (< 8 %). These values are in accordance with the known internalization capacity of NTS_2 upon agonistic stimulation. An early efflux was observed, increasing from 45.28 ± 6.85% at 5 min to 66.06 ± 8.55 % at 45 min. JMV7488 was characterized as a full agonist reaching 90.88 ± 11.49 % of normalized levocabastine maximum intracellular Ca^{2+} mobilization (EC_{50} respectively 431 nM and 118 nM). In vivo [^{68}Ga]Ga-JMV7488 showed a moderate but promising tumor uptake of 0.5 %ID/g at 90 min post-injection. Kidneys (21.32 ± 7.04% ID/g) and prostate (4.56 ± 4.66% ID/g) demonstrated the highest normal uptake. Dynamic µPET/CT data are currently under analysis. **Conclusion:** We have synthesized and characterized radiolabelled [^{68}Ga]Ga-JMV7488, a full agonist at the NTS_2, which binds to NTS_2 with high affinity and moderate selectivity. Compared with the literature (2), this novel analogue provides higher tumor uptake at later time point offering the potential to image and/or treat tumors over-expressing NTS_2. The uptake in normal prostate represents a caveat for the use of NTS_2 for diagnostic procedures in primary prostate cancers. We appeal for more studies aiming at deciphering the expression profile of NTS_2 in human tumors. **References:** (1) Swift SL et al. Cancer Res. (2010) ; (2). Maschauer S et al. Bioorg Med Chem. (2015)

1309

Wednesday, October 20 - Saturday, October 23, 2021

on-demand pool, release on Wednesday, October 20 at 09:00

Cutting Edge Science Track - Featured Session: Harmonisation and Standardisation

OP-0722

The Importance of Harmonisation and Standardisation

Á. Krizsán; *ScanoMed Nuclear Medicine Centers, Translational Imaging Laboratory, Budapest, HUNGARY.*

OP-0723

The Canadian PET Phantom for Prostate Oncology (C3PO) - A Multimodality Imaging Phantom for ^{18}F-PSMA Harmonization

R. Fedrigo[1,2], *R. Coope*[3], *A. Rahmim*[1,2,4], *F. Bénard*[1,2,4], *C. Uribe*[2,4];
[1]*BC Cancer Research Institute, Vancouver, BC, CANADA,* [2]*University of British Columbia, Vancouver, BC, CANADA,* [3]*Genome Science Institute, Vancouver, BC, CANADA,* [4]*BC Cancer, Vancouver, BC, CANADA.*

Aim/Introduction: Prostate-specific membrane antigen (PSMA) PET is an imaging modality that allows for enhanced detection of metastatic prostate cancer (mPCa). Due to its potential, multiple phase III clinical trials using PSMA PET are ongoing worldwide. Improved quantification and harmonization of clinical trials can enable development of more robust multi-centre studies and has the potential to build predictive and prognostic models for mPCa. Conventionally, the NEMA Image Quality phantom is used to evaluate scanner performance, in which [^{18}F]FDG is injected into 10-37mm spheres. However, these experiments do not realistically model the high-contrast, focal lesions that are characteristic of mPCa. This encourages the development of standardized phantoms that are more relevant to PSMA PET imaging. In this study, we developed the Canadian PET Phantom for Prostate Oncology (C3PO), a PET/CT/MRI-compatible phantom designed for quantification and harmonization of ^{18}F-PSMA PET. **Materials and Methods:** As a proof-of-concept, two C3PO prototypes (h=18.5cm, d=20cm) were machined from acrylic. In the main cavity, C3PO contains 3-16mm ^{22}Na (sodium-22) epoxy spheres to simulate prostate cancer metastasis [1]. ^{22}Na has similar decay properties to ^{18}F but a longer half-life ($T_{1/2}$=2.6yrs vs. 109.7min), allowing for it to simulate lesions imaged with ^{18}F-PSMA PET. [^{18}F]FDG is injected into the background and a bladder-simulating compartment to establish realistic PSMA uptake distributions. Polyurethane filter foam creates small air pockets to displace radioactivity and increase image heterogeneity, which is more realistic to a patient image. In a separate region, C3PO contains 6 spherical inserts (3-37mm) that can be injected with [^{18}F]FDG. This component evaluates the upper-bound accuracy for each scanner, in which background activity is not present and lesions are observed under "ideal" conditions. A study protocol was designed using realistic activity concentrations determined from an analysis of [^{18}F]-DCFPyL PSMA PET images. Results: ^{22}Na epoxy spheres were cast and embedded in the polyurethane foam. The total activity of the epoxy spheres is less than 1MBq (due to their small sizes), which allows it to be shipped under "exempt" status by the Canadian Nuclear Safety Commission (CNSC). The protocol was tested using a GE MI PET/CT scanner and required <60min preparation and 9min scan time, making it feasible for a large-scale study. **Conclusion:** A standardized imaging phantom was developed for improved quantification of ^{18}F-PSMA PET images. C3PO has the potential to improve comparison between clinical trials, which may lead to more robust predictive metrics and prognosis for prostate cancer. **References:** [1] Fedrigo et al., EJNMMI,vol.47,S259,2020

OP-0724

Acquisition and reconstruction protocols revisited for F18 PSMA imaging

T. Hekimsoy, H. Porger, C. Lohrmann, A. Reinhardt, F. Lahner, C. Meisinger, M. Eiber, W. A. Weber, S. G. Nekolla;
TU München, München, GERMANY.

Aim/Introduction: The recent introduction of digital PET/CT system with superior time-of-flight and spatial resolution offers the opportunity to adjust acquisition and reconstruction protocols. Especially F18-labelled PSMA ligands are attractive as the target is small, the uptake is intense and shows low unspecific uptake. Thus, we aimed to identify an improved protocol in such a specific setting. **Materials and Methods:** We acquired PET whole body F18-PSMA data in listmode step and shoot mode with a frame duration of 120s (Vision, Siemens). In 25 patients (mean weight adjusted injected dose: 310MBq, 4MBq/kg) we reconstructed data with 10, 30, 60 and 90s frame duration. Lesion and background analysis resulted in mean and max SUV as well as PET derived volume. In addition, we used EARL certification measurements data to identify the protocol with the highest resolution/recovery as well as EARL compatible reconstruction parameters. Finally, we used latter parameters to reconstruct the 120s data as comparison. Results: The reconstruction protocol with the highest resolution used a matrix of 440x440, PSF and TOF, and no post recon filter, the EARL settings were 220x220, PSF+TOF, Gaussian 4mm. Especially for the small spheres, recovery coefficients were above the EARL upper limit (d=10mm: +45%, d=13mm: +19%). For the higher resolution, SUV mean, SUV max and volume in the lesions showed no significant difference for 60, 90 and 120s data. The shorter reconstructions showed significant differences due to increased noise levels (30s: Vol: -14±22%, mean: +7±12%, max: +9±10%, 10s: Vol: -42±29%, mean: +33±32%, max: +37±26%). The background showed consistent values with the exception of the SUVmax in the 10s (+97±29%) and the 30s data (+8±7%). The target lesion was not detectable in 20% of the cases for the 10s data. Using the EARL compatible reconstructions in the full data, the linear regression with the higher resolution mode showed a marked underestimation in the lesion using EARL compatible settings (mean: slope: 0.39, R2:0.84, max: slope: 0.37, R2:0.89) while the background remained unchanged (slope: 1.02, R2:0.99). The same lesions which disappeared in the 10s data were still visible but dropped below the local threshold of 5. **Conclusion:** The use of the recent PET/CT system has the potential to reduce the injected dose. However, larger studies are necessary to define this value. Using the capabilities of this generation of PET/CT points to the need to balance sensitivity and harmonization in data acquisition and reconstruction especially for this class of radiotracers. **References:** None

OP-0725

Comparison of quantitative measures between EARL1 and EARL2 specifications in PET/CT studies using Gallium-68

R. Oliveira[1,2,3], F. Oliveira[1], C. Constantino[1], L. Vieira[4], M. Costa[1,3], D. Costa[1];
[1]Champalimaud Centre for the Unknown, Champalimaud Foundation, Lisbon, PORTUGAL, [2]Instituto Superior de Engenharia de Lisboa, Instituto Politécnico de Lisboa, Lisbon, PORTUGAL, [3]Mercurius Health, Oeiras, PORTUGAL, [4]Health and Technology Research Center, Escola Superior de Tecnologia da Saúde de Lisboa, Instituto Politécnico de Lisboa, Lisbon, PORTUGAL.

Aim/Introduction: Gallium-68 (^{68}Ga) usage has increased significantly in PET/CT studies in the last years. However, there is a lack of harmonization in the acquisition and reconstruction protocols. EARL1 and EARL2 are now well-established standards for Fluorine-18 (^{18}F), but the performance of these specifications on ^{68}Ga is not sufficiently studied. This study has two aims: to compare the recovery coefficients (RC) with ^{68}Ga using protocols that fulfill EARL1 and EARL2 specifications; to compare the differences in terms of SUV and patients' lesion volumes in [^{68}Ga]Ga-PSMA-11 studies between reconstructions that fulfill these specifications. **Materials and Methods:** A two-stage study was conducted: (1) nine $^{68}GaCl_3$ filled PET/CT NEMA-IEC Body Phantom acquisitions were performed using exactly the ^{18}F protocol; (2) retrospective evaluation of [^{68}Ga]Ga-PSMA-11 PET/CT data from 20 male patients (mean age 68±8 years old, 40 lesions) with prostate cancer metastases. All acquisitions were performed with the same equipment (Philips Vereos Digital PET/CT), which has both EARL1 and EARL2 accreditations. For each acquisition, two reconstructions were performed, one fluffing EARL1 and other EARL2 specifications. The SUVmax, SUVmean and SUVpeak of all phantom's spheres were compared between reconstructions. For the patients' study, the volume of the lesions was also compared. Results: Overall, RC obtained with ^{68}Ga were inferior to the expected values for ^{18}F, both for EARL1 and EARL2 reconstruction protocols. However, they are very close to the acceptable values for ^{18}F and within the limits in most cases. Mean SUVmax, SUVmean and SUVpeak increased significantly in all phantom's spheres when images were reconstructed with EARL2 specifications comparatively to EARL1. For the spheres with 10, 13, 17, 22, 28 and 37mm of diameter, the mean SUVmax increased 55%(SD=±6%), 58%(±4%), 40%(±3%), 22%(±3%), 16%(±3%) and 14(±3%); the mean SUVmean increased 52%(±10%), 58%(±8%), 37%(±4%), 22%(±1%), 16%(±1%), 11%(±1%); and the mean SUVpeak increased 27%(±1%), 32%(±1%), 30%(±1%), 20%(±1%), 10%(±1%), 6%(±1%), respectively. The results found in the phantom studies were confirmed in real patients' lesions. Mean increases in the SUVmax, SUVmean and SUVpeak from EARL1 to EARL2 reconstructions were 52%(±19%), 36%(±24%) and 33%(±19%) respectively. Regarding the lesions' volume, there was a mean decrease of 20%(±19%). **Conclusion:** The SUVmax, SUVpeak, SUVmean and lesions' volume varied considerably among reconstruction protocols, especially in small lesions with high affinity for ^{68}Ga-labeled radiopharmaceuticals. Since these features are widely used during clinical staging and follow-up, special attention needs to be taken regarding harmonization of PET reconstruction protocols. Otherwise these features may contribute to inaccurate assessments. **References:** None

OP-0726

The Effect of Residual Counts from Medical Materials Used for ^{18}F-FDG Injection on Quantitative Parameters of PET/CT Imaging in Pediatric Oncology Patients

N. Gülaldi, B. Cagdas;
Department of Nuclear Medicine, Ministry of Health, Ankara City Hospital, Ankara, TURKEY.

Aim/Introduction: Pediatric Oncology patients routinely followed up with ^{18}F-FDG PET/CT scan for staging and treatment response purposes. SUVMax and SUVPeak calculations are derived from patient weight, time of injection, and injected activity dose. We aim to reveal the importance of residual activity left within the medical pieces used for the injection such as i.v. line and 3-way stop cock plastic other than the empty syringe. **Materials and Methods:** Fifty-four children aged 6 months-old-17 years old (mean=9,5∓4,9) at the time of imaging were included in the study. PET/CT scans were performed for staging, treatment response, or relapse evaluation purposes. Diagnoses of the children were; 10 Ewing's sarcoma, 26 lymphomas, 2 Langerhans cell histiocytosis, 5 neuroblastoma, 1 renal cell carcinoma, 5 osteosarcomas, and 5 rhabdomyosarcoma. ^{18}F-FDG was given 45 minutes of injection 0.1 MBq/kg intravenously using i.v. line and 3-way stop-cock device. Full syringe and empty syringe counts were noted to calculate SUVMax, SUVpeak values. In addition, we measured i.v line pieces such as plastic tubes and 3-way stop cock plastic pieces after injection and recorded them as an implement to the empty syringe. Paired samples T-test comparison to reveal any statistical significance between two measurements for the SUVMax lesion, SUVpeak lesion, SUVMax liver, and SUVMax mediastinum values. Lesions with the highest ^{18}F-FDG within the patients were used as a comparison. Injected dose parameters were changed within the PET/CT scanner according to values obtained. Voxel-based calculations were recorded and the same VOI's were used between the 2 measurements. Results: Two SUVMax values of the lesion with the highest activity were significantly different in paired-samples T-test comparison (p = .001). However, the difference of SUVPeak and SUVMax values from mediastinum and liver were not statistically significant, although SUVPeak values of the lesion gave borderline results. **Conclusion:** Various corrections were postulated affecting the quantitative parameters of PET/

CT scan. SUVMax, SUVPeak values of the lesions, and the liver-mediastinum in patients with malignancy especially in a pediatric age group are important for the correct interpretations of the scan findings. Mediastinum and liver uptake are used as self-standard sites for the comparison of the lesion uptake. Our study showed that resultant SUVMax values change significantly when medical materials used during ^{18}F-FDG injection are measured and subtracted from full syringe counts and entered into the PET/CT scanner acquisition information page. **References:** None

OP-0727

Negative-Cast Modelling for Oncology (NCMO) - Development of a Novel Technique for Casting Radioactive Tumour Models

R. Fedrigo[1,2], R. Coope[3], I. Bloise[1], C. Gowdy[4], A. Rahmim[1,2,5], C. Uribe[2,5];
[1]BC Cancer Research Institute, Vancouver, BC, CANADA, [2]University of British Columbia, Vancouver, BC, CANADA, [3]Genome Science Institute, Vancouver, BC, CANADA, [4]BC Children's Hospital, Vancouver, BC, CANADA, [5]BC Cancer, Vancouver, BC, CANADA.

Aim/Introduction: Positron emission tomography (PET) is used within oncology to stage and assess treatment response. There is evidence that quantitative imaging metrics can enhance the prognostic value of PET and its ability to guide treatment decisions. Conventionally, the accuracy of PET images is evaluated using the NEMA Image Quality phantom, in which 10-37mm spheres simulating lesions are injected with [^{18}F]FDG. However, this approach is not realistic for heterogeneous tumour shapes. We aimed at developing a template-based approach for accurate and reproducible casting of tumour models. We present Negative-Cast Modelling for Oncology (NCMO) and, as a proof-of-concept, we apply NCMO to model primary mediastinal B-cell lymphoma (PMBCL) tumours. **Materials and Methods:** Tumours were segmented by an experienced nuclear medicine physician from a set of PET/CT PMBCL images. Seven lesions (2.7mL to 171mL) were saved in a stereolithography (stl) file format and 3D-printed (Stratasys uPrint SE Plus). Negatives of the 3D-printed tumours were cast using silicone-based molding materials (Smooth-On, USA). To minimize formation of air pockets, aluminum rods were secured to the models to establish injection and breathing holes subsequently used in the casting process. Tumour models were cast using liquid plastic (Smooth-On, USA), fluorescent red pigment, and [^{18}F]FDG (200:5:1 ratio-by-volume). [^{18}F]FDG concentration was selected based on the 50th percentile of an analysis of 22 lesions from 13 PMBCL patients. Images of lesions were acquired using the GE MI PET/CT scanner (10min bed-duration) to determine the ground truth for lesion radioactivity and radiomics features. True tumour volume was determined by mass (ρ=1.15g/mL for liquid plastic). Results: Mean absolute error (MAE) comparing TMTV ground truth and theoretical value was determined to be 13.8%, indicating that the casting method is accurate. The high viscosity of the liquid plastic used in the casting process causes radioactivity within the lesion to be heterogeneous. PET images using the NCMO method were determined to be highly realistic by an experienced nuclear medicine physician, due to the heterogeneous shapes and radioactivity distributions of the tumours. **Conclusion:** We developed a negative tumour casting method for use in oncology, which accepts PET/CT segmentations of real patient images as the template. NCMO has the potential to enable improved studies related to traditional image metrics as well as radiomics-based features within PET imaging. This method is generalizable and has the potential to be translated to other imaging modalities (e.g. SPECT, CT). **References:** none

OP-0728

Development of a patient-specific kidney phantom with inhomogeneous activity distribution using only a single fillable compartment

A. Theisen, M. Lassmann, A. K. Buck, J. Tran-Gia;
Department of Nuclear Medicine, University of Würzburg, Würzburg, GERMANY.

Aim/Introduction: 3D-printed phantoms have become increasingly important for assessing quantitative SPECT/CT. Inhomogeneous activity distributions are typically achieved by multiple compartments separately filled with stock solutions of different activity concentration, complicating phantom filling and increasing the error susceptibility. The aim of this work was the design of a single-compartment phantom mimicking inhomogeneous spatial activity distributions by internal filling structures of different volume fractions. This leads to apparently inhomogeneous activity distributions if the structure size is smaller than the SPECT resolution. **Materials and Methods:** Two kidney phantoms with different internal structures in cortex and medulla were designed based on a contrast-enhanced CT of a patient. After segmentation, internal structures of different volume fractions were achieved through a Boolean "AND" operation with gyroid structures [1] of different wall thickness. In consequence, the two phantoms had medulla:cortex volume fraction ratios of 1:1 (gyroid wall thickness 0.5 mm) and 1:5 (gyroid wall thickness 0.5 mm [cortex] and 2.65 mm [medulla]). After 3D printing using a Form 2 (Formlabs) and leakage testing, the phantoms were filled with 95 MBq ^{177}Lu based on a 24 h peri-therapeutic ^{177}Lu-DOTATATE SPECT/CT of the same patient. The 1:1 and 1:5 phantoms (filling volumes 158 mL and 135 mL) were filled with activity concentrations of 0.60 MBq/mL and 0.70 MBq/mL, respectively. Quantitative SPECT/CT imaging was performed on a Siemens Intevo Bold camera (medium-energy collimator, 120 views of 10 s, non-circular orbit, xSPECT Quant reconstruction: 48

iterations, 1 subset, no postfilter). Results: A good agreement between phantom designs, fabricated phantoms (high-resolution CT), and patient kidney (clinical low-dose CT) was found. The internal structures were invisible in the SPECT images, indicating a sufficiently small wall thickness. While the voxel-based activity distribution of the 1:1 phantom showed the expected peak around 0.52 MBq/mL (activity concentration times volume fraction not filled by the gyroid), the peak was wider for the 1:5 phantom (two merging activity concentration peaks at 0.61 MBq/mL and 0.27 MBq/mL for cortex and medulla, respectively). In comparison, the patient showed the most inhomogeneous activity distribution. **Conclusion:** The proposed method provides printable phantoms mimicking inhomogeneous activity distributions while using a single stock solution, thus simplifying the filling process and reducing uncertainties in the activity determination. By changing the wall thickness of an internal gyroid structure, different activity distributions can be realized, enabling phantom-based modeling of inhomogeneous activity distributions for assessing and reducing uncertainties in internal dosimetry. **References:** [1] Schoen, NASA Technical Note 1970.

OP-0729

Accuracy of thyroid uptake calibration method: a multi-centric study with realistic phantoms

T. Beaumont[1], F. Bouchet[2], D. Broggio[1], G. Brouquieres[3], B. Farman[4], A. Forbes[5,6], C. Jaudet[7], G. Le Rouzic[8], J. Maisonobe[9], F. Maurel[10], C. Murat[11], Y. Petegnief[12], B. Piron[13], L. Santoro[14], B. Serrano[15], P. Tylski[16], N. Varmenot[17], M. Demonchy[18];
[1]IRSN/SDOS/LEDI, Fontenay-Aux-Roses, FRANCE, [2]CHU Angers, Angers, FRANCE, [3]CHITS-Hôpital Sainte Musse, Toulon, FRANCE, [4]CHU La Timone, Marseille, FRANCE, [5]AP-HP Hôpital Bicêtre, Le Kremlin-Bicêtre, FRANCE, [6]AP-HP Hôpital Antoine Béclère, Clamart, FRANCE, [7]Centre François Baclesse, Caen, FRANCE, [8]Centre Hospitalier Régional d'Orléans, Orléans, FRANCE, [9]Groupe Hospitalier Pité-Salpêtrière, Paris, FRANCE, [10]CHU de Nice, Nice, FRANCE, [11]Centre Hospitalier d'Avignon, Avignon, FRANCE, [12]CHRU Jean MINJOZ, Besancon, FRANCE, [13]CHU Nîmes, Nîmes, FRANCE, [14]ICM Val d'Aurelle, Montpellier, FRANCE, [15]Centre Hospitalier Princesse Grace, Monaco, FRANCE, [16]Hospices Civils de Lyon, Bron, FRANCE, [17]Institut de cancérologie de l'Ouest R. Gauducheau, Saint-Herblain, FRANCE, [18]CHI Fréjus Saint-Raphael, Fréjus, FRANCE.

Aim/Introduction: measurement of the thyroid uptake is of interest in diagnostic and for treatment of benign thyroid disease. The sensitivity obtained from measurement in air or in a standard neck phantom does not take into account the real thyroid anatomy. The goal of this multi-centric study was to assess the accuracy of thyroid uptake measurement using a set of realistic thyroid phantoms of varying size. These measurements were carried-out according to the site-specific local procedure (Local) and according to a standardized protocol (Std). In this preliminary report sensitivities obtained with routine calibration objects were compared with those obtained with the set of phantoms, for both protocols. **Materials and Methods:** measurements were carried-out from October 2020 to June 2021 on 20 NaI gamma-cameras and 3 CZT cameras with parallel and pinhole collimators. Radionuclides were Tc-99m and I-123. Five thyroid phantoms between 3 and 30 mL were used. Images were centrally analyzed, a 3DSlicer module has been developed for automatic segmentation and calculation of the sensitivity. The mean sensitivity over five thyroid volumes $<S_{vol}>$ was compared with the routine calibration factor (S_{rout}) and with the sensitivity in air, obtained with a unique syringue (S_{air}). The three sensitivities were measured for both protocols. Results: 25 configurations have been analyzed (58% of final set). For pinhole Tc-99m measurements, the mean sensitivities S_{air} were 101 ±45 counts/MBq/s (Std, n=7) and 148 ±91 counts/MBq/s (Local, n=7). The difference being mainly due to different measurement distances in the protocols. For I-123 measurements with parallel collimators, the mean sensitivities S_{air} were 73 ±13 counts/MBq/s (Std, n=10) and 72 ±14 counts/MBq/s (Local, n=9). S_{air} was almost independent of radionuclides and protocol. For pinhole collimator the sensitivity decreased when the thyroid volume increased, whatever the radionuclide and protocol. For the 30 mL phantom, on mean, the sensitivity was 12% lower than <Svol>. Considering the local protocol and both radionuclides the relative difference between S_{rout} and $<S_{vol}>$ was greater than 15% in 43% of the cases. The standard protocol did not reduce this difference. For parallel collimators the difference between S_{rout} and $<S_{vol}>$ was always less than 17%, almost independently of the protocol, radionuclide and parallel collimator model. **Conclusion:** with parallel collimators, the sensitivity was relatively independent of the thyroid volume and the routine calibration was suitable for thyroid uptake estimation. For pinhole collimators the calibration was strongly influenced by the volume and quantitative measurement were of limited accuracy. **References:** None

OP-0730

Radioiodine uptake measurement on planar scintigraphic images: an automatic process reducing thyroid volume effect

T. Beaumont[1], A. Forbes[2,3], E. Durand[2], A. Castilla-Lièvre[3], D. Broggio[1];
[1]IRSN/SDOS/LEDI, Fontenay-Aux-Roses, FRANCE, [2]AP-HP Bicêtre Hospital, Le Kremlin-Bicêtre, FRANCE, [3]AP-HP Antoine Béclère Hospital, Clamart, FRANCE.

Aim/Introduction: Dosimetry-based therapy of benign thyroid diseases requires the assessment of the radioiodine uptake (RIU) at least at one time-point before therapy. For that purpose, a planar scintigraphic image can be acquired with a gamma-camera after administration of a tracer activity of I-123. The aims of this systematic study is to investigate the

accuracy of a standard RIU calibration method using a clinical routine phantom compared with a set of five realistic thyroid phantoms. **Materials and Methods:** The planar images were acquired with two gamma-cameras, Siemens Symbia T2 and S, with LEHR collimators. The thyroid phantoms, with volumes ranging from 3 to 30 mL and the routine phantom were filled with I-123 solution (10 MBq). The phantoms were imaged at two measuring distances (20 and 30 cm). In this systematic study, six measurements of reproducibility were performed for each geometry. The influence of the following parameters has been evaluated: distance, phantom type, thyroid volume, image processing and calibration protocol. A new automatic method, independent of the region of interest (ROI) chosen by the user was evaluated. Results: The standard calibration procedure generally underestimated the thyroid activity when compared to the realistic phantoms calibration factor. Precisely, at 30 cm, the difference in activity was at most 12% for Symbia T2 and 20% for Symbia S. Experiments showed limited impact of thyroid volume (<6%) and distance on uptake assessment but the standard image processing method influenced greatly RUI estimates. Therefore, the systematic study enabled implementing a new automatic procedure based on a fixed thresholding of planar images. For I-123, an optimum threshold, independent of the gamma-camera and measuring distance, and minimizing the thyroid volume effect was obtained with value of 10%. Using this image processing, the bias on measured activity was 3% for Symbia T2 and 2% for Symbia S. **Conclusion:** In the investigated clinical practice, the RIU was often inaccurately determined at any thyroid volume. An underestimation of 20% of the uptake indicated that the therapeutic activity given to patients could have been reduced by that much. The automatic calibration method considerably reduced the thyroid volume effect. Currently, this method and realistic thyroid phantoms are used in a French multi-centric study to evaluate the accuracy of thyroid uptake calibration. In a future work, the quantification of RIU for patients with multinodular diseases will be studied with a new pathologic phantom including two nodules enabling to mimic hyper- or hypo-uptake. **References:** None

OP-0731

Myocardial Perfusion Imaging and Extra-Myocardial Uptake: The Effect of Post-Processing Decisions on Left Ventricular Contraction Quantitative Parameters for a Dedicated Cardiac SPECT Camera

J. Kennedy[1], *T. Hasdai*[2], *Z. Keidar*[1];
[1]*Rambam - Health Care Campus, Haifa, ISRAEL,* [2]*B. and R. Rappaport School of Medicine, Technion – Israel Institute of Technology, Haifa, ISRAEL.*

Aim/Introduction: A solid-state cadmium zinc telluride (CZT) SPECT device with multiple-pinhole collimation provides ultrafast myocardial perfusion imaging (MPI). This study aims at determining the effect on MPI quantitative analysis when excluding extra-myocardial uptake using masking software for this device. **Materials and Methods:** 200 ^{99m}Tc-sestamibi gated MPI studies performed on a CZT device using a same-day rest/stress protocol were retrospectively analyzed. The data were post-processed under 3 conditions: no masking (NM), loose masking (LM), and tight masking (TM). For LM, masking was sufficient to exclude extra-myocardial uptake but with a margin between the edges of the myocardium and the mask edge. For TM, the mask edge was set to give no margin. Ejection fractions (EF) were calculated using 3 different quantitative software packages originally developed by a hospital (HEF), a university (UEF), and the camera manufacturer (MEF). Subgroups were created by considering MPI studies (n=54) read as not normal (EF≤45% or ischemia or scar) and by considering those with no margin between extra-myocardial uptake and the inferior wall (n=31). Results were compared using rank sum tests. The number of studies needing masking for the automated estimation of EF was also evaluated (χ^2 test). Results: Compared to NM, LM caused average reductions of < 3.7 percentage points (60.4±13.6 to 56.8±12.9, mean±SD) while TM caused average reductions of 7.5 percentage points (60.4±13.6 to 52.8±12.6), for HEF stress studies (p<0.0001). For UEF, all differences were small (< 2% points) with LM providing the smallest differences from NM. For MEF, all differences were small (< 1.5 % points) with LM providing the smallest differences from NM, with generally no statistically significant difference between masking and NM populations (p≥0.07). Between the software packages, the biggest differences were for NM (>6.0 % points), with LM providing smaller differences (<1.7 % points) on the whole (p<0.0001). There was little difference in results by dividing into subgroups. Compared to NM, LM generally provided for a statistically significant (p<0.05) increase in the number of studies (e.g. from n=181 to n=200, MEF rest) whereby the software packages could automatically estimate EF. **Conclusion:** Masking is a necessary part of MPI post-processing in some studies. Overall, masking did not greatly affect the quantitative results of MPI for this CZT device. However, for some ejection fraction estimates, light masking provides more consistency and tight masking causes substantial reductions that may lead to an inaccurate left ventricular contraction assessment. **References:** none

OP-0732

Towards a comprehensive validation for Monte Carlo SPECT simulations

S. Pells[1,2], D. M. Cullen[1], A. P. Robinson[2,1,3], B. Pietras[1], D. Deidda[2], A. Fenwick[2,4], K. Ferreira[2], A. Fish[1], D. Hamilton[3], W. Heetun[2], P. Julyan[3], G. Needham[1], E. Page[3], E. Price[1], J. Tipping[3];
[1]The University of Manchester, Manchester, UNITED KINGDOM, [2]The National Physical Laboratory, Teddington, UNITED KINGDOM, [3]The Christie NHS Foundation Trust, Manchester, UNITED KINGDOM, [4]Cardiff University, Cardiff, UNITED KINGDOM.

Aim/Introduction: Monte Carlo (MC) simulations directly track the interactions of each gamma ray emitted from a source and record all instances of scatter and attenuation. They are therefore a valuable tool for the optimisation of acquisition protocols and image corrections in Single-Photon Emission Computed Tomography (SPECT). Accurate image corrections are becoming increasingly important due to the need for quantitative SPECT, and their methodologies are frequently based on results from MC. The results of MC simulations are often used as a 'ground-truth', but this is only the case if the simulation is fully validated against experimental data. This work aims to establish a comprehensive validation for a MC SPECT simulation. **Materials and Methods:** A full MC simulation of the Mediso AnyScan SPECT system installed at the National Physical Laboratory has been developed in the GATE (Geant4 Application for Tomographic Emission) toolkit [1]. The simulation models the components of each detector head and the collimators according to technical specifications provided. The simulation can run in both dual- and triple-head acquisition modes. Experimental measurements of detection efficiency for a range of energies were collected, permitting an energy-dependent camera efficiency to be modelled and applied to the simulation. Validation data have been collected in a range of geometries, including commercial and 3D-printed phantoms, for Lu-177 and Tc-99m. Experimental observables have been considered to verify the simulation output is comparable to that of the physical SPECT system; these include the sensitivity, energy spectra, tomographic acquisition and movement of the detector heads, and the projection images. Results: Quantitative analysis has confirmed that the simulated acquisitions are equivalent to the physical SPECT acquisitions based on the given observables. **Conclusion:** This work provides a validation protocol which can be applied to any MC SPECT simulation. The validated simulation is now being used to optimise clinical imaging protocols and corrections for the novel isotopes Tb-155 and Tb-161. **References:** Jan S. 2004, 49:4543-61 Phys. Med. Biol.

1310

Wednesday, October 20 - Saturday, October 23, 2021

on-demand pool, release on Wednesday, October 20 at 09:00

Clinical Oncology Track - TROP Session: Prostate BC Recurrence

OP-0734

Diagnostic Performance and Prognostic Value of Combined ^{68}Ga-PSMA and ^{68}Ga-DOTA-RM2 PET/MRI in Recurrent Prostate Cancer

P. Mapelli[1,2], S. Ghezzo[1], E. Preza[2], A. Samanes Gajate[2], V. Cucchiara[1], G. Brembilla[1], C. Bezzi[1], R. Rigamonti[2], P. Magnani[2], E. Toninelli[2], V. Bettinardi[2], A. Savi[2], A. Palmisano[3], N. Suardi[4], L. Gianolli[2], P. Scifo[2], A. Briganti[1,4], A. Esposito[1,3], M. Picchio[1,2];
[1]Vita-Salute San Raffaele University, Milan, ITALY, [2]Nuclear Medicine Department, IRCCS San Raffaele Scientific Institute, Milan, ITALY, [3]Department of Radiology, IRCCS San Raffaele Scientific Institute, Milan, ITALY, [4]Department of Urology, IRCCS San Raffaele Scientific Institute, Milan, ITALY.

Aim/Introduction: To investigate the combined role of ^{68}Ga-PSMA PET/MRI and ^{68}Ga-DOTA-RM2 PET/MRI in prostate cancer (PCa) recurrence and the prognostic value of PET parameters. **Materials and Methods:** Thirty-five patients with biochemical recurrence of PCa underwent ^{68}Ga PSMA PET/MRI, with 31/35 also undergoing ^{68}Ga-DOTA-RM2 PET/MRI scan within 3 days, to restage the disease. Qualitative assessment of the scans by comparing the global and location-specific findings on ^{68}Ga-PSMA and ^{68}Ga-DOTA-RM2 PET/MRI was performed, and Wilcoxon-signed rank test was used to test for the differences. SUVmax, SUVmean at 40-50-60% threshold of SUVmax were calculated. Spearman correlation was used to study the association between PET parameters and multi-tracer PET positive lesions. The sample was subdivided according to PSA concentration in three groups (PSA≤0.5 ng/ml, 0.5<2, ≥2). Fisher's exact test was performed to study the association between PSA and multi-tracer PET positive findings. Mann-Whitney U test was used to investigate whether higher levels of PSA were related to a higher number of PET positive lesions. P-values were corrected for multiple testing by false discovery rate and significance was defined below the .05 level. Results: Patients' mean age was 70 years (range: 44-89) and mean PSA concentration was 2.8 ng/ml (range: 0.21-14.4). ^{68}Ga-PSMA PET/MRI was positive in a higher number of patients and detected more lesions compared to ^{68}Ga-DOTA-RM2 PET/MRI (26/35, 94 lesions vs 15/31, 40 lesions; p=.002 and .002). ^{68}Ga-PSMA detected more lesions in all the examined locations (pelvis, lymph-nodes, bones and visceral) than ^{68}Ga-DOTA-RM2 (p=.007, .008, .002, .028, respectively). ^{68}Ga-PSMA and ^{68}Ga-RM2 PET/MRI positive findings were concordant in 12/31 patients, partially concordant in 8/31 patients and discordant in 11/31

patients. Among the 11/31 discordant findings, 10/11 were ^{68}GaPSMA positive and ^{68}Ga-DOTA-RM2 negative, and 1/10 was ^{68}Ga-PSMA negative and ^{68}Ga-DOTA-RM2 positive. ^{68}Ga-PSMA SUVmax, SUV40, SUV50 and SUV60 correlated with the amount of ^{68}Ga-PSMA PET/MRI positive lesions (ρ=0.41, 0.40, 0.42, 0.42; p=.048). PSA level was not significantly associated with disease detected by PET/MRI, although patients with high levels of PSA were 5.5 and 4 times more likely to be ^{68}Ga-PSMA and ^{68}Ga-DOTA-RM2 PET positive than individuals with low levels of PSA. Furthermore, patients with higher levels of PSA presented more lesions on ^{68}Ga-PSMA PET/MRI (p=.001). **Conclusion:** ^{68}Ga-PSMA is more sensitive than ^{68}Ga-DOTA-RM2 in detecting lesions in recurrent PCa. The numerosity of PET positive lesions correlates with ^{68}Ga-PSMA PET/MRI SUV at different thresholds and is associated with higher levels of PSA, unravelling potential prognostic factors. **References:** None

OP-0735

^{68}[Ga]PSMA-11 PET/TC in prostate cancer: accurate localization for an accurate treatment management

R. Viglialoro[1], L. Marzorati[1], A. Marciano[1], G. Aghakhanyan[1], E. Esposito[1], F. Bartoli[1], R. Zanca[1], M. Sollini[2,3], P. A. Erba[1,4];
[1]Regional Center of Nuclear Medicine, Department of Translational Research and New Technology in Medi, Pisa, ITALY, [2]Regional Center of Nuclear Medicine, Department of Translational Research and New Technology in Medi, Pieve Emanuele, ITALY, [3]IRCCS humanitas Research Hospital, Rozzano (Milan), ITALY, [4]Regional Center of Nuclear Medicine, Department of Translational Research and New Technology in Medicine, Groningen, NETHERLANDS.

Aim/Introduction: Many PET radiopharmaceuticals have been used in the biochemical recurrence (BCR) of prostate cancer (Pca), including [^{18}F]FMCH and [^{68}Ga]PSMA-11, the last is recommended at PSA level < 1.0 ng/mL. We presented the initial results of the prospective double arm trial, [^{68}Ga]PSMA and/or [^{18}F]FMCH PET/CT, conducted in patients with BRC to predict clinically relevant information using radiomics and machine-learning (ML) approaches. **Materials and Methods:** We assessed 89 patients who were enrolled in the [^{68}Ga]PSMA-11 arm (mean age 72 years ± 34 years) and 33 patients (mean age 73 years ± 7 years) who were enrolled in 2nd arm encountering both [^{68}Ga]PSMA and [^{18}F]FMCH PET/CT scans. All studies were performed with PET/CT Discovery 710 (GE Healthcare). The administered activity of [^{68}Ga]PSMA-11 was 1.8-2.2 MBq/kg according to the EANM guidelines and 2.8-7 MBq/Kg for [^{18}F]FMCH. Region-of-interests (ROIs) were delineated using 40% SUVmax threshold (PETVCAR tool, GE Advantage 4.6), while the LifeX software was used for radiomics analysis. Grouping variables were define (a) with the lesion burden using oligometastatic/plurimetastatic categorization (either with 3 or 5 lesions cut-off) and (b) with Gleason Score (GS) labels, such as class-0 representing GS = 6, 7; class-1, GS = 8,9 etc.). Data were split into 80% for training and validation, while 20% for test-set and cross-validation using 5, 7, 10 K-folds. Logistic regression was used as a classifier after applying Lasso algorithm for data-dimensionality reduction. Area Under Curve (AUC) was obtained to validate the model accuracy. Results: Overall, 53/36 patients with oligometastatic/plurimetastatic disease were defined using 3 lesions cut-off, while 74 oligometastatic/plurimetastatic patients with a cut-off 5. A different distribution in PSA and SUVmax values was only found with the cut-off 3. No association was found with bone disease phenotype, although a trend was noted with higher PSA. ML able to classify GS 6 vs GS 7-8-9 groups (AUC of 0.87). The subgroups of GS 7, 8 and 9 show similar signature. Treatment decisions were changed after [^{68}Ga]PSMA-11 PET/CT for the patients in the 2nd arm. **Conclusion:** This preliminary data confirms the potential of PET/CT driven ML-approaches to predict clinically relevant information in BCR. These data can be expanded to new patients and lesions, that will allow us to verify the analysis pipeline and to select parameters for adaptive personalized treatment. **References:** none

OP-0736

Oncological Outcomes after 68Ga-PSMA-11 PET/CT performed in Hormone-Sensitive Prostate Cancer (HSPC) patients for Biochemical Recurrence and eligible for Salvage Therapy

F. Ceci[1], G. Rovera[1,2], G. C. Iorio[3], A. Guarneri[3], V. Chiofalo[3], R. Passera[1], M. Oderda[4], S. Dall'Armellina[1], A. Giordano[2], P. Gontero[4], U. Ricardi[3], D. Deandreis[1];
[1]Nuclear Medicine, Department of Medical Sciences, University of Turin, Turin, ITALY, [2]Section of Nuclear Medicine, University Department of Radiological Sciences and Haematology, Università Cattolica del Sacro Cuore, Rome, ITALY, [3]Radiation Oncology, Department of Oncology, AOU Città della Salute e della Scienza di Torino, Turin, ITALY, [4]Urology, Department of Surgical Sciences, AOU Città della Salute e della Scienza di Torino, Turin, ITALY.

Aim/Introduction: Prostate-Specific-Membrane-Antigen/Positron Emission Tomography (PSMA-PET) detects with high accuracy disease-recurrence, significantly improving the clinical management of biochemically-recurrent (BCR) prostate cancer (PCa). However, there is lack of data regarding the oncological outcomes of patients who performed PSMA-PET. Objective: to evaluate the incidence of clinically-relevant events during follow-up in patients who performed PSMA-PET for BCR. **Materials and Methods:** this analysis was performed in a cohort of consecutive, hormone-sensitive, hormone-free, recurrent PCa patients enrolled through a prospective single-arm study [1]. All patients were considered eligible for salvage therapy, having at least 24 months of follow-up after PSMA-PET. Outcome Measurements and Statistical Analysis: the primary end point was the Event-Free Survival (EFS), defined as the time between the PSMA-PET and the date of event/last follow-up. The Kaplan-Meier method was used to estimate

the EFS curves, comparing the effect of different predictors by the log-rank test. EFS was also investigated by the uni- and multi-variate Cox proportional hazards regression. Event was defined as: a) death; b) radiological progression assessed by PET (PSMA or choline or fluciclovine) or whole-body MRI, bone scan, contrast-enhanced CT; c) PSA recurrence after systemic and/or loco-regional therapy. Results: 176 patients were analyzed (median PSA 0.62 [IQR:0.43-1.00] ng/mL; median follow-up of 35.4 (IQR:26.5-40.3) months). Events after PSMA-PET were observed in 79/176 patients (44.9%). The proportion of event-free patients was 78.8% (1-year), 65.2% (2-years), and 52.2% (3-years). Patients with clinically-relevant events had a significantly higher median PSA (0.81 [IQR:0.53-1.28] vs 0.51 [IQR:0.36-0.80] ng/mL) and a lower PSAdt (5.4 [IQR:3.7-11.6] vs 12.7 [IQR:6.6-24.3]) (p<0,001). The Kaplan-Meier curves showed PSA>0.5 ng/mL, PSAdt≤6 months and a positive PSMA-PET result were associated with a higher event rate (p<0.001). No significant differences of event rates were observed in patients who received changes in therapy management after PSMA-PET vs. patients who did not receive therapy changes. Finally, PSA> 0.5 ng/mL and PSAdt≤ 6months were statistically-significant event-predictors in multi-variate model (p<0.001). **Conclusion:** This study evaluated the incidence of clinically-relevant events during follow-up in HSPC patients who performed PSMA-PET for BCR. Events were detected in 44.9% of patients and event rates differed among specific clinical settings. Besides PSA and PSAdt, negative PSMA-PET scans were associated with longer event-free survival, while events were equally distributed regardless changes in therapy management. PSMA-PET might help to stratify patients by oncological outcomes, leading to a more cost-effective management, namely during early recurrence. **References:** [1] Eur J Nucl Med Mol Imaging. 2020 Nov;47(12):2804-2815.

OP-0737

Pattern of failure in patients with biochemical recurrence after PSMA-radioguided surgery

L. Schweiger[1], T. Maurer[2], R. Simon[3], T. Horn[3], M. Eiber[1], W. Weber[1], I. Rauscher[1];
[1]Department of Nuclear Medicine, Klinikum rechts der Isar, Technical University of Munich, Munich, GERMANY, [2]Martini-Clinic Prostate Cancer Center at University of Hamburg-Eppendorf (UKE), Hamburg, GERMANY, [3]Department of Urology, Klinikum rechts der Isar, Technical University of Munich, Munich, GERMANY.

Aim/Introduction: Prostate-specific membrane antigen (PSMA)-targeted radioguided surgery (RGS) has become a powerful tool for removing small or atypically localized lesions through radioactive labelling of tumor tissue in patients with localized recurrent prostate cancer (PC). Nevertheless, the pattern of failure (locoregional or systemic) after PSMA-RGS remains unknown. Therefore, the aim of this retrospective analysis was to evaluate the pattern of metastases using PSMA-ligand PET in patients developing a second biochemical recurrence (BCR) after PSMA-RGS. **Materials and Methods:** For this study, 80 patients were retrospectively included undergoing PSMA-ligand PET because of BCR (Median PSA: 0,9 ± 1.93 ng/mL; range: 0.2 - 14.2 ng/mL) after prior PSMA-RGS for PSMA-ligand PET positive recurrent PC. Only patients with ≥1 histopathological proven soft tissue metastases removed during PSMA-RGS were included. One nuclear medicine physician evaluated all PSMA-ligand PETs. All suspicious lesions for recurrent PC were grouped as following: 1) local recurrence 2) lymph node metastases (pelvic, retroperitoneal and supradiaphragmatic) 3) bone and 4) visceral metastases. Detection rates and lesion localization were determined and stratified by PSA-values. Results: The median time between PSMA-RGS and PSMA-ligand PET for secondary BCR was 13,5 ± 12,3 months (range: 5,0- 25,6 months). In total, 62/80 (77.5%) patients showed PSMA-ligand positive findings. PSMA-ligand PET detection rates were 58.3% (14/24), 72.2% (13/18), 83.3% (15/18) and 100% (20/20) for PSA-levels of 0.2-<0.5 ng/mL, 0.5-<1 ng/mL, 1-<2 ng/mL and ≥2 ng/mL, respectively. More than half of the patients (53,2%; 33/62) showed local recurrence and/or pelvic lymph node metastases. 41.9% presented with local and/ or only distant metastases with a combination of pelvic and retroperitoneal lymph nodes (7/62), as well as a combination of local recurrence and pelvic lymph nodes (7/62) occuring most frequently. **Conclusion:** PSMA-ligand PET is a useful method to detect and localize recurrent disease in patients with secondary BCR after PSMA-RGS with more than half of the patients presenting with loco-regional recurrence offering the potential for a second local therapy (e.g. radiation therapy, further resection). **References:** none

OP-0738

Head-To-Head Comparison Between wb-MRI And ^{68}Ga-PSMA PET/CT In Restaging Biochemical Recurrent Prostate Cancer

R. Mei[1], M. Moscarino[1], A. Farolfi[1], P. Castellucci[1], L. Calderoni[1], F. Mattana[1], S. Telo[1], F. Serani[1], F. Ceci[2], S. Fanti[1];
[1]Nuclear Medicine Policlinico S.Orsola-Malpighi IRCCS, Bologna, ITALY, [2]IEO European Institute of Oncology IRCCS, Milano, ITALY.

Aim/Introduction: Imaging detection of prostate cancer (PC) recurrence is crucial for the best treatment strategy. Positron emission tomography/computed tomography (PET/CT) with ^{68}Ga-prostate-specific membrane antigen (^{68}Ga-PSMA) has become an essential tool in re-staging PC, showing unprecedent detection rate as compared to other standard techniques, even for prostate-specific antigen (PSA) values lower than 0.2 ng/mL. Another important diagnostic tool is magnetic resonance imaging (MRI) including diffusion-weighted imaging, which has several advantages in re-staging PC patients, especially in those with pelvic anatomical alterations as consequence of previous surgery.

To date, only few studies with small cohorts compare the diagnostic performances of ^{68}Ga-PSMA PET/CT and whole-body (wb) MRI.In this retrospective, multi-center, single-arm study we aimed to compare the diagnostic performances of wb-MRI and ^{68}Ga-PSMA PET/CT in restaging PC patients with biochemical recurrence after radical prostatectomy. **Materials and Methods:** Patients who had undergone radical prostatectomy for PC and with newly occurrence of biochemical relapse of disease (PSA ≥ 0.2 ng/mL) were included. All patients had undergone wbMRI and ^{68}Ga-PSMA PET/CT scans within a period not superior to 4 weeks and without changes of treatment. Reference standard was either histopathology (when available), or follow-up imaging (i.e., a confirmation of the finding was considered as malignancy), or PSA levels (i.e., a decrease in PSA level after or under therapy will be considered as malignancy). Results: Overall, 14 patients were included, median aged 69 (IQR:64-72); 6/14 (43%) had high-risk PC, while median PSA at the time of the scans was 1.87 ng/mL (IQR:1.11-4.18 ng/mL). On a patient-based analysis, wb-MRI resulted positive in 10/14 (71%) patients, while ^{68}Ga-PSMA PET/CT only in 7/14 (50%). On a lesion-based analysis, wb-MRI found more lesion than ^{68}Ga-PSMA PET/CT (n= 21 vs 18), being able to detect more local recurrence (28% vs 7%), pelvic nodal metastases (50% vs 36%) and bone metastases (57%vs 28%); on the contrary, wb-MRI detected fewer extra-pelvic nodal metastases (7% vs 50%). Interestingly, detection rate of ^{68}Ga-PSMA PET/CT was superior to wb-MRI for grouped pelvic and extrapelvic nodes (p=.021) and for PSA values <1.0ng/mL (7% vs 0%). **Conclusion:** Although preliminary, this study demonstrated the complementary role of both wb-MRI and ^{68}Ga-PSMA PET/CT in restaging PC. Particularly, wb-MRI detected more local recurrence, pelvic nodal metastases and bone metastases, while ^{68}Ga-PSMA PET/CT was superior for node metastases and with low PSA values. **References:** None.

OP-0739

Safety of [^{68}Ga]Ga-PSMA-11 prepared with the Sterile Cold Kit used in a pivotal clinical trial

L. Ravasi[1], S. Chowdhury[2], C. Hayward[3], D. Kryza[4], A. Giraudet[4];
[1]Telix pharmaceuticals, Herstal, BELGIUM, [2]Medical Oncology Guy's Hospital, London, UNITED KINGDOM, [3]Telix Pharmaceuticals, Indianapolis, IN, UNITED STATES OF AMERICA, [4]Centre Léon Bérard, Lyon, FRANCE.

Aim/Introduction: Combination of treating molecularly selected patients with a targeted radiolabeled diagnostic and therapeutic gave birth to the theragnostics concept. With regards to prostate, an International, Prospective, Open-label, Multicenter, Randomized Phase 3 Study in the Treatment of Patients with Progressive PSMA-positive Metastatic Castration-resistant Prostate Cancer (mCRPC), named Vision, has been carried out. The eligibility of the patients in Vision has been made by assessing the expression of PSMA via [^{68}Ga]Ga-PSMA-11 mostly reconstituted with Telix cold kit. **Materials and Methods:** We here report the interim safety data of the report from the Vision trial integrated into the dossier submitted to the FDA. Results: For the Safety population, there were 48 (23.3%) subjects that reported 109 events after receiving Ga-68 PSMA-11. The majority of events were in the Musculoskeletal and Connective Tissue Disorders, General Disorders and Administration Site Conditions, Gastrointestinal Disorders, Blood and Lymphatic System Disorders, Nervous System Disorders, Infections and Infestations, Renal and Urinary Disorders, and Injury, Poisoning, and Procedural Complications. The most frequently reported AEs include anaemia, asthenia, arthralgia, constipation, haematuria, bone pain, and acute kidney injury. There were 2 (4.2%) patients that reported events assessed as possibly related to study drug, including asthenia and constipation. There was 1 (2.1%) patient that reported hot flush which was assessed as probably related to study drug. There were 2 (4.2%) patients that reported events assessed as definitely related to study drug, including injection site warmth and cognitive disorder. **Conclusion:** The safety results from this study are consistent with what is reported in the literature regarding other investigations of Ga-68 PSMA-11 in patients diagnosed with BCR, and the class of diagnostic radiopharmaceutical imaging agents more broadly (Fendler et al., 2019).The safety report from the Vision trial about the Telix's Kit for the preparation of Ga-68 PSMA-11 meets the safety requirements for a NDA submission to the FDA. **References:** Fendler WP, Eiber M, Beheshti M, Bomanji J, Ceci F, Cho S, Giesel F, Haberkorn U, Hope TA, Kopka K, Krause BJ, Mottaghy FM, Schöder H, Sunderland J, Wan S, Wester HJ, Fanti S, Herrmann K. 68Ga-PSMA PET/CT: Joint EANM and SNMMI procedure guideline for prostate cancer imaging: version 1.0. Eur J Nucl Med Mol Imaging. 2017 Jun;44(6):1014-1024.

OP-0740

First experiences with late acquisition [^{68}Ga]Ga-PSMA-11 PET/CT using a long axial field-of-view PET/CT scanner for the diagnosis of recurrent prostate cancer

I. Alberts[1], G. Prenosil[1], C. Mingels[1], K. Bohn[1], M. Viscione[1], H. Sari[2], A. Rominger[1], A. Afhsar-Oromieh[1];
[1]Institut für Nuklearmedizin, Bern, SWITZERLAND, [2]Advanced Clinical Imaging Technology, Lausanne, SWITZERLAND.

Aim/Introduction: While acquisition of images in [^{68}Ga]Ga-PSMA-11 following longer uptake times can improve lesion uptake and contrast, resultant imaging quality and count statistics are limited by the isotope's half-life (68 minutes). Here, we present the first experiences with a new long axial field-of-view (LAFOV) PET/CT system, demonstrating late imaging is feasible and can even provide improved image quality compared to regular acquisitions. **Materials and Methods:** In these preliminary data we report our initial

experiences with 10 patients who underwent standard imaging at 1h p.i. following administration of 192±36 MBq [^{68}Ga]Ga-PSMA-11 with additional late imaging performed at 4h p.i. Images were acquired in a single bed position for 6 min at 1h p.i. and 16 min p.i. at 4h p.i. using a LAFOV scanner (106 cm axial FOV). Two experienced nuclear medicine physicians reviewed all scans in consensus and evaluated overall image quality (5-point Likertscale), lesion uptake in terms of standardised uptake values (SUV), tumour to background ratio (TBR) and target-lesion signal to background noise (SNR). Results: Subjective image quality as rated on a 5-point Likert-scale was only modestly lower for late acquisitions (4.2/5 at 4h p.i.; 5/5 1h p.i.) TBR was significantly improved (4h: 3.41 vs 1h: 1.93, p<0.001) and SNR was improved with borderline significance (4h: 33.02 vs 1h: 24.80, p=0.062) at later imaging. Images were obtained with total acquisition times comparable to routine examinations on standard axial FOV scanners. **Conclusion:** Late acquisition in tandem with a LAFOV PET/CT resulted in improvements in TBR and SNR and were associated with only modest impairment in subjective visual imaging quality. These data show that later acquisition times for [^{68}Ga]Ga-PSMA-11 may be preferable when performed on LAFOV systems. **References:** None

OP-0741

How to deal with a negative Gallium-68 prostate-specific membrane antigen positron emission tomography/computed tomography (^{68}Ga-PSMA PET/CT) during biochemical recurrence?

H. Lanzafame[1], F. Serani[2], A. Farolfi[2], C. Malizia[2], S. Fanti[2,3], R. Mei[4], G. Aluisio[5], F. Medici[6,7];

[1]Nuclear Medicine Unit, Department of Biomedical and Dental Sciences and Morpho-Functional Imaging, University of Messina, Messina, ITALY, [2]Nuclear Medicine, IRCSS, Azienda Ospedaliero-Universitaria di Bologna, Bologna, ITALY, [3]Nucleare Medicine-Department of Experimental, Diagnostic and Specialty Medicine, University of Bologna, Bologna, ITALY, [4]Nuclear Medicine, IRCSS, Azienda Ospedaliero- Universitaria di Bologna, Bologna, ITALY, [5]Radiation Oncology, Azienda Ospedaliero-Universitaria di Ferrara, Ferrara, ITALY, [6]Department of Experimental, Diagnostic and Specialty Medicine - DIMES, S. Orsola-Malpighi Hospital, University of Bologna, Bologna, ITALY, [7]Radiation Oncology IRCSS Azienda Ospedaliero- Universitaria di Bologna, Bologna, ITALY.

Aim/Introduction: 68Ga-PSMA PET/CT is used in patients with biochemical relapse (BRC) after radical prostatectomy (RP). Despite the attested efficacy of salvage radiotherapy (sRT), there is still no unanimous consent on the best time to treat definition. Various Authors, taking into consideration possible prognostic risk factors, tried to identify a precise subset of patients who could benefit from the "wait and see" approach. In this context, we investigated any significant correlation between clinical features and longer relapse-free survival. **Materials and Methods:** We retrospectively analyzed men with prostate cancer who underwent PSMA PET with negative findings from 2016 to 2019 for BCR (two consecutives serum PSA values > 0.2 ng/ml) after RP. Images were reviewed independently by two blinded nuclear medicine physicians, disagreement was resolved with consensus. Patients who received androgen deprivation therapy (ADT) prior or after PET, and/or undergoing ADT at time of observation were excluded. We recorded iPSA, ISUP score, risk classification, PSA persistence, PSA kinetics, time gap between surgery and recurrent disease, PSA before PET (<0.5 ng/ml/ >0.5 ng/ml), PET scan results, following management (SRT +/-). Treatment response was defined as PSA ≤ 0.1 ng/ml. Time to progression was defined by PSA relapse (two consecutives serum PSA values > 0.2 ng/ml with undetectable PSA after sRT or persistence) or further PSA rise. Multivariate logistic regression analysis was performed to identify determinants for differences in patients subgroups. Results: No significant differences in risk factors were found between treated and non treated patients. Median follow up after PSMA was 17 months (IQR 11-29 mo).Of all 151 patients (median age 68y) with negative scan, 66.8% (101/151) received sRT, whereas 55% (50/151) underwent a "watch and wait" approach. Among all patients with negative PSMA who received sRT, 81.1% (82/101) demonstrated treatment response, compared with further PSA increase in 100% (50/50) of non treated. The median of disease progression was 8 months. Cox proportional hazards analysis attested relative risk of progression 5 times higher in non treated PET negatives, compared to those who received sRT. Of all examined factors, only PSA persistence proved predictive of biochemical failure (p=0.02) . **Conclusion:** In negative PSMA, sRT allows to achieve treatment response in the majority of patients. With the exception of PSA persistence, no clinical feature holds significant prognostic value for progression disease. According to our preliminary results, there's no reasonable evidence that supports a surveillance approach. **References:** None.

OP-0742

Potential value of ^{68}Ga-PSMA-11 PET to predict biochemical recurrence in primary prostate cancer after radical prostatectomy

H. Wang[1], T. Amiel[2], T. Langbein[1], I. Rauscher[1], T. Horn[2], M. Heck[2], T. Maurer[3,4], W. Weber[1], M. Eiber[1];

[1]Department of Nuclear Medicine, Klinikum rechts der Isar, Technical University Munich, Munich, GERMANY, [2]Department of Urology, Klinikum rechts der Isar, Technical University Munich, Munich, GERMANY, [3]Martini-Klinik Prostate Cancer Center, University Hospital Hamburg-Eppendorf, Hamburg, GERMANY, [4]Department of Urology, University Hospital Hamburg-Eppendorf, Hamburg, GERMANY.

Aim/Introduction: Prostate-specific membrane antigen (PSMA)-ligand positron emission tomography (PET) has been applied successfully for primary staging in prostate cancer patients. Associations between PSMA-immunohistochemistry and outcome hold promise indicate the potential of PET-imaging to serve as a noninvasive imaging biomarker to predict disease outcomes after radical prostatectomy (RP). Recently the molecular imaging TNM classification (miTNM) was introduced to standardize PSMA-ligand PET interpretation. We aimed to investigate the predictive value of ^{68}Ga-PSMA-11 PET findings for time to biochemical recurrence (BCR) in primary prostate cancer after RP. **Materials and Methods:** In a retrospective analysis, 186 primary prostate cancer patients treated with RP who had undergone a ^{68}Ga-PSMA-11 PET up to three months prior to the surgery were included. Maximum standardized uptake value (SUV_{max}), SUV_{mean}, tumor volume (TV) and total lesion (TL) were collected from PET-imaging. Uni- and multivariate logistic regressions were used to analyze associations between PET-findings and pathological parameters (Gleason Score [GS] and surgical margin). Uni- and multivariate Cox regression were used to assess the correlation between time to BCR and clinicopathological information, including age, serum prostate-specific antigen (PSA) level, ^{68}Ga-PSMA-11 PET findings, and pathological characteristics. Kaplan-Meier curves were used to display BCR-free survival rates at time intervals. A molecular staging system was established and a cutoff of SUV_{max} 5.4 was applied for IA and IB stage separation. A p-value < 0.05 was considered statistically significant. Results: At a median follow-up after RP of 38 months (IQR: 22-53), BCR was observed in 58/186 patients during the follow-up period. A significant association between a positive surgical margin and miN status (miN1 vs. miN0, OR: 5.428, p=0.004) was detected. miT status (miT≥3a vs. miT<3, OR: 2.696, p=0.003) was identified as an independent predictor for aggressive GS (GS≥8). Multivariate Cox regression analysis indicated that PSA level (HR: 1.024, p=0.014), advanced GS (GS≥8 vs. GS<8, HR: 3.253, p<0.001) and miT status (miT≥3a vs. miT<3, HR: 1.941, p=0.035) were independent predictors for BCR. In the miT2 subgroup, shorter BCR-free survival was observed in the patients with higher SUV_{max} (IB vs. IA stage, log-rank, p=0.022). **Conclusion:** Preoperative miTNM classification from ^{68}Ga-PSMA-11 PET correlates with postoperative GS, surgical margin status and time to BCR. The association between miTNM staging and outcome proposes ^{68}Ga-PSMA-11 PET as a novel imaging biomarker and potentially serves for ancillary pre-treatment stratification. Prospective studies are necessary to fully determine its use including primary prostate cancer patients with different treatments and risk categories. **References:** None

OP-0743

Therapy impact of ^{18}F-PSMA PET/CT in biochemical recurrence of prostate cancer patients with PSA< 1 ng/ml postprostatectomy and ^{18}F-Choline PET/CT negative

M. Cózar Santiago[1], J. García Garzón[1], J. Pastor Peiro[2], P. Bassa Massanas[1], A. Canoves Llombart[1], J. Aguilar Barrios[1], R. Sanz Llorens[1], V. Faus Rodrigo[1], M. Soler Lopez[1], J. Ferrer Rebolleda[1]; [1]ASCIRES-Nuclear Medicine Department. General Hospital Universitary, Valencia, SPAIN, [2]ASCIRES-Radiotherapy Department. General Hospital Universitary, Valencia, SPAIN.

Aim/Introduction: To evaluate the rate of recurrence detection on ^{18}F-PSMA PET/CT in postprostatectomy patients with PSA< 1 ng/ml and a negative ^{18}F-Choline PET/CT (Spanish regulatory requisite to authorize an ^{18}F-PSMA study), and to assess its impact on therapy strategies provided **Materials and Methods:** Prospective study including 27 consecutive prostate cancer (PC) patients with PSA< 1 ng/ml, initially treated with prostatectomy (mean time of 19 months since radical treatment), and with a negative ^{18}F-Choline PET/CT study performed < 1 month before. A dual-phase PET/CT scan was performed after iv injection of 185±10% MBq of ^{18}F-FDCFPyL: 1) early imaging (immediately after tracer administration) of prostate area, and 2) whole-body imaging 1h after tracer injection. Two experienced readers, using visual and quantitative analysis, assessed PET/CT images. Lesions detected were categorized into four regions: prostate bed recurrence (Tr), pelvic lymph nodes (N1), extrapelvic lymph nodes (M1a) and bone/visceral metastases (M1b). Based on ^{18}F-PSMA PET/CT findings, the Oncology Committee decided most adequate therapy strategy: radiotherapy, radiotherapy volume, androgen deprivation therapy (ADT) associated, and other systemic treatments Results: Mean patient age was 68.6-year-old. Mean PSA level was 0.29 ng/mL and mean PSADT was 8 months. ^{18}F-PSMA PET/CT was negative in 11 out of 27 (40.7%) patients. Sixteen out of 27 (59.3%) per-patient positive ^{18}F-PSMA PET/CT were classified as TrN0M0 (n:2); T0N1M0 (n:11); T0N0M1a (n:2); and TrN0M1a (n:1). Regarding lesion site, patients with Tr (n:3); patients with N1 (n:11); patients with M1a(n:3); patients with M1b (n:0). All lymph-node uptake corresponded with infracentimetric lesions on CT. Regarding patient-stratification, 10 had solitary lesions, 4 oligometastases (< 5 lesions) and 2 multimetastases. Based on ^{18}F-PSMA PET/CT positive results, change in therapy approach was as follows: change in radiotherapy volume in 7 patients, change in radiotherapy volume and ADT in 6, no change in therapy management in 2, and radiotherapy contraindication in 1 patient (systemic treatment instead) **Conclusion:** ^{18}F-PSMA PET/CT allowed disease detection in 59.3% of prostate cancer patients with PSA levels <1 ng/ml postprostatectomy and negative ^{18}F-Choline PET/CT. Disease location and patient stratification provided a tailored treatment strategy, guidance for salvage radiotherapy, indication for ADT, and even radiotherapy contraindication in 1 patient **References:** None

OP-0744

Detection rate of 18F-Choline positron emission tomography/computed tomography in patients with non-metastatic hormone sensitive and castrate resistant prostate cancer

P. Artioli[1], F. Zattoni[2], M. Burei[3], A. Chiaravalloti[4], D. Donner[5], S. Panareo[6], L. Evangelista[1];
[1]University of Padova, Padova, ITALY, [2]University of Udine, Udine, ITALY, [3]IOV, Padova, ITALY, [4]University of Rome, Rome, ITALY, [5]Hospital of Trento, Trento, ITALY, [6]University of Ferrara, Ferrara, ITALY.

Aim/Introduction: To assess the detection rate of 18F-choline PET/CT in non-metastatic hormone-sensitive prostate cancer (hsPCa) and non-metastatic castrate resistant prostate cancer (CRPCa), based on the criteria proposed in the phase III SPARTAN trial and with high Gleason Score (GS). **Materials and Methods:** Between October 2008 and September 2019, data from a retrospective multicenter study, involving patients undergoing ^{18}F-choline PET/CT scans for a biochemical recurrence of PCa, were collected. The following inclusion criteria were used: 1) histologically proven PCa, 2) a non-metastatic disease in accordance with conventional imaging findings; 3) a PSA doubling time (PSAdt) $\leq$10 months, 4) a GS $\geq$ 8 and 5) no pelvic node $\geq$ 2 cm. the group of hsPCa and CRPCa patients, were compared by using a non-parametric statistical analysis. Moreover, a logistic regression analysis and ROC curves were used. Results: 140 patients were included. Of these, 82 patients were affected by hsPCa, and 58 had a CRPCa. Overall, 18F-Choline PET/CT was positive in 99/140 (70.7%). It was positive in 55/82 (67.1%) hsPCa patients and in 44/58 (75.9%) CRPCa subjects, respectively. The site of recurrence at 18F-Choline PET/CT were: 16 (27.6%) and 20 (24.4%) in prostatic bed, 25 (43.1%) and 24 (29.3%) in loco-regional lymph nodes and in 27 (46.6%) and 28 (34.1%) in distant organs, respectively for CRPCa and hsPCa patients. The optimal cut-off values for PSA at the time of PET/CT for the prediction or recurrence were 0.5 vs. 2.5 ng/mL for all site of recurrence (AUC: 0.70 vs. 0.72), 0.48 vs. 3.4 ng/mL for prostatic bed (AUC: 0.60 vs. 0.59), 0.5 vs. 1.5 for loco-regional lymph nodes (AUC: 0.62 vs. 0.57) and 2.2 vs. 2.8 ng/mL for distant metastasis (AUC: 0.74 vs. 0.71), respectively in CRPCa and hsPCa (all p=NS). **Conclusion:** The rate of positive 18F-Choline PET/CT is similar in patients with a hsPCa and CRPCa, in case of low PSAdt and high GS. Therefore, non-metastatic PCa patients should be assessed by molecular imaging, in order to adapt the most appropriate therapeutic approach. **References:** Fendler, et al. Clin Cancer Res. 2019; 25:7448-7454. Zattoni et al. Clin Nucl Med. 2020; 45:594-603.

OP-0745

The detection rate of PSMA-PET is still preserved in a low probability setting of a positive scan in patients with biochemical recurrence: a dual phase protocol with diuretic enhancement

A. Miceli[1], V. Feudo[2], C. Baiocco[3], S. Genovese[3], P. Scalzi[3], A. Trevisan[3], G. Sambuceti[1], C. Poti[3];
[1]DISSAL, Genoa, ITALY, [2]Section of Nuclear Medicine, University Department of Radiological Sciences and Hematology, Università Cattolica del Sacro Cuore, Rome, ITALY, [3]Unit of Nuclear Medicine, Aosta Regional Hospital, Aosta, ITALY.

Aim/Introduction: Biochemical recurrence is an age-old problem for patients after radical treatments for prostate cancer. Indeed, the sooner salvage therapies are performed, the better are the results. In this scenario, Prostate-Specific Membrane Antigen Positron Emission Tomography (PSMA-PET) has firmly entered the clinical practice to localize disease recurrence in the presence of very low Prostate-Specific-Antigen (PSA) serum levels (0.2-1 ng/mL). In addition to the absolute value of PSA, PSA doubling-time (DT), Gleason Score (GS), and androgen-deprivation-therapy (ADT) at the time of PET contribute to predict a positive result from the scan. In a low-risk setting, however, the pre-test probability is considered insufficient to justify the exam (1). Optimizing the acquisition protocol may potentially improve the PSMA-PET detection rate, even in this context. **Materials and Methods:** We retrospectively analyzed 97 patients who underwent 68Ga-PSMA-PET from March 2018 to April 2021 for biochemical recurrence. Our protocol provides the administration of 3 MBq/Kg of 68Ga-PSMA-11, 60 minutes of uptake-time and a 4 min/bed vertex-to-knees scan. Furosemide 20 mg i.v. is then administered, inviting the patient to void the bladder (3 urinations) before the late scan (120-140 minutes post tracer-injection), of the pelvic region (2-3 beds with acquisition time of 5 min/bed). Patients were divided into two groups according to the pre-test probability (45 with ≥ 40% and 52 with < 40%, respectively) based on a well-validated prediction nomogram (1). Results: The overall PSMA-PET detection rate was 69%. No statistically significant differences were observed between the low and the high pre-test probability subgroups (63,5%, and 71%, respectively, p=0.3). Stratifying anatomically no differences were seen, but it is worth noting that in the prostatic bed the detection rate was higher in the low-risk group (30,8% vs 22%; p=0.3), while in the lymphatic pelvic region was higher in the high-risk one (30,7% vs 46,6%; p= 0.1) indicating a less and a more advanced disease, respectively. We also reported a clear change in clinical management in 27% of patients in the low-risk group. **Conclusion:** With our scan protocol, the detection rate of PSMA-PET is preserved even in patients with a low probability of a positive scan (e.g. PSA value < 0.8 ng/ml, GS ≤7, DT > 6 months), demonstrating its straightforward utility in the clinical management of patients, especially

with localized disease. **References:** 1. Ceci F. et al. Prediction nomogram for ^{68}Ga-PSMA-11 PET/CT in different clinical settings of PSA failure after radical treatment for prostate cancer. doi: 10.1007/s00259-019-04505-2.

1311

Wednesday, October 20 - Saturday, October 23, 2021

on-demand pool, release on Wednesday, October 20 at 09:00

Featured Session: Brain Tumor Imaging - More than Amino Acids in Gliomas

OP-0747

CXCR4 and SSTR Imaging of Brain Tumours

T. Traub-Weidinger; Department of Biomedical Imaging and Image-Guided Therapy, Medical University of Vienna, Vienna, AUSTRIA.

OP-0748

Quantitative Parameters from 18F-FDG PET/MRI Reveal Intratumoral Heterogeneity in Primer Brain Tumors Confirmed by Pathology

K. Seker[1], E. Çeltikçi[2], U. Aydos[1], S. Gülbahar Ateş[3], M. A. İnan[4], Ü. Ö. Akdemir[1], L. Ö. Atay[1];
[1]Gazi University Faculty of Medicine, Department of Nuclear Medicine, Ankara, TURKEY, [2]Gazi University Faculty of Medicine, Department of Neurosurgery, Ankara, TURKEY, [3]Abdurrahman Yurtaslan Oncology Training and Research Hospital, Department of Nuclear Medicine, Ankara, TURKEY, [4]Gazi University Faculty of Medicine, Department of Medical Pathology, Ankara, TURKEY.

Aim/Introduction: To evaluate the relationship between regional tumor metabolism, cellularity, perfusion and histopathological grade of primary brain tumors. **Materials and Methods:** A total of 29 biopsy data and imaging parameters obtained from 13 patients (mean age: 53.4±18.4; 9 males, 4 females) with primary or recurrent brain tumors who underwent 18F-FDG PET/MRI between 2019-2021 were evaluated, retrospectively. In quantitative analysis, normalized SUV values were calculated by proportioning the maximum standardized uptake values (SUVmax) of the intratumoral foci for identified biopsy areas, and the SUVmax and the mean SUV value (SUVmean) measured from the contralateral gray matter (GM) and white matter (WM) at the centrum semiovale level (SUV1: lesion/GM SUVmaks; SUV2: lesion/GM SUVmean; SUV3: lesion/WM SUVmaks; SUV4: lesion/WM SUVmean). The minimum apparent diffusion coefficient (ADC) (b=1000) values of the lesions were calculated from the MR images taken in the same session. In patients with ASL (arterial spin labeling) images, the normalized perfusion index was calculated (lesion region of interest value/ipsilateral cerebellar region of interest value). Biopsy results obtained from identified areas using stereotaxic and neuro-navigation techniques were recorded. Results: Four biopsy focus was evaluated in two patients, three in one patient, two in eight patients, and one in two patients. Necrosis and granulation tissue were detected in two foci, grade 2 tumors in 7 foci, grade 3 in 9 foci, and grade 4 in 11 foci. There were a significant difference in SUVmax, normalized SUV and ADCmin between histopathological tumor grades (Table 1). When grade 4 tumor foci and other tumor foci were compared, only a significant difference was found between the groups in SUVmax and normalized SUV (Table 2). In correlation analysis, a moderate significant negative correlation was found between SUV values and ADCmin (R: (-0.73)-(-0.65); p<0.001). Perfusion indeces were found to have a highly significant negative correlation only with ADCmin (R: (-0.80); p=0.004). In ROC analysis, optimum threshold values for discriminating grade 4 tumors were calculated as 9.4, 0.62, 0.84, 2.99 and 3.79 for SUVmax, SUV1, SUV2, SUV3 and SUV4, respectively. The sensitivity and specificity levels were calculated as 72.7% and 72.2% for SUVmax, 91% and 67% for SUV1, and 82% and 72.2% for SUV2, SUV3 and SUV4, respectively. **Conclusion:** In the single-session PET/MR imaging of brain tumors, quantitative metabolic data provided by PET images and cellularity and perfusion data provided by MR images enable the determination of intra-tumor heterogeneity and appropriate biopsy areas. **References:** none

OP-0749

Brain metabolic changes in patients with disseminated malignant melanoma receiving immunotherapy

M. Sizova[1], F. Sampedro[2], V. Camacho[1], S. Abouzian[1], F. Fuentes-Ocampo[1], A. Teixido[1], A. Fernandez[1], D. López-Mora[1], J. Duch[1], A. Flotats[1], M. Estorch[1], I. Carrio[1];
[1]Hospital de la Santa Creu i Sant Pau, Universitat Autònoma de Barcelona, Barcelona, SPAIN, [2]Institut de Recerca de l'Hospital de la Santa Creu i Sant Pau, Barcelona, SPAIN.

Aim/Introduction: To evaluate brain metabolic changes in patients with disseminated malignant melanoma after 3-6 months of receiving immunotherapy, and to investigate whether these changes correlate with the exposure to the immunotherapy regimen. **Materials and Methods:** Seventeen patients (12 males; 68 ± 17 years) with disseminated malignant melanoma (15 cutaneous; 1 conjunctival; 1 vulvar) were prospectively included from May 2017 to February 2021. Fourteen patients were treated with anti PD-1 therapy and 3 patients with combined immunotherapy (anti PD-1 and anti CTLA-4). Exclusion criteria included brain metastases and neurological diseases. All patients underwent two brain [18F]FDG PET/CT examinations, before (19 ± 20 days) and after 3-6 months of the start of immunotherapy. Voxelwise SUVratios were measured using the protuberance as the reference region. Using the SPM12 software, FDG-PET images were then normalized to 2mm MNI space and smoothed

with a Gaussian kernel of 12 mm FWHM . Longitudinal changes in brain metabolism were assessed by comparing pre vessus post-treatment FDG images using a voxelwise paired t-test. Additionally, we performed a longitudinal regression analyses to investigate whether the time under immunotherapy influenced the longitudinal loss of brain metabolism. The following potential confounding factors were taken into consideration: different PET/CT scanners, days between PET/CT examinations and days between the start of immunotherapy and PET/CT examinations. Results: None of the patients presented cognitive impairment or other neurological alterations between pretreatment and postreatment (3-6 months) PET/CT examinations. Three patients required opioid treatment for pain control during the study period. The statistical analysis revealed a significant SUVratio decrease in temporoparietal regions ($p < 0.01$, FDR-corrected).A tendency to greater SUVratio decrease was observed in parieto-temporal and occipital regions in patients with a longer duration of immunotherapy ($p < 0.005$ uncorrected). **Conclusion:** Patients with disseminated malignant melanoma receiving immunotherapy presented a significant decrease of brain metabolism in temporoparietal regions after 3-6 months of treatment initiation. Further studies are needed to better characterize the effect of immunotherapy on brain metabolism and its clinical implications. **References:** None

OP-0750

Dual-time point brain FDG PET to differentiate tumor progression from radionecrosis after stereotactic radiotherapy for brain metastases

H. Otman[1], J. Farce[2], F. Le Jeune[2], D. Mariano Goulart[3], F. Cachin[1], M. Chawki[4], M. Chanchou[1], A. Girard[2];
[1]Centre Jean Perrin, Clermont Ferrand, FRANCE, [2]Centre Eugene Marquis, Rennes, FRANCE, [3]CHU Montpellier, Montpellier, FRANCE, [4]CHU Nancy, Nancy, FRANCE.

Aim/Introduction: Dual phase 18[F]-FDG brain PET (dual-PET) is useful to distinguish tumor recurrence (TR) from radionecrosis (RN) after stereotaxic radiosurgery (SRS) of brain metastases, when contrast-enhanced MRI is inconclusive. We aimed to compare six different visual and quantitative interpretation criteria to enhance diagnostic performances. **Materials and Methods:** In this retrospective french multicentric study (Clermont-Ferrand, Montpellier, Rennes), we evaluated 45 patients previously treated with SRS for BM, addressed for a dual-PET by the local neuro-oncological committees for an evolving lesion on MRI inconclusive between TR and RN, at least 3 months after the last SRS session. Dual-PET included both an "early" and a "delayed" acquisition, respectively 30 to 60 minutes and 4 to 5 hours after 18[F]-FDG injection. After measuring SUVmax values of both lesion (L) and mirror contralateral grey matter (GM) at early (1) and delayed (2) acquisitions, three quantitative metrics were calculated : ratios of L SUVmax to GM SUVmax at "early" (L1/GM1) and "delayed" (L2/GM2) acquisitions and the retention index which is the variation over time of the standardized SUVmax ratio (RI = [(Delayed-Early)/Early]). Visual analysis was also conducted using a subjective 6 points visual scale of the lesion uptake at both acquisitions. The five interpretation criteria were compared according to their area under the ROC curve (AUC), and to their diagnostic accuracy applying the best cut(off value (maximizing the Youden's index) by the Cochran Q test. The final diagnosis was based on pathology, or by default radiological and clinical follow-up criteria after at least 6 months. Results: Final diagnoses were TR for 24 patients and RN for 21 patients. There was no statistically significant difference regarding AUC between the different interpretation methods. AUC ranged from 0.78 [95%CI 0.63; 0,89] with the L1/GM1 Ratio, to 0.85 [95%CI 0.72; 0.94] with the L2/GM2 ratio. Visual analyses AUC were excellent at both early (0.835 [95%CI 0.7; 0.93]) and delayed acquisitions (0.83 [95%CI 0.69; 0.92]). There was no statistically significant difference between accuracies ($p=0.87$) ranging from 0.71 with the RI ratio to 0.80 with both the "delayed" visual and quantitative analyses. **Conclusion:** Dual-PET protocol distinguishes RN and TR after SRS with robust diagnostic performances in case of doubtful MR, with an accuracy up to 80%. **References:** none

OP-0751

Differential alterations in tumoral and extra-tumoral cerebral blood flow in grades III and IV glioma patients using quantitative [^{15}O]H_2O PET

A. J. Gonçalves[1], M. Alotaibi[1], A. R. Carlin[1], Y. Chen[1], C. Y. Wong[1], I. K. Djoukhadar[2], G. Krokos[3,1], A. Jackson[1], D. Coope[2], M. C. Asselin[1];
[1]The University of Manchester, Manchester, UNITED KINGDOM, [2]Salford Royal NHS Foundation Trust, Manchester, UNITED KINGDOM, [3]King's College London, London, UNITED KINGDOM.

Aim/Introduction: Clinical management of gliomas remains challenging, with grade IV gliomas (glioblastoma) associated with treatment resistance and poor prognosis. Alterations in perfusion (cerebral blood flow, CBF) in the tumour and throughout the brain likely influence the effectiveness of radiotherapy and drug delivery. PET with radiolabelled water ([^{15}O]H_2O) is considered the gold standard to accurately measure absolute CBF. The aim of this study is to quantify CBF in glioma patients, compared against measurements in healthy controls, to assess CBF heterogeneity in the tumour and the surrounding brain. **Materials and Methods:** Dynamic [^{15}O]H_2O PET data were acquired using the high-resolution research tomograph (HRRT, Siemens) in 14 controls (43.4±5.7 years, 8 females) and 13 patients (49.8±12.4 years, 3 females) of which the first 3 WHO grade III and 5 grade IV gliomas have been analysed to date. Parametric maps of absolute CBF estimates were generated using the 1-tissue compartment model with a sampled arterial blood input function. Tumour-

related abnormalities were manually delineated from gadolinium-enhanced T1-weighted MR and FLAIR images. Extra-tumoral white matter (WM) and grey matter (GM) were segmented from structural T1-weighted MRIs using FSL. Groups were statistically compared using the Mann-Whitney U-test and regions using the Wilcoxon signed-rank test with the level of significance set at p<0.05. Results: From the controls, the normal CBF range (95% confidence interval) was determined to be 0.254-0.396 and 0.316-0.480 ml/min/cm^3 in WM and GM, respectively. For grade III gliomas, CBF for WM and GM laid within these ranges. Tumour regions with and without gadolinium enhancement were found to have either diminished or elevated CBF compared to WM with marked heterogeneity. Conversely, for grade IV gliomas, CBF in both WM and GM were significantly reduced by 31.4% and 29.1% (p=0.00017 and p=0.005), respectively. CBF in the enhancing rim (0.211±0.036 ml/min/cm^3) was not elevated compared to WM in these patients. Regions defined as necrotic core were depleted of CBF by 47.3% compared to WM. FLAIR regions in both grades III and IV gliomas had CBF values not significantly different from their respective WM regions. **Conclusion:** Grade III gliomas have relatively preserved CBF in normal appearing WM and GM. The significant reduction in global CBF in grade IV gliomas may be a result of the increase in intracranial pressure, a common feature in grade IV gliomas. The different CBF between grades III and IV in FLAIR regions may be indicative of differing underlying biology and cellularity. **References:** none

OP-0752

The rise of metabolism: Expression of pentose phosphate pathway enzymes in treatment-naïve gliomas

E. Klebermass[1,2], A. Woehrer[3], G. Ricken[3], N. Poetsch[1], S. Bucconi[1], A. Miller[4,5], A. Haschemi[4], T. Balber[6], M. Hacker[1], H. Viernstein[2], M. Mitterhauser[6], T. Traub-Weidinger[1];
[1]Department of Biomedical Imaging and Image-guided Therapy, Division of Nuclear Medicine, Medical University of Vienna, Vienna, AUSTRIA, [2]Department of Pharmaceutical Technology and Biopharmaceutics, University of Vienna, Vienna, AUSTRIA, [3]Institute of Neurology, Medical University of Vienna, Vienna, AUSTRIA, [4]Department of Laboratory Medicine, Medical University of Vienna, Vienna, AUSTRIA, [5]Department of Neurobiology, Harvard Medical School, Boston, MA, UNITED STATES OF AMERICA, [6]Ludwig Boltzmann Institute Applied Diagnostics, Vienna, AUSTRIA.

Aim/Introduction: Genomic profiling of glioblastoma multiforme (GBM) has promoted interest in metabolic reprogramming in gliomas (1). In tumors, the pentose phosphate pathway (PPP) is a major regulator of redox homeostasis and biosynthetic metabolism. Glucose-6-phosphate dehydrogenase (G6PD) is the first and rate-limiting enzyme of the oxidative PPP-branch (oxPPP), controlling the generation of NADPH and ribulose-5-phosphate, a precursor for nucleotide synthesis. The non-oxidative PPP-branch, with sedoheptulokinase (SHPK) as a key enzyme, replenishes the oxPPP and regulates glucose metabolism (2). To advance research on glioma metabolism, we aimed at evaluating SHPK and G6PD expression in treatment-naïve glioma patients that had undergone [^{11}C] methionine ([^{11}C]MET) PET-scans. **Materials and Methods:** Immunohistochemical staining with anti-SHPK (ab69920) or anti-G6PD antibody (ab210702) was performed on tumor biopsies of a heterogeneous cohort of 100 glioma patients (59 male). Expression was semi-quantitatively assessed with the Histoscore (H-score), using the formula [(intensity 1 * % area stained) + (intensity 2 * % area stained)], with 1 depicting weak and 2 depicting strong staining. H-scores were compared with tumor-to-noise (T/N) ratios of the patients' [^{11}C]MET-PET-scans, IDH1 status and proliferation rate (MIB-1 score). Statistical tests were performed with SPSS 25.0 for Mac with p-values <0.05 considered statistically significant. Results: G6PD and SHPK expression was found in tumor and microenvironmental cells. Median G6PD H-score was significantly higher in GBM compared to lower-grades (107 vs. 52), while SHPK expression was very heterogeneous. In general, a higher MIB-1 score corresponded to a higher G6PD expression and higher [^{11}C]MET-PET T/N ratios. Patients with a G6PD H-score >69 (median) had a significantly shorter median survival (35 vs. 159 months, p<0.001), while survival was not related to SHPK. G6PD expression in high-grade astrocytomas (grade 3 (n=21)+GBM (n=25)) was significantly lower in tumors with IDH1-R132H mutation (p=0.015). Calculated over all tumors, there was a significant correlation between expression of SHPK and T/N ratio (p=0.03), as well as G6PD and T/N ratio (p<0.001). **Conclusion:** Our data reinforce the proposed prognostic value of G6PD in gliomas and its relation to tumor aggressiveness and growth. Both the PPP and methionine can drive tumor growth and counter-balance redox-stress by glutathione production. Though causalities still need to be proven, our data suggest that enhanced [^{11}C]MET accumulation in tumors might not only be a readout for increased amino acid metabolism, but could also mirror other metabolic pathways. **References:** (1)Libby C.J., et al. Biochim Biophys Acta Rev Cancer. 2018 Apr; (2)Ge T., et al. Front. Endocrinol. 2020 Jun

OP-0753

Role of 64CuCl2 in the diagnosis and in the dosimetry assessment in paediatric high-grade gliomas

F. Fiz[1], M. Ugolini[2], G. Ferrarazzo[3], A. Cistaro[2], G. Bottoni[2], S. Righi[2], M. Massollo[2], A. Cirone[2], A. Piccardo[2];
[1]Humanitas Clinical and Researhc Center - IRCCS, Milan, ITALY, [2]E.O. "Ospedali Galliera", Genoa, ITALY, [3]A.S.L. 3, Genoa, ITALY.

Aim/Introduction: Paediatric high-grade gliomas (HGG) are aggressive tumour entities presenting diagnostic challenges, especially when the anatomy is distorted by previous

treatments. Tumour-specific PET tracers could overcome this issue. Cooper is an important co-enzyme in energy-producing processes, whose turnover is increased in tumour cells. ^{64}Cu is a positron-emitting cooper radioisotope with a long half-life of 12,3 hours, fit for diagnostic purposes with potential theranostics implication. In this study, we tested the HGG $^{64}CuCl_2$ uptake and dosimetry using multiple time-points PET/CT **Materials and Methods:** Ten paediatric HGG subjects (median age: 9 years; range: 6-15) underwent a cerebral $^{64}CuCl_2$ PET/CT and an MRI (T1 contrast-enhanced and FLAIR). PET acquisition was repeated at three time points (1, 24, and 72 h p.i.). Tumour volumes were assessed in PET and in the two MR series by two expert readers. Uptake intensity was calculated from the PET volume as SUVmean and TBR. The dose to the tumour lesions was computed using the OLINDA method. Results: Out of the ten patients, eight presented a diffuse intrapontine glioma or a diffuse midline glioma with H3K27M mutations; one was affected by a glioblastoma and one by an anaplastic astrocytoma. A total of twelve lesions were identified, nine of them (75%) showed a visible $^{64}CuCl_2$ uptake. Intensity of accumulation was very variable (median SUV: 0.92, range 0.28-2.22; median TBR 3.41, range 1.6-10). The tracer showed a progressive accumulation over time (median SUV of 1.36 and 2.06 at the second and third time point, $p<0.05$ and $p<0.01$ respectively; median TBR of 6.24 and 10.87, $p<0.01$). The PET-based volumes were more similar to the T1- than to the FLAIR-derived ones (median of 2.95, 6.31, and 2,67 ml for T1, FLAIR, and PET, respectively). The mean effective dose was 0.0051 mGy/MBq. **Conclusion:** $^{64}CuCl_2$ is able to visualize the HGG metabolism, especially in the perfused parts of the lesions, featuring an excellent contrast with the background tissue and an accumulating pattern over time. **References:** None.

OP-0754

Meningiomas as Incidentalomas Visualized on ^{68}Ga-DOTATOC-PET/CT

E. Alevroudis[1], T. Liotsou[2], M. Metaxas[2], M. Tsoli[3], E. Anagnostou[3], G. Kaltsas[3], S. N. Chatziioannou[1,2];
[1]2nd Department of Radiology, Nuclear Medicine Unit, National and Kapodistrian University of Athens, General University Hospital "Attikon", Athens, GREECE, [2]Nuclear Medicine Division, Biomedical Research Foundation Academy of Athens, Athens, GREECE, [3]1st Department of Propaedeutic Internal Medicine, Endocrine Unit, National and Kapodistrian University of Athens, Athens, GREECE.

Aim/Introduction: Meningiomas constitute the most common primary brain neoplasms representing about one third of all intracranial tumors. The vast majority are benign (WHO grade 1) occurring more frequently in women. Meningioma cells overexpress somatostatin receptors (SSTR), especially subtype-2. This feature allows their incidental detection with ^{68}Ga-DOTA conjugated peptides PET/CT imaging performed for the diagnosis and staging of neuroendocrine tumors (NET) [1,2]. The aim of this study was to determine the prevalence incidentally discovered meningiomas in a cohort of NET patients who underwent ^{68}Ga-DOTATOC-PET/CT imaging. **Materials and Methods:** We retrospectively reviewed 398 consecutive patients with histopathologically confirmed gastroenteropancreatic and lung NET, who underwent ^{68}Ga-DOTATOC-PET/CT for staging/restaging purposes between 2019-2020. PET/CT whole-body scans were performed 60 minutes post ^{68}Ga-DOTATOC injection. Focally increased brain uptake, clearly greater than background brain uptake, except pituitary uptake, was considered indicative of a meningioma. ^{68}Ga-DOTATOC-PET/CT imaging was interpreted by an experienced nuclear medicine physician. Results: 6/398 (1.5%) patients with at least one brain finding were considered positive for meningioma. The median age was 65 years (range:29-73 years), 5 were female while all had well-differentiated NET (5 pancreatic and one lung NET). The SUVmax range was 1,1-32,7, median value:3,5. One patient had multiple brain foci in left frontal and left parietal lobe and near sella turcica. In the remaining patients single focal uptakes were noted in the right cavernous sinus, right temporal area, frontal lobe, by right hemisphere of the cerebellum and the frontal lobe respectively. Notably, in 4 patients the brain finding was the only body finding, while in the remaining 2 patients there was only additional uptake in the primary malignancy without any other lesions. Although no additional histopathological or conventional imaging evidence of a meningioma was available, the presence of other than meningioma brain tumors expressing high SSTR was clinically highly unlikely as well as the possibility of secondary neuroendocrine tumor depositions as the disease in our patients was localized and none presented with other metastases. **Conclusion:** Incidental ^{68}Ga-DOTA-PET/CT focal brain uptake, most likely due to meningioma, although rare, should always be considered and careful examination of the brain should be part of the interpretation of ^{68}Ga-DOTA scans. **References:** 1. Fathi AR, Roelcke U. Meningioma. Curr Neurol Neurosci Rep. 2013 Apr;13(4):337. 2. Galldiks N, Albert NL, Sommerauer M, et al. PET imaging in patients with meningioma-report of the RANO/PET Group. Neuro Oncol. 2017;19(12):1576-1587.

OP-0755

Imaging of primary glial tumor using [^{68}Ga]Ga-PSMA-11 PET/CT - preliminary experience

K. Pelka[1,2], K. Koczyk[3], L. Królicki[1], J. Kunikowska[1];
[1]Nuclear Medicine Department, Medical University of Warsaw, Warsaw, POLAND, [2]Department of Methodology, Laboratory of Centre for Preclinical Research, Medical University of Warsaw, Warsaw, POLAND, [3]Department of Neurosurgery, Medical University of Warsaw, Warsaw, POLAND.

Aim/Introduction: Primary glial tumors are the most prevalent type of brain tumors in adults with heterogenous histology. According to the WHO classification, gliomas should be classified according to the degree of malignancy: grade I-II (low-grade glioma), grade III (anaplastic astrocytoma or oligodendroglioma or oligoastrocytomas) and grade IV (glioblastoma). The one of most important questions is how to differentiate low- and high-grade glioma before surgery. Prostate specific membrane antigen (PSMA) originally discovered in prostate cancer has been found in other tumors, such as gliomas. The aim of the study was to compare [^{68}Ga]Ga-PSMA-11 PET/CT results with post-operative histopathological examination. **Materials and Methods:** 28 patients (pts) with revealed tumors in MRI were enrolled in single-institution study. All patients underwent contrast-enhanced MRI and [^{68}Ga]Ga-PSMA-11 PET/CT. PET/CT from apex to mid high was performed on Biograph 64 (Siemens) 60 min, after 2 MBq/kg injection of [^{68}Ga]Ga-PSMA-11. PET/CT findings were compared visually as well as semi- quantitatively using maximized standardized uptake values (SUVmax). At the time of preliminary analysis 24 pts aged 44.2±14.7 years, had undergone histopathological verification of lesions. Results: No radiopharmaceutical-related adverse events were noted. The images showed a very low background activity of the normal brain. Among 24 operated patients, 21 had glioma tumors : grade II - 9 pts, grade II/III - 2 pts, grade III - 2 pts, and grade IV - 8 pts, with final histopathological result with genetic examination in 13 of them. [^{68}Ga]Ga-PSMA-11 PET/CT showed no uptake in all grade II pts. Both grade II/III and III showed slightly increase uptake only in 50 % of pts with SUVmax 1.9. All grade IV pts showed clearly visible uptake in tumors, in total we found 12 lesions in 8 patients. Histopathology was available from 8 primary grade IV lesions with the highest uptake in [^{68}Ga]Ga-PSMA-11 PET/CT with SUVmax 7.2±1.4. 3/24 pts had different histopathological diagnosis: one - metastasis from lung cancer with SUVmax 3.5, and 2 pts inflammatory disease with SUVmax 2.5-3.2. **Conclusion:** Early results of [^{68}Ga]Ga-PSMA-11 PET/CT show high uptake in primary high-grade gliomas. The preliminary data shows promising possibility of pre-operative differentiation between low- and high-grade glioma. Further investigation of the clinical utility of this method in differentiation low- and high-grade glioma is warranted. **References:** none

OP-0756

Role of Gallium 68 PSMA PET CT in evaluating recurrence in previously treated patients with glioma of the brain

P. U N, *A. R. Bharathi, S. M. Desai, K. Rishi, G. GV, B. Srinath, H. Mohan;*
Sri Shankara Cancer Hospital and Research Center, Bangalore, INDIA.

Aim/Introduction: Glioblastoma multiforme (GBM) is one of the most aggressive and fatal primary tumor of the brain. Recurrent rate after initial treatment is upto 80-90% at the site of surgical margins. Routinely these patients are followed with contrast-enhanced Magnetic Resonance Imaging (MRI) and 2-deoxy-2-[18F] fluoro-D-glucose positron emission tomography (FDG-PET/CT). Recently studies have shown that prostate specific membrane antigen (PSMA) is expressed in vascular endothelium of various solid tumors, including GBM. Thus, the purpose of this study is to apply the recently introduced technology Ga68 PSMA PET/CT in the diagnosis of the suspected recurrence at the surgical margins of treated case of glioblastoma. **Materials and Methods:** In this study, a total of 11 consecutive patients with a history of glioblastoma, post-surgery and chemoradiation status were referred for assessment of recurrent disease versus radiation necrosis. Other primary brain tumours and metastases to the brain are excluded. All patients underwent MRI and Ga-68 PSMA PET/CT as per standard clinical protocol within a time window of 1 week. Results: Of the 11 patients, Ga68 PSMA PET/CT showed increased uptake in 8 patients. The mean SUV max of 8 patients who showed increased uptake was 2.7 and mean tumor to background ratio of 8.9 ± 5. The remaining 3 patients did not show increased uptake and the mean SUV max and mean TBR were 1.3 and 2.8. On comparison with MRI, 8 patients who showed increased uptake in Ga68 PSMA PET/CT were diagnosed as recurrent disease. 2 patients who did not show increased uptake in Ga68 PSMA scan were also diagnosed as recurrent disease in MRI. Remaining 1 patient with negative Ga68 PSMA scan result was diagnosed as post-operative changes in MRI. Of the 11 patients, only 4 patients underwent biopsy and were proved as recurrent disease (3 true positive and 1 false negative). 3 patients died during the evaluation. Remaining patients did not undergo biopsy because of the associated morbidity and mortality. **Conclusion:** The results are exploratory and there is a possible role of Ga68 PSMA PET/CT in the diagnosis of recurrent disease in a suspected case of glioblatoma. However, further larger studies are needed to assess the accuracy of Ga68 PSMA PET/CT with surgical histopathology and follow up **References:** Kunikowska J et al., 68Ga-Prostate-Specific Membrane Antigen-11 PET/CT: A New Imaging Option for Recurrent Glioblastoma Multiforme? Clin Nucl Med. 2020 Jan;45(1):11-18

OP-0757

The Role of 68Ga-PSMA PET/CT Imaging in Intracranial Metastases

E. Arslan[1], N. Ergül[1], R. Şahin[1], Y. Karagöz[2], Y. Bozkaya[3], T. F. Çermik[1]; [1]Istanbul Training and Research Hospital,Clinic of Nuclear Medicine, Istanbul, TURKEY, [2]Istanbul Training and Research Hospital,Department of Radiology, Istanbul, TURKEY, [3]Istanbul Training and Research Hospital,Department of Medical Oncology, Istanbul, TURKEY.

Aim/Introduction: Detection of intracranial metastases with F-18 FDG PET/CT imaging is unsatisfactory due to the high physiologic radiopharmaceutical uptake of normal parenchyma. The aim of this study was to investigate the diagnostic efficacy and clinical contribution of Ga-68 PSMA PET/CT in cases with known or suspected intracranial metastases. **Materials and Methods:** A total of 21 cases (9 F, 12 M), with a mean age of 56.4±14.5 were included in the study. F-18 FDG and Ga-68 PSMA PET/CT scans and cranial MRI were performed to all patients in the same week. The number and distribution of intracranial metastases obtained on both PET/CT images were assessed and SUVmax was calculated from each lesion. PET findings were compared with other clinical features of the patients, such as primary tumoral focus and histopathological data. Results: The most common indications for PET/CT imaging were breast cancer with 38% (n:8), lung cancer with 19% (n:4), and colon cancer with 19% (n:4). These were followed by gastric signet ring cell adenocarcinoma, pancreatic neuroendocrine tumor, thyroid papillary cancer, laryngeal cancer, and diffuse large B-cell non-Hodgkin lymphoma, each with a rate of 4.8% (n:1). The mean axial diameter of the most prominent metastatic lesions in the patients was 2.06±0.85 cm. However, the smallest metastatic focus detected with Ga-68 PSMA PET/CT imaging was 0.22 cm in axial diameter, also confirmed by MRI. In 8 cases (38%), intracranial metastatic lesions that could not be detected by F-18 FDG PET/CT were successfully detected by Ga-68 PSMA PET/CT imaging, and also all metastatic lesions detected by Ga-68 PSMA PET/CT were confirmed by cranial MR imaging. **Conclusion:** The absence of PSMA expression in normal brain parenchyma is an advantage for Ga-68 PSMA PET/CT imaging in detecting intracranial metastases compared to FDG with physiologic parenchymal uptake. We think that this advantage will be contribute to MRI in the diagnosis of intracranial metastasis and also it may have a new potential role in the treatment of intracranial tumors with PSMA, which is a theragnostic radioligand. **References:** None

1401

Friday, October 22, 2021, 10:45 - 12:15

Channel 1

CME 10: Radionuclide Therapies - Management of Side Effects and Complications

OP-0760

Radioiodine Therapy in Thyroid Cancer

M. Luster; University Hospital Marburg, Department of Nuclear Medicine, Marburg, GERMANY.

OP-0761

Peptide Receptor Radionuclide Therapy in Neuroendocrine Tumours

G. Gnanasegaran; Royal Free London NHS Foundation Trust, Department of Nuclear Medicine, London, UNITED KINGDOM.

OP-0762

^{177}Lu and ^{225}Ac PSMA Therapy for Prostate Cancer

S. Schwarzenböck; Rostock University Medical Center, Department of Nuclear Medicine, Rostock, GERMANY.

1402-1

Friday, October 22, 2021, 10:45 - 11:30

Channel 2

Interview with the Expert 10 - Running a Preclinical Lab in New York City

OP-0924

Interview - Running a Preclinical Lab in New York City

J. Lewis; Memorial Sloan Kettering Cancer Center, New York, UNITED STATES OF AMERICA.

OP-0925

Interview - Running a Preclinical Lab in New York City

TBA; New York, UNITED STATES OF AMERICA.

1402-2

Friday, October 22, 2021, 11:30 - 12:15

Channel 2

Interview with the Expert 11 - New PET Tracers in Oncology

OP-0247

Interview - New PET Tracers in Oncology

H. Minn; University of Turku, Clinical Oncology, Turku, FINLAND.

OP-0248

Interview - New PET Tracers in Oncology

TBA; Turku, FINLAND.

1404

Wednesday, October 20 - Saturday, October 23, 2021

on-demand pool, release on Wednesday, October 20 at 09:00

Technologists - TROP Session: Sharing Technologist's Experience 3

OP-0767

Multiple-Time-Point 2-[^{18}F]FDG PET/CT: Adrenal Glands Normal Metabolic Pattern Characterization

I. Rodrigues[1], A. Martins[1], S. Carmona[2], M. J. Vieira[2], L. Oliveira[1]; [1]Grupo Joaquim Chaves Saúde - Lisbon, Portugal/ Portuguese Red Cross Health School - Lisbon, Portugal, Lisbon, PORTUGAL, [2]Grupo Joaquim Chaves Saúde - Lisbon, Portugal, Lisbon, PORTUGAL.

Aim/Introduction: To characterize the normal metabolic behavior of the adrenal glands over time. **Materials and Methods:** Retrospective analysis of 90 adrenal glands (AG) from 45 oncological patients (27 males) with mean age (±SD) of 63.42±2.26 years without adrenal or hepatic pathology and blood glucose levels<150mg/dL. For each patient, two PET/CT studies were acquired: all the 45 patients performed a wholebody image 70 minutes after the 2-[^{18}F]FDG administration; a second abdominal image was acquired at 3 different time points for 3 different groups (15 patients each) at 120 minutes (G1), 180 minutes (G2) or 240 minutes (G3). For each time point left (LAG) and right adrenal gland (RAG) characterizations was based on a visual score (3 point scale, comparing AG vs liver uptake) and on semi-quantitative analysis that included the determination of AG SUVmax and adrenal gland-to-liver SUVmax ratio (AG/L ratio). Results: The comparison between the visual score and the AG/L ratio showed a moderate correlation for LAG (R^2=0.6277 p=0.000) and a weak correlation for RAG (R^2=0.3459 p=0.000). Mean AG SUVmax values were at 70 minutes (45 patients) for left AG=3.01±0.51 and right AG=2.74±0.45; at 120 minutes (15 patients), left AG=3.06±0.46 and right AG=2.88±0.49; at 180 minutes (15 patients) left AG=3.10±0.42 and right AG=2.82±0.38 and at 240 minutes (15 patients) left AG=3.59±0.61 and right AG=3.32±0.54. At all time points LAG and RAG mean SUVmax was lower than liver mean SUVmax (all groups p=0.000). Mean SUVmax and mean AG/L ratios for LAG were higher than the ones for RAG (all groups p=0.000). Analyzing these parameters over time, there was no significant difference of mean right and left AG/L ratio values in different time points (p>0.05) but there was an increase in mean SUVmax values for LAG and RAG respectively of 5.5% and 4.7% in G1 (p<0.05); 9.9% and 10.6% in G2 (p<0.05) and 8.5% and 13.4% in G3 (p<0.05). **Conclusion:** In our series, AG/L ratio seems the most robust parameter for assessing normal AG, as AG metabolic pattern over time is characterized by a mean SUVmax value increase and a stable AG/L ratio. This semiquantitative parameter should not be replaced by visual assessment, as they seem to have no strong correlation. The knowledge of the evolution of these parameters over time is important, and can be especially useful when differentiating borderline uptake patterns of small benign and malignant lesions. **References:** None

OP-0768

Feasibility of 3D TOF PET/CT scanning with reduced [^{18}F]-FDG activity obtaining equivalent clinical and semi-quantitative parameters

J. Pilz, L. Hehenwarter, G. Schweighofer-Zwink, G. Rendl, M. Beheshti, C. Pirich;
Department of Nuclear Medicine and Endocrinology, University Hospital Salzburg, Paracelsus Medical University, Salzburg, AUSTRIA.

Aim/Introduction: A recent published retrospective study by our group demonstrated the feasibility of PET/CT imaging with short acquisition time (57seconds per bed position (s/BP)) and equivalent clinical and semi-quantitative parameters to standard acquisition. This study aimed to translate the finding of "short acquisition" to "dose reduction" and evaluates the equivalence of PET/CT performance with 25% reduced injected [^{18}F]-FDG activity comparing PET acquisition times of 100 and 75s/BP. **Materials and Methods:** So far, 49 patients with melanoma, lung or head & neck cancer underwent a standard whole-body, vertex-to-tigh or skull-base-to-tigh [^{18}F]-FDG PET/CT examination using our EARL accredited 3D TOF Ingenuity TF scanner. As routine standard [^{18}F]-FDG PET protocol in our department, 4 MBq/kg bw will be applied with a PET acquisition time of 75s/BP. In this study 25% dose reduction has been applied and each patient received 3 MBq/kg bw of [^{18}F]-FDG. In order to simulate our standard the PET acquisition time was increased to 100s/BP. Afterwards, a second PET dataset per patient with a short acquisition time of 75s/BP was reconstructed using PET list-mode data. PET data were reconstructed using a 3D OSEM TOF algorithm. Two experienced nuclear medicine physicians analysed PET/CT studies, two datasets per patient (100s and 75s), using the Intellispace software version 10.1. PET-positive lesions per body region (head&neck, thorax, abdomen, bone, extremity) and image quality (grade 1-5) were evaluated. Semi-quantitative parameters e.g. SUVs were calculated using 3D VOI in order to be able to compare the [^{18}F]-FDG-positive lesions between the 100 and 75s datasets per patient. Statistical analyses were performed by equivalence testing (TOST) using the R software version 3.6.3 and Bland-Altman Plots were created with graph pad prism version 6. Results: Equal report results were found in >95% of the 245 investigated body regions (5 body regions

per patient) for both readers comparing 100s and 75s PET/CT studies. The overall subjective image quality was described as equal or superior in 81.6% by reader 1 and 87.8% by reader 2. Equivalence was established in 32 PET-positive lesions matched per patient between the 100s and 75s PET/CT studies for SUVmax (mean of differences: -0.109, equivalence bounds +-0.28, 90%CI -0.277-0.059, p=0.047). **Conclusion:** The primary results of this study showed comparable clinical and semi-quantitative finding of [^{18}F]-FDG PET studies applying 25% less activity by standard acquisition time. These findings seem to be of clinical relevance, especially in cancerous patients who undergo multiple PET/CT examinations for treatment monitoring. **References:** None

OP-0769

The effect of patient's body mass indices on PET/CT images with 68Ga PSMA

Y. Parlak, D. Goksoy, G. Gumuser, E. Sayit;
Celal Bayar University, Manisa, TURKEY.

Aim/Introduction: Positron emission tomography/computed tomography (PET/CT) with 68Ga-PSMA imaging is a common imaging method that provides early treatment opportunity in patients with prostate cancer. Scanning time, especially in overweight patients considering the short half-life of the radionuclide, has a significant impact on image quality. The aim of our study is to determine the appropriate scanning time for 68Ga PSMA PET/CT imaging by using body mass index (BMI) of the patient. **Materials and Methods:** Fifty seven patients (mean age; 68.73±8.8 years) who were admitted to our department for 68Ga PSMA PET/CT imaging were included in the study. Patients were divided into 4 groups according to the body mass index (BMI) values. (1st group BMI≤24.9, 2nd group BMI between 25-29.9, 3rd group BMI between 30-34.9 and 4th group BMI≥35). Approximately 60 min later, imaging was performed from mid thigh to skull base with a Truflight Select PET/CT system (Philips Medical Systems, USA). A second imaging focused on the patient's liver was additionally performed, as a reference image at 360 s/bp. PET images were reconstructed from the reference image obtained for the images at 60, 90, 120, 180, 240, 300 seconds / bed position (s / bp). In order to measure the PET/CT with 68Ga PSMA image quality, normalized SNR was calculated using the signal to noise ratio (SNR) in the liver due to the relative homogeneous 68Ga uptake. The correlations and differences between scaning time and activity according to the patient's BMI were statistically calculated. Results: The SNRs of reconstructed images for 60, 90, 120, 180, 240, 300, 360 s/bp was obtained as 7.95 ± 1.34, 8.85 ± 1.63, 9.3 ± 1.8, 9.8 ± 1.6, 10.9 ± 2.14, 11.77 ± 2.48, 12.41 ± 2.94, respectively. Our results showed a significant increase in SNR with scaning time and a decrease in SNR when patient's body mass index increased. **Conclusion:** When the calculated normalized SNRs are evaluated, the scanning time of at least 180 s/bp in the first 3 groups and 240 s/bp for the patients in the 4th group will significantly increase the image quality. It has been concluded that this protocol is applicable for patients with good general condition, considering the patient movement conditions depending on longer imaging time. **References:** none

OP-0770

Image quality of ^{18}F-FDG for patients with different body mass index

B. Olsson[1], E. Trägårdh[1,2], J. Oddstig[2,3], S. Leide-Svegborn[4];
[1]Clinical Physiology and Nuclear Medicine, Lund, SWEDEN, [2]Wallenberg Center for Molecular Medicine, Lund, SWEDEN, [3]Radiation Physics, Lund, SWEDEN, [4]Radiation Physics, Malmö, SWEDEN.

Aim/Introduction: Due to photon absorption and scatter the image quality may vary for patients with different body mass index (BMI) that undergoes ^{18}F-FDG PET examinations. Our clinical protocol, patients are administered with 4MBq/kg body-weight, maximum 500MBq. The acquisition time is 1.5min/bedposition and reconstructed with Q.Clear, beta-value 550. This according to previous study [ref]. The aim was to investigate if there is any difference in image quality for patients with a BMI above 30kg/m^2 respectively below 20kg/m^2. **Materials and Methods:** The study included 34 patients with low BMI (<20 kg/m^2) and 29 patients with high BMI (≥30 kg/m^2). The patients were imaged after 60 minutes on Discovery MI, GE Healthcare, PET-CT. Sex patients with low BMI and 29 patients with high BMI, the acquisition time was 4 min/bedposition, acquired in listmode, which allowed the studies to be truncated to six different acquisition times of 1.5 - 4min/bedposition. Three regions-of-interest (ROIs) in the liver were drawn in each patient. Using the ROIs in the liver, the average signal-to-noise ratio (SNR) was calculated for each patient. The image quality was evaluated by experienced nuclear medicine physicians. Results: Patients with low BMI had a mean BMI of 16 (range14-18), patients with high BMI had mean BMI of 34 (range30-49) and patients with normal BMI of 24 (range21-29). At acquisition 1.5min/bed position, patients with low BMI had mean SNR of 11.1, patients with high BMI had mean SNR of 10.1. Previous study showed mean SNR of 10.3 for patients with normal BMI. SNR increased with increasing acquisition time, ranging from 8.1 to 15.9 for low BMI and from 8.3 to 16.7 for high BMI. SNR also increased when BMI increased for a given acquisition time. The evaluation of image quality showed a need to increase the acquisition time to 2.5min/bed position to reach acceptable image quality for 80% of the patients with high BMI. Patients with low BMI had an acceptable image quality at 1.5min/bed position. **Conclusion:** The quantitative analysis showed no significant difference in SNR between

patients with different BMI. However, the evaluation of the image quality showed a need to increase time/bed position for patients with high BMI. The image quality for patients with low BMI were acceptable at our standard acquisition time. **References:** E Trägårdh et al. Impact of acquisition time and penalizing factor in a block-sequential regularized expectation maximization reconstruction algorithm on a Si-photomultiplier-based PET-CT system for ^{18}F-FDG. EJNMMI Res. 2019;9(1):64.

OP-0771

The influence of metal artifacts on PET data

M. Jensen;
Bispebjerg/Frederiksberg Hospital, Copenhagen, DENMARK.

Aim/Introduction: Metal artifacts from a hip replacement may interfere with interpretation of PET imaging and reduce the diagnostic accuracy. The aim of this study was to evaluate if CT reconstruction of a phantom based on Metal Artifact Reduction (MAR) would reduce artifacts in the reconstructed PET images. **Materials and Methods:** A phantom with two hip prostheses was suspended in a [^{18}F] FDG and tap water solution in a tub (≈1MBq/L). The phantom was scanned in a GE Discovery MI PET/CT scanner. Two scans were performed with a CT tube current of 50 mA and 500 mA as they are the extreme limits used for PET/CT scans of the hips at our department. The PET scans were reconstructed using Ordered Subset Expectation Maximization (OSEM) and Block Sequential Regularized Expectation Maximization (BSREM) based on CT attenuation with and without the MAR. The scans covered the acetabular cup/femur head part of the prostheses. A region beyond the prosthesis was used as s reference region. The regions were 11.51 cm^2 and 13.41 cm^2, respectively. Results: The 50mA scan without MAR showed a 22 % and 21% decrease in activity measurement on OSEM and BSREM respectively as compared to the reference region. With MAR reconstruction, the reduction was 13 % and 6 % respectively. The 500 mA without MAR showed a 24 % and 38% decrease in activity measurement for OSEM and BRSEM respectively. With MAR, the reduction was 14 % and 24 % respectively. **Conclusion:** MAR reconstructions had a lower deviation to the reference region then the reconstructions without MAR. The OSEM reconstructions were not as affected by the tube current, as the BSRAM reconstructions, which showed an increased deviation from the control images with increased current. The results are promising for implementing MAR in attenuation correction of PET reconstruction. **References:** None

OP-0772

Mouse Handling for ^{18}F-FDG PET Imaging: Preparing the Way for a Future Guideline

F. Ribeiro[1], A. Santos[2], J. Veloso[1];
[1]Institute for Nanostructures, Nanomodelling and Nanofabrication (i3N), Department of Physics, University of Aveiro (DFis-UA), Aveiro, PORTUGAL, [2]Institute for Clinical and Biomedical Research (iCBR), Faculty of Medicine of the University of Coimbra (FMUC), Area of Environment Genetics and Oncobiology (CIMAGO), Center for Innovative Biomedicine and Biotechnology (CIBB), Coimbra, PORTUGAL.

Aim/Introduction: Positron Emission Tomography (PET) scanners dedicated to small-animals emerged as animal model-based research of human disease proved to be an essential and extensively used research tool. However, many physiological, technical and physical factors influence the experimental outcomes. In small animals, factors such as diet, ambient temperature, and anaesthesia strongly impact ^{18}F-FDG (Fluoro-18-labeled fluorodeoxyglucose) uptake by normal tissues. Hence, it is of utmost importance to select the appropriate methodology to achieve repeatable, reproducible and reliable data. Several works have been published to improve research reporting, and guidelines to amplify the quality and reliability of published research. Though these works provide valuable information to plan and conduct animal studies, trying to ensure reproducibility, manuscripts describe different methodologies - standardization does not exist. They even mention the need to develop specific animal handling protocols for a particular biomarker. Wide differences in protocols for preclinical PET imaging can explain the outcome variations in the literature. Hence, not only standardization of procedures does not exist, but also there are not many resources or guidelines providing researchers with valuable tools to ensure accurate and reproducible data extraction. In this contribution, a literature review of recommendations and good practices is presented, aiming to provide an adequate and detailed description of the relevance of animal handling specifically for mouse PET imaging with ^{18}F-FDG. **Materials and Methods:** The proposed guideline follows the recommendations and good practices described in the literature. It also agrees with experimental findings on the influence of animal handling in preclinical PET imaging. The report of adequate animal preparation and care for ^{18}F-FDG PET imaging favors the standardization of this specific procedure. Results: The proposed guideline includes procedures for mouse preparation and care prior, during and after ^{18}F-FDG PET scanning, such as housing conditions, circadian cycle, diet, temperature, blood sample, radiotracer administration and anaesthesia. Recommendations specific for Oncologic, Cardiac and Neurologic studies are also included. **Conclusion:** The present overview represents a key milestone in the effort to enhance standardization of

mouse handling for ^{18}F-FDG PET imaging. It could be the first step for a guideline to enhance reproducibility, repeatability and reliability of future research. Authors are encouraged to follow the recommendations outlined herein during the planning and conducting of their research, assuring that it is robustly designed. **References:** doi.org/10.1161/CIRCRESAHA.114.303819; doi.org/10.1038/nrd3439-c1; doi.org/10.1007/s00259-018-4194-x; Journal of Nuclear Medicine Jun 2006, 47 (6) 999-1006; doi.org/10.2310/7290.2013.00055; doi.org/10.1186/s40658-015-0135-y.

OP-0773

Improving patient experience during [18F]FDG PET-CT scan using an audiovisual scenarios intervention

S. Abouzian, A. Flotats, A. Domènech, M. Sizova, A. Teixidó, F. Fuentes, A. Bagües, R. Berlanga, M. Izquierdo, I. Liarte, R. Ramil, R. Vila, A. Fernández, J. Duch, V. Camacho, D. López-Mora, M. Estorch, I. Carrió;
Nuclear Medicine Department. Hospital Santa Creu i Sant Pau, Barcelona, SPAIN.

Aim/Introduction: Our aim was to assess the effects ofan audiovisual scenarios interventionon the anxiety status of cancer patients during [^{18}F]FDG PET/CT scanning. **Materials and Methods:** We prospectively studied 120 patients who were referred to the Nuclear Medicine department for[^{18}F] FDG PET/CT scanning (63 women, 57 men; 64±11 years), from May 2020 to December 2020, andwere distributed in 4 groups of 30 according to the exposure to an audiovisual scenarios intervention (Philips Ambient Experience, AE): Group 1: regular conditions (no AE) during injection and scan scanning, group 2: AE only in the injection room, group 3: AE only in the scan room, and group 4: AE both in the injection and scan rooms. In order to assess the anxiety status before and after the scan, the patients answered the State-Trait Anxiety Inventory (STAI), which includes a state anxiety test (S-anxiety) that refers to how a person is feeling at the time of the scan and a Trait anxiety (T-anxiety) that refers to how a person feels across typical situations on a daily basis. We compared both tests results among groups. Variables are expressed as mean ± standard deviation. Results: The anxiety status across typical situations on a daily basis of the 4 groups was comparable (p= NS). Group 1: the mean STAI sumscore was 17.43±8,67 at pre scan and 17.27±8.59 at post scan; p= 0.80. Only 16.6% (5/30) of patients had a better result after scan. Group 2: the mean STAI sumscore was 17.37±10.51 at pre scan and improved to 15.83±9.65 at post scan, p= 0.145. The AE improved the anxiety status in 46.6% of patients (14/30). Group 3: the mean STAI sumscore was 17.53±11.67 at pre scan and significantly improved to 15.13±9.76 at post scan, p= 0.019. The AE improved the anxiety status in 50% of patients (15/30). Group 4: the mean STAI sumscore was 17.4±9.75 at pre scan and significantly improved to 14.87±8.11 at post scan, p= 0.028. The AE improved the anxiety status at post scan in 66.6% of patients (20/30). **Conclusion:** Audiovisual scenarios intervention decreases anxiety levels of patients during [^{18}F]FDG PET/CT scanning,in particular when applied either in the injection and scan rooms or only in the scan room. **References:** none

OP-0774

Clinical Feasibility of dual-phase ^{18}F-NaF PET/CT (Dynamic NaF)

M. Al-Daas, R. Alhemaidani, A. Esmail, F. Marafi;
Jaber Al-Ahmad Center for Molecular Imaging, Shuwaikh, KUWAIT.

Aim/Introduction: Three-Phase bone scintigraphy has been traditionally used in the diagnosis of inflammatory bony conditions as well as metastatic disease involvement. The lack of three-dimensional image acquisition and hybrid study the first two phases are limitations of this modality. 18F-Sodium Fluoride (NaF) PET/CT overcomes these limitations due tohigher spatial resolution, tomographic data and combined acquisition with CT-Scan. In addition, post-injection waiting uptake time on NaF (1:30 hours) is less than the bone scintigraphy (3 hours).In this study our aim is to determine clinical feasibility of the dual-phase 18F-NaF PET/CT. **Materials and Methods:** A total of 30 patients complaining of lower limb joints pain (hip, knee or ankle/foot) or with hip/knee prosthesis were included in the study (20 females, 10 males). Scout and CT images were first obtained to determine the region of interest. Then all patients were injected under the camera using automatic injector with 0.06 mCi/KG of 18F-NaF. Dynamic images were directly taken post injection for 5min (the same region of the CT). Delayed images were obtained after 1-hour post injection at the same region of interest, images were static for 5 min. Results: Early dynamic 18F-NaF PET/CT data acquired over first 5 minutes demonstrated early increased flow and hyperemiaat sites of pathological tissue with good contrast and accurate localization.Delayed images were consistent with the early findings in most of the cases due to suspected pathology. **Conclusion:** Dual-Phase 18F-NaF PET/CT is a feasible nuclear medicine modality for imaging bony disorders especially inflammatory etiologies. **References:** 1. Freesmeyer M, Stecker FF, Schierz JH, Hofmann GO, Winkens T. First experience with early dynamic (18)F-NaF-PET/CT in patients with chronic osteomyelitis. Ann Nucl Med. 2014 May;28(4):314-21. doi: 10.1007/s12149-014-0810-4. Epub 2014 Jan 29. PMID: 24474597.2. Lee JW, Yu SN, Yoo ID, Jeon MH, Hong CH, Shim JJ, Chang SH, Lee SM. Clinical application of dual-phase F-18 sodium-fluoride bone PET/CT for diagnosing surgical site infection following orthopedic surgery. Medicine (Baltimore). 2019 Mar;98(11):e14770. doi: 10.1097/MD.0000000000014770. PMID: 30882648; PMCID: PMC6426471.3. Cheng C, Alt V, Pan L, Thormann U, Schnettler R, Strauss LG, Heinemann S, Schumacher M, GelinskyM, Nies B, Dimitrakopoulou-Strauss A. Application of F-18-sodium fluoride (NaF) dynamic PET-CT (dPET-CT) for defect

healing: a comparison of biomaterials in an experimental osteoporotic rat model. Med Sci Monit. 2014 Oct 15;20:1942-9. doi: 10.12659/MSM.891073. PMID: 25317537; PMCID: PMC4210358.

OP-0775

The effect of TOF on image quality and its correlation with patient BMI using 18F NAF PET/CT

Y. Aldowaisan[1], L. Ali[2], F. Marafi[1];
[1]Jaber Alahmad Center for Molecular Imaging, Kuwait, KUWAIT, [2]Allied health sciences-Kuwait University, Kuwait, KUWAIT.

Aim/Introduction: ^{18}F-Sodium Fluoride (^{18}F-NaF) PET/CT scanning is used to detect abnormal osseous lesions of metastatic cancers or benign inflammatory processes. It is a pivotal part of the diagnosis and management of patients to deliver the best possible treatment course. ^{18}F-NaF PET/CT can provide high-quality images with great spatial resolution evidently exceeding conventional bone scintigraphy. Current PET/CT scanners use Time of flight (TOF) as an essential part of modern PET technology.The aim is to determine the effect of TOF on image quality and lesion detectability as well as its relation to Body Mass Index (BMI). **Materials and Methods:** The data was obtained from a total of 28 oncology patients and two patients complaining of bone pain. 21 patients had a BMI ≤33 and seven had a BMI ≥ 33. The NaF protocol is composed of scout and CT images followed by a PET whole body scan. All patients were injected with 0.06 mCi/kg of 18F-NaF and uptake time ranged between 62 and 77 minutes (mean = 70 minutes) post injection. The imaging protocol was determined based on the BMI of the patients (60 seconds/bed for a BMI of 33 or less, 75 sec/bed for 33.1 to 39.9 and 90 sec/bed for 40-50). All images were obtained using GE Discovery MI PET/CT. Both TOF and non-TOF images were acquired for all patients. A signal-to-noise-ratio (SNR) was measured for both the TOF and non-TOF images. A total of four regions of interest were drawn: iliac crest, 5th lumbar vertebral body of (L5), and two random abnormal legions. Results: The SNR for images reconstructed with non-TOF was significantly decreased compared to TOF (P value < 0.001) using Wilcoxon signed-Rank Test. The improvement of SNR in TOF images was seen regardless of the position of the lesion in the chest, the abdomen, or the pelvis. The mean SNR gain using TOF was 1.14±0.20. No correlation was found between SNR gain and the BMI of the patients. **Conclusion:** TOF has improved the SNR and detectability of different lesions regardless of its region. No correlation was found between the improvement of SNR and BMI of patients. **References:** 1. Surti S, Karp JS. Update on latest advances in time-of-flight PET. Phys Med. 2020 Dec;80:251-258. doi: 10.1016/j.ejmp.2020.10.031. Epub 2020 Nov 16. PMID: 33212421; PMCID: PMC7749844.

OP-0776

Feasibility of Fast NaF PET/CT Study in Assessing Metastatic Bone Diseases Using Digital PET Detectors.

M. Al-Daas[1], R. Alhemaidani[1], L. Ali[2], A. Eilaghi[3], F. Marafi[1], A. Esmail[1];
[1]Jaber Al-Ahmad Center for Molecular Imaging, Shuwaikh, KUWAIT, [2]Allied Health Science - Kuwait University, Shuwaikh, KUWAIT, [3]Australian College of Kuwait, Kuwait City, KUWAIT.

Aim/Introduction: NaF PET/CT is used for assessing bone metastasis with a high sensitivity and high-resolution PET images. Digital PET/CT systems have high sensitivity that make fast scanning possible. We aimed to evaluate the feasibility of acquiring NaF PET/CT in a fast mode using the available digital PET/CT equipment. Image analysis using Signal to Noise Ratio (SNR) is one robust quantitative parameter of lesion assessment across different imaging protocols. **Materials and Methods:** 15 patients (age 46- 83) had NaF PET/CT to detect osteoblastic bony lesions. Injections were done as per departmental protocol 2.22 MBq/kg (132.8- 230.1 MBq) using automatic PET injector. Imaging started after an average of 77.9min (63-100 min) post tracer injection using Discovery MI (GE Health care Digital system). Whole body CT scan for attenuation correction and localization purposes was done. A fast and routine whole body PET emission scans were done as per proposal (table 1). Regions of interest (ROI) were drawn on normal areas (vertebra (L5), right iliac bone and head of femur) and abnormal areas. Mean Standard Uptake Value (SUV mean), standard deviation (std) of selected lesions and a SUV mean of a background (BKG) were obtained to calculate (SNR) of all ROI. Mann-Whitney Rank Sum (MWRS) test was used to compare SNR between routine and fast protocols. Spearman correlation (SC) was used to study correlation between SNR values in routine and fast protocol. Results: The proposed fast NaF required about 3-4 minutes in total. Qualitative assessment of both scan modes revealed almost identical images. No single lesion was missed when fast NaF acquisition was assessed for reporting the findings. SNR analysis of all regions is seen (Table 2). Using (MWRS) test, the hypothesis that there is a significant change in SNR in routine vs fast protocol was rejected (P > 0.050) in all ROIs except head of femur (P=0.008). Strong and statistically significant correlation between SNR values in routine and fast protocol is found between any pair of variables in the comparative study using (SC) test. **Conclusion:** Results suggest the possibility to reduced imaging time by 80% using digital PET/CT. Comparable SNR between the 2 protocols is demonstrated. Adopting fast NaF protocol will allow the performance of more cases in busy PET/CT clinics. In this small group patient comfort is maximized without the loss of important image information. Larger sample is needed to consolidate this concept. **References:** None

1405

Wednesday, October 20 - Saturday, October 23, 2021

on-demand pool, release on Wednesday, October 20 at 09:00

Joint Symposium 19 (EANM/EFOMP): Harmonisation and Standardisation

OP-0778

The Need for Harmonisation and Standardisation in Nuclear Medicine

S. Barrington; King's College London and Guy's and St Thomas' PET Centre, School of Biomedical Engineering and Imaging Sciences, London, UNITED KINGDOM.

OP-0779

PET Harmonisation Beyond EARL

R. Boellaard; VU University Medical Centre, Department of Radiology and Nuclear Medicine, Amsterdam, NETHERLANDS.

OP-0780

Towards Harmonisation of SPECT/CT

S. Peters; Radboud University Medical Centre, Department of Radiology and Nuclear Medicine, Nijmegen, NETHERLANDS.

OP-0781

Reproducible Radiomics Through Image Biomarker Standardisation

A. Zwanenburg; National Center for Tumor Diseases, Partner site Dresden, Dresden, GERMANY.

1406

Wednesday, October 20 - Saturday, October 23, 2021

on-demand pool, release on Wednesday, October 20 at 09:00

Joint Symposium 20 (EANM/AAPM): Artificial Intelligence for Image Processing and Quantification

OP-0783

Introduction

M. Hatt; LaTIM, INSERM, UMR 1101, Univ Brest, Brest, FRANCE.

OP-0784

Modern A.I. Methods for Image Reconstruction

I. Häggström; MSKCC, Physics department, New York, UNITED STATES OF AMERICA.

OP-0785

A.I. Algorithms in Detection and Segmentation Tasks

P.-H. Conze; IMT-Atlantique, Brest, FRANCE.

OP-0786

A.I. Applied to Image Triaging and Predictive Modelling

A. Gafita; UCLA, Department of molecular and medical pharmacology, Los Angeles, UNITED STATES OF AMERICA.

1407

Wednesday, October 20 - Saturday, October 23, 2021

on-demand pool, release on Wednesday, October 20 at 09:00

Teaching Session 4: Immunotherapy - Assessing Organs and Events on [^{18}F]FDG PET/CT

OP-0788

Immune Activation on PET - Beneficial or Detrimental?

C. Lasnon; François Baclesse Cancer Centre, Nuclear Medicine, Caen, FRANCE.

OP-0789

Hunting Down Immune Activation and irAEs

N. Aide; CHU de Caen, Service de Médecine Nucléaire, Caen, FRANCE.

OP-0790

Tricky Cases from Daily Routine Activity

R. J. Hicks; The Sir Peter MacCallum Cancer Center, Department of Oncology, Molecular Imaging and Therapeutic Nuclear Medicine, Melbourne, AUSTRALIA.

1409

Wednesday, October 20 - Saturday, October 23, 2021

on-demand pool, release on Wednesday, October 20 at 09:00

Cutting Edge Science Track - TROP Session: Data Analysis

OP-0792

Visual reading and centiloid scaling for the evaluation of brain amyloid PET imaging

E. Prieto, V. Puente, J. F. Bastidas, J. J. Rosales, L. Irazola, B. Echeveste, M. Riverol, J. Arbizu;
Clínica Universidad de Navarra, Pamplona, SPAIN.

Aim/Introduction: Centiloid scale is a standardized metric for quantification of amyloid PET tracers. The aim of this study was to investigate the agreement of centiloid scale with visual reading. **Materials and Methods:** 78 patients (50 males, 28 females) aged 71.6 ± 6.0 years diagnosed with Amnestic Mild Cognitive Impairment who underwent an amyloid PET at our institution (13 florbetaben, 22 florbetapir, 43 flutemetamol) and a structural MRI were retrospectively

reviewed. PET images were classified as positive or negative by consensus between two trained nuclear medicine physicians using tracer-specific visual reading procedures. A local SPM8-based process pipeline was implemented in our site and verified using the GAAIN dataset. This pipeline was then run in our series to calculate SUVratio between the global cortical region and the whole cerebellum using the GAAIN volumes of interest. Then, the SUVratio values were converted to centiloid scale using linear conversion equations obtained from the literature. A receiver operating characteristic analysis (ROC) was conducted to discriminate patients in agreement with the visual reading, and centiloid cut-off was calculated as that that maximized the Youden's J Index. Results: The 23 (29%) patients visually classified as positive presented centiloid values of 70.8 ± 33 while those classified as negative (71%) obtained centiloid values of -2.2 ± 15.3 (Wilcoxon test $p<0.05$). Comparison of centiloid values with expert visual read (positive or negative) yielded an AUC of 0.968, and 25.5 was calculated as the optimal CL threshold to discriminate patients according to the visual reading classification. **Conclusion:** Centiloid scale seems to be a promising quantitative tool to unify data from different amyloid PET tracers that has demonstrated an outstanding discrimination power for positive and negative patients according to the standardized visual reading of PET imaging. **References:** None

OP-0793

Interpretation of discordances among amyloid biomarkers: the role of semiquantitative methods in cerebral amyloid load determination

M. Nerattini[1], F. Rubino[1], A. Arnone[1], C. Polito[2], S. Mazzeo[2], G. Lombardi[3], B. Nacmias[2], G. Puccini[4], S. Sorbi[2], M. De Cristofaro[1], R. Sciagrà[1], V. Bessi[2], V. Berti[1];
[1]Nuclear Medicine Unit - Azienda Ospedaliero-Universitaria Careggi, Florence, ITALY, [2]Department of Neuroscience, Psychology, Drug Research and Child Health (NEUROFARBA) - Azienda Ospedaliero-Universitaria Careggi, Florence, ITALY, [3]IRCCS Fondazione Don Carlo Gnocchi - IRCCS Fondazione Don Carlo Gnocchi, Florence, ITALY, [4]Nuclear Medicine Unit - S. Stefano Hospital of Prato, Prato, ITALY.

Aim/Introduction: Discordances among amyloid biomarkers often occur in Alzheimer Disease (AD). Semiquantitative methods are useful in overcoming diagnostic uncertainties in Nuclear Medicine. We aim to interpret discordances among Amyloid Positron Emission Tomography (Amy-PET) and cerebrospinal fluid (CSF) $A\beta_{42}$ results, using Amy-PET semiquantitative evaluation and supported by CSF $A\beta_{42/40}$ Ratio. **Materials and Methods:** Thirty-six subjects with dementia or mild cognitive impairment, assessed by neuropsychological tests, structural and functional imaging and amyloid CSF assays ($A\beta_{42}$, $A\beta_{42/40}$) were retrospectively examined. Amy-PET scans were analyzed by visual assessment, voxel-based statistical maps analysis and Standardized Uptake Value ratio (SUVR) measurement. Results: We extracted from our sample subjects with discordant amyloid biomarkers. Implementing CSF $A\beta_{42}$ (A) and Amy-PET (P) evaluations with CSF $A\beta_{42/40}$ Ratio (R) as an independent parameter, we obtained three groups: A+R+P-, A-R+P+ and A+R-P-. The Amy-PET SUVR analysis showed a decreasing pattern from A-R+P+ to A+R+P- to A+R-P-, with amyloid regional load in A-R+P+ and A+R-P- comparable to positive and negative concordant subjects, respectively. These findings led us to hypothesize that CSF $A\beta_{42}$ outcome in A-R+P+ and A+R-P- groups is a false-result. Moreover, A-R+P+ cases presented amyloid tracers binding in posterior cingulate cortex (PCC) and Orbitofrontal Cortex significantly higher than concordant negatives subjects at Amy-PET voxel-based analysis. These regions are part of the Default-Mode Network, known to be early affected by AD. So, when CSF $A\beta_{42}$ disagrees with Amy-pet, Ratio could be resolutive, unmasking $A\beta_{42}$ as a false-result. Interestingly, $A\beta_{42}$ false-positive subjects showed $A\beta_{42}$ levels close to the cut-off. In A+R+P- group, SUVR regional analysis demonstrated values in Precuneus, PCC, and Dorsolateral-Inferior-Frontal-Cortex (DLIFC), higher than in the other regions, even no significantly different from concordant positives subjects. It's well known that precuneus and PCC are typical AD areas, whereas the importance of the result in DLIFC is understandable considering the usual frontal lobes sparing until late stages of AD. The less atrophy and perfusion reductions in these areas could have allowed the radiotracers to reach DLIFC without being masked by neurodegeneration phenomena and partial volume effects. **Conclusion:** Amyloid discordant cases could be overcome by integrating CSF $A\beta_{42}$ and Amy-PET with the Ratio. The concordance of any 2 out of the 3 biomarkers seems to reveal the remaining one as a false-result. A cut-off points review could avoid CSF $A\beta_{42}$ false-negative results. The regional semiquantitative Amy-PET analysis in AD areas, such as precuneus and PCC, could increase the accuracy in AD diagnosis. **References:** None

OP-0794

Image-level trajectory inference of tau pathology using variational autoencoder for Flortaucipir PET

J. Hong[1], K. Shi[1], A. Rominger[1], H. Choi[2];
[1]University of Bern/Inselspital, Bern, SWITZERLAND, [2]Seoul National University Hospital, Seoul, KOREA, REPUBLIC OF.

Aim/Introduction: The hyperphosphorylation and abnormal aggregation of tau protein is a key hallmark for Alzheimer's disease (AD). The post mortem analysis demonstrated that tau accumulates in a certain pattern in the AD brain, namely Braak staging. However, the quantification of tau PET has not yet reached a consensus, as the question lies in 'where', as well as 'how much.' In addition, recent studies revealed conflicting results contrary to Braak staging. We

believe that tau PET images inherently conceives the hidden feature, and by exploiting variational auto-encoder (VAE) we intended to derive the tau distribution of representative stages in the progress of AD and the quantification method. **Materials and Methods:** 1080 pairs of T1 MRI image and AV-1451 PET were recruited in total (78 AD, 483 MCI, 519 CN) from ADNI. PET images were spatially normalized to the Montreal Neurological Institute (MNI) space using SPM8. VAE was built with 5 layers in both encoder and decoder, with a latent feature unit of 100. Agglomerative clustering was performed in latent space resulting in 4 clusters. Assuming clusters adjacent to one another shares more than the ones apart and the progression from one stage to another is more likely to take place in the direction where the total distance is the shortest, MST method was implemented by defining vertices as the centre of each cluster and edge weight as the euclidean distance between each cluster centres. Results: AD was prevalent in cluster 3 and CN in cluster 2. Among clusters, cluster 3 displayed the highest SUVr in the temporal and cingulate region, except for the hippocampus. MST resulted in the cluster sequence of 2-0-1-3, and the tau progression was reproduced by drawing trajectory along the sequence in latent space followed by VAE generator. The result resembled Braak staging and the tau progress was quantified between 0 and 100 by projecting each latent vector onto the trajectory. The SUVr of the amygdala increased from the score of 40 onwards, and temp_inf, fusiform and cingulum_post followed. **Conclusion:** The tau progress with VAE latent representation conformed well with Braak staging and the proposed tau quantification method appeared to have the potential. **References:** [1]Cho, H. C. (2016a). In vivo cortical spreading pattern of tau and amyloid in the Alzheimer disease spectrum. Ann. Neurol., 80, 247-258[2]H Braak, E. B. (1991). Neuropathological staging of Alzheimer-related changes. Acta Neuropathol., 82(4):239-59.

OP-0795

Impact of meningeal uptake and partial volume correction techniques on differences in [^{18}F]MK-6240 binding between healthy controls and aMCI patients

N. Mertens[1], L. Michiels[2,3], G. Vanderlinden[1], R. Lemmens[2,3], M. Vandenbulcke[4], K. Van Laere[1], M. Koole[1];
[1]Nuclear Medicine and Molecular Imaging, University Hospital and KU Leuven, Leuven, BELGIUM, [2]UZ Leuven/KU Leuven, Neurology, Neurosciences, Experimental Neurology, Leuven, BELGIUM, [3]VIB, Center for Brain & Disease Research, Laboratory of Neurobiology, Leuven, BELGIUM, [4]Old-Age Psychiatry, University Hospital and KU Leuven, Leuven, BELGIUM.

Aim/Introduction: [^{18}F]MK-6240 is a second-generation tau PET tracer for neurofibrillary tangles in the brain. Although [^{18}F]MK-6240 displays very low aspecific signal in the brain, varying levels of meningeal tracer uptake can be noticed thay may induce cortical spill-in effects. The aim of this study was to evaluate the impact of meningeal uptake on differences in [^{18}F]MK-6240 binding between healthy controls (HC) and patients with amnestic mild cognitive impairment (aMCI) and to incorporate an extracerebral compartment for partial volume correction (PVC) to reduce the meningeal effect. **Materials and Methods:** 20 HCs and 10 age-matched aMCIs underwent a [^{18}F]MK-6240 plus volumetric T1 PET-MR scan (GE Signa), acquired 90-120min post tracerinjection. Standardized uptake values (SUV) were calculated with and without PVC. First, Müller-Gartner (MG) PVC was implemented, using white and gray matter probability maps (CAT12) and assuming homogeneous white matter uptake, without taking extracerebral spill-in effects into account. Second, region-based voxelwise (RBV) PVC was used based on anatomical parcellations (Freesurfer7.1), which included skull, skin and extracerebral cerebrospinal fluid as additional compartments to model partial volume effects. Next, SUV ratio (SUVR) maps were calculated relative to cerebellar gray matter. Finally, HCs were classified into two groups (10 HC each) with "low" ("HC-low") and "high" ("HC-high") meningeal uptake based on the skull SUVR which includes meningeal uptake, using a k-means clustering algorithm. Group differences between "HC-low", "HC-high" and 10 aMCIs were compared and assessed using VOI- (Freesurfer7.1; $p_{uncor}<0.05$) and voxel-based (SPM12; $p_{height,uncor}<0.001$) analysis. Results: Mean extracerebral [^{18}F]MK-6240 SUVR was 1.01±0.11 for "HC-low" and 1.43±0.10 for "HC-high". "HC-high" controls showed significant differences in cortical SUVR with "HC-low" when no PVC was applied. For MG-PVC several cortical regions remained different, while for RBV-PVC, no significant differences beween HC groups were found. All cortical regions were significantly different between aMCI and HC, independent of the HC group after MG- or RBV-PVC. Effect size (mean SUVR aMCI/HC) increased between aMCI and both HC groups after PVC, and were highest for RBV-PVC (see Table2), despite a slight increase in variance. All results were confirmed by voxelwise analyses where especially peripheral cortical influx effects due to meningeal uptake were abolished by RVB-PVC. **Conclusion:** Varying meningeal uptake can have significant impact on cortical differences in [^{18}F]MK-6240 SUVR between HC and aMCI. Appropriate PVC with correction for extracerebral spill-in effects homogenizes the control groups and produces a higher, more robust effect size that is independent of meningeal [^{18}F]MK-6240 uptake. **References:** none

OP-0796

Image-Derived Input Functions From Dynamic ^{15}O-Water Positron Emission Tomography Scans Using Penalised Reconstruction

P. Young[1,2], L. Appel[3], A. Tolf[4], S. Kosmidis[3], J. Burman[4], A. Rieckmann[5,6], M. Schöll[1,2,7], M. Lubberink[3];
[1]Department of Psychiatry and Neurochemistry, University of Gothenburg, Gothenburg, SWEDEN, [2]Wallenberg Centre for Molecular and Translational Medicine, Gothenburg, SWEDEN, [3]Radiology & Nuclear Medicine, Department of Surgical Sciences, Uppsala University, Uppsala, SWEDEN, [4]Neurology, Department of Neurosciences, Uppsala University, Uppsala, SWEDEN, [5]Department of Radiation Sciences, Umeå University, Umeå, SWEDEN, [6]Munich Center for the Economic of Aging, Max Planck Institute for Social Law and Social Policy, Munich, GERMANY, [7]Dementia Research Centre, UCL Queen Square Institute of Neurology, London, UNITED KINGDOM.

Aim/Introduction: Accurate quantification of positron emission tomography (PET) tracer kinetics requires an input function. The gold standard for this in brain-PET is arterial blood sampling, however, this technique entails clinical difficulties with it being time-consuming, burdensome and associated with certain risk of adverse events. The use of image-derived input functions (IDIFs) would overcome this, but limited spatial resolution and poor signal to noise ratio of PET during the first pass of the bolus has prohibited accurate measurements in the carotid arteries. Here, we use penalised reconstruction and an optimized partial volume correction to improve identification of the carotid arteries for a novel image-derived input function for ^{15}O-water PET. **Materials and Methods:** Sixteen subjects underwent two 10-minute ^{15}O-water PET scans with arterial blood sampling on a digital time-of-flight PET/CT scanner at baseline and after administration of acetazolamide. Images were reconstructed using block-sequential regularised expectation maximisation with a regularisation parameter value β of 300. Using a thresholding technique, the carotid arteries were isolated in the early frames of the dynamic image. This mask was then applied to the dynamic images to generate an input function. This input function was corrected for partial volume errors using an iterative method accounting for spill-in and spill-out corrections. The accuracy of the IDIF was established by comparison of area under the curve (AUC) and derived parametric images against blood-sampled input functions (BSIFs). Results: AUC measures demonstrated good agreement between BSIF and IDIF with average differences for peaks at 4% (±5.6%) and tails (up to 300s) at 1.2% (±11.2%). Whole-brain grey matter CBF values typically showed good agreement with a correlation (R^2) of 0.92 and an average difference between the BSIF- and IDIF-based CBF values of 2% (±7%). Regional CBF values also showed good agreement with an average correlation (R^2) of 0.99 between corresponding regions. **Conclusion:** State-of-the-art PET reconstructions and corrections for partial volume effects allow for robust IDIF for a dynamic ^{15}O-water using only the dynamic PET scan images. This can provide a practical alternative to arterial blood sampling or the need for additional image acquisition from MRI. This technique may therefore remove the associated difficulties when performing clinical studies. Future research will investigate the feasibility of the approach for other tracers and patient populations. **References:** None

OP-0797

Evaluation of partial volume correction and comparison of PET normalization methods in PET/MR myocardial viability assessment for recovery prediction of left ventricular contractility after percutaneous revascularisation of coronary chronic total occlusions

A. Villagran Asiares[1], T. Vitadello[2], E. L. Solari[1], T. Ibrahim[2], S. G. Nekolla[1];
[1]Nuklearmedizinische Klinik und Poliklinik, Klinikum rechts der Isar der Technischen Universität München, München, GERMANY, [2]Klinik und Poliklinik für Innere Medizin I, Klinikum rechts der Isar der Technischen Universität München, München, GERMANY.

Aim/Introduction: Accurate prediction of myocardial contractility recovery after revascularisation is crucial for interventional risk stratification in coronary chronic total occlusions (CTO). The indication to revascularization is based on the viability assessment through cardiac imaging. Previous studies reported the benefits in recovery prediction of using fluorodeoxyglucose (FDG) and late gadolinium enhancement through a semi-quantitative analysis from PET/MR images. However, to increase reproducibility and reduce impact of PET partial volume effects, a quantitative approach is needed. This study aims to evaluate a PET quantitative analysis considering different uptake normalization methods and PVE on contractility recovery prediction after CTO revascularization. **Materials and Methods:** Myocardial viability and contractility were assessed with PET/MR imaging in 22 patients before revascularisation of a CTO. After 6 months, contractility was evaluated from a cardiac MR exam. Segmental contractility recovery based on wall motion abnormalities was predicted using FDG PET quantitative models based on different uptake normalizations (50% maximum, maximum, mean, and z-score) and compared with a 5-point scale semi-quantitative analysis. PVC was implemented adapting an algorithm based on anatomical references for PET/CT [1] to PET/MR images using LGE based masks. Recovery prediction was performed with a random forest classifier. Training and testing data were selected through stratified random sampling with replacement. Prediction was assessed with balanced accuracy (bAcc), ROC AUC, and Precision-Recall AUC (PR AUC), and Wilcoxon's tests with a Bonferroni's correction were used for model comparison. Results: From 13/22 patients, FDG PET quantitative models using absolute uptake value

(bAcc 0.52± 0.12, ROC AUC 0.57±0.14, PR AUC 0.46±0.10) or relative to the maximum uptake value (bAcc 0.55±0.11, ROC AUC 0.59±0.14, PR AUC 0.48±0.11) were the most similar models to the reference 5-points scale FDG (bAcc: 0.55±0.09, ROC AUC 0.56±0.11, PR AUC 0.43±0.06). PVC PET models underestimated the recovery prediction in bAcc, ROC AUC, and PR AUC (bAcc<0.49, ROC AUC<0.49, and PR AUC<0.38, p-value<0.008). **Conclusion:** This study evaluated the clinical impact of PVC and the normalization selection of FDG PET uptake for quantitative analysis. In this cohort PVC based on anatomical references underestimated contractility recovery prediction. Further evaluation with different algorithms is encouraged. Quantitative analysis based on absolute or relative to the maximum FDG uptake presented similar prediction to current semi-quantitative analysis, illustrating the potential application on the standardization in cardiac PET analysis. **References:** [1] Du, Yong, et al. "Compensation for spill-in and spill-out partial volume effects in cardiac PET imaging." Journal of Nuclear Cardiology 20.1 (2013): 84-98.

OP-0798

Textural Analysis of 18F-FDG PET Images to Evaluate Treatment Response

X. Hu[1], S. Han[1], L. Wang[2], Q. Chu[2], N. D'Ascenzo[1,3], Q. Xie[1,3];
[1]Department of Biomedical Engineering, Huazhong University of Science and Technology, Wuhan, CHINA, [2]Department of Oncology, Tongji Hospital, Tongji Medical College, Huazhong University of Science and Technology, Wuhan, CHINA, [3]Department of Medical Physics and Engineering at the Istituto Neurologico Mediterraneo NEUROMED I.R.C.C.S, Pozzilli, ITALY.

Aim/Introduction: Textural analysis of PET images has shown encouraging prospect in making treatment plan and predicting treatment response or survival for certain types of cancer in recent years. Tumor volume was commonly used to evaluate treatment response in clinic. Here we aim to find useful parameters from PET images which have potential ability to improve treatment response and prognosis. **Materials and Methods:** Ten male six weeks old BALB/c-nude mice xenografted with A549 cells were randomly divided into two groups when the tumor volume were close to 20mm^3. After the baseline scanning, one group was treated weekly with Cisplatin (5mg/kg). All mice were scanned 10 min using the digital small animal PET/CT Trans-PET Discoverist180 after a 60 min uptake period of ^{18}F-FDG every 3-4 days. All images were reconstructed using 3D OSEM algorithm. The tumor size were measured at each time before PET scanning. After the 7th PET scanning, tumors were cut off from the mice after euthanization. Tumor tissues were stained using TUNEL kit following fixing, paraffin embedding and section. SUV_{max}, SUV_{mean} and 89 textural indices were extracted from PET images of each mouse at each scanning time. Results: Results showed that the tumors of treated group grew obviously slower than the control group and there was significant difference between the volume of control group and treated group after the 3rd cisplatin treatment which corresponding to the 7th PET scanning. No significant difference was found in SUV_{max} and SUV_{mean} between the two groups at each scanning time. There were 5 textural indices derived from GLZSM (Size Zone Non-Uniformity, Size Zone Non-Uniformity Normalized and Small Area Emphasis) and NGTDM (Coarseness and Complexity) have significant difference between the treated group and control group after the 3rd cisplatin treatment. TUNEL staining showed that a large number of tumor cells were apoptosis in the treatment group and significantly higher than the control group. In addition, these 5 textual indices and tumor volumes were highly correlated with the extent of cell apoptosis. **Conclusion:** Our results indicated that these 5 textural indices have the same potential ability as tumor volume to evaluate the treatment response and may improve treatment response and prognosis. **References:** none

OP-0799

Image quality assessment of low dose ^{68}Ga DOTA-TOC PET using traditional semi-quantitative metrics, clinical assessment and radiomic feature extraction

A. McCann[1], S. Cournane[2], E. Loughnane[1], A. Stone[1], R. Killeen[1], L. León Vintró[2], J. Lucey[1];
[1]St Vincents University Hospital, Dublin, IRELAND,
[2]University College Dublin, Dublin, IRELAND.

Aim/Introduction: Dose optimisation can result in reduced radiation dose to the patient and may increase the number of possible administrations for each ^{68}Ge/^{68}Ga generator elution. However, there is no consensus as to which quantitative metric best identifies the minimum administered activity that will still achieve adequate image quality. The aim of this study was to identify the most appropriate objective metrics for assessing image quality for reduced dose PET images. **Materials and Methods:** 20 ^{68}Ga-DOTA-TOC PET/CT patient images acquired on a Siemens Biograph Horizon PET/CT scanner were iteratively reconstructed using time-of-flight imaging. Listmode acquisition facilitated the simulation of reduced activity images, with reconstructions ranging from 100% to 10% activity equivalents, in 10% increments. For each lesion, $SUV_{max,}$ SUV_{mean} , SUV_{peak}, volume and total lesion somatostatin avidity (TLSA) were measured. Uptake in the Liver and Spleen was analysed and the SNR calculated. Tumour-to-normal tissue uptake was analyzed and lesion-CNR assessed. Clinical image quality was visually assessed by a Nuclear Medicine radiologist and rated using the Likert scale. Phantom studies were acquired, with their reduced-dose images simulated and analysed to determine the impact of reduced counts on Recovery Coefficients (RC), sphere-CNR, SUV and volume accuracy for varying target sizes. NECR and pNECR were also determined for each reconstruction. Radiomic feature extraction was performed for phantom

spheres and patient lesions, using PyRadiomics Toolbox to identify count-sensitive metrics. Results: In the phantom study the most count-sensitive metrics were found to be SNR and CNR. While a decrease in both CNR and SNR was observed at the 40% count images, a statistically valid difference for these metrics was only noted for images with counts ≤20%. Even at these low levels the CNR still exceeded the Rose Criterion of CNR 3-5 for adequate detection. There was no statistical difference found in the RC for each reconstruction. For the patient images analysed to date, a reduction in SNR and CNR was noted at 40%; however, even at 30% activity equivalent the lesion-to-liver CNR was adequate. Of the 125 radiomic features extracted from the patient images, on average 99 features were found to be count-sensitive, of these 7 features had a coefficient of variation >10% across all reconstructions. Further analysis is on-going. **Conclusion:** The results analysed to date suggest that the administered activity may be substantially reduced, by up to 50% in some cases, without a loss of clinically relevant information. Further results will be presented. **References:** None

OP-0800

A 3-minute semi-automated PSMA PET organ segmentation method to use in the clinic and train neural networks

G. Chaussé[1], I. Bloise[1], N. Colpo[1], I. Klyuzhin[1], F. Yousefi[1], J. Brosch-Lenz[1], S. Probst[2], A. Rahmim[1], C. Uribe[1], F. Bénard[1];
[1]BC Cancer / Research Institute, Vancouver, BC, CANADA,
[2]Jewish General Hospital, Montreal, QC, CANADA.

Aim/Introduction: With the rising demand for personalized radionuclide therapies treatment, whole body segmentation for dosimetry has become a daily problem of many clinical nuclear medicine departments. Prostate-specific membrane antigen radionuclide targeted therapy (PRLT) is a major contributor due to the sheer number of prostate cancers in the Western world and therefore of candidates for this therapy. A fully automated segmentation would provide accurate reproducible results for dosimetry and ease the load on the personnel. However, using artificial intelligence (AI) requires a lot of training data and great expertise to achieve reliable results for patient care. This project aimed at testing a semi-automated method as an alternative to manual or AI-based methods to answer today's clinical needs for organ segmentation. **Materials and Methods:** [18F]-DCFPyL PSMA PET images from 80 patients were selected from two prospective single-arm clinical trials (NCT02899312, NCT03459820) based on the absence or low number of pathological lesions on imaging and PET scanner model used (20 patients/model, 4 models across two institutions). Contours were drawn on PET images by three observers (two nuclear physicians and one technologist) around organs using whole-body SUV thresholding and cluster analysis sequentially, then optimized with edge detection and manual drawing tools as provided in a commercially available imaging software. The fourteen segmented organs were labelled as 'Left/Right Kidney', 'Bladder', 'Spleen', 'Right/Left Lacrimal', 'Sublingual', 'Right/Left Parotid', 'Right/Left Submandibular', 'Tubarial Gland', 'Liver', 'Bowel'. Labels were generated by a homemade program (using Visual Basics) based on the relative location of the contours and verified by a nuclear physician. Similarity of contours between pairs of observers was evaluated per organ using the Dice similarity coefficient (DSC) representing a percentage of overlap between 3D contours. Results: For most scans, the segmentation process, labelling of organs and verification was achieved in approximately 3 minutes. Averaged DSCs between observers were 86.3±10.9% and improved to 91.2±2.5% when low-uptake and non-solid organs (Sublingual, Tubarial Gland, and Bowel) were excluded. Observers were instructed to provide a contour for all organs, even when no uptake was present, which can explain lower agreement for those. The bladder was most reproducible (DSC= 94.6±0.2%). **Conclusion:** The presented method quickly segments PSMA PET organs, and has high reproducibility between observers for various PET scanners and institution protocols. Such method can enable routine implementation of PET-based dosimetry and allow rapid generation of large datasets for AI training. Applicability for other radiopharmaceuticals and SPECT images remains to be verified. **References:** None

OP-0801

Fuzzy c-means clustering in input function and wash-in parameter derivation for dynamic SPECT cardiac study

A. Studen[1,2], M. Bunc[3], M. Mrak[3], S. Rep[4,5], L. Ležaić[4,6];
[1]Faculty of Mathematics and Physics, University of Ljubljana, Ljubljana, SLOVENIA, [2]Jožef Stefan Institute, Ljubljana, SLOVENIA, [3]Department of Cardiology, UMC Ljubljana, Ljubljana, SLOVENIA, [4]Department of Nuclear Medicine, UMC Ljubljana, Ljubljana, SLOVENIA, [5]Medical Imaging and Radiotherapy Department, Faculty of Health Sciences, University of Ljubljana, Ljubljana, SLOVENIA, [6]Faculty of Medicine, University of Ljubljana, Ljubljana, SLOVENIA.

Aim/Introduction: Dynamic cardiac SPECT (DC-SPECT) allows for absolute quantification of myocardial perfusion which is particularly important in patients with symmetrically developed cardiac disease. DC-SPECT images require complex analysis due to deteriorating factors including short frame collection time associated statistical errors and motion artifacts. Data driven unsupervised machine learning algorithms such as fuzzy c-means clustering (FCC) can reduce impact of noise on obtained results [1]. The aim of the study was to verify the arterial input function (AIF) calculation based on clustered time-activity curves (TAC) and determine statistical reliability of cluster derived physiology parameters compared to parameters extracted via conventional means. **Materials and Methods:** 6 patients suffering from three-

vein cardiac disease were imaged at the SIEMENS Symbia SPECT/CT camera using [^{99m}Tc]tetrofosmin (600 MBq) and 20 interval measurement protocol [2]. The stability of FCC was evaluated by a repetitive random selection of N most common TAC and associated partition matrix in the torax region covered by the camera, where N equals 10, 20 or 30. TAC with the largest amplitude was considered an AIF sample parameterized by finite rise- and fall-times. Fifteen myocardium regions were manually segmented by an experienced nuclear medicine specialist. Regional wash-in parameter was determined by one-compartmental fit to regional TACs and compared to cluster fit, where partition matrix was used to identify cluster associated with the selected region. Results: The cluster based algorithm yielded a reliable AIF estimate that was used in TACs fitting, allowing for single pixel fits to converge in all cases. Cluster based wash-in estimates were able to reproduce regional TACs values with Pearson R^2 value of 0.88 for a 30 sample cluster. **Conclusion:** Clustering algorithm can reproduce complexity of a dynamic SPECT scan. The whole thorax clustering allows for reliable and robust AIF identification and a set of 30 most common responses per patient reproduces the tissue parameters in standard myocardium regions. **References:** [1] H. Bal et al. IEEE Trans Nuc Sci 50 (5) 2003 [2] Shrestha U et al. J Nucl Cardiol 24 (1) 2017

OP-0802

A simulation study to compare cross-validation versus holdout or external testing to assess the performance of machine learning based clinical prediction rules

R. Boellaard[1], J. J. Eertink[1], P. J. Lugtenburg[2], G. J. Zwezerijnen[1], S. E. Wiegers[1], H. C. de Vet[1], J. M. Zijlstra[1];
[1]Amsterdam University Medical Centers, Amsterdam, NETHERLANDS, [2]Erasmus MC Cancer Institute, Rotterdam, NETHERLANDS.

Aim/Introduction: FDG PET/CT radiomics with machine learning (ML) are explored to develop prognostic or predictive models. ML requires large datasets for training, (cross-)validating and testing. PET studies typically have small sample sizes (n<500) and lack external datasets. In this study we used a clinical data simulator to validate the performance of ML models by cross-validation (CV) versus holdouts and/or external testing. **Materials and Methods:** Simulated clinical data were generated using distributions of baseline FDG PET/CT on metabolic tumor volume (MTV), SUV, the maximal distance between the largest lesion and any other lesion (Dmaxbulk), WHO status and IPI of 296 diffuse large B-cell lymphoma (DLBCL) patients. These data were used to predict time to progression (TTP) within 2 years using an existing logistic regression model. False positive and negative events were simulated per stage (2, 3 and 4) to achieve an ROC equal to the clinical study. Using this simulated datasets we trained and cross-validated several ML models: (a) cross-validation only (n=500); (b) CV-training (n=400) with outcome-stratified testing-holdouts (n=100); (c) CV-training (n=500) with newly simulated external testing data (n=100); (d) as in (c) but with test data sizes of 100, 200, 500 and; (e) as in (c) but simulating testing datasets with stage 2 or 4 patients only. All simulations were repeated 100 times. Logistic regression (LR), linear discriminant analysis (LDA), support vector machine (SVM) and random forest (RF) models were CV-trained and tested. Results: CV area under the ROC curves were 0.70±0.04, 0.70±0.03, 0.69±0.03 and 0.68±0.04 for LR, LDA, SVM and RF, respectively. In all cases mean and SD of CV AUC-ROCs were not different to those seen across 100 holdout and/or external tests having the same size as the CV-folds. Increasing the external testing dataset size resulted in more precise AUC-ROC estimates. Finally, test datasets containing 100% stage 2 or stage 4 patients resulted in different AUC-ROCs, e.g 0.62±0.07 and 0.72±0.06 for LR. **Conclusion:** When testing ML methods in case of small sample sizes (n<500) there is no added value using holdout or very small external datasets (n<100). A single small testing dataset suffers from a large uncertainty suggesting that repeated CV using the full training dataset is preferred instead. Our simulations also demonstrated that it is important to consider the impact of differences in patient population between training, cross-validation and testing data, which may ask for adjustment of relevant variables. **References:** None

OP-0803

A novel methodology for assessing reproducibility of heterogeneity metrics in PET radiomics using noise-equivalent count rate, Monte Carlo simulation and 3D-printed patient-specific tumour phantoms

G. Needham[1,2], P. Julyan[2], D. M. Cullen[1], J. Tipping[2], D. Hamilton[2], S. Pells[1,2,3], A. Fish[1,2];
[1]University of Manchester, Manchester, UNITED KINGDOM, [2]The Christie NHS Foundation Trust, Manchester, UNITED KINGDOM, [3]National Physical Laboratory, Teddington, UNITED KINGDOM.

Aim/Introduction: The advent of accessible machine-learning software has inspired a great interest in research around radiomics in PET. There is little of this research dedicated to establishing the reproducibility of the hundreds of metrics extracted using radiomics software. This work suggests a framework for validating these metrics, specifically those quantifying heterogeneity, by comparison with how they and the noise-equivalent count rate (NECR) are affected by increasing activity within the field of view (FOV). **Materials and Methods:** The NECR is a measurement of collected PET data after removing the effects of scatter and random coincidences. Comparing the characteristic curve of the NECR against activity in the scanner FOV against similar curves for heterogeneity metrics can provide a robust method for determining whether any given heterogeneity metric is exaggeratedly affected by noise in the data. The

NECR plotted against activity exhibits a characteristic peak, beyond which any increased activity disproportionately increases random coincidences; if a heterogeneity metric is unduly influenced by data noise, its curve against activity will manifest a stationary point at this NECR peak. Physical PET data is collected from phantoms; included in this study are a 20 cm diameter cylindrical phantom, the NEMA Image Quality phantom and a series of 3D-printed tumour phantoms created from patient data. These phantoms are filled with an ^{18}F solution of activity around 500 MBq and data is acquired for 12 hours. Once validated, a Monte Carlo simulation is used to predict the behaviour of metrics at a range of activity values to determine repeatability and uncertainty, with suggestions for clinical applications. Results: Pilot studies using the cylindrical and NEMA IQ phantoms have been conducted and compared to simulation results. Data is to be acquired for the 3D-printed tumour phantoms and presented. **Conclusion:** The NECR provides inspiration for a novel methodology for verifying the susceptibility of heterogeneity-based image metrics to noise. The hypotheses and initial work presented here have an exciting potential for guiding a more reliable use of radiomics metrics in the clinical environment. **References:** none

1410

Wednesday, October 20 - Saturday, October 23, 2021

on-demand pool, release on Wednesday, October 20 at 09:00

Clinical Oncology Track - TROP Session: Local Radionuclide Therapy and Other Oncological Treatments

OP-0805

Holmium-166 radioembolization as adjuvant treatment after radiofrequency ablation of early-stage hepatocellular carcinoma up to 5 cm: a dose escalation study (HORA EST HCC trial)

P. Hendriks[1], D. D. Rietbergen[1], A. R. van Erkel[1], M. J. Coenraad[1], M. Arntz[2], R. Bennink[3], A. E. Braat[1], A. L. Crobach[1], O. M. van Delden[3], T. van der Hulle[1], H. Klumpen[3], R. W. van der Meer[1], F. Nijsen[2], C. S. van Rijswijk[1], J. Roosen[2], B. N. Ruijter[1], F. Smit[1], M. K. Stam[1], B. Takkenberg[3], M. E. Tushuizen[1], F. H. van Velden[1], L. de Geus-Oei[1], M. C. Burgmans[1];

[1]Leiden University Medical Center, Leiden, NETHERLANDS,
[2]Radboud UMC, Nijmegen, NETHERLANDS,
[3]Amsterdam UMC, Amsterdam, NETHERLANDS.

Aim/Introduction: Recurrence rates after thermal ablation of hepatocellular carcinoma (HCC) are higher for lesions >2 cm[1]. The aim of this study was to investigate the distribution of holmium-166 microspheres (Ho-166-MS) as adjuvant treatment after radiofrequency ablation (RFA) in early stage HCC, and to establish an administration dose to the affected liver segments that would result in a dose of ≥120 Gy in the hyperemic zone around the ablation volume (i.e. target volume). **Materials and Methods:** This was a multicenter, prospective, dose-escalation study in HCC patients with a single lesion 2-5 cm or a maximum of 3 lesions of ≤3 cm each, who were deemed too high risk for surgical resection. Patients underwent RFA on day 1, followed by a diagnostic angiography procedure with a contrast-enhanced cone-beam CT (ce-CBCT) and injection of Technetium-99m macroaggregated albumin into the (sub)segmental artery of the tumor-bearing liver segment(s) (not exceeding 50% of the liver volume) on the next day. The perfused treatment volume was segmented from the ce-CBCT. The dose escalation study design allowed for a maximum of 3 cohorts up to 10 patients that would receive 60, 90 or 120 Gy of Ho-166-MS (Quiremspheres) radioembolization to the perfused treatment volume within day 5-10 after RFA. Subsequently, a SPECT/CT was acquired for post-treatment dosimetry. The primary endpoint was met when a dose of ≥120 Gy was reached in the target volume in at least 9/10 patients, based on post-treatment Ho-166 SPECT dosimetry. Secondary endpoints were toxicity, local recurrences, disease-free survival and overall survival. Results: Twelve patients were treated (male 10, median age: 66 y/o (35-79), mean tumor size: 25 mm (11-45)). Two patients received 60 Gy on the treatment volume, but in both patients the target dose was <120 Gy so the endpoint was not met. Subsequently, 10 patients received 90 Gy on the treatment volume. ≥120 Gy was reached in 9/10 patients in this cohort, with a mean target volume dose of 143 Gy (102-213), so the end point was met. A single grade 3 complication was reported (infection of ablation area). No local recurrences were found (mean follow-up: 11 months). **Conclusion:** Combined RFA and Ho-166 radioembolization for HCC 2-5 cm is feasible and safe with a treatment volume dose of 90 Gy. **References:** 1. Galle P et al. EASL Clinical Practice Guidelines: Management of hepatocellular carcinoma. Journal of Hepatology, vol69.1;182-236

OP-0806

The first steps to fully personalized selective internal radiation therapy: intraprocedural MRI-based dosimetry of holmium-166 microspheres

J. Roosen[1], M. A. Arntz[1], M. Janssen[1], C. G. Overduin[1], M. W. Konijnenberg[1,2], J. J. Fütterer[1], J. F. Nijsen[1];

[1]Radboud University Medical Centre, Nijmegen, NETHERLANDS,
[2]Erasmus Medical Centre, Rotterdam, NETHERLANDS.

Aim/Introduction: Selective internal radiation therapy (SIRT) is a locoregional treatment for liver tumours during which radioactive microspheres are injected in the hepatic arterial system. To investigate the potential of fully personalized MRI-guided SIRT, we prospectively studied the microsphere

distribution and dosimetry with radioactive holmium-166 microspheres (QuiremSpheres®), using intraprocedural MRI. **Materials and Methods:** Ethical committee approval was obtained for this feasibility study, in which 6 patients with unresectable liver tumours were treated. The SIRT procedure was split up: the catheter was placed under X-ray guidance as per usual, after which the patient was moved to an MRI scanner that is positioned directly adjacent to the hybrid OR. The total activity for each of the identified catheter positions was split in 4 predefined fractions per hemiliver. MRI was performed during and after the administration of each fraction. All fractions for one catheter position were injected within one hour. Quantitative imaging was performed after each fraction and converted to dose maps using Q-Suite software to establish the tumour to liver ratio (T/L ratio) and perform voxel-based dosimetry. Two days after treatment, ^{166}Ho SPECT/CT imaging was performed to confirm the dose distributions found on MRI. Results: Six patients with a variety of liver tumours were treated (breast cancer (n=2), cholangiocarcinoma (n=1), colorectal cancer (n=1) and hepatocellular carcinoma (n=2)), adding up to a total of 11 injection positions. Feasibility of performing the procedure in the MRI bore was established in 9/11 injection positions (1 procedure took too long, 1 catheter position was too unstable for transport to MRI scanner). Imaging quality was sufficient for intraprocedural dosimetry in all patients. Dosimetry analysis is currently ongoing, but intermediate results show that the intrahepatic distribution of microsphere fractions is not necessarily consistent between different fractions. In a single tumour (colorectal cancer) saturation with microspheres was observed, in which the last fraction of microspheres hardly lead to an increase in mean tumour dose. In some cases the T/L ratio decreased through administering more microspheres, whereas the opposite is seen in others. **Conclusion:** This is first study worldwide to demonstrate feasibility of intraprocedural dosimetry during SIRT with ^{166}Ho microspheres in human patients. This serves two direct purposes: it is an important step to better understand SIRT fundamentally, and it paves the way towards an image-guided approach to SIRT in a follow-up study. **References:** None

OP-0807

Dose-response for yttrium-90 resin microesphere radioembolization in Hepatocellular carcinoma

M. Rodríguez-Fraile[1], *A. Cabrera*[1], *J. Rosales*[1], *J. Bastidas*[1], *F. Grisanti*[1], *M. Sanchez*[2], *A. Martínez de la Cuesta*[1], *M. Iñarrairaegui*[1], *J. Bilbao*[1], *B. Sangro*[1];
[1]*Clínica Universidad de Navarra, Pamplona, SPAIN,*
[2]*Universitat de València, Valencia, SPAIN.*

Aim/Introduction: To determine the capacity of 99mTc-MAA and 90Y-PET/CT dosimetric parameters to predict tumor response to radioembolization (RE) with 90Y-resin-microspheres. **Materials and Methods:** Patients with Hepatocellular carcinoma (HCC) lesions suitable for repeat measurement and treated with lobar RE in our institution from 2013 to 2017, were restrospectively evaluated. Dosimetric parameters (Dmean, D98, D70, D50, V120, V100, V70 and V40) were obtained for each lesion in both 99mTc-MAA and 90Y-PET/CT studies using a 3D-voxel based dosimetry software (Planet Dose, Dosisoft). Tumor response was assessed using mRECIST criteria in radiologic images at time-1 (within 3 months after RE), time-2 (3-6) and time-3 (6-9). Dose and tumor relationship was determined for lesion and for patient. To assess agreement between 99mTc-MAA and 90Y-PET/CT dosimetric parameters, the Lin Concordance Correlation Coefficient (CCC; 95% CI) was used. Spearman Rs, Median and Mann-Whitney tests were used to study association and differences between variables. Progression-free-survival (PFS) and overall survival (OS) were analyzed using Kaplan-Meier method and Cox regression analysis. Results: Twenty-eight patients (mean age 65.2 ±11 years) with intermediate or advanced HCC (46 lesions) were included. Median PFS and OS were 11 (7.4-14.6) and 33 months (0-67), respectively. Liver surgery, favoured by RE, was performed in seven patients (25%). In 31/35 lesion studied at time-1 there was a decreased in the longest viable diameter compared to baseline imaging (median: -24.6%; 16.7 to -100), in 28/29 at time-2 (median -40%; 0 to -100) and in 26/27 at time-3 (mean:-60.9% ± 32). A moderate (0.4-0.6) or substantial (≥0.6) CCC for all dosimetric parameters between 99mTc-MAA and 90Y-PET/CT studies was found. Lesions were divided in responders (partial and complete response) and non-responders (stable or progressive). The median V100 obtained in 99mTc-MAA was 16% (0-72) for responders and 1.2% (0-63) for non-responders ($p<0.02$) at time-2. For 90Y-PET/CT parameters, median D70 was significantly different ($p<0.05$) between responders and non-responders lesions: 40.4 Gy (13.1-81.7) and 25 Gy (1.4-89), respectively. Nevertheless, no dosimetric parameters were able to discriminate between groups in Kaplan-Meier curves or in Cox regression. **Conclusion:** Dosimetric parameters obtained both in 99mTc-MAA (V100) and 90Y-PET/CT (D70) studies are predictive of tumor response in HCC patients treated with 90Y-resin-microspheres. **References:** None

OP-0808

Suggested protocol for Y-90 PET/CT dosimetry in liver therapy with Y-90 microspheres

K. Knesaurek;
Icahn School of Medicine at Mount Sinai, New York, NY, UNITED STATES OF AMERICA.

Aim/Introduction: The aim of this study is to find the optimal clinical method for Y-90 PET/CT based dosimetry, using two slightly different approaches. **Materials and Methods:** As part of a continuing study, 31 patients were taken to a PET/

CT suite (mCT, Siemens Medical) following therapy with Y-90 microspheres. The low mA, non-diagnostic CT images were used for attenuation correction and localization of the Y-90 microspheres in the PET/CT studies. The acquisition time was 15 min, the reconstruction matrix size was 200x200x75 mm and voxel size 4.07x4.07x3.00 mm. The commercially available software package, MIM 6.8 (MIM Software Inc., Cleveland, Ohio), was utilized to calculate Y-90 dosimetry from the PET images. Two methods were used for voxel-based dosimetry calculations; the Local Deposition Method (LDM) and LDM with scaling (LDMwS) for known injected activity. Results: The average total liver dosimetry values (mean ± SD) were 49.93 ± 24.79 Gy and 56.08 ± 21.54Gy for LDM and LDMwS, respectively. In most cases, the LDMwS method produced slightly higher dosimetry values than the LDM method. Bland-Altman analysis calculated a mean difference of 6.20 ± 3.85 Gy. The repeatability coefficient was 7.55 (14.2 % of the mean). **Conclusion:** The slightly higher values produced by LDMwS compared to the LDM method is due to the difference between dose calibrator scaling, and the quantitative accuracy of Y-90 PET imaging. Although, the differences are not great, they should be diminished by better quantifiable Y-90 PET imaging and improved dose calibrator quality control. The optimal method of Y-90 dosimetry calculation should use both, LDMwS and LDM values and if the differences between these two approaches are more than 15%, further investigation should be applied. **References:** None

OP-0809

Feasibility and Therapeutic Potential of 177Lu-Fibroblast Activation Protein Inhibitor (FAPI) for Patients With Relapsed or Refractory of Various Cancers: A preliminary study

M. Assadi[1], S. Rekabpour[1], G. Divband[2], B. Nikkholgh[2], H. Ahmadzadehfar[3], E. Jafari[1], N. Shakibazad[1], N. Jokar[1], I. Nabipour[1]; [1]Bushehr University of Medical Sciences (BUMS), Bushehr, IRAN, ISLAMIC REPUBLIC OF, [2]Khatam PET-CT center, Khatam Hospital, Tehran, IRAN, ISLAMIC REPUBLIC OF, [3]Department of Nuclear Medicine, Klinikum Westfalen, Dortmund, GERMANY.

Aim/Introduction: In this study, we aimed to evaluate the feasibility, biodistribution, safety and dosimetry data of 177Lu-FAPI-46 in numerous types of malignancies. **Materials and Methods:** In total, 21 advanced adenocarcinoma patients had non-operable tumor or refractory to conventional therapy were enrolled in this study included ovarian (n=2), sarcoma (n=2), colon (n=3), breast (n=5), pancreas (n=2), prostate (n=2), cervix (n=1), round-cell tumor (n=1), lung (n=1) , anaplastic thyroid cancers (n=1) and cholangiosarcoma (n==1). For evaluation of FAP expression, all patients underwent ^{68}Ga-FAPI PET/CT scan or ^{177}Lu-FAPI-46 scintigraphy scintigraphy with a diagnostic dose (370 MBq). Patients received 1.85-4.44 GBq per cycle of ^{177}Lu-FAPi-46 in each cycle. The time interval between each cycle was 4-6 weeks. For evaluation of biodistribution and dosimetry, whole body scan was acquired at 2 (without voiding), 24-, 48-, 72-, 96-, 120-, 144- and 168-hours post-injection (p.i.). The ECOG status performance was evaluated, monthly. Also, the CTCAE v4.03 was used for measurement of PTRT-associated toxicity. Results: 18 cases showed positive FAP expression, which had been selected to perform PTRT. The median number of PTRT cycles was 2 (range: 1-4) and the median total injected dose was 6.1 GBq . The median injected dose in each cycle was 3.7 GBq (range: 1.85-4.44). The median overall survival time from the primary diagnosis (OS-d) was 25.0 months (range: 6.0-110.0) and from the diagnosis of the recurrence/refractory (OS-r) was 9.0 months (range: 5.0-30.0). According to the follow up results, 12 of patients showed stable disease with no significant change in clinical condition but 6 showed progressive disease. From the start of treatment with 177Lu-FAPI , the median PFS was 3.0 months (range: 1.0-6.0), and the OS-t was 4.0 months(range: 1.0-6.0) . The median ECOG and KPS before PTRT were 1 (0-2) and 75 (50-100), respectively, which no change were observed after PTRT. According to the dosimetric analysis, the median absorbed dose to whole-body was 0.026 (range: 0.023-0.034), liver was 0.136 (range: 0.001-0.2), kidneys were 0.886 (0.076-1.39) and spleen was 0.02 (0.002-0.2) mGy/MBq. **Conclusion:** This preliminary study may demonstrate potential feasibility and safety of PTRT using 177Lu-FAPI-46 in several types of cancers for the patients who have relapsed or are refractory to conventional treatment options. In addition, this phase I,II FAPI theranostic pair study might help in identifying the dose limiting toxicity (DLT) and also recommended phase 2 dose (RP2D) of 177Lu-DOTA-FAPI . **References:** none

OP-0810

Radioimmunotherapy for relapsed or refractory B cell non-Hodgkin lymphoma: 3-year follow-up of 66 patients

K. Maruyama, K. Utsunomiya, Y. Kono, Y. Ueno, N. Tanigawa; Kansai Medical University, Osaka, JAPAN.

Aim/Introduction: Yttrium-90 ibritumomab tiuxetan is an antibody radionuclide conjugate targeting the CD20 antigen. CD20 antigen is expressed on more than 90% of B cell non-Hodgkin lymphoma. Aim of this retrospective study was to assess the efficacy of radioimmunotherapy with Yttrium-90 ibritumomab tiuxetan (^{90}Y-IT) for relapsed or refractory B cell non-Hodgkin lymphoma (NHL). **Materials and Methods:** We examined 66 patients (median age 68 years, range 45-87 years) with NHL who received ^{90}Y-IT between October 2012 and November 2017. Histologies included 46 Follicular lymphoma (FL), 14 Mucosa associated lymphoid tissue lymphoma (MALT), and 6 Mantle cell lymphoma (MCL). Response, and by using Kaplan-Meier method overall survival (OS) and progression-free survival (PFS) were analyzed. Results: After ^{90}Y-IT, an overall response rate (ORR) was 86% and included

a 62% complete response (CR) rate (41 patients) and a 24% partial response (PR) rate (16 patients). ORRs were 87% in FL, 100% in MALT, and 50% in MCL, respectively. With a median follow-up of 58 months (range 0.9 to 101 months) after ^{90}Y-IT, Kaplan-Meier estimated OS and estimated PFS rates were 90.5 % and 60.3 % at 3 years, and 86.7% and 50.6% at 5 years, respectively. Overall, ^{90}Y-IT was relatively well tolerated instead of hematologic toxicities. During follow-up, 10 patients (15%) died: one died of multiple brain infarction and nine of disease progression. Only one patient (1.5%) developed second malignancy: endometrial adenocarcinoma of uterus at 58 months after ^{90}Y-IT. **Conclusion:** Yttrium-90 ibritumomab tiuxetan was well tolerated and demonstrated clinically meaningful antitumor activity in relapsed or refractory B cell NHL, particularly notable for FL and MALT. **References:** none

OP-0811

Cosmetic Outcome after Brachytherapy with Not-sealed 188Rhenium-resin in Patients with Non-Melanoma Skin Cancers

L. Vetrone[1], P. Castellucci[2], F. Savoia[3], A. Farina[1], S. Vichi[4], F. Zagni[5], A. Patrizi[3], L. Strigari[5], A. G. Morganti[6,7], S. Fanti[1,2];
[1]Nuclear Medicine, Department of Experimental, Diagnostic and Specialty Medicine, University of Bologna, Bologna, ITALY, [2]Nuclear Medicine, IRCCS, Azienda Ospedaliero-Universitaria di Bologna, Bologna, ITALY, [3]Dermatology Department, IRCCS Azienda Ospedaliero-Universitaria di Bologna, Bologna, ITALY, [4]Clinical Engineering Department, IRCCS, Azienda Ospedaliero-Universitaria di Bologna, Bologna, ITALY, [5]Medical Physics Department, IRCCS Azienda Ospedaliero-Universitaria di Bologna, Bologna, ITALY, [6]Radiation Oncology Department, IRCCS Azienda Ospedaliero-Universitaria di Bologna, Bologna, ITALY, [7]Radiation Oncology Department, Department of Experimental, Diagnostic and Specialty Medicine, University of Bologna, Bologna, ITALY.

Aim/Introduction: High dose-personalized brachytherapy with a non-sealed 188Rhenium-resin (OncoBeta®GmbH for Rhenium-SCT®) is a new treatment option for non-melanoma skin cancer (NMSC) especially in elderly patients (pts) and for those whom surgical approach could be difficult or contraindicated. The aim of this retrospective study is to evaluate the cosmetic outcome after treatment and to correlate it with acute and late toxicity. **Materials and Methods:** From September2017 to April 2021, 83 pts (28F,55M, age56-97, mean 83 yo) showing 93 histologically proven NMSC (60BCC; 33SCC) were treated. Lesions were located on ears (9/93), nose (21/93), scalp (32/93), cheeks (13/93), extremities (11/93) and trunk (7/93). Mean surface area was 7.3cm2 (range 1-60cm2). Mean thickness invasion 1.2mm (range 0.2-3.0mm). Mean treatment's time was 79 minutes (range 21-285). Mean applied activity 302MBq (range 36-1300MBq) and mean radiation dose delivered to the whole lesion's volume (GTV) 54Gy (range 18-126 Gy). Pts were followed after 14, 30, 60, 90 and 180 days when dermoscopy and biopsy were performed. Acute and late side effects were classified using Common Terminology Criteria for Adverse Events 5.0 (CTCAE) within the first 30 days and at 90. Radiation Therapy Oncology Group (RTOG) Cosmetic Scale (CS) was used to evaluate cosmetic results after at least 6 months of follow-up. Cosmetic outcomes were evaluated after 6 months in 74/93 lesions. Results: At 6 months follow-up, CS1 (excellent) was present in 56/74 lesions; CS2 (good) was present in 18/74 lesions. Nobody showed fair (CS3) or poor (CS4) cosmetic results. CS1 results were most frequently observed on head (50/56) than extremities and trunk (6/56). CS2 was mostly present on extremities and trunk (11/18) than head (7/18). After 30 days, 88 lesions were evaluated: 51/88 lesions showed CTCAE grade-1; 33/88 lesions showed CTCAE grade-2; 4/88 were CTCAE grade-3. After 90 days, late toxicity was evaluated in 83 lesions: 82/83 lesions showed CTACE grade1-2; only 1 lesion showed CTCAE grade-3. Excellent cosmetic results (CS1) were mostly correlated to late toxicity CTCAE grade-1, while CS2 was more frequently correlated with CTCAE grade-2. **Conclusion:** High dose brachytherapy with a not-sealed 188Rhenium-resin resulted to be a safe and promising treatment in terms of cosmetic outcome for NMSC. The location of the lesion (trunk or extremities) seems to play a role in determining cosmetic results. Further studies are required to better understand which factors may influence cosmetic outcome. **References:** None.

OP-0812

High Dose Brachytherapy with 188Re-(Rhenium) Resin in Patients with Non-Melanoma Skin Cancers

L. Vetrone[1], F. Savoia[2], A. Farina[1], S. Vichi[3], F. Zagni[4], L. Strigari[4], A. G. Morganti[5,6], A. Patrizi[2], S. Fanti[1,7], P. Castellucci[7];
[1]Nuclear Medicine, Department of Experimental, Diagnostic and Specialty Medicine, University of Bologna, Bologna, ITALY, [2]Dermatology, IRCCS Policlinico di Sant'Orsola, Department of Experimental, Diagnostic and Speciality Medicine (DIMES), Alma Mater Studiorum, University of Bologna, Bologna, ITALY, [3]Clinical Engineering Department, IRCCS, Azienda Ospedaliero-Universitaria di Bologna, Bologna, ITALY, [4]Medical Physics Department, IRCCS Azienda Ospedaliero-Universitaria di Bologna, Bologna, ITALY, [5]Radiation Oncology Department, IRCCS Azienda Ospedaliero-Universitaria di Bologna, Bologna, ITALY, [6]Radiation Oncology, Department of Experimental, Diagnostic and Specialty Medicine, University of Bologna, Bologna, ITALY, [7]Nuclear Medicine, IRCCS, Azienda Ospedaliero-Universitaria di Bologna, Bologna, ITALY.

Aim/Introduction: High-dose brachytherapy using a non-sealed 188Re-resin (188Rhenium SCT®) is a new treatment option for Non-Melanoma Skin Cancer (NMSC) for those patients where surgery could result difficult in terms of efficacy and cosmetic results. The aim of this study is to assess the efficacy and the safety of a single application of 188Rhenium SCT® for the treatment of NMSC, in a large population of patients with NMSC. **Materials and Methods:**

From September2017 to April2021, 83 patients (28F,55M, age56-97, mean 83yo) underwent 188Re-brachytherapy in our Centre. Overall, 93 histologically proven NMSC (60BCC; 33SCC) were treated. Inclusion criteria were: presence of NMSC assessed with biopsy; lesions difficult to treat with surgery; patients with co-morbidities who might contra-indicate surgery; lesion's thickness lower than 3mm; lesion's area smaller than 60cm2; Seventy-five out of ninety-three (81%) lesions were located on head: 9/75 ears, 21/75 nose, 32/75 scalp, 13/75 other sites; 11/93 were located on the extremities and 7/93 on the trunk. Mean surface area was 7.3cm2 (range 1-60cm2); mean thickness invasion 1.2mm (range 0.2-3.0mm). Treatment's parameters were: treatment time (mean 79 minutes; range 21-285 minutes); administered activity (mean 302MBq; range 36-1300MBq); delivered dose to Gross Tumour Volume (GTV; mean 54Gy; range 18-126 Gy). After treatment, follow up check points were at: 14, 30, 60, 90 and 180 days, when a dermoscopy and biopsy (if needed) were performed. Common Terminology Criteria for Adverse Events 5.0 (CTCAE) scale was used to evaluate the early and late side effects (14-30/90 days). Mean follow up was 19 months (range 6-44 months). Results: Efficacy: after 6 months, 74 lesions were available for evaluation and 73/74 (99%) lesions showed complete healing while persistence was detected in 1/74 (1%). After 12 and 24 months, respectively two patients showed relapse. Early toxicity was evaluated after 30 days in 88 lesions: 51/88 lesions showed CTCAE grade-1; 33/88 lesions showed CTCAE grade-2; 4/88 CTCAE grade-3. After 90 days, late toxicity was evaluated in 83 lesions: CTACE grade1-2 was present in 82/83 lesions; CTCAE grade-3 in 1 lesion. Side effects lasted up to 2-12 weeks (mean 4 weeks) with complete healing after 90 days in all cases. **Conclusion:** High-dose brachytherapy using 188Rhenium SCT is a promising alternative treatment for NMSC. After six months, 99% of the treated lesions showed complete histological response after a single application. Recurrence rate after one or two years resulted to be low; toxicity resulted to be transient and acceptable. **References:** None.

OP-0813

Initial clinical experience with [^{90}Y]Y-FAPI-46 radioligand therapy for advanced stage solid tumors

J. Ferdinandus[1], P. Fragoso Costa[1], L. Kessler[1], M. M. Weber[1], N. Hirmas[1], K. Kostbade[1], S. Bauer[1], M. Schuler[1], M. Ahrens[2], H. U. Schildhaus[1], C. Rischpler[1], J. T. Siveke[1], K. Herrmann[1], W. P. Fendler[1], R. Hamacher[1];
[1]University Hospital Essen, Essen, GERMANY, [2]University Hospital Frankfurt, Frankfurt, GERMANY.

Aim/Introduction: Fibroblast activation protein (FAP) is overexpressed in several solid tumors and therefore represents an attractive target for radiotheranostic applications. Recent investigations demonstrated rapid and high uptake of small-molecule inhibitors of FAP ([^{68}Ga]Ga-FAPI-46) for PET imaging. Here, we report our initial experience with [^{90}Y]Y-labelled FAPI-46 ([^{90}Y]Y-FAPI-46) for radioligand therapy (RLT) of heavily pretreated patients with solid tumors. **Materials and Methods:** Patients were considered for [^{90}Y]Y-FAPI-46therapy in case of (a) exhaustion of all approved therapies based on multidisciplinary tumor board decision and (b) high FAP expression, defined as SUVmax ≥ 10 in more than 50% of all lesions. If tolerated, post-therapeutic PET scans were performed to determine absorbed dose to organs at risk and tumor lesions. Blood-based dosimetry was used to determine bone-marrow absorbed dose. Adverse Events were graded using CTCAE v.5.0. Results: Nine patients received a median of 3.8 (IQR 3.25-5.40) GBq for the first cycle and three patients received subsequent cycles with a median of 7.4 (IQR 7.3-7-5) GBq. Post-treatment scintigraphy demonstrated sufficient [^{90}Y]Y-FAPI-46 uptakein tumor lesions in 7 of 9 patients (78%). Mean absorbed dose was 0.52 Gy/GBq (IQR 0.41-0.65) in kidney, 0.04 Gy/GBq (IQR 0.03-0.06) in bone marrow and below 0.26 Gy/GBq in the lung and liver. Measured tumor lesions received up to 2.28 Gy/GBq (median 1.28 Gy/GBq). Hematologic G3/G4 toxicities were noted in four patients (44%), of which thrombocytopenia was most prevalent (N = 6; 67%), whereas other G3/G4 laboratory-based adverse events were N ≤ 2. No acute toxicities attributed to [^{90}Y]Y-FAPI-46 were noted. Radiographic disease control was noted in four patients (44%). **Conclusion:** FAP-targeted RLT with [^{90}Y]Y-FAPI-46was well tolerated with a low rate of attributable adverse events. Low radiation doses to organs at risk suggest feasibility of repeat cycles of [^{90}Y]Y-FAPI-46. We observe signs of clinical activity, but further studies are warranted to determine efficacy and toxicity profile in a larger cohort. **References:** none

OP-0814

Efficacy and safety of 124-I-MIBG guided high activity 131-I-MIBG therapy of metastatic pheochromocytoma and neuroblastoma

I. Maric[1], M. M. Weber[1], W. Jentzen[1], J. Schmitz[1], N. Unger[2], T. D. Poeppel[1], A. Prochnow[1], K. Herrmann[1], W. P. Fendler[1];
[1]Department of Nuclear Medicine, University of Duisburg-Essen and German Cancer Consortium (DKTK), University Hospital Essen, Essen, GERMANY, [2]Department of Endocrinology, Diabetes and Metabolism, University of Duisburg-Essen and German Cancer Consortium (DKTK), University Hospital Essen, Essen, GERMANY.

Aim/Introduction: We aim to evaluate the efficacy and safety of 124I-MIBG dosimetry guided high-activity 131I-MIBG therapy of metastatic pheochromocytoma or neuroblastoma. **Materials and Methods:** Fourteen patients with advanced pheochromocytoma or neuroblastoma, age 9 to 69 years, underwent pre-therapeutic 124I-MIBG dosimetry with subsequent 131I-MIBG therapy. After application 124I-MIBG serial whole-body retention measurements and serial PET/CT scans allowed an estimation of a whole-body dose as a

surrogate of bone marrow toxicity and absorbed doses to kidneys and liver and hematological toxicity. Response was evaluated by baseline to follow-up change in 124I-MIBG-PET/CT, defined by RECIST as well as decrease in number and/or intensity of lesions and change in SUV, and, in two cases, by computed tomography/magnetic resonance imaging. Results: The therapy activity ranged from 3.5 to 50 GBq. Median overall survival was 85 months (min. 5 months, max. 164 months), median progression free survival was 25 months (min. 2 months, max. 115 months). The overall response (CR, PR) rate was 35 %. Stable disease was observed in 57 % and 50 % of patients for greater than 12 and 24 months, respectively. Only 1 patient exceeded the estimated whole body dose of 2 Gy after receiving a single therapy infusion with 50 GBq and demonstrated manageable grade 3 hematological toxicity, which resolved within 12 months after the therapy. None of the patients showed liver function deterioration. **Conclusion:** 124I-MIBG dosimetry guided high activity 131-MIBG therapy for pheochromocytoma or neuroblastoma is feasible, resulted in durable responses with a low rate of manageable adverse events. Efficacy of 124I-MIBG guided dose escalation should further be assessed in prospective trials. **References:** None.

OP-0815

Potential theranostic approach of 177Lu-trastuzumab and 177Lu-FAPI in metastatic breast cancer: An ongoing study

M. Assadi[1], S. Rekabpour[1], N. Jokar[1], H. Ahmadzadehfar[2], E. Jafari[1]; [1]Bushehr University of Medical Sciences (BUMS), Bushehr, IRAN, ISLAMIC REPUBLIC OF, [2]Department of Nuclear Medicine, Klinikum Westfalen, Dortmund, GERMANY.

Aim/Introduction: Breast cancer is the most frequent invasive malignancy and the second major cause of cancer death in females mostly due to the considerable diagnostic delay and failure of therapeutic strategies. In the line of precision oncology in breast cancer, clinical translation of ^{177}Lu-trastuzumab (Herceptin), and ^{177}Lu-FAPI-46 was followed in this multidisciplinary design study . **Materials and Methods:** At first , treatment recommendations are classified according to the expressed genes: Luminal A (ER+/PR+/HER-2-negative/lowKi-67); Luminal B including two subtypes HER-2-negative (ER+/PR+/HER-2-negative/highKi-67) and HER-2-overexpressed (ER+/PR+/any Ki-67/HER-2+); HER-2 positive or non-luminal (ER and PR absent/HER-2 over-expressed); and basal-like or triple-negative breast cancers (TNBC) (ER-/PR-/HER-2-negative). HER2 test result was considered as positive if: (a) IHC 3+ based on circumferential membrane staining or (b) FISH assay be positive using either a single-probe or dual-probe FISH. If IHC result is 2+ then a confirmation by FISH is required for the selection of trastuzumab treatment . Preliminary clinical studies performed in 2 cancer patients with IHC 3+ proven HER2 positive metastatic breast cancer revealed preferential localization of 177Lu-trastuzumab in breast cancer lesions. Three non 3+ HER2 but FAP presenting patients examined by PET or SPECT also considered for 177Lu-FAPI-46 therapy Results: We present five patients with breast cancer who were refractory or relapsed after conventional therapy while presumably responded to the molecular radiotherapy with ^{177}Lu-trastuzumab (Herceptin), and ^{177}Lu-FAPI-46. **Conclusion:** This preliminary study may help in developing ^{177}Lu-trastuzumab (Herceptin) and 177Lu-FAPI theranostic approach in breast cancer patients with potential to translate into conventional treatment strategies alone or in combination with other common treatment especially in aggressive and resistant types of breast cancer. In addition to other critical aspects such as the regulation, standardization of the radiopharmaceutical production, clinical examination procedure and evaluation, training of the colleagues with breast oncology should put in list of things to do. However, further well-designed trials are highly warranted. **References:** Goldhirsch, A., et al., Strategies for subtypes—dealing with the diversity of breast cancer: highlights of the St Gallen International Expert Consensus on the Primary Therapy of Early Breast Cancer 2011. Annals of oncology, 2011. 22(8): p. 1736-1747. 6. Al-thoubaity, F.K., Molecular classification of breast cancer: A retrospective cohort study. Annals of Medicine and Surgery, 2020. 49: p. 44-48.

OP-0816

Targeted Radionuclide Therapy with Lu 177-Dotatate, Iodine 131-Mibg and RAI in Children: Applicability and Efficacy

U. Korkmaz, S. Soyluoglu; Trakya University Medical Faculty, Department of Nuclear Medicine, Edirne, TURKEY.

Aim/Introduction: Advances in molecular technologies have made Radionuclide therapy (RNT) an effective part of targeted therapy. Although RNT is widely used for adults, has limited use in children. Iodine ablation (RAI) constitutes the majority of pediatric applications. However, the use of Lu-DOTATATE (DOTA) and I-131 MIBG (MIBG) is increasing. In this study, applicability and effectiveness of DOTA, MIBG and RAI treatments in pediatric patients was investigated. **Materials and Methods:** Patients who received DOTA, MIBG or RAI treatment and followed for at least two years were included in the study. Treatment specifications were collected from patient files. Post-treatment and control images were captured from the archive. Treatments were divided into groups as DOTA, MIBG and RAI. Widespread of the tumors, status of achievement of the treatment goal (ATG), progression-free survival (PFS) and disease-free survival (DFS) were determined. Side effects were identified. Results: 33 treatments were included in the study (17 were RAI, 12 were DOTA and 4 were MIBG). The highest mean age was in the RAI group (15.2), and the lowest was in the DOTA group (10.5). Majority of the patients was female (60.6%). The

gender difference was most pronounced in the RAI group (88% female, 12% male), the most balanced group was the DOTA (42% female and 58% male). For the entire cohort, the complete response rate (CRR) was 42%, the partial response rate (PRR) was 15.2%, the stable disease rate (SDR) was 36.4% and the progressive disease rate (PDR) was 6.1. CRR was higher in females (60% vs 15.8). The highest CRR was seen in the RAI group (82.3%), majority of the DOTA treatments (83.3%) was resulted in SD. PD was observed only in DOTA group (Figure 1). ATG rates were high in all groups (84.8% for all cohort, 80% for females and 92% for males). 82% of the RAIs, 83% of the DOTAs and 100% of the MIBGs reached the treatment goal (Figure 2). No major complications occurred. PFS was high in all groups. DFS was high only in the RAI group. **Conclusion:** RNT use in childhood is less than adults, but its frequency and indications are increasing. Most common indication is still DTC. Neuroblastoma and paragangliomas are in the second place. RNT is a safe and effective treatment that can be used in all three disease. Contributes to both quality of life and lifespan with a dose/number of administration model that is correctly selected. **References:** none

1411

Wednesday, October 20 - Saturday, October 23, 2021

on-demand pool, release on Wednesday, October 20 at 09:00

Featured Session: Novel Molecular Brain Imaging Applications

OP-0818

No Novel Applications Without Quantification

J. C. Price; *Harvard Medical School, Department of Radiology, Cambridge, UNITED STATES OF AMERICA.*

OP-0819

Simultaneous [^{18}F]FDG PET/MR in visual snow syndrome: multimodal findings and diagnostic accuracy of [^{18}F]FDG PET

*J. Gebruers**[1], J. Ceccarini*[2], K. Goffin[1,2], E. Boon[3], K. Van Laere[1,2]; [1]Nuclear Medicine, UZ Leuven, Leuven, BELGIUM, [2]Nuclear Medicine and Molecular Imaging, Department of Imaging and Pathology, KU Leuven, Leuven, BELGIUM, [3]Division of Neurology and Psychiatry, UPC Kortenberg and UZ Leuven, Leuven, BELGIUM. (*shared first authors)*

Aim/Introduction: Visual snow (VS) syndrome is a chronic neurologic condition characterized by the constant perceiving of tiny flickering dots over the entire visual field. The underlying pathophysiology of this condition is still largely unknown, and VS patients are often misdiagnosed due to the lack of objective diagnostic measures. Using simultaneous [^{18}F]FDG PET/MR, we investigated regional cerebral metabolic activity and voxel-based morphometry (VBM) associated with VS, in comparison to healthy controls. Secondly, the diagnostic accuracy of quantitative volume-of-interest (VOI) [^{18}F]FDG analysis in comparison with visual accuracy in clinical practice was evaluated. **Materials and Methods:** Simultaneous [^{18}F]FDG PET and structural MR imaging (GE Signa 3T PET/MR) was performed on 7 patients with VS syndrome (24.6 ± 5.7 yrs; 5M/2F) and 15 screened age-matched healthy controls (CON) (28.0 ± 5.3 yrs; 8M/7F). PET data were quantitatively analyzed both by a voxel- (SPM12) and VOI-based (Hammers N30R83 atlas PMODv4.1) approach. Voxel-based morphometry was performed to determine grey matter (GM) changes. To assess classification accuracy, first a discriminant analysis was performed using relative VOI [^{18}F]FDG data. Moreover, a visual analysis was done by two experienced readers in a blinded fashion. Diagnostic performance in terms of sensitivity, specificity, and accuracy was calculated. Results: Increased regional glucose metabolism was found in VS patients compared to CON in the primary and secondary visual cortex, including the calcarine sulcus, lingual gyrus and cuneus ($p_{cluster\text{-}FWE} < 0.05$, max VOI changes +10%), together with hypometabolism in the mesotemporal cortex ($p_{cluster} < 0.001$, -13%). VS patients also had increased GM volume in the corticolimbic system bilaterally ($p_{cluster\text{-}FWE} < 0.05$), in the left secondary and associative visual cortex, and in the left lingual gyrus ($p_{cluster} < 0.001$). All CON and VS cases were correctly classified using the mesotemporal VOI (ROC AUC 1.00), while for the entire occipital lobe, lingual gyrus and the cuneus, values ranged from 0.92 to 0.96. Visual analysis for differentiating VS and CON cases resulted in heterogeneous findings between observers with sensitivity 14-71% and specificity 60-100%. **Conclusion:** Patients with VS syndrome show both structural and metabolic abnormalities that are not only confined to the visual system. Semiquantitative [^{18}F]FDG PET using mesotemporal and occipital lobe VOIs has high diagnostic accuracy (92-100%). This outperforms visual analysis even for experienced observers, in line with the moderate metabolic alterations averaging around 10-13%. **References:** None

OP-0820

Association of neuroinflammation and myelin content with functional disability in multiple sclerosis: a multi-tracer PET/MR study

M. Pitombeira[1], M. Koole[2], A. M. de Souza[3], F. L. Duran[4], K. R. Campanholo[1], D. J. Fontoura Solla[5], C. M. Rimkus[6], M. F. Mendes[1], S. L. Apóstolos-Pereira[1], G. Busatto Filho[7], D. Callegaro[1], C. A. Buchpiguel[3], D. de Paula Faria[3];
[1]Department of Neurology, Faculdade de Medicina FMUSP, Universidade de Sao Paulo, São Paulo, BRAZIL, [2]Division of Nuclear Medicine, Department of Imaging and Pathology, University Hospitals Leuven and KU Leuven, Leuven, BELGIUM, [3]Laboratory of Nuclear Medicine (LIM43), Department of Radiology and Oncology, Faculdade de Medicina FMUSP, Universidade de Sao Paulo, São Paulo, BRAZIL, [4]Laboratory of Psychiatric Neuroimaging (LIM-21), Department and Institute of Psychiatry, Faculdade de Medicina FMUSP, Universidade de Sao Paulo, São Paulo, BRAZIL, [5]Division of Neurosurgery, Department of Neurology, Faculdade de Medicina FMUSP, Universidade de Sao Paulo, São Paulo, BRAZIL, [6]Department of Radiology and Oncology, Faculdade de Medicina FMUSP, Universidade de Sao Paulo, São Paulo, BRAZIL, [7]Department of Psychiatry, Faculdade de Medicina FMUSP, Universidade de Sao Paulo, São Paulo, BRAZIL.

Aim/Introduction: Neuroinflammation and myelin injury occurs simultaneously in multiple sclerosis (MS) and the pathological profile differs widely according to clinical phenotype which poses a challenge in identifying biomarkers to predict MS-related disability. Positron emission tomography (PET) using TSPO, and myelin-specific tracers have the potential to address specific underlying in vivo pathology and broaden the understanding of the heterogeneity in this disease. Our aim was to investigate the associations between neuroinflammation and myelin content with functional disability in patients with MS. **Materials and Methods:** ^{11}C-PK11195 and ^{11}C-PIB PET images and magnetic resonance (MR) were acquired in a hybrid PET/MR system from 47 patients with MS (28 RRMS and 19 PMS) and 18 healthy controls (HC). PNEURO tool of PMOD software was used to define volumes of interest (VOIs), ^{11}C-PK11195 distribution volume (Vt) using Logan graphical method with metabolite-corrected plasma input function and ^{11}C-PIB distribution volume ratio (DVR) with Logan method using a reference region extracted for each subject by a supervised clustering algorithm. Functional disability was assessed using the Expanded Disability Status Scale (EDSS). Results: Patients and HC did not differ in age and gender. As expected, RRMS were younger (mean age 35.8 years, P<0.001) and PMS had a higher disability (median EDSS 6.5, P<0.001). ^{11}C-PK11195 uptake was overall higher in all studied regions in MS patients, with higher means of Vt in PMS, but these differences were not significant. ^{11}C-PIB uptake differed in MS patients and HC in the corpus callosum (P=0.004) and caudate (P=0.002) with overall lower DVR observed in PMS. Linear regression models adjusted for age, gender, and phenotype, demonstrated that higher EDSS was associated with higher ^{11}C-PK11195 uptake and low ^{11}C-PIB uptake in corpus callosum (P=0.038, β=0.19; P=0.022, β=- 0.21), caudate (P=0.046, β=0.18; P=0.018, β=-0.21) and total T2-lesion (P=0.007, β= 0.24; P=0.012, β=- 0.24), and exclusively with higher ^{11}C-PK11195 in cortical grey matter (GM) (P=0.026, β=0.20), cerebellar cortex (P=0.022, β=0.20), thalamus (P=0.016, β=0.23) and normal-appearing white matter (NAWM) (P=0.022, β=0.19). **Conclusion:** Higher functional disability was associated with neuroinflammation in several GM regions and NAWM along with low myelin content in the corpus callosum and caudate, which may be related to the classic periventricular location of MS lesions. Our findings indicate that widespread innate immune cell activation, beyond demyelination, can contribute to functional disability in the RRMS and PMS phenotypes. **References:** none

OP-0821

Pharmacodynamic effects of padsevonil using simultaneous [^{11}C]-UCB-J PET-MR Arterial Spin Labeling perfusion measurements

M. Koole[1], B. Lacroix[2], M. Devrome[1], H. Chanteux[2], R. P. Maguire[2], K. Van Laere[1,3];
[1]KU Leuven, Leuven, BELGIUM, [2]UCB Pharma, Braine l'Alleud, BELGIUM, [3]UZ Leuven, Leuven, BELGIUM.

Aim/Introduction: PET-MR imaging can measure simultaneously tracer binding, downstream cerebral blood flow (CBF) and neuronal activation. We explored whether SV2A occupancy and effects on CBF could be detected simultaneously after single dose Padsevonil (PSL). Baseline and post dose MR Arterial Spin Labeling (ASL) perfusion measurements were compared to determine the effects of PSL and changes were compared with [^{11}C]-UCB-J PET measured SV2A occupancies. **Materials and Methods:** PET-MR scanning was performed in 10 healthy volunteers (8M/2F; age 27.6±10.0 yrs) at baseline, and at two timeponts (2–24 hr, N=10) and (6–30h, N=7) post single dose of PSL (6.2–100mg) Dynamic [^{11}C]-UCB-J PET scan with arterial blood sampling was performed distribution volumes (V_T) and corresponding SV2A occupancies at these timepoints. Simultaneously, MR ASL data were acquired and perfusion estimates calculated. ASL data were spatially normalized to Montreal Neurological Institute (MNI) space for voxelwise analysis while brain Volume-Of-Interest (VOI) were defined using a simplified Hammers atlas. Results: [^{11}C]-UCB-J PET data showed an occupancy range of 57–98% (avg=82%) and 16–63% (avg=41%) for the post1 and post2, respectively. The VOI-based analysis detected a statistically significant decrease in brain perfusion post1 compared to baseline in thalamus, insula, cerebellum, posterior cingulate cortex and brainstem. These findings

were confirmed by the voxel-wise analysis which identified significantly different clusters between baseline and post1 ASL measurements (p_{uncorr}<0.001, k_{ext}>500 voxels) covering the same regions of interest. In addition, we demonstrated a recovery of brain perfusion in these specific brain regions for the post2 ASL relative to baseline. For thalamus, posterior cingulate cortex, insula and parietal cortex, a VOI-based correlation analysis detected a statistically significant correlation between decrease of brain perfusion relative to baseline and PSL plasma concentration. These findings were confirmed by a voxel-wise regression analysis including all scans (n=27) and using the PET-based SV2A occupancy as a covariate where additionally a significant cluster was observed in the cerebellum (p_{uncorr}<0.001, k_{ext}>500 voxels). **Conclusion:** We observed a pattern of local decreased CBF and SV2A occupancy following administration of PSL and demonstrated a dose dependent effect. These findings may present a potential of PET-MR and ASL perfusion measurements for future research to follow the time course of drug effects during PET RO studies and to differentiate between the efficacy of different drugs in patient groups. **References:** none

OP-0822

Learning results in metabolically driven adaptations of brain connectivity

S. Klug[1], L. Rischka[1], G. M. Godbersen[1], W. Wadsak[2,3], V. Pichler[2,4], M. Hacker[2], R. Lanzenberger[1], A. Hahn[1];
[1]Department of Psychiatry and Psychotherapy, Medical University of Vienna, Vienna, AUSTRIA, [2]Department of Biomedical Imaging and Image-guided Therapy, Division of Nuclear Medicine, Medical University of Vienna, Vienna, AUSTRIA, [3]Center for Biomarker Research in Medicine (CBmed), Graz, AUSTRIA, [4]Department of Pharmaceutical Chemistry, University of Vienna, Vienna, AUSTRIA.

Aim/Introduction: Based on the assessment of the brain's glucose metabolism via PET, an earlier study discovered decreases in region-specific glucose metabolism after practicing a challenging visuospatial task, suggesting higher metabolic efficiency after learning (1). On the other hand, forming new connections via synaptic plasticity seems to result in increased metabolic costs (2). The technique of metabolic connectivity mapping (MCM) (3) combines functional connectivity with glucose metabolism to assess directional brain connectivity, thereby exploiting the fact that energy demands mainly arise postsynaptically. With this framework, we aimed to investigate if learning leads to metabolically cost-intensive formation of connections between different brain regions. **Materials and Methods:** 41 healthy subjects divided into training and passive control groups underwent two PET/MRI measurements separated by 4 weeks. During the scans, glucose metabolism (CMRGlu from [^{18}F]FDG functional PET) and functional connectivity (FC from BOLD fMRI) were acquired simultaneously at rest and while playing the video game Tetris®. After defining target regions by distinct neuronal activation during task performance (frontal eye field, intraparietal sulcus, occipital cortex) (4), individual MCM maps were calculated by spatial correlations between the CMRGlu pattern of the target region and the voxel-wise FC pattern generated in the target region. To assess, if learning-induced changes in directional brain communication are primarily driven by metabolic changes, the training effect was re-calculated after removing voxels based on their CMRGlu or FC values. Results: Comparison of training and control group after the 4-week training period revealed MCM changes for the primary visual cortex (V1), insula (Ins) and dorsal anterior cingulate cortex (dACC) with the occipital cortex (OCC) as target region (group*time*condition interaction, all p<0.05 FWE-corrected). Post-hoc analysis displayed a training-induced increased input from these regions to OCC at rest. Simulated deletion of voxels based on CMRGlu eliminated these training effects, which was not the case for FC. **Conclusion:** Learning resulted in higher input from brain regions primarily involved in attention (salience network, Ins+dACC), error monitoring (dACC), and network switching (Ins). These effects were distinctly dependent on CMRGlu. We interpret our results as an increased synapse formation between higher-order (Ins, dACC) and lower-order brain regions (OCC), potentially arising from metabolically costly insertion of postsynaptic AMPAR receptors (5). These findings emphasize the high potential of integrating PET in multimodal approaches to evaluate learning-induced metabolic changes and their role in modifying brain connectivity. **References:** (1) Haier et al.(1992)BrainRes.20;570(1-2):134-43. (2)Plaçais et al.(2017)NatCommun.5;8(1):15510. (3)Riedl et al.(2016) ProcNatlAcadSci.12;113(2):428-33. (4)Hahn et al.(2020) eLife.21;9:e52443. (5)Harris et al.(2012)Neuron.6;75(5):762-77.

OP-0823

Relationships between different measures of brain connectivity

I. Yakushev, A. Lizarraga, I. Ripp, A. Sala, W. Weber;
Technical University of Munich, School of Medicine, Klinikum rechts der Isar, Department of Nuclear Medicine, Munich, GERMANY.

Aim/Introduction: Functional magnetic resonance (fMRI) and diffusion weighted imaging (DWI) have so far made a major contribution to delineation of the human brain connectome. While structural connectivity of DWI appears to determine functional connectivity of fMRI to a certain degree, their spatial relationships are yet unknown. Even less clear are links with measures of brain connectivity from positron emission tmography (PET) data. In contrast to fMRI and DWI, PET data are typically available for analyses as one single image per subject. Thus, PET-based connectivity modelling commonly relies on identification of intersubject covariance patterns at a group level. Here, we assessed relationships between the

established MRI-based measures of brain connectivity and intersubject covariance patterns of f18-fluorodeoxyglucose (FDG) uptake (PET_{cov}) and regional grey matter volume (GM_{cov}). **Materials and Methods:** Multi-modal imaging was performed in 56 healthy middle aged individuals on a hybrid PET/MR scanner. Structural MRI, fMRI, DWI, and FDG-PET data underwent state of the art preprocessing. Measures of interest were derived from 106 grey matter regions covering the whole brain. Probabilistic tractography was utilized to reconstruct white matter tracts between the above regions, in terms of structural connectivity. Global relationships between weights from 4 modalities were calculated using Spearman's correlations. Spatial overlap for the whole brain was calculated using convergence ratio (CR), the percentage of overlapping connections relative to detected one. Adjusted CR refers to CR accounted for connections by chance. Results: Spearman's correlation coefficients were 0.38 for PET_{cov} and structural connectivity, 0.30 for PET_{cov} and functional connectivity, and 0.29 for structural and functional connectivity. Correlations with GM_{cov} were weaker, with the coefficient of 0.15 for GM_{cov} and structural connectivity. Mean adjusted CRs at sparsity levels of 55 to 80 % were 31 % for structural and functional connectivity, 26 % for PET_{cov} and structural connectivity, and 25 % for PET_{cov} and functional connectivity. CRs for GM_{cov} were again lower, with the lowerst one of 14 % again for GM_{cov} and structural connectivity. **Conclusion:** Structural connectivity is related to functional connectivity and PET_{cov} to a similar degree. GM_{cov} overlap poorly with all connectivity measures. These results strongly support PET_{cov} as sovereign index of brain connectivity. Analyses of the relationships for anatomical and functional subdivisions of the brain are under way. **References:** none

OP-0824

Longitudinal metabolic brain connectivity analysis after acute unilateral vestibulopathy

M. Grosch[1], S. Becker-Bense[1], P. Bartenstein[2], M. Dieterich[3], S. Ziegler[2], A. Zwergal[1];
[1]German Center for Vertigo and Balance Disorders, LMU Hospital, München, GERMANY, [2]Department for Nuclear Medicine, LMU Hospital, München, GERMANY, [3]Department of Neurology, LMU Hospital, München, GERMANY.

Aim/Introduction: Symptoms of acute unilateral vestibulopathy (AUV) partially recover due to adaptive brain plasticity. In this study, we analyzed whole-brain metabolic connectivity changes after AUV by longitudinal [^{18}F]-FDG PET imaging. **Materials and Methods:** 22 patients with AUV underwent resting state [^{18}F]-FDG PET scans (static, 30-60 min after injection, 150 ± 20 MBq) in the acute phase (mean: 6d) and after partial behavioral compensation (mean: 6m). PET data were compared to 22 age-matched controls. Images were registered elastically, smoothed with a 12-mm 3D-Gaussian filter, normalized to the whole brain, and segmented with AAL3 atlas. Pearson's correlations between all segmented brain regions were calculated group-wise to determine connections ($|r|>0.5/p<0.001$). The resulting metabolic connectome was quantified between and within hemispheres, and vestibular/multisensory/motor/cognitive networks were analyzed. Additionally, homotopic connections were quantified. Results: Patients had severe vestibular asymmetry in the acute stage (mean horizontal slow-phase velocity (SPV): 9.9°/sec, subjective visual vertical (SVV): 7.6°), which recovered until 6m after AUV (SPV: 0.7°/sec, SVV: 1.7°). In the acute stage and as compared to controls, whole-brain metabolic network analysis indicated a significant drop in the total number of connections, and specifically in interhemispheric homotopic connections. In the chronic stage, the low number of interhemispheric connections of homotopic regions persisted. The distribution of connections between/within hemispheres reformed to the control cohort state, but the total number of connections remained on a lower level. Compared to the early stage, multisensory network connectivity relatively increased in the ipsilesional hemisphere. **Conclusion:** AUV disrupts the symmetry of metabolic networks between hemispheres persistently. These data may be important for the understanding of higher sensory network dysfunction and conversion risk to functional dizziness after AUV. Furthermore, metabolic brain connectivity is often studied in healthy control cohorts or for neurodegenerative diseases. This study analyzed healthy brains with an erroneous vestibular input and the experimental setup therefore may be suited to understand the methodic backgrounds of metabolic brain connectivity more in detail. **References:** none

OP-0825

Quantification of P-glycoprotein function at the human blood-brain barrier using [^{18}F]MC225 and PET

P. Mossel[1], A. T. Willemsen[1], L. Garcia Varela[1], W. Arif[1,2], R. Boellaard[1,3], P. H. Elsinga[1], P. de Deyn[4,5,6], R. A. Dierckx[1], A. A. Lammertsma[1,3], A. L. Bartels[4], G. Luurtsema[1];
[1]Department of Nuclear Medicine and Molecular Imaging, University Medical Center Groningen, Groningen, NETHERLANDS, [2]Department of Radiological Sciences, King Saud University, Riyadh, SAUDI ARABIA, [3]Department of Radiology & Nuclear Medicine, Amsterdam UMC, Vrije Universiteit Amsterdam, Amsterdam, NETHERLANDS, [4]Department of Neurology, University Medical Center Groningen, Groningen, NETHERLANDS, [5]Faculty of Medicine and Health Sciences, University of Antwerp, Antwerp, BELGIUM, [6]Department of Biomedical Sciences, Neurochemistry and Behaviour, Institute Born-Bunge (IBB), University of Antwerp, Antwerp, BELGIUM.

Aim/Introduction: P-glycoprotein (P-gp) is an efflux transporter located at the endothelial cells of the blood-brain barrier (BBB), which is involved in the transport of various neurotoxic substances out of the brain. Alterations in P-gp function

play an essential role in the pathophysiological mechanisms underlying neurodegenerative disorders, drug resistance, and drug-drug interactions. Currently used tracers to measure P-gp function are in general avid substrates and suffer from low brain uptake at baseline P-gp levels, which hamper evaluation of increases in P-gp function. To overcome this limitation, [^{18}F]MC225 was developed. [^{18}F]MC225 is a weak P-gp substrate, which has shown higher brain uptake than (R)-[^{11}C]verapamil at P-gp baseline levels in preclinical studies [1]. The higher uptake at baseline enables measurements of both increases and decreases in P-gp function. This pilot study aimed to determine the best pharmacokinetic model to describe [^{18}F]MC225 kinetics in the human brain. Moreover, the ability of [^{18}F]MC225 to measure changes in human BBB P-gp function was evaluated by blocking P-gp function using cyclosporine. **Materials and Methods:** Three healthy subjects were scanned twice using a 60 minute dynamic scan protocol with arterial sampling. Scans were performed at baseline and after inhibition of P-gp function by continuous intravenous administration of 2.5 mg·kg^{-1}·h^{-1} cyclosporine, starting 30 minutes prior to the scan. Plasma data were corrected for labelled metabolites and then tissue data were fitted to both reversible and irreversible compartmental models. The goodness of fit was determined based on a visual assessment of the fits together with the Akaike Information Criterion (AIC). Kinetic parameters were obtained using the whole brain grey matter as volume of interest. Results: A reversible two-tissue compartment model with an additional blood volume parameter was selected as model of choice based on lowest AIC scores for all subjects and V_T was used to estimate P-gp function. Plasma input curves (areas under the curve) were similar at baseline level and after P-gp inhibition (p=0.61). Whole brain grey matter V_T values increased from 5.6±1.2 at baseline P-gp level to 9.8±3.4 after administration of cyclosporine. **Conclusion:** A reversible two-tissue-compartment model is the preferred model to quantify [^{18}F]MC225 kinetics in humans. The preliminary results show clear differences between [^{18}F]MC225 V_T under baseline P-gp conditions and after P-gp inhibition with cyclosporine. Thus, [^{18}F]MC225 seems a promising novel PET-tracer to measure changes in human BBB P-gp function. **References:** 1.García-Varela L, et al. Mol Pharm(2020);17:3477-86.

OP-0826

First-in-human mapping of the GluN2B subunits of the N-methyl-D-aspartate receptor using (R)-[^{11}C]Me-NB1 and PET

L. Rischka[1], *C. Vraka*[2], *V. Pichler*[2,3], *S. Rasul*[2], *L. Nics*[2], *G. Gryglewski*[1], *P. Handschuh*[1], *M. Murgaš*[1], *G. M. Godbersen*[1], *L. R. Silberbauer*[1], *J. Unterholzner*[1], *C. Wotawa*[1], *A. Haider*[4], *H. Ahmed*[4], *R. Schibli*[4], *T. Mindt*[2,5,6], *M. Mitterhauser*[2,5], *W. Wadsak*[2,7], *A. Hahn*[1], *R. Lanzenberger*[1], *M. Hacker*[2], *S. M. Ametamey*[4];
[1]Department of Psychiatry and Psychotherapy, Medical University of Vienna, Vienna, AUSTRIA, [2]Department of Biomedical Imaging and Image-guided Therapy, Division of Nuclear Medicine, Medical University of Vienna, Vienna, AUSTRIA, [3]Department of Pharmaceutical Chemistry, University of Vienna, Vienna, AUSTRIA, [4]Centre for Radiopharmaceutical Sciences ETH-PSI-USZ, Institute of Pharmaceutical Sciences ETH, Zurich, SWITZERLAND, [5]Ludwig Boltzmann Institute Applied Diagnostics, Vienna, AUSTRIA, [6]Institute of Inorganic Chemistry, Faculty of Chemistry, University of Vienna, Vienna, AUSTRIA, [7]Center for Biomarker Research in Medicine (CBmed), Graz, AUSTRIA.

Aim/Introduction: The N-methyl-D-aspartate receptor (NMDAR) plays a key role in pathophysiological processes [1]. More precisely, GluN2B-enriched NMDAR are associated with neuropsychiatric disorders, including neurodegenerative diseases [2]. Targeting these receptors would enable specific drug development and treatment monitoring. Recently, the radioligand (R)-[^{11}C]Me-NB1 was introduced in rodents, showing high specific binding to the GluN2B subunits [3]. Here, we investigated the potential of (R)-[^{11}C]Me-NB1 for imaging GluN2B-enriched NMDAR for the first time in humans. **Materials and Methods:** Six healthy subjects (all male) underwent two measurements on a fully-integrated PET/MRI scanner lasting for 120 min. The radioligand (R)-[^{11}C]Me-NB1 was administered as bolus via a cubital vein. Standardized uptake values (SUV) were computed to assess brain uptake and pharmacokinetics of the radioligand. Regions-of-interest included cortical, subcortical and white matter structures. In an exploratory approach, the total volume of distribution (V_T) was quantified with the Logan plot using an arterial input function. Test-retest reliability was investigated for SUV and V_T with the coefficient of variation (COV) and the absolute percentage difference (APD). Results: (R)-[^{11}C]Me-NB1 passed the blood-brain-barrier and showed reversible binding within the scan duration. The radioligand featured high brain uptake, which was similar across cortical regions but heterogeneous in subcortical areas. Interestingly, the white matter structures showed markedly different kinetics compared to grey matter regions. Test-retest reliability was high for SUV with COV ranging from 4.9 - 6.0% and APD from 6.8 - 8.5%. Slightly higher results were achieved with V_T (mean COV: 7.4%, mean APD: 10.5%). SUV and V_T exhibited a moderate correlation (rho = 0.44). **Conclusion:** We successfully translated the GluN2B-specifc radioligand (R)-[^{11}C]Me-NB1 to humans and demonstrated favourable characteristics such as heterogeneous uptake and high test-retest reliability. Except for the cerebellum, similar uptake patterns compared to rodent studies were obtained, indicating a high selective binding to the GluN2B subunits [3]. The opportunity to map GluN2B-enriched NMDAR in humans opens novel possibilities in terms of drug development and treatment of neurodegenerative and other neuropsychiatric diseases. **References:** [1] Sattler et al. (2000) J.Mol.Med 78:3-13 [2] Schreiber et al. (2019) Commun.Biol. 2:420 [3] Haider et al. (2019) J.Nucl.Med 60:1167-1173

OP-0828

Role of [18F]FDG and [18F]Florbetapir PET/CT to predict Alzheimer's disease development in patients with Down syndrome

S. Abouzian[1], R. Valverde[2], J. Pegueroles[3,4], M. Sizova[1], F. Fuentes[1], A. Fernández[1], J. Duch[1], D. López-Mora[1], M. Estorch[1], I. Barroeta[3,4], M. Carmona-Iragui[3,4], A. Lleó[3,4], I. Carrió[1], A. Flotats[1], J. Fortea[3,4], V. Camacho[1];

[1]Nuclear Medicine Department. Hospital de la Santa Creu i Sant Pau, Biomedical Research Institute Sant Pau, Universitat Autònoma de Barcelona, Barcelona, SPAIN, [2]Nuclear Medicine Department. Hospital de Cruces, Bilbao, SPAIN, [3]Sant Pau Memory Unit, Department of Neurology, Hospital de la Santa Creu i Sant Pau, Biomedical Research Institute Sant Pau, Universitat Autònoma de Barcelona, Barcelona, SPAIN, [4]CIBERNED, Madrid, SPAIN.

Aim/Introduction: Down syndrome (DS) is a genetically determined form of Alzheimer's disease (AD). In patients with DS, the physiopathological changes of AD can be detected with PET/CT imaging. The aim of this study was to evaluate the continuum of AD in subjects with DS using [18F]Florbetapir and [18F]FDG PET/CT imaging. **Materials and Methods:** We retrospectively analysed 51 subjects with DS (32 men; mean age 40±11 years) distributed in 4 groups according to the level of cognitive decline: 35 without cognitive decline (asymptomatic DS), 8 with prodromal AD (prodromal DS), 6 with AD dementia (dementia DS) and 2 with non-degenerative cognitive decline (non-degenerative DS). All patients underwent [18F]Florbetapir and [18F]FDG PET/CT imaging, with both visual and quantitative analyses. [18F]FDG images were intensity-scaled relative to the pons-vermis region and spatially normalized using SPM12. The standardized uptake value ratios (SUVr) were extracted from Landau's region of interest. [18F]Florbetapir images were spatially normalized using MRI transformations computed with Advanced Normalization Tools (ANTs) and scaled using the whole cerebellum as reference region. Results: Among the asymptomatic DS subjects, 97% (34/35) presented preserved brain metabolism on [18F]FDG (SUVr 1.37±0.10) and 77% (27/35) presented absent cortical [18F]Florbetapir uptake (SUVr 1.17±0.13). All patients with prodromal DS presented cortical [18F]Florbetapir uptake, and 5/8 (62%) of them presented parietotemporal hypometabolism. In comparison with the asymptomatic DS group, prodromal DS patients showed significant lower [18F]FDG SUVr (1.15±0.15 vs 1.37±0.10, p= 0.002) and significant higher [18F]Florbetapir SUVr (1.35±0.13 vs 1.17±0.13, p= 0.003). All patients with dementia DS presented cortical [18F]Florbetapir uptake, and 5/6 (83%) of them presented parietotemporal hypometabolism. In comparison with the asymptomatic DS group, dementia DS patients showed significant lower [18F]FDG SUVr (0.95±0.19 vs 1.37±0.10, p= 0.001) and significant higher [18F]Florbetapir SUVr (1.34±0.09 vs 1.17±0.13, p= 0.002). In comparison with prodromal DS group, dementia DS patients showed significant lower [18F]FDG SUVr (0.95±0.19 vs 1.15±0.15, p= 0.036) and no significant different [18F]Florbetapir SUVr (1.34±0.09 vs 1.35±0.13, p=ns). The two patients with non-degenerative DS presented normal metabolism on [18F]FDG PET/CT and absence of [18F]Florbetapir cortical uptake. In comparison with the asymptomatic DS group, there were no significant different SUVr of [18F]FDG (1.33±0.10 vs 1.37±0.10, p=ns) or [18F]Florbetapir SUVr (1.14±0.09 vs 1.17±0.13, p=ns). **Conclusion:** In adults with DS, the sequential changes observed on [18F]FDG and [18F]Florbetapir PET/CT imaging may be useful to evaluate the clinical phases of AD, and may be used to predict the development of AD dementia. **References:** none.

1413

Friday, October 22, 2021, 13:10 - 13:30

Channel 1

Plenary Quiz (for Plenary 4)

OP-0831

Plenary Quiz

M. Benesova; *DKFZ Heidelberg, Molecular Biology of Systemic Radiotherapy, Heidelberg, GERMANY. &* ***G. Bakos;*** *German Cancer Research Center (DKFZ), Molecular Biology of Systemic Radiotherapy (E270), Heidelberg, GERMANY.*

1501

Friday, October 22, 2021, 13:30 - 14:50

Channel 1

Plenary 4: Isotopes' Past and Future

OP-0833

The Importance of the Isotope

J. Sosabowski; *Queen Mary University of London, Barts Cancer Institute, Centre for Molecular Oncology, London, UNITED KINGDOM.*

OP-0834

Clinical Applications of Alpha vs Beta

M. Eiber; *Technical University Munich, Department of Nuclear Medicine, Munich, GERMANY.*

OP-0835

New Isotopes on the Blocks

U. Köster; *Institut Laue-Langevin (ILL), Grenoble, FRANCE.*

OP-0836
Isotopes' Availability
V. Pichler; Department of Pharmaceutical Sciences, Vienna, AUSTRIA.

OP-0837
Zr and Friends
D. Vugts; VUmc Imaging Center Amsterdam Radiology & Nuclear Medicine, Amsterdam, NETHERLANDS.

OP-0838
Beta Emitters for Surface Therapy
P. Castellucci; IRCCS Azienda Ospedaliero-Universitaria di Bologna, Nuclear Medicine Unit, Bologna, ITALY.

OP-0839
The Best has yet to Come
P. Laverman; Radboud University Nijmegen Medical Center, Department of Radiology and Nuclear Medicine, Nijmegen, NETHERLANDS.

1601

Friday, October 22, 2021, 15:05 - 16:35

Channel 1

CME 11: New Concepts for Imaging and Therapy of Bone Metastases

OP-0849
Nuclear Imaging of Bone Metastases
H. Zacho; University Hospital, Department of Nuclear Medicine, Aalborg, DENMARK.

OP-0850
Radionuclide Therapy of Bone Metastases
A. Afshar-Oromieh; University Hospital Insel-Spital, Department of Nuclear Medicine, Bern, SWITZERLAND.

OP-0851
Radiation Therapy of Bone Metastases
P. Dirix; University of Antwerp, Radiation Oncology, iridium network, Antwerp, BELGIUM.

1602

Friday, October 22, 2021, 15:05 - 16:35

Channel 2

The Top 3 Trials Sessions - 3 - New Tracers

OP-0853
18F-Fluoroglutamine PET as a Promising Prognostic Tool in IDH Mutant Glioma
S. Krebs, M. S. Graham, M. Grkovski, A. Mauguen, R. Goel, S. B. Thakur, L. R. Schaff, I. K. Mellinghoff, R. J. Young, T. Kaley, M. P. Dunphy;
Memorial Sloan Kettering Cancer Center, New York, NY, UNITED STATES OF AMERICA.

Aim/Introduction: ^{18}F-(2S,4R)-4-Fluoroglutamine (^{18}F-FGln) is a promising new imaging biomarker of tumor metabolism in malignant brain glioma. We herein provide the first report of the prognostic value of ^{18}F-FGln PET in glioma patients from analysis of our first in-human trial data. **Materials and Methods:** This prospective study included 31 treated patients with high- and low-grade glioma (NCT 01697930). All patients underwent a 30-min dynamic ^{18}F-FGln PET immediately post-injection and a 10-min static ^{18}F-FGln PET at 90 min post-injection. 19/31 patients had a delayed 10-min static scan at 180 min post-injection. ^{18}F-FGln uptake was quantified by volumes-of-interest analysis of static and dynamic PET data in terms of standardized uptake value (SUV_{max}), ^{18}F-FGln volume of distribution (V_T; Logan analysis), and ^{18}F-FGln transport (K_1; reversible 2-tissue compartment model). We analyzed the relationship between PET parameters and mutation status, overall survival (Cox models), and 3-month progression (Mann-Whitney-Wilcoxon tests). Results: Thirty-one patients underwent ^{18}F-FGln PET—thereof 20/31 with concern for progression, 6/31 with stable disease, and 5/31 with new lesions—to differentiate low-grade from high-grade glioma. Twelve patients (41%) had been diagnosed with IDH mutant tumors, 17 with IDH wildtype, and two were unknown. Fourteen tumors (52%) showed MGMT promoter methylation.A total of 40 lesions were identified in 30/31 patients on PET (n=4, 1 pt; n=2, 8 pts; n=1, 22 pts) (median 1, range: 0-4). One patient had no measurable disease on PET, concordant with the lack of abnormal enhancement and perfusion on MRI. Another patient had a clearly ^{18}F-FGln-avid lesion correlating with rim-enhancement without elevated perfusion on MRI, subsequently biopsied and reported as IDH wild type, MGMT unmethylated GBM. SUV_{max} at 30, 90, and 180 min were significantly associated with the risk of progression (p=0.03, 0.02, and 0.04, respectively); however, V_T and K_1 were not significantly associated. To predict the 3-month progression status, receiver operating characteristic (ROC) analysis at 180 min SUV_{max} revealed a cut-off value of 1.46, which was associated with a sensitivity of 0.91 and a specificity

of 0.80. In IDH mutant patients univariable analysis showed that a one-unit increase of SUV_{max} at 30 min corresponds to doubling the risk of death (HR=2.35, p=0.01), while a one-unit increase of SUV_{max} at 90 min corresponds to tripling the risk of death (HR=3.07, p=0.01). **Conclusion:** In a heterogeneous treatment population, we found that higher tumor-avidity for ^{18}F-FGln portends worse outcomes for IDH mutant glioma patients. **References:** None

OP-0854

Phase I safety and bioimaging trial of ifabotuzumab in patients with glioblastoma

A. Scott[1,2,3], L. Cher[1,2], P. Inglis[4], Z. Lwin[4], E. Lau[2], C. Wichmann[1], U. Ackermann[1,2], A. Gunjur[2], A. McDonald[1], N. Coombs[2], K. Remen[2], N. Guo[1], S. Lee[1,2,3], S. Gong[2], J. Palmer[1,3], K. Pathmaraj[2], G. O'Keefe[2], F. Scott[1,3], B. Day[5], A. Boyd[1,4], O. Ahmed[6], D. Chappell[6], P. Thomas[4], C. Durrant[6], H. Gan[1,2,3];

[1]Olivia Newton-John Cancer Research Institute, Melbourne, AUSTRALIA, [2]Austin Health, Melbourne, AUSTRALIA, [3]La Trobe University, Melbourne, AUSTRALIA, [4]Royal Brisbane and Women's Hospital, Brisbane, AUSTRALIA, [5]QIMR Berghofer Medical Research Institute, Brisbane, AUSTRALIA, [6]Humanigen Inc, Burlingame, CA, UNITED STATES OF AMERICA.

Aim/Introduction: Glioblastoma multiforme (GBM) is the most frequent and lethal primary brain neoplasm, with only 10% of patients surviving 5 years. EphA3 is a tumour restricted antigen expressed in various solid tumors and the tumour vasculature of 100% of GBM. Ifabotuzumab is a non-fucosylated IgG1κ humaneered antibody targeting the EphA3 receptor. A Phase I study of ifabotuzumab (targeting EphA3) in haematological malignancies showed it was well tolerated and clinically active. Here we report on a Phase I dose escalation and biodistribution study of ifabotuzumab in recurrent GBM. **Materials and Methods:** The primary objective was to determine the safety and recommended Phase II dose of ifabotuzumab in GBM patients (pts). Secondary objectives were to determine the biodistribution and pharmacokinetics (PK) of ^{89}Zr- ifabotuzumab, the frequency of EphA3 positive GBM and response rates. On day 1, eligible pts with measurable tumors received a trace (5mg) dose of zirconium labelled ifabotuzumab (^{89}Zr-ifab) followed by sequential PET imaging over 1 week to determine its biodistribution, frequency of in situ EphA3 expression and quantitative tumour uptake. Safety assessments and PK sampling were also undertaken. On day 8, pts commenced weekly ifabotuzumab infusions in one of two cohorts (3.5mg/kg, 5.25 mg/kg). On day 36, pts received both ^{89}Zr-ifab and ifabotuzumab, allowing assessment of receptor occupancy. Response rate (RANO) and survival data were collected. Pts then continued on ifabotuzumab until progression. Results: A total of 12 pts were enrolled in the study. Mean age was 51.6 years (±14.24) and 7/12 pts were male. Treatment emergent adverse events included infusion reactions in 4 pts, seizures in 3 pts, cerebral oedema in 1, rash in 1, headaches in 8, eye disorder in 1. Most were considered related to study drug except seizure in 2 pts, headaches and eye disorder. The best response was stable disease for 23 weeks. ^{89}Zr-ifab PET scans showed rapid, tumour-specific targeting at all known tumour sites and in all pts, but with no normal tissue uptake. MRI scans showed predominant T2/FLAIR changes, occasionally marked, which were consistent with treatment effect of ifabotuzumab on tumour vasculature. **Conclusion:** Ifabotuzumab demonstrates highly sensitive, specific and reproducible targeting of the tumour and tumour microenvironment in all patients in this study. The imaging changes suggest direct modulation of the tumour vasculature. Additional studies are planned to evaluate ifabotuzumab as part of an antibody-drug conjugate in various solid tumour types. **References:** none

OP-0855

Use of SPECT with "99mTc-1-thio-D-glucose" for the Diagnosis of Brain Tumors

R. Zelchan[1], A. Medvedeva[1], O. Bragina[1], A. Ribina[1], E. Stasyuk[2], V. Chernov[1], E. Mishina[3];

[1]Cancer Research Institute is a subdivision of the Federal State Budgetary Scientific Institution "To, Tomsk, RUSSIAN FEDERATION, [2]National Research Tomsk Polytechnic University, Tomsk Polytechnic University, TPU., Tomsk, RUSSIAN FEDERATION, [3]Siberian State Medical University , SSMU, Tomsk, RUSSIAN FEDERATION.

Aim/Introduction: to study the possibility of using SPECT "99mTc-1-thio-D-glucose" for the diagnosis of primary brain tumors. **Materials and Methods:** the study included 70 patients diagnosed with a brain tumor (Grade II-IV) who underwent SPECT with "99mTc-1-thio-D-glucose"(99mTc-TG) at the stages of combined treatment. The study also included 10 patients with benign brain diseases (cysts). All patients underwent 99mTc-TG SPECT 2 hours after intravenous administration of the radiopharmaceutical at a dose of 500 MBq. The study was performed according to standard protocols; 32 projections were recorded in a matrix of 256x256 pixels without hardware magnification. During processing, the tumor/background index was calculated as the ratio of the intensity of radiopharmaceutical accumulation in the area of interest and the symmetric zone of the intact brain tissue. MRI with contrast and PET / CT were used as reference methods. Results: The brain tumor was visualized in all patients included in the study. The sensitivity of the method was 100%. None of the patients with benign pathology showed accumulation of 99mTc-TG in the brain. The specificity was 100%. When analyzing the results, it was found that the tumor/background index correlated with the tumor grade and the Ki-67 marker. For Grade II tumors, the tumor/background was 2.40 (2.10-2.72), for Grade III 3.89 (3.52-4.10) and for Grade IV 7.20 (6.80-7.40). After dynamic observation of patients after treatment, it was found that the survival rate of patients with brain tumors in whom the tumor/background was below 5.940 before treatment, the

overall survival was more than 100 months. Patients with a tumor/background index higher than 5.940 according to SPECT with 99mTc-TG had an overall survival of less than 70 months. **Conclusion:** The results of the study indicate a high diagnostic efficiency of SPECT with 99mTc-TG in the imaging of brain tumors. The tumor / background index allows differentiating tumors of a low degree of malignancy (Grade II) and a high degree of malignancy (Grade III-IV). In addition, the tumor / background has a predictive role in the prognosis of the course of the disease in these patients. Thus, SPECT with 99mTc-TG is a promising method for diagnosing brain tumors, which is easy to perform and low cost of the procedure. **References:** None

OP-0856

^{68}Ga-ABY-025 PET Predicts the Metabolic Response in Breast Cancer Patients: Preliminary Results From a Phase II Study

A. Alhuseinalkhudhur[1,2], H. Lindman[2], M. Lubberink[1], V. Iyer[3], P. Liss[3], T. Sundin[4], F. Y. Frejd[2,5], J. Hartman[6], I. Velikyan[1], J. Sörensen[1];
[1]Nuclear Medicine and PET, Department of Surgical Sciences, Uppsala University, Uppsala, SWEDEN, [2]Department of Immunology, Genetics and Pathology, Uppsala University, Uppsala, SWEDEN, [3]Department of Surgical Sciences, Radiology, Uppsala University, Uppsala, SWEDEN, [4]Clinical Research and Development Unit, Uppsala University Hospital, Uppsala, SWEDEN, [5]Affibody AB, Solna, SWEDEN, [6]Department of Oncology and Pathology, Karolinska Institute, Stockholm, SWEDEN.

Aim/Introduction: A previous Phase I study indicated that positron emission tomography (PET) measurements with the novel HER2-binding tracer ^{68}Ga-ABY-025 correlated with HER2-status determined by immunohistochemistry (IHC) of tumour biopsies. The objectives of this Phase II trial were to determine an optimal imaging protocol for clinical use and define ^{68}Ga-ABY-025 uptake cut-off measured in standardized uptake value (SUV) for accurate comparison with IHC results in terms of treatment response prediction. **Materials and Methods:** This study intended to include 40 patients with advanced breast cancer and known positive HER2-status. Automated production of ^{68}Ga-ABY-025 was conducted using a disposable cassette system. PET examinations were performed at 2+3 h or 3+4 h after injection of ^{68}Ga-ABY-025 at baseline to define optimal acquisition time point. FDG PET/CT was performed at baseline and after 2 cycles of therapy to assess treatment response. Selected lesions (up to 5 lesions per patient) were followed in all scans recording SUVs. The results from ^{68}Ga-ABY025 were compared to IHC HER2-status and the metabolic response (fractional change of FDG total lesion glycolysis between the scans) by ROC analyses. Results: Thirty-two patients were included. Trial biopsies were HER2-positive in 25, negative in 4, and borderline positive in 3 patients. Mean 149±38 MBq radioactivity with mean 322±29 microgram ABY-025 peptide was injected. ^{68}Ga-ABY025 SUV plateaued at 3h post-injection, no significant gain observed at the later 4 h p.i. time point. ^{68}Ga-ABY-025 PET predicted metabolic tumour response with 69% sensitivity and 60% specificity using SUVmax 7.6 as a cut-off value (AUC=0.66, p=0.01) in all patients, and with 82% sensitivity and 81% specificity using SUVmax 6.0 as best cut-off in soft tissue lesions (n=23, AUC=0.81, p=0.002) compared with IHC having 84% sensitivity and 38% specificity (n=23, AUC=0.61. p=0.08). Using SUVmax 7.6 as a threshold, ^{68}Ga-ABY-025 SUV and biopsy results were discordant in 12 out of 32 patients (37.5%) with no significant association. **Conclusion:** ^{68}Ga-ABY-025 PET at SUVmax cut-off value of 6.0 predicted metabolic tumour response to HER2-targeted treatment more accurately, compared with IHC-staining. PET images with optimal image contrast were obtained at 3 h p.i. **References:** none

OP-0857

Preliminary results of a pilot study with [^{18}F]-DPA-714 PET-CT to explore Tumor-Associated-Macrophages in triple negative breast cancer

C. Rousseau[1], N. Arlicot[2], O. Kerdraon[3], J. Vercouillie[4], L. Ferrer[5], I. Doutriaux-Dumoulin[3], R. Movassaghi[3], L. Ouldamer[6], F. Boiffard[3], C. Renaudeau[3], M. Colombié[3], V. Fleury[3], M. Le Thiec[3], B. Maucherat[3], A. Morel-Thierry[3], D. Rusu[3], N. Allam[3], M. Santiago-Ribeiro[7], F. Kraeber-Bodéré[8];
[1]ICO René Gauducheau, F-44800 Saint-Herblain, France; Université de Nantes, CNRS, Inserm, CRCINA, F-44000, Nantes, FRANCE, [2]UMR 1253, iBrain, Université de Tours, Inserm CIC 1415, University Hospital, F-37000, Tours, FRANCE, [3]ICO René Gauducheau, F-44800, Saint Herblain, FRANCE, [4]UMR 1253, iBrain, Université de Tours, Inserm, F-37000, Tours, FRANCE, [5]ICO René Gauducheau, F-44800 Saint-Herblain, France; CNRS, Inserm, CRCINA, F-44000, Nantes, FRANCE, [6]CHRU de Tours, Hôpital Bretonneau, F-37000 Tours, France ; Laboratoire "Nutrition, Growth and Cancer", Université de Tours, INSERM UMR1069, F-37000, Tours, FRANCE, [7]UMR 1253, iBrain, Université de Tours, Inserm, CHRU de Tours, Hôpital Bretonneau, F-37000, Tours, FRANCE, [8]Université de Nantes, CHU de Nantes, CNRS, Inserm, CRCINA, F-44000, Nantes, FRANCE.

Aim/Introduction: Triple-negative breast cancer (TNBC) tends to exhibit aggressive and metastatic behavior lacking from targeted therapies. Tumor-associated-macrophages (TAMs) could change phenotype in response to signals from micro-environment: kill tumor cells (M1) or promote their growth and metastases (M2). TAMs are targets of interest in TNBC. The mitochondrial translocator protein (TSPO) is sensitive marker for macrophages and could be interesting for TNBC stratification. Non-invasive [^{18}F]-DPA-714 PET-CT is valuable to assess their expression. This pilot prospective multicenter study (NCT04320030) aims at assessing correlation between TAMs and [^{18}F]-DPA-714 PET-CT pattern in 12 TNBC patients. Preliminary results are presented here. **Materials and Methods:** Patients underwent TSPO genotyping, [^{18}]-FDG PET-CT, breast MRI and [^{18}F]-DPA-714 PET-CT. Immediately

after [^{18}F]-DPA-714 injection (3.5MBq/kg), 30min dynamic thorax PET-CT (DPA_1) is acquired, followed by 15min identical examination (DPA_2) 30min later, followed by a whole body PET-CT. Tumor SUV_{max}, SUV_{mean}, TLG and MTV are measured. SUV_{max}, SUV_{mean} ratios from tumour to contralateral breast (TC) are determined. Macrophages immunochemistry, in vitro [^{3}H]-DPA-714 autoradiography and TSPO genotyping will be carried out at the final study stage. Results: A total of 11 patients has been included and imaging data were available for analysis for 6 patients (mean age 66.1). All patients were IIA stage, with median CEA and Ca15-3 of 1.8 (0.8-2.2) and 21.8 (13-21) µg/L respectively. Median clinical tumor size was 20.5mm (11-32), with 4 SBR II cases, and median Ki67 8% (8-25). Breast MRI showed 19mm (13-31) as median tumor size, 0.7 (0.1-0.9) as median ADC and four patients presented a tumor washout. For FDG PET-CT, median SUV_{max}, SUV_{mean}, TLG and MTV were 6.3 (4.1-29.0), 3.7 (2.3-18.7), 6.6 g (1.9-26.9) and 1.4 cm^3 (0.5-3.1), respectively. For [^{18}F]-DPA-714 PET-CT, median DPA_1 and DPA_2 SUV_{max} were significantly different (4.5 ; 2.2-5.8 and 6.6 ; 3.1-8.9 respectively ; p<0.03), as well as between DPA_1 and DPA_2 SUV_{mean} (2.9 ; 1.3-3.5 and 4.0 ; 1.8-5.) respectively ; p<0.03) ; DPA_1 and DPA_2 TLG (6.9 g ; 1.8-12.5 and 10.4 g ; 2.8-17.4 respectively ; p<0.03). A significant decrease was observed between time 1 and 2 for T/C_{SUVmax} (1.4 ; 1.3-1.6 and 0.2 ; 0.01-0.10 respectively ; p<0.03). No adverse events occured after [^{18}F]-DPA-714 injection. **Conclusion:** Over time, [^{18}F]-DPA-714 uptake seems to increase with some variations over our TNBC patients. Contreversely, quantitative measured contrast decreases overtime without noticeable qualitative effect on $DPA_{1,2}$ images. Study is ongoing and supplementary data will be presented at the congress. **References:** None

OP-0858

Tumor uptake of the anti-LAG-3 tracer [89Zr]Zr-BI 754111 in HNSCC and NSCLC patients progressing on previous anti-PD-1 treatment

I. H. C. Miedema[1], M. C. Huisman[1], G. J. Zwezerijnen[1], A. Thiele[2], R. Grempler[2], A. P. Pitarch[2], D. J. Vugts[1], T. D. de Gruijl[1], C. W. Menke-van der Houven van Oordt[1];

[1]Amsterdam UMC, location VUmc, Amsterdam, NETHERLANDS, [2]Boehringer Ingelheim, Ingelheim am Rein, GERMANY.

Aim/Introduction: Lymphocyte-activation gene 3 (LAG-3) is an inhibitory receptor expressed on tumor-infiltrating lymphocytes, and might play a role in developing resistance to anti-PD-1 therapy. Combination treatment of anti-PD1 with anti-LAG-3 is a novel strategy currently under clinical investigation[1]. In this clinical imaging study, we have evaluated LAG-3 expression in head and neck squamous cell carcinoma (HNSCC) and non-small cell lung cancer (NSCLC) patients, who previously progressed on anti-PD-1 containing treatment, using [89Zr]Zr-BI 754111 (anti-LAG-3), and compared tumor uptake with three different doses of BI 754111. **Materials and Methods:** Patients were given 240 mg BI 754091 (anti-PD-1), followed 8 days later by administration of [89Zr]Zr-BI 754111 (37 MBq, 4 mg). PET/CT scans were obtained 2, 96 and 144 h post-injection (p.i.). Three weeks later, patients received 240 mg of BI 754091 and 40 or 600 mg of BI 754111 followed by [89Zr]Zr-BI 754111 (37 MBq, 4 mg) with scans 96 and 144 h p.i.. Lesions were scored positive when exceeding local background, and delineated on PET for quantification. Venous blood samples for radioactivity concentration (% injected activity (IA)/L) were obtained at various timepoints. Tumor-plasma-ratio (TPR) was calculated by dividing tumor uptake (%IA/L) by plasma %IA/L. Patients continued 3-weekly combination treatment until disease progression or unacceptable toxicity. Results: We included 6 patients: two with metastatic HNSCC, and four with metastatic NSCLC. 20 tumor lesions were analyzed, each patient had ≥2 positive lesions. Tumor uptake was heterogeneous between and within patients. Median TPR for tracer dose (4 mg) BI 754111 was 2.70 (IQR 0.78 - 4.62) after 144 h. With the 44 mg dose the TPR was significantly decreased to median 0.67 (IQR 0.50 - 0.85, $p \leq 0.0001$) and similarly to median 0.60 (IQR 0.42 - 0.75, $p \leq 0.0001$) for the 604 mg dose, with no significant difference between the 44 and 604 mg dose. Correlation with LAG-3 immunohistochemistry scores will be presented. **Conclusion:** Using [89Zr]Zr-BI 754111 PET/CT imaging that contained 4 mg of anti-LAG3 antibody, we can visualize and quantify tumor uptake in HNSCC and NSCLC patients, who progressed on previous anti-PD-1 containing treatment. Administering higher doses of antibody significantly decreased TPR in both the 44 and the 604 mg dose. **References:** 1. Ascierto et al. Initial efficacy of anti-lymphocyte activation gene-3 (anti-LAG-3; BMS-986016) in combination with nivolumab (nivo) in pts with melanoma (MEL) previously treated with anti-PD-1/PD-L1 therapy. Journal of Clinical Oncology 35, no. 15_suppl (May 20, 2017) 9520-9520.

OP-0859

Pilot phase study of ^{18}F-FP-$R_0$1-MG-F2 PET in pancreatic cancer patients

***R. Nakamoto**, V. Ferri, H. Duan, N. Hatami, M. Goel, J. Rosenberg, R. Kimura, M. Wardak, T. Haywood, R. Kellow, B. Shen, W. Park, A. Iagaru;*

Stanford University, Stanford, CA, UNITED STATES OF AMERICA.

Aim/Introduction: A novel cystine knot peptide PET tracer, ^{18}F-FP-$R_0$1-MG-F2 (knottin), was developed to selectively bind to human integrin $\alpha_v\beta_6$, which is over-expressed in pancreatic cancer. The purpose of this study is to evaluate the safety, biodistribution, dosimetry and lesion uptake of ^{18}F-FP-$R_0$1-MG-F2 in patients with pancreatic cancer. **Materials and Methods:** Fifteen patients (6 men, 9 women) with histologically confirmed pancreatic cancer were prospectively enrolled and underwent knottin PET/CT between March 2017 and February 2021. Vital signs and laboratory results

were collected before and after the imaging scans. Maximum standardized uptake values (SUV_{max}) and mean SUV (SUV_{mean}) were measured in 24 normal tissues and pancreatic cancer lesions for each patient using whole-body of knottin PET/CT images. From the biodistribution data, the organ doses and whole-body effective dose were calculated using OLINDA/EXM software. Tumor-to-normal tissue (T/N) SUV_{mean} ratios of pancreatic lesions considered positive by visual analysis were also calculated. The SUV_{mean} of non-diseased areas in pancreas, ascending aorta, lung, intra-abdominal fat, and liver were utilized to calculate T/N ratios. Results: There were no significant changes in vital signs or laboratory values that qualified as adverse events. At 1 hour post-injection, areas of high ^{18}F-FP-$R_0$1-MG-F2 uptake (included the pituitary gland, stomach, duodenum, kidneys, and bladder (average SUV_{mean}, 9.7 - 14.5). Intermediate uptake was found in the normal pancreas (average SUV_{mean}, 4.5). Mild uptake was found in the lungs and liver (average SUV_{mean} < 1.0). The effective dose was calculated to be 2.538×10^{-2} mSv/MBq. Knottin PET/CT detected all known pancreatic tumors in the 15 patients, although it did not detect small peri-pancreatic lymph nodes in two of three patients who were found to have lymph node metastases at surgery. Knottin PET/CT detected distant metastases in the lungs (n = 5), peritoneum (n = 2), and liver (n = 4), as confirmed by biopsy and/or contrast-enhanced CT. At 1 hour post-injection, average T/N ratios of primary tumor (n = 15) were 1.5 ± 0.5, ranging from 0.6 - 2.4. Average T/N ratios of metastatic lesions [lymph node (n = 15), lung (n = 40), peritoneum (n = 22), and liver (n = 58)] were all above 2, ranging from 3 - 10. **Conclusion:** ^{18}F-FP-$R_0$1-MG-F2 is a safe PET radiopharmaceutical with high uptake in primary and metastatic pancreatic cancer lesions. **References:** Nat Commun. 2019 Oct 14;10(1):4673. doi: 10.1038/s41467-019-11863-w.

OP-0860

PSMA-PET/CT and additional PET/MRI using [F-18] siPSMA-14: Improvement in local tumour detection in prostate cancer patients with biochemical recurrence after radical prostatectomy and prior to salvage therapy

J. Miksch[1], *Y. Funk*[1], *W. P. Thaiss*[1], *J. P. Steinacker*[1], *M. Grunert*[2], *D. Di Carlo*[3], *F. Zengerling*[4], *C. Solbach*[1], *M. Beer*[5], *T. Wiegel*[6], *V. Prasad*[1], *H. J. Wester*[3], *A. J. Beer*[1];
[1]*Department of Nuclear Medicine University Hospital Ulm, Ulm, GERMANY,* [2]*Department of Nuclear Medicine, German Armed Forces Hospital, Ulm, GERMANY,* [3]*Pharmaceutical Radiochemistry, Technical University Munich, Garching, GERMANY,* [4]*Department of Urology and Pediatric Urology, University Hospital Ulm, Ulm, GERMANY,* [5]*Department of Radiology, University Hospital Ulm, Ulm, GERMANY,* [6]*Department of Radiation Oncology and Therapy, University Hospital Ulm, Ulm, GERMANY.*

Aim/Introduction: In staging prostate cancer (PCa) patients with Ga-68- and F-18-labelled PSMA ligands in early stages of biochemical recurrence (BCR) low tumour burden and tracer kinetics can complicate tumor detection. By combining a whole body PSMA-PET/CT with an additional pelvic PET/MRI using a silicon-based F-18 labelled PSMA (siPSMA) compound we tried to minimize equivocal lesions and improve tumour detection. **Materials and Methods:** In 17 PCa patients (64 ± 15 y; GS 7 - 9) after radical prostatectomy (R0 / R1 15 / 2) without systemic treatment or salvage therapy and a BCR of median (range) PSA 0.30 (0.03 - 0.64) ng/ml PET/CT images were acquired 90 min. p.i. of 343 ± 17.6 MBq siPSMA-14 from head to mid-thigh with an additional pelvic PET/MRI, each with intravenous contrast agent and without forced diuresis. Images were evaluated by a nuclear medicine physician and radiologist using a score system C1-C5 (C1/C2: Definitely / probably benign; C3: equivocal; C4/C5: probably / definitely malignant) for local, lymphatic and bone findings. Results: All but one patient had locoregional recurrence of PCa detected by PET/CT and pelvic PET/MRI evaluation: PET/CT / PET/MRI detected 59% (10 / 17) / 94% (16 / 17); local, lymphatic and bone malignant findings in PET/CT / PET/MRI presented 47% (8 / 17) / 88% (15 / 17), 6% (1 / 17) / 6% (1 / 17) and 6 % (1 / 17) of patients. In PET/MRI higher number of local lesions were classified as C4/C5 (32% (19 / 60)) as compared to in PET/CT (17% (10 / 60)) with 76% (13 / 17) of patients showing at least mild local tracer uptake with SUV mean / max ranging between 1.5 / 1.8 - 3.7 / 5.8. PET/MRI imaging reduced local equivocal findings by 80% (PET/CT: 10 / 16; PET/MRI: 2 / 4). **Conclusion:** Additional pelvic PSMA-PET/MRI to whole body PSMA-PET/CT without forced diuresis reduces equivocal findings and improves tumour detection prior salvage treatment in early stages of biochemical recurrence of prostate cancer patients. **References:** None

OP-0861

First results of biodistribution and tumour targeting of ^{68}Ga-DOTA-MGS5 PET/CT in advanced medullary thyroid cancer patients

C. Uprimny*, S. Bayerschmidt, G. di Santo, M. Klingler, A. Hörmann, B. Warwitz, C. Rangger, E. von Guggenberg, I. Virgolini;*
Medical University of Innsbruck, Innsbruck, AUSTRIA.

Aim/Introduction: The majority of medullary thyroid cancers (MTC) show a high expression of cholecystokinin-2 receptors (CCK2R). We have recently introduced a new CCK2R targeting peptide analogue derived from human minigastrin, DOTA-DGlu-Ala-Tyr-Gly-Trp-(N-Me)Nle-Asp-1-Nal-NH_2 (DOTA-MGS5). In preclinical studies ^{68}Ga-labelled DOTA-MGS5 (^{68}Ga-DOTA-MGS5) showed high resistance against proteolytic digestion in vivo and enhanced tumour targeting. We here report on our first clinical data on biodistribution and tumour targeting with ^{68}Ga-DOTA-MGS5 in advanced MTC patients. **Materials and Methods:** Seven patients with advanced MTC (mean calcitonin level: 1128.1 ng/L) were administered with a mean activity of 177.0 MBq of ^{68}DOTA-MGS5. PET/CT

scans were performed one and two hours after radiotracer injection (p.i.). PET images were judged visually. In addition, SUV-measurements of tissues with physiologic uptake and of lesions with increased accumulation rated positive for malignancy were performed. Results: All seven patients showed at least one lesion with pathologic radiotracer uptake considered malignant. MGS5-positive local recurrence was detected in two patients (median SUV_{max} one and two h p.i.: 3.7 and 6.2). Six patients showed a total of nine lymph nodes with pathologic uptake (median SUV_{max} one and two h p.i.: 3.8 and 3.9), 27 pathologic liver lesions were found in three patients (median SUV_{max} one and two h p.i.: 5.0 and 5.3), whereas 50 MGS5-avid bone lesions were present in two patients (median SUV_{max} one and two h p.i.: 4.0 and 4.6). Physiologic tracer accumulation was highest in urinary bladder, renal pelvis, stomach and gall bladder with a median SUV_{max} one/two h p.i. of 101.9/118.6, 27.3/35.3, 20.4/26.2 and 5.8/6.5, respectively. Physiologic tracer uptake was low in blood pool, liver, bowel and spleen showing a median SUV_{max} one/two h p.i. of 3.3/2.7, 2.5/2.1, 2.5/1.7 and 1.4/1.3, respectively. **Conclusion:** Preliminary results of our study suggest that ^{68}Ga-DOTA-MGS5 PET/CT has the potential to identify tumour lesions in advanced MTC patients, and might become an alternative molecular imaging method in MTC-patients with elevated calcitonin levels in whom standard diagnostic work-up fails to detect tumour recurrence. **References:** none

OP-0862

First in human biodistribution and first imaging results of ^{68}Ga- EMP-100 PET - a novel ligand for imaging c-MET-expression in metastatic renal cell carcinoma

L. Mittlmeier[1], A. Todica[1], F. Gildehaus[1], M. Unterrainer[2], L. Beyer[1], M. Brendel[1], H. Ilhan[1], S. T. Ledderose[3], M. Schott[4], S. Rodler[4], L. Rath[4], J. Marcon[4], C. C. Cyran[2], C. G. Stief[4], M. Staehler[4], P. Bartenstein[1];
[1]LMU Munich, Department of Nuclear Medicine, Munich, GERMANY, [2]LMU Munich, Department of Radiology, Munich, GERMANY, [3]LMU Munich, Department of Pathology, Munich, GERMANY, [4]LMU Munich, Department of Urology, Munich, GERMANY.

Aim/Introduction: The receptor tyrosin kinase c-MET is upregulated in renal cell carcinoma (RCC) and its expression is negatively correlated with overall survival in metastatic RCC (mRCC). Prediction of treatment response to therapy with tyrosin kinase receptor inhibitors targeting c-MET such as cabozantinib is highly desirable to improve patient management. ^{68}Ga-EMP-100 is a novel PET ligand that directly targets c-MET expression. In this pilot analysis, we present the first in-human data of ^{68}Ga-EMP-100 in mRCC patients comparing the intra- and interindividual biodistribution and evaluating uptake characteristics in mRCC tumor lesions. **Materials and Methods:** Twelve patients with mRCC either prior to anticipated cabozantinib therapy or at assessment of further last line therapy options underwent ^{68}Ga-EMP-100 PET/CT imaging. We compared the biodistribution in normal organs and tumor uptake of mRCC lesions by SUV_{mean} and SUV_{max} measurements. Additionally, metastatic sites were compared between PET and contrast enhanced CT visually and the respective, quantitative PET-parameters were assessed and compared inter- and intra-individually. Results: The highest physiological ^{68}Ga-EMP-100 accumulation was present in the urinary bladder content, followed by high uptake in the kidneys, moderate uptake in the liver and the spleen, whereas significantly lower uptake intensity was e.g. observed in the pancreas body or the intestines. Overall, 87 tumor lesions were included: Of these, 68/87 (79.3 %) were visually rated c-MET positive with a median SUV_{max} of 4.4 and SUV_{mean} of 2.5. Comparing different tumor sites, highest uptake intensity was present in tumor manifestations at the primary site (SUV_{max} 9.1 (4.9 - 29.2)), followed by bone metastases (SUV_{max} 5.6 (1.0 - 15.9)), lymph node metastases (SUV_{max} 3.9 (2.1 - 6.3)) and visceral metastases (SUV_{max} 3.8 (0.1 - 16.2)). The occurrence of visually PET-negative lesions was distributed heterogeneously intra- and interindividual. with the highest number of PET-negative metastatic manifestations in the lung and the liver. **Conclusion:** Targeting c-MET expression, ^{68}Ga-EMP-100 shows distinctly elevated uptake in mRCC patients with high inter- and intraindividual differences comprising both c-MET-positive and -negative lesions. Our preliminary clinical results indicate that ^{68}Ga-EMP-100 is a promising molecular imaging tool and warrant further systemic studies on its clinical use in different tumor entities potentially expressing c-MET, as well as for the use of c-MET ligands as a diagnostic and theragnostic tool. **References:** none

OP-0863

First clinical experience with Zr-89-Df-IAB22M2C PET/MRI in patients with metastatic cancer

J. Schwenck[1,2,3], D. Sonanini[2,4], D. Seyfried[2], W. Ehrlichmann[2], G. Kienzle[2], G. Reischl[2,3], I. Wilson[5], W. Le[5], G. Smith[5], R. Korn[5], F. Seith[6], A. Forschner[7], T. Eigentler[7], M. Röcken[7,3,8], L. Zender[4,3,8], B. Pichler[2,3,8], L. Flatz[7], M. Kneilling[2,3,7], C. la Fougere[1,3,8];
[1]Department of Nuclear Medicine and Clinical Molecular Imaging, Eberhard Karls University, Tübingen, GERMANY, [2]Werner Siemens Imaging Center, Department of Preclinical Imaging and Radiopharmacy, Eberhard Karls University, Tübingen, GERMANY, [3]Cluster of Excellence iFIT (EXC 2180) "Image-Guided and Functionally Instructed Tumor Therapies", Eberhard Karls University, Tübingen, GERMANY, [4]Department of Medical Oncology and Pneumology (Internal Medicine VIII), Eberhard Karls University, Tübingen, GERMANY, [5]ImaginAb, Inc, Inglewood, CA, UNITED STATES OF AMERICA, [6]Department of Diagnostic and Interventional Radiology, Eberhard Karls University, Tübingen, GERMANY, [7]Department of Dermatology, Eberhard Karls University, Tübingen, GERMANY, [8]German Cancer Consortium (DKTK), German Cancer Research Center (DKFZ) Partner Site Tübingen, Tübingen, GERMANY.

Aim/Introduction: Despite the spectacular success of immune checkpoint inhibitor therapy (ICT) in selected cohorts of patients with metastatic cancer, only a limited proportion of patients benefit from ICT overall. $CD8^+$ cytotoxic T cells are key players in ICT mediated therapeutic responses as they destroy MHC class I-dependent tumor cells. Tumor-infiltrating $CD8^+$ T cells are therefore a surrogate for response to ICT. The radiolabeled minibody [^{89}Zr]Zr-Df-IAB22M2C has a high affinity for human $CD8^+$ T cells and was already successfully tested in a phase I study. Here, we aimed to gain first clinical experience with the non invasive assessment of the CD8 T cell infiltration in cancer patients by in vivo [^{89}Zr]Zr-Df-IAB22M2C PET/MRI. **Materials and Methods:** We investigated in total 8 patients with metastasized cancers (5 x malignant melanoma; 1 x choroidal melanoma, 1 x NSCLC and 1 x sarcoma) before (n = 3) or during (n = 5) ICT. Radiolabeling of Df-IAB22M2C with Zr-89 was performed according to Good Manufacturing Practice. Multiparametric PET/MRI was performed 24 h after injection of 74.2±17.9 MBq [^{89}Zr]Zr-Df-IAB22M2C (1.1 - 1.8 mg Df-IAB22M2C) on a Siemens Biograph mMR System (SiemensHealthineers, Erlangen, Germany). We analyzed the [^{89}Zr]Zr-Df-IAB22M2C uptake within the tumors/metastases and primary and secondary lymphatic organs. Results: [^{89}Zr]Zr-Df-IAB22M2C was well tolerated without any noticeable side effects. The PET/MRI acquisitions 24h p.i. of [^{89}Zr]Zr-Df-IAB22M2C revealed an excellent image quality with a rather low background signal due to minor retention in the blood pool and a low unspecific tissue uptake. Interestingly, only one metastasis clearly showed an intense tracer uptake in this patient cohort. Nevertheless, we observed a high interpatient variability in the tracer uptake within the primary and secondary lymphoid organs. Four out of five patients treated with ICT exhibited a relatively high [^{89}Zr]Zr-Df-IAB22M2C uptake in the bone marrow. Two of these four patients as well as two other patients yielded a pronounced [^{89}Zr]Zr-Df-IAB22M2C uptake within non metastatic lymph nodes. Strikingly, a low [^{89}Zr]Zr-Df-IAB22M2C uptake in the spleen compared to the liver (liver/spleen ratio < 10) was associated with cancer progression during ICT in 4 out of the 5 patients. **Conclusion:** Our first clinical experiences revealed the feasibility of [^{89}Zr]Zr-Df-IAB22M2C PET/MRI to assess potential immune-related changes in the metastasis and the primary and secondary lymphatic organs. According to our results we hypothesize that alteration in the [^{89}Zr]Zr-Df-IAB22M2C uptake in primary and secondary lymphoid organs might be associated with the response to ICT. **References:** None

1604

Wednesday, October 20 - Saturday, October 23, 2021

on-demand pool, release on Wednesday, October 20 at 09:00

Mini Course 1: Safety in PET/MRI

OP-0842

Safety in Magnetic Resonance

V. Silva; *Centro Hospitalar Universitário São João, Magnetic Resonance Department, Porto, PORTUGAL.*

OP-0843

Safety in the Hybrid PET/MR System

M. Federspiel; *Copenhagen University Hospital, Rigshospitalet, Dept. of Nuclear Medicine & PET, Copenhagen, DENMARK.*

1605

Wednesday, October 20 - Saturday, October 23, 2021

on-demand pool, release on Wednesday, October 20 at 09:00

Joint Symposium 21 (EANM/AAPM): Numerical and Computer Phantoms

OP-0868

Digital Human Phantoms for Dosimetry in Nuclear Medicine Imaging and Therapy - Historical Development and Recent Advances

W. Bolch; *University of Florida, Advanced Laboratory for Radiation Dosimetry Studies, Gainesville, UNITED STATES OF AMERICA.*

OP-0869

The Use of Computer Phantoms in Nuclear Medicine Imaging

K. Sjögreen Gleisner; *Lund University, Department of Medical Radiation Physics, Lund, SWEDEN.*

OP-0870

Computing Models for Dosimetry, and Beyond

M. Bardiès; *U1194 INSERM/ICM/Montpellier University, Cancer Research Institute of Montpellier, Montpellier, FRANCE.*

1606

Wednesday, October 20 - Saturday, October 23, 2021

on-demand pool, release on Wednesday, October 20 at 09:00

Joint Symposium 22 (EANM/EURAMED): The MEDIRAD Project - Impact on Nuclear Medicine Practice

OP-0873

Introduction - The MEDIRAD Project

G. Flux; *Royal Marsden Hospital and Institute of Cancer Research, Radioisotope Physics, Sutton, UNITED KINGDOM.*

OP-0874

Multi-Centre Clinical Trials Involving Dosimetry of Radioiodine Treatment for Thyroid Cancer

J. Taprogge; *Royal Marsden Hospital and Institute of Cancer Research, Radioisotope Physics, Sutton, UNITED KINGDOM.*

OP-0875

DNA Damage and Repair during Radioiodine Therapy within the MEDIRAD Project

U. Eberlein; *University Hospital Würzburg, Department of Nuclear Medicine, Würzburg, GERMANY.*

OP-0876

Hybrid Imaging in Nuclear Medicine - Results from the MEDIRAD Project

K. Bacher; *Ghent University, Division of Medical Physics, Ghent, BELGIUM.*

1607

Wednesday, October 20 - Saturday, October 23, 2021

on-demand pool, release on Wednesday, October 20 at 09:00

Teaching Session 5: Radiation Detection and Measurement

OP-0845

Radiation Detectors - Which is the Right One for the Task?

A. Mackenzie; *University College London Hospitals, Institute of Nuclear Medicine, London, UNITED KINGDOM.*

OP-0846

The Importance of Quality Control and Instrumentation Performance

R. Freudenberg; *Universitätsklinikum Dresden, Klinik und Poliklinik für Nukleamedizin, Dresden, GERMANY.*

OP-0847

What and When to Measure? Establishing Standard Operating Procedures

T. Kracmerova; *University Hospital Motol, Nuclear medicine, Prague, CZECH REPUBLIC.*

1609

Wednesday, October 20 - Saturday, October 23, 2021

on-demand pool, release on Wednesday, October 20 at 09:00

Cutting Edge Science Track - Featured Session: PET Reconstructions and Corrections

OP-0882

Developments in PET Reconstructions and Corrections

B. Hutton; *University College London (UCL), Institute of Nuclear Medicine, London, UNITED KINGDOM.*

OP-0883

Optimization of reconstruction parameters of a block sequential regularized expectation maximization algorithm for ^{68}Ga-DOTOTAC PET/CT studies

T. Christensen[1], A. L. Nielsen[2], M. H. Vilstrup[2], P. Braad[2]; *[1]Department of Clinical Engineering, Region of Southern Denmark, Esbjerg, DENMARK, [2]Department of Nuclear Medicine, Odense University Hospital, Odense, DENMARK.*

Aim/Introduction: Image reconstruction in nuclear medicine has widely been using the ordered-subset-expectation-maximum (OSEM) algorithm. In recent years, a commercially available block sequential regularized expectation maximization (BSREM) algorithm was introduced to improve reconstruction convergence with suitable noise control. The aim of the present study was to investigate the impact of the BSREM penalizing factor (β) on image noise and activity quantitation, and to investigate if optimizations might facilitate lower scan times or activity administrations in ^{68}Ga-DOTOTAC PET/CT. **Materials and Methods:** The background of a NEMA/IEC torso phantom was filled with a homogeneous aqueous ^{68}Ga-solution at an activity concentration corresponding to that of the liver in clinical ^{68}Ga-DOTOTAC examinations. Spherical inserts (diameters: 10-37 mm) were filled at a 5:1 sphere-to-background activity contrast. Scans were performed on a Discovery MI 25 cm axial field-of-view PET/CT scanner (GE Healthcare) at acquisition times of 10, 20, 35, 60 and 90 seconds/bed and reconstructed using either PSF-OSEM (4 iterations, 17 subsets, 5 mm Gaussian post-filter) or BSREM with β-values in the interval 300-3000. Contrast recovery curves (RC) were calculated for each sphere. Four 50 mm VOIs was placed in the background and image noise compared across scan and reconstruction settings. Six anonymized clinical ^{68}Ga-DOTOTAC-examinations were acquired in listmode at 90 s per bed-position and retrospectively reframed and

reconstructed similar to phantom studies. The image quality in blinded patient and phantom scans were visually graded by two experienced nuclear medicine physicians. Results: BSREM with a β-value of 550 showed similar RC to PSF-OSEM while lower or higher β-values resulted in, respectively, superior or inferior RC's, especially in larger spheres. In phantom studies, the noise at an acquisition time of 90 s was significantly lower for BSREM (β: 550) than for PSF-OSEM. Similar noise levels to 90 s PSF-OSEM, was obtained at 35 s with BSREM with no change to the RC's. Visual grading analysis by the physicians confirmed the results. Diagnostic confidence of BSREM-reconstructed (β: 550) patient studies at acquisition times of 60 s was graded similar to PSF-OSEM studies at 90 s. In both phantom and patient studies, the physicians preferred β-values in the interval 550-800. **Conclusion:** Optimized β-values in BSREM image reconstructions might lead to improved activity quantification and image quality in ^{68}Ga-DOTOTAC PET/CT examinations or be utilized to lower scan times or administered activities compared to standard PSF-OSEM image reconstruction. **References:** none

OP-0884

Optimization of Q.Clear β Penalization Factor for Dynamic PET Imaging

E. Lysvik[1], L. G. Mikalsen[1,2], T. Hjørnevik[1];
[1]Oslo University Hospital, Oslo, NORWAY, [2]Oslo Metropolitan University, Oslo, NORWAY.

Aim/Introduction: Q.Clear, a Bayesian penalized likelihood (BPL) reconstruction algorithm, allows for full convergence of the iterative reconstruction without the added noise found in traditional iterative reconstruction methods. BPL contains a β penalization factor which controls the strength of the penalty term controlling the noise in the image [1]. The goal of this study is to optimize the β penalization factor for time frames of variable lengths as used in dynamic PET imaging. **Materials and Methods:** Seven hollow spheres (volume range: 0.0063-8 mL) in a Flangeless Esser PET Phantom was filled with 23.3 MBq/mL [18F], against a water filled background and scanned on a GE Discovery MI 4 PET/CT system (GE Healthcare) for 25 min in list mode. Data was reconstructed in to 5 sets of 5 repetitions with variable frame duration (10 s, 30 s, 1 min, 2 min, 5 min) using Q.Clear with 18 β-values ranging from 100 to 3500 (30 cm FoV, 256x256x71 matrix). All images were analyzed using PMOD 4.0 (PMOD Technologies). A Volume of Interest (VOI) of predefined size was automatically placed over each sphere where the max average signal was measured for the middle of the five repeated scans. The resolution recovery coefficient (RC) and the coefficient of variance (CV) for the maximum signal was calculated as a measure of accuracy and precision, respectively. Results: For all frame durations and sphere sizes, the RC is overestimated for small β-values (<300). Increasing β beyond 900 does not significantly impact RC for the larger spheres (≥0.5 mL) for frame durations ≥ 30 sec. For smaller spheres (≤0.25 mL) increasing β beyond 900 decreases RC. For the 10-s frame, a larger β-value (>1400) would be more optimal for all lesion sizes. Inter-scan variability (CV) increases with shorter frame durations and smaller sphere sizes. For β=900, the variability increases from <3% to <15% with shorter frame durations for larger spheres, and from <6% to <25% for small spheres. Increasing β to 1400 would increase precision, however, decrease RC for small spheres. **Conclusion:** The choice of β-value depends on frame duration and sphere sizes. In a complex dynamic dataset with variable frame durations, the optimal β-value provides a balance between accuracy and precision for all time frames. We here suggest a β penalization factor of 900 for dynamic PET imaging. **References:** [1] Ross, S. (2014). Q.Clear [White paper]. GE Healthcare.

OP-0885

BSREM for Brain Metastases Detection with [18F]FDG PET/CT in Lung Cancer Patients

V. Liberini[1,2], D. A. Pizzuto[3,2], M. Messerli[2], E. Orita[4,2], H. Grünig[2], A. Maurer[2], C. Mader[2], L. Husmann[2], D. Deandreis[1], F. Kotasidis[5,2], J. Trinckauf[2], A. Curioni[6], I. Opitz[7], S. Winklhofer[8], M. W. Huellner[2];
[1]UNITO - University of Turin, Turin, ITALY, [2]Department of Nuclear Medicine, University Hospital Zürich, University of Zürich, Zürich, SWITZERLAND, [3]Nuclear Medicine Unit, Fondazione Policlinico Universitario A. Gemelli IRCCS, Rome, ITALY, [4]Department of Radiology, Nippon Medical School, 1-1-5 Sendagi, Bunkyo-ku, Tokyo, JAPAN, [5]GE Healthcare, Waukesha, WI, UNITED STATES OF AMERICA, [6]Department of Medical Oncology and Hematology, University Hospital Zurich, University of Zurich, Zürich, SWITZERLAND, [7]Department of Thoracic Surgery, University Hospital Zurich, Zürich, SWITZERLAND, [8]Department of Neuroradiology, Clinical Neuroscience Center, University Hospital Zurich, Zürich, SWITZERLAND.

Aim/Introduction: Novel iterative Bayesian penalized likelihood reconstruction algorithms, such as block sequential regularized expectation maximization (BSREM), have improved the detectability of small-sized, faintly FDG-avid lesions with low TBR, which holds true for a proportion of brain metastases. The aim of our study was to compare block sequential regularized expectation maximization (BSREM) with different β-values and ordered subset expectation maximization (OSEM) algorithms, in order to define which reconstruction algorithm is most appropriate for brain metastases detection in digital [18F]FDG PET/CT in lung cancer patients. **Materials and Methods:** We retrospectively analyzed staging/restaging [18F]FDG PET/CT scans of 40 consecutive lung cancer patients with new brain metastases, confirmed by MRI. PET images were reconstructed using BSREM (β-values of 100, 200, 300, 400, 500, 600, 700) and OSEM. Two independent blinded readers (R1 and R2) evaluated each reconstruction using a 4-point scale for general image quality, noise and lesion detectability.

SUVmax of metastases, brain background, target-to-background ratio (TBR) and contrast recovery (CR) ratio were recorded for each reconstruction. Among all reconstruction techniques, differences in qualitative parameters were analyzed using non-parametric Friedman test, while differences in quantitative parameters were compared using analysis of variances for repeated measures. Finally, Cohen's kappa (k) was used to measure inter-reader agreement. Results: The overall number of BM detected retrospectively with PET/CT were 67, 69, 70, 65, 59, 53, 48, 49 at $BSREM_{100}$, $BSREM_{200}$, $BSREM_{300}$, $BSREM_{400}$, $BSREM_{500}$, $BSREM_{600}$, $BSREM_{700}$ and OSEM, respectively. The mean number of BM detected was 1.63±1.48 (median=1; 0-7) per patient at clinical 18F-FDG PET/CT with $BSREM_{400}$ reconstruction versus 4.42±5.93 (median=2; 1-30; total 177) at MRI. The overall detectability of brain metastases was highest for BSREM200 (R1:2.83±1.17; R2:2.68±1.32) and BSREM300 (R1:2.78±1.23; R2:2.68±1.36), followed by BSREM100, which had lower accuracy owing to noise. The highest median TBR was found for BSREM100 (R1:2.19±1.05; R2:2.42±1.08), followed by BSREM200 and BSREM300. Image quality ratings were significantly different among all different reconstruction ($p<0.001$). The median quality score was higher for BSREM100-300, and both noise and metastases' SUVmax decreased with increasing β-value. Inter-reader agreement was particularly high for the detectability of photopenic metastases and blurring (all $k>0.65$). **Conclusion:** BSREM200 and BSREM300 yielded the best results for the detection of brain metastases, surpassing both BSREM400 and OSEM, typically used in clinical practice. **References:** None

OP-0886

Clinical feasibility and assessment of impact of data-driven respiratory motion-correction studied in 659 whole-body 18F-FDG PET/CT scans

A. H. Dias[1], P. Schleyer[2], M. H. Vendelbo[1], K. Hjorthaug[1], L. C. Gormsen[1], O. L. Munk[1];
[1]Aarhus University Hospital, Aarhus, DENMARK, [2]Siemens Medical Solutions USA, Inc., Knoxville, TN, UNITED STATES OF AMERICA.

Aim/Introduction: In clinical PET scanning, respiratory motion may cause blurred PET images that effectively reduces image resolution and potentially hinders lesion evaluation. Traditional methods for motion compensation require prolonged PET scan time and an external device. In this work, we evaluate the feasibility and clinical impact of a new device-less method for data-driven gating (DDG) that requires no additional scan time. **Materials and Methods:** 659 patients were PET/CT scanned on Siemens Biograph Vision 600 (Siemens Healthineers) with a strain-gauge belt (Anzai Medical Corporation). Three PET images were reconstructed for each study: a standard uncorrected image, a belt-gated motion-corrected image (OncoFreeze with Anzai), and a DDG motion-corrected image (OncoFreezeAI). The technologists registered problems related to the placement of the belt, the quality of the respiratory waveforms, and the reconstruction of gated images. 200 patients with FDG avid lesions in the torso were selected for image evaluation. Images were anonymized and randomized before being analysed by 3 experienced nuclear medicine physicians blinded for gating method. The clinicians were requested to fill out a survey regarding image quality, the presence of motion blurring or artifacts, preference in terms of image quality and readability, and presence of additional clinically relevant information in any of the scans. Inter-user agreement was evaluated by Fleiss-Kappa. Results: NM technologists reported moderate to difficult belt placement in 27% of patients. Physician assessment showed that nearly all images were of diagnostic quality (kappa=1), with only 1 belt-gated reconstruction being unusable. Blurring was reported in about 10% of images (181/1800 assessments), although with only fair inter-rater agreement (kappa=0.24). However, only in 2.5% (15/600) was blurring considered a clinical problem for image evaluation, with good inter-rater agreement (kappa=0.76). Overall, the physicians preferred the gated reconstructions with a slight preference for the DDG reconstructions over the belt-gated reconstructions. In less than 2% of cases did one of the images yield additional diagnostic information, but these findings were mostly of uncertain aetiology and with poor inter-rater agreement (kappa=0.17) **Conclusion:** In this study around one-tenth of images contained motion artefacts which could be compensated by a motion corrected reconstruction. Motion compensation using DDG proved easy to use in clinical practice, DDG images were of good quality and were overall slightly preferred by physicians over belt-gated images. Since the complications of using belt-based gating methods are quite prevalent in clinical routine, DDG is an alternative that should be considered when available. **References:** None

OP-0887

Improvement of myocardial perfusion images with data-driven corrections of motion and respiration: Comparison between retrospective and prospective gating methods

K. Nakajima[1], T. Shibutani[1], F. Massanes[2], H. A. Vija[2], T. Shimizu[2], S. Yoshida[1], H. Yoneyama[1], M. Onoguchi[1], S. Kinuya[1];
[1]Kanazawa University, Kanazawa, JAPAN, [2]Siemens Medical Solutions USA, Hoffman Estate, IL, UNITED STATES OF AMERICA.

Aim/Introduction: Prospective electrocardiographic (ECG) gating has been a common procedure for myocardial perfusion imaging. However, few studies investigated applications of corrections for attenuation, scatter, respiratory motion and tomographic consistency combined with data-driven retrospective gating. The aim of this study was to apply all these corrections using a list-mode data and to compare the image quality of perfusion and function with

conventional SPECT images. **Materials and Methods:** A total of 15 patients (age 73±9 years) with coronary heart disease who underwent myocardial perfusion scan with ^{99m}Tc-MIBI/tetrofosmin at resting condition were studied. The SPECT data were acquired with a dual-detector SPECT using prospective ECG gating (conventional method; 6-degree step-and-shoot, 6.6 mm/pixel, 16 ECG gates, beat length with a 20% window, and Flash3D reconstruction) and list mode data acquisition with X-ray computed tomography (xSPECT cardiac method; continuous rotation, 2.4 mm/pixel, 16 ECG gates). CT-based attenuation and scatter corrections, data-driven respiratory motion corrections were applied to improve tomographic consistency. Images were reconstructed with ordered subset expectation maximization algorithm for both methods. All beat lengths during acquisition were analyzed with histograms. Image quality was visually assessed including segmental count distribution, myocardium to cavity contrast, and perfusion defect. The images were also analyzed quantitatively with profile curves, polar perfusion maps, left ventricular functional parameters (end-diastolic volume [EDV], end-systolic volume ([ESV], ejection fraction [EF], and volume curves) for prospective and retrospective gating. Results: In conventional prospective gating based on acquisition of 20% window allowance, >25% of the beats were rejected in 5 patients, whereas retrospective gating used average of 98% beats for reconstruction. When patients without perfusion defect were analyzed with polar map (n=10), the inferior-to-anterior count ratio was 0.79±0.13 for Flash3D and 1.01±0.08 for xSPECT (p=0.0003).Myocardial walls were thinner and cavity counts were lower in all patients with xSPECT than the Flash3D method. In patients with myocardial infarction, the defect contrast was always higher with the xSPECT images than Flash3D images by 10% (p=0.0096). The mean EDV and ESV were slightly higher in retrospective gating by 4 mL (p=ns) and 6 mL (p=0.017),respectively, and mean EF was lower by 5% compared with prospective gating (p=0.025). The volume curve shape by retrospective gating was improved without fluctuation caused by motion and variation of the beat length. **Conclusion:** Retrospective gating incorporating data-driven motion and respiratory corrections provided higher image resolution, homogeneous distribution in walls, and higher defect contrast compared with conventional imaging. **References:** none

OP-0888

Regularized Reconstruction in Combination with Quiescent Phase Respiratory Gating on a Time-of-Flight PET/MR Scanner for ^{18}F-FDG Examinations in Patients with Esophageal Cancer

N. Korsavidou Hult, S. Kvernby, J. Hedberg, G. Linder, H. Ahlström, T. Bjerner, M. Lubberink;
Uppsala University, Uppsala, SWEDEN.

Aim/Introduction: Block-sequential regularized expectation maximization (BSREM) is an iterative reconstruction method that allows for full convergence, which improves lesion detection and quantitative accuracy in small lesions. This can be of importance in esophageal cancer because of small lymph nodes located near the tumor which can obscure small avid lesions. The aim of this study was to evaluate the quantitative accuracy of BSREM, as well as the combination with quiescent phase respiratory gating (QPRG), in a fully integrated digital PET-MR system in esophageal cancer patients. **Materials and Methods:** 15 single bed position 30-min ^{18} FDG examinations were conducted on a PET-MR system. Images were reconstructed using TF-OSEM with 2 iterations, 28 subsets and a 5 mm post filter, as well as BSREM with penalization factor b of 50, 100, 150 and 300, both without and with quiescent phase gating using QPRG. For static reconstructions, only the first 15 min of data was used, whereas the full 30 min was used for QPRG reconstructions, ensuring similar count statistics. Volumes of interest were drawn over tumors using 41% isocontours and SUVmax was calculated. Signal to noise ratio (SNR) was estimated as tumor SUVmax divided by the standard deviation in a approximately 3 cm diameter spherical VOI over the liver. Statistical differences between OSEM and the different b values with and without QPRG were tested. Results: Background noise levels declined significantly with increasing b factor and were lower than for TOF-OSEM for b > 100. SUVmax values increased significantly compared to TOF-OSEM for b 50 and 100, but decreased for b 150 and 300. SNR increased by 43% for b 300 compared to TOF-OSEM. QPRG resulted in an increase in SUVmax of 5-13% depending on reconstruction method, but also in > 20% increased background noise compared to equivalent static reconstructions, resulting in a decrease in SNR levels by 10-15% compared to equivalent static scans **Conclusion:** Depending on the value of the penalization factor b, BSREM can dramatically improve SNR levels in examinations of esophagus cancer patients. Although QPRG results in higher SUVmax values and likely improves quantitative accuracy, it also increases noise as defined in this work, resulting in lower SNR values. This will be investigated further in clinical observer studies. **References:** none

OP-0889

Prostate cancer imaging with PSMA PET/MRI: The effects of data-driven bulk patient motion and its compensation

B. Bogdanovic, E. Solari, A. Villagran Asiares, S. Schachoff, M. Eiber, W. Weber, S. Nekolla;
Klinikum rechts der Isar der Technischen Universität München, Munich, GERMANY.

Aim/Introduction: The whole-body PSMA PET/MRI a well-known clinical assessment tool in prostate cancer (PCa) diagnostics and therapy. One particularly beneficial application is the biopsy planning PET/MRI protocol used to target PCa lesions for the prospective biopsy. Time and again, however, final PET images acquired from lengthy scans feature spontaneous bulk patient motion, the artefacts of which tend to lead to reduced spatial resolution that could be the reason for some biopsy mismatches with, presumably, very small lesions. Thus, the aim of this study was to assess the effects of and correct for bulk patient motion in a prostate biopsy planning PET/MR protocol. **Materials and Methods:** Twenty-five PCa patients injected with 311±45 MBq of ^{18}F-PSMA were scanned 15 min in a single bed position covering the prostate in the PET/MR scanner. Axial and transversal motion were detected in the single-slice rebinned sinograms using a technique based on centre-of-mass (CoM) tracking every 250 ms. Upon filtering the CoM signal for noise and respiration artefacts, CoM shifts in axial coordinates (1) as well as the (transversal) offsets (2) and projection angles (3) were detected and divided into rapid and gradual displacements. The entire PET raw data were accordingly divided into motion frames based on each of the three parameter dynamics, which were then separately reconstructed and co-registered, thus generating a motion-corrected PET image. SUV_{mean} was computed from the lesions before and after motion correction. Results: Seventeen patient scans featured rapid or gradual movements. On average, 3.5±1.5 frames were considered for each patient, resulting in mean frame duration of 3.60 min (to ensure a sufficiently high SNR, no frame was to be shorter than 3 min). A mean SUV_{mean} change of 11.3% was found, going as high up as 19% in one patient scan. Maximal detected displacement was an axial displacement of 1.3 mm in one patient scan. **Conclusion:** Patient bulk motion is common in lengthy prostate PET examinations and can affect PET quantitation as well as the final representation of lesion size and location.
References: none

OP-0890

Zero-TE vs 2-point Dixon MRI-based Attenuation Correction for Chest FDG PET/MRI with Deep Learning: Comparison of Quantitative Values on Pseudo CT and Reconstructed PET data

M. Nogami[1], H. Matsuo[1], M. Nishio[1], M. Tachibana[1], J. Inukai[1], F. Zeng[1], T. Kurimoto[2], K. Kubo[1], T. Murakami[1];
[1]Kobe University Hospital, Kobe, Hyogo, JAPAN,
[2]GE Healthcare, Hino, Tokyo, JAPAN.

Aim/Introduction: Zero echo-time (ZTE) is a suitable proton-density magnetic resonance imaging (MRI) for bone imaging. Conventional 2-point Dixon is available for four-tissue segmentation in MRI-based attenuation correction (AC) map (MRAC) but has yet to be evaluated whether the Dixon could generate pseudo-computed tomography (pCT) with bone component by unsupervised generative adversarial networks (GANs) in the chest. The purpose was to generate chest pCT from ZTE and Dixon, and to assess the difference in quantitative values of pCT and positron emission tomography (PET). **Materials and Methods:** Three hundred and sixty patients who underwent chest FDG PET/MRI with central-frequency-adjusted ZTE and Dixon were retrospectively analyzed. Unpaired training data included bias-corrected ZTE or Dixon and CT component of PET/CT and were utilized for training unsupervised GANs with a modality independent neighborhood descriptor (U-GAT-IT/MIND) model. A pCT-based AC map with bone ($pCTAC_{ZTE}$ and $pCTAC_{Dixon}$) was created by merging the segmented bone map onto a conventional MRAC and was applied to PET reconstruction on the offline workstation. 38 cases with ZTE and Dixon PET/MRI and PET/CT in the same patients were used to compare between $pCTAC_{ZTE}$, $pCTAC_{Dixon}$ and CT-based AC map (CTAC) and to validate the model for pCT histogram and standardized uptake values (SUV) after AC. Fixed region of interests (ROI) were placed in the spine and the rib on the AC maps for histogram comparison and in the spine and liver on reconstructed PET for mean SUV (SUVmean) comparison. The similarity of the histogram by $pCTAC_{ZTE}$, $pCTAC_{Dixon}$ and MRAC to CTAC was assessed by the correlation coefficients. Wilcoxon's signed rank test were used to compare the correlation coefficients and SUVmeans between AC maps. Results: The correlation coefficients of the histogram for $pCTAC_{ZTE}$ were significantly higher than MRAC in the spine and rib ($p<0.0001$), and those for $pCTAC_{Dixon}$ were higher in the spine ($p<0.0001$). The coefficients for $pCTAC_{ZTE}$ in the rib (0.705±0.229) was significantly higher than that for $pCTAC_{Dixon}$ (0.670±0.230) ($p=0.032$). Spine and liver SUVmean by $pCTAC_{ZTE}$ (1.44±0.37 and 2.45±0.44, respectively) and $pCTAC_{Dixon}$ (1.45±0.38 and 2.45±0.44, respectively) were significantly larger than that by MRAC (1.34±0.37 and, 2.42±0.44, respectively) ($p<0.0001$).

Conclusion: Deep-learning (DL) -based AC map generation with bone component was feasible by both ZTE and Dixon. ZTE shows higher correlation with CT in the histogram of the rib than Dixon. AC maps by DL with both ZTE and Dixon yield higher SUV in the bone and liver to those by conventional MRAC. **References:** none

OP-0891

Influence of Spatial Resolution and SNR of Attenuation Correction Maps on Breast PET images in a Fully-Hybrid PET/MR system

I. Neri[1], M. Emendi[1], C. Canevari[1], A. Savi[1], V. Bettinardi[1], C. Losio[2], R. Menichini[1], N. Ferjani[1], L. Presotto[1], R. Di Micco[3], O. Gentilini[3], M. Picchio[1,4], L. Gianolli[1], P. Scifo[1];
[1]Nuclear Medicine Department, IRCCS San Raffaele Scientific Institute, Milan, ITALY, [2]Radiology Department, IRCCS San Raffaele Scientific Institute, Milan, ITALY, [3]Breast Surgery Unit Department, IRCCS San Raffaele Scientific Institute, Milan, ITALY, [4]Vita-Salute San Raffaele University, Milan, ITALY.

Aim/Introduction: Hybrid PET/MR is an innovative technique that combines morphologic and functional data. Reliable estimation of PET Attenuation Correction (AC) MR-based is a fundamental issue in PET/MRI and the standard method for generating AC-maps is the segmentation of Lava Flex sequence into different tissue classes. Due to the patient's prone position during acquisition and the small FOV in MRI, truncations occur, leading to incomplete AC-maps. In this work, we investigate how AC-maps change, after modifying the acquisition parameters of the AC sequence, and how much the final PET images are affected. **Materials and Methods:** Forty-six women (mean age: 50.44±12.7ys) with breast cancer underwent 18F-FDG PET/MR study using a SIGNA PET/MR (GE Healthcare) scanner. During breast prone PET scan, standard MRAC acquisition (pixel size 1.95mmx1.95mm, matrix 256x128, 120 slices, slice thickness 2.6mm, FOV=50cmx50cm, TR/TE=4ms/1.7ms, NEX=0.7) has been collected. Additionally, four different MRAC sequences were acquired with the same parameters of the standard MRAC (Ref) except for: A) NEX=1; B) matrix 256x256, NEX=1; C) NEX=2; D) matrix 256x256, NEX=2; E) improved dorsal region localized shimming. Using GE offline Duetto Toolbox, six PET reconstructed images were obtained with different MRACs. An expert Nuclear Medicine physician defined the VOIs on the breast lesions and Lymph Nodes (LN). SUV_{max} and SUV_{mean} were calculated together with the percentage differences (SUV_{diff}) and the Root Mean Squared Error (RMSE) between the new set of images and the reference. Results: Eighty-three lesions were identified: 46 breast lesions and 37 active LN. The RMSE calculation suggests that both for AC-maps and PET the highest differences are found between Ref and E) acquisitions (RMSE_AC-map= $3{,}88{\cdot}10^{-2} \pm 9{,}97{\cdot}10^{-3}$, RMSE_PET=$5{,}82{\cdot}10^{-3} \pm 2{,}17{\cdot}10^{-3}$). The lowest differences in average are related to acquisition A) (RMSE_AC-map= $3{,}55{\cdot}10^{-2} \pm 9{,}06{\cdot}10^{-3}$, RMSE_PET= $5{,}26{\cdot}10^{-3} \pm 1{,}73{\cdot}10^{-3}$). Both for breast lesions and for LN, C) shows the highest SUV_{diff} value (2.34±2.08%) while B) the lowest (1.84±1.67%). For axillary LN the highest differences are found in E) (SUV_{diff}=2.47±2.85%), while the lowest are in B) (SUV_{diff}=2.13±2.80%). Nevertheless, none of them is statistically significant. **Conclusion:** From results, spatial resolution and SNR acquisition parameters modifications in MRAC sequences seem to affect SUV_{mean} and SUV_{max} of the corresponding corrected PET images, but not significantly. Using improved shimming on the dorsal side has shown the highest effect on the RMSE both for AC maps and for PET images. **References:** none

OP-0892

A concept for quality assurance of PET/MRI attenuation correction with B_0-maps

***E. Wallstén**, J. A. Lundman, M. Bylund, M. Adjeiwaah, A. Larsson, T. Nyholm;*
Umeå University, Umeå, SWEDEN.

Aim/Introduction: Quantification in PET/MRI relies on attenuation correction estimates based on MR sequences, commonly introduced as substitute CTs (sCTs). The sCT is not a perfect representation of the physical reality, and errors can for example derive from metal implants or misclassification of air. There is yet, to our knowledge, no method that facilitates detection of possible misclassifications or presence of material, e.g. implants, incompatible with the sCT generation algorithm. The patient- induced distortions of the B_0-field can be measured on the MRI scanner or simulated from an sCT (Lundman et al., 2017). This provides two independent quantifications of the B_0- field distortions. In this work, we propose a concept for patient-specific quality assurance of sCTs based on these quantifications. **Materials and Methods:** Patients that underwent radiotherapy in the pelvic region and the brain region were selected. All patients were scanned on a GE Signa PET/MR with an IDEAL-sequence for measurements of the patient-induced distortions of the B_0-field. The pelvic patients underwent T2-weighed MRI-scans for calculation of sCTs with a statistical decomposition algorithm (Wallstén et al., 2020). For the brain region, zero echo time scans (ZTE) were applied for conversion to sCTs with a method under development from GE Healthcare. The sCTs were used for simulation of the patient- induced distortions of the B0-field. From the images of the measured and the simulated B_0- fields, new images of the standard deviations (Stdev-images) were calculated. Stdev-images for simulated and measured B_0-fields were compared with visual interpretation of the squared error images. Results: The method clearly highlights pockets of air present at the time of acquisition that are not transferred to the sCT. Titanium represented in the sCT but not in the patient is also captured clearly. Patients with metal implants are entering the study. In the brain images, nasal cavities and the ear canal are known

problematic areas where bone and air can be misclassified, and these areas are marked by the method. **Conclusion:** The proposed method can identify material differences where there is a clear variation in magnetic susceptibility, which includes many non-body-specific materials and air cavities. **References:** Lundman, J. A. et al. (2017) 'Patient-induced susceptibility effects simulation in magnetic resonance imaging', Physics and Imaging in Radiation Oncology, 1, pp. 41-45. doi: 10.1016/j.phro.2017.02.004. Wallstén, E. et al. (2020) 'Improved PET/MRI attenuation correction in the pelvic region using a statistical decomposition method on T2-weighted images', EJNMMI Physics. EJNMMI Physics, 7(1). doi: 10.1186/s40658-020-00336-5.

1610

Wednesday, October 20 - Saturday, October 23, 2021

on-demand pool, release on Wednesday, October 20 at 09:00

Clinical Oncology Track - Featured Session: Prostate Cancer Therapy

OP-0894

The Visions Beyond VISION

B. Hadaschik; Universitätsklinikum Essen, Urology, Essen, GERMANY.

OP-0895

Minimally Invasive Robot-Assisted PSMA-Guided Salvage Surgery in Recurrent Prostate Cancer Using DROP-IN Radioguidance - A Prospective Feasibility Study

H. de Barros[1], M. N. van Oosterom[1,2], M. L. Donswijk[3], J. J. Hendrikx[3,4], F. W. van Leeuwen[1,2], T. Maurer[5], H. G. van der Poel[1], P. J. van Leeuwen[1];
[1]Department of Urology, Netherlands Cancer Institute-Antoni van Leeuwenhoek Hospital, Amsterdam, NETHERLANDS, [2]Interventional Molecular Imaging Laboratory, Department of Radiology, Leiden University Medical Center, Leiden, NETHERLANDS, [3]Department of Nuclear Medicine, Netherlands Cancer Institute-Antoni van Leeuwenhoek Hospital, Amsterdam, NETHERLANDS, [4]Department of Pharmacy & Pharmacology, Netherlands Cancer Institute-Antoni van Leeuwenhoek Hospital, Amsterdam, NETHERLANDS, [5]Martini-Klinik Prostate Cancer Center and Department of Urology, University Hospital Hamburg-Eppendorf, Hamburg, Hamburg, GERMANY.

Aim/Introduction: Prostate-Specific Membrane Antigen (PSMA)-targeted radioguidance was proven to be valuable for the detection of prostate cancer (PCa) recurrences during open salvage surgery. Rapid extension of robot-assisted surgery has increased the need for robot-compliant radioguided surgery (RGS) techniques. Here we aim to evaluate the feasibility and short-term outcomes of robot-assisted ^{99m}Technetium (^{99m}Tc)-Investigation & Surgery (I&S)-based PSMA-RGS with a DROP-IN gamma probe in patients with recurrent PCa. **Materials and Methods:** This ongoing prospective feasibility study (NCT03857113) included eighteen patients with a biochemical recurrence (PSA ≥ 0.2 ng/ml) after radical prostatectomy or radiotherapy with up to 2 pelvic PCa recurrences (either nodal or local) on PSMA positron emission tomography (PET)/CT. Patients received an intravenous injection of ^{99m}Tc-PSMA I&S (median activity 541 MBq, interquartile range [IQR] 516-579). Approximately 17 hours post-injection, patients received a preoperative single-photon emission CT (SPECT)/CT as a quality control for tracer injection and distribution. Robot-assisted ^{99m}Tc-PSMA-RGS was performed using the tethered DROP-IN gamma probe 21 hours post-injection. The primary endpoint was feasibility to identify and resect PCa recurrences with robot-assisted ^{99m}Tc-PSMA-RGS. Secondary endpoints included the concordance between radioactive ratings of removed specimens and final histopathology results, the frequency of a >50% prostate-specific antigen (PSA) reduction and a complete biochemical response (cBR; PSA < 0.2 ng/ml) 6 weeks postoperatively. Results: At surgery, median age was 69 years (IQR 66-72) and median PSA was 0.97 ng/ml (IQR 0.50-2.34). In total, 19 out of 20 (95%) preoperatively identified lesions on PSMA PET/CT could be localized and resected during robot assisted surgery using the DROP-IN gamma probe (median metastasis size: 8.7 mm, IQR 3.8-15.0). One suspicious lymph node on preoperative PSMA PET/CT could not be pursued intraoperatively due to extensive intestinal adhesions. On a specimen basis, overall diagnostic sensitivity and specificity of ^{99m}Tc-PSMA-RGS was 86% and 100%, respectively. Postoperative PSA measurements were available for 15 men. A >50% PSA reduction and cBR was seen in 10 (67%) and 3 (20%) patients, respectively. No high-grade complications (Clavien-Dindo ≥ grade 3) were observed. **Conclusion:** The preliminary results of this ongoing prospective trial suggest that robot-assisted ^{99m}Tc-PSMA-RGS using the DROP-IN probe is feasible and useful for the intraoperative detection and resection of nodal or local PSMA-avid PCa recurrences. **References:** None

OP-0896

Development of a novel framework for treatment response evaluation using PSMA-PET/CT in patients with metastatic castration-resistant prostate cancer (RECIP): an international multicenter study

A. Gafita[1], I. Rauscher[2], M. Weber[3], B. Hadaschik[3], H. Wang[2], W. R. Armstrong[1], R. Tauber[2], T. R. Grogan[1], J. Czernin[1], M. B. Rettig[1], K. Herrmann[3], J. Calais[1], W. A. Weber[2], M. R. Benz[1], W. P. Fendler[3], M. Eiber[2];
[1]UCLA, Los Angeles, CA, UNITED STATES OF AMERICA, [2]Technical University Munich, Munich, GERMANY, [3]University of Duisburg-Essen, Essen, GERMANY.

Aim/Introduction: Lutetium-177-labeled prostate-specific membrane antigen (LuPSMA) is a novel therapeutic option for men with metastatic castration-resistant prostate cancer (mCRPC). The prognostic role of PSMA-targeted PET/CT for treatment monitoring was not established and standardized criteria for response evaluation are yet to be developed. This study aimed to develop a novel framework for Response Evaluation Criteria In PSMA-imaging (RECIP) and a composite response classification which combines responses by PSA measurements and by RECIP (PSA+RECIP). **Materials and Methods:** This was an international, multicenter, retrospective study. 124 men with mCRPC who underwent LuPSMA and received PSMA-PET/CT at baseline (bPET) and at interim after two cycles of LuPSMA (iPET) were included. PSA changes were recorded at interim from baseline and categorized as: response (≥50% decrease) and progression (≥25% increase) (PCWG3). Pairs of bPET and iPET were interpreted by consensus among three blinded readers for appearance of new lesions. Tumor lesions were segmented and total PSMA-positive tumor volume (PSMA-VOL) was obtained. Appearance of new lesions and changes in PSMA-VOL on iPET were combined to develop RECIP, which was defined as: complete response (RECIP-CR) as absence of any PSMA uptake on iPET; partial response (RECIP-PR) as response in PSMA-VOL without appearance of new lesions; progressive disease (RECIP-PD) as progression in PSMA-VOL and appearance of new lesions; stable disease (RECIP-SD) as any condition which does not qualify for RECIP-CR, -PR, or -PD. PSA+RECIP was defined as: response (PSA response and/or RECIP-PR) and progression (PSA progression and/or RECIP-PD). The primary outcome was the prognostic value of RECIP for overall survival (OS). Secondary outcome was the prognostic ability (by Harrell's C-index) of PSA+RECIP compared to PSA only. Results: The median OS was 13.5 months (95%CI, 11.6-15.4). No patients achieved RECIP-CR. Median OS of RECIP-PD (n=39; 8.3 [95%CI, 7.4-9.2] mo) was significantly shorter compared to RECIP-SD (n=47; 13.1 [95%CI, 9.9-16.3] mo) and to RECIP-PR (n=38; 21.7 [95%CI, 18.7-24.7] mo; p<0.001). PSA+RECIP had superior C-indices in identifying responders and progressors compared to PSA only: 0.65 vs 0.62 (p=0.028) and 0.66 vs 0.63 (p=0.044), respectively. **Conclusion:** PSMA-PET/CT by RECIP is prognostic for OS and can be used as a response biomarker to monitor efficacy of LuPSMA in men with mCRPC. PSA+RECIP is proposed as a novel composite efficacy endpoint for clinical trials of mCRPC. Validation of these findings in a prospective setting is warranted. **References:** none

OP-0897

The prognostic role of inflammatory indices from peripheral blood and clinical factors in metastatic castration-resistant prostate cancer (mCRPC) patients treated with Radium-223 (BIO-Ra-223 study)

M. Donegani[1], S. E. Rebuzzi[2,3], M. Ponzano[1], M. Bauckneht[4], V. Frantellizzi[5], E. Lodi Rizzini[6], M. Mascia[7], V. Lavelli[8], A. Gaudiano[8], M. L. Stazza[9], M. Licari[10], V. Murianni[2,3], A. Signori[1], L. Cavallini[6,11], V. Laghi[6,11], L. Cindolo[12], R. P. Costa[10], A. Spanu[9], G. Rubini[8], F. Monari[6], G. De Vincentis[5], G. Fornarini[2];

[1]Department of Health Sciences (DISSAL), University of Genoa, Genoa, ITALY, [2]Medical Oncology Unit 1, IRCCS Ospedale Policlinico San Martino, Genoa, ITALY, [3]Department of Internal Medicine and Medical Specialties, University of Genoa, Genoa, ITALY, [4]Nuclear Medicine, IRCCS Ospedale Policlinico San Martino, Genoa, ITALY, [5]Department of Radiological Sciences, Oncology and Anatomical Pathology, Sapienza University of Rome, Rome, ITALY, [6]Radiation Oncology, IRCCS Azienda Ospedaliero-Universitaria di Bologna, Bologna, ITALY, [7]Unit of Nuclear Medicine, Spirito Santo Hospital, Pescara, ITALY, [8]Nuclear Medicine Department, University of Bari "Aldo Moro", Bari, ITALY, [9]Unit of Nuclear Medicine, Department of Medical, Surgical and Experimental Sciences, University of Sassari, Sassari, ITALY, [10]Unit of Nuclear Medicine, Biomedical Department of Internal and Specialist Medicine, University of Palermo, Palermo, ITALY, [11]Department of Experimental Diagnostic and Specialty Medicine-Alma Mater Studiorum Bologna University, Bologna, ITALY, [12]Department of Urology, Villa Stuart Private Hospital, Rome, ITALY.

Aim/Introduction: The survival benefit of Radium-223 in mCRPC patients has been observed to be lower in real-life compared to that reported in the ALSYMPCA trial. This is probably due to a suboptimal selection of patients with poor prognostic features in the clinical practice. Consequently, the identification of prognostic factors to select mCRPC patients most likely to benefit from Radium-223 is needed. The multicentre retrospective BIO-Ra-223 study investigates the prognostic role of peripheral blood indices and clinical factors aiming to develop a novel prognostic score for mCRPC patients treated with Ra-223. **Materials and Methods:** Complete blood count was assessed before the first cycle of Radium-223 calculating neutrophil-to-lymphocyte ratio (NLR), derived NLR (dNLR), lymphocyte-to-monocyte ratio (LMR), platelet-to-lymphocyte ratio (PLR), systemic inflammation index (SII). Clinical factors included pre-treatment Eastern Cooperative Oncology Group performance status (ECOG PS), Gleason Score (GS) group, number of bone metastases, alkaline phosphatase (ALP), line of therapy, previous chemotherapy, and the presence of lymphadenopathies. Overall Survival (OS) and the treatment completion rates were the main endpoints. Results: 519 mCRPC patients received Radium-223 in seven Italian centres between 2013 and 2020. The median OS

(mOS) of the entire cohort was 19.9 months. All inflammatory indices and clinical factors (except for GS group) significantly predicted OS at the univariable analyses. In the multivariable ones, all indices, ECOG PS, number of bone metastases and ALP significantly correlated with OS. The multivariable model with NLR (<3.1 vs ≥3.1), ECOG PS (0-1 vs 2-3), number of bone metastases (<6, 6-20, >20) and ALP (<220 vs ≥220) showed the highest c-index (0.711), which was maintained after internal validation (bootstrap re-sampling) (c-index: 0.707). Using the Schneeweiss scoring system, ten categories were identified in 494 pts with complete data and merged in two prognostic groups with distinctive OS: score 0-4 (337 patients, mOS: 27.8 months) and score 5-10 (157 patients, mOS: 9.7 months) (HR 4.03, p<0.001). Group 0-4 was associated with a statistically higher percentage of treatment completion compared to group 5-10, both first three cycles (96% vs 73%; p < 0.001) and all six cycles (75% vs 36%; p < 0.001). **Conclusion:** Although external validation is needed, these preliminary results showed that the BIO-Ra-223 score represents a widely applicable tool in the clinical practice to identify two distinctive prognostic groups of mCRPC patients showing different rates of treatment completion. This novel prognostic score is promising and could potentially improve the patients' selection for Radium-223 treatment. **References:** none

OP-0898

Oncological and postoperative outcome of salvage PSMA-radioguided surgery in recurrent prostate cancer

T. Maurer[1], *S. Knipper*[1], *M. Irai*[1], *D. Köhler*[2], *I. Rauscher*[3], *F. W. van Leeuwen*[4], *P. van Leeuwen*[5], *H. de Barros*[5], *L. Budäus*[1], *T. Steuber*[1], *M. Graefen*[1], *M. M. Heck*[6], *R. Simon*[6], *T. Horn*[6], *M. Eiber*[3];
[1]*Martini-Klinik Prostate Cancer Center, University Hospital Hamburg-Eppendorf, Hamburg, GERMANY,* [2]*Department of Radiology and Nuclear Medicine, Hamburg-Eppendorf, GERMANY,* [3]*Department of Nuclear Medicine, Technical University of Munich, Munich, GERMANY,* [4]*Interventional Molecular Imaging Laboratory, Department of Radiology, Leiden, NETHERLANDS,* [5]*Department of Urology, Antoni van Leeuwenhoek Hospital – the Netherlands Cancer Institute, Amsterdam, NETHERLANDS,* [6]*Department of Urology, Technical University of Munich, Munich, GERMANY.*

Aim/Introduction: Positron-emission tomography (PET) directed against the prostate-specific membrane antigen (PSMA) allows detection of even small and/or atypically localized metastatic prostate cancer (PCa) lesions at low PSA values. In a subset of patients with recurrent oligometastatic localized PCa salvage surgery might be of value. Poor outcomes may partly be due to incomplete resection of metastatic lesions, which occurs in up to two third of salvage lymph node dissections. To facilitate such surgery, we recently introduced the concept of PSMA-targeted radioguided surgery (PSMA-RGS). In this retrospective analysis, we present the outcome and follow-up data in a large patient series obtained from two centers. **Materials and Methods:** We assessed 336 patients treated with PSMA-RGS between 04/2014 and 12/2020, using the radiopharmaceutical ^{111}In-PSMA I&T and ^{99m}Tc-PSMA I&S. All patients included presented with biochemical recurrence after radical prostatectomy (RP) and displayed soft-tissue lesions on PSMA PET. Lesions were resected guided by preoperative PET/CT and/or SPECT/CT images and intraoperative use of a gamma-probe. Biochemical recurrence (BCR)-free survival (PSA < 0.2ng/ml) and therapy-free survival (TFS) were calculated using Kaplan-Meier. Moreover, Clavien-Dindo complications were evaluated. Results: Median age was 67 years (interquartile range [IQR]: 61-71 years) with a median of 55.4 months (IQR: 26.7-94.7 months) between RP and PSMA-RGS. Prior to PSMA-RGS, overall median PSA was 1.1 ng/ml (interquartile range [IQR]: 0.5-2.1 ng/ml). Metastatic soft-tissue PSMA-positive lesions could be removed in 319 (94.9%) patients. During the median follow-up of 20.1 months (IQR: 5.7-37.7 months), 215 patients experienced BCR and 125 patients received further therapy. Median BCR-free survival was 7.8 months (IQR: 5.3-11.3 months) and median TFS was 32.7 months (21.6-43.0 months). At one year of follow-up, BCR-free survival rate was 42.9% and TFS rate was 67.2%. Three patients died during follow-up. 22 (6.5%) suffered from Clavien-Dindo complications grade III-IV within three months from surgery. Limitations are the retrospective design and lack of a control group. **Conclusion:** PSMA-RGS provides a promising tool to guide the surgical resection of soft tissue recurrences identified on PSMA-PET. It presents an opportunity in selected patients with PCa recurrence to prolong BCR-free survival and therefore possibly increase therapy-free survival with an acceptable rate of high grade complications. Further studies are needed to confirm our findings. **References:** none

OP-0899

Pain response and clinical outcomes in patients with metastatic castration-resistant prostate cancer (mCRPC) treated with radium-223 (Ra-223): Final results from a prospective, noninterventional study (PARABO)

H. Palmedo[1], *H. Ahmadzadehfar*[2], *S. Eschmann*[3], *I. Selkinski*[4], *A. Niesen*[5], *J. Schönberger*[6], *V. Barsegian*[7], *K. Liepe*[8], *F. M. Mottaghy*[9], *R. Guan*[10], *J. Pinkert*[11], *S. Buetikofer*[11], *K. Herrmann*[12];
[1]*Institute of Radiology and Nuclear Medicine Kaiser-Passage and PET/CT Centre Johanniter Hospital, Bonn, GERMANY,* [2]*Klinikum Westfalen, Dortmund, GERMANY,* [3]*Marienhospital Stuttgart, Stuttgart, GERMANY,* [4]*Radiomedicum, Frankfurt, GERMANY,* [5]*Diakovere Henriettenstift, Hannover, GERMANY,* [6]*Klinikum Weiden, Weiden, GERMANY,* [7]*Helios Kliniken Schwerin, Schwerin, GERMANY,* [8]*Klinikum Frankfurt (Oder) GmbH Nuklearmedizin, Frankfurt, GERMANY,* [9]*University Hospital RWTH Aachen University, Aachen, GERMANY,* [10]*Bayer HealthCare Pharmaceuticals, Whippany, NJ, UNITED STATES OF AMERICA,* [11]*Bayer AG, Berlin, GERMANY,* [12]*Universitätsklinikum Essen, Essen, GERMANY.*

Aim/Introduction: Ra-223 was associated with significantly prolonged overall survival (OS), reduced symptomatic skeletal events (SSEs) and a favourable safety profile vs placebo in patients with mCRPC in a phase 3 trial. PARABO (NCT02398526), a prospective, single-arm, observational study, assessed pain outcomes in patients with mCRPC who received Ra-223 in real-life clinical practice settings in Germany. **Materials and Methods:** Patients with mCRPC were enrolled in the PARABO study and received Ra-223 between March 2015 and December 2017. The primary outcome was clinically meaningful pain response, ie, a ≥2-point improvement in Brief Pain Inventory short form (BPI-SF) worst pain score. Secondary outcomes included OS, SSEs and safety. Results: In total, 354 patients were evaluable for effectiveness and 356 for safety; 214 patients (60.1%) completed 6 Ra-223 cycles - the most common reasons for early termination were adverse events (AEs; n=43, 12.1%) and disease progression (n=36, 10.1%). At baseline, most patients had Eastern Cooperative Oncology Group performance status 0/1 (73.4%), >6 metastatic lesions (86.5%), ≥1 prior systemic anticancer therapy (68.4%, median 1 prior therapy overall, median 2 prior therapies in the 242 patients with prior therapy), and no or mild pain (68.6%). 52.5% received concomitant bone-health agents (BHAs; denosumab or bisphosphonates). During Ra-223 therapy, 59.3% of 216 patients with baseline worst pain score >1 had a pain response; response was greater in patients who completed 5-6 vs 1-4 cycles of Ra-223 (67.1% [98/146] vs 42.9% [30/70]). Mean BPI-SF component scores improved or were maintained from baseline during Ra-223 treatment. By cycle 6, 24.0% of patients reported 80-100% pain relief. Median OS was 17.2 months (95% CI 15.3-19.0) and was longer in patients who completed 5-6 vs 1-4 cycles (20.7 vs 5.7 months). 25.8% of patients experienced drug-related treatment-emergent AEs (TEAEs), most often anaemia (9.3%), diarrhoea (4.8%), and fatigue (2.8%); 11.2% experienced grade ≥3 drug-related TEAEs. In total, 14.7% of patients experienced SSEs during the study, including new pathologic fractures in 7.3%. **Conclusion:** In this real-life study, 60% of patients had a clinically meaningful pain response. A pain response was achieved in 2/3 of patients who received 5-6 cycles and 42.9% of men who had received 1-4 injections. The overall clinical outcomes with radium-223, including pain response and OS, were consistent with previous observations. Overall safety is comparable to the established safety profile of radium-223. **References:** none

OP-0900

Tumor-to-liver ratio (TLR) by ^{68}Ga-PSMA-11 PET/CT for response assessment and prediction of progression-free survival in patients with mCRPC undergoing ^{177}Lu-PSMA-617 radioligand therapy

F. Khreish[1], M. Wiessner[1], F. Rosar[1], Z. Ghazal[1], A. Sabet[2], S. Maus[1], J. Linxweiler[3], M. Bartholomä[1], S. Ezziddin[1];
[1]Department of Nuclear Medicine , Saarland University, Homburg, GERMANY, [2]2)Dept. of Nuclear Medicine, Frankfurt University, Frankfurt am Main, GERMANY, [3]Department of Urology , Saarland University, Homburg, GERMANY.

Aim/Introduction: To date little is known about the molecular imaging-based response assessment of prostate-specific membrane antigen (PSMA)-targeted radioligand therapy with ^{177}Lutetium (^{177}Lu-PSMA-617 RLT) in metastatic castration-resistant prostate cancer (mCRPC). We analyzed the correlation between molecular imaging-based response and biochemical PSA response in mCRPC patients treated with ^{177}Lu-PSMA-617 and their potential prediction of survival. **Materials and Methods:** Respective analysis of 51 mCRPC patients given two 2 of ^{177}Lu-PSMA-617 RLT at 6-week intervals. ^{68}Ga-PSMA-11 PET/CT was obtained about 2 weeks prior to the first cycle and 4-6 weeks after the second cycle. Response assessment using SUV_{peak} and tumor-to-liver ratio (TLR) was determined by modified PERCIST criteria. PET-derived parameters were compared to biochemical response using serum PSA. Concordance and correlation analyses were performed. Progression-free survival (PFS) in relation to the PET-parameters, patient characteristics and PSA results were analyzed using Kaplan-Meier curves, log-rank test at $p<0.05$ significance, and Cox proportional-hazards modeling. Results: ΔTLR and ΔSUV_{peak} were significantly correlated with ΔPSA ($p<0.001$, each). ΔSUV showed minor inferiority correlation ($r_{SUV} = 0.57$ vs. $r_{TLR} = 0.63$). Median PFS (95% CI) was 8.0 (5.9-10.1). In univariate analysis, responders showing partial remission (PR_{PSA} and PR_{TLR}) had significantly ($p<0.001$, each) longer PFS (median: 10.5 and 9.3 months) than non-responders showing either stable or progressive disease (median: 4.0 and 3.5 months). Response assessment using SUV_{peak} failed to predict survival. In multivariable analysis, TLR was independently associated with PFS ($p<0.001$), as was good performance status ($p=0.002$). Biochemical response assessment using serum PSA was not contributed to regression analysis ($p=0.090$). **Conclusion:** Our study indicates the superiority of using liver-normalized tumor SUV values for molecular response assessment in this setting over mere use of tumor SUV measurements as until yet widely practiced. **References:** none

OP-0901

[^{225}Ac]Ac-PSMA-617 augmented [^{177}Lu]Lu-PSMA-617 RLT in challenging advanced mCRPC patients

F. Rosar[1], J. Krause[1], M. Bartholomä[1], S. Maus[1], T. Stemler[1], I. Hierlmeier[1], J. Linxweiler[2], S. Ezziddin[1], F. Khreish[1];
[1]Department of Nuclear Medicine, Saarland University - Medical Center, Homburg, GERMANY, [2]Department of Urology, Saarland University - Medical Center, Homburg, GERMANY.

Aim/Introduction: The use of the alpha emitter ^{225}Ac in prostate-specific membrane antigen (PSMA)-targeted radioligand therapy (RLT), either as monotherapy or in combination with ^{177}Lu, is a promising therapy approach in patients with metastatic castration-resistant prostate carcinoma (mCRPC). We report on the efficacy and safety profile of [^{225}Ac]Ac-PSMA-617 augmented [^{177}Lu]Lu-PSMA-617 RLT in challenging ^{177}Lu-naive mCRPC patients who were attributed with poor prognosis. **Materials and Methods:** Retrospective analysis of n=15 advanced mCRPC patients attributed with poor prognosis by presence of visceral metastases, high total tumor burden with diffuse bone metastases or short PSA doubling time < 2 months. Biochemical and molecular imaging response was assessed after two cycles of [^{177}Lu]Lu-PSMA-617 RLT with at least one [^{225}Ac]Ac-PSMA-617 augmentation. Biochemical response was evaluated according to PCWG3 criteria using PSA serum value. Molecular imaging-based response was assessed by modified PERCIST criteria using the whole-body total lesion PSMA (TLP) and molecular tumor volume (MTV) derived from [^{68}Ga]Ga-PSMA-11 PET/CT. Furthermore, PSA-based progression-free survival (PSA-PFS), overall survival (OS) and toxicity according to Common Terminology Criteria for Adverse Events (CTCAE) were analyzed. Results: At baseline, mean PSA, MTV and TLP was 667 ± 895 ng/ml, 1291 ± 1210 ml, and 9558 ± 9476 ml x SUV, respectively. After two cycles of [^{177}Lu]Lu-PSMA-617 RLT with at least one [^{225}Ac]Ac-PSMA-617 augmentation, mean PSA, MTV and TLP was 249 ± 398 ng/ml , 887 ± 1047 ml, and 5214 ± 6381 ml x SUV, respectively. Biochemical and molecular imaging-based partial remission was observed in 53.3% (8/15) and 66.7% (10/15) of treated patients, respectively. The median PSA-PFS and OS was 9.1 and 14.8 months, respectively. No serious acute adverse events were recorded. 2/15 patients experienced CTCAE grade 3 anemia. No other CTCAE grade 3 or 4 toxicities were observed. RLT-related xerostomia (CTCAE grade 1/2) was recorded in 2/15 patients. **Conclusion:** Our data revealed high efficacy of [^{225}Ac]Ac-PSMA-617 augmented [^{177}Lu]Lu-PSMA-617 RLT, with a favorable side effects profile, in our challenging cohort of patients. **References:** none

OP-0902

PSMA-targeted photodynamic therapy in surgical prostate tumor samples

Y. Derks[1], M. Schilham[1], S. van Lith[1], M. Sedelaar[1], D. Somford[2], M. Gotthardt[1], D. Löwik[3], S. Lütje[4], S. Heskamp[1], M. Rijpkema[1];
[1]Radboud university medical center, Nijmegen, NETHERLANDS, [2]Canisius Wilhelmina Hospital, Nijmegen, NETHERLANDS, [3]Radboud University, Nijmegen, NETHERLANDS, [4]University Hospital Bonn, Bonn, GERMANY.

Aim/Introduction: Incomplete resection of prostate cancer (PCa) is associated with recurrent disease and worse prognosis. Photodynamic agents have the potential of combining fluorescence-guided surgery with ablation of cancer cells by photodynamic therapy (PDT). PSMA-N064 is a prostate specific membrane antigen (PSMA) ligand coupled to the photosensitizer IRDye700DX. Previously, we have demonstrated that PSMA-N064 allows tumor-specific fluorescence imaging in preclinical studies. Now, we aim to evaluate the potential of PSMA-N064 for targeted PDT (tPDT) on surgically obtained human PCa samples. **Materials and Methods:** So far, 15 PCa patients were included (total 20 patients). Immediately after resection of the prostate, one healthy tissue sample and four tumor samples were collected. Samples were incubated with 0.05 nmol/ml PSMA-N064 in binding buffer (4 hrs, 37°C). After washing, fluorescence flatbed scanning was performed to evaluate ligand uptake. Subsequently, samples were illuminated with 690nm light (50 J/cm^2) using a light-emitting diode. Sixteen hours post illumination, samples were fixed, embedded, sectioned (4µm) and stained (H&E, PSMA). Therapeutic efficacy was evaluated by caspase-3 (apoptosis) and γH2AX (DNA damage) staining. Viability of the treated tumor sample was compared to the treated normal prostate sample and control tumor samples (light only, ligand only or no treatment). Results: Macroscopic fluorescence imaging showed higher accumulation of the ligand in tumor tissue samples (mean fluorescence intensity (MFI) 67,877 ± 24,385) compared with normal prostate tissue samples (MFI 20,586 ± 10,714, $p < 0.001$). Preliminary results of caspase-3 and γH2AX stainings suggest more profound apoptosis and double strand DNA breaks in the treated tumor samples compared to the healthy control sample. However, near-infrared light alone might also induce some degree of apoptosis and DNA double strand breaks compared with the other control tumor samples. Upon completion of all patients (expected June 2020), differences in caspase-3 and γH2AX will be evaluated quantitatively. **Conclusion:** Preliminary results of our study indicate that tumor-targeted PDT using the IRDye700DX-conjugated PSMA-N064 ligand induces apoptosis and double strand DNA breaks in human PCa-samples, suggesting therapeutic efficacy. In the future, this ligand may improve surgical outcome of PCa patients as it allows intraoperative tumor detection and targeted PDT of undetected or unresectable tumor rests. **References:** None

OP-0903

Factors that could predict tumour sink effect: Experience with Lu177 Prostatespecific membrane antigen therapy

M. Tuncel[1], T. Telli[1], M. Tuncalı[1], E. Karabulut[2]; [1]Hacettepe University, Department of Nuclear Medicine, Ankara, TURKEY, [2]Hacettepe University, Department of Biostatistics, Ankara, TURKEY.

Aim/Introduction: Tumour sink effect (TSE) has been defined as; decreased uptake in healthy tissue with increased tumoural sequestration of the radiopharmaceuticals. In this study, we investigated the factors that could predict the tumour sink effect in an extended group of patients who received 177LuProstate-specific membrane antigen (PSMA) therapy due to progressive metastatic castration-resistant prostate cancer (mCRPC). **Materials and Methods:** We have retrospectively analysed the pre-therapy 68Ga-PSMA positron-emission tomography (PET)-computed tomography (CT) and post-therapy planar whole-body scans of patients who received at least two cycles of 7.4 GBq of 177Lu-PSMA therapy due to mCRPC. Age, previous therapies, International Society of Urological Pathology (ISUP) score, and pre-therapy serum tumour marker levels were recorded. Post 177Lu-PSMA therapy images were analysed for TSE. 68Ga-PSMA PET-CT images were used to calculate SUVmax in malignant & healthy tissues, metabolic tumour volume (MTV) and total lesion PSMA index (TLPI). Results: Seventy-eight patients with mCRPCa were referred to 177Lu-PSMA-617 therapy. The cohort's median age was 74 ± 9 years(56-86 years). Among these, 79% had high-grade disease with an ISUP score of 4 or 5. Based on the post-therapy scans, TSE was detected in 22/78 (28.2%) patients. Age, height, weight, body mass index(kg/m2), and body surface area(m2) failed to predict TSE. In univariate analysis, patients with TSE had higher pre-therapy PSA, PSA velocity, and ALP ($p < 0.0001$). In regard to PET parameters, patients with TSE had higher 68Ga-PSMA MTV, 68Ga-PSMA TLPI and lower pretherapy renal SUVmax ($p < 0.0001$), pretherapy liver SUVmax(p:0.01), pretherapy parotid gland SUVmax (p:0.03), and pretherapy parotid gland SUVmean (p:0.038). In the multivariant analysis, 68Ga-PSMA TLPI, pre-therapy PSA, and PSA velocity were found to be statistically significant. When analysed according to Youden index, pretherapy PSA level of 143 ng/ml (sensitivity 0.765 and 0.875), PSA velocity of 251 ng/ml/ year (sensitivity 0.765 and 0.833), and 68Ga-PSMA TLPI of 3019 g (sensitivity 0.765 and 0.875) was found to be the best cut-off points to predict TSE. **Conclusion:** The tumor sink effect was seen in 28.2% of patients. 68Ga- PSMA TLPI, pre-therapy PSA, and PSA velocity was found to be the predictors of TSE. Clinical trials that consider this effect as a part of a dose algorithm may further increase therapeutic efficacy. **References:** none

OP-0904

Tumor regression and response of local tumor in mCRPC patients after two cycles of [^{177}Lu]Lu-PSMA-617

F. Khreish, P. Flach, M. Bartholomä, S. Maus, S. Ezziddin, F. Rosar; Department of Nuclear Medicine , Saarland University, Homburg, GERMANY.

Aim/Introduction: Prostate-specific membrane antigen (PSMA)-targeted radioligand therapy (RLT) with [^{177}Lu]Lu-PSMA-617 is an effective therapy option in patients with metastatic castration-resistant prostate carcinoma (mCRPC). While several studies have shown the efficacy for various sites of metastases, data for local tumor regression (primary tumor or local recurrence) is still lacking. We investigated local tumor regression in mCRPC patients treated with [^{177}Lu]Lu-PSMA-617 RLT. **Materials and Methods:** Retrospective analysis of n=45 mCRPC patients showing a primary tumor or local recurrence on baseline [^{68}Ga]Ga-PSMA-11 PET/CT and treated with at least two cycles of [^{177}Lu]Lu-PSMA-617 RLT. Local tumor regression and response were assessed by [^{68}Ga]Ga-PSMA-11 PET/CT after two cycles PSMA-RLT using molecular imaging parameters (SUV_{max}, total lesion PSMA (TLP)) and modified PERCIST criteria. Results: At baseline mean SUV_{max} and TLP of local tumor was 34 ± 27 and 231 ± 399 ml, respectively. After two cycles PSMA-RLT, mean SUV_{max} and TLP were 23±16 and 86±140 ml; both significantly lower ($p < 0.001$) than at baseline. Median decrease was 25% and 43%, respectively. Based on modified PERCIST criteria on SUV_{max}partial remission (PR), stable disease (SD) and progressive disease (PD) was observed in 20/45 (44%), 21/45 (47%) and 4/45 (9%), respectively. Accordingly, PR, SD, and PD was noted in 27/45 (61%), 12/45 (26%) and 6/45 (13%), respectively based on modified PERCIST criteria on TLP. **Conclusion:** Our data indicate the efficacy of [177Lu]Lu-PSMA-617 RLT for local disease control of prostate cancer, which is encouraging to investigate RLT in earlier stages of disease. **References:** none

OP-0905

^{68}Ga-PSMA-11-PET/MRI radiomics in patients receiving ^{177}Lu-617-PSMA-therapy

W. Roll, P. Schindler, M. Masthoff, R. Seifert, M. Bögemann, M. Weckesser, K. Rahbar; University Hospital Münster, Münster, GERMANY.

Aim/Introduction: ^{177}Lutetium PSMA-617 (Lu-PSMA) therapy is efficacious for the treatment of patients with metastasized castration-resistant prostate cancer (mCRPC) and has gained visibility through ongoing phase III trial. Prior to therapy ^{68}Ga-PSMA-11-PET is used for evaluation of uptake. Data on prediction of therapy outcome and survival out of pretherapeutic imaging parameters is still sparse. In this study the predictive and prognostic value of radiomic imaging features from ^{68}Ga-PSMA-11-PET/MRI are analyzed.

Materials and Methods: 21 patients with mCRPC underwent ^{68}Ga-PSMA-11-PET/MRI before Lu-PSMA therapy. PET positive volume was extracted and transferred to whole body T2-, T1- and contrast enhanced T1-weighted MR-sequences. Radiomic features from PET and MR-sequences were extracted by two independent readers. Stepwise reduction of radiomic features was performed and the balanced dataset was split into a training (70%) and a testing dataset (30%). Single and multiple logistic regression models were used for selecting variables that allow classification of biochemical response (PSA decrease >50%). For their correlation to overall survival (prognostic value) relevant parameters are tested. Results: Eight patients achieved biochemical response (PSA decline >50%) after a median of 3 cycles of Lu-PSMA therapy. Ten PET, T1 post Gd and T2 parameters differentiated well between responders and non-responders. Logistic regression model revealed highest accuracy (AUC = 0.83) for T2 interquartile range for the prediction of biochemical response after Lu-PSMA-therapy. Within the final model patients with biochemical response (p=0.003) and high T2 interquartile range (p=0.038) in pretherapeutic imaging survived significantly longer. **Conclusion:** This pilot study provides first evidence on a potential predicitve and prognostic value of ^{68}Ga-PSMA-11-PET/MRI radiomics prior to Lu-PSMA therapy. Beyond imaging based parameters, blood based biomarkers and previous treatments should be included in future studies. **References:** none

OP-0906

Efficacy and Safety of Lu-177 PSMA in Heavily Pretreated Population with mCRPC; Experience from King Hussein Cancer Center (KHCC) in Jordan

A. Al-Ibraheem, D. Sweedat, F. Anwer, N. Al-Hajaj, Y. Saleh, A. Mohamedkhair, M. Shahait, R. Abu-Hijlih, A. Abufara, S. Salah; King Hussein Cancer center, Amman, JORDAN.

Aim/Introduction: Radioligand prostatic specific membrane antigen (PSMA) by Lu-177 (PRLT) is a promising new radionuclide therapeutic agent for patients with metastatic castration-resistant prostate cancer (mCRPC). The purpose of this retrospective analysis is to evaluate the efficacy and safety of 177Lu-PSMA-617 in KHCC's patients who received this radioligand therapy by analyzing the biochemical response, quality of life, and toxicity profile. **Materials and Methods:** Fifty-nine cycles of PRLT were given in 23 consecutive mCRPC patients who progressed after receiving the best available standard of care treatments. Those patients who received at least one cycle of PRLT were included in this analysis. Mean number of prior therapies = 3.5 (range: 1-7) All patients received prior abiraterone or enzalutamide, 14 received both, 6 received only abiraterone and 3 received only enzalutamide, 6 patients received one agent chemotherapy , 8 patients received two agents chemotherapy, while the other 9 patients received ≥three agents. In addition, 17 patients recieved radiotherapy. All patients had undergone PSA tests before Lu-177 PSMA therapy. Patients were treated with a dose (4-7.4 GBq) of Lu-177 PSMA at eight weeks intervals. 2 patients received 7 cycles, 3 patients received 4 cycles, 6 patients received 3 cycles, 3 patients received 2 cycles and 9 patients received one cycle. PSA response was evaluated at least two weeks after every cycle. According to the Prostate Cancer Workgroup 3 Criteria, a PSA decline ≥ of 50% was considered as a response. On the basis of blood levels, toxicity was categorized using the Common Toxicity Criteria for Adverse Events. Quality of life for pain was assessed for each patient. Results: A decline in PSA of any amount was observed in fourteen out of 23, sixty (61%) of patients after the first cycle. After the last cycle, a decline in PSA ≥50% and of any amount was seen in (40%) and (60%) of patients, respectively. Grade 3-4 hepatotoxicity and nephrotoxicity were observed in two patients (8.6%) for both. Eighteen patients (78 %) reported significant improvement in their pain. **Conclusion:** Lu-177 (PRLT) demonstrated significant activity, achieved significant pain palliation, and had a favorable toxicity profile in this heavily pretreated population with mCRPC. Serum PSA level during PRLT remains a clinically significant predictor of response. Overall survival of those patients will be analyzed in the next stage of this project in light of the biochemical response **References:** none

1611

Wednesday, October 20 - Saturday, October 23, 2021

on-demand pool, release on Wednesday, October 20 at 09:00

TROP Session: Paediatric Nuclear Medicine

OP-0908

Metabolic [^{18}F]FDG-PET parameters at diagnosis are prognostic for overall survival in pediatric sarcoma patients

M. Fosbøl, L. L. Hjalgrim, A. K. Berthelsen, L. Borgwardt; Rigshospitalet, Copenhagen, DENMARK.

Aim/Introduction: Pediatric sarcoma is a heterogeneous group of tumors, where osteosarcoma (OS), Ewing sarcoma (ES) and rhabdomyosarcoma (RMS) constitute the most frequently occurring subtypes. Although [^{18}F]FDG PET/CT is an integrated part of staging and monitoring disease, the prognostic value of metabolic parameters derived from [^{18}F]FDG PET is still debated. The aim of this study was to investigate quantitative pretherapeutic [^{18}F]FDG parameters; metabolic tumor volume (MTV) and total lesion glycolysis (TLG) for primary tumor (P-MTV and P-TLG) and whole-body tumor burden (Total-MTV and Wb-TLG) in regards to prediction of overall survival. **Materials and Methods:** Retrospective, single-center study of children diagnosed with OS, ES or RMS

in the period 2005-2020 with a pretheraputic staging [^{18}F] FDG-PET/CT. Semiautomatic isocontour volumes of interest (VOI) of primary tumor and metastases were drawn using following SUV thresholds: SUV 2.0, SUV 2.5, SUV 40%max, SUV 60%max, SUVmean liver + 1SD and SUVmean liver + 2SD. P-MTV, P-TLG, Total-MTV and Wb-TLG were calculated for each threshold. SUV_{max} and SUV_{peak} were registered in all tumors. Outcome data regarding overall survival were collected from the Danish register of pediatric cancer (DBCR). Results: A total of 66 patients had pretherapeutic [^{18}F]FDG-PET/CT (OS: n=18, ES: n=24, RMS: n=24). Median age was 11 years (range: 0.4-17.8). Five-year overall survival was 74.2 %. In univariate Cox regression analysis of Log2 transformed variables with overall survival as outcome, $Log2\text{-}Total\text{-}MTV_{Liver1SD}$ resulted in the highest hazard ratio (HR) of 1.45 (95% CI:1.15-1.82, P=0.002). $Log2\text{-}Wb\text{-}TLG_{40\%}$, $Log2\text{-}Wb\text{-}TLG_{Liver1SD}$, $Log2\text{-}Total\text{-}MTV_{Liver2SD}$, $Log2\text{-}Wb\text{-}TLG_{Liver2SD}$ were also significantly associated with overall survival (P <0.05). Divided into tumor subgroups the same parameters were also significant predictors of overall survival for RMS patients, where $Log2\text{-}Total\text{-}MTV_{Liver1SD}$ showed a HR of 1.79 (95% CI:1.25-2.57, P=0.002). In OS and ES patients there was a tendency of higher HR in the liver-normalized parameters, however this was not significant. **Conclusion:** This is to our knowledge the first study investigating the prognostic value of total body quantitative [^{18}F]FDG parameters including both primary tumor and metastases in pediatric sarcoma. We found Total-MTV and Wb-TLG based on SUV thresholds normalized to mean liver uptake associated with overall survival, whereas SUV_{max} and SUV_{peak} were not significant predictors. These results suggest that total tumor volume as well metabolic parameters should be combined for optimal risk stratification in these patients. **References:** None

OP-0909

^{18}F-DOPA PET imaging in pediatric brain tumors: clinical applications and radiation safety profile

M. Pizzoferro[1], C. Polito[2], G. Megaro[3], S. Sollaku[4], C. Altini[1], M. F. Villani[1], E. Casciani[4], A. Napolitano[2], D. Ciucci[2], F. Martire[2], S. Donatiello[2], S. Colafati[5], V. Cannatà[2], A. Cacchione[3], M. A. De Ioris[3], A. Mastronuzzi[3], M. C. Garganese[1];
[1]IRCCS Bambino Gesù Children's Hospital, Nuclear Medicine Unit/Imaging Department, Rome, ITALY, [2]IRCCS Bambino Gesù Children's Hospital, Physics Unit, Rome, ITALY, [3]IRCCS Bambino Gesù Children's Hospital, Department of Oncohematology, Rome, ITALY, [4]Private Hospital Pio XI, Nuclear Medicine Unit/Imaging Department, Rome, ITALY, [5]IRCCS Bambino Gesù Children's Hospital, Neuroradiology Unit/Imaging Department, Rome, ITALY.

Aim/Introduction: Brain tumors are the most common cause of death among all childhood, with a wide range of histological classification and survival times. Building on advances in medical imaging and on a heavy clinical need, new applications of ^{18}F-di-idrossi-fenil-alanina (^{18}F-DOPA) PET are under development for the evaluation and management of pediatric brain tumors without defined practice guidelines. Describing our experience, the aim of the present study is to provide a comprehensive assessment of the clinical applications of ^{18}F-DOPA PET in pediatric population affected by brain tumors, considering clinical benefits and radiation safety profile. **Materials and Methods:** We retrospective assessed 49 ^{18}F-DOPA PET scans in 44 pediatric patients referred to our institution for the presence of primary, residual or recurrent brain tumors (25 boys, 19 girls; mean age 8.9 years: 1 month-21 years; mean weight 38Kg: 3-102Kg). ^{18}F-DOPA PET/CT and brain MRI were co-registered to obtain a more accurate PET image evaluation. ^{18}F-DOPA uptake parameters (lesion-to-normal background -T/N- and lesion-to-striatum ratios -T/S) were compared with histology and correlated to WHO tumor grade (Pearson's test). Dosimetric impact of ^{18}F-DOPA PET/CT was assessed considering PET tracer (administered activity: from 37 to 340MBq) and X-ray radiation dose contribution. Results: Histological data were obtained for all patients: 27/44(61%) high-grade glioma, 9/44(20%) low-grade glioma, 8/44(19%) others. Considering WHO tumor grade we had 34(77%) and 10(23%) patient with high and low-grade tumor, respectively. 20 ^{18}F-DOPA-PET were performed for diagnostic purpose, 3 for suspected relapse, 23 for post-treatment evaluation and 3 for follow-up. We observed heterogeneous patterns of ^{18}F-DOPA uptake according to different histological type of tumor, showing a linear correlation between T/S and T/N for both high (r=0.88) and low grade tumors (r=0.94). Mean effective and absorbed doses to brain and bladder from the use of PET tracer resulted respectively: 5.09±2.18 mSv, 2.59±1.11 mGy, 60.48±26.04 mGy(≤ 5 years), 4.47±1.34 mSv, 1.74±0.52 mGy, 63.30±18.92 mGy(>5 -10 years), 5.11±2.00 mSv, 1.78±0.70 mGy, 77.63±30.44 mGy(>10 -15 years), 4.54±1.54 mSv, 1.59±0.54 mGy, 68.10±23.09 mGy(>15 years). Additional radiation dose delivered by low-dose CT was simulated resulting in: 1.31 mSv (≤ 5 years), 1.28 mSv (>5 -10 years), 0.58 mSv (>10 -15 years), 0.74 mSv (>15 years). **Conclusion:** ^{18}F-DOPA PET imaging provides useful information about tumor metabolism in different steps of oncologic disease (diagnosis, residual, relapse and progression), resulting fully justified in terms of radiation exposure. It remains crucial to define ^{18}F-DOPA PET guideline, specifically standardized for pediatric patients. **References:** None

OP-0910

Preliminary investigation into use of 18F-fluorethyltyrosine PET (18F-FET-PET) within the paediatric population for stratification and prognostication of brain gliomas

P. Francis, Y. Shvarts;
Royal Children's Hospital, Melbourne, AUSTRALIA.

Aim/Introduction: 18F-FET-PET is utilised in diagnosis and progression of brain gliomas.We set out to identify the correlation between data derived from image analysis of 18F-FET-PET imaging and histopathology findings in the grading of paediatric brain gliomas. **Materials and Methods:** We retrospectively searched for all historic 18F-FET-PETs since the installation of a positron emission tomography-magnetic resonance imaging (PET-MRI) in April 2016. 10 paediatric patients with brain glioma were identified from this pool as having both undergone 18F-FET-PET imaging and histopathology analysis. Scores for SUVmax, tumour to brain ratio (TBR) and time activity curves (TAC) were derived from imaging. WHO grading (WHO I-IV) and Ki67 index percentages were noted from histopathology reports. Imaging was performed with Seimens Biograph mMR. Derivation of SUVmax and tumour-brain ratio (TBR) was performed using Seimen's Syngovia analysis software. A TAC was also generated for each patient and overall six curve types were identified: rapid uptake with plateau (I), rapid uptake with decline (II), rapid uptake with slow increase (III), rapid uptake (IV), progressive uptake (V), plateau with slow increase (VI). Histopathology grades were acquired from the histopathology reports from either stereotactic biopsy (n=2 (20%)) or surgically resected speci-mens (n=8 (80%)). Results: The mean SUVmax value was greater in the patient pool with a high-grade WHO glioma (4.23 95%CI 0.34-8.11 vs 6.06 95%CI 3.94-8.18). An SUVmax of >4 provided sensitivity (75%) and (specificity 0.33) for predicting high-grade WHO lesions,. The TBR of individual patients was categorised into that of a HG (TBR>2) or a LG lesion (TBR <2). There was a trend to a higher value of WHO grading from histopathology (2.31, 95% CI 0.78-3.83 vs 3.03, 95% CI 2.20-3.83), in the patient group considered to have HG lesions as per TBR. The correlation of a TBR >2 being indicative of a WHO high-grade lesion showed sensitivity (88%) (specificity 0.33). **Conclusion:** FET imaging in paediatric gliomas may provide valuable information in the grading of tumours and help guide decision making in the need for further investigation. Further research needs to be undertaken as there are discrepancies between correlations to WHO grading in this small sample and previous adult studies. **References:** none

OP-0911

Role of 18F FDG PET/CT In Pediatric Malign Melanoma

E. Isik[1], S. Kuyumcu[1], D. Has Şimşek[1], S. Büyükkapu Bay[2], R. Kebudi[2], S. N. Ünal[1];
[1]Istanbul University Istanbul Faculty of Medicine Nuclear Medicine Department, Istanbul, TURKEY, [2]Istanbul University Oncology Institute, Department of Pediatric Hematology-Oncology, Istanbul, TURKEY.

Aim/Introduction: We aimed to evaluate the role of 18F-FDG PET-CT in the detection of pediatric malign melanoma(MM). **Materials and Methods:** In this retrospective study, 17 pediatric patients with MM were evaluated with staging and restaging 18F-FDG PET/CT scan. Patients under the age of 18 with a diagnosis of MM who had staging or restaging FDG imaging were included in the study. Pathological findings, lesion localizations, demographic data and PET/CT findings of the patients were evaluated and compared with pathology reports and clinical follow-up. Localization of the primer disease (head&neck, upper or lower extremities and trunk), presence of lymph node and distant metastasis were evaluated. Results: Seventeen children and adolescents (9females and 8males; mean age,11.2years; age range, 4-17years) were included in the study. Tumor sites were divided into four groups which were lower extremities(n:7), upper extremities(n:4), head and neck(n:2) and trunk(n:4). All, except one patient with mucosal (conjunctival) melanoma, had cutaneous melanoma. Three patients had congenital melanocytic nevi. The average dose administered in F18-FDG PET/CT was 8.6±2.6 mCi. A total of 27 scans were evaluated; 15 for staging and 12 for restaging. While no pathological findings were detected in 17 of the scans, positive findings in 7 and suspicious findings -in terms of disease recurrence in 3 patients were observed. Four in 5 patients with positive findings had positive lymph nodes, only two of them had inflammatory findings proven by pathology. One patient had no FDG uptake but micro-metastases in one lymph node proven by the pathology. All of the suspected FDG uptake areas were lymph nodes and all of them were confirmed as metastatic. Multiple metastatic diseases was observed in 2 patients and these patients died due to progressive disease. The overall sensitivity, specificity, PPV, NPV and accuracy were 87.5%, 84,2%, 70%, 94,1%, 85,1% respectively. In restaging imaging sensitivity, specificity, PPV, NPV and accuracy were 100%, 75%, 100%, 66,6%, 83,3% respectively. **Conclusion:** F18 FDG PET-CT is a very sensitive imaging method in staging and restaging in pediatric MM. Any abnormal metabolic activity detected on FDG PET/CT should be further investigated. In addition, considering its sensitivity, negative predictive value and the advantage of whole-body imaging in a single session, it can be used in the follow-up of the disease in patients with suspected recurrence. **References:** Bay, S.B., Ö. Görgün, and R. Kebudi, Children with malignant melanoma: a single center experience from Turkey. Turk Pediatri Ars, 2020. 55(1): p. 39-45.

OP-0912

[^{18}F]metafluorobenzylguanidine (MFBG) PET-CT vs. [^{123}I]metaiodobenzylguanidine (MIBG) imaging in neuroblastoma patients

A. Samim[1,2], G. A. Tytgat[1], T. Blom[1], A. J. Poot[1,2], N. Tolboom[1,2], A. J. Braat[1,2], M. M. van Noesel[1], M. G. Lam[2], B. de Keizer[1,2]; [1]Princess Máxima Centre for Paediatric Oncology, Utrecht, NETHERLANDS, [2]University Medical Centre Utrecht, Utrecht, NETHERLANDS.

Aim/Introduction: [^{18}F]metafluorobenzylguanidine (MFBG) is a new PET tracer for imaging of neuroblastoma. Compared to standard [^{123}I]metaiodobenzylguanidine (MIBG) imaging, MFBG PET-CT offers the advantages of faster acquisition, single-day imaging, no need for thyroid protection and higher resolution PET imaging. The aim of this study was to evaluate the feasibility and diagnostic performance of MFBG PET-CT compared to MIBG imaging in neuroblastoma patients. **Materials and Methods:** In this prospective pilot study from July 2020 to May 2021, we aimed to perform paired MFBG PET-CT and MIBG scans. All paediatric neuroblastoma patients referred for standard MIBG imaging were eligible for inclusion. MIBG imaging consisted of administration of 4 MBq/kg [^{123}I]MIBG (range 80-300 MBq), followed by next-day whole-body planar scintigraphy (including focused field-of-view SPECT-CT). Patients underwent additional MFBG PET-CT within two weeks, which consisted of administration of 2 MBq/kg [^{18}F]MFBG (range 21-166 MBq), followed by a total-body PET-CT at 60 minutes post-injection. For comparison of skeletal involvement on paired scans, the SIOPEN score was used. Results: Eighteen paired MFBG and MIBG scans were performed in a total of twelve patients (11/12 stage M). No adverse events related to MFBG injection were observed. The majority (8/10) of patients who required sedation for MIBG scanning, were able to undergo MFBG PET-CT without sedation. MFBG had a lower estimated effective dose than MIBG (median 0.84 mSv [IQR 0.76-1.22] vs. 3.22 mSv [IQR 3.03-3.83], respectively). In almost all paired scans, MFBG PET-CT detected equal or more skeletal disease compared to MIBG imaging. On patient-based analysis, MFBG PET-CT detected a higher total SIOPEN score in 67% (12/18), an equal score in 28% (5/18), and a lower score in 5% (1/18) of the scans. On skeletal segment-based analysis, MFBG PET-CT detected a higher SIOPEN score in 27% (58/216), an equal score in 70% (153/216), and a lower score in 3% (5/216) of the segments. In 67% (12/18) of the paired scans MFBG PET-CT detected additional lesions in 38 skeletal segments that were negative on MIBG imaging. **Conclusion:** MFBG PET-CT is considered a safe and feasible imaging method in paediatric neuroblastoma patients. MFBG PET-CT has many practical advantages and provides excellent imaging quality at a lower radiation exposure. Preliminary results indicate that MFBG PET-CT may have higher tumour detection capability compared to MIBG imaging. In almost all cases (95%), MFBG PET-CT detected equal or more skeletal disease. MFBG PET-CT has the potential to replace MIBG imaging in neuroblastoma patients. **References:** None

OP-0913

Evaluating the Diagnostic Utility of 68Ga-DOTA-TOC PET/CT and 18F-FDG-PET PET/CT in High-Risk Neuroblastoma Pediatric Patients Compared to the standard Modalities (123I-MIBG, Bone Scans and CT)

A. Al-Ibraheem[1], U. Al-Rasheed[1], N. Hirmas[2], H. Halalsheh[1], F. Ajlouni[1], A. Mohamedkhair[1], N. Mashahdani,[1], I. Sultan[1]; [1]King Hussein Cancer center, Amman, JORDAN, [2]Universitätsklinikum Essen, Essen, GERMANY.

Aim/Introduction: Accurate staging of pediatric patients with high-risk Neuroblastoma is essential and has implications for prognosis and the treatment plan. The standard modalities for detection of the extent of metastasis in Neuroblastoma patients are 123I MIBG, CT, MRI, and bone scans. 18F-FDG-PET/CT and 68Ga-DOTA-TOC PET/CT scans are new promising modalities for the evaluation of metabolic status and somatostatin receptors, respectively in neuroendocrine tumors. The aim of this study is to find if 18F-FDG-PET/CT and 68Ga-DOTA-TOC PET/CT scan detection rate of Neuroblastoma metastatic lesions are equal to or better than the aforementioned standard modalities and if they may be used as complementary, or even alternative modalities in the staging of patients with high-risk Neuroblastoma. **Materials and Methods:** 8 pediatric patients with a pathologically confirmed high-risk Neuroblastoma (According to COG protocol) who are younger than 12 years of age at the time of initial diagnosis, with no prior systemic therapy, were included. SIOPEN scoring system was used as a comparative scoring system for assessing medullo-skeletal lesions of all the 8 patients who were examined by bone, 123I MIBG, 18F-FDG-PET/CT, and 68Ga-DOTA-TOC PET/CT scans. While soft tissue primary and metastatic lesions were assessed based on visual detection and SUVmax values obtained by both 18F-FDG-PET/CT and 68Ga-DOTA-TOC PET/CT scans and this was compared to the standard modalities, CT scan, and I-123 MIBG scan. Results: In all patients and across all segments assessed through SIOPEN score, 68Ga-DOTA-TOC PET/CT scan scored equal or higher scores than the other scanning modalities regarding the detection of bone metastases. The concordance in a bone scan, 123I MIBG, and 18F-FDG-PET/CT with the 68Ga-DOTA-TOC PET/CT were 18%, 57%, and 71% respectively. Particularly for segment1 (the head), 68Ga-DOTA-TOC PET/CT scan shows significantly higher detection capacity compared to the other modalities. In regard to primary and metastatic soft tissue detection, both18F-FDG-PET/CT and 68Ga-DOTA-TOC PET/CT scans have higher sensitivity (92.9% and 96.2% respectively) compared to the current standard examination modalities, the CT scan (84.6%) and 123I MIBG (65%). **Conclusion:** 68Ga-DOTA-TOC PET/CT

scan shows equal or higher detection capacities for medullo-skeletal metastatic lesions of high-risk Neuroblastoma in the pediatric age group compared to the standard imaging modalities. Both 68Ga-DOTA-TOC PET/CT and 18F-FDG-PET/CT scans superseded the standard imaging modalities (CT and I-123 MIBG) in detecting soft tissue metastatic lesions. Interpretation confidence was higher in 68Ga-DOTA-TOC PET/CT when compared to 18F-FDG-PET/CT due to a higher target to background uptake and SUVmax. values. **References:** none

OP-0914

Evaluation of Physiological Thymic, Splenic and Hepatic Activity with ^{18}F-FDG PET/CT: Exploration of Normal Range among Pediatric Patients

G. April, R. Lambert, S. Turpin;
CHU Ste-Justine, Montreal, QC, CANADA.

Aim/Introduction: ^{18}F-FDG PET/CT applications in pediatrics have increased considerably in the last decade. However, few studies have addressed normal standardized uptake values (SUVs) of referral organs such as mediastinal blood pool (MBP), thymus (T), liver (L), spleen (S) and bone marrow (BM) in children. The purpose of this study is to assess those values in a cohort of pediatric patients. **Materials and Methods:** Two-hundred-eighty-nine ^{18}F-FDG PET/CT scans performed in children staged for non-hematological neoplasms were retrospectively reviewed. Imaging was performed without sedation, following standard protocol and pediatric dosimetry optimization. Quantitative (SUVmax) assessment of metabolic activity was performed using ROIs for MBP, T, L, S and BM, with calculation of L/MBP, L/S, BM/L ratios. One-way ANOVA analysis was performed to evaluate differences in uptake times and blood sugar level (BGL) between age groups. SUVmax mean and standard deviation for each region was obtained, and correlation coefficients (r) in relation with age, weight and body-surface area (BSA) were calculated. Results: Cohort mean age was 12.9 ± 5.24 years. Mean uptake time was 78.5 ± 15.6 minutes and BGL was 4.93 ± 0.79 showing no statistical differences between age groups. Mean MBP SUVmax was 1.26 ± 0.37, increasing with age (r =0.74), weight and BSA (r = 0.82-0.84). Mean liver SUVmax was 1.60 ± 0.48, increasing with age (r=0.74, reaching a plateau around age 14), weight and BSA (r =0.82-0.85). Mean spleen SUVmax was 1.49 ± 0.39, showing little variation with age (r=0.5), weight or BSA (r=0.64-0.69). Mean thymus SUVmax was 2.3 ± 0.6. Thymic activity tended to increase with age, maximized around 11 years-old, followed by involution. Mean bone marrow SUVmax was 1.94 ± 0.54, increasing with age (r=0.64, peak around age 15), weight and BSA (r=0.73-0.75). Liver-to-spleen mean ratio was 1.08 ± 0.22, increasing from 0.5 to reach the unity around 4 years-old and remaining stable afterwards. Bone marrow/liver mean ratio was 1.21 ± 0.27, with negative correlation with increasing age, weight and BSA. **Conclusion:** Referral organs ^{18}F-FDG uptake varies significantly from birth to adulthood following a relationship between SUVmax (MBP, L, S and BM) and weight/BSA, more than with age. Hepatic immaturity in infants may explain lower liver-to-spleen ratio, suggesting that hepatic referral may be less reliable in young children for neoplastic follow-up. Cut-off values for splenic, bone marrow and thymic SUVmax, as well as related ratios for the detection of inflammation/infection remains to be determined. **References:** None

OP-0915

Weight based optimization of administered activity for [^{18}F]FDG PET/CT in paediatric patients

C. P. Cox, D. M. van Assema, F. A. Verburg, T. Brabander, M. Konijnenberg, M. Segbers;
Erasmus MC, Rotterdam, NETHERLANDS.

Aim/Introduction: The role of 2-[^{18}F]fluoro-2-deoxy-D-glucose ([^{18}F]FDG) Positron emission tomography / computed tomography (PET/CT) in children is still expanding. Optimized paediatric dosage regimens are needed to keep the patient's absorbed dose as low as reasonably achievable. The 2020 SNMMI & EANM paediatric guidelines are derived from adult-based protocols, and both focus on absorbed dose without taking image quality into account. At this moment, only a few dedicated paediatric optimization studies are published. The aim of this study is to propose a dedicated optimized paediatric dosage regimen based on patient size that provides constant and clinical sufficient image quality. **Materials and Methods:** Retrospective analysis was performed on 102 children (54 boys and 48 girls) that underwent a diagnostic [^{18}F]FDG PET/CT scan between January 2017 and July 2020. The image quality of the PET scans was measured by the signal-to-noise ratio (SNR) in the liver. The SNR liver was normalized (SNRnorm) for administered activity and acquisition time by assuming Poisson statistics. Curve fitting of SNRnorm with body weight, body height, body mass index, body weight/body height and body surface area was performed using a non-linear 2-parameter model $\alpha\ p^{-d}$ and a linear single parameter model $\alpha\ p^{-0.5}$. Three independent nuclear medicine physicians reviewed the PET scans to establish a SNR that yielded at least moderate or good image quality. An optimal dosage regimen was derived based on this SNR value for the preferred model. Results: Body weight demonstrated the highest coefficient of determination for the non-linear (R^2 = 0.81) and linear (R^2 = 0.80) models. The non-linear model was preferred by the Akaike's corrected information criterion. The review of the nuclear medicine physicians yielded a SNR of 6.5 for at least moderate or good image quality. The optimal dose regimen was based on the non-linear model as a function of body weight with α = 2.23 (95% CI 1.90 to 2.51), d = 0.46 (95% CI 0.43 to 0.50). This dosage regimen showed a reduction of 41% (NACG) and 63% (EANM) for the amount

of administered activity and consequently in absorbed dose compared to the current guidelines. **Conclusion:** An optimal dosage regimen based on body weight and SNR will reduce paediatric absorbed dose with at least 41% for [^{18}F]FDG PET in comparison to the current EANM and SNMMI guidelines at satisfactory image quality. **References:** None

OP-0916

Evaluation of semi-quantitative scoring systems for metaiodobenzylguanidine (mIBG) scans in patients with stage 4 neuroblastoma: A single-center experience

M. Tuncel, M. E. Mavi, P. Ö. Kıratlı;
Hacettepe University, Department of Nuclear Medicine, Ankara, TURKEY.

Aim/Introduction: Semi-quantitative analysis of I-123-MIBG scans with modified-Curie and The International Society of Paediatric Oncology Europe Neuroblastoma(SIOPEN) scoring systems have been shown to be helpful in the evaluation of disease extent and have a prognostic impact in stage-4 neuroblastoma.In this study we aimed to evaluate the diagnostic and prognostic value of these scoring-systems and reveal the additional value of SPECT-imaging in neuroblastoma. **Materials and Methods:** Thirty-one patients, with stage-4 or 4S, diagnosed between January-2009 and December-2020 were included in this retrospective study. Cross-sectional analysis of baseline and post-induction chemotherapy I-123-MIBG scans were performed. Planar and SPECT I-123-MIBG scans were assessed for Curie and SIOPEN scores and correlated with event free survival(EFS). Results: There were 14/31(45%)males and 17/31(55%) females with an age of 50±38 months(7-185 m).SPECT-images were available for14/31(45%)patients in baseline and 15/31(48%)in post-induction chemotherapy.SPECT-scores were higher than planar-scores(mainly in SIOPEN). The mean baseline SIOPEN-planar vs SPECT-scores were,14.4 vs 16,4(p:0,028),and in post-induction these were 1,7 vs2.7(p:0,04). The mean Curie-scores of baseline-planar vs SPECT-scores were:14.4 vs16,4(p:0,028) and in post-induction these were 2,2 vs3,3 respectively(p:0,086). On baseline study analysis,SPECT-imaging demonstrated an additional value in 7/14(%50)patients primarily in region 2 for Curie-scoring, whereas in SIOPEN-scoring it showed an added value in regions 2 and 8, in 4/7(57%) patients.In the post-induction setting,SPECT had additional value in 10/15(67%) patients for Curie and in 9/15(60%) patients for SIOPEN.These were primarily located in region 4 for Curie and in region 2 for SIOPEN.In prediction of EFS; Youndex analysis revealed, a cut-off-value of≥2(AUC:0,746, sensitivity:77,specificity:70) for post induction planar Curie-scoring, wheras≥3 for SPECT(AUC:0,724,sensitivity:71,specificity:58).For SIOPEN planar and SPECT scoring a cut-off of≥2(AUC:0,77 sensitivity:77 specificity:78) was found.Using these cut-off values,3 year EFS was 70% with planar SIOPEN<2, and 30% with SIOPEN score≥2(p:0,022). Likewise with the cut-off values it was 78% for planar-Curies-scores and 28% for SPECT-Curie-scores(p:0.023).Youndex analysis of baseline studies, showed cut-off value of ≥16(AUC:0,697 sensitivity:69,specificity:70) for Curie-planar and ≥18 for Curie SPECT(AUC:0,66, sensitivity:84, specificity:70), where it was≥13(AUC:0,695 sensitivity:81,5 specificity:62) for SIOPEN-planar and≥22 for SIOPEN-SPECT (AUC:0,713 sensitivity:67 specificity:84).Using these thresholds 3 year EFS was %72 for patients with planar SIOPEN<13, wheras %28 for SIOPEN score ≥13-(p:0,023) and for Curie-scoring-system these values were 68% and 28% for planar imaging respectively(p:0.05), **Conclusion:** I-123-mIBG Curie and SIOPEN scores have prognostic value in stage 4 neuroblastoma. SPECT imaging could increase these scores by detecting additional lesions missed by planar imaging. Optimal cut-off points for prognostication should be tested in larger patient series. **References:** none

OP-0917

[^{99m}Tc]Tc-MAG3 Renal Scintigraphy and Relative Renal Function: C-shaped or inferior background ROI?

S. Fontão de Castro[1], I. Próspero[1], I. Lopo[2], L. Violante[1], R. Silva[2,3], T. Saraiva[2,3], H. Duarte[1], G. Costa[2];
[1]Instituto Português de Oncologia do Porto Francisco Gentil, EPE, Porto, PORTUGAL, [2]Centro Hospitalar e Universitário de Coimbra, Coimbra, PORTUGAL, [3]Instituto de Ciências Nucleares Aplicadas à Saúde (ICNAS), Coimbra, PORTUGAL.

Aim/Introduction: Absolute and relative renal function (RRF) are important quantitative parameters, with impact on the clinical decision, that can be easily estimated by dynamic Tc-MAG3 renal scintigraphy. However, many technical aspects, such as the design of the regions of interest (ROI) for background subtraction, are indispensable to ensure the accuracy of both measurements. The aim of this study was to assess which background ROI, C-shaped or inferior, maximizes RRF measurement accuracy. **Materials and Methods:** Retrospective study comprising 56 children referred for [^{99m}Tc]Tc-DMSA and [^{99m}Tc]Tc-MAG3 renal scintigraphy within 1 year, between 01/01/2012 and 28/02/2021, in a general Nuclear Medicine department. Twenty-four patients were excluded due to pyelonephritis (N=7) and surgery (N=5) between scans, single kidney (N=8) and technical issues (N=4). A total of 32 children were included (median age 2.30 [0.15;17.86] years; 53% females [N=17]). Standard dynamic [^{99m}Tc]Tc-MAG3 renal scintigraphy studies were reviewed and both C-shaped and inferior background ROI RRF measurements recorded (integral method). Posterior static [^{99m}Tc]Tc-DMSA renal scintigraphy studies were re-processed and RRF calculated and regarded as the gold standard. C-shaped and inferior background ROI [^{99m}Tc]Tc-MAG3 renal scintigraphy RRF measurements were compared between them and with the gold-standard through paired samples T-test. A Pearson correlation test was also performed. Results: Statistical analysis showed a strong

and statistically significant correlation between the RRF obtained through the 3 different methods used (C-shaped and inferior ROI: Pearson´s coefficient 0.995; C-shaped and DMSA: Pearson´s coefficient 0.967; inferior ROI and DMSA: Pearson´s coefficient 0.969). A statistically significant difference was also found between the RRF obtained through the C-shaped and inferior background ROI in the standard dynamic [^{99m}Tc]Tc-MAG3 renal scintigraphy ($p<0.001$). There were no statistically significant differences between the RRF obtained through [^{99m}Tc]Tc-MAG3 renal scintigraphy, using either background ROI, and [^{99m}Tc]Tc-DMSA. The mean [95% confidence interval] renal function asymmetry (left-right difference) was 9.24% [0.11; 17.84] for [^{99m}Tc]Tc-DMSA, and 10.50% [0.43; 20.89] and 7.54% [-2.01; 17.15] for C-shaped and inferior [^{99m}Tc]Tc-MAG3 renal scintigraphy background ROI, respectively. **Conclusion:** Although a statistically significant difference was found between the RRF obtained through both background ROI [^{99m}Tc]Tc-MAG3 renal scintigraphy, neither significantly differed from the gold standard. This highlights the importance of using the same background subtraction methodology for RRF assessment, despite the preferred background ROI, especially in follow-up studies. Limitations of this study include its retrospective nature, small sample and age dispersion. **References:** None.

1701

Friday, October 22, 2021, 16:50 - 18:20

Channel 1

CME 12: Nuclear Medicine in the Evaluation of Child Abuse

OP-0920

Child Abuse Clinical Features, Diagnosis and Management

H. Yechiam; Meir Medical Center, Emergency Medicine department and Beit Lyn Child Advocacy Center, Kfar Saba, ISRAEL.

OP-0921

Nuclear Medicine in the Diagnosis of Child Abuse

L. Drubach; Boston Children's Hospital, Division of Nuclear Medicine, Boston, UNITED STATES OF AMERICA.

OP-0922

Radiological Aspects of Child Abuse

C. Giraudo; University Hospital of Padova, Institute of Radiology Department of Medicine DIMED, Padua, ITALY.

1702-1

Friday, October 22, 2021, 16:50 - 17:25

Channel 2

Interview with the Expert 12 - Radiopharmacy Running

OP-0926

Interview - Radiopharmacy Running

S. Fanti; University of Bologna, Radiological Sciences - Nuclear Medicine, Bologna, ITALY.

OP-0927

Interview - Radiopharmacy Running

C. Decristoforo; Medical University Innsbruck, Department of Nuclear Medicine, Innsbruck, AUSTRIA.

1704

Wednesday, October 20 - Saturday, October 23, 2021

on-demand pool, release on Wednesday, October 20 at 09:00

Mini Course 2: Case Studies (PET/CT & PET/MRI)

OP-0865

Clinical Cases in PET Radiopharmaceutical Production

G. Kodahl; Aarhus University Hospital, Nuclear Medicine & PET, Aarhus, DENMARK.

OP-0866

Clinical Cases in PET/CT & PET/MR

A. Dias; Aarhus University Hospital, Nuclear Medicine & PET, Aarhus, DENMARK.

1705

Wednesday, October 20 - Saturday, October 23, 2021

on-demand pool, release on Wednesday, October 20 at 09:00

Joint Symposium 23 (EANM/EURADOS): Extremity Dosimetry - It's in Your Hands!

OP-0931

European Survey on Extremity Dosimetry

L. Cunha; IsoPor-Azores, Nuclear Medicine and Molecular Imaging, Azores, PORTUGAL.

OP-0932

Pilot Studies on New Radionuclides

A. McCann; St. Vincent's University Hospital, Department of Medical Physics and Clinical Engineering, Dublin, IRELAND.

OP-0933
Skin Contamination Dose on the Fingers
P. Covens; Vrije Universiteit Brussel, Department of Radiation Protection, Brussels, BELGIUM.

OP-0934
Technologist's Experience
A. Geão; Hospital CUF Descobertas, Nuclear Medicine Department, Lisbon, PORTUGAL.

1706

Wednesday, October 20 - Saturday, October 23, 2021

on-demand pool, release on Wednesday, October 20 at 09:00

Joint Symposium 24 (EANM/ESMO): Theranostics in Thyroid Cancer Beyond Radioactive Iodine

OP-0936
Molecular Basis of Differentiated Thyroid Cancer
S. Leboulleux ; Nuclear Medicine and Endocrine Oncology, Gustave Roussy, Villejuif, FRANCE.

OP-0937
New Targets for Thyroid Cancer in Pre-Clinical Research
C. D'Alessandria; Head of Radiopharmacy, Nuclear Medicine Department, Klinikum rechts der Isar of Technical University of Munich, Munich, GERMANY.

OP-0938
PSMA in Thyroid Cancer
M. Sollini; Humanitas University, Nuclear Medicine Division, Milan, ITALY.

OP-0939
PRRT and Alpha Emitters in Thyroid Cancer
D. Deandreis; Director of Nuclear Medicine Division, Department of Medical Sciences, University of Turin, AOU Città della Salute e della Scienza, Turin, ITALY.

1707

Wednesday, October 20 - Saturday, October 23, 2021

on-demand pool, release on Wednesday, October 20 at 09:00

Teaching Session 6: Animal Models - Technical Considerations and Recommendations

OP-0878
Animal models: general aspects
C. Baun; Department of Nuclear Medicine, The Preclinical Imaging Facility, Odense University Hospital , Odense, DENMARK.

OP-0879
Animal models for the evaluation of radiopharmaceuticals
M. Toussaint; Department of Neuroradiopharmaceuticals, Institute of Radiopharmaceutical Cancer Research in the Helmholtz-Zentrum Dresden-Rossendorf, Leipzig, GERMANY.

OP-0880
How to avoid errors in translation?
T. Balber; Ludwig Boltzmann Institute Applied Diagnostics, Applied Translational Research, Vienna, AUSTRIA.

1709

Wednesday, October 20 - Saturday, October 23, 2021

on-demand pool, release on Wednesday, October 20 at 09:00

Cutting Edge Science Track - TROP Session: Data/Image Processing Based on Deep Learning

OP-0941
Deep Learning for Predicting Gamma-Ray Interaction Positions in LYSO Detector
C. Clement[1], G. Birindelli[1], M. Pizzichemi[2], F. Pagano[2], A. Rominger[1], E. Auffray[2], K. Shi[1];
[1]Inselspital, Bern, SWITZERLAND, [2]CERN, Geneva, SWITZERLAND.

Aim/Introduction: Organoids, stem-cell-derived three-dimensional tissue cultures, find increasing applications ranging from disease modelling to drug discovery and personalized medicine. These growing numbers of uses lead to strong demand for novel measurement capabilities. In this abstract, we present the first steps of developing an on-chip PET system capable of imaging organoids. We evaluate the prediction of gamma-ray interaction positions with deep learning methods trained on simulated data. **Materials and Methods:** For this purpose, we designed a Geant4 based Monte Carlo simulation of a tentative detection block consisting of three continuous LYSO crystals with silicon photomultipliers (SiPMs) added to multiple sides of the detector. We created a large dataset of light pattern images of a wide range of gamma-ray incidence positions and angles with the simulation. The dataset is used to train a Convolutional Neural Network (CNN) based reconstruction network learning the nonlinear relationship between gamma-ray interaction positions and their resulting surface light patterns. We also established a centroiding based baseline method for comparison with the deep learning based approach. Results: We determined the optimal number of surfaces covered with SiPMs needed to predict the interaction position with various experiment runs. The experiments showed that some surfaces encode significantly more information compared to others. The best network achieved a mean average error (MAE) of 1.48 mm

when trained on a dataset of 110,000 samples and tested on 14,000 samples. The baseline method achieves a MAE of 6.16 mm on the same test set. **Conclusion:** The results indicate a promising direction for deep learning based gamma-ray interaction position prediction for a detector block of continuous crystals. With a larger dataset and an extensive hyperparameter search, the results will be further improved. In successive experiments, we will compare the results achieved with simulated data to experimental data. **References:** none

OP-0942

Monte Carlo-based assessment of a deep learning-based method for acceleration of SPECT imaging by generating synthetic projections

J. Leube[1], M. Salas-Ramirez[1], M. Lassmann[1], J. Gustafsson[2], J. Tran-Gia[1];
[1]Department of Nuclear Medicine, University of Würzburg, Würzburg, GERMANY, [2]Department of Medical Radiation Physics, Clinical Sciences Lund, Lund University, Lund, SWEDEN.

Aim/Introduction: Recently, Rydén et al. presented a deep learning-based approach to reduce SPECT/CT acquisition times by generating synthetic projections [1]. They used a small dataset of ~400 SPECT/CT patient acquisitions to train and assess their approach. This study applies an extensive database of simulated SPECT data to investigate this idea under well-defined conditions (e.g., regarding noise) and with considerably more data. **Materials and Methods:** We generated a database of 10,000 simulated low-noise SPECT projection datasets (120 projections, 128x128 matrices, 0.48×0.48 cm^2 pixels, 20% energy window at 208 keV) for a clinical SPECT/CT system using SIMIND [2]. The activity distributions were based on randomly distributed random-shapes placed in a Jaszczak cylinder. Three u-shaped convolutional neural networks (u-nets) based on the fastMRI architecture [3] were trained to generate 60 synthetic projections shifted by 3° with respect to 60 input projections (separated by 6° angular steps). A: 10,000 datasets with Poisson noise, split into 9000/500/500 pairs for training/validation/testing using 40 epochs. B: same as A, but for a different Poisson noise realization. C: 440 datasets randomly selected from A, split into 400/40 pairs for training/validation using 200 epochs (setup of [1]). Training was based on an L1 loss function between simulated (input) and synthetic projections (output). For all 500 test datasets, synthetic projections were generated using the trained u-nets A-C. The similarity between simulated and synthetic projections was assessed based on structural similarity index measure (SSIM) and normalized root mean square error (NRMSE). Results: No significant differences (paired t-test) in SSIM (p=0.196) and NRMSE (p=0.677) were observed between u-nets A and B with SSIM values of 0.982±0.009 (mean±standard deviation) and 0.982±0.008, and NRMSE values of 1.42%±0.23% and 1.44%±0.34%, respectively. In contrast, both SSIM (0.880±0.155) and NRMSE (7.81%±12.31%) were significantly lower/higher for u-net C (p<0.001). In addition, a comparison between synthetic and low-noise projections showed high SSIM (0.997±0.003) and low NRMSE (0.42%±0.13%), demonstrating the method's denoising effect. In contrast, significantly lower SSIM (0.983±0.008, p<0.001) and NRMSE (1.14%±0.16%, p<0.001) values were found between noisy and low-noise projections. **Conclusion:** Rydén et al. showed that deep learning can accelerate SPECT imaging. In continuation, our analysis demonstrates the denoising effect of the methodology. Additionally, we found that a small dataset of ~400 may not be sufficient for reliable training of the u-net. **References:** [1] Rydén et al. (2021), J Nucl Med 62:528-535. [2] Ljungberg et al. (1989), Comput Meth Prog Bio 29:257-72. [3] Zbontar et al. (2018) arXiv:abs/1811.08839.

OP-0943

Deep learning-based time-of-flight (TOF) PET image enhancement of non-TOF PET/CT scans

A. Mehranian[1], S. D. Wollenweber[2], M. D. Walker[3], K. M. Bradley[4], P. Fielding[5], M. W. Huellner[6], F. Kotasidis[7], K. Su[2], R. Johnsen[2], F. Jansen[2], D. R. McGowan[8,3];
[1]GE Healthcare, Oxford, UNITED KINGDOM, [2]GE Healthcare, Waukesha, WI, UNITED STATES OF AMERICA, [3]Oxford University Hospitals NHS FT, Oxford, UNITED KINGDOM, [4]Wales Research and Diagnostic PET Imaging Centre, University Hospital of Wales, Cardiff, UNITED KINGDOM, [5]Department of Radiology, University Hospital of Wales, Cardiff, UNITED KINGDOM, [6]Zurich University Hospital, Zurich, SWITZERLAND, [7]GE Healthcare, Zurich, SWITZERLAND, [8]Department of Oncology, University of Oxford, Oxford, UNITED KINGDOM.

Aim/Introduction: To enhance the quantitative accuracy and diagnostic value of FDG PET images from non-TOF PET scanners, to emulate the performance achieved using TOF, via use of deep convolutional neural networks (DCNN). **Materials and Methods:** List-mode data from 240 FDG PET/CT scans, from six PET centres using Discovery MI PET scanners, with a timing resolution of 385 ps, were split into 210 training, 15 validation and 15 testing sets. The data were reconstructed using the block-sequential regularised expectation-maximisation (BSREM) algorithm with and without TOF, using three sets of regularisation parameters to cover different levels of smoothness (smooth, standard, and sharp). Three DCNN models were trained to map the input non-TOF BSREM images to their corresponding target TOF image. The resulting models were evaluated using the testing set based on standardised uptake value (SUV) quantification in lesions, liver, and lungs. Three experienced readers rated the PET/CT images (75 series) blinded to reconstruction method in a six-point Likert scale based on diagnostic confidence, lesion detectability and overall image quality. Results: Quantitative analysis of 47 identified test lesions showed

that the non-TOF, smooth, standard and sharp DCNN images resulted in -42±17%, -35±22%, -22±24%, -6±24% difference in SUV_{max} compared to target TOF-BSREM image. In lungs, the SUV_{mean} errors, averaged over 5 volumes-of-interest (VOIs) per exam, were 13±12%, 4±9%, 2±12%, 3±10% respectively. In liver, the VOI-based SUV_{mean} errors were 8±5%, 3±4%, 2±4% and 1±4%, respectively. Visual inspection showed that our DCNN improved feature sharpness and convergence (e.g. ribs, vertebra, lesions) towards TOF reconstruction. Clinical readings averaged for all readers and metrics showed that non-TOF, DCNN-smooth, DCNN-standard, DCNN-sharp and TOF images scored 2.9, 3.5, 3.6, 3.9 and 3.5 - in other words, DCNN-enhanced images scored as well as, or better than, TOF images. **Conclusion:** Deep learning-based image enhancement models may provide TOF-equivalent image quality without TOF information. The model is general and could hence be applied to non-TOF images from BGO-based PET/CT scanners. **References:** none

OP-0944

Whole body non-rigid PET/CT alignment using synthetic CT generation from non-attenuation corrected ^{18}F-FDG PET images with a 3D CycleGAN

S. Khushu[1], C. CA von Gall[2], M. Reymann[3], L. Sibille[2], B. Spottiswoode[2], P. Ritt[4], T. Kuwert[4], V. Shah[2];
[1]FAU Erlangen, Erlangen, GERMANY, [2]Siemens Medical Solutions USA, Inc., Knoxville, TN, UNITED STATES OF AMERICA, [3]Siemens Healthcare GmbH, Erlangen, Germany, Erlangen, GERMANY, [4]Clinic of Nuclear Medicine University Hospital Erlangen, Erlangen, GERMANY.

Aim/Introduction: Despite the advancement in hybrid scanner technology, misregistration between PET and AC-CT still presents as a challenge because of patient motion between consecutive independent acquisitions. Similarity based non-rigid registration algorithms may work in some cases but robustness is inherently limited by the orthogonality of PET and CT images. We investigated if a) the visual image quality of the NAC PET-derived synthetic-CT(sCT) created by a 3D cycleGAN was comparable to the original-CT(oCT); b) registered-CT(rCT) images created by deformable registration of oCT to sCT has visually improved alignment with NAC-PET compared to oCT for use in attenuation correction; c) sCT-aligned to oCT in multi-timepoint registration impacts the dice-score coefficient. **Materials and Methods:** A 3D cycleGAN was trained using 30x30x30 cm image patches from 168 NAC-PET and CT datasets (Siemens Biograph Vision and Biograph Truepoint). For qualitative evaluation, an additional 25 test datasets were randomly selected from a 200 independent datasets obtained from two different sites. An expert evaluated the quality of the sCT images on a score of 1 (lowest) to 5 (highest). Non-rigid registration between oCT and sCT resulted in the creation of a registered CT (rCT). The expert evaluated the visual quality of rCT versus oCT images fused to the NAC-PET. A score of 1 (acceptable) was given by nuclear medicine (NM) expert if the visual alignment between NAC-PET/rCT was better than NAC-PET/oCT, or 2 if unacceptable. Quantitative evaluation was performed based upon dice-score coefficient for 10 segmented organs using multi-timepoint registration of 38 patient follow-up scan pairs from the independent dataset pool. Ground truth was defined as the dice-score coefficient from registration of CT2 (CT-from-timepoint2) to CT1 (CT-from-timepoint1). To evaluate the accuracy of a sCT for PET/CT alignment, sCT was registered to CT1, which resulted in sCT*. Next, CT2 was registered to sCT* and dice score coefficient was re-calculated. Results: Qualitative evaluation demonstrated (score:#dataset) (1:6),(2:11),(3:8),(4:0),(5:0). All cases demonstrated acceptable alignment for rCT with the NAC-PET (1:25),(2:0). Even when quality of sCT was poor, the resulting registration image (rCT) was considered acceptable for use in attenuation correction by the NM expert. Dice-coefficient calculation revealed close agreement when CT2 was registered to sCT*: a)CT2-registered-to-CT1(ground truth): 0.875±0.073b)CT2-registered-to-sCT*: 0.837±0.077c) CT2-registered-to-sCT: 0.791±0.080 **Conclusion:** This work offers initial evidence that cycleGAN-generated CT derived from NAC-PET, together with CT-to-CT non-rigid registration, improves CT/NAC-PET alignment irrespective of image quality.A quantitative assessment (dice-score) demonstrated close agreement between sCT and ground truth, supporting the idea of non-inferiority. **References:** none

OP-0945

The clinical performance of artificial intelligence based PET denoising on a digital PET/CT

K. Weyts, C. Lasnon, R. Ciappuccini, J. Lequesne, E. Quak, A. Corroyer Dulmont, B. Clarisse, L. Roussel, S. Bardet, C. Jaudet;
Centre François Baclesse, Caen, FRANCE.

Aim/Introduction: In the context of an increasing PET/CT demand and delay, we aimed to investigate the clinical performance of an artificial intelligence (AI) based PET denoising while simulating a 50% [^{18}F]fluorodeoxyglucose ([^{18}F]FDG) PET acquisition time reduction. **Materials and Methods:** One hundred and ninety four consecutive patients referred for an [^{18}F]FDG PET/CT to our cancer centre were prospectively included in january-february 2021. The original [^{18}F]FDG PET studies (3MBq/kg, 90 sec/bed position, 3D-OSEM + PSF reconstruction-VEREOS SiPM PET/CT, Philips Healthcare) were reconstructed on half of the acquisition time data (45 sec/bed position) and subsequently denoised by Subtle PET® (50% denoised PET), a FDA approved software based on deep learning with deep convolutional neural networks. Five nuclear medicine physicians compared side to side the masked original gold-standard and 50% denoised PET, displayed in a random order. The visual detectability and semi-quantitative parameters of lesions/ foci with

increased FDG uptake (malignant or benign), and of the liver as a reference, were collected. For each PET serie a 3-point global image quality score (IQ) per patient was given (1: bad to 3: good). Results: Of 194 PET examinations, 33 were normal on both PET series. In the remaining 161, 857 FDG avid lesions/foci were visually detected in either of both series. The concordance rate was 98%. There were seven false negative lesions in six patients on the 50% denoised PET, leading to a 99.2% lesion-based sensitivity. False negative lesions showed a small lesion size on CT (median and maximum long axis 5 and 9mm vs 15 and 130mm for true-positive lesions, p≤0.009) and moderate SUL on original PET (median SUL_{peak} 1.5 vs 2.7g/ml, p=0.0008). The per-patient and per-lesion false positive rate on 50% denoised PET was 5% and 1.5%, respectively. Thirteen false positives were found in the liver (n=10), bone (n=2) and spleen (n=1) corresponding to small, indeterminate lesions. Standard and harmonized EARL-1 lesional SUL_{max} , SUL_{peak}, MTV, hepatic SUL_{mean} were not significantly different and highly correlated (intraclass correlation coefficients-ICC ranging from 0.863 (for MTV) to 0.996 (for standard and EARL-1 SUL_{peak} and EARL-1 SUL_{max}) between original and 50% denoised PET. The mean visual IQ was similar in the original and 50% denoised PET, 2.94 vs 2.91. **Conclusion:** This prospective and comparative study demonstrates similar performances of 50% denoised and original [^{18}F]FDG PET in a digital PET/CT. These data may allow reducing PET acquisition time by half in clinical practice. **References:** none

OP-0946

Sparse deep-learning: Multi-organ objective segmentation (MOOSE) for 18F-FDG PET/CT total body datasets

L. Shiyam Sundar, O. Kulturer, B. Fueger, T. Nakuz, D. Kifjak, M. Hacker, T. Beyer;
Medical University of Vienna, Vienna, AUSTRIA.

Aim/Introduction: Total-body PET/CT systems open up the possibility of examining the physiological status of multiple organs simultaneously. There is a rising interest in using 18F-FDG PET for assessing multi-organ interactions in healthy and pathological cohorts. Multi-organ delineation is a prerequisite for quantifying metabolic activity in different organs. However, manual segmentation of organs is untenable both in clinical and research environment. To bypass the manual labour, we have adopted a self-optimizing 3D-unet based deep learning solution for automated multi-organ segmentation from 18F-FDG PET/CT datasets to enable high-throughput data analysis. **Materials and Methods:** A sparse retrospective dataset of 20 whole-body 18F-FDG PET/CT datasets (Siemens TPTV PET/CT system) and their corresponding brain T1-MRI were used for our deep-learning endeavours. We performed a random 50-50 split on the datasets to generate training (n=10) and testing datasets (n=10). Both PET and CT images were synergistically used for segmenting various organs. 18F-FDG PET datasets were used for directly segmenting Hammersmith brain regions and low-dose CT images were used for segmenting non-cranial organs. Four expert clinicians delineated reference segmentations for organs such as thyroid, aorta, inferior vena cava, heart, lung, liver, pancreas, spleen, adrenal glands, kidneys, bladder, and bones (n=13) from the low-dose CT. Simultaneous Truth and Performance Level Estimation algorithm was used for generating ground truth volumes from the segmentations of the different clinicians. To create the reference segmentations of 83 hammersmith atlas brain regions for PET, we normalized the individual subject's T1-MR to the MNI-space. The inverse transforms were used to bring the atlas to the native T1-MR space. Subsequently, the subject's T1-MR was coregistered with their PET, and the transformation matrices were applied to the atlas to generate reference delineations for the PET-brain regions. For training, the PET/CT datasets and their segmentations were passed to the self-adapting 3D u-net. After 1000 epochs, we concluded the training, and the resulting model was used for inferring the test data. Results: The resulting segmentations had a DICE coefficient of >0.85 for all the organs except adrenal glands ~0.70%, therefore attesting to the possibility of generating a whole-body atlas directly from the PET/CT datasets using sparse deep learning. **Conclusion:** Our results indicate that the derived deep-learning model can effectively be used for high-throughput multi-organ analysis in both whole-body and total-body 18F-FDG PET/CT datasets. **References:** None

OP-0947

Evaluation of a Deep Learning Skeleton Segmentation Method to Aid in the Identification of PSMA-positive Bone Lesions

V. Gopalakrishnan, P. Soroush, K. Dong, C. Halley, M. Bending, A. Kruzer, A. S. Nelson;
MIM Software, Beachwood, OH, UNITED STATES OF AMERICA.

Aim/Introduction: Literature demonstrates the utility of prostate-specific membrane antigen (PSMA) with PET/CT imaging to determine the extent of prostate cancer (PCa) and associated metastases. Accurate measurement of tumor burden in bone, the most frequent site of extra-nodal metastases, is fundamentally important in PCa staging and treatment. However, identification of osseous lesions can be arduous for clinicians, especially in patients with advanced disease. Manual and atlas-based skeleton segmentation is especially problematic compared to other organs, due to its size and spatial complexity. In this study, we created a convolutional neural network-based artificial intelligence (AI)

model to automatically segment the skeleton in CT scans. We then quantitatively compared the outputs of the AI model to the outputs of an atlas-based segmentation method. **Materials and Methods:** Whole-body CT scans with clinically generated bone segmentations were reviewed and fine-tuned by trained physicians. These 82 scans and associated segmentions constitute the ground-truth volumes of interest. The AI model was trained with 3D U-Net architecture1 using 57 of the 82 scans. This model generates a probability map which is thresholded to create output segmentations. Simultaneously, a bone atlas was generated with the same 57 scans. Following training, segmentations were generated on the remaining 25 scans by both AI and atlas-based models for testing. Overlap statistics between the ground-truth and each of the test segmentations were calculated. Comparisons of the AI and atlas segmentation overlaps were performed with one-tailed t-tests. Results: The Dice similarity coefficient of the AI-based segmentations (mean: 0.95) was significantly higher than the atlas-based segmentations (mean: 0.77), $p < 0.01$. The Mean Distance to Agreement of the AI-based segmentations (mean: 0.55 mm) was significantly lower than the atlas-based segmentations (mean: 6.18 mm), $p < 0.01$. The maximum Hausdorff distance of the AI-based segmentations (mean: 50.93 mm) was significantly lower than the atlas-based segmentations (mean: 88.93 mm), $p = 0.014$. **Conclusion:** Clinically useful bone segmentation can be performed automatically through the use of an AI-based model. Our results demonstrate superior model accuracy compared to an atlas-based approach. We plan to apply these AI-generated skeleton segmentations to whole body PET lesion segmentations to determine the PCa tumor burden in the bone. **References:** 1. Çiçek Ö, Abdulkadir A, Lienkamp SS, Brox T, Ronneberger O. 3D U-Net: Learning Dense Volumetric Segmentation from Sparse Annotation. ArXiv160606650 Cs. Published online June 21, 2016. http://arxiv.org/abs/1606.06650

OP-0948

Automated analysis of total tumour burden on Ga-68 PSMA PET/CT using convolutional neural network and novel watershed filtering

L. McIntosh[1,2], J.P. Buteau[3], P. Jackson[1,4], J. Ferdinandus[5], N. Hardcastle[1,6,7], R. Franich[2,1], M. Hofman[3,6];

[1]Department of Physical Sciences, Peter MacCallum Cancer Centre, Melbourne, AUSTRALIA, [2]School of Science, RMIT University, Melbourne, AUSTRALIA, [3]Prostate Cancer Theranostics and Imaging Centre of Excellence, Molecular Imaging and Therapeutic Nuclear Medicine, Peter MacCallum Cancer Centre, Melbourne, AUSTRALIA, [4]Molecular Imaging and Therapeutic Nuclear Medicine, Peter MacCallum Cancer Centre, Melbourne, AUSTRALIA, [5]Department of Nuclear Medicine, University Hospital Essen, Essen, GERMANY, [6]Sir Peter MacCallum Department of Oncology, University of Melbourne, Melbourne, AUSTRALIA, [7]Centre for Medical Radiation Physics, University of Wollongong, Wollongong, AUSTRALIA.

Aim/Introduction: Quantitative parameters derived from total tumour burden (TTB) segmentation on 68Ga prostate-specific-membrane-antigen (PSMA) PET/CT are prognostic indicators for patients with metastatic castration-resistant prostate cancer [1]. Standardised reporting guidelines for PSMA-PET have recently been published, however, work remains to improve accuracy and time required for TTB delineation. We aimed to develop a fully automated algorithm to delineate TTB on PSMA PET/CT by implementing convolutional neural network (CNN) followed by a purpose-designed watershed technique to discriminate between physiological and non-physiological uptake. We compared our results to manually defined TTB contours from trained nuclear medicine physicians on 50 unseen cases from a clinical trial. **Materials and Methods:** 48 (31 metastatic, 17 normal) PSMA PET/CT images were used to train CNN to detect physiological uptake with standard uptake value (SUV) > 3 using fused PET and CT images concatenated as input. Model training was implemented using physiological contours that were generated by subtracting clinician-defined TTB from a whole-body SUV > 3 map on fused PET/CT dataset. To improve segmentation accuracy near tissue boundaries, final classification was performed using watershed technique according to local maxima location designated as either malignant or physiological by CNN. Fifty unseen PSMA PET/CT images were used to compare dice score coefficient, PSMAvol, PSMAmean (SUV), and PSMAmax (SUV) metrics derived from the combined model against manually defined clinician contours. Dice score coefficient was used to compare contours, and Bland-Altman mean difference and Pearson's correlation to compare quantitative parameters. Results: In the fifty patient validation cohort, the trained model and watershed filtering achieved a median dice score coefficient of 0.93 (0.30-0.99). PSMAmean, PSMAmax and PSMAvol calculated from manual contour and automated method agreed with a mean difference (Bland-Altman) of -0.2 SUV, -1.6 SUV and -153 mL, and Pearson's correlation of 0.98, 0.97, and 0.93 respectively. Two cases had a dice score of 0.30, both attributed to metastatic disease in the liver. **Conclusion:** We developed a fully automated algorithm to delineate TTB on PSMA PET/CT using CNN and novel watershed filtering. Performance against unseen data was comparable to that of a trained nuclear medicine physician. Implementation may enable routine reporting of whole body quantitative parameters with potential to improve standardisation or reporting, assessment of suitability for LuPSMA therapy and response assessment. **References:** [1] Ferdinandus, et al. (2020). Prognostic biomarkers in men with metastatic castration-resistant prostate cancer receiving [177Lu]-PSMA-617. EJNMMI, 47(10), 2322-2327.

OP-0949

Comparison of Deep Learning-Based Glioma Segmentation Using [^{18}F]FET PET Data With Clinically Established Threshold Methods

B. Kotulski, A. Holzgreve, J. Brosch-Lenz, A. Gosewisch, G. Böning, P. Bartenstein, N. L. Albert, S. Ziegler, L. Kaiser;
Department of Nuclear Medicine, University Hospital, LMU Munich, Munich, GERMANY.

Aim/Introduction: For the diagnosis and treatment planning of gliomas a reliable tumour delineation is required. For [^{18}F]FET PET-based glioma segmentation, a threshold of 1.6 x background intensity is clinically established, but it does not always accurately reflect the real tumour boundaries. In contrast, deep learning segmentation algorithms delineate tumours based on more sophisticated, self-learned features. For model optimization, validation and comparison of both approaches, ground truth activity distributions were generated in this study based on real PET data and used as input for PET simulations. **Materials and Methods:** Lesion-free images were artificially generated from static [^{18}F]FET PET images of 314 glioma patients by mirroring the healthy cerebral hemispheres. Each image was divided into connected sub-volumes with defined intensity ranges. This was followed by the application of a VOI-based partial volume effect correction. Gliomas extracted randomly from [^{18}F]FET PET data were then inserted. Artificial PET images with homogeneous and heterogeneous tumours were simulated from these ground truth data using dPETSTEP [1]. Multiple intensity-thresholds were evaluated and optimized for delineation by maximizing the mean Dice coefficient using repeated 5-fold cross validation based on background intensity (I_{BG}), maximum intensity (I_{Max}), and contrast ($I_{Cont}=I_{Max}-I_{BG}$): $F_{BG}xI_{BG}$, $F_{Max}xI_{Max}$, and $(I_{Max}-I_{BG})xF_{cont}+I_{BG}$. For the deep learning-based approach the segmentation performance of a convolutional neural network [2] was validated accordingly using the same dataset splits. Results: The cross validated Dice coefficients of the optimized thresholds were 0.84 ± 0.16, 0.83 ± 0.20 and 0.86 ± 0.16 for homogeneous and 0.84 ± 0.16, 0.63 ± 0.26 and 0.79 ± 0.19 for heterogeneous tumours for background-, maximum- and contrast-based methods, respectively. Dice coefficients for the clinically established F_{BG} of 1.6 were 0.79 ± 0.23 and 0.78 ± 0.21 for homogeneous and heterogeneous tumours while the deep learning-based approach yielded 0.93 ± 0.08 in both cases. **Conclusion:** When simple threshold-based methods are used, contrast-based segmentation yields best performance for homogeneous tumours and background-based for heterogeneous tumours. Deep learning performs best, for both homogeneous and heterogeneous tumours and might thus be applicable in a wider range of glioma-types. **References:** [1] Haggstrom, I. et al., Dynamic PET simulator via tomographic emission projection for kinetic modeling and parametric image studies. Med Phys, 2016. 43(6): p. 3104-3116.[2] Kamnitsas, K. et al., "Efficient Multi-Scale 3D CNN with Fully Connected CRF for Accurate Brain Lesion Segmentation", Medical Image Analysis, 2016.

OP-0950

Automatic lesion detection and segmentation in PSMA PET/CT images using deep neural networks

Y. Xu[1], I. Klyuzhin[1,2,3], S. Harsini[2], A. Ortiz[1], A. Rahmim[2,3], J. Lavista Ferres[1];
[1]Microsoft AI for Good Research Lab, Redmond, WA, UNITED STATES OF AMERICA, [2]BC Cancer Research Institute, Vancouver, BC, CANADA, [3]University of British Columbia, Vancouver, BC, CANADA.

Aim/Introduction: Recent studies demonstrate that total tumor volume (TV) computed from PET/CT images of cancers especially metastatic prostate cancer is a strong prognosticator of therapy response and survival. To compute TV, it is essential to detect and segment lesions. When performed manually, it requires considerable amount of time and thus cannot be easily implemented in routine clinical practice. In this work, we aim to develop a convolutional neural networks-based framework for lesion detection and segmentation of prostate cancer metastases in PET/CT images, enabling a fully-automated computation of TV. **Materials and Methods:** 526 whole-body PET/CT images of patients with metastatic prostate cancer were available for the study, acquired with the [18F]-DCFPyL radiotracer that targets prostate-specific membrane antigen (PSMA). Transaxial PET image size was 192 x 192 pixels (3.64 x 3.64 mm/pixel), and the CT images were downsampled to the same size. In each image, up to 5 lesions were manually delineated by a nuclear medicine physician, and the mean number of lesions was 2.23 (standard deviation 1.87). 418 images were used for model training, 30 for model validation, and 78 for model testing. Two models were tested: a fully convolutional network with a ResNet-101 backbone and a U-Net. The models were trained to identify lesions for each pair of PET/CT slices. The inputs included the PET/CT slices, the two neighboring slices to incorporate the 3D contextual information, and the axial position of the central slice. Oversampling was used to address class imbalance. Results: Model performance was evaluated using the Intersection over Union (IoU) metric. The ResNet-101 and U-net architectures produced a similar IoU of 0.22-0.25. The mean sensitivity was 0.44 and specificity >0.9999. Both models generalized well to new data, as the validation and test sets produced similar IoU values. At least one lesion was detected correctly in 79.5% of the test images. Near the bladder, 78% of lesions were detected. Away from the bladder, 92% of lesions with SUVmax>5 were detected, with mean Dice score 0.52. Conversely, only 17% of lesions with SUVmax<5 were detected. **Conclusion:** Our results demonstrate the feasibility of performing simultaneous

lesion detection and segmentation using convolutional neural networks. The models were good at detecting lesions with SUVmax>5. Lesion intensity and proximity to bladder were found to be especially important in detectability. Future work will focus on improving the detection of lesions with lower SUV values by designing custom loss functions and data augmentation techniques. **References:** none

OP-0951

Development of a Deep Learning Natural Language Processing Model for Classification of Lung Cancer Radiology Reports

S. Mithun[1,2,3], A. K. Jha[1,2,3], U. B. Sherkhane[1,2], V. Jaiswar[2], A. Nautiyal[2,3], N. C. Purandare[2,3], V. Rangarajan[2,3], A. Dekker[1], L. Wee[1]; [1]Department of Radiation Oncology (Maastro), GROW School for Oncology, Maastricht University Medical Centre+, Maastricht, NETHERLANDS, [2]Tata Memorial Hospital, Mumbai, INDIA, [3]Homi Bhabha National Institute (HBNI), Deemed University, Mumbai, INDIA.

Aim/Introduction: Natural Language Processing (NLP) is useful for cohort building by automatically selecting studies for various conditions. Specifically, for cancer research NLP might be useful as it requires handling of Big Data for information extraction. Manual data retrieval is both cumbersome and impractical from such a huge corpus. Use of NLP tools to extract data from radiology reports can make it less time consuming as well as more effective. In this study, we have developed and compared deep learning models for classification of lung cancer radiology reports from a corpus of radiology reports. **Materials and Methods:** This study was approved by IEC of the hospital as a retrospective study with waiver of consent. 3902 reports radiology reports, including CT and PET/CT of thoracic disease management group were used. Reports were anonymized and cleaned by using a python script where patient identification information was removed and text lowercased. We performed a balanced train-test split(70:30) of the corpus. The training set was used to train 2 different deep learning models using bidirectional long short term memory neural networks. The test set was then used to test the model. The two models used and compared were-1) Bi-LSTM_simple: Input layer, text embedding layer, Bi-LSTM layer(units = 32), output dense layer and 2) Bi-LSTM_dropout: Input layer, text embedding layer, SpatialDropout1D layer (0.5), Bi-LSTM layer (units = 32), GlobalAveragePooling1D layer, GlobalMaxPooling1D layer, concatenate, Dropout layer (0.5), Dense layer (activation="relu"), Dropout layer (0.5), Dense layer (activation="relu"), Dropout layer (0.5), output Dense layer. We calculated and compared the precision, recall, F1 score and accuracy of the models for the test set. We also compared the AUC for both models using predicted class probabilities. Results: The models used for classification, Bi-LSTM_simple had precision=0.91, recall=0.91, F1 score=0.91, accuracy=0.91, AUC using predicted class probabilities=0.963 whereas Bi-LSTM_dropout had precision=0.95, recall=0.95, F1 score=0.95, accuracy=0.94, AUC using predicted class probabilities=0.991. **Conclusion:** Both the deep learning models showed good performance for classification of lung cancer reports from the corpus. However, the overall accuracy was better for the Bi-LSTM model with dropout layers. **References:** None

OP-0952

^{18}F-FDG dynamic brain PET study estimating the arterial plasma radioactivity curve using a convolutional neural network (CNN)

K. Kawauchi, C. Katoh;
Hokkaido University, Sapporo, JAPAN.

Aim/Introduction: Metabolism quantitative images can be calculated from dynamic PET images. However, the conventional method requires arterial blood sampling as an input function and is highly invasive. Therefore, we have developed a method to estimate the input function from a dynamic PET image using a convolutional neural network (CNN). To verify the usefulness of this algorithm, we analyzed ^{18}F-FDG dynamic brain PET images while performing arterial blood sampling. We aimed to make it possible to analyze arterial blood sampling by the conventional method without using blood sampling data on CNN. **Materials and Methods:** 29 patients with neurological diseases (37.3±13.2 years old, 11 males, 18 females) were employed. For each patient, 185MBq of18F-FDG was infused intravenously, arterial blood sampling and dynamic PET data acquisition were performed at 20, 50, 70, 100, 140, 180, 220, 270, 330, 390, 450, 570, 750, 930, 1110, 1350, 1650, 1950, 2250, 2550, 2850, 3150 seconds after infusion. Sampled arterial blood was centrifuged and the radioactivity of the plasma was measured with a well-counter to obtain the time-activity curve of the arterial plasma. The 22-frame PET images in one axial plane was used where internal cervical artery was taken most clearly. Twenty-nine cases were divided into 28 train cases and 1 test case. Using the dynamic PET images of train case and sampled arterial plasma curves, a CNN was trained. The CNN estimated the time-activity curve of the arterial plasma by using dynamic PET images of test case. After that, the estimated value and the measured value were compared. The test cases were changed in order and repeated 29 times (Leave-One-Out method). Results: Estimated time-activity curves by CNN using the Leave-One-Out method had no difference statistically by Wilcoxon test at any sampled time compared with those from sampled arterial plasma. In each test-group patient, 100 ROIs were positioned in the brain and time-activity curves in the brain tissue were obtained and cerebral metabolic rate of glucose (CMRGlc) was calculated. Correlation coefficients between CMRGlc from the sampled blood and from the CNN yielded a significantly high correlation coefficient is 0.97. **Conclusion:** The time-activity curve of arterial plasma

was estimated from ^{18}F-FDG dynamic brain PET data using CNN. CNN has enabled non-invasive measurements of input functions from dynamic PET data. This method is a means that can be applied to various dynamic medical image data quantitative analysis. **References:** none

1710

Wednesday, October 20 - Saturday, October 23, 2021

on-demand pool, release on Wednesday, October 20 at 09:00

Clinical Oncology Track - Featured Session: Neuroendocrine Therapy

OP-0954

What is coming after NETTER-1?

V. Prasad; *Department of Nuclear Medicine, Uniklinik Ulm, Ulm, GERMANY.*

OP-0955

Comparison Between Standard and Intensive Radionuclide Therapy with 177LU-DOTATATE in Advanced Neuroendocrine Tumors: Preliminary Results from a Randomized Phase II Study

I. Grassi[1], *M. Monti*[2], *S. Nicolini*[1], *M. Sansovini*[1], *F. Foca*[2], *M. Caracciolo*[3], *A. Corrado*[1], *L. Fabbri*[4], *V. Fausti*[5], *S. Severi*[1], *G. Paganelli*[1];

[1]*Nuclear medicine department IRST "Dino Amadori" IRCCS Meldola, Meldola Fc, ITALY,* [2]*Unit of Biostatistics and Clinical Trials IRST "Dino Amadori" IRCCS Meldola, Meldola Fc, ITALY,* [3]*Nuclear Medicine Unit, University of Ferrara, Ferrara, ITALY,* [4]*Unit of Biostatistics and Clinical Trials IRST "Dino Amadori" IRCCS, Meldola Fc, ITALY,* [5]*Osteoncology and Rare Tumors Center IRST "Dino Amadori" (IRST), IRCCS, Meldola Fc, ITALY.*

Aim/Introduction: To compare safety and efficacy of intensive (every 5 weeks) versus standard (every 8 weeks) treatment with 177LU-DOTATATE (Lu- PRRT) in advanced gastroenteropancreatic (GEP) and bronchial NETs **Materials and Methods:** Consecutive patients with advanced GEP (G1/G3 Ki67<55%) and bronchial NETs were enrolled in a prospective randomized phase II study from may 2016 till september 2019. Patients were scheduled to receive a total cumulative activity (TCA) of 18.5 or 27.8 GBq of Lu- PRRT according to kidney and bone marrow parameters and were randomly assigned to be treated every 5 weeks or 8 weeks. To assess safety, patients were monitored at each hospitalization, 3-4 weeks after each cycle and once a month every 4 months during follow up according to Common Terminology Criteria for Adverse Events 4.0 (CTCAE). To assess efficacy, anatomic imaging was performed every 4 months since randomization and evaluated according to the Version 1.1 of Response Evaluation Criteria in Solid Tumors (RECIST) Results: One hundred twenty patients were enrolled (one hundred three GEP and seventeen bronchial NETs). Sixty-one received the intensive treatment and fifty-nine the standard one. 4 pateints had grade 3 hematological toxicity (neutropenia, anemia and thrombocytopenia) with no difference between intensive and standard treatment. Other grade 3 toxicities regarded creatinine (one patient), alanine aminotransferase (ALT, one patient), nausea (one patient) and fatigue (four patients). Seventy-nine patients (sixty-eight GEP and eleven bronchial NETs) who did at least 3 cycles were also evaluable for objective response, thirty-six received the intensive treatment and fourty-three the standard ones. Patient showed a comparable disease control rate (DCR) 63.9% vs 69.8% between intensive and standard treatment. Objective response rates (ORR) for intensive and standard treatments were 26,6% vs 11.8% when 27.8 GBq TCA was administered and 21.7% vs 10% when 18.5 TCA was used. (p-value: 0.769). **Conclusion:** Lu-PRRT every 5 weeks is safe and effective when the activity/cycle is personalized according to kidney and bone marrow parameters. In this randomized study, a reduced gap between cycles did not increase toxicity maintaining the same DCR in GEP and bronchial advanced NET tumors. However, preliminary data suggest a tendency toward a better ORR in patients who received intensive treatments. **References:** none

OP-0956

A Phase I/II Clinical Trial for High-dose ^{131}I-meta-iodobenzylguanidine Therapy for High-risk Neuroblastoma Preceding Single Myeloablative Chemotherapy and Hematopoietic Stem Cell Transplantation

H. Wakabayashi[1], *R. Kuroda*[2], *R. Araki*[2], *A. Inaki*[1], *R. Nishimura*[2], *Y. Ikawa*[2], *K. Yoshimura*[3], *T. Murayma*[4], *Y. Imai*[5], *T. Funasaka*[5], *T. Wada*[2], *S. Kinuya*[1];

[1]*Dept of Nuclear Medicine, Kanazawa University Hospital, Kanazawa, JAPAN,* [2]*Dept of Pediatrics, Kanazawa University Hospital, Kanazawa, JAPAN,* [3]*Medical Center for Translational and Clinical Research, Hiroshima University Hospital, Hiroshima, JAPAN,* [4]*Dept of Clinical Development, Kanazawa University Hospital, Kanazawa, JAPAN,* [5]*Innovative Clinical Research Center, Kanazawa University, Kanazawa, JAPAN.*

Aim/Introduction: High-risk neuroblastoma is a childhood cancer with a poor prognosis despite modern multimodality therapy. This Phase I/II study was performed to determine the safety, dose-limiting toxicity (DLT), and efficacy of high-dose ^{131}I-meta-iodobenzylguanidine (^{131}I-mIBG) therapy combined with single high-dose chemotherapy (HDC) and hematopoietic stem cell transplantation (HSCT) for high-risk neuroblastoma patients. **Materials and Methods:** Patients received 666 MBq/kg of ^{131}I-mIBG and, after safety evaluation, single HDC and HSCT. Autologous and allogeneic stem cell sources were accepted. After engraftment, we evaluated

the safety and response. The primary endpoint was DLT. DLT was defined as any adverse events associated with ^{131}I -mIBG that comprised a significant obstacle to subsequent HDC. Secondary endpoints were incidence of adverse event/reaction, hematopoietic stem cell engraftment, and responses according to the Response Evaluation Criteria in Solid Tumors (RECIST) and ^{123}I -mIBG scintigraphy. Results: We enrolled eight high-risk neuroblastoma patients (M/F, 2/6; median age 4 years; range, 1 - 10 years). Although all patients had adverse events/reactions in high-dose ^{131}I-mIBG therapy, we found no DLT. Neuroblastoma patients with newly diagnosed received CEM (carboplatin, etoposide, and melphalan) (n=5) or BuMel (busulfan and melphalan) (n=1) and autologous peripheral blood stem cell transplantation. Two relapsed neuroblastoma patients had BuMel and Killer-cell immunoglobulin-like receptor ligand mismatched cord blood transplantation (KIR-L-MM-CBT). Patients had adverse events and adverse reactions in 100.0% and 25.0% during single HDC and 100.0% and 12.5% during HSCT. No patients had Grade 4 complications except myelosuppression during single HDC and HSCT. All patients were evaluated for response assessment after engraftment. The response rate based on RECIST was 87.5% (7/8) in stable disease (SD) and was 12.5% (1/8) in not evaluated (NE). The scintigraphic response was 62.5% (5/8) in complete response and was 37.5% (3/8) in SD. There was no progression of disease (observation period; median 60 days, range 45 - 86 days) and death (observation period; median 1.6 years, range 0.5 - 2.5 years). **Conclusion:** We showed the safety and efficacy of ^{131}I-mIBG therapy with 666MBq/kg followed by single HDC and autologous or allogeneic SCT in high-risk neuroblastoma patients, and DLT was not observed, indicating that the combination therapy has tolerability. High-dose ^{131}I-mIBG therapy combined with KIR-L-MM-CBT could be performed without severe adverse events in two relapsed neuroblastoma patients. Further studies are needed to elucidate the long-term efficacy of the therapy protocol incorporating of ^{131}I-mIBG therapy. **References:** none

OP-0957

Health-related quality of life during and the years after peptide receptor radionuclide therapy in patients with neuroendocrine tumors

C. Andersson[1], P. Hellman[1], D. Granberg[2], P. Lagergren[2], E. Thiis-Evensen[3], A. Sundin[1], K. Edfeldt[1];
[1]Dept. of Surgical Sciences, Uppsala University, Uppsala, SWEDEN, [2]Dept. of Molecular Medicine and Surgery, Karolinska Institutet, Stockholm, SWEDEN, [3]Dept. of Gastroenterology, Oslo University Hospital, Oslo, NORWAY.

Aim/Introduction: The aim of this study was to assess health-related quality of life (HRQoL) in patients' with neuroendocrine tumors (NETs) at cycle one and four during peptide receptor radionuclide therapy (PRRT). A further aim was to examine patients perceived HRQoL some years after completing PRRT. **Materials and Methods:** HRQoL was assessed by the European research and treatment of cancer quality of life questionnaire core-30 (EORTC QLQ-C30) and tumor-specific module QLQ-GINET.21 at baseline (cycle one) and cycle four of PRRT in 204 patients (men n=134, women n=70). The diagnosis were SI-NETs (n=124), P-NET (n=45) and other NETs (n=35). Patients' perceived HRQoL was compared with a matched control cohort. HRQoL for the follow-up cohort was measured 1-4 years (n=26) and 4-8 years (n=19) after PRRT. Results: During PRRT HRQoL improved for all patients regarding global quality of life, role, social and emotional functioning together with symptom relief for fatigue, nausea/vomiting, pain, insomnia, appetite loss, diarrhoea and treatment related worries. Patients with normal weight and <65 years experienced more improvement than those with overweight and >65 years. In the follow-up cohort (1-4 years), several aspects regarding HRQoL increased. However, 4-8 years after PRRT there was a decrease for i.e. physical and social functioning, fatigue and disease related worries ($p \leq 0.05$). **Conclusion:** PRRT improve HRQoL in patients with NET. However, older patients and those with overweight may experience lower HRQoL. The improved HRQoL seems to persist a few years after PRRT and then decrease. The study results may be helpful to improve the patient care for patients with NETs. The long-term HRQoL the years following PRRT needs to be further investigated in larger patient cohorts. **References:** None

OP-0958

Survey of Challenges in Access to Diagnostics and Treatment for Neuroendocrine Tumor (NET) Patients (SCAN): PRRT in the Treatment of Neuroendocrine Tumor (NET) Patients

S. Dureja[1], T. Kolarova[2], M. McDonnell[3], D. Van Genechten[4], C. Bouvier[5], E. Gellerman[6], D. O'Toole[7], H. Singh[8], J. Chen[9], J. Howe[10], S. Singh[11], M. Pavel[12], C. Rodien-Louw[13], S. Leyden[14], R. Hicks[15];
[1]SMH Cancer Centre, New Delhi, INDIA, [2]International Neuroendocrine Cancer Alliance (INCA), Boston, MA, UNITED STATES OF AMERICA, [3]NET Patient Network, Dublin, IRELAND, [4]vzw NET & MEN Kanker Belgium, Kortrijk, BELGIUM, [5]Neuroendocrine Cancer UK, Leamington Spa, UNITED KINGDOM, [6]NET Research Foundation (NETRF), Boston, MA, UNITED STATES OF AMERICA, [7]National Centre for Neuroendocrine Tumours, St. Vincent's University and Department of Clinical Medicine, St. James Hospital and Trinity College, Dublin, IRELAND, [8]Prince Court Medical Centre, Kuala Lumpur, MALAYSIA, [9]Department of Gastroenterology, the First Affiliated Hospital Sun Yat-Sen University, Guangzhou, CHINA, [10]University of Iowa Carver College of Medicine, Iowa City, IA, UNITED STATES OF AMERICA, [11]Sunnybrook Odette Cancer Centre, University of Toronto, Toronto, ON, CANADA, [12]Department of Endocrinology, Friedrich Alexander University Erlangen-Nuremberg, Erlangen, GERMANY, [13]APTED France, Lyon, FRANCE, [14]NeuroEndocrine Cancer Australia, Blairgowrie, AUSTRALIA, [15]Peter MacCallum Cancer Center, Melbourne, AUSTRALIA.

Aim/Introduction: The Survey of Challenges in Access to Diagnostics and Treatment for Neuroendocrine Tumor Patients (SCAN) measured the delivery of healthcare to NET patients. This analysis focused on the group of NET patients undergoing peptide receptor radionuclide therapy (PRRT) compared to the global survey group. **Materials and Methods:** During Sept-Nov 2019, 2359 NET patients, including 259 (11%) who had received PRRT, and 436 healthcare professionals (HCPs) from 68 countries, completed an online self-report survey available in 14 languages disseminated by INCA and its partner organizations. Results: After initial clinical evaluation and investigation, NET was the first diagnosis for 26% of patients undergoing PRRT (69/259) vs. 27% Global (640/2359). Importantly, 50% of patients subsequently undergoing PRRT were initially misdiagnosed at least once with another condition, with a higher rate of multiple misdiagnosis vs. the global sample: 38% (129/259) vs 31% (720/2359), p<0.0001. Of PRRT patients, 65% (169/259) had Stage IV disease at diagnosis, which was significantly higher than the percentage reported by patients globally (46%, 1077/2359, p<0.0001). Patients receiving PRRT reported prior or concurrent treatments including somatostatin analogs (SSA) (58%, 151/259), surgery (10%, 27/259), and oral chemotherapy (10%, 25/259). They declared a significantly higher usage of specialized NET services, including consultation with NET specialists (81%, 210/259 vs 53%, 1250/2359, p<0.0001), discussion of their management by a multidisciplinary team (49%, 126/259 vs 33%, 766/2359, p<0.0001, interaction with a clinical nurse specialized in NETs (43%, 112/259 vs 26%, 602/2359, p<0.0001), and involvement in patient support group (42%, 109/259 vs 32%, 750/2359, p<0.0001) compared to the global survey population. Although not all patients surveyed were aware of the availability of PRRT in their own country of residence, it was known to be available within the country of residence in 91% of patients undergoing PRRT (235/259) but only in 52% (1183/2275, p<0.0001) globally. According to HCPs, 64% (277/431) indicated that PRRT was available in the country in which they worked, with significant differences between advanced economies (AE) and emerging and developing economies (EDE) at 77% (165/218) vs 53% (112/213, p<0.0001). **Conclusion:** NETs are often initially misdiagnosed, patients frequently have advanced disease by the time of definitive diagnosis. Access to advanced treatment tools for NET patients is required to optimize disease management and improve patient outcomes. Access to specialised NET services seems to impact the likelihood of patients receiving PRRT, which is more limited in less economically-advanced countries. **References:** Dasari A, et al. JAMA Oncol 2017;3:1335-42

OP-0959

Lutetium177 in patients with stage IV neuroendocrine tumours of any origin. Data from 321 patients of the multicenter national registry

M. Mitjavila Casanovas[1], P. Belló[2], V. Pubul[3], A. García[4], J. Arbizu[5], T. Navarro[6], D. Marin[7], M. Castellón[8], C. Duran[9], C. Field[10], B. Llana[11], B. Miguel[12], M. Estorch[13], J. Hernando[14], A. Custodio[15], A. Repetto[16], J. Vercher-Conejero[17], A. Muros[18], J. Cano[19], E. Caballero[20], P. García[21], C. Blanco[22], J. Aller[1], A. Carmona[23], P. Jimenez-Fonseca[11];
[1]Hospital Universitario Puerta de Hierro Majadahonda, Madrid, SPAIN, [2]Hospital Universitario La Fe, Valencia, SPAIN, [3]Hospital Universitario Santiago Compostela. , Santiago de Compostela, SPAIN, [4]Hospital Universitario Vall d´Hebron, Barcelona, SPAIN, [5]Clínica Universitaria Navarra., Pamplona, SPAIN, [6]Hospital Universitario Ramón y Cajal, Madrid, SPAIN, [7]Hospital Universitario 12 de Octubre, Madrid, SPAIN, [8]Hospital Virgen de la Arrixaca, Murcia, SPAIN, [9]Hospital General Universitario Gregorio Marañón, Madrid, SPAIN, [10]Hospital Madrid Sanchinarro, Madrid, SPAIN, [11]Hospital Universitario Central de Asturias, Oviedo, SPAIN, [12]Hospital Universitario de Burgos, Burgos, SPAIN, [13]Hospital Sant Pau, Barcelona, SPAIN, [14]Hospital Universitario Vall d´hebron, Barcelona, SPAIN, [15]Hospital Universitario La Paz, Madrid, SPAIN, [16]Hospital Universitario Son Espases, Palma de Mallorca, SPAIN, [17]ICO - Hospital Universitario Bellvitge, Barcelona, SPAIN, [18]Hospital Universitario Virgen de las Nieves, Granada, SPAIN, [19]Hospital General Universitario Ciudad Real, Ciudad Real, SPAIN, [20]Hospital Universitario Doctor Peset, Valencia, SPAIN, [21]Hospital Universitario Getafe, Madrid, SPAIN, [22]Hospital Universitario Príncipe de Asturias, Madrid, SPAIN, [23]Hospital General Universitario Morales Meseguer, Murcia, SPAIN.

Aim/Introduction: NETTER I and ERASMUS clinical trials have led to Lutetium177 (Lu177) approval in Spain for the treatment of unresectable G1-2 well-differentiated SSTR-overexpressing GEP-NET, that have progressed with somatostatin analogues. The aim of this study is to determine the effectiveness of Lu177 in stage IV NETs regardless of its location and line of treatment, as well as the toxicity profile and the main predictors of progression free survival (PFS). **Materials and Methods:** Patients with advanced NET, including paragangliomas and pheochromocytomas, neuroendocrine carcinoma (G3) who had received or were receiving treatment with Lu177 were included. PFS and overall survival (OS) were estimated by the Kaplan-Meier method and compared by log-rank test and Cox regression. Results: A total of 321 cases were recruited in 21 centers included in the national registry SEPTRALU. The median age was 58 years (range, (18-88), 55% were men and 90% had ECOG-PS 0-1. The most frequent location of the tumor was pancreas (36%) and small intestine (26%) and of the metastases, liver (82%), and lymph nodes (60%). Lung NETs (8%), pheochromocytomas&paragangliomas (5%), grade 3 (9%), and heavily pretreated (≥3 previous lines) (11%) were included. The response rate was 24%, PFS was 27.1 months (95% CI, 24.0-44.8). and OS was 43.2 months (95% CI,

29.5-NA). The main toxicity was nausea (20%), emesis (15%), myelosuppression (15%), rash (3%), and nephrotoxicity (3%) with less than 4% of grade 3-4 toxicity. Performance status (ECOG-PS), HR 1.16 (95% CI, 1.06-1.27, p=0.001); Ki67 index, HR 3.01 (95% CI, 1.87-6.49, p<0.005); gender, HR 1.32 (95% CI, 1.20-1.49, p=0.042); line of treatment HR 2.37 (95% CI, 1.25-3.48, p=0.004), and previous everolimus, HR 2.63 (95% CI, 1.18-5.88, p=0.004) were predictors of PFS. Primary tumor site or functionality had no predictive value. **Conclusion:** In this clinical practice series, Lu177 was active in NETs irrespective of primary tumour site with effectiveness comparable to that of the phase III NETTER I trial in midgut tumours. Predictors of PFS were ECOG-PS, Ki67, line of treatment, gender, and previous treatment with everolimus. **References:** none

OP-0960

Peptide Receptor Radionuclide Therapy (PRRT) as neoadjuvant therapy in neuroendocrine tumors - one center experience

M. Opalinska[1], A. Sowa-Staszczak[2], A. Grochowska[3], H. Zwinczewska[2], A. Hubalewska-Dydejczyk[1];
[1]Nuclear Medicine Unit, Endocrinology Department, University Hospital in Krakow, Krakow, POLAND, [2]Chair and Department of Endocrinology, Jagiellonian University Medical College, Krakow, POLAND, [3]Department of Radiology, University Hospital, Krakow, POLAND.

Aim/Introduction: Neuroendocrine neoplasms including neuroendocrine tumors (NET) are often diagnosed as primary metastatic or inoperable. In those cases as a 1st line systemic therapy usually are used long acting somatostatin analogues or chemotherapy regimens, but seldom it enables radical treatment. In patients with good somatostatin receptor expression in tumors tissue Peptide Receptor Radionuclide Therapy (PRRT) may be used as 2nd or 3rd line of treatment. However, as described in literature, in some selected cases PRRT may be used as a first line/neoadjuvant therapy giving a chance for subsequent surgery which correspond with improvement of final outcomes. Aim: Assessment if neoadjuvant PRRT could be a treatment option for selected patients with initially unresectable NETs. **Materials and Methods:** Among the group of 114 patients treated with PRRT in 2005-2020 years, in about 30 cases PRRT was the first line therapy mainly due to massive disease burden at the moment of diagnosis. Among this group 9 patients received PRRT as an 1 line treatment because of primary inoperable tumors with the intention of preoperative reduction of the tumor size leading to potential subsequent surgical treatment. In this group the chance for any and curative surgery as well as the change of tumor diameter and volume was calculated. Additionally the influence of potencial clinical and radiological features on the chance of surgery, after application of PRRT as a neoadjuvant therapy, was assessed. Results: Neodjuvant PRRT enabled surgery with the intention of radical cure in 4 of 9 (45%) patients. Finally in two cases (22%) the radical surgery were performed. After the PRRT, the mean tumour diameter changed by -1,0cm (range from -3.7 to 0.3cm). The mean tumour volume decreased by 57.6 cm3 (range from -186.2 to 34.7 cm3) whereas attenuation decreased by 6.4 HU (range from -17,6 to 17,9 HU). According to RECIST 1.1 criteria, stabilization of the disease (SD) and partial response (PR) were observed in 6 and 1 patient respectively, and progressive disease (PD) was seen in 2 patients. No clinical and radiological features of NETs was found as statistically important in the assessment of the potential chance for subsequent surgery after neodjuvant PRRT application. **Conclusion:** PRRT may be considered not only as a palliative but also as a neoadjuvant therapy in primary inoperable NETs. There are no clinical or radiological features which give a fully unambiguous answer to the question whether neodjuvant PRRT may allow for radical surgical treatment. **References:** none

OP-0961

Effects of simplifications of absorbed dose calculation to the kidneys in later therapy sessions in patients with neuroendocrine tumours receiving ^{177}Lu-Octreotate therapy

M. Sandstrom[1,2], M. Lubberink[1,2], K. Fröss-Baron[1], U. Garske-Román[1], A. Sundin[1];
[1]Nuclear medicine & PET, Department of Surgical Sciences, Uppsala University, Uppsala, SWEDEN, [2]Medical Physics, Uppsala, SWEDEN.

Aim/Introduction: Fractionated therapy with ^{177}Lu-octreotate is an effective treatment option for patients with generalized neuroendocrine tumors. Different imaging protocols to calculate the absorbed doses (AD) to solid organs have been suggested in the attempt to optimize the treatment. The current aim was to study the influence of possible simplifications on absorbed dose calculations. **Materials and Methods:** Three hundred and fifty-three patients (133 female and 220 male) with neuroendocrine tumors with high somatostatin receptor expression were included. All patients received at least 4 cycles of treatment with 7.4 GBq ^{177}Lu-octreotate. SPECT/CT over the abdomen were, for both therapy session 1 and 4, acquired at 24, 96 and 168 h after infusion of ^{177}Lu-octreotate. Both the AD and the effective half-lifes (t_{eff}) in kidneys were calculated for both therapy session 1 and 4. As an attempt to simplify the AD calculation at the fourth session, the AD was also calculated using only a single measurement point at either 24, 96 or 168 h and the t_{eff} from the first session resulting in three different estimates AD_{24} (using the point at 24 h and the t_{eff} from session 1), AD_{96} (using the point at 96 h and the t_{eff} from session 1) and AD_{168} (using the point at 168 h and the t_{eff} from session 1). These results were than compared to $AD_{24,96,168}$, which is the AD value calculated using all three scans in session 4. Difference and agreement between the simplified

calculations and $AD_{24,96,168}$ were assessed by regression and Bland-Altman analysis. Results: For all comparisons the bias was quite small (less than ±5%) while the standard deviation of the bias (SD_{bias}) was 23% between the $AD_{24,96,168}$ of session 1 and 4 and for t_{eff} it was 14%. Between both AD_{24} and AD_{96} versus $AD_{24,96,168}$ the SD_{bias} was about 10%. For AD_{168} versus $AD_{24,96,168}$ it was a quite clear deterioration where the SD_{bias} was almost 20%. It was observed (for measurement points at 24 h and 96 h) that the estimated AD generally deviated less than 10% from the reference value using only one time point with an earlier determined t_{eff}. If the single point was later (168 h) a larger difference was observed. **Conclusion:** The observed difference using earlier determined t_{eff} and a one-point measurement was found to be result in acceptable values for the absorbed dose estimation of the kidneys. **References:** none

OP-0962

Treatment of metastatic paragangliomas with 177Lu-DOTATATE: outcomes from a single centre experience

I. Próspero, S. F. Castro, C. Costa, J. Oliveira, H. Duarte, I. L. Sampaio, G. Ferreira;
Instituto Português de Oncologia do Porto, Porto, PORTUGAL.

Aim/Introduction: Paragangliomas (PGL) are rare and clinically heterogeneous neuroendocrine tumours arising from the extra-adrenal autonomic paraganglia. Patients with malignant PGL show a markedly variable clinical course, and treatment options for progressive disease are limited. Recent evidence suggests peptide receptor radionuclide therapy (PRRT) with ^{177}Lu-DOTATATE as a promising modality of treatment for patients with malignant or inoperable PGL. The aim of this study was to evaluate the outcomes of PRRT in a population of patients with metastatic PGL. **Materials and Methods:** Retrospective study involving 11 patients with progressive metastatic PGL, who received PRRT in our Institution between 2011 and 2018 (median 3 cycles; median cumulative activity 18.14 GBq). Patients were followed until last observation or death. Data were collected and analysed regarding disease characteristics, clinical presentation, best morphologic response (according to RECIST 1.1), progression free survival (PFS), overall survival (OS), best symptomatic response and treatment-related toxicity. LogRank tests and Cox Regression analysis were performed to investigate factors associated with PFS and OS (α=0.05). Results: The population median age was 32 years (IQR 11), with male gender predominance (7/11 patients). The majority of patients had SDHB mutations (8/11 patients) and functional tumours (7/11 patients). Abdomen was the predominant PGL location (6/11 patients). The most common locations of metastasis were bone (all patients) and lymph nodes (6 patients); 4 patients had visceral metastasis. During a median follow-up period of 57.7 months (IQR 30.4), disease control rate was 60% (6 patients had stable disease as best treatment response, 4 had early progressive disease and 1 patient had non-measurable bone lesions according to RECIST); 4 deaths occurred. Clinical response was favourable, with only 2 patients revealing worsening of symptoms following PRRT, related with disease progression; 2 had pain relief, 2 had stable symptoms and 5 remained asymptomatic. Median PFS was 24.58 months; median OS was not reached. Male gender was associated with worse PFS (p=0.047) and OS (p=0.009). The presence of visceral metastasis also tended to be associated with worse OS (p=0.057). The most frequent treatment-related toxicity was haematological, mostly G1/G2 lymphopenia (45.5% and 36.4%, respectively). **Conclusion:** PRRT can be considered an appropriate therapeutic resource in metastatic paraganglioma, by contributing to achieve disease stabilization in a patient population where few treatment options are available. These results suggest that treatment effectiveness may be affected by factors associated with the underlying disease aggressiveness. The safety profile also sustains ^{177}Lu-DOTATATE regimen as a valid therapeutic option. **References:** None.

OP-0963

Prospective evaluation of glucose metabolism variations assessed with FDG PET/CT in a cohort of NET patients treated with PRRT

L. Urso[1], S. Panareo[1], A. Castello[1], M. Caracciolo[1], I. Zamberlan[1], N. Ortolan[1], A. Nieri[1], E. Tonini[1], C. Morotti[2], G. Valpiani[2], L. Uccelli[1], C. Cittanti[1], M. Bartolomei[1];
[1]Nuclear Medicine Unit, Oncological Medical and Specialists Department, University Hospital of Ferrara, Ferrara, ITALY, [2]Research Innovation Quality and Accreditation Unit, University Hospital of Ferrara, Ferrara, ITALY.

Aim/Introduction: besides ^{68}Ga-DOTA-peptides PET/CT, FDG PET/CT is emerging as a relevant diagnostic and prognostic tool in NET. "Flip-flop" phenomenon, consisting in simultaneous decrease of ^{68}Ga-DOTA-peptides and increase of FDG uptakes, and correlation between the FDG lesional avidity and proliferation index (Ki-67) have been observed during natural history of these tumors. The aim of our study was to evaluate the variations on FDG PET/CT in NET patients treated with 2 different schemes of PRRT and to correlate them with clinical-pathologic variables. **Materials and Methods:** we prospectively evaluated 108 lesions referring to 56 patients (33 males, 23 females; median age 64.5 years) affected by NET of various origin (28 pancreatic, 13 gastrointestinal, 9 bronchial, 6 unknown primary and 1 pheochromocytoma) and grading (median Ki67=9%); 32 patients were treated with MONO-PRRT (5 ^{177}Lu-DOTATOC cycles) and 24 with DUO-PRRT (3 ^{177}Lu-DOTATOC alternated with 2 ^{90}Y-DOTATOC cycles), within phase II clinical trial FENET-2016 (CTID:NCT04790708). SUVmax variations of a maximum of 3 target lesions per patient (58 for MONO-PRRT and 50 for DUO-PRRT) were compared between

baseline and 3 months post-PRRT FDG PET/CT. Results: at least one pathological FDG uptake was demonstrated in 35 (62.5%) patients before PRRT but only in 29 (52%) after PRRT. Twenty/50 lesions treated with DUO-PRRT were FDG avid before therapy, while only 14 were confirmed after PRRT (p=0.03). None of the 30 FDG negative lesions showed an increased FDG uptake after therapy. Moreover, in patients treated with MONO-PRRT, 14 lesions showed a decreasing trend in SUVmax after therapy, although not statistically significant. Regarding primary origin, lesion from pancreas and with unknown primary origin demonstrated a significant reduction of SUVmax after DUO-PRRT compared to MONO-PRRT scheme (p=0.03 and p=0.04 respectively). A mild positive correlation was found between grading and MONO-PRRT (r=0.39, p<0.02), while no evidence was detected with DUO-PRRT. **Conclusion:** our results suggest that PRRT, mostly with DUO scheme, could be effective in changing NET lesions glucose metabolism. In particular, this aspect seems more evident in patients affected by pancreatic and unknown primary NET, regardless of their Ki-67 index. We can speculate that an association of ^{90}Y, characterized by both higher energy emission and crossfire effect, with ^{177}Lu-labelled peptides, which have longer half-life and greater safety for organs at risk, might represent a valid option in FDG positive NET addressed to PRRT. Studies with larger cohorts of patients are required to validate our preliminary findings. **References:** Oh S. et al. Int_J_Mol_Imaging 2011;2011:524130.

OP-0964

Predictive factors of adverse events onset in GEPNET patients treated with PRRT

F. Scalorbi[1], G. Argiroffi[1], A. Lorenzoni[1], M. Baccini[2], L. Gherardini[2], V. Fuoco[1], N. Prinzi[1], S. Pusceddu[1], G. Calareso[1], E. M. Garanzini[1], S. Mazzaglia[1], M. Milione[1], C. Chiesa[1], E. Seregni[1], M. Maccauro[1]; [1]Istituto Nazionale Tumori Milano, Milan, ITALY, [2]Department of Statistics, University of Florence, Florence, ITALY.

Aim/Introduction: To predict real-life adverse events occurrence in a series of consecutive GEPNET patients treated with PRRT. **Materials and Methods:** G1-G2 metastatic GEPNETs patients treated in our centre with PRRT (^{177}Lu-Oxodotreotide, 4 administrations,7.4 GBq/each) from April 2019 to December 2020 were considered. Patients were all previously treated with SSA followed by radiological disease progression (PD). Haematopoietic, liver and renal toxicities were collected every 14 days during PRRT and graded according to CTCAE v5 (G0, G1-G2, G3-G4). The population was subdivided as midgut/foregut and G1/G2, according to WHO2019. Patients were categorical grouped according with ECOG-PS, number of metastatic sites, previous treatment lines (1,>=2) and the therapies received before PRRT (splenectomy, Everolimus, alkylating chemotherapy). To test independence between CTCAE onset and patient characteristics Pearson/Fisher and Kruskal-Wallis test were assessed. Logistic regression with Firth correction (R Puhr, Stat Med2017) and bootstrap were performed to determine predictability of clinical features and previous therapies for CTCAE onset. Results: Eighty-six patients were treated, 19 were excluded due to ongoing PRRT therefore 67 (31(46.3%) males, 36(53.7%) female, mean age 63) were selected. Thirty-eight (56.7%) were classified as midgut, 29(43.3%) as foregut, 24(35.8%) G1 and 43(64.2%) G2. Alkylating chemotherapy and Everolimus were the previous treatments in 13(19.4%) patients, in both cases. Patients were treated with PRRT as third or further lines in 34.3% (23) of the whole population, 48.3% (14) of foregut cohort. All the patients showed at least one G1-G2 CTCAE during PRRT, in particular anaemia (46,68.6%), thrombocytopaenia (32,47.8%) and leukopaenia (30,44.8%). G3-G4 were rare events, reported in 5(7.5%) cases considering haematological alterations (2 neutropaenia, 1 anaemia, 2 thrombocytopaenia) and 2(3%) cases for liver (1 ALT/GPT and 1 INR alteration). Anaemia and thrombocytopaenia occurred in the same patient, causing discontinuation. In all the other cases G3-G4 were transitional. No G3-G4 renal toxicities were reported. Logistic regression showed that line of PRRT administration was the most powerful predictor of thrombocytopaenia (log Odds Ratio (logOR): 1.54,SE 0.71,CI 0.24 -3.03, p:0.019), anaemia (logOR 5.63,SE 3.07,CI 1.19-12.84, p:0.004) and GGT alteration (logOR 1.88, SE0.85, CI 0.29-3.53,p: 0.022). Furthermore, primary tumor histology (midgut versus foregut) was a good predictor of ALT/GPT (logOR 1.24,SE 0.63, CI 0.045-2.48, p: 0.04) and GGT (logOR 1.34,SE 0.73,CI -0.02- 2.87, p: 0.053) alterations. **Conclusion:** Line of PRRT administration is a strong predictor of haematological CTCAE onset during PRRT. These results, if confirmed in large-cohort studies, can have a huge impact on everyday PRRT decision-making process. **References:** None

OP-0965

Diagnostic 68Ga-DOTATOC imaging parameters and correlations with absorbed dose from 177Lu-DOTATATE treatment in GEP-NET-patients

R. Bruvoll[1,2], J. Blakkisrud[1,2], L. Mikaelsen[2,3], J. Connelly[2], C. Stokke[1,2]; [1]Department of Physics, University of Oslo, Oslo, NORWAY, [2]Division of Radiology and Nuclear Medicine, Oslo University Hospital, Oslo, NORWAY, [3]Department of Life Sciences and Health, Oslo Metropolitan University, Oslo, NORWAY.

Aim/Introduction: Peptide receptor radionuclide therapy (PRRT) is a radionuclide treatment used for gastroenteropancreatic neuroendocrine (GEP-NET) tumours that express somatostatin receptors (SSTRs). High expression of SSTRs as assessed on 68-Ga-DOTATOC PET/CT-images is a crucial part of deciding patient eligibility for PRRT with 177Lu-DOTATATE. The exact uptake correlation between the two radiolabeled somatostatin analogues is however not clear. The purpose of this study was to investigate the possibility to predict the resulting therapeutic absorbed

dose to individual tumours based on diagnostic PET/CT-parameters acquired pre-treatment. **Materials and Methods:** Thirty-two patients (27 male, 5 female) with GEP-NET were included in this retrospective study. Patients received 7.4 GBq (7288-7907 MBq, one patient received 4195 MBq) of 177-Lu-DOTATATE and data from the initial treatment fraction were included for analysis. 146 (3-12 per patient) tumors were segmented on pre-therapeutic 68-Ga-DOTATOC PET/CT images and post-therapeutic 177-Lu-DOTATATE SPECT/CT images acquired 24h and 168h post injection. A threshold-based segmentation method with a threshold of 40 % of the maximum tumour value was used both for PET and SPECT segmentation. A recovery coefficient curve found from spherical phantom inserts was used for partial volume correction. A volume cut-off of 8ml was also included to avoid substantial partial volume effect. A model to predict absorbed dose to the tumours was developed using an assumed linear relationship between the 68-Ga-DOTATOC -SUV and 177-Lu-DOTATATE activity concentration together with a fixed effective tumour half-life based on the population average. Calculated absorbed doses were compared to their diagnostically predicted counterpart. Results: Liver metastases represented the majority of the included tumours with 79% incidence. Mean SUV_{mean} from the 68-Ga-DOTATOC PET/CT scans was 25.9 (7.1-84.4), with corresponding mean absorbed dose, effective half-life and tumor volume derived from 177-Lu-DOTATATE SPECT/CT scans 24.7Gy (2.2-69.4), 92.8 hours (42.9-151.6) and 52ml (8-844). The linear fit between 177-Lu-DOTATATE activity concentration and SUV was poor (R^2 = 0.17). The ratio between estimated and calculated absorbed dose was on average with standard deviation 1.10+/-0.75. **Conclusion:** Somatostatin receptor 68Ga-DOTATOC PET imaging is inadequate for predicting absorbed dose from 177Lu-DOTATATE on the lesion level. This is partly due to differences in effective half-life and a high deviation between the SUV-values on diagnostic 68Ga-DOTATOC PET/CT-images vs 177-Lu-DOTATATE activity concentration. This stresses the need to measure the absorbed dose to tumours post-therapeutically with imaging over multiple time points. **References:** None

OP-0966

Investigation of miRNAs as outcome predictors in midgut NET treated with PPRT

F. Scalorbi, L. Roz, G. Pollaci, G. Centonze, V. Lagano, F. Facchinetti, G. Calareso, E. M. Garanzini, L. Cattaneo, M. Maccauro, M. Gariboldi, E. Seregni, M. Milione;
Istituto Nazionale Tumori Milano, Milan, ITALY.

Aim/Introduction: To evaluate miRNA expression in paraffin samples (FFPE) from midgut NET to predict early disease progression after PRRT. **Materials and Methods:** Tissue samples from G1-G2 midgut patients treated with PRRT (^{177}Lu-DOTATATE, 7.4 GBq/each, 4 administrations, every 8 weeks) from April 2019 to November 2020 were considered. Only FFPE samples collected before PRRT, with at least 60% cellularity and no protein/solvent contamination, were selected. Two CT or MRI scans per patient were collected, performed within 3 months before and 3 months after the treatment. RECIST1.1 criteria were applied to evaluate the response to PRRT (progression versus non-progression). The expression of 3 miRNAs (miR-375, miR-196a, miR-21-5p) were quantified by qRT-PCR, after housekeeping normalisation (RNU48, U6), comparing progressive and non-progressive groups. One biological and 2 technical replicates were performed (SD<0,5) and DDCT (Delta Delta CT) formula was applied to quantify miRNA expression. Fifteen (53.8%) samples were obtained from metastatic lesions. The association between clinical features (gender, age, sample localisation: primary versus metastatic lesions), miRNA expression and disease progression was assessed using the Chi/Fisher exact test for categorical variables and Kruskal-Wallis test for continuous variables (age and DDCT). Logistic regression models were performed to determine predictability of clinical features and miRNA expression for disease progression. Results: Twenty-eight FFPE samples (mean cellularity 80%, range 60-95%) were selected (10 males, 18 females, mean age 64.8, SD+/-11,2, CI 60.6-69 years). Five patients were diagnosed as progressive disease (PD), mean age in PD patients was 67.4 (SD+/-11.4, CI 63.2-71.6) versus 64.3 (SD+/-11.2, CI 60.1-68.3) in non-PD. MiRNA196 and miRNA21-5p showed slightly increased expression in PD patients (mean DDCT: -4.9 vs -4.6 and-4.6 vs -4.4, respectively) meanwhile miR-375 showed decreased expression (mean DDCT: -2.7 vs -3.1). Chi/Fisher and K-Wallis test did not reach statistical significance for any of the aforementioned covariates (included DDCT), while logistic regression showed an OR of 4.04 for miR375 (SE 2.62, 95%CI 1.13-14.44, p 0.032) for PD patients. **Conclusion:** Evaluation of miRNA expression is a feasible procedure in FFPE from midgut NET, with good reproducibility. MiRNA-375 can be a useful independent predictor of early disease progression after PRRT, showing OR equal to 4.04. External validation of the results on larger cohort has been planned. **References:** None

1711

Wednesday, October 20 - Saturday, October 23, 2021

on-demand pool, release on Wednesday, October 20 at 09:00

TROP Session: General Nuclear Medicine

OP-0968

Diagnostic value of early and late postvoid static imaging after diuretic renogram with [^{99m}Tc] Tc-MAG-3

L. Del Barco Diez Canseco, S. Álvarez Ruíz, L. de la Cueva Barrao, P. Navarro Beltran, G. Guzman Prudencio, M. Calderon Calvente, N. Canchumanya Huatuco, M. Falgas Lacueva, M. Sangrós Sahún, D. Abós Olivares;
Hospital Universitario Miguel Servet, Zaragoza, SPAIN.

Aim/Introduction: The dynamic diuretic renogram complemented with postvoid static images, performed 5 and 60 minutes after its completion, is a frequently used diagnostic test in the assessment of the diuretic renogram, which reduces the number of indeterminate renograms and false positives for obstruction The objective of this study is to evaluate the diagnostic contribution of post-void imaging in the interpretation of the results of the dynamic diuretic renogram. **Materials and Methods:** A retrospective study was carried out, of the diuretic renograms performed in our department from January 2018 to December 2019, selecting those studies in which early and late postvoid images were performed. Each renographic curve was classified, according to the pattern of response to the diuretic, as obstructive, non-obstructive and indeterminate, constituting our initial diagnosis. Subsequently, it was counted whether after viewing the postvoid images there was a change in diagnostic criteria and in what sense. Results: A total of 332 patients of any age were analyzed, of which 99 (30%) had postvoid images (study group). Of this group: a) 63 had an indeterminate pattern in the diuretic renogram, of which 37 (59%) were reclassified as non-obstructive when additional elimination was observed; b) 22 patients had an obstructive pattern in the renogram, 13 (59%) of them reclassified, after the portmiccinoal, as non-obstructive; c) 14 had a non-obstructive pattern in the renographic curve, of which 11 (79%) were also classified as non-obstructive (the other 3 had distal ureter pathology that distorted the interpretation of the results). In summary, in our study group after performing postvoid images, 50 (50.5%) patients were reclassified as non-obstructive. **Conclusion:** The performance of postvoid images after the diuretic renogram allowed in our study to modify the initial diagnostic impression, based on the morphological analysis of the renographic curves, ruling out obstruction in 50.5% of cases. Post-void images were equally useful in patients with obstructive and indeterminate diuretic renogram, reducing uncertainty in the diagnosis of the clinical report and the number of false obstructive patterns. **References:** None

OP-0969

The Impact of Background ROI on Relative Renal Function in Different Patients Subsets

S. Fontão de Castro[1], I. Póspero[1], I. Lopo[2], L. Sobral Violante[1], R. Silva[2], T. Saraiva[2], H. Duarte[1], G. Costa[2];
[1]Instituto Português de Oncologia do Porto Francisco Gentil, EPE, Porto, PORTUGAL, [2]Centro Hospitalar e Universitário de Coimbra, Coimbra, PORTUGAL.

Aim/Introduction: Measurement of absolute and relative renal function is an essential part of dynamic renal scintigraphy. Background region of interest (ROI), by appraising the effect of several extra-renal sources of activity, such has the liver, spleen and blood pool, play an important influence on renal function measurements. Through this work, we aim to explore the impact of the background ROI on relative renal function in different subsets of patients. **Materials and Methods:** Retrospective study of 181 consecutive patients with a clinical suspicion of decreased renal function or obstructed kidney referred for [^{99m}Tc]Tc-MAG3 renal scintigraphy between 01/10/2020 and 28/02/2021 in a general Nuclear Medicine department. Twenty-eight patients were excluded due to pediatric age (N=11), single kidney (N=13) or transplanted kidney (N=4). A total of 153 patients were analyzed: 54% women (N=82); mean age 62.1±16.1 years; mean body mass index (BMI) 270.7±5 Kg/m^2 and mean [^{99m}Tc]Tc-MAG3 administered activity 153.9±25.9 MBq. Standard dynamic renal scintigraphy studies were reviewed and the absolute and relative renal function obtained with C-shaped and inferior background ROI were recorded (integral method). A Pearson correlation test was performed and a paired samples t-test used to determine if there were significant differences ($p<0.05$) in the relative renal function obtained with C-shaped and inferior background ROIs. Patients were also divided into groups regarding absolute renal function (normal/impaired) and BMI and were compared using the same set of statistical tests. Results: There was a strong correlation between the relative renal function obtained with both background ROIs (Pearson's Coefficient 0.968), despite a statistical significant difference between them ($p<0.020$). These results remained in patients with normal absolute renal function and BMI inferior to 30 ($p<0.001$ and $p<0.014$, respectively). However, no statistically significant difference was found in obese (≥30kg/m^2) or patients with impaired renal function ($p=0.150$ and $p=0179$, respectively). **Conclusion:** According to our results, and despite an excellent correlation, relative renal function obtained with C-shaped and inferior background ROI was statistically different. However, in obese and patients with impaired absolute renal function, no statistically significant differences were found based on background ROI, which may be explained by a higher and more evenly distributed background activity in these subsets of patients. **References:** None.

OP-0970

Is diuretic renography useful in patients with Bricker procedure?

D. Vega Perez, M. D. Marin Ferrer, A. Galiana Moron, P. Zaragoza Ballester, S. Ruiz Solis, A. Saviatto, E. Martinez Albero, V. M. Godigna Guilloteau, P. Pilkington Woll, P. Sarandeses Fernandez, A. Gomez Grande, M. J. Tabuenca Mateo;
Hospital 12 de Octubre, Madrid, SPAIN.

Aim/Introduction: To determine the usefulness of the (99mTc)-MAG3 diuretic renography (DR) in the follow-up and detection of complications of oncological patients(p) who underwent ileal conduit urinary diversion (Bricker procedure). **Materials and Methods:** We carried out a retrospective study between the years 2016-2020 selecting 48p with Bricker who had undergone DR study with F+10 protocol (injection of Furosemide 10 min post-tracer-injection). The mean age was 71.6±8 years, 85% had bladder cancer and 42p were men. In all 48p the following parameters were analyzed: Morphological imaging techniques (29p CT and 19p Ultrasound) assessing urinary tract dilation and atrophy; time since Bricker procedure; indication for the DR study and serum creatinine values. In the DR studies, renal function (RF) was categorized into: preserved parenchyma RF≥45%, mild-moderate deterioration RF45%-20% and severe RF≤20%. The elimination curve was categorized into: obstructive, non-obstructive and flat curve. The posterior urological management (nephrostomy/ureteral dilation, antibiotic treatment and others) information was collected. DR results as obstruction or non obstruction/atrophy were correlated with urological management; results of morphological imaging tests as dilated/not dilated were correlated with urological management. Results: Range of time since Bricker: 1 month-23 years (average 3.6 years). Indication for study: Isolated urinary tract dilation on CT/Ultrasound 25p(52.08%), fever and urinary tract dilation 14p(29.16%), impaired renal function 7p(14.58%), sepsis and impaired renal function 1p(2.09%) and control 1p(2.09%). Mean creatinine: 1.63 mg/dL ± 0.98 (range 0.74-5.28mg/dL). A total of 95 renal units were evaluated (1 patient had previous nephrectomy). CT/ultrasound findings: isolated hydronephrosis in left kidney(LK) 25p, in right kidney(RK) 21p; renal atrophy: LK(6) 2 of them with hydronephrosis, RK(5) 3 with hydronephrosis; Lithiasis: LK(1), RK(1); 36 kidneys without notable findings. DR function analysis: RF≥45%: LK(21), RK(35); RF 45%-25%: LK(19), RK(8) and RF≤20%: LK(7) and RK(5). Elimination curve patterns: non-obstructive LK(25), RK(39); obstructive LK(15,) RK(4) and flat curve LK(7), RK(5). Urological management: followed-up 16p(33.33%), established renal atrophy 7p(14.58%), interstitial nephropathy treatment 1p(2.09%), antibiotic treatment 4p(8.33%), nephrostomy/ureteral dilation 8p(16.66%), nephrostomy and antibiotics 11p(22.92%), and nephrectomy 1p(2.09%). Of the 43 patients with hydronephrosis on CT/ultrasound, the DR showed that 8p(18.6%) also had severe renal deterioration not detected on CT/ultrasound. The statistical analysis between imaging tests and interventional urological management, obtained a sensitivity of 90% and specificity of 96% for DR; and 100% and 17.85% for CT/ultrasound. **Conclusion:** Our results confirm the use of diuretic renography as gold standard to determine interventional or conservative urological management in patients with Bricker procedure. **References:** None

OP-0971

Dose Reduced [^{18}F]PSMA-1007 PET is Feasible for Functional Imaging of the Renal Cortex

K. Valind[1,2], G. Brolin[1,3], J. Jögi[1,2], D. Minarik[1,3], E. Trägårdh[1,2];
[1]Wallenberg Centre for Molecular Medicine, Lund University, Lund, SWEDEN, [2]Clinical Physiology and Nuclear Medicine, Skåne University Hospital, Lund and Malmö, SWEDEN, [3]Radiation Physics, Skåne University Hospital, Lund and Malmö, SWEDEN.

Aim/Introduction: Prostate Specific Membrane Antigen (PSMA) has become the main target for Positron Emission Tomography (PET) imaging in prostate cancer. PSMA-ligand radiotracers show a significant renal uptake [1], and their use for functional imaging of the renal cortex have been suggested [2]. The standard for such imaging is scintigraphy with ^{99m}Tc labelled dimercaptosuccinic acid (DMSA). The aim of this study was to determine if the effective dose from [^{18}F]PSMA-1007 PET could be reduced to the level of a [^{99m}Tc]Tc-DMSA scintigraphy, with sufficient image quality for evaluation of the kidneys. **Materials and Methods:** 12 patients underwent PET/CT imaging at 1h, 2h and 5.5h after injection of 3.9±0.2 MBq/kg [^{18}F]PSMA-1007 (range 3.4 - 4.2). List-mode data was binned into series with acquisition times of 10s, 20s, 30s, 60s, 90s, and 120s per bed position (bp) for each of the 3 acquisitions. The quality of each series was rated by 3 observers using a 5-point Likert scale, taking into account image noise, contrast, and level of detail. Results: For two patients, list mode files for the 2h post-injection (p.i.) acquisitions were lost, with only 120s/bp data available. Thus, 206 series were evaluated. At least acceptable image quality (3/5) for >90% of the images was achieved for acquisition times of at least 90s for 1h p.i. images, 60s for 2h p.i. images and 120s for 5.5h p.i. images. [^{99m}Tc]Tc-DMSA scintigraphy is often performed with an acquisition time of 15 minutes. Increasing PET acquisition time at 2h p.i. from 60s to 15 minutes results in a possible reduction of administered activity to 0.27 MBq/kg. For a 1 year-old child weighing 10 kg, this corresponds to an effective dose of 0.3 mSv (unpublished biokinetic data). An additional low-dose CT of 0.3 mSv yields an effective dose of 0.6 mSv. The effective dose for a [^{99m}Tc]Tc-DMSA scan using 18 MBq (according to the EANM dosage card for children) is 0.67 mSv. **Conclusion:** Image acquisition at 2h after injection of [^{18}F]PSMA-1007 is feasible for renal cortical imaging. An acquisition time of 15 minutes per bed position corresponds to a similar effective dose as a [^{99m}Tc]Tc-DMSA scintigraphy.

References: 1. Giesel FL, Hadaschik B, Cardinale J, et al. F-18 labelled PSMA-1007: biodistribution, radiation dosimetry and histopathological validation of tumor lesions in prostate cancer patients. Eur J Nucl Med Mol Imaging. 2017;44:678-88. 2. Sarikaya I, Alqallaf A, Sarikaya A. Renal Cortical (68) Ga-PSMA-11 PET and (99m)Tc-DMSA Images. J Nucl Med Technol. 2021;49:30-3.

OP-0972

Evaluation of Dynamic Renal ^{68}Ga-DOTA PET/CT to Monitor the Urinary Efflux and to Estimate the Glomerular Filtration Rate Using a Compartmental Kinetic Modelling Approach

D. Kersting[1], M. Sraieb[1], R. Seifert[1], P. Fragoso Costa[1], S. Kazek[1], L. Umutlu[2], M. Nader[1], W. Fendler[1], W. Jentzen[1], K. Herrmann[1], C. Rischpler[1];
[1]Department of Nuclear Medicine, University Hospital Essen, University of Duisburg-Essen, Essen, GERMANY, [2]Department of Diagnostic and Interventional Radiology and Neuroradiology, University Hospital Essen, University of Duisburg-Essen, Essen, GERMANY.

Aim/Introduction: Renal scintigraphy using ^{99m}Tc-DTPA is well-established to evaluate urinary efflux and to monitor kidney function prior to radionuclide therapy. During renal scintigraphy, repeated blood sampling is required to calculate the glomerular filtration rate (GFR). Alternatively, dynamic PET imaging alone using glomerular filtrated tracers like ^{68}Ga-labelled 1,4,7,10-Tetraazacyclododecane-1,4,7,10-tetraacetic acid (^{68}GA-DOTA) can be performed. Potential advantages of PET-based renal function assessment are shorter examination times and direct GFR calculation from PET data (GFR_{PET}) without additional blood sampling by compartmental kinetic modelling. In this study, we compared imaging results of ^{68}GA-DOTA PET in 12 patients who previously underwent renal scintigraphy examinations. Serum creatine-derived GFR measurements were compared to PET-based GFR estimations. **Materials and Methods:** Dynamic list-mode PET data (mean applied activity: 112 MBq of ^{68}Ga-DOTA) were acquired for 30 min using a Siemens Biograph Vision PET/CT system and reconstructed in 12 frames of 30 seconds and 18 frames of 90 seconds. All PET images were interpreted in a consensus read by three nuclear medicine physicians. To obtain renal time-activity-curves (TACs), the renal cortex was segmented; the arterial input function was estimated from the abdominal aorta. Single compartmental modelling was performed using complete 30-min and reduced 15-min PET data sets to calculate GFR_{PET-30} and GFR_{PET-15}, respectively. The CKD-EPI-formula was used as reference standard for GFR estimation (GFR_{crea}). Renal scintigraphies were used as reference standard for visual interpretation. GFR results were compared using the Pearson correlation coefficient (PCC) and the interclass correlation coefficient (ICC). Results: Visual interpretation of PET images and TACs revealed both-sided urinary obstruction in 2/12, right-sided urinary obstruction in 1/12 and normal urinary efflux in 9/12 patients. These were the same findings as in pretherapeutic renal scintigraphy examinations. Regarding all patients, GFR_{Crea} and GFR_{PET-30} were poorly correlated with an ICC of 0.43 and a PCC of 0.51 (95%-confidence interval: 0.10-0.84). For a subgroup of patients with undisturbed urinary efflux (n=9), GFR_{Crea} and both GFR_{PET-30} and GFR_{PET-15} were well correlated with an ICC of 0.78 and 0,76, respectively, and a PCC of 0.82 (0.34-0.97) and 0.76 (0.19 - 0.95), respectively. **Conclusion:** Assessment of urinary efflux and GFR calculation by dynamic ^{68}Ga-DOTA PET without blood sampling is feasible at a short acquisition time of 15 minutes. However, GFR calculation by single compartmental modelling failed in patients with disturbed urinary efflux. Further studies evaluating the potential of dynamic renal PET imaging are warranted. **References:** none

OP-0973

Pulmonary embolism - a diagnostic dilemma with perfusion only SPECT/CT during the COVID 19 pandemic

O. Evbuomwan, G. Engelbrecht;
University of The Free State, Bloemfontein, SOUTH AFRICA.

Aim/Introduction: Lung perfusion abnormalities is not a rarity in COVID 19 infected patients. It could be associated with pulmonary embolism, pulmonary infiltrates from COVID pneumonia or perfusion shunting. A VQ SPECT/CT study has a very high sensitivity and specificity in diagnosing pulmonary embolism. However most nuclear medicine facilities had to rely initially on a perfusion only SPECT CT study because of the fear of potential spread of the infection during the process of ventilation. However, a perfusion only study is not as specific as a VQ study, and we found out in our facility that this lead to an initial increase in false positive rates of pulmonary embolism in COVID 19 infected patients. **Materials and Methods:** We retrospectively reviewed the data of all the COVID-19 infected patients who had a perfusion only SPECT/CT study in our facility between July and September 2020. Ten of these patients had a VQ SPECT/CT study performed 3 months after their initial perfusion only study and we reviewed these images too. Results: Forty-seven patients who had perfusion only SPECT/CT study within the study period were included in the study. Fifteen (31.9%) of them had perfusion defects associated with some form of mosaic hypoattenuation on CT. Ten of the 15 (66.6%) were initially diagnosed with pulmonary embolism due to the nature of the defects (at least one large, wedge shaped segmental defect). All 10 patients had a follow up VQ SPECT/CT study performed 3 months after commencing therapeutic anticoagulation. Fifty percent of these patients had matching ventilation studies with little or no reduction in the size of their perfusion defect. The other 50% showed some form of defect resolution with unmatched ventilation,

thereby confirming the diagnosis of pulmonary embolism. **Conclusion:** We confirm that pulmonary embolism is not the only cause of perfusion defects with a near normal CT in patients with COVID 19 infection. These defects could also be due to a shunting process that is thought to be associated with COVID 19 pneumonia. We suggest that if perfusion studies alone are to be performed, a very careful look at the CT to identify mosaic hypoattenuation is advised. However, this mosaic hypoattenuation is not too evident on most of our non-diagnostic CT studies, thereby increasing the chances of having a false positive scan for pulmonary embolism in the absence of a ventilation study. **References:** None

OP-0974

Contribution of Ventilation/Perfusion SPECT/CT in alternative diagnosis for pulmonary embolism suspicion

L. Besson[1], V. Habouzit[1], M. Castan[2], A. Viallon[2], L. Bertoletti[3], N. Prévôt-Bitot[1], P. Bonnefoy[1];
[1]Nuclear medicine department, Hôpital Nord, CHU de Saint-Etienne, Saint-Etienne, FRANCE, [2]Emergency department, Hôpital Nord, CHU de Saint-Etienne, Saint-Etienne, FRANCE, [3]Department of vascular and therapeutic medicine, Hôpital Nord, CHU de Saint-Etienne, Saint-Etienne, FRANCE.

Aim/Introduction: Since twenty years, SPECT/CT allows to optimize nuclear medicine protocols and improve performances of techniques. In acute pulmonary embolism (PE), SPECT/CT is widely used although it still requires clinical validation in randomised studies. Many studies focused on sensibility or specificity improvements but few have evaluated its potential in alternative diagnosis, even though the prevalence of PE is low. The aim of this study was to evaluate the impact of Ventilation/Perfusion (V/Q) SPECT/CT in alternative diagnosis to PE compared to planar scintigraphy. **Materials and Methods:** We retrospectively evaluated V/Q lung scan in patients referred from the emergency department of our institution with suspected PE. We compared a cohort of adult patients explored with planar scintigraphy (2013-2015) versus a cohort evaluated with SPECT/CT (2020). The primary objective is to compare the number of cases in which lung scan is able to propose an alternative diagnosis in absence of PE for each modality. The secondary objective is to describe alternatives diagnoses potentially observed. Results: A total of 171 patients were included in the study (81 with planar imaging and 90 with SPECT/CT). Patients explored with planar V/Q scan were significantly older (mean age 78.6 vs 73.3 years, p=0.02) but did not differ in terms of clinical presentation or comorbidities except for the presence of chronic lung disease (23% vs 11% respectively for SPECT/CT and planar groups, p=0.04). Lung scans were suggestive of PE in 15 patients with planar lung scan and 14 with SPECT/CT (p=0.54). Among the 142 patients without pulmonary embolism, 68 alternative diagnoses could be identified: 19 patients (29.2%) in the planar group versus 49 patients (64.5%) in the SPECT/CT group (p<0.0001). The most common lesions seen on SPECT/CT were pleural effusions (n=25), signs of cardiac decompensation (n=23) or pulmonary infections (n=11), COPD lesions (n=9) and/or thoracic neoplasia (n=6). The most common lesions found on planar scans were signs of pulmonary injection (n=6), pleural effusions (n=4), signs of cardiac decompensation (n=4), emphysema (n=4) or COPD lesions (n=3) and atelectasis (n=1). **Conclusion:** When lung scintigraphy rules out PE, SPECT/CT currently allows an alternative diagnosis to explain the symptomatology in many situations, which is an evolution compared to planar scintigraphy. This ability must be known and exploited to improve patient management and limit number of imaging examinations. **References:** none

OP-0975

Diagnosis of pulmonary embolism during COVID-19 pandemic: comparison of perfusion SPECT/CT to CTPA

J. C. Ferro, S. Carmona, R. T. Ferreira, A. I. Santos;
Hospital Garcia de Orta, E.P.E., Almada, PORTUGAL.

Aim/Introduction: Ventilation/perfusion single-photon emission computed tomography (V/P-SPECT) and computed tomography of the pulmonary arteries (CTPA) are well-established for pulmonary embolism (PE) diagnosis. COVID-19 pandemic introduced the use of perfusion SPECT with low-dose computed tomography (P-SPECT/CT), avoiding ventilation SPECT. Our aim was to compare P-SPECT/CT and CTPA results in patients with clinical suspicion of PE. **Materials and Methods:** Retrospective analysis of 30 patients (mean age: 60.1±17.7 years, 60.0% female), with clinical suspicion [23 patients (76.7%)] or in follow-up for previously PE [7 patients (23.3%)], who underwent P-SPECT/CT and CTPA (April-December 2020). The median time interval between tests was 6.0 [P25:2.8;P75:13.0] days. Tests were classified as PE positive, PE negative and inconclusive. Positive tests were paired and compared regarding the number and location of pulmonary lobes/arteries involved. Statistical analysis was performed using IBM SPSS Statistics (v26). Results: P-SPECT/CT was PE positive in 23/30 (76.6%), negative in 5/30 (16.7%) and inconclusive in 2/30 (6.7%) patients, whereas, CTPA was PE positive in 12/30 (40.0%), negative in 11/30 (36.7%) and inconclusive in 7/30 (23.3%) patients. 14/30 (46.7%) patients had concordant results, mostly regarding positive PE results [11 patients (36.7%)]. 16/30 (53.3%) patients had discordant results: for the 3 patients with a negative PE P-SPECT/CT, 1 (3.3%) had a positive and 2 (6.7%) had an inconclusive CTPA; for the 12 patients with a positive PE P-SPECT/CT, 8 (26.7%) had a negative and 4 (13.3%) had an inconclusive CTPA; and the 1 patient (3.3%) with an inconclusive P-SPECT/CT had a negative CTPA. There was no association between P-SPECT/CT and CTPA results (Fisher's Exact Test, p>0.05). The median

number of pulmonary lobes/arteries involved by PE in both tests was 2.5 [P25:1.0;P75:4.0]. Considering the 16 patients with non-negative results on both tests, P-SPECT/CT was the test that identified more lesions in 9/16 (56.3%) patients versus CTPA in 4/16 (25.0%). Regarding the 9 most discordant results (8 patients with a positive P-SPECT/CT and a negative CTPA and 1 patient with the inverse result): 6/9 (75%) patients started therapeutic anticoagulation and 3/9 (25%) did not. **Conclusion:** We have found no association between P-SPECT/CT and CTPA results for PE diagnosis, P-SPECT/CT identified more positive cases and a higher number of lobes involved. Care must be taken when interpreting these results due to the small size of the sample, as well as, according to some authors, they may reflect false positive results which might have important impact on therapeutic management. **References:** None

OP-0976

Pre-surgical Prognostic Assessment by Mebrofenin 99mTc Scintigraphy in Patients Undergoing Resective Liver Surgery

J. Uña, J. Valderrey Pulido, A. Allende Riera, C. Cárdenas Negro; Servicio Canario Salud, Santa Cruz de Tenerife, SPAIN.

Aim/Introduction: We use hepatobiliary scintigraphy with 99mTc-mebrophenin (HBS-M) as a quantitative method for evaluating global liver function and future liver remnant function (LRF) in a series of patients candidates for resective liver surgery and its result as a prognostic method in the prediction of post-surgical liver failure. **Materials and Methods:** The results are analyzed in 46 patients who were submitted to a hepatobiliary scintigraphy with 99mTc-mebrophenin with initial dynamic acquisitions and hybrid tomography (SPECT / CT) before to liver resection. The global liver function and that of the future liver remnant were obtained from the analysis of the initial dynamic phase of the scintigraphy. The liver volume to be preserved was expressed as a percentage of the total liver volume, both measured from the CT sections. We take the value of 2.69%/min/m2 as the functional limit of future liver remnant. Patients below this threshold were rejected and/or referred to portal embolization as a method of increasing the remaining functional liver volume. The liver function analytical data were compared before and on the 5th postoperative day. Results: None of the patients undergoing resective surgery whose future remnant liver function value exceeded the established threshold suffered liver failure. Bilirubinemia values remained, in all cases, within normal limits. INR values were altered in two patients to return to normal later. **Conclusion:** The hepatobiliary scintigraphy with 99mTc-mebrofenin seems to be consolidated as a prognostic method of great value in estimating the postoperative risk of liver failure in all patients who are candidates for liver resection surgery, being superior to liver volumetry by CT by including in its assessment areas of liver tissue with normal structure and appearance but hypo or non-functional for the study with 99mTc-mebrofenin. **References:**

OP-0977

Quantitative approaches to selective spleen detection in Technetium-99m-labelled denatured red blood cells scintigraphy - a quantitative single centre analysis

A. Holzgreve[1], F. Völter[1], A. Gosewisch[1], M. P. Fabritius[2], M. Brendel[1], N. L. Albert[1], P. Bartenstein[1], M. Unterrainer[2], L. M. Mittlmeier[1]; [1]Department of Nuclear Medicine, University Hospital, LMU Munich, Munich, GERMANY, [2]Department of Radiology, University Hospital, LMU Munich, Munich, GERMANY.

Aim/Introduction: Scintigraphy with administration of technetium-99m (^{99m}Tc)-labelled denatured red blood cells (RBCs) is a commonly applied tool for detection of unclear bleeding sites. However, due to physiological RBC molting, RBC scintigraphy could also be used for detection of ectoptic spleen tissue or splenules. Therefore, we conducted a single-center analysis investigating the uptake characteristics in suspected splenic lesions in direct quantitative correlation to physiologic uptake in sites of physiological uptake in order to objectify the visual, clinical read out of RBC scintigraphy for unclear abdominal lesions suggestive of splenic tissues. **Materials and Methods:** Consecutive patients with ^{99m}Tc-labelled RBC scintigraphy (median 145 MBq) for assessment of suspected splenic tissue from 2013 to 2021 were included. A planar image of the abdomen (10 min p. i.) and a SPECT/low dose CT (30 min p. i.) were acquired. Firstly, scans were reviewed and rated either as vital splenic or non-splenic lesions by 4 nuclear medicine physicians. Then, lesions' uptake characteristics were quantified using a volume-of-interest (VOI)-based approach, hepatic uptake served as reference tissue. Uptake within target lesions and physiologic uptake of mediastinum, bone marrow and, if available, pancreas and suspected splenic tissue were quantified. Results: 43 abdominal lesions in 18 patients were investigated. 35 lesions were rated as vital splenic tissue. 7 lesions were rated as metastasis or other tissue. The median uptake ratio was significantly higher in splenic tissues (3.90 (range, 0.58-8.74)) compared to other lesions (0.61 (range, 0.01-0.87)), $p<0.001$. 1 lesion was excluded (spill-in from adjacent spleen). 5 new, priorly unnoted lesions were discovered due to increased uptake in RBC-scintigraphy. The median ratio of physiologic uptake in the pancreas was 0.16 (range 0.03-0.67), mediastinum 0.25 (0.04-2.37), bone marrow 0.17 (0.03-0.45) and orthotopic spleen 10.25 (0.61-29.82). Compared to orthotopic spleen tissues, pancreatic uptake showed the lowest uptake characteristics (median 0.16 vs. 10.25, $p<0.001$). **Conclusion:** RBC is highly feasible for assessment of suspected splenic tissues with detection of additional,

previously unknown sites of splenus. As the uptake in distinct extra-splenic reference regions such as the pancreas is invariably low compared to orthotopic spleen tissues, these areas can be used as both visual and quantitative comparator for the evaluation of suspected ectopic, recurrent or even intra-pancreatic splenic tissues. A histologically verified quantitative cutoff standardization for detection of splenic tissue is underway. **References:** none

OP-0978

Colorectal scintigraphy and abdominal ultrasound to assess bowel peristalsis during transanal irrigation in spinal cord injury patients: preliminary results

G. Rubini[1], A. Branca[1], G. Frasca[2], R. Sinisi[2], D. F. Altomare[3], A. Gaudiano[1];
[1]Section of Nuclear Medicine, DIM, University "Aldo Moro", Bari, ITALY, [2]Physical and Medicine Rehabilitation Departement of Basci Science, Neuroscience and Sense Organs, University "Aldo Moro", Bari, ITALY, [3]Department of Emergency and Organ Transplantation, University of Bari., Bari, ITALY.

Aim/Introduction: Bowel dysfunction is one of the most widespread clinical comorbidities associated with spinal cord injury (SCI), significantly impacting patients' quality of life. Transanal irrigation (TAI) system is a valid treatment that allows intestinal empting, when conservative treatment fail. Colorectal scintigraphy (CRS) during TAI with 99mTc-DiethylAminoPentaceticAcid Saline Solution (99mTc-DTPA-SS) allows to visualize the progression of the solution along entire colon. This prospective study aims to detect the different pattern of peristalsis activation with CRS and abdominal ultrasound (US). **Materials and Methods:** we enrolled 7 patients with SCI (6 traumatic, 1 non traumatic) who underwent a TAI (Peristeen®) session with dynamic CRS (1 frame/0.5 sec) to detect the 99mTc-DTPA-SS progression throughout the bowel; simultaneously whirlpools created from the solution transit were visualized on US, providing a qualitative score (normovalid-hypovalid), considering splenic flexure as anatomic landmark. 99mTc-DTPA-SS pumping system was stopped at T=30 sec (T0). Qualitative evaluation of post-evacuation images were done at CRS. Colon was divided into six segments corresponding to a Region of Interest (ROI) at dynamic CRS: cecum, ascending, transverse, splenic flexure, descending, rectosigmoid. Time activity curves (TAC) were obtained for each ROI and counts at 30sec time intervals were evaluated. Results: In 5/7 patients TAC suggested the presence of preserved peristalsis: decreasing counts in ROI drawn on distal colon segment, followed by increasing counts on proximal one, corresponded to a spike on the TAC, suggesting retrograde peristalsis activation. An opposite trend was suggestive of anterograde peristalsis. In these patients, at T0, both splenic flexure and ileocecal valve were detected with CRS and US showed normovalid whirlpools. In 2/7 patients, TAC showed a plateau in each ROI, suggesting a passive retrograde progression of 99mTc-DTPA-SS due to its pushing within the pump system and a single peak at the end of the dynamic exam corresponded to an anterograde peristalsis, coinciding with the evacuative stimulus. In this group, at T0, only splenic flexure was detected with CRS, while ileocecal valve was displayed later; US showed hypovalid whirlpools. Qualitative evaluation of post-evacuation images showed complete intestinal emptying in the first group, incomplete in the second one. **Conclusion:** Our preliminary results suggest that CRS is an imaging method able to evaluate progression of 99mTC-DTPA-SS along the entire colon during TAI. CRS could examine the peristalsis activation in SCI patients and could predict the treatment response. **References:** none

OP-0979

Clinical usefulness of ^{99m}Tc-labelled heat-denatured red blood cell SPECT/CT in the investigation of suspected ectopic splenic tissue

S. Georga, A. Kalaitzoglou, D. Katsampoukas, G. Arsos;
3rd Dept. of Nuclear Medicine, Aristotle University Medical School, Papageorgiou General Hospital, Thessaloniki, GREECE.

Aim/Introduction: Characterization of abdominal masses as ectopic splenic tissue may be unsuccessful by contrast enhanced CT or MRI. ^{99m}Tc-labelled heat-denatured red blood cell (^{99m}Tc-HDRBC) scintigraphy, based on the ability of the spleen to rapidly sequester injured erythrocytes, is highly accurate in detecting functional splenic tissue. The study is aiming to report on the use of ^{99m}Tc-HDRBC-SPECT/CT in the characterization of abdominal masses, suspected as ectopic splenic tissue, in various clinical settings. **Materials and Methods:** Nine ^{99m}Tc-HDRBC-SPECT/CTs performed to our department between 9/2014 and 1/2021 were retrospectively reviewed. Planar and SPECT/CT images, acquired 2 hours p.i of 2 mCi ^{99m}Tc-HDRBC, were visually and semiquantitatively evaluated. Post-^{99m}Tc-HDRBC-SPECT/CT imaging, included somatostatin receptor scintigraphy (SSRS, 3 cases), ^{18}F-FDG-PET/CT (1), dynamic pancreas CT (2), CT (2) and MRI (2). ^{99m}Tc-HDRBC-SPECT/CT findings were correlated with additional imaging, surgical results or clinical follow-up. Results: Nine adult patients (6 men, aged 53.4±14.6 years) with a total of 11 (seven with single, two with double) abdominal lesions, suspected of ectopic splenic tissue or splenosis by CT and/or MRI were involved. Three patients had previous splenectomy (one along with left hemicolectomy for colon cancer and two for refractory immune thrombocytopenia - ITP). ^{99m}Tc-HDRBC-SPECT/CT identified 6 of the 11 known abdominal lesions as functioning splenic tissue (4 splenosis, 2 accessory spleens / one intrapancreatic) and was negative in the rest five. One additional, previously undetected, small ectopic splenic mass was detected by SPECT/CT in a patient

with splenosis. Median lesion diameter was 1.8 cm. Eight lesions were located in the left upper abdomen and 4 were intrapancreatics. Among the ^{99m}Tc-HDRBC positive lesions, 3/7 were more intense than the liver and 4/7 fainter. All four patients with ^{99m}Tc-HDRBC confirmed splenic lesions avoided surgery and remained asymptomatic, apart from one with ITP who was submitted to splenectomy. In the 5 patients with ^{99m}Tc-HDRBC negative lesions, final diagnosis was NET in 3 (2 by surgery/histopathology, 1 by positive SSRS), GIST in 1 (by surgery/histopathology) and no diagnosis in 1 with an intrapancreatic mass, being anoperated and asymptomatic with stable MRI findings over one year. **Conclusion:** ^{99m}Tc-HDRBC scintigraphy is a clinically valuable noninvasive imaging modality for correct characterization of abdominal masses suspected as ectopic splenic tissue by CT or MRI, thus optimizing further patients' management. SPECT/CT increases the sensitivity of planar imaging for small lesions and those adjacent to native spleen and provides precise anatomic localization of the ectopic splenic tissue. **References:** None

1801

Saturday, October 23, 2021, 09:00 - 10:30

Channel 1

CME 13: Immunotheranostics

OP-0982

Immunotherapy and Nuclear Medicine diagnostics - Where do we Stand?

E. G. E. de Vries; *University Medical Center Groningen (UMCG), Department of Medical Oncology, Groningen, NETHERLANDS.*

OP-0983

Combining Immunotherapy and Radiation - Is the Whole more than the Sum of its Parts?

F. Herrera; *Centre Hospitalier Universitaire Vaudois (CHUV), Department of Oncology, Division of Radiation Oncology, Lausanne, SWITZERLAND.*

OP-0984

Nuclear Medicine Immunotheranostics - Synergisms and Antagonisms

N. Schaefer; *Centre Hospitalier Universitaire Vaudois (CHUV), Department of Nuclear Medicine and Molecular Imaging, Lausanne, SWITZERLAND.*

1802-1

Saturday, October 23, 2021, 09:00 - 09:45

Channel 2

Interview with the Expert 13 - A Life in NM

OP-0986

Interview - A Life in NM

I. Carrio; *Research Institute, Hospital Sant Pau, Barcelona, SPAIN.*

OP-0987

Interview - A Life in NM

TBA

1802-2

Saturday, October 23, 2021, 09:45 - 10:30

Channel 2

Interview with the Expert 14 - Prostate Cancer Imaging

OP-0988

Interview - Prostate Cancer Imaging

D. Oprea-Lager; *Amsterdam University Medical Centers, Department of Radiology & Nuclear Medicine, Amsterdam, NETHERLANDS.*

OP-0989

Interview - Prostate Cancer Imaging

J. Adam; *Amsterdam University Medical Center, Department of Radiology and Nuclear Medicine, Amsterdam, NETHERLANDS.*

1804

Wednesday, October 20 - Saturday, October 23, 2021

on-demand pool, release on Wednesday, October 20 at 09:00

Mini Course 3: Case Studies (Conventional Nuclear Medicine)

OP-0928

Interesting Cases in Conventional Nuclear Medicine

C. Pestean; *Ion Chricuta" Oncology Institute, Nuclear Medicine Department, Cluj Napoca, ROMANIA.*

OP-0929

How Clinic Affects the Image and its Interpretation

M. Gazzilli; *Spedali Civili, Nuclear medicine unit, Brescia, ITALY.*

1805

Wednesday, October 20 - Saturday, October 23, 2021

on-demand pool, release on Wednesday, October 20 at 09:00

Joint Symposium 25 (EANM/ESES/ESSO): Global Cost-Effectiveness of Different DTC Management Strategies

OP-0990

Costs of OVER - Diagnosis, Treatment and Follow-up of DTC Patients. How to Get Out of "a Vicious Circle"?

T. Geliashvili; N.N. Blokhin National Medical Research Center of Oncology (N.N. Blokhin NMRCO), Department of radionuclide therapy department, Moscow, RUSSIA.

OP-0991

Is Active Surveillance of Micro-Differentiated Thyroid Carcinoma Really Cheaper than Surgical Approach?

M. Raffaelli; Fondazione Policlinico Universitario Agostino Gemelli IRCCS, Università Cattolica del Sacro Cuore, Division of Endocrine and Metabolic Surgery, Department of Medical and Surgical Sciences, Rome, ITALY.

OP-0992

Cost-Effectiveness of Different Surgical Approaches in Differentiated Thyroid Cancer Patients

K. Lorenz; Martin Luther University, Halle, GERMANY.

OP-0993

Cost-Effectiveness of Postsurgical Pretreatment Radioiodine Imaging

J. Mihailovic; Oncology institute of Vojvodina, Department of Nuclear Medicine, Sremska Kamenica, SERBIA.

1806

Wednesday, October 20 - Saturday, October 23, 2021

on-demand pool, release on Wednesday, October 20 at 09:00

Joint Symposium 26 (EANM/ESMI/WMIS): Imaging Mitochondria and Mitochondrial Dysfunction

OP-0995

Imaging Mitochondrial Dysfunction in the Context of Neuroinflammation

C. Barca; Westfälische Wilhelms-Universität Münster, European Institute for Molecular Imaging (EIMI), Münster, GERMANY.

OP-0996

Value of TSPO Imaging in Cardiac Disease

J. Thackeray; Hannover Medical School, Department of Nuclear Medicine, Translational Cardiovascular Molecular Imaging, Hannover, GERMANY.

OP-0997

Imaging Oxidative Stress in Neurodegenerative Diseases

H. Okazawa; University of Fukui, Biomedical Imaging Research Center, Fukui, JAPAN.

OP-0998

In Vivo Imaging of Mitochondrial Membrane Potential in Cancer

M. Han; UCLA, David Geffen School of Medicine, Division of Pulmonary and Critical Care Medicine, Los Angeles, UNITED STATES OF AMERICA.

1809

Wednesday, October 20 - Saturday, October 23, 2021

on-demand pool, release on Wednesday, October 20 at 09:00

Cutting Edge Science Track - TROP Session: Artificial Intelligence - Clinical Applications

OP-1000

PBPK Model Based Voxel-wise Prediction of Post-therapy Dosimetry for ^{177}Lu-PSMA I&T Therapy

S. Xue[1], A. Gafita[2], M. Drobnjakovic[1], Y. Zhao[2], G. Birindelli[1], A. Afshar-Oromieh[1], M. Eiber[2], A. Rominger[1], K. Shi[1]; [1]University of Bern, Bern, SWITZERLAND, [2]Technical University of Munich, Munich, GERMANY.

Aim/Introduction: PSMA-directed radioligand therapy (RLT) has become one of the effective treatment options for metastatic castration-resistant prostate cancer (mCRPC). In EANM 2020, we proposed a deep learning method for voxel-wise prediction of post-therapy dosimetry from pre-therapy positron emission tomography (PET) images. However, the accuracy is still less satisfactory due to limited data. In this study, we propose to integrate physiologically based pharmacokinetic (PBPK) model in the pretraining of the deep learning methods to improve the prediction. **Materials and Methods:** 23 patients with mCRPC treated with ^{177}Lu-PSMA I&T RLT and 11 patients treated with ^{177}Lu-PSMA-617 were retrospectively included in this study. Only those cycles with pre-therapy PET imaging before the treatment and at least 3 post-therapeutic SPECT/CT dosimetry imaging were selected. Totally 48 treatment cycles from ^{177}Lu-PSMA I&T and 11 cycles from ^{177}Lu-PSMA-617 were considered for this proof-of-concept study. 3D RLT DoseGAN were developed with a 3D U-net generator and a

convolutional neural network (CNN) based discriminator. For pretraining, 266 digital phantoms were generated based on the PBPK modeling on XCAT phantoms to simulate a variety of pretherapy PET and the spatiotemporal distribution of therapy ligands. A forward projection PET simulator was employed to simulate PET imaging on digital phantoms and dose-kernel methods were applied to generate post-therapy dosimetry. Results: The preliminary results showed that, the PBPK pre-trained 3D RLT Dose GANs achieved the voxel-wise normalized root mean squared error (NRMSE) of 3.2±0.7% (mean±std.) (3.8±0.7% without pre-training) and peak signal-to-noise ratio (PSNR) of 30.1±1.8 (28.5±1.6% without pre-training) on ^{177}Lu-PSMA I&T. As for PSMA-617, it achieves 2.1±0.8% NRMSE (2.2±0.7% without pre-training) and PSNR of 34.0±3.8 (34.0±3.9% without pre-training) on ^{18}F dataset, and 1.8±0.9% NRMSE (1.9±0.8% without pre-training) and PSNR of 35.0±2.5 (34.5±3.9% without pre-training) on ^{68}Ga dataset. Furthermore, clinical assessment with coronal maximum intensity projection (MIP) and dose volume histogram (DVH) also confirmed that our proposed model achieved similar performance on examples from these two datasets in terms of image quality. The AI-generated dosimetry images achieved a general mean absolute error (MAE) of 21.2±10.8% (24.0±10.0% without pre-training) to the ground truth, in terms of DVH. **Conclusion:** Our experimental results demonstrate the incorporation of PBPK model may improve the development of artificial intelligence methods for dosimetry prediction and accelerate the implementation of dosimetry-guided treatment planning for RLT. **References:** none

OP-1001

A Neural Network Add-on to Classify I^{123}-Ioflupane Images

J. McCormick, R. Staff;
NHS Grampian, Aberdeen, UNITED KINGDOM.

Aim/Introduction: The use of semi-quantitative analysis of Ioflupane (I^{123}) imaging to aid diagnosis is increasing available. Extracting the specific binding ratios (SBR) which represent the DaT uptake in the caudate and putamen is commonly used with an age-matched normal database to distinguish between diseases and controls. These quantitative extraction tools frequently generate multiple metrics, such as symmetry, caudate to putamen ratios along with striatal to background ratios of varying utility. How these measures should be aggregated to reach a diagnostic conclusion is unclear. In this study we developed and validated a neural network (NN) approach using SPSS®, to classify DaT images using these extracted values and compared them with the individual quantitative measures and published estimates of expert visual interpretation. **Materials and Methods:** 200 local patient and 131 healthy control DaT datasets from the Parkinson's Progression Markers Initiative were used. The datasets were classified by expert opinion of visual interpretation. The semi-quantitative data was extracted using DaTQUANT™. The data was randomised to either the discovery or validation set. A NN was created using the discovery set and tested using the validation set, producing a validation ROC curve. This was repeated 10 times using data randomly assigned to the discovery or validation set and the average area under the curve (AUC) estimated. The process was repeated introducing demographic data, added to the NNs to assess discriminatory value of gender, age and referral type. The NN used a 70:30 partition between discovery and validation. The hidden layer architecture was automatic, the training was batch type and the optimisation algorithm was scaled conjugate gradient. Results: The highest average AUC ROC using one DaTQUANT™ extracted value was 0.8852 (s.e. 0.020). The NN AUC achieved was 0.9357 (s.e. 0.0153). The NN significantly improves the AUC ROC ($p<0.05$). The NN had a specificity of 88% for a sensitivity of 84% (95%CI of 77-89%). Expert visual interpretation of a similar study had a sensitivity of 84% and specificity of 71% [1]. The addition of age into the NN did not significantly improve the AUC ROC ($p>0.05$), 0.9360 (s.e. 0.0156). **Conclusion:** The use of AI in conjunction with semi-quantitative analysis performs well for the diagnostic task. The NN performed as well as expert visual interpretation and better than quantification alone. **References:** [1] Kenneth J. Nichols, et al, Interpreting ^{123}I-ioflupane dopamine transporter scans using hybrid scores, Eur J Hybrid Imaging. 2018; 2(1): 10

OP-1002

Prediction of Major Adverse Cardiac Events after Myocardial Perfusion Imaging using multi-task deep neural network and time-to-event data

K. Pieszko[1], A. Singh[1], A. Killekar[1], Y. Otaki[1], T. Sharir[2], A. J. Einstein[3], M. B. Fish[4], T. D. Ruddy[5], P. Kaufmann[6], A. J. Sinusas[7], E. J. Miller[7], T. M. Bateman[8], S. Dorbala[9], M. Di Carli[9], D. Dey[1], J. Liang[1], D. S. Berman[1], P. J. Slomka[1];
[1]Department of Imaging (Division of Nuclear Medicine), Medicine, and Biomedical Sciences, Cedars-Sinai Medical Center, Los Angeles, CA, UNITED STATES OF AMERICA, [2]Department of Nuclear Cardiology, Assuta Medical Centers, Tel Aviv, ISRAEL, [3]Division of Cardiology, Department of Medicine, and Department of Radiology, Columbia University Irving Medical Center and New York-Presbyterian Hospital, New York, NY, UNITED STATES OF AMERICA, [4]Oregon Heart and Vascular Institute, Sacred Heart Medical Center, Springfield, OR, UNITED STATES OF AMERICA, [5]Division of Cardiology, University of Ottawa Heart Institute, Ottawa, ON, CANADA, [6]Department of Nuclear Medicine, Cardiac Imaging, University Hospital Zurich, Zurich, SWITZERLAND, [7]Section of Cardiovascular Medicine, Department of Internal Medicine, Yale University School of Medicine, New Heaven, CT, UNITED STATES OF AMERICA, [8]Cardiovascular Imaging Technologies LLC, Kansas City, MT, UNITED STATES OF AMERICA, [9]Department of Radiology, Division of Nuclear Medicine and Molecular Imaging, Brigham and Women's Hospital, Boston, ME, UNITED STATES OF AMERICA.

Aim/Introduction: Multiple studies evaluated the use of machine learning algorithms to predict major adverse cardiac events (MACE) using clinical and imaging variables, but the time-to-event is often neglected during training and evaluation of models. We evaluated the prediction of both composite MACE endpoint as well as prediction of its individual components by the DeepHit model that uses a deep neural network to learn the distribution of survival times directly and can handle competing risks. Prognostic performance was compared with that of XGBoost model, which was previously applied to MACE prediction in similar scenarios. **Materials and Methods:** From the multi-center REgistry of Fast Myocardial Perfusion Imaging with NExt generation SPECT (REFINE SPECT), 20414 patients (64±8 years, 56% male) undergoing stress Tc-99m SPECT-MPI were followed for 4.5±1.7 years for MACE. Patients who underwent early revascularization (<90 days from scan) were excluded from analysis (n=698). MACE consisted of all-cause death, nonfatal myocardial infarction, unstable angina, or late revascularization (≥90days). Two competing events were defined: death and acute coronary syndrome (ACS) or late revascularization. A single DeepHit model was trained to predict distribution of survival of these events. The DeepHit model was compared with XGBoost classifier in terms overall concordance of predictions, area under receiver operating curve (AUC) and model calibration using Brier score. Results: For the prediction of death within 1 year from scan DeepHit outperformed XGBoost (AUC 0.841 vs. 0.819, p=0.02; Brier score 0.02 vs. 0.05). Similarly for the prediction of ACS or late revascularization within 1 year from scan DeepHit provided better performance (AUC 0.747 vs. 0.722; Brier score 0.03 vs 0.05). For the prediction of 1-year MACE DeepHit AUC was comparable to XGBoost (0.772 vs 0.763,p=0.17) but Brier score was better (0.04 vs 0.09, respectively). For long-term prediction XGBoost performed better than DeepHit (AUC 0.769 vs 0.751, p<0.0001 for MACE within 3 years from scan. The concordance index for the prediction of overall MACE probability of the DeepHit and XGBoost models were 0.74 and 0.76, respectively. **Conclusion:** The use of a multi-task survival model allows for more accurate prediction of events within a-1-year from the scan. The ability to handle competing risk scenarios allows for selecting patients at the highest risk of a specific event. This approach could allow adjust the management to the individual patient's risk profile more precisely. Unlike standard classification models, DeepHit allows to estimate the survival probability at any chosen time from scan. **References:** none

OP-1003

A convolutional neural network-based program to predict nodal metastasis of non-small cell lung cancer in ^{18}F-FDG PET

***E. Kidera**, S. Koyasu, T. Ishimori, Y. Nakamoto;*
Department of Diagnostic Imaging and Nuclear Medicine, Graduate School of Medicine, Kyoto University, Kyoto, JAPAN.

Aim/Introduction: To develop a convolutional neural network (CNN)-based program to predict nodal metastasis of non-small lung cell cancer (NSCLC) in ^{18}F-FDG PET. **Materials and Methods:** We obtained PET images for the initial staging of NSCLC from six datasets in The Cancer Imaging Archive (TCIA) and included 435 patients with nodal staging available. We generated 36 maximum intensity projection (MIP) images of the thoracic region from the PET images for each patient. A residual network (ResNet)-based CNN was trained using MIP images of 304 (70%) patients to predict whether nodal metastasis was present. We tested the performance of the trained CNN using the rest 131 (30%) patients. Accuracy, precision, recall and F-score were calculated in an image-based analysis and in a patient-based analysis. In the patient-based analysis, a patient was classified as positive for nodal metastasis when more than 18 out of 36 MIP images were classified as positive referring to previous research [1]. We used Gradient-weighted Class Activation Mapping (Grad-CAM) to confirm that the CNN extracted information mainly from hilar or mediastinal regions. One radiologist also classified the patients as positive or negative for nodal metastasis using MIP images and accuracy, precision, recall and F-score were calculated. To quantify the agreement of the CNN and the radiologist, the Cohen's kappa was also calculated. Results: 235 (51%) of the patients had regional nodal metastasis (N1, N2 or N3). In the image-based analysis, accuracy, precision, recall and F-score were 0.706, 0.728, 0.678 and 0.702, respectively. In the patient-based analysis, accuracy, precision, recall and F-score were 0.756, 0.797, 0.701 and 0.746, respectively. Grad-CAM highlighted hilar or mediastinal regions in all of the MIP images classified as positive in visual evaluation. In the patient-based classification by one radiologist, accuracy, precision, recall and F-score were 0.771, 0.803, 0.731 and 0.766, respectively. The Cohen's kappa between the classification by the CNN and that by the radiologist was 0.631. **Conclusion:** A CNN-based program using MIP images of PET predicted nodal metastasis of NSCLC with comparable reliability to one radiologist. Our preliminary results suggested that the CNN-based program could be a promising tool to support radiologists to detect lymph node metastasis. **References:** [1] Kawauchi K et al. "A convolutional neural network-based system to classify patients using FDG PET/CT examinations." BMC Cancer. 2020 Mar 17;20(1):227.

OP-1004

Artificial Intelligence based outcome classification from baseline ^{18}F-FDG PET/CT in de novo diffuse Large B-cell lymphoma patients

R. Boellaard[1], D. Wesseling[1], C. Eertink[1], B. de Vries[1], E. Lugtenburg[2], B. Zwezerijnen[1], S. Wiegers[1], R. Vet[1], S. Golla[1], J. Zijlstra[1];
[1]Amsterdam University Medical Centers, Amsterdam, NETHERLANDS, [2]Erasmus MC Cancer Institute, Rotterdam, NETHERLANDS.

Aim/Introduction: Diffuse large B-cell lymphoma (DLBCL) is the most common type of aggressive non-Hodgkin's lymphoma. At present clinical information, such as IPI and age, as well as baseline PET uptake metrics, such as metabolic tumor volume, are used or investigated for prognostication. The aim of this study was to develop an artificial intelligence (AI) based prediction of 2-year time to progression (TTP) for DLBCL patients using maximum intensity projections (MIPs) of baseline ^{18}F-FDG PET images. **Materials and Methods:** A convolutional neural network (CNN) was developed, trained and cross-validated to predict outcome using ^{18}F-FDG MIP PET scans of 296 DLBCL patients. The CNN was used to generate a probability score for outcome < 2 year TTP ($prob^{cnn}$). Next, logistic regressions were performed using these $prob^{cnn}$. These regressions were extended by including clinical data (age, LDH/ULN, IPI) as well as standard PET parameters (total metabolic tumor volume (MTV)) and maximum distance between the largest lesion and any other lesion (Dmaxbulk). Performance of the models were assessed by the area under the curve of the receiver operating characteristic curves (ROC-AUC) using 5-fold cross-validation. Results: The logistic regression model based on only clinical data and standard PET metrics yielded a cross-validated ROC-AUC of 0.71±0.11. Using the CNN alone provided a 2-year TTP prediction with a cross-validated ROC-AUC of 0.69±0.07. The combined logistic regression model using clinical prognostic factors together with $prob^{cnn}$ resulted a cross-validated ROC-AUC of 0.79±0.08. **Conclusion:** The predicted probability from a CNN can be successfully combined with patient-specific characteristics in a logistic regression model for prediction of the 2-year TTP of DLBCLs. The inclusion of a CNN estimated probability during logistic regression improved the ROC in terms of higher AUC and better cross-validated variabilities. **References:** None

OP-1005

Bone scintigraphy classification: a comparison between machine learning and deep learning classifiers using imaging data only

M. Silva[1,2,3], F. Oliveira[1], J. Castanheira[1], Â. Silva[1], L. Vieira[4], D. Costa[1];
[1]Champalimaud Centre for the Unknown, Champalimaud Foundation, Lisbon, PORTUGAL, [2]Instituto Superior de Engenharia de Lisboa, Instituto Politécnico de Lisboa, Lisbon, PORTUGAL, [3]Mercurius Health, Oeiras, PORTUGAL, [4]Health and Technology Research Center, Escola Superior de Tecnologia da Saúde de Lisboa, Lisbon, PORTUGAL.

Aim/Introduction: Computer-aided diagnosis to classify bone scintigraphy (BS) is more and more used with variable results. Variability is, most likely, due to: dataset, features used (image and/or demographic), type of classifier and algorithms implementation. This impacts on independent evaluation of the potential of each technique and BS images to clearly identify bone metastases (BM). Our aim was to compare common classification techniques, based on machine/deep learning, in the identification of BM using BS images only. **Materials and Methods:** A sample of 432 patients (mean age 65 years, 247 female) was retrospectively selected: 156 prostate cancer, 222 breast cancer, 35 other oncological pathologies and 19 unknown oncological disease. BS whole-body acquisitions were performed in a Philips BrightView gamma camera (matrix 512x1024, pixel size 2x2mm^2). Patients were injected with 650-750MBq of [^{99m}Tc]HDP, and the images obtained 2-4h post-injection. Malignant and doubtful lesions were identified by a nuclear medicine physician based on patient's BS and all clinical information available. Any other bone "hotspot" was considered benign. Images' intensity was normalized by the median value of the main bone structures of each patient [1]. The classifiers selected were: decision trees (DT), support vector machines (SVM), k-nearest neighbor (kNN), artificial neural network (ANN) and convolutional neural network (CNN), available in the Matlab R2019a software. The DT, SVM, kNN and ANN classifiers were fed with lesion's intensity and geometric features extracted from the BS images after lesions segmentation [2]. The CNN classifier was fed with image patches (32x32 pixels) centered on each lesion. Classifiers were compared based on the balanced accuracy (mean of sensitivity and specificity) obtained from leave-one-out cross-validation method. Results: In total, 1308 malignant lesions and 856 benign hotspots were identified. The balanced accuracy values obtained were: 65%, 70%, 69%, 69% and 66%, for DT, SVM, kNN, ANN and CNN classifiers, respectively. CNN optimizer was harder to optimize than all other classifiers. **Conclusion:** The classifiers reached very close results, SVM being the best of all. CNN classifier performed worse than most of the others and was the hardest to optimize, despite the advantage of not requiring segmentation. The obtained balanced accuracies were inferior to some of those already published, mainly due to the use of BS imaging features only - any other patients' information was not considered. Funding: BTSCAD project, ref.: LISBOA/NORTE-01-0247-FEDER-017685 **References:** [1] Oliveira et al, EJNMMI 2018;45:S44-S5; [2] Constantino et al, Eur Radiol 2021;31:3071-9

OP-1006

Estimation of FAZA-uptake regions in high-grade glioma from MR images: a preliminary transfer learning artificial intelligence study

L. Presotto[1], C. Bezzi[2], V. Bettinardi[1], S. Ghezzo[2], P. Mapelli[2,1], F. Fallanca[1], B. Catalfamo[3], A. Castellano[4,2], G. Conte[5], I. Neri[1], C. Monterisi[1], A. Panzacchi[1], P. Scifo[1], L. Gianolli[1], N. Anzalone[4,2], P. Maria[1,2];

[1]Nuclear Medicine Unit, IRCCS Ospedale San Raffaele, Milan, ITALY, [2]Vita-Salute San Raffaele University, Milan, ITALY, [3]University of Messina, Messina, ITALY, [4]Department of neuroradiology, IRCCS Ospedale San Raffaele, Milan, ITALY, [5]Mayo Clinic, Rochester, MN, UNITED STATES OF AMERICA.

Aim/Introduction: To investigate whether convolutional neural networks can predict hypoxic regions on MRI scans in patients with high-grade glioma (HGG), based on ^{18}F-labeled fluoroazomycinarabinoside (^{18}F-FAZA) PET data, thanks to the use of transfer learning. Specifically, a network learnt features specific of glioma on a massive public database, so that these features could be exploited to predict hypoxia despite the availability of a small sample of subjects **Materials and Methods:** In this monocentric study 18 patients (13 males, 5 females; mean age: 65, range: 1-81) with brain MRI suggestive for HGG underwent 18F-FAZA PET/CT before treatment between April 2016 and October 2017 for hypoxia assessment. Regions of interests (ROIs) identifying tumour's hypoxic areas were manually drawn by an expert nuclear medicine physician on PET scans. For each patient, T1, T2, Flair and Gadolinium contrast enhanced T1 MRI sequences were retrieved, co-registered to PET scans and resampled to isotropic 2x2x2 mm^3 pixel size. A modified 2.5D U-Net, with residual blocks, was initially trained on the publicly available Brain Tumor Segmentation (BraTS) database. It differentiated three sub-regions (contrast-enhancing area, peritumoral edema, necrotic core and non-enhancing area), given in input the listed MR sequences with a Dice Similarity Coefficient (DSC) of 0.89, 0.64 and 0.74 for whole tumor, core and contrast enhancing area respectively), the model was saved. In this work it was assumed that the layer before the output convolution contains all relevant features characterizing the glioma environment, and a new model was created taking this as its input to a single 1x1 convolution layer. The weights from the first model were fixed. In a leave-one-out approach the second model was trained on 17 patients and evaluated on the remaining one, to predict the hypoxic ROI determined on PET. DSC was used to evaluate model performance. Results: The transfer learning approach proposed resulted in a CNN with only 33 free parameters to be trained, thus avoiding overfitting. Furthermore, training took only 250s on a CPU. The DSC was higher than 0.62 in 88% of the patients. The mean and median dice were 0.69 and 0.73, respectively. **Conclusion:** This exploratory study suggests that artificial intelligence can estimate the regions determined to be hypoxic by FAZA-PET, by combining information extracted from MR sequences in novel ways. Further validation will be performed to best investigate the regions characterized by false positives and negatives. It also highlight the potential of transfer learning for rare pathologies. **References:** none

OP-1007

An exploratory study of the application of convolutional neural networks to ^{99m}Tc-DPD scans for amyloidosis classification

E. Sousa[1,2], A. Tweddel[2], G. Avery[2], A. Turner[3], S. J. Archibald[1,2];

[1]Positron Emission Tomography Research Centre, University of Hull, Cottingham Road, Hull, HU6 7RX, Hull, UNITED KINGDOM, [2]Castle Hill Hospital, Hull University Teaching Hospitals NHS Trust, Castle Road, Cottingham, East Yorkshire, HU16 5JQ, Hull, UNITED KINGDOM, [3]School of Computer Science, University of Nottingham, Computer Science Building, Wollaton Rd, Lenton, Nottingham NG8 1BB, Nottingham, UNITED KINGDOM.

Aim/Introduction: The application of convolutional neural networks (CNNs) in medical image classification is increasing. However, the performance of CNNs is dependent on the quality of data available. In ^{99m}Tc-3,3-diphosphono-1,2-propanodicarboxylic acid (^{99m}Tc-DPD) examinations for amyloidosis diagnosis, there can be variations in tracer uptake that can interfere with the classification accuracy of the CNNs. The aim of this study was to evaluate the applicability of CNNs in the classification of amyloidosis assessing the interfering factors in classification. **Materials and Methods:** Two different CNNs, one with 15 layers (CNN15) and the other with 27 Layers (CNN27) were designed and applied to ^{99m}Tc-DPD scans in patients for binary classification of the images as healthy or non-healthy in terms of the presence of amyloidosis. The scans were previously classified by an expert following the Perrugini Grade (PG) classification for amyloidosis where healthy is PG=0, and unhealthy is PG>0. Whole Body (WB) and segmented region images(heart(H), kidneys(K), heart and kidneys (HK)) were used. Some of the databases used for training and testing of the system were enlarged by symmetrically rotating the images. The accuracy of the classification was evaluated for each variation in region analysed, the size of the database, the projection used (Anterior/Posterior), the presence or absence of images with unusual uptake profiles, the different distributions between training/testing data, and the presence or absence of cases that had early diagnosis of amyloidosis. Results: CNN27 performed better than CNN15 in classifying the WB images, achieving results of accuracy, in most of the cases, above 0.75 and, in some cases, above 0.90, compared with only 0.50 to 0.80 for CNN15. CNN15 showed better accuracy in the segmented regions where unusual uptake cases and borderline values were not included, and even with the augmentation of the databases the accuracy could not be improved for CNN15. Both databases performed better when

only PG > 1 images were included in the unhealthy database. Using CNN15 to analyse the segmented regions accuracy values ranging between 0.55 in HK (as the lowest) and 1 (as the highest) in H were obtained. **Conclusion:** This exploratory study of application of CNNs to clinical amyloidosis images showed promising results. Although results are limited due to the small size of the databases used, CNN15 was demonstrated to have good discriminatory ability when classifying images of the segmented heart region of ^{99m}Tc-DPD in amyloidosis patients. CNN27 demonstrated good results in classification of WB images. **References:** none

OP-1008

Fully Automated Detection and Segmentation of Hypermetabolic Lesions in Pretherapeutic [^{18}F]FDG PET / CT Images of Lymphoma and Sarcoidosis Patients

A. Iantsen[1], P. Lovinfosse[2], M. Ferreira[3], A. Jadoul[2], N. Withofs[2], C. Derwael[2], A. Frix[4], J. Guiot[4], D. Visvikis[1], M. Hatt[1], R. Hustinx[2,3];
[1]LaTIM, INSERM, UMR 1101, Univ Brest, Brest, FRANCE, [2]Division of Nuclear Medicine and Oncological Imaging, University Hospital of Liège, Liège, BELGIUM, [3]GIGA-CRC in vivo Imaging, University of Liège, Liège, BELGIUM, [4]Pneumology Department, University Hospital of Liège, Liège, BELGIUM.

Aim/Introduction: Automated detection and segmentation of pathological uptakes in [^{18}F]FDG PET images can be useful to derive clinically relevant metrics such as total tumor burden for diagnosis and prognosis purposes. It remains a challenging task given the large possible range of number, location, size and heterogeneity of lesions. Semi-automated delineation such as the use of manually adjusted thresholds applied to visually detected lesions by an expert, remains time-consuming and subjective, and a fully automated approach is thus desirable for improved robustness and reproducibility. The goal of this work was to evaluate the feasibility of achieving fully automated detection and delineation by training a deep convolutional neural network. **Materials and Methods:** A cohort of 419 patients who underwent pretherapeutic [^{18}F]FDG PET and associated low-dose CT scans was retrospectively collected for the purpose of developing and testing the proposed algorithm. The ground-truth for each PET/CT scan was determined semi-automatically by one of four physicians following the same procedure, i.e. standardized uptake value (SUV) threshold of 3, volume > 2 cc and manual correction whenever deemed necessary. The seminal U-Net architecture was applied "off the shelf" to develop the model on 397 patients and evaluate it on 22 test patients. In addition, the test subset was annotated by all experts independently to evaluate inter-observer variability. Dice similarity coefficient (DSC), Sensitivity (SE) and Positive Predictive Value (PPV) computed on a patient basis (i.e., all lesions considered together) were used for the first stage evaluation. A lesion by lesion analysis was then performed applying different detection criteria. An ablation study was carried out to identify main factors affecting segmentation results. Results: The model obtained good average accuracy for all metrics on the patient basis (DSC=0.84±0.16) with SE (0.84±0.21) and PPV (0.90±0.12). On the lesion basis, the performance varied (DSC between 0.61 and 0.77; SE 0.60 - 0.75; PPV 0.66 - 0.83) depending on the chosen detection criteria. The analysis of the inter-observer variability demonstrated insignificant differences between the ground-truth annotations of all experts (e.g., the patient-wise DSC=0.96±0.15) and ensured the reproducibility of the procedure for establishing the ground-truth. Visual inspection confirmed the relevance of the model predictions and revealed the limitations inherent to the evaluation method. **Conclusion:** The proposed approach achieved good overall results and might provide a robust and accurate fully automated solution for future works investigating the clinical prognostic and predictive value of metrics derived from these segmentation masks. **References:** none

OP-1009

A Fully Automated Method For Bladder Segmentation In PSMA PET/CT Scans

Y. Farag[1], R. de Schaetzen[1], G. Chaussé[2], F. Yousefirizi[1], I. Klyuzhin[2], A. Rahmim[2,3], C. Uribe[2,3];
[1]BC Cancer Research Institute, Vancouver, BC, CANADA, [2]BC Cancer, Vancouver, BC, CANADA, [3]Department of Radiology, University of British Columbia, Vancouver, BC, CANADA.

Aim/Introduction: Current methods for reliable organ segmentation from medical scans often require physician supervision, introducing variability and labour. In prostate cancer, standardization of prostate segmentation and precise lesion reporting would facilitate comparison between prostate imaging and biopsies, with the potential to improve targeted biopsies and thereby diagnostic accuracy. Prostate-specific membrane antigen (PSMA) PET/CT imaging allows for relatively low-noise scans of the pelvis with high prostate lesion uptake, but suffers from urinary excretion resulting in high bladder uptake adjacent to the prostate gland. We aim to develop a fully automated method for bladder segmentation to potentially subtract it from PSMA PET/CT scans without altering local prostate cancer detection. We believe this first step to be paramount in developing accurate tools to segment prostate glands and prostate lesions for standardized lesion reporting. **Materials and Methods:** To this end, we proposed a fully automated deep segmentation model for the bladder. A labelled dataset was created from a cohort of 59 PET/CT PSMA scans. Images were segmented by a nuclear medicine physician using semi-automated tools available with MIM (MIM Software USA) to identify the prostate gland, the seminal vesicles, PSMA-positive prostate lesions, the bladder, and the urethra (when urine-containing). A training dataset (n=40) of randomly selected samples was used to train a 3D U-Net model in a multi-class setting with a per-class Dice similarity coefficient (DSC) objective to predict labels of tumor, bladder, or background for each pixel in a

PET scan. The model was then evaluated on the test data (n=19). The performance of the methods was quantified using the DSC. Results: Our model achieved a mean DSC score of 0.911 ± 0.096, with a median of 0.937 on the test data. The predicted bladder segmentations had an average overlap of 1.58 pixels with respect to the ground truth tumor segmentations. A threshold value of 40% on predicted bladder probabilities showed minimal impact on DCS score (0.900 ± 0.101 mean, 0.927 median) and reduced tumor overlap to 0 pixels. This demonstrates predicted bladder segmentations can be safely masked from PET scans without impacting the accuracy of subsequent tumor detection. **Conclusion:** Our automated method, based on the U-Net architecture, accurately segments the bladder from PET PSMA scans. The method, in combination with fixed threshold post-processing, was able to achieve zero tumor overlap. The proposed approach is a critical step towards automating prostate lesion detection and improving standardization of clinical reporting. **References:** none

OP-1010

Classification of the image embeddings extracted from pretrained CNNs using tree-based models: a proof-of-concept study in medical imaging

N. Gozzi[1], E. Giacomello[2], M. Sollini[3,1], M. Kirienko[4], C. Jones[5], P. Lanzi[2], D. Loiacono[2], A. Chiti[3,1];
[1]IRCCS Humanitas Research Hospital, Rozzano - Milan, ITALY, [2]Dipartimento di Elettronica, Informazione e Bioingegneria, Politecnico di Milano, Milan, ITALY, [3]Department of Biomedical Sciences, Humanitas University, Pieve Emanuele - Milan, ITALY, [4]Fondazione IRCCS Istituto Nazionale Tumori, Milan, ITALY, [5]Dipartimento di Biotecnologie Mediche e Medicina Traslazionale, Università degli Studi di Milano, Milan, ITALY.

Aim/Introduction: CNNs achieve great performances thanks to high computational power and large publicly available datasets. Transfer learning, i.e. leveraging patterns learned on a large dataset to improve generalization for another task, is an effective approach for computer vision tasks on small datasets. However, in medical imaging we still lack of pretrained machine learning models that could be easily adapted to new tasks. In this work, we propose: 1) the development of feature extractor CNN models, trained using large publicly available datasets of labeled medical images 2) the classification of the image embeddings extracted from the pretrained CNNs using tree-based models, validated on an independent local dataset. We tested this proof-of-concept approach on chest radiographs (CXRs). **Materials and Methods:** Seven CNNs (DenseNet121, DenseNet169, DenseNet201, InceptionResNetV2, Xception, VGG16, VGG19) were trained on CheXpert[1], a public dataset composed of 223316 CXRs with 14 major-findings labels. Then, we applied the trained networks as a feature extractor stage to an independent dataset composed of 941 CXRs collected at IRCCS Humanitas Research Hospital. Based on radiological report, each image was labeled as normal/abnormal and abnormalities were further classified as cardiac, lung, pneumothorax, pleura, bone, device. To obtain semantically strong high-level features, we extracted the output of each CNN (image embeddings) before the classification layer. The extracted embeddings for each CNN (70% training, 30% test) were used to train a Random Forest (RF) model, to perform multi-label classification. Ensembling of the results was performed using simple and entropy-weighted averaging. Model performance was assessed by using the area under the curve (AUC). Results: The best RF model, obtained with simple averaging of the predictions, achieved for each label the following AUC values: normal 0.86, cardiac 0.85, lung 0.72, pneumothorax 0.92, pleura 0.94, bone 0.85, device 0.86 (average of 0.856). The training time was in the order of few minutes. **Conclusion:** CNNs pre-trained on a large public dataset of medical images can be exploited as feature extractor for a task of interest even if different from the original one. The extracted image embeddings contain relevant information to train an additional classifier with good performance on an independent dataset. This overcomes the need for large private datasets, high computational resources and long training times. Further studies on different image modalities, including nuclear medicine and molecular imaging, are planned to confirm our findings. **References:** [1] Irvin et al., "Chexpert: A large chest radiograph dataset with uncertainty labels and expert comparison" 2019

OP-1011

Automatic PET image quality control using Convolutional Neural Networks

E. Pfaehler;
University of Augsburg, Augsburg, GERMANY.

Aim/Introduction: Machine learning studies require a large number of images often acquired at different PET/CT systems. When combining images from different systems, the use of harmonized image quality is essential, i.e. following EARL standards. However, for retrospective data EARL accreditation may not have initially been in place. An automated quality control gives the opportunity to retrospectively check if images meet certain quality standards. The aim of this study was to develop a convolutional neural network (CNN) that can identify if an image is EARL compliant. **Materials and Methods:** 106 PET images acquired on three PET/CT systems (Philips Gemini, GE Discovery, Siemens Biograph mCT40) were included in the study. All images were reconstructed with the locally clinical preferred, EARL1, and EARL2 compliant reconstruction protocols and 120s scan duration. First, an edge-enhanced image was generated by subtracting a PET image from the 6 mm Full-Width-At-Half-Maximum Gaussian smoothed image. These 'edge' images were then used to train two sparse CNNs: One CNN was trained to distinguish clinical and EARL compliant reconstructions. Images found to be EARL compliant were then consecutively used in a second CNN

optimized to identify EARL1 and EARL2 compliant images. The accuracy of both CNNs was assessed using 10-fold cross validation. Next, the CNNs were trained on the whole dataset. To test the final CNN on an independent dataset and to assess the impact of image noise on the CNN decision, the CNNs were applied to 30 images acquired at a Siemens Biograph Vision reconstructed with 30, 60, 120, and 180 s scan duration. Results: In the cross-validation, the first CNN classified 100% of the clinical, 100% of the EARL1 compliant, and 95% of the EARL2 compliant images correctly. When using the second CNN specialized on distinguishing between EARL1 and EARL2 compliant images, the CNN classified 95% of EARL1 compliant images and 85% of EARL2 compliant images correctly. The accuracy in the independent dataset was comparable to the accuracy in the cross-validation for both CNNs. The scan duration had no impact on the results. **Conclusion:** We developed two consecutive CNNs that can automatically identify if an image is meeting EARL standards. In this way, images that are not EARL compliant can retrospectively be adjusted (by adding additional smoothing). This gives the opportunity to retrospectively include studies in a multi-center setting in which harmonization of images from different PET systems is essential. **References:** None.

1810

Wednesday, October 20 - Saturday, October 23, 2021

on-demand pool, release on Wednesday, October 20 at 09:00

Clinical Oncology Track - TROP Session: Lymphoma and Other Hematological Tumours

OP-1013

Reliability of Deauville Scale for Lymphoma PET assessment in FIL and IELSG multi-center clinical trials

F. Bergesio[1], L. Guerra[2], F. Fallanca[3], M. Gregianin[4], S. Morbelli[5], U. Ficola[6], S. Peano[7], G. Storto[8], A. Franceschetto[9], L. Melis[10], E. Borsasti[11], G. Treglia[12], L. Ceriani[12], A. Versari[13], S. Chauvie[1]; [1]Medical Physics Division, S. Croce e Carle Hospital, Cuneo, ITALY, [2]Nuclear Medicine Division, S. Gerardo Hospital, Monza, ITALY, [3]Nuclear Medicine Division, S. Raffaele Hospital, Milan, ITALY, [4]Nuclear Medicine Division, Istituto Oncologico Veneto IRCCS, Padua, ITALY, [5]Nuclear Medicine Division, S.Martino Hospital, Genova, ITALY, [6]Nuclear Medicine Division, La Maddalena Hospital, Palermo, ITALY, [7]Nuclear Medicine Division, S. Croce e Carle Hospital, Cuneo, ITALY, [8]Nuclear Medicine Division, IRCCS CROB, Rionero in Vulture, ITALY, [9]Nuclear Medicine Division, AO Universitaria, Modena, ITALY, [10]Nuclear Medicine Division, A. Businco Hospital, Cagliari, ITALY, [11]Nuclear Medicine Division, CRO Hospital, Aviano, ITALY, [12]Nuclear Medicine Division, IOSI Hospital, Bellinzona, SWITZERLAND, [13]Nuclear Medicine Division, S. Maria Nuova Hospital, Reggio Emilia, ITALY.

Aim/Introduction: According to the Lugano classification, Deauville scale (DS) is the recommended scoring system for reporting of interim (iPET) and end-of-therapy (ePET) Positron Emission Tomography (PET/CT) in FDG-avid lymphoma.In this work we evaluated the reliability of the DS used in multi-center trials of Italian Foundation Lymphoma (FIL) and of International Extranodal Lymphoma Study Group (IELSG). **Materials and Methods:** Five trials were included in this analysis: HD0607 (Advanced-stage Hodgkin Lymphoma);FOLL12 (Follicular Lymphoma);DLCL10 (Diffuse Large B-Cell Lymphoma);ROUGE (Advanced-stage classical Hodgkin Lymphoma);IELSG37 (Primary Mediastinal Large B-Cell Lymphoma).PET/CT images were independently reviewed by a group of nuclear medicine physicians blinded to patient history, clinical data and treatment outcome. The reference lesion (i.e. the location of the most active residual lesion) was visually scored according to DS. For each study we evaluated the reliability among all reviewers and the mean for each couple of reviewers using:the Krippendorff Alpha (KA) and the Cohen Kappa (CK), both calculated on the discrete (D) 5-point scale and on the binary (B) PET positive/negative scale using different trial-related threshold of positivity; the percentage overall agreement (OA), the positive agreement (PA), the negative agreement (NA) as the ratio of number of concordant cases plus half of the number of discordant cases respect to the number of cases. Results: 753iPET (603PET-/150PET+) included in the HD0607 trial were reviewed by 6 expert nuclear physicians. For iPET the KAd, KAb, OAb, PAb, NAb values were 0.39,0.78,0.90,0.89,0.91 respectively. 733ePET (647PET-/86PET+) included in the FIL-FOLL12 trial were reviewed by 6 expert nuclear physicians. For iPET the KAd, KAb, OAb, PAb, NAb values were 0.30,0.62,0.92,0.77,0.94 respectively. 108ePET (86PET-/22PET+) included in the FIL-DLCL10 trial were reviewed by 5 expert nuclear physicians. For iPET the KAd, KAb, OAb, PAb, NAb values were 0.37, 0.63,0.88,0.75,0.91 respectively.455ePET (239PET-/216PET+) included in the IELSG37 trial were reviewed by 6 expert nuclear physicians. For iPET the KAd, KAb, OAb, PAb, NAb values were 0.49,0.75,0.86,0.86,0.87 respectively.444 iPET (366PET-/78PET+) and 369ePET (324PET-/45PET+) included in the FIL-ROUGE trial were reviewed by 5 expert nuclear physicians. For iPET the KAd, KAb, OAb, PAb, NAb values were 0.36,0.74,0.93,0.87,0.95 respectively. For ePET the KAd, KAb, OAb, PAb, NAb values were 0.28,0.73,0.95,0.88,0.96 respectively. **Conclusion:** The Deauville Score is a reproducible scoring system in clinical trials using FDG-PET/CT for response assessment in several lymphomas diseases. Notably, inter-observer agreement on 5-point scale among different pathologies and different time-points is consistent. DS4 confirm to be the most reproducible DS. **References:** none

OP-1014

The superiority of [^{18}F]-FDG over ^{68}Ga-FAPI-04 PET/CT in diagnosis of various types of lymphoma

X. Chen, T. Yuan, M. Wei, X. Wang;
Department of Nuclear Medicine, Peking University Cancer Hospital & Institute, Beijing, CHINA.

Aim/Introduction: To compare the diagnostic efficacy of [^{18}F]-FDG PET/CT and ^{68}Ga-FAPI-04 PET/CT for various types of lymphoma. **Materials and Methods:** We prospectively evaluated 123 patients with various types of lymphoma, all those who underwent contemporaneous ^{68}Ga-FAPI-04 and [^{18}F]-FDG PET/CT from December 2019 to December 2020. The uptake values and tumor-to-liver ratios of involved nodal stations and extranodal lesions were compared between [^{18}F]-FDG and ^{68}Ga-FAPI-04 PET/CT, using the Wilcoxon Signed Ranks test or Mann-Whitney U test. Results: The study cohort consisted of 15 patients with Hodgkin lymphoma (HL) and 108 with non-Hodgkin lymphoma (NHL) (62 males and 61 females; median age, 54 years; age range, 21-79 years). No statistically significant difference was found between the SUVmax of HL and NHL, whether in [^{18}F]-FDG PET/CT (12.9 ± 6.7 vs 14.5 ± 10.0, P = 0.814) or ^{68}Ga-FAPI-04 PET/CT(9.5 ± 3.7 vs 8.1 ± 5.1, P = 0.120). The tracer uptake of involved lymph stations (14.3 ± 9.6 vs 8.3 ± 4.9, P =0.000) and extranodal lesions (14.9 ± 10.3 vs 8.8 ± 5.1, P = 0.000) was higher with [^{18}F]-FDG PET/CT than with ^{68}Ga-FAPI-04 PET/CT. Of them, 86 patients showed higher [^{18}F]-FDG uptake than ^{68}Ga-FAPI, while no statistically significant difference was found between the tumor-to-liver ratios of nodal and extranodal lesions (5.2 ± 4.0 vs 5.5 ± 4.5, P =0.603; 5.4 ± 4.2 vs 5.7 ± 4.0, P =0.704) because of the low background activity in ^{68}Ga-FAPI-04 PET/CT (average SUVmax of liver: 1.71 ± 0.56). All involved nodal and extranodal lesions exhibited a high interindividual and intralesional SUV variation with ^{68}Ga-FAPI-04 PET/CT, compared with [^{18}F]-FDG PET/CT. Meanwhile, ^{68}Ga-FAPI-04 PET/CT showed a much lower uptake than [^{18}F]-FDG PET/CT in the detection of small lymph nodes (size <10mm in diameter). **Conclusion:** we conclude that [^{18}F]-FDG PET/CT is advantageous over ^{68}Ga-FAPI-04 PET/CT in clearly detecting various types of lymphoma, with higher tracer uptake in most extranodal and nodal lesions, which results in more reliable diagnosis, staging, and response evaluation. **References:** none

OP-1015

2-[^{18}F]FDG-PET/CT imaging and radiomics as predictors of early response in patients with lymphoma undergoing chimeric antigen receptor T-cell therapy (CAR-T)

A. Paccagnella, A. Farolfi, G. Paolani, G. Della Gala, M. Santoro, C. Malizia, B. Casadei, S. Mattoni, L. Strigari, P. Zinzani, S. Fanti;
IRCCS Azienda Ospedaliero-Universitaria, Bologna, ITALY.

Aim/Introduction: CAR-T cell therapy has revolutionized the treatment of relapsed/refractory lymphomas. Unfortunately, non-responder-rate is around 30-60% and almost 35% of patients develop moderate/severe toxicity, i.e., Cytokine Release Syndrome (CRS) and Immune Effector Cell-Associated Neurotoxicity syndrome (ICANS). Therefore, it is of critical importance the early identification of refractory patients and those at high risk of developing moderate/severe toxicity. Primary aim was to early predict the response to CAR-T based on metabolic and Radiomics-PET-features extracted from the baseline 2-[^{18}F]FDG-PET/CT. Secondary aim was to determine a possible correlation between those features and the severity of toxicity. **Materials and Methods:** From September 2019 to March 2021, patients with relapsed/refractory lymphoma treated with CAR-T-cell therapy were prospectively enrolled. Allpatients underwent 2-[^{18}F]FDG-PET/CT evaluation at baseline (PET_0) and 1 month after CAR-T-cell infusion (PET_1). PET_0 semi-quantitative parameters, namely SUVmax, metabolic-tumor-volume (MTV) and total-lesion-glycolysis (TLG), were calculated. 105 Radiomics-PET-features were extracted. Univariate analysis was performed. A generalized linear model (GLM) was trained to predict the outcome and its performance was estimated using the area under ROC curve (AUC). Correlation among radiomics, MTV, TLG and toxicity was investigated. Results: 29 patients were enrolled (mean age=52; range: 19-68). 12/29 patients (41%) achieved a complete (CR) and 17/29 (59%) a partial response (PR) at PET_1. 9/17 PR patients (53%) underwent re-evaluation at 3 months: 2 converted to CR, 3 had a progression (PD) and 4 maintained PR. At the time of last follow-up, 3 patients died due to PD and 1 due to neurotoxicity. Baseline SUVmax, MTV and TLG were significantly associated with tumor response at PET_1 (all p<0.05). Three Radiomics-PET-features (i.e., Kurtosis, SurfaceVolumeRatio and SumAverage) were significantly associated with early response. In the GLM, Kurtosis and SUVmax were prognostic factors of response, with an AUC of 0.80 (95%CI: 0.63-0.94). Significant associations were found between the severity of CRS and baseline MTV (p<0.05, AUC: 0.79; 95%CI: 0.61-0.93) and TLG (p<0.05, AUC: 0.77; 95%CI: 0.61-0.92). Four Radiomics-PET-features (i.e., MajorAxisLength, MCC, MaximumProbability and Busyness) were associated with CRS grade (p<0.05). Moreover, PET_0 parameters were not significantly associated with severity of ICANS (p=0.3). **Conclusion:** Baseline 2-[^{18}F]FDG-PET/CT semiquantitative-parameters, i.e. MTV, TLG and SUVmax, and Radiomics-PET-

features were significantly associated with early response in lymphoma patients treated with CAR-T cell therapy. Radiomics-PET-features were mostly related to lesion-shape and inhomogeneity, suggesting the prognostic role of image-texture. Interestingly, 2-[^{18}F]FDG-PET/CT parameters and Radiomics-PET-features were also associated with the severity of CRS but not with ICANS. **References:** None

OP-1016

Lesion dissemination feature (Dmax) calculated at baseline PET/CT improves risk stratification of ABVD treated Hodgkin Lymphoma patients

R. Durmo[1,2], A. Cottereau[3], L. Rebaud[4], C. Nioche[4], A. Ruffini[5], F. Fioroni[1], S. Luminari[1], F. Merli[1], M. Meignan[6], I. Buvat[4], A. Versari[1]; [1]AUSL-IRCCS of Reggio Emilia, Reggio Emilia, ITALY, [2]PhD program in Clinical and Experimental Medicine (CEM), University of Modena and Reggio Emilia, Modena, ITALY, [3]Department of Nuclear Medicine, Cochin Hospital, AP-HP, University of Paris, Paris, FRANCE, [4]LITO laboratory, UMR 1288 Université Paris Saclay/Inserm/Institut Curie, Orsay, FRANCE, [5]GRADE Onlus, Reggio Emilia, ITALY, [6]Lysa Imaging, Henri Mondor University Hospital, AP-HP, University Paris East, Creteil, FRANCE.

Aim/Introduction: Identifying factors that could help to predict disease relapse or therapy resistance in patients with Hodgkin Lymphoma (HL) is an open research question. Recently, the largest distance between two lesions (Dmax), a simple imaging feature measured from 18F-FDG PET scans and reflecting lesions dissemination, has been introduced as a new prognostic factor in diffuse large B cell lymphoma. The aim of this study was to investigate the prognostic value of Dmax in newly diagnosed HL patients and to define interaction of Dmax with other available prognostic factors. **Materials and Methods:** We conducted a retrospective review of patients with stage I-IV HL who were treated with doxorubicin, bleomycin, vinblastine, and dacarbazine (ABVD) chemotherapy regimen between 2007 and 2020. Available baseline 18F-FDG PET/CT scan were required for inclusion. From the baseline PET images, the centroid of each lesion was automatically obtained and considered as the lesion location. The distances between all pairs of lesions were calculated and Dmax was obtained for each patient. Dmax was dichotomized according to the median value within our cohort. Early Metabolic response with 18F-FDG-PET was reported according to the five-point Deauville scale (DS1-5) and considered positive for DS4-5 (iPET+). Main study endpoint was Progression Free Survival. Results: 183 patients were included in the study, median age was 40 years (15-81), 48% had stage III-IV. Dmax was calculated in155/183 patients, median value was 20cm (range 2.6-77.8). iPET was available in 172/183 patients and was positive in 31 cases (DS4-5; 18%). 41% had a IPS score more than 2. Higher Dmax values were observed for males, for patients with low serum albumin, low LDH, elevated ESR, and high MTV. 5 year PFS was 77% (95% CI 70-82%). In univariate analysis, IPS>2 (HR 2.20 CI 1.26-3.87) and Dmax>20 (HR 2.38 CI 1.21-4.72) were associated with lower PFS rates. Dmax>20 was confirmed as an independent prognostic factor in multivariate analysis (HR 2.14 CI 1.04-4.38). Combining Dmax with iPET, Dmax had a meaningful role for identification of patients at different risk of progression among iPET- cases. Using iPET- and Dmax<20cm as a reference group, the iPET- and Dmax>20cm showed a HR of 2.58 (CI 1.24-5.37). **Conclusion:** Dmax, a PET feature reflecting the spread of disease allows better risk stratification of HL patients treated with ABVD and in particular for patients with early complete metabolic response. Accordingly, combining Dmax and iPET might contribute to refine initial staging and tailor therapy. **References:** none

OP-1017

The role of ^{18}F-FDG PET/CT parameters in predicting outcome of patients with aggressive B cell lymphoma treated with anti-CD19 CAR-T-cell

A. Lorenzoni, A. Guidetti, G. Argiroffi, A. Dodero, M. Kirienko, S. Pizzamiglio, M. Pastori, B. Padovano, A. Chiappella, E. Seregni, P. Verderio, P. Corradini, A. Alessi;
Fondazione IRCCS Istituto Nazionale Tumori, Milan, ITALY.

Aim/Introduction: To evaluate the role of metabolic parameters derived from ^{18}F-FDG PET/CT in predicting clinical outcome in patients with aggressive B cell lymphoma treated with CD19-targeting CAR-T-cell therapy. **Materials and Methods:** All patients underwent a baseline ^{18}F-FDG PET/CT (PET1) before CAR-T-cell therapy and received PET-based response assessment at 30 days (PET2) and 90 days (PET3). Following CAR-T-cell therapy, treatment response was assessed with PET2 and PET3 according to the Lugano classification criteria. Quantitative PET parameters were computed with PET-VCAR software (GE Healthcare) on dedicated workstations. Contours of pathological lesions were delineated using two semiautomatic contouring system: 41% SUVmax threshold and an iterative adaptive algorithm. SUVmax, SUVmean, metabolic tumor volume (MTV) and total lesions glycolysis (TLG) were automatically recorded. Total MTV (TMTV) and total TLG (TTLG) were calculated as the sum of all individual lesions. A quantitative measure of intratumoral heterogeneity, heterogeneity index (HI) was also recorded. The association between PET parameters and response at 1 month or 3 months, categorized as (CR + PR) vs (PD + SD), was evaluated using the univariate logistic regression model. The association between PET parameters and PFS was evaluated using the univariate Cox regression model. Results: Twenty-nine patients were evaluated (median age 51 years; range 22-70): 20 affected by diffuse-large B-cell lymphoma and 9 by primary mediastinal B-cell lymphoma. Patients received treatment with axi-cel (n=18) or tisa-cel (n=11) at physician discretion. At a median follow-up of 343 days (interquartile range, 214-482 days) 24 patients are alive

and 5 died of disease progression with an estimated 1-year PFS and OS of 39% (95% CI, 20%-58%) and 78% (95%CI, 55%-91%) respectively. Clinical response at PET2 was observed in 55% of the patients (n=8 CR, n=8 PR); progressive disease at PET3 occurred in 2 pt in PR e in 3 pt with SD. Baseline SUVmax, SUVmean, TTLG, TMTV, HI were not correlated with clinical response and PFS. The variation of HI between PET1 and PET2 were significantly associated with response at 1 month (OddsRatio: 1.41; 95%CI: 1.02-1.93; p 0.035). **Conclusion:** Baseline metabolic parameters on ^{18}F-FDG PET/CT did not correlate with clinical outcome suggesting that several factors could influence the response to CAR T-cells. The variation of metabolic heterogeneity is associated with response suggesting an important role of early evaluation of disease after CAR T-cells infusion. A larger cohort of patients and a validation group are needed in order to verify these observations. **References:** None

OP-1018

Prognostic role of baseline ^{18}F-FDG PET/CT metabolic parameters in primary gastric DLBCL

D. Albano, F. Dondi, A. Mazzoletti, P. Bellini, M. Gregorelli, A. Calabrò, L. Camoni, F. Bertagna, R. Giubbini;
University of Brescia and Spedali Civili of Brescia, Brescia, ITALY.

Aim/Introduction: The aim of our study was to investigate whether the metabolic baseline ^{18}F-FDG PET/CT parameters may predict treatment response (at end of first-line treatment) and prognosis in primary gastric diffuse Large-B cell lymphoma (DLBCL). **Materials and Methods:** Between January 2010 and January 2020, 57 patients with histologically proven primary gastric DLBCL were retrospectively included; all patients underwent baseline ^{18F}-FDG-PET/CT before any treatment and end of treatment PET/CT after 6 cycles of chemotherapy (R-CHOP). The PET images were analyzed visually and semi-quantitatively by measuring the maximum standardized uptake value body weight (SUVbw), the maximum standardized uptake value lean body mass (SUVlbm), the maximum standardized uptake value body surface area (SUVbsa), lesion to liver SUVmax ratio (L-L SUV R), lesion to blood-pool SUVmax ratio (L-BP SUV R) of gastric lesion. Moreover, metabolic tumor volume and total lesion glycolysis of gastric lesion (gMTV and gTLG) and total MTV (tMTV) and TLG were measured. For the entire population, receiver operating characteristic curve analysis was used to identify the optimal cutoff point of semiquantitative parameters in the light of progression free survival (PFS) and overall survival (OS). Survival curves were plotted according to the Kaplan-Meier method. Results: All baseline PET/CT were positive showing increased ^{18}F-FDG uptake in gastric lesions. Extragastric disease was registered in ten patients with intestinal involvement in 5 cases, pulmonary in 3, bone in 2 and multi-organ disease in one. At a median follow up of 80 months, the median PFS and OS were 69 and 80 months with 5-year PFS of 49% and 5-year OS of 59%. Baseline gMTV, gTLG, tMTV and TLG were significantly higher in patients with incomplete response (partial response and progression) compared to complete response group at end of treatment (p 0.019, p 0.004, p 0.013 and 0.004, respectively), while no significant differences were found considering SUVbw, SUVlbm, SUVbsa, L-L SUV R and L-BP SUV R. In univariate analysis, SUVbw, SUVlbm, SUVbsa, L-L SUV R, L-BP SUV R, gMTV and gTLG were not related to outcome survival. Instead, tMTV and TLG were confirmed to be independent prognostic factors both for PFS (p=0.023 and p=0.038) and OS (p=0.038 and p=0.026). **Conclusion:** In conclusion, in our study we demonstrated that metabolic tumor features (tMTV and TLG) were significantly correlated with PFS and OS and were significantly lower in patient with complete response after therapy compared to incomplete response group. **References:** None

OP-1019

Interim FDG PET/CT Predicts Response to Treatment and Outcome in Hodgkin's Lymphoma Patients; Experience from KHCC Tertiary Cancer Center in Jordan

A. Al-Ibraheem[1], F. M. Anwer[1], Q. Shagera[2], M. Juweid[3], A. N. Khalaf[1], M. Ma'koseh[1];
[1]King Hussein Cancer center, Amman, JORDAN, [2]Institute Jules Bordet, Université Libre de Bruxelles (ULB), Brussels, BELGIUM, [3]Jordan University, Amman, JORDAN.

Aim/Introduction: The goal of this study is to assess the impact of interim FDG PET's (iPET) in patients with Hodgkin's lymphoma (HL) treated with ABVD chemotherapy. **Materials and Methods:** We retrospectively searched our database for patients with de novo HL between 31 December 2013 and 31 December 2017, treated with upfront ABVD, who had undergone baseline and iPET (after 2 or 4 ABVD cycles) and had at least 6 months follow-up after therapy. The response assessment on iPETs was based on the Deauville scores (DS). Patients were classified as having a complete metabolic response (CMR, DS 1-3) and non-CMR (DS≥4). The response at the end of ABVD was assessed by FDG PET/CT and biopsy confirmation for patients with residual FDG uptake. The association between iPET and end of therapy response status was investigated using logistic regression analysis. Survival analysis was performed using the Cox regression hazard model and Kaplan-Meier methods. Results: A total of 245 patients were included in the study. The median age of patients was 29 years (range, 18-83), and the follow-up time was 32 months (range, 6-81 months). Sixty-nine patients underwent iPET-2 and 176 iPET-4. There was no association between the timing of iPET and the iPET -response status (p=0.71). Among the total, 201 patients (82%) had iPET-CMR and 44 (18%) iPET-nCMR. iPET was strongly correlated with the end of therapy response status; 194/201 of iPET-CMR had CR and 29/44 of iPET-nCMR had no CR at the end of

chemotherapy (p<0.0001). iPET-CMR patients had better outcome with 91% 3-y EFS and 95% 3-y OS than patients with iPET-nCMR (41% 3-y EFS and 86% 3-y OS, p<0.0001 for both). In univariate analysis, the baseline risk factors such as patient age ≥45 and disease stage IV were statistically significant prognostic factors (p<0.05 for EFS and OS). In multivariate analysis, the disease stage remained independent only for EFS (p=0.006) and patient age for OS (p<0.0001) while iPET remained significant for EFS and OS (p<0.0001 and p=0.001, respectively). **Conclusion:** Interim PET is highly predictive of the outcome of patients with HL treated with ABVD chemotherapy. iPET's early and accurate assessment of the response might help tailor therapy to the individual patient. **References:** None

OP-1020

Automatic lymph lesion quantification by artificial intelligence in lymphoma patients examined with [^{18}F] FDG PET/CT

M. Sadik[1], J. López-Urdaneta[1], J. Ulén[2], O. Enqvist[3], P. Andersson[4], E. Trägårdh[5], L. Edenbrandt[1];
[1]Nuclear Medicine, Gothenburg, SWEDEN, [2]Eigenvision AB, Malmö, SWEDEN, [3]Eigenvision AB and Electrical Engineering, Malmö and Gothenburg, SWEDEN, [4]Haematology and Medicine, Borås and Gothenburg, SWEDEN, [5]Clinical Physiology and Nuclear Medicine, Malmö, SWEDEN.

Aim/Introduction: Several studies demonstrates that tumor lesion glycolysis (TLG) is associated with progression-free survival, and sometimes with overall survival in lymphoma patients. Our aim was to develop an artificial intelligence (AI) based quantification of TLG, restricted as a first step to lymph node lesions, in lymphoma patients examined with [^{18}F]FDG PET/CT. **Materials and Methods:** One hundred and one lymphoma patients were selected, of whom 71 were included in the training of the AI-system, 20 patients were included in validation and 10 as test. In order to present a mix of patients to the AI, i.e. patients with lymph node lesions and those with only physiological uptake, 67% of the cohort were Hodgkin´s lymphoma at staging, while the rest were patients with lymphoma examined after treatment with no active disease. In the training process, all lesions were manually segmented by a trained technologist and a nuclear medicine physician using the final report sent to the referring department. All patients were examined at Sahlgrenska University Hospital between 2011-2016, mean age 44 years (rage 14-85) in the training/validation and 47 years (range 16-70) in test. TLG was calculated as total metabolic tumor volume multiplied by the SUVmean in the entire lesion volume. The AI was trained to segment the lymph node lesions directly using the CT image, the PET image, and an automatically generated organ mask similar to [1], but with one important modification: to get an accurate TLG estimate, all pixels were assigned a loss, whereas [1] marked some pixels as "don't care". Results: Seven patients in the test group were at the staging phase, i.e. having an active disease, while three were at a post-treatment phase. Spearman's rank coefficient showed a correlation for lymph uptake TLG of 0.988 between AI versus manual segmentations. Median lymph uptake TLG values for AI was 442 g (range 0-1324) versus manual segmentation 401 g (range 0-1432), respectively. **Conclusion:** This pilot study indicate that lymph TLG in lymphoma patients can accurately be quantified using AI. The system has potential to facilitate the workflow for nuclear medicine physicians in the near future by automatically quantifying lesions. **References:** Artificial intelligence-based detection of lymph node metastases by PET/CT predicts prostate cancer-specific survival. Borrelli P , Larsson M, Ulén J, Enqvist O, Trägårdh E, Hvid Poulsen M, Mortensen MA, Kjölhede H, Høilund-Carlsen PF, Edenbrandt L. Clin Physiol Funct Imaging. 2021;41(1):62-67.

OP-1021

The prognostic significance of ^{18}F-FDG PET/CT in multiple myeloma according to novel interpretation criteria (IMPeTUs)

C. Sachpekidis[1], M. Merz[2], V. Weru[3], A. Kopp-Schneider[3], A. Jauch[4], H. Goldschmidt[2], A. Dimitrakopoulou-Strauss[1];
[1]Clinical Cooperation Unit Nuclear Medicine, German Cancer Research Center (DKFZ), Heidelberg, GERMANY, [2]Department of Internal Medicine V, University Hospital Heidelberg and National Center for Tumor Diseases (NCT), Heidelberg, GERMANY, [3]Division of Biostatistics, German Cancer Research Center (DKFZ), Heidelberg, GERMANY, [4]Institute for Human Genetics, University of Heidelberg, Heidelberg, GERMANY.

Aim/Introduction: ^{18}F-FDG PET/CT is the preferred imaging modality for treatment monitoring and response evaluation in multiple myeloma (MM). However, MM is a heterogeneous disease from an imaging point of view, raising serious issues on the reporting and interpretation of the PET/CT scans. With the current study we investigated the prognostic role of the newly introduced, visual Italian Myeloma criteria for PET Use (IMPeTUs) in MM patients undergoing high-dose chemotherapy (HDT) followed by autologous stem cell transplantation (ASCT). **Materials and Methods:** Forty-seven patients with newly diagnosed, symptomatic MM underwent whole body ^{18}F-FDG PET/CT before commencement of treatment (baseline PET/CT). Thirty-four of these patients (72.3%) were also examined after completion of ASCT (follow-up PET/CT). ^{18}F-FDG PET/CT data analysis was based on the IMPeTUs criteria, which take into consideration - among others - the metabolic state of the bone marrow based on the 5-point Deauville score (DS), the number and metabolic state of focal ^{18}F-FDG-avid lesions, as well as the presence of extramedullary disease (EMD) and paramedullary disease (PMD). We analyzed whether parameters from IMPeTUs at baseline and/or follow-up PET/CT are correlated to clinically

relevant parameters and patients' outcome, as assessed by progression-free survival (PFS). Results: Median follow up from baseline and follow-up PET/CT was 85.1 months and 76.7 months, respectively. The number of focal, ^{18}F-FDG-avid medullary lesions on PET/CT significantly correlated with the bone marrow infiltration rate and the R-ISS stage, while the presence of PMD was associated with LDH plasma levels. At univariate survival analysis the number of focal, ^{18}F-FDG-avid, medullary lesions both before and after therapy, as well as the presence of EMD and PMD at baseline imaging adversely affected PFS. Multivariate Cox regression analysis for baseline parameters confirmed that the number of focal, ^{18}F-FDG-avid, medullary lesions and the presence of EMD are associated with adverse prognosis, irrespective of the presence of high-risk cytogenetic abnormalities and the R-ISS stage. The 5-point DS of ^{18}F-FDG uptake in reference bone marrow and focal lesions showed a significant decrease as response to treatment, but it did not affect patient survival. **Conclusion:** Several parameters utilized in IMPeTUs predict PFS in patients with newly diagnosed MM undergoing ASCT. Our results suggest the significant role of the new criteria in patient stratification and response assessment. Additional studies are warranted for the further evaluation of IMPeTUs in the direction of establishment of robust cut-off values with a prognostic significance in the disease. **References:** None.

OP-1022

The Relationship Between Bone Marrow Involvement on ^{18}F-Fluorodeoxyglucose Positron Emission Tomography/Computed Tomography and Bone Marrow Biopsy in Patients with Multiple Myeloma

K. Gebreslassie[1], F. Bassa[2], J. Warwick[1], Z. Chapanduka[3];
[1]Stellenbosch University, Tygerberg Hospital, Nuclear Medicine Division, Cape Town, SOUTH AFRICA, [2]Stellenbosch University, Tygerberg Hospital, Haematology Division, Cape Town, SOUTH AFRICA, [3]Stellenbosch University, Tygerberg Hospital, Hematopathology Division, Cape Town, SOUTH AFRICA.

Aim/Introduction: Multiple myeloma is a plasma cell neoplasm characterized by unrestrained monoclonal proliferation of malignant plasma cells, which develop from B lymphocytes within the bone marrow. Bone marrow biopsy plays a crucial role in the diagnosis and assessment of treatment response in myeloma. ^{18}F-fluorodeoxyglucose positron emission tomography/computed tomography (^{18}F-FDG PET/CT) has been shown to be a complementary measure of marrow involvement in lymphomas, particularly in Hodgkin lymphoma and diffuse large B cell lymphoma. However, only limited information is available on its potential role in the assessment of bone marrow involvement and its relationship with bone marrow biopsy in patients with multiple myeloma. Therefore, this study is aimed to compare these two modalities in assessing bone marrow involvement and/or tumor burden. **Materials and Methods:** From a retrospective review of 190 patients with multiple myeloma from January 2013 to July 2020, 103 patients were included. Plasma cell infiltration (PCI) on bone marrow biopsy was compared for three visual patterns of ^{18}F-FDG bone marrow uptake (irregular, diffuse less than or equal to the liver, and diffuse greater than liver). The PCI was based on bone marrow biopsy and aspiration results. The ^{18}F-FDG uptake at the site of bone marrow biopsy was assessed visually and semiquantitatively. A Kruskal-Wallis rank test and quantile regression were used to compare the percentage of plasma cell bone marrow infiltration across the three described patterns of bone marrow ^{18}F-FDG uptake. Results: Eighty-four patients had diffuse bone marrow uptake. Of these 25/84 had uptake greater than liver, all having PCI ≥60% and a median value of 85%. Of the 84 patients, the 59 patients with uptake less than or equal to liver had PCI <10% in 57.6% (34/59), and ≥10% in 42.4% (25/59) with a median value of 8%. Nineteen patients had irregular bone marrow uptake. Of these 4/19 (21.1%) had PCI of <10% and 15/19 (78.9%) ≥10%, with a median value of 23%. The median percentage of PCI across the three described patterns of FDG uptake was significantly different (P=0.0001). **Conclusion:** Bone marrow biopsy and ^{18}F-FDG PET/CT showed a good concordance in patients with diffuse bone marrow ^{18}F-FDG uptake in assessing the tumor burden in patients with multiple myeloma. However, bone marrow biopsy may underestimate the tumour burden in patients with an irregular pattern of ^{18}F-FDG uptake with a potential risk of undertreatment of the patient. **References:** None

OP-1023

Semi-automated extraction and histogram analysis of physiological uptake in bone marrow with 18F-FDG PET/CT

Y. Satoh[1,2], S. Funayama[2], M. Imai[1], H. Onishi[2];
[1]Yamanashi PET Imaging Clinic, Chuo, JAPAN, [2]University of Yamanashi, Department of Radiology, Chuo, JAPAN.

Aim/Introduction: BM biopsy is the gold standard for diagnosis of hematopoietic disorders, but it is highly invasive and contains many sampling errors. ^{18}F-fluorodeoxyglucose (FDG)-positron emission tomography/computed tomography (PET/CT) has been reported to be able to visualize glucose metabolism in bone marrow (BM) throughout the body less invasively, which was difficult with conventional morphological imaging such as CT and magnetic resonance imaging. Although previous reports have proposed several BM segmentation methods using computational approaches to FDG-PET/CT images [1,2], the method that can be easily applied to clinical practice has not been standardized, and

the quantitative method for evaluating the physiological FDG uptake pattern in BM has not been clarified. The aim of this study was to establish a semi-automatic BM extraction from FDG-PET/CT with fewer steps using deep learning-based organ segmentation and provide FDG-uptake patterns in healthy adults using a histogram analysis, which will be useful as a database of hematological disorders and have an impact on their management. **Materials and Methods:** Consecutive healthy adults who underwent FDG-PET/CT between May 2017 and March 2020 were retrospectively analyzed. Whole-spine and pelvic bone marrow CT was automatically extracted using an algorithm for automatic bone segmentation based on multi-task three-dimensional fully convolutional neural networks (3D-FCN). The correlation between clinical indicators (age, sex, body mass index (BMI), white blood cell count (WBC), etc.) and PET-derived parameters of mean standardized uptake value (SUV_{mean}) and histogram features were evaluated. Multiple regression analyses provided predictive formulas for the PET parameters. Results: A total of 118 healthy adults (68 men, 50 women) were analyzed. The volume of the extracted bone marrow PET was 1129.38 ± 154.8 cm^3 and 793.38 ± 107.64 cm^3 in men and women ($p< 0.0001$), respectively. There were no significant differences in the PET parameters between the sexes. Multiple regression analysis following univariate analysis showed that SUV_{mean} was predicted with BMI and WBC in men ($R=0.59$, and $p < 0.0001$), and SUV_{mean}, entropy, and variance were predicted with age and BMI in women ($R=0.85$, 0.71, and 0.69, respectively; all $p<0.0001$). All PET parameters increased as BMI and WBC increased, and decreased as age increased. BMI correlated with entropy in men and with uniformity in both sexes. **Conclusion:** A simplified FDG-PET/CT bone marrow quantification method presented revealed uptake patterns in healthy adults using histogram analysis. **References:** 1. Sambuceti G, Eur J Nucl Med Mo Imaging 2012 2. Takahashi MES, Sci Rep 2019

OP-1024

Correlation between Baseline PET/CT Findings and Clinical Parameters in Multiple Myeloma Patients

A. Arçay[1], F. Aydın[1], C. N. Dündar Çağlayan[1], E. Vural[2], U. Iltar[2], M. N. Engin[1], Z. G. Kıprak[1], A. Boz[1];
[1]Akdeniz University Hospital, Department of Nuclear Medicine, Antalya, TURKEY, [2]Akdeniz University Hospital, Department of Internal Medicine, Antalya, TURKEY.

Aim/Introduction: FDG PET/CT is considered a valuable tool for the visualization of disease activity in both newly diagnosed and relapsed multiple myeloma(MM) patients.PET parameters have also been designated as important surrogate markers for predicting prognosis.The objective of this study is to compare the initial clinical characteristics of MM patients with baseline PET parameters. **Materials and Methods:** A total of 105 newly diagnosed MM patients were enrolled in this study, who were diagnosed at our hospital between February 2015 and May 2020. Patients' clinical parameters at diagnosis (serum albumin,β2-microglobulin,creatinine,calcium,lactate dehydrogenase(LDH),hemoglobin levels,International Staging System(ISS),immunohistochemical markers,Ig subtypes and age) and baseline PET parameters(presence of positive PET findings,number of focal hypermetabolic bone lesions(FLs),SUVmax of the lesion showing highest FDG uptake,presence of extramedullary disease(EMD) and/or plasmacytoma) were retrospectively analyzed. Results: 105 patients which consisted of 38 women and 67 men patients with a median age of 64(42-84) years were reviewed. At diagnosis,the distribution of the patients according to ISS was I(n=20,19.4%);II(n=37,35.9%);III(n=46,44.7%), respectively. Based on PET/CT findings at diagnosis; 43(41%) patients had no FLs. There were 15(14.3%) patients with ≤3 FLs, 19(18.1%) patients with 4-9 FLs and 28(26.7%) patients with ≥10 FLs. The mean SUVmax value of the lesion that had the highest FDG uptake was 9.56±7.64(2.9-47). Plasmacytomas were detected in 25 patients and 7 patients had EMD which varied in origin, including soft tissue,lymph nodes,muscles,lung,pleural tissue and pancreas. Groups of clinical characteristics were formed according to the presence or absence of anemia,azotemia,hypercalcemia,elevated β2-microglobulin,hypoalbuminemia,elevated LDH levels and also to the ISS,immunohistochemical markers and Ig subtypes.SUVmax values revealed no significant difference between these groups (Mann-Whitney U,p>0,05 in all groups).However, when comparing clinical characteristics based on the number of FLs, Ig subtype groups revealed significant differences (Pearson's chi-squared,p=0,002). Out of 28 IgA subtype patients, 42.9% had ≥10 FLs, besides among IgG subtype patients(n=49) 14.3% had ≥10 FLs.When comparing clinical characteristics based on the presence/absence of the plasmacytoma; anemia, azotemia and CD19 immunohistochemical marker groups showed significant differences (Pearson's chi-squared,p=0,019;0,012;0,004,respectively). In the patients without plasmacytoma; anemia, azotemia and CD19 absence percentages were significantly higher than the group with plasmacytoma. **Conclusion:** Regarding PET parameters, FLs are more likely to be related to the prognostic clinical parameters compared to the SUVmax values. Immunologically different Ig subtypes can predict prognostic significance and we observed that these subtypes were associated with the number of FLs. Besides, the results revealed that CD19 immunohistochemical marker could be related to the plasmacytoma presence. **References:** None.

1811

Wednesday, October 20 - Saturday, October 23, 2021

on-demand pool, release on Wednesday, October 20 at 09:00

TROP Session: Nuclear Thyroidologist and Thyroid Cancer Management - Current Update and Future Perspectives

OP-1026

^{68}Ga-FAPI PET/CT Accuracy In Patients With Recurrent Papillary Thyroid Carcinoma

U. Elboga, Z. Sayıner, E. Sahin, S. Ozturk, Y. Cayirli, Y. Celen, E. Akarsu;
Gaziantep University, Gaziantep, TURKEY.

Aim/Introduction: Papillary thyroid carcinoma (PTC) is the most common endocrine tumor with an increasing incidence worldwide whereas its mortality is stable or even decreasing. PTC has a relatively good prognosis with mortality rates less than 10%, but with an overall risk of recurrence of about 30%. We aimed to evaluate the use of ^{68}Ga-FAPI PET/CT in localizing PTC foci in patients with biochemical relapse. **Materials and Methods:** This is a retrospective study. Patients who were previously diagnosed with PTC and achieved biochemical recovery after the first operation followed by consequent treatment and whose thyroglobulin (Tg) levels significantly increased in the last follow-up were included in the study. ^{68}Ga-FAPI PET/CT and ^{18}F-FDG PET/CT were performed for comparative purpose and detection of recurrence foci. Results: 29 patients having well or poorly papillary thyroid carcinomas have been enrolled to the study. Pathologic subgroups were papillary (n=26) and poorly differentiated (n=3) thyroid carcinomas. Anti-Tg antibody positivity were noted in 5 of the patients, while all 29 of them were Tg positive and had been consist of three groups as follows: 2-10 ng/mL (n=4), 11-300 ng/mL (n=14), 301 ng/mL and above (n=11). Recurrence was detected in 72.4% (n=21) and 86% (n=25) of the patients via ^{18}F-FDG PET/CT and ^{68}Ga-FAPI PET/CT, respectively. Accuracy of detection noted as 100% (5/5), 75% (3/4), and 92.9% (13/14) in groups with the anti-Tg antibody positivity, Tg levels of 2-10 ng/mL and 11-300 ng/mL, respectively, when the two imaging modalities were utilized together. Furthermore, accuracy of ^{68}Ga-FAPI PET/CT was 100% (11/11) in the group with Tg levels of 301 ng/mL and above, whereas accuracy of ^{18}FDG PET/CT was 81.8% (9/11). Lastly, median SUVmax of recurrent lesions detected by the ^{68}Ga-FAPI PET/CT (medianSUVmax: 6.0) were statistically higher than the ones detected by the ^{18}FDG PET/CT (Median SUVmax: 3.7) (p=0.002). **Conclusion:** In the presence of biochemical disease in patients with recurrent PTC especially in case of higher Tg levels, ^{68}Ga-FAPI PET/CT can be used in patients whose results could not be obtained via ^{18}F-FDG PET/CT imaging in the detection of metastatic foci. Moreover, current results suggest that ^{68}Ga-FAPI PET/CT and ^{18}F-FDG PET/CT can be used as complementary modalities to detect recurrent foci in patients with PTC. **References:** none

OP-1027

Diagnostic Radioiodine Scintigraphy After the First Radioiodine Treatment in High-risk Thyroid Cancer: Is it Necessary?

A. Bay[1], K. Vase Jepsen[1], N. Møldrup Jakobsen[1], O. Gerke[1], L. Bastholt[2], M. Grubbe Hildebrandt[1], P. Grupe[1];
[1]Department of Nuclear Medicine, Odense University Hospital, Odense, DENMARK, [2]Department of Oncology, Odense University Hospital, Odense, DENMARK.

Aim/Introduction: The role of diagnostic whole-body scintigraphy (DxWBS) as part of the response evaluation after the initial radioiodine (RAI) therapy of patients with high-risk differentiated thyroid cancer (DTC) is increasingly questioned. Few studies have investigated this issue. This retrospective analysis aimed to investigate the value of DxWBS in combination with TSH-stimulated Thyroglobulin (TSH-Tg) in evaluation of initial treatment efficacy. **Materials and Methods:** Between 2015-2020 we evaluated 162 patients with high-risk DTC, who had a total thyroidectomy followed by ^{131}I therapy (3.7 GBq - except four patients who initially received 1.1 GBq, but then reclassified from intermediate to high-risk DTC). Four months later, the response to therapy was evaluated using TSH-Tg and DxWBS. Patients with positive DxWBS and/or elevated TSH-Tg received a second dose of ^{131}I therapy (3.7 GBq). Accuracy analyses of the DxWBS were obtained using the therapeutic whole-body scintigraphy (TxWBS) at second ^{131}I therapy as the reference standard. Results: A total of 55/162 patients (34%) were allocated to a second ^{131}I therapy. Of these, 35 patients (64%) had an elevated TSH-Tg only, 12 (22%) had positive DxWBS only, and eight patients (14 %) had both elevated TSH-Tg and positive DxWBS. In eight of the 12 patients who were DxWBS positive only, the following TxWBS (with SPECT/CT) also revealed ^{131}I uptake considered to be related to their thyroid cancer. As a consequence RAI treatment was continued past the second course. The sensitivity and specificity of DxWBS was 58% and 78%, respectively.The agreement between stratification based on TSH-Tg combined with DxWBS compared Tg alone was 93%. - with no significant difference between subgroups with and without TgAb (p= 0.07). **Conclusion:** The sensitivity of DxWBS is low. However 12 out of the 162 patients were selected for further RAI therapy based on DxWBS alone and eight of these actually continued RAI therapy also past the second course. Omitting DxWBS in the diagnostic work-up may cause residual thyroid cancer not to be detected in 7%

of the patients. These patients may have residual non-Tg producing cancer cells, remaining sensitive to RAI therapy. So based alone on these data we cannot omit DxWBS as part of the evaluation of efficacy after the first course of RAI therapy in patients with high-risk DTC. **References:** None.

OP-1028

Targeting the Amyloid with [^{18}F]AV-45 for Medullary Thyroid Carcinoma PET/CT Imaging

C. Li[1], P. Zhang[2], R. Nie[1], X. Gong[1], J. Xie[1], Z. Yu[3], R. Yan[3], Z. Lu*[1];*
[1]Department of Nuclear Medicine, First Affiliated Hospital of Dalian Medical University, Da Lian, CHINA, [2]Department of Pathology, First Affiliated Hospital of Dalian Medical University, Da Lian, CHINA, [3]King's College London, School of Biomedical Engineering and Imaging Sciences, St. Thomas' Hospital, SE1 7EH, London, UNITED KINGDOM.

Aim/Introduction: Amyloid plaques formed from the misfolding of calcitonin is the key characteristics of medullary thyroid carcinoma(MTC). we applied the β-amyloid specific radiotracer, [^{18}F]AV-45 to image MTC with PET, and Compared [^{18}F]FDG and [^{18}F]AV-45 PET/CT imaging in the same patient. **Materials and Methods:** One MTC patient with recurrent neck lymph node metastasis underwent [^{18}F]FDG and [^{18}F]AV-45 PET/CT imaging. Consecutive human MTC tissue samples from five patients, Consecutive lymph node and paratumor muscle tissue sections form a Post-operative MTC patient and one healthy human thyroid tissue sample were stained by hematoxylin and eosin, Congo Red, respectively. The tissue sections were also incubated with [^{18}F]AV-45 with and without its reference compound for autoradiography. Results: The amyloid plaque in MTC and metastasis neck lymph node tissue was observed in hematoxylin and eosin, Congo Red staining. Similar amyloid distribution were observed clearly in the [^{18}F]AV-45 autoradiography, which was largely blocked by its reference compound. In the PET/CT scans, the [^{18}F]FDG PET/CT imaging detected elevated radioactivity uptake by multiple neck lymph nodes, In contrast, only one of these lymph nodes showed increased [^{18}F]AV-45 uptake. And the radioactivity distribution patterns in this [^{18}F]FDG and [^{18}F]AV-45 positive lymph node were different. **Conclusion:** [^{18}F]AV-45 has selective and specific uptake by the amyloid plagues in MTC tissue samples. [^{18}F]AV-45 PET/CT imaging successfully detected MTC lymph node metastasis in a recurrent MTC patient. In contrast, [^{18}F]FDG gave false positive results for multiple lymph node metastasis. **References:** none

OP-1029

^{99m}Tc-Hynic-TOC Scan in Differentiated Thyroid Cancer Patients with Negative ^{131}I Whole-Body Scan: low cost but relatively effective method

A. Aghaei, *K. Aryana, E. Askari, P. Jahan Panah, N. Ayati, S. Shafiei, S. Zakavi;*
Nuclear medicine research center, Mashhad university of Medical Sciences, Mashhad, IRAN, ISLAMIC REPUBLIC OF.

Aim/Introduction: Negative whole body iodine (^{131}I) scan (WBIS) with elevated serum thyroglobulin (Tg) levels are found in 20% of patients with differentiated thyroid cancer (DTC). Several studies have reported the expression of somatostatin receptors in DTC patients. Therefore, we evaluated the efficacy of ^{99m}Tc-Hynic-TOC somatostatin receptor scintigraphy (SRS) for detection of non-iodine-avid metastases in these patients. We also assessed the impact of SRS on staging and management of these patients **Materials and Methods:** The study population consisted of 35 DTC patients (25 women; PTC = 88.2%, FTC = 11.8%), with mean age of 54.8 ±15.56 years, who had elevated Tg levels despite of negative post-ablation WBIS. All patients underwent whole body SRS, 3-4 hours after intravenous injection of 20-25 Megabequrel (MBq) of ^{99m}Tc-Hynic-TOC. Sites of suspicious radiotracer accumulation were correlated with anatomic imaging and changes in the staging and management were recorded. Results: : The overall TNM staging (8th AJCC) of the patients were as follows: 35.3%, 17.6%, 14.7%, 5.9% and 26.5% as T_1, T_2, T_3, T_{4a} and T_{4b}, respectively. Also, 70.6% of patients were in N_{1b} group and 35% had distant metastasis (M_1). SRS was positive in 26 (76.5%) of cases. Patients with positive scan had significantly higher Tg levels at the time of scan, compared to those with negative scans (154.5±188.6 vs. 28.2±32.7 ng/mL, p-value = 0.005). Interestingly, previous history of neck external beam radiation therapy (EBRT) was significantly correlated with ^{99m}Tc-HYNIC-TOC avidity. Addition of SSTR scintigraphy changed overall staging and management in 11% and 32.4% of the patients, respectively. Five patients were candidates for peptide-receptor radionuclide therapy (PRRT) due to sufficient SSTR expression. **Conclusion:** The study showed SSTR scintigraphy as useful adjunct imaging modality in DTC patients with highly elevated Tg and negative WBIS. It may also be helpful for choosing the optimal treatment as well as referring patients for PRRT. The likelihood of positive findings on ^{99m}TcHynicTOC is higher in cases with previous history of EBRT or high Tg levels (i.e. suppressed-Tg >80 ng/mL) at the time of scan. **References:** none

OP-1030

Multivariate analysis of initial prognostic factors in pediatric differentiated thyroid carcinoma after RAI: a multicentric Italian experience

D. Albano[1], N. Quartuccio[2], F. Dondi[1], A. Campenni[3,4], M. Siracusa[3], S. Panareo[5], L. Urso[5], M. Bartolomei[5], S. Scotti[6], D. De Palma[6], A. Piccardo[7], M. Massollo[7], M. Garganese[8], M. Villani[8], M. Pizzoferro[8], C. Altini[8], A. Grossi[9], S. Baldari[3], F. Bertagna[1], R. Giubbini[1], A. Cistaro[10,11]; [1]University of Brescia and Spedali Civili of Brescia, Brescia, ITALY, [2]A.R.N.A.S. Ospedale Civico Di Cristina Benfratelli, Palermo, ITALY, [3]Unit of Nuclear Medicine, Department of Biomedical and Dental Sciences and Morpho-Functional Imaging, University of Messina, Messina, ITALY, [4]Thyroid Committee, European Association of Nuclear Medicine, Vienna, AUSTRIA, [5]Nuclear Medicine Department, Azienda Ospedaliero-Universitaria di Ferrara, Ferrara, ITALY, [6]Nuclear Medicine Unit, ASST-Settelaghi, Varese, ITALY, [7]Nuclear Medicine Unit, Ente Ospedaliero Ospedali Galliera, Genova, ITALY, [8]Diagnostic Imaging Department - Nuclear Medicine Unit, IRCCS Bambino Gesù Pediatric Hospital, Rome, ITALY, [9]DPUO, Endocrine Unit, IRCCS Bambino Gesù Pediatric Hospital, Rome, ITALY, [10]Nuclear Medicine Division, Salus Alliance Medical, Genova, ITALY, [11]Pediatric Study Group Committee, Italian Association of Nuclear Medicine and Molecular Imaging, Milan, ITALY.

Aim/Introduction: Differentiated Thyroid Carcinoma (DTC) is the most frequent endocrine pediatric carcinoma. Several variables have been studied in literature with the aim to predict treatment response and survival in pediatric DTC, but low and controversial evidences are available. The primary aim of this multicentric retrospective study was to identify factors associated with treatment response at one-year after the first radioactive iodine (RAI) therapy. The secondary aim was to reveal the clinical features correlated to a higher risk of persistence disease at the last follow-up. **Materials and Methods:** All consecutive patients≤21 years treated for DTC in 6 Italian centers in the period 1980-2020 were recruited for a total of 330 patients: 222 females (67%) and 108 male, age 15.2 ± 3.5 years (range 4-21 years). All, except nine with papillary microcarcinoma, underwent total thyroidectomy followed by RAI. For the present study, the risk of persistence/recurrent disease of our patients was scored according to 2015 ATA guidelines. The response to initial therapy was assessed at 12 months by thyroglobulin levels measurement and morpho and/or functional imaging according to 2015 ATA criteria. Moreover, at the last follow-up patients were dichotomized in subjects with not evidence of disease (NED) and persistent/progressive disease. Results: At 1-year after the first RAI, 170 children showed excellent response, 41 indeterminate response and 104 incomplete response (15 patients were lost during the follow-up). Children with excellent response were significantly younger, had less frequently capsular and vascular invasion, had lower tumor size and stimulated-Thyrogobulin (sTg), and presented more frequently low-risk disease. At multivariate analysis, only sTg confirmed to be an independent predictor of treatment response (p<0.001). ROC analysis showed that a pre-ablation sTg≥27.2 ng/ml was the best threshold to discriminate excellent response from incomplete response (sensitivity 73.6%, specificity 92.1% and AUC of 0.858). After a median follow-up of 108 months (range 12-480), NED was present in 277 cases (88%), while persistent disease was observed in the remaining 38 (12%). At multivariate analysis, sTg and 1-year treatment response categories were significantly associated with the risk of persistent disease (p=0.010 and 0.001, respectively). **Conclusion:** In pediatric DTC, pre-ablation sTg≥27.2 ng/mL is significantly associated with 1-year treatment response and with the risk of long-term persistent disease and may therefore be use as a marker to identify patients who may need more intensive surveillance. 1-year response may also serve to predict the disease status at the last control. **References:** none

OP-1031

Clinical Analysis of Differentiated Thyroid Cancer in Pediatric Age Group: A Single Medical Institution Experience of 33 Years

H. Nalbant, S. Gülbahar Ateş, B. B. Demirel, G. Uçmak; Dr. Abdurrahman Yurtaslan Ankara Oncology Training and Research Hospital, Ankara, TURKEY.

Aim/Introduction: The incidence of pediatric differentiated thyroid cancer(DTC) is relatively lower compared to adults. The aim of this study was to present the clinical experience data in our institution on pediatric DTC patients. **Materials and Methods:** One hundred-two children and adolescents with DTC(≤21years) who were followed at our institution between 1988 and 2021 were included in this study. Patients' ages, follow-up duration, histopathology results, radiological and laboratory findings, presence of lymph node and distant metastases, iodine uptake status on the first radioactive iodine (RAI) therapy, and follow-up data were evaluated. Logistic regression analysis was performed in prediction of persistent disease. Results: The median age of total 102 patients' at diagnosis was 17 years(5-21y, 16.5 ±3.7) (27 male,75 female) and the median follow-up duration was 9.5years(3 30y,10.1±5.3).Histopathology results of 102 patients contained 89(87.2%) papillary, 8(7.8%) follicular, 4(3.9%) hurtle cell, and 1(1%) papillary and follicular carcinoma. Median stimulated thyroglobulin level was 23,3 ng/ml(0,2-6300). Four patients had anti-thyroglobulin positivity. The total numbers of patients with positive lymph node metastases and with lung metastases at diagnosis was observed in 42(41.2%) and in 17(16.7%), respectively. While all of the patients received at least one dose RAI therapy, the total numbers of the patients with thyroid bed uptake, with neck lymph node uptake, and with lung uptake on the first radioactive therapy (RAI) were 70(68.6%), 26(25.5%),

13(12.7%),respectively. In the follow-up, 57(55.9%) patients were disease-free, while 22patients had stable-persistent disease and 3 patients had progressive biochemical and/or structural disease. However, the follow-up data of 20 patients could not be reached. Distant metastasis and recurrence were not observed during follow-up. Second primary malignancy was observed in 2 patients (bladder carcinoma and glioblastoma multiforme) in the follow-up. Univariate analysis revealed significant differences between presence of lymph node metastasis and/or lung metastasis at diagnosis and lung uptake on the first RAI therapy among disease-free and with persistent disease patients. We found that presence of lymph node metastasis had 5 times greater risk to develop persistent disease in the follow-up (p=0.034, ORR: 5.07, 95% CI: 1.14-22.70). **Conclusion:** We found high incidence of lymph node and lung metastasis in pediatric DTC patients in consistent with the literature. We suggest that accurate staging continued with RAI therapy and hormone replacement therapy provide substantially disease-free survival and prevent progression in pediatric DTC. Thus, by rational approach long disease-free and overall survival can be provided even with distant metastasis in pediatric DTC patients. **References:** None

OP-1032

Mapping of Iodine Avidity in Papillary Thyroid Cancer Reveal Associations with Thyroglobulin Expression and Tissue Proliferation

J. Nilsson, J. Siikanen, C. Hedman, C. Juhlin, C. Ihre Lundgren; Karolinska Institutet, Stockholm, SWEDEN.

Aim/Introduction: Papillary thyroid cancer is treated with radioiodine to ablate thyroid remnants and to treat spread disease. Adequate iodine accumulation in cancer tissue, iodine avidity, is important for successful treatment. The iodine avidity in a specific patient is often unknown at the point of initial treatment. This study investigated which histological tumour characteristics correlate with avidity, adding useful information for individualised treatment. **Materials and Methods:** In order to quantify avidity in cancer tissue, tracer amounts of iodine-131 was given to 45 patients with cytologically confirmed papillary thyroid cancer ahead of surgery. At pathology grossing, representative samples of tumour, lymph nodes and normal thyroid tissue were taken and subjected to radioactivity quantification ex vivo, to determine avidity. Afterwards, samples underwent routine and extended pathology work-up and analysis. Results: Our data show that tumoural Tg expression was correlated to avidity with a Pearson correlation coefficient ρ=0.51 (95% CI 0.32 - 0.66). The correlation between Tg expression and avidity was similar for both primary tumours and for lymph node metastases. Ki-67 index was negatively correlated to avidity in primary tumours ρ=-0.55 (95% CI -0.74 - -0.27), but not in lymph node metastases. Neither primary tumour size nor pT-stage ≥3 were significantly correlated to avidity. **Conclusion:** This work provides new information on which tumours that have low iodine avidity pre-therapeutically. The lower avidity in tumours associated poor Tg expression and high Ki-67 index can in part explain the worse prognosis for those patients. Our findings also suggest that radioiodine dosage could be adapted to Tg expression and Ki-67 index along with pT stage, potentially improving the efficacy of radioiodine therapy. **References:** none

OP-1033

Ablative treatment with ^{131}I in low-risk papillary thyroid cancer: is low-dose as effective as high-dose?

A. Roteta Unceta Barrenechea[1,2], A. Andrés Gracia[1,2], L. Tardin Cardoso[1], Y. Saker Diffalah[1], P. Razola Alba[1], T. Escalera Temprado[1], M. Delgado Castro[1], E. Prats Rivera[1], M. Abós Olivares[1]; [1]UCMHMNA - Clinic Hospital "Lozano Blesa", Zaragoza, SPAIN, [2]IIS-Aragón, Zaragoza, SPAIN.

Aim/Introduction: To compare the results of low-dose and high-dose radioiodine therapy in low-risk papillary thyroid cancer (PTC). **Materials and Methods:** 190 patients with low-risk PTC (T1N0M0, T2N0M0 and T1/2N1M0) treated with 30mCi, 50mCi or 100mCi of ^{131}I (01/01/2008-12/31/2017). Thyroglobulin, Antithyroglobulin Antibodies levels and imaging tests were reviewed at one year and at present (March-2021). Responses to treatment were classified into (Tuttle's criteria): Excellent response (ER) and Non-Excellent Response (Incomplete structural -ISR-, Incomplete biochemical -IBR- and Indeterminate -IR-). Twenty-five patients were excluded (not enough data). Results: 165 patients: 103 T1N0M0 (7 treated with 30mCi, 87 with 50mCi and 9 with 100mCi), 14.6% men, mean age 49.1 years and mean follow-up 6.65 years (3, 11-13.01), and 62 T2N0M0-T1/2N1M0 (13 treated with 30mCi, 38 with 50mCi and 11 with 100mCi), 22.5% men, mean age 46.3 years and follow-up mean 6.52 (2.93-12.22) years. T1N0M0 stage:- 30mCi: 6 patients (86%) ER, 1 (14%) non-excellent response (1 ISR) at one year. At present 100% ER.- 50mCi: 65 (75%) ER, 22 (25%) non-excellent response (13 ISR, 7 IBR, 2 IR) at one year. 3 patients were retreated: 1 ISR, 1 IR, 1 ER. Currently, 77 patients (89%) ER (including 1 ISR, 1 IR retreated) and 10 (11%) non-excellent response (4 ISR -1 retreated-, 6 IBR).- 100mCi: 7 (78%) ER, 2 (22%) non-excellent response (1 ISR, 1 IBR) at one year. Currently 9 (100%) ER. T2N0M0-T1/2N1M0 stage:- 30mCi: 8 patients (62%) ER, 5 (38%) non-excellent response (1 ISR, 2 IBR, 2 IR) at one year. One IR patient was retreated. At present, 10 (77%) ER (including 1 IR retreated) and 3(23%) not excellent response (1 ISR, 2 IBR).- 50mCi: 21 (55%) ER, 17 (45%) non-excellent response (7 ISR, 7 IBR, 3 IR) at one year. 4 patients were retreated: 1 by IBR, 3 by IR. Currently, 34 patients (89%) ER (including 1 IR, 2 IR retreated) and 4 (11%) had non-excellent response (2 IR, 2 IR -including 1 IR retreated-). - 100mCi: 6 (55%) ER at one year, 5 (45%) non-excellent

response (4 IBR, 1 IR) at one year. The patient with IR was retreated. At present, 8 (73%) ER (including the IR retreated) and 3 (27%) not excellent response (2 ISR, 1 IBR). **Conclusion:** It seems effective to give a low dose of ^{131}I to low-risk PTC for ablative treatment. However, a study with greater statistical significance should be carried out to confirm these results. **References:** None

OP-1034

Prospective, observational study on radioiodine treatment in DTC patients with intermediate risk or micro lymph node metastases

A. Ledwon, A. Blewaska, E. Paliczka-Cieslik, T. Olczyk, A. Sygula, A. Kropinska, E. Lewandowska-Jablonska, D. Handkiewicz-Junak; Maria Sklodowska-Curie National Research Institute of Oncology, Gliwice branch, Department of Nuclear Medicine and Endocrine Oncology, Gliwice, POLAND.

Aim/Introduction: Since the publication of ATA guidelines on thyroid cancer in 2016 much controversies arouse around indications and results of adjuvant radioiodine treatment in intermediate or low-risk patients with lymph node micrometastases. The first, preliminary results of ESTIMABL2 the prospective trial showed no radioiodine benefit in low-risk DTC. However, intermediate patients were not included in the study. THE AIM of our prospective, observational study was to evaluate the effects of radioiodine therapy in intermediate-risk DTC patients or patients with lymph node micrometastases. Here we present preliminary results in the first 146 DTC patients **Materials and Methods:** There were 125 women (85%) and the median age at diagnosis was52 years. Majority of patients, 116 (79%) were diagnosed with papillary cancer, the mean tumor diameter was 12 mm, in 46 (31%) there was an extrathyroid extension, in 97 (66%) vascular invasion and in 75 (51%) lymph node metastases. The median diameter of lymph node metastases was 2 mm. All patients had total thyroidectomy and in case of lateral lymph node metastases lateral lymphadenectomy. Median 131-I activity was 100 mCi and all patients were treated after rhTSH stimulation. Median time from the first operation to radioiodine therapy was 5 months. After radioiodine treatment patients were in follow up with diagnostic scintigraphy planed 18-24 months after treatment, unless unexpected results of radioiodine therapy indicated other procedures. The study was conducted from 06.2018 do 12.2019. Herein we present group of 146 treated from 06.2018 do 06.2019. Results: In posttherapy scintigraphy, only in two patients, there was suspicion in regional lymph nodes and no distant metastases. In none of these patients persistent disease was confirmed. Median thyroglobulin on 1st and 3rd day of rhTSH stimulation was 0.53 ng/ml and 7.6 ng/ml respectively. Unfortunately due to the COVID-19 situation from 112 planned diagnostic follow-up scintigraphy, only 69 were performed - 3 (4%) of patient had a structural recurrence and in another 3 (4%) and in another 3 (4%) the biochemical persistent disease was diagnosed. **Conclusion:** Our preliminary results show that in a selected group of patients with intermediate risk, there are excellent treatment results. However, the question of whether radioiodine adjuvant therapy could be omitted in this group of patients should be addressed in a prospective randomized trial. **References:** None

OP-1035

Ablation rate after radioactive iodine therapy in patients with differentiated thyroid cancer at intermediate or high risk of recurrence: a systematic review and a meta-analysis

L. Piscopo[1], M. Klain[1], C. Nappi[1], E. Zampella[1], V. Gaudieri[1], V. Cantoni[1], R. Green[1], F. Volpe[1], M. Manganelli[1], E. Caiazzo[1], M. De Risi[1], M. Petretta[2], M. Schlumberger[1], A. Cuocolo[1]; [1]Department of Advanced Biomedical Sciences, University Federico II, Naples, ITALY, [2]IRCCS SDN, Naples, ITALY.

Aim/Introduction: After total thyroidectomy with or without lymph-node dissection for differentiated thyroid cancer (DTC), radioactive ^{131}I (RAI) therapy may be administered for 3 main goals: remnant ablation, adjuvant therapy, or therapy. Although literature offers a huge armamentarium of data on survival benefit of RAI administration in patients with DTC at intermediate-high risk of recurrence, to our knowledge a meta-analysis on successful rate in these patients has not yet been performed. We performed a systematic review and a meta-analysis to investigate the successful ablation rate after RAI administration in patients with DTC at intermediate-high risk of recurrence. **Materials and Methods:** A comprehensive literature search of the PubMed, Scopus and Web of Science databases was conducted according to the PRISMA statement using the following key words: "differentiated thyroid cancer" OR "DTC", "thyroid neoplasm", "prognosis", "outcome", "follow-up", "radioactive iodine therapy" OR "RAI therapy", "I-131 ablation", "thyroglobulin" OR "Tg". A study was considered eligible if all of the following criteria were met: 1) data were available on age, gender and administered RAI activity, histopathology and extent of surgery; 2) the study presented data of adult subjects with differentiated thyroid cancer at intermediate or high risk of recurrence after RAI therapy according to American Thyroid Association risk classification; 3) the study included at least 100 subjects; 4) follow-up after RAI therapy for at least 1 year; and 5) the study provided data on successful ablation after RAI therapy defined as absence of abnormal findings at neck ultrasonography and undetectable serum Tg in the absence of anti-Tg antibodies. Results: The final analysis included 9 studies accounting for 3103 patients at intermediate-high risk of recurrence. In these patients, the successful ablation rates ranged from 51% to 94% with a 71% pooled successful ablation and was higher in intermediate (72%) than in high (52%) risk patients with a relative ratio of 1.22 (95% confidence interval 1.05-1.42,

P<0.01). Pooled recurrence rate in intermediate risk patients achieving successful ablation was only 2% during the subsequent 6.4-year follow-up while the pooled recurrence rate was 14% in patients who did not achieve a successful ablation. **Conclusion:** In a large sample of 3103 patients at intermediate-high risk of persistent/recurrent disease, 71% of them achieved a successful ablation. In these intermediate-risk patients, the probability of subsequent recurrence is low and most recurrence occurred in those with already abnormal findings at the first control. **References:** None

OP-1036

Recurrence-free survival and prognostic factors after adjuvant therapy with radioactive iodine-131 in patients with differentiated thyroid carcinoma

Y. Iizuka[1,2], T. Katagiri[2], K. Ogura[2], M. Inoue[2], K. Nakamura[2], T. Mizowaki[2];
[1]Shizuoka City Shizuoka Hospital, Shizuoka, JAPAN, [2]Kyoto University, Kyoto, JAPAN.

Aim/Introduction: Adjuvant therapy (AT) with radioactive iodine (RAI) is performed to reduce the risk of recurrence and prolong the survival rate in patients with differentiated thyroid carcinoma (DTC) after thyroidectomy. The purpose of this study was to evaluate the recurrence-free survival (RFS) rate and factors related to recurrence. **Materials and Methods:** Patients who underwent AT in our hospital for DTC without macroscopic residual lesions or metastatic lesions after surgical resection were retrospectively evaluated. Between January 2011 and July 2020, 343 patients underwent AT. Patients whose metastases were confirmed during AT and whose AT results were unknown were excluded; thus, 284 patients were evaluated. Recurrence was defined in the following cases: patients with visible recurrent tumours on image analysis or with pathologically established recurrent tumours during re-operation. RFS rates were estimated using the Kaplan-Meier method, and Cox regression analysis. Besides, inverse probability of treatment weighting (IPTW) analysis was performed for age, sex, histology, performance status, the American Thyroid Association (ATA) risk classification, and thyroglobulin levels higher than 4 ng/dL before AT without thyroid hormone stimulation (pre-Tg) in terms of the treatment dose because these factors affected the decision of the treatment dose. P-values less than 0.05 were defined as significant. Results: The median observation period was 38.7 months (range, 3-280 months). The patients' median age was 54 years (range, 9-85). Ninety-two patients were male, and 192 patients were female. The treatment doses were 1,110 MBq in 111 patients, 1,850 MBq in 16 patients, and 3,700 MBq in 157 patients. There were 36 cases of recurrence. The first recurrence sites were as follows: the thyroid bed in 2 patients, cervical lymph nodes (LNs) in 16 patients, mediastinal LNs in 3 patients, other LN sites in 2 patients, and lungs in 16 patients (including overlap). The estimated 3-year RFS rate was 84.5% (95% confidence interval: 78.1-89.2%). Twenty-eight patients exhibited recurrence within three years. The histology (excluding that of papillary carcinoma), treatment dose, and pre-Tg were found to be significant factors that worsened the RFS in univariate analysis. The treatment dose and pre-Tg were also significant factors related to worsening RFS in multivariate analysis. However, IPTW analysis showed that the treatment dose was not a significant factor worsening the RFS (p=0.7). **Conclusion:** The estimated 3-year RFS rate was 84.5% in patients treated with AT with RAI. Pre-Tg was found to be a significant factor for recurrence. **References:** none

OP-1037

Anxiety And Depression In Patients With Differentiated Thyroid Carcinoma (DTC) Treated With Radioiodine In The Pandemic Year

***B. Pérez López[1]**, Á. Sánchez-Anguita Muñoz[2], E. Martín Gómez[3], F. Pulido López[3], J. De la Torre Laso[2], A. Álvarez Delgado[3], R. Ruano Pérez[1];*
[1]Hospital Clínico Universitario de Valladolid, Valladolid, SPAIN, [2]University of Salamanca, Salamanca, SPAIN, [3]Hospital Clínico Universitario de Salamanca, Salamanca, SPAIN.

Aim/Introduction: Cancer diagnosis is associated with an increased prevalence of psychopathological disorders,anxiety and depression.Patients treated with radiopharmaceuticals present prior concerns related to ignorance of the therapy,radiation protection standards or radiation fear that increases psychological distress.Our aim was to know the state of mental health and mental discomfort of patients who have been treated with radioiodine during the year of COVID19 pandemic and identify barriers to meet the needs of psychological care. **Materials and Methods:** Patients diagnosed with DTC referred for 131I-treatment from January-2020 to January-2021 in 2 hospitals.Data collection was made by standardized questionnaires for mental health assessment(STAI test, BDI Depression test),demographic and social data (age, sex, number of children...),relevant pathological history, histological type,tumor stage (TNM scale) and specific data on 131I-treatment. Results: 52 patients were included, 17 men and 35 women, mean age of 55.31 years±13.27. 55.8% from Hospital-A and 44.2% from Hospital-B.The 76.9% of the patients were diagnosed with papillary carcinoma,7.7% papillary oncocytic variant,9.8% follicular carcinoma and 3.8% Hürtle cell carcinoma.The majority of them showed no lymph node involvement at diagnosis,T1N0 (44.2%) and T3N0 (9.6%), and 7.7% M1.In the 82.7% of cases, this was the first 131I-treatment,13.5% the second and 1.9% the third, with a relationship between the number of admissions and TNM stage (p=0.041).In 82.4% of cases, rhTSH was administered prior to treatment. The mean dose administered was 3561.2±1396.9MBq with a mean duration of admission of 3.7 days, being males the

group with the highest dose and duration of admission. There was no significant correlation between the type of preparation for treatment and patients degree of depression or anxiety.A positive correlation was observed between the duration of hospitalization, the degree of depression (p=0.048) and the 131I-dose (p=0.001).Face-to-face medical consultation was performed in 57.7% of the cases and by telephone in 42.3%.The duration of the consultation had an influence on the patients degree of anxiety,the longer the interview the less anxiety (p=0.002) without affecting the degree of depression.The degree of overall satisfaction with the process was rated as low in 13.5%(all in the telephone consultation group),appropriate in 44.2% and very good in 44.2%. **Conclusion:** According to our results, there is a direct relationship between the duration of hospitalization and the degree of depression of the patients, since it is associated with a higher dose and stage.Likewise, the time we dedicate to our patients has an impact on the reduction of anxiety and on the degree of global satisfaction. **References:** None

1901

Saturday, October 23, 2021, 10:45 - 12:15

Channel 1

CME 14: Probing Tumour Metabolism - An Update

OP-1040

Imaging Nucleoside Transport for Monitoring Targeted Therapy in Cancer

F. Iommelli; *National Research Council, Institute of Biostructures and Bioimages, Naples, ITALY.*

OP-1041

Illuminating Metabolic Heterogeneity and Vulnerabilities in Lung Cancer

D. Lewis; *Cancer Research UK Beatson Institute, Glasgow, UNITED KINGDOM.*

OP-1042

Imaging Tumour Metabolism and its Heterogeneity with MRI

F. Gallagher; *Department of Radiology, University of Cambridge, Cambridge, UNITED KINGDOM.*

1902-1

Saturday, October 23, 2021, 10:45 - 11:15

Channel 2

Special Talk by Declan Murphy

OP-1045

Prostate Cancer along the Yellow Brick Road

D. Murphy; *Consultant Urologist & Director of Genitourinary Oncology, Peter MacCallum Cancer Centre, Melbourne, AUSTRALIA.*

1902-2

Saturday, October 23, 2021, 11:30 - 12:15

Channel 2

Interview with the Expert 15 - Reflections on the Development of PET and Theranostics Downunder - A 25-Year Journey into the Light

OP-1046

Interview - Reflections on the Development of PET and Theranostics Downunder - A 25-Year Journey into the Light

R. Hicks; *The Sir Peter MacCallum Cancer Center, Department of Oncology, Molecular Imaging and Therapeutic Nuclear Medicine, Melbourne, AUSTRALIA.*

OP-1047

Interview - Reflections on the Development of PET and Theranostics Downunder - A 25-Year Journey into the Light

J. J. Morigi; *Royal Darwin Hospital, PET/CT centre, Darwin, AUSTRALIA.*

1905

Wednesday, October 20 - Saturday, October 23, 2021

on-demand pool, release on Wednesday, October 20 at 09:00

Joint Symposium 27 (EANM/JSNM): Advances in Molecular Imaging of Neurodegenerative Disorders

OP-1049

Advances in Tau Imaging

L. Beyer; *Ludwig Maximillian University Munich, Department of Nuclear Medicine, Munich, GERMANY.*

OP-1050
Advances in MAO-B Imaging
R. Harada; Tohoku University Graduate School of Medicine, Department of Pharmacology, Sendai, JAPAN.

OP-1051
Advances in Synaptic Density Imaging
K. Van Laere; Catholic University Leuven, Department of Nuclear Medicine, Leuven, BELGIUM.

OP-1052
Advances in Alpha-Synuclein Imaging
M. Ono; National Institutes for Quantum and Radiological Science and Technology, Department of Functional Brain Imaging Research, Chiba, JAPAN.

1906

Wednesday, October 20 - Saturday, October 23, 2021

on-demand pool, release on Wednesday, October 20 at 09:00

Joint Symposium 28 (EANM/IAEA): Lancet Oncology Commission on Medical Imaging and Nuclear Medicine

OP-1095
The Lancet Oncology Commissions
D. Collingridge; The Lancet Oncology, London, UNITED KINGDOM.

OP-1096
Goals and Scope of the Lancet Oncology Commission on Medical Imaging and Nuclear Medicine
D. Paez; Division of Human Health, International Atomic Energy Agency, Vienna, AUSTRIA.

OP-1097
Global Utilization of Imaging and Nuclear Medicine in Oncology
A. Scott; Department of Molecular Imaging and Therapy, Austin Health, Melbourne, AUSTRALIA.

OP-1098
Health Economic Analysis of Cancer Imaging
R. Atun; Centre for Health Decision SCience, Harvard TH Chan School of Public Health, Boston, UNITED STATES OF AMERICA.

OP-1099
Overview and Recommendations
H. Hricak; Department of Radiology, Memorial Sloan Kettering Cancer Center, New York, UNITED STATES OF AMERICA.

1909

Wednesday, October 20 - Saturday, October 23, 2021

on-demand pool, release on Wednesday, October 20 at 09:00

Cutting Edge Science Track - TROP Session: Radiomics - Methodology and Clinical Applications

OP-1054
How to improve the transportability of radiomic models?
F. Orlhac[1], C. Nioche[1], M. Soussan[1,2], I. Buvat[1]; [1]LITO, U1288 Inserm/Institut Curie, Orsay, FRANCE, [2]AP-HP, Université Paris 13, Hôpital Avicenne, Department of Nuclear Medicine, Bobigny, FRANCE.

Aim/Introduction: To investigate the impact of the composition of the training cohort on the performance of radiomic models when applied to external databases. **Materials and Methods:** Four public [1-4] and one private databases of non-small cell lung cancer patients were included, for a total of 642 patients who underwent a baseline 18F-FDG PET/CT scan. For each patient, the primary lesion was segmented using a threshold set to 40% of SUVmax and 42 radiomic features were extracted using LIFEx [5]. We evaluated the performance of radiomic models to differentiate between adenocarcinoma (ADK) and other subtypes (OTH) using Linear Discriminant Analysis. Models were established after feature selection, consisting in keeping only features that had a Spearman correlation with others less than 0.80. We trained a model using one of the 5 databases and tested its performance on another database, yielding 20 training/testing set combinations. To train the model, either all patients were included, or only the most "typical" patients based on prior knowledge. Since it is known that ADK lesions tend to be less metabolically active than other lesions, the typical ADK (respectively OTH) were defined as those with SUVmax lower (higher) than the median of SUVmax in all ADK (all OTH) lesions. The model performances were evaluated using the Area under the ROC curve (AUC). Results: A total of 327 patients were identified as ADK, corresponding to between 41% and 70% of patients depending on the database. When using all patients of the training set, the AUC on the test set varied between 0.492 and 0.842. When using only the most typical patients of the training set (corresponding to keeping 50% of the patients), the performance of the resulting model on the test set improved in 15 out of 20 training/testing combinations (Wilcoxon test $p<0.05$, AUC=[0.534-0.887]), suggesting the models were more generalizable. The classification on testing set was improved for 62±10% of patients, i.e. 81±17% of typical patients and 44±15% of other patients. **Conclusion:** As expected, the performance of a model on an independent

set largely depends on the size and composition of the training set. When a prior is available, training a radiomic model using only the typical patients identified using that prior led to better generalizability of the model performance, in particular for typical patients. **References:** [1] Kirienko. EJNMMI 2018. [2] Kirk & Albertina. TCIA 2016. [3] Li. TCIA 2020. [4] Bakr. TCIA 2017. [5] Nioche. Cancer Res 2018.

OP-1055

Comparison of multicentre harmonization strategies: ComBat harmonization vs. pre-selection based on robustness

R. Da-ano[1], F. Lucia[1,2], I. Masson[1,3], R. Abgral[4], J. Alfieri[5], C. Rousseau[6], A. Mervoyer[3], C. Reinhold[7,8], O. Pradier[1,2], U. Schick[1,2], D. Visvikis[1], M. Hatt[1];
[1]INSERM - DR GRAND OUEST/ LaTIM U1101, Brest, FRANCE, [2]Radiation Oncology Department, University Hospital, Brest, FRANCE, [3]Department of Radiation Oncology, Institut de cancérologie de l'Ouest René-Gauducheau, Saint-Herblain, FRANCE, [4]Department of Nuclear Medicine, University of Brest, Brest, FRANCE, [5]Department of Radiation Oncology, McGill University Health Centre, Montreal, QC, CANADA, [6]Department of Nuclear Medicine, Institut de cancérologie de l'Ouest René-Gauducheau, Saint-Herblain, FRANCE, [7]Department of Radiology, McGill University Health Centre, Montreal, QC, CANADA, [8]Augmented Intelligence & Precision Health Laboratory of the Research Institute of McGill University Health Centre, Montreal, QC, CANADA.

Aim/Introduction: Radiomic features are potential imaging biomarkers for prognosis and predictive modeling in oncology and are notoriously sensitive to imaging factors variability (scanner model, acquisition protocols and reconstruction algorithms. Our goal was to compare two approaches to suppress the center-effecct in radiomic predictive modelling relying on machine learning (ML) algorithms with embedded feature selection methods: pre-selecting features based on their robustness to these factors or ComBat a posteriori harmonization. **Materials and Methods:** ninety-two IBSI-compliant radiomic features were extracted from FDG-PET and MRI sequences (T1, T1c, T2 and ADC maps) of 189 cervical cancer patients treated with radiochemotherapy in 3 centers (Brest, n = 117 and Nantes, n = 44 in France, and Montreal, n = 28, in Canada). For the first strategy, features exhibiting an interclass correlation coefficients (ICC) above 0.90 across scanners and centers were considered highly robust. For the second strategy, the distributions of all features were harmonized using the standard ComBat and the improved version recently developed (BM-ComBat)[1]. After splitting the data 70/30% in training and testing sets, the two strategies were then compared by training and validating models predictive of local failure through three different machine learning pipelines: LASSO for multivariate regression (MR) and embedded feature selection associated with Random Forest (RF) and Support Vector Machine (SVM). They were compared using Matthews correlation coefficient (MCC) and Area under the curve (AUC). Results: The performance of models trained using the subset of features selected for their robustness showed very poor performance (AUC 0.45-0.59, MCC 0.05-0.19) with or without harmonization, hinting at the fact that most predictive features were eliminated beforehand due to their sensitivity to the scanner and center effects. Using a different threshold for ICC (>0.7 or 0.8) did not modify significantly the results. Of note, results using all features as input were good, even without harmonization (AUC 0.79-0.84, MCC 0.48-0.86), which shows that the ML algorithms were able to combine predictive features in an efficient way. **Conclusion:** Feeding all available features to any ML pipeline relying on embedded features selection techniques led to models with much better predictive performance than pre-selecting a smaller set of highly robust features. This means, at least in our dataset, that predictive features were the ones sensitive to changes in imaging properties of the multicentre data and they were eliminated during the pre-selection. **References:** [1] https://www.nature.com/articles/s41598-020-66110-w

OP-1056

Linking imaging to genetic patterns in head and neck squamous cell carcinoma

C. Spielvogel[1], S. Stoiber[1], M. Grahovac[1], D. Krajnc[1], J. Schnöll[1], B. J. Jank[1], V. Bystry[2], M. Hacker[1], L. Papp[1], L. Kenner[1], A. R. Haug[1];
[1]Medical University of Vienna, Vienna, AUSTRIA, [2]Central European Institute of Technology, Brno, CZECH REPUBLIC.

Aim/Introduction: Personalized cancer medicine is highly dependent on the utilization of genetic information to guide targeted therapy. Currently, genetic information is mainly assessed using invasive acquisition of tissue via biopsies. The goal of this study was to evaluate non-invasive quantitative PET/CT imaging markers for the prediction of genetic tumor characteristics with a focus on pathway disruption in head and neck squamous cell carcinoma (HNSCC) patients. **Materials and Methods:** The study cohort consisted of 70 patients with HNSCC. For all patients, whole exome sequencing (WES) data from formalin-fixed paraffin-embedded tissue samples as well as 18F-FDG-PET/CT was acquired. For a total of 50 cancer related pathways, binary scores were created, indicating the disruption of each pathway. Pathway disruption scores were derived based on Ensembl variation consequences and PolyPhen scores of the WES mutational variations. Quantitative imaging patterns were derived using an established radiomics feature extraction workflow. Potential associations between pathway disruption scores and radiomic features were examined using a statistical approach based on Mann-Whitney U test and a machine learning approach based on a random forest classifier with stratified 250-fold Monte Carlo cross-validation. Results: The two most significant pathways identified to be associated with radiomic features, according

to the univariate statistical approach, were p53 signaling and hippo signaling. p53 signaling was associated with two PET-based radiomic texture features corresponding to intra- and inter-lesion heterogeneity (p value 0.0005 and 0.0002). Hippo signaling was associated with one PET/CT hybrid feature and one CT-based feature (p value 0.0009 and 0.0009). Using the machine learning-based analysis, the two most predictable pathways were mTOR signaling (AUC 0.64) and chemokine signaling (AUC 0.63), while p53 and hippo signaling were among the six most predictable pathways (AUC 0.59 and 0.57). Kernel density estimation showed differences in per-label distributions for the most significant radiomic features. **Conclusion:** This study supports the assumption that imaging features are indicative of genetic patterns of tumors. However, with radiomic features alone, the predictive performance is still poor. Kernel density estimation suggests that there is a clear difference in the distribution of radiomic features for functional versus disrupted pathways. Nonetheless, the large overlap between the distributions highlights a potential reason why the radiomic features have limited predictability. Further investigations on combining imaging features with complementary, non-invasive markers may increase the predictive performance to a clinically applicable level. **References:** none

OP-1057

A radiomic signature based on features extracted from baseline 18F-FDG PET/CT predicts 2-year PFS in Hodgkin Lymphoma patients

R. Durmo[1,2], V. Trojani[1], M. Casali[1], F. Fioroni[1], A. Ruffini[3], S. Luminari[1], F. Merli[1], M. Iori[1], A. Versari[1], M. Bertolini[1]; [1]AUSL-IRCCS of Reggio Emilia, Reggio Emilia, ITALY, [2]PhD program in Clinical and Experimental Medicine (CEM), University of Modena and Reggio Emilia, Modena, ITALY, [3]GRADE Onlus, Reggio Emilia, ITALY.

Aim/Introduction: Hodgkin Lymphoma (HL) is one of the most curable cancer. However, relapse or refractory disease in a subset of patients who then require salvage therapy and treatment-related toxicity still represents an unsolved clinical problem. Identifying factors that could improve the early detection of these refractory patients is very important to improve risk stratification and individualize treatment. The aim of this study was to assess whether a baseline 18F-FDG PET-based radiomic model could predict relapsed or refractory disease in HL patients. **Materials and Methods:** We selected a retrospective cohort of stage I-IV HL patients treated in our institute between 2007-2020. Available baseline 18F-FDG PET/CT scans were required for inclusion. From the baseline 18F-FDG PET/CT images all lesions were semiautomatically segmented using a 41% SUVmax threshold. Radiomic features were extracted using an in-house software employing the pyradiomics library. Lesions with less than 64 voxels were excluded from the analysis. Least absolute shrinkage and selection operator (LASSO) regression was used for feature selection and constructing a radiomic model. Receiver operating characteristic (ROC) curves were used to test the predictive performance of this signature. Main endpoint of the study was 2-year progression free survival (PFS). Results: We identified a study population of 173 patients. Median age was 39 years (15-88) and 45% had stage III-IV. Median follow up was 54.0 months (range 27.2 - 91.5) and 2-year PFS was 74.9% (95% CI 72.7% - 77.2%). A total of 1503 radiomic features were extracted, including shape-based features, first-order histogram features, high-order textural features, and waveled-filtred features. Based on the LASSO regression analysis, 6 wavelet image-filtered features resulted significant and selected to establish the radiomic signature. The radiomics model showed an AUC of 0.67 (CI 0.64-0.71) with true positive rate of 0.96 and false positive rate of 0.70. The optimal signature threshold identified through ROC analysis divided the population in two distinct groups (log-rank test p-value < 0.01) with 2-year PFS of 24.0% (CI 18.0-32.4) and 80.3% (CI 78.2% - 82.5%) respectively. **Conclusion:** The baseline 18F-FDG PET-based radiomic signature has the potential to be used as a non-invasive prognostic factor in HL patients. This could help clinicians to improve patient-specific therapy strategies. **References:** none

OP-1058

From multidimensional (PET radiomics, clinical and semantic) to patient-based "short-format" fingerprint for Hodgkin Lymphoma outcome prediction

F. Gelardi[1], N. Gozzi[2], L. Cavinato[3], M. Sollini[1,2], M. Kirienko[4], M. Biroli[1], F. Ricci[2], F. Ieva[3,5], A. Santoro[1,2], C. Carlo-Stella[1,2], A. Chiti[1,2]; [1]Humanitas University, Pieve Emanuele, ITALY, [2]IRCCS Humanitas Research Hospital, Rozzano, ITALY, [3]MOX–Modelling and Scientific Computing lab, Department of Mathematics, Politecnico di Milano, Milan, ITALY, [4]Fondazione IRCCS Istituto Nazionale Tumori, Milan, ITALY, [5]CADS–Center for Analysis, Decision, and Society, Human Technopole, Milan, ITALY.

Aim/Introduction: Hodgkin Lymphoma (HL) typically presents with a number of lesions. High inter-patient and intra-patient HL lesion heterogeneity represent the major challenge in applicability of advanced imaging analyses. We aimed to establish a predictive model based on clinical data and aggregated radiomic features (namely, short-format/patient-based representation) to predict HL refractoriness at baseline. **Materials and Methods:** [18F]FDG-PET/CT images for staging purposes of 136 newly diagnosed HL patients were retrospectively evaluated. [18F]FDG-avid lesions greater than 64 voxels were semi-automatically segmented and radiomic features were extracted with LIFEx (Nioche C, et al. Cancer Research. 2018; 78:4786-4789; www.lifexsoft.org). To reduce feature redundancy, a correlation criterion was used (elimination threshold >|80%|). For each feature remained in the set of potential predictors, we calculated mean, standard

deviation, maximum and minimum of all segmented lesions within a patient. Different univariate and multivariate models were tested to identify and select the most robust features to be plugged into the model. Finally, a "short-format" fingerprint including clinical data, semantic and radiomic features was established. Easy ensemble classifier was used to test the predictive power of the short-format fingerprint. Interim and follow-up (FU) [18F]FDG-PET/CT images defined patients' outcome (refractory/relapsing and responders) according to the Deauville score. P-value ≤0.05 was considered for statistical significance. Results: Interim-PET resulted positive in 9/136 patients; 20/136 patients were refractory or relapsed at the end of first-line chemotherapy or during follow-up. Overall, 1210 lesions (893 nodal and 317 extra-nodal) were segmented. Clinical data and radiomic features resulted uncorrelated. Semantic and radiomics features were finally retained in the short-format fingerprint. The short-format fingerprint predicted responders vs patients with positive interim-PET with 0.69 AUC, 0.73 accuracy, and 0.64 sensitivity. In the FU outcome prediction, the model achieved an AUC of 0.72, accuracy of 0.72 and sensitivity of 0.72 in classifying responder vs refractory/relapsing patients. **Conclusion:** The model based on "short-format" PET radiomic fingerprint achieved promising results in first-line chemotherapy outcome prediction. The higher performance in identifying relapsing patients at last FU-PET compared to refractory at interim-PET may be related to a greater number of positive findings suggesting that a larger dataset would increase the predictive model performance. The "short-format" PET radiomic fingerprint allowed a patient-based approach, overcoming the limitations related to inter-patient and intra-patient lesion heterogeneity. Baseline HL risk stratification can be improved including PET-derived radiomic data. **References:** None

OP-1059

[^{18}F]FDG PET radiomics for the prediction of genetic clusters in pheochromocytomas and paragangliomas

W. A. Noortman[1,2], D. Vriens[1], E. H. Aarntzen[3], A. van Berkel[3], H. J. Timmers[3], L. F. de Geus-Oei[1,2], F. H. van Velden[1];
[1]Leiden University Medical Center, Leiden, NETHERLANDS, [2]University of Twente, Enschede, NETHERLANDS, [3]Radboud University Medical Center, Nijmegen, NETHERLANDS.

Aim/Introduction: Pheochromocytomas and paragangliomas (PPGLs) are rare neuroendocrine tumours. Up to 40% harbour an underlying germline mutation. Furthermore, somatic mutations are found in at least one-third of sporadic PPGLs. Hereditary PPGLs can be segregated into 2 clusters based on their transcription profiles: cluster 1 (SDH, VHL) is enriched for genes that are associated with hypoxic response, and cluster 2 (RET, NF1) implicates gene mutations that activate kinase signaling. Cluster 1 PPGLs are associated with increased [^{18}F]FDG accumulation (i.e. SUV_{max}). This study compared the use of radiomics, SUV_{max} and biochemical profile for the prediction of genetic clusters of PPGLs. **Materials and Methods:** Sixty-nine patients underwent a [^{18}F]FDG-PET/CT scan prior to surgery. Seventy-two lesions (13 cluster 1, 19 cluster 2, 40 no or unknown somatic mutation) were delineated using an adaptive threshold of 41% SUV_{peak}, wherefrom 105 radiomic features were extracted. Stratified 5-fold cross-validation for the prediction of the genetic cluster (one-versus-rest) was performed using binomial logistic regression. Dimensionality reduction using redundancy filtering of the Spearman correlation matrix and factor analysis was incorporated in the folds; 1 factor was obtained for every 10 patients in the training set. Predictive performances were presented as mean areas under the receiver operating characteristic curves (AUC) over the five folds for the test sets. Results were validated by sham data, i.e. replacing the radiomic features with random numbers without distribution. AUCs of the biochemical profile (noradrenergic, adrenergic and dopaminergic), SUV_{max} and the radiomics model were compared to sham data. Results: Cluster 1 could be predicted using biochemistry alone with a mean AUC for the test set of 0.84. SUV_{max} resulted in a mean test AUC of 0.95 (0.96 combined with biochemistry). The five radiomic factors reached an AUC of 0.91 (0.85 with biochemistry). The AUC of sham data was 0.66 (0.77 with biochemistry). For cluster 2, the mean AUCs were 0.61, 0.78 (0.80), 0.84 (0.84) and 0.63 (0.61) for biochemistry, SUV_{max}, radiomic factors and sham data, respectively (with biochemistry in brackets). No or unknown mutation was predicted with AUCs of 0.60, 0.62 (0.49), 0.76 (0.72) and 0.59 (0.64) for biochemistry, SUV_{max}, factors and sham data, respectively. **Conclusion:** Identification of cluster 2 PPGLs and PPGLs with no or unknown mutation might be better achieved by radiomics when compared to biochemistry, SUV_{max} or sham data. SUV_{max} could already predict cluster 1 PPGLs with high certainty, therefore radiomics could not enhance the classification performance for this cluster. **References:** None

OP-1060

Context-aware saliency guided PET/CT radiomics: joint prediction of phenotype and outcome in multi-center head and neck cancer

W. Lv, J. Ma, L. Lu;
Southern Medical University, Guangzhou, CHINA.

Aim/Introduction: Characterizing intra-tumor heterogeneity is critical for outcome prediction and individualized treatment planning in head and neck cancer. Motivated by saliency detection in computer version, we hypothesis that tumor sub-regions with higher/lower saliency maybe represent different phenotype and more responsible for tumor progression. Thus, this multi-center study aims to investigate the prognostic value of context-aware saliency guided PET/CT radiomics.

Besides, considering human papilloma virus (HPV) positive oropharyngeal carcinoma (OPC) showed better prognosis, while high grade poorly differentiated cancer showed worse prognosis, the prognostic value of features that predictive to HPV and/or grade was also evaluated. **Materials and Methods:** 806 HNC patients with FDG-PET/CT images from 9 centers were collected from The Cancer Imaging Archive (TCIA). Among which, 507 (63%) patients are with OPC. Training and testing cohorts were divided by a ratio of 3:2 (597 patients from 5 centers vs. 209 patients from 4 centers). HPV status and histopathology grade are available for 100 and 228 patients in training cohorts respectively. Context-aware saliency detection was adopted to generate saliency maps. 497 radiomics features were extracted from the whole ROI, sub-ROI with saliency >=0.5 or saliency <0.5 in PET and CT images respectively. Feature harmonization (comBat) was implemented under center-, voxel size-, scanner-based batch divisions. Top 10 features with higher concordance index (C-index) for outcome prediction and/or higher AUC for HPV and/or grade prediction were selected, and multivariate Cox model was constructed by Akaike information criteria (AIC). Results: Most models (15/20) showed better performance are constructed by using features from high/low saliency ROI. In the whole testing cohort, models containing both prognostic features and predictive features of grade showed similar performance for outcome prediction (C-index: 0.664-0.819 vs. 0.676-0.805) compared to models only containing prognostic features. In the subset of OPC in testing cohort, when incorporating predictive features of HPV and/or grade into outcome prediction model, higher C-index were achieved to 0.653-0.662 vs. 0.634, 0.760-0.841 vs. 0.734, 0.647-0.672 vs. 0.656, and 0.683 vs. 0.669 compared with models only built with prognostic features for RFS, MFS, OS and PFS predictions, respectively. More models (7 vs. 1 vs. 1) showed better performance by using comBat with voxel-dased division than that of center-based and scanner-based division. **Conclusion:** Saliency guided radiomics showed better performance than conventional radiomics. Features predictive to HPV and/or grade are also helpful for outcome prediction. Feature harmonization based on different batch division methods showed varying performance improvement. **References:** none

OP-1061

Predicting the presence of targetable molecular alterations with clinico-metabolic ^{18}F-FDG PET radiomics in non-Asian lung adenocarcinoma patients

C. Lasnon[1], K. Weyts[1], R. Gervais[1], N. Aide[2];
[1]François Baclesse Cancer Centre, Caen, FRANCE, [2]CHU de Caen, Caen, FRANCE.

Aim/Introduction: In non-small cell lung cancer, and in particular in lung adenocarcinoma, the next generation sequencing (NGS) at diagnosis is increasingly carried out because first line-of treatment depends on multiple molecular targets (1) but no consensus has been reached until now. The current hot topic is to determine who will benefit from NGS panels and when in the care time-line. The aim was therefore to investigate if combining clinical characteristics with pre-therapeutic ^{18}F-FDG PET radiomics could predict the existence of molecular alterations in key molecular targets in lung adenocarcinoma in order to screen patients who are more likely to benefit from a molecular testing. **Materials and Methods:** This non-interventional mono-centric study prospectively included patients with newly-diagnosed lung adenocarcinoma referred for baseline PET and who had tumoral molecular analyses for the following targets: EGFR, BRAF, KRAS, NRAS, MET, STK11, PIK3CA, ALK and ROS1. Tumoral volumes of interest were analysed using LifeX software. A logistic regression was performed, including sex, age, smoking history, AJCC stage and thirty-one PET variables. A validation process was used by randomly splitting the data in training and validation datasets. Results: Eighty-seven patients were analysed. Forty-seven patients (54.0%) had at least one molecular alteration. Based on the training dataset (n=67), five variables were included in the logit model: age, sex, AJCC stage, correlation$_{_GLCM}$ and GLNU$_{_GLZLM.}$ More molecular alterations were observed in women: 88.0% in women versus 40.3% in men (p<0.0001). Others clinical and PET variables were different between patients with and without molecular alterations. There was a moderate correlation between correlation$_{_GLCM}$ and GLNU$_{_GLZLM}$ (p <0.0001, ρ = 0.591). The ROC analysis for molecular alteration prediction using this model found an AUC equal to 0.891 (p<0.0001). A cut-off value set to 0.38 led to a sensitivity of 97.4%, a NPV of 80.4% and a LR+ equal to 3.1. Applying this cut-off value in the validation dataset of patients (n=20), the test presented a sensitivity equal to 88.9%, a NPV equal to 87.5% and a LR+ = 2.4. **Conclusion:** A clinico-metabolic ^{18}F-FDG PET phenotype allows detecting key molecular target alterations with high sensitivity and NPV thus opening the way to the selection of patients for molecular analysis. **References:** 1. L. Schwartzberg, E.S. Kim, D. Liu, D. Schrag, Precision Oncology: Who, How, What, When, and When Not?, American Society of Clinical Oncology educational book. American Society of Clinical Oncology. Annual Meeting 37 (2017) 160-169

OP-1062

Prognostic value of radiomics features extracted from ^{18}F-FDG PET/CT image in Diffuse Large B-Cell Lymphoma (DLBCL) patients

L. Travaini, G. Lo Presti, F. Botta, S. Raimondi, S. Mazzara, M. Ferrari, E. Derenzini, S. Pileri, M. Cremonesi, F. Ceci;
IEO, European Institute of Oncology, Milan, ITALY.

Aim/Introduction: ^{18}F[FDG]-PET/CT is currently used to stage Diffuse large B-cell lymphoma (DLBCL). Up to 40% of patients, develop refractory disease with a poorer prognosis. The early identification of patients with unfavourable prognosis allows to improve patient therapeutic management. The extraction of radiomic features (RFs) through quantitative PET/CT image might identify reliable imaging biomarkers predictive of prognosis. Aim: to evaluate the association between ^{18}F[FDG]-PET/CT RFs and patients' outcome assessed by disease-free survival (DFS) and overall survival (OS). **Materials and Methods:** We retrospectively analysed clinical records of newly diagnosed DLBCL patients investigated with baseline ^{18}F[FDG]-PET/CT at our institution. Radiomics analysis (LifeX package) was performed by applying regions of interest (ROIs) semi-automatically, using a fixed 2.5 SUV threshold. Shape, first and second order features were calculated for the lesion with the highest uptake. Reproducibility of RFs according to different acquisition parameters was assessed with ANOVA test. A radiomic score was obtained by multivariable LASSO Cox model. Univariate analysis of clinical variables and radiomic score was performed by Log-rank test. A clinical model was obtained by Cox regression including the following predictors: IPI, TMTV and lesion volume. Finally, a clinical-radiomic model was obtained adding the radiomic score to the clinical model. The performance of the models was evaluated by C-index. Results: One-hundred and twelve patients were considered in this analysis (55 females, 57 males. Median age 58.1 years). Stage-I was diagnosed in 9.5% of cases, stage-II in 22.4%, stage-III in 9.5% and stage-IV in 58.6%. The median follow-up was 42 months. Eighteen patients died during follow-up. Fifty-four RFs were extracted for each target lesion. After reproducibility test, 44 RFs were considered robust. Radiomic score resulted significantly associated with both DFS and OS at multivariable analysis ($p<0.001$). Among clinical variables, only IPI resulted associated with DFS at univariate ($p=0.008$), but not at multivariate analysis ($p=0.19$). Otherwise, IPI score was associated with OS both at univariate and multivariable analysis ($p<0.001$). C-index to measure the prediction accuracy of DFS for the clinical, radiomic and clinical-radiomic models were 0.67 (0.57-0.77), 0.77 (0.70-0.85) and 0.79 (0.71-0.87), respectively. C-index (95%CI) to measure the prediction accuracy of OS for the three above referenced models were 0.78 (0.69-0.87), 0.82 (0.72-0.92) and 0.87 (0.79-0.96), respectively. **Conclusion:** The combination of clinical and radiomic parameters was able to predict DFS and OS with a high accuracy. Thus, ^{18}F[FDG]-PET/CT-based RFs might be proposed as baseline parameters to stratify high- vs. low-risk in DLBCL patients. **References:** None.

OP-1063

MIRAS: an end-to-end solution with a graphical user interface for radiomics

F. Tixier[1,2], B. Laurent[1], V. Jaouen[1], O. Tankyevych[3,1], C. Cheze-Le-Rest[3,1], M. Hatt[1], D. Visvikis[1];
[1]INSERM, LaTIM, Brest, FRANCE, [2]Brest University Hospital, Radiation Therapy Department, Brest, FRANCE, [3]University Hospital of Poitiers, Nuclear medicine department, Poitiers, FRANCE.

Aim/Introduction: The extraction of image biomarkers, commonly named radiomics, has become a very useful tool to build prognostic and predictive models for cancer patients. However, training models maximizing the predictive value of radiomics and validating them efficiently in multi-institutional datasets represents a true challenge. There is a need for tools facilitating the extraction of radiomics from robust pipelines. For this reason, we aimed at developing a software with a graphical user interface allowing the processing of the images from segmentation to the extraction of radiomics features, together with image pre-processing options. **Materials and Methods:** MIRAS (Multimodality Imaging for RAdiomics Software) was developed in C++ from the source code of ITK-SNAP v3.6 [1]. This software includes already existing tools in ITK-SNAP such as c3d and adds the possibility to integrate modules for other specific image processing tasks. The current version of the software includes a module for the segmentation providing the algorithms Fuzzy C-Means and Fuzzy Locally Adaptive Bayesian (FLAB) algorithm [2], as well as a module allowing extraction of Image biomarker standardisation initiative (IBSI) compliant [3] radiomic features. Results: MIRAS runs successfully on Windows and Linux. C3d is used for the resampling of the images from anisotropic voxels and the software provides an intuitive graphical user interface for fast segmentation of metabolic tumor volumes on PET images. Once segmented, these volumes can be directly processed for radiomic features extraction, including the use of wavelet-filtered images, currently under standardization by the IBSI [3]. In addition, a batch mode allows applying the same process on a list of images. The modules used in MIRAS take the form of external libraries (.dll or .so) and consequently, their integrations are easy, which also allows users to integrate their own personalized modules. A number of recently published radiomic studies have relied on MIRAS [4-6]. **Conclusion:** MIRAS provides an end-to-end solution with a graphical user interface for the image analysis dedicated to radiomics. This makes easier the implementation of robust pipelines for the extraction of radiomic features that are useful to build predictive or prognostic models. **References:** [1]: http://www.itksnap.org/ [2]: Hatt M et al. A fuzzy locally adaptive Bayesian segmentation approach for volume determination in PET.

IEEE transactions on medical imaging 2009 [3]: Zwanenburg A et al. Image biomarker standardisation initiative. arXiv 2019 [4] Tankyevich O. et al. Methods 2021 [5] Bourbonne V. et a. Radiotherapy and Oncology 2021 [6] Sepehri S. et al. Diagnostics 2021

OP-1064

Postsurgical Gleason score prediction enhanced by PSMA PET/MRI radiomics

E. Solari[1], A. Gafita[2], S. Schachoff[1], B. Bogdanović[1], A. Villagrán Asiares[1], I. Rauscher[1], D. Visvikis[3], W. Weber[1], N. Navab[4], M. Eiber[1], M. Hatt[3], S. G. Nekolla[1];

[1]Technical University of Munich, Department of Nuclear Medicine, Klinikum rechts der Isar, München, GERMANY, [2]Department of Molecular and Medical Pharmacology, University of California, Los Angeles, CA, UNITED STATES OF AMERICA, [3]LaTIM, INSERM, UMR 1101, Univ Brest, Brest, FRANCE, [4]Technical University of Munich, Computer Aided Medical Procedures & Augmented Reality, School of Informatics, München, GERMANY.

Aim/Introduction: Gleason score (GS) is a reliable tool in prostate cancer (PCa) patient management, is a proxy for PCa aggressiveness, and closely correlates with patient outcome. Not all patients undergo radical prostatectomy (RP) and therefore postsurgical GS (psGS) is usually estimated through a biopsy-based GS (bGS), which differs from psGS in around 30% of the cases. In this study, we compare the predictions of psGS from a previously developed radiomics model to the use of bGS. **Materials and Methods:** A retrospective study was performed, including 68Ga-PSMA PET/MR primary staging PCa studies from a single PET/MRI scanner. Only patients with available psGS and bGS were included. A support vector machine (SVM) model was trained with IBSI-compliant whole-prostate radiomics from PET and ADC studies, to predict psGS in three groups (G1: GS<8, G2: GS=8, G3: GS>8). From a 6-fold cross-validation with 2:1 train vs validation samples, the best performing SVM model (highest balanced accuracy in the validation) was selected. The predictions of our model were compared to bGS through accuracy (Acc), balanced accuracy (bAcc), sensitivity (sens) and specificity (spec). Results: An unbalanced cohort of 131 patients (G1: 59% (n=77); G2: 23% (n=30); G3: 18% (n=24)) was used to train and select our best model. 101 patients with both available psGS and bGS were selected for the comparison (G1: 62% (n=63); G2: 20% (n=20); G3: 18% (n=18)). The comparisons (radiomics model vs bGS) show that our model outperformed bGS in predicting psGS overall (Acc: 78.7% vs 70.3%; bAcc: 83.2% vs 72.2, respectively) and within each group (sens: G1: 73.0% vs 68.3%; G2: 85.0% vs 65.0%; G3: 91.7% vs 83.3%, respectively). Only the specificity for the lower GS group was higher using bGS (spec: G1: 92.1% vs 97.4%; G2: 83.3% vs 82.7%; G3: 93.4% vs 83.1%, respectively), which agrees with bGS underestimating the psGS more often than our model (underestimated: 17.8% vs 25.7%, overestimated: 3.5% vs 4.0%, respectively). **Conclusion:** Compared to bGS, combined PSMA-PET and ADC map radiomics featured a better performance in the prediction of psGS by groups. This suggests a potential clinical value of PET/MRI radiomics as an alternative to invasive biopsy-based GS in PCa grading, especially in patients who do not undergo RP. **References:** *This project is funded by the European Union's Horizon 2020 research and innovation programme under the Marie Sklodowska-Curie grant agreement No 764458

OP-1065

The performance of ^{18}F-PSMA-1007 PET/CT Radiomics on risk stratification discrimination and distant metastases prediction in newly diagnosed prostate cancer

Z. Wang[1], A. Zheng[1], W. Dong[1], Y. Li[1], J. Gao[1], Q. Nie[2], C. Ding[2], X. Duan[1];

[1]The First Affiliated Hospital of Xi'an Jiaotong University, Xi'an, CHINA, [2]Philips Healthcare, Shanghai, CHINA.

Aim/Introduction: To evaluate the performance of ^{18}F-PSMA-1007 PET/CT Radiomics on risk stratification discrimination and distant metastases prediction in primary prostate cancer. **Materials and Methods:** The prediction model was developed in a retrospective cohort that consisted of 179 patients admitted consecutively between March 2019 and June 2020 with biopsy or radical prostatectomy proven prostate cancer (PCa). Radiomic features were extracted from ^{18}F-PSMA-1007 PET/CT of PCa. Lasso regression model was used for data dimension reduction, feature selection, and radiomics signature building. Logistic regression analysis was used to develop the predicting model, we incorporated the radiomics signature, total prostate-specific antigen (tPSA), distant metastasis status, Gleason Score, and this was presented with a radiomics nomogram. The performance of the nomogram was assessed with respect to its calibration, discrimination, and clinical usefulness. Internal validation was assessed. Results: The radiomics signature, which consisted of 10 selected features, was significantly associated with tPSA level, Gleason Score (P<0.001 for both primary and validation cohorts). Predictors contained in the individualized prediction nomogram included the radiomics signature, tPSA level (tPSA≥20 vs tPSA<20) and distant metastasis status. The model showed good discrimination with a receiver operating characteristic (ROC) curve of 0.719 (95% CI, 0.751 to 0.867) for Gleason Score. Decision curve analysis demonstrated that the radiomics nomogram was clinically useful. **Conclusion:** This study presents an ^{18}F-PSMA-1007 PET/CT radiomics nomogram that incorporates the radiomics signature, tPSA level, and distant metastasis status, which can be conveniently used to facilitate the preoperative individualized prediction of Gleason Score in patients with PCa. **References:** None

1910

Wednesday, October 20 - Saturday, October 23, 2021

on-demand pool, release on Wednesday, October 20 at 09:00

Clinical Oncology Track - TROP Session: Gynaecological and Melanoma

OP-1067

18F-FDG PET/MRI for Preoperative Assessment of Endometrial Cancer: Diagnostic Performance and Predictive Value

P. Mapelli[1,2], G. Ironi[3], F. Fallanca[2], A. Bergamini[4], C. Bezzi[1], L. Monaco[5], G. Mathoux[5], F. Baldassi[5], S. Ghezzo[1], A. Samanes Gajate[2], N. Ferjani[2], G. Candotti[4], V. Bettinardi[2], G. Taccagni[6], P. Rancoita[7], G. Mangili[4], L. Bocciolone[4], L. Gianolli[2], P. Scifo[2], M. Picchio[1,2], F. De Cobelli[1,3];

[1]Vita-Salute San Raffaele University, Milan, ITALY, [2]Nuclear Medicine Department, IRCCS San Raffaele Scientific Institute, Milan, ITALY, [3]Radiology Department, IRCCS San Raffaele Scientific Institute, Milan, ITALY, [4]Unit of Obstetrics and Gynaecology, IRCCS San Raffaele Scientific Institute, Milan, ITALY, [5]University of Milano-Bicocca, Milan, ITALY, [6]Unit of Pathology, IRCCS San Raffaele Scientific Institute, Milan, ITALY, [7]University Centre of Statistics in the Biomedical Sciences, Vita-Salute San Raffaele University, Milan, ITALY.

Aim/Introduction: To investigate the diagnostic performance and predictive value of fully hybrid 18F-FDG PET/MRI in patients with endometrial cancer (EC) candidate to surgery. **Materials and Methods:** Prospective monocentric study including 35 patients with biopsy-proven EC undergoing preoperative 18F-FDG-PET/MRI (December 2018-April 2021) for staging purpose. Histological examination was the reference standard. PET (SUVmax, SUVmean40, MTV40, TLG40) and MRI (Volume index-VI, Volume, tumour volume ratio-TVR, ADCmean, ADCmin) parameters were calculated on the primary tumour and their role in predicting EC risk group, the presence of lymphovascular space invasion (LVSI), myometrial invasion (MI) was assessed. ROC analysis was used to assess the predictive value of PET and MRI parameters on EC characteristics. P-values of AUC test were adjusted for multiple testing with Bonferroni's correction. Results: Patients' mean age was 66.57 years (SD: 10.21). 18F-FDG PET/MRI identified the primary tumour in all patients. 22/35 patients had medium-high risk EC and 13/35 low risk disease; 13/35 presented LVSI and 22/35 had MI at histological examination. The accuracy of 18F-FDG PET/MRI in detecting pathological lymphnodes was 91.4%, with a sensitivity, specificity, PPV and NPV of 85.7%, 92.9%, 75.0% and 96.3%, respectively. The accuracy in detecting myometrial invasion was 77.1%, with a sensitivity, specificity, PPV and NPV of 72.7%, 84.6%, 88.9% and 64.7%, respectively. MRI VI, Volume and TVR were predictors of EC risk group (p-value: 0.006, 0.024 and 0.018, respectively) and LVSI (p-value: 0.002, 0.007 and 0.007 respectively). For EC risk group prediction, an MRI VI >15.39 corresponded to a sensitivity and specificity of 90.9% and 76.9%, a Volume >7.85 corresponded to a sensitivity and specificity of 81.8% and 76.9% and a TVR >8.22 corresponded to a sensitivity and specificity of 86.4% and 69.2%. For LVSI prediction, MRI VI >25.45 corresponded to a sensitivity and specificity of 92.3% and 81.8%, a Volume >14.35 corresponded to a sensitivity and specificity of 76.9% and 86.4% and a TVR >21.08 corresponded to a sensitivity and specificity of 76.9% and 77.3%. MTV40 and TLG40 were predictors of LVSI (p-value: 0.003 and 0.014, respectively). A MTV40 >8.12 corresponded to a sensitivity and specificity of 100% and 72.7%; a TLG40 >131.40 corresponded to a sensitivity and specificity of 84.6% and 68.2%. **Conclusion:** 18F-FDG PET/MRI has good accuracy in preoperative staging of EC; PET and MRI parameters has synergic role in preoperatively predicting LVSI, with MRI parameters being also predictive for EC risk group. **References:** None

OP-1068

Relation Between SUV_{max} And ADC Values Of Primary Cervical Tumor And Their Correlation With Lymph Node Metastasis Detected By PET/MRI

F. Aghazada, R. L. Uslu Besli, M. S. Sager, K. Sonmezoglu;

Istanbul University-Cerrahpasa, Cerrahpasa Faculty of Medicine Department of Nuclear Medicine, Istanbul, TURKEY.

Aim/Introduction: We aimed to determine the correlation between the apparent diffusion coefficient (ADC) value and maximum standardized uptake value (SUV_{max}) of the primary tumor and to assess the relationship between these values and lymph node metastasis status using positron emission tomography / magnetic resonance imaging (PET/MRI) for primary staging of patients with cervical cancer. **Materials and Methods:** Thirty-seven patients with biopsy-proven cervical cancer who underwent F-18 FDG PET/MRI for primary staging prior treatment between August 2017 and November 2020 were included in the study and their imaging data were evaluated retrospectively. SUV_{max} and ADC values of the primary tumor and lymph node metastasis status were recorded for each patient. Enlarged lymph nodes with short axis diameter of >1cm and with increased FDG uptake that can be distinguished from background activity, were accepted as metastasis. The relationship between the ADC and SUV_{max} values and the lymph node metastasis status was investigated. Statistical analysis was performed with the SPSS program. Logistic regression analysis was performed for detection of correlation between lymph node metastasis status and SUVmax and ADC values, whereas linear regression analysis was performed for comparison of SUV_{max} and ADC values. Results: The median age of the patients were 50 years (range: 28-69 years). Mean SUVmax value of the primary tumor was 18.1 ± 6.4 (range: 6.5-32; 95% CI: 15.9-20.3) and

the mean ADC value was 0.94x10-3 ± 0.24 x10-3 mm2/s (range: 0.63x10-3 - 1.57x10-3 mm2/s; 95% CI: 0.85-1.02x10-3 mm2/s). Correlation between SUVmax and ADC values was evaluated by Linear Regression analysis. There was a negative correlation between SUVmax and ADC values ($p<0.01$), whereas there was not any significant correlation between SUVmax and ADC values and lymph node metastasis ($p=0.129$ and $p=0.125$, respectively). **Conclusion:** In the present F-18 FDG PET/MRI study performed for primary staging of cervical cancer patients, we detected a negative correlation between SUV_{max} value and ADC value in the primary tumor. SUV_{max} or ADC value could not give prognostic information about lymph node metastasis status. **References:** none

OP-1069

Prognostic value of pretreatment ^{18}F-FDG PET/CT metabolic parameters in advanced high grade serous ovarian cancer

***D. Travaglio Morales**, M. Coronado Poggio, C. Huerga Cabrerizo, D. Monachello Araujo, E. López Llobet, Y. Abadi Sedraoui, J. Cordero García, S. Rodado Marina, C. Lancha Hernandez, C. Escabias del Pozo, S. Rizkallal Monzón, L. Dominguez Gadea;*
Hospital Universitario La Paz, Madrid, SPAIN.

Aim/Introduction: To evaluate the prognostic value of pretreatment ^{18}F-FDG PET/CT quantitative parameters in patients with advanced high grade serous ovarian cancer. **Materials and Methods:** A review of 37 patients diagnosed of advanced high grade serous ovarian cancer between 2016 and 2019 in our center was carried out, evaluating pretreatment ^{18}F-FDG-PET/CT metabolic parameters: maximum standardized uptake value (SUVmax), total lesion glycolysis (TLG) and metabolic tumoral volume (MTV).Two Nuclear physicians evaluated the quantitative parameters semiautomatically using the Volume Viewer v13.0 GE software, which classifies ROIs as target(t), non target(nt) and total (t+nt) according to PERCIST criteria. Follow up was made recording relapses and final status (exitus/alive). Disease-free survival (DFS) and overall survival (OS) were calculated. Correlation between metabolic parameters and DFS/OS was made using multivariate analysis. Results: Descriptive analysis: average age: 62.70 years. Mean quantitative values: SUVmax: 13.21g/ml; TLG (t+nt): 2738g/ml x cm^3; TLG(t) 2205g/ml x cm^3; TLG(nt): 532g/ml x cm^3; MTV(t): 708cm^3; MTV(nt): 662 cm^3; MTV(t+nt): 1370 cm^3. Median DFS was 7.6 months (5-11) and OS 30.6 months (18-39). TLG(t+nt) and MTV(t) were significantly associated with DFS (p 0.044 and p0.013, respectively): higher TLG(t+nt) and MTV(t) increased the risk of relapse. TLG(t) was near to be significantly associated with DFS (p0.054). None of the metabolic parameters were significantly correlated with OS. **Conclusion:** In patients with high grade advanced serous ovarian cancer, pretreatment metabolic parameters TLG(t+nt) and MTV(t) have prognostic value, being able to predict higher risk of relapse. **References:** None

OP-1070

Can 2-[^{18}F]FDG PET/CT predict cervical cancer response to chemoradiotherapy?

***M. Monteiro**[1], P. Lapa[1,2], T. Saraiva[1], G. Costa[1,2], J. Pedroso de Lima[1,3];*
[1]Centro Hospitalar e Universitário de Coimbra, Coimbra, PORTUGAL, [2]Faculdade de Medicina da Universidade de Coimbra, Coimbra, PORTUGAL, [3]Instituto de Ciências Nucleares Aplicadas à Saúde, Coimbra, PORTUGAL.

Aim/Introduction: Chemoradiotherapy (CRT) has been the standard of care for patients with uterine cervical cancer with bulky IB2-IVA disease for almost two decades, demonstrating an improvement in both disease free survival and overall survival over standard radiotherapy/hydroxyurea. 2-deoxy-2-[^{18}F]fluoro-D-glucose positron emission tomography/computed tomography (2-[^{18}F]FDG PET/CT) plays an important the imaging workup and treatment planning in patients with advanced uterine cervical cancer who are scheduled to undergo curative CRT. 2-[^{18}F]FDG based metabolic tumor volume (MTV) is a prognostic parameter, mainly for highly 2-[^{18}F]FDG avid tumors. In this retrospective work, we aim to assess whether there is a radiomic parameter that could predict response to CRT. **Materials and Methods:** A total of two hundred and fifty 2-[^{18}F]FDG PET/CT scans, performed between January 2015 and October 2020 on patients with diagnosed cervical cancer, were reviewed. Thirty-two patients with advanced uterine cervical cancer who underwent curative CRT that were submitted to initial staging 2-[^{18}F]FDG PET/CT were selected. MTV, total lesion glycolysis (TLG), maximum standardized uptake (SUVmax) and mean standardized uptake (SUVmed) were quantified. Treatment response was classified as negative, meaning there was partial or no response on follow-up, or positive, meaning there was complete response on follow-up, according to all clinical data available, such as analytical values, magnetic resonance imaging and 2-[^{18}F]FDG PET/CT results. All relevant demographic and clinical data were recorded. Statistical analysis was performed using SPSS version 25.0. Results: Thirty-two patients were included (age: 56.0±11.4 years, 38-79). Eight patients were classified as negative responders and 24 as positive. The median MTV on negative responders was 128 cm^3 (interquartile amplitude=48.8; 54.1-206.2), whereas on positive responders was 61.9 cm^3 (interquartile amplitude=60.8; 21.8-141.2). For a significance level of 5%, the observed difference is statistically significant (H Kruskal-Wallis, p=0.01). The area under the ROC curve for MTV was 0.81 (95% confidence interval (CI) 0,644-0,976, p=0.01). A cut-off point of 92.6 had a sensitivity of 88% and a specificity of 71%. The cut-off point for maximal (100%) sensitivity was 52.1, which had a specificity of 38%; whereas the cutoff point for maximum specificity (100%) was 143.6, which had a sensitivity of 25%. TLG, SUVmax and SUVmed had no statistically significant different values between responders and no responders. **Conclusion:** Despite further larger and

prospective studies are warranted, in our series, MTV seems to be a potential predictor for CRT outcome on patients with advanced uterine cervical cancer. **References:** none

OP-1071

Predictive Role of 18F-FDG PET/CT in Gestational Trophoblastic Neoplasia

C. Bezzi[1], P. Mapelli[1,2], L. Monaco[3], G. Mathoux[3], A. Bergamini[1,4], E. Zambella[1], F. Fallanca[2], S. Ghezzo[1], A. M. Samanes Gajate[2], L. Presotto[2], G. Sabetta[4], G. Mangili[4], R. Cioffi[4], V. Bettinardi[2], L. Gianolli[2], P. Scifo[2], M. Picchio[1,2];
[1]Vita-Salute San Raffaele University, Milan, ITALY, [2]Nuclear Medicine Department, IRCCS San Raffaele Scientific Institute, Milan, ITALY, [3]University of Milano-Bicocca, Milan, ITALY, [4]Unit of Obstetrics and Gynaecology, IRCCS San Raffaele Scientific Institute, Milan, ITALY.

Aim/Introduction: To investigate the predictive role of 18F-FDG PET/CT in patients affected by gestational trophoblastic neoplasia. **Materials and Methods:** This retrospective monocentric study included 28 female patients (median age: 30 years, range: 18-46) who underwent to 18F-FDG PET/CT for staging assessment of gestational trophoblastic neoplasia. Semi-quantitative PET parameters were derived on the primary lesions and used for the analysis: maximum standardized uptake value (SUVmax), SUV mean, metabolic tumour volume and total lesion glycolysis calculated at 40% threshold (SUVmean40, MTV40, TLG40). The nonparametric Spearman's correlation coefficient was used to evaluate correlations between PET parameters and tumor's types (non molar trophoblastic vs. post molar trophoblastic tumors), as well as between high vs. low risk groups defined according to the FIGO score. Area under the curve (AUC) of the receiver operating characteristic (ROC) curve was used to evaluate parameters' performance in predicting both tumor's types and FIGO score classes. The nonparametric Mann-Whitney U test was used to investigate the potential of PET parameters in differentiating patients according to both tumor's types and FIGO score classes. Results: Eleven patients had a non molar trophoblastic tumor and 13 patients had a post molar trophoblastic tumour. Among these, 14 patients with a FIGO score <6 were grouped as "low risk", while the remaining 10 patients were classified as "high risk". SUVmax showed a low correlation with tumor's types, (rho=0.489, P=0.015), while SUVmean40 a moderate correlation (rho=0.537, P=0.006). These two PET parameters also showed a low correlation with FIGO score (rho=0.439, P=0.031 and rho=0.451, P=0.026, respectively); a moderate correlation was observed between TLG40 and FIGO score (rho=0.512, P=0.010). According to ROC analyses, SUVmax resulted a fair predictor of both tumor's types (AUC: 0.783; CI: 0.55-0.94) and FIGO score (AUC: 0.242; CI: 0.04-0.48), while SUVmean40 resulted a fair predictor of FIGO score (AUC: 0.235; CI: 0.04-0.46) and a good predictor of tumor's type (AUC: 0.811; CI: 0.60-0.97). Finally, the Mann-Whitney U test demonstrated the discriminative ability of the following PET parameters: distributions of SUVmax and SUVmean40 resulted significantly different between both non molar trophoblastic and post molar trophoblastic tumours (P=0.020 and P=0.010, respectively) and risk classes (P=0.037 and P=0.032, respectively). Moreover, TLG40 distribution resulted significantly different between the two groups defined by the FIGO score (P=0.015). **Conclusion:** 18F-FDG PET parameters showed both a predictive and discriminative role in assessing tumor's type and FIGO score in patients affected by gestational trophoblastic neoplasia. **References:** None

OP-1072

Comparison of FDG-PET/CT findings and quantitative parameters and tumor markers in Ovarian Ca patients with peritoneal metastasis

C. Dündar Çaglayan[1], F. Aydin[1], M. Engin[1], A. Arçay Öztürk[1], Z. G. Kiprak[1], S. Sezgin Göksu[2], A. Boz[1];
[1]Akdeniz University Hospital Nuclear Medicine Department, Antalya, TURKEY, [2]Akdeniz University Hospital Medical Oncology Department, Antalya, TURKEY.

Aim/Introduction: Among gynecological malignancies,ovarian cancer is the 3rd in the world and the 2nd in Turkey(1).Hematogenous spread is rare,in approximately 89% of the patients,it is diagnosed at an advanced stage because the tumor cells metastasize to the peritoneum and therefore has a poor prognosis(2).Peritoneal invasion starts with ovarian capsule penetration and direct invasion to adjacent organs and pelvic peritoneum and progresses by spreading(3).Ca-125 is frequently used as a tumor marker in the follow-up of treatment response and recurrence in ovarian carcinoma with low sensitivity and specificity(4).In a study comparing CT,MRI,and FDG PET/CT in detecting,PET/CT sensitivity was 95%and specificity was 96%(5).To investigate the relationship between PET/CT quantitative parameters and Ca-125 values in patients with ovarian carcinoma with peritoneal involvement in FDG-PET/CT. **Materials and Methods:** Retrospective FDG PET/CT images of 30 patients(histological subtype; 25 serous carcinoma,1 endometroid carcinoma,4 unknown)diagnosed with ovarian carcinoma with peritoneal metastasis taken between 01.2019 and 01.2021 in Akdeniz University Hospital Nuclear Medicine Department has been examined.FDG PET/CT findings were correlated with histopathological findings or radiological/clinical follow-up.Peritoneal metastasis patterns were grouped as acid, peritoneal thickening, implant,and mass lesion; extensity was grouped visually from 1 to 4.SPSS Statistics 23 program was used to compare the levels,SUVmax values of lesions and peritoneal metastasis patterns. Results: The mean age of patients was 58.8(38-77).Ca-125 values of 5 patients were within normal limits,and 25 patients were higher(>35U/mL).The mean SUVmax value of peritoneal lesions was 15.4(± 8).The correlation was performed by

histopathology in 9 patients and by clinical and radiological follow-ups in 21 patients.Nodular implants were observed in 22 patients,peritoneal thickening in 15 patients,mass in 13 patients,and ascites in 9 patients.21 patients had more than one pattern.Statistical analysis revealed a significant relationship between mass lesions(>1cm) and SUVmax value(p=0.01)and the mean SUVmax value was 21.16(± 8.46). There was no significant relationship between Ca-125 level and different peritoneal uptake patterns(p>0.05).Although 83.3%(25/30)of patients with peritoneal metastases had an elevation of Ca-125,no significant relationship was found between SUVmax values and Ca-125 levels(p=0.48). Significant relationship was found between the extensity and SUVmax(p=0.03). **Conclusion:** Although Ca-125 elevation is a frequently encountered marker in patients with peritoneal metastasis,it did not contribute to the prediction of disease extent and uptake patterns.SUVmax value was found to be significantly higher in patients with widespread metastasis and peritoneal mass lesions. **References:** 1. htpp://kanser.gov.tr/daire-faaliyetleri/kanser-istatikleri.html 2. Ozols RF. Treatment goals in ovarian cancer. Int J Gynecol Cancer. 2005; 5 Suppl.1:3-11.3. Onkolojide PET/BT, Jinekolojik tümörlerde PET/BT, Dr. Yasemin Şanlı 4. Lutz AM, WIllmann JK, Drescher CW, Ray P, Cochran FV, Urban N, et al. Early diagnosis of ovarian carcinoma: isasolution in sight? Radiology. 2011; 259:329-45.5. Sabine Schmidt, MD, Reto Antoine Meuli, MD, PhD, Chahin Achtari, MD, and John Olivier Prior, MD, PhD. Peritoneal Carcinomatosis in Primary Ovarian Cancer Staging Comparison Between MDCT, MRI, and18F-FDGPET/CT. Clin Nucl Med 2015; 40: 371-377

OP-1073

Prognostic significance of follow-up ^{18}F-FDG PET/CT in uterine sarcoma

***A. K Majeed**, R. Kumar, A. Sharma, S. T. Arunraj, C. Bal;*
All India Institute of Medical sciences, Delhi, INDIA.

Aim/Introduction: Uterine sarcomas are rare mesenchymal tumors with poor outcomes. This retrospective study aimed to evaluate the prognostic role of follow-up 18F-FDG(Fluorodeoxyglucose) PET/CT in predicting the overall survival. **Materials and Methods:** A total of 15 patients with pathologically proven uterine sarcoma [leiomyosarcoma(n=9), low-grade endometrial stromal sarcoma(n=4), and undifferentiated uterine sarcoma(n=2)] were retrospectively included in the study. All patients underwent an 18F-FDG PET/CT scan either to rule out suspected recurrence (n=10) or for post-therapy surveillance (n=5). PET/CTs were evaluated visually and semi-quantitatively by using SUVmax (maximum standardized uptake value), and the sum of metabolic tumor volumes(MTV total). Kaplan-Meier curves were computed to assess the PET/CT findings on overall survival. Results: The median age of enrolled patients was 45 years (range: 30-82 years) and the median follow-up period was 16.6months (range: 3-47 months). Residual or recurrent disease was present in 8 patients on PET/CT. Median SUVmax and MTV total were 17.8(range:9.9-39) and 100.2(range: 11-370) respectively. The median overall survival (OS) of patients with lesions was significantly lesser than the patients without lesions (11.33 months, range: 3-20 months Vs 25.63 months, range: 9-47 months, p=0.004). It was found that all the patients with no evidence of residual or recurrent lesion on the scan were alive at the end of the study, whereas, 6 out of 8 patients with lesions died during the follow-up. In PET/CT positive patients, no difference in median SUVmax value was noted between the event group(17.8, range: 9.9-39.0) and the live group (19.4, range: 16.1-22.7), whereas MTV total was higher in the event group(187.9, range: 18.8-370.0) Vs 28.5, range: 11.0-46.0). **Conclusion:** Follow up 18F FDG PET/CT is useful for predicting the prognosis of patients with uterine sarcoma. **References:** none

OP-1074

Sentinel Node Mapping in Patients with Ovarian Tumors: A Study Using Intraoperative ^{99m}Tc-Phytate Gamma Probing and Post-Operative SPECT/CT Lymphoscintigraphy

***S. Ataei**, M. Farazestanian, S. Mostafavi, K. Sadri, A. Azad, N. Jahani, M. Esmaeil Poor, Z. Yousefi, M. Hassanzadeh, R. Sadeghi;*
Mashhad university of medical science,
Mashhad, IRAN, ISLAMIC REPUBLIC OF.

Aim/Introduction: Early ovarian cancer (EOC) requires a complete surgical staging. This involves a radical lymphadenectomy up to the level of renal vessels [1], which implies the subsequent risk of complications and morbidity [2]. Sentinel lymph node mapping has been presented as a procedure in EOC staging in an attempt to reduce radical lymphadenectomy-related morbidities. Previous research on sentinel node mapping in ovarian tumors is limited in size and scope [3]. In order to determine the ovarian lymphatic mapping in ovarian tumors for subsequent sentinel node biopsy, we used intra-operativeTc-99m-Phytate injection and postoperative SPECT/CT lymphoscintigraphy imaging. **Materials and Methods:** Twenty patients with an ovarian mass were included in the study. The radiotracer was injected just after laparotomy and before removal of the tumor in the utero-ovarian and suspensory ligaments of the ovary just beneath the peritoneum. In all patients, the sentinel nodes were identified using a hand-held gamma probe. Then, standard pelvic and para-aortic lymphadenectomy was performed for malignant masses on frozen section, and lymph nodes were harvested separately for histopathological examination. In case of benign pathologies or borderline ovarian tumors on frozen section, lymphadenectomy was not performed. For all patients, abdominal and pelvic SPECT/CT lymphoscintigraphy was performed within 24 hours. Results: SPECT/CT identified sentinel nodes in para-aortic

only area in 3 (15%), pelvic/para-aortic areas in 9 (45%), and pelvic only area in 5 (25%) patients. In 3 (15%) patients, no sentinel lymph nodes could be identified by SPECT/CT, but were detected by gamma probing. Also, there were additional unusual location of sentinel nodes in the peri renal and inferior gluteal region in two patients. As well, SPECT/CT showed hotspot in one patient at the site where sentinel nodes were resected. **Conclusion:** Sentinel node mapping using intra-operative injection of the radiotracer is safe and feasible in ovarian tumors. SPECT/CT lymphoscintigraphy appears to well identify ovarian lymphatic mapping and can potentially have an important role in preventing unnecessary lymphadenectomy in patient with early stage ovarian cancer.Keywords: Ovarian tumor, Sentinel lymph nodes, Lymphoscintigraphy, SPECT/CT, Lymphatic mapping. **References:** 1.Holschneider CH, Berek JS. Ovarian cancer: epidemiology, biology, and prognostic factors. Semin Surg Oncol. 2000; 19(1):3-10. 2. Nyberg RH, Korkola P, Maenpaa J. Ovarian sentinel node: is it feasible? Int J Gynecol Cancer. 2011; 21(3):568-72. 3. Uccella S, Zorzato PC, Lanzo G, Fagotti A,Cianci S, Gallina D, Scambia G. The role of sentinel node in early ovarian cancer: A systematic review. Minerva Medica. 2019; 110: 358-366

OP-1075

Metabolic imaging with FDG-PET and time to progression in patients discontinuing immune-checkpoint inhibition for metastatic melanoma

J. Ferdinandus, A. Zaremba, L. Zimmer, L. Umutlu, R. Seifert, F. Barbato, S. Ugurel, E. Chorti, V. Grünwald, K. Herrmann, D. Schadendorf, W. P. Fendler, E. Livingstone;
University Hospital Essen, Essen, GERMANY.

Aim/Introduction: The optimal duration of immune checkpoint blockade (ICB) therapy is not well established. Active residual disease is considered prohibitive for treatment discontinuation and its detection by diagnostic CT imaging is limited. Here, we set out to determine the potential added value of 2-[18F]fluoro-2-deoxy-D-glucosepositron emission tomography (FDG-PET) to identify patients at higher risk of relapse following discontinuation of immunotherapy in advanced melanoma. **Materials and Methods:** Metastatic melanoma patients who discontinued CPI therapy were identified retrospectively. All patients received FDG-PET and diagnostic CT within four months of discontinuation due to durable response and/or toxicity. Morphologic response was assessed according to RECIST v1.1. Complete metabolic response (CMR) at time of discontinuation was defined as uptake in tumor lesions below background, whereas any site of residual, FDG-avid disease was rated as non-CMR. Our primary endpoint was time to progression (TTP) after therapy discontinuation stratified by morphologic and metabolic imaging response using Kaplan-Meier estimates and log-rank test. As secondary endpoint, we report overall survival (OS) outcomes. Results: Forty-three patients were eligible for analysis. Reasons for discontinuation were either durable response (n=27) or unacceptable toxicity (n=16). Median follow-up was 24.2 months since ICB discontinuation. Median TTP in the overall cohort was not reached. A greater proportion of patients reached CMR in PET (n=35, 81.4%) as compared to complete responses (CR) in CT (n=13, 30.2%). Median TTP for CMR vs. non-CMR patients was reached for non-CMR (9.89 months, 95%CI 2.4-not reached,p<0.001) but not for CMR patients. Twenty-five patients had non-progressive, residual disease by RECIST v1.1 criteria (five with stable disease, 20 with partial response). Of these, 21 patients had CMR (84%), median TTP not reached), and 4 (16%) non-CMR (mean TTP 12.7 months; 95%CI 4.4-NR, p<0.001). **Conclusion:** Complete metabolic response to ICB therapy is an important treatment outcome that identifies melanoma patients with a low risk of recurrence and favourable prognosis.Our data recommend prospective evaluation of FDG-PET to select patients for ICB discontinuation. **References:** none

OP-1076

An externally validated nomogram to predict 1-year PFS of patients with metastatic melanoma before anti-PD-1 therapy, based on clinical, biological and [18] F-FDG PET-derived features

A. Girard[1], C. Pontoizeau - Guery[1], M. Paquet[2], X. Palard-Novello[1], A. Devillers[1], O. Humbert[2,3];
[1]Centre Eugène Marquis, Rennes, FRANCE, [2]Department of Nuclear Medicine, Centre Antoine-Lacassagne, Université Côte d'Azur (UCA), Nice, FRANCE, [3]TIRO-UMR E 4320, UCA/CEA, Nice, FRANCE.

Aim/Introduction: We aimed to develop and externally validate a model to predict the 1-year PFS in patients with metastatic melanoma based on clinical, biological and [18F]-fluorodeoxyglucose positron emission tomography data routinely available before the initiation of anti-PD-1 therapy. **Materials and Methods:** Patients with metastatic melanoma who started an anti-PD-1-based immunotherapy between 2015 and 2019 were retrospectively included in two different centers. In the training set from a first center, variable reduction was performed from fourteen measured features. A nomogram was then built with a survey-weighted Cox model based on selected predictors. In the external validation set, predicted 1-year PFS were calculated using the previously made nomogram. Observed Kaplan-Meier survival curves were compared between groups of patients regarding their predicted PFS. Results: Eighty-one patients were included in the training set, and 21 in the validation set. Median follow-up were 17.7 months [range 0.3,64.9] and 22.4 months [range 1.5,54.9], respectively. Fifty-four (66.7%) and thirteen (61.9%) patients had progressive disease during follow-up, respectively. The three selected predictors for the final model were the presence of active brain metastases, the total metabolic tumor volume and the performance status. The

concordance-indexes were 0.71 in both sets. In the training set, the group of patients predicted with good prognosis (predicted 1-year PFS probability>0.5) had an observed PFS of 23.7 months versus 3.1 months for patients predicted with poor prognosis (p<0.001). In the external validation set, observed median PFS was "unreached" versus 6.5 months, respectively (p=0.012). Regarding overall survival, medians were "unreached" versus 6.1 months, respectively (p<0.001) in the training set; and "unreached" versus 27.9 months, respectively (p=0.056) in the validation set. **Conclusion:** We developed and externally validated a model to discriminate, at baseline, patients with high against low risk of progression 1 year after initiation of anti-PD-1 therapy, providing an easily usable tool to personalize treatment. **References:** None

OP-1077

Predictive value of baseline [^{18}F]FDG PET/CT for response to systemic therapy in patients with advanced melanoma

V. Liberini[1], R. Mimmo[2], R. Passera[1], E. Califaretti[1], F. Ceci[1], P. Fava[3], M. Rubatto[3], L. Tonella[3], G. Polverari[1,4], S. Ribero[1], M. Bellò[1], V. Arena[4], P. Quaglino[3], D. Deandreis[1];
[1]Nuclear Medicine Unit, Department of Medical Sciences, University of Turin, Turin, ITALY, [2]UNITO - University of Turin, Turin, ITALY, [3]Dermatology Clinic, University of Turin, Turin, ITALY, [4]PET Center, Affidea IRMET, Turin, ITALY.

Aim/Introduction: To evaluate the association between baseline [^{18}F]FDG-PET/CT tumor burden parameters and early (3 months) and late (12 months) disease progression rate after first-line target therapy or immunotherapy in advanced melanoma patients. **Materials and Methods:** 50 advanced melanoma patients that performed baseline [^{18}F]FDG-PET/CT before first-line target therapy (32/50) or immunotherapy (18/50) were retrospectively analyzed. A semi-automatic segmentation was performed by one operator using LifeX. Lesions were detected setting a standardized uptake value (SUV) threshold >2.5 and segmented using a 41%-isocontour volumes of interests (VOIs). Whole-body and per-district (soft tissue, lymph nodes, lung, liver and bone) metabolic tumor volume (MTV) and total lesion glycolysis (TLG) were calculated for each patient. Therapy response was assessed according to RECIST 1.1 criteria on CT scan at 3 (early) and 12 (late) months and classified as follows: complete/partial response and stable disease (responders) and progression (non-responders). PET parameters were compared with Mann-Whitney test for the entire cohort, target therapy (A) and immunotherapy subgroup (B), respectively. Optimal cut-offs for predicting progression were defined using the ROC curve. Results: Fifty patients (F:M=30:20; median age=62y) with advanced melanoma (stage II=1, III=14 and IV=35 pts) were included. 33/50 patients were BRAFV600 mutated. For the entire cohort, MTVwb and TLGwb were 10.6 cm^3 [0-329.5] and 50.75 [0-1732.9], respectively. Soft tissue, lymph nodes, lung, liver and bone metastases were detected in 12/50 (group A:B=9/32:3/18), 31/50 (A:B=22/32:9/18), 17/50 (A:B=5/32:12/18), 3/50 (A:B=2/32:1/18) and 6/50 (A:B=4/32:2/18) patients.For the entire cohort, group A and B, patients were classified as non-responders in 44/50, 30/32 and 14/18 respectively at early evaluation, and in 39/50, 25/32 and 14/18 respectively at late evaluation.Significant differences of metabolic parameters between responders vs non-responder status were found only at late evaluation for MTVwb, TLGwb, MTVbone and TLGbone (all p<0.03) in the entire cohort and in group A and also for MTVlfn and TLGlfn (all p<0.05) in group A. No significant differences were found for group B. At late evaluation, the following optimal cut-off values to separate responders vs non-responder pts have been found: MTVwb=13cm^3 (p=0.03; AUC=0.71, sensitivity=64%, specificity=64%) and TLGwb=53 (p=0.02; AUC=0.73, sensitivity=73%, specificity=60%) for the entire cohort; MTVwb=14cm^3 (p=0.02; AUC=0.81, sensitivity=83%, specificity=69%) and TLGwb=86 (p=0.005; AUC=0.87, sensitivity=83%, specificity=73%) for group A. **Conclusion:** In advanced melanoma higher values of whole-body and bone metabolic parameters were correlated with non-responder outcome, especially in patients treated with target therapy. Baseline [^{18}F]FDG-PET/CT before systemic treatment might be an important tool to predict response to treatment. **References:** None

OP-1078

^{18}F-FDG-PET/CT in the Staging, Follow-up and Treatment Tailoring of Malignant Melanoma - First "Full-Digital" Experience in a Single Instituition

L. Chavdarova[1], I. Gavrilova[2], E. Piperkova[1];
[1]University Specialized Hospital for Active Treatment in Oncology, Clinic of Nuclear Medicine, Sofia, BULGARIA, [2]University Specialized Hospital for Active Treatment in Oncology, Clinic of Dermatooncology, Sofia, BULGARIA.

Aim/Introduction: Contemporary treatment of malignant melanoma (MM) including immune- and targeted approaches leads to an increased need of correct staging and treatment monitoring. Although well known as usually FDG-avid and helpful, there is still no strong evidence for the standard use of FDG-PET/CT in the routine work-up of melanoma. Because of that, the aim of our investigation was the evaluation of diagnostic input of the new generation, full-digital PET/CT scanning for the precise staging and treatment tailoring of MM. **Materials and Methods:** Since the initiation of our "full-digital", newest generation, PET/CT-scanner in the Clinic of Nuclear medicine in June 2020, we collected prospective data from 121 adult patients with MM (53 female, 68 male), with last scan of the assessed series on 15.04.2021. SUVmax, TLG, MTV and number of lesions were calculated where applicable, influence and change in therapy was assessed. If available, the reports were compared

with following histologic results. Results: 121 patients (pts) received at least one (PET-1) scan, 57 negative and 64 positive for pathologic lesions. In 24 pts a second (PET-2) scan was performed in the follow-up (9 negative, 15 positive), one patient received a third (PET-3) (positive) scan. SUVmax ranged from 57,26 in PET-1 to 29,9 in PET-2, to 4,75 in PET-3. Good treatment response was evaluated with decreasing TLG, MTV and number of lesions. PET-1 helped further treatment tailoring in 77 pts - 28 received targeted therapy, 27 received immune check-point inhibitors, 7 - BCG, 9 - radiotherapy, 13- surgery. PET-2 changed further therapy in 15 pts: 8 - target-, 4- immune-, 3- surgery. Histology proved 7 true-positive, 2 true-negative and 2 false-positive (reactive lymph nodes) results. True-negative based on follow-up imaging were 6 studies. PET/CT assessed 9 pts with a second malignancy - 6 in remission, 1 - progressive and 2 newly diagnosed. In single pts PET/CT detected distinctive lesions in the bowels and in the brain. **Conclusion:** FDG-PET/CT is high-promising in the clinical staging and treatment tailoring of MM and should take place in the routine algorithm of this disease. Additional data collection and assessment from our study follows for statistical significance. **References:** None

1911

Wednesday, October 20 - Saturday, October 23, 2021

on-demand pool, release on Wednesday, October 20 at 09:00

TROP Session: Nuclear Medicine Imaging and Therapy in Thyroid and Parathyroid Disorders

OP-1080

Quantitative classification and radiomics of [^{18}F]FDG-PET/CT in indeterminate thyroid nodules

M. Mostert[1,2], E. J. de Koster[3], W. A. Noortman[1,4], L. de Geus-Oei[1,3,4], F. H. van Velden[1], W. J. Oyen[5,6,3], D. Vriens[1];
[1]Leiden University Medical Center, Leiden, NETHERLANDS, [2]Delft University of Technology, Delft, NETHERLANDS, [3]Radboud University Medical Center, Nijmegen, NETHERLANDS, [4]University of Twente, Enschede, NETHERLANDS, [5]Rijnstate Hospital, Arnhem, NETHERLANDS, [6]Humanitas University, Milan, ITALY.

Aim/Introduction: Only 20-30% of thyroid nodules with indeterminate cytology (Bethesda III/IV) are malignant. Although [^{18}F]FDG-PET/CT can rule out malignancy in visually [^{18}F]FDG-negative thyroid nodules, a visually positive [^{18}F]FDG-PET/CT does not differentiate between benign or malignant, requiring surgery to obtain a definite diagnosis. This concerns Hürthle cell nodules in particular, which are almost exclusively strongly [^{18}F]FDG-positive. We evaluated whether quantitative assessment of [^{18}F]FDG-PET/CT, including radiomics and machine learning of [^{18}F]FDG-positive nodules, could further improve the preoperative differentiation and diagnostic yield of [^{18}F]FDG-PET/CT. **Materials and Methods:** We prospectively included [^{18}F]FDG-PET/CT scans of 132 patients with an indeterminate thyroid nodule. Receiver operating characteristic (ROC) curve analysis was performed for SUV_{max}, SUV_{peak}, SUV_{max}-ratio, and SUV_{peak}-ratio values, including assessment of threshold values at which malignancy was reliably ruled out (≥95% sensitivity). Subgroup analysis was performed for Hürthle cell nodules (n=31). Of the 91 [^{18}F]FDG-positive nodules, 80 (88%) EARL-compliant scans were subsequently included in a radiomics and machine learning assessment. After volumetric segmentation at 50% SUVpeak, 108 standardized radiomic features were extracted from [^{18}F]FDG-PET and low-dose CT images. Elastic Net Regression classifiers were trained and evaluated in a 20-times repeated random split. Dimensionality reduction using redundancy filtering and factor analysis was incorporated in the splits, retaining one factor for every 10 patients in the training sets. Predictive performance of radiomics was presented as mean AUC across test sets; 95% confidence intervals (CI) were constructed using a corrected resampled t-test. Results: Thirty-four of 132 (26%) patients had borderline or malignant tumors on histopathology; 32 were [^{18}F]FDG-positive. The SUV_{max}-ratio differentiated best between benign and borderline/malignant nodules (AUC 0.73 [95% CI, 0.64-0.82]); at a threshold of ≤1.2, 97.1% sensitivity and a 28% benign call rate were observed. Thirty of 31 (97%) oncocytic nodules were visually [^{18}F]FDG-positive; 9 (29%) were borderline/malignant. If higher thresholds were applied than in non-oncocytic nodules, all four [^{18}F]FDG-PET/CT-parameters accurately differentiated between benign and borderline/malignant oncocytic nodules. A SUV_{max}-ratio ≤3.4 showed 100% sensitivity and a 23% benign call rate (AUC 0.60 [95% CI, 0.39-0.81]). Radiomics analysis of [^{18}F]FDG-positive nodules showed a mean test set AUC of 0.50 [95% CI, 0.29-0.71] and 0.49 [95% CI, 0.32-0.66] for PET features and PET/CT features, respectively. **Conclusion:** Quantitative [^{18}F]FDG-PET/CT assessment may aid the pre-operative differentiation of indeterminate thyroid nodules. Different SUV-thresholds should be applied in oncocytic and non-oncocytic nodules to optimize diagnostic yield. Radiomic analysis with machine learning did not contribute to further differentiation of [^{18}F]FDG-positive nodules. **References:** None

OP-1081

Do ultrasound elastography and thyroid imaging reporting and data systems correctly classify hyperfunctioning nodules on thyroid scintigraphy?

***M. Tuncel**, B. S. Turan, Z. Işık;*
Hacettepe University, Department of Nuclear Medicine, Ankara, TURKEY.

Aim/Introduction: Ultrasound elastography and thyroid imaging reporting and data systems(TI-RADS) are commonly used to classify thyroid nodules as benign or malignant and

guide further management. However, the performance of these methods in hyperfunctioning nodules on thyroid-scintigraphy is yet to be evaluated. Here we report our experience with ultrasonographic and elastographic imaging of hyperfunctioning nodules **Materials and Methods:** We prospectively collected the clinical and ultrasonographic data from patients with hyperfunctioning nodules on thyroid-scintigraphy. These hyperfunctioning nodules were analysed according to the American College of Radiology(ACR)-TIRADS, European(EU)-TIRADS, Korean Society of Thyroid Radiology(K)-TIRADS, American Thyroid Association ultrasound nodule classification, systems and elastography. Elastographic images were analysed with 5-point Rago& 4-point Asteria scoring systems and strain-ratio. Nodules with Rago-scores of 4 and 5 and Asteria-scores of 3 and 4 were regarded as suspicious for malignancy. A strain ratio of >3.7 was accepted as a cut-off point to differentiate between benign and malignant nodules. Results: Twenty-one patients(age:58±15,F/M: 13/8) were included in our study.Six patients had clinical, eleven had subclinical hyperthyroidism, and four patients had low to normal TSH values (between0.36-2µIU/mL)& normal T4 levels.A total of twenty-five hyperfunctioning nodules with a median size of 22 mm (range:11-55 mm) were analysed from these patients. ACR-TIRADS scores were ≥3 in 17/25(68%) nodules whereas ≥3 in 22/25(88%) nodules for both EU and K-TIRADS. According to ATA classification,10/25 (40%) nodules had ≥ intermediate suspicion for malignancy.None of the nodules had 4 or 5 scores for the Rago-scoring system, but 12/25(48%) nodules had ≥3scores for Asteria.When correlated with the size, fine nodule aspiration biopsy was indicated in; 12/25(48%) nodules according to ACR TIRADS,16/25(64%) nodules with EU-TIRADS,20/25(80%) nodules with K-TIRADS, and 21/25(80%) nodules with ATA ultrasound-nodule-classification system. None of the nodules with the Rago scoring system, 11/25(44%) nodules with Asteria scoring system, and 9/25(36%) nodules with strain ratio had an indication for biopsy. Among these hyperfunctioning nodules, one was biopsied with a benign cytology result. Fourteen of them were treated with radioiodine. Others were followed with anti-thyroid medication with no additional sign of malignancy (median-follow-up:12 months,range:6-18 months). **Conclusion:** Malignancy in hyperfunctioning nodules is exceedingly rare, so no fine-needle aspiration biopsy is necessary. However, currently available TI-RADS and ATA nodule classification systems could not correctly classify hyperfunctioning nodules, as seen with our study. Elastographic parameters, except for Rago scoring systems, also lack diagnostic accuracy. Thyroid scintigraphy is still needed in patients with hyperthyroidism or low to normal TSH levels. **References:** None

OP-1082

Evaluation of treatment efficiency in 301 patients with hyperthyroidism treated with a single dose of I-131 as outpatient

B. Ince, A. Namazova, S. Bilgic, A. Nazari, A. Kibar, F. Aghazada, S. Asa, R. Uslu Besli, M. Sager, K. Sonmezoglu;
Istanbul University-Cerrahpasa, Department of Nuclear Medicine, Istanbul, TURKEY.

Aim/Introduction: It was aimed to compare the treatment efficiency rates in patients with hyperthyroidism who received a single dose of I-131 treatment according to etiological origin. **Materials and Methods:** Having diagnosis of hyperthyroidism totally 301 patients who were treated with radioactive iodine (RAI) two years ago or more, were retrospectively analyzed. Patients who received RAI treatment in the last 2 years were excluded from the study. The average age of the patients was 54±13.4 (18-86) and 207 (69%) were female while 94 (31%) were male. 225 (75%) patients were diagnosed with Graves (150 female, 75 male); 45 (15%) patients (34 female, 11 male) were diagnosed with toxic adenoma and 31 (10%) patients (23 female, 8 male) were diagnosed with toxic multinodular goiter (MNG). The I-131 dose was determined empirically by an experienced nuclear medicine specialist, mainly considering the patient's clinical symptoms and I-131 uptake % values. Patients who become euthyroid or hypothyroid after RAI treatment were classified as "treatment-effective group"; on the other hand, patients with persistent hyperthyroidism or recurrence during follow-up were classified as "treatment-resistant group". Results: I-131 treatment doses applied to the patients were ranged from 5-23 mCi (median=13), and the follow-up durations after treatment were 24-394 months (mean=116 months). There was no statistical difference between the mean I-131 doses given to the treatment-effective group and the treatment-resistant group (12.45 vs 12.5; p=0.9). However there was a significant difference on the mean I-131 uptake % values before treatment between the two groups (%26.9±12.9 & 33.8±17.5; p=0.001 at 2 hour and %55.5±19.2 & 62±21.6; p=0.03 at 24 hour). While 81% (n=244) of all patients had an effective response to treatment, 57 patients (19%) remained resistant to treatment. The treatment efficiency and resistance rates according to the etiology of the disease are given in Table 1. RAI treatment was applied again to 98% (n=56) of the treatment-resistant patients and antithyroid drug treatment was applied to 2% (n=1). **Conclusion:** RAI is the most effective outpatient treatment modality for hyperthyroidism. When it is evaluated according to etiological subtypes, the highest treatment efficiency rated patient group was toxic adenoma (89%), while the lowest treatment efficiency rated was observed as toxic MNG (71%). On the other hand, the patient group with the highest rate of becoming euthyroid was toxic MNG (35.5%), while the lowest was Graves' patients (8%). **References:** No references.

OP-1083

Does functional heterogeneity play a role in Graves' Disease response to RAI treatment? A retrospective decade-long radiomic analysis

M. Monteiro[1], A. P. Moreira[1,2], G. Costa[1,3], J. Isidoro[1], P. Gil[1], J. Pedroso de Lima[1,2,3];
[1]Centro Hospitalar Universitário de Coimbra, Coimbra, PORTUGAL, [2]Instituto de Ciências Nucleares Aplicadas à Saúde (ICNAS), Coimbra, PORTUGAL, [3]Faculdade de Medicina da Universidade de Coimbra, Coimbra, PORTUGAL.

Aim/Introduction: An undeniably expanding interest in recent nuclear medicine research has been directed towards analysing radiomic features extracted from functional imaging, especially positron emission tomography - computed tomography (PET-CT) studies in the field of oncology, in which tumor heterogeneity is usually associated with poor treatment response. However, some widely used conventional molecular imaging modalities, such as thyroid scintigraphy (in which heterogeneity, despite being usually interpreted in a subjective manner, may influence clinical evaluation and treatment selection), still lack relevant uses for radiomics. The aim of this study is to assess, looking back at data from the last decade, whether radiomic features commonly used as heterogeneity markers can help predict the outcome of radioactive iodine (RAI) treated Graves' Disease (GD), based on pre-treatment [^{99m}Tc]$NaTcO_4$ - thyroid scintigraphies. **Materials and Methods:** Clinical data was collected from the charts of 244 patients (n=244) treated for GD with RAI between 2010 and 2019. Treatment outcome was defined based on information from the patients' follow-up records and/or thyroid hormone (TH) profile (measured roughly one year after the therapy day). Subjects were labeled as either R - responsive (n=187); or U - unresponsive (n=57). Anterior projection imaging studies from [^{99m}Tc] $NaTcO_4$ - thyroid scintigraphies obtained for each patient as part of pre-treatment work up were then retrieved and processed using specific software (Medical Image Processing, Analysis, and Visualization). Regions of interest (ROIs) were drawn around the observed thyroid parenchyma in a semi-automatic manner. Eight radiomic features were extracted and used as functional heterogeneity markers: circularity, solidity, standard deviation of pixel intensity, pixel intensity coefficient of variation, difference between geometric center and center of gravity, eccentricity, coefficient of skewness and coefficient of kurtosis. Finally, the correlation significance between outcomes recorded and each marker was statistically assessed. Results: Differences in circularity between the two groups nearly missed significance (mean(U) = 0,46 vs mean(R)=0,44; p=0,053, Independent Samples T Test). No statically significant association was shown between RAI responsiveness and solidity, standard deviation of pixel intensity, pixel intensity coefficient of variation, difference between geometric center and center of gravity, eccentricity, coefficient of skewness and coefficient of kurtosis. **Conclusion:** Our findings suggest that, even though heterogeneity plays an important role in predicting treatment outcomes in oncological diseases, nuclear medicine practitioners should not be hampered from selecting GD candidates for RAI based on apparent functional heterogeneity, since no clear correlation seems to exist between its radiomic expression and treatment response. **References:** none

OP-1084

The Incidence of Radioiodine-Induced Graves' Disease Following Treatment of Thyroid Autonomous Tissue

Ž. Rot[1], T. Zaletel[2], D. Krković[3], S. Gaberšček[1,4], K. Zaletel[1,4];
[1]Department of Nuclear Medicine, University Medical Centre Ljubljana, Ljubljana, SLOVENIA, [2]School of Clinical Medicine, University of Cambridge, Cambridge, UNITED KINGDOM, [3]Department of Nuclear Medicine, University Medical Centre Maribor, Maribor, SLOVENIA, [4]Faculty of Medicine, University of Ljubljana, Ljubljana, SLOVENIA.

Aim/Introduction: Radioiodine (I-131) therapy is an effective treatment for thyroid autonomy, but may induce Graves' disease (GD), which is characterised by antibodies against TSH receptor (TSHRAb), in up to 5% of patients. We set out to evaluate the incidence and risk factors of I-131-induced GD in patients with thyroid autonomy in an iodine sufficient area. **Materials and Methods:** We retrospectively reviewed 883 patients (145 males and 738 females) aged 14 to 92 years (mean 68.4±13.9 years) with solitary toxic adenoma or toxic nodular goiter who received I-131 between January 2013 and December 2015. Prior to treatment, antibodies against thyroid peroxidase (TPOAb), thyroglobulin (TgAb) and TSHRAb were measured. All patients were negative for TSHRAb. Additionally, the uptake of iodine-123 (I-123) at 20-hours or technetium-99m-pertechnetate (Tc-99m) was determined. Patients were treated with median activity of 745 MBq I-131 (range 478-1140 MBq) and followed up for 12 months. Patients were monitored for de novo occurrence of GD by measuring thyroid function and TSHRAb concentration. Patients' characteristics influencing the occurrence of I-131-induced GD were analysed; p-value of <0.05 was considered statistically significant. Results: Prior to I-131 therapy, TPOAb and/or TgAb concentration was increased in 16.4% (145/883) of patients with median TPOAb and TgAb concentrations of 30.8 KU/L and 15 KU/L, respectively. The median I-123 uptake, measured in 62.9% (555/883) of patients, was 27.0%, and the median Tc-99m uptake, measured in 37.1% (328/883) patients, was 0.87%. An increase in TSHRAb concentration was observed in 4.3% (38/883) patients at 3.8±2.0 months following I-131 application; of those, 68.4% (26/38) presented with overt hyperthyroidism. Compared to those with negative TSHRAb, patients with de novo occurrence of GD were significantly more likely to be positive for TPOAb and/or TgAb before I-131

application (52.6% vs 14.8%, p<0.001). Furthermore, they had significantly higher median concentrations of TPOAb (45.6 KU/L vs 30.6 KU/L, p<0.001) and TgAb (15.1 KU/L vs 15.0 KU/L, p<0.01). Similarly, the median uptake of I-123 before treatment was significantly higher (32.5% vs 27.0%, p=0.028), but their Tc-99m uptake did not differ (0.97% vs 0.87%, p=0.69). There was no significant difference with respect to applied activity of I-131 (median, 744.5 vs 745.5 MBq, p=0.92), age (66.5±14.9 vs 68.5±13.9 years, p=0.38) or gender (p=0.58). **Conclusion:** We show that patients with increased TPOAb and/or TgAb levels prior to I-131 therapy are at a higher risk of developing GD post-treatment. We therefore recommend monitoring these patients closely following I-131 application. **References:** None.

OP-1085

Effectiveness of Radioactive Iodine Therapy of Immune Reconstitution Inflammatory syndrome Associated-Associated Graves Disease in People Living with HIV infection

I. Lawal[1], K. Mokoala[1], G. Popoola[2], A. Orunmuyi[3], T. Lengana[1], N. Mokgoro[1], M. Sathekge[1];
[1]University of Pretoria, Pretoria, SOUTH AFRICA, [2]University of Ilorin, Ilorin, NIGERIA, [3]University of Ibadan, Ibadan, NIGERIA.

Aim/Introduction: Graves disease (GD) is one of the manifestations of immune reconstitution inflammatory syndrome seen in patients with human immunodeficiency virus infection effectively treated with anti-retroviral therapy. No study has described the effectiveness of radioactive iodine therapy (RAIT) in this GD phenotype. We aimed to describe the clinical characteristics and the response to RAIT of immune reconstitution inflammatory syndrome-associated Graves disease (IRIS-GD) in comparison to GD seen in HIV-uninfected patients. **Materials and Methods:** We retrospectively reviewed the medical records of patients treated with RAIT for GD. We obtained clinical, biochemical, and HIV-related information of patients from their medical records. We compared patient characteristics and response to RAIT between patients with IRIS-GD and GD seen in HIV-uninfected patients. Results: A total of 253 GD patients, including 51 patients with IRIS-GD, were included. Among IRIS-GD patients, CD+ T-cell nadir was 66 cells/µL (range=37-103) with a peak HIV viral load of 60,900 copies/mL (range=36,542-64,500). At the time of diagnosis of IRIS-GD, all patients had a completely suppressed HIV viremia with a CD+ T-cell count of 729 cells/µL (range=350 - 1279). The median interval between the commencement of HIV treatment and the onset of GD was 63 months. At 3-months follow-up, the proportion of patients with IRIS-GD achieving successful RAIT outcome (euthyroid/hypothyroid state) was lower than HIV-uninfected patients (40.9% versus 63.4%, respectively, p=0.006). The response rate to RAIT was similar between the two groups at 6-month follow-up (73.8% versus 80.2%, respectively, p=0.354). After correcting for differences in age, gender, and pretreatment thyroid-stimulating hormone level, there was no significant difference in RAIT response at 3- or 6-month follow-up between the two groups. **Conclusion:** After correcting for possible confounders, the response to RAI treatment is not different between patients with IRIS-GD and GD in HIV-uninfected patients. **References:** None

OP-1086

Parathyroid scintigraphy in hyperparathyroidism: the added value for radioguided parathyroidectomy

***R. T. Ferreira**, J. C. Ferro, C. R. Santos, S. Carmona, I. Nascimento, A. F. Gomes, R. R. Marques, P. M. Costa, A. I. Santos;*
Hospital Garcia de Orta, E.P.E., Almada, PORTUGAL.

Aim/Introduction: Radioguided parathyroidectomy (RP) is a minimally invasive surgery which results depend on the correct localization of hyperfunctioning parathyroid gland(s) (HPG) preoperatively. Our aim was to evaluate the role of [99mTc]Tc-MIBI parathyroid scintigraphy (PS) in patients who underwent RP. **Materials and Methods:** A retrospective sample of PS performed prior to RP (January/2004-December/2020) was collected and analysed. For the scintigraphic studies, a dual-phase protocol was used, consisting of two planar acquisitions (at 20 and 180 minutes post-administration of the radiopharmaceutical) and an initial SPECT imaging using [99mTc]Tc-MIBI. PS were scored for number and location of the HPG in planar and SPECT images and classified as the type of washout. PS findings were compared with the results obtained with RP. Statistical analysis was performed with IBM SPSS Statistics(v26). Results: 63 scans, from 61 patients, were evaluated (two patients repeated PS for persistent disease after subtotal parathyroidectomy). The median age was 61[P25:53.0;P75:70.0] years' old, (range 13-85), with female preponderance (65.1%). 41/63 (65.1%) studies were referred for primary HPT and the remaining for secondary HPT. The median level of parathyroid hormone in primary HPT was 188.5 [P25:134.3;P75:313.7]pg/mL and serum calcium was 11.4[P25:10.5;P75:12.0]mg/dL, whereas in secondary HPT was 1760.0[P25:1407.8;P75:2187.8] pg/mL and 9.4[P25:8.6;P75:10.0] mg/dL, respectively. For both parameters there was a statistically significant difference between values in primary and secondary HPT (for PTH levels - Mann-Whitney's test, p<0.001; and for serum calcium levels - t-Student Test, p<0.001). Fast washout was present in 14/63 (22.2%), and SPECT allowed HPG identification in 10 of them. There was a statistically strong association between the fast washout and the additional value of SPECT (Fisher's exact test, p<0.001). PS showed a total agreement with the number of glands removed on surgery in 45/63 (71.4%) studies and a partial agreement in the remaining. There was a statistically strong association between this agreement and primary HPT (Chi-Square test, p<0.001). All the HPG identified on PS were removed on RS and confirmed on histopathology

examination. **Conclusion:** PS has a valuable role in identifying and localizing HPG in RP with, as expected, better results on primary HPT. In this process SPECT introduces an incremental value versus planar images in fast washout HPT, improving identification. **References:** None

OP-1087

Parathyroid Histopathology and [18F]F-Choline Uptake in PET/MR in Primary Hyperparathyroidism

V. Liberini[1,2], G. B. Morand[3], N. J. Rupp[4], E. Orita[5], D. Deandreis[1], M. Broglie Däppen[3], M. Hofbauer[2], A. Maurer[2], L. Husmann[2], C. E. Mader[2], H. Grünig[2], A. A. Alharbi[2], M. Messerli[2], M. W. Huellner[2]; [1]UNITO - University of Turin, Turin, ITALY, [2]Department of Nuclear Medicine, University Hospital Zürich, University of Zürich, Zürich, SWITZERLAND, [3]Department of Head & Neck Surgery, University Hospital Zurich, University of Zurich, Zürich, SWITZERLAND, [4]Department of Pathology and Molecular Pathology, University Hospital Zurich, Zürich, SWITZERLAND, [5]Department of Radiology, Nippon Medical School, 1-1-5 Sendagi, Bunkyo-ku, Tokyo, JAPAN.

Aim/Introduction: Mechanisms responsible for [18F] F-choline uptake in hyperfunctioning parathyroid glands are not clearly understood. The aim of our work was to assess the relationship between the histopathological structure of hyperfunctioning parathyroids and parathyroid [18F] F-choline uptake. **Materials and Methods:** A total of 31 parathyroid adenomas were retrospectively analyzed in patients with primary hyperparathyroidism and preoperative [18F]F-choline PET/MR. PET/MR parameters of parathyroid glands (maximum standardized uptake value (SUVmax) and target-to-background ratio (TBR)) in early-phase (EP) and late-phase (LP), MRI volume), preoperative PTH serum concentration, and postoperative histopathology (predominant cell type and growth pattern of adenoma cells, location and size of adenoma) were assessed. The relationship of PET/MR parameters, PTH and histological parameters was determined using Mann-Whitney U, Spearman correlation and Kruskal-Wallis test. Results: Adenomas were predominantly composed of chief cells, water-clear cells and oncocytic cells in 27/31, 2/31 and 2/31 cases, respectively. The growth pattern was predominantly solid, follicular and trabecular in 18/31, 8/31 and 5/31, respectively. The SUVmax was 6.71±3.39 in EP and 6.91±3.97 in LP. Follicular growth pattern had slightly higher EP SUVmax (trabecular: 4.12±0.56; solid: 6.62±3.19; follicular: 8.56±3.96; p=0.046). Spearman's correlation showed a strong positive correlation between volume and both EP and LP SUVmax (0.626; p=0.0001 and 0.576; p=0.0001, respectively). Linear regression analysis revealed a significant correlation between PTH level and EP and LP SUVmax (both p=0.001). **Conclusion:** Our findings suggests that [18F]F-choline uptake depends on the histological growth pattern of the adenoma, with higher uptake in follicular and solid patterns compared to a trabecular pattern. **References:** None

OP-1088

Role of ^{18}F-Fluoromethylcholine PET/CT in addition to conventional imaging techniques in patients with primary hyperparathyroidism candidate to radioguided surgery

***S. Casanueva Eliceiry**, N. Sánchez Izquierdo, M. Manyalich Blasi, P. Domínguez Garijo, A. Fritsch Medina, M. Mora Porta, F. Hanzu, M. Rodrigo-Calvo, S. Vidal-Sicart, O. Vidal-Pérez, D. Fuster Pelfort; Hospital Clínic Barcelona, Barcelona, SPAIN.*

Aim/Introduction: Primary hyperparathyroidism (PHPT) is diagnosed biochemically and treated mainly through surgery. Minimally invasive procedures are preferred over conventional open explorations. Preoperative localization of the hyperfunctioning parathyroid tissue (HFPT) is an essential aspect for minimally invasive parathyroidectomy (MIP) to prevent recurrence of disease. Parathyroid scintigraphy with 99mTc-MIBI in two phases (early and late acquisition), performed as a planar, tomographic (SPECT) or hybrid (SPECT/CT) is the most widely used technique. ^{18}F-Fluoromethylcholine (^{18}F-FCH PET/CT) has been proposed as a promising tool for the detection of HFPT, especially in cases where other methods have been unsuccessful to localize the pathological parathyroid gland. The aim of this study was to determine the efficacy of ^{18}F-FCH PET/CT in locating HFPT and to compare it with that of 99mTc-MIBI and neck ultrasonography (USG). **Materials and Methods:** A group of 35 consecutive patients (28 women and 7 men) diagnosed with PHPT were referred to our department for an assessment with imaging studies.Early and delayed planar images were acquired for dual-phase 99mTc-MIBI scintigraphy at 15 and 120 minutes post-injection (p.i.) of 888 MBq, respectively. SPECT/CT images were obtained 90 minutes p.i. with 120 projections for anatomic references.18F-FCH PET/CT images were obtained 60 minutes p.i. of approximately 100 MBq. 5-6 beds, caudo-cranial, 2,5 min per bed. Regional uptake not associated with thyroid disease was considered positive for HFPT.Nuclear medicine Images were analyzed by a Nuclear Medicine physician specialist and a resident physician having reached a consensus on the location of the suspected HFPT. Neck USG images were analyzed by an experienced Radiologist. All patients underwent a MIP, obtaining surgical biopsies that were subsequently analyzed by a pathologist. Findings of all the 3 preoperative imaging modalities were correlated with histopathology and were analyzed patient-wise (35 patients) and lesion-wise (38 lesions). Results: Neck USG, 99mTc-MIBI and 18F-FCH PET/CT localized pathological parathyroid glands in 10 (10/31, 32.3%), 20 (20/35, 57.1%) and 31 (31/35, 88.6%) patients, respectively. In a patient basis, these 3 imaging techniques yielded a sensitivity of 32.4%, 57.9% and 92.1%; PPV of 78.6%, 84.62% and 94.6%; and an accuracy rate of 79.0%, 85.7% and 96.4% respectively. On a lesion-wise analysis specificity was similar in the 3 modalities but showed a NPV of 79.1%,

86.0% and 97.1% respectively. **Conclusion:** 18F-FCH PET/CT demonstrated a higher diagnostic performance compared to the other imaging modalities, proving to be an excellent alternative for HFPT preoperative detection in patients with PHPT candidate to MIP. **References:** none

OP-1089

Interobserver agreement and utility of [^{18}F] fluorocholinePET/CT for the assessment of parathyroid adenomas (preliminary results)

I. Sánchez Rodríguez[1], M. Suárez-Piñera[1], A. Sabaté-Llobera[1], I. Gil-Viciano[1], J. Vercher-Conejero[1], P. Moreno-Llorente[2], A. Palomar-Muñoz[1], A. Benítez-Segura[1], M. Cortés-Romera[1];
[1]PET-Unit. Department of Nuclear Medicine, L'Hospitalet De Llobregat., Barcelona, SPAIN, [2]Endocrine Surgery Unit, Department of Surgery, Hospital Universitari de Bellvitge-IDIBELL, Barcelona, SPAIN.

Aim/Introduction: Parathyroid adenomas are the most common cause of primary hyperparathyroidism (pHPT) and surgery is the only curative treatment. Localization workup is often challenging due to the small size and variable localization of parathyroid adenoma. [^{18}F]fluorocholine PET/CT seems to be an effective method to detect these adenomas. This study aimed to: 1. Determine the interobserver agreement; 2. Assess the diagnostic performance of [^{18}F]fluorocholine PET/CT in patients with suspected pHPT; 3. Evaluate the correct acquisition time; and 4. Correlate PET/CT findings with PTH level. **Materials and Methods:** [^{18}F]fluorocholine PET/CT was performed on 41 patients (30 females, 26-76 years) with a diagnosis of pHPT and candidate to a curative surgery. All patients had been previously studied with other imaging techniques such as: ultrasound, [^{99m}Tc]Tc-sestamibi SPECT/ CT and/or MRI, with negative or inconclusive results. The imaging protocol consisted of a 10 minute dynamic study and of static images at 10 and 60 minutes after injection of 3.7 ± 1.2 MBq/kg of [^{18}F]fluorocholine. PET studies were analyzed independently by two nuclear medicine specialists (observers 1 and 2). Doubtful cases were assessed jointly. Preoperative parathyroid hormone (PTH) levels were collected. PET findings were compared with the surgical outcome (n =7) or with the clinical follow-up. Kappa concordance coefficient was used to evaluate the reproducibility among observers. Results: Hyperfunctioning glands were better or exclusively detected on late images than in the dynamic acquisition. Observer 1 found: 18 positive, 21 negative and 2 inconclusive PET results. Observer 2 found: 15 positive, 24 negative and 2 no conclusive results. Interobserver agreement was 82%, moderate agreement using Kappa coefficient. All pathologically confirmed adenomas were detected by [^{18}F]fluorocholine PET/CT. One surgical pathology specimen was negative (no adenoma) in agreement with negative PET result. Preoperative PTH levels were slightly higher in the positive PET/CT studies (median: 160 pg/mL) than in the negative studies (median: 121.4 pg/mL). **Conclusion:** The interpretation of [^{18}F]fluorocholine PET/CT for the detection of parathyroid adenomas is consistent among observers. The dynamic acquisition did not provide any additional information. PTH levels were slightly higher in patients with positive PET/CT. These preliminary results suggest that [^{18}F]fluorocholine PET/CT can be used for the detection and localization of parathyroid adenomas in patients with undetected lesions on conventional imaging techniques. Further studies are needed to know the exact value of this technique in these patients. **References:** None.

OP-1090

Evaluation of C-11-methionine-PET/MRI in primary hyperparathyroidism

N. Eberhardt[1], J. P. Steinacker[1], A. Hillenbrand[2], A. Müller-Reinartz[3], C. Michalski[3], P. Korf[4], M. Beer[5], C. Solbach[1], T. Kull[1], A. J. Beer[1];
[1]Ulm University Medical Center, Department of Nuclear Medicine, Ulm, GERMANY, [2]Surgical and Orthopedic Practice Clinic SI, Riedlingen, GERMANY, [3]Ulm University Medical Center, Department of General and Visceral Surgery, Ulm, GERMANY, [4]Siemens Healthcare GmbH, Erlangen, GERMANY, [5]Ulm University Medical Center, Department of Diagnostic and Interventional Radiology, Ulm, GERMANY.

Aim/Introduction: In primary hyperparathyroidism, C-11-methionine-PET/CT is a highly sensitive method for the preoperative localization of parathyroid adenomas. However, the correlation between PET findings and corresponding anatomical structures in CT is often difficult. In this respect PET/MRI is a promising method as it combines the superior sensitivity of molecular imaging with PET and the advantages of excellent soft tissue contrast and functional imaging in MRI. Moreover, PET/MRI reduces radiation exposure compared to PET/CT. Thus, we evaluated the performance of C-11-methionine PET/MRI for localization of parathyroid adenomas in patients with hyperparathyroidism. **Materials and Methods:** 15 PET/MRI scans (Siemens Biograph mMR, 3 T) of patients with laboratory evidence of primary hyperparathyroidism were evaluated retrospectively (9F, 6M, median age 55 years). The scans were acquired 20 min p. i. of approx. 500 MBq C-11-methionine from the skull base to the diaphragm (native + contrast enhanced, Gadovist 0.1 ml / kg BW; scan time approx. 35 min). The protocol consisted of the following sequences: axial T1-Flash CAIPI, T2-Haste STIR, T2-TSE, DWI, dynamic contrast enhanced T1-Flash; sagittal + coronal: T2-TSE Dixon. First we rated the level of certainty of findings in PET alone and secondly for the combined analysis of PET and MRI on a Likert scale from 1 to 5 (1 = uncertain diagnosis, 5 = certain diagnosis). Results: In all cases there was at least one suspicious finding for a parathyroid adenoma detected by PET. Two suspicious findings were found in one patient. In PET alone, 11/16 results were rated with 4, 3/16 with 5 and 2/16 with 3. By combining PET and MRI, the

ratings improved to 5 in 12/16, most of them could be best identified morphologically by early arterial enhancement in the dynamic contrast enhanced sequence. In 3/16 cases there was no change by combined PET and MRI analysis. No clear anatomical correlate was detectable in MRI in 1/16. The diagnosis could be confirmed histopathologically after operation without false positive findings for 7 cases. In comparison to equivalent PET/CT protocols, radiation exposure could be reduced by 65-80 %. **Conclusion:** For preoperative localization of parathyroid adenomas in primary hyperparathyroidism C-11-methionine-PET/MRI is a promising method with a high detection rate of adenomas combined with excellent anatomical correlation and a substantial reduction of radiation exposure compared to PET/CT. **References:** None

OP-1091

C11-Choline PET/CT usefulness in patients with primary hyperparathyroidism and negative or inconclusive 99mTc-MIBI scan

Á. Gutiérrez-González*, O. Cuenca-Vera, I. Martínez-Rodriguez, F. Gómez-de la Fuente, M. De Arcocha-Torres, A. Sánchez-Salmón, N. Martínez-Amador, S. Ruiz-Llama, J. Jiménez-Bonilla, J. Andrés-Pacheco, R. Quirce;*
Nuclear Medicine Service. Marqués de Valdecilla University Hospital. Molecular Imaging Group (IDIVAL). University of Cantabria, Santander, SPAIN.

Aim/Introduction: To determine the contribution of C11-Choline PET/CT (CHOL) to the localization of pathological parathyroids glands in patients with primary hyperparathyroidism and 99mTc-MIBI scan (MIBI) negative or inconclusive. **Materials and Methods:** Three-year prospective study involving 31 consecutive patients (26 women; mean age: 62.87 ± 10.52 years) with primary hyperparathyroidism (serum intact PTH: 163.45 ± 85.56 pg/ml) and suspected adenoma with negative or inconclusive MIBI scan who underwent CHOL. C11-Choline was produced in an in-house cyclotron and using and automated synthesis system. Cervical-thoracic PET/CT images were acquired 20 minutes after iv injection of 6.3 MBq/kg of C11-Choline. Any cervical or thoracic focal accumulation of the radiotracer higher than the background was considered as positive. Results: MIBI was negative in 27 out of the 31 (87.1%) patients included (PTH levels: 154.85 ± 64.41 pg/ml). CHOL was positive in 17 of these patients (62.96%) and negative in 10 (37.04%). In the remaining 4 patients (12.1%) MIBI showed doubtful positive findings, considered as inconclusive results (PTH: 221.5 ± 182.22 pg/ml). In these 4 patients CHOL showed matching positive findings in the same location. Overall, a total of 21 out of the 31 (67.74%) patients were CHOL positive, 17 of them (80.95%) showed a focal uptake located in cervical region, and 4 (19.05%) in extracervical region. Ten out of the 21 patients with positive CHOL underwent surgery (including 3 of the 4 patients with matching MIBI and CHOL findings). In 8 patients surgery confirmed the presence of a parathyroid adenoma at the same location as CHOL findings (7 in the cervical region and 1 extracervical). In the other 2 patients no adenoma was found at surgery (reported on CHOL as a cervical and an extracervical adenoma). PTH levels were not significant different between positive and negative CHOL (181.24 ± 97.53 vs. 126.10 ± 31.22 pg/ml, respectively, p = 0.083). **Conclusion:** Regardless of PTH levels, CHOL was useful in the localization of parathyroid adenomas in patients with primary hyperparathyroidism and negative MIBI scan. CHOL was also useful to solve doubts in patients with inconclusive MIBI scans, showing a complementary role of both techniques. **References:** None.

2001

Saturday, October 23, 2021, 12:25 - 12:45

Channel 1

Closing Session

OP-1094

Closing Session

S. Fanti; *EANM Congress Chair, Bologna, ITALY.*

212

Wednesday, October 20 - Saturday, October 23, 2021

on-demand pool, release on Wednesday, October 20 at 09:00

e-Poster Presentation Session 1: The Nuclear Cardiovascular World at its Best

EPS-001

Myocardial blood flows and reserves on solid state camera; correlations with coronary history and cardiovascular risk factors

J. Pinaquy*, P. Ferenczi, F. Debordeaux, H. Douard, Y. Pucheu, T. Couffhinal, Q. Ceyrat, L. Bordenave;*
University Hospital of Bordeaux, Bordeaux, FRANCE.

Aim/Introduction: Study designed to test association between stress-induced myocardial blood flow (sMBF), resting MBF (rMBF), and MBF reserve (MFR) and coronary artery disease (CAD) in a population of CAD and non-coronary patients. Secondary objectives were to confront visual analysis and dynamic analysis and to explore potential association between MBF and several cardiovascular risk factors **Materials and Methods:** Retrospective analysis of 155 patients (80 with known CAD and 75 without CAD). We randomly screened them among all patients referred to the

CHU of Bordeaux (Haut Lévêque Hospital) from December 2018 to June 2020 for a dynamic MPI with an evaluation of stress and rest MBF and MFR. Coronary patients had to present a recent positive ICA defined as at least one >50% stenosis in at least one coronary territory. Cardiovascular risk was assessed. Results: Significantly lower total sMBF and MFR were observed in coronary patients (1.49mL·g-1·min-1) vs. non-coronary patients (1.95mL·g-1·min-1) with a mean difference of +0.49mL·g-1·min-1 (0.29; 0.65; p<0.0001). The same results were obtained for MFR (2.12 vs. 2.61, +0.49 [0.20; 0.78], p = 0.0009). No difference was found in rMBF between coronary and non-coronary patients (0.74 and 0.82, respectively; p = 0.12). In comparison with visual analysis, lower sMBF were found in pathologic territory, lower rMBF in necrotic territory and lower MFR in necrotic ones. Rest and stress flows were significantly lower in the RCA territory (p < 0.0001 compared to Cx and LAD). A significant correlation between total sMBF, rMBF and diabetes was found. **Conclusion:** This exploratory study is concordant with previous recently published results regarding quantitative assessment of myocardial blood flows and reserves using CZT gamma-cameras. It reinforces the utility of this measurement to differentiate coronary and non-coronary patients in global analyses and by territory. The correlations found between several cardiovascular risks factors with flows and reserves values will require further investigations especially for diabetic patients. **References:** Shiraishi S et al. Clinical usefulness of quantification of myocardial blood flow and flow reserve using CZT-SPECT for detecting coronary artery disease in patients with normal stress perfusion imaging. Journal of Cardiology. avr 2020Acampa W et al. Quantification of myocardial perfusion reserve by CZT-SPECT: A head to head comparison with 82Rubidium PET imaging. J Nucl Cardiol. 7 mai 2020de Souza et al. Quantification of myocardial flow reserve using a gamma camera with solid-state cadmium-zinc-telluride detectors: Relation to angiographic coronary artery disease. J Nucl Cardiol [Internet]. 20 juin 2019

EPS-002

Influence of Music During Cardiac Stimulation for Myocardial Perfusion Imaging Studies

J. Prieto Prieto[1,2], M. Guiote Moreno[1,2], B. Luque Espejo[1], F. Maza Muret[1,2], R. Zurera Pareja[2], J. Vallejo Casas[1,2];
[1]University Hospital Reina Sofia, Córdoba, SPAIN,
[2]IMIBIC. Maimonides Biomedical Research Institute of Córdoba, Córdoba, SPAIN.

Aim/Introduction: The aim of our study was to determine whether, during pharmacological stimulation for 99mTc-Tetrofosmin myocardial perfusion SPECT/CT scans, music could be a relevant factor by contributing to improve patients clinical perception of well-being during the test. **Materials and Methods:** Since February 2020, 118 patients were consecutively recruited, 48 male (40.7%) and 70 female (59.3%) (mean age 68.77 years, standard deviation 10.13 years). In 84 cases (71.2%) patients were referred for diagnosis of inducible myocardial ischemia, while 34 of them (28.8%) for prognostic evaluation of known ischemic heart disease. Of these patients, 35 (29.7%) were stimulated with adenosine, and 83 (32.2%) with regadenoson due to COVID-19 pandemic and clinical comorbidities including obesity or respiratory pathologies. Patients were randomly classified into two groups: the test group listened to Claude Debussy's "Clair de Lune" during drug administration, whereas patients in the control group were stimulated without music. All of them were given a survey with the following variables: tolerability, presence of palpitations, sweating, nausea, headache, central chest pain, abdominal pain, dyspnea, cough and tingling sensation. Test group patients were asked whether they were positively influenced by the music. Blood pressure (BP), heart rate (HR) and peripheral blood oxygen saturation (SpO2) parameters were taken before and after pharmacological stimulation. Other symptoms such as fatigue or dizziness were also collected. Chi-square test was performed for qualitative variables, while bilateral t-test was performed for quantitative parameters. A p-value <0.05 was considered statistically significant. Results: Music was played to 57 patients (48.3%), whereas 61 patients (51.7%) were included in control group. Although 97 patients (82.2%) had some adverse effect, cardiac stimulation was subjectively well or very well tolerated by 92 patients (78%). Dyspnea, sweating and headache were the predominant adverse effects in 71 (60%), 55 (46.6%) and 39 (33%) patients, respectively. Among the 57 patients subjected to music, 44 (72.1% of them) reported a positive influence of music exposition during cardiac stimulation (p<0.01), and 35 (57%), 25 (41%) and 20 (33%) patients presented those symptoms respectively. Given the small sample size, no statistically significant differences were obtained between occurrence of adverse effects or clinical parameters and exposure to music in both groups. Further patient recruitment is required and will be carried out in our department. **Conclusion:** Music is a useful tool for patients to subjectively better tolerate adenosine and/or regadenoson administration during cardiac stimulation for the acquisition of myocardial perfusion SPECT/CT studies with 99mTc-tetrofosmin. **References:** none

EPS-003

^{99m}Tc-HMDP Quantification in Cardiac Amyloidosis: the Heart to Whole-Body Ratio

A. Marques, B. M. Rocha, M. Cruz, M. Paiva, S. Maltês, P. Lopes, J. Carvalho, F. Abreu, C. Aguiar, M. Mendes, S. Pintão;
Centro Hospitalar de Lisboa Ocidental, Lisboa, PORTUGAL.

Aim/Introduction: Transthyretin Amyloid Cardiomyopathy (ATTR-CM) is a condition often diagnosed by means of a non-invasive algorithm using bone scintigraphy. Our main goal was to characterize the Heart to Whole-Body (H/WB)

ratio in an ATTR-CM cohort. **Materials and Methods:** This is a study of consecutive patients with ATTR-CM followed in our centre. As per site protocol, these patients are routinely assessed at least thrice yearly, including a yearly transthoracic echocardiography (TTE). All data is systematically recorded in the medical electronic chart. In our institution, we use the ^{99m}Tc-HMDP radiotracer and acquire an early (5 min) and a late (3 h) planar whole-body image. The H/WB ratio was measured by tracing the regions of interest of the whole body, heart, kidneys and bladder on late planar images. The Spearman method was used to assess the correlation between the variables of interest. Results: Overall, 18 patients were included (mean age 82 ± 5 years; 78% male, 56% atrial fibrillation; hATTR-CM in 4 cases; tafamidis in 7 cases), most of whom were diagnosed by the non-invasive algorithm (Perugini grade 2 or 3 in 12 and 2 cases, respectively). The median H/WB ratio was 3.53 (2.60-4.37). There was a tendency towards higher H/WB ratio in patients with Perugini grade 3 vs. grade 2 [9.49 (4.37-14.61) vs 3.18 (2.57-3.97); p=0.078). The strongest correlation between the H/WB ratio and variables of interest were moderate at best - i.e. diastolic blood pressure (r=-0.421; p=0.082), Sokolow-Lyon index (r=-0.451; p=0.070), and the interventricular septum thickness (r=0.492; p=0.038) and the E/A ratio by ETT (r=0.628; p=0.029). No correlation was noted with left ventricular ejection fraction, left atrial volume, right ventricular function indices nor laboratory evaluation (including NT-proBNP and cardiac troponin). There was a tendency towards higher risk of hospitalization for Heart Failure with increasing H/WB ratio (HR 1.18; p=0.078). **Conclusion:** Our preliminary findings suggest that the H/WB ratio might associate with surrogate markers of cardiac amyloid infiltration and increased risk of hospitalization for Heart Failure. Whether this variable further adds prognostic value over that of traditional variables is worth being prospectively assessed in a larger ATTR-CM prospective cohort. **References:** None.

EPS-004

Utility of Hybrid Imaging SPECT/CT VS Planar Imaging in ATTR Cardiac Amyloidosis

O. Bourogianni[1], *N. Kapsoritakis*[1], *I. Zaganas*[2], *A. Patrianakos*[1], *M. Stahaki*[1], *A. Tsaroucha*[1], *S. Koukouraki*[2];
[1]*University Hospital of Crete, Heraklion, GREECE,* [2]*School of Medicine, University of Crete, Heraklion, GREECE.*

Aim/Introduction: Amyloidosis is a group of protein folding disorders in which more than one organ is infiltrated by proteinaceous deposits known as amyloid. One of the most common organ involved is cardiac with myocardial amyloid deposits. There are two most common types, the light chain (AL) and transthyretin (ATTR) cardiac amyloidosis (CA). CA if left undiagnosed and untreated is a life threatening disease. The most commonly used radioisotopic imaging technique is planar cardiac scintigraphic imaging. The purpose of this study is to evaluate the role of hybrid cardiac imaging SPECT/CT in addition to planar imaging in the diagnosis of ATTR-CA. **Materials and Methods:** 89 patients suspected for ATTR-CA were referred in our department. All of them underwent clinical investigation, echocardiography, MRI cardiac imaging, serum light chain immunoglobulin measurements and gene tests. 46/89 patients showed echo and MRI inconclusive results and serum measurements negative for light chain immunoglobulins. 99mTc Pyrophosphate (PYP) planar, SPECT and SPECT/CT cardiac scintigraphic imaging was performed 1hr and 3hrs post injection. Using a reconstruction station, qualitative and quantitative analysis was performed. For qualitative analysis on planar imaging the Perugini scores was used. Semiquantitative analysis was based on the method of ROIs (heart/ contralateral mediastinum ratio). Qualitative and quantitative analysis for SPECT and SPECT/CT was performed. For SPECT visual analysis was based on the evaluation of myocardial uptake and quantitative analysis on a polar map (17 segments). For SPECT/CT "Q metrix" software provided by GE Medical Systems was used for evaluating the standardized uptake value (SUV). Results: 99mTc PYP planar qualitative analysis: Grade 0 (negative for ATTR): 10/46 (21,7%), Grade 1 (equivocal): 15/46 (32,6%) and Grade 2 or 3: 21/46 pts (45,65%) based on Perugini score and H/CL ratio (≤1,5 for grade 1 and ≥ 1,5 for grade 2 or 3). SPECT/CT for pts with grade 1 on planar imaging showed that 45,65% were classified as grade 2 or 3, and the rest remained equivocal. **Conclusion:** SPECT/CT is a very promising tool for the accurate diagnosis of ATTR-CA because of its ability to better defining the myocardial boundaries vs planar imaging, to distinguish blood pool from cardiac uptake, to offer attenuation corrected images and a more accurate quantitative analysis based on SUV. **References:** None

EPS-005

Transthyretin Cardiac Amyloidosis: The Utility of Cardiac Scintigraphy with 99mTc-HDP

M. Tagliatori Nogueira, *C. Paniagua Correa, M. de la Rubia Marcos, B. Manzarbeitia Arroba, M. Álvarez Moreno, C. Sandoval Moreno, A. Herrero Muñoz, L. Castillejos Rodriguez, M. Balsa Bretón;*
Hospital Universitario de Getafe, Madrid, SPAIN.

Aim/Introduction: This is a review of 99mTc-HDP Cardiac Scintigraphy (CS) of patients with suspected cardiac transthyretin amyloidosis (ATTR-CA), its prevalence and relationship with cardiovascular risk factors, echocardiography, cardiovascular magnetic resonance (CMR) and biopsy. **Materials and Methods:** Retrospective analysis of 73 CS of patients with suspected Cardiac Amyloidosis (CA) between 2014 and 2019, 49 men and 24 women with a mean age of 76.9 (44-90). 740 MBq of 99mTc-HDP were administered obtaining planar images (A-P and LAO view) and a chest SPECT/CT. Cardiac uptake was interpreted according to the visual scale (0 absence / 1<bone / 2=bone / 3>bone), being

2-3 suggestive of ATTR-CA and its myocardial extension according to SPECT/CT. The results were compared with echocardiography, CMR, endomyocardial biopsy and their relationship with left ventricular ejection fraction (LVEF) and heart failure. Results: Of the 73 studies, 25 (34.2%) were positive (CS-P) and 48 (65,8%) were negative (CS-N). 100% of CS-P showed a visual scale of 3, of which 100% had hypertrophic cardiomyopathy, 92% preserved LVEF, and 64% infiltrative cardiomyopathy by echocardiography/CMR. The SPECT/CT showed an 80% of unique left ventricle (LV) involvement, 12% LV+RV, 4% LV+LA, and 4% LV+LA+RV, without being associated with a greater number of cardiovascular risk factors, heart failure or LVEF diminished. No patient with CS-P underwent endomyocardial biopsy and only one patient with CS-N and high suspicion presented a positive biopsy for AL (light-chain amyloidosis). **Conclusion:** Cardiac Scintigraphy as a non-invasive method is adequate to avoid the morbidity and mortality of endomyocardial biopsy. The prevalence of ATTR-CA in our center is 34.2% and always shows LV involvement, without finding a relationship with less LV ejection fraction or more CV risk factors/heart failure decompensations in cases of extension to other cardiac chambers. **References:** none

EPS-006

Global and Regional Coronary Flow Reserve assessed by routine perfusion SPECT improves the interpretation of the final report

L. Philippe, C. Prunier-Aesch, Y. El. Yaagoubi;
Medecine Nucleaire Tourangelle, Chambray-les-Tours, FRANCE.

Aim/Introduction: Coronary Flow Reserve (CFR) is usually performed by dynamic SPECT or PET. Routine 99mTc-tetrofosmin (1 day Stress-Rest protocol) can also be used to assess global and regional CFR. The purpose of this study is to evaluate an expected added value of the CFR to the final report. **Materials and Methods:** We assess the CFR by means of a Coronary Reserve Index (CRI) obtained with routine 99mTc tetrofosmin SPECT. We use the counts ratio Stress/Rest on short axis slices, after application of five corrective factors. The routine gated tetrofosmin SPECT was reported as consistent with Coronary Artery Disease (CAD), or not. These results were compared to Invasive Coronary Angiography (ICA). Analysis efficiency of SPECT perfusion for CAD diagnosis was compared to CRI results in order to check if the CRI is an added value. We applied this processing to a series of 48 patients addressed to our institution for routine myocardial Stress/Rest (exercise, dipyridamole, or regadenoson), for suspicion of CAD. Patients with previous revascularization were excluded. Among this population, we observed 43 patients with diabetes, 38 patients with High Blood Pressure (HBP), 18 patients having both risk factors. Results: ICA is considered as gold standard, although ICA provides different information when compared with perfusion SPECT. Considering ICA results, 9 patients had no significant CAD, and 41 patients had significant CAD. Gated SPECT found 13 patients with CAD, and 37 patients with no significant CAD. CRI indicated 6 patients with normal coronary reserve (CRI > 3), and 42 patients with low coronary reserve. Diagnostic performances were assessed for standard perfusion gated SPECT (A), for CRI evaluation (B), and for SPECT completed by CRI (C). Sensitivity: (A) 77%. (B) 97%. (C) 98%. - Specificity: (A) 44%. (B) 56%. (C) 50% - Positive Predictive Value: (A). 86% (B) 90%. (C). 91% - Negative Predictive Value:(A) 31% (B) 83%. (C) 80% . The CRI evaluation allowed to correct the initial diagnosis of 7 patients (15% of patients series): 7 false negative converted in 7 true positive. Some disagreement between CRI and ICA, are probably related to the difference of data obtained with both methods: microvascular disease for SPECT-CI vs epicardial lesions for ICA. **Conclusion:** CRI evaluation (fully automatic process) computed for each patients is an incremental diagnostic value over standard myocardial gated SPECT. Consideration of this parameter decreases the number of false negative SPECT (mainly due to multivessel disease). **References:** none

EPS-007

Performance Of Different Myocardial Suppression Protocols For Assessing Inflammation

B. Rodriguez-Alfonso, F. Dominguez-Rodriguez, A. Prieto-Soriano, D. de Castro-Campos, S. Guzman-Ortiz, M. Mitjavila-Casanovas;
Hospital Universitario Puerta De Hierro, Majadahonda, SPAIN.

Aim/Introduction: Adequate suppression of myocardial physiological uptake is mandatory to avoid false-positive results when evaluating active myocardial inflammation with ^{18}F-FDG-PET/CT. Different protocols and success rates, specially combining heparin and dietary modification have been published. Our aim was to compare the performance of two suppression strategies in patients under evaluation for dilated myocardiopathy. **Materials and Methods:** All patients referred to PET/CT to rule out inflammation in the context of a dilated myocardiopathy were included. We analyzed the level of physiological uptake suppression achieved by combining different myocardial suppression protocols, consisting of dietary modification (High-fat low-carbohydrate protein-free (HFLC) diet for 3 days), 16-hours fasting period and intravenous bolus of unfractionated heparin (uH). The quality was categorized as optimal (complete), suboptimal (mild uptake) and null (hot myocardium). Results: Thirty-two patients were included. All patients followed the 16-hours fasting period and all except for one the 3-days HFLC diet. Optimal suppression was achieved in 26 patients (81%), suboptimal in 5 (16%) and null in 1 (3%). Heparin was administered 15 minutes before the intravenous injection of ^{18}F-FDG in 15 patients (47%) and suppression was optimal in 12/15 (80%) and suboptimal in 3/15 (20%). No heparin was given in 14 patients and 12 accomplished for an optimal

suppression (86%). The only patient who followed exclusively the 16-hours fasting period was the only one with hot myocardium. No adverse effects were observed with any of the protocols used. **Conclusion:** The use of heparin does not appear to add benefits over the 3-days HFLC diet followed by a long fasting period.Previous dietary modification is probably necessary, beside the long fast, to obtain higher rates of success in myocardial suppression strategies. **References:** none

EPS-008

Reliability of [^{123}I]I-metaiodobenzylguanidine cardiac SPECT assessment in postinfarction heart failure patients

A. Teresinska, J. Wnuk, O. Wozniak, A. Maciag, E. K. Biernacka; National Institute of Cardiology, Warsaw, POLAND.

Aim/Introduction: Planar imaging, evaluating global cardiac [^{123}I]I-metaiodobenzylguanidine (MIBG) uptake, is a standard method for prognosis in heart failure (HF). SPECT imaging is expected to be superior, especially for prediction of life-threatening arrhythmias, by providing information on regional heterogeneity of cardiac adrenergic system. This study aimed to determine the quality and reproducibility of MIBG SPECT in postinfarction HF patients without diabetes, qualified for implantable cardioverter defibrillator (ICD) in primary prevention of sudden cardiac death. **Materials and Methods:** Consecutive subjects, qualified for ICD, were prospectively included. Late planar MIBG studies were followed by SPECT; low-energy-high-resolution collimators and filtered-back-projection reconstruction were applied. The analysis was based on visual assessment of the quality of SPECT images ("unacceptable" or "quantitative") by 2 independent experienced readers. Additionally, consensus qualitative assessment of planar images was conducted; the relative uptake intensity among heart (Heart), left lung (Lung) and liver (Liver) was connected with SPECT results. To evaluate intra- and interobserver reproducibility, the coefficient of variation (CV%) was used for planar heart/mediastinum (HMR) and SPECT summed defect score (SDS). Results: Fifty subjects were enrolled (43 M: age 67±14y, LVEF 27±5%). Planar images were interpretable in all patients. In 13 patients (26%), the assessment of SPECT was impossible because of very high lung (in 7 patients), liver (2) or lung and liver uptake (4). Reproducibility of HMR was high: intraobserver and interobserver CV% was 2.8% and 3.2%. Reproducibility of SDS was lower: 9.4% and 10.5%. LVEF>30 was observed in 22% cases of 'quantitative' and in none case of 'unacceptable' SPECT. Assessment of planar MIBG images showed Liver much higher than Lung and Heart in all the 50 patients. In 'unacceptable' SPECT group, Lung in planar imaging was higher than Heart in 77% and comparable to Heart in 23% of patients. In 'quantitative' SPECT group the proportions were significantly different: Lung was higher than Heart in 19% and comparable or lower in 81% of patients. **Conclusion:** Reliability of MIBG SPECT imaging, at least with conventional imaging protocols, in postinfarction HF patients is limited. In our study, in approximately a quarter of patients SPECT assessment of cardiac denervation was impossible, even without additional damage from diabetic cardiac neuropathy. Intra- and interobserver reproducibility of SPECT assessment was low. The criteria predisposing the patient to good quality MIBG SPECT were: high values of LVEF (i.e. close to 35%) and left lung uptake intensity in planar images comparable or lower to heart uptake. **References:** none

EPS-009

Insulin loading for optimal cardiac Fluorine-18 fluorodeoxyglucose positron emission tomography: an easier and more efficient preparation

Y. Chen;
Quanzhou 1st hospital, Quanzhou, CHINA.

Aim/Introduction: Efficacy of intravenous insulin injection for improving the image quality of cardiac Fluorine-18 -fluorodeoxyglucose (^{18}F-FDG) positron emission tomography (PET) was evaluated in this study. **Materials and Methods:** Sixty-seven patients (55 male and 12 female; average age 59.6 ± 12.5 years) with ischemic heart diseases were enrolled between November 2017 and June 2019 in this retrospective study. The qualities of cardiac ^{18}F-FDG PET/CT images were evaluated with optimal preparation protocols including standardized glucose loading (n = 29) and insulin loading (n = 38). Standardized uptake values (SUVs) of the left ventricular myocardium and liver were recorded. And the preparation time, i.e. the interval time between glucose/insulin administration and ^{18}F-FDG injection, was also recorded. Uninterpretable PET images were defined as the ratio of SUVmyo/SUVliv < 1. Data were analyzed with t- or Chi-square test. Results: The ratios of the interpretable cardiac PET images were significantly more in the insulin loading group than in the glucose loading group (38/38 vs. 25/29, P = 0.03). Among these interpretable images, the SUVs of the myocardium and liver, and ratios of SUVmyo/SUVliv were similar between these two groups. The preparation time was significantly shorter in the insulin loading group than in the standardized glucose loading group (22 ± 5 min vs. 109 ± 29 min, P < 0.01). **Conclusion:** Insulin loading protocol is easier and more efficient than standardized glucose loading preparation for the high-quality of cardiac ^{18}F-FDG PET image. **References:** [1] Dilsizian V, et al. J Nucl Cardiol. 2016;23:1187-226.[2] Tarakji KG, et al. circulation. 2006;113:230-7.[3] Anavekar NS, et al. J Am Coll Cardiol. 2016;67:2874-87.[4] Vitale GD, et al. J Nucl Med. 2001;42:1730-6. [5] Bax JJ, et al. Eur J Nucl Med Mol Imaging. 2002;29:452-7.[6] Martin WH, et al. Eur J Nucl

Med. 1997;24:1291-7.[7] McCrary JR, et al. The Egyptian Heart Journal. 2013;65:123-9.[8] Schinkel AF, et al. J Nucl Med. 2003;44:877-83. [9] Sarikaya I, et al. J Saudi Heart Assoc. 2018;30:75-85.[10] Valentin RC, et al. J Nucl Cardiol. 2018.[11] Augustin R. IUBMB Life. 2010;62:315-33. [12] Liepinsh E, et al. Metabolism. 2014;63:127-36.[13] Yakisich JS, et al. Stem Cells Int. 2019: 6254269.[14] Boellaard R, et al. Eur J Nucl Med Mol Imaging. 2015;42:328-54. [15] Welch BT, et al. Adv Radiat Oncol. 2018;4:79-89.

EPS-010

Radiomic assessment of epicardial adipose tissue and cardiac innervation imaging in prognosis of catheter ablation of atrial fibrillation

Y. Varlamova[1], E. Popov[1], S. Sazonova[1], N. Nikitin[2], S. Minin[3], A. Romanov[3], I. Kisteneva[1], R. Batalov[1], S. Popov[1];
[1]Cardiology Research Institute, Tomsk NRMC, Tomsk, RUSSIAN FEDERATION, [2]Medical Center "Avicenna", Novosibirsk, RUSSIAN FEDERATION, [3]E. Meshalkin National Medical Research Center of the Ministry of Health of the Russian Federation, Novosibirsk, RUSSIAN FEDERATION.

Aim/Introduction: Previous studies shown that epicardial adipose tissue volume ratio and cardiac sympathetic activity might be independently associated with late atrial fibrillation (AF) recurrence after catheter ablation (CA). The aim of current study was to investigate the ability of cardiac innervation imaging and radiomic assessment of epicardial adipose tissue to predict late AF recurrence after CA. **Materials and Methods:** Cardiac metaiodobenzylguanidine (123I-mIBG) scintigraphy and cardiac CT imaging were performed before CA in 26 patients with persistent AF. Radiomic characterization of epicardial adipose tissue were measured from computed tomography scans by 3D Slicer (version: 4.13.0). Patient was followed for 12 months. Results: During a median follow-up arrhythmia recurrence was observed in 8 patients. Patients with AF recurrence had a significantly lower baseline late heart-to-mediastinum ratio (1.51(1.34-1.64 vs 1.83(1.6-1.91), p<0.05) and significantly higher washout rate (WR) (35.9(25-40) vs 11.7(7.7-20.9), p<0.05) compared to patients without AF recurrence. There were no significant differences in radiomic characterization of epicardial adipose tissue in patients with and without AF recurrence. Multivariable analysis demonstrated that the WR (OR: 2.37, 95%CI 1.12-5.04, p<0.023) was independent predictor of AF recurrence after CA. **Conclusion:** In AF patients the incidence of arrhythmia recurrence after CA is associated with impaired cardiac sympathetic nervous activity. **References:** None

EPS-011

Coronary flow reserve in patients with preserved left ventricle ejection fraction and non-obstructive coronary artery disease

A. Mochula, K. Kopeva, A. Maltseva, K. Zavadovsky, E. Grakova;
Cardiology Research Institute, Tomsk NRMC, Tomsk, RUSSIAN FEDERATION.

Aim/Introduction: The objective of our study was to evaluate association of dynamic CZT-SPECT indices and course of heart failure with preserved left ventricle ejection fraction (HFpEF) in patients with non-obstructive coronary artery disease. **Materials and Methods:** A total of 48 patients and baseline LVEF of 62 (56; 67)% were enrolled in the study. Thirty-six (75%) patients had HF of NYHA class I-III diagnosed. NT-proBNP levels did not exceed normal for HF (>125 pg/mL) in 12 patients (25%). All patients had a non-obstructive CAD that was confirmed by ICA. Serum levels NT-proBNP were measured using an enzyme immunoassay. Stress and rest myocardial blood flow (MBF), coronary flow reserve (CFR) parameters were evaluated by dynamic CZT-SRECT [1]. Net-retention model with motion and attenuation correction were used [2]. Results: In heart failure patients the values of CFR significantly correlated with NT-proBNP levels (r=-0.387; p=0.014), NYHA classes (r =-0.819; p<0.001) and LVEF (r =-0.256, p=0.049). According to NYHA classes, values of CFR were different (p<0.001). In patients with NYHA class 1 (n=16) values of CFR 2.88 (2.52; 3.3) and levels of NT-proBNP were 184 (129.4; 457.8) pg/mL. In patients with NYHA class 2 (n=8) values of CFR were 1.8 (1.55; 2.08) and levels of NT-proBNP were 459 (187.6; 881.1) pg/mL. In patients with NYHA class 3 (n=12) values of CFR were 1.31 (1.23; 1.49) and levels of NT-proBNP were 2137 (442.4; 3508.65) pg/mL. Values of CFR were higher by 27.6% in patients without HF in comparison to patients with HF (3.01 [2.86; 3.15] vs. 2.18 [1.97; 2.88], respectively). **Conclusion:** Our data suggest that values of CFR were associated with NYHA classes in patients with HFpEF and non-obstructive coronary artery disease. It requires further study with inclusion of more patients to prove this association and prognostic role CFR parameters in HF progression in patient with HFpEF. This study was supported by the Russian Federation President Grant MK-1347.2020.7. **References:** 1. Zavadovsky K.V., Mochula A.V., Boshchenko A.A., Vrublevsky A.V., Baev A.E., Gulya M.O., Nesterov E.A., Liga R., Gimelli A. Absolute myocardial blood flows derived by dynamic CZT scan vs invasive fractional flow reserve: Correlation and accuracy Journal of Nuclear Cardiology. - 2019. 2. Zavadovsky K.V, Mishkina A.I., Mochula A.V., Lishmanov Yu.B. The method for correction of motion artefacts to improve myocardial perfusion imaging. REJR. 2017; No. 7 (2), pp. 56-64 (In Russ.)].

EPS-012

Quantification of Cardiac 99mTc-bisphosphonates (DPD) uptake using SPECT-CT images in Amyloidosis Transthyretin patients

M. Solá, G. Moragas, M. Salcedo Pujantell, J. Deportos, M. N. Torres, M. H. Olivares, S. Lafuente, V. Vallejos, M. Domingo;
Hospital Universitari Germans Trias i Pujol, Badalona, SPAIN.

Aim/Introduction: To assess whether cardiac single-photon emission computed tomography (SPECT/CT) quantification of 99mTc-3,3-diphosphono-1,2-propanodicarboxylic acid (DPD) would improve diagnostic accuracy. **Materials and Methods:** This study was carried out at GermansTrias i Pujol Universitary Hospital between 2017 and 2020. It was a prospective analysis of DPD planar and SPECT-CT studies requested to patients with suspected cardiac amyloidosis. Scans were reported using a visual grading system (0 to 3 increasingly; 2-3 positive) on planar images (anterior, left oblique anterior and lateral). Cardiac uptake and vascular activity over mediastinic vessels were quantified from drawn VOIs on SPECT/CT transaxial sections. A cardiac/ mediastinic index (C/M) was calculated. Inter-observer variability of planar and tomographic results, and correlation among them were analyzed. Also, a cut off-point was calculated from mean and SD of C/M index of patients considered negative on visual analysis (grade 0-1). Patients with discordance between visual and quantitative evaluations were revisited. The study was approved by the ethical commission of our hospital. Results: A total of 226 DPD scans were analyzed (patient mean age 78,1 ± 10,7 years; 46% male). Inter-observer variability of planar analysis (r2 0,897; p<0,001) and C/M index (r2 0,884; p<0,001) correlated well. On visual analysis 108 were grade 0; 77 were grade 1; 6 were grade 2; and 35 were grade 3. C/M index correlated well with visual grading: for grades from 0 to 3, mean ± SD C/M index were 0,93 ± 0,15; 1,01 ± 0,22; 1,87 ± 1,24; and 6,79 ± 2,97, respectively. A cut off C/M index of 1,35 was determined to classify a SPECT/CT as positive (0-1 vs 2-3 on visual grading). Discordance between visual and quantitative index was found in 7 studies (corresponding to visual grades 1 or 2), however visual revaluation of SPECT-CT images allowed to resolve discordation in 6 of them (based on intraventricular vascular activity, 3 negatives and 3 positives; study 7 was difficulted by its small cardiac size). **Conclusion:** SPECT/CT quantification in DPD scintigraphy is possible and outperforms visual analyses on planar images. Differentiation of grade 1 or 2 migth be confused by vascular uptake specially on small sized hearts, which can difficult to draw the VOI. This index can help in the diagnosis of cardiac amyloidosis and improve diagnostic accuracy. **References:** none

EPS-013

The value of CZT SPECT myocardial blood flow and reserve assessment in terms of identifying high-risk patients after surgical treatment of ischemic cardiomyopathy

V. Shipulin, A. Pryakhin, S. Andreev, A. Mochula, M. Gulya, K. Zavadovsky, V. M. Shipulin;
Cardiology Research Institute, Tomsk National Research Medical Centre, Russian Academy of Sciences, Tomsk, RUSSIAN FEDERATION.

Aim/Introduction: Myocardial blood flow (MBF) and myocardial flow reserve (MFR) obtained by dynamic SPECT (dSPECT) on CZT gamma camera are rather new, rapidly developing but yet not really well-established parameters [1]. Even less information exists about their prognostic values, especially in patients with ischemic cardiomyopathy (ICM) [2]. Our purpose was to access the value of MBF and MFR obtained by dSPECT on CZT gamma camera in evaluating high-risk patients after surgical treatment of ICM. **Materials and Methods:** 30 patients with ICM were enrolled. Before surgical treatment, all patients underwent dSPECT (Tc99m-MIBI; 2 days stress-rest protocol, adenosine 140mkg/kg/min). After surgical treatment, patients were divided into 2 groups: with (death, intra-aortic balloon pump, extra inotropic support) (n=10) and without (n=20) complications in early postoperative period. Results: According to the preoperative data groups were comparable in majority of basic parameters except LV EF (%) (28 (IQR25; 32) vs. 34 (31;37), p=0.002), LV ESV(ml) (181 (136;198) vs. 140 (121; 162), p=0.006) and the number of coronary arteries with stenosis ≥ 75% (CA≥ 75%) (p=0.02). Neither of intraoperative parameters (cross-clamp time, cardio-pulmonary bypass time etc.) showed differences between groups. According to dSPECT significant differences were revealed between groups for MFR (1.27 (0,97; 1.98) vs. 0.88 (0.72; 1.17), p=0.01). Multivariate logistic regression analysis showed that age (odds ratio [OR] 1.3, 95% confidence interval [CI] 1.13-2.09, p <0.001), ESV LV (OR 1.07, CI 1.02-1.1.2, p<0.001) and MFR (1.46, CI 1.46-2.03, p<0.001) were independent predictors of the complicated course of early postoperative period. ROC-analysis showed that MFR (cut-off value >1.13) had a sensitivity of 71% and a specificity of 75% in field of prediction the adverse early postoperative course. Moreover, MFR had higher AUC value than ESV LV and age (AUC 0.833, 0.740 and 0.714 respectively). **Conclusion:** The value of MFR, assessed by preoperative dSPECT, is associated with adverse course of early postoperative period in patients with ICM. **References:** 1. Shipulin V.V., Saushkin V.V., Pryakhin A.S., Andreev S.L., Vesnina Zh.V., Zavadovsky K.V. The value of myocardium perfusion imaging in assessment of patients with ischemic cardiomyopathy. REJR 2019; 9(3):155-175. DOI:10.21569/2222-7415-2019-9-3- 155-175. 2. Zavadovsky, K.V., Mochula, A.V., Maltseva, A.N. et al. The current status of CZT SPECT myocardial blood flow and reserve assessment: Tips and tricks. J. Nucl. Cardiol. (2021). https://doi.org/10.1007/s12350-021-02620-y

EPS-014

The Clinical-Diagnostic Relevance of Visual Score 1 at [99mTc]Tc-2,3-dicarboxypropane-1,1-diphosphonate Scintigraphy ([99mTc]Tc-DPD) for Cardiac Amyloidosis

L. Vetrone[1], N. Fraccascia[1], G. Argalia[1], E. Fortunati[1], A. Giovannetti[2], R. Bonfiglioli[3], E. Tabacchi[3], S. Longhi[4], C. Gagliardi[4], E. Biagini[4], N. Galiè[4,5], S. Fanti[1,3];

[1]Nuclear Medicine, Department of Experimental, Diagnostic and Specialty Medicine, University of Bologna, Bologna, ITALY, [2]Cardiology Unit, Department of Experimental, Diagnostic and Specialty Medicine, University of Bologna, Bologna, ITALY, [3]Nuclear Medicine, IRCCS, Azienda Ospedaliero-Universitaria di Bologna, Bologna, ITALY, [4]Cardiology Unit, IRCCS, Azienda Ospedaliero-Universitaria di Bologna, Bologna, ITALY, [5]DIMEC, IRCCS, Azienda Ospedaliero-Universitaria di Bologna, Bologna, ITALY.

Aim/Introduction: The presence of heart involvement in patients (pts) with amyloidosis is the major determinant of survival. There are two most frequent types of cardiac amyloidosis (CA): acquired monoclonal immunoglobulin light-chain form (AL) and transthyretin-related (familial and wild-type) form (ATTR). An important diagnostic tool for CA is the [99mTc]Tc-DPD where the cardiac retention of the tracer can be classified in a visual score (VS). The VS has four grades of severity (0-3) rating the tracer's distribution among heart, bone and soft tissues. VS2-3 is suggestive for ATTR, after the exclusion of serum and urine immunofixation electrophoresis for AL. VS1 cannot provide a specific diagnostic orientation. The aim of this preliminary study is to assess the clinical-diagnostic relevance of VS1. **Materials and Methods:** 19 pts (3/19 female, 16/19 male, median age 73.4 yo) with VS1 who underwent [99mTc]Tc-DPD from January 2016 to February 2021 at Our Center, were retrospectively selected. Clinical, laboratory, histological data and conventional imaging (echocardiography-ECHO, cardiac magnetic resonance-CMR), performed before [99mTc]Tc-DPD, were collected. Results: ATTR was diagnosed in 11/19 pts. Among them, ECHO was highly suggestive for CA in 8/11 and negative in 3/11; CMR was performed and suspected of CA in 2/11. Further performed investigations were: 1/11 endomyocardial biopsy, 1/11 abdominal subcutaneous fat aspiration, 1/11 bone marrow biopsy and 8/11 genetic tests (GT). Among GT group, 3/8 showed hereditary mutations (1/3Thr59Lys, 1/3Ile68Leu, 1/3Ala47) with mean age 48,7 yo (range 38-56), while 5/8 were positive for wild-type mutations with mean age 74,5 yo (range 49-85). Despite the absence of certain diagnosis, 6/19 pts were highly suspected for CA due to the presence of multiple typical ECHO CA-features. Within this group of pts, 3/6 presented also hemodynamically significant aortic stenosis. Only 1/19 pt was positive for AL at further investigations. 1/19 pt was negative for CA, but during other investigations Tako-Tsubo and Acute Coronary Disease were diagnosed. **Conclusion:** According to the results VS1 can lead towards a diagnosis of CA more than expected. Further studies are needed to explore, in a larger population, the clinical-diagnostic relevance of VS1. **References:** None.

EPS-015

[99mTc]Tc-2,3-dicarboxypropane-1,1-diphosphonate (99mTc-DPD)-SPECT/CT in patients with low mediastinal uptake in the assessment of Transthyretin Cardiac Amylodosis: an Italian single center experience

N. Fraccascia[1], R. Bonfiglioli[2], E. Tabacchi[2], G. Argalia[1], L. Vetrone[1], C. Malizia[2], S. Fanti[2,3];

[1]Nuclear Medicine, DIMES, Alma Mater Studiorum, University of Bologna, Bologna, ITALY, [2]IRCCS Azienda Ospedaliero-Universitaria di Bologna, via Massarenti 9, Bologna, ITALY, [3]Nuclear Medicine, DIMES, Alma Mater Studiorum, University of Bologna, via Massarenti 9, Bologna, ITALY.

Aim/Introduction: Transthyretin-Cardiac Amylodosis (CA-ATTR) is a group of diseases caused by abnormal extracellular deposition of insoluble proteins that involve myocardium. Due to unknown calcium-mediated mechanism, scintigraphy with bone tracers like ^{99m}Tc-DPD, are used for non-invasive diagnosis of CA and are able to differentiate different subtypes with high diagnostic precision. Nowadays, mayor guidelines recommend performing ^{99m}Tc-DPD-SPECT/CT only in cases of proven Myocardical Uptake (MU), and there is no consensus about it's utility for evaluation of patient negative or doubtful at Planar Imaging (PI), especially in those patient with low mediastinal uptake. The aim of our study was to describe our experience with ^{99m}Tc-DPD-SPECT/CT in patient that resulted doubtful at Perugini Scoring (PS) with low grade (PS=1) at PI and to search for any clinical or technical factor related with mediastinal uptake in pts that were confirmed negative at the ^{99m}Tc-DPD-SPECT/CT. **Materials and Methods:** A retrospective study of pts who underwent ^{99m}Tc-DPD for clinical suspicion of CA-ATTR, was conducted. 99MTc-DPD bone scan was performed according standard procedures. In pts with PS=1 at PI a low-dose SPECT/CT was performed on chest. According to SPECT/CT images, pts were referred as negative (PS=0) in case of diffuse blood-pool activity, or doubtful (PS=1) in case of low MU with normal bone uptake. Records Criteria (RC) like age, gender, BMI, administered activity, uptake-time (in minutes) and the presence of minimal extravasation of ^{99m}Tc-DPD at images were collected whenever possible. Results: Out of 173 pts that underwent ^{99m}Tc-DPD bone scan from between January 2016 to February 2021, 60 pts performed a 99MTc-SPECT/CT for low mediastinal uptake: 49 pts were PS=0 and 11 pts had PS=1 for presence of true MU. RC were retrievable only in 37 pts (10 M and 27 F; mean age: 70,1 , mean BMI: 25,3, mean administered activity: 700,35 MBq, mean uptake time: 172,5', 99MTc-DPD extravasation reported in 21 cases). In pts reported PS=0 at SPECT/CT, we searched any statistical correlation, using logistic regression, with mean value of age, BMI, administered activity and uptake-time. However no statistical correlation was proved, with the lowest p-value (0,3037) observer with age. **Conclusion:** SPECT/CT has proven to be, in our experience, a useful tool to discriminate between negative and doubtful pts results on PI. Indeed,

we didn't find any correlation between faint mediastinal uptake and RC that could explain the presence of doubtful mediastinal uptake at PI. **References:** None.

EPS-016

Transient Ischemic Dilatation with Adenosine Tc-Sestamibi Stress: Prognostic Significance In Patients with Normal Myocardial Perfusion

A. Alhouri*, B. Baniissa, M. Safi, M. Akkawi, O. Obeidat, M. Juweid;*
University of Jordan, Amman, JORDAN.

Aim/Introduction: To determine the significance of transient ischemic dilatation (TID) in patients with normal perfusion on adenosine stress/rest. **Materials and Methods:** We analyzed 430 consecutive patients with normal perfusion on 2-day adenosine stress/rest 99mTc-sestamibi. A group of 70 patients with Framingham 10-year coronary heart disease risk < 10% was used to derive abnormal TID thresholds (derivation group). The significance of TID at these thresholds was validated in the remaining 360 patients (validation group) followed for cardiac events for 31.2 ± 9.7 (mean ± SD) months. Results: Transient ischemic dilatation in the derivation group was 1.05 ± 0.13. Three definitions of an abnormal TID were used: > mean + 2SD (TID ≥ 1.32), > mean + 1SD (TID ≥ 1.19) and a TID in the group's highest quartile (TID ≥ 1.15). Of the 360 validation group patients, 12 (3.3%), 48 (13.3%) and 70 (19.4%) had TID ≥ 1.32, 1.19 and 1.15, respectively. Age, gender, family history of coronary artery disease (CAD), known CAD, smoking, hypertension, diabetes, dyslipidemia, rest LVEF, post-stress LVEF, ΔLVEF, ≥ 5% or 10% decrease in LVEF did not predict TID ≥ 1.32. However, TID ≥ 1.19 was predicted by rest LVEF and ≥ 5% decrease in LVEF (P = 0.04 and 0.02, respectively) and TID ≥ 1.15 was predicted by ≥ 5% decrease in LVEF (P = 0.02). Cardiac event-free survivals were similar in patients with a TID ≥ and < 1.32 (P = 0.68), ≥ and < 1.19 (P = 0.40) and ≥ and < 1.15 (P = 0.79). **Conclusion:** Transient ischemic dilatation does not confer adverse prognosis in patients with normal perfusion on adenosine stress/rest 99mTc-sestamibi irrespective of the threshold used for its definition. **References:** None

EPS-017

Molecular imaging in diagnosis of cardiovascular and lung damage in patients with COVID-19

A. Kudryavtsev*, M. M. Beregov, A. K. Kondakov, D. S. Kharina, D. Y. Mosin, I. A. Znamenskiy, A. E. Nikitin;*
CCH of RAS, Moscow, RUSSIAN FEDERATION.

Aim/Introduction: Due to the spread of COVID-19, the number of patients with viral pneumonia undergoing myocardial SPECT/CT and PET/CT has increased. COVID-19 associated pneumonia can influence the results of molecular imaging tests and hence cause unnecessary treatment. **Materials and Methods:** 10 patients with a moderate course of COVID-19, aged 55 to 75 years (6 male, 4 female) without previously known cardiovascular pathology undergone PET/CT with FDG and SPECT/CT with 99mTc-MIBI in accordance with established guidelines [1]. Patients enrolled in this study were treated according to the guidelines approved by the Ministry of Health of the Russian Federation. A cardiac ECG-gated PET scan was performed after intravenous administration of 400-450 MBq FDG. SPECT scan was performed in rest state after intravenous administration of 250-400 MBq 99mTc-MIBI. FDG distribution was evaluated with the subsequent semi-quantitative assessment of its accumulation in pulmonary and myocardial tissue. In SPECT/CT study, myocardial perfusion, as well as a lung-to-heart ratio (LHR), were calculated in all patients. Results: The most remarkable feature of SPECT/CT with 18-FDG in patients with COVID-19 was increased LHR in 7 of 10 patients (mean 0.62, SD 0.1) due to inflammatory changes of pulmonary tissue. Those changes may simulate multivessel coronary artery disease (CAD) which usually causes LHR raise because of diffuse myocardial hypoperfusion [2]. Myocardial PET/CT however showed no significant reduction of FDG uptake and, therefore, no myocardial viability decline. The highest FDG uptake was found in pulmonary "ground glass" opacities and mediastinal lymph nodes which is a typical manifestation of viral pneumonia, including COVID-19 [3]. On the other hand, consolidation showed less FDG uptake, probably due to a decrease in an inflammatory response. **Conclusion:** In this study, we have found that myocardial SPECT/CT in patients with COVID-19 may lead to false-positive results in diagnostics of multivessel coronary artery disease due to increased uptake in pulmonary tissue, as it also manifests as the lung-to-heart ratio increase. FDG PET/CT may provide valuable diagnostic information about inflammatory process in lung parenchyma. **References:** [1] Castelluci P., Deandereis D., Krizan, A., Mirzaei, S., Prior J.,Sattler, B. European Nuclear Medicine Guide 2020, 2020; available at https://www.nucmed-guide.app/#!/home. [2] Kumar SP, Brewington SD, O'Brien KF, Movahed A. Clinical correlation between increased lung to heart ratio of technetium-99m sestamibi and multivessel coronary artery disease. Int J Cardiol. 2005;101(2):219-222. doi:10.1016/j.ijcard.2004.03.020 [3] Minamimoto R, Hotta M, Ishikane M, Inagaki T. FDG-PET/CT images of COVID-19: a comprehensive review. Glob Health Med. 2020;2(4):221-226. doi:10.35772/ghm.2020.01056

312

Wednesday, October 20 - Saturday, October 23, 2021

on-demand pool, release on Wednesday, October 20 at 09:00

e-Poster Presentation Session 2: Dosimetry

EPS-018

Potential Limitations of Established Blood-Dosimetry Models for Lu-177 Therapy

P. Ritt[1], C. Jobic[1], A. Grings[1], M. Beck[1], C. Schmidkonz[1], T. Kuwert[1], M. Uder[2], M. Brand[2];
[1]Clinic for Nuclear Medicine, Erlangen, GERMANY,
[2]Department of Radiology, Erlangen, GERMANY.

Aim/Introduction: DNA double-strand breaks (DSBs) in blood lymphocytes of radionuclide-treated patients can be quantified by γ-H2AX immunofluorescence microscopy to determine radiation-induced foci (RIF). Based on this, we compared excess RIF side-by-side in patients undergoing Lu-177-DOTATOC or - PSMA therapy for gaining insight into potential limitations of dosimetry models. **Materials and Methods:** We obtained venous blood samples from 48 patients subjected to Lu-177-radioligand therapy (DOTATOC, 26; PSMA, 22) to quantify blood lymphocyte RIF and blood activity concentration at various time points post injection (PI). Based on currently used standard dosimetry models [1], absorbed doses and dose rates to blood were derived from sequentially assessed blood activity concentrations and gamma camera imaging. Results: PI RIF counts were significantly higher than baseline values (0.25 ± 0.15), with a peak at 5 min (3.93 ± 2.51). RIF declined for subsequent time points. Compared with RIF counts of Lu-177-DOTATOC, those of Lu-177-PSMA were significantly higher at 5 min PI and significantly lower at 72 h PI (both $p<0.05$). These differences could not be fully explained by blood doses and dose rates, which were significantly higher for PSMA than for DOTATOC treatment at every time point. RIF counts overall correlated with dose rates across all time points (Pearson's $r=0.78$; $p<0.01$) and with absorbed dose until 4 h PI (Pearson's $r=0.42$; $p<0.01$). **Conclusion:** Although dose values generated by currently established blood dosimetry model correlated with RIF counts, the difference observed in DOTATOC and PSMA treatment groups was unexplained. Significantly more RIFs were found in Lu-177-DOTATOC patients, despite lower dose rates and blood doses, exposing a potential limitation of the dosimetry model. **References:** [1] Eberlein U, Nowak C, Bluemel C, Buck AK, Werner RA, Scherthan H, et al. DNA damage in blood lymphocytes in patients after 177Lu peptide receptor radionuclide therapy. Eur J Nucl Med Mol Imaging. 2015;42(11):1739-49.

EPS-019

Patient-specific dosimetric workflow with a reduced number of time-points for 177Lu treatments

L. Vergnaud[1], A. L. Giraudet[2], A. Moreau[2], T. Baudier[1], D. Kryza[2], J. N. Badel[2], D. Sarrut[1];
[1]Centre Léon Bérard / CREATIS, Lyon, FRANCE,
[2]Centre Léon Bérard, Lyon, FRANCE.

Aim/Introduction: Patients with unresectable neuroendocrine tumors can be treated by internal radiation therapy administrating 7.4 GBq of Lu177-labeled somatostatin analog. Image-based absorbed dose estimation to organs requires several time-points acquisitions but their number is limited by clinical and logistical constraints. The goal of this work was to propose an adaptive dosimetric workflow for estimating absorbed doses from a reduced number of acquisitions. **Materials and Methods:** Thirteen patients with neuroendocrine tumors received four injections of 7.4 GBq of ^{177}Lu-DOTATATE except one patient because of haematological toxicity. Three SPECT/CT acquisitions were performed after the first cycle at 1h, 24h and 96h or 144h and a single acquisition after three latter cycles at 24h for estimating absorbed doses by kidneys, liver and intrahepatic tumors, spleen and bone marrow. Monte Carlo simulations were used to estimate dose rates for each acquisition to take into account self- and cross- doses. These dose rates were then integrated at the organ level (ODR). Time dose rate curves (TDC) were fitted with a tri-exponential function to respect the patients' physiology. For cycles with less than three acquisitions, three methods were proposed and evaluated. If the acquisition at 24h of cycle 1 was missing, the ODR was approximated by the next first ODR at 24h scaled according to the injected activities at each cycle. When only one acquisition was available, two cases were distinguished. Absorbed doses were estimated from the TDC of a previous cycle for the same patient scaled to the ODR available. Otherwise, TDC of other patients were scaled to the ODR and their integrals were averaged to obtain absorbed doses as proposed by Jackson and al. (1) with time activity curves. Results: Estimated errors when the ODR at 24h was replaced was inferior to 15.9% except for one patient. With only one acquisition, the lowest error was obtained for acquisitions at 96h or 144h with two methods: less than 11% for liver and spleen and less than 20% for kidneys. These methods are being tested for bone marrow dose estimation. Absorbed doses estimated with this workflow were: 2.5±0.9 Gy (left kidney), 2.7±1.2 Gy (right kidney), 2.8±1.7 Gy (liver) and 3.4±1.6 Gy (spleen) all cycles taken together. **Conclusion:** The proposed workflow allows the estimation of organ doses from a reduced number of acquisitions for patients treated with ^{177}Lu. **References:** (1) Jackson and al. JNM 2020

EPS-020

Assessing neuroendocrine tumour response to peptide receptor radionuclide therapy with ^{177}Lu-DOTATATE using voxel-based dosimetry

L. Ram, S. Bissell, S. Hughes, E. Ross, I. Geh;
Queen Elizabeth Hospital Birmingham, Birmingham, UNITED KINGDOM.

Aim/Introduction: Peptide receptor radionuclide therapy (PRRT) with ^{177}Lu-DOTATATE is a standardised therapy administered over 4 cycles with 7400MBq given at each. The 2013/59/Euratom Directive requires that target radiation doses are individually planned. Compliance is achieved by performing retrospective dosimetry. This project aims to establish a clinical dosimetry service, calculate tumour absorbed dose (AD) and assess tumour response with radiological, biochemical and maximum standardised uptake value (SUVmax) data. **Materials and Methods:** Dosimetry was applied to 20 patients undergoing PRRT. After cycle 1, patients underwent quantitative SPECT/CT (QSPECT/CT) 4 hours post-administration and SPECT-only imaging on days 1, 4 and 7. After cycles 2-4, only QSPECT/CT was performed 4 hours post-administration meaning dosimetry could not be applied. Tumour deposits were selected based on RECIST criteria, maximum axial diameter (MAD) on the pre-PRRT contrast enhanced CT (CECT) of at least 20mm and SUV of at least 6. AD was calculated with voxel-based dosimetry for selected tumour deposits and both kidneys. Tumour SUVmax was calculated for each cycle. SUVmax values at cycle 1 were compared with tumour AD. MAD of tumour deposits were measured on pre- and post-PRRT CECTs. Biochemical data (chromogranin A (CgA) and 5-hydroxy-indole-acetic acid (5-HIAA)) were monitored for response. Results: Mean AD and SUVmax for 37 suitable tumour deposits were calculated across 18 patients: mean AD (± standard deviation) was 14.4(± 10.3)Gy, mean SUVmax was 21.4(± 11.6). There is weak correlation between AD and SUVmax (R=0.46). Mean kidney AD was 3.5(± 1.1)Gy for the left kidney and 3.9(± 1.3)Gy for the right; four-cycle mean AD estimates were 14.0Gy and 15.7Gy, respectively. Neither of these exceed the external beam radiotherapy (EBRT) dose limit of 23Gy. This limit has shown to be inappropriate for PRRT, however. Mean percentage change (MPC) of SUVmax between cycles 1 and 4 for 14 tumours was -19.8(± 18.2)%. MPC of MAD for 20 tumours was -6.8(± 9.3)%; this reduction in measurable size may explain the reduction in SUVmax. Biochemical levels also reduced: MPC for CgA was -12.8(± 37.5)% (8 patients) and MPC for 5-HIAA was -7.6(± 25.4)% (7 patients). **Conclusion:** Cycle 1 AD and SUVmax have been found for 37 tumour deposits. SUVmax in QSPECT/CT images should not be used to estimate tumour AD. Kidney AD does not exceed the 23Gy EBRT dose limit. Tumours respond to PRRT biochemically, physically and in terms of ^{177}Lu-DOTATATE uptake. Relationships between these parameters need further investigation. **References:** none

EPS-021

Experimental Validation of Monte Carlo Beta and Gamma Depth Dose and Bone Equivalent Attenuation for Lu-177

B. Van, Y. Dewaraja, J. Niedbala, M. Kazmierski, D. Hubers, S. Wilderman, J. Mikell;
University of Michigan, Ann Arbor, MI, UNITED STATES OF AMERICA.

Aim/Introduction: Dosimetry software, such as Monte Carlo (MC) codes for patient specific dose calculations, should be commissioned prior to implementation in the clinic. For low and medium energy beta emitters, this is challenging due to the short range of betas. We designed a simple 3D-printed phantom capable of both single radiochromic film (RF) absorbed dose measurements as well as reproducible depth dose (DD) measurements. These measurements were used to validate our dedicated radiopharmaceutical therapy Dose Planning Method (DPM) MC code. **Materials and Methods:** Liquid ^{177}Lu sources were distributed in either saline or bone equivalent (K2HPO4 salt) solution and injected into 3D-printed half-cylinders sealed with 25.4μm thick tape. RF strips were secured between 2 half-cylinders. For DD measurements five strips were placed back-to-back with activity in only one half-cylinder and secured against a water equivalent backing. For DD, the first measurement point was 179μ from the activity surface and subsequent measurements were additional multiples of 278μ. For bone equivalent measurements, a single strip of RF was positioned between both half-cylinders filled with activity. Films were removed after 48hour exposures and absorbed dose was measured using triple channel dosimetry that was calibrated using a 6MV beam. The average dose to the central 1cm^2 of each RF was used for validation and compared to DPM absorbed dose estimates scaled based on the injected activity. Results: The RF measured doses in the 2 sets of 5 films DD were on average 803, 160, 63, 51, and 49 cGy, respectively and both measurement runs showed excellent agreement with each other. Measured doses were within 0.2% to 8.6% of DPM at the 5 depths. All experiments measured less dose to the RF than predicted by DPM. MC predicted that absorbed dose from betas was 93%, 65%, 15%, 1.5% and 1.2% of the total (betas + others) going from the DD film closest to the ^{177}Lu to the furthest, indicating a large component of the beta dose was measured/validated across our design. For the measurement with bone liquid, the underestimation relative to DPM was 11.5%. **Conclusion:** We demonstrated direct validation of absorbed dose calculations with DPM for ^{177}Lu. Agreement between measurement and simulation was within 9% across all measured DD and 12% for ^{177}Lu in bone equivalent liquid. Simulation sensitivity to material composition/thickness is under investigation. The 3D-printed phantom designed for liquid sources demonstrate a practical setup for experimentally validating radiopharmaceutical dose calculation algorithms. **References:** none

EPS-022

Optimization of the voxel-based ^{90}Y-PET SIRT dosimetry: definition of clinical and technical margins around the anatomical target to establish the therapeutic reference isodose and DVHs of tolerance

C. Ouardek[1,2], N. Ghazzar[2], M. Bernardini[2];
[1]Université Grenoble Alpes, Grenoble, FRANCE, [2]Hôpital Européen Georges Pompidou, Paris, FRANCE.

Aim/Introduction: We recently acquired a software platform allowing the 3D personalized voxel-based calculations for SIRT treatments. The aim of this work was to define clinical and technical margins around the target volume (TV) and to correlate the therapeutic response with its isodose, as well as the observed side effects of OARs with their DVHs. These correlations will permit to establish a reliable dose-response relationship for SIRT treatments, as in external beam radiotherapy (EBRT), in term of therapeutic reference isodose for the TV and DVHs of tolerance for the OARs. **Materials and Methods:** First, using several ^{90}Y phantoms acquisitions we optimized reconstruction parameters for volume delineation and absolute quantification of ^{90}Y-PET to ensure accuracy of absorbed dose computation and reproducibility in the definition of volumes of interest (VOIs). Then, 15 patients were retrospectively analyzed: contrast enhanced CT (ceCT), ^{18}FDG-PET/CT and ^{90}Y-PET/CT series were co-registered to allow delineating anatomical volumes, the gross tumor volume (GTV), and functional target volume (FTV), respectively. Then, for the first time in the published literature to our knowledge, margins were added around GTV to define the clinical tumor volume (CTV), as in EBRT. Furthermore, technical differences in spatial resolution between the anatomical (CT) and functional (PET) images were taken into account. Dose maps were computed to obtain isodoses and DVHs metrics. Results: In the cohort of patients we retrospectively analyzed, we observed side effects, like radiation-induced failure (RIF) on gallbladder, lungs and healthy liver. The correlation between these side effects and the calculated DVHs on ^{90}Y-PET images will permit to establish the DVH of tolerance for one particular OAR to predict and reduce such complications in the future treatments. In the same way, the positive response to the treatment will be correlated with the TV isodose found on ^{90}Y-PET dose map to obtain the therapeutic reference isodose predicting the local response. **Conclusion:** 3D personalized voxel-based dose distribution, allowed to determined retrospectively the therapeutic reference isodose for the TV, and the DVHs of tolerance for the OARs in SIRT treatments. These metrics, as in EBRT, will allow optimization of the treatment planning and the prediction of the therapeutic local response in a more reliable way than the mean absorbed dose. Nevertheless, this retrospectively dosimetric analysis on a little cohort should be extended on a larger group of patients to achieve more robust references. **References:** None

EPS-023

Automatic evaluation of patient biokinetics based on hybrid planar/SPECT imaging using OEDIPE software for 3D dosimetry in radionuclide therapy

M. Bensiali[1], N. Anizan[2], S. Lamart[1], E. Davesne[1,3], D. Broggio[1], A. Desbrée[1], D. Franck[1];
[1]Institut de Radioprotection et de Sûreté Nucléaire (IRSN), Fontenay-aux-Roses, FRANCE, [2]Institut de Cancérologie Gustave Roussy, Villejuif, FRANCE, [3]INSTN, Gif-sur-Yvette, FRANCE.

Aim/Introduction: The OEDIPE software has been continuously developed and applied to carry out personalized 3D dosimetry using Monte Carlo simulation in nuclear medicine [1]. Further improvement of this software was necessary to account for the patient-specific biokinetics of radiopharmaceuticals, which may greatly influence patient absorbed dose. Therefore, new functionalities based on SPECT and planar (hybrid) images have been implemented in OEDIPE and validated. **Materials and Methods:** To quantify the biokinetics of the radiopharmaceutical, features based on the analysis of planar and SPECT images have been integrated into OEDIPE: (i) image registration with the voxel-phantom created from the patient anatomical image, (ii) extraction of counts from the SPECT image within each volume of interest (VOI) and (iii) projection of the VOIs onto the planar images to retrieve counts included in the projected regions. Activities in VOIs are calculated using the SPECT calibration factor defined by the user, eventually accounting for recovery coefficients. Counts from the planar images may be corrected from dead-time by user-defined values, and are converted to activities using the SPECT quantification data. Cumulated activities are calculated from fitting time-activity curves. To validate these developments, hybrid images of a JASZCZAK phantom containing spheres (1 mL to 16 mL) filled with I-131 were used. The estimated activities and cumulated activities were compared with the reference values. To evaluate the clinical applicability of this approach, time-integrated activity coefficients (TIACs) were estimated with OEDIPE using four planar and one SPECT images of a patient treated with I-131 for metastatic differentiated thyroid cancer. Results were compared with TIACs derived from the patient whole-body counting and the activities quantified from the SPECT image. Results: The activity at each time-point and cumulated activity estimated by OEDIPE in the phantom spheres agreed well with the reference values, with relative errors ranging from -11% to 10%. TIACs estimated in the patient lesions were comparable with those derived from the whole-body counts, with less than 10% difference. **Conclusion:** These new features in OEDIPE enable automatic evaluation of patient-specific biokinetics from a series of planar and SPECT (hybrid) images, and thus improvement of the personalization of dose estimation in nuclear medicine. **References:** [1] A. Petitguillaume

et al, "OEDIPE, a software for personalized Monte Carlo dosimetry and treatment planning optimization in nuclear medicine: Absorbed dose and biologically effective dose considerations," Radioprotection, vol. 49, no. 4, pp. 275-281, 2014, doi: 10.1051/radiopro/2014021.

EPS-024

Voxel-wise Dosimetry of [^{68}Ga]Ga-PSMA-11 and Comparison With the Literature

J. Morgado[1], P. Ferreira[2], S. Di Maria[3], F. P. Oliveira[2], R. Vigário[4], D. C. Costa[2];
[1]Institute for Systems and Computer Engineering, Technology and Science, Porto, PORTUGAL, [2]Champalimaud Centre for the Unknown, Champalimaud Foundation, Lisbon, PORTUGAL, [3]Centre for Nuclear Sciences and Technologies, Lisbon, PORTUGAL, [4]NOVA School of Science and Technology, Almada, PORTUGAL.

Aim/Introduction: While the use of radioactively labeled drugs for diagnostic purposes brings tremendous benefits to the population, the associated risks due to ionizing radiation effects make it necessary to protect patients from potential harm. ^{68}Ga-prostate-specific membrane antigen positron emission tomography/computed tomography ([^{68}Ga]Ga-PSMA-11 PET/CT) imaging has rapidly gained notoriety in the nuclear medicine (NM) field. Therefore, knowledge of clinical safety and dosimetry of this radiopharmaceutical is crucial for its routine use in clinics. This study aimed to perform patient-specific dosimetry using the medical internal radiation dose (MIRD) method at the voxel level in the kidneys, liver, spleen, and red bone marrow. **Materials and Methods:** Whole-body PET/CT images of six prostate cancer patients were acquired after a single injection of [^{68}Ga]Ga-PSMA-11. All PET images were registered in the same coordinate space and calibrated for radioisotope concentration at the time of image acquisition. The organs of interest were manually segmented based on CT images, and the corresponding masks were resampled to the PET voxel size. The voxel S-values were computed using the Monte-Carlo N-Particle transport 6.1 code. The convolution of the S-values with the PET activity images resulted in absorbed dose rate distributions. These were subsequently time-integrated, taking into account all decay events to obtain the voxel-wise absorbed dose distributions. Dose values were computed and compared with the literature. Results: In our group of patients, the kidneys received the highest overall mean and median absorbed doses (mean: 0.0561 mGy/MBq, median: 0.0499 mGy/MBq), whilst the red bone marrow had the lowest values (mean: 0.0015 mGy/MBq, median: 0.0013 mGy/MBq). Tracer uptake in the liver resulted in a mean and median absorbed dose of 0.0132 mGy/MBq and 0.0126 mGy/MBq, respectively. Mean and median spleen doses were 0.0114 mGy/MBq and 0.0102 mGy/MBq, respectively. Our voxel-wise dosimetry values are significantly lower than those reported in the literature, ranging from -38.1% (in the liver) to -91.3% (in the red bone marrow). **Conclusion:** Our voxel-based approach considers the non-uniform biodistribution of the radiopharmaceutical in organs, rather than conventional organ-based dosimetry estimates, which are likely to overestimate absorbed dose values. The reasonably low absorbed doses calculated in the four organs studied corroborate the use of [^{68}Ga]Ga-PSMA-11 in NM clinics routine imaging in terms of radiation safety. **References:** None

EPS-025

Accuracy and reproducibility assessment of commercially available Dosimetry Toolkit software: A phantom study

A. Nautiyal[1,2], A. K. Jha[1,2], A. Konuparamban[1,2], S. Mithun[1,2], V. Rangarajan[1,2];
[1]Tata Memorial Hospital, Mumbai, INDIA, [2]Homi Bhabha National Institute(HBNI), Deemed University, Mumbai, INDIA.

Aim/Introduction: Increasing role of radionuclide therapy in oncology has increased the necessity of dosimetry software in nuclear medicine. Several vendors have developed dosimetry softwares which is commercially available for use. These softwares need to be validated properly prior to its implementation in routine clinical application. The aim of our study was to validate commercially available Dosimetry Toolkit software installed on Xeleris 4.1 workstation prior to its routine clinical applications. **Materials and Methods:** Dosimetry Toolkit installed on Xeleris 4.1 workstation calculates normalized cumulated activity (NCA) by using three methods i.e. 1) Planar, 2) SPECT and 3) Hybrid methods. Planar method requires sequential planar studies; SPECT method requires sequential SPECT/CT studies and Hybrid method requires sequential planar studies and single point SPECT study acquired on Discovery 670 SPECT/CT scanners. We performed a Toolkit validation study for planar method using NEMA IQ PET phantom and Lutetium-177 isotope. Largest sphere (37mm) of IQ phantom was used to mimic an organ. Phantom was prepared to create a target-to-background activity concentration ratio 8:1 (69.90 kBq/ml: 8.74 kBq/ml). Anterior & posterior planar views images were acquired at 0, 90 and 180 h post phantom preparation using Discovery 670 pro SPECT/CT scanner. Sensitivity of the SPECT system for Lutetium-177 was calculated as per vendor protocol using Petri dish and prescribed amount of Lutetium-177 activity. NCA was calculated by the mono-exponential fitting method using semi-automated processing on Dosimetry Toolkit software for 10 times. Similarly, NCA was also theoretically calculated using physical half-life and initial activity (NCA = 1.44 * T_p*As_0/A_0 ; where, T_p=Physical half life of Lutetium-177, As_0= initial activity in sphere, A_0 = Total initial activity in phantom) and considered as gold standard. NCA calculated by using Toolkit was compared with the gold standard. Simultaneously, reproducibility was assessed by calculating coefficient of variance (COV) for

repeated measurements using Toolkit. Results: Standard NCA value derived from theoretical calculation was 4.94 h. Measured NCA values for Toolkit method was 3.14 ± 0.03 h. The Toolkit underestimates NCA by 37% in comparison with gold standard. Reproducibility study shows COV of 0.9%. **Conclusion:** Our study shows that the Toolkit method generates the reproducible results and underestimates NCA in comparison with gold standard. **References:** None

EPS-026

PET-CT-based dosimetry for Y-90 Selective Internal Radiation Therapy (SIRT)

M. Kuc[1], A. Budzyńska[2,3], A. Kubik[2], M. Maciak[1], M. Konior[4], P. Piasecki[5], M. Dziuk[2,3], E. Iller[4];
[1]Radiological Metrology and Biomedical Physics Division (H2), National Centre for Nuclear Research, Otwock, POLAND, [2]Department of Nuclear Medicine, Military Institute of Medicine, Warsaw, POLAND, [3]Affidea Mazovian PET/CT Medical Centre, Warsaw, POLAND, [4]National Centre for Nuclear Research, Radioisotope Centre POLATOM, Otwock, POLAND, [5]Department of Interventional Radiology, Military Institute of Medicine, Warsaw, POLAND.

Aim/Introduction: The aim of the work is elaboration of a dosimetry method that allows the verification of the therapeutic doses evaluation in SIRT (Selective Internal Radiation Therapy) therapy. The method consists in analysing the patient's PET-CT images after administering a radiopharmaceutical in the form of Y-90 microspheres. The administered isotope, apart from beta$^-$ decay, shows beta$^+$ radioactivity, the share of which is high enough to be useful in the PET-CT examination. The subject of the presentation is the analysis of the distribution of activity and dose absorbed in a dedicated water phantom with vials containing $^{90}YCl_3$ solution with volumes and activities similar to the therapeutic ones. **Materials and Methods:** For the purposes of the work, a water phantom was designed and constructed, in which small-volume vials were placed to test the scanner's response to Y-90 activities. Dedicated software was developed for the analysis of image data. Using the software, the user can determine the spatial distribution of the activity and the absorbed dose over a wide area, and for specific volume of interest the absorbed dose and the homogeneity of the activity distribution. The development of the tool is consulted with the clinical community so that it can ultimately be used not only for scientific purposes, but also clinically. The presented results relate to measurement sessions for various concentrations of the Y-90 solution from 1 to 50 MBq/ml and various vial volumes from 2 to 25 ml. Additionally, the dependence of the quality of determining the sensitivity of the apparatus on the duration of the PET scan was investigated. Results: Processing the image data into the spatial distribution of activity required the development of DICOM files using Python3 libraries, including PyDicom, PyQtGraph and NumPy. The dependence of the apparatus sensitivity on the activity and volume of the samples was determined. The average sensitivity of the apparatus for 2 ml vials with an activity of 21 MBq was approximately 67% ± 6% and increased with increasing volume. The standard deviation of the apparatus sensitivity values for the above activities and volumes did not decrease with increasing PET scan time. **Conclusion:** The result of the work is the demonstration of a dosimetric method based on PET-CT examination, which will increase the accuracy of the absorbed dose assessment. The method consists in determining the activity of the Y-90 solution inside the analysed volume and converting this value into the absorbed dose. **References:** none

EPS-027

Independent Validation of Monte Carlo Simulations within In-House Dosimetry Software Using ICRP 110 Phantoms

P. Gape, D. Rushforth, J. Gear, G. Flux;
The Royal Marsden Hospital NHS Foundation Trust, Sutton, UNITED KINGDOM.

Aim/Introduction: This work aimed to validate voxel-based dosimetry software, incorporating the EGSnrc Monte Carlo code, developed as a 3D Slicer application. A secondary aim was to assess the need for full Monte Carlo simulations of beta decay in Ga-68 dosimetry. **Materials and Methods:** Photon simulations of a spherical activity distribution within a unit density scatter medium were modelled. Mono-energetic photons (140 - 662 keV) were simulated for spheres of 1 - 1000 ml. The calculated absorbed fractions were compared to published data [1]. Similar simulations were performed for a uniform distribution of Ga-68 within a 100 ml sphere. Beta decay was also modelled and calculated S-values were compared with published values form OLINDA v1.1 and IDAC. Ga-68 particle transport was finally simulated within the ICRP 110 Adult Female phantom for a series of organs (liver, kidneys and spleen). Data were simulated using the full beta decay and simulating only the photon transport (assuming local deposition of the beta particles). Absorbed doses were calculated to the source organ and the four organs receiving the highest cross-dose. These results were compared against those of the OpenDose collaboration [2]. Results: For mono-energetic photons, absorbed fractions were found to agree to within 2.2%. The calculated S-value for the Ga-68 sphere was within 3.4% and 2.2% of the respective OLINDA and IDAC S-values. For simulations within the ICRP phantom, a full simulation gave results to within 1.2% (self-dose) and 2.8% (cross-dose) of that of the Open Dose collaboration. A partial simulation, assuming only local deposition of the energy of the beta particles, gave results within 6.1% (self-dose) and 32.1% (cross-dose). **Conclusion:** Good agreement was demonstrated between the in-house software and published results, demonstrating suitability for future use. The value of

full beta particle simulation is demonstrated, particularly for cross-dose. Further work will extend validation to additional isotopes. **References:** 1. Stabin, M.G. and M.W. Konijnenberg, J Nucl Med, 2000. 41(1)(0161-5505). 2. Chauvin, M., et al., Journal of Nuclear Medicine, 2020. 61(10): p. 1514.

EPS-028

Dosimetry of iodine-125 eye plaque in brachytherapy of retinoblastoma tumor in animal model of rabbit

S. Moradi[1], S. Sheibani[1], M. Mokhtari Dizaji[2], F. Ghassemi[3], M. Arjmand[3];
[1]Radiation Application Research School, Nuclear Science and Technology Research Institute, Tehran, IRAN, ISLAMIC REPUBLIC OF, [2]Department of Medical Physics, Faculty of Medical Sciences, Tarbiat Modares University, Tehran, IRAN, ISLAMIC REPUBLIC OF, [3]Eye Research Center, Farabi Eye Hospital, Tehran University of Medical Sciences, Tehran, IRAN, ISLAMIC REPUBLIC OF.

Aim/Introduction: The aim of this study was to estimate the dose of iodine-125 plaque in brachytherapy treatment of ocular tumors of retinoblastoma for performing animal experiments of rabbits. **Materials and Methods:** In this study, autoradiographic test was performed using EBT3 Gafchromic film. In these experiments, the films were irradiated on eye plaque with diameter of 10mm containing five ^{125}I seeds in two positions (0.5 and 3mm from the inner surface of plaque). Also, the dose rate calculations were estimated at distances up to 10mm which were obtained from plaque simulator software in this study [1]. First, the experimental dose rate was obtained by film and compared with the dose rate values obtained from Sagoo et al [1]. In this study, the activity value of each seed and the total activity of plaque was 2.38mCi and 11.9mCi, respectively. Results: The dose rate was extracted using film at distances of 0.5 mm and 3 mm from the inner surface of the ocular plaque, was equal to 0.140 Gy/h.mCi and 0.078 Gy/h.mCi, respectively. While the dose rate using plaque simulator software obtained from Sagoo et al [1] at distances of 0 and 3 mm is equal to the value of 0.148 Gy/h.mCi and 0.069 Gy/h.mCi, respectively, which it almost corresponds to the dosimetry results of the film. Therefore, to apply a specified dose at a definite distance, the time of implantation of ocular plaque can be estimated using these dose rates. In this study, the time required to implant ocular plaque on the eyes of rabbits was estimated using these dose rate values [2]. **Conclusion:** The results of this study showed that the difference between the experimental dose rate with the results of the calculations of plaque simulator software obtained from the reference [1] is equal to 11%, which is an acceptable difference and is consistent with the reference report [3]. **References:** 1. Sagoo MS, Shields CL, Mashayekhi A, Freire J, Emrich J, Reiff J, Komarnicky L, Shields JA. Plaque radiotherapy for choroidal melanoma enerireling the optic disc. Arch Ophthalmol 2007; 125(9): 1202-1209. 2.Moradi S, Mokhtari-Dizaji M, Ghassemi F, Sheibani Sh, Asadi Amoli F. Increasing the efficiency of the retinoblastoma brachytherapy protocol with ultrasonic hyperthermia and gold nanoparticles: a rabbit model. International Journal of Radiation Biology, 2020; 96(12): 1614-1627. 3. Krintz A, Hanson WF, Ibbott GS, Followill DS. Verification of plaque simulator dose distributions using radiochromic film. Med Phys 2002; 29(6): 1220-1221.

EPS-029

Retrospective Single Time Point Spinal cord and Lesional Dosimetry for Radioiodine Treatment of Thyroid Cancer with High-Uptake in Vertebral Lesions

R. Gregory[1], H. McMeekin[1,2], R. Lewis[1], K. Beaton[3], M. Burniston[1];
[1]Barts Health NHS Trust, London, UNITED KINGDOM, [2]Hermes Medical Solutions Ltd., London, UNITED KINGDOM, [3]Barking, Havering and Redbridge University Hospitals NHS Trust, Barking, Havering and Redbridge, UNITED KINGDOM.

Aim/Introduction: For radioiodine treatment of thyroid cancer it is assumed that due to the short I-131 beta particle range, only organs that physiologically uptake the radioiodine are at risk of radiation damage. However organs at risk may receive a significant radiation dose from lesions adjacent to them. This case based-study originated from concern over radiation exposure of the spinal cord from radioiodine treatments with high uptake in lesions in the vertebral bodies, in planning subsequent external beam radiotherapy (EBRT) to treat cord compression from a vertebral lesion. Molecular radiotherapy dosimetry is not in routine clinical practice in this centre. Therefore based on the available patient data and resources within the department retrospective absorbed radiation dose estimates were made. **Materials and Methods:** All calculations had to be made on the single-time point SPECT/CT scan acquired as standard of care 2 days after each I-131 treatment. Quantitative SPECT reconstruction was performed using Hybrid Recon™ (Hermes Medical Solutions). Published Medical Internal Radiation Dose (MIRD) voxel S-values were used in a spread sheet, along with the measured activities to estimate absorbed doses in 6mm voxels around the lesions[1]. Hermes Voxel Dosimetry was also used to create Monte-Carlo based dose maps of the SPECT/CT scans. Oversized volumes-of-interest (VOIs) were used to determine the lesions' activities. These activities were constrained within VOIs defined about the lesions' contours on the CTs for dosimetry calculations. The same activities and CT volumes were used for each method. These estimates were summed over the 6 therapies. Results: The maximum cumulated absorbed radiation dose to the spinal cord was measured adjacent to a T11 vertebral body, at 6.9 Gy and 4.6 Gy using the voxel S-values and Hermes dosimetry package respectively, assuming a 2 day effective half-life. The T11 lesion estimated cumulated dose was 236.5 Gy and 174.9 Gy using the voxel S-values and the dosimetry package respectively, assuming a 2 day effective half-life. These doses would be a factor of 2.5 times higher if

the effective half-life of 8 days (the physical half-life of I-131) were assumed. **Conclusion:** The two methods gave radiation absorbed dose estimates of the same order of magnitude showing a measurable total absorbed dose to the spinal cord, of up to 17.3 Gy. The significance of these absorbed dose estimates compared to the effective EBRT dose is yet to be determined. **References:** 1. MIRD pamphlet 17

512

Wednesday, October 20 - Saturday, October 23, 2021

on-demand pool, release on Wednesday, October 20 at 09:00

e-Poster Presentation Session 3: More on Infection & Inflammation Imaging and NM in COVID-19

EPS-030

Reliability of ^{18}F-FDG PET/CT qualitative and semi-quantitative analysis in patients with suspicion of cardiac implantable electronic device infection

V. Lavelli, R. Ruta, F. Iuele, A. G. Nappi, A. Gaudiano, A. R. Pisani, G. Rubini;
Section of Nuclear Medicine, DIM, University "Aldo Moro", Bari, ITALY.

Aim/Introduction: Cardiac implantable electronic devices infection (CIEDI) is a frequent sequela in clinical experience and generally requires surgical CIED removal. Early diagnosis is of primary importance in order to promptly define the most accurate and specific therapeutic plan for each patient. Whole-body ^{18}F-FDG-PET/CT plays an important role in the management of patients with suspected CIEDI, allowing to detect even eventual septic dissemination. Several semi-quantitative parameters have been proposed in disease assessment, but a unique value has not been defined yet.This study aims to assess the ^{18}F-FDG-PET/CT reliability in the early diagnosis of CIEDI by considering the consistency of different semi-quantitative parameters. **Materials and Methods:** We retrospectively evaluated 35 patients with clinical suspicion of CIEDI who referred to our Nuclear Medicine Unit to perform ^{18}F-FDG-PET/CT. Microbiological results after CIED removal and/or clinical follow-up, considered as reference gold-standard, identified two groups (CIEDI+/CIEDI-). Both qualitative and quantitative analysis were performed on PET images. The following semi-quantitative PET/CT parameters were collected: SUV_{max}, semi-quantitative ratio (SQR) and target-to-background ratio (TBR). ^{18}F-FDG-PET/CT sensibility, specificity, positive predictive value (PPV), negative predictive value (NPV) and diagnostic accuracy (DA) were calculated. T-student's test was performed to establish if a statistically significant difference existed between each semi-quantitative parameter into two groups. ROC curves were employed in order to estimate the best semi-quantitative parameters cut-off values able to predict CIEDI. Results: ^{18}F-FDG-PET/CT resulted positive in 25/35 patients (71.4%) and negative in the remnants 10/35 (28.6%). Considering the gold standard, among positive PET, 22/25 (88%) were true positive while 3/25 (12%) were false positive; among negative PET, 3/10 (30%) were false negative, while the remnants 7/10 (70%) true negative. Se, Sp, PPV, NPV and DA of ^{18}F-FDG PET/CT resulted 95.7%, 75%, 88%, 90% and 88.6% respectively. After ROC curve analysis, exploratory cut-off values resulted: 2.56 for SUV_{max} (AUC=0.853; ES=0.073; CI=0.210% to 0.496; p<0.05); 3.37 for SQR (AUC=0.808; ES=0.093; CI=0.126% to 0.490; p<0.05); 1.20 for TBR (AUC=0.851; ES=0.084; CI=0.187% to 0.516; p<0.05). A statistically significant difference resulted for the mean value of SUV_{max}, SQR and TBR in patients with CIEDI+ and CIEDI- (p<0.05). **Conclusion:** Our results confirm the role of ^{18}F-FDG-PET/CT in the management of patients with suspicion of CIEDI and its reliability in the early diagnosis. In addition to SUV_{max}, other semi-quantitative parameters could be used as suggestive of clinical outcome. Further studies are mandatory to assess the accuracy of these results in larger populations and to standardize these parameters. **References:** None.

EPS-031

Role Of [^{18}F] FDG PET/CT In Infective Endocarditis On Prosthetic Valve And Intracardiac Devices

N. Alvarez Mena[1], C. Ponce Herrera[2], A. Gutiérrez Cardo[2], S. Martín Aguilar[2], M. Nicolás Aguado[2], E. Espinosa Muñoz[2], V. Marín Parrilla[2], D. Ramírez Ocaña[2], M. Puentes Zarzuela[2];
[1]Hospital Clínico Universitario de Valladolid, Valladolid, SPAIN,
[2]Hospital Regional Universitario de Málaga, Málaga, SPAIN.

Aim/Introduction: In the diagnosis of infective endocarditis (IE), the new modified Duke criteria of the European Society of Cardiology (ESC) 2015 include prosthetic perivalvular anomalous activity in [^{18}F]FDG PET/CT as the major criterion in a prosthesis implanted more than 3 months ago. Our objective is to assess the diagnostic yield of [^{18}F]FDG PET/CT in this disease. **Materials and Methods:** Retrospective series of 31 patients with suspected infective endocarditis (IE) who were performed [^{18}F]FDG PET/CT between June 20th of 2017 and March 25th of 2021.Variables such as sex, age, site of infection, semi-quantification of uptake (median SUVmax and median SUVratio of area under suspicion/mediastinal blood pool), classification according to modified Duke criteria, result of [^{18}F]FDG PET/CT and classification according to the new modified Duke criteria from ESC 2015 were analyzed. Results: 61% males. Median age: 69 years (4-86). 28 with suspected prosthetic valve infection and 3 in pacemaker leads. PET+: median SUVmax 5.30(3.27-11.96); median SUVratio 2.39(1.35-4.24). Inconclusive PET: median SUVmax 4.57(3.07-21.91); median SUVratio 2.15(1.68-3.69).Classification according to modified Duke criteria: 12 definite(39%), 12 possible(39%) and 7 rejected(22%). [^{18}F]FDG PET/CT shows positivity in 13 patients (4 with inconclusive echocardiography). 6

inconclusive PET (2 with surgery<3 months and 4 suboptimal preparation), although 2 presented vascular phenomena. Vascular phenomena in 6 patients: spondylodiscitis(2), pulmonary embolisms(2) and cerebral, splenic and/or renal embolisms(2). Other significant findings: 4 with intestinal uptake (1 rectal adenocarcinoma and 1 tubulovillous adenoma in histology), 1 thyroid nodule (papillary carcinoma in histology) and 1 with bilateral pulmonary infection. Classification according to new modified Duke criteria from ESC 2015: -In 12 possible: 4 definite with PET+(3 confirmed by echocardiography and 1 vegetation PCR (T. Whipplei)). 5 were ruled out after PET-. 3 inconclusive but vascular phenomena.-In 12 definite: support for diagnosis in 8. Negative in 2 in relation to good therapeutic response(radiological concordance). 2 inconclusive/negative but vascular phenomena.-In 7 rejected: 3 possible.That means that:14 defined(45%), 6 possible(19%) and 11 rejected(36%).Therefore, in our sample there is a reclassification of up to 45% of all patients (14/31), S=86%, E=100%, PPV=100%, NPV=92%. **Conclusion:** [^{18}F]FDG PET/CT is a tool of suitable diagnostic value in prosthetic valve IE and in intracardiac devices, increasing sensitivity of modified Duke criteria. In the cases of possible IE a negative PET/CT safely rules out the infectious diagnosis, leading to a great clinical impact by avoiding prolonged admissions, with unnecessary antibiotic and surgical treatment. Furthermore, whole-body imaging provides additional information of clinical relevance. **References:** none

EPS-032

Semiquantitative [^{18}F] FDG PET/CT Analysis In infective Endocarditis On Prosthetic Valve And Intracardiac Devices

N. Alvarez Mena[1], C. Ponce Herrera[2], A. Gutiérrez Cardo[2], S. Martín Aguilar[2], M. Nicolás Aguado[2], E. Espinosa Muñoz[2], V. Marín Parrilla[2], D. Ramírez Ocaña[2], M. Puentes Zarzuela[2];
[1]Hospital Clínico Universitario de Valladolid, Valladolid, SPAIN, [2]Hospital Regional Universitario de Málaga, Málaga, SPAIN.

Aim/Introduction: Our objective is to analyze the pathological uptakes found in [^{18}F]FDG PET/CT on valve prostheses and intracardiac devices when infective endocarditis is suspected. **Materials and Methods:** Retrospective series of 31 patients with suspected infective endocarditis (IE) who were performed [1^{8}F]FDG PET/CT between June 20th 2017 and March 25th 2021.Variables such as age, sex,site of infection,[^{18}F]FDG PET/CT result, uptake pattern(focal or diffuse), semi-quantification of uptake (median SUVmax of the area under uptake, median SUVratio of lesion-to-mediastinal blood pool and median SUVratio of lesion-to-liver) and their correlation with the definitive diagnosis of IE were analyzed. Results: Median age: 69 years(4-86).61% males.28 with suspected prosthetic valve infection and 3 in pacemaker leads.[^{18}F]FDG PET/CT was positive in 13 patients:4 inconclusive echocardiography and 1 negative blood cultures. 6 inconclusive PET:2 surgery<3 months and 4 suboptimal preparation, presenting 2 blood cultures(-).Focal uptake pattern in 12 patients (11 PET+). Diffuse in 7 patients (5 inconclusive PET). In all of them a persistence of the uptake in the uncorrected image is observed.1)PET+(42%):-Median SUVmax 5.30(3.27-11.96):focal 5.37;diffuse 4.70. -Median SUVratio of lesion-to-mediastinal blood pool 2.39(1.35-4.24):focal 2.62;diffuse 2.00. -Median SUVratio of lesion-to-liver 1.33 (0.81-2.42):focal 1.33;diffuse 1.18.2) Inconclusive PET(19%):-Median SUVmax 4.57(3.07-21.91):focal 4.73;diffuse 4.41.-Median SUVratio of lesion-to-mediastinal blood pool 2.15(1.68-3.69):focal 2.49; diffuse 1.81.-Median SUVratio of lesion-to-liver 1.37(0.94-1.97):focal 1.58; diffuse 1.15.Therefore, in the ROIs analyzed, we found a median SUVmax 4.73 (3.07-21.91). The distribution according to percentile(p):SUVmax 4.10 (p25),SUVmax 4.73 (p50) and SUVmax 6.82 (p75).89% of patients with PET uptakes show hypermetabolic foci with SUVmax>SUVmax in liver. However, only 21% of them doubled their uptake (3 confirmed by PET+ and 1 inconclusive PET by surgery<3 months although finally IE confirmed by echocardiography).Taking a value of SUVmax 5.50 as a cut-off point: S=83%,E=100%,PPV=100%,NPV=50%. In addition, of the 6 cases with inconclusive PET by visual analysis,3 of them had a diffuse pattern and SUVratio>median SUVratio of PET+ in our sample. Finally, IE was confirmed by echocardiography(2) and vegetation culture(1). **Conclusion:** According to our results, higher uptakes and focal distribution are more frequently associated with infection, achieving a specificity of 100% for a SUVmax cut-off value around 5.50 in our sample. However, these results must be interpreted with caution due to the limited number of patients studied. Furthermore, due to the distribution of the SUVmax value in the sample, it would be appropiate a combined assessment with other PET parameters (SUVratio, uncorrected image) as well as other diagnostic parameters, being particularly useful in inconclusive diagnosis. **References:** none

EPS-033

The effectiveness of the combination of extended fasting with dietary manipulation for suppressing physiologic myocardial 18-fluorodeoxyglucose uptake in patients undergoing positron emission tomography for sarcoidosis

A. Georgakopoulos[1], E. Manali[2], A. Papaioannou[2], H. Gialafos[3], M. Metaxas[4], L. Kolilekas[5], S. Papiris[2], S. Chatziioannou[1,4];
[1]2nd Department of Radiology, General University Hospital "Attikon", Medical School, National and Kapodistrian University, Athens, GREECE, [2]2nd Pulmonary Medicine Department, General University Hospital "Attikon", Medical School, National and Kapodistrian University, Athens, GREECE, [3]Aiginitio Hospital, Medical School, National and Kapodistrian University, Athens, GREECE, [4]Foundation for Biomedical Research of the Academy of Athens, Nuclear Medicine Division, Athens, GREECE, [5]7th Pulmonary Department, Athens Chest Hospital "Sotiria", Athens, GREECE.

Aim/Introduction: Optimal patient preparation is essential when using 18-fluorodeoxyglucose (^{18}F-FDG) positron emission tomography/ computed tomography (PET/CT) to evaluate for cardiac sarcoidosis. Unfortunately, despite the several methods that have been proposed to achieve suppression of physiologic ^{18}F-FDG uptake, approximately 30% of potential cardiac sarcoidosis patients have an inconclusive nondiagnostic scan. The aim of this study is the evaluation of the efficacy of prolonged fasting combined with a low-carbohydrate high-fat diet for suppression of physiologic myocardial ^{18}F-FDG uptake, in patients undergoing PET/CT for sarcoidosis. **Materials and Methods:** ^{18}F-FDG PET/CT was performed prospectively in consecutive patients with biopsy proven sarcoidosis, following adequate preparation with low-carbohydrate, high-fat diet for 24 hours, followed by 18 hours of fasting to suppress radiotracer's uptake by normal myocardial cells. Blood glucose levels was < 180 mg dL^{-1}in all patients prior to the injection. A whole body PET/CT scan (WBS) was obtained in order to reveal the total metabolic active disease followed by a 10 min cardiac extra bed scan. For the evaluation of cardiac images we used a visual interpretation with three imaging patterns: no ^{18}F-FDG uptake, diffuse uptake and focal ^{18}F-FDG uptake. The presence of focal ^{18}F-FDG uptake was consistent with cardiac inflammation from sarcoidosis while diffuse uptake was attributed to poor suppression of normal myocardial glucose uptake. Results: Study included 195 Caucasian sarcoidosis patients, median age (IQR) of 51 years (41-60), 51.8% females. Absence of ^{18}F-FDG uptake by the myocardium was obtained in 181 (92.8%) of the patients. In 14/195 patients a diffuse radiotracer uptake in the left ventricle was observed possibly due to incomplete preparation. Findings compatible with myocardial involvement were observed in 21/195 (10.8%) of patients with at least one focal radiotracer uptake. **Conclusion:** Prolonged fasting protocol combined with a low-carbohydrate, high-fat diet seems to be very effective for suppressing physiologic myocardial ^{18}F-FDG uptake in patients undergoing PET/CT for cardiac sarcoidosis. **References:** 1. Tang R, Wang JT, Wang L, Le K, Huang Y, Hickey AJ, Emmett L. Impact of Patient Preparation on the Diagnostic Performance of 18F-FDG PET in Cardiac Sarcoidosis: A Systematic Review and Meta-analysis. Clin Nucl Med. 2016;41(7):e327-39. 2. Maccarone MT. FDG-PET Scan in Sarcoidosis: Clinical and Imaging Indications.Curr Med Imaging Rev. 2019;15(1):4-9.

EPS-034

Lung Segmentation and Measurements of Pulmonary Metabolic Activity with FDG-PET/CT is Reproducible in Patients with COPD

A. Dogan[1,2], T. Christensen[3], T. Jensen[1], O. Hilberg[4], C. Juhl[1,5,2], S. Hess[6,2];

[1]Department of Medicine, Hospital South West Jutland, Esbjerg, DENMARK, [2]Department of Regional Health Research, Faculty of Health Sciences, University of Southern Denmark, Odense, DENMARK, [3]Department of Clinical Engineering, Region of Southern Denmark, Esbjerg, DENMARK, [4]Department of Medicine, Lillebaelt Hospiltal, Vejle, DENMARK, [5]Steno Diabetes Center, Odense, DENMARK, [6]Department of Radiology and Nuclear Medicine, Hospital South West Jutland, Esbjerg, DENMARK.

Aim/Introduction: The degree of pulmonary inflammation in chronic obstructive pulmonary disease (COPD) and any changes following successful or failed intervention may be difficult to ascertain, especially in pharmacologic trials. Despite increasing use of FDG-PET/CT in a multitude of infectious and inflammatory settings, the use in COPD is still limited. One potential advantage is the possibility to assess the degree of metabolic activity as a surrogate for pulmonary inflammation, but limited data are available on quantification and reproducibility of lung segmentation. The aim of this study was to investigate the reproducibility of quantitative measures of pulmonary inflammation by FDG-PET/CT in people with COPD. **Materials and Methods:** As part of a randomized double-blinded, placebo-controlled pharmacological trial of a potential novel weight-reducing and anti-inflammatory drug, 27 COPD-patients (13 receiving treatment and 14 receiving placebo), underwent 4D-respiratory-gated FDG-PET/CT before (scan one) and after (scan two) treatment on a Discovery 710(GE Healthcare) PET/CT. Using AW-server 2.0 (GE Healthcare) a medical doctor and a physicist blinded to all information independently segmented the lungs from the CT images and obtained mean standard uptake values (SUVmean) corrected for lean-body-mass in the phase-matched PET images of the whole segmented lung volume and total lesion glycolysis (TLG; SUVmean multiplied by volume). Inter-reader reliability was analyzed with Bland-Altman analysis and correlation plots using Matlab (MathWorks). Results: Bland-Altman analysis showed good agreement between the two raters with no bias for SUV values with a mean difference of 0.24 % and 0.65 % for scan one and two, respectively, and a 95 % limit of agreement range of -7.6 % to 8.1 % and -2.4 to 3.7 %. A bias for one reader was observed in the TLG values with a mean difference of 3.9 % and 4.5 % for scan one and two. Limit of agreements was 15 % and 6.4 % giving a range of -11 % to 19 % and -2 % to 10 % for scan one and two, respectively, indicating bias introduced in

the lung segmentation and a need for rigorous guidelines. Differences in measurements were uniformly distributed with no dependence with magnitude of values. **Conclusion:** Lung segmentation and subsequently derived quantitative parameters of metabolic activity in the lungs expressed as SUV and TLG are reproducible and warrants further studies as a surrogate measure of pulmonary inflammation. **References:** None

EPS-035

Staging of Alveolar Echinococcosis with PET/CT: Prediction of the Length of Benzimidazole Therapy in Inoperable Patients

L. Husmann[1], H. Gruenig[1], C. S. Rainer[2], A. Deibel[3], B. Ledergerber[4], U. J. Muehlematter[1], F. Grimm[5], M. Messerli[1], B. Hasse[4], B. Muellhaupt[3], M. W. Huellner[1];
[1]Department of Nuclear Medicine, University Hospital of Zurich / University of Zurich, Zurich, SWITZERLAND, [2]Institute of Diagnostic and Interventional Radiology, University Hospital Zurich, University of Zurich, Zurich, SWITZERLAND, [3]Division of Gastroenterology and Hepatology, University Hospital Zurich, University of Zurich, Zurich, SWITZERLAND, [4]Division of Infectious Diseases and Hospital Epidemiology, University Hospital Zurich, University of Zurich, Zurich, SWITZERLAND, [5]Institute of Parasitology, University of Zurich, Zurich, SWITZERLAND.

Aim/Introduction: To determine the role ^{18}F-fluorodeoxyglucose (FDG) positron emission tomography/computed tomography (PET/CT) in staging of patients with alveolar echinococcosis and to identify quantitative imaging parameters related to the length of benzimidazole therapy. **Materials and Methods:** We retrospectively analysed 47 PET/CT performed for staging in patients with confirmed alveolar echinococcosis. Quantitative imaging parameters were measured in the lesion with the highest FDG-uptake (i.e. maximum and peak standardized uptake values (SUVmax and SUVpeak)) and compared to normal liver tissue (SUVratio). Results: Median SUVmax in echinococcosis manifestations with the highest FDG-uptake was 5.4 (3.7-11.8), and 3.1 (2.5-9.0) in non-infected liver tissue. Thirteen patients (28%) were operated with a curative approach. In 43/47 patients (91%) benzimidazole therapy was initiated, and was successfully stopped after a median of 870 days (766-2517) in 14/43 patients (33%). Tests for trend of survivor functions displayed clear trends for longer benzimidazole therapy duration (p=0.05; n=25), and for longer time intervals to reach no detectable levels of Em-18 antibodies (p= 0.01, n=15) across tertiles of SUVratio in inoperable patients. **Conclusion:** In inoperable patients with alveolar echinococcosis, PET/CT performed for staging may predict the duration of benzimidazole therapy. **References:** None.

EPS-036

In polyadenopathy cases, is PET-CT reliable to differentiate sarcoidosis from lymphoma ?

G. Lades;
Centre Hospitalier Universitaire Dupuytren, Limoges, FRANCE.

Aim/Introduction: Sarcoidosis and lymphoma are frequent pathologies that can be associated and mimic each other. The final diagnosis is based on histopathological analysis, but many cases of errors are due to a non-optimal biopsy site. The objective of this study was to establish a reliable PET-CT based diagnostic score to improve the result of histopathology. **Materials and Methods:** From 2015 to 2020, 463 patients with histologically proven polyadenopathy, were retrospectively considered in our institution, and among them, only 127 underwent FDG-PET/CT. Two groups were selected, a derivation cohort of 79 patients which was used to determine the criteria that are statistically correlated to sarcoidosis, and a validation cohort of 48 patients which was used to elaborate the score. Results: 23 variables associated to sarcoidosis were identified. We isolated 2 items with clinical application: the small axis of the most hypermetabolic lymph node and the symmetry of lymph nodes involvement. Combining these 2 parameters in a score gave good diagnosis performance in predicting sarcoidosis with: sensitivity 90%, specificity 94% and accuracy 92%. Inter-reader agreement was appropriate with an ICC of 0,794. **Conclusion:** Using selected criteria, FDG PET-CT might be a reliable tool to specify the diagnosis between sarcoidosis and lymphoma in tricky polyadenopathy cases. **References:** none

EPS-037

Added Diagnostic Value of Lung Perfusion Scintigraphy In Admitted COVID-19 Patients

M. Algarni;
KFMMC, Dhahran, SAUDI ARABIA.

Aim/Introduction: To make describe radiographic imaging findings of perfusion single-photon emission computed tomography (SPECT)/CT for diagnosing pulmonary embolus (PE) and other important imaging finding in patients hospitalized with Coronavirus disease 2019 (COVID-19). **Materials and Methods:** This retrospective study was carried in the Nuclear Medicine Department, King Fahad Military Medical Complex, Dhahran between March to December 2020 (10 months). All patients undergoing evaluation for suspected PE admitted with COVID-19 imaged with Lung Perfusion SPECT/CT where CT angiogram was contraindicated (such patient with a renal problem or severe contrast reaction). Imaging findings were interpreted by 2 dual qualification physicians in both clinical radiology (CR) and nuclear medicine and consensus reporting was made.

Results: Out of 53 patients, majority were males (n=41, 77.4%). Lung Perfusion SPECT/CT demonstrate multiple segmental pulmonary in 6 (8.8%) of patients. Twenty-three patients (43.3%) had other abnormal imaging findings in associated CT of SPECT/CT with mostly peripheral GGO (56.5%), followed by consolidations (34.7%), and others imaging finding (such as atelectasis, reticulation, peribronchovascular thickening, lymphadenopathy, plural effusion and pneumomediastinum) (26%). All patients with unfavorable outcomes were above 65 years having comorbidities or complications (p<0.0005). **Conclusion:** Coronavirus disease 2019 is seen mostly affecting males. Elderly patients with co-morbidities may show unfavorable outcomes. Lung Perfusion SPECT/CT had important role during this time in diagnosis PE as well as interrupting other associated SPECT CT scan finding with peripheral ground glass opacities are the most common imaging findings. **References:** None

EPS-038

Role of Perfusion Lung Scan in discharged patients post SARS-CoV2 pneumonia

*M. L. De Rimini[1], **D. D'Arienzo**[1], G. Fiorentino[2], A. Annunziata[2], M. Flora[2], T. Valente[3], G. Borrelli[1], M. Bifulco[1], G. Mazzarella[1], M. Scarpato[1];*

[1]Nuclear Medicine Unit AO Ospedali dei Colli - Monaldi, Naples, ITALY, [2]Respiratory Pathophysiology and Rehabilitation AO Ospedali dei Colli - Monaldi, Naples, ITALY, [3]Radiology Unit AO Ospedalidei Colli - Monaldi, Naples, ITALY.

Aim/Introduction: Respiratory dysfunction is the main source of morbidity and mortality in patients (pts) with SARS-CoV2 disease. However, the inflammatory cascade further fuels pulmonary embolism (PE) occurrence, producing arterial vascular disease and venous thrombosis of small vessels that evolves into serious/permanent pulmonary lesions. So, a targeted functional definition can develop a positive management feedback for the outcome of pts and also for their costs on the Health System. We aim to evaluate the role of Pulmonary Perfusion (Q) Scintigraphy in COVID-19 discharged pts and its clinical impact in planning and monitoring therapy. **Materials and Methods:** Population: 27 pts discharged after COVID-19. Almost complete resolution of the symptoms (19/27), residual dyspnea (8/27: 5 at minimal motor activity - 3 after prolonged effort). All pts underwent Q scan at T0 (1-3 month after acute disease); at T1 (6 month later). Conventional planar and Q-SPECT/CT images were obtained for evaluation of lobar or segmental or subsegmental peripheral perfusion defects for each bronchopulmonary segment. Perfusion images were qualitatively and semiquantitatively analiysed (Q-Lung GE software) and compared with Angio-CT and HRCT obtained during hospitalization. Significant pulmonary perfusion defects at Q scan was considered for targeted therapy. Results: At T0: - Normal lung perfusion in 15/27 asymptomatic pts; -Perfusion Defects in 12/27 pts as follows: -Severe (at least one wedge-shaped peripheral defect estimated as ≥ 50% of a pulmonary segment without corresponding CT image abnormality) in 5 pts with dyspnea at minimal motor activity; -Moderate: consisting in multiple (> than 3) Sub-Segmental Defects in 3 pts with dyspnea after prolonged effort; -Mild Perfusion Defect (egual/less than 3) in 4 asymptomatic pts. At T1: lung perfusion improvement was observed in 6 out of the 12 pathological pts at T0 as follows: -1 pt with Severe Defects at T0; - 2 pts with Moderate Defect at T0; - 3 pts with Mild Defect at T0, suggesting the stop of therapy. **Conclusion:** In patients with recent COVID 19 disease, Q Scan and its quantification can be considered an added value to better understand the pulmonary pathophysiology induced by the disease, to better contextualize its symptoms by making a differential diagnosis between previous PE or pulmonary microembolism vs respiratory disease and to define a suitable therapeutic strategy centered for each patient. **References:** Parry AH et al. Pulmonary embolism in coronavirus disease-19 (COVID-19): rational and stepwise use of clinical data and imaging in its diagnosis. Clinical and Translational Imaging (2020) 8:299-301

EPS-039

Pulmonary Perfusion SPECT/CT Results in Thromboembolism Diagnosis in Patients at Post-COVID-19 Infection Period

***H. Nalbant**, S. Demirtaş Şenlik, B. B. Demirel, G. Uçmak; Dr. Abdurrahman Yurtaslan Ankara Oncology Training and Research Hospital, Ankara, TURKEY.*

Aim/Introduction: The aim of this study is to share perfusion SPECT/CT results in the diagnosis of pulmonary thromboembolism(PE) and follow-up findings of patients who had COVID-19 in the last 6 months without having any other PE risk factors. **Materials and Methods:** Fifty one patients without other risk factors for PE were included in the study. Patients' demographic features, PA chest radiography(CR), D-dimer values at the time of scintigraphy and COVID-19 diagnosis were recorded. Scintigraphy results were classified as negative(no perfusion defect or perfusion defect with parenchymal disorder in CT sections[match defect]), low probability(≤2 small subsegmental defects),suspicious(>2 small subsegmental defects or 1 large subsegmental defects), non-diagnostic(intensive parenchymal disorders with non-segmental perfusion defects) and high probability(multipl large subsegmental/segmental defects). Negative and low probability results were defined as non-PE group(NPEG); while suspicious and high probability results defined as PE group(PEG). Clinicians' final diagnosis, patients' treatments and follow-up findings were recorded. Results: Mean age was 57±12, majority of patients were women(34F,17M). Median time for scintigraphy after COVID-19 was 77±58 days. According to scintigraphy results, 36 of 51(70,5%) patients

were estimated as NPEG, 12 patients(23,5%) were estimated as PEG. Three patients(6%) were reported as non-diagnostic. Thirteen patients' final diagnosis couldn't be reached. 38 patients' follow-up evaluations are noted: 6 of 29(21%) NPEG, 7 of 7(100%) PEG, 1of 2(50%) non-diagnostic patients were diagnosed PE and treatment were initiated. All of these patients' D-dimer values were high(median: 1030ng/mL [520-3800]). Median follow-up time after initiating treatment for PE was 54 days(12-90d). Except 2, all patients' D-dimer values were decreased(median:410[190-1680]. Thirteen patients have been hospitalized during COVID-19. The PE diagnosis were higher in those patients(46%) than nonhospitalized ones. 9 of those had diagnostic CT for COVID, all had diffuse parenchymal involvment. Most of the patients with match defects on SPECT/CT were in this group(75%); the reason for this was the sequel changes after COVID-19. **Conclusion:** In this study, we detected 21% PE scintigraphically in the patient group with no risk factors other than having COVID-19. However, 37% of the patients received treatment with clinical acceptance of PE, mostly due to extremely high D-dimer values. In COVID-19 pandemic, because of high contamination risk ventilation scintigraphy couldn't be performed in many centers. SPECT/CT increases diagnostic accuracy by showing parenchymal sequel changes after COVID-19 pneumonia and probable false positivity can be prevented. **References:** None

EPS-040

Diagnostic Contribution Of Lung Perfusion SPECT/CT Imaging During The COVID-19 Pandemic

***N. Alvarez Mena**, F. Sebastián Palacid, P. Turbay Eljach, C. García García, B. Pérez López, C. Gamazo Laherrán, M. Alonso Rodríguez, A. Sainz Esteban, M. González Soto, M. Ruiz Gómez, R. Ruano Pérez; Hospital Clínico Universitario de Valladolid, Valladolid, SPAIN.*

Aim/Introduction: Due to the current health emergency (COVID-19 pandemic), it has been decided not to perform lung ventilation scintigraphy in most medicine nuclear units when pulmonary embolism (PE) is suspected.This work aims to assess the additional information of lung perfusion SPECT/CT scan. **Materials and Methods:** Retrospective series of 388 patients with suspected PE who were performed a lung perfusion scintigraphy from March 19th 2020 to March 25th 2021. We analysed variables such as age, sex, scan result, laterality, time of evolution and positivity for COVID-19. Data were also collected for patients who were performed lung perfusion SPECT/CT in case of inconclusive diagnosis: scan result, visualisation of more defects and other radiological findings. Results: Median age: 76 years (range 19-101). 208 women and 181 men. PE+ in 167 patients (43%), PE- in 214 (55%) and inconclusive diagnosis in 7 (2%, without SPECT/CT scan). 15 COVID-19+ (6 with acute PE confirmed by SPECT/CT scan).Of those diagnosed with PE, 62 were bilateral (37%) and 105 unilateral (63%). 75 patients with acute/subacute PE (45%) and the remaining 92 with chronic PE (55%).In 214 patients with inconclusive diagnosis a SPECT/CT scan was performed showing the following results: 63% with PE (59 acute/subacute and 76 chronic). In 10 patients more defects were found with SPECT/CT scan.Of the 79 patients without PE (confirmed by SPECT/CT scan), other clinically relevant radiological findings were observed in up to 60 patients (76%): pleural effusion (15), fibrosis (8), emphysema (7), bilateral infiltrates compatible with COVID-19 (6, with confirmatory CRP), pulmonary consolidations (5), atelectasis (5), air trapping (5), post-COVID-19 reticular interstitial pattern (3), pulmonary metastases (3), solitary pulmonary nodule suspicious for malignancy (2), arterial malformation (1). **Conclusion:** Lung perfusion SPECT/CT scan has an excellent diagnostic yield associated with planar imaging for suspected PE, with suitable sensitivity and specificity in the absence of a lung ventilation scintigraphy. Furthermore, low-dose CT provides additional information of great clinical utility, reducing false positives. **References:** none

EPS-041

Pulmonary embolism in non-hospitalized COVID-19 infected patients without severe disease

***O. Evbuomwan**, G. Engelbrecht;*
University of The Free State, Bloemfontein, SOUTH AFRICA.

Aim/Introduction: Pulmonary embolism is a well-known complication of COVID-19 infection. It has well been demonstrated and documented in hospitalized patients with the severe form of the disease. However, a few case reports have reported its occurrence in non-hospitalized patients with a milder form of the disease. In view of the limited data in this cohort of patients, we decided to assess the prevalence of pulmonary embolism in this group of patients in our environment. **Materials and Methods:** We retrospectively reviewed the data of all the COVID-19 infected patients who had a VQ SPECT/CT study or a perfusion only SPECT/CT study in our facility between July 2020 and January 2021. We excluded all the hospitalized patients and those patients diagnosed with severe disease. Sixty-five patients in total were included in the study and they all had raised D dimer levels, with persistent or new onset cardiopulmonary symptoms after de isolation. Results: The median (IQR) age of the study population was 46 (41-54) years and majority (88.2%) were females. All the participants had lung perfusion studies performed after de-isolation, 10-90 days after the diagnosis of COVID-19 infection. Forty-seven (72.3%) of them had perfusion only SPECT/CT study, while 18 (27.7%) had a VQ SPECT/CT study. There were 22 (33.8%) patients with lung perfusion defects in keeping with pulmonary embolism, with two patients having a false negative CTPA study. Of the 65 participants, 12 (18.5%) of them had a follow up VQ SPECT/CT study 3 months after their initial study. These follow up studies showed either

a partial or a complete resolution of earlier seen perfusion defects. **Conclusion:** We confirm that pulmonary embolism is not an uncommon occurrence in a certain category of non-hospitalized patients with COVID-19 infection. However, we recommend a multi-center prospective study should be done to show the true prevalence of pulmonary embolism in this particular cohort of patients. Some of the symptoms of post-acute COVID-19 infection might be due to undiagnosed pulmonary embolism and a modality that can detect both acute and chronic pulmonary embolism might play a vital role in these patients. **References:** None

EPS-042

Incremental values for Perfusion SPECT/CT in detection of PE in COVID-19 patients with deteriorating respiratory functions. Pilot Study

H. Elzeftawy, D. Omran, W. Waggas, A. El-Zeftawy;
King Faisal Specialist Hospital and Research Center, Jeddah, SAUDI ARABIA.

Aim/Introduction: To study the clinical value of SPECT/CT perfusion imaging for detection of PE in patients with Covid-19 pneumonia. **Materials and Methods:** A retrospective pilot study performed during the period from February 1, 2019 till March 31, 2021 for patients with COVID-19 PCR and SPECT/CT perfusion scan for PE. Results: 83 patients (22 M & 31 F with average age of 54 Ys) with Polymerase Chain Reaction (PCR) swab and SPECT/CT perfusion imaging were studied. 30 patients had their PCR swab more than 3 days from their scans and were excluded.38 patients had -ve PCR and showed no Covid-19 related pneumonia. 15 patients had +ve PCR swab and positive Covid-19 pneumonia at their SPECT/CT scans, 2 of them had CT PE scan for confirmation. 8 of the 15 PCR +ve and Covid-19 pneumonia had no PE signs (2 were in the ICU with high D Dimers); all received VTE prophylaxis only. The remaining 7 patients had +ve PE (3 were in the ICU) received therapeutic anticoagulant treatment for an average of 10 days. All 15 patients were discharged after showing clinical and serologic improvements. 2 patients deceased 7 and 12 months later due to other comorbid conditions. **Conclusion:** The beneficial outcome of targeting anticoagulant therapy to PE positive Covid-19 patients and avoiding its unnecessary use should drive the attention to the pivotal benefit of this technique in diagnosis and follow up of those patients. **References:** 1. Diagnosis and Treatment of Pulmonary Embolism During the Coronavirus Disease 2019 Pandemic A Position Paper From the National PERT Consortium, Rachel P. et al. Pulmonary and Cardiovascular Special Features. Chest 2020. 2. Massive pulmonary embolism following recovery from COVID-19 infection: inflammation, thrombosis and the role of extended thromboprophylaxis. Vadukul P, et al. BMJ Case Rep 2020;13: e238168. doi:10.1136/bcr-2020-238168. 3. Pulmonary embolism in patients with coronavirus disease2019 (COVID19) pneumonia: a narrative review. Sakr et al. Ann. Intensive Care (2020) 10:124. 4. Pulmonary Embolism in Patients with COVID-19 Awareness of an Increased Prevalence. Julien P. et al, Circulation. 2020; 142:184-186. DOI: 10.1161/CIRCULATIONAHA.120.047430. 5. The prevalence of pulmonary embolism in patients with COVID-19 and respiratory decline: A three-setting comparison. R.A.G. Brüggemann et al. Thrombosis Research 196 (2020) 486-490. 6. Potential of hybrid V/P SPECT-low-dose CT in lung diagnostics. Marika B, Breathe September 2012 Volume 9 No 1. 7. V/Q Scanning Using SPECT and SPECT/CT. Roach P.et al, J Nucl Med 2013; 54:1588-1596.

EPS-043

FDG PET-CT Imaging Of Immune Activation Post COVID Vaccination In Oncology Patients

S. Ali, A. Hussien, M. Kula, W. Ibrahim;
King Hamad University Hospital, AlSayh, BAHRAIN.

Aim/Introduction: On assessment of oncology patients with 18F-FDG PET-CT, vaccination may cause transient inflammation of lymph nodes demonstrating positive findings on PET scans. FDG-avid axillary lymph node(s) are common in patients receiving vaccines against SARS-CoV-2, influenza virus, or human papillomavirus, reflecting regional immune response. Recognition of such vaccination-related regional immune response prevents further needless examinations or costly biopsies in cancer patients. This preliminary study was designed to define the pattern, magnitude and duration of lymph node activation following vaccination. **Materials and Methods:** Thirty patients aged 23 - 84 years participated in this study. Of those who were included, there were 17 females and 13 males who received COVID 19 vaccine & were referred for oncologic FDG PET-CT imaging during 2021. Results: 4/30 had focal enhanced FDG activity over the vaccine injection site & ipsilateral axillary lymph nodes. 3/30 had ipsilateral axillary lymph nodes without detected activity at injection site. 3/30 had bilateral axillary lymph nodes activity with no demonstrated activity at injection site. In the ten patients with positive axillary lymph nodes, six patients were diagnosed as unilateral breast cancer in whom vaccination site was on the contralateral arm, one had renal lesion, one appendicular tumor, one head & neck cancer and one referred for characterization of pulmonary nodules. In those ten patients with hypermetabolic axillary nodes, the time interval between vaccine administration & PET scan was 13.1 ± 8.9 days (1 - 26 days). SUVmax range was 2.5 ± 0.9 (1.2 - 4.3). All those lymph nodes were benign looking with preserved fatty hilum & size ranged from 0.4 x 0.9 to 1.1 x 1.6 cm. 2/30 patients referred with initial diagnosis of lymphoma stage III showed multiple bilateral sizable hypermetabolic

axillary nodes which were considered to be likely related to disease involvement. The remaining 18/30 patients, had no detected abnormal nodal activity at axillae or cervical regions. **Conclusion:** Our results advocate performing PET-CT at least 2 weeks after vaccination especially if such immune response will affect interpretation. If not possible, record details regarding vaccination time and site and keep in consideration imaging patterns of immune response to vaccination especially in the current era of COVID-19 pandemic. **References:** none

EPS-044

Our experience in the assessment of pulmonary embolism with lung perfusion SPECT/ CT in COVID-19 patients

M. Salcedo Pujantell*, J. Deportós, M. Solà, V. Vallejos, S. Lafuente Carrasco, M. Olivares, M. Torres, G. Moragas;*
Hospital Universitari Germans Trias i Pujol, Badalona, SPAIN.

Aim/Introduction: To review the clinical utility of perfusion SPECT/CT for diagnosing pulmonary embolism (PE), without ventilation scan, in Covid-19 patients **Materials and Methods:** Between March and May 2020 we performed a prospective review of patients with perfusion SPECT/CT at Germans Trias i Pujol Universitary Hospital. Perfusion patterns were described as: no defects; single subsegmental defect; single segmental defect; multiple subsegmental defects; multiple subsegmental and segmental defects; heterogeneous distribution; and concordant CT/ perfusion defects. A positive result was considered when a single segmental defect or multiple subsegmental and/or segmental defects were found, compared with imaging findings on CT (normal, covid infiltrates and other findings). Results: 146 patients (69 women; mean age 61 years) were studied with perfusion SPECT/CT. All of them had a laboratory confirmed diagnosis of COVID-19, 110 were hospitalized while 36 were assessed after discharge (post-covid patients). Perfusion SPECT/CT was positive in 59 (39%) of patients. Nondiagnostic results were observed in 17 studies (13%). PE pattern was multiple subsegmental and/or segmental pulmonary defects in 45/59 (76%) and single segmental defect in 14/59 (24%). PE was diagnosed in 39 (36%) of 110 patients who showed Covid findings on CT. Furthermore , 18 (53%) out of 34 patients with normal CT were PE positive. Two more patients had other CT findings **Conclusion:** Despìte the inability to perform ventilation scans and the severe pulmonary involvement , we consider that perfusion SPECT/CT has clinical utility in the assessment of PE in COVID-19 patients, in the pandemic era. **References:** Bajc M, et al. Eur J Nucl Med Mol Imaging. 2019;46: 2429-2451. Batkia KD, et al. J Med Imaging Radiat Oncol. 2016; 60: 492-97.Palmowski K, et al. Respiration. 2014; 88: 291-297.Vöö, et al. Nul Med Commun.2020;41:991-993. Burger I, et al. Eur J Nucl Med Mol Imaging. doi.org/10.1007/s00259-020-0483-4. Lu Y ,et al. Eur J Nucl Med Mol Imaging. doi.org/10.1007/s00259-020-04835-6. Das JP, et al. Eur J Nucl Med Mol Imaging. doi.org/10.1007/s00259-020-05043-y. Sciagra R ,et al: Eur J Nucl Med Mol Imaging. doi.org/10,1007/s00259-020-04868-xCapaccione KM et al. Blood Res 2020;55:275-282. Léonard-Lorant I et al. Radiology 2020; 296:E189-E191. Kammetzky M et al .Radiology: Cardiothoracic Imaging 2020; 2(4):e200308

EPS-045

Ventilation/Perfusion Scintigraphy in the Assessment of Pulmonary Sequelae in COVID-19 Patients with Pneumonia and Pulmonary Embolism

C. Soldevila Lozano*[1], J. Mora-Salvadó[1], M. Bajén-Lázaro[1], A. Benítez-Segura[1], G. Reyes-Junca[1], P. Notta[1], S. Bondia-Bescós[1], L. Fernández-Romero[1], A. Riera-Mestre[2], A. Iriarte-Fuster[2], J. Mora-Lujan[2], M. Cortés-Romera[1];*
[1]Nuclear Medicine-PET (IDI). Hospital Universitari de Bellvitge, L'Hospitalet De Llobregat, SPAIN, [2]Internal Medicine Department. Hospital Universitari de Bellvitge, L'Hospitalet De Llobregat, SPAIN.

Aim/Introduction: SARS-CoV-2 infection (COVID-19) can cause respiratory sequelae. COVID-19 can cause thrombotic events too, being the most frequent pulmonary embolism (PE). The aim of this study was to evaluate pulmonary sequelae in patients (p) with COVID-19 pneumonia and PE by ventilation/perfusion (V/P) scintigraphy. **Materials and Methods:** We prospectively studied twenty-seven patients (9 women; mean age: 55 years) diagnosed with moderate-severe COVID-19 pneumonia, who presented a PE during the infection. A V/P scintigraphy (planar images and SPECT) with [^{99m}Tc]Tc-macroaggregated albumin for perfusion and Technegas® for ventilation was performed three months later. Scintigraphy was classified as normal (normal ventilation and perfusion), PE (normal ventilation and abnormal perfusion with segmental defects), pulmonary infarction (abnormal ventilation and perfusion with matched segmental defects) and pneumonia sequelae (abnormal ventilation and perfusion with mismatched defects or abnormal ventilation and normal perfusion). Results: V/P scintigraphy was normal in 14p (52%). V/Q scintigraphy showed pulmonary sequelae in 13p (48%): PE in 4p, pulmonary infarction in 4p, pneumonia sequelae in 3p, PE with pulmonary infarction in 1p and pulmonary infarction with pneumonia sequelae in 1p. **Conclusion:** Pulmonary sequelae is observed in almost half of the patients with COVID-19 pneumonia and PE three months after the infection. These sequelae are due to PE and/or pulmonary infarction in most patients. **References:** none

EPS-046

Preliminary study of quantitative evaluation for lung glucose metabolism using ^{18}F-FDG PET imaging in patients with pulmonary arterial hypertension related to congenital heart disease

X. Wang[1], L. Wang[2], W. Fang[2], C. Yan[1];
[1]Center of Structural Heart Disease, Fuwai Hospital, National Center for Cardiovascular Diseases, Chinese Academy of Medical Sciences and Peking Union Medical College, Beijing, CHINA, [2]Department of nuclear medicine, Fuwai Hospital, National Center for Cardiovascular Diseases, Chinese Academy of Medical Sciences and Peking Union Medical College, Beijing, CHINA.

Aim/Introduction: To investigate the value of ^{18}F-fluorodeoxyglucose (FDG) PET imaging in evaluating the ^{18}F-FDG uptake of lungs and its relationship with pulmonary hemodynamics in patients with pulmonary arterial hypertension (PAH) related to congenital heart disease (PAH-CHD). **Materials and Methods:** From January 2018 to June 2019, a total of 16 PAH-CHD patients (6 males, 10 females, age (29.2±10.6) years) and 22 health controls (8 males, 14 females, age (45.4±3.8) years) were respectively enrolled. All cases underwent dynamic ^{18}F-FDG PET imaging for lung ^{18}F-FDG influx rate (presented as Ki) . Right heart catheterization was performed to evaluate pulmonary hemodynamic parameters such as pulmonary vascular resistance (PVR), mean pulmonary vascular pressure (mPAP) in PAH-CHD patients after imaging within one week. Independent-sample t test was used to compare Ki of two groups. Pearson correlation analysis was used to test the relationship between Ki and PVR, mPAP in PAH-CHD patients. In addition, Glut1 expression was assessed immunohistochemically in lung specimens from five PAH-CHD patients with surgical correction and five health specimen from specimen bank. Results: Ki of the lungs was significantly higher in PAH-CHD patients than that of health controls ((0.0006±0.0003) vs (0.0004±0.0003) ml·g^{-1}·min^{-1}; t=2.15, P=0.038). In addition, Ki was not correlated with PVR and mPAP in PAH-CHD patients (r values: 0.202 and 0.006, both P>0.05). **Conclusion:** Pulmonary vascular remodeling could lead the increased lung ^{18}F-FDG uptake in patients with PAH-CHD. ^{18}F-FDG PET may have the ability in monitoring and evaluating pulmonary vascular remodeling in PAH-CHD. **References:** 1. Zhao L, Ashek A, Wang L, et al. Heterogeneity in lung ^{18}FDG uptake in pulmonary arterial hypertension: potential of dynamic ^{18}FDG positron emission tomography with kinetic analysis as a bridging biomarker for pulmonary vascular remodeling targeted treatments. Circulation. 2013 Sep 10;128(11):1214-24. doi: 10.1161/CIRCULATIONAHA.113.004136. 2. Marsboom G, Wietholt C, Haney CR, et al. Lung ^{18}F-fluorodeoxyglucose positron emission tomography for diagnosis and monitoring of pulmonary arterial hypertension. Am J Respir Crit Care Med. 2012 Mar 15;185(6):670-9. doi: 10.1164/rccm.201108-1562OC.

612

Wednesday, October 20 - Saturday, October 23, 2021

on-demand pool, release on Wednesday, October 20 at 09:00

e-Poster Presentation Session 4: Radiochemistry

EPS-047

The importance of precursor concentration for PET diagnostics with Ga-68-PSMA-11

***N. Nithack**, Y. Zhao, A. Helm, U. Lützen, M. Zuhayra;*
Universitätsklinikum Schleswig-Holstein, Klinik für Nuklearmedizin, Molekulare Bilddiagnostik und Therapie, Kiel, GERMANY.

Aim/Introduction: Positron emission tomography (PET) is becoming increasingly important in the diagnosis of prostate carcinoma. In the synthesis of the radiopharmaceutical used for this purpose, Ga-68 is coupled to the precursor PSMA-11. An increasing tumor to background activity ratio is associated with better contrast of PET images. The aim of this work was to determine plasma protein binding and prostate cancer cell uptake of Ga-68-PSMA-11 at different precursor concentrations and to determine the most beneficial in vitro PSMA 11 concentrations for PET. **Materials and Methods:** Ga-68-PSMA-11 was prepared with precursor concentrations ranging from 1 µg/GBq to 1 mg/GBq. Plasma protein binding was tested in vitro by ultrafiltration using human plasma. Cellular uptake of the radiopharmaceutical was studied on PSMA-positive LNCaP cells in relation to the precursor concentration. Results: Plasma protein binding of Ga-68-PSMA-11 was in nearly the same range at concentrations between 7.5 and 100 µg PSMA-11/GBq (42.0-42.6%). There was a small, but not significant, decrease in plasma protein binding only at very high PSMA-11 concentrations (≥ 500 µg/GBq). Cell uptake decreased significantly with increasing precursor concentrations. Compared with 10 µg PSMA-11/GBq, cellular uptake decreased by more than half at 1 mg PSMA-11/GBq (3.4 vs. 1.4 %). The ratio of cell uptake to plasma protein binding was highest at PSMA-11 concentrations of 7.5-15 µg/GBq. At higher concentrations (≥ 100 µg/GBq), the ratio was significantly decreased. **Conclusion:** Plasma protein binding of Ga-68-PSMA-11 is barely affected by the precursor concentration. In contrast, cellular uptake is much more dependent on this concentration. Low PSMA-11 concentrations between 7.5 and 15 µg/GBq showed the highest ratio of cellular uptake to plasma protein binding and thus the theoretically most favorable in vitro properties for PET diagnosis of prostate carcinoma. **References:** none

EPS-048

^{68}Ga-radiolabeling and pharmacological characterization of a kit-based formulation of the Gastrin-Releasing Peptide Receptor (GRP-R) antagonist RM2 for convenient preparation of [^{68}Ga]Ga-RM2

C. Morgat[1,2], A. Chastel[1,2], D. Vimont[2], S. Claverol[3], M. Berndt[4], M. Zerna[4], S. Chaignepain[3], E. Hindié[1,2];
[1]Nuclear Medicine Department - University Hospital of Bordeaux, Bordeaux, FRANCE, [2]University of Bordeaux, CNRS, EPHE, INCIA, UMR 5287, Bordeaux, FRANCE, [3]Proteome Platform, Univ Bordeaux, Bordeaux, FRANCE, [4]Life Molecular Imaging, Berlin, GERMANY.

Aim/Introduction: [^{68}Ga]Ga-RM2 is a potent Gastrin-Releasing Peptide-receptor (GRP-R) antagonist for imaging prostate cancer and breast cancer, currently under clinical evaluation in several specialized centers around the word. Targeted radionuclide therapy of GRPR-expressing tumors is also being investigated. We here report the characteristics of a kit-based formulation of RM2 that should ease the development of GRP-R imaging and make it available to more institutions and patients **Materials and Methods:** Stability of the investigated kits over one year was determined using LC/MS/MS and UV-HPLC. Direct ^{68}Ga-radiolabelling was optimized in terms of buffer (pH), temperature, reaction time and shaking time. Conventionally prepared [^{68}Ga]Ga-RM2 using an automated synthesizer was used as comparator. Finally, the [^{68}Ga]Ga-RM2 product was assessed as regards hydrophilicity, affinity, internalization, membrane bound fraction and efflux, which is a useful add to the literature given the paucity of in vitro data Results: The kit-based formulation, kept between 2°C and 8°C, was stable over one year. Using acetate buffer pH 3.0 in 2.5-5.1mL total volume, heating at 100°C during 10 minutes and cooling down for 5 minutes, [^{68}Ga]Ga-RM2 produced by kit complies with the requirement of the European Pharmacopoeia. Compared with the module production route, [^{68}Ga]Ga-RM2 produced by kit was faster and displayed higher yields, higher volumetric activity and was devoid of ethanol. In vitro, [^{68}Ga]Ga-RM2 displayed sub-nanomolar affinity (Kd = 0.25 ± 0.19nM), receptor specific and time dependent membrane-bound fraction of 42.0 ± 5.1% at 60 min and GRP-R mediated internalization of 24.4 ± 4.3% at 30 min. Finally, the efflux of internalized activity was 64.3 ± 6.5% at 5 minutes Finally, [^{68}Ga]Ga-RM2 displayed improved properties compared to its ^{111}In and ^{177}Lu counterparts **Conclusion:** The kit-based formulation of RM2 is suitable to disseminate GRP-R imaging and therapy to distant hospitals without complex radiochemistry equipment **References:** None

EPS-049

Securing Gallium-68 availability with liquid target production on mid-energy cyclotrons: Users' experience and scaling up

C. Gameiro[1], V. H. Alves[2], A. Abrunhosa[2], F. Alves[2], D. Goblet[1], B. Nactergal[1], A. Uhlending[3], V. Hugenberg[3], T. Ortgies[3], G. Hoeger[3], J. Manrique-Arias[4], R. Freifelder[5], K. Hye-Yeong[5], M. Bhuiyan,[5], A. Kucharski[5];
[1]IBA, Louvain-La-Neuve, BELGIUM, [2]Institute for Nuclear Sciences Applied to Health (ICNAS), Coimbra, PORTUGAL, [3]Department of Radiology, Nuclear medicine and Molecular Imaging, Bad Oeynhausen, GERMANY, [4]Cyclotron Department, Doctors Hospital, Monterrey, MEXICO, [5]Department of Radiology, University of Chicago, Chicago, IL, UNITED STATES OF AMERICA.

Aim/Introduction: It is redundant to say that the use of Gallium-68 (^{68}Ga) has grown exponentially in recent years with about 400 ongoing clinical trials[1] for multiple indications. The recent US FDA approval of [^{68}Ga]GaPSMA-11 in two academic institutions, together with the inclusion of PSMA-PET into several international guidelines will further consolidate the increasing demand. In this context, an uninterrupted supply of ^{68}Ga is key. Production from liquid targets using mid-energy cyclotrons can be a stable and cost-effective alternative for many centers worldwide. In this paper, several users share their experience on the liquid target production and scaling up of ^{68}Ga through labelling and QC testing in GMP (good manufacturing practices) compliance. **Materials and Methods:** The ^{68}Ga is produced in a cyclotron via ^{68}Zn(p,n)^{68}Ga nuclear reaction, where an enriched Zinc-68 (^{68}Zn) nitrate solution (^{68}Zn amounts ranging from 100-400 mg) in a conical liquid target is irradiated for about 1h [2]. Subsequently, the irradiated solution is post-processed via two-step solid phase extraction)[3] to obtain [^{68}Ga]$GaCl_3$ in <35 min, which is ready to be used for labelling of peptides (DOTA-NOC, DOTA-TOC, DOTA-TATE, DOTA-Ubiquicidin and PSMA-11) in an online, automated process. Quality control of the finished drug product is performed according to current European Pharmacopoeia and a shelf-life is established Results: On average, for 1-hour irradiations, sites have been able to produce 120-180 mCi of ^{68}Ga at EOB (end of bombardment) when low to medium amounts of enriched ^{68}Zn (100-200 mg) are used, while for higher amounts of enriched ^{68}Zn (400 mg), greater than 300 mCi of ^{68}Ga at EOB is obtained. For these runs, the currents varied from 40-90 µA, depending on the target size. The post purification resulted in >70% n.d.c. (non-decay corrected) yields and labelling yields were > 70% n.d.c. for both [^{68}Ga]GaPSMA-11 and [^{68}Ga]GaDOTA-NOC. Both compounds were compliant with current European Pharmacopoeia requirements over its entire shelf-life (4-5 h at end of purification=EOP). **Conclusion:** Production of ^{68}Ga via liquid targets using mid-energy cyclotrons is performed routinely in several GMP sites worldwide, which provides an economical viable and sustainable alternative to

the production of ^{68}Ga for local use and potential distribution when ramping up the manufacturing with higher amounts of target material. **References:** [1]https://www.clinicaltrials.gov/ct2/results/details?term=gallium+68:search date April, 2021[2] F. Alves et al, Modern Phys. Lett A, vol 32 (17), 2017.[3] V. Alves et al, Instruments vol 2 (17), 2018.

EPS-050

Production of Sm-153 with high specific activity for targeted radionuclide therapy

M. Van de Voorde[1], C. Duchemin[2,3], R. Heinke[2,3], L. Lambert[2], E. Chevallay[2], T. E. Cocolios[3], T. Cardinaels[1,3], B. Ponsard[1], M. Ooms[1], T. Stora[2], A. Burgoyne[1];
[1]SCK CEN, Mol, BELGIUM, [2]CERN, Geneva, SWITZERLAND, [3]KU Leuven, Leuven, BELGIUM.

Aim/Introduction: Samarium-153 (^{153}Sm) poses a high potential for targeted radionuclide therapy because of its favorable decay characteristics. ^{153}Sm has a half-life of 1.93 d, decays into a stable daughter nuclide (^{153}Eu) and emits β^- particles (E = 705 keV (30%), 635 keV (50%)) which are suitable for therapy. ^{153}Sm also emits γ photons (103 keV (28%)) with characteristics that also allow SPECT imaging, making ^{153}Sm a high-potential theranostic radioisotope. However, the full potential of ^{153}Sm in nuclear medicine is currently not being exploited because of the limited specific activity available as a result of the carrier added production method. Therefore, in this work, a new production method was developed to produce ^{153}Sm with high specific activity, suitable for radiolabeling. **Materials and Methods:** ^{153}Sm was efficiently produced via neutron irradiation of a highly enriched ^{152}Sm target (98.7% enriched, σ_{th} = 206 b) in the BR2 reactor at SCK CEN. Irradiated target materials were shipped to CERN-MEDICIS, where ^{153}Sm was isolated from the ^{152}Sm target via mass separation (MS) in combination with laser resonance enhanced ionization to drastically increase the specific activity. Further radiochemical purification steps were developed at SCK CEN to recover the ^{153}Sm from the MS target to yield a solution ready for radiolabeling. Gamma spectrometry and inductively coupled plasma mass spectrometry (ICP-MS) were used to characterize the produced $^{153}SmCl_3$. Proof of concept radiolabeling studies were performed with multiple concentrations of p-SCN-Bn-DOTA to confirm the quality of the produced $^{153}SmCl_3$. Results: The production process of high specific activity (HSA) ^{153}Sm was found efficient, yielding ^{153}Sm with a specific activity of 1.87 TBq/mg at end of purification. An overall mass separation efficiency of 4.5% was reached on average. The radiochemical process following the mass separation was found to be highly efficient, reaching an overall recovery rate of 84%. The HSA $^{153}SmCl_3$ was produced with a very high radiochemical (98.9 ± 0.24%.) and radionuclidic purity (>99.99%). Radiolabeling with the produced HSA ^{153}Sm was efficient, even at low concentrations of p-SCN-Bn-DOTA. **Conclusion:** In this proof-of-concept study, we demonstrated the potential to combine neutron irradiation with mass separation to supply high specific activity ^{153}Sm. Using this process, $^{153}SmCl_3$ suitable for radiolabeling, was produced with a very high specific activity allowing application of ^{153}Sm in targeted radionuclide therapy. Further studies to incorporate ^{153}Sm in radiopharmaceuticals for targeted radionuclide therapy are ongoing. **References:** None

EPS-051

Optimization of the Radiolabeling of Silk Fibroin Nanoparticles with Tc-99m by a direct method

M. Asensio Ruiz[1,2], Á. Alonso García[1], J. Cenis Anadón[3], A. Lozano Pérez[2,3], M. Martínez Martínez[1,2];
[1]Unidad de Radiofarmacia, Hospital Clínico Universitario Virgen de la Arrixaca, Murcia, SPAIN, [2]Instituto Murciano de Investigación Biosanitaria (IMIB)-Arrixaca, Murcia, SPAIN, [3]Departamento de Biotecnología, Genómica y Mejora Vegetal, Instituto Murciano de Investigación y Desarrollo Agrario y Alimentario, 30150-La Alberca, Murcia, SPAIN.

Aim/Introduction: Silk fibroin nanoparticles(SFN) have been revealed as a promising drug delivery system(DDS) not only due to their biocompatibility and low toxicity but also for their high binding capacity and stability. But its development as a DDS has been hampered by the lack of knowledge about the biodistribution of nanoparticles in the body.(1) The aim of this work is to optimize the radiolabeling of SFN with Tc-99m, a commonly used radionuclide with good physical properties and chemical versatility, in order to overcome the limitations of the formation of the "hydrolyzed-reduced" technetium species. Here, a "one step" radiolabeling approach is proposed, in which nanoparticles are labeled by a direct method. **Materials and Methods:** SFN were prepared by a rapid desolvation following our previous method(2) and characterized by dynamic light scattering(DLS) prior to radiolabeling as control. The procedure of radiolabeling was optimized by varying the amount of acidified $SnCl_2$ added to the SFN prior to the addition of Tc-99m sodium pertechnetate eluted from a Mo-99/Tc-99m generator. The mixtures were incubated at room temperature for 10 minutes and the radiolabeled nanoparticles were recovered by centrifugation and washed with ultrapure water. Radioactivity of pellets and supernatants were measured for Radiolabeling efficiency(RLE%) determination. The radiochemical purity(RCP%) was analyzed by instant-Thin Layer Chromatography(iTLC). The in vitro stability of the radiolabeling was evaluated by measuring the RCP% for 6 hours. DLS was performed after a decay period of at least 12 half-lives. Results: When 1 mg of SFN(4×10^{11} nanoparticles/mg; Zave=142.5±2.2nm; PdI=0.148±0.006 and ζ= -21.5±1.6mV) was radiolabeled with 37 MBq of Tc-99m sodium pertechnetate, in the presence of 7, 12, 20 or 250 µg of $SnCl_2$ in HCl 0.33M, the RLE% increased with the

$SnCl_2$ concentration from 88.34±1.11% to 96.38±0.29% with RCP of >95% in all cases. When 250 µg of $SnCl_2$ were added, a white precipitate was observed and the Z_{ave} increased from 142.5±2.2nm to 167.1±4.0nm, without a significant change in the values of PdI or in ζ. The Tc-99m-SFN were stable for 6h in NaCl(0.9%) releasing less than 10% of the Tc-99m. **Conclusion:** This direct, reproducible and affordable radiolabeling procedure paves the way for new biodistribution studies of this nanoparticles. **References:** (1)Martínez Martínez, T, et al. Fluorescent DTPA-Silk Fibroin Nanoparticles Radiolabeled with 111In: A Dual Tool for Biodistribution and Stability Studies. ACS Biomaterials Science & Engineering. 2020,6(6),3299-3309. (2)Lozano-Perez,A.A, et al. Silk Fibroin Nanoparticles: Efficient Vehicles for the Natural Antioxidant Quercetin. Int. J. Pharm. 2017, 518(1–2), 11–19.

EPS-052

18F-PSMA-1007 Synthesis: a production upgrade that enabled a federal experience in Argentina

M. Agolti[1], G. Messina[2], G. Casale[2], L. Solari[1], J. Sandobal[2], S. Fila[2]; [1]Centro de Medicina Nuclear Clinica Modelo, Parana, ARGENTINA, [2]Laboratorios Bacon, Buenos Aires, ARGENTINA.

Aim/Introduction: The logistics of PET radiotracers in Argentina is very complicated. Sites of image acquisition are sometimes more than 2500 km away from production centers. Naturally, the large pre-calibration activities needed to cross such distances raises additional challenges, specially for those tracers sensitive to radiolysis. The present article shows adjustments needed to avoid radiolytic impurities production during 18F-PSMA-1007 labeling that enabled us to increase activity batch productions to hold two independent clinical trials performed at distant sites. **Materials and Methods:** From November 2018 to April 2021 we have synthesized 27 batches in Synthera V0 module according to: 1) IBA-Synthera native method for 18F-PSMA-1007 synthesis and 2) Improved method reducing temperature (form 110°C to 95°C) and labeling times (from 480 to 300 seconds). Chemical and Radiochemical Purities (RCP) were controlled by High Performance Liquid Chromatography (HPLC)according to European Pharmacopoeia method for 18F-PSMA-1007. Chemical and radiochemical stabilities were controlled at different time points 10 hours after synthesis with the same HPLC method. Results: With IBA-Synthera native method two batches were rejected due to radiolytic impurities higher than the 10% limit. Even with higher initial activities the second method demonstrated to be more reliable. Taking in consideration just the approved batches obtained with IBA-method, the 18F-PSMA-1007 final activity increased from a mean activity of 790 mCi to a mean activity of 1330 mCi (1.68 times) with the second synthesis method. The mean value of the RCP increased slightly with the improvements, but more important, the dispersion of these values decreased significatively, giving a mean RCP Standard Deviation (SD) of 2.43% against 12.99% obtained with IBA-method, 5.3 times lower with the milder labeling conditions. **Conclusion:** Comparison of the batches synthesized with two different methods strongly suggests that milder labeling conditions are necessary to increase the 18F-PSMA-1007 activity produced as radiolytic byproducts are kept under control. With the improved method, higher activities were produced in a sustainable manner with less dispersion in the final radiochemical purities obtained and no batches rejected. Making it possible to perform nuclear medicine diagnostics with this tracer at distant acquisition places. **References:** None

EPS-053

Targeted alpha therapy with Actinium-225 radiopharmaceuticals: In-house preparation and quality control

R. Vatsa, S. Pandey, A. Chhabra, B. R. Mittal, J. Shukla; Postgraduate Institute of Medical Education and Research, Chandigarh, INDIA.

Aim/Introduction: ^{225}Ac labeled radiopharmaceuticals are gaining worldwide interest as a treatment of choice in refractory cancers. Short range and high toxicity associated with alpha particles make them an ideal candidate for targeted therapy. The present study describes the preparation and quality control of ^{225}Ac labeled PSMA-617 and DOTATATE for targeted alpha therapy in patients with prostate cancer and neuroendocrine tumors. **Materials and Methods:** Non carrier added ^{225}Ac as $^{225}AcCl_3$ was procured for radiolabeling of PSMA-617 and DOTATATE. Ascorbate buffer (pH 5-5.5), peptide (0.4-0.9 µg/µCi) and $^{225}AcCl_3$ were incubated at 90/95 for 30 min. The volume of reaction mixture was restricted to <0.5 mL. Radiolabeling yield and radiochemical purity were tested by thin later chromatography using 0.5 M sodium citrate as mobile phase. Purification if required was done by SPE based C-18 cartridge. Sterility was tested by incubating the samples in FTM and Soya broth for upto 14 days. Apyrogenecity was tested by kinetic chromogenic method using LAL reagent. Radiopharmaceuticals were administered within 30 min post preparation and imaging was performed 24 h post administration for observing the biodistribution. Results: A total of 52 doses (n=33 PSMA-617, n=19 DOTATATE) of ^{225}Ac tagged radiopharmaceuticals were prepared. Greater that 99% radiolabeling and radiochemical yield was achieved by incubating 0.6 µg/µCi of peptide with 150-350 µCi of $^{225}AcCl_3$ for 30 min. Radiolabeling yield was observed to be improved at pH 5.5 in comparison to pH 5.0. Purification was required mainly when less than 0.6 µg/µCi peptide was used at 5.0 pH. The Rf of ^{225}Ac-PSMA-617/DOTATATE and Free ^{225}Ac was observed to be 0.0 and 0.9-1.0. All preparations were observed to be sterile on sterility test. Endotoxin content was observed to be less than 0.6 EU/mL which was well below the permissible limits (175 EU). The ^{225}Ac-PSMA-617 (27 µCi/

Kg/Cycle, 10 mL) and ^{225}Ac-DOTATATE (27 µCi/Kg/Cycle, 20 mL) were administered intravenously with flow rate of 40 mL/h. A combination of arginine and lysine (25 gm each/2L saline) was also administered over 4 h, starting 30-60 min prior to administration of ^{225}Ac-DOTATATE for renal protection. **Conclusion:** DOTA-PSMA-617 and DOTATATE both can be tagged with ^{225}Ac with good radiolabeling yield at hospital radiopharmacy set up. **References:** None

EPS-054

Production of one or three patient doses (in one batch) of [^{177}Lu]Lu-PSMA-I&T on a fully-automated synthesis module

A. Cankaya, M. Balzer, H. Amthauer, W. Brenner, S. Spreckelmeyer; Charité - Universitätsmedizin Berlin, corporate member of Freie Universität Berlin, Humboldt-Universität zu Berlin, and Berlin Institute of Health, Department of Nuclear Medicine, Berlin, GERMANY.

Aim/Introduction: [^{177}Lu]Lu-PSMA is widely used for radioligand therapy of recurrent prostate cancer. To minimize the radiation dose for staff members and increase reliability and reproducibility of the production process while ensuring GMP-compliant production conditions, fully automated synthesis modules are an applicable tool. To our knowledge, the production of [^{177}Lu]Lu-PSMA-I&T has only been reported for different automated synthesis modules than the one we used for this study[1,2]. Here, we report and compare the results of the synthesis of [^{177}Lu]Lu-PSMA-I&T on the Modular Lab (ML) eazy from Eckert & Ziegler using one or three patient doses (in one batch) for clinical application. **Materials and Methods:** 14 µg/GBq PSMA-I&T GMP-grade (1 mg/mL in TraceSelect water) in 2.5 mL sodium ascorbate buffer (pH 4,5) were reacted with 6.8 GBq or 25.9 GBq [^{177}Lu]Lutetium chloride at 90 °C for 15 minutes. The crude product was purified via passing through a CM cartridge. After the synthesis, the following quality control parameters were determined: The radiochemical purity was evaluated using radio-HPLC and iTLC. Endotoxin concentration was determined via LAL-test. The pH of the product solution was measured. Sterility was evaluated referring to the Ph. Eur. method. Results: All syntheses were successful. The radiochemical yield for one patient dose (n = 3) ranged between 77.8% and 96.7%. The radiochemical purity determined by radio-HPLC was 99.7 ± 0.1% and by iTLC 99.7 ± 0.3%. The pH value of the product solution was 4.47 ± 0.26. For 3 patient doses in one batch the radiochemical yield was 97.5%. The radiochemical purity was 98.7% (HPLC) and 99.9% (iTLC). The pH of the product solution was 4.46. All samples showed an endotoxin concentration <5 IE/mL and were sterile. **Conclusion:** The fully-automated productions of [^{177}Lu]Lu-PSMA-I&T were successfully performed on the ML eazy module. Both, single dose and multi-dose synthesis, provided the product in excellent radiochemical yield and purity. Therefore, the synthesis module can be used for convenient, reliable and safe production of [^{177}Lu]-PSMA-I&T in a GMP environment for clinical application. The precursor amount of 40 µg/GBq recommended by the manufacturer could significantly be reduced to 14 µg/GBq to enable a more cost-effective production of the radiopharmaceutical. **References:** 1. Sørensen MA, et al. Automated synthesis of ^{68}Ga/^{177}Lu-PSMA on the Trasis miniAllinOne. J Labelled Comp Radiopharm. 2020;63(8):393-403. 2. Weineisen M, et al. ^{68}Ga- and ^{177}Lu-Labeled PSMA I&T: Optimization of a PSMA-Targeted Theranostic Concept and First Proof-of-Concept Human Studies. J Nucl Med. 2015;56(8):1169-76.

EPS-055

Validation of an analytical method on HPLC for ^{177}Lu-PSMA-1

***C. Brentot**, A. Revy, L. Batret, S. Levesque, F. Cachin, M. Tempier; Centre de lutte contre le cancer Jean Perrin, Clermont-Ferrand, FRANCE.*

Aim/Introduction: The prostate-specific membrane antigen (PSMA) is a type II glycoprotein which is over-expressed in prostate cancer tissue. Radioligand therapy using PSMA ligands labeled with lutetium-177 (^{177}Lu-PSMA) is the subject of many publications, particularly concerning castration-resistant prostate carcinoma. In France, in order to provide access to this treatment while awaiting marketing, the drug authorities have set up a compasionate use for ^{177}Lu-PSMA-1. In order to obtain this authorisation, the drafting of an Investigational Medicinal Product Dossier (IMPD) containing, in particular, the preparation and control steps of the finished product is required.The objective of this study is to show the different steps of the analytical control by HPLC of ^{177}Lu-PSMA-1 for the writing of our IMPD. **Materials and Methods:** On our radio-HPLC, a 150mm x 3mm C18 column is heated to 40°C. The solvents used are Water/TFA 0.1% and Acetonitrile/TFA 0.1%. The analysis time is approximately 28 minutes. In accordance with the EANM and the ICH (International Council for Harmonisation) guidelines, the analytical procedures tested with their Acceptance criteria (AC) were: linearity (coefficient of determination (R^2)≥0.99), detection (1%) and quantification limit, repeatability (CV<2%). Linearity of 177LuCl3 detection was also tested (R^2≥0.99). Linearity was determined over a concentration range of 2.5 to 25µg/mL, on 3 different days (D). The integration of the ^{177}Lu-PSMA-1 peak was performed identically on all 5 concentration points. The limit of detection and quantification was measured by integrating blanks over the same retention time as the final product peak. The repeatability was done by measuring at the same concentration, 6 consecutive times on 3 different days. Finally, the linearity of detection of $^{177}LuCl_3$ was tested from 3 samples over 3 different days in 5 points. Results: The linearity of the standard reference was validated with an R^2 of 0.9943 with a non-zero slope tested by a 5% Fisher test.

The limits of detection and quantification are 1.55µg/mL and 1.62µg/mL respectively over our linearity range. The CV of repeatability is 1.76%, which means that our method is repeatable. Finally, the linearity of detection of $^{177}LuCl_3$, was validated with R^2 at D1, D2, D3 respectively of 0.9996, 0.9998 and 0.9997. **Conclusion:** The validation of this analytical method allowed us to identify but also to precisely quantify the ^{177}Lu-PSMA-1 synthesised on 3 batches to finalise our IMPD. **References:** None

EPS-056

EU vs US radiopharmaceutical manufacturing and dispensing modalities

C. Ignace[1], O. Koper[2], L. Augustine[3];
[1]Cardinal Health, Mesa, AZ, UNITED STATES OF AMERICA, [2]Cardinal Health Nuclear and Precision Health Solutions, Dublin, OH, UNITED STATES OF AMERICA, [3]Cardinal Health Nuclear and Precision Health Solutions, Omaha, NE, UNITED STATES OF AMERICA.

Aim/Introduction: Radiopharmaceuticals are a hyper-regulated segment of the drug market across the world, as multiple agencies guarantee their safety and efficacy, as well as the safety of personnel handling isotopes. To ensure rapid and successful clinical development and commercialization of diagnostic and therapeutic nuclear drugs, it is important to have strong awareness of the compliance requirements within various territories. This presentation highlights differences between the US and European radiopharmaceutical spaces that must be integrated into the development process. **Materials and Methods:** This presentation will look at the control points behind nuclear drug product manufacturing and patient dose dispensing across both territories. We will cover briefly International Council for Harmonisation (ICH) Guidance regarding pre-commercial development and the interpretation of Good Manufacturing Practice requirements. We will discuss and compare the role of nuclear pharmacies in patient dose preparation and dispensing across both geographic areas, looking at regulatory control points and associated limitations and advantages. Results: This review shows that the pharmaceutical manufacturing control points are similar between the EU and US, which supports a unified development of clinical programs and Chemistry, Manufacturing and Controls (CMC) information. The patient dose preparation and dispensing modalities are where most differences between EU and US are noted, especially regarding the practice of pharmacy. At its core, the EU regulations emphasize the role of local/hospital radiopharmacies about extemporaneous preparation and dispensing of patient unit doses from a drug product vial. The US model allows the same practices, however, US clinical/medical centers may also operate without the full functionality of an on-site radiopharmacy and instead rely on 3rd party local, regional or centralized radiopharmacies for the preparation and dispensing of patient-ready doses in dedicated vial(s) or syringe(s). US radiopharmacies can also play a critical role in a clinical site waste management program, which is especially important for long lived isotopes. Differences in dispensing modalities between the EU and the US can challenge a drug development program, such as decisions regarding product dosage form, as well as impact product level utilization, customer acceptance, market penetration, operating costs and ultimately profitability. **Conclusion:** Understanding the latitude afforded by the Board of Pharmacy to US radiopharmacies is critical for EU drug developers to make optimal design and commercial decisions upfront. Beyond supporting compliance and ensuring product market acceptance, this is also key to ensuring a program profitability and mitigation of unique liabilities for both diagnostic cand therapeutic (theranostic) nuclear drugs. **References:** None

EPS-057

Time-dependent sterility testing to determine the viability of microorganisms and autosterilisation in radiopharmaceutical therapeutics

A. Gummesson[1], G. Schwenk[2], S. Knolle[2], S. Protze[2], S. Weißflog[2], M. Joksch[1], B. J. Krause[1], C. Bergner[1];
[1]Department of Nuclear Medicine, Rostock University Medical Center, Rostock, GERMANY, [2]CUP Laboratorien Dr. Freitag GmbH, Radeberg, GERMANY.

Aim/Introduction: Sterility testing is used to assess the presence or absence of microorganisms in products made for human use. Most products can usually be tested directly after production, radiopharmaceuticals mostly with a significant time delay. Only few laboratories are equally authorized to handle radioactivity, and are also equipped to carry out sterility tests. According to the Radiation Protection Regulations, samples can only be sent from the manufacturing laboratory to a test laboratory without an authorization to handle radioactive materials after reaching the legal limit for unrestricted release of a particular nuclide ([^{177}Lu]Lutetium: 100 Bq/g). For the usual range of [^{177}Lu]Lutetium-activities applied in the synthesis of radiopharmaceuticals this would correspond to a decay time of 20 to 22 weeks. The aim of this project is to develop a concept for monitoring the sterility over the mentioned period of sample storage under varying storage conditions. **Materials and Methods:** Different sample compositions starting from the pure sample matrix to the manufactured [^{177}Lu]Lu-DOTATOC sample were used. According to USP and EP regulations, the inoculation of ultimately nine different types of microorganisms in two different amounts varying from 10 to 150 CFU was used. Bioburden or sterility tests was carried out for samples with varying activity concentrations between 0.07 GBq/mL and 0.49 GBq/mL. Individual batches were stored at 4 °C or at room temperature, respectively, and tested at least three points over time. Results: Time-dependent bioburden or sterility testing was used to determine the impact

of the radiopharmaceutical matrix to autosterilisation during long term storage of [^{177}Lu]Lutetium-containing radiopharmaceuticals. It was shown that in addition to the impact of radioactivity the non-radioactive buffered matrix of the radiopharmaceutical preparation significantly limits the survival of microorganisms. **Conclusion:** The survival rate of microorganisms in radiopharmaceutical preparations is very low, so that early sterility tests are required. Further research is necessary to address these effects either to a non- or poor-nutritive situation or to certain components of the matrix. Additionally, the time window has to be validated in which a sterility testing is reliable and will not lead to false negative results. Apart from this, the question of transferability to other nuclides and radiopharmaceutical preparations will have to be addressed. **References:** [1] StrSchV, 29.11.2018, p. 111. [2] EP, Chapter 2.6.1, Sterility, 8th edn, 2014. [3] USP, Chapter 71, Sterility, US Pharmacopeial Convention, Rockville, MD, 2014. [4] Technische Regeln für Biologische Arbeitsstoffe 460. [5] Technische Regeln für Biologische Arbeitsstoffe 466.

EPS-058

New radiopharmaceutical synthesis : Stability study of ^{177}Lu-PSMA-1

***L. Batret**, C. Brentot, A. Revy, S. Levesque, M. Tempier;*
Centre Jean Perrin, Clermont Ferrand, FRANCE.

Aim/Introduction: ^{68}Ga/^{177}Lu theranostic pair is a promising pathway of targeted therapy in prostate cancer treatment. French health authorities have allowed compassionate use concerning PSMA-1 which involves redaction of an investigational medicinal product dossier (IMPD) including synthesis of 3 validation batches and stability study of ^{177}Lu-PSMA-1. **Materials and Methods:** ^{177}Lu-PSMA-1 synthesis was developed on miniAIO (TRASIS). Stability study was performed on each batch 3, 24 and 48 hours after radiolabelling (conservation at room temperature: 23°C +/- 2°C). For each batch, quality controls were realized at each time and results were compared with T_0 and expected specifications: solution aspect, pH determination and radiochemical purity (RCP) by HPLC. In addition, volume activity decay corrected (A_{vol}) has been quantified by aliquoting each batch at each time and compared to initial results. Results: The three batches of ^{177}Lu-PSMA-1 were conformed with IMPD specifications at T_0. At each time, pH solution was the same for each batch (5 +/- 0.5, expected values: [4; 8]). Regarding RCP, minimum value observed was 97,58% for batch 1 (T_{+48h}) vs 99.53% at T_0, 98.69% for batch 2 (T_{+48h}) vs 99.44% at T_0 and 97.52% for batch 3 (T_{+48h}) vs 99.44% at T_0. All RCP results are higher than our IMPD limit (> 95%). Part of free Lutetium was always under 0.2% (max 0.14% for batch 1, 0.08% for batch 2 and 0.14% for batch 3), also attesting to the stability of ^{177}Lu-PSMA-1 and no dissociation of ^{177}Lu from the PSMA-1. About alteration of final product due to conservation in glass vial : A_{vol} measurement allowed us to say that there was no sorption process between the solution and the container. Indeed the A_{vol} variation was at maximum 3.28% for batch 1 (T_{+48h}), 5.34% for batch 2 and 4.35% for batch 3 (T_{+3h}). **Conclusion:** Stability is sufficient to allow ^{177}Lu-PSMA-1 conservation during 48h after synthesis. ^{177}Lu-PSMA-1 could be prepared the day before the administration to the patient, allowing easy and efficient planning within the Radiopharmacy unit. In each case, a last HPLC will be run just before injection. Results were included in our IMPD and send to French authorities who reviewed and validated it in March 2021. **References:** None

EPS-059

Optimization of Radiolabelling of [^{68}Ga]Ga-Macroaggregated Albumin

***P. Bhardwaj**[1,2], S. Mithun[1,2], A. K. Jha[1,2], P. Kamble[1,2], K. Chitnis[1,2], A. Nautiyal[1,2], V. Rangarajan[1,2];*
[1]Tata Memorial Hospital, Mumbai, INDIA, [2]Homi Bhabha National Institute (HBNI), Deemed University, Mumbai, INDIA.

Aim/Introduction: Ventilation and Perfusion (V/Q) scans are performed to diagnose pulmonary embolism (PE). [^{68}Ga]Ga-MAA is the most appropriate PET alternative of [99mTc]Tc-MAA to perform lung perfusion study, which can provide better image quality and resolution with improved diagnostic quality. Our study aimed to optimize labelling efficiency of [^{68}Ga]Ga-MAA with respect to number of particles and amount of activity and assess the in-vitro stability over a period of time. **Materials and Methods:** [^{68}Ga]Ga-MAA was labelled using commercially available lyophilized MAA kit with [^{68}Ga]$GaCl_3$ from ^{68}Ge/68Ga-Generator. MAA kit was reconstituted in saline and centrifuged at 3000rpm for 3min. Supernatant was discarded to remove $SnCl_2$ and free albumin from the mixture. This step was repeated four times and precipitated MAA was reconstituted in saline, fractionated and stored in freezer. Formulation of [^{68}Ga]Ga-MAA was performed by heating the mixture of [^{68}Ga]$GaCl_3$ and MAA fraction (pH:4-5) for 20 min at 85°C as protocol mentioned by S. Mithun et al. (1) using differential amounts of particles and activity. The radiochemical purity (RCP) of [^{68}Ga]Ga-MAA was performed using ITLC with 0.1M Tri-Sodium Citrate as mobile phase. RCP of [^{68}Ga]Ga-MAA formulation was assessed with 50K,100K,200K and 250K particles of MAA and 3mCi [^{68}Ga]$GaCl_3$ as well as for 200k particles and 3,6,9, 12,15,20 and 23mCi [^{68}Ga]$GaCl_3$ to optimize the [^{68}Ga]Ga-MAA formulation with respect to the number of particles and amount of activity. Then in-vitro stability of [^{68}Ga]Ga-MAA was assessed post formulation. Results: The overall labelling efficiency was found to be 97.97 ± 1.17%. The mean RCP of 50k,100k,200k and 250k particles using average [^{68}Ga]$GaCl_3$ activity 3.19±0.21 were 92.8±0.04, 95.5±1.2, 93.3±0.24 and 94.4±0.72 respectively. The 0,1,2,3 and 4hour average radiochemical purities using 200k particles with varying amounts of activities

were 97.97±1.17, 98.18±1.20, 97.81±1.63, 97.57±1.84, and 97.55±1.93 respectively. The detailed average RCP over a period of time is shown in table1. **Conclusion:** Our study shows the formulation is stable with as low as 50K particles and as high as 200K particles. We also found that the radiochemical purity was consistent for the activity range mentioned above. Our study also shows that formulation remains stable upto 4 hours post formulation. **References:** 1)Sneha Mithun, Ashish K. Jha, Pradip Chaudhari, Bhabani Shankar Mohanty, Sharada Sawant, Nilendu C. Purandare, Archi Agrawal, Sneha Shah, Venkatesh Rangarajan. Optimization of in-house formulation of 68 Ga macroaggregated albumin using commercially available macro aggregated albumin cold kit. Indian J Nucl Med [serial online] 2016;31, Suppl S1:4-28. O-18.

EPS-060

Production of W-188/Re-188 generator based on Al_2O_3

M. Karamivand, F. Johari, M. Davarpanah;
Pars Isotope, Tehran, IRAN, ISLAMIC REPUBLIC OF.

Aim/Introduction: Rhenium-188 is a beta and gamma emitter with a 16.98 hour half-life, it may form complexes. It allows synthesizing radiopharmaceuticals for diagnostics and therapy of malignant tumors, bone metastases, rheumatoid arthritis and other diseases. The parent isotope is W-188.The advantage of this generator is the presence of both beta and gamma radiation components (2.11 MeV, 0.155 MeV). **Materials and Methods:** For radioactive works, the hot cells were used. The beginning of tungsten activity was transferred into Hot cell. The preparation conditions of an alumina based $^{188}W/^{188}Re$ generator are reported. Initially, the W and Re sorption behavior on alumina in NaCl and HCl medium was performed evaluating the following parameters: medium pH, alumina size particle, and Column (7 mm × 120 mm). Results: The activity of W-188 loaded in the generator was 310 mCi.Data on W-188/Re-188 generator efficiency and quality control(Duration of observation 2 week) To show that the Re-188 can be used for radiolabeling, we performed radiolabeling experiments with octreotide and Bombesin developed chelator. **Conclusion:** We have developed and optimized an W-188/Re-188 generator to provide more than 300 mCi amounts of Re-188 on a daily basis. **References:** None

EPS-061

Comparison of the performance of four purification cartridges in the synthesis of 68Ga-PSMA-11

J. Stein[1], Q. Citerne[1], N. Veran[1], B. Demoré[1,2];
[1]Nancy University Hospital, Pharmacy Department, Vandoeuvre-lès-Nancy, FRANCE, [2]Lorraine University, EA 4360 APEMAC, Nancy, FRANCE.

Aim/Introduction: Gallium 68 (Ga-68) is currently the essential radionuclide for peptide labeling in PET imaging, including 68Ga-PSMA-11 (Prostate Specific Membrane Antigen) for the detection of prostate cancer recurrence. Ga peptide labeling usually requires four steps: generator elution, radiolabeling, purification on a solid phase extraction (SPE) cartridge and sterilizing filtration. The reaction mixture purification through the cartridge is a critical step in the synthesis for removal impurities as "unvectorized" Ga-68 which can be found in several chemical forms. The objective of this study is to compare the purification performance of different SPE cartridges by the behavior of unvectorized Ga-68. **Materials and Methods:** Four cartridges are tested: C18, tC18, HLB and HLB Prime. A mixture of Ga-68 (in 0.1M hydrochloric acid from generator elution) and acetate buffer 0.8M (pH = 4.5) are injected through a SPE cartridge using the 68Ga-PSMA-11 synthesis as method : SPE activation (according to supplier), radionuclide deposit, rinsing with water for injection (WFI), dropping out with a mixture (50/50 v/v) of WFI and ethanol and reformulation with sodium chloride. Activities are measured and decay corrected after each step. The manipulations are carried out in triplicate. Results: After the rinsing with WFI step, the unvectorized Ga-68 mostly remains bounded on the SPE for C18 (96.8%) and HLB Prime (98.9%) and in a lower proportion for tC18 (64.7%) instead of HLB cartridge where most of Ga-68 is eliminated (64.2%). For the latter, a higher standard deviation is observed (5.5%) against C18 (0.8%), HLB Prime (0.2%) and tC18 (2.4%). To the end product after dropping out and reformulation, the C18 cartridge appears to be the best performing SPE with only 0.8% unvectorized Ga-68 release from the cartridge. HLB Prime and tC18 give good purification performances too with 1.6% of unvectorized Ga-68 for each. To finish, HLB shows the lowest unvectorized Ga-68 elimination performance with 13.9% to the end product. Again, a higher standard deviation is observed (1.7%) than for the other cartridges (0.1% for C18 and tC18 and 0.2% for HLB Prime). The HLB cartridge appears to be the least effective and least reproducible SPE. **Conclusion:** With the lowest amount of unvectorized Ga-68 released in the final product, C18 offers the highest performances for Ga-68 labeling peptide purification. HLB prime and tC18 can be alternatively used according to the peptide behavior on the SPE. HLB shows inferior results and should be used only with high efficiency Ga-68 labeling. **References:** None.

EPS-062

Quality Control of [^{68}Ga]Ga-PSMA-11 injectable solutions: preparation of a long-term stable PSMA-11 reference solution (3 µg/mL) for Chemical Purity determination

A. Iudicello[1], F. Genovese[2], S. Boschi[3];
[1]Pharmaceutical Department, Azienda USL of Modena and Nuclear Medicine Unit, Azienda Ospedaliero-Universitaria of Modena, Modena, ITALY, [2]Centro Interdipartimentale Grandi Strumenti, University of Modena and Reggio Emilia, Modena, ITALY, [3]Department for Life Quality Studies, University of Bologna, Bologna, ITALY.

Aim/Introduction: The [^{68}Ga]Ga-PSMA-11 is the radiopharmaceutical of choice for imaging of Prostate Cancer. While performing the QC of the [^{68}Ga]Ga-PSMA-11 injectable solutions according to Ph. Eur. Monograph "Gallium (^{68}Ga) PSMA-11 injection" we observed a lack of long-term stability of the PSMA-11 reference solution b (3µg/mL) stored at -25°C. The aim of this study was to investigate the causes of PSMA-11 instability to obtain a long-term stable (> 30 days) reference solution b. **Materials and Methods:** A series of analyses were performed to investigate if the side product formation was due to an impurity, an acidic degradation caused by TFA, or to the HBED-CC tendency of chelating metal ions already at room temperature. Initially, the PSMA-11 reference solution b was prepared only with metal-free water. Since the obtained chromatograms showed the side product presence also in this solution during the storage at -25°C, the role of HBED-CC chelator in the side product formation was investigated. The HBED-CC is an acyclic chelator based on an EDTA-type structure. A large excess of EDTA was added to a PSMA-11 reference solution b, prepared with metal-free water and TFA, showing the contaminant compound, with and without heating at 50°C after adding EDTA. Clarified the role of the HBED-CC in the side product formation, a long-term stable PSMA-11 reference solution b was finally prepared by dissolving the PSMA-11 in a solution obtained by adding EDTA (10mg/mL) to the solvent mixture of metal-free water and TFA (0.1% v/v), which has been incubated for one night at 50°C to remove the metallic contaminants from the environment. Results: After adding EDTA to a PSMA-11 reference solution b showing the contaminant compound, the chromatographic peak area of the side product decreased over time in favor of the chromatographic peak area of PSMA-11. The complete transchelation effect of EDTA required 48 hours without heating and 5 hours with heating the solution after adding EDTA (the percentage of the side product decreased from an average of 70% to an average of 0.8%). The role of the HBED-CC in the side product formation was confirmed by a UHPLC-HRMS analysis which showed that the side product is likely a complex between HBED-CC and environmental Fe(III). **Conclusion:** The Added EDTA to PSMA-11 reference solution b permitted to prepare a long-term stable reference solution (until 12 months) and to implement Ph. Eur. analytical method for PC determination, that is suitable, fast, and routinely reproducible. **References:** none

EPS-063

Development of ^{211}At and ^{125}I Radiopharmaceuticals for Pretargeted Radioimmunotherapy of Disseminated Cancer

C. Timperanza[1], H. Jensen[2], E. Aneheim[1,3], S. Lindegren[1];
[1]Department of Medical Radiation Science, Institute of Clinical Sciences, Sahlgrenska Academy, University of Gothenburg, Gothenburg, SWEDEN, [2]Cyclotron and PET Unit, KF-3982, Rigshospitalet, Copenhagen, DENMARK, [3]Region Västra Götaland, Sahlgrenska University Hospital, Department of Oncology, Gothenburg, SWEDEN.

Aim/Introduction: To enhance the therapeutic efficacy of radioimmunotherapy of cancer, several pretargeting strategies have been developed. In pretargeted radioimmunotherapy, the tumour is pretargeted with a modified monoclonal antibody that has affinity for both, tumour antigen and radiolabelled carrier. A big challenge in cancer treatment is the elimination of occult disseminated tumour cells, in this context alpha emitter Astatine-211 has drawn attention due to its physicochemical characteristics. The aim is to design new molecules for pretargeting applications and to evaluate these substances to optimize the pharmacokinetics. It comprises development of a new pretargeting drug delivery strategy based the Diels Alder click chemistry system (Tetrazine/Trans-cyclooctene) adopting Astatine-211 and Iodine-125 as radionuclides. **Materials and Methods:** The effector molecule was synthesized first attaching N-Succinimidyl-3-(trimethylstannyl)-benzoate, Tetrazine-NHS ester and Succinic Anhydride to a poly(L)lysine (PL) scaffold (HTzPL or MeTzPL) in carbonate buffer pH 8,5. Then a dry astatine residue was activated with N-iodosuccinimide followed by electrophilic substitution of the trimethyl-tin group on the H(or Me)TzPL precursor, resulting in an Astatinated product. Purification was performed eluting the product in PBS on illustra NAP-5 column. Radiochemical purity of the product was determined within radio-TLC using 75% Methanol/Ethyl acetate elution. Finally, Tco-Agarose beads were used to assess the Tetrazine/Tco binding after radiolabelling. Results: Astatinated HTzPL resulted in 78% of radiochemical yield and 95% of radiochemical purity, determined after radio-TLC measuring on a gamma counter. It is also possible to iodinate both, HTzPL and MeTzPL, with ~82% of radiochemical yield and 99% of radiochemical purity. Preliminary studies on Tco-beads have shown a binding >93% using an excess of Tco over Tetrazine in the first 30 minutes to reach a value >97% after one hour. Unspecific protein binding, ~30%, has been noticed to the membrane of the centrifuge tube, therefore, different filters need to be used. **Conclusion:** A protocol for

the synthesis and radiolabelling of the PL based tetrazine-effector molecule has been developed. High radiochemical yield and radiochemical purity can be obtained in the astatination and iodination of the TzPL, resulting in a good binding to Tco. H-Tetrazine is reported to react faster than the Me-Tetrazine with Tco, which would be a great advantage when administered in vivo, but it is also less stable. Comparative studies are thus being performed to assess the characteristics of each compound. Additional in vitro and in vivo studies will be carried out for the full evaluation and optimization of the different Tetrazine effectors. **References:** None.

812

Wednesday, October 20 - Saturday, October 23, 2021

on-demand pool, release on Wednesday, October 20 at 09:00

e-Poster Presentation Session 5: Theranostics

EPS-064

Synergy when treating ovarian cancer cell lines with Radium-224 and PARP inhibitors

M. Malenge, T. B. Bønsdorff;
Oncoinvent AS, Oslo, NORWAY.

Aim/Introduction: Ovarian cancer is the leading cause of gynaecological cancer mortality. Despite the efficacy observed after cytoreductive surgery and first-line chemotherapy, disease relapse is reported in the majority of patient subsets. PARP inhibitors are prescribed as maintenance therapy for patients with ovarian cancer after first-line therapy to decimate residual disease. The inhibitors have demonstrated improved therapeutic value particularly in patients with characteristic mutational signatures. However, the therapeutic value is often transient due to the development of resistance. PARP inhibitors are known to sensitize cells to radiation due to prolonged modulation of DNA damage repair. This highlights the interest in combining PARP inhibitors with radionuclide therapy. Improved therapeutic effect of alpha therapy in combination with PARP inhibitors has been demonstrated in non-clinical studies. Alpha emitting radionuclides deliver high energy radiation to the target cells inducing irreversible double-strand DNA breaks. In this study we evaluate the potential of combining radium-224 (^{224}Ra), an alpha-emitter with 3.6 days half-life and the PARP inhibitors olaparib and niraparib for inhibition of growth of ovarian cancer cell-lines. **Materials and Methods:** The combination effect of ^{224}Ra with olaparib and niraparib was evaluated in two human non-BRCA-mutated ovarian cancer cell-lines: ES-2 and SKOV-3. The cells were simultaneously treated with ^{224}Ra and PARP inhibitors at escalating concentrations, inversely-proportioned concentrations and at one-point concentrations of one drug with escalating concentrations of the combining drug. Cell proliferation was measured 72, 96 and 120 hours after initiation of treatment. The combination index (CI) was calculated using the Chou-Talalay method for drug combination based on the median-effect principle where CI<0.9 is synergistic, 0.9<CI<1.1 is additive and CI>1.1 is antagonistic. Results: The CI between the 2 cell-lines was heterogenous across the tested range depending on the PARP inhibitor used in the combination, the concentrations of the combined drugs and the timepoint of assessment. The SKOV-3 cells were more resistant to all the individual treatments when compared to the ES-2 cells. The cells were more sensitive to niraparib treatment compared to olaparib. Synergism was attained in both ES-2 and SKOV-3 cell lines. The CI values representing the attained synergism for both the PARP inhibitors in combination with ^{224}Ra were between 0.4-0.85. **Conclusion:** We have shown that combination treatment with ^{224}Ra and PARP inhibitors is synergistic in non-BRCA-mutated ovarian cancer cell-lines. These findings highlight the need for further non-clinical evaluation of the potential translation value for ovarian cancer in patients with no mutational signatures. **References:** none

EPS-065

Theranostic Approach of CD38 and IL-1RAP Positive Haematological Malignancies Based on Radiolabelled Antibodies

J. Frenay[1], P. Bellaye[1], M. Moreau[2], C. Rossi[3], O. Casasnovas[3], L. Ringenbach[4], C. Ferrand[5,6], B. Collin[1,2];
[1]Centre Georges François Leclerc, Dijon, FRANCE, [2]Institut de Chimie Moléculaire de l'Université de Bourgogne, ICMUB, Dijon, FRANCE, [3]CHU Dijon Bourgogne - Hôpital François Mitterrand, Dijon, FRANCE, [4]Diaclone, Besançon, FRANCE, [5]CanCell Therapeutics, Besançon, FRANCE, [6]Etablissement Français du Sang de Bourgogne Franche-Comté, Besançon, FRANCE.

Aim/Introduction: Haematological malignancies define highly heterogeneous diseases with highly variable prognosis. Resistance to currently available therapies is a hallmark of leukaemia and lymphoma, and significantly accounts for treatment failure. Thus, discovery of novel therapies in association with novel companion biomarkers is crucial to promote personalized medicine and improve patient outcome. Thus, our preclinical work aims at developing two probes with theranostic capabilities, based on radiolabelled monoclonal antibodies targeting IL-1RAP and CD38, two biomarkers overexpressed in acute myeloid leukaemia (AML), myeloma and some lymphomas. **Materials and Methods:** MonoMac-6 (MM6), Ramos (Ra-1) and SU-DHL-5 cell lines were used as subcutaneous tumour models of IL-1RAP$^+$ leukaemia, CD38$^+$ lymphoma and CD38$^-$ lymphoma respectively. A total of 10x10^6 MM6, Ra-1 or SU-DHL-5 cells were implanted subcutaneously in the right flank of irradiated NOD-SCID mice. An anti-IL-1RAP

antibody (clone B-L43) and Daratumumab targeting CD38 were bioconjugated with DTPA and DOTAGA respectively, for radiolabelling with 111-Indium (^{111}In-DTPA-IL1RAP and ^{111}In-DOTAGA-Daratumumab). In vitro binding assays were performed to ensure that bioconjugation did not alter the affinity of antibodies for their respective targets. ^{111}In-DTPA-IL-1RAP and ^{111}In-DOTAGA-Daratumumab were injected i.v. in MM6-, RA-1- or SU-DHL-5-tumour bearing mice respectively (10MBq per mice in 100µl, n=6). For ^{111}In-DTPA-IL-1RAP, a blocking experiment (mice receiving a 100x excess of cold anti-IL1RAP antibody). Mice underwent SPECT/CT imaging at (24h/48h/72h and 144h post-injection and ex vivo gamma counting was performed after sacrifice. Results: SPECT imaging of ^{111}In-DTPA-IL-1RAP showed the highest tumour uptake at 144h post-injection (29.7 ± 1.6 %ID/g) with a significantly lower uptake in tumours receiving ^{111}In-DTPA-IL-1RAP and a 100x excess of cold anti-IL1RAP antibody (blocking experiment: 9.2 ± 1.0 %ID/g). These results were confirmed by ex vivo gamma counting. SPECT imaging of ^{111}In-DOTAGA-Daratumumab showed significantly higher uptake in CD38$^+$ tumours (RA-1) compared with CD38$^-$ tumours (SU-DHL-5). **Conclusion:** Our SPECT imaging probe targeting IL1-RAP was found to be a promising imaging agent to detect IL-1RAP$^+$ tumours and may be of interest as a companion diagnostic for a recently designed anti-IL-1RAP CAR-T cells therapy that will be evaluated in a future first in man clinical trial. Similarly, ^{111}In-DOTAGA-Daratumumab revealed to be a promising tool for specific detection of CD38$^+$ tumours and hold promises as a diagnostic tool to improved patient selection and monitoring in CD38$^+$ malignancies. Moreover, both of these probes have another theranostic feature based on the possibility to switch for other radionuclides suitable for PET (translational relevance, e.g. copper-64) or therapy (e.g. lutetium-177). **References:** None

EPS-066

^{99m}Tc-Tilmanocept SPECT Imaging As A Potential Non-Invasive Method To Quantify CD206$^+$ Tumor Associated M2-Like Macrophages

A. Bouchard[1,2], H. Sikner[1,2], M. Moreau[3], E. Limagne[2], P. Bellaye[1,2], E. Kohli[1,4,5], B. Collin[4,2,3];
[1]UMR INSERM/uB/AGROSUP 1231, Team 3 HSP-Pathies, labellisée Ligue Nationale contre le Cancer and Laboratoire d'Excellence LipSTIC, Dijon, FRANCE, [2]Centre anti-cancéreux Georges François Leclerc, Dijon, FRANCE, [3]UMR uB/CNRS 6302, Institut de Chimie Moléculaire, Dijon, FRANCE, [4]UFR des Sciences de Santé, Université de Bourgogne, Dijon, FRANCE, [5]CHU, Dijon, FRANCE.

Aim/Introduction: In the era of personalized medicine in oncology, progress regarding the modulation of tumor microenvironment (TME) and its follow-up by molecular imaging is of crucial importance because of its central role in the development of cancer. Among TME immunosuppressive cells, M2-like macrophages have been associated with cancer aggressiveness, therapy resistance and poor prognosis. The aim of our study was to assess if M2-like macrophages (i) could be tracked in vivo into the TME with SPECT imaging and (ii) could be modulated by inhibition of Gp96, an endoplasmic reticulum chaperone involved in inflammatory processes that we have previously shown to be expressed at the cell membrane of human primary M2 macrophages (1) **Materials and Methods:** Tissues from mouse triple negative breast cancer (4T1 cell line) and colon cancer (CT26 cell line) were analyzed by immunohistochemistry (IHC) to detect the presence of Gp96 and CD206 (marker of M2 macrophages) into the TME. Specific CD206 in vivo imaging on 4T1- and CT26-tumor bearing mice receiving or not a specific inhibitor of Gp96 (PU-WS13) was performed with ^{99m}Tc-Tilmanocept SPECT (i.v injection, 15MBq/mouse). Images were performed at 1h, 4h and 24h post-injection. Ex vivo gamma counting of tumors was performed after the last imaging. Radioactivity content measured with gamma counting or on images was expressed as percentage of injected dose per gram of tissue (%ID/g). For 4T1 tumors, tumor growth and collagen content were assessed. Results: IHC experiments demonstrated an overexpression of Gp96 in tumor cells as well as the presence of M2-like macrophages expressing both CD206 and Gp96 in 4T1 tumors while CT26 tumors only showed an upregulation of Gp96. In addition, ^{99m}Tc-Tilmanocept tumor uptake was significantly higher in 4T1- compared to CT26-tumor bearing mice (2.53 %ID/g and 1.08 %ID/g respectively, p=0.009). Interestingly, PU-WS13 induced significant decrease in ^{99m}Tc-Tilmanocept tumor uptake compared to untreated mice (1.12 %ID/g and 0.78 %ID/g respectively, p=0.0011) and a lower number of CD206$^+$ M2-like macrophages compared to untreated mice. These results correlated with reduced tumor growth and collagen content in 4T1 tumors. **Conclusion:** ^{99m}Tc-Tilmanocept SPECT imaging might represent an innovative non-invasive strategy to quantify CD206$^+$ tumor-associated macrophages as a biomarker relevant for prognosis, therapeutic prediction and/or monitoring of solid tumors. The potential effects of PU-WS13 on modulation of M2-like macrophages are currently investigated. **References:** (1) Chaumonnot et al. The HSP GRP94 interacts with macrophages intracellular complement C3 and impacts M2 profile during ER stress. Cell Death Dis. 2021

EPS-067

In Vitro and nanoSPECT/CT Imaging of Long-acting Radiolabeled PSMA Peptide in Animal Model of Prostate Cancer Bone Metastasis

***Y. Huang**, M. Chen, S. Chen, S. Lo, S. Lo, S. Li, L. Chen, M. Li, C. Chang, S. Farn;*
Institute of Nuclear Energy Research, Taoyuan, TAIWAN.

Aim/Introduction: Prostate-specific membrane antigen (PSMA) is highly expressed in prostate tumors and metastases. Duo to the expression pattern, PSMA-based

radiopharmaceuticals have become the new theranostic approach for metastatic castration-resistant prostate cancer (mCRPC), and ^{177}Lu-PSMA-617 is the leading PSMA-targeting radiotherapeutic agent in the field. The PSMA-INER-56, a molecule with PSMA-617 targeting activity and a novel albumin-binding motif, was designed to extend the blood retention time. Aims of this study were to evaluate binding affinity and cell uptake of PSMA-INER-56 peptide, and nanoSPECT imaging performance of ^{111}In-PSMA-INER-56 in LNCaP animal model of prostate cancer bone metastasis **Materials and Methods:** The binding affinity of the PSMA-617 and PSMA-INER-56 peptides for the PSMA was tested in a competition assay against ^{111}In-PSMA-617. The sum of the PSMA-bound fraction and the internalized fraction of ^{111}In-PSMA-INER-56 were determined on LNCaP and PC-3 cells. The final radioligand concentration was 0.2 nM. Animal model of prostate cancer bone metastasis was established by intra-femoral injection, and nanoSPECT/CT images were acquired at 1, 4, 24, 48, 72, 96 h postinjection of ^{111}In-PSMA-INER-56 (~500 µCi). Results: The radiochemical purity of radioligands was more than 90% analyzed by using radio-TLC and radio-HPLC. The cell uptake and internalization of ^{111}In-PSMA-INER-56 on LNCaP cells increased over time, reaching a maximum value at 24 h after incubation with values 33.0 ± 3.4% and 12.6 ± 2.3% total radioactivity, respectively. Uptake in PC-3 cells was below 2% at every time point. In LNCaP cells, PSMA-INER-56 showed a higher binding affinity than PSMA-617 (3.35 nM vs. 10.36 nM). The results of nanoSPECT/CT imaging presented that high bone metastasis uptake of ^{111}In-PSMA-INER-56 reached a plateau at 4-24 h and retained at least 96 h. **Conclusion:** These results indicated that the high binding affinity and specificity of PSMA-INER-56. And novel albumin-binding motif, p-methyl-phenyl group, could improve circulation time of PSMA-INER-56, and the slow release of ^{111}In-PSMA-INER-56 from albumin might allow continual uptake in prostate cancer bone metastasis. For future preclinical studies, we are going to evaluate whether ^{177}Lu-PSMA-INER-56 has better therapeutic efficacy in metastatic prostate cancer compared to ^{177}Lu-PSMA-617 at equal treated dose. **References:** none

EPS-068

Assessing potential damage to the healthy vascular endothelium from targeted radiopharmaceutical therapeutics

R. Ramadan[1], *L. Geenen*[1], *N. Daems*[1], *A. Aerts*[1], *S. Baatout*[1,2]; [1]*Radiobiology Unit, Blegian Nuclear Research Centre (SCK CEN), Mol, BELGIUM,* [2]*Department of Molecular Biotechnology, Ghent University, Ghent, BELGIUM.*

Aim/Introduction: External beam radiotherapy (EBRT) is an effective treatment for many thoracic cancers; however, it is also associated with an increased risk for developing cardiovascular disease, especially atherosclerosis. Next to EBRT, more recently, systemic administration of targeted radionuclide therapy (TRT) is considered a promising cancer treatment and the number of patients treated by TRT is progressively increasing. For example, [^{177}Lu]Lu-DOTA-TATE, targeting somatostatin subtype 2 receptors ($SSTR_2$), was approved for gastroenteropancreatic neuroendocrine tumors treatment. Internal radiation exposure from TRT may affect the heart and the blood vessels. However, the possible cardiotoxicity risks from TRT have not been investigated before. We previously showed that endothelial connexin43 hemichannels contribute to radiation-induced endothelium damage, the first event in the atherosclerotic process, by mediating ROS, cell death, inflammation, and senescence. These events could be protected by blocking these hemichannels. Here, we investigate the potential cytotoxic effect of [^{177}Lu]Lu-DOTA-TATE on the vasculature, at the cellular and the molecular level, focusing on the role of connexin43 hemichannel. **Materials and Methods:** Since endothelial cells are the first contact with the radiopharmaceuticals after systemic administration, and endothelium dysfunction is the first event in the atherosclerotic process, two endothelial cell lines, Telomerase-immortalized human Coronary Artery (TICAE) and Microvascular Endothelial cells (TIME) were used. $SSTR_2$ expression in confluent TICAE and TIME cells were assessed via western blotting. Steady state analysis was performed on TICAE and TIME cells at 30 min, 1h, 4h, 24h and 48h incubation time with [^{177}Lu]Lu-DOTA-TATE. Further, membrane binding and internalization of [^{177}Lu]Lu-DOTA-TATE in TICAE and TIME cells were investigated after 2h incubation. In addition, cell metabolic activity (MTS assay) and hemichannel function (ATP release assay) were assessed at various time points for different added activities (0.1-20 MBq/ml). Results: Preliminary results indicate that quiescent TICAE and TIME cells do not express $SSTR_2$. TICAE and TIME cells showed neglectable binding and internalization characteristics for [^{177}Lu]Lu-DOTA-TATE. However, higher activities of [^{177}Lu]Lu-DOTA-TATE treatment, 10 MBq/ml and 20 MBq/ml, affected cell metabolic activity and connexin43 hemichannel opening in TICAE and TIME cells. **Conclusion:** These preliminary results indicate that the unbound radioactivity present in the culture medium may contribute to endothelial cell responses. Since opening of connexin43 hemichannel was observed, it would be interesting to further investigate the role of these channels in endothelial cell responses, such as apoptosis, DNA damage and senescence, after [^{177}Lu]Lu-DOTA-TATE treatment, and whether blocking these channels may provide potential radioprotective properties, as observed with EBRT. **References:** None

EPS-069

A local (para)sympathetic blockage to overcome PSMA ligand uptalke in salivary glands

V. Nail[1,2,3], P. Garrigue[1,2,3], A. Moyon[1,2,3], B. Louis[1,3], L. Balasse[1,3], S. Fernandez[1,3], G. Hache[1,2,3], D. Taïeb[1,2,3], B. Guillet[1,2,3];
[1]Aix-Marseille University, Centre Européen de Recherche en Imagerie Médicale (CERIMED), Marseille, FRANCE, [2]Assistance Publique-Hôpitaux de Marseille, CHU La Timone, CHU Nord, Nuclear medicine department, Marseille, FRANCE, [3]Aix-Marseille University, INSERM, INRA, Centre de Recherche en Cardiovasculaire et Nutrition (C2VN), Marseille, FRANCE.

Aim/Introduction: Radioligand therapy (RLT) coupled with nuclear imaging targeting for the prostate-specific membrane antigen (PSMA) have known a growth using beta or alpha emitter radionuclides. However, physiological salivary gland uptake appears to be a limiting-factor involving severe side effects such as xerostomia. Firstly, we investigated the ability of anticholinergic[1] and α-adrenergic drugs to decrease non-specific salivary gland uptake[1] using [^{99m}Tc]TcO_4^- radiotracers. Then, the accumulation into the salivary glands using [^{68}Ga]Ga-PSMA-11 has been evaluated with the best identified protocol. **Materials and Methods:** Balb/c mice were treated with atropine (1 or 15 mg.kg^{-1}, intraperitoneal route (i.p). or 15 mg.kg^{-1}, sublingual route (s.l.)), scopolamine (1 or 5 mg.kg^{-1}, i.p.), ipratropium (4 mg.kg^{-1}, s.l.) and phenylephrine (5 mg.kg^{-1}, i.p.) 15 minutes prior to [^{99m}Tc]TcO_4^- or [^{68}Ga]Ga-PSMA-11 injection. MicroSPECT/CT imaging (NanoSPECT/CT camera, Mediso, Budapest, Hungary) were performed 45 minutes post-injection (p.i.) (n≥3) and [^{68}Ga]Ga-PSMA-11 PET/CT (NanoSPECT/CT camera, Mediso, Budapest, Hungary) study was performed 90 minutes p.i. (n=7). Salivary gland SPECT ant PET signals were compared using a paired t-test. Statistical significance was defined as P≤0.05. Results: Regarding microSPECT/CT studies, total salivary gland uptake using atropine (15 mg.kg-1, s.l or i.p.) and scopolamine (5 mg.kg-1, i.p.) were significantly reduced compared to control groups, respectively from 41.35±10.68 %ID/g to 26.39±6.93 %ID/g (***P=0.0006), from 44.57±4.17 %ID/g to 30.31±6.03% ID/g (*P=0.0145) and from 35.78±7.64 %ID/g to 26.67±6.79 %ID/g (**P=0.0021). Other studied conditions did not show any significant effect on the salivary gland accumulation. The translation to [^{68}Ga]Ga-PSMA-11 using atropine (15 mg.kg-1, s.l.) showed a reduction from 171.07±56.05 %ID/g to 84.04±24.07 %ID/g (***P=0.0009) in the salivary glands. **Conclusion:** Screening experiments using [^{99m}Tc]TcO4- imaging showed that atropine based strategies have the better potential for decreasing salivary glands uptake. Sub-lingual atropine strategy showed a halving of salivary glands retention of [^{68}Ga]Ga-PSMA-11 opening up encouraging prospects for the protection of the salivary glands for PSMA vectorised internal radiotherapy. These results must now be evaluated in prostate cancer model to prove that the decrease of the salivary uptake has low impact on the tumor's as well. **References:** [1]Baum RP et al. Injection of Botulinum Toxin for Preventing Salivary Gland Toxicity after PSMA Radioligand Therapy: an Empirical Proof of a Promising Concept. Nucl Med Mol Imaging. 2018 Feb;52(1):80-1. [2]Rupp NJ, et al. First Clinicopathologic Evidence of a Non-PSMA-Related Uptake Mechanism for 68 Ga-PSMA-11 in Salivary Glands. J Nucl Med. 2019 Sep;60(9):1270-6.

EPS-070

Performance characterization of a multi pin-hole SPECT for preclinical imaging

L. Irazola[1], E. Prieto[1], M. Collantes[2], M. Ecay[3], I. Peñuelas[4], J. M. Martí-Climent[1];
[1]Medical Physics, Clínica Universidad de Navarra, Pamplona, SPAIN, [2]Translational Molecular Imaging Unit. Universidad de Navarra. IdiSNA & Nuclear Medicine Department, Clínica Universidad de Navarra, Pamplona, SPAIN, [3]2Translational Molecular Imaging Unit. Universidad de Navarra. IdiSNA, Pamplona, SPAIN, [4]Translational Molecular Imaging Unit. Universidad de Navarra. IdiSNA & Unidad de Radiofarmacia. Clínica Universidad de Navarra. IdiSNA, Pamplona, SPAIN.

Aim/Introduction: To characterize the U-SPECT6/E-class (MILabs, The Netherlands) with two stationary NaI detectors using preclinical protocols suggested by the manufacturer. **Materials and Methods:** System performance was evaluated for two different collimators with 75 pinholes: UHS-M (Phi_{FOV}=7 mm, 0.35 mm pin-hole) and UHR-RM (Phi_{FOV}=28 mm, 1 mm pin-hole).·Energy resolution: Point sources of 5 MBq of ^{99m}Tc,^{67}Ga,^{123}I and ^{177}Lu were prepared in an Eppendorf cup and acquired within 2 beds for UHR-RM and 5 beds for UHS-M. FWHM was calculated for each photo peak. Mean values for both collimators were obtained.·Sensitivity: Same experimental setting as that of energy resolution was used. Sensitivity of the system was calculated as total detected events subtracting background (counts) divided by activity at scan time (MBq) and total acquisition time (s).·Uniformity: 60 minutes acquisitions were performed for a 30 mL syringe filled up to 12 mL with 300 MBq of ^{99m}Tc for the UHR-RM (7beds), a 12 mL syringe filled up to 3 mL with 120 MBq of ^{99m}Tc for the UHS.M (19 beds), and four 12 mL syringes with 100 MBq each, placed in a multi-mouse bed with UHR-RM. A cylindrical VOI was centrally placed in the phantom (r=5 mm, L=8 mm for the 3 mL syringes, r=8 mm, L=8 mm for the 12 mL syringe). Uniformity was calculated as: (max-min)/(max+min)x100.·Spatial resolution: Visual inspection of the rods in a 60 min Jaszczak acquisition for 55.5 MBq and 229.4 MBq of ^{99m}Tc for UHS-M and UHR-RM, respectively, was performed. All images were reconstructed using typical parameters in daily routine: SROSEM algorithm, 4 iterations and 128 subsets. Voxel size of 0.4 mm and Gaussian filter with FWHM of 0.7 mm was used for UHR-RM while 0.8 voxel size and 1.2 mm filter was used for UHR-RM. Results: ·Energy resolution: For photon energies between 95 keV and 208 keV,

energy resolution was below 12%FWHM and remained stable while for lower energies resolution worsened up to 25% for 25 keV.·Sensitivity: 463 cps/MBq was obtained for UHR-RM and 2968 cps/MBq for UHS-M collimator for ^{99m}Tc.·Uniformity: a 39.0% and 34.2% uniformity was obtained for UHS-M and UHR-RM collimators, respectively. In the case of the multi-mouse bed, uniformity in each syringe ranged from 31.0% to 33.4%.·Spatial resolution: a 1.2 mm and 0.75 mm resolution was found for UHR-RM and UHS-M, respectively. **Conclusion:** The investigated U-SPECT6/Eclass systems has demonstrated to provide good performance for preclinical use. **References:** None

EPS-071

Extensive in vitro and in vivo evaluation of SSTR2-mediated uptake and biodistribution of radiolabeled somatostatin analogues after treatment with HDAC inhibitor valproic acid

M. Klomp, L. J. Hofland, L. van den Brink, P. M. van Koetsveld, F. Dogan-Oruç, L. W. de Kreij - de Bruin, C. M. de Ridder, D. C. Stuurman, M. de Jong, S. U. Dalm;
Erasmus MC, Rotterdam, NETHERLANDS.

Aim/Introduction: Increased SSTR2-mediated uptake of [^{111}In]In-DOTATATE after histone deacetylation inhibitor (HDACi) treatment has already been demonstrated in neuroendocrine tumor (NET) cell lines. Based on our own analysis, valproic acid (VPA) is one of the most promising HDACis for this purpose. However, the effect of VPA has only been demonstrated in vitro; the effect in vivo remains unknown. Therefore, our aim is to examine the effect of VPA on SSTR2-mediated uptake of radiolabeled DOTATATE in vitro and in vivo. **Materials and Methods:** NCI-H69 small-cell lung cancer cells were treated for 8, 16, 24, 40 and 48 hours with 0.96 mM VPA. Hereafter, internalization studies were performed by incubating cells with 1 nM [^{111}In]In-DOTATATE, +/- 1 µM unlabeled DOTATATE. Moreover, SSTR2 upregulation was examined using RT-qPCR. NCI-H69-tumor bearing NMRI-Foxn1 nu/nu male mice were intraperitoneally injected with VPA (200 or 400 mg/kg) or vehicle. Four and eight hours afterwards, mice were intravenously injected with 10 MBq/200 pmol [^{177}Lu]Lu-DOTATATE. Subsequently, biodistribution studies were performed 4 hours after radiotracer injection to determine %ID/g tissue. Tissues were collected for mRNA and immunohistochemistry analysis. Results: VPA rapidly increased [^{111}In]In-DOTATATE uptake in vitro. After 24 hours, enhanced uptake levels (1.9-fold, $p<0.0001$) and increased SSTR2 mRNA (1.7-fold, $p<0.0001$) were observed. Tumor uptake of [^{177}Lu]Lu-DOTATATE was only significantly increased in animals injected with VPA 8 hours prior to radiotracer injection; 8.03 ± 0.63, 15.93 ± 5.72 and 21.74 ± 9.88 %ID/g for vehicle, 200 mg/kg and 400 mg/kg, respectively. However, further analysis also demonstrated significant increased %ID in normal organs. No statistically significant differences in SSTR2 mRNA expression levels were found in tumors and other tissues (i.e. spleen and liver). A higher %ID in the blood circulation was demonstrated, indicating an increased clearance half-life of [^{177}Lu]Lu-DOTATATE after HDACi-treatment. This is presumably a consequence of renal tubular damage, which was observed using both VPA concentrations. **Conclusion:** In NCI-H69 cells, VPA treatment increased SSTR2 expression levels in vitro but not in vivo, and increase uptake of radiolabeled DOTATATE in vitro and in vivo. The VPA dose was most likely insufficient to reach required tumoral levels enabling SSTR2 upregulation. However, since kidney damage was observed, increasing the VPA dose is not recommended. The observed increase in [^{177}Lu]Lu-DOTATATE tumor uptake was presumably a consequence of increased blood circulation caused by renal tubular damage. However, VPA-induced SSTR2 upregulation in humans remains open for investigation, as VPA is well-tolerated for long-term use in humans. **References:** None.

EPS-072

Validation of [^{18}F]-(2S,4R)-4-Fluoroglutamine in Multiple Myeloma Mouse Models

S. Valtorta[1,2]*, M. Chiu*[3]*, D. Toscani*[3]*, A. Sartori*[4]*, A. Coliva*[2]*, A. Brevi*[5,6]*, G. Taurino*[3]*, M. Grioni*[5]*, L. Ruffini*[7]*, F. Vacondio*[4]*, F. Zanardi*[4]*, M. Bellone*[5]*, R. M. Moresco*[1,2,8]*, O. Bussolati*[3]*, N. Giuliani*[3]*;*
[1]Department of Medicine and Surgery and Tecnomed Foundation - University of Milano - Bicocca, Monza, ITALY, [2]Department of Nuclear Medicine, San Raffaele Scientific Institute, IRCCS, Milan, ITALY, [3]Department of Medicine and Surgery, University of Parma, Parma, ITALY, [4]Department of Food and Drug, University of Parma, Parma, ITALY, [5]Division of Immunology, Transplantation and Infectious Diseases, San Raffaele Scientific Institute IRCCS, Milan, ITALY, [6]Università Vita-Salute San Raffaele, Milan, ITALY, [7]Nuclear Medicine; "Azienda Ospedaliero-Universitaria di Parma", Parma, ITALY, [8]IBFM-CNR, Segrate, ITALY.

Aim/Introduction: Positron Emission Tomography (PET) with 18F-fluorodeoxyglucose ([18F]FDG) is used to detect high glycolytic activity of multiple myeloma (MM) cells of both medullary and extramedullary disease but there is a good portion of MM patients who are false-negative. Besides enhanced glycolysis, glutamine (Gln) addiction has been recently described as a metabolic feature of MM. Here, we evaluated the possible use of Gln as a PET tracer in MM compared to [18F]FDG in MM preclinical models. **Materials and Methods:** We synthesized enantiopure (2S,4R)-4-Fluoroglutamine (4-FGln) and validated it as a Gln analogue in human MM cell lines (RPMI8226 and JJN3) comparing its uptake with that of 3H-labelled Gln. We then in vivo evaluated [18F]4-FGln uptake in two different murine models comparing it with that of [18F]FDG. JJN3 cells were subcutaneously injected in NSG mice and Vk12598 cells were injected intravenously in C57BL/6 mice to mimic bortezomib (BOR)-resistant MM model. Tumor growth was weekly

monitored with [18F]FDG and [18F]4-FGln PET. Finally, JJN3 mice were treated with BOR to evaluate the potential use of [18F]4-FGln to monitor anti-MM treatment. Mice were acquired with PET before and after BOR treatment. Images quantification was performed to obtain metabolic tumor volume, uptake value, total lesion glycolysis (TLG) and total lesion glutaminolysis (TLGln). Results: Both Gln and 4-FGln were actively accumulated by MM cells and exhibited a strong reciprocal competition. Inhibition analysis revealed that ASCT2 was the major entry route of both compounds. In vivo, all the JJN3 tumors displayed [18F]FDG and [18F]4-FGln uptake. As expected, BOR reduced tumor size as compared to vehicle. With both radiotracers, BOR treated animals displayed SUVmax, metabolic volume and TLG and TLGln values significantly lower than those of vehicle-treated animals at post-treatment PET. Regarding BOR-treated mice, [18F]FDG metabolic tumor volume increased after treatment and [18F]FGln parameters were able to distinguish responder from non-responder mice. Upon injection into C57BL/6 mice, Vk12598 cells colonized the BM without lytic lesions and the spleen. Four weeks after MM cells injection a significant increase of both [18F]4-FGln and [18F]FDG uptake was detected in spleens. **Conclusion:** Our data indicate that [18F]-(2S,4R)-4-Fluoroglutamine can give complementary information to that of [18F]FDG and can be a potential PET tracer in pre-clinical MM models either in a BOR-sensitive or in a BOR-resistant context. **References:** None

EPS-073

Preclinical Utility of Molecular Imaging in the Evaluation of Protective Effect of Telmisartan against Radiation-Induced Bone Marrow Injury

M. Fooladi[1,2], M. Cheki[3], A. Shirazi[1], P. Sheikhzadeh[1], M. Amirrashedi[1], F. Ghahramani[1], M. Khoobi[1];
[1]Tehran University of Medical Sciences, Tehran, IRAN, ISLAMIC REPUBLIC OF, [2]Department of Medical Physics and Biomedical Engineering, Tehran, IRAN, ISLAMIC REPUBLIC OF, [3]Ahvaz Jundishapur University of Medical Sciences, Ahvaz, IRAN, ISLAMIC REPUBLIC OF.

Aim/Introduction: The present study was aimed to investigate the ability of molecular imaging with ^{18}F-Fluro-deoxy-glucose (^{18}F-FDG) micro-positron emission tomography (microPET) to evaluate radioprotective efficacy of telmisartan, a highly selective angiotensin II receptor blocker (ARB) [1] in cellular recovery of bone marrow after in vivo irradiation. **Materials and Methods:** Male Wistar rats were randomly divided into four groups: Control, Telmisartan, Irradiated, Telmisartan+Irradiated. Telmisartan solution in phosphate buffered saline (PBS) was administrated orally at 12 mg/Kg body weight fro seven consecutive days prior to whole body exposing to a single sub-lethal dose of 5Gy X-rays [2,3]. The rats were imaged using ^{18}F-FDG microPET at 9 and 30 days post-irradiation. The ^{18}F-FDG uptake in femur bone marrow was determined according to the mean standardized uptake value (SUVmean) index. Bone Marrow were also processed in similar time points for histological examination. Results: Molecular imaging with ^{18}F-FDG microPET confirmed efficacy of telmisartan as a potent radioportective agent against ionizing radiation-induced injury of bone marrow in rat model. The results were also in line with the histological analysis indicating that pre-treatment with telmisartan significantly improves the number of different hematopoietic cell types in bone marrow compared to irradiated and non-treated group from day 9 to 30 after irradiation. **Conclusion:** The results showed that ^{18}F-FDG microPET as a kind of molecular imaging could be a good candidate to replace time-consuming and invasive biological techniques for screening radioprotector agents. **References:** [1]. Al-Hejjaj WK, Numan IT, Al-Sa'ad RZ, Hussain SA. Anti-inflammatory activity of telmisartan in rat models of experimentally-induced chronic inflammation: Comparative study with dexamethasone. Saudi Pharm J. 2011;19(1):29-34. doi: 10.1016/j.jsps.2010.10.004. PubMed PMID: 23960739. PubMed PMCID: PMC3745173. [2]. Cristina Schwarz F, da Silva Mansano N, Bruno Chies A, Arruda Viani G, Angélica Spadella M. Potential Radioprotective Effect of AT 1 Receptor Antagonists Against Morphological and Ultrastructural Changes in the Testes Induced by Ionizing Radiation. Int J Morphol. 2017;35(3). doi:10.4067/S0717-95022017000300005.[3].Suman S, Maniar M, Fornace AJ, Datta K. Administration of ON 01210. Na after exposure to ionizing radiation protects bone marrow cells by attenuating DNA damage response. Radiat Oncol. 2012;7(1):1-9. doi: 10.1186/1748-717X-7-6. PubMed PMID: 22264334. PubMed PMCID: PMC3275448.

EPS-074

Study of the gadolinium salt dose-enhancement In vitro effect as a promising agent for neutron capture therapy

M. Anikin[1], E. Plotnikov[1], V. Zhuk[2], N. Smolnikov[1], I. Lebedev[1], A. Naymushin[1];
[1]Tomsk Polytechnic University, Tomsk, RUSSIAN FEDERATION, [2]MedContrastSynthesis, Tomsk, RUSSIAN FEDERATION.

Aim/Introduction: Neutron capture therapy is promising beam therapy with great potential for selective destroying of tumor cells based on nuclear reactions. However, besides well-known boron-10 another advantage isotope is ^{157}Gd that has extraordinarily large cross section to thermal neutrons. Advantage over BNCT is intracellular presence of gadolinium because of the photons and electrons. In present paper some results of using gadolinium salt for in vitro studies are presented. **Materials and Methods:** We investigated effect of Gadolinium-based complex (Gd-DTPA). Studied Gd-DTPA initially was developed for MRI imaging, however, we use it as dose-enchantment drug in our in vitro Gd-NCT tests. The SKBR-3 (ATCC HTB-30) cell line was used as a biological

object. We applied MTT test to assess the viability of cancer cells after neutron irradiation and the possible dose-enhancement effects of the tested Gd preparation. Briefly, cells were cultured in DMEM/F12 complete medium and the Gd preparation was added in the appropriate concentration 1 hour before neutron irradiation. After irradiation all cell samples were plated in a 96-well plate (10,000 cells per well). After 48 hours of incubation (5% CO_2; 37C) the MTT reagent were added for 4 hours and replaced by DMSO. Cell viability was recalculated from the optical density compare to untreated control and expressed as a percentage of living cells As made viability tests has shown the optimal intracellular drug concentration is in range of 0.117 - 4.82 mg/ml for gadolinium salt where ^{157}Gd concentration is from 7 to 200 ppm. Cell lines were irradiated on IRT-T research reactor external beam port with thermal flux density of 5E8 $cm^{-2}s^{-1}$. Results: The use of Gd-DTPA as dose-enhancer in neutron irradiation of breast cancer cells in vitro leads to dose-dependent decrease in cell viability. Where for cells irradiated up to 12 Gy with 200 ppm 157Gd viability is 82±4 %. On the other hand, the same dose delivering but 7ppm of 157Gd leads to 99±6 % cells viability. **Conclusion:** It was found that the use of Gd-DTPA leads to a decrease in the viability of the culture after neutron irradiation, despite the relatively high radio-resistance of SKBR-3 cells. However, this cytotoxic effect is reliably observed only at a concentration of 200 ppm of the 157Gd isotope ($p < 0.05$). At lower concentrations of gadolinium, it is noted a slight tendency towards a decrease in cell viability after irradiation ($p > 0,05$). Further extensive testing is required to investigate this effect. **References:** none

EPS-075

Preclinical investigation of a novel luteinizing hormone-releasing hormone antagonist for triple negative breast tumor-bearing model by SPECT/CT imaging

M. Weng, S. Lo, S. Wang, Y. Shih, M. Weng, C. Ho, S. Farn;
Institute of Nuclear Energy Research, Taoyuan City, TAIWAN.

Aim/Introduction: Triple-negative breast cancer (TNBC) was clinically considered a subtype of human breast cancer that lacks diagnostic and effective therapeutic agents. Receptors for luteinizing hormone-releasing hormone (LHRH-R) were previously reported as potential targets for TNBC in vitro. However, as we know probes or drugs specific to LHRH-R are still under investigation as yet. In this research, we developed a novel LHRH peptide-based antagonist, DOTA-LHRH, which has been proved an effective strategy for in vivo uses by SPECT/CT imaging. **Materials and Methods:** The LHRH antagonist was first conjugated with a DOTA chelator; after radiolabeled with In-111, Ga-68, and Lu-177, the radiochemical purity (R.C.P.) was analyzed by both radio-TLC and radio-HPLC systems, respectively. Two kinds of TNBC cell lines, HCC 1806 and MDA-MB-231, were subcutaneously inoculated on mice. After intravenous (i.v.) injection of ^{111}In-DOTA-LHRH, both HCC 1806 and MDA-MB-231-bearing mice were anesthetized and imaged at 1, 4, and 24 h by a SPECT/CT, respectively. The bio-distribution test of ^{111}In-DOTA-LHRH in HCC1806-bearing mice was also investigated at 4 and 24 h. Results: The R.C.P. of ^{111}In-DOTA-LHRH, ^{68}Ga-DOTA-LHRH, and ^{177}Lu-DOTA-LHRH were all determined >90% by both radio-TLC and radio-HPLC, respectively. The SPECT/CT imaging data showed that ^{111}In-DOTA-LHRH was first collected in the liver, kidney, and both tumors at 1 h; the activity in both tumors decreased at 4 h and showed clearance performance at 24 h. In results of bio-distribution, ^{111}In-DOTA-LHRH was mainly collected in kidney, spleen, liver, and HCC 1806 tumors at 4 and 24 h; besides, there found many signals in urine and feces. The tumor-to-muscle count ratio (T/M) was calculated as 5.80 ± 3.33 and 3.88 ± 0.34 and the tumor-to-brain count ratio (T/B) were 19.03 ± 6.22 and 17.23 ± 0.25 at 4 and 24 h, respectively. **Conclusion:** This research has explored the characteristics of a novel LHRH peptide-based antagonist for LHRH-R over-expressive tumors in vivo. We suggested that DOTA-LHRH for further diagnostic research and may also provide innovative information for the development of TNBC patient's treatment strategies in the future in Taiwan. **References:** None

EPS-076

Simultaneous Biodistribution Studies of ^{99m}Tc/^{131}I Labeled Antibody with HPGe Gamma Spectrometry

M. Tassano[1], M. Cabrera[1], X. Camacho[1], M. Fernandez[1], M. Garcia[1], J. Gambini[2,3], P. Cabral[1];
[1]Facultad de Ciencias - Universidad de la Republica, Montevideo, URUGUAY, [2]Facultad de Medicina - Universidad de la República, Montevideo, URUGUAY, [3]CUDIM – Centro Uruguayo de Imagenología Molecular, Montevideo, URUGUAY.

Aim/Introduction: Biodistribution studies (BD) of radiopharmaceuticals are usually measured in single channel gamma detectors. Hyperpure germanium detectors (HPGe) enable efficient and high-resolution detection of different gamma energies, allowing simultaneous detection of multiple gamma-emitting samples. Also, if suitable shielding is available, such detectors can measure at low detection limits. Increased vascular endothelial growth factor (VEGF) expression has been found in many tumor types. Bevacizumab (Bmab) is a humanized, monoclonal antibody that recognizes VEGF. The aim of this study was to investigate the simultaneous biodistribution and lower detection limit of ^{99m}Tc-Bmab and ^{131}I-Bmab labeled antibody, using HPGe detector in order to determine the biodistribution profile of both labeling simultaneously. **Materials and Methods:** Briefly, 100 µg Bmab was incubated in a iodogen coated tube with ^{131}I. ^{99m}Tc-Bmab was prepared using Suc-HYNIC. Radiochemical purity was determined by HPLC. Three BD times (n=3) were performed in normal C57 mice. Co-injections of ^{99m}Tc-Bmab and ^{131}I-Bmab were in the following

ratios (µCi): BD 4h, 6:8; 24h, 60:8; 48h, 150:8. BD analyses were performed using a HPGe detector with 20% efficiency (at 1332 keV). Shielding arrangement consisted of: 10 cm thick external lead with low 210Pb content, and cadmium (5mm)/copper (1mm) as internal shielding. Results: The radiolabeling efficiency for both complexes was ≥90%, remaining above 85% and 90% 48 h post labeling ^{131}I and ^{99m}Tc Bmab respectively. Maintaining an error <5% for 60s measurements, it was possible to measure organs with lower limit of detection of: 182 Bq for ^{99m}Tc (140.5 keV) and 1424 Bq for ^{131}I (364.5 keV); minimum detection activity was: 500.0 Bq.g^{-1} (13.5 nCi.g^{-1}) for ^{99m}Tc, and 4500.0 Bq.g^{-1} (121.6 nCi.g^{-1}) for ^{131}I. In order to detect all organs (with <5% error in 60s), the minimum activity calibration found to be 0.6 µCi (22.2 kBq) for ^{99m}Tc, and 4.6 µCi (170.2 kBq) for ^{131}I, prior to sacrifice the animal. Similar BD patterns were found. Most notable differences appear at 48h with 2.5 fold uptake in thyroid by ^{131}I-Bmab than ^{99m}Tc-Bmab, while ^{99m}Tc-Bmab uptakes 2 fold in the spleen and liver. **Conclusion:** Detection of different radiolabeling strategies is possible using a HPGe detector, making it possible to study different BD profiles simultaneously. With suitable shielding and detector, much longer BD times can be achieved, enabling long-term studies. It also allows to reduce the number of mice involved in BD studies. **References:** none

EPS-077

Radioactive and near-infrared fluorescence in vivo imaging of Non-Hodgkin Lymphoma using 99mTc/Cy7-Fab(Bevacizumab)

X. Camacho[1], C. Perroni[1], C. Carneiro[2], M. Junqueira[2], D. Faria[2], M. García[1], M. Fernández[1], C. Buchpiguel[2], H. Cerecetto[1], R. Chammas[3], E. Riva[4], P. Cabral[1], J. Gambini[5];
[1]Universidad de la República-Facultad de Ciencias-Centro de Investigaciones Nucleares-Area de Radiofarmacia, Montevideo, URUGUAY, [2]Universidade de Sao Paulo-Nuclear Medicine Medical Investigation Laboratory LIM43-Hospital das Clínicas da Faculdade de Medicina, Sao Paulo, BRAZIL, [3]Universidade de Sao Paulo-Laboratório de Oncologia Experimental, Faculdade de Medicina, Sao Paulo, BRAZIL, [4]Universidad de la República-Clínica Hematológica. Hospital de Clínicas-Facultad de Medicina, Montevideo, URUGUAY, [5]Universidad de la República-Centro de Medicina Nuclear e Imagenología Molecular-Hospital de Clínicas-Facultad de Medicina, Montevideo, URUGUAY.

Aim/Introduction: Tumor angiogenesis is a crucial process in the growth, development and metastasis of many types of tumors, including NHL. One of its main inducers is vascular endothelial growth factor (VEGF) and its overexpression has been shown to be associated with poor prognosis in this pathology. Bevacizumab is a humanized monoclonal antibody that binds VEGF with high affinity, blocking its action. When we labeled Bevacizumab with 99mTc or Cy7 for tumor imaging, elevated hepatic uptake was observed [1-4]. Therefore, Fab fragments of antibodies are more attractive for tumor imaging because they are rapidly cleared from blood and normal tissue (except kidneys) and exhibit rapid tumor uptake [5,6]. With these aspects in mind, the aim of this work was to label and evaluate Fab(Bevacizumab) as potential radioactive or fluorescent imaging agent to assess VEGF expression in NHL. **Materials and Methods:** VEGF expresión was analyzed by Flow cytometry in human NHL cell line (Toledo). Fab(Bevacizumab) was produced by digestion of Bevacizumab with papain for 6 h at 37°C, derivatized with NHS-HYNIC-Tfa and radiolabeled with 99mTc. Radiochemical stability and in vitro cell assays were evaluated. Biodistribution and SPECT/CT análisis were performed in normal and Toledo tumor-bearing Nude Balb/C mice up 24 h p.i. Also, Fab(Bevacizumab) was labeled with Cy7 for in vivo fluorescence imaging up to 96 h. Results: By Flow cytometry análisis we demostrate that Toledo cell line present high leve lof VEGF expresión. Incubation with papain resulted in complete digestion of Bevacizumab and exhibited goog purity. Radiolabeling with 99mTc via NHS-HYNIC-Tfa was found to be easy, fast and stable, revealing high radiochemical purity. Biodistribution and SPECT/CT studies showed a quick blood cleareance and significant kidney and NHL engrafted tumor uptake. Cy7-Fab(Bevacizumab) flurescence imaging allowed NHL tumor identification up to 96 h p.i. **Conclusion:** In vivo visualization of VEGF expresión by 99mTc- or Cy7-labeled Fab(Bevacizumab) represents a potential tool that could be empleoyed in clinical setting in patients with NHL for staging, folllow-up, evaluation of tissue simples and to guide surgical excision if necessary. **References:** 1. Camacho X, et al. Joural of Anal Oncol. 2014,3:53-64. 2. Camacho X, et al. Oncology. 2013, 82,200-209. 3. Camacho X, et al. Curr Radiopharm. 2013, 6(1);12-19. 4. Camacho X, et al. Blood. 2017, 130(1): 5202. 5. Camacho X, et al. Anticancer Agents Med Chem. 2021, Epub ahead of print. 6. Calzada V, et al. Anticancer Agents Med Chem. 2016, 16(9):1184-1189.

EPS-078

Comparison Study of [^{111}In]In-DTPA-HL, [^{68}Ga]Ga-NOTA-HL and [^{18}F]AlF-NOTA-HL for Imaging of asialoglycoprotein receptor in Mice

H. Yu, C. Chan, C. Yang, K. Lin, C. Chien, C. Kuo, M. Wang;
Institute of Nuclear Energy Research, Taoyuan, TAIWAN.

Aim/Introduction: Hexavalent lactoside (HL), a multivalent glycoconjugate, has beneficial properties for imaging of liver function reserve by targeting the asialoglycoprotein receptor in liver. This ligand has been labeled with In-111 for use in pre-clinical evaluation. However, the availability and imaging quality of In-111 may hinder the widespread usage of this tracer. The recent development of ^{68}Ge/^{68}Ga generator and ^{18}F-aluminum fluoride ([^{18}F]AlF) labeling method provides simplified strategies for the PET radiotracer

synthesis. The purpose of this study was to prepare [^{111}In]In-DTPA-HL, [^{68}Ga]Ga-NOTA-HL and [^{18}F]AlF-NOTA-HL and to compare their pharmacokinetics and tumor imaging properties using small animal PET/SPECT. **Materials and Methods:** The radioligands were prepared by labeling the DTPA-HL/NOTA-HL conjugates with In-111, Ga-68 or F-18. Radiochemical purity of the radioligands was determined by radio-TLC and radio-HPLC. PET/SPECT/CT imaging of normal Balb/c mice were performed after intravenous injection of the radiotracers. ROIs analysis was performed with Pmode software. Results: All three compounds were prepared in high specific radioactivity and high radiochemical purity. All compounds showed rapid and high tracer uptake ([^{111}In]In-DTPA-HL > [^{68}Ga]Ga-NOTA-HL > [^{18}F]AlF-NOTA-HL) in the liver with high target-to-background ratios. The uptake in the other organs were similar for all three tracers. These compounds showed predominant renal clearance. **Conclusion:** [^{68}Ga]Ga-NOTA-HL and [^{18}F]AlF-NOTA-HL have targeting properties and pharmacokinetics comparable to those of [^{111}In]In-DTPA-HL. Considering their good imaging qualities and ease of accessibility, [^{68}Ga]Ga-NOTA-HL and [^{18}F]AlF-NOTA-HL are promising radiotracers for imaging of asialoglycoprotein receptor. **References:** 1. Lee RT, Lee YC. Affinity enhancement by multivalent lectincarbohydrate interaction. Glycoconj J. 2000;17(7-9):543-551. https://doi.org/10.1023/A:1011070425430 2. Decristoforo C, Pickett RD, Verbruggen A. Feasibility and availability of 68Ga-labelled peptides. Eur J Nucl Med Mol Imaging. 2012;39(Suppl 1):S31-S40. https://doi.org/10.1007/s00259-011-1988-5 3. Velikyan I. 68Ga-Based radiopharmaceuticals: production and application relationship. Molecules. 2015;20(7):12913-12943. https://doi.org/10.3390/molecules200712913 4. McBride, W.J., D'Souza, C.A., Karacay, H., Sharkey, R.M., Goldenberg, D.M., 2012a. New lyophilized kit for rapid radiofluorination of peptides. Bioconjugate Chem. 23, 538-547. https://doi.org/10.1021/bc200608e. 5. McBride, W.J., D'Souza, C.A., Sharkey, R.M., Karacay, H., Rossi, E.A., Chang, C.-H., Goldenberg, D.M., 2010. Improved 18F labeling of peptides with a fluoridealuminum-chelate complex. Bioconjugate Chem. 21, 1331-1340. https://doi.org/10.1021/bc100137x.

EPS-079

Syntheses of the ^{11}C-labeled thymine-carborane conjugates for PET imaging-guided boron neutron capture therapy (BNCT)

Z. Zhang[1,2], M. Suzuki[2,3];
[1]RIKEN Center for Biosystems Dynamic Research, Kobe, JAPAN,
[2]RIKEN Center for Molecular Imaging Science, Kobe, JAPAN,
[3]National Center for Geriatrics and Gerontology, Nagoya, JAPAN.

Aim/Introduction: Boron neutron capture therapy (BNCT), based on a neutron capture reaction (^{10}B(n,α)^{7}Li) to produce high LET alpha particle (α) and lithium-7 (^{7}Li) ion to kill cancer cells, has attracted much attention as a promising tumor-selective treatment.[1] However, the current BNCT still remains several challenges, such as efficient and selective delivery of boron agent into tumor tissue, non-invasive evaluation of boron agent distribution profile in vivo, as well as optimization of the spatiotemporal parameter of neuron-beam irradiation. For addressing these issues, we proposed a strategy of PET imaging-guided BNCT combined with the use of PET nuclide labeled tumor-targeting boron-rich agent. Here we designed and synthesized several prototypes of PET nuclide labeled tumor-targeting boron-rich agents, ^{11}C-labeled thymine-carborane conjugates. **Materials and Methods:** 5-Tributyl-2'-deoxyuridine and 5-tributyl-4'-thio-2'-deoxyuridine were conjugated with carborane via different linkers to give the precursors of PET nuclide labeled tumor-targeting boron-rich agents. These precursors were reacted with [^{11}C]methyl iodide to generate ^{11}C-labeled thymine-carborane conjugates, by using one-pot Pd/Cu co-mediated rapid ^{11}C-methylation.[2] Results: Since thymidine kinase I (TK1) involved in the DNA synthesis and proliferative activity of tumor cells, several thymidine analogues have been developed as TK1-targeting agents for tumor therapy or diagnostic imaging. Here, several derivatives of thymidine and 4'-thiothymidine conjugated with carborane, were designed and prepared as tumor-targeting boron-rich agents. For introducing PET nuclide carbon-11 into these boron-rich agents, the derivatives of 5-tributyl-2'-deoxyuridine and 5-tributyl-4'-thio-2'-deoxyuridine conjugated with carborane, were prepared as PET-tracer precursors. By one-pot Pd/Cu co-mediated rapid ^{11}C-methylation, these precursors were coupled with [^{11}C]methyl iodide to produce efficiently the ^{11}C-labeled thymidine carborane conjugates and 4'-thio-thymidine carborane conjugates, respectively. **Conclusion:** Several prototypes of ^{11}C-labeled thymidine analogues conjugated with carborane, have been successfully synthesized as tumor-targeting PET nuclide-labeled boron-rich agents for imaging guided BNCT. **References:** [1] Barth RF, et al. Clin Cancer Res. 2005; 11: 3987-4002. [2] Zhang Z, et al. J Labelled Comp Radiopharm. 2014; 57:540-549.

912

Wednesday, October 20 - Saturday, October 23, 2021

on-demand pool, release on Wednesday, October 20 at 09:00

e-Poster Presentation Session 6: Molecular Brain Imaging

EPS-080

The effect of reduced administered activity and image reconstruction on SUVR quantification in [^{18}F] flutemetamol amyloid PET-MR scanning

J. Anton Rodriguez[1,2], K. Herholz[3], S. F. Carter[4,5], J. C. Matthews[2];
[1]The Christie NHS Foundation Trust and University of Manchester,

Manchester, UNITED KINGDOM, [2]Division of Informatics, Imaging and Data Sciences, MAHSC, Manchester, UNITED KINGDOM, [3]Division of Neuroscience and Experimental Psychology, Faculty of Biology, Medicine and Health-University of Manchester, Manchester, UNITED KINGDOM, [4]WMIC, University of Manchester, UK, Manchester, UNITED KINGDOM, [5]Deparment of Psychiatry, University of Cambridge, Cambridge, UNITED KINGDOM.

Aim/Introduction: Quantification of brain amyloid deposits and the classification of patients as amyloid positive or negative has potential value in Alzheimer research and clinical diagnosis [1]. Suitable radiotracers have been developed together with methods to standardize quantification across patients and radiotracers [2]. The use of reduced administered activity may enable applications such as repeat longitudinal scanning and screening. We evaluate whether significant reductions in injected activities are possible without significant changes in amyloid deposit quantification and to evaluate the role of different reconstruction algorithms. This evaluation was conducted by subsampling full dose [^{18}F] flutemetamol (FLUT) PET-MR data and using commercially available reconstruction algorithms. **Materials and Methods:** PET data acquired on a PET-MR GE Signa of 7 scans (6 healthy elderly participants), corresponding to 90-110minutes post-injection of ~185MBq of FLUT was subsampled 10 times to mimic 10% injected activity.PET reconstructions: Three reconstruction algorithms were assessed: VPFX (OP-OSEM-TOF) with/without resolution modelling (SharpIR) (both 4 iterations-28 subsets) and Q.Clear regularised reconstruction. For VPFX a variety of Gaussian post-reconstruction filters and for Q.Clear a variety of beta values were assessed using Flangeless Esser-PET-phantom™ (visual and quantification assessment). Optimal β values resulted in β=250 (full-dose) and β=1000 (10% dose).Analysis: The images, full-dose OP-OSEM-TOF with 4mm-Gaussian (clinical standard) and QClear β=1000 for 10% dose, were read by an expert neurologist to determine the amyloid classification and confidence of classification. Statistical parametric mapping (SPM12) and centiloid regions were used to calculate SUVR values of cortical to cerebellum grey matter (GM) concentrations. Spatial normalisation was conducted using a T_1-weighted MPRAGE MR sequence and to refine regions to predominantly GM voxels, with both non-refined and GM-refined SUVR values assessed. Results: Five participants were classified as amyloid negative and one positive. All images were found to return high diagnostic-confidence levels with exception of one participant (intermediate confidence) at 10% dose (Qclear β=1000), a participant that displayed some significant atrophy. Quantitatively, very small differences in SUVR values were observed between dose levels and different reconstructions that were notably less than the differences between participants and regions (non-refined or GM-refined). Estimates of imprecision from resampling at a 10% dose were also small. **Conclusion:** Large reductions of the doses are possible without significant deterioration in SUVR accuracy and precision. Furthermore, although some deterioration is visible, images can still be read and classified with confidence. Further work is necessary with a larger more clinically relevant cohort. **References:** [1]Chételat et al. 2020;[2]Klunk et al. 2014

EPS-081

Model Based Data Driven Attenuation Correction for Brain Imaging with High Resolution Multifocal Collimator

X. Ding[1], *F. Massanes*[1], *G. Platsch*[2], *M. Reymann*[2], *H. Vija*[1]; *[1]Siemens Medical Solutions USA Inc., Molecular Imaging, Hoffman Estates, IL, UNITED STATES OF AMERICA, [2]Siemens Healthcare GmbH, Molecular Imaging, Forchheim, GERMANY.*

Aim/Introduction: We present a fully automated data driven model-based attenuation map generation approach ("MBDL-mumap") for brain SPECT using parallel hole and high resolution SMARTZOOM collimator "SZHRX", from them emission data alone. The SZHRX design allows for a non-local PSF approximation and thus iterative reconstruction with distance dependent 3D collimator response, attenuation and scatter correction is possible. **Materials and Methods:** The method is based on reconstruction of the emission only data to obtain the shape of the skull, and to replace the interior with age dependent cortical and brain tissue linear attenuation coefficients at the emission energy to yield the MBDL-mumap [1]. We acquired 10 patients on a Siemens Symbia T2 system using both a clinical protocol PARA (LEHR or MELP) and a SZHRX collimator for either brain perfusion studies using Tc99m or for I123-DaTscan studies. We performed two SPECT reconstructions: OSEM and OSCG. SPECT with SZHRX was brain centered with a 28 cm radius-of-rotation. Only one CT (130 kVp, 30 mAs effective, H31s) was performed for the clinical part of the study and established the reference mu-map. We determined reconstruction parameters for reliable shape-fitting and then compare mumaps and reconstructions visually, and quantitatively, using the transmittance of radially sampling projections to compare between the CT mumap and MBDL-mumap and random sampling of the activity concentration (kBq/mL) with spherical VOI varying volumes and locations within the brain. Results: Reconstruction parameters to generate a stable segmentation are 20 (OSEM) and 10 (OSCGM) updates and 20mm 3D Gaussian FWHM post-smoothing. Relative errors of transmittance between MBDL and CT mumap are (ave, std): -1.8%, 4.6% for SZHRX DaTscan; -0.3%, 5.1% for SZHRX Perfusion; -3%, 4.3% for PARA DaTscan; -0.2%, 5.1% for PARA perfusion. Wilcox tests show that there are no significant differences between the CT mumaps and the MBDL mumaps using either SZHRX collimators (p-value = 0.98), or PARA collimators (p-value = 0.65). The relative errors between the corresponding reconstructions are (ave,

std): 4.8%, 3.2% for SZHRX DaTscan; 4.0%, 5.4% for SZHRX Perfusion; 4.7%, 3.7% for PARA DaTscan; 0.6%, 6.0% for PARA perfusion. The p-values of Wilcox tests for the distributions are: 0.07(SZHRX DaTscan), 0.04(SZHRX perfusion), 0.87(PARA DaTscan), 0.1(PARA perfusion). **Conclusion:** Fully automated data-driven attenuation correction from brain SPECT data alone allows to mitigate the cupping artifact improving visual appearance. **References:** [1] X. Ding, A. H. Vija Quantitative SPECT Neuro imaging using an Attenuation Map from the Projection Data Alone. EANM2017 SPECT Quantification: OP-152

EPS-082

Hypometabolism and Atrophy Patterns Associated with Niemann-Pick type C

J. Silva-Rodríguez[1], C. Castro[1], J. Cortés[2], M. Arias[3], J. Gascón[4], M. Sobrido[5], P. Aguiar[6];
[1]Health Research Institute of Santiago de Compostela, Santiago de Compostela, SPAIN, [2]Nuclear Medicine Department, University Hospital of Santiago de Compostela, Santiago de Compostela, SPAIN, [3]Neurology Department, University Hospital of Santiago de Compostela, Santiago de Compostela, SPAIN, [4]Neurology Department, Hospital Universitari de Bellvitge, Barcelona, SPAIN, [5]Neurology Department, University Hospital of A Coruña, A Coruña, SPAIN, [6]University of Santiago de Compostela, Santiago de Compostela, SPAIN.

Aim/Introduction: Niemann-Pick disease type C (NP-C) is a rare genetic lysosomal lipid storage disease with progressive neurological impairment. On the basis of previous findings showing that MRI abnormalities are detected only in advanced stages of the NP-C disease and evidence supporting that PET hypometabolism might precede anatomical damage on several conditions, we conducted a crossectional and longitudinal imaging study to investigate whether (1) FDG-PET provides a distinctive hypometabolic pattern in NP-C, (2) these abnormalities precede anatomical findings revealed by MRI and (3) FDG-PET can measure longitudinal changes in NP-C. **Materials and Methods:** A multicenter observational study was conducted. Twenty-two patients with a genetically confirmed NP-C diagnosis were included. All of them underwent MRI and FDG-PET imaging on the same or consecutive days, and a wide range of demographic and clinical data was collected. A reduced number of patients (12) completed yearly follow-up visits for up to 4 years. Previously validated image harmonization strategies were applied to account for the use of different MRI and PET scanners. MRI volumetric analysis (both voxel and region-based) was performed with CAT12, while the PET analysis was performed using SPM (voxel-based) and in-house developed tools (region-based). Image analysis was performed comparing the NP-C cohort with a healthy subject cohort (67). In addition to group analysis, we performed individual analysis using previously published single-subject analysis strategies. Results: Voxel-wise atrophy patterns were restricted to the cerebellum and thalamus ($p<0.01$), confirming the MRI abnormalities summarized in the current recommendations for the diagnosis of NP-C. In contrast, PET hypometabolism spread through the whole cerebellum and limbic system and revealed large bilateral areas of affectation in cortical regions of the frontal and temporal lobes ($p<0.001$). These results were confirmed by the region-based analysis. Single-subject patterns revealed moderate heterogeneity, especially for the level of frontal affectation. Regarding longitudinal findings, glucose metabolism significantly decreased yearly in the cerebellum insula, thalamus, putamen, precentral gyrus, and anterior orbital gyrus (annual decrease of 4-12%, $p<0.01$). **Conclusion:** Our cross-sectional analysis revealed a distinctive hypometabolism pattern of NP-C. In addition, several areas of hypometabolism were not accompanied by atrophy, but were in good agreement with progression defined using animal models. This suggests that PET might provide a tool for earlier differential diagnosis. In addition, our longitudinal analysis revealed that the progression of neurodegeneration as measured by FDG-PET may constitute an imaging biomarker to assess the progression and possible treatment responses in NP-C. **References:** none

EPS-083

Amyloid PET imaging: impact on Alzheimer's Disease Diagnostic Work-up and patient management

C. Ferrari, P. Caputo, A. R. Pisani, A. Branca, G. Rubini;
Section of Nuclear Medicine, DIM, University of Bari "Aldo Moro", Bari, ITALY.

Aim/Introduction: Alzheimer's disease (AD) is the most common form of early onset senile dementia, with a strong social impact. 18F-Florbetapir, 18F-Florbetaben and 18F-Flutemetamol are amyloid PET (AMY-PET) tracers that allow the "in vivo" detection or exclusion of neuritic amyloid plaques. Because of its significant impact on patient management and cost of care, early and differential diagnosis of AD is essential in order to perform the correct therapeutic path and the adequate social-economic support. The study aims to assess the impact of AMY-PET response on the following clinical, therapeutic and psychological patient management, as well as of all involved family members. **Materials and Methods:** from February 2018 to February 2021, 76 patients (41/76 <=65y; 35/76 >65y; 27/76 XY, 49/76 XX) with suspected AD performed AMY-PET/CT at our Nuclear Medicine Unit. Forty-eight/76 patients were previously clinically evaluated by MMSE (average score 21.4; range 3-30).All patients and/or their caregivers were subsequently recalled for a follow-up survey administration which investigated: diagnosis change/confirmation, beginning/change of therapy, change in the patient management (adhesion to home-care program or to Alzheimer's Evaluation Unit (AEV) centres), possible caregiver

recruitment, AD-related healthcare-cost exemptions. Sensitivity, specificity, likelihood ratio positive (LR+) and likelihood ratio negative (LR-) were calculated to assess the AMY-PET performance by considering the final clinical diagnosis as gold standard. Univariate logistic regressions were performed to evaluate the correlation among AMY-PET and MMSE results, home-care program/AEV centre adhesion, caregiver recruitment and AD-related healthcare-cost exemptions. Data analysis was performed using R Studio software. Results: A total of 51/76 AMY-PET were positive and 25/76 were negative, with an overall concordance with the final clinical diagnosis of 96.1% (73/76). AMY-PET had a sensitivity and specificity of 96.2% and 95.8% respectively. LR+ was 23 (95%CI 3.38-157) and LR- was 0.04 (95%CI 0.01-0.16). Diagnostic Odds Ratio was 575 (40.6-21223.9 IC). A strong correlation between AMY-PET results and the inclusion of the patient in a home-care program (p=0.008), or in a AEV centre (p=0.017), as well as caregiver recruitment (p=0.001) and AD-related healthcare-cost exemptions, was found. Almost significant was the correlation between AMY-PET results and beginning/change of therapy (p=0.05). Instead, no significant correlation between AMY-PET result and the MMSE score was reached. **Conclusion:** Our preliminary results confirmed the high reliability of AMY-PET in the evaluation of patient with suspected AD, as an examination that alone can guide clinician even in the early diagnosis of AD with the consequently strong impact on the therapeutic/social-economic patient management. **References:** none

EPS-084

Machine Learning Radiomics for Prediction of Cognitive Deficits by Using Amyloid Pet Images

G. Giovacchini, E. Giovannini, V. Duce, S. Pastorino, O. Ferrando, F. Foppiano, C. Passera, A. Mannironi, A. Tartaglione, A. Ciarmiello;
S. Andrea Hospital, La Spezia, ITALY.

Aim/Introduction: This study was aimed to assess the correlation between radiomic features of amyloid PET and cognitive deficits in amnestic mild cognitive impairment (aMCI) and Alzheimer's disease (AD). **Materials and Methods:** 328 subjects from Alzheimer's Disease Neuroimaging Initiative database and EudraCT 2015-001184-39 trial (159 males, 169 females), mean age 72±7.4 years underwent PET/CT with [^{18}F]-Florbetaben. Study cohort consisted of normal controls (n=149), subjects with aMCI (n=144) and with AD (n=35). A total of 42 radiomic features and standardized uptake values (SUV) were extracted from PET studies. SUVr was obtained by normalization of cortical to cerebellar activity. Feature selection occurred with a 3-step process consisting of: 1) Spearman's rank correlation versus clinical diagnosis; 2) least absolute shrinkage and selection operator (LASSO) regression model; 3) evaluation of model predictive performance with bootstrap resampling and area under the curve (AUC). Results: The variable combination with the best diagnostic performance for group discrimination included 6 textural features of 3 different types (GLCM, GLRLM, GLSZM) and SUVr. This model increased the AUC in whole cortex in comparison to the model based only on SUVr (AUC: 0.86 vs. 0.66, P<0.05). SUVr and combined model including radiomic features and SUVr predicted the performance at neuropsychological tests. **Conclusion:** Predictive model based on SUVr and radiomic features provides better diagnostic performance than SUVr alone. Since single biomarker will probably not be able to improve the diagnosis of Alzheimer's disease, machine learning by analyzing multiple parameters extracted from the images and derived from clinical setting will be able to support the identification of a panel of different markers able to ensure an earlier and more accurate diagnosis. **References:** None

EPS-085

Differential Diagnosis of Atypical Parkinson Disorders from Parkinson's Disease using dual-phase F-18 FP-CIT PET/CT

M. Cheon, S. Kim, S. Ha, J. Yoo;
VHS Medical Center, Seoul, KOREA, REPUBLIC OF.

Aim/Introduction: Accurate differential diagnosis of atypical Parkinson disorders (APD) from Parkinson's disease (PD) is important for deciding on treatment regimens, providing a prognosis, clarifying etiology and pathogenesis, and developing new therapeutic strategies. A previous study showed a poor diagnostic result of the presynaptic dopamine transporter (DAT) imaging to differentiate APD. This study aimed to evaluate the usefulness of dual-phase F-18 FP-CIT positron emission tomography/computed tomography (PET/CT) imaging in the differential diagnosis of APD from PD. **Materials and Methods:** One hundred seventy-two subjects who underwent dual-phase F-18 FP-CIT PET/CT imaging for workup for parkinsonism were included. The diagnosis of PD was made according to the UK Parkinson's Disease Society Brain Bank Clinical Diagnostic Criteria. Two sequential PET/CT scans were acquired 5 min (early phase) and 3 h (late phase) after injecting 185 MBq of F-18 FP-CIT/CT. PET/CT images were interpreted by using quantitative analysis. Quantitative analysis was based on volumes of interest (VOI) using mean standardized uptake values (SUVmean). We compared subregional DAT binding potential (BP), putamen-to-caudate nucleus ratio of binding potential, asymmetry of the DAT binding, and degree of washout between APD and PD. Results: PD, 26 subjects; progressive supranuclear palsy, 8 subjects; corticobasal degeneration, 1 subject; multiple system atrophy (MSA)-parkinson type, 8 subjects; MSA-cerebellar type, 9 subjects; dementia with Lewy body, 15 subjects, and normal, 105 subjects were analyzed. In differentiate APD from PD, all BPs on both early and late phase and all factors of the percent change except for putamen were significantly different (all, P < 0.05). When

classified as APD when both the cutoff value of the $BP_{cerebellum}$ in the early phase (≤ 0.79), which is the best quantitative factor for discriminating between APDs and PD, and the striatal BP of the late phase are simultaneously satisfied, the sensitivity, specificity, positive predictive value, negative predictive value, and accuracy were 61.0%, 95.8%, 96.2%, 95.8%, and 73.9%, respectively. Diagnostic performances were significantly higher when the early phase was performed together than in the case of judging only the factors of the late phase. **Conclusion:** Our data indicate that no significant difference between PD and APD in the pattern and degree of CIT uptake in the late phase, but there was a significant difference in the early phase. Moreover, discrimination using quantitative analysis factors can further improve diagnostic performance. We propose that the application of dual-phase F-18 FP-CIT PET/CT would be beneficial for differentiating APD from PD. **References:** none

EPS-086

Regional Brain Amyloid Load Assessed by ^{11}C-PIB PET/CT and Cognitive Performance in Patients with Mild Cognitive Impairment: A Longitudinal Study

J. Jiménez-Bonilla[1], M. De Arcocha-Torres[1], J. Martín-Arroyo[2], O. Cuenca[1], I. Martínez-Rodriguez[1], A. Sánchez-Salmón[1], N. Martínez-Amador[1], F. Gómez-De la Fuente[1], S. Ruiz-Llama[1], A. Pozueta[2], M. Gómez[2], S. López-García[2], C. Lage[2], E. Rodríguez[2], P. Sánchez-Juan[2], R. Quirce[1];

[1]Nuclear Medicine Service. Marqués de Valdecilla University Hospital. Molecular Imaging Research Group-IDIVAL. University of Cantabria, Santander, SPAIN, [2]Neurology Service. Marqués de Valdecilla University Hospital., Santander, SPAIN.

Aim/Introduction: To evaluate the relationship between regional brain amyloid load (rBAL) and cognitive performance in patients with mild cognitive impairment (MCI) at diagnosis and 5-year follow-up. **Materials and Methods:** In 30 MCI patients (24 amnestic; 4 non-amnestic and 2 multi-domain; mean age 72 ± 5,07 years ; 13 men;) we evaluated at diagnosis their cognitive performance in 5 cognitive domains (language, visuospatial abilities, executive function, episodic memory and inmediate memory) by neuropsychological tests: Total free recall (RAL); Total recall (RAT); Delayed free recall (RALDf); Delayed total recall (RATDf);Rey figure memory (Rey-C); Digits span forward; Digits span backward, Trail Making Test-A; Boston Naming Test and VOSP; and regional brain amyloid deposition with a static ^{11}C-PIB PET/CT after 555Mbq of ^{11}C-PIB. At five-year, all were clinically re-examined using the same tests.^{11}C-PIB-PET/CTs were semiquantitatively analyzed obtaining SUV índices in cortical regions. Using the cerebellum as reference region, regional SUV ratios (SUVr) were obtained and rBAL was calculated as a SUVr averaging left and rigth SUVr values in frontal, parietal, temporal and occipital areas for each patient. Pearson's correlations between rBAL and cognitive scores were obtained; significant level were set at p< 0,05. Results: At diagnosis, 24 patients were PIB positive and 6 negative. At five-year, 22 progressed to Alzheimer dementia (10 mild and 12 severe) and 8 remained as MCI. In the study population, memory scores sligthly correlated at diagnosis with rBAL in temporal cortex (RAL r= -0,192; RAT =- 0,352; RLDf r= -0,122; RTDf= -0,129) but at 5-year, the scores obtained from these domains showed a stronger high correlation with initial temporal rBAL (RAL r= -0,587; RAT r= -0,587; RLDf r= - 0,352; RTDf r= -0,585). Visuoespatial abilities also improved their correlations with initial temporal rBAL 5-years later (VOSP r=-0,389 vs -0,462; Rey-C r= -0,373 vs - 0,523). Parietal rBAL showed a better high correlation at 5-years than at MCI diagnosis in memory and visuoespatial domains (RAT r= -0,260 vs - 0,544; RAT r= -0,373 vs -0,585; RATDf r=-0,332 vs - 0,585; VOSP r= - 0,332 vs -0,585). Frontal rBAL highly correlated with visuoespatial abilities at diagnosis and 5-year later (Rey-C r= -0,628) and with language domain (Boston r= -0,148 vs - 0,313). Occipital rBAL only correlated with visuoespatial abilities (Rey-C r= -0,512 vs -0,563). **Conclusion:** Initial rBAL showed a relationship with cognitive performance in MCI patients, predicting the degree of cognitive impairment, specially for temporal and parietal r BAL. **References:** None

EPS-087

Optimal Cut-off Value for Automated Semiquantitative Analysis of ^{123}I-beta-CIT SPECT in the Diagnosis of Idiopathic Parkinson's Disease

T. Laitinen[1,2], J. Miettinen[1], N. Vartiainen[2], H. Gröhn[2], T. M. Laitinen[2];

[1]University of Eastern Finland, Kuopio, FINLAND,

[2]Kuopio University Hospital, Kuopio, FINLAND.

Aim/Introduction: ^{123}I-beta-CIT uptake decreases in idiopathic Parkinson's disease (IPD) but also with normal aging. Therefore, when applying semiquantification, age-specific reference values are used. It is still unclear what would be optimal cut-off value to distinguish between patients with and without IPD. If the cut-off value is set as two standard deviations below the age specific expected value (-2 Z), 2.5% of healthy subjects would be false positives. Common practice is to look striatum and striatal subregions from both sides at the same time along with occipital reference region. In the case of several regions picked according to -2 Z, proportion of false positives increases with the number of analyzed regions. Furthermore, possible overlap between distributions of striatal specific binding ratio (SBR) in patients with and without IPD may result in false negatives. **Materials and Methods:** The study population was formed from 172 patients who were referred for ^{123}I-beta-CIT SPECT. An analysis program was used that fits the patient data to 3D normal templates containing volumes of interest for the left and right striatum, caudate, and putamen and calculates SBR values as well as corresponding Z-values. At the 3-4 years clinical follow-up, medical records and neuroimaging data

were evaluated to find out patients with clinical diagnosis of IPD (n=82) and those with no diagnosis of any movement disorders and no signs of any other clinically significant brain diseases (n=90). The ability of SBR in striatum and its substructures to identify IPD was evaluated by the receiver operating characteristic (ROC) curve analysis. Optimal cut-off value was determined using the maximum Youden Index (defined as sensitivity+specificity-1). Results: SBR values in the right and left striatum were lower in IPD as compared with the reference group (Right striatum: 2.62±0.74 vs 4.22±0.38, Left striatum: 2.45±0.65 vs 4.09±0.38, P<0.001 for both). The area under the ROC curve for identifying IPD by SBR was 0.996 for striatum, 0.967 for caudate, 0.993 for putamen and 0.999 for their combination. Optimal cut-off value for SBR was -2.9 Z (sensitivity 95% and specificity 99%) in striatum, -1.8 Z (sensitivity 88% and specificity 94%) in caudate, -3.1 Z (sensitivity 98% and specificity 100%) in putamen and -3.2 Z (sensitivity 98% and specificity 100%) in their combination. **Conclusion:** When several regions are taken into account in the quantification of striatal ^{123}I-beta-CIT uptake -3 Z, as a cut-off value, suits best to distinguish between patients with and without IPD. **References:** none

EPS-088

Additional value of 2-[^{18}F]FDG PET/CT in detection of malignancy in patients with paraneoplastic neurological syndromes having negative results of conventional radiological imaging

M. Opalinska[1], A. Sowa-Staszczak[2], K. Wężyk[3], A. Słowik[4], A. Hubalewska-Dydejczyk[2];
[1]Nuclear Medicine Unit, Endocrinology Department, University Hospital in Krakow, Krakow, POLAND, [2]Chair and Department of Endocrinology, Jagiellonian University Medical College, Krakow, POLAND, [3]Department of Neurology , University Hospital, Krakow, POLAND, [4]Chair and Department of Neurology, Jagiellonian University Medical College, Krakow, POLAND.

Aim/Introduction: Paraneoplastic neurological syndromes (PNS) affecting central nervous system are rare, presenting in less than 1% of all patients with cancer. The pathogenesis of PNS is presumed to result from autoimmune attack on the underlying malignancy and it is often connected with the presence of onconeural antibodies. Unfortunately, early imaging using classical radiological procedures (CT or MRI) often does not bring satisfactory results in finding underlying pathology. Prompt identification and treatment of tumor is recommended to remove the antigenic source which leads to lowering of the immune response and it is connected with better outcome. Among widely available methods a whole-body 2-[18F]F-FDG PET/CT may bring additional benefit in detection of underlying malignancy in patients with PNS who have negative or unremarkable conventional radiological findings. Aim: An evaluation of [18F]F-FDG PET/CT usefulness in detection of malignancy in PNS patients with positive onconeural antibodies and negative results of conventional (CT or MRI) radiological imaging. **Materials and Methods:** Among all patients diagnosed in Neurology Department in 2016-2020 because of PNS with different types of onconeural antibodies and negative results of conventional radiological imaging who underwent 2-[18F]-FDG PET/CT 19 cases were eligible to the study (1 case each: myasthenia gravis, neuromyelitis optica, primary angiitis of central nervous system, sensory polyneuropathy, sensorimotor and motor neuron disease, 4 cases each: polyneuropathy, autoimmune encephalitis, cerebellar degeneration). Results: In 42% (8 out 19) cases (in 1 case of myasthenia gravis, neuromyelitis optica and autoimmune encephalitis, 2 cases of axonal polyneuropathy and 3 cases of cerebellar degeneration) 2-[18F]F-FDG PET/CT enabled localization of metabolically active tumors non previously detected by conventional (CT or MRI) radiological imaging. **Conclusion:** 2-[18F]F-FDG PET/CT allow for neoplastic tumor detection in 42% of PNS cases with negative or unremarkable conventional radiological findings. Those results accelerated the diagnostic process and enabled faster initiation of casual treatment. **References:** none

EPS-089

A meta-analysis of brain glucose hypo-metabolism in patients with disorders of consciousness

A. Sala[1,2], B. Kaan Ok[1,3], A. Thibaut[1,2], O. Gosseries[1,2], S. Laureys[1,2], J. Annen[1,2];
[1]University of Liège, Liège, BELGIUM, [2]Centre du Cerveau2, University Hospital of Liege, Liege, BELGIUM, [3]Kadir Has University, Istanbul, TURKEY.

Aim/Introduction: The present study aims to synthesize existing studies on cerebral hypo-metabolism in patients with disorders of consciousness (DOC). **Materials and Methods:** A systematic review and meta-analysis was conducted in February 2021. Two independent assessors searched PubMed for voxel-wise, whole-brain, resting-state [18F]FDG-PET studies involving >16years-old patients with prolonged DOC. Coordinate-based meta-analysis was performed via activation likelihood estimation in GingerALE (statistical threshold: p<0.001, voxel-level; p<0.05 FWE-corrected, cluster-level). Distribution of hypometabolism was compared to the topography of neurocognitive and sensorimotor resting-state networks, based on the FINDlab atlas. Results: Of the resulting 265 studies, 12 met inclusion criteria, with 245 patients (Unresponsive Wakefulness Syndrome (UWS), n=107; Minimally Conscious State (MCS), n=138); and 259 healthy controls. Meta-analysis revealed hypo-metabolism in DOC patients in precuneus, posterior/middle cingulate gyrus, angular gyrus, inferior/superior parietal lobule, precentral gyrus, middle frontal gyrus, thalamus and caudatum. Among 14 resting state networks, hypo-metabolism was found preferentially in the default mode (40% of the assigned voxels), the executive control (27%) and the basal ganglia/thalamus (24%) networks.

Separate meta-analysis of UWS and MCS subgroups, revealed hypometabolism in superior parietal lobule uniquely in UWS patients, and hypometabolism in the caudatum uniquely in MCS patients. **Conclusion:** Cerebral hypo-metabolism in patients with DOC preferentially affects regions belonging to the default mode, executive and basal ganglia/thalamus networks. **References:** None

EPS-090

Association of periodontitis with Intracerebral Beta-Amyloid Plaque Deposition measured by ^{18}F-Florbetaben PET/CT

M. Rashki[1], E. Triviño-Ibáñez[1], T. Rudolphi Solero[1], M. Gerez Muñoz[2], I. Gómez Cartes[2], M. Gómez-Río[1];
[1]Department of Nuclear Medicine, University Hospital Virgen de las Nieves, Granada, SPAIN, [2]School of Dentistry, Granada Biohealth Research Institute, Granada, SPAIN.

Aim/Introduction: Recent studies suggest a direct relationship between periodontitis, an oral chronic inflammatory condition, and neurodegenerative disease of the central nervous system. Even though the mechanism underlying this association has not been confirmed, is generally accepted. We aimed to determine the possible association between periodontitis and the presence of Beta-amyloid plaque in patients with cognitive impairment. **Materials and Methods:** A prospective study of patients with mild cognitive impairment was performed, we explored the presence of Beta-amyloid plaque by [^{18}F]Florbetaben PET/CT. Periodontal disease was evaluated by oral examination performed by a dentist determining loss of teeth; rates of bleeding and/or cavities; probing depth of the gingival pocket and clinical insert loss. Results: Sixty-nine patients were included (mean age 63.22 ± 6.83; 33.3% men), 12 of them were toothless. Amyloid-PET was positive in 32 patients (46.4%). A complete oral examination was obtained in 56 cases (81%). The patients were grouped according to the severity of periodontal disease in two categories excluding the toothless patients: A) absence of periodontal disease or mild periodontitis (28 patients; 50%) and B) those with moderate or severe periodontal disease (28 patients). The bivariate analysis showed a statistically significant association between the degree of periodontitis and the result of the Amyloid PET (OR: 3.8; p <0.018), which means that the probability/risk of having a positive Amyloid-PET result was 3.8 times higher in the group with severe periodontitis compared to the mild periodontitis group. This association was maintained if edentulous patients were excluded from the analysis, as cause of tooth loss was not clear. **Conclusion:** The preliminary results of this study showed an association between the severity of the periodontal disease and the existence of amyloid plaque deposits detected by PET-Amyloid. **References:** None

EPS-091

Perfusion-like images based on [^{18}F]florbetaben PET correlate well with brain metabolism in patients with inherited transthyretin-related amyloidosis

S. Ferreira[1,2,3], P. Alves[4,5], I. Conceição[4,5], I. P. Martins[4,5], F. Oliveira[1], M. Silva[1], N. Matela[3], D. C. Costa[1];
[1]Champalimaud Centre for the Unknown, Champalimaud Foundation, Lisbon, PORTUGAL, [2]Philips Portuguesa S.A, Lisbon, PORTUGAL, [3]Institute of Biophysics and Biomedical Engineering, Faculty of Sciences of the University of Lisbon, Lisbon, PORTUGAL, [4]Department of Neurosciences, CHULN, Hospital de Santa Maria, Lisbon, PORTUGAL, [5]Instituto de Medicina Molecular, Faculdade de Medicina, Universidade de Lisboa, Lisbon, PORTUGAL.

Aim/Introduction: Transthyretin-related amyloidosis (ATTR) is the most common hereditary form of amyloidosis, with the most prevalent TTR mutation being Val30Met associated with a mixed or neuropathic phenotype (ATTRv-NP). Liver transplantation replaces the variant TTR gene with the wild-type gene in the liver. However, it cannot prevent the TTR deposition in the central nervous system (CNS), as choroid plexus and retina continue to produce variant TTR. Due to continued TTR deposition, some patients develop CNS disorders. CNS amyloid deposition can be mapped with [^{18}F]florbetaben PET/CT, among other radiotracers. [^{18}F]FDG is used to map brain metabolism, which is frequently a biomarker of neurodegeneration. This work aims to investigate if [^{18}F]florbetaben-derived perfusion-like images can also be used as a proxy for brain metabolism such as in other brain disorders. **Materials and Methods:** Nine patients with ATTRv-NP (6 females, mean age 52±3 years) were retrospectively studied. Each patient underwent three PET/CT acquisitions: [^{18}F]FDG started 45 minutes post-injection (p.i.) for 15 minutes, dynamic [^{18}F]florbetaben for 60 minutes duration started immediately p.i. and [^{18}F]florbetaben late acquisition started 90 minutes p.i. for 20 minutes. Both [^{18}F]florbetaben acquisitions were obtained after the same injection. Four perfusion-like images were obtained from [^{18}F]florbetaben dynamic acquisitions: early phase (sum of the counts between 1 and 9 min p.i.), relative delivery ratio R_1 from MRTM2 and SRTM2 kinetic models, and V_0 from Patlak method. All studies were acquired in the Philips Vereos Digital PET/CT. For each patient, perfusion-like images and [^{18}F]florbetaben late acquisitions were registered to [^{18}F]FDG images. Voxelwise within-subject correlation was assessed in all brain voxels between [^{18}F]FDG and the four perfusion-like images; and also, with [^{18}F]florbetaben late acquisitions (used to assess amyloid burden). Results: Very high correlation was obtained between [^{18}F]FDG and perfusion-like images. Mean (min-max) brain voxelwise within subject correlations were 0.96 (0.95-0.99), 0.96 (0.94-0.97), 0.96 (0.94-0.97) and 0.96 (0.95-0.97), for [^{18}F]florbetaben early phase images, R_1-MRTM2, R_1-SRTM2 and V_0-Patlak images, respectively. No significant correlation was found between the metabolism

([18F]FDG) and the amyloid burden (late [18F]florbetaben). **Conclusion:** According to our preliminary results, perfusion-like [18F]florbetaben-derived images can be used as a proxy for brain metabolism in patients with ATTRv-NP, similar to patients with other diseases. This ongoing work with increasing number of patients will attempt to obtain more robust validation, and assess whether these results can be extrapolated to patients with other types of cerebral amyloid angiopathy. **References:** None

EPS-092

The role of amyloid PET-CT with 18F-Flutemetamol in patients with mild cognitive impairment: Identification of the group at risk of developing Alzheimer's Disease

L. Rodriguez-Bel[1], M. Martínez de Bourio-Allona[1], J. Campdelacreu-Fumado[2], R. Reñé-Ramírez[2], I. Rico-Pons[3], P. Notta[1], J. Vercher-Conejero[1], G. Reynés-Llompart[1], J. Fernandez-Barrionuevo[1], M. Cortés-Romera[1];
[1]PET Unit, Department of Nuclear Medicine-IDI. Hospital Universitari de Bellvitge-IDIBELL, L'Hospitalet de Llobregat (Barcelona), SPAIN, [2]Department of Neurology. Hospital Universitari de Bellvitge-IDIBELL, L'Hospitalet de Llobregat (Barcelona), SPAIN, [3]Neuropsychology Unit. Department of Neurology. Hospital Universitari de Bellvitge-IDIBELL, L'Hospitalet de Llobregat (Barcelona), SPAIN.

Aim/Introduction: The definition of mild cognitive impairment (MCI) applies to people with cognitive impairment detected by standardized tests but without significant deterioration in activities of daily living. MCI can be caused by multiple etiologies, highlighting Alzheimer's disease (AD). Given the inherent heterogeneity of clinical MCI, more specific biomarkers are needed for detection of underlying AD pathology. Amyloid imaging provides an in vivo quantitative estimate of Aβ pathology that may serve this role. The aim of this study was to assess the role of amyloid-PET with 18F-Flutemetamol in identifying MCI patients who would clinically progress to Alzheimer's disease. **Materials and Methods:** We included 140 patients with MCI (mean age: 70; range: 54-80 years), 96 females. Most of them (74.5%) with amnestic-MCI subtype (a-MCI). All patients underwent neurological and neuropsychological assessment and PET amyloid imaging. Global cognitive status was assessed with the Mini-Mental-State Examination (MMSE) and severity of dementia was rated on the Clinical Dementia Rating (CDR) scale. The diagnosis of MCI was established using the revised Petersen criteria and CDR scale of 0,5. The interpretation of PET images was visual and semi-quantitative (Z scores) and individuals were classified as amyloid-positive (Z>2,5) or amyloid-negative (Z<2,5). Results: Amyloid PET was positive in 70 patients (50%), most of them with an amnesic multidomain MCI. In the subsequent follow-up (3 years), 41 patients progressed to AD, 19 remained stable, and the rest 10 patients presented other dementing processes non-AD. The conversion rate of MCI due to AD was 37 % within the first year, 43% within the second and 20% within the third year of follow-up. In both groups, the neocortical amyloid deposit was diffuse in nature, but in patients with MCI due to AD was higher (Z:7.5 ±2.6) than in non-converters group (Z:5.5±2,4). We found statistically significant differences in amyloid deposition intensity between the two groups using Student's t-test (p<0,05). **Conclusion:** Amyloid-PET will be a useful diagnostic tool, in combination with information on cognitive function and neuroimaging, in identifying patients with MCI at high risk for AD development. While our current cohort is modest in number, limiting statistical inference, elevated cortical uptake is associated with predictors of conversion to AD and eventual clinical progression. If effective anti-amyloid therapy becomes available for the treatment of MCI, it will be especially important to distinguish those patients who would benefit from it. Amyloid PET could help to make this distinction. **References:** None

EPS-093

Texture Quantification Parameters for Alzheimer's disease diagnosis measured by 11C- (R)- PK11195 PET images

M. Lapo Pais[1,2], L. Jorge[1,2], R. Martins[1,2], N. Canario[1,2,3], C. Xavier[1,2], A. Abrunhosa[1,2], I. Santana[3,4], R. Bernardes[1,2,3], M. Castelo-Branco[1,2,3];
[1]Coimbra Institute for Biomedical Imaging and Translational Research (CIBIT), University of Coimbra, Coimbra, PORTUGAL, [2]Institute for Nuclear Sciences Applied to Health (ICNAS), University of Coimbra, Coimbra, PORTUGAL, [3]Faculty of Medicine, University of Coimbra, Coimbra, PORTUGAL, [4]Department of Neurology, Coimbra University Hospital, Coimbra, PORTUGAL.

Aim/Introduction: Alzheimer's disease is the most common neurodegenerative disease and its triggers remain poorly understood. The golden standard imaging biomarker used in the clinical diagnosis of Alzheimer's disease is the 11C-Pittsburgh Compound B. As activated microglia have been associated to mediated neuroinflammation in neurodegenerative diseases and 11C- (R)- PK11195 translates its degree, this tracer might represent an alternative key biomarker in the study of Alzheimer's disease pathogenesis. The methods used to quantify PET data related to neurodegeneration are most often based on tracer kinetic modeling. The present study hypothesizes that textural quantitative parameters may be an alternative or complement to kinetic modeling in PET neuroimaging studies. Thus, we aimed to investigate both the potential of PK as an imaging biomarker and of the textural descriptors as quantitative parameters for the clinical diagnosis of Alzheimer's disease. **Materials and Methods:** Kinetic and textural quantification parameters of 11C-Pittsburgh Compound B and 11C- (R)-PK11195 PET images were submitted to classification using support vector machines and combined using the majority voting method ensemble technique. 11C-Pittsburgh

Compound B PET images were used as a ground truth, to create the label dataset. Results: The individual classifier built using the golden standard reference - $^{PiB}SUVR_{CER}$ images - yielded the best classification accuracy for Alzheimer's disease diagnostic (accuracy: 0.9250; sensitivity: 1; specificity: 0.8636 and balanced accuracy: 0.9286). Regarding 11C- (R)- PK11195 the best result was achieved using the ensemble technique (accuracy: 0.7250; sensitivity: 0.7083; specificity: 0.7500 and balanced accuracy: 0.7206). Although this classifier did not overperform, as expected, the standard reference, the measures of test performance and balanced accuracy were overall good and consistent with the ones obtained using the golden standard 11C-Pittsburgh Compound B and textural metrics. **Conclusion:** It was found clinically relevant quantitative information regarding Alzheimer's disease in the binding pattern of tracers measured by textural metrics. Textural whole-brain based approaches may be an alternative and complement to the most often used ROI based kinetic modeling quantification, particularly in PET neuroimaging studies using tracers as measures of diffuse physiological phenomena, such as microglia activation/neuroinflammation. Moreover, being PK an indirect measure of chronic inflammation, it represents a potential imaging biomarker not only for the clinical diagnosis of Alzheimer's disease but also in assessing the pathogenesis of this disorder, and in the finding of novel treatment strategies. **References:** none

EPS-094

^{18}F-FDOPA PET/CT diagnostic accuracy study in suspected brain tumors recurrence

***D. Lisei Coscia**, C. Salvat Dávila, C. Vigil Díaz, B. Fernández Llana, M. Domínguez Grande, M. López Carballo, A. Laverde Mächler, N. Martín Fernández, F. Gonzalez García;*
HUCA, Oviedo, SPAIN.

Aim/Introduction: PET/CT is being increasingly used to supplement MR Imaging in the clinical management of glioma, particularly in challenging cases. We investigated the diagnostic accuracy of PET/CT 3,4-Dihydroxy-6-[18F] fluoro-L-phenylalanine (PET-FDOPA) in brain tumors treated patients, in suspected recurrence during follow-up with MR. **Materials and Methods:** We performed an observacional retrospective single-center analysis of 19 patients/32 lesiones (9 females) (mean age 55, r13-64), from December 2016 to November 2019. All patients were referred due to suspected but not confirmed recurrence during MR follow-up. In total, 17 were primary brain tumors (10 glioblastoma, 3 astrocytomas, 2 oligodendroglioma grade II, 1 meningioma, 1 anaplastic medulloblastoma) and 2 brain metastasis. PET-FDOPA diagnostic accuracy of lesion analysis, sensitivity (Se), specificity (Sp), positive predictive value (PPV) and negative predictive value (NPV) were obteined. Maximal tumor standard uptake value-to-mean contralateral healthy cortex ratios (T/H) were recorded. Thresholds of T/H values were determined by receiver operating characteristic (ROC) analysis. Results: 32 brain lesions were found in 19 PET-FDOPA studies. Diagnostic confirmation was by surgery in 16/19 and in 3/19 by clinical/radiological follow-up (mean 10 months, r2-37). 27/32 lesions were compatible with tumor recurrence in PET-FDOPA, presenting values of Se, Sp, PPV and NPV of 99%, 83.3%, 96.3% and 99%, respectively. In lesion analysis confirming or not recurrence, the mean T/H values were 3.47 (CI95% 3.01-3.93) and 1.57 (CI95% 1.24-1.91) ($p<0.001$). ROC analysis yielded a threshold of 2.13 for T/H in confirming recurrence with a Se 96.3% and Sp 99%, area under the curve 0.978 ($p=0.001$). **Conclusion:** PET-FDOPA has a high diagnostic accuracy in detecting brain tumor recurrence, in patients with undetermined findings in MR. **References:** none

EPS-095

Technical improvements implemented in a PET dedicated to the brain (CaremiBrain) in its technical validation phase

***P. Nespral Torres**[1], A. Abadía-Ruiz[1], A. Delgado-Cano[1], M. Cabrera-Martín[1], G. González-Pavón[2], C. Morera-Ballester[2], M. Sanchís-Hernández[2], J. Matías-Guiu[3], J. Carreras-Delgado[1];*
[1]Nuclear Medicine Department, Health Research Institute of Hospital Clínico San Carlos. Madrid, SPAIN, [2]Oncovision, General Equipment for Medical Imaging S.A., Madrid, SPAIN, [3]Neurology Department, Health Research Institute of Hospital Clínico San Carlos. Madrid, SPAIN.

Aim/Introduction: The goal of developing a PET dedicated to the brain (CareMiBrain) has evolved from its initial approach to diagnosis and monitoring of dementias, to the more ambitious of creating a revolutionary clinical pathway for the knowledge and personalized treatment of neurological diseases. The main innovative feature of CareMiBrain is the use of detectors with continuous crystals, which allow a high resolution determination of the depth of annihilation photons interaction within the thickness of the scintillation crystal, with improved ergonomics and low tracer dose as added values. Our objective is to describe technical validation phase of PET CareMiBrain, project financed with funds from the European Union (Horizon 2020 innovation program, 713323). **Materials and Methods:** The technical validation consisted of a pilot, prospective and observational study whose objective was to obtain the first images (40 patients), analyze them and introducing clinically-relevant adjustments in acquisition, reconstruction and correction parameters after comparing the image quality of CareMiBrain with that of PET-CT Siemens Biograph. Inclusion criteria were: a) patients>18 years, b) with neurological diseases for whom a brain ^{18}F-FDG PET-CT study had been prescribed, c) signature of informed consent.Two nuclear physicians observed independently images acquired with PET CareMiBrain and with PET-CT on 22 specific brain

regions, without knowledge of the clinical data. Results: Caremibrain images showed sufficient quality for diagnosis. Thanks to team meetings and the joint analysis of the images, it was possible to detect its weak points and its causes. After initial evaluation, priorities for technical improvements were: 1) images were different from the current standard (more saturated); 2) image quality was superior in the frontal lobe vs. occipital, and in the parietal cortex vs. basal ganglia; 3) the third ventricle and the lateral ventricles were better seen on PET-CT; 4) CareMiBrain's attenuation correction could be improved; 5) possible improvements in reconstruction.The calibration, acquisition and processing processes, as well as the reconstruction, were optimized, the number of iterations was set to achieve the best signal-to-noise ratio, the random estimation was improved for more precise correction, attenuation map generation and attenuation correction were also improved and image post-processing filters were adjusted for CareMiBrain and included in the reconstruction algorithm. **Conclusion:** In conclusion, CareMiBrain has shown sufficient performance for its clinical use, its main advantage being the high spatial resolution, although it still has an horizon for improvement in the ongoing clinical phase II of this study, adding also quantification assessment. **References:** None.

EPS-096

F-18-FET and F-18-choline PET/CT imaging in primary diagnosis of low-grade gliomas with impact on therapy

A. Golubic[1], M. Hodolic[2,3], A. Misir Krpan[4], M. Zuvic[1], M. Baucic[4], G. Mrak[5,6], J. Nemir[5], D. Huic[1,6];
[1]Department of Nuclear Medicine and Radiation Protection, University Hospital Centre Zagreb, Zagreb, CROATIA, [2]Nuclear Medicine Department, Faculty of Medicine and Dentistry, Palacký University Olomouc, Olomouc, CZECH REPUBLIC, [3]Nuclear Medicine Research Department IASON, Graz, AUSTRIA, [4]Department of Oncology, University Hospital Centre Zagreb, Zagreb, CROATIA, [5]Department of Neurosurgery, University Hospital Centre Zagreb, Zagreb, CROATIA, [6]University of Zagreb School of Medicine, Zagreb, CROATIA.

Aim/Introduction: The aim of this prospective pilot study was to evaluate diagnostic accuracy and impact on therapy of F-18-FET and F-18-FCH in patients with brain lesions suggestive of low-grade gliomas (LGG). **Materials and Methods:** Eleven patients, 21 to 80 years of age, six of them women, have been included in this pilot study. Initial suspected LGG was reported with 3T magnetic resonance brain imaging. All patients underwent both F-18-FET and F-18-FCH PET/CT brain scan within one week. Brain imaging was performed according to standard protocol 20 minutes after intravenous injection 185 MBq of F-18-FET (O-(2-[F-18]-fluoroethyl)-L-tyrosine) and 185 MBq F-18-FCH (fluoromethyl-(F-18)-dimethyl-2-hydroxyethyl-ammonium chloride). Biopsy or surgical lesion ablation with the pathohistological diagnosis have been performed in the following month in nine patients, and a year-long clinical follow-up was reported in all patients. Results: Nine patients had a F-18-FET positive lesion, with SUVmax values ranging from 1,3 to 3,1. Four patients had F-18-FCH uptake in lesions that were also F-18-FET positive, SUVmax ranging from 0,5 to 3,9. Two patients were F-18-FET and F-18-FCH negative, conventional imaging was suggested in follow-up. Six patients had surgery and maximal tumour reduction. Histologically, grade IV glioblastoma was reported in two patients, who were both F-18-FET and F-18-FCH positive, with higher SUVmax values of metabolically active brain lesions. Diffuse astrocytoma was reported in four patients, anaplastic astrocytoma in one and two patients had gangliogliomas. Lesions histologically reported as lower grade, also had lower values of SUVmax F-18-FET uptake and were either F-18-FCH negative or had only faint F-18-FCH uptake (SUVmax 0,5 - 0,8).In a year-long clinical follow-up period, one patient, negative on both F-18-FET and F-18-FCH, has no morphological evidence of disease progression, any new therapy, or clinical signs of any brain disorder. One of the patients with aggressive grade IV glioblastoma and the highest SUVmax values of both F-18-FET and F-18-FCH has clinical and morphological progression of the disease. Chemoradiotherapy was included after surgery in five patients, with astrocytoma and glioblastoma histological diagnosis. **Conclusion:** Preliminary results of this pilot study on a small patient sample suggest functional imaging provides valuable additional information, necessary for individual patient management and further treatment. Amino acid and protein synthesis imaging gives important data on lesion volume and spread, while increased lipid synthesis seems to correlate with higher grade and more aggressive gliomas. **References:** None

1012

Wednesday, October 20 - Saturday, October 23, 2021

on-demand pool, release on Wednesday, October 20 at 09:00

e-Poster Presentation Session 7: An Overview on Endocrine Disease

EPS-097

Frequency of Malignancy in Incidental Thyroid Nodules Detected by F-18 FDG PET/CT

S. Kesim, H. T. Turoglu, S. Ozguven, S. Inanir, C. O. Sahin, N. Filizoglu, K. Niftaliyeva, T. N. Kissa, Z. C. Balaban Genc, F. Dede, K. Oksuzoglu, F. Sen, T. Ones, T. Y. Erdil;
Marmara University School of Medicine, Istanbul, TURKEY.

Aim/Introduction: Thyroid incidentalomas, asymptomatic thyroid nodules, are relatively common incidental findings detected during imaging studies. Herein, we aimed to evaluate the malignancy rate of nodular thyroid incidentalomas detected on FDG PET/CT studies, and their association with standardised uptake value (SUV) of FDG. **Materials and Methods:** Whole body FDG PET/CT scans performed from October 2013 to August 2020 for cancer evaluation (staging, monitoring of the disease, or treatment response) were retrospectively reviewed, selecting those that showed nodular thyroid foci. Glands with diffuse increased FDG uptake and patients whose fine-needle aspiration biopsy (FNAB) results were lacking in our database were excluded. Bethesda score of biopsy results and SUVmax values were correlated. Results: Eighteen patients with varying malignancies (i.e., breast, colon, lung, gastric cancer, and multiple myeloma) and increased focal FDG uptake on thyroid nodules and investigated using the FNAB procedure after PET/CT were included in the study. Of 18 patients, 6 were men and 12 were women. The average age of the patients was 61.9 years (range of 40-73 years; standard deviation of 8 years). The average SUVmax value was 12.5 ± 14.9. As specified by the Bethesda System for reporting thyroid pathologies, benign lesions were reported in 15 cases (83.3%) with an average SUVmax of 8.17 ± 9.15. Two patients with SUVmax values of 10.3 and 44.7 had papillary thyroid carcinoma, which is the most common histological type. The malignancy rate was found to be 11.1%. In one case, the result was suggestive for a thyroid nodule of follicular lesion of undetermined significance (Bethesda category III). There was no significant correlation found between SUVmax values and the Bethesda scores of the nodules ($p>0.05$). **Conclusion:** The incidence of malignancy of the thyroid incidentalomas shows high variation in the literature. Former studies indicate that a thyroid nodule with a SUVmax value greater than 5.0, regardless of its size, suggests malignancy. However, in our case series, it was not feasible to distinguish malignant from benign lesions using SUVmax values. While SUVmax is a predictive factor for malignancy, the FNAB remains the primary diagnostic tool for the clinical management of these patients. **References:** none

EPS-098

^{18}F-FDG thyroid incindental uptakes: can semiquantitative and volumetric parameters predict the final diagnosis?

F. Dondi[1], A. Mazzoletti[1], P. Bellini[1], A. Calabrò[1], M. Gregorelli[1], D. Albano[1], R. Rinaldi[1], M. Gazzilli[2], E. Cerudelli[2], L. Camoni[2], R. Giubbini[1], F. Bertagna[1];
[1]Università degli Studi di Brescia, Brescia, ITALY,
[2]Spedali Civili di Brescia, Brescia, ITALY.

Aim/Introduction: Incidental thyroid uptakes are frequent findings in ^{18}F-fluorodeoxyglucose positron emission tomography/computed tomography (^{18}F-FDG PET/CT) imaging. Correct assessment of these findings is mandatory given the possible presence of differentiated thyroid cancer (DTC). The aim of this retrospective study was to investigate a possible relationship between PET/CT parameters and the final diagnosis of thyroid incidentalomas detected at ^{18}F-FDG PET/CT. **Materials and Methods:** ^{18}F-FDG PET/CT scans of 221 patients with incidental thyroid uptakes were retrospectively analyzed. Maximum and mean standardized uptake value body weight max (SUVbwmax, SUVbwmean), maximum SUV lean body mass (SUVlbm), maximum SUV body surface area (SUVbsa), metabolic tumor volume (MTV) and total lesion glycolysis (TLG) of hypermetabolic lesions were collected. Furthermore, data about radiological follow-up, citology and histology were collected and compared to PET/CT parameters. Results: On follow up, the presence of DTC was demonstrated in 71 (32%) while 150 incidental thyroid uptakes were classified as benign. A significant correlation ($p<0,05$) between SUVbwmax, SUVbwmean, SUVlbm and SUVbsa values with final diagnosis was reported. In contrast, no correlation between MTV and TLG values and the final diagnosis was reported. Furthermore, receiver operating characteristic (ROC) curve analysis revealed values of 4.72 for SUVbwmax, 3.54 for SUVbwmean, 3.48 for SUVlbm and 1.3 for SUVbsa as the best values for discriminate between malignant and benign thyroid incidental uptakes. Areas under curve (AUC) were respectively 0.739, 0.720, 0.733 and 0.733. At multivariate analysis including age, size of the lesion and PET/CT semiquantitative parameters, only advanced age demonstrated to be an independent predictor for the final diagnosis. **Conclusion:** In conclusion with this study, we have demonstrated PET/CT semiquantitative parameters such as SUVbwmax, SUVbwmean, SUVlbm and SUVbsa are significantly correlated with the final diagnosis of thyroid incidental uptake at ^{18}F-FDG scans. However, at multivariate analysis only age of patients showed to be an independent predictor for final diagnosis. **References:** none

EPS-099

BRAFV600E mutational status in thyroid carcinoma patients - single center study

T. Makazlieva[1], N. Manevska[1], S. Stojanoski[1], A. Jankulovska[1], B. Stoilovska[1], A. Eftimov[2], R. Jovanovic[2];
[1]Institut of pathophysiology and nuclear medicine, Skopje, NORTH MACEDONIA, [2]Institut of pathology, Skopje, NORTH MACEDONIA.

Aim/Introduction: Thyroid carcinomas (TCs) are one of the most genetically evaluated carcinomas. The BRAFV600E mutation is the most frequent genetic alteration, but it isn`t still routinely recommended in the initial evaluation of the TCs patients. The aim of our study was to evaluate BRAF mutational status in TCs patients and to correlate it with clinical features: initial stage, age at diagnosis and post ablative ^{131}I scan in relation to presence or absence of BRAFV600E mutation. **Materials and Methods:** Fifty-two patients with TCs were evaluated for BRAFV600E mutational status from the primary tumor tissue. Retrospective analysis of the medical data and postoperative histopathology reports were performed to determine the histopathological type of tumor and the initial stage. Three nuclear medicine physicians with more than 10 years' experience reviewed the post ablative radioiodine whole body scans (WBS). Patients were followed for average 4 years (SD ± 2.7years). Results: We found that 32 out of 52 TCs patients or 63.46% were BRAFV600E + mutation and all of them were papillary thyroid carcinomas (PTC), or 21 typical variants, 9 follicular variants and one patient each were: Warthin like, tall cell and Hurthle cell variants of PTC. BRAFV600E - were 19 (36.54%) patients (4 being follicular thyroid carcinomas and 15 patients PTC). The average age at the moment of diagnosis was similar in both groups, or 45 years ±15.25 in BRAFV600E - group and 48 ± 13.26 years in BRAFV600E + group. Regarding the initial stage in BRAFV600E - group, 55% were TNM stage I, 25% stage II, 10% stage III and 10% Stage IV and BRAFV600E + group were 53.125% Stage I, 21.875% Stage II, 21.875% Stage III and 3.125% Stage IVa. Post ablative WBS scan detected remnant thyroid tissue accumulation in all BRAFV600E + patients. In four BRAFV600E - patients the scan revealed distant metastases in 3 patients, while accumulation in neck lymph nodes in 1 patient. **Conclusion:** Analysis hasn't revealed significant difference in age at diagnosis, initial staging and post ablative ^{131}I WBS scans among BRAFV600E + and - groups. Longer follow-up is recommended to discover the true meaning of BRAFV600E in the prognostication. **References:** Zhang M, Lin O. Molecular Testing of Thyroid Nodules. Arch Pathol Lab Med. 2016;140:1338-1344. Tang KT, Lee CH. BRAF Mutation in Papillary Thyroid Carcinoma: Pathogenic Role and Clinical Implications. Journal of the Chinese Medical Association, 2010;73(3):113-128.

EPS-100

Postoperative basal serum thyroglobuline (TG) prior to radioiodine therapy as a predictive factor of recurrence in patients with differentiated thyroid cancer (DTC)

***R. Núñez Muñoz**, Y. Carreres Ortega, M. A. Astudillo Sarmiento, R. Valverde Jorge, M. Nevares Herrero, J. Genollá Subirats, J. Santamaría Sandi, M. Badiola Molinuevo;*
Osakidetza, Bilbao, SPAIN.

Aim/Introduction: To assess the role of post-surgery serum thyroglobulin and prior to iodine-131 therapy as a prognostic factor for locoregional or distant recurrence. **Materials and Methods:** We conducted a retrospective study of 242 patients (81% women, 19% men, mean age: 50.5 ± 14.2 years) with differentiated thyroid cancer (90.9% papillary, 9.09% follicular), non-metastatic debut and treated with total thyroidectomy. 142 patients (58.7%) underwent lymphadenectomy (43% prophylactic, 15.7% therapeutic), 40.7% of which resulted in pathological lymphadenopathies. Serum TG was determined 6-8 weeks after surgery, using the Immunulite 2000 Siemens method, with a functional sensitivity of 0.5 ng/ml. All patients subsequently received iodine-131 therapy, followed by a post-treatment whole-body scan and cervicothoracic SPECT/CT acquired 7 days after radioiodine administration. Uptake was observed only in the thyroid bed in 88.8% of the studies and extrathyroid uptake in 8.26%. The median follow-up was 8 years (P25: 5.98, P75: 10.8). Data on both locoregional and distant recurrence were collected from the clinical history during follow-ups. Statistical software R Core Team version 4.0.1 was used for statistical analysis. Patients with positive antithyroglobulin antibodies were excluded. Results: 29 of the 242 patients (12%) presented recurrence (75.9% lymph node, 24.1% Bone/ Lung), with median time to recurrence of 1.36 years (P25: 0.65; P75: 2.75). Patients with relapse in follow-up presented a median serum TG value after surgery of 2.3 ng/ml, compared to 0.5 ng/ml of the non-recurrence patients. TG was categorized taking the value 2.5 ng/ml as a cut-off point, which corresponds to the P95 of the group of patients with no recurrence during follow-up. 14 (48.3%) of the patients who relapsed had post-surgery thyroglobulin values >2.5 ng/ml, compared to 5.2% (11/213) in the non-recurrence group. Performing a univariate analysis with this cut-off point, we have observed statistically significant differences between the patients who did relapse and those who did not ($p<0.001$). We observed that serum TG values >2.5 ng/ml implies a 17-fold higher risk of presenting recurrence (OR: 17.1, CI95% [6.73-45.5], AUC: 0.716 [0.0622-0.809]). When applied a multivariate logistic regression model, post-surgery serum thyroglobulin was shown as an independent variable. **Conclusion:** Basal serum thyroglobulin after surgery and prior to radioiodine therapy is an independent predictive factor of recurrence in patients with DTC. A serum thyroglobulin value >2.5 ng/ml implies a 17 times higher risk of suffering a recurrence, either lymph node or distant metastasis. 48.3% of patients who relapsed had thyroglobulin values >2.5 ng/ml. **References:** None

EPS-101

Low Radioiodine Dose in Postoperative Ablation of Residual Thyroid Tissue in Patients with Differentiated Thyroid Carcinoma

O. Bourogianni[1], N. Kapsoritakis[1], A. Tsaroucha[1], M. Stahaki[1], E. Papadaki[1], S. Koukouraki[2];
[1]University Hospital of Crete, Heraklion, GREECE, [2]School of Medicine, University of Crete, Heraklion, GREECE.

Aim/Introduction: Radioactive iodine131 (RAI) has been widely reported in the treatment of patients with differentiated thyroid cancer (DTC) since 1960's. Selecting an optimal dose of radioiodine for successful ablation is a continuous challenge in low risk patients. The aim of this study was to compare the success rate of low and high activities of 131-I for postoperative remnant ablation using 60mCi or 100mCi 131-I in well differentiated thyroid cancer patients and to assess clinical outcome 36months after RAI therapy. **Materials and Methods:** In order to achieve these targets a retrospective study took place in Therapy Unit of Nuclear Medicine. The sample of the study was consisted of 229 low risk patients (52 males, 177 females) who have undergone thyroidectomy, with histological diagnosis of low-risk well differentiated thyroid cancer. 118 patients received a low dose (60mCi) and 111 patients received a high dose (100mCi) of 131-I. The response to remnant ablation was defined as successful or unsuccessful according to post-therapy ultrasonography of the neck, diagnostic Whole Body Scan, serum thyroglobulin (Tg), and anti-Tg. The follow up completed 36 months after RAI therapy and recurrence rates were assessed. Results: Successful ablation was 95,7% in the low dose and 97,2 % in the high dose group (no statistically significant difference in ablation rates). The recurrence rates were 0,8% in the low dose group and 2,7% in the high dose group. The differences were not statistically significant between the two groups. Further evaluations within the groups based on demographical factors (age, sex) and the interval between the RAI therapy and referral to the assessment of the ablation efficacy did not reveal any statistically significant associations to the successful ablation rate and the recurrence rate. **Conclusion:** Our findings suggest that remnant thyroid tissue in patients with low-risk, well-differentiated thyroid cancer can be ablated with low radioiodine dose. The success and recurrence rate is not different from that obtained with high dose. **References:** None

EPS-102

The efficacy of radioactive iodine with cumulative activities over 600 mCi for the treatment of Differentiated Thyroid Carcinoma

A. Mazzoletti, D. Albano, F. Dondi, P. Bellini, A. Calabrò, M. Gregorelli, F. Bertagna, R. Giubbini;
ASST Spedali Civili of Brescia, University of Brescia, Brescia, ITALY.

Aim/Introduction: Radioactive iodine (RAI) has been used as adjuvant treatment for intermediate and high-risk differentiated thyroid carcinoma (DTC) after thyroidectomy. Previous studies suggested that the efficacy of RAI was obtained with cumulative activity equal to or lower than 600 mCi, higher activities were associated with increased risk of leukemia.The aim of this retrospective study was to investigate the treatment outcomes and the long-term follow-up after using cumulative activities of RAI>600 mCi for the treatment of DTC. **Materials and Methods:** We have retrospectively enrolled 178 patients (106 women; mean age 50.9) affected by DTC and treated with a cumulative activities of RAI>600 mCi in our Centre from 1998 to 2015. The response to therapy was assessed by thyroglobulin levels measurement and morpho and/or functional imaging according to 2015 ATA criteria. The average follow-up was 168 months (range 21-592). Results: Among 178 patients included, 126 had papillary DTC, 33 follicular DTC, 11 aggressive variants of papillary DTC and 7 Hurthle cell carcinoma. Twenty patients (11%) had distant metastases at presentation, while 80 (47%) showed nodal involvement. Mean number of RAI therapies received during years was almost 6 cycles with a median I131 cumulative dose received of 42,7 Gb. Ninety patients received a total amount of RAI between 600 mCi and 1000 mCi, while the remaining 88 a cumulative activity higher than 1000 mCi. After the last RAI cycle, excellent response was obtained in 24% of patients, indeterminate response in 10%, incomplete in 66%; finally, iodine refractoriness was present in 38%. Death occurred in 33 patients (18,5%), while second malignancy developed in 6 (3%). Comparing the two groups (600-100 mCi vs >1000 mCi) no significant differences were found considering the treatment response, risk of death and secondary malignancies, despite a high number of excellent response (31% vs 17%). When exceeding 1500 mCi the efficacy of RAI resulted very low with only 2% of excellent response. Male, advanced age, high Thyroglobulin, presence of distant metastases, ATA class risk at diagnosis, iodine refractory and the final response were statistically correlated to the risk of death; but at multivariate analysis only iodine refractoriness and age were confirmed to be independent factors for OS. **Conclusion:** RAI therapy provided to be an effective for DTC patients even when exceeding 600 mCi if appropriately selected and with low risk of secondary cancer. However, the decision to administer high cumulative RAI activities should be made on an personalized basis. **References:** none.

EPS-103

131I-SPECT/CT at the first radioiodine ablation and during follow-up in patients with differentiated thyroid carcinoma (DTC)

S. Nuvoli, A. Marongiu, I. Gelo, M. Luciana, M. L. Stazza, M. Rondini, A. Spanu, G. Madeddu;
University of Sassari, Sassari, ITALY.

Aim/Introduction: 131I-SPECT/CT has dramatically improved whole body scan (WBS) image interpretation in DTC patients after thyroidectomy. We further investigated SPECT/CT after first radioiodine ablation and during long-term follow-up to obtain the best management of affected DTC patients. **Materials and Methods:** We retrospectively evaluated 106 consecutive thyroidectomized DTC patients at primary radioiodine ablation; 24 patients were at high risk (H), 61 at low risk (L) and 21 at very low risk (VL). Both WBS and SPECT/CT were performed 5-7 days after 1.85-5.66 GBq oral therapeutic dose using hybrid dual-head gamma camera with high energy, parallel hole collimators. Eight-six patients could be monitored in the follow-up repeating both WBS and SPECT/CT after radioiodine diagnostic dose (185 MBq) together with thyroglobulin assay. Results: SPECT/CT concordantly with WBS detected 172 residues, only it characterizing other 36 residues unclear (n.24) or occult (n.12) at WBS. Moreover, SPECT/CT correctly classified 49 malignant foci in 17/106 patients (8H, 7L, 2VL) with significant ($p<0.001$) more elevated number than WBS which evidenced 32/49 foci in 13/17 patients. WBS classified as unclear 17/32 foci and wrongly classified other 2/32 foci correctly classified as metastases by SPECT/CT which also characterized 17/49 further malignant foci occult at WBS. SPECT/CT had an incremental value over WBS in 25.5% of the 106 patients and changed classification and therapeutic management in 16.03% of cases. Only SPECT/CT also changed neck lymph node and distant metastasis classification performed at surgery in 11 cases. The 86 patients monitored during follow-up also included 13 of 17 patients with metastases at post-therapeutic scans. Four/13 patients underwent disease progression with metastasis number increase as ascertained by diagnostic SPECT/CT and with persistently high thyroglobulin levels; other 4/13 patients had stable disease with unmodified metastatic lesions and thyroglobulin levels, while the remaining 5/13 patients showed disease improvement with reduction or absence of metastases and significant decrease of thyroglobulin levels. Moreover, other 13/86 patients (4H, 6L, 3VL) with only residues at post-therapeutic scan, showed 16 metastatic lesions in the follow-up, 13 unclear and 8 occult at WBS, only characterized by SPECT/CT; thyroglobulin levels were undetectable or very low in 5/13 patients, two of whom VL-T1aN0M0, while these increased in the remaining 8/13 cases. **Conclusion:** 131I-SPECT/CT proved higher performance than WBS in both post-radioiodine therapy and follow-up phases of DTC patients to establish correctly stage and risk stratification and to evaluate disease progression and regression. Routine SPECT/CT use is suggested in DTC protocol. **References:** None

EPS-104

Our Experience in the Use of Iodine-123 in the Diagnosis and Monitoring of Thyroid Cancer

M. Atalay[1], B. Ural[1], A. Yıldırım[1], B. Okudan Tekin[1,2];
[1]Ankara City Hospital, Ankara, TURKEY, [2]University of Health Sciences, Ankara, TURKEY.

Aim/Introduction: In differentiated thyroid cancer (DTC), local or distant metastases cause poor prognosis and early detection of these lesions contributes to overall survival with appropriate clinical judgment.[1] Radioiodine imaging in DTC is an invaluable method in personalized medicine to characterize each lesion in patients. In diagnosis and follow-up of DTC, Iodine-123 is preferred with its low radiation dose and appropriate energy, which does not have a stunning effect.[2] **Materials and Methods:** Thirty-six patients (28F, 8M, 45±3 years) diagnosed with DTC who were admitted to our clinic for radioactive iodine therapy and follow-up were included in that study. I-123 whole-body scan (WBS) was planned for 20 patients as routine follow-up who received RAI treatment 8-12 months ago, 7 patients in suspicion of recurrence or metastasis who received RAI treatment between 2012-2019 and 9 patients for diagnostic purposes. After 3 mCi I-123 iv application, WBS and neck spot images were obtained at the 4th and 24th hours, and SPECT/CT images at the 24th hour. F18 FDG PET/CT imaging was performed in 17 patients due to clinical suspicion. Results: Pathological involvement was detected in 10 patients (27%). In 2 of the 9 patients who underwent F18 FDG PET/CT, additional pathological involvements were detected in I-123 WBS, which were not detected in FDG PET/CT. Pathological involvement was detected on PET/CT imaging in 6 of 8 patients who were negative for I-123 WBS and had clinical suspicion (increase in Tg/AntiTg titer, lymph nodes with pathological appearance on USG). With I-131 WBS taken after treatment, additional foci were seen in the lung in 2 patients, in the bone in 1 patient and in the thyroid gland with a lymph node in 1 patient. Stunning was observed in 1 patient who was given RAI treatment at 3 weeks after the I-123 scan, but exogenous iodine intake could not be ruled out. **Conclusion:** In 9 patients who underwent diagnostic I-123 screening, the dose amount was changed according to the screening results. We think that I-123 is suitable for screening with high Tg and AntiTg and medium-high risk factors, with low radiation and no risk of stunning in post-treatment scans. **References:** 1)Su, Deng-Huang et al. "The impact of locoregional recurrences and distant metastases on the survival of patients with papillary thyroid carcinoma." Clinical endocrinology vol. 82,2 (2015): 286-94.2)Ferris, Trevor et al. "Use of radioiodine in nuclear medicine-A brief overview." Journal of labelled compounds & radiopharmaceuticals vol. 64,3 (2021): 92-108.

EPS-105

^{68}Ga-FAPI PET/CT Accuracy In Patients With Recurrent Medullary Thyroid Carcinoma

U. Elboga, Z. Sayıner, E. Sahin, S. Ozturk, Y. Cayirli, Y. Celen, E. Akarsu;
Gaziantep University, Gaziantep, TURKEY.

Aim/Introduction: Medullary thyroid cancer (MTC) is rare tumor of thyroid gland. Postoperatively persistently elevated basal calcitonin levels can be seen. Location of residual, recurrent, o rmetastatic disease is crucial to treatment management. We aimed to evaluate the use of ^{68}Ga-FAPI PET/CT in localizing MTC foci in patients with biochemical relapse. **Materials and Methods:** This is a retrospective study. Patients who were previously diagnosed with MTC and achieved biochemical recovery after the first operation and whose calcitonin levels significantly increased in the last follow-up were included in the study. ^{68}Ga-FAPI PET/CTand ^{18}F-FDG PET/CT were performed for comparative purpose and detection of recurrence localization. Results: Recurrence localization was detected in 3 of 7 patients with ^{18}F-FDG PET/CT, while ^{68}Ga-FAPI PET/CT was detected in 5 of 7 patients. Recurrence focus was detected with ^{68}Ga-FAPI PET/CT in three patients whose recurrence focus was not detected by ^{18}F-FDG PET/CT. The sensitivity was 71.43% with ^{68}Ga-FAPI PET/CT, while it was 42.86% with ^{18}F-FDG PET/CT. **Conclusion:** In the presence of biochemical disease in patients with recurrent MTC, ^{68}Ga-FAPI PET/CT can be used in patients whose results are not obtained with 18F-FDG PET/CT imaging in the detection of metastatic focus. ^{68}Ga-FAPI PET/CTand ^{18}F-FDG PET/CT can be used as complementary technics. **References:** None

EPS-106

Knowing like the Back of one's Hand the ^{99m}Tc-sestamibi Uptake Mechanism: Could a Simple Parathyroid Scan Be an Essential Tool for Studying BAT?

W. Jalloul[1], I. Roata[2], C. Archip[2], A. Tarca[2], R. Tibu[2], S. Chiper[1], I. Grierosu[1,2], T. Ionescu[1], C. Stolniceanu[1], M. Gutu[1,2], V. Ghizdovat[1], M. Moscalu[1], A. Naum[1,3], C. Stefanescu[1,2];
[1]University of Medicine and Pharmacy U.M.F „Grigore T. Popa", Iasi, ROMANIA, [2]Nuclear Medicine Laboratory, County Emergency Hospital „Sf. Spiridon", Iasi, ROMANIA, [3]Nuclear Medicine Laboratory, Regional Institute of Oncology, Iasi, ROMANIA.

Aim/Introduction: Brown Adipose Tissue (BAT) is an endocrine tissue whose metabolic effects and pathological implications are not entirely elucidated. Considering the ^{99m}Tc-sestamibi uptake mechanism in BAT, this retrospective study aims to emphasise the contribution of Parathyroid Scan (PS) to BAT detection, quantification and a better interpretation of this tissue's biodistribution in patients with endocrine pathologies. **Materials and Methods:** 441 patients were referred to our Laboratory (2015-2020) to perform the dual-phase ^{99m}Tc-sestamibi PS (neck and chest). After analysing the total number of 986 scans (493 for each early and delayed scans - some patients underwent more than one PS during this period), we identified images with hyperfunctional BAT. We studied this tissue's pattern through measuring the total counts and pixels by drawing a ROI in every BAT localisation. Each ROI_{BAT} was reported to an equal ROI in a non-BAT reference area (right hemithorax). We also performed statistical analysis in order to elucidate potential correlations between BAT biodistribution and patients' clinical parameters. Results: The accumulation of ^{99m}Tc-sestamibi in active BAT mitochondria was adequate to be visualised in 56 delayed scans (5.68% total images, 11.36% delayed scans) in 55 patients with mean age of 53.18 years. We noticed the preponderance of females (85.7%). The BMI mean value (mv) was 25.3±4.9 with 21.4% obese and 10.7% diabetic subjects. 19.6% of cases were reported in winter. 60.7% of patients had thyroid pathologies, predominantly nodular goiter (35.7%). Hyperparathyroidism was recorded in 87.5% of subjects (69.6% primary). PTH ranged between 14 and 3826 with a mv=456.71 pg/mL, and 80.4% of cases had osteoporosis. A statistically significant ρ (medium intensity, Sig=0.008<0.05) was found between PTH and BMI values. We noticed the presence of parathyroid adenoma(s) in 82.1% of images. BAT had symmetric distribution in 92.9%, homogeneous in 42.9%. This tissue was recorded in cervical and supraclavicular regions with single localisation in 73.2% of scans (87.8% cervical), whereas all the rest being multiple. The highest $ROI_{BAT}/ROI_{reference}$ and total $counts_{BAT}/pixels_{BAT}$ ratios were identified in the cervical region with respectively, 2.72 (mv=1.45) and 73.58 (mv=31.34) vs 2.58 (mv=0.55) and 48.24 (mv=10.06) in the supraclavicular area. **Conclusion:** In a time when quickness and efficiency of diagnostics matter most, sometimes simple approaches to novel studies is key. Through its tropism for tissues with high density in mitochondria, and for large differences in mitochondrial transmembrane potential, ^{99m}Tc-sestamibi complements ^{18}F-FDG in BAT analysis considering that SPECT technologies remain less expensive and more available. **References:** None

EPS-107

The role of parathyroid hormone and neck ultrasound in predicting positivity of parathyroid scintigraphy

D. Bezzi[1], E. Tabacchi[2], A. Scrivo[3], A. Cingolani[3], L. Calderoni[1], R. Bonfiglioli[2], C. Malizia[2], S. Fanti[1,2];
[1]Nuclear Medicine, Department of Experimental, Diagnostic and Specialty Medicine, University of Bologna, Bologna, ITALY, [2]Nuclear Medicine, IRCCS, Azienda Ospedaliero-Universitaria di Bologna, Bologna, ITALY, [3]Nephrology, Dialysis and Transplantation, Department of Experimental, Diagnostic and Specialty Medicine, University of Bologna, Bologna, ITALY.

Aim/Introduction: in this study we tried to evaluate whether parathyroid hormone value (PTH) and neck ultrasound (US) can predict the positivity of parathyroid scintigraphy and

whether it is possible to identify a cut-off value of parathyroid hormone that can predict its positivity. The goal was to refer patients to parathyroid scintigraphy, in case of PTH values above the cut-off, or to alternative imaging methods such as 11C-methionine PET or 11C-choline PET, in case of PTH values below the cut-off. **Materials and Methods:** this study was conducted on a pool of 261 patients with suspected hyperparathyroidism who performed the MIBI-SPECT/CT imaging protocol at our Nuclear Medicine Centre between 1st Nov, 2016 to Mar 31st, 2021. We excluded those without PTH assay performed within 12 weeks from scintigraphy and those without US. We thus obtained 197 cases that were grouped, according to scintigraphic results, into positives for enlarged parathyroid glands (n=68) or negatives (n=129). Univariate and multivariate logistic regressions were performed using US and PTH as variables to predict scintigraphic outcome. We also attempted to identify the PTH cut-off value by means of a ROC curve. Results: univariate and multivariate logistic regressions showed statistical significance for both the ultrasound variable and the PTH levels in predicting the positivity of scintigraphy with SPECT (US: p value <0,0001 with OR=11,3272; PTH: p value =0,0012 with OR=1,0017), with a concordance rate between US and MIBI-SPECT/CT of 78.7%. The ROC curve identified 430 pg/mL of PTH as a cut-off value capable of predicting positivity on scintigraphy (Sens 48.5%, Spec. 74.4%, AUC: 0.6327), which showed low sensitivity and is therefore not reliable. Considering that we had a good agreement between the US and the scintigraphic outcome but not perfectly overlapping, we subsequently evaluated the cut-off values in the two subgroups US negatives (n= 133) and US positives (n=64). In the US positives group a cut-off value of 258 pg/mL was reached (Sens. 71.1%, Spec. 52.6% PV+ 78%, AUC: 0.6053), however this value is limited by the small sample size. **Conclusion:** the results suggest that neck ultrasound, compared with PTH value, is a better predictor of positivity to parathyroid scintigraphy. The cut-off value identified for PTH (258 pg/mL) is significant in predicting a positive scintigraphy only for the subgroup of patients who already have a positive US, suggesting future uses in a diagnostic flow charts. **References:** none

EPS-108

Accuracy of Choline PET/CT vs Tc 99m Sestamibi SPECT/CT Parathyroid Imaging in Comparison to Histopathology in the Diagnosis of Parathyroid Adenoma: A Meta-Analysis

B. Tecson;
Philippine Heart Center, Quezon City, PHILIPPINES.

Aim/Introduction: In the advent of the use of Choline in Parathyroid PET/CT, we assessed its accuracy in diagnosing parathyroid adenoma in comparison to Tc 99m Sestamibi SPECT/CT parathyroid imaging, with histopathology as the reference standard. **Materials and Methods:** Cross-sectional studies from 2014 to 2019 were identified through MEDLINE, Pubmed, clinicaltrials.gov, and Google scholar. Literature search yielded 13 articles, 3 of which met the set inclusion and exclusion criteria. Results: Three published cross-sectional studies were included with a total of population of 157 patients. Choline PET/CT was found to have a pooled sensitivity of 0.99 (0.96-1.00), pooled specificity of 0.45 (0.17-0.77), positive likelihood ratio of 1.79 (1.1-2.9), negative likelihood ratio of 0.03 (0.0-0.1), positive predictive value of 96.0% (93.4-97.7%) and negative predictive value of 83.3% (39.0-97.6%), estimated with 95% CI. Tc 99m Sestamibi SPECT/CT parathyroid imaging had a sensitivity of 0.77 (0.70-0.84), pooled specificity of 0.45 (0.17-0.44), positive likelihood ratio of 1.43 (0.8-2.4), negative likelihood ratio of 0.49 (0.2-1.4), positive predictive value of 96.0% (93.4-97.7%) and negative predictive value of 83.3% (39.0-97.6%), estimated with 95% CI. **Conclusion:** Choline PET/CT showed superior sensitivity, negative predictive value and negative likelihood ratio over Tc 99m Sestamibi SPECT/CT parathyroid imaging. Pooled specificities, positive predictive values and positive likelihood ratios of both modalities were found to be similar. **References:** 1. Greenspan B, et al. SNM Practice Guideline for Parathyroid Scintigraphy 4.0. Journal of Nuclear Medicine Technology. 2012;40(2):111-118.2. Ziessman H, et al. Nuclear medicine. Philadelphia, PA: Elsevier/Mosby; 2014.3. Mettler F, et al. Essentials of nuclear medicine and molecular imaging. 7th ed. 2019.4. Huber G, et al. Benefit of 18F-fluorocholine PET imaging in parathyroid surgery. European Radiology. 2018;28(6):2700-2707.5. Beheshti M, et al. 18F-Fluorocholine PET/CT in the assessment of primary hyperparathyroidism compared with 99mTc-MIBI or 99mTc-tetrofosmin SPECT/CT: a prospective dual-centre study in 100 patients. European Journal of Nuclear Medicine and Molecular Imaging. 2018;45(10):1762-1771.6. Thanseer N, et al. Comparative Effectiveness of Ultrasonography, 99mTc-Sestamibi, and 18F-Fluorocholine PET/CT in Detecting Parathyroid Adenomas in Patients With Primary Hyperparathyroidism. Clinical Nuclear Medicine. 2017;42(12):e491-e497.7. Orevi M, et al. Localization of Parathyroid Adenoma by 11C-Choline PET/CT. Clinical Nuclear Medicine. 2014;39(12):1033-1038.8. Treglia G, et al. Diagnostic performance of choline PET for detection of hyperfunctioning parathyroid glands in hyperparathyroidism: a systematic review and meta-analysis. European Journal of Nuclear Medicine and Molecular Imaging. 2018;46(3):751-765.

EPS-109

Kinetic analysis of [^{18}F]CETO in subjects with adrenocortical pathologies and validation of simplified quantification methods

L. O'Sullivan[1], M. Lubberink[2], I. Silins[2], A. Sundin[2], M. Gurnell[3], F. Aigbirhio[4], M. Brown[5], A. Wall[2], T. Åkerstrom[2], S. Roslin[6], P. Hellman[2], G. Antoni[6];

[1]Medical Physics, Uppsala University Hospital, Uppsala, SWEDEN, [2]Department of Surgical Sciences, Uppsala University, Uppsala, SWEDEN, [3]Department of Medicine, Wellcome Trust-MRC Institute of Metabolic Science, University of Cambridge, Cambridge, UNITED KINGDOM, [4]Wolfson Brain Imaging Centre, Department of Clinical Neurosciences, University of Cambridge, Cambridge, UNITED KINGDOM, [5]Clinical Pharmacology, William Harvey Heart Centre, Queen Mary University of London, London, UNITED KINGDOM, [6]Department of Medicinal Chemistry, Uppsala University, Uppsala, SWEDEN.

Aim/Introduction: Existing PET tracers for imaging adrenocortical pathologies, such as [^{11}C]MTO, suffer from high liver uptake which complicates visualisation and quantification of uptake. [^{18}F]CETO is a promising, novel radiotracer for improved PET imaging of such pathologies without high liver uptake[1]. The aim of this study was to assess the kinetics of [^{18}F]CETO in subjects with adrenocortical pathologies and to validate simplified quantification methods. **Materials and Methods:** Fifteen subjects with either an adenoma (n=12), carcinoma (n=1), myelolipoma (n=1) or calcifications (n=1) in one or both adrenals underwent a 90 min dynamic [^{18}F]CETO PET scan. Arterial blood was sampled for metabolite analysis and measurement of blood radioactivity. One and two-tissue reversible (1T2k and 2T4k) and irreversible (1T1k and 2T3k) compartment models were fitted to adrenal TACs using a blood-sampled input function (BSIF) and image-derived input functions with patient-specific (IDIF) and population-averaged (IDIF-PA) corrections. The optimal model was determined based on the Akaike information criterion (AIC), the Schwarz criterion (SC) and robustness of parameter estimates. VOI and voxel-based Patlak K_i values, SUV_{60-70} and results from the IDIF-PA were validated against the optimal model parameters by means of regression and Bland-Altman analysis. Results: Modelling with a BSIF and IDIF produced comparable parameter estimates. For the IDIF, the 2T3k model was preferred (11/26 adrenals) followed by the 1T1k model (10/26 adrenals) according to the AIC, but unlike the 1T1k model, the 2T3k model did not produce robust parameter estimates. 1T1k-K_1 and 2T3k-K_i correlated and agreed strongly for normal adrenal tissue (R^2=0.99, bias=-0.01) and adenomas (R^2=0.98, bias=0.01), but not for carcinoma and calcifications. High agreement and correlation were demonstrated between 1T1k- K_1 using an IDIF and an IDIF-PA (R^2=0.96, bias=-0.01) as well as with voxel-based Patlak K_i values (R^2=0.91, bias=-0.01). The correlation for VOI-based Patlak K_i values was strongest when fitted to the 10-90 min data. A linear relationship between SUV_{60-70} and K_1 was demonstrated (R^2=0.71). **Conclusion:** For normal adrenal tissue and adenomas, the 2T3k model was preferred but the 1T1k model was more robust and obtained similar parameter estimates, thus was determined as the optimal model. As this possibly indicates that [^{18}F]CETO uptake is entirely flow-limited, studies should be conducted comparing [^{18}F]CETO uptake to adrenal perfusion with [^{15}O]water. Simplified quantification methods can be used to accurately quantify [^{18}F]CETO uptake **References:** [1] I. Silins et al., Int J Med Sci 2021.

EPS-110

Relation between Striatal to Pancreatic Dopaminergic Activity Ratio and Glycated Hemoglobin in Diabetic and Non-diabetic Patients

P. Kalmar[1], C. Gstettner[1], G. Schwantzer[2], R. M. Aigner[1];

[1]Department of Radiology, Division of Nuclear Medicine, Graz, AUSTRIA, [2]Institute for Medical Informatics, Statistics and Documentation, Graz, AUSTRIA.

Aim/Introduction: ^{18}F-FDOPA (6-[18F]-L-fluoro-L-3, 4-dihydroxyphenylalanine)-based PET/CT imaging is used routinely in the management of various tumor entities. ^{18}F-FDOPA enters cells via the neutral amino acid transporter (LAT1/4F2hc). In patients with diabetes, an increase in blood glucose levels leads to a decrease in LAT1 expression. This study investigates the relation between the newly defined Striatal to Pancreatic Dopaminergic activity Ratio (SPDR) and glycated hemoglobin (HbA1c) in both diabetic and non-diabetic patients. **Materials and Methods:** We conducted a retrospective analysis of all patients who underwent whole body ^{18}F-DOPA -PET/CT from 01/01/2010 to 01/31/2021. Exclusion criteria were a history of pancreatic or cranial surgery, pancreatic and peripancreatic lesions, neurological disorders, metformin-containing medication and a post-injection interval of <20 minutes. Examination date HbA1c level was obtained. Pancreatic SUVmean, striatal SUVmean and pancreatic volume were computed. To normalize interpatient variability, SPDR was calculated as the ratio of striatal SUVmean to pancreatic SUVmean. The diabetic and non-diabetic patient groups were compared using chi^2-test. Spearman correlation coefficient was used to assess the correlation between all metric parameters. A linear regression modell adjusted for age and sex was used to predict HbA1c based on SPDR. Results: We included 76 patients: 22 diabetics (28%), and 54 non-diabetics (72%). Between the diabetic and non-diabetic group there was a significant difference in age (p = 0.006), pancreatic SUVmean (p =0.001) and SPDR (p < 0.001). There was no significant difference in sex, striatal SUVmean, and pancreatic volume. For each 1 unit increment in SPDR HbA1c increases 11.77 mmol/mol (95% CI 4.46-19.08). **Conclusion:** An SPDR > 0.95 for female and > 1.08 for male patients corresponds to a

HbA1c value greater than 42 mmol/mol and could therefore indicate suspected diabetes. **References:** 1. Calabria, F. F. et al. 18F-dopa pet/ct physiological distribution and pitfalls: Experience in 215 patients. Clin. Nucl. Med. 41, (2016). 2. Shah, A. S. et al. The effects of obesity and type 2 diabetes mellitus on cardiac structure and function in adolescents and young adults. Diabetologia 54, (2011). 3. Santhanam, P. & Taïeb, D. Role of 18F-FDOPA PET/CT imaging in endocrinology. Clinical Endocrinology vol. 81 789-798 (2014).

EPS-111

Concomitant lithium increases radioiodine uptake and absorbed doses per volume-adjusted administered activity in Graves' disease: Comparison of conventional versus lithium-augmented radioiodine therapy

F. Khreish[1], *A. Schaefer-Schuler*[1], *L. Roth*[1], *F. Rosar*[1], *H. Aladwan*[1], *A. Sabet*[2], *M. Schreckenberger*[3], *S. Ezziddin*[1];
[1]*Department of Nuclear Medicine , Saarland University, Homburg, GERMANY,* [2]*Department of Nuclear Medicine Goethe University, Frankfurt am Main, GERMANY,* [3]*Department of Nuclear Medicine, University of Mainz, Mainz, GERMANY.*

Aim/Introduction: It is known that Lithium inhibits iodine and thyroid hormone release from thyroid cells, possibly increasing radioiodine retention and anti-hyperthyroid efficacy when given adjunctively to radioiodine therapy (RAI) of Graves' disease (GD). However, literature contains limited dosimetric data regarding the influence of concomitant lithium in this setting. **Materials and Methods:** Retrospective study of 104 patients with GD compared dosimetric variables in patients undergoing RAI with/without adjunctive lithium (n=52 each). Thyroidal radioiodine uptake (RAIU) was measured about 24 h after diagnostic testing. Patients received individualized RAI activities 24 h later. Using ≥3 RAIU daily measurements started 24 h post-RAI, effective radioiodine half-life and absorbed dose in the thyroid were determined. Cure rates of GD, defined as reaching euthyroidism or hypothyroidism post-RAI, were evaluated. Results: Lithium patients and controls had similar average "diagnostic" RAIU (51.1% ± 15.7% vs. 50.6% ± 13.8%, p=0.820), but the former had significantly higher RAIU post-RAI (56.3% ± 13.5% vs. 49.1% ± 13.5%, p=0.002), reflecting significantly greater change in the former (+16.2% ± 30.4% vs. -1.8% ± 16.1%, p=0.001). Radioiodine effective half-life was non-significantly longer in lithium patients (5.43 ± 1.50 d vs. 5.08 ± 1.16 d, p = 0.192). The mean RAI administered activity was 27% less in lithium patients (677 ± 294 MBq vs 930 ± 433 MBq, p=0.001), but GD cure rates were comparable (80% [33/41] vs. 86% [30/35), p=0.840). **Conclusion:** Lithium augmentation may increase the RAIU and potentially may permit decreased RAI activities without sacrificing efficacy. **References:** none

EPS-112

Lutetium-177 Labelled MAA Imaging and Therapy in Cystic and Solid Thyroid Nodules

S. Sager, *A. Aygün, E. Karayel, H. Pehlivanoğlu, M. Abuqbeitah, K. Sönmezoğlu;*
Istanbul University-Cerrahpasa, Istanbul, TURKEY.

Aim/Introduction: Lutetium-177 can be labelled with macroaggregated albümin and can be imaged in SPECT camera. Our aim was to see the images and therapy effect of Lu-177 labelled MAA in cystic and solid thyroid nodules. **Materials and Methods:** For this study, 15 cystic and solid thyroid nodules were used in 14 patients (mean age 53,6+16,4). Fine needle aspiration biopsy was performed on each nodule and benign nodules were included for this study. After Lu-177 MAA injection, 1 hour and 24 hour later SPECT/CT images were performed to see whether the activity was limited only in the nodule. Thyroid nodule volumes were performed with USG before application and 1 week, 1 month and 3 months after the Lu-177 MAA injection. Nodule volumes were calculated using the formula for the volume of a ellipse (L × W × D × 0.479). Results: Nine pure cystic, 3 solid and 3 mix nodules in 14 patients were included in this study. Mean Lu-177 activity was 1,40+0,7. Mean TSH result of the patient was 1,44. Mean nodule volume was calculated as 15,12 ml before application. All thyroid nodules significantly decreased in size and in volume after Lu-177 MAA injection. The mean nodule volume was calculated as 6,44 ml one week later. One month and 3 months later mean nodule volume was calculated as 4,18 ml and 2,24 ml respectively. There was no extranoduler activity extensions was seen in all nodules. There was no complication or infection was noted in any patients. **Conclusion:** Lutetium-177 labelled macroaggregated albumin imaging and therapy can be used in cystic or solid thyroid nodules for nodule size and volume reduction. **References:** none

EPS-113

Yttrium-90 Radiation Synovectomy in Knee-Activated Osteoarthritis: A Prospective Evaluation of almost a decade follow-up (115 months)

I. Iakovou[1], *J. Kotrotsios*[1], *K. Badiavas*[2], *M. Potoupnis*[1];
[1]*Aristotle University, Thessaloniki, GREECE,*
[2]*Papageorgiou Hospital, Thessaloniki, GREECE.*

Aim/Introduction: To assess the outcome of yttrium-90 radiation synovectomy (RS) in patients with knee activated osteoarthritis in a decade follow-up period. **Materials and Methods:** We prospectively evaluated 52 patients, aged 64 yrs (42-86) old, with osteoarthritic (Kellgreen-Lawrence grade I to III) knee pain resistant to conventional therapy referred for intraarticular yttrium-90 treatment in 2011, due to

synovial inflammation, as demonstrated by early-phase bone scintigraphy. All patients were offered a long term follow up to almost a decade after initial treatment at 6,12,60 months and then every year up to 115 months (only 13/52 pts finally managed to participate). Treatment outcome was evaluated by assessing the variation of a composite index (CCi) calculated in terms of a patient subjective Visual Analogue Scale (VAS) reporting knee pain in combination with a scoring system of objective clinical and functional parameters at rest and under load (joint edema/hyperthermia, pain in load, flexion, ability to walk, intraarticular therapies after RSO, knee surgery), ranging from 0 (no change - worsening) to 35 (excellent response). Results: After first RSO 21 pts underwent no other intraarticular treatment, with a range of 1-6 knee punctures for the rest of pts. The overall response rate for all treated joints was 65% at 12 months and 54% at 115 months (p = ns), as shown in the attached table The mean improvement rate for early stage (Kellgreen-Lawrence grade I/II) treated joints was higher than the one achieved by all patients in total. **Conclusion:** Yttrium-90 radiation synovectomy exerts a beneficial therapeutic effect in patients suffering of knee synovial inflammation due to osteoarthritis. Long term results are excellent/good in many patients, almost ten years after initial therapy, with better results succeeded in the cases of radiological minimal changes (early Kellgreen-Lawrence stage). **References:** none

1112

Wednesday, October 20 - Saturday, October 23, 2021

on-demand pool, release on Wednesday, October 20 at 09:00

e-Poster Presentation Session 8: Imaging in Recurrent Prostate Cancer

EPS-114

Predictive value of 68GA-PSMA PET/CT in men with biochemical relapse after radical prostatectomy, undergoing salvage radiotherapy

F. Serani[1], H. Lanzafame[2], A. Farolfi[1], C. Malizia[1], R. Mei[1], F. Medici[3,4], G. Aluisio[5], S. Fanti[1];

[1]Nuclear Medicine, IRCCS, Azienda Ospedaliero-Universitaria di Bologna, Bologna, ITALY, [2]Nuclear Medicine Unit, Department of Biomedical and Dental Sciences and Morpho-Functional Imaging, University of Messina, Messina, ITALY, [3]Radiation Oncology, Department of Experimental, Diagnostic and Specialty Medicine, University of Bologna, Bologna, ITALY, [4]Radiation Oncology, IRCCS, Azienda Ospedaliero-Universitaria di Bologna, Bologna, ITALY, [5]Radiation Oncology, Azienda Ospedaliero-Universitaria di Ferrara, Ferrara, ITALY.

Aim/Introduction: Gallium-68 prostate-specific membrane antigen positron emission tomography/computed tomography (^{68}Ga-PSMA PET/CT) has shown to be a valid diagnostic tool in men with biochemical recurrence (BCR) after radical prostatectomy (RP); its long-term prognostic or predictive potential is still unclear. The aim of this retrospective study was to evaluate the predictive value of PSMA PET in men with BCR after RP undergoing salvage radiotherapy (sRT). **Materials and Methods:** We enrolled patients with prostate cancer who underwent PSMA PET from 2016 to 2019 for BCR (two consecutives serum PSA values > 0.2 ng/ml) after RP and who received sRT or no treatment. Patients who received androgen deprivation therapy (ADT) prior or after PSMA scan, and/or were undergoing ADT at time of observation were excluded from the study. Data collected included tumor stage, iPSA, ISUP score, risk classification, PSA kinetics, PSA before PET (stratified in <0.5 ng/ml - >0.5 ng/ml), PET scan results, following management (sRT +/-). Time to progression was defined by PSA relapse (two consecutives serum PSA values >0.2 ng/ml with undetectable PSA after sRT or persistence). Patients with PET-positive findings outside the pelvis (M1) were excluded. Results: The median follow-up was 19 months (IQR, 13-27,25). PET positive showed disease confined to fossa in 9,5% (20/210), in pelvic nodes ± fossa in 18,6% (39/210). All these patients received sRT, according to PET results. PSMA showed negative results in 71,9% (151/210). Among these patients, 66,9% (101/151) underwent sRT to fossa and 33,1% (50/151) received no treatment. Overall treatment response after sRT was 83,1% (49/59) in patients with positive PSMA PET and 81,1% (82/101) in negative scans (p=0.7). Of those who had a negative PET and received no treatment, 100% (50/50) had a PSA failure at follow-up, with a median of 8 months at the Mantel-Haenszel curve. Cox proportional hazards analysis was performed attesting a PSA failure relative risk of 5 in non-treated PSMA negatives, compared to PSMA negatives who underwent sRT (p=0.06). On logistic regression, in both PET positive and PET negative groups treated with sRT that presented PSA relapse at follow up (29/160), there were no significantly correlated variables (low/intermediate or high risk, PSA persistence, time gap between surgery and recurrent disease, PSA kinetics and age). PSA failure relative risk after sRT was twice higher in those patients with serum PSA pre sRT>0,5 ng/ml, regardless of PSMA findings. **Conclusion:** ^{68}Ga-PSMA PET alone best predicts sRT response, regardless other risk factors. **References:** None.

EPS-115

Role of 18F-fluorocholine PET/CT for guiding and monitoring response in oligometastatic recurrence prostate cancer patients treated with stereotactic body radiotherapy

E. Noriega-Álvarez[1], L. García Zoghby[1], M. Amo-Salas[2], L. Calahorra Fernández[3], P. V. Rios[4], M. de Cabo Ripoll[5], F. Leal Hernández[6], M. V. Villas Sánchez[7], M. J. Donate Moreno[8], A. M. García Vicente[1], Á. M. Soriano Castrejón[1];
[1]Nuclear medicine physician. University Hospital of Ciudad Real, Ciudad Real, SPAIN, [2]Department of Mathematics, University of Castilla-La Mancha, Ciudad Real, SPAIN, [3]Urologist University General Hospital, Ciudad Real, SPAIN, [4]Radiation Therapy Oncologist. University Hospital of Ciudad Real, Ciudad Real, SPAIN, [5]Urologist Virgen de la Luz Hospital, Cuenca, SPAIN, [6]Urologist University General Hospital, Guadalajara, SPAIN, [7]Radiation Therapy Oncologist. University General Hospital, Albacete, SPAIN, [8]Urologist University Hospital of Ciudad Real, Albacete, SPAIN.

Aim/Introduction: To assess the role of 18F-Fluorocholine (FCH) PET/CT for guiding and monitoring stereotactic body radiotherapy (SBRT) in patients with oligometastatic recurrent prostate cancer (ORPCa). **Materials and Methods:** Thirty-six patients with biochemical recurrent PCa after radical treatment and oligometastatic disease detected in FCH-PET/CT (baseline study), treated with SBRT (43 procedures), were retrospectively enrolled. The inclusion criteria were: 1) ≤ 3 bone or lymph node metastases; 2) FCH-PET/CT performed at a mean of 3 months after SBRT (control study) and 3) available follow-up (biochemical monitoring with/without a follow-up FCH-PET/CT) of at least 6 months after SBRT. Five patients underwent several SBRT procedures separated in time. Thirty-nine SBRT treatments with curative intention and 4 palliative. Among other clinical variables, local response (progression or not) in irradiated lesions using EORTC[1] criteria in control FCH-PET/CT, PSA increased or not (≥ 25% respect to baseline), PCa risk classification and PSA kinetics before SBRT were obtained. Progression free survival (PFS) was biochemically (PSA increase ≥ 25% in two consecutive measures) and/or metabolically (appearance of new lesions in control or follow-up FCH-PET/CT) determined. Correlations between biochemical (PSA) and metabolic progression were analysed using Chi-squared test. Relations of PFS, PSA and metabolic progression with clinical characteristics were evaluated using Kaplan-Meier and Mann-Whitney analyses. Results: PSA increased in a short time after 12 SBRT procedures, whereas local progression was detected in only 4 control FCH-PET/CT (no statistical association, p=0.573). During a median follow-up of 16 months, biochemical and/or metabolic progression was observed in 30/43 SBRT procedures; with a significant association between both parameters (p<0.001). The median PFS was 9 months (4.13-13.9, 95%CI). Furthermore, unfavourable PSA kinetics showed statistical association with biochemical progression, being doubling time (p=0.022) and PSA velocity (p=0.027) significant variables. **Conclusion:** Despite our limited sample, FCH-PET/CT does not seem an optimal diagnostic imaging to guide SBRT in ORPCa patients based on the high rate of progression and short PFS observed in our patient population. On the other hand, for monitoring response, the main advantage of FCH-PET/CT is the diagnosis of progression in other locations, being of very limited value in the local response evaluation of irradiated locations. **References:** 1. Young H, Baum R, Cremerius U, et al. Measurement of clinical and subclinical tumour response using [18F]-fluorodeoxyglucose and positron emission tomography: review and 1999 EORTC recommendations. European Organization for Research and Treatment of Cancer (EORTC) PET Study Group. Eur J Cancer. 1999;35:1773-82.

EPS-116

Utility of 18F-choline PET/CT images in real-time transrectal US-guided prostate biopsy

A. Laverde Mächler, M. Domínguez Grande, G. Fernández Rivero, D. Lisei Coscia, B. Fernández Llana, C. Vigil Díaz, J. Suárez Fernández, J. Maraña González, A. Álvarez, L. Rodríguez Díaz, N. Martín Fernández, F. González García;
HUCA, Oviedo, SPAIN.

Aim/Introduction: Transrectal ultrasound-guided biopsy is the standard approach for histopathologic diagnosis of prostate cancer. Disadvantages of this modality include the fact that ultrasonography (US) is operator dependent, as well as the inability to directly visualize and target prostate lesions. These problems can be solved using magnetic resonance imaging (MRI)-targeted biopsy, nevertheless multiparametric MRI is not always available. Suspicious-appearing regions within the prostate seen on ^{18}F-choline PET/CT studies can be biopsied using ^{18}F-choline PET/CT-targeted biopsy, which can improve the diagnostic accuracy of prostate biopsy. **Materials and Methods:** We retrospectively reviewed 36 prostate cancer patients who underwent transrectal US-guided biopsies according to positive findings on ^{18}F-choline PET/CT recurrence studies in the 3 past years. The multidisciplinary team fused the real time transrectal US with the previous PET/CT images in order to improve the accuracy of the diagnostic procedure. Patient's age, Gleason Score, previous treatments and prostate-specific antigen (PSA) at the time of imaging were collected. Afterwards, we compare PET/CT findings with the definitive histopathology report. Results: The mean age of the 36 patients was 70 years (range 61 to 80 years). Gleason Score mean was 6 (range 6 to 9) and PSA median was 3.5 ng/mL (range 0.58 to 12.84). Comparing PET/CT findings with the respective histopathology report, we found 17 false positive results (FP) and 19 true positives (TP). We did not find statistically significant differences between PSA of patients with TP and FP biopsy results (mean 3.71ng/mL por TP patients and median of FP 3.73ng/mL; choosing different measures of central tendency because

of extreme values in the second group). **Conclusion:** Co-registration of previously acquired ^{18}F-choline PET/CT images with real-time transrectal US-guided prostate biopsy shows promise when MRI-targeted biopsy is not available. **References:** Schoots IG, Roobol MJ, Nieboer D, Bangma CH, Steyerberg EW, Hunink MG. Magnetic resonance imaging-targeted biopsy may enhance the diagnostic accuracy of significant prostate cancer detection compared to standard transrectal ultrasound-guided biopsy: a systematic review and meta-analysis. Eur Urol. 2015 Sep;68(3):438-50.Drost FH, Osses D, Nieboer D, Bangma CH, Steyerberg EW, Roobol MJ, Schoots IG. Prostate Magnetic Resonance Imaging, with or Without Magnetic Resonance Imaging-targeted Biopsy, and Systematic Biopsy for Detecting Prostate Cancer: A Cochrane Systematic Review and Meta-analysis. Eur Urol. 2020 Jan;77(1):78-94. Simopoulos DN, Natarajan S, Jones TA, Fendler WP, Sisk AE Jr, Marks LS. Targeted Prostate Biopsy Using ^{68}Gallium PSMA-PET/CT for Image Guidance. Urol Case Rep. 2017 Jun 3;14:11-14.

EPS-117

^{18}F-fluciclovine PET/CT in recurrent prostate cancer: detection rate, image interpretation using PROMISE staging system and impact on clinical management

L. Filippi[1], A. Fontana[2], P. Basile[1], G. Spinelli[3], O. Bagni[2];
[1]Department of Nuclear Medicine, Santa Maria Goretti Hospital, Latina, ITALY, [2]Department of Radiotherapy, Santa Maria Goretti Hospital, Latina, ITALY, [3]Oncology Unit, AUSL Latina (District 1) Sapienza University of Rome, Aprilia, ITALY.

Aim/Introduction: The aim of this retrospective, single-center clinical study was to assess the detection rate and the impact of 18F-fluciclovine positron emission computed tomography (PET/CT), interpreted according to the image-based TNM staging system (PROMISE), on the clinical management of men with biochemical recurrence (BCR) of prostate cancer (PCa) following initial radical therapy. **Materials and Methods:** Nonmetastatic PCa patients treated by curative-intent treatment (radiotherapy or prostatectomy) and referred for 18F-fluciclovine PET/CT due to BCR were included. PET/CT images were interpreted using PROMISE staging system and were classified as follows: prostate bed/seminal vesicle remnants (Tr), pelvic lymph nodes (N1), extrapelvic lymph nodes (M1a), bone (M1b), and visceral organs (M1c). The therapeutic strategy was decided by a pool of referring clinicians through multidisciplinary consensus meetings: an intended therapy was proposed by clinicians before being informed of PET/CT results; subsequently therapeutic decision was revised (implemented therapy) after the collegial discussion of PET/CT results. Clinical impact of 18F-fluciclovine PET/CT was defined as significant when it entailed a change in the treatment modality (e.g. from an intended systemic therapy to a loco-regional treatment). Results: Thirty-one patients were submitted to 18F-fluciclovine PET/CT at a mean of 4.7 years post-initial diagnosis, with a mean PSA of 1.64 ng/mL. Twenty-four had previously undergone radical prostatectomy, while 7 had received radiotherapy (± other therapy). The overall number of positive PET/CT scan was 25 (detection rate = 80%). Patients with positive PET/CT scan were classified according to PROMISE image-reading as: Tr in 10 cases (40%), TrN1 in 5 cases (20%), M1a in 3 cases (12%), M1b in 2 patients (8%), TrN1M1b in 2 cases (8%), TrM1aM1b in 3 patient (12%). PET/CT scan significantly impacted on disease management in 13 patients (i.e. 42%). When analyzing the different PROMISE subgroups, 18F-fluciclovine PET/CT scan significantly impacted in 9/15 (60%) patients with loco-regional recurrence (Tr or TrN1 stage) and in 4/5 (80%) patients with localizations to extrapelvic lymph nodes (M1a) or bone (M1b). **Conclusion:** PET/CT with 18F-fluciclovine represents a useful tool for the detection of BCR in PCa patients, with a considerable impact on disease management. PROMISE-based image reading may be helpful for identifying those subjects (TrN1 or M1a/M1b) who are more likely to gain a therapeutic benefit from PET/CT results. **References:** None

EPS-118

Comparison of 18F-Fluciclovine and 18F-Flurocholine PET/CT diagnostic performance in recurrent prostate cancer patients

C. Ferrari, A. G. Nappi, V. Lavelli, P. Mammucci, N. C. Merenda, G. Rubini;
Section of Nuclear Medicine, DIM, University "Aldo Moro", Bari, ITALY.

Aim/Introduction: 18F-Fluorocholine PET/CT has a well-established role in the evaluation of prostate cancer (PCa) recurrence in patients with biochemical relapse (BCR), even if its detection rate (DR) decreases for low PSA values. 18F-Fluciclovine has been recently approved to investigate BCR PCa, showing a promising DR also when PSA level is still low (PSA<1ng/ml).The study aims to compare diagnostic performance of 18F-Fluorocholine and 18F-Fluciclovine PET/CT in PCa patients with BCR, according to clinical and biochemical features. **Materials and Methods:** Between September 2019 and January 2021, a homogeneous cohort of 68 PCa patients with BCR (mean age 71 years, range: 51-84 years; mean PSA: 1.4 ng/mL, range: 0.2-5.67), randomized for PSA value, underwent 18F-Fluciclovine or 18F-Fluorocholine PET/CT. The following clinical features were included: Gleason Score (GS: <7 or ≥7), EAU risk group (low risk/intermediate-high risk) and biochemical parameters (PSA value: <1, ≥1 ng/mL; PSA doubling time: <6 or ≥6 months).Differences in DR between two methods were statistically compared with an analysis patient-based, lesion-based and other clinical features-based, using Chi-Square test and McNemar's test. A p<0.05 was considered statistically significant. Results: In patient-based analysis, the overall 18F-Fluciclovine DR was 21/34 (62%) and 18F-Fluorocholine DR 9/34 (26%), with a statistically significant

difference (x^2=8.589, p=0.003).Per lesion analysis showed a total of 27 positive findings in 18F-Fluciclovine group and 9 in 18F-Fluorocholine group; the DR in prostate bed, lymph node and bone site was 16/27 (59%), 9/27 (33%) and 2/27 (7%) respectively in the first group and of 3/9 (33%), 5/9 (56%) and 1/9 (11%) in the second group, without a statistically significant difference (p=0.114).Regarding the clinical features-based analysis, DR of the two radiopharmaceuticals resulted statistically significant according to GS (p<0.001), EAU risk group (p=0.002), PSAdt (p<0.001) and PSA value (p=0.013).Particularly, for PSA <1 and ≥1, DR were 44% and 78% in 18F-Fluciclovine group, and of 18% and 35% in 18F-Fluorocholine group respectively. If a further stratification of PSA values was performed (PSA <1, 1-2 and >2ng/mL), the DR was 44%, 70% and 88% in 18F-Fluciclovine group and of 18%, 20% and 63% in 18F-Fluorocholine group respectively, without demonstrating a significant difference. **Conclusion:** Our data confirmed the better diagnostic performance of 18F-Fluciclovine PET/CT in terms of DR compared to 18F-Fluorocholine PET/CT, particularly in the evaluation of prostate bed, also due to low urinary excretion. The significant difference of DR based on PSA value emphasized the use of 18F-Fluciclovine for low PSA level (<1ng/ml). **References:** None.

EPS-119

18F-DCFPyL PET/CT in biochemically recurrent prostate cancer with low prostate specific antigen (PSA) rates (<1.1 ng/mL). Searching for a suitable lower cut-off

P. Plaza López[1], *B. Domenech Brasero*[1], *P. Pifarre*[1], *N. Romera*[1], *F. Racca*[1], *O. Coronil*[1], *M. Suarez-Piñera*[2], *J. Torices Caballero*[1];
[1]*Hospital Quironsalud Barcelona, Barcelona, SPAIN,*
[2]*Hospital del Mar Barcelona, Barcelona, SPAIN.*

Aim/Introduction: To assess the usefulness of 18F-DCFPyL in patients with biochemical recurrence of prostate carcinoma and low PSA values <1.1 ng/mL. Find a suitable lower cut-off point **Materials and Methods:** Retrospective descriptive study. The first 37 patients with localized prostate carcinoma, treated with radical prostatectomy with curative intent and biochemical recurrence with low PSA values (range: 0.15 - 1.1 ng/mL) were selected. All the patients underwent 18F-DCFPyL PET/TC. Images were evaluated by 2 nuclear medicine experts and classified as positive (unequivocal pathological uptake) or negative (inconclusive or no uptake). Results: Overall, 15 of the 37 patients (40.5%) were positive. When patients with PSA ≤0.5 ng/mL were chosen alone, the detection percentage was reduced to 13.3%, being 60% for values >0.5 ng/mL. Two statistical methods were performed to select the cut-off point for PSA. Using the Chi Square test, the point = 0.52 ng/mL was the one that best differentiated patients eligible to undergo 18F-DCFPyL PET / CT from that ineligible. The ROC Curve established the point 0.57 ng/mL as the best, with a sensitivity of 0.87 and a Specificity of 0.64, and an AUC: 0.77. **Conclusion:** 18F-DCFPyL PET / CT has a high sensitivity to detect early tumor relapse of prostate cancer, however at very low PSA values its efficiency is questionable. We recommend a lower cut-off value between 0.52 - 0.57 ng/mL. **References:** Fanti, S., Goffin, K., Hadaschik, B.A. et al. Consensus statements on PSMA PET/CT response assessment criteria in prostate cancer. Eur J Nucl Med Mol Imaging 48, 469-476 (2021). https://doi.org/10.1007/s00259-020-04934-4 Esther Mena, Maria Liza Lindenberg, Ismail Baris Turkbey, Joanna H. Shih, Stephanie A. Harmon, Ilhan Lim, Frank Lin, Stephen Adler, Philip Eclarinal, Yolanda L. McKinney, Deborah Citrin, William Dahut, Bradford J. Wood, Venkatesh Krishnasamy, Richard Chang, Elliot Levy, Maria Merino, Peter Pinto, Janet F. Eary and Peter L. Choyke Journal of Nuclear Medicine June 2020, 61 (6) 881-889; DOI: https://doi.org/10.2967/jnumed.119.234799Diagnostic Performance of 18F-DCFPyL-PET/CT in Men with Biochemically Recurrent Prostate Cancer: Results from the CONDOR Phase III, Multicenter Study Michael J. Morris, Steven P. Rowe, Michael A. Gorin, Lawrence Saperstein, Frédéric Pouliot, David Josephson, Jeffrey Y.C. Wong, Austin R. Pantel, Steve Y. Cho, Kenneth L. Gage, Morand Piert, Andrei Iagaru, Janet H. Pollard, Vivien Wong, Jessica Jensen, Tess Lin, Nancy Stambler, Peter R. Carroll and Barry A. Siegel; CONDOR Study Group DOI: 10.1158/1078-0432.CCR-20-4573; CONDOR Study Group

EPS-120

Impact of 68Ga-PSMA PET-CT on radiotherapy planning in recurrent prostate cancer after radical prostatectomy

C. Varela Pinto, *B. Martins, V. Sousa, T. Antunes, C. Loewenthal;*
Hospital da Luz Lisboa, Lisbon, PORTUGAL.

Aim/Introduction: To evalute the impact of 68Ga-PSMA-11 PET-CT on radiotherapy planning at restaging of prostate carcinoma in patients submitted to radical prostatectomy as primary treatment. 68Ga-PSMA-11 PET-CT is a very sensitive and specific exam for detecting primary and metastatic lesions of prostate adenocarcinoma. At restaging, early and accurate detection of disease ensures the most appropriate treatment is instituted in a timely manner. In some patients with disease recurrence after radical prostatectomy, salvage radiotherapy can be offered as a possible curative therapy. **Materials and Methods:** Retrospective analysis of the clinical records of 23 patients (mean age 65.87 years, 47-93) with prostate cancer recurrence after radical prostatectomy. Patients underwent 68Ga-PSMA-11 PET-CT before planning external radiotherapy, between February 2017 and April 2021. Evaluation of clinical, biochemical, pathological and imaging results. Results: Twenty-three patients were submitted to radical prostatectomy as initial treatment and, following recurrence of prostate carcinoma, underwent 68Ga-PSMA-11 PET-CT in order to plan radiation therapy. Gleason score was 7(3+4) in 4 patients, 7(4+3) in 11, 8(4+4) in 3, 9(4+5) in 4 and unknown in 1 patient. Median time until recurrence of prostate cancer was 6 months (range 2-228 months). The

median PSA value at recurrence was 0.60 ng/mL (range 0.16-14.78 ng/mL). PSMA PET-CT was positive in 15/23 patients (65%). Five patients had disease confined to the prostatic bed, 7/15 had locoregional disease, whereas 3/15 had distant lesions (1 lymph nodes and 2 bone lesions). In 13/23 (57%) 68Ga-PSMA-11 PET-CT changed the radiation therapy plan (irradiation prostatic bed and pelvic lymph nodes). PET-CT identified lesions with increased radiopharmaceutical uptake that led to additional irradiation field. Radiation boost was performed in 1 patient due to recurrence in ureterovesival anastomosis. Stereotactic body radiation therapy was performed in 10 patients due to lymph nodes and in another 2 patients due to bone lesions. In these 13 patients the median PSA value before PET-CT was 1.09 ng/mL (range 0.2-14.78 ng/mL). In the remaining 10 patients (43%), the 68Ga-PSMA-11 PET-CT did not alter the radiotherapy field. **Conclusion:** 68Ga-PSMA-11 PET-CT resulted in additional relevant information when planning treatment with external radiotherapy in patients with prostate cancer recurrence after radical prostatectomy. In 57% of patients, therapeutic strategy was altered, due to the addition of new irradiation fields. **References:** None

EPS-121

Diagnostic accuracy of [^{18}F]-PSMA-1007 PET/CT in biochemical recurrent prostate cancer patients - a retrospective analysis

C. Mingels, J. Hünermund, K. P. Bohn, A. Rominger, A. Afshar-Oromieh, I. L. Alberts;
Department of Nuclear Medicine, Inselspital, Bern University Hospital, University of Bern, Bern, SWITZERLAND.

Aim/Introduction: Despite increasing use for the detection of biochemically recurrent prostate cancer (rPC), the diagnostic accuracy of [^{18}F]-PSMA-1007 is yet to be established. The aim, therefore, is to determine, the sensitivity (SE), specificity (SP), positive predictive value (PPV) and negative predictive value (NPV) for PC-local recurrence and metastases on a per-region basis. **Materials and Methods:** 177 consecutive patient undergoing [^{18}F]-PSMA-1007 PET/CT for rPC were analysed. An experienced nuclear medicine resident and a board-certified consultant interpreted all scans. The PET/CT was counted as positive if at least one PSMA-avid lesion suspicious for PC was reported. The patient-level detection rate was calculated. Details regarding further treatment, response, histology or confirmatory imaging were available of 152 patients. A region (prostate fossa, pelvic lymph nodes (LN), retroperitoneal LN, supradiaphragmatic LN, bones and soft tissue) was counted positive if at least one PSMA-positive lesion was confirmed. Confirmation of a true positive PSMA-avid lesion was defined as positive histopathology, fall in serum PSA (>50%) after targeted therapy or further CT, MRI, PET/CT or bone scan imaging with confirmation of the lesion. Regions were no PSMA-avid PC lesion was reported were counted as negative. Where additional imaging was able to confirm the absence of PC lesions or regions outside exclusively targeted RT with serum PSA decline (>50%) were counted as true negative regions. SE, SP, PPV and NPV were calculated for all six regions. Results: The overall detection rate was 91%. Conclusive follow up for affirmation or refutation of a PSMA-positive lesion was available for 81 of 152 patients on a per-region basis. In this subgroup (n=81) patient-based sensitivity was 95.6%. Overall sensitivity, specificity, PPV and NPV were 95%, 87%, 83% and 96% respectively. On a region basis PPV was 89% for local recurrence, 87% for pelvic LN, 87% for retroperitoneal LN, 82% for supradiaphragmatic LN, 79% for bone lesions. The number of solid organ metastases (n=6) was too small for an accurate PPV analysis. **Conclusion:** The known high detection rate for [^{18}F]-PSMA-1007 PET/CT in rPC patients was confirmed with a high PET positivity rate (91%), with corresponding high (>90%) sensitivity and NPV on a per-region basis. However, PPV was limited (overall 83%), particularly for bone lesion (79%), where bone lesions are a potential diagnostic pitfall. Knowledge of the reported accuracy and potential pitfalls of [^{18}F]-PSMA-1007 is essential in reading PET/CTs in patients with recurrent PC for clinic routine and further studies. **References:** none

EPS-122

Diagnostic performance of ^{68}Ga-P16-093 PSMA PET/CT compared to ^{18}F-fluciclovine PET/CT and ^{99m}Tc-MDP scintigraphy in prostate cancer: a pilot study

H. Lee[1], M. Daube-Witherspoon[1], J. Scheuermann[1], A. Young[1], R. Doot[1], E. Schubert[1], D. Alexoff[2], H. Kung[2], D. Pryma[1];
[1]University of Pennsylvania Perelman School of Medicine, Philadelphia, PA, UNITED STATES OF AMERICA, [2]Five Eleven Pharma Inc., Philadelphia, PA, UNITED STATES OF AMERICA.

Aim/Introduction: ^{68}Ga-P16-093, a small molecule PSMA ligand, previously showed equivalent diagnostic performance and less urinary radiotracer excretion compared to ^{68}Ga-PSMA-11 PET/CT in a pilot study of prostate cancer patients with biochemical recurrence (BCR)[1]. We performed a pilot study to examine the diagnostic performance of ^{68}Ga-P16-093 PET/CT compared to ^{18}F-fluciclovine PET/CT and ^{99m}Tc-MDP scintigraphy in prostate cancer patients. **Materials and Methods:** Prostate cancer patients with suspected disease were eligible. Following the administration of 150 ± 32 MBq (4.05 ± 0.86 mCi) of ^{68}Ga-P16-093 intravenously, a whole body PET scan with low-dose attenuation CT was obtained at approximately 90 minutes. Clinical ^{18}F-fluciclovine PET/CT and ^{99m}Tc-MDP scintigraphy were reviewed for lesion-by-lesion comparison. Each lesion was classified as benign or malignant based on all available clinical imaging, laboratory values, treatment response, and change over time. Results: Thirteen subjects were enrolled, 12 with BCR and one with primary disease. ^{18}F-fluciclovine PET/CT was available for comparison in 9 patients with 28 malignant lesions, acquired 107 ± 116 days from ^{68}Ga-P16-093 PET/CT (mean ± SD). ^{68}Ga-

P16-093 PET/CT showed per-lesion sensitivity of 83% (24 out of 28 lesions) without false positive findings, compared to 61% for ^{18}F-fluciclovine PET/CT. Two of the missed lesions were in the prostatectomy bed and the remaining two were in pelvic lymph nodes. In addition, ^{68}Ga-P16-093 PET/CT was able to exclude 6 benign osseous lesions found on 18F-fluciclovine PET/CT; five of them were not identified on subsequent clinical imaging and one patient's PSA became undetectable after salvage radiation to the prostatectomy bed without treatment of the putative bone lesion. 99mTc-MDP scintigraphy was available in 5 patients with 20 osseous metastases, acquired 46 ± 21 days from ^{68}Ga-P16-093 PET/CT. ^{68}Ga-P16-093 PET/CT was positive in all 20 metastases without false positive findings. In comparison, ^{99m}Tc-MDP scintigraphy only identified 16 lesions as positive; two of the missed lesions were successfully treated with salvage radiation and the remaining two missed lesions were identified on future ^{99m}Tc-MDP scintigraphy. **Conclusion:** ^{68}Ga-P16-093 PET/CT is able to identify prostate cancer lesions with high sensitivity. Given its robust diagnostic performance compared to ^{18}F-fluciclovine and ^{99m}Tc-MDP, ^{68}Ga-P16-093 merits further clinical investigation. **References:** 1. Green MA, Hutchins GD, Bahler CD, et al. [^{68}Ga] Ga-P16-093 as a PSMA-Targeted PET Radiopharmaceutical for Detection of Cancer: Initial Evaluation and Comparison with [^{68}Ga]Ga-PSMA-11 in Prostate Cancer Patients Presenting with Biochemical Recurrence. Mol Imaging Biol. 2020;22:752-763.

EPS-123

Incidental finding of Ga68-PSMA uptake in covid-19 induced pneumonia

A. Aghaei[1], *S. Soltani*[2], *S. Zakavi*[1], *N. Norouzbeigi*[3], *M. Esmatinia*[1], *G. Gholami*[1], *H. Dadgar*[3], *A. Masoudifard*[1];
[1]*Nuclear medicine research center, Mashhad university of Medical Sciences, Mashhad, IRAN, ISLAMIC REPUBLIC OF,* [2]*Uro-oncology research center, Mashhad university of Medical Sciences, Mashhad, IRAN, ISLAMIC REPUBLIC OF,* [3]*Nuclear medicine research center, Razavi international university of Medical Sciences, Mashhad, IRAN, ISLAMIC REPUBLIC OF.*

Aim/Introduction: Covid-19 pandemic is the global health crisis in our time and the resulted pneumonia is not infrequently seen in lung CT scanning performed for other reasons in asymptomatic patients.To our knowledge, this is the first report of PSMA uptake in covid-19 induced pneumonia and interestingly this occurred in an asymptomatic patient. **Materials and Methods:** A 68 years old man with prostate carcinoma was referred for Ga68-PSMA PET/CT scan because of recent significant rise of PSA.(more than tripled in recent 4 months). He had underwent external beam radiotherapy of the prostatic bed as the initial treatment 4 years ago and had been received[v1] androgen deprivation[v2] therapy till now. He complained of muscle weakness and fatigue, since 3 weeks before the scan, without dyspnea or shortness of breath. Results: In his Ga68-PSMA-611 PET/CT study, widespread skeletal metastasis, as well as liver involvement were noticed.Worth notably, multiple bilateral and patchy areas of ground glass opacity and consolidation was evident in the lung window of the CT scan performed for attenuation correction, which were located mostly in the peripheral areas of the lung, and were typical for covid-19 pneumonia . Interestingly, these lesions showed considerable PSMA uptake, which was about twice of the liver uptake (SUV max =4.1, mean SUV of the liver= 2.22). for confirmation of the Covid-19 infection, serology tests were ordered and elevated IGM level was confirmed. **Conclusion:** Our case, describes a rare case of PSMA uptake in covid-19 induced pneumonia in an asymptomatic patient. This highlights the importance of paying attention to these uncommon findings, while interpreting PET/CT scans and considering the false positive patterns of uptake, especially in the present covid-19 pandemic. **References:** none

EPS-124

Diagnostic performance of 18F-Fluciclovine PET/CT in biochemical recurrent prostate cancer patients with low PSA values

V. Lavelli, *A. G. Nappi, C. Ferrari, N. C. Merenda, G. Santo, C. Scaltrito, G. Rubini;*
Section of Nuclear Medicine, DIM, University "Aldo Moro", Bari, ITALY.

Aim/Introduction: 18F-Fluciclovine PET/CT is recommended for the detection of prostate cancer (PCa) recurrence in patients with biochemical relapse (BCR) after primary treatment. The present study investigates the diagnostic performance of 18F-Fluciclovine PET/CT in this setting of patients, with particular reference to low PSA values and the impact of other histological and clinical features on the detection rate (DR). **Materials and Methods:** Between September 2019 and January 2021, 34 PCa patients with BCR (mean age 71 years, range: 51-82 years; mean PSA: 1.4 ng/mL, range: 0.2-5.67) underwent 18F-Fluciclovine PET/CT at our Nuclear Medicine Unit for disease restaging. Clinical follow-up data of all patients were collected (mean 8.8 months, range 2-18), including: further PSA values, other diagnostic investigations, start/change treatment. The following PET-based semi-quantitative parameters were extracted: SUVmax of the reference lesion ($SUVmax_{RL}$) and the related Tumor to Background Ratio (TBR_{RL}), using abdominal aorta or bone marrow as background. Patients were stratified into groups according to Gleason Score (GS<7, GS≥7), EAU risk group (low risk, intermediate/high risk) and biochemical features (PSA value <1 or ≥1, PSA doubling time <6 or ≥6 months). Fisher's exact test and Mann-Whitney non-parametric test were employed to analyze correlation between 18F-Fluciclovine PET/CT DR and its semi-quantitative parameters into groups respectively. A $p<0.05$ was considered statistically significant. In addition, considering clinical follow-up as the reference gold standard, sensitivity, specificity, accuracy, positive and negative predictive value (PPV, NPV) of 18F-Fluciclovine PET/CT were calculated. Results:

18F-Fluciclovine PET/CT resulted positive in 21/34 (62%) patients with a total of 27 lesions detected, distributed per-site basis as follows: 16/27 (59%) were localized in prostate bed, 9/27 (33%) lymph nodes and 2/27 (7%) in bone. Considering PSA-stratification groups, a DR of 44% and 78% was found for PSA<1 and ≥1 respectively, with a statistically significant difference (p=0.046). No other significant difference was found for DR in the remnant groups. Similarly, $SUVmax_{RL}$ (p=0.012) and TBR_{RL} (p=0.036) resulted statistically significant only in the PSA<1 and ≥1 groups. 18F-Fluciclovine PET/CT reached a sensitivity of 84.21%, specificity of 76.92%, PPV of 84.21%, NPV of 76.92% and accuracy of 81.25%. **Conclusion:** 18F-Fluciclovine PET/CT is a reliable tool in the evaluation of PCa patients with BCR for the detection of local and distant recurrence, especially in the prostate bed, also due to low urinary excretion. Our results confirmed literature data about PSA value impact on 18F-Fluciclovine PET/CT DR, which remains significant also in patients with a low PSA. **References:** None.

EPS-125

Influence of Initial Treatment in the Performance of [11C]Choline PET/CT in the Follow-up of Prostate Cancer

F. Gomez-De La Fuente, I. Martínez-Rodríguez, O. Cuenca-Vera, A. Sánchez-Salmón, M. de Arcocha-Torres, S. Ruiz-Llama, N. Martínez-Amador, J. Jiménez-Bonilla, J. Andrés-Pacheco, R. Quirce;
Nuclear Medicine Service. Marqués de Valdecilla University Hospital. Molecular Imaging Group (IDIVAL). University of Cantabria., Santander, SPAIN.

Aim/Introduction: Despite the success of new available PET tracers, [11C]Choline remain as the main tracer available in our country for the assessment of prostate cancer (PCa). Our aim was to analyse the differences in the performance of [11C]Choline PET/CT depending on the initial treatment that the patients received, in order to detect groups with more benefit from this expensive test. **Materials and Methods:** The study included 120 [11C]Choline PET/CT examinations performed in 103 patients with PCa (68.4±7.5 years) requested for active surveillance or suspected relapse of PCa. The total of 120 PET/TC examinations included two subgroups of 60 examinations as per their initial treatment: radical prostatectomy (RP), with or without adjuvant treatment (Group 1), and other forms of treatment (radiotherapy, chemotherapy, hormonotherapy) (Group 2). PET/CT scans were acquired 20 minutes after administration of 555-740 MBq of [11C]Choline. The examinations were randomly selected and retrospectively evaluated. The minimum follow-up was 12 months. Results: From the 60 [11C]Choline PET/CT examinations performed in the group 1 of patients, 11 (18.3%) were positive and 49 (81.7%) negative. From the 11 positive examinations, 4 (36.46%) showed local recurrence and 7 (63.6%) distant recurrence (bone in 3 examinations, distant lymph nodes in 3 and both in 1). From the 60 [11C]Choline PET/CT examinations performed in the subgroup 2 of patients, 42 (70%) were positive and 18 (30%) negative. From the 42 positive examinations, 33 (78.6%) showed local recurrence, 4 (9.5%) distant recurrence (bone in 4 examinations, bone plus lung in 1) and 5 (11.9%) local plus distant recurrence (prostate plus distant lymph nodes in 4 examinations, prostate plus lung in 1). The difference between the percentage of positive [11C]Choline PET/CT results in both subgroups of patients (18.3% and 70%) was statistically significant (p<0.05). There were also significant differences in the Gleason index (7.0±0.9 in the group 1 and 6.7±1.2 in the group 2, (p=0.03). Mean serum PSA at the time of PET/CT was significantly higher (p<0.05) for the group 2 (3.9±4.6 ng/ml) compared to group 1 (0.7±0.8 ng/ml). **Conclusion:** Our results suggest that patients will benefit from [11C]Choline PET/CT regardless initial treatment, although [11C]Choline PET/CT diagnostic performance was different depending on the initial treatment, with 18.3% of positive results in the patients treated with RP vs 70% with other treatments. The uptake pattern was also different, with local recurrence in 36.46% of treated with RP vs 78.6% of treated with other treatments. **References:** None

EPS-126

Retrospective analysis of PET / CT with 18F-Choline for the evaluation of recurrence in prostate cancer

M. Cruz, J. Rodríguez-Rubio Corona, M. de Bonilla Candau, Y. Santaella Guardiola, M. Pajares Vinardell, J. Freire Macías;
Hospital Puerta del Mar, Cádiz, SPAIN.

Aim/Introduction: In the context of an increasing availability and evidence of Prostate-specific membrane antigen tracers (PSMA), it is proposed to evaluate the results of 18F-choline PET/CT to localize local, regional or distant disease in prostate cancer (PCa) patients in our population and according to its recurrence pattern. **Materials and Methods:** We have retrospectively analyzed 18F-choline PET/CT scans from 149 patients with PCa history with a follow up based on prostate-specific antigen (PSA) levels (mean, 25.12 ng/ml; median, 12.5ng/ml; range, 0.53-213ng/ml) and suspected recurrence. 58 patients had undergone primary radical prostatectomy (RP) (43/58 had secondary radiotherapy), 57 had undergone primary radiotherapy and 4 had persistent PSA increasement after receiving initial treatment (all after RP). 49 developed castrate-resistance to androgen deprivation. The level of suspicion for recurrence on 18F-choline PET/CT (scored as positive or negative) were evaluated by two professionals. Analyzed variables were: disease location (local, locoregional, regional and distant), correlation between positive 18F-choline PET/CT and initial treatment, PSA recurrence levels, PSA doubling time, Gleason score, D'Ámico risk classification and PET imaging. Results: Both professionals agreed on the positivity of 80.83% of the 18F-choline PET/CT scans. When sorted by PSA recurrence levels, 50% of patients

with a PSA level of less than 0.5ng/mL, 55.5% of patients with a PSA level of 0.5-0.99ng/mL, 75% of patients with a PSA level of 1-1.99ng/mL and 83.1% of patients with a PSA level of at least 2ng/mL scored a positive result on 18F-choline PET/CT scans. In multivariable analysis, PSA recurrence levels and Gleason score have been associated with scan positivity. Pattern analysis showed that distant disease was the most frequent disease location. **Conclusion:** 18F-choline PET/CT scans can detect CaP recurrence even in patients with low PSA levels. In addition to that, the clinical context may give us a certain pretest probability. Until prostate-specific membrane antigen are fully approved for PCa, choline PET/CT is really useful in order to get some results. **References:** None

EPS-127

Impact of Ga68-PSMA11 PET/CT on the Treatment of Patients with Recurrent Prostate Cancer After Radical Prostatectomy: a Single Center Experience

S. Grimaldi[1], S. Dall'Armellina[1], G. Rovera[2], F. Ceci[3], V. Chiofalo[1], G. Iorio[1], I. Bonavero[1], R. Parise[1], S. Bartoncini[1], V. Richetto[1], B. Lillaz[1], M. Oderda[1], P. Gontero[1], A. Guarneri[1], U. Ricardi[1], D. Deandreis[3];
[1]AOU Città della Salute e della Scienza, Turin, ITALY,
[2]Università Cattolica del Sacro Cuore, Rome, ITALY,
[3]Università degli Studi di Torino, Turin, ITALY.

Aim/Introduction: To evaluate the impact of Ga68-PSMA11 PET/CT in the management of patients with recurrent prostate cancer following radical prostatectomy (RP). **Materials and Methods:** We retrospectively analyzed data of patients with biochemical recurrence (BCR) post-RP (defined as PSA ≥0.2 ng/ml) who underwent Ga68-PSMA11 PET/CT at our institute. The primary endpoints were the biochemical progression-free survival (bPFS) rate after PET/CT guided radiotherapy and the bPFS after prostate bed salvage RT (SRT) following a negative PET/CT. The secondary endpoints included the change in the treatment plan, the interval to androgen deprivation therapy (ADT) initiation in patients treated exclusively with stereotactic body radiation therapy (SBRT). Results: 95 patients with BCR following RP (pN0-pNx) who underwent a Ga68-PSMA11 PET/CT between November 2016 and March 2019 were included. The time from PET/CT to the last follow-up was 36 months (range 11-50). The median PSA at PET/CT was 0.5 ng/ml (range 0.13-8.9). Twenty-six patients (27.3%) had a positive PET/CT (pathological findings in prostate bed in 9 patients, regional lymph nodes in 7, distant lymph nodes in 6, bone in 8). PET/CT findings lead to a change of RT planning in 17 patients (65.3% among positive PET/CT; 17.8% among all patients). Fifteen out of 26 patients (57.6%) treated with PET/CT guided RT experienced a recurrence after 1-32 months (median interval 9 months). Seven patients (26.9%) underwent SBRT only and 6 of them experienced a recurrence with a median bPFS of 15 months (range 3-30). In the SBRT group the median interval to ADT initiation was 8 months. PET/CT was negative in 69 patients. In this group, 57 patients received prostate bed SRT, 3 prostate bed SRT and ADT, 2 ADT only, and 7 underwent simple follow-up. Among the 60 patients who underwent SRT, 13 (21.6%) experienced a recurrence after 1-28 months (median 6 months). PET/CT negative patients treated with SRT (n=57; 3 patients lost at follow-up) had a longer bPFS than PET/CT positive patients treated with PET/CT guided RT (n=24; 2 patients lost at follow-up) (p<0.001). At 12 months, bPFS were 81.2% vs 54.2% respectively. **Conclusion:** In this retrospective study, Ga68-PSMA11 PET/CT influenced the delivered RT planning in a high proportion of patients with first BCR following RP. Moreover, PET/CT was able to provide prognostic information in terms of bPFS. **References:** none

EPS-128

Evaluation of ^{68}Ga-PSMA PET/CT in patients with Biochemical Recurrence of Prostate Cancer

M. Dyankova[1,2], T. Stoeva[1], Z. Dancheva[1], T. Yordanova[1], S. Chausheva[1], B. Chaushev[1], A. Klisarova[1];
[1]Medical University Varna "Prof. Dr. Paraskev Stoyanov", Department of Nuclear Medicine, Varna, BULGARIA,
[2]St Marina University Hospital, Varna, BULGARIA.

Aim/Introduction: The introduction of ^{68}Ga-PSMA PET/CT has significantly changed the prospect of prostate cancer (PC), especially for the early diagnosis and localization of disease recurrence. The aim of this study was to analyze the diagnostic value of ^{68}Ga-PSMA- PET/CT in patients with PC undergoing imaging for biochemical failure after radical therapy and to define the predictive factors of ^{68}Ga-PSMA positivity in this context. **Materials and Methods:** We performed a retrospective analysis of 133 consecutive patients with biochemical recurrence (BCR) after radical treatment for PC (surgery, radiotherapy (RT) or High-intensity focused ultrasound (HIFU)) who underwent PSMA PET/CT between July 2019 and August 2020. Potential influences of several factors such as age, International Society of Urological Pathology (ISUP) grade, T stage, actual PSA (aPSA) value,- and androgen deprivation therapy (ADT) were evaluated. Univariate and multivariate statistical analyses were performed to assess parameters associated with PSMA PET/CT positivity. The detection rates were correlated with the above mentioned factors, as well with initial PSA (iPSA), PSA doubling time (PSAdt) and European Association of Urology (EAU) risk groups. Results: The median iPSA and aPSA of the patients were: 13 ng/ml and 2 ng/ml, respectively. PSMA-PET detected recurrent disease in 90 patients (67.7%). In 43 patients (32.3 %) a local recurrence was revealed. Metastatic lymph nodes incidence was 37 (27.8%). Bone metastases were observed in 43 patients (32.3%) and visceral metastases in 5 patients (3.7%). Local recurrence was most commonly found in patients after HIFU 66.7% and RT 54.1% and distant bone metastases in patients after RT 54.2%. In multivariate

analysis, aPSA levels at the time of the PSMA scan was the only significant predictor of a positive PET/CT study (p = 0.020). Tumor-detection was positively associated with iPSA and aPSA levels, whereas ISUP grade, T stage and EAU risk groups showed only a positive tendency. Studies were positive in 50.0% of patients with iPSA <10ng/ml, 65.1% of patients with iPSA between 10 and 20 ng/ml, 54.5% of patients with iPSA between 20 and 50 ng/ml (p=0.002) and in 90.9% studies in patients with iPSA values ≥50 ng/ml (p=0.035). **Conclusion:** ^{68}Ga-PSMA PET/CT is an excellent tool for the detection of recurrent PC after radical treatment even at low aPSA levels. The aPSA value at the time of the examination appear to be the main predictor of ^{68}Ga-PSMA PET/CT positive findings. Tumor detection is positively associated with iPSA and aPSA levels. Keywords: ^{68}Ga-PSMA, biochemical recurrence **References:** None

EPS-129

A Preliminary Retrospective Experience on 18F-DCFPYL PSMA PET/CT Imaging in Biochemical Recurrence of Prostate Cancer

V. Lopez Prior, F. Manchón-Adsuar, R. Díaz-Expósito;
Valencian Oncologic Institution (IVO), Valencia, SPAIN.

Aim/Introduction: 18F-DCFPyL, a prostate-specific membrane antigen-targeting radiotracer, has shown promise as a prostate cancer imaging radiotracer. We retrospectively evaluated our preliminary experience, the sensitivity and impact on patient management of ^{18}F-DCFPyL in the setting of biochemical recurrence of prostate cancer. **Materials and Methods:** Subjects with prostate cancer and biochemical recurrence after radical prostatectomy or curative-intent radiotherapy were included. The subjects underwent ^{18}F-DCFPyL PET/CT imaging between july 2020 to march 2021. The localization and number of lesions were recorded. The uptake characteristics were measured. Lastly, we assess the change in treatment and impact on management. Results: 64 subjects (age 69 y; range: 62-73y IQR) with a median baseline PSA of 0,79 ng/ml (range: 0,61-1,18 ng/ml IQR) were evaluated. Findings on ^{18}F-DCFPyL PET/CT were considered negative (29,69%; 19/64), positive (60,94%; 39/64) or indeterminate (9,38%; 6/64). ^{18}F-DCFPyL PET/CT localized recurrent prostate cancer in 7,69% (3/39) of cases with a prostate-specific antigen (PSA) level of ≥0.4 to <0.5, 48,72% (19/39) with a level of ≥0.5 to <1.0, 41,03% (16/39) with a level of ≥1.0 to <2.0, and 2,56% (1/39) with a level of ≥2.0. Active disease was most often identified in regional/distant nodes (61,54%), followed by prostate bed/seminal glands (33,33%), bone (23,08%), lung (2,56%) and other sites (2,56%).Many subjects had few lesions (1 lesion in 41,03%, 2 in 17,95%, 3 in 17,95%, and more than 3 lesions in 23,08%). There was a trend towards significance for greater number of lesions with higher PSA level but the trend did not reach statistical significance. The median SULmax across all lesions was 4,41 (range 2,73-9,37 IQR). A change in treatment intent occurred in 69,80% of subjects (to palliative 36,50%; to curative 33,30%), disease stage changed in 61,90% (upstaged), imaging results changed plans for surgery or biopsy in 25,00% (added), imaging results changed plans for systemic therapy in 29,69% (started), imaging results changed plans for radiotherapy in 48,44% (40,63% added; 7,81% cancelled), and management plans changed in 68,30%. **Conclusion:** ^{18}F-DCFPyL PET/CT is sensitive for the localization of biochemical recurrence of prostate cancer. This test changed management plans for most subjects. **References:** None

EPS-130

First clinical application of a novel PSMA-11-derived hybrid molecule for preoperative PET/CT imaging and fluorescence-guided surgery of prostate cancer

A. Eder[1,2,3], M. A. Omrane[1,2,3], S. Stadlbauer[4,5], M. Roscher[4,6], W. Y. Khoder[7], C. Gratzke[7], K. Kopka[4,5,8], M. Eder[1,2,3], P. T. Meyer[1,9], C. A. Jilg[7], J. Ruf[1,9];
[1]Department of Nuclear Medicine, University Medical Center Freiburg, Freiburg, GERMANY, [2]Division of Radiopharmaceutical Development, German Cancer Consortium (DKTK), partner site Freiburg, Freiburg, GERMANY, [3]German Cancer Research Center, Heidelberg, GERMANY, [4]Radiopharmaceutical Chemistry, German Cancer Research Center, Heidelberg, GERMANY, [5]Helmholtz-Zentrum Dresden-Rossendorf, Institute of Radiopharmaceutical Cancer Research, Dresden, GERMANY, [6]Division of Radiooncology/ Radiobiology, German Cancer Research Center, Heidelberg, GERMANY, [7]Department of Urology, University Medical Center Freiburg, Freiburg, GERMANY, [8]German Cancer Consortium (DKTK), partner site Dresden, Dresden, GERMANY, [9]German Cancer Consortium (DKTK), partner site Freiburg, Freiburg, GERMANY.

Aim/Introduction: For treatment of localised prostate cancer (PCa) radical prostatectomy with lymph node dissection is an established curative strategy. However, the precise intraoperative localisation and delineation of tumour margins and metastases remain challenging. Targeted hybrid molecules featuring a radio- and fluorescent label might overcome these limitations and support intraoperative navigation. Here, we report the first clinical application of preoperative PET/CT imaging and subsequent fluorescence-guided surgery with a PSMA-11-derived peptidomimetic PSMA-targeting hybrid molecule. **Materials and Methods:** After giving written informed consent, 4 patients with high-risk prostate cancer (Gleason Score >8) underwent preoperative PET/CT imaging 1 h and 2 h after intravenous injection of approximately 200 MBq ^{68}Ga-PSMA-914 (^{68}Ga-Glu-urea-Lys-$(HE)_3$-HBED-CC-IRDye800CW) on a compassionate-use basis. One to six days after PET/CT, fluorescence-guided surgery was performed with PSMA-914 administration 1 h prior to surgery. Verification of intraoperative findings was done by postoperative ex situ fluorescence analysis and histopathology. Results: Preoperative ^{68}Ga-PSMA-914 PET/CT

imaging revealed high tracer uptake in the primary tumours at 1 h (mean SUV_{max} 21.6 ± 19.5 g/ml; range 6.1 - 49.0 g/ml), slightly increasing at 2 h (mean SUV_{max} 26.9 ± 25.8 g/ml; range 6.6 - 63.3 g/ml). Lymph node metastases were additionally found on PET imaging in three patients. Intraoperatively, the fluorescence signal of PSMA-914 specifically visualised primary tumour tissue and lymph node metastases with a high contrast to surrounding healthy structures and resections were performed under fluorescence-guidance. The PSMA-specific enrichment of the hybrid molecule in malignant tissue was additionally confirmed by ex situ fluorescence detection and histopathology. **Conclusion:** This first clinical translation demonstrates a successful proof-of-concept highlighting the potential of PSMA-targeting hybrid molecules. The novel PSMA-11-derived hybrid molecule PSMA-914 supports the precise pre- and intraoperative detection of PSMA-expressing tumour manifestations. Further studies need to explore its impact on surgical treatment and outcome in prostate cancer patients. **References:** none

1212

Wednesday, October 20 - Saturday, October 23, 2021

on-demand pool, release on Wednesday, October 20 at 09:00

e-Poster Presentation Session 9: Imaging in Primary Prostate Cancer

EPS-131

^{68}Ga-PSMA-PET/CT for staging high risk prostate cancer patients suitable for radical treatments: effective clinic implication and preliminary diagnostic performance

F. Mattana[1], L. Bianchi[2], E. Balestrazzi[2], F. Costa[2], R. Mei[1], A. Farolfi[1], M. Droghetti[2], A. Morganti[3], R. Schiavina[2], E. Brunocilla[2], P. Castellucci[1], S. Fanti[1];
[1]IRCCS Azienda Ospedaliero-Universitaria di Bologna, Metropolitan Nuclear Medicine, Bologna, ITALY, [2]IRCCS Azienda Ospedaliero-Universitaria di Bologna, Division of Urology, Bologna, ITALY, [3]IRCCS Azienda Ospedaliero-Universitaria di Bologna, Radiation Oncology Department, Bologna, ITALY.

Aim/Introduction: Prostate Specific Membrane Antigen-PET/CT(PSMA-PET/CT) might overcome limits of conventional imaging for staging high-risk prostate cancer (PCa) patients. Accurate staging of patients suitable for radical treatments may have a significant impact on the treatment management. We aimed to assess the management changes after PSMA-PET/CT in high-risk patients before the scheduled radical prostatectomy+extended pelvic lymph node dissection (RP+ePLND) or radiotherapy (RT). In a subgroup of patients who subsequently underwent RP, we aimed to evaluate the diagnostic performance of PSMA to detect lymph node metastases (LNM), using histology as reference standard. **Materials and Methods:** Patients were enrolled according to the following criteria:1)histopathologic diagnosis of PCa, treatment naïve, high-risk according to D'Amico, suitable for radical treatment (RP or RT); 2)^{68}Ga-PSMA-PET/CT performed for staging proposal. We analyzed the impact of PSMA-PET/CT on the intention to treat (ITT) based on a MDT decision before and after PSMA-PET/CT. The diagnostic performance of PSMA PET/CT in the detection of LNM was evaluated in a subgroup of 27 patients who underwent RP+ePLND, using histology as reference standard. ROC curve analysis was employed to calculate the Area Under the Curve (AUC) of PSMA-PET/CT to predict LNM. Results: Overall, 88 patients were enrolled (mean age 66yo and mean PSA level 13.1ng/ml). Before PSMA PET/CT the scheduled treatment were: 66 RP+ePLND and 22 RT, respectively. Overall, PSMA-PET/CT was positive for metastatic disease in 51 patients(58%): LNM in 12 patients(14%), skeletal lesions in 24(27%), LNM+skeletal lesion 12(14%) and visceral metastases in 3(3%). After PSMA-PET/CT, the following treatments were performed: 48(55%) RP+ePLND; 7(8%) RP+PLND+stereotactic RT (SBRT); 13(15%) whole pelvis RT+Androgen Deprivation Therapy (ADT); 8(9%) whole pelvis RT+SBRT, 2(2%) ADT, 10(11%) Docetaxel+ADT. Overall, 12(14%) patients had major treatment's change; from planned RP+ePLND or whole pelvis RT to ADT or Docetaxel+ADT); while 15(17%) had minor treatment's change: RP+ePLND+SBRT or whole pelvis RT+SBRT. In the subgroups of 27 who underwent RP+ePLND, 8 (30%) had LNM on histology. On a patient-based analysis, PSMA-PET/CT showed 57% sensitivity, 95% specificity, 86% NPV and 80% PPV and with AUC of 0.72 in the detection of LNM. **Conclusion:** PSMA-PET/CT had a major impact on management in 14% and a minor impact on 17% of the population. These results confirm the published literature in the same setting of patients and might encourage the extensive use of PSMA in this setting of patients. PSMA-PET/CT showed good accuracy (especially specificity) in the detection of LNM. **References:** None

EPS-132

Preoperative Evaluation of Prostate Cancer by Positron Emission Tomography / Computed Tomography (PET-CT) with PSMA-68Ga: Correlation with Prostate Magnetic Resonance and Histopathological Findings

C. Stachera Stasiak[1,2], A. Cardillo[3], S. Altino de Almeida[1], D. B. Parente[1,2], R. Souza Rodrigues[1,2], P. Rosado-de-Castro[1,2];
[1]Instituto D'Or de Ensino e Pesquisa - IDOR, Rio de Janeiro, BRAZIL, [2]Universidade Federal do Rio de Janeiro, Rio de Janeiro, BRAZIL, [3]Universidade Federal do Estado do Rio de Janeiro, Rio de Janeiro, BRAZIL.

Aim/Introduction: PET-CT image with Gallium-68 is a non-invasive diagnostic method to assess the biological behavior of prostate cancer. This method is already used to detect biochemical recurrence and has the potential to be used to

diagnose high-risk tumors and for staging. The objective of this study is to evaluate the accuracy of preoperative PET-CT with 68Ga-PSMA to detect and stage prostate cancer, as well as to compare PET-CT with 68Ga-PSMA with prostate magnetic resonance imaging (MRI) using postoperative histopathological findings as the reference standard. **Materials and Methods:** Sixty-five patients with prostate cancer were included in this retrospective study. All patients underwent PET-CT with 68Ga-PSMA and prostate MRI followed by radical prostatectomy. Results: The mean age of the patients was 70.1 ± 8.3 years. The mean PSA before PET-CT with 68Ga-PSMA was 13.0 ± 21.0 ng/mL. PET-CT with 68Ga-PSMA showed radiotracer uptake in the prostate in 92.3% patients. The average SUVmax in the prostate was 10.7 ± 9.4. Thirteen (22%) patients had one or more lymph nodes with radiotracer uptake. In addition, PET-CT with 68Ga-PSMA identified 4 patients with bone uptake. PET-CT and MRI showed similar results in 35 patients (54%). Overall, PET-CT with 68Ga-PSMA had an accuracy of 42% to detect the site of the primary tumor and MRI had an accuracy of 22% compared to the post-operative histopathological findings. The positivity rate of PET-CT with 68Ga-PSMA in the prostate was 92% and prostate MRI identified at least one lesion classified as PI-RADS 3 or more in 91% of patients. In the evaluation of metastatic lymph nodes, PET-PSMA correctly diagnosed 67% of the negative and 63% of the positive lymph nodes, with an accuracy of 66%. The accuracy of MRI to detect positive lymph nodes was 69%, with identification of 85% of true positive lymph nodes and 25% of true negative lymph nodes. **Conclusion:** The performance of PET-PSMA was similar to MRI to detect the tumor site. PET-PSMA was superior to MRI to detect true positive lymph nodes, and MRI was superior to detect true negative lymph nodes. PET-PSMA is a promising tool to detect the primary tumor and to identify positive lymph nodes and distant metastases, which may change treatment. **References:** none

EPS-133

Comparing Q.Clear & OSEM algorithms in detecting biochemical recurrence of prostate cancer in^{68}Ga-PSMA PETCT

P. Tansey[1], A. Nasoodi[2];
[1]Center for Advanced Medical Imaging (CAMI), St James's Hospital & Trinity College, Dublin, IRELAND, [2]St James's Hospital Nuclear Medicine department, Dublin, IRELAND.

Aim/Introduction: ^{68}Ga-PSMA-PETCT has become the standard of care in the management of bio-chemical recurrence (BCR) of prostate cancer. Utilising BPL is a paradigm shift enabling a more sophisticated reconstruction platform, commercially available on the new generation of PET/CT scanners (QCLear-GE Healthcare). By allowing effective convergence, BPL avoids excessive noise resulting in higher quality imaging. We introduced BPL to our practice in January 2021 following installation of a GE-Discovery-MI-PETCT. We investigated the advantage of using QCLear (2021) in our practice over the OSEM (2020) with the primary end point of the detection rate of BCR. **Materials and Methods:** This retrospective study was carried out at St James's Hospital. A search was conducted using National Integrated Medical Imaging System (NIMIS) to identify patients who underwent ^{68}Ga-PSMA-PETCT in the first quarter of the years 2020 and 2021 respectively. The PET images were acquired with 150-200MBq; Scan time 3 mins; Recon with QCLear (beta 1000). Patient Records was used to confirm the prostatectomy status, PSA, Gleason score (GS) and any non-surgical treatment the patients had received. Statistical analysis was carried out on SPSS. Results: 83 patients with BCR were included. 46/83 were scanned with QCLear in 2021. 37/46 (80%) (PSA 3.81±3.48,median 2.3) were positive. 37/83 were scanned with OSEM in 2020. 26/37 (70%) (PSA 3.95±4.21, median 2.5) were positive. Using the Mann-Witney-U-score, we demonstrated that the PSA was not a contributing factor in detecting the recurrence between the two algorithms (p-value 4.532), attributing higher detection rate in 2021 subgroup to the QCLear. 90% of the prostatectomy patients had recurrence detected with PSA>0.5ng/ml in the QCLear subgroup compared to 69% in the OSEM subgroup. Concordant with the literature, a detection rate of 57% was shown in prostatectomy patients with PSA<0.5ng/ml. Of note, QCLear had a 100% detection rate in the non-prostatectomy subset in 2021, compared to OSEM with an 86% detection rate in the non-prostatectomy subset in 2020 with diverging results observed with higher GS. **Conclusion:** This small retrospective study demonstrates a higher detection rate in the setting of BCR in routine clinical practice, by utilising QCLear algorithm independent of PSA. QCLear performed better in the prostatectomy subgroup especially at low PSA (PSA>0.5ng/ml) and identified the recurrence in 100% of patients in the non-prostatectomy group, owing to its higher performance at higher GS. We propose routine use of QCLear in the evaluation of ^{68}Ga-PSMA-PETCT although larger studies with more robust methodology are needed. **References:** none

EPS-134

Ga 68 PSMA PET/CT at the initial staging of high-risk patients with prostate cancer

***T. Pipikos**, M. Vogiatzis, J. Andreou, D. Kechagias, V. Fillipi, E. Oikonomou, K. Gogos, S. Merisoglou, D. Papoutsani, K. Dalianis, R. Efthimiadou, V. Prassopoulos;*
PET/CT Department, Hygeia hospital, Athens, GREECE.

Aim/Introduction: Ga68 PSMA is a specific PET agent for the investigation of prostate cancer patients. Although it is not routinely used at initial staging, in selected cases it can be of great value. Aim of this study is to evaluate the results of Ga68 PSMA PET/CT study in high-risk prostate cancer

patients at initial staging **Materials and Methods:** The data of 95 patients who underwent a Ga68 PET/CT study between 1/2019 and 03/2021 were retro prospectively evaluated. They were categorized as high risk based on their Gleason score (8 or higher). The area from the base of the skull to the mid-thigh was covered in the scan. SUVmax values in the prostate gland as well as in possible other sites of abnormal uptake were calculated Results: Fifty-eight patients (58/95-61%), had abnormal extra prostatic uptake, with thirty-one of them showing only lymph node lesions (31/58,53%), twenty (20/58, 34%) mixed lymph node and bone foci, while seven (7/58, 12%) patients had only bone lesions. Usual sites of abnormal lymph node uptake were the inner inguinal lymph nodes, lymph nodes in the anatomic space by the prostatic bed, the outer inguinal lymph nodes, the pre-sacral area and less frequently the para-aortic lymph nodes. Mean SUVmax of the lymph nodes foci was 23,5 (4,1 to 44). In most of the cases the lymph nodes were not abnormal using CT criteria alone (40/51, 78%). Mean SUVmax of the bone lesions was 22,3 (5,5 to 33), with most usual sites of pathology the spine and the pelvis. Thirty-seven patients had only uptake in the prostatic gland lesions, with mean SUVmax of 15,2, while the mean SUVmax in the prostate lesions in the group of patients with also extra-prostatic abnormal uptake was 27,35. There was no significant statistical difference of the SUVmax between the two groups (p=0,35). On the contrary when comparing the mean PSA values, the extra-prostatic group showed significantly higher PSA values compared to the prostate limited only group (58,9 to 10,9 respectively, p=0,006). **Conclusion:** Ga68 PSMA PET/CT study can be of great value in the initial staging of patients with high-risk prostate cancer. In the majority of patients extra prostate pathology can be identified, with a great impact in the therapy planning. **References:** none

EPS-135

Ga68 PSMA PET/CT in the restaging of patients with prostate cancer. Correlation to PSA levels

T. Pipikos, J. Andreou, M. Vogiatzis, D. Kechagias, V. Fillipi, E. Oikonomou, K. Gogos, K. Dalianis, S. Merisoglou, D. Papotsani, R. Efthimiadou, V. Prassopoulos;
PET/CT Department, Hygeia hospital, Athens, GREECE.

Aim/Introduction: In the follow up of prostate cancer patients, a usual diagnostic problem is biochemical recurrence with elevated PSA and no discovered underlying pathology in the conventional imaging. Ga68 PSMA is a specific agent for the investigation of prostate cancer. Aim of this study is to evaluate the effectiveness of Ga68 PSMA PET/CT in prostate cancer patients with biochemical recurrence **Materials and Methods:** The data of 221 patients that underwent a Ga68 PSMA PET/CT study in our department because of elevated PSA were evaluated. Results: Mean time after surgery was 5,5 years (0,3 to 26 years) with a mean patients' age of 70,4 years. One hundred fifty-five of these patients showed abnormal uptake (155/221-70%). Thirty-three had uptake only in the prostatic bed indicative of local recurrence, with a mean SUVmax value of 38,68 (6,1-94), while 132 patients had extra-prostatic abnormal findings with mean SUVmax value of 18,5. In the latter patient group the most common site of abnormal uptake was lymph nodes (100/132-76%) with mean SUVmax 12,1 (2,5-70). 54 patients (54/132-41%) had abnormal bone uptake with mean SUVmax of 27,9 (3,6-94), 3 patients had peritoneal implantations, 6 patients were presented with uptake indicative of liver metastasis, while three had lung foci. When categorizing the patients based on PSA levels, in the group of patients with PSA levels up to 0,5 ng/dl (61 patients) PET/CT pathology was discovered in 22/61(37%), while in the group with PSA values 0,51-0,99 ng/dl (35 patients) in 22/35(62%). Overall, in the group of patients with PSA values up to 0,99 ng/dl abnormal lesions were found in 44/96(46%) of the patients. In the group with PSA values of 1ng/dl or higher the rate of positive studies was 114/125(91%). **Conclusion:** Ga68 PSMA PET/CT study can be of great value in the restaging of patients with elevated PSA, especially in the group with PSA levels over 1 ng/dl. Although abnormal foci detection rate is lower in PSA levels<1 ng/dl, in the majority of the patient's abnormal findings in the Ga68 PSMA PET/CT study are detected, with a great possible impact in the therapy planning especially in the early treatment. **References:** none

EPS-136

Effective dose of for medical workers operating in a PET/CT with the use of synthesis module

K. Dalianis[1], K. Gogos[1], G. Kollias[1], R. Efthimiadou[2], V. Prassopoulos[2];
[1]Medical Physics Deparment, Hygeia Hospital, Athens, Marousi, GREECE, [2]PET/CT Deparment, Hygeia Hospital, Athens, Marousi, GREECE.

Aim/Introduction: The PET/CT applications have been continuously increasing for diagnostic procedures. Although such an increase is a positive trend for the benefit of patients, the associated risk of radiation exposure of staff needs to be properly evaluated. The aim of this study was to measure the radiation exposure of the staff and evaluate the doses in the first PET/CT department in Greece at Hygeia Hospital. **Materials and Methods:** To estimate the effective dose from external exposure all 6 members of the staff (2 nurses, 2 medical physicists, 2 technologists, had TLD badges worn at the upper pocket of their overall, TLD rings on the second finger of each hand constning of disk measuring diameter by 0,9 mm thickness. The basics stages for the PET/CT procedures involve 4 steps: segmentation of the dose, injection of the radiopharmaceutical, nursing care during uptake and positioning of the patient. Results: The results of our study for the average cumulative whole-body dose for 100 patients (μSv±SD) at different stages were: segmentation

of the dose 189±7,23, injection of the radiopharmaceutical 245±6,67, nursing care during uptake 70±5,63, positioning of the patient 146±12,3. The statistical analysis showed small differences between stages 1, 2 and 4 (p>0,05) but a great statistical difference was observed between stages 2,3 p=0,023. The results for the finger doses (μSv±SD) regarding the same stages were: segmentation of the dose 284±77.4, injection of the radiopharmaceutical 225±62.3, positioning of the patient 26,79±5.87. **Conclusion:** The personnel dose results are significantly lower than the recommended annual dose by International Commission for Radiological Protection. However, a greater effort should be made to reduce the doses further in line with the ALARA principal **References:** Normal 0 false false false EL X-NONE X-NONE /* Style Definitions */ table.MsoNormalTable {mso-style-name:"Table Normal"; mso-tstyle-rowband-size:0; mso-tstyle-colband-size:0; mso-style-noshow:yes; mso-style-priority:99; mso-style-parent:""; mso-padding-alt:0cm 5.4pt 0cm 5.4pt; mso-para-margin-top:0cm; mso-para-margin-right:0cm; mso-para-margin-bottom:10.0pt; mso-para-margin-left:0cm; line-height:115%; mso-pagination:widow-orphan; font-size:11.0pt; font-family:"Calibri",sans-serif; mso-ascii-font-family:Calibri; mso-ascii-theme-font:minor-latin; mso-hansi-font-family:Calibri; mso-hansi-theme-font:minor-latin; mso-bidi-font-family:"Times New Roman"; mso-bidi-theme-font:minor-bidi; mso-ansi-language:EL;} 1. Occupational Radiation Exposure to Workers Used18F-FDG May 2019 DOI: 10.23851/mjs.v29i4.489License CC BY-NC Project: Dose Measurements for Worker Used 8F-FDG 2. Statistical analysis of the occupational radiation doses in three different positron emission tomography-computed tomography centers in Egypt July 2019 DOI:10.4103/wjnm.WJNM_42_18 License CC BY-NC-SA Lab: Ibrahim Elsayed Saad's Lab 3. Currently Available Radiopharmaceuticals for Imaging Infection and the Holy Grail March 2018 Seminars in nuclear medicine 48(2):86-99 DOI:10.1053/j.semnuclmed.2017.10.003

EPS-137

[68Ga]PSMA-11 PET findings in intermediate/high risk prostate cancer patients at staging

A. Scarale[1], S. Capitanio[1], A. Franchini[2], M. A. Potami[1], M. Longoni[1], S. Tappero[1], E. Gay[1], G. Cabrini[1], M. Milella[1], P. Dell'Oglio[1], A. Galfano[1], A. M. Bocciardi[1], C. Rossetti[1];
[1]ASST Grande Ospedale Metropolitano Niguarda, Milan, ITALY, [2]University of Milano-Bicocca, Milan, ITALY.

Aim/Introduction: The use of [68Ga]PSMA11 PET in prostate cancer patients is becoming common in clinical practice. An increasing amount of data on the positive correlation between prostate specific antigen (PSA) and standardized uptake value (SUVmax) is accumulating on high risk prostate cancer patients at staging. Conversely, less data is available on upper intermediate risk prostate cancer patients. The aim of the present pilot study was to investigate the association between PSA and SUVmax even in the intermediate risk patients. **Materials and Methods:** A cohort of patients with a diagnosis of high and intermediate risk prostate cancer prior to any specific therapy (n=49; mean age=68 years; all patients with Gleason score ≥6) was used to evaluate the association between PSA levels at PET and SUVmax. Correlation between PSA and SUVmax was assessed by Kendall correlation, more appropriate for small samples. Because of the skewed distribution, values of PSA levels and SUVmax were log-transformed and then standardized. In order to assess the association between exposure and outcome unadjusted and adjusted regression models were performed. Age at recruitment, smoking habit, BMI, primary Gleason, number of prior biopsies, hypertension, cardiovascular heart disease (CHD) were considered as possible confounders in the fully-adjusted model. Association values were reported as beta (SE) per 1-SD increase in standardized log SUVmax levels. Results: Kendall correlation between PSA levels and SUVmax was moderately positive (i.e. 0.2, p-value=0.04). In a linear regression model, the association between PSA levels and SUVmax was weakly not significant (beta=0.24; SE=0.12; p-value=0.06). After an adjustment for general confounders (i.e. age, BMI, smoking habit), the association became stronger (beta=0.57; SE=0.17; p-value=0.003). A larger significant association was observed when primary Gleason, number of prior biopsies, hypertension and CHD were considered (beta=8.63; SE=3.6; p-value=0.03). **Conclusion:** In a cohort of 49 prostate cancer patients with Gleason score more than or equal to 6, PSA levels and SUVmax values were positively associated. Further investigations in larger samples are needed to replicate these findings and to further address the role of clinical risk factors on this association. **References:** None

EPS-138

A Randomised Controlled Diagnostic Trial Comparing [^{18}F]PSMA-1007 PET/CT with Conventional Imaging in Primary Staging of Prostate Cancer

K. Buch-Olsen[1], M. H. Vilstrup[1], S. Hansen[2], S. Hess[3], P. C. Holdgaard[4], M. H. Poulsen[5], J. H. Dam[1], S. S. Madsen[6], M. G. Hildebrandt[1];
[1]Department of Nuclear Medicine, OUH Odense, Odense, DENMARK, [2]Department of Oncology, OUH Odense, Odense, DENMARK, [3]Department of Nuclear Medicine, Hospital South West Jutland, Esbjerg, DENMARK, [4]Department of Nuclear Medicine, Hospital Lillebaelt, Vejle, DENMARK, [5]Department of Urology, OUH Odense, Odense, DENMARK, [6]Department of Urology, Hospital South West Jutland, Esbjerg, DENMARK.

Aim/Introduction: PSMA-PET/CT is not yet introduced in the European Guidelines for staging primary prostate cancer (PCa). We hypothesize that more sensitive imaging such as PSMA-PET/CT will lead to more correct staging, and hence enabling a more targeted/individualized treatment. This

study aims to evaluate the accuracy of PSMA-PET for staging and its impact on treatment strategy as well as progression-free survival (PFS) and improved quality of life (QoL) in primary PCa patients. **Materials and Methods:** Patients will be enrolled at five centres in the Region of Southern Denmark. Patients eligible for the study have newly diagnosed PCa with intermediate or high risk of metastases. The study is planned in a prospective randomized multicenter design. Patients will be randomized into two groups 1:1: A) a control group staged with conventional CE-CT and [^{18}F]fluoride-PET/CT and B) an interventional group staged with [^{18}F]PSMA-1007 PET/CT. The study has been approved by the local ethical committee and it is currently under evaluation at the Danish Medicines Agency (EudraCT number 2021-000123-12). Patients will be asked to fill in QoL questionnaires during the study period. Treatment strategies will be planned and registered in multidisciplinary team conferences based on the results of the scans and according to current guidelines. The endpoints will be compared for group A vs. B with primary endpoints being treatment strategies, PFS, and QoL measures. Results: A total of 448 patients i.e. 224 in group A and 224 in group B will be included in the study from September 2021-September 2024. We expect to find longer PFS in patients staged with [^{18}F]PSMA-1007 PET/CT because of detection of small metastases initially. We expect to see fewer prostatectomies in the interventional group, because detection of metastases will exclude patients from local curative treatment. PFS is expected to be longer because of more accurate staging enabling an even more targeted therapy than possible when using the less sensitive conventional imaging. **Conclusion:** There is a knowledge gap regarding the benefit for patients of using PSMA-PET/CT for staging patients with primary prostate cancer. This study intends to provide this knowledge to improve clinical evidence based decision making. **References:** none

EPS-139

Association Between Prostate-Specific Antigen (PSA) Levels And Metabolic Findings In Bone Scintigraphy (BS) In Prostate Adenocarcinoma. Stratification In Groups According To PSA Levels

***J. Badell**, F. Gomez-Caminero, E. Martin, S. Lopez, J. Cañadas, A. C. Peñaherrera, J. G. Villanueva, B. Lucas, E. Martin, L. Diaz, P. Garcia-Talavera, C. Riola, P. Tamayo;*
Hospital Universitario de Salamanca, Salamanca, SPAIN.

Aim/Introduction: Establish the relationship between serum PSA levels and the presence/absence of bone metastases in the staging bone scintigraphy (BS) in patients with a diagnosis of prostate adenocarcinoma (PAC) and define the indication of it as an extension study. **Materials and Methods:** We performed a retrospective analysis of 141 patients with a diagnosis of PAC, referred to our service between January and May 2019 for a first staging BS, comparing scintigraphic findings and PSA levels. Patients were stratified into 4 groups according to their serum PSA levels: group 1 (0-10 ng/ml; 74 patients), group 2 (10.1-20 ng/ml; 20 patients), group 3 (20.1-100 ng/ml; 25 patients), and group 4 (≥ 100.1 ng/ml; 22 patients). The scintigraphic results were defined following a dichotomous variable: evidence/no evidence of bone metastases. Results: The percentage of scintigraphic scans with evidence of bone metastases and their distribution according to the previously defined groups were: 16.21% (12/74) in group 1 patients, 25% (5/20) in group 2 patients, 44% (11/25) in group 3 patients, and 90.90% (20/22) in group 4 patients. A PSA cut-off point was set at 10 ng-ml, with a sensitivity and specificity of 75% and 67%, respectively, and a negative predictive value of 84%. **Conclusion:** A direct relationship was observed between increased serum PSA levels and the identification of bone metastases in patients of group 2 and later groups. BS would be recommended in patients with PAC and serum PSA levels ≥ 10.1 ng-ml, with a questionable recommendation in those patients with lower PSA levels. BS is an effective screening technique for bone staging in patients with a diagnosis of PAC and elevated PSA levels. **References:** none

EPS-140

Bladder hernia in the inguinal canal mimicking pubic metastasis on MDP and PSMA whole body scans

***V. Roshanravan**, S. Soltani, M. Esmatinia, K. Aryana, A. Aghaee;*
Mashhad University of Medical Sciences,
Mashhad, IRAN, ISLAMIC REPUBLIC OF.

Aim/Introduction: Bladder diverticulum is a common entity in urology and it's prevalence may reach up to 31.6% in men (1). Diversity in diverticulum position can be falsely contributed to different pelvic metastasis such as pubis(2), SI joint(3) on bone scan, Ga-68-PSMA-11 PET/CT(4) or 18F-FDG PET/CT(5-6) even mimicking a pelvic(7) or abdominal(8) metastasis or a soft tissue mass(9). **Materials and Methods:** A 73 y/o male with first presentation of urinary retention from two months ago referred to our department by an urologist for prostate cancer staging. The patient had Gleason score of 5+4 and total PSA of 79. He underwent Tc-99m-MDP and Tc-99m-PSMA scans on two different days. The bone study revealed diffuse uptake in sacrum and a focus of abnormal MDP activity in the right SI joint. Another focus was also noted in right pubic region best seen on anterior projection which later on SPECT/CT was confined to a bladder diverticulum with tracer accumulation protruding into the right inguinal canal forming a hernial sac. following a few days, Tc-99m-PSMA scan was carried out and depicted high uptake in sacrum and right pubic region as well. The uptake was again localized to the bladder hernia on dedicted SPECT/CT acquisition. The findings denotes an important differential diagnosis of the pubic metastases as well as added value of SPECT/CT imaging in aforementioned scans. Results: The simplest method to rule out osseous metastasis

is acquisition of a lateral view on bone scan, in this case we also carried out PSMA scan in which the lateral view did not help. This is probably where the SPECT/CT imaging is next best step to prevent false positive findings. **Conclusion:** Bladder diverticulum is relatively a common entityand may be a challenge in interpreting the scan for nuclear physicians. Our findings denotes an important and not uncommon finding which can mimic pubic metastases and highlights added value of SPECT/CT imaging in aforementioned scans. **References:** none

EPS-141

^{68}Ga-PSMA PET/CT in primary staging of prostate cancer (PC) patients: risk of metastatic disease

M. Dyankova[1,2], T. Stoeva[1], Z. Dancheva[1], T. Yordanova[1], S. Chausheva[1], B. Chaushev[1], A. Klisarova[1];
[1]Medical University Varna "Prof. Dr. Paraskev Stoyanov", Department of Nuclear Medicine, Varna, BULGARIA,
[2]St Marina University Hospital, Varna, BULGARIA.

Aim/Introduction: Accurate primary staging of prostate cancer (PC) is one of the most important issues for clinical management of patients. The aim of this study was to analyze the association between PSA values, clinical T stage, European Association of Urology (EAU) risk groups and International Society of Urological Pathology (ISUP) grade in locoregional nodal (N) and distant (M) staging of PCa with ^{68}Ga-PSMA PET/CT detection rate and metastatic lesions incidence in patients with intermediate and high risk disease. **Materials and Methods:** We performed a retrospective analysis of 109 consecutive patients with diagnosed biopsy-proven intermediate and high risk PCa who underwent staging ^{68}Ga-PSMA PET/CT between July 2019 to June 2020. The mean age of the patients was 68.3 years. The chi-squared test was used for testing association between two categorical variables. Results: The median PSA level was 12.5 ng/ml and median International Society of Urological Pathology (ISUP) grade was 3 with high-risk disease in 94 (86.2%). There was a significant relationship between the PSA level ($p<0.001$), ISUP grade ($p<0.001$), EAU risk ($p<0.05$) and the ability of ^{68}Ga-PSMA PET/CT to reveal the metastatic involvement. In males with intermediate-risk PC, metastases were identified in 1 (6.6%), compared to 40 (42.6%) with high-risk disease. Oligometastatic disease (≤5 lesions) was detected in 7 (6.4%) of patients, including 4 (3.7%) with a PSA level of <10 ng/ml and ISUP grade 4-5. Regional metastatic lymph nodes incidence was identified in 29 (26.6%) of males, including 20 (18.3%) with a PSA level of >20 ng/ml and 23 (21.1%) with ISUP grade 4-5. Distant lymph nodes were most commonly found in patients with a PSA level of >20 ng/mL ($p <0.001$) and clinical T 3-4 ($p= 0.083$). Bone metastases were identified in 23 (21.1%) of patients, including 15 (13.8%) with a PSA level of >20 ng/mL and 17 (15.6%) with ISUP grade 4-5. Visceral metastases were detected in 4 (3.7%) of males with a PSA level of >20 ng/mL and ISUP grade 4-5. Distant metastases as a whole were seen most commonly in patients with high levels of PSA and ISUP grade 4-5. **Conclusion:** This study confirms that ^{68}Ga-PSMA PET/CT is an excellent tool for the detection of metastatic lesions, oligometastatic disease in the initial staging of patients with high-risk PC. The detection of locoregional nodal and distant metastatic spread of PCa is positively associated with PSA levels, ISUP grade and EAU risk groups. **References:** None

EPS-142

Is there an ideal tracer for pre-surgical nodal staging primary PCa? Monocentric experience of [68Ga]PSMA and [18F]Fluciclovine performance in two high-risk populations

F. Mattana[1], L. Bianchi[2], E. Balestrazzi[2], F. Costa[2], A. Farolfi[1], R. Mei[1], C. Malizia[1], M. Droghetti[2], P. Castellucci[1], R. Schiavina[2], E. Brunocilla[2], L. Zanoni[1], S. Fanti[1];
[1]IRCCS Azienda Ospedaliero-Universitaria di Bologna, Metropolitan Nuclear Medicine, Bologna, ITALY, [2]IRCCS Azienda Ospedaliero-Universitaria di Bologna, Division of Urology, Bologna, ITALY.

Aim/Introduction: In patients with Prostate Cancer (PCa), conventional imaging may fail in correctly detecting lymph node metastasis (LNM). An accurate N staging in patient with high-risk PCa have a paramount impact in the patients management. In the latest years, these two tracers have been used also for staging patients with high risk PCa with promising results but data deriving from a comparison of the two tracers is still lacking. We aim to evaluate the diagnostic performance of [68Ga]Prostate-Specific-Membrane-Antigene ([68Ga]PSMA) for nodal staging high-risk primary PCa (with histological validation) and to present the performance of [^{18}F]Fluciclovine in a comparable setting. **Materials and Methods:** Patients were selected from an electronic archive (ongoing electronic archive for [68Ga] PSMA patients and completed investigational trial for [18F] Fluciclovine patients) and retrospectively included according to the following criteria: 1) histopathologic diagnosis of PCa, treatment naïve, high-risk according to D'Amico, eligible for radical prostatectomy; 2) conventional imaging negative for bone/distant metastases; 3) [68Ga]PSMA PET/CT (group A) or [18F]Fluciclovine PET/CT (group B) performed with staging proposal 4)availability of extended lympho-adenectomy (at least 8 ln). All the PET/CT images were reviewed from two Nuclear Medicine physician and all the lymph nodes findings were classified as positive or negative for metastatic localization on a visual analysis. The performance of the two tracers was calculated on a patients-based analysis using histology as reference standard. Results: Overall 99 patients were included (35 group A; 64 group B); patients characteristics were for group A and group B respectively: median age (67y; 66y), median PSA value (7,35 ng/ml; 7,4 ng/ml), median time between PET/CT and surgery (58;45 days).

No significant difference were found between group A and B when considering pISUP, pTNM, pN (chi-square p-value: 0,698; 0,924; 0,564 rispectively). For group A and group B respectively: N1 patients were 12 (34%)vs17 (27%) and N0 were 23(66%)vs47(73%) with total lymphonodes retrieved 645vs1671, positive 23 (3,6%)vs45 (2,7%) and negative 622 (96,4%)vs1627 (97,3%) at pathology. ON a patient based analysis the diagnostic performance (visual analysis) for detection of LNM for [68Ga]PSMA and [18F]Fluciclovine were respectively: sensitivity (41%; 47%), specificity (95%, 83%), PPV (83%; 50%), NPV (75%; 81%). **Conclusion:** On a patient based analysis, [68Ga]PSMA showed higher specificity and PPV for the detection of LNM in high-risk prostate cancer patients when compared to [18F]Fluciclovine. Both tracers showed inadequate sensitivity and NPV. Further region-based analysis (SUVmax, TBR) with [68Ga]PSMA (group A) and [18F] Fluciclovine(groupB) are on-going and will be presented. **References:** none

EPS-143

The impact of (68Ga)-Ga-PSMA-11 PET/CT in primary staging of prostate cancer

***F. Weitzer**, B. Pernthaler, E. Plhak, R. Riedl, R. M. Aigner;*
Medical University of Graz, Graz, AUSTRIA.

Aim/Introduction: The emerging PET tracer (68Ga)-Ga-PSMA-11 (prostate specific membrane antigen) has shown the clinical value for prostate cancer (PCa) staging although the value of semi-quantitative parameters has not been reported. Aim of this study was to determine the value of a two-time point imaging protocol in patients with untreated prostate cancer. **Materials and Methods:** We included 100 patients with newly diagnosed untreated PCa who underwent (68Ga)-Ga-PSMA-11 PET/CT from January 2017 to October 2019. The two-time point imaging protocol consisted of an early static PET/CT scan of the pelvis (6 min p.i.) and a late whole-body PET/CT scan (60 min p.i). We also investigated associations of semi-quantitative parameters derived via manually drawn volumes of interest (VOI) with Gleason grade group and PSA levels. Results: In 94/100 patients (94%) the primary tumor was detected in both scans. In 29/100 patients (29%) previously unknown nodal and distant metastases were detected at a median PSA level of 32.2 ng/ml (range 0.41 - 503 ng/ml), significantly higher than in the remaining 71/100 patients (71%) without metastasis at a level of 10.1 ng/ml (range 0.57 - 103 ng/ml, p=<0.001). Higher SUVmax and SUVmean were associated with higher Gleason grade group (p=0.004 and p=0.003, respectively) and higher PSA levels (p=<0.001). In 18/100 patients (18%) PET/CT findings led to an intensified therapeutic regime, while in 21/100 patients (21%) a less aggressive therapeutic regime was preferable due to a down staging in PET/CT. **Conclusion:** Two-time point (68Ga)-Ga-PSMA-11 PET/CT demonstrates a high detection rate for primary tumor of untreated PCa of 94% and previously unknown nodal and distant metastasis in up to 29%. Therefore, (68Ga)-Ga-PSMA-11 PET/CT improves diagnostic accuracy in primary staging of PCa. **References:** Uprimny C, Kroiss AS, Decristoforo C, Fritz J, von Guggenberg E, Kendler D, et al. 68Ga-PSMA-11 PET/CT in primary staging of prostate cancer: PSA and Gleason score predict the intensity of tracer accumulation in the primary tumour. Eur J Nucl Med Mol Imaging. 2017 Jun 1;44(6):941-9.

EPS-144

Correlation of Intraprostatic Malignant Lesions Using F18-Prostate Specific Membrane Antigen Positron Emission Tomography (F-18 PSMA1007 PET/CT) with Magnetic Resonance Imaging (MRI) and Transrectal Ultrasound (TRUS) Biopsy Results in Initial Staging of Prostate Cancer, Single Institution Experience

***A. Sadeq**, W. Moftah, A. Esmail, F. Marafi, M. Alfeeli;*
Jaber AlAhmad center for Molecular Imaging,
Shuwaikh Medical area, KUWAIT.

Aim/Introduction: PSMA PET imaging is emerging standard of care in prostate cancer. Originally, it was used to evaluate biochemical recurrence, however, in recent practice its clinical use was extended to detection, staging, and assessing therapy response. Due to unfavorable characteristic of Gallium-68 labeled PSMA, fluorine-18 PSMA1007 with high labelling yields, high tumor extraction, and non-urinary clearance was attractive alternative for clinical use. The latter feature allows better local visualization and therefore better intraprostatic malignant lesions assessment. We aimed to evaluate the ability of F18-PSMA1007 in accurately localizing intraprostatic lesions with comparison to current standard care MRI. Additional locoregional and distant disease involvement were considered as a secondary objective. **Materials and Methods:** 18 patients diagnosed with prostate cancer by TRUS biopsy, had MRI and F18-PSMA1007 PET/CT within median period of 3 weeks. F18-PSMA1007 PET/CT was performed in one center, reviewed by two nuclear medicine physicians using 30 MBq/Kg of F18-PSMA1007 uptake period median of 91 minutes post-injection. Images were obtained from the vertex to below-knee using GE PET/CT scanners. TRUS and MRI were done at different centers. MRI was reviewed by experienced radiologist. The results of F18-PSMA1007 PET/CT and MRI were compared with TRUS biopsy histopathological result. Results: 15 patients had excellent correlation between F18-PSMA1007 PET/CT and MRI findings. One of mismatched cases, F18-PSMA1007 highlighted lesion identified by TRUS as Gleason score of 7(4+3) with 40% of tissue involvement while MRI highlighted another ipsilateral lesion (not visualized on PET) identified by TRUS as Gleason score 7(3+4) with 50% of tissue involvement. Another Patient had no significant MRI lesion while both F18-PSMA1007 PET/CT highlighted abnormality corelated to TRUS finding of 20-30% tissue involvement with

Gleason score of 6(3+3). The last patient F18-PSMA1007 PET/CT findings revealed the malignant intraprostatic lesion in addition to another lesion which was labeled by both MRI and TRUS as benign prostatic hyperplasia. F18-PSMA1007 was also able to recognized local invasion in 11 lesions out of 12 lesions identified by MRI and showed equivocal result in one lesion. F18-PSMA1007 extra-pelvic views upstaged 4 patients with extra-pelvic lymph nodes, 5 cases extra-pelvic bone and 1 case with pulmonary involvement. **Conclusion:** F18-PSMA1007 PET/CT shows promising cost-effective result in assessing intraprostatic lesions as well as locoregional invasion when compared to MRI because of its main feature of negligible urinary excretion. Metastatic lesions out-side the standard MRI field is another essential advantage that adds to the role of F18-PSMA1007 PET/CT. **References:** none

EPS-145

Gallium-68 [68Ga] labeled prostate specific membrane antigen (PSMA)-11 PET/CT in primary nodal and distant staging of prostate cancer (PC) patients compared to conventional imaging modalities (CT, MRI, bone scintigraphy): a retrospective single center study

M. Dyankova[1,2], Z. Dancheva[1], T. Stoeva[1], T. Yordanova[1], S. Chausheva[1], B. Chaushev[1], A. Klisarova[1];
[1]Medical University Varna "Prof. Dr. Paraskev Stoyanov", Department of Nuclear Medicine, Varna, BULGARIA,
[2]St Marina University Hospital, Varna, BULGARIA.

Aim/Introduction: Accurate clinical staging have a major importance for prognosis assessment and treatment recommendations for patients with PC. The prostate-specific membrane antigen (PSMA) is a cell surface glycoprotein that is highly expressed by prostate epithelial cells and is a promising target for PC. The aim of this study was to assess the performance of ^{68}Ga-PSMA-PET/CT for primary locoregional nodal (N) and distant (M) staging of intermediate and high-risk PC compared with conventional imaging techniques, as well to estimate the risk of metastatic involvement based on PSMA PET/CT findings. **Materials and Methods:** We performed a retrospective analysis of 69 consecutive patients with newly diagnosed biopsy-proven PC who had been staged with a conventional staging protocol including magnetic resonance imaging (MRI), computed tomography (CT) and bone scintigraphy (BS). They additionally underwent PSMA PET/CT between July 2019 and June 2020. The mean age of the patients was 68.2 years. Imaging findings from imaging modalities were categorized as negative, equivocal and positive. Results: The median PSA level was 14.4 ng/ml and median International Society of Urological Pathology (ISUP) grade was 3. Regional metastatic incidence was identified in 29 (42.0%) of males with high-risk PC, including 24 (34.8%) with a PSA level of >10 ng/ml and 23 (33.3%) with ISUP grade 4-5. Distant metastatic disease was identified in 31 (44.9%) of males including 24 (34.8%) with a PSA level of >10 ng/ml and 25 (36.2%) with ISUP grade 4-5. Based on conventional imaging, 14 patients (20.3%) were staged as positive, 9 (13.0%) as equivocal and 46 patients (66.7%) as negative for nodal metastases. With additional information of the PSMA PET/CT, N status was upstaged in 16 (23.2 %) and downstaged in 5 (7.2 %). Based on conventional imaging, 22 patients (31.9%) were staged as positive, 11 (16.0%) as equivocal and 36 (52.2%) as negative for distant metastases. With additional information of the PSMA PET/CT, M status was upstaged in 18 (26.1%), and downstaged in 8 (11.6%). Significant differences in N and M staging frequencies were found for CT, MRI and BS compared to PSMA PET/CT. **Conclusion:** ^{68}Ga-PSMA PET/CT is a promising molecular imaging technique that outperformed conventional imaging in the detection of nodal and distant metastases in the initial staging of patients with intermediate and high-risk PC. The detection of locoregional nodal and distant metastatic spread of PC is positively associated with PSA levels and ISUP grade. **References:** None

EPS-146

The Role of PSMA PET/CT in Primary Staging of Prostate Cancer according PSMA-RADS scale and correlation with prognostic staging from AJCC 8th

***S. Medina-Ornelas**, F. Garcia-Pérez, E. Gomez-Argumosa, J. Vargas-Ahumada;*
Instituto Nacional de Cancerologia, Mexico City, MEXICO.

Aim/Introduction: Currently, changes in the PSMA-group recommend avoiding PSMA-RADS and they recommend 5 point scale; meanwhile, before the introduction of new criteria, PSMA-RADS was a good method for evaluation PSMA-PET/CT. We evaluated the association of initial PSMA-PET/CT findings according to PSMA-RADS scale with prognostic staging according to the 8th edition of the AJCC in prostate cancer (pCa) **Materials and Methods:** 32 patients with newly diagnosed pCa who underwent baseline PSMA-PET/CT were reviewed retrospectively. PSA, Gleason scores, Grade, stage groups c-TNM, therapy decisions were documented. SUVmax of the primary tumor (SUVmax/T), regional nodes (SUVmax/N), and metastases (SUVmax/M) were evaluating. Scales according to PSMA-RADS were determined. Correlations between parameters from PSMA- PET/CT and PSA at diagnosis, Grade, stage groups, and PSMA-RADS on staging were determined. Results: Mean PSA was 81.32±7.12 ng/ml. Mean GS was: 8 ± 1 (Grade 1-5). 2 patients were stage-group-IIC, 3 group-IIIA, 4 IIIB, 5 IIIC, 8 group-IVA, and 10 patients were group- IVB, according to the AJCC 8th edition. Mean SUVmax/T 12.5±8.8, SUVmax/N, 12.7±3.4 and SUVmax/M 15.7±4.5. PSMA-RADS were 3C in one patient, PSMA-RADS 4 in 15 patients, and PSMA-RADS 5 in 16 patients. No PSMA-RADS 1 or 2 were visualized. SUVmax/T, SUVmax/N, SUVmax/M were correlated with PSA, Grade, and prognostic stage groups, (Pearson correlation; r:0.630-p<0.001, r:0.590-p<0.001, r:0.601-p=0.006, respectively). 11 patients

were upstaged with PSMA-RADS (7 patients from EC IIIC to IVA; and 4 patients from EC IVA to EC IVB). Patients with PSMA-RADS 5 had a higher SUVmax value compared with patients with PSMA-RADS 4 ($p < 0.045$). **Conclusion:** Our preliminary results suggest that parameters of baseline PSMA-PET/CT correlate with risk stratification of the 8th edition of AJCC Staging. Identify metastatic disease is crucial for patients with the high-risk-localized disease, and define a better treatment. In addition, the PSMA-RADS scale may be hopeful to upstaging patients. **References:** none

EPS-147

^{18}F-Florastamin PET/CT for the initial staging of patients with high-risk prostate cancer

W. H. Choi[1], S. Boo[1], Y. Choi[2], H. Kim[2], S. Lee[2];
[1]Department of Nuclear Medicine, College of Medicine, The Cathoic University of Korea, Seoul, KOREA, REPUBLIC OF, [2]Department of Urology, College of Medicine, The Cathoic University of Korea, Seoul, KOREA, REPUBLIC OF.

Aim/Introduction: ^{18}F-Florastamin, which was previously called FC303, is a newly developed ^{18}F-labelled PET tracer for PSMA imaging. This prospective study assessed the clinical utility of ^{18}F-Florastamin PET/CT in the initial staging of patients with high-risk prostate cancer. **Materials and Methods:** We recruited 10 patients with newly diagnosed high risk prostate cancer. ^{18}F-Florastamin PET/CT were acquired within two week of conventional imaging (prostate MRI, contrast-enhanced abdominal CT, and whole body bone scintigraphy). ^{18}F-PET/CT findings were compared to conventional imaging and histopathological reports. Results: All patients had ^{18}F-PSMA uptake in the prostate gland. In four out of 10 patients, additional metastatic lesions were detected by PSMA PET/CT, which were missed on the conventional imaging. Equivocal findings on bone scintigraphy could be finally determined based on additional of the PSMA PET/CT. **Conclusion:** ^{18}F-Florastamin PET/CT shows promise as a relevant staging procedure by identifying nodal and/or distant metastasis in patients with initial diagnosis of high risk prostate cancer. **References:** None

1312

Wednesday, October 20 - Saturday, October 23, 2021

on-demand pool, release on Wednesday, October 20 at 09:00

e-Poster Presentation Session 10: Lymphoma and Other Hematological Diseases

EPS-148

Prognostic role of end-of-treatment Fluorine-18 Fluorodeoxyglucose (^{18}F-FDG) Positron Emission Tomography/Computed Tomography (PET/CT) in diffuse large B cell lymphoma (DLBCL): a pilot study application of neural networks to predict time-to-event

E. Triumbari[1], S. Annunziata[2,1], A. Pelliccioni[3], S. Hohaus[4,5], E. Maiolo[5], A. Giordano[1,2];
[1]Section of Nuclear Medicine, University Department of Radiological Sciences and Hematology, Università Cattolica del Sacro Cuore, Rome, ITALY, [2]Nuclear Medicine Unit, Department of Radiology, Radiotherapy and Hematology, Fondazione Policlinico Universitario A. Gemelli, IRCCS, Rome, ITALY, [3]INAIL-DiMEILA, Monte Porzio Catone, Rome, ITALY, [4]Section of Hematology, University Department of Radiological Sciences and Hematology, Università Cattolica del Sacro Cuore, Rome, ITALY, [5]Hematology Unit, Department of Radiology, Radiotherapy and Hematology, Fondazione Policlinico Universitario A. Gemelli IRCCS, Rome, ITALY.

Aim/Introduction: To retrospectively evaluate the prognostic role of end-of-treatment (EoT) ^{18}F-FDG-PET/CT parameters in a large monocentric population of DLBCL patients and develop a Neural Network model (NNm), in comparison with conventional multi-regression models (MMm), in a pilot study designed to predict time-to-event in patients with residual ^{18}F-FDG uptake. **Materials and Methods:** ^{18}F-FDG-PET/CTs of DLBCL patients who concluded first-line chemo-immunotherapy between 2010 and 2017 were evaluated for target lesions' visual assessment (according to Deauville Score, DS) and semiquantitative parameters (when DS>1) that could be correlated to follow-up (FUP) data and estimate survival curves. Dataset of patients with residual ^{18}F-FDG uptake and an adverse event during FUP was split into a training (26/37) and a test (11/37) subset to build unbiased feedforward artificial NNm and conventional MMm for time-to-event prediction. Pearson correlation coefficient "R", mean absolute error and mean relative error between observed and forecasted time-to-event were calculated as performance indexes of MMm and NNm. Results: Patients meeting inclusion criteria were 308, 145 of which had DS>1. Median FUP time was 30 months. 62 adverse events were observed at a median time-to-event of 16 months. At univariate analysis, visual DS and qPET (target SUVpeak to liver SUVmean ratio) showed prognostic impact, with qPET=2.36 being the optimal cut-point with respect to progression free survival (PFS). PFS at 3 years was 85% for DS

1-3 and 55% for DS 4-5, respectively. Positive and negative predictive values were 55% and 83% for DS 4-5, 89% and 82% for positive qPET, respectively. For the 37 patients with residual ^{18}F-FDG uptake and an adverse event during FUP, NNm showed a higher predictive power for time-to-event than MMm: mean absolute and relative error of NNm were 6 months and 58%, respectively, and 8 months and 67% in MMm. "R" between observed and forecasted time-to-event was 0.63 for the NNm and 0.49 for MMm. **Conclusion:** EoT ^{18}F-FDG-PET/CT parameters had a strong impact on outcome in a large cohort of DLBCL patients. DS demonstrated to be a powerful outcome predictor. qPET may increase PET/CT's positive predictive value, thus potentially becoming a tool to better discern patients who would benefit from further treatment. A pilot NNm applied on residual ^{18}F-FDG uptake parameters seemed to predict time-to-event with lower error and higher correlation coefficient than MMm. The use of these parameters and models could hold the promise to allow better timing of intervention and better application of patient-tailored treatment strategies. **References:** None

EPS-149

18F-FDG PET/CT Volumetric and Radiomic Features predict Histological Types of Bulky Mediastinal Lymphoma

E. Abenavoli[1], F. Linguanti[1], B. Puccini[2], F. Mungai[3], S. Cristin[4], I. Romano[2], V. Miele[4], R. Sciagrà[1,5], V. Berti[1,5];
[1]Department of Nuclear Medicine, Azienda Ospedaliero-Universitaria Careggi, Firenze, ITALY, [2]Lymphoma unit,Hematology department, Careggi Hospital and University of Florence, Firenze, ITALY, [3]Department of Radiology, Azienda Ospedaliero-Universitaria Careggi, Firenze, ITALY, [4]Department of Radiology, Azienda Ospedaliero-Universitaria Careggi, L, Firenze, ITALY, [5]Nuclear Medicine Unit, Department of Experimental and Clinical Biomedical Sciences, Firenze, ITALY.

Aim/Introduction: This study was performed to assess the diagnostic value of 18F-FDG PET and CT volumetric and texture parameters in the histological differentiation of mediastinal bulky due to grey zone lymphoma (MGZ), primary diffuse large B-cell lymphoma of the mediastinum (MDLCBL) and primary mediastinal Hodgkin lymphoma (MHL). **Materials and Methods:** We retrospectively reviewed 110 patients (28 MDLCBL,71 MHL, 11 MGZ) with histopathological diagnosis (gold standard), who underwent 18F-FDG PET/CT and contrast-enhanced CT (CE-CT) at staging. Lesions were delineated using a fully automated preselection of 18F-FDG avid structures defined by a SUV ≥ 2.5. Volumetric and radiomic parameters were measured using LIFEx software both for bulky lesion (BL) and for all lesions (AL, nodal and extranodal) on both CE-CT and 18F-FDG PET/CT. Results: We found a significant difference ($p<0.05$) between the 3 groups for SUVmax, SUVmean, SUVpeak, BL/AL-MTV and BL/AL-TLG. Among CE-CT features, there was a significant difference between groups only for mean BL Hounsfield units, few grey-level run length matrix (GLRLM)and generalized linear models (GLZLM) features. Interestingly, PET textural features both of first order, such as Skewness, Kurtosis and Histogram, and of second order grey-level, such as the majority of features fromgray-level co-occurrence matrix (GLCM), neighborhood grey-level difference matrix (NGLDM), GLRLM and GLZLM showed significant differences between the 3 groups. Several of those features resulted predictive of the histological group with statistical significance ($p<0.001$). **Conclusion:** Radiomics features, extracted in particular from 18F-FDG PET, could be discriminating for different mediastinal bulky lymphoma histologies. These features could have a complementary role in staging evaluation and help identify potential histologic inhomogeneity and transformations. **References:** none

EPS-150

Predicting Time to Treatment in Follicular Lymphoma on Watchful Waiting using Baseline Metabolic Tumor Burden

D. Maccora[1], L. Leccisotti[1,2], R. Malafronte[3], F. D'Alò[3], S. Annunziata[2], S. Hohaus[3], V. Rufini[1,2];
[1]Section of Nuclear Medicine, University Department of Radiological Sciences and Haematology, Università Cattolica del Sacro Cuore, Rome, ITALY, [2]Nuclear Medicine Unit, Fondazione Policlinico Universitario Agostino Gemelli IRCCS, Rome, ITALY, [3]Hematology Unit, Fondazione Policlinico Universitario Agostino Gemelli IRCCS, Rome, ITALY.

Aim/Introduction: Initial management of follicular lymphoma (FL) with low tumor burden includes watchful waiting (WW). Approximately 25-40% of patients managed with WW will develop progression of disease within 24 months. Clinical prognostic models currently used at staging, including the follicular lymphoma international prognostic index (FLIPI), are not reliable to identify patients at high risk of progression. The aim of the study is to evaluate the prognostic value of baseline metabolic tumor burden in FL patients on WW. **Materials and Methods:** From 2010 to 2019, 54 patients with histologically confirmed FL (grade 1-3), initial WW approach, who underwent staging FDG PET/CT, with a follow-up≥24 months were retrospectively included. Total metabolic tumor volume (tMTV) and total lesion glycolysis (tTLG) were calculated using an automatic whole-body segmentation (LesionID, MIM Software Inc.). Time to treatment (TTT) was calculated from the date of diagnosis until the date of start of systemic therapy. Receiver operating characteristic (ROC) analysis was used to define the optimal cutoff for TTT within 24 months prediction for PET parameters. Survival functions were calculated by Kaplan-Meier estimates. Cox regression model was applied to evaluate PET prognostic power and Wilcoxon-Mann Whitney test for the multivariable analysis. A p value <0.05 was considered statistically significant. Results: Patient mean age was 61±12 years, 52% were males,

57% with stage III-IV, 52% with intermediate-high FLIPI (≥2). With a median follow-up of 33 months, 22 (41%) patients started immuno-chemotherapy due to disease progression and 32 (59%) were on WW. The median tMTV and tTLG were 7cm^3 and 43, respectively. Metabolic tumor burden was 0 in 9 (17%) patients since lesion SUV was less than reference background. The optimal cut-points identified for TTT within 24 months were 14cm^3 for tMTV (AUC 0.70, 95% CI 0.51-0.88) and 64 for tTLG (AUC 0.71, 95% CI 0.52-088) (p<0.005). The expected probability of not starting treatment at 24 months after diagnosis was 87% (95% CI, 69-95) in patients with tMTV≤14cm^3 and 53% (95%, CI, 28-74) for tMTV>14cm^3 (p<0.005). The median TTT was 28 months for tMTV>14cm^3, while it was not reached for tMTV≤14cm^3. Similar results were obtained for tTLG. On multivariable analysis, patients with both tMTV>14cm^3 and intermediate-high FLIPI had 18% probability of not having starting treatment at 36 months. **Conclusion:** Baseline metabolic tumor burden has the potential to predict the outcome of FL patients on WW. In combination with FLIPI score, baseline tMTV and tTLG may drive clinical decisions. **References:** None

EPS-152

Can ^{18}F-FDG PET/CT early detect treatment-related cardiotoxicity in patients with lymphoma

M. Wei, T. Yuan, X. Chen, X. Wang;
Peking university cancer hospital, BeiJing, CHINA.

Aim/Introduction: To explore the role of ^{18}F-fluorodeoxyglucose (FDG) PET/CT in early detection of therapy-associated cardiotoxicity (TACT) in lymphoma patients and to analyze the diagnostic efficacy of different evaluation criteria. **Materials and Methods:** Consecutive patients between November 2009 to October 2018 were retrospectively enrolled. All patients underwent standard chemotherapy. Myocardial uptake of ^{18}F-FDG pre- and post-treatment were analyzed by visual interpretation and semi-quantitative (maximum standardized uptake value, SUVmax) methods. The value of pre-treatment SUVmax-heart -post-treatment SUVmax-heart (ΔSUVmax), %ΔSUVmax, and post-treatment SUVmax-heart/SUVmax-mediastinum, SUVmax-heart/SUVmax-liver and SUVmax-heart/SUVmax-background (left gluteal muscle) ratios were calculated. Receiver operating characteristic (ROC) curve analysis was performed to determine optimal cut-off values of those PET/CT imaging criteria for evaluating early TACT of lymphoma, taking electrocardiogram (ECG) positive as the end point. Independent-sample t test and χ2 test were performed. Results: A total of 274 patients (median age was 36-year old), with the male-to-female ratio of 1.85□1, were included, and 78.1% (214/274) of them had non-Hodgkin□s lymphoma (NHL). After treatment, 55.1% (151/274) of the patients had high myocardial uptake of ^{18}F-FDG (compared with liver uptake), 20.4% (56/274) of them had moderate myocardial uptake (between liver uptake and blood-pool uptake), and 24.5% (67/274) were with equal uptake (less than blood-pool uptake).There were significant differences in myocardial uptake between ECG-positive group (n=71) and ECG-negative group (n=203) (SUVmax: 7.77±4.06 vs 5.91±3.04; t=4.045, P<0.01). In ECG-positive group, there was statistically significant difference between equal intake and high intake (χ2=6.308, P=0.012). ROC curves showed that optimal thresholds of post-treatment SUVmax-heart, Δ SUVmax-heart, %ΔSUVmax-heart, and post-treatment SUVmax-heart/SUVmax-mediastinum, SUVmax-heart/SUVmax-liver and SUVmax-heart/SUVmax-background ratios were 9.4, 4.8, 1.4, 5.0, 2.3, 7.0 respectively. The corresponding areas under the curves (AUC) were 0.653, 0.637, 0.612, 0.655, 0.649 and 0.650, respectively. The sensitivity, specificity, positive predictive value, negative predictive value and accuracy of post-treatment SUVmax-heart/SUVmax-background ratios were 40.85% (29/71),82.76% (168/203),45.31%(29/64),80.00% (168/210)and 71.90%(197/274). **Conclusion:** ^{18}F-FDG PET/CT can early detect TACT in patients with lymphoma, and if using 7.0 as the threshold of post-treatment SUVmax- heart/SUVmax- background ratio, the specificity and negative predictive value of ^{18}F-FDG PET/CT for early prediction of TACT are up to 80%. **References:** [1]Kim J, et al. Association between FDG uptake in the right ventricular myocardium and cancer therapy-induced cardiotoxicity[J]. J Nucl Cardiol, In press 2019.[2]Bauckneht M, et al. Doxorubicin effect on myocardial metabolism as a prerequisite for subsequent development of cardiac toxicity: a translational 18F-FDG PET/CT observation[J]. J Nucl Med, 2017, 58(10): 1638-1645.

EPS-153

Impact of ^{18}F-FDG-PET / TC for Assessing Response to Chimeric Antigen Receptors T Cell Therapy (CAR-T Cells) in the Treatment of Refractory Non-Hodgkin Lymphoma

J. Ardila Mantilla, I. Gómez Fernández, M. Baquero Oliveros, A. Rotger Regí, J. Orcajo Rincón, C. Durán Barquero, M. Kwon, M. Bastos Oreiro, M. Toscano Sánchez, J. Alonso Farto;
Hospital General Univeristario Gregorio Marañón, Madrid, SPAIN.

Aim/Introduction: CD19-targeting chimeric antigen receptor T-cell therapy (CAR-T) has shown excellent efficacy in the treatment of relapsed/ refractory NHL. Our objective is to assess the usefulness of ^{18}F-FDG-PET / CT in monitoring response to CAR-T therapy and to determine the predictive value of volumetric and metabolic parameters of baseline ^{18}F-FDG-PET / CT. **Materials and Methods:** Ambispective observational study; We included 24 patients with CAR-T therapy who underwent baseline ^{18}F-FDG-PET / CT, at 30, 100, and 180 days post-infusion. The following parameters were calculated: Metabolic tumor volume (MTV), total lesion glycolysis (TLG), SUVmax, spleen/liver ratio (SLR), bone/liver ratio (BLR), and SUVmax of the thymus. The clinical response was described in terms of clinical benefit (BC) and non-

clinical benefit (NBC) and PET / CT in complete remission, partial remission, pseudoprogression, progression, and or hyperprogression. Results: 11 women and 13 men, the average age being 55.3 years; 13 DLBCL, 8 other types of NHL and 3 high-grade NHL. Statistically significant differences were found as predictors of the response in the following parameters: SUVmax at 30 days ($F = 3.4$, $p = 0.05$); MTV at 90 days (not significant, eta squared (η^2) 0.142) and especially at 180d MTV ($F = 3.89$ with $p = 0.04$ and $\eta^2 = 0.280$ and BLR ($F = 6.56$, $p = 0.01$ and $\eta^2 = 0.396$). **Conclusion:** Metabolic parameters such as MTV, SUVmax, or BLR index measured in baseline ^{18}F-FDG-PET / CT could identify patients who would obtain clinical benefit from CAR-T therapy, thus predicting metabolic response. **References:** None

EPS-154

Utility of serial PET imaging by Peking criteria to prospectively predict prognosis in patients with diffuse large B-cell lymphoma

T. Yuan, M. Wei, X. Chen, X. Wang;
Peking University Cancer Hospital & Institute, Beijing, CHINA.

Aim/Introduction: In order to confirm the predictive and prognostic value ofserialFDG PET by Peking criteria and compare it with another 2 common methods of interpretation: the Deauville visual 5-point scale (5-PS) and SUV_{max} reduction (ΔSUV). **Materials and Methods:** Patients with newly diagnosed DLBCL underwent pretreatment PET and PET-2, PET-4 or PET-end ^{18}F-FDG PET/CT evaluation were prospectively enrolled in our study (NCT02928861). The PET response of patients was classified as either positive or negative by using Peking criteria, 5-PS and ΔSUV_{max}method. The optimal threshold of Peking criteria is 1.6-fold of $SUV_{max\text{-}liver}$ for PET-2 and PET-4, 1.4-fold of $SUV_{max\text{-}liver}$ for PET-end[1-3]. PET-2, PET-4 and PET-end results were assessed for the ability to predict progression-free survival (PFS) and overall survival (OS). Results: Of 291 patients, 245 had PET-2, 233 had PET-4 and 219 had PET-end. Better prognostic accuracy, positive predictive value (PPV) and specificity was found by using Peking criteria (PFS: 77.82%, 65.63%, 93.99% and OS: 84.68%, 34.38%, 90.45%, respectively), compared with 5-PS criteria (PFS: 70.28%, 44.00%, 77.17% and OS: 69.35%, 17.57%, 72.27% respectively) and 66%ΔSUV_{max}criteria (PFS: 70.16%, 42.37%, 81.42% and OS: 74.60%, 20.34%, 78.64% respectively). As in the PET-4 and PET-end, the superior of Peking criteria for prognostic accuracy, PPV and specificity of the Peking criteria still existed. The PET-4 prognostic accuracy of Peking criteria, 5-PS and ΔSUV_{max} method was 77.82%, 70.28%, 70.16% for PFS and 84.68%, 69.35%, 74.60% for OS, respectively. With PET-6, accuracy of different methods was 81.53%, 77.48%, 74.77% for PFS and 86.04%, 80.18%, 80.18% for OS. Uni- and multivariate analyses shown that Peking criteria was independent predictor for PFS and OS ($p<0.01$). **Conclusion:** Serial FDG PET/CT by using Peking criteria could estimating prognosis effectively. Comparison results suggested it seems a great alternative interpretation of PET/CT imaging. Further multicenter, larger-scale trials are needed **References:** 1. Zhang Y, Fan Y, Ying Z, et al. Can the SUVmax-liver-based interpretation improve prognostic accuracy of interim and posttreatment (18)F-FDG PET/CT in patients with diffuse large B-cell lymphoma? Leuk Lymphoma. 2018; 59:660-669.2. Meignan M, Cottereau AS. Interim PET in lymphoma: from Deauville to Peking criteria. On the road, again. Leuk Lymphoma. 2018; 59:523-525.3. Fan Y, Zhang Y, Yang Z, et al. Evaluating early interim fluorine-18 fluorodeoxyglucose positron emission tomography/computed tomography with the SUVmax-liver-based interpretation for predicting the outcome in diffuse large B-cell lymphoma. Leuk Lymphoma. 2017; 58:1-9.

EPS-155

Quantification of whole-body [^{18}F]FDG avid lymphoma lesions: advantages of semiautomatic over manual segmentation

***C. S. Constantino**, S. Leocádio, F. Oliveira, M. Silva, C. Oliveira, J. C. Castanheira, Â. Silva, S. Vaz, R. Teixeira, M. Neves, P. Lúcio, C. João, D. C. Costa;*
Champalimaud Centre for the Unknown,
Champalimaud Foundation, Lisbon, PORTUGAL.

Aim/Introduction: [^{18}F]FDG PET/CT imaging is essential for lymphoma patients staging and follow-up. Robust segmentation algorithms are paramount for the quantification of [^{18}F]FDG avid lesions in clinical practice and research. Our aim is to validate and compare a semiautomatic segmentation algorithm against manual segmentation of whole-body lymphoma lesions in [^{18}F]FDG PET/CT images. **Materials and Methods:** We randomly assigned whole-body [^{18}F]FDG PET/CT images from 31 previously untreated patients (median age 60 y.o., range 21 to 82) with confirmed lymphoma (12 Hodgkin Lymphoma, 11 Follicular non-Hodgkin Lymphoma, and 8 Diffuse Large B-cell Lymphoma). [^{18}F]FDG avid lesions were identified by experienced nuclear medicine physicians. Two experienced observers (Obs1 and Obs2) drew a large 3D region of interest (ROI) around each lesion to be used for automated segmentation using a Bayesian classifier [1] (semiautomatic method). Each lesion was also manually segmented by the two observers (manual method) originating four segmentations per patient. The proportion of overlap between segmentations was calculated using Dice coefficient (DC). Clinically relevant imaging features – SUV_{max}, SUV_{mean}, SUV_{peak}, metabolic tumor volume (MTV), and total lesion glycolysis (TLG) – were extracted from manual and semiautomatic lesions segmentation. The intraclass correlation coefficient (ICC) for absolute agreement was calculated between the extracted features using both segmentation approaches. Results: 276 lymphoma lesions (single and/or conglomerated) were

identified. The median time spent on manual segmentation and ROI delineation was 45 minutes (range 8 to 158) and 10 minutes (range 2 to 57) per patient, respectively. The median DC achieved between observers' manual segmentation and between semiautomatic segmentations was 0.81 and 0.95 (Wilcoxon test, $p < 0.001$), respectively. Between manual and semiautomatic segmentation, a DC of 0.87 and 0.84 was obtained for Obs1 and Obs2 segmentations, respectively. Considering the total tumor burden of each patient, an excellent agreement between the extracted features was achieved for all segmentations (SUV_{max}: ICC=1.00; SUV_{peak}: ICC=1.00; SUV_{mean}: $0.93 \leq ICC \leq 1.00$; MTV: $0.90 \leq ICC \leq 0.99$; TLG: $0.98 \leq ICC \leq 1.00$). Considering the most representative lymphoma lesion on each patient (higher TLG), the five features extracted from that lesion also showed an excellent agreement ($0.92 \leq ICC \leq 1.00$) between the four segmentations independently. **Conclusion:** Semiautomatic segmentations were four times faster and more reliable (higher DC) than manual segmentations. An excellent agreement between manual and semiautomatic segmentations was found for all lesions' features. Our semiautomatic segmentation method can replace the manual segmentation of lymphoma lesions, contributing to more reliable quantitative measures, with potential positive impact on patients' assessment. Funding: LyRaCAD project (Ref.:LISBOA-01-0247-FEDER-039885). **References:** [1] doi:10.1007/s00330-020-07390-8

EPS-156

Role of ^{18}F-FDG-PET / TC in Predicting the Adverse Effects of Chimeric Antigen Receptors T Cell Therapy (CAR-T Cells) In The Treatment of Refractory Non-Hodgkin Lymphoma

I. Gomez Fernandez, J. Ardila Mantilla, M. Baquero Oliveros, A. Rotger Regí, J. Ardila Manjarrez, Y. Henao Celada, D. Zamudio Rodríguez, M. Kwon, M. Bastos Oreiro, M. Toscano Sánchez, J. Alonso Farto;
HGU Gregorio Marañon, Madrid, SPAIN.

Aim/Introduction: CD19-targeting chimeric antigen receptor T-cell therapy (CAR-T) has shown excellent efficacy in the treatment of relapsed/ refractory NHL. However, a serious adverse effect of this treatment is cytokine release syndrome (CRS). Our objective is to assess the usefulness of baseline 18F-FDG-PET / CT as a prognostic factor in CRS development. **Materials and Methods:** Ambispective observational study; we included 24 patients with CAR-T therapy. The following parameters used to monitor response to immunotherapy are recorded at baseline ^{18}F-FDG-PET / CT: Metabolic tumor volume (MTV), total lesion glycolysis (TLG), SUVmax of the target lesion, and spleen/liver ratio (SLR). We monitored for the presence of CRS graded as absent, mild (grades 1-2), or severe (grade 3-4) over the following 180 days post-infusion according to de CRS severity scale. Results: 11 women and 13 men, mean age 55.3 years; 13 DLBCL, 8 other types of NHL, and 3 high-grade NHL. 18 patients (75%) developed CRS; 16 mild (66.6%) and 2 severe (8.3%). Mean values for absence, mild and severe CRS were as follows MTV = 941.83 cm^3, 1721.97 cm^3 and 2687.67 cm^3, TLG = 7036.17,20865.5 and 18893.78, SUVmax= 13.85, 18.67 and 19.26, SLR =1.0, 0.84 and 2.0 (where a value <1,1 is considered to be of good prognosis). Statistically significant differences were observed between groups with MTV, TLG and SLR. SUV max of the target lesion did not show differences across the groups. **Conclusion:** Baseline 18F-FDG-PET / CT before CAR-T therapy seems to predict the appearance of serious adverse effects. MTV, TLG, and SLR are significantly higher in those patients with severe cytokine release syndrome than in those with mild or absent CRS. Baseline SUVmax does not seem to predict the appearance of CRS. **References:** None

EPS-157

Series interim ^{18}F-FDG PET/CT stratify the prognosis of patients with Hodgkin lymphoma:based on Peking Criteria

M. Wei, X. Chen, T. Yuan, X. Wang;
Peking university cancer hospital, BeiJing, CHINA.

Aim/Introduction: In the previous studies, we proved that the interim ^{18}F-FDG PET/CT effectively predicts the outcome in patients with the diffuse large B-cell lymphoma using the Peking Criteria ($SUV_{max\text{-}liver}$-based interpretation).This study was to investigate whether the Peking Criteria could improve prognostic accuracy of interim PET/CT, and whether series interim ^{18}F-FDG PET/CT using Peking Criteria could stratify the prognosis of patients with Hodgkin lymphoma. **Materials and Methods:** The response was evaluated using the revised criteria of Lugano et al. Peking Criteria(SUV_{max}/ SUVliver) was used to interpret PET-2 and PET-4 imaging. Receiver operator characteristics (ROC) curve analysis was performed for continuous variables to determine optimal cut-off values. A residue SUV_{max} higher than the optimal threshold or new ^{18}F-FDG-avid lesions indicated a positive lesion. For 5-PS, a score of more than or equal to 4 was defined as positive.$\%\Delta SUV_{max}$ was calculated as follows: $\%\Delta SUV_{max} = (SUV_{baseline} - SUV_{treated})/SUV_{baseline} \times 100\%$. Prognostic value of PET/CT findings evaluated using the three methods were compared on survival analysis. The outcome of PET-2 and PET-4 were stratificed and compared on survival analysis.Time-to-event end points were evaluated by Kaplan-Meier estimates and survival rates were compared by log-rank test. Univariate and multivariate analyses of outcomes were performed using other prognostic factors and PET-2/ PET-4 scans. Results: A total of 150 patients were recruited. 125 patients had undergone PET-2; 115 patients had undergone PET-4; 99 patients had undergone PET-2 and PET-4 . For progression-free survival(PFS),ROC analysis revealed the optimal threshold is 1.2 fold of $SUV_{max\text{-}liver}$ for PET-2, 1.0 fold of $SUV_{max\text{-}liver}$ for PET-4. Peking Criteria had a higher prognostic accuracy and

positive predictive value than 5-point scale,%SUV_{max} criteria. Dramatic differences in the outcomes between patients with positive and negative PET-2/PET-4 were demonstrated using Kaplan-Meier survival curves (p<.01). The outcomes of PET-2/PET-4 were stratified into three groups: [positive and positive], [(positive and negative) or (negative and positive)], [negative and negative],and showed significant differences on Kaplan-Meier survival analysis(p<.01). Univariate and multifactor analysis found PET-2 /PET-4 were independent prognostic factors for the outcome of HL. **Conclusion:** Peking Criteria were superior to 5-point scale and % SUV_{max} criteria in analyzing the PET-2 /PET-4 for the prognosis of HL patients,and Series interim ^{18}F-FDG PET/CT using Peking Criteria could stratify the prognosis of patients with Hodgkin lymphoma. **References:** Zhang Y, et.all. Can the $SUV_{max-liver}$-based interpretation improve prognostic accuracy of interim and posttreatment ^{18}F-FDG PET/CT in patients with diffuse large B-cell lymphoma? Leuk Lymphoma. 2018 Mar;59(3):660-669.

EPS-158

Evaluation of the volumetric parameters calculated with the 2-[^{18}F]FDG PET/CT and the molecular characteristics in patients with diffuse large B cell lymphoma, not otherwise specified

S. Guzmán Ortiz[1,2], J. Mucientes Rasilla[1], J. A. Vargas Nuñez[1,2], J. L. Rodriguez Carrillo[1], A. Dotor de Lama[1], M. B. Navarro Matilla[1], M. Mitjavila Casanovas[1];
[1]Puerta de Hierro University Hospital, Madrid, SPAIN,
[2]Autonoma University of Madrid, Madrid, SPAIN.

Aim/Introduction: Diffuse large B-cell lymphoma, not otherwise specified (DLBCL-NOS) is considered a group with a high mortality rate, therefore, studies have been carried out to improve risk stratification in terms of prognosis, such as the evaluation of total tumor burden, through volumetric parameters such as metabolic tumor volume (MTV) and total lesion glycolysis (TLG), assessment of molecular characteristics such as germinal center B-cell (GCB) and non-GCB and the chromosomal translocations. The objective is the evaluation between the baseline volumetric parameters calculated with 2-[^{18}F]FDG PET/CT and the molecular characteristics in patients with DLBCL-NOS. **Materials and Methods:** Retrospective study of 40 patients with DLBCL-NOS from the Hematology service, who underwent baseline 2-[^{18}F]FDG PET/CT between January 2012 and December 2018. MTV and TLG were calculated with the SUV 2.5 threshold. The immunohistochemical study evaluated CD10, BCL6 and MUM1 taking as a cut-off point for a positive result, the staining of at least 30% of the neoplastic cells. The technique used for the analysis of chromosomal translocations was fluorescent in situ hybridization. A descriptive analysis of the quantitative variables was carried out, using the median, 25th and 75th percentiles, as well as the absolute and relative frequencies for the qualitative variables. Excel 2016. Results: The mean age was 65 years, with 25(62.5%) being male and 15(37.5%) female. Regarding the molecular study, 28(70%) patients presented the GCB molecular phenotype and 12(30%) a non-GCB phenotype. The MTV and TLG according to the GCB phenotype were 304.43cm3(82.38;724.72) and 1728.84cm3(499.05;4643.77) respectively and according to the non-GCB phenotype they presented 565.65cm3(99;1557) and 4318.61cm3(781.54;10600.63) respectively, these being higher with respect to the GCB phenotype. In the analysis of the volumetric parameters and chromosomal translocations, regarding the GCB phenotype, it was observed that 1 patient had a triple translocation (BCL2+BCL6+MYC) with MTV 83.19cm3 and TLG 368.82cm3, 2 patients a double translocation (BCL2+MYC) with MTV 63.37cm3(53.45;73.28) and TLG 430.81cm3(399.82,461.81) and 1 with a double translocation (BCL6+MYC) with MTV 83.19cm3 and TLG368.82cm3. However, the non-GCB phenotype presented only the chromosomal translocation of the BCL6 gene in 5 patients with MTV 602.81cm3(136.48;1405.71) and TLG 4318.61cm3(939.91;9011.84), these volumes being higher tumor metabolic rates compared to combinations of chromosomal translocations of the GCB phenotype. **Conclusion:** Patients with DLBCL-NOS with a less aggressive molecular phenotype such as GCB have a lower MTV and TLG value, even in the presence of chromosomal translocations, compared to the more aggressive molecular phenotype such as non-GCB. **References:** None

EPS-159

The role of ^{18}F-FDG PET/CT in Erdheim-Chester Disease

***M. Pudis[1]**, A. Palomar-Muñoz[1], K. López-Aldabe[2], X. Solanich-Moreno[2], J. J. Robles-Barba[1], E. Llinares-Tello[1], I. E. Sánchez-Rodríguez[1], L. Rodríguez-Bel[1], S. Bondía-Bescos[1], M. Cortés-Romera[1];*
[1]Nuclear Medicine-PET (IDI) department, Bellvitge University Hospital-IDIBELL, L'Hospitalet de Llobregat, Barcelona, SPAIN,
[2]Internal Medicine department, Bellvitge University Hospital-IDIBELL, L'Hospitalet de Llobregat, Barcelona, SPAIN.

Aim/Introduction: Erdheim-Chester disease (ECD) is a rare multisystemic disorder characterized by excessive production and accumulation of histiocytes within multiple tissues. ECD diagnosis is based on characteristic clinical, radiological and histopathological features. The aim of this study was to analyse the importance of 18F-FDG PET/CT in the initial diagnosis and staging. Additionally, we analysed the correlation of BRAF V600E mutation on maximum standardized uptake value (SUVmax) and organ involvement. **Materials and Methods:** A retrospective review of a cohort of patients in our database between years 2009 and april 2021, searching for those with pathologically proven ECD and 18F-FDG PET/CT. The variables collected were age, gender and PET findings at staging (extension of the disease and SUVmax of the most active disease). We classified the patients by the presence of

BRAF V600E mutation. The SUVmax values between these two groups were compared using Student's t-test. Results: We reviewed 17 patients (12 men, mean age of 60y), 9 of them with BRAF V600E mutation. In this group of patients the mean SUVmax was 13,1 (SD 11,33) and the highest uptake was observed in the long-bones of legs and central nervous system (CNS). The most common site involved in these patients was the skeletal system (100%) and all patients had long bones of legs involved. Other organs frequently affected were CNS (78%), cardiac and/or aortic disease (56%), skin (56%), retro-orbital space (44%), retroperitoneal fibrosis (33%) and kidneys (33%). The BRAF V600E wild type patients (7) presented mean SUVmax of 6,8 (SD 5,2). The most common site involved in these patients was the skeletal system (88%) with long bones of legs involved in 63%. Other organs involved include the skin (38%), cardiac and/or aortic disease (25%), retroperitoneal fibrosis and kidneys. The Student's t-test of SUVmax values between these two groups reveals that the two-tailed P value equals 0.1745 (IC 95% from -3.09 to 15.56). Incidental tumour findings on FDG-PET/CT in ECD patients identified a lung and a prostate cancer in one of these patients. **Conclusion:** A whole body 18FDG-PET/CT (from the cranial vertex to the feet) should be considered in all the patients at the initial diagnosis of ECD to assess the extent of disease and the metabolic activity, particularly in patients with BRAF V600E mutation, who associate greater organ involvement. Despite the tendency towards higher SUVmax values in patients with BRAF V600E mutation, this difference is not considered to be statistically significant. **References:** None

EPS-160

[18F]-FDG PET-CT in the diagnosis and management of plasma cell disorders

M. Muzaffar, A. Hassan, B. Ahsan, T. Zafar;
Shaukat Khanum Memorial Cancer Hospital & Research Centre, Lahore, PAKISTAN.

Aim/Introduction: Plasma cell disorder (PCD) in its early phase, is determined commonly by the presence of a monoclonal heavy chain and light chain restricted antibody, called a paraprotein or M protein. The hallmark of MM is bone disease which occurs in almost all patients as disease progresses, causing increased morbidity and mortality. The International Myeloma Working Group (IMWG) has confirmed that one or more lytic bone lesions on PET-CT, CT or MRI suggests bone damage requiring therapy. The most significant advantage of [^{18}F]-FDG PET-CT over other imaging modalities is to differentiate between metabolically active and inactive lesions. **Materials and Methods:** Retrospective review of 52 patients with plasma cell disorders between January 2009 and April 2020. Patients were classified into PCD subtypes using serum protein electrophoresis, serum free light chains, bone marrow biopsy, tissue biopsy and the findings on PET-CT and other imaging modalities. The role of PET-CT in diagnosis and management of PCD was determined. Results: Of 52 patients, 36 males and 16 females. Age range 23-79 years (mean 54.9 years). Out of 88 scans; 20 were staging scans, 52 restaging scans, 4 each interim and end of treatment scans and 2 surveillance scans. Solitary plasmacytoma with normal Bone Marrow (BM) were 5(9.6%), solitary plasmacytoma with minimal BM involvement 2(3.8%), MM secretory 25 (48.1%), MM non-secretory 8(15.4%), MM with no data for BM involvement 6(11.5%). Suspicion of PCD 6(11.5%), of which no lytic lesion was found in 3. Of 88 scans 67% revealed avid skeletal lesions. SUV range 2.5-23.5 (mean=6.3). Non-avid lytic lesions in 21.6%, No lesion in 11.4%. 18.1% had visceral metastases and 26.1% had nodal metastases. PET-CT confirmed initial diagnosis in 70% of staging scans, altered diagnosis based on additional lesions 25%. Additional skeletal lesions were found in 70% leading to change in the management of 8(40%). In patients with solitary plasmacyotma with or without BM involvement, PET-CT identified and confirmed diagnosis in 93%, identified additional bone lesions in 47% and altered treatment plan in 53%. In patients with secretory MM PET-CT helped change management in 56% by identifying additional bone lesions. **Conclusion:** [18F] FDG PET-CT not only has a promising role in determining the disease burden of PCD by identifying localized and advanced disease, but also by confirming metabolically active disease process it alters the treatment plan. **References:** none

1412

Wednesday, October 20 - Saturday, October 23, 2021

on-demand pool, release on Wednesday, October 20 at 09:00

e-Poster Presentation Session 11: Neuroendocrine and Lymphoma

EPS-161

Concordance between baseline 68Ga-DOTATOC PET/CT and first post-dose 177Lu-oxodotreotide SPECT/CT (177Lu-DOTATATE-SPECT/CT) images in patients with neuroendocrine tumors (NETs) treated with peptide receptor radionuclide therapy (PRRT)

A. Cardozo Saavedra, M. Simó-Perdigó, A. García-Burillo, D. Villasboas-Rosciolesi, J. Hernando, J. Capdevila, S. Menéndez-Sánchez, R. Bellviure-Meiró, F. Dellepiane-Clarke, S. Aguadé-Bruix;
Hospital Universitari Vall d'Hebron, Barcelona, SPAIN.

Aim/Introduction: The correlation between post-dose 177Lu-DOTATATE-SPECT/CT and pre-treatment 68Ga-DOTATOC-PET/CT is still unclear, and discrepancies between both techniques could condition efficacy of PRRT. Our aim is to compare both baseline 68Ga-DOTATOC-PET/

CT and 177Lu-DOTATATE-SPECT/CT after the first dose of PRRT (FD-PRRT) in patients with NETs. **Materials and Methods:** We performed a comparative analysis of baseline 68Ga-DOTATOC-PET/CT versus 177Lu-DOTATATE-SPECT/CT images after the FD-PRRT in patients with metastatic NETs who underwent treatment with 177Lu-oxodotreotide from May 2019 to March 2021 at our center. Non-gastroenteropancreatic-NETs and those cases with more than three months between baseline 68Ga-DOTATOC-PET/CT and the FD-PRRT were excluded. We assessed subjective differences in the number of lesions (NOL) and objective semi-quantitative differences in the NOL and their "Krenning score" between the baseline 68Ga-DOTATOC-PET/CT and the 177Lu-DOTATATE-SPECT/CT. The lesions were grouped by discrete ranges (1, 2-3, 4-6, 6-10 and >10 lesions) and six locations: primary tumor (PT), lymph nodes (LN), liver, spleen, peritoneum and bone. Results: 28 patients and 168 locations were included (39% women, mean age 62 years). The interval between baseline 68Ga-DOTATOC-PET/CT and the FD-PRRT was 36.5 days (2-77). 21 patients (75%) showed discrepancies in any subjective or objective assessment. Of these, 90.5% in favor of 68Ga-DOTATOC-PET/CT images and 9.5% in favor of both techniques (but different locations). None of them disagreed exclusively in favor of 177Lu-DOTATATE-SPECT/CT images.Subjective NOL analysis: 21 global discordances (75%), 95.2% in favor of 68Ga-DOTATOC-PET/CT, and only 1 patient in favor of both techniques. 40 locations (23.8%) showed disagreement: 39 (97.5%) in favor of 68Ga-DOTATOC-PET/CT (11 LN, 10 liver, 9 peritoneum, 4 bone, 4 PT, 1 spleen) and only 1 location in favor of both techniques (more bone lesions evident with 177Lu-DOTATATE-SPECT/CT). Objective NOL analysis: 20 global discordances (71.4%), 95% in favor of 68Ga-DOTATOC-PET/CT, and only 1 patient in favor of both techniques. 34 locations (20.2%) showed disagreement: 33 locations (97%) in favor of 68Ga-DOTATOC-PET/CT (10 LN, 6 liver, 8 peritoneum, 4 bone, 4 PT, 1 spleen) and only 1 location in favor of both techniques (more liver lesions evident with 177Lu-DOTATATE-SPECT/CT in 1/168 case). Krenning score analysis: 4 global discordances (14.3%), all exclusively in favor of 68Ga-DOTATOC-PET/CT. 5 locations (2.9%) showed disagreement, all in favor of 68Ga-DOTATOC-PET/CT (2 LN, 1 peritoneum, 1 bone, 1 PT). **Conclusion:** 68Ga-DOTATOC-PET/CT is a reliable predictor for PRRT-targetable lesions. Most of the observed discrepancies are probably related to the differences in spatial resolution. **References:** None

EPS-162

Assessment of PRRT Response from SUV-SPECT & PET, Personal Dosimeter and Biochemical Metrics

T. Alkahtani[1,2,3], L. Livieratos[1,2], V. Lewington[1,2];
[1]King's College London, London, UNITED KINGDOM, [2]Guy's & St Thomas' Hospitals NHS Foundation Trust, London, UNITED KINGDOM, [3]Princess Nourah bint Abdulrahman University, Riyadh, SAUDI ARABIA.

Aim/Introduction: SPECT and PET imaging are routinely used to verify radiopharmaceutical distribution in patients undergoing peptide receptor radiotherapy (PRRT). Pre- and post-treatment quantitative imaging combined with patient-led whole-body dose rate measurements were performed in a cohort of neuroendocrine tumour (NET) patients undergoing PRRT. These data were compared with clinical metrics to investigate whether serial changes in PET and SPECT derived standardised uptake values (SUV) and whole-body retention correlated with clinical response. **Materials and Methods:** Pre- and post-treatment data from nineteen patients (mean age 62, SD 9.0) with histologically confirmed, unresectable metastatic NET were analysed retrospectively. All patients received 4 cycles of 7.4 GBq Lutetium-177 (^{177}Lu) DOTATATE therapy in accordance with approved guidelines. SUV was measured in 99 individual lesions and in normal tissues using Gallium-68 (^{68}Ga) DOTATATE PET CT (prior to PRRT cycle 1 and 3 months after cycle 4) and Lu-177 DOTATATE SPECT CT images (24 hr post PRRT cycles 1 and 4). Whole-body dose-rate measurements were recorded for 28 days after cycles 1 and 4. Haematological parameters and biochemical markers (Chromogranin A & Chromogranin B) were assessed prior to cycles1 and 4. Wilcoxon Signed-Rank test was applied for testing of SUV changes. Paired sample t-test was used to evaluate differences for non-target organs and Spearman for correlation. Results: A significant correlation was shown between SPECT and PET-derived SUV measurements (r_s=0.8, p<0.01). Lu-177 DOTATATE SPECT SUV and functional lesion volumes decreased between PRRT cycles 1 and 4 (p <0.01). The mean of total lesional SPECT SUVmean, SUVmax, and SUVpeak declined by approximately 50%. Average lesion to spleen (LTS) and lesion to liver (LTL) SUV ratios between PRRT cycles 1 and 4 decreased from 3:1 to 1.5:1 and from 14:1 to 8:1 respectively. Ga-68 PET-derived LTS and LTL SUV decreased by 29% and 38%, respectively. No clinically significant haematological toxicity was observed (National Cancer Institute Common Terminology Criteria for Adverse Events, NCI CTCAE grade 0-1). External whole-body dose rate measurements at cycle 4 correlated significantly with observed reductions in SPECT& PET SUV and CgA. Reductions in CgA and CgB correlated well (r_s =0.5) with decreases in PET and SPECT functional volume and SUV values. **Conclusion:** Measurement of SUV changes derived from quantitative SPECT and PET/CT is useful to evaluate PRRT response. SPECT-SUV combined with patient-led whole-body dose rate measurements have potential as early indicators of prospective response in patients undergoing molecular radiotherapy. **References:** none

EPS-163

Dynamic changes of SUVs in 68Ga-somatostatin analogue PET/CT in response to PRRT as a predictive factor in patients with neuroendocrine tumours

M. Opalinska[1], A. Sowa-Staszczak[2], A. Kania-Kuc[1], I. Al Maraih[1], K. Morawiec-Sławek[2], A. Hubalewska-Dydejczyk[2];
[1]Nuclear Medicine Unit, Endocrinology Department, University Hospital in Krakow, Krakow, POLAND, [2]Chair and Department of Endocrinology, Jagiellonian University Medical College, Krakow, POLAND.

Aim/Introduction: Despite significant progress in the diagnosis and treatment of neuroendocrine tumors(NETs), searching for novel predictive and prognostic factors is crucial, because already used ones are not sensitive enough, for actual assessment of response to therapy, including PRRT. The high heterogeneity of the somatostatin receptors density in different NET lesions and inside single tumours may influence an clinical outcome. Recent studies indicate that the response to PRRT assessed on the basis of imaging of somatostatin receptors may be a potentially useful tool for prediction of overall PRRT effect. Aim:Assessment if SUVs change in 68Ga-somatostatin analogue PET/CT in response to PRRT may have a predictive value in patients with NET and if their changes depend on the tissue where the metastases are located. **Materials and Methods:** 13 patients treated with PRRT due to NET dissemination who underwent [68Ga] Ga-DOTA-TATE PET/CT in 6months before and after PRTT were selected to the study. A total number of metastatic lesions suitable for analysis was 83. Lesions were divided into 6groups depending on the location: 1.liver, 2.pancreas, 3.bones, 4.lymph nodes of abdomen and pelvis, 5.lung, 6.lymph nodes of chest and neck. For every lesion in both PET/CT SUVmax were measured and were standardized against SUVmax of normal liver (corrected SUVmax). Further a change of corrected SUVmax expressed as a percent value were calculated. Finally, those results were complied with the result of PRRT assessed after mean follow-up time 8.9months as: 1. Partial response (PR) 2. Stabilization(SD) 3.Progression(PD). Results: During follow-up time, progression was diagnosed in 3, regression in 4and disease stabilization in 6patients. Among PR patients, a change of total corrected SUVmax was -277% with the highest decrease in lymph nodes of abdomen and pelvis, and the lowest in pancreas. Among patients with SD, corrected SUVmax decreased by 181%, with highest response in bones and the lowest in lymph nodes of abdomen and pelvis. Among PD patients the change of corrected SUVmax was on average 6% with the highest response in lungs and with highest progress in lymph nodes of abdomen and pelvis. The average decrease of corrected SUVmax of lesions in whole patients was 157,81%. **Conclusion:** A decrease of the mean value of corrected SUVmax in metastatic NET lesions may have a predictive value in estimation of NET outcome after PRRT. Different changes of SUVmax in different tissues may indicate a tissue dependent response to PRRT and determinate the overall PRRT effect. **References:** none

EPS-164

Evaluation of 177Lu-DOTATATE treatment in patients with metastasic or unresectable paragangliomas and pheochromocytomas

J. Cañón Sánchez, S. G. Prado Wohlwend, P. Bello Arques, J. C. Bernal Vergara, A. Utrera Costero;
Hospital Universitario I Politécnico La Fe, Valencia, SPAIN.

Aim/Introduction: Assessment of response and adverse events in patients with metastatic or unresectable paragangliomas and pheochromocytomas treated with 177Lu-DOTATATE. **Materials and Methods:** We treated 9 patients (5 women) from October 2014 until present, mean age 45.7 years (20 - 72), with a follow-up of 29.7 months (4 - 81). 5 patients received 4 cycles, 3/9 patients 3 cycles (due to partial response to treatment) and 2/9 1 cycle (due to exitus). 3 cases were pheochromocytomas and 6 were paragangliomas (5 abdominal and 1 cervical), with 3 cases related to an SDH mutation (2 SDHB and 1 SDHD) and 6 sporadic cases. 8 cases were functioning tumors. Metastases location was liver in 4 cases, lymph nodes in 6, bones in 8 and lungs in 3 cases. 3 patients were previously treated with chemotherapy, 2 with radiotherapy, 3 with somatostatin analogs, 2 with 131I-MIBG and 1 with tyrosine kinase inhibitors. Biochemical, clinical and radiological response and progression-free survival were evaluated. Results: We observed grade 1 haematological toxicity in 2 patients and grade 3 in 1. 2 patients presented gastrointestinal discomfort. 4/8 functioning tumors had biochemical response and in 4 it could not be evaluated. Radiologically, 4 showed partial response (1 get worse 10 months later, and 5 remained stable). Clinically, 5 patients remained stable, one progressed, 2 had not follow up due to early death, and 1 was not monitored in our hospital. Median disease progression-free survival was 28.8 months. Of the 3 death patients , 2 were in a very advanced stage of the disease and 1 had grade 3 haematological toxicity secondary to previous treatments. **Conclusion:** 177Lu-DOTATATE treatment in patients with metastatic paragangliomas and pheochromocytomas can be a safe and an effective therapeutic option with a good radiological, clinical and symptomatic response. Improves the progression-free survival disease, the quality of life and suggests better results in early stages of the disease. It would be interesting to review its positioning in the therapeutic algorithms, although larger series of patients are required. **References:** none

EPS-165

Role of Interim CT Scan in Patients with Neuroendocrine Tumors (NETs) Treated with 177Lu-oxodotreotide (177Lu): Love it or List it

S. Menendez-Sanchez, A. Garcia-Burillo, J. Hernando, D. Villasboas-Rosciolesi, A. Cardozo-Saavedra, M. Simo, J. Capdevila, S. Aguade;
Hospital Universitario Vall d'Hebron, Barcelona, SPAIN.

Aim/Introduction: Efficacy evaluation during ^{177}Lu therapy can be challenging in some patients (p), especially those CT scan performed interim between cycles. In the present study we evaluate the role of interim CT scan in NET patients treated with ^{177}Lu. **Materials and Methods:** All p with gastroenteropancreatic, lung and paraganglioma NETs treated in our institution between 2016 and 2020 with ^{177}Lu were reviewed. P were selected after case presentation in a multidisciplinary committee and somatostatin receptors overexpression in a ^{68}Ga-DOTA-PET-CT. According to our institution protocol, interim CT scan was performed between cycle two and three of ^{177}Lu. Responses were classified as partial response (PR), stable disease (SD) or progressive disease (PD) according to RECIST v1.1 criteria. A further morphological or functional imaging was performed 3 months after completion of ^{177}Lu therapy and p were reclassified as PR/SD/PD. Results: 39 p were included (41% female, age 59.2 years). Interim CT scan classification was: 12 (30.8%) PR, 20 (51.3%) SD, 7 (18%) PD. Final CT scan or Ga68-DOTA-PET-CT showed 26 (66.7%) PR, 7 (18%) SD and 6 (15.3%) PD. It was shown that most of the patients were classified as SD in the interim CT meanwhile 3 months after therapy 14 (35.2%) were reclassified as PR. Interim-CT showed pseudo-progression in one of the patients who was reclassified as SD in the post-therapy control. Only 3 (7%) p interrupted treatment due to interim CT scan PD. **Conclusion:** Interim CT scan may not reflect final result of ^{177}Lu therapy. Decisions related to continuation of ^{177}Lu should be made considering clinical situation and toxicity. In some cases, interim morphological imaging tests could be avoided, but further studies are needed. **References:** None

EPS-166

Evaluation and improvements of small VOI method for kidney dosimetry in patients undergoing radionuclide targeted therapy with ^{177}Lu-DOTATATE

J. Khan[1], T. Rydèn[2], M. Van Essen[3], J. Svensson[4], P. Bernhardt[5];
[1]Department of Medical Physics and Biomedical Engineering (MFT), Sahlgrenska University Hospital, Gothenburg, SWEDEN, [2]1Department of Medical Physics and Biomedical Engineering (MFT), Sahlgrenska University Hospital, Gothenburg, SWEDEN, [3]Department of Clinical Physiology, Sahlgrenska University Hospital,, Gothenburg, SWEDEN, [4]3Department of Oncology, Institution of Clinical Sciences, Sahlgrenska Academy at University of Gothenburg, Gothenburg, SWEDEN, [5]Department of Medical Radiation Sciences, Institute of Clinical Gothenburg Sciences, Sahlgrenska Academy at University of Gothenburg, Gothenburg, SWEDEN.

Aim/Introduction: Fractionated peptide receptor radionuclide therapy (PRRT) with ^{177}Lu-DOTATATE has shown good results in treatment of neuroendocrine tumours (NETs). The efficacy of ^{177}Lu-DOTATAE therapy can be further improved by allowing individualized protocols, based on dosimetry to dose limiting organs such as the kidneys. However, accurate kidney dosimetry with manual segmentation of the whole kidneys is time consuming compared to measuring only a fraction of the kidney with a small standardised spherical volume of interest (VOI). The aim of this study was to compare kidney dosimetry based on small VOI method to manually segmented kidneys. In addition, improvements in small VOI method for kidney dosimetry was evaluated. **Materials and Methods:** Eighteen patients (n=18) with NETs underwent ^{177}Lu-DOTATATE therapy. Monte Carlo based reconstruction was used for obtaining attenuation, scatter and collimator detector response (CDR) corrected SPECT images. The recovery coefficients (RCs) for the manually segmented kidneys (n=36) performed in the CT images were determined by Monte Carlo simulations. The kidney absorbed doses were calculated based on SPECT images with and without post-filtration using gaussian filter. Small VOI method accuracy was analysed by placing up to five small VOI of 2 ml or 4 ml volume at representative locations in kidney parenchyma. Results: The mean RCs of segmented kidney volumes (range = 31-243 ml) was equal to 0.85 (range = 0.73-0.90, standard deviation (SD) = 2.9%). Pearson correlation coefficient showed strong relationship (r =0.90-0.97) of estimated absorbed doses between the small VOIs and the whole segmented kidney methods. The SD obtained from the Bland-Altman analysis when using one 4 ml VOI or five small VOIs of 4 ml was 15% and 9.7%, respectively. With application of Gaussian post filtering the corresponding SD was decreased to 13% and 9.1%, respectively. Furthermore, by using 2 ml instead of 4 ml improved the accuracy of

the small VOI method; SD decreased in non-filtered SPECT images to 8.7% and in post-filtered images 8.5%. **Conclusion:** The study demonstrated that patient specific RCs are needed for improved kidney activity quantification. In addition, increasing number of small VOIs increases the accuracy of absorbed dose estimation and almost complied with the method of using manually segmented kidney and patient specific RCs. **References:** none

EPS-167

Evaluation of thyroid function in patients receiving Lu-177 DOTATATE treatment

A. Kibar, B. Ince, A. Nazari, K. N. Toplutas, S. Bilgic, S. Asa, R. L. Uslu Besli, M. S. Sager, H. B. Sayman, K. Sonmezoglu;
Istanbul University-Cerrahpasa, Cerrahpasa Faculty of Medicine, Istanbul, TURKEY.

Aim/Introduction: We aimed to investigate whether Lu-177 DOTATATE treatment has an effect on basal TSH values and to evaluate the reliability of this treatment in terms of thyroid function. **Materials and Methods:** 41 patients who received four or more cycles of Lu-177 DOTATATE treatment between 2011-2020 in our department were retrospectively examined. Patients with a history of thyroidectomy, taking levothyroxine or whose basal TSH values were outside the reference range were not included in the study. Laboratory reference value for TSH measurement was 0.27-4.2 µIU/ml. TSH values were measured before the treatment (Basal TSH), between the treatment cycles (interim-TSH) and after ending of the treatment, as well (end-TSH)" It was thought that patients whose interim-TSH values or end-TSH values were found to be outside the reference range were affected by Lu-177 DOTATATE treatment. Results: 22 (53.7%) of the patients were male and 19 (46.3%) were female. 10 patients were treated for pancreatic NET, 8 patients for ileum NET, 6 patients for liver NET, 6 patients for lung carcinoid, 3 patients for paraganglioma, 2 patients for gastric NET, 2 patients for pheochromocytoma, 2 patients for colon NET, 1 patient for gastrinoma and 1 patient for jejunum NET. The mean age of the patients at the time of the last treatment cycle was 57.5 $\pm$ 12.5 years. Patients received a median of 1001 mCi (526-2535) of Lu-177 DOTATATE in total. In 33 (80%) patients, none of the TSH values were out of the reference range in both interim and end measurements. In contrast, interim-TSH levels were out of the reference range (increase in five patients; decrease in three patients) in a total of 8 (20%) patients. While the change in two of the patients (one increase, one other decrease) showed persistence in the end-TSH measurements, other six patients'TSH values returned to normal limits in the subsequent measurements. **Conclusion:** Although it has accumulation to some extent in the thyroid gland, it has been observed that Lu-177 DOTATATE treatment is a quite safe procedure in terms of thyroid functions. However, it should be kept in mind that it may cause temporary and rarely permanent changes in TSH in some patients. Thyroid function tests should be checked in the routine follow-up of these patients. **References:** None

EPS-168

Simulation of selective ablation of liver metastases in neuroendocrine tumor patients

V. Santoro-Fernandes[1], B. Schott[1], D. Huff[1], T. Perk[2,3], A. Deatsch[1], S. Perlman[4], R. Jeraj[1,5,6];
[1]University of Wisconsin-Madison, Department of Medical Physics, Madison, WI, UNITED STATES OF AMERICA, [2]University of Wisconsin-Madison, Department of Radiology, Madison, WI, UNITED STATES OF AMERICA, [3]AIQ Global, Inc., Madison, WI, UNITED STATES OF AMERICA, [4]University of Wisconsin School of Medicine and Public Health, Department of Radiology, Section of Nuclear Medicine and Molecular Imaging, Madison, WI, UNITED STATES OF AMERICA, [5]University of Wisconsin-Madison, Carbone Cancer Center, Madison, WI, UNITED STATES OF AMERICA, [6]University of Ljubljana, Institute of Physics, Ljubljana, SLOVENIA.

Aim/Introduction: Patients with metastatic neuroendocrine tumors (NET) can have heterogenous lesion-level response to ^{177}Lu-DOTATATE treatment, with some lesions resisting treatment. Ablation of resistant lesions could achieve meaningful disease burden reduction, delay progression, and improve quality of life. Here we simulated the impact of selective ablation on reduction in liver tumor burden of NET patients. **Materials and Methods:** Seven NET patients with liver metastases were treated with ^{177}Lu-DOTATATE and imaged with ^{68}Ga-DOTATATE PET/CT at three timepoints (PET1:baseline, PET2:month6, PET3:month18). Liver lesions were delineated via SUV>10 threshold. Lesions were automatically matched longitudinally enabling lesion-level analysis. Four lesion-specific metrics were extracted: SUV_{total}, SUV_{mean}, SUV_{max}, and functional volume. For each metric, resistant (new and progressive) lesions were selected for simulated ablation (SA), with progressive lesions defined as >30% increase in that metric from PET1 to PET2. We simulated ablation of lesions at the time of PET2 as 100% reduction in lesion uptake on PET3. Two SA scenarios were investigated: selecting all new and progressive lesions (unlimited scenario) and selecting up to five lesions with the greatest relative increase in each PET metric (limited scenario). To evaluate SA benefit, the relative reduction in disease burden on PET3 and the change in disease burden from PET2 to PET3 were calculated. Results: An average of 8 liver metastases per patient was observed at PET2 (range:2-19). Lesion selection based on functional volume resulted in the greatest median burden reduction for both scenarios. 71% (5/7) of patients had at least one lesion selected for SA. In these patients, the median disease burden reduction resulting from SA in the unlimited scenario was 42% (range:1%-96%). Limiting lesion selection to five lesions yielded very similar results, with identical median burden reduction. 43% (3/7) of patients had burden reduction above 30% in both scenarios, deemed as clinically significant. Under SA, the median change in disease burden from PET2 to PET3 decreased 37%, in contrast to no SA, where disease burden increased 8%. **Conclusion:** Simulation shows that selective lesion ablation can reduce liver tumor

burden for about half of selected NET patients. Selecting up to five lesions for ablation was adequate. Functional volume derived from ^{68}Ga-DOTATATE was the most promising metric for lesion selection. Ablative therapies could be an important additional treatment to consider in NET patients. **References:** none

EPS-169

Toxicity evaluation of ^{177}Lu-DOTATATE for advanced neuroendocrine tumors

J. Bonilla Plaza, A. Martinez Lorca, T. Navarro Martinez, O. Ajuria Illarramendi, I. Lopez Villar, P. Azpeitia Hernandez, M. Gutierrez Guerrero, P. Paredes Rodriguez, M. Orduña Diez;
Hospital Ramón y Cajal, Madrid, SPAIN.

Aim/Introduction: Peptide receptor radionuclide therapy(PRRT) has become a vital treatment option in the management of advanced neuroendocrine tumors. ^{177}Lu-DOTATATE is a radiolabeled somatostatin analog indicated for the treatment of somatostatin receptor-positive neuroendocrine tumors(NETs) in adults.The treatment is usually limited by the kidney toxicity, where the radiopharmaceutical is reabsorbed and retained, or bone marrow by evident hematological toxicity or in the liver even though ^{177}Lu-DOTATATE does not undergo hepatic metabolism, some patients develop hepatotoxicity and/or steatosis.Our aim is to evaluate kidney injuries by evaluating creatinine, the development of hematological toxicity by measuring blood cells levels and liver toxicity during PRRT treatment. **Materials and Methods:** This study included 116 stand-alone ^{177}Lu-DOTATATE doses administered to 30 patients with an advanced neuroendocrine tumors(Grade1-Grade2)Ki-67<20% who underwent treatment between 2013-2021. An average activity of 7.3GBq ^{177}Lu-DOTATATE per dose(7.2- 7.4GBq) was administered at intervals of 8-10 weeks in four cycles, unless clear progression or grade 3 toxicity was detected. Patient baseline health status according to renal, liver and bone marrow function, tumors burden and medical history including prior treatment were recorded. Renal, liver and bone marrow function were then monitored during treatment at a mean of 13 days post ^{177}Lu-DOTATATE administration. Renal, liver and bone marrow function were evaluated by standard blood works; rubin(Br),AST,ALT,Albumina(Al),Platelets(Plt),Leukocytes(Leu) and hemoglobin(Hb). Results: During this follow-up of 30 patients 17male(56.6%), 13 female(43.3%) of ages 25 -76 years(mode 58 years)116 doses were analyzed, we excluded 4 doses(1 for progression, 2 for non related to treatment deaths and 1 pending for administration). Primary tumor locations were identified(Midgut 30%, pancreas 26.7%, unknow origin16.7%, lung 13.3%, colon 6.7% and rectum 6.7%) with a mean Ki67 of 10.26%(SD 7.1)We found anemia after 34 doses(G1 23.27%,G2 6.03%), thrombocytopenia (grade 1) in 3.44% of doses, leukocytopenia in 12 doses(G1 6.03%,G2 3.44%,G3 0.86%), elevated creatinine levels after 11 doses(9.48%), AST in 9 doses(7.75%), ALT in 11 doses(9.48%), bilirubin 1 dose(0.86%) and albumin 12(10.34%). Statistical analysis was performed, comparative mean values of studied variables after each treatment were obtained PLT 190.939(p=0,001), LEU 5466(p=0,001), Creatinine 0.922(p=0,001) Hb 12.65(p=0,001).In general, lower platelet counts were observed in males(p=0.024), higher bilirubin rates were observed after the 4th cycle in males(p=0.038), and a direct correlation between age and leucopenia is described (R=-0.528; p<0.003) **Conclusion:** Patients who underwent 177Lu-DOTATATE treatment didn't present a significant toxicity as described by the mean values obtained presenting a valid significance. **References:** None

EPS-170

Extended field imaging in F-18 FDG PET/CT in Multiple Myeloma; is it necessary?

Z. Koc, P. P. Özcan, A. Akdeniz, Z. S. Sağlam;
Mersin University, Mersin, TURKEY.

Aim/Introduction: Previous studies suggested the prognostic significance of the number of involvement sites in F-18 FDG PET/CT imaging in Multiple Myeloma (1, 2). Thus there is a trend towards extended field imaging in these patients. The aim of this study was to evaluate the diagnostic significance of the findings that could be observed in case of Whole body imaging is performed in F-18 FDG PET/CT in Multiple Myeloma patients. **Materials and Methods:** The imaging findings of 34 patients (20 F, 14 M; mean 63,8±10,7 years old) with diagnosis of Multiple Myeloma who were referred for staging, restaging or treatment response evaluation to the F-18 FDG PET/CT were evaluated retrospectively. The patients were divided into control (n=15) and patient groups (n=19); who do not have pathologic findings (lythic lesions with maximum standardized uptake value of >4) beyond the mid thigh and who does respectively. Results: The comparison of the two groups revealed no statistical significant difference between the bone marrow, two major lythic lesions in the standard field uptake values (P>0.01). In the mean 37,3±39,5 months follow up total of 11 patients were progressive among which 5 was in control and 6 in patients groups. **Conclusion:** The comparison of the two groups revealed no statistical significant difference between the bone marrow, two major lythic lesions in the standard field uptake values (P>0.01). In the mean 37,3±39,5 months follow up total of 11 patients were progressive among which 5 was in control and 6 in patients groups. **References:** 1. Walker R, Barlogie B, Haessler J, Tricot G, Anaissie E, Shaughnessy JD Jr, et al. Magnetic resonance imaging in multiple myeloma: diagnostic and clinical implications. J Clin Oncol. 2007;25:1121-1128.2. Walker RC, Brown TL, Jones-Jackson LB, De Blanche L, Bartel T. Imaging of multiple myeloma and related plasma cell dyscrasias. J Nucl Med. 2012; 53: 1091-101.

EPS-171

Importance of non attenuation corrected 18F PET/CT images in multilple myeloma (MM) vertbroplasty treated patients to avoid false positive reported images

M. Agolti, L. Solari;
Centro de Medicina Nuclear Clinica Modelo, Parana, ARGENTINA.

Aim/Introduction: Vertebroplasty is a frequently done procedure in MM patients for it is very effective to relieve pain in compression fracture, which is a very painful and common situation in these patients. For this procedure, physicians use image guidance, to inject a cement mixture into the fractured bone through a hollow needle. During kyphoplasty, a balloon is first inserted into the fractured bone through the hollow needle to create a cavity or space. MM si increasingly evaluated through 18F PET/CT, due to the excellent diagnostic performance in initial staging, evaluation of treatment response, investigation of residual disease and early relapse. **Materials and Methods:** We review 21 18F PET/CT, done in our center between April 2020 and April 2021 in a Phillips Gemini TF PET/CT with an integrated 16-slice CT, the dose was 7 mCi (average) according to Body Mass Index (BMI) to evaluate treatment response in MM. We found 3 patients with initial and after treatment PET CT. They were treated with autologous bone marrow transplant and vertebroplasty in 2 of them and kyphoplasty in 1 for compression fractures. The cement used in this procedure generates hyperdense images in CT. We review 7 hyperdense images in attenuation corrected images (ACI), corresponding to vertebroplasty/Kyphoplasty treatment. We report these studies according to the 5-point Deauville scale (DS) adopted for PET scans in lymphomas, with measures of FDG uptake by the liver and mediastinal blood pool and identical method for bone focal lesions. Results: The 7 lesions were hypermethabolyc in basal studies (Deauville 4). We reported in ACI and 6 remained Deauville 4, (85,7%) in post therapy study and 1 of them was Deauville 3. However all of them (100%) had no increased uptake in non attenuation corrected images (NACÍ). The uptake of these vertebrae was similar to other vertebraes. High density material could generate PET/CT artefacts due to incorrect calculations of attenuation coefficients. This is even more important considering FDG imaging can detect with high sensitivity the persistence of residual active clonal plasma cells within residual lytic lesions, maybe this finding could be included in MM reporting guidelines. **Conclusion:** Nuclear medicine physicians should be aware of hyperdense artefacts in ACI. We concluded NACI should be seen routinely in MM vertebroplasty/Kyphoplasty treated patients **References:** None

EPS-172

Image quality assessment of [68Ga]-Gallium-CXCR4-PET/CT in multiple myeloma and diffuse large B-cell lymphoma

A. Lambertini[1], P. Hartrampf[1], A. Haug[2], A. K. Buck[1];
[1]Department of Nuclear Medicine - Würzburg University Hospital, Würzburg, GERMANY, [2]Division of Nuclear Medicine - Medical University of Vienna, Vienna, AUSTRIA.

Aim/Introduction: [68Ga]-Gallium-labeled CXCR4-specific ligands are an emerging class of radiotracers in the theranostic imaging of human solid cancers. This retrospective study aimed at visually and semi-quantitatively evaluate CXCR4-PET/CT imaging in patients with multiple myeloma (MM) or diffuse large B-cell lymphoma (DLBCL) and to investigate the impact of scan protocol variabilities on image quality. **Materials and Methods:** 81 MM and 15 DLBCL patients who underwent 118 CXCR4-PET/CT scans were considered. A nuclear medicine physician, experienced in CXCR4-PET/CT, analyzed the images . VOIs were drawn around a target lesion to generate semiquantitative data and within the aortic arch to estimate blood-pool tracer retention. Tumor-to-Background ratios (TBRs) were extrapolated and visual rating of image quality was performed using a 5-point scale (0=no detectable lesions; 1=very poor; 2=poor; 3=moderate; 4=good; 5=very good). Starting peptide mass, synthesis activity, injected activity and time intervals between synthesis and injection as well as injection and start of PET/CT scanning were recorded. Additionally, injected peptide mass was calculated for each patient. Results: Within the MM group, no target lesions were detectable in 41/100 cases, while 59/100 showed enhanced lesion uptake. Forty-nine/59 (83%) scans were rated as „good" or „very good" while 3/59 (5%) as "moderate". Seven/59 (12%) scans showed poor uptake, but target lesions were still detectable at a visual inspection. Within the DLBCL group no lesions were detectable in 8/18 cases, while 10/18 scans were assessable. Ten/10 (100%) were ranked as either „good" or „very good". Visual and semi-quantitative analyses were concordant, showing MM-TBRs ≥3 in 52/59 (88%), <3 but ≥2 in 6/59 (10%) of cases, while TBR <2 were detected only in 1/59 (2%) of cases (average: 19). All DLBCL-TBRs (10/10, 100%) were ≥3 (average: 9). In the MM sub-cohort, uptake times averaged 68 minutes while injected activities averaged 122 MBq. Injected peptide mass averaged 7 µg (range: 3.7-20.0 µg). In DLBCL patients, uptake times averaged 70 minutes while injected activities averaged 121 MBq, respectively. Injected peptide mass averaged 7.7 µg (range: 4.7-15.2 µg). We observed no clear influencence of individual scan variations on image quality in terms of injected activities, uptake times or injected peptide mass. **Conclusion:** Our preliminary analysis suggests a consistently high image quality within the parameters of the employed imaging protocols. We were not able to detect any significant influence of individual protocol variabilities on final image quality in terms of injected activity, uptake time as well as injected peptide mass. **References:** None

EPS-173

Correlation of histopathological and ^{18}F-FDG-PET/CT data in patients with symptomatic multiple myeloma

M. Türk[1], C. Sachpekidis[2], S. Sauer[3], J. Hillengass[4], A. Dimitrakopoulou-Strauss[2];
[1]Ruprecht Karl University of Heidelberg, Heidelberg, GERMANY, [2]German Cancer Research Center (DKFZ), CCU Nuclear Medicine, Heidelberg, GERMANY, [3]University Hospital Heidelberg, Department of Hematology, Oncology and Rheumatology, Heidelberg, GERMANY, [4]Roswell Park Comprehensive Cancer Center, Buffalo, NY, UNITED STATES OF AMERICA.

Aim/Introduction: To investigate the correlation of histopathological data and semiquantitative parameters gained from ^{18}F-FDG-PET/CT studies in patients with symptomatic multiple myeloma (MM) before and after therapy with high-dose chemotherapy (HDT) and autologous stem cell transplantation (ASCT). **Materials and Methods:** Fifty-three transplant eligible patients with MM were examined with whole-body ^{18}F-FDG-PET/CT before treatment (T1). Forty-five of them also had a follow-up scan after HDT and ASCT (T2). In addition to bone-marrow (BM) samples, which were obtained from the iliac crest during routine diagnostics (reference lesions), BM biopsies of focal, myelomatous lesions (focal lesions) were obtained which were previously identified with help of low-dose CT. PET/CT data-analysis included semiquantitative evaluation (SUV calculations) performed in the locations of the biopsies/aspirations. If a focal lesion happened to be at site of biopsy/aspiration for the reference lesion, SUV of the contralateral site of the iliac crest was evaluated. Results: In total 131 BM samples were obtained, and the extend of plasma cell infiltration (PCI) was analysed. Wilcoxon-signed-rank test showed that PCI was significantly higher in focal lesions than reference at T1 ($p = 0.019$), but not at T2 ($p = 0.109$). SUV_{max} was significantly higher in focal lesions compared to reference lesions before and after therapy. ($p_{t1} < 0.0001$; $p_{t2} = 0.004$). The decline of SUV_{max} from T1 to T2 was significant in reference ($p < 0.0001$) as well as in focal lesions ($p < 0.0001$). The clinical data indicate a good response to therapy, with over 50% (out of 45 patients at T2) attaining a complete response (n=5) or near complete response (n=19), based on IMWG response criteria. Eleven patients achieved a very good partial response, nine patients had a partial response and only one patient a minimal response. No patients were categorized as having stable or progressive disease. **Conclusion:** In the baseline study, lesions identified by PET/CT showed significantly higher BM infiltration rates than those biopsies from the iliac crest. Moreover, the focal lesions demonstrated significantly higher FDG-uptake (SUV_{max}) than reference lesions. In the follow-up study the FDG-decrease was significant in both focal and reference lesions. **References:** none

1612

Wednesday, October 20 - Saturday, October 23, 2021

on-demand pool, release on Wednesday, October 20 at 09:00

e-Poster Presentation Session 12: Head Neck / Breast / Lung

EPS-174

Comparison of FDG PET/CT and MRI Imaging in the Evaluation of the Treatment Response in Patients with Head and Neck Cancer

M. Engin[1], F. Aydin[1], A. Arcay[1], C. Dundar Caglayan[1], E. Tezel[2], K. Karaali[2], A. Tatli[3], M. Genc Ozay[4];
[1]Akdeniz university faculty of medicine nuclear medicine department, Antalya, TURKEY, [2]Akdeniz university faculty of medicine radiology department, Antalya, TURKEY, [3]Akdeniz university faculty of medicine medical oncology department, Antalya, TURKEY, [4]Akdeniz university faculty of medicine radiation oncology department, Antalya, TURKEY.

Aim/Introduction: Treatment of primary head and neck cancer is often multi-disciplinary and encompasses combination of surgery, radiotherapy and chemotherapy. Choice of the method to evaluate the treatment response is difficult due to postsurgical and radiation-induced changes. In this study, we aimed to reveal the sensitivity and specificity of FDG PET/CT and MR imaging in evaluating the treatment response of the primary tumor in patients with head and neck cancer and to compare PET and MR parameters. **Materials and Methods:** The FDG PET/CT and MR images of 37 patients (10 females, 27 males) for staging and treatment response evaluation between November 2015 and March 2020 were evaluated retrospectively. Treatment response with both FDG PET/CT and MR images; classified as complete response, partial response, stable disease, and progression. SUVmax, SUVmean, MTV and TLG parameters of the primary tumor based on the FDG PET / CT and ADC_{mean} values based on the MR images were calculated. Data was processed using IBM SPSS Statistics version 23. The findings was confirmed by pathology in 13(35%) patients and by clinical and radiological follow-up findings in the others. Results: Of the 37 patients included in the study, 15(40%) were nasopharynx, 10(27%) were oral cavity, 7(18%) were oropharynx, 3(8%) were hypopharynx and 2(5%)) were laryngeal carcinoma. In 30(81%) of 37 patients, chemotherapy and radiotherapy combination, in 3(8%) patients, only radiotherapy, and in 4(11%) patients only chemotherapy protocols have been preferred in treatment, and primary tumor was surgically removed in 14(37%) patients.The average time between FDG PET/CT and MR images was 24(0-95) days. According to the pathological and follow-up correlation results, the sensitivity for FDG PET CT and MRI were 100% and 97%, and the specificity were 94% and 97%, respectively. A moderate

(p: 0.031) negative correlation was found between MTV and ADC_{mean} values in images taken for staging, and a strong negative correlation was found in post-treatment imaging (p: 0.042). Staging SUVmax and SUVmean values were found to be significantly higher in the group with progression after treatment compared to the group with complete response (p: 0.033). **Conclusion:** Although both FDG PET/CT and MR imaging are sensitive and specific in evaluating the treatment response in patients with head and neck cancer, it has been concluded that the interpretation of MRI is difficult due to frequently seen artifacts in this area, and FDG PET / CT is a method that can be safely preferred in this sense. **References:** none

EPS-175

18FDG PET-CT in the assessment of primary head and neck cancers: Our First Experience

B. Khrouf*, F. Hamza, M. Maaloul, W. Touila, H. Noomen, W. Amouri, S. Charfeddine, K. Chtourou, F. Guermazi;*
Habib Bourguiba Hospital, Sfax, TUNISIA.

Aim/Introduction: 18F-FDG PET/CT has rapidly become a widely used imaging modality for evaluating a variety of malignancies, including head and neck tumors. Given the complex anatomy of this region, 18F-FDG PET-CT is particularly advantageous in a few well-established indications such as tumor staging, radiotherapy planning, detection of unknown primary tumor site and detection of residual or recurrent disease. The aim of this study is to report PET-CT findings in head and neck cancer patients in order to assess its value in head and neck oncology. **Materials and Methods:** 19 patients (12 males and 7 females) with head and neck primary tumors were studied. FDG PET-CT scan, from the base of the skull to the mid thigh, was carried out in all patients, 1h after FDG injection. Patient-based and lesion-based analyses were performed in comparison with conventional CT findings. Results: The most common primary tumor site was the nasopharynx (58%). All cases were related to Undifferentiated Carcinomas of the Nasopharynx (UCNT). 4 patients were referred for laryngeal squamous cell carcinoma and 4 patients for well differentiated thyroid carcinoma. The main indications were restaging, including treatment response assessment, and detection of recurrent disease. On patient based analysis, PET-CT led to the upstaging of 10 patients (53%) in comparison with CT findings: 6 patients (31%) had distant metastases and more important loco-regional involvment was noted in 4 patients (21%). PET-CT and CT showed the same results in 4 patients (21%) while CT detected more lesions in 4 patients (21%). In 2 cases (10%), PET-CT led to a downstaging when showing no FDG uptake of pulmonary nodules detected in CT. On lesion based analysis, PET-CT detected a total of 10 lesions not seen in CT. PET-CT identified 11 local recurrences compared to 7 lesions detected by CT. PET-CT and CT detected 8 and 5 lymph node involvements respectively. 8 metastatic lesions were present in PET-CT scans versus 5 in CT. **Conclusion:** FDG PET-CT is a useful imaging technique with several clinical applications and has a significant impact on the management of patients with head and neck cancer thanks to its high sensitivity and specifity. Nevertheless, PET CT findings should be interpreted carefully due to the variable physiologic FDG uptake patterns in the head and neck area. **References:** none

EPS-176

Clinical Effectiveness Of Sentinel Node Biopsy In Early Oral Cavity Carcinoma

Y. Herrera-Martinez*, Á. De Bonilla-Damiá, V. Pachón-Garrudo, R. Álvarez-Pérez, J. Jiménez-Hoyuela;*
Hospital Universitario Virgen del Rocío, Seville, SPAIN.

Aim/Introduction: This study investigates the effectiveness of sentinel lymph node biopsy (SNLB) in patients with early oral carcinoma without clinically and radiographically cervical lymph nodes involvement. **Materials and Methods:** Prospective study in 85 patients with T1-T2N0M0 squamous cell carcinoma of the oral cavity. Lymphoscintigraphy was performed after the administration of four peritumoral injections of 3 mCi of ^{99m}Tc-nanocolloid. The sentinel lymph node (SLN) was detected by the acquisition of dynamic, early, delayed and SPECT/CT images. The day after the SLN detection, its intra-operative recognition was carried out using a Navigator GPS® scintigraphic probe. The sentinel nodes were excised, and subsequently elective deferred lymphadenectomy was performed if tumor infiltration of the nodes were observed. Follow-up was performed on average 24 months (range 7-42 months). Results: Eighty-five patients (37 men and 48 women) were included in the study with an average age of 62 ±12 years. Lesions were localized in the tongue in 48 cases (56,5%), 26 (30,6%) in the floor of the mouth, 8 (9,4%) in the gum and 3 in other locations. A mean of 2,5 SLN was excised per patient. The bilateral drainage of the radiotracer was observed in 25 patients (29,4%). The SLN was localized in most of the patients (97,6%). Metastases were found in 19 of the 85 patients (22,3%); in those patients with initial negative SLN, recurrence was observed in only two cases (3%) during the follow-up. Cervical lymphadenectomy was avoided in 77,7 % of the patients. **Conclusion:** SLNB allows a correct cervical staging of oral cavity carcinomas, avoiding unnecessary cervical lymphadenectomy. **References:** None

EPS-177

The utility of multiparametric imaging with 18F-FDG PET and MRI in predicting survival outcome of patients with nasopharyngeal carcinoma

S. Chan[1], C. Yeh[2], S. Ng[2], J. T. Chang[2];
[1]Hualien Tzu Chi Hospital, Hualien, TAIWAN, [2]Linkou Chang Gung Memorial Hospital, Taoyuan, TAIWAN.

Aim/Introduction: To prospectively evaluate the prognostic value of multiparametric imaging parameters from diffusion-weighted imaging (DWI), dynamic contrast-enhanced MRI (DCE-MRI), and 18F-FDG PET/CT in nasopharyngeal carcinoma (NPC). **Materials and Methods:** Patients with a histological diagnosis of primary NPC were deemed eligible. The patients underwent DWI, DCE-MRI, and 18F-FDG PET/CT before treatment. The relationships of PET and MRI radiomic parameters with overall survival (OS) and recurrence-free survival (RFS) were evaluated by Kaplan-Meier and Cox-regression analyses. We further used independent prognosticators to establish the models for survival prediction. Results: Eighty-one patients were recruited into the study. The median follow-up period was 3.79 years for the entire cohort and 4 years for the surviving patients. Thirteen patients (21.3%) expired while 20 (32.8%) developed recurrence. A univariate analysis revealed that the T classification, total lesion glycolysis (TLG), volume transfer constant (Ktrans), flux rate constant (Kep), and initial area under the curve (iAUC) were significantly associated with OS while the T classification, Epstein-Barr virus (EBV) DNA load, TLG, minimum apparent diffusion coefficient (ADCmin), extracellular volume fraction (Ve), and TLG/iAUC were associated with RFS. Via a multivariate analysis, iAUC ($p = 0.04$) and TLG ($p = 0.002$) were identified as independent prognosticators of OS, while Ve ($p = 0.03$), TLG/iAUC ($p = 0.02$), and EBV DNA ($p = 0.03$) remained as significant predictors of RFS. The c-indices of the prognostic models incorporating iAUC with TLG in predicting OS and incorporating Ve + TLG/iAUC + EBV DNA in predicting RFS were higher than the corresponding indices of the traditional staging system (0.79 versus 0.62 and 0.76 versus 0.61, respectively); further, they were also higher than those of models without either MRI or PET biomarkers alone. **Conclusion:** Integrating the PET metabolo-volumetric parameter with the MRI biomarkers demonstrated a higher prognostic performance than the traditional staging system or the prognostic model with single imaging modality alone. Multiparametric MRI and PET imaging information may help clinicians in designing a comprehensive management strategy. **References:** None

EPS-178

Delayed complete metabolic response assessed with 18F-FDG-PET/CT in two time-points in patients with malignant epithelial head and neck tumor after radiotherapy with or without systemic chemotherapy-three clinical cases

T. Yordanova, A. Klisarova, T. Stoewa, S. Chausheva, M. Dyankova, Z. Dancheva, B. Chaushev;
Medical University Prof. dr. P. Stoyanov, Deparment of nuclear medicine, Varna, BULGARIA.

Aim/Introduction: We present three patients with malignant epithelial head and neck cancer (MEHNC) treated with radiotherapy with or without chemotherapy. We assessed the treatment response with FDG-PET/CT in two time-points, after end of therapy and after folow-up period. The timing of post-treatment response assessment represents balance between allowing time for completion of tumour response and resolution of radiotherapy-related inflammation versus the need to assess response early enough post-treatment to allow potential surgical intervention in the event of an incomplete response. The challenge of determining the presence or absence of viable tumour following radiotherapy provides a powerful rationale for the incorporation of functional imaging into response assessment protocols. (1) **Materials and Methods:** We report three patients with biopsy confirmed squamous cell carcinoma of MEHNC, staged with FDG-PET/CT (2015-2016): carcinoma of the nasopharynx T2N0M0, of the maxillary gingiva T4N0M0 and in maxillary sinus T4N0M0. The first patient is 62 years-old-female, treated with radiotherapy. The second two patients are males respectively 48 and 38 years-old treated with chemoradiotherapy plus Cisplatin. Clinicopathological findings and clinical follow-up provided the reference standard. Results: All of the patients achieved noncomplete (partial) metabolic response on the PET/CT at assessment-1 by 3-4 months. We consulted the patients with specialists (ENT), the endoscopy and biopsy results revealed post-Radiotherapy inflammation. No treatment was prescribed only follow-up. The patients underwent control PET/CT-2 after meantime 12 months (7-16) after end of treatment and all of them achieved delayed complete metabolic response (delay CMR). **Conclusion:** The study of Li WF et al. demonstrates that nearly half of the patients with nasopharyngeal carcinoma not have a complete clinical response (cCR) at 3-4 months after radiotherapy actually achieve cCR by 6-9 months and delay cCR was not poor prognostic factor (2). Our three clinical cases demonstrate that we must careful monitoring with FDG-PET/CT the completion of treatment in two-time points to ensure timely initiation of salvage therapy for persistent or progressive disease. We advise careful observe responding tumor after therapy for meantime 12 months to enable patients with delayCMR to avoid unnecessary

treatment. **References:** 1. Cliffe H, Patel C, Prestwich R, Scarsbrook A. Radiotherapy response evaluation using FDG PET-CT-established and emerging applications. Br J Radiol.2017;90(1071):20160764. doi:10.1259/bjr.20160764 2. Li WF, Zhang Y, Liu X, Tang LL, Tian L, Guo R, Liu LZ, Sun Y, Ma J. Delayed clinical complete response to intensity-modulated radiotherapy in nasopharyngeal carcinoma. Oral Oncol. 2017 Dec;75:120-126. doi: 10.1016/j.oraloncology.2017.10.020. Epub 2017 Nov 10. PMID: 29224808

EPS-179

Quantitative assessment of bone metastases in breast cancer patients

***M. Mutuleanu**, A. Lazar, I. Irimescu, M. Gherghe;*
National Institute of Oncology "Prof.Dr.Alexandru Trestioreanu", Bucharest, ROMANIA.

Aim/Introduction: In recent years the extensive use of SPECT-CT for oncology purposes has led to improvement in detecting and assessing oncological lesion such as bone metastases. This is a preliminary study aiming to compare SUV max 99m-Tc-HDP tracer uptake value in metastatic bone lesions in breast cancer patients with SUV max value of degenerative bone lesions using SPECT-CT quantitative analysis. **Materials and Methods:** A number of 63 female patients diagnosed with breast cancer were scanned using bone scan SPECT-CT using 99mTc-HDP from October 2020 to the April 2021. The scanning was performed using the following protocol parameters: 60 views, 20 seconds per view, dual energy window with to energy peaks 140± 10 KeV and 120±5 KeV respectively. All patients were scanned 2 to 3 hours after the injection of the radiotracer. Multiple lesions from every patient were assessed and the ones with the highest SUV max were taken into consideration in order to compare them. The lesions were identified on the SPECT images and were manually delineated using the CT images in order to obtain a precise contour of the margins and to avoid spill-over from adjacent bone structures. A total of 126 lesions were assessed and were characterized into degenerative bone lesions or bone metastases based on their morphological appearance on the low-dose CT images. Quantitative analysis of every lesion was then performed using SUV max based on lean body mass. Results: The mean SUVmax value for degenerative bone lesions and for metastatic bone lesions, was 15.20±6.50 and 45.14±32.30 respectively. The value of the SUVmax in bone metastatic lesions was significantly higher than the one in degenerative bone lesions (p value <0.001). The cut-off value of SUVmax > 18.6 had a sensitivity of 94.4% and a specificity of 80.6% in differentiating between bone metastatic lesions and degenerative bone lesions. In order to determine the diagnostic accuracy a receiver operating characteristic (ROC) curve was performed obtaining an area under the curve of 0.923 with a 95% CI of 0.835-0.973. **Conclusion:** The SUVmax value obtained using the information from the SPECT-CT bone scan performing quantitative analysis of the bone metastatic lesions, were significantly greater than the values of the degenerative bone lesions, but extensive studies are necessary in order to use this findings as baseline for bone lesions assessment. **References:** none

EPS-180

Metabolic Parameters By FDG PET-CT As Predictor Of Poor Prognosis In Breast Cancer Patients

***S. Ali**[1], M. ELahmadawy[1], H. Fathy[2];*
[1]National Cancer institute, Cairo, EGYPT,
[2]National Cancer Institute, Cairo, EGYPT.

Aim/Introduction: Breast cancer is a very heterogeneous tumor with prognosis depending on various histopathological and immunohistochemical factors such as histopathological type, grade, hormone receptor status, HER2neu status, ki-67 value. Breast cancer is classified into four types based on immunohistochemistry (IHC): Luminal A, Luminal B, triple negative, HER2neu positive. Triple-negative breast cancer which represent around 20% of patients, have aggressive histology and poor prognosis compared to other types. FDG PET/CT scan is a useful imaging modality in baseline evaluation of breast cancer. Higher FDG uptake is noted in tumors with aggressive biology predicting poorer prognosis. Aim of this study is to correlate FDG uptake (SUVmax) in primary breast cancer with various immunohistochemical subtypes & other prognostic factors. **Materials and Methods:** Retrospective study including 47 patients undergoing initial staging FDG PET/CT. All were females with 66% above 45 years. On histopathological examination (HPE), 43 (91.5%) patients were of invasive ductal carcinoma type and 4 of lobular type. Most of them were Grade II/III (89.4%) and staged T2/T3 (76.6%) with positive metastatic lymph nodes in 83% of patients. Regarding molecular categorization: 3 were luminal A, 24 were Luminal B, 6 were ERBB2 positive and 14 were triple negative. SUVmax was compared to histopathological grades, IHC types, and ki-67 values. Results: The mean SUV_{max} of the population was 11.6 (±7.9). The mean SUV_{max} in different HPE grades was Grade 1 = 6.18 ± 2.5, Grade 2 = 8.47 ± 4.8 and Grade 3 = 15.7 ± 9.1. The mean SUV_{max} values in different IHC types in Luminal A = 10.9 ± 7.5, Luminal B = 9.5 ± 6.2, triple negative = 16.3 ± 9.7, and HER2neu positive = 9.3 ± 1.7. The mean SUV_{max} in high ki-67 patients was 12.56 ± 8.52 compared with 9.34 ± 5.12 in low ki-67. Mean SUVmax in patients with positive axillary lymph node was 10.71 ± 6.48 compared to 15.95 ±11.45. On multivariate analysis, significant higher SUV_{max} in triple negative (P = 0.015) & IDC patients (P =0.014). **Conclusion:** High SUV_{max} values were noted in high-grade, high ki-67 & triple-negative breast cancer. **References:** none

EPS-181

Incidental detection of breast cancer on [18F] fluorocholine PET/CT: a retrospective analysis

A. Androjna[1], M. Hocevar[2,3], S. Rep[1,4], K. Zaletel[1,3], L. Lezaic[1,3];
[1]Department for Nuclear medicine, University medical centre Ljubljana, Ljubljana, SLOVENIA, [2]Oncological Surgery, Oncology institute Ljubljana, Ljubljana, SLOVENIA, [3]Faculty of medicine, Ljubljana, SLOVENIA, [4]Faculty of health sciences, Ljubljana, SLOVENIA.

Aim/Introduction: Choline (and consequently [^{18}F] fluorocholine) is a nonspecific cell proliferation and signaling marker. In addition to the primary indication for PET/CT imaging, incidental findings of potential clinical relevance can occasionally be observed. The aim of this retrospective review was to evaluate the clinical relevance of incidental findings in the breast tissue of patients referred for [^{18}F]fluorocholine PET/CT imaging for various indications. **Materials and Methods:** We reviewed the medical documentation of patients in whom [^{18}F]fluorocholine PET/CT scan performed between December 2014 and September 2019; patients in whom incidental finding of a breast lesion(s) was reported on either PET or low-dose CT of the examination were evaluated further. Cytological or histological verification of lesions was used as a standard of truth. Results: We found 11 breast lesions in eight patients. The average age of the patients was 72 years. Nine lesions were confirmed as malignant and two lesions as benign. Six malignant lesions were confirmed by core-needle biopsy (CNB), one malignant lesion was confirmed by fine-needle aspiration biopsy (FNA) and one malignant lesion underwent direct excision. Definitive diagnosis of eight malignant lesions was confirmed by histological examination after surgery, one malignant lesion was not surgically removed (the patient underwent systemic treatment). Invasive ductal carcinoma (IDC) was diagnosed in 8 lesions (7 IDC were hormone dependent and Her-2 negative, 1 IDC was hormone independent and Her-2 positive), 1 lesion was diagnosed as invasive lobular carcinoma (ILC, hormone dependent, Her-2 negative). All nine malignant lesions exhibited focal uptake on [^{18}F]fluorocholine PET/CT scan. The mean SUVmax of malignant lesions was 5,0 (range 2,5-7,2) and the mean size on low-dose CT was 1,3 cm (range 0,6-3,5 cm).The benign lesions had no significant focal uptake over the background on the [^{18}F]fluorocholine PET/CT scan. CNB showed hyaline hypocellular stroma with SUVmax 0,6 in one case, and typical ductal hyperplasia as part of fibroadenoma, with SUVmax 1,4 in the other case. The mean size of benign lesions was 1,2 cm (range 0,8-1,7 cm). Both benign breast lesions were suspicious for malignancy on ultrasound. Typical ductal hyperplasia as part of fibroadenoma was mammographically suspicious, while retromammary stroma was mammographically unsuspicious. **Conclusion:** Incidentally detected breast lesions on [^{18}F]fluorocholine PET/CT scan are clinically important and require further evaluation. **References:** none

EPS-182

Differences between supine and prone images in 18F-PET/CT in restaging breast cancer. Development of a soft material device to acquire prone images with better resolution

M. Agolti, L. Solari;
Centro de Medicina Nuclear Clinica Modelo, Parana, ARGENTINA.

Aim/Introduction: Breast cancer is one of the most frequent causes of death in young women. Prone imaging is the ideal arrangement for breast imaging as it allows good separation between the breast tissue and the chest wall, and It minimizes breathing artefact, according to published bibliography. We started using an MRI device to perform prone images, however we had to many metal artefacts. **Materials and Methods:** We designed a Styrofoam device with soft mattress, totally horizontal with two holes to allow the breast being pendular. We made 45 PET CT between December 2019 and March 2021 for restadification/response to treatment evaluation in breast cancer. We discharged 8 PET CT for we had metallic artefact. The FDG dose was calculated considering the Body Mass Index (BMI), the imaging protocol was from skull base to superior thighs, performed in a Philips Gemini TF 16 PET CT 60 minutes after injection and after this we did prone images in our dispositive just from the thorax , the studies were seen by two experienced Nuclear Medicine physicians. We considered SUV Max, and the size of the hypermethabolic image in both positions in PET CT. Results: We identified 17 lesions. The average SUV in conventional images was 3,5 and in prono images was 3,9 with an average variation of less than 10%. Applying Wilcoxon Sign Rank test p=0,495; which has no statistical significance. Regards the size of the lesion, we measured at least two longest axial diameters, we found higher values in at least one of the axial measures in prone images in 14 of the evaluated patients, this represents 82,35%, regards Wilcoxon Sign Rank test p=0,044; statistically significant, we think this could be due to a better separation between structures ,and probably a better resolution, and in some patients, 5 of them, allowed us to report a mild hypermethabolic image, that wasn't seen in supino images. We found no change in the measurement of three patients, all of them underwent radical mastectomy, 1 of them with breast reconstruction. **Conclusion:** Prone images generated better resolution images in restaging breast cancer, which was evidenced through higher axial lesions´ length values , improving diagnosis. We found no significant differences in SUV .18FPET CT prone images with appropriate device are easy, they don't involve more radiation exposure when doing the hole study prono and allows better space resolution in restaging breast cancer, except in radical mastectomy **References:** None

EPS-183

Submandibular gland involvement, as an unusual and the only site of breast cancer metastasis, detected in FDG PET/CT study

A. Aghaei[1], G. Gholami[1], F. Nesari[1], F. Emami[2], B. Rasoulian[3], H. Dadgar[2];
[1]Nuclear medicine research center, Mashhad University of Medical Sciences, Mashhad, IRAN, ISLAMIC REPUBLIC OF, [2]Razavi Cancer research center, Razavi Hospital, Imam Reza international University, Mashhad, IRAN, ISLAMIC REPUBLIC OF, [3]Sinus and surgical Endoscopic research center, Mashhad University of Medical Sciences, Mashhad, IRAN, ISLAMIC REPUBLIC OF.

Aim/Introduction: : A 40 years old woman with history of invasive breast ductal carcinoma treated with previous right mastectomy and chemo-radiation therapy, was referred to our department for evaluation of recurrence. She complained of swelling in her left submandibular region that has occurred since 1 year ago. High resolution computed tomography (CT) scan of the abdomen and chest with intravenous contrast, and bone scanning with Tc99m-Methylen diphosphonate (MDP) were unremarkable. **Materials and Methods:** whole body FDG PET-CT scan shows an FDG avid lesion in the left submandibular gland with relatively high standardized uptake value (SUV max= 6.6) with no other abnormal finding Results: Fine needle biopsy of the left submandibular gland was performed which confirmed metastatic ductal carcinoma of the breast origin. Immunohistological study were positive for estrogen and progesterone receptors, and negative for human epidermal growth factor receptor 2 (HER2). Salivary gland cancers are relatively rare and metastases to submandibular gland are less common. Asymmetric focal FDG uptake in submandibular glands needs ultrasound and fine needle biopsy. (3) our case showed relatively significant uptake in the left submandibular gland with SUV more than triple of the liver mean SUV. As we know, this is the first case in the literature which showed solitary submandibular gland metastasis , with no other site of metastasis, detected in FDG-PET/CT study of a breast cancer patient. **Conclusion:** Although FDG uptake in salivary glands and tonsils are known as a normal variant in FDG PET/CT studies, attention should be paid when the uptake is asymmetrical or intense, even when the underlying malignant disease is not in the head and neck region **References:** 1. Flint PW, Haughey BH, Robbins KT, Thomas JR, Niparko JK, Lund VJ, et al. Cummings otolaryngology-head and neck surgery e-book: Elsevier Health Sciences; 2014. 2. Rawet T, Jegannathen A, Soumian S. Parotid gland: an unusual site of breast cancer metastasis. Case Reports. 2017;2017. 3. Purohit BS, Ailianou A, Dulguerov N, Becker CD, Ratib O, Becker M. FDG-PET/CT pitfalls in oncological head and neck imaging. Insights into imaging. 2014;5(5):585-602.

EPS-184

FDG Uptake in Breast Cancer and Quantitative Assessment of Breast Parenchymal Uptake on 18F-FDG PET/CT: Association with Histopathological, Hormonal Status, and Clinical Features

G. Alçin, E. Arslan, T. Aksoy, T. F. Çermik;
University of Health Sciences, Istanbul Training and Research Hospital, Clinic of Nuclear Medicine, Istanbul, TURKEY.

Aim/Introduction: The study was designed to evaluate breast tumors' predictive value of the 18F-FDG PET/CT parameters on the histopathological features, receptor expression status, and molecular markers of proliferation, such as the Ki-67 index. Also, to assess the metabolic activity (BPU) of the ipsilateral and contralateral breast normal fibroglandular tissue (FGT) on primary breast cancer. **Materials and Methods:** 287 patients were included in our study, 198 (69.0%) patients with breast cancer and 89 (31.0%) patients with normal breast parenchyma (control group). The SUVmax of breast carcinomas were compared with histopathologic and immunohistochemically defined subtypes (luminal A, luminal B, human epidermal growth factor receptor-2 (HER2) positive and triple-negative), as well as Ki-67 expression status, tumor size, axillary nodal involvement, and distant organ metastasis. We also analyzed the BPU of normal fibroglandular tissue in the BC and CG. Results: 42 cases (21.2%) luminal A, 119 cases (60.1%) luminal B, 18 cases (9.1%) as triple-negative, and 19 cases (9.6%) were HER2 types. 19.7% (n=39) of the primary lesions had low Ki-67 expression (<15%), and 80.3% (n=159) had high expression of Ki-67 (≥15%). There was a positive correlation between primary tumor SUVmax and tumor size (p=0.001), high Ki-67 expression (p<0.001), axillary nodal involvement (p<0,001), distant organ metastases (p=0.026), ER and PR negativity, and HER2 positivity (p=0.000, 0.001, and 0.021, respectively). The average SUVmax in the luminal A group was 6.84±3.32, 13.96±7.83 in the luminal B, 18.02±9.14 in the triple-negative, and 17.12±6.62 in the HER2 type group. Accordingly, the change in mean SUVmax in molecular subtypes was statistically significant (p<0,001). The SUVmax value of 0.5 cm from the tumor in the same quadrant is higher than the background parenchymal regions in the opposite quadrant and contralateral breast, suggesting that the distance to the tumor increases, the FDG uptake decreases (p<0.001 and 0.001, respectively). We found a statistically significant relationship between high mean SUVmean and ER-PR negativity, HER2 positivity, increased tumor diameter, high Ki-67 rates, and axillary LN involvement. Similarly, high mean MTV, increased tumor diameter, high Ki-67 rates, axillary LN involvement, and distant organ metastasis were statistically significantly associated. **Conclusion:** Strong relationships were detected between the ER and PR negativity, HER2 positivity, high Ki-

67 expression, tumor size, axillary lymph node involvement, distant metastases, and SUVmax. Therefore, we believe that metabolic parameters obtained with 18F-FDG PET/CT may provide relevant information about breast cancer tumor biology and suggest a potential role in identifying more aggressive behavior. **References:** none

EPS-185

18F-FDG PET/CT In The Characterization Of The Different Histological Subtypes Of Pulmonary Neuroendocrine Tumors And Its Prognostic Value

A. Peñaherrera Cepeda, P. García-Talavera San Miguel, J. Villanueva Curto, J. Cañadas Salazar, S. López Puche, J. Badell Martínez, C. Riola Parada, B. Lucas Velazquez, F. Gómez-Caminero López, P. Tamayo Alonso;
Complejo Asistencial Universitario de Salamanca, Salamanca, SPAIN.

Aim/Introduction: To analyze the differences of ^{18}F-FDG uptake in the different pulmonary neuroendocrine tumor (PNET) subtypes (small cell lung cancer -SCLC-, large cell neuroendocrine carcinoma -LCNEC- and carcinoid tumors), as well as its influence in the overall survival (OS) and progression free survival (PFS). **Materials and Methods:** Fifty- five patients (60 ± 16 years old) with PNET (17 SCLC, 5 LCNEC and 33 carcinoid tumors; staging I 46%, II 12 %, III 27%, IV 15%). A ^{18}F-FDG PET-CT was acquired in all patients. U Mann-Whitney test and Kruskal-Walls test to evaluate the differences in uptake among subtypes were performed. For OS and PFS analysis, ROC curve and Kaplan-Meier plots were used. OS could only be calculated in the SCLC group, because there were no deaths in the other two groups. Average follow up time was 27,13 ± 16, 05 months. Results: There was no statistically significant differences in uptake between typical and atypical carcinoid tumor, so they were analysed together. Significant differences in uptake (SUVmax) were obtained among carcinoid tumors (4.6±2.7), SCLC (12.9 ±8.6), and LCNEC (15.5 ± 5.6) (p=0.000). Comparing LCNEC and SCLC with carcinoid tumors, respectively, there were statistically significant differences (p=0.000). For OS, in the SCLC group, a cut-off point of SUVmax of 13.8 was obtained, being 8 months for SUVmax ≥ 13.8 and 14 months for SUVmax < 13.8 although no statistically significant differences were observed. Furthermore, the same SUVmax cut-off point of 13.8 was obtained for the PFS, being 3 months for SUVmax ≥ 13.8 and 14 months for SUVmax < 13.8, this difference was statistically significant (p=0.037). PFS in LCNEC was 10.5 months for SUVmax ≥ 15.6 and 29.7 months for SUVmax < 15.6. And in carcinoid tumors it was 42 months for SUVmax ≥ 4.2 and 56 months for SUVmax < 4.2. None of these differences were significant. **Conclusion:** The uptake of LCNEC and SCLC was found to be higher than that of carcinoid tumors. ^{18}F-FDG PET/CT could be a predictor of OS and PFS in PNET, although larger sample is needed to reach statistically significant differences. **References:** None

EPS-186

Dynamic whole-body ^{18}F-FDG PET/CT in patients with unclear lung tumors - evaluation of multiparametric dynamic imaging in a clinical setting

M. Weissinger[1], M. Atmanspacher[2], H. Dittmann[2], S. Gatidis[1], L. Zender[3], C. la Fougère[2];
[1]Department of Radiology, University Hospital Tuebingen, Tuebingen, GERMANY, [2]Department of Nuclear Medicine and Clinical Molecular Imaging, University Hospital Tuebingen, Tuebingen, GERMANY, [3]Internal Medicine VIII, University Hospital Tuebingen, Tuebingen, GERMANY.

Aim/Introduction: ^{18}F-FDG-PET/CT is the method of choice for staging of non-small-cell lung cancer. However, unclear FDG-positive lesions should be evaluated histopathologically due to the limited specificity of ^{18}F-FDG. The aim of this study was therefore to evaluate additional whole-body dynamic PET parameters to improve diagnostic accuracy. **Materials and Methods:** In this ongoing prospective study, 24 patients with unclear pulmonary lesions underwent dynamic PET acquisition 0-60min after injection of 300 MBq ^{18}F-FDG using a multi-bed-multi-timepoint technique. The acquisition of a standard of care static PET/CT was performed immediately afterwards as a reference. Static PET/CT scans were evaluated prospectively by an expert consensus. Performance of multiparametric PET data (SUV, Patlak slope, Patlak intercept) were evaluated based on retrospectively optimized cut-off values. Results: So far, pulmonary lesions of 22 patients have been validated (14 histologically, 7 follow-up). One patient received radiation therapy immediately after PET/CT. 13 pulmonary lesions were classified as malign, 9 as (post) inflammatory. Expert consensus identified malign lesions with a sensitivity of 100% (13/13), specificity of 45% (4/9), and accuracy of 77% (17/22). For static PET/CT parameters, a retrospectively defined optimal cut off value (SUVpeak 2.6) slightly improved the accuracy to 82% with a higher specificity (78%) but lower sensitivity (85%) than expert consensus. FDG-influx calculated by Patlak slope performed with a comparably good discriminatory power (AUC: 0.81) and very strong correlation with SUVpeak (r=0.98). Patlak intercept barely failed to differentiate malignant from benign with significant power (p=0.057, AUC: 0.74). However, Patlak intercept presented with a more heterogeneous distribution pattern and correlates only moderate with SUVpeak (r=0.73). The combination of dynamic and static PET parameters did not improve the accuracy significantly. **Conclusion:** Patlak slope can identify malign lung tumors with comparable precision as visual evaluation of experts or a SUVpeak based cut-off and has a strong correlation with static 60min p.i. SUV values. Patlak intercept might be a useful additional parameter, as the uptake pattern differs considerably from the SUV und Patlak slope. However, an additional value could not be confirmed in the interim analysis and needs to be investigated in a larger patient cohort. **References:** none

EPS-187

Incidental Renal Mass on PET/CT in Lung Cancer Patients, Evaluation With Histopathological Radiological And Clinical Findings: Pearls, Pittfals and False Positivities

B. Özdemir[1], S. Soyluoglu[1], U. Korkmaz[1], B. Gunay[2], B. Uslu[2], G. Durmus-Altun[1];
[1]Trakya University Department of Nuclear Medicine, Edirne, TURKEY, [2]Trakya University Department of Radiology, Edirne, TURKEY.

Aim/Introduction: The detection rates of incidental renal masses have increased in recent years due to the increased use of imaging modalities such as CT, MRI, and PET/CT. These incidental masses must be evaluated in a consistent manner.Because of its unique structure, F-18 FDG is mainly excreted via the kidneys, and unlike glucose, it is not fully reabsorbed. Physiological excretion of F-18 FDG in kidneys may complicated the evaluation of malignant lesions. The aim of this study was to assess the characteristics of F-18 FDG patterns of incidental renal masses and to establish the clinical utility of F-18 FDG PET/CT in clinical practice. **Materials and Methods:** From 2010 to 2020, patients who underwent PET/CT for the assessment of solitary pulmoner nodules, staging and evaluation of response to the treatment for lung cancer and also at the same time who had incidental FDG avid renal masses on PET/CT were included in this study. Patients' clinical-radiological data and histopathological results were correlated with PET/CT findings. Results: In 52 patient, that FDG uptake was related with malignancy (45 metastasis and 7 renal cell carcinoma). There was false positivity due to infectious process in 3 patients, polycystic disease in 11 patients and renal calculi in 3 patients. The size and number of lesions provided no useful information in distinguishing between malignant and benign disease. SUVmax ≥ 9.9 cut-off value was found to distinguish malignant-benign lesions with 72% sensitivity, 71% specificity, 72% diagnostic accuracy, 63% positive predictive value and 65% negative predictive value. **Conclusion:** Contrary to popular opinion, PET/CT make a significant contribution in the detection of incidental kidney lesions. All the lesions that SUVmax 9.9 g/ml and above, must be carefully evaluated as a malignant lesions. **References:** 1) Herts BR, Silverman SG, Hindman NM, Uzzo RG, Hartman RP, Israel GM, Baumgarten DA, Berland LL, Pandharipande PV. Management of the Incidental Renal Mass on CT: A White Paper of the ACR Incidental Findings Committee. J Am Coll Radiol. 2018 Feb;15(2):264-273. doi: 10.1016/j.jacr.2017.04.028. Epub 2017 Jun 23. PMID: 28651987 2) Goldberg MA, Mayo-Smith WW, Papanicolaou N, Fischman AJ, Lee MJ. FDG PET characterization of renal masses: preliminary experience. Clin Radiol. 1997 Jul;52(7):510-5. doi: 10.1016/s0009-9260(97)80327-3. PMID: 9240703. 3) Kochhar R, Brown RK, Wong CO, Dunnick NR, Frey KA, Manoharan P. Role of FDG PET/CT in imaging of renal lesions. J Med Imaging Radiat Oncol. 2010 Aug;54(4):347-57. doi: 10.1111/j.1754-9485.2010.02181.x. PMID: 20718915.

EPS-188

Evaluation of Two Thoracic Dedicated Imaging Techniques for Lung CT Stabilisation Applied to PET/CT in Lung Nodule Assessment: High-Frequency Non-Invasive Ventilation (HF-NIV) and Breath-Hold (BH)

M. Jreige, E. Darçot, M. Pappon, M. Nicod-Lalonde, N. Schaefer, C. Beigelman-Aubry, J. O. Prior;
Lausanne University Hospital, Lausanne, SWITZERLAND.

Aim/Introduction: To evaluate the effect of lung stabilisation using High-Frequency Non-Invasive Ventilation (HF-NIV) and Breath-Hold (BH) techniques on lung nodule detection and morphologic characterisation in PET/CT compared to a free-breathing (FB), standard lung CT acquisition. **Materials and Methods:** Six patients aged of 65±7 years addressed for initial assessment of suspicious lung nodules with ^{18}F-FDG PET/CT underwent three consecutive lung PET/CT acquisitions in FB, HF-NIV and BH conditions. [1] Lung nodules were assessed on all three CT acquisitions and characterised for number, size, volume and texture. Results: BH detected a significantly higher number of nodules (n=422) compared to HF-NIV (n=368) and even much higher number compared with FB (n=191) ($p<0.001$). The mean nodule size (mm) was 2.4±2.1 in BH, 2.6±1.9 in HF-NIV and 3.2±2.4 in FB for long axis and 1.5±1.3 in BH, 1.6±1.2 in HF-NIV and 2.1±1.7 in FB for short axis. There was a statistically significant difference between FB and BH ($p<0.001$ and $p<0.001$) and between FB and HF-NIV ($p=0.008$ and $p<0.001$) for long and short axis diameters, but no significant difference between BH and HF-NIV. A trend for higher measured volume was shown in FB compared to BH ($p=0.055$) and HF-NIV ($p=0.068$) without significant difference between BH and HF-NIV. A significant difference in detectability of sub-solid nodules was observed between the three acquisitions with BH showing a higher number of sub-solid nodules (n=128) compared to HF-NIV (n=72) and FB (n=44) ($p=0.002$). **Conclusion:** The highest detection rate of pulmonary nodules on CT was found in BH PET/CT. BH and HF-NIV demonstrated comparable 2D and 3D assessment of pulmonary nodule and performed better than FB. BH showed a better performance for detecting sub-solid nodules compared to HF-NIV and BH. BH PET/CT improves the detection and characterisation of lung nodules, with no inferiority compared to HF-NIV PET/CT, and may contribute to optimize oncological lung disease assessment. **References:** [1] Péguret N , Ozsahin M , Zeverin M, et al.Apnea-like suppression of respiratory motion: First evaluation in radiotherapy. Radiother Oncol. 2016 Feb;118(2):220-6.

EPS-189

Predictive value of quantitative metabolic tumor volume and metabolic index analysis in lung cancer stereotactic radiotherapy with F-18 FDG PET / CT

F. Aras[1], *A. Olmezoglu*[2];
[1]*Celal Bayar University, School of Medicine, Department of Nuclear Medicine, Manisa, TURKEY,* [2]*Celal Bayar University, School of Medicine, Radiation oncology, Manisa, TURKEY.*

Aim/Introduction: The objective of this study was to investigate . **Materials and Methods:** Overall, 94 early stage nonsmall cell lung cancer (NSCLC) patients who were administered stereotactic radiotherapy were included in the study. Results: Most of the study patients were male (91.5%). Mean age of the patients was 68.5 ± 9.0 years. The primary lung tumor was located centraly and peripherally in 25 (26.6%) and 69 (73.4%) of the patients, respectively. The median gross tumor volume (GTV) was 16.2 cc (interquartile range (IQR): 7.1- 32.9). Whereas all patients who had peripheral tumurs survived, 17 patients with central tumors (70.8%) died during the study period (p=0.001). Biologically effective dose (BED_{10}) values were significantly higher in patients who had peripheral tumors compared with patients with central tumors (p=0.001). Significantly more patients died in patients who had BED values below 100 Gy compared to patients who had BED values over 100 Gy (p=0.001). The survival distributions for the two groups were significantly different (p <0.001). Only GTV and Pretreatment SUVmean appeared as significant predictors of mortality. BED_{10} values showed a significant and strong positive correlation with total radiation dose, whereas it showed a significant strong negative correlation with number of fractions. **Conclusion:** Because of the limitations of sectional radiological diagnostic methods during therapy response assessment after chemotherapy or radiotherapy, the use of PET/CT for this indication has increased in the last years. The high uptake of F-18 FDG in most lung cancers and the demonstration that successful treatment reduces uptake have led to increasing enthusiasm for the use of PET/CT to assess the therapeutic response. **References:** None.

EPS-190

Renal metastasis of primary lung carcinoma is associated with death and progression predicted by F-18 FDG PET/CT

Z. Koc, *P. P. Özcan, V. Erçolak, Y. Karabulut;*
Mersin University, Mersin, TURKEY.

Aim/Introduction: Renal metastasis of a primary malignancy is not rare in autopsy series (1). Unfortunately, the F-18 FDG PET/CT imaging of kidneys is hampered because of urinary excretion of the radiopharmaceutical. Aim of this study was to analyze the outcome of the patients with the renal metastasis of lung cancer determined by F-18 FDG PET/CT. **Materials and Methods:** The F-18 FDG PET/CT images of seventeen patients (1 F, 16 M; mean: 61,6±9,3 years old) with renal metastasis of the primary lung carcinoma were evaluated retrospectively. The initial and follow up F-18 FDG PET/CT images of the patients as well as outcome results were analyzed retrospectively. Results: The patient and lesion characteristics as well as additional metastatic sites are summarized in Table 1. BT and/or Ultrasound examination was performed to the patients after the suggestion in the PET/CT report. Biopsy confirmation was required in five cases with oligo-metastatic involvement and one patient underwent nephrectomy operation. The pathology revealed severe involvement of the kidney. The follow up PET/CT examination of the patients have shown progressive disease despite proper treatment. **Conclusion:** The FDG accumulation associated with renal metastasis of lung carcinoma has been previously reported in case basis (3). However, the imaging features of the renal metastatic lesions might be similar with primary tumors (4). Previous studies have demonstrated sensitivity of as high as 100% in renal metastasis in series including also renal cell carcinoma and lymphoma (5). The results of this study indicated the worse prognostic features of the patients with renal metastasis of lung carcinoma indicated with FDG PET/CT. The worse prognosis of the patients with this finding might need more aggressive treatment regimens and follow up by means of metabolic imaging. **References:** 1. Kochhar R[1], Brown RK, Wong CO, Dunnick NR, Frey KA, Manoharan P.Role of FDG PET/CT in imaging of renal lesions. J Med Imaging Radiat Oncol. 2010 Aug;54(4):347-57. 2. Takahashi M, Kume H, Koyama K, Nakagawa T, Fujimura T, Morikawa T, Fukayama M, Homma Y, Ohtomo K, Momose T. Preoperative evaluation of renal cell carcinoma by using 18F-FDG PET/CT. Clin Nucl Med. 2015 Dec;40(12):936-40. 3. Nakhoda Z[1], Torigian DA, Saboury B, Hofheinz F, Alavi A. Assessment of the diagnostic performance of (18)F-FDG-PET/CT for detection and characterization of solid renal malignancies. Hell J Nucl Med. 2013 Jan-Apr;16(1):19-24.

1712

Wednesday, October 20 - Saturday, October 23, 2021

on-demand pool, release on Wednesday, October 20 at 09:00

e-Poster Presentation Session 13: Image Acquisition / Reconstruction / Processing 1

EPS-191

Determination of Partial-Volume Effect in Patient-Individual Kidney Phantoms for Tc-99m SPECT/CT

A. Grings, *T. Kuwert, P. Ritt;*
Clinic of Nuclear Medicine, Erlangen, GERMANY.

Aim/Introduction: Due to the limited spatial resolution of SPECT, activity concentration (AC) at a certain location of the resulting image could be over- or under-estimated, relative to true AC. This commonly is referred to as partial volume effect (PVE). It is recommended that PVE needs to be controlled for and corrected, especially for small structures and for applications relying on quantitative accuracy such as, e.g., dosimetry. One such correction method involves deriving PVE factors from phantom measurements. However, most studies using this approach so far have applied simplified geometries. In our study, we aim to determine kidneys' PVE for patient-individual geometries. **Materials and Methods:** Based on CT data, kidneys of 11 patients were segmented semi-automatically and post-processed in computer-aided-design (CAD) software. Fillable phantoms were generated using a commercially available 3-D-printer. By this, nine cortex-only phantoms (six patients) and ten whole-parenchyma phantoms (five patients) were obtained. For comparison, one phantom with ellipsoidal shape was generated. For measuring PVE, phantoms were fixed in a torso phantom. Kidneys were filled with an AC of 102 kBq/mL of Tc-99m, the background compartment was filled with inactive water. The recovery coefficient (RC) for all phantoms was determined from fully quantitative SPECT/CT acquisitions (Siemens Symbia Intevo Bold, low-energy high-resolution collimation, 3° angular sampling, 10 s per view) and subsequent standard SPECT reconstructions (ordered-subset conjugate-gradient algorithm, 1 subset, 72 iterations, no post-reconstruction smoothing, CT-based attenuation correction, dual energy window scatter correction). The RC was measured for volumes-of-interest based on segmentations of the CT image. Results: Our workflow resulted in fillable and watertight kidney phantoms for all patients. Average RC was 77.1 ± 1.4 % (range 74.5 - 78.9 %) and 49.8 ± 7.9 % (range 38.0 - 60.6 %) for whole-parenchyma and cortex-only phantoms, respectively. RC for the ellipsoidal phantom was 85.4%. The RC for whole-parenchyma phantoms was significantly higher than for cortex-only ($p<0.01$). Furthermore, variance of RC was significantly higher for cortex-only phantoms ($p<0.01$). **Conclusion:** Patient-individual extent of kidneys' PVE was successfully determined by measurements on 3-D printed phantoms. Generally, this extent varies considerably for different intra-renal uptake patterns. For geometries that are complex (renal cortex), inter-patient variability of PVE is significantly higher. This most likely complicates PVE correction based on measurements with simple geometries, as previously proposed in literature [1]. **References:** [1] Tran-Gia J, Lassmann M. Optimizing Image Quantification for ^{177}Lu SPECT/CT Based on a 3D Printed 2-Compartment Kidney Phantom. Journal of Nuclear Medicine. 2018;59(4):616-24.

EPS-192

Patient-Specific Phantoms for Tc-99m Brain Perfusion Imaging with SPECT/CT

A. Grings[1], M. Reymann[2], A. H. Vija[3], T. Kuwert[1], P. Ritt[1]; [1]Clinic of Nuclear Medicine, University Hospital, Erlangen, GERMANY, [2]Siemens Healthineers GmbH, Forchheim, GERMANY, [3]Siemens Medical Solutions USA, Inc., Molecular Imaging, Hoffman Estates, IL, UNITED STATES OF AMERICA.

Aim/Introduction: Interpreting brain perfusion SPECT scans is a difficult diagnostic task. It is encumbered by significant partial volume effect (PVE) due to the resolution of clinical SPECT, potentially obscuring the true activity uptake distribution. Recent technical advances aim at improving SPECT's spatial resolution or at correcting for PVE during or post-reconstruction. For evaluation of such novel technology knowledge of ground truth is mandatory and 3D printing opens new possibilities [1]. Unlike [2][3] we aimed to develop a high resolution, patient specific, fillable 3D-printed phantom for brain perfusion imaging for technology evaluation. This approach is extensible to other organs. **Materials and Methods:** We developed methods to create 3D-printed structures by using high resolution MRI patient data. For this test, we used data from a patient who underwent brain perfusion imaging with Tc-99m-HMPAO SPECT/CT and MRI due to suspected neurodegeneration. The MRI image of the patient's brain was segmented into two compartments (grey and white matter). A 3D printed fillable phantom was generated using an Ultimaker 3 with custom settings defined in a research project. For determining the phantom's imaging properties, SPECT/CT data were acquired on a Siemens Symbia T2 after filling the phantom with an Tc-99m activity concentration of 110.8 and 53.9 kBq/mL for grey and white matter, respectively. A fully quantitative SPECT reconstruction was performed using xSPECT Quant with standard parameters[4]. Images were visually evaluated by an experienced reader for plausibility, occurrence of artefacts and similarity to actual patient images. Additionally, SPECT recovery coefficient in each compartment was measured. Results: Visual analysis found a plausible uptake pattern as compared to the actual patient images. Measured quantitative uptake is reasonable, with 94.5 and 46.4 kBq/ml in grey and white matter using sampling VOIs, presumably showing expected PVE. **Conclusion:** Realistic and patient-specific brain phantoms can be manufactured based on 3D printing. Our results show the phantoms' potential for evaluating technology, aiming at improving image quality in SPECT/CT brain perfusion imaging. **References:** [1] Filippou V et al., Recent advances on the development of phantoms using 3D printing for imaging with CT, MRI, PET, SPECT, and ultrasound. Med. Phys.; 2018 [2] Läppchen T et al., 3D printing of radioactive phantoms for nuclear medicine imaging. EJNMMI Phys, 2020 [3] Tran-Gia J et al., Optimizing

Image Quantification for 177Lu SPECT/CT Based on a 3D Printed 2-Compartment Kidney Phantom, JNM, 2018 [4] Vija A.H., Introduction to xSPECT technology. Siemens Medical Solutions USA, Inc.; 2013

EPS-193

The potential of 18F-FDG PET/CT for monitoring disease progression of malignant PEComa

A. Martini[1,2], *A. Coppola*[1], *A. Arena*[1], *M. Dona*[1], *G. Baldi*[3], *S. Sestini*[1]; *[1]Hospital Santo Stefano, Nuclear Medicine Unit, Prato, ITALY, [2]University of Florence, AUOC Careggi Nuclear Medicine Department, Florence, ITALY, [3]Hospital Santo Stefano, Oncology Unit, Prato, ITALY.*

Aim/Introduction: PEComa has been shown to be rare tumor, especially the malignant type originating from the lung. For this reason, diagnostic criteria and treatment strategies of such tumor have not been fully established. We describe the potential of bio-molecular imaging in a case of patient affected by a malignant pulmonary PEComa undergoing a fluorine-18-fluorodeoxyglucose positron emission tomography/computed tomography (^{18}F-FDG PET/CT) for post-therapy purposes. **Materials and Methods:** A woman (73 y old) was admitted at Nuovo Ospedale Santo Stefano of Prato Italy due to right subclavicular swelling incidentally detected. A subsequent CT scan showed large mass in right superior pulmonary lobe slightly attached to mediastinal pleura. Several nodules were also detected in the medium and lower right pulmonary lobes. A mild enlargement of mediastinal lymph nodes was an additional morphological finding. CT-guided biopsy of the lung mass showed features favored a diagnosis of PEComa of the lung. At beginning patient underwent at therapy with sirolimus (5 mg) but due to pulmonary toxicity after three months the therapy was modified with sirolimus therapy (4 mg) and exemestane.A further CT scan after treatment revealed lesion in right superior pulmonary lobe to present with significant increase of dimensions (49 mm vs 39 mm). Besides, number of secondary nodules in the medium and lower right pulmonary lobes was found to be significantly increased. Several lesions suggestive of metastasis were also found in mediastinal and latero-cervical lymph nodes, hepatic parenchyma and left adrenal glands. No lesions were detected in bones. Results: Along with CT scan, the patient underwent a ^{18}F-FDG PET scan showing solid mass on the right superior lung to present with a high radioligand concentration (SUV max 19.06). A significant hypermetabolism was observed on mediastinal and latero-cervical as well as on supraclavicular axillary, celiac, para aorto-caval and hepatic hilar lymph nodes. Increased concentration of radioligand was also present on six hepatic lesions (SUV max:15) and on left adrenal nodule. The PET scan also detected multiple hypermetabolic metastatic lesions in almost all bone segments (SUV max 14.87 vertebral bodies and SUV max 10.93 pelvis), with the only exclusion of the skull case. Importantly, none of the bones showing a pathological increase of glucose metabolism presented with morphological abnormalities on diagnostic CT scan. **Conclusion:** In this contest, results of this case and previous studies suggest that ^{18}F-FDG PET could have a key-role in the diagnostic and therapeutic management of patients affected by this mesenchymal neoplasm. **References:** none

EPS-194

Application of PET/CT Studies in Radiotherapy Using Deformation Algorithms

S. Pena Vaquero, *Á. del Castillo Belmonte, M. Martín Veganzones, C. Andrés Rodríguez, M. Agulla Otero, A. Hurtado Romero, N. Álvarez Mena, I. Conles Picos, D. Miguel Pérez, L. Gómez Heras, D. Alonso Hernández, J. de Frutos Baraja, R. Torres Cabrera; Hospital Clínico Universitario, Valladolid, SPAIN.*

Aim/Introduction: Medical imaging, especially metabolic studies, plays an essential role in radiation therapy, since the information provided by planning CT often needs to be supported by this type of complementary studies. It is common for these studies to come from other centers or to be part of the set of images of the patient's history, with no link to the radiotherapy process. It is in this context that image deformation tools acquire great importance. The aim of this work is to compare two Deformable Image Registration (DIR) algorithms using segmented structures by uptake threshold in lung PET/TC studies. **Materials and Methods:** Ten patients treated for non-small-cell lung carcinoma with a single lung lesion and diagnostic PET/TC are retrospectively selected. The software for deformable fusion are Eclipse v15.6 (accelerated Demons) and Velocity v4.1 (extended multipass B-Spline). Structures are automatically generated in the deformed PET for each algorithm using a common relative threshold of the maximum SUV. To compare them, the Sørensen-Dice coefficient (DSC) and the relative variation of the generated volumes of each with respect to the union of the two are used. Results: The average DSC is 0.8 ± 0.1 and average junction volume to total volume is 82.6% and 80% for Velocity (V) and Eclipse (E) respectively. **Conclusion:** The differences between the transformation matrices generated by Demons and B-Spline algorithms produce changes in positions and slight variations in the uptake values both in maxima and in thresholds defining the boundaries, causing misalignment between the segmented contours. The results of both DIR algorithms with respect to the applied method of relative SUV threshold segmentation, are compatible and no bias is observed between them. **References:** None

EPS-195

Dynamic PSMA PET/MRI imaging: initial results

M. Gammel, I. Rauscher, M. Eiber, W. A. Weber, S. G. Nekolla; TU München, München, GERMANY.

Aim/Introduction: PSMA ligands changed image based diagnosis of prostate carcinoma in the last decade. However, imaging and analysis employ static acquisitions and quantification used for conventional tracers. Thus, we evaluated a dynamic acquisition in patients undergoing F18-PSMA PET/MR for biopsy planning. **Materials and Methods:** In 19 patients undergoing F18-PSMA PET/MR for biopsy planning, tracer was injected in the scanner and data was acquired for 20 minutes in one bed positioned center over the prostate. Then the patient was allowed to rest for 40 minutes outside the scanner. Finally, the regular PET/MRI imaging protocol was executed. Activity curves in tumor, blood , and bladder were generated. Dynamic data analysis was performed using a Patlak model and influx constant (Ki) , volume of distribution and R2 of the linear fit as quality control was assessed. Matching regions were analyzed (SUVmean, SD, max) in the late dynamic data (15-20min) and in the 60 min scan. PSA and Gleason-Scores (GS) were obtained pre and after prostatectomy, respectively. Results: The cohort showed a marked inhomogeneity: GS score distribution was 7a (33%), 7b(25%), 8 (8%), and 9 (33%). The PSA was 19.2±9.3 ng/ml. The PET derived tumor volumes were 3.8ml±5.7 ml (Min: 0.3 ml ,max.:21 ml). Comparing the early and the late SUV values, a good correlation (R2: 0.76) and a modest increase (8.6±3.5 vs. 13±5.1, slope: 1.2) was observed. The average R2 of the Patlak regression was 0.99±0.01 indicating proper fits. The correlation between Ki and early SUV was moderate (R2:0.53) but only poor (R2:0.2) for late SUV, with SUVmax showing the same trend. In general, GS and PSA correlated only poorly with SUV and Patlak parameters . We noted a marked variability in the blood and the urine dynamics. For blood, we delineated variabilities of 86%±36% between injection and 120s which was reduced to 28%±2% in the later phase. The urine signal was more complex and showed three phases: 98% ±29% (0.. 120s), 48% ±12% (120..500s),and 54%±22% (500..1200s). Compared with the blood signal in the first 20min, the urine surpassed the latter in 75% of the patients (806±247s) while in 25% the urine signal was below the blood indicating a complex clearance pattern. **Conclusion:** The analysis of dynamic F-PSMA data in a selected cohort showed substantial individual variability in blood, tumor, and urine. This needs to be accounted for in kinetic models with the goal of improving their predictive capabilities. **References:** None

EPS-196

A novel approach using 3D-registered datasets reduces distortions and artifacts in diffusion weighted imaging for improved fusion and analysis of multiparametric data in PET/MR

J. Steinacker[1], N. Eberhardt[1], P. Korf[2], C. Lisson[3], R. Grimm[2], W. Thaiss[1], G. Lang[4], C. Kropf-Sanchen[5], B. Grüner[6], M. Beer[3], A. J. Beer[1]; [1]Department of Nuclear Medicine, Ulm, GERMANY, [2]Siemens Healthcare GmbH, Erlangen, GERMANY, [3]Department of Radiology, Ulm, GERMANY, [4]Department of Cardiothoracic surgery, Ulm, GERMANY, [5]Department of Pulmonology, Ulm, GERMANY, [6]Department of Infectiology, Ulm, GERMANY.

Aim/Introduction: Hybrid PET/MR opens new aspects in multimodal multiparametric (m^2p) image analysis. However even with both PET and MRI acquired (near) simultaneously, voxel-by-voxel coregistration of PET and MRI data might not be 100% precise, as e. g. organ movement and intrinsic distortions especially in diffusion-weighted MR (DWI) intrinsically limit the precision of coregistration. However, a precise coregistration is a prerequisite for meaningful voxel-by-voxel analysis of m^2p data. Thus, our aim was to reduce distortions in DWI by using a novel algorithm with elastic 3D registration for optimization of fusion of DWI and PET data. **Materials and Methods:** In 12 patients scanned on a 3T PET/MR (Siemens Biograph mMR) datasets from thorax and abdomen were analyzed. We used a combination of rigid and non-rigid 3D registration with a volume preserving constraint (Multiparametric Analysis prototype, Siemens Healthcare GmbH), referenced to the T1w DIXON sequence used for attenuation correction (AC) to reduce distortions in DWI. We compared the results of this novel approach with the original fused DWI and PET data produced by the scanner. The concordance of DWI with the data sets for attenuation correction as ground truth was visually assessed and rated on the basis of defined anatomical landmarks (8 for abdomen, 6 for thorax) by three blinded, experienced nuclear medicine specialists and radiologists using the Likert scale (0 to 5 points). Results: The impression of all (n = 12) thorax examinations showed significant improvement in the correspondence between DWI and morphological landmarks in 3D-registered data sets (original data set overall 4.3 / 5 points ± 0.2, 3D-registered data set overall 4.6 / 5 points ± 0.2, p = 0.009). The most pronounced differences were noted for the chest wall (p = 0.006), followed by the tumor (p = 0.007) and the skin contour (p = 0.014). For the abdomen, our data sets showed no significant difference between original data sets and 3D-registered data sets. **Conclusion:** Our novel approach with volume-preserving elastic 3D registration of DWI using the T1w DIXON AC data significantly reduced distortions in DWI data and improved the precision of fusion with anatomical sequences. Regions and lesions in the thorax profited most, as they are more affected by susceptibility artifacts and /or respiratory movement. Thus

our novel approach is promising for improving voxel-by-voxel correlations of quantitative m^2p DWI and PET data in regions prone to movement and distortion artefacts in DWI. **References:** None.

EPS-197

How refinements in the DROP-IN design improve surgical dexterity and surgical decision-making during radioguided surgery

S. Azargoshasb[1], S. van Alphen[2], L. J. Slof[2], G. Rosiello[3], S. Puliatti[4], S. I. van Leeuwen[2], K. M. Houwing[2], M. Boonekamp[5], J. Verhart[5], P. Dell'Oglio[6], J. van der Hage[7], M. N. van Oosterom[2], F. W.B. van Leeuwen[2];
[1]Leiden University Medical Center, Leiden, NETHERLANDS, [2]Interventional Molecular Imaging-Laboratory, Department of Radiology, Leiden University Medical Center, Leiden, NETHERLANDS, [3]Department of Urology and Division of Experimental Oncology, Urological Research Institute IRCCS San Raffaele Scientific Institute, Milan, ITALY, [4]Department of Urology, University of Modena and Reggio Emilia, Via del Pozzo, Modena, ITALY, [5]Instrumentele zaken ontwikkeling, facilitair bedrijf, Leiden University Medical Center, Leiden, NETHERLANDS, [6]Department of Urology, ASST Grande Ospedale Metropolitano Niguarda, Milan, ITALY, [7]Department of Surgery, Leiden University Medical Center, Leiden, NETHERLANDS.

Aim/Introduction: Decision-making and dexterity, features that become increasingly relevant in (robot-assisted) minimally-invasive surgery, are considered the hallmarks for improving the surgical performance. Recently, DROP-IN gamma probes were introduced to facilitate radioguidance in robotic surgery. We now studied if robotic DROP-IN radioguidance can be further improved using tethered Click-On designs, which further integrate the detection modality with the robotic instruments themselves. **Materials and Methods:** Using computer-assisted drawing software, 3D printing and precision machining, we created a miniaturized gamma probe that can be "clicked" onto a robotic instrument. Using fiducials that could be tracked via the robotic Firefly laparoscope and a custom computer-vision algorithm we were then able to register the trajectory of movement. Using a dexterity phantom, the duration of the specific-tasks and the irregularities in movement could be quantified and used to compare tasks performed with the Click-On to those performed using the parental DROP-IN probe. To study the impact of radioguidance on surgical decision-making, we also performed a blinded study during porcine surgery, wherein surgeons had to identify a hidden ^{57}Co-source using either palpation or Click-On radioguidance. Results: When assembled onto a robotic instrument, the grasping function and rotational freedom of the instrument could be maintained, while preserving a diameter < 12mm. With both the Click-On and DROP-IN probes, the surgeons had full control of probe placement while optimally exploiting the maneuverability of the wristed robotic instruments. In dexterity-assessments the Click-On required 40% less movements to perform the task when compared to the DROP-IN. This converted into a reduction in time, path length, and increase in straightness index. During porcine surgery, radioguidance also improved decision-making: task-completion rate increased by 60%, procedural time reduced, and movements became more focused. **Conclusion:** The integration of gamma probes with surgical instruments provides a next step forwards in optimizing minimal-invasive surgery using radioguidance. The value of this concept was underlined by the impacts observed on surgical dexterity and decision-making. **References:** None

EPS-198

Dexterity and performance analysis in PET-navigated biopsies

I. Boekestijn, S. Azargoshasb, L. Pronk, A. R. van Erkel, M. N. van Oosterom, F. W. van Leeuwen, D. D. Rietbergen;
Leiden University Medical Center, Leiden, NETHERLANDS.

Aim/Introduction: In daily practice, at interventional radiology (IR), needle-based interventions (e.g. biopsy and ablation) for soft-tissue organs are commonly performed under guidance of morphological imaging (US, CT, MRI). Unfortunately, these imaging modalities are only able to identify disease at an advanced stage and provide limited information on a molecular level. Here nuclear medicine, and in particular PET imaging, can create benefit; targeting needles to the most metabolic-active sections of a lesion could improve accuracy. We studied in a phantom set-up if, computer-assisted navigation strategies help guide percutaneous needle placement by both experts and novices. **Materials and Methods:** Using a custom abdominal biopsy phantom we performed PET/CT guided needle placements under US guidance. Needle placements were monitored using a fiducial-based optical tracking system. To see how computer-assisted navigation impacts different users groups we studied the dexterity of experts (e.g. interventional radiologists) vs. novices. Needle trajectories were quantified for total pathlength, speed, acceleration, smoothness, angular dispersion and straightness index. Results: In all cases it was possible to record the traveled paths of both the ultrasound probe and the biopsy needle. The paths travelled, either with or without navigation could be visualized in 4D (i.e., x, y, and z over time) and with a time resolution of 20 Hz. Computer-assisted quantification of movement features indicated that the features, total pathlength, speed and straightness index had most impact. Comparing the groups indicated that computer-assisted navigation was most beneficial for novices. **Conclusion:** Using dedicate movement analysis we were able to quantify value of PET-navigated biopsies over using ultrasound only. These preclinical findings underline the potential that PET/CT guided biopsies could provide. Something that needs to be further validated in clinical follow-up studies. **References:** None

EPS-199

Selective sentinel lymph node biopsy (SLNB) in infiltrating breast cancer and neoadjuvant therapy

S. Perez Quiros, L. Fuentes Moreno, A. Prieto Soriano, M. Ramírez Medina, G. Silvestre Egea, J. Cardona Arboniés, S. Guzmán Ortíz, V. Spinelli René, M. Mitjavila Casanovas;
Hospital Universitario Puerta de Hierro, Majadahonda, SPAIN.

Aim/Introduction: To review the results in the implementation of selective sentinel lymph node biopsy in patients with infiltrating breast carcinoma who have an indication for neoadjuvant treatment **Materials and Methods:** Retrospective descriptive study from January-2016 to November-2020. We studied 29 patients with a diagnosis of infiltrating breast carcinoma and indication for neoadjuvant therapy. Selective sentinel lymph node biopsy was performed post-neoadjuvant in all patients with clinically positive axilla (cN1), and in patients with clinically negative axilla at diagnosis (cN0), it was performed pre- or post-neoadjuvant, according to the decision of the multidisciplinary committee Results: The mean age was 52.3 years. The most common immunohistochemical profile was triple negative (45%) and the neoadjuvant treatment received was chemotherapy, hormone therapy or immunological therapy, according to oncological criteria. At diagnosis, 27/29 patients were cN0, with selective sentinel lymph node biopsy performed pre-neoadjuvant in 40.7% and post-neoadjuvant in 59.3%. In the 2 patients categorised as cN1 at diagnosis, SLNB was performed post-neoadjuvant. We analysed the results according to whether the technique was performed pre (11/29) or postneoadjuvant (18/29). Of the SLNB performed pre-neoadjuvant in patients with cN0 axilla (11/27), macrometastatic lymph node involvement (pN1) was detected in four of them and they were treated with axillary lymphadenectomy post-neoadjuvant. A complete axillary pathological response was observed in two of these patients and no axillary lymph node involvement in two others. Of the 18 patients with SLNB post-neoadjuvant, 16 were cN0, with nodal involvement detected in 3; the 2 patients with axillary cN1 at diagnosis had negative biopsy (0/5 and 0/3). Of the 3 patients with positive SLNB, one was treated with lymphadenectomy after neoadjuvant treatment and the other two with adjuvant radiotherapy. **Conclusion:** Failure to perform selective sentinel node biopsy pre-neoadjuvant in patients with clinically negative axillae at diagnosis (cN0) may underdiagnose axillary involvement. Selective sentinel node biopsy post-neoadjuvant is necessary as it provides information on axillary lymph node staging and response to the treatment. Studies with a larger number of patients and follow-up are needed for the definitive implementation of this technique in clinical practice. **References:** none

EPS-200

3D digital reconstruction of anatomical models integrating PET/CT data for pre-operative planning in gynecologic oncology surgery: a preliminary study

L. Muraglia[1,2], P. Castellucci[2,1], B. Bortolani[3], S. Lodi[3], P. De Iaco[4,1], M. Perrone[4,1], L. Cercenelli[3], E. Marcelli[3], S. Fanti[2,1];
[1]Università di Bologna, Bologna, ITALY, [2]Metropolitan Nuclear Medicine, IRCCS Policlinico Sant'Orsola-Malpighi, Bologna, ITALY, [3]eDIMES Lab - Laboratory of Bioengineering, Department of experimental, diagnostic and specialty medicine (DIMES), Università di Bologna, Bologna, ITALY, [4]Department of Obstetrics and Gynecology, Unit of Oncologic Gynecology, IRCCS Policlinico Sant'Orsola-Malpighi, Bologna, ITALY.

Aim/Introduction: The aim of our study is to assess the feasibility and the usefulness of integrating PET-CT images to reconstruct 3D anatomical models for preoperative planning in gynecologic oncology surgery complex cases. **Materials and Methods:** Image segmentation was made with a dedicated software (Mimics Medical, Materialise, Leuven, Belgium) and it was fused with other anatomic structures adjacent to the lesion, that were segmented from previously acquired contrast enhanced-CT (ce-CT) scan.Finally, we reviewed the reconstructed 3D anatomical model with the surgeons before and after the surgery discussing the results. Results: The integration of PET images with ce-CT data for 3D anatomical model reconstruction provided detailed 3D images useful for tumor localization. Up to now, we segmented a metabolically active lesion from a 18F-FDG PET/CT scan of a patient referred to our Center with the diagnosis of uterine sarcoma relapsed after the primary treatment and elected for secondary surgery. This allowed the surgeons to predict some procedural issues during the pre-operative analysis of the images and to carefully plan complex surgical maneuvers. The reconstructed 3D digital models proved to be beneficial also during surgery. The usefulness of digital 3D models was then confirmed in a post-surgery meeting when we compared video fragments of the operation with the 3D rendered images. **Conclusion:** Integration of PET images in a 3D digital model was feasible. By our experience, surgeons obtained valuable information from our images in terms of surgery planning and reported a good correspondence between the reconstructed 3D digital model and the intraoperative anatomy. Therefore, we promote this technique for future development and routine use in selected cases. **References:** none

EPS-201

Semi-Automated Analysis Of Amyloid-PET Images Allows To Shorten Acquisition Time With Accuracy ComparableTo Standard Time

P. Guglielmo, M. Scarlattei, G. Baldari, G. Serreli, S. Migliari, A. Sammartano, A. Pennacchio, L. Ruffini;
University Hospital of Parma, Parma, ITALY.

Aim/Introduction: Clinical use of amyloid PET relies on visual interpretation of scans, which consists of comparing the signal intensity of "target-rich" brain regions to that of "target-poor" regions, e.g. subcortical white matter. In recent years, there have been increasing interest in coupling the traditional visual reading with (semi)automatic semi-quantification methods. The added value of these tools is increasing confidence in diagnostic conclusions, even though the resulting statistical maps still need to be interpreted by the reader. Amyloid-PET data are typically collected over 5 minutes periods for up to 10 or 20 minutes to record enough counts resulting in two to four frames of PET data (static scans); these frames can be inspected separately for evidence of movement during the scan, and acceptable frames are then combined to form the complete emission data file. Aim of our study is to evaluate whether the results of semi-quantitative analysis of PET data acquired for 10 minutes are similar to those of a 20 minutes acquisition. **Materials and Methods:** We performed [^{18}F]Flutemetamol PET/CT scans in 84 patients (37 F: 47 M), mean age 71 years, with a suspect of amyloid-related dementia. The 3-dimensional iterative reconstruction "Vuepoint" images acquired for both 10 (VP10) and 20 (VP20) minutes were analysed with the software Cortex-ID Suite® in comparison to age-matched healthy subjects, obtaining quantitative maps for each of the 19 anatomical brain regions defined by the software. The results of the two series were then correlated using the Student's t-test (p-values) and the Pearson correlation coefficient (Pcc). Results: The values obtained from the analysis with the software Cortex-ID Suite® showed a mean p-value of 0,75 (range 0,55-0,94) and a mean Pcc of 0,87 (range 0.81-1), demonstrating a good correlation between VP10 and VP20 values. The best correlations were found in the prefrontal regions (for both, p-value 0.92 and Pcc 0.99), in the right temporal lateral region (p-value 0.94; Pcc 0.99) and in the left precuneus (p-value 0.89; Pcc 0.98). The lowest values were observed, instead, in the right temporal mesial region (p-value 0.55; Pcc 0.81). **Conclusion:** Our data show that semi-automated analysis using only the first 10 minutes of acquisition provides results comparable to those obtained from a standard 20'-acquisition; this could lead to a shorter examination time, improving patient's comfort and avoiding motion artifacts. Nevertheless, larger studies with a wider patients population are encouraged to confirm these first data. **References:** None

EPS-202

Optimization of cardiac atrial metabolism quantitative analysis with digital TOF-PET/CT

M. Hesse, S. Marchandise, B. Gerber, R. Lhommel, V. Roelants;
Cliniques Universitaires Saint-Luc, Brussels, BELGIUM.

Aim/Introduction: Evaluation of left atrial (LA) remodeling, characterized partly by metabolic changes, is becoming increasingly relevant in understanding several pathological cardiac conditions. PET/CT with 18F-FDG is currently the gold standard for metabolic evaluation of the left ventricle. Recently, it has been suggested that, despite the thinness of the LA wall, LA metabolism evaluation is also feasible using the latest PET camera technologies. Therefore, we sought to perform a cardiac phantom study in order to determine which images advanced reconstruction algorithm is the most appropriate to use in this context. **Materials and Methods:** An anthropomorphic Heart/Thorax phantom was used, whose liver, heart cavity and walls were filled with typical patient 18F-FDG activity concentrations of about 5, 3.8 and 15 kBq/ml respectively. One bed position acquisitions of 10 minutes were performed, first using an analog TOF-PET/CT and then, immediately after, using a digital TOF-PET/CT. Raw data were reconstructed with a 2mm voxel size using standard manufacturer OSEM algorithms with different numbers of iterations and subsets, without resolution recovery (RR), with a third-party post-reconstruction PSF RR, and with the manufacturer PSF RR correction for the digital PET acquisition. Volumes of interest were manually drawn around the right and left atria and ventricles on the CT image from the PET/CT acquisition, then transferred to the PET image, from which 18F-FDG concentrations were extracted and compared to exact values. Results: When reconstructing with 4 iterations and 15 subsets without RR, the 18F-FDG concentration recoveries in the left atrium and the ventricles wall were 58% and 74% for the analog PET/CT, and 56% and 72% for the digital one, respectively. Third-party post-reconstruction RR was unable to improve the concentration recovery without markedly increasing the noise level, resulting in images with no medical value, especially in the case of the analog PET/CT. For the digital PET/CT, the manufacturer PSF RR using 5 iterations and a level 6 regularization provided an improved recovery of about 68% in the atria while preserving an acceptable noise level and images of diagnostic quality. **Conclusion:** The digital TOF-PET/CT combined with the manufacturer 4 iterations/15 subsets OSEM reconstruction and PSF RR with 5 iterations/6 regularization can be used to quantitatively analyze the left atrium uptake in patient 18F-FDG heart studies while still preserving image reading quality. This may lead to more precise analyses and identifications of patient cardiac diseases. **References:** none

EPS-203

Motion Correction in 15O-water Cardiac PET

N. Christensen[1], J. Nordström[2], M. Lubberink[3], L. Poulsen Tolbod[1];
[1]Department of Nuclear Medicine & PET, Aarhus University Hospital, Aarhus N, DENMARK, [2]Centre for Research & Development , Gävleborg, Gävle, SWEDEN, [3]Department of Surgical Sciences/ Nuclear Medicine & PET, Uppsala University, Uppsala, SWEDEN.

Aim/Introduction: Patient motion constitutes a limitation to cardiac PET imaging. In clinical practice, it is estimated that approximately 3% of ^{15}O-water cardiac PET exams are repeated due to severe motion artefacts (based on 500 exams at Aarhus University Hospital). Since ^{15}O-water is not retained in the myocardium, motion correction techniques established for ^{82}Rb cannot be readily applied. In this study, we examined the ability of image readers to visually detect and correct patient motion using data with simulated motion. **Materials and Methods:** A subset of simulated motion data from Nordström et al[1] was motion-corrected by two independent observers in a blinded fashion (Obs1 and Obs2). The data set consisted of 16 motions with an amplitude of 5-20 mm applied to data from 10 motion-free scans yielding 170 scans. Obs1 assessed motion by reviewing the dynamic PET images, whereas Obs2 reviewed the pre-motion-correction parametric images and polar maps as part of the assessment process. Motion correction was performed by manually shifting image volumes frame-by-frame with an overlay of the pre-motion-correction segmentation of the myocardial wall. Data were analyzed pre and post motion correction and MBF for each coronary territory was reported. Scans with large motion artefacts were defined as having > 20% deviation in MBF in one or more coronary territories compared to the original motion-free scan. Results: Obs1 and Obs2 motion-corrected 94% and 64% of the scans, respectively. Obs1 corrected 91% of the scans with large motion artefacts, whereas Obs2 only corrected 74%. The maximum motion-corrected shift of any frame only exceeded 10 mm in approximately 20% of the cases. In scans without motion, Obs1 wrongly identified motion in 8/10 scans and Obs2 in one scan. The median deviation introduced by erroneous correction was -0.1% (max 14%). In all scans, motion correction reduced artefacts in MBF in 56% (Obs1) and 58% (Obs2) of the scans. In coronary territories with large motion artefacts, the deviation from the original motion-free scan was reduced in 84% (Obs1) and 87% (Obs2) of the territories (median relative reduction 46%, 95% inter-percentile range -16% to 96%). **Conclusion:** Frame-by-frame motion correction after visual inspection can be used to reduce motion artefacts in cardiac ^{15}O-water PET. Using pre-correction results to assess motion, did not help the reader identify large motion, but reduced corrections in motion-free scans. **References:** Nordstrom et al. Influence of patient motion on quantitative accuracy in cardiac (15)O-water positron emission tomography. J Nucl Cardiol. 2021.

EPS-204

Adaptive Regularized Reconstruction Enabling High Resolution Brain PET Images from Whole Body FOV PET/CT Imaging

Y. Hsieh[1], K. Binzel[1], C. L. Wright[1], B. Zhang[2], P. Maniawski[2], M. V. Knopp[1];
[1]The Ohio State University Wexner Medical Center, Columbus, OH, UNITED STATES OF AMERICA, [2]Philips Healthcare, Cleveland, OH, UNITED STATES OF AMERICA.

Aim/Introduction: The image quality of Brain PET imaging has been stagnant since the introduction of whole body PET/CT, as reconstruction parameters are optimized for whole body. With the introduction of regularized reconstruction, we focused on refining an adaptive regularized reconstruction (AR) algorithm using a trained neural network to adjust the parameters to control image noise and optimize convergence. This study evaluates the feasibility of this approach to obtain high resolution brain PET images from whole body datasets. **Materials and Methods:** Whole body FOV datasets were acquired (90s/bed) within clinical trials using the Philips Vereos digital PET system after injecting either Standard of Care dose (~480MBq) or Low Dose (~185MBq). LD images were simulated by 33s/bed reconstruction of the SOC dose datasets. Using the clinical acquisitions, Adaptive Reconstruction and AR_Brain images were generated by using the default AR protocol, and the AR algorithm with optimized penalty factor for the brain, respectively. The optimized AR_Br was trained to choose lower penalty factors in order to obtain higher resolution brain images. Results: For SOC dose imaging, both AR_90s and AR_33s images reconstructed by using the default AR reconstruction algorithm for 90s/bed and 33s/bed data had fully diagnostic, high image quality from the neck to knee with smooth liver texture. AR_90s images presented slightly sharper resolution, while AR_33s image were smoother with lower resolution in the brain. The penalty factor used in the brain for the AR_90s images was close to 1, while the penalty factor for the AR_33s images was around 1.8. Using adjusted penalty factors below 0.5 to reconstruct AR_90s_Br and AR_33s_Br images, both image sets had similar sharp resolution in the brain. For low dose data, the AR_90s image reconstructed by using the default AR reconstruction algorithm also had good image quality from neck to knee with a smoother liver, but lower resolution in the brain compared to the clinical images. Using the penalty factors of 0.7 to reconstruct AR_90s_Br image, the image quality improved and led to consistent high resolution brain images. The results demonstrate that the brain PET reconstruction requires optimization and lower penalty factors in order to obtain high resolution in the brain. **Conclusion:** High resolution brain imaging from whole body FOV acquisitions can be obtained, if a proper penalty factor is chosen trained. Fine tuning the whole body PET neural network of AR algorithm can further improve the whole body image, especially the brain. **References:** none

EPS-205

Using prone position to reduce motion induced artefacts during SPECT myocardial perfusion imaging

I. Polycarpou[1,2], G. Charitou[3], S. Panagi[3,4], D. Kaolis[5], I. G. Petrou[6], Y. Parpottas[3,4];

[1]European University Cyprus, Nicosia, CYPRUS, [2]E.U.C. Research Center, Nicosia, CYPRUS, [3]Frederick Research Center, Nicosia, CYPRUS, [4]Frederick University, Nicosia, CYPRUS, [5]Department of Medical Physics, State Health Services Organisation, Nicosia, CYPRUS, [6]Department of Nuclear Medicine, Nicosia General Hospital, State Health Services Organisation, Nicosia, CYPRUS.

Aim/Introduction: In SPECT myocardial perfusion imaging (MPI), diaphragmatic attenuation and patient motion is a common source of false positives. Few studies in clinical data have shown that prone imaging may reduce these effects and can achieve similar sensitivity but better specificity compared to supine imaging. This study used an anthropomorphic phantom that allows to simulate different patient characteristics in order to understand the influence of patient positioning on cardiac motion artefacts. **Materials and Methods:** An anthropomorphic phantom assembly which enclosed thoracic moving phantoms able to perform different dynamic respiratory phases was used. The thoracic phantoms are an ECG beating cardiac, inflatable lungs and a liver, that all can oscillate in the cranio-caudal direction for different respiratory amplitudes. Tc99m was injected within the liver and the myocardial wall cavity. SPECT/CT data have been acquired for different scenarios (i.e. without and with perfusion defects; without patient motion and with normal or extreme motion). Data have been reconstructed using the OSEM algorithm with and without attenuation correction. Results: In SPECT MPI cardiac motion due to respiration induces artefacts, mainly in the anterior and inferior walls and can be a source of false-positive findings or affect the ability to detect defects. Prone imaging reduces these artefacts and increases counts and defect detectability, especially in the inferior wall. Although respiratory gating reduces motion blurring, it does not fully recover the exact extent and contrast of the perfusion defects, as it reduces counts, thus indicating the importance of correcting the cardiac respiratory motion. **Conclusion:** This study provides supporting evidence that prone position has a potential to limit cardiac motion induced artefacts in SPECT MPI especially under extreme breathing conditions. This study was co-funded by the European Regional Development Fund and the Republic of Cyprus through the Research and Innovation Foundation (Project: EXCELLENCE/1216/ 0085). **References:** None

EPS-206

Development and Validation of a novel image software for automatic semiquantitative analysis Tc-99m Trodat-1 SPECT in patients with suspicious Parkinsion's Disease

C. Hung[1], P. Kao[2,3], J. Weng[3], K. Lin[4], R. Liu[5];

[1]Department of Occupational Therapy and Graduate Institute of Behavioral Sciences, College of Medicine, Chang Gung University, Taoyuan, TAIWAN, [2]School of Medicine, Chung Shan Medical University, Taichung, TAIWAN, [3]Department of Nuclear Medicine, Chung Shan Medical University Hospital, Taichung, TAIWAN, [4]Department of Electrical Engineering, Chung Yuan Christian University, Taoyuan, TAIWAN, [5]School of Medicine, Department of Biomedical Imaging and Radiological Sciences, National Yang Ming Chiao Tung University, Taipei, TAIWAN.

Aim/Introduction: Neuroscience scientists have demonstrated many evidence-based studies by functional brain neuroimaging in recent decades. Comparison with detection of clinical symptoms, it is easier to reflect the neuropathology early by using non-invasive nuclear medicine images to understand the related alterations of brain function. Thus, functional brain imaging plays an increasingly important role in clinical research and application. ^{99m}Tc-Trodat-1 single-photon emission computed tomography (SPECT) had been widely used in Asia to assist clinical diagnosis of Parkinson's Disease (PD) and evaluate the severity of parkinsonism. However, it is subjective and time-consuming to calculate specific uptake ratio (SUR) by manual fusion of magnetic resonance imaging (MRI)/SPECT images in clinical settings. QTRODAT is a software for semiquantitative analysis of ^{99m}Tc-Trodat-1 image. The purpose is to compare the difference of SURs of striatum and putamen to occipital background generated by traditional manual fusion of MRI/SPECT and QTRODAT respectively to validate whether QTRODAT a proper substitute for traditional manual fusion method. **Materials and Methods:** One hundred patients who had prior ^{99m}Tc-Trodat-1 SPECT studies were recruited in this study. Each case of ^{99m}Tc-Trodat-1 SPECT was analyzed by both manual fusion of MRI/SPECT and QTRODAT. Regions of interest (ROI) were placed in both (right and left) striatum, putamen, caudate, and the background of the occipital lobe. The SURs are the count ratios of respective ROI to background. Then, there were 6 SURs yielded from both methods. Pearson linear correlation (r) was used to evaluate correlations between each SUR of the two methods. Moreover, Paired-Sample T test was applied to compare the SUR of the two methods. Statistical significance was set at $p < 0.05$. Statistical analyses were performed by SPSS (version 26.0). Results: Medium correlations were found between QTRODAT and the 6 SURs of the method of manual analysis($r>0.548$), whereas the Paired-Sample T test showed significant differences in the results of 6 SURs ($p<0.05$). Moreover, 6 SURs reported by the software were higher than that by manual analysis.

Conclusion: QTRODAT in dealing with SUR is not significantly different than manual analysis. High correlation was found between QTRODAT and manual analysis. QTRODAT can be applied for improving the efficiency to evaluate the severity of PD and the possible response after treatment intervention by ^{99m}Tc-Trodat-1 SPECT. Therefore, it may assist nuclear medicine physician to improve the clinical efficiency with confidence. However, the diagnostic accuracy by means of SURs of ^{99m}Tc-Trodat-1 SPECT with parkinsonism may need further investigation. **References:** none

EPS-207

Putamen-to-caudate (P/C) ratio is a parameter not affected of different methods of Dopamine transporter (DAT) brain SPECT quantification

J. Koutsikos, S. Giourgouli, V. Pantzou, M. Stathopoulou, T. Petropoulos;
Nuclear Medicine Department, Henry Dunant Hospital Center, Athens, GREECE.

Aim/Introduction: Dopamine transporter (DaT) imaging is useful for the differential diagnosis of Parkinson's syndrome from essential tremor. Visual evaluation of DaTSCAN images represents the generally accepted diagnostic method, but semiquantification can assist visual reading, especially in doubtful or borderline cases. Our aim was to compare a widely distributed free tool (Standard Processing - SP) with a commercial software (provided by Siemens - CS). **Materials and Methods:** DaT imaging studies, were analyzed visually by two nuclear medicine consultants, blind to clinical information, who agreed to classify the negative scans. Images were then processed using the two different softwares. The SP performs a tomo backprojection reconstruction method using a butterworth 0.40 filter. After the completion of the reconstruction, the number of axial images that display a clear image, are selected. The images are then summed up and are ready for quantification. The quantification uses normal patient ROIS', imported in the protocol, to aid the correct basal ganglia segmentation and are adjusted for each examination. For the CS, the raw data from the tomography are reconstructed using the backprojection method with a Butterworth 0.50 filter. The reconstructed data are loaded to the segmentation program, which detects, depending on intensity, the best image for quantification. The software automatically idetifies the basal ganglia and applies the ROIs on axial and sagittal planes. For the finalization of the quantification, the ROIs are fine adjusted for each patient on both planes. A specific-to-non-displaceable binding ratio (SBR) by normalizing counts on an occipital ROI and the putamen-to-caudate (P/C) ratio were then calculated for these two softwares. Results: 24 males and 36 females were visually interpreted as normal (mean age 69.9+/-8.9 y.o.). All the SBRs' were highly correlated between the two softwares with Pearson's 'r' correlation coefficients ranging from 0.394 to 0.796 (P<0.001), even CS values were statistically higher compared to SP ones (P<0.005). P/C ratio was unaffected of the software with comparable values (1.004+/-0.081 and 0.926+/-0.066 for right and left basal ganglia for SP and 0.929+/-0.046 and 0.927+/-0.038 respectively for the CS, P=NS). **Conclusion:** Both softwares work well and similarly one another in semi-quantification of DaT SPECT. The higher values of CS should be taken into account, especially in borderline studies. The P/C ratio is an independent quantification parameter. **References:** Morbelli S, Arnaldi D, Cella E, et al. Striatal dopamine transporter SPECT quantification: head-to-head comparison between two three-dimensional automatic tools. EJNMMI Res. 2020 Nov 7;10(1):137.

1812

Wednesday, October 20 - Saturday, October 23, 2021

on-demand pool, release on Wednesday, October 20 at 09:00

e-Poster Presentation Session 14: Image Acquisition / Reconstruction / Processing 2

EPS-208

On the Combination of a Dedicated HF Readout Circuit and the TOFPET2 ASIC to Push the Timing Performance of PET Systems

V. Nadig[1], S. Gundacker[1], H. Radermacher[1], D. Schug[1,2], B. Weissler[1,2], V. Schulz[1,2,3];
[1]Department of Physics of Molecular Imaging Systems, Institute of Experimental Molecular Imaging, RWTH Aachen University, Aachen, GERMANY, [2]Hyperion Hybrid Imaging Systems GmbH, Aachen, GERMANY, [3]Fraunhofer Instiute for Digital Medicine MEVIS, Aachen, GERMANY.

Aim/Introduction: Exploring new methods to improve the coincidence time resolution (CTR) of positron emission tomography (PET) systems is essential to increase the signal-to-noise ratio of a PET image. Maintaining a constant image quality, exploiting this increase leads to reduced radiation exposure or a higher throughput at clinical sites. Benchtop setups employing high-frequency (HF) readout and signal filters between detector pixels and readout electronics have shown exceptionally low CTRs over the past years. This study aims to combine these dedicated setups with a commercially available application-specific integrated circuit (ASIC) treated as a promising candidate to digitize events in PET systems. **Materials and Methods:** A dedicated HF readout circuit [1] was adapted to be used in combination with the TOFPET2 ASIC (version 2c, PETsys Electronics S.A.). Two single pixels of Hamamatsu S14160-3050 photo-sensors with an active area of 3 mm x 3 mm and two LYSO:Ce crystals (3 mm x 3 mm x 20 mm) manufactured by EPIC were optically coupled using

Cargille Meltmount and set up for coincidence experiments. A Na-22 point source with an activity of 0.67 MBq was used. Data were acquired for 120 s at an overvoltage of 7.8 V, triggering on different thresholds. Energy and timing are digitized in separate ASIC channels. Dark count scans were performed to monitor the trigger level at various thresholds. Results: Using the PETsys TOFPET2 Evaluation Kit as a reference, the Hamamatsu sensors in combination with the LYSO:Ce needles achieved CTRs of 200 ps. The energy resolution was in the range of 12 %. Employing the dedicated HF circuit in combination with the TOFPET2 ASIC, the CTRs could be improved to 191 ps. The energy resolution was in the range of 15 % for LYSO:Ce. **Conclusion:** Front-end modifications, e.g., using the HF readout circuit in combination with the TOFPET2 ASIC, have shown to be an effective method to push the CTR for the applied LYSO:Ce detector pixels. These changes either can, and finally should, be implemented in the ASIC or can be realized with an amplification stage before the ASIC input, as it was done in this case. This could potentially re-inforce the usage of BGO, coming along with a higher detection efficiency and lower costs, in PET systems as well. **References:** [1] Stefan Gundacker et al 2019 Phys. Med. Biol. 64 055012

EPS-209

3D-printed Source Holder for Dose Calibrators Enables Quantification of the Geometrical Effect of Source Position in Activity Measurements

T. Miettinen[1], S. Pekkarinen[1], L. Koivula[1], V. Reijonen[1], E. Hippeläinen[2];
[1]Department of Oncology, University of Helsinki and Helsinki University Hospital, Helsinki, FINLAND, [2]Clinical Physiology and Nuclear Medicine, HUS Medical Imaging Center, University of Helsinki and Helsinki University Hospital, Helsinki, FINLAND.

Aim/Introduction: When measuring activity with a dose calibrator, manufacturer's source holder is designed to position the radiopharmaceutical vials and syringes at fixed position inside the ionization chamber. However, the position of the source may still have some inaccuracy. For measuring this positional dependence of activity reading in dose calibrators of different manufacturers, we introduce a 3D-printed source holder made of polylactic acid with manufacturer-specific sockets. It enables positioning the source in a 1.5 ml microcentrifuge tube at 1 cm intervals at the vertical axis of the ionizion chamber and 0.3-0.6 cm intervals at the radial axis with a possibility of rotation across the horizontal plane. The aim was to test the source holder with different dose calibrators and radionuclides. **Materials and Methods:** We measured activity response of dose calibrators in 2 cm intervals at the central axis between 5.5-25.5 cm from the opening of the chamber. Response on the horizontal plane was measured at the depth of observed maximum activity reading of each dose calibrator. We compared two chambers from Veenstra (VDC-505 and VDC-603), two from Biodex (both Atomlab 500), and one from Capintec (CRC-25R). Two radionuclides were measured: Lu-177 (6.8-8.4 MBq, 0.15-0.25 ml) and Tc-99m (7.1-23.2 MBq, 0.05 ml). Measured activities were decay corrected and normalized to the maximum activity reading at central axis of each dose calibrator for comparison of the results. Results: With all dose calibrators, the activity reading differed from the maximum reading less than 2% at depths 17.5-21.5 cm and less than 5% at depths 13.5-23.5 cm. We observed the largest relative differences in normalized activity reading at 5.5 cm depth: for Lu-177, Veenstra VDC-603 had 16.4% higher reading than Capintec chamber; and for Tc-99m, Veenstra VDC-603 had 6.3% higher reading than Biodex chamber. Activity response curves were nearly identical between the dose calibrators of the same manufacturer: all readings were within 2.2% for Lu-177 and within 0.7% for Tc-99m. At the measurement point closest to the chamber wall, median activity reading of all dose calibrators was 3.9% higher (range 2.9-7.3%) than the maximum reading at the central axis. When repeating the measurements, mean and maximum deviations between the readings were 0.4% and 1.4%, respectively. **Conclusion:** We studied the effect of positional dependence of activity reading in dose calibrators using in-house designed 3D-printed source holder and point sources. We observed slight differences between dose calibrators of different manufactures when using Lu-177 and Tc-99m. **References:** none

EPS-210

Australian preclinical PET QA audit: a pilot study

*A. Scott[1], **G. Cowin**[2], K. Mardon[2], T. Hung[3], W. Lakshantha[4], M. DeVeer[5], G. Angelis[6], H. Hamze[7], A. Narayaran[2], G. O'Keefe[1], C. Dixson[2], S. Meikle[6];*
[1]Austin Health, ONJCRI, La Trobe Uni and University of Melbourne, Melbourne, AUSTRALIA, [2]Queensland NIF node, University of Queensland, Brisbane, AUSTRALIA, [3]UNSW NIF node, University of New South Wales, Sydney, AUSTRALIA, [4]SAHMRI NIF node, South Australian health and medical research institute, Adelaide, AUSTRALIA, [5]Monash NIF node, Monash University, Melbourne, AUSTRALIA, [6]University of Sydney-ANSTO NIF node, University of Sydney, Sydney, AUSTRALIA, [7]University of Sydney-ANSTO NIF node, ANSTO, Sydney, AUSTRALIA.

Aim/Introduction: PET is intrinsically a quantitative imaging procedure. However, the accuracy and precision is critically dependent on regular calibration of the instrument and the dose calibrator. Results also depend on acquisition, reconstruction and analysis methods and human input. Therefore, variability across facilities may be affected. This project aims to establish a national quality assurance (QA) audit for preclinical PET systems in Australia, coordinated by the National Imaging Facility (NIF) Molecular Imaging theme. Conducting such an audit on a regular (e.g. annual) basis and

reporting its outcomes will ensure research conducted using NIF preclinical PET systems throughout Australia is performed to the highest standards of reliability and reproducibility. **Materials and Methods:** Six QA phantoms were machined from solid acrylic rods at the Centre for Advanced Imaging. Defined NEMA NU 4 acquisition and analysis protocols were first performed on the 6 phantoms using a single PET camera (UQ Inveon, Siemens). Distribution to pilot sites throughout Australia was completed with local filling of the phantom, acquisition and analysis. FBP reconstruction was performed where available or the method available on the system. The data was uploaded to a central repository on the research data manager (RDM) system. Results: Reproducibility for the calculated recovery coefficient was demonstrated by the small SD for the 6 phantoms imaged on the UQ Inveon system. Results from the initial 7 systems showed relatively good agreement with the outliers not using FBP. **Conclusion:** The first pilot study for a national QA audit has been completed. Future directions include assessing 3D printing for phantom manufacture, developing automated analysis software and expanding the program to additional preclinical PET cameras in Australia. **References:** none

EPS-211

Evaluation of Inter-user Variability and Time-savings for a Semi-automated Segmentation Method of Planar Gallbladder and Renal Exams

K. Krawiec[1], J. Taylor[2], T. Martin[2], S. McGurk[2], S. Whitmarsh[3], A. S. Nelson[1];
[1]MIM Software Inc, Cleveland, OH, UNITED STATES OF AMERICA, [2]Sheffield Teaching Hospital NHS Foundation Trust, Sheffield, UNITED KINGDOM, [3]Beth Israel Deaconess Medical Center, Boston, MA, UNITED STATES OF AMERICA.

Aim/Introduction: Segmentation methods can often vary widely between institutions or users in planar nuclear medicine studies. This can lead to variability in clinical results and potentially impact patient care. The aim of this study was to evaluate a commercially available semi-automatic segmentation method for planar gallbladder and renal exams across multiple users at two institutions to assess the effect on inter-user variability and overall time-savings of segmentation. **Materials and Methods:** Eleven Gallbladder EF and sixteen Renal MAG3 exams were collected from multiple institutions. Motion correction was applied to studies prior to analysis to eliminate potential discrepancies. Testers included physicists and a technologist: three from Institution 1 and one from Institution 2. For each exam, two testers initially processed the cases with the automatic segmentation method and reviewed the contours. They assigned a quality score (1-3) and then edited the contours to be clinically acceptable. The testers evaluated the same cases 24 to 96 hours later and performed manual segmentation. Time-savings was evaluated by comparing manual segmentation to automatic segmentation with user edits (Auto-Edited). All time measurements were recorded automatically. Manual and auto-edited contours were processed for Renal MAG3 and Gallbladder EF analysis to obtain the split function percentage and ejection fraction. Results were compared between contouring methods and testers. Results: Evaluation of the Gallbladder EF results showed an average quality score of 2.45. The auto-edited contours resulted in a time-savings of 16.02 seconds compared to manual segmentation (19.0% decrease). Average absolute difference in auto-edited EF was 0.82% (R2= 0.99) compared to manual contours. Absolute difference between users was 2.02% (R2= 0.94) for manual contours and 0.69% (R2= 0.99) for auto-edited contours. Renal MAG3 results showed an average quality score of 2.29 with a time savings of 54.51 seconds (27.6% decrease). The split function of the auto-edited contours resulted in a 2.06% difference (R2= 0.98). Absolute difference between users was 1.72% (R2= 0.99) for manual contours and 1.02% (R2= 0.99) for auto-edited contours. **Conclusion:** Semi-automated segmentation of planar gallbladder and renal exams reduced user variability and required minimal edits, leading to significant time savings in a clinical workflow. **References:** None

EPS-212

Dose Reduction Strategies for Optimizing [89ZR]Zr-Df-IAB22M2C PET Scans Using Virtual Reconstruction (VR) Techniques

R. Korn[1], A. Abbott[1], J. Sunderland[2], I. Wilson[1], W. Le[1];
[1]ImaginAB, Inglewood, CA, UNITED STATES OF AMERICA, [2]University of Iowa, Iowa City, IA, UNITED STATES OF AMERICA.

Aim/Introduction: Tumor-infiltrating CD8 T-cells are critical for effective treatment in patients receiving immunotherapy (IOT). ^{89}Zr-Df-IAB22M2C (CD8 PET) is a novel 80 kDa minibody that binds to CD8+ cell receptor and can be used to non-invasively detect CD8+ cells in tumors and reference tissues. During Phase I and Phase II studies, a 3.0 mCi dose of ^{89}Zr-Df-IAB22M2C at 1.5mg API was selected for use because it provided optimal whole body (WB) PET image quality (IQ) and quantitative CD8 PET correlation with CD8+ cell densities. Although the radiation dose of 3.0 mCi is acceptable (EDE=2.4 rem/mCi; spleen critical organ), there is a desire to minimize radiation exposure while maintaining IQ and quantitative robustness (QR). Herein we report the potential impact of CD8 PET tracer dose reduction on IQ and QR from VR CD8 PET scans obtained from Phase II studies. **Materials and Methods:** All centers in the Phase II trial underwent PET scanner phantom harmonization prior to patient enrollment and maintained image acquisition and reconstruction parameters throughout. List mode (LM) acquired WB CD8 PET scans were processed and reconstructed to simulate VR doses (0.8 mCi - 2.0 mCi) by randomly discarding events in each LM stream according to predefined fractions of

original 3.0 mCi doses. Standard data corrections included attenuation, randoms, dead-time, and scatter. Volumes-of-interest were selected for lesions and reference tissues (at identical locations on each simulated scan). Count-based readouts were used to determine Signal-to-Noise (SNR), Contrast-to-Noise (CNR) and % SUVmean bias (%SB) at each simulated dose compared to original scans. Results: Three subjects with five LM WB PET/CT scans (two pre-IOT, three IOT) from three institutions were available for VR simulation. Tumor SNR, CNR and %SB at 1.0 mCi compared to original dose changed by 11.8%, 27.5% and 1.4%, respectively, Lower changes in these metrics were noted in reference tissues with known high CD8 cell densities including the spleen (3.7%, 6.7% and -0.7%) and bone marrow (4.7%, 0.6% and -3.4%) likely due to the high natural CD8 uptake in these organs. The IQ at 1.0 mCi was deemed acceptable, while QR had minimal impact at the lower doses. **Conclusion:** VR of CD8 PET scans at lower doses did not result in a substantial change in image quality nor quantitative robustness. These encouraging results led to adoption of 1.0 mCi doses (1.5mg API) for CD8 PET studies. **References:** None

EPS-213

Assessing quantitative threshold with FES PET/CT imaging in metastatic breast cancer

L. Ferrer[1,2], B. Maucherat[1], T. Carlier[3,2], M. Lacombe[4], S. Girault[4], A. Leduc-Pennec[5], F. Kraeber-Bodéré[3,2,6], C. Rousseau[1,2,6];
[1]ICO René Gauducheau, St Herblain, FRANCE, [2]CRCINA UMR 1232 INSERM, Nantes, FRANCE, [3]University Hospital, Nantes, FRANCE, [4]ICO Paul Papin, Angers, FRANCE, [5]University Hospital, Brest, FRANCE, [6]Nantes University, Nantes, FRANCE.

Aim/Introduction: We are conducting a multicentric study (NCT03442504) to determine the predictive value of 16α-18Fluoro-17β-Oestradiol (FES) PET-imaging in hormonotherapy response for metastatic breast cancer (MBC) patients. Among recent litterature [1, 2], several quantitative thresholds based on SUVmax or SULmean were proposed ranging from 1.5 to 2.0 to associate positiveness of lesions identified on FES examination. The aim of this study was too assess these threshold in relation with the positive or negative FES lesion score. **Materials and Methods:** One fluoro-desoxyglucose (FDG) and FES PET examinations were performed 2 weeks apart on 28 MBC patients from march 2017 to july 2020. A fully trained nuclear physician used Oncoplanet (Dosisoft) to delineate all metastatic sites, liver metastasis excepted, on both FDG and FES images with an unambiguous coding to insure a one-to-one relationship for each lesion. Delineation was performed with a semi-automatic algorithm (40% SUVmax) when possible or manually otherwise (lesions visible only in one of both examinations). SUV(max.,mean), SUL(max.,mean) was recorded for all lesions. Additionally, a binary visual score was attributed to each of them according to the expert's experience and was considered as the gold standard. Results: 636/879 (72%) were visually classified as FES positive. Minimal and maximal values for SUV/L(max.,mean) are reported in table 1, highlighting a clear overlap between maximal and minimal values of negative and positive lesions respectively. This overlapping region was smaller for SUL than for SUV values. Conversely, the wider is the region, the fewer data are included (123, 154, 134 & 166 for SUVmax., SUVmean, SULmax. and SULmean respectively). Cumulative distribution of both negative & positive datasets showed that 1.5 as SUVmax threshold misclassified negative and positive lesions in 16% and 1% respectively, whereas this threshold set to 2.0 lead to almost 0% and 5% misclassification of the formers respectively. In addition, SULmean threshold set to 1.5 lead to 0% and 21% misclassification for negative and positive lesions. **Conclusion:** This study seems to validate the use of SUVmax with a threshold of 2 to quantify FES examinations instead of SULmean as it lead to fewer lesion misclassifications. Further investigations need to be perform to investigate the best trade-off between sensitivity and specificity of the FES examination at the lesion level. **References:** 1. Kurland BF et al Oncologist. 2020 Oct;25(10):835-844. doi: 10.1634/theoncologist.2019-0967. 2. Boers J et al. Eur J Cancer. 2020 Feb;126:11-20. doi: 10.1016/j.ejca.2019.10.024.

EPS-214

A new fully automated method for lung segmentation using low-dose CT

S. Urbán[1], E. Szabó[2], Z. Mikó[1], J. Csirik[2], Z. Besenyi[1], L. Pávics[1];
[1]Department of Nuclear Medicine, University of Szeged, Szeged, HUNGARY, [2]Institute of Informatics, University of Szeged, Szeged, HUNGARY.

Aim/Introduction: Identification of the lung lobes and segments are important in the assesment of lung diseases. Most nuclear medicine clinicians use visual evaluation for the determination of the lobes and segments. On the usually used low-dose CT lobe fissures frequently appear partially and blurred due to partial volume effects and patient and breading motion. Furthermore, lung segments do not have visual borders which makes the computer-aided segment detection challenging. This work presents a fully automatic approach for lung segmentation motivated by the V/Q SPECT clinical protocols using low-dose CT images. **Materials and Methods:** The proposed method consists of five main steps: 1) lung segmentation; 2) trachea segmentation and labeling; 3) vessel segmentation; 4) fissure enhancement; 5) detection of the segments combining the results from the previous steps using marker based watershed algorithm, which uses the points of detected and labeled segmental bronchi as markers. The validation process was based on the comparison of manually defined and automatically detected segments by radiologists and specialists in nuclear medicine. The analyzed segments were rated as small volume difference (<10%) or

large volume difference (>10%) objects. 22 patients' (10 men, 12 women, mean age: 60 years) low-dose CT images (120 KeV, 50-100 mA, slice thickness: 2.5 mm) were evaluated. Results: The automatically detected lung segments according to Boyden's nomenclature were the followings (small volume difference in percentage of all cases): RU1 (72.7), RU2 (77.2), RU3 (90.9), RM4-5 (95.5), RL6 (72.7), RL7 (50), RL8 (59.1), RL9 (90.9), RL10 (90), LU1-2 (86.4), LU3 (81.8), LU4-5 (77.3), LL6 (90.9), LL7-8 (72.7), LL9 (100), LL10 (100). In some cases adjacent segments were segmented as mixed region as follows: LL9-10 (31.8%), LL7-10 (4.5 %), RU1-2 (18.2 %) and RL9-10 (22.7 %). RL7 (in 31.8 % of cases), RL8 (in 18.2 % of cases), LU4-5 (in 22.7 % of cases) and LL7-8 (in 18.2 % of cases) segments contained the largest volume errors (>10% volume difference). **Conclusion:** A new, fully automated method for lung segment identification was developed. Based on the evaluation the proposed segmentation method can facilitate and speed up the localization of the lung segments using low-dose CT images. **References:** none

EPS-215

Evaluation of Tumour Volume and Activity using New Tumour Modelling Method: Application to Non-Hodgkin's Lymphoma

R. Fedrigo[1,2], *R. Coope*[3], *I. Bloise*[1], *C. Gowdy*[4], *A. Hart*[5], *A. Rahmim*[1,2,6], *C. Uribe*[2,6];

[1]*BC Cancer Research Institute, Vancouver, BC, CANADA,* [2]*University of British Columbia, Vancouver, BC, CANADA,* [3]*Genome Science Institute, Vancouver, BC, CANADA,* [4]*BC Children's Hospital, Vancouver, BC, CANADA,* [5]*University of Victoria, Vancouver, BC, CANADA,* [6]*BC Cancer, Vancouver, BC, CANADA.*

Aim/Introduction: [^{18}F]FDG PET is frequently used to stage Non-Hodgkin's lymphoma and evaluate treatment response. However, the disease varies within the population and each patient responds differently to treatment, making disease management particularly challenging. There is evidence that quantitative imaging metrics, such as total metabolic tumour volume (TMTV) can enhance the prognostic value of PET and its ability to guide treatment decisions. There is significant motivation to implement automated segmentation of TMTV, as manual segmentation is time-consuming and not feasible within a clinical setting. In this study, we evaluate fixed threshold (FT) and gradient-based segmentation algorithms using Negative-Cast Modelling for Oncology (NCMO). This work is applied to primary mediastinal B-cell lymphoma (PMBCL), although these methods can be easily translated to other forms of lymphoma and cancer. **Materials and Methods:** Negative-Cast Modelling for Oncology (NCMO) was used to cast tumour models using segmented lesions from 5 PMBCL patients (2.7mL to 76mL). [^{18}F]FDG concentration was based on an analysis of 22 lesions from 13 PMBCL patients. Tumour models were inserted into the Probe-IQ phantom (without background activity) and imaged using the GE MI PET/CT scanner (2x10min bed positions), to determine the radioactivity ground truth. Next, the Probe-IQ liver and background was injected with [^{18}F] FDG to achieve target concentrations determined from the patient analysis (11.0kBq/mL and 3.7kBq/mL, respectively). 2x30min bed positions were acquired in list-mode. Images were reconstructed using OSEM (4 iterations, 8 subsets) with time-of-flight (ToF) and point-spread function modelling (PSF). Images were segmented using MIM (MIM Software, USA) with 20%,25%,30%,40%,50% fixed threshold (FT) and MIM's gradient-based algorithm (PET Edge+). Total metabolic tumour volume (TMTV) and total lesion glycolysis (TLG) was determined for each tumour. Results: For images unlisted for 1min bed duration, TMTV percent bias using 25% FT was -7.6% (3mL), -14.5% (21mL), and 2.3% (71mL). TMTV percent bias using gradient method was -3.5% (3mL), -32.5% (21mL), and -24.0% (71mL). TLG percent bias using the 25% FT had a percent bias of -18.3% for the 3mL lesion and 6.6% for the 71mL lesion. TLG percent bias with gradient method was -17.3% for the 3mL lesion and -11.6mL for the 71mL lesion. **Conclusion:** Our results suggest that 25% FT is best for TMTV quantification of PMBCL tumours, which is consistent with previously performed simulations [1]. Care should be taken with the gradient algorithm as it failed to accurately delineate tumour boundaries for some cases. **References:** [1] Fedrigo,et al, Proc. JNM, 2021

EPS-216

Comparison of atlas-based and manual segmentation versus simple ROI placement for quantification of liver and spleen metabolism in FDG-PET/CT

T. Kotwal, *G. Krokos, A. Malaih, S. F. Barrington, P. Marsden, B. M. Fischer;*

King's College London, London, UNITED KINGDOM.

Aim/Introduction: 18F-FDG PET is routinely used to assess response following cancer treatment. FDG uptake in tissues not directly involved in disease can provide additional information on response and side-effects, but its clinical utility is largely unassessed due to the impracticality of manually segmenting entire organs. As a step towards a time-efficient whole-body metabolic survey, we applied an atlas-based segmentation method and compared the accuracy of the extracted PET SUV metrics against those from manually segmented organs and volumes of interest (VOI) placed on the PET/CT images which are routinely used in clinic. **Materials and Methods:** Manual segmentations of the liver and spleen were performed on the PET and CT component of 50 PET/CT scans. Manual PET segmentations were used as the reference standard, with manual CT segmentations used to train the atlas using the 'leave one out' method. The atlas was trained on CT data to assess if algorithms trained on CT can be directly applied to PET and generate accurate SUV metrics. Clinically realistic PET measurements (e.g. as applied

with Deauville and PERCIST criteria[1]) were extracted from 3cm VOI's placed in the liver and the spleen. Results: Compared to the reference standard for the liver, the atlas-based method on average produced a 104% higher SUV_{max}, 4% lower SUV_{mean}, and 80% lower SUV_{peak}. The liver 3cm VOI's produced a 22% lower SUV_{max}, 4% higher SUV_{mean} and 17% lower SUV_{peak}. For the whole spleen, the atlas-based method produced a 15% higher SUV_{max}, 9% lower SUV_{mean}, and 4% higher SUV_{peak}. The Spleen 3cm VOI produced an 11% lower SUV_{max}, 11% higher SUV_{mean} and 9% lower SUV_{peak}. **Conclusion:** The atlas-based and VOI methods performed consistently well on this dataset with regard to SUV_{mean}. For SUV_{max} and SUV_{peak} larger discrepancies were observed, particularly in the case of the liver atlas, due to the extension of the CT segmented regions beyond the boundaries of the organs on PET leading to isolated large changes. As the VOI's were confined within the organ there was no risk of overlap, however the small area assessed compared to whole-organ segmentation methods may exclude regions of higher uptake. Overall, more accurate segmentations may be required for quantification which combines both functional and anatomical information from PET and CT respectively. **References:** 1. O J et al. Practical PERCIST: A Simplified Guide to PET Response Criteria in Solid Tumors 1.0. Radiology. 2016:576-584.

EPS-217

Social Media for Scientific Research: a preliminary evaluation of the impact of Publicization on Number of Citations of Medical Imaging Publications

A. Forcina Barrero[1], G. Converso[1], S. Di Giorgio[1], M. Grondelli[1], B. Maizza[1], S. Tarchi[1], M. Sollini[1,2], N. Gozzi[2], A. Chiti[1,2];
[1]Department of Biomedical Sciences, Humanitas University, Milan, ITALY, [2]IRCCS Humanitas Research Hospital, Milan, ITALY.

Aim/Introduction: Demand for open access papers and widespread use of social media increases: more than ever, scientific literature is accessible to a broader, less specialized population. Following this trend, countless scientific journals and authors have tried to increase the visibility of their works through social media. The use of these channels could have an exponentially increasing impact on the success of published papers, making of extreme interest and significance the attempt to gauge the true effects of social media advertising. This work aims to test the impact of social media publicization on number of citations of medical imaging publications. **Materials and Methods:** Via Embase, we selected papers assigned to a volume in 2018 in the following six journals: European Radiology, Radiology, Journal of Nuclear Medicine, European Journal of Nuclear Medicine and Molecular Imaging, Radiotherapy and Oncology, and International Journal of Radiation Oncology, Biology and Physics. Reviews were excluded from the analysis. Scopus and Altmetric were employed to extract information of interest for each paper including the number of scientific citations, the Altimetric score, and its details. Spearman and Kendall's correlation coefficients were utilized to test correlation between variables. Random Forest (RF) and Boosted Regression Tree (BRT) models were employed to investigate a potential predictor-response relation between the number of citations and all covariates with whom a correlation had been previously identified. Analysis was performed using R and Python by the MEDTEC School's students listed among the authors, under the supervision of NG, MS and AC. Results: We found a significant correlation between the number of citations and several predictors, including Mendeley (p-value=0.0003). Classifying the dataset in two subsets, depending on the citations, only the class with low citations proved to be significantly correlated to several predictors including the reads on Mendeley, the number of Twitter accounts, and Facebook.BRT was trained and achieved a RMSE of 17.40 with the residuals increasing exponentially with the number of citations. BRT found Mendeley, number of Twitter accounts and the sum of all 'cited_by' entries (profile per data source) to be highly influential in terms of citation count, explaining more than the 85% of the influence. **Conclusion:** Our findings suggested that article publicization may influence citations of papers within a certain range. We'll aim to foretell the number of citations considering a new metric based only on the predictors that proved significant, but citations exceeding a certain threshold could be harder to predict. **References:** None

EPS-218

An automated bladder/lesion separation method using 99mTc-PSMA SPECT/CT images

S. Urbán[1], V. Rácz[2], I. Farkas[1], J. Csirik[2], Z. Besenyi[1], L. Pávics[1];
[1]Department of Nuclear Medicine, University of Szeged, Szeged, HUNGARY, [2]Institute of Informatics, University of Szeged, Szeged, HUNGARY.

Aim/Introduction: Distinction of the bladder from nearby lesions on SPECT image has important applications in assessment of prostate cancer. Most nuclear medicine clinicians use visual evaluation for this task. On 99mTc-PSMA SPECT images high bladder activity can suppress lesions with much lower activities in its surrounding. This work presents an automated approach which could facilitate the localization of active lesions in the pelvic region using 99mTc-PSMA/CT images. **Materials and Methods:** The automated method needs a seed point inside the bladder for the localization, then consists of two main steps: 1) regional maxima detection on the SPECT image around the seed point 2) segmentation of the bladder using the fast marching segmentation method; the method is based on a hybrid image, which contains information from both SPECT and CT and also from the previously located regional maximas as potential lesions. The method finally segments the bladder and marks the potential lesions in the region. The validation process contained two

steps. First, the bladders were manually segmented and was compared to the result of the method. Second, lesions in the surroundings were also manually segmented and tested for localization. The proposed method was evaluated on 12 histologically verified prostatic cancer patiens with SPECT/CT. Results: Bladder segmentation was feasible in all of the cases using a manually determined seed point. The median Dice metric of the segmented and manually created bladder contours was 81.7% (min.: 62%, max.: 90.6%). 10/12 lesions were successfully marked as a separate lesion using local maxima. There were two cases, where the lesions were not marked: they were inseparable from the bladder based on the image information. **Conclusion:** A new, automated method for lesion/bladder separation was developed. Based on the evaluation the bladder can be segmented with high accuracy. Furthermore, most of the potential lesions can be detected and marked for a better diagnosis. **References:** none

EPS-219

Effects of dedicated uniformity map for narrow energy window

R. Hirvilammi[1,2], M. Seppänen[1,3], T. Noponen[1,2];
[1]Department of Clinical Physiology and Nuclear Medicine, Turku University Hospital, Turku, FINLAND, [2]Department of Medical Physics, Turku University Hospital, Turku, FINLAND, [3]Turku PET Centre, Turku University Hospital, Turku, FINLAND.

Aim/Introduction: Narrowing energy window can act as an effective scatter compensation in single photon emission computed tomography (SPECT) studies. However when using narrow energy window we have observed distortions of uniformity correction maps used to correct spatial non-uniformities in SPECT images. This phenomenon indicates that there may be a need for calibration of uniformity maps for each energy window separately. In this phantom study we investigated the effects of individual uniformity correction maps with narrow energy window for SPECT image quality. **Materials and Methods:** Intrinsic calibration of dedicated uniformity correction maps for ± 3 % energy window was done for both gamma camera detectors with digital Discovery 670 CZT SPECT/CT camera (GE Healthcare, Tirat Hacarmel, Israel) using 220 MBq ^{99m}Tc-point-source. SPECT QA phantom was imaged to evaluate effects of these dedicated uniformity correction maps. QA phantom included cold defects with different diameters and it was filled with 470 MBq of ^{99m}Tc. The phantom was imaged with ± 3 % energy window using original uniformity correction maps optimized for ± 7.5 % energy window and uniformity correction maps dedicated to ± 3 % energy window. Following imaging parameters were used: 33-36 s time-per-angle, matrix size 128x128 and zoom of 1.5. Reconstructions were carried out using Hermes Oncology software (Hermes Medical Solutions, Stockholm, Sweden) with 4 subsets, 16 iterations and Gaussian filter with FWHM of 7.0 mm. The volume of interests (VOI) of cold defects were delineated using CT images and the VOIs were transferred to SPECT images using Hermes Affinity Viewer 2 (Hermes Medical Solutions, Stockholm, Sweden). Noise was determined from areas surrounding the defects and contrast and contrast-to-noise ratios (CNR) were calculated for each defect. Student's t-test was used to evaluate the statistical differences between the mean values of CNRs. Results: Noise decreased (19.41 % vs. 15.42 %), contrast increased slightly (0.42 ± 0.14 vs. 0.43 ± 0.14) and CNR significantly increased (1.58 ± 0.73 vs. 2.82 ± 0.92 (p = 0.01))) when using dedicated uniformity correction maps acquired with ± 3 % energy window instead of original maps acquired with ± 7,5 % energy window. **Conclusion:** Default uniformity correction maps of SPECT devices can be distorted when applied to studies acquired with narrower energy windows. This study showed that uniformity correction maps generated with energy window matching the windows used for imaging may be useful to optimize image quality and gain the benefits of narrow energy window. **References:** none

EPS-220

[^{123}I]FP-CIT SPECT reconstruction: FBP versus OSEM with resolution recovery - a quantitative and qualitative comparison

R. Teixeira[1], J. Castanheira[1], Â. Silva[1], S. Vaz[1], M. Silva[1,2], A. Canudo[1,2], R. Oliveira[1,2], J. Correia[1,2], H. Delgado[1,2], M. Andrade[1,2], B. Freitas[1,2], S. Teixeira[1,2], V. Vieira[1,2], M. Machado[1], C. Constantino[1], F. Oliveira[1], D. C. Costa[1];
[1]Champalimaud Centre for the Unknown, Champalimaud Foundation, Lisbon, PORTUGAL, [2]Mercurius Health, Oeiras, PORTUGAL.

Aim/Introduction: This work investigates the differences in quantitative indices of striatal uptake and qualitative visual evaluation between FBP and OSEM with resolution recovery (OSEM-RC) reconstruction algorithms in brain [123I]FP-CIT SPECT. **Materials and Methods:** Data from fifty patients (mean age 68±10 years old, 26 males), referred to [123I]FP-CIT brain SPECT, were retrospectively investigated. All acquisitions were performed with a Philips BrightView gamma camera. For each patient, four image reconstruction protocols were applied: FBP, FBP with attenuation correction (FBP-AC), OSEM-RC (Astonish algorithm, Philips Healthcare), and OSEM-RC with attenuation correction (OSEM-RC-AC). Attenuation correction was performed using Chang's method with μ=0.12cm-1. All images were reconstructed with identical matrices (128x128), isotropic voxel size of 4.66 mm width, and post-reconstruction smoothing with Hanning filter (cutoff=1). For OSEM-RC and OSEM-RC-AC reconstructions, 3 iterations and 8 subsets were defined. For quantitative comparison, striatal uptake (caudate binding potential - CBP; and putamen binding potential - PBP), volume and length of the striatal region with normal uptake

were computed as in Oliveira et al (2018)[1]. For qualitative evaluation, four experienced nuclear medicine physicians classified, anonymously and independently, all images as "normal", "abnormal symmetric" and "abnormal asymmetric", knowing only which reconstruction protocol was used. Results: Mean uptake indices were generally higher when OSEM-RC was used in comparison with FBP, both for AC and non-AC reconstructions. For non-AC images, the mean increase was 0.19±0.17, 0.05±0.09 and 578±617mm3, for CBP, PBP, and volume, respectively (paired t-test, p<0.001 for all). For AC corrected images, the mean increase was 0.24±0.21, 0.08±0.11, and 541±814mm3, respectively (p<0.001 for all). There was no statistically significant difference regarding the length, between both types of algorithms. For reference, mean values for CBP, PBP and volume in healthy subjects are 2.38, 1.76 and 10300mm3, respectively [1]. Regarding qualitative evaluation, full agreement amongst the four raters was achieved in 82%, 82%, 80%, and 92% of the images for FBP, OSEM-RC, FBP-AC, and OSEM-RC-AC reconstructions, respectively. However, the differences were not statistically significant (Cochrane Q test, p=0.300). Images reconstructed with FBP were noisier than those reconstructed with OSEM-RC, both for AC and non-AC reconstructions. **Conclusion:** OSEM-RC algorithm, both with non-AC and with AC originated higher uptake indices in the striatum than FBP, which should be taken into consideration when comparing data from different reconstruction algorithms. Results from the visual evaluation are not conclusive. However, a trend for higher agreement using OSEM-RC-AC seems to exist. **References:** [1] Oliveira et al, EJNMMI 2018;45:1052-62, doi:10.1007/s00259-017-3918-7

EPS-221

Validation of PET data resampling methods to simulate lower injected doses on a multimodality PET-MR scanner

J. Anton Rodriguez[1,2], T. W. Deller[3], J. C. Matthews[2];
[1]The Christie NHS Foundation Trust, Manchester, UNITED KINGDOM, [2]Division of Informatics, Imaging and Data Sciences, MAHSC, Manchester, UNITED KINGDOM, [3]GE Healthcare, Waukesha, WI, UNITED STATES OF AMERICA.

Aim/Introduction: PET data resampling techniques [1,2] can be used to predict image quality changes with the reduced injected activities or reducing acquisition times using existing full-dose PET data. Methods to resample PET data acquired on the multimodality GE Signa PET-MR scanner has been developed and validated using scanner manufacture offline reconstruction tools. **Materials and Methods:** A Flangeless Esser-PET-phantom™ containing a series of cold rods of varying diameters and refillable cylindrical inserts of varying diameters of 8, 12, 16, and 25(x3)mm and one solid cylinder made of Teflon (25mm diameter) was scanned for 60 min with a total of 40 MBq of fluorine-18 at the start of scan and a contrast ratio of 4:1 in "hot cylinders" to background. Resampling of PET projection time-of-flight (TOF) data (10 replications) was performed using random resampling of a Poisson distribution (Matlab function "poissrnd") at different resampling fractions (RF): RF<1 to simulate lower scanning times/injected doses and RF=1 to assess precision of the data. Theoretical justification for this approach is a consequence of the Poisson limit theorem. Scanner reported singles at each crystal-block (used to estimate the distribution of random events), were also resampled with square root of RF. Reconstruction of data was performed using GE-offline-reconstruction Duetto_v02.06 with OP-OSEM-TOF (2it-28subsets). For RF=1, a time frame of 150sec from the start of acquisition was resampled. For RF<1, we resampled the full 3600sec time frame with an RF of 1/10.14, 1/20.13, 1/40.11 to simulate times from of 300, 150 and 75sec respectively from the start of acquisition. Additionally, acquisition replications without resampling were obtained by splitting original LM in similar time frames (increasing the frame durations to account for radioactivity decay). Analysis of the phantom images was performed using background image roughness (IR), background variability (BV) and contrast recovery of the inserts (CRC). Results: Differences in the activity background measurements, BV and CRC of the phantom inserts between acquisition and resampled replications were not statistically significant (95% confidence interval) with maximum difference (4%) found in the mean CRC_{8mm} values 3600/75 sec. Image roughness was found to increase when RF=1 by a factor of square root of 2 and in smaller increments when RF<1 simulations. **Conclusion:** Poisson resampling of TOF-sinograms is a valid approach to simulate lower doses or shorter acquisition times. Main differences were found for IR and which is a consequence of additive simulated and acquisition voxel variance. **References:** [1]Lartizien et al. 2010;[2]Markiewicz et al. 2015

EPS-222

Effect of Attenuation Correction CT Parameters on PET Image Quality and Quantification

K. Binzel, C. L. Wright, M. V. Knopp;
The Ohio State University Wexner Medical Center, Columbus, OH, UNITED STATES OF AMERICA.

Aim/Introduction: To demonstrate, in vivo, the validation of equivalence of PET reconstruction results with the use of an ultra-low dose or thin slice CT for attenuation correction. **Materials and Methods:** Six canines underwent ^{18}F-FDG PET imaging on a next-generation digital photon counting system (Philips Vereos). 75 minutes post-injection a 90 second/bed PET acquisition was performed over the whole body. Multiple CT series were acquired for validation. First, the standard protocol utilizing 120kVp, 150mAs, 4 and 2 mm slice thicknesses followed by an ultra-low dose (uLD) acquisition with 80kVp, 20 (n=4) or 25 (n=2) mAs, at 4mm.

The same PET listmode data were reconstructed using each of the three different CT series. Results: Blinded review found no significant differences in image quality or hot spot conspicuity among the differently reconstructed PETs. Using the full dose 4mm CT corrected PET images as reference, there was an average of 0.8% and 0.1% difference in SUV_{mean} for background regions measured on the uLD 4mm and full dose 2mm corrected PET images, respectively. One subject had two hot lymph nodes with SUV_{max} measurements of 4.56, 4.49, and 4.56 for the first and 4.35, 4.31, and 4.35 for the second, for the full dose 4mm, uLD 4mm, and full dose 2mm corrected PET images, respectively. **Conclusion:** To enable CT radiation dose reduction in PET, the use of ultra-low dose CT in this in vivo intra-individual analysis revealed a negligible impact on PET visualization and quantification. Neither was the use of a 2mm voxel PET reconstruction matrix affected by the choice of CT slice thickness, either 4 or 2mm. **References:** none

EPS-223

Key considerations when undertaking PSF acquisitions for use in I-131 post-therapy planar imaging deconvolution

W. Turner[1], F. Barrack[2], J. Scuffham[2], D. McGowan[1];
[1]Oxford University Hospitals, Oxford, UNITED KINGDOM, [2]Royal Surrey County Hospital, Guildford, UNITED KINGDOM.

Aim/Introduction: Septal penetration star artefacts occur when high energy photons pass through gamma camera collimation, causing detection of the attenuated photons. This effect is common in I-131 post-therapy imaging due to its high energy emissions. Deconvolution using a relevant Point Spread Function (PSF) has been seen in previous research to be an effective method for the removal of septal penetration artefacts in I-131 imaging [1]. This research aims to investigate the key considerations when obtaining PSF images for use in Richardson-Lucy deconvolution in post therapy imaging for optimal removal of septal penetration artefacts to improve quantification and assessment of activity for use in dosimetry calculations. **Materials and Methods:** PSF images of an I-131 point source were acquired on a GE Infinia gamma camera with Triple Energy Windows (TEW), allowing for TEW scatter correction to be undertaken, at multiple collimator-source distances. A range of patient images obtained with TEWs containing septal penetration artefacts underwent deconvolution using the acquired PSFs with Richardson-Lucy deconvolution and total variance regularisation. Results: It was observed in the PSF acquisitions that increasing collimator-source distance led to longer septal penetration spoke lengths. Using theoretical calculations, it was seen that the septal penetration spoke increases linearly with distance. For this reason, the collimator source distance of patient and PSF images must be closely matched before deconvolution can be undertaken to create an accurate estimate image. PSF background counts were seen to lead to a region of no counts around hot objects, causing a donut artefact post deconvolution. To rectify this, PSFs need undergo thresholding in order to remove background counts from the PSF image. **Conclusion:** In summary, when acquiring PSF images for use in the deconvolution of I-131 imaging, the user must consider the collimator-source distance of the PSF and the patient images and the background counts of the PSF image. Mismatches in the PSF and patient collimator-source distance leads to images with too much or not enough artefact removal which can impact qualitative and quantitative accuracy. The PSF image background must be removed, ideally using a background threshold, in order to ensure that deconvolution is undertaken correctly without the introduction of image artefacts into the image estimate. Optimising the PSF acquisitions allows for image estimates to be of suitable qualitative and quantitative accuracy. **References:** 1. F. Barrack, J. Scuffham, and S. McQuaid, "Septal penetration correction in I-131 imaging following thyroid cancer treatment," Phys. Med. Biol., 2018.

EPS-224

Towards Automatic Detection of Enlarged Parathyroid glands in 3D Images of 99mTc-MIBI / 99mTc-pertechnetate SPECT/CT

I. Marikova[1], L. Stablova[1], J. Trnka[1,2], M. Samal[1], D. Zogala[1];
[1]Institute of Nuclear Medicine, First Faculty of Medicine, Charles University and the General University Hospital, Prague, CZECH REPUBLIC, [2]Department of Radiation Protection, General University Hospital, Prague, CZECH REPUBLIC.

Aim/Introduction: The aim of the study was to extend application of principal component analysis (PCA) of simultaneously recorded 99mTc-MIBI/123-iodine parathyroid scintigraphy to 99mTc-MIBI/99mTc-pertechnetate (MIBI/Tc) image pairs obtained in two separate examinations recorded at different times. Additional difficulty was accurate and reproducible positioning of the patient under the camera, subsequent image registration, identification of residual misregistration artefacts and their differentiation from pathological lesions of parathyroid glands. **Materials and Methods:** Retrospective data of 18 consecutive patients indicated to MIBI/Tc parathyroid scintigraphy were analyzed using standard subtraction procedure (a reference method controlled visually by a user). MIBI and pertechnetate examinations were performed in 2 different days with 1-7 days interval. Position of each patient in camera gantry was carefully set using laser crosshair and standardized table shift. PCA of individual pairs of MIBI/Tc 3D data sets was performed after additional registration. The results were visualized as maximum intensity projections of individual components presented in transverse, sagittal and frontal planes. The images were examined visually for the presence of enlarged parathyroid glands. Results: Correlation coefficients between

the recorded volumes of MIBI and Tc images with standard positioning of the patient were below 0.50. Improved positioning increased their average value to 0.66 ± 0.12 and subsequent registration procedure (applied to the volume of interest including thyroid) to above 0.70. Average count in Tc images was about half of that in MIBI images. Reference procedure identified 13 enlarged parathyroid glands and 5 negative findings. New procedure using PCA recognized correctly all negative (100 %) and 12/13 (92 %) positive findings. In 7/12 (58 %) positive findings there was a complete agreement on both the presence and location of enlarged parathyroid glands. In the remaining 5/12 (42 %) positive patients, there was an agreement on the presence of pathology and the side (left / right lobe) but slight disagreement on the lesion location along craniocaudal direction (probably a consequence of residual misregistration). **Conclusion:** In retrospective MIBI and Tc data recorded at different times, PCA resulted in agreement with standard manual procedure in 17/18 (94 %) findings. An advantage of PCA is user-independent automatic scaling of subtracted images and calculation of proper subtraction weights. Assessment of PCA performance in parathyroid scintigraphy now continues in a prospective study including subsequent validation by surgery with the aim to extract diagnostic indices potentially useful for machine learning. **References:** EJNMMI 2020; 47(Suppl 1): S482, OP-968

1904

Wednesday, October 20 - Saturday, October 23, 2021

on-demand pool, release on Wednesday, October 20 at 09:00

Technologists' e-Poster Presentation Session - Sharing Technologist's Experience

TEPS-01

Effective half-life, excretion and radiation exposure of 177 Lu PSMA

Y. Parlak, D. Goksoy, G. Mutevelizade, G. Gumuser, E. Sayit; Celal Bayar University, Manisa, TURKEY.

Aim/Introduction: Lutetium-177 PSMA is increasingly used in targeted therapy in patients with prostate cancer. Therefore, radiation protection and radiation safety are very important for 177Lu-PSMA therapy. The aim of the study is to evaluate the radiation safety conditions by detecting the urine excretion rate, to calculate the effective half-life and to determine the retention of Lu-177 PSMA in the body as a function of time. **Materials and Methods:** Ten patients (mean age: 68 ± 10 years) treated with 177Lu PSMA were included in the study.The high-performance liquid chromatography (Scintomics 8100, Germany) system was used for quality control and radiochemical purity test was performed before administration. The patients treated with mean 6.88±0.9 GBq dose of Lu-177-PSMA. Urine samples of all patients were collected for 24 hours (6, 12, 18 and 24 hour) following the infusion and then counted. Activities were determined, then excretion rate and retention of 177Lu PSMA were calculated. Dose rate measurements were taken with Geiger Muller at 5th, 15th, 30th, 60th, 90th, 120th, 150th, 180th minutes and 24th, 48th and 72th hours from a distance of 1m at the abdominal level. External dose rate measurement regarding retained body activity were calculated. Results: Effective half life calculated from dose rate measurements was found as 18.5 ± 11 h within the first 24 h and 48.1 ± 22.8 h between 48 and 72 h. Excreted activity in urine was found as 33.8±20.7, 40.4±20.3, 46.1±22.4 and 53.3±21.5% of total doses at 6, 12, 18 and 24 h after administration, respectively. External dose rate measurements for 4h and 24h were 24.51 µSv/h, 16.14 µSv/h, respectively. **Conclusion:** Our results showed that 177Lu-PSMA therapy was suitable for outpatient treatment protocol in terms of radiation safety, as the dose rate decreases below the determined threshold of 30 µSv/h. **References:** none

TEPS-02

Reconstruction with 2 mm voxel size improves the detection of small parathyroid adenomas with [18F] fluorocholine PET/CT

S. Rep[1,2], M. Hocevar[3,4], P. Tomse[1], K. Zaletel[1,4], A. Cuderman[1], L. Lezaic[1,4];

[1]Department for Nuclear medicine, University Medical Centre Ljubljana, Ljubljana, SLOVENIA, [2]Faculty of health sciences, Medical imaging and radiotherapy department, Ljubljana, SLOVENIA, [3]Oncological Surgery, Institute of oncology, Ljubljana, SLOVENIA, [4]Faculty of medicine, Ljubljana, SLOVENIA.

Aim/Introduction: [18F]fluorocholine PET/CT has emerged as an excellent method for localization of hyperfunctioning parathyroid glands (HPG). Because of the relatively poor spatial resolution and partial volume effect of PET/CT imaging technique the detection of small lesions is limited. The aim of our research was to investigate the effect of 4 mm and 2 mm voxel size on the detection of small hyperfunctioning parathyroid glands in PET/CT images in a preclinical and clinical setting. **Materials and Methods:** In the first part, the NEMA phantom was scanned where spheres and background were filled with a solution of [18F]fluorocholine in activity ratio of 5:1. The second part included retrospective analysis of 45 patients with biochemically confirmed primary hyperparathyroidism. The images were reconstructed using 4 mm and 2 mm voxel dimensions. We evaluated contrast recovery coefficient (CRC), contrast to noise ratio (CNR), lesion volume, and performed quantitative analysis of the obtained data (SUVmax and SUVmean) on NEMA phantom and the patient group, the latter also evaluated visually. Results: In comparison to 4 mm voxel size, 2 mm voxel size reconstruction resulted in increased contrast (CRC, CNR) most significantly in

small spheres and lesions, while decreasing in larger spheres and lesions. For patient analysis, both in the early (10 minute pi.) and delayed (1 hour pi.) phase the average SUV (mean and max; 4.42 vs 4.14, 3.62 vs 3.36 and 6.35 vs 5.89, 5.19 vs 4.71), CNR (mean and max; 1.63 vs 1.14, 3.71 vs 2.61 and 4.81 vs 3.61, 7.23 vs 6.19) were significantly higher when using 2 mm voxel size compared to 4 mm voxel size reconstruction (Wilcoxon signed-rank p<0,001). Additionally, visual analysis of patient images confirmed better lesion delineation in 2 mm voxel size images, agreement between two interpreting nuclear medicine physicians being almost perfect (kappa, 0.84). Diagnostic yield of 2 mm voxel size improved the sensitivity over 4 mm voxel size by 5 % (94.3 vs 89.3 % for both phases). **Conclusion:** Voxel size in [18F]fluorocholine PET/CT imaging has an important role for precise lesion localization, sensitivity and image quality for diagnostic assessment of hypoerfunctioning parathyroid glands. **References:** none.

TEPS-03

PET/CT reconstruction study using 2 mm voxel size for improved image quality

S. Rep[1,2], P. Tomse[1], L. Jensterle[1,3], K. Zaletel[1,3], L. Lezaic[1,3];
[1]Department for Nuclear medicine, University Medical Centre Ljubljana, Ljubljana, SLOVENIA, [2]Faculty of health sciences, Medical imaging and radiotherapy department, Ljubljana, SLOVENIA, [3]Faculty of medicine, Ljubljana, SLOVENIA.

Aim/Introduction: Because of the relatively poor spatial resolution of PET imaging technique in comparison to computed tomography (CT), the detection of small lesions is limited, in part due to partial volume effect (PVE) which negatively affects images both visually and quantitatively. The aim of our research was to investigate the effect of 4 mm and 2 mm voxel size on image quality and on detection of small lesions. **Materials and Methods:** We used the NEMA body phantom with six fillable spheres and the Micro Hollow Sphere phantom with four fillable spheres. The spheres and background were filled with a solution of [18F]fluorodeoxyglucose, in spheres-to-background ratio of 2:1, 3:1, 4:1 and 8:1. Both phantoms were imaged and reconstructed with 2 mm and 4 mm voxel size and the contrast recovery coefficient (CRC), contrast to noise ratio (CNR) were evaluated for each ratio. Results: For phantom spheres ≤ 13 mm, we found significantly higher CRC and CNR using 2 mm voxel reconstructions (Wilcoxon signed-rank, p <0.05). CRC did not differ for large spheres (≥ 17 mm) using 2 mm and 4 mm voxel size. On the other hand, CNR for large spheres (≥ 17 mm) was significantly lower in 2 mm voxel size images compared to the 4 mm voxel size (Wilcoxon signed-rank, p <0.001). **Conclusion:** The reconstruction with 2 mm voxel size can improve precise lesion localization, image contrast, and image quality. **References:** none

TEPS-04

Evaluation and optimization 18F-choline PET/CT protocol

F. Evers, H. Stevens, E. Telenga, P. Jager;
Department of nuclear medicine Treant, Emmen, NETHERLANDS.

Aim/Introduction: Different guidelines are used to preform 18F-Choline-PET-CT (FCH-PET/CT) for detection of parathyroid adenomas. At our epartment in the Scheper Hospital (Emmen, The Netherlands), scans are performed after an injection of 2 MBq/kg 18F-Choline at 2 minutes post injection (p.i), 30 minutes p.i. and 60 minutes p.i.. The aim off the present study is to evaluate the adenoma detection rate at the different time points and to determine if it is possible to reduce the number of time points without a reduction in overall detection rate. **Materials and Methods:** We retrospectively analyzed all the patients that were reffered to our department for FCH-PET/CT between 2016 and 2020. Fifty-six patients were included. All scans were reviewed and reported by an experienced nucleair medicine physians. Each scan report was checked for visability of parathyroid adenomas at the three different time points. Results: Results: In 43 studies a parathyroid adenoma was detected on both the 30 min and 60 minute image (76.8%). In no patients a parathyroid adenoma was detected on the 60-minute image if the 30-minute image was negatieve (10/56 patients (17.8%)). In contrast, in 1 patient a paratyhroid adenoma was visible on the 30-min image, but not on the 60-minute image (1.8%). In two cases a paratyroid adenoma was detected on the 30-minute image the 60-minute image was omitted (3.6%). **Conclusion:** This study shows that the 60-minute image FCH-PET-CT examination does not contribute any additional information. This confirms earlier studies showing maximal uptake at 20 minutes. Accordingly, we have adjusted our scan protocol, with scan time points at 2 and 30 minutes p.i.. **References:** none

TEPS-05

Radiolabeling of a glucose derivative with technetium-99m for the diagnosis of brain cancer

E. Stasyuk[1], V. Skuridin[1], A. Rogov[1], E. Nesterov[1], R. Zelchan[2], V. Sadkin[1], E. Shelikhova[1];
[1]Tomsk Polytechnic University, Tomsk, RUSSIAN FEDERATION, [2]Tomsk National Research Medical Center, Tomsk, RUSSIAN FEDERATION.

Aim/Introduction: The detection of malignant neoplasms in the early stages of development is one of the most pressing problems of modern medicine. Scintigraphy with radioactively labeled glucose derivatives is one of the promising approaches to the early and high-precision diagnosis of cancer tumors, because cancer cells, in comparison with normal cells, have an increased level of glucose metabolism. In this work, an original approach was

developed for introducing a radioactive label of technetium-99m isotope into a glucose derivative containing thio groups. The resulting radiopharmaceutical allows early diagnosis of cancer, including brain cancer. **Materials and Methods:** : Substance 1-thio-B-glucose and other reagents were purchased from Sigma-Aldrich ACS grade. Obtaining a labeled radiopharmaceutical was carried out in 2 stages. At the first stage, the composition of the drug was developed based on the substance 1-thio-glucose, the reducing agent of tin dichloride dihydrate and the stabilizer of ascorbic acid. The resulting mixture was lyophilized without prior freezing in a freeze dryer. Subsequent radiolabeling was performed by adding 4 ml of sodium pertechnetate solution with an activity of 1.0 GBq and incubation at room temperature for 30 min. Radiochemical purity (RCP) control and complex formation were performed by TLC on silica gel using two different mobile phases. The in vitro stability of radioactively labeled glucose derivatives in aqueous solution was determined by adding a 1000-fold molar excess of cysteine, followed by monitoring the radiochemical purity using TLC. Tumor model creation was performed in mice using the C57B1 / 6j cell line (Lewis carcinoma). The radiopharmaceutical was administered to mice intravenously at a dose of 0.1 ml with a volumetric activity of 200 MBq / ml. Whole body scintigraphy of animals was performed on an E.CAM Signature 1800 gamma camera (Siemens, Germany) 15, 40 and 120 min after injection. Results: : Substance 1-thio-glucose - has been successfully labeled with 99mTc using a reducing agent and stabilizer. The radiochemical yield of 99mTc-1-thio-glucose was 91%, and the radiochemical purity was over 98%. Stability analysis, including analysis in the presence of excess cysteine, showed no adverse effect on radiochemical purity. 40 minutes after the injection of the drug, SPECT scanning of the animals showed a clear visualization of the implanted tumor of the right thigh. **Conclusion:** Substance 1-thio-D-glucose was successfully labeled with Tc-99m with high radiochemical purity (<98%) and stability. Scintigraphy with the obtained preparation provided high-precision detection of the implanted tumor, Lewis carcinoma, in mice. **References:** none

TEPS-06

Obtaining radiopharmaceuticals based on somatostatin analogs for imaging neuroendocrine tumors

***E. Shelikhova**, E. Stasyuk, E. Nesterov, A. Rogov, V. Sadkin, M. Larkina;*
Tomsk Polytechnic University, Tomsk, RUSSIAN FEDERATION.

Aim/Introduction: Neuroendocrine tumors (NET) are a heterogeneous group of oncological diseases with a variety of clinical and morphological symptoms and biological characteristics. Despite the fact that NET is a periodic recurrent disease, pathology. For and treatment of NETs, radiopharmaceuticals are used based on somatostatin analogs, for example, octreotide labeled with radionuclides such as 111In, 99mTc, 188Re, 177Lu, etc. **Materials and Methods:** To obtain a radiopharmaceutical were used methods of fine organic synthesis with the use of chelating agents based on DPAH. The products were purified and identified using high performance liquid chromatography. The radiochemical purity of the resulting complex was determined by thin layer chromatography. Results: A unique technology was developed for obtaining a complex based on DPAH-modified octreotide labeled with a radioactive isotope technetium-99m. The developed method makes it possible to obtain a product with a high yield and high rates of radiochemical purity (a patent was received in 2019). The yield of DPAH-modified octreotide (DPAH-octreotide) is 60.15%, and the radiochemical purity of the finished product (technetium-99m complex with DPAH-octreotide) is 96.2%. **Conclusion:** Preclinical studies have confirmed the safety of the drug and have shown that the developed complex accumulates rather intensively in the tumor and allows obtaining scintigraphic images of proper quality. **References:** none

TEPS-07

Results Of The Initial Examinations With MIBITop 1 mg Freeze Dried Kit

***S. Keresztes**[1], T. Mándoki[1], G. Nagy[2], S. Barna[2], M. Antalffy[1];*
[1]Institute of Isotopes Co., Ltd., Budapest, HUNGARY,
[2]Scanomed Ltd., Debrecen, HUNGARY.

Aim/Introduction: To formulate a new version of freeze dried sestamibi cold kit for radiopharmaceutical preparation which is suitable for routine use in nuclear medicine laboratories, for diagnostic imaging of myocardial perfusion, detection and localisation of coronary artery disease, for application of scintimammography and for examination of hyperfunctioning parathyroid tissue. **Materials and Methods:** The tested MIBITop 1 mg cold kit was subjected to the hospital application after the quality control and releasing procedures and the marketing authorization approval. The quality control tests were carried out to establish the compliance of specifications regarding the pH value, the tin(II) content, the loss on drying, the API assay and the radiochemical purity of injection. A simple, end-user method for 'on-the-spot' testing of radiolabeling has been developed as well. The first application was carried out by a known Hungarian hospital, where the quality of the product was also studied. Results: The quality was compliant to the European Pharmacopoeia specifications [01/2008:1926] and the product was successfully labelled with ^{99m}Tc. The initial clinical application demonstrated the high utility of ^{99m}Tc-sestamibi (^{99m}Tc-[tetrakis(1-isocyanide-2-methoxy-2-methylpropyl-)copper(I)] tetrafluoroborate) in diagnostic imaging of patients with myocardial perfusion diseases and parathyroid tissue tumors. The new composition allows

twenty or more patient examinations with one piece of cold kit. **Conclusion:** The formulated kit has comprehensive and economical application possibilities in hospitals. **References:** none

TEPS-08

Fully-automated production of 68Ga-FAPI-46 in TRASIS mini AIO and quality control with TLC and HPLC methods

R. Shukurov[1], Z. Dadashov[1], M. Valiyev[1], M. Balashov[1], C. Isayev[1], K. Eryilmaz[1], F. Valla[2], F. Novruzov[1];
[1]Azerbaijan National Centre Of Oncology, Department of Nuclear Medicine, Baku, AZERBAIJAN, [2]SOFIE, Totowa, NJ, UNITED STATES OF AMERICA.

Aim/Introduction: 68Ga-FAPI-46 is one of the most advantageous radiopharmaceuticals that have been successfully applied to PET imagining used in the examination of (FAPs) Fibroblast activation protein. This article discusses the fully automated synthesis of 68Ga-FAPI-46 in the TRASIS Mini AIO and the methods of quality control before clinical use. **Materials and Methods:** The synthesis of 68Ga-FAPI-46 radiopharmaceutical was conducted on the commercial labeling synthesis modules TRASIS Mini AIO was equipped with a disposable single-use cassette and reagent kit. The transfer line of the 68Ga radionuclide generator (IRE ELiT) is connected to the cassette. Gently dissolve 60 mg of FAPI-46 precursor (The precursor was obtained by SOFIE) in a buffer solution consisting of a mixture 1 ml 0.5 M Acetate buffer and 100 µl 0.2 M sodium ascorbate. The obtained mixture is loaded in the appropriate place at the cassette. The automated synthesis process continues elution of 1.2 ml of 68Ga radionuclide from the generator and dissolved precursor in the buffer solution mixed up in the reaction vial and heated to 95° C for 10 min. The product is trapped on the HLB cartridge and eluted with 5 ml of ethanol solution. Radiochemical purity was evaluated by radio-HPLC and radio-TLC. XDB-C18 (4.6x150mm) column is used for HPLC analysis. Radio-HPLC was performed with the following method: Acetonitrile/water/ 0.1% trifluoroacetic acid (TFA) (30:70:0.1) (Rf-3.0). A mixture of methanol/ammonium acetate 5M (75:25%) is used as the TLC mobile phase (Rf- 5.5-6.5). Results: The yield of the synthesized crude 68Ga-FAPI-46 sample was more than 75%. The radiochemical purity of the final product was observed to be >99%. **Conclusion:** Based on the obtained results, the proposed method for conducting the fully automated synthesis process of 68Ga-FAPI-46 radiopharmaceutical on the TRASIS mini AIO device has been proved to be reliable and suitable. This process could be applied for routine 68Ga-FAPI-46 GMP production for clinical applications. **References:** 1. Sarah Spreckelmeyer, Matthias Balzer, Simon Poetzsch, Winfried Brenner Fully-automated production of [^{68}Ga] Ga-FAPI-46 for clinical application. EJNMMI Radiopharm Chem. 2020 2. Clemens Kratochwil, Paul Flechsig, Thomas Lindner ett. all. ^{68}Ga-FAPI PET/CT: Tracer Uptake in 28 Different Kinds of Cancer. Journal of Nuclear Medicine, 2019 3. Frederik L. Giesel1, Sebastian Adeberg, Mustafa Syed ett, all. FAPI-74 PET/CT Using Either 18F-AlF or Cold-kit 68Ga-labeling: Biodistribution, Radiation Dosimetry and Tumor Delineation in Lung Cancer Patients. Journal of Nuclear Medicine, 2020

TEPS-09

Technical validation of myocardial flow reserve measurement using a dynamic cadmium-zinc-telluride camera

T. Niimi[1], K. Unno[1], S. Yoshida[2];
[1]Nagoya Daini Red Cross Hospital, Nagoya, JAPAN, [2]Nagoya University, Nagoya, JAPAN.

Aim/Introduction: A cadmium-zinc-telluride (CZT) camera allows for the evaluation of myocardial blood flow (MBF) and myocardial flow reserve (MFR) without positron emission tomography (PET). Many papers have shown a correlation with the numerical value obtained by PET regarding the measurement; however, these measurements are affected by collection timing, region of interest (ROI) size, and set sampling position of blood flow, making it difficult to consistently calculate accurate values. Regarding the ROI setting position, it seems that the influence on the measurement is largely dependent on the measurer. The effects of the ROI sampling position of blood flow on MBF and MFR were investigated by fixing the collection conditions, ROI size, and analysis conditions of the CZT camera. **Materials and Methods:** We evaluated 29 patients with suspected or known coronary artery disease who underwent dynamic CZT single-photon emission computed tomography (SPECT) after injection of 250 MBq and 820 MBq of 99mTc-sestamibi for rest and stress imaging, respectively. Nuclide injection was performed at 1 cm^3/s using an automatic injector and flushed with 30 ml of saline. Dynamic SPECT imaging data was analyzed using commercially available software. The ROI (2 pixels wide in the short axis and 30 mm long in the long axis) setting positions for the blood pool consisted of the left atrium (LA), left ventricle (LV), basal valve plane (within the LV and LA blood pool), and the peak count of the blood pool. Results: The global MBF (mean value of stress and rest) was 14.4% for the LA, -10.9% for the LV, and -15.9% for the peak count of the blood pool relative to the valve position including blood flow in the LA and LV ($p<0.05$). The peak count of the blood pool was all within the LV except for 3 cases (position across the LA and LV). MFR was -0.62% for the LA, 8.5% for the LV, and 7.4% for peak counts in the blood pool ($p>0.05$). **Conclusion:** The effect of the ROI sampling position of blood flow on MBF and MFR was confirmed. MBF tended to be lower in the LV and higher in the LA relative to the valve position including blood flow in the LA and LV. However, there was no significant difference in the MFR due to the difference in the ROI setting position. **References:** none

TEPS-10

Influence of low counts on clinical images of brain perfusion SPECT

A. Sugiura[1,2], M. Onoguchi[1], T. Shibutani[1], T. Aoki[2], Y. Kouno[2]; [1]Department of Quantum Medical Technology, Institute of Medical, Pharmaceutical and Health Sciences, Kanazawa University, Kanazawa, JAPAN, [2]Department of Radiological Technology, Kariya Toyota General Hospital, Kariya, JAPAN.

Aim/Introduction: The counts per pixel of brain perfusion single photon emission computed tomography (SPECT) images depend on the administration dose, acquisition time or patient condition, and it sometimes becomes poor acquisition counts in clinical practice. Therefore, when clinical limitations result in low acquisition counts, it is necessary to evaluate whether the images are diagnosable for clinical use. The aim of this study was to determine the lowest acquisition counts that can be diagnosed in qualitative images and statistical imaging analysis. **Materials and Methods:** We performed a brain phantom experiment simulating normal accumulation of ^{99m}Tc-ethyl-cysteinate dimer (^{99m}Tc-ECD) with brain uptake of 5.5 %. A Hoffman 3D brain which simulates gray and white-matter structures was used as the phantom. The SPECT data were acquired in a continuous repetitive rotation with a dual-head gamma camera equipped with a low-energy high-resolution (LEHR) collimator. Ten types of SPECT images with different acquisition counts (123.6, 92.3, 61.0, 30.8, 23.6, 19.9, 16.0, 12.0, 7.9 and 4.0 counts/pixel, respectively) were created by varying the addition of the number of rotations on a workstation. We used the normalized mean squared error (NMSE) and visual analysis scored on a 5-point scale. Then, the reference acquisition counts that assured image quality sufficient for diagnosis was defined. In the clinical study, we used 25 patients acquired in a continuous repetitive rotation. Furthermore, we created five brain images with lower acquisition counts than the reference by varying the number of rotations added from 1 to 5. The contrast-to-noise ratio (CNR) was calculated from the mean counts with ROIs in gray and white matter. In addition, the severity, extent and ratio of disease-specific regions were analyzed using easy Z-score imaging system (eZIS). Results: In the phantom study, the curve of NMSE showed a tendency of convergence from approximately 16.0 counts/pixel. The visual score increased as increasing acquisition counts, and showed that images with 30 counts/pixel or more were sufficient for diagnosis. The CNR was significantly decreased at one third of the reference acquisition counts (11.5 counts/pixel) or less. Severity and extent tended to increase as decreasing acquisition counts, and showed a significant increase at 5.9 counts/pixel. On the other hand, ratio did not vary significantly among the different acquisition counts. **Conclusion:** We conducted phantom and clinical studies, and determined that the image of 11.5 counts/pixel or more was necessary to ensure the reliability of both qualitative images and statistical imaging analysis. **References:** none

TEPS-11

The contribution of Artificial Intelligence for the Diagnosis of Alzheimer's Disease in PET: Systematic Review

P. Ferreira[1], F. Afonso[1], J. Saraiva[1], S. Figueiredo[1,2], L. Vieira[1,2,3]; [1]Escola Superior de Tecnologia da Saúde de Lisboa, Lisbon, PORTUGAL, [2]H&TRC-Health & Technology Research Center, ESTeSL- Escola Superior de Tecnologia da Saúde, Instituto Politécnico de Lisboa, Lisbon, PORTUGAL, [3]Centro de Investigação em Modelação e Optimização de Sistemas Multifuncionais, Escola Superior de Tecnologia da Saúde, Instituto Politécnico de Lisboa, Lisbon, PORTUGAL.

Aim/Introduction: Alzheimer's Disease (AD) is a progressive and irreversible neurodegenerative disease. The Positron Emission Tomography (PET) has contributed to the detection of pathological processes years before the appearance of clinical symptoms. The assessment of PET studies for AD is particularly challenging, since cognition involves a continuum spectrum between normal cognition (NC) and dementia, which includes Mild Cognitive Impairment (MCI) as the major state between normal cognitive decline and a dementia. Presently, the image interpretation is performed using conventional methods. Furthermore, new approaches based on Artificial Intelligence (AI) techniques, such as Deep Learning or Convolutional Neural Networks (CNN) are being applied. The present review aims to evaluate the contribution of AI in PET as a predictor of progressive MCI to the AD's course. **Materials and Methods:** This systematic review was performed using the Science Direct, PubMed and SciELO databases as resources, accordingly to PRISMA methodology. The articles included in the analyses were based on the English language and dated from 2011 to 2021. The keywords Alzheimer; FDG PET; Amyloid PET; Deep Learning; Artificial Intelligence; Predict were used. Review articles and high-complexity detailed mathematical algorithms were excluded. From a total of 335 analyzed articles, 25 were included. Results: The preliminary results suggest that AI-based PET methods can increase the accuracy of the prediction of the disease course in individuals with MCI. Choi H et al, show that their CNN-based approach was able to predict MCI progression to AD, marked as a sensitivity value of 81.0%, a specificity of 87.0% and an accuracy of 84.2%.[(1)] More recently, Yang Z et al., suggest that their deep learning model achieved 91.02% sensitivity and 77.63% specificity when it comes to predicting the conversion from MCI to AD using FDG-PET.[(2)] **Conclusion:** Although these results are preliminary, we believe that, based on these findings, AI holds an increasing contribution not only in the classification within the cognitive spectrum, but also in the early diagnosis and MCI conversion prediction. **References:** 1. Choi H, Jin KH. Predicting cognitive decline with deep learning of brain metabolism and amyloid imaging. Behav Brain Res. 2018;344(2010):103-9. 2. Yang Z, Liu Z. The risk prediction of Alzheimer's disease based on the deep learning model of brain 18F-FDG positron emission tomography. Saudi J Biol Sci. 2020;27(2):659-65.

TEPS-12

Optimization of becquerel calibration factor for quantitative bone SPECT without attenuation and scatter correction in the lumbar spine: Head-to-head comparison with attenuation and scatter correction

H. Ichikawa[1,2], M. Onoguchi[2], T. Shibutani[2], T. Ito[3], H. Shimada[1]; [1]Toyohashi Municipal Hospital, Toyohashi, JAPAN, [2]Department of Quantum Medical Technology, Graduate School of Medical Sciences, Kanazawa University, Kanazawa, JAPAN, [3]Department of Radiological Technology, Faculty of Medical Technology, Teikyo University, Itabashi-ku, JAPAN.

Aim/Introduction: Quantitative bone single-photon emission computed tomography (SPECT) with computed tomography (SPECT/CT) is known to afford improved diagnostic performance; although SPECT-alone systems are used widely, accurate quantitative bone SPECT with these systems is challenging. This study aimed to improve the accuracy of quantitative bone SPECT of the lumbar spine with a SPECT-alone system. **Materials and Methods:** The becquerel calibration factor (BCF) was measured using a cylindrical phantom, body phantom, and SIM^2 bone phantom, and the optimal values were determined by comparing the actual radioactivity concentrations with the quantitative SPECT values of a custom-designed bone phantom. The absolute recovery coefficient (RC) with and without attenuation and scatter correction (ACSC) were compared using the custom-designed bone phantom. SPECT/CT was performed on 93 consecutive patients with prostate cancer who underwent bone scintigraphy to obtain SPECT data with and without ACSC, and quantitative SPECT values were compared using the respective BCFs. The first 60 patients were classified according to body weight, and the correlation coefficient between standardized uptake values (SUVs) with and without ACSC were calculated, and the slopes were defined as body weight-based coefficients (BWCs). In the remaining 33 patients, the SUV was adjusted according to the BWC, and the accuracy of the adjustment was verified. Correlations between SUVs with and without ACSC were assessed using Pearson correlation coefficients, and paired values were analyzed using Wilcoxon signed-rank tests. Results: The optimal BCF value without ACSC was 40938.2. The peak quantitative SPECT values (QSVs) obtained from the BCF using SBP showed almost accurate radioactivity concentrations, even without ACSC. The absolute RCs with and without ACSC were similar. Unadjusted SUVs with and without ACSC were strongly correlated ($r = 0.927$); however, SUVs without ACSC was significantly higher than those with ACSC ($p < 0.0001$). The mean difference between the SUVs with and without ACSC disappeared when the SUVs without ACSC were adjusted by BWC ($p = 0.9814$). **Conclusion:** Our becquerel calibration method for quantitative bone SPECT enables interpretation with a harmonized SUV even in SPECT-alone systems. **References:** None

TEPS-13

Post COVID-19 vaccination reactive lymphadenopathy on 18F-FDG PET

A. Nasr, A. Akbari, J. Hagerman; Skåne University Hospital, Lund, SWEDEN.

Aim/Introduction: After the onset of the mass COVID-19 vaccination globally, numerous case reports have been published regarding fluorodeoxyglucose (18F) avid lymph nodes associated with the vaccination. According to The Society of Nuclear Medicine and Molecular Imaging (SNMMI), FDG-avid lymphadenopathy can be visualized up to 4-6 weeks post COVID-19 vaccination. This study aimed to investigate if COVID-19 vaccines lead to reactive FDG-avid lymph nodes and the duration of the avidity. Moreover, to compare this phenomenon among different types of vaccines (Pfizer/BioNTech, Moderna, and AstraZeneca). **Materials and Methods:** During March and April 2021, a total of 39 patients were included in the study. All patients with at least one dose of vaccine administered during the last two months were included. During the examination, patients were interviewed regarding COVID-19 vaccination (vaccination type, date, and injection site for the vaccination). The authors reviewed the images and the examination reports concerning the presence of reactive FDG-avid lymph nodes (positive findings). Results: 8 of 21 patients vaccinated with Pfizer/BioNTech, 2 of 8 patients with Moderna, and 4 of 9 patients with AstraZeneca had positive findings. The number of days between vaccination and the FDG-PET examination was 5.5 (2-27) for Pfizer/BioNTech, 10.5 (7-14) for Moderna, and 13.5 (4-14) for AstraZeneca, for the positive cases. **Conclusion:** Reactive FDG-avid lymph nodes can be visualized after COVID-19 vaccination, regardless of the vaccination type, for at least four weeks post-vaccination. Therefore it is crucial to report this information to the physician interpreting the FDG images. **References:** 1. Society of Nuclear Medicine and Molecular Imaging. SNMMI Statement: The Effect of COVID-19 Vaccination on FDG PET/CT [Internet]. Virginia: SNMMI; 2021 [cited 2021 April 30] Available from: https://www.snmmi.org/NewsPublications/NewsDetail.aspx?ItemNumber=36729

TEPS-14

Investigation of Optimal Reconstruction Conditions Using the Bayesian Penalized-Likelihood Algorithm in [^{18}F]fluciclovine PET Imaging for Brain Tumors

K. Tsuzura[1,2,3], K. Wagatsuma[3], N. Yokotsuka[2], K. Miwa[4], Y. Kamitaka[3], K. Tanimoto[1], R. Nishii[5], K. Ishii[3];
[1]QST Hospital, Chiba, JAPAN, [2]Teikyo University, Tokyo, JAPAN, [3]Tokyo Metropolitan Institute of Gerontology, Tokyo, JAPAN, [4]Fukushima Medical University, Fukushima, JAPAN, [5]Institute for Quantum Medical Science, Chiba, JAPAN.

Aim/Introduction: [^{18}F]fluciclovine is an amino acid positron emission tomography (PET) tracer that can help achieve better image contrast and lesion detectability for brain tumors than [^{11}C]methionine. Using [^{18}F]fluciclovine combined with the Bayesian penalized-likelihood (BPL) algorithm Q.Clear is expected to produce better image quality and quantification than that using the ordered subset expectation maximization reconstruction method. The BPL algorithm suppressed image noise to adjust the β value as a penalty function. The present study aimed to optimize the reconstruction parameters of the BPL algorithm in [^{18}F] fluciclovine. **Materials and Methods:** Six spheres (diameters of 38, 27, 16, 10, 7.5, and 5 mm) were placed in a brain tumor (BT) phantom. The background radioactivity and hot sphere-to-background ratio of the BT phantom were set at 1.1 kBq/mL and 3:1, respectively, as estimated from a previous report. The BT phantom was acquired for 20 min using a Discovery MI PET/CT system in list mode. All images were reconstructed under the following algorithm and parameters: BPL with time-of-flight (TOF), β = 100-1,000; 256 × 256 matrix size; and 1.0 mm/pixel. Contrast (% contrast), image noise as indicated by the coefficient of variation (CV), and recovery coefficient (RC) were calculated from the phantom images generated. The visual evaluation was assessed by the visibility of the 7.5-mm sphere. Results: The % contrast was stable regardless of β value for >16-mm spheres but decreased as the β value increased for ≤10-mm spheres. The CV decreased as a function of β-value and was <10% when β = 300. The RC was stable regardless of β-value for >16-mm spheres. The RC of ≤10-mm spheres decreased with increasing β-value. The accumulation of the 5-mm sphere did not recover due to the partial volume effect, whereas the 7.5-mm sphere was detected in all conditions. However, statistical noise on the phantom background was unable to distinguish the small hot sphere at β = 100 and 200. **Conclusion:** Contrast and quantification were improved when smaller β values were used; however, image noise appeared on the phantom background when β = 100 and 200. The optimal β-value for the BPL algorithm in [^{18}F]fluciclovine PET imaging for BT was β = 300, which provided the best balance between contrast and image noise. **References:** none

TEPS-15

The Imaging Performance of 89Zr in TOF PET/CT system

Y. Parlak[1], D. Goksoy[1], C. Sezgin[1], I. Medine[2], G. Gumuser[1], O. Aras[3], E. Sayit[1];
[1]Departmant of Nuclear Medicine, Celal Bayar University, Manisa, TURKEY, [2]Department of Nuclear Applications, Institute of Nuclear Sciences, Ege University, Izmir, TURKEY, [3]Department of Radiology, Memorial Sloan Kettering Cancer, New York, NY, UNITED STATES OF AMERICA.

Aim/Introduction: Zirconium 89 is a new radionuclide that plays an important role in immuno-positron emission tomography imaging. Due to its long half-life, it has an advantage in transfer and preparation processes, but disadvantageous in terms of radiation dose. The imaging characteristics of the 89Zr radionuclide were evaluated in this study. Our aim is to evaluate the image quality of 89Zr in the study. **Materials and Methods:** A point source in a capillary tube for spatial resolution measurements and a nonuniform cylindrical phantom containing hot/cold lesions for other measurements were prepared with 89 Zr. These sources were placed in the axial FOV center of PET/CT (Philips, TruFlight Select, 16-slice CT). The images were acquired at different time periods in the single bed position. Scaning time was 4 minutes for spatial resolution measurements and images with the duration of 1 min, 2 min, 3 min, 4 min, 5 min, 8 min and 10 minutes were also acquired for image characteristics. Signal to noise ratio, percent contrast and background variability were calculated as image characteristics. All images were reconstructed with the OSEM technique for 33 subset and 3 iterations. Results: According to our results, the spatial resolution of 89Zr was calculated as approximately 4.9 mm. The signal to noise ratio was calculated between 1.4-3.1 for different scanning times and various sphere sizes. The highest image contrast measured was 62% and the background variability was calculated in the range 5-13% for 89Zr. **Conclusion:** Our results have shown that 89Zr is an ideal radionuclide for immuno PET imaging. **References:** none

TEPS-16

Hand-foot contamination monitoring in hospital radiopharmacy laboratory: 2020 follow-up data

K. Levänen[1], C. Lehtinen[1], M. Kullberg[1], J. Ketola[2], J. Heikkinen[2];
[1]Department of Radiology and Nuclear Medicine, Social and healtcare joint authority of South Savo, Mikkeli, FINLAND, [2]Department of Medical Physics, South Savo Social and Health Care Authority, Mikkeli, FINLAND.

Aim/Introduction: Last year, we presented our hand-foot monitor contamination data from between February 2019 and February 2020. In this study, we present follow-up data obtained during the rest of 2020. Contamination control

is important in reducing unneeded doses to personnel or patients. A hand-foot monitor is useful in detecting possible contaminations in gloves or shoes. The hand-foot monitor was connected to cloud service, allowing real-time monitoring of measurements, easy record keeping, and data collection. **Materials and Methods:** Measurements were recorded during 8 months from May 2020 to December 2021. During that time, radiopharmacy laboratory was mainly used by four radiographers. After each visit to the lab, they measured the dose rate of their gloves and shoes with hand-foot monitor from eight target areas: right/left hand palm/back, right/left foot front/back. All targets were measured simultaneously in one measurement. Radiographers identified their measurements by personal label. Results: Threshold of contamination of clothes of personnel or environment outside radiopharmacy laboratory is defined as a dose rate of 4 Bq/cm^2 or more (Radiation and Nuclear Safety Authority STUK Finland). In total, the radiographers completed 125 measurements, of which in 14 % of cases (17 instances) contamination threshold was exceeded in at least one target area. Some activity was detected in 76 % of measurement cases (95 instances). The most common contamination target was right hand (76 % or 13 of cases above threshold, 46 % or 44 of cases of any activity). One instance of foot contamination was recorded (6% of cases above threshold). When threshold was exceeded, average dose rate was 59 Bq/cm^2 (median 17 Bq/cm^2, range from 4.1 to 570 Bq/cm^2). There were two incidents where the dose rate exceeded 100 Bq/cm2. Overall, average dose rate was 14 Bq/cm^2 (median 0.5 Bq/cm^2) when any activity was detected. Usually when one target was contaminated, some others were too. **Conclusion:** Right hand was the most commonly contaminated target; all radiographers were right-handed. Average dose rate of 59 Bq/cm^2 represented a 32% increase from previous data. Some outlier activities skew the distribution as the median, which we believe is a more realistic estimate, was only 17 Bq/cm^2. Average dose rate of 14 Bq/cm^2 in measurements where any activity was detected represents a 37% decrease from previous data. Number of contamination incidents has decreased by 2%. Overall, during the period our facility has used the hand-foot monitor, the average activity in measurements has declined. **References:** None

1912

Wednesday, October 20 - Saturday, October 23, 2021

on-demand pool, release on Wednesday, October 20 at 09:00

e-Poster Presentation Session 15: AI and Radiomics

EPS-225

Comparison of cross-combinations between feature selection and machine-learning classifier methods based on 18F-PET/CT radiomic features for prediction of the metabolic response in metastatic breast cancer

O. Gomez Lopez, J. López Herraiz, J. Udías Moinelo;
Complutense University of Madrid, Madrid, SPAIN.

Aim/Introduction: to identify an optimal combination between feature selection methods and machine learning (ML) classifiers based on 18F-PET/CT radiomic features, to predict metabolic response to the systemic treatment, in patients with recurrent/metastatic breast cancer. **Materials and Methods:** 48 patients with histologically confirmed recurrent/metastatic breast cancer, who received systemic treatment between 2010 and 2015, were enrolled. All patients had an 18F-FDG-PET/CT before and after the systemic therapy administration. A total of 228 tumor lesions were identified in the pre-treatment PET/CT; from these 127 were classified as responders (complete or partial metabolic response) and 101 as non-responders (stable or progressive metabolic response), by using PERCIST criteria. For each lesion, 202 image features from PET and CT were extracted. These features along with clinical and pathological information were used to construct prediction models of metabolic response, by using several combinations of feature selection and classification methods. The lesions were randomly divided into two groups with a ratio of 80:20. The bigger was used to create the models and 6-fold cross-validation, and the other to validate. Seven feature selection methods: ANOVA with F-score, mutual information (MI), least absolute shrinkage and selection operator (LASSO), Wilcoxon test, hierarchical clustering (HC), principal component analysis (PCA), and independent component analysis (IPA); in cross-combination with other seven classification methods: support vector machines (SVM), random forest (RF), Gaussian naive Bayes (GNB), logistic regression (LR), k-nearest Neighborhood (KNN), adaptative boosting (AdaBoost) and neural network (NN); were compared for their performance in predict the metabolic response to the treatment. Model performances were investigated via area under the receiver-operating characteristic curve (AUC) and accuracy (ACC) analysis. Results: selection method LASSO+classifier SVM or RF, ICA+SVM had the highest AUC in the cross-validation, with 0.91±0.05, 0.90±0.02, 0.90±0.05 respectively. The selection method LASSO+classifier RF had the highest AUC and ACC

in the validating set, with 0.83 and 0.80 respectively, followed by LASSO+KNN (AUC=0.83, ACC=0.71). MI+NB or AdaBoost, as well as Wilcoxon+NB or RF, had good performance with an AUC of 0.80. SVM had the best mean performance in the cross-validation and validation cohort (only accuracy). RF had the best mean of AUC in the validation cohort. **Conclusion:** this study showed that image features obtained from a pre-treatment 18F-FDG-PET/CT could predict the metabolic response in recurrent or metastatic breast cancer, by their incorporation in a ML model, which performance depends largely on the feature selection and ML classifier methods selected. LASSO+SVM/RF had the better performance. **References:** None

EPS-226

Reproducibility of a semi-automatic gradient-based segmentation approach for lymphoma PET

F. Yousefirizi[1], I. Bloise[2], P. Martineau[2], D. Wilson[2], F. Benard[2], T. Bradshaw[3], A. Rahmim[1,4], C. Uribe[2,4];
[1]BC Cancer Research Institute, Vancouver, BC, CANADA, [2]BC Cancer, Vancouver, BC, CANADA, [3]Department of Radiology, University of Wisconsin, Madison, WI, UNITED STATES OF AMERICA, [4]Department of Radiology, University of British Columbia, Vancouver, BC, CANADA.

Aim/Introduction: Metabolic tumor volume (MTV) and total lesion glycolysis (TLG) are identified as prognostic metrics for survival analysis and treatment planning in lymphoma. However, these values are not routinely reported due to the time-consuming task of segmentation. Artificial intelligence (AI) methods have shown promise in performing automatic segmentation but their performance is limited to the size of training data that requires reliable labels. However, manual delineations suffer from inter-observer variability, even when using semi-automatic methods (e.g. fixed thresholding). We aim to develop a semi-automatic workflow that is robust and reproducible between observers to simplify the development of an extensive training dataset for automatic TMTV reporting on diffuse large B-cell lymphoma (DLBCL) PET scans. **Materials and Methods:** A semi-automatic workflow was created using the gradient-based segmentation method (MIM Software, USA). Three experienced nuclear medicine physicians independently segmented nine cases from a cohort of DLBCL PET scans. Lesions were labeled with 15 prepopulated anatomical regions (cervical lymph nodes, thoracic, etc.) as the variant site/size of lymphoma lesions can affect the performance of AI techniques. Physicians were informed that delineations would be used for TMTV calculations. Intraclass correlation coefficient (ICC) for the different segmentations was calculated for MTV, total lesion glycolysis (TLG), max and mean standard uptake (SUV) values. Additional features such as Standard deviation to mean ratio (Std_Mean), Kurtosis, Skewness were considered (for heterogeneity assessment). The segmentation results were also evaluated using the STAPLE algorithm that provides an estimation of true segmentation. Results: We observed high repeatability (ICC ≥ 95%) with respect to a number of quantitative measures (i.e. MTV, TLG, and SUVmax) between physicians. The measured ICC values were MTV=98%, TLG=99%, SUVtot=99%, SUVmax=96% (ICC>95%), SUVmean=92% (ICC>90%), Std_Mean=71% (ICC>70%). Based on the ICC values, Skewness=29% and Kurtosis=0.43 (ICC<50%) had significantly low repeatability among the physicians. The Dice scores compared to the ground truth (estimated by STAPLE) were 0.88, 0.79, and 0.88; the Jaccard values were 0.83, 0.72, and 0.82, and the Hausdorff Distances were 3.06, 4.18, and 3.95 respectively. **Conclusion:** Our initial results suggest that our workflow is reproducible for MTV and a number of quantitative metrics. While some features such as Kurtosis and Skewness depicted poor reproducibility. The segmentation evaluation also showed that the delineated regions were relatively close to one another. This has the potential of facilitating the creation of a multi-institutional dataset to develop reliable AI models and to facilitate routine reporting of TMTV and other features. **References:** none

EPS-227

Integrating gene mutation mutual exclusion logic and radiomics to improve the efficacy of predicting EGFR mutation in non-small cell lung cancer

J. Wang, F. Kang, J. Wang;
Department of Nuclear Medicine, Xijing Hospital, Fourth Military Medical University, Xi'an, Shaanxi, CHINA.

Aim/Introduction: Gene mutations are mutually exclusive in non-small cell lung cancer(NSCLC). To clarify the significance of mutation mutual exclusion information in the optimization of radiomics algorithms, this study aimed to take EGFR and KRAS as examples, to explore the influence of KRAS mutation information on the accuracy of radiomics algorithms for predicting EGFR mutation. **Materials and Methods:** We retrospectively analyzed 218 NSCLC patients with 18F-FDG PET/CT scans and results of EGFR and KRAS gene mutations. Patients were randomly divided into training and testing cohorts. The Pyradiomics toolkit was used for radiomics feature extraction. The gradient boosting decision tree (GBDT) algorithm was used to select features and develop a radiomics score(RS). A composite nomogram model combining PET/CT RS and KRAS mutation information were developed using logistic regression. The area under curve (AUC), specificity, sensitivity, accuracy, and precision were calculated for the model performance evaluation on the training and testing cohort. Results: Among the three models, the composite model exhibited the best performance. The composite nomogram model demonstrated highest AUC, accuracy and specificity in both training and testing cohort (AUC: 0.882 and 0.882, accuracy: 0.809 and 0.758, specificity: 0.868 and 0.879), significantly higher than CT RS model (AUC: 0.784 and

0.778, accuracy: 0.73 and 0.712, specificity: 0.632 and 0.636) and PET/CT RS model (AUC: 0.817 and 0.791, accuracy: 0.77 and 0.712, specificity: 0.789 and 0.788). By adding the KRAS exclusive mutation information, the composite nomogram model respectively corrected 37.4% and 42.9% false positive cases produced by the PET/CT RS model, without sacrificing its sensitivity (0.809 and 0.758). **Conclusion:** Adding the KRAS exclusive mutation information can significantly improve the accuracy of radiomics in predicting EGFR mutations, indicating that combining mutually exclusive logic of genetic mutation is a potential method for improving the radiomics model for predicting gene mutations. **References:** none

EPS-228

Methodological Framework for AI-assisted diagnosis of Active Aortitis using Radiomic Analysis of FDG PET-CT

L. Duff[1,2], A. Scarsbrook[3,4], S. Mackie[5,6], M. Bailey[1,7], R. Frood[3,4], A. Morgan[1,8], C. Tsoumpas[1,9,10];
[1]University of Leeds, LICAMM, Leeds, UNITED KINGDOM, [2]University of Leeds, CDT TERM iMBE, Leeds, UNITED KINGDOM, [3]University of Leeds, Leeds Institute of Medical Research, Leeds, UNITED KINGDOM, [4]St. James University Hospital, Department of Radiology, Leeds, UNITED KINGDOM, [5]University of Leeds, University of Leeds, Leeds Institute of Rheumatic and Musculoskeletal Medicine, Leeds, UNITED KINGDOM, [6]NIHR Leeds, Biomedical Research Centre, Leeds Teaching Hospitals NHS trust, Leeds, UNITED KINGDOM, [7]Leeds General Infirmary, The Leeds Vascular Institute, Leeds, UNITED KINGDOM, [8]NIHR Leeds, Biomedical Research Centre, Leeds Teaching Hospitals NHS trust, Leeds, UNITED KINGDOM, [9]Icahn School of Medicine at Mount Sinai, Biomedical Engineering and Imaging Institute, New York, NY, UNITED STATES OF AMERICA, [10]Invicro, London, UNITED KINGDOM.

Aim/Introduction: The aim of this study was to explore the feasibility of assisted diagnosis of active (peri-)aortitis using radiomic imaging biomarkers derived from [^{18}F]-Fluorodeoxyglucose Positron Emission Tomography - Computed Tomography (FDG PET-CT). This could have potential utility as a clinical decision-making tool facilitating objective and standardized assessment. **Materials and Methods:** The entire aorta was manually segmented on FDG PET-CT scans of patients with active aortits (n=50) and a control group (n=25). Pyradiomics and Simple ITK were used to extract 107 radiomic features (RF) and Standardised Uptake Value (SUV) metrics from the segmented aorta and harmonised using the ComBat technique. Mann Whitney U test and Logistic Regression (LR) classifiers were used to evaluate the diagnostic utility of extracted RF and SUV parameters. Diagnostic utility of RFs, SUV metrics and independent grading of aortic wall activity by an experienced radiologist according to EANM/SNMMI procedural recommendations were compared. Three fingerprints were built to explore the diagnostic ability of clusters of RFs and SUV metrics. Fingerprint A - features had to meet the following criteria: AUC≥0.5, accuracy ≥0.7, Mann Whitney U test p value ≤ where n = number of features. Fingerprint B - Fingerprint A criteria plus features were removed to reduce inter-feature correlation. Fingerprint C was formed with Principal Component Analysis (PCA). Results: Several RFs were shown to have high area under the receiver operating characteristic curve (AUC) scores 0.90 (0.83-0.97 95% Confidence Interval (CI)) when used individually in LR classifiers. RFs were also shown to have higher diagnostic ability than conventional SUV metrics. The radiomic fingerprints performed similarly with AUCs of A 0.84 (0.65-1.00 95% CI), B 0.91 (0.80-1.00 95% CI), C 0.87 (0.77-1.00 95% CI). **Conclusion:** Diagnosis of active aortitis based on radiomic analysis of FDG PET-CT is feasible. Radiomic features, individually and collectively had superior diagnostic performance than SUV metrics. **References:** none

EPS-229

Prognostic value of radiomic parameters derived from initial PET/CT in head and neck cancers

C. Latappy[1], N. Antonorsi[1,2], F. Trousset[1], A. Filali[1], R. Perdrisot[1], O. Tankyevych[1,2], C. Cheze-Le Rest[1,2];
[1]CHU de Poitiers, Department of Nuclear Medicine, Poitiers, FRANCE, [2]INSERM UMR 1101, LATIM, Brest, FRANCE.

Aim/Introduction: ^{18}F-FDG PET/CT often used for the initial staging of head and neck cancer can be used to extract many quantitative parameters. Our objective was to study the ability of radiomic parameters derived from a pre-therapeutic 18-FDG PET to predict the overall survival of patients with head and neck cancer. **Materials and Methods:** 148 patients with locally advanced head and neck squamous cell carcinoma treated by surgery or radiotherapy between 2012 and 2019 were included retrospectively. All patients underwent an ^{18}FDG PET/CT as part of routine pre-therapeutic staging. The metabolic tumor volume was determined by an automatic segmentation method (FLAB) and 9568 parameters were extracted from the PET and CT images. The correlation betweeen clinical features, PET and CT radiomics with the therapeutic response, recurrence and overall survival were analyzed. Their predictive value was determined by univariate logistic regression. A multivariate analysis with a selection of parameters by the LASSO method and classification by random forests was carried out on a subgroup of the population (75%) and the developed models (combining clinical data +/- radiomics PET +/- radiomics CT) were tested on the remaining population. The corresponding Kaplan-Meier curves were compared by log-rank test. Results: Amongst clinical parameters, only WHO status and TNM stage (8th edition) were correlated with loco-regional response. PET and CT radiomics were more efficient than clinical parameters in predicting response, recurrence, and overall survival. For all clinical endpoints considered the SUVmax performed worse compared to the texture parameters. The most efficient multivariate model for

predicting response and survival was obtained by combining clinical data with PET and CT texture parameters (AUC 0.87). **Conclusion:** PET/CT derived parameters demonstrated better performances- than the clinical parameters in predicting the response and overall survival confirming the interest in considering a radiomics based approach for the optimization of therapy management in patients with head and neck cancer. **References:** none

EPS-230

Prediction of CT radiomic features using PET radiomic features and vice versa

A. Jha[1,2,3], S. Mithun[1,2,3], U. B. Sherkhane[1,2], V. Jaiswar[2], G. Mehta[2,3], A. Nautiyal[2,3], N. Purandare[2,3], V. Rangarajan[2,3], A. Dekker[1], L. Wee[1];
[1]Department of Radiation Oncology (Maastro), GROW School for Oncology, Maastricht University Medical, Maastricht, NETHERLANDS, [2]Tata Memorial Hospital, Mumbai, INDIA, [3]Homi Bhabha National Institute (HBNI), Deemed University, Mumbai, INDIA.

Aim/Introduction: Qualitative and semi-quantitative parameters of PET and CT images are used to assist decision making for cancer treatment. In initial studies PET and CT radiomic features have shown promising results in disease prognostication and treatment outcome prediction in cancer. These features are specific to the outcome and different features show association with different outcomes. Hence finding the scalability of radiomic features from one modality to another can have promising impact. In our study we have tried to check the scalability of radiomic features across the modalities, PET and CT. We have performed a study to predict CT radiomic features using PET radiomic features and vice versa. **Materials and Methods:** This study was approved by the institutional ethics committee as retrospective study. 104 NSCLC patients who underwent pre-treatment PET-CT scan were included in this study. Primary lung tumor was delineated by SUV cut-off (42%) method on PET images and saved as RTStructure for PET and CT series. These Images and RTStructures were used for radiomic extraction using bin-width of 25 and 5 for CT and PET respectively using pyradiomic 2.1.0 software and in-house developed python script. Subsequently, concordance correlation coefficient (CCC) was calculated between PET and CT features and top 25 correlated features (excluding shape features) were selected to develop a prediction model. Entire set of data was split into training and validation sets (70:30). For each PET radiomic feature; a set of CT features were selected and vice versa using Recursive Feature Elimination(RFE). For individual feature prediction across modalities, a multivariate linear regression model was developed using selected features. Model performance was assessed based on accuracy of prediction (C-index) on validation set. Results: Around 54% and 46 % radiomic features show positive and negative correlation across PET and CT respectively. Only 91(8.33%), 69(6.3%) and 51(4.67%) features have $0.5<CCC<0.7$, $0.7\leq CCC<0.9$ and $CCC\geq 0.9$ respectively. Top 25 selected radiomic features had CCC equal to or more than 0.99. The average C-Index and p-value in validation set for 25 PET radiomic features prediction was found to be 0.988(±0.019) and <0.0001 respectively. Similarly, average C-Index value and p-value in validation set for 25 CT radiomic features prediction was found to be 0.987(±0.016) and <0.0001 respectively. **Conclusion:** As per our findings, very few radiomic features have good correlation between PET and CT. These features show excellent capability to predict features across these modalities. **References:** none

EPS-231

Understanding omics data of lung cancer patients: Correlations between metabolomics and radiomics

L. Mesotten[1,2], L. Deckers[2], R. Truyens[2], E. Derveaux[1,2], P. Adriaensens[2], M. Thomeer[1,2], R. Boellaard[3];
[1]ZOL, Genk, BELGIUM, [2]Uhasselt, Hasselt, BELGIUM, [3]Amsterdam UMC, Amsterdam, NETHERLANDS.

Aim/Introduction: Treatment of lung cancer remains challenging, partly due to the late-stage diagnosis of patients. With a strong focus on non-small cell lung cancer (NSCLC), this pilot study examines the diagnostic and prognostic potential of combining specific metabolic biomarkers from blood plasma (metabolomics) with features out of medical images (radiomics). This way, metabolomics and radiomics might be at the base of developing a more personalized treatment plan for lung cancer patients. This study aims to combine a metabolomics and radiomics dataset from lung cancer patients and to unravel the underlying correlations between the techniques. **Materials and Methods:** The initial patient cohort consisted of 32 patients, all diagnosed with early-stage NSCLC. All patients underwent a lobectomy as part of their standard-of-care treatment plan. The PET-CT images of all the patients were collected using ^{18}F-FDG (Biograph Horizon camera, Siemens). The PET-CT images were then segmented using a semi-automatic tool (ACCURATE), creating specific volumes of interest (VOIs) of the lung lesions for each patient. By loading the VOIs into the second tool (RADIOMICS), 486 radiomics parameters were extracted from each VOI (Both tools developed by R.B.) Simultaneously, 238 metabolic parameters representing 62 plasma metabolites were determined from the same patients using proton nuclear magnetic resonance (^{1}H-NMR) spectroscopy. A correlation coefficient test was used on the total omics-dataset to find a correlation between these two sets of parameters. Results: The correlation values found between the radiomics and metabolomics parameters showed R^2 values between 0.5 and 0.65 (positive correlation) or between -0.5 and -0.65 (negative correlation). The positive correlations found in the metabolomics dataset were mainly related to the concentration of plasma glucose. The radiomics

features positively correlated to glucose were identified as: center of mass shift, large zone low grey level emphasis, joint maximum, and angular second moment. The negative correlations found in the metabolomics dataset were mainly related to glycerol and phospholipids. The radiomics features that were negatively correlated to these metabolites were identified as coefficient of variation and quarter coefficient. **Conclusion:** For the first time, these results might suggest that the concentrations of at least some plasma metabolites are directly correlated with radiomics features that are extracted out of PET-CT images of the same patients. By increasing the patient cohort or focusing solely on PET images, correlations with other plasma metabolites might become apparent. **References:** none

EPS-232

Diagnostic value of baseline FDG PET/CT skeletal features in follicular lymphoma

J. Faudemer[1], N. Aide[1], G. Damaj[1], A. Gac[1], J. Vilque[2], C. Lasnon[2]; [1]CHU de Caen, Caen, FRANCE, [2]Centre François Baclesse, Caen, FRANCE.

Aim/Introduction: At present, ^{18}FDG-PET/CT can't be used to omit bone marrow biopsy (BMB) among initial staging procedures in follicular lymphoma (FL) (1). The additional diagnostic value of skeletal TFs on baseline ^{18}FDG-PET/CT in DLBCL patients has given promising results (2). The aim is therefore to evaluate the value of ^{18}FDG-PET/CT radiomics for the diagnosis of bone marrow involvement (BMI) in FL patients. **Materials and Methods:** This retrospective bicentric study enrolled newly-diagnosed FL patients addressed for baseline ^{18}FDG-PET/CT. For visual assessment, examinations were considered positive in cases of obvious bone focal uptakes. For textural analysis, the skeleton VOIs were automatically extracted from segmented CT images and analysed using LifeX software. BMB and visual assessment were taken as gold standard: BMB−/PET− patients were considered as Bone-$_{NEGATIVE}$ patients whereas BMB+/PET-, BMB−/PET+ and BMB+/PET+ as Bone-$_{POSITIVE}$ patients. A LASSO regression algorithm was used to select features of interest and build a prediction model. Results: Sixty-six patients were included: 36 Bone-$_{NEGATIVE}$ (54.5%) and 30 Bone-$_{POSITIVE}$ (45.5%). The LASSO regression found variance$_{GLCM}$, correlation$_{GLCM}$, joint entropy$_{GLCM}$ and busyness$_{NGLDM}$ to have non-zero regression coefficients. Based on ROC analysis a cut-off equal to - 0.190 was found to be optimal for the diagnosis of BMI. Corresponding sensitivity, specificity, PPV and NPV values equal to 70.0%, 83.3%, 77.8% and 76.9%, respectively. When comparing the ROC AUCs with using BMB alone, visual PET assessment or PET pred.score, a significant difference was found between BMB versus visual PET assessments (p=0.010) but not between BMB and PET pred.score assessments (p=0.097). **Conclusion:** Skeleton texture analysis is worth exploring to improve the performances of ^{18}FDG-PET/CT for the diagnosis of BMI at baseline in FL patients. **References:** 1. Luminari S, Biasoli I, Arcaini L, et al. . The use of FDG-PET in the initial staging of 142 patients with follicular lymphoma: a retrospective study from the FOLL05 randomized trial of the Fondazione Italiana Linfomi. Ann Oncol. 2013;24(8):2108-2112 2. Aide N. Talbot M. Fruchart C. Damaj G. Lasnon C. Diagnostic and prognostic value of baseline FDG PET/CT skeletal textural features in diffuse large B cell lymphoma. Eur J Nucl Med Mol Imaging. 2018 May;45(5):699-711.

EPS-233

The Effect of Increasing the Number of Iterations on the Stability of PET Radiomic Features: A Phantom Study

E. Alsyed[1], R. Smith[2], L. Bartley[2], C. Marshall[2], E. Spezi[1]; [1]Cardiff University, Cardiff, UNITED KINGDOM, [2]Wales Research & Diagnostic PET Imaging Centre, Cardiff, UNITED KINGDOM.

Aim/Introduction: The term radiomics is generally understood to mean a method of extracting quantitative features from medical images that cannot be seen by the human eye . Recently, researchers have shown an increased interest in using radiomic features extracted from positron emission tomography (PET) images which may serve as biomarkers to monitor cancer prognosis and treatments. However, more research on the stability of features under varying ordered subsets expectation maximization (OSEM) reconstruction settings needs to be undertaken before adopting radiomic features as key prognostic indicators clinically. This study set out with the aim of assessing the stability of PET image radiomic features over the number of OSEM iteration. **Materials and Methods:** Twenty radioactivity filled syringes were used to construct four artificial tumour inserts (7 in total for each tumour) with different degrees of heterogeneity. GE690 PET/CT scanner was utilized to scan the cylindrical uniform water filled phantom that contain the tumour inserts. Images were reconstructed with 6 different number of OSEM iteration (1, 2, 3, 4, 5, 6). Region of interests (ROI) were segmented in the default settings image (iteration = 2) and copied to all other subsequent images. To extract 78 3D-radiomic features for each number of iterations, SPAARC (Spaarc Pipeline for Automated Analysis and Radiomic Computing) was used. To assess feature stability against number of iterations, the Coefficient of Variation (COV) was calculated for each feature and categorized into four groups based to their COV values. Groups include unstable (COV > 20%), poorly stable (10% < COV ≤ 20%), moderately stable (5% < COV ≤ 10%) and stable (COV ≤ 5%) [1]. Results: 69.5% (54) of features were found to have high stability (COV ≤ 5%) whilst varying the number of iterations. Such features include GLCM_sum_average and NGTDM_coarseness. Seventeen (22%) and 5 (6%) features showed moderately stability (5% < COV ≤ 10%) and poor stability (10% < COV ≤ 20%) when varying the number of iterations, respectively. Only two features were found to have large variability (COV > 20%)

against numbers of iterations. **Conclusion:** Radiomic features may be affected by increasing the number of OSEM iterations. It is recommended that features with high variability against different parameters must be removed from further radiomic studies. **References:** [1] F. Gallivanone, M. Interlenghi, D. D. Ambrosio, I. Castiglioni, and G. Trifir, "Parameters Influencing PET Imaging Features : A Phantom Study with Irregular and Heterogeneous Synthetic Lesions," vol. 2018, 2018.

EPS-234

Phantom with Heterogenous Tumour Inserts to Explore the Impact of Varying Number of OSEM Subsets on PET Radiomic Features

E. Alsyed[1], R. Smith[2], L. Bartley[2], C. Marshall[2], E. Spezi[1];
[1]Cardiff University, Cardiff, UNITED KINGDOM, [2]Wales Research & Diagnostic PET Imaging Centre, Cardiff, UNITED KINGDOM.

Aim/Introduction: Positron emission tomography (PET) imaging plays an important role in the management of cancer. The iterative reconstruction of PET imaging is computationally expensive and to accelerate the reconstruction process, the ordered subsets expectation maximization (OSEM) algorithm is commonly used. However, there is a trade-off between image noise and the number of OSEM subsets. Therefore, radiomics which refers to a method of extracting quantitative features from medical images may be influenced by OSEM subsets and the subsequent degradation of the image quality (e.g. noise). This phantom study was undertaken to evaluate the stability of PET image radiomic features with varying number of OSEM subsets. **Materials and Methods:** An array of radioactivity filled syringes (7 in total for each tumour) were used to construct an artificial tumour insert. Four tumours were modelled with varying degrees of heterogeneity. The inserts were placed into a cylindrical uniform water filled phantom and imaged for 80 minutes using a GE690 PET/CT. Images were reconstructed with 5 different number of OSEM subsets (12, 16, 18, 24, 32). The segmentation was performed in the default settings (24 Subsets) and overlaid to all other subsequent images. 78 3D-radiomic features were extracted for each tumour volume at each number of subsets using SPAARC (Spaarc Pipeline for Automated Analysis and Radiomic Computing). The stability of radiomic features with varying number of OSEM subsets were assessed using the Coefficient of Variation (COV). Features were divided into four groups including stable (COV≤5%), moderately stable (5%<COV≤10%), poorly stable (10%<COV≤20%) and unstable (COV>20%) [1]. Results: Only five (6%) features had high instability (COV > 20%) with changing number of OSEM subsets. Five other features including GLRL_Run_length_variance, GLSZM_Zone_size_non_uniformity, and GLDZM_Large_distance_low_grey_level_emphasis were poorly stable (10% < COV ≤ 20%). Fifteen features (19%) were found to be moderately stable (5% < COV ≤ 10%). Fifty three (68%) features showed high stability (COV ≤ 5%). All NGTDM features were found to be very stable (COV ≤ 5%) against number of OSEM subsets. **Conclusion:** One major issue effecting confidence in adopting PET images radiomic features as clinical biomarker is their stability over varying number of OSEM subsets. Unstable radiomic features (with high COV) should be used with extreme caution in radiomic studies. **References:** [1] F. Gallivanone, M. Interlenghi, D. D. Ambrosio, I. Castiglioni, and G. Trifir, "Parameters Influencing PET Imaging Features : A Phantom Study with Irregular and Heterogeneous Synthetic Lesions,"vol.2018,2018.

EPS-235

Feasibility and Optimization of Radiomic Settings for Differentiation of HC and AD using ^{18}F-FDG and ^{11}C-PIB PET Scans

D. Peretti[1], G. Kolinger[1], E. Pfaehler[1], F. Reesink[1], B. de Jong[1], P. De Deyn[1,2], R. Dierckx[1], D. Vállez García[3,1], R. Boellaard[3,1];
[1]University Medical Center Groningen, Groningen, NETHERLANDS, [2]University of Antwerp, Antwerp, BELGIUM, [3]Amsterdam University Medical Center, Amsterdam, NETHERLANDS.

Aim/Introduction: Radiomics is an established method for identifying image features for computer-aided diagnosis and has been vastly applied to oncological studies. This study aimed to assess the feasibility of applying radiomic features to neurodegenerative diseases. A secondary aim was to optimize this methodology for the case of Alzheimer's disease (AD) patients using 2-[^{18}F]-fluoro-2-deoxy-D-glucose (FDG) and ^{11}C-labelled Pittsburgh Compound B (PIB) PET scans. **Materials and Methods:** 26 patients diagnosed with AD and 18 healthy controls (HC) underwent FDG and PIB PET scans. Per subject, the T1-MRI scans were used for delineation of cortical and cerebellar grey matter (GM) and cortical white matter (WM) tissues. PET images were registered to the MRI (subject space) and then transformed into the MNI space. All images were normalized to average cerebellar uptake (SUVR). All possible combinations of the following settings were considered: (1) tracer: FDG or PIB; (2) space: subject or MNI space; (3) discretization: fixed bin number (BN) of 64, fixed bin sizes of 0.05 or 0.25; and (4) volume of interest (VOI): cortical GM, cortical WM or BRAIN (union of cortical GM and WM). A total of 479 radiomics features were extracted for each configuration. Features that correlated (higher than 0.9) to the traditional metrics of average VOI uptake or volume in any configuration were removed from the analysis. A Wilcoxon signed-rank test was used to assess whether the features were significantly different between AD and HC. Results were corrected for multiple comparisons using Bonferroni and considered statistically significant if p-value < 0.05. Results: Different configurations resulted in different feature values. 241 features were removed due to their correlations with either VOI volume or average uptake. In general, PIB resulted in more features being significantly different between AD and HC subject than FDG images.

Meanwhile, independently of the tracer, a fixed BN of 64 and the GM VOI resulted in more features that discriminated between subject groups when compared to the remaining setting options. Except for a few features (e.g., features that were normalized by intensity range), subject and MNI spaces yielded similar numbers of discriminative features. **Conclusion:** These preliminary results suggest that radiomic features extracted from brain PET images may be used to differentiate AD and HC subjects. Further research is needed to assess the optimal combination of settings that maximizes feature repeatability, and to address radiomic features from brain regions that are known to be affected by neurological diseases. **References:** none

EPS-236

Robustness of Radiomic Features against Reconstruction Settings in [^{18}F]FET and [^{18}F]GE180 PET Imaging of Gliomas

A. J. Zounek, A. Holzgreve, F. Vettermann, J. Brosch-Lenz, A. Gosewisch, G. Böning, P. Bartenstein, N. L. Albert, S. Ziegler, L. Kaiser; Department of Nuclear Medicine, University Hospital, LMU Munich, Munich, GERMANY.

Aim/Introduction: Radiomic feature analysis and machine learning applications rely on large datasets to enable meaningful predictions that support clinical decisions. For both training of models and a subsequent clinical application, datasets often originate from multiple sources. However, heterogeneities in the datasets such as different image reconstruction settings can hinder this process. In this study, the influence of common PET image reconstruction settings on non-invasive glioma quantification using radiomic features was examined in order to identify the settings with the highest impact. **Materials and Methods:** The available image data consisted of amino acid ([^{18}F]FET) and TSPO ([^{18}F]GE180) PET acquisitions of 19 patients diagnosed with glioma. Image reconstruction was performed with 10 different settings per acquisition. The parameters being varied were type of reconstruction algorithm (filtered backprojection/OSEM2D/OSEM3D/TrueX), matrix size (128/168/336), number of subsets (8/16/21) and filter type (2/4/5 mm Gaussian). The number of iterations was held constant at a value of 4. Lesions were automatically segmented based on a threshold value which was obtained by multiplying the background signal by a factor of 1.6 according to the clinical standard. The PyRadiomics package was employed to extract 107 features per image. Statistically significant differences of features between different reconstruction settings were evaluated using the Friedman test, where the percentage of features with $p<0.001$ and the average test statistic were assessed. Results: The choice of filter (FET: 85% of features with $p<0.001$ and average test statistic of 29; GE180: 85%, 25) had the highest impact on glioma quantification using radiomic features for both tracer types, followed by the choice of algorithm (59%, 20; 53%, 17). The variation of matrix size (33%, 11; 24%, 9) and number of subsets (36%, 11; 48%, 13) resulted in a lower number of significantly different features. **Conclusion:** Results of the statistical analysis suggest that feature extraction is highly sensitive to image reconstruction settings in [^{18}F]FET as well as [^{18}F]GE180 PET imaging of glioma patients. Notably, even first-order features were strongly affected by a variation of settings. Overall, only very few features were found to show sufficient robustness. Thus, one should be cautious when dealing with data from multiple sources. Careful selection of suitable features and feature harmonization should be considered when uniformity of reconstruction settings is not given. **References:** none

EPS-237

18F-FDG PET radiomics predicts pathological data and survival of intrahepatic cholangiocarcinoma

F. Fiz[1], C. Masci[2], M. Sollini[1], G. Costa[1], G. Torzilli[1], F. Ieva[2], A. Chiti[1], L. Viganò[1];
[1]Humanitas Clinical and Research Center - IRCCS, Milan, ITALY, [2]MOX - Modelling and Scientific Computing Lab, Department of Mathematics, Politecnico di Milano, Milan, ITALY.

Aim/Introduction: Intrahepatic cholangiocarcinoma (IHC) is a rare disease at increasing incidence and poor prognosis. Surgery is the only potentially curative treatment, but adequate preoperative assessment of tumor biology and prediction of survival are unmet needs. The IHC SUV at ^{18}F-FDG PET/CT has shown some association with prognosis, but a limited capability to predict the pathology data. Recently, texture analysis (TA) has been applied to non-invasively predict the biology of tumors. We applied TA to preoperative PET/CT of IHC patients to ascertain if PET/CT-based radiomics are associated with the pathology data and survival. **Materials and Methods:** All consecutive patients with histologically proven IHC undergoing complete surgery between 2010 and 2019 with a pre-operative ^{18}F-FDG PET/CT were considered. A manual IHC slice-by-slice segmentation was performed, and textural features were extracted (LifeX®). Radiomic features were combined with: 1) the clinical data into a logistic regression model to predict the pathology data, i.e. IHC grading and microvascular invasion; 2) the clinical and pathological data into a Cox regression model to predict overall and progression-free survival (OS and PFS). Results: 74 patients (43 females, mean age 67 years, range 40-88) were included. SUVmean was not predictive of tumor grading and microvascular invasion. At the multivariate analysis, among the textural features, GLCM_Energy was associated with the IHC grading ($p=0.037$), while GLCM_Homogeneity ($p=0.005$), NGLDM_Coarseness ($p=0.005$) and GLZLM_LZE ($p=0.018$) with the microvascular invasion. The combined clinical/radiomic model had an AUC=0.78 for tumor grading prediction, and AUC=0.89 for microvascular invasion. After a median follow-up of 24 months, 3-year OS and PFS were

49% and 25%, respectively. SUVmean was not associated with OS and had a borderline-significant association with PFS at the univariate analysis (p=0.072), not confirmed at the multivariate one. In the multivariate model, GLRLM_LRE was associated with OS (HR=2.04, p=0.05) together with age (HR=2.32, p=0.003), type-3 tumor pattern (HR=3.14, p=0.034), lymph-node metastases (HR=15.71, p<0.001), and adjuvant chemotherapy (HR=0.30, p=0.031). GLRLM_LRE was also associated with PFS (HR=3.83, p=0.003) together with type-3 tumor pattern (HR=5.78, p=0.006), lymph-node metastases (HR=8.47, p<0.001), microvascular invasion (HR=2.72, p=0.031), and adjuvant chemotherapy (HR=0.13, p<0.001). **Conclusion:** In the present series, SUV was not a reliable IHC biomarker, while PET/CT-based radiomics describing general or zonal voxel homogeneity were associated with the tumor grading and microvascular invasion. Linear voxel patterns were associated with survival. In combination with standard clinical data, radiomics have the potential to improve non-invasive assessment of the IHC biological characteristics and prognosis. **References:** None.

EPS-238

Effect of change of gross tumour volume on CT radiomic features

G. Mehta[1,2], A. K. Jha[1,2,3], S. Mithun[1,2,3], V. Jaiswar[1], U. B. Sherkhane[1,3], N. Purandare[1,2], V. Rangarajan[1,2], A. Dekker[3], L. Wee[3];
[1]Tata Memorial Hospital, Mumbai, INDIA, [2]Homi Bhabha National Institute (HBNI), Deemed University, Mumbai, INDIA, [3]Department of Radiation Oncology (Maastro), GROW School for Oncology, Maastricht University Medical Centre+, Maastricht, NETHERLANDS.

Aim/Introduction: Radiomics is the extraction of high throughput quantitative features from medical images like CT, MRI, PET or SPECT. Radiomic features can be largely classified as shape-based, first order, textural, Laplacian of Gaussian (LOG) and wavelet features [1]. The radiomics workflow involves image segmentation i.e. Gross tumour volume (GTV) delineation, Image pre-processing, feature extraction, feature selection and model development. The image segmentation is manually performed by qualified and experienced imaging professionals, subjected to individual bias. The variation in image acquisition and GTV delineation impacts the radiomics feature value largely. Various studies have been performed to find the robustness of radiomics features and volume confounding effects[2]. In our study we have tried to find out the effect of change in volume on radiomics features. **Materials and Methods:** Study was approved by institutional ethics committee of our institution. The CT scan of 50 NSCLC patients who underwent diagnostic PET/CT scan in our department during 2015-17 was used in this study. GTV (GTV-100) was manual segmented over primary lung tumour by 15 year experienced physicist and checked by 30 years experienced nuclear medicine physician. Subsequently, two more GTV was delineated inside the original GTV-100 i.e. GTV-70 (70% of GTV-100) and GTV-30 (30% of GTV-100) by other physicist. In house developed python script and pyradiomics 2.1.0 was used for radiomics feature extraction. 1093 features were extracted for all three GTVs i.e. GTV-100, GTV-70 and stored as three subsets. The inter-class correlation (ICC-3) was calculated by using R software for three subsets of radiomic features to find effect of change in GTV volume. ICC value 0.9 and above was considered as robust correlation among three groups. Results: 21.59% (236/1093) radiomic features were highly correlated with each other ICC≥ 0.90. Out of 236 robust correlating features 10, 44, 182 features were original, LOG and wavelet features respectively. **Conclusion:** Our study shows that significant amount of features present high correlation despite considerable change in GTV. **References:** 1. Jha, A K, Mithun, S, Rangarajan, V, Wee, L, Dekker, A, Emerging role of artificial intelligence in nuclear medicine, Nuclear Medicine Communications: March 1, 2021 - Volume Publish Ahead of Print - Issue -doi.10.1097 MNM.0000000000001381 2. Jha, A.K., Mithun, S., Jaiswar, V. et al. Repeatability and reproducibility study of radiomic features on a phantom and human cohort. Sci Rep 11, 2055 (2021). doi.10.1038 s41598-021-81526-8

EPS-239

Non-invasive prognostic assessment of patients with NET liver metastases treated with PRRT: a ^{68}Ga-DOMITATE PET-based radiomics evaluation

G. Centurioni, C. la Fougère, F. Fiz;
Nuclear Medicine and Clinical Molecular Imaging, University Hospital Tübingen, Tübingen, GERMANY.

Aim/Introduction: Liver metastases (LM) from neuro-endocrine tumors (NET) can be managed by peptide-receptor radiotherapy (PRRT). However, the response duration in terms of time-to-progression (TTP) can show significant variations, ranging from weeks to months, also depending on the NET grading. Standard assessment of somatostatin-receptor (SSR) PET images is suboptimal in predicting TTP and grading. In this study, we tested whether additional analysis of PET patterns, termed "radiomics" can estimate TTP and assess the grading non-invasively. **Materials and Methods:** The institutional database was searched to identify NET patients with LM and treated with PRRT (Feb 2013 to Jan 2018). VOIs were constructed on each LM on the pre-PRRT 68Ga-DOTATATE PET (PET1) and on their counterparts on the same examination after two PRRT cycles (PET2). Radiomics analysis was carried out with LifeX®. Patients were sorted in long- and short responders (LR and SR) according to their TTP median. Results: Sixty-one patients (38 males, age 65±11, range 30-84) were identified. At the latest observation point (March 2021), forty-nine of them (80%) progressed with a median TTP of 27 months (range 4-73 months).At PET1, G3 LM had a higher SUVmean than G1/2 (13.6±3.6 vs 10.9±4.6, p<0.01) a less positive skewness (0.28±0.49 vs 0.71±0.49,

p<0.001), as well as greater levels of radiomics indicators of linear and zonal high-SUV patterns GLRLM_HGRE (2017±817 vs 1290±754, p<0.001) and GLZLM_HGZE (1935±720 vs 1244±655, p<0.001). Even though the radiomics indices showed no significant difference between LR and SR, the twelve patient that did not experience any progression had a higher SUVmean (p<0.01) and lower levels of GLRLM_LGRE/SRLGE as well as of GLZLM_LGZE/SZHGE (p<0.01) than those who progressed.At PET2 (after two PRRT cycles), SR had a higher drop of SUVmean (2.8±4.5 vs 0.7±4.8, p<0.001) as well as in different radiomics parameters: GLRLM_HGRE (p<0.01), NGLDM_Contrast (p<0.001), GLZLM_HGZE (p<0.01), and GLZLM_SZHGE (p<0.001). **Conclusion:** Semi-quantitative and PET radiomics assessments after two cycles might predict PRRT effectiveness in liver-metastasized NET patients, which were not reliably assessable with conventional imaging. In addition, our study revealed that both G3 NETs and short-term responders present a pattern characterized by high SSR density, with abundance of linear and zonal high uptake patterns in radiomics analysis. Interestingly, reduction of these indices after the first two PRRT correlated with a shorter time to progression, which might hint to a PRRT-driven selection of more aggressive clones, with lower SSR expression. **References:** None.

EPS-240

Artificial Intelligence Applications in SSTR Targeted PET/CT Images: Prediction of Response Assessment in GEP-NETs Undergoing PRRT with [^{177}Lu]DOTATOC

R. Laudicella[1,2,3], A. Vento[1], A. Spataro[1], A. Comelli[2], A. Stefano[4], L. Crocè[1], S. Baldari[5], M. Bambaci[6], D. Arico[6], M. Ippolito[5], M. Gaeta[7], I. A. Burger[3,8], F. Minutoli[1], S. Baldari[1];
[1]Nuclear Medicine Unit, Department of Biomedical and Dental Sciences and Morpho-Functional Imaging, University of Messina, Messina, ITALY, [2]Ri.MED Foundation, Palermo, ITALY, [3]Department of Nuclear Medicine, University Hospital Zürich, University of Zürich, Zurich, SWITZERLAND, [4]Institute of Molecular Bioimaging and Physiology, National Research Council (IBFM-CNR), Cefalu', ITALY, [5]Nuclear Medicine Department, Cannizzaro Hospital, Catania, ITALY, [6]Department of Nuclear Medicine, Humanitas Oncological Centre of Catania, Catania, ITALY, [7]Section of Radiological Sciences, Department of Biomedical Sciences and Morphological and Functional Imaging, University of Messina, Messina, ITALY, [8]Department of Nuclear Medicine, Kantonsspital Baden, Baden, SWITZERLAND.

Aim/Introduction: PRRT is a well-established option for progressive, metastatic neuroendocrine tumors (NET). However, almost 30% of patients do not respond to this approach and no well-established criteria are suitable for PRRT response assessment. Radiomics aims at identifying features contained in biomedical images, analyzing them in various scenarios such as the patients' outcome prediction. Therefore, we aimed to develop a radiomics predictive model of response to PRRT in gastroenteropancreatic (GEP) progressive, metastatic NET analyzing [^{68}Ga]DOTA-peptide PET/CT images pre-PRRT. **Materials and Methods:** We examined 324 SSTR-positive lesions, after a retrospective analysis of 38 GEP-NETs (9 G1 - 27 G2 - 2 G3) who underwent restaging [^{68}Ga]DOTA-peptide PET/CT before complete PRRT with [^{177}Lu]DOTATOC. Clinical, laboratory and radiological follow-up data were collected for a period of at least 6 months after the last cycle. We used LifeX software, through which 65 features were extracted from PET data for each lesion based on a manually placed region of interest (ROI) with standardized size. Additionally, pre-PRRT Chromogranine A values and histological grading were also considered as additional clinical features. Radiologic follow-up determined the status (progression vs response in terms of stability/reduction/disappearance) for each lesion. All features (PET and clinical) were correlated to the response data, and for features significantly associated with response, the delta-radiomics was assessed on follow-up [^{68}Ga]DOTA-peptide PET/CT performed until 9 months post-PRRT. A new statistical system was implemented based on the point-biserial correlation coefficient and the logistic regression analysis for the reduction and selection of the features; the Discriminant Analysis was used, instead, to obtain the predictive model. Results: From the reduction and selection process, the combination of 3 features, 2 from PET HISTO_Skewness; HISTO_Kurtosis) and one clinical (Grading), was able to predict the disease status at follow-up with sensitivity, specificity, and accuracy of 84.0%, 66.6%, and 78.1%, respectively. Percentage variations of delta HISTO_Skewness and delta HISTO_Kurtosis of 548.1% and 69.3%, respectively, were able to distinguish between progression vs response; at ROC analysis, HISTO_Skewness and HISTO_Kurtosis variations cut-offs reached an AUC, sensitivity, and specificity of 0.76, 88.8%, 61.4%, and 0.77, 88.8%, 60.3%, respectively. **Conclusion:** The presented preliminary radiomics model proved to be potentially useful in the prediction of response of GEP-NETs patients treated with [^{177}Lu]DOTATOC PRRT. **References:** none

EPS-241

Evaluation of Parametrial Infiltration in Cervical Cancer by Radiomics Analysis of ^{18}F-FDG PET

Z. Tan[1], F. Shang[1], T. Wang[2], X. Tang[1], H. Sun[2], S. Liu[1];
[1]School of Life Science, Beijing Institute of Technology, Beijing, CHINA, [2]Department of Radiology, Shengjing Hospital of China Medical University, Shenyang, CHINA.

Aim/Introduction: The presence of parametrial infiltration (PMI) is significantly associated with the recurrence of cervical cancer[1]. ^{18}F-FDG PET/MR functioned well on diagnosis of PMI in cervical cancer[2]. In the present study, a radiomics model for automatically assessing PMI in cervical cancer. **Materials and Methods:** The study included 64 female patients (24 with and 40 without PMI) with pathologically proven cervical

cancer (FIGO stage IB to IIA) from 2017 to May 2018. Each patient underwent 18F-FDG PET/MRI scan after signed informed consent. The contour of tumor was manually delineated by an experienced physician at the largest tumor level on the T2W-MR image. A region with the boundary inside and outside 2 pixel of the contour was generated for feature extraction. A total of 864 features (863 radiomics features and age) were used in the present study. The feature selection was conducted as follows: 1) The top 400 features were retained according to F-value in ANOVA; 2) Pearson correlation coefficient matrix was calculated. If the feature pairs with Pearson correlation coefficient was over 0.92, the feature with highest accuracy in univariate logistic regression was retained; 3) Random forest was used in recursive feature elimination to select out 90 features. Monte Carlo cross validation (MCCV) was conducted 500 times to reduce the influence from the bias of data distribution (training set vs. test set = 8:2). The top 10 features were selected according to the appearance frequency in MCCV, and was used to build model with random forest. The accuracy, sensitivity and negative predictive value was calculated to evaluate the performance of the model. Results: The evaluation of PMI using radiomics analysis was in good agreement with pathological result (accuracy = 78.88%, sensitivity = 66.9% and negative predictive value = 80.67%). **Conclusion:** The radiomics analysis of ^{18}F-FDG PET is a potential method to evaluate the parametrial infiltration. **References:** [1] Matsuo K , Mabuchi S , Okazawa M , et al. Utility of risk-weighted surgical-pathological factors in early-stage cervical cancer.[J]. British Journal of Cancer, 2013, 108(6):1348-1357. [2] Wang T , Sun H , Han F , et al. Evaluation of parametrial infiltration in cervical cancer with voxel-based segmentation of integrated 18F-FDG PET/MRI images: A preliminary study[J]. European Journal of Radiology, 2019, 118.

EP-01

Wednesday, October 20 - Saturday, October 23, 2021

e-Poster Area, release on Wednesday, October 20 at 09:00

Preclinical Studies -> Medical Preclinical -> Preclinical Oncology

EP-001

Pioglitazone sensitises human breast cancer cells to the TRAIL-induced cell death

Y. Zhao, *M. Marx, M. Zuhayra, U. Lützen; Department of Nuclear Medicine, Molecular Imaging, Diagnostics and Therapy, University Hospital of Schleswig-Holstein, Kiel, GERMANY.*

Aim/Introduction: TRIAL (tumor necrosis factor-related apoptosis-inducing ligand) and the anti-diabetic drug, pioglitazone (Pio), have been demonstrated to induce apoptosis in various types of cancer cells. We investigated whether: 1) Pio affects the proliferation of breast cancer cells, 2) which mechanisms mediate this effect, and 3) the combination Pio with TRAIL more effectively kills breast cancer cells than Pio or TRIAL alone. The uptake of ^{18}F-FDG and ^{99m}Tc-MIBI into breast cancer cells treated with Pio / TRIAL was employed to assess the cell metabolism and the mitochondrial status, respectively. **Materials and Methods:** Breast cancer cells, the MDA-MB-231 cell line, cultured up to 70-80 % confluence, were exposed to different concentration of TRAIL (10-50 ng/ml), Pio (25-100 µM) and 15d-PGJ_2, a natural PPARγ ligand (2-10 µM), in the presence or absence of the PPARγ antagonist, GW 9662 (2 µM) for 24 h. The cell death was evaluated using lactate dehydrogenase (LDH) and the cell proliferation was assessed by incubation of cells with WST-1 reagent. Cancer cells incubated in a glucose-deprived medium were exposed either to ^{18}F-FDG (80 Kbq/well, 20 min) or to ^{99m}Tc-MIBI (80 Kbq/well, 10 min). The radioactivity in cell pellets was quantified with γ-counter and expressed as cpm/mg of protein. Results: TRAIL and Pio, but not 15d-PGJ_2, promoted cell death dose-dependently, as evidenced by increased LDH release into the culture medium. The simultaneous treatment with Pio and the lowest dose of TRAIL further potentiated the rate of cell death. Pio, but not TRAIL, decreased the cell proliferation determined by WST-1 assay. GW 9662 did not reverse this effect indicating a PPARγ - independent mechanism. Increased uptake of ^{18}F-FDG into breast cancer cells treated with loweest concentrations of TRAIL (10ng/ml), Pio (25µM) and 15d-PGJ_2 (2µM) points to accelerated cell metabolism. Exposure of cancer cells to higher concentrations decreased the mitochondrial membrane permeability as evidenced by ^{99m}Tc-MIBI uptake. The PPARγ presumably interfered with the TRAIL-induced uptake of ^{18}F-FDG but not with that of ^{99m}Tc-MIBI. **Conclusion:** Pio enhances the TRAIL- induced breast cancer cell death independently of the PPARγ activation. The additional anti-proliferative effects and impairments of the mitochondrial membrane integrity by Pio may provide an effective therapeutic strategy for the treatment of breast cancer. Patients suffering from chemo-resistant breast cancer may benefit from the additional treatment with Pio in terms of a better response and longer progression-free survival. **References:** 1. Del Veccgui S, et al, 2004; 2. Moretti J et al, 2005

EP-002

Evaluation of amino acid PET imaging in a head and neck cancer model

J. Verhoeven, S. Piron, B. Descamps, C. Vanhove, I. Goethals; Ghent university, Ghent, BELGIUM.

Aim/Introduction: Amino acid PET is mainly applied in neuro-oncology. However, this could be of value in some peripheral cancer types. In this preclinical study we are interested to evaluate the uptake of amino acid PET tracers compared to conventional [^{18}F]FDG PET imaging in a sqamous head and neck cancer model. **Materials and Methods:** The study was approved by the Ghent University ethics committee for animal experiments (ECD 19/50). Five mice (C3H/HeJ, Charles River), were inoculated with SCC VII cells in the floor of mouth region using a sublingual approach. After tumor growth confirmation, PET/CT scans were acquired on three consecutive days using ±10 MBq 2-[^{18}F]FELP, [^{18}F]FET or [^{18}F]FDG. One hour after injection of the radiotracer, static PET scans were performed for 15 minutes. An additional PET image was acquired 4 hours after [^{18}F]FDG injection. All tumors and two background regions (floor of mouth and neck) were delineated and standardized uptake values (SUV_{mean} and SUV_{max}) as well as tumor-to-background ratios (TBR_{mean} and TBR_{max}) were determined using PMOD. A p-value of <0.05 was considered significantly different. Results: Tumor growth was visual in the neck region, inferior to the mandible after a waiting period of fourteen days. When comparing the different control regions (floor of mouth versus neck), only a significant difference could be found when using [^{18}F]FDG. Comparison of the tracers themselves led to the following results. There is a significant difference in SUV_{mean}, SUV_{max}, TBR_{mean} and TBR_{max} values between 2-[^{18}F]FELP and [^{18}F]FET. This is also the case for the comparison of the [^{18}F]FELP and [^{18}F]$FDG_{conventional}$ or [^{18}F]$FDG_{delayed}$. No significant differences could be found between [^{18}F]FET and [^{18}F]FDG (except for the TBR_{max}). Between [^{18}F]$FDG_{conventional}$ and [^{18}F]$FDG_{delayed}$, no significant differences were observed. **Conclusion:** These initial results suggest that amino acid PET could be of value in the delineation of head and neck cancer due to lower background uptake when compared to [^{18}F]FDG. Further studies are needed to evaluate amino acid PET in head and neck cancer imaging. **References:** None

EP-003

Targeting CD-20 antigen expression in Melanoma with ^{99m}Technetium-labeled Rituximab

C. Perroni[1], X. Camacho[1], M. Tassano[1], M. García[1], M. Cabrera[1], M. Fernández[1], J. Benech[2], H. Cerecetto[1], J. Gambini[3], P. Cabral[1]; [1]Centro de Investigaciones Nucleares-Facultad de Ciencias-Universidad de la República, Montevideo, URUGUAY, [2]Laboratorio de Señalización Celular y Nanobiología, Instituto de Investigaciones Biológicas Clemente Estable, Montevideo, URUGUAY, [3]Centro de Medicina Nuclear e Imagenología Molecular, Hospital de Clínicas, Facultad de Medicina, Universidad de la República, Montevideo, URUGUAY.

Aim/Introduction: In melanoma there is a cellular subpopulation that possesses self-renewal, differentiation, tumorigenicity, drug resistance capacity and overexpresses the CD20 antigen. Therefore, these cells could be a crucial factor for the progression of this disease. The Rituximab antibody specifically recognizes this antigen and blocks its action. The aim of this work was to radiolabel and evaluate Rituximab with ^{99m}Technetium as novel Melanoma imaging agent. **Materials and Methods:** CD-20 antigen expression was analyzed by laser confocal microscopy (LCM) and flow cytometry in murine Melanoma cell lines (B16F1 and B16F10). Rituximab was derivatized with NHS-HYNIC-Tfa and radiolabeled with 99mTc. Radiochemical stability and in vitro cell assays were evaluated. Biodistribution analyses were performed in normal and B16F1 and B16F10 tumor-bearing C57bl/6 mice up to 24 h p.i., using a high purity germanium detector (HPGe) (Canberra) with 20% counting efficiency (at 1332 keV). Spectra were analyzed off-line using Genie 2000 v 3.2. SPECT/CT studies were also evaluated in normal and Melanoma tumor-bearing C57bl/6 mice up 24 h p.i. Results: We demonstrate that murine melanoma cells lines present high expression of CD-20 antigen. Radiolabeling with ^{99m}Tc via NHS-HYNIC-Tfa was found to be easy, fast and stable, revealing high radiochemical purity without interfering with CD-20 recognition. Biodistribution and SPECT/CT analysis in melanoma bearing C57bl/6 mice showed high liver and discrete tumor uptake. **Conclusion:** ^{99m}Tc-HYNIC-Rituximab led to highly pure radiolabeled compound in an easy, fast and stable way, preserving its biological activity. This new molecular imaging agent could potentially be used for the visualization of CD-20 antigen expression in Melanoma patients. **References:** None

EP-004

Evaluation of Radiotherapy associated with Temozolomide plus Metformin in a GBM immunocompetent microenvironment

D. Salvatore[1,2], S. Valtorta[1,2], G. Bertoli[3], S. Todde[1,3], M. Iannone[1], A. Coliva[2], E. Toninelli[2], A. Spinelli[4], F. Zerbetto[5], S. Villa[5], N. Di Muzio[5], R. Moresco[1,2,3];
[1]Department of Medicine and Surgery and Tecnomed Foundation, University of Milano—Bicocca, Monza, ITALY, [2]Nuclear Medicine Department, San Raffaele Scientific Institute (IRCCS), Milan, ITALY, [3]Institute of Molecular Bioimaging and Physiology (IBFM), National Research Council (CNR), Segrate, ITALY, [4]Experimental Imaging Centre, San Raffaele Scientific Institute (IRCCS), Milan, ITALY, [5]Department of Radiation Oncology, San Raffaele Scientific Institute (IRCCS), Milan, ITALY.

Aim/Introduction: Glioblastoma (GBM) is the mostly encountered astrocytic brain tumour in adults and, although the standard therapy based on surgical resection associated with radiation therapy (RT) and concomitant Temozolomide (TMZ)-based chemotherapy, it presents a severe prognosis. We previously observed that Metformin (MET) addition to TMZ prolonged the survival of mice orthotopically injected with human derived EGFR-mutated and -amplified cell lines. Here we evaluate the MET add-on effect in an immunocompetent GBM model. RT efficacy in GBM in triggering a prompt immune response activation was studied. **Materials and Methods:** In vitro assays (survival, proliferation, migration, invasion, gene expression profile about proliferation, cell cycle and glucose metabolism) were performed by treating commercial murine cells GL261 with doses of TMZ and MET at different times. In vivo mice model was set up by orthotopically injecting GL261 in C57Bl/6 mice. Mice were divided in treatment groups: vehicle, MET, TMZ and TMZ+MET. Tumour response was monitored by using MRI and PET with [18F]FLT (Thymidine Kinase 1 for cell proliferation) and [18F]VC701 (TSPO receptor for cell inflammation). Radiotherapy was evaluated in further separate animal groups alone or in association with TMZ and/or MET. IHC and molecular studies for both the cohorts are ongoing. Results: MET and TMZ 25 μM combination at 24 hours affected survival, proliferation and cell cycle, as observed by the decreased expression of cyclin and kinase genes. MET plus TMZ 100 μM raised the expression levels of Pyruvate kinase and Hexokinase enzymes. Cell migration was significantly reduced by adding MET to TMZ. GL261 tumours are hyperproliferative and display a high uptake of [18F]VC701. MET alone did not significantly increase overall survival (median: 27 days) in comparison with vehicles (25 days) and TMZ alone (44.5 days) or in association with MET (48 days) presented time-limited efficacy. No significant change of [18F]FLT and [18F]VC701 uptake was detected. Radiation treatment slowed down tumour growth compared to vehicles, as indicated by the reduced tumour volume and [18F]FLT uptake in MRI and PET, respectively, but the efficacy was time-limited (median survival: 40 days). **Conclusion:** In vivo the administration of radiotherapy alone or the TMZ and MET association delayed tumour growth but with a time-limited efficacy. In the therapy early phases we observed a tumour volume reduction only after radiotherapy alone. The association of RT and TMZ and MET is under evaluation, we are also investigating the role of tumour microenvironment (immune cells) in tumour-response to therapy. **References:** None

EP-02

Wednesday, October 20 - Saturday, October 23, 2021

e-Poster Area, release on Wednesday, October 20 at 09:00

Preclinical Studies -> Medical Preclinical -> Preclinical Therapy

EP-005

Efficacy of ^{18}F-fluorothymidine and ^{18}F-fluorodeoxyglucose Positron Emission Tomography in Determining a Radiotherapy Effect

T. Otani, H. Ikushima, Y. Bando, K. Kuwahara, H. Otsuka, K. Kondo, H. Miyoshi;
Tokushima University, Tokushima, JAPAN.

Aim/Introduction: After radiotherapy, inflammatory cells, such as macrophages around the lesion, cause false positives in 2′-[^{18}F]fluoro-2′-deoxy-D-glucose (^{18}F-FDG) positron emission tomography (PET), which may decrease the accuracy of determining a therapeutic effect. 3′-deoxy-3′-[^{18}F]fluorothymidine (^{18}F-FLT) has been shown to suppress the effects of inflammation caused by radiation therapy more so than ^{18}F-FDG and thus may be used as a quantitative imaging marker for radiation therapy. The utility of ^{18}F-FLT in the diagnosis of malignancy has been reported, but studies on the prediction and determination of the radiotherapy effect are limited. Our aim was to clarify the utility of ^{18}F-FLT PET in determining the radiotherapy effect. **Materials and Methods:** Non-small cell lung cancer cell lines A549 and FT821 transplanted into mice were divided into 20 Gy X-ray irradiation and non-irradiation groups when tumors reached approximately 10 mm in diameter. ^{18}F-FLT and ^{18}F-FDG PET/CT measurements were performed before (pre) and 13 days (post) after irradiation. The standardized uptake value (SUV) was used for the quantitative tumor analysis of PET images. Following PET/CT measurements, tumor volume was measured over time to evaluate the anticancer effect of irradiation. Ki-67 was evaluated histopathologically. Results: Irradiation was performed at 20 and 50 days after transplantation for A549 and FT821, respectively. For A549, ^{18}F-FLT showed a significantly greater decrease post-

irradiation compared with pre-irradiation (SUV of 2.67 and 1.56 for pre- and post-irradiation, respectively). For FT821, ^{18}F-FLT uptake showed a slight decrease post-irradiation compared with pre-irradiation (SUV of 1.39 and 1.21 for pre- and post-irradiation, respectively). ^{18}F-FDG uptake showed a slight decrease post-irradiation compared with pre-irradiation for both A549 and FT821. Regarding tumor volume, both A549 and FT821 showed slower tumor growth in the irradiated group than in the non-irradiated group. At 13 days after irradiation, tumor volumes were 36% and 47% lower in the irradiation group compared with the non-irradiation group for A549 and FT821, respectively. Ki-67 showed a significantly greater decrease in the irradiated group compared with the non-irradiated group (48% and 52% decrease for A549 and FT821, respectively). **Conclusion:** Results of tumor volume and Ki-67 demonstrated anticancer effects in both A549 and FT821. A549 had higher proliferation than FT821 on the basis of the results of ^{18}F-FLT uptake and doubling-time of tumor volume. Significant ^{18}F-FLT uptake decrease was observed in A549 only, which suggests that ^{18}F-FLT may be more effective than ^{18}F-FDG in determining an anticancer effect in highly active tumors. **References:** none

EP-006

Evaluation of treatment process in reducing retinoblastoma tumor size using iodine-125 plaque brachytherapy in animal model of rabbit

S. Moradi[1], S. Sheibani[1], M. Mokhtari Dizaji[2], F. Ghassemi[3], F. Asadi Amoli[4], M. Arjmand[3];
[1]Radiation Application Research School, Nuclear Science and Technology Research Institute, Tehran, IRAN, ISLAMIC REPUBLIC OF, [2]Department of Medical Physics, Faculty of Medical Sciences, Tarbiat Modares University, Tehran, IRAN, ISLAMIC REPUBLIC OF, [3]Eye Research Center, Farabi Eye Hospital, Tehran University of Medical Sciences, Tehran, IRAN, ISLAMIC REPUBLIC OF, [4]Department of Pathology, Eye Research Center, Farabi Eye Hospital, Tehran University of Medical Sciences, Tehran, IRAN, ISLAMIC REPUBLIC OF.

Aim/Introduction: In this study, brachytherapy with iodine-125 eye plaque was used to treat retinoblastoma in an animal model of a rabbit in such a way that the tumor apex received a dose of 20 Gy. The aim of this study was to estimate tumor size and evaluate the process of tumor treatment with a dose lower than the prescribed dose of 40 Gy in order to reduce radiation complications for combination therapy of brachytherapy with other treatments to evaluate the synergistic effect in future studies. **Materials and Methods:** In this study, to treat induced retinoblastoma in 10 male New Zealand white rabbits, eye plaque with a diameter of 10 mm containing five I-125 seeds was used. The eye plaque is implanted inside the eye for a few days so that the apex of the tumor receives the prescribed dose, then the plaque is removed from the eye. Plaque implantation requires the animal to be placed under general anesthesia. To control and evaluate the tumor growth process before and after treatment, tumor measurement was performed using indirect ophthalmoscope and B-mode ultrasound images at the beginning of treatment and the third week after treatment. Tumors were also evaluated pathologically. Results: The results of this study indicated that evaluation of tumor growth showed that three weeks after brachytherapy, the tumor size decreased to its initial size of 0.49. **Conclusion:** It can be concluded that a dose range of 20Gy for irradiating the tumor was effective in shrinking the tumor. Due to the fact that the prescribed dose of 40Gy, which is usually prescribed in eye plaque brachytherapy for retinoblastoma and a lower dose has been used in this study, so it has less side effects of radiation and can be used in future studies of combination therapies with plaque brachytherapy. **References:** none

EP-03

Wednesday, October 20 - Saturday, October 23, 2021

e-Poster Area, release on Wednesday, October 20 at 09:00

Imaging Clinical Studies -> Oncological Imaging Clinical Study -> Breast

EP-007

[^{18}F]Sodium fluoride-PET/MRI monitoring of chemotherapy response in breast cancer bone metastases- Proof of concept

M. Zia, E. Lundström, J. Mårtensson, M. Lubberink, A. Sundin;
Department of Surgical Sciences, Uppsala University, Uppsala, SWEDEN.

Aim/Introduction: RECIST 1.1 tumour size measurements on CT/MRI is the mainstay of cancer therapy monitoring. However, bone metastases are not measured and are consistently difficult to evaluate for a response. When responding to chemotherapy, these metastases show osteosclerosis, initially in the form of micro-calcification within the bone marrow, which generally escapes CT detection. This study aimed to assess dynamic and static PET/MRI with [^{18}F]sodium fluoride ([^{18}F]NaF) by combining the standardized uptake value (SUV) and net influx rate (K_i) from PET with the apparent diffusion coefficient (ADC), fat fraction (FF) and effective transverse relaxation rate (R_2*) from MRI, to monitor the effect of chemotherapy on bone metastases. **Materials and Methods:** In this prospective study, three breast cancer patients (mean age 73y) diagnosed with bone metastases on CT underwent a 60-minutes dynamic whole-body [^{18}F]NaF-PET/MRI at baseline and following 3-6 months of chemotherapy (Letroxole n=2, Tamoxiphen n=1). In the PET images, pelvic and spine metastases with high/intermediate uptake were delineated (approximately n=12/patient), applying an adaptive threshold algorithm (50%

of maximum cut-off) to provide SUV_{mean} and SUV_{max}. Tracer kinetic modeling was performed on a 60-minute dynamic PET of the pelvis and the net uptake rate K_i was calculated using a two-tissue reversible model, which provided the best fit. MRI comprised anatomical sequences, six-point Dixon MRI and diffusion-weighted imaging (b=50-800 s/mm^2). VOI measurements of ADC, FF and R_2* utilized the OLEA medical software. The changes between baseline and follow-up data were calculated and tested (Wilcoxon signed-rank) and correlations between data utilized linear regression. Results: The [^{18}F]NaF uptake in the bone metastases decreased from PET/MRI at baseline to follow-up median SUV_{mean} -27.1% (P=0.0015) and median SUV_{max} -26.6% (P=0.0001). The changes in K_i similarly decreased, median K_i -38.7% (P=0.00034) and were in agreement with the changes in SUV_{mean} (R^2=0.706, P=0.0001) and SUV_{max} (R^2=0.685, P=0.00002). The ADC showed therapy response with a median 8.2 % increase, consistent with necrosis. The FF increase was median 9.2%, consistent with conversion to fattier marrow and the R_2* increase was median 11.9 %, possibly due to the development of micro-calcification and new bone formation. **Conclusion:** In this feasibility study, [^{18}F]NaF-PET/MRI provided a powerful method to monitor chemotherapy response in breast cancer bone metastases, as reflected by the parallel significant decreases in SUV and K_i. MRI showed changes in ADC, FF and R_2*, consistent with the response, although not reaching statistical significance. **References:** None

EP-008

Utility of 18F-FDG PET-CT metrics predicting lymph node involvement in locally advanced breast cancer

Q. Pitalua Cortes[1], O. Garcia Perez[1], L. Torres Agredo[2], N. Esparza Arias[1];
[1]Instituto Nacional de Cancerologia, Mexico city, MEXICO, [2]Universidad Autónoma de Bucaramanga, Bucaramanga, COLOMBIA.

Aim/Introduction: Predictive models of lymphatic infiltration have been created in patients diagnosed with breast cancer, since it has been shown to be one of the factors that most intervenes in the recurrence prognosis and survival, so this information becomes important when defining treatments; for example, the nomogram performed by the Memorial Sloan Kettering Cancer Center, where characteristics such as the age of the patients, tumor size, histological lineage, location, lymphovascular invasion, multifocality, tumor grade, and estrogen and progesterone receptor status are considered.The aim of this study is to evaluate the ability of staging 18F-Fluorodeoxyglucose (18F-FDG) PET-CT to predict lymphatic spread of breast cancer. **Materials and Methods:** A retrospective cohort of patients attended at "Instituto Nacional de Cancerología México" between 2016-2020 was analyzed, diagnosed with breast carcinoma, who underwent to staging 2-[18F]-FDG PET-CT and subsequently they were taken to surgical treatment with sentinel lymph node and/or lymphadenectomy. The SUVmax, tumor metabolic volume, total lesion glycolysis and size of the breast tumor and axillary lymph nodes were analyzed. The data obtained were analyzed with the statistical program STATA 14.0. A univariate analysis was performed with the clinical and histological variables of the tumor; and a bivariate analysis evaluating the discriminatory capacity of the PET-CT findings by calculating the area under the ROC curve. Results: Fifty-eight patients were included, 75.8% (n=44) presented positive sentinel lymph nodes confirmed by histopathology. The mean age was 56 +/- 12.6; 65.62% (n=44) were T1 and T2, 39.6% (n=23) presented T4. According with the immunophenotype the highest frequency corresponded to luminal b with 43.1% (n=25), 72.41% (n=42) had ductal carcinoma histology, with high grade ki67 67.3% (n=9). In the bivariate analysis, an association was found between T1-T2 tumor size [RR 1.78 CI (95% 1.13-2.81) p=0.0008] and nodal size in PET with a diameter of 10 mm [RR 1.56 CI (95% 1.2-1.9) p=0.0027]. No other significant variables were found to predict axillary metastatic spread. **Conclusion:** No metabolic characteristics of the primary tumor were found to predict lymphatic spread, only an association was found between tumor size (less than 5 cm), as well as lymph node size measured in the short axis greater than 10 mm. These findings could be correlated with specific cancer hallmark biomarkers, such as angiogenesis (RGD) or those that characterize the tumor microenvironment, such as CXCR4 or FAPI. **References:** Ann Surg Oncol. 2017 Aug;24(8):2174-2181. doi: 10.1245/s10434-017-5860-0Nucl Med Commun. 2019 Nov;40(11):1112-1121. doi: 10.1097/MNM.0000000000001085.

EP-04

Wednesday, October 20 - Saturday, October 23, 2021

e-Poster Area, release on Wednesday, October 20 at 09:00

Imaging Clinical Studies -> Oncological Imaging Clinical Study -> Lung (including Mesothelioma)

EP-009

FDG PET/CT vs. PET/MRI with zero-echo time (ZTE): Comparing the capability of detection of lung metastasis and differentiating it from other lesions and the precision in fused images

J. Inukai[1], M. Nogami[2], F. Zeng[2], M. Tachibana[1], K. Kubo[2], T. Kurimoto[3], T. Murakami[1];
[1]Kobe University Graduate School of Medicine, Kobe, JAPAN, [2]Kobe University Hospital, Kobe, JAPAN, [3]GE Healthcare, Hino, JAPAN.

Aim/Introduction: This study aimed to compare the capability of detection of lung metastasis and differentiating

it from other lesions and precision in fused images between fluorodeoxyglucose positron emission tomography/computed tomography (FDG PET/CT) and PET/magnetic resonance imaging (MRI) with zero-echo time (PET/ZTE). **Materials and Methods:** In this matched case-control study, 1242 and 229 patients who underwent FDG PET/CT and PET/ZTE, respectively, were retrospectively evaluated. Age, sex, height, body weight, affected regions in the lung fields (upper and lower) and lesions' diameters (< 1 cm and ≥ 1 cm) were matched, to ensure that the study population had an equal distribution of similar patients in the PET/CT (patients, n = 266; lung fields, n = 448) and PET/ZTE (patients, n = 224; lung fields, n = 448) groups, using multivariate analysis. To assess the capability of PET/ZTE and PET/CT to detect lung metastasis and differentiate it from other lesions, images were separately evaluated by two readers using a 5-point visual scoring system and compared using the receiver operating characteristic analysis followed by the McNemar's test. The reference standards of the lesions were acquired using histopathological results and/or at least 1-year radiological follow-up. Inter-reader agreement was tested using Cohen's kappa coefficient. To evaluate precision in the fused images, the largest FDG-avid lung lesions of the matched patients were assessed between PET/ZTE (patients, n = 52; lesions, n = 78) and PET/CT (patients, n = 68; lesions, n = 78) images. The distances of the lesions between PET and ZTE (dist-PET/ZTE), and between PET and CT (dist-PET/CT) images, were calculated by measuring the distance between the centres of the regions of interest, and compared by Wilcoxon's signed rank test. Results: No significant differences were observed between PET/ZTE and PET/CT in the detection and differentiation between lung metastasis and other lesions in both fields. An almost perfect agreement was observed in the inter-rater assessments (weighted kappa = 0.89 and 0.86, respectively).The degrees of lesion misregistration with PET/ZTE (3.626 ± 2.012 mm) were significantly smaller than that with PET/CT images (5.478 ± 2.990 mm) (p = 0.0028) for lower lung fields. No significant difference in misregistration was found for the upper fields. **Conclusion:** The capability of PET/MRI with ZTE to detect lung metastasis and differentiate it from other lesions was identical to PET/CT. Precision in fused images with PET/MRI with ZTE was significantly better than PET/CT for lesions in the lower lung field. **References:** none

EP-010

Perfusion only SPECT CT only as a surrogate for VQ imaging in the COVID-19 era; a single centre experience

T. Hussain, M. Vadrucci;
Barts Health NHS Trust, London, UNITED KINGDOM.

Aim/Introduction: Due to the COVID19 pandemic and the uncertain transmissibility of the virus in the early stages of the pandemic, scientific societies such as SNMMI and EANM initially suggested to omit ventilation imaging in VQ SPECT imaging in the diagnosis of pulmonary embolism (PE). This was to reduce the risk of exposure to staff and to limit the time spent within the nuclear medicine department by patients attending the department. Since March 2020, we therefore implemented perfusion-only SPECT CT as a surrogate for ventilation imaging, in a cohort of patients that were to be continued to require perfusion imaging in the diagnosis of pulmonary emboli, including patients with contrast allergy, pregnancy and impaired renal function. Our aim is to retrospectively look at our predictive values for PE using perfusion SPECT imaging only and also determine whether SPECT CT has been a useful surrogate. **Materials and Methods:** We interrogated local clinical records for patients undergoing perfusion-only SPECT or SPECT/CT imaging from the initial lockdown in London in March 2020 up until March 2021. A total of 100 studies in 92 patients were identified from our RIS and PACS software, including 23 pregnant women. Clinical records, biochemical and other radiological findings were also reviewed retrospectively for confirmation or exclusion of pulmonary embolism diagnosis. Results: 20/100 (20%) scans were reported as having positive perfusion scans for pulmonary emboli. Of these, 16 of which had concurrent SPECT CT, which demonstrated no matching pulmonary parenchymal CT abnormalities. In 1/20 (false positive rate 5%), PE was excluded by analysis of subsequent clinical records. **Conclusion:** In our centre, perfusion SPECT CT imaging has been a useful tool in the assessment of PE in the COVID19 pandemic, particularly in those patients unable to undergo CTPA and minimises COVID-19 exposure in patients and staff. **References:** None

EP-011

Prognostic and predictive value of radiomic parameters in 18F-FDGPET/CT in non-small cell lung cancer patients treated with immunotherapy

F. Trousset[1], N. Antonorsi[1,2], A. Filali Razzouki[1], C. Latappy[1], O. Tankyevych[1,2], C. Cheze-Le Rest[1,2];
[1]CHU de Poitiers, Poitiers, FRANCE, [2]INSERM U1101 Latim, Brest, FRANCE.

Aim/Introduction: Identifying reliable predictive biomarkers of response to immunotherapy is a major challenge. The purpose of this study was to investigate the ability of radiomics derived from pre-treatment and follow-up PET/CT images to predict response to therapy, durable clinical benefit (DCB) and survival in non-small cell lung cancer (NSCLC) patients treated with immunotherapy. **Materials and Methods:** 64 NSCLC patients eligible for immunotherapy were retrospectively included between 2016 and 2020 in this single-center study. All patients underwent an 18F-FDG PET/CT scan before treatment. Response was assessed after 8 weeks treatment based on PET/CT (n=54) or after 12 weeks using diagnostic CT (n=10). 23 patients had an additional PET/CT scan 12 weeks after therapy initiation. Response was

assessed according to PERCIST, iPERCIST and RECIST criteria. Radiomic parameters were extracted from the metabolic primary tumor volume, determined by an automatic segmentation method (FLAB). Response to therapy, durable clinical benefit (DCB) and progression-free survival were the endpoints considered. Correlation with clinicopathological and metabolic parameters was examined using a Cox multivariate proportional hazards model. Results: Median follow-up was 1055 days. 48% of patients achieved at least a partial response or stable disease, leading to a DCB rate of 42%. Pseudo-progressions were identified in 4 patients who eventually achieved a DCB. Performance status (PS) and tumor stage were significantly associated with DCB. Lower PS and TLG were associated with longer survival ($p = 0.0097$ and $p = 0.0397$). SUV was not discriminatory for therapeutic response or survival. PET and CT baseline radiomics and delta-radiomics were more effective than clinical parameters, SUV, MTV and TLG in predicting survival, therapy response and clinical benefit. **Conclusion:** Radiomic parameters extracted from pre-treatment and follow-up PET/CT scans and their variation during treatment may play a role in predicting therapeutic response, clinical benefit and survival in NSCLC patients treated with immunotherapy. Further prospective studies are now needed to validate these results and ultimately help clinicians to personalize immunotherapy treatment. **References:** none

EP-012

Serial change of functional volume of non-transplanted lung before and after unilateral lung transplantation

S. Nagamachi[1], T. Shiraishi[2], S. Miyahara[2], R. Waseda[2], K. Yochimitsu[1];
[1]Department of Radiology, Faculty of Medicine, Fukuoka University, Fukuoka Prefecture, JAPAN, [2]Department of Thoracic Surgery, Faculty of Medicine, Fukuoka University, Fukuoka City, JAPAN.

Aim/Introduction: The unilateral lung transplantation is curative surgical method for chronic respiratory dysfunction. However, few studies have reported about the course of respiratory function in the residual non-transplanted lung. We evaluated the serial change of non-transplanted lung functional volume before and after unilateral lung transplantation using scintigraphy and CT volumetric. **Materials and Methods:** We analyzed retrospectively 23 patients undertaken unilateral lung transplantation due to chronic refractory respiratory failure. All patients were classified into two groups, emphysema group (n=12) and fibrosis group (n=13). They were undertaken both Tc-99m MAA perfusion scintigraphy, Kr-81m ventilation scintigraphy and CT volumetric before and after lung transplantation. After the transplantation, these three examinations were evaluated annually within 2 years. On the posterior planar images, the count ratios of non-transplanted lung to the transplanted lung (N/T ratio) were obtained. The lung volume ratios of the non-transplanted lung to the transplanted lung (N/T volume ratio) were obtained by the CT volumetric study. Results: In the emphysema group, the mean values of N/T ratio were 0.91 in ventilation, 0.82 were in perfusion and 0.88 in the CT volumetric before the transplantation. After the transplantation. the mean value of N/T ratio were 0.43 in ventilation, 0.42 in perfusion and 2.3 in CT volume metric after 1 year. And 2 years after, N/T ratios were 0.25 in ventilation and 0.22 in perfusion and 2.4 in CT volume metric. In the fibrosis group, the mean values of N/T ratio were 0.72 in ventilation, 0.83 were in perfusion and 0.83 in the CT volumetric before the transplantation. After 1 year, the mean value of N/T ratio was 0.63 in ventilation, 0.16 in perfusion and 0.46 in the CT volumetric. After 2 years, the mean value of N/T ratio was 0.17 in ventilation, 0.03 in perfusion and 0.11 in the CT volumetric. After the unilateral lung transplantation, anatomical volumetric change in residual lung was dependent on underlying diseases. If the residual lung was emphysema, it increases progressively, in contrast to decrease of functional volume in the residual lung. While in the fibrosis group, anatomical volume decreases progressively in accord with the decrease of functional volume of residual lung. **Conclusion:** After the unilateral lung transplantation, residual anatomical volume increase in emphysema and decrease in fibrosis. In contrast, both perfusion and ventilation were gradually and continuously decreased in non-transplanted lung. These phenomena would affect the prognosis of respiratory function of unilateral lung transplantation. **References:** none.

EP-013

Correlation between bone scintigraphy and HE4 serum values with bone metabolism in lung cancer patients

J. Weissensteiner[1], E. Babusikova[2];
[1]Department of Nuclear Medicine, Hospital Poprad, Poprad, SLOVAKIA, [2]Comenius University in Bratislava, Jessenius Faculty of Medicine in Martin, Department of Medical Biochemistry, Martin, SLOVAKIA.

Aim/Introduction: Primary lung cancer is one of the most common types of cancer. Osteocalcin (OC) is marker of bone formation, beta-carboxyterminal cross-linking telopeptide of type I collagen (ß-CTx) is maker of bone resorption and human epididymis protein 4 (HE4) is a potential useful tumour marker. The aim of this study was to compare serum concentration of OC, ß-CTx, HE4 in lung cancer patients with bone scintigraphy. **Materials and Methods:** We estimated serum concentration of biochemical markers of bone metabolism (OC, ß-CTx) and HE4 in 60 patients with lung cancer. The mean age was 66.65 years (range: 50-84 years). In healthy controls were 10 persons without malignant disease (mean age 52.3, and range 34-67 years). All participants of study were examined by whole-body bone scintigraphy using a hybrid SPECT/CT scanner with 99mTc-MDP. The study populations included

50 non-small-cell lung cancers (NSCLC), 9 small-cell lung cancers (SCLC), 1 patient with typical carcinoid of lung. NSCLC included 21 squamous cell carcinomas, 20 adenocarcinomas, 3 large cell carcinomas, 3 non-small-cell lung cancers with neuroendocrine component, and 3 undetermined non-small-cell lung carcinomas. Results: The bone metastases were detected in 15 cases (25 %), probably bone metastases were detected in 11 cases (18.33 %) and 34 patients (56.67 %) were without bone metastases. In healthy persons were serum concentrations of OC, ß-CTx, HE4 in reference range; only in one case was serum concentration of OC and ß-CTx below reference range. We did not find significant difference of OC concentration in patients with bone metastases in comparison with healthy control (p=0.60). The significant difference in β-CTx concentration between patients with bone metastases and healthy control were found (p=0.02). We observed significant difference in HE4 concentration between lung cancer patients and healthy control (p<0.0001). Patients with small-cell lung cancer had the most increased serum concentration of HE4. **Conclusion:** Beta-carboxyterminal cross-linking telopeptide of type I collagen could be a diagnostic marker of bone metastases in correlation with bone scintigraphy in lung cancer patients. Osteocalcin does not have diagnostic importance. The increasing serum concentrations of human epididymis protein 4 can be useful in the diagnosis of bone metastases in patients with small-cell lung cancer. **References:** none

EP-014

^{18}F-FDG in suspected non-small cell lung carcinoma recurrence

P. García-Talavera San Miguel[1], M. Mellado[2], F. Gómez-Caminero[1], B. Lucas[1], J. G. Villanueva[1], C. Peñaherrera[1], C. Riola[1], M. E. Martín[1], P. Tamayo[1];
[1]Nuclear Medicine department. Hospital Clínico Universitario de Salamanca, Salamanca, SPAIN,
[2]Universidad de Salamanca, Salamanca, SPAIN.

Aim/Introduction: To evaluate the role of ^{18}F-FDG PET-CT in the diagnosis of non-small cell lung cancer (NSCLC) recurrence, compared with CT, as well as its prognostic value. **Materials and Methods:** 29 patients with NSCLC were included (70.1±8.0 years old; 26 men). ^{18}F-FDG PET-CT for suspicion of recurrence (27) or re-staging (12) was performed in all patients (in 7 patients several PET-CT were performed at different times). Histology: adenocarcinoma (14), squamous cell carcinoma (12), large cell carcinoma (3).Staging: IA (4 patients), IB (1), IIA (2), IIB (4), IIIA (10), IIIB (6), IV (2). Endovenous contrast CT was performed in all patients. Results were confirmed through radiological follow-up and/or histology. Spearman's Rho to assess the correlation between size and SUVmax of lesions and Mann-Whitney's U-test to establish if there are differences in uptake between histological types were used. ROC curve to calculate the optimal cut-off value of SUVmax for overall survival (OS) and progression free survival (PFS) prediction was conducted. Survival analysis by means of Kaplan-Meier method was performed. Results: 28 (71.80%) out of 39 CT and PET-CT were concordant and 11 (28,20%) non-concordant. Of the latter, PET-CT was positive in 7 and CT in 4 (sensitivity: 100% for PET and 77% for CT, and PPV: 100% and 86%, respectively). CT and PET-CT detected 58 concordant lesions (45.31%). In the non-concordant cases, CT detected 19 lesions and PET-CT 51 (128 detected lesions). Out of 77 lesions detected by CT, 65 were TP, 12 FP and 39 FN. Out of 109 lesions detected by PET-CT, 104 were TP and 5 FP. The sensitivity to detect lesions was 63% for CT and 100% for PET-CT. PET-CT changed therapeutic management in 15 cases. PET-CT found 7 synchronic tumors (6 in colon, 1 in thyroid). A significant correlation (p=0.000) between SUVmax and size of the lesions and significant differences in uptake between adenocarcinoma and squamous cell carcinoma were found. In survival analysis, Long-Rank test showed significant differences for PFS (p=0.006) between SUVmax ≥3.15 (26.03±4.08 months) and SUVmax <3.15 patients (56.67±4.35 months); it showed significant differences (p=0.004) for the OS between patients with SUVmax ≥8.15 (16.06±4.69 months) and with SUVmax <8.15 (61.73±5.45 months). **Conclusion:** ^{18}F-FDG PET-CT showed better results compared to contrast CT in the suspicion of recurrence of NSCLC. It has an impact on therapeutic management in 38,5% of cases, and could play an important role in prognostic assessment, both in PFS and OS. **References:** None

EP-05

Wednesday, October 20 - Saturday, October 23, 2021

e-Poster Area, release on Wednesday, October 20 at 09:00

Imaging Clinical Studies -> Oncological Imaging Clinical Study -> Gastro-Intestinal (including Liver and Non-Endocrine Pancreas)

EP-015

The Value of Future Remnant Liver Function Assessment in Pediatric Patients Before Extended Liver Resection

E. Kireeva, K. Chaurasiya, D. Akhaladze, Y. Likar;
Dmitry Rogachev National Research Center of pediatric Hematology, Oncology and Immunology, Moscow, RUSSIAN FEDERATION.

Aim/Introduction: Surgical resection is still the most effective treatment method for hepatic malignancies in adults as well as in children. Postoperative outcomes mainly depend on the quality of the residual liver segment, which requires accurate preoperative assessment of future remnant liver function (FRL-F). Hepatobiliary scintigraphy (HBS) with ^{99m}Tc-

Mebrofenin is widely used for assessment of FRL-F. It has been shown in adults that the threshold value of FRL-F >2.7%/min/m^2 minimizes the postoperative liver failure but there is no any data available about pediatric patients.Aim: The value of HBS with ^{99m}Tc-Mebrofenin in assessment of preoperative FRL-F in pediatric patients with liver tumors. **Materials and Methods:** Fifty-five pediatric patients (33 boys, 22 girls, aged from 1-month to 18 years) with liver malignancies most of them with hepatoblastoma were included in this study. All patients underwent surgical treatment ranging from segmental to extended liver resection. HBS with ^{99m}Tc-Mebrofenin was performed in all patients before surgery using standard protocol with two dynamic phases and SPECT/CT. The obtained FRL-F values were normalized to body surface area and expressed in %/min/m^2. Results: The value of FRL-F measured in 55 pediatric patients ranged from 1.81 to 31.8 %/min/m^2.24 patients underwent various segmental or atypical liver resections, the FRL-F value ranged from 4.53 to 31.8 %/min/m^2. 9 patients underwent left-sided hemihepatectomy and extended left-sided hemihepatectomy. The FRL-F value ranged from 4.47 to 30 %/min/m^2. None of the patients have developed liver failure after surgery.22 patients underwent right-sided hemihepatectomy and extended right-sided hemihepatectomy. The FRL-F value ranged from 1.81 to 22.64 %/min/m^2. Two patients of this group with FRL-F values of 1.81 and 3.4 %/min/m^2, have developed transient postoperative hepatic failure. **Conclusion:** In our study the value of FRL-F for most of the patients were more than 2.7%/min/m^2 before surgery, which can be explained by lack parenchymal diseases such as steatosis and cirrhosis in children and the higher possibilities of liver regeneration. In the postoperative period, only two patients who had low FRL-F values and undergone extended right-sided hemihepatectomy developed transient hepatic failure, which was subsequently resolved safely. To obtain reliable data it is necessary to continue the study with further recruitment and analysis. **References:** none

EP-06

Wednesday, October 20 - Saturday, October 23, 2021

e-Poster Area, release on Wednesday, October 20 at 09:00

Imaging Clinical Studies -> Oncological Imaging Clinical Study -> Neuroendocrine (Pancreatic and Others)

EP-016

Significance of [68Ga]Ga-DOTA-NOC uptake in the pancreatic tail

D. Fraga, *R. Sousa, M. Silvestre, D. Ferraz, I. Vitorino, D. Rombo, M. R. Carvalho, F. Brandão, I. P. Carvalho, P. Ratão, T. C. Ferreira, L. Salgado;*
Instituto Português de Oncologia de Lisboa Francisco Gentil, Lisbon, PORTUGAL.

Aim/Introduction: [68Ga]Ga-DOTA-peptides specifically bind to somatostatin receptors, which are overexpressed in Neuroendocrine Tumors (NETs). [68Ga]Ga-DOTA-peptides Positron Emission Tomography / Computed Tomography (PET/CT) has demonstrated superiority in the imaging of NETs compared to other modalities. During our practice with [68Ga]Ga-DOTA-NOC PET/CT, we noticed that, in addition to the well known physiological uptake, several scans showed uptake in the pancreatic tail of equivocal meaning, leading to further investigations. To our knowledge, only Delbeke et al (2019) reported frequent uptake in the pancreatic tail. The aim of our study is to understand the significance of this uptake. **Materials and Methods:** From the 290 [68Ga]Ga-DOTA-NOC PET/CT studies performed in our department between November 2018 and February 2021, we selected the ones in which pancreatic tail uptake was reported (54), corresponding to 36 patients. Of them, 21 were male and 15 were female, aged between 23 and 81 years old (average of 63.3). Only the patient's first scan was considered. The maximum Standardized Uptake Value (SUVmax) of the pancreatic tail uptake was measured and compared to that of the healthy liver. Patients' medical history and additional tests (mostly imaging and endoscopic studies) were reviewed to determine the most likely nature of the pancreatic tail uptake. The statistical evaluation was performed using the Pearson's Chi-square test. Results: Of the 36 patients, 15 showed evidence of disease in the pancreatic tail, while in 21 no clear evidence of disease was found. The SUVmax of the pancreatic tail ranged from 4.05 to 112.40. In 19 patients, this value was higher than that of the liver and in the other 17 patients, the opposite happened. In the 15 patients with confirmed disease in the pancreatic tail, the SUVmax was superior to that of the liver in all cases; in the remaining 21 patients, only 4 had SUVmax higher than that of the liver (p=0.000002). We also found a significant correlation between the presence of disease and SUVmax greater than 10 in the pancreatic tail (p=0.0000007). **Conclusion:** Our results show that in 41,7% of patients, the uptake of [68Ga]Ga-DOTA-NOC in the pancreatic tail corresponds to disease, suggesting that additional assessment is needed.We also found that uptake in the pancreatic tail with SUVmax greater than that of the liver and greater than 10, seem to be strong indicators of presence of disease. **References:** none

EP-017

Impact of Different βlevels Q.Clear Reconstructions on [68Ga]Ga-DOTANOC PET/CT Image Quality in Overweight NEN Patients: Preliminary Results

G. Argalia[1], *E. Fortunati*[1], *L. Zanoni*[2], *V. Allegri*[2], *C. Malizia*[2], *D. Calabrò*[1], *S. Civollani*[2], *D. Campana*[3,4], *S. Fanti*[1,2], *V. Ambrosini*[1,2];
[1]*Nuclear Medicine, Department of Experimental, Diagnostic and Specialty Medicine, University of Bologna, Bologna, ITALY,* [2]*Nuclear Medicine, IRCCS, Azienda Ospedaliero-Universitaria di Bologna, Bologna, ITALY,* [3]*Oncology, IRCCS, Azienda Ospedaliero-Universitaria di Bologna, Bologna, ITALY,* [4]*DIMEC, IRCCS, Azienda Ospedaliero-Universitaria di Bologna, Bologna, ITALY.*

Aim/Introduction: Digital PET/CT allows Q.Clear image reconstruction with different Beta-levels (β), although no definitive standard β for [68Ga]68Ga-DOTANOC PET/CT has been established yet. As patient's body mass index (BMI) can affect image quality, the aim of the study was to visually and semi-quantitatively assess three β compared to standard OSEM in overweight patients. **Materials and Methods:** Inclusion criteria: 1) patients with neuroendocrine tumour (NEN) included in a prospective CE-approved electronic archive (131/2017/O/Oss); 2) [68Ga]68Ga-DOTANOC PET/CT performed on a digital tomograph between September-2019 and March-2021; 3) BMI≥25. Images were acquired following EANM guidelines and reconstructed with OSEM and Q.Clear with three β (800, 1000, 1600). Scans were revised by 3 expert readers, unaware of clinical data, who independently chose the preferred reconstruction for visual image quality. Semi-quantitative analysis was performed on each scan (SUVmax-T of the highest uptake lesion, SUVmean-L of the liver background, SUVmax-T/SUVmean-L, Signal-to-noise ratio-SNR, Contrast-to-noise ratio-CNR). Results: Overall, 75 patients (median age: 63yo [23-87]) were included: pre-obesity sub-group (25≤BMI<30, n=50) and obesity sub-group (BMI≥30, n=25). [68Ga]68Ga-DOTANOC PET/CT was positive for disease in 45/75 (60.0%) cases (14 obese and 31 pre-obese patients). Agreement among readers' visual rating was high (Kscore=0.88) and the β1600 was preferred in most cases (in 96% of obese patients and in 53.3% of pre-obese cases). OSEM was considered visually equal to β1600 in 44.7% of pre-obese cases and in 4% of obese patients. In a minority of pre-obese cases, OSEM was preferred (2%). β800 and β1000 were always rated inferior. Overall, CNR (p<0,0001) and SNR (p<0,0001) were significantly different between OSEM (CNR: mean 38.6±29.6, median=32.5; SNR: mean=8.1±2.0, median=8.1) and β1600 (CNR: mean 59.3±51.5, median=52.3; SNR: mean=11.1±2.7, median=12.2), conversely to SUVmean-L (non-significant); these results were also confirmed when calculated separately for the pre-obesity and obesity sub-groups. SUVmax-T, SUVmax-T/SUVmean-L resulted significantly different among all reconstructions in the whole population as well as in the pre-obese sub-group, while no differences were observed in the obese sub-group between β1600 and OSEM. **Conclusion:** This preliminary study showed that β1600 Q.Clear improves overall image quality in obese patients, while its impact in pre-obese cases is less relevant compared to standard OSEM. Considering that semi-quantitative analysis was limited to the highest uptake lesion, further larger studies including lesion-based analysis and head-to-head comparison with conventional radiological procedures are warranted to establish the best β in other clinical settings (e.g. small lesions, normal weight patients). **References:** None.

EP-018

Modified TGR: a new strong radiological marker to accurately predict early response to PRRT in GEPNETs

F. Scalorbi, G. Calareso, E. Garanzini, G. Argiroffi, V. Fuoco, A. Marchianò, E. Seregni, M. Maccauro;
Istituto Nazionale Tumori Milano, Milan, ITALY.

Aim/Introduction: To investigate the added value of modified TGR (tumor growth rate) as radiological predictor of early response to PRRT, in GEPNET patients. **Materials and Methods:** Progressive metastatic G1-G2 GEPNET patients treated with PRRT (^{177}Lu-DOTATATE 4 administrations, 7.4 GBq/each) at our centre from 04/2019 to 10/2020 were considered. Inclusion criteria were 3 CT/MRI scans per patient: one(i) performed within 3 months before PRRT to assess disease burden and confirm radiological progression, one(ii) interim evaluation after 2 PRRT administrations and one(iii) within 4 months after the end of treatment to assess early response, according to RECIST1.1. All the scans were centrally re-evaluated by 2 dedicated radiologists. TGR was calculated in 2 ways: assuming that the volume of the lesions can be calculated applying the volume of a sphere formula(TGR_ sphere, classical TGR formula, Dromain,BMC2019) or the volume of an elliptical cylinder (TGR_ elliptical_cylinder, new model). In both cases, to assess TGR, baseline versus interim evaluations were compared and the values were expressed as % increase/month. Patients were subdivided as responders(CR,PR,SD) and non-responders(PD), according to RECIST. Performance status was evaluated by ECOG v.5, lines of previous therapies were calculated as possible confounders. Chi/Fisher and K-Wallis test were applied to assess independence between response to treatment and patient characteristics. Logistic regression was performed to determine predictability of both TGR models and clinical features for disease progression. ROC analysis was applied to assess the performance of the two models and evaluate optimal TGR_sphere and TGR_elliptical_cylinder cut-off. Results: According to inclusion criteria, 27 patients (12 males, 15 females, mean age 63.9, range 37-80, SD 10.8) were analysed. Fifteen (55.6%) were midgut, 12(44.4%) foregut, 24(88.8%) ECOG 0, three (11.2%) ECOG 1 or 2. PRRT was applied in second line in 18(66.6%), in third or further in 9(33.4%) in patients. Considering RECIST, 4(14.8%) patients were non-responders. Chi/Fisher and K-Wallis test didn't show statistical significance. Logist regression showed OR equal to 5.9(SE 9.4) with AUC 0.95(Sensitivity 75%, Specificity 95%) for TGR_elliptical model and OR 1.05(SE 0.07) with AUC 0.75(Sensitivity 25%, Specificity 75%), for TGR_spherical model. The optimal cut-off value for progression prediction was 5.5% volume increase/month for TGR_elliptical_cylinder (Sensitivity 100%,Specificity 86.4%) and 5.3%/month for TGR_sphere (Sensitivity 75%, Specificity 81.8%). **Conclusion:** Interim TGR_elliptical_cylinder is a strong and accurate predictor of early progression of GEPNET disease after PRRT.

The optimal TGR_elliptical_cylinder cut-off value to predict early progression is 5.5%/month, with optimal sensitivity and specificity. External validation is on course. **References:** None

EP-019

New ^{99m}Tc Exendin (9-39)/Tyr3-Octreotide radioligand improves sensitivity and specificity for the diagnosis of benign and malignant insulinomas, in comparison to ^{111}In-pentetreotide

E. Cortes-Mancera[1], J. Gonzalez Díaz[2], J. Soto Andonaegui[2], G. Ferro Flores[3], B. Ocampo García[3];
[1]Hospital Angeles del Pedregal, Mexico City, MEXICO, [2]UMAE Hospital de Especialidades. Centro Médico Nacional Siglo XXI, Mexico City, MEXICO, [3]Instituto Nacional de Investigaciones Nucleares (ININ), Mexico City, MEXICO.

Aim/Introduction: Benign insulinomas express the glucagon-like peptide 1 receptor (GLP-1R) in high density and show low levels of expression of somatostatin receptor (SSTR2). In malignant insulinomas, the opposite happens. The radiolabeled GLP-1R antagonist Exendin (9-39) has potentially shown greater affinity than the Exendin-4 agonist. ^{99m}Tc Exendin (9-39)/Tyr3-Octreotide is a new lyophilized preparation that has affinity for both GLP-1 and SST2 receptors. The aim of the study was to compare the sensitivity of SPECT ^{99m}Tc-Exendin (9-39)/Tyr3-Octreotide vs ^{111}In-pentetreotide for the diagnosis of insulinomas. **Materials and Methods:** Patients with endogenous hyperinsulinemic hypoglycemia were selected. The presence and type of tumor were confirmed by histopathology. 2 hours after injection of 370 MBq of ^{99m}Tc Exendin (9-39)/Tyr3-Octreotide an abdomen SPECT was acquired. One week later, 222 MBq of 111In-pentetreotide were administered and SPECT was acquired at 4 and 24 hours after injection. Semi-quantitative analyzes were performed. The maximum target- background ratio (TBRmax) was calculated using the contrast capture of healthy pancreatic tissue as background. Results: 18 patients were included with the stated criteria, aged between 21 and 63 years and with a histopathological diagnosis of insulinoma (14 benign and 4 malignant insulinomas). The 14 benign insulinomas were surgically removed (dimensions: 20.2 ± 9.1 mm). Symptoms of hypoglycemia were resolved immediately after surgery in 14/14 patients whose tumors were detected by ^{99m}Tc Exendin (9-39)/Tyr3-Octreotide, whereas in studied patients with ^{111}In-pentetreotide only 11/14 patients were detected. A significant difference between SPECT TBRmax was observed in favor of ^{99m}Tc Exendin (9- 39)/Tyr3-Octreotide compared to ^{111}In-pentetreotide. (TBRmáx 9,82 ± 4 vs 4,48 ± 3; p <0,001). In the 4 patients with malignant insulinomas with metastases in the liver and retroperitoneum studied with both ^{111}In- pentetreotide and ^{99m}Tc Exendin (9-39)/Tyr3- Octreotide, both drugs detected 10/10 injuries (TBRmáx de 10±2.1 vs 14.6 ± 3; p<0.001). The sensitivity of ^{99m}Tc Exendin (9-39)/Tyr3-Octreotide was 96.67% compared to ^{111}In- pentetreotide, of 83.09%. The specificity of ^{99m}Tc Exendin (9-39)/Tyr3-Octreotide was 92% compared to ^{111}In-pentetreotide, of 72%. **Conclusion:** ^{99m}Tc Exendin (9-39)/Tyr3-Octreotide SPECT is an excellent specific agent for molecular imaging of GRP-1R/SSTR positive insulinomas. Being a new hybrid ligand, it allows the diagnosis of both benign and malignant insulinomas with better dosimetry, shorter acquisition time, high availability and low cost in comparison to ^{111}In-pentetreotide. **References:** None

EP-020

Radiomic Model Discriminating Low Grade Pancreatic Neuroendocrine Tumours Assessed by Biopsy of the Primary Lesion

G. Argalia[1], E. Fortunati[1], D. Calabrò[1], S. Malavasi[2,3], D. Campana[4,5], R. Casadei[6,5], C. Ricci[6,5], A. Bevilacqua[2,7], S. Fanti[1,8], V. Ambrosini[1,8];
[1]Nuclear Medicine, Department of Experimental, Diagnostic and Specialty Medicine, University of Bologna, Bologna, ITALY, [2]Advanced Research Center for Electronic Systems (ARCES), University of Bologna, Bologna, ITALY, [3]Research Institute on Global Challenges and Climate Change (Alma Climate), University of Bologna, Bologna, ITALY, [4]Oncology, IRCCS, Azienda Ospedaliero-Universitaria di Bologna, Bologna, ITALY, [5]DIMEC, IRCCS, Azienda Ospedaliero-Universitaria di Bologna, Bologna, ITALY, [6]Surgery, IRCCS, Azienda Ospedaliero-Universitaria di Bologna, Bologna, ITALY, [7]Department of Computer Science and Engineering (DISI), University of Bologna, Bologna, ITALY, [8]Nuclear Medicine, IRCCS, Azienda Ospedaliero-Universitaria di Bologna, Bologna, ITALY.

Aim/Introduction: Grade 1 (G1) and grade 2 (G2) pancreatic neuroendocrine tumours (pNET) may show different clinical behaviour. Tumour grade can be assessed by either histology of the whole excised primary lesion or its biopsy. Even though bioptical specimens may not be representative of the whole lesion, they are much more available in clinical practice. The aim of this study is to evaluate whether [68Ga]Ga-DOTANOC PET/CT derived radiomic features can be employed to discriminate pNET grade, assessed by biopsy of the primary lesion. **Materials and Methods:** Patients (pts) were selected from a prospective CE-approved electronic archive collecting cases of pts with neuroendocrine lesions who underwent [68Ga]Ga-DOTANOC PET/CT. Pts with a pNET lesion bigger than 1cm^3 and with a [68Ga]Ga-DOTANOC PET/CT scan performed at staging were included. Tumour grade was assessed on bioptical samples (WHO 2019). [68Ga]Ga-DOTANOC PET/CT was performed and interpreted following standard EANM procedure. Segmentation of the whole tumour volume was manually performed by the nuclear medicine physician on the fused [68Ga]Ga-DOTANOC PET/CT images. 12 first-order and 48 second-order radiomic features were then computed on the SUV maps over the regions of interest, considering four distances (d). Linear discriminant analysis was applied on couples of radiomic features showing low linear correlation and high statistical power. The Wilcoxon rank-sum test and the Area Under the Curve (AUC) of the receiver operating characteristic were evaluated to assess radiomic models performance. The

couple showing the lowest p-values and the highest AUC was finally selected. Results: 26 pts (18 G1 and 8 G2) met the inclusion criteria. The radiomic model made of second-order normalized homogeneity (d=2) and joint maximum (d=4) features showed the highest significant performance (p-value=0.0014) with sensitivity=75%, specificity=89%, accuracy=85%, AUC=90%, true negative=16, false positive=2, false negative=2, true positive=6. Among the four pts misclassified, one G2 lesion lay very far from the discrimination line, showing features more similar to G1 than G2. Noteworthy, this pt had borderline ki67 index (equal to 3), thus leading to questioning whether this lesion was originally correctly discriminated by the bioptical sample examination. **Conclusion:** This preliminary model, although on a limited sample size, showed that biopsy results can be used to generate a radiomic model to discriminate pNET grade. Further data are needed on larger samples and performance should be compared to radiomic models derived from histological results. **References:** None.

EP-021

[68Ga]Ga-DOTANOC PET/CT in Neuroendocrine Tumours: Results of Data Collection in a Three-Years Electronic Archive

E. Fortunati[1], G. Argalia[1], L. Zanoni[2], S. Telo[1], D. Calabrò[1], D. Campana[3,4], R. Casadei[5,4], C. Ricci[5,4], C. Mosconi[6], S. Fanti[1,2], V. Ambrosini[1,2];

[1]Nuclear Medicine, Department of Experimental, Diagnostic and Specialty Medicine, University of Bologna, Bologna, ITALY, [2]Nuclear Medicine, IRCCS, Azienda Ospedaliero-Universitaria di Bologna, Bologna, ITALY, [3]Oncology, IRCCS, Azienda Ospedaliero-Universitaria di Bologna, Bologna, ITALY, [4]DIMEC, IRCCS, Azienda Ospedaliero-Universitaria di Bologna, Bologna, ITALY, [5]Surgery, IRCCS, Azienda Ospedaliero-Universitaria di Bologna, Bologna, ITALY, [6]Radiology, IRCCS, Azienda Ospedaliero-Universitaria di Bologna, Bologna, ITALY.

Aim/Introduction: Neuroendocrine tumours (NEN) are rare and heterogeneous for both primary tumour site and behaviour (either at first diagnosis or during the natural disease course). The collection of clinical and imaging data of patients (pts) undergoing [68Ga]Ga-DOTANOC PET/CT in a prospective electronic archive (PEA), may provide valuable information for clinical management as well as for a better employment of [68Ga]Ga-DOTANOC PET/CT in the diagnostic flow-chart. **Materials and Methods:** All pts, both with pathologically proven NEN or only suspected NEN, who underwent [68Ga]Ga-DOTANOC PET/CT at Our Centre (September 2017-September 2020), were prospectively enrolled in a CE-approved PEA (131/2017/O/Oss). Collected information included pts' clinical, laboratory and imaging data. [68Ga]Ga-DOTANOC PET/CT was performed and interpreted (visually and semi-quantitatively) according to the EANM-guidelines. Results: In the study period, 1353 [68Ga]Ga-DOTANOC PET/CT scans were performed. Most NEN were well-differentiated (1056/1353) while suspected NEN were 297/1353. Most pathologically confirmed primary tumours were detected in the gastro-entero-pancreatic tract (51.7%) and in the lungs (10.4%); less frequent forms included paragangliomas (1.1%), insulinomas (0.4%), pheochromocytomas (0.9%), meningiomas (0.5%) and medullary thyroid cancer (0.8%). A minority of cases were MEN1-2 (3.4%). Unusual primary tumour localizations included: ears (n=10), thymus (n=7), breast (n=6), ovary (n=3) and skin (n=3, Merkel-cell carcinoma). Indications to [68Ga]Ga-DOTANOC PET/CT included: staging (11.5%), post-surgical staging (11.4%), PRRT selection (1.7%), ad interim evaluation (20.3%), restaging after therapy (4%), suspected relapse (9.6%), follow-up (14.7%), unknown primary tumour (4.8%) and suspected NEN without pathological confirmation (22%). In the latter subset (n=297), [68Ga]Ga-DOTANOC PET/CT was positive only in about half of them (n=166/297, 55.9%). [68Ga]Ga-DOTANOC PET/CT was positive for NEN lesions in 865/1353 scans and in 300/1353 (22.2%) the disease was limited to the primary tumour site. Metastasis were present in 565/1353 scans: nodal-only involvement was described in 148/565 (26.2%) while diffuse metastatic spread was present in 417/565 scans (73.8%), with or without nodal involvement. The most frequent metastatic sites were the liver, the bones and the lungs. PET-positive non-malignant findings were frequently observed (660/1353, 48.8%) and were described as: physiological uptake in the pancreas-uncinate process, accessory spleens, inflammatory/infectious processes. **Conclusion:** Most pts presented metastatic spread at [68Ga]Ga-DOTANOC PET/CT images, GEP and lung primary tumour and frequent false positive non-malignant findings. Considering NEN rarity as well as their heterogeneous clinical presentation and behaviour, clinical and imaging data collection in a PEA is crucial for a more tailored employment of [68Ga]Ga-DOTANOC PET/CT in the diagnostic flow-chart. **References:** None.

EP-07

Wednesday, October 20 - Saturday, October 23, 2021

e-Poster Area, release on Wednesday, October 20 at 09:00

Imaging Clinical Studies -> Oncological Imaging Clinical Study -> Colorectal

EP-022

FDG PET/CT and Diffusion-Weighted MRI in Primary Staging of Rectal Cancer

A. Arçay[1], F. Aydın[1], A. Keven[2], Z. G. Kıprak[1], M. N. Engin[1], C. N. Dündar Çağlayan[1], A. Boz[1];

[1]Akdeniz University Hospital, Department of Nuclear Medicine, Antalya, TURKEY, [2]Akdeniz University Hospital, Department of Radiology, Antalya, TURKEY.

Aim/Introduction: The study aims to compare FDG PET/CT findings and parameters with diffusion-weighted MRI findings and parameters and postoperative pathology findings in primary staging before treatment in rectal cancer patients. **Materials and Methods:** A total of 27 rectal cancer patients whose postoperative pathological results, FDG PET/CT, MRI images before treatment and operation between 2016 and 2019 were available in our hospital were included in the study. SUVmax, SUVmean, MTV, and TLG parameters from the primary tumor lesion in FDG PET/CT imaging and ADC values from MRI images were recorded. Pathological stage, stage according to MRI findings and lymph nodes presented in PET/CT were retrospectively evaluated. Results: 27 patients which consisted of 11 women and 16 men patients with a mean age of 60 (31-82) years were reviewed. The median days between FDG PET/CT and MRI scans that were performed before the operation were 5 (0-25) days. When the relationship between FDG parameters and MRI ADC values was examined, a negative moderate significant correlation (Spearman, ρ=-0.390; p=0.044) was found between MTV and ADC. Although there were negative weak-moderate correlations between other PET parameters and ADC, they were not statistically significant (p>0.05). When we analyze the difference between the primary tumor PET and MRI parameters in the patient groups with lymph node-positive and negative in PET/CT, no significant difference was observed in SUVmax and SUVmean values, while TLG and MTV values were significantly higher in the lymph node-positive (Mann-Whitney U,p=0.026 and p=0.02). Also, ADC values were higher in the lymph node-negative group than in the positive group (Mann-Whitney U,p=0.03). The sensitivity, specificity and accuracy of MRI and PET/CT for lymph node detection were 71.4%, 23.1%, 48.1% and 78.6%, 30.8%, 55.5%, respectively. PET/CT findings of 21 patients with locally advanced disease (pathological T3 and T4 stage) showed clouding in the surrounding fatty tissue in 12 patients. Besides, distant metastases were detected in 2 patients out of 21 patients without clouding in the surrounding fat tissue, which contributed to the staging of the patient. In 19 of 21 patients with pathological T3 and T4 stage, the MRI T stage was also observed similarly. **Conclusion:** MRI is superior to FDG PET/CT in local staging of the tumor; however, the sensitivity of MRI and FDG PET/CT were similar for lymph node detection. The negative correlation between ADC and MTV in pre-treatment primary tumors confirms the relationship between tumor cellularity and metabolic activity. **References:** None.

EP-023

Quantitative Parameters of 18F-FDG PET/CT as a biomarker of KRAS expression in Metastatic Colorectal Cancer

S. Moustafa[1], S. Khallaf[2], A. Rayan[3], A. Tawakol[4], M. Makawy[1], N. M. Mostafa[1];

[1]Assiut university. Clinical Oncology and Nuclear medecine, Assiut, EGYPT, [2]Medical clinical Oncology, SECI. South Egypt cancer Institute, Assiut, EGYPT, [3]Assiut university. Clinical Oncology, Assiut, EGYPT, [4]Cairo University. Clinical Oncology and Nuclear medecine, Cairo, EGYPT.

Aim/Introduction: Colorectal cancer (CRC) is the third most common cancer. It develops through accumulation of genetic alterations in oncogenes and tumor suppressors. Mutations in the KRAS gene occur in approximately 40% of CRCs. CRC most commonly metastasizes to the liver, then to the lung . Currently new drugs called oral tyrosine kinase inhibitors inhibit proliferation and angiogenesis may be beneficial in those patients depending on the KRAS type. KRAS mutational tests have two limitation first the heterogenesity either within the tumour or discordant between tumour and metastatic site, second the biopsy of metastatic site is difficult and need invasive proceduresThere are conflicting results of few published 18F-fluorodeoxy glucose positron emission tomography/computed tomography (18F-FDG PET/CT) studies about relationship between KRAS mutational status and metabolic activity of metastatic CRC. The aim of the study was to evaluate the association between KRAS types and the level of metabolic activity of metastatic CRC demonstrated by18F-FDG PET/CT to give anon invasive predictors of the therapeutic response to targeted therapy in these patients. **Materials and Methods:** Thirty-six patients with metastatic CRC who had mutational analysis for their tumor specimen were prospectively included in our study. Baseline 18F-FDG PET/CT was performed for all patient before starting treatment. Quantitative parameters including SUVmax and TLG (Total lesion Glycolysis) extracted from FDG-PET/CT study. Results: Twenty-three males and thirteen females, the mean age was 51.2±14.8. The mean of maximum standardized uptake value (SUVmax) of metastatic lesions was significantly higher in patients with mutant KRAS (11.5) than that of those with wild type (5.3), (P= 0.03). In the contrast, there was no significant association between total lesion glycolysis (TLG) and KRAS status, (P= 0.2). **Conclusion:** SUVmax extracted from 18F-FDG PET/CT was significantly higher in metastatic CRC patients with mutant KRAS. So, high SUVmax is suggested to be a potential non-invasive negative predictive biomarker for response to anti-EGFR in metastatic CRC. **References:** None.

EP-024

Evaluation of incidental gastrointestinal accumulations in 18F-FDG PET to differentiate malignant lesions from benig ones

D. Dezso, K. Zámbó, Z. Ritter, Z. Bán, Z. Szabó, E. Schmidt;
University of Pécs, Medical School, Department of Medical Imaging Diagnostic, Division of Nuclear Medicine, Pécs, HUNGARY.

Aim/Introduction: Colorectal cancer is one of the most common malignancies in the Western world. The aim of our study was to find the best parameter of 18F-FDG PET examination to differentiate focal accumulations of malignant from benign gastrointestinal diseases in patients with other oncological indications. **Materials and Methods:** Five hundred and six patients were investigated retrospectively with oncological indications. They underwent 18F-FDG PET/CT examination between June 2016 and January 2017. Incidental accumulations of 18F-FDG were evaluated in the gastrointestinal system. The PET/CT data were compared with the endoscopic and histopathological findings. SUVmax, entropy, homogeneity, intensity variability was measured with Interview Fusion software (Mediso), and the results were evaluated with the help of SPSS software. The SUVmax was corrected with the mean SUVmax of the liver and mediastinal blood-pool. Results: In our ongoing study endoscopic results were available in 44 examined patients (23 women, mean age 58±9 and 21 men, mean age 60±14) with 56 focal FDG accumulations, 8 patients treated with metformin. Ten lesions were identified as malignant diseases. Inflammatory and other benign GI lesions were observed in the other 46 cases. Based on our early results, corrected ($p<0.001$; $r=0.519$,$p<0.001$) and uncorrected ($p<0.001$; $r=0.499$,$p<0.001$) SUVmax values and entropy ($p<0.05$; $r=0.301$,$p<0.05$) were significantly higher in malignancies, and they were correlated with histological findings. There was no significant difference between the homogeneity ($p=0.164$) and intensity variability ($p=0.211$) of malignant and benign lesions. Based on the ROC analysis, the optimal cut-off values for differentiating malignant lesions from benign ones were uncorrected SUVmax>13,0 (sensitivity 70.0%, specificity 97.7%). **Conclusion:** Considering other studies, SUVmax may be the most usable PET parameter to differentiate incidental FDG accumulations in the gastrointestinal system, but other PET parameters may also help, such as entropy of the lesion. **References:** 1 Project no. TKP2020-IKA-08 has been implemented with the support provided from the National Research, Development and Innovation Fund of Hungary, financed under the 2020-4.1.1-TKP2020 funding scheme.

EP-08

Wednesday, October 20 - Saturday, October 23, 2021

e-Poster Area, release on Wednesday, October 20 at 09:00

Imaging Clinical Studies -> Oncological Imaging Clinical Study -> Prostate Other

EP-025

Effect of cold intervention on ^{68}Ga-PSMA uptake of salivary glands

F. Görtan, N. Coşkun, N. C. Gülaldı;
Turkish Ministry of Heath, Ankara City Hospital, Department of Nuclear Medicine, Ankara, TURKEY.

Aim/Introduction: Due to high expression of prostate specific membrane antigen (PSMA) on salivary glands, xerostomia is a well known side effect of peptide receptor radionuclide therapies (PRRT's) utilised with ^{177}Lu and ^{225}Ac for castration-resistant prostate cancer. Our study aims to determine the effect of external cooling on the degree of ^{68}Ga-PSMA uptake in salivary glands. **Materials and Methods:** Sixty five patients referred to our institution for ^{68}Ga-PSMA imaging were prospectively enrolled in the study. Thirty minutes prior to i.v. radiopharmaceutical injection, cooling material containing ice was placed on the right side of patient's face, to meae sure to cover area of salivary glands. The cooling material was replaced with a new one in every thirty minutes to be able to obtain sufficient cooling. PET/CT images were acquired from vertex to midthigh after 60 minutes of i.v. injection of 2 MBq/kg ^{68}Ga-PSMA at 2 minutes/bed position. SUVmax, SUVmean, SUVmin and SUVstd values of parotid and submandibulary glands were measured for both sides of each patient. Results: Comparing values right versus left parotid gland ^{68}Ga-PSMA uptake; SUVmax: 18.88±6.74 versus 19.78±7.49 p=0,47, SUVmean: 11.75±4.34 versus 12.31±4.75 p=0,48, SUVmin: 7.60±2.72 versus 7.97±3.09 p=0,48, SUVstd: 2.59±1.02 versus 2.74±1.08 p=0,44 and submandibular gland ^{68}Ga-PSMA uptake SUVmax: 23,15±7.21 versus 24.10±7.07 p=0,45, SUVmean: 14.61±4.57 versus 15.19±4.60 p=0,48 SUVmin: 9.20±2.91 versus 9.62±2.84 p=0,40, SUVstd: 3.39±1.08 versus 3.47±1.07 p=0,65. Although right sided salivary glands showed lower radiopharmaceutical uptake for all sixty five patients with 4.7% reduction for SUVmax and 4.1% for SUVmean, results did not differ significantly for any of investigated parameters statistically. Although right sided salivary glands showed lower radiopharmaceutical uptake for all 65 patients with 4.7% reduction for SUVmax and 4.1% for SUVmean, results did not differ significantly for any of the investigated parameters statistically. **Conclusion:** Given the successful and increased use of ^{177}Lu-PSMA and ^{225}Ac-PSMA PRRT's for the castration-resistant prostate cancer, preventive strategies for side effects are needed to be investigated. According to our data, the effect of cold intervention to reduce radioligand uptake on salivary glands is limited and therefore seems to be insufficient to prevent xerostomia. **References:** None

EP-026

Impact of the 18F-PSMA PET/CT in the evaluation of response to androgen deprivation therapy in prostate cancer, a single center experience

S. Medina-Ornelas, F. Garcia-Pérez, M. Alvarez-Avitia, N. Sobrevilla-Moreno, M. Jimenez-Rios;
Instituto Nacional de Cancerologia, Mexico City, MEXICO.

Aim/Introduction: Prostate-Specific Membrane Antigen (PSMA) is very useful in the evaluation of recurrence of prostate cancer (PC) and high accuracy in the evaluation of metastatic sites; meanwhile patterns of disease the response is not fully studied, many patients only had monitoring disease with PSA values, but the correlation with the overall disease in vivo with PET/CT is poor. Our objective is to determine the value of 18F-PSMA PET/CT in the evaluation of response to androgen deprivation therapy (ADT) in patients with PC non-castration resistance. **Materials and Methods:** We enrolled 28 patients between October 2018 and December 2020 with confirmed PC hormone-sensitive with 18F-PSMA PET/CT, who underwent a baseline scan, followed by a follow-up scan after ADT, with mean an interval of 6.4 months between 2 scans. Treatment response on 18F-PSMA PET/CT based on quantitative parameters SUVmax and MTV, response criteria were defined according to increase or decrease of 50% of overall uptake and was compared with a biochemical response based on PSA levels; the correlation was made with Spearman rank. Results: Overall PET-based response with SUVmax and MTV showed partial response in 73% and stable disease in 20 % of the patients with a complete biochemical response and we found a correlation with PSA decrease (r = 0.789). Only 6% of patients who had biochemical responses showed discordant results on 18F-PSMA PET/CT. 1% of patients showed progressive disease complete biochemical response. The sites of response was prostate gland (r= 0.809),lymph nodes (r = 0.768) and metastatic sites in bone (r = 0.502) **Conclusion:** we conclude that 18F-PSMA PET/CT is a good imaging method in evaluating response to ADT with a strong correlation with PSA values. Both parameters are useful for determining partial response or stable disease; not only visual analysis. The discordance between 18F-PSMA and PSA maybe represent mutations in clone cells. More studies are necessary to validate this observation **References:** none

EP-027

Discrepancy between serum PSA and tumour burden in PSMA PET/CT: can we find an explanation?

L. Lemos[1], P. Soeiro[1], R. Silva[1,2], R. Ferreira[1,2], G. Costa[1,3], J. Pedroso de Lima[1,2,3];
[1]Centro Hospitalar e Universitário de Coimbra, Coimbra, PORTUGAL, [2]Instituto de Ciências Nucleares Aplicadas à Saúde (ICNAS), Faculdade de Medicina, Universidade de Coimbra, Coimbra, PORTUGAL, [3]Faculdade de Medicina, Universidade de Coimbra, Coimbra, PORTUGAL.

Aim/Introduction: Serum prostate-specific antigen (PSA) is the main cornerstone in the follow-up of prostate cancer patients after local therapy. However, some patients presenting with high serum PSA apparently have an unexpectedly low tumour volume on PSMA PET and vice-versa. One hypothesis for such discrepancy is that PSA level is dependent on other variables besides tumour volume alone. Therefore, we propose to investigate other clinical and metabolic variables that might influence PSA values. **Materials and Methods:** We retrospectively reviewed a total of 714 [^{68}Ga]Ga-PSMA PET/CT scans performed between November/2015 and March/2021 and selected all patients who underwent radical prostatectomy and had a serum PSA measurement within 30 days of the scan. Patients who underwent any form of hormonal therapy or chemotherapy were excluded. Semi-automatic tumour VOI were defined through the application of a SUV threshold of 2.5g/ml, and volume (PSMA-TV), SUVmax and SUVmean measurements were recorded. Total lesion PSMA expression (PSMA-TL) was obtained by multiplying PSMA-TV by SUVmean. Demographical and histological data were also recorded, and PSA-doubling time was calculated. Results: Thirty-one patients fulfilled the inclusion criteria, with an average age of 70.23±5.43 [58-82] years. ISUP scores 1, 2, 3, 4 and 5 displayed a frequency of 6.5%, 19.4%, 48.4%, 6.5% and 3.2%, respectively. In 16.0% of patients ISUP grade was unknown. Fourteen patients underwent additional radiotherapy (45.2%). Median PSA at the time of the scan was 1.89ng/mL [0.12-47.30]. PSMA PET/CT derived parameters were as follows: median PSMA-TV 2.432cm3 [0.144-69.058]; median PSMA-TL 9.847 [0.096-297.989]; median SUVmax 5.734 [0.998-24.449]; median SUVmean 3.538 [0.667-8.969]. A strong and statistically significant correlation was found between PSA values and PSMA-TV (Spearman's rho 0.715, $p<0.01$) and PSMA-TL (rho 0.690, $p<0.01$). A significant, albeit weaker, correlation with SUVmax was also discovered (rho 0.477, $p=0.012$). In a multivariate model, only PSMA-TV and PSMA-TL remained statistically significant, whereas SUVmax did not. PSA doubling time did not correlate with any of the PSMA PET/CT derived parameters. We also did not find statistically significant differences in any of these variables between Gleason scores or ISUP grade groups. **Conclusion:** In our sample, besides PSMA-TV, only PSMA-TL showed a statistically significant correlation with PSA values, which persisted in a multivariate model. No other clinical and metabolic variables showed correlation with PSA or remained statistically significant following a multivariate analysis. **References:** none

EP-028

The cause of high [^{18}F]PSMA-1007 uptake in the urinary bladder in some of the [^{18}F]PSMA-1007 patients: an explorative, retrospective study

Y. Allach, B. Privé, W. van Gemert, M. Schilham, L. R. Perk, M. Gotthardt, J. Nagarajah, M. Janssen;
Radboudumc, Nijmegen, NETHERLANDS.

Aim/Introduction: Positron emission tomography (PET) targeting prostate-specific membrane antigen (PSMA) to image prostate cancer allow accurate diagnosis and staging. Compared to the other PSMA-PET tracers available, [^{18}F]PSMA-1007 is metabolized by the hepatobiliary tract resulting in low renal excretion. This allows an excellent evaluation of the pelvic area. However, some patients do show high excretion of [^{18}F]PSMA-1007 by the renal system. Yet, this discrepant pharmacokinetics of [^{18}F]PSMA-1007 by some patients remains poorly understood. Hence, the present study aimed to investigate this by evaluating [^{18}F]PSMA-1007 PET scans from prostate cancer patients. **Materials and Methods:** In this single centre retrospective study, patients that underwent [^{18}F]PSMA-1007 PET imaging between July 2018 and January 2021 were included. All data regarding the PET scan, production of batch and individual patient characteristics were archived and analysed. As a model for the urinary uptake of [^{18}F]PSMA-1007, a 20 mm ROI was placed in the bladder for SUV values. A SUVmax of > 7.5 in the bladder was considered as high urinary excreting. Results: To date, we have evaluated 125 of the in total 514 [^{18}F]PSMA-1007 PET scans in 344 patients. Seventy-eight patients received two [^{18}F]PSMA-1007 PET scans (n= 156 scans), whereas 37 patients received three or more scans (n= 125 scans). The mean age was 69 years (±7.8). The mean administered activity of [^{18}F]PSMA-1007 was 251 MBq, and a mean of 88 minutes was in between injection and the PET/CT scan. The mean SUVMax and mean SUVMean of the bladder were 6.9 (±5.0) and 4.5 (±3.5), respectively. Of the 125 evaluated PSMA PET scans, high urinary uptake (SUVmax > 7.5) was observed in 42 cases (35%). Of the 37 patients that had ≥ 3 scans, six patients (16%) showed high urinary excretion (SUVmax >7.5) in one scan while the other scans showed low urinary uptake (SUVmax ≤7.5). Between these scans, no differences were observed in medication, kidney function, application of contrast, scan time, day of scanning, presence of aspecific bone uptake and risk factors. However, the high excreting cohort more frequently used diuretics (17.1% vs 6.4%) and had a slightly shorter time between the injection and scan (84 min (±18.0) vs 92 min (± 20.8)). **Conclusion:** In this ongoing study, we have not yet observed a direct influencing factor that may result in high renal excretion of [^{18}F]PSMA-1007. Thus, the definitive conclusions are still pending at time of submission. **References:** None

EP-029

Radiopharmaceutical Biodistribution and the Factors Affecting Biodistribution in Ga^{68}-PSMA PET/CT

A. Arçay Öztürk, A. Boz, M. Erkılıç, G. G. Bural, F. Aydın;
Akdeniz University Hospital, Department of Nuclear Medicine, Antalya, TURKEY.

Aim/Introduction: The aim of our study is to determine the physiological and pathophysiological distribution of the pharmaceutical(Ga^{68}-PSMA-617) by determining the range of uptake in the normal organs,tissues,pathological lesions and investigate whether there are differences in distribution according to the laboratory,histopathological and clinical findings that can affect image evaluation. Also,we aimed to determine cut-off values to distinguish pathological lesions from physiological uptake. **Materials and Methods:** 229 prostate cancer patients who underwent Ga^{68}-PSMA-PET/CT at our department between January and May 2018 were retrospectively analyzed.The patients were grouped as negative/positive groups according to the absence/presence of pathological activity on PET/CT.In the positive group, subgroups were formed according to Gleason score,treatments received before imaging,metastatic status,serum PSA, ALP, LDH, and creatinine values.The SUV values of the organs and lesions of the patients in these subgroups were compared among themselves and also with the negative group. Results: The highest uptake of Ga^{68}-PSMA-617 was observed in the renal cortex, bladder lumen, submandibular gland(SMG),parotid gland,lacrimal gland and jejunum sorted in descending order.There was no significant difference in the physiological uptake of lymph nodes and bone between the groups.In the group with patients that received androgen deprivation therapy, the bone metastasis SUV values were found to be higher and the SUV values of the SMG and renal cortex were found to be lower (Mann-Whitney U,p=0.043;0.004;0.01,respectively).In the group with patients that received radiotherapy, the normal prostate tissue SUV values were determined to be higher (Mann-Whitney U,p=0.009).The SUV values of the SMG, cerebellum, breast, testis, muscle, liver and blood pool were determined to be lower in the group of patients with high serum LDH values.The cut-off SUVmax value was determined to be 6,945 (sensitivity 89.6%,specificity 98.1%) for primary prostate lesion; 4,72 for lymph node metastasis; 4,25 for bone metastasis. The serum PSA values were higher in the positive group and the PSA cut-off value to distinguish the negative/positive groups was found to be 1,505 (sensitivity 79.7%,specificity 77.3%). **Conclusion:** PSMA-617 demonstrates similar biodistribution with other PSMA ligands(PSMA-11 and PSMA-I&T).The physiological uptake of lymph nodes and bone which were mostly metastasized in prostate cancer, are not affected by the factors we examined.It should be kept in mind that the normal prostate tissue SUV values may increase in patients receiving radiotherapy,the physiological and pathological

uptake of the organs may differ due to the changes in PSMA expression in patients receiving androgen deprivation therapy and tumor burden may affect the biodistribution. **References:** None.

EP-030

[11C]C-Choline, [68Ga]Ga-PSMA, [18F]F-FACBC PET/CT in Castration Resistant Prostate Cancer Patients: Which Is the Most Suitable To Assess the Therapy Response?

G. Argalia[1], E. Tabacchi[2], S. Vichi[3], C. Malizia[2], F. Massari[4], V. Mollica[4], V. Di Nunno[5], E. Nobili[4], C. Nanni[2], S. Fanti[2,1];
[1]Nuclear Medicine, Department of Experimental, Diagnostic and Specialty Medicine, University of Bologna, Bologna, ITALY, [2]Nuclear Medicine, IRCCS, Azienda Ospedaliero-Universitaria di Bologna, Bologna, ITALY, [3]Clinical Engineering Department, IRCCS, Azienda Ospedaliero-Universitaria di Bologna, Bologna, ITALY, [4]Medical Oncology, IRCCS, Azienda Ospedaliero-Universitaria di Bologna, Bologna, ITALY, [5]Medical Oncology, Azienda USL/ Institute of Neurological Sciences of Bologna, Bologna, ITALY.

Aim/Introduction: This study evaluates, on preliminary data, which PET/CT-radiotracer, among [11C]C-Choline, [68Ga]Ga-PSMA, [18F]F-FACBC, is the most suitable for therapy assessment in metastatic castration resistant prostate cancer (mCRPC) patients (pts). **Materials and Methods:** In the contest of a wider prospective interventional monocentric explorative study (granted project RF-2016-02364809), we evaluated mCRPC pts enrolled from January2019 to January2021 who have been randomly assigned to receive [11C]C-Choline, [68Ga]Ga-PSMA or [18F]F-FACBC PET/CT respectively. Each pt underwent two PET/CT scans: one before therapy onset with Abiraterone or Enzalutamide and one two months later. No therapeutic changes derived from PET/CT results. On each scan we evaluated the Metabolic Tumour Volume (MTV), calculated with a fixed threshold set at 40% of SUV max with a licensed software (GE-VCAR), and the Total Lesion Activity (TLA:MTVxSUVmean). Correlation between PSA-value, highest SUVmax, MTV, TLA and therapy-response assessed through the variation of PSA-value at first and second scan, for the three different radiotracers, was calculated. In particular the therapy-response was assessed by the increase (bad response) or the decrease (good response) of PSA-value and by the PSA-value variation>50%, among the two scans. For statistical analysis we used SPEARMAN and FISHER tests. Results: We enrolled 23 mCRPC pts randomized for [11C]C-Choline(8pts), [68Ga]Ga-PSMA(8pts) and [18F]F-FACBC(7pts). For [11C]C-Choline group we found a strong significant correlation between PSA-value and MTV (SPEARMAN:Rho=0.8748;p-value<0.0001) and PSA-value and TLA (SPEARMAN:Rho=0.9441;p-value<0.0001). No significant correlation was found between PSA-value and SUVmax. For [68Ga]Ga-PSMA group we found a moderate correlation between PSA-value and SUVmax (SPEARMAN:Rho=0.5357;p-value=0.0422), PSA-value and MTV (SPEARMAN:Rho=0.5246;p-value=0.0447) and PSA-value and TLA (SPEARMAN:Rho=0.5571;p-value=0.0336). For [18F]F-FACBC group we found a moderate correlation between PSA-value and SUVmax (SPEARMAN:Rho=0.6795;p-value=0.0151). No significant correlation was found between PSA-value and MTV and PSA-value and TLA. In the [68Ga]Ga-PSMA group we found a significant correlation between therapy-response and variation of SUVmax (FISHER:p-value=0.02857) and between therapy-response and variation of TLA (FISHER:p-value=0.02857). Furthermore, the therapy-response considered as the increase/decrease>50% of PSA-value among the two scans, due to the small number of data, showed no significant correlation with SUVmax, MTV and TLA. Nevertheless, in the [68Ga]Ga-PSMA group, there seems to be a correlation between PSA-value variation>50% and SUVmax, MTV and TLA. **Conclusion:** Limited to the small number of pts, [11C]C-Choline and [68Ga]Ga-PSMA are the radiotracers that provide parameters which better correlate with PSA-value, giving a more accurate representation of the volume of active disease. [68Ga]Ga-PSMA is the radiotracer that provides parameters which better correlate with therapy-response. Further validation is required. **References:** None.

EP-031

Predictors of ^{68}Ga-PSMA-11 PET/CT tumour burden in castration resistant prostate cancer patients: a single center experience

S. Telo[1], L. Vetrone[1], A. Giordano[1], C. Malizia[2], A. Farolfi[2], L. Calderoni[1], S. Mattoni[1], R. Mei[1], P. Castellucci[2], S. Fanti[3];
[1]Nuclear Medicine, Department of Experimental, Diagnostic and Specialty Medicine, University of Bologna, Bologna, ITALY, [2]Nuclear Medicine, IRCCS, Azienda Ospedaliero-Universitaria di Bologna, Italy, Bologna, ITALY, [3]Nuclear Medicine, Department of Experimental, Diagnostic and Specialty Medicine, University of Bologna;Nuclear Medicine, IRCCS, Azienda Ospedaliero-Universitaria di Bologna, Italy, Bologna, ITALY.

Aim/Introduction: To evaluate ^{68}Ga-PSMA-11-PET/CT tumour-burden in a cohort of'early'CRPC(castration-resistant-prostate-cancer) patients in relation to initial PSA(iPSA) before radical prostate-cancer(PC) therapy, PSA Velocity(PSAV), PSA at time of ^{68}Ga-PSMA-11-PET/CT(PSAPET), PSA Doubling Time(PSADT), ISUP and presence of local vs distant disease. **Materials and Methods:** We reviewed all PC patients who were referred to our Center(April2016-December2019) to perform ^{68}Ga-PSMA-11-PET/CT. Inclusion criteria:1)patients who underwent ^{68}Ga-PSMA-11-PET/CT with the indication of CRPC; 2)previous PC radical therapy (radical surgery or radical radiation) 3)patients who underwent up to a line of therapy after becoming CR. ^{68}Ga-PSMA-11-PET/CT findings were categorized as positive and negative by two experienced Nuclear Medicine Physicians. Doubtful findings were re-evaluated and categorized by consensus. Positive

findings were categorized as: local disease (local relapse in prostate bed/pelvic lymph-nodes) and distant disease (distant lymph-nodes/bone/visceral disease). Patients were divided in 3 outcome groups: Negative (negative ^{68}Ga-PSMA-11-PET/CT), Oligometastatic (a maximum of 3 lesions at ^{68}Ga-PSMA-11-PET/CT), multimetastatic (>3 lesions at ^{68}Ga-PSMA-11-PET/CT). Mann-Whitney U test was employed to compare each variable (ISUP, PSAPET, iPSA, PSADT, PSAV, local vs distant disease) between two groups (Oligometastatic/Multimetastatic) after Kruskal-Wallis test. Fisher's exact test was used to analyze multimetastatic/oligometastatic patients vs distant localizations of disease. A univariate logistic regression model was used to evaluate the relationship between the outcome groups vs all variables. Results: 84/2272 patients matched the inclusion criteria. ^{68}Ga-PSMA-11-PET/CT resulted negative in 6/84 and positive in 78/84 cases. Oligometastatic disease was detected in 40/78 patients: mean age=73(range:55-91); mean iPSA= 13,3 ng/ml(range:3,4; 103); mean PETPSA=2,6 ng/ml(range:0,3-22,1); mean PSADT=9,5 months(range:0,7-91,3); mean PSAV=4,3 ng/ml/year(range:0,1-65,7); mean ISUP=3(range:1-5); mean SUVmax of the positive lesions=25,9(range:2-138). 11/40 pts had only local disease, 29/40 pts had also distant disease. Multimetastatic disease was detected in 38/78 patients: mean age=72(range:55-88); mean iPSA= 19,3 ng/ml(range:2-90); median PETPSA=13,5 ng/ml(range:0,4-103,3); mean PSA DT=5,6 months(range:0,8-29); mean PSAV=16,7 ng/ml/year(range:0,1-161,5); mean ISUP=3(range:2-5); mean SUVmax of the positive lesions=30,35(range:5,4-110). 3/38 pts had only local disease, 35/38 pts had also distant disease. The difference among iPSA, PETPSA and PSAV values in the oligometastatic vs multimetastatic groups resulted statistically significative(all $P < 0.05$). Furthermore, distant localizations of disease were observed in multimetastatic patients more than in oligometastatic patients(P value=0.037). On logistic regression, PSAV and PSAPET were only independently predictive of outcome(P values<0.05). **Conclusion:** In our population of 'early' CRPC patients a higher number of PET-positive-lesions (multimetastatic condition) was associated to increased iPSA, PSAV and PETPSA values. Furthermore, distant metastatic disease was observed more frequently in multimetastatic patients. **References:** none

EP-032

Response assessment to second-line systemic therapies in advanced prostate cancer using ^{68}Ga-PSMA-11 PET/CT

L. Calderoni[1], A. Farolfi[2], P. Castellucci[2], F. Serani[2], S. Telo[2], S. Mattoni[2], F. Mattana[1], R. Mei[2], E. Maietti[3], S. Fanti[2];
[1]Nuclear Medicine University of Bologna DIMES, Bologna, ITALY, [2]Nuclear Medicine University of Bologna IRCCS, Bologna, ITALY, [3]Department of Biomedical and Neuromotor Sciences, University of Bologna, Bologna, ITALY.

Aim/Introduction: Assessment of response to therapy leads to treatment optimization in patient with advanced castration-resistant prostate cancer (CRPC). With some limitations, prostate-specific membrane antigen PET/CT (PSMA PET) can fill in the gaps left by conventional imaging methods and biomarkers including identification of predictors of response, adequate monitoring to implement a change in therapy, and parameters associated with overall survival (OS). To evaluate which PSMA PET parameters predict response to systemic therapy and to assess which are associated with OS **Materials and Methods:** We retrospectively evaluated the PSMA PET in 45 patients with a biochemical diagnosis of CRPC performed before and after a second line of systemic treatment. We compared the predictive accuracy of response with PSMA PET with that of biochemical response with serum PSA. We investigated whether PSMA expression on PET/CT correlates with PSA parameters (serum level, doubling time and velocity) and whether PSMA expression on PET/CT at baseline is a predictive marker of treatment response Results: PMSA PET and biochemical response were concordant in 65.1% of cases; 3/43 cases (7%) had a PSMA PET downstaging; 12/43 cases (27.9%), had an upstaging (k=0.39, p-value<0.001) with PSMA PET. The difference in PSA change between PET response categories was significant (P=0.0021). No statistically significant association was found between the number of lines of therapy and PSMA PET response(P=0.547).There is a moderate positive correlation between SUVmax and PSA value at baseline (r=0.477, p=0.003); as PSA increases, SUVmax increases, although the relationship does not appear linear. There is a moderate positive correlation between SUVmax and PSA value at baseline (r=0.477, p=0.003), as PSA increases SUVmax increases, but also between SUVmax and velPSA (r=0.373, p=0.033), although not linear. The correlation between SUVmax and dtPSA was not significant (r=-0.202, p=0.260). The correlation with OS was low (<0.3) and not significant for all SUV and PSA parameters **Conclusion:** Evaluation of PSA variation in PET response categories allowed for a better definition of the limitations of biochemical assessment. PSMA PET was able to better define responses where PSA, seeing at least a 50% reduction in PSA, would be identified as progression and where, seeing a change between +24% and -49%, would be identified as stable disease. PSMA PET

is therefore more reliable than PSA, especially in patients with PSA values not in clear progression. The correlation between OS and PET parameters was low and not significant, probably due to short follow-up time (median=28 months) **References:** none

EP-033

Influence of 68Ga-PSMA-11-PET/CT on Clinical Management in Castration Resistant Prostate Cancer Patients: a Single Centre Experience

L. Vetrone[1], S. Telo[1], A. Giordano[1], A. Spagnoletti[2], A. Farolfi[3], L. Calderoni[1], R. Mei[1], P. Castellucci[3], S. Fanti[1,3];
[1]Nuclear Medicine, Department of Experimental, Diagnostic and Specialty Medicine, University of Bologna, Bologna, ITALY, [2]Medical Oncology Department 1, Fondazione IRCCS Istituto Nazionale dei Tumori, Milan, ITALY, [3]Nuclear Medicine, IRCCS, Azienda Ospedaliero-Universitaria di Bologna, Bologna, ITALY.

Aim/Introduction: To evaluate the role of 68Ga-PSMA-11-PET/CT in the clinical management of early CRPC(castration-resistant-prostate-cancer) patients. **Materials and Methods:** All PCa patients referred to our Center (April2016-December2019), to perform 68Ga-PSMA-11-PET/CT were reviewed. Inclusion criteria: 1)patients who underwent 68Ga-PSMA-11-PET/CT with the indication of CRPC; 2) previous PC radical therapy 3)patients who underwent up to a line of therapy after becoming CR. 68Ga -PSMA-PET/CT were categorized as positive and negative, oligometastatic (a maximum of 3 lesions at 68Ga-PSMA-11-PET/CT) and multimetastatic (>3 lesions at 68Ga-PSMA-11-PET/CT) by two experienced Nuclear Medicine Physicians. Doubtful findings were re-evaluated and categorized by consensus. Positive findings were categorized as: local disease (local relapse in prostate bed and/or pelvic lymph-nodes) and distant disease (distant lymph-nodes, bone and visceral disease). Patients' clinical and conventional imaging data (ISUP, iPSA, PSA at time of PET, clinical condition, comorbidities, previous/ongoing therapies, available conventional diagnostics carried out within 3 months) were evaluated by an oncologist. It was then determined whether 68Ga-PSMA-11-PET/CT result was able to change patients' management in comparison to clinical data according in particular to the presence of visceral disease and bone multimetastatic and multifocal disease. Results: 84/2472 matched the inclusion criteria. 68Ga-PSMA-11-PET/CT was negative in 6/84(7%) and positive in 78/84(93%); 40/78 were oligometastatic and 38/78 were multi-metastatic. Biochemical features of the PET-positive population were: median ISUP:3(IQR1-5), median iPSA:9,1ng/ml(IQR:5,9-14,7), median PSAdoubling-time:4,2 months (IQR:2,2-7,5), medianPSAvel :2,4ng/ml/yr(IQR:1-8,5), median PSA-PET:1,84 ng/ml (IQR:0,7-5). 12/22 were multimetastatic: 6/12 had lymph-node disease, 1/12 had lymph-node+visceral liver disease, 5/12 had bone disease(1/5 just bone disease, 3/5 bone and lymph-node disease, 1/5 bone and visceral lung disease), while 10/22 were oligometastatic: 3/10 had bone disease, 1/10 had bone and lymph-node disease, 2/10 had visceral disease (lung), 3/10 had just lymph-node disease, 1/10 had local relapse+lymph-node disease.In 22/84 (26%) patients 68Ga-PSMA-11 PET/CT results determined a change in patients'management. After 68Ga-PSMA-11-PET/CT 5/22(23%) pts changed therapy from androgen deprivation therapy(ADT) to systemic chemotherapy; 7/22(32%) pts were eligible for ADT+bicalutamide/enzalutamide after previous ADT therapy and 10/22(45%) were eligible for ADT+enzalutamide/abiraterone after previous ADT.Despite the lack of imaging-guidelines consensus in the management of CRPC patients this preliminary study showed that 68Ga-PSMA-11-PET/CT changed the management in 26% of patients. **Conclusion:** In our population of 'early' CRPC patients 68Ga-PSMA-11-PET/CT changed patients' management in a significant part of the studied CRPC-cohort. Further studies are needed to assess the role of 68Ga-PSMA-11 PET/CT in this field. **References:** None.

EP-034

Assessing correlation between ^{68}Ga-PSMA-11 renal PET parameters and renal function tests

J. Schierz[1], I. Sarikaya[2], A. Albatineh[3], A. Sarikaya[4];
[1]Municipal Hospital Dresden, Department of Radiology, Dresden, GERMANY, [2]Kuwait University Faculty of Medicine, Department of Nuclear Medicine, Kuwait City, KUWAIT, [3]Kuwait University, Faculty of Medicine, Department of Community Medicine and Behavioral Sciences, Kuwait City, KUWAIT, [4]Trakya University, Faculty of Medicine, Department of Nuclear Medicine, Edirne, TURKEY.

Aim/Introduction: ^{68}Ga -PSMA ligands are used for prostate cancer but also show high renal cortical uptake. In this study, we aimed to assess if there is any correlation between renal PSMA PET parameters and renal function tests using the images of prostate cancer patients. **Materials and Methods:** ^{68}Ga-PSMA-11 PET/CT images of the patients with prostate cancer were retrospectively evaluated. The following PET parameters were obtained: SUV_{max}, SUV_{mean}, SUL_{max}, SUL_{mean}, volume, TLG_{SUL} and counts of both kidneys as well as SUV_{mean} of liver, blood pool and spleen. Total TLG_{SUL}, total volume, kidney to liver and kidney to blood pool ratios were calculated. Patient's creatinine values were obtained and GFR was calculated using the MDRD formula. Statistical analysis was performed to understand if there is a correlation between above parameters and renal function tests. Results: Twenty five patients were included in this study. GFR was significantly/positively correlated and creatinine was significantly/negatively correlated with renal SUV/liver SUV and renal SUV/blood pool SUV ratios. GFR was marginally positively correlated with renal SUL_{mean} and creatinine was marginally negatively correlated with total TLG_{SUL}. Total renal parenchymal volume was significantly and

directly (positively) associated with GFR and significantly and inversely (negatively) associated with creatinine. **Conclusion:** Renal ^{68}Ga-PSMA uptake appears to be correlated with renal function tests. Our method of measuring approximate renal parenchymal volume on PET image appears to be reliable. **References:** none

EP-035

68Ga-PSMA-11 PET/CT for Bone Lesions in Early Castration Resistant Prostate Cancer Patients: a Single Centre Experience

L. Vetrone[1], S. Telo[1], A. Giordano[1], A. Spagnoletti[2], A. Farolfi[3], L. Calderoni[1], S. Mattoni[1], R. Mei[1], P. Castellucci[3], S. Fanti[1,3]; [1]Nuclear Medicine, Department of Experimental, Diagnostic and Specialty Medicine, University of Bologna, Bologna, ITALY, [2]Medical Oncology Department 1, Fondazione IRCCS Istituto Nazionale dei Tumori, Milan, ITALY, [3]Nuclear Medicine, IRCCS, Azienda Ospedaliero-Universitaria di Bologna, Bologna, ITALY.

Aim/Introduction: To evaluate the concordance/discordance between 68Ga-PSMA-11-PET/CT and Low Dose Computed Tomography (LDCT) for detection-rate of bone lesions in early-CRPC(castration resistant prostate cancer) cohort. **Materials and Methods:** We reviewed all PCa patients who were referred to our Center, from April 2016 to December 2019, to perform 68Ga-PSMA-11-PET/CT. Inclusion-criteria:1) patients who underwent 68Ga-PSMA-11-PET/CT with CRPC-indication;2) previous PC-radical therapy(radical surgery/radiation) 3) patients who underwent up to a line of therapy after becoming CR. 68Ga-PSMA-11-PET/CT findings were categorized as positive and negative by two experienced Nuclear Medicine Physicians. Doubtful findings were re-evaluated and categorized by consensus. Positive findings were categorized as: local relapse in prostate bed, pelvic lymph-nodes, distant lymph-nodes, bone and visceral. Bone lesions were evaluated using both LDCT of PET and 68Ga-PSMA-11-PET/CT by two Nuclear Medicine Physicians. Concordance and discordance were evaluated in terms of number and localization of bone lesions at respectively LDCT and 68Ga-PSMA-11-PET/CT. Results: 84pts matched the inclusion-criteria. Mean age was 75yo(range 55-91). 68Ga-PSMA-PET/CT was positive in 78/84(93%) pts. Among them, 40/78(51%)pts reported bone lesions(13/40 without bone's remodeling, 25/40 osteo-thickened, 2/40 osteo-lytic). Biochemical features were: median iPSA=9 ng/ml (IQR:5,5-14,5); median PETPSA=1,75 ng/ml(IQR:0,9-6,4), median PSAdt=4,2 months(IQR:1,8-5,6), median PSAvel=2,45 ng/ml/yr(IQR:1-14,8). LDCT vs 68Ga-PSMA-11-PET/CT concordance was detected in 23/40 pts(concordance-group), while LDCT vs 68Ga-PSMA-11-PET/CT discordance was registered in 17/40 pts(discordance-group). This group included all the lesions without tissue's remodeling(13/40), one osteo-lytic pattern and three sclerotic patterns. Among the discordance-group, in 13/17pts 68Ga-PSMA-11-PET/CT detected bone disease while LDCT was negative in bone(group1); in 1/17pt 68Ga-PSMA-11-PET/CT registered more bone lesions than LDCT(group2); in 3/17pts LDCT revealed more lesions than 68Ga-PSMA-11-PET/CT(group3). In discordance-group, 8/17 were oligometastatic(4/8 only bone lesions, 1/8 lung and bone, 1/8 prostate relapse and bone, 1/8 local lymph-nodes and bone, 1/8 local and distant lymph-nodes and bone) and 9/17 were multimetastatic(4/9 presented bone, distant and local lymph-nodes, 3/9 only bone lesions, 1/9 bone and distant lymph-nodes, 1/9 prostate relapse, distant lymph-nodes and bone). 68Ga-PSMA-11-PET/CT led to up-staging in 17%(13/78) of patients, detecting bone lesions not seen by LDCT. There was no LDCT upstaging. According to the available follow-up data, 3/13pts changed therapy after 68Ga-PSMA-11-PET/CT. **Conclusion:** In our experience, 68Ga-PSMA-11-PET/CT detected more bone lesions than LDCT in a significant part of CRPC-cohort. Even if there is no consensus, it could be useful to better analyze the role of 68Ga-PSMA-11-PET/CT in restaging and follow-up CRPC-population. Further investigations are required to evaluate the relevance of 68Ga-PSMA-PET/CT in the management of CRPC-patients. **References:** None.

EP-036

Incidentalomas on PET-CT with 68Ga-PSMA

C. Varela Pinto, B. Martins, V. Sousa, C. Loewenthal; Hospital da Luz Lisboa, Lisbon, PORTUGAL.

Aim/Introduction: Description and follow-up of incidental findings in patients who underwent PET-CT with 68Ga-PSMA at initial staging or restaging of prostate carcinoma. 68Ga-PSMA PET-CT detects lesions avid for PSMA and is currently one of the most sensitive and specific exams for detecting primary and metastatic prostate carcinoma lesions. Increase in PSMA expression also occurs in tumors other than prostate origin. Incidental findings of neoplasms of the colon, esophagus, thyroid, lung, kidney and brain have been described in the literature. **Materials and Methods:** Retrospective evaluation of clinical electronic records of 402 patients (mean age 68.5 years, range 39-93) who underwent 68Ga-PSMA PET-CT for initial staging and restaging of prostate carcinoma between February 2017 and March 2021. Biochemical, clinical, imaging and pathological findings were reviewed. Results: Four hundred and two patients underwent PET-CT with 68Ga-PSMA for staging and restaging prostate carcinoma. In 16 patients (4%) PET-CT showed incidental findings of lesions not related to prostate disease. Nine patients had lung lesions with SUVmax between 0.82 and 5. Three of these patients had pathological confirmation of primary lung cancer. Two patients were followed up, 1 patient with 18F-FDG PET-CT suggestive of primary lung carcinoma and 1 patient with chest CT compatible with granulomatous disease. Four patients had increased radiopharmaceutical uptake in the thyroid gland with SUVmax between 3.37 and

11.16, 2 of whom underwent fine needle aspiration cytology, resulting in follicular thyroid carcinoma in 1 patient (SUVmax 8.55). Two patients had increased radiopharmaceutical uptake in soft tissue with SUVmax 3.68 and 3.15, with a pathological result of Masson's hemangioma and fusocellular lipoma, respectively. In one patient, PET-CT detected left supraclavicular lymph nodes (SUVmax 5.22 and 2.62), without other changes. These infracentimetric nodes were not biopsied and have been submitted to SBRT, with no resultant change in PSA values. **Conclusion:** 68Ga-PSMA PET-CT is a very sensitive exam for detecting primary and metastatic lesions of prostate carcinoma. However, overexpression of PSMA is not specific to prostate cancer. These incidental findings allowed the detection of lung, thyroid, soft tissue and lymph nodes lesions. In several cases, this allowed for initial detection of second tumors, which would otherwise have remained undiagnosed. **References:** none

EP-037

True nmCRPC in high-risk patients on ^{18}F-Choline PET/MRI as compared with diagnostic imaging techniques accepted in international guidelines

J. Garcia, A. Compte, P. Bassa, S. Mourelo, S. Ortiz, M. Soler, M. Buxeda, E. Valls, A. Blanch, E. Riera;
CETIR ASCIRES Grupo biomédico, Barcelona, SPAIN.

Aim/Introduction: Nonmetastatic castration-resistant prostate cancer (nmCRPC) is defined by an increasing PSA level despite androgen deprivation therapy (ADT), with no evidence of distant metastases on bone scan and chest, abdomen and pelvic CT. The low detection rate associated to diagnostic imaging techniques in accepted guidelines and nonspecific fluctuations in PSA difficult early diagnosis of CRPC. We aimed to determine the true nmCRPC cases on ^{18}F-Choline PET/MRI in patients with high-risk CRPC. **Materials and Methods:** This retrospective study included 20 CRPC patients at high risk for developing metastases, defined by PSA value > 3 ng/mL and PSA doubling time (PSAdT) < 10 months with ongoing ADT, and with no significant lesions detected on CT and bone scan. Patients underwent ^{18}F-Choline PET/MRI to rule out metastases. All patients were previously treated with radical prostatectomy, as well as salvage radiotherapy in 8 patients.A dual-phase study was acquired after intravenous administration of 185±10% MBq of ^{18}F-Choline: 1) early imaging (immediately after tracer administration) of prostate area (emission PET/Multiparametric MRI). 2) whole-body imaging 1 h after tracer injection (emission PET/MRI: T1, T2, STIR, diffusion).Two blinded readers, using visual and quantitative PET and MRI criteria time (SUV, size, CDE, ADC), interpreted PET/MRI images. Lesions detected were categorized into four regions: prostate bed (T), pelvic lymph nodes (N1), extrapelvic lymph nodes (M1a) and bone metastases (M1b). Results: Median patient age was 74 y. Median PSA level was 5 ng/mL and median PSADT was 4 months.^{18}F-Choline PET/MRI was negative in 5 out of 20 (25%) patients, thus being qualified as true nmCPRC. Fifteen out of 20 (75%) per-patient positive ^{18}F-Choline PET/MRI were classified as: TrN0M0 (n:1); T0N1M0 (n:1); TrN1M0 (n:1); T0N0M1a (n:3); T0N0M1b (n:1); T0N0M1aM1b (n:2); TrN0M1a (n:1); TrN0M1b (n:1); TrN0M1aM1b (n:1); T0N1M1a (n:1); T0N1M1b (n:1); TrN1M1aM1b (n:1).Regarding lesion site, detection confidence increased with joint interpretation of PET & MRI findings: 6 patients with T (MRI better in 4), 6 patients with N1 (PET better in 2), 7 patients with M1a (PET better in 5), and 7 patients with M1b (PET better in 1).Regarding patient-stratification, 4 had solitary lesions, 4 oligometastases (< 5 lesions) and 4 multimetastases. **Conclusion:** ^{18}F-Choline PET/MRI showed a high prevalence of lesions in otherwise classically known nmCRPC patients. Adequate early staging allowed detection of more targetable local and oligometastatic disease, which may provide value for individualized treatment strategies.These aspects warrant further study on CRPC imaging (PSMA) and targeted therapy fields. **References:** None

EP-038

Impact of ^{18}F-PSMA-11 PET/CT on Management of Biochemical Recurrence and High Risk Prostate Cancer Staging

K. De Man[1], S. Piron[2], N. Van Laeken[1], L. Delrue[1], V. Fonteyne[1], N. Lumen[1], B. Van den Broeck[1], K. Kersemans[1], P. Ost[1], V. Schelfhout[1];
[1]University Hospital Ghent, Ghent, BELGIUM,
[2]Laboratory of Radiopharmacy, Ghent, BELGIUM.

Aim/Introduction: In this study, we evaluated the impact of ^{18}F-PSMA-11 PET/CT on the patient management plan in patients with primary or recurrent disease. Furthermore, the sensitivity of this new PET/CT tracer was investigated. **Materials and Methods:** In this prospective observational study, 60 prostate cancer patients (9 primary staging, 51 biochemical recurrence) were imaged with ^{18}F-PSMA-11 PET/CT. Pre- and post-scan questionnaires were completed by the treating physician to observe changes in therapy intent. Follow-up data (histological confirmation, MRI imaging and PSA values after radiotherapy without implementation of systemic therapy) was correlated with the ^{18}F-PSMA-11 findings. Results: The patient-based detection rate was 82% and a management change was seen in 52% of the cases. The heterogeneous characteristics of the included patients resulted in a widely varying treatment change, mostly originating from an increase of disease extent on ^{18}F-PSMA-11 PET/CT. Follow-up data revealed a per-patient sensitivity for ^{18}F-PSMA-11 of 69%. **Conclusion:** ^{18}F-PSMA-11 PET/CT showed to be a highly promising method for the detection of prostate cancer lesions. **References:** None.

EP-09

Wednesday, October 20 - Saturday, October 23, 2021

e-Poster Area, release on Wednesday, October 20 at 09:00

Imaging Clinical Studies -> Oncological Imaging Clinical Study -> Thyroid

EP-039

Possibly coexistence of Hashimoto thyroiditis (HT) and papillary thyroid carcinoma (PTC): data from two institute

K. Zaplatnikov[1], *V. Sukhov*[2];
[1]*MVZ Nuklearmedizin Mögeldorf, Nürnberg, GERMANY,*
[2]*Nikiforov Russian Center for Emergency and Radiation Medicine, St Petersburg, RUSSIAN FEDERATION.*

Aim/Introduction: HT is an offen autoimmune thyroid disease, known to be the most common cause of hypothyroidism in nonendemic goitrous areas. It is usually characterized by symmetric, painless, and diffused but sometimes localized swelling of the thyroid gland with features of hypothyroidism. **Materials and Methods:** The coexistence of the two diseases is possible but not common, in this situation is diagnostic is several, where many pseudonodul with hypoechogenic. The fine needle aspiration is not for all possible, we estimated algoorithmus for diagnosis. Patients with HT/PTC (Gr.A) and PTC without HT (Gr.B) were studied In prospective way. In algorithm of initial investigation 99mTc-scitigraphy, thyroid hormone (fT4, fT3, TSH) and anti-TPO/anti-Tg antibodies levels estimation were performed along with clinical examination, thyroid sonography with Doppler DS and FNAC. Every case of PTC was confirmed by patho-histological examination. Age, sex, geographic anamnesis, tumour features (dimensions, angioinvasion, capsular infiltration, multifocality and lymphnode metastases), nuclear medicine examination data, therapy history and estimated total effective doses received by former inhabitanats of contaminated areas were analysed. Results: Statistically significant (P=0.001) difference in tumour size was found in two Groups: the average diameter was found to be 1.721+/-0.5812 and 1.145+/-0.871 cm in Gr.A and in Gr.B, respectively. Capsular infiltration was present only in Gr.A in 3 cases. The angioinvasion was found in 8 cases of Gr.A and 1 cases in Gr.B (P=0.310). Multifocality was found in 19 patients in Gr.A and in 2 in Gr.B (P=0.0009). There were no statistical differences in sex (P=0.423) and age (P=0.330). All pts in Gr.A had HT with high levels of thyroid Abs (TgAb/TPOAb). 51.5% autoantibody positive pts with US suspicious multifocal non-uniform thyroid goiter revealed scintigraphic cold lesion (pic.3), in Gr.B 60% nodes were undetectable in scans. Unfortunately, no thyroid gland and collective thyroid doses were available and estimated total effective doses were found for less than half of Gr.A with no cases of documented high over-doses. **Conclusion:** Statistically proven high prevalence (100%) of HT and multifocal PTC in Gr.A compared to Gr.B in our study might be related to the fact, that a majority of patients were previously residents of North-Eastern regions of Kazakhstan (probability of extensive radiation exposure). Our results justify a necessity of screening for PTC in population group exposed to external radiation and with concomitant HT. **References:** none

EP-040

The use of FDG PET/CT in patients with recurrent differentiated thyroid cancer

O. Ekmekcioglu;
University of Health Sciences, Sisli Etfal Education and Research Hospital, Nuclear Medicine Dept., Istanbul, TURKEY.

Aim/Introduction: Differentiated thyroid cancer might lost the ability to keep iodine and get de-differentiated. FDG PET/CT is used for searching recurrence in thyroid cancer patients when there is suspicion for metastases. Especially de-differentiated lesions become FDG avid and more aggresive clinical behaviour is seen. The aim of this study is to investigate the use of FDG PET/CT in differentiated thyroid cancer. **Materials and Methods:** Fourty-six patients either with iodine negative scan or clinical progression and suspicious for metastases with differentiated thyroid cancer, has been referred to our department for FDG PET/CT scan, evaluated retrospectively. PET/CT findings were correlated with the characteristics of the patients and prognostic factors of the disease. Results: Twenty-six patients (56,2%) have showed positive findings for recurrence in FDG PET/CT images. Positive FDG PET/CT findings were significantly correlated with stage and thyroglobulin levels. SUVmax values did not show a significant relation with other findings of the patients. Cut off value for Thyroglobulin was found 52,5 ng/ml with levels of %73,08 sensitivity, %75,00 specificity, %79,17 positive predictive value and %68,18 negative predictive value for FDG PET/CT imaging. **Conclusion:** FDG PET/CT seems to be useful detecting recurrence in differentiated thyroid cancer. Increased thyroglobulin levels and stage of the disease has shown a significant relation with FDG positivity. Even the degree of SUVmax did not show a significant relation, it gives idea for aggressive clinical behaviour and should be considered in treatment protocol of the recurrent disease. **References:** none

EP-041

Health-related quality of life analysis in differentiated thyroid carcinoma patients: a Tunisian study

S. Mensi[1], *M. Ben Fredj*[1], *M. Ben Rejeb*[2], *T. Dardouri*[1], *A. Ezzine*[1], *K. Chatti*[1];
[1]*Departement of nuclear medecine, Sousse, TUNISIA,* [2]*Department of Community Health and Epidemiology, Sousse, TUNISIA.*

Aim/Introduction: Differentiated thyroid cancer (DTC) can compromise the quality of life of patients. Our purpose is to assess the factors that influence the health-related quality of life (HRQOL) of Differentiated thyroid cancer (DTC) patients after surgery and radioiodine treatment. **Materials and Methods:** From January 2018 to december 2019,eighty-nine DTC patients who underwent surgery and received radioiodine treatment were recruited. The patients were invited to answer the Short-Form 36-Item Health Survey in its arabic version (Tunisian dialect) including multiple aspects of physical and social functioning. Descriptive and bivariate analysis between domain scores and variables of interest were performed. Results: This study revealed that majority (sex ratio =0,15) of respondents was female, married (84,3%), unemployed (66,3%), with urban residence (67,4%). Mean (± SD) age of the respondent was 45,03(±13,71) years, 65% had secondary education or more. Out of 89 cases, 83(93.3%) was papillary and 6 (6,7%) was follicular carcinoma. Bivariate logistic regression analysis showed that male gender, higher level of education, early TNM stage, low risk of tumour recurrence, patient aged <18years at diagnosis, a cumulative dose of iodine-131<5550MBq, use of Liothyronine Sodium, complete remission and surgery for locoregional recurrence had a positive impact on HRQoL in DTC patients. Factors with a negative impact on HRQoL were advanced age and hypothyroidism after discontinuing treatment with levothyroxine(TSH stimulation for radioiodine administration). **Conclusion:** HRQoL is significantly influenced by many sociodemographic and clinical factors. More attention should be given to DTC patients after surgery and radioiodine treatment to improve quality of life. **References:** none

EP-10

Wednesday, October 20 - Saturday, October 23, 2021

e-Poster Area, release on Wednesday, October 20 at 09:00

Imaging Clinical Studies -> Oncological Imaging Clinical Study -> Gynaecological

EP-042

Can Delayed Pelvic FDG PET/CT Scan Improve Lesion Detection and Differentiation?

K. Afanasenka, *D. Vaitkiene, I. Kulakiene, S. Sediene, I. Simeliunaite; Lithuanian University of Health Sciences, Kaunas, LITHUANIA.*

Aim/Introduction: Gynecological malignancies are a group of debilitating oncologic ailments frequently affecting women in Europe and Worldwide. Currently, a wide array of structural and molecular imaging modalities are available for evaluating disease spread. 18F-FGD PET/CT being one of them, has one of the highest rates of sensitivity and specificity. Nevertheless, physiological activity in pelvic structures and lesions that are smaller than designated resolution of the PET scanner, hinder primary tumour extent and pathological lymph node evaluation. The purpose of this study was to evaluate if an additional delayed pelvic scan improves lesion characterization, detection rates compared to whole body PET/CT images and can it help differentiating malignant lesions from physiological surrounding tissue activity. **Materials and Methods:** All patients were provided with written consent form approved by regional ethics committee. A total of 155 patients (age median 56), histologically proven gynecological malignancies (uterine, cervical and ovarian cancer, FIGO stages I-IV), were investigated between November 2018 and November 2020. Two PET/CT scans were completed: whole body (approx. 60 min after FDG injection; low dose CT, 3 min/per bed position) and delayed pelvic (approx. 120 min after injection, diagnostic non-enhanced CT, 5 min/per bed position). Three independent readers of varying experience in nuclear medicine (two with at least 5 year of experience and one less than one year) evaluated images, surveyed and classified lesions by assigning a Likert type scoring (5-point scale: ranging from 1 - benign to 5 - malignant) and looked for possible new lesions in delayed pelvic scan. Descriptive statistics, interobserver weighted kappa values were calculated. Results: A total of 465-589 lesions were evaluated on whole body PET/CT images. On delayed pelvic scan 26.5 and 14.5 percent of lesions had their scores changed by one point when evaluated by experienced readers while 30.4 percent of lesions were changed by inexperienced reader; the score change by two points were 8.5%, 8.1% and 5.6% of lesions respectively. Additionally 94 to 124 new, previously unseen lesions with average size of 0.7 cm (SD=0.2) were detected in delayed pelvic images. The mean kappa value between readers for malignant lesion was 0.68–0.74, while on delayed pelvic images it increased to 0.76–0.83. Other assigned lesion scores had worse agreement strength which varied from poor to moderate. **Conclusion:** Delayed pelvic FDG PET/CT scan allows more confidant lesion categorization and is helpful in detecting new lesions. **References:** none

EP-043

Breast and Bilateral Axillary Lymph Nodes Metastases from Serous Ovarian Carcinoma and Treatment Response Demonstrated on ^{18}F-FDG PET/CT

C. Sahin, *S. Ozguven, T. Y. Erdil, N. Filizoglu, S. Kesim, K. Niftaliyeva, T. N. Kıssa, Z. C. Balaban, K. Oksuzoglu, F. Sen, T. Ones, H. T. Turoglu, S. Inanir;*

Marmara University Pendik Training and Research Hospital, Department of Nuclear Medicine, Istanbul, TURKEY.

Aim/Introduction: Serous ovarian carcinoma generally spreads to pelvic and/or para-aortic lymph nodes and the peritoneal cavity. Metastasis of ovarian carcinoma to the breast and axillary lymph nodes are extremely rare and

this event can mimics primary breast carcinoma. Herein, we presented a 48-year-old woman with history of stage IV ovarian cancer was found to have breast lesions and lymph nodes on follow-up magnetic resonance imaging, suspicious for primary breast tumor. **Materials and Methods:** A 48-year-old woman with diagnosed serous ovarian carcinoma treated with TAH+BSO followed by chemotherapy. There was no evidence of local recurrence at the follow-up of 2.5 years. Physical examination showed palpable right breast masses and bilateral axillary nodal enlargement. The lesions were correlated with MRI and the patient was referred to FDG PET/CT. Results: FDG PET/CT revealed FDG-avid two lesions in the lower quadrants of the right breast and bilateral metastatic axillary lymph nodes (A, B and C). A moderate to intense hypermetabolic right parasternal, mediastinal, anterior diaphragmatic, hepatogastric, and peripancreatic lymph nodes were also noted. Serum CA-125 and CA 15-3 levels were 83.9 U/mL and 50 U/mL, respectively. The patient underwent biopsy for the breast lesions and pathology confirmed serous carcinoma metastasis morphologically similar to the previously diagnosed ovarian cancer. The patient received eight cycles of combined paclitaxel and carboplatin chemotherapy. The second FDG PET/CT was performed for the evaluation of treatment response depicted marked regression of the disease. The hypermetabolic bilateral axillary lymph nodes and breast lesions were not observed on PET/CT imaging after chemotherapy (D, E and F). **Conclusion:** Breast metastasis from malignancies is extremely rare, accounting for only 0.33% to 6.3% of breast tumors and mostly originates from melanomas, sarcomas, leukemia, lymphoma, lung cancer, renal carcinomas, and ovarian tumors. Although ovarian cancer metastasis to the breast and/or axillary lymph nodes is an uncommon condition, it is associated with a poor prognosis. Accurate diagnosis of the origin of the breast lesions during the early stages of the disease can prolong the expected survival time, because treatment differs considerably for patients with ovarian metastasis to the breast, as compared with patients with primary breast carcinoma. It should be kept in mind in the differential diagnosis when staging or restaging for any patient with a history of ovarian carcinoma. **References:** None

EP-044

Valuing 18-FDG PET/CT Efficiency in Examining Patients with Cervical Cancer

J. Stojanovic, I. Grozdic Milojevic;
Centre for Nuclear medicine, Clinical Center of Serbia, Faculty od Medicine University of Belgrade, Belgrade, SERBIA.

Aim/Introduction: The aim of this study was to examine the role of 18-FDG PET / CT in the evaluation of patients with cervical cancer. **Materials and Methods:** Data from 56 patients (mean age 52.05 ± 10.9) with diagnosis of cervical cancer was used in the retrospective analysis. A criterion for including patients in the study was confirmed pathohistological diagnosis of squamous cell carcinoma. Patients with other carcinomas, with active infection/inflammation and with glucose level above 11mmol/l, were excluded from the study. All patients underwent PET/CT scan, 60 minutes after 18F-FDG injection. Maximum standardized uptake value (SUVmax) is used for measuring FDG uptake. Using International Federation of Gynecology and Obstetrics (FIGO) cervical cancer staging scheme 7 patients were diagnosed with stage I, 29 patients with II, 14 with III, 6 patients with stage IV of cervical cancer. Spearman's correlation coefficient was used to evaluate the correlations between FIGO stage and PET/CT finding (normal/pathologic), p values of < 0.05 were indicators of statistical significance. Results: In 53.6 % of the patients PET/ CT indicated present disease. In 37.5% PET/CT result showed less advanced disease and in 8.9% PET/CT results were indecisive, and required additional diagnostic procedures (MR diagnosis, hysteroscopy..). Based on results, average SUVmax value was 8.70 ± 8.62. Values of SUVmax in FIGO stages I-IV were 6.6 ± 13.07; 7.1 ± 5.78; 8.7± 7.07; 18.8 ± 11.4. Assessment of distant areas showed active proliferative process present predominantly in the pelvic lymph nodes in 41.1% (SUVmax12.05 ± 9.55) followed by retroperitoneal lymph nodes in 33.9% (SUVmax 10.04 ± 6.63) and mediastinal lymph nodes in 32.1% patients (SUVmax 5.92 ± 2.85). The disease was identified in the lungs in 17.9% (SUVmax 7.87 ±6.04), in the bones in 10.7% (SUVmax 5.23 ±1.99),in the liver in 5.4% (SUVmax 4.93 ± 1.85) and in the inguinal lymph nodes in 5.4% patients (SUVmax 7.33 ± 2.13).There was no significantcorrelation between FIGO staging and PET/CT result (p=0.207). **Conclusion:** This study further shows favorable role that 18-FDG PET/CT has for determining distant lymph node involvement and evaluation of patients with recurrent cervical cancer. **References:** none

EP-11

Wednesday, October 20 - Saturday, October 23, 2021
e-Poster Area, release on Wednesday, October 20 at 09:00

Imaging Clinical Studies -> Oncological Imaging Clinical Study -> Lymphoma

EP-045

Prognostic Value of 18F-FDG PET/CT biomarkers in patients with diffuse large B-cell lymphoma treated with Chimeric Antigen Receptor T Cell Therapy, preliminary results

J. Cañadas Salazar, L. G. Díaz González, J. G. Villanueva Curto, F. Gomez-Caminero López, P. García-Talavera San Miguel, A. C. Peñaherrera Cepeda, C. Riola Parada, B. Lucas Velázquez, S. López Puche, J. Á. Badell Martínez, E. Martín Gómez, C. Montes Fuentes, L. Granado Alonso, M. E. Alonso Sarasquete, M. D. Caballero Barrigon, A. Martin Garcia-Sancho, P. Tamayo Alonso;
Sacyl, Salamanca, SPAIN.

Aim/Introduction: To evaluate the prognostic value of PET biomarkers such as metabolic tumor volume (MTV), total lesion glycolysis (TLG) and maximum standard uptake value (SUVmax), in the outcome of patients diagnosed with diffuse large B-cell lymphoma treated with Chimeric Antigen Receptor T Cell (CART). **Materials and Methods:** We prospectively analyzed patients diagnosed of diffuse large B cell lymphoma who received CD19- targeting CAR-T cell therapy at our center, between March 2019 and April 2021. The patients underwent 18F-FDG PET/CT studies prior to the treatment and at 28 days post infusion. Pretreatment values of serum lactate dehydrogenase (LDH) and presence of a bulky tumor (<7 cm) were defined. Treatment response was evaluated by 18F-FDG PET/CT at 28 days post infusion using the Deauville criteria. PET biomarkers were measured using MIM software (v7.0.6) by two nuclear medicine specialists at each time point, and statistical analysis was carried out using IBM SPSS statistics software (v.24). Results: A total of 28 patients were selected, 16 men and 12 women, mean age of 60yrs (range 32-76). Prior to treatment 19 (68%) patients presented an advanced stage, 14 (50%) an increased level of LDH and 10 (36%) had bulky disease. Mean follow-up was 6,5 months (0,8-20,8), in this period 12 patients developed recurrence of their disease, and 7 patients perished in a mean time of 7 months (1-13). The median values for baseline PET/CT biomarkers were acquired from the complete response group were MTV_{cr}: 47,57ml, TLG_{cr}: 528,3 and $SUVmax_{cr}$: 17,87; and from the group that did not achieve complete response MTV_{pr}: 234,03ml, TLG_{pr}: 1041,24 and $SUVmax_{pr}$: 20,06 demonstrating higher values in the groups that did not achieve a complete response. The Mann-Whitney U test was performed on each biomarker for the presence or absence of a complete metabolic response, indicating statistical significance in the TLG (p=0,038) and SUVmax (p=0,029) but not in the MTV (p=0,068). **Conclusion:** PET biomarkers seem to demonstrate an association in the prediction of response to CART therapy, although MTV does not show a significant relationship, which may be due to the small sample size. Further follow-up and patient numbers are required. **References:** None

EP-046

Prognostic value of interim ^{18}F-FDG PET/CT evaluation methods in peripheral T-cell lymphoma: a prospective, diagnostic accuracy study

T. Yuan, Y. Zhang, X. Chen, M. Wei, X. Wang;
Peking University Cancer Hospital & Institute, Beijing, CHINA.

Aim/Introduction: ^{18}F-FDG PET/CT has been recently demonstrated as an effective predictor of therapeutic responses and outcomes in patients with PTCL, nevertheless there was lack of agreed-upon standardized response criteria. **Materials and Methods:** We performed prospective trail (NCT03051568) to further investigate the prognostic value of total metabolic tumor volume (TMTV) and whether the Peking criteria ($SUV_{max\text{-}liver\text{-}based}$ Interpretation) is superior to Deauville visual 5-point scale (5-PS) and change in SUV (ΔSUV_{max}) for evaluation of early interim (PET-2) and interim (PET-4) scan in PTCL. 74 Patients with newly diagnosed PTCL who had performed an FDG PET/CT at baseline (PET-0), after the second cycle(70 patients) or forth cycle (49 patients) of CHOP/CHOP-like treatment were prospectively enrolled in this study. Receiver-operating-characteristic analysis was performed to determine optimal cutoff value of TMTV and Peking criteria. The PET response of patients was classified as either positive or negative by using Peking criteria, 5-PS and ΔSUVmax method. PET-2 and PET-4 results were assessed for the ability to predict progression-free survival (PFS). Results: ROC analysis revealed the optimal threshold of Peking criteria is 1.8-fold of $SUV_{max\text{-}liver}$ for PET-2 and 1.4-fold of $SUV_{max\text{-}liver}$ for PET-4. The optimal cutoff of TMTV is 98.54% for PET-2 and 99.83% for PET-4. Peking criteria (84.29% 76.47% and 91.49%, respectively) had a higher prognostic accuracy, positive predictive value (PPV) and specificity than 5-PS criteria (57.14%, 41.46% and 48.94%, respectively), 66%ΔSUV_{max} criteria (67.14%, 45.16% and 68.09%, respectively) and ΔTMTV (71.43%, 50.00% and 78.00%, respectively) in PET-2. As in the PET-4 the accuracy, PPV and specificity of the Peking criteria (71.43%, 58.33% and 84.85%, respectively) to predict 3-year PFS was higher than that with use of the 5-PS criteria (71.43%, 40.33% and 64.71%, respectively), 70%ΔSUV_{max} scale (65.32%, 47.06% and 72.73%, respectively). The accuracy of 99.83% ΔTMTV (73.47%)was a little higher than Peking criteria. The PPV and specificity for predicting 3-year PFS by using Peking criteria were much better than those using the other two interpretations. Markedly differences in the outcome between patients with positive and negative PET-

2/PET-4 were demonstrated using ΔTMTV and three image interpretation methods ($p<0.05$). Univariate and multifactor analysis found PET-2 and PET-4 were independent prognostic factors for the outcome of PTCL. **Conclusion:** In PTCL, iPET can predict unfavorable PFS following treatment by ΔTMTV and Peking criteria. Peking criteria were superior to 5-PS and ΔSUV_{max} method in analyzing the PET-2 and PET-4 for the prognosis of PTCL patients. **References:** none

EP-047

Metabolic tumor burden and cytokine release syndrome (CRS) in patients with diffuse large cell B lymphoma (DLCBL) treated with CTL019 chimeric antigen receptor -T-cell (CAR-T): preliminary experience

C. Mantarro[1], M. Donegani[2], M. Bauckneht[3], S. Raffa[2], S. Chiola[4], A. A. Miceli[2], F. Lanfranchi[2], F. D'Amico[2], G. Sambuceti[2], A. Raiola[5], C. Ghiggi[6], E. Angelucci[7], S. Morbelli[2];
[1]Department of Biomedical and Dental Sciences and Morphological ad Functional Images, University of Messina, Messina, ITALY, [2]Department of Health Sciences (DISSAL), University of Genoa, Genoa, ITALY, [3]IRCCS Ospedale Policlinico San Martino, Genoa, ITALY, [4]Humanitas Clinical and Research Center–IRCCS, Milan, ITALY, [5]UOC Ematologia e Trapianto di Midollo Osseo, IRCCS Ospedale Policlinico San Martino, Genoa, ITALY, [6]Hematology and Transplant Center Division, IRCCS Ospedale Policlinico San Martino, Genoa, ITALY, [7]Hematology, Ospedale Policlinico San Martino, Genoa, ITALY.

Aim/Introduction: CAR-T therapy has demonstrated a high complete remission (CR) rate and durable response in patients with relapsed/refractory diffuse large B cell lymphoma (DLBCL). CAR-T cell therapy is associated with unique adverse effects, including CRS and neurologic toxicities. A potential role of tumor burden has been advocated to predict both the occurrence of CRS as well as poorer response. Preliminary data has shown that FDG PET might capture response to CAR-T as early as 30 days after treatment however role of metabolic tumor volume to predict occurrence of CRS and interference of CRS on FDG PET reading still need to be clarified. **Materials and Methods:** Eight patient who underwent CAR-T therapy at our institution were submitted to FDG PET at baseline and 30 days after treatment (PET1). 5-point Deauville score was used to classify PET response on PET1 and the presence of CRS was based on the Penn grading scale. SUVmax, SUVmean and Metabolic Tumor volume (MTV) for all lesions were measured at baseline PET. Similarly, signs of systemic immune activation on PET1 were evaluated in non-target organs visually and by computing SUVmax in spleen, bone marrow, thyroid, Waldeyer's ring, joints. Results: 4/8 patients experienced CRS (2 CRS=2 and 2 CRS=4); 6/8 patients showed a DS score ≤3 while one patients was classified as DS 4 and one patients as DS 5. Of note all patients showing CRS had a DS1 (no signs of local immune activation interfering with PET visual reading). Patients experiencing CRS had a significantly higher MTV (555.6±100) with respect to the two patients not showing CRS (61.1±73) while no differences were highlighted for the other PET-based parameters (SUVmax 19.1±10.5; SUVmean 4.6±1.1 for CRS group and SUVmax 12.1±4; SUVmean 4.5±1; MTV 61.1±73 for the remaining patients). Two of the patients experiencing CRS were also showing signs of systemic immune activation (increased tracer uptake in the joints resembling a pattern similar to polymyalgia rheumatic in one case; and increased thyroid tracer uptake in another case). **Conclusion:** Patients' higher metabolic tumor burden was associated with higher frequency and severity of CRS. Patients with CRS might also show sign of systemic immune activation while CRS did not affect tracer uptake in disease sites or in surrounding tissue thus suggesting that 30 days after CAR-T, FDG PET reading is not hampered by the presence of CRS. **References:** none

EP-048

Prognostic significance of FDG-PET derived conventional and textural parameters in high grade B cell lymphoma

Z. Ritter[1], K. Zámbó[1], D. Dezső[1], Z. Szabó[1], Z. Bán[1], K. Szigeti[2], D. Szöllősi[2], D. Veres[2], K. Farkas[3], Á. Szomor[4], D. Máthé[2], A. Hussain[4], E. Schmidt[1];
[1]University of Pécs Clinical Centre, Department of Medical Imaging, Division of Nuclear Medicine, Pécs, HUNGARY, [2]Semmelweis University Faculty of Medicine, Department of Biophysics and Radiation Biology, Budapest, HUNGARY, [3]University of Pécs Institute of Bioanalysis, Pécs, HUNGARY, [4]University of Pécs 1st Department of Internal Medicine, Pécs, HUNGARY.

Aim/Introduction: Diffuse large B cell lymphoma (DLBCL) is the most common subtype of non-Hodgkin Malignant Lymphomas. There is a need to distinguish the high-risk patients as early as possible for further intense therapy. For this, we aimed to evaluate the prognostic significance of conventional and textural PET parameters derived from baseline FDG-PET/CT. Furthermore, we analyzed which VOI should be used for calculation of textural parameters. **Materials and Methods:** The baseline PET/CT scans were performed between 2014-2019 in 87 patients(age: 23-81, median:59) diagnosed with DLBCL before the initial therapy. TLG(Total lesion glycolysis), MTV(Metabolic Tumor Volume), and SUV(Standardized uptake value) max were segmented semi-automatically by Interview Fusion (global threshold package). For further evaluation by each patient, the biggest VOI or the VOI with the highest SUV max value were selected. From each VOI the features were calculated by histogram analysis or texture-based approaches such as neighborhood gray-tone difference matrix (NGTDM), gray-level co-occurrence matrix (GLCM), grey-level run-length matrix (GLRLM), and grey-level size zone matrix (GLSZM). All patients received standard R-CHOP treatment. Cell of origin (COO) and revised international prognostic index (R-IPI)

were also determined before the initiation of the therapy. Event-free survival was defined as the time from registration date to disease relapse, progression, and death related to lymphoma. Data were analyzed using SPSS statistical software. Results: After completing standard treatment, 57 patients had complete metabolic remission, and 30 patients had detectable metabolically active tumor tissue or relapse within 24 months. Based on these findings, we divided the patients into two groups. Using Chi-square test there was significant association between COO, R-IPI, and the groups ($p<0.05$). Using Mann Whitney test, there was significant difference between the groups, with TLG, MTV ($p<0.001$) and SUVmax ($p<0.05$). In case of textural parameters the significance depended on which VOI was used for feature calculation. In 24 patients, not the largest VOI was the most active. For the extraction of textural parameters, the largest VOI proved to be more applicable. After preselection by Mann Whitney test Receiver Operating Characteristic curve analysis were performed to predict progression or relapse within two years, and the highest diagnostic accuracy had MTV. **Conclusion:** Based on our results, conventional and also textural PET parameters could be useful for prognosis assessment together with clinical data. We suggest to use the largest VOI for extraction of textural parameters in case of many foci in patients with DLBCL. **References:** None.

EP-049

Association between Baseline Total Metabolic Tumor Volume, Interim Deauville 5-Point Scale and Progression Free Survival in Patients with Diffuse Large B-Cell Lymphoma

P. Kalmar[1], S. Hatzl[2], E. Schulz[2], T. Schwarz[1], P. Neumeister[2], C. Beham-Schmid[3], C. Gstettner[1], R. M. Aigner[1];
[1]Department of Radiology, Division of Nuclear Medicine, Graz, AUSTRIA, [2]Department of Internal Medicine, Division of Hematology, Graz, AUSTRIA, [3]Institute of Pathology, Graz, AUSTRIA.

Aim/Introduction: ^{18}F-FDG-PET/CT is the standard imaging modality for disease staging and end of treatment assessment of diffuse large B-cell lymphoma (DLBCL). However, its use for response prediction has not been standardized, yet. Baseline total metabolic tumor volume (TMTV) ≥220 cm^3 and ΔSUVmax after two cycles of rituximab plus cyclophosphamide, doxorubicin, vincristine, and prednisone (R-CHOP) have been reported to be superior to the visual Deauville 5-point scale (DS). Our aim was to assess the prognostic value of TMTV, ΔSUVmax and DS in contemporary "real-world" DLBCL patients uniformly treated with R-CHOP given every 21 days (R-CHOP21). **Materials and Methods:** We conducted a retrospective analysis of 144 patients with DLBCL who were diagnosed and treated with R-CHOP21 at our institution during January 1st 2015 and December 31st 2019. All patients underwent ^{18}F-FDG-PET/CT at diagnosis and after four cycles of R-CHOP21 (i-PET4). SUVmax and TMTV were computed. Primary endpoint for all time-to-event analyses was 5-year progression free survival (PFS), estimated with Kaplan-Meier estimators, and compared between groups using log-rank tests. Uni- and multivariable modeling of PFS functions was performed with Cox proportional hazards models. Harrell's concordance index was calculated to evaluate model fit of different PET parameters. Results: Estimated 5-year PFS and overall survival (OS) were 63% (95% CI, 51-73) and 75% (95% CI, 63-84), respectively. Higher baseline TMTV predicted for higher risk of progression and death. Baseline TMTV threshold of >220cm^3 could be confirmed. At i-PET4, TMTV, SUVmax, and DS comparably predicted PFS with a good discriminatory performance (c-indices between 0.76 and 0.80). Five-year cumulative incidences of primary disease progression or relapse were 32% and 76% in patients with DS of 1-3 points (n=67) and 4-5 points (n=34), respectively (Gray's test $p<0.0001$). Complete metabolic response (CMR), composite of interim TMTV of 0 and SUVmax of 0 (n=60 patients), showed 5-year PFS of 83% and 31% in patients with and without a CMR (log-rank $p<0.0001$). ΔSUVmax was predictive of PFS but not superior to DS. **Conclusion:** DLBCL patients with baseline TMTV >220cm^3 and DS of ≥4 have an inferior PFS and are therefore prime candidates for new treatment strategies. **References:** Bartlett NL et al. J Clin Oncol. 2019;37(21):1790-1799. Sehn LH et al. Blood. 2018;132 (Supplement 1):783. Cheson BD et al. J Clin Oncol. 2014;32(27):3059-3068. Zhou Z et al. Blood. 2014;123(6):837-842. Montalbán C et al. Br J Haematol. 2017;176(6):918-928.

EP-050

The role of 18F-FDG PET/CT in evaluation of bone marrow involvement in patients with diffuse large B-cell lymphoma

C. Sandoval Moreno, B. Manzarbeitia Arroba, M. De la Rubia Marcos, M. Tagliatori Nogueira, M. Álvarez Moreno, P. García Alonso, A. Herrero Muñoz, A. Ortega Valle, M. Balsa Bretón;
Hospital Universitario de Getafe, Getafe, SPAIN.

Aim/Introduction: We aimed to evaluate the efficacy of 18F-FDG in detection of bone marrow involvement in Diffuse Large B-cell Lymphoma (DLBCL). **Materials and Methods:** We reviewed records of all patients with newly diagnoses of DLBCL during 7 years. Bone marrow biopsy (BMB) and 18F-FDG PET/CT were performed (time interval between both procedure less than 30 days) before treatment. We evaluated 72 patients (35 women and 37 male), the median age was 61.1 years (range 24 - 85 years). 18F-FDG PET/CT was performed using a standard protocol and BMB was doing in posterior left iliac crest. Visual evaluation was performed for 18F-FDG PET/CT scan and we classified 18F-FDG PET/CT results in negative (non bone uptake), positive (focal bone uptake) and diffuse positive (diffuse bone uptake). Finally, PET results were compared with histological data. Results: In

our series, 48 patients (66.6%) had a negative 18F-FDG PET/CT study: 43 of them had a negative BMB (true negatives) and 5 were false negative (non focal bone uptake and positive BMB). These gave us a negative predictive value of 89.6%. On the other hand, 18 patients (25%) had focal bone uptake: 8 of them had positive BMB (true positive) and 10 patients had negative BMB. In these cases, 18F-FDG PET/CT was negative in left iliac crest and all of them had a negative 18F-FDG PET/CT control after chemotherapy, so we considered them as a PET/CT true positive for bone marrow involvement. Finally, in our series, we classified 6 patients as a diffuse positive uptake, only one of them had a positive BMB. **Conclusion:** According to our results, the BMB could have been avoided when focal positive bone uptake was observed in PET/TC. Furthermore, the BMB couldn't be safely avoided in negative PET/TC studies. However, prospective and analytic studies are needed to prove this hypothesis, especially in negative and diffuse positive cases. **References:** None.

EP-051

The Utility of Metabolic Parameters on Baseline F-18 FDG PET/CT in Predicting Survival in Paediatric Lymphoma: A Preliminary Review

J. Reed[1,2], A. Masenge[3], M. Vorster[1,2], M. Sathekge[1,2]; [1]University of Pretoria, Pretoria, SOUTH AFRICA, [2]Steve Biko Academic Hospital, Pretoria, SOUTH AFRICA, [3]Department of Statistics, University of Pretoria, Pretoria, SOUTH AFRICA.

Aim/Introduction: Lymphoma is the third most common paediatric cancer. Early detection of high-risk patients is necessary in order to anticipate those who will benefit from intensive therapy and follow-up. Current literature shows that residual tumor avidity on PET following chemotherapy corresponds with lower overall survival (OS) and progression-free survival (PFS). However, the value of various metabolic parameters on baseline F-18 FDG PET as predictors of OS and PFS have not been adequately investigated. The aim of this study is to evaluate the prognostic value of tMTV, TLG and SUV_{max} on baseline F-18 FDG PET/CT in predicting OS and PFS in paediatric lymphoma. A secondary objective is to determine whether various biochemical and imaging risk indicators are predictive of OS and PFS. **Materials and Methods:** A total of 21 male and 7 female paediatric patients (mean age 11.2 years; range: 4-20 years) with histologically-proven lymphoma who were referred to the department of Nuclear Medicine between January 2013 and December 2018 were included in this analysis. 24 patients had Hodgkin Lymphoma (HL) and 4 patients Non-Hodgkin Lymphoma (NHL). Baseline F-18 FDG PET/CT images were retrospectively reviewed and tMTV, TLG and SUVmax values were recorded, as well the presence of bone marrow, splenic, liver or lung involvement and the presence or absence of effusions or bulky disease. Follow-up records on hospital databases were reviewed and baseline biochemistry (Hb, LDH, albumin, ESR) was recorded. All patients received therapy in accordance with standard regimes. Patients who received any therapeutic intervention prior to baseline imaging, who did not complete therapy or who were lost to follow-up were excluded. Results: Mean follow-up period was 42.5 months (median 39.5 months; range: 7 - 95 months). Significant negative correlation was observed between baseline tMTV and PFS ($r = -0.455$, $p=0.017$). The presence of bone marrow involvement on baseline PET (N=10) was associated with shorter mean PFS (25.90 months) compared with those with no bone marrow involvement (N=17; 42.06 months). Likewise, the presence of pleural or pericardial effusion (N=6) was associated with a mean PFS of 17.33 months versus 41.43 months in those with no effusions (N=21). **Conclusion:** tMTV on baseline F-18 FDG PET/CT demonstrates significant negative correlation with PFS in paediatric lymphoma. In addition, the presence of bone marrow involvement or effusion(s) on baseline imaging are associated with shorter mean PFS. Further evaluation of a larger sample size is necessary in order to confirm these preliminary findings. **References:** None.

EP-052

Prognostic Value of [^{18}F]FDG PET/CT at the End of Treatment in Follicular Lymphoma

C. Soldevila Lozano[1], M. Cortés-Romera[1], E. Llinares-Tello[1], A. Palomar-Muñoz[1], S. Mercadal-Vílchez[2], E. González-Barca[2]; [1]PET/CT Unit (IDI)- Department of Nuclear Medicine. Hospital Universitari de Bellvitge, L'Hospitalet De Llobregat, SPAIN, [2]Department of Hematology. ICO. Hospital Duran i Reynals-IDIBEL, L'Hospitalet De Llobregat, SPAIN.

Aim/Introduction: Although Follicular lymphoma (FL) is indolent, it is [^{18}F]FDG avid. PET/CT has an impact on the treatment response assessment in Hodgkin lymphoma and in aggressive non-Hodgkin lymphoma. However, this is more controversial in FL. The aim of this study was to evaluate the prognostic value of [^{18}F]FDG PET/CT at the end of treatment (EOT) in patients with FL. **Materials and Methods:** Sixty-four patients (28 women; mean age 57 years) diagnosed with FL (grade 1, 2 or 3A) underwent an [^{18}F]FDG PET/CT before treatment and EOT. Forty-four patients were treated with six cycles of R-CHOP. EOT PET/CT was reported using Deauville score (DS) and Lugano Classification and the results were considered as negative (DS 1-3) or positive (DS 4-5) and as complete metabolic response (CMR), residual metabolic response (RMD), no metabolic response (NMR) and/or progression metabolic disease (PMD). The median follow-up was 50 months. Events (relapse and exitus), overall survival (OS) and progression free-survival (PFS) were analyzed. Results: According to Deauville score, EOT PET/CT was negative in 41 patients (64%) and positive in 23 (36%); the median OS was 57 months in negative patients and 47 months in positive patients; the median PFS was 34 months in negative patients (12 events) and 24 months in positive

patients (12 events). According to Lugano Classification, EOT PET/CT was categorized as CMR in 41 patients (64%), RMD in 17 (26%) and PMD in 6 (10%); the median OS was 57 months in CMR, 52 months in RMD and 31 months in PMD; the median PFS was 34 months in CMR (12 events), 31 months in RMD (6 relapse) and 17 months in PMD (6 relapse). **Conclusion:** Positive EOT PET/CT indicates a worse prognosis than negative EOT PET/CT. CMR and RMD demonstrate a higher OS and PFS than PMD. However, similar results are observed between CMR and RMD. Therefore, [^{18}F]FDG PET/CT at the end of treatment for FL has significant prognostic value. **References:** none

EP-053

Efficacy of 18F-FDG PET/CT in evaluation of Bone marrow involvement in patients with non Hodgkin Lymphoma and the influence of analytic parameters

C. Sandoval Moreno, M. De la Rubia Marcos, M. Tagliatori Nogueira, B. Manzarbeitia Arroba, M. Álvarez Moreno, P. García Alonso, A. Herrero Muñoz, C. Paniagua Correa, M. Balsa Bretón;
Hospital Universitario de Getafe, Getafe, SPAIN.

Aim/Introduction: We aimed to evaluate the efficacy of ^{18}F-FDG in the detection of bone marrow involvement in Non-Hodgkin Lymphoma (NHL) and the influence of tumors markers. **Materials and Methods:** We reviewed records of all patients with newly diagnosed NHL over a 7-year period. Bone marrow biopsy (BMB), ^{18}F-FDG PET/CT and blood analysis were performed (time interval between them less than 30 days) before treatment. ^{18}F-FDG PET/CT was performed using a standard protocol and BMB was doing in posterior left iliac crest. Visual evaluation was performed for ^{18}F-FDG PET/CT scan and we classified ^{18}F-FDG PET/CT results in negative (non bone uptake) and positive (focal bone uptake). Cases with diffuse bone uptake were excluded. Data of tumors markers (β2-microglobulin and lactate dehydrogenase (LDH)) were gathered. Finally, PET results were compared with histological data and analytic parameters using T-Student test. Results: We evaluated 131 patients (61 women and 70 male), with median of age was 62.3 years (range 24 - 85 years). In our series, 98 patients had a negative ^{18}F-FDG PET/CT study: 75 of them had a negative BMB (true negatives) and 23 were false negative (non focal bone uptake and positive BMB). We excluded the false negative from statistical analysis. On the other hand, 33 patients had focal bone uptake: 17 of them had positive BMB (true positive) and 16 patients had negative BMB. In these 16 cases, ^{18}F-FDG PET/CT was negative in left iliac crest and all of them had a negative ^{18}F-FDG PET/CT control after chemotherapy, so we considered them as a PET/CT true positive for bone marrow involvement. We do not find significant differences between PET/CT results and β2-microglobulin values. However, that was found when we compare PET/CT results and LDH (p 0.00005). If we divide patients in aggressive and indolent NHL, we find statistical significant differences between PET/CT results and LDH levels in aggressive cases (p 0.0001) and between PET/CT results and β2-microglobulin levels in indolent ones (p 0.04). **Conclusion:** According to our results, the BMB could have been avoided when focal positive bone uptake was observed in PET/CT. In addition, patients with aggressive NHL and elevated LDH and patients with indolent NHL and increased β2-microglobuline levels seem to have more probability of bone marrow involvement in PET. However, prospective and analytic studies are needed to prove this hypothesis. **References:** None

EP-054

Role of [^{18}F]FDG PET/CT in the evaluation of bone marrow at the initial staging of Non-Hodgkin Lymphoma patients

M. Calderón Calvente, M. Falgás Lacueva, L. De la Cueva Barrao, N. Canchumanya Huatuco, G. Guzmán Prudencio, L. Del barco Diez Canseco, M. Sangrós Sahún, P. Navarro Beltrán, S. Álvarez Ruiz, D. Abós Olivares;
Hospital Universitario Miguel Servet, Zaragoza, SPAIN.

Aim/Introduction: To evaluate the role of [^{18}F]FDG PET/CT in the diagnosis of bone marrow (BM) infiltration of patients recently diagnosed with non-Hodgkin Lymphoma (NHL) in our setting. **Materials and Methods:** Consecutive patients with NHL who had [^{18}F]FDG PET/CT scan for initial staging from January to December 2020 were selected. We gathered data about BM metabolism, as assessed by Nuclear Medicine professionals at our hospital at the time of the test. Studies were classified as positive or negative, and in the case of presence of positive uptake, whether it was diffuse or focal in order to relate them to BM histopahological results. To evaluate the results, contingency tables were constructed for all the patients, and also for the most prevalent histopathological subtypes, assigning values for TP, TN, FP and FN in order to calculate sensitivity (SE), Specificity (SP), Positive Predictive Value (PPV) and Negative Predictive Value (NPV). Finally, positive predictive values (PPV) were calculated for the two groups of positive uptake: diffuse or focal. Results: Of the 43 patients collected 6 were excluded due to the lack of available histopathological results and 1 was excluded because of known EPO treatment at the time of the test, a stablished cause of false positive results. When evaluating all NHL, regardless of the histopathological subtype, prevalence of positive BM in our sample was 25%, obtaining SE 0.88, E 0.59, PPV 0.42 and NPV 0.94. Prevalence of positive BM in follicular lymphoma (FL) was 36.3%, with SE 1, E 0.57, PPV 0.57, NPV 1. Data of the diffuse large B-cell lymphoma (DLBCL) sample showed prevalence of positive BM of 12.5%, with SE 1, E 0.64, PPV 1 and NPV 1. When analysing the type of BM uptake, we found PPV 0.66 for focal uptake and PPV of 0.33 for diffuse uptake. **Conclusion:** Although PPV is higher in patients with focal BM uptake than in patients with

diffuse uptake in [^{18}F]FDG PET/CT studies, neither show data that support avoiding BM biopsy in the case of positive BM findings. Although the size of our sample is small, the fact that we obtained high NPVs (especially in the most frequent histopahological subgroups) indicates that negative BM findings could be diagnostic, thus avoiding the performance of BM biopsy in a group of patients. **References:** None

EP-12

Wednesday, October 20 - Saturday, October 23, 2021

e-Poster Area, release on Wednesday, October 20 at 09:00

Imaging Clinical Studies -> Oncological Imaging Clinical Study -> Melanoma

EP-055

The Role of 18F-FDG PET-CT for the Follow up of Tumor Response to Immunotherapy with Checkpoint Inhibitors in Patients with Advanced Melanoma

I. Kostadinova;
Clinic of nuclear medicine, University Hospital Acibadem City Clinic, Mladost, Sofia, BULGARIA.

Aim/Introduction: Immune checkpoint inhibitors nowadays have become a strength treatment in patients with metastatic melanoma, as they have led to longer progression free and overall survival. As a main difference with conventional treatment is the longer tumor response and appearance of immune related adverse events. The aim of the study was to follow up of the treatment response of patients with metastatic malignant melanoma to check point inhibitors, using 18F-FDG PET-CT. **Materials and Methods:** We have studied prospectively 42 patients (24 women and 18 men), treated with pembrolizumab (39 patients) and with nivolumab (3 patients) for the period 2016-2020, performing 172 18F- FDG PET-CT investigations (on the average 4.1 per patients), before and after beginning of the immunotherapy (the first follow up scan was performed on 3 month in order to escape visualization of eventual early pseudoprogression).We have used metabolic criteria PERCIST and morphological criteria- RECIST 1.1 and irRC for treatment response evaluation. Results: Progression was registered in 12/42 patients (29%) with 40.5% metabolic increase of activity of the target lesions on average (including new lesions) and the treatment was discontinued; complete response in 17/42 patients (40%) (including four patients with pseudoprogression which was proved during the follow up investigations and clinical status); partial response in 6/42 patients(14%) with 42% metabolic decrease of activity of the target lesions on average and stable disease was registered in 7/42 patients (17%). In 15 of the patients (36%), the therapeutic answer was visualized earlier on PET than on CT or additional lesions were registered (in some normal sized lymph nodes, bone marrow, peritoneum, muscles or subcutaneous tissue). Seven of the patients with negative PET findings and residual lesions on CT (17%) had no signs of progression in the following 3 years. Six of the patients showed adverse effects of the treatment- most often pneumonitis, sarcoidosis, hypophisitis, colitis, skin changes. **Conclusion:** We consider PET-CT as a very promising tool for follow up of the patients with metastatic melanoma under treatment with checkpoint inhibitors in order to optimize therapeutic algorithm. The effect of the immunotherapy and the adverse reactions could be visualized earlier on the basis of the changed metabolism, compared to usage of CT only. **References:** none

EP-13

Wednesday, October 20 - Saturday, October 23, 2021

e-Poster Area, release on Wednesday, October 20 at 09:00

Imaging Clinical Studies -> Oncological Imaging Clinical Study -> Any Other Malignant (including Primary of Unknown Origin)

EP-056

The potential added value of SPECT/CT in the management of patients

D. Grigolato*, S. Rossetto, A. De Lucchi, U. Tebano, G. Napoli, N. Luca, M. Gabbani, F. Fiorica;*
Azienda Scaligera Verona, Ospedale Mater Salutis Legnago, ITALY.

Aim/Introduction: To evaluate if single-photon emission computed tomography/computed tomography (SPECT/CT) scanning can give additional information in the work up of patients beyond the clinical query **Materials and Methods:** We retrospectively assessed a total of 181 patients (64 males, 117 females, age range 31-87 years, mean 65.7) who were referred to the nuclear medicine unit between 1st July 2020 and 31th December 2020 and performed one or two SPET/CT scans as a completion of their scintigraphy (Optima, CT 640 GE, 120 KeV 30 mA). 116/181 patients with previous diagnoses of cancers underwent bone scintigraphy for staging or restaging (108) and ^{99m}Tc-nanoalbumon lymph node scintigraphy for lymph node mapping (8) while 65 patients had suspicious benign diseases and performed perfusion lung scintigraphy for suspected pulmonary embolism (21), bone scintigraphy for unexplained bone pain (19), ^{99m}Tc-MIBI scintigraphy for iperparathyroidsm (8) and myocardial perfusion scintigraphy for suspected ischemic heart disease (27) Results: The diagnostic contribution of SPECT/CT was established during multi-disciplinary team meetings, after biopsies, MR, PET/CT and/or CT imaging. Among the 116 oncologic patients, there were 43 cases of prostate cancer and 39 of breast cancer, 9 lung cancers, 8

malignant melanomas and 12 patients with other cancer types. In 77/116 patients SPET/CT found out some findings unrelated to type of scintigraphy and/or to the known pathology. CT showed unexpected synchronous tumours in 3 patients (breast, laryngeal and oral cancer). At restaging with bone scintigraphy, 7 men with prostate cancer and 2 women with breast cancer, had large, suspicious lymph nodes at CT, confirmed as recurrent disease at biopsy or with other examinations (MRI and PET/CT). Three patients showed high HDP uptake in the heart, and SPET/CT described these findings as highly suspicious of cardiac amyloidois. In 62/77 cases CT depicted benign lesions (gallbladder stones, intra-thoracic goitre, adrenal adenomas, pleural, pericardial and abdominal effusions, kidney cysts, aneurysms). In eleven patients CT showed millimetric pulmonary nodules which are still in follow up. SPET/CT was found to have decisive additional information that changed the management of 15 patients (8.3%), adding prompted surgical treatment (2) and/or radiotherapy (7) or redirecting the patient to conservative management (6) **Conclusion:** Adding a SPECT/CT scan to the standard scintigraphic examination not only can give precise information on the pathology under investigation but also brings benefits in the personalized management of the patient **References:** None

EP-14

Wednesday, October 20 - Saturday, October 23, 2021

e-Poster Area, release on Wednesday, October 20 at 09:00

Imaging Clinical Studies -> Other Oncological Clinical Study -> Radioguided Surgery and Radiation Therapy Planning

EP-057

ROLL with Freehand-SPECT for assessment of surgical margins in breast cancer

J. Orozco Cortés, Á. Badenes Romero, G. Garrigos, Á. Esteban Hurtado, M. Navas de la Cruz, I. Latorre Agraz, E. Martinez Lopez, P. Abreu Sánchez, T. Mut Dolera, D. Reyes Ojeda, B. Cueto Cañadas, D. Balaguer Muñoz, N. Estelles, R. Martinez Garcia, E. Caballero Calabuig;
Hospital Universitario Dr Peset, Valencia, SPAIN.

Aim/Introduction: To compare the effectiveness of Freehand-SPECT and mammography vs Pathological Anatomy (AP) for the assessment of surgical margins with ROLL (Radioguided Occult Lesion Localization) technique in breast cáncer. **Materials and Methods:** Prospective longitudinal study in 36 patients (39 lesions) diagnosed with breast cancer (BC) with criteria for SNOLL/ROLL. A pre-surgical study is performed, after echo-guided administration of 99mTc-nanocolloid/ 99mTc-macroaggregates of albumin, in the tumor. Hybrid images (optical + SPECT) and three-dimensional navigation images with gamma probe are obtained by means of Freehand-SPECT. In the operating room 4-5 images are obtained with Freehand-SPECT, I) on the skin for tumor localization, II) after exposure of the bed for resection guide, III) of the bed after excision, IV and V) to the surgical specimen in anterior-posterior and lateral. A decision is made whether or not to widen the margins considering: a) residual activity (cps) at the margins of the resection bed; b) visual analysis of the uptake in the specimen; c) a minimum distance of 10mm + the radius of the lesion from the margins of the specimen to the center of greatest uptake. We evaluate the concordance of: The surgical margins between Freehand-SPECT vs mammography of the piece, being the reference technique PA; and the surgical time employed with Freehand-SPECT and mammography. Results: Tumor localization in the operating room with Freehand-SPECT: 100%. The results are evaluated for each of the six edges of every lesion removed. With the described criterio to widen margins, concordance of surgical specimen edges between Freehand-SPECT and mammography: 94.5%. Between Freehand-SPECT and PA: 93.1%. Between mammography and PA: 93.5%, all being statistically significant (p-value <0.000), so we can affirm that both techniques are related to or dependent on the reference technique, PA. Negative predictive value (NPV: probability of negative border in piece without affected borders) with Freehand-SPECT: 95.9%, with mammography: 96.07%. Positive predictive value (PPV: probability of positive border in piece with affected border) with Freehand-SPECT: 41.7%, with mammography: 42.8%. Median total operating room time: 60.25 minutes (30-145). Mean intraoperative Freehand-SPECT time: 5 scans=10 min. Time for mammography: 20 min. **Conclusion:** The probability of ruling out affected margins with Freehand-SPECT is not inferior to mammography. This method would not increase operating room time. **References:** none

EP-058

Long term follow-up of patients with Small Intestine Neuroendocrine Tumors submitted to Ex Vivo Beta-Radioguided Surgery with Y-90-DOTATOC

C. Grana[1], M. Colandrea[1], M. E. Ferrari[1], E. Bertani[1], F. Collamati[2], R. Faccini[3], S. Morganti[2], S. Papi[1], N. Fazio[1], F. Spada[1], L. Funicelli[1], E. Pisa[1], E. Solfaroli-Camillocci[2], U. Fumagalli Romario[1];
[1]European Institute of Oncology, IRCCS, Milan, ITALY, [2]Istituto Nazionale di Fisica Nucleare, Rome, ITALY, [3]Dipartimento di Fisica, Universita` di Roma Sapienza, Rome, ITALY.

Aim/Introduction: Complete surgery is the milestone of treatment of Small Intestine (SI) Neuroendocrine Tumors (NET) and could improve the prognosis in these patients. As we recently published, radioguided surgery (RGS) with beta-radioisotopes probe, provides a clearer delineation of the lesions with low radiation exposition for surgeons. **Materials**

and Methods: Five SI-NET patients with liver and abdominal lymph node metastases (4 male and 1 female, median age 61.8 years (range 51-71 years) were enrolled in our protocol receiving 5 mCi of Y-90-DOTATOC and subsequently operated, with the the ex-vivo analysis of their surgical specimens After surgery, patients received the standard and periodical follow up with morphological and functional imaging, blood examinations and clinical visits Results: 1 patient, operated on March 2017, remained stable for 2 years and when progressed, he received PRRT with Lu-177-oxodotreotide (800 mCi) obtaining a stabilization of disease; his blood examinations did not showed any long term toxicity 1 patient, operated on May 2017, has a stable disease at the last follow up of December 2020; he is in therapy with SSA; his blood examinations do not show any haematological or renal impairment. 1 patient, operated on July 2017, has a stable disease at the last follow up of December 2020; he is in therapy with SSA; his blood counts and kidney function are normal. 1 patient, operated on January 2018, has a stable disease at the last follow up of April 2021; he is in therapy with SSA, with normal blood examinations. 1 patient, operated on November 2018, presented a systemic progression of disease, after 4 months from surgery, and died few months after (this patient had also an important carcinoid syndrome with carcinoid cardiopapathy) All the patients tolerated very well the administration of Y-90-DOTATOC and the following surgery; there were no surgical complications or late side effects (no kidney funcion alteration, normal values on blood counts) during all the follow up period. **Conclusion:** This multidisciplinary approach that includes radioguided surgery with Y-90-DOTATOC administration is a safe procedure; we believe the importance of going on with the trial with the in-vivo application of the technique. **References:** First Ex vivo Results of Beta- Radioguided Surgery in Small Intestine Neuroendocrine Tumors with Y-90-DOTATOC. Cancer Biother Radiopharm. 2021 Feb 18

EP-059

Utilization of radioguided occult lesion localization (ROLL) method in thyroid and parathyroid surgery

A. Jankulovska, S. Stojanoski, N. Manevska, T. Makazlieva, V. Majstorov, D. Miladinova;
Institute of pathophysiology and nuclear medicine, Faculty of Medicine, Skopje, NORTH MACEDONIA.

Aim/Introduction: Assessment of the feasibility and effectiveness of radioguided occult lesion localization (ROLL) technique in patients undergoing surgical intervention for excision of hyperfunctional parathyroid tissue and remnant thyroid tissue or lymph node (LN) dissection in patients with confirmed thyroid carcinoma (TC). **Materials and Methods:** The study group consisted of 18 patients undergoing ROLL from January 2017 to December 2018. 11 patients (54±13,91 years, five females and six males) were diagnosed with primary hyperparathyroidism (confirmed by laboratory tests for PTH, calcium and phosphorus levels and parathyroid ultrasound performed before surgery). All underwent dual phase ^{99m}Tc-MIBI parathyroid SPECT/CT scintigraphy for correct preoperative parathyroid adenoma localization. Another 7 patients (52,83±11,68 years, five females and two males) with histologically proven thyroid carcinoma were scheduled for reoperation (5 patients due to papillary TC remnant tissue, 1 patient due to recurrent papillary TC and 1 patient due to LN metastasis of medullary TC). Ultrasound guided injection of 7 Mbq ^{99m}Tc-macroagregate in each lesion on the day of the surgery had been applied. Subsequently ROLL technique with gamma probe had been used intraoperatively to correctly identify the tissue for excision. Results: Parathyroid adenomas were confirmed histologically in all 11 patients. Mean PTH and total calcium levels were measured prior to parathyroid surgery and were 1599,21±912,59 pg/ml and 2,89±0,67 mmol/L, respectively. Parathyroid adenoma's size ranged from 8 to 21 mm. In patients operated due to the remnant thyroid tissue, lesions ranged from 21 to 27 mm in diameter, measured postoperatively. In 1 patient who underwent excision of recurrent papillary TC total of 3 foci were excised, ranging 7-17 mm in diameter. Lymph node dissection was performed in 1 patient with medullary TC and 2 LN were extracted, 8mm and 18 mm in diameter. Histological confirmation was obtained for all the extracted lesions. **Conclusion:** ROLL should be used as an effective technique for minimal invasive parathyroid and thyroid surgery. The ROLL method seems to be very helpful to the surgeons for precise localization of the small lesions. At the same time, shortening the time of the surgical intervention is another significant accomplishment of the technique. **References:** None

EP-060

Lung shunt fraction (LSF) evaluation in microspheres liver radioembolization pre-therapy Technetium 99mTc albumin aggregated (99m-Tc MAA): comparison between planar scintigraphy, SPECT/CT and post-therapy Yttrium-90 microspheres PET/CT (90Y PET/CT)

F. Serani[1], G. Della Gala[2], M. Santoro[2], G. Paolani[2], S. E. Prisco[1], N. Bonazzi[1], G. Battisti[1], S. Strolin[2], E. Tabacchi[3], L. Calderoni[1], L. Strigari[2], S. Fanti[1,3];
[1]Nuclear Medicine- Department of Experimental, Diagnostic and Specialty Medicine, University of Bologna, Bologna, ITALY, [2]Medical Physics Department, IRCCS Azienda Ospedaliera Universitaria Bologna, Bologna, ITALY, [3]Nuclear Medicine, IRCCS, Azienda Ospedaliero-Universitaria di Bologna, Bologna, ITALY.

Aim/Introduction: Radioembolization treatment with 90Y for unresectable liver malignancies, both primitive or metastatic, is preceded by a 99mTc-MAA procedure, which is used to estimate the lung shunt fraction (LSF) and the radiopharmaceutical distribution. The LSF is

normally evaluated by contouring the liver and lungs on the geometric mean of planar scintigraphy (PS), which suffers both from operator and methodology errors.The aim of this retrospective analysis is to evaluate the LSF estimation interobserver variability with SPECT/CT and the correlation between LSF estimation on PS, SPECT/CT and post-treatment Y90 PET/CT using a Bayesian penalized-likelihood (BPL) reconstruction algorithm. **Materials and Methods:** All patients consecutively treated at our Institution between June 2020 and February 2021 were retrospectively evaluated. LSF was calculated as the ratio between the total lungs counts divided by the total lungs and liver counts. LSF calculated from PS, performing contouring operation with clinical workstation tools, were collected from the clinical database. Two nuclear medicine physicians contoured lungs and liver on CT images of the SPECT/CT acquisitions using 3D-contouring tools on the same workstation independently in a blinded fashion. One additional operator contoured lungs and liver on CT images of the post-treatment PET/CT using an additional software.Statistically significant differences in LSF estimation between the described methodologies were assessed (Wilcoxon test, $p<0.05$).Patients were dichotomized between LSF higher/lower than 5% for all datasets (PS, SPECT/CT for both operators, PET/CT). Inter-operator variability in SPECT/CT was evaluated with Cohen's K-coefficient. To evaluate the agreement in LSF estimation between PS and PET/CT and between SPECT/CT and PET/CT the confusion matrix was evaluated, considering PET/CT as gold standard and assessing performance with McNemar test. Results: 36 patients (17 male, 19 female; mean age: 67+/-12 years) were enrolled. 28 patients presented hepatocellular carcinoma, 8 patients other malignancies (metastases or cholangiocellular carcinoma). Median[ranges] LSF were 6%[1.8-15], 1.5%[0.2-20.0], 1.5%[0.2-17.8] and 2.8%[0.8-19.5] for PS, SPECT/CT operators, and PET/CT respectively. Differences were statistically significant for PS vs. PET/CT only. SPECT/CT inter-observer agreement was good (K=0.65). PS accuracy in predicting BPL-based PET/CT LSF>=5% was lower than SPECT/CT (0.32 and 0.84 respectively). The confusion matrix showed that PS systematically overestimated LSF ($p<0.001$). **Conclusion:** SPECT/CT LSF assessment was reproducible between operators. Agreement with post-treatment BPL-based PET/CT LSF assessment was higher with SPECT/CT than PS. **References:** None.

EP-061

Targeted Axillary Dissection by marking the positive lymph node with ^{99m}Tc-MAA and sentinel lymph node biopsy in breast cancer patients after neoadjuvant chemotherapy. Initial experience

M. Pudis[1], A. Benítez-Segura[1], J. G. Reyes-Junca[1], M. T. Bajén-Lázaro[1], A. García-Tejedor[2], R. Ortega-Martínez[3], C. Soldevila-Lozano[1], A. Petit-Montserrat[4], M. Cortés-Romera[1];
[1]Nuclear Medicine-PET (IDI) department, Bellvitge University Hospital-IDIBELL, L'Hospitalet de Llobregat, Barcelona, SPAIN, [2]Gynecology department, Bellvitge University Hospital-IDIBELL, L'Hospitalet de Llobregat, Barcelona, SPAIN, [3]Radiology department, Bellvitge University Hospital-IDIBELL, L'Hospitalet de Llobregat, Barcelona, SPAIN, [4]Pathology department, Bellvitge University Hospital-IDIBELL, L'Hospitalet de Llobregat, Barcelona, SPAIN.

Aim/Introduction: To analyze the reliability of Targeted Axillary Dissection technique using ^{99m}Tc-MAA (TAD-MAA) and sentinel lymph node biopsy (SLN) in patients with cN1 breast cancer who after neoadjuvant chemotherapy (NACT) result to be ycN0. **Materials and Methods:** A prospective study (from july 2018 to april 2021) of 24 patients (34-79 years old), diagnosed with invasive ductal breast carcinoma, cT1-T3N1 that after NACT became ycN0. Before NACT, the affected axillary lymph node was marked with a clip. The day before surgery, an ultrasound-guided labeling of the clipped lymph node (CLN) was performed with ^{99m}Tc-MAA (CLN*) (1 patient had 2 CLN). A preoperative lymphoscintigraphy was performed with SPECT-CT. Surgical detection of the sentinel lymph node by ^{99m}Tc-nanocolloid and Patent blue V dye was performed in 16 patients (4 patients only received ^{99m}Tc-nanocolloid). If the CLN* presented metastasis, axillary lymph node dissection (ALND) was performed. The average follow-up of these patients was 13,5 months (0-33 months). We analyzed the correct labeling of CLN* (by SPECT-TC), surgical detection of CLN* and SLNB; presence of metastases in CLN* and SLN and presence of axillary recurrence during follow-up these patients. Results: Correct labeling of CLN* was performed in 24 out of 25 CLN. In one patient an ultrasound-guided labeling failed and the CLN was marked with a harpoon. It is excluded from the study. Surgical detection of CLN* was successful in all of the patients (24 CLN* detected). 17/24 CLN* were considered sentinel nodes (they dyed blue). Keep in mind that in 5 patients we did not administer a blue dye and we do not know if the radioactivity comes from ^{99m}Tc-MAA or ^{99m}Tc-nanocolloid. Surgical detection of SLN was also successful in all of the patients and we detected 2 SLN (including CLN*) in 10 patients and 3 or more (including CLN*) in 14 patients. Metastatic lymph-node involvement was present in 6 CLN*. One of these 6 patients with CLN* involved also presented metastasis in 1 SLN. An ALND was performed and 2 of these patients presented more lymph nodes affected. The average follow-up of these patients was during 13,5 months (0-33 months). None of these

patients presented axillary recurrence during the follow-up. **Conclusion:** TAD-MAA technique is simple and reliable (even if only 2 SLN are removed). ALND was avoided in 70% of the patients. SPECT-CT should be performed in all of these patients in order to confirm the correct labeling of the CLN. **References:** none

EP-15

Wednesday, October 20 - Saturday, October 23, 2021

e-Poster Area, release on Wednesday, October 20 at 09:00

Imaging Clinical Studies -> Other Oncological Clinical Study -> Sentinel Node

EP-062

Reduction of anxiety in patients undergoing lymphoscintigraphy for breast cancer without adequate information from the surgeon

L. Burroni, D. Luconi, D. Celani, G. Scuppa, C. Lucarini, M. Damico; Nuclear Medicine, Ancona, ITALY.

Aim/Introduction: Anxiety is a state of agitation of strong apprehension due to fear, uncertainty, waiting for something. In the taxonomy NANDA is defined as a vague sense of unease or fear accompanied by autonomous responses whose source is often unspecified or unknown to the person. It is a sense of apprehension caused by the forecast of danger. It has been observed that women who have to undergo pre-operative breast cancer lymphoscintigraphy, manifest a heightened state of anxiety related to poor information. A comparative descriptive study to evaluate the effectiveness of nursing interventions aimed at reducing anxiety began in June 2020 and ended in March 2021. **Materials and Methods:** 100 women (aged 30-70 yrs) without cognitive impairment were divided into 2 study groups: 50 without information about the diagnostic examination and the other with an empathic communication approach, active listening and a calming technique. In all patients were performed:• Detection of vital signs (VS): blood pressure, heart rate, respiratory rate and PO_2 value • Administration of the reduced Hamilton Scale (sweating, agitation, dry mouth, crying, change in tone of voice) with clinical evaluation for the severity of anxiety symptoms, with a score from 0 (not present) to 4 (severe). Total score ranges 0-24, where <8 indicates mild, 9-16 mild to moderate, and 17-24 from moderate to severe. The first group had no informative approach but only detection of the VS of the Hamilton scale before and after the procedure. The second group detected the VSs and administered the reduced Hamilton scale with the nursing intervention of empathic communication, active listening and calming technique. Results: The data collected show that 90% of patients have an increase in HR in the pre-treatment phase, with a 70% reduction in the post-treatment phase in both groups. In the first group, the Hamilton scale found that 33% experienced mild to moderate anxiety before the procedure, with 52% persisting after the scintigraphic examination. In the second group, the Hamilton scale finds that 20% experience mild to moderate anxiety before the procedure, with a reduction to 8% after the diagnostic procedure. **Conclusion:** An empathic approach through effective communication, active listening, with calming and distraction techniques allow a reduction of anxiety objectively confirmed by the detection of VS and data obtained with the Hamilton scale. This allows for greater compliance of patients, with better acceptance of the exam and the ability to maintain immobility during acquisition. **References:** none

EP-063

Are magnetic nanoparticles combined with ICG a valuable alternative to ICG-99mTc-nanocolloid in sentinel lymph node surgery? - introduction of intraoperative 3D freehand magnetic particle imaging

S. Azargoshasb[1], L. Molenaar[2], G. Rosiello[3], T. Buckle[4], D. M. van Willigen[4], M. M van de Loosdrecht[5], M. M. Welling[4], L. Alic[6], F. W.B. van Leeuwen[4], A. Winter[7], M. N. van Oosterom[4];
[1]Leiden University Medical Center, Leiden, NETHERLANDS, [2]Magnetic Detection & Imaging group, Technical Medical Centre, University of Twente, Enschede, NETHERLANDS, [3]Department of Urology and Division of Experimental Oncology, URI, Urological Research Institute, IRCCS San Raffaele Scientific Institute, Milan, ITALY, [4]Interventional Molecular Imaging-Laboratory, Department of Radiology, Leiden University Medical Center, Leiden, NETHERLANDS, [5]Magnetic Detection & Imaging group, Technical Medical Centre, University of Twent, Enschede, NETHERLANDS, [6]Magnetic Detection & Imaging group, Technical Medical Centre, University of Twente, Enschede, NETHERLANDS, [7]University Hospital for Urology, Klinikum Oldenburg, School of Medicine and Health Sciences, Carl von Ossietzky University Oldenburg, Oldenburg, GERMANY.

Aim/Introduction: Sentinel lymph node biopsy is a routine procedure for nodal staging in penile cancer. Most commonly, this procedure is guided by radiocolloids that help to provide various forms of preoperative mapping and intraoperative guidance. More recently, hybrid radio- and fluorescence-tracers, such as ICG-99mTc-nanocolloid extended the procedure with intraoperative fluorescence imaging. In parallel, magnetic-particle based approaches that use superparamagnetic iron-oxide nanoparticles (SPIONs) in combination with a handheld-magnetometer-detection probe have emerged. In the current study, we investigate a 3D magnetic particle imaging (MPI) and navigation modality (freehand MPI) in procedures that use a combination of magnetic and indocyanine-green (ICG) fluorescence guidance. **Materials and Methods:** The freehand MPI setup was constructed around a surgical navigation

device, optical tracking system, magnetometer probe and dedicated software. Before injection of the magnetic tracer, ICG was added, forming a cocktail of both tracers. Both the 3D freehand MPI modality and tracer mixture were characterized in phantoms, on human skin explants and during porcine surgery. Results: Studies on phantom and human skin explants illustrated that the current freehand MPI modality had a sensitivity of $2.2*10^{-2}$ mg/mL SPIONs, a resolving power of at least 7 mm and a depth penetration up to 1.5 cm. Evaluation during porcine surgery showed that freehand MPI could improve target identification by allowing for an augmented reality image overlay of the tracer distribution on the surgical field. Furthermore, the sites of SPION accumulation could be used as target for navigation in virtual reality. This boosted surgical confidence, as opposed to using magnetic tracing only. Furthermore, in analogy to the hybrid approach, fluorescence imaging provided an additional visual confirmation of sentinel nodes during their excision. **Conclusion:** 3D freehand MPI is feasible in vivo, providing the ability to better identify SPION accumulation and by facilitating surgical navigation. Furthermore, the use of ICG provides the ability to confirm correct localization. **References:** None

EP-064

Value of sentinel lymph node biopsy in vulvar cancer

A. Sainz Esteban, P. Turbay Eljach, N. Álvarez Mena, F. Sebastián Palacid, C. García García, C. Gamazo Laherrán, B. Pérez López, M. Gónzalez Soto, R. Ruano Pérez;
Hospital Clinico Universitario, Valladolid, SPAIN.

Aim/Introduction: The aim of the study was to determine the detection rate and negative predictive value (NPV) of sentinel lymph node biopsy (SLNB) in vulvar cancer. **Materials and Methods:** A retrospective study from 2007 and 2021 has been performed in women with vulvar cancer who underwent SLNB in our service. A total of 21 women were studied (age: 69±11): one with adenocarcinoma of the bartholino gland, 19 with epidermoid carcinoma and one with sebaceous carcinoma. Twenty-one patients presented a stage IB. Ten patients had tumours in the midline. None of the patients had clinically suspicious inguinofemoral lymph nodes or previous treatment with surgery, chemotherapy or radiotherapy. Acquisition of static planar images was performed after the intradermal administration of 37-148 MBq of 99mTc-nanocoloidal albumin. A SPECT/CT was performed in 18 patients and acquisition of dynamic planar images was performed in 15. In 5 patients excision of sentinel lymph nodes (SLN) was followed by an inguinofemoral lymphadenectomy (IFL) (bilateral or unilateral depending on tumour localization) because the SLNB in this centre was under the validation period at that moment. All patients were observed with follow-up for at least 9 months. Results: Planar images detected 38 SLN in the 21 patients (detection rate: 100%). SPECT/CT did not detect additional SLN but improved the anatomical localization of all the SLN. Eight patients with a midline tumour presented bilateral drainage. Unilateral drainage was obtained in 13 patients, 11 with lateral tumour localization and 2 with midline tumour. SLN was positive for metastasis in 5 patients and negative in 16. Of the 16 patients with negative SLN, the IFL was negative in 4 and the follow-up in 12. The last patient with a midline tumour presented a SLN in the right groin that was negative for metastasis and did not show other lymph node affected. However, the left IFL showed several metastatic lymph nodes (false positive) (NPV: 15/16). **Conclusion:** SLNB seems to be a useful technique for the detection of nodal involvement in early stages vulvar malignancies. **References:** None

EP-065

Sentinel lymph node in endometrial cancer and its impact on clinical practice

Y. Saker Diffalah, A. Roteta Unceta Barrenechea, P. Razola Alba, T. Escalera Temprado, A. Andrés Gracia, M. Delgado Castro, L. Tardín Cardoso, E. Prats Rivera, M. Abós Olivares;
Hospital Clínico Universitario Lozano Blesa, Zaragoza, SPAIN.

Aim/Introduction: Sentinel lymph node biopsy is a technique that has proven to be effective in the surgical and clinical management of numerous tumors. In endometrial carcinoma, there is currently no consensus on the indications or the possibility of avoiding lymphadenectomy in patients with negative sentinel lymph node. Aim: to analyze sentinel lymph node biopsy results in endometrial cancer patients who has been treated in our hospital. **Materials and Methods:** Descriptive retrospective study of 77 patients treated in our hospital for endometrial cancer in pre-surgical stages IA, IB and II, who underwent scintigraphic detection of sentinel lymph node with 99mTc-nanocoloid, from April 2015 to June 2020. Scintigraphic images and pelvic SPECT-CT were taken after periferical injection of the radiotracer in uterine cérvix. Surgical treatment was hysterectomy and lymphadenectomy by laparoscopic surgery. In addition patients received injection of indocyanine green or methylene blue. Results: 67 patients have been finally included. In 10 cases it was decided not to perform lymphadenectomy during surgery due to surgical risk. The mean age was 65.89 years. The histological types were 56 endometrioid adenocarcinomas, 8 serous and 3 carcinosarcomas. Regarding the pre-surgical stage, 16 cases were stage IA (23.88%), 34 were stage IB (50.74%) and 5 were stage II (7.46%). In 24 patients, the postoperative diagnosis was different from the initial one. The histological degrees were: 21 cases grade 1 (27.27%), 34 cases grade 2 (44.15%), and 22 cases grade 3 (28.57%). The scintigraphic detection rate was 67.53%. At least, one sentinel node has been detected in 45 patients, which 22 of them had bilateral drainage and 23 unilateral. In patients with unilateral drainage, the result of the contralateral lymphadenectomy did not modify the staging.

In 35 patients the sentinel node and lymphadenectomy were negative. In 9 cases sentinel lymph node was positive and 8 of them had not other lymph node involved. A single case showed a negative sentinel node with affectation of a para-aortic lymph node. The surgical detection rate, taking into account only those detected by lymphoscintigraphy, was 95.55%. The sensitivity was 90% in cases with positive sentinel lymph node, with only one false negative case. The negative predictive value was 97.22%. **Conclusion:** Sentinel lymph node biopsy with scintigraphic detection can be useful in the surgical staging of endometrial cancer in initial stages, being able to perform less invasive surgery, a guided surgical procedure and thus avoid the morbidity associated with lymphadenectomy. **References:** None.

EP-066

Concordance Between FREEHAND-SPECT and Conventional Scintigraphy for Sentinel Node Detection in Breast Cancer

J. Orozco Cortés, Á. Esteban Hurtado, M. Navas de la Cruz, Á. Badenes Romero, I. Latorre Agraz, P. Abreu Sánchez, T. Mut Dólera, D. Reyes Ojeda, D. Balaguer Muñoz, B. Cueto Cañadas, A. Abella Tarazona, C. Plancha Mansanet, E. Caballero Calabuig; Hospital Universitario Dr Peset, Valencia, SPAIN.

Aim/Introduction: Freehand-SPECT (declipse SPECT®; SurgicEye, Munich, Germany) has recently become a viable alternative for sentinel node biopsy. In addition to the planar conventional scintigraphy images, it allows for direct visualization of the distribution of radioactivity and improves navigation to radioactive target lesions providing accurate lesion depth measurements after a few minutes scan. The aim of the study was to evaluate the correlation between the number of sentinel node detected between Freehand-SPECT and planar conventional scintigraphy images. **Materials and Methods:** A total of 100 patients with an initial diagnosis of invasive breast cancer and no clinical evidence of nodal involvement, prospectively underwent sentinel lymph node biopsy. The preoperative study included Freehand-SPECT images at 15 minutes postinjection and conventional gamma camera images at 25 (early) and 60 (late) minutes postinjection. A concordance study was performed between the number of sentinel nodes detected with Freehand-SPECT and planar scintigraphy images; as well as sentinel nodes detection in early and late scintigraphy. Results: There was a high overall concordance between Freehand-SPECT and scintigraphy (72% for Freehand-SPECT and early scintigraphy; and 85% between Freehand-SPECT and late scintigraphy). In the concordance study, a moderate concordance was recorded between Freehand-SPECT and early scintigraphy (kappa coefficient: 0.42) and a moderate to high concordance between Freehand-SPECT and late scintigraphy (kappa coefficient: 0.60) showing no significant differences between them (p-value=0.16). **Conclusion:** Freehand-SPECT could be a valid alternative for the performing of the presurgical study of sentinel node in breast cancer since a moderate to high concordance with conventional studies has been obtained. **References:** 1.Bluemel, C., Schnelzer, A., Okur, A., Ehlerding, A., Paepke, S., Scheidhauer, K., & Kiechle, M. (2013). Freehand SPECT for image-guided sentinel lymph node biopsy in breast cancer. European Journal of Nuclear Medicine and Molecular Imaging, 40(11), 1656-1661. doi:10.1007/s00259-013-2473-0 2. Federica Orsini, Federica Guidoccio, Sergi Vidal-Sicart, Renato A. Valdés Olmos, and Giuliano Mariani. General Concepts on Radioguided Sentinel Lymph Node Biopsy: Preoperative Imaging, Intraoperative Gamma-Probe Guidance, Intraoperative Imaging, and Multimodality Imaging. En Mariani, G., Manca, G., Orsini, F., Vidal-Sicart, S., & Valdés Olmos, R. A. (Eds.). (2013). Atlas of Lymphoscintigraphy and Sentinel Node Mapping.

EP-067

Is the sentinel lymph node biopsy (SLNB) an adequate technique for axillary staging in patients with locally advanced breast cancer (LABC)?

J. Espejo Niño, R. Valverde Jorge, M. Nevares Herrero; Hospital Universitario Cruces, Barakaldo, SPAIN.

Aim/Introduction: Analyze if sentinel lymph node biopsy(SLNB) allows adequate axillary staging in patients with locally advanced breast cancer(LABC) treated with neoadjuvant chemotherapy(nCT) . **Materials and Methods:** Retrospective study (January/12-January/21) in patients with LABC selected for nCT with: initial clinical and radiological tumor and lymph node staging (TNM-AJCC-7-Edition), histological types, tumor markers, therapeutic protocols, submitted to SLNB, with evaluation of the tumor and lymph node radiological and pathological post-nCT response. We obtained: SLNB detection rate(DR), false negatives(FN), relapse and death. Results: 113 patients with LABC met the inclusion criteria: 104-IDC, 5-ILC, 1-DCIS, 1-tubular, 1-medullary and 1-colloid. 20-SLNB before therapy(pre-nCT) and 93-SLNB after therapy(post-nCT). From the pre-nCT group: 5-SLNB-positive(SLNB+), 13-SLNB-negative(SLNB-), 2-SLNB with micrometastasis(SLNBmic). In the evaluation after neoadjuvant treatment by MRI, 2 presented complete response(CR), 1 progression(PP), 3 stable disease(SD), 12 major partial response(MPR) and 2 minor partial response(mPR). We performed lymphadenectomy(LDN) at the 5-SLNB(+): 2 were LDN(+) with 1-EE and 1-PP; and 3 were LDN(-): 2-MPR and 1-SD. 2-SLNB(-) passed away, 2-MPR, 1 with LDN (-) and another without LDN. The DR for pre-NQT-SLNB was 100%. From the post-nCT group 52 were cN(+) and 41-cN(0) before therapy. 33 were SLNB(+) that in evolution presented: 5-CR, 15-MPR, 10-mPR, 1-SD and 2-PP. In 9 patients there was no migration(NM): 1-CR, 4-mPR, 1-SD and 3-MPR. The 51-SLNB(-) presented: 19-CR, 23-MPR, 7-mPR, 1-SD and 1 without MRI. We carried out 71/93 LDN including 33-SLNB(+) and 9 NM.

We obtained 27LDN(+): 18-SLNB(+), 4-NM and 5-SLNB(-). We obtained 44-LDN(-): 24-SLNB(+), 5-NM and 15-SLNB(-). Thus, the DR for post-NQT-SLNB was 100%. 4 patients with distant relapse died: 3 with MPR: 2-NM and 1 SLNB(-); 1 with mPR and BSGC(+). Out of 71 SLNB with LDN, we obtained 12,7% FN taking into account the NM and 8% of the FN without NM. **Conclusion:** Our DR for SLNB-pre-nQT was 100% and post-nQT was 90.3%. The FN in the post-nQT-SLNB were 12.7%, taking into account the NM and 8% of the FN without NM, there being no false positives in SLNB. **References:** Giuliano AE, Ballman KV, McCall L, Beitsch PD, Brennan MB, Kelemen PR, Ollila DW, Hansen NM, Whitworth PW, Blumencranz PW, Leitch AM, Saha S, Hunt KK, Morrow M. Effect of Axillary Dissection vs No Axillary Dissection on 10-Year Overall Survival Among Women With Invasive Breast Cancer and Sentinel Node Metastasis: The ACOSOG Z0011 (Alliance) Randomized Clinical Trial. JAMA. 2017 Sep 12;318(10):918-926. doi: 10.1001/jama.2017.11470. PMID: 28898379; PMCID: PMC5672806.

EP-068

Non-Identification of Sentinel Lymph Nodes in Head and Neck Melanoma: Clinical Predictors and Outcome

***M. Punda**, M. Romić, M. Pastorčić Grgić, D. Vagić, I. Jakšić, T. Jukić, A. Fröbe;*
UHC Sestre Milosrdnice, Zagreb, CROATIA.

Aim/Introduction: The performance of sentinel lymph node (SLN) lymphoscintigraphy in head and neck melanoma (HNM) is challenging due to complex lymphatic drainage in that area. Furthermore, peritumoral radioactivity may overlap the draining node resulting in non-identification (NI) of SLNs. The reported incidence of NI of SLNs in HNM is up to 9.95 %, however the literature that provides the management in such cases is scarce. We aimed to determine the occurrence and clinical predictors of NI of SLNs and consequent outcome among our HNM patients. **Materials and Methods:** The study included clinically node-negative patients with melanoma who underwent SLN scintigraphy from January 2014 to January 2020. After peritumoral injection of 99mTc-nanocolloid, dynamic and static planar imaging followed by SPECT/CT was performed. In case of non-visualization of SLNs, delayed planar imaging up to 2 hours was done prior SPECT/CT. Results: Out of 780 melanoma patients examined, 130 (16.7%) had HNM. SLNs were identified in 122/130 patients: unilateral and bilateral neck and axillar SLNs were found in 106, 16 and 4 patients, respectively. The SLNs were NI in 8 (6.2%) patients (6 women, 2 men) aged 76.5 (mean, range 63-82) years. The median (range) Breslow thickness was 2.58 (1.59- 4) mm and median (range) mitotic rate was 8.14 (2-15) mitoses/mm^2. Of the 8 patients, 7 underwent wide local excision of melanoma only, the scars were free of tumor. In one patient with preauricular melanoma (4 mm thickness) superficial parotidectomy and ipsilateral neck dissection was done: histopathology revealed residual melanoma with negative lymph nodes and the patient was free of tumor after 36 months of follow-up. Three patients (melanoma on the cheek, auricular and infraauricular) developed ipsilateral neck lymph node metastases within 5-7 months. One patient with neck melanoma (2 mm thickness, 12 mitoses/mm^2) developed distant metastases seven months after SLN scintigraphy. The remaining three patients (submandibular, temporal and zygomatic melanoma) were free of disease after follow-up between 14 to 54 months. **Conclusion:** We found NI of SLNs in 6.2 % of our patients with HNM, mainly associated with older age and unfavorable histopathological features of primary melanoma. Three patients developed ipsilateral neck nodal disease close to the primary melanoma and one patient developed distant metastases, soon after SLN scintigraphy. Therefore, our results revealed that the management of HNM patients with NI of SLNs should consider careful closer clinical follow-up and the use of additional modalities to enhance SLN identification. **References:** None

EP-069

Re-injection of the tracer in cases of no sentinel node visualization in lymphoscintigraphy for breast cancer, increases the detection rate of sentinel nodes and therefore high number of unnecessary axillary lymph node dissections can be avoided

***A. Aghaei**[1], R. Sadeghi[1], E. Soltani[2], S. Jangjoo[1], M. Asadi[2], V. Dabbagh[1];*
[1]Nuclear medicine research center, Mashhad university of Medical Sciences, Mashhad, IRAN, ISLAMIC REPUBLIC OF, [2]Onco-surgery research center, Mashhad university of Medical Sciences, Mashhad, IRAN, ISLAMIC REPUBLIC OF.

Aim/Introduction: Sentinel node biopsy is considered the standard of care in early stage breast cancer and can obviate the need for axillary lymph node dissection in patients without axillary nodal involvement. In this study we evaluated the effect of radiotracer re-injection in case of sentinel node non-visualization on pre-operative lymphoscintigraphy of breast cancer patients. **Materials and Methods:** 1850 early stage breast cancer patients (clinically N0) were referred to our department for sentinel node mapping. All patients received a single dose of Tc-99m phytate (0.5mCi/0.2 cc for single day protocol and 1 mCi/0.2 cc for two day protocol) in the peri-areolar area of the index lesion using an insulin syringe in an intradermal fashion. Lymphoscintigraphy images of the patients were done 1 to 2 hours post injection in anterior and lateral views.Overall, 255 patients had sentinel node non-visualization. Our strategy for patients with axillary sentinel node non-visualization differed for two periods of time. Between March 2017 and September 2017, sentinel node non-visualization was reported to the surgeon without any re-injection of the radiotracer. For the rest of the study

period, the patients received another dose of the radiotracer five centimeters apart from the first injection (again intradermal and peri-areolar). Immediately following the second injection, another lymphoscintigraphy images were taken (with same parameters). In addition, in case of sentinel node harvesting failure, axillary lymph node dissection was done. Results: Overall 255 patients entered our study. Fifty five patients were in group I without any re-injection. The remainder of the patients (200 patients) was in group II with re-injection of the radiotracer.155 out of 200 (77.5%) patients of group II, a sentinel node could be visualized following re-injection of the radiotracer. Sentinel node could be found in all these patients intra-operatively. Detection rate was 15 out of 45 and 15 out of 55 in group I and patients without sentinel node visualization even after re-injection respectively all of which were detected by blue dye (12 and 13 patients with blue dye only respectively). Axilla was involved in 5 out of 40 (12.5%) patients in group I with intra-operative sentinel node mapping failure. On the other hand, axilla was involved in 27 out of 30 (90%) group II patients with sentinel node non-visualization and intraoperative mapping failure. **Conclusion:** Re-injecting of the tracer increases the detection rate of sentinel nodes and therefore high number of unnecessary axillary lymph node dissections can be avoided. **References:** none

EP-070

Challenging visualization of sentinel lymph nodes in upper urinary tract urothelial carcinoma

W. Cytawa, W. Polom, A. Polom, M. Frankiewicz, E. Szurowska, P. Lass, M. Matuszewski;
Medical University of Gdansk, Gdansk, POLAND.

Aim/Introduction: The aim of this study was to assess the possibility of performing the analysis of lymphatic outflow and detecting sentinel lymph nodes (SLNs) in patients with suspicion of upper urinary tract urothelial carcinoma (UTUC) with the use of radioisotope-based technique. **Materials and Methods:** A prospective study was conducted on 19 patients (mean age 73.4 years, 7 male) between March 2018 and January 2021 with suspected UTUC, in whom diagnostic ureterorenoscopy (URS) was performed. During the procedure tumor biopsy for staging purposes was carried out, with additional injection of ^{99m}Tc-labeled nanocolloid into the healthy urothelium mucosa around the tumor (4 portions of 9.25 MBq per injection). Hybrid SPECT/CT lymphoscintigraphy was performed 24±3 hours after radiotracer injection using a SPECT/CT dual-head gamma-camera. Any focal activity of radiotracer detected in the local lymphatic outflow region, apart from the site of injection, was considered SLN. Results: Pathological staging obtained from the biopsy was: T0 in 8 (42 %) patients, Ta - 7 (36 %), and T1 - 4 (21 %). In 4 (21 %) patients concomitant bladder cancer was found. SLNs were detected in 2 (10.5%) patients. In the first patient a single, unilateral SLN in the paraaortic region was visualized. In the second patient two unilateral SLNs were detected - one with clear focal uptake located behind the left external iliac artery and the other with faint focal uptake located slightly higher. In the remaining 17 cases (89.5 %) no clear SLNs were observed, however in 5 cases (26.3%) SPECT/CT imaging revealed diffused outflow of radiotracer from the injection site caudally, through the retroperitoneal space, outside the urinary tract, along the ipsilateral iliopsoas muscle. **Conclusion:** Lymphatic outflow assessment in UTUC using SPECT/CT lymphoscintigraphy is possible yet challenging, with SLNs visualization in about 10% of cases. In about 25% of patients the imaging revealed spillage of the radiotracer outside the urinary tract which could result from the accidental tracer injection into the retroperitoneal space due to the very thin wall of the ureter. SPECT/CT lymphoscintigraphy in UTUC may provide valuable information about patients individual anatomy and the direction of potential metastatic cells spread from the tumor. **References:** None

EP-071

Inguinal Lymph Node Relapse in Vulvar Carcinoma After Negative Sentinel Lymph Node Biopsy

C. Soldevila Lozano[1], M. Bajén-Lázaro[1], J. Mora-Salvadó[1], A. Benítez-Segura[1], J. Suils-Ramón[1], E. Llinares-Tello[1], I. Sánchez-Rodríguez[1], G. Reyes-Junca[1], M. Martí-Cardona[2], L. Fernández-Romero[1], M. Cortés-Romera[1];
[1]Nuclear Medicine-PET (IDI). Hospital Universitari de Bellvitge, L'Hospitalet De Llobregat, SPAIN, [2]Department of Gynecology and Obstetrics. Hospital Universitari de Bellvitge, L'Hospitalet De Llobregat, SPAIN.

Aim/Introduction: The aim of this study was to analyze the incidence of inguinal lymph node relapse in patients (p) with squamous vulvar carcinoma and negative sentinel lymph node biopsy (SLNB). **Materials and Methods:** We retrospectively reviewed forty-eight patients (mean age: 71 years) with vulvar squamous cell carcinoma (stage I-II), who underwent SLNB between 2010 and 2019. Lymphoscintigraphy (planar images and SPECT/TC) was performed the day prior to the surgical procedure by injecting 5mCi of [^{99m}Tc]Tc-Nanocolloid. SLN was detected at surgery with a gamma probe. Lymphadenectomy was not performed in patients with negative SLNB. The follow-up period was from 12 months to 108 months (median: 40 months). The location of primary tumor (lateral or midline lesions), inguinal lymph node relapse, progression-free survival (PFS) and SLN detection rate were analyzed. Results: Lateral lesions were observed in 19/48 patients: lymphoscintigraphy showed 1p with bilateral drainage and 18p with unilateral drainage; SLN detection rate was 100% (70% with negative SLNB); inguinal lymph node relapse was not observed in any patients with lateral lesions. Midline

lesions were observed in 29/48 patients: lymphoscintigraphy showed 2p unilateral drainage and 27p bilateral drainage; SLN detection rate was 96% (80% with negative SLNB); inguinal lymph node relapse was observed in 3p (2p with negative SLNB and 1p without ipsilateral drainage); mean PFS was 13 months. **Conclusion:** Vulvar squamous cell carcinoma has a low incidence of inguinal lymph node relapse. Recurrence only appears in patients with midline lesions and his median PFS is one year. SLNB is very useful for staging regional lymph nodes in patients with vulvar squamous cell carcinoma stage I-II. **References:** none

EP-072

Detection of disseminated prostate cancer cells in sentinel lymph node by dielectrophoretic technology: proof-of-concept

C. Rousseau[1], E. Moranton[2], D. Cochonneau[2], G. Aillet[3], T. Rousseau[4], A. Morel-Thierry[2], D. Heymann[5];
[1]ICO René Gauducheau, F-44800 Saint-Herblain; Université de Nantes, CNRS, Inserm, CRCINA, F-44000, Nantes, FRANCE, [2]ICO René Gauducheau, F-44800, Saint Herblain, FRANCE, [3]Institut d'HistoPathologie, F-44000, Nantes, FRANCE, [4]Urologic Clinic Nantes-Atlantis, F-44800, Saint Herblain, FRANCE, [5]ICO René Gauducheau, F-44800 Saint-Herblain; Université de Nantes, F-44000, Saint Herblain, FRANCE.

Aim/Introduction: This work used patients data from a previous cohort (231 patients) constituted to validate the accuracy of the isotopic sentinel lymph node (SLN) technique correlated with extensive pelvic lymph node dissection (ePLND) in patients with localized prostate cancer (PCa). All of them had an intermediate or high risk of lymph node metastases according to D'Amico and 193/231 (83.5%) were lymph node invasion free (pN_0 and SLN_0). Among these patients, with a median follow-up of 7.1 years (95% CI: [6.6-7.5]), 53/193 (27.4%) of them presented an early recurrence of their disease. Consistent with this, we hypothesize that these patients presented an onset of lymph node invasion by tumor cells which was below the threshold of detection by conventional histological approaches. We then propose to re-analyze these samples using dielectophoretic microfluidic approach to detect rare metastatic prostate cancer cells. **Materials and Methods:** Biological cohort: First, 5 involved SLN patient samples extracted from the entire cohort, were used for the calibration of the technique. Then, retrospective Formalin-fixed paraffin-embedded sentinel lymph nodes (samples fixed and included in parrafine) from 53 patients (pN_0 and SLN_0) will be analyzed. The number of nodes available varies from one patient to another. Histological assessment defined sentinel lymph nodes invaded ("positive") and non invaded by cancer cells ("negative"). Preparation of samples: For each node, a section 20 micrometers thickness was prepared. After deparaffinization, enzymatic digestion and antigen retrieval, cell suspensions were immunostained for pan-cytokeratin, vimentine, PSA/PSMA, CD45 and DAPI. Cancer cell enumeration : pan-cytokeratin$^+$, PSA/PSMA$^+$, vimentin$^{+/-}$, DC45$^-$ were considered as cancer cells and enumerated by using dielectrophoretique approach (DEPArray®). Results: As expected, pan-cytokeratin$^+$, PSA/PSMA$^+$, vimentin$^{+/-}$, DC45$^-$ prostate cancer cells were detected in the "positive" sentinel lymph node group. Interestingly, pan-cytokeratin$^+$, PSA/PSMA$^+$, vimentin$^{+/-}$, DC45$^-$ were also detected in sentinel lymph nodes initially labeled "negative" (pN0 and SN0) after the histological investigation. **Conclusion:** Recurrent disease in pN_0 and SN_0 prostate cancer patients may be explained by an early dissemination of cancer cells in sentinel lymph nodes which were below the threshold of detection by conventional histological approaches. Dielectrophoretic technology may complete the panel of diagnostic tools in pathology for detecting rare disseminating cancer cells. Study is ongoing and supplementary data will be presented at the congress. **References:** Rousseau et al, EJNMMI. 2016; 43:1849-56; Bolognesi et al, Sci Rep 2016; 6: 20944; Gabriel et al, Clin Chem 2016; 62: 571-81

EP-073

Performance of lymphoscintigraphy and intraoperative sentinel node mapping in patients with prior breast surgery

*L. Ferreira, **V. Alves**, J. Pereira;*
Centro Hospitalar Universitário de São João, Porto, PORTUGAL.

Aim/Introduction: It is already known that patients with previous breast treatments may have altered drainage patterns. The purpose of this study was to assess the feasibility of lymphoscintigraphy in patients with prior breast surgery and to investigate the factors related to the detection of sentinel lymph node. **Materials and Methods:** Between January 2008 and April 2020, 138 patients who had undergone previous breast surgery were submitted to breast lymphoscintigraphy with ^{99m}Tc-nanocolloids to identify a sentinel lymph node preoperatively. Presence of drainage and its pattern, history of previous axillary node dissection, radiotherapy (RT), chemotherapy (QT) and type of previous surgery (benign, conservative or non-conservative) were assessed. Results: Lymphoscintigraphy was successful in 91 (65.9%) patients. Lymphoscintigraphy and intraoperative identification (if performed) of sentinel lymph nodes was positive in 71.0% of patients. The median of lymph nodes removed per patient was 1.8. Lymph node metastases were detected in 26.5% of patients with sentinel node biopsy. Lymphoscintigraphy was positive in 94.9% of patients submitted to prior benign breast surgery (all of them had homolateral migration); in 50% of patients who underwent prior conservative surgery (33.8%, 5.9% and 10.3% corresponded, respectively, to homolateral, contralateral and bilateral migration); and in 64.5% of patients who have had previous non-conservative surgery (migration was

41.9% homolateral, 9.7% contralateral and 12.9% bilateral). Among patients who had undergone previous axillary node dissection, lymphoscintigraphy was positive in 45.9% (21.6% homolateral, 8.1% contralateral and 16.2% bilateral migration) of patients, while it was positive in 73.3% of patients without previous axillary node dissection (64.4% was homolateral migration). In those who were submitted to prior RT, 41.4% had a positive lymphoscintigraphy (22.4% homolateral, 7.0% contralateral and 12.1% bilateral migration), versus 83.8% in those not submitted to RT (75.0% had homolateral migration). In bivariate analysis, the presence of previous RT, axillary node dissection and type of prior surgery (benign and conservative versus non-conservative) were statistically significant ($p<0.05$) for the identification of a sentinel lymph node, both in lymphoscintigraphy and intraoperatively; while in multiple logistic regression, RT was the only independent predictor ($p<0.001$ and odds ratio=0.67). **Conclusion:** Lymphoscintigraphy seems to be feasible in patients with prior breast surgery and plays an important role in identifying atypical lymphatic flow patterns. Prior irradiation of the breast (and axilla) seems to greatly influence lymphatic migration. **References:** None

EP-074

Initial experience from a multicentre clinical trial evaluating the safety and performance of a drop-in gamma probe for sentinel lymph node biopsy in prostate cancer

L. Fumadó Ciutat[1], J. Walz[2], B. Hadaschik[3], J. Adshead[4], W. Everaerts[5], K. Goffin[5], M. Grootendorst[6], F. Oldfield[6], A. Mestre Fusco[7], S. Vidal-Sicart[1], J. Abascal Junquera[1];
[1]Hospital del Mar, Barcelona, SPAIN, [2]Institut Paoli-Calmettes Cancer Centre, Marseille, FRANCE, [3]University Hospital Essen, Essen, GERMANY, [4]The Lister Hospital, Stevenage, UNITED KINGDOM, [5]KU Leuven, Leuven, BELGIUM, [6]Lightpoint Medical Ltd., Chesham, UNITED KINGDOM, [7]Hospital University Dr Josep Trueta, Girona, SPAIN.

Aim/Introduction: Conventional rigid laparoscopic gamma probes (RLGPs) used for minimally invasive sentinel lymph node biopsy (SLNB) procedures have limited manoeuvrability and control which restricts identification of sentinel lymph nodes (SLNs). To address these limitations drop-in gamma probes (DIGPs) have been developed by different groups with each probe having different design and performance features[1]. Here we present the initial results from our DIGP as part of an ongoing prospective multicentre clinical trial that evaluates the performance and safety of this device for SLNB in prostate cancer (ClinicalTrials.gov: NCT04632251). **Materials and Methods:** The DIGP consists of a Tethered Probe connected to a Control Unit. The Tethered Probe is 40 mm long, fits through a standard 12 mm laparoscopic port and contains a Grip Feature that is compatible with standard tissue graspers used for minimally invasive surgery. The Control Unit provides visual and audio feedback of the activity levels, and can be connected to an additional display (e.g. da Vinci TilePro). After ethics approval was obtained, patient recruitment commenced in Hospital Del Mar, Barcelona. A transrectal ultrasound-guided ^{99m}Tc-nanocolloid injection of 240 MBq was given into each quadrant of the prostate. Planar lymphoscintigraphy scans were acquired 30-minutes and 2-hours post-injection. A laparoscopic radical prostatectomy was performed followed by SLNB and ePLND the morning of the next day. Suspected SLN locations were scanned in vivo with the DIGP probe and subsequently with a RLGP. All excised SLNs and non-SLNs were measured ex vivo with both probes. All specimens were sent subsequently for post-operative histopathology. Results: 2 SLNs were identified by the DIGP and the RLGP in each patient (Table 1). In one patient a paraaortic SLN was identified on preoperative imaging but this SLN was not deemed suitable for excision during surgery. The DIGP recorded a higher count rate than the RLGP in all in vivo and 3/4 ex vivo measurements. All SLNs and non-SLNs removed were negative on histopathology. No device-related adverse events occurred. **Conclusion:** These early results show that our DIGP can successfully detect SLNs with excellent sensitivity compared to the RLGP and identify SLNs outside of the ePLND template. Data from patients undergoing robot-assisted and open surgery are awaited and interim results after N = 10 patients are expected in July 2021. Future applications include the use of the DIGP in combination with ^{99m}Tc-PSMA for intraoperative detection of lymph node metastases. **References:** [1].Valdés Olmos et al. Clinical Nuclear Medicine. 2020.

EP-075

Lymphoscintigraphy in the Time of COVID-19: Effect of Molybdenum-99 Shortage on Feasibility of Sentinel Node Mapping

R. Sadeghi, K. Sadri, V. Dabbagh, A. Mahdi;
Mashhad University of Medical Sciences, Mashhad, IRAN, ISLAMIC REPUBLIC OF.

Aim/Introduction: In the current study, we reported our experience on sentinel node mapping of breast cancer patients during the extreme shortage of Mo99-Tc99m generators using Tc-99m phytate. **Materials and Methods:** During the period from March 7, 2019, to April 18, 2020, due to disruption of molybdenum supply chain, we used low specific activity Tc-99m pertechnetate elute (0.5-2 mCi of 99mTcO4 in 5 mL) for each kit preparation. Two or three intradermal periareolar injections were done for each patient (0.02-0.1 mCi/0.2 mL for each injection). Immediately following injection, dynamic lymphoscintigraphy was done. Surgery was done the same day of injection and the axillary sentinel node was sought using a gamma probe. Results: Overall, 35 patients were included in the study. The specific activity of the Tc-99m elute (in 5 mL) used for kit preparation was 2 mCi/10

mg in four, 1.5 mCi/10 mg in eight, 1.25 mCi/10 mg in eight, 1 mCi/10 mg in three, 0.75 mCi/10 mg in five, and 0.5 mCi/10 mg of 99mTc-Phytate in seven patients. For the first four groups of patients, we used two 0.2 mL injections, while in the latter two groups, three 0.2 mL injections were used. At least one sentinel node was detected in all patients but three in whom axilla was involved. **Conclusion:** Sentinel node biopsy can be achieved with low specific activity of Tc-99m elute at the time of Mo99-Tc-99m generator shortage. If special personal protection is used, sentinel node mapping can be done in nuclear medicine departments with excellent results despite the COVID-19 pandemic and disruption of generator shipment. **References:** None

EP-076

The accuracy of sentinel node biopsy by99mTc-sodium phytate in patients with pancreatic cancer

***R. Sadeghi**, M. Aliakbarian, S. Hamed, B. Memar;*
Mashhad University of Medical Sciences, Mashhad, IRAN, ISLAMIC REPUBLIC OF.

Aim/Introduction: Pancreaticoduodenectomy is the only potentially curative treatment for pancreatic cancer. The identification of the first nodal drainage site (sentinel node) may improve the detection of metastatic nodes and can contribute to a less invasive surgery. We aimed to determine the accuracy of sentinel node mapping in patients with pancreatic cancer using intraoperative radiotracer injection technique. **Materials and Methods:** At surgical exposure, peritumoral injection of 0.4-0.5 mci/0.5 ml of 99mTc- sodium phytate was performed. After tumor resection, sentinel nodes were investigated in the most common areas using a hand-held gamma probe. Any lymph node with in vivo count twice the background was considered as sentinel node, thus, it was removed and sent for pathological assessment. Then a standard lymph node dissection was performed for all patients. Results: Fourteen patients with cancer in the head of the pancreas were included in this study. Overall, 180 lymph nodes were harvested with a mean of 11.6±4.7 lymph nodes per patient. In eight patients, at least one sentinel node could be identified (detection rate about 64%). False negative rate of the study was 3/5 (60%). **Conclusion:** Our study revealed insufficient diagnostic accuracy and high false negative rate for sentinel lymph node mapping with 99mTc- sodium phytate in pancreatic cancer. **References:** None

EP-077

Radioactive and Fluorescence (Hybrid) Imaging in Breast Sentinel Node Procedures

***J. Gambini**[1], E. Silvera[1], F. Portugal[1], R. J. Ortega[1], G. Yang[2], T. Quinn[3], J. C. Hermida[1], O. Alonso[1], P. Cabral[1];*
[1]Centro De Medicina Nuclear e Imagenología Molecular, Hospital de Clínicas, Montevideo, URUGUAY, [2]Shanghai Jiao Tong University, Shanghai, CHINA, [3]University of Missouri, Columbia, Missouri., MO, UNITED STATES OF AMERICA.

Aim/Introduction: Breast sentinel node (SN) biopsy has been validated and allows us to identify the node that is most likely to harbor metastases. In this way, it is possible to avoid performing axillary dissection with its associated morbidities to those patients where no disease is found. Recently fluorescent and radioactive (hybrid) tracers have been incorporated to SN procedures. The most studied one is 99mTc nanocoloid - indocyanine green (99m Tc NC ICG) who provides a visual component enabling precise SN removal. The objective of our work is to describe our experience with this hybrid marker in GC breast biopsy. **Materials and Methods:** 99mTc NC ICG was prepared as described by Brower et al. in 2012 (1). Twenty five breast cancer bearing female patients were injected subcutaneously in the periareolar region in the same cuadrant where the breast lesion was identified with 3 mCi of 99m Tc NC ICG. Afterwards planar scintigraphic and SPECT/CT (Mediso AnyScan 16) were performed. During surgical procedures a gamma probe (Europrobe) and our portable ICG fluorescence detection system was used for SN localization. In this way, the surgeon could be guide towards the SN using the acoustic cue provided from the gamma probe and when close to the suspected node find the SN with fluorescence images. Once SNs were found, they were removed and examined by pathologists. Results: The hybrid tracer 99mTc NC ICG was easily prepared. 99m Tc NC ICG allowed SN preoperative identification through scintigraphy and SPECT CT. Surgeons use this information to plan their surgeries. During surgeries, gamma probe guides the surgeons towards the SN through their acoustic cues, and fluorescence images allows precise SN removal, because of high fluorescence spatial images. Fifty six nodes were removed, all nodes were radioactive and fluorescent. **Conclusion:** All procedures were carried out without complications or adverse effects. The hybrid tracer adds a visual component to the procedure that helps surgeons locate and remove SN. It´s use will allow surgeons to gain confidence and experience in intraoperative fluorescence imaging and will open the path to the use of novel hybrid tracers such as hybrid PSMA in prostate cancer surgery **References:** 1. Brouwer OR, Buckle T, Vermeeren L et al. Comparing the hybrid fluorescent-radioactive tracer indocyanine green-99mTc-nanocolloid with 99mTc-nanocolloid for sentinel node identification: a validation study using lymphoscintigraphy and SPECT/CT. J Nucl Med . 2012 Jul;53(7):1034-40.

EP-16

Wednesday, October 20 - Saturday, October 23, 2021

e-Poster Area, release on Wednesday, October 20 at 09:00

Imaging Clinical Studies -> Cardiovascular Imaging Clinical Study -> Perfusion

EP-078

Myocardial Perfusion SPECT Defects and Left Ventricular Ejection Fraction Accuracy

I. Lopo[1], R. Silva[1,2], M. Cunha[1], P. Lapa[1,3], G. Costa[1,3], J. Pedroso de Lima[1,3,2];

[1]Centro Hospitalar e Universitário de Coimbra, Coimbra, PORTUGAL, [2]Instituto de Ciências Nucleares Aplicadas à Saúde (ICNAS), Coimbra, PORTUGAL, [3]Faculdade de Medicina da Universidade de Coimbra, Coimbra, PORTUGAL.

Aim/Introduction: Left ventricular ejection fraction (LVEF) is a common and useful measure of left ventricular systolic function. Equilibrium radionuclide angiocardiography (ERNA) is widely considered the technique of choice for LVEF assessment, due to its accuracy, operator independency, nominal cost and low radiation burden. Myocardial perfusion SPECT (MPS) can also be used to determine LVEF, however this method hinges upon automatic ventricular wall detection and complex volume calculation algorithms that might be hindered by severe perfusion defects, contrary to ERNA. For that reason, we aim to explore the influence, if any, of perfusion defects on MPS LVEF accuracy. **Materials and Methods:** Patients submitted to ERNA and rest MPS from 2012 to 2020, within a maximum time interval of 6 months, were retrospectively selected. Patients who underwent cardiac procedures or suffered major adverse cardiovascular events between scans were excluded. ERNA and rest MPS LVEF measurements were determined using Ejection Fraction Analysis and Myovation protocols for Xeleris (GE Healthcare), respectively. ERNA LVEF was considered as the gold standard. Perfusion defects were visually quantified through Summed Rest Score (SRS) calculation, according to international guidelines. Patients were also arbitrarily divided, according to SRS, into two groups (Group 1: SRS <20; Group 2: SRS ≥20). Results: A total of 63 patients were included (mean age: 65.25 ±10.68 years; 82.5% men). Median (interquartile range) SRS was 13 (3-27). Thirty-nine patients had a SRS <20 and 24 a SRS ≥20. A statistical significant correlation between the LVEF measurement error (LVEF MPS - LVEF ERNA) and SRS was not found (Spearman coefficient 0.083, p=0.516). Also, no statistically significant differences were found between the LVEF obtained through ERNA and MPS when considering all patients (p=0.065), in Group 1 (p=0.212) or in Group 2 (p=0.120) (Wilcoxon signed-rank test). Additionally, LVEF measurement error was no statistically different between groups (p=0.766). **Conclusion:** These results imply that the extent of perfusion defects in rest MPS does not significantly influence LVEF accuracy. Thus, patients with significant perfusion defects should have accurate MPS LVEF measurements. **References:** none

EP-079

Higher negative predictive value on seven years follow up of normal gated myocardial perfusion imaging in diabetic patients with HBA1c ≤7.3

N. Fatima[1], M. Zaman[1], S. Zaman[2], A. Zaman[2];

[1]Aga Khan University, Karachi, PAKISTAN, [2]Dr Ruth Pfau (CHK), Karachi, PAKISTAN.

Aim/Introduction: This prospective study was carried out to find the negative predictive value (NPV) of normal gated myocardial perfusion imaging (GMPI) in diabetics with a predefined cut-off value of HBA1c ≤7.3. **Materials and Methods:** This study was conducted at Karachi Institute of Heart Disease (KIHD) after prior approval from ethical committee. Total 257 diabetics who had a normal GMPI from June 2011 till March 2012 were included. These patients were followed up on telephone for seven years for cardiac events like fatal myocardial infarction (FMI) and nonfatal myocardial infarction (NFMI). Followup was not available in 33 patients, leaving a cohort of 224 participants. Mean HBA1c was calculated for seven years. Patients were subdivided according to predefined cut-off value of HBA1c 7.3 as determined in previously published study by same group (57 in group A with HBA1c >7.3 and 167 in in group B with HBA1c ≤ 7.3). Results: No statistically significant difference was found in age, gender, body mass index, hypertension, dyslipidemia, family history, LV function, Bruce and vasodilator stress protocol in both groups except metabolic equivalent of task (METS) was significantly higher in group B (<0.05). Overall mean survival was significantly higher in group B with HBA1c ≤7.3 (Mean=80 vs. 71; CI=78-83 vs. 64-78 months in Group B and A respectively; logrank value=5.576; p <0.05). Significantly higher fatal and non-fatal cardiac events during seven years follow-up were recorded in group A with HBA1c >7.3 with lower METS <7 (3 vs. 0 FMI and 11 vs. 9 NFMI and annualized event rate 0.75% vs. 0% and 2.8% vs. 0.76% group A and Group B respectively; p<0.05). **Conclusion:** We conclude that NPV of a normal GMPI is higher in diabetic patients having a good glycemic control (mean HBA1c ≤ 7.3) and better functional capacity (≥7 METS). **References:** none

EP-080

Prevalence and Age-related Differences in the Occurence and Severity of Adverse Effects to Vasodilators Used in Myocardial Perfusion Imaging

J. Momodu, A. Ayeni, K. Purbhoo, M. Vangu;
University of Witwatersrand, Parktown, SOUTH AFRICA.

Aim/Introduction: In myocardial perfusion imaging (MPI); a widely used non-invasive imaging technique for evaluating coronary artery disease, maximal myocardial hyperemia is typically achieved with physical stress (1). However, in patients who are unable to tolerate exercise, pharmacological stress can be achieved using intravenous coronary vasodilators (2). This study assesses the prevalence of adverse effects and age-related differences in patient tolerance to coronary vasodilators (intravenous adenosine and dipyridamole) in a South African population cohort. **Materials and Methods:** Between August 2018 and November 2019, patients with known or suspected coronary artery disease referred for pharmacological stress MPI (n=264) were closely monitored for adverse effects during or immediately after termination of the intravenous vasodilator infusion. Adverse effects were graded using a four-point scale as follows: 0= no adverse effects; 1= less than 3 adverse effects (mild); 2= 3-6 adverse effects (moderate); 3= more than 6 adverse effects (severe) or adverse effects requiring reversal with intravenous aminophylline. One hundred and forty seven patients (55.7%) received adenosine while 117 patients (44.3%) received dipyridamole. Using the mean age of 60 years, the study population was divided into two groups; <60 years (Group A) and ≥60 years (Group B). Results: The most common adverse effect was headache, occuring in 16% of the study population. Other reported adverse effects include: chest pain, wheezing, dyspnea, dry mouth, nausea, abdominal discomfort and vomiting. Adverse effects occurred in 62.1% of the study population (69.3% in Group A and 56.7% in Group B), majority were mild to moderate. Only 3 patients (1%) developed severe adverse effects requiring reversal with intravenous aminophylline. Older patients (Group B) were 42% less likely to develop adverse effects compared to younger patients (Group A) {OR=0.58; 95% CI=0.35-0.97; p=0.036}. We found no statistically significant difference when the age groups were compared with different grades of adverse effects. **Conclusion:** Younger patients are more likely to develop adverse effects associated with intravenous adenosine and dipyridamole in pharmacological stress MPI. **References:** 1. Einstein AJ, Pascual TB, Mercuri M, Karthikeyan G, Vitola J V., Mahmarian JJ, et al. Current worldwide nuclear cardiology practices and radiation exposure: Results from the 65 country IAEA nuclear cardiology protocols cross-sectional study (INCAPS). Eur Heart J. 2015;36(26):1689-96. 2. Verberne HJ, Acampa W, Anagnostopoulos C, Ballinger J, Bondt P De, Buechel RR, et al. EANM procedural guidelines for radionuclide myocardial perfusion imaging with SPECT and SPECT / CT. European Association of Nuclear Medicine. 2015. p. 1-78.

EP-081

The role of stress-rest myocardial scintigraphy in patients who are candidate to organ transplantation

L. Vendramin[1], C. Sarais[2], P. Artioli[3], S. Padoan[3], D. Cecchin[3], L. Evangelista[3];
[1]University of Padua, Padua, ITALY, [2]Department of Cardio-Thoraco-Vascular Sciences and Public Health, University of Padua, Padua, ITALY, [3]Nuclear Medicine Unit, Department of Medicine DIMED, University of Padua, Padua, ITALY.

Aim/Introduction: In patients candidates for organ transplantation the value of myocardial perfusion imaging (MPI) is still uncertain, indeed, it is unknown if this test is better than the most common imaging techniques in predicting major adverse cardiovascular events and the overall mortality rate. The aim of the study is to provide evidence on the clinical value of MPI in pre-transplant evaluation, assessing the difference between the overall mortality rate and the cardiovascular mortality rate, in two cohorts of patients with normal or abnormal MPI. **Materials and Methods:** From 2014 to 2018, rest and stress MPI images of 43 patients candidates for organ transplantation (n=19 for liver, n=17 for kidneys, n=2 lung and n=5 others), were reassessed and interpreted by two nuclear medicine physicians. MPI was considered positive in case of a defect of perfusion compatible with ischemia and/or necrosis. In all patients, data about follow-up period was collected in order to evaluate the overall mortality rate and the cardiovascular mortality rate. Results: Out of 43 patients (median age: 59 years; 23-74), 30 (70%) had a positive MPI scan. Myocardial ischemia was found in 22 (73%) patients, 6 (20%) necrosis and 2 (2%) both (ischemia+necrosis). During a median follow up period of 58 months (2-83 mo.), 16 patients died. Out of them, 3 died for a major cardiovascular event. The death was registered in 12/30 (40%) patients with a positive MPI and in 4/13 (31%) with a negative MPI. At Kaplan-Meier analysis, no difference was found for the all-cause mortality between patients with a positive and a negative MPI (p=0.638). Conversely, the presence of dialysis or cirrhosis showed a trend of significance for overall mortality rate (p=0.298). **Conclusion:** MPI cannot stratify the risk of mortality due to the transplantation. Given the low number of deaths relative to cardiovascular causes, it was not possible to define if the MPI could be a predictor of them. **References:** De Lima, et al. Nephrol Dial Transplant. 2012;27(7):2979- 84.Doukky, et al. Journal of Nuclear Cardiology. 2018;25(6):2058-68.

EP-082

Higher cardiac events with impaired exercise tolerance (METS <7) and lower ejection fraction <45% in patients with medium to large size fixed perfusion defect(s) on gated myocardial perfusion scintigraphy with prior coronary revascularization

M. Zaman[1], N. Fatima[1], S. Zaman[2], A. Zaman[2];
[1]AKUH, Karachi, PAKISTAN, [2]Dr Ruth Pfau (CHK), Karachi, PAKISTAN.

Aim/Introduction: This prospective study was carried out to find the predictive value of fixed perfusion defect(s) for future cardiac events on follow-up gated myocardial perfusion imaging (GMPI) after coronary revascularization (graft surgery and coronary stenting). **Materials and Methods:** This study was conducted at Karachi Institute of Heart Disease (KIHD) after prior approval from ethical committee. Total 330 patients who were referred for GMPI for chest pain evaluation after coronary revascularization from June 2015 till December 2016 were selected. 186 out of 330 patients with fixed perfusion defects on GMPI were included as study population. These patients were followed for 06 years for cardiac events both fatal myocardial infarction (FMI) and nonfatal myocardial infarction (NFMI). Followup was not available in 11 patients, leaving a cohort of 175 participants. Patients were subdivided according to stress protocol (Bruce protocol in 84 and vasodilators in 91 patients). Results: Mean age of population was 58 years without statistically significant difference in age, body mass index, diabetes mellitus, hypertension, dyslipidemia, family history and smoking in exercise and vasodilator stress groups (except male dominance in exercise group). No significant Odd ratio (OR) was found for cardiac events in exercise and vasodilators groups with medium to large size fixed perfusion defects on GMPI. In exercise group, metabolic equivalent of task (METS) less than 7 (METS <7) had significant OR and Hazard ratio for future cardiac events in patients with medium to large size perfusion defects as an independent factor (OR=9; CI=1.07-75.5, HR=8.61; CI=2.49-29.75 p=<0.05; and OR=10.1) and as cofounding factor for ejection fraction less than 45% (CI=1.13-90.9; HR=5.66; CI=1.76-18.14; p=<0.05). **Conclusion:** Medium to large sized fixed perfusion defects with LVEF <45% are associated with higher cardiac events rate in patients after coronary revascularization. A lower exercise effort tolerance (<7 METS) is an independent and confounding factor for patients with LVEF <45%. Exercise GMPI has better predictive value for future cardiac events in patients with coronary revascularization. **References:** none

EP-083

Aspects of myocardial gated-SPECT in dextrocardia with situs inversus totalis

H. Haba[1], A. Chirilă[2], D. Piciu[1], L. Strîmbu[2];
[1]"Prof. Dr. Ion Chiricuta" Institute of Oncology, Cluj-Napoca, ROMANIA, [2]"Niculae Stăncioiu" Heart Institute, Cluj-Napoca, ROMANIA.

Aim/Introduction: Situs inversus totalis is a rare autosomal recessive congenital pathology, mostly diagnosed incidentally (approximately 1 case from 10.000) by an imagistic investigation performed for other reasons. Dextrocardia - as a part of situs inversus totalis - is an anatomical position anomaly of the heart situated in the right hemithorax with its base-to-apex axis pointed towards posterior and right. At these patients the incidence, physiopathology, clinical/imagistic workup and treatment of cardiovascular events are identical with the general population. **Materials and Methods:** In this report we present the case of a 60 year-old woman with dextrocardia associated with situs inversus totalis, essential arterial hypertension under oral treatment, and family medical history of cardiovascular pathology, who was suffering from atypical effort-related chest pain. She was admitted to our clinic for myocardial perfusion scintigraphy gated-SPECT using the Tc^{99m}-Tetrofosmin radiotracer in order to investigate her eligibility for coronarography. Results: We performed two different acquisitions and analyses, carried out by using a 180° noncircular orbit: clockwise from -45° (left anterior oblique - LAO) to 135° (right posterior oblique - RPO), and counterclockwise from RPO to LAO. The raw images were reconstructed using Cedars-Sinai software and the quantitative-semiquantitative analyses were shown by the QPS (Quantitative Perfusion SPECT) and QGS (Quantitative Gated SPECT) software. Particularity of this case: Due to swapping of the lateral and septal walls on SPECT-images, a visual analysis and a manual quantitation is possible - but operator-dependent; the automatic quantification is substantially limited by reporting to the database made of patients with normally positioned heart. **Conclusion:** Myocardial perfusion gated-SPECT imaging is a helpful diagnostic tool in patients with situs inversus totalis with dextrocardia, but it requires an increased attention and precaution both at the acquisition and the processing/interpreting side. **References:** none

EP-084

The evaluation of myocardial perfusion of dynamic SPECT CZT in patients with non-obstructive coronary artery disease: comparison with blood lipid levels

A. Maltseva, K. Kopeva, A. Mochula, S. Belyaeva, E. Grakova, K. Zavadovsky;
Cardiology Research Institute, Tomsk National Research Medical Center, Russian Academy of Sciences, Tomsk, RUSSIAN FEDERATION.

Aim/Introduction: At present 2/3 of patients with non-obstructive coronary artery disease suffer from microvascular dysfunction. The risk factors of cardiovascular diseases, such as dyslipidemia, can play important role in the pathogenesis of microvascular dysfunction. Previous positron emission tomography results partly confirmed that, but the available data regarding myocardial blood flow (MBF), myocardial flow reserve (MFR), and blood lipid levels are controversial. The purpose of the study is to assess the feasibility of dynamic SPECT CZT for the identification of lipid-induced microvascular dysfunction in patients with non-obstructive coronary artery disease. **Materials and Methods:** Based on coronary computed tomography angiography results, patients with non-obstructive coronary artery disease (stenosis <50%) were included in the study. All patients underwent dynamic SPECT on Cadmium-Zinc-Telluride (CZT) cardiac gamma-camera. Standard indexes of myocardial perfusion (SSS, SRS, SDS), stress left ventricular ejection fraction (sLVEF), and quantitative parameters (stress/rest MBF (s/r MBF), MFR) were assessed. The 1-tissue-compartment model without attenuation correction was used for quantitative analysis. Additionally, the blood lipid levels (total cholesterol (TC), low-density lipoprotein (LDL), triglycerides (TG)) were assessed. Based on MFR results two groups were created: 1. with reduced MFR ≤2.0 (n=14), 2. with a normal value of MFR >2.0 (n=18). Results: The study included 32 patients (24 men, age 50.9±9.4 years) with cardiac pain and/or exertional dyspnea. The maximum coronary artery stenosis was 25.0(0.0;35.0)%. Standard myocardial perfusion indexes and sLVEF did not differ significantly in two groups: SSS 3.0(0.0;4.0) vs 0.0(0.0;1.0), SRS 0.0(0.0;0.0) vs 0.0(0.0;0.0), SDS 3.0(0.0;3.0) vs 0.0(0.0;1.0), sLVEF 61.0(55.0;67.0) vs 64.0(61.0;67.0)%, respectively. Quantitative analysis demonstrated sMBF 0.64(0.32;0.88) vs 1.22(0.95;1.39) ml/min/g, rMBF 0.54(0.49;0.77) vs 0.38(0.35;0.46) ml/min/g, MFR 1.6(1.29;1.93) vs 2.94(2.64;4.25), respectively. Blood lipid levels did not differ significantly: TC 4.9(4.7;5.7) vs 4.7(4.3;5.3) mmol/l, LDL 3.1(1.8;3.6) vs 2.7(2.2;3.3) mmol/l, TG 1.1(0.9;2.1) vs 1.6(0.9;2.4) mmol/l, respectively. Nevertheless the first group had the trend to higher blood lipid levels. The Spearman correlation in patients with reduced MFR showed that MFR had strong negative relationships (p<0.05) with TC (ρ=-0.937), LDL (ρ=-0.793), TG (ρ=-0.757) and sLVEF with TC (ρ=-0.786), meanwhile sMBF и rMBF did not correlate with blood lipid levels. **Conclusion:** In patients with non-obstructive coronary artery disease dynamic SPECT CZT showed feasibility for the assessment of lipid-induced reduction of myocardial flow reserve in contrast to visual (semi-quantitative) analysis. Dynamic SPECT CZT might be used for the assessment of lipid-induced microvascular dysfunction. This study was supported by the Russian Federation President Grant MK-1347.2020.7. **References:** none

EP-085

Incidence of Pathological Morphological Findings on Myocardial Perfusion SPECT/CT

S. Kesim*, H. T. Turoglu, S. Ozguven, S. Inanir, N. Filizoglu, C. O. Sahin, K. Niftaliyeva, T. N. Kissa, Z. C. Balaban Genc, K. Oksuzoglu, F. Sen, T. Ones, T. Y. Erdil;*

Marmara University School of Medicine, Istanbul, TURKEY.

Aim/Introduction: Non-contrast computed tomography (CT) for attenuation correction in myocardial perfusion imaging (MPI) has become widely used due to the development of hybrid SPECT/CT systems. Herein, we aimed to investigate the incidence of abnormal morphological findings detected on CT images acquired for attenuation correction. **Materials and Methods:** Between October 2020 and February 2021, a total of 109 patients with suspected coronary artery disease (50 women and 59 men) who underwent rest/stress Tc-99m sestamibi (MIBI) myocardial perfusion imaging with an integrated SPECT/CT device were included in this study. Results: The average age of the patients was 51.6 years (range of 30-81 years; standard deviation of 9.87 years). Myocardial ischemia was observed in 25.7% of the patients, while fixed perfusion defect suggestive of scarring accounted for 1.8% of all patients. Detection of cardiomegaly, dilatation of the ascending aorta, dilatation of main pulmonary artery, pericardial effusion, coronary artery calcification and pulmonary nodule on attenuation correction CT was 45.9%, 12.8%, 7.3%, 5.5%, 19.3% and 4.6%, respectively. **Conclusion:** Myocardial perfusion imaging (MPI) with SPECT/CT is a useful modality to assess suspected or known CAD. Because of the technological advancement accompanied by the increased availability of hybrid SPECT/CT scan, many facilities perform myocardial perfusion SPECT with CT attenuation correction to improve diagnostic accuracy and reliability. This additional imaging data permits the detection of several benign and malignant findings, not apparent on the merely myocardial perfusion SPECT images. These incidental findings may have an impact on patient management. The detection and reporting of such abnormalities necessitates a meticulous evaluation of the raw SPECT images and the CT images acquired for attenuation correction. Therefore, the interpretation of MPI should not be restricted to only perfusion of the heart muscle. **References:** Zadro C, Roussel N, Cassol E, et al. Prognostic impact of myocardial perfusion single photon emission computed tomography in patients with major extracardiac findings by computed tomography for attenuation correction. J Nucl Cardiol. 2018;25(5):1574-1583.

EP-17

Wednesday, October 20 - Saturday, October 23, 2021
e-Poster Area, release on Wednesday, October 20 at 09:00

Imaging Clinical Studies -> Cardiovascular Imaging Clinical Study -> Heart Failure (including Sarcoidosis and Amyloidosis)

EP-086

Utility of ^{99m}Tc-Diphosphonates scintigraphy in the diagnosis of cardiac amyloidosis by transthyretine: experience in our hospital

M. Negre[1], N. Ferran[1], A. Mestre[1], C. Tapias[1], V. Pineda[2], A. Armengou[3], P. Vilardell[4], E. Torrent[1], A. Rubió[1];
[1]IDI-Nuclear Medicine Department. Hospital Universitari de Girona Dr. Josep Trueta, Girona, SPAIN, [2]IDI-Radiology Department. Hospital Universitari de Girona Dr. Josep Trueta, Girona, SPAIN, [3]General Internal Medicine Department. Hospital Universitari de Girona Dr. Josep Trueta, Girona, SPAIN, [4]Cardiology Department. Hospital Universitari de Girona Dr. Josep Trueta, Girona, SPAIN.

Aim/Introduction: Cardiac amyloidosis is an infiltrative disease caused by protein deposition. The most common forms are primary amyloidosis, caused by immunoglobulin light chain deposition (AL), or transthyretin amyloidosis (ATTR), in its hereditary variant (ATTRv) or natural (ATTRwt). The aim of the study was to evaluate the utility of cardiac scintigraphy with 99mTc-diphosphonates in the differential diagnosis between the different sub-types of cardiac amyloidosis, especially the ATTR variant. **Materials and Methods:** We performed a retrospective analysis of 74 patients (58 men, mean age: 77.6±12.8 years) with suspected cardiac amyloidosis. Whole-body scintigraphy was completed after administration of 925MBq of 99mTc-DPD (44 patients) or 99mTc-HMDP (30 patients). If there was myocardial diphosphonate uptake in the planar image, a cardiac SPECT study was made. Patients with a myocardial uptake equal to or greater than bone uptake were considered positive for ATTR (Perugini score 2-3). Results were correlated with other available techniques: imaging studies, immunoelectrophoresis (IEF), genetic study and clinical assessment. Results: Thirty-six patients had suggestive uptake of ATTR (32 men; mean age 82±7.2 years). Score 2: six patients; Score 3: thirty patients. Twenty-four patients had biventricular involvement and eight had extracardiac uptake. All 36 patients had an echocardiogram (18 with a compatible result, 18 suggestive, 2 negatives). Seventeen had an MRI (15 with compatible result; two negatives). In 15, a genetic study was performed: positive in four; negative in 11. In 28 patients, immunoelectrophoresis was performed: negative result in 26; doubtful in two. Taking into account the scintigraphic results, imaging studies, IEF, genetic study and clinical assessment, 29 patients were diagnosed with ATTR: ATTRv in 4 patients (positive mutation; IEF not available in 3, negative in one; 2 with negative echocardiogram); ATTRwt in 11 patients (negative mutation; negative IEF, one patient with negative MRI) and 14 patients without being able to define sub-type of ATTR (negative IEF; one patient with negative MRI). Diagnosis of ATTR was probable in 2 patients (doubtful result of IEF in one, not available in another, both patients with extracardiac uptake and carpal tunnel syndrome). Diagnosis of AL in 1 patient (doubtful IEF, positive cardiac biopsy). It was not possible to differentiate between different forms of amyloidosis in 4 patients due to the lack of IEF, lack of suggestive clinic or extracardiac uptake. **Conclusion:** Diphosphonate cardiac scintigraphy is useful for detecting the ATTR variant in patients with suspected cardiac amyloidosis, conditioning a real impact on its clinical management. **References:** None

EP-087

Myocardial uptake in patients with malignant prostate neoplasia: Is there a relationship with transthyretin cardiac amyloidosis?

A. Roteta Unceta Barrenechea[1,2], A. Andrés Gracia[1,2], L. Tardin Cardoso[1], Y. Saker Diffalah[1], T. Escalera Temprado[1], M. Delgado Castro[1], P. Razola Alba[1], J. Melero Polo[3,2], P. Revilla Marti[3,2], M. Aibar Arregui[3,2], A. Gracia Gutierrez[4,2], E. Bueno Juana[3,2], I. Moreno Gázquez[3], R. Pérez Palacios[2], S. Atienza Ayala[3,2], C. Lahuerta Pueyo[3,2], S. Menao Guillén[3,2], E. Prats Rivera[1], M. Abós Olivares[5];
[1]UCMHMNA - Clinic Hospital "Lozano Blesa", Zaragoza, SPAIN, [2]IIS-Aragón, Zaragoza, SPAIN, [3]Clinic Hospital "Lozano Blesa", Zaragoza, SPAIN, [4]Hospital General de la Defensa de Zaragoza, Zaragoza, SPAIN, [5]UCMHMNA, Zaragoza, SPAIN.

Aim/Introduction: To analyse incidental myocardial uptake in diphosphonate scintigraphy in patients with prostatic neoplasia and to check whether these patients present risk factors (RF) related to cardiac transthyretin amyloidosis (c-ATTR) or not. **Materials and Methods:** We analysed 99m Tc-diphosphonate scintigraphy in patients with prostatic neoplasia (01/01/2017-31/03/2021). Patients with previous scintigraphy under the suspicion of c-ATTR were excluded. In those patients with incidental myocardial uptake, gammagraphic characteristics (Perugini score), cardiological clinical features, prostate biopsies, echocardiographic parameters and laboratory values were assessed. Subsequently, they were classified into two groups: patients without RF for c-ATTR and patients with RF for c-ATTR. Results: A total of 1050 scintigraphies were evaluated. Of these, 21 (2%) showed myocardial deposition of the radiotracer. Two studies were excluded because of a previous diagnosis of ATTR-c.On the one hand, 6 patients (29%) had no risk factors for ATTR-c: mean age 86.7, Perugini score (grade 1 = 2, grade 2 = 2 and grade 3 = 2), Gleason (5 - 9), PSA (at diagnosis 114.2 ng/ml and in the scan 15.4 ng/ml) and NT-proBNP (<2000 ng/l).On the other hand, 13 patients (71%) had risk factors for ATTR-c (6 carpal tunnel syndrome, 6 heart failure with

preserved LVEF, 4 AVB and 2 Dupuytren's disease): mean age 80.7 years (7/12 Perugini score 1 and 6/12 score 2-3), Gleason (5 - 9), PSA (at diagnosis 46.4 ng/ml and on scan 25.2 ng/ml) and NT-proBNP (2 patients with >2000 ng/l).In none of these patients a cardiological evaluation, such as echocardiography, or a determination of free light chains in serum or urine was performed in order to confirm c-ATTR. **Conclusion:** In the presence of myocardial uptake in patients with prostatic neoplasia, although it has been attributed to prostate cancer, cardiological evaluation for c-ATTR is recommended. **References:** None.

EP-088

Cardiac Uptake of 99m-Tc DPD as a Predictive Factor of Left Ventricular Wall Thickness in Patients with Transthyretin Cardiac Amyloidosis

N. Martínez-Amador*, O. Cuenca-Vera, J. Andres-Pacheco, A. Gutierrez-Gonzalez, M. Pombo-Lopez, A. Bota-Bota, F. Gomez-De La Fuente, J. Jimenez-Bonilla, I. Martinez-Rodriguez, A. Sanchez-Salmon, M. De Arcocha-Torres, S. Ruiz-Llama, R. Quirce;*
Nuclear Medicine Service. Marqués de Valdecilla University Hospital. Molecular Imaging Group (IDIVAL). University of Cantabria, Santander, SPAIN.

Aim/Introduction: To assess the cardiac left ventricular wall distribution of Technetium-99m-3,3-diphosphono-1,2-2 propanodicarboxylic acid (99m-Tc DPD) in patients with transthyretin cardiac amyloidosis (ATTR) as an early predictor of left ventricular wall involvement, anticipating to the echocardiographic changes. **Materials and Methods:** This is a retrospective study in 46 consecutive patients with clinical and echocardiographic suspicious of ATTR, 7/46 women (15%). A whole body scintigraphy with 99m-Tc DPD and thorax SPECT were performed. All included patients showed cardiac uptake of 99m-Tc DPD and were classified followed the Perugini score (S0-S3), S2 (moderate intensity uptake) in 4/46 (8.7%), and S3 (high intensity uptake) in 42/46 (91.3%). The semi-quantitative analysis was determined in each of the left ventricular walls using polar maps, made from the cross-sections of the thorax SPECT. The findings were correlate with echocardiographic data of left ventricular ejection fraction (LVEF) and thickness of the interventricular septum (IVS). Results: The highest 99m-Tc DPD uptake in both groups was found in the IVS than in the others ventricular walls (S2: 59.0±9.2%; S3: 72.2±4.9%) p=0.059. Statistically significant differences were found between IVS uptake for each group and the remaining ventricular walls, anterior wall (S2: 39.5±7.5; S3: 53.3±10.2), lateral wall (S2: 43.5±17.3; S3: 53.9±10.2), inferior wall (S2: 39.7±15.8; S3: 56.0±9.1) and apex (S2: 38.0±21.6, S3: 55.5±14.9) (p <0.0001). The echocardiographic analysis showed a mean value of LVEF for group S2 of 51.2±15.3 and for S3 of 46.9±13.2 (p=0.417) and an IVS thickness value of 18.5±5.9mm and 18.8±3.2mm for S2 and S3 group respectively (p=0.462). **Conclusion:** Non-invasive diagnosis of ATTR it had a progress with the introduction of scintigraphy in the diagnostic algorithm. Our results showed that the cardiac uptake of 99m-Tc DPD is not symmetrical in the left ventricle walls, being statistical significantly higher in the IVS in patients with Perugini criteria (S2 and S3) of ATTR. On the other hand, the echocardiography findings do not found differences in LVEF and thickness of the IVS between both groups, showed septal hypertrophy and disturbance of LVEF in both groups. These findings suggest than the cardiac uptake of 99m DPD-Tc can be a predictor of amyloid fibber deposition in the myocardium and can be an early predictor of heart dysfunction. **References:** None

EP-089

Diagnostic performance of ^{99m}Tc-DPD scintigraphy for ATTR cardiac amyloidosis: single center experience and integration in the diagnostic workflow

B. Martins*, C. V. Pinto, V. Sousa, L. Raposo, C. Loewenthal;*
Hospital da Luz, Lisbon, PORTUGAL.

Aim/Introduction: Amyloidosis comprises a group of diseases caused by extracellular deposition of insoluble polymeric proteins, causing loss of function. Heart is the second most affected organ. Prognosis is dire, heart-failure being the main cause of death. Since clinical course, treatment and prognosis vary, characterization of disease sub-type, systemic extension and treatment response is essential. Scintigraphy with ^{99m}Tc-DPD has recently gained importance, namely for the identification of amyloidosis subtype. **Materials and Methods:** A retrospective assessment of patients who underwent ^{99m}Tc-DPD scintigraphy for suspected ATTR cardiac amyloidosis between 2015 and 2021 was undertaken [N = 25, mean age 79 (38-90), 15 male-gender and 10 female]. Images were acquired using standard protocols; relative cardiac uptake was retrospectively reviewed and blindly classified according to the Perugini Scale by three different physicians. Concordance between the final interpretation and NT-proBNP, echocardiogram and cardiac magnetic resonance, performed as part of the diagnostic workup, was assessed. Results: Of the 25 patients, 14 were positive for cardiac amyloidosis (56%): 12 were classified as grade 3 on the Perugini scale and 2 as grade 2. Stratification was 100% concordant between interpreting physicians. Eleven patients also showed ^{99m}Tc-DPD uptake suggestive of systemic amyloid involvement in one or more extra-cardiac sites: abdominal muscles (n=10), shoulder girdle (n=5) and lungs (n=2). Four patients with baseline NT-proBNP measurements below the exclusion cutoff underwent scintigraphy (1 with suspicious echocardiogram and MRI, 1 with LVH on echocardiogram, 1 with inconclusive MRI and another due to clinical criteria); all were negative for cardiac amyloidosis by scintigraphic criteria, and all are still alive in 2021 (including a patient studied in 2017, positive on MRI). Seventeen patients underwent echocardiography prior

to scintigraphy; 14 had suspicious criteria: 9 of these were positive on scintigraphy and 5 negative (64.3% agreement). Nine patients underwent MRI prior to scintigraphy, all suggestive of cardiac amyloidosis: 7 of wich also were positive on scintigraphy (77.8% agreement). As it is a relatively recent sample, of the 14 positive patients, 12 are still alive and under surveillance. **Conclusion:** In this single centre cohort, stratification of relative cardiac uptake showed excellent concordance between interpreting physicians. We found a significant discrepancy between echocardiogram, cardiac MRI and ^{99m}Tc-DPD scintigraphy concerning the diagnosis of cardiac amyloidosis. **References:** none

EP-090

Diagnosis of Transthyretin Cardiac Amyloidosis by ^{99m}Tc-diphosphonate Scintigraphy

M. Pudis[1], *L. M. Gràcia-Sánchez*[1], *A. Palomar-Muñoz*[1], *P. C. Notta*[1], *M. Buaki-Sogo*[2], *G. Reynés-Llompar*[3], *C. Díez-López*[4], *S. Bondía-Bescos*[1], *M. Cortés-Romera*[1];
[1]*Nuclear Medicine-PET (IDI) department, Bellvitge University Hospital-IDIBELL, L'Hospitalet de Llobregat, Barcelona, SPAIN,* [2]*Radiopharmacy department, Bellvitge University Hospital-IDIBELL, L'Hospitalet de Llobregat, Barcelona, SPAIN,* [3]*Medical Physics department, Bellvitge University Hospital-IDIBELL, L'Hospitalet de Llobregat, Barcelona, SPAIN,* [4]*Cardiology department, Bellvitge University Hospital-IDIBELL, L'Hospitalet de Llobregat, Barcelona, SPAIN.*

Aim/Introduction: Scintigraphy is a noninvasive method that facilitates early diagnosis of transthyretin cardiac amyloidosis (ATTR-CA), an infiltrative cardiomyopathy caused by extracellular deposition of transthyretin-derived insoluble amyloid fibrils.The aim of this study is to analyze the prevalence of ATTR-CA in patients, either with a clinical suspicion and/or predisposing genetic mutation. **Materials and Methods:** We retrospectively analyzed the patients with suspicion of ATTR-CA and performed [^{99m}Tc] Tc-DPD scintigraphy, between 2016 and 2018.The patients were classified into three groups: Group A: clinical suspetion of senile ATTR (ATTRwt). Group B: carriers of ATTR-associated genetic mutation (ATTRm). Group C: recipients of Domino Liver Transplant (DLT) from donors diagnosed with familial amyloidotic polyneuropathy (FAP). We reviewed the age, sex, presence of hypertension and cardiac symptoms, scintigraphy finding of cardiac (CA) and/or extracardiac (ECA) amyloid deposits, visual/qualitative Perugini score (PS) and mean cardiac semiquantification (CS) comparing mean counts in the heart ROI-to-contralateral chest ROI. Results: Group A (92p): 60 male and 32 female, 84% diagnosed with arterial hypertension and heart failure. We detect CA in 20 out of 92p (22%) and 6 out of these 20p (30%) also present ECA. Out of all the CA patients, 11 present PS 3 (CS 3,4); 7 with PS 2 (CS 2,8) and 2 with PS 1 (CS 1,9). Group B (28p): 14 male and 14 female, 36% of them diagnosed with hypertension. We detected CA in 4 out of 28p (14%) and one of them presented ECA (25%). Out of all the CA patients, 3 presented PS 3 (CS 2,6); 1 with PS 2 (CS 2,2). Group C (17p): 10 male and 7 female, all of them diagnosed with hypertension. Median of 10,5 years after DLT (from 2 to 26 years). We detect CA in 1 out of 17 patients (6%) and none of them present ECA. This patient presents PS 2 and CS 1,6. **Conclusion:** All of the patients with CA presented CS greater than 1,5. The highest prevalence of CA is observed in patients with clinical suspetion of senile ATTR (ATTRwt). Most of the patients in this group were diagnosed with hypertension and heart failure. The PS, CS and ECA are also higher in this group of patients compared with the rest of the groups. We detected CA only in one recipient of DLT with a mean of 10,5 years after surgery. **References:** none

EP-091

99mTc-HDMP scintigraphy detects transthyretin-related cardiac amyloidosis; a substitute for biopsy?

A. Cimino, *E. Rizza, L. Luongo, A. Mita;*
Nuclear Medicine Unit, Lecce, ITALY.

Aim/Introduction: Systemic amyloidosis is heterogeneous disease characterized by extracellular deposition of protein-derived fibrils, namely amyloid, in different tissue and organs, like heart. Two types of amyloid commoly infiltrate the heart: immunoglobulin light-chain (AL) amyloid and transthyretin (TTR) amyloid. Imaging with cardiac US/MRI provides nonspecific findings. Gold standard for etiological diagnosis of cardiac amyloidosis (CA) is endomyocardial biopsy combined with immunohistochemical parameters/mass spectroscopy, both high-cost and invasive procedures. Technetium-99m hydroxymethylene diphosphonate (99mTc-HMDP) scintigraphy is a impoortant tool for defining CA, specifically transthyretin subtype (ATTR), Our work underlines the role of nuclear medicine in CA diagnosis and patients management. **Materials and Methods:** From July 2020 to February 2021 we retrospectively analysed eighteen patients [14 males, 4 females; aged 32-86y] with suspected ATTR, underwent myocardial scintigraphy 150 minutes after iv administration of 740 MBq 99mTc-HMDP. Myocardial radiotracer uptake was assessed optically based on Perugini Score: (0: absent cardiac uptake and normal bone uptake; 1: mild cardiac uptake, inferior to bon uptake; 2 : moderate cardiac uptake with attenuated bone; 3: high cardiac uptake with decreased or absent bone uptake) Diagnosis was confirmed by biopsy and/or laboratory investigation Results: Diffuse intense myocardial uptake (score 3) verified in 5 patients by 99mTc-HDMP scintigraphy, was consistent with ATTR suspect. In 3 patients whole-body scintigraphy showed a moderate cardiac upatke (Score 2), biopsy was necessary to confirm. In ten patients cardiac radiotracer uptake was absent (Score 0), so invasive procedure was avoid, like biopsy. Detection of ATTR in our study population by 99mTc-HDMP scintigraphy was accomplished with 100% sensitivity and specificity.

Conclusion: Our data indicate that 99mTc-HDMP scintigraphy has a key role in the early diagnosis but even more in the exclusion of patients with the ATTR subtype. 99mTc-HDMP scintigraphy confirms to be a simple, non-invasive, low-cost and widely available modality. It does not require preparation and has no side effect so it can be performed in all types of patients including hemodynamically complicated patients. This examination, optimizing the management of pts who do not require admission to procedures with high costs and more invasive, is useful for earlier diagnosis and screening of CA. **References:** None

EP-092

Incidental findings of extra osseous Tc99m DPD uptake, in unselected patients undergoing bone scintigraphy

A. Doumas[1], F. Spyroglou[1], E. Papanastasiou[1], G. Gerasimou[1], E. Giannoula[1], D. Boundas[2], I. Iakovou[1];
[1]Aristotle University, AHEPA hsp, Thessaloniki, GREECE,
[2]Ippokratis, Nucl Med Centre, Thessaloniki, GREECE.

Aim/Introduction: Due to our department involvement in a multicentric study on cardiac amyloidosis, bone scintigraphy is performed in all our patients using exclusively ^{99m}Tc-3,3-diphosphono-1,2-propanodicarboxylic acid (^{99m}Tc-DPD). Main target of the study is to describe experience acquired using ^{99m}Tc-DPD in our daily scintigraphic bone imaging, in patients investigated for bone metastatic disease existence or for various orthopedic reasons. **Materials and Methods:** Whole bone scan was performed in 332 consecutive patients, 181 men and 151 women, aged 72+/-16 years, from August to December 2020. Of these patients, 23 (7%) were investigated for suspected cardiac amyloidosis, while the rest, 178 (53%) for the exclusion of metastatic bone disease and 131 (40%) for orthopedic reasons. Results: Of the 23 patients investigated for cardiac amyloidosis 7 (30%) actually had increased uptake at the myocardial area, (5 patients assessed as Grade 2 or 3 and 2 as Grade 1).Additionally, in other 4 (1.2%) patients, cardiac uptake also appeared as a incidental finding. These patients were all men and over 78 years.Another interesting finding is the uptake of ^{99m}Tc-DPD at the liver or spleen in 14 (4%) patients, uptake at the soft tissue of the thighs in 9 patients and finally at the periarticular areas of the shoulders, carpal joints in a large percentage of patients. This finding was attributed to degenerative osteoarthritis, but amyloid deposition at the above mentioned areas cannot be excluded. **Conclusion:** ^{99m}Tc-DPD is considered to be a suitable radiopharmaceutical for the everyday bone scintigraphy use. Additionally, it may provide useful information in detecting unsuspected cardiac amyloidosis, possible localization of amyloid at the soft tissue and joints, whilst it is not inferior in bone uptake quality, as in the case of PYP. Therefore, it is highly recommended for the entire bone scintigraphic workup in nuclear medicine laboratories, and not only for the confirmation or exclusion of cardiac amyloidosis. **References:** none

EP-093

Absolute in vivo SPECT-CT quantification of myocardial amyloid ATTR deposit in patients with a positive ^{99m}Tc-DPD scan

***F. Sebastián Palacid**, N. Álvarez Mena, B. Pérez López, C. Gamazo Laherrán, P. Turbay Eljach, M. Alonso Rodríguez, A. Sáinz Esteban, C. F. García García, M. J. González Soto, M. Á. Ruiz Gómez, R. Ruano Pérez;*
Hospital Clínico Universitario Valladolid, Valladolid, SPAIN.

Aim/Introduction: To quantify in SPECT-CT studies the ATTR-myocardium deposit of visual Perugini grade 2 and 3 patients submitted for a ^{99m}Tc-DPD scan. **Materials and Methods:** We included all consecutive patients with visual Perugini's grade 2 and 3 positive ^{99m}Tc-DPD scan in the last six months. Planar whole-body and chest images were acquired 3 hours after the intravenous injection of 740 MBq of ^{99m}Tc-DPD. SPECT-CT images (120 projections 360º and 12 seconds / projection) were processed with Qmetrix for SPECT GE Healthcare. SPECT system sensitivity was 180 cnts/sec/MBq. SUVmax and percentage of the injected dose in the cardiac ventricles were registered. Results: 19 patients have been evaluated (17 males and 2 females; mean weight 73.5 ± 7.29 kg). Of these, 13 were classified according to grade 3 of the Perugini's visual scale and 14 had biventricular uptake of the radiopharmaceutical. Mean SUVmax for the left ventricle was 9.92 ± 2.96 (2.26 ± 1.08% total injected dose), while for the right ventricle a mean SUVmax of 6.04 ± 1.99 (0.68 ± 0.33% total injected dose) was calculated.We found significant differences when comparing grade 2 and grade 3 patients in terms of SUVmax and percentage of injected dose in both ventricles: Patients with ATTR grade 3 amyloidosis have a mean SUVmax, which is 2.2 times higher than patients with grade 2, both in left and right ventricles.In turn, the total injected dose in both left and right ventricles was 4 times higher in patients with grade 3 than in the other group. **Conclusion:** In vivo quantification of myocardial ^{99m}Tc-DPD uptake is a promising tool complementary to Perugini's visual scale. It is possible to establish cut-off values between grade 2 and 3, and also might permit a quantitative parameter in the follow up of ATTR cardiac amyloidosis patients. **References:** None

EP-18

Wednesday, October 20 - Saturday, October 23, 2021

e-Poster Area, release on Wednesday, October 20 at 09:00

Imaging Clinical Studies -> Cardiovascular Imaging Clinical Study -> Other Cardiovascular Imaging (including Plaque)

EP-094

Differentiation ST-elevation from non-ST-elevation myocardial infarction on cardiac end-systolic Fluoro-18-fluorodeoxyglucose PET images using insulin intravenous preparation

Y. Chen;
Quanzhou 1st hospital, Quanzhou, CHINA.

Aim/Introduction: We aim to differentiate ST-elevation myocardial infarction (STEMI) from non-ST-elevation myocardial infarction (NSTEMI) based on cardiac electrocardiogram (ECG)-gated Fluoro-18-fluorodeoxyglucose (^{18}F-FDG) PET images. **Materials and Methods:** Consecutive patients with acute myocardial infarction (AMI) early after coronary angiography with significant non-infarct related artery lesion scheduled for cardiac ECG-gated ^{18}F-FDG PET/CT through insulin intravenous procedure between 15, June 2018 and 20, July 2020 were included in this retrospective study. Segmental ^{18}F-FDG uptake at end-systolic phase (ES) were automatically calculated and normalized to the highest uptake using the Quantitative Gated SPECT 2012 version (Cedars-Sinai Medical Center, USA). The probability of STEMI was rated on those polar maps using a 5-point scale. Receiver operating characteristics (ROC) analysis and the optimal sensitivity and specificity were calculated. ***Results:*** Thirty-eight patients (STEMI 17, NSTEMI 21) were included. The area under curve (AUC) of ROC was equal to 0.89±0.06 (95%CI 0.77, 1.00). At the optimal threshold, i.e. any segment with ^{18}F-FDG uptake reducing >50% and its gradient descend ≥50%, the sensitivity, specificity was 0.94±0.06 (95%CI 0.83, 1.00), 0.76±0.09 (95%CI 0.58, 0.94) respectively. **Conclusion:** End-systolic ^{18}F-FDG PET images obtained with insulin intravenous preparation had been potential to differentiate STEMI from NSTEMI early after AMI. **References:** 1. Roffi M, et al. Eur Heart J. 2016; 37:267-315.2.Ibanez B, et al. Eur Heart J 2018; 39:119-177.3. Kendziora B, et al. BMJ Open. 2020;10:e034359.4. Eitel I,et al. J Am Coll Cardiol. 2014; 64:1217-26.5. Nordlund D, et al. BMC Cardiovasc Disord. 2019; 19:161.6. Feistritzer HJ, et al. Eur Heart J Cardiovasc Imaging. 2020; 12:67-76.7. Symons R, et al. JACC Cardiovasc Imaging. 2017;11:813-825.8. Pontone G, et al. Circ Cardiovasc Imaging. 2017;10:e006428.9. Bøtker HE, et al. Cardiovasc Res 2012; 94:266-75.10. Nensa F, et al. Radiology 2015 ;276:400-7.11. Mehta SR, et al. N Engl J Med. 2019; 381:1411-1421.12. Rischpler C, et al. Eur Heart J Cardiovasc Imaging 2015; 16:661-9.13. Anavekar NS, et al. J Am Coll Cardiol. 2016; 67:2874-87. 14. Chen YC, et al. J Nucl Cardiol. 2020.15. Akbar H, et al. In: StatPearls. Treasure Island (FL): Stat Pearls Publishing; August 8, 2020.

EP-19

Wednesday, October 20 - Saturday, October 23, 2021

e-Poster Area, release on Wednesday, October 20 at 09:00

Imaging Clinical Studies -> Endocrinological Imaging Clinical Study -> Endocrinology (including Thyroid Benign)

EP-095

Evaluation of single only sestamibi positive foci in patients with secondary hyperparathyroidism

A. Aktas*, A. Gencoglu, G. Moray, M. Haberal;*
Baskent University, Ankara, TURKEY.

Aim/Introduction: Parathyroid scintigraphy is an established diagnostic imaging modality for the preoperative evaluation of patients with hyperparathyroidism. A single hot foci respresenting an adenoma is common in patients with primary hyperparathyroidism. In secondary hyperparathyroidsm, hyperplasia in parathyroid glands is generally reflected as activity in several parathyroid glands on parathyroid scintigraphy. In this study, we evaluated histopathologic evidence of final diagnosis in patients with secondary hyperparathyroidism who had a single hot foci on parathyroid scintigraphy. **Materials and Methods:** This study was approved by Baskent University Institutional Review Board (Project No: KA21/236). This study included 24 patients with secondary hyperparathyroidism who had a single hot foci on parathyroid scintigraphy. All patients had surgery within 1 month of imaging. Parathyroid scintigraphy was performed using 15-20 mCi Tc-99m sestamibi. Planar neck and mediastinal images were acquired at 15 minute (early-phase), and 2 hour (delayed-phase) after injection. All patients had ultrasonography. Results: Histopathologic evaluation revealed: hyperplasia (n= 8; 3 with diffuse and 5 with nodular hyperplasia), typical adenoma (n=5), atypical adenoma (n=2), amyloid infiltration (n=1). In the remaining 8 patients, 6 had a hot foci which was due to 2 or 3 glands coming close to each other and creating a single hot foci. In these 6 patients, hot foci had an inferior location adjacent to the lower pole of the thyroid. Final diagnosis in the remaining 2 patients was a thyroid pathology: one on the upper pole and the other one located more centrally. **Conclusion:** The results suggest that a single hot foci on parathyroid scintigraphy in secondary hyperparathyroidism commonly represent hyperplasia in the form of a single gland or multiple glands coming close to each other adjacent to the lower pole of thyroid. Location, size, uptake intensity and distance of the foci from the thyroid

gland and correlation with ultrasonography findings may be helpful for a correct interpretation of sestamibi scan findings. **References:** None

EP-096

Thyrotropin value reached 20 days after levothyroxine withdrawal in Follow-up of Differentiated Thyroid Cancer

M. Torres Negreira[1], G. Sierra[1], P. Orellano[1], G. dos Santos[2], J. Hermida[2], B. Mendoza[1], O. Alonso[2];
[1]Endocrinology and Metabolism Centre, Hospital de Clínicas, Montevideo, URUGUAY, [2]Molecular Imaging Centre, Hospital de Clínicas, Montevideo, URUGUAY.

Aim/Introduction: Acute hypothyroidism induced by withdrawall of thyroid hormone in patients with differentiated thyroid cancer (DTC) during disease follow-up affects multiple organs, systems, and quality of life. It can produce adverse cardiovascular effects, especially in those patients with underlying disease and particularly in older adults. Alters the lipid profile and exacerbates neuropsychiatric disease. In Uruguay, raising Thyroid Stimulating Hormone (TSH) to ≥30 uIU/ml for the performance of whole body radioiodine scintigraphy (RIS) and/or serum thyroglobulin (Tg) dosage, in the absence of recombinant human TSH (rhTSH) is achieved by suspension of Levothyroxine (LT4) for 4 to 6 weeks with the possible repercussions mentioned. **Materials and Methods:** We carried out a prospective, observational and analytical study in patients from the public system who required evaluation of DTC follow-up. TSH was dosed on day 20 after the suspension of LT4 and on day 30 prior to performing RIS. Age, sex and body mass index (BMI) were analyzed as possible factors that could influence the TSH value. Quality of life was assessed on day 20 and day 30 with the SF-12 Health Questionnaire. Results: We included 20 patients with treated DTC with 2 to 20 years of evolution, 18 female and 2 male. The median age was 46.1 years (Range: 40.41-51.79). The median BMI was 27.5 (Range: 25.75-30). The mean dose of LT4 they received was 150 ug/day (Range: 125-150). The TSH prior to the suspension of LT4 had a mean value of 0.9uIU/ml, standard deviation ± 0.67. On the 20th day, 19 patients increased TSH to ≥30 uIU/ml, with a mean of 62.6 uIU / ml (Range: 48.54-76.66). On day 30, all patients had a TSH >100 uIU/ml. There was no association between TSH elevation and sex (P=0.595), age (P= 0.207), BMI (P=0.459) or the initial TSH value. The symptoms of hypothyroidism registered on day 30 were significantly more severe in relation to day 20, with a decrease in the score of the SF-12 questionnaire, score, mean of 85.1 (SD: 14.1; R: 60-100) at 20 days vs one mean of 48.7 (SD: 19-5; R: 20-79) at 30 days. **Conclusion:** According to our results, suspending LT4 20 days prior to DTC evaluation is enough to raise TSH to a value ≥30 uIU/ml, and can reduce the undesirable symptoms of acute hypothyroidism that occurs after 30 days. **References:** none

EP-097

Usefulness of Elastography in the Assessment of Cold Solid Thyroid Nodules

A. Štrok[1], K. Bajuk Studen[1], E. Pirnat[1], N. Bedernjak Bajuk[1], S. Gaberšček[1,2], K. Zaletel[1,2];
[1]Department of Nuclear Medicine, University Medical Centre Ljubljana, Ljubljana, SLOVENIA, [2]Faculty of Medicine, University of Ljubljana, Ljubljana, SLOVENIA.

Aim/Introduction: The prevalence of thyroid nodules detected by ultrasound (US) is up to 50% in general population and approximately 5–10% of them is malignant. Diagnostic assessment includes laboratory tests, thyroid US and thyroid scintigraphy, where suspicious nodules are characteristically cold when using Tc-99m pertechnetate as a tracer. A useful tool for US-based risk stratification of thyroid nodules is Thyroid Imaging Reporting and Data System (TIRADS). Recently, a complementary role of elastography was shown. Our aim was to evaluate a diagnostic value of elastography using carotid artery pulsation in the assessment of cold solid thyroid nodules. **Materials and Methods:** In 39 patients, 31 females and 8 males (mean age 51.9±16.8 years), we evaluated solitary or dominant solid thyroid nodule that was cold on scintigraphy with Tc-99m pertechnetate. In every patient, thyrotropin (TSH) was measured, thyroid and nodule volume were calculated using standard formula and TIRADS score was estimated on the basis of US characteristics. Elastography using carotid artery pulsation was performed and elasticity contrast index (ECI) of thyroid nodule and paranodular tissue was assessed. In every nodule, fine needle biopsy was performed and cytology was reported using Bethesda classification system. Patient and nodule characteristics were compared according to cytology result. Results: Mean TSH level was 1.73±1.13 mIU/L. Mean thyroid volume was 29.6±18.9 ml and mean nodule volume was 13.4±14.9 ml. Males had significantly larger nodule volume than females (28.4±22.7 vs 9.6±9.3 ml, p=0.05). Mean ECI of thyroid nodules was significantly higher compared with mean ECI of paranodular tissue (1.81±0.84 vs 1.09±0.34, p<0.001). Suspicious Bethesda category (4 or 6) was confirmed in 20.5% (8/39) of patients. Compared with unsuspicious nodules, nodules with suspicious Bethesda category were confirmed in significantly younger patients (38.6±18.8 vs 55.4±14.6 years, p=0.01), their proportion was significantly higher in males than in females (p=0.02) and their TIRADS score was significantly higher (p<0.001). Patients with suspicious or unsuspicious cytology did not differ with respect to mean ECI of thyroid nodule (2.2±1.3 and 1.7±0.6, p=0.33), nodule volume (p=0.71) or TSH concentration (p=0.87). **Conclusion:** Our results show a significantly higher ECI in cold solid thyroid nodules than in surrounding thyroid tissue. However, elastography with ECI evaluation does not seem to contribute significantly to the assessment of malignant potential of those nodules. Data based on larger number of nodules is needed to further evaluate the value of elastography. **References:** none

EP-098

[^{18}F]-Fluorocholine PET/CT in primary hyperparathyroidism: Initial experience

J. Fernández Fernández, M. Muros de Fuentes, E. Triviño Ibañez, M. Lopez de la Torre Casares;
Virgen de las Nieves University Hospital, Granada, SPAIN.

Aim/Introduction: The [^{18}F]-Fluorocholine PET/CT could be a good alternative to other imaging techniques in the localization of the hyper-functioning parathyroid tissue given its better spatial resolution, ability to detect ectopic glands, and the conjunction of the molecular and anatomical image.The objetive of this study is to evaluate the utility of [^{18}F]-Fluorocholine PET/CT as a localization method in primary hyperparathyroidism and to compare with the routine imaging protocol in our hospital. **Materials and Methods:** Observational and retrospective study. We studied 32 patients with primary hyperparathyroidism between 2020-2021. We performed [^{18}F]-Fluorocholine PET/CT using the usual protocol of Nuclear Medicine Department. We considered three options: positive PET/CT studies (if we have positive findings in neck or out of neck), Negative PET/CT studies (without any uptake) or inconclusive results. The number of lesions, and their location, in the early and late images were analysed. The results were compared to conventional methods (neck US, [^{99m}Tc]Tc-MIBI SPECT/CT and CT with intravenous contrast). Medical record was revised for surgery and pathology reports in operated patients (6/32). Results: 32 patients (56,3 mean years, 81,3% female). 23 patients showed a positive18F-choline PET/CT study, 3 negative and 6 inconclusive study. 61.9% (13/21) of patients with negative [^{99m}Tc]Tc-MIBI SPECT/CT was [^{18}F]-Fluorocholine PET/CT positive. 66,7% (16/24) of patients with negative neck US was [^{18}F]-Fluorocholine PET/CT positive. 77.8% (7/9) with negative CT was [^{18}F]-Fluorocholine PET/CT positive. All negative [^{18}F]-Fluorocholine PET/CT studies had negative neck US and negative [^{99m}Tc]Tc-MIBI SPECT/CT. Pathological parathyroid gland was correctly identified by [^{18}F]-Fluorocholine PET/CT in all patients who underwent surgery 100% (6/6). **Conclusion:** [^{18}F]-Fluorocholine PET/CT allows detect more pathological parathyroid gland in hyperparathyroidism patients than routine imaging protocol in our hospital (neck US, [^{99m}Tc]Tc-MIBI SPECT/CT and CT with intravenous contrast). Pending confirmation with a greater number of operated patients, [^{18}F]-Fluorocholine PET/CT shows a high detection rate. **References:** none

EP-099

Scintigraphic features of atypical parathyroid adenoma

A. Aktas[1], N. Torun[2], G. Nursal[2], A. Gencoglu[1], H. Ozdemir[1];
[1]Baskent University, Ankara, TURKEY, [2]Baskent University, Adana, TURKEY.

Aim/Introduction: Atypical parathyroid adenoma is a tumor of unknown malignant potential that has features intermediate between typical adenoma and parathyroid carcinoma. Its diagnosis is established by histopathologic evaluation of the surgical material. Although invasive potential is absent in atypical parathyroid adenoma, close follow-up may be needed after diagnosis. There is no way to predict its presence before and during the operation. The aim of this study was to evaluate . **Materials and Methods:** This study was approved by Baskent University Institutional Review Board (Project No: KA21/237) . In this retrospective study, we evaluated 5-year data of parathyroid scintigraphy images of patients referred for the evaluation of hyperparathyroidism who had undergone postscan parathyroid surgery. There were 5 patients with parathyroid carcinoma and 10 patients with atypical parathyroid adenoma. Parathyroid scintigraphy was performed after 15-20 mCi Tc-99m sestamibi injection. Planar neck and mediastinal images were acquired at 15-minute (early image), and 2-hour (delayed image) after injection. Images were interpreted in relation to location, size, uptake and retention intensity of parathyroid lesion. Scintigraphy findings in atypical parathyroid adenoma were compared to those of typical parathyroid adenoma and carcinoma. Results: All patients with parathyroid carcinoma had early phase intense foci with persistent activity on delayed images. On planar image, hyperactive foci occupied whole thyroid length in 4 and 2/3 of lobe in 1 patient. In all patients with carcinoma, remaining parts of the thyroid had a suppressed appearance on early images. In half of the patients with atypical adenoma, scintigraphic features resembled to that of carcinoma. In the remaining 5 patients, atypical adenoma had a resemblance to that of typical adenoma with a relatively smaller size and moderate uptake. **Conclusion:** Atypical parathyroid adenoma exhibited scintigraphic features that have similarities to both carcinoma and typical adenoma. The value of scintigraphic pattern in predicting recurrence or malignant transformation needs to be determined with follow-up evaluation. **References:** None

EP-20

Wednesday, October 20 - Saturday, October 23, 2021

e-Poster Area, release on Wednesday, October 20 at 09:00

Imaging Clinical Studies -> Infection and Inflammation -> Vasculitis and Endocarditis

EP-100

The additional role of ^{18}F-FDG PET/CT in the evaluation of suspected prosthetic valve infective endocarditis

C. Ferrari, R. Ruta, F. Iuele, A. Sciacqua, C. Altini, A. Gaudiano, G. Rubini;
Section of Nuclear Medicine, DIM, University "Aldo Moro", Bari, ITALY.

Aim/Introduction: European Society of Cardiology (ESC) guidelines have recently been modified by the addition of ^{18}F-FDG PET/CT as a major criterion in the diagnosis of infective endocarditis (IE). A systematic comparison between updated ESC criteria and traditional modified Duke's Criteria (mDC) has not been evaluated yet, to assess the additional value of ^{18}F-FDG PET/CT, in particular in prosthetic valve endocarditis (PVE). Validated semi-quantitative parameters with standardized methodology have not been defined yet. In addition, diffuse splenic uptake has been investigated, but its relevance has to be ascertained.The aims of this study were the evaluation of ^{18}F-FDG PET/CT additional role in patients with suspected PVE, the assessment of semi-quantitative parameters and the description of the diffuse splenic uptake finding. **Materials and Methods:** We retrospectively included 16 patients with clinical suspicion of PVE who referred to our Nuclear Medicine Unit in the last 2 years to perform ^{18}F-FDG PET/CT. All patients were classified as possible PVE at admission, according to mDC. After ^{18}F-FDG PET/CT qualitative analysis, patients were reclassified as definite PVE or rejected PVE. The final diagnosis, considered as gold-standard, was based on the Endocarditis Team's evaluation, established 3 months after hospitalization. The following semi-quantitative PET parameters were collected: maximum standardized uptake value (SUV_{max}), semi-quantitative ratio (SQR) and target-to-background ratio (TBR). Mean values of splenic uptake were also collected. Sensibility (Se), specificity (Sp), positive predictive value (PPV), negative predictive value (NPV) and diagnostic accuracy (DA) of ^{18}F-FDG PET/CT were calculated. t-student's test was performed to establish if a statistically significant difference between values, in patients confirmed for PVE and not, existed. Results: ^{18}F-FDG PET/CT resulted positive in 10/16 (62.5%) patients and negative in 6/10 (37.5%). After Endocarditis Team's evaluation during follow-up, 8/16 (50%) patients were confirmed for PVE (all True Positive at PET examination), while the remnants 8/16 (50%) were rejected for PVE (6/8 True Negative, 2/8 False Positive at PET examination). Se, Sp, PPV, NPV and DA of ^{18}F-FDG PET/CT resulted 100%, 75%, 80%, 100% and 87.5% respectively. Differences of mean values of SUV_{max}, SQR, TBR and splenic uptake between the two groups (confirmed PVE and rejected PVE) resulted statistically significant ($p<0.05$). **Conclusion:** Our preliminary results confirm the additional role of ^{18}F-FDG PET/CT in patients with suspected PVE and evaluate the usefulness of semi-quantitative parameters, collected with a reproducible methodology, as well as the possible relevance of a diffuse splenic uptake. Further studies are mandatory in larger populations. **References:** None.

EP-101

Variations of myocardial uptake suppression and infective endocarditis detectability between a first conventional fasting-based FDG-PET and a second one scheduled on the next day after an Atkins diet

M. Germaini, C. Boursier, F. Goehringer, C. Selton-Suty, B. Lefevre, V. Roch, L. Imbert, M. Claudin, E. Chevalier, P. Marie;
CHRU Nancy, Nancy, FRANCE.

Aim/Introduction: Complete suppression of the myocardial FDG uptake is not always achieved with conventional fasting diet protocols, thereby affecting the FDG-PET detection of inflammatory and infectious heart diseases. However, several days of low carbohydrate diets, such as the Atkins diet, may also suppress the myocardial FDG uptake. This study aimed to assess whether myocardial uptake suppression and endocarditis detectability are further improved on FDG-PET repeated the day after a first conventional fasting-based FDG-PET in patients fed with an Atkins diet between the two investigations. **Materials and Methods:** Eighteen patients with preexisting definite infective endocarditis according to Duke-Li criteria (age: 73±16 years, 3 women, 13 with cardiac prosthesis), were recruited (ClinicalTrials.gov Identifier: NCT03465098) and underwent: (i) a 1st FDG-PET after a conventional metabolic preparation (≥ 12-hours fasting after a low-carbohydrate diner) and (ii) a 2nd FDG-PET on the next day, after an immediate switch to a 12-hours Atkins regimen (≤ 3 g of carbohydrate), which was followed by an additional ≥ 12-hours fasting period. The visual detection of the endocarditis foci was compared between the 2 PET, together with the SUV from myocardial and endocarditis areas and with blood biomarkers. Results: A shift toward a ketogenic metabolism was evidenced through an increase in the plasma beta-hydroxybutyrate level between the 1st and 2nd PET (p=0.022), in association with a decrease in insulinemia (p=0.043) and a stable glycemia. The myocardial suppression of FDG uptake was incomplete (i.e., with myocardial areas showing a higher activity than the left ventricular blood cavity) on the 1st PET of 10 patients (56%). For these 10 patients, myocardial SUV uptake decreased between the 1st and 2nd PET (SUVmax: 6.0±3.1 vs. 4.4±3.3, p=0.017), and the endocarditis/myocardium SUVmax ratio increased (0.87± 0.35 vs. 1.30±0.69, p=0.038), resulting in a relevant enhancement in endocarditis detection on the 2nd PET in 4 cases (significant

increases in diagnostic confidence in 2 cases and endocarditis visualized on only the 2nd PET in the 2 other cases). By contrast, none of these changes was observed in the 8 patients for whom the myocardial uptake suppression was complete on the 1st PET. **Conclusion:** In patients affected by infective endocarditis and showing an incomplete myocardial uptake suppression on a conventional fasting-based FDG-PET, further enhancements in myocardial uptake suppression and endocarditis detectability may be achieved by an additional FDG-PET prescribed on the next day together with an Atkins diet between the two investigations. **References:** none

EP-21

Wednesday, October 20 - Saturday, October 23, 2021

e-Poster Area, release on Wednesday, October 20 at 09:00

Imaging Clinical Studies -> Infection and Inflammation -> Other Infections and Inflammatory Diseases

EP-102

The role of 18F-FDG PET/CT in patients with IgG4 related disease. Our experience

C. Sandoval Moreno, B. Manzarbeitia Arroba, M. Tagliatori Nogueira, M. De la Rubia Marcos, M. Álvarez Moreno, L. Castillejos Rodríguez, A. Ortega Valle, M. Balsa Bretón;
Hospital Universitario de Getafe, Getafe, SPAIN.

Aim/Introduction: IgG4 related disease is a systemic disease characterized by tissue infiltration of plasmatic cells, fibrosis and IgG4 cells present in tissues. Elevated serum IgG4 level is present in most patients. The aim of this paper is to evaluate the efficacy of 18F-FDG PET/TC in the detection of inflammatory activity in patients with diagnosed or suspected of IgG4 related disease and the different patterns that we can observe. **Materials and Methods:** We reviewed records of patients referred to our Nuclear Medicine Department with diagnosis of IgG4 related disease in the last year. We evaluated 5 patients (all of them were males), the median age was 55.8 years. Whole body 18F-FDG PET/CT and visual evaluation was performed. Results: All of our patients had a positive result with different patterns: - - Mural thickening of the abdominal aorta. - - Bilateral granulomatous inflammation of perirenal fat. - - Pleuromediastinal thickening and increased periaortic density. - - Increased prevascular density in mediastinum. - - Areas of diffuse ground glass, reticular pattern and alveolar consolidation in both lungs. All of them had uptake in 18F-FDG PET/TC study and we observed 5 completely different results. In this series, perivascular involvement seems to be more frequent. Although pancreas involvement is one of the most common patterns described in bibliography, we haven't observed pancreas involvement in ours patients. **Conclusion:** 18F-FDG PET/CT is useful for evaluating inflammatory activity and it also helps to locate the most accessible lesions for biopsy. Perivascular involvement seems to be more common in our series. However, bigger scale studies are needed to prove this hypothesis. **References:** None

EP-22

Wednesday, October 20 - Saturday, October 23, 2021

e-Poster Area, release on Wednesday, October 20 at 09:00

Therapy Clinical Study -> Oncological Therapy Clinical Study -> Neuroendocrine Therapy

EP-103

Adverse Prognostic Factors in Patients Refractory Pheochromocytoma and Paraganglioma After ^{131}I-metaiodinebenzylguanidine (^{131}I-mIBG) Therapy

T. Hiromasa, H. Wakabayashi, D. Kayano, A. Inaki, A. Toratani, N. Akatani, S. Watanabe, T. Yamase, Y. Kunita, H. Mori, S. Saito, A. Takata, S. Kinuya;
Kanazawa University Hospital, Kanazawa, JAPAN.

Aim/Introduction: Pheochromocytoma and paraganglioma (PPGL) are rare diseases, and knowledge of following the clinical course is limited. In Japan, surgery and external beam radiation mainly have been performed as local treatment for patients with refractory PPGL. ^{131}I-metaiodinebenzylguanidine (^{131}I-mIBG) therapy and chemotherapy with cyclophosphamide, vincristine, and dacarbazine (CVD) have been performed as a systemic treatment for them. We aimed to describe whether baseline characteristics at initial ^{131}I-mIBG therapy and the best response based on Response Evaluation Criteria in Solid Tumors guideline (version 1.1) to ^{131}I-mIBG treatments could predict the outcome of patients with refractory PPGL. **Materials and Methods:** A retrospective review was performed of all patients [n=58 (male/female =34/24), median age 49.2] with refractory PPGL who received ^{131}I-mIBG therapy at our institution between September 2009 and September 2019. Overall survival was estimated by the Kaplan-Meier method. We examined the effect of the following factors on overall survival: age, sex, hypertension, diabetes mellitus, palpitations, constipation, cancer pain, catecholamines values, past-history of operation, past-history of CVD therapy, past-history of external beam radiation for bone metastasis, sites of metastases and response to MIBG treatments. The Cox proportional hazards model was used to evaluate independent prognostic factors on overall survival. Multivariable Cox regression analysis was performed on significant parameters in univariable Cox regression analysis. The overall survival curves were compared using the log-rank test. Results: In the follow-up period, 18 patients died from exacerbation of their diseases. The estimated 5-year

and 10-year survival rates from initial diagnoses of refractory PPGL were 79.0% and 66.3%, respectively. Those rates from the first ^{131}I-mIBG therapy were 68% and 49.5%, respectively. The multivariate Cox proportional hazards model showed that constipation [hazard ratio (HR) 7.7, P = 0.014], past-history of external irradiation for bone metastasis (HR 17.4, P = 0.048) and progressive disease (PD) in response to ^{131}I-MIBG therapy (HR 69.1, P = 0.017) were adverse prognostic factors for overall survival after first ^{131}I-mIBG therapy. The log-rank test demonstrated that constipation (P = 0.0086), past-history external beam radiation for bone metastasis (P < 0.0001) and PD in response to ^{131}I-mIBG therapies (P < 0.0001) were correlated with poor the survival rates. **Conclusion:** The response to ^{131}I-mIBG treatment is a strong predictor for prognosis after the first ^{131}I-mIBG therapy in patients with refractory PPGL and is better suited than baseline characteristics. **References:** None

EP-104

177Lu-DOTATATE efficacy and safety in functioning neuroendocrine tumors: a joint analysis of phase II prospective clinical trials

A. Bongiovanni[1], S. Nicolini[2], F. Foca[3], T. Ibrahim[1], M. Sansovini[2], I. Grassi[2], C. Liverani[1], N. Riva[1], M. Bocchini[1], A. Moretti[4], F. Matteucci[2], L. Fabbri[3], M. Signoretti[5], C. A. Pacilio[6], R. Galassi[7], G. Paganelli[2], S. Severi[2];

[1]Osteoncology and Rare Tumors Center, IRCCS Istituto Romagnolo per lo Studio dei Tumori (IRST) "Dino Amadori", Meldola, ITALY, [2]Nuclear Medicine and Radiometabolic Unit, IRCCS Istituto Romagnolo per lo Studio dei Tumori (IRST) "Dino Amadori", Meldola, ITALY, [3]Unit of Biostatistic and clinical trials, IRCCS Istituto Romagnolo per lo Studio dei Tumori (IRST) "Dino Amadori", Meldola, ITALY, [4]Nuclear Medicine Unit, Morgagni Pierantoni Hospital, Forli, ITALY, [5]Unit of Gastroenterology and Digestive Endoscopy, Forli-Cesena Hospital, AUSL Romagna, Forli, ITALY, [6]General and Oncology Surgery, Morgagni-Pierantoni Hospital, Forli, ITALY, [7]Nuclear Medicine Unit, Morgagni Pierantoni Hospital, Forli, ITALY.

Aim/Introduction: Neuroendocrine tumors (NETs) are rare malignancies with different prognosis. At least 25% of metastatic patients have functioning neuroendocrine tumors (F-NETs) that secrete bioactive peptides, causing specific debilitating and occasionally life-threatening symptoms such as diarrhea and flushing. Somatostatin analogs (SSAs) are usually effective but beyond them few treatment options are available. We evaluated the clinical efficacy of 177Lu-DOTATATE in patients with progressive metastatic F-NETs and SSA-refractory syndrome. **Materials and Methods:** A non pre-planned joint analysis was conducted in patients enrolled in phase II clinical trials on metastatic NETs. We extrapolated data from F-NET patients with ≥1 refractory sign/symptom to octreotide, and ≥1 measurable lesion. Syndrome response (SR), overall survival (OS), progression-free survival (PFS), tolerance and disease response were analyzed.[177] Lutetium dosage was 3.7 GBq for the LUNET protocol (GEP-NET G1/2 with FDG-negative PET/CT) in which patients were randomized to have 5 or 7 cycles of therapy 8 weeks apart. The LUTHREE protocol (basket protocol with Ki-67 <35% patients) was stratified by the presence of risk factors for renal and bone marrow toxicity. Patients at risk were treated with a 3.7 GBq repeated for 5 cycles, while not at-risk cases underwent 5.5 GBq repeated for 5 cycles. In both cases, patients were randomized to receive treatment every 5 or 8 weeks to evaluate potential differences in terms of toxicity and efficacy. Results: Sixty-eight patients were enrolled, the majority (88.1%) with a SR. According to RECIST criteria, one (1.5%) patient showed a CR, 21 (32.3%) had a PR and 40 (61.5%) SD. At a median follow-up of 28.9 months (range 2.2-63.2) median PFS was 33.0 months (95%CI: 27.1-48.2). Median OS (mOS) had not been reached at the time of the analysis; the 2-year OS was 87.8 months (95%CI: 76.1-94.1). Syndromic responders showed better survival than non responders, with a mOS of 93.9 (95%CI: 92.2-98.0) vs 40.0 months (95%CI: 6.6-73.4), respectively. Median time to syndrome response was 5.0 months (95% CI 4.0-6.5). Time to best tumor response was 7.3 months (95%CI: 5.8-7.9). 233 adverse events were recorded. Grade 1-2 haematological toxicity was the most frequent. **Conclusion:** ^{177}Lu-DOTATATE improved symptoms and disease control in patients with F-NETs. Treatment was well tolerated. The syndrome had an impact on both quality of life and OS. **References:** none

EP-105

Associated with PRRT change of corrected SUVs max values in NET metastatic lesions assessed on [68Ga]Ga-DOTA-TATE PET/CT

M. Opalinska[1], A. Sowa-Staszczak[2], A. Kania-Kuc[1], I. Al Maraih[1], M. Buziak-Bereza[2], A. Hubalewska-Dydejczyk[2];

[1]Nuclear Medicine Unit, Endocrinology Department, University Hospital in Krakow, Krakow, POLAND, [2]Chair and Department of Endocrinology, Jagiellonian University Medical College, Krakow, POLAND.

Aim/Introduction: Peptide receptor radionuclide therapy (PRRT) is an effective treatment regimen for metastatic or inoperable NETs with good somatostatin receptor expression. Increasingly often, research focuses on the heterogeneity of metastatic lesions in NETs, which is probably related to the final treatment response Aim: Assessment of corrected SUV max change associated with PRRT in metastatic NET lesions in [68Ga]Ga-DOTA-TATE PET/CT. **Materials and Methods:** 13 patients treated with PRRT using 177Lu and 177Lu/90Y DOTA-TATE in 2017-2019 due to dissemination of G1 and G2 neuroendocrine neoplasm were eligible for study. In this group [68Ga]Ga-DOTA-TATE PET/CT was performed in average 4.5 months before and 3.6 months after PRRT. A total of 83 metastatic lesions were evaluated and they were

located in the liver, bones, lungs and lymph nodes of the neck, chest, abdominal and pelvic cavity. For every lesion in both PET/CTs (before and after PRRT) SUVmax, mean value of SUV, and ROI volume were measured. SUVmax in target lesion was compared to the mean value of SUV in the lesion volume to assess the homogeneity of the lesions. Further for all lesion corrected SUVmax was counted, taking into account individual for each patients SUV max of reference organs (normal liver). Finally corrected SUVmax change (before and after PRRT) was counted. The change of SUVs value in every organ of every patient were counted and compared between individual patients. Results: The mean change of corrected SUVmax value counted on [68Ga]Ga-DOTA-TATE after PRRT was significantly lower than on images before PRRT. Mean change of corrected SUV max of all metastatic lesion was -161,96% (range -1385,85% to 57,92%). The mean change of corrected SUV max value in liver, lymphnodes and bones were -99,08% (range -316,19% to 23,56), -307,53% (range -1385% to 31,98%) and -187,21% (range - 702,70% to 57,92%) respectively. In 12 patients, regardless of the location of the metastatic lesions, the mean corrected SUVmax change had the same direction. Only in 1 patient corrected SUV max direction were different in vary locations of metastatic lesions. **Conclusion:** There are a significant changes of corrected SUVmax in metastatic lesions obtained from routine [68Ga]Ga-DOTA-TATE PET/CT. In most patients the changes of corrected SUVmax in all types of metastatic lesions have the same direction. The possible impact of those findings as predictive factor to PRRT response will be investigated. **References:** none

EP-106

Body mass index and prior therapy lines conditioning response to [177Lu]Lu-DOTATATE therapy in neuroendocrine tumours

J. Fernández Fernández, M. Muros de Fuentes, E. Triviño Ibañez, M. Lopez de la Torre Casares, E. Gonzalez Flores;
Virgen de las Nieves University Hospital, Granada, SPAIN.

Aim/Introduction: To analyze the influence of body mass index (BMI) and prior therapy lines on the response to 177Lu-DOTATATE therapy in neuroendocrine tumours (NETs). **Materials and Methods:** Observational and prospective study including 28 patients with NETs (gastroenteropancreatic, pulmonary and others locations), grade 1 to 3, in disease progression to prior therapies: somatostatin analogues (SSA), everolimus, transarterial chemoembolization (TACE) or other therapies, referred for therapy with [^{177}Lu]Lu-DOTATATE. Patients were classified into group I (more than three prior therapies) and into group II (three or less prior therapies). We analyzed the association between BMI, disease extension, years of disease evolution, prior therapies, radiological response (RECIST v1.1 criteria) and [^{177}Lu]Lu-DOTATATE therapy response, hematological complications and overall survival. Results: Outcome of 28 patients (53% male), mean age was 56.4 ± 10.98 years and mean time of disease evolution was 4.7 ± 4.18 years. The mean of prior therapy lines was 2.88 ± 1.18. 18 patients received more than three prior therapies and 10 patients received three or less prior therapies. 42% of patients presented mild, moderate, or severe hematological alterations during treatment. More frequent in women (53.8%) than in men (33.3%), although not statistically significant (p = 0.274).The presence of hematological alterations did not show association with age, time of evolution, extension of the disease and type of response.There were more hematological alterations in patients treated with >3 prior therapies (70%) compared to those treated with ≤3 prior therapies (28.4%; p=0.038); in patients treated with TACE (66.7%) rather than in those patients not treated with TACE (21.4%, p=0.03). Overall survival was statistically significant lower in patients who presented hematological alterations compared with patients who did not (HR: 8.9; p= 0.016). **Conclusion:** Patients with lower BMI and higher number of prior therapies present more hematological alterations during [^{177}Lu]Lu-DOTATATE therapy, this was statistically significant associated with a lower overall survival (HR: 8.9). **References:** none

EP-23

Wednesday, October 20 - Saturday, October 23, 2021

e-Poster Area, release on Wednesday, October 20 at 09:00

Therapy Clinical Study -> Oncological Therapy Clinical Study -> Prostate Cancer Therapy

EP-107

Combined bone scintigraphy and ^{18}F-fluorocholine PET/CT predicts response of bone metastases to radium-223 treatment in patients with castration-resistant prostate cancer

F. Volpe[1], *M. Klain*[1], *V. Gaudieri*[1], *M. Petretta*[2], *E. Zampella*[1], *C. Nappi*[1], *G. Storto*[3], *R. Gallicchio*[3], *L. Piscopo*[1], *M. Manganelli*[1], *V. Parisella*[1], *L. Pace*[4], *M. Schlumberger*[1], *A. Cuocolo*[1];
[1]*Department of Advanced Biomedical Sciences, University Federico II, Naples, ITALY,* [2]*IRCCS SDN, Diagnostic Imaging, Naples, ITALY,* [3]*Nuclear Medicine Unit, IRCCS, Referral Cancer Center of Basilicata, Rionero in Vulture, ITALY,* [4]*Dipartimento di Medicina, Chirurgia e Odontoiatria "Scuola Medica Salernitana"/DIPMED, Salerno, ITALY.*

Aim/Introduction: Bone metastases burden evaluation is essential before radium-223 therapy. The aim of this study was to assess the value of combined bone scintigraphy and 18F-fluorocholine PET/CT in predicting the clinical outcome in patients with castration-resistant prostate cancer and bone metastases treated with radium-223. **Materials and Methods:** A retrospective analysis of 48 patients who received radium-223 therapy between 2015 and 2017 was

performed. The treatment protocol included six courses of radium-223 and treatment failure was defined as less than six treatment courses. The endpoints were pain relief and overall survival. Bone scintigraphy and 18F-fluorocholine PET/CT were performed in all patients before radium-223 therapy. Results: The follow-up was 15±10 months (range 2-43 months). Thirty-four patients died during the follow-up and nine patients prematurely discontinued the treatment. After radium-223 therapy, pain relief was observed in 27 (56%) patients (P<0.001). Among patients without pain relief, 71% had more bone lesions at 18F-fluorocholine PET/CT than at bone scintigraphy (pre-therapy imaging mismatch) (P<0.05). At univariable analysis, variables associated with a poor overall survival were Gleason score (P<0.05), treatment failure (P<0.001), baseline ALP level (P<0.05), post-therapy ALP level (P<0.005), persistent or worsened post-therapy pain (P<0.05), and pre-therapy imaging mismatch with more lesions seen on PET/CT than on bone scintigraphy (P<0.05). At multivariable analysis, only treatment failure and post-therapy ALP level were independent predictors of a poor overall survival (both P<0.05). In the sub-group of 39 patients who had completed treatment protocol, post-therapy ALP level and pre-therapy imaging mismatch with more lesions at 18F-choline PET/CT than at bone scintigraphy were independent predictors of a poor overall survival (both P<0.05). **Conclusion:** After radium-223 therapy, patients with more lesions at 18F-fluorocholine PET/CT than at bone scintigraphy had a poor prognosis, suggesting that a combined imaging approach could be useful to predict outcome after radium-223 therapy. **References:** none

EP-108

The value of osteoblastic activity from prostate cancer in efficacy and safety of radium-223 dichloride therapy

I. Lopo[1], P. Lapa[1,2], G. Costa[1,2], J. Pedroso de Lima[1,2,3];
[1]Centro Hospitalar e Universitário de Coimbra, Coimbra, PORTUGAL, [2]Faculdade de Medicina da Universidade de Coimbra, Coimbra, PORTUGAL, [3]Instituto de Ciências Nucleares Aplicadas à Saúde (ICNAS), Coimbra, PORTUGAL.

Aim/Introduction: Radium-223-Dichloride ([^{223}Ra]$RaCl_2$) is an alpha-emitter indicated in the treatment of bone metastases secondary to castrate-resistant prostate cancer (mCRPC). Despite the short path of the alpha particle in tissues, the truth is that bone marrow toxicity is a concern and should be monitored. Bone scintigraphy (BSc) plays a major role in the evaluation of bone involvement but also in the selection of patients to [^{223}Ra]$RaCl_2$ therapy. We aimed to evaluate the impact of the extent and intensity of osteoblastic expression of metastatic bone disease (^{OE}Mbd), measured by BSc, in bone marrow activity and quality of life. **Materials and Methods:** We performed a retrospective study with mCRPC patients that have concluded [^{223}Ra]$RaCl_2$ therapy at our institution until February 2021. Before the treatment, either BSc and blood count (haemoglobin, platelets and neutrophils) were checked. The ^{OE}Mbd, defined as the percentage of osteoblastic activity of skeleton derived from tumour, was quantified by applying a semi-automatic method, using the geometric mean image obtained with whole-body planar BSc. Based on arbitrarily established ^{OE}Mbd cut off, patients were divided in two groups (G1: ^{OE}Mbd≤30%; G2: ^{OE}Mbd>30%). All relevant clinical data available were collected (Gleason score, haematological profile, quality of life questionnaire - EORTC QLQ-C30 -, date of death). Using SPSS for statistical analysis, we compared blood count levels before and after treatment in both groups, as well as efficacy, determined by effects in quality of life (Wilcoxon test). Results: A total of 24 patients (G1: N=10; G2: N=11) were selected (mean age=71.3±9.0 years; Gleason score ≥7 in 92.8% of patients; mean PSA level at 1st cycle =122.6±157.1ng/dL; 11 patients completed the 6 cycles). The median ^{OE}Mbd was 19.8% (2.3-27.5) in G1 and 44.0% (35.8-76.7) in G2. Surprisingly, statistically significant lower values of haemoglobin after treatment (18.2±11.1 days after last cycle) were found in both groups (G1: p=0.024; G2: p=0.05) but no difference was found regarding to neutrophils (G1: p=0.50; G2: p=0.236) and platelets (G1: p=0.086; G2: p=0.477). Our analysis showed no differences in quality of life reported by patients between the 1st (before treatment) and last questionnaire (before last cycle) in both groups (G1: p=0.393; G2: p=0.160). The median overall survival after the 1st cycle in G1 and G2 was 6 (4-19) and 7 (2-33) months, respectively. **Conclusion:** Our study suggests that patients with more severe bone disease do not have worse response or be more susceptible to haematological adverse events. **References:** none

EP-109

[68Ga]FAPI-46, [18F]FDG and [68Ga]PSMA-11 PET/CT findings in advance stage castration resistant metastatic prostate carcinoma treated with tandem radionuclide [225Ac]/[177Lu]PSMA-617: Two case reports

F. Novruzov[1], E. Mehdi[1], Z. Dadashov[1], M. Moore[2], F. Valla[2], T. Tahirov[3], F. Giammarile[4,1], F. Guliyev[5], J. Aliyev[6];
[1]Azerbaijan National Centre of Oncology, Department of Nuclear Medicine, Baku, AZERBAIJAN, [2]SOFIE, Totowa, NJ, UNITED STATES OF AMERICA, [3]The National Centre of Oncology, Department of Medical Oncology, Baku, AZERBAIJAN, [4]International Atomic Energy Agency, Vienna, AUSTRIA, [5]Azerbaijan National Centre of Oncology, Department of Uro-Oncology, Baku, AZERBAIJAN, [6]Azerbaijan National Centre Of Oncology, Department of General Surgery, Baku, AZERBAIJAN.

Aim/Introduction: The aim of our study is to determine normal and cancer distribution of 68Ga-FAPI-46 in patients with prostate cancer treated with targeted radionuclide treatments, and to compare [68Ga]-PSMA-11, [68Ga]FAPI-46 and [18F]FDG biodistribution. In prostate cancer patients,

[18F]FDG may be performed in order to assess disease aggressivity. **Materials and Methods:** Two patients with advanced stage metastatic castration resistant prostate carcinoma in progression after hormone therapy were addressed for PSMA targeted therapy. [68Ga]PSMA-11 PET/CT showed multiple axial and appendicular skeleton sclerotic lesions with pathological and intense uptake. Single-agent PSMA-targeted radioligand therapy with alpha-emitter showed promise results against disseminated prostate carcinoma but may cause severe xerostomia, which may substantially impair patients' quality-of-life. To minimize xerostomia severity we used tandem therapy with low-activity [225Ac]PSMA-617 plus low-activity the [177Lu]-PSMA-617. Post-treatment evaluation was performed after 3 cycles of radionuclide treatment with cocktails tandem protocol with [225Ac]/[177Lu]PSMA-617 (4 MBq/4 GBq respectively). [68Ga]FAPI-46 and [18F]FDG PET/CT performed after treatment. Results: In a 60-year old male, the PSA level went down from 212.9 to 1.13 ng/mL; [68Ga]PSMA-11, [68Ga] FAPI-46 and [18F]FDG PET/CT confirmed complete regression in all bone lesions. In a 75-year old male, the PSA level initially went down from 185 to 35 ng/mL and [68Ga]PSMA-11 images showed regression in all bone lesions. Because of subsequent PSA progression [18F]FDG and [68Ga]FAPI-46 PET/CT scan were performed, showing intense uptakes in all bone lesions.In both cases, [18F]FDG and [68Ga]FAPI-46 images were concordant. Both exams correctly identified the patient with aggressive lesions, presumably resistant to the PSMA targeted therapy. **Conclusion:** In advanced stage metastatic prostate carcinoma resistant to the PSMA targeted therapy, [18F]FDG and [68Ga]FAPI-46 pathologic uptake may indicate potential for FAPI targeted radionuclide treatment with beta and/or alpha emitters. **References:** 1. Clemens Kratochwil, Paul Flechsig, Thomas Lindner ett. all. ^{68}Ga-FAPI PET/CT: Tracer Uptake in 28 Different Kinds of Cancer. Journal of Nuclear Medicine, 20192. Khreish F, Rosar F, Kratochwil C, Giesel FL, Haberkorn U, Ezziddin S. Positive FAPI-PET/CT in a metastatic castration-resistant prostate cancer patient with PSMA-negative/FDG-positive disease. Eur J Nucl Med Mol Imaging. 2020

EP-24

Wednesday, October 20 - Saturday, October 23, 2021

e-Poster Area, release on Wednesday, October 20 at 09:00

Therapy Clinical Study -> Oncological Therapy Clinical Study -> Thyroid Therapy

EP-110

The Role of Early- and Late-Stimulated Thyroglobulin in Predicting Treatment Response One Year After RAIT in Low-Intermediate Risk DTC

A. Calabro', D. Albano, F. Dondi, A. Mazzoletti, P. Bellini, M. Gregorelli, F. Bertagna, R. Giubbini;
ASST Spedali Civili of Brescia, University of Brescia, Brescia, ITALY.

Aim/Introduction: Measurement of recombinant human thyrotropin (rhTSH)-stimulated thyroglobulin (Tg) is generally recommended 24 h (early) and 72-96 h (late) after the second rhTSH injection in patients affected by low-intermediate risk Differentiated thyroid carcinoma (DTC) who received 131-radioiodine therapy (RAIT). Usually late-Tg is considered to evaluate status of disease and to choose RAIT activities to administer, but recent initial evidences underlined the superior accuracy of early-Tg in predicting treatment efficacy and prognosis. Our aim was to investigate the role of early and late-stimulated Tg after rh-TSH injections in predicting treatment response one year after RAIT in patients affected by low-intermediate risk Differentiated thyroid carcinoma and to compare these two time-point Tg measurements at 24 and 72-96h to find the most accurate one. **Materials and Methods:** We evaluated 197 patients (F:M=150:47; mean age 52.2) with DTC who underwent rhTSH-aided RAIT (average 1.5 GBq) after total thyroidectomy between 2012 and 2015. SerumTg level was measured before rhTSH administration (basal Tg), 24 h after the second rhTSH administration (early-stimulated Tg), and 96 hours days after the second rhTSH administration (late-stimulated Tg). The response to initial therapy was assessed at 12 months by thyroglobulin levels measurement and morphologic and/or functional imaging according to 2015 ATA criteria. ROC analysis was performed for basal Tg, early Tg and late Tg with the aim to predict 1-year treatment response. Univariate and multivariate analyses were performed for basal Tg, early Tg, late Tg, and other clinical variables. Results: One hundred and forty-two patients (72%) had an excellent response one-year after RAIT, 40 (20%) indeterminate response and 15 (8%) an incomplete response. The best threshold value to predict 1-year excellent response was 1.2 ng/mL (AUC = 0.681, p value 0.007) for basal Tg, 1.1 ng/mL (AUC = 0.761, p value<0.001) for early Tg, and 3.3 ng/mL for late Tg (AUC =0.752, p<0.001). In the multivariate analysis, only early Tg (OR 11.515; 95%CI 2.959-44.786; p 0.0004) and late Tg level (OR 11.387; 95%CI 2.980-43.508, p 0.0004) independently predicted excellent

response. Applying the nonparametric method described by DeLong, the comparison between the ROC curves of early Tg and late Tg showed no significant differences. **Conclusion:** Both early and late-stimulated Tg are optimal diagnostic tools for predicting the response to primary treatment of DTC with similar performances. **References:** none

EP-111

Postoperative outcome in patients with low-risk differentiated thyroid cancer treated without radioactive iodine ablation

P. Dong, L. Wang, L. Xiao, L. Yang, R. Huang, L. Li;
West China Hospital of Sichuan University, Chengdu, CHINA.

Aim/Introduction: To evaluate postoperative outcomes of Chinese patients with low-risk differentiated thyroid cancer (DTC) treated with total thyroidectomy (TT) or lobectomy but did not undergo radioactive iodine (RAI) ablation. **Materials and Methods:** Between July 2015 and September 2016, we retrospectively enrolled adult patients with low-risk DTC who underwent TT or lobectomy without RAI therapy. Follow-up consisted of trends of serum thyroglobulin (Tg), anti-thyroglobulin antibody (TgAb) levels, and neck ultrasonography (US) every 6-24 months. Clinical outcomes at last follow-up were defined as no evidence of disease, biochemical, structural, and indeterminate abnormalities according to the follow-up findings. No evidence of disease was defined as negative neck US and a stable or decreasing trend of suppressed serum Tg and negative TgAb levels. Results: A total of 543 patients were followed up. At a median follow-up of 49 months (range 31-64 months), 517 (95%) had no evidence of disease, while the other 26 had either an increasing trend of suppressed serum Tg levels (n=9, biochemical abnormality), an increasing trend of TgAb levels (n=3, biochemical abnormality) or a stable or decreasing trend of suppressed serum Tg levels, but a positive trend of TgAb levels (n=14, indeterminate abnormality). No patients had structural abnormalities or no deaths related to thyroid cancer. The risk of abnormalities was significantly higher in lobectomy than in TT (P<0.001). **Conclusion:** TT without RAI ablation therapy might be the suitable approach for patients with low-risk DTC. Determining trends of suppressed serum Tg and TgAb levels, and neck US findings could be appropriate methods for follow-up. **References:** None.

EP-25

Wednesday, October 20 - Saturday, October 23, 2021

e-Poster Area, release on Wednesday, October 20 at 09:00

Therapy Clinical Study -> Oncological Therapy Clinical Study -> Other Oncological Treatments

EP-112

Feasibility and Therapeutic Potential of 177Lu-rituximab for patients with histologically confirmed relapsed or refractory CD20-positive B-cell lymphoma : A preliminary study

M. Assadi[1], S. Rekabpour[1], H. Ahmadzadehfar[2], R. Nemati[1], E. Jafari[1], N. Jokar[1];
[1]Bushehr University of Medical Sciences (BUMS), Bushehr, IRAN, ISLAMIC REPUBLIC OF, [2]Department of Nuclear Medicine, Klinikum Westfalen, Dortmund, GERMANY.

Aim/Introduction: The aim of this study was to assess the feasibility and therapeutic potential of 177Lu-rituximab in the treatment of patients with histologically confirmed relapsed or refractory CD20-positive B-cell lymphoma (follicular lymphoma with or without transformation). **Materials and Methods:** Patients were premedicated with analgesic/antipyretic (paracetamol) and antihistaminic (diphenhydramine) . Within 4h of completion of the rituximab infusion, 177Lu-Rituximab was injected over a 10 min period. Weekly blood counts and chemistry to week 8 or after resolution of nadir, then monthly. Restaging (FDG PET/CT) after 1-2 months. Results: The first case was a patient with follicular lymphoma suffering from relapsing disease after 4 previous regimens. He was treated with 50mCi (1850 MBq) of 177Lu-Rituximab. 18FDG PET shows multiple hypermetabolic tumoral residues especially in the lung . 177Lu scintigram up to two days after 177Lu-DOTA-rituximab depicts distribution of 177Lu throughout the body. Repeated 18FDG PET about 1 month after radioimmunotherapy shows partial response. Case two was a patient with refractory primary cerebral lymphoma to standard therapy. He received 50mCi (1850 MBq) of 177Lu-Rituximab . On follow up , progression of the huge brain mass was seen and the patient died. **Conclusion:** This preliminary study might demonstrate feasibility and therapeutic potential of 177Lu-Rituximab in patients with relapsed follicular lymphomas; however, further studies preferentially well-designed multicenter international clinical trial especially with the emerging of highly efficient non-radionuclide drugs are warranted. **References:** Flavio Forrer , Catharina Oechslin-Oberholzer, Benedetta Campana, Richard Herrmann, Helmut R Maecke, Jan Mueller-Brand, Andreas Lohri. Radioimmunotherapy with 177Lu-DOTA-rituximab: final results of a phase I/II Study in 31 patients with relapsing follicular, mantle cell, and other indolent B-cell lymphomas. 2013 Jul;54(7):1045-52.

EP-26

Wednesday, October 20 - Saturday, October 23, 2021

e-Poster Area, release on Wednesday, October 20 at 09:00

Technical Studies -> Radiation Protection -> Radiation Exposure and Protection

EP-113

Establishment of National DRL for CT (PET) Hybrid Imaging Studies for Kuwait Population "The Second Phase National Dose Audit -2020"

M. Masoomi[1], I. Al-Shammeri[1], L. Al-Kandari[1], H. Elrahman[1], J. Al-Shammeri[2];

[1]Medical Imaging Department, ADAN Hospital - MOH, Hadiya, KUWAIT, [2]Department of Nuclear Medicine, Faculty of Medicine, Kuwait University, Jabriya, KUWAIT.

Aim/Introduction: DRLs for CT part of PET/CT examinations are limited. Published DRLs from other countries may not be directly relevant to the state of Kuwait. This study aimed to execute the second phase of the national DRL in support of dose optimisation in the State of KW. **Materials and Methods:** In this multicenter collaborative study, with participation of 8 PET/CT centers, 309 oncology patients in comparison to 197 patients in 2019 were collected and analyzed to set up a NDRL base line. Each center upper limit of entries was set to 40 and data was restricted to adult oncology patients as per the Kuwait Ethical Committee recommendation and the limitation of the other studies. The UK-IPEM Methodology, was adopted as per 2019 audit. The CTDLvol, DLP and scan length (SL) were recorded and Median, Mean, SD, 75th, 25th percentiles as well as WB effective dose (ED) were calculated. All centers had an integrated 64 slices CT. Results: Dose and scan length statistics for the half body (HB) and whole body (WB) scans which were 65% and 35% of the total (309) respectively, and the combined (WB +HB) examinations were presented together with the Proposed local DRLs and the Achievable doses. Patient dose varied, with a maximum of two and half fold variation in DLP. The ratio of maximum to minimum mean doses for the HB and the WB scans in centers for the same clinical studies varied between 2.3-7.3 for HB and 2.1-7.3 for WB. Third quartile DLP (mGy x cm) and CTDIvol (mGy) values (set for NDRL) for the HB PET/CT was (537, 5) which was higher than the current UK NDRL (400, 4.3) but were lower than the Swiss National NDRL (620, 6) and the France National NDRL (762, 7.7). Comparatively, the Proposed NDRLs for (WB) was (684, 4.1) which was lower than Swiss National Data (720, 5.0). The results were in reasonable agreement with the centers, though, Swiss had about 5000 (HB) & 706 (WB), the UK had 370 (HB) and France had 1000 (HB) entries. The calculated mean ED varied from 4.3 to 10.5 mSv, for HB and from 3.1 to 7.6 mSv for WB scans. The NDRL for the second phase was lower in comparison to the NDRL for 2019. **Conclusion:** Although, there was 9.1% improvement in NDRL for 2020 in comparison to 2019, there is a continuous need for improving the NDRL. **References:** none

EP-114

Assessment of extremitiesand eye doses to staff involved in radionuclide therapy procedures in Kuwait

M. Alnuaimi;

Kuwait Cancer Control Center, AL Sabah Medical Area - Shweikh, KUWAIT.

Aim/Introduction: There has been growing use of theranostic agents in nuclear medicine. Currently, no information is available on eye and extremities doses for staff working in nuclear medicine in Kuwait and there is similar lack of information from the region. With increasing emphasis on radiation induced health effects and reduction in threshold dose for eye lens, there is a need to assess the radiation doses to staff working during nuclear medicine therapeutic procedures. The objective of this study is to assess the occupational eye lens and extremities doses during theranostic applications in Kuwait and promotes optimization by providing the required scientific data and inputs for developing related guidelines for the healthcare professionals. **Materials and Methods:** The ED3 (Rotunda) active personal dosemeters were used to provide real time measurement for the doses. The ED3 makes use of Silicon diodes technology to measure Hp(0.07) radiation over the range of 60 keV up to 1.25 MeV. Two ED3 dosemeters were placed one on the left side of the eyes using a head strap and the other clipped to the index finger of the dominant hand. The eye lens and extremities doses were monitored during a sample of 100 radionuclide therapy procedures at Kuwait Cancer control center. The median doses values were taken. Results: The dose to the eye lens and the extremities of staff administering the 131I radioiodine (3700 MBq) capsules were 3.4 and 59.9 µSv respectively. The dose during 177Lu-PSMA (7400 MBq) administration were 13 and 418 µSv for the eye lens and the extremities, respectively. The estimated annual doses based on the annual workload of 100 radionuclide patients in Kuwait compared against annual ICRP dose limits . The annual eye lens dose is 0.34 mSv from 131I therapy and 5.9 mSv from 177Lu procedures. The annual extremities dose is 1.3 mSv from 131I therapy and 41 mSv from 177Lu procedures. The estimated annual doses received during radionuclide therapy procedures are lower than the dose limits. **Conclusion:** In this study, the eye lens and extremities doses to nuclear were measured for the first time in Kuwait during radionuclide therapy procedures. The results show that the eye lens doses can potentially exceeded the annual ICRP dose limit with increasing workload which necessitate additional radiation protection optimization measures. In addition, regular radiation protection training and awareness for radionuclide therapy staff needs to be highlighted to reduce occupational doses. **References:** none

EP-115

Estimation of radiation exposure of workers in radionuclide therapy using ^{131}I and ^{177}Lu

J. Hudzietzova[1], M. Fülöp[2], J. Sabol[3], A. Vondrák[4], O. Kraft[5];
[1]Czech Technical University in Prague, Kladno, CZECH REPUBLIC, [2]ABRS, s.r.o., Samorin, SLOVAKIA, [3]Faculty of Security Management PACR in Prague, Prague, CZECH REPUBLIC, [4]IZOTOPCENTRUM, s.r.o., Nitra, SLOVAKIA, [5]Department of Nuclear Medicine, University Hospital Ostrava, Ostrava, CZECH REPUBLIC.

Aim/Introduction: The aim of the paper is to estimate the radiation exposure of workers when working with ^{131}I and ^{177}Lu, where the routine procedure in the administration of radionuclide therapy activities can lead to greater skin exposure, or to whole-body exposure of the worker. **Materials and Methods:** Employees of two nuclear medicine departments involved in therapeutic treatment with ^{131}I and ^{177}Lu-labeled radiopharmaceuticals have been monitored. The preparation and administration of both radiopharmaceuticals differed as to the type of technological equipment used. The ^{131}I-NaI solution was prepared manually. The ^{131}I administration was manual and involved working with both ^{131}I-NaI solution and capsules of activities of 3.7 GBq or 7.4 GBq. In the case of ^{177}Lu, an automatic filling station was used and the application was also carried out using an automatic applicator. Workers were monitored during the experiments using 13 pairs of thermoluminescent dosimeters placed on the roots and fingertips and palms. The personal dose equivalent, $H_p(10)$, was also monitored using electronic dosimeters during selected radionuclide therapy procedures. Results: During the preparation of ^{131}I, the average skin exposure was approximately 2.1 mSv/GBq (the contamination was not taken into account), while in the case of the application, the average skin exposure was approximately 0.045 mSv/GBq. For pharmacists preparing a ^{131}I-NaI solution, the exposure ratio between the index finger and fingertip was also estimated to be approximately 2.3. As to the use of ^{177}Lu, the experiments are still going on. From the preliminary results it was found that in 1 day of working with ^{177}Lu (according to the profession) the average exposure of a worker in terms of $H_p(10)$ was about 4 μSv. **Conclusion:** In almost all ^{131}I cases, the maximum exposure values were found at the fingertips. Preliminary results show the influence of technological equipment in the administration of radionuclides for the therapy. The paper is also stressing the importance of compliance with radiation protection requirements related to the administration of radionuclides in therapy. Acknowledgments: The paper was partially supported by the project SGS18/100/OHK4/1T/17. **References:** None

EP-116

Relative Contributions to Patient Effective Dose in SPECT-CT Hybrid Imaging

J. Dixon, J. Dennis, A. Nicol;
NSH Greater Glasgow and Clyde, Glasgow, UNITED KINGDOM.

Aim/Introduction: Medical imaging with ionising radiation is commonplace in healthcare. Whilst beneficial, the use of radiation has an associated risk of cancer induction. ICRP principles enshrine exposure optimisation. Effective Doses (ED) from administration of radiopharmaceuticals are generally well established, but exposure from the Computed Tomography (CT) component of hybrid imaging is often at lower levels than in diagnostic radiology and the resulting EDs are less well known. There has been recent work to establish National Diagnostic Reference Levels (NDRLs) in the UK for CT examinations performed during hybrid imaging (PHE, 2019) but these are given in terms of Computed Tomography Dose Index Volume ($CTDI_{vol}$) and Dose-Length Product (DLP) which makes evaluation of ED across imaging modalities difficult. This work aims to assess the absolute and relative contributions to total ED resulting from radiopharmaceutical administration and CT in hybrid imaging to assist with optimisation. **Materials and Methods:** Radiopharmaceutical and CT EDs were estimated for several common hybrid imaging procedures. Radiopharmaceutical EDs were found by comparing intended administered activities with the NDRLs (ARSAC, 2021) and scaling quoted EDs accordingly. ED for the CT component was calculated using the ImPACT CT dosimetry tool (ImPACT, 2011). A departmental audit collected $CTDI_{vol}$ data for a range of procedures and averages were calculated. For each scanner, over-ranging and displayed $CTDI_{vol}$ accuracy were assessed. Typical scan ranges were matched against the mathematical anatomical model in ImPACT and adjusted for over-ranging. Protocol settings and corrected $CTDI_{vol}$ were then entered into the ImPACT calculator to give the ED for each scan type. Results: Relative contributions to total ED from SPECT and CT imaging respectively were estimated to be: •Tc-99m colloid head & neck sentinel lymph node 0.2mSv/1.7mSv (10%/90%) •Tc-99m MAA/Kr-81m V/Q 2.4mSv/3.3mSv (42%/58%) •Tc-99m EDDA/HYNIC-TOC 3.7mSv/4.3mSv (46%/54%) •I-123 mIBG 5.2mSv/3.7mSv (59%/41%) •Tc-99m DPD cardiac amyloid 4.8mSv/1.7mSv (74%/26%) •Tc-99m Tetrofosmin myocardial perfusion (two-day protocol) 8.9mSv/1.3mSv (87%/13%) •Tc-99m Sestamibi/I-123 Sodium Iodide parathyroid 14.2mSv/1.2mSv (92%/8%) •Tl-201 Chloride brain 14.0mSv/0.4mSv (97%/3%) **Conclusion:** This single centre survey of EDs from the SPECT and CT components of SPECT-CT imaging reveal a wide range of absolute and relative contributions to total dose. Significant efforts for optimisation are required for both SPECT and CT components. **References:** ARSAC. (2021). Notes for guidance on the clinical administration of radiopharmaceuticals

and use of sealed radioactive sources. ImPACT CT scanner evaluation group. (2011). ImPACT's ct dosimetry tool. PHE. (2019). National Diagnostic Reference Levels (NDRLs) from 19 August 2019.

EP-27

Wednesday, October 20 - Saturday, October 23, 2021

e-Poster Area, release on Wednesday, October 20 at 09:00

Technical Studies -> Dosimetry and Radiobiology -> Preclinical Dosimetry and Radiobiology

EP-117

Evaluation of a custom-made software to calculate I-131 dose for ablation of small sizes of thyroid remnants from diagnostic I-123 SPECT/CT images

I. Iakovou[1], S. Frangos[2], I. Petrou[3], A. Hadjiconstanti[4], K. Michael[5,6], T. Leontiou[5,4], E. Ttofi[5,7], E. Kyriacou[5,4], M. Lyra[4], Y. Parpotas[5,4]; [1]Aristotle University, Thessaloniki, GREECE, [2]Department of Nuclear Medicine, Bank of Cyprus Oncology Center, Nicosia, CYPRUS, [3]Department of Nuclear Medicine, Nicosia General Hospital, State Health Services Organisation, Nicosia, CYPRUS, [4]Frederick Research Center, Nicosia, CYPRUS, [5]Frederick University, Nicosia, CYPRUS, [6]Department of Medical Physics, Bank of Cyprus Oncology Center, Nicosia, CYPRUS, [7]Department of Medical Physics, German Oncology Center, Limassol, CYPRUS.

Aim/Introduction: Diagnostic thyroid I-131 or I-123 SPECT/CT imaging can provide information on the actual presence of remnants after surgery for thyroid cancer. It is important to determine the sizes of remnants for the implementation of individualized treatment for ablation. The purpose of this study was to evaluate a custom-made software that calculates I-131 dose for ablation of each thyroid remnant from diagnostic I-123 SPECT/CT images. **Materials and Methods:** I-123 and I-131 scattered corrected SPECT/CT images were acquired using a neck-thyroid phantom and the clinical protocols. The phantom encloses trachea, oesophagus, cervical spine and a removable section with small sizes of thyroid remnants. Radiopharmaceuticals could be injected within the phantom and the remnants to simulate different background-to-remnant activity ratios. A custom-made software was used to calculate the volume of each remnant and the corresponding I-131 dose for ablation from I-123 diagnostic SPECT/CT images. The volume and the count-volume ratio for each remnant was calculated from common ROIs in SPECT (uptake) and in CT (HU values) matrices. For the dose calculations, I-123 count matrices were transformed to activity matrices and then translated to I-131 activity matrices taking into account their different decay rates. Acquisitions at different time-points were utilized to calculate the I-131 cumulative activity, and subsequently, the dose matrices using the S-factors. An individual acquisition could also be utilized to calculate the dose from the residence time. The dose can be calculated for different chosen I-131 activities and it is based on the remnant' volume. Results: The software was evaluated by using the acquired images and the phantom with different sizes of small known thyroid remnants. The software could calculate all examined volumes of thyroid remnants (1-10 mL) with an average error of 5%. It can also calculate the dose for ablation of each remnant (1-3) from diagnostic I-123 images. The dose can be calculated for different % ROIs of a remnant. Radiobiological models, based on the calculated doses and guidelines, can also be extracted. **Conclusion:** A fast and user-friendly software to calculate I-131 dose for ablation of thyroid remnant from diagnostic I-123 SPECT/CT images was evaluated and it was considered to be useful for the medical physicists and nuclear medicine physicians of the consortium. This study was co-funded by the European Regional Development Fund and the Republic of Cyprus through the Research and Innovation Foundation (Project: EXCELLENCE /1216/0088). **References:** none

EP-118

Biodistribution and dosimetry after intraperitoneal injection of ^{224}Ra-labeled microparticles in rats

S. Westrøm[1], J. Fonslet[2], C. H. Nielsen[2], C. Stokke[3,4], T. B. Bønsdorff[1]; [1]Oncoinvent AS, Oslo, NORWAY, [2]Minerva Imaging ApS, Ølstykke, DENMARK, [3]Division of Radiology and Nuclear Medicine, Oslo University Hospital, Oslo, NORWAY, [4]Department of Physics, University of Oslo, Oslo, NORWAY.

Aim/Introduction: Radium-224-labeled calcium carbonate microparticles (^{224}Ra-$CaCO_3$-MP) have been developed to treat micrometastases located in the abdominal cavity. The degradable microparticles function as carriers of the alpha-emitter to ensure intraperitoneal (i.p.) retention. The aim of the present work was to assess the ex vivo biodistribution in rats, of ^{224}Ra-$CaCO_3$-MP representative of a radiopharmaceutical currently tested in two clinical phase I trials. In addition, dosimetry was calculated and extrapolated to the absorbed doses to human. **Materials and Methods:** Female Wistar rats were administered i.p. with ^{224}Ra-$CaCO_3$-MP (89 kBq/animal, 30 mg $CaCO_3$) or a solution of $^{224}RaCl_2$ (97-220 kBq/animal). The ex vivo biodistribution was assessed at time points ranging from 2 to 336 hours post injection. Blood for clinical pathology was collected. The activity per gram tissue of ^{224}Ra and the daughter nuclide ^{212}Pb was measured. For dosimetry calculations, the cumulated activity was determined by linear interpolation between the measured values. Due to the short half-lives of ^{220}Rn and ^{216}Po, these were assumed to decay in the same tissue as ^{224}Ra. The radionuclides ^{212}Bi, ^{208}Tl and ^{212}Po were assumed to decay in the same tissue as ^{212}Pb. The contributions from gamma and x-rays were disregarded. The dosimetry results were extrapolated to humans and scaling

with relative biologically effectiveness (RBE) factors was performed. Results: A fundamental shift in skeletal uptake was seen when ^{224}Ra was adsorbed onto the microparticles compared to when given as the free cation, indicating that the majority of ^{224}Ra was retained i.p. after administration of ^{224}Ra-$CaCO_3$-MP. A similar distribution pattern of ^{224}Ra and the progeny ^{212}Pb supports that ^{212}Pb is mainly located at the site of ^{224}Ra decay. Analyses of clinical pathology showed no treatment-related adverse effects, apart from a transient depression of neutrophils. For rats, bone, kidneys, and bladder were among the organs receiving the highest absorbed doses from ^{224}Ra-$CaCO_3$-MP. The RBE-adjusted absorbed dose values for human were well below 0.5 Gy/MBq for all tissues. **Conclusion:** The biodistribution of ^{224}Ra-$CaCO_3$-MP showed how the majority of the radioactivity was retained in the peritoneal cavity of rats after i.p. injection. Further, based on the low absorbed doses for all tissues, administration of up to 7 MBq ^{224}Ra-$CaCO_3$-MP - the maximum activity in the phase I studies - is most likely safe in the clinical setting. However, there are various uncertainties associated with extrapolations from preclinical experiments and it is therefore necessary to perform dose-effect investigations also in human. **References:** None

EP-119

Development of a digital three-dimensional rodent model for production of small laboratory animal phantoms

I. Miloichikova[1,2], A. Bulavskaya[1], Y. Cherepennikov[1], E. Gargioni[3], A. Grigorieva[1], S. Stuchebrov[1], M. Wegner[3,4];
[1]Tomsk Polytechnic University, Tomsk, RUSSIAN FEDERATION, [2]Cancer Research Institute of Tomsk National Research Medical Center of the Russian Academy of Sciences, Tomsk, RUSSIAN FEDERATION, [3]University Medical Center Hamburg-Eppendorf, Hamburg, GERMANY, [4]Hamburg University of Technology, Hamburg, GERMANY.

Aim/Introduction: Preclinical studies in nuclear medicine and radiation therapy are based on experiments on small laboratory animals. However, the use of animals for medical purposes is an important internationally recognized ethical issue. Considering that scientific progress requires in-vivo experiments, such studies should aim to limit the number of involved animals to a minimum and to reduce their suffering. In addition, the use of living animals causes certain difficulties connected with individual anatomy of every particular animal and demands to meet the requirements for their maintenance, nutrition and disposal. The possible solution of this problem is to use artificial animal models (phantoms) with a well defined density distribution to imitate interactions with ionizing radiation, so that experiments on animals can be reduced and even avoided in some cases. From this point of view, creation of phantoms using the rapid prototyping technologies seems to be the most efficient. For this purpose, an anatomically accurate digital 3D model of a rodent phantom was developed in this work, which design allows loading radiopharmaceuticals into the area of interest. **Materials and Methods:** We propose to produce zoomorphic small laboratory animal phantoms by using the Fused Deposition Modeling method on the basis of animal computed tomography data with materials of the corresponding X-ray density. To create these phantoms, volumetric digital models of rodent bodies have to be created taking into account normal and pathological anatomy. For this purpose, computed tomography data was converted from the DICOM format to three-dimensional STL data, suitable for rapid prototyping systems. Volumetric digital models of rodent phantoms were designed to allow the placement of radiopharmaceuticals and dosimeters in different regions of the body. Results: A tree-dimensional digital model of a male mouse was designed and constructed. The model includes separated volumes corresponding to muscles, skeleton, brain, lungs, organs of the gastrointestinal tract, kidneys, bladder, and testicles. The model was designed to allow the locating of a radiopharmaceutical or a dosimeter in the area of interest. **Conclusion:** This study proposes a concept for creating small laboratory animal phantoms by means of additive manufacturing. A three-dimensional model of a male mouse was developed for this purpose. The designed solution allows for a flexible use of radiopharmaceuticals and the positioning of dosimeters in the areas of interest. Future work will involve the validation of this model for Monte Carlo simulations. This work is supported by the Russian Science Foundation, project No. 19-79-10014. **References:** None.

EP-28

Wednesday, October 20 - Saturday, October 23, 2021

e-Poster Area, release on Wednesday, October 20 at 09:00

Technical Studies -> Dosimetry and Radiobiology -> Clinical Dosimetry

EP-120

Comparison of 3D dosimetry methods in hepatic radioembolisation with ^{90}Y microspheres

N. Carrasco Vela[1], N. Tejedor[2], P. Bello[2], F. Blazquez[3], C. Olivas[2], V. Gimenez-Gomez[4], B. Luna[5], D. Perez-Enguix[2], I. Torres-Espallardo[2];
[1]Hospital Universitario Dr. Peset, Valencia, SPAIN, [2]Hospital Universitario y Politecnico La Fe, Valencia, SPAIN, [3]Hospital Universitario y Politécnico La Fe, Valencia, SPAIN, [4]Universidad de Valencia, Valencia, SPAIN, [5]Hospital Universitari Son Espases, Palma de Mallorca, Illes Balears, SPAIN.

Aim/Introduction: PET image plays a key role in quantitative image-based dosimetry for hepatic Y90 radioembolization. It is usually argued that the blurring introduced by the

PET is larger than the one due to the convolution kernel in a Voxel-S-Value (VSV) method so that Local Deposition Method (LDM) provides sufficiently precise results. The aim of this retrospective study is to compare LDM and VSV with Monte Carlo (MC) simulations to establish when MC could offer relevant information. **Materials and Methods:** Ten cases treated with Therasphere™ were included in the study. Liver, perfused region, healthy tissue and tumor structures were contoured in post-treatment images from a Gemini TF 64 PET/CT scanner. Moreover, synthetic PET images generated with self-developed Matlab programs were also included in the analysis. Gaussian kernels with 4, 7 and 10 mm FWHM were applied to these images. MC simulations generated with GATE v8.2 were evaluated against LDM and VSV dose maps obtained from MIM SurePlan™ LiverY90 either assuming absolute calibration or scaling the activity distribution so that the measured activity matches the injected activity (relative calibration). Results were compared through DVHs, isodose maps and gamma test using the PythonPyMedPhys library. Results: The % of local Γ(4mm/1%)<1 obtained when comparing MC with LDM using relative calibration was 80-99% for patient images and 100% for synthetic images with blurring. In general, differences between LDM and VSV mean dose decrease for larger blurring and both methods tend to MC results with VSV mean doses always closer to MC. When comparing VSV with LDM for patients with absolute calibration 100% of Γ<1 was obtained. Isodose maps and gamma matrices showed that differences in dose distributions were mostly located at liver-lung interface. **Conclusion:** Spatial resolution of current PET is on the interval 7-10 mm while modern PET/CT are expected to reach 4 mm. In this range, dose at voxel level are in good agreement at 1% level among the several methods but special care must be taken when considering mean doses. Significant differences are observed between absolute and relative differences due to activity outside the FOV. At this point, Y90 PET/CT calibration is essential for image-based dosimetry. We find differences in MC dose distributions in patients with hepatic dome tumors caused by heterogeneities at liver-lung interface and the breathing motion spread. Because of that, a gating protocol should be considered. **References:** None

EP-121

Determination of effective intra-renal half-life in radioligand therapy with ^{177}Lu-PSMA-617: Comparison of different approaches

C. Happel, *L. Völler, W. T. Kranert, B. Bockisch, D. Gröner, N. Mader, A. Sabet, F. Grünwald;*
University Medical Center Frankfurt, Frankfurt, GERMANY.

Aim/Introduction: In radioligand therapy (RLT) with ^{177}Lu-PSMA-617 the kidneys should be monitored dosimetrically as they are presumed vulnerable organs. An accurate dosimetry requires the absolute quantification of the intra-renal activity and the determination of the effective half-life (EHL) in the kidneys. While SPECT/CT-imaging is mandatory for absolute quantification, EHL can be estimated via VOI-evaluation of sequential SPECT-examinations (A) or a ROI-evaluation of either posterior views (B) or the geometric mean of conjugated views (C) of sequential whole body images. Aim of the presented study is to compare method B and C to method A, which is defined as standard procedure. **Materials and Methods:** Scintigraphic SPECT and whole body images of 100 consecutive patients (mean age: 73.8 (54 - 86.2) years) who received RLT for metastatic castration resistant prostate cancer (mCRPC) were evaluated retrospectively. Mean administered activity was 7.6 ± 1.1 GBq per cycle. Scintigraphic abdominal SPECT and conjugated whole body imaging were performed 24, 48 and 72 h post administration in each patient. EHL of the kidneys was calculated by a mono exponential fit of the temporal development of the countrate according to method A, B and C. Results: Mean EHL calculated according to method A was 28.9 ± 7.8 h for the left kidney (lk) and 30.5 ± 9.4 h for the right kidney (rk). The calculation according to method B revealed a mean EHL of 48.9 ± 71.4 h (lk) and 39.9 ± 18.8 h (rk) and 61.9 ± 59.9 h (lk) and 57.0 ± 72.4 h (rk) according to method C. The determination coefficient R^2 was calculated to compare the different methods. Mean R^2 was 0.981 (lk) and 0.977 (rk) for method A, 0.935 (lk) and 0.952 (rk) for method B and 0.882 (lk) and 0.892 (rk) for method C respectively. **Conclusion:** EHL determined by ROI-evaluation of posterior views (B) and the geometric mean of conjugated views (C) differed significantly from EHL determined by VOI-evaluation of sequential SPECT-examinations (A). This is due to the high fluctuation range of method B and C caused by a sagittal overlap of the colon, other organs as well as metastases. The results indicate that an exact determination of intra-renal EHL by ROI-evaluation of scintigraphic whole body images is not possible. Therefore, the determination of intra renal EHL has to be performed by a VOI-evaluation of sequential SPECT-examinations. **References:** none

EP-122

Dosimetry of Metastases in Treatments with ^{177}Lu-DOTATATE - Comparison Between two Calculation Software

T. Monserrat Fuertes[1], *N. Montenegro Iglesias*[1], *D. Álvarez Llorente*[1], *D. San José Olmedo*[1], *C. Arroyo Sánchez*[1], *M. A. Peinado Montes*[1], *P. Mínguez Gabiña*[2];
[1]*Hospital Universitario Central de Asturias, Oviedo, SPAIN,*
[2]*Hospital Universitario Cruces/Gurutzeta, Bilbao, SPAIN.*

Aim/Introduction: The aim of this study is to compare the absorbed doses in metastases obtained with the commercial voxel-level dosimetry software PLANET®Dose (DOSIsoft SA, Cachan, France) with those obtained with the free software IDACDose2.1. **Materials and Methods:** Absorbed doses were calculated in a total of 45 liver metastases from 19 patients

after the first ^{177}Lu-DOTATATE treatment cycle.To determine the time-integrated activity, three SPECT/CT of each patient were acquired, at approximately 24 h, 48 h and 168 h post-administration, in a gamma camera Discovery NM/CT 670 (General Electric). The volume of each lesion was obtained by delineation on a contrast-enhanced CT image acquired within three months prior to treatment. Absorbed dose calculation with IDACDose2.1 The contour delineated in the contrast-enhanced CT was manually transferred to the in-house developed software ViDi to quantify the activity of each lesion in the three SPECT/CT acquisitions. Each measurement was corrected for partial volume effect (PVE) dividing the activity by a recovery coefficient, previously calculated with phantom images. For each lesion, the three measurements were fitted to a monoexponential curve and the time-integrated activity calculated. This time-integrated activity, together with the lesion volume, was entered into the IDACDose program to obtain the mean absorbed dose. Absorbed dose calculation with PLANET®Dose All three SPECT/CT acquisitions were elastically registered. Each metastasis was delineated in one of the acquisitions, either by hand or with the threshold method, but always trying to match the lesion volume with the volume measured in the contrast-enhanced CT. Then, this structure was propagated to the other two acquisitions. To calculate the absorbed dose, the activity in each voxel was convolved with the S-voxel factors to obtain the absorbed dose-rate. This absorbed dose-rate was averaged, adjusted to a monoexponential and integrated to obtain the absorbed dose in each lesion. PLANET®Dose does not include the PVE correction, so the result obtained was subsequently corrected by the corresponding recovery coefficient. Results: The root mean square deviation value of the mean absorbed doses obtained with the two calculation methods was 8.7%. The Lin's concordance correlation coefficient was 0.99. The Bland-Altman plot analysis showed that the difference between the mean absorbed doses ranged from -5.1 Gy to 1.4 Gy for 95% of the lesions. **Conclusion:** PLANET®Dose results are consistent with those from IDACDose2.1 as long as they are independently corrected by PVE. **References:** None

EP-123

A Monte Carlo Based Tool for Skin Dose Assessment in ^{188}Re Treatment of Non-Melanoma Skin Cancer

S. Vichi[1], *F. Zagni*[2], *M. Ruscillo*[3], *L. Vetrone*[4], *A. Farina*[4], *D. Mostacci*[3], *F. Savoia*[5], *P. Castellucci*[6], *S. Fanti*[6,4], *L. Strigari*[2];
[1]*Clinical Engineering Department, IRCCS Azienda Ospedaliero-Universitaria di Bologna, Bologna, ITALY,* [2]*Medical Physics Department, IRCCS Azienda Ospedaliero-Universitaria di Bologna, Bologna, ITALY,* [3]*Department of Industrial Engineering, University of Bologna, Bologna, ITALY,* [4]*Nuclear Medicine, Department of Experimental, Diagnostic and Specialty Medicine, University of Bologna, Bologna, ITALY,* [5]*Dermatology, IRCCS Azienda Ospedaliero-Universitaria di Bologna, Bologna, ITALY,* [6]*Nuclear Medicine Department, IRCCS Azienda Ospedaliero-Universitaria di Bologna, Bologna, ITALY.*

Aim/Introduction: An innovative medical device has been recently approved for the therapy of non-melanoma skin cancer (NMSC) using ^{188}Re (Rhenium-SCT®, OncoBeta GmbH, Munich, Germany). ^{188}Re is a beta (2.1MeV, 85%) and gamma (115keV, 15%) emitter with a half-life of 17 hours. The treatment is based on the application of a ^{188}Re-based resin over the tumor. The treatment goal is to deliver a personalized absorbed dose to the deepest point of neoplastic infiltration (prescribed dose). In this work we developed a tool, based on Monte Carlo simulation, for a personalized calculation of treatment parameters. **Materials and Methods:** The Monte Carlo code FLUKA was used to simulate the treatment. A geometrical model of the skin and the applied resin was implemented considering the density and chemical composition of all the involved materials. Radioactive decay was activated in order to model the decay scheme of ^{188}Re. The dose was scored considering different dimensions of the lesion, varying consequently the source dimension. To validate the implemented MC model, calculations were performed also using Varskin, a software approved by the US-NRC as a reference tool for skin dosimetry. With the results obtained a Lookup Table (LUT) was implemented containing the absorbed dose, per unit activity and time, as a function of depth and lesion dimension. Based on this LUT, a dedicated tool in Matlab was developed for the automatic calculation of the treatment time entering as input parameters the area and depth of the lesion, the target dose and the ^{188}Re activity applied on the sheet covering the target. The tool was also implemented for an immediate estimation during the treatment of the dose in-depth profile, the DVH, the average and the maximum dose to the lesion. Results: The results of skin absorbed dose obtained with the two codes were consistent within the 10% in the range of 0.05-3mm and within the 3% in the range of 0.5 to 2mm. The tool was used for the treatment of 93 NMSC lesions in 83 patients. Mean thickness invasion 1.2mm (range 0.2-3.0mm); mean surface area 7.3cm2 (range 1-60cm2); mean treatment time 79 minutes (range 21-285 minutes); mean applied activity 302MBq (range 36-1300MBq); mean prescribed dose 26Gy (range 10-55Gy), while the average absorbed dose was 54Gy (range 18-126Gy). **Conclusion:** The developed software provides a powerful, MC-based, tool for real-time estimation of treatment parameters (i.e. activity and time), personalized depending on the prescribed dose and lesion characteristics. **References:** None

EP-29

Wednesday, October 20 - Saturday, October 23, 2021

e-Poster Area, release on Wednesday, October 20 at 09:00

Technical Studies -> Radiopharmacy/ Radiochemistry -> New Radiopharmaceuticals - SPECT

EP-124

Evaluation of new ^{99m}Tc-labeled enrofloxacin derivatives as potential infection- or tumor-specific imaging agents

D. Papagiannopoulou[1], G. Tzovas[1], L. Papadopoulou[1], M. Kakafika[1], I. Iakovou[2];
[1]Aristotle University of Thessaloniki, School of Pharmacy, Thessaloniki, GREECE, [2]Aristotle University of Thessaloniki, Medical School, Thessaloniki, GREECE.

Aim/Introduction: ^{99m}Tc is a useful radionuclide with suitable properties in SPECT imaging and low cost for widespread use. Infection-specific radiopharmaceuticals are useful tools in nuclear medicine and as a result a series of ^{99m}Tc-fluoroquinolones have been evaluated in the past. Also, fluoroquinolones functionalized at the 3-carboxylate position were shown to have antitumoral properties. In this work, a series of 3-carboxylate-enrofloxacin derivatives labeled with the ^{99m}Tc-tricarbonyl core were evaluated in vitro and in vivo for the ability to target oedema due to bacterial infection as well as tumors. **Materials and Methods:** Three enrofloxacin derivatives erx-dpa, erx-ida and erx-pama were labeled with [^{99m}Tc][Tc(CO)$_3$] precursor. For the in vitro uptake studies, a) Escherichia Coli bacteria (2x10^8 cells/0,2 mL saline), alive and heat-killed, were incubated with the ^{99m}Tc-tracers for 1 h at 37 °C and b) attached murine CT26 tumor cells (1x10^6 cells/ mL) were incubated with the ^{99m}Tc-tracers for 15 min, 1, 2, 4 h at 37 °C. The percent cell uptake was calculated after centrifugation of the cells from the supernatant. For the in vivo experiments, two groups of BALB/c mice were used, the first with bacterial infection by Escherichia coli (group A) and the second group of BALB/c mice (group B), bearing subcutaneously syngeneic murine CT26 tumors. The ^{99m}Tc-tracers were injected intravenously and the mice were euthanized at 0.5h and 2h in Group A and at 0.5 min, 1, 2 h in Group B. Results: In the in vitro studies the alive Ecoli cell uptake was found to be 2.74±0.25% for ^{99m}Tc-erx-dpa, 0.52±0.03% for ^{99m}Tc-erx-ida, 0.91±0.29% for ^{99m}Tc-erx-pama (p-values: 0.048, 0.136, 0.050). The CT26 cell uptake at 4 h was found to be 5.70±0.92% for ^{99m}Tc-erx-dpa, 0.05±0.01% for ^{99m}Tc-erx-ida, 1.05±0.15% for ^{99m}Tc-erx-pama(p-values: 0.004, 0.004, 0.009). Concerning the in vivo experiments, in group A, the inflamed/normal muscle ratio of the tracers were 0.61±0.15 for ^{99m}Tc-erx-dpa, 1.36±0.69 for ^{99m}Tc-erx-ida, 1.02±0.39 for ^{99m}Tc-erx-pama, at 2h p.i.. In group B, the CT26 tumor/blood ratio of the tracers were 0.66±0.21 for ^{99m}Tc-erx-dpa, 0.61±0.26 for ^{99m}Tc-erx-ida, 2.54±0.29 for ^{99m}Tc-erx-pama at 2h p.i.. **Conclusion:** The ^{99m}Tc-tracers accumulation in bacteria (both alive and dead) as well as in the CT26 cells is related to their lipophilicity (^{99m}Tc-erx-dpa>^{99m}Tc-erx-pama>^{99m}Tc-erx-ida). No accumulation at the site of E. coli infection was observed. Furthermore, tracer ^{99m}Tc-erx-pama exhibited favorable pharmacokinetic profile and increasing CT26 tumor/blood ratio and therefore appears to be more promising as a tumor-imaging agent. **References:** None.

EP-30

Wednesday, October 20 - Saturday, October 23, 2021

e-Poster Area, release on Wednesday, October 20 at 09:00

Technical Studies -> Radiopharmacy/ Radiochemistry -> New Radiopharmaceuticals - PET

EP-125

Synthesis of 68-Ga-NOTA-(Fab')$_2$-Trastuzumab, New PET Radiopharmaceutical for Imaging of Breast Cancer Expressing HER-2 Receptor

B. Shetye[1,2], S. Mithun[1,2], M. Pathan[1,2], P. Monteiro[1,2], M. Kameshwaran[1,2], S. Shah[1,2], S. Gupta[3,2], V. Rangarajan[1,2];
[1]Dept of Nuclear Medicine and Molecular Imaging,Tata Memorial Hospital, Mumbai, INDIA, [2]Homi Bhabha National Institute (HBNI), Deemed University, Mumbai, INDIA, [3]Department of Medical Oncology, Advanced Centre for Treatment Research & Education in Cancer, Tata Memorial Centre, Navi, Mumbai, INDIA.

Aim/Introduction: Radioimmunoconjugate of monoclonal antibody has been used for diagnostic and therapeutic purposes. Large size of antibody results in slow blood clearance, low pharmacokinetics, low tumor wall penetration and nonspecific interaction of F_c component with other cells. To overcome these drawbacks fragmented antibodies are used for synthesis of radioimmunoconjugate. PET-CT imaging system offers images with better resolution and reliable personalized attenuation correction by CT. Epidermal growth factor receptors (EGFR) are over expressed on various cancerous cells. Trastuzumab humanized IgG1 monoclonal antibody shows high affinity for human epidermal growth factor 2 (HER-2) receptors. It is used for treatment of breast cancer. The aim of our study was to perform a synthesis of of fragmented Trastuzumab antibody (Fab')$_2$ and its radiolabeling with 68-Ga using NOTA as a chelating agent. Advantages of 68Ga radionuclide are its availability in in-house radio-pharmacy and ease of synthesis which can be done as per patient requirement. **Materials and Methods:** Purification of Trastuzumab (22mg/ml) was done using PD-10 column. It was digested by immobilized pepsin. For the preparation of Trastuzumab-(Fab')$_2$ 20mM sodium acetate

(pH= 4.5) used as digestion buffer. Purified Trastuzumab and immobilized pepsin were equilibrated in digestion buffer separately. Digestion was carried out by mixing both of them together, kept in an incubator shaker water bath for 24 to 30 hrs. Purification of the product was done using 50 kilodalton ultra centrifugal filter devices by centrifugation at 1500 RPM. Its concentration was measured in spectrophotometer at 280nm. Conjugation of fragment with CHX-A-NOTA was performed keeping 1:10 molar concentration using standard protocol (1). pH of $68GaCl_3$ obtained from 68Ge/68Ga generator was adjusted to 4.5 using 0.1M sodium acetate buffer (pH= 6). 3mg of Trastuzumab-$(Fab')_2$ and $68GaCl_3$ were mixed together and incubated for 15 min at room temperature. Reaction mixer was purified in a PD-10 column using 0.05M phosphate buffer (pH= 7.4). Final product was passed through 0.22µ Millipore filter. Radiochemical purity was determined using 10mM sodium citrate as a mobile phase. Stability was determined till 2 hours. Results: Fragmentation of Trastuzumab to (Fab'-2) using immobilized pepsin and its purification resulted in a yield of 60-70%. Radiochemical purity was >98%. Stability till 2hrs was 98%. **Conclusion:** Our work resulted in efficient fragmentation of Trastuzumab to (Fab'-2). 68Ga-NOTA(Fab'2)- Trastuzumab showed impressive radiochemical purity and stability. **References:** Kameswaran M, Pandey U, Gamre N, Sarma HD, Dash A. Preparation of 177Lu-Trastuzumab injection for treatment of breast cancer. Applied Radiation and Isotope148(2019) 184-190

EP-126

Preparation and preclinical studies of ^{64}Cu-NOTA-antiCD20 for clinical use in PET imaging of B-cell Non-Hodgkin's Lymphoma

B. Alirezapour[1], S. Shahhosseini[2], E. Aslani[2], M. Hashemizadeh[3], H. Yousefnia[1], G. Aslani[1];
[1]Nuclear Science and Technology Research Institute (NSTRI), Tehran, IRAN, ISLAMIC REPUBLIC OF, [2]School of Pharmacy, Shahid Beheshti University of Medical Sciences, Tehran, IRAN, ISLAMIC REPUBLIC OF, [3]Pars Isotope Company, Tehran, IRAN, ISLAMIC REPUBLIC OF.

Aim/Introduction: Radiolabeled monoclonal antibodies have shown great promise for cancer diagnosis and therapy. Rituximab is a monoclonal chimeric antibody which has been approved by US FDA for immunotherapy of Non-Hodgkins' lymphoma (NHL). In the present study, we prepared Rituximab as an anti-CD20 antibody via identical novel chelator, NOTA (p-SCN-Bn-NOTA) labeled with ^{64}Cu ($T_{1/2}$ = 12.8 h, β+ = 17%, β− = 39%, EC = 43%) and performed preliminary biodistribution studies in mouse bearing tumor. **Materials and Methods:** Rituximab (5 mg) was conjugated with NOTA (Macrocyclics B-605), the average number of the chelator conjugated per mAb was calculated and total concentration was determined by spectrophotometrically. NOTA-Rituximab was labeled with 64Cu (10 mCi, 0.37 GBq) then Radiochemical purity and immunoreactivity by Raji cell line and serum stability of 64Cu- NOTA-Rituximab were determined. The biodistribution studies and radioimmunoscintigraphy were performed in SCID/Nude mice bearing Raji cell (64Cu - NOTA- Rituximab i.v., 100 µl, 20±5 µg mAb , 6, 12, 24 and 48). Results: 64Cu-NOTA-Rituximab was prepared (RCP= 99.0% ± 0.4, Specific activity 4.9 ± 0.7 µCi/µg). Conjugation reaction of chelator (25 molar excess ratio) to antibody resulted in a product with the average number of chelators attached to a mAb (c/a) of 2.6 ± 0.4. Immunoreaction of 64Cu- NOTA-Rituximab complex towards CD20 antigen was determined by RIA and the complex showed high immunoreactivity towards CD20. In vitro and in vivo stability of radioimmunoconjugate was investigated respectively in PBS and blood serum by RTLC method. In vitro stability showed more than 97% ± 1.5 in the PBS and 90% ± 2.2 in the serum over 24 h. The Immunoreactivity of the radiolabeled anti-CD20 towards Raji cell line was done by using Lindmo assay protocol. Under these conditions, the immunoreactivity of the radioimmunoconjugate was found to be 0.84. The biodistribution of 64Cu-NOTA-Rituximab complex in normal and SCID/Nude tumor bearing mice at 6, 12, 24 and 48 after intravenous administration, expressed as percentage of injected dose per gram of tissue (%ID/g). Biodistribution and imaging studies at 24 and 48 h post-injection revealed the specific localization of complex at the site of tumors. **Conclusion:** 64Cu-NOTA-Rituximab is a potential compound for PET imaging of Non-Hodgkin's Lymphoma (NHL) in oncology. **References:** None

EP-31

Wednesday, October 20 - Saturday, October 23, 2021

e-Poster Area, release on Wednesday, October 20 at 09:00

Technical Studies -> Radiopharmacy/ Radiochemistry -> Radiopharmaceutical Preparation and Quality Control

EP-127

In vitro stability assessment of in-house labeled [^{68}Ga] Ga-EDTA

K. Chitnis[1,2], A. K. Jha[1,2], S. Mithun[1,2], A. Nautiyal[1,2], P. Bhardwaj[1,2], V. Rangarajan[1,2];
[1]Tata Memorial Hospital, Mumbai, INDIA, [2]Homi Bhabha National Institute (HBNI), Deemed University, Mumbai, INDIA.

Aim/Introduction: GFR study is performed using [^{99m}Tc] Tc-DTPA to assess renal function by gamma camera or plasma sampling method. [^{68}Ga]Ga-EDTA is another radiopharmaceutical which can be used as an alternative of [^{99m}Tc]Tc-DTPA to perform GFR study on Positron Emission Tomograpy and plasma sampling method [1]. Aim of our study was to optimize the formulation of [^{68}Ga]Ga-EDTA and assess the stability of EDTA stock solution and [^{68}Ga]Ga-EDTA

preparation. **Materials and Methods:** The reconstitution of 0.125M Ethylenediamine Tetra Acetic Acid (EDTA) was performed by adding 2.3265 g of anhydrous EDTA (>99.99% purity) in 50 ml of ultra-pure water under aseptic conditions and mixed well to dissolve completely, was called stock solution. The formulation of [^{68}Ga]Ga-EDTA was performed in two steps ; first 0.1ml of 0.125M EDTA was added in 0.9ml 0.1M Sodium Acetate buffer and mixed well; subsequently mixture was aseptically transferred in freshly eluted [^{68}Ga]$GaCl_3$ in 4 ml of 0.05M HCl. The reaction mixture was incubated for 10 min at room temperature to complete the reaction. Radiochemical purity (RCP) was performed using ITLC strips as stationary and 0.1M Tri-Sodium Citrate as mobile phase.Stability of stock solution was assessed by performing RCP of [^{68}Ga]Ga-EDTA formulation post 1, 10, 20, 40, 76 days post reconstitution of stock solution. Stability of [^{68}Ga]Ga-EDTA formulation was assessed by performing RCP of [^{68}Ga]Ga-EDTA at 0hr, 1hr, 2hr, 3hr and 5hr post formulation. Results: Stability study of stock solution was performed for two stock solutions and RCP was performed 10 times at each time point. The average RCP across all the time points for two stock solutions was found to be 98.36% (±0.60%). The average decrease in RCP from the first day to last day was found to be 1.69%.Stability of [^{68}Ga]Ga-EDTA formulation was performed for both the stock solutions 2 times at each time point. The average RCP across all time points post formulation was found to be 96.91% (±1.7%). Average RCP at 5 hour post formulation was found to be 94.18% (±1.2%) which is 4.7% less than 0hr RCP which is 98.91% (±0.8%). **Conclusion:** Through our study we are able to demonstrate the stability of EDTA stock solution up to 76 days post reconstitution and [^{68}Ga]Ga-EDTA formulation up to 5-hours post synthesis. **References:** 1.Jha AK, Mithun S, et.al., Optimization of in-house synthesis of [^{68}Ga]Ga-ethylenediaminetetraacetic acid for glomerular filtration rate estimation by positron emission tomography and plasma sampling method, Indian J Nucl Med 2016; 31: 5 (Sup): 1-61

EP-128

Preparation and optimization of the radiolabeling method of111In-PSMA-INER-56

S. Chen[1], *S. Lo*[2], *S. Lo*[2], *M. Li*[2], *M. Chen*[2], *W. Lo*[2], *S. Li*[2];
[1]*Institute of nuclear energy research, Taoyuan, TAIWAN,*
[2]*Institute of Nuclear Energy Research, Taoyuan, TAIWAN.*

Aim/Introduction: Prostate cancer is the second popular cancer for men and the vast majority of patients with clinically advanced prostate cancer are found to have cancer cells metastasized to the bones. The prostate-specific membrane antigen (PSMA) is being recognized as over-expressed in the primary and metastasized state of prostate cancer and low-expressed in normal tissues in recent research. Therefore, it is a target for prostate cancer to be used for diagnostic and therapy. We design^{111}In-PSMA-INER-56, a long-acting, targeted drug for prostate cancer, which has higher affinity and absorption into LnCaP cells. Our goal is to optimize reaction conditions for the radiolabeling of ^{111}In-PSMA-INER-56. We expect the kinetic result will be applied for future clinical translation. **Materials and Methods:** The albumin-binding PSMA precursor PSMA-INER-56 was analyzed by HPLC to have a purity of 90%. During the radiolabeling process, the PSMA-INER-56 precursor (10~40μg/μL, dissolved in DMSO) was added with 1M NaOAc buffer (PH 6), then mixed with 0.1N HCl $^{111}InCl_3$ solution (6mCi, eluted from INER). Incubate a total volume of 300 μL reactive vials in a 95℃ temperature-controlled heater for 5-20 min. Finally, the radiolabeling efficiency of ^{111}In-PSMA-INER-56 was determined by ITLC (Instant Thin Layer Chromatography), and the radio purity was analyzed by the HPLC system. Results: In our research, we observed that radioactivity and precursor concentration are the main factors in the radiolabeling of the experiment of ^{111}In-PSMA-INER-56. The kinetics of PSMA-INER-56 labeled with ^{111}In is the best at pH6. Using 10μg of PSMA-INER-56 precursor can be completely radiolabeled with ^{111}In at 95℃ in 5min when the specific activity of ^{111}In was up to 280μCi/μL. The radiochemical yield can reach more than 90%. When the specific activity of ^{111}In is 100~280μCi/μL, only the increased amount of PSMA-INER-56, more than 30μg, can obtain a greater than 90% radiochemical yield of ^{111}In-PSMA-INER-56. **Conclusion:** ^{111}In-PSMA-INER-56 is a potential radiopharmaceutical candidate for prostate cancer. We investigated that ^{111}In-PSMA-INER-56 has a better labeling yield at pH 6 (1M NaOAc buffer). The best labeling condition for ^{111}In-PSMA-INER-56 is to use 30μg of PSMA-INER-56 precursor, added to pH6 (1M NaOAc buffer), and mixed with radioactivity 6mCi(280μCi/μL)of ^{111}In, react in 95℃ within 10 min. We can obtain 90% of the radiochemical purity of ^{111}In-PSMA-INER-56. The radiosynthesis conditions can be provided for the subsequent stability test of ^{111}In-PSMA-INER-56. **References:** [1].W.A.P.B. EJNMMI 2003 Jun;30(6):917-20[2]. M.W. J Nucl Med 2015; 56:1169-1176[3]. A.S. ACS Omega 2018, 3, 8278−8287

EP-129

^{188}Re-glucoheptonate for targeted radiotherapy

M. Karamivand*, M. Davarpanah;*
Pars Isotope, Tehran, IRAN, ISLAMIC REPUBLIC OF.

Aim/Introduction: The aim of this study was to develop the kit-based synthesis of the agent on a therapeutic scale, to assess its stability in vivo, and to obtain preliminary biodistribution, prior to evaluation of its potential as a targeted radiotherapy agent. **Materials and Methods:** Dissolve 3 mg of stannous chloride dihydrate using 0.5 ml of 0.2N HCl just before it is added to the final solution. Dissolve 5 g of calcium glucoheptonate in approximately 0.5 mL of water for injection, Slowly add solution stannous chloride dihydrate to the GH solution and stirring. Adjust the pH to between 3.5 and 5.5 using 1N NaOH or 1N HCl and heat in a

boiling water bath for 15 min. Reconstitute the freeze-dried kit using 2 mL of freshly eluted $^{188}ReO4^-$ solution containing a maximum of 80 mCi of activity.Stir for 1 min and use after 20 min. Results: The results showed aselective attachment to tumor tissues, particularly to metastaticbone cancer originating from prostatic carcinoma, similar to that of the technetium analog. In this study, ^{188}Re-GH was synthesized, factors influencing the yield of ^{188}Re-GH were optimized, and finally a freeze-dried kit was formulated which gave a radiolabeling yield of 97%. The pharmacokinetics behavior of ^{188}Re-GH and ^{99m}Tc-GH in rats was identical, hence it is concluded that ^{188}Re-GH is quite suitable for intracoronary radiation therapy and the dose to critical organs be minimal in case of balloon rupture. **Conclusion:** Radionuclides ^{188}Re play a considerable role in the development of new target-specific therapeutic radiopharmaceuticals. **References:** None

EP-32

Wednesday, October 20 - Saturday, October 23, 2021

e-Poster Area, release on Wednesday, October 20 at 09:00

Covid Studies -> Clinical Study

EP-130

Comparative Study Before And During The SARS-CoV-2 Pandemic In Breast Cancer With SLNB After Neoadjuvant Chemotherapy

N. Alvarez Mena, F. Sebastián Palacid, P. Turbay Eljach, C. García García, B. Pérez López, C. Gamazo Laherrán, M. Alonso Rodríguez, A. Sainz Esteban, M. González Soto, M. Ruiz Gómez, R. Ruano Pérez; Hospital Clínico Universitario de Valladolid, Valladolid, SPAIN.

Aim/Introduction: To evaluate the impact of the COVID-19 pandemic situation on breast cancer candidates for sentinel lymph node biopsy (SLNB) after neoadjuvant chemotherapy (NAC). **Materials and Methods:** Comparative study of women with breast cancer undergoing NAC and intraoperative detection of SLNB (eco and MRI negative axilla involvement after NAC) between the 12 months prior to the pandemic (February 2019 to February 2020) and the 12 months influenced by the pandemic (March 2020 to March 2021).Variables such as age, reason for referral, pre-NAC tumour size and axillary involvement (cTN status), post-NAC axillary pathological response (ypTN), SLNB result and type of surgery were analysed. Results: Group A (prepandemic): 44 women. Median age 51 years (33-73), 27% from screening programme (7 positive axilla), 73% self examination. cT status: 5cT1c; 33 cT2; 6 cT3-T4. cNstatus: 18 cN0; 26 cN+. After surgery 64% pathological complete response (pCR). 29 (66%) breast conservative surgery.Group B (pandemic): 44 women. Median age 52 years (27-73), 9% from screening programme. cT status: 9cT1c; 29cT2; 6 cT3-T4. cNstatus: 29 cN0; 15 cN+. After surgery 57% pathological complete response (pCR). 31 (72%) breast conservative surgery.Comparing both periods, during SARS-CoV2 pandemic we significantly observed less cancer detection by screening (9% vs. 27%; x^2 $p<0.05$), and a lower percentage of patients with pre-NAC axillary involvement (34% vs. 59%; x^2 $p<0.05$). No statistical differences in % SN visualization and detection, % of axillary dissection, % post-NAC pathological complete response (57% vs. 64%; p=0.6). **Conclusion:** The COVID-19 pandemic has diminished the early detection of breast cancer subsidiary to SLNB after NAC. The lower number of patients referred with initial axillary involvement could indicate a higher tumour aggressiveness at the time of diagnosis and, consequently, a lower pathological response to chemotherapy, not being suitable candidates for SLNB. **References:** none

EP-131

^{18}F-FDG brain PET in post-SARS-CoV-2 infection with neurological involvement:time-dependent severity of hypometabolism after the acute infection

A. Martini[1,2], G. Carli[3], L. Kiferle[4], P. Piersanti[4], P. Palumbo[4], S. Morbelli[5], D. Perani[3], S. Sestini[1];
[1]Hospital Santo Stefano, Nuclear Medicine Unit, Prato, ITALY, [2]University of Florence,AUOC Careggi Nuclear Medicine Unit, Florence, ITALY, [3]University Vita Salute San Raffaele, Nuclear Medicine Unit Division of Neuroscience, Milan, ITALY, [4]Hospital Santo Stefano Neurology Unit, Prato, ITALY, [5]University of Genoa, Hospital San Martino, Genoa, ITALY.

Aim/Introduction: Although clinical reports have established that coronaviruses have neuro-invasive potential, little evidence exists that primary cerebral infection is a significant contributing factor. Aim of study was to characterize the time-dependent functional impairment of brain areas in SARS-CoV-2 patients with newly originated neurological symptoms and to provide deeper understanding of physiopathology underlying central nervous system involvement. **Materials and Methods:** we included nine patients with newly originated neurological symptoms due to past SARS-CoV-2 acute infection and five patients with neurological symptoms and ongoing acute SARS-CoV-2 infection. All patients with past SARS-CoV-2 infection underwent baseline PET scan together with neurological cognitive assessment at different time-points from the acute phase. All patients with acute SARS-CoV-2 infection underwent a PET scan during disease acute phase but without assessment of neurological performance due to critical conditions. One patient also performed follow-up PET scan after significant remission of clinical symptoms. Brain metabolism was analysed using an optimised and validated voxel-based SPM method at the single-subject level ($p = 0.01$), based on comparisons with a large and well-selected dataset of healthy control. Results: The five patients with ongoing SARS-CoV-2 infection featured widespread hypometabolism affecting almost all

brain cortices. Five patients undergoing PET scan within two months to SARS-CoV-2 acute infection showed extended hypometabolism and pathological MMSE values, involving the orbito- and pre-frontal cortex, and temporo-parietal cortex. The three patients undergoing PET scans five months later from SARS-CoV-2 acute phase featured a rather normal PET and cognitive scores. Results of scans performed in the patient respectively closed to the acute phase and during clinical remission showed an ongoing infection-like pattern with extended and severe hypometabolism affecting almost all brain cortices at first acquisition and only a slight hypometabolism in orbitofrontal and medial frontal cortices at second acquisition. **Conclusion:** results show that patients with ongoing SARS-CoV-2 infection featured a widespread hypometabolism affecting almost all brain cortices, while the scans of patients with post SARS-CoV-2 infection show that a rather extended cortical hypometabolism continues to be present immediately after the acute phase and that, along with remission of clinical neurological symptoms, such hypometabolism reduces progressively as a function of time from the onset of acute phase. These findings suggest that cortical functional impairment observed in patients with neuro-SARS-CoV-2 infection is likely to be transient and almost reversible, possibly due to synergistic effects of systemic virus-mediated inflammation sustained by systemic cytokine release and transient hypoxia inducing local microglial activation. **References:** none

EP-132

Can FDG PET Predict Covid 19 Disease Severity and Discharge Time

F. Beytur[1], S. Sager[1], A. N. Aktaş[2], R. Karaali[2], A. Nazari[1], F. Aghazada[1], S. Asa[1], L. Uslu-Beşli[1], H. B. Sayman[1], K. Sönmezoğlu[1]; [1]Cerrahpasa Faculty of Medicine, Nuclear Medicine Department, Istanbul, TURKEY, [2]Cerrahpasa Faculty of Medicine, Infectious Diseases Department, Istanbul, TURKEY.

Aim/Introduction: Covid19 disease(CD) has spread among the world and infected millions of people. It affects most commonly the lungs and makes ground-glass opacity(GGO) nodules that contain inflammatory cells. At our hospital, many patients have been hospitalized because of CD. Some of these patients had malignancies or were suspected of malignancies and they underwent F-18 FDG PET for their malignancies. Inflammatory cells express GLUT-1 receptors more than normal cells thus shows high FDG avidity. We aimed to evaluate the prognosis of CD with FDG PET results. **Materials and Methods:** We evaluated 10 Covid19 patients' data retrospectively who undergone FDG PET scan between April 2020 and March 2021 while being hospitalized for CD at our hospital. 6 patients' Covid19 PCR tests were positive, 4 of them were negative. These 4 patients diagnosed as CD with thorax CT. 4 of these 10 patients are lymphoma, 2 of them are lung cancer, 1 is SLL/CLL, 1 is larynx cancer, 1 is ovarian cancer and 1 is gastric cancer. These patients were followed with daily inflammatory blood parameters such as CRP, ferritin, fibrinogen, D-dimer, lymphocyte count while being hospitalized. We compared SUVmax values of lung lesions with these inflammatory parameters on the day of the FDG PET scan done and the patients' discharge time after the FDG PET scan. None of these lung lesions were associated with the patients' primary malignancy. Results: SUVmax values of the lung lesions ranged from 1,1 to 17,03. Comparison of SUVmax and discharge time were found statistically significant (p=0.003). So, lower SUVmax predicts less hospitalization time. And also at one patient, SUVmax was the second-highest as 13,23 and this patient died 3 days after PET scan at ICU. Another patient's SUVmax was less than this (6,14) and this patient died 38 days after the PET scan. Comparison of any of these inflammatory parameters with SUVmax was not found to be significant. **Conclusion:** At CD patients FDG PET might predict discharge time and if the disease will be lethal. However, prospective trials should be done to determine this accurately. **References:** None

EP-133

Aspects of FDG-avid lymph nodes on FDG PET/CT following COVID-19 vaccines

P. Grecu[1,2], H. Tissot[1], A. M. Bettaieb[1], T. Kamoun[1], C. Garcia[1]; [1]Nuclear Medicine Section, Diagnostic Imaging Department, Gustave Roussy, Villejuif, FRANCE, [2]Nuclear Medicine Laboratory, "Sf. Spiridon" County Emergency Hospital, Iasi, ROMANIA.

Aim/Introduction: FDG-avid reactive axillary lymph nodes following H1N1 or influenza vaccines are a known pitfall (1, 2). Recently, FDG-avid reactive lymphadenopathy on Positron Emission Tomography-Computed Tomography (PET/CT) has also reported in patients following COVID-19 vaccination (3). The aim of our study was to describe the distribution pattern for these findings following three different COVID-19 vaccines. **Materials and Methods:** This is a retrospective study. We analyzed 32 consecutive patients who were referred to perform a FDG PET/CT for oncological indications and who have previously received the COVID-19 vaccine. Results: The patients were vaccinated with two types of mARN vaccine (Pfizer/BioNTech or Moderna) and one viral vector vaccine (AstraZeneca/Oxford). Two patients vaccinated more than 4 weeks prior to FDG-PET/CT had normal loco-regional FDG-avidity lymph nodes. The rest of them (n=30) had a variable FDG-avidity lymph nodes (mean SUV 4.45 ± 2.59). The uptake intensity varying according to the time between vaccination and FDG-PET/CT (mean SUV 5.83 ± 3.25 for the first week vs mean SUV 2.57 ± 0.94 after 4 weeks) and the number of doses (mean SUV 5.07 ± 3.30 for the first dose vs mean SUV 6.20 ± 3.60 for the second dose, evaluated in the first week). All the reactive lymph nodes were located axillary and less frequent on supraclavicular stations ipsilateral of the vaccine's site. All had preserved fatty hilum and ovoid

shape (mean small diameter 7.87 mm ± 3.65). **Conclusion:** In our small cohort of patients, we found a high variability of FDG-avidity reactive loco-regional lymph nodes following three different COVID-19 vaccines. All vaccines have the same distribution pattern with ipsilateral FDG-avid reactive axillary lymph nodes and less frequently on supraclavicular stations, FDG uptake decreasing gradually over time and preserving normal anatomical features. This data could be important when interpreting the FDG-PET/CT images in an oncologic setting of patients. **References:** 1. Ayati, Narjess et al. "Generalized Lymph Node Activation after Influenza Vaccination on ^{18}F FDG-PET/CT Imaging, an Important Pitfall in PET Interpretation." Asia Oceania journal of nuclear medicine & biology vol. 5,2 (2017): 148-150. doi:10.22038/aojnmb.2017.8702 2. Burger, Irene A et al. "Incidence and intensity of F-18 FDG uptake after vaccination with H1N1 vaccine." Clinical nuclear medicine vol. 36,10 (2011): 848-53. doi:10.1097/RLU.0b013e3182177322 3. Özütemiz C, Krystosek LA, Church AL, Chauhan A, Ellermann JM, Domingo-Musibay E et al. Lymphadenopathy in COVID-19 Vaccine Recipients: Diagnostic Dilemma in Oncology Patients. Radiology. 2021 Feb 24. https://doi.org/10.1148/radiol.2021210275

EP-134

Management of differentiated thyroid cancer through nuclear medicine facilities during Covid-19 emergency: the telemedicine challenge

M. Manganelli, *M. Klain, C. Nappi, E. Zampella, V. Gaudieri, S. Maurea, M. De Risi, F. Volpe, E. Caiazzo, D. De Lucia, R. Bologna, L. Piscopo, M. Schlumberger, A. Cuocolo;*
Department of Advanced Biomedical Sciences, University Federico II, Naples, ITALY.

Aim/Introduction: From March 11, 2020 when the World Health Organization characterized the novel coronavirus Covid-19 outbreak as a pandemic, healthcare services were suddenly called to deal with new critical issues including the need to maintain the planned therapeutic management and cancer patient surveillance using all available tools, including new technologies. We investigated whether a telemedicine service (TMS) carried out during Covid-19 pandemic impacted on differentiated thyroid cancer (DTC) patient management. **Materials and Methods:** We retrospectively reviewed the number and findings of outpatient visits in DTC subjects referred at our Radiometabolic Unit between March 11, 2020, and May 31, 2020, during Covid-19 pandemic. Office visits scheduled between March and May 2020 were converted in teleconsultation advising all patients planned for an in-ward access to use TMS for all clinical necessity. The number and findings of DTC patients evaluated by in-ward access in the corresponding period of 2019 were also assessed for direct comparison. Results: During Covid-19 pandemic 445 TMS visits were performed. As compared with the corresponding period of 2019 by in-ward access (n=525), only 15% of outpatient evaluations were missed. A 28% numeric decrease of first accesses for newly diagnosed DTC cases was observed, from 75 in 2019 to 54 during the corresponding period in 2020. While the mean age and percentage of male gender during Covid-19 did not differ compared with the corresponding period of 2019 (50±15 vs. 49±14 years and 23% vs. 20% male gender respectively, both P=NS), patients' proportion with classical papillary histology was significantly lower during the pandemic compared with those evaluated in the corresponding months of 2019 (60% vs. 68%, P<0.02). Follow-up visits results obtained in outpatients by TMS during the emergency and by in-ward access during the corresponding period of 2019 were analyzed according to three subgroups of patients: 1) those requiring a further RAI or surgical treatment (8/450 vs. 7/391); 2) those requiring further tests (28/450 vs. 34/391); and 3) those with unremarkable findings (414/450 vs. 350/391). Patients' proportion in each subgroup did not differ between the two considered periods (all P=NS). All scheduled RAI therapies during the pandemic were performed after telephone triage and pharyngeal swab. **Conclusion:** Our findings demonstrate the telemedicine tools utility to avoid the potential negative impact of interruption or diagnostic and/or therapeutic procedures postponement. Therefore, investments in medical network system development, including implementation of telehealth approaches, should be encouraged at national and international levels. **References:** none

EP-135

Nuclear medicine lung perfusion imaging after COVID-19: review of a patient cohort

B. Martins, *C. V. Pinto, V. Sousa, C. Loewenthal;*
Hospital da Luz, Lisboa, PORTUGAL.

Aim/Introduction: In addition to fibrotic pulmonary sequelae after severe symptomatic disease, another important cause of morbidity is increased likelihood of thromboembolic events in systemic and pulmonary circulations, especially in patients who required hospitalization, but also in less severe and even asymptomatic patients. A few months after the first wave, first cases of "post-covid syndrome" began to appear; in this context, in October 2020 we received the first patient for pulmonary thromboembolism (PTE) exclusion. **Materials and Methods:** Retrospective analysis of the clinical file of patients who underwent pulmonary perfusion scintigraphy with ^{99m}Tc-albumin macroaggregates, to exclude post-COVID PTE, between October 2020 and April 2021 [N = 13, mean age 47 years (min 25, max 71), 4 men, 8 women]. Personal history, acute illness symptoms, need for hospitalization and all images and reports were reviewed, comparing the results with previous radiological exams. In patients diagnosed with PTE on scintigraphy, we confirmed that therapy had been instituted and inquired about persistence of symptoms.

Results: Of the 13 patients studied, 6/13 (46%) were positive for PTE on scintigraphy (3 subsegmental; 3 segmental, 3 unilateral, 3 bilateral; mean age 47 - min. 25, max. 71 -, 3/6 below 35 years old). This assessment was blindly compared during the review, having been 100% concordant. At the time of pulmonary perfusion scintigraphy, all patients reported tiredness for small efforts and one had dyspnea. Of the 6 positive patients on scintigraphy, 4 were female, 3 had a relevant personal history [(DM2(3), obesity(3), ex-smokers(2), high blood pressure(1)]. Eighty percent (5/6) had acute symptomatic disease [tiredness(3) cough(2), fever(2), headache(2), dyspnea(1), diarrhea(1) and anosmia(1)] and 2/6 required hospitalization out of the ICU. Four of them (4/6) had previously undergone radiological examinations (chest X-ray or CT), with 3/6 having findings compatible with COVID acute disease. The 6 patients diagnosed with PTE all began anticoagulation [rivaroxaban (5), apixaban (1)] after perfusion scintigraphy, currently under surveillance and monitoring of therapeutic efficacy. **Conclusion:** Forty six percent of studied patients were positive for PTE (even with negative chest CT and the majority with mild acute disease) leading to changes in therapeutic management. Bearing in mind that Portugal was much more affected by the 2nd wave of the pandemic (that peaked in the beginning of 2021), it is expected that complications after acute illness increase significantly in the coming months, so we will continue studying the relationship between the disease and development of pulmonary thromboembolic sequelae. **References:** none

EP-136

Molecular Imaging Findings Update on the NCI-NCTN Clinical Trial: Natural History of COVID-19 in Cancer Patients

M. Knopp[1], C. Nealer[1], P. Robson[1], E. Huang[2], B. Rini[3], L. A. Korde[4], L. K. Shankar[4];

[1]The Ohio State University Wexner Medical Center, Columbus, OH, UNITED STATES OF AMERICA, [2]National Cancer Institute, Rockville, MD, UNITED STATES OF AMERICA, [3]Vanderbilt Ingram Cancer Center, Nashville, TN, UNITED STATES OF AMERICA, [4]National Cancer Institute, Bethesda, MD, UNITED STATES OF AMERICA.

Aim/Introduction: In order to better understand the biologic sequela of COVID-19 as a growing co-morbidity in cancer patients, the National Cancer Institute initiated a natural history clinical trial (NCI-COVID) via its National Clinical Trial Network and its National Community Oncology Research Program. Clinical data, bio specimens, CT, MRI and PET/CT imaging performed as part of clinical care within the initial 6 months after COVID-19 diagnosis are being collected to assess the impact of COVID-19 on lesions, such as flare, nodal status or accelerated progression, and to determine the potential diagnostic difficulties in evaluating cancer burden due to associated abnormalities from COVID-19. **Materials and Methods:** Images collected pre-COVID infection are being used as reference. COVID-19 management-related imaging which document organ involvement and complications are being collected via the NCI Imaging and Radiation Oncology Core. This report focuses on the related findings there are being observed in molecular imaging studies performed during the continued oncology care of the patients in all age ranges including pediatric. Results: At the time of this submission, 1172 patients were enrolled in the trial from 253 unique sites, of which 826 had submitted imaging data. Of this imaging data, 127 were PET/CT studies, 93 performed prior to COVID-19 infection, 13 during active infection, and 21 post-infection. At the time, 16 patients had repeated imaging, 9 prior to and during active infection and 7 before and after infection. The most recent information shareable will be presented just in time at EANM 2021, along with the reporting of any challenges or learning points from the organization of such a study. Information will also be provided on how limited imaging data may be made available and timelines of the NCI The Cancer Imaging Archive. **Conclusion:** This report will provide the current status of experience, organization, and assessment plans of the NCI-NCTN Clinical Trial: Natural History of COVID-19 in Cancer Patients and present update on relevant observations in those patients having received a molecular imaging study. **References:** none

EP-137

GSMPI can predict early cardiac dysfunction in elderly high-risk DTC patients after TSH suppression treatment

Y. Liu;

Zhengzhou University, Zhengzhou, CHINA.

Aim/Introduction: To investigate the relationship between cardiac dysfunction and duration of treatment after TSH suppression therapy in elderly high-risk DTC patients. **Materials and Methods:** GSMPI data of elderly high-risk DTC patients with aged 60-64 years from September 2015 to September 2016 at the First Affiliated Hospital of Zhengzhou University were collected. Patients were arranged for GSMPI as a baseline one month after total thyroidectomy, subsequently 131-iodine treatment and TSH suppression treatment were performed. Patients were divided into 2 groups according to the duration of TSH suppression treatment. GSMPI were performed after the 12th month treatment for group A and 18 months after treatment for group B. Left ventricular systolic and diastolic function parameter, and myocardial perfusion were obtained. Results: A total of 46 elderly high-risk DTC patients with 60-64 years old were enrolled. The peak filling rate of group A and group B decreased significantly with the increase of TSH suppression time, from 3.28±0.59 to 2.59±0.51 after treatment for 12 months , and decreased to 2.03 ± 0.47 for 18 months. One-way analysis of variance showed that there was a significant difference in PFR between different groups (P = 0.01). There were no significant

differences in the peak ejection rate, LVEF, the phase angle, phase standard deviation , entropy, the total score of resting perfusion and the total perfusion defect between different groups (P > 0.05). **Conclusion:** TSH suppression therapy can induce cardiac dysfunction in 60-64 years old high-risk DTC patients. Peak filling rate can predict cardiac dysfunction early and provide a basis for individualized diagnosis and treatment and prognosis evaluation. **References:** 1. HAUGEN BR, ALEXANDER EK, BIBLE KC, et al. 2015 American Thyroid Association management guidelines for adult patients with thyroid nodules and differentiated thyroid cancer: The American thyroid association guidelines task force on thyroid nodules and differentiated thyroid cancer[J]. Thyroid, 2016,26(1):1-133.2.Betancur J, Otaki Y, Motwani M, et al. Prognostic value of combined clinical and myocardial perfusion imaging data using machine learning[J].JACC Cardiovasc Imaging, 2017: 2406.

EP-33

Wednesday, October 20 - Saturday, October 23, 2021

e-Poster Area, release on Wednesday, October 20 at 09:00

Covid Studies -> Other Study (incl. Organisation)

EP-138

Impact of COVID-19 pandemic on diagnostic Nuclear Medicine practice in Greece - a biannual survey (2019-2020)

J. Koutsikos[1,2], P. Georgoulias[3], S. Koukouraki[4], L. Lamprakos[5], I. Iakovou[6], S. Tsiouris[7], D. Apostolopoulos[8], T. Paschalis[9], A. Fotopoulos[7];

[1]Nuclear Medicine Department, 401 General Military Hospital, Athens, GREECE, [2]Nuclear Medicine Department, Henry Dunant Hospital Center, Athens, GREECE, [3]Nuclear Medicine Laboratory, University of Thessaly, University Hospital of Larissa, Larissa, GREECE, [4]Department of Nuclear Medicine, School of Medicine, University of Crete, Heraklion, Crete, GREECE, [5]Nuclear Medicine Department, Iatropolis Medical Center, Athens, GREECE, [6]2nd Department of Nuclear Medicine, Aristotle University, AHEPA hsp, Thessaloniki, GREECE, [7]Nuclear Medicine Department, University Hospital of Ioannina, Ioannina, GREECE, [8]Department of Nuclear Medicine, University Hospital of Patras, Rion Patras, GREECE, [9]Greek National Organization for the Provision of Health Services, Strategic Planning Division, Athens, GREECE.

Aim/Introduction: The COVID-19 pandemic in Greece is part of the worldwide pandemic of coronavirus disease 2019 caused by the severe acute respiratory syndrome coronavirus 2 (SARS-CoV-2). The first case in Greece was confirmed on February 26, 2020 while the first death report was a 66-year-old man on March 12, 2020. As of mid April 2021, there have been 308,000 confirmed cases and 9,239 deaths. The purpose of this study is to evaluate the impact of the pandemic on inpatient and outpatient nuclear medicine operations, on public and private Nuclear Medicine departments and to provide actual data for future evidence-based decisions regarding public health crises by quantifying the change in Nuclear Medicine utilisations in Greece. **Materials and Methods:** The Hellenic Society of Nuclear Medicine & Molecular Imaging (HSNM&MI), with the contribute of the Greek National Organization for the Provision of Health Services, gathered all the data regarding Nuclear medicine procedures, made at 2019 and 2020 on public and private nuclear medicine departments in Greece; the relevant data of the preceding year (2019) served are reference for comparison. The analysis included all of the faculty's diagnostic procedures by category; the prescribed number of each procedure was calculated and used for the analysis. Results: An average decline of 13% in diagnostic procedures performed in 2020 in comparison to these of 2019 (159.031 vs 138.424) was reported. March, April, and May 2020 were the most affected months. Private nuclear medicine departments had an average of 5% decline, while public nuclear medicine department an average of 27% decline. Myocardial studies decreased by an average of 18%, bone scans by 12%, thyroid studies by 19%, lung scans by 26%, kidney scan by 21% and the remaining studies by 18%. Positron emission tomography / computed tomography (PET/CT) was the only procedure that had an average increase by 8% in total, resulting as the average of 17% decline in public and 26% increase in private practice. **Conclusion:** The COVID-19 pandemic brought an annual decline in the diagnostic procedures in both public and private nuclear medicine departments. March, April, and May 2020 were the most affected months, due to restrictions announced by the Greek authorities. Public nuclear medicine departments presented a higher decline in comparison with private nuclear medicine departments due to the reduced turnout of patients in public hospital units. The private sector recorded the only reverse trend concerning PET exams that increased compared to 2019. **References:** none

EP-34

Wednesday, October 20 - Saturday, October 23, 2021

e-Poster Area, release on Wednesday, October 20 at 09:00

Bone & Joint Malignant and Benign Diseases

EP-139

Phase 1a intra-individual comparison trial of 10x ultrafast whole-body Na^{18}F digital PET/CT for assessing non-malignant and malignant osteoblastic lesions

C. Wright, K. Binzel, Y. Hsieh, E. Folefac, D. A. Diaz Pardo, D. G. Stover, M. V. Knopp;
The Ohio State University, Columbus, OH, UNITED STATES OF AMERICA.

Aim/Introduction: In patients with symptomatic bony disease, whole-body Na^{18}F PET image acquisition times (60 - 120 s/bed) are longer than desired and new approaches to markedly reduce PET image acquisition times are needed. The aim of the study is to assess an ultrafast (10x), whole-body, Na^{18}F PET imaging approach using digital PET/CT technology for the detection and assessment of osteoblastic lesions. **Materials and Methods:** This intra-individual comparison trial of whole-body dPET/CT (Vereos, Philips) was performed using target Na^{18}F doses of 185 MBq in 70 oncologic patients. Investigational dPET acquisitions were performed at a 10x faster rate of 9 s/bed (1/10 of the standard PET acquisition time starting at ~79 min post injection) and then at the standard 90 s/bed (~83 min post injection). All dPET image data sets were reconstructed using standard definition voxel volumes (4x4x4 mm^3) and Time-of-Flight. All matched and individual data sets were reviewed by a blinded reader panel using an Intellispace Portal workstation to assess image quality and lesion detectability. Results: All 70 patients had evaluable dPET datasets (n = 140) for qualitative and quantitative assessment. Qualitatively, ^{18}F uptake within normal bone, non-malignant and malignant osteoblastic lesions was visually comparable on the 9 and 90 s/bed acquisitions and no discordant lesions were identified. A total of 419 discrete Na^{18}F-avid lesions were detected on the 9 and 90 s/bed acquisitions (247 non-malignant and 145 malignant). Non-malignant lesions (often degenerative change) were noted in 69 patients and 27 patients demonstrated malignant lesions. Quantitatively, there was excellent linear correlation (R^2 = 0.97) between the SUVmax values for all 419 NaF-avid lesions between the 9 and 90 s/bed acquisitions. For both dPET acquisitions, malignant lesions demonstrated higher average SUVmax values (33.7 ± 28.1 for 90 s/bed and 28.7 ± 26.5 for 9 s/bed) than non-malignant lesions (23.2 ± 12.5 for 90 s/bed and 20.1 ± 11.4 for 9 s/bed, p<0.05). Average SUVmean values were comparable for the 9 and 90 s/bed acquisitions in terms of normal vertebral bone (5.9 ± 1.1 and 6.5 ± 1.2, respectively) and background skeletal muscle (0.65 ± 0.10 and 0.68 ± 0.12, respectively). **Conclusion:** An unmet clinical need for shorter PET acquisition times for patients with symptomatic non-malignant and/or malignant disease remains and this study demonstrates that 10x faster whole-body Na^{18}F digital PET imaging (~3 min total PET time) is achievable with no loss of overall image quality, lesion detectability or quantitative accuracy. **References:** None

EP-140

Prognostic value of quantitative [18F]FDG-PET features in patients with metastatic soft tissue sarcoma

G. Kalisvaart, W. Grootjans, J. V. Bovée, H. Gelderblom, J. A. van der Hage, M. A. van de Sande, J. L. Bloem, L. de Geus-Oei;
Leiden, Leiden University Medical Center, NETHERLANDS.

Aim/Introduction: Patients with metastatic soft tissue sarcoma (STS) have a poor prognosis. The major aim of treatment in these patients is disease control in combination with preservation of quality of life. In this regard, patient prognosis plays a pivotal role in selecting treatment strategies. Quantitative [^{18}F]FDG-PET features have shown high prognostic value in patients with non-metastatic STS and in patients with other types of malignancies. Therefore, this study aimed to determine the association between frequently used quantitative [^{18}F]FDG-PET parameters and overall survival in metastatic STS patients. **Materials and Methods:** This retrospective study included patients with STS, who received an [^{18}F]FDG-PET/CT for (re)staging, on which metastatic disease was detected. Only scans which were performed according to EANM procedure guidelines for tumour imaging: version 2.0, were included. For all STS lesions a volume of interest was determined using Philips Intellispace Portal software. For this purpose, an adaptive algorithm was applied using a threshold of 41% of the standardized uptake value (SUV) peak corrected for local background. SUVmax, SUVpeak, SUVmean, metabolic tumour volume (MTV), and total lesion glycolysis (TLG) were calculated. Clinical variables included age, gender, histologic grade, location of the primary tumour, time between diagnosis of the primary tumour and metastatic disease, and the number of tumour lesions. Cox proportional regression analysis was used to assess the prognostic value. Overall survival served as the standard of reference. Univariable analysis as well as multivariable analysis with forward variable selection was performed. P values < 0.05 were considered statistically significant. Results: A total of 29 patients were included in this study. Median follow-up in survivors was 25 months. The 2-year survival rate was 49%. Univariable analysis showed a significant association between the total number of lesions (p=0.046), SUVmax (p=0.003), SUVpeak (p=0.003), and SUVmean (p=0.01) and overall survival. SUVmax (p=0.004), SUVpeak (p=0.004), and SUVmean (p=0.006) remained the only independent predictors of overall survival after all three were separately analysed in multivariable analysis with clinical variables.

Hazards ratios for a 1 unit increase in SUVmax, SUVpeak, and SUVmean were 1.28 (95%CI = 1.08-1.51), 1.36 (95%CI = 1.11-1.68), and 2.14 (95%CI = 1.24-3.68), respectively. **Conclusion:** SUVmax, SUVpeak, and SUVmean on [^{18}F]FDG-PET/CT are predictors of overall survival in patients with metastatic STS. In these patients, [^{18}F]FDG-PET/CT scans can, therefore, be used as a valuable informative tool in the personalisation of treatment strategies. **References:** None

EP-141

Myocardial Uptake As A Casual Finding In Tc-99m HMDP Bone Scintigraphy And Its Relationship With Pathological History, Analytical Parameters And Tumor Markers

S. Lopez Puche, G. Felipe, M. María Esther, C. José Cristobal, P. Andrea Carolina, B. José Ángel, V. Juan Gabriel, D. Luis, G. Paloma, L. Blanca, R. Cristina, T. Pilar;
Hospital Universitario de Salamanca, Salamanca, SPAIN.

Aim/Introduction: To analyze myocardial uptake in patients who underwent bone scintigraphy (BS) with 99m-Tc HMDP and to establish its relationship with the personal history, analytical parameters, and tumor markers of the patients. **Materials and Methods:** All the 99m-Tc HMDP BS procedures conducted in our center from January 2013 to April 2021 were reviewed. The study included only those with positive myocardial uptake, and it registered its intensity using a visual grading scale (1-3), personal history, age, sex, levels of calcium and alkaline phosphatase (AP), tumor markers (PSA, CEA, estrogen and progesterone receptors, HER-2), and presence of absence of bone metastasis and cardiac amyloidosis. Results: In total, 57 patients with positive myocardial uptake were identified from a global sample of 15,804 BS procedures. The average age was 88 years (67-96 years). 47 patients were men and 10 were women. 30 patients presented prostate carcinoma (PC), 7 had breast carcinoma (BC), 5 had Paget's disease (PD), 8 had other types of cancer (O), and 7 did not present any oncological disorder. In total, 79% of the patients in the final sample presented oncological disease. 55 patients showed myocardial uptake grade 2, 1 patient showed grade 1 uptake, and 1 showed grade 3 uptake. Calcium levels were normal in all patients. 7 patients presented elevated AP levels. 12 patients presented elevated PSA levels. 2 patients presented elevated CEA levels (CEA values were analyzed in 14 patients). Hormone receptors were positive, and HER-2 was negative in all patients with BC. 9 patients presented bone metastasis and no patients presented known cardiac amyloidosis. Analytical values could not be obtained in 11 patients. **Conclusion:** The presence of myocardial uptake in BS was not related with elevated levels of bone turnover markers or tumor markers, or with the presence of cardiac amyloidosis in the patients in our study. The cause of positive myocardial uptake could not be ascertained in patients with no known oncological history and with normal bone turnover markers. However, considering the fact that 79% of the patients presented tumor pathology, (mainly prostate carcinoma), it could be useful to screen for oncological disease in patients with positive myocardial uptake as a casual finding in BS conducted for other causes, particularly in elderly patients. **References:** 1. Poblete García VM, Rodado Marina S, García Vicente A, Soriano Castrejón A. Benign myocardial uptake of 99mTc-HMDP in prostate carcinoma: based on three cases. Rev Esp Med Nucl. 2003 Jan-Feb;22(1):35-9.

EP-142

Normal Values of Skeletal Tc-99m-labelled Bisphosphonate Uptake in SPECT/CT

P. Ritt, P. Heim, A. Grings, M. Beck, T. Kuwert;
Clinic for Nuclear Medicine, Erlangen, GERMANY.

Aim/Introduction: Up to now, little is known about the uptake of Tc-99m-labelled bisphosphonates (DPD) measured by single-photon emission computed tomography/ X-ray computed tomography (SPECT/CT) in healthy skeleton. Knowledge on normal uptake values could facilitate the diagnosis of diseases by enabling a better differentiation between pathological and physiological bone processes, similar to many applications in positron emission tomography. Consequently, the purpose of this study was to determine mean and maximum standardized uptake values (SUVmean and SUVmax) for Tc-99m-DPD in morphologically healthy bone tissue. **Materials and Methods:** SPECT/CT data were acquired in 81 patients (57 women and 24 men; mean age 68.8 ± 13.5 years), with a field-of-view from lower spine to proximal femur. The CT parts of the retrieved scans were automatically segmented by neural networks [1] into six separate regions, namely left and right femur, left and right pelvis, sacrum, and lower spine. The segmentations were transferred to the reconstructed quantitative SPECT images and uptake in the respective segmentations quantified as SUVmean and SUVmax. Segmented bones harboring abnormalities and pathologies were excluded from further analysis. Results: Lowest uptake was measured in proximal left and right femur with (average ± standard deviation) an SUVmean of 2.8 ± 0.7 (SUVmax 7.4 ± 3.3) and 2.8 ± 0.7 (SUVmax 7.1 ± 2.5), respectively. In sacrum and lower spine, SUVmean was 4.0 ± 0.8 (SUVmax 11.3 ± 3.7) and 4.6 ± 1.4 (SUVmax 9.7 ± 2.5), respectively. Furthermore, SUVmean of the left and right pelvis were 4.1 ± 0.8 (SUVmax 10.3 ± 5.4) and 4.2 ± 0.9 (SUVmax 10.8 ± 6.5). Uptake was significantly different between regions ($p<0.01$), e.g., between left femur and sacrum, between right femur and sacrum, or between right femur and right pelvis. **Conclusion:** Our results are in same range as reported by others, e.g. by Qi et al. for normal DPD uptake of vertebrae [2]. Uptake in bone is heterogeneous so that regional normal values of this variable should be determined when capitalizing on SUV quantitation to establish diagnosis in skeletal SPECT/CT. **References:** [1]

Trägårdh E, et al. RECOMIA-a cloud-based platform for artificial intelligence research in nuclear medicine and radiology. EJNMMI Phys. 2020:4;7:51. [2] Qi N, et al. Standardized uptake values of 99mTc-MDP in normal vertebrae assessed using quantitative SPECT/CT for differentiation diagnosis of benign and malignant bone lesions. BMC Med Imaging. 2021;21(1):39.

EP-143

Asymptomatic Elastofibroma Dorsi: prevalence, morphological and metabolic characteristics of 18F-FDG PET/CT in oncological patients

G. Arsos, A. Georgiou, A. Kalaitzoglou, P. Exadaktylou, D. Katsampoukas, S. Georga, V. Mpalaris, M. Moralidis; 3rd Dept of Nuclear Medicine, Aristotle University of Thessaloniki School of Medicine, Thessaloniki, GREECE.

Aim/Introduction: Elastofibroma dorsi (ED) is a benign soft tissue lesion of the chest wall, typically located infrascapulary, commonly bilateral. The pathologically proven prevalence among the elderly is considerably high, particularly in females. ED is usually moderately hypermetabolic and must be differentiated from primary or secondary malignant chest wall lesions. The aim of the study is to investigate the prevalence, distribution and morphological and metabolic features of ED incidentally detected by 18F-FDG PET/CT. **Materials and Methods:** From a database of 9,760 (98% oncological) 18F-FDG PET/CT scans, 7,247 first-occurrence studies were retrospectively investigated for ED. A detailed medical history was obtained from all patients. Assuming a semiellipsoid shape, ED volume was estimated from 3 diameters in 2 planes, radiodensity was measured in axial CT sections and metabolic activity by SUVmax, with the ipsilateral infraspinatus muscle as control. Results: A total of 193 asymptomatic ED lesions were found in 124 patients. All lesions were grossly semiellipsoid in shape and located under the tip of the scapula in close contact to the ribs, apart from 3 located periscapullary. As no ED lesion was identified in patients aged less than 50 years, further analysis included patients aged or older than 50 years only (5,782 studies). In this group, ED prevalence was maximum among females (4.3% vs 1.1% in males, $p<0.05$). Age and female sex prevalence significantly differ between those with and without ED (70.1±9.1 years vs 66.5±8.9 years, $p<0.05$ and 68.3% vs 33.4%, $p<0.05$, respectively). Sixty-eight (54.8%), 40 (32.3%) and 16 (9.3%) of the patients had bilateral, right only and left only lesions respectively, $p<0.005$ in all paired comparisons). Three patients had 3 lesions each. Two patients had a history of excision of preoperatively undiagnosed ED lesions during ipsilateral thoracotomy for lung cancer, before PET/CT. Median ED volume was 22.4 ml (range 0.7 - 185.4). Density and SUVmax significantly differ between ED and ipsilateral infraspinatus muscle (2.6±0.6 g/ml vs 1.1±0.2 g/ml, $p<0.05$ and 30.4±13.6 HU vs 54.3±5.7 HU, $p<0.05$, respectively). **Conclusion:** Incidental detection of ED by 18F-FDG PET/CT is not uncommon in older females. The lesion is located almost always infrascapulary in close contact to the ribs, is semiellipsoid in shape, and is hypodense and moderately hypermetabolic in comparison to normal adjacent musculature. Awareness of the entity and its features when reporting 18F-FDG PET/CT helps to avoid false-positives and unneedded further diagnostic procedures. **References:** None

EP-144

Usefulness of bone metastasis evaluation by bone scintigraphy using AI diagnosis support system in plurality of cancers

K. Nomura, M. Nakayama, A. Okizaki; Department of Radiology, Asahikawa Medical University, Asahikawa, JAPAN.

Aim/Introduction: In bone scintigraphy for plurality of cancers, we compare the analysis results of the artificial intelligence (AI) diagnostic support system (VSBONE BSI) utilizing deep learning with the diagnostic results by nuclear medicine experts. **Materials and Methods:** Cancer patients who underwent bone scintigraphy at our hospital from April 2014 to December 2019 were randomly selected and evaluated retrospectively. The extracted cases were 62 breast cancer patients, 20 prostate cancer cases, and 2 bladder cancer cases. There were 33 cases clinically diagnosed with bone metastases and 51 cases without bone metastases. The results of bone metastasis diagnosis and EOD score by VSBONE BSI and nuclear medicine experts are the subjects of this study. These results were evaluated statistically. Nuclear medicine experts made a diagnosis of bone metastasis by referring to various images such as CT or MRI. Since VSBONE BSI does not have an EOD score calculation function, the EOD score was counted from the accumulated lesions analyzed by this diagnostic support system as suspected metastasis. Results: The detection ability of bone metastasis by VSBONEBSI was 0.879 for sensitivity, 0.901 for specificity, 0.852 for positive predictive value, and 0.920 for negative predictive value. Bone metastasis detection ability by nuclear medicine experts was 100%. Regarding the EOD score in patients clinically diagnosed with metastasis, there was a significant correlation between VSBONE BSI and nuclear medicine experts in Spearman's rank correlation coefficient ($r = 0.834$; $P < 0.01$). **Conclusion:** Regarding bone scintigraphy using the AI diagnosis support system, it was suggested that it may have the same diagnostic ability as nuclear medicine experts in plurality of cancers. **References:** none

EP-145

Asymptomatic Elastofibroma Dorsi : Detectability by diagnostic CT and 18F-FDG PET/CT in oncological patients

G. Arsos, A. Georgiou, P. Exadaktylou, A. Kalaitzoglou, D. Katsampoukas, S. Georga, V. Mpalaris, E. Moralidis;
3rd Dept. of Nuclear Medicine, Aristotle University of Thessaloniki School of Medicine, Papageorgiou Gen. Hospital, Thessaloniki, GREECE.

Aim/Introduction: Elastofibroma dorsi (ED) is a slow growing, usually asymptomatic, commonly infrascapular/bilateral, benign soft tissue lesion of the chest wall. Despite a high (25%) pathological prevalence among older females, it is only sporadically recognized in routine thorax CT. Regular diagnostic review of 18F-FDG PET/CT improves ED detection, but may still miss the majority of the lesions. ED awareness is mandatory to avoid false-positive 18F-FDG PET/CT reports and further diagnostic procedures. The aim of the study is to investigate the detectability of ED by diagnostic thorax CT, routine 18F-FDG PET/CT reviewing and ad hoc search of oncological 18F-FDG PET/CT scans. **Materials and Methods:** Our 18F-FDG PET/CT reports database (9,760 scans of 7,247 patients) was first investigated for the term "elastofibroma dorsi" (group A) and then the rest of the studies were thoroughly reviewed for ED lesions (group B). Medical history and available reports of previous imaging were obtained from all patients. In cases of patients with sequential PET/CT studies, only the first ones were included in analysis. Assuming a semiellipsoid ED shape, volume was estimated from 3 diameters in 2 planes, radiodensity was measured in the axial sections of the low-dose CT of PET/CT and metabolic activity by SUVmax. Results: A total of 193 ED lesions were found in 124 patients (mean age 70.3±9.0 years, 68% females, all asymptomatic for ED). ED prevalence exceeded 4% (84/1959) in females aged over 50 years. Ninety-nine (79.8%) of the patients had a diagnostic thorax CT prior to PET/CT, none reporting the presence of ED. Number of patients, number of lesions, mean age, female sex prevalence, frequency of prior thorax CT, ED volume and ED radiodensity and SUVmax in groups A and B were (mean±SD or median [IQR]) respectively: 34 vs 90, B/A ratio 2.64, $p<0.05$; 57 vs 136, B/A ratio 2.39, $p<0.05$; 70.9 ± 7.8 years vs 70.0 ± 9.4 years; 73.5% vs 65.6%; 73.5 vs 82.2%; 34.0 [34.5] vs 17.9 [22.4] ml, $p<0.05$, 35.6 ± 11.6 HU vs 28.3 ± 13.8 HU, $p<0.05$ and 3.1 ± 0.6 vs 2.4 ± 0.6 g/ml, $p<0.05$. **Conclusion:** ED practically remains unrecorded by diagnostic thorax CT. Routine 18F-FDG PET/CT may detect a minority of ED lesions, namely the larger and/or more opaque and active of them. When systematically searched for, ED is a not uncommon18F-FDG PET/CT finding, particularly in older females. **References:** None

EP-146

FDG PET / CT And MRI As Predictor Of Histological Response To Neoadjuvant Chemotherapy In Patients With Osteosarcoma And Ewing Sarcoma

Z. Kiprak, F. Aydin, A. Arçay Öztürk, A. Keven, E. Bilek, M. N. Engin, C. N. Dündar Çağlayan, A. N. Akınel, E. Güler;
Akdeniz University, Antalya, TURKEY.

Aim/Introduction: To compare FDG PET / CT and MRI findings based on pathology findings in the evaluation of preoperative neoadjuvant chemotherapy response in patients diagnosed with osteosarcoma and ewing sarcoma. **Materials and Methods:** The PET / CT, MRI and pathology results of 86 patients admitted to the PET / CT unit of our hospital between 2016-2020 with the diagnosis of osteosarcoma and ewing sarcoma were retrospectively analyzed. Staging and response to treatment after neoadjuvant chemotherapy 16 patients with pathology results with PET / CT and MRI examinations were included in the study. The size of the primary mass-residual tumor areas observed in the staging and treatment response of the patients in PET / CT and MRI and the primary tumor SUVmax values observed in the staging PET / CT were measured. Results: Pathological diagnosis was accepted as the gold standard in evaluating the response to treatment after neoadjuvant chemotherapy. The sensitivity of PET / CT in evaluating the treatment response was 33.3%, and the specificity was 100%. The sensitivity of MRI in evaluating the treatment response was 28.5%, and the specificity was 100%. In comparison to the dimensions of primary mass-residual tumor areas monitored in PET/CT and MRI, the values measured in PET/CT and MRI were strongly correlated with each other. When the SUVmax values measured in PET/CT studies of patients who responded to treatment and had residual tumors were met; the average SUVmax values of patients who responded to treatment were 8.9, while the average SUVmax: 15.1 was found in patients with residual tumors, and no significant differences were found between these two values. The average time between staging and post-treatment PET/CT examinations of patients was 3.6 months, and the average time between MRI examinations was 3.7 months. In addition, PET/CT examinations of patients showed nodular lesions compatible with multiple metastases in the lung in 3 patients, regional metastatic lymph nodes in 3 patients, additional bone metastasis in 2 patients, and bone marrow metastasis in 1 patient. 2 patients had nodular lesions with suspected millimetric metastases in the lung. **Conclusion:** In evaluating treatment response after neoadjuvant chemotherapy in osteosarcoma and ewing sarcoma, PET / CT and MRI have low sensitivity but high specificity. PET / CT study; allows the detection of additional metastatic foci as it provides whole body evaluation. **References:** none

EP-147

Skeletal metastasis detection with 99mTc-MDP bone scan and 18-F-FDG PET/CT scan in breast cancer patients

N. Manevska[1], S. Besliev[2], N. Bozinovska[1], T. Makazlieva[1], S. Stojanoski[1], D. Miladinova[1], A. Ugrinska[1,2];
[1]Medical Faculty, Skopje, NORTH MACEDONIA, [2]Institute of Positron Emission Tomography, Skopje, NORTH MACEDONIA.

Aim/Introduction: Breast cancer is the most commonly-diagnosed cancer worldwide in females. Skeleton is the most common site of metastasis spread (for breast cancer). Bone scan (BS) is a widely used, non-invasive nuclear medicine diagnostic tool for detecting bone metastasis (BM) in the early phase of the disease as well as after therapy. Although hybrid PET/CT imaging are more considered for staging and restaging the disease as well as evaluating treatment response, BS is still keeping its position as a highly sensitive method in detecting bone metastasis. The aim of our study was to compare the findings of bone scan and FDG-PET/CT scan for detection of BM in breast cancer patients at initial staging of the disease. **Materials and Methods:** We retrospectively analyzed 25 patients with breast cancer who underwent both BS and PET/CT scan for detecting BM in the period 2019-2020. Whole body BS was performed 3 hours after iv injection of 740 MBq 99mTc-MDP. PET/CT was performed after 60 minutes of iv injection of 18F-FDG in accordance with standard protocols. Results: 25 patients were included in the study (age 53,56±11,55 years). BM affected both axial and appendicular skeleton in (n=7, 38,88%), axial skeleton only was affected in 8pts, while appendicular only in (n=4, 22,2%). Solitary metastases were detected in 5 pts, 3pts had 2 BM, 10pts had three or more BM. From all 25 patients, 7 pts (41,17%) had negative findings for BM with both methods, while 18 patients had positive findings with both methods. Among these positive findings, 10 patients (n=10/18; 55,55%) had identical metastatic bone foci detected with both methods. On the other hand, PET/CT scan revealed more foci of bone metastasis than BS in (n=7/18 patients; 38,88%), depicting BM in scapula, spine, sternum and iliac bones in different patients, that were not seen on bone scan. Bone scan presented more BM foci in only (n=2/18 patients; 11,1%). Patients with normal findings on BS did not reveal BM on PET/CT scan which means there is a good correlation regarding false negative findings with both methods. **Conclusion:** BS and 18F-FDG-PET/CT are complementary modalities that are highly sensitive in evaluating BM in breast cancer patients. Hybrid imaging (SPECT/CT and PET/CT) because of the complementary value of CT may contribute to the diagnosis of BM. Bone scan is widely used, low cost, easy to perform diagnostic modality and remains the method of choice for detection of bone metastasis. **References:** none

EP-148

Quantitative Assessment of Enthesis Patients with Ankylosing Spondylitis

N. Dizdar[1], M. Cagli[2], A. Akbulut[3], B. Duyur Çakit[2], G. Koca[3], H. Genc[2], M. Korkmaz[3];
[1]Department of Nuclear Medicine, University of Health Sciences, Gulhane Training and Research Hospital, Ankara, TURKEY, [2]Department of Physical Medicine and Rehabilitation, University of Health Sciences, Ankara Training and Research Hospital, Ankara, TURKEY, [3]Department of Nuclear Medicine, University of Health Sciences, Ankara Training and Research Hospital, Ankara, TURKEY.

Aim/Introduction: Enthesitis, characteristic feature of ankylosing spondylitis (AS), is the inflammation of the origin and insertion of ligaments, tendons, aponeuroses, annulus fibrosis, or joint capsules. We investigated relationship between ultrasonographic findings and bone scintigraphy parameters in major peripheral enthesis of lower extremity in AS patients. **Materials and Methods:** Twentypatients diagnosed with AS (AS Group) according to modified-NewYork-Criteria, were referred to our department and 20 patients without rheumatological diseases or pathological findings (Control Group) on bone scintigraphy were included retrospectively. Lower extremity major peripheral enthesis regions were evaluated with ultrasonography for increased tendon thickness, enthesophytes and bone erosions, which are characterized findings of enthesitis (1). Enthesitis indexes for 4 major peripheral enthesitis regions in lower extremity were evaluated by bone scintigraphy in all cases. A standard-sized circular ROI was drawn on region of enthesitis and non-enthesitis region on same extremity, and calculated counts of ROIs were proportioned to each other (Enthesal region/Non-enthesal region) (Figure 1). The enthesitis indexes of the groups were analyzed statistically (Mann-Whitney-U-test, $p < 0.05$). Results: Age, gender, disease duration, HLA-B27 positivity, CRP and sedimentation values of are given in Table-1. Superior and inferior patella, tuberositas tibia and calcaneus posterior regions were evaluated as the most common affected enthesis region. In the physical examination, 24 regions out of 160 regions in 12 patients out of 20 AS patients, had symptoms of tenderness, edema or pain in enthesis regions. At ultrasonographic evaluation, tendon thickening, enthesophytes and bone erosion were observed in 59 enthesis regions out of 160 regions. Mean enthesitis index, calculated in AS Group was 1.36±0.23 whereas in Control Group it was 1.23±0.17 and there was a significant difference between groups ($p < 0.05$). In our study, superior right and left patella and right calcaneus posterior were the most common enthesis regions whereas the differences were statistically significant between the groups (Table-2). **Conclusion:** In AS patients, regions where enthesitis was diagnosed by physical examination and ultrasound, bone scintigraphy presented focal increased radioactivity uptake due to local inflammation, bone erosion

and ossification in enthesitis, and calculated enthesitis index was found to be significantly higher than Control Group (2). Therefore, enthesitis index calculated in bone scintigraphy seems to be a valuable method to assist clinician for diagnosis of enthesopathy. **References:** 1. D'Agostino MA. Ultrasound imaging in spondyloarthropathies. Best Pract Res Clin Rheumatol. 2010;24(5):693-700.2. Groshar D, Rozenbaum M, Rosner I. Enthesopathies, inflammatory spondyloarthropathies and bone scintigraphy. J Nucl Med. 1997;38(12):2003-5

EP-149

Clinical use of three-phase bone scintigraphy in identifying complications after knee replacement in patients with deforming osteoarthrosis with COVID-19

P. Korol[1], *O. Shcherbina*[2], *M. Kostylev*[1];
[1]*Shalimov's National Institute of Surgery of Transplantation, Kiev, UKRAINE,* [2]*Shupik's National University of Health of Ukraine, Kiev, UKRAINE.*

Aim/Introduction: To evaluate the prognostic value of the kinetic parameters of three-phase bone scintigraphy in identifying complications after knee joint replacement in patients with deforming osteoarthrosis (DO). **Materials and Methods:** 215 patients (88 men and 127 women) aged 29 to 77 years were imaged by three-phase bone scintigraphy: I stage - angiographic phase, II stage - early static phase, III stage - delayed static phase. Intestinal uptake was observed visually 3 hours after the intravenous administration of 740 MBq ^{99m}Tc MDP. Results: The first cohort included 83 patients with DO of the knee joints without COVID-19, the second - 132 patients with COVID-19. Significant increase in the indicators of arterial inflow ($t = 2.67$; $p < 0.05$) and integral perfusion ($t = 2.94$; $p < 0.05$) in the angiographic phase of patients with COVID-19, due to increased osteoblastic activity and angiogenesis , in comparison with the indicators of patients without COVID-19. The kinetics of 99mTc MDP in patients with COVID-19 is characterized by a significant predominance of retention ($t = 3.22$; $p < 0.05$) and specific accumulation of the drug in the early static phase ($t = 2.53$; $p < 0.05$) and delayed static phase of scintigraphy ($t = 2.41$; $p < 0.05$) compared with the parameters of patients without COVID-19. According to the results of kinetic analysis, patients with COVID-19 showed a gradual increase in the percentage of accumulation of the radiological index in the lesion focus, which is associated with increased integral perfusion, increased vascular permeability due to the action of infectious agents, activation of resorption factors and the synthesis of mineral components. **Conclusion:** The use of three-phase bone scintigraphy contributes to early detection of paraendoprosthetic complications in the postoperative period, a reduction in the number of revision endoprostheses and a reduction in the rehabilitation period after knee replacement in patients with COVID-19. **References:** None

EP-150

Effectiveness of F18-FDG PET/CT in Initial Assessment of Necrotizing Otitis Externa (NOE) and Evaluation of Anti-Microbial Response

A. Hussien, S. Ali, M. Kula, O. Sabra, W. Ibrahim;
King Hamad University Hospital, Muharraq, BAHRAIN.

Aim/Introduction: Necrotizing (malignant) otitis externa (NOE) represents invasive infection of external auditory canal and skull base mainly affecting diabetic elderly patients and aggravated by compromised immunity. Treatment of NOE is challenging employing long-term intravenous antibiotics. NOE may progress to cranial nerve palsies and temporomandibular joint osteomyelitis with uncommon but fatal complications like meningitis, brain abscess, and dural sinus thrombophlebitis. Aim of this study is to evaluate the effectiveness of F18-FDG PET/CT in detecting soft tissue and bone infection in patients with suspected NOE and to assess response after anti-microbial treatment. **Materials and Methods:** Case series were collected from 2018 to 2020 in which 15 patients were diagnosed with NOE based on clinical features and temporal bone CT. The mean age was 69.1 yr ± 10.4; 60% of patients were male, and all patients were diabetic. Eight patients were evaluated with PET/CT in which 5 patients underwent both initial (PET1) and evaluation of therapy (PET2) scans. Two patients only had an initial scan (PET1) and one had a baseline bone scan and PET2 to evaluate therapy response. Results: In the seven patients who had a baseline PET1, infection was located in the following areas: mastoid (7/7), external ear (5/7), middle ear (3/7), temporal bone (2/7), nasopharynx (2/7), Eustachian tube (2/7), sphenoid (1/7), and parotid gland (1/7). PET1 diagnosed two patients with bilateral NOE. Hybrid PET/CT in initial assessment of NOE provides both metabolic and anatomical data, exhibiting more involved sites & earlier than CT temporal. Compared to bone scan, PET1 demonstrated soft tissue involvement besides the osseous structures usually seen in bone scan. Six patients underwent PET2 after receiving a course of antibiotics for at least 6 weeks. PET2 demonstrated a good response to treatment in four of the patients with improvement of symptoms. Meanwhile, PET2 detected mild metabolic regression after treatment in two of the patients who continued the antibiotic regimen; one of them died after venous thrombosis and stroke while the other one had NOE relapse. For assessment of therapy response PET2 showed better results compared to bone scan & CT as the former remains positive for longer periods with persistent osteoblastic activity and the CT changes persist even after clinical improvement. **Conclusion:** 18F-FDG PET/CT should be considered as imaging modality of choice to diagnose NOE, to evaluate disease extent, and to assess response to anti-microbial therapy. Larger and controlled studies are advised. **References:** None

EP-151

Relationship of F-18 FDG PET/CT Imaging Findings with Bone Trauma Age

S. Orun, U. Korkmaz, S. Soyluoglu, G. Durmus Altun;
Trakya University, Edirne, TURKEY.

Aim/Introduction: FDG,which is mainly used in oncological imaging in nuclear medicine and has become widespread in infection imaging,is a glucose analogue.FDG uptake reflects cellular glucose metabolism.Increased FDG uptake occurs in regions where glucose consumption is increased due to increased metabolic activity or inflammation in the relevant tissue.Osteoclasts disrupt bone structure by pumping HCl to dissolve calcium salts.This process requires intense energy,and the main source of energy is glucose.The aim of this study is to reveal the parameters of the recovery process after bone trauma and to determine the relationship between trauma time and F-18 FDG PET/CT imaging findings in order to distinguish between physiological uptake and infection in patients with surgical trauma or prosthesis in the bone. **Materials and Methods:** All patients who applied to the Department of Nuclear Medicine for F-18 FDG PET/CT imaging between 2010 and 2020 were retrospectively screened.176 patients(mean age:68±12 years;92 M,84 K) who met the inclusion criteria were included in the study. The time-dependent relationship of the patients with trauma time,trauma type,prosthesis shape,SUVmax and SUVmean values was determined.In addition,subgroup analyzes were performed on the basis of prosthesis application and surgical bone trauma. Results: 43 patients had knee prosthesis(KP:Group1),84 had hip prosthesis(HP:Group2),27 had a history of sternotomy(Group3) and 22 had prosthesis in other bone areas (vertebra,humerus,femur,shoulder) (Group4).The average age of bone trauma was calculated as 80±84 months(1-480).The mean SUVmax value determined from the trauma site was calculated as 4.05±2.45(0.90-12.27;±95%:3.79-5.30).There was a difference between the SUVmax values of the groups in the study,and it was seen that Group 3 had the lowest SUVmax value(2.8±2.08,1.2-9.1;±95%:2.00-3.65)(p:0.002).A reverse linear relationship was found between trauma age and SUVmax-SUVmean values(r:-0.24,p:0.009 for SUVmax and r:-0.23,p:0.006 for SUVmean).In patients with bone surgery duration of 12 months or less,SUVmax(4.9 vs 3.6) and SUV mean(1.7 vs 1.1) values were found to be significantly higher(p:0.01 and p:0.001). **Conclusion:** Depending on the bone prosthesis application and the recovery period after osteotomy,the metabolic activity is above the critical value in the first year.In addition,in clinical cases where the age of bone trauma should be known,it seems possible to have an idea for the first year following the trauma.Standardized interpretation criteria are not defined for FDG-PET/CT to be evaluated as positive or negative in prosthetic infection. For this reason,FDG-PET/CT is not routinely used today in the diagnosis of prosthetic infection.After determining the relationship between bone trauma age and FDG metabolism,further research is needed in terms of its use in prosthetic infection. **References:** none

EP-152

Evaluation of human anti-mouse antibodies prior to the administration of ^{99m}Tc-Besilesomab

***P. Guardia Jimena**, R. Arenas Aguaza, M. Martínez del Valle Torres, D. Becerra García;*
Hospital Universitario Clínico San Cecilio, Granada, SPAIN.

Aim/Introduction: Besilesomab is a anti-granulocyte monoclonal antibody type IgG BW 250/183 produced in murine cells, which may produce human anti-mouse antibodies (HAMA), due to this it is necessary to confirm the absence of these antibodies prior to administration [1]. The aim of this study was to provide our experience in the determination of HAMA antibodies in serum prior to the administration of ^{99m}Tc-Besilesomab. **Materials and Methods:** We retrospectively studied 94 patients with age ranges from 26 to 89 years who underwent a ^{99m}Tc-Besilesomab scintigraphy for suspected osteoarticular infection between 2017 and 2021, who the presence of HAMA antibodies in serum was previously determined. Rapid HAMA tests were performed in 89 patients that were carried out and interpreted according to the manufacturer's instructions; in 6 of these patients the result was confirmed by blood analysis with quantification of HAMA antibodies in serum in an external laboratory, the result being positive from index higher than 1.00. In the remaining 5 patients the HAMA determination was performed in the laboratory. Finally, all patients underwent the ^{99m}Tc-Besilesomab scintigraphy without any documented adverse reaction. Results: Of the 89 HAMA rapid tests, 84 negative results, 1 borderline result and 4 positive results were obtained. These 4 positive patients, the doubtful one and a sixth patient with a negative result but who was going to receive a second dose of ^{99m}Tc-Besilesomab were confirmed in the laboratory, all determinations being negative for the presence of HAMA antibodies in serum, HAMA ranges <0.1 -0.73. The 5 patients with laboratory determination had negative results for the presence of HAMA antibodies in serum, ranges <0.1-0.58. The prevalence of HAMA positive patients prior to the administration of ^{99m}Tc-Besilesomab was 0%. **Conclusion:** The low prevalence of human anti-mouse antibodies in our study population makes the ^{99m}Tc-Besilesomab scintigraphy safe for the evaluation of osteoarticular infection in patients who have not previously had contact with this radiopharmaceutical, and even in those who have performed this study previously. The use of HAMA rapid tests is highly sensitive to ensure the detection of positive patients, which simplifies the use of ^{99m}Tc-Besilesomab. **References:** 1. Signore A, Jamar F, Israel O, Buscombe J, Martin-Comin J, Lazzeri E. Clinical indications,

image acquisition and data interpretation for white blood cells and anti-granulocyte monoclonal antibody scintigraphy: an EANM procedural guideline. Eur J Nucl Med Mol Imaging. 2018;45(10):1816-31.

EP-153

Influence of tocilizumab therapy on osteoarticular inflammatory activity assessed by [18F]FDG PET/CT in patients with refractory polymyalgia rheumatica

I. Martínez-Rodríguez[1], D. Prieto-Peña[2], Á. Gutiérrez-González[1], M. De Arcocha-Torres[1], O. Cuenca-Vera[1], J. Andrés-Pacheco[1], F. Gómez-de la Fuente[1], N. Martínez-Amador[1], A. Sánchez-Salmón[1], J. Jiménez-Bonilla[1], S. Ruiz-Llama[1], M. Pombo-López[1], A. Bota-Bota[1], M. A. González-Gay[2], R. Quirce[1];
[1]Nuclear Medicine Service. Marqués de Valdecilla University Hospital. Molecular Imaging Group (IDIVAL). University of Cantabria., Santander, SPAIN, [2]Rheumatology Service. Marqués de Valdecilla University Hospital. Genetics and atherosclerosis research group on systemic inflammatory diseases (IDIVAL)., Santander, SPAIN.

Aim/Introduction: To evaluate the influence of tocilizumab (TCZ) on osteoarticular inflammatory activity assessed with [18F]FDG PET/CT (PET/CT) in patients with refractory or atypical polymyalgia rheumatica (PMR) and its association with the clinical outcome of patients. **Materials and Methods:** We retrospectively included 12 consecutive patients (10 women, 67.0±8.6 years-old) with refractory PMR and concomitant large vessel vasculitis with initial PET/CT prior to TCZ treatment and follow-up PET/CT (interval: 15.1±6.0 months). All patients were symptomatic and 11 were on corticosteroids/corticosteroids plus methotrexate therapy at the time of initial PET/CT. PET/CT were obtained 180' after injection of [18F]FDG (7 MBq/Kg). Osteoarticular uptake was visually analyzed in comparison to liver (grade 0: no uptake to grade 3: higher than liver uptake). Eight regions were evaluated for each patient: shoulders, sternoclavicular joints, cervical and lumbar spinous processes, ischial tuberosities, hip joints, greater trochanters, and knees (total regions evaluated: 96). Clinical outcome of the patients was recorded. Results: We observed osteoarticular uptake (grade>0) in 39/96 regions (40.6%) at the initial PET/CT and 36 regions (37.5%) at the follow-up PET/CT. The intensity of uptake at the initial PET/CT was grade 1 in 15 regions (38.5%), grade 2 in 9 (23%) and grade 3 in 15 (38.5%) and at the follow-up was grade 1 in 19 regions (52.7%), grade 2 in 9 (25%) and grade 3 in 8 (22.3%). Intense uptake (grade 3) was most frequently observed at the initial PET/CT at the lumbar spinous processes (33.3% of patients) and ischial tuberosities (25%) and, at the shoulders, sternoclavicular joints, and lumbar spinous processes at the follow-up PET/CT (16.7% of patients in all three regions). After TCZ a clinical complete response (CP) was observed in 7 patients and partial response (PR) in 5. The mean osteoarticular uptake decreased from 0.55±0.91 to 0.45±0.81 in patients with CP and from 1.25±1.33 to 0.9±1.10 in PR (non-significant differences). In the 7 patients with CR the intensity decreased in 48.1% of the initially uptake regions and increased/not changed in 51.9%. In the 5 patients with PR the uptake decreased in 59.1% of the regions and increased/not changed in 49.9%. **Conclusion:** Overall [18F]FDG PET/CT showed a decrease in the osteoarticular inflammatory activity in patients with refractory PMR treated with TCZ. Although the differences were not significant, there was a trend for patients with PR to have a higher osteoarticular uptake by PET/CT both initially and during follow-up compared to those with CR. **References:** None

EP-35

Wednesday, October 20 - Saturday, October 23, 2021

e-Poster Area, release on Wednesday, October 20 at 09:00

General Isotopic Imaging

EP-159

Quantification of Lung Ventilation/Perfusion SPECT (V/Q_{SPECT}): A Helping Tool in Pulmonary Embolism

S. Menendez-Sanchez, R. Bellviure-Meiro, A. Cardozo-Saavedra, M. Boronat-Ferrater, S. Asadurova, F. Velazquez-Krisch, F. Dellepiane-Clarke, S. Aguade;
Hospital Universitario Vall d'Hebron, Barcelona, SPAIN.

Aim/Introduction: The Q.LUNG TEP program available in the GE Xeleris workstation produces a V/Q discordance percentage. The aim of our study was to determine what percentage of discordance gave the highest sensibility (Sn) and specificity (Sp) values for the diagnosis of pulmonary embolism (PE). **Materials and Methods:** 84 patients (p) with symptoms and suspected PE were sent to the Nuclear Medicine department for a final diagnosis. They underwent multiple planar imaging and V/Q lung SPECT right after inhalation of 99mTc-Technegas and after iv administration of 260 MBq 99mTc-MAA (Macroaggregated human albumin).A GE Discovery 670 Gammacamera was used for imaging acquisition and the Q.LUNG TEP program for image processing. The final PE diagnosis was obtained after the qualitative evaluation of the planar and SPECT V/Q studies. 2x2 contingency tables and Chi-square test were performed with the mismatch quantification percentages obtained by the Q.LUNG TEP program and the diagnostic (qualitative) results. Results: 43/84 (51.2%) of the patients were classified as negative for PE after the visual evaluation while 41/84 (48.8%) were deemed positive for PE. As per the Q.LUNG TEP quantification all studies SPECT studies showed V/Q discrepancy, with values ranging between 2% and 49%. Contingency table analysis was performed with ascending values of the discordance percentage and calculating the Sn

and Sp for each percentage. With the help of a ROC curve a cutting point of 13% was set as having the higher Sn (80%) and Sp (79%) values (p<0.001).It should be mentioned that a 20% mismatch value or higher was also able to correctly classify 95% of the PE patients (Sp:95%; Sn: 79%; p<0.001). **Conclusion:** Q.LUNG TEP (V/Q_{SPECT}) quantitative analysis correctly classifies most of the patients with suspected PE. It is a very useful tool for patients with non-diagnostic "undetermined" qualitative V/Q scans. 13 % is the quantitative percentage value with higher Sn and Sp in our study. **References:** None

EP-160

Clinical values of DMSA SPECT in follow-up evaluation of renal injuries after conservative management

***S. Cho**, S. Yu, H. Jang, J. Kim, K. Park, H. Song;*
Chonnam National University Hospital,
Gwangju, KOREA, REPUBLIC OF.

Aim/Introduction: Tc-99m dimercaptosuccinic acid (DMSA) scan can visualize cortical integrity of the kidneys. We sought to evaluate the clinical values of 3-dimensional analysis of Tc-99m DMSA scintigraphy in patients with renal injuries after conservative treatment using single-photon emission computed tomography (SPECT). **Materials and Methods:** From June 2020 to February 2021, consecutive 12 patients with at least ≥grade 1 renal injury were prospectively enrolled. They underwent DMSA planar and SPECT scans for the follow-up evaluation of cortical integrity following conservative management for renal injuries. Serum biomarkers of renal function were also measured on the same day to obtain glomerular filtration rate (GFR). Split renal function (SRF) was measured for the injured kidney using planar and SPECT images, respectively. On SPECT images, renal cortex was delineated with a threshold of ≥40% global maximum uptake; SRF was measured as the ratio of preserved cortical volume of the injured kidney to total cortical volume (TCV). TCV was divided by patients' body surface area to obtain TCV index. Mutual correlations were analyzed for parameters from planar and SPECT images, and GFR. Results: The median interval between index trauma and DMSA scan was 17 weeks. SRF of the injured kidney (right 7, left 5) significantly correlated between planar and SPECT images (rho = 0.958, p <0.001). However, SRF values were significantly lower for SPECT images, as compared to planar images (bias -1.58%, p = 0.034). Bland-Altman plot revealed an overestimation of SRF in severer cortical damage (lower SRF values). Among planar and SPECT parameters, TCV index showed the best correlation with GFR (rho = 0.817, p = 0.011). **Conclusion:** Planar DMSA images overestimate the SRF of injured kidney. TCV index measured by DMSA SPECT shows the best correlation with GFR. **References:** Reichkendler et al. Eur J Nucl Med Mol Imaging 2020;47:729-33.Cao et al. Am J Roentgenol 2016;207:1324-8.Brenner et al. Am J Roentgenol 2009;193:333-7

EP-161

Value of renal transplant scintigraphy: comparison with surgical occurrences and Doppler ultrasound resistive index

***A. Marques**, F. Abreu, J. Carvalho, S. Pintão;*
Centro Hospitalar de Lisboa Ocidental, Lisbon, PORTUGAL.

Aim/Introduction: The value of renal scintigraphy has long been recognized in the early post-transplant period alongside with resistive index (RI) measured by Doppler ultrasound (DUS). We analyzed our hospital's renal transplant population and compared renographic evaluation results with surgical occurrences and DUS RI. **Materials and Methods:** We retrospectively analyzed epidemiological data, surgical occurrences, DUS RI and up to 5 day post-transplant renal scintigraphy results of all the patients submitted to renal transplantation since 2010 until now. Renographic studies were acquired with ^{99m}Tc-MAG_3 and a normal scan was considered one to show normal perfusion and time-activity curve. DUS, epidemiological and surgical data were gathered from patient files. Results: 523 renal transplant recipients were studied, being 63.2% male, with a median age of 51 years (20-77) and mainly caucasian (82.5%). The donors were 54% female, with a median age of 55 (4-77) and 79.1% of the renal grafts came from a cadaver donor. Median time of cold ischemia for live donor was 1.5 hour; for cadaver donor was 17.3 hours (1-25); median number of graft arteries was 1 (1-3); 78.2% didn't experience hypotension during surgery; 81.6% had immediate diuresis; median post-transplant creatinine was 5.62 mg/dL (0.89-12.7 mg/dL). 86% of the patients were submitted to DUS: 37.1% RI above 0.7. In renographic studies, 37.4 % of the transplant recipients had decreased perfusion and 60.7% showed signs of Acute Tubular Necrosis (ATN). Median Effective renal plasma flow (ERPF) was 187 (20-528). Median ERPF changed according to donor status [221 (living donor) vs 205 (cadaver donor)]. Receiving a living donor kidney represents a higher likelihood of a normal renal scan [OR 7,8 (4.4-13.6), p<0,001]. No significant statistical relation was found between longer cold ischemia time (CIT) and lower ERPF (Spearman correlation - 0.104, p=0.069). Median ERPF changed according to the presence of immediate diuresis [median ERPF 190.8 (immediate diuresis) vs 159.8 (not immediate diuresis), p=0.01]. Median ERPF did not change according to body mass index and surgery duration. Significant statistical correlation was found between renographic perfusion and Doppler US RI [Spearman correlation - 0.113, p=0.026]. **Conclusion:** Early post-operative renal scan is a valuable method to provide graft information, such as kidney transplant blood flow which correlated well with the Doppler ultrasound resistive index. Graft function was better in living donor kidneys and in the presence of immediate diuresis, however it did not change significantly according to cold ischemia time and surgery duration. **References:** None.

EP-162

Role of follow-up quantitative bone SPECT-CT in active condylar hyperplasia

D. Cáceres Silva, L. Mohamed Salem, T. E. Rodríguez Locarno, T. Moreno Monsalve, A. S. De Agrela Serrao, A. M. Leiva Montejo, M. I. Castellón Sánchez, J. L. Navarro Fernández, L. Frutos Esteban, J. F. Contreras Gutiérrez, M. A. Claver Valderas;
Hospital Clínico Universitario Virgen de la Arrixaca, Murcia, SPAIN.

Aim/Introduction: Condylar hyperplasia is a disorder characterized by excessive and progressive growth of the mandibular condyle. The aim was to determine the value of follow-up bone SPECT-CT (QB SPECT-CT) in the diagnosis of active condylar hyperplasia (CH). **Materials and Methods:** We studied prospectively 121 patients, 82 (66.1%) women and 39 (33.9%) men, mean age 28.1 ± 10.0 years. Cranial SPECT/CT study was performed 2 hours postinjection of 740 Mbq Tc99m-HMDP I.V., in a LEHR collimator, zoom: 1, matrix size: 128x128, 22 sec/frame every 4º, 360º aquisition orbit. Average activity was calculated in 2 ROIS drawn on both mandibular condyles in three successive axial slices. Condyle differential uptake was calculated using the following formula: ROI activity in study/ right ROI + left ROI x 100 We consider an active CH when the differential quantification is greater than or equal to 55% in one of the condyles. A total of 180 tests were performed between 2009 and 2020. A follow-up study was done with an interval of 8.08 ± 5.53 months in 44 patients (26 positive and 18 negative). 8 patients who have undergone "condylar shave" surgery were excluded from the analysis. Results: Of the 36 patients with follow-up, 19 were positive, 11 women (78.9%) and 8 men (21.1%), with a mean age 28.7 ± 9.3 years. 17 studies were negative: 13 (76.5%) women and 4 (23.5%) men, mean age 27.5 ± 8.2 years. In the follow-up study, 12 of the previously positive (63.1%) remain positive, of which 6 were women and 6 were men (50% respectively), mean age 29.9 ± 9.5 years. 7 of the previously positive (36.9%) became negative, in which surgery was avoided. In the follow-up of the 17 negatives, the absence of active condylar hyperplasia was confirmed in 16 patients (94.1%), 8 were women and 8 were men (50% respectively), mean age 27.6 ± 9.5 years. **Conclusion:** Quantitative bone SPECT-CT follow-up is a very useful technique in the management of patients with mandibular condylar hyperplasia. A normal initial study practically rules out active condylar hyperplasia. Follow-up SPECT-CT avoids unnecessary surgery in 36.9% of patients. **References:** none

EP-163

Evaluation of clinical response to cholestyramine in patients affected by chronic diarrhoea undergoing 75-selenium homocholic acid taurine (sehcat) scintigraphy: preliminary results

I. Bossert[1], A. Schiepatti[2,3], M. Cincotta[4], D. D'Ambrosio[5], A. Marchetto[1], F. Lusetti[3], F. Biagi[2,3], G. Trifirò[1];
[1]Nuclear Medicine Service, Istituti Clinici Scientifici Maugeri SpA SB IRCCS, Pavia, ITALY, [2]Gastroenterology Unit, Istituti Clinici Scientifici Maugeri SpA SB IRCCS, Pavia, ITALY, [3]Gastroenterology Unit, University of Pavia, Pavia, ITALY, [4]University of Pavia, Pavia, ITALY, [5]Medical Physics Unit, Istituti Clinici Scientifici Maugeri SpA SB IRCCS, Pavia, ITALY.

Aim/Introduction: Chronic diarrhoea (lasting >4 weeks) is a common cause for patients to seek medical advice. We have recently shown that up to one third of patients suffering from chronic diarrhoea had a short-term clinical response to cholestyramine, thus potentially confirming bile acid malabsorption (BAM) [1]. However, the correlation between clinical response to cholestyramine and results of 75-Selenium Homocholic Acid Taurine (Sehcat) scintigraphy were not evaluated [1]. Moreover, data on the correlation between Sehcat results and long-term response to cholestyramine in patients affected by BAM are lacking. This study provides preliminary results on the relationship between Sehcat results and clinical response to cholestyramine in patients affected by chronic diarrhoea. **Materials and Methods:** Between February and April 2021, patients with chronic diarrhoea attending our Gastroenterology outpatients clinic were prospectively proposed to undergo Sehcat test followed by a trial of cholestyramine 8g/day regardless from Sehcat results. Sehcat uptake values <15% was considered positive, whereas between 15% and 17% were considered borderline. Preliminary clinical response to cholestyramine was evaluated after 1 month. Data on continuity of treatment and reasons for discontinuing cholestyramine were also collected. Results: Nineteen patients (14F, mean age 41±14 years) with chronic diarrhoea were enrolled. Four patients were affected by an organic disease (2 Crohn's disease with ileal involvement, 1 coeliac disease with persistent diarrhoea despite histological response to a strict gluten-free diet, and type 1 refractory coeliac disease). In this group, one patient was lost to follow-up. In the remaining three, one had borderline values of Sehcat uptake with clinical response to cholestyramine at one month, while 2 had negative Sehcat (one clinical response, one not). The group of functional diarrhoea included 15 patients (5 cholecystectomy). Data about follow-up at one months were available for 8 patients in this group. Two of them had positive Sehcat scan and complete response to cholestyramine, and six a negative scan result (three had complete clinical response to cholestyramine and three did not). **Conclusion:** Our preliminary data show that although Sehcat can be helpful

in identifying BAM, some patients can have clinical response to bile acid sequestrants despite negative Sehcat results. Further data are needed to identify predictors of long-term clinical response to cholestyramine despite negative Sehcat. **References:** 1. Costa S, et al. Prevalence and clinical features of bile acid diarrhea in patients with chronic diarrhea. J Dig Dis. 2021.

EP-164

Salivary Scintigraphy in the evaluation of xerostomia in patients treated with Intensity Modulated Radiotherapy for head and neck malignancy

P. U N, V. G, K. Rishi, G. GV, B. Srinath, H. Mohan;
Sri Shankara cancer hospital and Research center, Bangalore, INDIA.

Aim/Introduction: IMRT with concurrent chemotherapy remains the mainstay of treatment for locally advanced Head & Neck Squamous cell carcinoma (HNSCC). The salivary glands are frequently exposed to radiation during treatment, leading to impaired function and xerostomia. This can be significantly debilitating for the patient affecting the quality of life. Salivary scintigraphy has been a reliable technique for assessing the salivary gland function. **Materials and Methods:** A total of 20 patients were included in this prospective study. Salivary Scintigraphy was performed using Tc-99m pertechnetate in patients with carcinoma nasopharynx, oropharynx, hypopharynx and larynx treated with Intensity Modulated Radiotherapy (IMRT). These tests were done at three separate occasions during the treatment course; 1 Baseline study before RT, 2. 15 days post RT (1st follow up) and 3. 3 months (2nd follow up) post RT. Salivary scintigraphy was evaluated visually using time activity curve (TAC) and semiqantitatively by calculating ejection fraction (EF) using a formula. Results: Out of 20 patients, 18 patients had an ejection fraction of 45% or more at baseline and 2 had decreased value. The baseline median Ejection Fraction value of right parotid and left parotid is 53.5% and 47% respectively. In 1st follow up, the median decrease in Ejection fraction value in the right parotid was 29.5% and in the left parotid was 27%, with 'p' value of <0.001. In 2nd follow up, the median decrease in Ejection fraction value in the right parotid is 11% and in the left parotid is 16%, with 'p' value of <0.001. Grade 1 xerostomia is seen in Number /20 (50%) of patients and Grade 2 in number / 20 (61%) (Is this correct grade 1 in 50% and grade 2 in 61%?) of patients. Salivary scintigraphy reliably identified the salivary gland dysfunction as early as 15 days post RT. Those who demonstrated a significant drop in salivary gland function and ejectinon fraction immediately at the first followup were seen to develop xerostomia later on with not much change in salivary gland function in the second follow up **Conclusion:** Salivary scintigraphy can be used to identify the patients who may be at risk of developing xerostomia following radiotherapy in carcinoma of nasopharynx, oropharynx, hypopharynx and larynx patients treated with IMRT **References:** Gupta T, et al. Prospective longitudinal assessment of parotid gland function using dynamic quantitative pertechnate scintigraphy and estimation of dose-response relationship of parotid.sparing radiotherapy in head-neck cancers. Radiat Oncol. 2015;10:67

EP-165

Detection of Thromboembolic Pulmonary Disease using Lung Perfusion SPECT/CT in the time of COVID-19: Outcome Analysis

T. H. Tan, R. Ismail;
Sunway Medical Centre, Bandar Sunway, MALAYSIA.

Aim/Introduction: In the current COVID-19 pandemics, most nuclear medicine centres have omitted the ventilation component of the V/Q SPECT and substituted it with low-dose CT (LDCT). Several publications have demonstrated comparable diagnostic performance between V/Q SPECT and Q-SPECT/CT in evaluation of pulmonary embolism (PE) or chronic thromboembolic pulmonary hypertension (CTEPH). However, higher false positive rate in Q-SPECT/CT has raised some concerns. Hence, the aim of this study is to evaluate the clinical outcome of Q-SPECT/CT in thromboembolic pulmonary disease **Materials and Methods:** From Jan 2020 to Dec 2020, 29 consecutive patients (M: F = 8: 21; median age= 52 year (21-89)) suspected of having PE or CTEPH were referred for non-contrasted Q-SPECT/CT. All patients were screened negative of COVID PCR tests. Positive findings were based on "MSKCC Q-SPECT/CT" and/or PISAPED criteria. The final diagnosis was established based on composite reference standard that included at least 2-months cardiorespiratory assessment; follow-up Q-SPECT/CT; D-dimer; ultrasound; CTPA; ECG; echocardiography; CXR; HRCT. Results: Q-SPECT/CT was positive in 19 patients; indeterminate in 1 and 9 were negative. Three false positive cases were observed during follow-up. Of the remaining 16 true positive patients, all patients' cardiorespiratory symptom were improved or stable after anticoagulants treatment. Complete or partial resolution of perfusion defect(s) were observed on follow-up Q-SPECT/CT. No anticoagulant was given to negative or indeterminate patients. Their conditions were not deteriorated after 2 months of follow-up and were considered true negative. The overall sensitivity, specificity, PPV, NPV and accuracy of Q-SPECT/CT were 100% (95% CI, 79.41%-100%), 76.92% (95% CI, 46.19%-94.96%), 94.55% (95% CI, 86.53%-97.91%), 100% and 95.38% (95% CI, 80.48%- 99.74%) respectively. **Conclusion:** In view of current COVID-10 outbreak, Q-SPECT/CT can substitute conventional VQ SPECT or SPECT/CT keeping in mind of the small number of false positivity. High NPV excludes thromboembolic pulmonary disease with high degree of certainty. **References:** None

EP-166

A novel, simple equation improving the accuracy of glomerular filtration rate (GFR) measurement with 99mTc-DTPA and two blood samples

G. Arsos, A. Kalaitzoglou, K. Lazaridis, D. Katsampoukas, E. Moralidis;
3rd Dept. of Nuclear Medicine, Aristotle University of Thessaloniki School of Medicine, Papageorgiou Gen. Hospital, Thessaloniki, GREECE.

Aim/Introduction: The convenient GFR measurement by the slope-intercept technique using two blood samples (GFR2), is known to overestimate systematically GFR and all the correction equations, including the most widely applied Brochner-Mortensen (BM), underestimate considerably higher GFR values. We have previously presented an empirical power function equation (PFE), outperforming BM correction in measurements with chromium-51 labeled ethylenediamine tetraacetic acid (51Cr-EDTA), offering results not differing from multisampling, full kinetic analysis (GFRMS), taken as the standard (1). A propos of the replacement of 51Cr-EDTA by 99mTc-diethylenetriaminepentaacetic acid (99mTc-DTPA), we have also shown that the two radiotracers give almost identical values of both GFRMS and GFR2 over a wide range of renal function (2). We aim to investigate the validity of the PFE in predicting GFRMS from GFR2 when 99mTc-DTPA is used for GFR measurement. **Materials and Methods:** GFR was measured for clinical purposes in 338 patients (aged 14-86 years, females 38.8%) by bolus i.v. injection of 99mTc-DTPA and plasma elimination analysis by two-compartment modelling of 10 blood samples obtained between 5 and 240 min p.i., (GFR10, ml/min). GFR2 (ml/min) was calculated from two samples at 120 and 240 min p.i and was properly corrected by the BM formula (GFR2-BM) and by the power function ($GFR2\text{-}PF = 1.5GFR2^{0.9}$). Body surface area was calculated according to Haycock formula. The correlation and agreement of GFR2, GRR2-BM and GFR2-PF with GFR10 were assessed by linear regression and Bland-Altman analysis. Significance was accepted for $p<0.05$. Results: The correlation of GRR2-BM and GFR2-PF with GFR10 was good and excellent respectively (r2, 0.984, 0.981; slope, 1.11, 0.99; constant, -0.2, 1.1 ml/min respectively) with only the slope of the GFR2-PF not differing from unity. Mean bias [95% confidence intervals] between GRR2-BM and GFR2-PF and GFR10 through the entire GFR10 range were minimal for GFR2-PF (-6.8 [-17.8 - 4.2] and -0.4 [-9.8 - 9.0] ml/min respectively, $p<0.05$ for paired bias comparisons). The same parameters for GFR10 higher than 100 ml/min were -13.1 [-26.7 - 0.1] and -0.6 [-14.7 - 13.5] ml/min respectively, $p<0.05$ for paired bias comparisons. **Conclusion:** Our power function equation provides corrected GFR2 values, measured with 99mTc-DTPA, very close to those of the multisampling full kinetic analysis and outperforms Brochner-Mortensen correction especially in higher GFR values. **References:** 1) G. Arsos et al. Eur J Nucl Med Mol Imaging 2017; 44 (Suppl 2): S174-S175. 2) G. Arsos et al. Eur J Nucl Med Mol Imaging 2019; 46 (Suppl 1): S510-S511

EP-167

Comparison of GFR measurement with two-blood sample technique using ^{99m}Tc-DTPA vs. MDRD4 and CKD-EPI equations in potential kidney donors

J. Carvalho, A. B. Marques, F. Abreu, S. Pintão;
Hospital de Santa Cruz - Centro Hospitalar de Lisboa Ocidental, Carnaxide, PORTUGAL.

Aim/Introduction: Accurate determination of glomerular filtration rate (GFR) in the evaluation of renal function is crucial for the selection of potential kidney donors. Nuclear medicine methods are considered accurate in measuring GFR but are not always easily available in every centre. The four-variable Modification of Diet in Renal Disease (MDRD4) and Chronic Kidney Disease Epidemiology Collaboration (CKD-EPI) formulas are two commonly used equations to estimate GFR. The aim of this study was to evaluate the performance of these GFR estimation equations when compared with technetium-99m diethylenetriaminepentaacetic acid (^{99m}Tc-DTPA) clearance. **Materials and Methods:** We compared ^{99m}Tc-DTPA clearance using a two-blood sample method with MDRD4 and CKD-EPI creatinine-based equations in a population of 195 healthy potential kidney donors, from January 2010 to March 2021. Results: A total of 195 potential kidney donors (68.2% female; median age 50 years, range 21 - 75 years) were included in this study. Mean ^{99m}Tc-DTPA measured GFR (mGFR) was 101.5 ± 19.1 mL/min/1.73 m^2, with median mGFR of 101 mL/min/1.73 m^2. Both equations underestimated the GFR value measured by ^{99m}Tc-DTPA (MDRD4: -11.50 ± 18.82 mL/min/1.73 m^2; CKD-EPI: -4.99 ± 17.41 mL/min/1.73 m^2). Pearson's correlation between the estimation equations and the measured method was superior for CKD-EPI ($r=0.525$; $p<0.001$) than for MDRD4 ($r=0.482$; $p<0.001$), even when differentiating between patients with a mGFR ≥90 mL/min/1.73 m^2 (CKD-EPI: $r=0.439$; $p<0.001$; MDRD4: $r=0.345$; $p<0.001$) and those with decreased renal function (CKD-EPI: $r=0.317$; $p=0.02$; MDRD4: $r=0.278$; $p=0.042$). Accuracy within 30% and 10% of the $mGFR_{99mTc\text{-}DTPA}$ value was highest for CKD-EPI (92.3% and 42.1%, respectively, $p<0.01$), especially in patients whose renal function was ≥90 mL/min/1.73 m^2 (95.7% and 47.5%, respectively, $p<0.001$). **Conclusion:** Both creatinine-based formulas tended to underestimate renal function when compared with two blood sample ^{99m}Tc-DTPA measured GFR. However, the CKD-EPI equation showed a better performance than MDRD4 in GFR estimation in healthy potential kidney donors with normal renal function, providing a more accurate tool in the absence of accessible Nuclear Medicine methods. **References:** none

EP-168

Recommending bone scan with Tc99m-MDP as the missing link but an effective method in the initial staging of patients with muscle invasive bladder carcinoma

A. Aghaei[1], A. Masoudifard[1], H. Ghorbani[2], S. Soltani[3], K. Aryana[1], S. Zakavi[1];
[1]Nuclear medicine research center, Mashhad University of Medical Sciences, Mashhad, IRAN, ISLAMIC REPUBLIC OF, [2]Uro-oncology research center, Mashhad university of Medical Sciences, Mashhad, IRAN, ISLAMIC REPUBLIC OF, [3]Urology research center, Mashhad University of Medical Sciences, Mashhad, IRAN, ISLAMIC REPUBLIC OF.

Aim/Introduction: Accurate staging plays a crucial role in determining the type of treatment for bladder cancer patients, especially in high-risk cases. Due to the relatively high prevalence of bladder cancer, which is the second most common malignancy of the urothelial system, and the increasing incidence of various cancers in recent years, it is necessary to be more careful in the initial examination of patients with this type of cancer and determine the appropriate treatment. Based on the results of the bone scan, in the presence of extensive skeletal metastases, patients undergo palliative treatment with chemoradiotherapy without performing unnecessary surgery, otherwise, they will undergo curative treatment with radical cystectomy. **Materials and Methods:** 52 patients with muscle invasive bladder cancer who referred to Ghaem Hospital, Mashhad, between 2018-2020 for bone scanning with Tc99m-MDP, enrolled in the study. 48 out of 52 patients were referred for initial staging and fulfilled our inclusion criteria. Their previous anatomical imaging findings such as abdominal and pelvic CT scans or pelvic MRI were completely evaluated. These patients underwent bone scintigraphy with pelvic SPECT/CT before radical cystectomy. Whole body scanning was performed 4 hours after injection of Technetium 99m-methyl diphosphonate (MDP) in both anterior and posterior views. Since the most common site of bone involvement in these patients Are the pelvic bones and the spine, so at least pelvic SPECT/CT was performed in all patients. Results: frequency of skeletal metastasis was 26.7 percent of which 19 percent was detected by previous pelvic CT/MRI. All the reported skeletal metastasis the previous anatomical imaging, were detected in the bone scan. Hydronephrosis existed in 55.6% of patients. The lymph nodes and bone metastasis Existed in 55.6% and 20.0% of the patients There was no statistically significant relation between bone metastasis with age, lymph nodes metastasis status, serum calcium and ALP levels. There was a significant correlation between hydronephrosis and existence of lymphnode metastasis. But, no relation was found between hydronephrosis and bone metastasis, as well as bone and lymph node metastasis. **Conclusion:** Bone scan has higher diagnostic performance than conventional imaging methods for detecting bone metastases, even after re-evaluation of the CT/MRI images retrospectively by focusing on the site of m,etastasis detected in bone scan images. It changed management in 8.8% of our patients, so we recommend bone scanning in the initial staging of muscle invasive bladder carcinoma patients. **References:** none

EP-169

Prognostic value of diuretic MAG3 renogram in acute kidney injury

***D. Cáceres Silva**, T. Rodríguez Locarno, T. Moreno Monsalve, A. Leiva Montejo, A. S. De Agrela Serrao, J. F. Contreras Gutiérrez, M. I. Castellón Sánchez, J. L. Navarro Fernández, L. Frutos Esteban, L. Mohamed Salem, M. A. Claver Valderas;*
Hospital Clínico Universitario Virgen de la Arrixaca, Murcia, SPAIN.

Aim/Introduction: The aim is to evaluate the usefulness of the renogram as a prognostic factor in acute kidney injury (AKI). **Materials and Methods:** A retrospective analytical study. We included 49 patients with AKI who underwent a Technetium-99m-MAG3 scintigraphy renogram in the acute phase. The patients had a mean age of 58.5 ± 14.5 years; 41 males. A logistic regression analysis was performed to predict the need for chronic hemodialysis (CHD) from sets of factors using cross-validation on 5 binders to obtain the coefficients. All combinations of these variables taken from a 1, 2, 3, 4, and 5 were tested. One-way ANOVAs were performed to compare the distributions of numerical and categorical variables. Multiple hypothesis adjustment factor = 78. For the statistical analysis were used statsmodels and sklearn for Python 3.8.0. Results: The logistic regression analysis showed as a notable result that the factors ('previous creatinine (Cr)', 'acute hemodialysis (AHD)', 'vascular phase') predict chronic hemodialysis (CHD) with a Receiver Operating Characteristic (ROC) curve with an area under the curve (AUC) 0,86. The factors ('previous chronic kidney disease, 'posterior Cr, 'AHD', 'curve morphology') predict CHD with a ROC curve with an AUC of 0.88. Factors ('Age', 'Previous Cr', 'Exitus",'AHD, 'vascular phase') predict CHD with a ROC curve with AUC 0.90. The ANOVAs showed as a remarkable result that the factors ('vascular phase, 'curve morphology') are correlated with a p-value of 0.0084 after using the Bonferroni correction for multiple hypotheses. The factors (' previous Cr', 'curve morphology') are correlated with a p-value of 0.02 and the factors ('Previous Cr', 'curve morphology') are correlated with a p-value of 0.01 without showing significance after the Bonferroni correction. **Conclusion:** There is a relationship between the renogram with respect to the need for CHD. There is a correlation between vascular phase in relation to morphology. There is no relationship between curve morphology and creatinine. It would be a useful technique in the prognosis of AKI. **References:** none

EP-170

Evolution of Renal Function in Living Kidney Donors with ^{99m}Tc-DTPA

P. Azpeitia Hernández, J. A. Pérez Iruela, M. V. Gómez Martínez, J. Bonilla Plaza, M. Gutiérrez Guerrero, I. López Villar, A. Martínez Lorca, O. Ajuria Illarramendi, M. P. Orduña Diez;
Hospital Universitario Ramón y Cajal, Madrid, SPAIN.

Aim/Introduction: Living Kidney Donation is an actual technique for patients in end-stage kidney failure. All possible donors are well screened, where estimated glomerular filtration rate (GFR) is an important parameter to determine actual kidney function. Our protocol included isotopic GFR from renal uptake of technetium [^{99m}Tc] Tc-DTPA (GFRi) and other methods for GFR determination based in creatinine serum. Our aim is to evaluate if there are pretransplant factors that predict increase creatinine levels after donation and the role of isotopic GFR. **Materials and Methods:** This study included 37 potential live donors studied between 2018 -2021. Eight patients were dismissed for comorbidities, 8 (22%) are in process completion and 21 (56%) donated. These 21 consecutive kidney donors (38% men; mean age 52.48 ± 7 years) had a main follow-up of 10 months [1-25] after nephrectomy, showing a creatinine increased (>1.1) in seven patients. We analyzed the possible factors associated with creatinine increased (Group A, normal Cr follow-up [<1.1mg/dl]; Group B lower Cr [> 1.1mg/dl]). Results: We compared group A (n = 14) and group B (n = 7). Group A were 93% female with main age 52.86 ± 8 years, that presented a normal pre-donation renal function of Cr 0.71 ± 0.11, GFR by MDRD-4 89.4 ± 9.6 and GFRi 105.20 ± 30.28 ml/min. Group B (100% male; main age 51.71 ± 5 years), presented normal range of Cr baseline 0.92 ± 0.14, MDRD-4 88.18 ± 15.14 and GFRi 96.42 ± 21.97 ml/min, having a mean creatinine increased of 1.47 ± 0.2 mg/dl. Predictors for creatinine increased were male sex ($p < 0.01$), weight ($p < 0.01$), height ($p < 0.01$) and baseline Cr ($p < 0.05$). The different methods to estimate the GFR, did not show correlation with creatinine increased. However, GFRi has been the method that shown more difference between the two groups. There is a trend of a lower GFRi value with a Cr follow-up increased (A vs B: 105.2 ± 20.28 vs 96.42 ± 21.97; p=0.5). This difference is not statistically significative, but this may change with a higher number of cases. **Conclusion:** Sex, weight, height and creatinine baseline are good predictors of creatinine increased in kidney transplant donors. In our study, the baseline isotopic GFR has shown lower values in donors who presented a creatinine elevation during the follow-up. This data needs to be confirmed in subsequent studies with a greater number of possible donors. **References:** None

EP-36

Wednesday, October 20 - Saturday, October 23, 2021

e-Poster Area, release on Wednesday, October 20 at 09:00

Technologist Digital ePoster

EP-171

The eye can see what the mind knows

A. Ghilardi[1], G. Medolago[2], B. Ondei[1];
[1]ASST-PG23, Bergamo, ITALY, [2]Humanitas Gavazzeni, Bergamo, ITALY.

Aim/Introduction: We wanted to point out the great development of nuclear cardiology procedures such as to allow a diagnostic prognostic multimodality approach in CAD. The appropriate use of non invasive procedures is a crucial issue in diagnosis prognosis and hence critical to manage CAD. Physicians can use many imaging tests: stress echocardiography [ECHO], stress myocardial perfusion [SPECT PET], CTA and CMR. Selecting the right best test may not be simple or even daunting. The knowledge of patient population and benefits limitations of each technology will enable medical imaging professionals to help clinicians in test selection. **Materials and Methods:** We distinguish anatomical [CTA CMR] and functional modalities [SPECT PET ECHO]: the former assess coronary stenosis, the latter ischemia. It's wellknown that anatomical stenosis does not reliably predict ischemia or hemodynamic significance. The choice between anatomical and functional modalities depends on clinical question at hand. Results: Normal perfusion SPECT has high negative predictive value [hard annual cardiac event rate <1%]. These patients benefit medical therapy and may be studied in follow up if symptomatic. Semiquantitative analysis identifies patients with significant perfusion defect [>10%] who need revascularization. In patients with known CAD or with high pretest probability Gated SPECT could be the first choice to determine prognosis and to identify culprit lesion. Phase analysis is helpful to differentiate artifacts due to attenuation, LBBB, Pacemaker and specifically to evaluate efficacy of CRT. To overcome pseudohomogeneous perfusion [balanced ischemia] in multivessels disease new CZT dedicated GC allows to calculate CFR as accurately as PET and to acquire simultaneously two different radionucluides [Tc_{99m}, I^{123}]. PET F^{18}DF is considered gold standard for viable myocardium susceptible to revascularization; recently it showed to be useful to study cardiac sarcoidosis, endocarditis and arterial inflammation. F^{18}DG injected close to peak exercise identifies ischemic anaerobic myocardium. CZT SPECT CT GC obtains a complete anatomical and functional evaluation of CAD, matching fusion images and calculating CFR. At last cardiac sympathetic imaging with MI^{123}BG due to its exceedingly high negative predictive value would identify patient at lower risk in whom a watch and wait strategy could be adopted for

ICD implantation. **Conclusion:** Nuclear Cardiology, in which the role of technologist both in acquisition and processing is relevant, still remains an effective and accurate quantitative multimodality procedure in the diagnostic, but mostly prognostic evaluation of CAD to help clinician in decision making for each patient. **References:** none

EP-172

The usefulness of ^{99m}Tc-Pertechnetate scintigraphy and SPECT/CT in the workup of goiter

A. Tavellin, D. Carazzato, S. Rossetto, D. Grigolato;
Ospedale Mater Salutis, Legnago, ITALY.

Aim/Introduction: To evaluate if adding a SPCT/CT to standard thyroid scintigraphy is feasible for patients with multinodular goiter and may add important information to the clinician **Materials and Methods:** From February 2021 a 99m-technetium thyroid scintigraphy has been performed with planar standard acquisition of the region of the neck for 10 minutes (150 MBq of pertechnetate, matrix) or after reaching 4 x 10^5 counts, immediately followed by a SPCT/CT (Optima, CT 640 GE,120 kV, 30 mA, pitch 1.25, matrix 128x128, 30 projections of 20s) of the neck and chest in all patients with thyroid proved nodules or when there is a suspicious of an intrathoracic development of the gland Results: We have recently started to apply this method to patients with enlarge goiters. Up to now, four patients were submitted to thyroid scintigraphy and SPECT/CT. A man of 50 years old, with a sub-clinical hyperfunctional multinodular goiter with a prominent, non-functional intrathoracic nodule of 8 cm causing a faint compression of the trachea. The second patient, a 83 year-old women, with normal thyroid function and without compressive symptoms of the airway and cervical or thoracic vessels, had surprising giant intra-thoracic goiter at SPECT/CT, which showed enlarge nodules with diffuse calcifications, mimicking a mediastinal bulky mass with moderate compression of the superior cava and trachea.In the remainig two cases, a 64 and a 61 year-old women with multifunctional goiters, SPET/CT correctly identified hot, cold and normal functioning nodules. None of these patients complained about the extra-time spent lying on the acquisition bed, a total of 20-25 minutes **Conclusion:** Hybrid imaging with SPECT/CT can play an interesting role in the workup of patients with intrathoracic thyroid nodules or in multinodular goiters, being useful in giving structural and functional information to the clinicians. The method is well tolerated and feasible in all patients. **References:** none

EP-173

Analytical method validation tests for the development of a new radiopharmaceutical drug : ^{177}Lu-PSMA-1

P. Orhon[1], M. Piquemal[1], P. Bedouch[2], J. Vuillez[3], L. Djaileb[3], M. Desruet[1], J. Leenhardt[1];
[1]Radiopharmacy, Grenoble Alpes University Hospital, Grenoble, FRANCE, [2]Pharmacy department, Grenoble Alpes University Hospital, Grenoble, FRANCE, [3]Nuclear Medicine, Grenoble Alpes University Hospital, Grenoble, FRANCE.

Aim/Introduction: The development of a new therapy using PSMA-1 ligand labeled with ^{177}Lutetium requires the submission of an Investigational Medicinal Product Dossier (IMPD). Beforehand, we had to validate the analytical methods in order to determine the radiochemical purity (RCP) by High Performance Liquid Chromatography (HPLC) and Thin Layer Chromatography (TLC) methods. The aim of these validations is to prove that both methods are suitable for the intended purpose. **Materials and Methods:** Lu-PSMA-1 (non-radioactive reference standard), ^{177}Lu-PSMA-1 and free ^{177}Lu (impurity) were injected in HPLC and TLC following the manufacturer instructions. Accuracy, precision, intermediate precision, specificity, linearity, robustness, detection limit (LoD) and quantification limit (LoQ) were evaluated. Means, standard deviations and variation coefficients (CV%) of the RCP, the retention time (Rt) and the retention factor (Rf) were calculated and linear regression coefficients (R^2) were determined for linearity and accuracy evaluations. Results: Identification test confirmed that Rt of the main peak of the radioactive product corresponded to the retention time of the non-radioactive reference standard. The analytical method was specific to properly separate potential impurities from the radiopharmaceutical ^{177}Lu-PSMA-1 (resolution = 18 in HPLC and 3.14 in TLC). The accuracy of the method was achieved by spiking a known amount of free ^{177}Lu with ^{177}Lu-PSMA-1, resulting in a percentage recovery of 100.94% for HPLC and 99.91% for TLC. The linearity of the radiodetectors was evaluated through linear regression coefficients (HPLC R^2= 0.9978 ; TLC R^2 = 0.9997). Precision results for retention time and radiochemical purity were conformed for HPLC (Rt : 17min32±1min, CV%=0.12% and RCP : 98.78%±0.72%, CV%=0.73%) and TLC (Rf : 0.918±0.03, CV%=3.16% and RCP : 99.12%±0.89%, CV%=0.90%). For each of the conditions tested in order to evaluate the robustness of the method we observed a variation of Rt (13min24±8, CV%=1.07% and 17min53±3 CV%= 0.28%) in HPLC and a modification of Rf (0.367±0.036, CV%=9.68%) in TLC. Finally, from background measurments, LoD and LoQ were defined as 12 and 34 kBq in HPLC and 20 and 62 kBq in TLC respectively. **Conclusion:** All these results demonstrated the robustness and reliability of our analytical method for the evaluation of ^{177}Lu-PSMA-1 radiochemical purity. This work will be annexed in the IMPD file and submitted to the French National Agency for the Safety of Medicines (ANSM) to obtain the authorization to carry out this automated preparation in our radiopharmacy laboratory. **References:** EANM guideline on the validation of analytical methods for radiopharmaceuticals

EP-174

Yttrium microspheres irradiated at the IRT-T reactor for radioembolization of liver cancer

V. Sadkin[1], E. Nesterov[1], A. Rogov[1], E. Stasyuk[1], K. Mayorov[2], S. Getia[2], N. Sashova[2], N. Markov[2];
[1]National Research Tomsk Polytechnic University, Tomsk, RUSSIAN FEDERATION, [2]BEBIG, Moscow, RUSSIAN FEDERATION.

Aim/Introduction: Tomsk Polytechnic University (TPU), together with an industrial partner (BEBIG), start produced yttrium microspheres at its research nuclear reactor this fall. This radiopharmaceutical is intended for the treatment of liver cancer in inoperable patients and, unlike analogs, it destroys the tumor in a targeted manner without affecting healthy organs and tissues. **Materials and Methods:** Microspheres are produced from yttrium-aluminosilicate glass with a composition in a mass ratio for oxides of 2: 1: 2, respectively. Irradiation of yttrium-89 microspheres will be carried out at the IRT-T reactor, power 6 MW, neutron flux $1.7 * 10^{14}$ neutron/cm^2 To obtain one dose of the final preparation, a weighed portion of 0.1 g of yttrium microspheres is irradiated. For 3.5 hours of irradiation, a therapeutic dose of 1 GBq sources with a three-day preliminary calibration is achieved in the reactor. Microspheres are processed using distilled water, alcohol and hydrochloric acid. An assessment of the radionuclide purity was carried out using a gamma spectrometer based on a semiconductor ultrapure germanium detector and a pulse analyzer with a resolution of 1.7 keV along the 1332 keV ^{60}Co line. The impurity of the main accompanying isotopes ^{88}Y / ^{89}Sr, ^{65}Zn and ^{152}Eu at the date of introduction is less than 10^{-4}%. Yttrium microspheres are injected into the patient's bloodstream, which delivers them directly to the tumor. After delivery, the microspheres block the access of blood with oxygen to the metastases, in parallel acting on them with beta radiation. In the Russian Federation, this method of treatment is not yet massively applied. Results: The industrial production of yttrium microspheres began in the fall of 2020. There have already been test deliveries to Moscow clinics. The drug is registered and has permits for use in clinical practice. **Conclusion:** April 9, 2021 at A. Tsyb Medical Radiological Research Center for the first time in Russia, clinical trials of the method of radioembolization of tumors with domestic microspheres produced by the Russian company "Bebig" began. Four operations were performed at once on patients with inoperable forms of liver cancer. **References:** none

EP-175

Dosimetry prior to I-131 therapy in hyperthyroidism using thyroid computed tomography value

H. Ikeda[1], N. Fujita[2], Y. Ochi[1], M. Nishio[1], Y. Asano[1], S. Abe[2], K. Kato[1];
[1]Department of Integrated Health Science, Nagoya University Graduate School of Medicine, Nagoya, JAPAN, [2]Nagoya University Hospital, Nagoya, JAPAN.

Aim/Introduction: The activity to be administered by I-131 therapy for hyperthyroidism is determined using the radiation absorbed dose necessary to cure the thyroid volume and the residence time (RT) of I-131 in the thyroid volume. It takes time and effort to determine the accurate RT of I-131 because multiple time measurements are required after the administration of test dose of I-131. If only one early measurement at 1-4 days is used to determine the RT of I-131, the effect of the effective half-life cannot be considered; this increases the measurement error. In past our study, thyroid computed tomography (CT) value correlates with the effective half-life. Therefore, we investigated the possibility of improving the estimation accuracy of I-131 thyroid RT using thyroid CT value. **Materials and Methods:** Seventy patients with Graves' disease were included in this retrospective study. Three uptake assessments including measurements 3 h, 24 h, and 4-7 days after oral administration of I-131 (3.7 MBq) were used to deduce the reference RT (RT_{ref}) according to EANM guidelines. We also determined RT_{24h} based on only one measurement at 24 h and the fixed effective half-life. A regression equation for estimating the effective half-life from the thyroid CT value was created using a single regression analysis of the effective half-life and thyroid CT value. RT_{CT} was calculated based on the 24-h uptake and the estimated effective half-life from the thyroid CT value. RT_{24h} and RT_{CT} were compared with RT_{ref}, and the errors were respectively calculated. Results: RT_{24h} determined from the 24-h uptake had an error of > 50%, with a mean absolute error of 33%. In patients with a long effective half-life, RT was underestimated, and in patients with a short effective half-life, RT was overestimated. Further, RT_{CT} based on the estimated effective half-life from the CT value resulted in an error of < 40%. The mean absolute error was 18% when using RT_{CT}, i.e., less error than that when using RT_{24h}. **Conclusion:** The RT_{CT} calculated using the 24-h uptake and effective half-life estimated from the CT value had a smaller maximum error and absolute mean error than the RT_{24h} calculated using only the 24-h uptake. The estimated effective half-life calculated from the thyroid CT value could be used to improve the estimation accuracy of the I-131 thyroid RT, if I-131 uptake was not measured multiple times. **References:** none

EP-176

Radiation safety in PET-CT preparation

T. Säilä[1], S. Lahti[1], T. Raita[1], J. Husari[2], T. Taatila[2];
[1]Tampere University of Applied Sciences, Tampere, FINLAND,
[2]Tampere University Hospital, Tampere, FINLAND.

Aim/Introduction: The aim of this study was to increase knowledge related to the radiation safety in 18F-FDG studies in the Department of Nuclear Medicine, which has been operating in the new premises for eight months. Research questions are: How distance and location in the room affect dose rate and how time spent on cannulation or positioning affects the radiation doses of the NM staff? **Materials and Methods:** The entire data comprises two parts: the first data were collected from five different points in the patient preparation room and the second data from the imaging room during F18-FDG imaging. The dose rate was measured at two different distances from the patient. The measurements were performed by several radiographer students. Therefore, detailed instructions and data collection forms were prepared in advance. The dose rates were measured with a radiation meter calibrated by the Radiation and Nuclear Safety Authority. Results: The study is currently in process, so only preliminary results are available. Based on the results of the measurements in the preparation room, it will be possible to assess at which point in the room it is safest to work and in what order the patients should be placed in the room. The results will be illustrated in relation to the floor plan of the room. Preliminary results suggest that the dose rate decreases more with increasing distance than when operating behind a lightweight wall. The results from the imaging room measurements determine how large the change in dose rate (%) is as the distance increases. In this study dose rates are also illustrated by describing the radiation dose relative to the time required for cannulation and patient positioning at various distances and locations in preparation and imaging rooms. The dose rates will be described using tables and graphs. **Conclusion:** The radiographers and nuclear medicine technologists working in the department of NM ought to understand the importance of distance and shielding material in their daily work especially when working with new equipment in new facilities. Based on the measurements a radiation safe workflow can be better designed and the effectiveness of structural radiation protection can be proved. **References:** None

EP-177

Operational Organization of a Clinical and Translational Research Environment using Today's Digital Technologies

L. Merrin[1], A. Pippin[1], M. M. Knopp[2], M. Timko[1], K. Binzel[1], M. V. Knopp[1];
[1]The Ohio State University Wexner Medical Center, Columbus, OH, UNITED STATES OF AMERICA, [2]Technical University of Munich, Munich, GERMANY.

Aim/Introduction: As clinical and translational research operations require rigorous documentation and organization even more than for clinical care due to extensive regulatory and compliance requirements in molecular imaging, we embarked on a systems engineering based approach to reorganize our operational processes embracing today's readily available digital technologies. We present our approach and experience focusing on all aspects relevant to clinical and translational molecular imaging. **Materials and Methods:** During a systems engineering analysis we identified essential process components and developed an approach we referred to as the Amazon- and Google-lization of all process steps. These tech giants extensively use and rely on unique identifiers / tags for everything and every step that enables creation of a unique fingerprint that can then be linked and processed out of any data lake approach using readily available tools like Microsoft Excel or Google sheets. The key is to create timestamped events, tasks, or items that create a continuous trail of tasks, procedures and events. The use of QR code labeling, that can be readily scanned by pocket-size QR barcode scanners, is essential and can be inexpensively accomplished with today's digital tools. The linkage of electronic capture forms with linearly structured spreadsheets enables readily implementable optimization with the ability to track and record every step, item, imaging, or facility process. Results: In this presentation we demonstrate how we have implemented this tag and processes fingerprinting approach. These tools can readily be created and adapted to ever changing environments. QR code labels are efficient and effective. They truly helped to revolutionize and enable a real-time documentation as well as task management for process steps from the acquisition of materials to scheduling to capture of radiation safety relevant information and image analysis. **Conclusion:** Operational workflow can be readily improved by leveraging today's digital technologies which can feedback real time dashboards. Most importantly, a flexible and readily adaptable / modifiable process management can be achieved which is of increasing importance in clinical and translational molecular imaging environments due to the ever-increasing requirements of documentation. We observed substantial improvements in efficiency and quality of documentation but also to assign process specific tasks which can guide team members also in research like what is in place for clinical radiology information

systems. We were actually surprised that such capabilities could be implemented without purchasing any major software utilizing available capabilities of Microsoft 365 and or Google G suite features. **References:** none

EP-178

Contribution of Listening to Music in Reducing Anxiety in Bone Scintigraphy

M. Boal[1], *E. Pereira*[2], *D. Branco*[3], *T. Guerreiro*[3], *L. Vieira*[4];
[1]*Instituto Superior de Engenharia de Lisboa/Escola Superior de Tecnologia da Saúde de Lisboa, Lisbon, PORTUGAL,* [2]*NuclearMed, Hospital Particular de Almada, Almada, PORTUGAL,* [3]*LASIGE, Faculdade de Ciências, Universidade de Lisboa, Lisbon, PORTUGAL,* [4]*H&TRC and CIMOSM, Lisbon, PORTUGAL.*

Aim/Introduction: Anxiety in cancer patients is very common, partially due to diagnostic procedures and to the uncertainty regarding examination results. There are many anxiety reducing methods described in literature, being the most studied listening to music. To our best knowledge, a study evaluating whether listening to music contributes to anxiety reduction in patients undergoing bone scintigraphy has not yet been carried out. The aim of this study is to assess the effect of listening to music during bone scintigraphy on breast cancer patient's anxiety level. **Materials and Methods:** Study carried out in patients with breast cancer, who underwent bone scintigraphy by clinical indication. These patients underwent a non-pharmacological strategy of listening to music during bone scintigraphy imaging. Physical activity (accelerometer), psychological (STAI) and physiological (heart rate, blood pressure, oximetry) measures were used. Physical activity was measured for 3 days prior to the procedure using a wrist accelerometer and physiological measurements were taken before and after imaging. A pre-examination questionnaire and a questionnaire about the procedure were also given to the patients and the short version of the STAI questionnaire was completed before and after the procedure. Results: Preliminary results show variations in blood pressure before and after the procedure and different sleep/wake patterns in the night before the exam, suggesting that these indicators can be used to assess anxiety, and the efficacy of future interventions. **Conclusion:** The efficacy of non-pharmacological interventions to reduce anxiety in examinations has been poorly evaluated. This study aims to provide objective evidence of the benefits of listening to music during bone scintigraphy. Preliminary analysis has focused on assessing face validity, revealing that the instruments are sensitive to change and applicable to assess the impact of an intervention. **References:** none

EP-37

Wednesday, October 20 - Saturday, October 23, 2021

e-Poster Area, release on Wednesday, October 20 at 09:00

Paediatrics

EP-154

Analysis of Pediatric Patients Requiring PET/CT and Additional Other Nuclear Medicine Methods in the management of cancer

S. Soyluoglu, *U. Korkmaz;*
Trakya University, Medical School, Edirne, TURKEY.

Aim/Introduction: The use of PET/CT in pediatric oncology has not been clarified by guidelines as in adult patients due to the lack of large-scale and multicenter studies. The reason for this may be that these tumors are less common and clinicians are more hesitant about the use of radiation in pediatric patients. The aim of this study is to retrospectively evaluate pediatric patients referred to PET/CT and additional Nuclear Medicine applications for diagnosis and follow-up of malignant diseases, and to analyze the contribution of these applications to patient management. **Materials and Methods:** Patients under the age of 18 who were referred to the PET/CT unit for oncological diagnosis between 2010 and 2020, whose data could be accessed from the patient archive system, were included in the study. The patient files were analyzed retrospectively, findings and their contribution to patient management were evaluated. Results: Over a ten-year period, 364 PET/CT (345 F-18 FDG, 17 Ga-68, 2 NaF) scans were performed in 171 pediatric patients for investigation of malignancy (96 boys, 75 girls, mean age: 9±5.5, min:4 months, max:17 years). While 102 patients had only PET/CT, 69 patients required at least one other Nuclear Medicine examination (Tc-99m MDP, I-123-MIBG, I-131, Tc-99m MIBI, Tc-99m pertechnetate, Tc-99m Mag3/DTPA/DMSA) during the staging or treatment process. The average number of PET/CT was 2.1±1.5 (min:1, max:9). When other Nuclear Medicine examinations were added, the average number of examinations per patient was found 3.1±2.6 (min:1, max:16). The highest total dose received by a pediatric patient was 78 mSv, an osteosarcoma patient followed for 11 years. The most common PET/CT indication was lymphomas (N=62) followed by soft tissue sarcomas (N=37). The most common group requiring multiple examinations was neuroblastoma and paragangliomas. The highest radiation exposure was seen in bone tumor patients due to multiple PET and bone scintigraphy studies. In 25 patients, multiple modalities provided guidance in making treatment decisions/changes or symptom management. No complications or malignancies secondary to radiation were detected during the follow-up period. **Conclusion:** F18 FDG PET/CT is the most commonly used imaging method in pediatric oncological diagnosis and

staging. Although PET/CT exposes relatively high radiation doses for pediatric patients, it stands out because of the benefits it provides. FDG, other Non-FDG PET agents and other scintigraphic methods step in when clinicians have come to a crossroad at the decision stage, and contribute significantly to the determination of the treatment protocol and patient management. **References:** None

EP-155

Slope-intercept vs. single-sample glomerular filtration rate in children

J. Holness, A. Brink;
University of Cape Town, Cape Town, SOUTH AFRICA.

Aim/Introduction: For measurement of glomerular filtration rate (GFR) in children, the European Association of Nuclear Medicine (EANM) guideline recommends using either the slope-intercept method (SI-GFR) or a single-sample technique (SS-GFR). The procedure can be traumatic for children who are young or have difficult venous access, therefore a clear advantage of SS-GFR is that it requires only one blood sample. However, the timing of the single sample is dependent on kidney function. When the GFR is high the sample can be taken at 2h, but in cases of kidney failure, the sample needs to be delayed to 6h or even 24h. This is inconvenient for patients and their caregivers. An additional problem is that one frequently does not know at the outset what the child's GFR will be for purposes of scheduling the blood sample. In our setting, changing from SI-GFR to SS-GFR will only be advantageous if the blood sample can be taken at one fixed time point, preferably at 2h, in all children. The aim of this study therefore was to compare SS-GFR (2h) and SS-GFR (4h) to SI-GFR. **Materials and Methods:** This was a retrospective analysis of GFR measurements performed using ^{51}Cr-EDTA or ^{99m}Tc-DTPA. Blood samples were taken at 2h and 4h. SI-GFR was calculated following the EANM and British Nuclear Medicine Society (2004) guidelines. The Jödal Bröchner-Mortensen correction was applied. SS-GFR was calculated using the Fleming equation at the two time points. Bland-Altman analyses were used to assess the agreement between the methods, and the proportions of measurements that differed by >10 ml/min/1.73m^2 were determined. Results: 318 GFR measurements were included, median GFR 92 ml/min/1.73m^2 (IQR: 72-111 ml/min/1.73m^2). The median differences (SS-GFR - SI-GR) were 1.9 ml/min/1.73m^2 (2h) and 5.4 ml/min/1.73m^2 (4h). The 95% limits of agreement were ±11.3 ml/min/1.73m^2 (2h) and ±22.3 ml/min/1.73m^2 (4h). SS-GFR (2h) differed from SI-GFR by >10 ml/min/1.73m^2 in 9.1% of cases and SS-GFR (4h) in 33.3% (P<0.001). In 3/318 (0.9%) of cases SS-GFR (2h) and SI-GFR were within 20 ml/min/1.73m^2 of each other. **Conclusion:** In the majority of patients there was good agreement between SI-GFR and SS-GFR (2h). Validation of these findings by comparing SS-GFR (2h) to GFR calculated from the area under the full plasma clearance curve would be useful. The agreement between SS-GFR (4h) and SI-GFR was poor, but this is likely to reflect errors common to both methods e.g. low counts for the 4h samples. **References:** none

EP-156

Evaluate the efficiency of SPECT/CT in the diagnosis of mandibular unilateral active condylar hyperplasia

J. Maraña González, J. Suárez Fernández, M. López Carballo, A. Laverde Mächler, L. Rodríguez Díaz, M. Domínguez Grande, N. Martín Fernández, D. Lisei Coscia, F. González García;
HUCA, Oviedo, SPAIN.

Aim/Introduction: Evaluate the contribution of SPECT/CT in the diagnosis of Mandibular Unilateral Active Condylar Hyperplasia (ACH) and comparation with SPECT. **Materials and Methods:** 27 consecutive patients referred for suspected ACH and explored by bone scan with SPECT/CT between June 2016 and November 2019 were retrospectively selected. 5 patients were excluded due to insufficient follow-up or surgery performed > 6 months after scintigraphy. Finally, 22 patients were analysed (10 men and 12 women, median of age 20 years old). A bone scintigraphy with SPECT/CT on the mandible area was performed 3 hours after the injection of 99mTc-DPD. A differential quantitative analysis of total events in condyles using regions of interest in grouped axial slices was done. Evaluating the SPECT images, those with a quantitative difference >10% between both condyles were considered positive for ACH and those with a difference <10% as negative. Considering the SPECT/CT studies same criteria were applied, but those whose CT image presented normal condylar morphology and/or pathological alterations of the temporomandibular joint were also classified as negative. The final diagnosis was based on the histological analysis of the resected specimens or on clinical and radiological criteria after a minimum follow-up of 3 months. Results: The sensitivity, specificity, positive and negative predictive values, and accuracy were 100%, 78%, 50%, 100% and 82% for the SPECT differential quantitative study and 100%, 89%, 67%, 100% and 91% for the SPECT/CT study, respectively. Two cases with false negative results in the SPECT study were correctly diagnosed by SPECT/CT (one with normal condylar morphology and the other with temporomandibular arthropathy). **Conclusion:** Bone scintigraphy with SPECT/CT is a useful imaging method for the diagnosis of ACH with a high negative predictive value, and which also increases the specificity, positive predictive value and accuracy of the quantitative differential SPECT study of the mandibular condyles. **References:** None

EP-157

Quantitative assessment of ^{123}I-MIBG uptake in children in determining the unfavorable histological type of neuroblastoma

M. Yadgarov[1], N. Matveev[2], K. Chaurasiya[1], E. Kireeva[1], Y. Likar[1]; [1]Dmitry Rogachev National Medical Research Center, Moscow, RUSSIAN FEDERATION, [2]Russian National Research Medical Univercity, Moscow, RUSSIAN FEDERATION.

Aim/Introduction: Scintigraphy with ^{123}I-MIBG plays an important role in the diagnosis and assessment of the tumor process in neuroblastoma. In recent years, data have emerged on the possible relationship between the degree of ^{123}I-MIBG accumulation and the histological variant of neuroblastoma. The aim of our work was to determine the significance of the quantitative assessment of SUVmax in the non-invasive determination of an unfavorable histological type of neuroblastoma, which is associated with a poor prognosis. **Materials and Methods:** The retrospective analysis included 153 pre-therapy patients with neuroblastoma; the median age was 17.7 months (range 1 to 125). 122 patients (79.7%) had a poorly differentiated (unfavorable) variant of neuroblastoma and 31 patients (20.3%) had a highly differentiated variant (ganglioneuroma). All patients underwent SPECT / CT scintigraphy, and the accumulation of the ^{123}I-MIBG in the primary tumor was assessed using the work station with the calculation of the SUVmax parameter. Intergroup analysis was performed using the Mann Whitney U-test, the optimal cut-off value for the SUVmax parameter was selected based on the optimal sensitivity / specificity ratio according to the results of the ROC analysis. Results: Patients with an unfavorable histological variant of neuroblastoma had significantly higher SUVmax values in comparison with patients with a favorable variant: median 5.5 [3.3; 8.3] versus 2.9 [1.6; 4.4], $p<0.001$. The AUC for SUVmax was 0.769 (95% CI: 0.642; 0.895), the optimal cut-off value was 3.74, allowing oncologists to classify patients according to the degree of tumor differentiation with 71.0% sensitivity and 70.6% specificity. **Conclusion:** Method of non-invasive determination of histological type of neuroblastoma, based on an SUVmax assessment, together with the additional data may have important implications for clinical management of patients with neuroblastoma. **References:** none.

EP-158

Prognostic Factors in Children with Hydronephrosis and Urinary Tract Infection

I. Grierosu[1,2], R. Tibu[2], A. Tarca[2], T. Ionescu[1], C. Stolniceanu[1], W. Jalloul[1], A. Statescu[2], M. Starcea[1,3], R. Russu[3], M. Munteanu[3], V. Ghizdovat[1,2], L. Teodoriu[1,2], C. Stefanescu[1,2]; [1]UMF "Grigore T. Popa", Iasi, ROMANIA, [2]County Emergency Hospital „Sf. Spiridon", Iasi, ROMANIA, [3]Hospital "Sf. Maria", Iasi, ROMANIA.

Aim/Introduction: Our experience is owing to 10 years of collaboration between two single centres from the North-East Region of Romania, Paediatric Nephrology and Nuclear Medicine. A radioisotopic nephrogram offers many functional information for clinicians. It is well known that T_{max} especially gives an orientation about parenchymal status. Therefore, it could be interesting to describe renal parenchyma from both points of view: functional and morphological. **Materials and Methods:** From 1123 paediatric cases (age range between 3 months and 17 years) referred to the Nuclear Medicine Department, we chose only 73 cases of hydronephrosis who underwent, not longer than 2-3 days apart, both radioisotopic investigations: ^{99m}Tc DTPA and ^{99m}Tc DMSA. There were preponderant male subjects (60.27%). All children had minimum one episode of urinary tract infection in their antecedents. Dynamic and static images were acquired with a Siemens Diacam double-headed gamma camera. Results: We compared T_{max} (obtained on nephrogram) with scintigraphically estimated GFR (glomerular filtration rate) and the number of scars (in renoisotopic scan) for each kidney, in a total of 146 kidneys. The children were divided in three age groups: group 1 = between 3 months and 1 year, group 2 = 1 to 12 years, and group 3 = 12 to 18 years old. We found a medium correlation only between T_{max} and the number of scars, between groups 1 and 2, $R_1 = 0.4746$ (p_1 value = 0.04658) and $R_2 = 0.4011$ (p_2 value = 0.00002). The other correlations, T_{max} compared with GFR and GFR with number of scars were not statistically significant. It looks that only the number of scars influence the parenchymal radiotracer transit and has inconsiderable influence on GFR. **Conclusion:** Our results conclude that the scars influence T_{max} but none of them influences GFR. In the absence of new episodes of urinary tract infection and with a good therapeutic approach, the scars will recede, even disappear. In these conditions, we recommend to repeat the radioisotopic investigations during the healing process, to observe the curve parameters evolution, such as the time of parenchymal transit. **References:** none

EANM22

WORLD LEADING MEETING

35th Annual Congress of the European Association of Nuclear Medicine

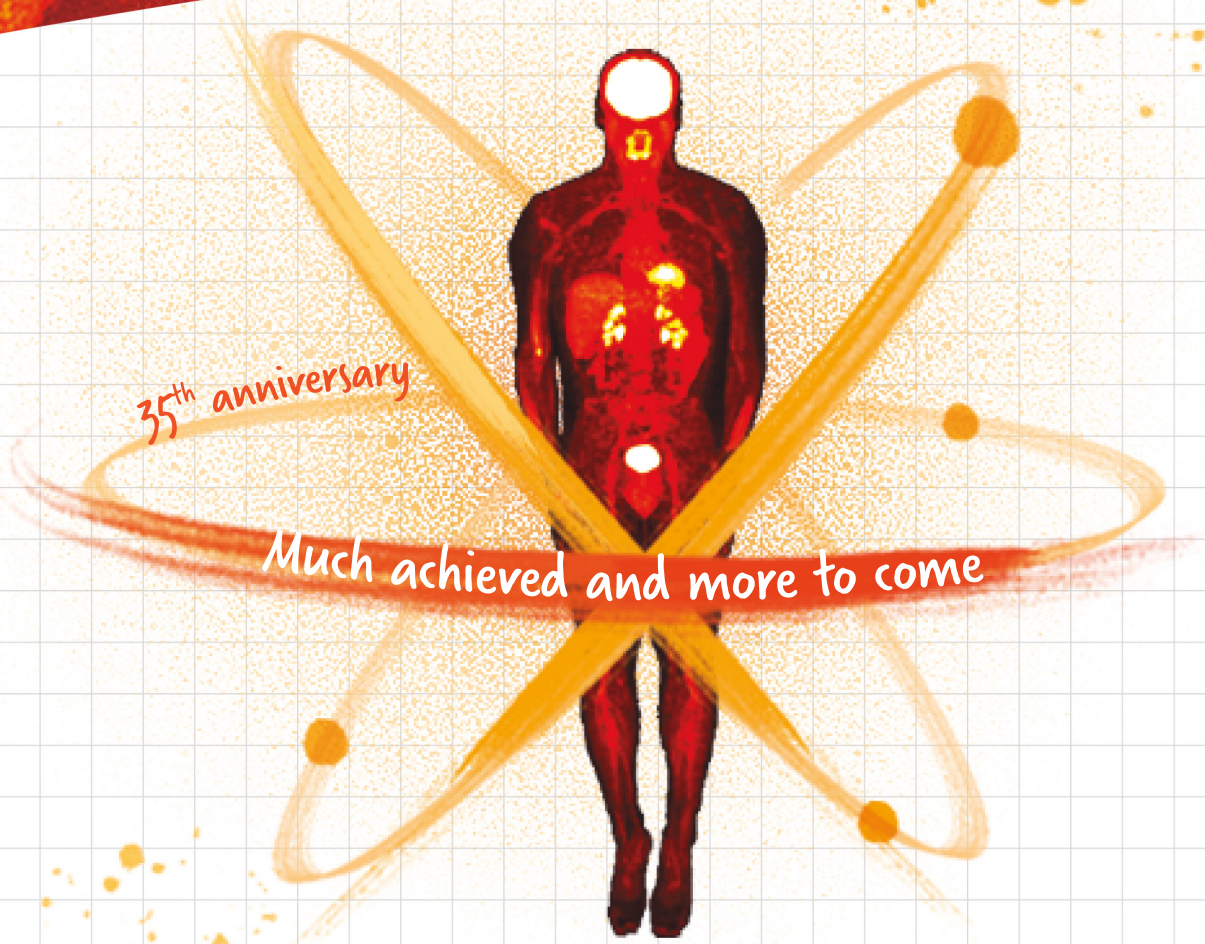

BARCELONA

Oct 15 - 19, 2022

eanm22.eanm.org

ESMIT

European School of Multimodality Imaging and Therapy

Course Programme 2022

In order to make it easier for our community to make the most of their Continuous Medical Education, ESMIT is expanding its educational offers.

Our 2022 programme will include:

4 new **Online Courses** | **15** new **Live Webinars** | **7** new **Advanced Courses** in Vienna

... organised in 5 Thematic Tracks:

- Artificial Intelligence and Quantification
- Clinical Nuclear Medicine
- Scientific Track
- Theranostics
- Cardiac Amyloidosis (EURO-LEARN)

Registration for 2022 will open during the EANM 2021 Congress. Do not forget to visit the ESMIT Booth!

Get your Dose of Education

More information at **eanm.org/esmit** or contact us at **esmit@eanm.org**

FOCUSMEETING.EANM.ORG

SEVILLE, SPAIN

FEBRUARY 3-5, 2022

EANM 4 FOCUS

MOLECULAR IMAGING AND THERAPY IN HAEMATOLOGICAL TUMOURS

EUROPEAN ASSOCIATION OF NUCLEAR MEDICINE